Correspondence

Evolution: students debate the debate

I asked my third- and fourth-year undergraduate students whether they thought that evolutionary theory needs rethinking (see *Nature* **514,** 161–164; 2014). More than two-thirds (26 out of 38) argued that it did not — because the synthesis proposed by Kevin Laland *et al.* has largely already occurred.

Far from being neglected as Laland and colleagues imply, topics such as developmental bias, plasticity, niche construction and extra-genetic inheritance are well established in basic courses on evolutionary theory. Students today recognize that these processes can be both outcomes and causes of evolution. There is also a large body of work on co-evolutionary dynamics and interacting phenotypes (see, for example, any of the 400 or so papers that cite J. B. Wolf *et al. Trends Ecol. Evol.* **13,** 64–69; 1998).

Although all of my students agreed that the phenomena discussed by Laland and colleagues warrant further study, they — like the authors of the counterpoint piece, Gregory Wray *et al.* — did not view the authors' ideas as an "alternative vision of evolution". There would therefore seem to be no "struggle for the very soul of the discipline".

Hope Klug *University of Tennessee, Chattanooga, USA.*
hope-klug@utc.edu

Evolution: viruses are key players

The debate on rethinking evolutionary theory (see *Nature* **514,** 161–164; 2014) should include viruses. By integrating into host DNA, viruses have markedly influenced the evolution and development of cellular organisms (see, for example, F. Baluška *Ann. NY Acad. Sci.* **1178,** 106–119; 2009).

Viruses are the most abundant genetic entities on the planet. Almost all genomes of cellular organisms contain viral sequences, elements of which are now essential in gene regulation.

Persistent endogenous retroviruses, for example, have contributed crucially to the evolution of the mammalian placenta. And the genetic variations that led to the evolution of adaptive immunity in vertebrates, or the equivalent system in prokaryotes, were not a result of random errors in DNA replication but of viral infection events (see L. P. Villarreal *Viruses* **3,** 1933–1958; 2011).

Guenther Witzany *Telos-Philosophische Praxis, Bürmoos, Austria.*
František Baluška *University of Bonn, Germany.*
baluska@uni-bonn.de

Evolution: networks and energy count

Standard evolutionary theory should incorporate the complexity of adaptive evolving systems — including species, niches and environment — as dynamic relationship networks (see *Nature* **514,** 161–164; 2014).

For example, epigenetic inheritance — which changes gene expression but not the DNA sequence — involves the storage of molecular information and its retrieval, transfer and processing at the supramolecular level. This involves transitory processes that are self-organized, self-assembled and dynamic.

DNA replication too is one of countless functional tasks of interest in the study of evolution: changes propagate through interlinked levels of organization, inducing connectivity and interaction at all scales of the multilevel system.

The process of natural selection is now being captured, by modelling fitness attractors that incorporate power laws and non-equilibrium steady states at the edge of chaos, with energy landscapes made of basins, valleys, floors, ridges and saddle points (see, for example, K. Friston *J. R. Soc. Interface* **10,** 20130475; 2013).

Arturo Tozzi *ASL Napoli 2 Nord, Naples, Italy.*
tozziarturo@libero.it

NATURE.COM
For more on the evolutionary theory debate, see: go.nature.com/gbqfv9

Anti-vivisectionists respond

Following our seven-month undercover investigation, the British Union for the Abolition of Vivisection (BUAV) strongly disagrees with your claim that the Max Planck Institute in Tübingen, Germany, has done a "good job" on its website in explaining its neuroscience research on macaques (see *Nature* **513,** 459–460; 2014).

Our investigation of the macaques' treatment and conditions was undertaken with SOKO-TS, a German animal-protection organization. The BUAV goes to enormous lengths to check facts and is extremely careful only to publish allegations that it believes are demonstrably true.

After rigorously scrutinizing footage and documentation from this investigation, the leading German television station Stern has called into serious question claims and images posted on the Max Planck Institute's website. For example, the institute makes what in our opinion is the bizarre claim on its website that the animals do not suffer.

Jane Goodall, the renowned primatologist, says she has seldom seen such sickening experiments. They have no place in a civilised society.

Following the Stern broadcast, the institute has identified a need for improvement in terms of staff organization and agreed to introduce overnight care for the animals following surgery and to improve veterinary attention.

We consider that the use of macaques in these experiments is unnecessary: the continued creative and ethical use of imaging techniques on patients and volunteers is, we believe, far more likely to produce improvements in neurological health.

It is not better PR that animal researchers need, as you argue, but a paradigm shift in thinking, a better appreciation of the suffering they cause animals and a commitment to genuine transparency.

Michelle Thew *BUAV, London, UK.*
michelle.thew@buav.org

Ice-bucket challenge should jolt funding

The Italian prime minister Matteo Renzi was among the vast number of people who accepted the 'ice-bucket challenge' this summer, helping to raise €2 million (US$2.5 million) in Italy for research into amyotrophic lateral sclerosis (ALS), also known as motor neuron disease (see *Nature* **514,** 403–404; 2014).

This sum exceeds his government's average annual budget for ALS research, which is still seriously underfunded — despite Italy ranking third in international ALS publications, after the United States and Japan.

ALS researchers worldwide are waiting to see how the sum of around $100 million that has been collected by this philanthropic phenomenon will be used, and whether it will boost governments' plummeting contributions towards basic research. I hope so: without such funds there can be no development of new drugs for this incurable disease.

Maria Teresa Carrì *University of Rome 'Tor Vergata', Italy.*
carri@bio.uniroma2.it

© 2014 Macmillan Publishers Limited. All rights reserved

Society for Chaos Theory in Psychology & Life Sciences

NEWSLETTER

Vol. 22, No. 3
April, 2015

Feature Article

NEURAL CODE & POWER LAWS

The road from spike frequency to mental states is paved with intermediate energetic steps which can be defined and quantified

Arturo Tozzi, MD, PhD
ASL Napoli 2 Nord, Distretto 45
Caivano, Naples, Italy

ABSTRACT

The brain electric activity exhibits a power law distribution which appears as a straight line when plotted on logarithmic scales in a log power versus log frequency plot. The slope of the line is given by a single constant, the power law exponent. Since a variation in slope may occur during different functional states, the brain currents are said to be multifractal, i.e. characterized by a spectrum of multiple possible exponents. A role for such non-stationary scaling properties in neural coding has scarcely been taken into account. Here we show that changes in fractal slopes and in the message content are correlated. Taking into account arguments concerning entropy, we illustrate that modifications in power law exponents are associated with variations in the Rényi's entropy, which is a generalization of Shannon's entropy. Changes in Rényi's entropy, in turn, are able to modify the information transmitted by spikes. Our results point up that multifractal systems lead to different probability outcomes based solely on increases or decreases of the fractal exponents. We offer new insights in the characterization of the forces required for transcranial stimulation, where doubts still exist about the parameters of the waveforms to employ. We indeed anticipate our essay to be a starting point for testing psychological correlates of the brain activity - such as sensations - under currents equipped with different power law slopes.

INTRODUCTION

The brain activity observed at many spatiotemporal scales exhibits fluctuations with complex scaling behavior (Newman, 2005), including not only cortical electric oscillations, but also membrane potentials and neurotransmitter release (Milstein et al., 2009; Linkenkaer-Hansen, et al., 2001). In particular, the frequency spectrum of cerebral electric activity displays a scale-invariant behaviour $S(f)= 1/f^n$, where $S(f)$ is the power spectrum, f is the frequency and n is an exponent that equals the negative slope of the line in a log power versus log frequency plot (Van de Ville et al. 2010; Pritchard, 1992). Pink noise can be regarded as an intrinsic property of the brain characterizing a large class of neuronal processes (de Arcangelis and Herrmann, 2010); moreover, power law distributions contain information about how large-scale physiological and pathological outcomes (Jirsa et al., 2014) arise from the interactions of many small-scale processes. It must be emphasized that the fractal slope is not invariant in brain, but is rather characterized by multiple possible exponents (He et al., 2010), summarized in a single value, the "generalized fractal dimension" **α**. It has been demonstrated that different functional states - spontaneous fluctuations, task-evoked, perceptual and motor activity (Buszaki and Watson, 2012), cognitive demands (Fetterhoff et al., 2014), ageing (Suckling et al, 2008) - account for variations in power law exponents across cortical regions (Tinker and Velazquez, 2014; Wink et al, 2008). Accordingly, we may view the multifractal cortex as an ensemble of intertwined (mono)fractals, each with its own dimension and scaling slope: the brain is thus regarded as a system of fractal geometry with a complex spectrum of self-exact similarity breakdown, in which scaling exponents mark dynamical transitions between different response regimes (Papo, 2014).

The aim of our paper was to evaluate, via a geometrical/mathematical model of synthetic power law oscillations, the relationships among brain scaling slopes, energy/ Rényi's entropy and psychological states. Do cortical fluctuations in power law exponents modify the energy of the system? The answer is positive. The metabolic activity of the brain is high, accounting for 20% of the energy consumed. Much of the brain's vast energy budget is reserved for spontaneous neuronal activity, but perceptual and motor activity, task performance and cognitive demands account for an additional energy consumption of 5%, often confined to small cortical areas (Sengupta et al., 2013). Indeed, local boosts in spike frequency (in particular beta and gamma waves) cause a transitory increase of energy

consumption and free energy production, with a metabolic cost of 6.5 μmol/ATP/gr/min for each spike (Attwell and Laughlin, 2001). Throughout the increases in free energy, the *1/f*^{n} exponent varies across brain regions. Recent papers start to uncover connections between the exponent of a fractal scaling in escape paths from energy basins and the activation free energy (Perkins et al., 2014). The ongoing fluctuations with complex scale-free properties can thus be absorbed into a free energy framework (Friston, 2010): the critical slowing implicit in power law scaling of dynamics is mandated by any system that minimizes its energetic expenditure.

It has been shown that the entropy is also linked with different psychological and cognitive states. As an example, analysis performed on emotionally online dialogues demonstrated the tendency towards a growing entropy (Sienkiewicz et al, 2013). Further, ensemble of supervised maximum entropy classifiers can accurately detect and identify sentiments expressed in notes (Wicentowski and Sydes, 2012), perceptual functions are correlated with thermodynamical entropy and free energy (Freeman et al., 2011) and Shannon's entropy is able to predict task performance (Guastello et al., 2013). Finally, the entropy has been recently proposed as a measure of semantic and syntactic information of multidimensional discrete phenomena (Štys et al., 2015). Our task was to evaluate if increases or decreases in the *1/f*^{n} power slope in multifractal systems, besides the above mentioned impact on energy efficiency, might play a role in information processing and emotions, or, in other words, if are we allowed to link probability outcomes with psychological states.

METHODS

Because our model relies on the so called "Rényi's entropy", we need to explain why this underrated construct is useful in the portrayal of multifractal systems. Indeed, the basic thermodynamic properties of multifractal systems may be discussed by extending the notion of the information Shannon's entropy into the more general framework of the Rényi's entropy. The Rényi's entropy of order β is defined to be (Baez, 2011):

$$H_\beta(X)=(1/1-\beta)\ \ln\Sigma_i\, p_i^\beta$$

Where $0 \leq \beta < \infty$. The term X is a random variable with *n* possible outcomes and and $p_i = P(X=i)$, for $i = 1, 2, 3, \ldots n$, is a probability distribution on a finite set.

The Rényi's entropy approaches the Shannon's entropy as β approaches 1, so that β=1 (i.e., the limit for β→1) is defined to be the Shannon's entropy:

$$\lim_{\beta\to 1} H_\beta = -\Sigma_i\, p_i\ \ln p_i$$

The Rényi's entropy is also closely related to the

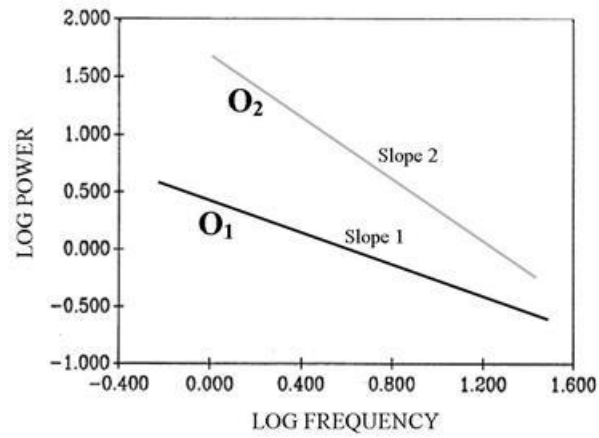

Fig. 1. Two series of free scale oscillations O1 and O2 with different power law exponents and slopes. See text for further details.

thermodynamical Gibbs' entropy and the free energy *F*, through the formula: $F = (1 - T)\ H_\beta$ in which T is the temperature. Mathematically, it is expressed as follows: the Rényi's entropy of a system is minus the "1/β-derivative" of its free energy with respect to a quantity. Because of its build–in predisposition to account for self–similar systems, the Rényi's entropy is an effective tool to describe multifractal systems (Jizba and Korbel, 2015). It has been demonstrated that the Rényi's entropy and the generalized fractal dimension **α** are interchangeable: the Rényi's parameter β is connected via a Legendre transformation with the multifractal singularity spectrum **α** (Jizba and Arimitsu, 2001). It means that, from the maximum entropy point of view, the power law exponent *n* and Rényi's parameter β exhibit a straight relation, therefore changes in *n* lead to changes in β (Słomczynski et al, 2000).

Here follows the procedure we carried out. We generated, in a log amplitude versus log frequency scatter plot, an artificial model of multifractal system (Figure 1), obtaining two series of free scale oscillations $\mathbf{O_1}$ and $\mathbf{O_2}$ with different power law exponents and slopes - slope 1 and slope 2, respectively - (Milstein et al. 2009; Pritchard, 1992).

Taking into account the two oscillations $\mathbf{O_1}$ and $\mathbf{O_2}$, we build, in touch with Shannon (1948), a system equipped with the random variable *p* in the case of two possibilities with probabilities *p* and (1-*p*) and calculated on the X-axis the values of Rényi's entropy (with β=1 corresponding to the slope 1 and β=2 corresponding to the slope 2), plotted as a function of *p* on the Y-axis (Figure 2A). In order to connect the probability *p* with psychological correlates, we plotted on the X-axis a diagram (Figure 2A) which summarized the emotions associated with the delivery of reward or punishment or a stimulus associated with them, or with the omission of a reward or punishment (Rolls).

In our simulation, the two possibilities with probabilities *p*=0 and *p*=1 were the utmost sensations of

terror and ecstasy, while the intermediate steps stood for the in-between emotions from the first to the second: fear, apprehension, relief, pleasure - each one characterized by its probability *p* -. The use of the Rolls' diagrams was just a proof of concept: other diagrams with different mental states (sensations, perceptions, cognitive abilities) could be tested instead. Furthermore, the difference Δ*p* between the curves β=2 and β=1 was plotted against a range of values of Rényi's entropy (Figure 2B).

RESULTS

The curves in Figure 2A illustrate the two cases of Rényi's entropy with exponents β=1 and β=2. The curve β=1 stands for the Shannon's entropy (under ergodic conditions). Note that, at a given value of *p*, a passage from the exponent β=2 to β=1 leads to an increase in Rényi's entropy, and vice versa. Furthermore, at a given value of Rényi's entropy, a variation in β exponent leads to a different probability distribution: as an example, the left right arrow shows the difference in *p* between the curves β=2 and β=1, at the fixed point of Rényi's entropy=.55. Figure 2B points up that different rates of Rényi's entropy are correlated with a wide spectrum of probabilities *p*: at each given value of entropy, the shift of the exponent from β=2 to β=1 causes different changes in Δ*p*. In other words, at each given value of Rénji entropy, a simple variation in power law exponent *n* from 2 to 1 modifies the value of *p*, and thus the content of the message.

In order to evaluate if changes in β exponent could be correlated with the occurrence of different emotions, we plotted the emotions described by Rolls on the X-axis of the probabilities and found that, in our model, a modification of the β exponent leads to different psychological states. In the above mentioned example, at the fixed value of Rényi's entropy=0.55, the variation in Rényi's exponent from 2 to 1 modifies the emotions from fear to terror (Figure 2A).

CONCLUSIONS

Our analysis led to an unexpected conclusion: the road from spike frequency to mental states is paved with intermediate energetic steps which can be defined and quantified. In order to optimize perceptions and thoughts, the brain is equipped with an intrinsic mechanism of fluctuations with complex temporal and spatial scaling properties: in this framework, changes in power law exponents play a crucial role in information processing, leading to variations not only in entropy and probability, but also in basic emotions.

The relation between stimulus, spike trains and transmitted inputs forms the neural code, the crucial tool by which neurons recognize and store the data. But where is the neural code? A range of different theories

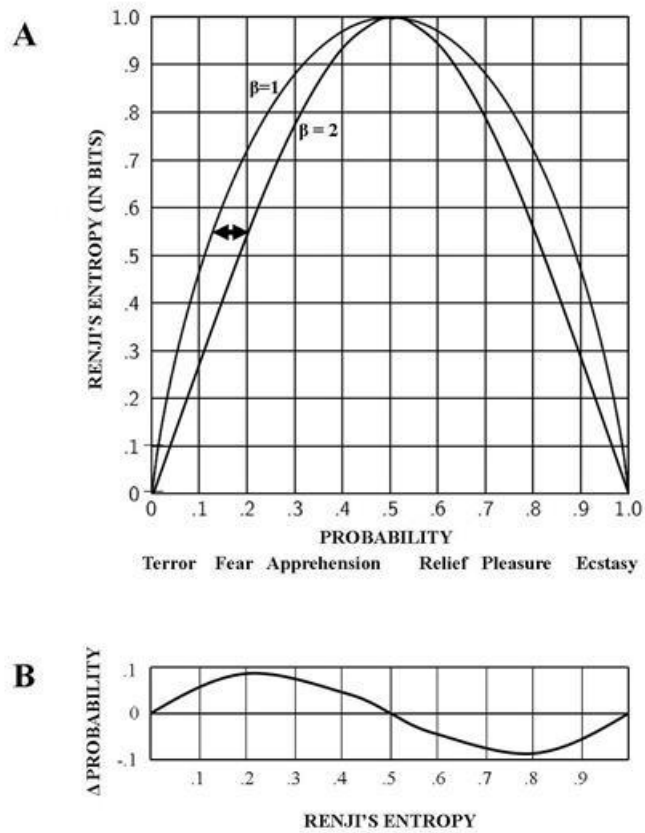

Fig. 2 A: Two cases of Rényi's entropy with exponents β=1 and β=2.

Fig. 2 B : Difference Δp between the curves β=1 and β=2 plotted against a range of values of Rényi's entropy. See text for further details.

has been offered over the years: rate or temporal codes, latency, relational, synchrony codes, mixtures of them (Gollisch, 2009). We hypothesize that another underrated mechanism might play a role in neural communication: the power law exponent. Based on the above mentioned energetic constraints, we indeed propose that variations in brain fractal slopes are correlated with changes in the content of the message. In such a framework, complex scale-free statistics are fixed points of a renormalization flow and can be understood as asymptotic behaviors emerging as the system is rescaled (Fraiman and Chialvo, 2012), while cognitive tasks are modulated by the $1/f^{n}$ exponents of the brain fluctuation probability function, leading to a shrinking of multifractal spectrum and/or transitions from mono- to multi-fractal distributions (Popivanov et al., 2006).

Our results pave the way for innovative therapeutic strategies. We conjecture that the electric fractal-like structures - setting aside their supposed relationships with self organized criticality (Bak et al., 1987), nonequilibrium steady-state dynamics or second order phase transitions (Papo, 2014) - could be modulated

through the superimposition of an external electric currents characterized by carefully chosen power law exponents. We suggest that the techniques of transcranial electrical stimulation need to take into account not only the amplitude and frequency of the applied waveforms (Reato et al., 2013), but also their scaling slope. A tenable field of application are the diseases that have been linked to disturbance of brain networks - Alzheimer's disease, depression, attention deficit hyperactivity disorder, autism (Fox and Raichle, 2007) -, meaning that they could be ameliorated, or even removed, by appropriate artificial fields - e.g., via selective application of electric waves of specific power law exponent on target micro-areas - able to "recovery" and restore the physiological brain activity (Sunderam et al., 2009).

BIBLIOGRAPHY

Attwell,D., & Laughlin, S.B. (2001). An energy budget for signaling in the grey matter of the brain. Journal of Cerebral Blood Flow Metabolism, 21(10), 1133-1145.

Baez, J.C. (2011). Entropy and Free Energy. arXiv:1102.2098 [quant-ph].

Bak, P., Tang, C., Wiesenfeld, K (1987). Self-organized criticality: An explanation of the 1/f noise. Physical Review Letters, 59(4), 381-384. PMID: 10035754.

Buzsáki, G., & Watson, B.O. (2012). Brain rhythms and neural syntax: implications for efficient coding of cognitive content and neuropsychiatric disease. Dialogues in Clinical Neurosciences, 4, 345-367.

de Arcangelis, L., & Herrmann, H.J. (2010). Learning as a phenomenon occurring in a critical state. Proceedings of the National Academy of Sciences, 107, 3977-3981.

Fetterhoff, D., Opris, I., Simpson, S.L., Deadwyler, S.A., Hampson, R.E., Kraft, R.A. (2014). Multifractal analysis of information processing in hippocampal neural ensembles during working memory under Δ9-tetrahydrocannabinol administration. Journal of Neuroscience Methods, pii: S0165-0270(14)00264-7. doi: 10.1016/j.jneumeth.2014.07.013.

Fox, M.D., & Raichle, M.E. (2007). Spontaneous fluctuations in brain activity observed with functional magnetic resonance imaging. Nature Review Neuroscience, 8, 700-711.

Fraiman, D., & Chialvo, D.R. (2012). What kind of noise is brain noise: anomalous scaling behavior of the resting brain activity fluctuations. Frontiers in Physiology, 3:307. doi: 10.3389/fphys.2012.00307.

Freeman, W. J., Livi, R., Obinata, M., Vitiello, G. (2011). Cortical phase transitions, non-equilibrium thermodynamics and the time-dependent Ginzburg-Landau equation. arXiv:1110.3677v1.

Friston, K. (2010). The free-energy principle: a unified brain theory? Nature Review Neuroscience, 11, 127-138.

Gollisch, T. (2009). Throwing a glance at the neural code: rapid information transmission in the visual system. Human Frontier Science Program Journal, 3(1), 36–46. doi: 10.2976/1.3027089.

Guastello, S.J., Gorin, H., Huschen, S., Peters, N.E., Fabisch, M., et al. (2013). The minimum entropy principle and task performance. Nonlinear Dynamics, Psychology, and Life Science, 17(3):405-423.

He, B.J., Zempel, J.M., Snyder, A.Z., Raichle, M.E. (2010). The temporal structures and functional significance of scale-free brain activity. Neuron, 66(3), 353-369. doi: 10.1016/j.neuron.2010.04.020.

Jirsa, V.K., Stacey, W.C., Quilichini, P.P., Ivanov, A.I., Bernard, C. (2014). On the nature of seizure dynamics. Brain, 137(Pt 8), 2210-2230. doi: 10.1093/brain/awu133.

Jizba, P., & Arimitsu, T.(2001). The world according to Renyi: thermodynamics of fractal systems. AIP Conference Proceedings, 597, 341-348.

Jizba, P., & Korbel, J. (2015). On q-non-extensive statistics with non-Tsallisian entropy. arXiv:1501.07386.

Linkenkaer-Hansen, K., Nikouline, V.V., Palva, J.M., Ilmoniemi, R.J. (2001). Long-range temporal correlations and scaling behavior in human brain oscillations. Journal of Neuroscience, 21(4), 1370-1377.

Milstein, J., Mormann, F., Fried, I., Koch, C. (2009). Neuronal shot noise and Brownian 1/f2 behavior in the local field potential. PLoS One, 4(2):e4338. doi: 10.1371/journal.pone.0004338.

Newman, M.E.J. (2005). Power laws, Pareto distributions and Zipf's law. Contemporary Physics, 46, 323-351.

Papo, D. (2014). Functional significance of complex fluctuations in brain activity: from resting state to cognitive neuroscience. Frontiers in Systems Neuroscience, 8, 112. doi: 10.3389/fnsys.2014.00112.

Perkins, T.J., Foxall, E., Glass, L., Edwards, R. (2014). A scaling law for random walks on networks. Nature Communications, 5, 5121. doi: 10.1038/ncomms6121.

Pritchard, W.S. (1992). The brain in fractal time: 1/f-like power spectrum scaling of the human electroencephalogram. International Journal of Neuroscience, 66, 119-129.

Popivanov, D., Stomonyakov, V., Minchev, Z., Jivkova, S., Dojnov, P., et al. (2006). Multifractality of decomposed EEG during imaginary and real visual-motor tracking. Biological Cybernetics, 94, 149–156.

Reato, D., Rahman, A., Bikson, M., Parra, L.C. (2013). Effects of weak transcranial alternating current stimulation on brain activity-a review of known mechanisms from animal studies. Frontiers in Human Neuroscience, 7:687. doi: 10.3389/fnhum.2013.00687.

Rolls, E.T. (2008). Emotion, higher-order syntactic thoughts, and consciousness. In L. Weiskrantz and M.K. Davies (Eds.), Frontiers of Consciousness (pp. 131-167). Oxford: Oxford University Press.

Sengupta, B., Stemmler, M.B., Friston, K.J. (2013). Information and efficiency in the nervous system - a synthesis. PLoS Computational Biology, 9(7):e1003157. doi: 10.1371/journal.pcbi.1003157.

Shannon, C.E. (1948). A Mathematical Theory of information. The Bell System Technical Journal, 27, 379-423, 623-656.

Sienkiewicz, J., Skowron. M, Paltoglou, G., Holyst J.A. (2013). Entropy growth in emotional online dialogues. Journal of Physics: Conference Series 410 012096. doi:10.1088/1742-6596/410/1/012096.

Słomczynski, W., Kwapien, J., Zyczkowski, K. (2000). Entropy computing via integration over fractal measures. Chaos, 10(1), 180-188.

Štys, D., Korbel, J., Rychtáriková, R., Soloviov, D., Císař, P., Urban, J. (2015). Point information gain, point information gain entropy and point information gain entropy density as measures of semantic and syntactic information of multidimensional discrete phenomena. arXiv:1501.02891.

Suckling, J., Wink, A.M., Bernard, F.A., Barnes, A., Bullmore, E. (2008). Endogenous multifractal brain dynamics are modulated by age, cholinergic blockade and cognitive performance. Journal of Neuroscience Methods, 174(2), 292-300. doi:10.1016/j.jneumeth.2008.06.037.

Sunderam, S., Chernyy, N., Peixoto, N., Mason, J.P., Weinstein, S.L., et al. (2009). Seizure entrainment with polarizing low-frequency electric fields in a chronic animal epilepsy model. Journal of Neural Engineering, 6(4):046009. doi: 10.1088/1741-2560/6/4/046009.

Tinker, J., & Velazquez, J.L. (2014). Power law scaling in synchronization of brain signals depends on cognitive load. Frontiers in Systems Neuroscience, 8:73. doi: 10.3389/fnsys.2014.00073.

Van de Ville, D., Britz, J., Michel, C.M. (2010). EEG microstate sequences in healthy humans at rest reveal scale-free dynamics. Proceedings of the National Academy of Sciences USA, 107(42), 18179-18184. doi: 10.1073/pnas.1007841107.

Wicentowski, R., & Sydes, M.R. (2012). Emotion Detection in Suicide Notes using Maximum Entropy Classification. Biomedical Informatics Insights, 5: 51–60. doi: 10.4137/BII.S8972.

Wink, A.M., Bullmore, E., Barnes, A., Bernard, F., Suckling, J. (2008). Monofractal and multifractal dynamics of low frequency endogenous brain oscillations in functional MRI. Human Brain Mapping, 29(7), 791-801. doi: 10.1002/hbm.20593.

Author's personal copy

Cogn Neurodyn
DOI 10.1007/s11571-015-9337-1

REVIEW PAPER

Information processing in the CNS: a supramolecular chemistry?

Arturo Tozzi[1]

Received: 23 June 2014 / Revised: 2 February 2015 / Accepted: 3 March 2015
© Springer Science+Business Media Dordrecht 2015

Abstract How does central nervous system process information? Current theories are based on two tenets: (a) information is transmitted by action potentials, the language by which neurons communicate with each other—and (b) homogeneous neuronal assemblies of cortical circuits operate on these neuronal messages where the operations are characterized by the intrinsic connectivity among neuronal populations. In this view, the size and time course of any spike is stereotypic and the information is restricted to the temporal sequence of the spikes; namely, the "neural code". However, an increasing amount of novel data point towards an alternative hypothesis: (a) the role of neural code in information processing is overemphasized. Instead of simply passing messages, action potentials play a role in dynamic coordination at multiple spatial and temporal scales, establishing network interactions across several levels of a hierarchical modular architecture, modulating and regulating the propagation of neuronal messages. (b) Information is processed at all levels of neuronal infrastructure from macromolecules to population dynamics. For example, intra-neuronal (changes in protein conformation, concentration and synthesis) and extra-neuronal factors (extracellular proteolysis, substrate patterning, myelin plasticity, microbes, metabolic status) can have a profound effect on neuronal computations. This means molecular message passing may have cognitive connotations. This essay introduces the concept of "supramolecular chemistry", involving the storage of information at the molecular level and its retrieval, transfer and processing at the supramolecular level, through transitory non-covalent molecular processes that are self-organized, self-assembled and dynamic. Finally, we note that the cortex comprises extremely heterogeneous cells, with distinct regional variations, macromolecular assembly, receptor repertoire and intrinsic microcircuitry. This suggests that every neuron (or group of neurons) embodies different molecular information that hands an operational effect on neuronal computation.

Keywords Information · Processing · Action potential · Neural code · Supramolecular · Macromolecule · Embodiment

Introduction

How does central nervous system (CNS) process information[1]? This crucial question forms part of the more general effort aimed at establishing causal relations between specific aspects of neuronal activity and system-level consequences (Gollisch 2009).

All the current paradigms in neuroscience, such as the computational models (Rumelhart et al. 1986; Qu et al. 2014; Kim and Lim 2013), the Bayesian brain and free-energy hypothesis (Friston 2010), the connectome (Sporns 2013), the fractal dimension analysis (Ibáñez-Molina and Iglesias-Parro 2014; Mattei 2014), the early multisensory

✉ Arturo Tozzi
Tozziarturo@libero.it

[1] ASL Napoli 2 Nord, Distretto 45, Via Santa Chiara, 80023 Caivano, Naples, Italy

[1] It is important to define what we mean by "information" and "information processing" in CNS. By "information" we will assume an ordered sequence of symbols from an input and an output alphabet. With the term "information processing" we will assume a function that maps any input sequence sample from an input alphabet into an output sequence from an output alphabet (Wicker and Kim 2003).

Published online: 10 March 2015

Author's personal copy

integration (Klemen and Chambers 2012), are based on two tenets:

(1) Information is contained in the electric currents generated by neurons. Neurons process information, which is passed by action potentials—the language by which neurons communicate with each other (Gollisch 2009). To give an example, all sensory data are initially encoded as voltage changes in sensory receptors; these noisy and ambiguous signals are processed by the peripheral nervous system and brain to produce percepts and qualia, experienced as sharp, certain and unambiguous (Brown H, Friston K: Resolving Uncertainty in Perception, Research topics 2013).

(2) The cells of neural circuits are not characterized computationally by their morphology or specific protein content, rather by the intrinsic and extrinsic connectivity they exhibit. In this view, cortex is generally regarded as homogenous, all areas being composed of a basic repeated circuit (Elston and Rockland 2002), sometimes referred to as a canonical microcircuit. Functional specificity is determined by the source of inputs and, implicitly, the axonal connectivity among neurons (Xiumin 2014). It follows that the information transmitted by the neuron must be contained in the temporal sequence of the spikes, the "spike train". The relationship between stimulus, spike trains and transmitted information forms the "neural code", the crucial tool by which neurons recognize, represent, store and transmit information (Gollisch 2009). The term "code" thus means the representation of the facts about the stimulus in terms of neuronal spiking activity.

In summary, there is a broad consensus based on the concepts of action potentials, neural code and canonical microcircuits that emphasise a singular level of message-passing in the brain; namely, those messages mediated by action potentials. Current theories consider self-evident the foremost role of action potentials in communication and highlight their function in establishing distributed neuronal interactions across several levels (including brain regions, functional circuits and large-scale networks), usually within a hierarchical or modular architecture.

However, in the last decade, neuroscience has witnessed major advances at the molecular and extra-neuronal level: multiple lines of evidence now shed new light on information processing in CNS. The aim of this (theoretical) paper—based on recent innovations—is therefore to point towards an alternative perspective. This paper comprises four sections. The first section suggests that the role of action potential/neural code in information processing is less prominent than thought. "When it comes to the brain, wiring isn't everything. Although neurobiologists often talk in electrical metaphors, the reality is that the brain is not nearly as simple as a series of wires and circuits" (Newswire 2014). We will show that action potentials—rather than just processing information—may mediate other functions in the CNS. Section two links information processing to mechanisms other than action potential/neural code, emphasizing the role of biologically active molecules and macromolecules. This section introduces a scenario based on "supramolecular chemistry". Section three considers other (potentially underrated) mediators of information processing in CNS from a more holistic perspective, emphasising the circular causality among different spatial and temporal scales: in particular, we will focus on extra-neuronal factors and the potentially important role of peripheral receptors. The final section shows how, contrary to the standard model, neuronal populations are heterogeneous and every cell (or group of cells) embodies specific and unique molecular information.

A different role for the action potential?

How does the neural code work? What do spike patterns mean? This is a topic of intense debate within the neuroscience community. A range of different theories has been offered over the years: the paradigms of the rate or temporal codes, latency, relational, synchrony codes, variations or mixtures of them, and so on (Gollisch 2009). We hypothesize that action potentials play a role in local–global communication, modulating and regulating the processing of information (that is mediated by local processes entailed by the infrastructure of single neurons and microcircuits at multiple scales of organisation).

The evidence points towards cortical oscillations, cross-frequency phase coupling and representation of multiple time scales as tools for mediating interactions among functional cell assemblies in distributed brain circuits (Buzsáki and Watson 2012). Synchronized neuronal activity does not seem to contain a specific code, rather to operate as a generic mechanism capable of binding together neural activities of spatially separated cortical areas and dynamically shaping task-relevant neural ensembles out of larger, overlapping circuits (Buschman et al. 2012).

The main function of electric pulses appears to be to regulate information processing. The brain uses synchronized activity to establish or select network connections and to organize complex information, such as sensory inputs. Recent studies are in accordance with in vivo observations related to the coordination of neuronal

Author's personal copy

processing and point towards the hypothesis that timing is crucial. To give some examples:

- Recent works underline the special role of neuronal synchrony in pattern recognition. A framework has been proposed in which inhibitory alpha oscillations limit and prioritize neuronal processing (Jensen et al. 2014). During spatially distributed representations in early visual regions, inhibition prevents neuronal firing. As the inhibition ramps down within a cycle, a set of neuronal representations will activate sequentially according to their respective excitability. Both top-down and bottom-up drives determine excitability; in particular, spatial attention constitutes a major top-down influence. On a shorter time scale, fast recurrent inhibition segments representations in slots 10–30 ms apart, generating gamma-band activity at the population level (Jensen et al. 2014). Other data suggest that, in the frontal cortex, beta-frequency synchrony selects the relevant rule ensemble, while alpha-frequency synchrony deselects a stronger, but currently irrelevant, ensemble (Buschman et al. 2012). Furthermore, 20–40-Hz oscillations have been identified as a mechanism for synchronizing evolving representations in dispersed neural circuits, during encoding and retrieval of olfactory-spatial associative memory (Igarashi et al. 2014).
- The study of temporal windows in visual perception (and attention) shows how oscillatory dynamics play a role in carving successive visual inputs into separate perceptions, with higher beta power associated with incorrect perception of the target and evoked alpha phase reset associated with correct target perception (Wutz et al. 2014).
- Rapidly changing brain states during learning may be encoded by the synchronization of oscillations across different brain regions. Waves originating from prefrontal cortex and striatum are involved in learning associations to form new communication circuits when monkeys learn to categorize different patterns of dots (Antzoulatos and Miller 2014). The role of waves, in this case, is to synchronize and enable faster learning.
- The sensitivity of neuronal activity to the timing of synaptic inputs suggests that synchrony determines the propagation of information and, in turn, regulation of synchrony is a critical element. The developing brain in Xenopus tadpolere wires and fine-tunes its connections differently depending on the relative timing of sensory stimuli (Munz et al. 2014). Asynchronous firing not only causes brain cells to lose their ability to make other cells fire, but induces a 60 % increase in axonal branching. The stabilization of retinal nerve cell branches caused by synchronous firing involves signalling downstream of the synaptic activation of the *N*-methyl-D-aspartate receptor. In contrast, the enhanced exploratory growth that occurs with asynchronous activity does not appear to require the activation of this receptor (Munz et al. 2014).
- The time scale of practice affects patterns of brain activity associated with motor skill acquisition. Activity in the striatum is consistently more rostral in the intermediate time scale and more caudal over longer time scales. These data support neurophysiological models that posit that systems are active, but at different time points, during motor learning (Lohse et al. 2014).

Gamma-band activity and the synchronization of neural activity in the gamma-frequency range, observed ubiquitously in different cortical and subcortical structures, have been associated with different cognitive functions and reflect neuronal network coordination involved in attention, learning and memory (Kucewicz et al. 2014; Brunet et al. 2014). However, it is still unknown whether gamma-band synchronization subserves a single universal function and reflects a global recognition signal, or a diversity of functions across the full spectrum of cognitive processes. This question has been addressed by Bosman et al. (2014), who stresses that gamma oscillations, associated with interplay between inhibition and excitation, originate from basic functional motifs that confer advantages for low-level system processing and multiple cognitive functions throughout evolution. The multifunctionality of gamma-band activity is confirmed by its role in neural systems for perception, selective attention, memory, motivation and behavioural control. Thus, gamma-band oscillations seem to support multiple cognitive processes, rather than a single one.

In summary, even under the standard model of neuronal message passing (through temporally coordinated action potentials), a picture emerges that speaks directly to circular causality among different temporal scales. Circular causality of this sort is a characteristic of self-organised dynamical systems (most formally characterised in synergetics). It suggests that any dynamical system can exhibit modes of behaviour which separate into slow and fast timescales. Typically, the fast modes are local and dissipate quickly; while slow modes are more global and decay more slowly (the amplitudes of these slow modes are known as order parameters). Crucially, the slow modes are simply the superposition or average of fast modes, while—at the same time—the slow modes enslave and contextualise the fast modes. This is the essence of circular causality between different timescales. In the context of the oscillatory brain dynamics considered in this section, one could regard distributed and synchronised (global) modes as the slow modes that contextualise standard (action potential) message passing to mediate the sorts of phenomena we

Author's personal copy

associate with attention and the gating (or selection) of particular patterns of connectivity (or interactions). If this view is correct, then simply equating neuronal codes with firing rates of action potentials is an incomplete description of neuronal dynamics; because it fails to accommodate the dynamic coordination implicit in self-organised activity—and evidenced by the neuromodulatory effects of distributed synchronous activity in the brain. In the next section, we extend this argument to cover not just different temporal scales, but also spatial scales of neuronal systems.

The function of biologically active molecules and/or macromolecules in information processing

Traditionally, in neuroscience the emphasis is on evaluating cognition from a computational point of view. However, studies in biologically inspired robotics and embodied intelligence provide strong evidence that cognition cannot be analyzed and understood by looking at computational processes as a single level, but that physical system–environment interaction needs to be taken into account. According to some authors, we need to build our understanding of cognition from the bottom up; that is, all the way from how our body is physically constructed (Pfeifer et al. 2014). A connection between cognition, body morphology and soft material properties has been pursued, showing how physics-based approaches have led to new insights into biological systems at all scales of space and time, at all levels of complexity, including information processing in CNS (Foffi et al. 2013).

The recent idea of "supramolecular chemistry" (the so called "chemistry beyond molecule"), has paved the way towards appreciating chemistry as an information science, the science of informed matter (Lehn 2007). Complex chemical entities can be reversibly constructed from molecular components bound together by labile non-covalent interactions. The novel concept of molecular information involves the storage of information at the molecular level and its retrieval, transfer and processing at the supramolecular level, via transitory molecular processes that are self-organized, self-assembled and dynamic (Lehn 2007). Sequential, hierarchical self-organization on increasing scale and constitutional dynamics in non-equilibrium systems can lead to the emergence of novel features/properties at each level, organization in space as well as in time and passage beyond reversibility. This perspective is particularly relevant for the brain that is probably the best example of an open system which maintains non-equilibrium steady-state (i.e., homoeostasis or allostasis) in the face of environmental fluctuations.

The complexity of the biological milieu calls for more refined descriptions when entering the domain of biological sciences. To what extent does the strong spatial inhomogeneity (clustering, cellular compartmentalization, and so on), diffusion, excluded volume, electrostatic and hydrodynamic interactions have to be taken into account? The experimental evidence is still controversial, but recent results suggest that interactions affect the kinetics of self-assembly reactions. Crowding-induced changes in the structure and dynamics of macromolecules describe a scenario of systems capable of generating well-defined functional supramolecular architectures by self-assembling from their components, thus behaving as programmed chemical systems. For example, it has been demonstrated that small variations in the genetic code—thought to be inconsequential (involving genes with diverse functions in endocytosis, oxidative stress response, RAS-cAMP signalling and transcriptional regulation of multicellular growth)—that have not previously been shown to exhibit functional relationships—and do not individually appear to have much effect—collectively lead to significant changes in an organism (Taylor and Ehrenreich 2014).

Incorporating this perspective appears to be crucial for understanding the dynamics of biological systems in vivo and suggests that this approach is also valid in neurobiology (Foffi et al. 2013). Indeed, the current day concepts about synaptic transmission, intraneuronal signaling and interactions between neuronal genome, proteome and metabolome are in line with the basic principles exposed by Lehn: hence, the ideas about supramolecular chemistry are implicitly incorporated in the recent neurobiological research. At present there are clues that speak to neuronal processing that rests on macromolecules, rather than just electric pulses. Scientists are starting to address the important problem of whether cellular signals can also travel long distances in a crowded environment (c.f., action potentials). There follows a list of recent papers (that pertain to the molecular neurobiology of cognitive functions), which demonstrates that gene expression within neuronal populations and changes in molecular/macromolecular conformation, number or synthesis, can mediate different neural functions:

- A recent "experimentum crucis" explains why different sets of the same protein variations occur in one neuron and how this contributes to the complex wiring. In the Drosophila, the neuron can create many isoforms from the same Dscam1 protein on its cell surface (He et al. 2014). The specific set of isoforms of Dscam1 receptor determines the neuron's unique molecular identity and plays an important role in establishing accurate connections and for neuronal self-recognition and self-avoidance. Different sets of Dscam1 isoforms occur also inside one axon and lead to dominant dosage-sensitive inhibition of branching. Thus, cell-

Author's personal copy

intrinsic use of surface receptor diversity is of general importance in regulating axonal branching during brain wiring (He et al. 2014).

- Neurexin isoforms are generated via alternative splicing at multiple independent sites and have power over cognitive functions (Treutleina et al. 2014). For instance, Neurexin 1a and 2 and CNTNAP2, all members of the neurexin superfamily of transmembrane molecules, have been implicated in neuropsychiatric disorders (Karayannis et al. 2014).
- Researchers reported changes in 352 proteins in rat brain 15 min after phencyclidine injections. The transitory modifications started a chain reaction of changes in the molecular network around the proteins, such as changes in cell metabolism and calcium balance, transport of substances into and out of cells and in the structure of the cytoskeleton, causing the rats to change their behaviour (Palmowski et al. 2014).
- An astonishing three-dimensional model of an "average" synapse has been generated, displaying 300,000 proteins in atomic detail. Copy numbers varied over more than three orders of magnitude between steps, from about 150 copies for the endosomal fusion proteins to more than 20,000 for the exocytotic proteins (Wilhelm et al. 2014).
- Researchers have identified key genes linked to people showing a higher tolerance for pain than others. The DRD1 gene variant was 33 % more prevalent in the low pain than in the high pain group. Among people with a moderate pain perception, the COMT and OPRK variants were 25 and 19 % more often found than in those with a high pain perception. The DRD2 variant was 25 % more common among those with a low pain threshold compared to people with a moderate threshold (Onojjighofia 2014).
- FoxP mutants take longer than wild-type flies to make decisions in odour discriminations of similar or reduced accuracy, especially in difficult, low-contrast tasks. RNA interference with FoxP expression in αβ core Kenyon cells, or the over expression of a potassium conductance channel in these neurons, is recapitulated the FoxP mutant phenotype. A mushroom body subdomain, whose development or function requires the transcription factor FoxP, supports the progression of a decision toward commitment (DasGupta et al. 2014).
- Mn2+ accumulates intracellularly on injection into the motor neurons in the buccal network of living Aplysia, its concentration increases when the animals are presented with a sensory stimulus (Radecki et al. 2014).
- Different types of neurons traffic microRNA to distinct membrane locations, affecting the functional response of neurons: Extracellular let-7b, a microRNA found in the CNS, affects neurons through its interaction with Toll-like receptor 7 (TLR7), but with divergent outcomes in different neurons. Indeed, let-7b stimulation of cortical and hippocampal neurons leads to neuronal apoptosis, whereas let-7b activation of TLR7 stimulated the cation channel transient receptor potential A1 (TRPA1) on the dorsal root ganglia sensory neurons and induced pain responses. The primary difference that influences these distinct responses is the localization of TLR7 to the endosome in the cortical and hippocampal neurons, or the plasma membrane in the sensory neurons (Winkler et al. 2014).

Different aspects of molecular signalling relevant to the formation of memories have been extensively studied. The most recent papers highlight the numerous molecular mechanisms that underlie memory processing:

- MAPK and PKA signalling cascades are spatiotemporally integrated in a single neuron, to support synaptic plasticity underlying memory formation (Ye et al. 2012).
- Prion-based mechanisms provide a durable molecular memory, involved in long-term memory formation (White-Grindley et al. 2014).
- Fatty Acid-binding Protein 5 (FABP5) enhances learning and memory functions in the brain hippocampus region, both by decreasing anandamide levels and by activating the Nuclear Receptor Peroxisome Proliferator-activated Receptor β/δ. FABP5 delivers endocannabinoids to cellular machinery that breaks them down and shuttles compounds to a transcription factor that increases the expression of cognition-associated genes (Yu et al. 2014).
- RGS7 plays a part in hippocampal synaptic plasticity. GABA shapes the activity of the output pyramidal neurons via RGS7, in cooperation with its binding partner R7BP. Deletion of RGS7 in mice dramatically sensitizes responses to GABAB receptor stimulation and markedly slows channel deactivation kinetics. As a result, mice lacking RGS7 exhibit deficits in learning and memory formation (Ostrovskaya et al. 2014).
- The retrosplenial cortex engages in the formation and storage of memory traces for spatial information: the spatial memory consolidation is enhanced by over expression of the transcription factor CREB with a viral vector (Czajkowski et al. 2014).
- The fruit fly Drosophila melanogaster has a dedicated mechanism for active forgetting: blocking the G-protein Rac leads to slower, and activating Rac to faster forgetting (Brea et al. 2014).
- The spatial positioning of proteins at specific areas around neurons predicts which memories are recorded (O'Donnell and Sejnowski 2014).

Author's personal copy

Finally, other types of neuronal infrastructures, apart from spikes, are used by neurons for information processing. These include the following examples:

- Neurons utilize secretory events, both to process information and to fine-tune the release of neuropeptides. For example, a localized intracellular store of calcium is needed to initiate the secretion of neuropeptides (McNally et al. 2014).
- Evaluating the spatial and temporal characteristics of vesicle transport has important implications for our understanding of cognitive pathways. In a neuronal culture system from Drosophila larval brains, scientists visualized the movement dynamics of several cargos/organelles along a 90 micron axonal neurite over time. All vesicles/organelles showed robust bi-directional motility at both day 1 and day 2. Reduction of motor proteins decreased the movement of vesicles/organelles, with increased numbers of neurite blocks and neuronal growth perturbation. Strikingly, all blockages were not fixed and permanent as previously thought, but some blocks were dynamic clusters of vesicles that resolved over time (Iacobucci et al. 2014).
- Mitochondria have a central role in neuronal physiology. Axonal mitochondria undergo spontaneous "contractions", accompanied by reversible redox changes. These contractions are amplified by neuronal activity and constitute respiratory chain-dependent episodes of depolarization coinciding with matrix alkalinization, followed by uncoupling (Breckwoldt et al. 2014). Furthermore, recent results indicate that adult hippocampal neurogenesis requires adaptation of the mitochondrial compartment. The development of new neurons from stem cells in the hippocampus of adult mice is paralleled by extensive changes to mitochondrial mass, distribution and shape. Genetic inhibition of the activity of the mitochondrial fission factor dynamin-related protein 1 (Drp1) inhibits neurogenesis under basal and exercise conditions. Conversely, enhanced Drp1 activity furthers exercise-induced acceleration of neuronal maturation (Steib et al. 2014).

In summary, based on recent data, we hypothesize that, although all neurons exhibit a common repertoire of macromolecules, each one embodies a specific, non-covalent and transitory supramolecular assembly. This explains why each neuron is apparently similar to others, but functionally different. An important question arises: if macromolecules play a part in neuronal information processing, why has this link not been emphasised by the current paradigms that focus on electric pulses? One answer is that there are still many unexplored aspects, because protein dynamics is more sensitive than structure to environmental factors such as crowding, solvent, temperature, pressure, confinement. While in vitro experiments remain the only way to investigate the intrinsic properties of molecules, this approach ignores the fact that—in their natural milieu—proteins are surrounded by other molecules of different chemical nature, and this crowded environment considerably modifies their behaviour (Foffi et al. 2013). At present, the complexity of functionally interacting structures is beyond our current knowledge: biological macromolecules live and operate in a structured and complex environment within the cell—and the interior of the cell is by no means a simply crowded medium (Foffi et al. 2013). Due to the absence of well defined technical contributions directed to sustain that the concept of neural code must be introduced in a largest framework, neuroscientists are just starting to investigate the overwhelming (and probably unexpected) complexity of this system. The recent drafts of the human proteome (proteins encoded by 17,294 genes were identified, accounting for 84 % of the annotated protein-coding genes) (Kim et al. 2014a, b, c; Chen et al. 2014) are promising tools to obtain a better comprehension of supramolecular chemistry and to complement available human genome and transcriptome data. An impressive array of new tools and technologies is going to expand on the network aspects of cellular neurobiology and molecular neuroanatomy (Pollock et al. 2014). As an example, recent papers focused on the mechanisms of the multifaceted molecular reorganization of the inhibitory synapse during postsynaptic plasticity, with special emphasis on the key role of protein dynamics to ensure prompt and reliable activity-dependent adjustments of synaptic strength (Petrini and Barberis 2014). Last but not the least, much insight will be gained from the novel big data efforts in neuroscience, consisting in collections of large, open, high-throughput sets (Choudhury et al. 2014).

Information processing: not just neurons!

Structures quite different from neurons may also play a role in information processing in CNS. As an example, the extracellular medium is crucial for neuronal activity; some important examples include: substrate patterning and stiffness influence neuronal development by regulating its dynamics. Biophysical cues, such as the mechanical properties of the extracellular matrix, are known to modify neuronal differentiation and maturation (Sur et al. 2013). As noted above, the spatial positioning of proteins at specific areas around neurons predicts which memories are recorded (O'Donnell and Sejnowski 2014). Finally, a novel pathway found in the amygdala links fear-associated extracellular proteolysis of EphB2 to anxiety (Attwood et al. 2011).

Author's personal copy

These examples suggest that the external milieu of neurons provides an embodiment that dictates their function. In this section, we pursue the notion of embodied neuronal computation by listing some key examples of a circular causality (reciprocal exchange) between neurons and the environment. To illustrate the diversity and ubiquity of this (generalised) embodiment, we will focus on the neuronal infrastructure (white matter) itself, the role of bacteria and pathogens, the role of physiology and finally, of peripheral receptors.

Embodiment in connectome

In a similar vein, myelin plasticity helps to explain how the brain adapts in response to different stimuli. For example: myelin coverage along axons is not uniform as previously supposed and changes in white matter distribution may constitute a form of neuronal plasticity. In mice, individual neurons have a distinct longitudinal distribution of myelin, including a new pattern where myelinated segments are interspersed with long, unmyelinated tracts (Yates 2014). Furthermore, it has been demonstrated that the profile of longitudinal distribution of myelin is an integral feature of neuronal identity and that variability in the thickness of the envelope is a structural feature affecting the conduction of neuronal signals (Tomassy et al. 2014). Indeed, neuronal activity causes an increase in the thickness of the myelin sheaths within the active neural circuit, by promoting adaptive oligodendrogenesis (Gibson et al. 2014). Furthermore, changes in white matter microstructure in the superior cerebellar peduncles and primary motor cortex contribute to motor expertise and individual differences in ability (Roberts et al. 2013). Finally, leptin receptors are expressed in hypothalamic astrocytes involved in feeding control and their conditional deletion leads to altered glial morphology and synaptic inputs. In mice with astrocyte-specific leptin receptor deficiency, leptin-regulated feeding was diminished, whereas feeding after fasting or ghrelin administration was elevated (Kim et al. 2014a, b, c).

Commensal and pathogenic embodiment

Intestinal bacteria are also involved in many functions within CNS. Recent findings show that commensal bacteria can activate neural pathways and CNS signalling systems (Foster and Neufeld 2013). Several mechanisms have been proposed:

- Gut microbes alter levels of neurotransmitter-related metabolites affecting gut-to-brain communication. For instance, certain bacteria produce homovanillate—the breakdown product of dopamine—and *N*,*N*-dimethylglycine, a building block for proteins and neurotransmitters (American Society for Microbiology's annual meeting in Boston, Mass., May 17 to 20, 2014).
- It is known that gut hormones, such as peptide YY and glucagon-like peptide-1, directly affect neurons within the hunger-regulating hypothalamus. However, other unexpected intestinal agents may also influence the hypothalamus. A link between fermentation in the colon and activity in the brain has been traced. Acetate, released following the fermentation of dietary fibre in the mouse gut, accumulates in the hypothalamus and affects appetite (Frost et al. 2014).
- Stress increases intestinal permeability, causing gut bacteria to move into the systemic circulation. It is thought that circulating bacteria, offering a major source of Lipopolysaccharide, activate toll-like receptor (TLR) signalling pathways in the brain and subsequently induce neuroinflammatory responses. This process has been investigated in a rat model, suggesting that increased stress causes TLR-4 up-regulation in frontal cortex (Gárate et al. 2014).
- Finally, pathogenic microorganisms may affect brain functioning. Astonishingly, bacterial pathogens produce pain by directly activating sensory neurons that modulate inflammation (Chiu et al. 2013). It has been discovered that Staphyloccocus aureus induces calcium flux and action potentials in nociceptor neurons, via bacterial N-formylated peptides and the pore-forming toxin α-haemolysin (aHL). N-formyl peptides activate nociceptors by binding to FRP1 and inducing calcium flux, while αHL forms pores in the nociceptive cell membrane, allowing cation exchange (Chiu et al. 2013).

These and other studies suggest that the relationships between the CNS and immune system are more extensive and intimate than previously appreciated. A complex regulation of gene expression in neural cells in response to peripheral inflammation has been discovered. Recent observations reveal the existence of a previously unrecognized mechanism, based on extracellular vesicles that transfer functional RNA directly from the hematopoietic system to brain neurons, in response to inflammation and peripheral infections (Ridder et al. 2014). Reporter gene expression in neurons is caused by intercellular transfer of functional Cre recombinase messenger RNA from immune cells into neurons, in the absence of cell fusion. Although Cre-mediated recombination events in the brain is highly restricted in the healthy animal, inflammatory injuries increase both the frequency of transfer and the range of the neuronal target populations, extending beyond Purkinje neurons (Ridder et al. 2014).

Recent findings shed new light on the epigenetic basis of gene expression and molecular adaptations in brain.

Author's personal copy

Specific epigenetic mechanisms are involved in the stress response (Stankiewicz et al. 2013). These mechanisms (DNA methylation, histone modifications and microRNA activity) not only stably determine cell phenotype, but are also responsible for dynamic molecular adaptations of the limbic–hypothalamic–pituitary–adrenal axis to chronic psychogenic stressors. Traumatic experiences in early life alter mouse microRNA expression and metabolic responses in the progeny, via a molecular process of non-genetic inheritance of behavioural symptoms (Gapp et al. 2014). We speculate that variations in neural proteins due to epigenetic factors could explain the differences in functions of neurons, despite their apparent uniformity.

Molecular chaperones prevent aggregation and misfolding of proteins in the cellular environment and are thus central to maintaining protein homeostasis. Mechanisms of binding enables chaperones to function as holdases and unfoldases, by exerting forces to retain proteins in the unfolded state and at the same time protect them from aggregation by shielding their exposed hydrophobic regions from the solvent (Saio et al. 2014). The multiple binding sites recognize and interact with a large number of substrates with unrelated primary sequences. The fast kinetics enables chaperones to interact with transiently exposed, aggregation-prone regions of unstable proteins in the cytosol: we hypothesize that it could be one of the general mechanisms for the supramolecular chemistry described in Sect. 'The function of biologically active molecules and/or macromolecules in information processing'.

Physiological embodiment

It is well-known that basic physiological inputs can influence cognitions and emotions. Because bodily signals are constantly relayed to the neocortex, neural responses to them are likely to shape ongoing information processing, which in turn engages autonomic reflexes to change physiological (interoceptive) inputs. For example:

- In recent years, there has been an overwhelming increase in research on how nutritional factors influence cognition and behaviour. Neurocognitive performance is influenced by nutritional factors, ranging from the dietary level (e.g., whole diet and meal composition) to effects of macronutrients (glucose and omega-3 fatty acids) and micronutrients (vitamins, iron) (Smith and Scholey 2014).
- Metabolite concentrations reflect the physiological states of tissues and cells and may influence CNS functions (Bozek et al. 2014). In most species, chronic energy imbalance impacts olfactory-driven behaviours in response to food (Badonnel et al. 2014) and a high-fat diet leads to long-lasting structural and functional changes in the olfactory system (Whalley 2014).
- Short-term interoceptive fluctuations enhance perceptual and evaluative processes related to the handling of fear and threat, countering the view that baroreceptor afferent signalling is always inhibitory to sensory perception. The processing of brief fear stimuli is selectively gated by their timing in relation to individual heartbeats and these interoceptive signals influence the detection of emotional stimuli at the threshold of conscious awareness, altering judgments of emotionality of fearful and neutral faces (Garfinkel et al. 2014).
- Beyond conscious vision, physiological inputs underlie behaviourally relevant differential activation in multifunctional cortical areas. In humans, neural events locked to heartbeats before stimulus onset predict the detection of a faint visual grating in the posterior right inferior parietal lobule and the ventral anterior cingulate cortex. Heartbeats therefore shape visual conscious experience, potentially by contributing to the neural representations of the organism that might underlie subjectivity and a sense of self (Park et al. 2014).

Receptor embodiment

An underrated actor plays a crucial role in information processing in the CNS; namely, the peripheral receptor. To date, scientists have identified only a few of the receptors present on different types of nerve cells. However, research is ongoing: for example, using a new method, a group identified more than 400 receptors active in the sole warm sensitive neurons (Eberwine and Bartfai 2011). About one-third of them were "orphan" receptors, meaning the chemicals they bind to are unknown. Furthermore, a screening identified 194 candidate olfactory receptor genes linked to 11 odorants in the nematode Caenorhabditis elegans (Taniguchi et al. 2014).

Previously unrecognized sensory abilities are ceaselessly reported in animals. With the identification of additional receptors, we are gaining deeper insight into the mechanisms through which they process information.

- A self-recognition peripheral mechanism between skin and suckers in octopus prevents their arms from interfering with each other, via chemical signals that inhibit the attachment reflex (Nesher et al. 2014).
- Bumblebees can detect and discriminate the variations in pattern and structure exhibited by floral electric fields (Clarke et al. 2013).
- Some birds perform remarkable feats of navigation, using their different compasses: a star, a sun and a magnetic compass. Scientists do not yet understand how the birds' magnetic compass works, but there is

Author's personal copy

evidence that they use the quantum phenomenon of electron spin to navigate (Engels et al. 2014).

- Nematodes have concentration-dependent odour-sensing mechanisms, segregated at the olfactory receptor and sensory neuron levels. These neurons responded to high diacetyl concentrations only, whereas another class of chemosensory neurons react to both low and high concentrations. Chemosensory neurons ectopically expressing SRI-14 responded to a high concentration of diacetyl, resulting in avoidance responses (Taniguchi et al. 2014).
- A chloroplast retrograde signal regulates nuclear alternative splicing in plants. Light/dark conditions affect splicing of a subset of Arabidopsis genes preferentially encoding proteins involved in RNA processing (Petrillo et al. 2014).
- The sea catfish Plotosus japonicas is able to detect tiny changes in the water's pH level, changes indicating that the surrounding seawater has become slightly more acidic. The catfish senses local pH-associated increases in $H(+)/CO_2$ equating to a decrease of ≤ 0.1 pH unit in ambient seawater. This ability allows the fish to sense the breathing of prey hidden in the seafloor (Caprio et al. 2014).

Also human senses are under close investigation. Amazing novel "qualities" of receptors have been recently discovered in Homo sapiens:

- Recent observations suggest that protons might act as neurotransmitters. Protons, in concert with classical electric mechanisms, act directly as a nonquantal chemical neurotransmitter at vestibular hair cell-calyx afferent synapses (Highstein et al. 2014). Another study demonstrate that, in amygdala, postsynaptic receptors are acid-sensing ion channels, Na+- and Ca_2+-permeable channels, activated by extracellular acidosis. This process facilitates synaptic plasticity, a critical requirement for amygdala-dependent learning and memory (Du et al. 2014).
- The critical role of light for cognitive brain responses has been recently underlined. There is evidence in favour of a cognitive role for melanopsin, which may confer a form of "photic memory" to human cognitive brain function, via its wavelength-dependent, light-driven dual states (Chellappa et al. 2014).
- Merkel cells are primary sites of tactile transduction, and not Aβ-afferent nerve endings as previously believed. Scientists identified the Piezo2 ion channel as the Merkel cell mechanical transducer. Piezo2 transduces tactile stimuli into Ca(2+)-action potentials in Merkel cells, which drive Aβ-afferent nerve endings to fire slowly adapting impulses (Ikeda et al. 2014).
- There is mounting evidence that touch has another dimension, providing not only its well-recognized discriminative input to the brain, but also an affective input. It has been proposed that a class of low-threshold mechanosensitive C fibres that innervate the hairy skin represents the neurobiological substrate for the affective and rewarding properties of touch. C-fibres could be therefore involved in affect and reward, not just in pain (McGlone et al. 2014).
- Human visual gender perception draws on subconscious chemosensory biological cues, an effect that has been hitherto unsuspected. Indeed, a recent study suggests the existence of human sex pheromones, with particular interest in two human steroids, androstadienone and estratetraenol, which communicate opposite gender information in a sex-specific manner (Zhou et al. 2014).
- Unexpectedly, glucocorticoid hormone receptors have been found in the tongue. The highest concentrations were found in Tas1r3 taste cells, which are sensitive to sweet and umami taste (Parker et al. 2014). It suggests that hormones play a role in the detection of specific sensory qualities.
- The presence of carbohydrate in the human mouth has been associated with the facilitation of motor output. Oral receptors for carbohydrates have been identified as a potential mode of afferent transduction for this novel form of nutrient signalling, distinct from taste. Oral carbohydrate signalling increases activation within the primary sensorimotor cortex during physical activity and enhances activation of neural networks involved in sensory perception (Turner et al. 2014).

Receptors set in motion not only action potentials, but also a cascade of biochemical events correlated with information processing:

- Three single-point mutations in a single protein have been identified that can invert temperature-sensitivity, turning a cold-sensitive TRPA1 ion channels receptor for thermal pain into one that senses heat. The single-point mutation produced a profound change in the temperature sensitivity of the protein, but it did not affect the chemical sensitivity (Jabba et al. 2014).
- Mutations in the human gene encoding the Nav1.7 sodium channel can lead to either the inability to sense pain, or pain hypersensitivity. An antibody that blocks the NaV1.7 voltage-gated sodium channel in the neuronal cell membrane and suppresses pain in mice has been found to also simultaneously suppress itching in mice, even though pain and itch sensations usually follow different paths (Lee et al. 2014).

Author's personal copy

- During odour learning, molecular regulation of olfactory receptor expression contributes to plasticity in the olfactory system (Claudianos et al. 2014).
- Spike-based approaches to feature selectivity in sensory pathways focus on the most active neurons. However, a subthreshold method has been able to identify feature selectivity in the rodent vibrissal system, regardless of spiking activity (Shephard and Stanley 2014).
- Netrin-1, an axon-guiding molecule, affects in different ways neurons that express different combinations of receptors. Netrin-1 has two separate binding sites on opposite ends, enabling it to simultaneously bind two sensing neogenin molecules on the axons. Neogenin slightly different splice isoforms provide a basis for diverse signalling outcomes (Xu et al. 2014).

Peripheral receptors may have cognitive effects… by themselves! An astonishing piece of evidence shows that sensations are not processed by the CNS, but by peripheral receptors. Most mammals have two types of cone cells: S and M, sensitive to blues and greens. The retinas of Old World monkeys and humans acquired a third cone, sensitive to longer wavelengths (L cone), that allows them to see the red. A group of scientists genetically engineered a strain of knock-in mice that had human L cones in addition to their M and S ones (Jacobs et al. 2007). Animals whose retinas contained both native mouse pigments and human L pigment acquired the capacity to see in combinations of three basic colours, instead of two. Thus the appearance of a new dimension of sensory experience was demonstrated, based solely on gene-driven changes in receptor organization. Unlike the malleable cortex of young animals, adult brains are far more rigid and tend to have a harder time rewiring themselves; it came thus a complete surprise that another experiment endowed adult squirrel monkeys—lacking L cones—colour vision (Mancuso et al. 2009). The scientists injected retinas with a virus that introduced the human gene for the red-detecting pigment into cone cells. Twenty weeks later, the monkeys began to identify red dots; 2 years later, they remained able to distinguish all colours. These remarkable experiments reveal that phenomenal knowledge is an intrinsic property of the peripheral receptor. Receptors have thus a prominent role in sensory pathways and the importance of cortical areas in perceptual synthesis needs to be properly contextualised in terms of the embodied interactions with the world (and internal millionaire) through sensory organs.

In summary, this section has emphasised that neuronal processing cannot be considered in isolation from an embodied neuronal infrastructure—including its own physical substrates. The examples chosen here show that nearly every aspect (from gut bacteria to peripheral receptors) of the embodied nervous system has a profound influence on the nature of neuronal computations and the implicit information processing. The final section considers the implications for the CNS itself in terms of its neuroanatomy and physiology.

Are neurons different from each other? A new phrenology

Some authors claim that each region of the neocortex represents an independent organ, dedicated to a complete and distinct function. This idea, first put forward by the phrenologists Gall and Spurzheim, is still tangible in many current mapping studies aimed at localizing functions—commonly referred to as functional segregation specialisation. Such functional cartography with the aid of neuroimaging techniques has been characterized as "neophrenology" (Nieuwenhuys et al. 2008). In our paper we go further, towards a novel phrenology: the cerebral cortex is composed not only of discrete organs or regions, but of distinct and unique neuronal assemblies that span the macromolecular to microcircuit scale.

Growing evidence confirms that cortex is not homogenous; all areas are not composed of a basic repeated circuit (Elston and Rockland 2002). The cortex has distinct regional variations in the structure of its circuitry and cellular components; it is not a simple assembly of the same canonical microcircuit, whose function depends solely on the axonal connections among them. Indeed, cortex is a collection of deeply heterogeneous cell assemblies. Rather than forming mere functional networks of cells transmitting an electromagnetic impulse, pyramidal neurons, inhibitory interneurons, astrocytes show morphological and biochemical variations (Haustein et al. 2014).

Several studies have revealed distinct specialisations in pyramidal cell phenotype and structure in different cortical layers and areas (Spruston 2008). As an example, the functional columnar organization of sensory cortices, once thought to be underpinned by a network of structurally uniform columns of neurons, clearly shows a different pattern: the number of neurons can differ markedly between the "barrel" columns in the vibrissal area of the rat somatosensory cortex (Yates 2013). These variations are not random, but systematic; that is, cells become more branched and more spinous when comparing primary sensory with sensory association and executive cortical areas. The extent of regional differences in cell structure is species dependent (Elston and Rockland 2002) and the distinct regional specifications are probably due to strict genetic constrains (Spruston 2008; Anderson and Coulter 2013; Southwell et al. 2014; Zhang 2004).

The more we investigate, the more we discover different roles and abilities in apparently homogenous populations

Author's personal copy

of neurons. We now list some recent studies linking neuronal types to specific active molecules and well-defined behaviours:

- A new neuron type within the area pretectalis helps zebrafish coordinates their eye and swimming movements, to compensate for self-motion (Kubo et al. 2014). These neurons are prevalently direction selective, either monocularly or binocularly driven, and hierarchically organized to distinguish between rotational and translational optic flow.
- Researchers have identified two types of neurons that enable the spinal cord to control skilled forelimb movement. The first is a group of excitatory interneurons needed to make accurate and precise movements; the second is a group of inhibitory interneurons necessary for achieving smooth movement of the limbs (Azim et al. 2014).
- With help from EyeWire, an online community of "citizen neuroscientists", it has been demonstrated that Off-type starburst amacrine cells in retina have dendrites with receptive fields oriented in space–time and therefore respond selectively to stimuli that move in the outward direction from the soma (Kim et al. 2014a, b, c).
- Researchers revealed a specific cell type and microcircuit underlying disinhibitory control in cortex and demonstrated that it is activated under specific behavioural conditions (Pi et al. 2013).
- De novo memory-involved protein expression can be restricted to specific neurons within a population, and to specific dendrites within a single neuron (O'Donnell and Sejnowski 2014).
- Mice virgin males—genetically impaired in vomeronasal sensing—exhibit an odd behaviour: they are parental and do not attack pups as usual. A subset of galanin-expressing neurons in the medial preoptic area is specifically activated during male and female parenting, while a different subpopulation is activated during mating. Thus, galanin neurons emerge as an essential regulatory node of male and female parenting behaviour and other social responses (Wu et al. 2014).
- Large proportion of prefrontal cortex neurons are multifunction, mixed selectivity neurons, specialized for one judgment or the other. They may be crucial in promoting complex, flexible behaviour (Cromer et al. 2010; Rigotti et al. 2013).

The complexity and cellular heterogeneity of neuronal circuitry presents a major challenge to understanding the role of discrete neural populations in controlling behaviour (Ekstrand et al. 2014). While neuroanatomical methods enable high-resolution mapping of neural circuitry, these approaches do not allow systematic molecular profiling of neurons based on their connectivity. New techniques may shed new light on these topics. For instance, it has been recently discovered that associative learning in the mouse is dynamically regulated by the stimulus-specific activation of two distinct disinhibitory microcircuits through precise interactions between different subtypes of local interneurons: in basolateral amygdala, interneurons expressing parvalbumin and somatostatin bidirectionally control the acquisition of fear conditioning (Wolff et al. 2014). Furthermore, as an example, a novel approach identified a number of markers specific to VTA dopaminergic projection neurons (Ekstrand et al. 2014).

Just as activity of individual neurons means different things in different brain areas, so does activity of other cells in CNS. Recent results have redefined microglia and help us to understand how different myeloid cell populations operate, based on their cell-specific gene expression signatures, distinct ontogeny and differential functions. This raises the possibility that astrocytes are not all the same and may serve various roles throughout the different areas of brain (Haustein et al. 2014). Humans also have more types of GABAergic interneurons than other model species—and studies are beginning to show differences in function (Clowry 2014).

Concluding remarks

Our brief theoretical account could be summarized with a seemingly antithetical definition: "supramolecular phrenology". The term "supramolecular" refers to the basic sentiment that information processing should be generalized to cover all metabolic and synaptic signalling in the brain, including the molecular basis of synaptic plasticity. We emphasize the dynamic coordination of information transfer in terms of action potentials contextualizing the exchange among cortical areas (as opposed to the content of the information). Furthermore, we place a holistic emphasis on macromolecules and molecular processes in encoding information. This seems consistent with the information encoded in synaptic connections that accumulates experience with the world through synaptic plasticity. In one sense, it highlights the distinction between perceptual inference (that is contextualised by action potentials) and perceptual learning (that relies upon macromolecular information storage) (Friston, personal communication).

On the other side, the term "phrenology" emphasizes the delicate and heterogeneous nature of cortical hierarchies with deep structure. This fits comfortably with hierarchical predictive coding and functional specialization in the brain, which again emphasizes the distribution of information coding over multiple levels and timescales. This

Author's personal copy

paper has tried to substantiate the importance of considering the circular causality or reciprocal interactions between separable scales—and between the nervous system and the world in which it is embodied. A proper consideration of this holistic aspect of information processing in the brain may necessarily rest upon a supramolecular phrenology, which can be construed as the ultimate form of embodied cognition.

Acknowledgments I would like to thank Karl Friston for commenting upon an earlier version of this manuscript.

References

Anderson S, Coulter D (2013) Neuronal birth to cortical circuitry. Science 340(6136):1058–1059. doi:10.1126/science.1235778

Antzoulatos EG, Miller EK (2014) Increases in functional connectivity between prefrontal cortex and striatum during category learning. Neuron S0896–6273(14):391–392. doi:10.1016/j.neuron.2014.05.005

Attwood BK, Bourgognon JM, Patel S, Mucha M, Schiavon E et al (2011) Neuropsin cleaves EphB2 in the amygdala to control anxiety. Nature 473(7347):372–375. doi:10.1038/nature09938

Azim E, Jiang J, Alstermark B, Jessell TM (2014) Skilled reaching relies on a V2a propriospinal internal copy circuit. Nature 508(7496):357–363. doi:10.1038/nature13021

Badonnel K, Lacroix MC, Monnerie R, Caillol M, Baly C (2014) Rat strains with different metabolic statuses differ in food olfactory-driven behavior. Behav Brain Res 270C:228–239. doi:10.1016/j.bbr.2014.05.011

Bosman CA, Lansink CS, Pennartz CM (2014) Functions of gamma-band synchronization in cognition: from single circuits to functional diversity across cortical and subcortical systems. Eur J Neurosci 39(11):1982–1999. doi:10.1111/ejn.12606

Bozek K, Wei Y, Yan Z, Liu X, Xiong J et al (2014) Exceptional evolutionary divergence of human muscle and brain metabolomes parallels human cognitive and physical uniqueness. PLoS Biol 12(5):61001871. doi:10.1371/journal.pbio.1001871

Brea J, Urbanczik R, Senn W (2014) A normative theory of forgetting: lessons from the fruit fly. PLoS Comput Biol 10(6):e1003640. doi:10.1371/journal.pcbi.1003640

Breckwoldt MO, Pfister FM, Bradley PM, Marinković P, Williams PR et al (2014) Multiparametric optical analysis of mitochondrial redox signals during neuronal physiology and pathology in vivo. Nat Med 20(5):555–560. doi:10.1038/nm.3520

Brunet NM, Bosman CA, Vinck M, Roberts M, Oostenveld R et al (2014) Stimulus repetition modulates gamma-band synchronization in primate visual cortex. Proc Natl Acad Sci USA 111(9):3626–3631. doi:10.1073/pnas.1309714111

Buschman TJ, Denovellis EL, Diogo C, Bullock D, Miller EK (2012) Synchronous oscillatory neural ensembles for rules in the prefrontal cortex. Neuron 76(4):838–846. doi:10.1016/j.neuron.2012.09.029

Buzsáki G, Watson BO (2012) Brain rhythms and neural syntax: implications for efficient coding of cognitive content and neuropsychiatric disease. Dialogues Clin Neurosci 4:345–367

Caprio J, Shimohara M, Marui T, Harada S, Kiyohara S (2014) Marine teleost locates live prey through pH sensing. Science 344(6188):1154–1156. doi:10.1126/science.1252697

Chellappa SL, Ly JQ, Meyer C, Balteau E, Degueldre C et al (2014) Photic memory for executive brain responses. Proc Natl Acad Sci USA 111(16):6087–6091. doi:10.1073/pnas.1320005111

Chen CY, Ho A, Huang HY, Juan HF, Huang HC (2014) Dissecting the human protein–protein interaction network via phylogenetic decomposition. Sci Rep 4:7153. doi:10.1038/srep07153

Chiu IM, Heesters BA, Ghasemlou N, Von Hehn CA, Zhao F et al (2013) Bacteria activate sensory neurons that modulate pain and inflammation. Nature 501(7465):52–57. doi:10.1038/nature12479

Choudhury S, Fishman JR, McGowan ML, Juengst ET (2014) Big data, open science and the brain: lessons learned from genomics. Front Hum Neurosci 8:239. doi:10.3389/fnhum.2014.00239

Clarke D, Whitney H, Sutton G, Robert D (2013) Detection and learning of floral electric fields by bumblebees. 340(6128):66–69. doi:10.1126/science.1230883

Claudianos C, Lim J, Young M, Yan S, Cristino AS et al (2014) Odor memories regulate olfactory receptor expression in the sensory periphery. Eur J Neurosci 39(10):1642–1654. doi:10.1111/ejn.12539

Clowry GJ (2014) An enhanced role and expanded developmental origins for gamma-aminobutyric acidergic interneurons in the human cerebral cortex. J Anat. doi:10.1111/joa.12198

Cromer JA, Roy JE, Miller EK (2010) Representation of multiple, independent categories in the primate prefrontal cortex. Neuron 66(5):796–807. doi:10.1016/j.neuron.2010.05.005

Czajkowski R, Jayaprakash B, Wiltgen B, Rogerson T, Guzman-Karlsson MC et al (2014) Encoding and storage of spatial information in the retrosplenial cortex. Proc Natl Acad Sci USA 111(23):8661–8666. doi:10.1073/pnas.1313222111

DasGupta S, Ferreira CH, Miesenböck G (2014) FoxP influences the speed and accuracy of a perceptual decision in Drosophila. Science 344(6186):901–904. doi:10.1126/science.1252114

Du J, Reznikov LR, Price MP, Zha X, Lu Y et al (2014) Protons are a neurotransmitter that regulates synaptic plasticity in the lateral amygdala. Proc Natl Acad Sci USA 111(24):8961–8966. doi:10.1073/pnas.1407018111

Eberwine J, Bartfai T (2011) Single cell transcriptomics of hypothalamic warm sensitive neurons that control core body temperature and fever response Signaling asymmetry and an extension of chemical neuroanatomy. Pharmacol Ther 129(3):241–259. doi:10.1016/j.pharmthera.2010.09.010

Ekstrand MI, Nectow AR, Knight ZA, Latcha KN, Pomeranz LE, Friedman JM (2014) Molecular profiling of neurons based on connectivity. Cell 157(5):1230–1242. doi:10.1016/j.cell.2014.03.059

Elston GN, Rockland KS (2002) The pyramidal cell of the sensorimotor cortex of the macaque monkey: phenotypic variation. Cereb Cortex 12(10):1071–1078

Engels S, Schneider NL, Lefeldt N, Hein CM, Zapka M et al (2014) Anthropogenic electromagnetic noise disrupts magnetic compass orientation in a migratory bird. Nature 509(7500):353–356. doi:10.1038/nature13290

Foffi G, Pastore A, Piazza F, Temussi PA (2013) Macromolecular crowding: chemistry and physics meet biology (Ascona, Switzerland, 10–14 June 2012). Phys Biol 10(4):040301

Foster JA, Neufeld KAMV (2013) Gut-brain axis: how the microbiome influences anxiety and depression. Trends Neurosci 36(5):305–312. doi:10.1016/j.tins.2013.01.005

Friston K (2010) The free-energy principle: a unified brain theory? Nat Rev Neurosci 11(2):127–138. doi:10.1038/nrn2787

Frost G, Sleeth ML, Sahuri-Arisoylu M, Lizarbe B, Cerdan S et al (2014) The short-chain fatty acid acetate reduces appetite via a central homeostatic mechanism. Nat Commun 5:3611. doi:10.1038/ncomms4611

Gapp K, Jawaid A, Sarkies P, Bohacek J, Pelczar P et al (2014) Implication of sperm RNAs in transgenerational inheritance of the effects of early trauma in mice. Nat Neurosci 17(5):667–669. doi:10.1038/nn.3695

Author's personal copy

Gárate I, García-Bueno B, Madrigal JL, Caso JR, Alou L et al (2014) Toll-like 4 receptor inhibitor TAK-242 decreases neuroinflammation in rat brain frontal cortex after stress. J Neuroinflammation 11:8. doi:10.1186/1742-2094-11-8

Garfinkel SN, Minati L, Gray MA, Seth AK, Dolan RJ, Critchley HD (2014) Fear from the heart: sensitivity to fear stimuli depends on individual heartbeats. J Neurosci 34(19):6573–6582. doi:10.1523/JNEUROSCI.3507-13.2014

Gibson EM, Purger D, Mount CW, Goldstein AK, Lin GL et al (2014) Neuronal activity promotes oligodendrogenesis and adaptive myelination in the mammalian brain. Science 344(6183): 1252304. doi:10.1126/science.1252304

Gollisch T (2009) Throwing a glance at the neural code: rapid information transmission in the visual system. HFSP J 3(1):36–46. doi:10.2976/1.3027089

Haustein MD, Kracun S, Lu XH, Shih T, Jackson-Weaver O et al (2014) Conditions and constraints for astrocyte calcium signaling in the hippocampal mossy fiber pathway. Neuron 82(2):413–429. doi:10.1016/j.neuron.2014.02.041

He H, Kise Y, Izadifar A, Urwyler O, Ayaz D et al (2014) Cell-intrinsic requirement of Dscam1 isoform diversity for axon collateral formation. Science 344(6188):1182–1186. doi:10.1126/science.1251852

Highstein SM, Holstein GR, Mann MA, Rabbitt RD (2014) Evidence that protons act as neurotransmitters at vestibular hair cell-calyx afferent synapses. Proc Natl Acad Sci USA 111(14):5421–5426. doi:10.1073/pnas.1319561111

Iacobucci GJ, Rahman NA, Valtueña AA, Nayak TK, Gunawardena S (2014) Spatial and temporal characteristics of normal and perturbed vesicle transport. PLoS One 9(5):e97237. doi:10.1371/journal.pone.0097237

Ibáñez-Molina AJ, Iglesias-Parro S (2014) Fractal characterization of internally and externally generated conscious experiences. Brain Cogn 87C:69–75. doi:10.1016/j.bandc.2014.03.002

Igarashi KM, Lu L, Colgin LL, Moser MB, Moser EI (2014) Coordination of entorhinal-hippocampal ensemble activity during associative learning. Nature 510(7503):143–147. doi:10.1038/nature13162

Ikeda R, Cha M, Ling J, Jia Z, Coyle D, Guemail JG (2014) Merkel cells transduce and encode tactile stimuli to drive aβ-afferent impulses. Cell 157(3):664–675. doi:10.1016/j.cell.2014.02.026

Jabba S, Goyal R, Sosa-Pagán JO, Moldenhauer H, Wu J et al (2014) Directionality of temperature activation in mouse TRPA1 ion channel can be inverted by single-point mutations in ankyrin repeat six. Neuron. doi:10.1016/j.neuron.2014.04.016

Jacobs GH, Williams GA, Cahill H, Nathans J (2007) Emergence of novel color vision in mice engineered to express a human cone photopigment. Science 315(5819):1723–1725

Jensen O, Gips B, Bergmann TO, Bonnefond M (2014) Temporal coding organized by coupled alpha and gamma oscillations prioritize visual processing. Trends Neurosci. doi:10.1016/j.tins.2014.04.001

Karayannis T, Au E, Patel JC, Kruglikov I, Markx S et al (2014) Cntnap4 differentially contributes to GABAergic and dopaminergic synaptic transmission. Nature. doi:10.1038/nature13248

Kim SY, Lim W (2013) Coupling-induced population synchronization in an excitatory population of subthreshold Izhikevich neurons. Cogn Neurodyn 7(6):495–503. doi:10.1007/s11571-013-9256-y

Kim JG, Suyama S, Koch M, Jin S, Argente-Arizon P et al (2014a) Leptin signalling in astrocytes regulates hypothalamic neuronal circuits and feeding. Nat Neurosci. doi:10.1038/nn.3725

Kim JS, Greene MJ, Zlateski A, Lee K, Richardson M et al (2014b) Space-time wiring specificity supports direction selectivity in the retina. Nature 509(7500):331–336. doi:10.1038/nature13240

Kim MS, Pinto SM, Getnet D, Nirujogi RS, Manda SS et al (2014c) A draft map of the human proteome. Nature 509(7502):575–581. doi:10.1038/nature13302

Klemen J, Chambers CD (2012) Current perspectives and methods in studying neural mechanisms of multisensory interactions. Neurosci Biobehav Rev 36(1):111–133

Kubo F, Hablitzel B, Dal Maschio M, Driever W, Baier H, Arrenberg AB (2014) Functional architecture of an optic flow-responsive area that drives horizontal eye movements in zebrafish. Neuron 81(6):1344–1359. doi:10.1016/j.neuron.2014.02.043

Kucewicz MT, Cimbalnik J, Matsumoto JY, Brinkmann BH, Bower MR et al (2014) High frequency oscillations are associated with cognitive processing in human recognition memory. Brain 137(8):2231–2244. doi:10.1093/brain/awu149

Lee JH, Park CK, Chen G, Han Q, Xie RG et al (2014) A monoclonal antibody that targets a NaV1.7 channel voltage sensor for pain and itch relief. Cell 157(6):1393–1404. doi:10.1016/j.cell.2014.03.064

Lehn JM (2007) From supramolecular chemistry towards constitutional dynamic chemistry and adaptive chemistry. Chem Soc Rev 36(2):151–160

Lohse KR, Wadden K, Boyd LA, Hodges NJ (2014) Motor skill acquisition across short and long time scales: a meta-analysis of neuroimaging data. Neuropsychologia 59C:130–141. doi:10.1016/j.neuropsychologia.2014.05.001

Mancuso K, Hauswirth WW, Li Q et al (2009) Gene therapy for red–green colour blindness in adult primates. Nature 461(7265):784–787. doi:10.1038/nature08401

Mattei TA (2014) Unveiling complexity: non-linear and fractal analysis in neuroscience and cognitive psychology. Front Comput Neurosci 8:17. doi:10.3389/fncom.2014.00017

McGlone F, Wessberg J, Olausson H (2014) Discriminative and Affective touch: sensing and feeling. Neuron 82(4):737–755. doi:10.1016/j.neuron.2014.05.001

McNally JM, Custer EE, Ortiz-Miranda S, Woodbury DJ, Kraner SD et al (2014) Functional ryanodine receptors in the membranes of neurohypophysial secretory granules. J Gen Physiol 143(6): 693–702. doi:10.1085/jgp.201311110

Munz M, Gobert D, Schohl A, Poquérusse J, Podgorski K et al (2014) Rapid Hebbian axonal remodeling mediated by visual stimulation. Science 344(6186):904–909. doi:10.1126/science.1251593

Nesher N, Levy G, Grasso FW, Hochner B (2014) Self-recognition mechanism between skin and suckers prevents octopus arms from interfering with each other. Curr Biol 24(11):1271–1275. doi:10.1016/j.cub.2014.04.024

Newswire (2014): http://newswire.rockefeller.edu/2014/05/22/researchers-profile-active-genes-in-neurons-based-on-connections/

Nieuwenhuys R, Voogd J, van Huijzen C (2008) The human central nervous system. Springer, Heidelberg

O'Donnell C, Sejnowski TJ (2014) Selective memory generalization by spatial patterning of protein synthesis. Neuron 82(2): 398–412. doi:10.1016/j.neuron.2014.02.028

Onojjighofia T (2014) Presented at the american academy of neurology's 66th annual meeting in Philadelphia, April 26 to May 3

Ostrovskaya O, Xie K, Masuho I, Fajardo-Serrano A, Lujan R et al (2014) RGS7/Gβ5/R7BP complex regulates synaptic plasticity and memory by modulating hippocampal GABABR-GIRK signalling. Elife 3:e02053. doi:10.7554/eLife.02053

Palmowski P, Rogowska-Wrzesinska A, Williamson J, Beck HC, Mikkelsen JD et al (2014) Acute phencyclidine treatment induces extensive and distinct protein phosphorylation in rat frontal cortex. J Proteome Res 13(3):1578–1592. doi:10.1021/pr4010794

Park HD, Correia S, Ducorps A, Tallon-Baudry C (2014) Spontaneous fluctuations in neural responses to heartbeats predict visual detection. Nat Neurosci 17(4):612–618. doi:10.1038/nn.3671

Author's personal copy

Parker MR, Feng D, Chamuris B, Margolskee RF (2014) Expression and nuclear translocation of glucocorticoid receptors in type 2 taste receptor cells. Neurosci Lett 571:72–77. doi:10.1016/j.neulet.2014.04.047

Petrillo E, Herz MA, Fuchs A, Reifer D, Fuller J et al (2014) A chloroplast retrograde signal regulates nuclear alternative splicing. Science 344(6182):427–430. doi:10.1126/science.1250322

Petrini EM, Barberis A (2014) Diffusion dynamics of synaptic molecules during inhibitory postsynaptic plasticity. Front Cell Neurosci 8:300. doi:10.3389/fncel.2014.00300

Pfeifer R, Iida F, Lungarella M (2014) Cognition from the bottom up: on biological inspiration, body morphology, and soft materials. Trends Cogn Sci. doi:10.1016/j.tics.2014.04.004

Pi HJ, Hangya B, Kvitsiani D, Sanders JI, Huang ZJ, Kepecs A (2013) Cortical interneurons that specialize in disinhibitory control. Nature 503(7477):521–524. doi:10.1038/nature12676

Pollock JD, Wu DY, Satterlee JS (2014) Molecular neuroanatomy: a generation of progress. Trends Neurosci 37(2):106–123. doi:10.1016/j.tins.2013.11.001

Qu J, Wang R, Yan C, Du Y (2014) Oscillations and synchrony in a cortical neural network. Cogn Neurodyn 8(2):157–166. doi:10.1007/s11571-013-9268-7

Radecki G, Nargeot R, Jelescu IO, Le Bihan D, Ciobanu L (2014) Functional magnetic resonance microscopy at single-cell resolution in Aplysia californica. Proc Natl Acad Sci USA 111(23):8667–8672. doi:10.1073/pnas.1403739111

Ridder K, Keller S, Dams M, Rupp AK, Schlaudraff J et al (2014) Extracellular vesicle-mediated transfer of genetic information between the hematopoietic system and the brain in response to inflammation. PLoS Biol 12(6):e1001874. doi:10.1371/journal.pbio.1001874

Rigotti M, Barak O, Warden MR, Wang X, Daw ND et al (2013) The importance of mixed selectivity in complex cognitive tasks. Nature 497(7451):585–590. doi:10.1038/nature12160

Roberts RE, Bain PG, Day BL, Husain M (2013) Individual differences in expert motor coordination associated with white matter microstructure in the cerebellum. Cereb Cortex 23(10):2282–2292. doi:10.1093/cercor/bhs219

Rumelhart DE, McClelland JL, PDP Research Group (1986) Parallel Distributed Processing. MIT Press, Cambridge

Saio T, Guan X, Rossi P, Economou A, Kalodimos CG (2014) Structural basis for protein antiaggregation activity of the trigger factor chaperone. Science 344(6184):1250494. doi:10.1126/science.1250494

Shephard CJ, Stanley GB (2014) The needle in the haystack. Nat Neurosci 17(6):752–753. doi:10.1038/nn.3730

Smith MA, Scholey AB (2014) Nutritional influences on human neurocognitive functioning. Front Hum Neurosci 8:358. doi:10.3389/fnhum.2014.00358

Southwell DG, Nicholas CR, Basbaum AI, Stryker MP, Kriegstein AR et al (2014) Interneurons from embryonic development to cell-based therapy. Science 344(6180):1240622. doi:10.1126/science.1240622

Sporns O (2013) Network attributes for segregation and integration in the human brain. Curr Opin Neurobiol 23(2):162–171. doi:10.1016/j.conb.2012.11.015

Spruston N (2008) Pyramidal neurons: dendritic structure and synaptic integration. Nat Rev Neurosci 9(3):206–221. doi:10.1038/nrn2286

Stankiewicz AM, Swiergiel AH, Lisowski P (2013) Epigenetics of stress adaptations in the brain. Brain Res Bull 98:76–92. doi:10.1016/j.brainresbull.2013.07.003

Steib K, Schäffner I, Jagasia R, Ebert B, Lie DC (2014) Mitochondria modify exercise-induced development of stem cell-derived neurons in the adult brain. J Neurosci 34(19):6624–6633. doi:10.1523/JNEUROSCI.4972-13.2014

Sur S, Newcomb CJ, Webber MJ, Stupp SI (2013) Tuning supramolecular mechanics to guide neuron development. Biomaterials 34(20):4749–4757. doi:10.1016/j.biomaterials.2013.03.025

Taniguchi G, Uozumi T, Kiriyama K, Kamizaki T, Hirotsu T (2014) Screening of odor-receptor pairs in Caenorhabditis elegans reveals different receptors for high and low odor concentrations. Sci Signal 7(323):ra39. doi:10.1126/scisignal.2005136

Taylor MB, Ehrenreich IM (2014) Genetic interactions involving five or more genes contribute to a complex trait in yeast. PLoS Genet 10(5):e1004324. doi:10.1371/journal.pgen.1004324

Tomassy GS, Berger DR, Chen HH, Kasthuri N, Hayworth KJ et al (2014) Distinct profiles of myelin distribution along single axons of pyramidal neurons in the neocortex. Science 344(6181):319–324. doi:10.1126/science.1249766

Treutleina B, Gokcec O, Quakea SR, Südhofc TC (2014) Cartography of neurexin alternative splicing mapped by single-molecule long-read mRNA sequencing. Proc Natl Acad Sci USA 111(13):E1291–E1299. doi:10.1073/pnas.1403244111

Turner CE, Byblow WD, Stinear CM, Gant N (2014) Carbohydrate in the mouth enhances activation of brain circuitry involved in motor performance and sensory perception. Appetite 80C:212–219. doi:10.1016/j.appet.2014.05.020

Whalley K (2014) Sensory systems: eat well to improve smell? Nat Rev Neurosci 15(7):428–429. doi:10.1038/nrn3771

White-Grindley E, Li L, Mohammad Khan R, Ren F, Saraf A et al (2014) Contribution of Orb2A stability in regulated amyloid-like oligomerization of Drosophila Orb2. PLoS Biol 12(2):e1001786. doi:10.1371/journal.pbio.1001786

Wicker SB, Kim S (2003) Fundamentals of codes, graphs, and iterative decoding. Kluwer Academic Publishers, Boston

Wilhelm BG, Mandad S, Truckenbrodt S, Kröhnert K, Schäfer C et al (2014) Composition of isolated synaptic boutons reveals the amounts of vesicle trafficking proteins. Science 344(6187):1023–1028. doi:10.1126/science.1252884

Winkler CW, Taylor KG, Peterson KE (2014) Location is everything: let-7b microRNA and TLR7 signaling results in a painful TRP. Sci Signal 7(327):pe14

Wolff SB, Gründemann J, Tovote P, Krabbe S, Jacobson GA et al (2014) Amygdala interneuron subtypes control fear learning through disinhibition. Nature 509(7501):453–458. doi:10.1038/nature13258

Wu Z, Autry AE, Bergan JF, Watabe-Uchida M, Dulac CG (2014) Galanin neurons in the medial preoptic area govern parental behaviour. Nature 509(7500):325–330. doi:10.1038/nature13307

Wutz A, Weisz N, Braun C, Melcher D (2014) Temporal windows in visual processing: "prestimulus brain state" and "poststimulus phase reset" segregate visual transients on different temporal scales. J Neurosci 34(4):1554–1565. doi:10.1523/JNEUROSCI.3187-13.2014

Xiumin L (2014) Signal integration on the dendrites of a pyramidal neuron model. Cogn Neurodyn 8(1):81–85. doi:10.1007/s11571-013-9252-2

Xu K, Wu Z, Renier N, Antipenko A, Tzvetkova-Robev D et al (2014) Structures of netrin-1 bound to two receptors provide insight into its axon guidance mechanism. Science 344(6189):1275–1279. doi:10.1126/science.1255149

Yates D (2013) Cerebral cortex: sizing up the columns. Nat Rev Neurosci 14(12):817. doi:10.1038/nrn3631

Yates D (2014) Myelination: a not so even distribution. Nat Rev Neurosci 15(6):351. doi:10.1038/nrn3755

Ye X, Marina A, Carew TJ (2012) Local synaptic integration of mitogen-activated protein kinase and protein kinase A signalling mediates intermediate-term synaptic facilitation in Aplysia. Proc Natl Acad Sci USA 109(44):18162–18167. doi:10.1073/pnas.1209956109

Author's personal copy

Yu S, Levi L, Casadesus G, Kunos G, Noy N (2014) Fatty acid-binding protein 5 (FABP5) regulates cognitive function both by decreasing anandamide levels and by activating the nuclear receptor peroxisome proliferator-activated receptor β/δ (PPARβ/δ) in the brain. J Biol Chem 289(18):12748–12758. doi:10.1074/jbc.M114.559062

Zhang ZW (2004) Maturation of layer V pyramidal neurons in the rat prefrontal cortex: intrinsic properties and synaptic function. J Neurophysiol 91(3):1171–1182. doi:10.1152/jn.00855.2003

Zhou W, Yang X, Chen K, Cai P, He S, Jiang Y (2014) Chemosensory communication of gender through two human steroids in a sexually dimorphic manner. Curr Biol 24(10):1091–1095. doi:10.1016/j.cub.2014.03.035

Journal of Theoretical Biology 377 (2015) 117–118

Contents lists available at ScienceDirect

Journal of Theoretical Biology

journal homepage: www.elsevier.com/locate/yjtbi

Letter to Editor

How to turn an oscillation in a pink one

HIGHLIGHTS

- Scale-free dynamics are an intrinsic feature of a large class of natural models.
- A fractal-like wave can be produced by summing a random oscillation to a chosen one.
- Fractal systems can be produced by choosing the appropriate oscillation to bring in.

ARTICLE INFO

Keywords:
Fractals
Scale-free
Oscillation
Power law

Scale-free dynamics – also called $1/f^n$ behavior, pink noise, power law, fractal-like distribution (Newman, 2005) – are an intrinsic feature of a large class of natural models, from earthquakes to brain activity (He et al., 2010). Assessing a geometrical/mathematical model of synthetic power law oscillations, we noticed that a wave containing a fractal-like structure can be produced by summing a random oscillation to a carefully chosen one. Here follows the procedure we carried out. First, we generated random numbers with power law distribution, obtaining a series of oscillations **1** in a log amplitude versus log frequency scatter plot (the solid line in Fig. 1A). The series exhibited a pink noise behavior: $A(f)=1/f^n$, where A was the amplitude of the oscillation, f was the frequency and n was the power exponent (Milstein et al., 2009). Second, we produced a non scale-free oscillation **2** (the dotted line in Fig. 1A) equipped with a random point $\mathbf{O_2}$. Third, we chose the point $\mathbf{O_1}$ characterized by the same frequency of $\mathbf{O_2}$, but a different amplitude. Fourth, we extrapolated the sine waves corresponding to the points $\mathbf{O_1}$ and $\mathbf{O_2}$ (Fig. 1B). Fifth, we looked for the required oscillation $\mathbf{O_3}$ which we had to superimpose upon $\mathbf{O_2}$, in order that the combination might be equal to the oscillation $\mathbf{O_1}$. We handled the sinusoidal oscillations through the classical formula (Booker, 1993) reported in Fig. 1B, where t denotes time.

In summary, we demonstrated that a pink noise can be obtained by adding a random sine wave to a proper one. This observation gives rise to countless applications: a “hidden” oscillation may cause a scale-free behavior in a random noise; a fractal system can be produced by simply choosing the appropriate oscillation to bring in; if power laws are involved in random walks, phase transitions and self-organized criticality (Bak et al., 1987), then the superimposition of a carefully chosen oscillation may lead to systems of increased complexity; “nested” waves from the central nervous system's spontaneous networks (Fox and Raichle, 2007) may be the source of the scale-free dynamics seen in EEG and fMRI; in the event of brain 1/f scaling disruption caused by illnesses such as Alzheimer's disease, an external wave – for instance, via transcranial stimulation (Reato et al., 2013) – could restore the broken symmetry.

http://dx.doi.org/10.1016/j.jtbi.2015.04.018
0022-5193/© 2015 Elsevier Ltd. All rights reserved.

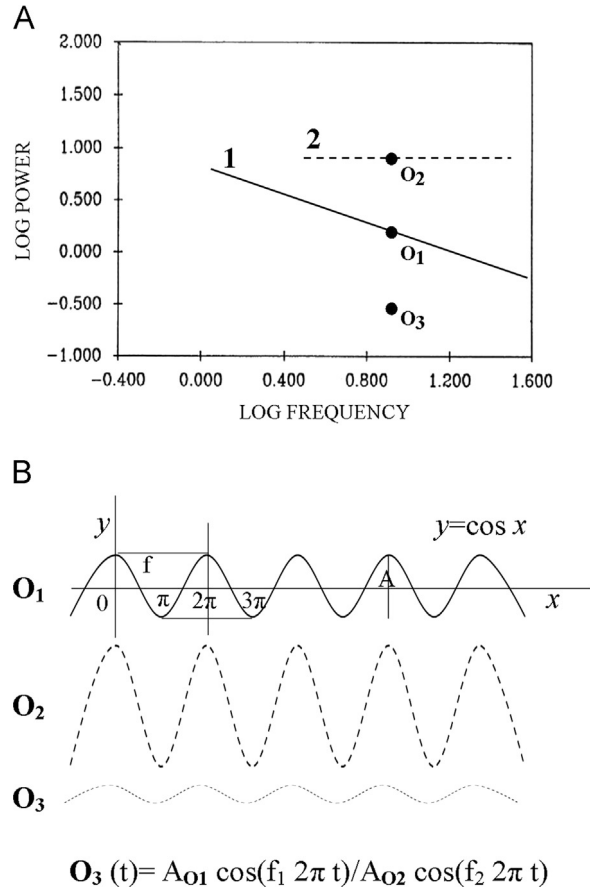

Fig. 1A. Power law distributions in a log power (amplitude) versus log frequency scatter plot. Fig 1B. Sine waves corresponding to the points O_1 and O_2.

References

Bak, P., Tang, C., Wiesenfeld, K., 1987. Self-organized criticality: an explanation of the 1/*f* noise. Phys. Rev. Lett. 59 (4), 381–384, PMID: 10035754.

Booker, H.G., 1993. A Vector Approach to Oscillations. Academic Press, London & New York.

Fox, M.D., Raichle, M.E., 2007. Spontaneous fluctuations in brain activity observed with functional magnetic resonance imaging. Nat. Rev. Neurosci. 8, 700–711.

He, B.J., Zempel, J.M., Snyder, A.Z., Raichle, M.E., 2010. The temporal structures and functional significance of scale-free brain activity. Neuron 66 (3), 353–369. http://dx.doi.org/10.1016/j.neuron.2010.04.020.

Milstein, J., Mormann, F., Fried, I., Koch, C., 2009. Neuronal shot noise and Brownian $1/f^2$ behavior in the local field potential. PLoS One 4 (2), e4338. http://dx.doi.org/10.1371/journal.pone.0004338.

Newman, M.E.J., 2005. Power laws, Pareto distributions and Zipf's law. Contemp. Phys. 46, 323–351.

Reato, D., Rahman, A., Bikson, M., Parra, L.C., 2013. Effects of weak transcranial alternating current stimulation on brain activity – a review of known mechanisms from animal studies. Front. Hum. Neurosci. 7, 687. http://dx.doi.org/10.3389/fnhum.2013.00687.

Arturo Tozzi

Center for Nonlinear Science, University of North Texas, Denton, Texas 76203, USA

Available online 25 April 2015

tion that there may be other patient groups in whom either short storage or long storage might have clinical effects, either beneficial or adverse. No significant between-group differences in acquired infections were noted in the three storage-duration trials cited. However, the hypothesis that transfusing red cells with a prolonged storage duration exacerbates established infection in humans would need to be tested.

Marie E. Steiner, M.D.
University of Minnesota
Minneapolis, MN
stein083@umn.edu

Susan F. Assmann, Ph.D.
New England Research Institutes
Watertown, MA

Christopher P. Stowell, M.D., Ph.D.
Massachusetts General Hospital
Boston, MA

1. Steiner ME, Ness PM, Assmann SF, et al. Effects of red-cell storage duration on patients undergoing cardiac surgery. N Engl J Med 2015;372:1419-29.
2. Lacroix J, Hébert PC, Fergusson DA, et al. Age of transfused blood in critically ill adults. N Engl J Med 2015;372:1410-8.
3. Fergusson DA, Hébert P, Hogan DL, et al. Effect of fresh red blood cell transfusions on clinical outcomes in premature, very low-birth-weight infants: the ARIPI randomized trial. JAMA 2012;308:1443-51.

DOI: 10.1056/NEJMc1505699

Oral Propranolol for Infantile Hemangioma

TO THE EDITOR: The article by Léauté-Labrèze et al. (Feb. 19 issue)[1] emphasizes the therapeutic efficacy and the short-term safety of propranolol in the treatment of infantile hemangiomas. However, recent studies raise concerns about potential long-term neurodevelopmental or cognitive effects of the highly lipophilic propranolol.[2] Indeed, lipophilic beta-blockers cross the blood–brain barrier, leading to sleep and memory disturbances.[3] For example, sleep disturbance, somnolence, and irritability have been observed in many infants treated with propranolol,[4] and this drug has been shown to decrease specific memory functions in adults.[5] A recent review suggested the possibility that blockage of neural pathways critical for learning and memory could be an unrecognized long-term side effect of propranolol in infants.[6] Further long-term studies are thus needed before clinicians routinely suggest the use of propranolol in the treatment of infantile hemangiomas.

Arturo Tozzi, M.D., Ph.D.
Azienda Sanitaria Locale Napoli 2 Nord
Naples, Italy
tozziarturo@libero.it

No potential conflict of interest relevant to this letter was reported.

1. Léauté-Labrèze C, Hoeger P, Mazereeuw-Hautier J, et al. A randomized, controlled trial of oral propranolol in infantile hemangioma. N Engl J Med 2015;372:735-46.
2. Langley A, Pope E. Propranolol and central nervous system function: potential implications for paediatric patients with infantile haemangiomas. Br J Dermatol 2015;172:13-23.
3. McAinsh J, Cruickshank JM. Beta-blockers and central nervous system side effects. Pharmacol Ther 1990;46:163-97.
4. Solman L, Murabit A, Gnarra M, Harper JI, Syed SB, Glover M. Propranolol for infantile haemangiomas: single centre experience of 250 cases and proposed therapeutic protocol. Arch Dis Child 2014;99:1132-6.
5. Kroes MC, Strange BA, Dolan RJ. Beta-adrenergic blockade during memory retrieval in humans evokes a sustained reduction of declarative emotional memory enhancement. J Neurosci 2010;30:3959-63.
6. Hoeger PH. Propranolol for infantile haemangiomas: certain chances, potential risks. Br J Dermatol 2015;172:3-4.

DOI: 10.1056/NEJMc1503811

THE AUTHORS AND A COLLEAGUE REPLY: Like Tozzi, we are very concerned about potential side effects of propranolol, as with any drug used in children. However, we found no evidence to indicate serious adverse effects of propranolol in our study.

The article by Langley and Pope that Tozzi cited is essentially theoretical, not evidence-driven. There are no data to suggest that the adverse events about which Tozzi is concerned are increased in children treated with propranolol. Moreover, it is uncertain how data from small studies involving healthy adults[1] relate to risks in developing children. Although historical comparisons are difficult and available studies of propranolol for infantile hemangioma (including ours) have not included formal neurocognitive evaluations, the rates of neurodevelopmental defect or delay observed among propranolol-treated patients[2,3] seem to be within

The New England Journal of Medicine
Downloaded from nejm.org on July 19, 2015. For personal use only. No other uses without permission.
Copyright © 2015 Massachusetts Medical Society. All rights reserved.

the range observed in the general population.[4] Thus far, data from more than 2000 propranolol-treated infants in clinical studies and a compassionate-use program in France have been reassuring, but we agree that there is a need for large studies assessing longer-term outcomes.

To date, propranolol is by far the best-studied beta-blocker in infants. We believe that any assessment of its benefits and potential risks should take into account that the efficacy and safety profiles of alternative drugs used for this condition are not as well documented.

Christine Léauté-Labrèze, M.D.
Centre Hospitalier Universitaire de Bordeaux
Bordeaux, France
christine.labreze@chu-bordeaux.fr

Jean-Jacques Voisard, M.D.
Pierre Fabre Dermatologie
Lavaur, France

Nicholas Moore, M.D., Ph.D.
Université de Bordeaux
Bordeaux, France

Dr. Moore reports receiving grants from Pierre Fabre, Novartis, Boehringer Ingelheim, and Bayer and consulting fees from Pfizer and Novartis. Since publication of their article, the authors report no further potential conflict of interest.

1. Button KS, Ioannidis JPA, Mokrysz C, et al. Power failure: why small sample size undermines the reliability of neuroscience. Nat Rev Neurosci 2013;14:365-76.
2. Phillips RJ, Penington AJ, Bekhor PS, Crock CM. Use of propranolol for treatment of infantile haemangiomas in an outpatient setting. J Paediatr Child Health 2012;48:902-6.
3. Gonski K, Wargon O. Retrospective follow up of gross motor development in children using propranolol for treatment of infantile haemangioma at Sydney Children's Hospital. Australas J Dermatol 2014;55:209-11.
4. Boyle CA, Boulet S, Schieve LA, et al. Trends in the prevalence of developmental disabilities in US children, 1997-2008. Pediatrics 2011;127:1034-42.

DOI: 10.1056/NEJMc1503811

Preoperative Testing in Patients Undergoing Cataract Surgery

TO THE EDITOR: I read the article by Chen et al. (April 16 issue)[1] with interest, because I have had several discussions with ophthalmologists at my institution about requests for unnecessary preoperative evaluations and testing (complete blood count, blood chemical profile, electrocardiography) before cataract extraction. The response has been, "Yes, I know they are not needed or recommended, but the hospital will not let me operate without them." At least in some situations, what looks like a provider-related practice pattern could be the result of institutional requirements that should be changed but so far have not been.

Barry G. Saver, M.D., M.P.H.
University of Massachusetts Medical School
Worcester, MA
Barry.Saver@umassmed.edu

No potential conflict of interest relevant to this letter was reported.

1. Chen CL, Lin GA, Bardach NS, et al. Preoperative medical testing in Medicare patients undergoing cataract surgery. N Engl J Med 2015;372:1530-8.

DOI: 10.1056/NEJMc1506125

THE AUTHORS REPLY: We agree with Saver that the ongoing use of routine preoperative testing in patients undergoing cataract surgery may result from institutional requirements rather than the practice patterns of individual providers. Other authors have reported that physicians order testing because of tradition, medicolegal concerns, or the belief that another physician expects testing before cataract surgery.[1,2] Although it may be difficult to change institutional dogma and entrenched practice patterns, we believe that physicians should feel empowered to question and update policies and protocols that have not kept up with current evidence-based recommendations in order to provide better and higher-value care to their patients. In 2000, the American Academy of Ophthalmology issued a clinical statement recommending against the use of routine preoperative testing in patients undergoing cataract surgery, and the organization updated this statement in 2014.[3] For low-risk elective ambulatory procedures such as cataract surgery, patients in their usual state of health should be allowed to proceed to the operating room without any further workup.[3-5]

Catherine L. Chen, M.D., M.P.H.
Adrian W. Gelb, M.B., Ch.B.
R. Adams Dudley, M.D., M.B.A.
University of California, San Francisco
San Francisco, CA
chenc1@anesthesia.ucsf.edu

The New England Journal of Medicine
Downloaded from nejm.org on July 19, 2015. For personal use only. No other uses without permission.
Copyright © 2015 Massachusetts Medical Society. All rights reserved.

Preprints (www.preprints.org) | NOT PEER-REVIEWED | Posted: 20 September 2018 doi:10.20944/preprints201809.0403.v1

RICHARD AVENARIUS' "KRITIK DER REINEN ERFAHRUNG" (CRITIQUE OF PURE EXPERIENCE): AN ENGLISH SUMMARY

Arturo Tozzi
Center for Nonlinear Science, Department of Physics, University of North Texas, Denton, Texas 76203, USA
Computational Intelligence Laboratory, University of Manitoba, Winnipeg, Canada
ASL Napoli 2 Nord, Distretto 45, Caivano, Naples, Italy
E-mail address: tozziarturo@libero.it

We provide the first English translation of Richard Avenarius' masterpiece, the "Kritik der Reinen Erfahrung" (1888-1890), to give the possibility to the (almost) unaware English speakers to appreciate such a neglected and innovative philosopher and his still topical epistemology.

KEYWORDS: philosophy; epistemology; empirio-criticism; neuroscience; brain

INTRODUCTION

The French-Swiss Professor in inductive philosophy Richard Avenarius (1843-1896), father of empirio-criticism together with Ernst Mach, is one of the most underrated and misunderstood philosophers ever. It mostly depends upon his terminology, which displays an insurmountable difficulty (Russo Krauss, 2015). However, influenced by the most innovative proposals of his times of transition between the Idealistic/Rationalist legacies and the new Materialistic/Scientific interpretation of reality – i.e, by cultural evolutionism, linguistics, biomechanics, entropy/energy and, above all, by the newborn experimental psychology -, Richard Avenarius produced a complete system of philosophy and innovative methods of investigation of the laws of knowledge (Tozzi and Peters, 2017). Chunks of his original ideas can be found not only in philosophers of mind after him - such as Gestalt, phenomenalism, behaviourism, functionalism and cybernetics (Marr 1982), autopoiesis, dynamical systems theory (Churchland 2007; Richardson et al., 2014; Tognoli and Kelso, 2014), embedded/embodied mind (Gibson 1986; Friston 2008), topology of the brain function (Lewin 1936; Tozzi e t al., 2017) – but also in countless neuroscientific theories and approaches – e.g., nervous transduction via electric spikes (Nieuwenhuys et al., 2008), neural code's cracking (Watanabe et al., 2014), consciousness (Tononi 2008); multisensory integration, Bayesian accounts (Friston 2010), symmetry breaks (Roldán et al., 2014; Tozzi and Peters, 2016; Sengupta et al., 2016) -. Our aim is to provide the first chronological English summary of his masterpiece, the "Kritik" (Avenarius 1908), to make English speakers aware of this ignored and pioneering thinker. The numbers in brackets provided below single out the original paragraphs of his book (Edition 1908).

© 2018 by the author(s). Distributed under a Creative Commons CC BY license.

Preprints (www.preprints.org) | NOT PEER-REVIEWED | Posted: 20 September 2018 doi:10.20944/preprints201809.0403.v1

CRITIQUE OF PURE EXPERIENCE (1888-1890)

PREFACE AND GENERAL INTRODUCTION [1-39]

Avenarius starts from **the two axioms of knowledge**. The first establishes that every human individual originally accepts over against him: a) a spatial environment composed of manifold parts which stand in relation of dependence to one another, and b) other human individuals making manifold describable statements; c) what-is-stated is in some way dependent upon the environment. **The second axiom** says that the scientific knowledge is just a development of the pure knowledge, i.e. the non-scientific, simple and natural possible knowledge.

It follows the **empiriocritic assumption**: when the human individual finds himself in the mist of the external environment, he states he's having an experience [1]. The concepts of matter, substance, soul, consciousness, causality, necessity, freedom, reality are not included in such assumption [38].

Follow then two (apparently) **interchangeable propositions**: if a statement comes from the environment, then the statement is an experience [2]; if a statement is an experience, then the statement comes from the environment [3]. **Three questions follow**: in what sense does the experience come from the environment [7]? In what sense is a statement an experience [8]? Do the two questions collimate or diverge [9]? The entire book will be devoted to the answers of these questions. Through analytic tools [14], a formal and **general theory** not only of the pure experience, but also of the human knowledge and action, can be displayed [11-13].

He includes no other **standpoint** than that where he stands. As the Greek philosopher, he stands in the turmoil of the market-place, not as buyer or seller, in order that he may just observe [16].

The next paragraphs explore the relationships among the tree members: the environment, the self and the human statements. The ever-changing **environment** displays variations in quality and quantity, space and time, simplicity and intricacy [20-23]. The environment is not just involved in experience, but is also regarded as threat, as disturbing influence capable of breaking down the maintenance of the individual. The environment must nevertheless be regarded also as favorable to maintenance, nourishment and protection [37].

The **individuals** who make statements are organisms who live in a linguistic community, are born, grow preserve for a while and die [24]. The **statements** are not sounds or noises, but words (or gestures, such as the lacrimal secretions which point to cry, or mimic movements) [25]. The sensations are the describable content of statements. The latter are not stationary, because they may change [29]. They are simple or complex, primitive or evolved. We cannot perceive the thoughts and the sensations of other men, but just assign to them thoughts and sensations analogous to ours. The human statements can be divided in **elements** (such as green, cold, hard, sweet) and in **characters** (qualifications like pleasant, nice, beneficial, unpleasant) [30].

The link between the environment and the statements is very dynamical [31-36]. When the environment changes (as an example, during a chemical-physical experiment), it follows a variation in the statement [31]. Further, the statements may vary even if the environment does not, and vice versa: as an example, if a child looks at the same figure, he can see each time something different. The same names or sounds may refer to different people or facts. Other times, the sensation from a sensory modality may evoke sensations from another: i.e., I see a fruit and feel its taste. Furthermore, the statements may change due to the different cultural background of every individual.

Preprints (www.preprints.org) | NOT PEER-REVIEWED | Posted: 20 September 2018 doi:10.20944/preprints201809.0403.v1

PART ONE: OUR ENVIRONMENT AND THE PARTIAL CENTRAL NERVOUS SYSTEM [40-435]

A system is formed of two variables connected in a way such that when one changes, the other changes [41]. The **initial state** occurs before the variation, the final state afterwards [44]. The changes can be either real or merely possible [46]. The **final state** depends on two settings: the initial state of the system and the external factors acting on the system [54].

The man is the only member of the empiriocritic assumption who stands as witness [58]. The environment of a single individual [59] is a system and can be divided into spatial and social environments [60]. The environment acts on the organisms in two ways: either gets into the organism causing a change in matter, or stimulates the nerves [62]. A peculiar kind of environment is the human being, in which a distinction can be done: the non-nervous and the nervous systems [66]. The **nervous system** can be divided in nerves and brain [67]. The statements made by human beings do not depend on the environment, nor by the nerves: when the nerves are damaged, is indeed possible to have sensations anyway (phantom limb syndrome, visual hallucinations during optic nerve atrophy) [68].

There is however a part of the more comprehensive system of nervous central organs in which are collected the afferences and the efferences [70], by which the statements depend on: we do not need to care about its precise anatomical and physiological structure, because it has not yet been sufficiently ascertained by the experimental trials to find a localization for brain functions; besides, we have no need of this information for our purposes [72]. (note of the translator: hereafter we will term, slight improperly, this unidentified subsystem with the broad **term of "brain"**), The only notable thing is that there is a division of functional subsystems in brain [73], irrespective of differences in coordination, morphological development, functional relationships [75-77].

When somebody accepts over against him that the statement depends on the environment, he accepts over against him that the statements depends on the brain [79], in particular on **changes in brain** [80]. The statements depend on the environment just in the sense that the environment is able to modify the brain [82]. The variations of the environment are studied by the special sciences [82-83], while the variations of the individual, and in particular of his brain, are noteworthy and deserve a better explanation [85]. The environment acts on the brain directly or indirectly, through physiological - awareness, sleep, fatigue, training - or pathological changes - hallucinations, illnesses - [102-117], or variations propagated by other parts of the organism, such as the movements of vocal organs. A very important variation is the **habituation**, which may exert on the brain a temporary functional action, or a permanent organic one [116.]

The statements do not directly depend on the environment, rather by brain variations, but the latter depend on the environment [127]. The whole psychical life is a function of the self-preservation of the organism within certain limits, or, in case itis becoming disorganized, is the function of the self-preservation of a partial system of the organism [130]. The brain tends **toward asserting itself**, either in the individual, or social, or global organisms. The ideal environment is the maternal womb, where the self-preservation is utmost [133].

The highest levels of conservation [139] are achieved when an energetic equilibrium occurs in the brain between two opposite forces: the stimulus (the excitation of a nerve) and the material exchange (the metabolism). In other words[155], our maintenance is conditioned by an highly dynamical equilibrium between two opposite customary processes: **work and nourishment**. The brain alternates between these states of equilibrium and breaks [160]: when changes take place, there are also at hand the conditions which annul the change; then the brain approximates again to its maximum-maintenance. It consists in **oscillations** [160] between two phases, in deviation from a preliminary value and in approximating to it again. A process of change is itself compounded from various oscillations, characterized by many features [163-176] treated extensively in part two, including the central habituation [173].

Psychical processes come along the physiological processes of the restoration of equilibrium in living organisms. When the equilibrium of a brain is disturbed, it is always on account of a

difference arising between the nutritive functions of the system and its work. It is unnecessary to deal further with the process of nourishment - we may even assume it to take place during the sleep [198, 200] -; then we have only to explain in what the work-process consists. The elementary physiological processes consist of a state of disturbance of the equilibrium of the brain and of a restoration of the difference. All the changes which lie between this beginning and end follow each other immediately; they form the **vital train** [181]. It is a complex process divided into three parts: the **introductive section**, where, starting from the quiet state, a disturbance (oscillation) is introduced which breaks the equilibrium [182]. Then follows the **intermediate** section, where compensation mechanisms are activated through mechanisms called variations counteracting the oscillations [223; 352 and following]. There are different types of **variations**: general and specific, significant and not significant, qualitative and quantitative [sleep and awakening: 190, then till 218], outside and inside the brain [241]. The **final state** is such that the oscillation is suppressed with return to the quiet and maximum preservation state [314]. Every vital train ends with phase three [189], but the vital trains are infinite, superimposed, cross-linked, hierarchical [184-185, 177]. The ideal equilibrium of the brain cannot be achieved, due to the continuous dynamics [186].

The following evolution is **towards more perfect series** [406]. The removal of the alteration toward the higher conservation occurs in two ways: either the return to the original stable state, or a different stable state. The environment is posed more times, leading to a final state, valid just for that individual in that moment.

There are also **systems ofhigher order**, in which the brain of different individuals joins together in higher social assemblies [328]. It is the tendency of the whole mass of human knowledge to become the highest degree adapted to the surrounding world. Humanity represents, in the whole, a kind of ultra-human organism, following the same basic rules of self-preservation of the individual [341].

An individual vital train is composed, e.g., of the following terms: (1) Habitual increase of nourishment; (2) Habitual increase of work, set for a short time; (3) Variation of work; (4) Compensating adjustments until the variation is completely annulled. The individual vital train is equipped with many processes [407-435] which progressively remove the useless terms, approximating to the final pure stages equipped with minimum energy and maximum stability, higher spatial and temporal unrestriction, indispensability [352, 389]. The role of habituation is once again crucial. The final state of the brain is a physiological configuration which does not vary when the environment changes [409]. It is unvaried towards every changing component of the environment. However, this final state is composed not only by the final pure state, but also by other variable, **accidental factors** [414], which need to be progressively abolished [432]. When the geographical and social environment widens to include the entire Earth surface and the entire mankind, the brain removes the accidental factors through a biomechanical process of progressive elimination.

The answer to the first question is thus the following: the environment is at the base of the experience only when he leads to variations in the individual brain, and only when a statement depends on environmental variations [435]. However, such values are valid just for a given individual, in a given moment: the individual final state changes from individual to individual, and also from place to place and from epoch to epoch.

PART TWO: SPECIFIC VITAL TRAINS [436-963]

Avenarius illustrates the particular cases of the general principles exposed in Part one, looking for the countless psychological correlates of the physiological vital trains. The general scheme is the following: when an individual makes a statement, a change in oscillations occurs in brain [455]. The statements depend upon the characteristics of the physiological variations in brain and its oscillations.

The oscillations in the brain display different characteristics, each one leading to different statements [162-175; 458-sgg]. We will go through a few case in points. The **form** of the oscillations affects all statements dependent upon the senses (touch, pressure, temperature, hearing, smell, taste and sight) [459]. The **magnitude** of the oscillation gives rise to the values of intensity, as "strong" or "weak" [461]. The **relevance** of the oscillation depends upon the significance which the partial system just affected has for the whole central organ, related to natural disposition and training. Although the magnitude may be the same, the oscillation will assume a different value if it affects a partial system which is or is not highly developed by its disposition and training. The varying relevance of the oscillation affects the feeling, moods, and so on, [464], while the **direction** is related to "pleasure" and "pain" [469]. The mode in which an oscillation is affected by practice and training is the familiarity, including the "real," "known," and "certain," and their variations. The **habituation** and its changes play once again a crucial role: they give rise to the "difference" [474] and the "identity" [476]: in other words, the more the same oscillation is repeated, the more the sensation is perceived as usual, the same [479]. Other values linked with changes in habituation are: the sure, the certain, the known, the familiar. The **opposition** of many oscillations gives rise to the sensation of prevalence and perception of finer details (discrimination), in which some sensations are highlighted by the attention, compared with the faded background sensations [505]. When the **connexions** of the oscillations vary, these latter become more active, more differentiated, more articulated. The concepts of thing, idea, arise from the mix of different oscillations [512; 535]. The things have a higher intensity than the ideas. When two oscillations are **similar** and the statement is perceived as the same, long chains of oscillations lead to: "all together", "always", "everywhere", progressively reaching the **general concept of the total reality**, the world. When the identical becomes rule, the rules become laws and the truths become sure, existing, while the different becomes exception [552 sgg]. In summary, to make an example: a statement as to its strength depends only upon the amplitude of the oscillations, as to its pitch depends upon the number, and as to its timbre depends upon the form.

The mental life falls into series, called the **specific vital trains**, with prearranged general features, characterized by **three sections** [775]. In the first section, at the start there is the expected value, stated by the individual as sure, true, known. Then enters a variation, stated as different, diverging, doubtful, unexpected, together with the feeling of pain, opposition, or uncertainty, inquietude, dissatisfaction [797, 842]. The second section is an effort to suppress the anomaly: the brain strives to remove this unpleasant experience, through complex mental processes or simple habitual actions. At the end, value is found in the final section, leading to the feelings of rest, satisfaction, certainty, truth and quiet of the brain [850]. The variations can be **removed either through** peripheral action (practical behavior) or through brain action (theoretical behavior). Avenarius stresses that each statement is influenced by type and magnitude of the individual's background [853], and that the final section **is independent** from the number or proceedings of the intermediate steps [857]. Furthermore, there are **three ways to suppress the variations**: (1) reduction of the unknown to the known; (2) gradual habituation to a change, so that the unknown becomes a known. (3) temporary substitution of one kind of change for another. However, due to the differences of the initial conditions among individuals, the ideas achieved in the third section could lead, after a while, once again from a known to an unknown. The ultimate suppression of variations occurs via the search for **universal laws** [888]. As times goes on, the individuals and the generations are in front of faster, simpler and unavoidable concepts [890]. The approximation will always be towards the identical highly generalized, unlimited concepts [891], independently from the initial steps. The universal concepts are characterized by simple, complete descriptions, by qualitative differences expressed in many ways and by formal equivalences expressed in different forms.

In a foremost paragraph, Avenarius examines **the experience regarded as character** [931], i.e. the variable form (emotions, sensations, perceptions and so on), in which we experience anything. The question is not what individuals mean for experience, but: what individuals state is an experience? [932]. Many examples are listed in which statements are referred as experience [933]: the appearance of the sun, the perceived temporal relationships among events, the difference between

sleep and arousal, the travel in far countries during dreams, the miracles, the presages of death, the causal connection, the footsteps of the animals, the things that man say each other, the logic, the calculations, the axioms, the mathematical laws. So, what is the experience? Is it always linked to the external environment [935]? Does it refer to entities, or simply to the cognition of their existence, or is it pure cognition without existence? [936]. The three solutions are not satisfactory [937], because the experience cannot be defined only in one way. The individual simply bumps into the components of the environment, and then describes what he met [938]. When a little girl states that she has seen angels, then the angels are an experience for her [938]. The individual who states: "it is an experience" is saying that he had a plurality of single perceptions [940]. Thus, the better, although incomplete, definition of experience could be: something perceived [940]. Also the ego, the I, is a statement, in which the perception is felt as the individual's own perception [943]. The more the thing and the perceiving individual are separated, the more the thing is perceived by the individual as active and as a factum of experience, while the individual perceives himself as a passive percipient [945, 946].

Then Avenarius evaluates **the experience regarded as content** [947], i.e. everything which is felt, sensed, perceived and so on. When individuals state they have an experience, what is the content of their experience [948]? The content depends on the modifications in the brain and on the current state and education of each individual [951]. It doesn't matter if the statements are related to existing or non-existing entities: all the values perceived by the individual in a given moment as experience are indeed a content of experience [952], and they may vary if the individual changes [953]. The difference between characters and contents is that the former are mutable and can be defined as forms, while the latter are permanent and can be defined as elements [955]. **The answer to the second question** is thus the following: the experience (in its narrower concept) is the perception by the brain of the things extracted from the environment [958-59]. A wider concept of experience does not involve the things, but the ideas. The ideas also look like existing, simply there, given, so that, even if a centaur is not an experience, its idea is an experience [961]. There is a passage from the perceived thing (the **narrower concept** of experience) to the represented idea (the **wider concept** of experience) [962-963].

PART THREE: THE MOST GENERAL CONCEPTS [964-1040]

Part three investigates the highest concepts, i.e. the final states corresponding to all the possible environment manifold parts, equipped with the maximum possible frequency and embracing all the possible historical contents of the statements [971]. The highest concept, expressed by the statement: "the whole is this" is the **concept of the world**. However, they still embrace not only the more general concepts, but also superfluous ones: indeed, many different concepts of the world were expressed during the history of mankind, because they were also related to genetic constrains, social groups and historical background [977]. Thus the concepts of the world are incomplete, because **include also unnecessary** components [979] and their historical development is not ended at this time. The three possible series of the concept of the world -logical, historical, critical- [980] are correlated: when the historical series increases together with the critical series, it occurs a further generalization [981].

The concept of the world is preserved by the individuals and left to posterity via communication and conditioning [982]. If the concept is transmitted unchanged through the generations, its strength decreases with the time due to habituation, until it cannot be recognized anymore [984]. The transformation of the concepts of the world leads from certainty to doubts about them: thus arises **the enigma of the world**, in place of the concept of the world [986]. The most the perplexity increase, the most is strong the need to solve the problems as soon as possible [988] and several new different satisfying concepts of the world may arise [990-991]. The solutions are however transitory and changing with the time, both in the individual and in the community [992]. Every

concept of the world is characterized by residual unneeded concepts, depending on the education of the individuals [993]. The number of superfluous concepts may either remain the same, or decrease, or increase [994]. The provisional solutions to the enigma of the world are countless and the only way to find more general concept is to **expunge the surplus components** [996]: the more the concept of the world is spatially enlarged, including many communities and then the whole mankind, the more the solution is general and definitive, approximating a purified and exclusive experience [997, 1030]. When the concepts of the world are many, if the space and time is long enough, they always tend towards the highest concept [998] and the brain is satisfied [1000].
During the cultural evolution, the concepts of the world are at first regarded as a positive experience, a perceived thing, an empiric knowledge; however, in a following phase of removal, they weaken and are regarded as non-empirical knowledge, pseudo-problems, until they gradually vanish and disappear [1022-1023]. The last phase is their reappearance in a distilled form, just as pure descriptions [1002-21, 1024, 1028]. The final, pure concepts of the world allow the brain to be entirely conditioned by the environment and the statements to be regarded as complete experience [1031, 1040]. **The answer to the third question** is thus the following: a primitive experience (knowledge=naturally perceived) leads to addition of non-experience (either knowledge=perceived and knowledge=not perceived) until a definitive, just described, exclusive experience takes place (knowledge= purified perceived) [1034]. More advanced social groups may be closer than others to the pure concepts of the world, at least in some fields of knowledge [1035]: indeed, evolution does not proceed linearly nor uniformly and small groups of more civilized individuals have an important role in pushing forward the changes towards possible solutions of the problems [1036-37].

REFERENCES

1) Avenarius R. 1908. Kritik Der Reinen Erfahrung von Richard Avenarius. Lepzig: C.R. Reisland.
2) Churchland PM. 2007. Neurophilosophy At Work. Cambridge Univ Pr ISBN-10: 0521864720. ISBN-13: 978-0521864725
3) Friston K. 2008. Hierarchical models in the brain. PLoS computational biology 4, e1000211
4) Friston K. 2010. The free-energy principle: a unified brain theory? Nat Rev Neurosci 11(2):127-138.
5) Gibson JJ. 1986. The ecological approach to visual perception. Boston: Houghton-Mifflin.
6) Lewin K. 1936. Principles of Topological Psychology, transl. F. Heider and G. M. Heider. McGraw-Hill, New York.
7) Marr D. 1982. Vision. A computational investigation into the human representation and processing of visual information. W. H. Freeman and Company.
8) Nieuwenhuys R, Voogd J, van Huijzen C. 2008. The Human Central Nervous System. Heidelberg: Springer.
9) Richardson MJ, Dale R, Marsh KL. Complex dynamical systems in social and personality psychology. In: Reis HT, Judd CM (eds), Handbook of Research Methods in Social and Personality Psychology. 2nd Edition, 2014. Cambridge University Press, Cambridge. ISBN: 9781107600751
10) Roldán É, Martínez I, Parrondo JMR, Petrov D. 2014. Universal features in the energetics of symmetry breaking. Nature Physics, 10(6), 457–461. http://doi.org/10.1038/nphys2940.
11) Russo Krauss C. 2015. L'empiriocriticismo di Richard Avenarius tra psicofisiologia e teoria della conoscenza, in R. Avenarius, Il concetto umano di mondo, Morcelliana, Brescia.
12) Sengupta B, Tozzi A, Cooray GK, Douglas PK, Friston KJ. 2016. Towards a Neuronal Gauge Theory. PLoS Biol 14(3): e1002400.

13) Tognoli E, Kelso JA. 2014. Enlarging the scope: grasping brain complexity. Front Syst Neurosci 8, 122.
14) Tononi G. 2008. Consciousness as integrated information: a provisional manifesto. Biol Bull. 215(3):216-42.
15) Tozzi A, Peters JF. 2016. A Topological Approach Unveils System Invariances and Broken Symmetries in the Brain. Journal of Neuroscience Research 94 (5): 351–65. doi:10.1002/jnr.23720.
16) Tozzi A, Peters JF. 2017. Towards Topological Mechanisms Underlying Experience Acquisition and Transmission in the Human Brain. Integr Psychol Behav Sci. 51(2), 303–323. doi: 10.1007/s12124-017-9380-z.
17) Tozzi A, Peters JF, Fingelkurts AA, Fingelkurts AA, Marijuán PC. 2017. Topodynamics of metastable brains. Physics of Life Reviews, 21, 1-20. http://dx.doi.org/10.1016/j.plrev.2017.03.001.
18) Watanabe T, Hirose S, Wada H, Imai Y, Machida T, Shirouzu I, Konishi S, Miyashita Y, Masuda N. 2014. Energy landscapes of resting-state brain networks. Front Neuroinform 25;8:12.

PLOS | BIOLOGY

ESSAY

Towards a Neuronal Gauge Theory

Biswa Sengupta[1]*, Arturo Tozzi[2], Gerald K. Cooray[3], Pamela K. Douglas[4], Karl J. Friston[1]

1 Wellcome Trust Centre for Neuroimaging, University College London, London, United Kingdom, **2** Center for Nonlinear Science, University of North Texas, Denton, Texas, United States of America, **3** Clinical Neurophysiology, Karolinska University Hospital, Stockholm, Sweden, **4** LINT Laboratory, University of California, Los Angeles, Los Angeles California, United States of America

* b.sengupta@ucl.ac.uk

Abstract

Given the amount of knowledge and data accruing in the neurosciences, is it time to formulate a general principle for neuronal dynamics that holds at evolutionary, developmental, and perceptual timescales? In this paper, we propose that the brain (and other self-organised biological systems) can be characterised via the mathematical apparatus of a gauge theory. The picture that emerges from this approach suggests that any biological system (from a neuron to an organism) can be cast as resolving uncertainty about its external milieu, either by changing its internal states or its relationship to the environment. Using formal arguments, we show that a gauge theory for neuronal dynamics—based on approximate Bayesian inference—has the potential to shed new light on phenomena that have thus far eluded a formal description, such as attention and the link between action and perception.

CrossMark
click for updates

OPEN ACCESS

Citation: Sengupta B, Tozzi A, Cooray GK, Douglas PK, Friston KJ (2016) Towards a Neuronal Gauge Theory. PLoS Biol 14(3): e1002400. doi:10.1371/journal.pbio.1002400

Published: March 8, 2016

Copyright: © 2016 Sengupta et al. This is an open access article distributed under the terms of the Creative Commons Attribution License, which permits unrestricted use, distribution, and reproduction in any medium, provided the original author and source are credited.

Funding: BS and KJF are supported by the Wellcome Trust (088130/Z/09/Z). BS is thankful to the Mathematical Biosciences Institute for hosting him, and facilitating communication with experts working on the symmetry perspective of dynamical systems. We thank John Ashburner for his comments on an initial draft of this paper. GKC is supported by a postdoctoral fellowship from the Swedish Brain Foundation (Hjärnfonden). PD is funded by the Klingenstein Foundation, and the Keck Foundation. The funders had no role in study design, data collection and analysis, decision to publish, or preparation of the manuscript.

Competing Interests: The authors have declared that no competing interests exist.

Introduction

Recent innovations such as optogenetics and neuroimaging enable us to characterise the relationship between the activity of neurons and their system-level behaviour. These technical innovations call for theories that describe neuronal interactions and reveal the underlying principles. In physics, electromagnetism, the general theory of relativity, and the quantum field theory have been consolidated within the rigorous and holistic framework of a gauge theory [1]. Here, we propose that a gauge-theoretic formalism in neurosciences might not only provide a quantitative framework for modelling neural activity but also show that neuronal dynamics across scales—from single neurons to population activity—are described by the same principle. This paper suggests that if we could formulate a gauge theory for the brain—or cast an existing theory as a gauge theory—then many aspects of neurobiology can be seen as consequences of fundamental invariance properties. This approach could clarify the intimate relationship between apparently distinct phenomena (e.g., action and perception) and, potentially, offer new tools for computational neuroscience and modelling.

This paper is comprised of three sections. The first provides an informal description of gauge theories in physics. The second focuses on the biological features required for a gauge

theory for the brain. In the third section, we discuss the three ingredients of a gauge theory: a system equipped with symmetry, some local forces, and one or more gauge fields. To illustrate the approach, we use the principle of variational free energy minimisation as a candidate for a neuronal gauge theory. This principle says that every aspect of the brain, from neuronal activity to synaptic connection strengths, can be described as a process that minimises variational free energy, where variational free energy measures the probability of sensory inputs, under the brain's model of how those inputs were caused. The variational aspect of variational free energy comes from its derivation from variational calculus, which is at the heart of gauge theories and information geometry, which are the focus of this article.

At its simplest, variational free energy reduces to prediction error or surprise in exactly the same way that estimating the parameters of a statistical model can be reduced to minimising the sum of squared error. We will see later that when physical laws, such as Hamilton's principle of least action, are applied to variational free energy, the resulting behaviour looks very much like statistical inference, lending the brain—and indeed any self-organising system—the look and feel of a system that is trying to estimate or infer the causes of its (sensory) exchanges with the world. In fact, advanced statistical analyses of data minimise variational free energy, where negative free energy approximates Bayesian model evidence. Effectively, minimising variational free energy corresponds to maximising model evidence. This means that if the brain minimises variational free energy it is inherently Bayesian; hence the Bayesian brain hypothesis [2–5].

We provide a glossary of technical terms (S1 Glossary) and series of appendices (S1 Appendix; S1–S5 Text) that offer a technical account of the free energy formalism, gauge theory, and their relationship. These appendices unpack the key conceptual points for technically-minded readers. Although formulating the free energy principle as a gauge theory may have important implications for new inference schemes that can be used to analyse data (i.e., infer the structure and parameters of models of empirical data), we focus on the implications for neurobiology.

I. Gauge Theories in Physics

A gauge theory is a physical theory that predicts how one or more physical fields interact with matter. Every gauge theory has an associated Lagrangian (i.e., a function that summarises the dynamics of the system in question), which is invariant under a group of local transformations [6]. Consider Newton's laws of motion in an inertial frame of reference (e.g., a ball in an empty room). These laws are valid at every point in the room. This means that the dynamics and the Lagrangian do not depend on the position of the ball. In this system, the dynamics will be invariant under translations in space. These transformations—that preserve the Lagrangian—are said to be equipped with gauge symmetry. In short, a symmetry is simply an invariance or immunity to changes in the frame of reference [7].

Take a rotating frame of reference (e.g., the Earth) and call it the system. During the rigid rotation of the Earth, the distances between every town remain invariant. As Earth rotates, one can say that we have a gauge transformation that does not change the distance between the cities (S1 Appendix). This means that the system preserves its symmetry (c.f., the laws of Nature), despite the action (or gauge transformations) of global forces (acting on every point of the system). This action corresponds to a global transformation of the system—a transformation that preserves invariances; in this instance, distances. There is, however, another possibility: for example, compare the Earth and moving objects on its surface (e.g., the water in the ocean). When the motion of water is described relative to the Earth, its inertia (that is, its tendency to move in a straight line) distorts its motion. This phenomenon is called the Coriolis effect: rather than flowing directly from areas of high pressure to low pressure—as they would in a

nonrotating world—currents tend to flow in a clockwise sense (with respect to the direction of travel) in the Northern hemisphere and counterclockwise in the Southern hemisphere. The Coriolis effect is thus a curvilinear motion in a rotating (noninertial) frame of reference. A gauge transformation that is not constant, i.e., varies with spatial location, is referred to as a local symmetry. One or more local forces acting on just a few parts of the system produce local transformations.

Why is the symmetry preserved, despite the perturbing action of local forces? This is because the local forces are balanced by another force—called the gauge field. Note that when the global symmetry of the system is preserved despite local forces, there is a local deformation, and the symmetry is said to be locally broken, or at best, hidden. In a system equipped with global symmetry, it is thus possible to find a local breaking of symmetry that can be "repaired" by the gauge field. Let us again take the example of the Coriolis forces. For someone who only uses inertial frames of reference, the Coriolis forces do not exist; they are just forces we invent to pretend we are in an inertial system when in fact we are not: they are practical, because they allow us to continue using Newton's laws. Albert Einstein discovered something similar; the laws of special relativity are not valid when gravitational forces (which are due to energy and momentum) are present. However, by allowing energy and momentum to bend space–time, he could retain special relativity, at least locally, making the gravitational forces disappear. For Einstein, gravitational forces are as unreal as the Coriolis forces; they are forces we have to invent when we choose an inappropriate frame of reference. See S1 Appendix that illustrates these ideas using a simple pendulum example.

In summary, gauge theory is relatively straightforward: one has a Lagrangian that prescribes equations of motion. These equations of motion are generally invariant under changes in a spatial frame of reference (e.g., a straight line is a straight line everywhere on a sheet of paper); however, if we stand back and see that motion (a line in space–time) changes with position (e.g., a straight line on a sheet of paper that has been bent), we can extend the global symmetry to a local symmetry by introducing compensatory fields or forces—the gauge fields. The notion of bending or curvature here is important, because manifolds that shape trajectories in the space of probability distributions are necessarily curved. This is important for systems that minimise variational free energy (S1 Text) and related Bayesian brain theories [8]. In fact, we shall see below that quintessentially cognitive faculties like "attention" can, in principle, be derived using gauge theory.

II. Gauge Theories for the Nervous System

Gauge theories originate from physics; however, they could be applied to countless fields of biology: cell structure, morphogenesis, and so on. Examples that lend themselves to a gauge-theoretic treatment include recent simulations of embryogenesis [9] and the self-organisation of dendritic spines [10]. Although these examples appear unrelated, both can be formulated in terms of a gradient ascent on variational free energy. In other words, we may be looking at the same fundamental behaviour in different contexts [11]. Here, we focus on the central nervous system (CNS). Can we sketch a gauge theory of brain function? The answer rests on identifying —in biological systems like the brain—the tenets of a gauge theory; namely,

1. A system equipped with a continuous symmetry that can be conserved.
2. The presence of local forces acting on the system (a group of local transformations), where a gauge field renders its Lagrangian invariant under such transformations.

When attempting to establish what aspect of CNS function might be understood in terms of a Lagrangian, the variational free energy looks highly plausible [12]. The basic idea is that any

self-organising system, at nonequilibrium steady-state with its environment, will appear to minimise its (variational) free energy, thus resisting a natural tendency to disorder. This formulation reduces the physiology of biological systems to their homeostasis (and allostasis); namely, the maintenance of their states and form, in the face of a constantly changing environment.

If the minimisation of variational free energy is a ubiquitous aspect of biological systems, could it be the Lagrangian of a gauge theory? This (free energy) Lagrangian has proved useful in understanding many aspects of functional brain architectures; for example, its hierarchical organisation and the asymmetries between forward and backward connections in cortical hierarchies [13]. In this setting, the system stands for the brain (with neuronal or internal states), while the environment (with external states) is equipped with continuous forces and produces local sensory perturbations that are countered through action and perception (that are functionals of the gauge field).

In summary, the free energy formalism rests on a statistical separation between the agent (the internal states) and the environment (the external states). Agents suppress free energy (or surprise) by changing sensory input, by acting on external states, or by modifying their internal states through perception [12,14]. In what follows, we try to show that the need to minimise variational free energy (and hence achieve homeostasis) acquires a useful logical mathematical formalism, when framed as a gauge theory.

The Utility of a Gauge Theory for the CNS

Whenever we posit a normative theory in neuroscience, we appeal to some objective function or Lagrangian—and the opportunity to develop a gauge theory. So what would this gauge theory tell us? Put simply, it would allow us to understand complex and apparently chaotic neuronal dynamics in much simpler yet formal terms. In the same way that we model and understand the gauge fields (e.g., Coriolis forces) driving our weather patterns, it may be possible to understand the driving effects of neuronal afferents on postsynaptic responses as a necessary consequence of much simpler invariances or symmetries. This prospect is particularly prescient if neuronal activity encodes representations or (Bayesian) beliefs, where the Lagrangian (i.e., variational free energy) becomes a function of probability distributions.

Minimising variational free energy describes how a system changes its (internal) states so that they are the most probable under the (external) states of the environment. The system does so by implicitly learning a generative model of its environment. A generative model is simply a model that generates sensory inputs. If the model can reproduce or predict sensory samples from the environment, then it implicitly infers how sensations were generated or caused. Clearly, a good model will make predictions with a very low prediction error (or variational free energy). Put another way, minimising variational free energy ensures the brain becomes a good model of its environment. If we add into this mix the fact that sensory input is actively sampled, then acting to minimise free energy will inevitably make the model's predictions come true. This is how action and perception are understood in terms of variational free energy minimisation.

Recall that a key ingredient of a gauge theory is a continuous symmetry that can be conserved. So what does gauge symmetry bring to the table? Here, we develop the idea that distinct classes of inference or behaviour are equivalent to pattern formation in the nervous system. For example, the perception of a visual object involves highly organised patterns of neuronal responses throughout the visual cortical hierarchy, reflecting a functional specialisation for colour and motion [15]—right down to the architecture of classical receptive fields [16,17]. Since patterns can be classified into a variety of groups, so can a system's behaviour. Specifically, the

gauge perspective enables us to specify an ontology of patterns or responses that is independent of the generative model. This does not mean that the generative model is irrelevant, but rather a great deal could be learnt by knowing about the symmetries (invariances) of that model. All models with a given symmetry explore the same range of pattern-forming behaviour—without reference to the underlying model [18]. For example, could experience-dependent or Hebbian plasticity [19] be an example of a symmetry that minimises variational free energy [20], and yet the products of experience lead to very different—but equally good—neuronal patterns and architectures. In other words, could we understand phenomena like bistable perception [21] and intersubject variability [22] in terms of a gauge theory.

In the animal kingdom, many aspects of behaviour are similar, yet the neural mechanisms that mediate such behaviours can be very different. For example, bees may forage using different neuronal mechanisms [19] from those used by a rat to explore a maze [23], or those we employ while foraging for information with visual saccades [24]. The difference emerges from the heterogeneity of evolutionary pressures from the ecological niche. A gauge theory that describes behaviour and establishes a mathematical framework to understand the gauge transformations that render behaviour invariant, within and between species, may be invaluable. Particularly because such an approach paves the way for a computational neuroethology, enabling us to study what properties of neuronal dynamics are conserved over species, and what constraints have caused certain neural network properties to diverge over evolution. For example, the minimisation of variational free energy may provide an explanation for foraging that transcends the ecological context: see [25] for an example of epistemic foraging that is formally equivalent to saccadic sampling of the visual field [26].

In the study of dynamical attractors and pattern formation, it generally makes sense to study model-independent generalities as a first step, adding the details later. For example, the Lorenz attractor has found a useful role in modelling a variety of systems; from catalytic reactions [27] to meteorology [28] and immunology [29]. A technical issue here is the distinction between phase and physical space [18]. Any system evolves in a physical space, wherein transformations to a phase-space involve an unspecified change of coordinates. Such coordinate transformations can disconnect variables of the dynamical system and the variables observed in physical space (e.g., the phase reduction techniques used to characterise rhythmic brain activity in terms of fluctuations in the phase of a neuronal oscillation at any given frequency [30] and other dynamical systems ranging from cell biology to cancer research [31]. See also S1 Appendix). The gauge-symmetry perspective alleviates the potentially problematic disconnect between physical and phase spaces: a symmetry property in phase space translates into a symmetry property in the physical space, and vice-versa, because this is the defining property of properly formulated gauge symmetries. A related benefit of understanding the symmetries of a dynamical system is that it enables one to map from one dynamical system to another, allowing us to identify a range of solutions with identical dynamics [32,33].

The second important question posed by framing a gauge theory is "how are symmetries related to gauge fields?" The answer to this question is that gauge fields are objects (compensatory fields) introduced to maintain symmetry and thus also the original equation of motion (S2 Text). In other words, one can imagine them as fields that ensure the Lagrangian is invariant to transformations. In the next section, we use these notions to formulate the variational free energy formalism as a gauge theory for the nervous system.

III. Sensory Entropy as a Lagrangian

The variational free energy formalism uses the fact that biological systems must resist the second law of thermodynamics (i.e., a tendency to disorder), so that they do not decay to

equilibrium. In a similar vein to Maxwell's demon, an organism reduces its entropy through sampling the environment—to actively minimise the self information or surprise of each successive sensory sample (this surprise is upper bounded by free energy). By doing so, it places a bound on the entropy of attributes of the environment in which it is immersed. Variational free energy operationalises this bound by ensuring internal states of the system become a replica (i.e., a generative model) of its immediate environment. This can be regarded as a formulation of the good regulator hypothesis [34], which states that every good regulator of a system must be a model of that system.

We know that a gauge theory would leave the Lagrangian invariant under continuous symmetry transformations. Therefore, a gauge theory of the brain requires the interaction among three ingredients: a system equipped with symmetry, some local forces applied to the system, and one or more gauge fields to compensate for the local perturbations that are introduced. The first ingredient is a system equipped with symmetry: for the purposes of our argument, the system is the nervous system and the Lagrangian is the entropy of sensory samples (which is upper-bounded by variational free energy, averaged over time). The local forces are mediated by the external states of the world (i.e., through sensory stimuli). The gauge fields can then be identified by considering the fact that variational free energy is a scalar quantity based on probability measures. Let us see how.

From differential geometry treatments of probability measures (S3 Text), it is known that the manifold traced out by sufficient statistics of a probability measure is curved in nature [35,36]; more specifically, it has negative curvature and is therefore endowed with a hyperbolic geometry. Barring technical details, it suffices to understand that a functional (e.g., variational free energy) of such probability measures is not flat but induces a curved (Riemannian) landscape. Moving along such a curved manifold requires a measure of distance that corresponds to the distance between two distributions. Again, differential geometry tells us that such a measure of distance is provided by the Fisher information metric (Cencov's characterisation theorem) that quantifies the amount of information that a random variable carries about an unknown parameter. Technically, the Fisher information represents the curvature of the relative entropy (Kullback-Leibler divergence). Put simply, distances in the curved geometry of sufficient statistics—that define variational free energy—correspond to the relative entropy in going from one point on the free energy manifold to another.

Instead of using classical results from differential geometry [35–39], we will motivate the gauge formulation of variational free energy by asking an empirical question: how does neuronal activity follow the steepest descent direction to attain its free energy minimum? In other words, how does it find the shortest path to the nearest minimum? As the free energy manifold is curved, there are no orthonormal linear coordinates to describe it. This means the distance between two points on the manifold can only be determined with the help of the Fisher information metric that accounts for the curvature. Algebraic derivations (S3 Text) tell us that, in such free energy landscapes, a Euclidean gradient descent is replaced by a Riemann gradient, which simply weights the Euclidean gradient by its asymptotic variance.

In the free energy framework, when the posterior probability is approximated with a Gaussian distribution (the Laplace approximation; S4 Text), perception and action simply become gradient flows driven by precision-weighted prediction errors. Here, prediction errors are simply the difference between sensory input (local perturbations) and predictions of those inputs based upon the systems internal states (that encode probability distributions or Bayesian beliefs about external states that cause sensory input). Mathematically, precision-weighted prediction errors emerge when one computes the Euclidean gradient of the free energy with respect to the sufficient statistics. In a curvilinear space, the precision-weighted prediction errors are replaced by dispersion- and precision-weighted prediction errors. This says something quite

fundamental—perception cannot be any more optimal than the asymptotic dispersion (inverse Fisher information) regardless of the generative model. In statistics, this result is known as the Cramér-Rao bound of an estimator. In other words, the well-known bound (upper limit) on the precision of any unbiased estimate of a model parameter in statistics emerges here as a natural consequence of applying information geometry. In the context of the Bayesian brain, this means there is a necessary limit to the certainty with which we can estimate things. We will see next, that attaining this limit translates into attention. See Box 1 for an overview.

Notice that the definition of a system immersed in its environment can be extended hierarchically, wherein the gauge theory can be applied at a variety of nested levels. At every step, as the Lagrangian is disturbed (e.g., through changes in forward or bottom-up sensory input), the precision-weighted compensatory forces change to keep the Lagrangian invariant via (backward or top-down) messages. In the setting of predictive coding formulations of variational free energy minimisation, the bottom-up or forward messages are assumed to convey prediction error from a lower hierarchical level to a higher level, while the backward messages comprise predictions of sufficient statistics in the level below. These predictions are produced to explain away prediction errors in the lower level. From the perspective of a gauge theory, one can think of the local forces as prediction errors that increase variational free energy, thereby activating the gauge fields to explain away local forces [40]. In this geometrical interpretation, perception and action are educed to form cogent predictions, whereby minimization of prediction errors is an inevitable consequence of the nervous system minimising its Lagrangian. Crucially, the cognitive homologue of precision-weighting is attention, which suggests gauge fields are intimately related to (exogenous) attention. In other words, attention is a force that manifests from the curvature of information geometry, in exactly the same way that gravity is manifest when the space–time continuum is curved by massive bodies. In summary, gauge theoretic arguments suggest that attention (and its neurophysiological underpinnings) constitutes a necessary weighting of prediction errors (or sensory evidence) that arises because the manifolds traced out by the path of least free energy (or least surprise) are inherently curved.

Conclusions

The importance of the reciprocal interactions among different scales and between the nervous system and the world has been repeatedly emphasised here and elsewhere. A quantitative formulation of this holistic aspect of information processing in the brain is clearly needed and has been framed in terms of variational free energy minimisation or, more simply, as a suppression of prediction errors encountered by an agent that is actively sampling its environment [12,14]. In this essay, we have reformulated the resolution of prediction error (or surprise) as a gauge theory for the nervous system. Such geometrical formulations endow variational inference with symmetry breaking, enabling invariance with respect to the generative model; irrespective of the model's parameterization [41,42].

The free energy formulation enables us (or our brains) to compare a variety of hypotheses about the environment given our sensory samples. So what does a gauge formulation add? After scoring a variety of models according to their variational free energy, one selects the best generative model that explains the data at hand. If symmetry transformations can be evaluated for the best performing model, afforded by the symmetry group, we can possibly go a step further and ask what other models could explain the data with the same model evidence? Such symmetry transformations therefore furnish us with a family of models that explain the data with equal probability [43–45]: see Fig 1 for a schematic illustration of this idea. The challenge of such an approach would be to deduce the symmetry groups of the probability distributions encoded by neuronal activity (S5 Text). If this was possible, one could identify the class of

Box 1. How Does Local Gauge Invariance Explain Neuronal Inference?

This essay considers the principle of free energy minimization as a candidate gauge theory that prescribes neuronal dynamics in terms of a Lagrangian. Here, the Lagrangian is the variational free energy, which is a functional (a function of a function) of a probability distribution encoded by neuronal activity. This probabilistic encoding means that neuronal activity can be described by a path or trajectory on a manifold in the space of sufficient statistics (variables that are sufficient to describe a probability distribution). In other words, if one interprets the brain as making inferences, the underlying beliefs must be induced by biophysical representations that play the role of sufficient statistics. This is important because it takes us into the realm of differential geometry (S2 Text), where the metric space—on which the geometry is defined—is constituted by sufficient statistics (like the mean and variance of a Gaussian distribution). Crucially, the gauge theoretic perspective provides a rigorous way of measuring distance on a manifold, such that the neuronal dynamics transporting one distribution of neuronal activity to another is given by the shortest path. Such a free energy manifold is curvilinear, and finding the shortest path is a nontrivial problem—a problem that living organisms appear to have solved. It is at this point that the utility of a gauge theoretic approach appears; suggesting particular solutions to the problem of finding the shortest path on curved manifolds. The nature of the solution prescribes a normative theory for self-organised neuronal dynamics. In other words, solving the fundamental problem of minimising free energy—in terms of its path integrals—may illuminate not only how the brain works but may provide efficient schemes in statistics and machine learning.

Variational or Monte Carlo formulations of the Bayesian brain require the brain to invert a generative model of the latent (unknown or hidden) causes of sensations (S3 Text). The implicit normative theory means that neuronal activity (and connectivity) maximises Bayesian model evidence or minimises variational free energy (the Lagrangian)—effectively fitting a generative model to sensory samples. This entails an encoding of beliefs (probability distributions) about the latent causes, in terms of biophysical variables whose trajectories trace out a manifold. In (deterministic) variational schemes, the coordinates on this manifold are the sufficient statistics (like the mean and covariance) of the distribution or belief, while for a (stochastic) Monte Carlo formulation, the coordinates are the latent causes themselves (S3 Text). The inevitable habitat of these sufficient statistics (e.g., neuronal activity) is a curved manifold (see S1 and S2 Figs).

This curvature (and associated information geometry) may have profound implications for neuronal dynamics and plasticity. It may be the case that neuronal dynamics—or motion in some vast neuronal frame of reference—is as simple as the pendulum (S1 Appendix). However, because the Lagrangian is a function of beliefs (probabilities), the manifold that contains this motion is necessarily curved. This means neuronal dynamics, in a local frame of reference, will (appear to) be subject to forces and drives (i.e., Levi-Civita connections). For example, the motion of synaptic connection strengths (sufficient statistics of the parameters of generative models) depends upon the motion of neural activity (sufficient statistics of beliefs about latent causes), leading to experience-dependent plasticity. A more interesting manifestation (highlighted in the main text) may be attention that couples the motion of different neuronal states in a way that depends explicitly on the curvature of the manifold (as measured by things like Fisher information). In brief, a properly formulated gauge theory should, in principle, provide the exact

form of neuronal dynamics and plasticity. These forms may reveal the underlying simplicity of many phenomena that we are already familiar with, such as event-related brain responses, associative plasticity, attentional gating, adaptive learning rates, and so on.

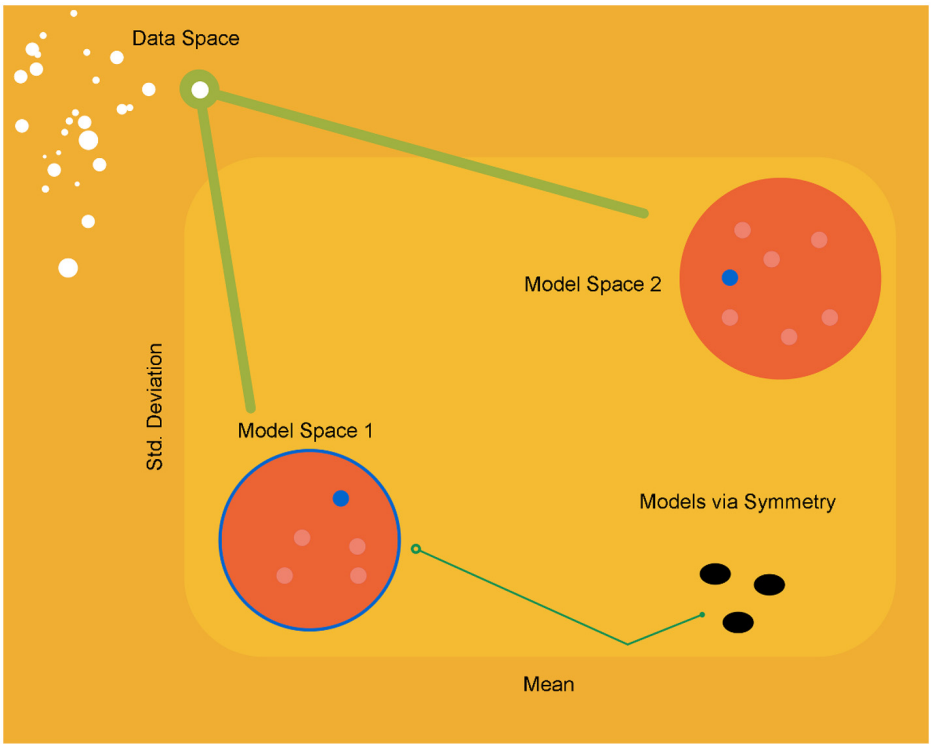

Fig 1. Invariance of inference—a proposal. A univariate normal model space (of the equivalent data space) whose coordinates are sufficient statistics. The orange circles represent two model spaces, where minimization of variational free energy leads to the appropriate model (blue circles in each case). It might be that one parameterisation (blue outer circle for model space 1) is more suitable than another. Notice that using the Riemann gradient instead of the Euclidean gradient automatically guarantees gauge-invariance by breaking the symmetry within a model. But what about between-model symmetries? After the optimal model has been selected, symmetry transformation could enable one to derive a range of models (black circles) that describe the data equally well (in terms of log model evidence or negative free energy). These can be obtained by using the intrinsic geometry of the gauge field (the Levi-Civita connection) and the symmetries afforded by the variational free energy.

doi:10.1371/journal.pbio.1002400.g001

models explaining data using a single inference methodology. From the perspective of biological self-organisation, this means that there are potentially many different models that do the same job of predicting sensory data. It is tempting to associate the equivalence classes afforded by symmetry groups above with the biological species—all doing an equally good job of modelling their (local) environments.

Supporting Information

S1 Appendix. Global and local gauge invariance.
(DOCX)

S1 Fig. Conjugate gradient-descent algorithm on manifolds. (A) New parameters (θ) are selected by performing gradient descent on orthogonal subspaces with gradient G and the descent direction H. (B) On a Riemannian manifold, minimization along lines (as in a Euclidean subspace described in A) is replaced by minimization along geodesics. This creates a problem, in that H_i and H_{i-1} are in two different tangent spaces and thus cannot be added together. (C) Vector addition as in Eqn. 12 (in S3.2) is undefined on a Riemannian manifold. Addition is replaced by exponential mapping followed with parallel transport described using a covariant gauge field (Levi-Civita connection; see text).
(TIFF)

S2 Fig. Parallel transport on Riemannian manifolds. (A) The Riemann exponential map is used to map a vector field H from $T\mathcal{M} \rightarrow \mathcal{M}$ whilst a logarithmic map is used to map the vector field from $\mathcal{M} \rightarrow T\mathcal{M}$. (B) Graphical illustration of parallel transporting a vector field H using a Schild's ladder (see text for details).
(TIFF)

S1 Glossary.
(DOCX)

S1 Text. Variational free energy.
(DOCX)

S2 Text. A tutorial on differential geometry.
(DOCX)

S3 Text. Dynamics on manifolds.
(DOCX)

S4 Text. The geometry of a univariate normal distribution.
(DOCX)

S5 Text. Symmetry-aware algorithms.
(DOCX)

References

1. O'Raifeartaigh L, Straumann N. Gauge theory: Historical origins and some modern developments. Rev Mod Phys. 2000; 72(1):1–23.
2. Knill DC, Pouget A. The Bayesian brain: the role of uncertainty in neural coding and computation. Trends Neurosci. 2004; 27(12):712–9. PMID: 15541511
3. Ma WJ, BJ M, Latham PE, Pouget A. Bayesian inference with probabilistic population codes. Nat Neurosci. 2006; 9(11):1432–8. PMID: 17057707
4. Dayan P, Hinton GE, Neal R. The Helmholtz machine. Neural Computation. 1995; 7:889–904. PMID: 7584891
5. Kersten D, Mamassian P, Yuille A. Object perception as Bayesian inference. Annu Rev Psychol. 2004; 55:271–304. PMID: 14744217
6. Zeidler E. Quantum Field Theory III: Gauge Theory: Springer; 2011.
7. Rosen J. Symmetry in Science: An Introduction to the General Theory: Springer-Verlag; 1995.
8. Doya K, Ishii S, Pouget A, Rao RPN, editors. Bayesian Brain: Probabilistic Approaches to Neural Coding: The MIT Press; 2011.
9. Friston K, Levin M, Sengupta B, Pezzulo G. Knowing one's place: a free-energy approach to pattern regulation. Journal of the Royal Society, Interface / the Royal Society. 2015; 12(105).
10. Kiebel SJ, Friston KJ. Free energy and dendritic self-organization. Front Syst Neurosci. 2011; 5:80. doi: 10.3389/fnsys.2011.00080 PMID: 22013413
11. Friston K. Life as we know it. Journal of the Royal Society, Interface / the Royal Society. 2013; 10 (86):20130475. doi: 10.1098/rsif.2013.0475 PMID: 23825119

12. Friston KJ. The free-energy principle: a unified brain theory? Nature reviews Neuroscience. 2010; 11 (2):127–38. doi: 10.1038/nrn2787 PMID: 20068583
13. Friston K. Hierarchical models in the brain. PLoS Comput Biol. 2008; 4(11):e1000211. doi: 10.1371/journal.pcbi.1000211 PMID: 18989391
14. Sengupta B, Stemmler MB, Friston KJ. Information and efficiency in the nervous system—a synthesis. PLoS Comput Biol. 2013; 9(7):e1003157. doi: 10.1371/journal.pcbi.1003157 PMID: 23935475
15. Zeki S. The Ferrier Lecture 1995 behind the seen: The functional specialization of the brain in space and time. Philos Trans R Soc Lond B Biol Sci. 2005; 360(1458):1145–83. PMID: 16147515
16. Olshausen BA, Field DJ. Emergence of simple-cell receptive field properties by learning a sparse code for natural images. Nature. 1996; 381:607–9. PMID: 8637596
17. Angelucci A, Bullier J. Reaching beyond the classical receptive field of V1 neurons: horizontal or feedback axons? J Physiol Paris. 2003; 97:141–54. PMID: 14766139
18. Golubitsky M, Stewart I. The Symmetry Perspective: From Equilibrium to Chaos in Phase Space and Physical Space: Birkhäuser; 2003.
19. Montague PR, Dayan P, Person C, Sejnowski TJ. Bee foraging in uncertain environments using predictive Hebbian learning. Nature. 1995; 377(6551):725–8. PMID: 7477260
20. Friston K. Hierarchical models in the brain. PLoS Comput Biol. 2008; 4(11):e1000211. doi: 10.1371/journal.pcbi.1000211 PMID: 18989391
21. Brascamp JW, Klink PC, Levelt WJ. The 'laws' of binocular rivalry: 50 years of Levelt's propositions. Vision research. 2015; 109(Pt A):20–37. doi: 10.1016/j.visres.2015.02.019 PMID: 25749677
22. de Vladar HP, Szathmary E. Neuronal boost to evolutionary dynamics. Interface focus. 2015; 5 (6):20150074. doi: 10.1098/rsfs.2015.0074 PMID: 26640653
23. Lisman J, Redish AD. Prediction, sequences and the hippocampus. Philosophical transactions of the Royal Society of London Series B, Biological sciences. 2009; 364(1521):1193–201. doi: 10.1098/rstb.2008.0316 PMID: 19528000
24. Wurtz RH, McAlonan K, Cavanaugh J, Berman RA. Thalamic pathways for active vision. Trends Cogn Sci. 2011; 5(4):177–84.
25. Friston K, Rigoli F, Ognibene D, Mathys C, Fitzgerald T, Pezzulo G. Active inference and epistemic value. Cognitive neuroscience. 2015:1–28.
26. Friston K, Adams RA, Perrinet L, Breakspear M. Perceptions as hypotheses: saccades as experiments. Front Psychol. 2012; 3:151. doi: 10.3389/fpsyg.2012.00151 PMID: 22654776
27. Poland D. Cooperative catalysis and chemical chaos: a chemical model for the Lorenz equations. Physica D. 1993; 65 (1):86–99.
28. Lorenz EN. Deterministic nonperiodic flow. J Atmos Sci. 1963; 20(2):130–41.
29. de Boer RJ, Perelson AS. Size and connectivity as emergent properties of a developing immune network. Journal of theoretical biology. 1991; 149(3):381–424. Epub 1991/04/07. 2062103. PMID: 2062103
30. Brown E, Moehlis J, Holmes P. On the phase reduction and response dynamics of neural oscillator populations. Neural Comput. 2004; 16:673–715. PMID: 15025826
31. Dinicola S, D'Anselmi F, Pasqualato A, Proietti S, Lisi E, Cucina A, et al. A Systems Biology Approach to Cancer: Fractals, Attractors, and Nonlinear Dynamics. Omics-a Journal of Integrative Biology. 2011; 15(3):93–104. doi: 10.1089/omi.2010.0091 PMID: 21319994
32. Bluman GW, Kumei S. Symmetries and Differential Equations: Springer New York; 1989.
33. Olver P. Applications of Lie groups to differential equations: Springer-Verlag; 1993.
34. Conant RC, Ashby WR. Every good regulator of a system must be a model of that system. Int J Systems Sci. 1970; 1(2):89–97.
35. Amari S. Information geometry of the EM and EM algorithms for neural networks. Neural Networks. 1995; 8(9):1379–408.
36. Tanaka T. Information geometry of mean-field approximation. In: Opper M, Saad D, editors. Advanced Mean Field Methods: Theory and Practice: The MIT Press; 2001. p. 259–73.
37. Ikeda S, Tanaka T, Amari S. Stochastic reasoning, free energy, and information geometry. Neural Computation. 2004; 16(9):1779–810. PMID: 15265322
38. Skovgaard LT. A Riemannian geometry of the multivariate normal model. Scand J Statist. 1984; 11:211–23.
39. Amari S, Nagaoka H. Methods of Information Geometry: Oxford University Press; 2000.

40. Tschacher W, Haken H. Intentionality in non-equilibrium systems? The functional aspects of self-organized pattern formation. New Ideas Psychol. 2007; 25(1):1–15.
41. Diaconis P, Gupta SS. Group representations in probability and statistics; 1988.
42. Eaton ML. Group Invariance Applications in Statistics: Institute of Mathematical Statistics; 1989.
43. Lauritzen SL. Statistical Manifolds. In: Amari S-I, Barndorff-Nielsen OE, Kass RE, Lauritzen SL, Rao CR, editors. Differential Geometry in Statistical Inference: IMS Monographs; 1987. p. 165–216.
44. Helland IS. Statistical inference under symmetry. International Statistical Review. 2004; 72(3):409–22.
45. Barndorff-Nielsen O. Information and Exponential Families in Statistical Theory; 2014.

ResearchGate

See discussions, stats, and author profiles for this publication at: https://www.researchgate.net/publication/297716108

PLOS Biol 2016 SUPPORTING INFO

Data · March 2016

CITATIONS
0

READS
130

5 authors, including:

Biswa Sengupta
Huawei Technologies
56 PUBLICATIONS **582** CITATIONS

SEE PROFILE

Arturo Tozzi
University of North Texas
170 PUBLICATIONS **740** CITATIONS

SEE PROFILE

Gerald Cooray
Karolinska University Hospital
55 PUBLICATIONS **347** CITATIONS

SEE PROFILE

Pamela K. Douglas
University of California, Los Angeles
46 PUBLICATIONS **517** CITATIONS

SEE PROFILE

Some of the authors of this publication are also working on these related projects:

Project My pediatric papers View project

Project Variational Neuroethology View project

All content following this page was uploaded by Arturo Tozzi on 10 March 2016.

The user has requested enhancement of the downloaded file.

Towards a Neuronal Gauge Theory
Sengupta B, Tozzi A, Cooray GK, Douglas PK, Friston KJ (2016)
PLoS Biol 14(3): e1002400. doi:10.1371/
journal.pbio.1002400

Supporting Information

S1 Appendix. Global and local gauge invariance

Consider a simple pendulum that oscillates with the same frequency ω in *x* and *y* coordinates. It is usually convenient to use polar coordinates, where $z = x + iy$, such that the motion can be described by a (second order) differential equation $\partial_{tt} z + \omega^2 z = 0$ and the direction or angle satisfies $\tan\theta = y / x$. In terms of the motion, the absolute coordinates (the *x* and *y* axes) are simply irrelevant; for example, we can rotate the axes by α to represent the motion in new coordinates x' and y'. The differential equation remains the same (although we need to replace θ by $\theta - \alpha$). This amounts to multiplying the differential equation by $e^{-i\alpha}$ and redefining $z' = ze^{-i\alpha}$. This means that although we have rotated the frame of reference, the equation of motion is unchanged. This is **global gauge invariance**. It is global because the entire frame of reference was rotated by the same amount, irrespective of where or when we describe the motion.

Now imagine we rotate the *x* and *y* co-ordinates by an angle that depends on time: i.e., the rotation α now becomes $\alpha(t)$. With this local transformation (local with respect to a particular time), multiplying by $e^{-i\alpha}$ does not ensure the invariance of the differential equation. How could we then retain the laws of motion? Remarkably, we can do so by replacing the time derivatives by $\partial_t - iA(t)$. The field $A(t)$ is the compensatory **gauge field** that ensures the equation of motion holds, locally. This is **local gauge invariance**. This amounts to rotating our coordinate system with an angular velocity $\partial_t \alpha(t)$ creating a fictitious force (like a Coriolis force). In short, the gauge field $A(t)$ induces compensatory yet fictitious forces, necessary to retain invariance under a local gauge transformation. From a local perspective, the pendulum will appear to move erratically in response to the gauge field; while, from a global perspective, nothing has changed.

S1 Glossary

- **Lagrangian mechanics**: It is an alternative way to look at Newton's laws of motion. Put simply, it describes the motion of an object by first formulating a function (the Lagrangian) that is the difference between the object's kinetic and potential energy, and then finding the minimum of this function over time (this is called action). Newton's laws of motion fall out as a result of this minimization– this is known as the principle of least action.

- **Invariance and equivariance**: A function f is invariant under a transformation g when $f(g(x)) = f(x)$. The function is equivariant when $f(g(x)) = |\partial g / \partial x| \, f(x)$. For example, the distances between points in a picture do not change when the picture is rotated (invariance), while the angles between the points do not change when the picture is enlarged (equivariance).

- **Gauge theory**: It is any field theory (i.e., a specification of how a field of quantities changes with time or other variables), where the field's Lagrangian is invariant under a continuous group of local transformations.

- **Gauge fields**: These can be viewed as fictitious forces (mathematically, an Ehresmann connection) that are introduced to compensate for a poorly chosen coordinate system; such that there exists no gauge (or coordinate) transformation that can make the gauge field vanish.

- **Group theory**: The study of algebraic structures known as groups. Put simply (everyday) objects such as fields or vector spaces are groups. The distinction between different sorts of groups rests on the types of operations and axioms that can be applied.

- **Riemann geometry**: It is a branch of differential geometry that studies smooth manifolds (i.e. surfaces) with a measure of distance instantiated as an inner product (metric).

- **Information geometry**: Using insights from Riemann geometry, information geometry studies the properties of statistical manifolds such as those defined by probability distributions.

- **Symmetry**: Symmetry is any property of a system that is invariant under certain transformations. For example, an equilateral triangle remains the same, when rotated by 60°.

- **Fisher information**: It quantifies the amount of information that an observable variable carries about an unknown (random) variable causing the observation.

- **Kullback-Leibler divergence**: A non-commutative measure (and non-negative) of the difference between two probability distributions.

- **Free energy**: An information theoretic measure that bounds or limits (by being greater than) the surprise (or self information) on sampling some data, under a model of how those data are generated.

- **Entropy**: The average surprise (self information) of outcomes sampled from a probability distribution. A distribution with low entropy means that, on average, the outcome is predictable. Entropy is therefore a measure of uncertainty.

- **Sufficient statistics**: These are quantities that are sufficient to parameterize a probability density (for example, the mean and covariance of a Gaussian distribution).

- **Generative model**: A probabilistic model (joint distribution) of the dependencies between causes and effects (data), from which samples can be generated. It is usually specified in terms of the likelihood of data, given their causes (parameters of a model) and priors over those causes.

- **Prior**: The probability distribution of the causes of data that encodes beliefs about those causes before observing the data.

- **Bayesian brain hypothesis**: The idea that the brain uses internal probabilistic (generative) models to update posterior beliefs, using sensory information, in a (approximately) Bayes-optimal fashion.

- **Laplace approximation**: A saddle-point approximation of the integral of a function that uses a second-order Taylor expansion. When the function is a probability density, the implicit assumption is that the density is approximately Gaussian.

S1 Text. Variational free energy

In these appendices (supporting information), we provide a brief overview of the ingredients required to establish a gauge-theoretic formulation of variational free energy minimisation. We start by describing the basics of variational free energy followed by a primer ondifferential (Riemann) geometry, and ending with the propagation of probability measures on a curved manifold.Throughout, Einstein summation over repeated indices is assumed.

The variational free energy formalism assumes that an agent minimizes the entropy of its sensory states $s \in S$ .Only through its sensory receptors can a biological system access the states of its environment; in other words, sensory states form a veil (technically, a Markov blanket) between the system's internal states $\theta \in \Theta$ and its environment (external states) $\psi \in \Psi$. By bounding the entropy of its sensory states, the system confinesthe entropy of its environment. Under the assumption of ergodicity, this entropy is the long-term average of surprise. Crucially, the system cannot calculate this quantity directly because it has to marginalize over the external states that cause sensory input.The objective then becomes to obtain a lower bound on the marginal likelihood $\ln p(s)$ by approximating it using a parametric probability distribution(for example, a Gaussian distribution) $q(\psi)$ over the (unknown) external states that are hidden behind the Markov blanket (i.e., hidden causes of sensations). In short, the Lagrangian $\mathrm{L} = -\ln p(s)$ is minimised by bounding the surprise using the variational free energy $\mathrm{F}(s,\theta) \square \mathrm{F}(s,q)$ of the distribution $q(\psi \mid \theta)$ where θ are the sufficient statistics or parameters of the variational distribution. In the case of a Gaussian distribution the sufficient statistics are simply the mean and the co-variances $\{\mu, \Sigma\} \subset \theta$.

The variational distribution that minimises free energy can be expressed in terms of anEuler-Lagrange action $\delta S(\mathrm{F}(s,q)) = 0 \Leftrightarrow \nabla \mathrm{F} = 0$, implying that the gradient descent on the variational free-energy manifold leads us to the most optimal representation of the external states.A numerical scheme to solve such a variational problem is generalised (Bayesian) filtering [1]. The Bayesian perspective follows because our Lagrangian is also known as (the negative logarithm of) Bayesian model evidence. In other words, minimising free energy is equivalent to maximising model evidence.

1. Friston KJ, Trujillo-Barreto N, Daunizeau J (2008) DEM: A variational treatment of dynamic systems. Neuroimage 41: 849-885.

S2 Text.A tutorial on differential geometry

In this section, we present a brief introduction to key concepts in differential (Riemann) geometry that are necessary to understand information geometry.Biological systems are immersed in a 4-dimensional world where 3-spatial and 1-time co-ordinates form the frame of reference. Fibre bundles are constructs from differential geometry that offers a general formulation of such frames of reference. Intuitively, a 2-dimensional sheet is sampled by gluing together a collection of identical 1-dimensional lines, stacked, say, on the x-axis. The lines are then called fibres (F) and the subspace that glues them together is called the base (B) – taken together, the lines form a fibre bundle ($\bar{F}$). Replacing the 2-dimensional sheet by a cylinder simply alters the base; wherein the fibres are attached to a circle and the co-ordinates of a line range between plus and minus infinity, while the co-ordinates on a circle take values between 0 and 2π . In such a case – where it is easy to find a global co-ordinate system – we call the corresponding bundle *trivial.* A non-trivial bundle would be a Möbius strip, where it is not possible to instantiate a global co-ordinate system. Such scenarios occur more often than not. In these cases, it is possible to use a web of local co-ordinate systems. The only requirement then becomes establishing some rules that describe how a local co-ordinate changes between adjoining patches. A connection field – also known as the gauge field – fulfils this requirement and reconciles the apparent disagreement between the coordinate systems of the fibres glued to nearby points of the base.

The gauge field is therefore a vector field comprised of independent coordinates in the base. For the comparison of two co-ordinate systems – of two local points – it suffices to construct a rule for frame adjustments along the independent coordinates of the base. The difference can be accounted by a series of transitions along the independent directions (say b).Mathematically, one calculates the scalar product of the difference between the points of the base db and the gauge field A

$$\Delta F(b) = db \cdot AF \equiv \sum_{i=1}^{\dim B} A^i F(b).db^i .$$

Here the gauge field A is a transformation between the coordinate systems of $F(b)$ and $F(b+db)$. The route between $F(b)$ and $F(b+db)$ defines a curve; along with the gauge field, these define a parallel transport along the curve. When we compare two distant elements of a fibre using a connection field – and do not find a difference – we can say that the second element is a result of parallel transport of the first element along the curve. Let us now formalize the concepts that we have described so far:

Definition 1. A **smooth fibre bundle** is a composite object made up of – (a) a smooth manifold $\bar{F}$ that is called the total (bundle) space, (b) a smooth manifold B called the base space, (c) a smooth mapping $w : \bar{F} \to B$ called the projection whose Jacobian is required to have maximal rank at every point, (d) a smooth manifold F called the fibre and (e) a group G of smooth transformations of the fibre F called the structure group of the

fibre bundle.**Tangent** and **co-tangent** bundles are special cases of a fibre bundle. The Lagrangian, summarizing the dynamics is the natural energy function on the tangent bundle whilst the Hamiltonian is the natural energy function on the co-tangent bundle. A **jet bundle** generalizes both the tangent and the cotangent bundle.

Definition 2.A fibre bundle is characterised as ***trivial*** if we can introduce a global co-ordinate system so that any point can be identified using a pair of co-ordinates (x, f) where f is a set of co-ordinates on the fibre and x is a set of co-ordinates on the base. Similarly, a ***principal fibre bundle*** is a special fibre bundle, whose fibre is the group G.

Definition 3. For a curve γ on the base, a **connection** is a map ϕ_γ of the fibre $F_{\gamma(a)}$ at point $\gamma(a)$ to fibre $F_{\gamma(b)}$ at point $\gamma(b)$ that satisfy the following requirements – (a) ϕ_γ depends continuously on $\gamma(t)$, (b) ϕ_γ is independent of the parameterization of the path – parallel transport is defined by the path rather than the function $\gamma(\cdot)$, (c) ϕ_γ is the identity map if $\gamma(t)$ is constant and (d) parallel transport along two consecutive curves is equivalent to transport along the combined curve; a corollary of which states that transport in opposite direction generates the inverse parallel transport. A connection is called a **G-connection** if the map ϕ_γ is an element of the structure group for any curve in the base. In summary, results of parallel transport with the same endpoint but different paths can be different. The **curvature** of the fibre bundle measures this difference.

For our purposes, we will confine ourselves to a Riemannian manifold – a manifold that is analytic and where each tangent space is equipped with an inner product, varying smoothly from point to point. This inner product takes the form of a metric on the tangent bundle that approximates the manifold locally. This enables us to define various notions such as length, angles, volumes, etc.

Definition 4. A **Riemannian metric** on a manifold M is a covariant 2-tensor g which associates each point on the manifold with an inner product $g = \langle -, - \rangle_x$ on the tangent space $\mathrm{T}_x\mathrm{M}$. The metric is not only bilinear but also symmetric and positive definite and therefore defines a Euclidean distance on the tangent space. In terms of local co-ordinates the metric is given by a matrix $g_{ij} = \langle X_i, X_j \rangle_x$ where X_i and X_j are tangent vectors to M at x and varies smoothly with x. A **geodesic** curve is a local minimiser of arc-length computed with a Riemannian metric.

Definition 5. In Riemann geometry, the **Levi-Civita connection** is the torsion or curvature free connection of the tangent bundle that preserves the Riemannian metric. More specifically, it is a unique affine connection ∇ such that it is

- compatible with metric i.e., $X.g(Y,Z) = g(\nabla_X Y, Z) + g(Y, \nabla_X Z)$

- has symmetry i.e., $\nabla_X Y - \nabla_Y X = [X, Y]$ where $[X, Y]$ is the Lie bracket

The compatibility condition can be expressed in terms of covariant derivative i.e., if $X(t) = X(\gamma(t))$ and $Y(t) = Y(\gamma(t))$ are two vector fields along the curve γ and D/dt is the co-variant derivative along γ then,

$$\frac{d}{dt} g\left(X(t), Y(t)\right) = g\left(\frac{DX(t)}{dt}, Y(t)\right) + g\left(X(t), \frac{DY(t)}{dt}\right) \qquad 1$$

Definition 6. In a manifold that has been parameterised and the curve $\gamma(t)$ is represented as $(x^1(t), \ldots, x^M(t))$, the co-variant derivative of a vector field v can be written as,

$$\frac{Dv}{dt} = \sum_m \left\{ \frac{dv^m}{dt} + \sum_{i,j} \Gamma_{ij}^m v^j \frac{dx^i}{dt} \right\} \frac{\partial}{\partial x_m} \qquad 2$$

Here, the coefficients of the connection Γ_{ij}^m are known as the **Christoffel symbols**. Simply, the parallel transport along the curve becomes a first order linear system,

$$\frac{dv^m}{dt} + \sum_{i,j} \Gamma_{ij}^m v^j \frac{dx^i}{dt} = 0, \text{ m=1,…,M} \qquad 3$$

In such a case the Christoffel symbols are given by,

$$\Gamma_{ij}^m = \frac{1}{2} \sum_l \left\{ \frac{\partial}{\partial x_i} g_{jm} + \frac{\partial}{\partial x_j} g_{mi} - \frac{\partial}{\partial x_m} g_{ij} \right\} g^{ml} \qquad 4$$

g^{ml} represents the metric inverse. The geodesic equation can now be written as a system of a second order system,

$$\frac{d^2 x^m}{dt^2} + \sum_{i,j} \Gamma_{ij}^m \frac{dx^i}{dt} \frac{dx^j}{dt} = 0, \text{ m=1,…,M} \qquad 5$$

This concludes our brief introduction to differential geometry.

S3 Text. Dynamics on manifolds

We will now use the concepts described in Section S2 to describe the geometry of the variational free-energy landscape (Section S1). We begin by formulating the evolution of parameters using Langevin equations (a stochastic formulation) before moving on to describe the evolution of the approximate probability distribution, as used in the variational free-energy framework (a deterministic formulation).

S3.1 Stochastic approach– parameters of the generative model form the co-ordinate basis

The evolution of parameters θ of a generative model can be characterised with a Langevin equation, whose ensemble densityminimises variational free energy[1],

$$d\theta(t) = \frac{1}{2}\nabla \mathrm{J}\ (\theta(t))dt + d\mathbf{b}(t) \qquad 6$$

where we define the quantity $\mathrm{J}\ (\theta) \equiv \log p(\psi = \theta \mid s) := \log p(\theta)$ and $\mathbf{b}$ denotes Brownian motion. It is important to realize that this Langevin equation describes the stochastic flow of parameters – and not of the sufficient statistics of the distribution that describes the parameters (see section S3.2). In theory such a stochastic differential equation (SDE) should converge to a unique and invariant ergodic density, which will approximate the posterior density of parameters given sensory data. Discretisation using numerical methods often lead to non-convergence or convergence to a 'wrong' ergodic density. An empirical solution amounts to probabilistically accepting solutions at each time step depending on the relative densities of the solution at the new and the old time-steps (e.g., Markov chain Monte Carlo procedures).

By virtue of the Nash embedding theorem, our aim here is to define the above (Langevin) diffusion process on a manifold M that is embedded on a higher dimensional Euclidean space $\mathbb{R}^n$. If we can do this, the evolution of the probability measure on the manifold simply becomes an Euler-Lagrange flow.

Before we start our derivation, let us generalise the Laplace operator to Riemannian manifolds. This linear operator is known as the Laplace-Beltrami operator, composed as the divergence of the covariant derivative[2]. Assume that M is an oriented Riemannian manifold, then the volume form on M indexed by the coordinate system θ^i is

$$\mathrm{vol_n} = \sqrt{|g|}\, d\theta^1 \wedge d\theta^2 \ldots d\theta^n \qquad 7$$

where $d\theta^i$ are the 1-forms forming a dual basis, g is the metric tensor and $\wedge$ is the familiar wedge product. The divergence of a vector field on a manifold $\widehat{\Theta}$ is then a scalar function with

$$(\mathrm{div}\widehat{\Theta})\mathrm{vol_n} = L_{\widehat{\Theta}}\mathrm{vol_n} \qquad 8$$

with L denoting the Lie derivative of the vector field $\widehat{\Theta}$. Such divergence can be written in local co-ordinates as,

$$\mathrm{div}\widehat{\Theta} = \frac{1}{\sqrt{|g|}}\partial_i\left(\sqrt{|g|}\, d\widehat{\Theta}^i\right) \qquad 9$$

Now for any scalar function J we can also define a vector field $\nabla\mathrm{J}$ on the manifold using inner products for all vectors v_θ at point v on the tangent space $T_\theta\mathrm{M}$,

$$\begin{aligned} \left\langle \nabla\mathrm{J}\ (\theta), v_\theta \right\rangle &= d\mathrm{J}\ (\theta)(v_\theta) \\ \left(\tilde{\nabla}\mathrm{J}\ \right)^i &= \partial^i\mathrm{J}\ = g^{ij}\partial_j\mathrm{J} \end{aligned} \qquad 10$$

With these identities, the Laplace-Beltrami operator (Δ) becomes,

$$\Delta\mathrm{J}\ = \frac{1}{\sqrt{|g|}}\partial_i\left(\sqrt{|g|}\, g^{ij}\partial_j\mathrm{J}\ \right) \qquad 11$$

The Langevin equation 6 comprises two terms – a drift term and a diffusion term; where the latter is represented by the Laplace-Beltrami operator (diffusion with 'constant' infinitesimal variance with respect to the metric) when diffusion occurs on a Riemannian manifold. While the gradient has the form in Eqn. 10, using Ito's calculus, one can show the non-linear mapping of the martingale $d\mathbf{b}(t)$ becomes,

$$d\tilde{\mathbf{b}}_t = \frac{1}{2}\frac{1}{\sqrt{|g(\theta)|}}\partial_i\left(\sqrt{|g|}\, g^{ij}\right)dt + \sqrt{g^{ij}}\, d\mathbf{b}_t \qquad 12$$

The probability density $p(\theta)$ also has to be altered to yield the correct invariant density on the manifold; this can be attained by the following transformation

$$\tilde{p}(\theta) = p(\theta)\frac{1}{\sqrt{|g(\theta)|}} \qquad 13$$

Combining all of the transformations we obtain the Langevin equation on the manifold,

$$d\theta(t) = \frac{1}{2}\tilde{\nabla}\mathrm{J}\ \ (\tilde{p}(\theta))dt + d\tilde{\mathbf{b}}(t) \qquad 14$$

Such flows are invariant under transformation of random variables and covariant under re-parameterisation.Specifically under the Bayesian framework, the metric becomes the expected Fisher information in combination with the negative Hessian of the log-prior[3].

S3.2 Deterministic approach– sufficient statistics of the generative model form the co-ordinate basis

The evolution of the variational free-energy could be described on a Riemann manifold by augmenting the first order gradient flow using a Fisher information metric [4,5]. On a Euclidean manifold, the minimization of variational free-energy involves

$$\frac{-\nabla\mathrm{F}}{\|\nabla\mathrm{F}\|} = \lim_{\varepsilon\to 0}\frac{1}{\varepsilon}\arg\min_{d\theta:\|d\theta\|\leq\varepsilon}\mathrm{F}\ (\theta + d\theta) \qquad 15$$

This simply says that the flow of parameters (e.g. means and co-variance of a Normal distribution; $\{\mu,\sigma,\ldots\}\in\theta$) will induce the largest change in free-energy under a unit change in parameters. Notice that the inner products are defined on a Euclidean manifold.

Classical results from information geometry (Cencov's characterisation theorem) tell us that, for manifolds based on probability measures,a unique Riemannian metric exists – the Fisher information metric. In statistics, Fisher-information is used to measure the expected value of the observed information.Whilst the Fisher-information becomes the metric for curved probability spaces, the distance between two distributions is provided by the Kullback-Leibler (KL)divergence. It turns out that if the KL-divergence is viewed as a curve on a curved surface, the Fisher-information becomes its curvature:

$$
\begin{aligned}
KL_{sym}(\theta,\theta') &= \mathrm{E}_{\theta}\left[\log\frac{q(\psi|\theta)}{q(\psi|\theta')}\right] + \mathrm{E}_{\theta'}\left[\log\frac{q(\psi|\theta')}{q(\psi|\theta)}\right] \\
&= d\theta^{T} g(\theta) d\theta + \mathrm{O}(d\theta^{3}) \\
g_{ij}(\theta) &= \int_{-\infty}^{+\infty} q(\psi,\theta)\frac{\partial \ln q(\psi,\theta)}{\partial\theta_i}\frac{\partial \ln q(\psi,\theta)}{\partial\theta_j} d\psi \\
KL[\theta_0+\delta\theta:\theta_0] &\approx \frac{1}{2} g_{ij}(\theta_0)(\delta\theta)^{2}
\end{aligned}
\tag{16}
$$

Gradient descent on such a manifold then becomes the solution of $\arg\min_{d\theta} \mathrm{F}\ (\theta + d\theta)$, subject to $KL_{sym}(\theta,\theta+d\theta) < \varepsilon$; i.e., the direction of the highest decrease in the free-energy, for the smallest change in the KL divergence. The solution of this optimization problem yields Amari's natural gradient that replaces the Euclidean gradient $\nabla \mathrm{F}$ by its Riemannian counterpart $\tilde{\nabla}\mathrm{F} = \mathrm{g}_{\mathrm{ij}}(\theta)^{-1}\nabla\mathrm{F}$. This derivative is invariant under re-parameterisation of the approximate probability distribution, thereby helping us to break symmetries on the variational free-energy manifold.

This formulation has two important consequences – (a) from classical results in statistics, pre-conditioning of the free-energy gradient by the Fisher-information tells us that the variance of the estimator is bounded from below by the Fisher-information (Cramér-Rao bound) and (b) under a Normal distribution approximation of the posterior distribution, precision-weighted prediction errors under a Euclidean manifold are replaced by asymptotic dispersion and precision-weighted prediction errors under a Riemannian manifold.

Such constructs are already instantiated in advanced Bayesian filtering schemes, such as the SPM code-base (available from http://www.fil.ion.ucl.ac.uk/spm/) using Fisher-scoring – the gradient of variational free-energy is pre-multiplied by the inverse Fisher information metric.Notice that the metric in Fisher-scoring is simply the variance of the score function, while our derivation of the metric includes not only the metric for the likelihood but also that of the prior (instantiated as the Hessian of the prior).

The question that we now ask is whether we can deduce an optimization scheme that enables us to traverse the free-energy landscape? In other words, find the geodesic to local minima in the sub-manifold. There are two routes one can take to increase the statistical efficiency of the implicit optimisation – first, we can formulate the Hessian operator on the Riemannian manifold in terms of the Laplace-Beltrami operator (Section S3.1) or we can retain a first-order approximation and formulate descent directions that are orthogonal to the previous descent directions. Such Krylov sub-spaces are well-known in numerical analysis with the *conjugate gradient-descent* algorithm providing one such example (Figure S1). Routinely used in optimization, conjugate gradient descent methods have been used for gradient descent on manifolds traced out by energy functions such as the variational free-energy [6,7]. Simply such a scheme amounts to,

$$\theta_i = \theta_{i-1} + \alpha H_i$$
$$H_i = -G_i + \beta H_{i-1} \qquad 17$$
$$\beta = \frac{\nabla_i^T \nabla_i}{\nabla_{i-1}^T \nabla_{i-1}} \xrightarrow{Riemannize} \frac{\tilde{\nabla}_i^T \nabla_i}{\tilde{\nabla}_{i-1}^T \nabla_{i-1}}$$

For β we have used the Fletecher-Reeves instantiation on a curved manifold; other update rules such as Polak-Ribière, Hestenes-Stiefel or Dai-Yuan can be similarly lifted to a Riemannian manifold[8]. Allof these conjugate gradient descent formulas have a problem – one cannot add two vector fields H_i and H_{i-1} on a Riemannian manifold. This is because they exist on different tangent manifolds. H_{i-1} should undergo parallel transport to the tangent manifold containing H_i using a connection (a gauge) field. In our case, this is the Levi-Civita connection described in Section S2.

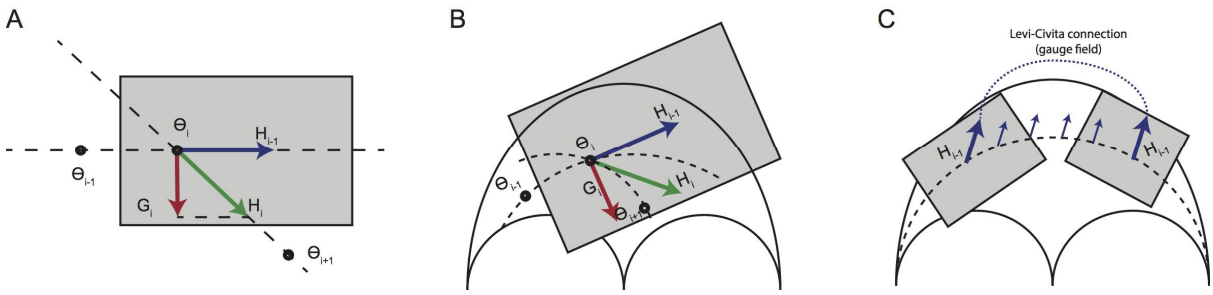

Figure S1

Parallel-transport requires the solution of a second-order differential equation. Analysis shows us that the natural gradient is simply the first order approximation of the parallel transport –that we pursue in terms of solving geodesic equations for the sufficient statistics. For the Laplace approximation, we could derive the Christoffelsymbols analytically (Section S4), while for more complicated probability distributions we need to resort to a generic transport procedure (Figure S2). Namely, we use the Riemann exponential map for mapping the vector field on the tangent manifold to the geodesic described on the manifold $(TM \rightarrow M)$, whereas a Riemann logarithmic map represents the transformations of vector-fields from the manifold to the tangent manifold $(M \rightarrow TM)$,

$$\exp_\theta(A) = \theta^{1/2} \exp(\theta^{-1/2} A \theta^{-1/2}) \theta^{1/2}$$
$$\log_\theta(A) = \theta^{1/2} \log(\theta^{-1/2} A \theta^{-1/2}) \theta^{1/2} \qquad 18$$

The geodesic is first approximated using standard projection method [9]. Then using the exponential and logarithm maps a Schild's ladder[10] is instantiated as following:Let θ_I and θ_F denote the initial and final points on the geodesic that the vector field is to be transported to. We start by calculating $n_1 = exp_{\theta_I}(H)$ and

the midpoint m_1 between the geodesic segment joining n_1 and θ_1. We then trace out the geodesic from θ_I through m_1 for twice its length, tracing out a new point n_2. This scheme is repeated until we reach θ_F. After the vector field H has been parallel transported to θ_F, we are in a position to useparameter updates as detailed in Eqn. 17. Numerical instantiation of this algorithm shall be presented elsewhere [11].

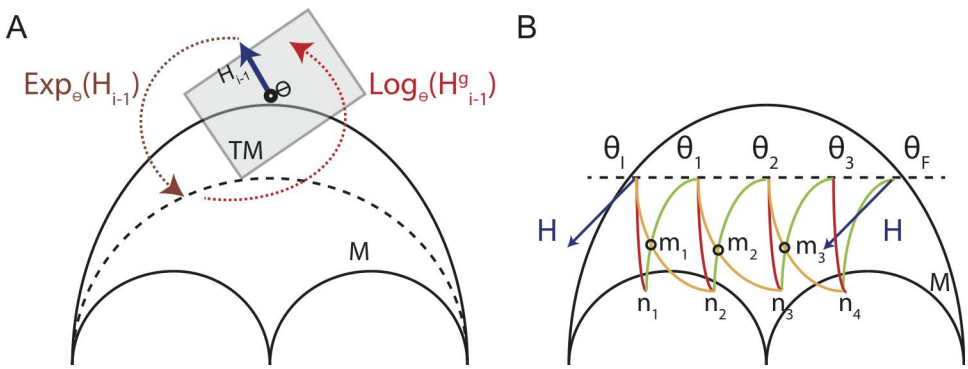

Figure S2.

1. Jordan R, Kinderlehrer D, Otto F (1999) The variational formulation of the fokker-planck equation. SIAM J Math Anal 29: 1-17.
2. Hsu E (2002) Stochastic Analysis on Manifolds: American Mathematical Society.
3. Sengupta B, Friston KJ, Penny WD (2015) Gradient-based MCMC samplers for dynamic causal modelling. Neuroimage.
4. Amari S (1995) Information geometry of the EM and EM algorithms for neural networks. Neural Networks 8: 1379-1408.
5. Tanaka T (2001) Information geometry of mean-field approximation. In: Opper M, Saad D, editors. Advanced Mean Field Methods: Theory and Practice: The MIT Press. pp. 259-273.
6. Honkela A, Raiko T, Kuusela M, Tornio M, Karhunen J (2010) Approximate Riemannian Conjugate Gradient Learning for Fixed-Form Variational Bayes. Journal of Machine Learning Research 11: 3235−3268.
7. Hensman J, Rattray M, Lawrence ND. Fast variational inference in the conjugate exponential family; 2012.
8. Nocedal J, Wright S (2006) Numerical Optimization: Springer.
9. Hairer E, Lubich C, Wanner G (2004) Geometric Numerical Integration: Structure Preserving Algorithms for Ordinary Differential Equations: Springer.
10. Misner C, Thorne K, Wheeler J (1973) Gravitation: W.H. Freeman.

11. Sengupta B, Penny WD, Friston KJ (2016) Information geometric variational learning. (under preparation).

S4Text. The geometry of a univariate Normal distribution

The normal distribution $\mathrm{N}\ (\mu,\sigma)$, a member of the exponential family, does not enjoy the geometry of a Euclidean manifold. The Laplace-approximation of a variational density (see Friston, Mattout et al. 2007) rests on approximating the posterior distribution with a Normal distribution. Therefore, it becomes instructive to understand its geometry.Calculation shows that the Riemannian metric (the Fisher information) simply reads $g(\mu,\sigma) = diag\left[\sigma^{-2}\ \ 2\sigma^{-2}\right]$ for a univariate Normal. Further algebra shows that the non-zero terms of the Levi-Civita connection for a univariate Normal distribution are

$$\Gamma^1_{1,2} = -\frac{1}{\sigma}, \Gamma^2_{1,1} = \frac{1}{2\sigma}, \Gamma^2_{2,2} = -\frac{1}{\sigma} \qquad 19$$

S5 Text. Symmetry-aware algorithms

A technically, prescient issue is how to use these notions to identify models via symmetry [1]. The (pure) mathematical tool that allows us to do this is topological group theory [2,3]. An important lead using group theory for statistical inference is the development of a novel class of Markov chains called *orbital Markov chains*[4], that could potentially be used to draw samples from the equivalence class of a probability measure. In the absence of symmetries, orbital Markov chains are equivalent to standard Markov chains. Unsurprisingly, taking symmetries of the proposal distribution into account leads to a faster convergence (rapid mixing) of the Markov chain [5,6]. Equivalence classes in such orbital Markov chains are deduced using a well-known product replacement algorithm [7]. Such an algorithm allows generating an approximately uniformly distributed random element of a finite group by instantiating a random walk on the group. Under a variational inference framework, our differential geometry algorithm instantiates a similar symmetry-awareness (see SectionS3). The challenge remains in understanding the symmetry groups for directed Bayesian networks via established tools of geometry and group theory, helping us forge a gauge theory that is not only useful for understanding biotic self-organizationbut also in the statistical analysis of data.

1. Nishihara R, Minka T, Tarlow D (2013) Detecting Parameter Symmetries in Probabilistic Models. arXiv preprint arXiv:1312.5386.
2. Diaconis P, Gupta SS (1988) Group representations in probability and statistics.
3. Eaton ML (1989) Group Invariance Applications in Statistics: Institute of Mathematical Statistics.
4. Niepert M. Markov chains on orbits of permutation groups; 2012.
5. Niepert M. Lifted probabilistic inference: An MCMC Perspective; 2012.
6. Shariff R, György A, Szepesvári C. Exploiting symmetries to construct efficient MCMC algorithms with an application to SLAM; 2015.
7. Pak I. The product replacement algorithm is polynomial; 2000. pp. 476-485.

View publication stats

frontiers in Human Neuroscience

REVIEW
published: 26 May 2016
doi: 10.3389/fnhum.2016.00247

New Perspectives on Spontaneous Brain Activity: Dynamic Networks and Energy Matter

Arturo Tozzi[1,2], *Marzieh Zare*[3]* and *April A. Benasich*[4]

[1] Center for Nonlinear Science, University of North Texas, Denton, TX, USA, [2] Computational Intelligence Laboratory, University of Manitoba, Winnipeg, MB, Canada, [3] School of Computer Science, Institute for Research in Fundamental Sciences (IPM), Tehran, Iran, [4] Center for Molecular and Behavioral Neuroscience, Rutgers University-Newark, Newark, NJ, USA

Spontaneous brain activity has received increasing attention as demonstrated by the exponential rise in the number of published article on this topic over the last 30 years. Such "intrinsic" brain activity, generated in the absence of an explicit task, is frequently associated with resting-state or default-mode networks (DMN)s. The focus on characterizing spontaneous brain activity promises to shed new light on questions concerning the structural and functional architecture of the brain and how they are related to "mind". However, many critical questions have yet to be addressed. In this review, we focus on a scarcely explored area, specifically the energetic requirements and constraints of spontaneous activity, taking into account both thermodynamical and informational perspectives. We argue that the "classical" definitions of spontaneous activity do not take into account an important feature, that is, the critical thermodynamic energetic differences between spontaneous and evoked brain activity. Spontaneous brain activity is associated with slower oscillations compared with evoked, task-related activity, hence it exhibits lower levels of enthalpy and "free-energy" (i.e., the energy that can be converted to do work), thus supporting noteworthy thermodynamic energetic differences between spontaneous and evoked brain activity. Increased spike frequency during evoked activity has a significant metabolic cost, consequently, brain functions traditionally associated with spontaneous activity, such as mind wandering, require less energy that other nervous activities. We also review recent empirical observations in neuroscience, in order to capture how spontaneous brain dynamics and mental function can be embedded in a non-linear dynamical framework, which considers nervous activity in terms of phase spaces, particle trajectories, random walks, attractors and/or paths at the edge of the chaos. This takes us from the thermodynamic free-energy, to the realm of "variational free-energy", a theoretical construct pertaining to probability and information theory which allows explanation of unexplored features of spontaneous brain activity.

Keywords: spontaneous activity, free energy principle, power law, phase transition, energetic constrains

OPEN ACCESS

Edited by:
Chrystalina A. Antoniades, University of Oxford, UK

Reviewed by:
Peter Jedlicka, Goethe University Frankfurt, Germany
Ramon Guevara Erra, Paris Descartes University, France
Haroldo Valentin Ribeiro, Universidade Estadual de Maringá, Brazil

***Correspondence:**
Marzieh Zare
marziehzare@ipm.ir

Received: *14 April 2015*
Accepted: *09 May 2016*
Published: *26 May 2016*

Citation:
Tozzi A, Zare M and Benasich AA (2016) New Perspectives on Spontaneous Brain Activity: Dynamic Networks and Energy Matter. Front. Hum. Neurosci. 10:247. doi: 10.3389/fnhum.2016.00247

INTRODUCTION

Neural oscillations are observed throughout the central nervous system (CNS) and at all levels. Here we are specifically concerned with "spontaneous brain activity", that is brain activity generated in the absence of an explicit task and frequently correlated with "resting-state or default-network activity" (Raichle et al., 2001). Much of what is known concerning

the intersection of brain anatomy and function comes from functional magnetic resonance imaging (fMRI) studies that highlight task-evoked responses. In general, fMRI studies focus on changes in the blood oxygenation level-dependent (BOLD) signal, which is induced by the neural response to an externally controlled stimulus/task (Damoiseaux et al., 2006). These experiments, as well as those employing a variety of other techniques, encourage the view that two different types of neuronal activity drive brain function: evoked and spontaneous. However, such an approach ignores an alternative possibility: that the brain's operations are *primarily spontaneous* and involve the acquisition and maintenance of information (Raichle, 2010; Barrett and Simmons, 2015). Multiple techniques, such as fMRI, electroencephalography (EEG) and magnetoencephalography (MEG), show that spontaneous, low-frequency fluctuations of cerebral activity, which cannot be attributed to the experimental design or other explicit input or output (Fox and Raichle, 2007), are temporally coherent within distributed, spatially independent, functional networks, and resemble those evoked by sensory, motor, and cognitive paradigms (de Pasquale and Marzetti, 2014). Spontaneous activity of the brain, first formally characterized 30 years ago, has received growing attention, as witnessed by the ever-increasing number of articles dedicated to this topic (Fox and Raichle, 2007; Buckner et al., 2008). Although sceptical researchers hold that BOLD signals mainly originate from cerebral blood flow (Tong and Frederick, 2010), it is widely believed that spontaneous signals are best correlated with spikes in the range of slow cortical potentials (Raichle et al., 2001). Indeed, spontaneous fluctuations have not only been observed in electric activity, but also in various hemodynamic and metabolic parameters, including spontaneous fluctuations in the membrane potential, spontaneous spikes and neurotransmitter release (O'Donnell and van Rossum, 2014). Multiple observations have documented the finding that fluctuations in spontaneous neurotransmitter release show a 1/f frequency distribution, similar to that of BOLD. Recent reports also suggest that such spontaneous neurotransmission release events have an autonomous role in intra-neuronal communication—as well as in the regulation of synaptic plasticity and homeostasis—distinct from that of evoked release and independent of presynaptic action potentials (Kavalali, 2015). Such findings highlight the realization that spontaneous brain activity has a vital functional role, is produced at all levels of the brain, and can, with the appropriate analytic and theoretical approaches provide unparalleled insights into dynamic brain function.

This review comprises five sections in which we hope to address this rapidly expanding area of research. The first section highlights the conceptual view that spontaneous fluctuations are the basic, standard architecture, not just of functional, but also of anatomical brain organization. Section two describes the high energetic requirements of the brain, but also emphasizes the fact that "spontaneous activity" requires *less* energy than "evoked activity". Starting from such an assumption, the following section aims to explain spontaneous activity using the framework of "energetic landscapes" and complex, nonlinear systems. Section four reviews the most recent experimental studies, which have explored the link between spontaneous brain activity and psychological states. The fifth section, starting from the ubiquitous phenomenon of power laws and its correlations, provides an overview of one of the most successful general brain frameworks, Friston's (2010) "Free Energy Principle", in order to explore the power of this theory to explain the role of spontaneous brain activity.

SPONTANEOUS ACTIVITY IS THE INTRINSIC ARCHITECTURE OF BRAIN ORGANIZATION

It is clear that spontaneous brain activity cannot be simply reduced to "background noise" uncorrelated to the system response, rather it occurs during unconstrained "resting states"; that is, in subjects who are lying quietly with eyes closed, or while fixating on a target, but with no explicit task instruction, directed to think of nothing in particular, but importantly, awake. Spontaneous signals detected and recorded by fMRI, EEG or MEG support the hypothesis that spontaneous fluctuations constitute the basic architecture of functional brain organization (Cole et al., 2014). Spontaneous cortical electric activity is already present in the foetus by the 34th week of gestation (Krueger and Garvan, 2014); the brain spontaneously pulsates during the fatal period, in the same manner as the heart spontaneously contracts. It has also been demonstrated that spontaneous fluctuations are more frequently observed in immature synapses as compared to those that are more mature (Kavalali et al., 2011). In addition, the vertebrate spinal cord and brainstem possess central pattern generator (CPG) circuits, which can produce meaningful functional output in the absence of sensory inputs. Neocortical circuits could be regarded as particularly plastic types of CPGs, as they have rich spontaneous dynamics that are powerfully modulated or engaged by sensory inputs, but can also generate output in their absence (Yuste et al., 2005). Recent results also demonstrate that gamma-band activity in the alert monkey is largely an emergent property of cortex, arising from the resting state waves (Bastos et al., 2014). These fluctuations in cortical excitability exert a remarkable effect on other elements of the field potential's activity, as well as on the spiking activity of neurons. In fact, this "coupling" or nesting of many spikes subserves an important coordinating role and provides a logical structure for the integration of functional activity (Buszáki, 2006). In sum, spontaneous fluctuations appear to represent the standard architecture of the nervous system's functional organization (Cole et al., 2014), have a critical functional role, are produced by brain circuits and provide a window into their dynamic operations.

Spontaneous activity has been shown to correlate with brain function, as well as with precise anatomical structures. Analyses of spontaneous fluctuations within fMRI signals have identified a number of large-scale intrinsic networks, that is, regions with similar functionality and synchronous activity, which tend to be dynamically correlated in their spontaneous BOLD activity. Current data support the hypothesis

that resting state networks have long-term stability, but in very flexible configurations (Gonzalez-Castillo et al., 2014). Among the networks exhibiting coherent fluctuations in spontaneous activity during rest, the "default-mode network" (DMN) is of particular interest. The DMN includes functionally and structurally connected regions that show high metabolic activity and blood flow at rest, but deactivate when specific goal-directed behavior or cognition is needed (Raichle et al., 2001). Despite recent, still controversial claims (Vatansever et al., 2015), a feature of the DMN is the inverse relationship of its neuronal activity with another intrinsic network, namely the "attentional network". The attentional network is activated during externally-directed cognition and is engaged during cognitive tasks that require focused attention; importantly, it is deactivated during internally-directed cognition, whereas the opposite is true of the DMN.

ENERGETIC REQUIREMENTS OF SPONTANEOUS ACTIVITY

The brain's energy consumption follows the traditional thermodynamic formula:

$$E = G + TS$$

where, E is the enthalpy, G is the free-energy, T is the temperature and S is the thermodynamic entropy. Note that the formula, contrary to our simplified account, does not talk about absolute values, but of their variation. In simpler words, enthalpy represents the "fuel" coming into the brain. Enthalpy grossly corresponds to the sum of the "useful" or "free-energy" (i.e., the energy that can be converted to do work) and energy dissipation (e.g., entropy).

The brain represents 2% of the human body mass yet it accounts for about 20% of total energy consumed (corresponding to the enthalpy E), a very substantial proportion by any measure (Raichle et al., 2001; Fox and Raichle, 2007). The metabolic activity of the brain, influenced by a balance between the energy costs incurred by its operation and the benefits realized by energy expenditure, is therefore high and remarkably constant over time (Sengupta et al., 2013). Why does the brain consume such remarkable amounts of enthalpy, despite the fact that evolution is geared toward minimizing very high metabolic costs? Almost 20–60% of the enthalpy allocated for the brain is used to support the specific metabolic rate of the cortical gray matter, primarily the restoration of transmembrane potentials, and for neuronal signaling purposes—e.g., action potentials and synapses (Sengupta et al., 2013). Although the brain as a whole consumes large amounts of enthalpy, there are important differences between the total energy required for spontaneous vs. evoked neural activity. Evoked activity (i.e., perceptual and motor activity, task performance and similar cognitive functions), requires an additional energy consumption of ∼5%, as compared with spontaneous activity. This is due to local increases in spike frequency (in particular beta and gamma waves) during evoked activity, which causes a transitory increase of energy consumption and free-energy production. A key point here is that increased spike frequency during evoked activity has a significant metabolic cost, specifically 6.5 μmol/ATP/gr/min for each additional spike, with an ATP consumption higher than the "typical" mean rate at 4 Hz (which is 3.29×10^9 molecules of ATP/neuron/s; Attwell and Laughlin, 2001). These observations strongly suggest that, although spontaneous brain activity consumes a significant proportion of the brain's vast energy budget (the enthalpy used by various neuronal processes produces an average of about four spikes/s), that amount is appreciably less than the more energy-intensive evoked activity (Attwell and Laughlin, 2001; Sengupta et al., 2013), Thus, it is clear that spontaneous brain activity exhibits a lower energetic level as compared with evoked activity. In sum, the fact that spontaneous brain energy has a lower energy level than evoked activity is clear in terms of spikes. Indeed, we know that each spike has a certain consumption of ATP. Each spike is formed by an oscillation, equipped with both amplitude and frequency. For Ohm's law, energy consumption due to the AMPLITUDE of the oscillation is negligible as compared with energy consumption due to the FREQUENCY of the oscillation. This means that evoked activity, equipped with a mean frequency of spikes higher than spontaneous activity, expends more energy, both in terms of enthalpy and free-energy. In the following sections, this noteworthy statement allows us to analyze how the complexity of such an adaptive system is best understood as a "dynamic network" that aims to decrease its free-energy via entropy transfer.

UNDER SPONTANEOUS ACTIVITY, THE BRAIN EXHIBITS COMPLEX DYNAMICS

Recent models of nervous activity are starting to incorporate the complexity of adaptive evolving systems as dynamic relationship networks (Fraiman and Chialvo, 2012). Indeed, brain function can be analyzed not only through old-fashioned cause/effect, linear paradigms typical of deterministic systems, but in other, more promising ways. The concept of a nonlinear brain needs to be framed into the energy landscape theory, a concept built for assessment of potential surfaces in proteins (Bryngelson and Wolynes, 1987; Tozzi et al., 2016). In such a framework, the brain stands for a "phase space", an abstract space where particle trajectories travel. In line with recent "nonlinear" neuronal theories (Friston and Ao, 2012), each brain function can be mathematically treated as a particle that crosses abstract, functional landscapes made of energy valleys, peaks and basins. Whirlpools (called attractors) are located within these landscapes and correspond to low-energy basins, which transport the particles (Watanabe et al., 2014). The particle movements occur through transitory, erratic, stochastic processes (called "random walks"), giving rise to self-organized, self-assembled and self-sustained structures (Bak et al., 1987; Strogatz, 2001; Vuksanovic and Hövel, 2014). Such nonlinear techniques are able to predict the evolution of trajectories in time; for each of the cycles around the attractor, there is a characteristic nonlinear scaling

law (Newman, 2005) that governs the amplitude and period of the orbit and that can be quantified via differential equations. Among the several models described in the literature, the fixed-point attractor—a funnel-like location in phase space where trajectories converge as time progresses, following the shortest path—is suggested by recent articles (Sengupta et al., 2016; Tozzi et al., 2016). However, several alternative neuronal models to fixed-point attractors have been proposed: for example, it has been suggested that brain function exhibits a stable sequence, called transient heteroclinic channel (Afraimovich et al., 2013) and that, at least during spontaneous brain activity, the brain might display a functional torus (Tozzi and Peters, 2016). Further, concepts like communication-through-coherence (Fries, 2005; Deco and Jirsa, 2012) must also be taken into account.

Apart from nonlinearity, brain activity retains the characteristics of a complex system with non-equilibrium dynamics. This means that a large number of interacting and inter-dependent components exhibit emergent properties (i.e., properties that cannot be found at the micro-level state of organization, but are typical of the macro-level state). Changes propagate through interlinked levels, inducing connectivity and interaction at all scales of the brain system. Thus cognitive processes become observable products of the underlying dynamical system, with macroscopic features emerging from the sum of high fluctuating elements. Accordingly, behavior emerges as a macroscopic property from the renormalization of microscopic brain events (Papo, 2014).

It has also been proposed that the brain operates near criticality (Beggs and Timme, 2012) at the edge of chaos. That is, it works within a narrow window between randomness and regularity, forming a functional regime where information processing occurs as rapidly as possible (Tognoli and Kelso, 2014). It has been suggested that the brain exists near a second-order phase transition (Afraimovich et al., 2013), a state characterized by peculiar dynamical features—such as the universal power laws described in the next paragraphs. Claims of brain criticality are still quite controversial (Beggs and Timme, 2012). For example, Priesemann et al. (2014) suggest that neural activity does not reflect a self-organized critical state, but a slightly sub-critical regime. Other researchers suggest that brain function does not exhibit erratic brain dynamics nor attractors, but rather exhibits a stable sequence (Afraimovich et al., 2013).

Another possibility is that the brain could be in phase transition during spontaneous activity, but be out-of-phase during evoked activity (i.e., while processing stimuli coming from the external world). Indeed, under spontaneous conditions, the CNS displays the slow dynamics associated with low free energy (Papo, 2014). This suggests that spontaneous brain activity might lie at the bottom of the energy landscapes' deep basins, in steep valleys where the free energy is (relatively) lower, as compared with the peaks. In such valleys, various dynamical phenomena might counteract the dissipation of brain energy. In particular, attractors could contribute to slowing the loss of energy and decreasing the entropy production typical of random systems (Gaspard, 2005). During spontaneous fluctuations, energy expenditure is thus balanced by homeostatic mechanisms—such as attractors and power laws (Vuksanovic and Hövel, 2014), in an effort to minimize free-energy. It has been proposed that, in the presence of attractors, resting-state networks emerge as "structured noise fluctuations" around a stable, low-firing equilibrium state (Deco and Jirsa, 2012). In contrast to spontaneous brain activity during rest, engaging in effortful cognitive tasks seems to modify brain function in a different manner. Neural systems can evolve from a subcritical regime of randomness to a critical state and then, beyond the critical value, to a supercritical regime, characterized by regularity and absence of complexity (Zare and Grigolini, 2013; Papo, 2014). This raises the possibility that evoked activity could lead to an exit from the phase transition that is typical of spontaneous activity. In sum, the spontaneous activity of the brain is an example of an "open system", partly stochastic due to intrinsic fluctuations, that maintains an interplay between structural bottlenecks and non-equilibrium steady-state dynamics (i.e., homoeostasis or allostasis), in the face of environmental fluctuations (Friston, 2010).

MENTAL FUNCTIONS AND SPONTANEOUS ACTIVITY

There is ongoing discussion as to whether spontaneous fluctuations reflect changes of the underlying brain physiology independent of neuronal function, or instead reflect the neuronal baseline activity of the brain, when goal-directed neuronal action and external input are absent (Damoiseaux et al., 2006). Despite some claims to the contrary (Fox et al., 2015; Vatansever et al., 2015), it is widely believed that intrinsic activity is associated with unconstrained, conscious cognition (i.e., mind-wandering or day dreaming propensities; Kucyi and Davis, 2014) and with higher cognitive functions, such as internally-oriented cognition, autobiographical memory (Conway and Pleydell-Pearce, 2000; Morewedge et al., 2014), self-referential processing, affective decision making and autobiographical memory (Philippi et al., 2015). Others hypothesize that spontaneous functional connectivity patterns at rest might well constitute a "signature of consciousness", reflecting a continuous stream of ongoing cognitive processes as well as random fluctuations shaped by a fixed anatomical connectivity matrix (Barttfeld et al., 2015). It has also been recently proposed that the DMN *is* the dreaming state (Domhoff and Fox, 2015).

Different DMN subsystems play an important role in aspects of internally-directed, spontaneous self-generated thought (characterized by their independence from external stimuli), such as accessing conceptual knowledge or autobiographical memories, conceptual processing, experiences focused on the future, construction of coherent mental scenes, retrieval of information related to self and other, to be reflected upon in a meta-cognitive manner (for a description of the terminology, see Andrews-Hanna et al., 2014) and open-monitoring meditation (Marzetti et al., 2014). Recent evidence suggests considerable overlap between the DMN and regions involved in self- and other-related mental processes—such

as social, affective and introspective processes—(Amft et al., 2015). In line with the celebrated experiments of Libet et al. (1983), our ability to make choices might arise from random fluctuations in the brain's background electrical noise; this suggests that individuals might well behave independently of cause and effect (Bengson et al., 2014).

If the above described brain functions are truly correlated with spontaneous activity, it means that they display lesser energetic requirements that other activities, such as sensation or perception. This testable proposition is an example of how our hypothesis about the lower energetic expenditure of spontaneous activity might be empirically proved. Some evidence already exists: e.g., it has been demonstrated that, during mind wandering, sensations and perceptions entrain the brain in a state of lower energy expenditure (Fox et al., 2015). In terms of the dynamical systems theory framework, this might correspond to the basins of the spontaneous networks, which form a temporary random walk for spontaneous thoughts.

In the general context of the brain as a whole, spontaneous activity provides a bridge that links different actors that come into play, for example among anatomic structures, energetic requirements and functional connectivity. Indeed, the low-energy activity constitutes such a conceptual bridge, because it exhibits both anatomical/functional (spontaneous brain activity and DMN) and psychological correlates (spontaneous, deliberate, self-generated thoughts; Andrews-Hanna et al., 2014).

FREE-ENERGY THEORY AND SPONTANEOUS BRAIN ACTIVITY

The brain activity observed at many spatiotemporal scales exhibits a $1/f^n$-like power spectrum (Newman, 2005), including not just macroscopic electric oscillations, EEG, MEG and fMRI signals (He, 2014), but also microscopic membrane potentials and fluctuations in neurotransmitter release (Linkenkaer-Hansen et al., 2001; Milstein et al., 2009). In particular, the frequency spectrum of cerebral electric activity displays a scale-invariant behavior $S(f) = 1/f^n$, where S(f) is the power spectrum, f is the frequency and n is an exponent that equals the negative slope of the line in a log power vs. log frequency plot (Pritchard, 1992; Van de Ville et al., 2010). Pink noise has been regarded as an intrinsic property of the brain characterizing a large class of neuronal processes (de Arcangelis and Herrmann, 2010); moreover, power law distributions contain information about how large-scale physiological and pathological outcomes (Jirsa et al., 2014) arise from the interactions of many small-scale processes. The emergence of power law distributions in the brain (i.e., the spontaneous neuronal "avalanches" occurring in the upper cortical layers) has been interpreted in terms of self-organized criticality (Beggs and Plenz, 2003); thus, spontaneous brain activity has been proposed as a source of ideal 1/f noise (Allegrini et al., 2009).

In addition, the connectome displays a free-scale structure, involving not just temporal power laws, but also geometric fractals (Reese et al., 2012): this interesting observation further supports the hypothesis that the brain is in phase transition. However, the presence of power-law scalings in the brain remains controversial (Beggs and Timme, 2012). It must be emphasized that the fractal slope is not invariant in brain, but is rather characterized by multiple possible exponents (He et al., 2010), summarized by a single value, the "generalized fractal dimension". Accordingly, we may view the multifractal cortex as an ensemble of intertwined (mono)fractals, each with its own dimension and scaling slope: the brain is thus regarded as a system of fractal geometry with a complex spectrum of self-exact similarity breakdown, in which scaling exponents mark dynamical transitions between different response regimes (Papo, 2014). With an increase in free-energy, the power law exponent varies across brain regions (Pritchard, 1992; He et al., 2010; Beggs and Timme, 2012; Tinker and Velazquez, 2014). The question that arises is: do cortical fluctuations in power law exponents modify the energy of the system? And the answer is yes. Recent articles have begun to uncover connections between such an exponent and activation free-energy, specifically in escape paths from energy basins (Perkins et al., 2014). Furthermore, it has been shown that fractals ensure an increase of production of entropy, when a system is close to equilibrium (Gilbert et al., 2000). The critical slowing implicit in power law scaling is mandated by any system that tries to minimize its energetic expenditure. For example, it has been demonstrated that brain regions with a larger fractal exponent are more expensive in their glucose metabolism (He, 2011).

Overall then, ongoing fluctuations with complex scale-free properties, such as spontaneous brain oscillations, can be absorbed into a free-energy principle (Friston, 2010), a theoretical framework that is of central importance in this context. In such a framework, a general theory of spontaneous brain function arises in a biologically informed fashion and has the potential to be operationalized and empirically assessed (Barrett and Simmons, 2015; Papadopoulou et al., 2015). The free-energy principle for adaptive systems (that is, biological agents, like the brain) attempts to provide a unified account of action, perception and learning. Any self-organizing system at equilibrium with its environment must minimize its free-energy, thus resisting a natural tendency to disorder/entropy. This formulation reduces the physiology of biological systems to their homeostasis, specifically, the maintenance of their states and form in the face of a constantly changing environment.

The brain operates at the edge of a delicate equilibrium and therefore appears to avoid minimizing its thermodynamic entropy production. It corresponds to the principle of minimizing the so-called "variational free-energy" at each point in time. The concept of variational free-energy is slightly different from the above mentioned "classical" thermodynamical free-energy, because the former refers to Helmholtz free-energy, which is a functional of some outcomes and a probability density over their (hidden) causes. Such a tenet supports the attempt to understand how subtle steady-state equilibrium is maintained through apparent resistance to the natural tendency to increase entropy, in order that the living beings restrict themselves to a limited number of states. The variational free-energy

construct is an information theoretic quantity, as opposed to a thermodynamic quantity, thus it has been exploited in machine learning and statistics to solve many inference and learning problems. (Friston, 2010). In this context, the "time average" of variational free-energy becomes a proxy for entropy.

From the point of view of the brain, the environment includes both the external and the internal milieu. The probability of sensory states (interoceptive and exteroceptive) must have low entropy and because entropy is also the average of self-information or "surprise", the brain implicitly avoids surprises (Friston, 2010). The free-energy principle separates the environment (the external states) from the agent (the internal states). Agents suppress free energy (or surprise) via changing sensory input by acting on external states, or by modifying their internal states through perception. This embodied exchange with the environment endeavors to maintain, as far as possible, an unsteady state that is the essence of survival and self-organization. In the framework of a logical-mathematical formalism, the variational free energy considered above pertains to probability and information theory—but what role does thermodynamic free-energy play? Crucially, minimizing variational free-energy necessarily entails a metabolically efficient encoding that is consistent with the principles of minimum redundancy and maximum information transfer (Picard and Friston, 2014). Maximizing mutual information and minimizing metabolic costs are two sides of the same coin; by decomposing variational free energy into accuracy and complexity, one can derive the principle of maximum mutual information as a special case of maximizing accuracy, while minimizing complexity translates into minimizing metabolic costs (Friston et al., 2015). Thus, the basic form of Friston's free-energy principle supports the idea that the energetic levels of spontaneous brain activity, which are lower when compared with evoked activity, allow the CNS to obtain two apparent contradictory achievements: to minimize as much as possible the metabolic costs, and to the largest extent possible, maximize mutual information.

In conclusion, every psychical state in living beings is a result of the self-preservative processes of the organism, a biological fact of the drive to maintain, as far as possible, a state close to a (more or less stable) equilibrium. This optimal point, around which the life of the organism moves in constant oscillation, also has a logical-mathematical significance when framed within an energetic theory of spontaneous brain activity. Thus, consideration of the energetic differences between spontaneous and evoked brain activity and the effect on dynamic cortical networks, when viewed using a non-linear dynamical framework, constitutes a new approach to better understanding spontaneous brain dynamics as a conceptual bridge between anatomical/functional and psychological correlates.

AUTHOR CONTRIBUTIONS

All authors had full access to all the data in the study and take responsibility for the integrity of the data and the accuracy of the data analysis. AT, MZ, AAB: Study concept and design. AT, MZ: Acquisition of data. AT, MZ, AAB: Analysis and interpretation of data. AT, MZ, AAB: Drafting of the manuscript. AAB: Critical revision of the manuscript for important intellectual content. AT, MZ, AAB: Statistical analysis. AAB: Obtained funding. AT, MZ, AAB: Administrative, technical, and material support. AT, MZ, AAB: Study supervision.

ACKNOWLEDGMENTS

The authors would like to thank Karl Friston for commenting upon an earlier version of this manuscript.

REFERENCES

Afraimovich, V., Tristan, I., Varona, P., and Rabinovich, M. (2013). Transient dynamics in complex systems: heteroclinic sequences with multidimensional unstable manifolds. *Int. J. Disc. Nonli. Complex.* 2, 21–41. doi: 10.5890/dnc.2012.11.001

Allegrini, P., Menicucci, D., Bedini, R., Fronzoni, L., Gemignani, A., Grigolini, P., et al. (2009). Spontaneous brain activity as a source of ideal 1/f noise. *Phys. Rev. E Stat. Nonlin. Soft. Matter Phys.* 80:061914. doi: 10.1103/physreve.80.061914

Amft, M., Bzdok, D., Laird, A. R., Fox, P. T., Schilbach, L., and Eickhoff, S. B. (2015). Definition and characterization of an extended social-affective default network. *Brain Struct. Funct.* 220, 1031–1049. doi: 10.1007/s00429-013-0698-0

Andrews-Hanna, J. R., Smallwood, J., and Spreng, R. N. (2014). The default network and self-generated thought: component processes, dynamic control and clinical relevance. *Ann. N Y Acad. Sci.* 1316, 29–52. doi: 10.1111/nyas.12360

Attwell, D., and Laughlin, S. B. (2001). An energy budget for signalling in the grey matter of the brain. *J. Cereb. Blood Flow Metab.* 21, 1133–1145. doi: 10.1097/00004647-200110000-00001

Bak, P., Tang, C., and Wiesenfeld, K. (1987). Self-organized criticality: an explanation of the 1/f noise. *Phys. Rev. Lett.* 59, 381–384. doi: 10.1103/physrevlett.59.381

Barrett, L. F., and Simmons, W. K. (2015). Interoceptive predictions in the brain. *Nat. Rev. Neurosci.* 16, 419–429. doi: 10.1038/nrn3950

Barttfeld, P., Uhrig, L., Sitt, J. D., Sigman, M., Jarraya, B., and Dehaene, S. (2015). Signature of consciousness in the dynamics of resting-state brain activity. *Proc. Natl. Acad. Sci. U S A* 112, 887–892. doi: 10.1073/pnas.1418031112

Bastos, A. M., Briggs, F., Alitto, H. J., Mangun, G. R., and Usrey, W. M. (2014). Simultaneous recordings from the primary visual cortex and lateral geniculate nucleus reveal rhythmic interactions and a cortical source for γ-band oscillations. *J. Neurosci.* 34, 7639–7644. doi: 10.1523/JNEUROSCI.4216-13.2014

Beggs, J. M., and Plenz, D. (2003). Neuronal avalanches in neocortical circuits. *J. Neurosci.* 23, 11167–11177,

Beggs, J. M., and Timme, N. (2012). Being critical of criticality in the brain. *Front. Physiol.* 3:163. doi: 10.3389/fphys.2012.00163

Bengson, J. J., Kelley, T. A., Zhang, X., Wang, J. L., and Mangun, G. R. (2014). Spontaneous neural fluctuations predict decisions to attend. *J. Cogn. Neurosci.* 26, 2578–2584. doi: 10.1162/jocn_a_00650

Bryngelson, J. D., and Wolynes, P. G. (1987). Spin glasses and the statistical mechanics of protein folding. *Proc. Natl. Acad. Sci. U S A* 84, 7524–7528. doi: 10.1073/pnas.84.21.7524

Buckner, R. L., Andrews-Hanna, J. R., and Schacter, D. L. (2008). The brain's default network. *Ann. N Y Acad. Sci.* 1124, 1–38. doi: 10.1196/annals.1440.011

Buszáki, G. (2006). *Rhythms of the Brain.* New York, NY: Oxford University Press.

Cole, M. W., Bassett, D. S., Power, J. D., Braver, T. S., and Petersen, S. E. (2014). Intrinsic and task-evoked network architectures of the human brain. *Neuron* 83, 238–251. doi: 10.1016/j.neuron.2014.05.014

Conway, M. A., and Pleydell-Pearce, C. W. (2000). The construction of autobiographical memories in the self-memory system. *Psychol. Rev.* 107, 261–288. doi: 10.1037/0033-295x.107.2.261

Damoiseaux, J. S., Rombouts, S. A., Barkhof, F., Scheltens, P., Stam, C. J., Smith, S. M., et al. (2006). Consistent resting-state networks across healthy subjects. *Proc. Natl. Acad. Sci. U S A* 103, 13848–13853. doi: 10.1073/pnas.0601417103

de Arcangelis, L., and Herrmann, H. J. (2010). Learning as a phenomenon occurring in a critical state. *Proc. Natl. Acad. Sci. U S A* 107, 3977–3981. doi: 10.1073/pnas.0912289107

de Pasquale, F., and Marzetti, L. (2014). "Temporal and spectral signatures of the default mode network," in *Magnetoencephalography: From Signals to Dynamic Cortical Networks*, eds S. Supek and C. J. Aine (Heidelberg: Springer Verlang), 451–476.

Deco, G., and Jirsa, V. K. (2012). Ongoing cortical activity at rest: criticality, multistability and ghost attractors. *J. Neurosci.* 32, 3366–3375. doi: 10.1523/JNEUROSCI.2523-11.2012

Domhoff, G. W., and Fox, K. C. (2015). Dreaming and the default network: a review, synthesis and counterintuitive research proposal. *Conscious. Cogn.* 33C, 342–353. doi: 10.1016/j.concog.2015.01.019

Fox, M. D., and Raichle, M. E. (2007). Spontaneous fluctuations in brain activity observed with functional magnetic resonance imaging. *Nat. Rev. Neurosci.* 8, 700–711. doi: 10.1038/nrn2201

Fox, K. C. R., Spreng, R. N., Ellamil, M., Andrews-Hanna, J. R., and Christoff, K. (2015). The wandering brain: meta-analysis of functional neuroimaging studies of mind-wandering and related spontaneous thought processes. *Neuroimage* 111, 611–621. doi: 10.1016/j.neuroimage.2015.02.039

Fraiman, D., and Chialvo, D. R. (2012). What kind of noise is brain noise: anomalous scaling behavior of the resting brain activity fluctuations? *Front. Physiol.* 3:307. doi: 10.3389/fphys.2012.00307

Fries, P. (2005). A mechanism for cognitive dynamics: neuronal communication through neuronal coherence. *Trends Cogn. Sci.* 9, 474–480. doi: 10.1016/j.tics.2005.08.011

Friston, K. (2010). The free-energy principle: a unified brain theory? *Nat. Rev. Neurosci.* 11, 127–138. doi: 10.1038/nrn2787

Friston, K., and Ao, P. (2012). Free energy, value and attractors. *Comput. Math. Methods Med.* 2012:937860. doi: 10.1155/2012/937860

Friston, K., Rigoli, F., Ognibene, D., Mathys, C., Fitzgerald, T., and Pezzulo, G. (2015). Active inference and epistemic value. *Cogn. Neurosci.* 6, 187–214. doi: 10.1080/17588928.2015.1020053

Gaspard, P. (2005). Brownian motion, dynamical randomness and irreversibility. *New J. Phys.* 7:77. doi: 10.1088/1367-2630/7/1/077

Gilbert, T., Dorfman, J. R., and Gaspard, P. (2000). Entropy production, fractals and relaxation to equilibrium. *Phys. Rev. Lett.* 85, 1606–1609. doi: 10.1103/physrevlett.85.1606

Gonzalez-Castillo, J., Handwerker, D. A., Robinson, M. E., Hoy, C. W., Buchanan, L. C., Saad, Z. S., et al. (2014). The spatial structure of resting state connectivity stability on the scale of minutes. *Front. Neurosci.* 8:138. doi: 10.3389/fnins.2014.00138

He, B. J. (2011). Scale-free properties of the functional magnetic resonance imaging signal during rest and task. *J. Neurosci.* 31, 13786–13795. doi: 10.1523/JNEUROSCI.2111-11.2011

He, B. J. (2014). Scale-free brain activity: past, present and future. *Trends Cogn. Sci.* 18, 480–487. doi: 10.1016/j.tics.2014.04.003

He, B. J., Zempel, J. M., Snyder, A. Z., and Raichle, M. E. (2010). The temporal structures and functional significance of scale-free brain activity. *Neuron* 66, 353–369. doi: 10.1016/j.neuron.2010.04.020

Jirsa, V. K., Stacey, W. C., Quilichini, P. P., Ivanov, A. I., and Bernard, C. (2014). On the nature of seizure dynamics. *Brain* 137, 2210–2230. doi: 10.1093/brain/awu133

Kavalali, E. T. (2015). The mechanisms and functions of spontaneous neurotransmitter release. *Nat. Rev. Neurosci.* 16, 5–16. doi: 10.1038/nrn3875

Kavalali, E. T., Chung, C., Khvotchev, M., Leitz, J., Nosyreva, E., Raingo, J., et al. (2011). Spontaneous neurotransmission: an independent pathway for neuronal signaling? *Physiology (Bethesda)* 26, 45–53. doi: 10.1152/physiol.00040.2010

Krueger, C., and Garvan, C. (2014). Emergence and retention of learning in early fetal development. *Infant Behav. Dev.* 37, 162–173. doi: 10.1016/j.infbeh.2013.12.007

Kucyi, A., and Davis, K. D. (2014). Dynamic functional connectivity of the default mode network tracks daydreaming? *Neuroimage* 100, 471–480. doi: 10.1016/j.neuroimage.2014.06.044

Libet, B., Gleason, C. A., Wright, E. W., and Pearl, D. K. (1983). Time of conscious intention to act in relation to onset of cerebral activity (readiness-potential). The unconscious initiation of a freely voluntary act. *Brain* 106, 623–642. doi: 10.1093/brain/106.3.623

Linkenkaer-Hansen, K., Nikouline, V. V., Palva, J. M., and Ilmoniemi, R. J. (2001). Long-range temporal correlations and scaling behavior in human brain oscillations. *J. Neurosci.* 21, 1370–1377.

Marzetti, L., Di Lanzo, C., Zappasodi, F., Chella, F., Raffone, A., and Pizzella, V. (2014). Magnetoencephalographic α band connectivity reveals differential default mode network interactions during focused attention and open monitoring meditation. *Front. Hum. Neurosci.* 8:832. doi: 10.3389/fnhum.2014.00832

Milstein, J., Mormann, F., Fried, I., and Koch, C. (2009). Neuronal shot noise and Brownian 1/f2 behavior in the local field potential. *PLoS One* 4:e4338. doi: 10.1371/journal.pone.0004338

Morewedge, C. K., Giblin, C. E., and Norton, M. I. (2014). The (perceived) meaning of spontaneous thoughts. *J. Exp. Psychol. Gen.* 143, 1742–1754. doi: 10.1037/a0036775

Newman, M. E. J. (2005). Power laws, Pareto distributions and Zipf's law. *Contemp. Phys.* 46, 323–351. doi: 10.1080/00107510500052444

O'Donnell, C., and van Rossum, M. C. (2014). Systematic analysis of the contributions of stochastic voltage gated channels to neuronal noise. *Front. Comput. Neurosci.* 8:105. doi: 10.3389/fncom.2014.00105

Papadopoulou, M., Leite, M., van Mierlo, P., Vonck, K., Lemieux, L., Friston, K., et al. (2015). Tracking slow modulations in synaptic gain using dynamic causal modelling: validation in epilepsy. *Neuroimage* 107, 117–126. doi: 10.1016/j.neuroimage.2014.12.007

Papo, D. (2014). Functional significance of complex fluctuations in brain activity: from resting state to cognitive neuroscience. *Front. Syst. Neurosci.* 8:112. doi: 10.3389/fnsys.2014.00112

Perkins, T. J., Foxall, E., Glass, L., and Edwards, R. (2014). A scaling law for random walks on networks. *Nat. Commun.* 5:5121. doi: 10.1038/ncomms6121

Philippi, C. L., Tranel, D., Duff, M., and Rudrauf, D. (2015). Damage to the default mode network disrupts autobiographical memory retrieval. *Soc. Cogn. Affect. Neurosci.* 10, 318–326. doi: 10.1093/scan/nsu070

Picard, F., and Friston, K. (2014). Predictions, perception and a sense of self. *Neurology* 83, 1112–1118. doi: 10.1212/wnl.0000000000000798

Priesemann, V., Wibral, M., Valderrama, M., Pröpper, R., Le Van Quyen, M., Geisel, T., et al. (2014). Spike avalanches *in vivo* suggest a driven, slightly subcritical brain state. *Front. Syst. Neurosci.* 8:108. doi: 10.3389/fnsys.2014.00108

Pritchard, W. S. (1992). The brain in fractal time: 1/f-like power spectrum scaling of the human electroencephalogram. *Int. J. Neurosci.* 66, 119–129. doi: 10.3109/00207459208999796

Raichle, M. E. (2010). Two views of brain function. *Trends Cogn. Sci.* 14, 180–190. doi: 10.1016/j.tics.2010.01.008

Raichle, M. E., MacLeod, A. M., Snyder, A. Z., Powers, W. J., Gusnard, D. A., and Shulman, G. L. (2001). Inaugural article: a default mode of brain function. *Proc. Natl. Acad. Sci. U S A* 98, 676–682. doi: 10.1073/pnas.98.2.676

Reese, T. M., Brzoska, A., Yott, D. T., and Kelleher, D. J. (2012). Analyzing self-similar and fractal properties of the *C. elegans* neural network. *PLoS One* 7:e40483. doi: 10.1371/journal.pone.0040483

Sengupta, B., Stemmler, M. B., and Friston, K. J. (2013). Information and efficiency in the nervous system—a synthesis. *PLoS Comput. Biol.* 9:e1003157. doi: 10.1371/journal.pcbi.1003157

Sengupta, B., Tozzi, A., Cooray, G. K., Douglas, P. K., and Friston, K. J. (2016). Towards a neuronal gauge theory. *PLoS Biol.* 14:e1002400. doi: 10.1371/journal.pbio.1002400

Strogatz, S. H. (2001). *Nonlinear Dynamics and Chaos: With Applications to Physics, Biology, Chemistry and Engineering (Studies in Nonlinearity).* Boulder, Colorado: Westview Press.

Tinker, J., and Velazquez, J. L. (2014). Power law scaling in synchronization of brain signals depends on cognitive load. *Front. Syst. Neurosci.* 8:73. doi: 10.3389/fnsys.2014.00073

Tognoli, E., and Kelso, J. A. (2014). Enlarging the scope: grasping brain complexity. *Front. Syst. Neurosci.* 8:122. doi: 10.3389/fnsys.2014.00122

Tong, Y., and Frederick, B. D. (2010). Time lag dependent multimodal processing of concurrent fMRI and near-infrared spectroscopy (NIRS) data suggests a global circulatory origin for low-frequency oscillation signals in human brain. *Neuroimage* 53, 553–564. doi: 10.1016/j.neuroimage.2010.06.049

Tozzi, A., Flå, T., and Peters, J. F. (2016). Building a minimum frustration framework for brain functions in long timescales. *J. Neurosci. Res.* doi: 10.1002/jnr.23748 [Epub ahead of print].

Tozzi, A., and Peters, J. F. (2016). Towards a fourth spatial dimension of brain activity. *Cogn. Neurodyn.* 10, 189–199. doi: 10.1007/s11571-016-9379-z

Van de Ville, D., Britz, J., and Michel, C. M. (2010). EEG microstate sequences in healthy humans at rest reveal scale-free dynamics. *Proc. Natl. Acad. Sci. U S A* 107, 18179–18184. doi: 10.1073/pnas.1007841107

Vatansever, D., Menon, D. K., Manktelow, A. E., Sahakian, B. J., and Stamatakis, E. A. (2015). Default mode network connectivity during task execution. *Neuroimage* 122, 96–104. doi: 10.1016/j.neuroimage.2015.07.053

Vuksanovic, V., and Hövel, P. (2014). Functional connectivity of distant cortical regions: role of remote synchronization and symmetry in interactions. *Neuroimage* 97, 1–8. doi: 10.1016/j.neuroimage.2014.04.039

Watanabe, T., Hirose, S., Wada, H., Imai, Y., Machida, T., Shirouzu, I., et al. (2014). Energy landscapes of resting-state brain networks. *Front. Neuroinform.* 8:12. doi: 10.3389/fninf.2014.00012

Yuste, R., MacLean, J. N., Smith, J., and Lansner, A. (2005). The cortex as a central pattern generator. *Nat. Rev. Neurosci.* 6, 477–483. doi: 10.1038/nrn1686

Zare, M., and Grigolini, P. (2013). Criticality and avalanches in neural network. *Chaos Solitons Fractals* 55, 80–94. doi: 10.1016/j.chaos.2013.05.009

Conflict of Interest Statement: The authors declare that the research was conducted in the absence of any commercial or financial relationships that could be construed as a potential conflict of interest.

Copyright © 2016 Tozzi, Zare and Benasich. This is an open-access article distributed under the terms of the Creative Commons Attribution License (CC BY). The use, distribution and reproduction in other forums is permitted, provided the original author(s) or licensor are credited and that the original publication in this journal is cited, in accordance with accepted academic practice. No use, distribution or reproduction is permitted which does not comply with these terms.

Author's personal copy

Cogn Neurodyn
DOI 10.1007/s11571-016-9379-z

REVIEW

Towards a fourth spatial dimension of brain activity

Arturo Tozzi[1] · **James F. Peters**[2]

Received: 26 October 2015 / Revised: 19 January 2016 / Accepted: 28 January 2016
© Springer Science+Business Media Dordrecht 2016

Abstract Current advances in neurosciences deal with the functional architecture of the central nervous system, paving the way for general theories that improve our understanding of brain activity. From topology, a strong concept comes into play in understanding brain functions, namely, the 4D space of a "hypersphere's torus", undetectable by observers living in a 3D world. The torus may be compared with a video game with biplanes in aerial combat: when a biplane flies off one edge of gaming display, it does not crash but rather it comes back from the opposite edge of the screen. Our thoughts exhibit similar behaviour, i.e. the unique ability to connect past, present and future events in a single, coherent picture as if we were allowed to watch the three screens of past-present-future "glued" together in a mental kaleidoscope. Here we hypothesize that brain functions are embedded in a imperceptible fourth spatial dimension and propose a method to empirically assess its presence. Neuroimaging fMRI series can be evaluated, looking for the topological hallmark of the presence of a fourth dimension. Indeed, there is a typical feature which reveal the existence of a functional hypersphere: the simultaneous activation of areas opposite each other on the 3D cortical surface. Our suggestion—substantiated by recent findings—that brain activity takes place on a closed, donut-like trajectory helps to solve long-standing mysteries concerning our psychological activities, such as mind-wandering, memory retrieval, consciousness and dreaming state.

Keywords Hypersphere · Brain · Central nervous system · Borsuk-Ulam theorem · Fourth dimension · Manifold

✉ Arturo Tozzi
tozziarturo@libero.it

James F. Peters
James.Peters3@umanitoba.ca

1 Center for Nonlinear Science, University of North Texas, 1155 Union Circle, #311427, Denton, TX 76203-5017, USA

2 Department of Electrical and Computer Engineering, University of Manitoba, 75A Chancellor's Circle, Winnipeg, MB R3T 5V6, Canada

How do thoughts flow in the brain? Current advances in neuroscience emphasize the role of energetic landscapes (Watanabe et al. 2014; Sengupta et al. 2013), a sort of functional linens equipped with peaks, valleys and basins made of free-energy, where thoughts move, following erratic and/or constrained trajectories (Afraimovich et al. 2013; Zare and Grigolini 2013; Fraiman and Chialvo 2012; Deco and Jirsa 2012). Such "dynamical systems" theories lack however an explanation of the possible physiological mechanisms underlying brain activity. General theories are thus needed to further improving our knowledge of central nervous system activity. This review, based on recent findings, introduces the concept of a spatial fourth dimension, where brain functions might take place, as a general device underlying our thoughts' dynamics. In particular, we hypothesize that brain activity is shaped in guise of a "3-sphere" which performs 4D movements on the cortical layers, giving rise to a functional "Clifford torus" where mental operations might take place. We will discuss how thoughts follow constrained, donut-like trajectories along preferential functional railways embedded in the very structure of the human brain connectome. This essay comprises five sections and an appendix organized as follows. The very first section will be devoted to give as simple as possible explanations of concepts from the far-

Published online: 03 February 2016

Author's personal copy

flung branch of topology. Because this method of investigation of the laws of biology diverges from what was previously familiar, we prefer to use a language addressed to a broad interdisciplinary audience which encompasses experts from different fields (neuroscientists, medical doctors, biologists, epistemologists). Sections two and three will aim to enclose the concept of the 3-sphere in the framework of brain activity, in order to demonstrate the feasibility of our theory and to sketch a four-dimensional brain model in a way that is empirically testable. Section four, taking into account suggestions from recent papers, will provide quantitative methods for an experimental assessment of our hypothesis, which could be of use to researchers that investigate network connectivity. The final section discusses how a brain hypersphere could lead to novel approaches to organized brain models, improving our understanding of cortical functions and paving the way to innovative research strategies. In order to show how our theory can be operationalized, we also provide an appendix as supporting information for technical readers. This latter material unpacks 3-spheres and fourth dimensions afforded by a mathematical point of view.

What is a hypersphere?

A *n*-sphere, also called S^n, is a n-dimensional structure embedded in a $n + 1$ space (Henderson 1996). For example, a 1-sphere (S^1) is the one-dimensional circumference surrounding a 2-dimensional disk, while a 2-sphere (S^2) is the 2-dimensional surface of a 3-dimensional space (a beach ball's surface is a good illustration) (Henderson and Taimina 2001). In mathematical terms, a 3-sphere (S^3), also called *glome* (from the Latin "glomus", meaning ball of string), or generically *hypersphere*, is an artificial convex structure enclosed in a Euclidean 4-dimensional space called a *4-ball* (Marsaglia 1972). The prefix "hyper" refers to 3- (and higher-) dimensional analogues of n-spheres. A 3-sphere is thus the surface of a 4-dimensional ball, while a 4-dimensional ball is the interior (the content) of a 3-sphere, in the same way as a bottle of water is made of a glass surface and a liquid content. How to build a glome? In topology, a glome can be attained by superimposing two 2-spheres (two beach balls) whose opposite edges are abstractly glued together: we obtain a structure called the *Clifford torus* (Manetti 2015). A Clifford torus reminds a lifebelt, with its donut-like shape (Fig. 1a), nevertheless with an important difference: the Clifford torus displays the same local geometry as an "ordinary" three-dimensional space, but its global topology is different (Willard 1970; Krantz 2009). Our torus is constantly in movement, because it is equipped with intricate rotations called *quaternionic movements* (Ozdemir and Özekes 2013; Lemaître 1948). Imagine a skein made of rope circles, where each rope takes a different rotation: the general shape of the skein is always the same, but an ever changing motion occurs inside it. The internal shape of the glome is in ceaseless activity, depending on the number of ropes

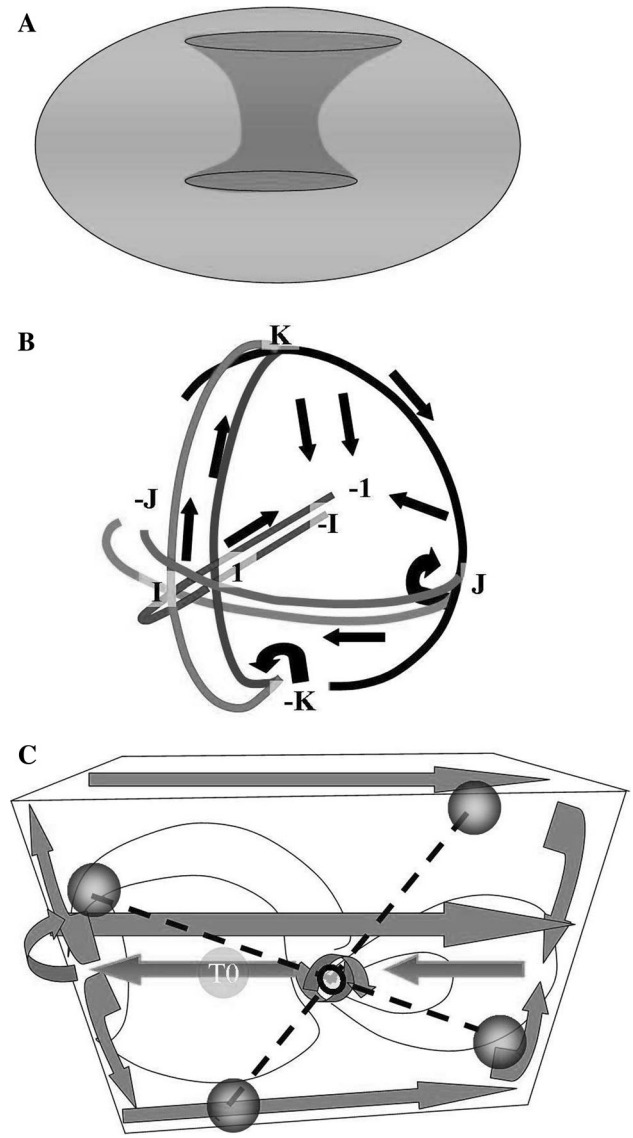

Fig. 1 Different ways to depict a hypersphere. **a** How two 2-spheres glued together along their spherical boundary give rise to a donut-shaped Clifford torus. **b** Another way to depict a hypersphere: the superimposition of two 2-spheres (which circumferences are glued together) gives rise to a glome. Some of the quaternion rotations are depicted by the straight and curved arrows. **c** 3D projection of a hypersphere. The *lines* on the left enlarge in diameter, forming a circle of increasing circumference on the left surface of the 3D space. Conversely, on the opposite right side, the *lines* shrink and give rise to a circle of decreasing circumference on the right surface of the 3D space. See text for further details. The *dotted lines* and the *black spheres* depict some of the possible antipodal points predicted by the Borsuk Ulam Theorem (to give another example, J and −J are antipodal points in **a**)

Author's personal copy

taken into account and their trajectories. Complicated motions occur indeed on a hypersphere: four pairs of points opposite each other (called antipodal points $1, -1, k, -k, j, -j$ and $i, -i$) give rise to the "quaternion group" (Hart and Segerman 2014), which displays two possible types of reciprocal 4D rotations (Fig. 1b). For a mathematical treatment of hyperspheres, quaternions and the correlated Lie groups, see Appendix, Section 1. The glome, requiring four dimensions for its definition just as an ordinary sphere requires three, is not detectable in the usual spatial 3-dimensions and is thus very challenging to assess. Figures 1a–c show the possible ways to cope with a 3D visualization of a glome: observe how opposite sections of the rim fit together, rather than trying to visualize the whole thing at once the way you would visualize a common sphere. Each apparent line segment is really two, one arching upward into the third dimension and the other arching downward. To better understand the concept of a 3-sphere, the images should be watched during their complicated movements: a list of very useful videos is provided in Appendix, Section 1.

Why an hypersphere to explain brain activity?

Experimental and theoretical clues allow us to conjecture that the brain activities (at least some of them) are embedded in a torus lying on the surface of a hypersphere. The theoretical claims of brain multidimensionality are widespread (Tononi 2008; Papo 2014; Ponce-Alvarez et al. 2015; Schoenberg and Speckens 2015). Models characterized by dimensionality reduction have been used in the study of human central nervous system, particularly through full-brain auto-regressive modelling (Garg et al. 2011). It has been demonstrated that high dimensionality spontaneous activity structures—termed "lag threads"—can be found in the brain, consisting of multiple, reproducible temporal sequences (Mitra et al. 2015). Moreover, it has been shown that the exceedingly diverse nonlinear selectivity in single-neuron activity in the prefrontal cortex, which encodes distributed information about all task-relevant aspects, is a signature of high-dimensional neural representations: crucially, this dimensionality is predictive of animal behaviour as it collapses in error trials (Rigotti et al. 2013). In addition, recent findings suggest that nervous structures process information through topological as well as spatial mechanisms. For example, it is has been hypothesized that hippocampal place cells create topological templates to represent spatial information (Dabaghian et al. 2014). We stated that a glome displays a donut-like shape: it means that the trajectory followed by a particle inside the torus is closed. To make an example, if you walk along one of the curves of a 4-ball, you think are crossing a straight trajectory, and do not recognize that your environment is embedded in an higher dimension. The torus may be compared with a video game with biplanes in aerial combat: when a biplane flies off one edge of gaming display, it does not crash but rather it comes back from the opposite edge of the screen. Mathematically speaking, the display edges have been "glued" together. Our brain exhibits similar behaviour, i.e., the unique ability to connect past, present and future events in a single, coherent picture (Fingelkurts and Fingelkurts 2014; Nyberg et al. 2010), as if we were allowed to watch the three screens of past-present-future glued together in a mental kaleidoscope. The same occurs during other brain functions, *e.g.*, memory retrieval, recursive imagination and mind wandering (Andrews-Hanna et al. 2014), in which concepts flow from a state to another and appear to be "glued" together. As stated above, the torus is naturally visualized intrinsically, by ignoring any extrinsic properties a surface may have: it is thought that all the movements onto a torus surface are performed just by trajectories *internal* to its structure. For example, take a sheet of paper and bend it into a half-cylinder: the extrinsic geometry of the paper has obviously changed, but the paper itself has not been deformed and its intrinsic geometry has not varied. What would you see if you lived in a closed 4-dimensional manifold? You should be able to see yourself, via the intrinsic structure provided by the glued surfaces of a hypersphere, in an otherwise unperceivable 4D space (Weeks 2002). In the same way, we humans perceive our thoughts intrinsically and naturally adopt "private", subjective standpoints.

How to demonstrate the presence of a brain hypersphere?

Brains equipped with a hypersphere is a counter-intuitive hypothesis, since we live in a 3D world with no immediate perception that 4D space exists at all. We need thus to evaluate indirect clues of the undetectable fourth dimension, such as signs of the glome rotations on a familiar 3D surface. In other words, rotations of a 4D torus embedded in a 4-ball can be identified through their "cross section" movements on a more accessible 3D surface (Fig. 1c), as if you recognized an object just from its shadow projected on a screen. In Fig. 1c, the arrows illustrate the trajectories followed by the 4D quaternionic movements of a Clifford torus, when projected onto the surface of the 3D space in which it has been artificially embedded. Note that the arrows (representing the quaternions' flows) follow the external and medial surfaces of the 3D space in a way that is predictable. It must be emphasized that just one of the possible directions of the quaternion movements is

Author's personal copy

displayed in Fig. 1c: the flow on a Clifford torus may indeed occur in each of the four planes. The small circle labelled T0 depicts one of the possible conventional starting points of the flow. In Fig. 1c we showed just the trajectory from right to left, starting from T0; however, also the opposite trajectory, from left to right, and countless others, can be exploited by the torus during its 4D movements.

The presence of a glome can be detected invoking the Borsuk-Ulam Theorem (BUT) from topology, which is characterized by very helpful features (Borsuk 1933; Matoušek 2003). BUT states that we can identify on a n-sphere two "antipodal points" (i.e., points directly opposite each other) (Fig. 2). To make an example, there always exist a pair of opposite points on the earth's equator (a 1-sphere) with the same temperature. It is worth of mention that the two antipodal points display similar characteristics and have matching descriptions (Cohen 1973; Giblin 2010). Such two opposite points can be used not just for the description of simple topological structures, but can also be generalized to the description of two antipodal shapes or signals. Thus, if you take into account physical and biological phenomena instead of "points", BUT leads naturally to the possibility of a region-based, not simply point-based, geometry, in which we view collections of signals as surface shapes, where one shape maps to another antipodal one (Peters 2014; Collins 2004; Borsuk 1958–1959; Borsuk 1969; Borsuk and Gmurczyk 1980). A point on S^2 (which is embedded in R^3) projects to two antipodal points on R^4. It means that the projection from a lower dimension R^n (equipped with just one point) to an higher one R^{n+1} gives rise to two opposite, symmetrical points. It also means that different phenomena (including brain activity) could be studied in terms of antipodal points, if we embed them in just one dimension higher than the usual one.

If we embed the brain in the 4D space of a Clifford torus, the presence of antipodal (opposite) points or shapes on 3D cortical surfaces could be evaluated (Fig. 3). We need to stress again that the hypersphere's location displayed in Fig. 3 is just one of the countless possible: being the glome a *functional* structure equipped with many rotations and trajectories, it can be placed in different points of the brain surface. The antipodal points in the fourth dimension evoked by BUT can be viewed as brain signals opposite each other on the three-dimensional brain. For example, when a surface "fires", the simultaneous firing of the opposite one is a proof of a perceivable "passing through" of the fourth dimension onto the brain 3D surface. The mechanism, elucidated in Fig. 3, is the following: the activation of a single point on the 3D brain S^2 surface (Fig. 3a) leads to the activation of two antipodal points on the 4D brain S^3 surface (Fig. 3b). In turn, the activation of two antipodal points on S^3 leaves on the 3D brain S^2 surface "hallmarks" (Fig. 3c) which can be detected by currently available neuroimaging techniques. For a mathematical treatment of the Borsuk-Ulam theorem, shapes, homotopies and their applications, see the Appendix, Section 2. In conclusion, the mathematical model of antipodal points can be casted in a biologically informed fashion, resulting in a framework that has the potential to be operationalized and assessed empirically.

Are there proofs or clues of brain hypersphere?

Our brain hypersphere hypothesis could be corroborated either by prospective investigations, or by retrospective evaluation of published resting-state fMRI data, looking for the hallmarks of the hypothesized BUT. Why resting- state studies are more feasible for an evaluation of the possible

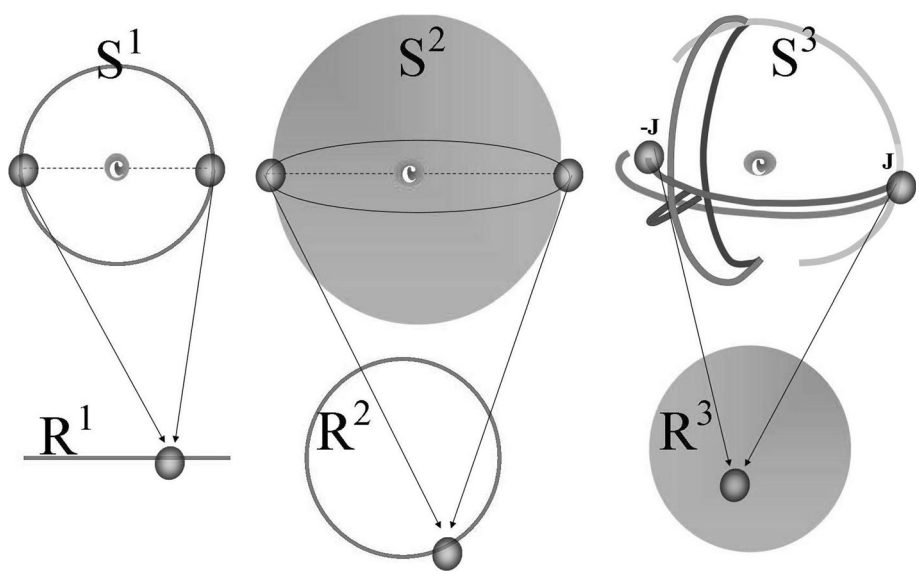

Fig. 2 The Borsuk-Ulam theorem for different values of S^n. S^1 depicts a circumference, S^2 a common sphere, S^3 a hypersphere, while R^1 portrays a line, R^2 a circumference and R^3 a common sphere. Note that the two antipodal points in every sphere S^n project to a single point in the corresponding space R^n, and vice versa

Author's personal copy

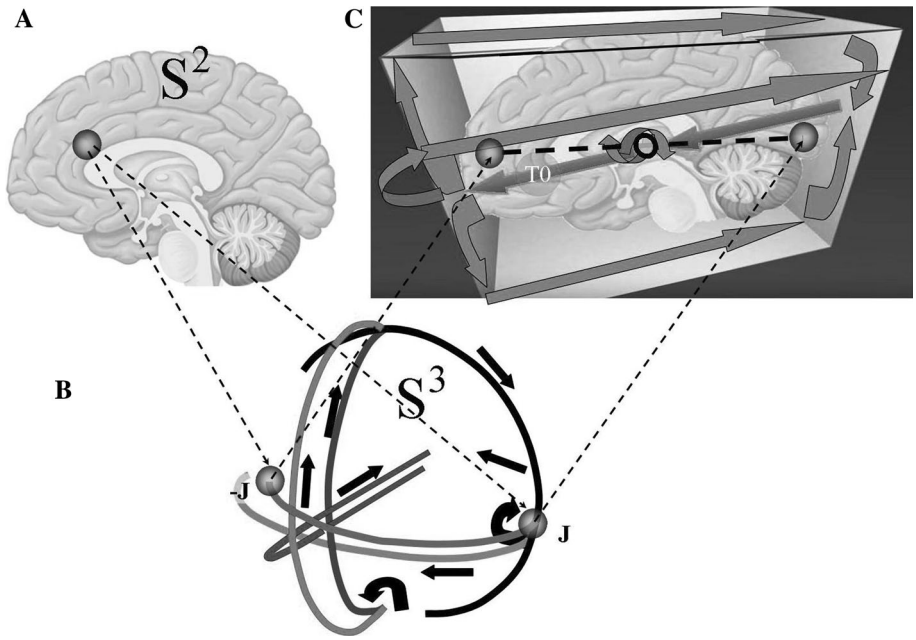

Fig. 3 The concept of hypersphere in the framework of brain functional activity. According to the Borsuk-Ulam theorem, the activation of a single point on the S^2 brain surface (Fig. 1a) leads to the activation of two antipodal points (corresponding in this case to the quaternionic points J and −J) on the S^3 brain surface (**b**). The simultaneous activation of the S^3 antipodal points displayed in **b** can be also evaluated on the 3D cortical surface (**c**), provided the brain is embedded in a 3D space containing the 4D Clifford torus (the same 3D space described in Fig. 1c). The nomenclature is borrowed from **c**

presence of a glome in brain activity? Spontaneous oscillations are intrinsic, low-frequency fluctuations of cerebral activity which cannot be attributed to the experimental design or other explicit input or output (Fox and Raichle 2007). Among the networks exhibiting coherent fluctuations in spontaneous activity, the "default-mode network" (DMN) is worth of mentioning, because it includes functionally and structurally connected regions that show high metabolic activity at rest, but deactivate when specific goal-directed behavior is needed (Raichle et al. 2001). Spontaneous oscillations recapitulate the topographies of fMRI responses to a wide variety of sensory, motor and cognitive task paradigms, providing a powerful means of delineating brain functional organization without the need for subjects to perform tasks (Mitra et al. 2014). To evaluate our BUT hypothesis, we favour studies focused on intrinsic, instead of task-evoked activity, because the former is associated with mental operations that could be attributed to the activity of a glome—mental "screens" are glued together and the trajectories of particles (or thoughts!) follow the internal surface of a Clifford torus. For example, spontaneous brain activity has been associated with mind-wandering or day dreaming propensities (Kucyi et al. 2014), construction of coherent mental scenes, autobiographical memories (Conway and Pleydell-Pearce 2000), experiences focused on the future and dreaming state (Domhoff and Fox 2015). Recent evidence also suggests overlap between the DMN and regions involved in self- and other-related mental operations—such as affective and introspective processes (Amft et al. 2015; Philippi et al. 2015; Morewedge et al. 2014)—for a description of the terminology, see Andrews-Hanna et al. (2014). It has also been hypothesized that spontaneous functional connectivity patterns at rest might constitute a "signature of consciousness", reflecting a stream of ongoing cognitive processes (Barttfeld et al. 2015). Spontaneous activity is highly variable among individuals, depending on local brain differences, somatosensory awareness, age span, race, culture and so on (Gorgolewski and al 2014; Sadtler et al. 2014). We speculate that such variability might be correlated with those differences in Clifford torus' structure and movements illustrated above. A brain 3-sphere has the potential to represent a conceptual bridge, because it exhibits both anatomical/functional (spontaneous brain activity and DMN) and psychological correlates (spontaneous, deliberate, self-generated thoughts).

Several data (movies, figures and temporal series) extrapolated from different available experimental studies and/or meta-analyses describing brain spontaneous activity seem to corroborate our hypothesis. To make some examples:

(a) High dimensionality spontaneous activity structures—"lag threads" -, consisting of multiple highly reproducible temporal sequences, showed the frequent occurrence of the antipodal points' activation at different times (Mitra et al. 2015) (Fig. 4).
(b) Decomposition of spontaneous brain activity into distinct fMRI co-activation patterns displayed a simultaneous activation of perisylvian and/or the opposite medial occipito-parietal areas (Liu et al. 2013) (Fig. 5a).
(c) Karahanoglu and Van De Ville (2015) decomposed resting-state fMRI using iCAPs, i.e. innovation-

Author's personal copy

driven co-activation patterns. Their results show once again that opposite brain areas activate together: in particular, the pattern was cleary visible in bilateral posterior-frontal antipodal areas and in bilateral perisilvian antipodal areas (Fig. 5b).

(d) Meta-analytic clusters of fMRI temporal activation associated with mind-wandering and related spontaneous thought processes (Fox et al. 2015) clearly displayed the simultaneous activation of two antipodal zones (Fig. 5c).

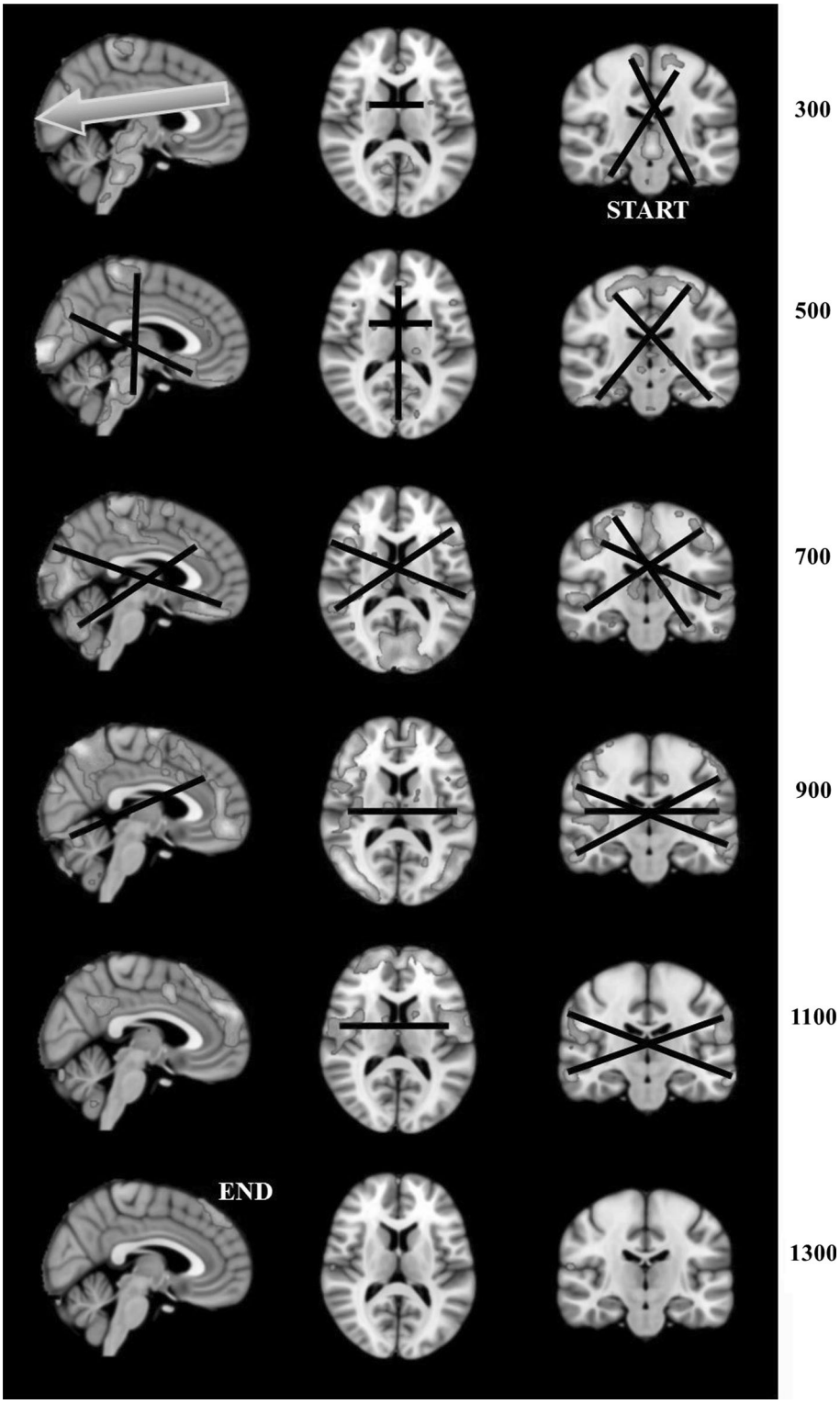

Fig. 4 Video frames, modified from Mitra et al. (2015), showing lag threads computed from real BOLD resting state rs-fMRI data in a group of 688 subjects, obtained from the Harvard-MGH Brain Genomics Superstruct Project (*see Mitra* et al. 2015 for further technical details). Note the widely diffused presence of BUT hallmarks (*black lines*) at different times and in different brain projections

Author's personal copy

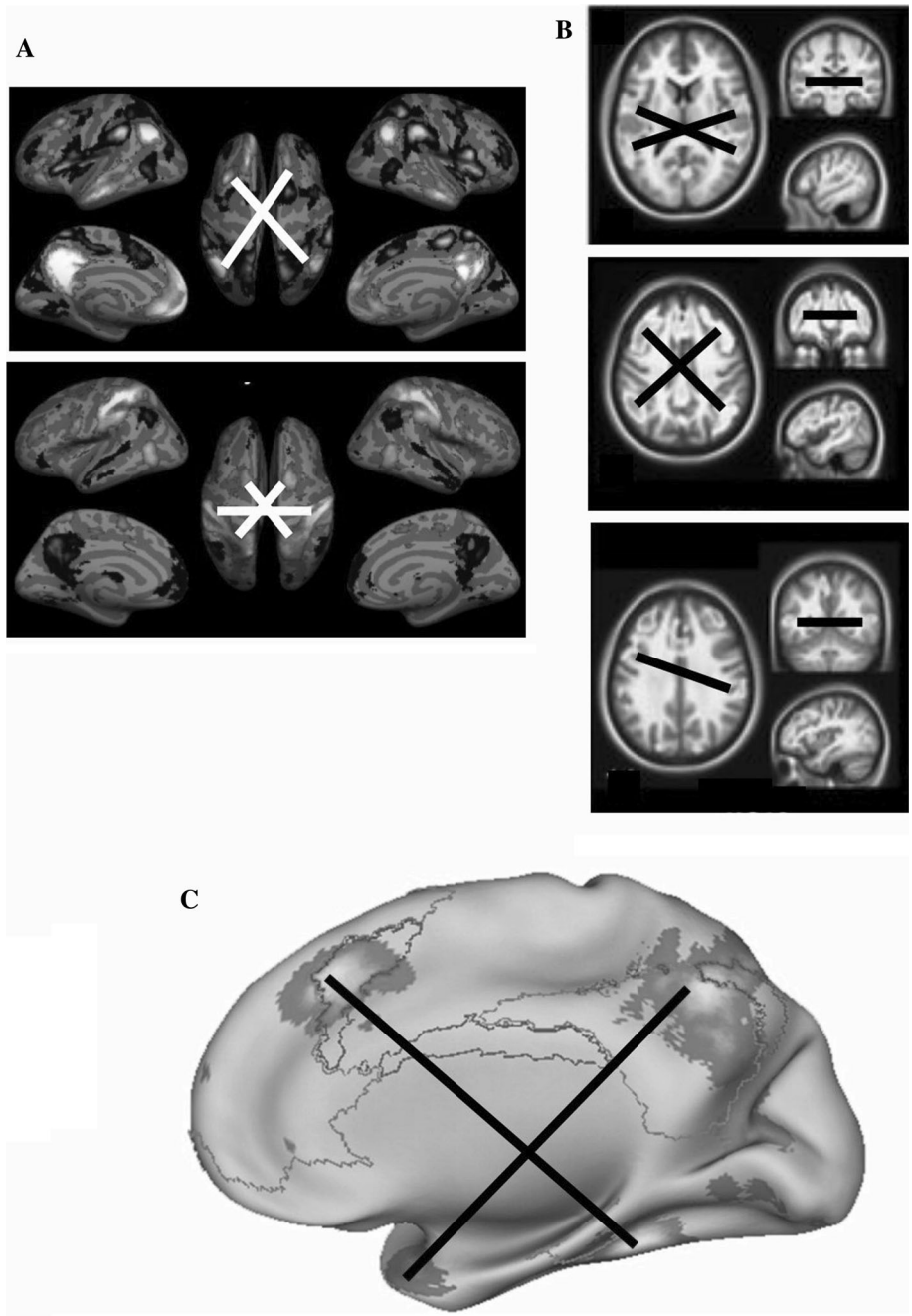

Fig. 5 Examples from functional neuroimaging real data showing how the predicted antipodal points can be correctly identified: given one point (a brain signal), there is a second point (another brain signal) at the opposite end of a straight line segment connecting them and passing for the center (*white* or *black lines*). **a** Decomposition of Spontaneous Brain Activity into Distinct fMRI Co-activation Patterns (Liu et al. 2013). **b** Different clusters during resting-state fMRI scanning, evaluated through innovation-driven co-activation patterns (called iCAPs) (Karahanoglu and Van De Ville 2015). **c** Significant meta-analytic clusters of fMRI temporal activation associated with mind-wandering and related spontaneous thought processes (Fox et al. 2015)

(e) Unnoticed features of antipodal points' activation can be found also in other data sets. For example, see Andrews-Hanna et al. (2014), Fox and Raichle (2007), Raichle (2009), Power et al. (2014), Mao et al. (2015), Harrison et al. (2015), Gusnard et al. (2001), Gravel et al. (2014), Barttfeld et al. (2015), Ajilore et al. (2013).

In sum, it is possible to find in literature several data confirming the occurrence of opposite brain zones' activation, which is the sign predicted by BUT. The fMRI sequences of brain region activations, apart from differences depending on slight methodological distinctions among the papers, exhibited a stereotyped topographical firing pattern, such that brain loci are activated together with their opposite zones. As a result, highly reproducible topography and propagation through subsets of regions that are shared across multiple trajectories can be found in different data sets: it corroborates the prediction of BUT linked with the presence of a brain hypersphere.

Author's personal copy

What now?

Our review uncovered evidence of hypersphere in experimental fMRI series obtained during spontaneous activity, raising the possibility that (at least some) brain functions lie on a glome enclosed in 4D space. Brain activity is thus temporally driven by a functional 3-sphere, intrinsic to the brain and (probably) embedded in the very anatomical structure of the connectome. Indeed, to evaluate glomes in terms of framework for brain functions, we first need to identify potential brain signal loci where quaternion rotations might take place. The natural candidate is the spatially embedded network of the human connectome (Sporns 2011; Jarman et al. 2014), a non-stationary, highly dynamical structure (de Pasquale et al. 2015; Fox et al. 2015) characterized by complex topological features and an ever-changing geometry (Roberts 2015). Me may thus state that a 4D cap surrounds the brain, equipped with trajectories which follow quaternion movements along the nodes of the connectome. The reproducibility of the BUT hallmarks in different Authors suggests that this organizational feature is essential to normal brain physiology and function.

Further studies are needed to evaluate what happens when other techniques are used, *e.g.*, EEG and diffusion tensor imaging. Does evoked, task-related activity exhibit the same features displayed by resting-state? Additional investigations will elucidate whether, following the stimulus onset (either external from the environment or internal from the body melieu and the brain), the multidimensional space outlined by cortical activity is invariant or reduced (Papo 2014). Human fMRI studies have recently revealed that a co-activation of sensory and fronto-parietal areas (in particular, simultaneous firing of activated antipodal points in somatosensory, lateral and medial frontal, posterior parietal and in the cingulate cortex) is crucial for conscious sensory perception in the several second time-scale of BOLD signal fluctuations (Hirvonen and Palva 2015).

If you are embedded in a 4D torus containing a doll, you see in front of you side-to-side reversal (and/or three-quarters turn) doll's images. To be into a glome looks like to stand in front of a weird mirror: if you raise your left hand, you see in infinitely many screens countless copies of yourself raising the left hand, while other copies raise the right one. Because such neighboring images of the same object are related by glide reflections translations (Weeks 2002), it remains to be seen what the implications of the glome would have for consciousness, perception of time and nature of reality. Going a step further, our "deterministic" account of linear transformations needs to be contextualized, taking into account the suggestions of the brain as an energy-sparing, complex, nonlinear system equipped with attractors and/or random walks (Beggs and Timme 2012; Friston 2010; Zhang et al. 2015). Also the role of electromagnetic currents needs to be re-evaluated, i.e., do spikes contain the message, or, as recently suggested (Tozzi 2015), they serve other kinds of functions? For example, it has been proposed that features of a brain signal with spectral peaks in preferred bands (gamma, beta and so on) provide a basis for feature vectors in a 4D Euclidean space (Padhy et al. 2011). Further, the hypersphere, due to different movements of the quaternionic system, relentlessly varies its intrinsic structure: in this context, it is reasonable to speculate that each mental state corresponds to a different glome's topological space. In conclusion, our original approach to brain activity, starting from such a completely new point of view, contains the promise of great fruitfulness in the mere fact that it directs us into new ways, opens out new perspectives and shows how it is possible to get quite a new light upon the old problems which are constantly being turned over and over in the same way. Indeed, a deeper knowledge of a fourth brain dimension via experimental confirm will lead to novel approaches to organized biological models, will improve our understanding of cortical functions and will also pave the way to innovative therapeutic strategies.

Appendix

Section 1

Movements of particles on 3-spheres

At first, we need to mathematically define a hypersphere. It is an n-sphere formed by points which are constant distance from the origin in $(n + 1)$-dimensions (Henderson and Taimina 2001; Giblin 2010). A 3-sphere of radius r (where r may be any positive real number) is defined as the set of points in 4D Euclidean space at distance r from some fixed center point **c** (which may be any point in the 4D space).

The notation S^n refers to an n-sphere, which is a generalization of the circle. A 1-sphere is a set points on the perimeter of a circle in a 2D space, while a 2-sphere is a sets of surface points in a 3D space and a 3-sphere is set of points on the surface of what is known as a "hypersphere". From a geometer's perspective, we have the following n-spheres, starting with the perimeter of a circle (S^1) and advancing to S^3, which is the smallest hypersphere, embedded in a 4-ball:

1-sphere $S^1 : x_1^2 + x_2^2$, *embedded in* R^2 (circle perimeter, the common circumference),
2-sphere $S^2 : x_1^2 + x_2^2 + x_3^2$, *embedded in* R^3 (surface of the common sphere, i.e. a beach ball),

Author's personal copy

3-sphere $S^3 : x_1^2 + x_2^2 + x_3^{2+} x_4^2$, *embedded in* R^4 (the smallest hypersphere surface),…,
n-sphere $S^n : x_1^2 + x_2^2 + x_3^{2+} \ldots + x_n^2$,*embedded in* R^n.

In technical terms, a map of a glome equipped with Sp(1) or SU(2) Lie groups can be projected onto a 3-D surface. The 3-sphere is parallelizable as a differentiable manifold, with a principal U(1) bundle over the 2-sphere. Apart S^3, the only other spheres that admit the structure of a Lie group are the 0-sphere $\mathbf{S}^0$ (real numbers with absolute value 1), the circle $\mathbf{S}^1$ (complex numbers with absolute value 1) and $\mathbf{S}^7$.

The 3-sphere's Lie group structure is Sp(1), which is a compact, simply connected symplectic group, equipped with quaternionic 1X1 unitary matrices. The glome $\mathbf{S}^3$ forms a Lie group by identification with the set of quaternions of unit norm, called versors (Ozdemir and Özekes 2013). The quaternionic manifold is a cube with each face glued to the opposite face with a one quarter clockwise turn. The name arises from the fact that its symmetries can be modeled in the quaternions, a number system similar to the complex numbers, but with three imaginary quantities, instead of just one (Lemaître 1948). For an affordable, less technical treatment of quaternions, see (Hart and Segerman 2014).

In addition: Sp(1) ≈ SO(4)/SO(3) ≈ Spin(3) ≈ SU (2).

Thus, Sp(1) is equivalent to—and can be identified with—the special unitary group SU(2).

List of useful videos

They are very helpful in order to understand the hypersphere's movements in four dimensions.

(a) The superimposition of two 2-spheres (with circumferences glued together) gives rise to a 3-sphere equipped with quaternionic movements: https://www.youtube.com/watch?v=XFW769hqa1U
(b) a stereographic projection of a Clifford torus, performing a simple rotation through the xz plane: https://en.wikipedia.org/wiki/Clifford_torus#/media/File:Clifford-torus.gif)
(c) 3-D Stereographic projection of the "toroidal parallels" of a 3-D sphere: https://www.youtube.com/watch?v=QlcSlTmc0Ts
(d) The shape of the 3-sphere is ever-changing, depending on the number of circles taken into account and their trajectories: http://nilesjohnson.net/hopf.html
(e) A video correlated with the above mentioned Hart and Segerman's paper (2014) illustrates the quaternions' movements of… a group of monkeys: http://blogs.scientificamerican.com/roots-of-unity/nothing-is-more-fun-than-a-hypercube-of-monkeys/

Section 2

The Borsuk-Ulam Theorem

Continuous mappings from object spaces to feature spaces lead to various *incarnations* of the Borsuk-Ulam Theorem, a remarkable finding about Euclidean n-spheres and antipodal points by K. Borsuk (Borsuk 1958–1959). Briefly, antipodal points are points opposite each other on a S^n sphere. There are natural ties between Borsuk's result for antipodes and mappings called homotopies. In fact, the early work on n-spheres and antipodal points eventually led Borsuk to the study of retraction mappings and homotopic mappings (Borsuk and Gmurczyk 1980).

The Borsuk-Ulam Theorem states that:

Every continuous map $f{:}S^n \to R^n$ must identify a pair of antipodal points.

Points on S^n are *antipodal*, provided they are diametrically opposite. Examples are opposite points along the circumference of a circle S^1, or poles of a sphere S^2. An *n*-dimensional Euclidean vector space is denoted by R^n. In terms of brain activity, a feature vector $x \in R^n$ models the description of a brain signal.

Borsuk-Ulam in brain signal analysis

In order to evaluate the possible applications of the Borsuk-Ulam Theorem in brain signal analysis, we view the surface of the brain as a n-sphere and the feature space for brain signals as finite Euclidean topological spaces. The Borsuk-Ulam Theorem tells us that for description $f(x)$ for a brain signal x, we can expect to find an antipodal feature vector $f(-x)$ that describes a brain signal on the opposite (antipodal) side of the brain. Moreover, the pair of antipodal brain signals have matching descriptions. Let$X$denote a nonempty set of points on the brain surface. A topological structure on$X$(called a brain topological space) is a structure given by a set of subsets τ of X, having the following properties:

(Str.1) Every union of sets in τ is a set in τ
(Str.2) Every finite intersection of sets in τ is a set in τ

The pair (X, τ) is called a topological space. Usually, X by itself is called a topological space, provided X has a topology τ on it. Let X, Y be topological spaces. Recall that a function or map f: $X \to Y$ on a set X to a set Y is a subset $X \times Y$ so that for each $x \in X$ there is a unique $y \in Y$ such that $(x, y) \in f$ (usually written $y = f(x)$). The mapping f is defined by a rule that tells us how to find $f(x)$. For a good introduction to mappings, see (Willard 1970).

A mapping f: $X \to Y$ is continuous, provided, when $A \subset Y$ is open, then the inverse $f^{-1}(A) \subset X$ is also open. For more about this, see Krantz (2009). In this view of

Author's personal copy

continuous mappings from the brain signal topological space X on the surface of the brain to the brain signal feature space R^n, we can consider not just one brain signal feature vector $x \in R^n$, but also mappings from X to a set of brain signal feature vectors $f(X)$. This expanded view of brain signals has interest, since every connected set of feature vectors $f(X)$ has a shape. The significance of this is that brain signal shapes can be compared.

A consideration of $f(X)$ (set of brain signal descriptions for a region X) instead of $f(x)$ (description of a single brain signal x) leads to a region-based view of brain signals. This region-based view of the brain arises naturally in terms of a comparison of shapes produced by different mappings from X (brain object space) to the brain feature space R^n. An interest in continuous mappings from object spaces to feature spaces leads into homotopy theory and the study of shapes.

Let f, g: $X \to Y$ be continuous mappings from X to Y. The continuous map H: $X \times [0, 1] \to Y$ is defined by

$$H(x, 0) = f(x), \quad H(x, 1) = g(x), \quad \text{for every } x \in X.$$

The mapping H is a *homotopy*, provided there is a continuous transformation (called a deformation) from f to g. The continuous maps f, g are called homotopic maps, provided $f(X)$ continuously deforms into $g(X)$ (denoted by$f(X) \to g(X)$). The sets of points $f(X)$, $g(X)$ are called shapes. For more about this, see Manetti (2015) and Cohen (1973).

For the mapping H: $X \times [0, 1] \to R^n$, where $H(X, 0)$ and $H(X, 1)$ are *homotopic*, provided $f(X)$ and $g(X)$ have the same shape. That is, $f(X)$ and $g(X)$ are homotopic, provided:

$$\| f(X) - g(X) \| < \| f(X) \|, \quad \text{for all } x \in X.$$

It was Borsuk who first associated the geometric notion of shape and homotopies. This leads into the geometry of shapes and shapes of space (Collins 2004). To make an example, a pair of connected planar subsets in Euclidean space R^2 have equivalent shapes, if the planer sets have the same number of holes (Krantz 2009). The letters e, O, P and numerals 6, 9 belong to the same equivalence class of single-hole shapes. In terms of brain signals, this means that the connected graph for $f(X)$ with, for example, an *e* shape, can be deformed into the 9 shape. This suggests yet another useful application of Borsuk's view of the transformation of shapes, one into the other, in terms of brain signal analysis. Sets of brain signals not only will have similar descriptions, but also dynamic character. Moreover, the deformation of one brain signal shape into another occurs when they are descriptively near (Peters 2014).

A remark concerning brain activity on hyperspheres

One of the formulations of BUT (the third one, in Borsuk 1933) states that there is no antipodal mapping $f : S^n \to S^{n-1}$. It is not completely true: in case of antipodal points not represented by shapes or feature spaces, but by Lie groups, we can detect the hints of the movements of S^4 on S^3, because the Lie group has at least one point $S^n \cap S^{n-1}$. The main benefit here is that, according to the BUT dictates, for each given brain signal we are allowed to find a counterpart in the cortical surface's antipodal position.

References

Afraimovich V, Tristan I, Varona P, Rabinovich M (2013) Transient dynamics in complex systems: heteroclinic sequences with multidimensional unstable manifolds. Discontin Nonlinearity Complex 2(1):21–41

Ajilore O et al (2013) Constructing the resting state structural connectome. Front Neuroinform 7:30

Amft M et al (2015) Definition and characterization of an extended social-affective default network. Brain Struct Funct 220:1031–1049

Andrews-Hanna JR et al (2014) The default network and self-generated thought: component processes, dynamic control, and clinical relevance. Ann NY Acad Sci 1316:29–52

Barttfeld P et al (2015) Signature of consciousness in the dynamics of resting-state brain activity. Proc Natl Acad Sci USA 112: 887–892

Beggs JM, Timme N (2012) Being critical of criticality in the brain. Front Physiol 7(3):163

Borsuk M (1933) Drei ¨satze ¨uber die n-dimensionale euklidische sp¨hare. Fundamenta Mathematicae XX:177–190

Borsuk M (1958–1959) Concerning the classification of topological spaces from the standpoint of the theory of retracts. Fund Math XLVI:321–330

Borsuk M (1969) Fundamental retracts and extensions of fundamental sequences. Fund Math 64(1):55–85

Borsuk M, Gmurczyk A (1980) On homotopy types of 2-dimensional polyhedra. Fund Math 109(2):123–142

Cohen MM (1973) A course in simple homotopy theory. Springer, New York

Collins GP (2004) The shapes of space. Sci Am 291:94–103

Conway MA, Pleydell-Pearce CW (2000) The construction of autobiographical memories in the self-memory system. Psychol. Rev 107:261–288

Dabaghian Y et al (2014) Reconceiving the hippocampal map as a topological template. eLife. doi:10.7554/eLife.03476

de Pasquale F, et al (2015) A dynamic core network and global efficiency in the resting human brain. Cereb Cortex. doi:10.1093/cercor/bhv185

Deco G, Jirsa VK (2012) Ongoing cortical activity at rest: criticality, multistability, and ghost attractors. J Neurosci 7:3366–3375

Domhoff GW, Fox KC (2015) Dreaming and the default network: a review, synthesis, and counterintuitive research proposal. Conscious Cogn 24(33C):342–353

Fingelkurts AA, Fingelkurts AA (2014) Present moment, past, and future: mental kaleidoscope. Front Psychol 5:395

Fox MD, Raichle ME (2007) Spontaneous fluctuations in brain activity observed with functional magnetic resonance imaging. Nat Rev Neurosci 8:700–711

Fox KC et al (2015) The wandering brain: meta-analysis of functional neuroimaging studies of mind-wandering and related spontaneous thought processes. Neuroimage 111:611–621

Fraiman D, Chialvo DR (2012) What kind of noise is brain noise: anomalous scaling behavior of the resting brain activity fluctuations. Front Physiol 3:307. doi:10.3389/fphys.2012.00307

Author's personal copy

Friston K (2010) The free-energy principle: a unified brain theory? Nat Rev Neurosci 11:127–138
Garg R et al (2011) Full-brain auto-regressive modeling (FARM) using fMRI. Neuroimage 58:416–441
Giblin P (2010) Graphs, surfaces and homology, 3rd edn. Cambridge University Press, New York
Gorgolewski KJ, et al (2014) A correspondence between individual differences in the brain's intrinsic functional architecture and the content and form of self-generated thoughts. PLoS One 13, 9(5):e97176
Gravel N et al (2014) Cortical connective field estimates from resting state fMRI activity. Front Neurosci 8:339
Gusnard DA et al (2001) Medial prefrontal cortex and self-referential mental activity: relation to a default mode of brain function. Proc Natl Acad Sci USA 98:4259–4264
Harrison SJ et al (2015) Large-scale probabilistic functional modes from resting state fMRI. Neuroimage 109:217–231
Hart V, Segerman H (2014) The Quaternion Group as a Symmetry Group. arXiv:1404.6596v1
Henderson DW (1996) Experiencing geometry on plane and sphere. Prentice Hall. ISBN 978-0-13-373770-7
Henderson DW, Taimina E (2001) Crocheting the hyperplane. Math Intell 23(2):17–28
Hirvonen J, Palva S (2015) Cortical localization of phase and amplitude dynamics predicting access to somatosensory awareness. Hum Brain Mapp. doi:10.1002/hbm.23033
Jarman N, Trengove C, Steur E, Tyukin I, van Leeuwen C (2014) Spatially constrained adaptive rewiring in cortical networks creates spatially modular small world architectures. Cogn Neurodyn 8(6):479–497. doi:10.1007/s11571-014-9288-y
Karahanoglu FI, Van De Ville D (2015) Transient brain activity disentangles fMRI resting-state dynamics in terms of spatially and temporally overlapping networks. Nat Commun 6:7751
Krantz SG (2009) A guide to topology. The Mathematical Association of America, Washington
Kucyi A et al (2014) Dynamic functional connectivity of the default mode network tracks daydreaming? Neuroimage 100:471–480
Lemaître G (1948) Quaternions et espace elliptique. Acta Pontif Acad Sci 12:57–78
Liu X et al (2013) Decomposition of spontaneous brain activity into distinct fMRI co-activation patterns. Front Syst Neurosci 7:101
Manetti M (2015) Topology. Springer, Heidelberg
Mao D et al (2015) Low-frequency fluctuations of the resting brain: high magnitude does not equal high reliability. PLoS One 10(6):e0128117
Marsaglia G (1972) Choosing a point from the surface of a sphere. Ann Math Stat 43(2):645–646. doi:10.1214/aoms/1177692644
Matoušek J (2003) Using the Borsuk-Ulam Theorem. Lectures on topological methods in combinatorics and geometry. Springer, Berlin
Mitra A et al (2014) Lag structure in resting state fMRI. J Neurophysiol 11:2374–2391
Mitra A et al (2015) Lag threads organize the brain's intrinsic activity. Proc Natl Acad Sci USA 112:E2235–E2244
Morewedge CK et al (2014) The (Perceived) Meaning of Spontaneous Thoughts. J Exp Psychol 143:1742–1754
Nyberg L et al (2010) Consciousness of subjective time in the brain. Proc Natl Acad Sci USA 107:22356–22359
Ozdemir F, Özekes H (2013) On the Homomorphisms of the Lie Groups SU(2) and S3. Abstract Appl Anal. doi:10.1155/2013/645848
Padhy PK et al (2011) Feature extraction and classification of brain signal. World Acad Sci Eng Tech 55:651–652
Papo D (2014) Functional significance of complex fluctuations in brain activity: from resting state to cognitive neuroscience. Front Syst Neurosci 8:112
Peters JF (2014) Topology of digital images. Visual pattern discovery in proximity spaces (Intelligent Systems Reference Library, 63), Springer
Philippi CL et al (2015) Damage to the default mode network disrupts autobiographical memory retrieval. Soc Cogn Affect Neurosci 10:318–326
Ponce-Alvarez A et al (2015) Task-driven activity reduces the cortical activity space of the brain: experiment and whole-brain modeling. PLoS Comput Biol 28:e1004445
Power JD et al (2014) Studying brain organization via spontaneous fMRI signal. Neuron 84:681–696
Raichle ME (2009) A paradigm shift in functional brain imaging. J Neurosci 29:12729–12734
Raichle ME et al (2001) A default mode of brain function. Proc Natl Acad Sci USA 98:676–682
Rigotti M, Barak O, Warden MR, Wang XJ, Daw ND, Miller EK, Fusi S (2013) The importance of mixed selectivity in complex cognitive tasks. Nature 497(7451):585–590. doi:10.1038/nature12160
Roberts JA, et al (2015) The contribution of geometry to the human connectome. Neuroimage 10:379–393
Sadtler PT et al (2014) Neural constraints on learning. Nature 512:423–426
Schoenberg PL, Speckens AE (2015) Multi-dimensional modulations of alpha and gamma cortical dynamics following mindfulness-based cognitive therapy in Major Depressive Disorder. Cogn Neurodyn 9(1):13–29. doi:10.1007/s11571-014-9308-y **(Epub 2014 Aug 29)**
Sengupta B, Stemmler MB, Friston KJ (2013) Information and efficiency in the nervous system–a synthesis. PLoS Comput Biol 9(7):e1003157. doi:10.1371/journal.pcbi.1003157
Sporns O (2011) The human connectome: a complex network. Ann NY Acad Sci 1224:109–125
Tononi G (2008) Consciousness as Integrated Information: a Provisional Manifesto. Biol Bull 215:216–242
Tozzi A (2015) Information processing in the CNS: a supramolecular chemistry? Cogn Neurodyn 9:463–477
Watanabe T, Hirose S, Wada H, Imai Y, Machida T, et al (2014) Energy landscapes of resting-state brain networks. Front Neuroinform 25, 8:12. doi:10.3389/fninf.2014.00012. **(eCollection 2014)**
Weeks JR (2002) The shape of space, 2nd edn. Marcel Dekker inc., New York
Willard S (1970) General topology. Dover Pub. Inc, Mineola
Zare M, Grigolini P (2013) Criticality and avalanches in neural network. Chaos Solitons Fract 55:80–94. doi:10.1016/j.chaos.2013.05.009
Zhang H, Zhang Y, Xu D, Liu X (2015) Deterministic convergence of chaos injection-based gradient method for training feedforward neural networks. Cogn Neurodyn 9(3):331–340. doi:10.1007/s11571-014-9323-z **(Epub 2015 Jan 1)**

1° Give an example of a pair of shapes A, B with either matching or strongly similar descriptions $\Phi(A), \Phi(B)$ so that one shape can deformed into the other shape.
2° Write a Mathematica script to illustrate Part 1.
3° Give a counterexample to disprove Conjecture 5.46 that, for all pairs of shapes A, B with matching or strongly similar descriptions $\Phi(A), \Phi(B)$, one shape can be deformed (mapped into) another shape, provided the shapes that have matching descriptions.
4° Write a Mathematica script to disprove Conjecture 5.46. ■

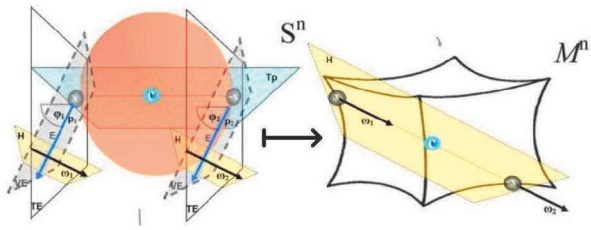

Fig. 5.20. $S^n \mapsto M^n$

5.10 Borsuk-Ulam Theorem Extended to hyperbolic surfaces by A. Tozzi

The Borsuk-Ulam theorem (BUT) tells that there exists a pair of antipodal points on convex n-sphere that are mapped to the same point in n-dimensional Euclidean space $\mathbb{R}^n$. In this section, let S^n be a convex manifold containing a pair of antipodal points that map to a single point in $\mathbb{R}^n$.

So far, the features of geometric regions in 2D and 3D digital images have features such as oblong, concave, diameter, perpendicular, circular that are mapped to real numbers that quantify region features. In this section, we consider image regions equipped with hyperbolic geometry characterized by sectional curvature -1, *i.e.*, regions with a concave shape. The question to consider now is where the antipodal points on flat or on concave surfaces (predicted by BUT) can also be found on image surfaces with negative curvature. In other words, is it possible to transport antipodal points found by BUT to corresponding vectors on a Riemannian manifold M^n with negative curvature?

The answer to this question is positive, provided we map (parallel transport) the antipodal points identified by BUT to points on a hyperbolic manifold. Although parallel transport requires the solution of a second-order differential equation, analysis shows us that we are allowed to have a first-order approximation of the parallel transport. In effect, we pursue parallel transport by solving geodesic equations for sufficient statistics [94] (see, also, an overview of the important aspects of geometric numeric integration by E. Hairer [93]). To solve the parallel transport problem, a number of options are available.

Parallel Transport Options

1° Ehresmann connection [68].
2° Levi-Civita connection [20].
3° We can formulate the Hessian operator on the Riemannian manifold in terms of the Laplace-Beltrami operator [111].
4° 4) We can also retain a first-order approximation and formulate descent directions that are orthogonal to the previous descent ones, through numerical analysis with the conjugate gradient-descent algorithm [112]. Routinely used in optimization, conjugate gradient descent methods have been utilized for gradient descent on manifolds traced out by energy functions such as the variational free-energy [218]. ■

Example 5.54 walks through the steps for parallel transport using the Ehresmann connection.

Example 5.54. **Antipodal points on S^n mapped to Riemannian manifold M^n.**
Parallel transport of antipodal points (predicted by BUT) on convex S^n to antipodal points on a concave Riemannian manifold M^n is illustrated in Fig. 5.20. This is accomplished with an Ehresmann connection (for the details, see C. Ehresmann [68]. After the Ehresmann connection has been performed and the vectors ω_1, ω_2 are found, then use the Riemannian exponential map $exp(\omega_i), i = 1, 2$ from S^n to M^n and the logarithmic map $log(\omega_i), i = 1, 2$ for the opposite mapping $M^n \mapsto S^n$. Let H in Fig. 5.20 be the plane on the Riemannian manifold M^n, containing the vectors ω_1, ω_2 that represent the antipodal points $x, -x$ on S^n. After this has been achieved, use the ham-sandwich theorem to find the center of the hyperbolic manifold (denoted by ◯).

Theorem 5.55. Ulam's Ham Sandwich Theorem.
For any three given sets in Euclidean space, each of finite outer Lebesgue measure, there exists a plane that bisects all three setss, i.e., *separates each of the given sets into two sets of equal measure.*

Proof. Assume that the Borsuk-Ulam Theorem holds and then the proof of the ham-sandwish follows (for the details, see [15]). □

■

In summary, the Borsuk-Ulam Theorem can be extended to concave surfaces, making it possible to look for antipodal points in images equipped with a negative curvature.

Author's personal copy

Int J Theor Phys (2016) 55:3689–3696
DOI 10.1007/s10773-016-2998-7

Quantum Entanglement on a Hypersphere

James F. Peters[1] · Arturo Tozzi[2]

Received: 1 December 2015 / Accepted: 23 March 2016 / Published online: 11 April 2016
© Springer Science+Business Media New York 2016

Abstract A quantum entanglement's composite system does not display separable states and a single constituent cannot be fully described without considering the other states. We introduce quantum entanglement on a hypersphere - which is a 4D space undetectable by observers living in a 3D world -, derived from signals originating on the surface of an ordinary 3D sphere. From the far-flung branch of algebraic topology, the Borsuk-Ulam theorem states that, when a pair of opposite (antipodal) points on a hypersphere are projected onto the surface of 3D sphere, the projections have matching description. In touch with this theorem, we show that a separable state can be achieved for each of the entangled particles, just by embedding them in a higher dimensional space. We view quantum entanglement as the simultaneous activation of signals in a 3D space mapped into a hypersphere. By showing that the particles are entangled at the 3D level and un-entangled at the 4D hypersphere level, we achieved a composite system in which each local constituent is equipped with a pure state. We anticipate this new view of quantum entanglement leading to what are known as qubit information systems.

Keywords Quantistic · Entanglement · Borsuk-Ulam theorem · Homotopy · Qubit

✉ Arturo Tozzi
tozziarturo@libero.it

James F. Peters
James.Peters3@umanitoba.ca

[1] Department of Electrical and Computer Engineering, University of Manitoba, 75A Chancellor's Circle, R3T 5V6, Winnipeg, MB, Canada

[2] Center for Nonlinear Science, University of North Texas, 1155 Union Circle, #311427, Denton, TX 76203-5017, USA

Author's personal copy

1 Introduction

Quantum entanglement is a widely accepted, experimentally verified physical phenomenon occurring when a system of particles interact as a whole, in a way such that the quantum state of each particle cannot be described independently and their physical properties - such as position or spin - are instantly correlated [1]. When a composite system is entangled, it is impossible to separate its components and attribute to each one a definite pure state. Quantum state cannot be factored as a product of states of its local constituents (e.g. individual particles) and one constituent cannot be fully described without considering the other(s) [2–4]. It gives rise to a paradoxical effect: it seems that one particle of an entangled pair "knows" what measurement has been randomly performed on the other, even though such information cannot be communicated between them. While a composite system is always expressible as a sum of products of states of local constituents, when the system is entangled the sum necessarily has more than one term. This means that we cannot recognize cause/effect relationships. In such a framework, the Borsuk-Ulam theorem (BUT) from topology comes into play, leading to a game-changing result: the hypersphere quantum information theorem. The BUT states that every continuous map from a *n*-sphere (denoted S^n) to a *n*-Euclidean space must identify on S^n a pair of antipodal points directly opposite each other [5] (Fig. 1). To make an example, the case n =1 says that there always exist a pair of opposite points on the earth's equator with the same temperature. An *3*-sphere (called a hypersphere) is a generalization of the circle: mathematically, it is a simply connected manifold of constant, positive curvature that maps to a *3*-dimensional Euclidean space [6]. When we examine a system equipped with quantum entanglement, we usually do not take into account a noteworthy feature: our measurements are on a S^2 manifold, which is a 3D world.

2 Theory

Our basic approach is to map entangled system signals in S^2 to S^3. Notice that our S^2 measurements illustrate just the "hints" of such an S^3 activity analogous to way one recognizes an object from its shadow projected on a screen. The spheres equipped with $n > 2$ are not detectable in the usual spatial 3-dimensions and are thus challenging to assess. If we look just at mappings on the surface of S^3 system, we find the puzzling picture of quantum entanglement, apparently incompatible with our perceptions. BUT also states that every continuous function maps each pair of antipodal n-sphere surface points into surface vectors on a Euclidean *n*-space. This means that entanglement (*i.e.*, a system not formed by two product states) can be seen as just 3D space surface points that have a corresponding pair of S^3 antipodal points (pure states!). We demonstrate that each of the two entangled particles may have a pure state, provided they are embedded in a dimension higher: the system is entangled at the S^2 level, but un-entangled at the S^3 hypersphere level. We thus obtain a 4D composite system, factored as a product of states of its local constituents.

In keeping with recent work on quantum computation, quantum distillation and quantum information science [1, 2], we propose an approach to entanglement which provides a new source of quantum information, by mapping entangled quanta on a 3D surface to unentangled quanta on the surface of a hypersphere. The old adage that opposites are attracted to

Author's personal copy

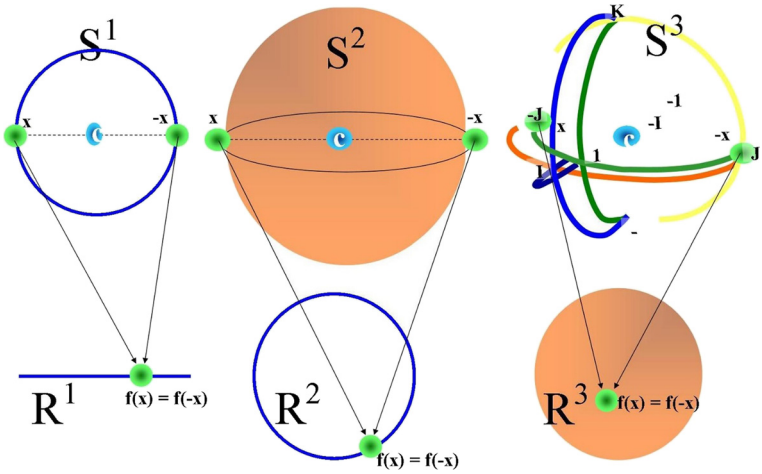

Fig. 1 The Borsuk-Ulam theorem for different values of S^n. Two antipodal points in S^n project to a single point in R^n, and vice versa. Remind that every S^n is embedded in a n+1-ball, and thus every S^n is one-dimension higher than the corresponding R^n

each other, applies here. This analogy, applied to the problem of extracting information from entangled quanta, gets it impetus from BUT, a discovery made by Borsuk [5] in 1933. If we start with entangled quanta with antipodal locations on the surface of a sphere, then a continuous mapping of surface particles to a higher level quanta on the surface of a hypersphere results in matching quantum information derived from the entangled quanta. This information is reversible for invertible continuous mappings of antipodal surface quanta into the surface of a hypersphere. Schrödinger [7][17] observed that we must gather information about the entangled quanta to achieve *disentanglement*. His work provides yet another solution to the disentanglement problem. In this instance, our proposed continuous mapping of surface quanta to hypersphere surface quanta is analogous to what Schrödinger calls a *programme of observations* as a means of finding representatives of entangled quanta. In our case, the quantum-mapping images are representatives of entangled quanta, with the added bonus that the images provide matching signatures of the entangled surface quanta.

3 Mathematical Model and Equations

The basic approach is to think in terms of a homotopic mapping of a 3D shape produced by one continuous function that can be deformed into another shape by a second continuous function. To do this, we first consider the BUT theorem. An n-dimensional Euclidean vector space is denoted by R^n. Thus, for example, a feature vector $x \in R^n$ models the description of a surface signal. BUT states that e*very continuous map* $f : S^n \rightarrow R^n$ *must identify a pair of antipodal points* – diametrically opposite points on an n-sphere [8–11]. Points are *antipodal*, provided they are diametrically opposite [9]. Examples of antipodal points are

Author's personal copy

the endpoints of a line segment, or opposite points along the circumference of a circle, or poles of a sphere.

BOX

The following notation and terminology is used in this paper:
Qubit stands for quantum information. ***Qubit system*** stands for a system that can be in one of an infinite number of states.
A space X is pathwise-connected, provided, for every two points $A, B \in X$, there is a path connecting them *(22)*. This means that each pair of points A, B are connected by a curve lying wholly within X.
1-sphere: S^1 stands for a 1-sphere (i.e, a collection of circles). Each $x \in S^1$ is a vector $(x1, x2)$ on the perimeter of a S^1 circle. $A \in S^1$, is a vector $(x1, x2)$ on the circumference of a 1-sphere.
2-sphere: S^2 is a 2-sphere (for example, a common beach ball). Each $x \in S^2$ is a vector $(x1, x2, x3)$. $(A, q(A))$ is a vector on the surface of a 2-sphere, in which $q(A) \in R$ is a real number that is a signal value. $\|q(A)\rangle_{q(A)}$ stands for a singlet state vector written as a **ket** $\|q(A)\rangle_{q(A)}$ of the signal $q(A)$ on a 2-sphere.
3-sphere: S^3 stands for a 3-sphere (the smallest hypersphere). Each $x \in S^3$ is a vector $(x1, x2, x3, x4)$. $f(q(A)) \in S^3$ is a vector $(A^c q(A)^c f(q(A)))$ on the surface of a hypersphere S^3, while $f(q(-A)) \in S^3$ is a vector $((-A^c q(-A)^c f(q(-A)))$. *Observe that* $f(q(A)) = f(q(-A))$ is predicted by BUT.
$\|f(q(A))\rangle_{q(A)}$ is a singlet state vector written as a **ket** $\|f(q(A))\rangle$ of the description of $q(A)$ on the 3-sphere.

We will follow the terminology displayed in **BOX**. The notation S^n designates an n-sphere. We have the following n-spheres, starting with the perimeter of a circle (this is S^1) and advancing to S^3, which is the smallest hypersphere:

1-sphere $S^1 : x_1^2 + x_2^2 \rightarrow R^2$ (circle perimeter),
2-sphere $S^2 : x_1^2 + x_2^2 + x_3^2 \rightarrow R^2$ (surface),
3-sphere $S^3 : x_1^2 + x_2^2 + x_3^{2+} x_4^2 \rightarrow R^2$ (smallest hypersphere surface), ...,
n-sphere $S^n : x_1^2 + x_2^2 + x_3^{2+} ... + x_n^2 \rightarrow R^2$

If we view the phase space of quantum entanglement as a n-sphere and the feature space for signals as a finite-dimensional Euclidean topological space, then BUT tells us that for each description $f(x)$ of a signal x, we can expect to find an antipodal feature vector $f(-x)$ that describes a signal on the opposite (antipodal) to x with a matching description (Fig. 2).

Let X denote a nonempty set of points on the surface of a 3D system. We assume that that is a topological space, which means that the unions and intersections of the subsets of x belong to X. Let X,Y be topological spaces. Recall that a function or map $f : X \rightarrow Y$ on a set X to a set Y is a subset $X \times Y$, so that for each $x \in X$ there is a unique $y \in Y$ such that $(x, y) \in f$ (usually written $y = f(x)$). The mapping f is defined by a rule that tells us how to find $f(x)$. A mapping $f : X \rightarrow Y$ is continuous, provided $A \subset Y$ is open, then the inverse $f^{-1}(A) \subset X$ is also open [8, 11, 12][14,19,22]. In this view of continuous mappings from a signals topological space X on the surface of a 3-sphere to the signal feature space R^n, we can consider not just one signal feature vector $x \in R^n$, but also mappings from X to a set of signal feature vectors $f(X)$. This expanded view of signals has interest, since every connected set of feature vectors $f(X)$ has a shape, which has direct bearing on the study of the shapes of space [13]. This means that signal shapes (in our case, mappings of sets of entangled particles) can be compared.

Author's personal copy

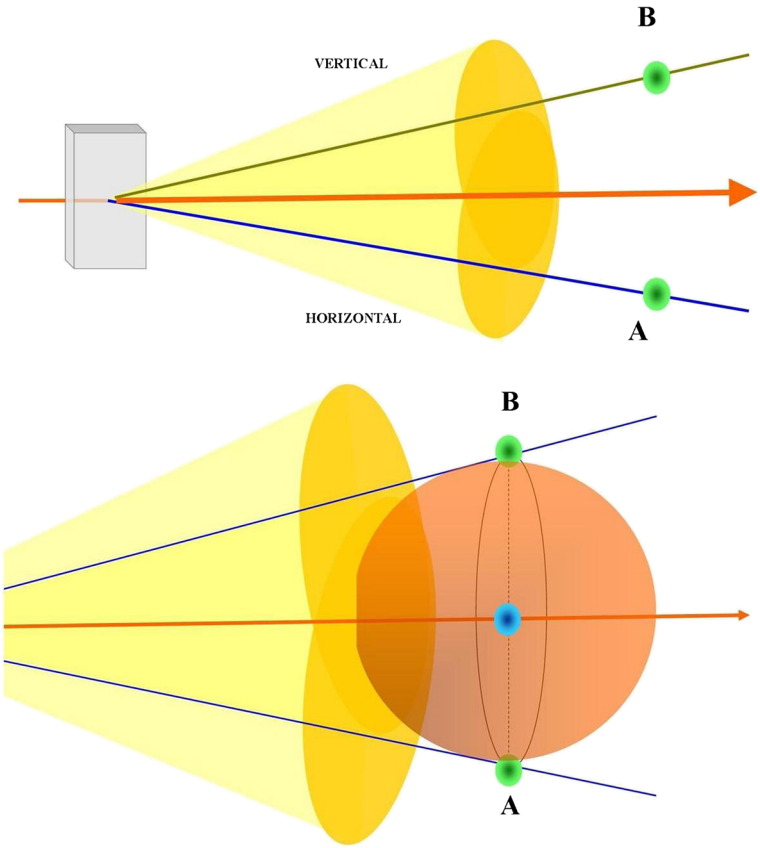

Fig. 2 Spontaneous parametric down-conversion, the commonest method used to create quantum entanglement, may generate a pair of photons entangled in polarisation [23, 24]. When a strong laser beam is conveyed through a nonlinear crystal, the most of photons continue straight through the crystal, while a small amount are splitted into photon pairs. The two photons may share the same polarization (type I correlation), or may be equipped with mutually perpendicular polarizations (type II correlation). In the latter case, displayed in Figure, we are in front of a pair of horizontally- and vertically- polarized entangled photons (**A** and **B**). These type II photons display trajectories, constrained within the two cones, which may exist simultaneously in the lines where the cones intersect. The two cones represent sources of pairs of photons that become entangled. We embedded the two points A and B (visually represented by blobs with dark centers), corresponding to the entangled particles of Fig. 1A, in a circumference centred in the laser beam. Such a circumference is one of the circles surrounding the sphere S^n. For the Borsuk-Ulam theorem, the two antipodal points A and B are described by the same function, provided they are embedded in S^n. The function stands for the physical properties corresponding to the quantum entanglement of the two particles A and B: in this framework, it becomes clear that the two points are strictly correlated. Note that the figure is just an oversimplification: the S^n sphere, which is actually a 3-sphere, is depicted as a simple 2-sphere, to make it easier to recognize

A consideration of $f(X)$ (set of region signal descriptions entangled on a n-sphere) instead of $f(x)$ (description of a single signal x) leads to a region-based view of signals, which arises naturally in terms of a comparison of shapes produced by different mappings from X (object space) to the feature space R^n.

Let $f, g : X \to Y$ be continuous mappings from X to Y . The continuous map $H : X \times [0, 1] \to Y$ is defined by $H(x, 0) = f(x)$, $H(x, 1) = g(x)$, for every $x \in X$.

Author's personal copy

The mapping H is a homotopy [6, 14, 15], if there is a continuous transformation (called a deformation) from f to g. The continuous maps f, g are called homotopic maps, provided $f(X)$ continuously deforms into $g(X)$ (denoted by $f(X) \rightarrow g(X)$). The sets of points $f(X), g(X)$ are called shapes [8, 13].

The mapping $H : X \times [0, 1] \rightarrow R^n$, where $H(X, 0)$ and $H(X, 1)$ are homotopic, provided $f(X)$ and $g(X)$ have the same shape. That is, $f(X)$ and $g(X)$ are homotopic, if: $\|f(X) - g(X)\| < \|f(X)\|$, for all $x \in X$.

4 Results and Discussion

Once achieved an association between the geometric notion of shape and homotopies, we introduce the following theorem:

Hypersphere Quantum Information Theorem Let $\{|\mathrm{f(q(-A))}\rangle\}$ be a set of pathwise-connected qubit vectors on the surface of a hypersphere S^3 in a normed linear space. The shape $\{|\mathrm{f(q(-A))}\rangle\}$ induced by the set of path-connected qubit state vectors can be deformed onto the shape $\{|\mathrm{f(q(A))}\rangle\}$ on a 3-sphere.

Proof The proof is an immediate consequence of the Borsuk-Ulam Theorem. From BUT, each $|\mathrm{f(q(A))}\rangle = |\mathrm{f(q(-A))}\rangle$. Hence the shape $\{|\mathrm{f(q(-A))}\rangle\}$ deforms into the shape $\{|\mathrm{f(q(A))}\rangle\}$.

Next, we investigate quantum entanglement on an n-Sphere embedded in a normed linear space X. Let E(A,B) denote the entanglement of vectors A,B on a normed linear space. Conventional entanglement is represented by:

$$\mathrm{E(A,B)} = 1/\sqrt{2}(|0\rangle_{\mathrm{A}} \otimes |1\rangle B - |1\rangle A \otimes |0\rangle_B).$$

Let $S^1 \in \boldsymbol{X}$ be the circumference (perimeter) of a 1-sphere circle, $A, -A \in X$the quanta (vectors) on X and, finally, let $A, -A$ be antipodal quanta on X. Let $q : X \rightarrow R$ be a mapping from a quantum A on X into the reals R and q(A), q(B) $\in R$ be real-valued antipodal entangled signals. In addition, let Q be a set of signal values originating from points A, B on the perimeter X of a 1-sphere circle. □

Remark 1 For A in S^{n}, the point A (also called a state) and the signal q(A) defines a vector (A, q(A)) on the surface of a 2-sphere. That is, $\mathrm{Sq(A)\rangle A} \in \mathrm{S}^2$. Signals on an S^2 surface are then mapped to feature vectors $\mathrm{f(q(A))} \in \mathrm{S}^3$ that describe the signals q(A). From this, we can rewrite the quantum entanglement model in the following way. Let E(A,−A) denote the quantum entanglement of states A,−A, defined by:

$$\mathrm{E(A, -A)} = 1/\sqrt{2}(|\mathrm{q(A)}\rangle_{\mathrm{A}} \otimes |\mathrm{q(B)}\rangle_{-\mathrm{A}} - |\mathrm{q(-A)}\rangle_{-\mathrm{A}} \otimes |\mathrm{q(A)}\rangle_{\mathrm{A}}).$$

Let Q be a set of signals on the surface of a 2-sphere, Y be a set of feature vectors S^3 on the surface of a 4-dimensional hypersphere and f : Q → Y be a continuous mapping on the set of signals Q into Y. Let q,−q ∈ Q be antipodal quantum signals.

Remark 2 f(q(A)) defines a feature vector (A, q(A), f(q(A))) on the surface of a hypersphere S^3. That is, $|\mathrm{f(q(A))\rangle q(A)} \in \mathrm{S}^3$. Each qubit provides information about a signal q(A). In addition, the Borsuk-Ulam Theorem predicts the presence of antipodal qubits f(q(A)), f(q(−A)), such that the information provided by f(q(−A)) matches the information provided by f(q(A)). From this, we obtain a new form of entanglement, at the information level on a

Author's personal copy

hypersphere. Let E(q(A), q(−A)) denote the quantum entanglement of states q(A), q(−A), defined by:

$$E(q(A), q(-A)) = 1/\sqrt{2}(|f(q(A))\rangle_{q(A)} \otimes |f(q(-A))\rangle_{q(-A)} - |f(q(-A))\rangle_{q(-A)} \otimes |f(q(A))\rangle_{q(A)}).$$

Let the qubit system $Y = \{Sf(q(A))\rangle\}$ be a set of pathwise-connected qubit vectors on the surface of a hypersphere S^3 in a Hilbert space, which defines a quantum information system. That is, the set of descriptions Y of signals provides a model for a process about a collection of signals. From the Hypersphere Quantum Information Theorem, we know that the shape $\{|f(q(-A))\rangle\}$ can be deformed into the shape Y. In addition, from the Borsuk-Ulam Theorem, we also know that:

$$|f(q(A))\rangle = |f(q(-A))\rangle.$$

This means that a definite pure state can be attributed to $|f(q(A))\rangle$. The system is thus entangled at the S^2 level, while is un-entangled at the S^3 hypersphere level.

The geometrical aspects of entanglement have been already investigated by offering a numerical approach, iteratively refining an estimated separable state towards the target state to be tested, and checking if the target state can indeed be reached [16][16]. We gave instead a different geometrical account of quantum entanglement, by exploring the possibility of a a correlation between it and the Borsuk-Ulam Theorem. We showed that there are striking analogies between the antipodal points evoked by BUT and the entangled particles evoked by quantistics, such that the phenomenon of quantum entanglement can be investigated in guise of an n-sphere embedded in a Hilbert Space. This leads naturally to the possibility of a region-based, instead of a point-based, geometry in which we view collections of signals as surface shapes, where one shape maps to another antipodal one [17–21]. We have developed a mathematical model of antipodal points and regions cast in a physically-informed fashion, resulting in a framework that has the potential to be operationalized and assessed empirically. The notion that information about particles resides on a hypersphere is a counter-intuitive hypothesis, since we live in a 3D world with no immediate perception that 4D space exists at all, e.g., if we walk along one of the curves of a 4-ball, we think are crossing a straight trajectory, not recognizing that our environment is embedded in higher spatial dimensions. The cause/effect relationships of the entangled system occurs in the fourth dimension: for this reason, we are not able to detect it by ordinary means. We are able to look just at at the 3D part part of the S^3 system and such an incomplete viewpoint gives us the false impression of a weird picture, apparently incompatible with our common sense. In conclusion, the Borsuk-Ulam theorem sheds new light on quantum entanglement. It explains how the two entangled particles on a hypersphere yield observations about particles that reside on a lower dimensional sphere, thus leading to a quantum information system.

References

1. Jaeger, G.: Quantum Information an Overview. Springer, New York (2007)
2. Gruska, J.: Quantum entanglement as a new information processing resource. N. Gener. Comput. **21**, 279–295 (2003)
3. Hauke, P., Tagliacozzo, L.: Spread of correlations in long-range interacting quantum systems. Phys. Rev. Lett. **111**(20), 207202 (2013)

Author's personal copy

4. Horodecki, P., Horodecki, M.: Entanglement and thermodynamical analogies. Acta Physica Slovaca **3**, 141–56 (1998)
5. Borsuk, K.: Drei saetze ueber die n-dimensionale euklidische sphaere. Fundam. Math. **XX**, 177–190 (1933)
6. Cohen, M.M.: A Course in Simple Homotopy Theory. Springer, New York (1973)
7. Schroedinger, E.: Discussion of probabilty relations between separated systems. Proc. Camb. Philos. Soc. **31**, 555–563 (1935)
8. Peters, J.F.: Computional Proximity. Excursions in the Topology of Digital Images, Intelligent Systems (Reference Library 102, Springer, 2015, doi:10.1007/978-3-319-30262-1)
9. Weisstein, E.W.: Antipodal points (http://mathworld.wolfram.com/AntipodalPoints.html. 2015)
10. Henderson, D.W.: Experiencing Geometry. In: Euclidean, Spherical, and Hyperbolic Spaces. 2nd edn. (2001)
11. Naimpally, S.A., Peters, J.F.: Preservation of continuity. Scientiae Mathematicae Japonicae **76**, 305–311 (2013)
12. Willard, S.: General Topology. Dover Pub., Inc., Mineola (1970)
13. Collins, G.P.: The shapes of space. Sci. Am. **291**, 94–103 (2004)
14. Borsuk, M., Gmurczyk, A.: On homotopy types of 2-dimensional polyhedral. Fundam. Math. **109**, 123–142 (1980)
15. Dodson, C.T.J., Parker, P.E.: A User's guide to algebraic topology. Kluwer, Dordrecht (1997)
16. Leinaas, J.M., et al.: Geometrical aspects of entanglement, arXiv:0605079v1, pp. 1–31 (2006)
17. Borsuk, M.: Concerning the classification of topological spaces from the standpoint of the theory of retracts. Fundam. Math. **XLVI**, 177–190 (1958)
18. Borsuk, M.: Fundamental retracts and extensions of fundamental sequences **64**, 55–85 (1969)
19. Krantz, S.G.: A Guide to Topology. The Mathematical Association of America, Washington (2009)
20. Manetti, M.: Topology. Springer, Heidelberg (2015)
21. Peters, J.F.: Topology of Digital Images. Visual Pattern Discovery in Proximity Spaces. Intelligent systems (reference library, **63** Springer, 2014)
22. Weisstein, E.W.: Pathwise-connected (Mathworld, http://mathworld.wolfram.com/Pathwise-Connected.html. 2015)
23. Zhang, Y., et al.: Simulating quantum state engineering in spontaneous parametric down-conversion using classical light. Opt. Express. **22**, 17039–17049 (2014)
24. Quesada, N., Sipe, J.E.: Time-ordering effects in the generation of entangled photons using nonlinear optical processes. Phys. Rev. Lett. **114**, 093903 (2015)

Journal of Neuroscience Research 00:00–00 (2016)

Review

A Topological Approach Unveils System Invariances and Broken Symmetries in the Brain

Arturo Tozzi[1]* **and James F. Peters**[2]

[1]Center for Nonlinear Science, University of North Texas, Denton, Texas
[2]Department of Electrical and Computer Engineering, University of Manitoba, Winnipeg, Manitoba, Canada

Symmetries are widespread invariances underscoring countless systems, including the brain. A symmetry break occurs when the symmetry is present at one level of observation but is hidden at another level. In such a general framework, a concept from algebraic topology, namely, the Borsuk-Ulam theorem (BUT), comes into play and sheds new light on the general mechanisms of nervous symmetries. The BUT tells us that we can find, on an n-dimensional sphere, a pair of opposite points that have the same encoding on an $n - 1$ sphere. This mapping makes it possible to describe both antipodal points with a single real-valued vector on a lower dimensional sphere. Here we argue that this topological approach is useful for the evaluation of hidden nervous symmetries. This means that symmetries can be found when evaluating the brain in a proper dimension, although they disappear (are hidden or broken) when we evaluate the same brain only one dimension lower. In conclusion, we provide a topological methodology for the evaluation of the most general features of brain activity, i.e., the symmetries, cast in a physical/biological fashion that has the potential to be operationalized. © 2016 Wiley Periodicals, Inc.

Key words: hidden symmetry; Central nervous system; Borsuk-Ulam theorem; invariance

Symmetry is a type of invariance occurring when a structured object does not change under a set of transformations (Weyl, 1982). Symmetries hold the key for understanding many of nature's intimate secrets because they are the most general feature of countless types of systems. Huge swathes of mathematics, physics, and biology, including the brain, can be explained in terms of the underlying invariance of the structures under investigation. In physics, symmetries can be "broken." Symmetry breaking consists of sudden change in the set of available states; the whole phase space is partitioned into nonoverlapping regions (Roldàn et al., 2014) so that small fluctuations acting on a system cross a critical point and decide which branch of a bifurcation is taken. In particular, in spontaneous symmetry breaking (SSB), the underlying laws are invariant under a symmetry transformation, but the system as a whole changes. SSB is a process that allows a system cast in a symmetrical state to end up in an asymmetrical one. SSB describes systems in which the equations of motion or the Lagrangian obey certain invariances, but the lowest energy solutions do not exhibit them. "Hidden" is perhaps a better term than "broken" because the symmetry is always there in such equations (Higgs, 1964). In the case of finite systems with metastable states, the confinement is not strict; the system can "jump" from one region to another (Roldàn et al., 2014). With respect to the brain, its activity is an example of an open system, partially stochastic resulting from intrinsic fluctuations but containing islands at the edge of the chaos, that maintains homeostasis or allostasis in the face of environmental fluctuations (Friston, 2010). The

SIGNIFICANCE

This Review provides a theoretical/methodological framework based on simple topological concepts that make possible the evaluation of brain parameters in terms of their dimensionality, symmetries, and symmetry breaking. The brain functional and anatomical organization may be better assessed if one considers how certain hidden symmetries, essential for shaping brain gradients and activity, may appear only under the lens of higher dimensional neural representations. We explain the computational and thermodynamic interest of such topologies and offer concrete examples of their possible applications to neuroscience. This Review emphasizes the role of a rigorous mathematical apparatus in unifying and operationalizing deep multidisciplinary theoretical questions.

*Correspondence to: Arturo Tozzi, Center for Nonlinear Science, University of North Texas, 1155 Union Circle No. 311427, Denton, TX 76203-5017. E-mail: tozziarturo@libero.it

Received 18 December 2015; Revised 14 January 2016; Accepted 26 January 2016

Published online 00 Month 2016 in Wiley Online Library (wileyonlinelibrary.com). DOI: 10.1002/jnr.23720

© 2016 Wiley Periodicals, Inc.

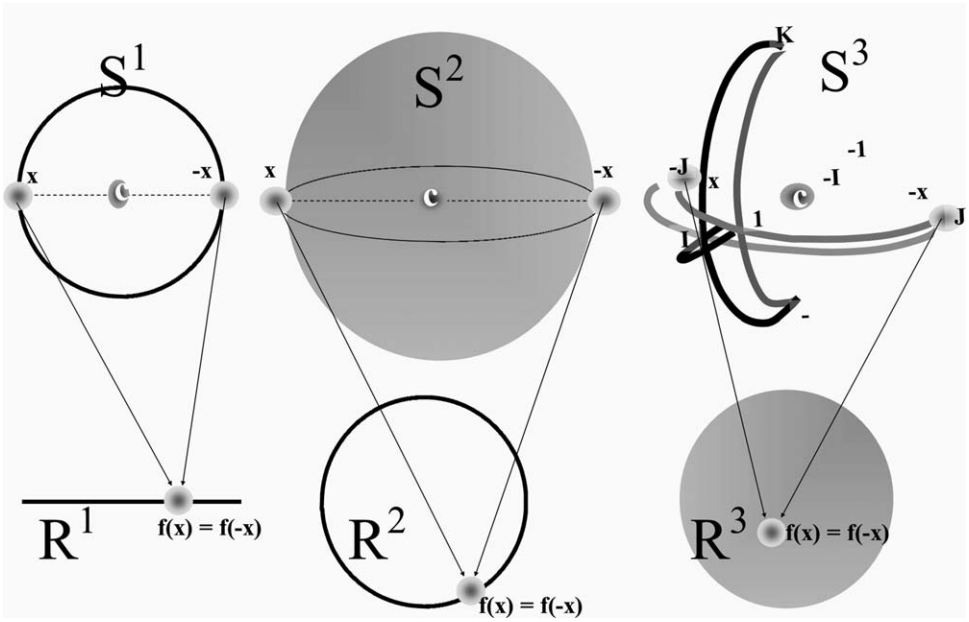

Fig. 1. The BUT for different values of S^n. Two antipodal points in S^n project to a single point in R^n and vice versa. Remember that every S^n is embedded in an $n + 1$-ball; thus, every S^n is one dimension higher than the corresponding R^n.

brain retains the characteristics of a complex, nonlinear system with nonequilibrium dynamics (Fraiman and Chialvo, 2012), equipped with random walks (Afraimovich et al., 2013). It operates at the edge of chaos (Tognoli and Kelso, 2014) and lives near a metastable state of second-order phase transition between micro- and macrolevels (Beggs and Timme, 2012), characterized by infinite correlation length, countless dimensions, slight nonergodicity, attractors (Deco and Jirsa, 2012), and universal power laws, evidenced by the presence of spontaneous neuronal avalanches (De Arcangelis and Herrmann, 2010).

In such a multifaceted framework, the Borsuk-Ulam theorem (BUT) is useful. This theorem tells us that, if a sphere is mapped continuously into a plane set, there is at least one pair of antipodal points having the same image; that is, they are mapped in the same point of the plane (Beyer and Zardecki, 2004). Here, we show that brain symmetries hidden at a lower level are detectable at a higher level of analysis and vice versa. In other words, a symmetry break occurs when the symmetry is present at one level of observation but hidden at another level.

This theoretical Review comprises six sections. In the first section, we show how brain symmetries can be studied in a topological fashion, i.e., in terms of antipodal points on a hypersphere. If we enclose symmetries equipped with antipodal self-similar points into the abstract spaces of n-spheres, they can be evaluated in the guise of projections on S^{n-1}, where they stand for the broken symmetry. The second through fourth sections explain how we are allowed to generalize the BUT to the study of all the types of brain symmetries. In particular, section 2 illustrates how the symmetries are not required to be framed only as antipodal points on spatial n-spheres, as stated by the "classical" BUT, but can also be embedded in every kind of n-sphere equipped with other types of dimensions. Section 3 further expands the possible use of the BUT in the study of symmetries by showing that they can also occur between two nonantipodal points embedded in an n-sphere. Section 4 is devoted to extending the concept of symmetries from systems formed by convex spheres to the concave, hyperbolic manifolds that are thought to be the natural frame of brain activity. The fifth section lists the best candidates that may represent a symmetry (and Lagrangian) to formulate a BUT theory for the nervous system. Throughout sections 1–5, we also provide concrete examples of applications of symmetry and symmetry breaking in neuroscience to show that our theory can be operationalized in the study of brain anatomy, function, and dynamics. The final section describes the methodological advantages of the topological approach to nervous symmetries.

NERVOUS SYMMETRIES AS ANTIPODAL POINTS ON AN *N*-SPHERE

The BUT is a remarkable finding by K. Borsuk (1933) about Euclidean n-spheres and antipodal points. It states that every continuous map, $f{:}S^n \rightarrow R^n$, must identify a pair of antipodal points (on S^n; Dodson and Parker, 1997; Fig. 1).

The sphere S^n maps to R^n, which is an n-dimensional Euclidean space. Another less technical definition is, if a sphere is mapped continuously into a plane set, there is at least one pair of antipodal points having the

same image; that is, they are mapped in the same point of the plane (Beyer and Zardecki, 2004). For other definitions of the BUT and its countless proofs, see Matoušek (2003) and Peters (2016).

The notation S^n denotes an n-sphere, which is a generalization of the circle (Weeks, 2002). An n-sphere is an n-dimensional structure embedded in an $n + 1$ space. For example, a 1-sphere (S^1) is the one-dimensional circumference surrounding a two-dimensional disk, whereas a 2-sphere (S^2) is the two-dimensional surface of a three-dimensional ball (a beach ball is a good example). An n-hypersphere (briefly, n-sphere or S^n) is formed by points that are constant distances from the origin in $n + 1$ dimensions (Marsaglia, 1972). For example, a 3-sphere (also called a *glome*) of radius r (where r may be any positive real number) is defined as the set of points in four-dimensional Euclidean space at distance r from some fixed center point c (which may be any point in the four-dimensional space; Moura and Henderson, 1996). A 3-sphere is a simply connected three-dimensional manifold of constant, positive curvature that is enclosed in a Euclidean four-dimensional space called a "4-ball." A 3-sphere is thus the surface or boundary of a four-dimensional ball, and a four-dimensional ball is the interior of a 3-sphere in the same way that a bottle of water is made of a glass surface and a liquid content.

Points on S^n are antipodal, provided that they are diametrically opposite (Weisstein, 2015). Examples of antipodal points are the endpoints of a line segment, the opposite points along the circumference of a circle, or the poles of a sphere. Furthermore, every continuous function from an n-sphere S^n into Euclidean n-space R^n maps some pair of antipodal points of S^n to the same point of R^n. For example, if we use the mapping $f{:}S^3 \rightarrow R^3$, then $f(x)$ in R^3 is only a signal value (a real number associated with x in S^3) and $f(x) = f(-x)$ in R^3. Furthermore, when $g{:}S^2 \rightarrow R^2$, the $g(x)$ in R^2 is a vector in R^2 that describes the x embedded in S^2. In other words, a point embedded in an R^n manifold is projected to two opposite points on an S^{n+1}-sphere and vice versa. The next sections highlight the versatility of the three main ingredients of the BUT, the antipodal points with matching description, the n-sphere, and the possibility to map into an $n - 1$ sphere.

DESCRIPTION OF A SIGNAL THROUGH THE BUT

In terms of activity, a feature vector $x \in R^n$ models the description of a signal. To elucidate the picture in the application of the BUT in signal analysis, we view the surface of a manifold as an n-sphere and the feature space for signals as finite Euclidean topological spaces. The BUT tells us that for description $f(x)$ for a signal x, we can expect to find an antipodal feature vector $f(-x)$ that describes a signal on the opposite (antipodal) side of the manifold S^n. Thus, the pair of antipodal signals has matching descriptions on S^n.

Let X denote a nonempty set of points on the surface of the manifold. A topological structure on X (called a "topological space") is a structure given by a set of subsets τ of X, having the following properties: Str1, every union of sets in τ is a set in τ; Str2, every finite intersection of sets in τ is a set in τ.

The pair (X,t) is called a topological space. Usually, X by itself is called a topological space, provided X has a topology τ on it. Let (X,Y) be topological spaces. Recall that a function or map $f{:}X \rightarrow Y$ on a set X to a set Y is a subset $X \times Y$ so that for each $x \in X$there is a unique $y \in Y$ such that $(x, y) \in f$ [usually written $y = f(x)$]. The mapping f is defined by a rule that tells us how to find $f(x)$. For a good introduction to mappings, see Willard (1970).

SHAPES AND HOMOTOPIES

A mapping $f{:}X \rightarrow Y$ is continuous, provided that, when $A \subset Y$ is open, then the inverse $f^{-1}(A) \subset X$ is also open. For more about this, see Krantz (2009). In this view of continuous mappings from the signal topological space X on the manifold's surface to the signal feature space R^n, we can consider not only one signal feature vector $x \in R^n$ but also mappings from X to a set of signal feature vectors $f(X)$. This expanded view of signals has interest because every connected set of feature vectors $f(X)$ has a shape. The significance of this is that signal shapes can be compared.

A consideration of $f(X)$ set of signal descriptions for a region (X) instead of $f(X)$ (description of a single signal x) leads to a region-based view of signals. This region-based view of the manifold arises naturally in terms of a comparison of shapes produced by different mappings from X (object space) to the feature space R^n. An interest in continuous mappings from object spaces to feature spaces leads to homotopy theory and the study of shapes.

Let $f,g{:}X \rightarrow Y$ be continuous mappings from X to Y. The continuous map $H{:}X \times [0,1] \rightarrow Y$ is defined by $H(x,0) = f(x)$, $H(x,1) = g(x)$, for every $x \in X$. The mapping H is a homotopy, provided that there is a continuous transformation (called a "deformation") from f to g. The continuous maps f,g are called "homotopic maps," provided that $f(X)$ continuously deforms into $g(X)$ [denoted by $f(X) \rightarrow g(X)$]. The sets of points $f(X)$, $g(X)$ are called "shapes." For more about this, see Manetti (2015) and Cohen (1973).

It was Borsuk who first associated the geometric notion of shape and homotopies. There are natural ties between Borsuk's result for antipodes and mappings called "homotopies." The early work on n-spheres and antipodal points eventually led Borsuk to the study of retraction and homotopic mappings (Borsuk, 1958–1959, 1969; Borsuk and Gmurczyk, 1980). This leads into the geometry of shapes and shapes of space (Collins, 2004). A pair of connected planar subsets in Euclidean space R^2 have equivalent shapes, provided that the planar sets have the same number of holes (22). For example, the letters e, O, P and the numerals 6, 9 belong to the same equivalence class of single-hole shapes. In terms of signals, it means that the connected graph for $f(X)$ with, for example, an *e*

shape can be deformed into the 9 shape. This suggests yet another useful application of Borsuk's view of the transformation of a shape into another, in terms of signal analysis. Sets of signals will have not only similar descriptions but also dynamic character. Moreover, the deformation of one signal shape into another occurs when they are descriptively near (Peters, 2014).

In sum, the concept of antipodal points can be generalized to countless types of system signals. The two antipodal points can indeed be used for the description not only of simple topological points but also of more complicated structures, such as shapes of space (spatial patterns), shapes of time (temporal patterns), thermodynamical parameters, movements, trajectories, and general symmetries (Peters, 2014).

If we evaluate simply CNS activity instead of signals, the BUT leads naturally to the possibility of a region-based, not simply point-based, brain geometry, with many applications. A brain region can indeed have features such as area, diameter, average signal value, trajectories, and so on (Peters, 2016). We are thus allowed to describe brain symmetries as antipodal points on an n-sphere. If we map the two points on an $n - 1$-sphere, we obtain a single point. Here, the symmetry is hidden; i.e., it is not visible in dimension $n - 1$. A spontaneous symmetry breaking occurs when a symmetry is not a property of the individual states of a system but is a property of the mathematical structure that models the physical system. This is the case with the antipodal points on an n-sphere that can be mapped to the same signal value. To restore the apparently broken symmetry, we are required to evaluate only the single point in a dimension higher, where the two antipodal points will appear and the symmetry, hidden in the lower dimension, will be refurbished. In conclusion, if we enclose brain symmetries, equipped with antipodal self-similar points, into the abstract spaces of n-spheres, the former can be evaluated in the guise of projections on S^{n-1}. The two antipodal points standing for symmetries are assessed at one level of observation, whereas the single point standing for the broken symmetry is assessed at a lower level of observation.

AN EXAMPLE: INTERPRETATION OF A TESSELLATION OF AN FMRI

Here we specify the nature of the observables and the mapping of signals into the feature space used for the analysis of brain activity, and we show an application to available data sets to explain why our proposed approach offers an advance over the current set of tools. To do this, we include an application showing a graphic analysis of a brain fMRI (a so-called Delaunay tessellation) to understand better some aspects of brain computation and/or function viewed in the context of the predictions of the BUT.

We must first build a Delaunay tessellation. Each key point signal is chosen because of its feature values, which sharply contrast with its neighboring signal values. The Delaunay triangulation connects with a pair of nearest key points with a straight edge, resulting in a collection of triangles covering an image (Edelsbrunner, 2014). In its simplest form, a key point is chosen based on dominant color intensity and pixel gradient. That is, the gradient orientation of a pixel is the angle of the tangent to the pixel. A pixel gradient dominates, provided that the gradient differs sharply from its neighbors. Consider Figure 2, which contains tessellations of four fMRI images from Fox et al. (2015). The triangle vertices in the four Delaunay triangulation fMRI images are dominant (key point) brain signals in a collection of 1-sphere surface values. The upper half of Figure 2 contains a Delaunay mesh in situ (Fig. 2A) and a Delaunay mesh projected onto a 1-sphere (Fig. 2B). The lower half of Figure 2 contains the Delaunay mesh plot by itself (Fig. 2C) and the Delaunay mesh projected onto a 2-sphere by itself (Frank and Hart, 2010; Fig. 2D). If we look at this key point-based Delaunay mesh in Figure 2, we see that 1) key points associated with brain signals with high intensity and gradient orientation differ from those of neighboring fMRI pixels; 2) the Delaunay mesh connects each pair of fMRI key point pixels nearest each other; 3) the Delaunay mesh includes connections between key points among the pairs of fMRI images; 4) the connections among the four fMRI images represent mappings predicted by the BUT; i.e., at least one pair of fMRI key points is connected to a key point on another image; 5) fMRI pixel intensity and gradient orientation of a fMRI key point constitute a feature vector in R^n (Fig. 2D).

In sum, we are able to predict the occurrence of antipodal points on different fMRI images by knowing the activated points on only one of them. In effect, this means that we can know in advance which brain areas are activated at the same time. Novel patterns of simultaneous (or sequential) activities of different (smaller or larger) brain zones could be discovered and transferred to a lower dimension R^n manifold.

SYMMETRIES CAN BE EMBEDDED IN DIFFERENT KINDS OF *N*-SPHERES

The BUT can be generalized to all types of brain symmetries. Although the BUT had originally been described just in the case of n being a natural number that expresses a spatial dimension, nevertheless the value of n in the brain, S^n, can also stand for a fractional or an irrational number. The n exponent is not required either to be a natural number or to be embedded in a spatial dimension. We are allowed to modify the BUT's exponent on an n-sphere and to change a natural number into a rational or irrational one to describe n in a brain symmetric system equipped with two antipodal points. We are allowed indeed, if we take into account a BUT on d-spheres with Hausdorff dimension d, which is a fraction between 0 and 1 and is an expression of the fractal dimension.

We used the following terminology. Metric space: let X be a metric space with the metric $\mu_d(X)$ defined on it. This means that $\mu_d(X) \geq 0$ and that μ_d has the usual symmetry and triangle inequality properties for all subsets

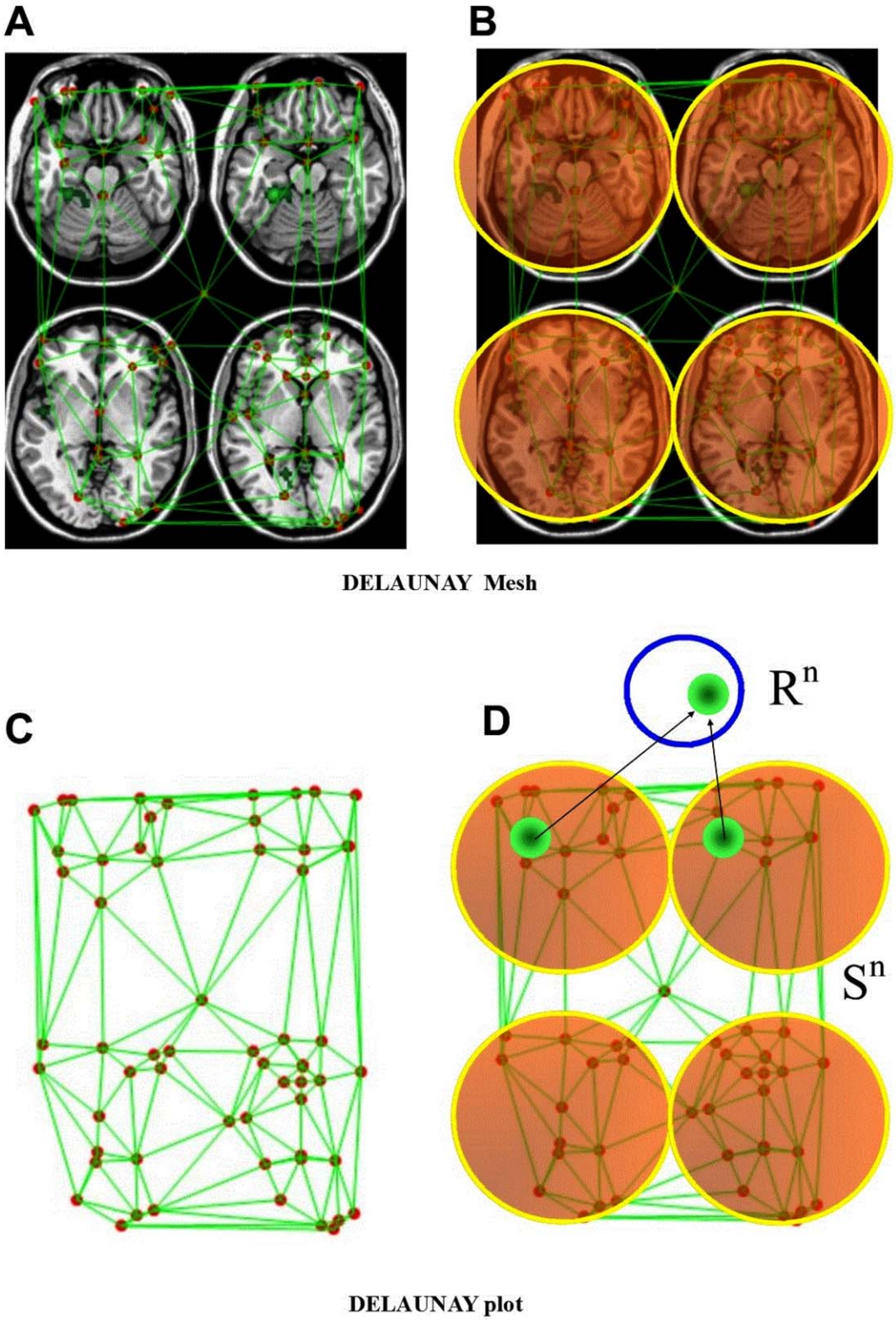

Fig. 2. Meta-analytic activations associated with mind wandering and related spontaneous thought processes throughout the entire brain. Horizontal slices are presented with 3-mm skip (modified from Fox et al., 2015). **A,C** show Delaunay tessellation; **B,D** show the same images embedded in S^n spheres, according to the BUT dictates. See article text for further details.

of X. Hausdorff measure: let d be either 0 or a positive real number in R_0^+. The Hausdorff measure $\mu_d(X)$ equals a real number for each number d in $X = R^d$. Hausdorff dimension (informal): the threshold value of d denoted by $\dim_H(X)$ is the Hausdorff dimension of X, provided that $\mu_d(X) = 0$ if $d > \dim_H(X)$ and $\mu_d(X) = \infty$ if $d < \dim_H(X)$.

Lemma

Schleicher boundedness lemma. Let d be any real number in R_0^+ and let Y be a metric space. If $X \subset Y$, then $\dim_H(X) \leq \dim_H(Y)$.

Proof: immediate from the definition of the Hausdorff dimension of a nonempty set. Assume that X is a nonempty subset (inner sphere) of an n-sphere and has the same center as S^n with the Hausdorff measure $\mu_d(X)$ defined on it, and assume that $\mu_d(X)$ satisfies the Schleicher lemma conditions. The inner sphere S^d of an n-sphere S^n can be any subsphere in S^n, including S^n itself. Then, the inner sphere S^d has dimension $d = \dim_H(X)$, $d \leq n$. In addition, assume that R^d is a d-dimensional space that is a subset of the n-dimensional Euclidean space R^n, $d < n$. This gives us a new form of the BUT (Borsuk, 1933).

Theorem

Hausdorff-Borsuk-Ulam theorem. Let S^d with Hausdoff dimension d be an inner sphere of an n-sphere and let $f{:}S^d \rightarrow R^d$ be a continuous map. There exists a pair of antipodal points on S^d that are mapped to the same point in R^d.

Proof. A direct proof that this theorem is symmetric with the proof of the BUT is given by Su (1997), given that we assume that S^d is an inner sphere of S^n symmetric around the center of S^n and, from the Schleicher boundedness lemma, $\dim_H(S^d) \leq \dim_H(S^n)$.

Summary. The BUT can be used not only for the description of spatial dimensions equipped with natural numbers but also for the description of antipodal points on brain d-spheres equipped with (fractal) Hausdorff dimension d. The same mechanism also stands for other kinds of n-spheres' dimensions other than fractals. It allows us to use the n parameter as a versatile tool for the description of CNS symmetries. The n exponent of S^n can be cast as an integer, a rational number (the above-mentioned case of self-similarity and fractal dimensions; see also paragraph 5), or an irrational number (in case we want to evaluate nonlinear, chaotic brain as embedded in a Feigenbaum constant's dimension; see example 2 below; Smith, 2013). The n exponent could stand for completely different parameters; for example, we might regard brain circadian rhythms as embedded in a sphere in which n stands for the time and not for a spatial dimension. In such a vein, we may also regard the temporal symmetries in EEG as antipodal points characterized by similarities in time occurrence and not in shape.

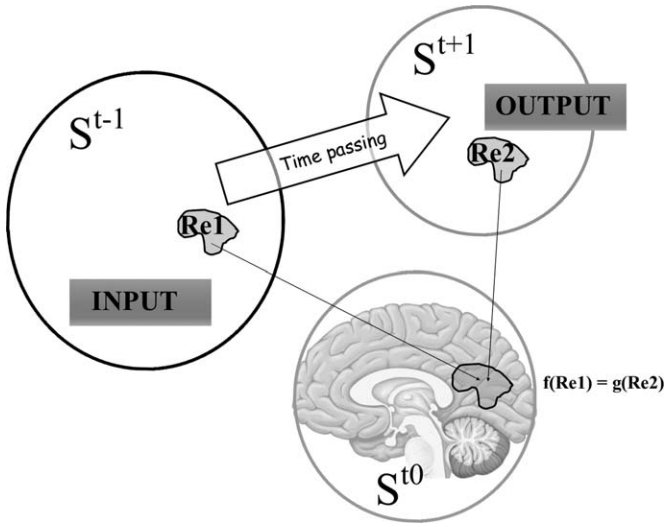

Fig. 3. A system formed by n-spheres in which n stands for a time dimension. The antipodal points Re1 and Re2 are located on a sphere equipped with a dimension of time $t - 1$ (the past) and with a dimension of time $t + 1$ (the future), respectively. The brain, equipped with time $t0$, stands for the present.

Example 1: From Stimuli to Brain Responses

The brain, in a topological framework, might stand for a system formed by two variables connected in a way such that when one changes the other changes. The initial state occurs before the variation, and the final state occurs afterward (Fig. 3). The changes can be either real or merely possible. The final state depends on two settings, the initial state of the system and the external factors acting on the system. Note that, in this case, in touch with dictates of the BUT variant, the system is formed by n-spheres equipped with time but not spatial dimensions.

Example 2: Phase Transitions and Nonlinear Dynamics in the Brain

The brain is believed to be an open system that maintains a nonequilibrium steady state (i.e., homoeostasis or allostasis) in the face of continuous environmental fluctuations (Van de Ville et al., 2010; Friston et al., 2014). It displays complex, nonlinear dynamic features and is equipped with a large number of interacting and interdependent components with random walks (Perkins et al., 2014), circular causality (Fraiman and Chialvo, 2013), and self-organized criticality (Bak et al., 1987). The brain is also said to operate at the edge of chaos (a regime characterized by dependence from initial conditions, positive Lyapunov exponents, and attractors) and tends to live near a metastable state of second-order phase transition (Afrahimovich et al., 2013; De Arcangelis et al., 2006). Sequential, hierarchical self-organization on an increasing scale leads to passage beyond reversibility in space as well as in time and to the emergence of novel features and properties at each level (Beggs and Timme, 2012; Taylor and Ehrenreigh, 2014). In this complex framework, the

BUT variant is able to elucidate (at least some of) the dynamics underlying the nonlinear brain. We must first introduce the "logistic map," which is a one-dimensional nonlinear difference equation widely used to study equations in the field of dynamic systems theory. For example, take into account the coupled equations (Richardson et al., 2014)

$$X_{(t+1)}=r_1x_{(t)}\left(1-x_{1(t)}\right)+\alpha r_2x_{2(t)}\frac{\left(1-x_{2(t)}\right)}{1+\alpha},$$

$$X_{2(t+1)}=r_2x_{2(t)}\left(1-x_{2(t)}\right)+\alpha_1r_1x_{1(t)}\frac{\left(1-x_{2(t)}\right)}{1+\alpha},$$

where x is a generic variable representing some observable behavior, r is a fixed behavioral parameter (the phase parameter), and t equals time from step 0 to step n. A logistic map may be simply plotted and visualized on a one-parameter bifurcation diagram as a function of the scaled parameter r (Fig. 4A). At the edge of criticality, a so-called Hopf bifurcation occurs. In general, every chaotic system that corresponds to a one-dimensional map with a single quadratic maximum will bifurcate at the same rate (Alligood et al., 1996); the limiting ratio of each bifurcation interval to the next between every period doubling is 4.6692 . . . . This value is called the first universal "Feigenbaum constant" (Smith, 2013); note that that such a constant is a transcendental number (Jordan and Smith, 2007).

Through our BUT variant, we achieve an n-sphere with an n-exponent corresponding to the Feigenbaum number. The next step is to locate the n-sphere on the above-mentioned logistic map to embed the topological antipodal points into the bifurcation diagram (Fig. 4A). After having achieved two antipodal points for every bifurcation, we are allowed to map them in the concentric layers of another n-sphere (Fig. 4B). We obtain a novel topological n-sphere that summarizes the whole behavior of a nonlinear system in phase transition, such as the brain. Note that the center of the sphere stands for a completely linear system, whereas, when we move along the circumference toward the sphere surface, we achieve antipodal points representing a progressively more chaotic system. In such a vein, knowledge of just the single central point and the first Feigenbaum constant leads to predictions about the temporal development of the phenomena occurring in the brain at the edge of chaos.

SYMMETRIES ARE NOT REQUIRED TO BE ANTIPODAL POINTS ON *N*-SPHERES

The applications of the BUT can be generalized not just for the evaluation of brain symmetries as antipodal points on an n-sphere but also as nonantipodal points. Indeed, a theorem derived from the BUT, the region-based version of the BUT (Re-BUT), is as follows. Let 2^{Sn} be a family of regions on an n-sphere. A region can have features such as area, diameter, average signal value, and so on.

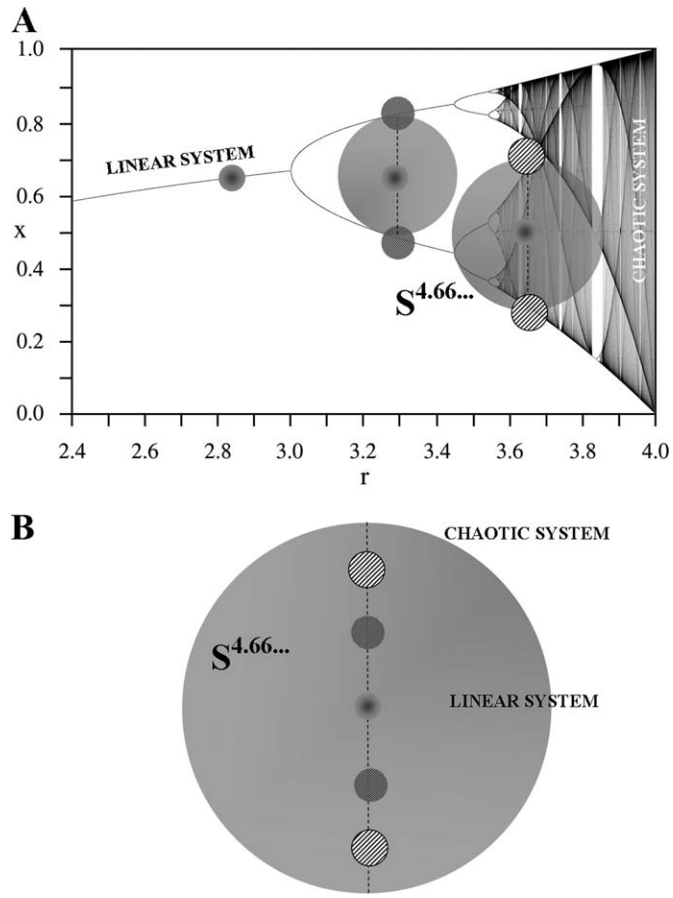

Fig. 4. **A:** Bifurcation diagram of a logistic map's nonlinear dynamic equation. The x axis displays the phase parameter. At the first Hopf bifurcation, the exponent n of the n-sphere corresponds to the first Feigenbaum constant. The same operation can be repeated at each of the following bifurcations; only the first and the second ones are displayed in the figure. Each sphere is equipped with two antipodal points that intersect the curves of the corresponding bifurcation and display the same value on the x axis. **B:** The antipodal points described for A are projected onto a single sphere that stands for A's spheres cast in a concentric way so that the center is the same for all of them.

Theorem

Re-BUT. If $f{:}2^{Sn}\rightarrow R^n$ is a continuous function, then f(Re1) = f(Re2) for a pair of regions Re1, Re2 on 2^{Sn} (Peters, 2016).

Proof. Given Re1 in 2^{Sn}, we know that there are many possible regions Re2 with matching feature values. The value of f(Re1) is a feature value of region Re1. From the fact that there is at least one other region Re2 descriptively the same as Re1 in 2^{Sn}, we have f(Re1) = f(Re2).

Example. Let f(Re1) equal the area of Re1 on an n-sphere. Because there are many regions of an n-sphere with area the same as Re1, let Re2 be one of those regions. Then, f(Re1) = f(Re2) (Fig. 5). This means that the antipodal points restriction from the classical BUT is no longer required. We can also consider homotopic

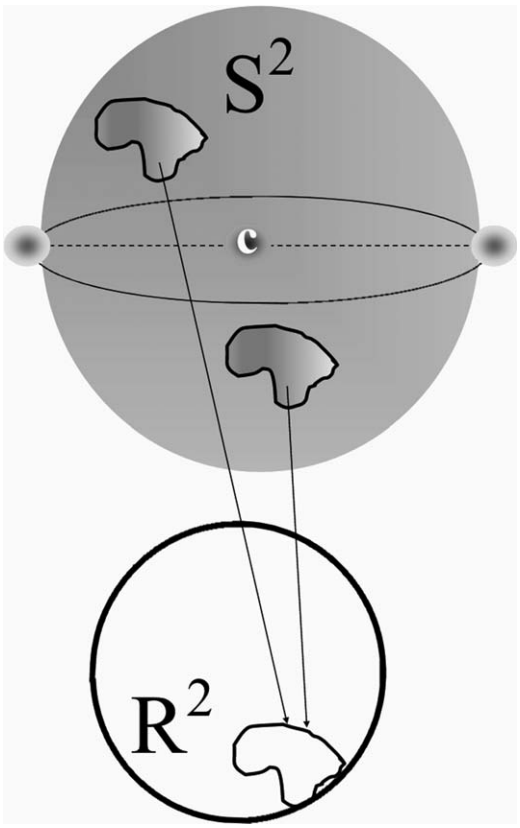

Fig. 5. Simplified sketch of the Re-BUT. The functions with matching description are not required to be antipodal. Thus, two signals, if equipped with a signal matching, may be embedded in every zone of the *n*-sphere.

brain regions on an *n*-sphere that are either adjacent or far apart, and the ReBUT applies provided that there is a pair of regions on *n*-sphere with the same feature values. We are thus allowed to say that the two points are not required to be antipodal to be described together. This makes it possible, for example, to evaluate matching signals from neuroimaging techniques, even if they are not opposite but near each other.

An Example Based on Multisensory Integration: Hierarchical Structures of the Brain

The Re-BUT applies nicely to multisensory integration (Klemen and Chambers, 2012); two environmental stimuli from different sensory modalities display similar features when mapped into cortical neurons. For example, an observer stands in front of the surrounding environment (Fig. 6), and a guitar player is embedded in the environment. The observer perceives, through his different sense organs such as his ears and eyes, the sounds and the movements produced by the player. The guitar player stands for an object embedded in a three-dimensional sphere. The two different sensory modalities produced by the player (sounds and movements) stand for nonantipodal points on the sphere's circumference. Even if objects belonging to different regions can be either different or similar depending on the objects' features (Peters, 2016), the two nonantipodal points must share the same features. In our case, both sounds and movements come from the same object embedded in the sphere, i.e., the guitar player. The two nonantipodal points project to an $n - 1$-dimensional layer, the brain cortex where multisensory neurons lie, and converge into a single multimodal signal. According to the dictates of the Re-BUT, such a single point contains "melted" messages from the two modalities, which takes into account the features of both.

The sequential processing of information is thought to be hierarchical such that the initial, low-level inputs are transformed into representations, and integration emerges at multiple processing cortical stages (Werner and Noppeney, 2009; Van den Heuvel and Sporns, 2011). Such processes of progressive message convergence could be fruitfully studied in terms of symmetries and antipodal points that converge toward a single manifold (Fig. 6). The observable brain anatomy would reside in the *n*-dimensional space (antipodal points are not glued), but, if we apply the BUT, we could hypothesize that there exists, at a certain level of abstraction, a functional space in which these homotopic regions are mapped as one single point/region, which could, for instance, make transparent the resilient redundancy of the homotopic regions at the relevant level of processing.

GENERALIZATION OF THE BUT TO SYMMETRIES OCCURRING ON HYPERBOLIC MANIFOLDS

The original formulation of the BUT describes the presence of antipodal points on spatial manifolds in every dimension, provided that the *n*-sphere is a convex, positive-curvature manifold. However, many symmetry breakings described in physics and biology (and, in particular, in the brain!) occur on manifolds equipped with another type of geometry, the hyperbolic one. The latter encloses complete Riemannian *n*-manifolds of constant sectional curvature −1 and concave shape. The models of hyperbolic space (i.e., the Klein model) share the same geometry in the sense that any of them can be related to others by a transformation that preserves the geometrical properties of the space, including isometry, though not with respect to the metric of a Euclidean embedding. From differential geometric treatments of probability measures, it is easy to see that brain manifolds traced out by sufficient statistics of a probability measure are negatively curved in nature (Watanabe et al., 2014) and therefore endowed with a hyperbolic geometry. Hyperbolic manifolds allow the study of energy gradients in brain energetic landscapes because they describe the descent to the lower energetic basins. For example, the proteins' final folded conformation is dictated by the minimum frustration principle on long time scales; proteins' energy decreases more than expected from thermodynamic claims because they assume conformations progressively more similar to the native state (Bryngelson and Wolynes,

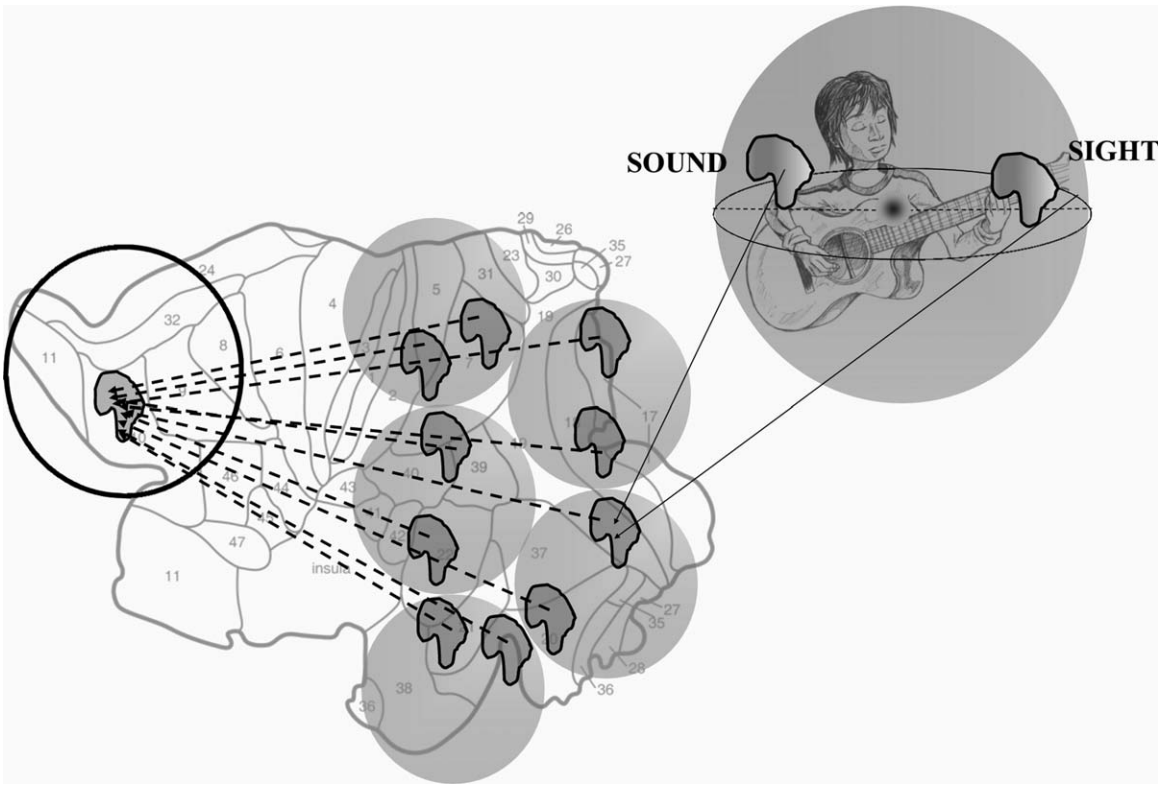

Fig. 6. Convergence of *n*-spheres' antipodal points with the same matching description. Cerebral hemispheres were unfolded and flattened into a two-dimensional reconstruction by computerized procedures (Van Essen, 2005). The final, pure abstractions achieved in the frontal lobes encompass countless different matching points from different, closely packed *n*-spheres coming from the sensory areas. The ideas (abstractions) link together antipodal points embedded in different *n*-spheres. Their projections to the "higher" areas give rise to the abstract concepts. See article text for further details.

1987; Sutto et al., 2007; Flå and Ahmed, 2011). Now the question is whether the antipodal points predicted by the BUT can be detected not only on positive-curvature manifolds, as stated by Borsuk, but also on manifolds equipped with negative curvature. In other words, is it possible to transport the BUT's antipodal points onto Riemannian manifolds with negative curvature? The answer is positive, if we perform a parallel transport of the two antipodal points of S^n onto the hyperbolic manifold (Hairer et al., 2004; Mitroi-Symeonidis, 2015). There are different routes one can take to achieve the goal. We must resort to one of the following generic transport procedures, Ehresmann connection (Ehresmann, 1950), Levi-Civita connection (Boothby, 1986), or Laplace-Beltrami operator (Jost, 2002). Also, we can retain a first-order approximation and formulate descent directions that are orthogonal to the previous descent ones through numerical analysis with the conjugate gradient-descent algorithm (Snyman, 2005). Routinely used in optimization, conjugate gradient-descent methods have been used in neuroimaging for gradient descent on manifolds traced out by energy functions (Sengupta et al., 2014). After a connection has been performed and the vectors corresponding to the antipodal points have been achieved on the hyperbolic manifold M^n, the standard projection method (Hairer et al., 2004) allows us to use the Riemann exponential map $\exp(\omega)$ to map the vector from $S^n \rightarrow M^n$ and the logarithmic map $\log(\omega)$ for the opposite mapping $M^n \rightarrow S^n$. Having achieved the center of the hyperbolic manifold M^n through the "ham-sandwich" theorem, we are allowed to map the two antipodal points from S^n to M^n and vice versa (Peters, 2016).

In summary, the BUT can also be generalized to symmetries occurring on concave manifolds. We are thus allowed to look for antipodal points and hidden symmetries on structures equipped with a negative curvature because this occurs for most brain symmetries and nervous energy landscapes.

LOOKING FOR SYMMETRIES IN THE BRAIN

The search for symmetry in the CNS is not an easy task; because of our lack of knowledge of brain function, we do not know exactly what (and where) the hidden symmetries are. Furthermore, it is unrealistic to think of obtaining in biology the mathematical accuracy of a physics experiment; i.e., athough a physics experiment isolates the object of study and excludes the surrounding confounding features, a biological trial must take into account countless hidden variables. As a matter of fact, recent studies have suggested that cognitive functions do

not depend solely on electrical pulses but also on intra- and extraneuronal causes, involving supramolecular interactions among biologically active macromolecules (Tozzi, 2015). Thus, the overwhelming complexity of the factors involved is beyond our current computational comprehension. It is also important to warn that descriptions cannot unambiguously characterize the etiology of fluctuation assets because similar symmetric properties may stem from qualitatively different generators that may be difficult to distinguish with our finite amount of data (Papo, 2014).

Power Laws

It has been demonstrated that the frequency spectrum of cerebral activity exhibits a scale-invariant behavior $S(f) = 1/f^n$, where $S(f)$ is the power spectrum, f is the frequency, and n is the power spectral density, the so-called dimension of the fractal (that equals the negative slope of the line in a log power vs. log frequency scatterplot; Pritchard, 1992; Milstein et al., 2009). The brain generates fluctuations with complex scaling properties even in the absence of exogenous perturbations or changes in parameters controlling its activity (Papo, 2014), and the scale-invariant behavior involves not only the cortical electrical activity but also spontaneous neurotransmitter release (Fox and Raichle, 2007). Indeed, studies have suggested that a universal scaling is a spatiotemporal property of the brain, characterizing a large class of cerebral models and physiological signals (De Arcangelis et al., 2006). The emergence of power-law distributions has been interpreted in terms of self-organized criticality (Lübeck, 2004), a successful framework that refers to a mechanism of slow energy accumulation and fast energy redistribution, driving the system toward a critical state (De Arcangelis and Herrmann, 2010). In analyzing the scaling properties, it has been proposed that cognitive processes can be framed in terms of complex generic properties of brain activity at rest and, ultimately, of functional equations, limiting distributions, symmetries, and possibly universality classes characterizing them (Sengupta and Stemmler, 2014). Power-law distributions contain information on how large-scale physiological and pathological outcomes arise from the interactions of many small-scale processes (Jirsa et al., 2014). The above-mentioned fractal dimension gives rise to a dimension greater than the classical one dimension, which is generally attributed to the normal curves embedded in a standard Euclidean space (Mandelbrot, 1967). More importantly, the fractal dimension encourages us to take another look at the mechanisms that give rise to the brain's power-law distributions. As stated above, the BUT variants can be used for the description of antipodal points on d-spheres equipped with Hausdorff (fractal) dimension d. It is thus suitable to make use of rational numbers, instead of integer ones, as n exponents in S^n. The mechanism of a slope corresponding both to the α exponent and the n-dimension is valid both for spatial fractals (Fig. 7A) and for temporal power-laws plots (Fig. 7B).

Equalizing Excitation–Inhibition Ratios Across Cortical Neurons

Another symmetry has recently been found in the CNS. An unexpected degree of order has been revealed in the spatial distribution of synaptic strengths. This is a mechanism by which the neurons equalize the strengths of excitation (E) and inhibition (I), and the brain maintains its internal balance not only in time but also in space (Xue et al., 2014). Specifically, there is a constant E/I ratio between the total amount of excitatory and inhibitory stimulation (Sengupta et al., 2013a; Sengupta and Stemmler, 2014). E/I ratio is stable, both in vitro and in the intact and spontaneously active cerebral cortex, not only for individual pyramidal neurons at a given time (Haider et al., 2006) but also across multiple cortical neurons (Xue et al., 2014) and during neural avalanches (Lombardi et al., 2012). E and I are always matched; an optimal E/I ratio across neurons is maintained, despite fluctuating cortical activity levels, through the appropriate strengthening or weakening of inhibitory synapses, carried out by an increased recruitment of parvalbumin-expressing inhibitory neurons (Xue et al., 2014). The relationship between the two opposing forces in the mammalian cerebral cortex affects many cortical functions, such as feature selectivity and gain (Sengupta et al., 2013a) or memory of past activity (Lombardi et al., 2012). It may allow for rapid transitions between relatively stable network states (Sengupta et al., 2013b), permitting the modulation of neuronal responsiveness in a behaviorally relevant manner. E/I ratio could be interpreted as evidence of a homeostatic mechanism among strengthening and weakening processes in the adaptation of real synapses, both at the single neuron level and at the network excitability level. Homeostatic systems induce a distinction between inhibitory and excitatory connections that could contribute to symmetry breaking, leading to directed coupling and information transfer (Tognoli and Kelso, 2014). E/I ratio could thus be regarded as the symmetry of the intact and spontaneously active cerebral cortex.

A Matter of Energy?

An issue of central importance in this context is the recently proposed free-energy principle for adaptive systems, which tries to provide a unified account of action, perception, and learning (Friston, 2010). Any self-organizing system at equilibrium with its environment must minimize its (variational) free energy, thus resisting a natural tendency to disorder/entropy. The Bayesian probability of sensory states (interoceptive and exteroceptive) must have low entropy, and, because entropy is also the average self-information or "surprise," the brain must avoid surprises. The feasibility of a calculation based on entropy has been demonstrated to be useful in the basic understanding of neural function (Friston, 2008). The

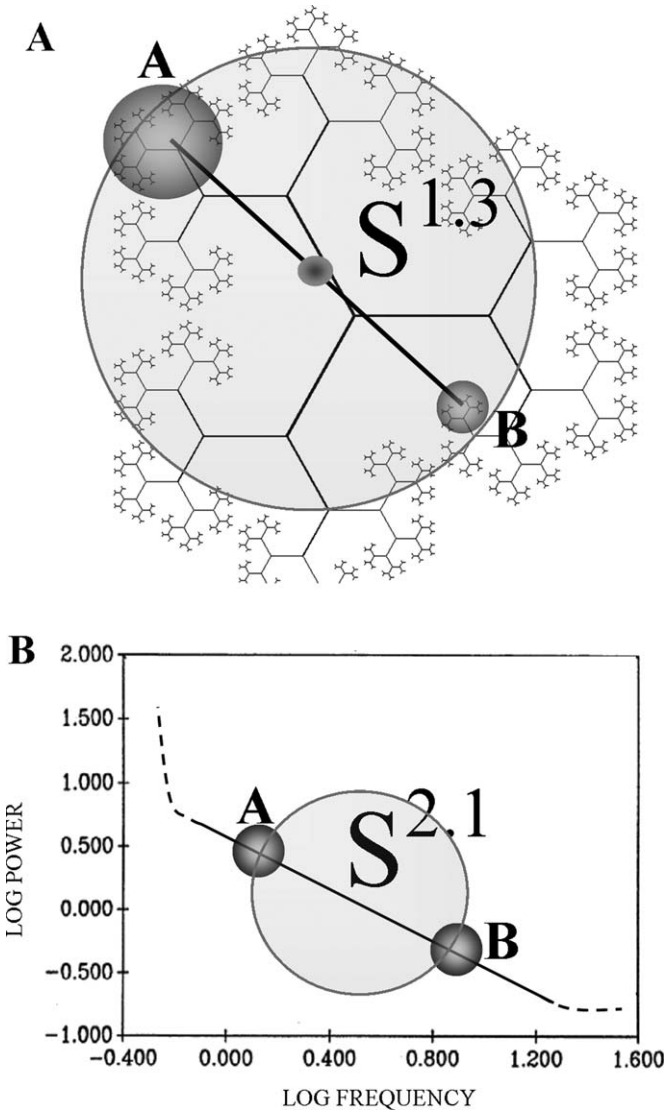

Fig. 7. Antipodal points on self-similar structures. **A:** Spatial fractals embedded in an n-sphere equipped with n corresponding to a rational number (in this case, 1.3). The circles labeled A and B depict fractals at lower and higher magnification, respectively. They have matching descriptions. **B:** The plot displays log power vs. log frequency of an electric wave along with the regression line (modified from Pritchard, 1992). The regression line's slope (in this case, $\alpha = 2.1$) is the linear alignment of the data points reflecting the dominant power law. The plot displays an example of the "temporal" variant of scale-free behavior (the so-called power laws) in the framework of the BUT; if we take into account a system with, i.e., a fractal dimension $D = 2.1$, we may regard the spatial $1/f^{\alpha}$ structure (equipped with antipodal points A and B) as embedded in a sphere $S^{2.1}$, which is equipped with a value of n corresponding to the fractal dimension α. Note that the BUT is not valid at the slope's tails, where the α exponent is lost (dotted lines at right and left of the main slope).

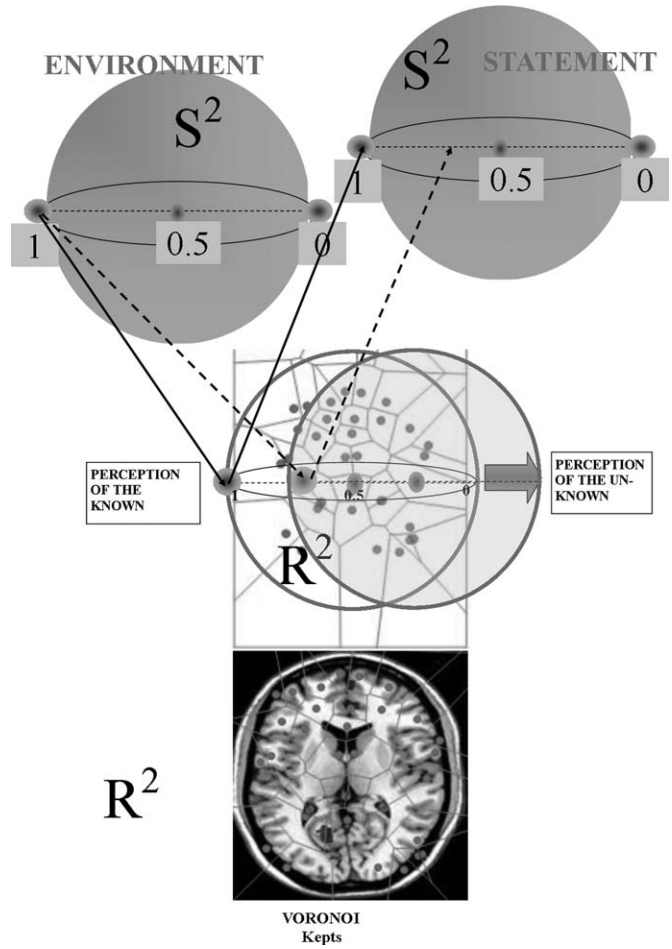

Fig. 8. The "oscillating" R^n manifold. The inputs (the environment) and outputs (in this case, the statement correlated with the environmental input) are located on two spatial n-spheres, each one equipped with antipodal points corresponding to 1 (on state) and 0 (off state) and with a center corresponding to 0.5 (fuzzy, uncertain state). The two antipodal points map to a point located on the diameter of a Euclidean manifold R^n that, in this case, stands for groups of neurons equipped with logic gates (prepared through another type of tessellation, the Voronoi). An input 1 is projected to R^n and then maps, for the Re-BUT theorem, to the output n-sphere in position 1. However, when the output (say, 0.3) is different from the input (say, 1), this means that the R^n sphere has moved horizontally and its center has moved. In this case, the input 1 does not map any longer to 1 on R^n but rather to 0.3 so that R^n projects to the output 0.3 even if the input is 1. If the input and the output are known (e.g., 1 and 0.3, respectively), we can calculate the change occurring in the R^n projection. To compare the two different projections on R^n, we are required to know only how much the center of the R^n sphere has moved. We can thus predict, given a known input, which cortical areas were activated when the output has changed; we are required to look at only the R^n tessellation and to see where the novel position of the point (corresponding to an activated zone) is located.

variational free-energy principle separates the environment (the external states) from the agent (the internal states; Friston, 2013). Agents can suppress free energy (or surprise) by changing the two things on which it depends; they can either change sensory input by acting on the world or modify their internal states via different perceptions (Sengupta et al., 2013b). Figure 8 displays the process of perception in Bayesian and topological terms. The

brain uses Bayesian beliefs to evaluate whether a matching description takes place. If it occurs, we achieve the "known" (i.e., "I see a cat"). When the description is, instead, not matching, a Kullback-Leibler divergence takes place and we attain the "unknown" (i.e., "I'm not sure whether I'm seeing a cat or a lynx"). There are two possible ways to compensate and achieve once again the known; either the R^n sphere moves, say, to the right (change in mental priors) or it moves to the left (body movements in search of the expected signals in the environment). Variations can thus be removed either through peripheral action (practical behavior) or through brain action (theoretical behavior).

The "ancient" Richard Avenarius (1907) and Ernst Mach (1897) indicated that the relation of the "I" (the corporeal presence of the human being) to the environment (the spatial presence of the object) is determined in such a way that both are present as common and inseparable elements. The "I" is found to be present just as much as the environment. This interconnection and inseparability of the "I" and its surroundings constitutes an essential association and homogeneity of the two coordinated values, setting in motion a circular process, from any point within which the whole complex of changes may start. In sum, the ideal point of rest, about which the life of the organism moves in constant oscillations, also has a logical–mathematical significance when framed as a topological theory.

The viability of the CNS is influenced by a balance between the metabolic cost incurred (in terms of ATP) by its operation and the information theoretic benefits realized by energy expenditure (Sengupta and Stemmler, 2014). The metabolic activity of the brain is remarkably constant over time (Raichle and Gusnard, 2002), and the energy budget (that is, the energy use by various neuronal processes) has been calculated (Sengupta et al., 2010). Minimizing variational free energy requires a metabolically efficient encoding that is consistent with the principles of minimum redundancy and maximum information transfer (Sengupta et al., 2013b). Maximizing mutual information and minimizing metabolic costs are two sides of the same coin; by decomposing variational free energy into accuracy and complexity, one can derive the principle of maximum mutual information as a special case of maximizing accuracy, whereas minimizing complexity translates into minimizing metabolic costs. Despite an apparent resistance to the natural tendency to increase entropy, nonequilibrium steady state is maintained (Sengupta and Stemmler, 2014). To solve this problem, one uses a (Bayesian) information theoretic construct called "variational free energy," which is a proxy for entropy; minimizing entropy production corresponds to the principle of minimizing variational free energy at each point in time. Variational free energy may be considered a sort of symmetry for systems that attain nonequilibrium steady state; accordingly, we can treat it exactly as a Lagrangian and, implicitly, as a way of minimizing entropy. Thus, the variational free energy is the Lagrangian, which is the expression of the underlying brain symmetry.

Quantum Mind Theories

Thus far, symmetrical theories of the CNS have been proposed in the framework of quantum mind theories (Freeman and Vitiello, 2008). Some of these models resemble lattice gauge theory of high-energy physics, whereas others are quantum systems, not in the sense that they consist of quantum components (such as any physical system) but that their macroscopic properties cannot be explained without recourse to an underlying quantum dynamics. Because it is not possible to test these hypotheses because of our lack of knowledge of the quantum effects in the brain, we will not go through these theories but will briefly summarize the most interesting concepts. Many models are based on the notion of spontaneous breakdown of symmetry (Freeman and Vitiello, 2008). The dynamic symmetry that gets broken is the rotational symmetry of the electric dipole vibrational field of the water molecules and other biomolecules present in the brain structures. The external input or stimulus acts on the brain as a trigger for the breakdown of the dipole rotational symmetry. When the system is not in the least-energy state, mathematical consistency requires the existence of massless particles, the Nambu-Goldstone quanta, that are normally observed in solid-state physics. It has been hypothesized that long-range correlations established by the coherent condensation of bosons may have a role in memory storage, learning, and consciousness (Matsui, 2001).

CONCLUSIONS: WHY?

This Review describes a general topological mechanism that explains the phenomenon of broken symmetries in the brain. The model is cast in an experimental fashion that has the potential of being operationalized. The question here is: why? What does a topologic reformulation help in the evaluation of brain hidden symmetries? First of all, it must be emphasized that the symmetries are widespread at every level of organization and may be regarded as the most general feature of systems, perhaps more general than free-energy and entropy constraints. Indeed, recent data suggest that thermodynamic requirements have close relationships with symmetries. The novel, interesting observation that entropy production is strictly correlated with symmetry breaking in quasistatic processes paves the way for using system invariances for estimation of the brain metastable states' free energy and the energy requirements of neural computations and information processing (Roldán et al., 2014). Thus, providing insights into symmetries provides a very general approach to every kind of brain function and dynamics. A shift in conceptualizations is evident in a brain theory of broken symmetries based on a BUT approach; the symmetries in this framework are hidden in a dimension and restored in a dimension higher and vice versa. For example, beyond the critical value, the "death" of complexity occurs, and the system falls into a supercritical regime or regularity (Zare and Gringolini, 2013). In such a vein, the fractal dimension characterizing the low-frequency spikes

of the spontaneous brain activity is lost when high-frequency spikes are activated by sensations and perceptions (Allegrini et al., 2009; Buszaki and Watson, 2012).

Furthermore, the invaluable opportunity to treat the elusive brain phenomena as topological structures allows us to describe symmetries in the language of powerful analytical tools, such as combinatorics, hereditary set systems (Matoušek, 2003), simplicial complexes, homology theory, and functional analysis. Also, generalizations of the BUT, such as the Grassmann manifolds (Dol'nikov, 1992) and the Bourgin-Yang-type theorems (Yang, 1954), could be fruitfully used in the study of nervous hidden symmetries. Embracing the BUT approach to symmetries means that the "real" brain activities can be described as paths or trajectories on abstract structures (called "topological manifolds"). This takes us into the powerful realm of algebraic topology, in which the abstract metric space (a projection of the environment's real geometric space) constitutes sufficient statistics. Moreover, attempts are being made to provide a systematic way of characterizing symmetries in the network structures of the connectome by inspecting the eigenvalues of different types of connectivity matrices (Esposito et al., 2014).

We conclude with a semantic consideration; the terms "symmetry" and "symmetry breaking" might appear somewhat arbitrary because it could be argued that the $n - 1$ space is more symmetrical than the n-dimensional space that it maps (in terms of group theory/theoretical physics), given that the antipodal gluing does not lead to opposite infinities/limits but only to a circular continuum that erases a discontinuity. We want to anticipate such possible hermeneutical confusion in some of the readership by emphasizing that our use of symmetries displays the invaluable advantage not only in treating the characteristic occurrence in cortical dynamics of complex fluctuations as a physical object (Tononi, 2008) but also in classifying measurable cognitive functions as operators acting on symmetries (Papo, 2014). By changing physical space into the dialectics symmetry/topology, paradoxes of nervous activity are more easily exposed; the BUT language opens up a virtual window into spaces beyond our brain's physical three-dimensional structure.

CONFLICT OF INTEREST STATEMENT

The authors do not have any known or potential conflicts of interest, including any financial, personal, or other relationships within three years of beginning the submitted work, with people or organizations that could inappropriately influence or be perceived to influence their work. No conflicts have been identified.

ROLE OF AUTHORS

Both authors had full access to all the data in the study and take responsibility for the integrity of the data and the accuracy of the data analysis. Study concept and design: AT, JFP. Acquisition of data: AT, JFP. Analysis and interpretation of data: AT, JFP. Drafting of the manuscript: AT, JFP. Critical revision of the article for important intellectual content: AT, JFP. Statistical analysis: AT, JFP. Obtained funding: AT, JFP. Administrative, technical, and material support: AT, JFP. Study supervision: AT, JFP.

REFERENCES

Afraimovich V, Tristan I, Varona P, Rabinovich M. 2013. Transient dynamics in complex systems: heteroclinic sequences with multidimensional unstable manifolds. Discontinuity Nonlinearity Complexity 2:21–41.

Allegrini P, Menicucci D, Bedini R, Fronzoni L, Gemignani A, Grigolini P, West BJ, Paradisi P. 2009. Spontaneous brain activity as a source of ideal 1/f noise. Phys Rev E Stat Nonlin Soft Matter Phys 80: 061914.

Alligood KT, Sauer, Yorke YA. 1996. Chaos: an introduction to dynamical systems. In: Banchoff T, Devlin K, Gonnet GH, Marsden JE, Wagon S, editors. Textbooks in mathematical sciences. New York: Springer.

Avenarius R. 1907. Kritik Der Reinen Erfahrung von Richard Avenarius. Berlin: O.R. Reisland.

Bak P, Tang C, Wiesenfeld K. 1987. Self-organized criticality: an explanation of the 1/f noise. Phys Rev Lett 59:381–384.

Beggs JM, Timme N. 2012. Being critical of criticality in the brain. Front Physiol 3:163.

Beyer WA, Zardecki A. 2004. The early history of the ham sandwich theorem. Am Math Monthly 111:58–61.

Boothby WM. 1986. An introduction to differentiable manifolds and Riemannian geometry. New York: Academic Press.

Borsuk M. 1933. Dreisätze über die n-dimensionaleeuklidischesphäre, Fund Mathematic XX:177–190.

Borsuk M. 1958–1959. Concerning the classification of topological spaces from the standpoint of the theory of retracts. Fundamenta Mathematicae XLVI:177–190.

Borsuk M. 1969. Fundamental retracts and extensions of fundamental sequences. Fund Mathematic 64:55–85.

Borsuk M, Gmurczyk A. 1980. On homotopy types of 2-dimensional polyhedral. Fundamenta Mathematicae 109:123–142.

Bryngelson JD, Wolynes PG. 1987. Spin glasses and the statistical mechanics of protein folding. Proc Natl Acad Sci U S A 84:7524–7528.

Buzsaki G, Watson BO. 2012. Brain rhythms and neural syntax: implications for efficient coding of cognitive content and neuropsychiatric disease. Dialog Clin Neurosci 14:345–367.

Cohen MM. 1973. A course in simple homotopy theory. New York: Springer-Verlag.

Collins GP. 2004. The shapes of space. Sci Am 291:94–103.

De Arcangelis L, Herrmann HJ. 2010. Learning as a phenomenon occurring in a critical state. Proc Natl Acad Sci U S A 107:3977–3981.

De Arcangelis L, Perrone-Capano C, Herrmann HJ. 2006. Self-organized criticality model for brain plasticity. Phys Rev Lett 96:028107.

Deco G, Jirsa VK. 2012. Ongoing cortical activity at rest: criticality, multistability, and ghost attractors. J Neurosci 32:3366–3375.

Dodson CTJ, Parker PE. 1997. A user's guide to algebraic topology. Dordrecht: Kluwer.

Dol'nikov VL. 1992. A generalization of the ham sandwich theorem. Math Notes 52:771–779.

Edelsbrunner H. 2014. A short course in computational geometry and topology. Berlin: Springer.

Ehresmann C. 1950. Les connexionsinfinit'esimalesdans un espacefibrée differentiable. Bruxelles: Colloque de Topologie. p 29–55.

Esposito U, Giugliano M, van Rossum M, Vasilaki E. 2014. Measuring symmetry, asymmetry, and randomness in neural network connectivity. PloS One 9:e100805.

Flå T, Ahmed S. 2011. Evolution of cold-adapted protein sequences. In: Fung GPC, editor. Sequence and genome analysis II: methods and applications. iConcept Press.

Fox KC, Spreng RN, Ellamil M, Andrews-Hanna JR, Christoff K. 2015. The wandering brain: meta-analysis of functional neuroimaging studies of mind wandering and related spontaneous thought processes. Neuroimage 111:611–621.
Fox MD, Raichle ME. 2007. Spontaneous fluctuations in brain activity observed with functional magnetic resonance imaging. Nat Rev Neurosci 8:700–711.
Fraiman D, Chialvo DR. 2012. What kind of noise is brain noise: anomalous scaling behavior of the resting brain activity fluctuations. Front Physiol 3:307.
Frank NP, Hart SM. 2010. A dynamical system using the Voronoï tessellation. Am Math Monthly 117:92–112.
Freeman WJ, Vitiello G. 2008. Dissipation and spontaneous symmetry breaking in brain dynamics. J Phys A Math Theor 41:304042.
Friston K. 2008. Hierarchical models in the brain. PLoS Comput Biol 4: e1000211.
Friston K. 2010. The free-energy principle: a unified brain theory? Nat Rev Neurosci 11:127–138.
Friston K. 2013. Life as we know it. J R Soc Interface 10:20130475.
Friston K, Sengupta B, Auletta G. 2014. Cognitive dynamics: from attractors to active inference. Proc IEEE 102:427–445.
Haider B, Duque A, Hasenstaub AR, McCormick DA. 2006. Neocortical network activity in vivo is generated through a dynamic balance of excitation and inhibition. J Neurosci 26:4535–4545.
Hairer E, Lubich C, Wanner G. 2004. Geometric numerical integration: structure preserving algorithms for ordinary differential equations. New York: Springer.
Higgs P. 1964. Broken symmetries and the masses of gauge bosons. Phys Rev Lett 13:508–509.
Jirsa VK, Stacey WC, Quilichini PP, Ivanov AI, Bernard C. 2014. On the nature of seizure dynamics. Brain 137:2210–2230.
Jordan DW, Smith P. 2007. Nonlinear ordinary differential equations: introduction for scientists and engineers, 4th ed. Oxford: Oxford University Press.
Jost J. 2002. Riemannian geometry and geometric analysis. Berlin: Springer-Verlag.
Klemen J, Chambers CD. 2012. Current perspectives and methods in studying neural mechanisms of multisensory interactions. Neurosci Biobehav Rev 36:111–133.
Krantz SG. 2009. A guide to topology. Washington, DC: The Mathematical Association of America.
Lombardi F, Herrmann HJ, Perrone-Capano C, Plenz D, de Arcangelis L. 2012. Balance between excitation and inhibition controls the temporal organization of neuronal avalanches. Phys Rev Lett 108:228703.
Lübeck S. 2004. Universal scaling behavior of nonequilibrium phase transitions. Int J Mod Phys B 18:3977–4118.
Mach E. 1897. The analysis of sensations. Mineola, NY: Dover.
Mandelbrot B. 1967. How long is the coast of Britain? Statistical self-similarity and fractional dimension. Science 156:636–638.
Manetti M. 2015. Topology. Heidelberg: Springer.
Marsaglia G. 1972. Choosing a point from the surface of a sphere. Ann Math Statist 43:645–646.
Matoušek J. 2003. Using the Borsuk-Ulam Theorem. Lectures on topological methods in combinatorics and geometry. Berlin Heidelberg: Springer-Verlag.
Matsui T. 2001. Gauge symmetry and neural networks. In: Janke W, et al., editors. Fluctuating paths and fields. Singapore: World Scientific. p 271–280.
Milstein J, Mormann F, Fried I, Koch C. 2009. Neuronal shot noise and Brownian 1/f2 behavior in the local field potential. PloS One 4:e4338.
Mitroi-Symeonidis F-C. 2015. Convexity and sandwich theorems. Eur J Res Appl Sci 1:9–11.
Moura E, Henderson DG. 1996. Experiencing geometry: on plane and sphere. Upper Saddle River, NJ: Prentice Hall.
Papo D. 2014. Functional significance of complex fluctuations in brain activity: from resting state to cognitive neuroscience. Front Syst Neurosci 8:112.
Perkins TJ, Foxall E, Glass L, Edwards R. 2014. A scaling law for random walks on networks. Nat Commun 5:5121.
Peters JF. 2014. Topology of digital images. Visual pattern discovery in proximity spaces. Intelligent Systems Reference Library, vol 63. Berlin: Springer.
Peters JF. 2016. Computational proximity. Excursions in the topology of digital images. Intelligent Systems Reference Library. Berlin: Springer (submitted).
Pritchard WS. 1992. The brain in fractal time: 1/f-like power spectrum scaling of the human electroencephalogram. Int J Neurosci 66:119–129.
Raichle ME, Gusnard DA. 2002. Appraising the brain's energy budget. Proc Natl Acad Sci U S A 99:10237–10239.
Richardson MJ, Dale R, Marsh KL. 2014. Complex dynamical systems in social and personality psychology. In: Reis HT, Judd CM, editors. Handbook of research methods in social and personality psychology, 2nd ed. Cambridge: Cambridge University Press.
Roldán E, Martínez IA, Parrondo JMR, Petrov D. 2014. Universal features in the energetics of symmetry breaking. Nat Phys 10:457–461.
Sengupta B, Stemmler MB. 2014. Power consumption during neuronal computation. Proc IEEE 102:738–750.
Sengupta B, Stemmler M, Laughlin SB, Niven JE. 2010. Action potential energy efficiency varies among neuron types in vertebrates and invertebrates. PLoS Comput Biol 6:e1000840.
Sengupta B, Laughlin SB, Niven JE. 2013a. Balanced excitatory and inhibitory synaptic currents promote efficient coding and metabolic efficiency. PLoS Comput Biol 9:e1003263.
Sengupta B, Stemmler MB, Friston KJ. 2013b. Information and efficiency in the nervous system—a synthesis. PLoS Comput Biol 9: e1003157.
Sengupta B, Friston KJ, Penny WD. 2014. Efficient gradient computation for dynamical models. Neuroimage 98:521–527.
Smith R. 2013. Period doubling, information entropy, and estimates for Feigenbaum's constants. Int J Bifurcation Chaos 23:1350190.
Snyman JA. 2005. Practical mathematical optimization: an introduction to basic optimization theory and classical and new gradient-based algorithms. New York: Springer.
Sutto L, Latzer J, Hegler JA, Ferreiro DU, Wolynes PG. 2007. Consequences of localized frustration for the folding mechanism of the IM7 protein. Proc Natl Acad Sci U S A 104:19825–19830.
Taylor MB, Ehrenreich IM. 2014. Genetic interactions involving five or more genes contribute to a complex trait in yeast. PLoS Genet 10: e1004324.
Tognoli E, Kelso JA. 2014. Enlarging the scope: grasping brain complexity. Front Syst Neurosci 8:122.
Tononi G. 2008. Consciousness as integrated information: a provisional manifesto. Biol Bull 215:216–242.
Tozzi A. 2015. Information processing in the CNS: a supramolecular chemistry? Cogn Neurodyn 9:463–477.
Van de Ville D, Britz J, Michel CM. 2010. EEG microstate sequences in healthy humans at rest reveal scale-free dynamics. Proc Natl Acad Sci U S A 107:18179–18184.
Van den Heuvel MP, Sporns O. 2011. Rich-club organization of the human connectome. J Neurosci 31:15775–15786.
Van Essen DC. 2005. A population-average, landmark- and surface-based (PALS) atlas of human cerebral cortex. Neuroimage 28:635–666.
Watanabe T, Hirose S, Wada H, Imai Y, Machida T, Shirouzu I, Konishi S, Miyashita Y, Masuda N. 2014. Energy landscapes of resting-state brain networks. Front Neuroinform 8:12.
Weeks JR. 2002. The shape of space, 2nd ed. New York: Marcel Dekker.

Weisstein EW. 2015. Antipodal points. http://mathworld.wolfram.com/AntipodalPoints.html
Werner S, Noppeney U. 2009. Superadditive responses in superior temporal sulcus predict audiovisual benefits in object categorization. Cereb Cortex 20:1829–1842.
Weyl H. 1982. Symmetry. Princeton, NJ: Princeton University Press.
Willard S. 1970. General topology. Mineola, NY: Dover.
Xue M, Atallah BV, Scanziani M. 2014. Equalizing excitation–inhibition ratios across visual cortical neurons. Nature 511:596–600.
Yang CT. 1954. On theorems of Borsuk-Ulam, Kakutani-Yamabe-Yujob, and Dynson, I. Ann Math 60:262–282.
Zare M, Grigolini P. 2013. Criticality and avalanches in neural network. Chaos Solitons Fractals 55:80–94.
Zeidler E. 2011. Quantum field theory III: gauge theory. New York: Springer.

Neuroscience Letters 626 (2016) 99–105

Contents lists available at ScienceDirect

Neuroscience Letters

journal homepage: www.elsevier.com/locate/neulet

Research paper

Brain tissue tessellation shows absence of canonical microcircuits

James F. Peters[a], Arturo Tozzi[b,*], Sheela Ramanna[c]

[a] Department of Electrical and Computer Engineering, University of Manitoba, 75A Chancellor's Circle, Winnipeg, MB R3T 5V6, Canada
[b] Center for Nonlinear Science, University of North Texas, 1155 Union Circle, #311427, Denton, TX 76203-5017, USA
[c] Department of Applied Computer Science, University of Winnipeg, Winnipeg, MB R3B 2E9, Canada

HIGHLIGHTS

- Tessellation techniques allows the detection of clusters of activity in 2D images.
- The technique is able detect functional information from morphological pictures.
- It shows that the anatomical brain micro-structure is constrained towards peculiar points in each layer.

ARTICLE INFO

Article history:
Received 14 January 2016
Received in revised form 25 March 2016
Accepted 28 March 2016
Available online 17 May 2016

Keywords:
Topology
Brain
Histology
Voronoi
Phrenology

ABSTRACT

We provide a novel, fast and cheap method for the morphological evaluation of simple 2-D images taken from histological samples. This method, based on computational geometry, leads to a novel kind of "tessellation" of every type of biological picture, in order to locate the zones equipped with very fine-grained differences in the tissue texture, compared with the surrounding ones. As an example, we apply the technique to the evaluation of histological images from brain sections and demonstrate that the cortical layers, rather than being a canonical assembly of homogeneous cells as usually believed, display scattered neuronal micro-clusters equipped with higher activity than the surrounding ones.

© 2016 Elsevier Ireland Ltd. All rights reserved.

1. Introduction

The current paradigms in neuroscience regard the cortex as homogenous, *i.e.*, all areas are composed of a basic, repeated assembly of the same canonical microcircuit [1–4]. However, novel data point towards an alternative hypothesis. Some authors claim that each neocortical region represents an independent organ, dedicated to a complete and distinct function [5,6]. This idea, first put forward by Gall and Spurzheim, is still tangible in many current mapping studies aimed at localizing functions, commonly referred to as functional segregation specialisation. Such functional cartography with the aid of neuroimaging techniques has been characterized as "phrenology" [7]. Contrary to the standard model, the cerebral cortex is composed not only of discrete organs or regions, but also of distinct and unique neuronal assemblies spanning from the macromolecular to microcircuit scale. The cortex comprises extremely heterogeneous cells, with distinct regional variations, receptor repertoire and intrinsic microcircuitry [8]: this suggests that every neuron (or group of neurons, of assemblies of neuronal/glial cells, or intra- extra-cellular ensembles) embodies different molecular information that has an operational effect on neuronal computation [9,10].

A morphological analysis of simple 2D images taken from stained histological samples gives insights into the micro-anatomical structure of tissues and enables high-resolution mapping of neural circuitry. However, such procedures lack the possibility to evaluate the neural functional states and do not allow systematic profiling of neurons based on their connectivity. Further, the conditions of regularity and isotropy, required by standard morphometric procedures, are not fulfilled in the central nervous system, where cells are distributed in a highly complex manner. The more we investigate, the more we discover different roles and abilities in apparently homogenous populations of neurons [11]: the complexity and cellular heterogeneity of neuronal circuitry presents a major challenge to understanding the role of discrete neural populations in controlling behaviour. Here we propose a modified Voronoï tessellation (Keypoint-based Voronoï

* Corresponding author.
E-mail addresses: james.peters3@umanitoba.ca (J.F. Peters), tozziarturo@libero.it (A. Tozzi), s.ramanna@uwinnipeg.ca (S. Ramanna).

http://dx.doi.org/10.1016/j.neulet.2016.03.052
0304-3940/© 2016 Elsevier Ireland Ltd. All rights reserved.

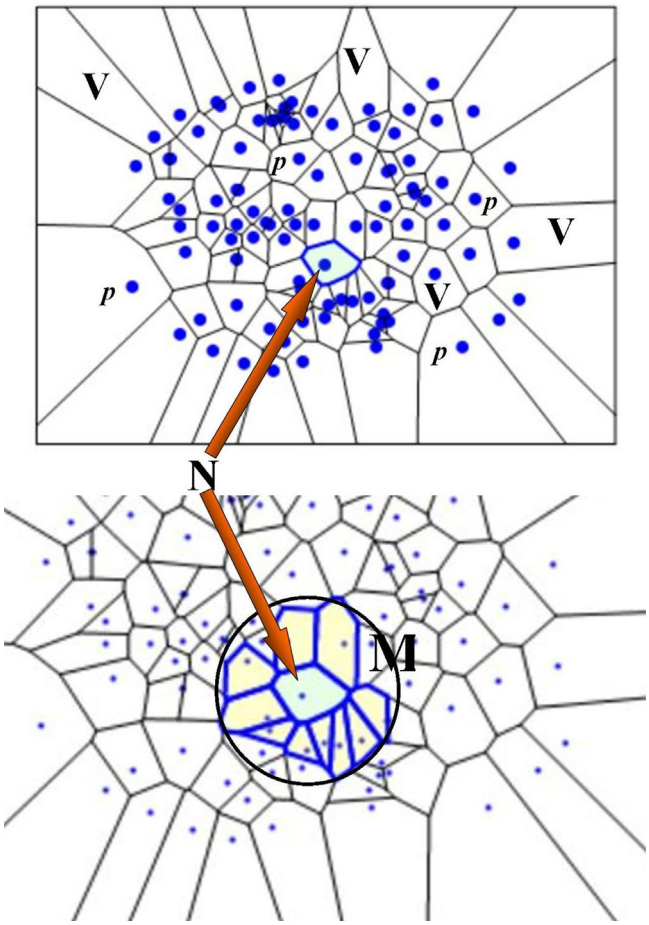

Fig. 1. A collection of Voronoï regions, called Voronoï mesh, at low and high magnification (at the top and the bottom, respectively). The figure illustrates, as an example, some generating keypoints (p), some Voronoï regions (V), a nucleus (N) and its corresponding maximal nucleus cluster (displayed into the circle M).

Tessellation, KVT) able to give insights into the physiological and pathological functional state of neural tissues too.

2. Materials and methods

2.1. Voronoï tessellation method using gradient orientation-based generating points

To establish a framework for the proposed approach to analysing images extracted from histological sample, we briefly introduce a Voronoï tessellation (tiling) of images (Fig. 1A) [12–14]. The story starts with the selection of a set *S* (a part of a histological picture) containing generating points (sites) (*p* in Fig. 1A), so that the characteristics (e.g., being part of an edge or a corner, having a distinctive gradient orientation or colour brightness) of each site is different from the characteristics of any other. In other words, the study of histological images is aided by identifying points (pixels) in each image where the angle of the tangent (gradient orientation) to a point is different from the gradient orientation of other pixels in the same image. Different gradient orientations reflect differences in the texture of a histological image. By detecting differences in the gradient orientations of the pixels in a histological image, we are able to identify very fine-grained differences in the tissue texture. We know that every pixel in an image has a gradient orientation (angle of a tangent to a pixel) [15]. And the latter is a good choice for a generating point, since pixel gradient orientations tend to fluctuate sufficiently to make it possible to find pixels that are not close together, and which reflect the characteristics of widely separated histological zones. Sites chosen based on their gradient orientation angle are a form of what are known as "keypoints". In this study, site pixels have been chosen so that each site has gradient orientation that is different from that of any other site.

After choosing a set of generating points *p* (*i.e.*, keypoints) as sites, the next task is to cover an image with non-overlapping convex polygons, called "Voronoï regions". A Voronoï region (V in Fig. 1A) is a set of points in an image that are closer to *p* than to any other site in *S*. The collection of polygons in a Voronoï tessellation is also called a "Voronoï mesh". A gradient orientation-based Voronoï tessellation provides insights concerning the physiological and pathological functional state of neural tissues. The Voronoï tessellation method has a 90-year history cogently explained in Ref. [16] with many variations [17]. Our study introduces an application of what is known as "maximal nucleus clustering" in Voronoi mesh [18]. A "nucleus cluster" is a collection of mesh polygons adjacent to a central polygon, called the "nucleus"(N in Fig. 1B). When the number of polygons adjacent to the nucleus is maximal, then the resulting "maximal nucleus cluster"(M in Fig. 1B) resides on those parts of an image having the greatest change and greatest accumulation of neighbouring Voronoï regions in close proximity to each other, in order that each site has a different gradient orientation.

Such tessellations of histological images provide information concerning spatial distribution, because the polygonal areas do not vary much when the cells are regularly distributed. On the contrary, smaller and larger polygons occur when cellular clusters (characterized by generating points with gradient orientations close to the gradient orientation angle of a nucleus) are displayed and may be identified by simple algorithms. Voronoï tessellation has been used to evaluate the numerical density and spatial distribution of neuronal and glial cells, because it takes into account the topographical features typical of the CNS [19]. It has been also used to investigate spatial relations between neural mosaics in retina, in order to evaluate possible constraints or connectivity between different co-localized cellular populations [20].

For technical readers, **Algorithm 1** gives the steps to find a maximal nucleus in a tessellated (tiled) histological image. Briefly, after a gradient orientation-based tiling of an image, those Voronoï polygons with the highest number of sides are maximal nuclei of clusters formed by each maximal nucleus and its adjacent polygons (one adjacent polygon for each edge of the nucleus).

Algorithm 1: Find Maximal Nucleus Cluster in a Voronoï tiling of a histological image by finding a Voronoï with the highest number of sides.

```
Input  : Histological Image img.
Output: Maximal Nucleus Clusters on histological image img.
/* img ⟼ TiledImg using Voronoï tessellation of img. */;
ngon ⟵⊣ TiledImg;
/* Choose a Voronoï region ngon in TiledImg. */;
NoOfSides ⟵⊣ ngon;
/* Count number of sides in ngon. */;
TiledImg := TiledImg ∖ ngon;
/* Remove ngon from TiledImg. */;
ContinueSearch := True;
while (TiledImg ≠ ∅ and ContinueSearch) do
    /* Check if ngon is a maximal nucleus in TiledImg. */;
    ngonNew ⟵⊣ TiledImg;
    /* Choose a Voronoï region ngonNew in TiledImg. */;
    TiledImg := TiledImg ∖ ngon;
    /* Remove ngon from TiledImg. */;
    NewNoOfSides ⟵⊣ ngonNew;
    /* Count number of sides in ngon. */;
    if (NewNoOfSices > NoOfSides) then
        ngon := gonNew;
        /* Replace ngon with ngonNew, since it has more adjacent polygons.
        */;
    else
        /* Otherwise ignore ngonNew. */;
    if (TiledImg = ∅) then
        ContinueSearch := False;
        /* Discontinue search when there are no polygons left to check. */;
/* ngon is the nucleus of a maximal nucleus cluster. */;
```

3. Are there relationships between morphology and function?

It is intuitively difficult to see any way to infer the degree of "functional activity" of neurons from the inhomogeneity of their distribution on histo slides. In this more theoretical paragraph, we evaluate the functional implications of our framework, introducing the concept of Borsuk-Ulam Theorem (BUT) and matching signals. The basic form of BUT tells us that there exist a pair of antipodal (opposite) points on the circumference that map to a single pointing a line [21–23]. The two antipodal points are indeed assessed at one level of observation, while the single point is assessed at a lower level [24,25]. This means that, if we embed a maximal nucleus cluster in a circumference, there exist two antipodal points with matching description (Fig. 2A). Furthermore, the two opposite points can be used not just for the description of simple topological points [26,27], but also of more complicated features, such as functions or signals [15,18,26]. If we evaluate central nervous system (CNS) "activity" instead of "points", this BUT variant (called ReBUT) leads naturally to the possibility of a region-based, not simply point-based, brain geometry. Therefore, reBUT provides a handy vehicle in expressing the relationship between Voronoï polygons that serve as cluster nuclei.

In the tiling of histological images, it may occur that more than one maximal nucleus cluster can be found, all of them equipped with the same number of sides (i.e., such maximal nucleus clusters have matching description). Thus, from reBUT, different maximal

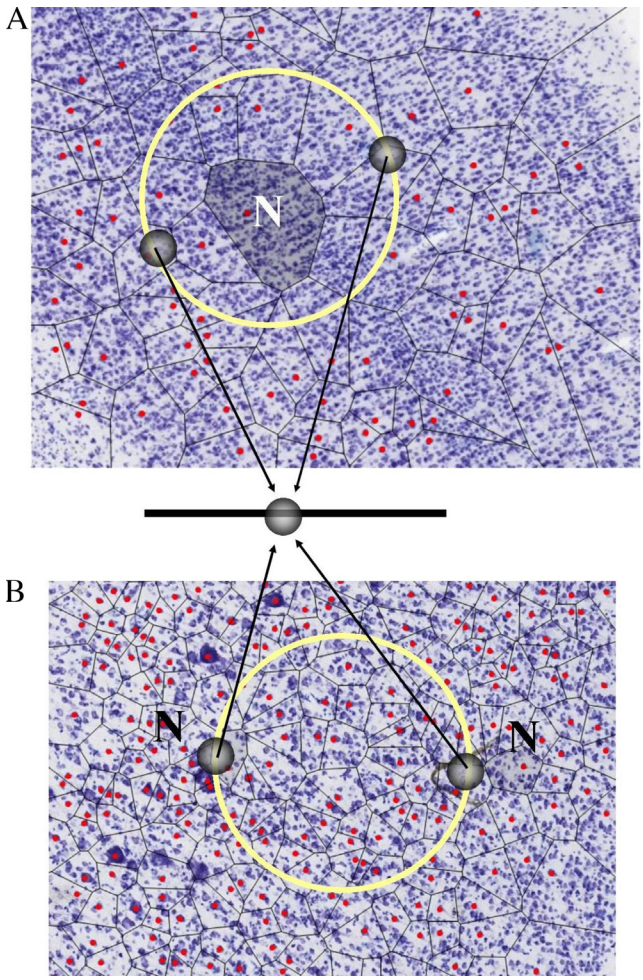

Fig. 2. (A) The Borsuk-Ulam theorem applied to histological brain tessellation. Note that a single maximal nucleus (N) displays two antipodal points with matching description. (B) The use of reBUT. Note that, this time, two different maximal nuclei display matching description.

nucleus clusters may be embedded in the same circumference and might have matching functional description (Fig. 2B). This means that systems phenomena (e.g., functions, or different types of activity) could be characterized as antipodal points with matching description, in order that the functions of signal shapes can be compared [18,27]. It might be objected that maximal nuclei polygons are not properly circular, because they display a polygonal shape and sometimes also a concave structure, different from the circumference's convexity required by the basic form of BUT. However, the BUT can be generalized also to symmetries occurring on flat or concave manifolds [18,28]. In other words, whether the system displays a concave, convex or flat shape, it does not count: we may always find the points with matching description predicted by BUT.

In conclusion, it might be speculated that changes in morphological features could be correlated with variations in physical functions. Thus, gradient differences in the various zones of the picture might be linked with different functional counterparts.

4. Materials

We achieved KVT tessellations on histological, whole-brain coronal slices from adult *Chlorocebus aethiops*. We took the brain images from the website Brain Maps.org (http://brainmaps.org/index.php). We assessed the Dataset ID 42, species *Chlorocebus aethiops*, adult, Nissl stain, embedded in gelatin, coronal plane, resolution 0.46 μm/pixel, section thickness 40 μm (http://brainmaps.org/ajax-viewer.php?datid=42&sname=385). We performed KVT on images at different magnifications, from 10× to 40×, and on separate or consecutive slices. Different cortical areas were examined.

5. Results

We found that, everywhere in the cortex, isolated small clusters of higher activity can be noticed in different layers (Figs. 3 and 4). The clusters are scattered, *i.e.*, some micro-areas of a specific layer are more active than the adjacent others embedded in the same layer. In most of the tessellations, more than one cluster is detectable.

We evaluated pictures taken from the following cortical areas: cingulate gyrus, area 4, area 3b, intraparietal sulcus, lateral sulcus, superior temporal gyrus, superior temporal sulcus and inferior temporal sulcus.

We performed KVT tessellations on 25 samples at four different magnifications (4×, 10×, 20×, 40×) and we found:

Absent clusters: (1/25 samples). Note that the absence of a cluster was localized in area 3b.

One maximal cluster: (10/25 samples). This feature was more frequent in higher magnification images (20 and 40×)

Two maximal clusters: (9/25 samples). This feature was scattered all over the magnifications.

More than two maximal clusters: (5/25 samples). This feature was more frequent in smaller magnification images (4 and 10×).

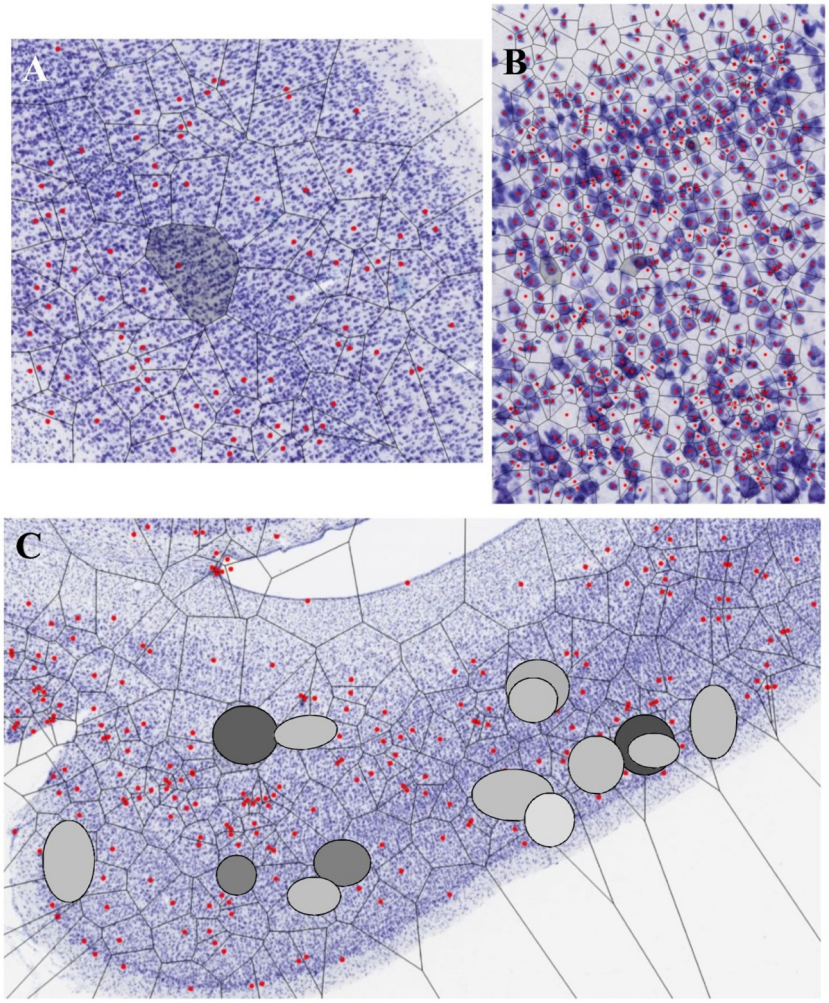

Fig. 3. Examples of keypoint-based Voronoï diagrams on images taken from cortical slices of *Chlorocebus aethiops* at different magnifications.
(A) an isolated cluster of activity (shaded in grey) is visible in layer IV of the inferior temporal sulcus at low magnification. This Voronoï diagram is characterized by one distinct nucleus and its surrounding mesh cluster.
(B) Two isolated clusters of activity are visible in layer II of the intraparietal sulcus at high magnification.
(C) Mesh clusters of activity on 10 superimposed, consecutive brain images from the inferior temporal sulcus at low magnification. The black circles refer to the presence of mesh clusters at high activity in the deepest slices, the grey circles in the intermediate slices and the white circles in the most superficial ones. Note the presence of many small, isolated clusters in all the brain layers.

The clusters were localized in all the layers from I to VI, but were more frequent in layers II–III (18/25 samples).

6. Conclusions

We showed that it is feasible to detect clusters of activity in tessellated 2D images. Given any image, it is possible to assess maximal nucleus clusters in a Voronoï tiling of histological images. The gradient orientation-based Voronoï regions outside the greatest clustering (mesh cluster around a maximal nucleus) are descriptively different, since each generating point has a different gradient orientation angle. In the language of proximity spaces, polygons outside the mesh cluster are *spatially far* from the nucleus, since no polygon outside the mesh cluster has any points in common with the nucleus, and *descriptively far* from the nucleus, since the description of the generating point for the Voronoï region is not the same as the description of the generating points of the polygons outside the mesh cluster.

Therefore, a Voronoï region that has the highest number of adjacent polygons indicates both a part of a histological image where there is the greatest clustering around a particular region, and the greatest "activity". These observations suggest that activity of the part of brain occupied by clusters is greater than the surrounding regions. Evidence comes from the fact that in all cases there are few nucleus clusters. The highest number of adjacency polygons surrounding a cluster nucleus indicates where there is the greatest concentration of symmetry among the regions of the brain images. As expected, at higher magnifications, fewer clusters are found. Smaller convex polygons are more interesting, because they belong to clusters of polygons surrounding small cluster nuclei: these clusters are important and serve as means of identifying those parts of a cortical image with more activity.

Our results show that the cortex is not a stereotyped sequence of homogeneous neurons as previously believed, but contains instead islands where the activity is higher than the surrounding ones. It is in touch with "phrenological" claims, against the standard version of canonical microcircuits view of the brain. The anatomical micro-structure of the brain is constrained towards peculiar points in each layer. Further, it is noteworthy that the activity clusters do not involve just the Nissl-stained neurons, but also their surrounding melieu. This means that other structures apart neurons contribute to the increase of activity found in specific brain micro-

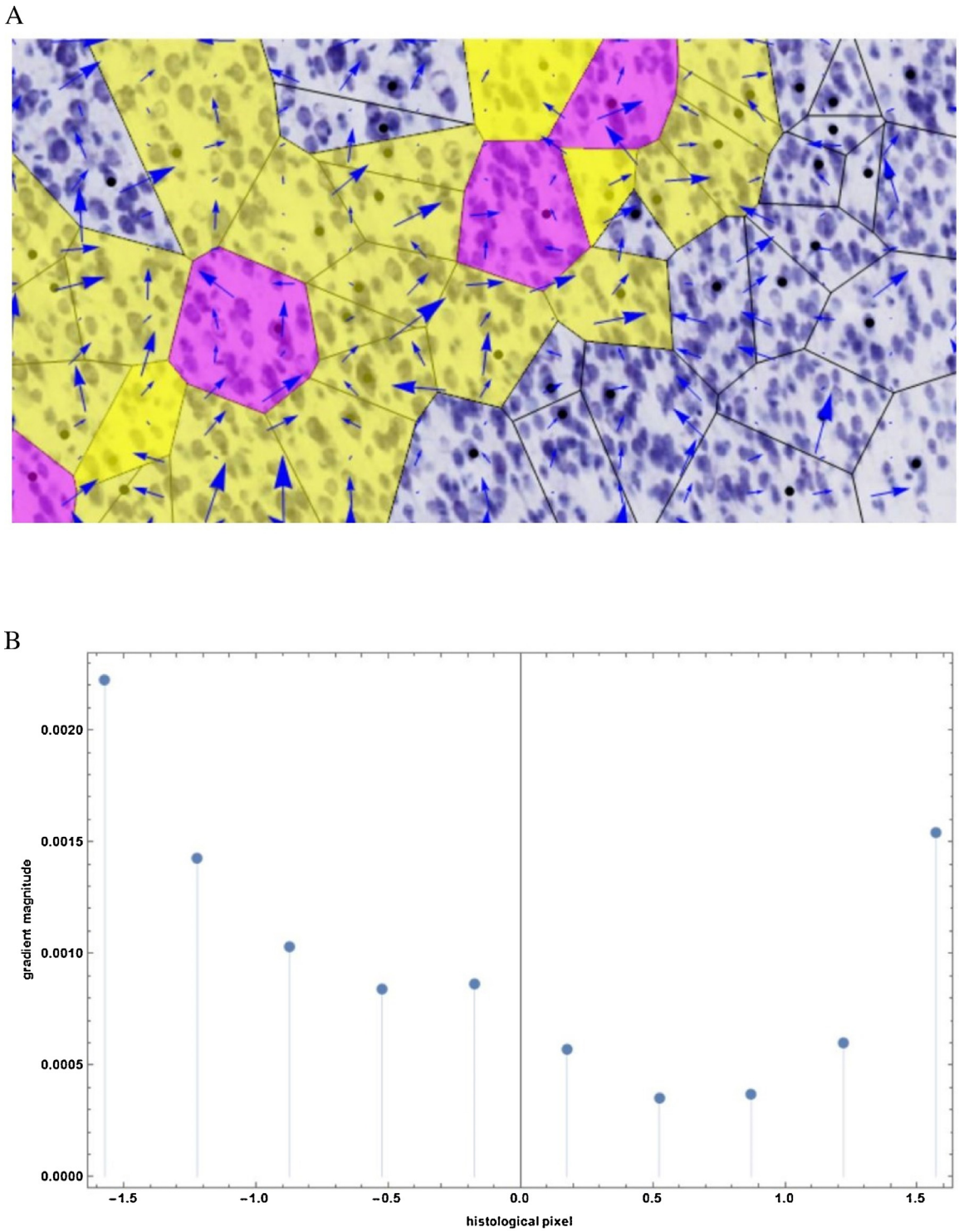

Fig. 4. (A) The tessellated image contains arrows of varying size that represent the gradient orientation of the tangent vectors for each of the different gradient orientations found. The thicker arrows indicate higher gradient magnitudes. A maximal nucleus cluster collects together those regions containing the highest number of pixels, each with a different gradient orientation. So it is entirely possible that some pixels outside the maximal nucleus cluster will have different gradient magnitudes: it tells that, although such pixels are not highly concentrated, they do reflect high gradient magnitudes. (B) presents histograms showing the number of pixels with different gradient orientations. Each histogram spike indicates those pixels with a particular gradient magnitude, such as 0.0035 for those pixels with gradient magnitudes slightly greater than 0.

areas. The gradient differences are associated with variations in the conformation of the otherwise apparently homogeneous neural assemblies: we hypothesize that they could stand, due to reBUT, for still unknown functional differences among cortical micro areas. In such a vein, the recognition of the most active cortical micro-areas through a simple morphological processing technique also allows a preliminary choice of the micro-zones to evaluate through more sophisticated techniques, such as immunohistochemistry.

In conclusion, we provide a method of physical/biological images evaluation which is easy to perform, fast (it takes 3–8 s for each KVT analysis), cheap, and able to give us information about the most “active” histological areas. We are thus allowed to detect

information from a morphological picture. In the case of histological brain tissue, our results could be summarized with a definition: "phrenology", a term which emphasizes the delicate and heterogeneous nature of cortical hierarchies with deep structures and the distribution of information coding over multiple levels and timescales [6,29]. Our study shows that 2D tessellations using algorithms that have been published [18] can be adapted to histological pictures, in the evaluation of medical and biological images.

References

[1] D.E. Rumelhart, J.L. McClelland, PDP Research Group, Parallel Distributed Processing, MIT Press, 1986, ISBN: 9780262181204.
[2] K. Friston, The free-energy principle: a unified brain theory? Nat. Rev. Neurosci. 11 (2) (2010) 127–138, http://dx.doi.org/10.1038/nrn2787.
[3] O. Sporns, Network attributes for segregation and integration in the human brain, Curr. Opin. Neurobiol. 23 (2) (2013) 162–171, http://dx.doi.org/10.1016/j.conb.2012.11.015.
[4] J. Klemen, C.D. Chambers, Current perspectives and methods in studying neural mechanisms of multisensory interactions, Neurosci. Biobehav. Rev. 36 (1) (2012) 111–133.
[5] N. Spruston, Pyramidal neurons: dendritic structure and synaptic integration, Nat. Rev. Neurosci. 9 (3) (2008) 206–221, http://dx.doi.org/10.1038/nrn2286.
[6] A. Tozzi, Information processing in the CNS: a supramolecular chemistry? Cogn. Neurodyn. 9 (2015) 463–477.
[7] R. Nieuwenhuys, J. Voogd, C. van Huijzen, The Human Central Nervous System, Springer, Heidelberg, 2008.
[8] G.N. Elston, K.S. Rockland, The pyramidal cell of the sensorimotor cortex of the macaque monkey: phenotypic variation, Cereb. Cortex 12 (10) (2002) 1071–1078.
[9] M.D. Haustein, S. Kracun, X.H. Lu, T. Shih, O. Jackson-Weaver, et al., Conditions and constraints for astrocyte calcium signaling in the hippocampal mossy fiber pathway, Neuron 82 (2) (2014) 413–429, http://dx.doi.org/10.1016/j.neuron.2014.02.041.
[10] D. Yates, Cerebral cortex: sizing up the columns, Nat. Rev. Neurosci. 14 (12) (2013) 817, http://dx.doi.org/10.1038/nrn3631.
[11] M.I. Ekstrand, A.R. Nectow, Z.A. Knight, K.N. Latcha, L.E. Pomeranz, J.M. Friedman, Molecular profiling of neurons based on connectivity, Cell 157 (5) (2014) 1230–1242, http://dx.doi.org/10.1016/j.cell.2014.03.059.
[12] N.P. Frank, S.M. Hart, A dynamical system using the Voronoïtessellation, Am. Math. Monthly 117 (2) (2010) 92–112.
[13] R. Szeliski, Computer Vision Algorithms and Applications, Springer, Berlin, 2011, http://dx.doi.org/10.1007/978-1-84882-935-0 (xx + 812 pp.).
[14] E.W. Weisstein, Voronoï Diagram, Wolfram MathWorld, 2015 (http://mathworld.wolfram.com/VoronoiDiagram.html).
[15] J.F. Peters, Topology of digital images Visual Pattern Discovery in Proximity Spaces, Intelligent Systems Reference Library, 63, Springer, 2014, 2014, ISBN 978-3-642-53844-5, pp. 1–342.
[16] H. Edelsbrunner, A Short Course in Computational Geometry and Topology, Springer, Berlin, 2014, 110 pp.
[17] R. Hettiarachchi, J.F. Peters, Multi-manifold LLE, learning in pattern recognition, Pattern Recognit. 48 (2015) 2947–2960, http://dx.doi.org/10.1016/j.patcog.2015.04.003.
[18] J.F. Peters, Computational proximity Excursions in the Topology of Digital Images, Intelligent Systems Reference Library, 102, Springer, 2016, pp. 1–468, http://dx.doi.org/10.1007/978-3-319-30262-1.
[19] G. Duyckaerts, G. Godefroy, Voronoï tessellation to study the numerical density and the spatial distribution of neurons, J. Chem. Neuroanat. 20 (1) (2000) 83–92.
[20] O.M. Mozos, Jose A. Bolea, Jose M. Ferrandez, Peter K. Ahnelt, Eduardo Fernandez, Reprint of: V-proportion: a method based on the Voronoï diagram to study spatial relations in neuronal mosaics of the retina, Neurocomputing 74 (March (8)) (2011) 1165–1174.
[21] M. Borsuk, Drei sätzeüber die n-dimensional euklidische sphäre, Fundam. Math. XX (1933) 177–190.
[22] E.W. Weisstein, Antipodal Points, 2015 http://mathworld.wolfram.com/AntipodalPoints.html.2015.
[23] A. Tozzi, J.F. Peters, Towards a fourth spatial dimension of brain activity, Cognit. Neurodyn. 10 (3) (2016) 189–199, http://dx.doi.org/10.1007/s11571-016-9379-z.
[24] W.A. Beyer, A. Zardecki, The early history of the ham sandwich theorem, Am. Math. Monthly 111 (1) (2004) 58–61.
[25] G. Marsaglia, Choosing a point from the surface of a sphere, Ann. Math. Stat. 43 (2) (1972) 645–646, http://dx.doi.org/10.1214/aoms/1177692644.
[26] A. Tozzi, J.F. Peters, A topological approach unveils system invariances and broken symmetries in the brain, J. Neurosci. Res. 94 (5) (2016) 351–365, http://dx.doi.org/10.1002/jnr.23720.
[27] J. Matoušek, Using the Borsuk–Ulam theorem, in: Lectures on Topological Methods in Combinatorics and Geometry, Springer-Verlag, Berlin Heidelberg, 2003.
[28] F.-C. Mitroi-Symeonidis, Convexity and sandwich theorems, Eur. J. Res. Appl. Sci. 1 (2015) 9–11.
[29] A. Tozzi, Tor Fla, J.F. Peters, Building a minimum frustration framework for brain functions over long time scales, J. Neurosci. Res. (2016), http://dx.doi.org/10.1002/jnr.23748.

BUILDING A MINIMUM FRUSTRATION FRAMEWORK FOR BRAIN FUNCTIONS IN LONG TIMESCALES

Arturo Tozzi [1], Tor Flå[2], James F. Peters[3]

[1] Center for Nonlinear Science, University of North Texas
1155 Union Circle, #311427 Denton, TX 76203-5017 USA
tozziarturo@libero.it

[2] Department of Mathematics and Statistics, Centre for Theoretical and Computational Chemistry, UiT, The Arctic University of Norway, N-9037 Tromsø, Norway

[3] Department of Electrical and Computer Engineering, University of Manitoba
75A Chancellor's Circle Winnipeg, MB R3T 5V6 CANADA and
Department of Mathematics, Adıyaman University, 02040 Adıyaman, Turkey
James.Peters3@umanitoba.ca

Running Head: from proteins folding to brain activity

Keywords: Minimum frustration principle, brain, nervous system, energy landscape, evolution, timescale

The minimum frustration principle is a computational approach which states that, in the long timescales of evolution, proteins' free-energy decreases more than expected by thermodynamical contraints as their aminoacids assume conformations progressively closer to the lowest energetic state. Here we show that this general principle, borrowed from protein folding dynamics, can be fruitfully applied to nervous function too. Highligting the foremost role of energetic requirements, macromolecular dynamics, and, above all, intertwined timescales in brain activity, the minimum frustration principle elucidates a wide range of mental processes, from sensations to memory retrieval. Brain functions are compared to trajectories which, in long nervous timescales, are attracted towards the low-energy bottom of funnel-like structures characterized both by robustness and plasticity. We discuss how the principle, as derived explicitly from evolution and selection of a funneling structure from microdynamics of contacts, is different from other brain models equipped with energy landscapes, such as the Bayesian and free-energy principle and the Hopfield networks. In sum, we make available a novel approach to brain function cast in a biologically informed fashion, with the potential to be operationalized and assessed empirically.

SIGNIFICANCE STATEMENT

The aim of this paper is to evaluate whether the minimum frustration principle (MFP), a powerful theory developed to solve the protein-folding problem, can also provide insights into brain functioning. MFP is a computational approach based on the fact that the proteins' free-energy decreases more than expected by simple thermodynamic costraints, as they assume conformations progressively closer to the native state. We consider the neuronal background for a MFP theory of the CNS, in the attempt to achieve a proper brain phase space where mental operations might take place.

Current advances in human neurosciences shed new light on questions concerning the functional architecture of the nervous system and the status of mental and its relation to the physical. Novel innovations such as optogenetics (Deisseroth, 2014) and transcranial stimulation (Filmer et al., 2014), focus on establishing causal relations between specific aspects of neuronal activity and system-level consequences. Many people, although emphasizing the molecular basis of synaptic plasticity, accept the idea that broad methodological investigation and general theories are needed to further advance our understanding of the brain, despite the intrinsic simplifications offered by such general frameworks. Several global theories have been developed recently about the nervous system's functions, such as the role of rhythms/oscillations (Buszaki and Watson, 2012), computational models (Magosso et al., 2008; Izhikevich, 2010), connectome (Van den Heuvel and Sporns, 2011), dynamical system theories, nonlinearity and metastability (Fraiman and Chialvo, 2012; Deco and Jirsa, 2012), Bayesian approaches and the free-energy principle (Friston, 2010), information theory and multidimensional manifolds (Tononi, 2008; Sengupta et al., 2016), reductionist approaches based on atomic or molecular changes (Freeman and Vitiello, 2008) and supramolecular chemistry (Tozzi, 2015).

Based on recent findings, the aim of this paper is to evaluate whether the *minimum frustration principle* (MFP), a powerful theory developed to solve the protein-folding problem and can also provide insights into brain functioning. MFP is a computational approach based on the fact that the proteins' free-energy decreases more than expected by simple thermodynamic costraints, as they assume conformations progressively closer to the ground (native) state (Bryngelson and Wolynes, 1987; Bryngelson et al., 1995).

This paper comprises six sections. The first section elucidates the minimum frustration principle in its natural framework, namely, protein folding. MFP has an energy funnel-like structure, equipped with a transitional ridge that ensures the fastest and more efficient protein activity. To build a theory with physiological bases, section two covers the mental and functional correlates of the minimum frustration principle in the context of brain activities. To achieve a proper brain phase space where mental operations might take place, the third section considers the neuronal background for a MFP theory of the central nervous system (CNS). Section four provides a mathematical treatment for technical readers. Section five elucidates the differences between MFP and the current, most successful models of brain activity. In the final sixth section, we

speculate about the hypothetical molecular mechanisms of MFP, namely, dewetting transitions and protein "knots".

1. THE MINIMUM FRUSTRATION PRINCIPLE FOR PROTEIN FOLDING

The concept of MFP, a statistical description of protein's potential surface, is framed within the energy landscape theory (Ferreiro et al., 2011; Sutto et al., 2007). The most efficient physical and biological systems tend towards levels of minimum free-energy and MaxEnt, or, in other words, try to reach the deepest valleys embedded in the energy landscape. The ideal, most efficient landscape is a *smooth*, funnel-like one, where the energy trajectory rapidly converges towards the lowest energy bottom. However, in most examples this is not the case and the systems are said to be "frustrated". The term *frustration* refers to systems where competing energy interactions occur and the energy landscape is *rough*, *i.e.*, it is not possible to reach the minimum level of energy due to the large number of peaks and asperities. The classical example is a spin glass, *i.e.*, a magnetic system in which spins are randomly arrayed in a dilute alloy. In a spin glass, the interactions between spins are equally often, with spins both at random ferromagnetic (spins tend to point in the same direction) and anti-ferromagnetic (spins tend to point in opposite directions). Hence, the two conflicting local tendencies (parallel spins versus alternating spins) cannot be satisfied completely in any arrangement of spin orientations (Bryngelson et al., 1995). Due to the intristic constraints given by the interactions among its components, the system is equipped with many local minima and cannot reach a single lowest possible energy level, *i.e.*, the steep funnel-like tunnel in which "minimum frustration" takes place. Thus, in most systems, the tendency towards low energy states go hand-in-hand with a residual degree of frustration (Rijito and Verkhiver, 1996). For technical readers, the next paragraph displays a mathematical treatment of frustrated systems' dynamics.

The Minimum frustration principle for protein folding. In a spin glass, let *m*, *x*, Ω, and *m*(*x*) be respectively: the magnetization, position, region occupied by the material, temperature dependent magnitude of ferromagnetic material, and potential, where $|m(x)| = f(\theta), x \in \Omega$, with $f(\theta) = 0,$ for $\theta \geq \theta_c$, where θ_c is the Curie point. The energy of a ferromagnetic material is assumed to have three parts, namely, exchange energy, anistropic energy and magnetostatic energy (James and Kinderlehrer, 1990; James and Kinderlehrer, 1991). The frustration in the system results from the competition between anistropic energy, that requires constant magnetization strength and direction, and an induced field energy that tends towards zero. The system's energy can be written as a Lagrange functional, expressed in terms of potential u and constant applied field h_o:

$$L(m,u) = \frac{1}{2}\int_{\square^3} |\nabla_u|^2 dx + \int_{\Omega} \left(m \cdot \left(h_o - \nabla_u \right) - \varphi(m) \right) dx$$

.

Then, for appropriate variations of *u*, total system energy $E(m) = -\inf_u L(m,u),$ *i.e.*, the negative greatest lower bound of the Lagrangian *L*(*m*,*n*) relative to varying potential *u*. Minimum system energy is then expressed in the following way: $-P^* = \inf_u E(m;h_o) = -\sup_m \inf_u L(m,u),$ and let $N \subseteq \{m(x) : |m(x)| = 1,$ almost equal in $\Omega\}, H = H^1(\square^3),$ so that $P_N^* = \sup_N \inf_H L(m,u),$ and $P_N = \inf_N \sup_H L(m,u),$ with $\mathrm{P}_N^* \leq \mathrm{P}_N$ (approximate minimum energy).

P_N^* represents approximate minimum system energy, provided *N* is not all functions m with $|m(x)| = 1.$ In general, ferromagnetic material is unstablein the single domain state. For mathematics underlying this view of system energy, see (James and Kinderlehrer, 1990). Isayev observes that there is a competition between ferromagnetic and anti-ferromagneic spin ordering (Isayev, 2003).

Minimum frustration's Hamiltonian in protein folding. Let m_i be a coarse grain variable with values 0 or 1. The folding pathways of proteins are described with the Hamiltonian *H* defined by $H = -\varepsilon \sum_{[i,j]} m_i m_{i+1} \ldots m_{j-1} m_j$ with the summation over native pairs $[i, j],\ i < j$.

H is a Go-Type Hamiltonian with minimal frustration (Itoh and Sasai, 2006), used by Munoz and Eaton (1999), Henry and Eaton (2004) to analyze free energy landscapes and rates of folding many proteins. Because foldability, due to the specific energetic constraints of minimum frustration (which requires specially shaped energy landscapes resembling a funnel and a transitional ridge: Wolynes, 1996), the effect of non-native interactions and energetic frustration is strongly minimized and the energy gap between native and misfolded structures is maximized (Das and Matysiak, 2005).

However, evidence from theory and from simulation in protein folding studies indicates that the more stable proteins are "minimally" frustrated heteropolymers, i.e., they are equipped with a *pure* rugged funnel-like landscape which molds the roughness underlying the detailed protein dynamics (Sutto et al., 2007; Frauenfelder et al, 1991; Hegler et al., 2008). Proteins are enriched by evolution to select amino-acidic sequences with the propensity to fold into the lowest possible energy structures, giving rise to very stable, minimally frustrated conformations. As a result, a strong energy bias towards the native basin occurs, overcoming both the asperities of the landscape and chain entropy (Onuchic et al., 1997). A positive correlation has been found between contacts with longer transition path lifetimes (the "native" contacts) and the number of residue contacts made in the native structure (the aminoacids that interact in the fully folded protein). The minimum level of energy (corresponding to the minimum frustration) is achieved when both a high number of native and residue interactions occur, leading to a faster and more efficient folding process (**Figure 1**). The "classical" funnel-like energy landscape used to describe protein folding is typically characterized by the energy, the fraction of native-like contacts and the entropy. However, in the present manuscript the x-axis displays the number of residue contacts instead of the entropy. Notice that, with a decrease in the number of residue contacts, each one quantitatively represented by numbers greater than 1, there is a corresponding decrease in entropy. For example, let 4,5,8 represent residue contacts with corresponding entropy 1.09861 and let 4,8 represent a reduction in the number of residue contact with correpsonding entropy 0.693147. In the 3rd section, we construct a brain phase space corresponding to the one characterized by residual contacts (on the x-axis) and native interactions (on the z-axis). It means that in our phase

space (without the use of entropy), the energy landscape still has the shape of funnel, because the entropy or the systems' size still shrinks down towards the zero.

It has been shown that a minimally frustrated folding process (overtaking the native contacts' inhomogeneity, the non-native interactions and the residual local frustration), passes through a very fast transitional state, called "trasversal ridge", and points towards the lowest possible energy levels. Minimal frustration is very important for protein function. It is a critical prerequisite for fast kinetics and thermodynamic protein stability (Verkhiver and Rejito, 1996). Timescales enter into the picture when we consider the duration of minimized frustration: the actual value of the energy difference needed to ensure a funnelled, ridged landscape depends on the biological constraints of the folding timescale (Wolynes, 1996). In sum, in the long timescales of evolution, proteins tend towards an energy state of "minimum frustration" (Bryngelson and Wolynes, 1987; Bryngelson et al., 1995).

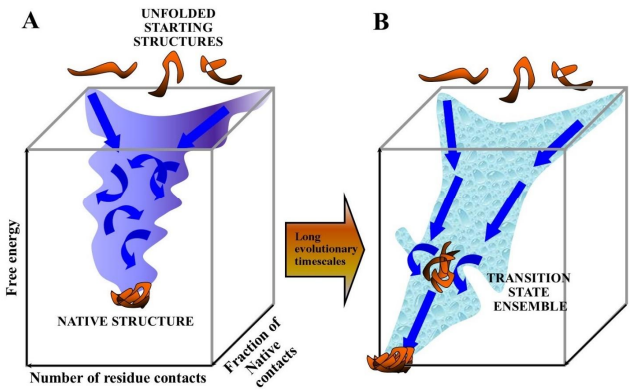

Figure 1. Protein folding (from the unfolded starting subunities to the native final structure) framed in the context of the energy landscape theory. The phase space is equipped with three parameters: the x-axis displays the number of residue contacts among the aminoacids endowed in the protein structure (e.g., the contacts among the aminoacids forming a protein). The y-axis displays the free-energy, while the z-axis the number of homogeneous "native" interactions among the aminoacids endowed in the protein structure. The arrows point towards higher values of the corresponding parameters. **Figure A** depicts a partially frustrated final conformation, while **Figure B** shows the minimum frustrated final conformation of a folded protein. Note that, when MFP taking place, the folding sequence dictated by long evolutionary timescales is pushed towards a funnel-like conformation of the energy landscape, equipped with a transitional "ridge" and with an ultimate very low level of free-energy. See the text for further details.

2. POSSIBLE FUNCTIONAL CORRELATES OF MFP FOR BRAIN ACVTIVITIES

The very general scheme of MFP might stand for a large repertoire of brain functions and activities such as sensations and perceptions, emotions, mood-state and affect, memory. For the meaning of these terms, refer to Andrews-Hanna et al. (2014). Recent data point towards the cortex as *phrenological*. That is, the cortex is comprised of extremely heterogeneous cells, with distinct regional variations, macromolecular assembly and intrinsic microcircuitry (Spruston, 2008; Yates, 2014). This suggests that every neuron (or group of neurons) embodies different molecular information and displays different types of spiking responses (Haustein et al., 2014; Tozzi 2015), even if they retain the same broad-spectrum of energy mechanisms. This also suggests that every different brain function depends on changes in the phase space which take place in different anatomical areas or subareas.

Many brain functions can be described in terms of trajectories falling into a funnel-like attractor, which is a steep tunnel located in a functional phase space where trajectories converge as time progresses. Looking for possible mental counterparts, we may hypothesize that, when the particle falls into a partially frustrated tunnel, the correlated mental activities could be either erratic patterns of movements or thoughts, or vanishing memories, or mind wandering, or unsure perceptions, in which different ideas are not properly melted together. In turn, when the particle falls into the frustrated steep, narrow, funnel-like tunnel, the correlated psychical activities could be, for example, preserved memories, or sharp sensations of "known" objects, or accurate motor patterns, or sure perceptions due to the confluence of different sensations, or disparate, unsure thoughts which converge towards a single, fixed idea.

As an example, during visual sensation, we may hypothesize that the energy is minimised in fixed point attractors, which modulate the free-energy and underwrite the perception of *known*, *unambiguous* spatial objects. When instead the trajectory falls in a rough landscape, it is not able to reach the lowest energy level, because it is trapped in the asperities of the *frustrated* funnel: it means that the perception is not *sure*, but problematic. Again, for example, recognition decision response to environmental stimuli, set in the many signalling timescales of brain function that are evolutionary constraints in protein folding, is subject to the MFP. An energy gap occurs in our fitness landscape between a well-defined global minimum state and a dynamic transitional one (the bridge), which simulates the stimuli system's behaviour before it settles into the global minimum. The sequences of stimuli are constrained: due to the continuous exposure to the same stimulus, the energy landscape becomes a funnel-like functional state. Amidst the valleys and peaks, larger variations in energy gap lead thus to deep funnels, which inexorably draw the neuronal recognition decision activities to themselves (Deco and Jirsa, 2012). In other words, the different signalling timescales occurring in brain during the processes of perception give rise to strictly constrained functional outcomes, conditioned only by long timescale statistics. The sensitive states are the possible stimuli sequences dictated by the functional constraints of the external environment and the interaction landscape. We obtain a quantifiable picture of stimuli's evolution under fitness fluctuations (Mustonen and Lassig, 2008): changes in the environmental stimuli cause effective network variations (for example, segregation in different receptors, or production of different neuronal phenothpes into the neural "niche:" we will describe them below) that modify the equilibria in an irreversible way and lead to new monomorphic decision states (distinct sensory neuron subsets). The importance of the MFP in a nervous context of sensation/perception lies in the different, robust functional brain timescales, which selection is determined by the evolution of stimuli presentation. When external stimuli reach the cortex, the corresponding perceptions become accurate just in case of trajectories on the free-energy landscape falling into funnels. MFP predicts that, overlong-term timescales, perception invariably falls in the funnels. This means that along-term exposition to the same sensation that occurs in infants and children during the first years of life, could lead to accurate perceptions.

Other mental states and operations can be hypothesized as endowed in the MFP framework. For example, stored patterns

could give rise to pattern recognition. More complex mental activities such as thinking and reasoning, might require harder work and network development on long timescales. To achieve the desired output, the time required might range from minutes (*e.g.*, simple changes in the "software" of molecular assembly are required to achieve the goal) to months (e.g., new architecture and hardware, *i.e.*, the genesis of new synapses or novel cells is required). In conclusion, it is important to state that the MFP, in our framework, is just one of the general mechanisms of brain function. Indeed, it is able to explain some brain activities, such as sensitization and memory retrieval, while other activities, such as sensory adaptation, mind wandering, self-generated thoughts, free thoughts, sequencing/planning, choice, judgement, creativity, might subtend other mechanisms. The alternative mechanisms are described in the sequel.

3. MFP FOR NERVOUS ACTIVITY: BUILDING THE REQUIRED BRAIN PHASE SPACE

In the attempt to build a brain theory based on MFP, one problem is obviously that we do not have an explicit model for mean interaction properties as for proteins, where we can use the well-known amino acids' properties. We need to take into account that MFP has been developed using tools from statistical mechanics and finite systems' phase transitions. Because the energy landscape theory is inspired by algorithms that quantify the degree of local frustration in molecules, it is equipped with a phase space. Therefore, we need at first to build a corresponding brain phase space, in which the MFP for nervous functions might take place.

Brain phase space: the free-energy on the y-axis. Concerning the parameter on the y-axis, the brain's free-energy is the nervous counterpart of the protein free-energy in the classical MFP for protein folding (**Figure 2**). An issue of central relevance in this context is the *free-energy principle* (FEP: Friston, 2010). The FEP is a general theory of brain function which arises in a biologically informed fashion and has the potential to be operationalized and assessed empirically. The free-energy principle for an adaptive system such as the brain tries to provide a *unified account of action, perception and learning*. That is, any self-organizing system at nonequilibrium steady state with its environment must minimize its free-energy, thus resisting a natural tendency to disorder (non-zero entropy). This formulation, which fits nicely with MFP, reduces the physiology of biological systems to their homeostasis, namely, the maintenance of system states in the face of a constantly changing environment. The brain is regarded as an active inference machine that functions according to Bayesian principles. That is, sensory inputs constrain estimates of prior probability from past experience, to create the posterior probabilities that serve as beliefs about the causes of such inputs in the present (Barrett and Simmons, 2015). From the perspective of the MFP, one can regard this belief updating as free-energy minimisation in terms of energy gradients and information flows. The activation of the peripheral receptor leads to feedforward electric oscillations towards the cortex, in order to increase the free-energy in the connectome landscape. For example, if one considers the visual system, the best known among sensory systems in Primates (Niewenhuys et al., 2008), he may note that simple localized bright stimuli related to the external world evoke high frequency oscillatory firing patterns along the entire sensory pathway: from the retinal ganglion cells (Shlens et al., 2009), to the optical layers, the lateral geniculate nucleus (Guido and Sherman, 1998; Mooney et al., 1996; Bastos et al., 2014) and the cortex.

When the energy stream crosses the cortex, the brain displays unstable dynamics (Papo, 2014). Crucially, for our argument, this neuronal activity is an example of an open-system, which, although partly stochastic due to intrinsic fluctuations, maintains an interplay between structural bottlenecks and non-equilibrium steady-state dynamics (i.e., homoeostasis or allostasis), in the face of environmental fluctuations. The brain function also retains the characteristics of a complex, non-linear system, formed by a large number of interacting and inter-dependent components which exhibit emergent properties, spontaneous self-organization, circular causality (Fraiman and Chialvo, 2012), divergent susceptibility and sensitivity to initial small changes. In short, the brain operates at the edge of chaos, ina metastable state near criticality, where the maximum information function lies between randomness and regularity (Zare and Grigolini, 2013). At the cortical level, minimising entropy production corresponds to minimising "variational free-energy" at each point in time (Sengupta et al., 2013a). This approach is about trying to understand how non-equilibrium steady-state is maintained, with an apparent resistance to the natural tendency to increase entropy. In this context, the average time of variational free-energy becomes a proxy for entropy. Furthermore, because variational and thermodynamic free-energy share a common minimum, one can link information processing (i.e., Bayesian belief updating) to metabolic efficiency by noting that minimising variational free-energy is the same as maximising Bayesian model evidence, which is also the same as minimising thermodynamic free-energy (and associated entropy).

The key thurst of FEP is that energy expenditure is balanced by homeostatic mechanisms, in an effort to minimize free-energy: the interplay between neuronal structure and activity at many different spatiotemporal scales gives rise to functional attractors (Watanabe et al., 2014a). In the context of MPF, a funnel-like functional structure is required: the best candidate is the "fixed-point attractor", a location in phase space where trajectories converge as time progresses. As we will see, the MFP framework takes into account the FEP. Accorting to both the models, a low energy basin lies at the bottom of the free-energy brain landscape, far from the peaks and close to the lower branches. The lowest energy levels give rise to dynamical phenomena that counteract the natural dissipation that would otherwise predominate in the nervous system: attractors impose transitory constraints on the landscape and attenuate the energy loss. The time-dependent, unexpected increase of entropy production typical of random systems (Gaspard, 2005) is thus counteracted by the presence of the attractors, acting as transitory constraints for random walks.

The funnel-like mechanism of brain activity is also suggested by a recent paper, where a novel gauge theoretic perspective of the brain provides a rigorous way of measuring distance on a manifold, such that the neuronal dynamics transporting one distribution of neuronal to another is given by the shortest path (Sengupta et al., 2016). In the context of physics, the MFP is rather close to Ising model and maximum entropy model. As described above, "frustration" was originally defined in behaviours of magnetic spins, which is well described by Ising model. This Ising model and maximum entropy model are, in addition, known to be well fitted to various empirical neural activities, ranging from neuronal spike activity and local field potential to fMRI signals (Schneidman et al., 2006). Moreover, energy landscape that was calculated by fitting Ising model to fMRI signals was shown to well account for individual difference in bistable visual perception and relevant anatomical differences (Watanabe et al., 2014b). Considering these close

relationships and accumulation of previous empirical evidence, the MFP attains solid ground.

However, it must be taken into account that countless neuronal models alternative to fixed point attractors have been proposed: for example, it has been suggested that brain function does not exhibit erratic brain dynamics nor attractors, rather a stable sequence, called transient heteroclinic channel (Afraimovich et al., 2013). According to some Authors, the neural network as an open system is not at equilibrium and may not always be described by fixed point attractors. Indeed, for example, line attractors (Seung 1996) and limit cycles (Yan et al., 2013) have been used to describe different brain functions. To make the picture also more complicated, it must be taken into account that many different functional regimes might occur in the brain: to make an example, it has been recently proposed that, at least during spontaneous brain activity, the brain might display a 4D functional Clifford torus (Tozzi and Peters, 2016). Further, crucial concepts like meta-stability and communication-through-coherence must be taken into account (Deco and Jirsa, 2012). Thus, the picture seems to be characterized by more than a single mechanism: it is possible that different functions are equipped with different kinds of attractors, or even linear and nonlinear dynamics. It is possible that the peculiar protein and macromolecular arrangements required for a nervous MFP and a subsequent funnel-like attractor are displayed just by some brain areas deputed to functions such as perception or memory storage, while other areas use other types of attractors which require - and are charachterized by - other types of protein conformations. In this paper, we limit our analysis just at the building of a "pure" MFP nervous network. We will limit our treatment to a broadening of the fixed-point attractor to a simple quasi-equilibrum picture, with a constrained long timescale variance. Here will not take into account more complex attractors that could also have a mental counterpart, such as strange attractors, nor nonlinear dynamics, perimeters regimes, nor even statistical phase transitions.

The connectome subtends the presence of an energy landscape in brain, equipped with quantifiable levels of energy. How such energy levels could be correlated with the parameter we used on the y axis, i.e., the free-energy? In order to answer to this crucial question, it must be kept into account that the high metabolic brain activity is remarkably constant over time (Fox and Raichle, 2007): what consumes such large amounts of energy? For our purposes, we notice that local increases in spike frequency cause a transitory boost of energy consumption and free-energy production, with a metabolic cost of 6.5μmol/ATP/gr/min for each spike (Attwell and Laughlin, 2001). Thus, the increase in thermodynamic free-energy during brain activity is mostly due to spiking. In sum, the electric oscillatory activity of the extended connectome– in particular, at the spike frequency – correspond to the *y*-axis of our free-energy landscape.

The x- and z-axes: building the required brain networks. In the last paragraph, we stated that brain computations take place on a phase space endowed into the nervous connectome, which is equipped with a potential energy surface characterised not just by stationary points where the gradient vanishes (individual local minima), by also by transition states and basins, low-energy valleys and high-energy peaks. Starting from this energy framework, the minimum frustration comes into play as the main actor. If the MFP brain framework closely resembles the theories of protein folding in terms of free-energy landscapes for contact network interactions between amino-acids, how does it operate in the brain? How one can build a model which accommodates the overwhelming complexity of the interactions among the countless components of the nervous milieu? We need to find a nervous counterpart to residual contacts (on the x-axis) and native interactions (on the z-axis), which are the two remnant ingredients of MFP.

The role of supra-molecular interactions is crucial in explaining how the CNS processes information and how MFP comes into play. Current theories are based on two tenets: a) information is transmitted by action potentials and b) homogeneous neuronal assemblies of cortical circuits perform operations characterized by the intrinsic connectivity among neuronal populations (Gollisch, 2009). In this view, the size and time course of any spike is stereotypic and the information is restricted to the temporal sequence of spikes (Buszaki and Watson, 2012). However, recent data point towards an alternative hypothesis: a) instead of simply passing messages, action potentials play a role in the dynamic coordination at multiple spatial and temporal scales, across several levels of a hierarchical modular architecture (Bosman et al., 2014) and b) information is processed at all levels, from macromolecules to population dynamics. For example, intra-neuronal - changes in protein conformation, concentration and synthesis (Kavalai et al., 2011) - and extra-neuronal factors –such as extracellular proteolysis, substrate patterning, myelin plasticity, microbes, metabolic status (Marcoli et al., 2015; Foster and McVey Neufeld, 2013) may have cognitive connotations by themselves. The concept of "supra-molecular chemistry" has been recently introduced (Tozzi, 2015), involving the storage of information at the molecular level and its retrieval, transfer and processing at the supra-molecular level, through transitory and labile non-covalent processes that are self-organized, self-assembled and dynamic (Lehn, 2007; Taylor and Ehenreich, 2014). Such a theory is a good starting point to evaluate a MFP for the nervous system: indeed, this operational approach, endowed in a macro-molecular framework, is, formally, very close to the protein-folding problem, where native interactions and residual contacts among molecular structures are of foremost prominence.

The simplest model of the cortical layers we can think of is a network of two-dimensional functional niches, i.e., basic local compartmental units including both "neuronal decision cells" (NDC) and their own local environment (glia, extracellular space, and so on). The NDC corresponds to the native contacts (on the x-axis) in the protein folding framework (**Figure 2**). The inputs to a niche could be external, i.e. coming from other cells, or local/internal. NDC produce an activity in quasi-equilbrium with electric signalling: this timescale is slower, compared with fast speed of proteic enzymatic reactions. These signals, interacting in a multitude of neuronal synaptic pathways and compartments, regulate the functional states of both NDC and its connections, due to a quasi-static equilibrium. In robust neuronal networks as the brain, the response of signal input/output relations often displays a *sigmoidal (S-shaped) form* (Eeckman and Freeman, 1991).

It must be emphasized that the parameter *t* determines the shape of the sigmoidal function: it elucidates the link between minimum frustration and long timescales (Laurenbacher and Sturmfels, 2009). For example, $g(z(t))$ is a sigmoidal response function for a single neuron at time *t* (Benardette et al., 2008) defined by

$g(z(t)) = \frac{1}{1+e^t}$ (single neuron sigmoidal response function at time *t*),

which can be typically expressed by simple logical decisions modelled by a history-dependent, bistable on-off state. This means that NDC could be in two functional states: *activated* (on) at time *t* and *deactivated* (off)at time $t+k, k \geq 1$. Such bistable response occurs when the sigmoidal activity is combined

with positive feedbacks. Indeed, in a bistable responsive system, there exist two states in a stimulus range, meaning that whether the system is in high- or low-activity state depends on its previous history (memory). Sometimes the on-state can also be maintained after stimulus removal, leading to an irreversible activation. Bistability and positive feedback can thus be mechanisms for noise-resistant cell-fate decisions.

Are we allowed hypothesize an on/off mechanism of brain activity? The answer is positive: such a device has been already demonstrated in brain. A homeostatic mechanism has been revealed in the spatial distribution of synaptic strengths, by which neurons balance excitation (E) and inhibition (I), not only in time, but also in space (Xue et al., 2014). Specifically, cortical circuits appear to maintain a constant E/I ratio between the total amount of excitatory and inhibitory stimulation (Sengupta et al., 2013a; Sengupta et al., 2013b). E/I balance has been described both in vitro and in the spontaneously active cortex, not only for individual pyramidal neurons at a given time (Haider et al., 2006), but also across multiple cortical neurons and during neural avalanches (Lombardi et al., 2012). An optimal E/I ratio across neurons is maintained, despite fluctuating cortical activity levels, through the appropriate strengthening or weakening of inhibitory synapses (Xue et al., 2014). The relationship between the two opposing forces affects many cortical functions, such as feature selectivity and gain (Sengupta et al., 2013b), or memory of past activity (Lombardi et al., 2012), or rapid transitions between relatively stable network states (Sengupta et al., 2013b), which allow the modulation of neuronal responsiveness in a behaviourally relevant manner (Haider et al., 2006). The E/I ratio in each area can be calculated, provided that total must give zero. The E/I ratio stand for the needed parameter on the x-axis (corresponding to the residue contact in the protein folding MFP framework): the less the E/I ratio deviates from zero, the less residue contacs occur, and the lesser is the frustration.

We need now to introduce the proper neural network, where the funnel-like attractor equipped with a transitional ridge might take place. Dynamical neural networks have been widely used in brain models. For example, the recurrent artificial Hopfield networks (Hopfield, 1982) display binary threshold nodes, meaning that the unit (i.e. the node in the graph which simulates the artificial neuron) may take just one of two different values: 1 and -1. The value depends on whether or not the units' input exceeds a threshold. Pairs of nodes are linked through symmetric connections charachterized by distinctive connectivity weights. Hopfield networks are equipped with an energy landscape, ruled by an effort to minimize energy. When units are repeatly updated through learning rules such as the Hebbian one (which states that "neurons that fire together, wire together"), the energy always decreases and tends to converge towards an attractor pattern, the final stable state of minimum energy level. However, we will see in the next sections that the networks predicted by MFP are both more plastic and stable that the Hopfield ones. The MFP network is also easy to parametrize, because frustration can be extracted from just a few parameters: the microdynamics of the niches, the on/off cells ratio, the cell contact density variance and the external fluctuations, which can be parameterized by external energy variance. In touch with protein folding, in which the minimum level of energy (minimum frustration) depends on the number of residual contacts and native interactions, a free-energy brain landscape equipped with minimum frustration can be naturally designed, by taking into account just two parametrizing factors: the NDC's on/off internal/external states (on the x- axis of our brain phase space) and the NDC's cell number (on the z-axis) (**Figure 2**). The estimation of the effective population is very useful, because it allows us to perform a simple linearization. Based on these two parameters (which can be compared to residual contacts and native interactions in the "classical MFP for protein folding), we can calculate both the mean free/energy activity in every point of the network and the gaps between the transition states (a technique called entropy pairwise fixation probabilities: Watanabe et al., 2014a). In the MFP model, thermodynamic free-energy is defined by informational entropy and pairwise probabilities - parametrized through partition function or by maximum of relative entropy - and compared with a mean entropy. The mean energy difference between on and off states accommodates an MFP lying transversal to a ridge in the joint distribution function: in other words, a transition ridge of minimum frustration, where trajectories are constrained to move, is embedded into the energy landscape (Best et al., 2013).

In short timescales, the NDC is thus allowed to decide wheter to read, write, or erase memory bits, or alternatively to send out excitatory/inhibitory electric spike signals. However, in long timescales, NDC can also choice to produce different neuronal phenotypes equipped with the lowest possible degree of frustration: such a feature is of outmost importance when a long-duration of stimulus exposition occurs (which can be compared to the long evolutionary timescales in the "classical" MFP for protein folding). Also, countless environmental, epigenetic and metabolic factors might be important for the parametrization of the on-off states. We would like to stress once again that the key to understand the concept of MFP and funnelling in a neural framework lies in the well-known suggestion that the brain displays diverse timescales with diverse functions (Papo, 2015; De Pasquale and Marzetti, 2014; Gonzalez-Castillo et al., 2014; Linkaeker-Hansen et al., 2001): from the one nanosecond of side chain rotation, to the 50 nanosecond of the small loops; from the one-ten milliseconds of small protein function, to the stochastic oscillations in neuronal synapses (Kavalali et al., 2011); from the high-frequency of ultra-fast electric spikes, to the intermediate frequency of neuronal spike trains; from the low-frequency on spontaneous BOLD fluctuations (Raichle, 2010), to the ultra-slow time changes (hours or days) in protein signals (Kravchick and Jordan, 2015). In order to show how our theory can be operationalized, we provide the next section as supporting information for technical readers.

Summarizing: the ensuing brain energy landscapes - formally equivalent to the well-studied landscapes in protein folding (Morcos et al., 2014; Wales, 2012) - can be compared to a lattice. The functional assemblies of neurons, including their sensory molecular machinery, electrical interactions, extracellular fields, cortical feedbacks and also environmental stimuli, can be studied through logic models of pluri-dimensional networks, equipped with a binary interaction between neurons which is a simple two-decision state based on on/off probability distributions (stimuli-yes/stimuli-not, for example). Starting just from the quantifiable changes in free-energy due to the above mentioned connectome's electric oscillations, we achieve a functional free-energy landscape, transiently equipped with different values in diverse brain areas and with various timescales. While the minimum frustration of protein folding is dictated by the long timescales of the evolution, the minimum frustration of brain function is dictated by the long timescales of nervous activity. On longer brain timescales, we achieve the mean thermodynamic free-energy level which can be embedded in the known equations talking about free-energy difference type rate which goes into a sigmoidal function.

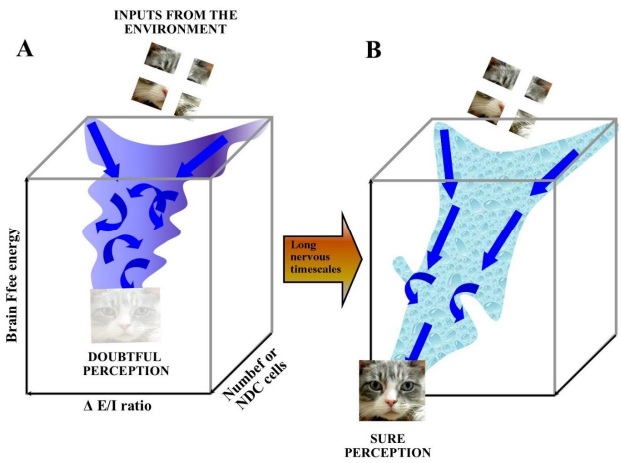

Figure 2. The nervous sensitive/perceptive counterparts of a theory of brain function based on the principle of minimum frustration. Modified from **Fig. 1**. The x-axis displays the Δ E/I ratio (the arrow points towards E/I = 0), while the z-axis shows the number of functionally well-adapted NDC. Note that in **Figure A** the asperities of the energy tunnel do not allow a "sure" perception of the object embedded in the external world (in this example, a cat). In turn, when the attractor is funnel-shaped and equipped with a transitional ridge (**Figure B**), the perception is sure and faster and requires lower energy expenditure. The evolutionary timescales in Figure 1 have been replaced here with long nervous timescales. Note that, after proper transversal averaging, the three parameters, according to MFP, should be globally, or even locally, related to longitudinal quantities following the ridge curve.

4. A LANDSCAPE MODEL WITH MINIMUM FRUSTRATION

As we stated in Section 3, our landscape brain model based on probabilistic and evolution fitness robustness/plasticity requires a "neuronal decision cells" (NDC) network. Here we show how a landscape model with minimum frustration can be naturally designed to populate the necessary functional/unfunctional brain states, thus leading to robust decisions that are parameterized by mean free "energy/activity" gaps between transition states. Here we show how the MFP is potentially useful in transcribing the underlying principles to experimental assessment, by describing the procedures for an estimation of the required three brain parameters (free-energy, effective NDC population and E/I ratio).

Local quasi-equilbrium for networks of regulated neuronal signals. Although a local quasi-equilibrium can be applied at all levels, from DNA to cell structure, we will focus on the level where we single out the brain memory/decision cells and their basic slow timescale. ("slow", when compared to the speed of molecular kinetics). We will assume that the network function is gauged through the activity of NDC, embedded in their network of niches, by the lumped sigmoidal function described by a single activity measure E, which is in terms of activity at time t:

$$E_t(f,Z): p(E_t(f,Z)) = \frac{f(E_t;\lambda)}{Z_t(\lambda)} = e^{\frac{-\beta E_t}{Z_t(\beta)}}.$$

E is a function of f and Z at time t. Then we have a means of connecting MFP and FEP relative to some timescale. Here $\lambda = \beta$ is supposed to be the inverse temperature, but we could also use other significant parameters - e.g. the total number of contacts - depending on which scaling we are using.
A clear correlation is self-evident between β and E on the one hand, and the statistical mechanics' inverse temperature and energylevel at time *t* on the other hand. When the average activity is measurable, the exponential model clearly leads to the MaxEnt principle. Because we have not modelled the activity in terms of decision network, a reasonable model would be to take into account the network of long-range contacts, combined with effective interaction weights symbolizing the unit states a cell can take. Many categories could be used to describe different types of division/death processes, cell states and so on: to simplify, we evaluated just a few *k* categoricals states, i.e. an alphabet *A* labeled $i \in \{1, 2, \dots, k\}$.

Bilinear interactions. We now introduce the effective bilinear interactions for neuronal decision cells in long-range contacts, described by the interaction contributionM_{ij}, i; $j \in \{1, \dots, k\}$and by the dynamic contact network (equipped as usual with nodes, positions, edges and distances) C_{st},s; t = 1, ..., N.
Here *s* and *t* stand for the positions of a cells' sequence in given compartments, corresponding -- for active cells -- to the labelling of a nonuniform grid of niches. But *s* and *t* also stand for those activity interactions parameterized by the signal constitutents (proteins, different types of RNA, small ligands such as drugs, DNA methylation, and so on). Since we are going to concentrate on NDC and their niches, we consider for simplicity the niches as equipped with a cell compartment containing different fractions of both active and quiescent neurons: the functional brain counterpart of active and quiescent neurons is the Excitatory/Inibitory ratio (described in Section 3 of the main text). It is therefore natural to fasten together in a sole effective unit both the state variables for each niche and its closest interacting neighbours. The effective population of such units, corresponding to $N_e = \langle N^{-1} \rangle^{-1}$, can be evaluated through the spatial and/or ensemble average inverse population included in an heterogenous NDC population.
The active cells in a network of cell niches and cell compartments C = (C_{st}) can be modelled through a simple bilinear interaction matrix:

$$E_t(C,M) = \sum_{s>t=1}^{N} C_{st} M_{i(s)k(t)} = C : Y^{(N)T} M Y^{(N)},$$

where $E_t(C,M)$ is functionof the dynamic networkat time *t*.*C* : $Y^{(N)}$ is a map from bilinear interactions to activity potential, given by the value $E_{(y)}$ which stands for the corresponding probability potential for decision activity. E is function of the independent variables C and M. Because it depends on neuronal activity and function, it allows us to cast a reasonable model for the distribution function of cell ensemble's activityat time *t*. If we consider an approximately additive interaction model -*i.e.*, just one neuronal cell species (normal) -, we obtain the simplest model:
$M_{ij} = m_0 + \varepsilon_0 (w_i + w_j)$,
and an effectively linear model of interactions at time t:

$$y(t) = K_{y(t)} c \cdot w^{(n)}$$

which can be parameterized in energy units for the acivity cueing the decision process. Here $c = (c_s = k_s/K)$ stands for the network's long-range contact density vector, defined as the number of contacts divided by the total number of contacts. In a simple model, the number of contacts for a given signalling channel are proportional to the compartmental cell numbers, so that:

$k_s = K_c n_s = K_c N_e x_s$
and
$c = k/K = (K_c N_e/K)x^{(n)} = \rho x^{(n)}$,
where K_c stands for the effective number of signalling channels for activity $y(t)$ per cell. Because we need a fast response system for each cell, the cell function's activity is given by:

$$y(t) = y_{t_0} K_e N_e w^{(n)} \cdot x^{(n)} \ .$$

$y = y_{t0} K_c N_e w^{(n)} \cdot x^{(n)}$.
If the compartment contains more than one cell type, we can generalize by assuming additive contribution to signals through our bilinear interaction model:

$$y(t) = \sum_{c=1}^{r} y_{t,c} = y_{t_0} K_e N_e \sum_{c=1}^{r} w_n^c \cdot x_c^{(n)} = y_{t_0} K_e N_e W^{(n)} \cdot X^{(n)}$$

For sake of simplicity, we will treat each NDC unit as a single ensemble merged into other identically distributed units, but with the extra catch that also local short-range interactions occur.

Introducing minimal frustration and deep funnels. The MFP for robust systems means that there must be a clear activity potential gap between:

a) A well-defined global minimum functional state in the activity potential $E_t(y(t)_f)$ at time t, and
b) A statistical dynamic network transition state, which simulates the behavior before it has settled into the global minimum.

The energy required by NDC units is proportional to a descrease of frustration at its minimal levels.
Moreover, if we want to achieve a robust functional behavior of the unit, we should appeal not just to the MFP, but also to other opportunitities, in order to achieve a plastic global network where a certain degree of fragility/disorder is helpful in order to improve performance.
Let:

$$\Delta E_t\left(y(t)\right) = E\left(y_{lm}(t)\right) - E\left(y_f(t)\right),$$

$\Delta E(y \mid y_{lm}) = E(y_{lm}) - E(y_f)$,
where $y_{lm}(t)$ at time t is defined by

$$y_{lm}(t) = F_{lm}(t) = E_{lm}(t) - TS, \text{ with } E_{lm}(t) = E_{lm}(t) + \frac{\Gamma^2}{T},$$

and

$$S = -\frac{\left(\frac{\Gamma^2}{T^2}\right)^2}{2} + S_0 \ ,$$

which stands for the mean free potential activity gap between:

a) the average potential activity in the functional state y_f with minimum activity potential, and
b) the statistical liquid-like transition ensembles occurring just above the functional minimum activity state.

A larger ΔE_t at time $t$gives rise to a deeper funnel, which isessential to achieve an operating mean activity (function). The liquid activity ensemble is thermodynamically stabilized either by a larger configurational entropy of the disordered phase (S_0), or by a larger ruggedness of its activity landscape, modulated by the activity potential mapping. The evolution of NDC and signalling and decision circuitry will try to avoid:

a) either dysfunctional locally trapped minimal activity states occurring in a disordered regime of negative entropy (where $T < T_g$),
b) or unstable equilibria (where $T > T_f$), which occur, for example, in potential activity maxima regime of negative free-activity potential energy differences.

Advantages of neural MFP. The MFP, as derived from evolution in the monomorphic fitness limit, gives a robust ridge approximation of the decision sigmoidal function/rates, in such a way that the mean free (activity) energy gap can be monitored and directly related to the contact density, multiplied by the activity weigth factors derived from the activity matrix. This is because, at the very slow evolutionary time scales, the evolutionary equilibrium distribution can be expressed as a MaxEnt principle for the selection of the functional constraints. The mean free-energy gap should be larger than zero (stable functional equilibrium in the lab frame) and the frustration should be small or (if you want the the inverse frustration) large. We define the non-dimensional quantities:

- The mesoscopic frustration : $\kappa = \Delta E/\Gamma$ 〖_〗
- The nondimensional energy standard deviation: $\gamma = \Gamma/T$
- The mean (free) energy gap : $e = \Delta E/T$, $f = \Delta F/T$

In terms of these variables, we find - by marginalizing the joint exponential distribution for the mean free-energy gap and the inverse frustration - that the problem in the (κ,γ) plane (or in any pair of the four nondimensional quantities above) has a ridge following a path: $\kappa = h(\gamma)$ which in principle can be linearized around any fixed point κ_0, γ_0, in order to give the relations $\delta\kappa = h'(\gamma_0)\delta\gamma$.
At the same time, the minimization of the proper mixture of NDC is ensured by the stable homeostasis in line equilibria, which guarantees that, if the number can be robustly controlled, the total energy is located in a ridge distribution, where several NDC distributions can be easily checked towards insults. It can be achieved in the Grand Canonical liquid activity ensemble, by optimizing the number of contacts through a mixture of chemical potential constraints together with an extra term. Again, we have to constrain the mean free potential activity difference and minimize both its frustration and each of the contacts' frustration. We expect, from the transversal minimization of the frustration parameter, an equilibrium ridge which now contains a variance contribution for each contact/cell type. Evolution therefore benefits from the natural stable equilibria occurring in the multispecies interacting neuronal cells' potential activity. Our model suggestsa mean probability for a NDC to have activated function F, given a signal y_f:

$$p_F\left(y_f(t) \mid E_t, Z_F\right) = \frac{e^{-\lambda \Delta E_t\left(y_f(t) \mid y_{lm}(t)\right)}}{Z_F},$$

$p_F\left(y_f(t) \mid E_t, Z_F\right)$ is a conditional probability that depends on E_t, Z_F.
for each cell function affecting both the active cells' net growth and their interaction with other compartments. In the simplest case, when y_{lm} is fixed, the active state's probability into the active local cell's mean ensemble (which is embedded in a cell niche compartment interacting with other cell compartments) is:

$$p_F\left(y_f(t) \mid E_t, Z_F\right) = \frac{e^{-\lambda E_t\left(y_{fm}(t)\right)}}{Z_F}.$$

In this case, y_{fm} suggests that the ensemble means over local niche compartments give rise to effective population scale and effective average weight factors for cell signalling.

Other possible models. In this section we just discussed the mean decision rates as a microscopic background for the commonly used Integrate and Fire (IF) neuronal model. Nevertheless, the model could also be applied to:

a) Brain/neuronal cells' networkscasted as a Markov model for global states of networks in an open environment, and/or:
b) Commonly used network approximations as, for example, the simplest case of a set of interacting decision hubs modelled as kernels *in time and space* for correlated decision hubs.

We believe that our essay is a starting point to evaluate brain decision-activity functions in terms of energy costs landscape. The state of minimum frustration described above is a novel theoretical framework available for both evolution and biological network signals (such as the brain), either in stochastic or mean models of decision activity rates over time.

5. MINIMUM FRUSTRATION PRINCIPLE: WHAT FOR IN BRAIN STUDIES?

The question now is: what does MFP theory bring into play in the evaluation of brain activity? How do predictions from the MFP approach differ from predictions from current dynamical models, such as FEP or Hopfield Networks?

As in the FEP, MFP too considers free-energy as a statistical average quantity including temperature, entropy and transition state mean energy. The perceived inputs will be thus averaged over transition states. However, MFP states that, if there is a large enough timescale, the perceived inputs will be also averaged, because the brain perceptual machinery is tuned by evolution to ensure precisely that. In MFP, what is very significant is that the perception/decision apparatus is constrained to recognize just in "long" timescales. Friston's prior probability becomes, in MFP terms, the rugged funnel-like landscape in which the predictions signals are conveyed by *long-standing* past experiences. If in Friston's model the input sequence of coded signals leads to increases or decreases of free-energy which is dissipated as the coding sequence has passed, such a concept does not matter in MFP: the entropy might decrease or increase after a single sensation to get higher order - which could mean both higher or lower free-energy – but, on average, after numerous sensations on long timescales, the outcome leads inexorably to a decrease of free-energy, otherwise it would not be a stable recognition process. MFP thus stresses that the outcome must lead to a more ordered structure at recognition, not necessarily through immediate changes in free-energy. Further, while FEP emphasizes macro-phenotype dynamics and scarcely takes into account micro-anatomy and neuronal melieu, the MFP, at least its protein counterpart, is clearly grounded on micro-dynamics and macromolecular interactions.

In touch with the Hopfield networks, also MFP describes the brain in terms of dynamical energy landscapes, which activity is ruled by an effort to minimize free-energy. Nevertheless, MPF displays important differences also with respect to Hopfield networks. Hopfield uses McCullough-Pitts' dynamical rules, in order to make the retrieval possible: activations of multiple neurons map onto the activation of a new neuron's firing rate and their weights strengthen the synaptic connections between the new activated neurons. However, in the original formulation of Hopfield networks, this process occurs in a repetitious fashion: an attractor pattern is a final stable state and, under updating, is not able to modify any value within it. In the Hopfield network, contrary to MFP, the dynamical rule will always modify the values of the state vector in the direction of one of the "fixed" stored patterns. Both MFP and Hopfield Network are able to change the minima: however, Hopfield Network achieves this result by changing the weights, while in MFP the change of minima is both more plastic and more stable, because it depends on the duration of non-zero Hamiltonian. Therefore, while the Hopfield networks retain a "rough", more "frustrated" landscape, the MFP tends sharply towards a smooth, more efficient funnelled trajectory.

The MFP network is less rigid: its niches are able to produce, after a long-duration of stimulus exposition, different neuronal phenotypes, equipped with the lowest possible degree of frustration. This means that MFP networks are allowed to modify their energy features in long timescales, dynamically changing either their function, or structure, or even morphology. It gives rise to a system equipped with robustness and plasticity: accordingly, the active populations' stability limits towards dysfunction or misfunction are better guaranteed, compared with Hopfield networks.

The MFP solves also a problem raised by Rabinovich: he hypothesizes a neural processing model based on transient dynamics as in "liquid state machines", with no need for classical attractors (Rabinovich et al., 2008). He emphasizes that, because neural phenomena occur on very short timescales, classical attractor states (i.e., fixed points) cannot be realistically reached. However, the very fast mechanisms of a funnel-like MFP attractor overtake this objection, in order that an attractor state can be reached in brain easier and faster than previously expected.

As we stated above, MFP requires a specially shaped energy landscape resembling a funnel. Because the funnel depends on the biological constraint of the evolution, timescales enter into the picture when we consider the duration of minimized frustration. The overwhelming role of timescales in the MFP context is once again emphasized: the standpoint here is the presence of long-lasting external environmental inputs which act on the organism's internal melieu. In sum, the MFP-based brain model is simply different from the others, as derived explicitly from evolution and selection of a funneling structure in a constrained free-energy valley, equipped with contacts' microdynamics (which allows the lowest possible energy level) and a transversal ridge path. Minimal frustration is a critical prerequisite for fast kinetics and thermodynamic protein stability; it means that a brain model based on minimal frustration gives rise to more stable, efficient and fast mechanisms of nervous activity.

6. POSSIBLE MOLECULAR CANDIDATES

An interesting question then arises, which can be approached speculatively, because of our current lack of knowledge: are there micro-molecular candidates for the MFP theory? We propose a hypothetical mechanism for many classes of brain receptors, including the well-studied mechanosensory channels (Anishkin and Sukharev, 2004); namely, a state of dewetting transition: a concept borrowed from fluid mechanics (Sharmaa and Reiterb, 1996; Thompson, 2012). When water and ions are enclosed within the narrowest sub-nanometer confines of an ion channel's hydrophobic pore, they exhibit an odd behaviour: in such a peculiar context, a stochastic liquid-vapour water phase transition occurs, near a critical point (Aryal et al., 2015). These transient vapour states are "dewetted", i.e. effectively devoid of

water molecules within all or part of the pore. The decreased amount of water molecules in liquid state leads to impaired conductance, energy barriers to ion transit and closure of the channel (corresponding to an increase of inhibition in the E/I ratio), in a process termed "hydrophobic gating". The principles underlying the metastable dynamical state of hydrophobic gating require a very small radius of the tube and interactions with a strongly hydrophobic lining (Boreyko et al., 2011; Lapierre et al., 2013). Dewetting transitions, characterized by such an unusual behaviour of water's supramolecular assembly, represent an increasingly important general principle that has been applied to countless morphological and/or functional biological structures, ranging from protein cavities (Young et al., 2010) to lipid droplets (Thiam et al., 2013) and opening of macroapertures in endothelial cells (Gonzalez-Rodriguez et al., 2012), from extracellular matrix and glycocalix (Tanaka et al., 2005), to cell adhesion (Sackmann and Bruinsma, 2002) and lipid bilayers (Vargas et al., 2014). We speculate that dewetting transition might have a role as physical/chemical, supramolecular and functional substrate for the mechanisms of E/I ratio decreases, leading to augmented neuronal inhibition and subsequent changes in MFP networks.

A possible molecular role for prefrontal methyltransferases in working memory, emotion and cognition has been recently suggested (Jakovcevski et al., 2015). Such an interesting observation throws an unexpected bridge between topology, molecular assemblies and brain function. Methyltransferases are among the rare enzymes exhibiting the weird property of "knot" in their backbone. In other words, they are proteins with structures that do not disentangle completely after being pulled from both ends (Virnau et al., 2011). A knot is indeed the embedding of a closed line in the 3-D space and cannot be reduced to a simple circle by a continuous deformation (Wu, 1992). The knot theory arises from topology and provides tools for cataloguing different types of knots, for possibly transforming one into another via a deformation of 3-D space upon itself and for summing different knots in assemblages equipped with commutative and associative properties (Cromwell, 2004). In turn, the "supramolecular chemistry" suggests that complex chemical entities can be reversibly constructed from molecular components bound together by labile non-covalent interactions (Lehn, 2007). Incorporating such different perspectives appears particularly relevant for understanding how the brain does represent the stimuli coming from the environment. Nevertheless, recent findings suggest that nervous structures could process information through topological, other than spatial, mechanisms: for example, it has been suggested that hippocampal place cells create a topological template to represent spatial information (Dabaghian et al., 2014). Further, structures quite different from spikes, such as macromolecular assemblies, may play a role in information processing in nervous system: we do not yet understand to what extent the diffusion and biophysical cues, such as the mechanical properties of the extracellular matrix (Sur et al., 2013), have to be taken into account when talking about the brain function. Thoughts could be metaphorically compared with open strings made of proteins and/or supramolecular assemblies, a sort of random walks wandering around in the viscous fluid of the nervous milieu, until they reach a steady attractor. The entanglement of their extremities may give rise to reversible or irreversible topological knots, respectively standing for labile or enduring perceptions and memories. The link with MFP becomes clearer when we consider that topology is anoter key factor governing folding reactions. Indeed, structures of transition state ensembles (Clementi et al., 2000; Koga and Takada, 2001), folding rates (Chavez et al., 2004), the existence of folding intermediates (Ferreiro et al., 2005) and dimerization mechanisms (Levy et al., 2004) are well-predicted in models where frustration has been removed and topological information of the native state is the sole input.

7. CONCLUSIONS

Every mental state is a result of an evolutionary self-preservative processes, a biological functional phenotype trying to maintain invariance or steady state. The ideal point about which the nervous activities of the organism moves in constant oscillations has a logical-mathematical significance when framed in MFP theory. The concept of energy landscape for bio-networks, combined with the evolutionary fitness and selection principles of minimum frustration, promises to shed new light on our understanding of brain function. In conclusion, this paper is an effort to unify current perspectives on brain function in a coherent framework that retains their most important tenets. We have emphasized that nervous system activity is characterized by peculiar energy requirements and constraints, based on its countless spatio-temporal levels. We have suggested a role of MFP, a concept borrowed from protein folding, to further advance our understanding of the self-organised brain.

ACKNOWLEDGEMENTS

The Authors would like to thank Karl Friston for commenting upon an earlier version of this manuscript.

REFERENCES

1) Afraimovich V, Tristan I, Varona P, Rabinovich M. 2013. Transient Dynamics in Complex Systems: Heteroclinic Sequences with Multidimensional Unstable Manifolds. Discontinuity, Nonlinearity Complexity 2(1): 21-41.
2) Andrews-Hanna JR., Smallwood J, Spreng RN. 2014. The default network and self-generated thought: component processes, dynamic control, and clinical relevance. Ann NY Acad Sci 1316:29-52.
3) Anishkin A, Sukharev S. 2004. Water dynamics and dewetting transitions in the small mechanosensitive channel MscS. Biophys J 86:2883-2895.
4) Aryal P, Sansom MS, Tucker SJ. 2015. Hydrophobic gating in ion channels. J Mol Biol 427:121-30.
5) Attwell D, Laughlin SB. 2001. An energy budget for signaling in the grey matter of the brain. J Cerebral Blood Flow Metabolism, 21:1133-1145.
6) Bak P, Tang C, Wiesenfeld K. 1987. Self-organized criticality: an explanation of the 1/f noise. Phys Rev Lett 59:381–384.
7) Barrett LF, Simmons WK. 2015. Interoceptive predictions in the brain. Nat Rev Neurosci 16:419-29.
8) Bastos AM, Briggs F, Alitto HJ, Mangun GR, Usrey WM. 2014. Simultaneous recordings from the primary visual cortex and lateral geniculate nucleus reveal rhythmic interactions and a cortical source for gamma-band oscillations. J Neurosci 34:7639-7644.
9) Beggs JM, Plenz D. 2004. Neuronal avalanches in neocortical circuits. J Neurosci 24:5216–5229.

10) Benardette DM, Noonburg VW, Pollina B. 2008. Qualitatitive tools for studying periodic solutions and bifurcations as applied to the periodially harvested logistic equation, Amer Math Monthly 115: 202-219.

11) Best RB, Hummer G, Eaton WA. 2013. Native contacts determine protein folding mechanisms in atomistic simulations. PNAS 110: 17874–1789.

12) Boreyko JB, Baker CH, Poley CR, Chen CH. 2011. Wetting and Dewetting Transitions on Hierarchical Superhydrophobic Surface. Langmuir, 27:7502-7509.

13) Bosman CA, Lansink CS, Pennartz CM. 2014. Functions of gamma-band synchronization in cognition: from single circuits to functional diversity across cortical and subcortical systems. Eur J Neurosci 39:1982-1999.

14) Bryngelson JD, Wolynes PG. 1987. Spin glasses and the statistical mechanics of protein folding. PNAS 84: 7524-7528.

15) Bryngelson JD, Onuchic JN, Socci ND, Wolynes PG. 1995. Funnels, pathways, and the energy landscape of protein folding: a synthesis. Proteins 21: 167-195.

16) Buzsaki G, Watson BO. 2012. Brain rhythms and neural syntax: implications for efficient coding of cognitive content and neuropsychiatric disease. Dialogues clin neurosci 14:345-367.

17) Chavez LL, Onuchic JN, Clementi C. 2004. Quantifying the roughness on the free-energy landscape: entropic bottlenecks and protein folding rates. J Am Chem Soc 126: 8426-8432.

18) Clementi C, Nymeyer H, Onuchic JN. 2000. Topological and energetic factors: what determines the structural details of the transition state ensemble and "en-route" intermediates for protein folding? An investigation for small globular proteins. J Mol Biol 19: 937-953.

19) Cromwell PR. 2004. Knots and Links. Cambridge, UK: Cambridge University Press.

20) Dabaghian Y, Brandt VL, Frank LM. 2014 Reconceiving the hippocampal map as a topological template. eLife 10.7554/eLife.03476. (doi: http://dx.doi.org/10.7554/eLife.03476)

21) Das P, Matysiak S. 2005. Balancing energy and entropy: A minimalist model for the characterization of protein folding landscape, PNAS 102:10141-10146.

22) de Arcangelis L, Herrmann HJ. 2010. Learning as a phenomenon occurring in a critical state. PNAS 107: 3977-3981.

23) de Pasquale F, Marzetti L. 2014. Temporal and Spectral Signatures of the Default Mode Network. Magnetoencephalography, 451-476.

24) Deco G, Jirsa VK. 2012. Ongoing cortical activity at rest: criticality, multistability, and ghost attractors. J Neurosci 32:3366-75.

25) Deisseroth K. 2014. Circuit dynamics of adaptive and maladaptive behaviour. Nature 505:309-317.

26) Eeckman FH, Freeman WJ. Asymmetric sigmoid non-linearity in the rat olfactory system. Brain Res. 1991 Aug 23;557(1-2):13-21.

27) Elston GN, Rockland KS. 2002. The pyramidal cell of the sensorimotor cortex of the macaque monkey: phenotypic variation. Cereb Cortex 12:1071-1078.

28) Ferreiro DU, Cho SS, Komives EA, Wolynes PG. 2005. The energy landscape of modular repeat proteins: topology determines folding mechanism in the ankyrin family. J Mol Biol 354: 679-692.

29) Ferreiro DU, Hegler JA, Komives EA, Wolynes PG. 2007. Localizing frustration in native proteins and protein assemblies. PNAS 104:19819-19824

30) Ferreiro DU, Hegler JA, Komives EA, Wolynes PG. 2011. On the role of frustration in the energy landscapes of allosteric proteins. PNAS 108: 3499-5303.

31) Filmer HL, Dux PE, Mattingley JB. 2014. Applications of transcranial direct current stimulation for understanding brain function. Trends Neurosci 37:742-753.

32) Foster JA, McVey Neufeld KA. 2013. Gut-brain axis: how the microbiome influences anxiety and depression. Trends Neurosci 36: 305-312.

33) Fox MD, Raichle ME. 2007. Spontaneous fluctuations in brain activity observed with functional magnetic resonance imaging. Nat Rev Neurosci 8: 700-711.

34) Fraiman D, Chialvo DR. 2012. What kind of noise is brain noise: anomalous scaling behaviour of the resting brain activity fluctuations. Front Physiol 3:307.

35) Frauenfelder H, Sligar SG, Wolynes PG. 1991. The energy landscapes and motions of proteins. Science 254: 1598-1603.

36) Freeman WJ, Vitiello G. 2008. Dissipation and spontaneous symmetry breaking in brain dynamics. J Phys A Math Theor 41, 304042: 1-17.

37) Friston K. 2010. The free-energy principle: a unified brain theory? Nat Rev Neurosci 11:127-138.

38) Friston K, Rigoli F, Ognibene D, Mathys C, Fitzgerald T, Pezzulo G. 2015. Active inference and epistemic value. Cogn Neurosci 13: 1-28.

39) Gaspard P. 2005 Brownian motion, dynamical randomness and irreversibility. New J Phys 7, 77.

40) Gonzalez-Castillo J, Handwerker DA, Robinson ME, Hoy CW, Buchanan LC, Saad ZS, Bandettini PA. 2014. The spatial structure of resting state connectivity stability on the scale of minutes. Front Neurosci. 2014; 8: 138.

41) Gonzalez-Rodriguez D, Maddugoda MP, Stefani C, Janel S, Lafont F, Cuvelier D, Lemichez E, Brochard-Wyart F. 2012. Cellular dewetting: opening of macroapertures in endothelial cells. Phys Rev Lett 25, 108(21):218105

42) Gollisch T. 2009. Throwing a glance at the neural code: rapid information transmission in the visual system. HFSP J 3: 36–46.

43) Guido W, Sherman SM. 1998. Response latencies of cells in the cat's lateral geniculate nucleus are less variable during burst than tonic firing. Vis Neurosci. 15: 231-7.

44) Haider B, Duque A, Hasenstaub AR, McCormick DA. 2006. Neocortical network activity in vivo is generated through a dynamic balance of excitation and inhibition. J Neurosci 26: 4535-4545.

45) Haustein MD, Kracun S, Lu XH, Shih T, Jackson-Weaver O, Tong X, Xu J, Yang XW, O'Dell TJ, Marvin JS, Ellisman MH, Bushong EA, Looger LL, Khakh BS. 2014. Conditions and Constraints for Astrocyte Calcium Signaling in the Hippocampal Mossy Fiber Pathway. Neuron, 82:413–429.

46) Hegler JA, Weinkam P, Wolynes PG. 2008. The spectrum of biomolecular states and motions. HFSP J. 2: 307-313.

47) Henry, E.R., Eaton, W.A., 2004. Chem Phys 307: 163-185.

48) Hopfield JJ. 1982. Neural networks and physical systems with emergent collective computational abilities. PNAS 79: 2554–2558.

49) Isayev AA. 2003. Competition between ferromagnetic and antiferomagnetic spin ordering in nuclear matter. JETP Letters l77: 251-255.

50) Itoh, K., Sasai, M., 2006. Flexibly varying folding mechanism of a nearly symmetrical protein: B domain of protein A. PNAS 103: 7298-7303.

51) Izhikevich EM. 2010. Hybrid spiking models. Philos Trans A Math Phys Eng Sci 368(1930):5061-5070.

52) James RD, Kinderlehrer D. 1990. Frustration in ferromagnetic materials, 2 Continuum Mech. Thermodyn 215-239.

53) James RD, Kinderlehrer D. 1991. An example of frustration in a ferromagnetic material. *in* J.-M. Coron et al, Eds., Nematics, 201-221. Berlin: Springer.

54) Jakovcevski M, Ruan H, Shen EY, Dincer A, Javidfar B, Ma Q, Peter CJ, Cheung I, Mitchell AC, Jiang Y, Lin CL, Pothula V, Stewart AF, Ernst P, Yao WD, Akbarian S. 2015.

Neuronal Kmt2a/Mll1 Histone Methyltransferase Is Essential for Prefrontal Synaptic Plasticity and Working Memory. J Neurosci, 35: 5097-5108.
55) Kavalali ET, Chung C, Khvotchev M, Leitz J, Nosyreva E, Raingo J, Ramirez DM. 2011. Spontaneous neurotransmission: an independent pathway for neuronal signaling? Physiology (Bethesda) 26:45-53.
56) Koga N, Takada S. 2001. Roles of native topology and chain-length scaling in protein folding: a simulation study with a Go-like model. J Mol Biol 313: 171-180.
57) Kravchick DO, Jordan BA. 2015. Presynapses go nuclear! EMBO J. 15:984-986.
58) Lapierre F, Coffinier J, Boukherroub R, Thomy V. 2013. Electro- (de)wetting on Superhydrophobic surfaces. Langmuir, 29: 13346-13351.
59) Laurenbacher R, Sturmfels B. 2009. Computer algebra in system biology. Amer Math Monthly 116: 882-891.
60) Lehn JM. 2007. From supramolecular chemistry towards constitutional dynamic chemistry and adaptive chemistry. Chem Soc Rev 36:151-160.
61) Levy Y, Wolynes PG, Onuchic JN. 2004. Protein topology determines binding mechanism. PNAS 101: 511-516.
62) Linkenkaer-Hansen K, Nikouline VV, Palva JM, Ilmoniemi RJ. 2001. Long-range temporal correlations and scaling behaviour in human brain oscillations. J Neurosci 21: 1370-1377.
63) Lombardi F, Herrmann HJ, Perrone-Capano C, Plenz D, de Arcangelis L. 2012. Balance between Excitation and Inhibition Controls the Temporal Organization of Neuronal Avalanches. Phys. Rev. Lett. 108, 228703.
64) Looi JC, Walterfang M, Nilsson C, Power BD, van Westen D, Velakoulis D, Wahlund LO, Thompson PM. 2014. The subcortical connectome: hubs, spokes and the space between - a vision for further research in_neurodegenerative disease. Aust N Z J Psychiatry. 48:306-309.
65) Lenglet C, Abosch A, Yacoub E, De Martino F, Sapiro G, Harel N. 2012. Comprehensive in vivo mapping of the human basal ganglia and thalamic connectome in individuals using 7T MRI. PLoS One. 7,e29153.
66) Mancuso K, Hauswirth WW, Li Q, Connor TB, Kuchenbecker JA, Mauck MC, Neitz J, Neitz M. 2009. Gene therapy for red-green colour blindness in adult primates. Nature 461: 784-787.
67) Magosso E, Cuppini C, Serino A, Di Pellegrino G, Ursino M. 2008. A theoretical study of multisensory integration in the superior colliculus by a neural network model. Neural Netw 21:817-829.
68) Marcoli M, Agnati LF, Benedetti F, Genedani S, Guidolin D, Ferraro L, Maura G, Fuxe K. 2015. On the role of the extracellular space on the holistic behaviour of the brain. Rev Neurosci 26(5):489-506.
69) Mooney R, Penn AA, Gallego R, Shatz CJ. 1996. Thalamic relay of spontaneous retinal activity prior to vision. Neuron 17: 863-874.
70) Morcos F, Schafer NP, Cheng RR, Onuchic JN, Wolynes PG. 2014. Coevolutionary information, protein folding landscapes, and the thermodynamics of natural selection. PNAS 111:12408-12413.
71) Munoz, V., Eaton, W.A., 1999. PNAS 96:11311-11316.
72) Mustonen V, Lässig M. 2008. Molecular evolution under fitness fluctuations. Phys Rev Lett 100(10):108101.
73) Nieuwenhuys R, Voogd J, van Huijzen C. 2008. The Human Central Nervous System. Heidelberg: Springer.
74) Xue M, Atallah BV, Scanziani M. 2014. Equalizing excitation-inhibition ratios across visual cortical neurons. Nature 511:596-600.
75) O'Donnell C, Van Rossum MC. 2014. Systematic analysis of the contributions of stochastic voltage gated channels to neuronal noise.. Front Comput Neurosci 8:105.
76) Onuchic JN, Luthey-Schulten Z, Wolynes PG. 1997. Theory of protein folding: the energy landscape perspective. Ann Rev Phys Chem 48:545-600.
77) Oh SW, Harris JA, Ng L, Winslow B, Cain N, et al. 2014. A mesoscale connectome of the mouse brain. Nature 508: 207-214.
78) Papo D. 2014. Functional significance of complex fluctuations in brain activity: from resting state to cognitive neuroscience. Front Syst Neurosci 8, 112.
79) Papo D. 2015. how can we study reasoning in the brain? Front Hum Neurosci 9, 222.
80) Picard F, Friston K. 2014. Predictions, perception, and a sense of self. Neurology 83:1112-1118.
81) Pruszynski JA, Johansson RS. 2014. Edge-orientation processing in first-order tactile neurons. Nat Neurosci 17:1404-1409.
82) Rabinovich M, Huerta R, Laurent G. 2008. Neuroscience. Transient dynamics for neural processing. Science 4;321(5885):48-50.
83) Raichle ME. 2010. Two views of brain function. Trends Cogn Sci 14:180-190.
84) Reese TM, Brzoska A, Yott DT, Kelleher DJ. 2012. Analyzing Self-Similar and Fractal Properties of the C. elegans Neural Network. PLoS ONE 7,(10): e40483.
85) Rijto PA, Verkhivker GM. 1996. Unraveling principles of lead discovery: From unfrustrated energy landscapes to novel molecule anchors. PNAS 93: 8945-8950.
86) Sackmann E, Bruinsma RF. 2002. Cell adhesion as wetting transition? Chemphyschem. 12:262-269.
87) Schmidt A, Denier N, Magon S, Radue E-W, Huber CG, et al. 2015. Increased functional connectivity in the resting-state basal ganglia network after acute heroin substitution. Translat Psychiatry 5, e533.
88) Schmithorst VJ, Vannest J, Lee G, Hernandez-Garcia L, Plante E, Rajagopal A, Holland SK. 2014. Neurovascular coupling underlying the BOLD effect increases with age during childhood. Hum Brain Mapp 6(1):1-15.
89) Schneidman E, Berry MJ, Segev R Bialek W. 2006. Weak pairwise correlations imply strongly correlated network states in a neural population. Nature 440:1007-1012.
90) Seung H S. 1996. How the brain keeps the eyes still. PNAS 93(23): 13339-13344.
91) Shlens J, Field GD, Gauthier JL, Greschner M, Sher A Litke AM, Chichilnisky EJ. 2009 The structure of large-scale synchronized firing in primate retina. J Neurosci. 29: 5022-5031.
92) Schmitt O, Eipert P, Hoffmann R, Morawska P, Klünker A, Meinhardt J, Lessmann F, Beier J, Kadir K, Karnitzki A, Jenssen J, Kuch L, Sellner L, Wree A. 2014. Central and peripheral monosynaptic, polysynaptic and collaterals connectivity in the rat. Front Neuroinform Conference Abstract: Neuroinformatics 2014.
93) Sengupta B, Stemmler MB, Friston KJ. 2013a. Information and efficiency in the nervous system--a synthesis. PLoS Comput Biol 9, e1003157.
94) Sengupta B, Laughlin SB, Niven JE. 2013b. Balanced excitatory and inhibitory synaptic currents promote efficient coding and metabolic efficiency. PLoS Comput Biol 9, e1003263.
95) Sengupta B, Stemmler MB. 2014. Power Consumption During Neuronal Computation. Proceedings IEEE 102: 738-750.
96) Sengupta B, Tozzi A, Cooray GK, Douglas PK, Friston KJ. 2016. Towards a Neuronal Gauge Theory. PLoS Biol 14(3): e1002400.
97) Sharmaa A, Reiterb G. 1996. Instability of Thin Polymer Films on Coated Substrates: Rupture, Dewetting, and Drop Formation. J Colloid Interface Sci 178: 383-399.
98) Spruston N. 2008. Pyramidal neurons: dendritic structure and synaptic integration. Nat Rev Neurosci 9:206-221.

99) Sur S, Newcomb CJ, Webber MJ, Stupp SI. 2013. Tuning supramolecular mechanics to guide neuron development. Biomaterials 34:4749-4757.
100) Sutto L, Latzer J, Hegler JA, Ferreiro DU, Wolynes PG. 2007. Consequences of localized frustration for the folding mechanism of the IM7 protein. PNAS 104:19825-19830.
101) Taylor MB, Ehrenreich IM. 2014. Genetic interactions involving five or more genes contribute to a complex trait in yeast. PLoS Genet 10,e1004324.
102) Tanaka M, Rehfeldt F, Schneider MF, Mathe G, Albersdorfer A, Neumaier KR, Purrucker O, Sackmann E. 2005. Wetting and dewetting of extracellular matrix and glycocalix models. Journal of Physics: Condensed Matter 17, 9.
103) Thiam AR, Farese Jr RV, Walther TC. 2013. The biophysics and cell biology of lipid droplets. Nat Rev Molecular Cell Biol 14: 775- 786.
104) Thompson CV. 2012. Solid-State Dewetting of Thin Films. Ann Rev Materials Res 42: 399-434.
105) Tong Y, Frederick BD. 2010. Time lag dependent multimodal processing of concurrent fMRI and near-infrared spectroscopy (NIRS) data suggests a global circulatory origin for low-frequency oscillation signals in human brain. Neuroimage. 53:553-64.
106) Tognoli E, Kelso JA. 2014. Enlarging the scope: grasping brain complexity. Front Syst. neurosci 8, 122.
107) Towlson EK, Vértes PE, Ahnert SE, Schafer WR, Bullmore ET. 2013. The rich club of the C. elegans neuronal connectome. J Neurosci 33:6380-6387.
108) Tononi G. 2008. Consciousness as Integrated Information: a Provisional Manifesto. Biol Bull 215:216-42.
109) Tozzi A. 2015. Information processing in the CNS: a supramolecular chemistry? Cogn Neurodyn 9:463-477.
110) Tozzi A., Peters JF. 2016b. Towards a fourth spatial dimension of brain activity. Cogn Neurodyn, in press. DOI: 10.1007/s11571-016-9379-z.
111) Van den Heuvel MP, Sporns O. 2011. Rich-club organization of the human connectome. J Neurosci 31:15775-15786.
112) Vargas JN, Seemannab R, Fleury JB. 2014. Fast membrane hemifusion via dewetting between lipid bilayers. Soft Matter 10: 9293-9299.
113) Verkhivker GM, Rejto PA. 1996. A mean field of ligand-protein interactions: Implications for the structural assessment of human immunodeficiency virus type 1 protease complexes and receptor-type binding, PNAS 93: 60-64.
114) Virnau P, Mallam A, Jackson S 2011. Structures and folding pathways of topologically knotted proteins. J Phys Condens Matter 23, 033101.
115) Vuksanovic V, Hövel P. 2014. Functional connectivity of distant cortical regions: Role of remote synchronization and symmetry in interactions. NeuroImage, 97: 1–8.
116) Yan H, Zhao L, Hu L, Wang X, Wang E, Wang J. 2013. Nonequilibrium landscape theory of neural networks. PNAS 110(45): 4185-4194.
117) Yates D. 2014. Myelination: A not so even distribution. Nat Rev Neurosci 15,351.
118) Young T, Hua L, Huang X, Abel R, Friesner R, Berne BJ. 2010. Dewetting transitions in protein cavities. Proteins 78:1856-1869.
119) Wales DJ. 2012. Decoding the energy landscape: extracting structure, dynamics and thermodynamics. Philos Trans A Math Phys Eng Sci 28: 2877-2899.
120) Watanabe T, Hirose S, Wada H, Imai Y, Machida T, Shirouzu I, Konishi S, Miyashita Y, Masuda N. 2014a. Energy landscapes of resting-state brain networks. Front Neuroinform 25:8:12.
121) Watanabe T, Masuda N, Megumi F, Kanai R, Rees G. 2014b. Energy landscape and dynamics of brain activity during human bistable perception. Nat Commun. 28, 5:4765.
122) Wolynes PG. 1996. Symmetry and the energy landscapes of biomolecules, PNAS 93: 14249-14255.
123) Wu FY. 1992. Knot theory and statistical mechanics. Rev Mod Phys 64:1099-1131.
124) Zare M, Grigolini P. 2013. Criticality and avalanches in neural network. Chaos Solitons Fractals 55: 80–94.

SCHOLARLY PAGES

Archives of Information Science and Technology

Original Research Open Access

Multidimensional Chaotic Dynamics and Entropies

Arturo Tozzi[1,2]*, James F Peters[3,4], Colin James III[5] and Eva Déli[6]

[1]*Center for Nonlinear Science, University of North Texas, Denton, USA*

[2]*Computational Intelligence Laboratory, University of Manitoba, Winnipeg, Canada*

[3]*Department of Electrical and Computer Engineering, University of Manitoba, Winnipeg, Canada*

[4]*Department of Mathematics, Adiyaman University, Adiyaman, Turkey*

[5]*Ersatz Systems Machine Cognition, LLC, USA*

[6]*Institute for Consciousness Studies (ICS), Hungary*

In Search of Hidden Dimensions

The possible presence of further dimensions hidden in our three-dimensional-plus time world might help to elucidate countless physical and biological systems' behaviors, from quantum entanglement to brain function. Nevertheless, suggestions concerning multidimensional arrangement of physical and biological systems do not deserve the role of scientific claims, unless the suggested additional dimensions can be verified via empirically testable hypotheses and experimental apparatus. Here we suggest that the widespread nonlinear dynamics and chaotic behavior of physical and biological collective systems might mirror further dimensions hidden in our world. Indeed, bringing together disparate knowledge from seemingly unrelated fields (brane cosmology, fluid dynamics, algebraic topology, computational topology, dynamic systems theory, logic and statistical mechanics), we show how, in logistic maps derived from nonlinear dynamical equations, the typical bifurcation diagrams might arise from linear flow paths, that intersect large-sized hidden dimensions at the canonical phase parameter's values between three and four. Therefore, chaotic dynamics suggests the existence of a further hidden dimension in our Universe. We also provide a thermodynamic framework which suggests that the cosmic entropy is encompassed in a multidimensional manifold.

Introduction

In brane cosmology, strings and branes theories are based on the hypothetical existence of hidden dimensions surrounding us [1-3]. Our Universe could either lie on a spatial three-dimensional brane embedded in a higher dimensional bulk, or could be flanked by one or more multi-dimensional branes of different possible sizes and shapes [4,5]. Nothing is known about the scale of such extra dimensions. There is no consensus among theoreticians: some believe that extra-dimensions are warped in microns-scale manifolds, while others suggest that they could be of the size of millimeters, or hypothesize an indeterminately high hidden dimension surrounding us [6-8]. In order to assess the issue, we start from a recently proposed topological model, which suggests that two particles entangled in an n-dimensional space are un-entangled, when assessed in one dimension higher [9]. Because quantum entanglement occurs also between particles light-years away from each other, this means that, if their disentanglement occurs onto a further hidden dimension, the extra-dimensional manifolds must be very large and must influence also our three-dimensional-plus time (space-time) Universe. This observation points towards elusive higher dimensions surrounding us, able to intersect our space-time world and to interact with it. Such invisible (e.g., hidden by our standpoint of

***Corresponding author:** Arturo Tozzi, Center for Nonlinear Science, Department of Physics, University of North Texas, 1155 Union Circle, #311427, Denton, Texas 76203-5017, USA; Computational Intelligence Laboratory, University of Manitoba, Winnipeg, Winnipeg R3T 5V6 Manitoba, Canada, E-mail: tozziarturo@libero.it

Received: June 09, 2017; **Accepted:** July 19, 2017; **Published online:** July 21, 2017

Citation: Tozzi A, Peters JF, Colin J III, et al. (2017) Multidimensional Chaotic Dynamics and Entropies. Arch Inf Sci Technol 1(1):10-19

Copyright: © 2017 Tozzi A, et al. This is an open-access article distributed under the terms of the Creative Commons Attribution License, which permits unrestricted use, distribution, and reproduction in any medium, provided the original author and source are credited.

observers embedded in a space-time structure), infinite curvilinear dimension(s) crosses and/or is embedded in the fabric of our world. In order to try to elucidate our rather speculative claim, we look for hints of hidden dimensions in natural phenomena occurring in our space-time world, starting from the premise that extra-dimensions might be emergent also in our lower-dimensional environment.

In particular, we evaluate the widespread complex, nonlinear physical and biological collective systems, equipped with non-equilibrium dynamics and characterized by a large number of interacting and inter-dependent components, spontaneous self-organization and self-organized criticality [10-14]. Many physical and biological collective nonlinear systems operate at the edge of chaos. A chaotic system displays dependence from initial conditions, positive Lyapunov exponents and attractors. They tend to live near a metastable state of second-phase transitions, characterized by infinite correlation length, countless functional dimensions [15], spontaneous avalanches and universal power laws [16-18].

Here we show, based on claims from far-flung disciplines that the typical bifurcation diagram of logistic maps' nonlinear dynamical equations might arise from the interaction of linear paths with large-sized hidden dimensions intersecting them. We introduce a multidimensional approach that offers an explanation of some aspects of dynamic systems theory, in particular Hopf bifurcations, in terms of hidden dimensions, and also a method in order to evaluate the consequences of this strategy. We also provide a framework able to solve a long-standing issue. Indeed, the second law of thermodynamics states that the thermodynamic entropy tends to increase in a closed system, so that the process is irreversible. We asked: why is thermodynamic entropy frequently unchanged, during nonlinear phase transitions?

Materials and Methods

In order to assess and operationalize our hypothesis that hidden dimensions, endowed in our space-time world, might give rise chaotic nonlinear dynamics, we need to develop the proper procedures. In search for hidden dimensions, we will proceed as follows: at first, we will provide a brief description of logistic plots. Then, we will describe four different approaches from far-flung disciplines. We will try to demonstrate that they stand for different clues converging towards our claim.

Premise: Chaotic bifurcations and logistic plots

As stated above, different physical and biological systems display nonlinear features. This form of dynamics is frequently studied through logistic maps equipped with bifurcations, which intervals are dictated by the Feigenbaum constants [19]. A logistic map is a one-dimensional nonlinear difference equation, widely used to study dynamic systems theory's issues [20]. It encompasses a generic variable representing an observable behavior and a fixed behavioral parameter (the phase parameter). Logistic maps can be plotted and visualized on a one-parameter bifurcation diagram, as a function of the scaled parameter *r*. Note that, at the edge of criticality, bifurcations occur.

The first universal Feigenbaum constant stands for the limiting ratio of each bifurcation interval to the next, between every period doubling [21]. It is applicable to one-parameter maps, where $f(x)$ is a function parameterized by the bifurcation parameter a:

$$x_{i+1} = f(x_i),$$

and also for other logistic maps, such as:

$$f(x) = ax(1-x),$$

and

$$f(x) = \alpha x - x^2$$

Therefore, every chaotic system, described by maps with a single quadratic maximum, will bifurcate at the same rate, i.e., the first Feigenbaum constant [22]. The latter is a transcendental number, given by the limit [23]:

$$\delta = \lim_{n\to\infty} \frac{a_{n-1} - a_{n-2}}{a_n - a_{n-1}} = 4.669201609...$$

Where a_n stands for discrete values of the variable a at the nth period doubling. Note that the ratio $\frac{a_{n-1} - a_{n-2}}{a_n - a_{n-1}}$ converges to the first Feigenbaum constant.

The second Feigenbaum constant, i.e,

α = 2.502907875095892822283902873218…,

is the ratio between the width of a tine and the width of one of its two subtines (except the tine closest to the fold). A negative sign is applied to α, when the ratio between the lower subtine and the tine width is measured.

The first approach: Detecting dimensions through flows assessment

When you watch from afar a circular structure, you may not be sure if it is a 2D disk or a 3D sphere, unless you go close and look for shadows or angles. There is however an indirect procedure, in order to detect objects' dimensions and shape. If you convey a laminar flux towards its surface, you can assess fluxes' trajectories (Figure 1). Therefore, looking at flows' behavior, you may assess whether the circular structure displays two or three dimensions. In other words, we are allowed to evaluate what happens to a water flow when we introduce a solid object that, being an interposed obstacle, is able to

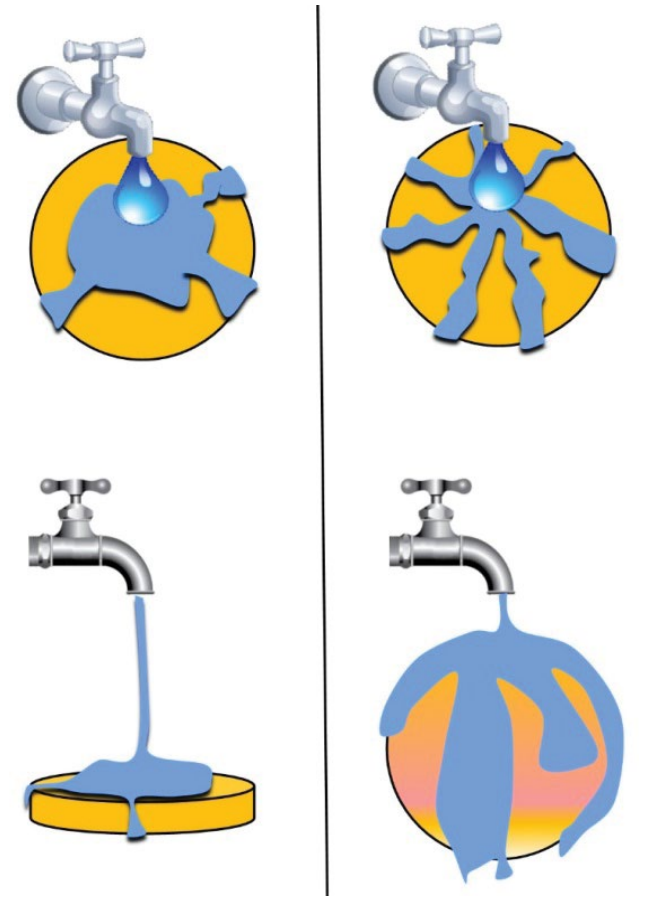

Figure 1: How to detect objects' dimensions and shape through a laminar flux. The left side of the Figure displays water flows in case of the object being a 2D disk, while the right side 3D sphere. A water stream intersecting the discoidal surface of an object allows us to understand whether the object is two-dimensional (a disk) or three dimensional (a sphere), in case we are not able to detect such feature from afar. The pattern of the water falling on the surface is different, according to the dimensionality of the object. The upper figures depict the upper surfaces of the 2D and 3D objects, respectively, while the lower figures display their lateral view.

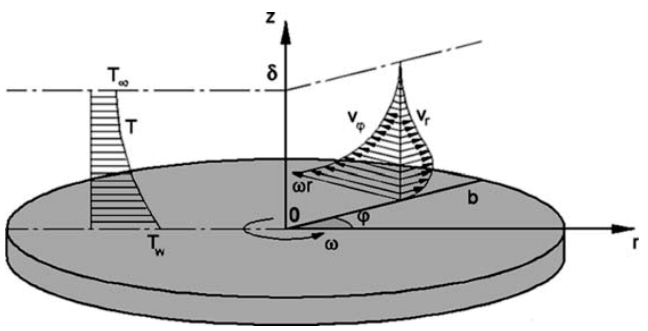

Figure 2: Provides, as an example, geometrical arrangement and main parameters of the problem of fluid flow and heat transfer over a rotating disk in still air [45].

modify the liquid paths. For example, if you use a funnel, the water will be conveyed in a very thin flow.

In Figure 2, for sake of simplicity, we described a water flow. Nevertheless, we are also allowed to use other kinds of streams, such as electromagnetic or sonic currents, and so on [24,25]. Every one of such fluxes obeys different types of well-established equations, following well-studied trajectories that could be visualized and quantified. For example, air fluxes on a disk have been widely investigated. The flux features will tell us about the shape of the hidden surface. Indeed, by knowing the disk's radius and the strength of the uniform field, we may evaluate the orientation and movements of the disk's surface and the presence of hidden obstacles (Figure 2), both for laminar or turbulent fluxes. As an example of previously unrecognized classes of flows, stochastic heat engines have been assessed, in particular a colloidal sphere diffusing in a conventional optical tweezer [26]. In this case, non-conservative optical forces bias the particle's fluctuations into toroidal vortexes, whose circulation can reverse direction with temperature or laser power.

These methods from fluid dynamics allows us to look (in physical and biological systems' phase spaces with superimposed "obstacles" to the flux) for hypothetical traces left by different kinds of fluxes, in order to indirectly assess possible hidden dimensions and their shapes. In particular, we might be able to assess what happens to a particle trajectory traveling in a n-spatial environment, when it interacts with an object not endowed in a further spatial dimension, but instead endowed in an abstract "super space" [27]. Super spaces have been introduced in the study of super symmetry, in order to compare the otherwise not assessable bosons and fermions' total behavior. The philosophy behind super spaces is to embed phase spaces both in spatial and non-spatial dimensions, in order to improve the detectability of otherwise invisible parameters. Here we use super spaces in guise of abstract, non-spatial dimensions superimposed to spatial systems, able to interfere with the trajectories occurring in classical spatial n-dimensions.

The second approach: Topology comes into play

The Borsuk-Ulam Theorem (BUT) states that, if a sphere S^n is mapped continuously into an n-dimensional Euclidean space R^n, there is at least one pair of antipodal points on S^n which map onto the same point of R^n [28,29]. See Tozzi and Peters [30] for further details and a mathematical treatment. The notation stands for an n-sphere [31], which is an n-dimensional, circular structure, embedded in an $n + 1$ space [32]. For example, a 2-sphere (S^2) is the 2-dimensional surface of a 3-dimensional space. Antipodal points are, *e.g.*, the poles of a sphere [33,34].

Several BUT variants have been developed in the very

last years. For example, we can consider regions on an *n*-sphere that are either adjacent or far apart. This means that pairs of points need not be antipodal, in order to have matching descriptions [35]. This BUT variant has utility, provided there are a pair of regions on an *n*-sphere which are *similar*. The concept of antipodal points can be used not just for the description of points, but also for more complicated structures, such as shapes of space (object contours), temporal intervals (temporal oscillations), functions, vectors and symmetries [36,37]. This leads to a particularly useful region-based BUT, dubbed re-BUT [35]. We are allowed to describe brain features on an *n*-sphere either as antipodal points, or antipodal regions. This means that antipodal signal shapes can be compared [35]. That is, feature-based descriptions of antipodes can be assessed at one level of observation, while their projections into a single shape can be analyzed at a lower level [37].

Although BUT was originally limited to an *n*-sphere where *n* is a natural number, nevertheless *n* can also be regarded as rational or irrational number [37]. For example, we might regard functions or shapes as embedded in a sphere in which *n* stands for number of instants in time. Hence, the parameter *n* becomes useful in the description of nonlinear and fractal dynamical systems.

The original formulation of BUT describes the presence of antipodal points on spatial manifolds in every dimension, provided the manifold is a convex, positive-curvature structure (e.g., a ball). However, the kind of geometry that best describes world dynamics is a matter of debate. Theoretical contenders include Euclidean, elliptic and hyperbolic geometry. This means that systems functions might occur on manifolds endowed with different types of geometry, for example the hyperbolic one encloses complete Riemannian *n*-manifolds of constant sectional curvature-1 and concave shape [38]. We are thus allowed to look for antipodal points also on structures equipped with kinds of curvature other than the convex one [39]. Or, in other words, whether the system under examination displays a concave, convex or flat functional appearance, it does not matter: we may always find the points with matching description predicted by BUT. For further details, see also Peters and Tozzi [37].

In sum, the BUT displays versatile features which can be modified in different guises: last but not least, the mapping of antipodal points into the lower level of a $n - 1$ sphere. In our case, we are allowed to use BUT in order to describe Hopf bifurcations, because the latter cannot occur in discrete-time systems or maps. However, because the intended meaning is related to a Poincare section, the argument about the hidden dimensions holds true. Precisely, a period-doubling bifurcation in the logistic map may correspond to a double-covering bifurcation of a limit-cycle in a higher dimensional space.

The third approach: Computerized tessellation of the image of the logistic plot

We assessed the logistic plot "classical" image of nonlinear, chaotic dynamics through a novel image analysis approach [40,41]. Indeed Peters, et al. [41] introduced a novel method for the measurement of information level in data sets, based on image subdivision in small polygons equipped with different entropic content. This method, called maximal nucleus clustering, is based on nucleus clustering in Voronoï tessellations [42]. In brief, a computerized program chooses the points of the image with the higher difference of orientation, compared with the others. The choice of such points, called generating points, allows us to build around them small polygons, called Voronoi tessellation regions. Such small polygons, depending on the number of their sides, display different levels of information. In particular, the polygons with the higher number of sides, called Maximum Nucleus Clusters (MNC), together with their surrounding polygons, might be an indirect clue of hidden dimensions in a two-dimensional Figure. Indeed, MNC reveals zones of the image characterized by different gradient orientation and diverse functional dimensions [40]. The fractal structure of the logistic map is believed to come from the stretch-and-fold process: therefore, why, in our framework, do MNCs imply hidden dimensions? In Peters, et al. [40] we hypothesized that every parameter correlated with the MNCs might stand for a functional dimension. In the previous paragraph, we introduced the concept of BUT and matching signals. The basic form of BUT tells us that there exists a pair of antipodal (opposite) signals on the circumference that maps to a single one on a line. The two antipodal signals are assessed at one level of observation, while the single one at a lower level. This means that, if we embed a MCN onto a circumference, there exist two antipodal signals with matching description. Therefore, BUT provides a handy vehicle in expressing the relationship between Voronoï polygons that serve as cluster nuclei. In the image tiling, more than one MCN can be found, all of them equipped with the same number of sides (i.e., these MCNs display matching description). Therefore, different MNCs may be embedded in the same circumference and may display matching functional description. In other words, systems features could be characterized as antipodal signals with matching description, in order that the functions of signal shapes can be compared. It might be speculated that changes in morphological features could be correlated with variations in physical functions. Thus, gradient differences might be linked with different functional and dimensional counterparts.

Although we live in a space-time world with no immediate perception that hidden spaces exists at all, the hints of a further dimension can be identified through their "cross section" movements on a more accessible three-dimensional surface, as if you recognized some object from its shadow projected on a screen. In such a vein, MNCs might be able to evaluate indirect clues of the undetectable fourth dimension, e.g., the hallmarks or signs on a familiar space-time surface.

The fourth approach: Logical validation

Here we asked whether it is feasible to validate as true, through logic tools, the possibility that a logistic plot is correlated with a hidden dimension that intersects linear behaviors of collective systems, when they phase parameter changes from 3 to 4. In general terms, we described a logical question in the format of: "if possibly A (with its logical parts), then B" to be validated true or validated not true. In our specific case, we asked whether the following two questions are logically tenable:

a) Is it possible that laminar fluxes can be unobstructed or bifurcated by interposition of the necessity of hidden dimensions implying visible dimensions?

b) The necessity of non-visible dimensions imply the possibility of laminar fluxes as either: 1) Not obstructed; or 2) Bifurcated by non-visible dimensions implying visible dimensions?

We used the following logic procedure. We mapped categorical subject parts into "literal" variables. The validation was performed by the logic model checker Meth8 (U.S. Patent pending). Meth8 is a logic model checker which requires each expression as a numbered equation to be validated true/not validated true in each case to constitute a well-formed and satisfiable proof. It is based on VŁ4, the variant that corrects and resuscitates the quaternary logic Ł4 of Łukasiewicz.

We used the 4 propositions < p, q, r, s >. We mapped action relations into respective lists for:

a) Connectives < And; Not and; Or; Not or; Equivalent; Not equivalent; Imply; Not imply >;

b) Common symbols with ~ for Not as the set { &, ~&, V, ~V, ↔, [ ], →, ← };

c) One letter symbols in Meth8 as the set { & , \ , + , - , = , @ , > , < }.

We also mapped modifiers in modal operators for possibility and necessity, using the following symbols:

a) Common symbols of the lozenge ◊ and box [];

b) One letter characters in Meth8 as % and #.

Predicate logic has two quantifiers, the existential ∃ as "at least one exists" and the universal ∀ as "for all". The quantifiers are based on (the misattributed) Aristotle's Square of Opposition which provably is not bivalent (not exact).

However, propositional logic has two modal operators that provably are bivalent (exact) and generally interchange with the two quantifiers, ◊ for ∃ and [] for ∀.

We also mapped expressions into the format of:

a) Named types in order of literal, operator, literal such as p & q;

b) Named parts in order of antecedent, connective, consequent.

Results

Here we show how the bifurcation diagram of 2D logistic maps' nonlinear dynamical equations might be shaped and deformed by an intersecting hidden dimension, e.g., a super space containing the first Feigenbaum constant.

The first approach: Detecting dimensions through flows assessment

In this logistic plot, x stands for the detectable trajectory followed by a particle in a space-time, and r stands for possible hidden dimensions. When the scaled parameter r is measured between 1 and 3, the particle behavior

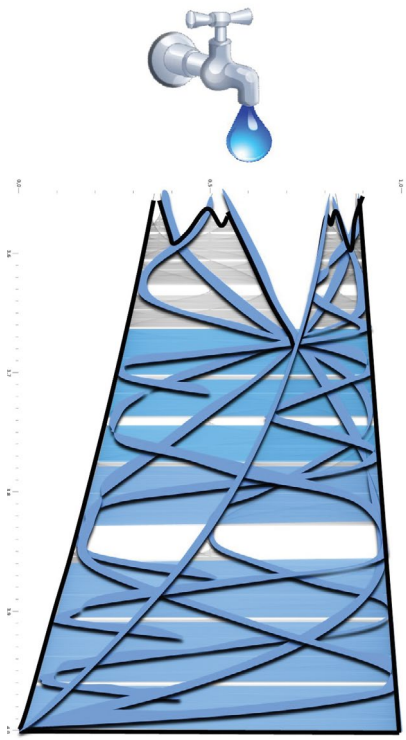

Figure 3: The hypothetical case of an obstacle hidden in the logistic map's bifurcations able? Is this a word? To modify water flows.

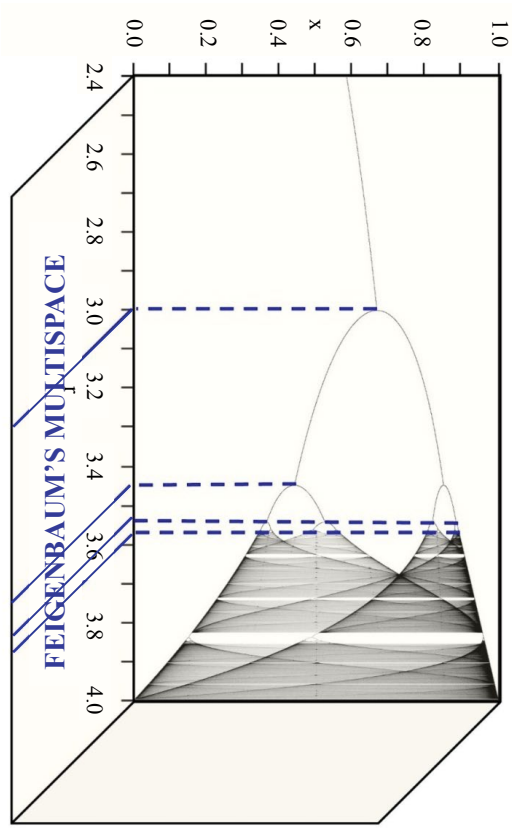

Figure 4: Illustrates how a Feigenbaum multi space might modify the trajectories in a logistic plot, leading to bifurcations when it interferes with the flow.

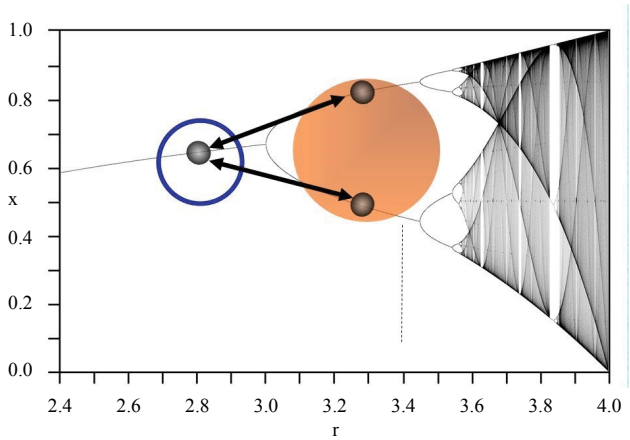

Figure 5: Bifurcation diagram of a simulated logistic map's nonlinear dynamical equation. The axis *x* displays a hypothetical phase parameter r, the axis *y* the probability of a generic variable. At the first Hopf bifurcation, the exponent *n* of the *n*-sphere stands for the first Feigenbaum constant. The same operation can be repeated at each of the following bifurcations: just the first one is displayed in Figure. Each n-sphere is equipped with two antipodal points which intersect the curves of the corresponding bifurcation and display the same value on the axis *x*. In sum, the irrational number of the Feigenbaum constant can be used in guise of a super space superimposed to a 2D chaotic logistic plot. Such super space is able to modify the linear trajectories, leading to a cascade of fractal bifurcations.

is linear. When the value 3 is reached, it looks like an obstacle to the flow occurs (Figure 3). At phase parameter's values between 3 and 4, the super space (e.g., one or more hidden dimensions) interferes with the plot and interacts with the traveling particles. When linear trajectories cross the super space, they split into progressively increasing fractal bifurcations, until a totally chaotic pattern is achieved. Interestingly, this further dimension(s) is somewhat correlated with the first Feigenbaum constant (Figure 4).

The second approach: Topology comes into play

Tozzi and Peters [30] demonstrated that embracing systems non-linearity in the framework of the Borsuk-Ulam theorem means that nervous bifurcation transformations (the antipodal points) can be described as paths or trajectories on abstract spheres equipped with Feigenbaum dimensions (Figure 5). Note that, from linearity to non-linearity, the number of points with matching description increases. This means, for the BUT theorem and its variants, that, going from phase parameter 3 to 4, it occurs an increase of n-dimensions. However, in this case, the term n does not stand for a natural number as in the classic BUT, but for an irrational number (the Feigenbaum constant). We could state that, in a logistic plot equipped with a hypothetical hidden dimension, the increase of bifurcations is given by the BUT dictates (e.g., a single feature in n-dimensions maps to two features or more in $n + 1$ dimensions). The concave trajectories are caused by the shape of the hidden dimension(s), because the bifurcation distortion could be due to a negative-curvature superimposed manifold(s). There must be a concave manifold that modifies the original linear curve, when, at the proper values of the phase parameter, trajectories pass through it. In sum, chaotic behavior might be correlated with the intersection between the linear path and a hidden dimension(s).

The third approach: Computerized tessellation of the image of the logistic plot

Figure 6 depicts MNCs in a tessellated logistic plot at different magnifications. Note that in this case MNCs and their surrounding polygons stand for the possible location of the hidden dimension interfering with linear trajectories.

The fourth approach: Logical validation

Our first question was:

"Is it possible that laminar fluxes can be unobstructed or bifurcated by interposition of the necessity of hidden dimensions implying visible dimensions?"

(Q1)

LET:

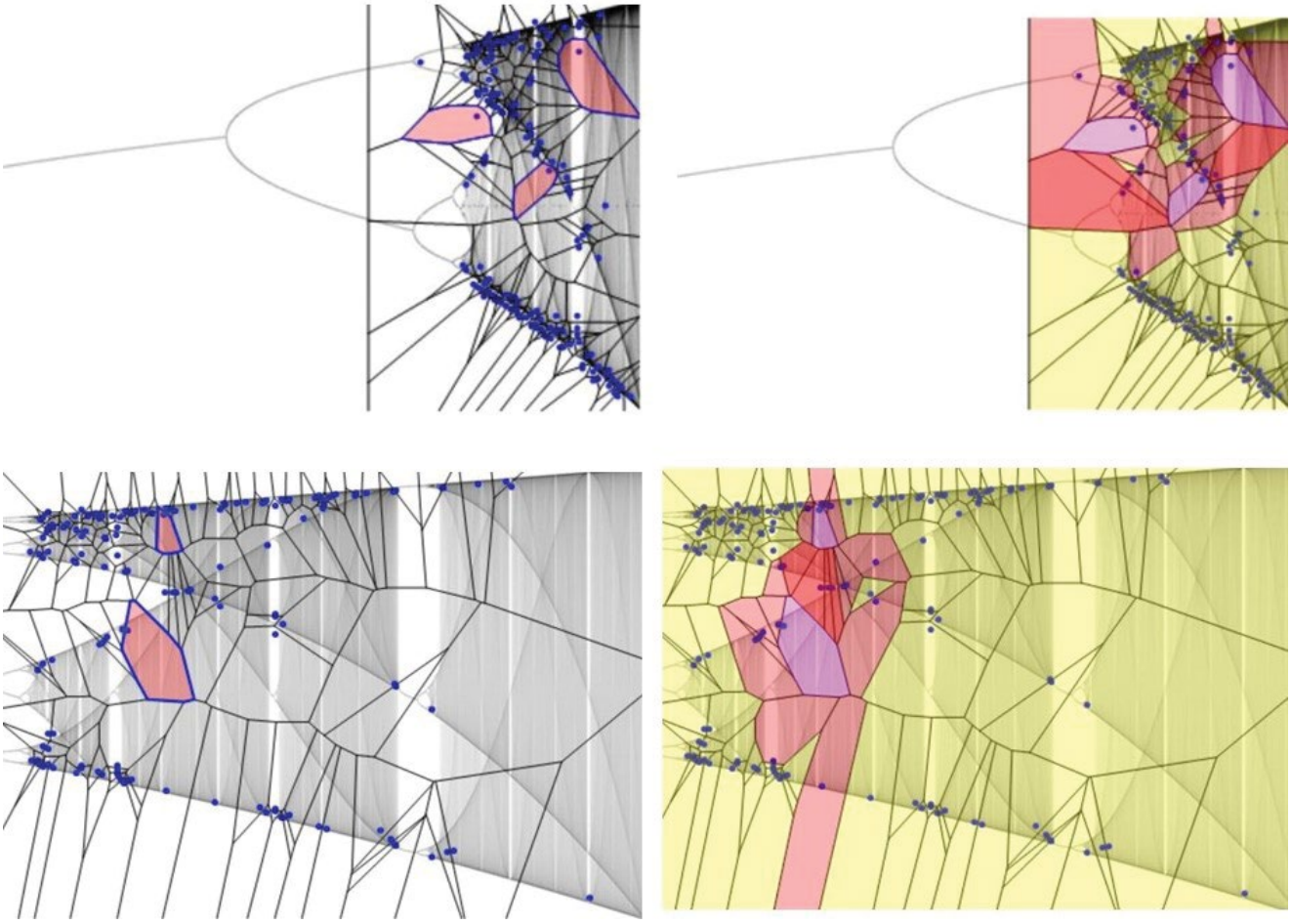

Figure 6: MNCs in logistic plots at different magnification levels (upper and lower figures). The figures on the left depict the MNCs, the figures on the right the MNCs plus their surrounding polygons.

p = dimensions; q = visibility; r = fluxes; s = laminar; ~ Not (negation);

% possibility; # necessity;

> Imply; < Not Imply; = Equivalent; @ Not Equivalent; + Or; & And;

(p@p) False (obstructed); ~(p@p) = (p = p) True (unobstructed); vt Validated true true.

Our second question was:

"Does the necessity of non-visible dimensions imply the possibility of laminar fluxes in Eq Q1 as either: 1. Not obstructed; or 2. Bifurcated by non-visible dimensions implying visible dimensions?"

(Q2)

#(p&~q) > %(((r&s) > ~(p@p)) + ((r&s) > ((p&~q) > (p&q)))); vt

Model 1 TTTTTTTTTTTTTTTT

Model 2.1 EEEEEEEEEEEEEEEE

Model 2.2 EEEEEEEEEEEEEEEE

Model 2.3.1 EEEEEEEEEEEEEEEE

Model 2.3.2 EEEEEEEEEEEEEEEE

The answer to the two questions is "yes", as proved by the truth table for Q1 with Q2 in Model 1.1.

In sum, we indirectly suggested, summoning clues from completely different approaches, the presence of an invisible, extra-large dimension intertwined with our space-time world and able to interact with it.

Conclusions

Claims from theoretical physics and, recently, also from neuroscience [30], suggest the possible presence of extra dimensions interacting with our three-dimensional-plus time physical and biological world. It has been hypothesized that elusive, higher dimensions of unknown curvature (either flat, or curved, or warped, and so on) surround us, intersecting our space-time world and interacting with it. Our aim was to propose a method in order to detect such hidden dimensions. We showed how their presence can be proofed by the occurrence of bifurcations, while their shape can be ex-

trapolated from the curves' deformation after every bifurcation. In particular, in logistic plots from nonlinear chaotic collective dynamics, we showed how it is possible to detect the hints of an unknown factor, able to vary the otherwise linear particle trajectories. The interaction between the usual space-time trajectories and the further dimension(s) occurs just when the proper angles allow their superimposition. Therefore, we find trajectory divergences that are detectable in our world.

Due to the current lack of knowledge, we were not able to elucidate the features of such a hidden dimension. Although we stated that possible hidden dimensions interfere with physical and biological processes, giving rise to nonlinear dynamics in our world, nevertheless we never talked about the nature of such dimension and about "spatial" features. Indeed, we are not allowed to say whether we are in front of one, or more than one, further spatial dimension. The concave shape of trajectories could also be provided by the curvature of a complex (real and imaginary) space, that displays, in a physical geometry, a dual mapping between: a) Visible regions embedded in an n dimensional real space and b) Hidden regions mapping to an $n + 1$ - dimensional imaginary space. Another possibility is that the hidden dimension stands for a "temporal" dimension, instead of a spatial one. Due to our above described quantum entanglement account; we might speculate that (in our space-time, zero curvature Universe) a further hidden, infinite dimension is endowed, in guise of an invisible rolled, tangled thread, or wire. We might hypothesize that a sort of one-dimensional rope surrounds us. Differently from other models that suggest particles trajectories travelling along different dimensions of a multidimensional phase space, we propose that particles move into our space-time phase space, but collide with such one-dimensional rope endowed in the cosmos. A one-dimensional rope cannot encompass a two-dimensional oscillation, but just a uni-dimensional force. Nevertheless, if such hypothetical one-dimensional force propagates into our space time cosmic dimensions, it would give rise to pluri-dimensional oscillations detectable by us. Which kind of force can be encompassed in a mono-dimensional rope? If we hypothesize that this dimension is made of negative time (an inverted arrow of our usual time), we solve a lot of puzzling experimental observations, with no need to further, problematic forces.

Is also feasible that the hidden dimension has something to do with the Feigenbaum constant, e.g., with an irrational number. In such a speculative vein, we need to remember an astonishing, unnoticed similarity between the numbers of the first Feigenbaum constant and the Zeeman Effect, which is correlated with magnetic fields. Indeed, the value of Zeeman Effect's constant is 4.66860 × 101 metre/tesla, a value that parallels the first four numbers of the first Feigenbaum constant, in particular for the highest values of bifurcations in logistic plots. Of course, caution is needed, for two reasons: a) We did not assess standard deviation or correlation statistic to show the corresponding similarity; b) The Zeeman constant depends on the arbitrary chosen unit system, while the Feigenbaum constant is a ratio; therefore, it could simply mean that such concurrence is purely random. Nevertheless, the coincidence is remarkable, and might point towards a hypothetical correlation between two widespread features of our world: nonlinear chaotic bifurcations and magnetic fields.

The phase transitions described in chaotic nonlinear logistic plot do not lead to changes in thermodynamic entropy. Our framework helps to better elucidate such issue, by providing a multidimensional account of thermodynamic entropy able to elucidate the second law of thermodynamics and to answer to a long-standing question: why does the thermodynamic entropy increase in our three-dimensional (plus time) Universe? Where the increase of entropy does comes from? Here the Bekenstein inequality comes into play. Let k be Boltzmann's constant, R the radius of a sphere that can encompass a given system, E the total mass energy (including any rest masses), $\hbar$ the reduced Planck constant and c the speed of light. The Bekenstein bound is an upper limit on the entropy S (or information I) encompassed into a finite region of space equipped with a finite amount of energy. In other words, the Bekenstein bound stands for the maximum amount of information required to describe a physical system down to the quantum level. This means that the information of a physical system, or the information necessary to describe it, must be finite, in case of both the region of space and the energy being finite. The universal form of the bound can be described as follows [43,44]: $S \leq \frac{2\pi RkE}{\hbar c} = \frac{2\pi Rk(hf)}{\hbar c} = \frac{2\pi Rk\left(\frac{hc}{\lambda}\right)}{\hbar c}$, Where f is the wave frequency of the particulate photon energy E and h is the quantum of action (Planck's constant).

A noteworthy consequence of the Berkenstein bound, *i.e.*, that the entropy contained in our space-time Universe is proportional to the two-dimensional border of the sphere enclosing the system, led some theoreticians to hypothesize the holographic principle. The latter states that the entire universe can be seen as two-dimensional information on the cosmological horizon, such that the three dimensions (plus time) we observe are an effective description only at macroscopic scales and low energies. The holographic principle was inspired by black hole thermodynamics, which conjectures that the maximal entropy in any region scales with the radius squared,

and not cubed as might be expected. Indeed, the Bekenstein-Hawking formula states that the black hole entropy is proportional to the area of its event horizon. The fact that the black hole entropy is also the maximal entropy that can be obtained by the Bekenstein bound (wherein the Bekenstein bound becomes equality) was the main observation that led to the holographic principle. Summarizing, the holographic model hypothesizes that the entropy endowed in our space-time Universe might be encompassed in a two-dimensional surface, because, in the case of a black hole, the informational content of the objects fallen into the hole might be entirely contained in surface fluctuations of the event horizon. Our goal is to "reverse" such idea: if we place a three-dimensional sphere instead of a two-dimensional one on the right side of the equation, we achieve on the left side the value of the entropy encompassed in FOUR dimensions. Put another way, the Bekenstein bound is the upper limit of the energy of a system at a particular time t defined by

$$S(t) \leq \frac{4\pi R(t)k\left(\frac{hc}{\lambda(t)}\right)}{\hbar c} = \frac{4\pi R(t)kh}{\hbar\lambda(t)}$$

Therefore, if we achieve thermodynamic entropy encompassed in a multidimensional Universe instead of the space-time one, we are able to explain why the entropy S seems to increase in our detectable Universe's linear paths, while it is kept invariant during nonlinear chaotic phase transitions. Indeed, if we keep the Universe enthalpy constant, we might hypothesize that the free-energy flows towards the further dimension, leaving in our space-time dimensions an apparent, relative increase in entropy. Therefore, free energy is "sucked" by, "drained" towards the hidden dimension. This apparent phenomenon disappears at the observation level of a higher dimension, where the entropy is left unchanged: this is the case of the logistic plot after bifurcations and of an hypothetical thermodynamic entropy embedded in a further, hidden dimension.

Our findings pave the way to future works and developments. Further mathematical studies are needed, in order to assess the shape of the hidden dimension(s). Our procedure allows not just to look for hints of veiled dimensions in our microscopic or macroscopic Universe, but also to use abstract dimensions in order to evaluate natural paths. Although we took into account the example of the Feigenbaum multi space, we can also use other multi spaces, e.g., dimensions containing physical constants, in order to evaluate happens when a dynamic system interferes with such dimensions. Furthermore, by measuring the curvature of laminar fluxes when they approach cosmic bodies, we could study solar winds, electromagnetic waves or cosmic wave's background, in order to assess whether hidden dimensions are endowed in our Universe, and where they are located.

References

1. Rubakov VA, Shaposhnikov ME (1983) Do we live inside a domain wall? Physics Letters B 125: 136-138.
2. Baulieu L, Green M, Picco M, et al. (2001) Progress in String Theory and M-Theory. Springer, Berlin.
3. Hashimoto K (2012) D-Brane: Superstrings and New Perspective of Our World. Springer-Verlag, Berlin.
4. Hitchin N (2003) Generalized Calabi-Yau manifolds. The Quarterly Journal of Mathematics 54: 281-308.
5. Burgess CP, van Nierop L (2013) Technically natural cosmological constant from supersymmetric 6D brane backreaction. Physics of the Dark Universe 2: 1-16.
6. Candelas P, Horowitz G, Strominger A, et al. (1985) Vacuum configurations for superstrings. Nuclear Physics B 258: 46-74.
7. Arkani-Hamed N, Dimopoulos S, Dvalic G (1998) The hierarchy problem and new dimensions at a millimeter. Physics Letters B 429: 263-272.
8. Randall L, Sundrum R (1999) A Large Mass Hierarchy from a Small Extra Dimension. Physical Review Letters 83.
9. Peters JF, Tozzi A (2016) Quantum Entanglement on a Hypersphere. Int J Theoret Phys 55: 3689-3696.
10. Bak P, Tang C, Wiesenfeld K (1987) Self-organized criticality: An explanation of the 1/f noise. Phys Rev Lett 59: 381-384.
11. Fraiman D, Chialvo DR (2012) What kind of noise is brain noise: Anomalous scaling behavior of the resting brain activity fluctuations. Front Physiol.
12. Perkins TJ, Foxall E, Glass L, et al. (2014) A scaling law for random walks on networks. Nat Commun 5: 5121.
13. Deco G, Jirsa VK (2012) Ongoing cortical activity at rest: criticality, multistability, and ghost attractors. J Neurosci 32: 3366-3375.
14. Tozzi A (2014) Evolution: Networks and Energy Count. Nature 515: 343.
15. Afraimovich V, Tristan I, Varona P, et al. (2013) Transient Dynamics in Complex Systems: Heteroclinic Sequences with Multidimensional Unstable Manifolds. Discontinuity, Nonlinearity and Complexity 2: 21-41.
16. de Arcangelis L, Herrmann HJ (2010) Learning as a phenomenon occurring in a critical state. Proceedings of the National Academy of Sciences 107: 3977-3981.
17. Beggs JM, Timme N (2012) Being critical of criticality in the brain. Front Physiol 3: 163.
18. Tozzi A (2015) How to Turn an Oscillation in a Pink One. Journal of Theoretical Biology 377: 117-118.
19. Strogatz SH (1994) Nonlinear Dynamics and Chaos, Studies in Nonlinearity. Perseus Books Publishing.
20. Richardson MJ, Dale R, Marsh KL (2014) Complex dynamical systems in social and personality psychology. In: Reis HT, Judd CM, (2nd edn), Handbook of Research Methods in Social and Personality Psychology. Cambridge University Press, Cambridge.

21. Smith R (2013) Period doubling, information entropy, and estimates for Feigenbaum's constants. International Journal of Bifurcation and Chaos 23.
22. Alligood KT, Sauer TD, Yorke JA (1996) Chaos: An Introduction to Dynamical Systems. Textbooks in Mathematical Sciences, Springer.
23. Jordan DW, Smith P (2007) Non-Linear Ordinary Differential Equations: Introduction for Scientists and Engineers. (4th edn), Oxford University Press.
24. Reynolds O (1883) An experimental investigation of the circumstances which determine whether the motion of water shall be direct or sinuous, and the law of resistance in parallel channels. Philosophical Transactions of the Royal Society 174: 935-982.
25. Tritton DJ (1988) Physical Fluid Dynamics. (2nd edn), Oxford University Press, UK.
26. Sun B, Grier DG, Grosberg AY (2010) Minimal model for brownian vortexes. Phys Rev E Stat Nonlin Soft Matter Phys 82.
27. Rogers A (2007) Supermanifolds: Theory and Applications. World Scientific.
28. Borsuk K (1933) Drei satzeuber die n-dimensional euklidische sphare. Fundamenta Mathematicae 20: 177-190.
29. Beyer WA, Zardecki A (2004) The early history of the ham sandwich theorem. American Mathematical Monthly 111: 58-61.
30. Tozzi A, Peters JF (2016) Towards a Fourth Spatial Dimension of Brain Activity. Cognitive Neurodynamics 10: 189-199.
31. Weeks JR (2002) The shape of space. (2nd edn), Marcel Dekker Inc, New York-Basel.
32. Marsaglia G (1972) Choosing a Point from the Surface of a Sphere. Ann Math Statist 43: 645-646.
33. Matousek J (2003) Using the Borsuk-Ulam Theorem. Lectures on Topological Methods in Combinatorics and Geometry. Springer-Verlag Berlin Heidelberg.
34. Collins GP (2004) The shapes of space. 291: 94-103.
35. Peters JF (2016) Computational Proximity: Excursions in the Topology of Digital Images. Intelligent Systems Reference Library 102.
36. Borsuk K (1969) Fundamental retracts and extensions of fundamental sequences. Fundamenta Mathematicae 64: 55-85.
37. Tozzi A, Peters JF (2016) A Topological Approach Unveils System Invariances and Broken Symmetries in the Brain. Journal of Neuroscience Research 94: 351-365.
38. Sengupta B, Tozzi A, Cooray GK, et al. (2016) Towards a Neuronal Gauge Theory. PLoS Biol 14: e1002400.
39. Mitroi-Symeonidis FC (2015) Convexity and sandwich theorems. European Journal of Research in Applied Sciences 1: 9-11.
40. Peters JF, Tozzi A, Ramanna S (2016) Brain Tissue Tessellation Shows Absence of Canonical Microcircuits. Neuroscience Letters 626: 99-105.
41. Peters JF, Ramanna S, Tozzi A, et al. (2017) BOLD-independent computational entropy assesses functional donut-like structures in brain fMRI image. Frontiers Hum Neurosci 11: 38.
42. Peters JF, Inan E (2016) Strongly near Voronoi nucleus clusters.
43. Bekenstein JD (1973) Black Holes and Entropy. Phys Rev D 7: 2333-2346.
44. Bekenstein JD (1974) Generalized second law of thermodynamics in black-hole physics. Phys Rev D 9: 3292-3300.
45. Shevchuk IV (2009) Modelling of Fluid Flow and Heat Transfer in Rotating-Disk Systems. In: Convective Heat and Mass Transfer in Rotating Disk Systems. Lecture Notes in Applied and Computational Mechanics. Springer, Berlin, Heidelberg, 45: 11-31.

information

MDPI

Review

Symmetries, Information and Monster Groups before and after the Big Bang

Arturo Tozzi [1,*] and James F. Peters [2,3]

1 Center for Nonlinear Science, University of North Texas, Denton, TX 76203, USA
2 Department of Electrical and Computer Engineering, University of Manitoba, 75A Chancellor's Circle, Winnipeg, MB R3T 5V6, Canada; james.peters3@umanitoba.ca
3 Mathematics Department, Adıyaman University, 02040 Adıyaman, Turkey
* Correspondence: tozziarturo@libero.it

Academic Editors: Pedro C. Marijuán, Abir (Andrei) U. Igamberdiev and Lin Bi
Received: 5 October 2016; Accepted: 14 December 2016; Published: 21 December 2016

Abstract: The Monster group, the biggest of the sporadic groups, is equipped with the highest known number of dimensions and symmetries. Taking into account variants of the Borsuk–Ulam theorem and a novel topological approach cast in a physical fashion that has the potential to be operationalized, the universe can be conceived as a lower-dimensional manifold encompassed in the Monster group. Our universe might arise from spontaneous dimension decrease and symmetry breaking that occur inside the very structure of the Monster Module. We elucidate how the energetic loss caused by projection from higher to lower dimensions and by the Monster group's non-abelian features is correlated with the present-day asymmetry in the thermodynamic arrow. By linking the Monster Module to its theoretical physical counterparts, it is then possible to calculate its enthalpy and Lie group trajectories. Our approach also reveals how a symmetry break might lead to a universe based on multi-dimensional string theories and CFT/AdS (anti-de Sitter/conformal field theory) correspondence.

Keywords: topology; entropy; energy; sporadic groups; universe

---

The Mode is an enclosed, detectable manifestation of the Substance... The Substance is equipped with infinite attributes (Spinoza, Ethica, pars I)

1. Introduction

The Fischer–Griess Monster group, the largest among the twenty-six sporadic groups, is equipped with 196,883 dimensions and an order of about 10^{54} elements [1]. It is noteworthy that the Monster Module displays the highest known number of symmetries [2]. It has been recently proposed that the symmetries, widespread invariances occurring at every level of organization in our universe, may be regarded as the most general feature of physical systems, perhaps also more general than thermodynamic constraints [3,4]. Therefore, giving insights into the Monster symmetries would provide a very general approach to systems function, universe evolution and energetic dynamics. Here we show how a novel symmetry-based, topological approach sheds new light on the Monster's features. We provide a foundation for the Monster's physical counterparts, cast in a fashion that has the potential to be operationalized, which can be used for the assessment of our universe's evolution and, in particular, pre-Big Bang scenarios.

This paper comprises six sections, including the introduction. In the second section, we describe a generalized version of the Borsuk–Ulam theorem, in order to provide the topological machinery for further evaluations of the Monster in the context of theoretical physics. The third section assesses the relationships between the Monster and the modular j-function. Section four explains how the universe

might originate from the Monster Module, due to a dimension loss, linking the Monster group to theoretical physics counterparts. Furthermore, taking into account energetic arguments dictated by topological dimensions decrease, the section explains why and how our universe is equipped with the symmetry breaks, which give rise to the thermodynamic arrow. Section five elucidates various physical features of the Monster. In the final sixth section, we raise a number of still open questions.

2. Topological Tools

2.1. The Standard Version of the Borsuk–Ulam Theorem (BUT)

The Borsuk–Ulam Theorem [5] is given in the following form by [6].

Borsuk–Ulam Theorem. *Let $f : S^n \to R^n$ be a continuous map. Then there exists $x \in S^n \subseteq R^{n+1}$ such that $f(x) = f(-x)$.*

Proof. A beautiful and concise proof of this theorem is given by [7], and not repeated here. □

This means that antipodal points on n-sphere S^n map to R^n, which is the n-dimensional Euclidean space [8,9]. Points on an n-sphere S^n are antipodal, provided the points are diametrically opposite [10]. The original formulation of BUT displays versatile ingredients that can be modified, resulting in BUT with different guises: proximally continuous mappings and antipodal (or non-antipodal) points with matching description and bijection mappings from a higher to a lower dimension.

In the sequel, the notion antipodal point is extended antipodal regions. A region on the surface of an n-sphere S^n is a part (subset) of S^n. A surface region $\neg x$ is the antipode of x, provided $x \neq \neg x$ and x has the same feature values (characteristics) as $\neg x$. For more about this, see [11]. From a physics perspective, a region is a relativistic mass in a slice of space swept out a moving particle. The particles on a physical n-sphere are moving at the same velocity. For every physical region with mass $x \in S^n$, we can always find $\neg x$ (the analog of the antipode $-x$ of a point on the surface of S^n) with the same characteristics (velocity and mass). In effect, for the relativistic energy $e_x = m_x c^2$, we can find its antipodal energy $e_{\neg x}$ for $\neg x \in S^n$. To be an antipodal energy $e_{\neg x}$, we weaken the original notion to antipodes, with $\neg x$ being a particle on S^n that has characteristics that match those of $x \in S^n$. This leads to an energetic form of BUT (energy-BUT) for antipodal particles$x, \neg x \in S^n$:

Energy-Borsuk–Ulam Theorem. *Let $f : S^n \to R^n$ be a continuous map. Then there exists $x \in S^n \subseteq R^{n+1}$ such that $f(x) = f(\neg x)$ and $e_x = e_{\neg x}$.*

Proof. $f(x) = f(\neg x)$ a feature vector in R^{n+1}. Since, for each $x \in S^n$ there is $\neg x \in S^n$ with the same velocity and mass, the result follows, i.e., $f(x) = f(\neg x)$ and $e_x = e_{\neg x}$. □

2.2. BUT Variants

We resume with some BUT variants described by Peters [12] and Tozzi and Peters [3]. The concept of antipodal points can be generalized to countless types of signals. Two opposite points encompass not just the description of simple topological points, but also of spatial and temporal patterns, vectors and tensors, functions, signals, thermodynamic parameters, trajectories, symmetries [3]. The two antipodal points standing for different systems features are assessed at one level of observation, while the single point is assessed at a lower level. The antipodal points restriction from the classical BUT is no longer needed, because the applications on an n-sphere can be generalized not just for the evaluation of diametrically opposite points, but also of non-antipodal ones. We are allowed to take into account homotopic regions on an n-sphere that are either adjacent or far apart. This means that the points (or regions) [13] with the same feature value do not need necessarily to be antipodal, in order to be described together [12]. The original formulation of BUT describes the presence of antipodal points on

spatial manifolds in every dimension, provided the n-sphere is a convex, positive-curvature structure. However, many physical functions occur on manifolds endowed with other types of geometry: for example, the hyperbolic one [14,15]. Whether the manifold displays a concave, convex or flat activity, this does not have an impact: we may always find the points with matching description predicted by BUT. Although BUT has been originally described just in case of n being a natural number that expresses a spatial dimension, its value in S^n can also stand for other types of numbers. The n value can be also cast as an integer, a rational or an irrational number. This allows us to use the n parameter as a versatile tool for the description of systems symmetries [3]. A BUT variant tells us that we can find a pair of opposite points an n-dimensional sphere, that display the same encoding not just on a R^n manifold, but also on an $n-1$ sphere. A symmetry break occurs when the symmetry is present at one level of observation, but hidden at another level [4]. This means that symmetries can be found when evaluating the system in a proper dimension, while they disappear (are hidden or broken) when the same system is embedded in just one dimension lower.

Here we introduce recently developed, unpublished BUT variants. The first is a BUT corollary, which states that a S^n manifold does not map just to a R^{n-1} Euclidean space, but straight to a S^{n-1} manifold. In other words, the Euclidean space is not mentioned in this formulation. Indeed, in many applications, e.g., in fractal systems, we do not need a Euclidean manifold at all. A manifold, in this case S^n, may exist in and on itself, by an internal point of view, and does not need to be embedded in any dimensional space [13]. Therefore, we do not need an S^n manifold curving into a dimensional space R^n: we may think that the manifold just does exist by itself. An important consequence of this BUT version is that a n-sphere may map on itself. The mapping of two antipodal points to a single point in a dimension lower can be a projection internal to the same n-sphere.

The second and foremost variant is the above mentioned termed energy-BUT.There exists a physical link between the abstract concept of BUT and the real energetic features of systems formed by two spheres S^n and S^{n-1}. An n-sphere S^n is equipped with two antipodal points, standing for symmetries according to BUT.BUT is enriched by considering an n-sphere S^n as a *manifold*, which is a Hausdorff space with a countable basis where each point has a neighbourhood that is homeomophic to some Euclidean space. Briefly, a space is Hausdorff, provided distinct points belong to disjoint neighbourhoods (distinct points live in separate houses [16]). A mapping $f : X \to Y$ is homeomorphic, provided f on X is 1-1, onto Y and has a continuous inverse. For the sake of intuition, we illustrate the notion of homeomorphic neighbourhoods in terms of planar homeomorphic energistic neighbourhoods. Let $p, x \in S^n$, radius $r > 0$ and $\|e_x - e_p\| = \sqrt{{e_x}^2 + {e_p}^2}$ (norm of energies associated with the points x, p) for an open neighbourhood $N(p, r)$ defined by

$$N(p,r) = \left\{ x \in R^2 : \|e_x - e_p\| < r \right\}.$$

Then a homeomorphic mapping $f : N(p,r) \to R^2$ is defined by

$$f(x) = \frac{e_x}{\sum_{i=1}^{|N(p,r)|} e_y}, \; x, y \notin N(p,r).$$

For more about manifolds, see [12]. When these opposite points map to an n-dimensional Euclidean manifold where S^{n-1} lies, a symmetry break/dimensionality reduction occurs, and a single point is achieved [11]. It is widely recognized that a decrease in symmetry goes together with a reduction in entropy and free-energy (in a closed system). This means that the single mapping function on S^{n-1} displays energy parameters lower than the sum of the two corresponding antipodal functions on S^n. Therefore, a decrease in dimensions gives rise to a decrease of energy and energy requirements. BUT no longer depends on thermodynamic parameters, but rather on topological features such as affine connections and homotopies. The energy-BUT concerns not just energy, but also information. Indeed, two antipodal points contain more information than their single projection in a lower dimension.

Dropping down a dimension means each point in the lower dimensional space is simpler, because each point has one less coordinate. In sum, energy-BUT provides a way to evaluate the decrease of energy in topological, other than thermodynamic, terms.

Another novel variant of BUT is the region-based BUT. This is a straightforward extension of what is known as region-BUT (briefly, reBUT).

Region-Based Borsuk–Ulam Theorem (ReBUT). *Let 2^{S^n} be a collection of nonempty surface regions of S^n and let there be a continuous map. Then there exists $x \in 2^{S^n} \subseteq R^{n+1}$ such that $f(x) = f(\neg x)$.*

Proof. $f(x), f(\neg x)$ a feature vector in R^{n+1}. We can always find region $\neg x \in 2^{S^n}$ that is antipodal to $x \in 2^{S^n}$, i.e., $\neg x \cap x = \varnothing$ and $\neg x, x$, have matching descriptions in R^{n+1}, minimally, equal velocity and mass while moving along the path through space swept out by S^n (called a world canal during the course of its history [17]). Hence,

$$f(x) = f(\neg x). \square$$

The usual continuous function required by reBUT (region-based BUT in [3]) is replaced by a proximally continuous function, which guarantees that, whenever a pair of strings (regions that are world lines) are close (near enough to have common elements), then we always know that their mappings will be also be close. A string is a region of space with non-zero width and either bounded or unbounded length. As a particle moves through space following a world line [18], interactions occur at the junctions of world lines. Let τ the proper time of a particle, measured by clock travelling with a particle and integration along the world line of the particle. The $action_{particle}$ of a freely moving particle is defined by

$$action_{particle} = -mc^2 \int d\tau.$$

As time evolves, a particle leaves a trace of its movements along a surface, which are "remembered". A string is then a remembered part of a hypersphere surface over which a particle travels. In terms of quantum theory, a string is a path defined by a moving particle. Put another way, a string is path-connected and its path is defined by a sequence of adjacent fat surface points. The points are fat because they are physical as opposed to abstract geometric points. In other words, a string A(briefly, str$A$) is a thin region of space that has describable features such as connectedness, length, open-ended or closed-ended, and shape. Strings str$A$, $\neg$str$A$ are antipodal, provided str$A$ and $\neg$str$A$ are disjoint and yet have the same description. Strings str$A$, $\neg$str$A$ are examples of antipodal sets [19]. The description of str$A$ (briefly, $\Phi(\text{str}A)$) is a feature vector in R^n, where each component of $\Phi(\text{str}A)$ is a feature value of str$A$.

2.3. Quantum String Axioms

1. Every string has an action.
2. If str$A$, $\neg$str$A$ are antipodal, then $action_{strA} = action_{\neg strA}$.
3. Separate strings with k features with the same description are antipodal.
4. There is a set $\{\neg\text{str}A\}$ of antipodal strings for every string str$A$.

Let X be a topological space equipped with descriptive proximityδ_Φ. str$A$ δ_Φ $\neg$str$A$ reads str$A$, and $\neg$str$A$ have the same description. Let 2^{S^n} denote the family of sets on the surface of a hypersphere S^n and str$A$, $\neg$str$A$ $\in 2^{S^n}$ are antipodal strings on S^n. A function $f : 2^{S^n} \to R^n$ is proximally continuous, provided str$A$ δ_Φ $\neg$str$A$ implies $f(\text{str}A)$ δ_Φ $f(\neg\text{str}A)$. With these observations about strings, we obtain the following results.

Lemma. [strBUT]. *If $f : 2^{S^n} \to R^n$ is proximally continuous, $f(\text{str}A) = f(\neg\text{str}A)$ for some* str$A$ *in* 2^{S^n}.

Proof. Case $n = 1$. Let each str$A$ have one feature, namely, action. Assume antipodal strings str$A$, $\neg$str$A$ with n features are descriptively close, i.e., str$A$ δ_Φ $\neg$str$A$. Since f is proximally continuous, we have $f(\text{str}A)$ δ_Φ $f(\neg\text{str}A)$. From Axiom 2, $action_{strA} = action_{\neg strA}$. Hence, from the definition of the descriptive proximity δ_Φ, $f(\text{str}A) = f(\neg\text{str}A)$.

Case $n > 1$. The proof is symmetric with case $n = 1$ and Axiom 3. □

Theorem 1. *If* $f : 2^{S^n} \to R^k$, $k > 0$ *is proximally continuous,* $action_{strA} = action_{\neg strA}$ *for some* str$A$ *in* 2^{S^n}.

Proof. We consider only the case for $k = 1$, for strings whose only feature is action. The desired result is immediate from the strBUT Lemma and Axiom 2. This result is easily extended to the case where $k > 1$ for strings with k features. □

Theorem 2. *If* $f : 2^{S^n} \to 2^{R^k}$, $k > 0$ *is proximally continuous,* $f(A) = f(\neg A)$ *for each* $\neg$str$A$ *in the set of antipodes* $\{\neg\text{str}A\} \in 2^{S^n}$.

Proof. Immediate from the Theorem 1. □

In order to map S^n to S^{n-1}, we need to work with lower dimensional spaces containing regions where each point in S^{n-1} has one less coordinate than a point in S^n.

Let X be a topological space equipped with Lodato proximity [12]. str$A$ δ $\neg$str$A$ reads str$A$ and $\neg$str$A$ are close. Dochviri and Peters [20] introduce a natural approach in the evaluation of the nearness of sets in topological spaces. The objective is to classify levels of nearness of sets relative to each given set. The main result is a proximity measure of nearness for disjoint sets in an extremely disconnected topological space. Let int(str$A$) be the set of points in the interior of str$A$. Another result is that if strings str$A$, $\neg$str$A$ are nonempty semi-open sets such that str$A$ δ $\neg$str$A$, then int(str$A$) δ int($\neg$str$A$) .

An important feature is that the manifolds M^d and M^{d-1} are topological spaces equipped with a strong descriptive proximity relation. Recall that in a topological space M, every subset in M and M itself are open sets. A set E in M is open, provided all points sufficiently near E belong to E [21]. The description-based functions in BUT are strongly proximally continuous and their domain can be mathematical, physical or biological features of world line shapes. Let A, B be subsets in the family of sets in M (denoted by 2^M) and let $f : 2^M \to R^n$, $A \in 2^M$, $f(A) =$ a feature vector that describes A. That is, $f(A)$, $f(B)$ are descriptions of A and B. Nonempty sets are strongly near, provided the sets of have elements in common. The function f is strongly proximally continuous, provided A strongly near B implies $f(A)$ is strongly near $f(B)$. This means that strongly near sets have nonempty intersection. From a BUT perspective, multiple sets of objects in M^d are mapped to $f(A \cap B)$, which is a description of those objects common to A and B. In other words, the functions in BUT are set-based embedded in a strong proximity space. In particular, each set is a set of contiguous points in a path traced by a moving particle. The path is called a world line. Pairs of world lines have squiggly, twisted shapes opposite each other on the surface of a manifold. Unlike the antipodes in a conventional hypersphere assumed by the BUT, the antipodes are now sets of world lines that are discrete and extremely disconnected. Sets are extremely disconnected, provided the closure of every set is an open set [20], is in the discrete space and the intersection of the closure of the intersection of every pair of antipodes is empty. The shapes of the antipodes are separated and belong to a computational geometry. That is, the shapes of the antipodal world lines approximate the shapes in conventional homotopy theory [22]. The focus here is on the descriptions (sets of features) of world line shapes. Mappings onsets with matching description, or, in other words, mappings on descriptively strongly proximal sets, here means that such mappings preserve the nearness of pairs of sets. The assumption made here is that antipodal sets live in a descriptive Lodato proximity (DLP) space. Therefore, antipodal sets satisfy the requirements for a DLP [12]. Let δ be a DLP and write A δ B to denote the descriptive nearness of antipodes A and B, and let f be a DLP continuous function. This means A δ B implies $f(A)$ δ $f(B) = f(A) \cap f(B) \neq \varnothing$.

Example. Assume that antipodes A and B have symmetries (shape, bipolar, color, overlap, path-connectedness), and f is DLP strongly continuous function, then $A\ \delta\ B\ \Rightarrow\ f(A)\ \delta\ f(B)$.

This means that whenever A and B are descriptively close, then A is mapped to $f(A)$ and B is mapped to $f(B)$ and $f(A)\ \delta\ f(B)$. If we include in the description of A and B the location of the discrete points in A and B, then the DLP mapping is invertible. That is,$f(A)$ maps to A, $f(B)$ maps to B and $f(A)\ \delta\ f(B)$ implies $A\ \delta\ B$.

Figure 1 provides an example of antipodal sets in case of a pair of closed regions, e.g., strings.

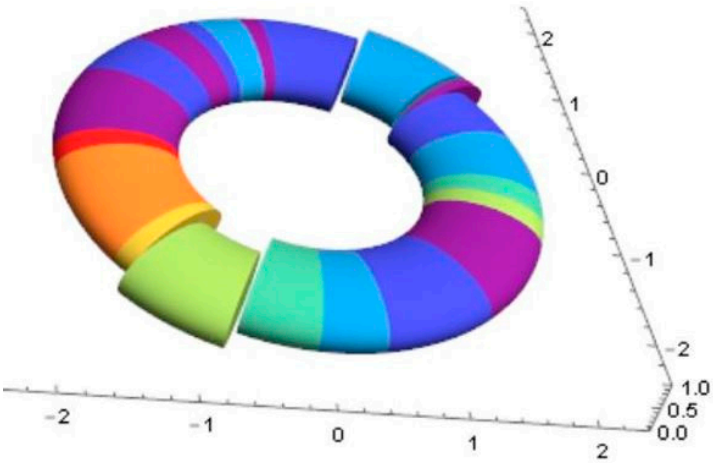

Figure 1. Torus Antipodal Strings. World lines with matching description preserve the nearness of pairs of sets. See text for further details.

2.4. Generalized BUT (genBUT)

We conclude this section by introducing a generalized version of BUT, which encompasses all the previously described variants. This version allows the study of the Monster in the context of theoretical physics. Gen-BUT states that: *Multiple sets of objects with matching descriptions in a d-dimensional manifold M^d are mapped to a single set of objects in M^{d-1} and vice versa.* The sets of objects, which can be mathematical, physical or biological features, do not need to be antipodal and their mappings need not to be continuous. The term matching description means the sets of objects display common feature values or symmetries. M stands for a manifold with any kind of curvature, either concave, convex or flat. M^{d-1} may also be a part of M^d. The projection from S to R in not anymore required, just M is required. The notation d stands for a natural, or rational, or irrational number. This means that the need for spatial dimensions of the classical BUT is no longer required. The process is reversible, depending on energetic constraints. Note that a force, or a group, an operator, an energetic source, is required, in order to project from one dimension to another.

3. Embedding the Monster Group in M^{d-1}

The Monstrous Moonshine conjecture suggests a puzzling relationship between the Fourier coefficients of the normalized elliptic modular invariant, e.g., the hauptmodul J, the value of which value is 19,884, and the simple sums of dimensions of irreducible representation of the Monster Group M, which is 196,883 [23]. It would seem that a relationship between the symmetries in the plot (range) of the j-function and symmetries in the Monster group products occurs. These symmetries can be visualized as shown in Figure 2.

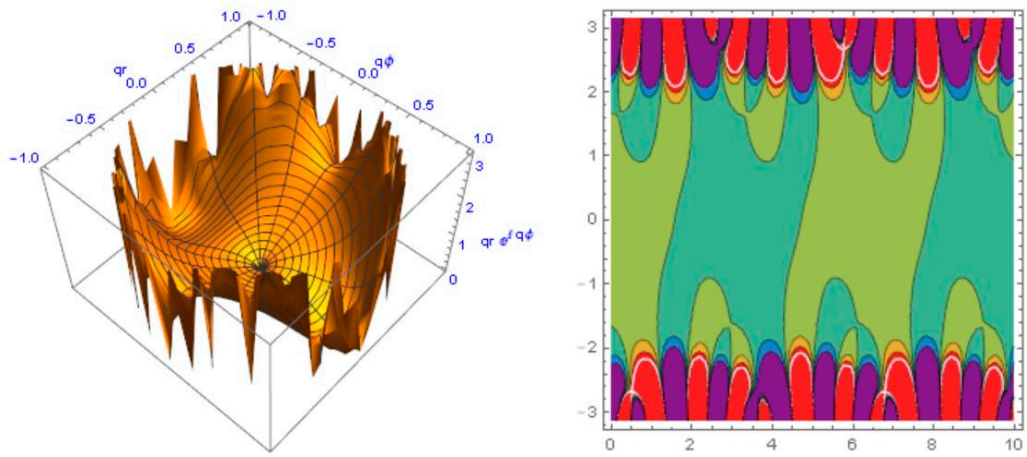

(**a**) (**b**)

Figure 2. (**a**) 3D plot of $qre^{iq\phi}$ with nome q; (**b**) 2D plot of real part of an elliptic module function $q = e^{i\pi\tau}$. Symmetries in (**a**) display a 3D plot and in (**b**) a 2D plot of an elliptic module function. The j-function is an elliptic module function such as an elliptic theta function. A sample elliptic theta plot is shown in this Figure. Such functions are expressed in terms of a nome $q = e^{i\pi\tau}$. Then, for a complex number z, Jacobi theta functions are defined in terms the nome q, e.g., $\vartheta_1(z,q) \equiv \sum_{n=-\infty}^{\infty} (-1)^{n-\frac{1}{2}} q^{\left(\frac{n+1}{2}\right)^2} e^{(2n+1)iz}$.

We might speculate that, in physical terms, the j-function could stand for an activity occurring in the Monster Module during the movements of the Lie Monster Group. In an infinite-dimensional space, the action of the j-function is correlated with the Monster vertex operator Virasoro algebra, e.g., the Monster Module [24].

A topological approach helps to elucidate such an unusual relationship. In the BUT framework, the j-function and the Monster Module are sets of objects with matching descriptions embedded in a M^d manifold, where d stands for their abstract dimension 196,884. Encompassing the two parameters in a M^d manifold allows us to provide a topological commensurability between the Monster Module and the j-function. When we reduce the dimensions to $S^{196,883}$, we achieve a single function, e.g., the Monster Lie group. It easy to see that if we map the two functions to a dimension lower, in this case $M^{196,883}$, we achieve a single function that retains the features of both. This single function stands for the Monster Group, which is the automorphic Lie group acting on the Monster Module (Figure 3, upper part). In topological terms, as always, two functions on a S^n sphere lead to a single function on a S^{n-1} sphere.

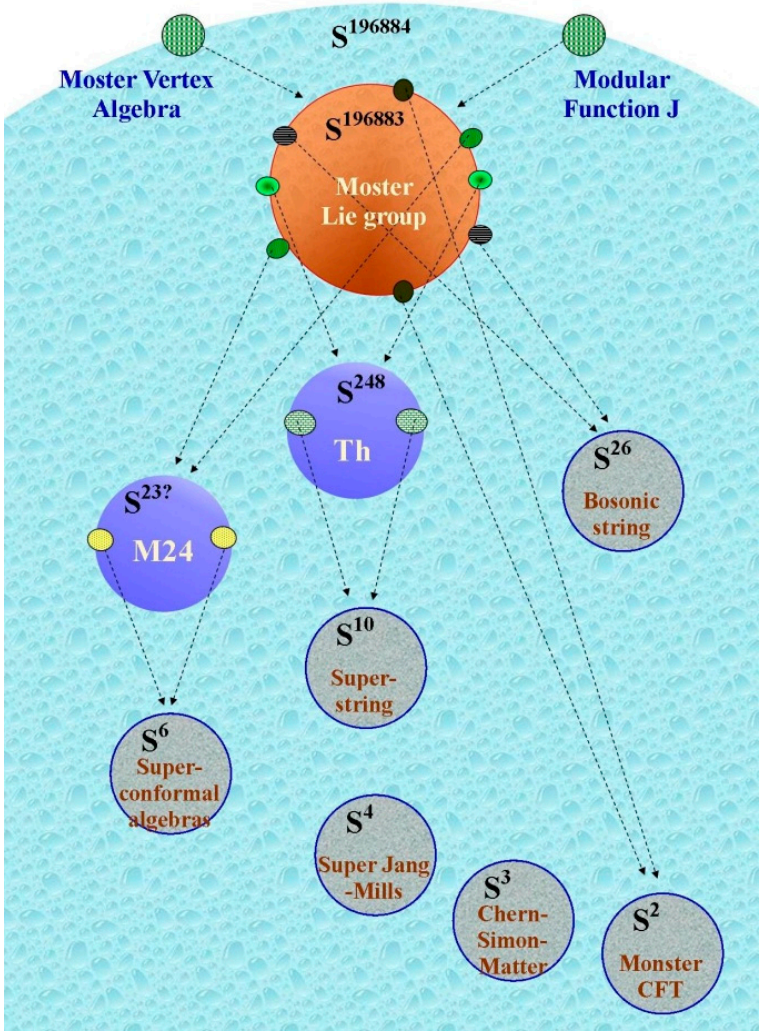

Figure 3. Progressive loss of dimensions in sporadic groups can be encompassed in a Borsuk–Ulam Theorem framework. Note also the loss of symmetries from the highest dimension levels to the lowest ones. The Figure also illustrates how every sporadic group might display a theoretical physical counterpart.

4. Of Monsters and Universes

4.1. Dimensions Reduction

We propose a BUT model that describes our universe as located inside the Monster Module. We argue, based on topological and energetic claims, that our universe might arise from a spontaneous loss of dimensions, e.g., an automorphism, occurring in the very structure of the supersymmetric, multidimensional Monster Module. If the Monster stood before the Big-Bang, we are in front of a manifold with the highest possible energy, because it displays the highest number of symmetries: indeed, according to energy-BUT, the more the symmetries, the more the energy. Therefore, every decrease in the symmetries of the original structure (the Monster) halves the energy of the subsequent, less symmetric level (occurring after the Big Bang). It is worthy of mention that the symmetries of the hypothetical M^d structure encompassing our universe do not need to be necessarily of the huge order of 10^{54}. Indeed, the Monster group includes several subgroups, classified into the sporadic groups (e.g., Mathieu groups, Leech lattice groups, and so on) [25]: this means that the universe might arise either from the Monster group, or one of its subgroups. In such a vein, one might think different possible physical scenarios:

(a) The Monster group is progressively formed starting from its subgroups, with a gradual building from blocks.
(b) The Monster group is the original structure giving rise to our universe.
(c) The Monster group, the original structure, splits in its subgroups, then one of the subgroups gives rise to our universe.

Because the entropy is increasing in the universe, the first hypothesis is less reasonable: since our universe is moving towards lower free-energy levels, it would be better to start with a higher energetic manifold before the Big Bang, and not vice versa. At the Big Bang, a loss of dimensions and thermodynamic free-energy took place. Going from a higher dimension to a lower one, a sort of quantum jump occurred, in guise of an electron orbit where electrons jump towards more internal levels. Note that the BUT dictates provide a testable hypothesis: every jump towards a lower symmetrical state must halve the previous energetic level. Because a loss of dimensions comes together with a loss of symmetries, just the symmetries embedded in our low-dimensional universe's dimensions are kept, while the others are apparently lost. The lost symmetries could in theory be restored by inverting the process from our universe's lower dimensions to the Monster Module's higher ones, but it would require a source of energy able to perform the inverse projection, and this is not the case of our cosmos.

4.2. Topological Relationships between the Monster and String Theories

The Monster group has been already correlated with well-known scenarios in theoretical physics. Moonshine can be regarded as a collection of related examples where algebraic structures have been associated with automorphic functions or forms, because it is also displays relationships with the Lie group $E^8(C)$ and a lattice vertex operator algebra equipped with a rank 24 Leech lattice [23,26]. Several features of the Monster, either its Module, or its group and subgroups, have been associated with different physical theories. Some examples are depicted in Figure 3 (lower part). For example, links between Monstrous Moonshine and string theories have been proposed: the Monster might stand for the symmetry of a string theory for a Z^2-orbifold of free bosons on a Leech lattice torus, in the context of a conformal field theory equipped with partition function j. Recent papers link other sporadic groups (e.g., Monster subgroups) with modular forms, suggesting a more central role for the Umbral Moonshine conjecture [27]. On the other hand, Witten proposed that pure gravity in AdS_3 (anti deSitter) space with maximally negative cosmological constant is AdS/CFT dual to a holomorphic CFT (conformal field theory), with the numbers of the Moonshine coming into play [28]. CFT/AdS is dual to string theories and is involved in many theoretical models: CFT, Chern-Simon-Matter, Super Jang–Mills, Superconformal algebras. The AdS/CFT correspondence means that conformal field theory is like a lower-dimensional hologram, which captures information about the higher-dimensional quantum gravity theory: this is one of the typical frameworks easily describable by a BUT topological apparatus.

4.3. The Problem of Singularity

A problem now arises: how to explain the event, commonly called singularity [29], which, according to our scenario, caused an apparent loss of dimensions in the Monster and gave rise to our universe? In order to answer to this crucial question, it must be taken into account that a particle trajectory on a hypersphere (or in general on every manifold), does not need to be closed: a particle not necessarily goes right through the whole surface, but could also travel just for a short path [30]. In such a vein, a hypothetical particle embedded into the Monster Module, which follows the movements dictated by the Monster Lie group, cannot travel everywhere on the Monster surface, due to the huge number of dimensions. In other words, ergodic pathways cannot be guaranteed when a particle travels on the Monster Module, due to the countless possible trajectories. When a particle travels into the huge Monster manifold's phase space, it might simply take a random path towards just a few of the countless dimensions. We provide an example from the 26D bosonic string theory. This well-studied

model, although partially dismissed, provides a good illustration in order to elucidate such issue. Furthermore, the 26D bosonic string theory takes place on the Leech lattice, e.g., a manifold that is almost ubiquitous in the description of sporadic groups. Bosons' trajectories in a 24D Leech lattice may follow paths encompassing 196,884 dimensions. The random trajectories followed by moving particles encompass just some of the total Monster's dimensions. When bosons' paths fall into lower dimensions, bosons lose energy, according to the energy-BUT dictates. The sudden loss of energy might explain the Big Bang, that arises when the particle moves towards preferential paths in lower dimensions, e.g., when they move towards our universe. Therefore, the singularity might be simply explained by random particles' movements occurring on small sub-parts of the Monster Module. The Big Bang might just have been occurred naturally, when a particle fell into a Monster's dimension instead of another. This also means that the chosen paths in low dimensions (our universe) are equipped with just a few of the Monster symmetries. In our universe, the residual Monster symmetries are lost, or, better, hidden, because they become visible when evaluated from a higher dimension. The loss of the other primeval Monster dimensions gives rise to symmetry breaking and the thermodynamic arrow. In order to elucidate why a decrease in symmetries and dimensions leads to our universe equipped with symmetry breakings, it must be also taken into account that almost all the finite groups are non-abelian. This explains why the cosmic rules in our universe are dictated by asymmetric laws: indeed, the intrinsic non-abelian structure of the Monster itself ensures the non-reversibility of the particle patterns. In sum, once taken a path, due to both non-abelian and energetic arguments, it is not possible to reverse the process in our universe, unless other energy is supplied. Note that, because random paths might occur everywhere on the Monster Module, this means that countless universe are allowed, every one equipped with just some of the primeval Monster symmetries. The presence of an ergodic, homogeneous Monster Module before the Big Bang solves the so-called horizon problem too. A few Planck times after the Big Bang, the universe consisted of 10^{90} Planckian size, disconnected regions [31]. Currently, those regions make up our observable universe and resemble one another. The presence of the homogeneous Monster Module before the Big Bang explains, together with the inflationary period, why all the initial disconnected regions displayed the same features.

4.4. The Monster and the Spacetime

The Monster is a manifold that, for the BUT variants, can be also described as a hypersphere. Therefore, our universe is internal to the Monster. The loss of dimensions occurs in the Monster, giving rise to the Big Bang. That is why the fossil background cosmic radiation comes from everywhere, when we look at it [32]. Another problem arises: how can a string-like manifold give rise and encompass the whole universe? A possible solution is that the Monster is not in the space, and the space is bent together with the universe. Concerning the time, the things are more complicated. Indeed, in touch with Veneziano's pre Big Bang scenarios [31], the time could exist before the singularity, and not arise together with the universe's spatial dimensions. Indeed, the Monster group needs to be embedded in the time, because it, acting as a Lie group, needs to perform symmetric movements, which may just occur in a given time. It might however be speculated that the time is not required at the Monster Module level, and the Wheeler–DeWitt equation might be valid at such level. This means that, while the Monster Module, embedded in a $S^{196,884}$ manifold, lies in infinite dimensions and is atemporal, the lower level, embedded in an $S^{196,883}$ manifold, requires the introduction of the parameter time.

5. Quantifying Physical Monster's Parameters

5.1. Towards the Monster's Enthalpy

The energy-BUT can be used in order to calculate the energetic requirements of Monster Modules in a physical context. Thermodynamics says that:

$$\mathrm{H} = \mathrm{F} + \mathrm{T} \times \mathrm{E}$$

where H is the Enthalpy, F the free-energy, T the temperature (trascurable) and E the entropy. We assume that our universe is closed. We will evaluate the possible values at the Big Bang (H_0, F_0, T_0, E_0) and at the present time (H_1, F_1, T_1, E_1). The current level E_1 of entropy in the universe is estimated in $2.6 \pm 0.3 \times 10^{122}$ K [33,34], while T_1 is neglectable. If the universe displays four dimension as currently believed, every dimension contains approximately an average entropy of: $E_1/4$.

As shown in [33], the current universe displays almost the highest possible values of entropy. Also in the future, the entropy will be just slightly larger than the current value E_1, because a monotonical increase already occurred. This means that E_1 is, more or less, the maximum value of entropy achievable in the whole life of the universe, and also means that the free-energy F_1 is currently very low. Therefore:

$$E_1 = H_1.$$

The current E_1 almost equals the total enthalpy H_1 of the universe. Vice versa, at the Big Bang, F_0 and T_0 were very high and E_0 close to zero. This means that, at the Big Bang:

$$F_0 = H_0 - T_0.$$

If the Monster occurred before the Big-Bang, we are in front of a manifold with the highest possible energy, because it displays the higher number of symmetries. If the Monster gave rise to our universe, and the Monster displays 196,883 dimensions, the Entropy of the Monster E_M is:

$$E_M = E_1/4 \times 196{,}883.$$

Thus, the enthalpy of the Monster H_M stands roughly for the same value:

$$H_M = E_1/4 \times 196{,}883$$

The loss of dimensions in the Monster Module, due to the non-abelian movements of the Monster Lie group and the energy-BUT, give rise to different universes with dimensions lower than the Monster, and equipped with less energy and information.

Through the Conway atlas of finite groups, we know the dimensions and the order of every group, including the sporadic ones. It is not difficult to calculate how many dimensions have been lost. We know this number, e.g., 196,883 less 4 (here 4 stands for the four space-time dimensions of our universe, we know how many symmetries are preserved, and we know, for energy-BUT, that every decrease of a single symmetric level denotes the loss of half of the energy. If the pre-Big Bang manifold, e.g., the Monster Module, is equipped with 196,884 dimensions and 10^{54} elements, and if our universe has four dimensions, we have 10^{50} elements in our universe.

Summarizing, once hypothesized a high-energy Monster Module before the rise of our universe, the next step is to reduce the symmetries from the Monster vertex operator to the Monster group, which is the Lie group acting on it. A further step gives rise to a dimensions and symmetries reduction until the emergence of our universe.

5.2. Information

The energy-BUT states that it is not possible to achieve higher information starting from a lower dimensional level. This means that we need to start from the Monster Module, and not vice versa. The process must be top-down, e.g., from the Monster to the universe, and not bottom-up. According to the energy-BUT, a loss of information occurs together with a decrease in dimensions. Therefore, from the Monster to our universe, it occurs a loss if information. You cannot move a particle in our universe from lower to higher dimensions, unless you, for energy-BUT, do not inject novel free-energy or enthalpy. You can just do it locally in the universe, for example when biological entities arise in limited niches, but not everywhere, because the total entropy increases together with a decrease in free-energy. Summarizing, from the highest to the lower levels there is a reduction, and not an emergence of information.

5.3. Watching the Monster: Vertex Algebra

In order to incorporate the *j*-function into a general context and to visualize the movements of the Monster Group on the Monster Module, we built a simplified 3D model equipped with a hypersphere and a vertex algebra operator. We achieved a low-dimensional model of *j*-function and its group, embedded into a vertex algebra's manifold. Briefly, a vertex algebra provides a mathematical formulation of the chiral part of 2-dimensional conformal field theory. The axioms of a vertex algebra are obtained from the properties of quantum field theories and operator product expansions (OPEs). The main tactic flowing from OPEs is that a product of local operators defined at nearby locations can be expanded in a series of local operations [35]. A graphical representation of an OPE is represented in Figure 4A. Let ω_1, ω_2 be periods of a doubly periodic function with $\tau \equiv \frac{\omega_1}{\omega_2}$. Then Klein's absolute invariant is defined by

$$J(\omega_1, \omega_2) = \frac{g_2^3(\omega_1, \omega_2)}{\triangle(\omega_1, \omega_2)},$$

where g_2 is the invariant of the Weierstrass elliptic function. If H is the upper half plane and $\tau \in H$, then

$$J(\tau) \equiv J(1, \tau) = J(\omega_1, \omega_2).$$

The function $J(\tau)$ is the *j*-function modulo a constant multiplicative factor [36,37]. A dynamical system with a strange attractor and invariant tori [38] initialized with the *j*-function is illustrated in Figure 4b.

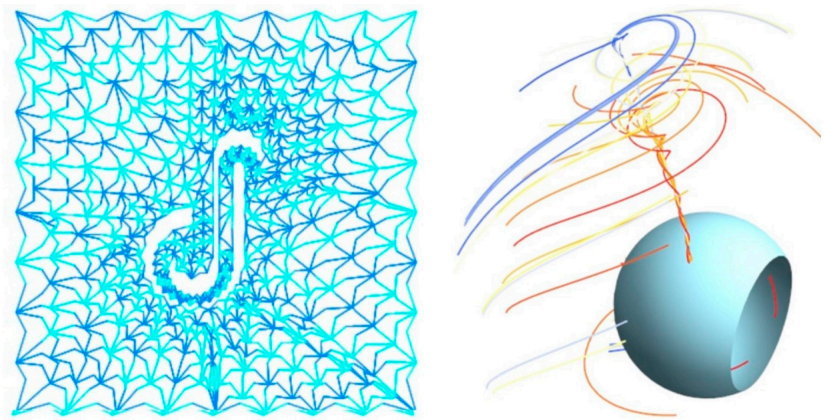

(**a**) (**b**)

Figure 4. Defining a vertex algebra on a torus helps us to visualize otherwise abstract structures. Starting from a vertex operator algebra (a very small portion is illustrated in (**a**)) we made use of the attractors and the corresponding ordinary differential equations described by [38]. In (**b**), the *j*-function on the attractor torus displays one coordinate initialized with a *j*-function value.

6. Questions and Conclusions

Starting from a Spinozian global system, shaped in the guise of a multidimensional and multi-symmetric manifold equipped with a structural order of relationships, we were able to analyse, through a loss of dimensions dictated by the algebraic features of the Monster Module and its Lie group, the individual history of the universe. The universe can be thus conceived of as a manifold at lower dimensions encompassed in higher ones. The Monster Module is a manifold equipped with absolutely the highest dimensions—that is, a manifold consisting in the highest number of symmetries. The Monster Moonshine manifold is prior to its modifications. This may mean that the nature and the flow of events in the universe is a Monster's self-projection towards less dimensions. The universe stands for a local symmetry, e.g., modifications of the Monster manifold. The Monster

Module cannot exist in, and cannot be conceived through, a higher manifold other than itself. Every manifold in the universe exists either in itself or in some higher manifold else, e.g., the Monster Module. The knowledge of a lower dimension manifold in the universe depends on and involves the knowledge of higher dimensions mapping the lower manifold. In the meantime, the Monster Module, which n-dimensions are untouched, is still there. If different trajectories on the Monster Module give rise to different local losses of dimensions, this means that countless universes are possible, each one equipped with different or overlapping symmetries.

We would like to bring to an end with a few unsolved problems.

(a) Where does the Monster take such a huge amount of enthalpy? It takes us in pre-, pre-Big Bang scenarios. This is the same problem with inflationist models, that do not explain where the energy of the required false vacuum comes from. A link between the Monster group and the false vacuum might be speculated.
(b) What is the role of the j-function in the pre Big Bang period? Does it provide energy?
(c) How does the Monstrous Moonshine look like? We could either imagine a timeless, immutable manifold where just the Monster Group movements take place, or as we did, a dynamical, time-dependent structure.
(d) Does the curvature of the Monster Module change with the passage of time? This could be a very useful information, in order to elucidate the hypothesized step from an ancient anti DeSitter hyperbolic universe to the current, flat one.
(e) Our universe might not arise directly from the Monster, but by one of its subgroups, e.g., the Th group (Figure 3), which is correlated with the successful superstring 10D theory. Is it possible to split the Leech lattice in which the Monster group is embedded, in order to achieve the lower dimensional E8 lattice where the Th group's movements take place? It is central to remind that the step from an E8 lattice to the Leech lattice requires $\times 3$ multiplication and peculiar rotations.
(f) The topological step from the vertex operator algebra to the Lie Monster Group requires a continuous function. Are we in front of a "super" gauge field? In other words, is there a gauge field that causes the first projection depicted at the top of Figure 3? In a topological framework, the feature that links the symmetries at a higher level with the single point at a lower level is the continuous function. If we assess two antipodal points as symmetries, and the single point as symmetry breaks and local transformations, a gauge field could be required, in order to restore the (apparently hidden) symmetry.

Conflicts of Interest: The authors declare no conflict of interest.

References

1. Conway, J.H.; Curtis, R.T.; Norton, S.P.; Parker, R.A.; Wilson, R.A. *Atlas of Finite Groups: Maximal Subgroups and Ordinary Characters for Simple Groups*; Conway, J.H., Ed.; Clarendon Press: Oxford, MS, USA, 1985.
2. Du Sautoy, M. *Finding Moonshine: A Mathematician's Journey through Symmetry*; Fourth Estate: London, UK, 2008.
3. Tozzi, A.; Peters, J.F. A Topological Approach Unveils System Invariances and Broken Symmetries in the Brain. *J. Neurosci. Res.* **2016**, *94*, 351–365. [CrossRef] [PubMed]
4. Roldán, E.; Martínez, I.A.; Parrondo, J.M.R.; Petrov, D. Universal features in the energetics of symmetry breaking. *Nat. Phys.* **2014**, *10*, 457–461. [CrossRef]
5. Borsuk, M. Drei Sätze über die n-dimensionale euklidische Sphäre. *Fundam. Math.* **1933**, *1*, 177–190. (In German)
6. Crabb, M.C.; Jawaworski, J. Aspects of the Borsuk–Ulam theorem. *J. Fixed Point Theory Appl.* **2013**, *13*, 459–488. [CrossRef]
7. Bredon, G.E. *Topology and Geometry (Graduate Texts in Mathematics)*; Springer: New York, NY, USA, 1993; p. 557.

8. Beyer, W.A.; Zardecki, A. The early history of the ham sandwich theorem. *Am. Math. Mon.* **2004**, *111*, 58–61. [CrossRef]
9. Matoušek, J. *Using the Borsuk-Ulam Theorem: Lectures on Topological Methods in Combinatorics and Geometry*; Springer: Berlin/Heidelberg, Germany, 2003.
10. Weisstein, E.W. Antipodal Points. 2016. Available online: http://mathworld.wolfram.com/AntipodalPoints.html (accessed on 19 December 2016).
11. Tozzi, A.; Peters, J.F. Towards a Fourth Spatial Dimension of Brain Activity. *Cogn. Neurodyn.* **2016**, *10*, 189–199. [CrossRef] [PubMed]
12. Peters, J.F. *Computational Proximity: Excursions in the Topology of Digital Images*; Intelligent Systems Reference Library, Ed.; Springer: Berlin, Germany, 2016.
13. Weeks, J.R. *The Shape of Space*, 2nd ed.; Marcel Dekker, Inc.: New York, NY, USA; Basel, Switzerland, 2002.
14. Watanabe, T.; Masuda, N.; Megumi, F.; Kanai, R.; Rees, G. Energy landscape and dynamics of brain activity during human bistable perception. *Nat. Commun.* **2014**. [CrossRef] [PubMed]
15. Sengupta, B.; Tozzi, A.; Cooray, G.K.; Douglas, P.K.; Friston, K.J. Towards a Neuronal Gauge Theory. *PLoS Biol.* **2016**, *14*, e1002400. [CrossRef] [PubMed]
16. Naimpally, S.A.; Peters, J.F. *Topology with Applications: Topological Spaces via Near and Far*; World Scientific: Singapore, 2013.
17. Weyl, H. *Space-Time-Matter*; Dutton Publishing: Boston, MA, USA, 1922.
18. Olive, D.I.; Landsberg, P.T. Introduction to string theory: Its structure and its uses. *Philos. Trans. R. Soc. Lond. A Math. Phys. Sci.* **1989**, *329*, 319–328. [CrossRef]
19. Petty, C.M. Equivalent sets in Minkowsky spaces. *Proc. Am. Math. Soc.* **1971**, *29*, 369–374. [CrossRef]
20. Dochviri, I.; Peters, J.F. Topological sorting of finitely near sets. *Math. Comp. Sci.* **2016**, *10*, 273–277. [CrossRef]
21. Bourbaki, N. *Elements of Mathematics. General Topology 1*; Éditions Hermann: Paris, France, 1966; Chapters 1–4.
22. Borsuk, M. Fundamental retracts and extensions of fundamental sequences. *Fundam. Math.* **1969**, *64*, 55–85.
23. Frenkel, I.; Lepowsky, J.; Meurman, A. A natural representation of the Fischer-Griess Monster with the modular function J as character. *Proc. Natl. Acad. Sci. USA* **1984**, *81*, 3256–3260. [CrossRef] [PubMed]
24. Duncan, J.F.R.; Griffin, M.J.; Ono, K. Moonshine. *Res. Math. Sci.* **2015**, *2*. [CrossRef]
25. Gannon, T. *Moonshine beyond the Monster: The Bridge Connecting Algebra, Modular Forms and Physics*; Cambridge University Press: Cambridge, UK, 2006.
26. Borcherds, R. Monstrous Moonshine and Monstrous Lie Superalgebras. *Invent. Math.* **1992**, *109*, 405–444. [CrossRef]
27. Eguchi, T.; Ooguri, H.; Tachikawa, Y. Notes on the K3 Surface and the Mathieu group M_{24}. *Exp. Math.* **2011**, *20*, 91–96. [CrossRef]
28. Witten, E. Three-dimensional gravity revisited. 2007; arXiv:0706.3359.
29. Chow, T.L. *Gravity, Black Holes, and the Very Early Universe. An Introduction to General Relativity and Cosmology*; Springer: New York, NY, USA, 2008; p. 280.
30. Collins, G.P. The shapes of space. *Sci Am.* **2004**, *291*, 94–103. [CrossRef] [PubMed]
31. Veneziano, G. A Simple/Short Introduction to Pre-Big-Bang Physics/Cosmology. 1998; arXiv:hep-th/9802057v2.
32. Fixsen, D.J. The Temperature of the Cosmic Microwave Background. *Astrophys. J.* **2009**, *707*, 916–920. [CrossRef]
33. Egan, C.A.; Lineweaver, C.H. A Larger Estimate of the Entropy of the Universe. 2010; arXiv:0909.3983v3.
34. Frampton, P.; Hsu, S.D.H.; Kephart, T.W.; Reeb, D. What is the entropy of the universe? 2008; arXiv:0801.1847.
35. Ekstrand, J. Lambda: A Mathematica package for operator product expansions in vertex algebras. *Comput. Phys. Commun.* **2011**, *182*, 409–418. [CrossRef]
36. Weisstein, E.W. Klein's Absolute Invariant. 2016. Available online: http://mathworld.wolfram.com/KleinsAbsoluteInvariant.html (accessed on 19 December 2016).
37. Frenkel, I.B.; Lepowsky, J.; Meurman, A. *Vertex Operator Algebras and the Monster*; Academic Press: Cambridge, MA, USA, 1988; Volume 134.
38. Sprott, J.C. A dynamical system with a strange attractor and invariant tori. *Phys. Lett.A* **2014**, *378*, 1361–1363. [CrossRef]

© 2016 by the authors; licensee MDPI, Basel, Switzerland. This article is an open access article distributed under the terms and conditions of the Creative Commons Attribution (CC-BY) license (http://creativecommons.org/licenses/by/4.0/).

information

MDPI

Review

A Symmetric Approach Elucidates Multisensory Information Integration

Arturo Tozzi [1,*] and James F. Peters [2]

[1] Center for Nonlinear Science, University of North Texas, 1155 Union Circle, Denton, TX 76203, USA
[2] Department of Electrical and Computer Engineering, University of Manitoba, 75A Chancellor's Circle, Winnipeg, MB R3T 5V6, Canada; James.Peters3@umanitoba.ca
* Correspondence: tozziarturo@libero.it; Tel.: +1-39-335-844-7399

Academic Editors: Pedro C. Marijuán, Abir U. Igamberdiev and Lin Bi
Received: 6 October 2016; Accepted: 22 December 2016; Published: 27 December 2016

Abstract: Recent advances in neuronal multisensory integration suggest that the five senses do not exist in isolation of each other. Perception, cognition and action are integrated at very early levels of central processing, in a densely-coupled system equipped with multisensory interactions occurring at all temporal and spatial stages. In such a novel framework, a concept from the far-flung branch of topology, namely the Borsuk-Ulam theorem, comes into play. The theorem states that when two opposite points on a sphere are projected onto a circumference, they give rise to a single point containing their matching description. Here we show that the theorem applies also to multisensory integration: two environmental stimuli from different sensory modalities display similar features when mapped into cortical neurons. Topological tools not only shed new light on questions concerning the functional architecture of mind and the nature of mental states, but also provide an empirically assessable methodology. We argue that the Borsuk-Ulam theorem is a general principle underlying nervous multisensory integration, resulting in a framework that has the potential to be operationalized.

Keywords: multimodal; heteromodal; integration; neuron; brain; Borsuk-Ulam theorem; antipodal

---

> "*A color is a physical object when we consider its dependence upon its luminous source; regarding, however, its dependence upon the retina, it becomes a psychological object, a sensation. Not the subject, but the direction of our investigation, is different in the two domains*" *(Mach 1885)*.

Current advances in human neurosciences shed new light on questions concerning the status of the mental and its relation to the physical. Multisensory neurons (we will also term them "heteromodal" or "multimodal") receiving convergent inputs from multiple sensory modalities (independent sources of information called "cues") integrate information from the five different senses [1]. When cues are available, combining them facilitates the detection of salient events and reduces perceptual uncertainty, in order to improve reactions to immediate dangers and to rapidly varying events [2]. Multisensory neurons are able as well to carry out complex brain activities, such as object categorization [3]. Heteromodal integration displays complicated temporal patterns: absent in the superior colliculus of newborn's brain, it arises in the earlier weeks/months of postnatal life [4,5]. As time goes on, neurons develop their capacity to engage in multisensory integration, which determines whether stimuli are to be integrated or treated as independent events. Multisensory integration's development is due to early sensory experience, extensive experience with heteromodal cues and, above all, maturation of cooperative interactions between superior colliculus and cortex [6,7]. The ability to engage in multisensory integration specifically requires cortical influences [8,9]: without the help of cortical activity, neurons become responsive to multiple sensory modalities, but are unable to integrate different sensory inputs [10]. To make the picture more intricate, multisensory experience is a plastic capacity

depending on dynamic brain/environment interactions [11]: neurons indeed retain sensitivity to heteromodal experience well past the normal developmental period, in order that the brain learns a multisensory principle based on the specifics of experience and is able to apply it to novel incoming stimuli [12].

In such a multifaceted framework, the Borsuk-Ulam theorem (BUT) from topology comes into play. This theorem tells us that two opposite points on a sphere, when projected on a one-dimension lower circumference, give rise to a single point displaying a matching description [13]. In this review, we will elucidate the underrated role of topology in multimodal integration, illustrating how simple concepts may be applied to brain processes of cues integration. This paper comprises four sections. In the first section, we will compare the traditional hierarchical view of multisensory integration with the very last developments: the latter talk about the nervous system as a sum of multisensory neurons that form extensive forward, backward and lateral connections at the very first steps of integration in the primary sensory areas. The second section provides a description of the BUT and its role in multisensory integration. Section three goes through the BUT's theoretical and experimental consequences in theory of knowledge and in the explanation of mental states' nature. The last section elucidates what the BUT brings on the table, when applied to multimodal neurons.

1. Classical vs. Current View

Traditional research on the basic science of sensation asks what types of information the brain receives from the external world. To elucidate the classical view, as an example we will go through the visual system, the best known and the most relevant among sensory systems in Primates. The retinal receptors are sensitive to simple signals related to the external world. The message is sent to the primary visual cortex V1, where specific aspects of vision such as form, motion or color are segregated in different parallel pathways. V1 projects to the associative areas termed "unimodal", since they are influenced by a sole sensory modality (in this case, the vision) [14]. The visual unimodal associative cortex (secondary visual cortex) is arranged in two streams, devoted to the control of action and objects perception. Processing channels, each serving simultaneously specialized functions, are also present in the central auditory and somatosensory systems. The message is then conveyed from unimodal to associative areas termed "heteromodal", since they are influenced by more than one sensory modality (visual, auditory, somatosensory, and so on) [15]. A high-order heteromodal area, the prefrontal cortex, collects the highly-processed inputs conveyed by other associative areas. In this classical view, the sequential processing of information is hierarchical, such that the initial, low-level inputs are transformed into representations and multisensory integration emerges at multiple processing cortical stages [3]. The hierarchical view is also embraced by the most successful model of cognitive architecture, i.e., the connectome, where hubs/nodes are characterized by preferential railways of information flows [16].

In the last decade, neuroscience has witnessed major advances, emphasizing the potentially vast underestimation of multisensory processing in many brain areas. New mechanisms, such as the "unimodal multisensory neurons" [17], have been demonstrated. In addition, multisensory interactions have been reported at system levels traditionally classified as strictly unimodal: both primary and secondary sensory areas receive substantial inputs from sources that carry information about events impacting other modalities [18–22]. In particular, it has been well established in the case of the human V1, which is inherently multisensory [23]. In adult mice, vision loss through one eye leads whiskers to become a dominant nonvisual input source which attains extensive visual cortical reactivation [24]. In blind individuals, when visual inputs are absent, occipital ("visual") brain regions respond to sound and spoken language [25]. A growing number of studies reports the presence of connectivity between V1 and primary auditory cortex (as well as other higher-level visual and auditory cortices). Non-visual stimuli have been shown to enhance the excitability of low-level visual cortices within the occipital pole. Research into cross-modal perception has also linked senses other than vision, such as taste with audition [26]. Escanilla et al. [27] demonstrated odor-taste convergence in the nucleus of

the solitary tract of the awake, freely licking rat. A multisensory network for olfactory processing, via primary gustatory cortex connections to primary olfactory cortex, once again suggests that sensory processing may be more intrinsically integrative than previously thought [28].

In sum, the current broad consensus is that the multimodal model is widely diffused in the brain and that most, if not all, higher- as well as lower-level neural processes are in some form multisensory. Information from multiple senses is integrated already at very early levels of processing, leading to the concept of the whole neocortex as multisensory in function. Forward, backward and lateral extensive connections support communication in a densely-coupled system, where multisensory interactions occur at all temporal and spatial stages [29]. The content of the single neuronal outputs turns out to be increasingly complex. The functional wheel has come full circle when the highest polymodal areas send feedback messages to the primary sensory cortices. From now on, a ceaseless pathway of feedbacks and feedforwards takes place among cortical areas. The functional importance of the so called "backward" connections is worth of mention. The effects of the projections from higher areas to multimodal neurons play an important role both in multisensory development and in complex brain functions, providing meaningful adjustments to the ongoing activity of a given area. It has been argued that backward connections might embody the causal structure of the world, while forward connections just provide feedback about prediction errors to higher areas [30]. That is, anatomical forward connections are functional feedback connections. For backward connections to effectively modulate lower level processing, higher order areas would need to begin their processing at approximately the same time as lower areas. While this was originally thought not to be the case, we know now that the cross-modal interactions' processing latencies are highly similar to the latencies at which initial sensory processing occurs in the respective primary cortices [29].

2. A Topological Model of Multisensory Integration

2.1. The Borsuk-Ulam Theorem.

Continuous mappings from object spaces to feature spaces lead to various variants of the Borsuk-Ulam Theorem [13,31,32]. Antipodal points are points opposite each other on a S^n sphere [33]. There are natural ties between Borsuk's result for antipodes and mappings called homotopies. In fact, the early work on n-spheres and antipodal points eventually led Borsuk to the study of retraction mappings and homotopic mappings [34].

The Borsuk-Ulam Theorem states that:

Every continuous map $f : S^n \to R^n$ *must identify a pair of antipodal points.*

Points on S^n are antipodal, provided they are diametrically opposite. Examples of antipodal points are the endpoints of a line segment S^1, or the opposite points along the circumference of a circle S^2, or the poles of a sphere S^3 [35]. An n-dimensional Euclidean vector space is denoted by R^n [36,37]. Put simply, BUT states that a sphere displays two antipodal points that emit matching signals. When they are projected on a circumference, they give rise to a single point which a description matching both antipodal points (Figure 1A). Here "opposite points" means two points on the surface of a three-dimensional sphere (the surface of a beach ball is a good example) which share some characteristics in common and are at the same distance from the center of the beach ball [38]. For example, BUT dictates that on the earth's surface there always exist two opposite points with the same pressure and temperature. Two opposite points embedded in a sphere project onto a single point on a circumference, and vice versa: this means that the projection from a higher dimension (equipped with two antipodal points) to a lower one gives rise to a single point (equipped with the characteristics of both the antipodal points). It is worth mentioning again that the two antipodal points display similar features: we will go through this central issue in the next paragraph.

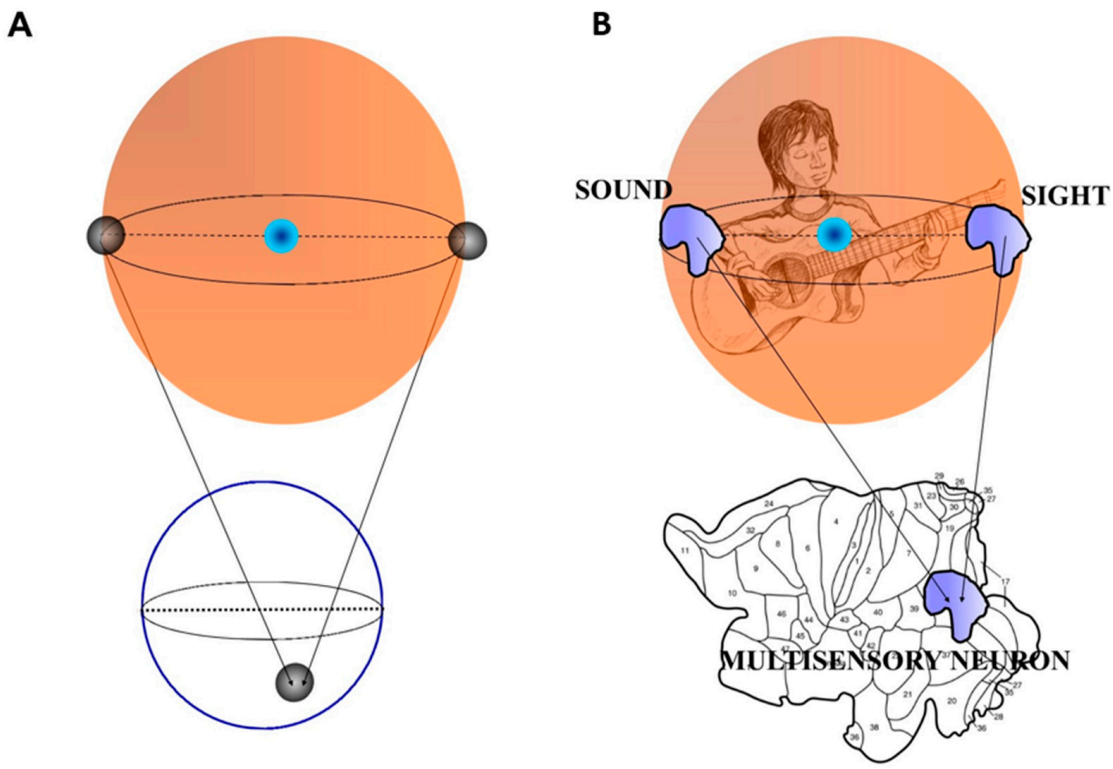

Figure 1. (**A**) A simplified sketch of the Borsuk-Ulam theorem: two antipodal points (black spheres) on a three-dimensional sphere project to a single point on a two-dimensional circumference. (**B**) The Figure shows what happens when an observer is in front of a guitar player. The environmental inputs from different sensory modalities (in this case sound and sight are depicted in guise of shapes instead of points) converge on a single group of multisensory neurons in the cortical layers of brain's observer. Note that the brain is flattened and displayed in 2D [39]. According to the dictates of the Borsuk-Ulam theorem, the single shape contains a melted message from the two modalities. Modified from Tozzi and Peters [37].

2.2. Borsuk-Ulam Theorem in Brain Signal Analysis.

What does BUT mean in a physical/biological context? How could BUT be helpful in the evaluation of brain function? The two antipodal points can be used not just for the description of simple topological points, but also of broad-spectrum phenomena: i.e., either two antipodal shapes, or functions, or signals, or vectors. For example, a "point" may be described as a collection of signals or a surface shape, where every shape maps to another antipodal one. Here we provide, for technical readers, the underlying mathematical treatment. In order to evaluate the possible applications of the BUT in brain signal analysis, we view the surface of the brain as an n-sphere and the feature spaces for brain signals as finite Euclidean topological spaces. In terms of brain activity, a feature vector $x \in R^n$ models the description of a brain signal. The BUT states that, for description $f(x)$ for a brain signal x, we expect to find an antipodal feature vector $f(-x)$ that describes a brain signal on the opposite (antipodal) side of the brain (or of the environment). The pair of antipodal brain/environmental signals have matching descriptions. Let X denote a nonempty set of points on the brain surface. Recall that an open set does not encompass its boundary or limit points. A topological structure on X (called a brain topological space) is a collection of open sets τ of X, having the following properties:

(Str. 1) Every union of sets in τ is a set in τ
(Str. 2) Every finite intersection of sets in τ is a set in τ

The pair (X, τ) is called a topological space. Also X by itself can be termed a topological space, provided X has a topology τ on it. Let X, Y be topological spaces. A function or map $f : X \to Y$ on a set X to a set Y is a subset $X \times Y$, so that for each $x \in X$ there is a unique $y \in Y$ such that $(x, y) \in f$ (usually written $y = f(x)$). The mapping f is defined by a rule telling us how to find $f(x)$.

Provided $A \subset Y$ is open, a mapping $f : X \to Y$ is continuous and the inverse $f^{-1}(A) \subset X$ is also open [40]. In this view of continuous mappings from the brain signal topological space X on the brain surface to the brain signal feature space R^n, we can consider not just one signal feature vector $x \in R^n$, but also mappings on X to a set of signal feature vectors $f(X)$. This expanded view of brain signals has interest, since every connected set of feature vectors $f(X)$ has a shape. In sum, this means that brain signal shapes can be compared. A consideration of $f(X)$ (set of brain signal descriptions for a region X) instead of $f(x)$ (description of a single brain signal x) leads to a region-based view of brain signals. This region-based view of the brain arises naturally in terms of a comparison of shapes produced by different mappings from X (brain object space) to the brain feature space R^n. An interest in continuous mappings from object spaces to feature spaces leads into homotopy theory and the study of shapes.

Let $f, g : X \to Y$ be continuous mappings from X to Y. The continuous map $H : X \times [0, 1] \to Y$ is defined by

$$H(x, 0) = f(x), H(x, 1) = g(x), \text{ for every } x \in X.$$

The mapping H is a homotopy, provided there is a continuous transformation (called a deformation) from f to g. The continuous maps f, g are called homotopic maps, provided $f(X)$ continuously deforms into $g(X)$ (denoted by $f(X) \to g(X)$). The sets of points $f(X)$, $g(X)$ are called shapes [41].

For the mapping $H : X \times [0, 1] \to R^n$, where $H(X, 0)$ and $H(X, 1)$ are homotopic, provided $f(X)$ and $g(X)$ have the same shape. That is, $f(X)$ and $g(X)$ are homotopic, in case of:

$$\|f(X) - g(X)\| < \|f(X)\|, \text{ for all } x \in X.$$

An interest in continuous mappings from object spaces to feature spaces leads into homotopy theory and the study of shapes: antipodal points on a sphere have the same shape [42]. It was Borsuk who first associated the geometric notion of antipodal shapes and mappings, called homotopies [34,43,44]. Borsuk's discovery paves the way for a geometry of shapes and shapes of space [45,46]. To make an example, a pair of connected planar subsets in Euclidean space R^2 have equivalent shapes, if the planer sets have the same number of holes [40]. This suggests yet another useful application of Borsuk's view of the transformation of one shape into the other, in terms of brain signal analysis. Sets of brain signals not only will have similar descriptions, but also similar dynamic character. Moreover, the deformation of one brain signal shape into another occurs when they are descriptively near [47,48]. This expanded view of signals has interest, since every connected couple of antipodal points has a shape: therefore, signal shapes can be compared. If we evaluate physical and biological phenomena instead of "signals", BUT leads naturally to the possibility of a region-based, not simply point-based, geometry, with many applications. In terms of activity, two antipodal regions model the description of a signal. The regions themselves live on what is known as a manifold, which is a topological space that is a snapshot (tiny part) of a locally Euclidean space. For a given signal on a sphere, we expect to find an antipodal region that describes a signal with a matching description. In sum, the mapping from the sphere to the circumference is defined by a rule which tells us how to find a single point/region [49]. The region-based view of the manifold arises naturally in terms of a comparison of shapes produced by different mappings from the sphere to the circumference [50].

2.3. Borsuk-Ulam Theorem and Multisensory Integration.

Multisensory integration could be evaluated in terms of antipodal points and BUT. Figure 1B depicts an example of multisensory integration in the BUT framework. Consider an observer who hears the strumming of a guitar standing in the surrounding environment. A guitar player is embedded in the environment. The observer perceives, through his different sense organs such as ears and eyes, the sounds and the movements produced by the guitar player. According to the BUT dictates, the guitar player stands for an object embedded in a three-dimensional sphere. The two different sensory modalities produced by the guitar player (sounds and movements) stand for the antipodal points on the sphere's surface. Objects belonging to antipodal regions can either be different or similar, depending on the features of objects [48]; however, the two antipodal points share the same features. Both sounds and movements come indeed from the same object embedded in the sphere, i.e., the guitar player. The two antipodal points are not true points, but instead shapes, or functions, which can also be portrayed as vectors containing all the features of the stimulus: in the case, for example, of the visual inputs, the vector contains information about the colours, the shape, the movements of the guitar player. The two antipodal points project at first to a two-dimensional layer, the brain cortex—where multisensory neurons lie—, then are integrated into a single multimodal signal, which takes into account the features of both. Cerebral hemispheres can be indeed unfolded and flattened into a two-dimensional reconstruction by computerized procedures [39]. We may think to a single vector, embedded in the two-dimensional brain, which contains the features of all the information from the two inputs.

A variant of the BUT theorem, called reBUT [50], states that the two points (or regions, or vectors or whatsoever) with similar description do not need necessarily to be antipodal, in order to be described together (Figure 2A). This means that different inputs from different modalities do not need to be perfectly antipodal on the n-sphere (the environment). Sets of signals not only will have similar descriptions, but also dynamic character; moreover, the deformation of one signal shape into another occurs when they are descriptively near [47]. This elucidates an important feature of multisensory integration. Although multisensory interactions' simulations at the neuronal level clearly show that the simple effect of heteromodal convergence is sufficient to generate multimodal properties, nonetheless the multisensory integration's occurrence almost never could be predicted on the basis of a simple linear addition of their unisensory response profiles: the interactions may indeed be super-additive, sub-additive, or display inverse effectiveness and temporal changes [1,5,51,52]. In the BUT's topological framework, this apparently bizarre behaviour is explained by the dynamical changes occurring at the antipodal points [48]. There is indeed the possibility that two inputs from different cues are not perfectly integrated. This means that the mapping of the two cues on the S^{n-1} sphere does not match perfectly, and the sensation is doubtful (Figure 2B). A superimposition of two spheres with slightly different centers occurs. The brain thus might "move" its spheres, in order to restore the coherence between the two signals. Therefore, by an operational point of view, we might be able to evaluate the distance between the central points of the two spheres, in order to achieve the discrepancy values between the two multisensory signals projected from the environment to the brain.

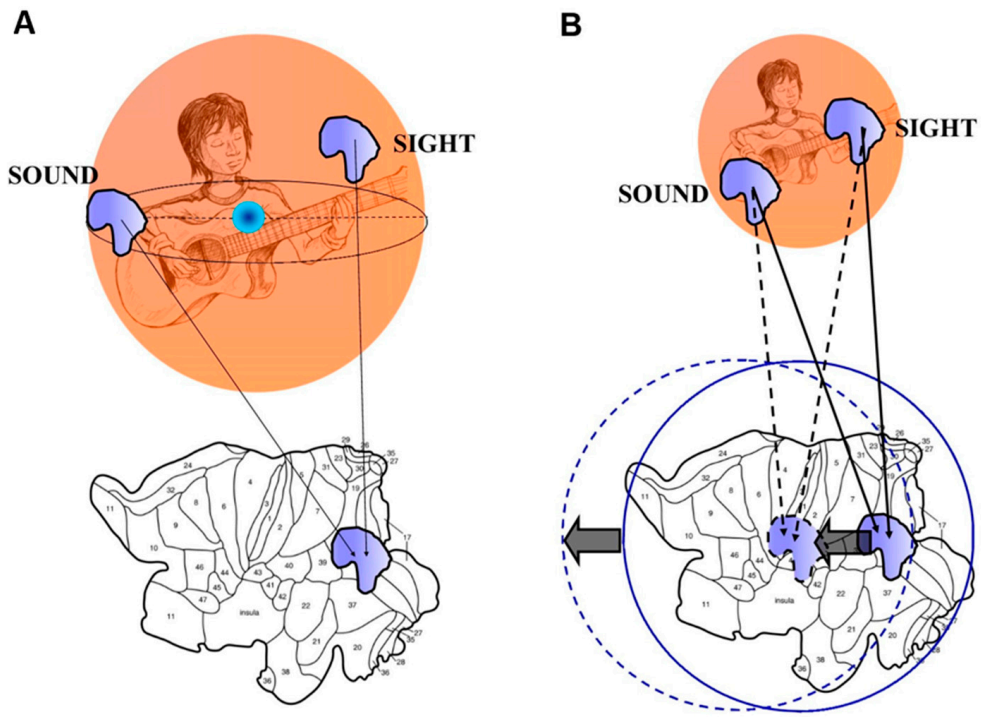

Figure 2. (**A**) A simplified sketch of the reBUT (a variant of the Borsuk-Ulam theorem). The functions with matching description do not need necessarily to be antipodal. Thus, the two inputs from different sensory modalities may arise from every point of the environment, if they are just equipped with a signal matching. (**B**) When the two inputs from different modalities do not match on the 2-D brain surface, a discrepancy occurs between two brain spheres, which can be quantified by evaluating the distance between their two centres. Modified from Tozzi and Peters [37].

The BUT is not simply a "metaphor", rather a real computational tool. Indeed, there is room to use the description of the BUT and its variants in order to assess computations involved in multisensory integration, therefore providing both mechanisms and explanatory hypotheses. A BUT variant, termed energy-BUT, is particularly useful in our context. There exists a physical link between the abstract concept of BUT and the energetic features of the system formed by two manifolds S^n and S^{n-1}. We start from a manifold S^n equipped with a pair of antipodal points. When these opposite points map to an n-Euclidean manifold (where S^{n-1} lies), a dimensionality reduction occurs, and a single point is achieved. However, it is widely recognized that a decrease in dimensions goes together with a decrease in information. Two antipodal points contain more information than their single projection in a lower dimension, because dropping down a dimension means that each point in the lower dimensional space is simpler: each point has one less coordinate. To make an example, a two-dimensional shadow of a cat encompasses less information than a three-dimensional cat. This means that the single mapping function on S^{n-1} displays informational parameters lower than the two corresponding antipodal functions on S^n. Because information can be evaluated in terms of informational entropy, BUT and its variants yield physical quantities: we achieve a system in which entropy changes depend on affine connections and homotopies. Entropies can be evaluated in fMRI functional studies through different techniques, e.g., pairwise entropy [53–55], Granger causality index, phase slope index, and so on [56]. Here we propose a topological procedure in order to assess changes in informational entropies in brain fMRI multisensory integration's studies. The method is described in Figure 3. In our example, the visual and auditory cues stand for a continuous function, from the sphere surrounding the individual to his cortical multisensory neurons. Informational entropy values can be identified in multisensory neurons after their activation: in the hypothetical case of Figure 3, we choose a putative entropy value of 1.02. According to the BUT's dictates, the same value 1.02 must be found both in

the environmental cues (a single value of 1.02 for every one of the two different cues), and in every other cortical area involved in multisensory processing. We might not know the entropy values of the sound and sight in the external environment. However, this is not important: if we identify a group of cortical multisensory neurons that fire when a visual and auditory cue are presented together, we need just to know the entropy values of such neuronal assembly. Therefore, by knowing the sole entropy values of a Blood Oxygenation Level Dependent (BOLD)-activated multisensory brain area, we are allowed to correlate different brain zones involved in multisensory integration (Figure 3). Indeed, neurons equipped with the same entropy values are functionally linked, according to BUT. Therefore, we are able to assess the cortical zones that display the same entropy values, shedding light on the pathways involved in multisensory integration. This methodology paves also the way to experimentally evaluate which model, e.g., either the traditional or the current view of multisensory integration, is valid. Note that, in the proposed fMRI context, BUT is related to a meso-level of observation that involves cortical circuits and inter-areal massive interactions, through "Communication through Coherence". Nevertheless, once neuro-techniques will be more advanced, BUT should be applicable also to micro-levels of observation, such as single-cell spiking activity.

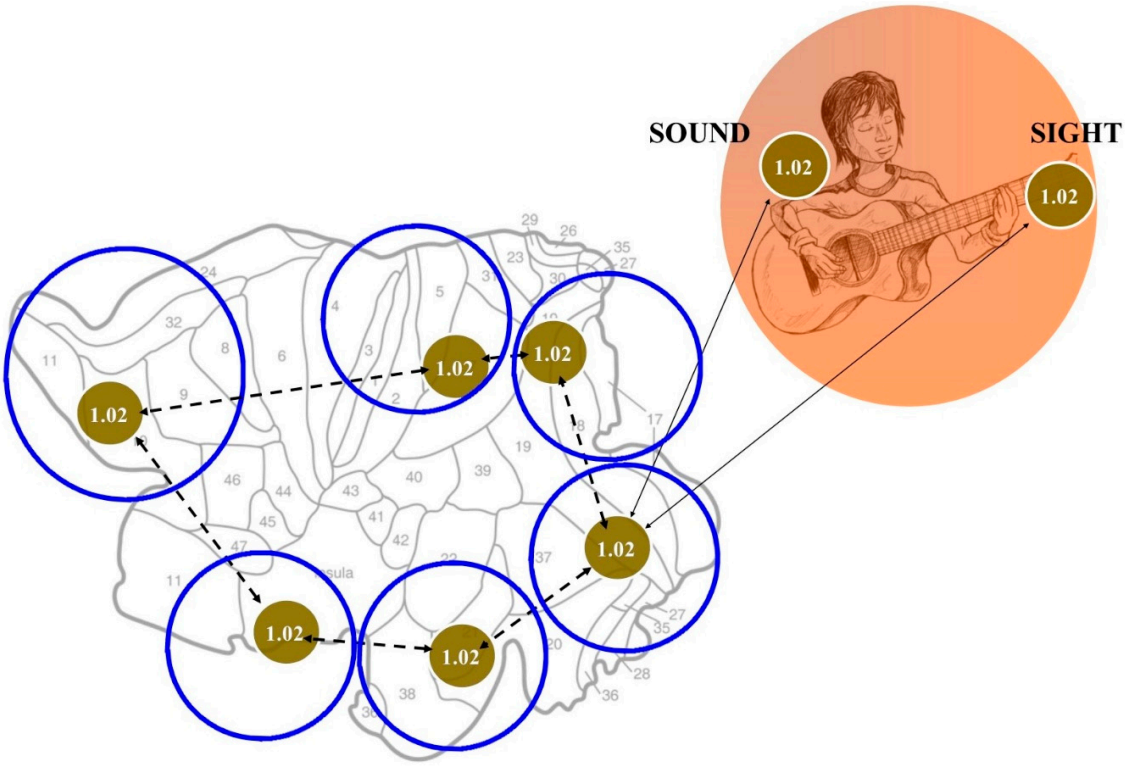

Figure 3. The use of BUT in the evaluation of brain computations during multisensory integration. The figure displays a hypothetical case for illustrative purposes. The red circles are equipped with a number standing for the corresponding entropy value (in this hypothetical case: 1.02). The right Figure displays the environment containing two cues with matching description, e.g., equipped with entropy values: 1.02. The same entropy value can be found in the corresponding multisensory neuronal assembly located in the brain sensory cortex (left figure). This means that there must be at least a cortical area (or micro-area) with the same entropy value of the two matching points encompassed in the environment. Because multisensory interactions occur at all temporal and spatial stages, their extensive cortical connections must have something in common: they must display the same values of entropy (in this case, 1.02). This allows us to recognize which zones of the brain are functionally correlated during multisensory integration.

3. An Answer for Current Issues

In this section, we will go through the issues of the nature of mental states and theory of knowledge, through the lens of topology. The BUT model takes into account the content-bearing properties of physical neural networks, by reducing representational states to construct of observables and by providing a mechanistic account of the neural processes which underlie the mental processes of knowledge. BUT integration works not just at the so-called low-level processes—such as perception, motor control and simple mnemonic processing—[57], but also at the high-levels—such as planning and reasoning—[58]. In the above-described recent model of multisensory integration, sensory modalities outline a broadly interconnected network with multiple forward, backward and lateral connections, rather than a hierarchical system of parallel sensory streams that converge at higher levels. The key difference between the traditional and the novel view is whether the hierarchy comprises distinct and parallel streams that converge at higher levels, or whether there are dense interactions between all sensory streams, even at lower levels [29]. The BUT approach supports a model that assume rich cross-modal interconnectedness at all processing levels, suggesting that functional interplay between the senses occurs at all anatomical levels and across a varied time course. For example, the connections between the two secondary cortex's visual pathways (the "where" and the "what" systems) provide evidence for a common and simultaneous neural substrate for action and perception.

The BUT allows us to establish the "metaphor" in a general cognitive theory. If a metaphor is a linguistic expression in which at least one part of the expression is transferred from one domain of application (source domain), where it is common, to another (target domain) in which it is unusual [59], there are striking formal analogies with the topological concept of antipodal points. We hypothesize that the metaphor is produced by the convergence on a multisensory neurons' assembly of both literal and figurative messages (corresponding to the antipodal points located in the environment). The heteromodal integration, aiming to gain insight through the metaphor that no literal paraphrase could ever capture, links together in a linguistic expression the domain of intuitive common-sense understanding of the "literal", and the domain of application of the "figurative". The peculiar nature of multisensory integration leads to a radical rethinking of mental representations. It takes into account the "cognitive" needs of theoretical representational states and provides a neuroanatomical frame to cognitive semantics. Can a single neuronal output contain more information than each of its countless inputs? The answer to this crucial question implies cognitive theoretical conclusions, concerned both with information and knowledge.

Multimodal neurons utilize the salient, meaningful information from different sensations and "melt" them into a novel message, which holds a "semantic" content. Consider the classical "leg of the table". The leg "appears to us at first a single, indivisible whole. One name designates the whole". But "the apparently indivisible thing is separated into parts" [60]: the world "leg" is not strictly a literal source domain, because it already contains the "merging" and integration of several features, such as the color, the shape, the temperature, the evoked feelings. In the framework of BUT, mental processes are not just cortical networks' computations operating on the "syntax" of representation (i.e., Boolean logic), but they also throw a bridge between the latter and the "semantic" notion of mental content. The countless inputs become thus able to solve not-computable functions and to "fabricate" a cognitive process. BUT mechanisms underlying multisensory integration let us hypothesize that our "naïve" thoughts are semantic [61], rather than syntactic, and that, during mental processes, the metaphor goes before the axiomatization and the formal syntax rules of the first-order predicate logic. Scientific data confirm heteromodal integration as "semantic" and show which cortical networks are most likely to mediate these effects, with the temporal area being more responsive to semantically congruent, and the frontal one to semantically incongruent audio-visual stimulation [62]. It has been suggested that multisensory facilitation is associated with posterior parietal activity as early as 100 ms after stimulus onset; as participants are required to classify heteromodal stimuli into semantic categories, multimodal processes extend in cingulate, temporal and prefrontal cortices 400 ms after stimulus onset [63].

The BUT model displays astonishing connections with Gärdenfors' [64] "cognitive semantics", which states that meanings are in the head, but are not independent of perception and bodily experience. Topology provides a conceptual bridge between "realistic" semantics (the meaning of an expression is something out there in the world) and "cognitive" semantics (meanings are expressions of mental entities independent of truth). Gardenfors states that semantic elements are based on spatial or topological rules [65,66], not on symbols: in touch also with BUT multisensory integration, cognitive models are primarily image-schemes transformed by metaphoric and metonymic operations [64]. Experimental data provide evidence for a complex inter-dependency between spatial location and temporal structure in determining the ultimate behavioral and perceptual outcome associated with paired multisensory stimuli [67]. This experience of time and two- or three-dimensional spatial configurations, together with the expressions pertaining to higher level of conceptual organization, can be easily explained by a topological mapping of the components onto the multisensory. The blending, a standpoint of cognitive semantics [68], refers to a "mental" space configuration in which elements of two input spaces are projected into a third space, the blend, which thus contains elements of both [69]. If we figure this space not as "mental" but as "biological", the blend turns out to be the BUT. Rather than just combining predicates, the semantic model/BUT structure blends behaviors from multiple (mental or anatomical) spaces and explains "apparently" emergent phenomena [70].

Inferring which signals have a hypothetical common underlying cause—and hence should be integrated—is a primary challenge for a perceptual system dealing with multiple sensory inputs. The brain is able to efficiently infer the causes underlying our sensory events. Experiments demonstrate that we use the similarity in the temporal structure of multisensory cue combinations, in order to infer from correlation the causal structure as well as the location of causes [71]. This capacity is not limited to the high-level cognition, rather it is performed recurrently and effortlessly in perception too [72]. In case of abnormal multisensory experience (visual-auditory spatial disparity), an atypical multisensory integration takes place (Stein 2009). We hypothesize that inferences form a sort of "niche construction", which shapes the common sense of a neural machinery operating in embodied/embedded interaction with the environment [73]. Our brain is also able of abstraction, i.e., to create its own representational endowment or potential, without recourse to external objects or states of affairs, such as causal antecedents or evolutionary history [74]. Truth conditions are not crucial for such a kind of representational content. How could multisensory neurons' outputs abstract both causal and not causal events, in order to introduce new multifaceted elements into the thinking process? Perhaps heteromodal neurons are able to re-evoke complex data also in absence of the original external stimulus, by comparing and integrating the countless novel semantic messages included in the single bi-dimensional point predicted by BUT, in order that the brain is able to "look without seeing, listen without hearing" (Leonardo da Vinci) [75]. The role of the highest cortical areas could be crucial in activating multisensory neurons of lower levels, also in absence of external stimuli. Data from literature suggest this possibility. Two important temporal epochs have been described in the visual, auditory and multimodal response to stimuli: an early phase, during which both weak/no-unisensory and defined multisensory responses occur, and a late period, after which the unisensory responses have ended and the multisensory one remains [76]. In sum, in view of the BUT principles, the higher brain activities may be explained by a sole factor: the presence of a multi-dimensional structure equipped with antipodal points. It astonishingly resembles Godel's suggestion of abstract terms more and more converging to the infinity in the sphere of our understanding.

4. What Does Topology Bring to the Table?

In conclusion, we provided a general topological mechanism which explains the elusive phenomenon of multisensory integration. The model is cast in a physical/biological fashion which has the potential of being operationalized and experimentally tested through fMRI studies. A shift in conceptualizations is evident in a theory of knowledge based on BUT multisensory integration: it is no longer the default position to assume that perception, cognition and motor control are unisensory

processes [77]. In agreement with Ernst Mach [60], objects are "combinations or complex of sensations". Our senses do not exist in isolation of each other and, in order to fully answer to epistemological queries, the processes in question must be studied in a multimodal context [29]. The question here is: What for? What does a topologic reformulation add in the evaluation of multimodal integration? The opportunity to treat elusive mental phenomena as topological structures takes us into the realm of algebraic topology, allowing us to describe brain function in the language of powerful analytical tools, such as combinatorics, hereditary set systems [32], homology theory and functional analysis. BUT and its extensions provide a methodological approach which makes it possible for us to study multisensory integration in terms of projections from real to abstract phase spaces. The importance of projections between environmental spaces, where objects lie, and brain phase spaces, where multimodal operations take place, is also suggested by Sengupta et al. [78], who provide a way of measuring distance on concave neural manifolds. Note that the BUT requires the function to be continuous, while the nervous activity is at most piecewise continuous. However, the projections dictated by BUT might occur just in the periods in which brain activity is piecewise continuous, e.g., during a single multisensory task, and then be broken when another different task occurs. A methodological approach has been proved useful in the evaluation of brain symmetries, in order to assess the relationships and affinities among BOLD activated areas [37] and among cortical histological images [79]. However, BUT and its variants are not just a *methodological* approach, but also display a *physical* meaning. Based on the antipodal cortical zones with co-occurring BOLD activation, it has been also recently suggested that brain trajectories might display donut-like trajectories [36].

The different animals' senses capture only bits and selected aspects of reality and display the world from limited points of view [80]. "The development of the human mind has practically extinguished all feelings, except a few sporadic kinds, sound, colors, smells, warmth, etc." [81]. However, a realistic fraction, albeit incomplete, reaches our brain from outside and gives rise, thanks to the BUT, to an isomorphism between sensations and perceptions. As stated above, the BUT perspective allows a symmetry property located in the real space (the environment) to be translated to an abstract space, and vice versa, enabling us to achieve a map from one dynamical system to another. "A truth is like a map, which does not copy the ground, but uses signs to tell us where to find the hill, the stream and the village" [82]. If symmetry transformations (antipodal points) can be evaluated, we are allowed to use the pure mathematical tools of topological group theory. Symmetry transformations therefore furnish us with a topologic family of models able to explain the data. In the study of multisensory integration, promising empiric advances are forthcoming: cutting edge methods have been recently proposed, from oscillatory phase coherence, to multi-voxel pattern analysis applied to multisensory research at different system levels, to the TMS-adaptation paradigm (for a review, see [29]). The last but not the least, two computational frameworks that account for multisensory integration have been recently established [83,84]. In the context of BUT, such advances might provide a considerable experimental support and a unifying computational account of multisensory neurons' features.

Conflicts of Interest: The authors declare no conflict of interest.

References

1. Krueger, J.; Royal, D.W.; Fister, M.C.; Wallace, M.T. Spatial receptive field organization of multisensory neurons and its impact on multisensory interactions. *Hear. Res.* **2009**, *258*, 47–54. [CrossRef] [PubMed]
2. Fetsch, C.R.; DeAngelis, G.C.; Angelaki, D.E. Visual-vestibular cue integration for heading perception: Applications of optimal cue integration theory. *Eur. J. Neurosci.* **2010**, *31*, 1721–1729. [CrossRef] [PubMed]
3. Werner, S.; Noppeney, U. Superadditive responses in superior temporal sulcus predict audiovisual benefits in object categorization. *Cereb. Cortex* **2009**, *20*, 1829–1842. [CrossRef] [PubMed]
4. Stein, B.E.; Rowland, B.A. Organization and plasticity in multisensory integration: Early and late experience affects its governing principles. *Prog. Brain Res.* **2011**, *191*, 145–163. [PubMed]

5. Royal, D.W.; Krueger, J.; Fister, M.C.; Wallace, M.T. Adult plasticity of spatiotemporal receptive fields of multisensory superior colliculus neurons following early visual deprivation. *Restor. Neurol Neurosci.* **2010**, *28*, 259–270. [PubMed]
6. Burnett, L.R.; Stein, B.E.; Perrault, T.J., Jr.; Wallace, M.T. Excitotoxic lesions of the superior colliculus preferentially impact multisensory neurons and multisensory integration. *Exp. Brain Res.* **2007**, *179*, 325–338. [CrossRef] [PubMed]
7. Stein, B.E.; Perrault, T.Y., Jr.; Stanford, T.R.; Rowland, B.A. Postnatal experiences influence how the brain integrates information from different senses. *Front. Integr. Neurosci.* **2009**, *3*. [CrossRef] [PubMed]
8. Stein, B.E.; Stanford, T.R.; Rowland, B.A. Development of multisensory integration from the perspective of the individual neuron. *Nat. Rev. Neurosci.* **2014**, *15*, 520–535. [CrossRef] [PubMed]
9. Johnson, S.P.; Amso, D.; Slemmer, J.A. Development of object concepts in infancy: Evidence for early learning in an eye-tracking paradigm. *Proc. Natl. Acad. Sci. USA* **2003**, *100*, 10568–10573. [CrossRef] [PubMed]
10. Xu, J.; Yu, L.; Rowland, B.A.; Stanford, T.R.; Stein, B.E. Incorporating cross-modal statistics in the development and maintenance of multisensory integration. *J. Neurosci.* **2012**, *15*, 2287–2298. [CrossRef] [PubMed]
11. Porcu, E.; Keitel, C.; Müller, M.M. Visual, auditory and tactile stimuli compete for early sensory processing capacities within but not between senses. *Neuroimage* **2014**, *97*, 224–235. [CrossRef] [PubMed]
12. Yu, L.; Rowland, B.A.; Stein, B.E. Initiating the development of multisensory integration by manipulating sensory experience. *J. Neurosci.* **2010**, *7*, 4904–4913. [CrossRef] [PubMed]
13. Borsuk, K. Drei Sätze über die n-dimensionale euklidische Sphäre. *Fundam. Math.* **1933**, *20*, 177–190. (In German)
14. Nieuwenhuys, R.; Voogd, J.; van Huijzen, C. *The Human Central Nervous System*; Springer: Heidelberg, Germany, 2008.
15. Pollmann, S.; Zinke, W.; Baumgartner, F.; Geringswald, F.; Hanke, M. The right temporo-parietal junction contributes to visual feature binding. *Neuroimage* **2014**, *101*, 289–297. [CrossRef] [PubMed]
16. Van den Heuvel, M.P.; Sporns, O. Rich-club organization of the human connectome. *J. Neurosci.* **2011**, *31*, 15775–15786. [CrossRef] [PubMed]
17. Allman, B.L.; Keniston, L.P.; Meredith, M.A. Not just for bimodal neurons anymore: The contribution of unimodal neurons to cortical multisensory processing. *Brain Topogr.* **2009**, *21*, 157–167. [CrossRef] [PubMed]
18. Hackett, T.A.; Schroeder, C.E. Multisensory integration in auditory and auditory-related areas of Cortex. *Hear. Res.* **2009**, *258*, 72–79. [CrossRef] [PubMed]
19. Shinder, M.E.; Newlands, S.D. Sensory convergence in the parieto-insular vestibular cortex. *J. Neurophysiol.* **2014**, *111*, 2445–2464. [CrossRef] [PubMed]
20. Reig, R.; Silberberg, G. Multisensory integration in the mouse striatum. *Neuron* **2014**, *83*, 1200–1212. [CrossRef] [PubMed]
21. Kuang, S.; Zhang, T. Smelling directions: Olfaction modulates ambiguous visual motion perception. *Sci. Rep.* **2014**, *23*. [CrossRef] [PubMed]
22. Kim, S.S.; Gomez-Ramirez, M.; Thakur, P.H.; Hsiao, S.S. Multimodal Interactions between Proprioceptive and Cutaneous Signals in Primary Somatosensory Cortex. *Neuron* **2015**, *86*, 555–566. [CrossRef] [PubMed]
23. Murray, M.M.; Thelen, A.; Thut, G.; Romei, V.; Martuzzi, R.; Matusz, P.J. The multisensory function of the human primary visual cortex. *Neuropsychologia* **2015**. [CrossRef] [PubMed]
24. Nys, J.; Smolders, K.; Laramée, M.E.; Hofman, I.; Hu, T.T.; Arckens, L. Regional Specificity of GABAergic Regulation of Cross-Modal Plasticity in Mouse Visual Cortex after Unilateral Enucleation. *J. Neurosci.* **2015**, *35*, 11174–11189. [CrossRef] [PubMed]
25. Bedny, M.; Richardson, H.; Saxe, R. "Visual" Cortex Responds to Spoken Language in Blind Children. *J. Neurosci.* **2015**, *35*, 11674–11681. [CrossRef] [PubMed]
26. Yan, K.S.; Dando, R. A crossmodal role for audition in taste perception. *J. Exp. Psychol. Hum. Percept. Perform.* **2015**, *41*, 590–596. [CrossRef] [PubMed]
27. Escanilla, O.D.; Victor, J.D.; di Lorenzo, P.M. Odor-taste convergence in the nucleus of the solitary tract of the awake freely licking rat. *J. Neurosci.* **2015**, *35*, 6284–6297. [CrossRef] [PubMed]
28. Maier, J.X.; Blankenship, M.L.; Li, J.X.; Katz, D.B. A Multisensory Network for Olfactory Processing. *Curr. Biol.* **2015**, *25*, 2642–2650. [CrossRef] [PubMed]
29. Klemen, J.; Chambers, C.D. Current perspectives and methods in studying neural mechanisms of multisensory interactions. *Neurosci. Biobehav. Rev.* **2012**, *36*, 111–133. [CrossRef] [PubMed]

30. Bastos, A.M.; Litvak, V.; Moran, R.; Bosman, C.A.; Fries, P.; Friston, K.J. A DCM study of spectral asymmetries in feedforward and feedback connections between visual areas V1 and V4 in the monkey. *Neuroimage* **2015**, *108*, 460–475. [CrossRef] [PubMed]
31. Dodson, C.T.J.; Parker, P.E. *A User's Guide to Algebraic Topology*; Kluwer: Dordrecht, The Netherlands, 1997.
32. Matoušek, J. *Using the Borsuk-Ulam Theorem*; Lectures on Topological Methods in Combinatorics and Geometry; Springer: Berlin/Heidelberg, Germany, 2003.
33. Weisstein, E.W. Antipodal Points. Available online: http://mathworld.wolfram.com/AntipodalPoints.html (accessed on 15 November 2016).
34. Borsuk, M.; Gmurczyk, A. On Homotopy Types of 2-Dimensional Polyhedral. *Fundam. Math.* **1980**, *109*, 123–142.
35. Moura, E.; Henderson, D.G. *Experiencing Geometry: On Plane and Sphere*; Prentice Hall: Englewood Cliffs, NJ, USA, 1996.
36. Tozzi, A.; Peters, J.F. Towards a Fourth Spatial Dimension of Brain Activity. *Cogn. Neurodyn.* **2016**, *10*, 189–199. [CrossRef] [PubMed]
37. Tozzi, A.; Peters, J.F. A Topological Approach Unveils System Invariances and Broken Symmetries in the Brain. *J. Neurosci. Res.* **2016**, *94*, 351–365. [CrossRef] [PubMed]
38. Marsaglia, G. Choosing a Point from the Surface of a Sphere. *Ann. Math. Stat.* **1972**, *43*, 645–646. [CrossRef]
39. Van Essen, D.C. A Population-Average, Landmark—And Surface-based (PALS) atlas of human cerebral cortex. *Neuroimage* **2005**, *28*, 635–666. [CrossRef] [PubMed]
40. Krantz, S.G. *A Guide to Topology*; The Mathematical Association of America: Washington, DC, USA, 2009; p. 107.
41. Manetti, M. *Topology*; Springer: Heidelberg, Germany, 2015.
42. Cohen, M.M. *A Course in Simple Homotopy Theory*; Springer: New York, NY, USA, 1973; p. MR0362320.
43. Borsuk, K. Concerning the classification of topological spaces from the standpoint of the theory of retracts. *Fundam. Math.* **1959**, *46*, 321–330.
44. Borsuk, K. Fundamental Retracts and Extensions of Fundamental Sequences. *Fundam. Math.* **1969**, *64*, 55–85.
45. Collins, G.P. The Shapes of Space. *Sci. Am.* **2004**, *291*, 94–103. [CrossRef] [PubMed]
46. Weeks, J.R. *The Shape of Space*, 2nd ed.; Marcel Dekker, Inc.: New York, NY, USA, 2002.
47. Peters, J.F. *Topology of Digital Images. Visual Pattern Discovery in Proximity Spaces, Intelligent Systems Reference Library*; Springer: Berlin, Germany, 2014; Volume 63, pp. 1–342.
48. Peters, J.F. *Computational Proximity. Excursions in the Topology of Digital Images, Intelligent Systems Reference Library*; Springer: Berlin, Germany, 2016; pp. 1–468.
49. Willard, S. *General Topology*; Dover Pub., Inc.: Mineola, NY, USA, 1970.
50. Peters, J.F.; Tozzi, A. Region-Based Borsuk-Ulam Theorem. *arXiv* **2016**, arXiv:1605.02987.
51. Perrault, T.J., Jr.; Stein, B.E.; Rowland, B.A. Non-stationarity in multisensory neurons in the superior colliculus. *Front. Psychol.* **2011**, *2*, 144. [CrossRef] [PubMed]
52. Benson, K.; Raynor, H.A. Occurrence of habituation during repeated food exposure via the olfactory and gustatory systems. *Eat Behav.* **2014**, *15*, 331–333. [CrossRef] [PubMed]
53. Schneidman, E.; Berry, M.J.; Segev, R.; Bialek, W. Weak pairwise correlations imply strongly correlated network states in a neural population. *Nature* **2006**, *440*, 1007–1012. [CrossRef] [PubMed]
54. Watanabe, T.; Kan, S.; Koike, T.; Misaki, M.; Konishi, S.; Miyauchi, S.; Masuda, N. Network-dependent modulation of brain activity during sleep. *NeuroImage* **2014**, *98*, 1–10. [CrossRef] [PubMed]
55. Wang, Z.; Li, Y.; Childress, A.R.; Detre, J.A. Brain entropy mapping using fMRI. *PLoS ONE* **2014**, *9*, 1–8. [CrossRef] [PubMed]
56. Kida, T.; Tanaka, E.; Kakigi, R. Multi-Dimensional Dynamics of Human Electromagnetic Brain Activity. *Front. Hum. Neurosci.* **2016**, *9*, 713. [CrossRef] [PubMed]
57. Sutter, C.; Drewing, K.; Müsseler, J. Multisensory integration in action control. *Front. Psychol.* **2014**. [CrossRef] [PubMed]
58. Drugowitsch, J.; de Angelis, G.C.; Klier, E.M.; Angelaki, D.E.; Pouget, A. Optimal multisensory decision-making in a reaction-time task. *Elife* **2014**. [CrossRef] [PubMed]
59. Jones, D.M.B. Models, Metaphors and Analogies. In *The Blackwell Guide to the Philosophy of Science*; Machamer, P., Silberstein, M., Eds.; Blackwell: Oxford, UK, 2002.
60. Mach, E. *Analysis of the Sensations*; The Open Court Publishing Company: Chicago, IL, USA, 1896.

61. Van Ackeren, M.J.; Schneider, T.R.; Müsch, K.; Rueschemeyer, S.A. Oscillatory neuronal activity reflects lexical-semantic feature integration within and across sensory modalities in distributed cortical networks. *J. Neurosci.* **2014**, *34*, 14318–14323. [CrossRef] [PubMed]
62. Doehrmann, O.; Naumer, M.J. Semantics and the multisensory brain: How meaning modulates processes of audio-visual integration. *Brain Res.* **2008**, *25*, 136–150. [CrossRef] [PubMed]
63. Diaconescu, A.O.; Alain, C.; McIntosh, A.R. The co-occurrence of multisensory facilitation and cross-modal conflict in the human brain. *J. Neurophysiol.* **2011**, *106*, 2896–2909. [CrossRef] [PubMed]
64. Gärdenfors, P. Six Tenets of Cognitive Semantics. 2011. Available online: http://www.ling.gu.se/~biljana/st1-97/tenetsem.html (accessed on 11 December 2016).
65. Gärdenfors, P. *Conceptual Spaces: The Geometry of Thought*; The MIT Press: Cambridge, UK, 2000.
66. Kuhn, W. *Why Information Science Needs Cognitive Semantics—And What It Has to Offer in Return*; DRAFT Version 1.0; Meaning and Computation Laboratory, Department of Computer Science and Engineering, University of California at San Diego: La Jolla, CA, USA, 31 March 2003.
67. Stevenson, R.A.; Fister, J.K.; Barnett, Z.P.; Nidiffer, A.R.; Wallace, M.T. Interactions between the spatial and temporal stimulus factors that influence multisensory integration in human performance. *Exp. Brain Res.* **2012**, *219*, 121–137. [CrossRef] [PubMed]
68. Langacker, R.W. *Cognitive Grammar—A Basic Introduction*; Oxford University Press: New York, NY, USA, 2008.
69. Fauconnier, G. *Mappings in Thought and Language*; Cambridge University Press: Cambridge, UK, 1997.
70. Kim, J. Making Sense of Emergence. *Philos. Stud.* **1999**, *95*, 3–36. [CrossRef]
71. Parise, C.V.; Spence, C.; Ernst, M.O. When correlation implies causation in multisensory integration. *Curr. Biol.* **2012**, *22*, 46–49. [CrossRef] [PubMed]
72. Körding, K.P.; Beierholm, U.; Ma, W.J.; Quartz, S.; Tenenbaum, J.B.; Shams, L. Causal inference in multisensory perception. *PLoS ONE* **2007**, *26*, e943. [CrossRef] [PubMed]
73. Friston, K. The free-energy principle: A unified brain theory? *Nat. Rev. Neurosci.* **2010**, *11*, 127–138. [CrossRef] [PubMed]
74. Grush, R. Cognitive Science. In *The Blackwell Guide to the Philosophy of Science*; Machamer, P., Silberstein, M., Eds.; Blackwell: Oxford, UK, 2002.
75. McLean, J.; Freed, M.A.; Segev, R.; Freed, M.A.; Berry, M.J.; Balasubramanian, V.; Sterling, P. How much the eye tells the brain. *Curr. Biol.* **2006**, *25*, 1428–1434.
76. Royal, D.W.; Carriere, B.N.; Wallace, M.T. Spatiotemporal architecture of cortical receptive fields and its impact on multisensory interactions. *Exp. Brain Res.* **2009**, *198*, 127–136. [CrossRef] [PubMed]
77. Méndez, J.C.; Pérez, O.; Prado, L.; Merchant, H. Linking perception, cognition, and action: Psychophysical observations and neural network modelling. *PLoS ONE* **2014**, *9*, e102553. [CrossRef] [PubMed]
78. Sengupta, B.; Tozzi, A.; Cooray, G.K.; Douglas, P.K.; Friston, K.J. Towards a Neuronal Gauge Theory. *PLoS Biol.* **2016**, *14*, e1002400. [CrossRef] [PubMed]
79. Peters, J.F.; Tozzi, A.; Ramanna, S. Brain tissue tessellation shows absence of canonical microcircuits. *Neurosci. Lett.* **2016**, in press. [CrossRef] [PubMed]
80. Holldobler, B.; Wilson, E.O. *Formiche—Storia di Un'Esplorazione Scientifica*; Adelphi: Milano, Italy, 2002.
81. Peirce, C.S. *Philosophical Writings of Peirce*; Buchler, J., Ed.; Courier Dover Publications: New York, NY, USA, 2011; p. 344.
82. Goodman, R.B. *Pragmatism: Critical Concepts in Philosophy*; Taylor & Francis: New York, NY, USA, 2005; Volume 2, p. 345.
83. Magosso, E.; Cuppini, C.; Serino, A.; di Pellegrino, G.; Ursino, M. A theoretical study of multisensory integration in the superior colliculus by a neural network model. *Neural Netw.* **2008**, *21*, 817–829. [CrossRef] [PubMed]
84. Ohshiro, T.; Angelaki, D.E.; DeAngelis, G.C. A normalization model of multisensory integration. *Nat. Neurosci.* **2011**, *14*, 775–782. [CrossRef] [PubMed]

© 2016 by the authors; licensee MDPI, Basel, Switzerland. This article is an open access article distributed under the terms and conditions of the Creative Commons Attribution (CC-BY) license (http://creativecommons.org/licenses/by/4.0/).

LFNN #1283618, VOL 0, ISS 0

Fullerenic-topological tools for honeycomb nanomechanics. Toward a fullerenic approach to brain functions

Arturo Tozzi, James F. Peters, and Ottorino Ori

QUERY SHEET

This page lists questions we have about your paper. The numbers displayed at left can be found in the text of the paper for reference. In addition, please review your paper as a whole for correctness.

Q1. Au: Please provide publisher name and location for Ref. 5.
Q2. Au: Please provide publisher name and location for Ref. 6.

TABLE OF CONTENTS LISTING

The table of contents for the journal will list your paper exactly as it appears below:

Fullerenic-topological tools for honeycomb nanomechanics. Toward a fullerenic approach to brain functions
Arturo Tozzi, James F. Peters, and Ottorino Ori

FULLERENES, NANOTUBES AND CARBON NANOSTRUCTURES
2017, VOL. 0, NO. 0, 1–7
http://dx.doi.org/10.1080/1536383X.2017.1283618

Taylor & Francis
Taylor & Francis Group

Fullerenic-topological tools for honeycomb nanomechanics. Toward a fullerenic approach to brain functions

Q1 Arturo Tozzi[a], James F. Peters[b], and Ottorino Ori[c]

[a]Center for Nonlinear Science, University of North Texas, 1155 Union Circle, #311427, Denton, TX, USA; [b]Department of Electrical and Computer Engineering, University of Manitoba, 75A Chancellor's Circle, Winnipeg, Canada; [c]Actinium Chemical Research, Via Casilina 1626/A, Rome, Italy

ABSTRACT
Fullerenic structures equipped with Stone-Wales transformations have been successfully utilized in the study of macromolecular assemblies. Here we show that this approach could be useful in the assessment of issues from a far-flung research area, i.e., neuroscience. Indeed, the basic morphological and functional unit of the brain, called the human microcolumn, is a tubular structure that can be flattened in the guise of a fullerene-like two-dimensional lattice. We describe this procedure in order to build a fullerene-like microcolumn, in which neuronal firing and electric signal propagation are assessed in terms of topological neural network modifications, instead of the canonical logic circuits. Every node stands for a neuron, where neural computations take place. This means that nervous activity, other than logic circuits, could instead depend on topological transformations and symmetry constraints dictated by Stone-Wales transformations occurring in the upper cortical layers. A two-dimensional fullerene-like lattice not only simulates the real microcolumn's microcircuitry, but also makes it possible us to build artificial networks equipped with robustness, plasticity and fastness. In this note, electric signal propagation is investigated in terms of pure topological modifications of the neural honeycomb network.

KEYWORDS
Brain topology; Fullerene-like lattice; Stone-Wales transformations; Topological efficiency, Simplicial complex

1. Introduction

Although fullerenes' primary application focuses on the assessment of carbon-networks in nanostructures, they also provide a mathematical framework that can be used in order to rank topological invariants in the portrayal of microcolumns, i.e., the stereotyped, column-like architecture representing the basic embryological/anatomical arrangement of the brain (1,2). Because architectonic relations among minicolumnar pyramidal cells are conserved under spatiotemporal changes (3), it is feasible to assess the tubular structure of the brain in terms of a 3D cylinder with the typical regular polygonal tiling of the fullerene. If we flatten the microcolumnar cylindrical structure to obtain of two-dimensional sheets, we achieve a lattice where generalized Stone-Wales transformations (or SW rotations) might occur (4,5). Therefore, it is possible to achieve a fullerene-like brain microstructure in which activity is dictated by transformations involving fullerene-like polygons. In a fullerene-like microcolumn, neuronal firing is assessed in terms of untangled topological neural network transformations. This structure can be compared to a barcode, or a biological matrix, in which every sequence of neuronal activation stands for a mental activity. We may also think of the bronze cup-shaped bells of a carillon, in which every sequence of diverse punchers gives rise to different melodies. In sum, we achieve a fullerene-like brain whose activity is dictated by topological transformations involving hexagons, pentagons, and other polygons. Such an approach not only allows us to build a model that faithfully simulates the biological brain activity, but also to assess neural computations in terms of topological relationships and transformations among spiking neurons, instead of series or parallel logic circuits. We also discuss the advantages of such an approach in terms of network fastness, robustness and plasticity.

Neuronal firing and electric signal propagation can be investigated in terms of SW topological modifications of the neural network. This assumption leads to a characterization of neurons as graph vertices and connections among neurons as bonds. Because such transformations are fully reversible, they provide a biological topological mechanism for neural signal annihilation or suppression. Concerning the mathematical apparatus related to symmetries and transformations on nanostructures, see the recent research article (6). Microcolumnar circuitry can be described in terms of fullerene-like 2D lattices with correlations between cell topology and computational models to describe circuitry functionalities (7). We are in fact allowed to build a biologically-plausible, fullerene-like lattice describing a microcolumn, equipped with hexagonal or pentagonal tiling. There are clues from the neuroscientific literature that suggests the feasibility of our hypothesis. Minicolumns are characterized by modular connectivity with invariant properties that resemble fullerene structures. Indeed, minicolumns display a translational symmetry across their central axis and rotational symmetry, i.e., displacement in different planes of each section. Furthermore, microcolumns are equipped with

Q1 **CONTACT** Ottorino Ori ottorino.ori@alice.it Actinium Chemical Research, Via Casilina 1626/A, 00133 Rome, Italy.
Color versions of one or more of the figures in the article can be found online at www.tandfonline.com/lfnn.
© 2017 Taylor & Francis Group, LLC

both transitive symmetry involving geometric scaling of morphometric relations in different cortical areas, and temporal symmetry involving morphometric relations during cortical maturation (29). Because architectonic relations among minicolumnar elements (pyramidal cells) are conserved under spatial and temporal variations (30), it is possible to assess the tubular structure of a microcolumn in terms of a 3D cylinder with the typical regular structure of the fullerene, e.g., a mesh of variously fused exagons and pentagons. Furthermore, it has been demonstrated that the microcortical assembly of pyramidal neurons exhibits the required fullerene-like stereotyped architecture. Indeed, neurons arranged in a parallel microcolumns' hexagonal lattice have been already described in literature (31). The hexagonal lattice is a reasonable assumption for microcolumns arrangement, based on studies of dendritic bundles and myelinated axons packing. Hexagonal spacing has been detected among bundles in the visual cortex' area 17 of rats (33), monkeys (34), and human medial prefrontal cortex (32)

In this graphical representation of the brain, nodes stand for microcortical pyramidal neurons linked by edges, e.g., neural dendritic connections. In cortical microcolumns, instead of SW flips on a fullerene surface, we need to evaluate the changes in firing activation of the neurons embedded in the nodes. In this case, SW permutations stand for a set of simple pyramidal neurons which fire simultaneously (Fig. 1). Therefore, it is possible to achieve a 2D fullerene-like lattice reproducing microcolumn's microcircuitry. We assume that the simultaneous firing of different neurons and specific activation sequences might give rise to *different topological isomeric conformations*, each one corresponding to a mental activity (perception, emotion, mind-wandering, calculation, and so on). The main difference from classical neural networks is that the brain functional activity is not based on logic nodes as it occurs in conventional networks, but on topological transformations, e.g., functional changes in the connectivity of firing neurons on a barcodelike structure. This model explains *countless* mental operations starting just from a relatively simple, stereotyped, highly preserved biological structure, such as the microcolumn. The extremely large number of SW rotations that may take place on the neural lattice permit an almost limitless set of moves, merely dictated by applying SW rotations on its bonds. In the same way as the tuning of the nanoparticle/substrate interaction provides unique ways of controlling the nanotube synthesis (8), fullerene-like, microcolumnar neural networks provide the fine-grain functional barcode's modularity required by different brain functions. This means that modifications in reciprocal connectivity among adjacent microcolumns allow a larger repertoire of barcode configurations and, therefore, of mental operations. In mental terms, a fullerene-like microcolumnar structure is associated with minimal wiring costs and fast synchronization/information transfer (9).

Topological and graph theoretical properties of fullerenes can be applied to the assessment of neural networks, in order to achieve a double task: improving our understanding of biological brain function in situ, and building more powerful artificial machines able to simulate cortical activities. This theoretical framework, cast in a biologically informed fashion (10–12), has the potential to be operationalized and assessed empirically. Indeed, the presence of a microcolumnar barcode

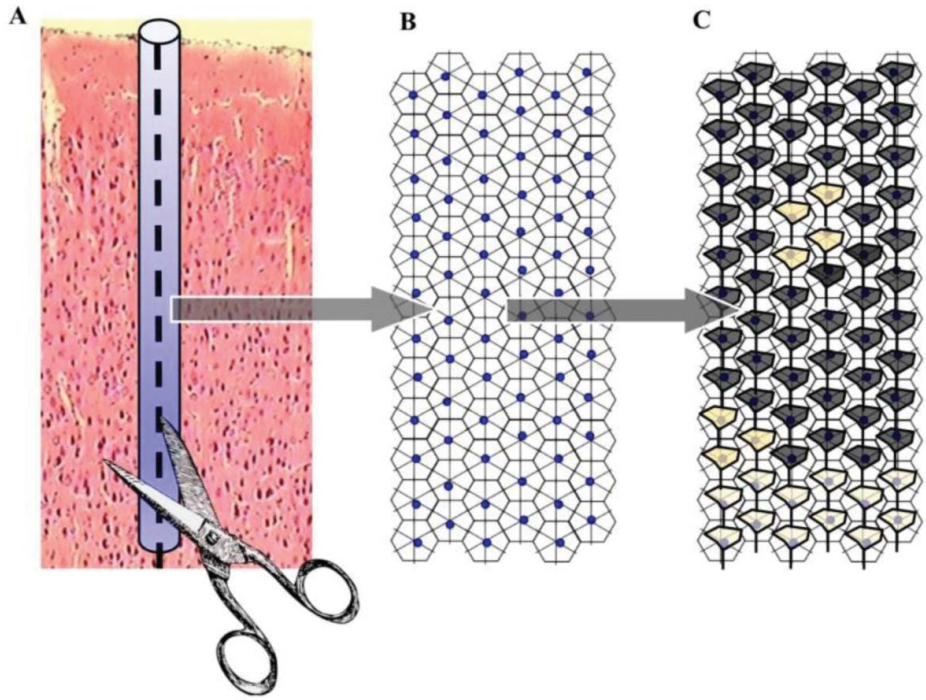

Figure 1. A fullerene-like cortical microcolumn. (A) The anatomical/functional basic structure of the brain, i.e., the tiny cortical microcolumn, is shaped in guise of a three-dimensional tubular armchair. If we cut the column through an edge, we achieve a flattened two-dimensional fullerene-like grid with exagonal tiling (B). In the hypothetical case of (B), provided just as an example, the molecular graph stands for a 2D zig-zag lattice, e.g., a flat, open visualization, made of 72 nodes with 6-bonds each. Panel (C) displays a set of possible topological transformations that might take place on this flattened microcolumn. Every node is filled with a pyramidal neuron which can be activated (yellow shapes) or deactivated (black shapes). Every set of activated/deactivated neurons gives rise to a different microcolumnar code, each one standing for a single mental activity among the countless possible.

predicted by a fullerene-like brain will be easily testable, once more powerful high density neurotechniques will be available, capable of capturing the simultaneous activity of large populations of microcolumnar pyramidal neurons. Graph theory tools have been proven to work quite effectively in simulating neuronal networks and relevant studies have been recently devoted to overcome what is considered to be a "critical simplifying assumption", i.e., that the basic unit in brain structure consists in just two nodes (a *dyad* of neurons or brain regions) connected by a graph edge. Generalized forms of graphs (*simplicial complexes*) based on algebraic topology recently appeared in literature (13) to model neural data and neural functions without the *dyadic limit*, aiming in such a way to "eclipse graph theory" in the near future of neural sciences. These sophisticated (somehow arbitrarily applicable) mathematical methods may be, in the opinion of the present authors, better applied by computing opportune nonlocal *topological invariants* (or *topological potentials*) that show the clear merits of carrying-on the influence of the structure of the whole neural network, keeping at the same time, uniquely defined computational rules. The present topological picture enlarges the horizon of recently reported methods that have been applied to simulate mechanical properties of zigzag honeycombs (see, e.g., (14)). In sum, original relationships between *neural signals and topological defects* are proposed in the following sections together with a specific theoretical framework that is able to describe the nanomechanics of 3-connected neural networks regardless of their structural regularities.

2. Topological method

In this section, we describe the procedure in order to build a fullerene-like microcolumn, in which neuronal firing and electric signal propagation are assessed in terms of pure topological neural network modifications, instead of the canonical ON/OFF logic circuits. At first, we illustrate how to shape a fullerene-like lattice through graph theoretical methods. Then, we evaluate the (*fully reversible*) topological moves taking place on such a lattice. Finally, we assess the neural biological counterparts of fullerenic structures, assessing microcolumns and neural spikings in terms of movements on proper 2D graphs. Furthermore, we provide, in the last section, a couple of simulations in order to test the feasibility of our fullerene-like microcolumnar framework.

Fullerene networks come into play. Fullerenes are 3-connected cubic planar graphs consisting of pentagons and hexagons; see the excellent recent update (15). Geometrically, a C_n fullerene is a closed trivalent polyhedral network in which n atoms are arranged in 12 pentagonal and $\left(\frac{1}{2}n-10\right)$ hexagonal rings (16–18). A regular 2D fullerene results therefore in a 3-regular (cubic) planar graph G_n generally describable as a mesh of exactly 12 variously fused pentagons, surrounded by distorted graphenic fragments. Signal propagation can be investigated via graph theoretical methods in this kind of cubic meshes. The basic assumption is that the evolution of microcircuits is ruled by the minimization of specific *topological invariants* (or *topological potential*) Ξ. Among the countless possible choices (19), we focus here on *distance-based* topological invariants capable of describing *long-range effects* involving *all pairs* of graph nodes.

The honeycomb microcircuit is described as a graph G_n with n nodes in which the d_{ij} integers stands for the number of graph edges connecting the two nodes i and j along the shortest path. In case of the distance $d_{ij}=k$, node j belongs to the k-th coordination shell of node i, and vice versa. By definition, $d_{ij}=d_{ji}$ and $d_{ii}=0$ for all nodes i,j. If we term $M=\max\{d_{ji}\}$ the length of the longest chemical distance in the graph—the integer M stands then for the graph *diameter*— and b_{ik} the number of k-neighbors of i, the effects of the long-range connectivity on a single node is summarized by the topological invariant w_i in (1).

$$w_i = \tfrac{1}{2}\sum_k k b_{ik} \quad k = 1,\ 2, \ldots, M-1,\ M, \tag{1}$$

where $n=\Sigma_k b_{ik}+1$ and $b_{i1}=6$ for any 6-fold node i. The symbols $\underline{w}$ and $\overline{w}$ indicate the smallest and the largest w_i values. Nodes with $w_i=\underline{w}$ (or $w_i=\overline{w}$) are the *minimal nodes* (or, conversely, the *maximal nodes*) in G_n. Integers $\{b_{ik}\}$ identify the Wiener-weights (WW) of node i. The Wiener index W, i.e., the first topological index applied in chemistry more than 60 years ago (19), derives from the half-summation of all d_{ij} entries given in (2).

$$W(n) = \tfrac{1}{2}\sum_{ij} d_{ij} = \sum_i w_i \quad i,j = 1,\ 2, \ldots,\ n-1,\ n. \tag{2}$$

The first topological modeling rule is the following: higher reactivity is assigned to a node with maximal w_i. Invariant W, providing the topological measure of the overall compactness of the system, is a good candidate for the topological potential $\Xi^W = W(G_n)$. This approach is grounded on relevant heuristic evidences, such as the fact that, among the 1812 nonisomorphic C_{60} fullerene isomers, just the physically stable isomer with icosahedral symmetry C_{60}-I_h and isolated pentagons corresponds to the cage with the minimum value $W=8340$ and it works well in marking stable isomers of C_{28}, C_{66} fullerenes (20, 21). The descriptor in (3)

$$\rho = W/n\underline{w} \tag{3}$$

measures instead the overall ability of the graph to evolve as a compact topological structure around its minimal nodes, which represent the most efficient nodes in G_n. For this reason ρ is called a *topological efficiency* index (20) and has been successfully tested to rank the *topological sphericity* of C_{50} fullerene graphs (22). From formula (3), an important inequality is derived, namely, the result in (4)

$$\rho \geq 1 \tag{4}$$

Many important chemical structures have $\rho=1$. Infinite cubic lattices or infinite graphene layers, together with icosahedral C_{60} molecules, are examples of perfectly spherical (topologically speaking) structures. And we formulate the second topological modeling rule: *the higher stability is assigned to structures with maximal sphericity*, e.g., minimal ρ. The two above mentioned modeling rules hold when similar topological

structures are compared. Lattice descriptor ρ represents in this approach the second form of topological potential $\Xi^{\rho} = \rho\,(G_n)$; both potentials Ξ^{W} and Ξ^{ρ} measure the collective effects exerted by G_n nodes on the nanomechanics of honeycomb mesh, including signal propagations effects.

3. Results and discussions

Preliminary simulations show how, starting from a fullerenic structure, it is possible to reversibly generate many alternative isomers (usually with a lower structural symmetry) by twisting two hexagons around a central bond (Fig. 2). The mechanism of signal generation is based on the preliminary activation of a pair of neurons both in the normal 6-fold status, followed by the creation of the *signal*, e.g., a *topological defect* of the pristine hexagonal mesh, that is represented by the 5|7 double pair (Fig. 2: step 0 and step 1, respectively). The 5|7 double pair (sometimes termed 5/7/7/5) is called the *SW defect* or *dislocation dipole*. Signal generation is achieved through the $SW_{6|6}$ rotation. The latter modifies the local connections of four neurons by rotating the bond between the two activated elements. After that change of local connections, nodes with 5- and 7-bonds appear in the network, making the topological structure of the system "naturally" ready for signal propagation that is easily obtained by applying a $SW_{6|7}$ rotation to the connection between the newly created 7-fold neuron and the activated one (Fig. 2, step 2), preserving the original 6-connectivity. As a result of the $SW_{6|7}$ action, the distance between the two 5|7 defects is increased by the insertion of one pair of hexagons, so that the signal has travelled for one step $\eta = 1$ in the honeycomb mesh. The two neurons that are brought back to the initial 6-fold condition (Fig. e 2, step 3) stand for the inactive status and their role will be briefly commented at the end of this section. Successive applications of $SW_{6|7}$ operators will split more and more of the two 5|7 pairs, allowing the signal to travel in the neural network with the typical wave mechanism of the SWw topological defect (23). Figure 2, step 4 shows the dislocation dipole with length $\eta = 2$; subsequent $SW_{6|7}$ rotations will further expand the dislocation dipole, allowing the topological signal to cover arbitrary distances η. According to the proposed approach, the large family of SW rearrangements introduced above, such as $SW_{6|6}$, $SW_{6|7}$ and so on, provide us with the basic tools in order to build a topological model able to describe the signal propagations in the neuron mesh. In summary, the topological mechanism describing the propagations of neural signals is based on the following graphical steps:

- The signal is considered to be a topological defect of the neural network. The "topological" benefits are straightforward: the signal does not change the number of neurons, be[illegible] easily annihilated by the reverse topological transformation able to restore the original status of the neural network. In principle, this fact also allows long duration of the network itself.
- The specific type of topological alteration proposed here as proper candidate for representing neural signal is the

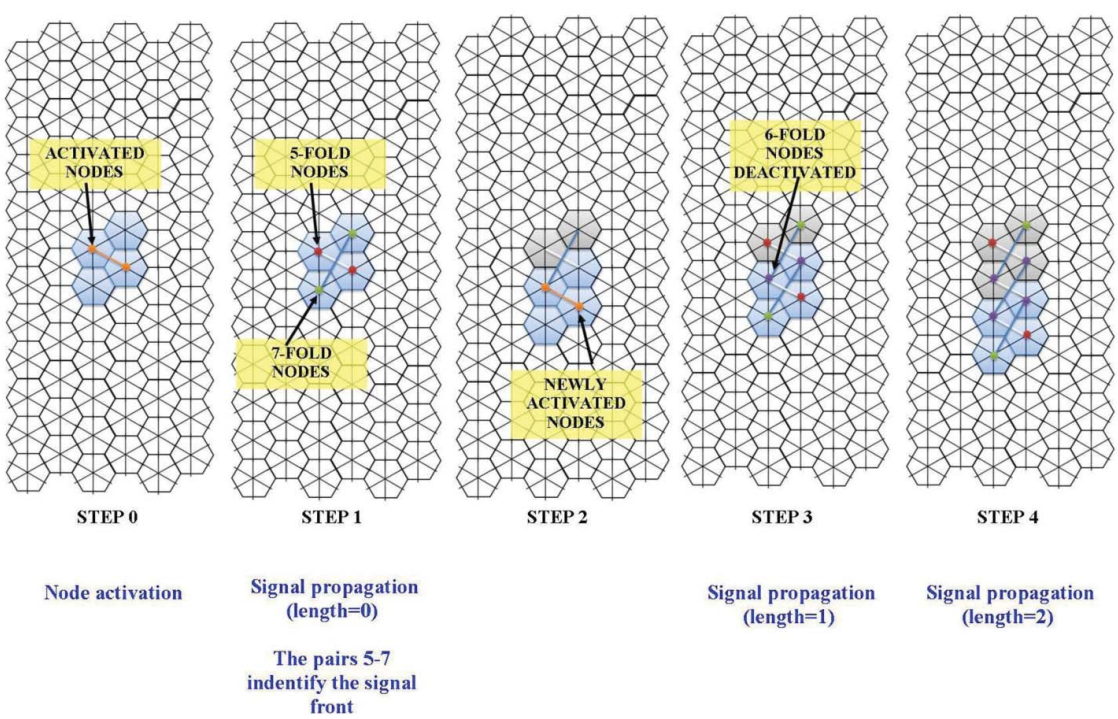

Figure 2. Simulation of a few possible transformations taking place on a flat exagonal lattice equipped with 72 nodes, 6-bonds each. The lattice stands for the cortical microcolumn containing 72 pyramidal neurons described in Figure 3C. Starting from the totally inactive state of 6-fold nodes on 6×12 lattice, some nodes gets activated (STEP 0). We may select whatever pair in the mesh. To make an example, after a visual input from the external environment, a few microcolumnar pyramidal neurons start to fire. STEP1 displays two 5|7 pairs, activated by just rotating the orange bond of STEP 0. Signal propagation gives rise to a sequential activation of novel front nodes (STEP 2), so that the activation wave propagates steps further (STEPS 3 and 4). Note that the purple balls, which identify hexagonal nodes deactivated after the passage of the wave, are ready for a possible reversible annihilation of the topological signal.

SW defect formed by two 5|7 pairs, whose creation involves 4 connected neurons under the action of the $SW_{6|6}$ operator.

- Multiple applications, for η-times, of the $SW_{6|7}$ operator produce the SWw defect with the expansion of the SW dislocation dipole and the linear propagation of the signal, in order to cover the distance η. The size η of the SW dislocation dipole (e.g., the signal) also corresponds to the number of pairs of inactive neurons included between the two 5|7 pairs. This topological modification of the network is also indicated as $5/7\{6/6\}_\eta 7/5$. SW defect has then $\eta = 0$.
- If needed, the η pairs of inactive neurons allow the complete topological annihilation of the SW dislocation dipole, by just applying η-times the reverse $rSW_{6|7}$ flip. The $rSW_{6|6}$ rotation will then restore the pristine hexagonal lattice.

The proposed correspondence between the neural signal and the linear SWw defect is just the simplest choice in the large family of topological modifications of the neuron lattice that may be built via SW rotations. The possible combinations of permutations (and therefore of simultaneously activated neurons in a fullerene-like microcolumn) are countless: in a lattice of 80 nodes and 2 activities (ON/OFF), we achieve the noteworthy number of 2^{80} possible permutations. Many operations, not shown in Figures, can be performed: edge sharing, interchanging the positions of two hexagons, rotation of a single edge, and so on. Because the switches are fully reversible, the edges can be rearranged in countless ways.

We do not know, due to our current lack of knowledge, whether the microcortical assembly of pyramidal neurons truly exhibits the required fullerene-like stereotyped conformation. The Borsuk-Ulam theorem (BUT) from algebraic topology, ideally suited for many applications (24), gives us a clue to solve this problem. The original formulation of BUT describes antipodal points on an n-sphere with matching descriptions on spatial manifolds in every dimension, provided the n-sphere containing the antipodes is a convex structure with positive curvature (i.e., a ball). However, BUT can be generalized to symmetries occurring either on flat manifolds, or on Riemannian hyperbolic manifolds of constant sectional curvature -1 and concave shape (i.e., a saddle) (12, 25). In other words, whether the system components are equipped with concave, convex or flat conformation, it does not matter: we can always find points with matching descriptions predicted by BUT (26).

The modifications of the *long-range structure of honeycomb network topology* depicted in Fig. 2, may be modeled by computing both topological potentials Wiener index $W(n)$ and topological efficiency index $\rho(n)$ introduced in the previous section (eqs. 3 and 4). The topological propagation of the signal has been simulated on the dual neural lattice G_n consisting of $n = 72$ nodes, all 6-connected, with $B = 216$ total edges due to periodic boundary conditions. That pristine graph G_n^* is then characterized by the starting values $W_n^* = 9864$; $\rho_n^* = 1$ of the two lattice descriptors (Fig. 3). Computation shows the 0.73% gain of the Wiener index when it passes to $W_n^0 = 9792$ after the creation of the SW defect with $\eta = 0$. The subsequent $SW_{6/7}$ initiates, by shifting one of the 5|7 pair in the lattice, the propagation of the signal further decreasing the topological potential $W_n^1 = 9771$ and $W_n^2 = 9728$ for $\eta = 1$ and $\eta = 2$, receptively. This behavior confirms that, at each propagation step, the expanding SWw defect increases the overall compactness of the neural network G_n^η, augmenting in such a way the *topological stability of the honeycomb system itself*. The global drop of the *topological potential* Ξ^W, shown in Fig. 3(a), demonstrates a linear trend favoring signal propagation. After the creation of the SW defect $\eta = 0$, the invariants w_i of the 72 neurons leave the uniform value $\underline{w} = 137$, assuming that different values depend on the respective topological stability. The two heptagons become the two stables nodes with $_{w_} = 130$; vice versa, the two pentagons are the less stable nodes of the neural mesh with maximal value $\overline{w_n^0} = 138$. As shown in Fig. 3b, the topological potential Ξ^ρ provides more details about topological rearrangements of the honeycomb mesh during signal propagation. The increased value of topological efficiency $\rho_n^0 = 1.0462$ stands for the barrier in the topological potential that competes against the signal creation. After this point, the topological potential Ξ^ρ shows a regular decrease, favoring in such way the smooth expansion of the SW dislocation dipole, e.g., the topological defect carrying the signal in the graph.

In this note, we showed how SW transformations might have a counterpart in the biological activity of brain microcircuitry. The results provided by the present study sustain the proposed original coincidence between *neural signal & topological defects*. We make available a novel approach that allows us to evaluate brain activity in terms of topological and graph theoretical properties of fullerenes. In touch with neural networks derived from the principle of minimum frustration for protein folding (27), the fullerene-like approach points towards a perception/decision apparatus constrained towards very low energetic levels, but just in long timescales, in order that predictions signals are conveyed by the sole long-standing past experiences. This is a very fertile field of research: current efforts focus on the unsolved mathematical problems concerning fullerenes, e.g., how to generate all possible non-isomorphic graphs for a fixed vertex count, or to calculate the number of distinct Hamiltonian cycles. Researchers are developing 2D graphs and 3D structures for many different fullerenes, ranging from $N = 20$ to 20,000 vertices, in order to evaluate various different graph-theoretical algorithms (28) and theorems and algorithms which allow a fast computation of topological indices for complex graphs, starting from their structural building elements (6). Future investigations will be carried out to correlate the sequences of SW topological transformations to the isomeric generation and propagation of 5|7 pairs or similar topological extended defects in the neural mesh.

Our framework also provides a link with human neurologic and psychiatric diseases. Experimental data and molecular dynamic simulations suggest that defects during the nucleation and growth of graphene alter the physical/chemical properties of carbon nanostructures (35), strongly deteriorating their functional state. An increase in energetic constraints, as it occurs, for example, during ageing or central nervous system's diseases, makes it easy to generate defects in the microcolumnar fullerene-like lattice, with subsequent decrease in system's free-energy and functional integrity. Our theoretical framework, cast in a biologically informed fashion, has the potential to be operationalized and assessed empirically. Indeed, the presence of a

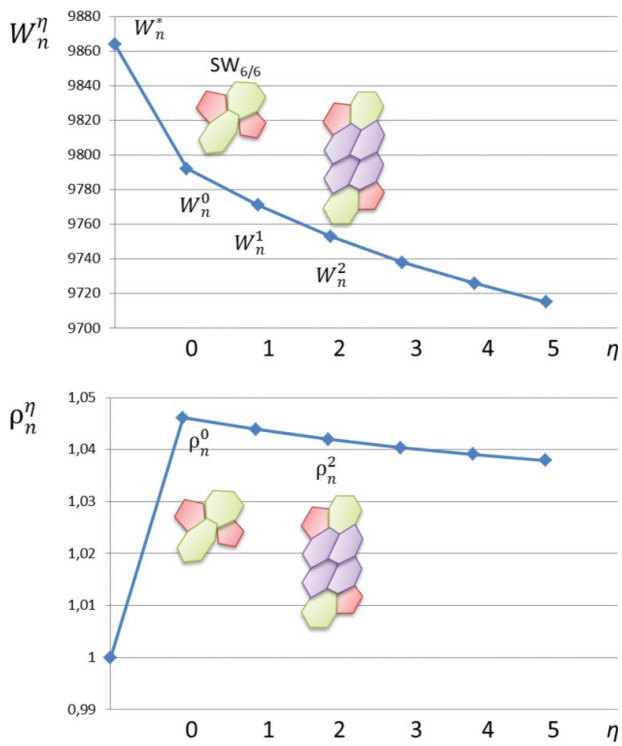

Figure 3. (a) Top. The topological potential W_n^η is computed for the SWw defect propagating in the hexagonal graph, in order to simulate the signal transmission in a neuron mesh equipped with $n = 72$ elements. $SW_{6/6}$ originates two 5|7 pairs at $\eta = 0$, then $SW_{6/7}$ splits them, by swapping one of the 5|7 two pairs with a pair of hexagons ($\eta = 1$). Further $SW_{6/7}$ rotation propagates the signal. Lattice configurations are depicted for $\eta = 0$ and $\eta = 2$; the initial value W_n^* corresponds to the pristine hexagonal mesh. (b) Bottom. Analogous variation of topological potential ρ_n^η for a SWw defect propagating in the periodic neuron mesh with $n = 72$ elements. The cost of the $SW_{6/6}$ rotation peaks at $\eta = 0$, whereas the $SW_{6/7}$ flips are followed by a gain favoring the propagation of the signal. The perfect symmetry of the pristine hexagonal mesh is testified by the value $\rho_n^* = 1$.

microcolumnar barcode predicted by a fullerene-like brain will be easily testable, once more powerful high density neurotechniques will be available, capable of capturing the simultaneous activity of large populations of microcolumnar pyramidal neurons (36). To make an example, if we were able to evaluate the microcolumnar pyramidal neurons that fire during every mental activity (e.g., visual tasks, emotions, and so on) we would achieve a fullerene-like structure filled with the corresponding activated nodes, therefore attaining a series of different grids or matrices (each one standing for a mental function).

Such powerful tools could be, in a near future, applied to the assessment of neural networks, in order to achieve a double task: improving our understanding of biological brain function in situ, and building more powerful artificial machines able to simulate cortical activities.

Conflict of interest

The authors declare that they have no conflict of interest.

References

1. Mountcastle, V. B. (1997) The columnar organization of the neocortex. *Brain*, 20 (4): 701–722.
2. Jones, E. G. (2000) Microcolumns in the cerebral cortex. *PNAS*, 97 (10): 5019–5021.
3. Casanova, M. F., El-Baz, A., and Switala, A. (2011) Laws of conservation as related to brain growth, aging, and evolution: symmetry of the minicolumn. *Front Neuroanat.* 26(5): 66.
4. Babic, D., Bassoli, S., Casartelli, M., Cataldo, F., Graovac, A., Ori, O., and York, B. (1995) Generalized Stone-Whales transformations. *Mol. Simul.*, 14: 395–401.
5. Ori, O., Putz, M. V., Gutman, I., and Schwerdtfeger, P. (2014) Generalized Stone-Wales transformations for fullerene graphs derived from berge's switching theorem. In *Ante Graovac — Life and Works*. Gutman, I., Pokric, B., Vukicevic, D. (eds.), 259–272. Q1
6. Koorepazan-Moftakhar, F., Ashrafi, A. R., Ori, O., and Putz, M. V. (2015) *Geometry and Topology of Nanotubes and Nanotori. Exotic Properties of Carbon Nanomatter.* Vol. 8 of the series Carbon Materials: Chemistry and Physics. pp 131–152. Q2
7. Turpin, A., Sampson, G.P., and McKendrick, A. M. (2009) Combining ganglion cell topology and data of patients with glaucoma to determine a structure–function map. *Invest Ophthalmol Vis Sci.* 50(7): 3249–3256.
8. Gomez-Ballesteros, J. L., Burgos, J. C., Lin, P. A., Sharma, R., Balbuena, P. B. (2015) Nanocatalyst shape and composition during nucleation of single-walled carbon nanotubes. *RSC Adv.* 5(129): 106377–106386.
9. Stam, C. J. and Reijneveld, J. C. (2007) Graph theoretical analysis of complex networks in the brain. *Nonlinear Biomed. Phys.*, 5; 1(1):3.
10. Köster, U., Sohl-Dickstein, J., Gray, C. M., and Olshausen, B. A. (2014) Modeling higher-order correlations within cortical microcolumns. *PLoSComputBiol*, 10(7): e1003684.
11. Singh, G., Memoli, F., Ishkhanov, T., Sapiro, G., Carlsson, G., and Ringach, D.L. (2008) Topological analysis of population activity in visual cortex. *J. Vision*, 8(8): 11–18.
12. Tozzi, A. and Peters, J. F. (2016) A topological approach unveils system invariances and broken symmetries in the brain. *J. Neurosci. Res.*, 94 (5): 351–65. doi:10.1002/jnr.23720.
13. Giusti, C., Ghrist, R., Bassett, D.S. (2016) Two's company, three (or more) is a simplex. Algebraic-topological tools for understanding higher-order structure in neural data. *J. Comput. Neurosci.* 41: 1–14.
14. Zhang, Z., Kutana, A., Yang, Y., Krainyukova, N.V., Penev, E.S., and Yakobson, B.I. (2016) Nanomechanics of carbon honeycomb cellular structures. *Carbon*, http://dx.doi.org/10.1016/j.carbon.2016.11.020.
15. Schwerdtfeger, P., Wirz, L., and Avery, J. (2015) The Topology of fullerenes. *Wiley Interdiscip. Rev.: Comput. Mol. Sci.*, 5: 96–145.
16. Chuang, C., Fan, Y-C., and Jin, B-J. (2009) Generalized classification scheme of toroidal and helical Carbon nanotubes. *J. Chem. Inf. Model.*, 2009, 49(2): 361–368. doi: 10.1021/ci800395r.
17. Fowler, P. W., Curl, R. F., and Murrell, J. N. (1993) Systematics of fullerenes and related clusters [and Discussion], philos. *Trans.: Phys. Sci. Eng.* 43(1667): 39–52.
18. Fowler, P. W., Rogers, K. M., Fajtlowicz, S., Hansen, P., and Caporossi, G. (2001) Facts and conjectures about fullerene graphs: Leapfrog, cylinder and Ramanujan fullerenes, In A. Benen et al. (Eds.), *Algebraic Combinatorics and Applications*, Springer.
19. Todeschini, R. and Consonni, V. (2000) *Handbook of Molecular Descriptors.* Wiley-VCH: Weinheim, Germany.
20. Ori, O., Cataldo, F., and Graovac, A. (2009) Topological ranking of C28 fullerenes reactivity. *Fullerenes, Nanotubes Carbon Nanostructures*, 17(3): 308–323. doi: 10.1080/15363830902782332.
21. Vukicevic, D., Cataldo, F., Ori, O., and Graovac, A. (2011) Topological efficiency of C66 fullerene. *Chem. Phys. Lett.*, 501(4–6): 442–445.
22. Graovac, A., Ashrafi, A. R., and Ori, O. (2014) Topological efficiency approach to fullerene stability—case study with C_{50}. *Advances in Mathematical Chemistry and Applications*, 2: 3–23. Subash C. Basak, Guillermo. Restrepo, and Jose L. Villaveces (Eds) Bentham Science Publishers.
23. Ori, O., Cataldo, F., and Putz, M. V. (2011) Topological anisotropy of stone-wales waves in graphenic fragments. *Int. J. Mol. Sci.* 12: 7934–7949; doi:10.3390/ijms12117934.
24. Matoušek, J. (2003) *Using the Borsuk-Ulam Theorem.* Springer-Verlag: Berlin, ISBN 978-3-540-00362-5.

25. Mitroi-Symeonidis, F-C. (2015) Convexity and sandwich theorems. *Eur. J. Res. Appl. Sci.*, 1: 9–11
26. Tozzi, A. (2016) Borsuk-Ulam Theorem Extended to Hyperbolic Spaces. In *Computational Proximity. Excursions in the Topology of Digital Images*, edited by J. F. Peters, 169–171. doi:10.1007/978-3-319-30262-1.
27. Tozzi, A., Fla, Tor, and Peters, J. F. (2016) Building a minimum frustration framework for brain functions in long timescales. *J. Neurosci. Res.* 94(8): 702–716.
28. Schwerdtfeger, P., Wirz, L., and Avery, J. (2013) Program FULLERENE a program for creating fullerene structures and for performing topological analyses. *J. Comput. Chem.*, 34: 1508–1526.
29. Opris, I. and Casanova, M. F. (2014) Prefrontal cortical minicolumn: From executive control to disrupted cognitive processing. *Brain.* 2014 Jul;137(Pt 7):1863–75. doi: 10.1093/brain/awt359.
30. Casanova, M. F., El-Baz, A., and Switala, A. (2011) Laws of conservation as related to brain growth, aging, and evolution: Symmetry of the minicolumn. *Front Neuroanat.* 26(5):66. doi: 10.3389/fnana.2011.00066.
31. Cruz, L., Urbanc, B., Inglis, A., Rosene, D. L., and Stanley, H. E. (2008) Generating a model of the three-dimensional spatial distribution of neurons using density maps. *Neuroimage.* 40(3): 1105–1115.
32. Peters, A. and Kara, D. A. (1987) Neuronal composition of area 17 of rat visual cortex. iv. the organization of pyramidal cells. *J. Comparative Neurology.* 260(4): 573–590.
33. Peters, A. and Sethares, C. (1991) Organization of pyramidal neurons in area-17 of monkey visual-cortex. *J. Comparative Neurology.* 1991;306(1): 1–23.
34. Gabbott, P. L. A. (2003) Radial organization of neurons and dendrites in human cortical areas 25, 32, and 32′. *Brain Res.* 992: 298–304.
35. Hashimoto, A., Suenaga, K., Gloter, A., Urita, K., Iijima, S. (2004) Direct evidence for atomic defects in graphene layers. *Nature*, 19;430 (7002): 870–3.
36. Köster, U., Sohl-Dickstein, J., Gray, C. M., and Olshausen, B. A. (2014) Modeling higher-order correlations within cortical microcolumns. *PLoSComputBiol.*, 10(7): e1003684.

Neuroscience Letters xxx (2017) xxx-xxx

Contents lists available at ScienceDirect

Neuroscience Letters

journal homepage: www.elsevier.com

Research article

Cracking the barcode of fullerene-like cortical microcolumns

Arturo Tozzi [a, b, *], James F. Peters [c, d, e, f], Ottorino Ori [g]

[a] Center for Nonlinear Science, University of North Texas, 1155 Union Circle, #311427 Denton, TX 76203-5017, USA
[b] Computational Intelligence Laboratory, University of Manitoba, Winnipeg R3T 5V6, MB, ASL NA2 Nord, Canada, Canada
[c] Department of Electrical and Computer Engineering, University of Manitoba, 75A Chancellor's Circle, Winnipeg, MB R3T 5V6, Canada
[d] Department of Mathematics, Adıyaman University, 02040 Adıyaman, Turkey
[e] Department of Mathematics, Faculty of Arts and Sciences, Adıyaman University 02040 Adıyaman, Turkey
[f] Computational Intelligence Laboratory, University of Manitoba, Winnipeg, MB, R3T 5V6, Canada
[g] Actinium Chemical Research, Via Casilina 1626/A, 00133 Rome, Italy

ARTICLE INFO

Article history:
Received 15 December 2016
Received in revised form 5 February 2017
Accepted 22 February 2017
Available online xxx

Keywords:
Brain circuitry
Cortical neuron
Neural code
Lattice
Artificial neural system

ABSTRACT

Artificial neural systems and nervous graph theoretical analysis rely upon the stance that the neural code is embodied in logic circuits, *e.g.*, spatio-temporal sequences of ON/OFF spiking neurons. Nevertheless, this assumption does not fully explain complex brain functions. Here we show how nervous activity, other than logic circuits, could instead depend on topological transformations and symmetry constraints occurring at the micro-level of the cortical microcolumn, *i.e.*, the embryological, anatomical and functional basic unit of the brain. Tubular microcolumns can be flattened in fullerene-like two-dimensional lattices, equipped with about 80 nodes standing for pyramidal neurons where neural computations take place. We show how the countless possible combinations of activated neurons embedded in the lattice resemble a barcode. Despite the fact that further experimental verification is required in order to validate our claim, different assemblies of firing neurons might have the appearance of diverse codes, each one responsible for a single mental activity. A two-dimensional fullerene-like lattice, grounded on simple topological changes standing for pyramidal neurons' activation, not just displays analogies with the real microcolumn's microcircuitry and the neural connectome, but also the potential for the manufacture of plastic, robust and fast artificial networks in robotic forms of full-fledged neural systems.

© 2016 Published by Elsevier Ltd.

1. Introduction

Current computational brain models, based on neural networks performing logic operations [1,2], are not able to fully elucidate a large repertoire of brain functions and mental faculties, such as attention and perception, emotions and cognition, memory and learning, decision making and goal-directed choice [3], mind wandering [4]. In order to build a versatile network able to simulate brain functions at micro-levels of observation, we introduce a cortical model, borrowed from fullerene's geometry, able to evaluate symmetry constraints and topological indices for micro-structures [5]. Although its primary application concerns the description of carbon-networks in chemical compounds, fullerene networks can be used in order to rank topological invariants in neural networks' assessment. In particular, the method applies to description of microcolumns, i.e., the fairly uniform, stereotyped, vertical column-like architecture believed to be the basic embryological/anatomical module and the fundamental processing unit of cortical arrangement [6–8]. Invariant, fullerene-like features are landmarks of microcolumnar modular connectivity. Indeed, minicolumns are characterized by translational symmetry across their central axis, rotational symmetry, transitive symmetry of morphometric relations and temporal symmetry during cortical maturation [9,10]. Therefore, it is feasible to evaluate tubular microcolumns in terms of three-dimensional cylinders equipped with exagonal and pentagonal fullerenic structures. By flattening cylinders into two-dimensional rectangles, we attain lattices that make it possible for us to investigate brain microcuircuitry according to translational procedures other than ON/OFF neural firing. A fullerene-like two-dimensional sheet might be compared to a barcode, where sequences of neuronal activations stand for mental specific functions. This approach not only allows us to build a fullerene-like model that simulates the real brain, but also to assess the vibrancy and inner workings of neural computations in terms of topological relationships among firing neurons.

2. Materials and methods

2.1. Stone-Wales transformations in neural networks

Two-dimensional fullerenes are 3-regular cubic planar graphs, describable as meshes of twelve variously fused pentagons [11–14]. Signal propagation on fullerenic networks can be investigated via graph theoretical methods. Among the possibile choices [15], we fo-

* Corresponding author at: Center for Nonlinear Science, University of North Texas, 1155 Union Circle, #311427 Denton, TX 76203-5017, USA.
Email addresses: tozziarturo@libero.it (A. Tozzi); james.peters3@umanitoba.ca (J.F. Peters); ottorino.ori@gmail.com (O. Ori)

http://dx.doi.org/10.1016/j.neulet.2017.02.064
0304-3940/© 2016 Published by Elsevier Ltd.

UNCORRECTED PROOF

cus on *distance-based* topological indices, able to describe long-range interactions involving all pairs of nodes. Neuronal firing and electric signal propagation are investigated in terms of pure topological network modifications. This assumption implies that the overall number of neurons (graph vertices) and connections among neurons (graph edges or bonds) are *fully preserved*, excluding neurons' creation or destruction along the process. The totally reversible topological permutations occurring on fullerene-like lattices' polygonal surfaces can be assessed and calculated. Methods based on vertex insertions or deletions and isomerisations on lattices have proven very useful, because they allow the formal derivation of one fullerene graph from another [16]. In particular, the so-called Stone-Wales (SW) transformations produce a rotated figure, with no changes in fullerene's external connectivity and molecular topology outside the denoted region of the lattice surface [17]. In sum, SW mechanisms extend transformations in the fullerenic mesh as a wave. They might play an important role in modifying not just the topology of carbon-based materials, like nanotubes and fullerenes [18], but also of neuronal circuits.

The general local Stone-Wales transformation $SW_{q/r}$ (Fig. 1A) is associated with the isomeric transformation that modifies the internal connectivity of four adjacent rings with *p, q, r, s* edges, producing four new rings with *p–1,q + 1,r–1,s + 1* edges, leaving unchanged the surrounding lattice regions. $SW_{p/r}$ reversibly rotates the central bond bridging *p* and *r* rings, leaving unaffected both the total number of nodes $k = p + q + r + s$-8 and the total number of edges k + 3. Fig. 1B–C illustrate the two most studied fullerenic forms, equipped with a rotation of a pentagon-hexagon double pair. SW rotations are able to generate fullerene isomers with different symmetries. In the case of the C_{60} fullerene, the *pyracylene* $SW_{5/6}$ rearrangements group the 1812 isomers in 13 inequivalent sets (Fig. 1C). Such limitation has been solved by using extended generalized SW transformations, in order to produce, starting from just one isomer, the whole C_{60} isomeric space [19].

Ori et al. [20], developed a convenient graphical tool, able to modify fullerene-like networks displayed as two-dimensional graphs made by *n* vertices (*carbon atoms or neurons*), through the isomeric insertion of different *r*-rings with $r > 2$. The case $r = 5,6$ stands for the regular fullerene. The graphical method's efficiency relies on the dual-representation of the graph, achieved by transforming the rings in nodes, and their edges in bonds. Fig. 1D–E provide examples of the interplay between direct and dual representations. The graphical tool allows, as a consequence of iterated SW rotations, the identification of a peculiar topological mechanism called the Stone-Wales wave (SWw) [20], e.g., the linear migration of the pentagon-heptagon 5|7 pair in the planar network. The first $SW_{6/6}$ rotation of the connection shared by the two neurons creates two 5|7 pairs (Fig. 1D). The second operator $SW_{6/7}$, by inserting the 6|6 couple of shaded hexagons between the two original 5|7 pairs, turns the bond between the heptagon and the shaded hexagon (Fig. 1E). This mechanism produces the overall effect of initiating the wave propagation along the dotted direction, because iterated $SW_{6/7}$ rotations will successively propagate the topological defect 5|7. For technical details, see Koorepazan-Moftakhar, et al. [5].

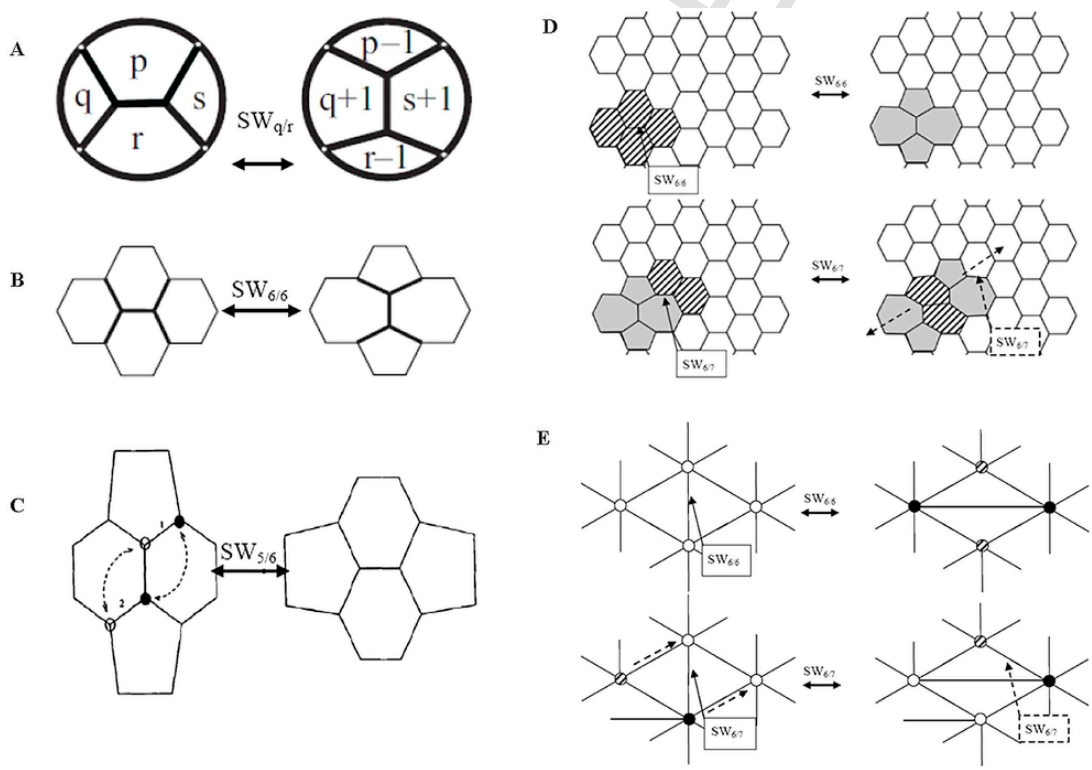

Fig. 1. A–C. Examples of Stone-Wales transformation $SW_{q/r}$. A: the general $SW_{q/r}$ rotation reversibly transforms four proximal polygons with p, q, r, s edges in four new rings with p–1, q + 1, r–1, s + 1 nodes. B: in the graphene p = q = r = s = 6, which stands for the $SW_{6/6}$ rotation normally encountered in carbon nanotubes, $SW_{6/6}$ flips four hexagons in a 5|7 double pair. Fig. 1C: the so-called "pyracylene rearrangement $SW_{5/6}$" displays a $SW_{5/6}$ rotation. D–E summarize the basic topological operations for generating and propagating SWw in lattices. D: in the direct graph, $SW_{6/6}$ originates two 5|7 pairs (gray), then $SW_{6/7}$ splits them, by swapping one of the 5|7 two pairs with a pair of hexagons (shaded); the dotted $SW_{6/7}$ propagates the SW wave in the dashed direction. E illustrates the same transformations in the dual plane. Hexagons, pentagons, heptagons are displayed by white, shaded, black circles respectively.

2.2. Building a fullerene-like microcolumn

Microcolumnar circuitry can be described in terms of biologically plausible fullerene-like two-dimensional lattices. A cortical microcolumn comprises 80–120 neurons, except in the primary visual cortex where the number doubles. About 80% are pyramidal neurons. This basic unit circuit forms a series of repeated items across the horizontal extent of the cortex, independent of area specializations [7]: in humans, the transverse diameter of each of the 2×10^7–2×10^8 microcolumns is about 28–50 μm [21,22]. Our knowledge of microcolumn organization is still largely incomplete, due to difficulties related to the physiological recording methods, as well as to data interpretation. However, despite few skeptical claims [23], several Authors [24–27] described microcolumnar exagonal arrangements in different cortical structures (neurons, dendritic bundles, myelinated axons packing) and in different areas and animals (monkeys, rats' area 17, human medial prefrontal cortex) and in artificial neural networks [28].

According to connectomics, cortical/subcortical structures form a hierarchical network equipped with winner-takes-all mechanisms and preferential pathways for fast communication [29,30]. The neural connectome is equipped with networks and energetic landscapes that can also be used for fullerene-like microcolumns' description. In the next paragraph, we will show how to build a neural network that takes into account SW connections for the 3465 isomers of the C_{64} Fullerene, using Mathematica. We will also assess fullerene-like neural networks in topological terms.

3. Results

Here we provide simulations showing how it is feasible to generate a neural network equipped with countless alternative isomers, starting from a simple fullerene-like structure. Fig. 2A depicts some topological transformations that might take place on microcolumns. A cortical microcolumn stands for a three-dimensional tubular armchair. By slicing at an angle to an edge, we achieve a flattened two-dimensional fullerene-like grid, a 30 μm-width lattice equipped with hexagonal (or pentagonal) tiling and about 80 nodes (Fig. 2A, left side). Such nodes, standing for the microcortical pyramidal neurons, are linked by edges (or bonds), e.g., dendritic/axonal connections. Every node is filled with a pyramidal neuron (activated or deactivated). A preliminary activation of a pair of neurons in the 6-fold status takes place, followed by the creation of the "signal", e.g. a topological defect of the hexagonal mesh, called SW defect. Signal generation is then achieved through further rotations (Fig. 2A, right side) that modify the local neuronal connections, by rotating the bond between the two activated elements. Additional applications of the SW operator will split more and more the neuronal pairs, allowing the signal to travel in the neural network according to the typical SWw wave mechanism.

In the nervous case, instead of SW flips on a fullerene surface, we assess changes in neuronal firing activation. Here "permutation" means which ones of the 80 pyramidal neurons are sequentially activated or deactivated. SW permutations may be regarded as a set of neurons which fire simultaneously. Every group of neural "permutations" might stand for a barcode, each one corresponding to a peculiar mental activity.

Our current lack of knowledge prevents us from assessing whether pyramidal neurons'assembly exhibits the required conformations. The Borsuk-Ulam theorem (BUT) from algebraic topology [31], helps us to solve this problem. The BUT describes antipodal points with matching description on spatial manifolds in every dimension, provided the n-sphere is a convex structure with positive curvature (*i.e.*, a ball). However, BUT can be generalized to symmetries occurring either on flat manifolds, or on Riemannian hyperbolic manifolds of concave shape (*i.e.*, a saddle) [32]. Whether the system components are equipped with concave, convex, flat or "stretched" conformation, we may always find the points with matching description predicted by BUT. This means that microcolumnar's neuronal activity can always be described in terms of transformations on two-dimensional lattices, although not perfectly arranged as a sterotyped fullerene-like structure (Fig. 2B).

We are allowed to build a 6-folded connectome-like network simulating microcolumns' behaviour. Fig. 3A provides the SW landscape of a fullerene-like microcolumn. Every point, standing for a C_{64} fullerene isomer, is connected with the first neighbour throw a single SW rotation (of order 0). In Fig. 3A, every single point stands for a neuronal assembly in a given configuration (say F1), while his neighbor lies in another configuration, e.g., F1 plus other faces, melted through a SW rotation. Every group is connected with others via topological deformations, depending on specific neural signals.

Fig. 3B and C illustrate the application of a novel topological concept, the biReBUT, on fullerenes. The details are provided in the Figure legend. This application arises from the observation of the neuronal symmetrical distribution in the left and right cortical hemispheres. That is, in brain with fullerene-like micro-structure, a pull-back from each neuron to its corresponding antipodes might occur.

4. Discussion

We achieved a two-dimensional fullerene-like lattice reproducing microcolumn's microcircuitry. In analogy with the chess game, a fullerene network resembles a chessboard, SW transformations are analogous to moves that chess pieces can perform, and single chess pieces are the neurons. When a piece moves on the chessboard, this is analogous to a neuron firing. Our results pave the way to answer to Mountcastle's question: what are the transforming operations imposed in a cortical column, upon its input, to produce its targeted outputs [6]? Although our lattice looks like a classical neural network at first sight, nevertheless it is faster, less energy-consuming, more plastic and stabler. It is easy to parametrize, because information can be extracted from just a few parametrizing factors. e.g., the simple topological operations taking place on networks. While other approaches emphasize macro- and meso- phenotype dynamics, our framework is grounded on operations occurring at nervous micro-levels. We assume that simultaneous firing of different neurons and specific activation sequences give rise to different topological conformations, each one corresponding to a mental activity (perception, emotion, and so on). The brain functional activity is not based on logic nodes as in conventional networks, but on topological transformations, e.g., functional changes in the firing neurons' sites.

Our model explains countless mental operations starting just from simple, stereotyped, highly preserved biological structures: the microcolumns. Fullerene-like models, involving any pair of connected nodes [33], unveil a very rich phenomenology, due to the almost infinite SW rotations that may take place. This makes possible a limitless set of moves, merely dictated by applying SW rotations on its bonds. Ubounded sets correspond to the series of mental operations taking place in our brain. During the synthesis/growth process of a C^n fullerene, the isomers with isolated pentagons often udergo SW interconversion. This may cause instability, because failures of some of its components are expected, in presence of high numbers of SW transformations. Nevertheless, the artificial implementation of the model itself grants for its stability through a simple expedient: by us-

UNCORRECTED PROOF

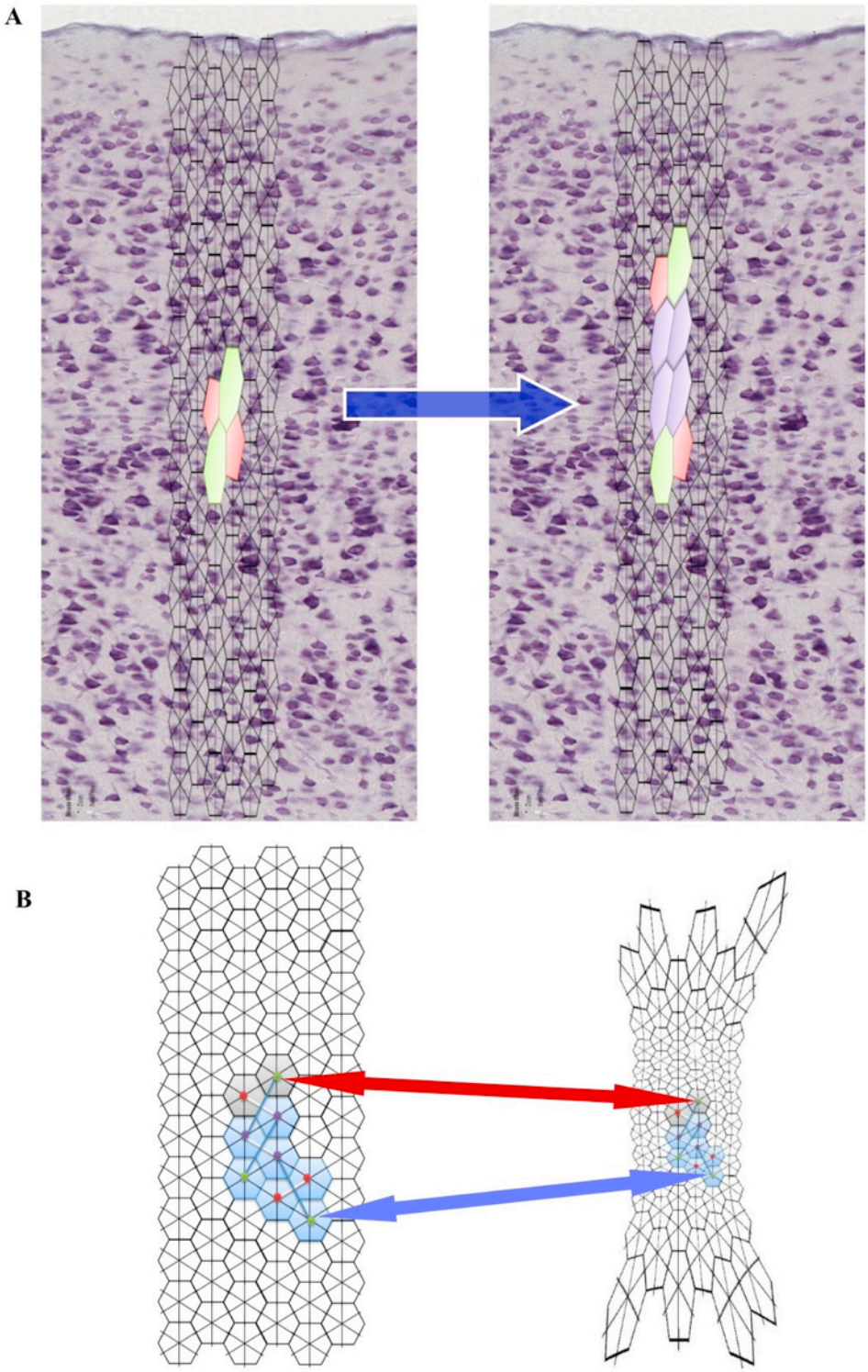

Fig. 2. A. Topological simulation of propagating signals on a fullerene-like grid, embedded in situ into a cortical micrococolumn. The stained exagons, depicting SW transformations in lattice's nodes, stand for activated pyramidal neurons. In this example, the flat hexagonal lattice, equipped with 72 nodes, 6-bonds each, stands for a cortical microcolumn containing 72 pyramidal neurons. Starting from the totally inactive state of 6-fold nodes on 6 × 12 lattice, some nodes (neurons) get activated (Fig. 2A, left side). We may select whatever pair in the mesh. In Fig. 2A, right side, signal propagation gives rise to a sequential activation of novel front nodes: the waves propagate steps further. B. Every deformation in fullerene-like lattices leaves the relationships among the single elements (the firing neurons) unchanged, due to the BUT dictates.

ing a given C_n isomer as a seed, a series of moves can be performed that give us the capability to build complete sets of fullerene isomers, by simple binding topological briges [9]. Therefore, both isomerization maps and complete isomer space's description can be achieved from a single known conformation. In the same way, the primal embryonal microcolumn gives rise to a huge amount of combinations in

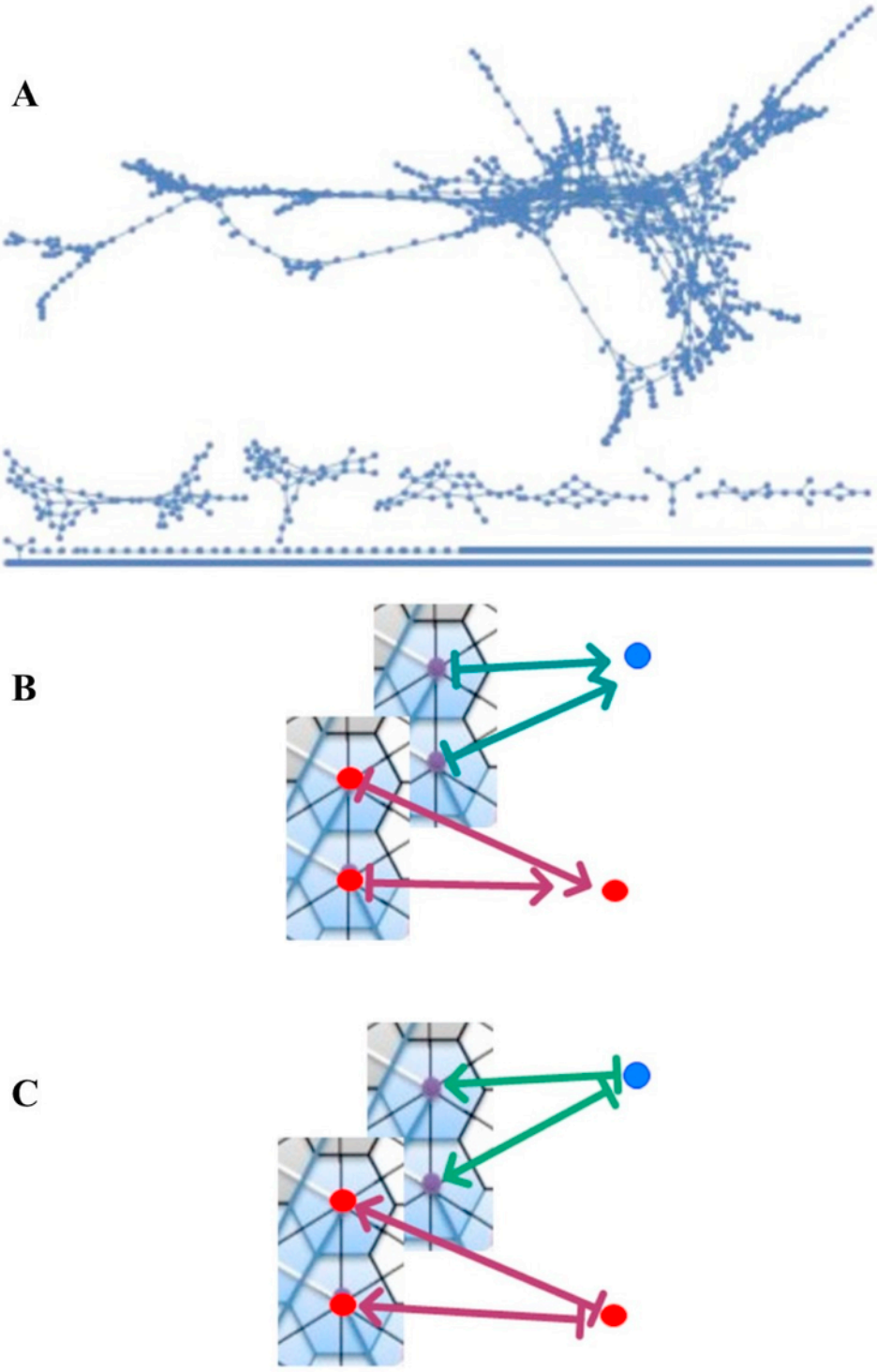

Fig. 3. A. Topological ranking of C_{64} isomers landscape. Signals can be connected by one up to 4 SW rotations. Here we provide, as an example, the graph defining the isomers that are connected by SW transformations of order G0 (i.e., a single SW rotation). Other graphs of different orders (G1, G2, G3) can be built. B. Region-based BUT (reBUT) results in a mapping of matching pyramidal neurons with matching descriptions (on a brain emisphere) to a single neuronal region ● (on the other emisphere). The neurons with matching description stand for activated neurons. reBUT comes into play by observing fullerene pyramidal neuronal regions with matching descriptions, and mapping the observed fullerene regions to a corresponding neuron in the other emisphere. For more about reBUT, see Peters [45] and Peters and Tozzi [46]. The bijective version of reBUT (**biReBUT**) states that if $f : 2^X \rightarrow 2^{R^k}$ is a continuous bijection from a collection of regions 2^X onto a collection of planar vectors 2^{R^k} in a k-dimensional space R^k, then:. 1) $f(A) = f(\neg A)$ for some $A \subset 2^X$ 2) there is a pullback $f^{-1}(A) = f^{-1}(\neg A) = A$. The proof of the first consequence of biReBUT is given in [45] and the second (pullback) consequence of this theorem results from the fact that the mapping f is a bijection (*i.e.*, 1-1 and onto).

the mature individual's microcircuitry. Starting from the single vertical template of about 80 pyramidal neurons that colonizes the whole cortex during embryonal life, countless barcodes might be built with time passing. In touch with catalysts that promote fullerene transformations and stabilize its transitions states, we hypothesize that the habituation to repeated stimuli during the first months/years of life could give rise to more stable and permanent transformations in microcolumns barcodes.

Fullerene-like networks are very fast, because they use simple transformations. Starting from each randomly built C_n fullerene structure, one may directly generate a certain number of new isomers using just SW flips, instead of searching for a new one. This improves computational speed, because the number of steps required by every operation is reduced. A simple increase in the order of SW transformations allows us to connect more microcolumns: dual structures, given by the combination of many microcolumns, can be easily built by joining the reciprocal space. As nanoparticle/substrate interaction's tuning provides unique ways of controlling nanotube synthesis [34], fullerene-like neural networks might provide the fine-grain functional barcode's modularity required by different brain functions.

Fullerene-like networks take time to become efficient, because SW transformations are less favoured by an energetic standpoint. The building of novel barcodes is a slow, time-consuming process. By a biological point of view, this is in touch with the slow development of mental operations' competence in young primates [35]. Vice versa, a fullerene-like neural network gives to adult primates unvaluable advantages, in terms of energy sparing. Pentagons incorporation, occurring at an early stage of nucleation pathway for single-wall nanotubes, leads to a very efficient system, because the number of dangling bonds is reduced, so that changes towards more entropic curvatures are achieved [36]. To make an example, fullerenes produced by the overlap of 12 nanocones which no direct pentagon fusion display very high thermodynamic stability, steady topological configurations and minimized graph invariants [37,16]. In mental terms, a fullerene-like microcolumnar structure might be associated with minimal wiring costs and fast synchronization/information transfer [38].

The concept of nervous connectome might be extended not just to the "classical" macro and meso- levels, but also to the microcolumnar level. Our observations suggest that connectome's nodes, hubs, energetic fluxes and trajectory paths are diffused along the entire neural pathway, including microcolumnar arrangement. This is in touch with the recently described micro-commectome, i.e., neural netwoks at cellular scale [39].

In terms of age-related mental decline and of a broad spectrum of neurologic and psychiatric disorders (autism, schizophrenia, Alzheimer disease, drug addiction), the results so far available point towards a loss of regularity and changes in the structural coherence of the microcolumnar organization and/or connectome modularity [40,10]. These features could be assessed in term of fullerene-like microcolumns. Indeed, defects of graphene nucleation/growth modify physical/chemical features of carbon nanostructures, generating lattice functional failures [41].

In sum, we make available a novel approach that allows us to evaluate topological brain activity in terms of fullerenes' graph properties. This powerful method could be, in a near future, applied to the assessment of neural networks, in order to achieve a double task: improving our understanding of biological brain function in situ, and building computers that simulate cortical activities. We would like to bring to an end with a methodological remark. Once high density neurotechniques will be able of capturing the simultaneous activity of larger populations [42], we suggest to analyize microcolumnar activity in primate temporal cortex or other associative cortices (instead of the "classical" rodents' barrel cortex or primates' visual cortex), because they display a notable sterotypy [7], which may prove to be a better model.

Uncited references

[43,44].

References

[1] O. Sporns, Structure and function of complex brain networks, Dialogues Clin. Neurosci. 15 (September (3)) (2013) 247–262.

[2] M. Ursino, C. Cuppini, E. Magosso, A neural network for learning the meaning of objects and words from a featural representation, Neural Netw. 63 (2014) http://dx.doi.org/10.1016/j.neunet.2014.11.009.

[3] M.S. Gazzaniga, The Cognitive Neurosciences, 4th ed., MIT Press, 2009. ISBN: 9780262013413.

[4] J.R. Andrews-Hanna, J. Smallwood, R.N. Spreng, The default network and self-generated thought: component processes dynamic control, and clinical relevance, Ann. N. Y. Acad. Sci. 1316 (2014) 29–52.

[5] Koorepazan-Moftakhar F., Ashrafi A.R., Ori O., Putz M.V., 2015, Geometry and Topology of Nanotubes and Nanotori. Exotic Properties of Carbon Nanomatter, Volume 8 of the series Carbon Materials: Chemistry and Physics, 131-152.

[6] V.B. Mountcastle, The columnar organization of the neocortex, Brain 20 (4) (1997) 701–722.

[7] E.G. Jones, Microcolumns in the cerebral cortex, PNAS 97 (10) (2000) 5019–5021, http://dx.doi.org/10.1073/pnas.97.10.5019.

[8] S. Ramaswamy, J.D. Courcol, M. Abdellah, S.R. Adaszewski, N. Antille, et al., The neocortical microcircuit collaboration portal: a resource for rat somatosensory cortex, Front Neural Circuits 9 (2015) 44, http://dx.doi.org/10.3389/fncir.2015.00044.eCollection 2015.

[9] M.F. Casanova, A. El-Baz, A. Switala, Laws of conservation as related to brain growth, aging, and evolution: symmetry of the minicolumn, Front. Neuroanat. 26 (5) (2011) 66, http://dx.doi.org/10.3389/fnana.2011.00066.

[10] I. Opris, M.F. Casanova, Prefrontal cortical minicolumn: from executive control to disrupted cognitive processing, Brain 137 (July (Pt 7)) (2014) 1863–1875, http://dx.doi.org/10.1093/brain/awt359.

[11] C. Chuang, Y.-C. Fan, B.-J. Jin, Generalized classification scheme of toroidal and helical carbon nanotubes, J. Chem. Inf. Model 49 (2) (2009) 361–368, http://dx.doi.org/10.1021/ci800395r. 2009.

[12] P. Schwerdtfeger, L. Wirz, J. Avery, J. Comput. Chem. 34 (2013) 1508–1526.

[13] A. Graovac, A.R. Ashrafi, O. Ori, Topological efficiency approach to fullerene stability-case study with C50, In: S.C. Basak, G. Restrepo, J.L. Villaveces (Eds.), Advances in Mathematical Chemistry and Applications, vol. 2, Bentham Science Publishers, 2014, pp. 3–23.

[14] Schwerdtfeger P., Wirz L., Avery J. 2015. The Topology of Fullerenes. Wiley Interdisciplinary Reviews: Computational Molecular Science 5, 96-145.

[15] R. Todeschini, V. Consonni, Handbook of Molecular Descriptors, Wiley-VCH, Weinheim, Germany, 2000.

[16] Ori O., Putz M.V., Gutman I., Schwerdtfeger P., 2014. Generalized Stone-Wales Transformations for Fullerene Graphs Derived from Berge's Switching Theorem. Ante Graovac – Life and Works. Gutman I, Pokric B, Vukicevic D (Eds.), 259-272.

[17] D. Babic, S. Bassoli, M. Casartelli, F. Cataldo, A. Graovac, et al., Generalized Stone-Whales transformations, Mol. Simul. 14 (1995) 395–401.

[18] J. Ma, D. Alfè, A. Michaelides, E. Wang, Stone-Wales defects in graphene and other planar sp2-bonded materials, Phys. Rev. B 80 (2009) 033407.

[19] O. Ori, F. Cataldo, A. Graovac, Topological ranking of C28 fullerenes reactivity, Fullerene Nanotube Carbon Nanostruct. 17 (3) (2009) 308–323, http://dx.doi.org/10.1080/15363830902782332.

[20] O. Ori, F. Cataldo, M.V. Putz, Topological anisotropy of Stone-Wales waves in graphenic fragments, Int. J. Mol. Sci. 12 (2011) 7934–7949, http://dx.doi.org/10.3390/ijms12117934.

[21] O. Sporns, G. Tononi, R. Kötter, The human connectome: a structural description of the human brain, PLoS Comput. Biol. 1 (4) (2005) e42.

[22] C. Johansson, A. Lansner, Towards cortex sized artificial neural systems, Neural Netw. 20 (1) (2007) 48–61. Elsevier.

[23] T.S. Skoglund, R. Pascher, C.H. Berthold, Aspects of the organization of neurons and dendritic bundles in primary somatosensory cortex of the rat, Neurosci. Res. 50 (2) (2004) 189–198.

[24] A. Peters, D.A. Kara, Neuronal composition of area 17 of rat visual cortex? iv. The organization of pyramidal cells, J. Comp. Neurol. 260 (4) (1987) 573–590.

[25] L. Cruz, B. Urbanc, A. Inglis, D.L. Rosene, H.E. Stanley, Generating a model of the three-dimensional spatial distribution of neurons using density maps, Neuroimage 40 (3) (2008) 1105–1115.

UNCORRECTED PROOF

[26] A. Peters, C. Sethares, 1991: Organization of pyramidal neurons in area-17 of monkey visual-cortex, J. Comp. Neurol. 306 (1) (1991) 1–23.
[27] P.L.A. Gabbott, Radial organization of neurons and dendrites in human cortical areas 25 32, and 32′, Brain Res. 992 (2003) 298–304.
[28] L. Yoder, Explicit logic circuits predict local properties of the neocortex's physiology and anatomy, PLoS One 5 (2) (2010) e9227, http://dx.doi.org/10.1371/journal.pone.0009227.
M.P. Van den Heuvel, O. Sporns, Rich-club organization of the human connectome, J. Neurosci. 31 (44), 2011, 15775–15786. 31.
[30] T.M. Reese, A. Brzoska, D.T. Yott, D.J. Kelleher, Analyzing self-similar and fractal properties of the C. elegans neural network, PLoS One 7 (10) (2012) e40483, http://dx.doi.org/10.1371/journal.pone.0040483.
[31] A. Tozzi, J.F. Peters, A topological approach unveils system invariances and broken symmetries in the brain, J. Neurosci. Res. 94 (5) (2016) 351–365, http://dx.doi.org/10.1002/jnr.23720.
[32] F.-C. Mitroi-Symeonidis, Convexity and sandwich theorems, Eur. J. Res. Appl. Scie. 1 (2015) 9–11.
[33] S. Maruyama, Y. Yamaguchi, A molecular dynamics demonstration of annealing to a perfect C60 structure, Chem. Phys. Lett. 286 (3–4) (1998) 343–349.
[34] J.L. Gomez-Ballesteros, J.C. Burgos, P.A. Lin, R. Sharma, P.B. Balbuena, Nanocatalyst shape and composition during nucleation of single-walled carbon nanotubes, RSC Adv. 5 (129) (2015) 106377–106386, http://dx.doi.org/10.1039/C5RA21877B.
[35] M.A. Skeide, A.D. Friederici, The ontogeny of the cortical language network, Nat. Rev. Neurosci. 17 (2016) 323–332, http://dx.doi.org/10.1038/nrn.2016.23.
[36] X. Fan, R. Buczko, A.A. Puretzky, D.B. Geohegan, J.Y. Howe, S.T. Pantelides, S.J. Pennycook, Nucleation of single-walled carbon nanotubes, Phys. Rev. Lett. 90 (2003) 145501.
[37] D. Vukicevic, F. Cataldo, O. Ori, A. Graovac, Topological efficiency of C66 fullerene, Chem. Phys. Lett. 501 (4–6) (2011) 442–445.
[38] C.J. Stam, J.C. Reijneveld, Graph theoretical analysis of complex networks in the brain, Nonlinear Biomed. Phys. 5 (1) (2007) 3. (1).
[39] M. Schröter, O. Paulsen, E.T. Bullmore, Micro-connectomics: probing the organization of neuronal networks at the cellular scale, Nat. Rev. Neurosci. (2017) http://dx.doi.org/10.1038/nrn.2016.182.
[40] L. Cruz, D.L. Roe, B. Urbanc, A. Inglis, H.E. Stanley, D.L. Rosene, Age-related reduction in microcolumnar structure correlates with cognitive decline in ventral but not dorsal area 46 of the rhesus monkey, Neuroscience 18 (4) (2009) 1509–1520. 158.
[41] A. Hashimoto, K. Suenaga, A. Gloter, K. Urita, S. Iijima, Direct evidence for atomic defects in graphene layers, Nature 19 (7002) (2004) 870–873. 430.
[42] U. Köster, J. Sohl-Dickstein, C.M. Gray, B.A. Olshausen, Modeling higher-order correlations within cortical microcolumns, PLoS Comput. Biol. 10 (7) (2014) e1003684.
[43] Blagojevic P.V.M., Ziegler G.M., 2016. Beyond the Borsuk-Ulam theorem: The topological Tverberg story, arXiv 1605.07321, 1-34.
[44] D.P. Buxhoeveden, M.F. Casanova, The minicolumn hypothesis in neuroscience, Brain 125 (5) (2002) 935–951.
[45] J.F. Peters, Computational Proximity. Excursions in the Topology of Digital Images, Intelligent Systems Reference Library, Springer-Verlag, Berlin, 2016http://dx.doi.org/10.1007/978-3-319-30262-1.
[46] Peters J.F., Tozzi A., 2016. Region-Based Borsuk-Ulam Theorem. arXiv.1605.02987

UNCORRECTED PROOF

frontiers in Human Neuroscience

ORIGINAL RESEARCH
published: 01 February 2017
doi: 10.3389/fnhum.2017.00038

Bold-Independent Computational Entropy Assesses Functional Donut-Like Structures in Brain fMRI Images

James F. Peters[1,2,3,4], *Sheela Ramanna*[5], *Arturo Tozzi*[6]* and *Ebubekir İnan*[3,4]

[1] Department of Electrical and Computer Engineering, University of Manitoba, Winnipeg, MB, Canada, [2] Department of Mathematics, Adıyaman University, Adıyaman, Turkey, [3] Department of Mathematics, Faculty of Arts and Sciences, Adıyaman University, Adıyaman, Turkey, [4] Computational Intelligence Laboratory, University of Manitoba, Winnipeg, MB, Canada, [5] Department of Applied Computer Science, University of Winnipeg, Winnipeg, MB, Canada, [6] Department of Physics, Center for Nonlinear Science, University of North Texas, Denton, TX, USA

We introduce a novel method for the measurement of information level in fMRI (functional Magnetic Resonance Imaging) neural data sets, based on image subdivision in small polygons equipped with different entropic content. We show how this method, called maximal nucleus clustering (MNC), is a novel, fast and inexpensive image-analysis technique, independent from the standard blood-oxygen-level dependent signals. MNC facilitates the objective detection of hidden temporal patterns of entropy/information in zones of fMRI images generally not taken into account by the subjective standpoint of the observer. This approach befits the geometric character of fMRIs. The main purpose of this study is to provide a computable framework for fMRI that not only facilitates analyses, but also provides an easily decipherable visualization of structures. This framework commands attention because it is easily implemented using conventional software systems. In order to evaluate the potential applications of MNC, we looked for the presence of a fourth dimension's distinctive hallmarks in a temporal sequence of 2D images taken during spontaneous brain activity. Indeed, recent findings suggest that several brain activities, such as mind-wandering and memory retrieval, might take place in the functional space of a four dimensional hypersphere, which is a double donut-like structure undetectable in the usual three dimensions. We found that the Rényi entropy is higher in MNC areas than in the surrounding ones, and that these temporal patterns closely resemble the trajectories predicted by the possible presence of a hypersphere in the brain.

Keywords: fMRI, hypersphere, nucleus clustering, strong proximity, temporal pattern, Voronoï tessellation

OPEN ACCESS

Edited by:
Chrystalina A. Antoniades, University of Oxford, UK

Reviewed by:
Dong-Hoon Lee, Yonsei University, South Korea
Zhen Yuan, University of Macau, China

***Correspondence:**
Arturo Tozzi
tozziarturo@libero.it

Received: *07 May 2016*
Accepted: *18 January 2017*
Published: *01 February 2017*

Citation:
Peters JF, Ramanna S, Tozzi A and İnan E (2017) Bold-Independent Computational Entropy Assesses Functional Donut-Like Structures in Brain fMRI Images. Front. Hum. Neurosci. 11:38. doi: 10.3389/fnhum.2017.00038

INTRODUCTION

In this paper, we introduce a novel technique of fMRI images analysis, called computational proximity method, i.e., nucleus clustering in Voronoï tessellations (Peters and Inan, 2016a). The images are subdivided in contiguous (without interstice or overlap) polygons, called the "Voronoï polygons." They yield a density map, called "tessellation," that makes it possible to make an objective measurement of the polygon areas' spatial distribution and helps to define "random," "regular," and

"clustered" distributions (Duyckaerts and Godefroy, 2000; Edelsbrunner, 2014). Tessellations have been already used in neuroscience, i.e., to investigate spatial relations and connectivity between neural mosaics in the retina (Mozos et al., 2011) or to evaluate histological cortical sections (Peters et al., 2016) and pattern recognition (Hettiarachchi and Peters, 2017). In a Voronoï tessellation of an fMRI image, of particular interest is the presence of maximal nucleus clusters (MNC), i.e., zones with the highest number of adjacent polygons (Peters et al., 2016). MNC reveals regions of the brain, independent from blood-oxygen-level dependent (BOLD) signals, characterized by different gradient orientation and diverse functional dimensions (Saye and Sethian, 2011).

To evaluate the power and potentialities of this novel approach, we used the Voronoï tessellation technique combined with Rényi entropy, in order to test the brain-hypersphere hypothesis. Indeed, it has been recently hypothesized that brain activity is shaped in the guise of a functional hypersphere, which performs complicated 4D movements called "quaternionic" rotations (Tozzi and Peters, 2016a). They give rise to the so-called "Clifford torus," a closed donut-like structure where mental functions might take place. The torus displays glued trajectories similar to a video game with spaceships in combat: when a spaceship flies off the right edge of the screen, it does not disappear but rather comes back from the left (Weeks, 2002). The human brain exhibits similar behavior, i.e., the unique ability to connect far-flung events in a single, coherent picture (Atasoy et al., 2016). During brain functions such as memory retrieval and mind-wandering, concepts flow from one state to another and appear to be "glued" together. It has also been recently proposed that the brain, when evaluated in the proper dimension (Kida et al., 2016), is equipped with symmetries in one dimension that disappear (said to be "hidden" or "broken") in just one dimension lower (Tozzi and Peters, 2016b). A symmetry break occurs when the symmetry is present at one level of observation, but "hidden" at another level: it suggests that a 4D hypersphere could be equipped with symmetries, of great importance in order to explain central nervous system (CNS) activities, undetectable at the usual 3D cortical level.

Although we live in a 3D world with no immediate perception that 4D space exists at all, the brain hypersphere rotations can be identified through their "cross section" movements on a more accessible 3D surface, as if you recognized some object from its shadow projected on a screen. We may thus evaluate indirect clues of the undetectable fourth dimension, such hypersphere rotations' hallmarks or signs on a familiar 3D surface. Here we show that, in temporal fMRI series from spontaneous and evoked brain activity, MNC discloses the typical patterns of quaternionic rotations and hidden symmetries.

MATERIALS AND METHODS

Here we describe the novel approach for fMRI neuroimages analysis. In brief, we show how fMRI images of the brain can be divided in small polygons, called tessellation regions, that display different levels of information. We elucidate how the differences amongst the small polygons make it possible for to evaluate otherwise hidden activities of the brain, and how such activities are the expression of transitory functional increases in nervous dimensions.

Samples

In order to validate the novel method via systematic analysis, we favored studies focused on intrinsic (also called spontaneous, or resting-state) instead of task-evoked activity, because the former is associated with mental operations that could be attributed to the activity of a torus (donut-shaped view of brain activity): "screens" are glued together and the trajectories of thoughts follow the internal toroid-shaped surface of a hypersphere. For example, spontaneous brain activity has been associated with day dreaming propensities, construction of coherent mental scenes, autobiographical memories, experiences focused on the future, dreaming state (for a description of the terminology, see (Andrews-Hanna et al., 2014).

We evaluated two published data sets of spontaneous, intrinsic activity, for a total of 64 images:

(a) Spontaneous activity structures of high dimensionality (termed "lag threads") can be found in the brain, consisting of multiple highly reproducible temporal sequences (Mitra et al., 2015). We retrospectively evaluated published video frames showing "lag threads" computed from real BOLD resting state rs-fMRI data in a group of 688 subjects, obtained from the Harvard-MGH Brain Genomics Superstruct Project. We assessed 4 sets of coronal sections (including a total of 54 Images) from the published videos (Threads 1, 2, 3, and 4): http://www.pnas.org/content/suppl/2015/03/24/1503960112.DCSupplemental
(b) We also analyzed 10 well-matched published pairs of networks, from the 20-component analysis of the 29,671-subject BrainMap activation database and (a completely separate analysis of) a 36-subject resting FMRI dataset (Smith et al., 2009).

Furthermore, we also evaluated 16 images from extrinsic (task-related) activity of the brain, in order to compare them with the intrinsic activity of the previous 64 images. We assesssed 16 fMRI images from visual tasks experiments, which illustrate the activity of different brain areas elicited by basic vision and object recognition (Mandelkow et al., 2016). In Mandelkow et al. (2016), a voxel-wise ANOVA F-statistic map (threshold $p < 1\%$, uncorrected) was superimposed on the T1 -weighted anatomical MRI of one representative subject (16 axial slices in radiological convention).

Each of the 80 tessellated images (64 from intrinsic and 16 from extrinsic brain activity) leads to the MNC mesh clustering described in the next paragraph. Such tessellations are also called tilings or meshes. This retrospective work was conducted in conformity with the ethical standards of the field and does not involve human subjects or animals.

Tessellations of Brain Images

This section explains how fMRI brain images can be subdivided into small polygons. In technical terms, we introduce nucleus clustering in Voronoï tessellations of plane surfaces (Edelsbrunner, 2006; Peters, 2016). A Voronoï tessellation is a tiling of a surface with various shaped convex polygons. Let E be

a plane surface such as the surface of an fMRI image and let S be a set of *generating points* in E. Each such polygon is called a Voronoï region $V(s)$ of a

$$V(s) = \left\{x \in E : \|x - s\| \leq \left\|x - q\right\| \text{ for all } q \text{ in } S\right\}.$$

In other words, a Voronoï region $V(s)$ is the set of all points x on the plane surface E that are nearer to the generating point s than to any other generating point on the surface (**Figures 1A,B**). In this investigation of fMRI images, each of the generating points in a particular Voronoï tessellation has a different description. Each description of generating point s is defined by the gradient orientation angle of s, i.e., the angle of the tangent to the point s.

Nucleus Clustering in Tessellated Images

This section elucidates why the small polygons described above are equipped with different, assessable characteristics. In very simple words, some polygons are different from the others, because they display higher number of sides. A *nucleus cluster* in a Voronoï tiling is a collection of polygons that are adjacent to (share an edge with) a central Voronoï region, called the cluster nucleus. In this work, the focus is on maximal nucleus clusters, which highlight singular regions of fMRI images. A pair

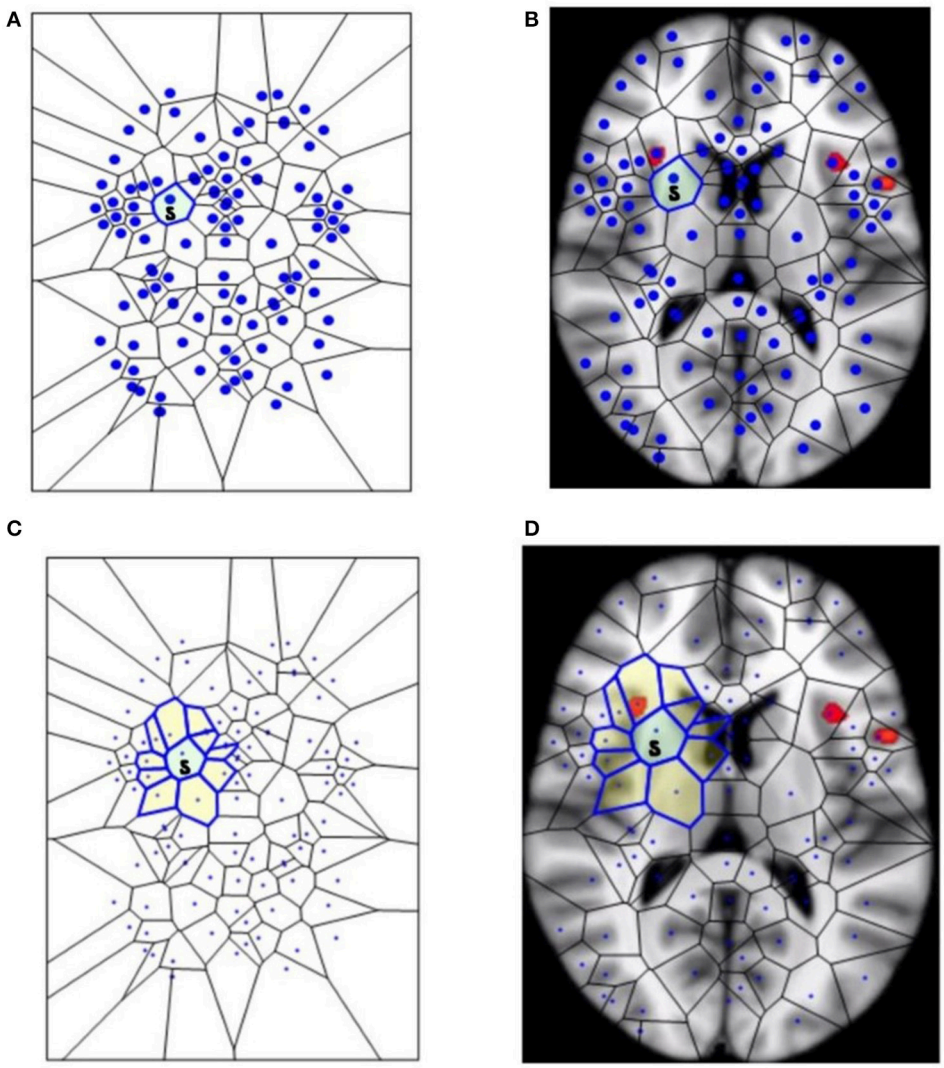

FIGURE 1 | The segmentation of fMRI images into small polygons, which makes it possible to compare the different morphological features displayed by the different groups. (A) Surface tiling of a sample Voronoï region $V(s) =$. Each region in the tiling represents a generating point with particular fMRI image features, such gradient orientation and brightness. It is also worth noting that no two regions have the same description. For this reason, every Voronoï region has a slightly different shape. This tiling is derived from the fMRI image in **(B)**, which displays Voronoï region $V(s)$ on a fMRI image taken from Mitra (11). **(C)** Displays a sample maximal nucleus cluster N for a particular generating point represented by the dot • in N. In this Voronoï tiling, the nucleus N has 10 adjacent polygons. Since N has the highest number of adjacent polygons, it is maximal. This cluster N is of particular interest, since the generating point • in N has *a gradient orientation that is different from the gradient orientation of any other generating point in this particular tiling*. In **(D)**, the maximal nucleus cluster N is shown *in situ* in the tiling of an fMRI image.

of Voronoï regions are considered *strongly near*, provided the regions have an edge in common (Peters, 2016; Peters and Inan, 2016b). A *maximal nucleus cluster N* contains a nucleus polygon with the highest number of strongly near (adjacent) Voronoï regions (**Figures 1C,D**).

For technical readers, the gradient orientation angle θ of a point (picture element) in an fMRI image is found in the following way. Let *img*(x,y) be a 2D fMRI image. Then:

$$G_x = \frac{\partial img}{\partial x},$$
$$G_y = \frac{\partial img}{\partial y},$$
$$\theta = \tan^{-1}\left[\frac{G_y}{G_x}\right] = \tan^{-1}\left[\frac{\frac{\partial img}{\partial y}}{\frac{\partial img}{\partial x}}\right] = \arctan\left[\frac{\frac{\partial img}{\partial y}}{\frac{\partial img}{\partial x}}\right].$$

In other words, the angle θ of the generating point of mesh nucleus is the arc tangent of the ratio of the partial derivatives of the image function at a particular point (x,y) in an fMRI image.

In sum, for each fMRI temporal frame, we produced tessellated images with one or more maximal mesh regions (i.e., a maximal region which contains the maximal number of adjacent regions). Furthermore, we produced tessellated images showing one or more MNC. Each maximal nucleus cluster N contains a central Voronoï region—the nucleus—surrounded by adjacent regions, i.e., Voronoï region polygons.

Also, for technical readers, we provide the steps for constructing a Voronoï tiling (regions) of an fMRI image, so that every generating point has gradient orientation (GO) angle θ that is different from the GO angles of each of the other points used in constructing the tiling on an fMRI image (see **Figure 2**). This form of construction guarantees that each nucleus of a mesh cluster is derived from a unique generating point. This is accomplished by weeding out all image pixels with non-unique GO angles. The end result is a collection of Voronoï regions that highlight different structures in a tessellated fMRI image. Each Voronoï region $V(s)$ is described by feature vector that includes the GO of the generating point s.

Since each s is unique (not repeated in the set of generating points in **Figure 2**), each nucleus mesh cluster N has a unique description. Taking this a step further, we identify maximal nucleus clusters on a tessellated fMRI image. In effect, each maximal N tells us something different about each region of a tiled fMRI image, since we include, in the description of a maximal nucleus, the number adjacent regions as well as the GO of the nucleus generating point.

Informational Entropy in fMRI Tessellations

Here we show why the fMRI polygons with more sides, called MNCs, display higher amounts of informational entropy, and therefore a higher informational content. Summarizing the previous paragraphs, the major new elements in the evaluation of fMRI images are: nucleus clusters, maximal nucleus clusters, strongly near maximal nucleus clusters, convexity structures that occur whenever maximum nucleus clusters intersect (Peters and Inan, 2016a). We showed in the above paragraphs that in a Voronoï tessellation of an fMRI image, of particular interest is the presence of ***maximal nucleus clusters*** (MNC), i.e., clusters with the highest number of adjacent polygons. In this section, we introduce a measure of the information that MNCs in fMRI images yield. We demonstrate that MNC reveal regions of the brain with higher levels of cortical information in comparison with non-MNC cortical regions, uniformly yield less information.

In a series of papers, Rényi (1961, 1966), introduced a measure of information of a set random events. Let X be a set random events such as the occurrence of polygonal areas in a Voronoï tessellation and let $\beta > 0, \beta \neq 1, p(x)$ the probability of the occurrence of x in X. Then Rényi entropy $H_\beta(X)$ is defined by

$$X = \{x_1, \cdots, x_n\},$$
$$H_\beta(X) = \frac{1}{1-\beta}\log_2 \sum_{i=1}^{n} p^\beta(x_i).$$

Because of the relationship between Rényi entropy of a set of events and the information represented by events, Rényi entropy and information are interchangeable in practical applications (Rényi, 1982; Bromiley et al., 2010). In fact, it has been shown that Rényi entropy $H_\beta(X)$ is a monotonic function of the information associated with X. This means that Rényi entropy can be used as a measure of information for any order $\beta > 0$.

Let X_{MNC}, X_{nonMNC} be sets of MNC polygonal regions and non-MNC polygonal regions in a random distribution of tessellation polygons. Also, let $p(x) = \frac{1}{x}, p(y) = \frac{1}{y}$ be the probability of occurrence of $x \in X_{MNC}, y \in X_{nonMNC}$. Notice that the nuclei in MNCs have the highest concentration of adjacent polygons, compared to all non-MNC polygons. Based on measurements of Rényi entropy for observed MNC vs. non-MNC polygons, we have confirmed that Rényi entropy of nucleus polygon clusters is consistently higher than the set of non-MNC polygons (**Figures 3**, **4**). This finding indicates that MNCs yield higher information than any of the polygon areas outside the MNCs.

In sum, Rényi entropy provides a measure of the information in maximal nucleus clusters and the surrounding regions of fMRI images. This means that the information from areas occupied by MNCs vs. non-MNC areas can be measured and compared. Furthermore, the maximal nucleus clusters are equipped with higher entropy values (and corresponding higher information), which contrasts with measure of information in the surrounding non-MNC regions. Hence, MNCs make it possible to pinpoint the sources of most information in fMRI images.

Borsuk-Ulam Theorem Comes into Play

Here we show how a simple theorem from topology is able to shed new light on the fMRI polygons equipped with different content of information. The Borsuk-Ulam Theorem (Borsuk, 1993; Dodson and Parker, 1997) states that:

Every continuous map $f : S^n \rightarrow R^n$ *must identify a pair of antipodal points* (*on* S^n) *with matching descriptions.*

Algorithm 2: Construct Gradient Orientation-Based Voronoï tiling on a Digital Image with a Set of Distinct Mesh Generators, i.e., every generator defines a unique nerve cluster $N := \{V(s)\}$, a collection of Voronoï regions

```
Input  : Read 2D fMRI image img.
Output: Gradient orientation-based Voronoï tiling on img.
Pixels := {pixel p : p ∈ img};
Generators := {s : s ∈ Pixels};
Select p ∈ Pixels;
Pixels := Pixels\p;
/* Remove p from Pixels. */ ;
Compute gradient orientation θ_p of p;
while (Pixels ≠ ∅) do
    Select pNew ∈ Pixels;
    Compute orientation angle θ_pNew;
    /* Next guarantee θ_pNew is not the same as θ_p. */ ;
    if (θ_p ≠ θ_pNew for all s in Generators) then
        Generators := Generators ∪ {pNew};
        /* i.e., add pNew to the set of Generators. */;
        Select p ∈ Pixels;
        Pixels := Pixels\p;
        /* i.e., remove p from Pixels. */ ;
        /* pNew defines a unique nerve cluster N := V(pNew). */ ;
        Compute Voronoï tiling using the set of Generators;
    else
        Ignore pNew;
    /* Continue looking for a unique mesh generator pNew */ ;
Superimpose V(Generators) on img;
```

FIGURE 2 | The steps in the method used to construct the mesh on an fMRI image shown in Figure 1D.

That is, each pair of antipodal points on an n-sphere maps to Euclidean space R^n (Beyer and Zardecki, 2004). Points on S^n are *antipodal*, provided they are diametrically opposite (Marsaglia, 1972; Weisstein, 2015). For further details, see Tozzi and Peters (2016a,b). The two antipodal points can be used not only for the description of simple topological points, but also for more complicated structures (Borsuk, 1969), such spatial or temporal patterns functions, signals, movements, trajectories and symmetries (Saye and Sethian, 2011; Peters, 2016). If we simply evaluate CNS activity instead of "spatial signals," BUT leads naturally to the possibility of a region-based, not simply point-based, brain geometry, with many applications (Tozzi and Peters, 2017). We are thus allowed to describe nervous systems functions or shapes as antipodal points on a n-sphere (**Figure 3**). This means that the activities under assessment (in this case, the 4D torus movements) can be found in the feature space derived from the descriptions (feature vectors) in a tessellated fMRI image.

If we map the two antipodal points on a n–1 –sphere, we obtain a single point. The signal shapes' functions can be compared (Weeks, 2002; Saye and Sethian, 2011): the two antipodal points representing systems features are assessed at one level of observation, while the single point is assessed at a lower level (**Figures 5A,B**). Although BUT was originally described in terms of a natural number n that expresses a structure embedded in a spatial dimension, nevertheless the n value can stand for

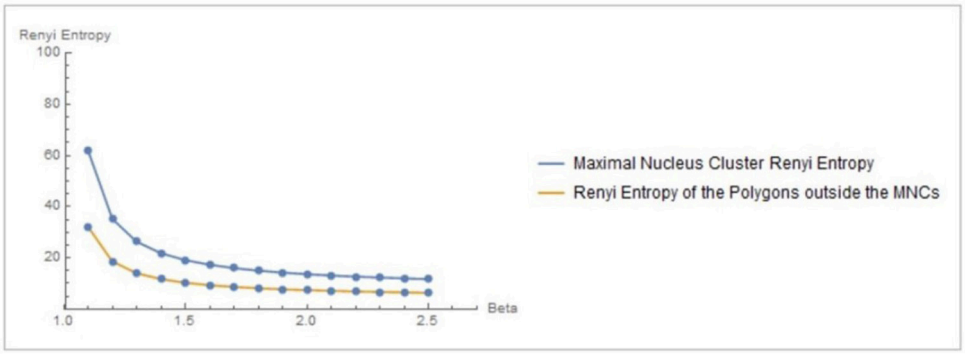

FIGURE 3 | Rényi entropy values of maximal nucleus clusters, compared with the surrounding areas of fMRI images. The *x* axis displays the values of the Beta parameter for $1.1 \leq \beta \leq 2.5$.

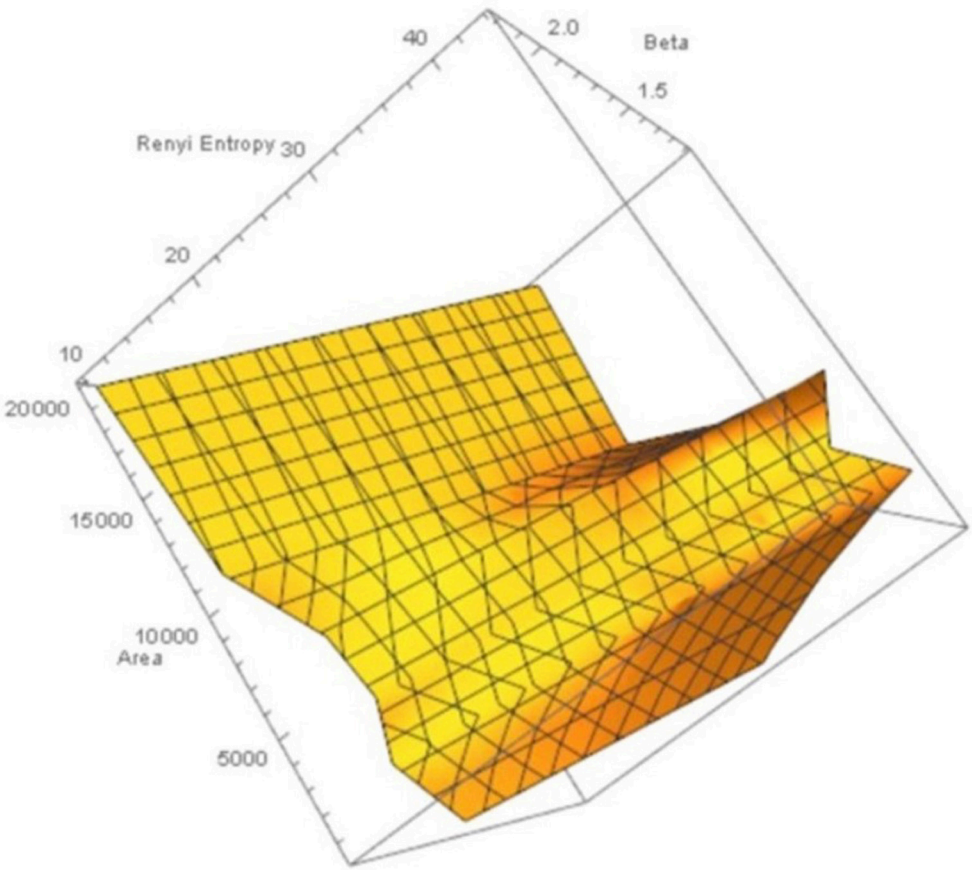

FIGURE 4 | Rényi entropy values vs. number polygon areas vs. $1.1 \leq \beta \leq 2.5$ of maximal nucleus clusters in fMRI images. MNC Nuclei surrounded by polygons with smaller areas have higher Rényi entropy, which tells us that smaller MNC areas yield more cortical information than MNCs with larger areas.

other types of numbers: it can be also cast as an integer, a rational or an irrational number (Tozzi and Peters, 2016b). We might regard functions or shapes as embedded in an *n*-sphere, where *n* stands for a temporal dimension instead of a spatial dimension. This makes it possible to use the *n* parameter as a versatile tool for the description of fMRI brain features (**Figure 5C**).

In sum, BUT and its variants say that:

(a) There exist regional spatial fMRI patterns (shapes, functions, vectors) equipped with matching description, e.g., they display the same features.
(b) We are allowed to assess the spatial patterns described by the MNC in terms of signals or temporal patterns (in our 4D case,

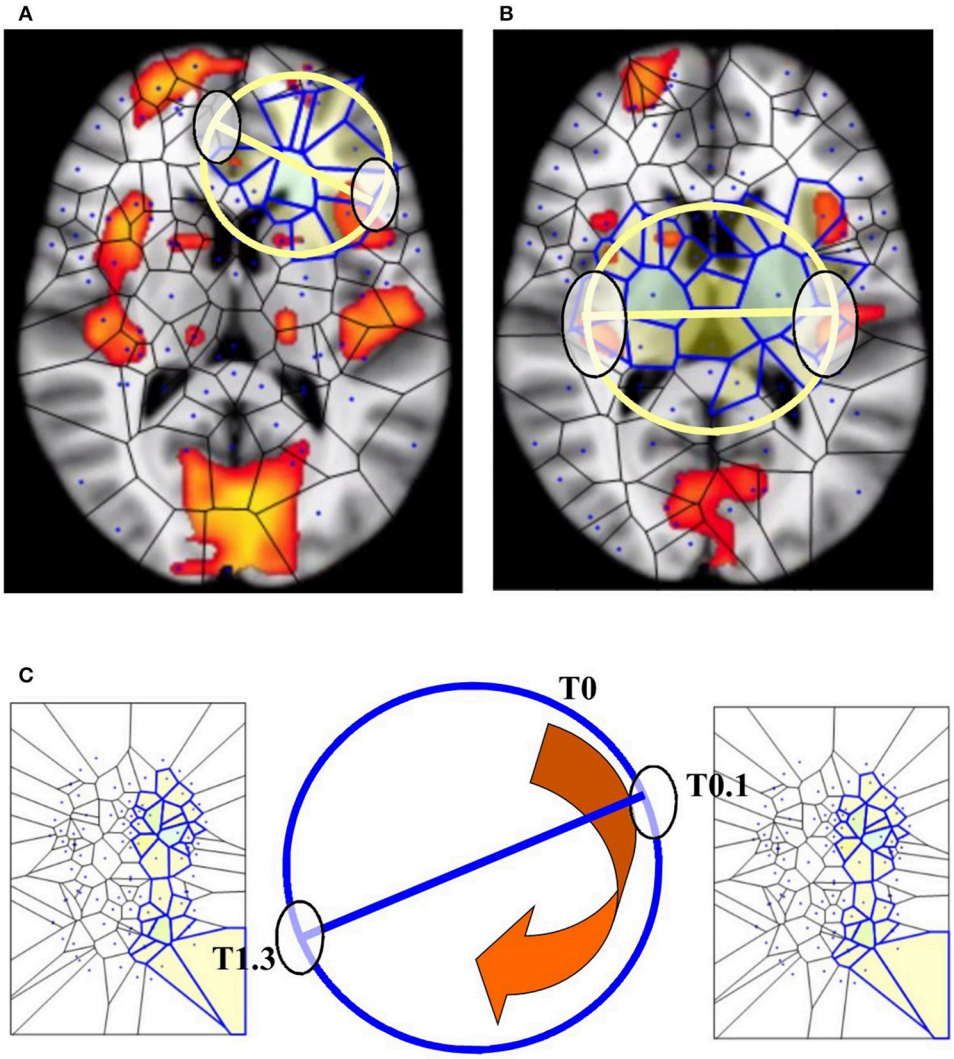

FIGURE 5 | BUT and its variants applied to fMRI neuroimages. (A,B) display respectively one and two maximal nuclei clusters ((11), Thread 2). Antipodal points with matching description (on a spatial circumference) can be detected in both the images. Note that the MNC do not necessarily correspond to the "traditional" BOLD activations (shown in red) detectable in fMRI neuroimaging studies. **(C)** displays a temporal matching description between two maximal nuclei clusters at time T0.1 and T1.3 seconds. Note that, in this Figure, the n-sphere number n refers to the time, and not to a spatial dimension. The curved arrow depicts the time conventionally passing clockwise along the circumference of the n-sphere.

the movements and trajectories on the 3D brain), in order to achieve a real-time description of the movements of the hypersphere.

Quaternionic Movements

In this paragraph, we describe the peculiar brain features that we expect our MNCs might help to elucidate and assess. In a previous study (Tozzi and Peters, 2016a), the presence of a hypersphere was detected invoking BUT: we viewed the antipodal points as brain signals opposite each other on a Clifford torus, i.e., we identified the simultaneous activation of brain antipodal signals as a proof of a perceivable "passing through" of the fourth dimension onto the nervous 3D surface.

Here we evaluated instead, in resting-state fMRI series, a more direct hallmark of the presence of a hypersphere: the trajectory and the temporal evolution of the signals on the 2D brain surface, in order to see whether they match the predicted trajectories of the Clifford torus. To evaluate a hypersphere in terms of a framework for brain activity, we first needed to identify potential brain signal loci where quaternion rotations might take place: we thus embedded the brain in the 3D space of a Clifford torus and looked for its hallmarks or hints (**Figure 6**).

RESULTS

In all the 80 assessed images, either from intrinsic or extrinsic activity of the brain, we found that clusters of higher activity,

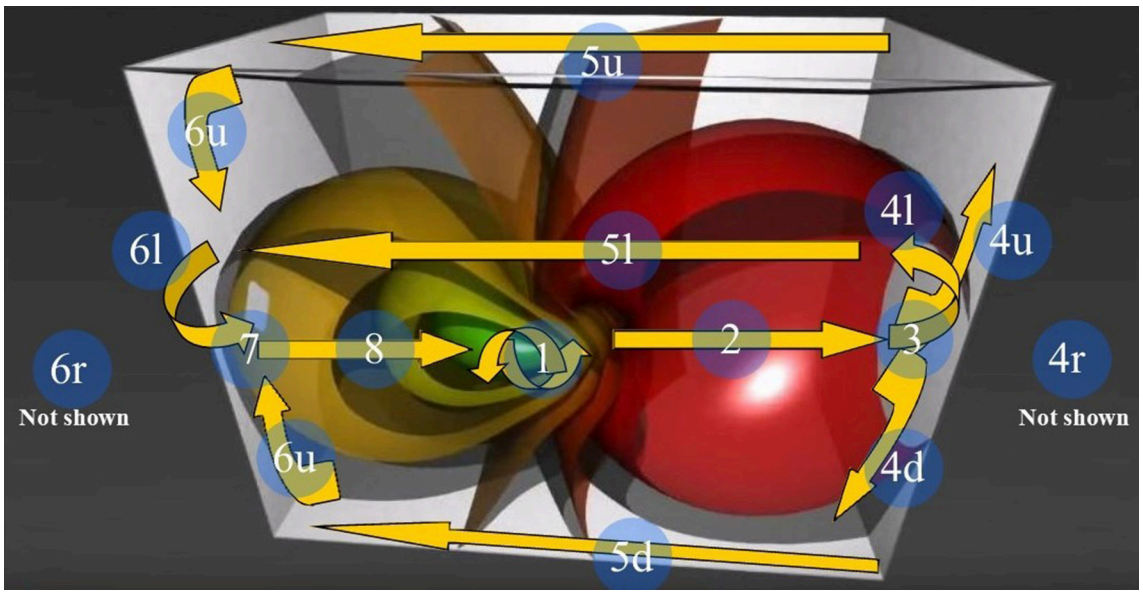

FIGURE 6 | The 3D Stereographic projection of the "toroidal parallels" of a hypersphere (from https://www.youtube.com/watch?v=QlcSlTmc0Ts; see also http://www.matematita.it/materiale/index.php?lang=en&p=cat&sc=2,745). The orange arrows illustrate the trajectories followed by the 4D quaternionic movements of a Clifford torus when projected onto the surface of the 3D space in which it is embedded. The circled numbers describe the trajectories, starting from the conventional point 1 (the letters u,d,r,l denote respectively the upper, down, right, and left trajectories on the surface of the 3D parallelepiped). Note that the arrows follow the external and medial surfaces of the 3D space in a way that is predictable. Just one of the possible directions of the quaternion movements is displayed: the flow on a Clifford torus may indeed occur in every plane. In this Figure, the spheres on the right grow in diameter, forming a circle of increasing circumference on the right surface of the 3D space. Conversely, on the opposite left side, the spheres shrink and give rise to a circle of decreasing circumference on the left surface of the 3D space.

which are equipped with higher Rényi entropy compared with the surrounding zones, are scattered throughout different nervous areas. Therefore, some micro-areas of a specific anatomical zones contain more information than the adjacent ones. In other words, the MNC approach detects regions in the brain with the higher Rényi entropy, compared with the surrounding ones. In 50% of the 80 analyzed images, more than one cluster is detectable.

Concerning the 64 images from spontaneous, intrinsic, resting state activity of the brain, the data analysis shows also that the MNC activity displays in 79.68% (51 of 64) the typical features of the Clifford torus' movements. This supports the hypothesis that a functional hypersphere occurs during resting state brain activity (**Figure 7**). At the beginning, the trajectory of spontaneous activity follows the median sections (see timeframes 0.1–0.3 in **Figure 7**), then moves toward the posterior part of the brain, where a reflexion of four trajectories along the lateral surfaces occurs (0.4). This pattern closely matches the one predicted by the model illustrating the quaternionic movements on a Clifford torus. The temporal sequence also show the hypersphere moves on the brain, and it moves relatively slowly. The hypersphere does not display a regular or continuous movement, rather it proceeds forward and then backward for a short time (time 0.5 and 0.6). From 0.7, the trajectory follows the patterns predicted by **Figure 6**.

In the four available temporal series of the 54 images of spontaneous activity from Mitra et al. (2015), the MNC movements follow a specular, repetitive temporal pattern of activation (**Figures 7**–**9**). For example, the pictures of the first and the last time display MNC activity with matching description. Note that, in the 64 rest-related images, the areas encompassing MNCs do not match those equipped with BOLD activity in 71.87% (46/64) (**Figure 9**).

Concerning the 16 images from evoked, task-related activity elicited by basic vision and object recognition (Mandelkow et al., 2016), they showed a widely distributed MNC pattern throughout the brain. Fifty percent (8/16) of the images displayed the pattern predicted by the presence of a hypersphere, against the above mentioned 79.68% of correspondence detected in images of intrinsic activity.

The results can be summarized as follows: MNCs sequences of brain region activations, apart from differences depending on slight methodological distinctions among the assessed papers, exhibit a stereotyped topographical firing pattern. The movements of a hypersphere are clearly detectable, and the MNC activity clearly displays antipodal points in a temporal sequence, independent from fMRI activation. Such features are more marked in images taken from intrinsic, rather than extrinsic, task-related activity of the brain.

CONCLUSIONS

There are two state-of-the-art approaches for understanding the communication among distributed brain systems using fMRI

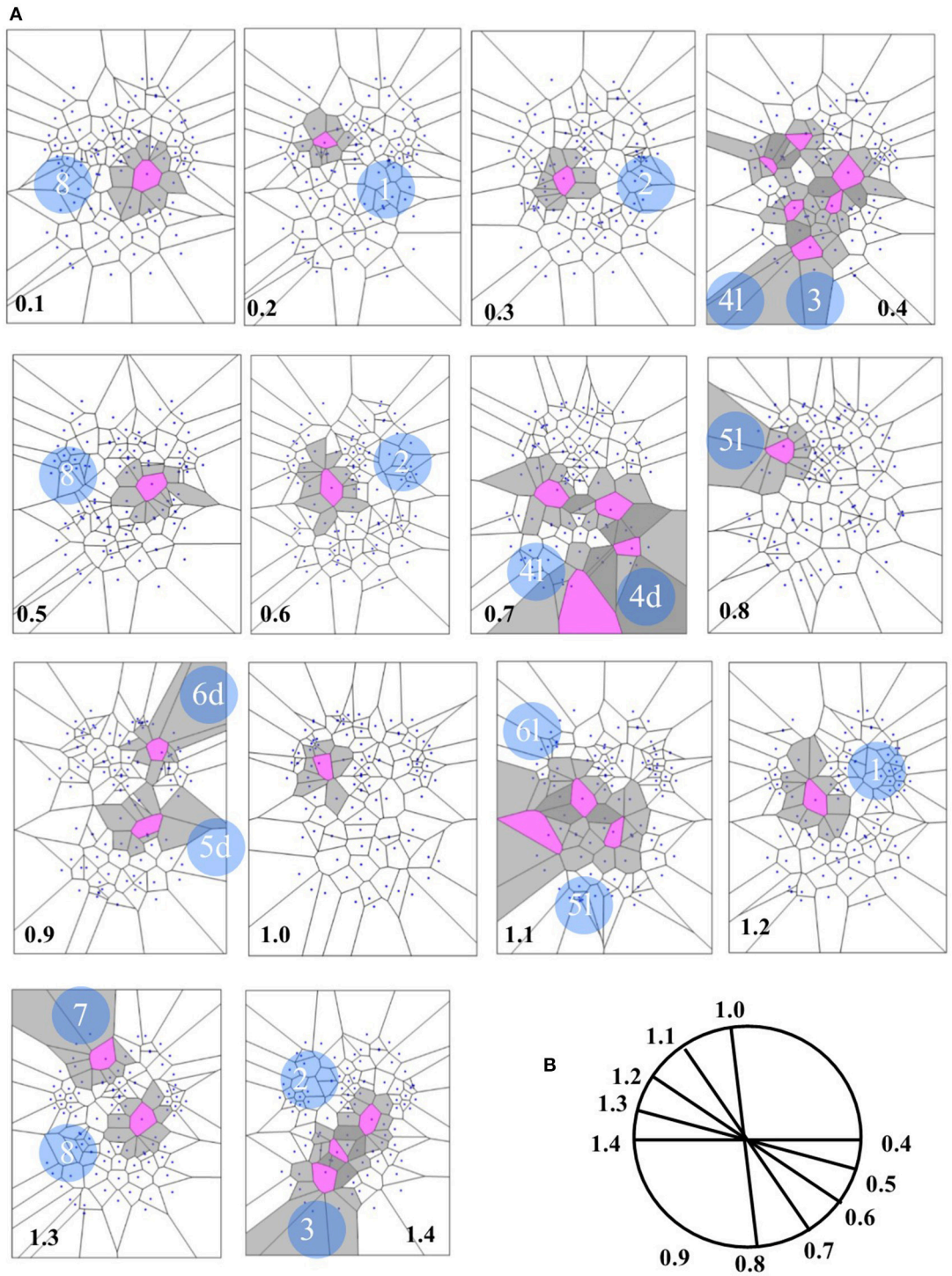

FIGURE 7 | (A) Depicts a real pattern of maximal nuclei clusters temporal activation (from Mitra et al., 2015, Thread 4). Note that the typical trajectories of a Clifford torus are clearly displayed (see **Figure 6** for comparison). If you look at the parallelepipedal 3D projections of the 4D quaternionic movements (**Figure 6**), the MNC embedded in the 2D brain surface stand for the 4D movements INTERNAL to the parallelepiped, while the MNC lying outside of the 2D brain surface stand for the 4D movements on the SURFACE of the parallelepiped in **(B)**. The movements described by maximal nucleus clusters are temporally specular. A matching description among temporal frames occurs, so that, for example, the frame 0.2 displays the same MNC features of 1.3. This means that the hypersphere moves in a stereotyped sequence and according a repetitive temporal sequence, following the trajectories predicted by the quaternionic model.

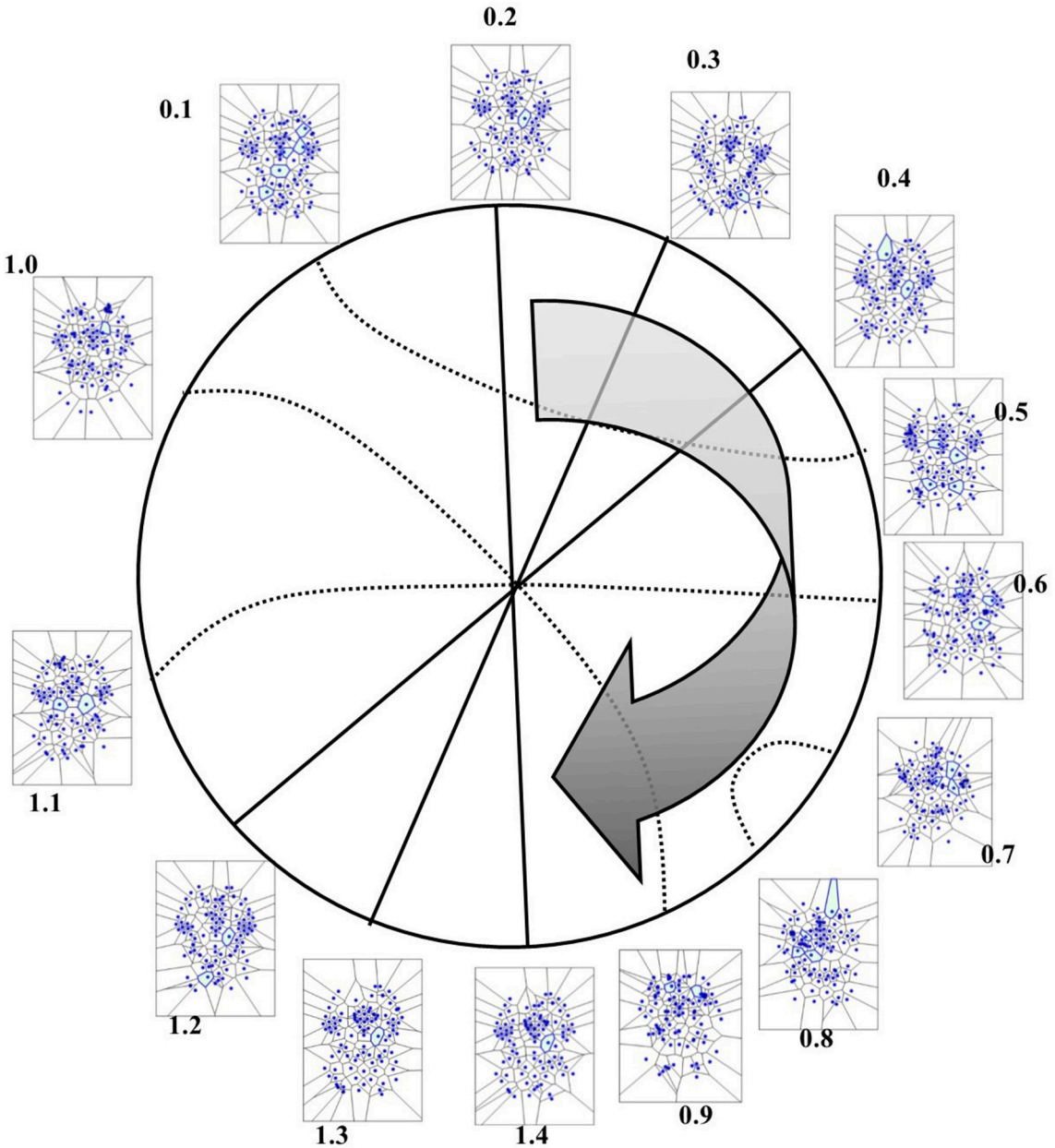

FIGURE 8 | Temporal antipodal points (from Thread 2 frames). The straight lines connecting opposite points on the temporal circumference depict "pure" antipodal points, while the curved lines depict non-antipodal points with matching description.

data. The first approach termed as *dynamic causal modeling* uses models of effective connectivity, while the second, called *Granger causal modeling,* uses models of functional connectivity (Friston, 2009, 2010). Our paper introduces a novel method, based on computational proximity (CP). This novelty can be expressed as follows: rather than being correlated with the "classical" BOLD activity, the CP method shows how spatial regions are correlated through their "proximity" (descriptive closeness to each other). From the experiments reported here, we are beginning to see different forms of brain function represented by the MNCs. We have demonstrated that computational proximity (i.e., strongly near nucleus mesh clusters) in 2D fMRI images is able to reveal hidden temporal patterns of Rényi entropy, enabling us to detect functional information from morphological data. The combination of tessellated images, topological framework provided by BUT, and Rényi entropy indicators of the information levels of image regions provide a systematic basis for the study of fMRIs. The validation of this approach to fMRI analysis stems from the mathematics of BUT and Rényi entropy. Central to this form of neural analysis

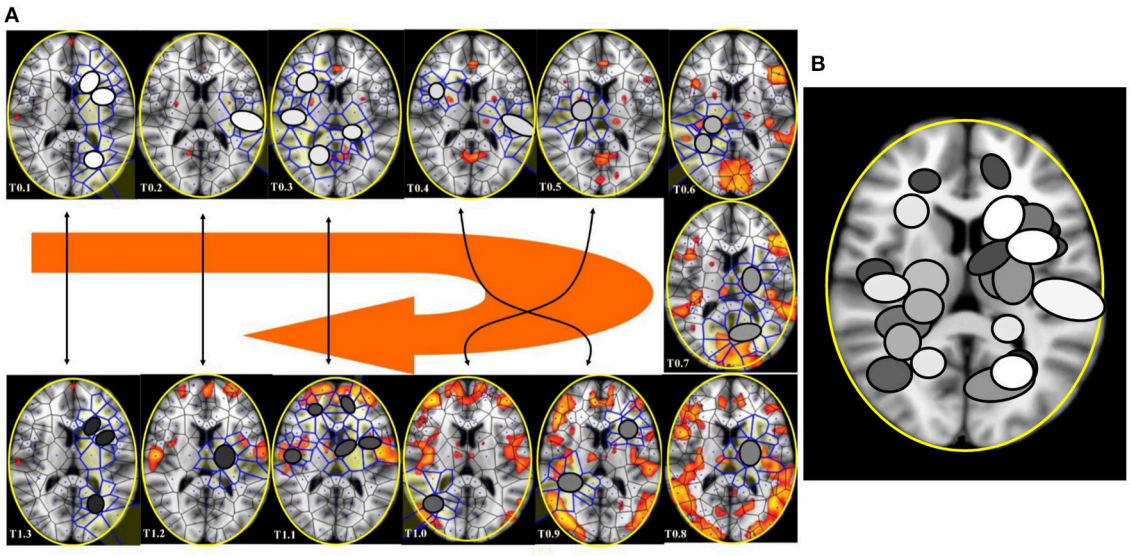

FIGURE 9 | (A) This figure (from Thread 1 timeframes) depicts another way to illustrate temporal antipodal points. The temporal sequences are displayed clockwise, from $T = 0.1$ to $T = 1.3$. The Voronoï regions embedded in MNC are depicted as circles. The white circles refer to the presence of mesh clusters at high activity in the initial times, the gray circles in the intermediate times and the darker circles in the later times. **(B)** MNC activity on 13 superimposed, consecutive brain images from Thread 1 (from time T0 to T13). Note that the areas of nuclei activation are scarcely superimposed to the "classical" zones of BOLD activation (shown in red).

is its introduction of tessellated fMRI images. Tessellation is a natural choice, since fMRI images by their nature both visual and geometric. There is a natural transition from a tessellated fMRI image to a consideration of those fMRI regions where the greatest changes occur. The greatest-change-regions are in the form of maximal nucleus clusters (MNCs) in each tessellated image. Detected MNCs in tessellated fMRI images are then subjected to analysis by BUT and the mechanics of Rényi entropy. The end result is a complete, verifiable, rigorous analysis fMRI images that are easily understood because of their visual character. The accuracy of the tessellated fMRI image approach stems from the computational geometry that leads to the detection of MNCs (Peters, 2016; Peters and Inan, 2016a; Peters et al., 2016; Tozzi and Peters, 2016b).

Here we have shown that a morphological analysis of simple 2D images taken from fMRI video frame sequences might give insights into the functional structure of neural processing. In a previous study, we evaluated the possible *hints* of a hypersphere on simple fMRI scans during resting state brain activity (Tozzi and Peters, 2016a). We showed how, due to the Borsuk-Ulam theorem (BUT), the fMRI activation of brain antipodal points could be a signature of 4D. The antipodal points predicted by BUT could be evaluated not just on images taken from fMRI studies, but also on datasets from other neuro-techniques, such as, for example, EEG. In the current study, we used a novel method, in order to confirm the data of the previous work with a completely different and more sophisticated approach. Indeed, looking at the sequences of maximal nucleus clusters and their entropy, we found experimental patterns compatible with the ones predicted by the hypersphere model. We detected on the 3D brain "shadows" of a 4D hypersphere rotating according to quaternion movements: these "hints" make it possible for us the possibility to visualize both the spatial arrangement and the movements of the corresponding Clifford torus. In other words, in particular during spontaneous brain activity, the apparently scattered temporal changes in MNCs follow a stereotyped trajectory which can be compared with the 4D movements of a hypersphere. Our study uncovered evidence of hypersphere during spontaneous activity, demonstrating that brain activity lies on a 3-sphere embedded in 4D space. How can be sure that the MNC reveals the presence of a brain hypersphere? Three cues talk in favor of this hypothesis. First, the MNC patterns, in particular during resting state fMRI data sets, closely resemble the theoretical trajectories predicted by Clifford torus movements. Second, temporal sequences of fMRI images display matching description, in agreement with the BUT dictates. Third, there is a difference in Rényi entropy between MNC and the surrounding zones, thereby pointing toward diverse levels of activity. The reproducibility of the hypersphere movements suggests that this organizational feature is essential to normal brain function. Because the Clifford torus incessantly changes its intrinsic structure, due to the different transformations of the quaternionic group, it is reasonable to speculate that each mental state corresponds to a different hypersphere's topological space. The concept of a hypersphere in the brain is also more noteworthy, if we frame it in the general picture of nervous symmetries (Tozzi and Peters, 2016b).

A shift in conceptualizations is evident in a brain theory of broken symmetries based on a hypersphere approach. It might be speculated that symmetries are hidden in a 3D dimension and restored in the higher dimension of the hypersphere, and

vice versa. This means that brain functional and anatomical organization may be better assessed if one considers how certain hidden "symmetries," essential to shaping brain gradients and activity, may only appear under the lens of higher-dimensional neural representations (Tozzi and Peters, 2016b), i.e., the hypersphere. We anticipate our essay to be a starting point for further evaluation, both in physiological and pathological conditions, of a neural fourth spatial dimension where other brain functions, such as perception, memory retrieval, might take place. It is also possible that every brain function displays a peculiar temporal pattern of such a novel entropic "activity." In sum, we operationalized a novel, fairly inexpensive, image-analysis technique useful in detecting hidden temporal patterns in the brain. We can assess the spatial patterns described by MNCs in terms of entropy variations. While, by our "subjective" and "private" viewpoint, we tend to watch an image inferring the semantic parts in order to give it a meaning, MNCs allow the detection of the "objective" entropy, which do not necessarily correspond to the zones of the figure that we view as more significant. This means that MNCs provide a basis for quantifying high-yield information areas in fMRI image features that are normally "hidden" from our attention.

AUTHOR CONTRIBUTIONS

All the authors equally contributed to: study concept and design, acquisition of data, analysis and interpretation of data, drafting of the manuscript, critical revision of the manuscript for important intellectual content, statistical analysis, obtained funding, administrative, technical, material support, and study supervision.

FUNDING

The research has been supported by the Natural Sciences & Engineering Research Council of Canada (NSERC) discovery grants 185986 and 194376.

REFERENCES

Andrews-Hanna, J. R., Smallwood, J., and Spreng, R. N. (2014). The default network and self-generated thought: component processes, dynamic control and clinical relevance. *Ann. N.Y. Acad. Sci.* 1316, 29–52. doi: 10.1111/nyas.12360

Atasoy, S., Donnelly, I., and Pearson, J. (2016). Human brain networks function in connectome-specific harmonic waves. *Nat. Commun.* 7:10340. doi: 10.1038/ncomms10340

Beyer, W. A., and Zardecki, A. (2004). The early history of the ham sandwich theorem. *Amer. Math. Month.* 111, 58–61. doi: 10.2307/4145019

Borsuk, M. (1969). Fundamental retracts and extensions of fundamental sequences. *Fund. Math.* 64, 55–85.

Borsuk, M. (1993). Drei sätze über die n-dimensional euklidische sphäre. *Fund. Math.* XX, 177–190.

Bromiley, P. A., Thacker, N. A., and Bouhova-Thacker, E. (2010). *Shannon Entropy, Rényi Entropy, and Information*. Tina 2004-004, Statistic and Inf Series, Imaging Science and Biomedical Engineering Division, University of Manchester.

Dodson, C. T. J., and Parker, P. E. (1997). *A User's Guide to Algebraic Topology.* Dordrecht: Kluwer.

Duyckaerts, G., and Godefroy, G. (2000). Voronoï tessellation to study the numerical density and the spatial distribution of neurons. *J. Chem. Neuroanat.* 20, 83–92. doi: 10.1016/S0891-0618(00)00064-8

Edelsbrunner, H. (2006). *Geometry and Topology for Mesh Generation.* Cambridge: Cambridge University Press.

Edelsbrunner, H. (2014). *A Short Course in Computational Geometry and Topology*. Cham: Springer Briefs in Applied Sciences and Technology, Springer.

Friston, K. (2009). Causal modelling and brain connectivity in functional magnetic resonance imaging. *PLoS Biol.* 7:e33. doi: 10.1371/journal.pbio.1000033

Friston, K. (2010). The free-energy principle: a unified brain theory? *Nat. Rev. Neurosci.* 11, 127–138. doi: 10.1038/nrn2787

Hettiarachchi, R., and Peters, J. F. (2017). Voronoï region-based adaptive unsupervised color image segmentation. *Patt. Recogn.* 65, 119–135. doi: 10.1016/j.patcog.2016.12.011

Kida, T., Tanaka, E., and Kakigi, R. (2016). Multi-dimensional dynamics of human electromagnetic brain activity. *Front. Hum. Neurosci.* 19:713. doi: 10.3389/fnhum.2015.00713

Mandelkow, H., de Zwart, J. A., and Duyn, J. H. (2016). Linear discriminant analysis achieves high classification accuracy for the BOLD fMRI response to naturalistic movie stimuli. *Front. Hum. Neurosci.* 10:128. doi: 10.3389/fnhum.2016.00128

Marsaglia, G. (1972). Choosing a Point from the Surface of a Sphere. *Ann. Math. Statist.* 43, 645–646. doi: 10.1214/aoms/1177692644

Mitra, A., Synder, A. Z., Blazey, T., and Raichle, M. E. (2015). Lag threads organize the brain's intrinsic activity. *Proc. Natl. Acad. Sci. U.S.A.* 112, 2235–2244. doi: 10.1073/pnas.1503960112

Mozos, O. M., Bolea, J. A., Fernandez, J. M., Ahnelt, P. K., and Fernandez, E. (2011). Reprint of: V-Proportion: a method based on the Voronoï diagram to study spatial relations in neuronal mosaics of the retina. *Neurocomputing* 74, 1165–1174. doi: 10.1016/j.neucom.2011.02.001

Peters, J. F. (eds.). (2016). "Computational proximity," in *Excursions in the Topology of Digital Images, Vol. 102* (Berlin: Springer, Intelligent Systems Reference Library), 169–171.

Peters, J. F., and Inan, E. (2016a). Strongly near Voronoï nucleus clusters. *arXiv* 1602, 1–7.

Peters, J. F., and Inan, E. (2016b). Strongly proximal Edelsbrunner-Harer nerves. Zbl 06665117. *Proc. Jangjeon Math. Soc.* 19, 563–582.

Peters, J. F., Tozzi, A., and Ramanna, S. (2016). Brain tissue tessellation shows absence of canonical microcircuits. *Neurosci. Lett.* 626, 99–105. doi: 10.1016/j.neulet.2016.03.052

Rényi, A. (1961). "On measures of entropy and information," in *Proceedings of the Fourth Berkeley Symposium on Mathematical Statistics and Probability, Vol. I*, (Berkeley, CA: University of California Press), 547–457.

Rényi, A. (1966). On the amount of information in a random variable concerning an event. *J. Math. Sci.* 1, 30–33.

Rényi, A. (1982). *Tagebuch über die Informationstheorie,* Vol. 173. Berlin: VEB Deutcher der Wissenschaften.

Saye, R. I., and Sethian, J. A. (2011). The Voronoi implicit interface method for computing multiphase physics. *Proc. Nat. Acad.* Sci. *U.S.A.* 108, 19498–19503. doi: 10.1073/pnas.1111557108

Smith, S. M., Fox, P. T., Miller, K. L., Glahn, D. C., Fox, P. M., Mackay, C. E., et al. (2009). Correspondence of the brain's functional architecture during activation and rest. *Proc. Natl. Acad. Sci. U.S.A.* 106, 13040–13045. doi: 10.1073/pnas.0905267106

Tozzi, A., and Peters, J. F. (2016a). Towards a fourth spatial dimension of brain activity. *Cogn. Neurodyn.* 10, 189–199. doi: 10.1007/s11571-016-9379-z

Tozzi, A., and Peters, J. F. (2016b). A topological approach unveils system invariances and broken symmetries in the brain. *J. Neurosci. Res.* 94, 351–365. doi: 10.1002/jnr.23720

Tozzi, A., and Peters, J. F. (2017). A symmetric approach elucidates multisensory information integration. *Information* 8:4. doi: 10.3390/info8010004

Weeks, J. R. (2002). *The Shape of Space, 2nd Edn.* New York, NY; Basel: Marcel Dekker, Inc.

Weisstein, E. W. (2015). *Antipodal Points*. Available online at: http://mathworld.wolfram.com/AntipodalPoints.html

Conflict of Interest Statement: The authors declare that the research was conducted in the absence of any commercial or financial relationships that could be construed as a potential conflict of interest.

Copyright © 2017 Peters, Ramanna, Tozzi and İnan. This is an open-access article distributed under the terms of the Creative Commons Attribution License (CC BY). The use, distribution or reproduction in other forums is permitted, provided the original author(s) or licensor are credited and that the original publication in this journal is cited, in accordance with accepted academic practice. No use, distribution or reproduction is permitted which does not comply with these terms.

TOWARDS TOPOLOGICAL MECHANISMS UNDERLYING EXPERIENCE ACQUISITION AND TRANSMISSION IN THE HUMAN BRAIN

Note: this manuscript is a previous version of the published paper:
Tozzi A, Peters JF. 2017. Towards Topological Mechanisms Underlying Experience Acquisition and Transmission in the Human Brain. J.F. Integr. psych. behav. doi:10.1007/s12124-017-9380-z

Arturo Tozzi (Corresponding Author)
Center for Nonlinear Science, University of North Texas
1155 Union Circle, #311427 Denton, TX 76203-5017 USA
Computational Intelligence Laboratory, University of Manitoba, Winnipeg, Canada
Winnipeg R3T 5V6 Manitoba
tozziarturo@libero.it

James F. Peters
Department of Electrical and Computer Engineering, University of Manitoba
75A Chancellor's CircleWinnipeg, MB R3T 5V6 CANADA and
Department of Mathematics, Adıyaman University, 02040 Adıyaman, Turkey
James.Peters3@umanitoba.ca

Keywords: Mind; Brain; Borsuk-Ulam Theorem; Sensation

ABSTRACT

Experience is a process of awareness and mastery of facts or events, gained through actual observation or second-hand knowledge. Recent findings reinforce the idea that a naturalized epistemological approach is needed to further advance our understanding of the nervous mechanisms underlying experience. This essay is an effort to build a coherent topological-based framework able to elucidate particular aspects of experience, *e.g.*, how it is acquired by a single individual, transmitted to others and collectively stored in form of general ideas. Taking into account concepts from neuroscience, algebraic topology and Richard Avenarius' philosophical analytical approach, we provide a scheme which is cast in an empirically testable fashion. In particular, we emphasize the foremost role of variants of the Borsuk-Ulam theorem, which tells us that, when a pair of opposite (antipodal) points on a sphere are mapped onto a single point in Euclidean space, the projection provides a description of both antipodal points. These antipodes stand for nervous functions and activities of the brain correlated with the mechanisms of acquisition and transmission of experience.

Current advances in human neurosciences shed new light on questions concerning the status of mental activity and its relation to physical function. Promising innovations such as transcranial stimulation (Filmer et al., 2014) and mind-to mind communication (Grau et al., 2014) call for broad methodological investigations in order to further advance our understanding of the brain. In this essay we will focus on *experience*, an active process of understanding, knowledge and mastery of facts or events which encompasses a different range of brain functions, such as thought, perception, memory, emotion, will, imagination, inter-individual communication and scientific theories (Cavell, 2002). Experience is gained through: a) the direct, actual observation of immediately perceived events and subsequent interpretation, b) or records or summaries from first-hand observers or experiencers c) or from instruments (Popper and Eccles, 1997).

In such a framework, simple concepts from algebraic topology, e.g., the Borsuk-Ulam theorem (BUT) and its variants, come into play, giving rise to a different approach that makes it possible to evaluate mental activities correlated with experience. In this essay, we will limit our topological evaluation to specific features of experience, *e.g.*, its acquisition and transmission. We will start from the pure, unmediated experience of the single individual and will proceed towards objects categorization and social experience through a plurality of shared experiences. In other words, we will investigate knowledge acquisition by an individual, a community and mankind at large. We will pursue the inductive approach introduced by the French Swiss philosopher Richard Avenarius (1843-1896). His *Kritik der reinen Erfahrung* (*Critique of Pure Experience*) (Avenarius, 1908) provides a useful high-level interpretation of physiological functions and psychological behavior, which works well in building a topological framework for experience (Russo Krauss, 2013; Russo Krauss, 2015).

This paper comprises six sections. The first section introduces BUT and its variants. Section two, devoted to objective evidence from experiments, shows how, despite our current lack of topological knowledge of the brain activity, a large number of papers tackled the issues of geometric representations of perceptual phenomena, relationships between geometrical shapes and nervous function, and changes in brain dimensions. The third section analyses the experiences of a single individual, who includes no other standpoint than that where he stands. As the case of the Greek philosopher, he is in the turmoil of the market-place, not as buyer or seller, in order that he may just observe. Particular cases are provided in sections four and five, in order to establish the psychological correlates of experience acquisition and transmission. In section six, we extend the experience onto social groups and a general human setting, where the most general concepts may arise. Section seven aims to answer the crucial question: what does a topological approach bring to the table, in the experimental evaluation of physiological mechanisms of experience?

1) THE BORSUK-ULAM THEOREM AND ITS VARIANTS

The Borsuk-Ulam Theorem (BUT) states that, if a sphere S^n is mapped continuously into an n-dimensional Euclidean space R^n, there is at least one pair of antipodal points on S^n which map onto the same point of R^n (Borsuk, 1933; Dodson, 1997; Beyer, 2004) (**Figure 1A**). See Tozzi and Peters (2016a) for further details and a mathematical treatment. The notation S^n stands for an n-sphere (Weeks, 2002), which is an n-dimensional, circular structure, embedded in an $n+1$ space (Marsaglia, 1972). For example, a 2-sphere (S^2) is the 2-dimensional surface of a 3-dimensional space (the exterior of a beach ball is a good illustration). Antipodal points are, *e.g.*, the poles of a sphere (Matousek, 2003; Collins, 2004).

We can consider regions on an n-sphere that are either adjacent or far apart (**Figure 1B**). This means that pairs of points need not be antipodal, in order to have matching descriptions (Peters, 2016). This BUT variant has utility, provided there are a pair of regions on an n-sphere which are *similar*. The concept of antipodal points can be used not

just for the description of points, but also for more complicated structures, such as shapes of space (object contours), temporal intervals (temporal oscillations), functions, vectors and symmetries (Borsuk, 1958-59; Borsuk, 1969; Peters, 2014; Tozzi and Peters 2016b) (**Figure 1C**). This leads to a particularly useful region-based BUT, dubbed reBUT (Peters, 2016). We are thus allowed to describe brain features on an *n*-sphere either as antipodal points, or antipodal regions. This means that antipodal signal shapes can be compared (Weeks, 2002; Peters, 2016). That is, feature-based descriptions of antipodes can be assessed at one level of observation, while their projections into a single shape can be analyzed at a lower level (Tozzi and Peters, 2016b).

Although BUT was originally limited to an *n*-sphere where *n* is a natural number, nevertheless *n* can also be regarded as rational or irrational number (Tozzi and Peters, 2016b). For example, we might regard functions or shapes as embedded in a sphere in which *n* stands for number of instants in time. Hence, the parameter *n* becomes useful in the description of dynamical systems such as the brain.

The original formulation of BUT describes the presence of antipodal points on spatial manifolds in every dimension, provided the manifold is a convex, positive-curvature structure (e.g., a ball). However, the kind of geometry that best describes human sensation, perception and higher mental processes, such as knowledge and consciousness, is a matter of debate. Theoretical contenders able to connect the stimulus and mental issues include Euclidean, elliptic and hyperbolic geometry. This means that brain functions might occur on manifolds endowed with other types of geometry: for example, the hyperbolic one encloses complete Riemannian *n*-manifolds of constant sectional curvature -1 and concave shape (*i.e*, a saddle) (Sengupta et al., 2016). We are thus allowed to look for antipodal points also on structures equipped with kinds of curvature other than the convex one (Mitroi-Symeonidis, 2015). Or, in other words, whether the brain displays a concave, convex or flat functional appearance, it does not matter: we may always find the points with matching description predicted by BUT (Tozzi, 2016). For further details, see also Peters and Tozzi (2016b).

In sum, the BUT displays four versatile ingredients which can be modified in different guises: a continuous mapping, two antipodal (or non-antipodal) points (or functions) with matching description, an *n*-sphere where the *n* value may change and, last but not least, the mapping of antipodal points into the lower level of a *n-1* sphere.

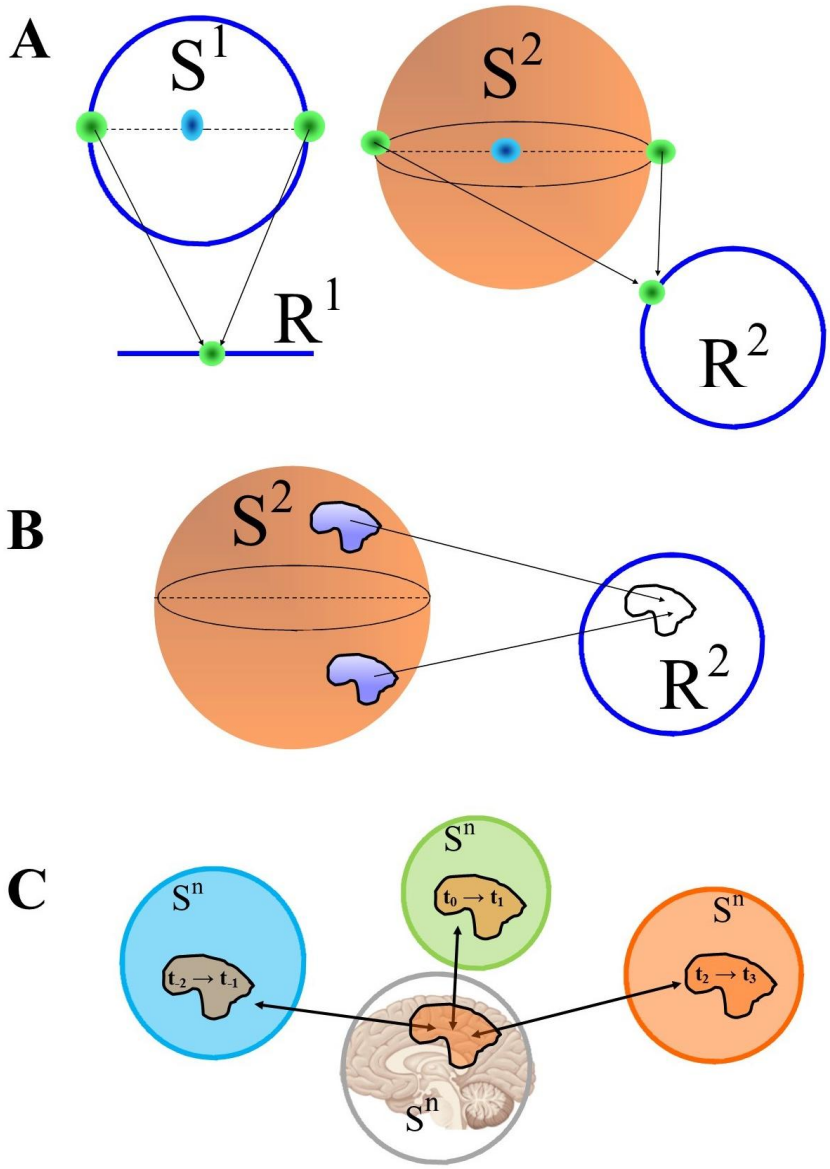

Figure 1A. *The Borsuk-Ulam theorem in case of S^n being a circle and a sphere. Two antipodal points in S^n project to a single point in R^n, and vice versa.* ***Figure 1B.*** *Simplified sketch of a BUT variant. Two functions with matching description do not need either to be antipodal (shown here), or embedded in the same n-sphere (shown in* **Figure 1C***), in order to be described together.* ***Figure 1C*** *displays an example of brain oscillations in a topological framework. In this case, the antipodal regions are three temporal intervals, embedded in different spatial n-spheres, which project to the brain surface. Therefore, the concept of similar antipodal signals can be used not just for the description of points or spatial features, but also of temporal sequences. This means that BUT allows us to compare not just motionless points or shapes, but also events.*

2) NEUROSCIENCE AND TOPOLOGY: STATE OF THE ART

The use of topological and geometrical tools (such as projections, shapes and vectors) for the assessment of mental phenomena dates back to the pioneering works of Alfred North Whitehead (Whitehead 1919) and Kurt Lewin (Lewin, 1935 and Lewin, 1936). In more recent times, such approach has been put forwards by "neuro-episthemological" scholars and pursued, among others, by eliminative materialism (Churchland, 2007), integration information theory (Tononi, 2008), while Suppes (2002) provides a setting for investigating problems of representation and invariance in

any systematic part of science. Due to the current lack of knowledge and the novelty of this field, it must be clearly stated that the "smoking gun" describing whether the invariant isomorphic structure between the brain and its function is effective or not, has not yet been found.

However, some studies assessed with proper experimental procedures the transformational relationship between the stimuli and the mechanisms of mental phenomena such as experience, knowledge, sensation, cognition, consciousness. They point towards a topological approach to mental phenomena as objective evidence, obtained either from actual experiments or results of computer simulations. Luneburg's task (1947) was to assess the mapping of physical space into visual space. This task can be fulfilled, if the metric of visual space can be expressed in guise of a physical bipolar coordinate system. The highly influential studies from Marr (1982) addressed the issue of visual information in terms of mathematical analysis and computational investigation. Findings suggest that nervous structures process information through topological as well as spatial mechanisms. For example, experiments on tachistoscopic perception of visual stimuli demonstrated that the visual system is sensitive to global topological properties, indicating their extraction as a basic factor in perceptual organization (Zeeman 1962). It is has been hypothesized that hippocampal place cells create topological templates to represent spatial information (Dabaghian et al., 2012; Dabaghian et al., 2014; Arai et al., 2014; Chen, 2014). Using a computational model based on Persistent Homology Theory, Milton et al. (2015) demonstrated that, in the physiological range, hippocampal place cells encode the topological features of the environment that serves as a basis of a cognitive map of space, spatial memory and spatial awareness. We will show in the next sections how the novel incarnations of the "classical" Borsuk-Ulam theorem lead to a better comprehension and assessment of several topological features of direct perception and imagination.

It has been argued that perception of persisting surfaces depends on the perception of specific structures, invariant over time (Gibson, 1971; Gibson, 1979). Gibson accounted for our knowledge of world objects by borrowing a concept of invariance in topology: a series of transformations can be endlessly and gradually applied to a pattern without affecting its invariant properties (Gibson,1950). Recognition (perceiving) objects entails continuous mappings between our representations of objects and in-the-world ones (Johnson-Laird, 2010). In effect, perception can be explained by equivalent configurations (form, shapes) of objects (Heft 1997; Rock, 1983). And, principal among the properties of world objects, is shape and acquisition of persistent perception of object shapes, which we explain with BUT variants.

The raising interest for topology in order to investigate neural structures is testified by a series of recent published papers. For example, Giusti et al. (2015) developed a novel approach to matrix analysis, called clique topology, in order to extract both random and geometric meaningful structures in pyramidal neurons in rat hippocampus, during non-spatial behaviors such as wheel running and rapid eye movement sleep. The Authors suggest that the geometric structure of correlations is shaped by the underlying hippocampal circuits, and does not stand merely for a consequence of position coding. Simas et al. (2015) devised a method that allows different operations between networks which share the same set of nodes, by embedding them in a common metric space and enforcing transitivity to the graph topology. They applied this method to construct an aggregated network from a set of functional graphs, each one from a different subject. Therefore, the comparison of aggregated functional topological network reveals emerging features, that could not be observed when the comparison is performed with the classical averaged functional network. Robinson et al. (2016) found that the eigenmodes of a single brain hemisphere's spatial structure are close analogues of spherical harmonics, which are the natural modes of the sphere. This last finding allows the use of the classical BUT in the description of neural field theory.

A foremost argument related to brain topology is the symmetry. Symmetries are invariances underlining physical and biological systems (Weyl, 1982). A symmetry break occurs when the symmetry is present at one level of observation, but "hidden" at another level (Roldàn et al., 2014). BUT tells us that we can find, on an n-dimensional sphere, a pair of opposite points that have the same encoding on an n-1 sphere. This means that symmetries can be found when evaluating the system in a proper dimension, while they disappear (are hidden or broken) when we assess the same system in just one dimension lower (Tozzi and Peters, 2016b). The term dimension, in our case, does not stand for a spatial dimension, rather reflects functional relationships of brain activities that take into account the dimensionality of the neural space. Connectivity and complex network analyses of neural signals allow the assessment of brain activity's dynamics, providing a novel insight into the multidimensionality of various neural functions' representations (Luce et al., 1995; Kida et al., 2016; Robinson et al. 2016). Apart from giving insights in neural dynamics in the *canonical* three dimensions (space, time, and frequency), complex network analyses are also able to evaluate other functional dimensions, e.g. categories of neuronal indices such activity magnitude, connectivity, network properties and so on (Kida et al., 2016). From a dynamical system perspective, one would expect that nervous dynamics can be described in terms of trajectories and/or manifolds in n-dimensional phase spaces (Lech et al., 2016). Mazzucato et al (2016) demonstrated that stimuli reduce the dimensionality of cortical activity. Clustered networks, such as default mode network, have instead a larger dimensionality, because the latter grows with ensemble size: the more neurons are recruited, the more the dimensions (Mazzucato et al., 2016). Singer et al. (2016) proposed that the low-dimensional cortical dynamics due to stimulus-induced synchronization in the visual cortex are sub-states that represent the results of computations performed in the high-dimensional state-space provided by recurrently coupled networks. Because dimension reduction and symmetry breaking display close relationships, symmetries are correlated with changes in

functional dimensions in the brain. Indeed, a key feature of dynamical approaches is that the dynamics they predict are characterized by non-equilibrium phase transitions, and therefore breaks of symmetries (Scholz et al., 1987; Jirsa et al., 1998). Brain symmetric states display dimensions higher than the asymmetric ones. In such a vein, Stemmler et al. (2015) proposed that animals can navigate by reading out a simple population vector of grid cell activity across multiple, different microscopic dimensions. While the spatial activity of a single grid cell does not constitute a metric, an ensemble of hierarchically organized grid cells does provide instead a distance measure (Stemmler et al., 2015).
In sum, the study of changes in brain dimensions proposed by BUT and its variant is a promising novel methodology. For example, Benson et al. (2016) recently developed an algorithmic framework for studying how complex networks are organized by higher-order connectivity patterns, revealing unexpected hubs and geographical elements. Furthermore, Kleinberg et al. (2016) demonstrated that real networks are not just random combinations of single networks, but are organized in specific ways dictated by hidden geometric correlation between layers. Such correlations allowed the detection of multidimensional communities, e.g., sets of nodes that are simultaneously similar in multiple layers. Crucial for our topological arguments, such multidimensionality also enables accurate trans-layer link assessment, meaning that connections in one layer can be predicted by observing the hidden geometric space of another layer. For example, when the geometric correlations are sufficiently strong, a multidimensional framework outperforms navigation in the single layers, allowing efficient targeted navigation simply by using local multilayer knowledge (Kleineberg et al., 2016).

3) EXPERIENCE ACQUISITION AT THE INDIVIDUAL LEVEL

Every human individual originally accepts:

a) an ever-changing spatial environment composed of manifold parts dependent on one another,
b) other human individuals making manifold describable statements and
c) these statements are dependent upon the environment.

When an individual becomes aware of some of the manifold parts of the environment outside him, he states he is having an experience. In a topological framework, we embed the environment in an *n*-sphere, the cortical layers in a *n*-Euclidean space and the describable statements in another *n*-sphere (**Figure 2**). The environmental *n*-sphere contains an object detected by the human individual, *e.g.*, manifold parts perceived together, while the other *n*-sphere contains statements which are not simple sounds or noises, but words (or gestures, such as the lacrimal secretions which point to crying or mimic movements) describing the object. A triad is accomplished, where a person is the only one of the three member who is a witness. The object and its verbal counterpart stand for two antipodal points, while their matching description is achieved in the brain of the human individual. It is noteworthy that the topological relationships among the three members do not exist out of the triad (**Figure 3**). We cannot perceive the thoughts and the sensations of other people, but just assign them thoughts and sensations analogous to ours. In topological words, we project our thoughts, emotions and statements to other people embedded in further environmental n-spheres. Our perception of an object continues, even when the object is out of sight. This can concisely explained by viewing regions on the surface of a S^n sphere as multiple representations of object shapes, mapped continuously to an object embedded in the environment that we have seen and continue to see. This occurs thanks to the continuous mapping from shapes in our memory to shapes in Euclidean space. In effect, persistence perception can be viewed as signals matching, i.e., real-scene visual signals that are collectively the umbra of physical shapes. Therefore, a mutual relationship occurs between the individual and the environment (Gibson, 1986). This perceptive experience is direct and immediate: information is directly taken from the environment, with no mediations. The topological concept of a smart mechanism able to extract the invariants from the input stream means that the active subject puts in relationships and connexions the objects through his senses, with no need for mental processing in order to build them. Topology nicely explains this interesting feature, which is common not just to perceptions, but also to higher mental activities (see the next paragraphs). Indeed, the antipodal points do not stand just for spatial features, such as an object, but also for temporal sequences (**Figure 1C**). Therefore, the brain links together not just spatial elements in an object, but also temporal events in a concept, an idea, a proposition, a hope, a desire and so on. Furthermore, the individual can be embedded not just in a spatial *n*-sphere, but also in an *n*-sphere in which *n* stands for the time, according to the dictates of the BUT variants. Many spheres with different times are possible: this means that the individual is able to link past and future events.

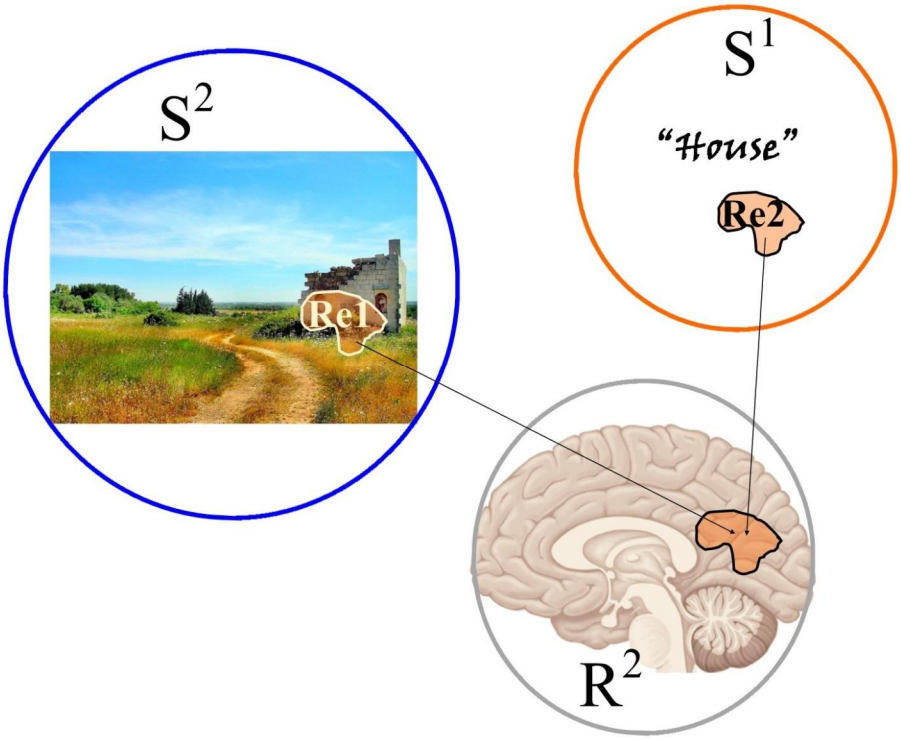

Figure 2. *Topological view of the individual experience evaluated through BUT variants. The environment is embedded in a S^n sphere, where the signal Re1, standing for an object, displays matching description with the signal Re2 embedded in a S^{n-1} sphere, standing for the word corresponding to the object. Both Re1 and Re2 project to a single signal, embedded in a manifold R^n, e.g., the brain.*

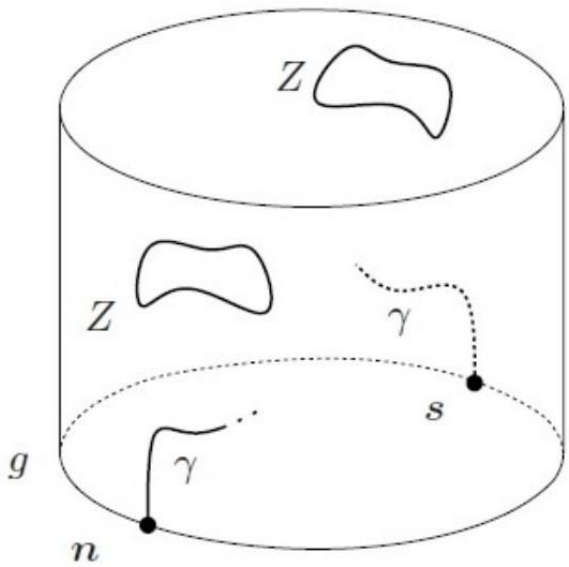

Figure 3. *The two figures Z with matching description project to the two functions γ on the g plane. It easy to see that, if we follow the two functions γ from n and s on, their ends cannot meet. Likewise, the two figures Z display similar features, but are disjoint. Modified from Matousek, 2003.*

Consider the following propositions, that are neither equivalent to each other nor are they interchangeable:

a) if a statement comes from the environment, then the statement is an experience;
b) if a statement is an experience, then the statement comes from the environment.

Indeed, the link between environment and statements is very dynamical. Sometimes, when environment changes, *e.g.*, during a chemo-physical experiment, a variation in statement follows. Other times statements may vary even if environment does not change, and vice versa: *e.g.*, over time, a child watching the same figure could detect modifications in the image, or the the same name may refer to different people. Statements may also change due to differences in the cultural background of individuals.

From this, we can ask the following three questions.

1) In what sense does an experience come from the environment?
2) In what sense is a statement an experience?
3) Do these two questions collimate or diverge?

The next Sections will be devoted to the answers of these three questions, via topological tools. The concepts of matter, substance, soul, consciousness, necessity, freedom, reality will not be included in our answers, nor the long-standing issue of causality. Indeed, the topological concept of proximity helps in elucidating the cause-and-effect problem in observing phenomena. Current scientific experience is grounded on the tenets of causality, *e.g.*, the relation between two processes where the first, the cause, is assumed to be responsible for the second, the effect. It is believed that the brain infers the causes underlying sensory events (Parise et al., 2011), or, in other words, is able to understand the causes when just the effects are known. This inferencing is not limited to conscious and high-level cognition, but it is also performed continually and effortlessly in unconscious perception (Körding et al. 2007). We argue that, if we evaluate different spatial and temporal (neural) phenomena in the light of the "sameness" and projections instead of causality, we achieve a novel view of brain events which has the potential to be operationalized and cast in an empirical way. Inference is replaced by affine connections, proximities, mappings and homotopies (i.e., perceived shapes are mapped into others, such as a coffee cup mapped to a torus). This is in touch with some philosophers (Hume, 1739-40) and scientists (Libet et al., 1987; Bengson et al., 2014) who believe that inference is just a trick of the mind, *i.e.*, the cause-effect relationships do not exist, but are merely apparent correlations among events dictated by our natural, evolutionary instinct of mental association among conjoined events. In Hume's words, we tend to believe that things behave in a regular manner to the extent that behavior patterns of objects seem to persist into the future, and throughout the unobserved present. Chicharro and Ledberg (2012) noticed that, because subsystems in the brain are often bidirectionally connected (Friston, 2008; Barrett and Simmons, 2015), this means that interactions rarely should be quantified in terms of cause-and-effect. A recently introduced concept, termed primitive chaos, is closely related to fundamental problems such as determinism, causality, free will and predictability (Ogasawara, 2010; Ogasawara and Oishi, 2012). Under some conditions, a new primitive chaos is constructed from the original primitive one, achieving a hierarchic structure. Such a picture implies that new events and causality are built from the old ones through a coarse-graining process. It is noteworthy that, under natural conditions, each primitive chaos leads to topological transitivity, while their infinite varieties are guaranteed by a non-degenerate Peano continuum, which typically might stand for a S^n sphere (Ogasawara and Oishi, 2014; Ogasawara, 2015).

4) EXPERIENCE MECHANISMS: BRAIN OSCILLATIONS TOWARDS UNSTABLE ENERGETIC EQUILIBRIA

A *system* is formed of two variables connected in a way such that when one changes, the other changes. The initial state occurs before the variation, the final state afterwards. **Figure 4** provides an example of how a topological formulation of a system allows an objective quantification of empirically testable features. The changes can be either real or merely possible. The final state depends on two settings, namely, the initial state of the system and the external factors acting on the system.

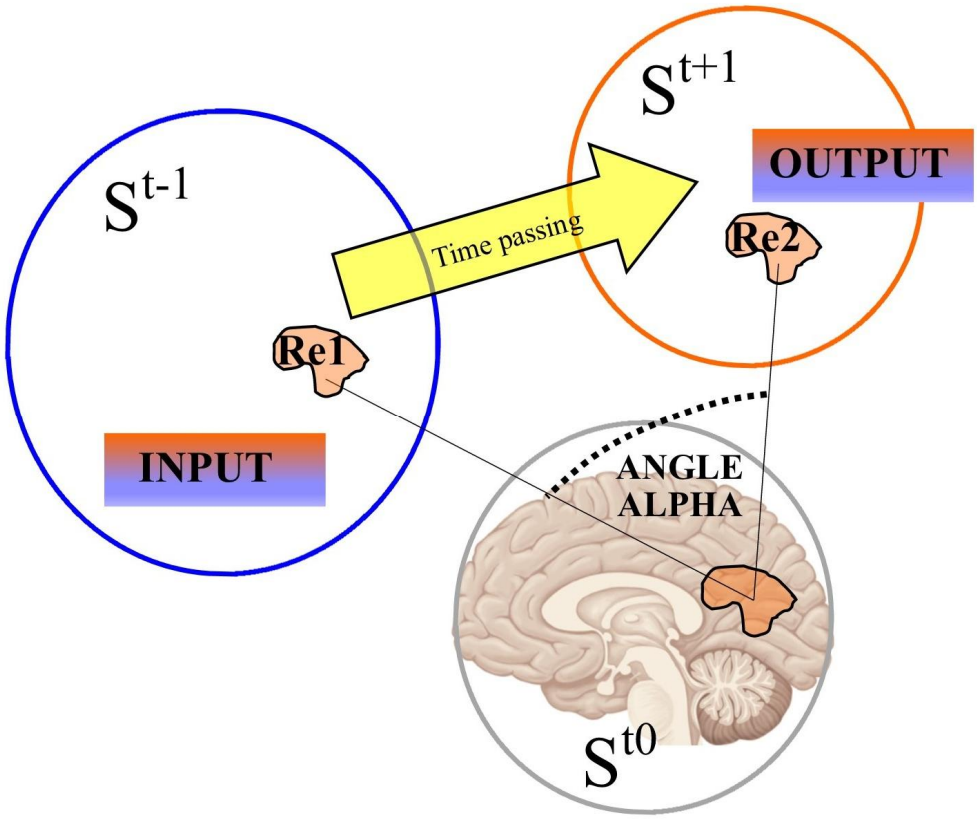

Figure 4*. A system formed by n- spheres made of time dimensions, according to one of the BUT variant. The antipodal regions Re1 and Re2 are located respectively onto a sphere equipped with a dimension of time T-1 (the past) and T+1 (the future). The brain occupies the present time T0. The angle alpha, corresponding to the temporal distance between the presentation of the stimulus and its word retrieval, can be measured. Modified from Tozzi and Peters (2016b).*

The environment of a single individual is also a system that can be divided into spatial and social environments. The environment acts on organisms in two ways, namely, impinging on an organism causing a material change, or stimulating the nerves. A human individual is the source of a peculiar environment, having both non-nervous and nervous systems. The nervous system, in turn, can be divided in peripheral and central nervous system (Nieuwenhuys et al, 2008). The statements made by human beings do not depend on the environment, nor by the peripheral nerves. Indeed, when nerves are damaged, it is still possible to have sensations such as phantom limb syndrome and visual hallucinations during optic nerve atrophy. Is there a part of the CNS which provides a basis for statements? We need not care about the precise anatomical and physiological structure, since experimental evidence has not sufficiently localized brain functions. Therefore, it makes sense to agree that there is a division of functional subsystems in the brain, irrespective of differences in morphological development and functional relationships. From this point forward, the term *brain* refers to unidentified subsystems that are the source of statements.

Acceptance that statements depend on the environment is tantamount to accepting that they depend on the brain and, particularly, on changes in brain. Statements depend on the environment just in the sense that the environment is able to modify the brain. While variations of the environment are studied by the special sciences, we will focus instead on variations of an individual, and in particular, of his brain. Statements do not directly depend on the environment but rather on brain variations. An entire psychical life is a function of self-preservation of the organism within certain limits. The highest levels of conservation are achieved when an energetic equilibrium occurs in the brain between two opposite dynamical forces, namely, brain activity and energy requirements. The brain alternates between these states of equilibrium and breaks into a process that consists of *oscillations* between the two phases, in the deviation from a preliminary value and in approximating to it again. When changes take place, the equilibrium of a brain is disturbed and conditions that annul the changes occur, so that the brain approximates once again to its maximum-maintenance. The functional phenomenon termed brain *oscillation* might encompass different mechanisms, *e.g.*, attractors (Tozzi, Fla, Peters 2016), transient heteroclinic channels (Afraimovich et al., 2013), networks with collective computational abilities

(Hopfield 1982; Izhikevich, 2010), nervous oscillators (Zlotnik et al., 2016) and so on. Despite the countless possible scenarios, the processes governing the brain *oscillations* may be generalized, when we take into account the second law of thermodynamics, which states that *every process occurring in nature proceeds in the sense in which the sum of the entropies of all bodies taking part in the process is increased* (Planck's formulation). An issue of central relevance in this context is the *free-energy principle* (FEP) (Friston, 2010). The brain is a self-organizing system at non-equilibrium steady state with its environment (Tognoli and Kelso, 2014) which has to minimize its free-energy, in order to resist a natural tendency towards disorderly state and high entropy. This formulation reduces the physiology of brain to its homeostasis, namely, the maintenance of system states confronted with a constantly changing environment. The brain is regarded as an active inference machine that works according to Bayesian principles: sensory inputs constrain estimates of prior probability from past experience, to create the posterior probabilities that serve as beliefs about the causes of such inputs in the present (Sengupta et al., 2013; Sengupta et al, 2014: Sengupta et al., 2016). The probability of sensory states must have low entropy and, since entropy is also the average self-information or "surprise", the brain implicitly avoids surprises (Friston et al, 2015). Agents suppress free-energy (or surprise) by changing: a) the sensory input, though an action on external states (the environment), or b) their internal brain states, through perception or attention. The imperative to maintain a non-equilibrium steady-state through exchanges with the environment acquires a logical-mathematical framework when evaluated through topological lenses. Indeed, one can regard belief-updating as free-energy minimisation in terms of energetic gradients and information flows (Sengupta et al., 2016) occurring in brain phase spaces embedded in n-spheres. We will be back on the operationalization of this energetic argument in Section five. The concepts of *proximity* (spatial as well as descriptive closeness) and affine connections are also helpful in solving one of the problems raised by *oscillations, e.g.*, how cooperation among so many "distant" sub-networks occurs seamlessly in real time. Thanks to the continuous mapping provided by BUT, we achieve a quantifiable explanation to the speed and balance of a system characterized by hierarchical and cross-hierarchical cooperating modules (Linkenkaer-Hansen et al., 2001).

5) VITAL TRAINS, CHARACTERS, ELEMENTS

In the previous Section, we argued that the elementary physiological processes consist of a state of disturbance of the equilibrium of the brain, followed by a restoration of the difference. All the changes which lie between this beginning and end of a physiological process are termed *vital train*. This is a complex three-stages process. The initial section emerges from a quiet state in which the oscillation, *e.g.*, a disturbance which breaks the equilibrium, is introduced. Follows then an intermediate section, where compensation mechanisms are activated via variations counteracting the oscillations. The final state is such that the oscillation is suppressed, with return to the quiet and maximum preservation state. The removal of the alteration, in order to achieve the highest level of conservation, may occur in two ways, namely, return to the original stable state or to a different stable state. Here we give an example which illustrates how mental life is arranged in three sections. At start, there is the expected value, stated by the individual as sure, true, known. When a statement is perceived as the same, long chains of oscillations lead to *all together*, *always*, *everywhere*, progressively reaching more general concepts. When the *identical* becomes a rule, the rules become laws and the truths become sure, existing, while the *different* becomes exception. Then enters a variation, stated as different, diverging, doubtful, unexpected. It comes together with the feeling of pain, opposition, or uncertainty, dissatisfaction. The second, following section is an effort to suppress the anomaly: the brain strives to remove the unpleasant experience. In touch with FEP, variations can be removed either through peripheral action (practical behavior), or through brain action (theoretical behavior). There are two ways to suppress the variations: (1) reduction of the unknown to the known; (2) gradual habituation to a change, so that the unknown becomes known. In the fifth Section we will describe how topology helps in elucidating these ways to suppress variations. A value is achieved in the final section which leads to feelings of rest, satisfaction, certainty, truth and quiet. It must be stressed that each statement is influenced by type and magnitude of an individual's background (Betzel et al., 2014). Although every vital train of thoughts ends with phase three, the ideal equilibrium of the brain can be never achieved, due to the continuous dynamics of infinite, superimposed, cross-linked, hierarchical vital trains. Indeed, the brain operates at the edge of chaos and tends to live near a metastable state of second-phase transition (Papo, 2014; Deco and Jirsa, 2012; Beggs and Timme, 2012; de Arcangelis and Herrmann, 2010). In other words, the brain displays nonlinear dynamics. As we will see in Section five, BUT and its variants give us the possibility to achieve linear dynamics from nonlinear ones.

A vital train is a process that progressively removes useless terms, approximating to the final pure stages equipped with: a) minimum energy and maximum stability, b) higher spatial and temporal unrestriction. The evolution of vital trains is towards more perfect series, *i.e.*, the lowest energetic basins, where the gradient descent values can be calculated by comparing angles between n-spheres.

The role of habituation and its changes is crucial, because they give rise to the *identity* and the *difference*. The more the same oscillation is repeated, the more the sensation is perceived as usual, and the same, certain, the known, the familiar. In an energetic context, habituation stands for the state equipped with the lowest possible energy (Tozzi et al., 2016). The final state of the brain is a physiological configuration which is unvaried towards every changing component of the environment. However, this final state embeds not just the final pure state, but also other accidental factors, which need to be progressively abolished. This occurs because minimal energy is difficult to reach. The answer to the first question in Section 2 is thus the following: the environment is at the base of the experience just in case it leads to variations in the individual brain, and just in case a statement depends on environmental variations. However, such values are valid just for a given individual, in a given moment: the individual final state varies from individual to individual, and also from place to place and from epoch to epoch (Barttfeld et al., 2015; Gorgolewski et al., 2014; Vuksanovic and Hövel, 2014).

In sum, the general scheme is the following: when an individual makes a statement, a change in oscillations occurs in brain. The statements depend upon the characteristics of the physiological variations in brain and its oscillations. Of utmost importance is the sensation of prevalence and perception of finer details (discrimination), in which some sensations are highlighted by the attention, compared with the faded background sensations. In topological terms, the prevalence plays an important role in deciding which parts of the environmental n-sphere must be taken into account: it means that the brain chooses from the external inputs the complex of elements of biological significance and marks them as *signals*. A possible role for visual attention and prevalence in an energetic gradient descent context has been recently hypothesized (Sengupta et al., 2016). Consciousness can be linked to our first BUT ingredient, namely, a continuous mapping. Indeed, brain activity needs continuous inputs from a source of enduringly active neurons. The ascending arousal system is a good candidate, because it contains tonic active neurons which guarantee a continuous electric stream towards the cortex, at least during alertness (Nieuwenhuys et al., 2008). In such a framework, consciousness stands both for physiological tonic neurons and for the continuous mapping required by BUT.

Human statements can be partitioned into characters (qualifications like pleasant, nice, beneficial, unpleasant) and elements (such as green, cold, hard, sweet). The difference between characters and elements is that the former are mutable and can be defined as forms, while the latter are permanent and can be defined as contents. At first, we examine experience regarded as character, *i.e*. the variable form (emotions, sensations, perceptions and so on), in which we experience anything. The question is not what individuals mean by an experience, but rather what individuals state is an experience. Many examples can be listed in which statements are referred as experience, *e.g*., the appearance of the sun, perceived temporal relationships among events, the difference between sleep and arousal, travel in far countries during dreams, miracles, presages of death, causal connections, footprints of animals, calculations and mathematical theorems. So, what is an experience? Is it always linked to the external environment? Does it refer to entities, or simply to the cognition of their existence, or is it pure cognition without existence? No one of the solutions proposed in answer to these questions is satisfactory, because experience cannot be defined in only in one way. The individual simply bumps into the components of the environment, and then describes what he has encountered. When a little girl states that she has seen angels, then the angels are an experience for her. The individual who states “it is an experience”, is equivalent to coalescing a plurality of single perceptions, explainable thanks to BUT and its variants.
Thus, a better although incomplete definition of experience could be: *something perceived*. Also the ego, the I, is a statement, in which perception is felt as the individual’s own perception. The more an observable and the individual are separated, the more the observable is perceived as active and a factum of experience, while the individual perceives selfhood as a passive percipient. Now we evaluate experience regarded as content, *i.e*., everything which is felt, sensed, perceived and so on. When individuals state they have an experience, what is the content of their experience? That content depends on modifications in the brain and on the current state and education of each individual. Regardless whether statements are about existing or non-existing entities, all the values perceived in a given moment as experience are indeed the content of experience, and may vary with individual changes. The answer to the second question raised in Section 2 is thus the following: experience, in a narrower definition, is the perception from the brain’s standpoint of the things extracted from the environment. A wider definition of experience does not involve things, but ideas. Ideas can also appear to be about existing, simply there or given entities, so that, even if a centaur is not an experience, its idea is an experience. Thus, a *continuous* flow occurs from the perceived thing (the narrower concept of experience) to the represented idea (the wider concept of experience). *Continuos*, in touch with one of the BUT ingredients.

6) EXPERIENCE TRANSMISSION AT INTER-INDIVIDUAL LEVELS

Brains of different individuals join together in higher order systems formed by social assemblies. The whole mass of human experience tends to become adapted as much as possible to the surrounding world. Humanity stands, as a whole, for a kind of ultra-human organism, following the same basic rules of self-preservation of the individual. When the geographical and social environment widens to include the entire Earth surface and all mankind, the brain removes the accidental factors via a process of progressive elimination. However, due to the differences of initial conditions among individuals, the ideas achieved in the third section could lead, after a while, once again from a known to an unknown. The ultimate suppression of variations occurs via the search for universal laws. Over time, individuals and the generations project faster, simpler and unavoidable concepts. This ongoing conceptualization of our experience is an approximation process that always tends towards identical highly generalized, unlimited concepts characterized by simple, complete descriptions, by qualitative differences expressed in many ways and by formal equivalences expressed in different forms.

The highest concepts, i.e. the final states corresponding to all the possible environment manifold parts, are equipped with the maximum possible frequency and embrace all the possible historical contents of the statements. For a topological explanation, see **Figure 5A**. Godel's suggestion of abstract terms more and more converging to the infinity in the sphere of our understanding take us straight to a comparison with systems equipped with BUT antipodal points and regions. The highest concept, expressed by the statement the *whole is this* is the *concept of the world* (e.g., an abstract idea). In terms of BUT, we achieve a progressive symmetry decrease. Starting from the countless symmetries endowed in the environment, we accomplish into the brain their substantial decrease (Tozzi and Peters, 2016b).

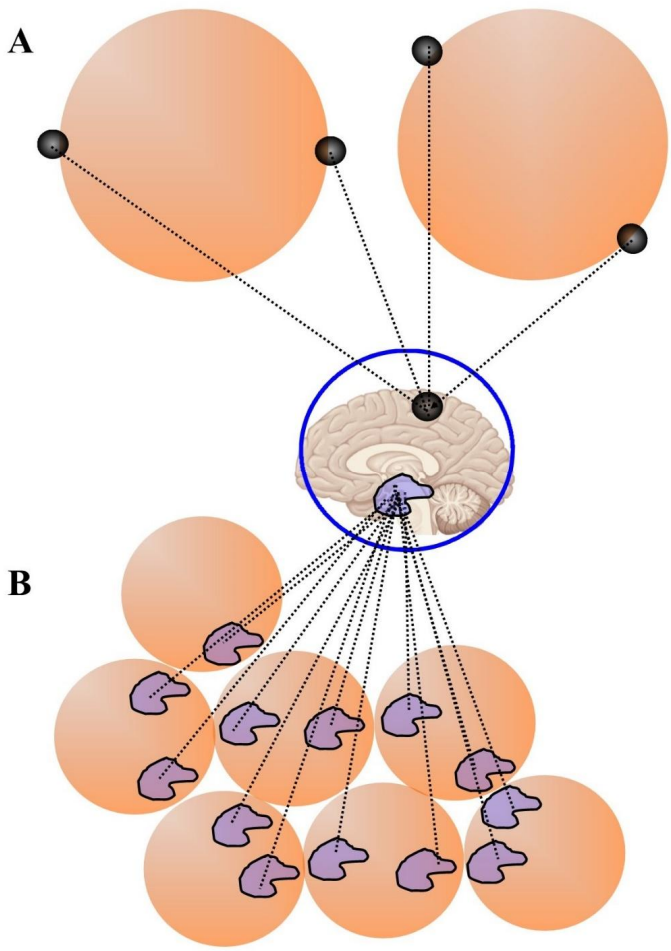

Figure 5*. Convergence of n-spheres' antipodal points with matching description.* ***Figure A****: the ideas (abstractions) link together antipodal points embedded in different environmental n-spheres. Their projections to the brain give rise to abstract concepts.* ***Figure B****: the final, pure abstractions encompass countless different matching functions from different, closely packed, environmental n-spheres.*

However, the concept of the world still embraces more general concepts as well as superfluous ones. Indeed, many different conceptualizations of the world result from genetic constraints, social groups and historical background. The concepts of the world are still incomplete, because they also include unnecessary components and their historical development has not ended at this time.
The concept of the world is preserved by individuals and left to posterity via communication and conditioning. If a concept is transmitted unchanged over generations, its strength decreases with the time due to habituation, until it cannot be recognized anymore. The transformation of the concepts of the world leads from certainty to doubts about them. Thus arises the *enigma* of the world, in place of the concept of the world. Confronted with the enigmas of our environment, the more perplexity increases, the more urgent is the need to solve the problems as soon as possible and several new different satisfying concepts of the world may arise. Solutions are however transitory and changing with the time, both within individuals and communities. Every concept of the world is characterized by residual unneeded concepts, depending on the education of the individuals. The number of superfluous concepts may either remain the same, or decrease, or increase. Provisional solutions to the enigma of the world are countless and the only way to find more general concepts is to expunge the surplus components. The more the concept of the world is spatially enlarged, the more the solution is general and definitive, approximating an exclusive experience. Increasingly over space and time, concepts of the world tend towards the higher level concepts and the brain is satisfied. During cultural evolution, the concepts of the world are at first regarded as a positive experience, a perceived thing, an empiric experience. However, in a following phase of removal, they weaken and are regarded as non-empirical experience, pseudo-problems, until they gradually vanish and disappear. The last phase is their reappearance in a distilled form, just as pure descriptions (**Figure 5B**). More mature, pure concepts of the world allow the brain to be entirely conditioned by the environment and mature statements are regarded as complete experience. There is an answer to the third question raised in Section 2. That is, a primitive experience (experience=naturally perceived) leads to addition of non-experience (either experience=perceived and experience=not perceived) until a definitive, just described, exclusive experience takes place (experience=purified perceived). More advanced social groups, *e.g.*, scientists, may be closer than others to pure concepts of the world, at least in some fields of experience. Indeed, evolution does not proceed linearly nor uniformly. Small groups of individuals have an important role in pushing forward changes that lead to possible solutions of the problems.

7) WHY BRING TOPOLOGY INTO THE ASSESSMENT OF EXPERIENCE?

The question here is: what does a topologic reformulation add in the evaluation of the nervous processes of experience? BUT and its extensions provide a methodological approach which makes it possible for us to study experience in terms of projections from real to abstract phase spaces. The importance of projections between environmental spaces, where objects lie, and brain phase spaces, where mental operations take place, is also suggested by a recent paper, which provides a rigorous way of measuring distance on concave neural manifolds (Sengupta et al., 2016). The real, measurable nervous activity can be described in terms of paths occurring on n-spheres. It leads to a consideration of affinities among nervous signals, characterized as antipodal points on multi-dimensional spheres embedded in abstract spaces. To provide an example, **Figure 4** shows how embedding brain activities in n-spheres allows the quantification of geometric parameters, such as angles, lengths, and so on, that could be useful in neuroimaging data optimization. BUT and its ingredients can be modified in different guises, in order to assess a wide range of nervous functions. Although this field is nearly novel and still in progress, with several unpublished findings, we may provide some examples. Such a methodological approach has been proved useful in the evaluation of brain symmetries, which allow us to perform coarse- or fine-grained evaluation of fMRI images and to assess the relationships, affinities, shape-deformations and closeness among BOLD activated areas (Tozzi and Peters, 2016b). Further, BUT has been proved useful in the evaluation of cortical histological images previoulsy treated with Voronoi tessellation (Peters et al., 2016).

A wide range of brain dynamics, ranging from neuronal membrane activity to spikes, from seizures to spreading depression (Wei; Bernard; Richardson), lie along a continuum of the repertoire of the neuronal nonlinear activities which may be of substantial importance in enabling our understanding of central nervous system function and in the control of pathological neurological states. Nonlinear dynamics are frequently studied through logistic maps equipped with Hopf bifurcations, where intervals are dictated by Feigenbaum constants. Tozzi and Peters (2016b) introduced an approach that offers an explanation of nervous nonlinearity and Hopf bifurcations in terms of algebraic topology. Hopf bifurcation transformations (the antipodal points) can be described as paths or trajectories on abstract spheres embedded in n-spheres where n stands for the Feigenbaum constant's irrational number (Kim; Schleicher). Although the paper takes into account just Hopf bifurcations among the brain nonlinear dynamics, this is however a starting point towards the "linearization" of other nonlinear dynamics in the brain. In sum, BUT makes it possible for us to evaluate nonlinear brain dynamics, which occur during knowledge acquisition and processing, through much simpler linear techniques.

BUT and its variants are not just a *methodological* approach, but also display a *physical*, quantifiable counterpart. To make an example, although anatomical and functional relationships among cortical structures are fruitfully studied, *e.g.*, in terms of dynamic causal modelling, pairwise entropies and temporal-matching oscillations (Friston, 2010; Watanabe et al., 2014), nevertheless *proximity* among brain signals adds information that has the potential to be operationalized. For example, based on the ubiquitous presence of antipodal cortical zones with co-occuring BOLD activation, it has been recently suggested that spontaneous brain activity might display donut-like trajectories (Tozzi and Peters 2016a).
BUT allows the evaluation of energetic nervous requirements too. There exists a physical link between the two spheres S^n and S^{n-1} and their energetic features. When two antipodal functions a n-sphere S^n, standing for symmetries, project to a *n*-Euclidean manifold (where S^{n-1} lies), a single function is achieved and a symmetry break occurs (Tozzi and Peters 2016b). It is known that a decrease in symmetry goes together with a decrease in entropy. It means that the single mapping function on S^{n-1} displays energy parameters lower than the sum of two corresponding antipodal functions on S^n. Therefore, in the system S^n and S^{n-1}, a decrease in dimensions gives rise to a decrease in energy. We achieve a system in which the energetic changes do not depend anymore on thermodynamic parameters, but rather on affine connections, homotopies and continuous functions. A preliminary example is provided by a recent paper, where BUT allows the detection of Bayesian Kullback-Leibler divergence during unsure perception (Tozzi and Peters, 2016b).

CONCLUSIONS

In conclusion, we have provided a topological approach to experience features which makes it possible to evaluate the interactions among environment, brain and human statements. A shift in conceptualizations is evident in the BUT approach. The interaction of neural signals is described in terms of *sameness*, *closeness* and their *feature value vectors* (*e.g.*, amplitude, duration, and so on). The invaluable opportunity to treat elusive mental activities in terms of topological structures makes it possible for us to describe experience in the language of powerful analytical tools. Embracing the approach provided by BUT and its variants in characterizing brain interactions means that the *real* neuronal activity can be described as paths or trajectories on *abstract* structures. This takes us into the realm of computational topology, a realm endowed with abstract metric spaces, *e.g.* projections of environmental spaces into geometric ones. It supplies us with richly sufficient statistics, that helps us to elucidate the mechanisms of human experience.
We conclude with a methodological remark. The symbolic logic approach to scientific experience, prevailing in the beginning of the twentieth century after Whitehead and Russell's influential book (1910) and the rise of logical positivism, was dismissed in the following decades. Our novel approach is paradoxically a return to the past, because it leads once again to emphasize the old weapons of logic thinking as methodologies able to inspire scientists in their experimental evaluation of physical/biological counterparts of human experience.

AKNOWLEDGMENTS

The Authors would like to thank Chiara Russo Krauss and Thomas Feldges for commenting on an earlier version of this manuscript.

REFERENCES

1) Afraimovich V, Tristan I, Varona P, Rabinovich M. 2013. Transient Dynamics in Complex Systems: Heteroclinic Sequences with Multidimensional Unstable Manifolds. Discont, Nonlin and Complexity 2(1): 21-41.
2) Arai M, Brandt V, Dabaghian Y. 2014. The Effects of Theta Precession on Spatial Learning and Simplicial Complex Dynamics in a Topological Model of the Hippocampal Spatial Map. PLoS Comput Biol 2014, 10(6):e1003651.
3) Avenarius R. 1908. Kritik Der Reinen Erfahrung von Richard Avenarius. Lepzig: C.R. Reisland.
4) Barrett LF, Simmons WK. 2015. Interoceptive predictions in the brain. Nat Rev Neurosci 16(7):419-429.
5) Barttfeld P, Uhrig L, Sitt JD, Sigman M, Jarraya B, Dehaene S. 2015. Signature of consciousness in the dynamics of resting-state brain activity. PNAS 112(3):887-892.
6) Beggs JM, Timme N. 2012. Being critical of criticality in the brain. Front Physiol 3:163.
7) Bengson JJ, Kelley TA, Zhang X, Wang J-L, Mangun GR. 2014. Spontaneous Neural Fluctuations Predict Decisions to Attend. J Cogn Neurosci. 26(11):2578-2584.
8) Benson AR, Gleich DF, Leskovec J. 2016. Higher-order organization of complex networks. Science 353, 6295: 163-166. DOI: 10.1126/science.aad9029.
9) Bernard C, Naze S, Proix T, Jirsa VK. Modern concepts of seizure modeling. Int Rev Neurobiol. 2014;114:121-53. doi: 10.1016/B978-0-12-418693-4.00006-6.

10) Betzel RF, Byrge L, He Y, Goñi J, Zuo X-N, Sporns O. 2104. Changes in structural and functional connectivity among resting-state networks across the human lifespan. NeuroImage 2:345–357.
11) Beyer WA, Zardecki A. 2004. The early history of the ham sandwich theorem. American Mathematical Monthly 1:58-61.
12) Borsuk M. 1933. Drei sätze über die n-dimensional euklidische sphäre, Fundamenta Mathematicae XX: 177–190.
13) Borsuk M. 1958-1959. Concerning the classification of topological spaces from the standpoint of the theory of retracts. Fundamenta Mathematicae XLVI:177–190.
14) Borsuk M. 1969. Fundamental retracts and extensions of fundamental sequences, Fundamenta Mathematicae 1:55–85.
15) Cavell S. 2002. “Knowing and Acknowledging", Must We Mean What We Say?. Cambridge University Press, 238–266.
16) Chen Z, Gomperts SN, Yamamoto J, Wilson MA. 2014. Neural representation of spatial topology in the rodent hippocampus. Neural Comput. 26, 1–39.
17) Chicharro D, Ledberg A. 2012. When two become one: the limits of causality analysis of brain dynamics. PLoS One 7(3):e32466. doi: 10.1371/journal.pone.0032466.
18) Churchland PM. 2007. Neurophilosophy At Work. Cambridge Univ Pr ISBN-10: 0521864720. ISBN-13: 978-0521864725
19) Collins GP. 2004. The shapes of space. Sci Am. 291: 94–103.
20) Dabaghian Y, Mémoli F, Frank L, Carlsson G: A Topological Paradigm for Hippocampal Spatial Map Formation Using Persistent Homology. PLoS Comput Biol 2012, 8(8):e1002581.
21) Dabaghian Y, Brandt VL, Frank LM. 2014. Reconceiving the hippocampal map as a topological template. Elife 3, e03476.
22) de Arcangelis L, Herrmann HJ. 2010. Learning as a phenomenon occurring in a critical state. PNAS 107:3977-3981.
23) Deco G, Jirsa VK. 2012. Ongoing cortical activity at rest: criticality, multistability, and ghost attractors. J Neurosci 7;32(10):3366-3375.
24) Dodson CTJ, Parker PE. 1997. A user’s guide to algebraic topology. Dordrecht, Netherlands: Kluwer.
25) Filmer HL, Dux PE, Mattingley JB. 2014. Applications of transcranial direct current stimulation for understanding brain function. Trends in neurosci 12:742-753.
26) Fraiman D, Chialvo DR. 2012. What kind of noise is brain noise: anomalous scaling behavior of the resting brain activity fluctuations. Frontiers in Physiology, 3:307.
27) Friston K. 2008. Hierarchical models in the brain. PLoS computational biology 4, e1000211
28) Friston K. 2010. The free-energy principle: a unified brain theory? Nat Rev Neurosci 11(2):127-138.
29) Friston K, Rigoli F, Ognibene D, Mathys C, Fitzgerald T, Pezzulo G. 2015. Active inference and epistemic value. Cogn Neurosci 13:1-28.
30) Gibson JJ. 1950. The Perception of the Visual World. Greenwood Press, Westpost, Conn.
31) Gibson JJ. 1971. The information available in pictures. Leonardo 4, 27-35.
32) Gibson JJ. 1979. The theory of affordance in the ecological approach to visual perception. Hillsdale, Erlbaum.
33) Gibson JJ. 1986. The ecological approach to visual perception. Boston: Houghton-Mifflin.
34) Giusti C, Pastalkova, Curto, Itskov. 2015. Clique topology reveals intrinsic geometric structure in neural correlations. Proc Natl Acad Sci U S A. 112(44):13455-60. doi: 10.1073/pnas.1506407112. Epub 2015 Oct 20.
35) Gorgolewski KJ, Lurie D, Urchs S, Kipping JA, Craddock RC, Milham MP, Margulies DS, Smallwood J. A correspondence between individual differences in the brain's intrinsic functional architecture and the content and form of self-generated thoughts. PLoS One 13;9(5):e97176.
36) Grau C, Ginhoux R, Riera A, Nguyen TL, Chauvat H, Berg M, Amengual JL, Pascual-Leone A, Ruffini G. 2014. Conscious Brain-to-Brain Communication in Humans Using Non-Invasive Technologies. PLoS One. 2014; 9(8): e105225. doi: 10.1371/journal.pone.0105225
37) Heft H. 1997. The relevance of Gibson’s ecological approach to perception for environment-behavior studies. In G.T. Hopfield JJ. 1982. Neural networks and physical systems with emergent collective computational abilities. PNAS 79: 2554–2558.
38) Hume D. 1739–40. A Treatise of Human Nature: Being an Attempt to introduce the experimental Method of Reasoning into Moral Subjects. Penguin Classics; New Ed edition (31 Oct. 1985)
39) Izhikevich EM. 2010. Hybrid spiking models.Philos Trans A Math Phys Eng Sci. 368(1930):5061-5070.
40) Jirsa VK, Fuchs A, Kelso JAS. 1998. Connecting Cortical and Behavioral Dynamics: Bimanual Coordination. Neural Computation archive, Volume 10 Issue 8, November 1998, 2019 - 2045.
41) Johnson-Laird PN. 2010. Mental models and human reasoning. PNAS, 107, 43: 18243–18250
42) Kida T, Tanaka E and Kakigi R. 2016. Multi-Dimensional Dynamics of Human Electromagnetic Brain Activity. Front. Hum. Neurosci. 9:713. doi: 10.3389/fnhum.2015.00713.
43) Kim I-S. Extensions Of The Borsuk ulam Theorem. J. Korean Math. Soc. 34 (1997), No. 3, pp. 599–222
44) Kleineberg K-K, Boguñá M, Serrano MA, Papadopoulos F. 2016. Hidden geometric correlations in real multiplex networks. Nature Physics, in press. doi:10.1038/nphys3812.
45) Körding KP, Beierholm U, Ma WJ, Quartz S, Tenenbaum JB, Shams L. 2007. Causal inference in multisensory perception. PLoS One 26;2(9):e943.
46) Lech RK, Güntürkün O, Suchan B. 2016. An interplay of fusiform gyrus and hippocampus enables prototype- and exemplar-based category learning. Behavioural Brain Research, doi:10.1016/j.bbr.2016.05.049
47) Lewin K. 1935. A dynamic theory of personality. McGraw_Hill Book Company, Inc. New York and London, 1935.
48) Lewin K. 1936. Principles of Topological Psychology, transl. F. Heider and G. M. Heider. McGraw-Hill, New York.
49) Libet B, Gleason CA, Wright EW, Pearl DK. 1983. Time of conscious intention to act in relation to onset of cerebral activity (readiness-potential). The unconscious initiation of a freely voluntary act. Brain 106 (Pt 3):623-642.
50) Linkenkaer-Hansen K, Nikouline VV, Palva JM, Ilmoniemi RJ. 2001. Long-range temporal correlations and scaling behavior in human brain oscillations. J Neurosci 21(4):1370-1377.

51) Luce, R. D., D'Zmura, M., Hoffman, D., Iverson, G. J., Romney, A. K. (eds) 1995 Geometric representations of perceptual phenomena. Papers in honor of Tarow Indow on his 70th birthday. Lawrence Erlbaum Associates.
52) Luneburg, R. K. 1947 Mathematical analysis of binocular vision. Princeton University Press.
53) Marr D. 1982 Vision. A computational investigation into the human representation and processing of visual information. W. H. Freeman and Company.
54) Marsaglia G. 1972. Choosing a Point from the Surface of a Sphere. Annals of Mathematical Statistics 43 (2): 645–646.
55) Matoušek J. 2003. Using the Borsuk–Ulam Theorem. Lectures on Topological Methods in Combinatorics and Geometry. Berlin Heidelberg: Springer-Verlag.
56) Mazzucato L, Fontanini A La Camera G. 2016. Stimuli Reduce the Dimensionality of Cortical Activity. Front. Syst. Neurosci, in press http://dx.doi.org/10.3389/fnsys.2016.00011.
57) Milton R, Babichev A, Dabaghian YA. 2015. A topological approach to synaptic connectivity and spatial memory. BMC Neuroscience201516 (Suppl 1):P44.
58) Mitroi-Symeonidis F-C. 2015 Convexity and sandwich theorems. European Journal of Research in Applied Sciences, vol. 1, pp. 9-11.
59) Moore, R.W. Marans, Adances in Environment, Behavior, and Design. Plenum Press, NY, 1997, 71-107.
60) Nieuwenhuys R, Voogd J, van Huijzen C. 2008. The Human Central Nervous System. Heidelberg: Springer.
61) Ogasawara Y. 2010. Sufficient Conditions for the Existence of a Primitive Chaotic Behavior, Journal of the Physical Society of Japan, 79 (2010) 15002.
62) Ogasawara Y, Oishi S. 2012. Consideration of a primitive chaos, Journal of the Physical Society of Japan, 81 (2012) 103001.
63) Ogasawara Y, Oishi S. 2014. Characteristic Spaces Emerging from Primitive Chaos, Journal of the Physical Society of Japan, 83 (2014) 014001
64) Ogasawara Y. 2015 A Structure behind Primitive Chaos, Journal of the Physical Society of Japan, 84 (2015) 064007.
65) Olver PJ. 1993. Applications of Lie groups to differential equations. Berlin: Springer-Verlag.
66) Papo D. 2014. Functional significance of complex fluctuations in brain activity: from resting state to cognitive neuroscience. Front Syst Neurosci, 8, 112.
67) Parise CV, Spence C, Ernst MO. 2011. When correlation implies causation in multisensory integration. Curr Biol 22(1):46-49.
68) Peters JF. 2014. Topology of Digital Images. Visual Pattern Discovery in Proximity Spaces, Intelligent Systems Reference Library. Berlin: Springer.
69) Peters JF. 2016 Computational Proximity. Excursions in the Topology of Digital Images. Intelligent Systems Reference Library 102. Switzerland: Springer Int. Pub.,*in press*. DOI: 10.1007/978-3-319-30262-1.
70) Peters JF, Tozzi A, Ramanna S. 2016. Brain Tissue Tessellation Shows Absence of Canonical Microcircuits. Neuroscience Letters 626: 99–105. doi:10.1016/j.neulet.2016.03.052.
71) Popper, Karl R.; Eccles, John C. (1977). The self and its brain. Berlin: Springer International. p. 425. ISBN 3-540-08307-3. You would agree, I think, that in our experience of the world everything comes to us through the senses [...]
72) Richardson MJ, Dale R, Marsh KL. Complex dynamical systems in social and personality psychology. In: Reis HT, Judd CM (eds), Handbook of Research Methods in Social and Personality Psychology. 2nd Edition, 2014. Cambridge University Press, Cambridge. ISBN: 9781107600751
73) Robinson PA, Zhao X, Aquino KM, Griffiths JD, Sarkar S, Mehta-Pandejee G. 2016. Eigenmodes of brain activity: Neural field theory predictions and comparison with experiment. Neuroimage. pii: S1053-8119(16)30090-8. doi: 10.1016/j.neuroimage.2016.04.050.
74) Rock I. 1983. The logic of perception. MIT Press, Cambridge, MA.
75) Roldán É, Martínez I, Parrondo JMR, Petrov D. 2014. Universal features in the energetics of symmetry breaking. Nature Physics, 10(6), 457–461. http://doi.org/10.1038/nphys2940.
76) Russo Krauss C. 2013. Il sistema dell'esperienza pura, Le Càriti, Firenze.
77) Russo Krauss C. 2015. L'empiriocriticismo di Richard Avenarius tra psicofisiologia e teoria della consocenza, in R. Avenarius, Il concetto umano di mondo, Morcelliana, Brescia.
78) Schleicher D, Hausdorff dimension, its properties, and its surprises, The American Mathematical Monthly 114 (2007), no. 6, 509–528, MR2321254.
79) Scholz JP, Kelso JAS, Schöner G. 1987. Nonequilibrium phase transitions in coordinated biological motion: Critical slowing down and switching time. Physics Letters A. Volume 123, 8, 390-394. doi:10.1016/0375-9601(87)90038-7Sengupta B, Stemmler MB, Friston KJ. 2013. Information and efficiency in the nervous system--a synthesis. PloS Comput Biol 9(7):e1003157.
80) Sengupta B, Friston KJ, Penny WD. 2014. Efficient gradient computation for dynamical models. Neuroimage. 98:521-527.
81) Sengupta B, Tozzi A, Cooray GK, Douglas PK, Friston KJ. 2016. Towards a Neuronal Gauge Theory. PLoS Biol 14(3): e1002400.
82) Simas T, Chavez M, Rodriguez PR, Diaz-Guilera A. 2015. An algebraic topological method for multimodal brain networks comparisons. Front Psychol. 6;6:904. doi: 10.3389/fpsyg.2015.00904. eCollection 2015.
83) Singer W, Lazar A. Does the Cerebral Cortex Exploit High-Dimensional, Non-linear Dynamics for Information Processing? Front. Comput. Neurosci., 22 September 2016 | http://dx.doi.org/10.3389/fncom.2016.00099
84) Stemmler M, Mathis A, Herz AVM 2015 Connecting multiple spatial scales to decode the population activity of grid cells. Sci. Adv. 1:e1500816 18 December 2015.
85) Suppes, P. 2002 Representation and invariance of scientific structures. Center for the Study of Language and Information Publication, Stanford.
86) Tognoli E, Kelso JA. 2014. Enlarging the scope: grasping brain complexity. Front Syst Neurosci 8, 122.

87) Tononi G. 2008. Consciousness as integrated information: a provisional manifesto. Biol Bull. 215(3):216-42.
88) Tozzi A. 2016. Borsuk-Ulam Theorem Extended to Hyperbolic Spaces. In Computational Proximity. Excursions in the Topology of Digital Images, edited by J F Peters, 169–171. doi:10.1007/978-3-319-30262-1.
89) Tozzi A., Peters JF. 2016a. Towards a fourth spatial dimension of brain activity. Cogn Neurodyn, *in press*. DOI: 10.1007/s11571-016-9379-z.
90) Tozzi A, Peters JF. 2016b. A topological approach unveils system invariances and broken symmetries in the brain. J Neurosci Res, in press. DOI: 10.1002/jnr.23720.
91) Tozzi A, Fla Tor, P. J. 2016. Building a minimum frustration framework for brain functions in long timescales. J Neurosci Res. *In press*.
92) Vuksanovic V, Hövel P. 2014. Functional connectivity of distant cortical regions: Role of remote synchronization and symmetry in interactions. NeuroImage, 97:1–8.
93) Watanabe T, Hirose S, Wada H, Imai Y, Machida T, Shirouzu I, Konishi S, Miyashita Y, Masuda N. 2014. Energy landscapes of resting-state brain networks. Front Neuroinform 25;8:12.
94) Weeks JR. 2002. The shape of space, IInd edition. New York-Basel : Marcel Dekker, inc.
95) Wei Y, Ullah G, Schiff SJ. Unification of neuronal spikes, seizures, and spreading depression. J Neurosci. 2014 Aug 27;34(35):11733-43. doi: 10.1523/JNEUROSCI.0516-14.2014.
96) Weyl H. 1982. Symmetry. Princeton: Princeton University Press. ISBN 0-691-02374-3.
97) Whitehead AN, Russell B. (1910). Principia mathematica (1 ed.), Cambridge: Cambridge University Press.
98) Whitehead AN. 1919. An enquiry concerning the principles of natural knowledge. Cambridge at the University Press.
99) Zeeman, E. C. 1962 The topology of the brain and visual perception. In Fort Jr., M. K. (ed.) Topology of 3-manifolds and related topics. Prentice-Hall, Pp. 240-256.
100) Zlotnik A, Nagao R, Kiss IZ, Li JS. 2016. Phase-selective entrainment of nonlinear oscillator ensembles. Nat Commun. 7:10788. doi: 10.1038/ncomms10788.

Author's personal copy

Cogn Neurodyn (2017) 11:283–292
DOI 10.1007/s11571-017-9431-7

RESEARCH ARTICLE

From abstract topology to real thermodynamic brain activity

Arturo Tozzi[1] · **James F. Peters**[2]

Received: 31 August 2016 / Revised: 14 February 2017 / Accepted: 8 March 2017 / Published online: 14 March 2017
© Springer Science+Business Media Dordrecht 2017

Abstract Recent approaches to brain phase spaces reinforce the foremost role of symmetries and energy requirements in the assessment of nervous activity. Changes in thermodynamic parameters and dimensions occur in the brain during symmetry breakings and transitions from one functional state to another. Based on topological results and string-like trajectories into nervous energy landscapes, we provide a novel method for the evaluation of energetic features and constraints in different brain functional activities. We show how abstract approaches, namely the Borsuk–Ulam theorem and its variants, may display real, energetic physical counterparts. When topology meets the physics of the brain, we arrive at a general model of neuronal activity, in terms of multidimensional manifolds and computational geometry, that has the potential to be operationalized.

Keywords Topology · Borsuk–Ulam theorem · Brain · Nervous system · Energetic landscape · Symmetry break

✉ Arturo Tozzi
tozziarturo@libero.it

James F. Peters
james.peters3@umanitoba.ca

[1] Center for Nonlinear Science, Department of Physics, University of North Texas, 1155 Union Circle, #311427, Denton, TX 76203-5017, USA

[2] Department of Electrical and Computer Engineering, University of Manitoba, 75A Chancellor's Circle, Winnipeg, MB R3T 5V6, Canada

Introduction

The brain is a complex, non-linear system operating at the edge of chaos, formed by inter-dependent components which exhibit spontaneous self-organization and emergent properties (Tognoli and Kelso 2013; Fraiman and Chialvo 2012; Zare and Grigolini 2013; Xu and Wang 2014). In such a vein, the brain is equipped with phase spaces where particle movements take place (Watanabe et al. 2013; Yan et al. 2013; Kim and Lim 2015; Wang et al. 2017). Such trajectories may display different paths. It has been suggested that the brain is equipped with funnel-like locations in phase space where trajectories converge as time progresses, following the shortest path (Tozzi et al. 2016a; Sengupta et al. 2016). Others proposed that brain function does not exhibit erratic brain dynamics nor attractors, but a stable sequence, the so-called transient heteroclinic channel (Afraimovich et al. 2013) and that a multidimensional functional torus might be displayed during spontaneous brain activity (Tozzi and Peters 2016a). Furthermore, crucial concepts like communication-through-coherence (Deco and Jirsa 2012) and collective movements (Touboul 2012; Tozzi 2015) must be taken into account. In sum, different functional regimes occurring in the brain phase space have been described, both in central nervous systems and in artificial neural networks, and they have been correlated with different brain functions (Tozzi et al. 2016a).

Despite the large number of possible trajectories, the processes governing brain paths may be unified when we take just into account energetic requirements and constraints. Indeed, the second law of thermodynamics states that e*very process occurring in nature proceeds in the sense in which the sum of the entropies of all bodies taking part in the process is increased* (Planck's formulation). This paper aims to evaluate brain energetic constraints in

Author's personal copy

the framework of algebraic topology, namely the Borsuk–Ulam theorem (BUT) (Borsuk 1933). We will take into account also another important topological ingredient, e.g., the symmetries, widespread at every level of nervous organization. Symmetries may be regarded as the most general feature of biological systems (including the brain), perhaps more general also than energetic requirements, so that giving insights into them might provide a general approach to nervous activities (Tozzi and Peters 2016b). Here we show how BUT and its variants may provide powerful insights into brain functioning, especially if we assess the noteworthy relationships between symmetry breaks, changes of neural dimensions, thermodynamic free-energy and informational entropy.

Abstract topology comes into play

The standard version of the Borsuk–Ulam theorem (BUT)

BUT states that (Dodson 1997):
Every continuous map $f : S^n \rightarrow R^n$ must identify a pair of antipodal points (on S^n).

In other words, if a sphere S^n is mapped continuously into a n-dimensional Euclidean space R^n, there is at least one pair of antipodal points on S^n which map onto the same point of R^n. For further details, see Tozzi and Peters (2016b). Examples of antipodal points are the opposite points along the poles of a sphere (Matoušek 2003). The notation S^n denotes an n-sphere of convex curvature, which is embedded in a $n + 1$ Euclidean space (Weeks 2002; Marsaglia 1972). The BUT's ingredients (antipodal points, a versatile use of the exponent n and projections from lower to higher dimensions) can be modified in different guises, in order to achieve a wide range of BUT variants (Tozzi and Peters 2016b; Peters and Tozzi 2016a, b). They provide not just a topological methodology for the evaluation of countless features of brain activity, cast in an empirical fashion that has the potential to be operationalized, but also a quantitative way to give a physical meaning to the otherwise *abstract* concept of BUT. The next paragraphs will go through recently described BUT variants and their applications to brain activity.

Brain regions instead of points

If we simply evaluate *nervous activities* instead of *points*, BUT leads naturally to the possibility of a region-based brain geometry. Indeed, the two opposite *points* could stand not just for the description of simple topological points (Marsaglia 1972), but also for the signals detected by different neuro-techniques, such as spatial or temporal patterns, vectors, particle trajectories, entropies, free-energies (Peters 2016). Therefore, we can describe brain features as antipodal points on $n+1$ –dimensional structures. This means that brain signals can be compared, because the two antipodal points can be assessed at higher-dimensional scales of observation, which can be pulled back to single points at lower-dimensional scales (Tozzi and Peters 2016b).

This approach makes it also possible to assess brain functions in the very general terms of particle trajectories taking place on manifolds, if we consider a nervous activity in a given cortical subarea as a geometric structure that has the characteristics of a *string*. By definition, a string on the surface of an n-sphere is a line that represents the path traced by a moving particle. In a geometric space, a string stands for a region of space with either bounded or unbounded lengths (Goddard and Olive 1985; Olive and Landsberg 1989). In evaluating brain strings, we need to take into account antipodal sets instead of antipodal points (Petty 1971). Indeed, in a point-free geometry (Di Concilio and Gerla 2006; Di Concilio 2013), regions replace points as the primitives. Therefore, in the evaluation of brain activities at every spatio-temporal scale, here we assess antipodal *regions* instead of antipodal *points* (Lenzen 1939; Disalle 1995; Peters and Naimpally 2012). There is however a difference between the strings embedded in structures of diverse dimensions. Strings contain more information than their projections in a lower dimensions. Indeed, the higher the dimension, the more the information encompassed in strings, because of the higher number of coordinates. This means that this BUT variant allows us to evaluate systems features in higher dimensions, in order to increase the amount of detectable information. To make an example, you might extract the three-dimensional shape of a cat, just looking at its shadow. Vice versa, dropping down a dimension means that each point in the lower dimensional space is simpler. It must be kept into account that, as BUT dictates, a single feature needs to project to TWO matching features, going one dimension higher. This means that a projection mapping contains multiple mappings in higher levels. Hence, BUT provides a way to evaluate changes of information among different anatomical and functional brain levels in a topological space.

Antipodality

The two points (or regions, or brain activities) do not need necessarily to be antipodal, in order to be described together (Peters 2016). Indeed, the BUT can be generalized not just for the evaluation of antipodal, but also of non-antipodal points on an n-sphere. We can consider regions on an n-sphere that are either adjacent or far apart (Tozzi and Peters 2016b). And this BUT variant applies to the brain,

Author's personal copy

provided there are a pair of regions on the cortex with the same feature value. (Peters 2016). This makes it possible to evaluate matching cortical signals, even if they are not "opposite", but "near" each other: the antipodal points restriction from the "standard" BUT is no longer needed.

Not just convex structures

The original formulation of BUT describes antipodal points on spatial manifolds in every dimension, provided the n-sphere is a *convex* structure with positive curvature (i.e., a ball). However, brain functions might occur on manifolds endowed with other types of geometry: for example, Sengupta et al. (2016) described brain functional activity in terms of trajectories taking place on hyperbolic Riemannian n-manifolds of constant sectional curvature -1 and concave shape (*i.e.*, a saddle). BUT can be generalized to symmetries occurring either on flat, or on concave structures (Mitroi-Symeonidis 2015; Tozzi 2016), making it possible for us to look for antipodal points on structures equipped with shapes other than the convex ones. In other words, whether the brain function displays a concave, convex or flat structure, it does not matter: we may always find the points with matching description predicted by BUT.

Not just spatial dimensions

Although BUT was originally described just in case of the term n of S^n being a natural number which expresses a structure embedded in a *spatial* dimension, nevertheless n can stand for other types of numbers too. Indeed, n can be also cast as an integer, a rational or an irrational number (Tozzi and Peters 2016b). This makes it possible to use the n parameter as a versatile tool for the description of brain features. In particular, this BUT version is useful in describing brain nonlinear dynamics, as we will see in the next chapters.

General BUT

In conclusion, we are allowed to provide a general version of BUT (Gen-BUT), that takes into account all the mentioned BUT variants that can be used in the topological study of the brain in the context of physics. Gen-BUT states that:

> Multiple sets of objects with matching descriptions in a d-dimensional manifold M^d are mapped to a single set of objects in M^{d-1} and vice versa.

The sets of objects, which can be mathematical, physical or biological features, do not need to be antipodal and their mappings need not to be continuous. The term *matching description* means the sets of objects display common feature values or symmetries. M stands for a manifold with any kind of curvature, either concave, convex or flat. The notation d stands for a natural, or rational, or irrational number. Note that a force, or a group, an operator, an energetic source, is needed, in order to project from one dimension to another. The process is reversible, depending on energetic constraints.

Systems' symmetry breaking: changes in brain dimensions

Symmetries are invariances underlining physical and biological systems (Weyl 1982). A symmetry break occurs when the symmetry is present at one level of observation, but "hidden" at another level (Roldán et al. 2014). BUT tells us that we can find, on an n-dimensional sphere, a pair of opposite points that have the same encoding on an $n-1$ sphere. This means that symmetries can be found when evaluating the system in a proper dimension, while they disappear (are hidden or broken) when we assess the same system in just one dimension lower (Tozzi and Peters 2016b).

There are two different ways to define and assess brain dimensions. Indeed, the term *dimension* may reflect either functional relationships of brain activities, or anatomical connections between cortical areas. The first approach takes into account the dimensionality of the neural space. Connectivity and complex network analyses of neural signals allow the assessment of the complex dynamics of brain activity, providing a novel insight into the multidimensionality of various neural functions' representations (Kida et al. 2016). From a dynamical system perspective, one would expect that brain activities are represented as, for example, some scalar quantity measured at different brain locations (say N locations) at different points in time. Then one could describe nervous dynamics as trajectories and/or manifolds in a N-dimensional phase space (Lech et al. 2016). Mazzucato et al. (2016) demonstrated that stimuli reduce the dimensionality of cortical activity. Clustered networks, such as default mode network, have instead a larger dimensionality, because the latter grows with ensemble size: the more neurons are recruited, the more the dimensions (Mazzucato et al. 2016). Apart from giving insights in neural dynamics in the *canonical* three dimensions (space, time, and frequency), complex network analyses are also able to evaluate other functional dimensions, e.g. categories of neuronal indices such activity magnitude, connectivity, network properties and so on (Kida et al. 2016). It must be taken into account that dimension reduction and symmetry breaking display close relationships, so that symmetries are correlated with changes in functional dimensions in the brain. Indeed, a key feature of

Author's personal copy

dynamical approaches is that the dynamics they predict are characterized by nonequilibrium phase transitions, and therefore breaks of symmetries (Scholz et al. 1987). Many studies emphasized how different levels of behavioral dynamics' organization take place in neural ensembles. To make some examples, Jirsa et al. (1998), focusing on the cortical left–right symmetry, derived a bimodal description of the brain activity that is connected to behavioral dynamics, while Jirsa et al. (1994) demonstrated that, when an acoustic stimulus frequency is changed systematically, a spontaneous transition in coordination occurs at a critical frequency, in both motor behavior and brain signals.

Concerning the second approach to brain dimensionality, it has been recently suggested that brain trajectories, at least during spontaneous activity, might display four spatial dimensions, instead of three (Tozzi and Peters 2016a). Brain symmetric states display dimensions higher than asymmetric ones, so that, in this case, the space of interest does not refer to dynamical neural spaces, but to detectable physical cortical locations. In such a vein, Stemmler et al. (2015) proposed that animals can navigate by reading out a simple population vector of grid cell activity across multiple spatial scales. Combining population vectors at different microscopic dimensions predicts indeed neural and behavioral correlates of multiscale grid cell readout, that transcend the known link between entorhinal grid cells and hippocampal place cells. While the spatial activity of a single grid cell does not constitute a metric, an ensemble of hierarchically organized grid cells does provide instead a distance measure (Stemmler et al. 2015). In our paper, the mapping of trajectories from high dimensional manifold to lower dimensions refers to both the above described definitions of dimensionality.

In sum, the study of changes in brain dimensions is a promising novel methodology. We need to take into account that, despite neural networks modelling complex systems are known to exhibit rich, lower-order connectivity patterns at the level of individual nodes and edges, however higher-order organization remains largely unknown. Benson et al. (2016) recently developed an algorithmic framework for studying how complex networks are organized by higher-order connectivity patterns, revealing unexpected hubs and geographical elements. In such a vein, Kleinberg et al. (2016) demonstrated that real networks are not just random combinations of single networks, but are instead organized in specific ways dictated by hidden geometric correlation between layers. Such correlations allowed the detection of multidimensional communities, e.g., sets of nodes that are simultaneously similar in multiple layers. Crucial for our topological arguments, such multidimensionality also enables accurate trans-layer link prediction, meaning that connections in one layer can be predicted by observing the hidden geometric space of another layer. For example, when the geometric correlations are sufficiently strong, a multidimensional framework outperforms navigation in the single layers, allowing efficient targeted navigation simply by using local multilayer knowledge (Kleineberg et al. 2016).

Abstract topology meets real physics: brain energetic requirements

A BUT variant, termed **energy-BUT**, is particularly useful in our context. There exists a physical link between the abstract concept of BUT and the energetic features of the system formed by two manifolds M^d and M^{d-1}. We start from a manifold M^d equipped with a pair of antipodal points, standing for a symmetry according to one of the above mentioned BUT variants. When these opposite points map to a n-Euclidean manifold (where M^{d-1}lies), a symmetry break/dimensionality reduction occurs, and a single point is achieved (Tozzi and Peters 2016b). However, it is widely recognized that a decrease in symmetry goes together with a decrease in entropy and free-energy, at least in a closed system. This means that the single mapping function on M^{d-1}displays energy parameters lower than the two corresponding antipodal functions on M^d. Therefore, decreases of dimensions give rise to decreases of energy and energy requirements (Fig. 1). In such a way, BUT and its variants yield physical quantities, because we achieve a system in which energetic changes do not depend anymore on thermodynamic parameters, rather on affine connections and homotopies.

It must be taken into account that energy-BUT concerns not just energy, but also information. Indeed, two antipodal points contain more information than their single projection in a lower dimension. Dropping down a dimension means that each point in the lower dimensional space is simpler, because each point has one less coordinate. In sum, energy-BUT provides a way to evaluate decreases in energy and information in topological, other than thermodynamic, terms.

In order to assess the energetic requirements of the brain in a topological fashion, we will provide two examples, the first assuming that the brain is a closed system, and the second that the brain is an open, nonequilibrium biological system.

The brain as a closed system

Here we provide an example in order to calculate the energy requirements of different functional states in the central nervous system. Changing the state of system necessarily entails a modification in thermodynamic free-energy, which is equivalent to the work done on the

Author's personal copy

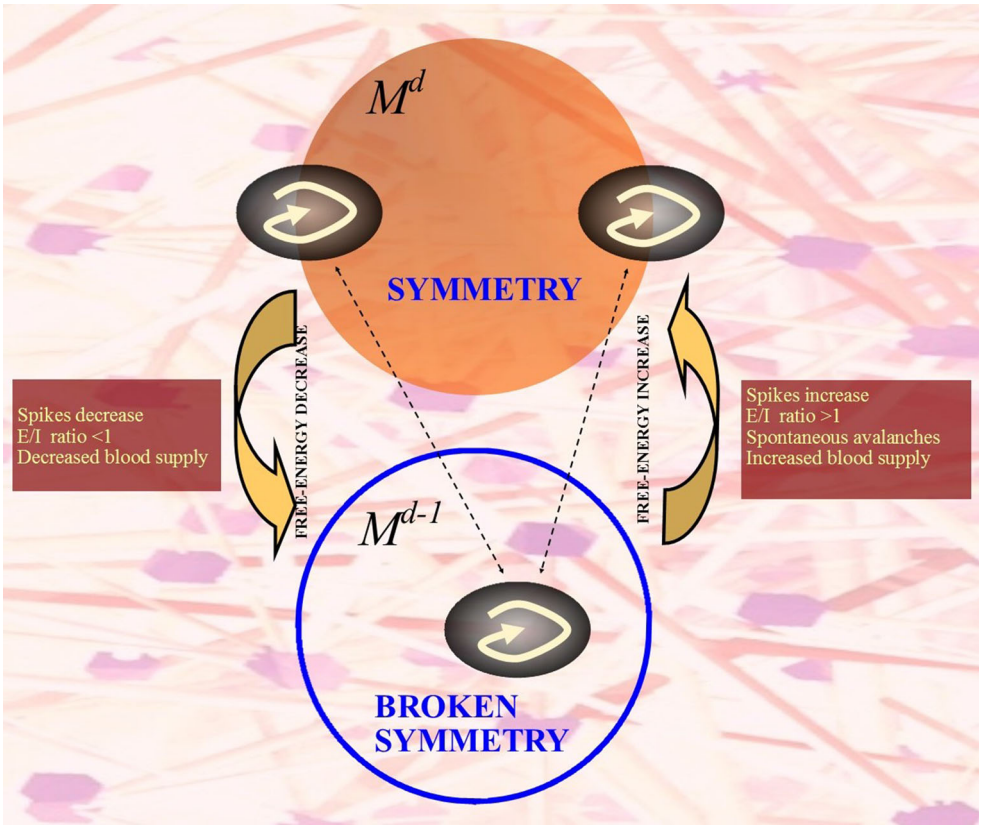

Fig. 1 The manifold M^d displays two antipodal points with matching description. It this case, according to BUT variants' dictates, the antipodal points stand for two symmetric functions equipped with the same energetic conformation (*black ovals* containing *curved arrows*). When a symmetry break occurs, the manifold M^{d-1} displays just a single function, equipped with an energetic level lower than the sum of the antipodal functions' ones. Therefore, dimension loss occurs together with a decrease of energy. The lateral *dark boxes* illustrate some hypothetical but plausible conditions which might cause increase or decrease of energy in the brain. In sum, the system displays a configuration with higher energy in M^d, and with lower energy when a symmetry break occurs. The background stands for a schematized structure of the brain phase space

system, and which can be regarded as the average uncertainty, or the information we have about the system's microscopic states (Sengupta et al. 2013a). We start from a nervous closed system, shaped in guise of a M^{d-1}equipped with a single physical function termed A and characterized, say, by a free-energy $= 1$ and an entropy $= 2$. For the gen-BUT, when we project the function to M^d, we achieve two antipodal functions B and C with matching description, forming a symmetric system. The question here is: which are the values of free-energy and entropy of each one of the two antipodal (symmetric) functions on M^d? And what happens to enthalpy? This question is crucial, because it calls attention to energy conservation and symmetries. In effect, this question leads to the Noether theorem (Noether 1918), which gives us a physical, testable counterpart to the otherwise *algebraic* topological BUT. Indeed, if we do not take into account the changes in free energy from A to B and C, there is no possibility to translate the abstract BUT to the physics of brain activity, and we have to use the BUT, as we already did, simply as a useful methodological tool (Peters et al. 2016).

The following scenario can be depicted. The projection (mapping) of the description of a pair of physical points (or regions, or functions) on M^d into a point in M^{d-1} occurs because we have found a continuous function between the two manifolds. This is a flexible situation, because we can vary the description of the pair physical points (regions, or functions) and achieve a mapping to various Euclidean spaces, depending on the number of features of the antipodes. From the gen-BUT perspective, the entropy of antipodal regions would be part of the description of the antipodes and would be the same for each antipode. This works for regions, since informational entropy is defined in terms of a set of events. Each regional antipode would be the culmination of a set of random events, leading to each antipode. Similarly, the free energy of each antipode would be the same. In sum, if the region A is characterized by free-energy $= 1$ and an entropy $= 2$, the regions B and C are both characterized by a free-energy $= 1$ and an entropy $= 2$. This means that the total free energy of the system $B + C$ is doubled, compared with A.

The brain as an open, nonequilibrium system

Several authors state that, being the brain an open, nonequilibrium biological system, nonlinear dynamics are of substantial importance in enabling our understanding of neuronal function and in the control of pathological neurological states (Tognoli and Kelso 2013; Fraiman and Chialvo 2012). As thermodynamic entropy measures the dispersion over microstates of a thermodynamic canonical ensemble, informational entropy plays the same role, but

Author's personal copy

over some phase functions or macroscopic variables that change with time (Sengupta et al. 2013a). This means that symmetry breaking in the brain may occur through the widely described phenomena of critical fluctuations and critical slowing (Scholz et al. 1987). Nonlinear dynamics and critical fluctuation can be studied through logistic maps equipped with Hopf bifurcations, where intervals are dictated by the Feigenbaum constants. The BUT variants introduce an approach that offers an explanation of nervous nonlinearity and Hopf bifurcations in terms of algebraic topology (Tozzi and Peters 2016b). Indeed, as reported by Tozzi and Peters (2016b), Hopf bifurcations can be described in terms of antipodal points encompassed in n-spheres. However, in this case, the term n does not stand for a spatial dimension, rather for the Feigenbaum constant's irrational number (Kim 1997; Schleicher 2007). Therefore, we achieve an abstract sphere made of irrational numbers, where nonlinear dynamics take place in guise of paths and trajectories with matching description. When going one dimension lower, the two antipodal points become just one, that can be described in linear terms. This means that BUT makes it possible for us to evaluate complex nonlinear brain dynamics through much simpler linear techniques.

Brain thermodynamic parameters: when but encompasses a physical quantity

This paragraph correlates thermodynamic and informational parameters with brain dynamical features, in order to analyze and quantify them. The paths described by BUT variants elucidate how the tight energetic coupling among different neural activities gives rise to brains that are in charge of receiving and interpreting signals from other cortical zones, in closely intertwined relationships at every spatio-temporal level. Therefore, topology plus energy becomes one of the central information processing strategies of the nervous system.

Free-energy

The brain represents 2% of the human body mass yet it accounts for about 20% of total energy consumed, a substantial proportion (Attwell and Laughlin 2001). The metabolic brain activity, influenced by a balance between the energy cost incurred by its operation and the benefits realized by energy expenditure, is therefore high and constant over time (Sengupta et al. 2013a). Why does the brain consume such remarkable amounts of energy, despite the fact that evolution is geared toward minimizing very high metabolic costs? Almost 20–60% of the energy allocated for the brain is used to support the metabolic rate of the cortical grey matter and for synapses and action potentials (Sengupta et al. 2013b). For our purposes, we limit our analysis to spike frequency. The free energy roughly corresponds to the electric spike frequency. See Tozzi et al. (2016b) for a technical explanation. It means that the increase in thermodynamic free-energy during brain activity is mostly due to spikes, and that we are allowed to evaluate variations in thermodynamic free-energy during brain activity just in terms of electric spiking. In the context of ongoing fluctuations with complex properties caused by variations in thermodynamic parameters, a foremost issue is the *free-energy principle* (Friston 2010). A self-organizing system like the brain, at nonequilibrium steady-state with its environment, needs to minimize its free-energy (and associated entropy), in order to resist a tendency towards disorder/entropy. The key thrust is that energy expenditure is balanced by homeostatic mechanisms, in an effort to minimize free-energy, and in an interplay between neuronal structure and activity at many different spatiotemporal scales. A subtle equilibrium takes place among actual sampled sensations, brain's predictions (e.g., the expected energy), expectation (e.g., the best possible guess), surprise (e.g. an improbable outcome caused by unknown quantities), accuracy (e.g., the surprise about the sensations that are expected) and complexity (e.g., the beliefs before and after observing data through sensory inputs). Such different mechanisms tend towards a main goal: minimising entropy production, which corresponds to minimising the so called *variational free-energy*. There is a strict correspondence between concepts in Friston's formalism and that of the thermodynamics. For example, the Gibb's thermodynamic free-energy stands, in Friston's framework, for the entropy of recognition density, or in other words, for the above mentioned actual sensation sampled by the brain. Further, because variational and thermodynamic free-energy share a common minimum, we are also allowed to link information processing (e.g., Bayesian belief updating) to metabolic efficiency (Sengupta et al. 2013b), so that the average time of variational free-energy becomes a proxy for entropy.

Temperature

The cortical temperature is not a stable parameter as currently believed. The brain displays instead thermal gradients observed at many spatiotemporal scales (Wang et al. 2014a). Local temperature fluctuations may act as a dynamic variable, modulating presynaptic and postsynaptic events, sensory stimuli, behavioral changes, memory encoding and fine-tune activity-dependent processes (Kalmbach and Waters 2012; Long and Fee 2008). In terms of symmetry breakings achieved during nervous second order phase-transitions, temperature might stand for one of

Author's personal copy

the critical control parameters which dictates how the brain evolves from one coordinated state to another. Therefore, brain temperature can be used as an order parameter to monitor the dynamics of the nervous collective state and deviations from the symmetrical state. Indeed, in terms of informational entropy, cortical temperatures contain information about how large-scale physiological and pathological outcomes arise from the interactions of many small-scale processes, in order that thermal brain variations may lead to different probability outcomes. In sum, non-stationary thermal cortical fluctuations, an underrated general mechanism of nervous function able to modify the energy of the brain and to influence psychophysical characteristics, can be assessed in topological terms.

Entropies

Entropies are evaluated in fMRI functional studies through different techniques, e.g., pairwise entropy (Schneidman et al. 2006; Watanabe et al. 2014; Wang et al. 2014b), Granger causality index, phase slope index, and so on (Kida et al. 2016). Such approaches also make it possible to analyze how the complexity of an adaptive system like the brain is best understood as a dynamic network that aims to decrease its free-energy, for example via entropy transfer. Here we propose a novel topological way to assess, in brain fMRI functional studies, changes in informational entropies. The method, referred here to changes in cortical spatial dimensions, is described in Fig. 2. The Figure shows how, by knowing just the entropy values for each BOLD-activated brain area, we are allowed to correlate two different brain states, e.g., a state with symmetry breaking and a state with preserved symmetries. During a symmetry break or vice versa, the brain may use different mechanisms in order to modify thermodynamic parameters. The possible mechanisms are displayed in Fig. 1. For example, when the system goes from symmetry to symmetry break, the enthalpy must be reduced of the half, via, e.g., a decrease of local blood flow (enthalpy), or a decrease of spike frequency (free-energy). When the system goes from a symmetry break towards a restored symmetry, the brain requires a surplus of *external* energy to *inject* into M^d, and vice versa. Brain spikes, in this framework, could stand for one of the thermodynamic parameters able to give rise to different attractors, and to supply the required enthalpy, in order to proceed from a symmetry to a symmetry breaking and vice versa. There are many good sources of data to test the claim that brain areas are energetically correlated during symmetry breaks. Indeed, unrestricted fMRI data sets are available in web repositories, such as The International Neuroimaging Data-sharing Initiative (INDI), that launched the 1000 Functional Connectomes Project (Biswal et al. 2010), or the

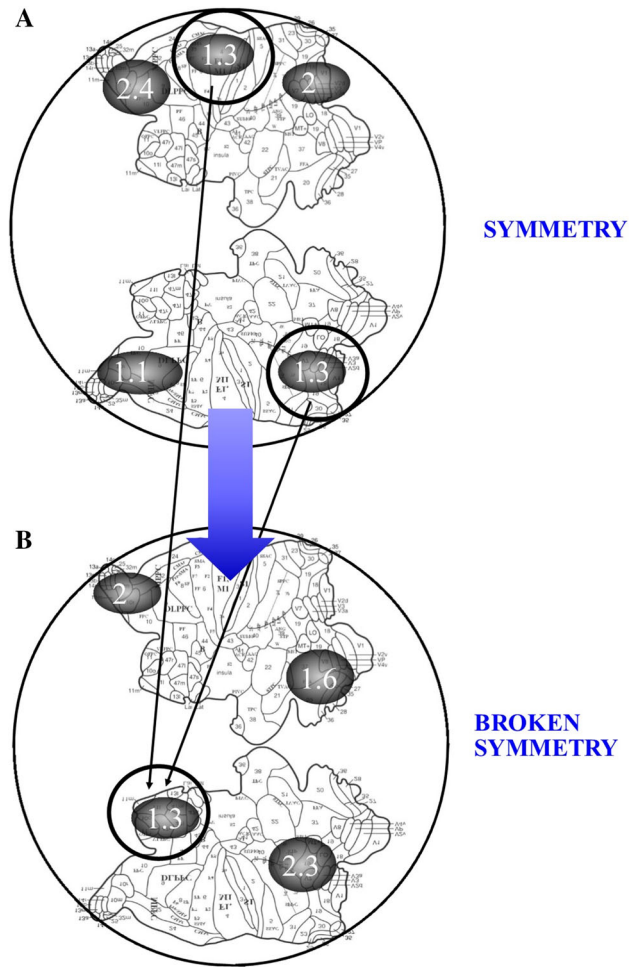

Fig. 2 The two brain hemispheres are flattened and displayed in 2D, according to Van Essen (2005). The *black circles*, depicting hypothetical micro-areas of *BOLD* signal during fMRI functional studies, contain a number which stands for the corresponding entropy value. **a** displays a functional state with preserved symmetry (e.g., mind wandering), while **b** one with symmetry breaking (e.g., a task-related activity). Note that two micro-areas with the same entropy values in **a** stand for two points with matching description. The latter necessarily project to a single point, in case the brain symmetry is broken, according to the dictates of gen-BUT. This means that in **b** there must be a micro-area with the same entropy value of the two matching points in **a**. It allows us to assess which zones of the brain could be correlated during functional symmetry breaks

Human Connectome Project (Glasser et al. 2016). We will provide an example, in order to demonstrate the feasibility of a combined energetic/topological approach and its aptitude of providing very accurate testable previsions. We have two mental states, one standing for a symmetry, and another for a broken symmetry. Imagine that the brain at rest displays a preserved symmetry, while the brain during a visual task displays a broken symmetry. Our proposed model may predict in fMRI series the energetic values for both the cases. Indeed, according to BUT, a single microarea with symmetry breaking necessarily projects to

Author's personal copy

TWO areas with preserved symmetry. The single area in lower dimensions and the two areas in higher dimensions must to display the same values of entropy. This allows us to recognize which zones of the brain are correlated during symmetry breaks, e.g., during the projective steps from higher to lower levels, and vice versa. Therefore, our framework may predict the following hypothetical results: if we find, during a visual task, say, three microareas with an entropy 1.08, we expect to find, during rest, six or more microareas with entropy = 1.08. In sum, by knowing just the entropy values for each BOLD-activated cortical sub-area, we are allowed to correlate two different brain states, e.g., a lower-dimensional state with symmetry breaking and a higher-dimensional state with preserved symmetries.

Conclusions

In this work, we proposed a framework that might be able to achieve, from an *abstract* topological assessment of brain activity, *real* thermodynamic parameters, in order to evaluate and correlate different cortical functions. BUT and its novel variants display very useful general features which help us to explain a wide-range of brain phenomena. By satisfying the requirements for BUT, it is possible for us to quantify increases and decreases of free-energy/entropy/enthalpy when going from one functional brain conformation to another, *e.g.*, from the functional 4D sphere of the default mode network during spontaneous brain activity (Tozzi and Peters 2016a), to the lower dimensional 3D manifold during evoked brain activity (Papo 2014). Therefore, the existence of one pair of mappings implies an overall change in thermodynamic and informational parameters. Despite BUT theorem states that it exists *at least a pair* of antipodal point that maps a dimension lower, nevertheless it does not say that *every antipodal pair* will be mapped to a single set, nor that *all* the two sets of objects in higher dimensions display matching descriptions with *all* the single sets of objects in lower dimensions. It means that we would neither specifically assess if a recorded brain state or a set of trajectories is the image of any antipodes, nor the accurate matching of the mapping from higher-dimension manifolds to lower-dimension ones. However, BUT is still very informative about brain dynamics in practice. Indeed, there exist some trajectories, even if we don't know which, that are mapped to a lower-dimensional space and imply a predictable energetic change. Because the brain functional micro-zones are countless, the use of BUT is helpful in achieving a drastic reduction and simplification of the areas to investigate. Instead of looking for a needle in a haystack, BUT makes it possible for neuro-researchers to remove the most of the straw and to increase the number of needles. The BUT approach also complements the claim of Simas et al. (2015), who suggested that the algebraic topological approach of embedding a brain network on metric spaces (of different dimensions) may reveal regions that are members of large areas or subsystems, rather than regions with a specific role in information processing. Indeed, Simas' framework is not restricted to the static aggregation, rather the multilayers assemblies can be seen as temporal brain windows, and their dynamics as a minimization of inter-level energy in an average time window. In sum, contrary to the classical averaging of connectivity matrices, the BUT approach reveals brain areas with a specific role in information processing.

A shift in conceptualizations is evident in a methodological approach based on BUT. That is, the opportunity to treat brain dynamics as topological structures gives us the invaluable chance to describe them through the tools of functional analysis (Dol'nikov 1992). The BUT perspective enunciates a symmetry property located in the physical space (the environment and the brain) to be translated to an abstract space and vice versa, enabling us to achieve maps from one system to another. This approach is in touch with recent proposals, which provide a rigorous way of measuring distance on brain manifolds (Sengupta et al. 2016). We might imagine the brain as a manifold, equipped with a high number of symmetries and with an internal, mathematically structured, holistic generative model of the external world. Depending on external stimuli (Tozzi et al. 2016a) and on individual background, symmetry breaks occur, giving rise to phase spaces equipped with a lower number of dimensions. This takes us into the realm of metric algebraic topology (Willard 1970), where multidimensional manifold describe the structural order of the relationships between nervous anatomical components and their functional paths.

References

Afraimovich V, Tristan I, Varona P, Rabinovich M (2013) Transient dynamics in complex systems: heteroclinic sequences with multidimensional unstable manifolds. Discontin Nonlinearity Complex 2(1):21–41

Attwell D, Laughlin SB (2001) An energy budget for signaling in the grey matter of the brain. J Cereb Blood Flow Metab Off J Int Soc Cereb Blood Flow Metab 21(10):1133–1145. doi:10.1097/00004647-200110000-00001

Benson AR, Gleich DF, Leskovec J (2016) Higher-order organization of complex networks. Science 353(6295):163–166. doi:10.1126/science.aad9029

Biswal BB, Mennes M, Zuo XN, Gohel S, Kelly C et al (2010) Toward discovery science of human brain function. Proc Natl Acad Sci USA 107(10):4734–4739. doi:10.1073/pnas.0911855107

Author's personal copy

Borsuk M (1933) Drei satze uber die n-dimensionale euklidische sphare. Fundam Math 20:177–190

Deco G, Jirsa VK (2012) Ongoing cortical activity at rest: criticality, multistability, and ghost attractors. J Neurosci 32(10):3366–3375. doi:10.1523/JNEUROSCI.2523-11.2012

Di Concilio A (2013) Point-free geometries: proximities and quasi-metrics. Math Comput Sci 7(1):31–42

Di Concilio A, Gerla G (2006) Quasi-metric spaces and point-free geometry. Math Struct Comput Sci 16(1):115137

Disalle R (1995) Spacetime theory as physical geometry. Erkenntnis 42(3):317–337

Dodson CTJ (1997) A user's guide to algebraic topology. Kluwer Academic Publishers, Dordrecht

Dol'nikov VL (1992) A generalization of the ham sandwich theorem. Math Notes 52:771–779

Fraiman D, Chialvo DR (2012) What kind of noise is brain noise: anomalous scaling behavior of the resting brain activity fluctuations. Front Physiol 3:1–11. doi:10.3389/fphys.2012.00307

Friston K (2010) The free-energy principle: a unified brain theory? Nat Rev Neurosci 11(2):127–138. doi:10.1038/nrn2787

Glasser MF, Smith SM, Marcus DS, Andersson JLR, Auerbach EJ et al (2016) The human connectome project's neuroimaging approach. Nat Neurosci 19:1175–1187. doi:10.1038/nn.4361

Goddard P, Olive D (1985) Algebras, lattices and strings. In: Lepowsky J, Mandelstam S, Singer IM (eds) Vertex operators in mathematics and physics. Mathematical Sciences Research Institute Publications, vol 3. Springer, New York, NY

Jirsa VK, Friedrich R, Haken H, Kelso JAS (1994) A theoretical model of phase transitions in the human brain. Biol Cybern 71:27. doi:10.1007/BF00198909

Jirsa VK, Fuchs A, Kelso JAS (1998) Connecting cortical and behavioral dynamics: bimanual coordination. Neural Comput Arch 10(8):2019–2045

Kalmbach AS, Waters J (2012) Brain surface temperature under a craniotomy. J Neurophysiol 108(11):3138–3146

Kida T, Tanaka E, Kakigi R (2016) Multi-dimensional dynamics of human electromagnetic brain activity. Front Hum Neurosci 9:713. doi:10.3389/fnhum.2015.00713

Kim I-S (1997) Extensions of the Borsuk–Ulam theorem. J Korean Math Soc 34(3):599

Kim SY, Lim W (2015) Frequency-domain order parameters for the burst and spike synchronization transitions of bursting neurons. Cogn Neurodyn 9(4):411–421. doi:10.1007/s11571-015-9334-4

Kleineberg K-K, Boguñá M, Serrano MA, Papadopoulos F (2016) Hidden geometric correlations in real multiplex networks. Nature Physics, in press. doi:10.1038/nphys3812

Lech RK, Güntürkün O, Suchan B (2016) An interplay of fusiform gyrus and hippocampus enables prototype- and exemplar-based category learning. Behav Brain Res. doi:10.1016/j.bbr.2016.05.049

Lenzen VF (1939) Physical geometry. Am Math Mon 46:324–334

Long MA, Fee MS (2008) Using temperature to analyse temporal dynamics in the songbird motor pathway. Nature 456(7219):189–194

Marsaglia G (1972) Choosing a Point from the Surface of a Sphere. Ann Math Stat 43(2):645–646. doi:10.1214/aoms/1177692644

Matoušek J (2003) Using the Borsuk–Ulam theorem. Lectures on topological methods in combinatorics and geometry. Springer, Berlin

Mazzucato L, La Fontanini A, Camera G (2016) Stimuli Reduce the Dimensionality of Cortical Activity. Syst. Neurosci, in press, Front. doi:10.3389/fnsys.2016.00011

Mitroi-Symeonidis F-C (2015) Convexity and sandwich theorems. Eur J Res Appl Sci 1:9–11

Noether E (1918) Invariante Variationsprobleme. Nachr. D. König. Gesellsch. D. Wiss. Zu Göttingen. Math-phys. Klasse 1918:235–257

Olive DI, Landsberg PT (1989) Introduction to string theory: its structure and its uses. Philos Trans R Soc Lond Ser A Math Phys Sci 329:319–328

Papo D (2014) Functional significance of complex fluctuations in brain activity: from resting state to cognitive neuroscience. Front Syst Neurosci 8:112. doi:10.3389/fnsys.2014.00112

Peters JF (2016) Computational Proximity. Excursions in the Topology of Digital Images. Edited by Intelligent Systems Reference Library. Springer, Berlin. doi:10.1007/978-3-319-30262-1

Peters JF, Naimpally SA (2012) Applications of near sets. Not Am Math Soc 59(4):536–542. doi:10.1090/noti817

Peters JF, Tozzi A (2016a) Region-Based Borsuk–Ulam Theorem. arXiv:1605.02987

Peters JF, Tozzi A (2016b) String-Based Borsuk–Ulam Theorem. arXiv:1606.04031v1

Peters JF, Tozzi A, Ramanna S (2016) Brain tissue tessellation shows absence of canonical microcircuits. Neurosci Lett 626:99–105. doi:10.1016/j.neulet.2016.03.052

Petty CM (1971) Equivalent sets in Minkowsky spaces. Proc Am Math Soc 29(2):369–374

Roldán É, Martínez I, Parrondo JMR, Petrov D (2014) Universal features in the energetics of symmetry breaking. Nat Phys 10(6):457–461. doi:10.1038/nphys2940

Schleicher D (2007) Hausdorff dimension, its properties, and its surprises. Am Math Mon 114(6):509–528

Schneidman E, Berry MJ, Segev R, Bialek W (2006) Weak pairwise correlations imply strongly correlated network states in a neural population. Nature 440:1007–1012

Scholz JP, Kelso JAS, Schöner G (1987) Nonequilibrium phase transitions in coordinated biological motion: critical slowing down and switching time. Phys Lett A 123(8):390–394. doi:10.1016/0375-9601(87)90038-7

Sengupta B, Stemmler MB, Friston KJ (2013a) Information and efficiency in the nervous system—A synthesis. PLoS Comput Biol. doi:10.1371/journal.pcbi.1003157

Sengupta B, Laughlin SB, Niven JE (2013b) Balanced excitatory and inhibitory synaptic currents promote efficient coding and metabolic efficiency. PLoS Comput Biol. doi:10.1371/journal.pcbi.1003263

Sengupta B, Tozzi A, Cooray GK, Douglas PK, Friston KJ (2016) Towards a neuronal gauge theory. PLoS Biol 14(3):e1002400. doi:10.1371/journal.pbio.1002400

Simas T, Chavez M, Rodriguez PR, Diaz-Guilera A (2015) An algebraic topological method for multimodal brain networks comparisons. Front Psychol. 6(6):904. doi:10.3389/fpsyg.2015.00904

Stemmler M, Mathis A, Herz AVM (2015) Connecting multiple spatial scales to decode the population activity of grid cells. Sci Adv 1:e1500816

Tognoli E, Kelso JS (2013) On the brain's dynamical complexity: coupling and causal influences across spatiotemporal scales. Adv Cognit Neurodyn (III), pp 259–265. doi:10.1007/978-94-007-4792-0

Touboul J (2012) Mean-field equations for stochastic firing-rate neural fields with delays: derivation and noise-induced transitions. Phy D Nonlinear Phenom 241(15):1223–1244. doi:10.1016/j.physd.2012.03.010

Tozzi A (2015) Information processing in the CNS: a supramolecular chemistry? Cogn Neurodyn 9(5):463–477. doi:10.1007/s11571-015-9337-1 (**Review**)

Tozzi A (2016) Borsuk–Ulam Theorem Extended to Hyperbolic Spaces. In: Computational Proximity. Excursions in the Topology of Digital Images, edited by JF Peters, pp 169–171. doi:10.1007/978-3-319-30262-1

Author's personal copy

Tozzi A, Peters JF (2016a) Towards a fourth spatial dimension of brain activity. Cogn Neurodyn 10(3):189–199. doi:10.1007/s11571-016-9379-z

Tozzi A, Peters JF (2016b) A topological approach unveils system invariances and broken symmetries in the brain. J Neurosci Res 94(5):351–365. doi:10.1002/jnr.23720

Tozzi A, Fla T, Peters PJ (2016a) Building a minimum frustration framework for brain functions in long timescales. J Neurosci Res. doi:10.1002/jnr.23748

Tozzi A, Zare M, Benasich AA (2016b) New perspectives on spontaneous brain activity: dynamic networs and energy matter. Front Hum Neurosci. doi:10.3389/fnhum.2016.00247

Van Essen DC (2005) A population-average, landmark- and surface-based (PALS) atlas of human cerebral cortex. Neuroimage 28:635–666

Wang H, Wang B, Normoyle KP, Jackson K, Spitler K (2014a) Brain temperature and its fundamental properties: a review for clinical neuroscientists. Front Neurosci 8(8):307

Wang Z, Li Y, Childress AR, Detre JA (2014b) Brain entropy mapping using fMRI. PLoS ONE 9(3):1–8. doi:10.1371/journal.pone.0089948

Wang Y, Wang R, Zhu Y (2017) Optimal path-finding through mental exploration based on neural energy field gradients. Cogn Neurodyn 11(1):99–111. doi:10.1007/s11571-016-9412-2

Watanabe T, Hirose S, Wada H, Imai Y, Machida T, Shirouzu I, Masuda N (2013) A pairwise maximum entropy model accurately describes resting-state human brain networks. Nat Commun 4:1370. doi:10.1038/ncomms2388

Watanabe T, Kan S, Koike T, Misaki M, Konishi S, Miyauchi S, Masuda N (2014) Network-dependent modulation of brain activity during sleep. NeuroImage 98:1–10. doi:10.1016/j.neuroimage.2014.04.079

Weeks JR (2002) The shape of space, 2nd edn. Marcel Dekker, inc, New York

Weyl H (1982) Symmetry. Princeton University Press, Princeton. ISBN 0-691-02374-3

Willard S (1970) General topology. Dover Pub. Inc, Mineola

Xu X, Wang R (2014) Neurodynamics of up and down transitions in a single neuron. Cogn Neurodyn 8(6):509–515. doi:10.1007/s11571-014-9298-9

Yan H, Zhao L, Hu L, Wang X, Wang E, Wang J (2013) Nonequilibrium landscape theory of neural networks. PNAS 110(45):4185–4194

Zare M, Grigolini P (2013) Chaos, Solitons & Fractals Criticality and avalanches in neural networks. Chaos, Solitons and Fractals: The Interdisciplinary Journal of Nonlinear Science, and Nonequilibrium and Complex Phenomena 55:80–94. doi:10.1016/j.chaos.2013.05.009

Author's personal copy

Cogn Neurodyn (2017) 11:391–394
DOI 10.1007/s11571-017-9428-2

BRIEF COMMUNICATION

The human brain from above: an increase in complexity from environmental stimuli to abstractions

James F. Peters[1,2,3] · Arturo Tozzi[3,4] · Sheela Ramanna[5] · Ebubekir İnan[2,3]

Received: 29 June 2016 / Revised: 7 February 2017 / Accepted: 23 February 2017 / Published online: 29 March 2017
© Springer Science+Business Media Dordrecht 2017

Abstract Contrary to common belief, the brain appears to increase the complexity from the perceived object to the idea of it. Topological models predict indeed that: (a) increases in anatomical/functional dimensions and symmetries occur in the transition from the environment to the higher activities of the brain, and (b) informational entropy in the primary sensory areas is lower than in the higher associative ones. To demonstrate this novel hypothesis, we introduce a straightforward approach to measuring island information levels in fMRI neuroimages, via Rényi entropy derived from tessellated fMRI images. This approach facilitates objective detection of entropy and corresponding information levels in zones of fMRI images generally not taken into account. We found that the Rényi entropy is higher in associative cortices than in the visual primary ones. This suggests that the brain lies in dimensions higher than the environment and that it does not concentrate, but rather dilutes messages coming from external inputs.

Keywords Entropy · Topology · fMRI · Tessellation

✉ Arturo Tozzi
tozziarturo@libero.it

James F. Peters
James.peters3@umanitoba.ca

Sheela Ramanna
s.ramanna@uwinnipeg.ca

Ebubekir İnan
einan@adiyaman.edu.tr

1 Department of Electrical and Computer Engineering, University of Manitoba, 75A Chancellor's Circle, Winnipeg, MB R3T 5V6, Canada

2 Department of Mathematics, Faculty of Arts and Sciences, Adıyaman University, 02040 Adıyaman, Turkey

3 Computational Intelligence Laboratory, University of Manitoba, Winnipeg, MB R3T 5V6, Canada

4 Center for Nonlinear Science, University of North Texas, 1155 Union Circle, #311427, Denton, TX 76203-5017, USA

5 Department of Applied Computer Science, University of Winnipeg, Winnipeg, MB R3B 2E9, Canada

Introduction

Sequential processing of information is hierarchical so that initial, low-level inputs of primary sensory areas are transformed into representations. Integration emerges at multiple processing associative cortical stages (Freeman 2007; Werner and Noppeney 2009; Nieuwenhuys et al. 2008). Sensory inputs are progressively concentrated, from the primary sensory areas to higher associative ones. As cortical distance from the input increases, brain functions organize messages in global gradients of abstraction, so that spatially progressive representation amalgamation emerges (Taylor et al. 2015). In sum, the current paradigm talks about a brain that, through the limited human sensory repertoire, extracts and concentrates information from the environment's overwhelming complexity, focusing just on what is useful for the individual preservation.

However, recent advances suggest that the brain is more complex than previously thought (Tozzi 2015) and displays a number of dimensions and symmetries higher than commonly believed (Tozzi and Peters 2016a, b; Xing et al. 2016; Peters et al. 2017). This means that external inputs progressively increase their complexity, when spikes cross the brain towards higher associative cortices. Here we hypothesize that sensory inputs are progressively diluted, when passing from the lower sensory areas to the higher associative ones. In other words, the "concept" (or the

Author's personal copy

"idea") could be more complex than the corresponding inputs from the external world. The brain activity might lead to increases, and not decreases, of complexity, compared with the surrounding environment. In order to test our claim, we evaluated, through novel neuroimaging techniques, the entropy values in different cortical areas after visual stimuli presentation and showed that the associative areas manifest more information than the primary sensory ones.

Materials and methods

Samples

We evaluated 16 fMRI images from visual tasks experiments, which illustrate the activity of different brain areas during vision. The images, taken from Mandelkow et al. (2016), display a widely distributed fMRI response throughout the brain, elicited by basic vision and object recognition. A voxel-wise ANOVA F-statistic map (threshold $p < 1\%$, uncorrected) was superimposed on the T1-weighted anatomical MRI of one representative subject (16 axial slices in radiological convention). Each tessellated image leads to the MNC mesh clustering described in the next paragraph.

Nucleus clustering in Voronoï tilings

Through computational techniques described in Peters et al. (2016, 2017), we detected, in the above-mentioned images, a set of keypoint sites S (also called generating points), each with a different orientation angle. Each site s is used to derive what is known as a Voronoï region of s, which is a polygonal shape contain all surface points that are nearer s than to any other site in S (Peters 2016; Edelsbrunner 2006; Duyckaerts and Godefroy 2000; Frank and Hart 2010). A Voronoï region $V(s)$ of a site s is defined by

$$V(s) = \left\{ x \in fMRI : \|x - s\| \underset{for\,all\,q \in S}{\leq} \|x - q\| \right\}.$$

A tessellated image results from finding all Voronoï regions on the image. The end result is a collection of convex Voronoï regions that reveal varying information levels in tessellated fMRI images. Each Voronoï region is the center of a cluster of polygonal regions called a nucleus cluster. A cluster with the highest number of adjacent Voronoï regions is called a maximal nucleus cluster (MNC) (Peters and Inan 2016; Peters 2016) (Fig. 1, left column). A MNC, which highlights singular regions of fMRI images, contains a nucleus polygon with the highest number of adjacent Voronoï regions (Fig. 1, central column). In effect, each maximal nucleus tells us something different about every region of a tiled fMRI image, since we include, in the description of a maximal nucleus, the number of adjacent regions as well as the orientation angles of the nucleus generating point. In sum, in a Voronoï tessellation of an fMRI image, of particular interest is the presence of MNCs, *i.e.*, clusters with nuclei having the highest number of adjacent polygons.

Information levels in fMRI nucleus clusters

MNCs reveal brain regions with higher levels of cortical information, in comparison with non-MNC cortical regions, that uniformly yield less information. Using Rényi entropy (Rényi 1961, 1966, 1982; Bromiley et al. 2010), as a measure of information, we previously demonstrated that the nuclei in MNCs have the highest concentration of adjacent polygons, compared to all non-MNC polygons (Peters et al. 2017). This finding points towards MNCs yielding higher information than any of the polygon areas outside the MNCs (Fig. 1, right column). In sum, Rényi entropy provides a measure of the information in MNCs and the surrounding zones of fMRI images. This means that the MNCs encompass higher entropy values, and therefore higher information, which contrasts with the lower information in the surrounding non-MNC zones.

Results

Each frame from Mandelkow et al. (2016) showed that stimulus-correlated fMRI activity is widespread in the occipital and ventral temporal cortices, consistent with their established involvement in basic vision and object recognition. For each frame, we produced tessellated images with one or more maximal mesh regions. Furthermore, we generated tessellated images showing one or more MNCs. The most of MNCs were found to be located in anterior or central brain zones, far from the posterior primary visual sensory areas. The entropy values were higher in the associative zones than in the primary sensory ones. This means that the associative brain areas, during vision, display more activity than the surrounding ones, including the primary visual area. See Fig. 1 for further details.

Discussion

The current paradigm describes a hierarchical landscape of cognition, where a relatively linear and continuous increase in symbolic content occurs over network-depth. A

Author's personal copy

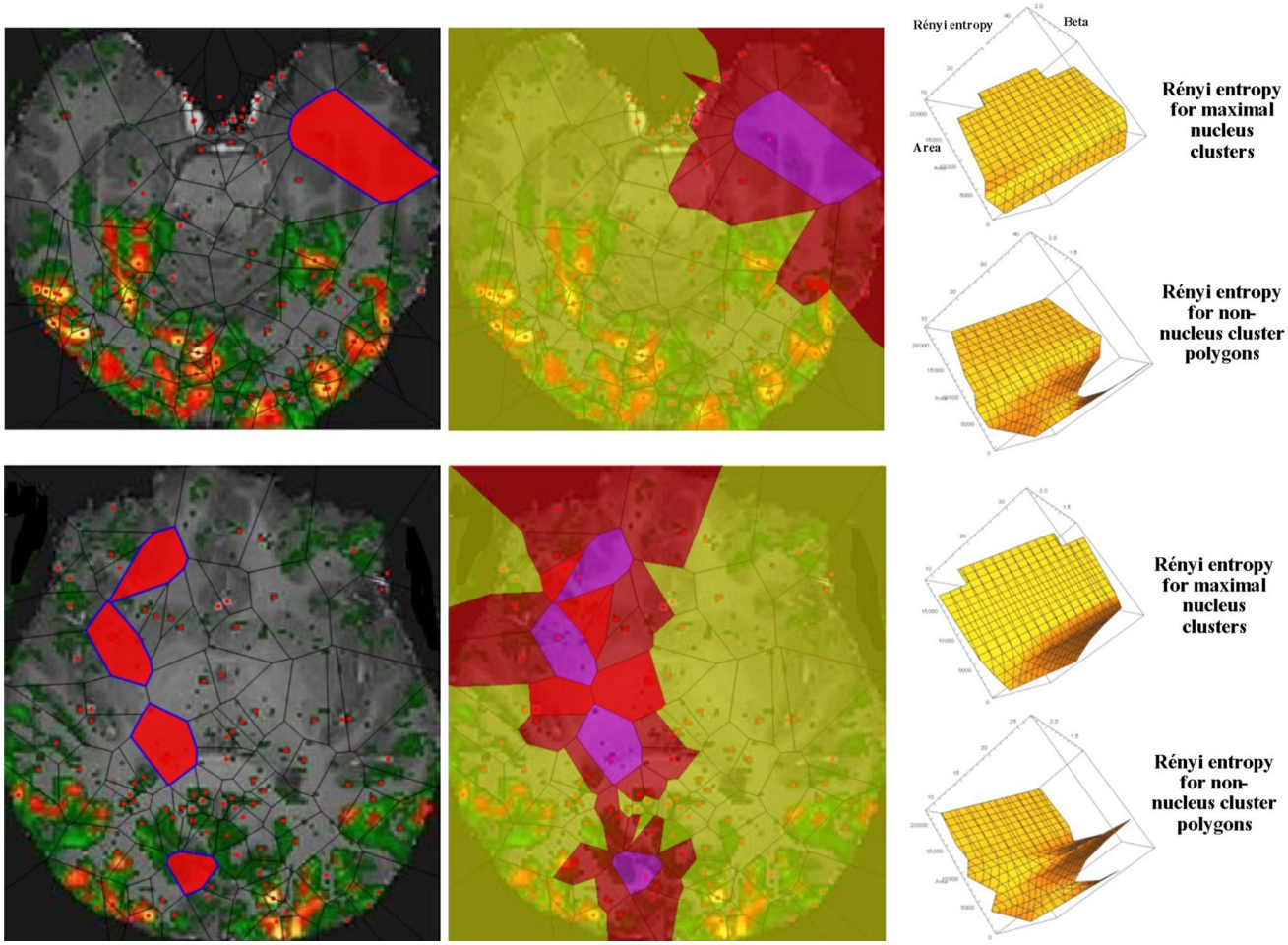

Fig. 1 Voronoï tessellation and MNCs in two fMRI images, taken from Mandelkow et al. (2016). The *left column* depicts Maximal Voronoi regions. Each *red dot* in the tiling stands for a generating point with particular features, such as gradient orientation angle and brightness. No two *red dots* have the same description. For this reason, every polygonal Voronoï region has a slightly different shape. Red polygons show MNCs. They are of particular interest, since their generating points have a gradient orientation that is *different from the gradient orientation of any other generating point in this particular tiling*. The *central column* displays cortical MNCs, i.e., the areas with the higher number of adjacent polygons. The *right column* illustrates informational levels in the two fMRI images, in particular the Rényi entropy values of the corresponding MNCs, compared with the surrounding areas. For every sample, the Rényi entropy values versus number polygon areas of MNC (*upper part*) and outside MNC (*lower part*) are displayed. MNC Nuclei surrounded by polygons with smaller areas have higher Rényi entropy, which tells us that smaller MNC areas yield more cortical information than MNCs with larger areas

continuum of stratified landscapes takes place in a hierarchical connectome, where a graded order of class is represented by a diagram of connected nodes. Starting from external inputs, an emergent aggregation of functions gives rise to abstractions processing, where *abstraction* is defined as a process creating general concepts of representation, by emphasizing common features (Taylor et al. 2015). A structural pyramid of the human connectome with gross network-depth directionality can be sketched. *Concrete* regions at the base of pyramid, connected to the outside world, are related to simple perceptions, sensory processing or physical actions. *Abstract* regions at the pinnacle of the pyramid, which are deepest in the brain network and least connected with the outside world, are related to more abstract concepts and symbols. Behavioral elements are conceptualized as brain functions, tasks or behaviors. This means that abstract behaviors start with sensory inputs and the information representation flow converges towards less complex schemes, e.g., the ideas (Pexman et al. 2013). In sum, unified concepts tend to compress and amalgamate the information content of an idea or an observable event, in order to retain only information which is relevant for an individualized goal or action (Taylor et al. 2015).

Here we proposed and tested an alternative hypothesis, where the above-mentioned pyramid of complexity is inverted: the abstract concepts are more intricate and contain more information than the external world. The brain does not *extract* and concentrate the meaning of

Author's personal copy

external objects in simple ideas, rather it *dilutes* the meaning of external objects in complicated ideas. The information is not *aggregated*, rather it is *scattered* in the brain. Recent papers suggest that the brain activity might be multidimensional and shaped in guise of a donut-like structure (see, for example, Tozzi and Peters 2016a). This means that the brain function lies in dimensions higher than the environment. Brain activity can be compared to a phase space where projections take place among regions temporarily equipped with different functional dimensions, each one mapping the other. In this powerful topologic framework, the world external to the observer *is* a single set of objects, while the world internal to the observer *is* many sets of objects with matching description (Tozzi and Peters 2016b). Single descriptions of biologically significant environmental inputs become matching descriptions in our thoughts. The object's concept lies in a dimension higher than the object. To make an example, mental images of cats are not pale copies of cats: while mental images are matching descriptions, real images are single descriptions. Thus, contrary to common belief, the object's concept is more intricate than the object.

This means that the primary sensory areas might display less entropy than the associative areas. To test our hypothesis, we needed to evaluate the changes in entropy values in fMRI images, in given timescales and in different areas. We used a novel image analysis technique. The major new elements in the evaluation of fMRI images are nucleus clusters, maximal nucleus clusters, strongly near maximal nucleus clusters, convexity structures that occur whenever max nucleus clusters intersect. We showed that in a Voronoï tessellation of an fMRI image, of particular interest is the presence of MNCs, *i.e.*, clusters with the highest number of adjacent polygons. We demonstrated that MNC reveal regions of the brain with higher levels of cortical information, in comparison with non-MNC cortical regions. We showed that, in touch with our hypothesis, such brain zones with higher levels of cortical information correspond to associative areas.

References

Bromiley, PA, Thacker, NA, Bouhova-Thacker, E (2010) Shannon entropy, Renyi entropy, and information. Tina 2004-004, Statistic and Inf Series, Imaging Science and Biomedical Engineering, The University of Manchester, UK

Duyckaerts G, Godefroy G (2000) Voronoï tessellation to study the numerical density and the spatial distribution of neurons. J Chem Neuroanat 20(1):83–92

Edelsbrunner H (2006) Geometry and topology for mesh generation. Cambridge University Press, Cambridge

Frank NP, Hart SM (2010) A dynamical system using the Voronoï tessellation. Am Math Mon 117(2):92–112

Freeman WJ (2007) Definitions of state variables and state space for brain-computer interface: part 1. Multiple hierarchical levels of brain function. Cogn Neurodyn 1(1):3–14. doi:10.1007/s11571-006-9001-x

Mandelkow H, de Zwart JA, Duyn JH (2016) Linear discriminant analysis achieves high classification accuracy for the BOLD fMRI response to naturalistic movie stimuli. Front Hum Neurosci 10:128. doi:10.3389/fnhum.2016.00128

Nieuwenhuys R, Voogd J, van Huijzen C (2008) The human central nervous system. Springer, Heidelberg

Peters JF (2016) Computational proximity. In: Intelligent Systems Reference Library (ed) Excursions in the topology of digital images. Springer, Berlin. doi:10.1007/978-3-319-30262-1

Peters JF, İnan E (2016) Strongly near Voronoï nucleus clusters. 1–7. arXiv:1602(03734)

Peters JF, Tozzi A, Ramanna S (2016) Brain tissue tessellation shows absence of canonical microcircuits. Neurosci Letters 626:99–105

Peters JF, Ramanna S, Tozzi A, Inan E (2017) BOLD-independent computational entropy assesses functional donut-like structures in brain fMRI image. Frontiers Hum Neurosci. doi:10.3389/fnhum.2017.00038

Pexman PM, Siakaluk PD, Yap MJ (2013) Introduction to the research topic meaning in mind: semantic richness effects in language processing. Hum Neurosci, Front. doi:10.3389/fnhum.2013.00723

Rényi A (1961) On measures of entropy and information. In: Proceedings of the fourth Berkeley symposium on mathematical statistics and probability, vol. I, University of California Press, Berkeley, pp 547–457 **(MR0132570)**

Rényi A (1966) On the amount of information in a random variable concerning an event. J Math Sci 1:30–33 **(MR0210263)**

Rényi A (1982) Tagebuch über die Informationstheorie. VEB Deutcher der Wissenschaften, Berlin **(MR0707097)**

Taylor P, Hobbs JN, Burroni J, Siegelmann HT (2015) The global landscape of cognition: hierarchical aggregation as an organizational principle of human cortical networks and functions. Sci Rep 5:18112. doi:10.1038/srep18112

Tozzi A (2015) Information processing in the CNS: a supramolecular chemistry? Cogn Neurodyn 9(5):463–477

Tozzi A, Peters JF (2016a) Towards a fourth spatial dimension of brain activity. Cogn Neurodyn 10(3):189–199. doi:10.1007/s11571-016-9379-z

Tozzi A, Peters JF (2016b) A topological approach unveils system invariances and broken symmetries in the brain. J Neurosci Res 94(5):351–365. doi:10.1002/jnr.23720

Werner S, Noppeney U (2009) Superadditive responses in superior temporal sulcus predict audiovisual benefits in object categorization. Cereb Cortex 20(8):1829–1842

Xing M, Ajilore O, Wolfson OE, Abbott C, MacNamara A et al (2016) Brain informatics and health. Ser Lect Notes Comput Sci 9919:149. doi:10.1007/978-3-319-47103-7_15

International Journal of Approximate Reasoning 86 (2017) 73–79

Contents lists available at ScienceDirect

International Journal of Approximate Reasoning

www.elsevier.com/locate/ijar

On normalization of inconsistency indicators in pairwise comparisons ☆

W.W. Koczkodaj [a,*], J.-P. Magnot [b], J. Mazurek [c], J.F. Peters [d,e], H. Rakhshani [f], M. Soltys [g], D. Strzałka [h], J. Szybowski [i], A. Tozzi [j]

[a] Computer Science, Laurentian University, Sudbury, ON P3E 2C6, Canada
[b] Lycée Jeanne D'arc, rue de grande Bretagne, 63000 Clermont-Ferrand, France
[c] Department of Informatics and Mathematics, School of Business Administration in Karvina, Silesian University in Opava, Univ. Square 1934/3, 73340, Czech Republic
[d] Computational Intelligence Laboratory, University of Manitoba, Winnipeg, Manitoba, R3T 5V6, Canada
[e] Department of Mathematics, Faculty of Arts and Sciences, Adiyaman University, 02040 Adiyaman, Turkey
[f] Department of Computer Science, Faculty of Mathematics, University of Sistan and Baluchestan, Zahedan, Iran
[g] California State University Channel Islands, Bell Tower West 2265, One University Drive, Camarillo, CA 93012, USA
[h] Faculty of Electrical and Computer Engineering, Rzeszów University of Technology, Al. Powstańców Warszawy 12, 35-959 Rzeszów, Poland
[i] AGH University of Science and Technology, Faculty of Applied Mathematics, al. Mickiewicza 30, 30-059 Kraków, Poland
[j] Center for Nonlinear Science, University of North Texas, Denton, TX 76203, USA

ARTICLE INFO

Article history:
Received 6 March 2017
Received in revised form 17 April 2017
Accepted 18 April 2017
Available online 21 April 2017

Keywords:
Pairwise comparisons
Inconsistency indicator
Normalization
Decision making

ABSTRACT

In this study, we provide mathematical and practice-driven justification for using $[0, 1]$ normalization of inconsistency indicators in pairwise comparisons. The need for normalization, as well as problems with the lack of normalization, is presented. A new type of paradox of infinity is described.

© 2017 Elsevier Inc. All rights reserved.

1. Preliminaries

Consistency in preferences (by pairwise comparisons) can be traced to [1], published by Kendall and Smith in 1939. By 1976, there were four articles listed in [2], with the inconsistency in the title. In [3], the consistency index (CI) was introduced. Many other definitions followed. All of them attempt to answer the most important question: how far have we departed from the consistent state which is well established by the consistency condition illustrated in Fig. 2 in this text. Briefly, every cycle of three interrelated comparisons: A/B, B/C, and A/C must be reducible to two comparisons, since the third comparison is a result of multiplication or division of these two comparisons. For example, given A/B and B/C, A/C should be equal to $(A/B) * (B/C)$. If A/B and A/C are given, B/C is equal to $(A/C)/(A/B)$. If B/C and A/C are given, A/B is equal to $(A/C)/(B/C)$. No other combination exists for a cycle of three comparisons. If all three ratios are given,

☆ Alphabetical order implies equal contribution.

* Corresponding author.
E-mail addresses: wkoczkodaj@cs.laurentian.ca (W.W. Koczkodaj), jean-pierr.magnot@ac-clermont.fr (J.-P. Magnot), mazurek@opf.slu.cz (J. Mazurek), rakhshani@pgs.usb.ac.ir (H. Rakhshani), msoltys@gmail.com (M. Soltys), strzalka@prz.edu.pl (D. Strzałka), szybowsk@agh.edu.pl (J. Szybowski).

http://dx.doi.org/10.1016/j.ijar.2017.04.005
0888-613X/© 2017 Elsevier Inc. All rights reserved.

inconsistency in such cycle may take place and usually, it does. Earlier definitions of inconsistency were based on the total count of inconsistent triads. Evidently, such cardinal inconsistency was imprecise.

This study proposes to regard the inconsistency in pairwise comparisons as a degree or extent of disagreement modelled on the concept of probability measure. Our study also demonstrates a problem shown in [4], where the normalization was not used.

2. Inconsistency indicator as a degree of disagreement in pairwise comparisons

The interval $[0, 1]$ (or discrete values between 0 and 1) is used in many theories and situations including:

- probability,
- multi-valued logic (as proposed by Lukasiewicz),
- fuzzy logic,
- rough set theory,
- theory of evidence.

There are also a number of zero–one laws of which the convergence of conditional expectations, known as "Lévy's zero–one law," can be summarized as "if we are learning gradually all the information that determines the outcome of an event, then we will become gradually certain what the outcome will be," which has application to the consistency-driven pairwise comparisons (recently used in [5], but based on inconsistency indicator introduced in [6]). The important interpretation of "Lévy's zero–one law" is "the gradual data gathering to determine the outcome of an event, then we will become gradually certain what the outcome will be" since it has the direct application to the reduction of inconsistency in pairwise comparisons.

According to [7], P. Lévy proved in 1937 (see [8]), that Kolmogorov's theorem follows from a more general property of conditional probabilities, which says that

$$\lim_{n\to\infty} P\{f(X_1, X_2, \ldots, X_n)|(X_1, X_2, \ldots, X_n)\}, \tag{1}$$

almost certainly equals 0 or 1 (depending on whether $f(X_1, X_2, \ldots X_n)$ is zero or not).

The use of interval $[0, 1]$ for inconsistency indicators is not only coming from the Occam's razor principle. The Section 3 shows that the lack of normalization in [4] leads to problems which this study attempts to correct. In this study, we will follow a business principle "change a problem into opportunity" and use it not only to correct [4] but to reason for an important axiom.

3. The need for normalization of inconsistency indicators

The fallacy of the Definition 3.6 on page 83 in [4]:

Let $X = \langle X, \cdot \rangle$ be a group. A $\mathcal{G}$-distance-based inconsistency indicator map (in abbreviation: a $\mathcal{G}$-inconsistency indicator map) on the group X is a function $T : X^3 \to G$ such that, for all $a, b, c, d, e \in X$, the following conditions are satisfied:

(i) $T(a, b, c) = 1_G \Leftrightarrow ac = b$;
(ii) $T(a, b, c) = T(b, ac, 1)$;
(iii) $T(a, de, c) \leq T(a, b, c) \odot T(d, b, e)$.

leads to a contradiction in the theory presented there.

The fallacy in the above definition is evidenced below by using the sequence of triads T_n converging to a consistent matrix when the limit of n, a natural number, is the infinity.

Formally, an inconsistency indicator (ii) is defined for a PC matrix, say M. So, $ii(M)$ should be used. However, a PC matrix:

$$M = \begin{bmatrix} 1 & x & y \\ 1/x & 1 & z \\ 1/y & 1/z & 1 \end{bmatrix}$$

is reduced to the three values: x, y, z which generate the entire matrix. For this reason, we will be using $ii(x, y, z)$ as a notation shortcut (to save on typing and space).

To make our point, all we need to do is demonstrate just one counter-example (for any particular distance). In particular, our goal is achieved when we construct all triads in the sequence T_n this way so that they have constant inconsistency greater than 0 (e.g., one or 2^{64}) and yet such sequence converges. In fact, it is enough to show the convergence for any sequence (e.g., Cauchy sequence). Evidently, T_n is a Cauchy sequence. The well-established consistency condition for PC matrix $M = [m_{ij}]$ is:

$$m_{ik} = m_{ij} * m_{jk} \quad \text{for } i < j < k \leq n \tag{2}$$

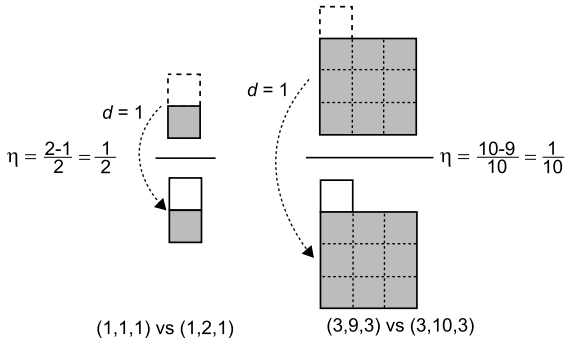

Fig. 1. Example of two triads with identical d.

These three PC matrix elements create a triad (m_{ij}, m_{ik}, m_{jk}) denoted here as (x, y, z). A triad is consistent when its middle value is equal to the multiplication of the first and third value. To show that Definition 3.6 in [4] leads to contradiction, consider the following sequence of triads:

$$T_n = (x^n, x^{2n} + 1, x^n) \quad \text{for natural } n = 1, 2, \ldots, \text{ and for } x > 1. \tag{3}$$

The Euclidean distance between the middle value in the triad T_n and the result of two other values after the group operation (multiplication) is constant and equals: $d(x^{2n} + 1, x^n \cdot x^n) = 1$. The relative error is defined as:

$$\eta = \left| \frac{y - y_{approx}}{y} \right|. \tag{4}$$

When the relative error definition, given by the equation (4), is applied to the middle value of the triad T_n, we get:

$$\frac{d(x^{2n} + 1, x^n \cdot x^n)}{x^{2n} + 1} = \frac{1}{x^{2n} + 1} \to 0 \quad \text{for } n \to \infty. \tag{5}$$

To illustrate that the distance (generalized or not) cannot serve as an inconsistency indicator, all we need to do is to produce just one counter-example. Fig. 1 shows that "one extra square" added to a consistent triad $(1, 1, 1)$ (hence "one of two") is worse than one extra square added to nine squares.

It is worthwhile to notice that the following triad:

$$(\infty, \infty^2, \infty)$$

is simply reduced to:

$$(\infty, \infty, \infty)$$

So, a triad may look like (x, x, x) but (x, x, x) is only consistent for $x = 1$, while (x, x^2, x) if consistent for any x (technically, $x > 0$ since PC matrix cannot contain zero or negative values).

From the point of view of the proof of convergence of T_n, it does not matter how the real limit looks like: (x, x^2, x) or (x, x, x) as long as the consistency condition holds for it.

Replacing 1 in T_n with any constant (e.g., 2^{64} which is a cosmic number) just increases n but the entire reasoning is unchanged. For the disbeliever in ∞, we can use three equal sticks of the length 1 which ratios were inaccurately estimated to $(1, 2, 1)$ giving the relative error of $|2 - 1|/1$, hence, 100%. Three other sticks, each 10 times shorter than the other stick, with the ratio estimations as $(10, 101, 10)$ give less than 1% relative error while the Euclidean distance is in both cases identical and equal to 1. The sequence of triads T_n converges to a consistent triad although each of its element has a constant inconsistency indicator making it inconsistent. Defining the inconsistency indicator as an unnormalized distance leads to the following contradiction:

> a sequence of triads converges to a consistent triad, however, each triad has (according to the theory in [4]) the inconsistency indicator which is equal to 1 for each triad in the sequence; therefore, 1 has to be the sequence limit.

The fallacy in the definition of inconsistency in pairwise comparisons as distance for the multiplicative case in [4] extends to the additive case as Fig. 2 illustrates it. Areas of triangles are proportional to ratios they represent: 2, 5, and 3. The layout of these values resembles their location in a PC matrix given as:

$$M = \begin{bmatrix} 1 & A & B \\ \frac{1}{A} & 1 & C \\ \frac{1}{B} & \frac{1}{C} & 1 \end{bmatrix}$$

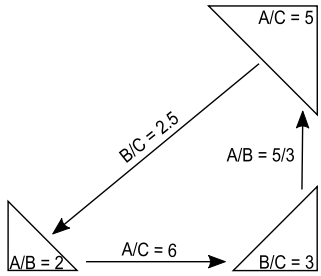

Fig. 2. Illustration of inconsistency concept.

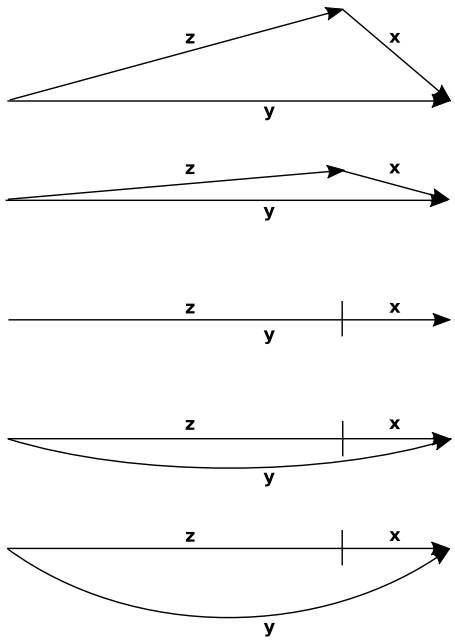

Fig. 3. Inconsistency in additive pairwise comparisons.

The first value in a triad (x, y, z) represents a ratio of entities A and B: $x = A/B$. The middle triad value $y = A/C$ is located in the same matrix row as x to the right of x. The third value in the triad $z = B/C$ is located in the same column as y below it. Values above the arrows represent the value for the third node to make the entire triad consistent. For example, if the value of 2.5 above the upper arrow is used for the replacement of value 3 in the third node (which this arrow does not connect), the triad becomes consistent (since $2.5 * 2 = 5$). Similarly, using the value of 6 above the arrow connecting x and y for $z = A/C = 5$ makes the triad (x, y, z) consistent.

The above reasoning demonstrates why using the distance, which is not normalized, as inconsistency is unacceptable. The distance between y and xz in a triad (x, y, z) remains constant (e.g. 1 or 2^{64}) for all triads in the sequence T_n while the limit of the relative error of approximation is converging to 0, hence, the triad becomes consistent at its limit with the expected inconsistency 0.

It is worthwhile to notice that the relative (hence, normalized) error was needed to make the point but it cannot be taken as a proof of the sufficiency. The analogy to probability provides enough reasoning for the sufficiency.

The above reasoning applies to [9]. In particular, [9] includes:

> "DEFINITION 6.1. The consistency index of the matrix in Equation 6.1 is given by $I_{\mathcal{G}}(A) = ||\rho_{123}|| = d_{\mathcal{G}}(a_{13}, a_{12} \odot a_{23})$. (6.2)"

which was analysed above.

The similar reasoning applies to the additive case of pairwise comparisons, where ratio ("how many times?") is replaced by difference ("by how much?") against the use of the unnormalized distance as an inconsistency indicator. Fig. 3 illustrates the interpretation of the inconsistency indicator as the area of the "triangle" which is reduced to the line for the consistent case. It is easy to see that the inconsistency for a triad (x, y, z), defined in [6] and finally simplified to $ii = 1 - \min(y/(x*z), x*z/y)$ in [10], does not suffer the above problem since the distance $d(y - x*z)$ is normalized and converges to 0. It is worth

mentioning that this may be an example for the need of normalization for applications since the distance normalization seems to be indispensable for the inconsistency indicator definition. The need for a normalized rating scale for pairwise comparisons has been shown in [11]. The lack of the rating scale normalization leads to a paradox. Similarly, the use of "central tendency" in the inconsistency indicator definition leads to deviations as demonstrated in [10] (Section 5 and 6). The two counter-examples and mathematical reasoning were provided that eigenvalue-based inconsistency, used in some customizations of pairwise comparisons, has no mathematical validity since it tolerates arbitrarily large errors when the size of a PC matrix increases to the infinity.

Our reasoning cannot be interpreted as "normalization will fix it all" since not every normalized distance can be used as inconsistency indicator, but whatever inconsistency indicator is defined, it has to be normalized for the reasons listed in the Section 4. Evidently, the list of reasons is, in all likeliness, incomplete, but sufficient to normalize all inconsistency indicators.

There is no question that we need to make risky moves in the absence of hard evidence and "stipulative" (more relevant term: "speculative") definitions may be proposed. However, such definitions should be clearly labelled so other researchers could be alerted and look for a validation or fallacy of such definitions. The theory, based on stipulative foundations, which are not properly labelled, becomes hard to invalidate as time passes and the progress of science suffers. One may only imagine that the eigenvalue-based inconsistency in [3] was "stipulative" since it was invalided in [10] in 2014.

Definition 3.6 in [4] could also be regarded as a stipulative definition. However, it was not labelled (or otherwise indicated) as "stipulative" in the text. The assumption that a generalized distance can be used as a map for inconsistency indicators was arbitrary, not rooted in the deep knowledge of pairwise comparisons, and unverified by real life examples. Not only is it corrected by this study, but has facilitated the discovery of the need for normalization which is a paradigm shift in the research of the inconsistency in pairwise comparisons.

It is worth to notice that all coefficients of T_n have the limit $+\infty$ hence we may wonder whether or not such limit is attainable. Observe that infinity is not a number and was rejected by the intuitionistic mathematics that was advocated by L.E.J. Brouwer. As it turns, the existence of infinity cannot be proved and it needs to be postulated (something that many of us often overlook to do).

One of the philosophical issues of applied mathematics is the approximation theory of real numbers. Most transcendental real numbers cannot be described since the set of transcendental real numbers is not countable, while a picture of one number after another can only show a countable set of numbers. Evidently, at various degrees of knowledge and applications, the idealized framework of mathematics may be questioned by the common sense with regard to the lack of effectiveness and/or feasibility of obtained results.

4. Why not [0, 1]?

The normalization has become so popular (especially in the applied science) that it's impossible to trace its origins. However, the probability is the high suspect, since it was already used (in its embryonic and partially mystic way) by Cardano, who was a gambler, in the 14th century. The probability has involved into one of the most powerful scientific methods universally used in most branches of applied and many theoretical sciences. The normalization in probability theory is related to two of three axioms proposed by Kolmogorov in 1933 hence it is of a considerable importance. However, normalization might have been in use for a few centuries. According to [12,13], the acceptance of Kolmogorov's axiomatization was not instantaneous but took tens of years (some researchers still try to relax some of his axioms).

The issue of normalization leads to the non-trivial mathematical theory of boundedness and bornology (as it is in [14] and in [15, §1.18], where it is related to compactification). A mathematical object A such as a set or function is *bounded*, provided that A has a value such that all members of the set or function are less than this bound. For example, the set of points in the half closed, half open interval $[0, 1)$ is bounded above by 1. Again, for example, the function $f(x) = \log(x)$, $0 < x \leq 2$ is bounded above by 1.

A *bornology* on a nonempty set X is a collection $\mathcal{B}$ of bounded sets B that cover X such that $X = \bigcup B$, and $\mathcal{B}$ is stable under inclusions and finite unions. The power set of a set X (denoted by 2^X) is the collection of the subsets of X, including X. The power set 2^X for $\bigcup\{x\}$, $x \in X$ is an example of a bornology. Boundedness and bornology are closely related to compactification. The bordification is related to compactification.

A subset A of a topological space X is *compact*, provided, for every open cover of A, there is a finite subcover of A [15, §11.0]. For example, every closed and bounded subset in $\mathbb{R}^n$, $n \geq 2$ is compact. However, $\mathbb{R}^1$ as well as any interval of $\mathbb{R}^1$ is not compact. For instance, let $X = [0, 1]$. Then 2^X is a topological space that is not compact, since 2^X has no finite subcover. Again, the set of all subsets of a geodetic line the plane is not compact for the same reason.

Let X be a locally compact space and $p \notin X$. Let $X^* = X \cup \{p\}$. Then the topology on X^* can be defined in the following way: $U \subseteq X^*$ is open if and only if $p \notin U$ and U is open in X, or $p \in U$ and $X \setminus U$ is compact. Then X^* is a (one-point) compactification of X.

One of the most important properties of normalization to $[0, 1]$ is the stability under multiplication defined as:

$$\text{for } \forall t, u \in [0, 1], t \cdot u \in [0, 1].$$

The maximality of $[0, 1]$ is evident in terms of the upper bound, since we cannot extend 0 to a negative value. If we extend 1 by the smallest positive value imaginable, say $\alpha > 0$, the multiplication gives:

$$(1+\alpha)\cdot(1+\alpha) = 1 + 2\alpha + \alpha^2 > 1 + \alpha. \tag{6}$$

It is worthwhile to notice that every non-generative subinterval of $[0, 1]$ is also stable under multiplication. However, it is not maximal. In other words, $[0, 1]$ is the only bounded (by two numbers excluding ∞) interval of the maximal size containing the multiplication of two non-negative real numbers belonging to it.

The "Zero One Infinity Rule" is attributed to Willem Louis van der Poel (a pioneering Dutch computer scientist, who is known for designing the ZEBRA computer). By the above elimination of ∞, our choice for the range of inconsistency indicators is reduced to 0 and 1.

Acting in this spirit of the probability axioms, we postulate the lower and upper bounds for inconsistency indicator as: $0 \le ii \le 1$ without the loss of generality. Unlike probability, inconsistency indicators do not need to reach the upper bound value. It reflects the reality that no one can be indefinitely inconsistent with some exceptions such as "0–1" inconsistency indicator with 0 for all consistent triads and 1 otherwise. Evidently, $ii = 1 - min(y/(xz), xz/y)$ for (x, y, z) cannot ever have a value of 1 since neither xz nor y can be 0 (x, y, z are ratios hence must be strictly positive).

Traditionally, most measures are constructed by setting two thresholds, namely, lower and upper bound. The lower bound is nearly always (if possible) assumed as 0. The upper bound is 10^c, where $c = 0$ for probability, fuzzy sets, rough sets, and more; $c = 1$ for various indicators such as school grades; $c = 2$ for percent values (hence approximation error and business).

There are a number of reasons why the interval $[0, \infty)$ is not as good as $[0, 1]$ but the most important reason is that the first half of $[0, \infty)$ is still $[0, \infty)$. In practice, the inconsistency in pairwise comparisons is unavoidable unless we decide to use the simplified version of pairwise comparisons as described in [16] with the minimum of $n - 1$ comparisons of so-called principal generators which allow us to compute the rest of PC matrix elements from the consistency condition ($a_{ij} * a_{jk} = a_{ik}$). When inconsistency exists (and it is nearly always as previously noticed), its degree is of great importance for the level of tolerance similar to p-value in statistics. The p-value interpretation is the probability that, using a given statistical model, the statistical summary is less than or equal to the chosen significance level (α) than the actual observed results (e.g., the difference between mean values of two compared groups). Needless to say that the value α in statistics is arbitrarily assumed for applications. In medical research, $\alpha = 0.05$ is frequently assumed as a reasonable significance level.

In pairwise comparisons, a similar level of "significance" for inconsistency indicators is needed. It should be called as the level of tolerance. Using an interval $[0, 1]$ is more convenient than $[0, \infty)$. For some inconsistency indicators (e.g., introduced in [6], called Kii here), the level of tolerance is set to $1/3$ since $Kii \in [0, 1)$, and it does not have easy interpretation in $[0, \infty)$. The related concepts in statistics are confidence levels and confidence intervals introduced by Neyman in 1937 in [17]. For the inconsistency in pairwise comparisons, the issue of a tolerance level is of as fundamental importance as the statistical significance in statistics.

The lack of "point of reference" in $[0, \infty)$ was a problem in [3], where a random inconsistency measure was introduced. It is in the direct contradiction of Stevens' observations in [18] stating that:

> "the assignment can be any consistent rule. The only rule not allowed would be random assignment, for randomness amounts in effect to a nonrule".

The interval $[0, 1]$ is used for most indicators and measures in applied sciences as well as in theoretical sciences. Keeping the values in the interval $[0, 1]$ may be the most natural way human brains process/assess concepts of nothing (0), a part of $(0, 1)$ and total/sum (which is 1). However, the most important reasoning for us is the following celebrated mathematical theorem.

Normalizing mappings is well researched and there are many functions mapping $\mathcal{R}^+$ onto $(0, 1)$. For example, generalized logistic function or curve, also known as Richards' curve, a Gompertz curve or Gompertz function, named after Benjamin Gompertz, a sigmoid function, and many other functions are normalized.

It is worth mentioning that the inconsistency indicator, proposed in [6] in 1993, is normalized. Recently, it was simplified in [16] to:

$$Kii = 1 - \min\left(y/(x\cdot z), x\cdot z/y\right) \text{ for } (x, y, z). \tag{7}$$

The equation (7) has an equivalent form

$$Kii = 1 - e^{-|ln(\frac{y}{x\cdot z})|}. \tag{8}$$

A different (and a bit unusual) type of normalization is needed to prevent a rating scale paradox (addressed in [11]).

The original title of this section was "Why $[0, 1]$?" but, after intensive study, it was changed to reflect the reality in the applied science. It is mostly pure mathematics and theoretical physics where ∞ reigns although the speed limit is observed even in the theoretical physics. Using ∞ in proofs is not only highly desirable but often necessary. However, variables of the indicators type are easier to process when they are normalized. For this reason, using $[0, 1]$ should be a rule. Such a rule should only be relaxed if there is a good reason not to follow it.

5. Conclusions

The best way is to avoid inconsistency as much as possible. Sometimes, it is possible as [16] demonstrates. A decision maker may choose to provide just $(n - 1)$ pairwise comparisons, which must be "principal generators" (e.g., located just

above or below the main diagonal and other strategic places specified in [16]). The remaining PC matrix elements can be reconstructed so the entire PC matrix is consistent. Using more than $(n-1)$ pairwise comparisons may (and usually does) lead to inconsistency, which is hard to manage without the use of heuristics.

However, avoidance of inconsistency has a reflection in the use of artificial levees in the river management. When the artificial levee is breached, the damage to properties and lives can be greater than flooding which occurs without an artificial levee constructed. When we enter more data and properly analyse their inconsistency to reduce it, the expectations are that the end result is improved. We hope that the $[0, 1]$ normalization of inconsistency indicators in pairwise comparisons may become one of "the best practices" of future knowledge management standards.

In conclusion, we have learned an important lesson here: when we use applied mathematics, we no longer have a complete freedom of using any term in any way we wish. The mathematical distance cannot serve as the inconsistency indicator as we demonstrated here by the use of the relative error.

Acknowledgments

The research has been supported in part by:

- the Polish Ministry of Science and Higher Education
- the Ministry of Education, Youth and Sports Czech Republic within the Institutional Support for Long-term Development of a Research Organization in 2017.

References

[1] M.G. Kendall, B.B. Smith, On the method of paired comparisons, Biometrika 31 (3/4) (1940) 324–345.
[2] R.R. Davidson, P.H. Farquhar, Bibliography on the method of paired comparisons, Biometrics 32 (2) (1976) 241–252.
[3] T.L. Saaty, Scaling method for priorities in hierarchical structures, J. Math. Psychol. 15 (3) (1977) 234–281.
[4] W.W. Koczkodaj, J. Szybowski, E. Wajch, Inconsistency indicator maps on groups for pairwise comparisons, Int. J. Approx. Reason. 69 (2016) 81–90.
[5] W. Koczkodaj, W. Kulakowski, A. Ligeza, On the quality evaluation of scientific entities in Poland supported by consistency-driven pairwise comparisons method, Scientometrics 99 (3) (2014) 911–926.
[6] W.W. Koczkodaj, A new definition of consistency of pairwise comparisons, Math. Comput. Model. 18 (7) (1993) 79–84.
[7] Zero–one law, Encyclopedia of Mathematics, www.encyclopediaofmath.org.
[8] P. Lévy, Théorie de l'addition des variables aléatoires, Gauthier-Villars, 1937.
[9] B. Cavallo, L. D'Apuzzo, A general unified framework for pairwise comparisons matrices in multicriterial methods, Int. J. Intell. Syst. 24 (4) (2009) 377–398.
[10] W.W. Koczkodaj, R. Szwarc, On axiomatization of inconsistency indicators for pairwise comparisons, Fundam. Inform. 132 (4) (2014) 485–500.
[11] W.W. Koczkodaj, Pairwise comparisons rating scale paradox, in: Transactions on Computational Collective Intelligence XXII, vol. 9655, 2016, pp. 1–9.
[12] G. Shafer, V. Vovk, The Origins and Legacy of Kolmogorov's Grundbegriffe, Working Paper 4, 2013.
[13] G. Shafer, V. Vovk, The sources of Kolmogorov's Grundbegriffe, Stat. Sci. 21 (1) (2006) 70–98.
[14] H. Hogbe-Nlend, Bornologies and Functional Analysis, vol. 26, 1st edition, North-Holland Pub., 1977.
[15] J.F. Peters, Computational Proximity, Excursions in the Topology of Digital Images, vol. 102, Springer International Publishing, Berlin, 2016.
[16] W.W. Koczkodaj, J. Szybowski, Pairwise comparisons simplified, Appl. Math. Comput. 253 (2015) 387–394.
[17] J. Neyman, Outline of a theory of statistical estimation based on the classical theory of probability, Philos. Trans. R. Soc. Lond. Ser. A, Math. Phys. Sci. 236 (767) (1937) 333–380.
[18] S.S. Stevens, Psychophysics, Wiley, New York, 1975.

Neuroscience Letters 653 (2017) 234–238

Contents lists available at ScienceDirect

Neuroscience Letters

journal homepage: www.elsevier.com/locate/neulet

Research article

A repetitive modular oscillation underlies human brain electric activity

Arturo Tozzi[a,f,*], James F. Peters[a,b,c,d], Norbert Jaušovec[e]

[a] Computational Intelligence Laboratory, University of Manitoba, Winnipeg R3T 5V6 Manitoba, Canada
[b] Department of Electrical and Computer Engineering, University of Manitoba, 75A Chancellor's Circle, Winnipeg MB R3T 5V6, Canada
[c] Department of Mathematics, Adıyaman University, 02040 Adıyaman, Turkey
[d] Department of Mathematics, Faculty of Arts and Sciences, Adıyaman University, 02040 Adıyaman, Turkey
[e] Department of Psychology, University of Maribor, Koroska Cesta 160, 2000 Maribor, Slovenia
[f] Center for Nonlinear Science, Department of Physics, University of North Texas, Denton, Texas 76203, USA, 1155 Union Circle, #311427, Denton, TX 76203-5017, USA

HIGHLIGHTS

- Modular functions are widespread in physics and biology.
- We examined a modular function in electric brain activity.
- We found a modular function, the J-function, embedded in human EEGs.

ARTICLE INFO

Article history:
Received 7 September 2016
Received in revised form 23 May 2017
Accepted 23 May 2017
Available online 26 May 2017

Keywords:
J-Function
Modular function
Nervous system
EEG
Complex numbers
Multidimensionality

ABSTRACT

The modular function j, central in the assessment of abstract mathematical problems, describes elliptic, intertwined trajectories that move in the planes of both real and complex numbers. Recent clues suggest that the j-function might display a physical counterpart, equipped with a quantifiable real component and a hidden imaginary one, currently undetectable by our senses and instruments. Here we evaluate whether the real part of the modular function can be spotted in the electric activity of the human brain. We assessed EEGs from five healthy males, eyes-closed and resting state, and superimposed the electric traces with the bidimensional curves predicted by the j-function. We found that the two trajectories matched in more than 85% of cases, independent from the subtending electric rhythm and the electrode location. Therefore, the real part of the j-function's peculiar wave is ubiquitously endowed all over normal EEGs paths. We discuss the implications of such correlation in neuroscience and neurology, highlighting how the j-function might stand for the one of the basic oscillations of the brain, and how the still unexplored imaginary part might underlie several physiological and pathological nervous features.
© 2017 Elsevier B.V. All rights reserved.

Significance statement

Our results point towards the brain as ubiquitously equipped with j-function's oscillations, which movements take place on the plane of the complex numbers. It means that there must be, in brain electric activity, also a veiled complex part, which can be assessed with the help of imaginary numbers. The modular j-function provides further dimensions to the real numbers, in order to enlarge their predictive powers: it suggests the possible presence of hidden (functional or spatial) brain extra-dimensions. Furthermore, j-oscillations could be disrupted during pathologies, paving the way to novel approaches to central nervous system's diseases.

1. Introduction

The j-function describes intertwined, repetitive elliptic trajectories taking place on the so-called *plane of the complex numbers* [1]. Such plane can be exemplified as a plot displaying on the x axis the real numbers (e.g., 1, 2, −1, −2) and on the y axis the imaginary part (e.g., a component that satisfies the equation $i^2 = -1$). The intersection of a real and an imaginary number in the graph is termed a *complex number* (Fig. 1A). The role of complex numbers in mathematics is to enlarge the concept of the one-dimensional number line

* Corresponding author.
E-mail addresses: tozziarturo@libero.it, tozziarturo@libero.i7 (A. Tozzi), james.peters3@umanitoba.ca (J.F. Peters), norbert.jausovec@um.si (N. Jaušovec).

http://dx.doi.org/10.1016/j.neulet.2017.05.051
0304-3940/© 2017 Elsevier B.V. All rights reserved.

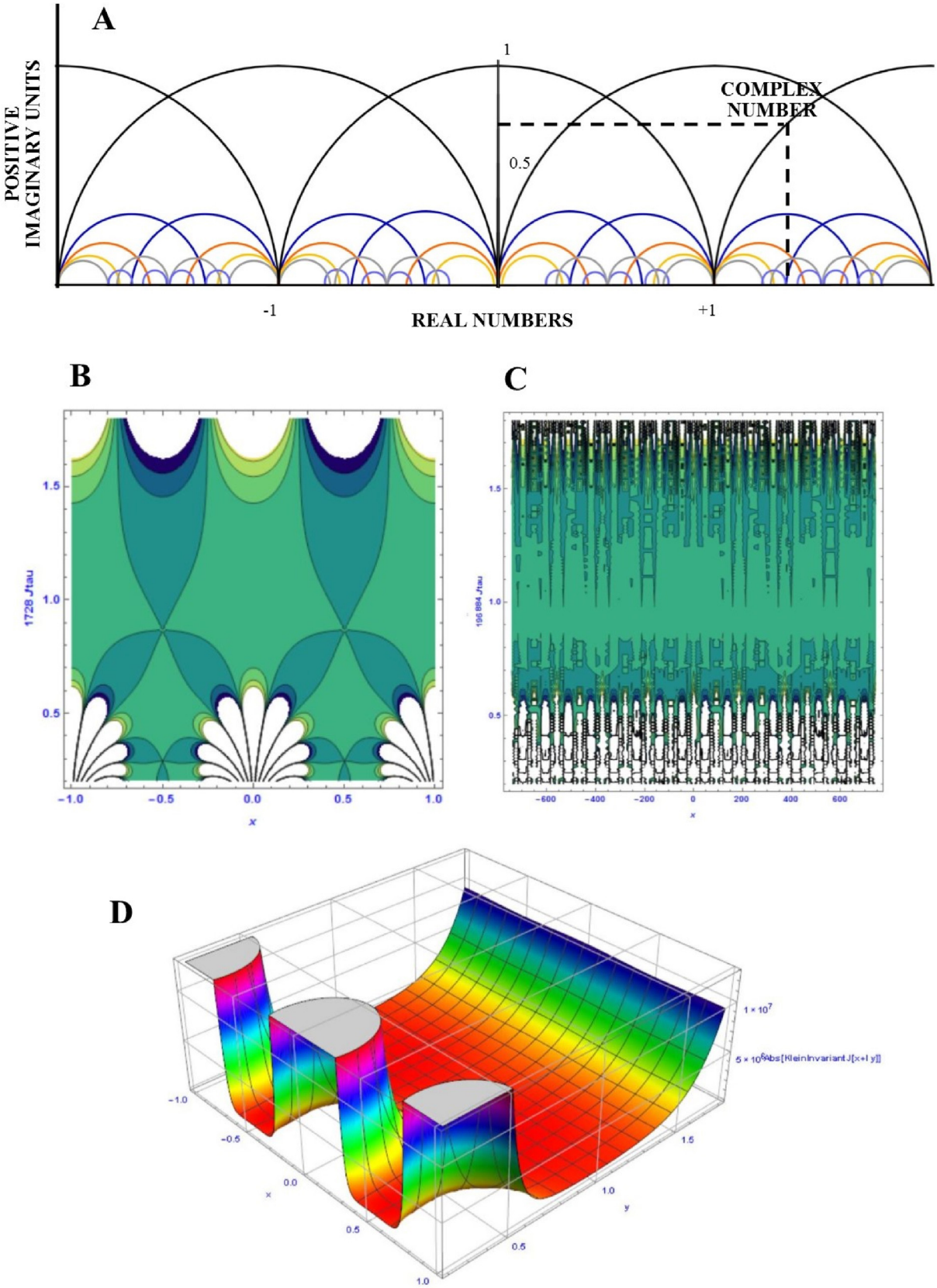

Fig. 1. Plots of Klein j-functions and their different possible paths. Fig. 1**A** depicts the general scheme of the elliptic oscillations on the upper half plane of the complex numbers. For sake of clarity, the locations of imaginary units and of real and complex numbers are provided. Fig. 1B and C shows the 2D plots achieved for $j = 1728$ and 196,884, respectively. Note the different coarse-grained appearance of the two plots. Fig. 1**D** displays the 3D plot, in case of $j = 196{,}844$. The plots in Figs. 1B–D were obtained using Mathematica® 10.

to the two-dimensional complex plane, allowing the description of real numbers with an additional coordinate. This trick is very useful not just in mathematics, but also in the other disciplines, from fluid dynamics to electrical engineering and computer graphics, from signal analysis to quantum mechanics, and so on [2,3].

The j-function is plotted on the upper half of the complex plane, e.g., it can be drawn just starting from positive imaginary numbers. The pattern depicted by the j-function is called modular, e.g. in simple terms, it looks like curved trajectories intersecting one each other in a recurrent and fractal pattern. The j-function exhibits the peculiarity that, contrary to other modular functions that can be mapped in all their points on planes, is equipped with cusps, e.g., single points where a trajectory starts to move backward.

It has been speculated that modular functions might have physical counterparts in our Universe, because they seem to be indirectly linked with string theories that describe the microscopic features of cosmos [4–7]. In particular, it has been suggested that the j-function might count the ways strings can oscillate at each one of their energy levels. Therefore, modular functions might be more widespread than thought and could be an underlying, hidden rhythm that dictates the oscillatory activities of different physical and biological systems. In this paper we evaluated the possibility that brain electric rhythms encompass the j-function. We chose, among the countless modular functions, the J one, because it is mathematically easier to treat and because it has been widely described in correlation with some physical phenomena. Indeed, j-function and brain activity display, at first sight, many common features: they are both modular, bot sinusoidal, both symmetric [8] and both can be described in terms of Fourier transform. In such a vein, we assessed EEG patterns collected from adult controls during eyes closed resting state, looking for the j-function's features. We demonstrated that the j-function is endowed in the very structure of human brain electric spikes, giving rise, at least in normal subjects, to reiterating oscillations equipped with a highly predictable pattern. Furthermore, we discuss the implications, both in basic neuroscience and in medical science, of our finding.

2. Methods

2.1. Subjects

The sample included 5 right-handed male students, undergraduates (age = 21 years). They were recruited from a large pool of individuals who participated in different experiments conducted at Department of Psychology, University of Maribor lab, in the last 2 years (e.g., [9]. The participants were tested with the WAIS-R test battery [10]; M = 100.60; SD = 1.14). The experiment was undertaken with the understanding and written consent of each subject.

2.2. Procedure, EEG recording and quantification

The participants were seated in a reclining chair while their resting eyes closed EEG was recorded for 5 min. Afterwards they solved several tasks which were part of different studies described above. A Quick–Cap with sintered (Silver/Silver Chloride; 8 mm diameter) electrodes was fitted to each participant. Using the Ten-twenty Electrode Placement System of the International Federation, the EEG activity was monitored over nineteen scalp locations (Fp1, Fp2, F3, F4, F7, F8, T3, T4, T5, T6, C3, C4, P3, P4, O1, O2, Fz, Cz and Pz). All leads were referenced to linked mastoids (A1 and A2), and a ground electrode was applied to the forehead. Vertical eye movements were recorded with electrodes placed above and below the left eye. Electrode impedance was maintained below 5 kΩ. EEG was recorded using NeuroScan Acquire Software and a SynAmps RT amplifier (Compumedics, Melbourne Australia), which had a band-pass of 0.15–100.0 Hz. At cutoff frequencies the voltage gain was approximately −6 dB. The 19 EEG traces were digitized online at 1000 Hz with a gain of 10× (accuracy of 29.80 μV/LSB in a 24 bit A to D conversion) and stored on a hard disk. Offline EEG analysis was performed using NeuroScan Scan 4.5 software (Compumedics, Melbourne, Australia). IAF for each subject was determined based on their resting EEG [11]. First, power spectra were calculated over the entire epoch length of 11 s (11,132 data points) and automatically screened for artifacts. Second, an automatic peak detection procedure found the highest peak (maximum alpha power) in a 7–14 Hz window (frequency steps of 0.09 Hz) separately for each lead. This method was used because it is more adequate for studying endophenotypic qualities during resting (eyes closed) EEG sessions [12,13] than the peak frequency center of gravity method proposed by [12], which is used for eyes open conditions. Third, IAF was computed for each channel and averaged over anterior (Fp1, Fp2, F3, F4, F7, F8, Fz), and posterior (T5, T6, P3, P4, O1, O2, Pz) locations (M = 9.88; SD = 0.34).

For our study, we examined artifact-free sequences of 5 s for every eye closed resting individual, from three scalp locations: CZ-, FZ- and PZ-. The EEG traces were filtered for different frequencies, in order to elucidate whether the j-function could be endowed in more than one brain rhythm. IAF between subjects did not differ significantly, therefore the resting eyes-closed EEG recordings were filtered in 5 fixed frequency bands: delta [1.0–3.9 Hz]; theta [4.0–7.9 Hz]; alpha [8.0–12.0 Hz]; beta [15.0–31.0 Hz] and gamma [32.0–49.0 Hz]. We used a band-pass Infinite Impulse Response (IIR) filter with a 48 dB/octave rolloff.

2.3. Looking for j-function in EEGs

The modular function j is the generator or hauptmodul of the genus zero function field (Fig. 1). The j-function was defined [14] by

$j(\tau) = 1728J(\tau)$, whose Fourier development is

$j(\tau) = e^{-2\pi ir} + 744 + 196884e^{2\pi ir} + 21493760e^{4\pi ir} + \cdots$, where

$\mathrm{I}[\tau] > 0$ is the half-period ratio and

$$\mathrm{J}(\tau) = \frac{4}{27}\frac{\left[1-\lambda(\tau)+\lambda^2(\tau)\right]^3}{\lambda^2(\tau)[1-\lambda(\tau)]^2}$$

is Klein's absolute invariant and$\lambda(\tau)$ is the eliptic lambda function (Piezas)

$$\lambda(\tau) \equiv \frac{\vartheta_2^4\left(e^{\pi ir}\right)}{\vartheta_3^4\left(e^{\pi ir}\right)}, \text{ where}$$

$\vartheta_i(0, q)$ are Jacobi theta functions and

$\mathrm{q} = e^{\pi ir}$ is the nome and $1728 = 12^3$.

In case of a j-function endowed in brain electric spikes, we would be able to detect just the waves depicting the real part of the modular function, because the imaginary part lies in a complex dimension (either numerical, or functional) that is undetectable by our senses and our technological tools, unless you explicitly look for it. In particular, our goal was to assess whether the EEGs' bidimensional lines match with the bidimensional real part of the j-function. At first, we built a bidimensional pattern of the j-function. The pattern (Fig. 2A) describes a curve conventionally moving from T0 to T1, from left to right. The most important parameter to take into account for our purposes is the distance between two peaks, that, being recursive, is the best testable feature of two-dimensional j-curves. The frequency and the amplitude

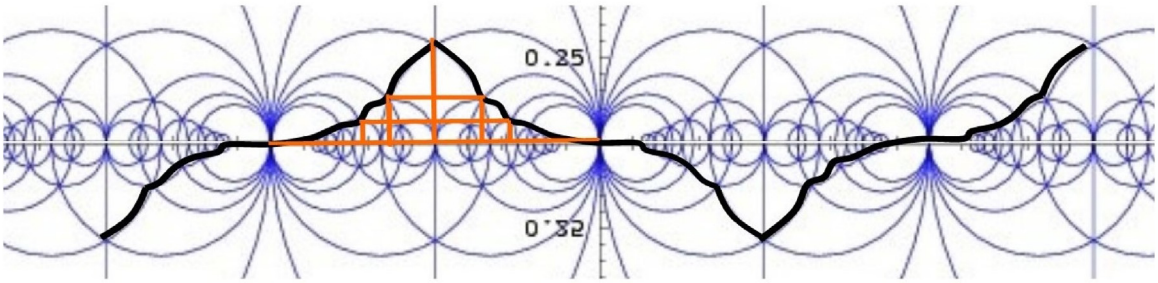

Fig. 2. Bidimensional pattern of a j-function, displaying the real part of j-oscillations. The black line depicts the j-pattern correlated with EEGs traces.

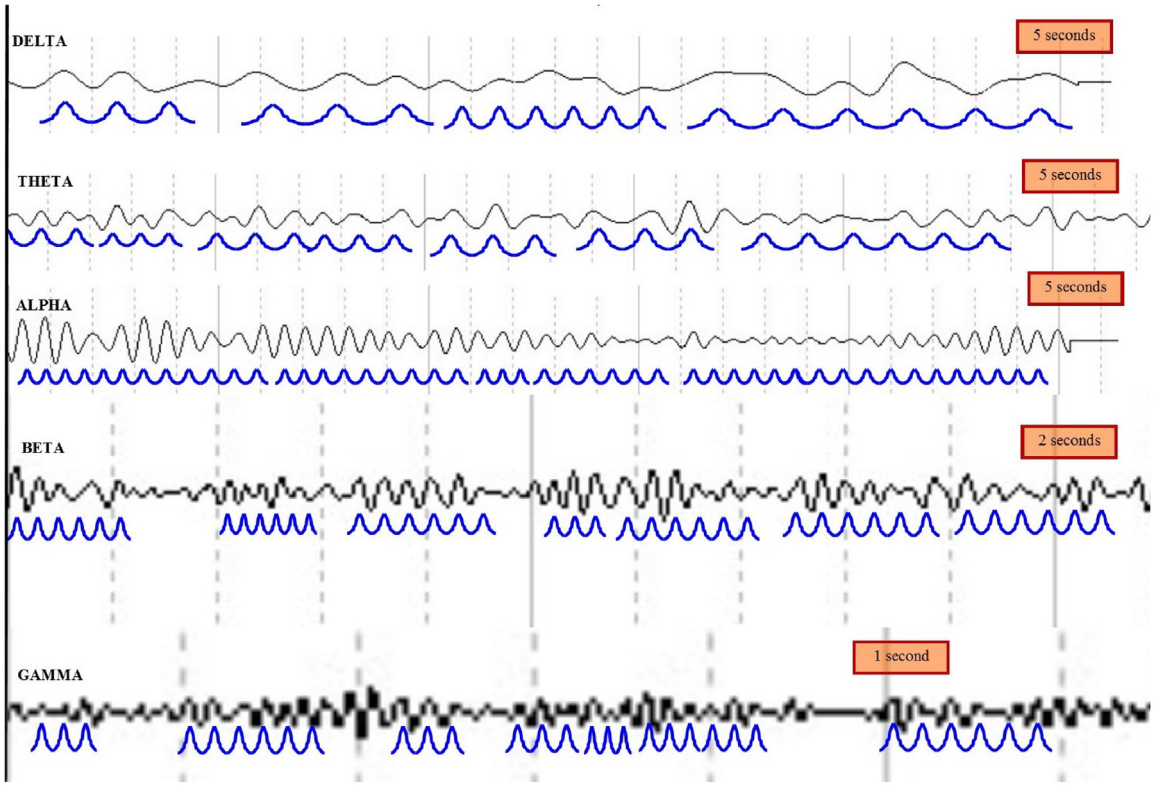

Fig. 3. Relationships between the j-function pattern (blue waves) and normal EEG rhythms (black waves) in the FZ- derivation of a single male control. The predicted blue curves match with the normal EEG oscillations almost everywhere. Delta, theta and alpha traces have the same resolution for the y (microV) axis, which gives a rather unclear view for the beta and gamma waves, usually in the <1 mV range. Therefore, beta and gamma frequencies are depicted in Figure at higher magnification and with a different temporal scale. (For interpretation of the references to colour in this figure legend, the reader is referred to the web version of this article.)

of the sinusoidal oscillations are less important, because, being the modular function fractal, it can be detected at different spatial and temporal coarse-grained scales. Likewise, because the EEG waves are equipped with multiple, unpredictable deformation arising by multiple intertwined interactions, the j-pattern could be nested in different amplitudes and frequencies.

We correlated the predicted j-pattern with the above mentioned EEG traces from adult controls. In particular, we evaluated the percentage of the two oscillations' superimposition. We used a t-student test for statistical analysis.

3. Results

The predicted j-pattern, standing for the real part of the j-function, matched the EEG plots recorded from all the normal healthy, resting, eyes-closed males (Fig. 3). In particular, the modular j-function is correlated with the distance among the peaks. J-function and EEG traces' superimposition was found in all the subjects and derivations. Taking into account all the frequencies and all the derivations, EEGs oscillations match the pattern of the predicted j-function in a high number of plots (Mean% ± SD: 87.6 ± 5.54). Although not significant, the slower waves (delta, theta and alpha) exhibited a slightly higher correlation (93% vs. 81%) than the faster ones (beta and gamma). It could depend on a more marked intertwining of oscillations in faster frequencies, that partially interferes with the detection of j-function's typical patterns. No statistical differences were found among different electrodes localizations. In sum, we found that the real part of the j-function's peculiar wave is ubiquitously endowed all over normal EEGs traces, independent of electric rhythms and electrode localizations.

4. Conclusions

We demonstrated that normal EEG's waves encompass the real part of a modular function. Our results suggest that the human brain displays a pattern resulting from elliptic, intertwined oscillations

resembling the waves described by the j-function. Such oscillations endowed in the brain spikes result from the delicate interaction of the countless moving trajectories that are at the very heart of modular functions. The presence in EEGs of the j-function, which movements take place on the so-called plane of the complex numbers, means that there must be, in brain electric activity, also a still unexplored complex part. While current neuro-techniques are able to detect and describe just the real part of nervous function, e.g., the part quantifiable through real numbers, the complex part is hidden from our observation, because it can be described just with the help of an imaginary component. It means that electric features linked with elusive brain functions, such as, e.g., long-distance interactions, consciousness and so on, could be unnoticed in the EEG traces. They could be assessable, if we add further parameters able to assess neural data sets not just in terms of real numbers, but also of complex ones. In such a vein, it must be taken into account that EEG techniques are able to assess just the part of the j-function that lies very close to the x axis, therefore missing the extensive part of the upper half plane of complex functions that lies farther away from the axis of real numbers.

The j-function is a mathematical tool which provides the real numbers with further dimensions, in order to enlarge their predictive powers. Therefore, it could be hypothesized that the mathematical superimposition between modular functions and EEG spikes might be correlated with the presence of further brain dimensions, undetectable by our 3D analyses. Indeed, the possibility of hidden functional or spatial nervous dimensions has been recently discussed [15]. The Authors described the occurrence, at least during spontaneous brain activity, of multi-dimensional toruses, where trajectories take place in guise of particles traveling on donut-like manifolds.

Although the possible presence of nested (real and the imaginary) parts of the j-function has not yet been explored in physical and biological phenomena, there are good reasons for hypothesizing that such j-oscillations could be widespread. For example, the Monstrous Moonshine conjecture suggests a puzzling relationship between one of the terms in the Fourier expansion of $j(\tau)$, which value is 19884, and the simple sums of dimensions of irreducible representation of the Monster group M, which is 196883 [16]. On the other hand, the Monster group has been correlated with physical features underlying our Universe [17,5]. Furthermore, the j-function displays both (spatial) fractal-like structure, and (temporal) power laws, in touch with the description of many physical and biological systems (including the brain) in terms of nonlinear systems equipped with scale-free behavior [18–22]. To give other examples, it has been recently proposed that symmetry breaks occur during brain function [8] and that the nervous activity might be described in terms of a gauge theory [23]. A gauge theory states that systems' general symmetries can be broken by local perturbations and then restored by the superimposition of gauge fields. The modular function j, with its repetitive and highly conserved pattern, is a very good candidate for the role of a general symmetry of the brain (and other systems).

Once established that the j-function's is ubiquitously endowed all over normal EEGs traces during resting state, eyes open conditions, the further steps could be: a) to evaluate task related EEGs, and b) to superimpose the j-pattern to nervous oscillations other than electric spikes, such as the ones detected by, e.g., fMRI or PET. Once elucidated the role of j-function in physiological brain oscillations, it will be worthwhile to look for possible j-function's alterations in pathological states. Indeed, it could be hypothesized that the recurring j-oscillations are disrupted during pathologies, paving the way to novel approaches to brain diseases.

References

[1] C.P. McKeague, Elementary Algebra, Brooks/Cole, 2011, p. 524, ISBN 978-0-8400-6421-9.
[2] R.A. Rankin, Modular Forms and Functions, Cambridge University Press, Cambridge, 1977, ISBN 0-521-21212-X.
[3] T.M. Apostol, Modular Functions and Dirichlet Series in Number Theory, Springer-Verlag, New York, 1990, ISBN 0-387-97127-0.
[4] T. Gannon, Moonshine Beyond the Monster: The Bridge Connecting Algebra, Modular Forms and Physics, 2006, ISBN 0-521-83531-3.
[5] J.F.R. Duncan, I.B. Frenkel, Rademacher sums, moonshine and gravity, Commun. Number Theory Phys. 5 (4) (2011) 1–128.
[6] T. Eguchi, H. Ooguri, Y. Tachikawa, Notes on the K3 Surface and the Mathieu groupM24, Exp. Math. 20 (2011) 91–96.
[7] J.F.R. Duncan, M.J. Griffin, K. Ono, Moonshine, Res. Math. Sci. 2 (2015) 11, http://dx.doi.org/10.1186/s40687-015-0029-6.
[8] A. Tozzi, J.F. Peters, A topological approach unveils system invariances and broken symmetries in the brain, J. Neurosci. Res. 94 (5) (2016) 351–365, http://dx.doi.org/10.1002/jnr.23720.
[9] S. Tement, A. Pahor, N. Jausovec, EEG alpha frequency correlates of burnout and depression: the role of gender, Biol. Psychol. 114 (2016) 1–12.
[10] D. Wechsler, Manual for the Wechsler Adult Intelligence Scale — Revised, Psychological Corporation, New York, NY, 1981.
[11] E. Angelakis, J.F. Lubar, S. Stathopoulou, J. Kounios, Peak alpha frequency: an electroencephalographic measure of cognitive preparedness, Clin. Neurophysiol. 115 (4) (2004) 887–897, http://dx.doi.org/10.1016/j.clinph.2003.11.034.
[12] W. Klimesch, H. Schimke, G. Pfurtscheller, Alpha frequency, cognitive load and memory performance, Brain Topogr. 5 (3) (1993) 241–251.
[13] G.S. Hooper, Comparison of the distributions of classical and adaptively aligned EEG power spectra, Int. J. Psychophysiol. 55 (2005) 179–189.
[14] A. Tozzi, J.F. Peters, Symmetries, Information and Monster Groups before and after the Big Bang, Information 7 (4) (2016) 73, http://dx.doi.org/10.3390/info7040073.
[15] A. Tozzi, J.F. Peters, A.A. Fingelkurts, A.A. Fingelkurts, P.C. Marijuán, Topodynamics of metastable brains, Phys. Life Rev. (2017), http://dx.doi.org/10.1016/j.plrev.2017.03.001.
[16] J.H. Conway, S.P. Norton, Monstrous moonshine, Bull. Lond. Math. Soc. 11 (3) (1979) 308–339, MR 554399(81j:20028).
[17] I. Frenkel, J. Lepowsky, A. Meurman, A natural representation of the Fischer-Griess Monster with the modular function J as character, Proc. Nat. Acad. Sci. U. S. A. 81 (10) (1984) 3256–3260, MR 747596 (85e:20018).
[18] K. Linkenkaer-Hansen, V.V. Nikouline, J.M. Palva, R.J. Ilmoniemi, Long-range temporal correlations and scaling behavior in human brain oscillations, J. Neurosci. 21 (4) (2001) 1370–1377.
[19] M.E.J. Newman, Power laws: pareto distributions and Zipf's law, Contemp. Phys. 46 (2005) 323–351.
[20] J. Milstein, F. Mormann, I. Fried, C. Koch, Neuronal shot noise and Brownian 1/f2 behavior in the local field potential, PLoS One 4 (2) (2009) e4338, http://dx.doi.org/10.1371/journal.pone.0004338.
[21] B.J. He, J.M. Zempel, A.Z. Snyder, M.E. Raichle, The temporal structures and functional significance of scale-free brain activity, Neuron 66 (3) (2010) 353–369, http://dx.doi.org/10.1016/j.neuron.2010.04.020.
[22] A. Tozzi, How to turn an oscillation in a pink one, J. Theor. Biol. 377 (2015) 117–118, http://dx.doi.org/10.1016/j.jtbi.2015.04.018, Elsevier.
[23] B. Sengupta, A. Tozzi, G.K. Coray, P.K. Douglas, K.J. Friston, Towards a neuronal gauge theory, PLoS Biol. 14 (3) (2016) e1002400, http://dx.doi.org/10.1371/journal.pbio.1002400.

Progress in Biophysics and Molecular Biology 131 (2017) 141–152

Contents lists available at ScienceDirect

Progress in Biophysics and Molecular Biology

journal homepage: www.elsevier.com/locate/pbiomolbio

Cellular gauge symmetry and the Li organization principle: General considerations

Arturo Tozzi [a, b], James F. Peters [c, d, e], Jorge Navarro [f], Wu Kun [g], Bi Lin [g, **], Pedro C. Marijuán [f, *]

[a] Center for Nonlinear Science, University of North Texas, 1155 Union Circle, #311427, Denton, TX 76203-5017, USA
[b] Computational Intelligence Laboratory, University of Manitoba, Winnipeg R3T 5V6 Manitoba, Canada
[c] Department of Electrical and Computer Engineering, University of Manitoba, 75A Chancellor's Circle, Winnipeg, MB R3T 5V6, Canada
[d] Department of Mathematics, Faculty of Arts and Sciences, Adıyaman University, 02040 Adıyaman, Turkey
[e] Computational Intelligence Laboratory, University of Manitoba, WPG, MB, R3T 5V6, Canada
[f] Grupo de Bioinformación / Bioinformation Group, Instituto Aragonés de Ciencias de la Salud (IACS), Instituto de Investigación Sanitaria Aragón (IISA), Edificio CIBA. Avda. San Juan Bosco, 13, 50009 Zaragoza, Spain
[g] International Center for Philosophy of Information, School of Humanities and Social Sciences, Xi'an Jiaotong University, Xi'an, China

ARTICLE INFO

Article history:
Received 28 April 2017
Received in revised form
6 June 2017
Accepted 13 June 2017
Available online 15 June 2017

Keywords:
Borsuk-ulam theorem
Cellular
Metabolic pathways
Torus
Topology
Gauge theory
Biology

ABSTRACT

Based on novel topological considerations, we postulate a gauge symmetry for living cells and proceed to interpret it from a consistent Eastern perspective: the *li* organization principle. In our framework, the reference system is the living cell, equipped with general symmetries and energetic constraints standing for the intertwined biochemical, metabolic and signaling pathways that allow the global homeostasis of the system. Environmental stimuli stand for forces able to locally break the symmetry of metabolic/signaling pathways, while the species-specific DNA is the gauge field that restores the global homeostasis after external perturbations. We apply the Borsuk-Ulam Theorem (BUT) to operationalize a methodology in terms of topology/gauge fields and subsequently inquire about the evolution from inorganic to organic structures and to the prokaryotic and eukaryotic modes of organization. We converge on the strategic role that second messengers have played regarding the emergence of a unitary gauge field with profound evolutionary implications. A new avenue for a deeper investigation of biological complexity looms. Philosophically, we might be reminded of the duality between two essential concepts proposed by the great Chinese synthesizer Zhu Xi (in the XIII Century). On the one side the *li* organization principle, equivalent to the dynamic interplay between symmetry and information; and on the other side the *qi* principle, equivalent to the energy participating in the process—both always interlinked with each other. In contemporary terms, it would mean the required interconnection between information and energy, and the necessity to revise essential principles of information philosophy.

© 2017 Elsevier Ltd. All rights reserved.

Contents

1. Introduction 142
   1.1. Introducing gauge symmetry and BUT 142
2. Topological cells 143
   2.1. Complexity index 143
   2.2. Energy considerations 143
   2.3. Biomolecular pathways are topological strings 144

* Corresponding author.
** Corresponding author.
E-mail addresses: tozziarturo@libero.it (A. Tozzi), james.peters3@umanitoba.ca (J.F. Peters), jnavarro.iacs@aragon.es (J. Navarro), wukun@mail.xjtu.edu.cn (W. Kun), bilin1001@qq.com (B. Lin), pcmarijuan.iacs@aragon.es (P.C. Marijuán).

http://dx.doi.org/10.1016/j.pbiomolbio.2017.06.004
0079-6107/© 2017 Elsevier Ltd. All rights reserved.

2.4. How to build a topological cell? . . . 145
3. A gauge theory for topological cells: fundamentals . . . 146
4. A topological gauge theory for living cells: what for? . . . 147
4.1. Visual interpretation of a gauge theory for energetic cellular paths . . . 147
5. Discussion . . . 148
6. Conclusion . . . 150
6.1. Philosophical coda . . . 150
References . . . 151

1. Introduction

The present paper is an attempt to extend a fundamental theory of modern physics, quite useful for the description of interactions between particles and fields, to the cellular dynamics of response to environmental signals and metabolites. Although a rigorous philosophical interpretation of this fresh and still tentative exploration of biological complexity cannot be properly framed yet (considering that the scientific exploration itself needs to be consolidated first), the work may provoke interesting philosophical-scientific and historical reflections as well—we will try to initiate them herein. Relevant names of modern physics have already made noticeable inroads about analogies between particle physics and Eastern thought: from Niels Bohr, to Werner Heisenberg, to Murray Gell-Mann. The arch famous book *The Tao of Physics* by Fritjof Capra (1975) popularized in the 1970's and 1980's a radical vision about that. But not many attempts have been made in biology or specifically in theoretical biology in that very direction (Ford, 2017; Torday and Miller, 2017). Finding a thinker of XIII Century in China who was proposing an explanatory framework which –arguably– is highly similar in abstract terms to the theoretical stance herein explored becomes rather surprising. But according to Joseph *Needham's* monumental work on *Science and Civilization in China* (1954–2015), we are in the forefront of the highest synthesizer, the truly Eastern equivalent to –and contemporary of– Thomas Aquinas' *Summa Theologicae* (cf. P. Kreeft, 2012). Indeed, the qualification of this work comes out far afield from the way of thinking that Western authors, both philosophers and scientists, were traditionally holding about the integration of life's processes, not to mention the "theories" during the medieval times or the mechanistic approaches during the scientific revolution (Chan, 1963). In another front, given that the gauge symmetry herein proposed implies a deep reconsideration of the informational dynamics of the living cell, putting it in a common framework with the basic gauge symmetry dynamics of the microphysical world, it would imply therefore rather complex information-symmetry-energy speculations that can be easily miscarried or misinterpreted because of their difficulty.

Therefore, in order to disentangle the different aspects involved, we will try to advance in a series of ordered discussion steps. Firstly, in the rest of this Introduction, we will attempt the direct presentation of gauge symmetry as based on new topological considerations, essentially the Borsuk-Ulam Theorem (BUT). Then, we will describe our theoretical construct of "topological cells", which will be based on a complexity index, energy considerations, and the interpretation of biomolecular pathways as "topological strings" (see below). Further, we will develop a more detailed gauge theory for these topological cells; we will discuss the results obtained and will extrapolate for the assessment of further biological complexity. We will see in the discussion that the mutual upholding between signals and mosaic gauge fields converge into the most robust dynamics via the emergence of second messengers, which really mark the transition from multiple proto-gauge fields to the genuine gauge field involving the response of the entire system. At the end of this technical presentation, we will retake the philosophical discussion, arguing that it is not just a matter of historical record, or an anecdotal comment about the *li* and the *qi* cleverly foreseen as organization principles many centuries ago; it is also an important concern in today's multidisciplinary dialogs around life, involving the relationships of information science (bioinformation in this case) and information philosophy (Wu, 1981, 2006, 2012; Brenner, 2011). Indeed, information appears as one of the main arenas where a new interpretation of life is nowadays attempted.

1.1. Introducing gauge symmetry and BUT

A gauge theory states that, in systems equipped with an internal symmetry and a preserved physical quantity, the local symmetry breaks due to external forces are counteracted by another force, called gauge field (Zeidler, 2011). Gauge theories, successfully developed in physics (Higgs, 1964), have been recently proposed for the evaluation of neuronal activities (Sengupta et al., 2016). Here we make an effort to operationalize a gauge theory also for cellular function. It is a very difficult task, because managing the astonishing numbers of molecular states and interactions continues to be a fundamental obstacle in building predictive models of biological systems (Sneddon et al., 2011); it is so despite pioneering works in bioenergetics and systems science which already obtained staggering figures for the minimal information describing the simplest cells (Morowitz, 1968; Riedl, 1978). Herein we will try to overtake the overwhelming complexity of cellular activity with the invaluable help of recently developed topological tools.

The Borsuk-Ulam theorem (BUT) states that, when a pair of opposite (antipodal) points on a 3D sphere are continuously mapped onto a 2D circumference, their projections have matching description (Tozzi and Peters, 2016a). Recently developed BUT variants can be summarized as follows: a single feature embedded in a n dimensions M^n manifold maps to two features with matching description on a M^{n+1} manifold (Tozzi and Peters, 2016b; Peters and Tozzi, 2016; Peters, 2016). In case of convex manifolds, such as, e.g., disks and spheres, we will term them S^n and S^{n+1}. Single features may stand for physical or biological characteristics, such as points, lines, surfaces, functions, vectors, spatial or temporal patterns, movements, particle trajectories, thermodynamic features, signals and, above all, symmetries. The manifold M may be equipped with every kind of curvature: concave, flat or convex (Tozzi, 2016; Peters et al., 2016). The number *n* may stand for different kinds of dimensions, *e.g.*, spatial, temporal, complexity, and for different numbers, *e.g.*, natural, rational, irrational, imaginary. Matching features can be described as characteristics of paths or trajectories on abstract structures and allow system features commensurability. It looks like a transparent glass sphere between a light source and your eyes. You watch two lights on the sphere surface instead of one. But the two lights are not just images; they

are also real. Matching features can be thus assessed at one level of observation, while single features stand at a lower level.

Symmetries are widespread invariances underlying the function and activity of physical and biological systems at every level of organization. Standing for the most general features of systems, even more general than the entropy constraints, symmetries provide a general approach to every kind of biological function (Tozzi and Peters, 2016b). Symmetry breaks are detectable at a lower level of observation—in other words, a single feature stands for broken symmetry, which can be restored at one level higher. Therefore, the above matching descriptions are restored symmetries. If we evaluate systems just one dimension higher, we are able to find the otherwise apparently hidden symmetries.

To sum up, our essential aim is addressed to build a gauge theory for *topological* cells, with potential to be used as a general methodology able to describe in depth the structural and functional complexity of living beings.

2. Topological cells

This section aims to apply the above-mentioned topological concepts to biological cellularity (i.e., *topological cells*). In a topological framework, biologically significant environmental single components become matching points into the cell. Every type of living cell displays maps with different function and description and lies in a dimension higher than the environment. In order to evaluate living cells in terms of features embedded in M^n manifolds, we need at first to search and define the parameter which stands for our n value, i.e., the complexity index.

2.1. Complexity index

Biological complexity has been widely discussed during recent decades from multiple points of view: evolutionary (Bonner, 1998); Boolean networks (Kauffman, 1993); cellular automata (Wolfram, 2002); Turing machine (Danchin, 2009); operating systems (Yan et al., 2010); and even different kinds of scalable computer models have also been described (Ayyadurai and Dewey, 2011; Helikar et al., 2012). Inspired by (Mariotti, 2008), we may say that an appropriate complexity index across biological scales should be evaluated in terms of a product of several factors, such as number of genes, average splicing events, number of differentiated cell types, and energy rate; and that product should be divided by the life span and the total mass, both expressed in adequate units. Notwithstanding that, herein we have decided to use the sole energy rate that, although not fully representative of the whole biological complexity, nevertheless is an important and very manageable general parameter.

Indeed, the *energy rate density* is the amount of energy across the system per unit time per unit mass (in CGS metric units erg/s/g; in MKS units joule/s/kg). Regardless of the units used, energy rate density, describing the flow of energy that circulates through any living system of a given mass, has been proposed as a proxy of systemic complexity along the evolutionary process (Chaisson, 2010, 2014). Energy rate density, equivalent to the specific metabolic rate in biology, has gained traction in recent years, with many diverse applications in various disciplines, including ecology, ethology, and behavioral science (Neubauer, 2012). The estimates of complexity metrics for plants and animals are provided in Fig. 1.

When we proceed towards more advanced cells, such as from archaea and prokaryotes to eukaryotes, we achieve biological systems with increasing complexity. For instance, prokaryotes stand for a S^n sphere and eukaryotes for a S^{n+1} sphere. Cellular pathways stand for single points on S^n and for matching points on S^{n+1}. The more the cell is complex, the more the corresponding metabolic patterns become *transmolecular,* being massively involved with the whole signaling, transcriptional, translational, transportation, and degradative apparatuses of the rest of the cell. Additionally, in more evolved cells, protein domain recombination equipped with higher levels of modularity gives rise to increased complexity of the system's molecular components themselves (Koonin, 2010). Just in signaling terms, eukaryotes are counting with around two dozen of major classes of signaling pathways, versus the three main classes of prokaryotes (Marijuán et al., 2010). These supernumerary pathways subsequently organize the multicellular developmental process by following the equivalent of a *signaling master plan* (Gerhart, 1999; Marijuán et al., 2013). Most of the developmental, morphological, and physiological correlated processes are based on a series of balances and symmetry breaks between opposed pathways, organized in circuits of astonishing complexity, but finally describable in symmetry terms. In sum, going from lower to higher complexity dimensions, we achieve not just an increase in matching, superimposed biomolecular and metabolic patterns, but also an exponential increase in the number of symmetries.

2.2. Energy considerations

From a higher to a lower dimension, a decrease of half of information and energy occurs, and vice versa—following "energy-BUT" considerations (Tozzi and Peters, 2017a, 2017b). There exists a physical link between the abstract concept of BUT and the real energetic features of systems formed by two spheres S^n and S^{n-1}. When two antipodal points on an n-sphere S^n map to a n-Euclidean manifold where S^{n-1} lies, a symmetry break/dimensionality reduction occurs, and a single point is achieved (Peters and Tozzi, 2016). It is widely recognized that a decrease in symmetry goes together with a reduction in entropy and free-energy (in a closed system) (Roldán et al., 2014). This means that the single mapping function on S^{n-1}displays energy parameters lower than the sum of the two corresponding antipodal functions on S^n. Therefore, a decrease in dimensions gives rise to a decrease of energy and energy requirements. BUT and its variants become physical quantities, because we achieve a system in which energetic changes do not depend anymore on thermodynamic parameters, rather on topological features, such as affine connections and homotopies. The energy-BUT concerns not just energy, but also information. Indeed, two antipodal points contain more information than their single projection in a lower dimension. Dropping down a dimension means that each point in the lower dimensional space is simpler, because each point has one less coordinate. In sum, energy-BUT provides a way to evaluate the decrease of energy in topological, other than thermodynamic, terms. Matching features display a doubled energy, compared with their corresponding single feature, in order that a *force* is required to go from the lesser dimension to the higher. It is in touch with biological claims. Indeed, with increase in evolutionary cellular complexity, the energy requirements become larger. To make an example, an average protozoan has nearly 5000 times more metabolic power than a single bacterium and can support a genome several thousand times larger (Lane and Martin, 2010). Successive levels of potency are organized along the evolutionary and developmental processes (Ford, 2017; Torday and Miller, 2017). In prokaryotic species, there exists an approximately quadratic relationship between the total number of genes and signaling components (Galperin, 2005), while the increase is exponential in eukaryotes (Marijuán et al., 2013). In the same vein, the information contained in a single feature embedded in a lower level is half the information contained in matching features embedded in the higher level. Because single features comprehend less information and less entropy than matching features, the environment encompasses less information and complexity than living beings.

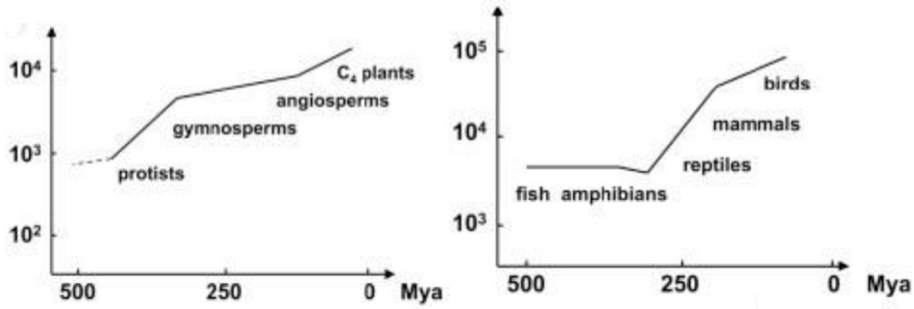

Fig. 1. Chaisson's complexity estimates for different biological organisms. Chaisson prefers to use the more familiar and traditional concept of energy, in particular the rate of energy produced or consumed per gram of the system being described, for his complexity metric. In the evolution of plants, let us note that angiosperms may comprise both C_3 and C_4 classes. In the evolution of animals, modern mammal species and birds have achieved similar energy rates. Modified from: http://www.informationphilosopher.com/solutions/scientists/chaisson/.

2.3. Biomolecular pathways are topological strings

A recently described BUT variant is particularly useful in our context, describing the topological existence of "strings" as paths defined by moving particles. That is, the pathway of bundles of particles moving through space form a collection X of Weyl world canals (curved worldsheets) with a topology on that collection. Each curved worldsheet draped over a Riemannian surface provides a history particle trajectories in the form of strings defined by paths followed by particles moving (wiggling, colliding, continuing) through space. Basically, this means that the intersection of sets of world canals is in X and the union of sets of world canals is also in X. In addition, X itself and the set containing no world canals (empty set) are also in the topology on X. Therefore, the Str-BUT variant may use particles with closed trajectories instead of points. The usual continuous function required by BUT (Peters and Tozzi, 2016) is replaced by a proximally continuous function, which guarantees that, whenever a pair of strings (regions that are called *world lines*) are close (near enough to have common elements), then we always know that their mappings will be also be close. A string is a region of space with either bounded or unbounded length. A region of space X is a worldsheet, provided X is covered with strings. By covered, we mean that if x is a point in X, then x belongs to at least one string. As a particle moves through space following a world line (Olive and Landsberg, 1989), interactions occur at the junctions of world lines. As time evolves, a particle leaves a trace of its movements along a surface that is *remembered*. One of the noteworthy features of strBUT is that strings can be described as movements on a donut-like torus. A string is then a remembered part of a hypersphere surface over which a particle travels. In order to map S^{n-1} to S^n, we need to work with higher dimensional spaces containing regions where each point in S^n has one more coordinate that a point in S^{n-1} (Fig. 2).

In our framework, the closed paths described by strBUT stand for biochemical pathways occurring in both prokaryotic and eukaryotic cells. Indeed, in all the living cells, molecular components and signal pathways are densely connected with the rest of systems. The tight coupling among different systemic activities, such as transcription, differential splicing, domain recombination, and cell differentiation gives rise to a ubiquitous signaling system that is in charge of receiving and interpreting all kind of inner/outer environmental inputs. Transmembrane molecular mechanisms continuously sense the external and internal milieu, leading to amplification cascades and mobilization of many different actuators (Gerhart, 1999; Marijuán et al., 2013). As an illustration, the way a real genome (pertaining to *E. coli K-12*) may react to very different kinds of environmental and inner stimuli can be evaluated both in genomic terms and in proteomic terms (Marijuán et al., 2015). An intertwined, ever changing play occurs between

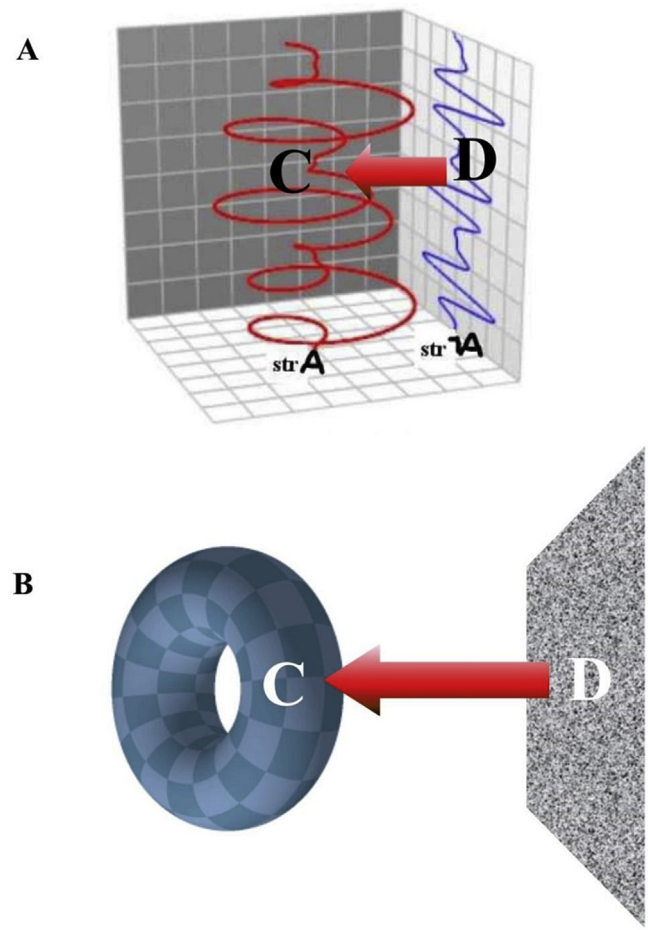

Fig. 2. StrBUT allows to proceed from linear to multidimensional paths. Fig. 2A illustrates two regions strA and [strA, where strA is embedded in a higher dimension C (a worldsheet) and [strA in a lower dimension D. strA and [strA stand for antipodal points with matching description. The path D stands for an environmental input reaching cell receptors, while C stands for cellular metabolic pathways. According to the dictates of strBUT, when we start from the evaluation of the linear pattern D, we could be able to assess its movements in C, e.g., one dimension higher. In Fig. 2B, because the more the dimensions, the more the information we achieve from the knowledge of the simpler pathway D, the more complex becomes C. As stated by strBUT, C may be described as a torus. Therefore, the movements of D become linear movements on a torus, equipped with information content higher than C.

incoming signals and inner controlling mechanisms. *Because the string paths are closed and therefore display a "hole" in their structure, this means that the massive networking of the whole biomolecular and metabolic patterns has to be amenable to description in abstract terms by means of trajectories traveling on donut-like structures*. Indeed, every single biomolecular pathway distinguishable in the cell may be taken as a closed string, either longer or shorter, and due to functional and topological proximity (Peters, 2016), it becomes intertwined with other strings in order to preserve the general homeostasis. Thereafter, the strBUT could be encompassed in the general context of cellular pathways, metabolic, signaling and otherwise. Metabolic responses encompass most of the genomic repertoire in prokaryotic cells, against approximately 10–20% in eukaryotes. Furthermore, because metabolic paths (the centrality of glucose degradation, and finally ATP production) are often the same in prokaryotes and eukaryotes, we may instead think in terms of difference in complexity when we also take into account signaling and controlling paths. Indeed, in eukaryotes, thanks to the enslaved mitochondria and their endless ATP supply, the bulk of complexity lies in the accompanying retinue of signaling, transcription, splicing, translation, transportation, and degradation processes. All these processes are functionally different, but all of them are crisscrossed and topologically interrelated into string paths. For instance, the qualitative difference between signaling and metabolic pathways was admirably described by Gerhart (1999, p. 228):

"As information transfer pathways, these signaling pathways are basically different from metabolic pathways, even though both are called 'pathways'. In a biosynthetic metabolic pathway, a carbon compound passes through a series of enzymatic steps, with appropriate energy inputs, undergoing modifications until it emerges as an end product ready for incorporation into a macromolecule or complex lipid. But in a signal transduction pathway, carbon atoms and energy are not passed along. Only an impulse is relayed by way of successive reversible changes of state of switch-like intermediates. At the end of the pathway, the transduced signal activates or inhibits some target protein […] the most frequent target of signaling is transcription, and some pathways affect only transcription."

Under our strBUT perspective, ALL biochemical, biomolecular, signaling, and metabolic pathways may be treated similarly. And that's a great analytical advantage.

2.4. How to build a topological cell?

We embedded the whole cells, their metabolic machinery and their DNA in different n-spheres, depending on their known degree of complexity, quantified through their energy rate density. An example is provided in Fig. 3. Few DNA segments (genes) and string-like metabolic pathways on a n-sphere give rise to many DNA segments and metabolic pathways on a n+1 sphere, in which n+1 means higher complexity. This also means that living cells display a higher number of symmetries, compared with the surrounding environment. The increase is transitory, because, in biological entities, a local diminution of entropy occurs, apparently against the second law of thermodynamics. When a biological structure increases its complexity dimensions in evolutionary timescales, then it displays antipodal points. Thus, biological structures increase symmetries and matching functions when their complexity rises. This also means that BUT is a general feature of biological systems. Fig. 3 shows how, with increases in complexity, the original single points (or strings) embedded in less complex S^n spheres become matching points on spheres of higher dimensions. Going towards higher dimensions, we achieve an exponential increase of matching points. This is in touch with the exponential growth of pathways and subsystems described in eukaryotic cells, compared with prokaryotic cells (Marijuán et al., 2010, 2013). According to the dictates of BUT variants, the single points stand for broken symmetries, while the two matching points stand for restored symmetries. The energy-BUT comes into play when cells equipped with high energetic levels due to their enlarged energetic machinery (via mitochondrial endocytosis) give rise to the route towards higher dimensions. Starting from the lower complexity of an inanimate environment, we achieve an enormous increase of complexity in living cells. The further evolution of biological systems, in touch with the concept of *bricolage,* which describes novel eukaryotic rearrangements of prokaryotic signaling systems (plus the incorporation of mitochondria, nuclear membrane, cytoskeleton, endocytic matrix, flagellum, etc.) makes possible the display of a finite, although enormously high, number of intrinsic symmetries. The latter, in touch with the Evo-Devo dictates, are the toolbox from where modular molecular assemblies are organized.

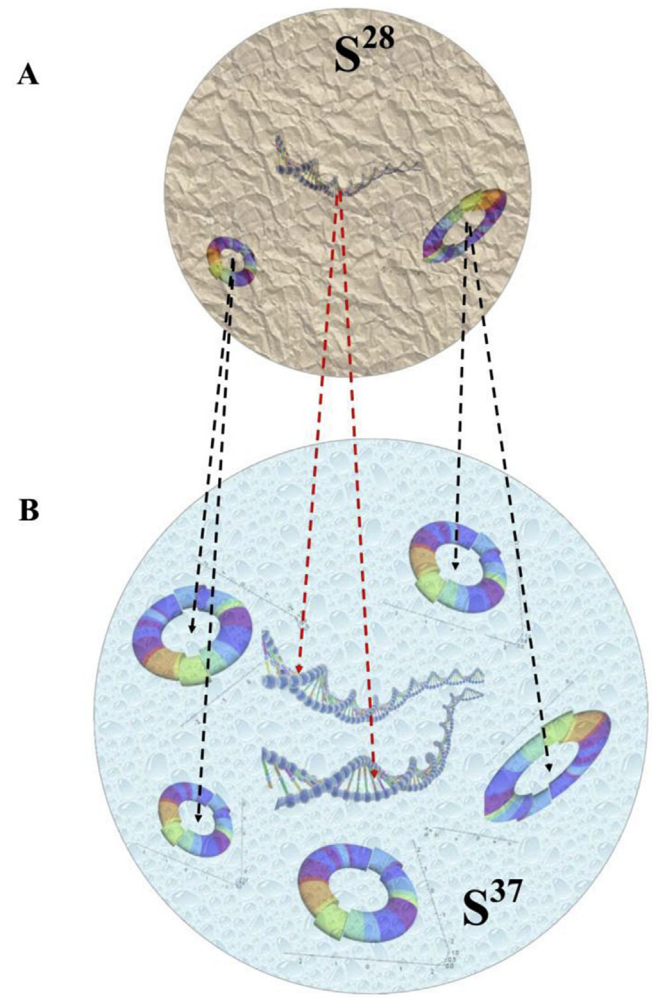

Fig. 3. Protists (Fig. 3A) and angiosperms (Fig. 3B), which were included in the complexity scheme of Fig. 1, are now contemplated in the framework of BUT and its variants. The two cells are embedded in n-spheres in which n stands for their energy rate density. Metabolic pathways are depicted as strictly interconnected string-like toruses that give rise to the intertwined multi-levels of activity typical of biological entities. The projection from the lower-dimensional sphere to the higher-dimensional one leads to an increase in number of metabolic pathways (black arrowhead lines) and DNA strands (red arrowhead lines).

3. A gauge theory for topological cells: fundamentals

Gauge theory in physics is a field theory, in which the Lagrangian, *e.g.*, a function that summarizes the dynamics of the system, is invariant under a continuous group of local transformations (Zeidler, 2011). What does it mean? We will try to explain what a gauge theory is, trying to convey the geometric intuition rather than the rigorous formalism. The underlying concept of gauge theories is quite simple: *gauge* means *choice*. A gauge is a *coordinate system* that varies depending on one's *location* with respect to some *base space*. When sketching a gauge theory, one can freely choose a symmetry *a priori*. By fixing a gauge, the model becomes easier to analyze mathematically. However, the tractability of the resulting problem can be heavily dependent on the choice of gauge that one introduces. A gauge theory is an abstract conjecture that needs to be tested by severe investigations (Tozzi et al., 2017; to appear). Gauge theories originate from physics; however, they could hypothetically be applied to countless fields of biology, including cell function. Here we hypothesize that cellular activity is due, at least partially, to a gauge theory. The most important question is the following: is it possible to transfer the powerful tools of gauge symmetries from their natural environment of physics particles to the soft and much more complex living structures? In other words, are we allowed to sketch a gauge theory of cellular function? The answer rests on the possibility to recognize in biological structures the tenets of a gauge theory:

1. The chance to apply differential geometry to living structures.
2. The presence of a living system equipped with a continuous symmetry and a physical quantity to preserve, *e.g.*, the Lagrangian, according to the Noether theorem;
3. The presence of local forces acting on the system, *e.g.*, in technical terms, a group of local continuous transformations.
4. The presence of a counterbalancing force, called gauge field, which is able to restore the general symmetry broken by the above mentioned local transformations.
5. In order to allow a comparison among the required forces, they all need to perform the same kind of movements. In technical word, the forces need to be equipped with a Lie group. To make an example, all the forces that travel along a circumference belong to the same Lie group, called U(1).

Therefore, we need to find at first biological counterparts of the above-mentioned tenets. The oversimplified Fig. 4 illustrates in plain words a possible gauge theory for cellular function involving biochemical pathways, concretely the concentrations of the second messengers of the cell. In more technical terms, the cellular biomolecular pathways, e.g., the topological strings moving in guise of torus trajectories, might stand for the required global symmetry. We can definitely bring strBUT into the picture. The trick here is to have a proximately continuous mapping f from a torus X to R^n, so that $f(strA)$ = feature vector of string *strA* in X. Let *sheetA* be a region of X that is a curved worldsheet. We introduce a second proximately continuous mapping g: from 2^X (family of strings on X) to R^n, so that $f(sheetA)$ = feature vector that describes worldsheet *sheetA* on X.

All the intertwined contiguous strings stand for the Lagrangian, which value is known, because it corresponds to Chaisson's energy rate density, expressed in erg s^{-1} g^{-1}. The global symmetry stands, in biological terms, for cellular homeostasis. The environmental stimuli acting on the cells receptors stand for the local transformations and give rise to local losses of symmetries within the cell. *The species-specific DNA stands for the required gauge field: the genome originates the "force" that counteracts the local environmental transformations acting on the cell.* Such a gauge field restores the locally-broken global cellular symmetry.

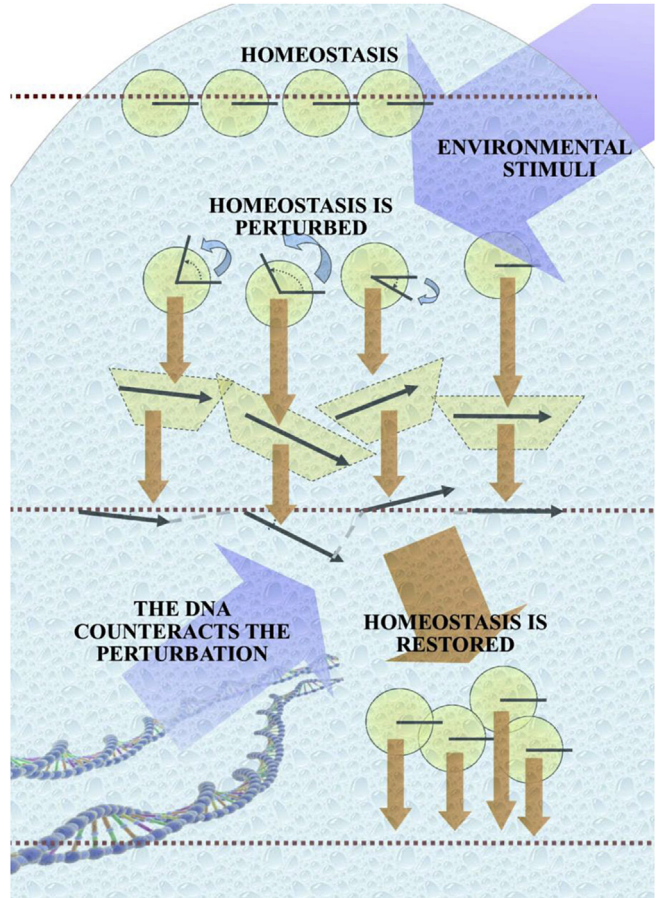

Fig. 4. A simplified sketch of a gauge theory for cellular function. The disks on the top stand for biochemical cellular pathways. Cellular homeostasis is displayed as a dotted, straight line. In gauge terms, the aligned disks stand for the cell's general symmetry. When an external input reaches the cell (left top), the pathways' perturbations can be described in terms of rotations taking place on every disk (middle figure). In gauge terms, such rotations stand for local losses of symmetries into the cell, that might be abstractly described as arrows that diverge from the homeostatic line. In order to restore the general symmetry (and therefore the cellular homeostasis), a continuous gauge field is required, which exerts a force opposite to the environmental perturbation. Such a gauge field originates from the DNA (right bottom of the figure). Note that all the forces are depicted in guise of torus-like abstract movements, and are thus comparable one each other.

In order to operationalize the whole procedure, we need that the three ingredients, e.g., global symmetry, local transformations, and gauge field, are equipped with the same kind of movements, so that they can be compared. Indeed, the particle movements on C (in Fig. 2B) may be described in terms of the proper Lie group. In Fig. 4, we used simple rotations on a disk, standing for changes in the homeostasis along cellular pathways. We may take into account also more complicated (and more realistic) a Lie group whatever movements, *e.g.*, trajectories taking which take place on torus, donut-like structures. A torus can have a topology defined on it (Calixto and Guerrero, 2006). The trick is to define a basis, so that the union and intersection of all sets in the basis gives us the members of the topology. In other words, we need to evaluate real external forces, metabolic and signaling cellular pathways, and DNA function in terms of abstract trajectories on a torus-like structure. In such a way, we are allowed to calculate the energetic values of the three ingredients. Fig. 4 illustrates how to build a gauge theory for cells. The differential geometry techniques for a

gauge theory are formally described in Sengupta et al. (2016) and in Tozzi et al. (2017, to appear).

4. A topological gauge theory for living cells: what for?

Topology, the mathematical branch that focuses on the proximity (nearness) of shapes preserved through deformations, stretching and twisting, allows the investigation of the most general activity features of biological systems. In particular, the biological incarnations of BUT and its variants allow an inquiry of the evolution from inorganic to organic structures and the comparison between prokaryotes and eukaryotes metabolisms/organizations. In order to elucidate the general mechanisms and the evolution of cellular functions, here we introduced a topological framework with keeps into account BUT variants. We showed how topological tools make it possible to assess the big divide of biological complexity in the framework of BUT variants. Therefore, the opportunity to treat *real* systems as *abstract* topological structures makes BUT a universal principle underlying natural phenomena.

The general BUT scheme leads to systems' properties in the real space that are translatable to abstract spaces, in guise of particles traveling on the surfaces of donut-like structures in *n*-dimensional spaces. This model encompasses a topological world, made of natural projections, where the connections among signals occur via proximities and mappings equipped with a structural order. There exist intertwined levels, correlated by maps, where different energy levels allow dimension increases or decreases. The world is a map from a level to another, and the cell is a rather constrained structure determined by factors external to itself. Life is a mapping, with a change of dimensions towards an increasing complexity, which leads, in living beings, to local increases of thermodynamic parameters and information levels.

The importance of a gauge theory for living beings accrues from the chance to predict and calculate unknown parameters. If we know the values of two of the three ingredients, we may achieve the value of the third, via the study of Riemannian manifolds (differential geometry). Briefly, a manifold is a topological space that is locally Euclidean. And a manifold that is Riemannian possesses a metric tensor, *i.e.*, a function that tells us how to compute the distance between any two points on a curved surface. To make an example, all the angles and vectors depicted in the oversimplified Fig. 4 can be accurately calculated, just starting from a few of them. The differential geometry techniques for a gauge theory are formally described in Sengupta et al. (2016) and in Tozzi et al. (2017, to appear).

The crucial question is how to use the proposed gauge field as an analytical tool in order to quantify real cellular phenomena, and how to figure out the upbringing of such a symmetry-restoring gauge field in the physicochemical cellular terms. Here the energy comes into play. A topological gauge theory makes it possible to quantify and assess the cellular energetic requirements. Indeed, from a higher to a lower dimension, a decrease of half of information and energy occurs, and vice versa (**energy-BUT**) (Tozzi and Peters, 2017b). In other words, there exists a physical link between the abstract BUT and the real energetic features of systems formed by two spheres S^n and S^{n-1}. When two antipodal points on an *n*-sphere S^n map to a local *n*-Euclidean manifold where S^{n-1} lies, a symmetry break or (in the inclusive sense) dimensionality reduction occurs, and a single point is achieved (Peters and Tozzi, 2016). Because a decrease in symmetry goes together with a reduction in entropy and free-energy (in a closed system) (Roldán et al., 2014), therefore the single mapping function on S^{n-1} must display energy parameters lower than the sum of the two corresponding antipodal functions on S^n. An increase in dimensions (as it occurs in eukaryotes compared with prokaryotes) gives rise to an increase energy and energy requirements. BUT and its variants become physical quantities, because we achieve a system in which energetic changes do not depend anymore on thermodynamic parameters, but rather on topological features, such as affine connections and homotopies. Therefore, energy-BUT provides a way to evaluate energetic changes in topological, other than thermodynamic, terms. Matching features display a doubled energy, compared with their corresponding single feature, so that a *force* is required to go from a lower dimension to a higher one. This topological paradigm is in touch with biological claims. Indeed, with an increase in evolutionary cellular complexity, the energy requirements become larger. To make an example, an average protozoan has nearly 5000 times more metabolic power than a single bacterium and can support a genome several thousand times larger (Lane and Martin, 2010). Successive levels of potency are organized along the evolutionary and developmental processes. In prokaryotic species, there exists an approximately quadratic relationship between the total number of genes and signaling components (Galperin, 2005), while the eukaryotic increase is exponential.

Therefore, a gauge theory allows us to quantify the energetic requirements of the cell metabolism and its developmental processes. The general symmetry values are known, because they correspond to the energy rate density typical of every cellular species.

The energy-BUT concerns not just energy, but also information. Indeed, two antipodal points encompass more information than their single projection in a lower dimension. Dropping down a dimension means that each point in the lower dimensional space is simpler, because each point has one less coordinate. In the same vein, the information contained in a single feature (embedded in a lower level of complexity) is half the information contained in matching features (embedded in a higher level). Because single features encompass less information and less entropy than matching features, the environment encompasses less information and complexity than living beings. We are therefore allowed to assess not just the energetic requirements, but also the information encompassed in living systems.

4.1. Visual interpretation of a gauge theory for energetic cellular paths

The central question to establish the gauge hypothesis in real molecular terms can be stated as follows: How can we transform the usual differential equations used in metabolic control theory, into the suggested string-paths? Is it possible to produce a realistic biomolecular description, even a partial one, of our global gauge problem, by depicting a concrete image of subsystems and describing how to transform them and obtain the topological strings? One of the possible applications is given here.

If we consider the "simple" *E. coli*, it is equipped with around 4000 genes and 200 transcription factors (TFs), and a complex signaling system. Interestingly, it has "second messengers" that relay the signals received from external receptors to the whole cell: Ca++, cAMP, cGMP, DAG, and a very few others. They make the local signal global for the whole cell, and they are the ones that activate the biggest retinues of TFs. And they do that just by varying their own concentration. Therefore, the second messengers could materialize the essential local "gauge transformations", to which the genome (the "gauge field") would respond with the greatest strength in some determined circumstances. We must note that the proposed gauge field is already latent in the existing functional loops. In other words, the specification of the gauge field proceeds without further referring to the on-going work of the multiple functional loops intervening in the cellular processes. It is by means of these functional loops that a coherent unitary response involving

all the cellular subsystems may be achieved (metabolic networking, signaling system, gene expression, degradation, organelles, etc.). But second messengers constitute the central "code" of any fast and flexible response of the whole cellular system, and the most important one, cAMP, directly "gauges" the energy level of the entire cell. Therefore, in order to proceed operationally, we need to record just the concentration of very few second messengers, and transform them into string paths trajectories in the torus. In terms of the simplified Fig. 4, concentration changes in one or more of the second messengers are measured and expressed in terms of rotations on a circle. The simple geometrical model shown in Figs. 5 and 6 illustrates a good example. See the Figures for further details. Therefore, through a gauge theory, it is feasible to measure the DNA energetic modifications required in order to restore the broken homeostasis.

5. Discussion

In touch with the concept of complex systems, defined as any system that cannot be fully understood by reducing it to its parts, we took into account the relational impacts of organization in natural systems, based on *organized* rather than on the sole *particulate* matter (Rosen, 1991). In a posthumous essay (Rosen, 2000): "The Schrodinger Question: What Is Life? Fifty Years Later", this author described the genome as a *force generator* acting upon the *inertial* enzyme and protein components of the cytoplasm (the whole scheme being developed via category theory and metabolic/repair systems), quite in line with the main idea herein developed. Indeed, a general gauge theory of cell function and biological complexity looks feasible to be cast in a testable fashion, in which symmetries and energetic constraints play a foremost role in order to operationally describe living beings' functionalities. We hypothesize that the general symmetries, equipped with a Lagrangian given by the internal homeostasis, stand for the whole cellular biomolecular network. Note that in this framework the general symmetries are more than local ones. The local transformations stand for the environmental inputs, which locally break the general cellular symmetries. In order to restore the broken symmetries, a gauge field is required. In this case, the gauge field might stand for the action of the cellular genome. Every species displays a different genetic repertoire, each one corresponding to a unique gauge field. The importance of a gauge theory for living beings lies on the chance to predict and calculate unknown parameters. If we know the values of two of the three ingredients, we may achieve the value of the third, via differential geometry. In our model, the general symmetry values are known, because they correspond to the energy rate density typical of every cellular species. Vice versa, given a vector value (say, an energetic value) for DNA and environmental

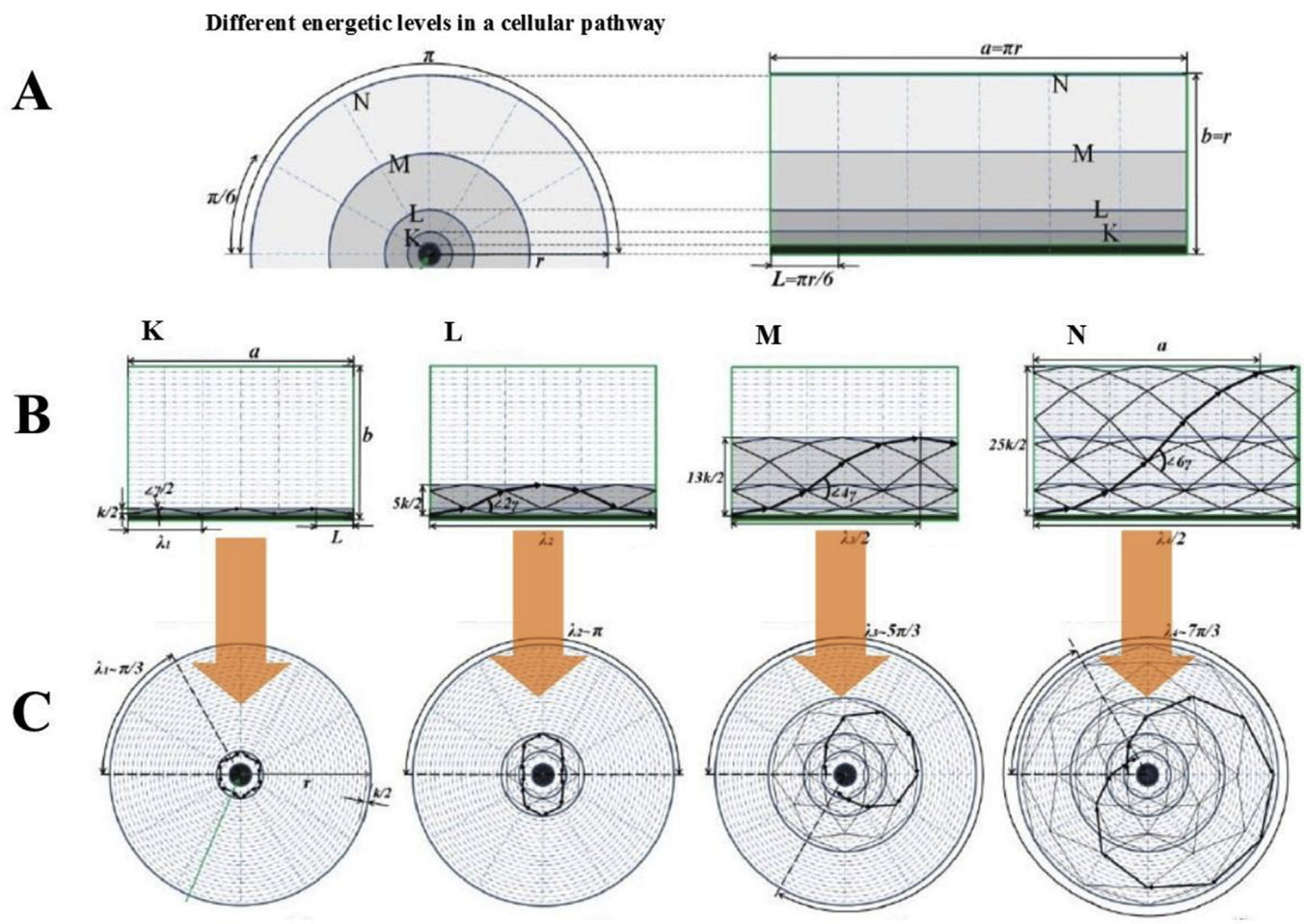

Fig. 5. Four-shells model of a cellular energetic pathway. Modified from Yurkin (2017). Despite Yurkin's model refers to the energetic atomic levels, so that the angles and energy are calculated based on the movements of electrons in different orbits, the same framework, with the due corrections, might be used for the evaluation of cellular metabolic paths. Fig. 5A, left: four energetic levels are displayed as rotations on a circle: K (the lowest energy), L, M, N (the highest energy). Fig. 5A, right: the four circular orbits can be mapped to a horizontal tape. Fig. 5B: the four energetic levels can be depicted as wavy trajectories extended along the horizontal tape. Trajectories intersect, forming angles γ, that vary according to the rays' inclination (dictated by specific parameters for every different system taken into account). Fig. 5C displays a view from above of Fig. 5B.

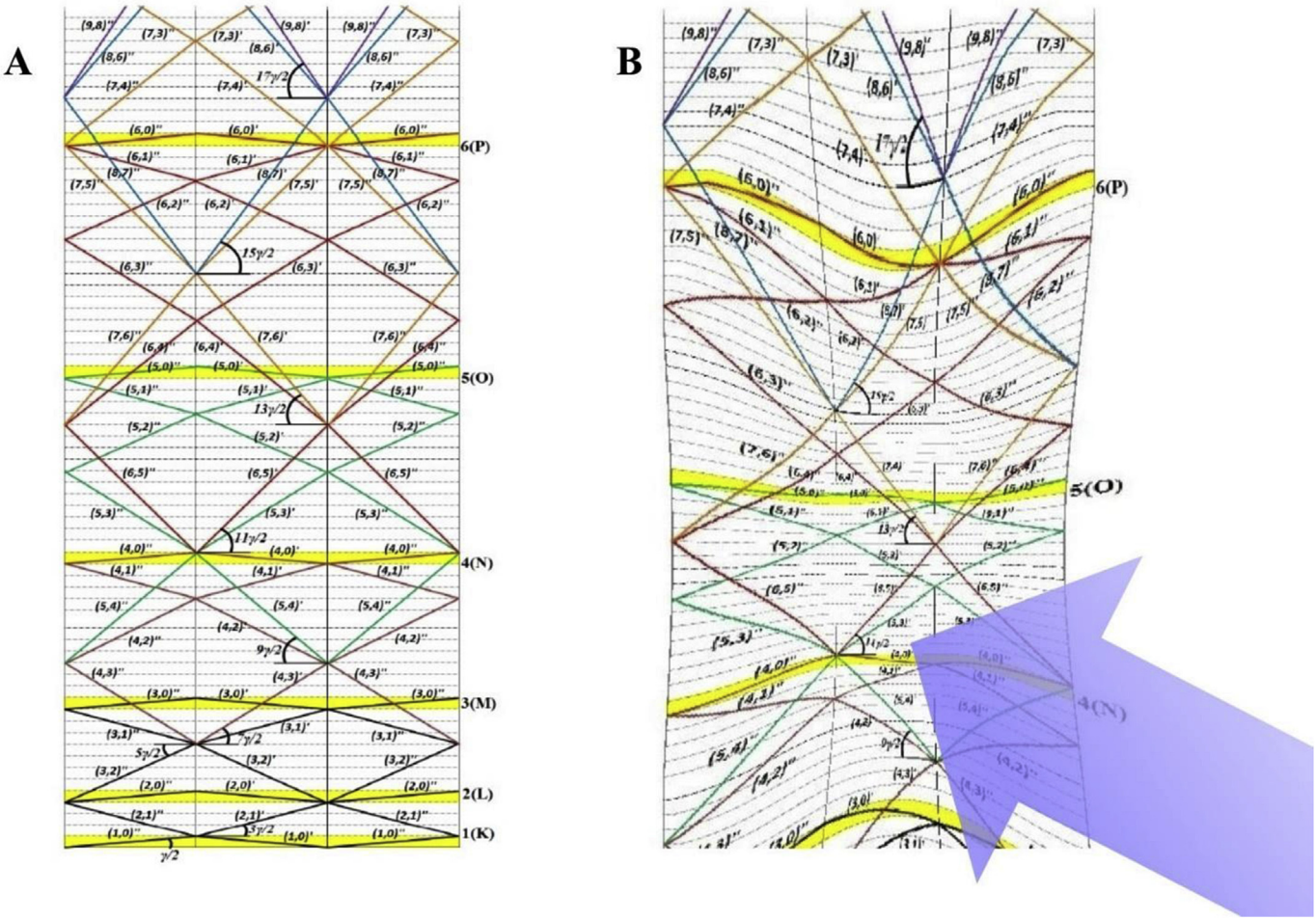

Fig. 6. A. The paths described in Fig. 5B and C can be projected onto a flattened rectangular coordinate grid. The Figure illustrates wavy trajectories of a multilevel cellular pathway, equipped with six increasing energetic levels (the lower energetic level K is placed at the bottom, the higher P at the top). The length of every line connecting two nodes stands for the average energy within two neighbor passes. Fig. 6B: when an external force (arrow) acts on the system, a grid deformation occurs, so that the angles γ and the energy lines are modified. The broken homeostasis can be restored by another force, the DNA gauge field. The DNA's angles γ and energetic levels able to "heal" the deformation can be calculated through a (relatively simple) gauge procedure.

stimuli, we could calculate the energy vector of the cellular symmetries. For example, we may assess which is the maximum external force which can be applied without destroying a given cell type. Through simulations that progressively increase the force of the external stimuli, it is also possible to know what is the minimum energy required for archaea, prokaryotes or eukaryotes.

Hutchison et al. (2016) recently described the minimal bacterial genome, e.g., the simplest artificial cell capable of autonomous growth. However, their cell is unrealistic, because they used a growth medium provided with an exceeding number of metabolites and micronutrients. A gauge theory might help to calculate the amount of DNA energy (and genes) required in order to build a more realistic and self-sustained minimal bacterial genome within a natural environment, without the help of any sophisticate artificial feeding. See recent computational explorations about that (Wagner, 2014). But, by far, the biggest challenge of the gauge approach would correspond to the framing of a new interpretation, topologically and symmetry based, of developmental processes. Actually, when eukaryotes dissociated their processes at the lower level and recombined or redeployed them at a higher level, via the organization of consistent modules interconnected by inner signals, they wide opened the topological theater (Nedelcu and Michod, 2004). Cellular functions were changed from a temporal level to a spatial one (both describable by BUT and its variants), and were restricted now to appear in specialized populations situated at the proper place and to interact with specific neighborhood relationships. More and more mappings equipped with a structural order became common in multicellulars (Barbieri, 2016), achieving further topological and developmental complexity. These mappings were always handled by the signaling and second messengers already commented. As new physical resources were incorporated, such as the force field and the electric field, the interconnection of cellular cytoskeletons with extracellular matrices and the interconnection of neurons via synapses could enter into the developmental-topological games (Marijuán et al., 2015). The amazing complexity of vertebrate bodies and brains was born … Then, the underlying decisive issue becomes the question of which is the first to come, either the gauge field or the second messengers. We argue that there is a big enigma related to the very origins of life, and how the internal regulation that brings about material self-organization was framed (Matsuno, 1984). In a similar way, the expression of genes was progressively organized according to "proto-gauge" fields in a mosaic form that gained cohesion and unitary dynamics via the emergence of second messengers, which really mark the transition from multiple proto-gauge fields to the genuine gauge field involving the response of the entire system.

The mutual upholding between signals and mosaic gauge fields converged into the most robust dynamics. For instance, in the response to the cAMP signal, from haphazard expression in oldest cells (*e.g.*, Archaea), we find that more than half of the genome of *E. coli* is involved in the response −direct and indirect− to cAMP via the corresponding transcription factor (crp) associated to the signal. Presumably, along the evolutionary process, once protocells stabilized the first code of life, the genetic code (Barbieri, 2016), there was a progressive advancement in the "encoding" or representation of the environment into the genome, so that the organization of gauge symmetries could take place.

We would like to bring this discussion to an end, with some caveats and warnings—and further biological speculations! Too many questions are still open. For instance, could we reconcile the gauge approach not only with the homeostasis, but also with the advancement of a life cycle, e.g., its *closure* with either reproduction or death? It would be very useful, both for the prokaryotic *simple* life cycle organization and for the eukaryotic *topology-laden* stages of cellular life, to encompass differentiation as well as quiescence/senescence/apoptosis/necrosis (Joo et al., 2016). Using the cycle as general symmetry reference would be a very fruitful step to take. The abstract *strings* constituting cell cycles might have also other features apart from the ones suggested in our paper. For example, the cycle advancement can be cast with different paths, depending either on environmental inputs, or disturbances, internal randomness, and so on. Maybe we could take into account multidimensional *attractors* equipped with basins of many possible states: see for instance the giant component that emerges for linked metabolic reactions in *E. coli*, with star-like topology (Almaas et al., 2004). Then the force arising from the genome, after receiving the appropriate *signals*, could modify some of the trajectory dimensions, so that the whole system is able to come back to the attractor/s. This can be seen in the way a real genome responds to external and internal disturbances (Marijuán et al., 2015). A few critical points, or multidimensional junctures, could be topologically important, as they become singularities leading to novel attractors or sub-basins. In the biomolecular literature, they are known as *checkpoints* (Marijuán et al., 2013). These cellular checkpoints become extreme *bottlenecks* that connect different regions of the same torus, or alternatively they could pertain to different toruses (e.g., in the case of cellular division leading to differentiation). Furthermore, if we take into account the whole *multicellular space*, would a global torus emerge from the fusion/mosaicism of the little cellular ones, via the massive information flow of shared signaling events? If we instead take into account a multicellular time, e.g., the structure of rhythms within rhythms (with a circadian central adaptive pattern), could we think on something like the "circadian torus" applied to the customary behavioral interlinked repertoires displayed by all animals into their natural environments?

In such a multifaceted context, the powerful strBUT approach displays the big advantage to treat all the trajectories as if they were embedded in a donut-like structure. This allows the comparison of completely different kinds of flows in a single, coherent scheme. In sum, the torus is the abstract space of the whole cell survival trajectories, carefully guarded by another torus, the genome. Indeed, the presence of a functional torus-like structure in the brain has been recently demonstrated (Tozzi and Peters, 2016a; Peters et al., 2017). So, all this stuff is quite intriguing, and points towards *a donut-like structure as a general principle underlying the abstract organization of biological systems.*

6. Conclusion

Gauge theories allow us to collect a huge amount of knowledge and data available in cellular biology, in order to formulate a general principle for cellular dynamics that holds at evolutionary, developmental, and homeostatic levels. A gauge-theoretic formalism in biology not only provides a quantitative framework for modeling cellular activity according to general principles, but also offers new tools for modeling and computational biology. Indeed, formulating cellular energetic requirements and constraints in terms of a gauge theory may have important implications for new inference schemes that can be used to analyze empirical data and to infer the structure and parameters of models (Sengupta et al., 2016).

This entails an encoding of cellular behaviours in terms of biophysical variables, whose trajectories trace out abstract manifolds. In variational schemes, the coordinates on such manifolds are the sufficient statistics and can be further complemented by Monte Carlo formulations. The manifolds are also able to assess ODEs, in terms, for example, of gradients in Langevin equations. In the Yurkin's model we explain in the Addendum, it means that we are allowed to assess the couplings of different cellular biochemical activities in a way that depends explicitly on the curvature of the manifold, that can be measured, e.g., in terms of Fisher information. For example, a model of invariance of inference based on gauge teories has been recently proposed in the neuroscience arena (Sengupta et al., 2016). A gauge formulation enabled the Authors to compare a variety of hypotheses about the environment detected by our sensory samples. Thus, symmetry transformations furnish us with a family of models that explain the available experimental data with equal probability. To make an example in terms of cellular biology, after scoring a variety of models according to their parameterized features, one may select the best and more suitable generative model that explains the biochemical data at hand.

If symmetry transformations can be evaluated for the best performing model, we can go a step further and ask what other models could explain the data with the same model evidence. If this was possible, one could identify the class of models explaining data using a single inference methodology. From the perspective of cellular organization, this means that there are potentially many different models that do the same job of keeping the homeostasis. After the optimal model has been selected, symmetry transformation could enable one to derive a range of models that describe the data equally well. Such equivalence classes could be theoretically associated with the biological species, all doing an equally good job of modeling their (local) environments and keeping the proper internal balance (Sengupta et al., 2016).

6.1. Philosophical coda

As the late Michael Conrad (1996) wrote about the laws of the microphysical world and the laws of biological systems: *"when we look at a biological system, we are looking at the face of the underlying physics of the universe."* In touch with this statement, some of the present authors (Tozzi et al., 2017) have also described a multisymmetric abstract torus in pre-Big Bang scenarios. Subsequently, the closing sentence of the above Section should be modified, in the sense that "all this stuff is quite intriguing, and points towards *a donut-like structure as a general principle underlying both physical and biological systems."* Further, our topological gauge framework encompasses intertwined levels, correlated by maps, where different energy levels permit dimension increases or decreases. The world is a map from a level to another, and the cell is a rather constrained structure determined by factors external to itself. In such a vein, life is a mapping, with a change of dimensions towards an increasing complexity, which leads, in living beings, to local increases of thermodynamic parameters and information levels.

These statements are quite close to Zhu Xi's cosmological vision.

Putting together central ideas of the different philosophical systems of his day (neither Taoism, nor Confucianism, nor Buddhism can be plainly identified with his ideas), he identified two essential aspects of the global reality, the *li* as organizing or rational principle, and the *qi* as the material or physical force. They integrate the *Taiji* or Supreme Ultimate, itself in a constant creative activity which promotes the emergence of the new (Chan, 1963). The *li* and *qi* operate in mutual interdependence, in continuous oscillations. They give rise to alternating phases, originating along their interdependence the yin and yang modes of energy (i.e., slow or contractive yin, versus rapid or expansive yang).

Therefore, in our gauge symmetry interpretation, we see how the *li* (the signaling information standing for the global symmetry and the genomic information) are coupled with the underlying *qi* (standing for the metabolic energy and the environmental symmetry breaks) so that they mutually generate the multiplicity of rhythms of the *Taiji* complex, unitary cell. This cellular existential process culminates in the generation of a reproductive cycle, emerging from the preexisting *Taiji* of the very cellular life (Scofield, 2011). It is worth to emphasize that the *li* and *qi* principles are more suitable for the approach developed in this manuscript than the categories of European philosophy. Along this view, neither energy nor information can be considered as a legitimization of monism for life—*e.g.*, neither the materialist stance so common in Western views, nor the idealism/vitalism of some schools in the past. Bottom-up and top-down flows of *li* influences (or information flows) always interlinked with the corresponding *qi* influences (energy flows) are passed in between the different existential realms, as another of the deepest implications of this doctrine.

Subsequently, when these views are extended to the social realm, the *li* principle also becomes the organizing dimension of individual behavior, always interrelated with the material part of life, but harmoniously integrated in the extent to which lives and societies can be managed successfully. So far, we have physical, biological, and also social issues framed into a consistent perspective of very advanced terms—"socioinformation" we may say about the latter. In this sense, one of the historical enigmas of Chinese science and philosophy, as pointed out by Joseph Needham (1954–2015), is how such advanced organismic philosophies were not capable of producing analytical science comparable to the Western world; and also the opposite could be argued, how the rich analytical science of the West was unable to develop interesting integrative thought around life, at least until the XIX Century—and, later on, arguably! In our case, it is not exaggerated to say that philosophical and scientific equivalents of terms that are essential in contemporary dialogs between scientific disciplines could be approximately pinpointed in this ancient XIII Century synthesis: information, energy, symmetry, oscillation, coherence, complexity, integration.

One of the many connections of the above –an important one that has been guiding the philosophy of this paper– refers to current debates around information. Certainly it is a relatively recent scientific, technologic, and philosophic term that has gained centrality: the *li* of our times! It has been claimed (Conrad, 1996; Marijuán, 1996) that a renewed information science transcending classical information theory and library science fields, as well as the limits of thermodynamics and computer science, would be able to connect the main achievements of the "information revolution" in very different areas (quantum information science, bioinformation, neuroinformation, social information science), and would provide us a novel *Weltanschaaung*. This was, in short, the "Foundations of Information Science" initiative. Close to that endeavor, one of the most active areas of enquiry has become the intersection between information science and information philosophy (Wu, 2006, 2012). Along the informational views of the latter author, the need for unification of critical disciplines and their formulation as a metaphilosophy are contributing to a new transdisciplinary paradigm, in which information has a central role in the approach to knowledge and to the classical split of academic disciplines (Wu, 1981). In fact, this approach establishes a new and necessary critique of the standpoints of modern philosophy as a whole. It provides the ontological basis for the kind of shift of perspective towards a dynamic, qualitative view of information of the kind that contemporary authors are exploring in a plurality of research fields: neither dualism nor monism, but informationalism. Interestingly, when looking for the qualitative-normative aspects of information and their implications for ethics and the information society, Wu Kun's ideas may be aligned and contrasted with some Western authors (Floridi, 2013), so that the road to an alternative and more integrative approach seems to be open. It is in this further integrative openness that Zhu Xi's ideas and the *li* organization principle strongly resonate.

The dialog between Eastern and Western worldviews have become a natural, implicit, and enriching aspect of today's global society and research. Herein, we have contributed with the gauge symmetry proposal for the living cell, and the subsequent informational commonalty of an integrative donut-like phase space. It is illustrative that the ancient *li* and *qi* principles become more suitable for the approach developed in this work than many other categories of European philosophy.

References

Almaas, E., Kovacs, B., Vicsek, T., Oltvai, Z.N., Barabási, A.L., 2004. Global organization of metabolic fluxes in the bacterium Escherichia coli. Nature 427, 839–843.

Ayyadurai, V.A., Dewey, C.F., 2011. CytoSolve: a scalable computational method for dynamic integration of multiple molecular pathway models. Springer Cell Mol. Bioeng. 4 (1), 28–45.

Barbieri, M., 2016. How did the eukaryotes evolve? October 2016 Biol. Theory. http://dx.doi.org/10.1007/s13752-016-0253-3.

Bonner, J.T., 1998. The Evolution of Complexity by Means of Natural Selection. October 1988. Princeton Univ Press.

Brenner, J.E., 2011. Wu Kun and the metaphilosophy of information. Inf. Theor. Appl. 18, 103–128.

Calixto, M., Guerrero, J., 2006. Wavelet transform on the circle and the real line: a unified group-theoretical treatment. Appl. Comput. Harmon. Analysis 21 (2), 204–229.

Capra, F., 1975. The Tao of Physics: an Exploration of the Parallels between Modern Physics and Eastern Mysticism. Shambhala Publications, Boulder (CO).

Chaisson, E.J., 2010. Energy rate density as a complexity metric and evolutionary driver. Complexity 16. http://dx.doi.org/10.1002/cplx.20323, p 27, 2011.

Chaisson, E.J., 2014. The natural science underlying big history. Sci. World J. 2014, 41. http://dx.doi.org/10.1155/2014/384912 pgs, 2014.

Chan, W.T., 1963. Trans. And comp., a Source Book in Chinese Philosophy.

Conrad, M., 1996. Cross-scale information processing in evolution, development and intelligence. BioSystems 38 (2), 97–109.

Danchin, A., 2009. Bacteria as computers making computers. FEMS Microbiol. Rev. 33, 3–26.

Floridi, L., 2013. The Ethics of Information. Oxford University Press.

Ford, Brian J., 2017. Cellular Intelligence: Microphenomenology and the Realities of Being (under review).

Galperin, M.Y., 2005. A census of membrane-bound and intracellular signal transduction proteins in bacteria: bacterial IQ, extroverts and introverts. BMC Microbiol. 5, R1–R19.

Gerhart, J., 1999. Warkany lecture 1998: signaling pathways in development. Teratology 60, 226–239.

Helikar, T., Kowal, B., Madrahimov, A., Shrestha, M., Pedersen, J., Limbu, K., et al., 2012. Bio-Logic Builder: a nontechnical tool for building dynamical, qualitative models. PLoS One 7 (10), e46417. http://dx.doi.org/10.1371/journal.pone.0046417.

Higgs, P., 1964. Broken symmetries and the masses of gauge bosons. Phys. Rev. Lett. 13, 508–509.

Hutchison 3rd, C.A., Chuang, R.Y., Noskov, V.N., Assad-Garcia, N., Deerinck, T.J., et al., 2016. Design and synthesis of a minimal bacterial genome, 2016 Mar 25 Science 351 (6280). http://dx.doi.org/10.1126/science.aad6253. aad6253.

Joo, J.H., Wang, B., Frankel, E., Ge, L., Xu, L., et al., 2016. The noncanonical role of ULK/ATG1 in ER-to-golgi trafficking is essential for cellular homeostasis, 2016 May 19 Mol. Cell. 62 (4), 491–506. http://dx.doi.org/10.1016/j.molcel.2016.04.020.

Kauffman, S., 1993. The Origins of Order: Self Organization and Selection in Evolution. Oxford University Press.

Koonin, E.V., 2010. The origin and early evolution of eukaryotes in the light of

phylogenomics. Genome Biol. 11 (5), 209.
Kreeft, P., 2012. Summa Philosophica. St. Augustine Press. South Bend (IN).
Lane, N., Martin, W., 2010. The energetics of genome complexity. Nature 467, 929–934.
Marijuán, P.C., 1996. First conference on foundations of information science: from computers and quantum physics to cells, nervous systems, and societies. BioSystems 38 (2), 87–96.
Marijuán, P.C., Navarro, J., del Moral, R., 2010. On prokaryotic intelligence: strategies for sensing the environment. BioSystems 99, 94–103.
Marijuán, P.C., del Moral, R., Navarro, J., 2013. On eukaryotic intelligence: signaling system's guidance in the evolution of multicellular organization. Biosystems 114 (1), 8–24. http://dx.doi.org/10.1016/j.biosystems.2013.06.005. Epub 2013 Jul 12.
Marijuán, P.C., Navarro, J., del Moral, R., 2015. How the living is in the world: an inquiry into the informational choreographies of life. Prog. Biophysics Mol. Biol. 119 (3), 469–480. http://dx.doi.org/10.1016/j.pbiomolbio.2015.07.002.
Mariotti, J.L., 2008. The Complexity Crisis. Platinum Press. Avon (MA).
Matsuno, K., 1984. Protobiology: a theoretical synthesis. In: Matsuno, K., Dose, K., Harada, K., Rohlfing, D.L. (Eds.), Molecular Evolution and Protobiology. Plenum Press, NY, pp. 433–464.
Morowitz, H.J., 1968. Energy Flow in Biology: Biological Organization as a Problem in Thermal Physics. Academic Press, New York. London.
Nedelcu, A.M., Michod, R.E., 2004. Evolvability, modularity, and individuality during the transition to multicellularity in volvocalean green algae. In: Schlosser, G., Wagner, G. (Eds.), Modularity in Development and Evolution. University of Chicago Press, Chicago, pp. 468–489.
Needham, J., 1954–2015. Science and Civilisation in China. Cambridge Univ. Press, Cambridge (UK).
Neubauer, R., 2012. Evolution and the Emergent Self. Columbia Univ. Press, New York.
Olive, D.I., Landsberg, P.T., 1989. Introduction to string theory: its structure and its uses [and discussion], 1989 Phil. Trans. R. Soc. Lond. A 319–328. http://dx.doi.org/10.1098/rsta.1989.0079, 1989 329.
Peters, J.F., 2016. Computational proximity. Excursions in the topology of digital images. In: Intelligent Systems Reference Library. Springer-Verlag, Berlin. http://dx.doi.org/10.1007/978-3-319-30262-1.
Peters, J.F., Tozzi, A., 2016. Region-based Borsuk-ulam Theorem arXiv.1605.02987.
Peters, J.F., Tozzi, A., Ramanna, S., 2016. Brain tissue tessellation shows absence of canonical microcircuits. Neurosci. Lett. 626, 99–105. http://dx.doi.org/10.1016/j.neulet.2016.03.052.
Peters, J.F., Ramanna, S., Tozzi, A., Inan, E., 2017. Frontiers Hum Neurosci. BOLD-independent Computational Entropy Assesses Functional Donut-like Structures in Brain FMRI Image. http://dx.doi.org/10.3389/fnhum.2017.00038.
Riedl, R., 1978. Order in Living Systems: a Systems Analysis of Evolution. Wiley, New York (Übersetzung von: Die Ordnung des Lebendigen).
Roldán, E., Martínez, I.A., Parrondo, J.M.R., Petrov, D., 2014. Universal features in the energetics of symmetry breaking. Nat. Phys. 10, 457–461. http://dx.doi.org/10.1038/nphys2940.
Rosen, R., 1991. Life Itself: a Comprehensive Inquiry into the Nature, Origin, and Fabrication of Life (Complexity in Ecological Systems). Columbia University press, New York, Chiclester, Ussex. ISBN-10: 0231075650.
Rosen, R., 2000. Essays on Life Itself. Columbia University Press.
Scofield, B., 2011. Cosmic rhythms of life. In: Margulis, L., Asikainen, C., Krumbein, W. (Eds.), Chimera and Consciousness: Evolution of the Sensory Self (151-159). MIT press, Cambridge. MA.
Sengupta, B., Tozzi, A., Cooray, G.K., Douglas, P.K., Friston, K.J., 2016. Towards a neuronal gauge theory. PLOS Biol. 14 (3), e1002400. http://dx.doi.org/10.1371/journal.pbio.1002400.
Sneddon, M.W., Faeder, J.R., Emonet, T., 2011. Efficient modeling, simulation and coarse-graining of biological complexity with NFsim. Nat. Methods 8 (2011), 177–183. http://dx.doi.org/10.1038/nmeth.1546.
Torday, John S., Miller Jr., William B., 2017. The Resolution of Ambiguity as the Basis for Life: Being is Doubt (under review).
Tozzi, A., 2016. Borsuk-ulam theorem extended to hyperbolic spaces. In: Peters, J.F. (Ed.), Computational Proximity. Excursions in the Topology of Digital Images, pp. 169–171. http://dx.doi.org/10.1007/978-3-319-30262-1.
Tozzi, A., Peters, J.F., 2016a. Towards a fourth spatial dimension of brain activity. Cogn. Neurodynamics 10 (3), 189–199. http://dx.doi.org/10.1007/s11571-016-9379-z.
Tozzi, A., Peters, J.F., 2016b. A topological approach unveils system invariances and broken symmetries in the brain. J. Neurosci. Res. 94 (5), 351–365. http://dx.doi.org/10.1002/jnr.23720.
Tozzi, A., Peters, J.F., 2017a. A symmetric approach elucidates multisensory information integration. Information 8, 1. http://dx.doi.org/10.3390/info8010004.
Tozzi, A., Peters, J.F., 2017b. From abstract topology to real thermodynamic brain activity. Cogn. Neurodynamics 11 (3), 283–292. http://dx.doi.org/10.1007/s11571-0-17-9431-7.
Tozzi, A., Sengupta, B., Peters, J.F., Friston, K.J., 2017. Gauge fields in the central nervous system. In: Opris, J., Casanova, M.F. (Eds.), The Physics of the Mind and Brain Disorders: Integrated Neural Circuits Supporting the Emergence of Mind. Springer; Series in Cognitive and Neural Systems, New York. Next to appear, on July 2017.
Wagner, A., 2014. Arrival of the Fittest: Solving Evolution's Greatest Puzzle. Penguin. NY. USA.
Wolfram, S., 2002. A New Kind of Science. Wolfram Media Inc., Champaign, IL.
Wu, K., 1981. The form of the philosophy of information. Potential Sci. J. 3, 33–35.
Wu, K., 2006. Formal proposal for a unified complex information theory. Stud. Dialectics Nat. 12, 96–99.
Wu, K., 2012. The essence, classification and quality of the different grades of information. Information 3 (3), 403–419.
Yan, K.K., Fang, G., Bhardwaj, N., Alexander, R.P., Gerstein, M., 2010. Comparing genomes to computer operating systems in terms of the topology and evolution of their regulatory control networks. PNAS 107 (20), 9186–9191.
Yurkin, A., 2017. New, binomial model of atom, trajectories and schemes of energy of splitting levels of atom. IOSR J. Eng. (IOSRJEN) 07 (02), 19–31.
Zeidler, E., 2011. Quantum Field Theory III: Gauge Theory. Springer.

Progress in Biophysics and Molecular Biology 131 (2017) 153–161

Contents lists available at ScienceDirect

Progress in Biophysics and Molecular Biology

journal homepage: www.elsevier.com/locate/pbiomolbio

Cellular Gauge Symmetry and the Li Organization Principle: A Mathematical Addendum. Quantifying energetic dynamics in physical and biological systems through a simple geometric tool and geodetic curves

Alexander Yurkin [a], Arturo Tozzi [b, c], James F. Peters [d, e, f, c], Pedro C. Marijuán [g, *]

[a] Russian Academy of Sciences, Moscow, Puschino, Russia
[b] Center for Nonlinear Science, University of North Texas, 1155 Union Circle, #311427, Denton, TX 76203-5017, USA
[c] Computational Intelligence Laboratory, University of Manitoba, Winnipeg R3T 5V6 Manitoba, Canada
[d] Department of Electrical and Computer Engineering, University of Manitoba, 75A Chancellor's Circle, Winnipeg, MB R3T 5V6, Canada
[e] Department of Mathematics, Adıyaman University, 02040 Adıyaman, Turkey
[f] Department of Mathematics, Faculty of Arts and Sciences, Adıyaman University, 02040 Adıyaman, Turkey
[g] Grupo de Bioinformación / Bioinformation Group, Instituto Aragonés de Ciencias de la Salud (IACS), Instituto de Investigación Sanitaria Aragón (IIS), Edificio CIBA. Avda. San Juan Bosco, 13, 50009 Zaragoza, Spain

ARTICLE INFO

Article history:
Received 28 April 2017
Received in revised form
9 June 2017
Accepted 16 June 2017
Available online 17 June 2017

Keywords:
Trajectories
Energy levels
Physics geometrization

ABSTRACT

The present Addendum complements the accompanying paper "Cellular Gauge Symmetry and the Li Organization Principle"; it illustrates a recently-developed geometrical physical model able to assess electronic movements and energetic paths in atomic shells. The model describes a multi-level system of circular, wavy and zigzag paths which can be projected onto a horizontal tape. This model ushers in a visual interpretation of the distribution of atomic electrons' energy levels and the corresponding quantum numbers through rather simple tools, such as compasses, rulers and straightforward calculations. Here we show how this geometrical model, with the due corrections, among them the use of geodetic curves, might be able to describe and quantify the structure and the temporal development of countless physical and biological systems, from Langevin equations for random paths, to symmetry breaks occurring ubiquitously in physical and biological phenomena, to the relationships among different frequencies of EEG electric spikes. Therefore, in our work we explore the possible association of binomial distribution and geodetic curves configuring a uniform approach for the research of natural phenomena, in biology, medicine or the neurosciences.

© 2017 Elsevier Ltd. All rights reserved.

Contents

1. A new geometric model 154
   1.1. Geometrical counterparts of quantum systems' energy levels 154
   1.2. Quantifying angles, quantum numbers and ratios 154
2. Possible applications of the model in biophysics, physiology (human disease), and neuroscience 156
   2.1. Timescales of protein folding 156
   2.2. The physiological underpinning of human disease 157
   2.3. Assessing brain oscillations 158
3. Conclusion 161
   Acknowledgements 161
   References 161

* Corresponding author.
E-mail addresses: alvl1yurkin@rambler.ru (A. Yurkin), tozziarturo@libero.it (A. Tozzi), james.peters3@umanitoba.ca (J.F. Peters), pcmarijuan.iacs@aragon.es (P.C. Marijuán).

http://dx.doi.org/10.1016/j.pbiomolbio.2017.06.007
0079-6107/© 2017 Elsevier Ltd. All rights reserved.

1. A new geometric model

Visual geometric models are widely used for the description of different phenomena in nature. In particular, the conception of a geodetic line or a geodetic curve was first considered long ago by Gauss (Bühler, 1981). To make a recent example, Yurkin (2017) provided a novel geometrical model of a structure of atomic electron shells, able to assess the main, azimuthal, magnetic, and spin numbers in terms of simple wavy trajectories, angles and distances. These parameters can be mapped onto a horizontal tape, making it possible us to assess difficult system structures by using an effortless MS Excel program, without additional proofs and assumptions.

Here follows a brief description of Yurkin's original geometric model for atomic shells (Yurkin, 2015). The geometrical steps in order to build atomic shells and subshells in the form of wavy trajectories (extended along horizontal tapes and connected with the image of circular atomic orbits) are summarized in Fig. 1 and Fig. 2. The paths are expressed in terms of wavy and circular trajectories of electron movements. Ratios between atomic models' features, as well as their quantum numbers and power levels, can be interpreted as trajectories of different shapes. In technical terms, Yurkin described a paraxial binomial (sharing in two) flat system of trajectories (Yurkin, 2016). This system consists of groups of rays, inclined under p angles that are a) are smaller than a given axis, and b) multiple to an angle γ:

$$p = \left(\frac{m+1}{2}\right)\gamma,$$

where

$$m = 0,\ \pm1,\ \pm2\ldots.$$

In addition, let us accept that:

$$p_0 = \left(\pm\frac{1}{2}\right)\gamma = s\gamma,$$

where

$$s = \pm\frac{1}{2}$$

in case of $m = 0$.

Points of ray branching are spaced by a symmetry axis on small distances of a q multiple to $k/2$ length:

$$q = \frac{jk}{2},$$

where $j = 0,\ \pm1,\ \pm2\ldots.$

We termed this rays system: "$[p = \left(\frac{m+1}{2}\right)\gamma, q = \frac{jk}{2}]$ – system", or *half-integer ray system*. This binomial system consists of groups of rays $\mathbb{N}$ equipped with links $\mathbb{K}$ (Yurkin, 2016).

We assume that the rays display an energy $\boldsymbol{E}$, extending along the branching $\mathbb{K}$ links. Therefore, the number of rays of $\mathbb{N}$ (and their energy $\boldsymbol{E}$) can be easily summarized. Generally, $\mathbb{N} \geq \mathbb{K}$. We designate number of passes of rays along links as. $0,\ 1,\ 2\ldots,\ n-1,\ n,\ n+1\ldots$

This ray system can be placed in a rectangular coordinate grid. The size of a cell grid displays height $= \frac{k}{2}$ and length $= L$. The configurations of this two-dimensional system matches the real electronic distribution in various atomic shells (Yurkin, 2016), therefore it demonstrated to be a very accurate model. In the present paper, we generalize the proposed geometric model by using geodetic curves.

1.1. Geometrical counterparts of quantum systems' energy levels

Consider the following designations. Let $\boldsymbol{E}(\boldsymbol{n},\boldsymbol{l})'$ denote the energy extending along the ray characterized by numbers $\boldsymbol{n}$ and $\boldsymbol{l}$ at each odd pass of n, and let $\boldsymbol{E}(\boldsymbol{n},\boldsymbol{l})''$ denote the energy extending along the ray characterized by numbers $\boldsymbol{n}$ and $\boldsymbol{l}$ at each even pass of $n-1$ or $n+1$. Here $n-1$, n and $n+1$ are numbers of rays passes. The numbers $\boldsymbol{n}$ and $\boldsymbol{l}$ characterize each one of the rays of our binomial system.

Let the average energy between two neighbor passes be represented by

$$\boldsymbol{E}(\boldsymbol{n},\boldsymbol{l}) = \frac{\left[\boldsymbol{E}(\boldsymbol{n},\boldsymbol{l})' + \boldsymbol{E}(\boldsymbol{n},\boldsymbol{l})'\right]}{2}$$

Generally,$\boldsymbol{n}$ and $\boldsymbol{l}$ accept the following values:

$$\boldsymbol{n} = 1, 2, 3, \ldots$$

$$\boldsymbol{l} = 0, 1, 2, \ldots.$$

1.2. Quantifying angles, quantum numbers and ratios

In quantum mechanics, every electron is characterized by four physical quantum numbers. Yurkin's atomic model, in touch with the literature (2017), utilizes the following values:

Principal: $\boldsymbol{n}$ corresponds to. $\boldsymbol{n} = 1, 2, 3, \ldots$

Azimuthal: $\boldsymbol{l}$ corresponds to. $\boldsymbol{l} = 0, 1, 2, \ldots$

Magnetic: $\boldsymbol{m_l}$ corresponds to. $m = 0, \pm1, \pm2\ldots$

Spin: $\boldsymbol{m_s}$ corresponds to. $s = \pm\frac{1}{2}$

Note that first expression:

$$p = \left(m + \frac{1}{2}\right)\gamma,$$

can be written also as:

$$p = \left(m + \frac{1}{2}\right)\gamma = \pm\left(l + \frac{1}{2}\right)\gamma.$$

If we accept that the quantum system contains a finite number of electrons, then the above mentioned expressions of the four physical quantum numbers can accept the minimum and maximum values$\boldsymbol{n}(min), \boldsymbol{n}(max), \boldsymbol{l}(max)$, and so on.

2. Possible applications of the model in biophysics, physiology (human disease), and neuroscience

In the previous Section, in touch with Yurkin (2015, 2016, 2017), we illustrated how to build a geometrical grid that makes possible us to describe systems equipped with various energetic levels. Visual geometric models are widely used for the description of different natural phenomena (Peters, 2016, 2017a, 2017b; Frankel, 2016). To make an example, the periodic table of chemical elements displays periodic regularities that can be visually illustrated in the form of circles, pyramids, spirals, and so on. In point of fact, Yurkin's model is different from others: although it has been developed in order to assess electrons' energetic levels in atomic orbits, it might be extended, with the due corrections, to countless, quite different physical and biological systems. In Yurkin's atomic model, the four sought-after values, i.e., m and s (that describe the

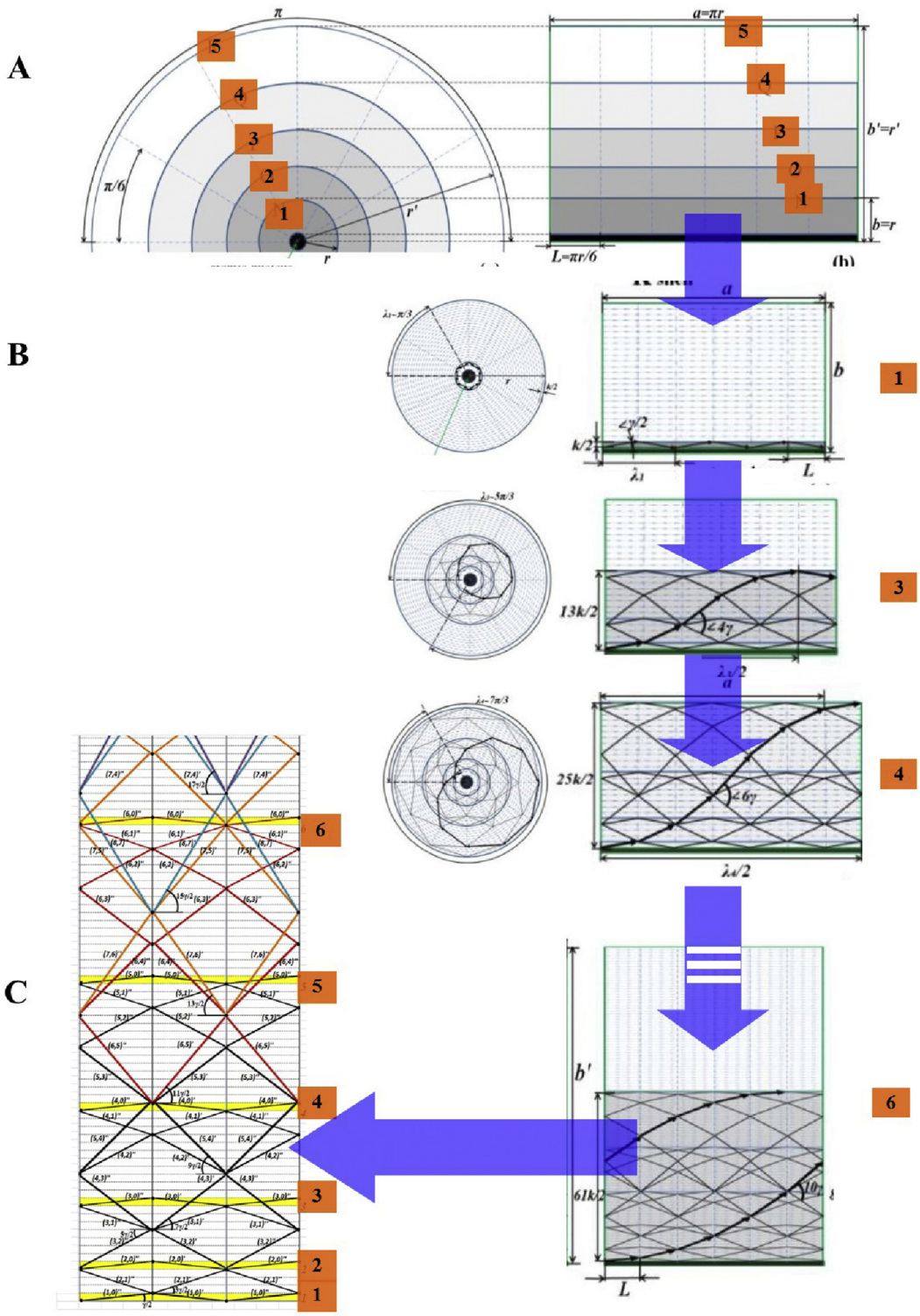

Fig. 1. Geometric model of atomic shells. Angles and energetic levels are calculated based on the movements of electrons in different orbits. Fig. 1A, **left**: five energetic levels are displayed as rotations on a circle: the lowest energy, close to the circle center, is numbered with 1, the highest with 5. Fig. 1A, **right**: the five circular orbits can be mapped onto a horizontal tape. Fig. 1B: the electronic movements on every energetic level can be depicted as wavy trajectories extended along the horizontal tape. Trajectories intersect, forming angles γ that vary according to ray inclination. The right and the left parts of Fig. 1B display views from different angulations. Fig. 1C, **right side**, displays the trajectories of a further, not shown level, the sixth one. Fig. 1C, **left side** illustrates a 2D geometrical picture of the 6-level atomic system, standing for the first six completely filled atomic shells. (Yurkin, 2017; modified).

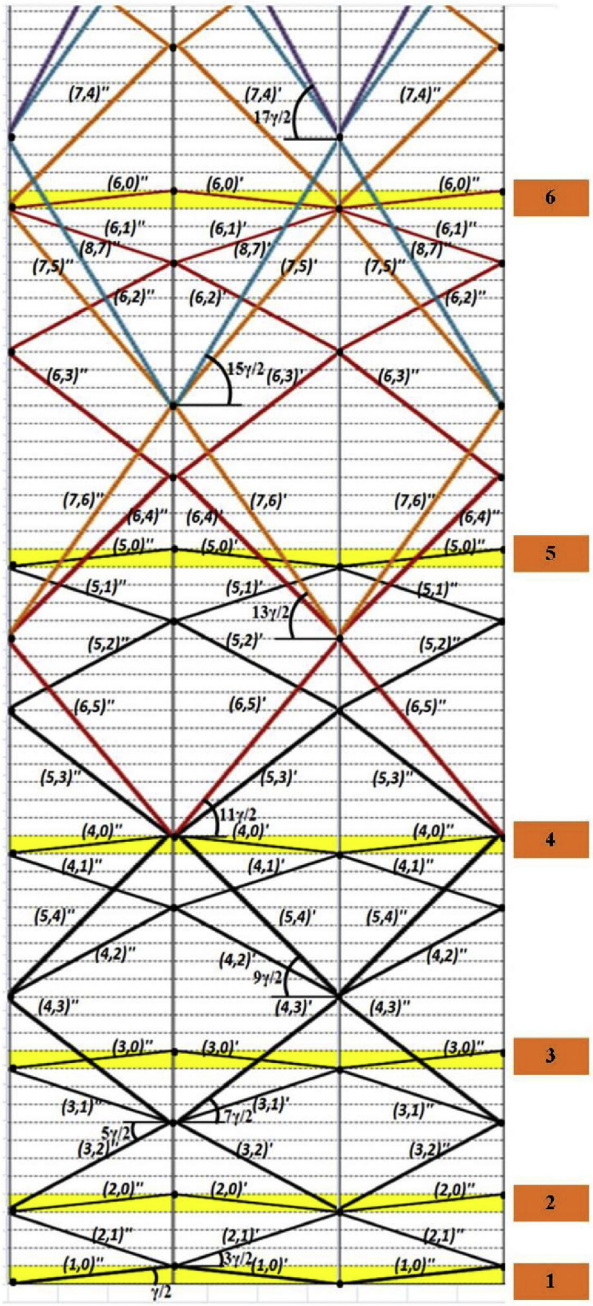

Fig. 2. Images of wavy trajectories of the first six completely filled atom shells and an of multilevel quantum system. To make an example, the first shell, termed with the squared number 1, consists of links inclined on angles $\gamma/2$ to an horizontal axis. The length of every line connecting two nodes stands for the average energy within two neighbor passes. Indeed, the energy $\boldsymbol{E}(\boldsymbol{n},\boldsymbol{l})'$ and $\boldsymbol{E}(\boldsymbol{n},\boldsymbol{l})''$ extending along these links is characterized by the numbers$\boldsymbol{n}=1$ and $\boldsymbol{l}=0$. The second shell, termed with the squared number 2, consists of links inclined on angles $\frac{\gamma}{2}$ and $\frac{3\gamma}{2}$ to a horizontal, while the energy $\boldsymbol{E}(\boldsymbol{n},\boldsymbol{l})'$ and $\boldsymbol{E}(\boldsymbol{n},\boldsymbol{l})''$ is characterized by the numbers $\boldsymbol{n}=1,2$ and $\boldsymbol{l}=0,1$.

required angles) and n and l (that describe the required energetic levels), stand for four physical quantum numbers such as systems of optical solitons. Nevertheless, the four parameters might stand for other systems' features too, according to the specific requirements of the phenomenon under evaluation. In the accompanying paper, we already raised the possibility to describe cellular metabolic paths in terms of angles and polygonal sides endowed in the Yurkin's geometric grid. In particular, we provided the example of second messengers (cAMP) and their correlated energetic pathways. Here we will make available other examples of physical and biological systems that can be described in terms of the geometrical Yurkin's grid. Furthermore, we will discuss its invaluable advantages in terms of the possibility to assess hidden interlevel system's correlations.

2.1. Timescales of protein folding

Our geometrical model is able to assess not just static "spatial" systems equipped with intertwined multi-levels of energy, but also the "temporal" energetic and entropic evolution of natural phenomena. In such a vein, every process described by Fokker-Planck equations, e.g., random processes that dissipate energy, may be located in a geometric grid which allows their easier assessment. The possibility to compare various angles and paths on the same grid allows us to evaluate the presence of unexpected correlations among features lying on different systems' energetic levels. In protein folding, for instance, if we equip every folding phase with the proper geometrical level, we could be able, by evaluating the current state in terms of angles and rays, to achieve information about the previous and future states.

The key to understanding the concepts of free-energy, entropy and funnelling in the mechanisms of protein folding lies in the well-known suggestion that an energetic gap occurs in their fitness landscape, between a well-defined global minimum state and a dynamic transitional one, which simulates the system's behaviour before it settles into the global minimum, *i.e.*, fixed-point attractors endowed by the landscape. Amidst the valleys and peaks, larger variations in energy gap lead to huge, deep funnels, which inexorably draw the protein folding activities to themselves, in long timescales (Tozzi et al., 2016a,b). The different timescales occurring in protein folding processes give rise to constrained functional outcomes, conditioned only by long time-scale statistics. Thus, the importance of topology in a protein context lies in the different timescales. Fig. 3 depicts the process of protein folding in terms of energy landscape theory, translated to our geometrical grids. The required values of *m* and *s* and *n* and l might stand, in this context, for the parameters that give rise to protein folding, depicted on the *x*, *y*, and *z* axes of Fig. 3A.

2.2. The physiological underpinning of human disease

The geometrical grid, when applied to biochemical paths occurring in our cellular assembly, or to whole body images, of to histological pictures of human normal and pathological samples, allows us to predict the real values in every point of the grid. A perturbation, *e.g.*, a disease, occurring in one of the points can be geometrically evaluated in terms of grid deformations that lead to local and global changes is angles and paths. The knowledge of the "normal", physiological geometrical grid of metabolic paths allows us to understand and predict where deformations might occur during pathological events. To make an example, if we detect a local grid deformation according with the shape of the geodetic curves, such as, e.g., a metastasis of unknown source, we could be able, by assessing the changes occurred in other parts of the grid, to understand where the primary source of the tumor is located (see Fig. 4). In other words, if we accurately know the angles and paths of the normal grid, we could be able to find hidden injuries, by just looking at a secondary alteration in another place of the grid.

2.3. Assessing brain oscillations

Brain electric activity displays a mean action potential rate of 4 Hz (Sengupta et al., 2013a,b), which is just a mean value

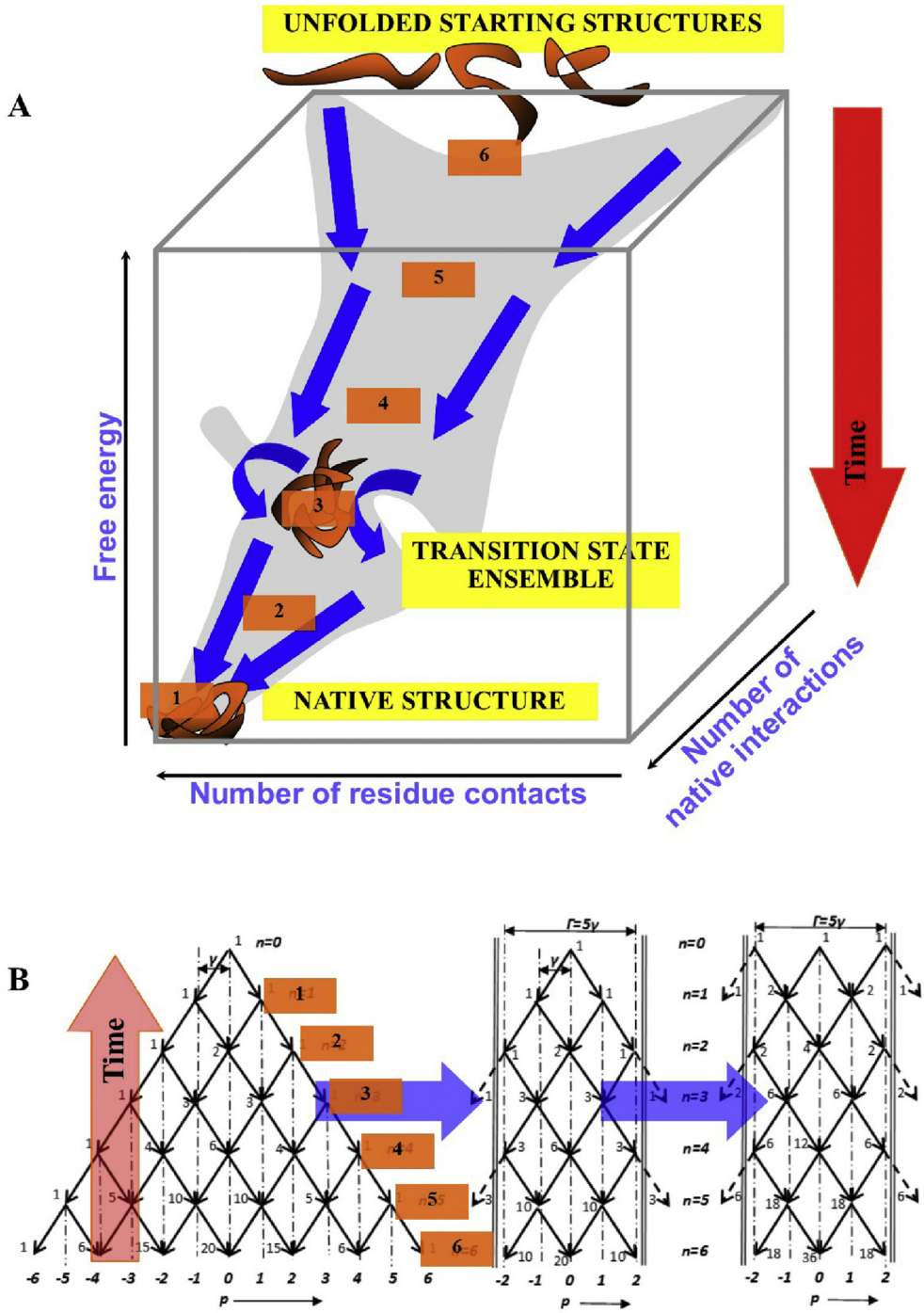

Fig. 3. Protein folding framed in the context o the energy landscape theory. Fig. 3A represents the folding sequence as equipped with a funnelling mechanism dictated by long timescales. (Modified from Tozzi et al., 2016a,b). Fig. 3B depicts regular, non-chaotic branching trajectories (of the first binomial type) of the energetic landscape depicted in Fig. 3A inside a neuronal network.

accounting for the diverse timescales of nervous activity. The coexistence of very low-frequencies (<2 Hz) and high frequencies (>10) is well established in neuroscientific studies (Buzsaki and Watson, 2012). It has been proposed that the different timescales are associated with unrelated functional activities (Raichle, 2010; de Arcangelis and Herrmann, 2010; de Pasquale and Marzetti, 2014). To make an example, it has been argued that the: a) anatomical, b) functional and c) psychological correlates of the very slow cortical potentials are respectively: a) the spontaneous brain activity (Raichle, 2010), b) the default mode networks and c) the unconstrained, conscious cognition (i.e. mind-wandering or day dreaming propensities) (Andrews-Hanna et al., 2014; Kucyi and Davis, 2014) or the dreaming state (Fox et al., 2015). It has been suggested that spontaneous low-frequency cerebral fluctuations are a neuronal activity that is intrinsically generated by the brain (Fox and Raichle, 2007). On the other hand, during stimuli-evoked activity or cognitive demands, the brain transitorily exhibits other functional conformations, linked with specific psychological correlates (Cole et al., 2014). For example, the brain high frequency activity has been associated with perceptual binding and feedback/

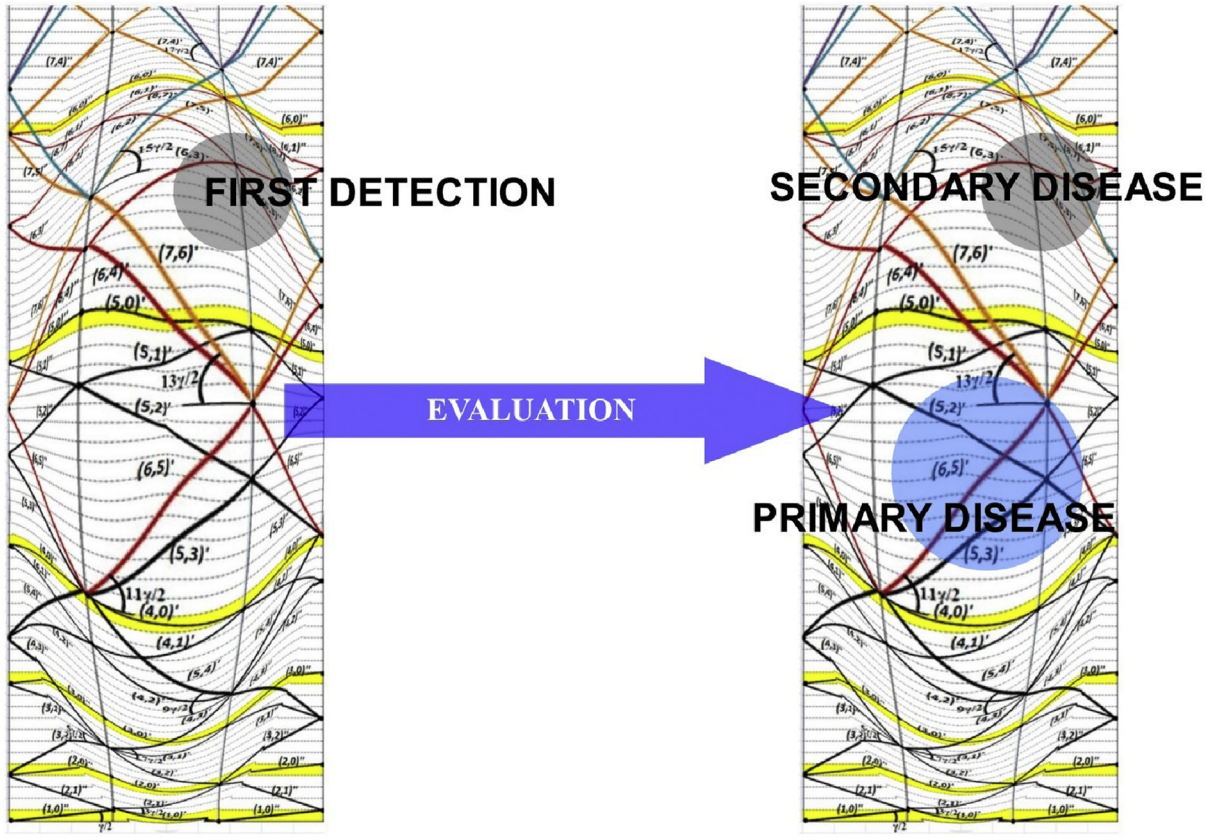

Fig. 4. Illustrating wavy trajectories of a multilevel cellular pathway, equipped with six increasing energetic levels. As always, the lower energetic level is placed at the bottom, the higher at the top. When an external force acts on the system (**left side**), a grid deformation according with the shape of the geodetic curves occurs, so that the angles γ and the energy lines are modified. The system's broken homeostasis, e.g., the grid deformation, is transmitted to other areas. The right part of the Figure shows how it is possible, starting from the initial detected perturbation, to derivate the primitive deformation.

feedforward waves able to improve the perception of external inputs (Buzsaki and Watson, 2012).

Given that the (environmental and internal) inputs provoke changes in spike frequency in diverse cortical areas, the brain exhibits a high number of possible source configurations, such as gamma oscillations in somatomotor cortex during states of enhanced vigilance, or alpha waves in posterior zones with eyes open, and so on (Bastos et al., 2014). Here we ask whether our geometrical model is able to detect hypothetical correlations between the functionally heterogeneous frequencies, and evaluate whether it is true that, when one changes, also the other modifies. Can the vast repertoire of brain electric spikes with different frequencies be evaluated in geometrical terms?

In order to build the proper grid, we need to start from the brain's energy requirements in different functional states. Evoked activity (i.e. perceptual and motor activity, task performance and similar cognitive functions), requires an additional energy consumption of ~5%, as compared with spontaneous activity. This is due to the local increases in spike frequency (in particular beta and gamma waves) that occur during evoked activity. The increased spike frequency during evoked activity has a significant metabolic cost, specifically 6.5 μmol/ATP/gr/min for each additional spike, with an ATP consumption higher than the "typical" mean rate at 4 Hz (which is 3.29×10^9 molecules of ATP/neuron/sec) (Attwell and Laughlin, 2001; Sengupta et al., 2013a,b). This led Tozzi et al. (2016a,b) to argue that the spontaneous brain activity consumes an amount of energy lower than the evoked activity. Indeed, each spike is equipped with an oscillation, characterized by two parameters: amplitude and frequency. For the Ohm's law, energy consumption due to the AMPLITUDE of the oscillation is negligible as compared with energy consumption due to the FREQUENCY of the oscillation. That means that evoked activity, equipped with a mean frequency of spikes higher than spontaneous activity, expends more energy. The higher the spike frequency, the higher the energetic level. This statement allows us to analyze brain spike frequencies in terms of a Yurkin's multilevel grid, where the lowest frequencies (<2) stand for the level 1 and the gamma spikes stand for the highest level (that in Fig. 5, is the level 6).

The amount of energy E can be calculated through the above mentioned ATP consumption for every spike. Other required parameters, such as m and s and n and l, might stand for different possible brain features, such as, to make an example, the spike orientation in the brain (feed-forward or feed-back), the trains of synchronized spikes of the same frequency, phase opposition, hierarchical or not hierarchical features, the interaction strength among the single neural nodes, and so on and so on (Fig. 6).

When encompassed in the proper geometrical grid, the different brain oscillations clearly exhibit correlations and energetic relationships, illustrated by angles' and side lengths'inter-levels matching descriptions. Indeed, a geometrical view of the brain spikes allows us to assess different frequencies in algebraic terms of homotopies and affine connections. Embracing brain spikes in the framework of geometry and topology (Dodson and Parker, 1997; Tozzi and Peters, 2016) means that biological brain timescales can be described as functions on grids: this perspective permits the nervous oscillations located in the "real" space (the 3D brain) to be

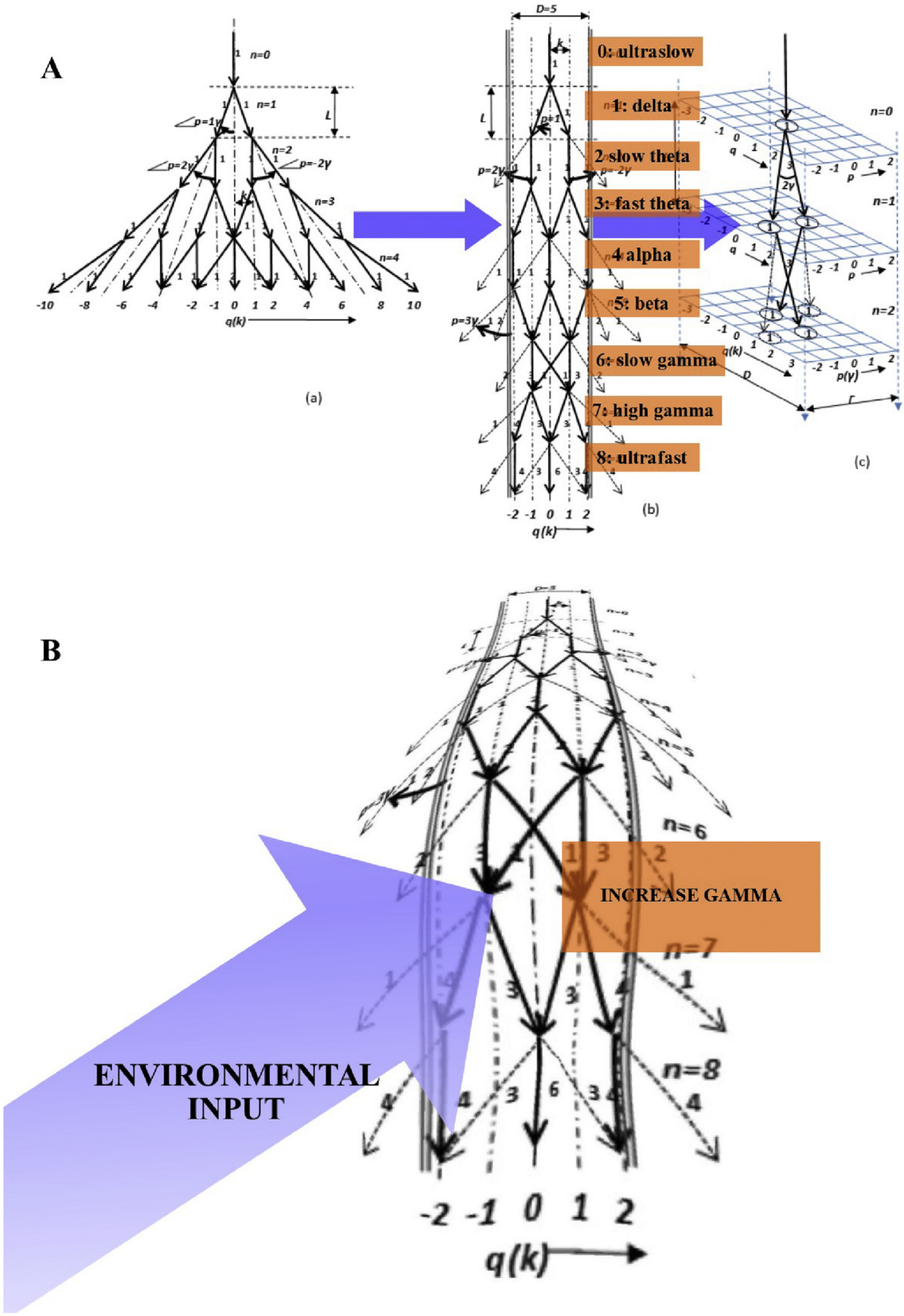

Fig. 5. Regular, non-chaotic and branching trajectories inside a neuronal network. The Figure displays neural trajectories of the second binomial type. Each neuron could connect with one, or two, or many other neurons. The hypothetical Fig. 5B depict what happens when an environmental input activates the higher brain frequencies. A grid deformation according with the shape of the geodetic curves takes place, starting from the higher frequencies, and extending to the lower frequencies in a predictable, testable and assessable way.

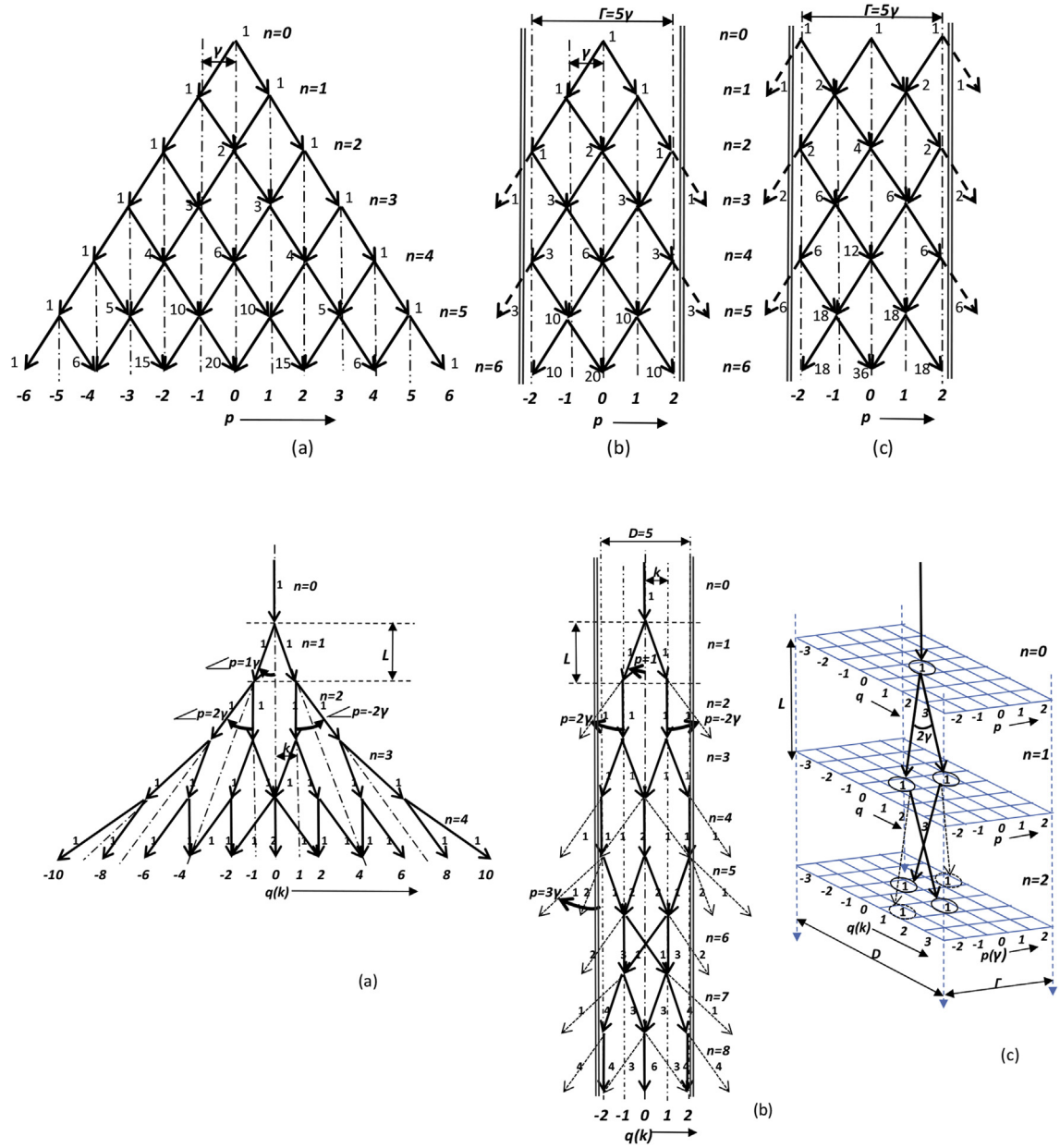

Fig. 6. Not chaotic, regular branching trajectories inside a neuronal network. **The upper part** illustrates neural trajectories of the first binomial type. **The lower part** displays neural trajectories of the second binomial type. Each neuron could connect with one, or two, or many other neurons.

translated to "abstract" spaces and *vice-versa,* enabling us to achieve maps from one level to another that allow the comparison of otherwise hidden features.

One of the main concerns in neuroscience is to try to understand how brain oscillations, frequencies and amplitudes are correlated. By inserting every range of spike frequencies in a different level of our geometric grid, we could be able to detect their hidden correlations, described by matching angles and the same paths lengths. To make a practical example, we could be able to study what happens to frequencies when just one of them is activated (Fig. 5B). It is well-established that perception is linked with trains of gamma and beta frequencies. In turn, gamma and beta frequencies, in our framework, stand for deformations in the higher energetic levels in the grid. In this case, for a more accurate description of real processes, we use geodetic curves, rather than straight lines.

Because we know the geometric relationships among the different spike frequencies at rest, we may be able to understand how the lower grid levels (i.e., the lower brain frequencies) respond to deformations in the higher levels (i.e., the task-related activation of the higher brain frequencies).

3. Conclusion

The ideal point of rest, about which the life of the organism moves in constant oscillations, has also a mathematical-logical significance when framed as a geometrical theory. Yurkin's approach allows us the possibility to compare various angles and paths on the same grid to evaluate the presence of unexpected correlations among features lying on different systems' energetic levels. If we equip every system with the proper geometrical level, we might be able, by evaluating the current state in terms of angles and rays, to achieve information about the previous and future

states. In particular, Yurkin's approach shows that spikes of different frequencies are correlated in the brain, because they display regular, comparable features and relationships. By knowing the values of a few grid points, the other ones can be detected and measured on other zones of the grid, because geometry provides a feasible way to link their reciprocal activities. Therefore, a theory from an apparent far-flung branch, the geometry, might help us to improve our knowledge of biomolecular and physiological phenomena, as well as the different nervous oscillations' relationships.

It could be asked whether a specific geometry of biological systems is feasible, and whether is it possible to cogently describe the cell based on very few first principles as geometry does. In this paper, we try to do that, and we even go further. By paraphrasing the influential paper from Wigner (1960), we highlight the "unreasonable power of mathematics in biology". Indeed, mathematical geometrical concepts turn up in entirely unexpected connections in the study of cellular function: they permit a surprisingly close and accurate description of biological phenomena in these connections. Indeed, in spite of the baffling complexity of the cell, geometry allows the discovery and the description of certain biological regularities and astonishing invariants properties that can be formulated in terms of accurate mathematical concepts.

We have showed in the accompanying paper and in this Addendum how gauge theories and geometry may play a sovereign role in the cellular affairs, so that the laws of a homeostatic living being can also be formulated directly in the language of mathematics, which seems to be the most universal language of science. Life does not abhor mathematical description, but demands the exploration of new biomathematical conceptualizations more congenial to biological complexity than the formal tools developed in the last two centuries. In the present work, starting from a top-down mathematical approach, we may be able to assess the apparently irreconcilable physical and biological coins of the cell without any reductionism. In sum, paraphrasing Wigner once again, we do not know why geometry works so well, but its accuracy seems to override the concerns about its truth and consistency.

Acknowledgements

To Raquel del Moral for her help in the preparation of this manuscript.

References

Andrews-Hanna, J.R., Smallwood, J., Spreng, R.N., 2014 May. The default network and self-generated thought: component processes, dynamic control, and clinical relevance. Ann. N. Y. Acad. Sci. 1316, 29–52. http://dx.doi.org/10.1111/nyas.12360. Epub 2014 Feb 6.

Attwell, D., Laughlin, S.B., 2001. An energy budget for signaling in the grey matter of the brain. J. Cereb. Blood Flow Metabolism 21 (10), 1133–1145.

Bastos, A.M., Briggs, F., Alitto, H.J., Mangun, G.R., Usrey, W.M., 2014 May 28. Simultaneous recordings from the primary visual cortex and lateral geniculate nucleus reveal rhythmic interactions and a cortical source for gamma-band oscillations. J. Neurosci. 34 (22), 7639–7644. http://dx.doi.org/10.1523/JNEUROSCI.4216-13.2014.

Bühler, W. Gauss, 1981. A Bibliographical Study. Springer-Verlag, N.Y. (chapter 9).

Buzsaki, G., Watson, B.O., 2012. Brain rhythms and neural syntax: implications for efficient coding of cognitive content and neuropsychiatric disease. Dialogues Clin. Neurosci. 14, 345–367.

Cole, M.W., Bassett, D.S., Power, J.D., Braver, T.S., Petersen, S.E., 2014 Jul 2. Intrinsic and task-evoked network architectures of the human brain. Neuron 83 (1), 238–251. http://dx.doi.org/10.1016/j.neuron.2014.05.014.

de Arcangelis, L., Herrmann, H.J., 2010. Learning as a phenomenon occurring in a critical state. Proc. Natl. Acad. Sci. 107, 3977–3981.

de Pasquale, F., Marzetti, L., 2014. Temporal and spectral signatures of the default mode network. Magnetoencephalography 451–476.

Dodson, C.T.J., Parker, P.E., 1997. A User's Guide to Algebraic Topology. Kluwer, Dordrecht, Netherlands xii+405 pp. ISBN: 0-7923-4292-5, MR1430097.

Fox, M.D., Raichle, M.E., 2007. Spontaneous fluctuations in brain activity observed with functional magnetic resonance imaging. Nat. Rev. Neurosci. 8, 700–711.

Fox, K.C.R., Spreng, R.N., Ellamil, M., Andrews-Hanna, J.R., Christoff, K., 2015 May 1. The wandering brain: meta-analysis of functional neuroimaging studies of mind-wandering and related spontaneous thought processes. Neuroimage 111, 611–621. http://dx.doi.org/10.1016/j.neuroimage.2015.02.039.

Frankel, T., 2016. The Geometry of Physics. An Introduction, third ed. Cambridge University Press, Cambridge,United Kingdom.

Kucyi, A., Davis, K.D., 15 October 2014. Dynamic Functional Connectivity of the Default Mode Network Tracks Daydreaming ?, vol. 100, pp. 471–480. http://dx.doi.org/10.1016/j.neuroimage.2014.06.044.

Peters, J.F., 18 Nov 2016. Two forms of proximal physical geometry. Axioms, sewing regions together, classes of regions, duality, and parallel fiber bundles. Adv. Math. Sci. J. 5 (2), 241–268. Preprint in arXiv:1608.06208v4 [math.GN].

Peters, J.F., 2017a. Foundations of Computer Vision. Computational Geometry, Visual Image Structures and Object Shape Recognition. Springer Int. Pub, AG. http://dx.doi.org/10.1007/978-3-319-52483-2.

Peters, J.F., 2017b. Proximal nerve complexes. arXiv 1841 A Comput. Topol. approach (1440), 1–16.

Raichle, M.E., 2010 Apr. Two views of brain function. Tre nds Cogn. Sci. 14 (4), 180–190. http://dx.doi.org/10.1016/j.tics.2010.01.008. Epub 2010 Mar 4.

Sengupta, B., Stemmler, M.B., Friston, K.J., 2013a. Information and efficiency in the nervous system–a synthesis. PLoS Comput Biol. 9 (7), e1003157. http://dx.doi.org/10.1371/journal.pcbi.1003157.

Sengupta, B., et al., 2013b. Balanced excitatory and inhibitory synaptic currents promote efficient coding and metabolic efficiency. PLoS Comput. Biol. 9, e1003263.

Tozzi, A., Peters, J.F., 2016. A topological approach unveils system invariances and broken symmetries in the brain. J. Neurosci. Res. 94 (5), 351–365. http://dx.doi.org/10.1002/jnr.23720.

Tozzi, A., Zare, M., Benasich, A.A., 2016a. New perspectives on spontaneous brain activity: dynamic networks and energy matter. Front. Hum. Neurosci. http://dx.doi.org/10.3389/fnhum.2016.00247.

Tozzi, A., Fla Tor, Peters, J.F., 2016b. Building a minimum frustration framework for brain functions in long timescales. J. Neurosci. Res. 94 (8), 702–716. http://dx.doi.org/10.1002/jnr.23748.

Wigner, E., 1960. The unreasonable effectiveness of mathematics in the natural sciences. In: Communications in Pure and Applied Mathematics, vol. 13. John Wiley & Sons, Inc, New York. No. I.

Yurkin, A.V., 2015. Symmetric Triangle of Pascal and Arithmetic Parallelepiped. On Possibility of New Evident Geometrical Interpretation of Processes in Long Pipes. Lambert Academic Publishing. ISBN: 978-3-659-38411-0 (ISBN: 978-3-8443-2275-0.

Yurkin, A.V., 2016. On descriptive geometrical interpretation of the principle of Pauli, elements of the table of Mendeleyev and the Newtonian laminar current of liquid. Prog. Phys. 12 (3), 149–169. April-July.

Yurkin, A.V., 2017. New, binomial model of atom, trajectories and schemes of energy of splitting levels of atom. IOSR J. Eng. (IOSRJEN) 07 (02), 19–31.

AUTHOR QUERY FORM

ELSEVIER	**Journal:** PLREV **Article Number:** 858	**Please e-mail your responses and any corrections to:** **E-mail:** corrections.esch@elsevier.vtex.lt

Dear Author,

Please check your proof carefully and mark all corrections at the appropriate place in the proof (e.g., by using on-screen annotation in the PDF file) or compile them in a separate list. Note: if you opt to annotate the file with software other than Adobe Reader then please also highlight the appropriate place in the PDF file. To ensure fast publication of your paper please return your corrections within 48 hours.

For correction or revision of any artwork, please consult *http://www.elsevier.com/artworkinstructions*

Any queries or remarks that have arisen during the processing of your manuscript are listed below and highlighted by flags in the proof. Click on the 'Q' link to go to the location in the proof.

Location in article	Query / Remark: click on the Q link to go Please insert your reply or correction at the corresponding line in the proof
Q1	Please confirm that the correct format of title has been used, in accordance with the format specified in the submission procedure in EES. (p. 1/ line 9)
Q2	The author names have been tagged as given names and surnames (surnames are highlighted in teal color). Please confirm if they have been identified correctly. (p. 1/ line 11)
Q3	Fig. 3 will appear in black and white in print and in color on the web. The caption of this figure contains references to color or the colors are mentioned in the main text. Based on this, the respective figure caption has been updated. Please check, and correct if necessary. (p. 4/ line 40)
Q4, Q5, Q6, Q7, Q8, Q9	If available, please complete and update the reference(s) given here: [69,72,79,108,112,113]. (p. 19/ line 27,31,41; p. 20/ line 26,32,34)
Q10	Page range in Ref. [81] was corrected. Please check and correct if necessary. (p. 19/ line 43)
	Please check this box if you have no corrections to make to the PDF file ☐

Thank you for your assistance.

Available online at www.sciencedirect.com

ScienceDirect

Physics of Life Reviews ••• (••••) •••–•••

PHYSICS of LIFE reviews

www.elsevier.com/locate/plrev

Review

Topodynamics of metastable brains

Arturo Tozzi [a,*], James F. Peters [b,c], Andrew A. Fingelkurts [d], Alexander A. Fingelkurts [d], Pedro C. Marijuán [e]

[a] *Center for Nonlinear Science, University of North Texas, 1155 Union Circle, #311427, Denton, TX 76203-5017, USA*
[b] *Department of Electrical and Computer Engineering, University of Manitoba, 75A Chancellor's Circle Winnipeg, MB R3T 5V6 Canada*
[c] *Department of Mathematics, Adıyaman University, 02040 Adıyaman, Turkey*
[d] *BM-Science – Brain and Mind Technologies Research Centre, Espoo, Finland*
[e] *Bioinformation Group, Aragon Institute of Health Science (IACS), Aragon Health Research Institute (IIS Aragon), Zaragoza, 50009 Spain*

Received 28 December 2016; received in revised form 11 January 2017; accepted 22 March 2017

Communicated by L. Perlovsky

Abstract

The brain displays both the anatomical features of a vast amount of interconnected topological mappings as well as the functional features of a nonlinear, metastable system at the edge of chaos, equipped with a phase space where mental random walks tend towards lower energetic basins. Nevertheless, with the exception of some advanced neuro-anatomic descriptions and present-day connectomic research, very few studies have been addressing the topological path of a brain embedded or embodied in its external and internal environment. Herein, by using new formal tools derived from algebraic topology, we provide an account of the metastable brain, based on the neuro-scientific model of Operational Architectonics of brain–mind functioning. We introduce a "topodynamic" description that shows how the relationships among the countless intertwined spatio-temporal levels of brain functioning can be assessed in terms of projections and mappings that take place on abstract structures, equipped with different dimensions, curvatures and energetic constraints. Such a topodynamical approach, apart from providing a biologically plausible model of brain function that can be operationalized, is also able to tackle the issue of a long-standing dichotomy: it throws indeed a bridge between the subjective, immediate datum of the naïve complex of sensations and mentations and the objective, quantitative, data extracted from experimental neuro-scientific procedures. Importantly, it opens the door to a series of new predictions and future directions of advancement for neuroscientific research.
© 2017 Elsevier B.V. All rights reserved.

Keywords: Topology; Borsuk–Ulam theorem; Nonlinear dynamics; Central nervous system; Mind

Abbreviations: BUT, Borsuk–Ulam theorem; FPT, fixed point theorem; IPST, internal physical space–time; OA, operational Architectonics; OM, operational module; OST, operational space–time; PST, phenomenal space–time; RTP, rapid transitive period.

* Corresponding author.
E-mail addresses: tozziarturo@libero.it (A. Tozzi), James.Peters3@umanitoba.ca (J.F. Peters), andrew.fingelkurts@bm-science.com (A.A. Fingelkurts), alexander.fingelkurts@bm-science.com (A.A. Fingelkurts), pcmarijuan.iacs@aragon.es (P.C. Marijuán).

http://dx.doi.org/10.1016/j.plrev.2017.03.001
1571-0645/© 2017 Elsevier B.V. All rights reserved.

UNCORRECTED PROOF

This research did not receive any specific grant from funding agencies in the public, commercial, or not-for-profit sectors.

0. Introduction

Over the last several decades, there has been an explosive development of new theories regarding brain and mind functioning as well as new powerful techniques that facilitate innovative experimental studies (see for example, [1–3]. However, none of these theories exploits in an *explicit* way the actual physical (brain) and subjective (mind) *operations* the human brain–mind performs in the course of behavior. The recently proposed Operational Architectonics (OA) framework of brain–mind functioning [4–10], by contrast to other theories, sets out with the explicit aim to describe, measure and model the brain and mind operations involved in the development of the most complex human behaviors, as governed by the brain. It is self-evident that both brain and mind functioning have intertwined temporal structure defined by their respective operations [11–13], where metastable changes of brain spatiotemporal patterns are isomorphic with cognitive and phenomenal levels [8,10].

This paper aims to throw a bridge between the above-mentioned OA model and the far-flung branch of algebraic topology. Indeed, topology, in assessing the properties that are preserved through deformation, stretching and twisting of objects, is an underrated methodological approach with countless possible applications [14–18]. In particular, the Borsuk–Ulam theorem (BUT), cast in a quantitative fashion which has the potential of being operationalized, stands for a universal principle underlying a number of natural phenomena [19]. BUT states that, if a single point on a circumference projects to a higher spatial dimension, it gives rise to two antipodal points with matching descriptions, and vice versa (Fig. 1A) [20–23]. Points on a sphere are *antipodal*, provided they are diametrically opposite [24], such as, for example, the poles of a sphere. This means, e.g., that there exist on the earth's surface at least two antipodal points with the same temperature and pressure. BUT looks like a translucent glass sphere between a light source and our eyes: we watch two lights on the sphere surface instead of one. But the two lights are not just imagined, they are also real with observable properties, such as intensity and diameter. This means that two antipodal points can be described at one level of observation, while relative to just a single point at a lower level [18,25]. Here we will show that BUT and its recently developed variants allow the assessment of brain functioning in terms of affinities and projections from real spaces to abstract ones.

This paper comprises four sections. The first section introduces the model of Operational Architectonics that considers the brain as a metastable system, thus placing the brain in the broader framework of dynamical systems theory. The second section illustrates, in plain terms accessible for a broader audience, the topological apparatus able to quantitatively describe the activity and function of the metastable brain. In particular, we will go through novel variants of the above mentioned BUT. The third, crucial, section throws a bridge between the two first parts, assessing the activities of the brain operational architectonics in terms of algebraic topology. We termed this novel approach "*brain topodynamics*". In the fourth section, we mention several predictions and new research directions that follow from the OA/topological framework. This section aims also to answer the most important question: in the context of OA, what does such topodynamical approach bring to the table, with respect to both conceptual and operational points of view? What new predictions can be established and what new research directions might be followed?

1. Brain metastability and brain–mind operational architectonics model

Recently a novel paradigm in relation to the brain–mind functioning is beginning to emerge—it stresses the dynamic balance between isolated functions of local neuronal assemblies and globally coordinated activity among them [8,12,13]. In this new view, the potential multivariability of the neuronal assemblies and their larger conglomerates (networks) appears to be far from continuous in time, but confined by the dynamics of short-term local and global *metastable* brain states [26]. As it has been proposed, metastability is an entirely new conception of brain functioning, where the individual parts of the brain exhibit tendencies to function autonomously at the same time as they exhibit tendencies for coordinated activity [11,26–28]. Specifically, *metastability* (when the system's degrees of freedom are restricted) is circumstantial for the interaction among the elementary neuronal systems (neuronal assemblies) in order to generate adaptive behavior within changing and not fully predictable environments: "By synchronizing the stable microstates of the 'microscopic variables' during certain periods, the neuronal systems (neuronal assemblies) have the possibility for interactive information exchange of the essential variables, which are important for the acceptance and

UNCORRECTED PROOF

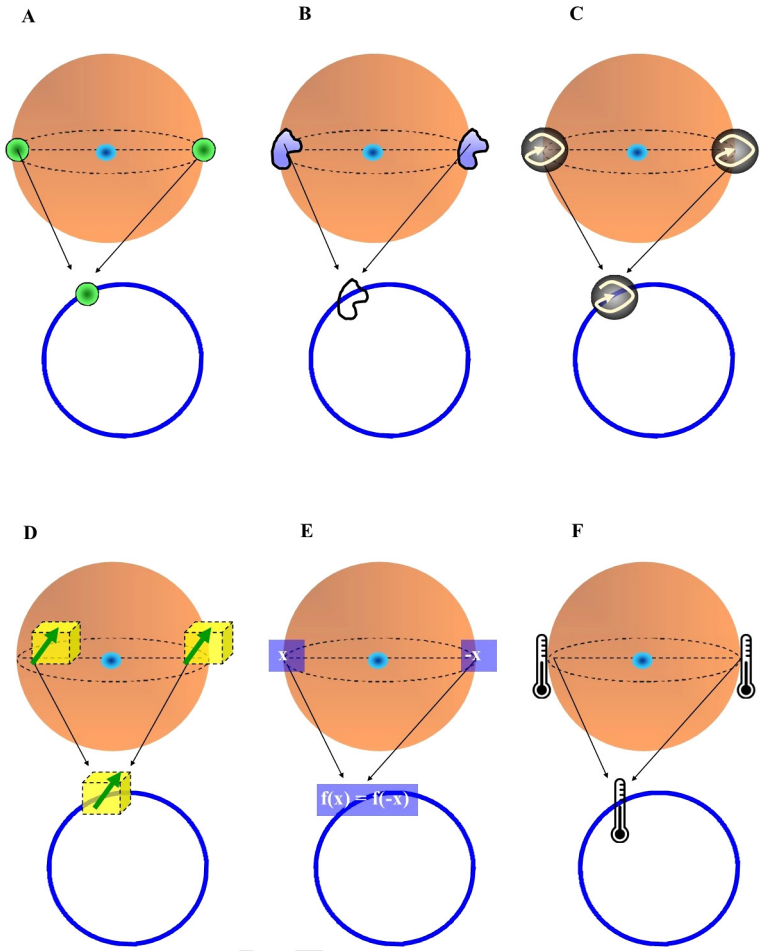

Fig. 1. Possible types of antipodal features in Borsuk–Ulam theorem (BUT). The original formulation of BUT, with two antipodal points, is illustrated in Fig. 1A. Figs. 1B–1F display, respectively, two antipodal shapes, trajectories, vectors, functions and temperatures. Each set of antipodal features on a sphere stands for a single feature on a circumference, if we evaluate it just one dimension lower.

expression of 'consensual decision' that is appropriate for the functional requirements engendered by each successive stage of behavioral/cognitive/mental performance" (p. 851 in Ref. [26]). In the metastable regime of brain functioning [26,28], the interplay of these two tendencies (autonomy and integration) represents the coexistence of a complementary and not antagonistic pair [29,30]. Thus, metastability in the brain refers to competition of complementary tendencies of cooperative integration and autonomous fragmentation among many distributed neuronal assemblies [11,26,28,31]. Importantly, metastability explicitly refers to transient, nonstationary processes; and in this respect it differs from synergetics [32], where the main principle is to compress the effective number of degrees of freedom in complex systems to a few "order parameters" or variables that adequately approximate system dynamics at large scales [33].

The metastability phenomenon in the brain is most clearly expressed and best observed at the level of an *electromagnetic field* which is highly nested, self-organized and structured in temporal and spatial domains [4,7,9,26]. Such a brain field is manifested as the interplay of multiple local oscillatory waves accessible through local electroencephalographic (EEG) measurements [7,34–36]. In that regard: What could be a model of brain–mind functioning especially well suited for studies of the nonstationary structure of the EEG field and which is uniquely capable of assessing the dynamic and metastable changes of brain spatial-temporal patterns that are isomorphic with cognitive and phenomenal levels [8,10]? Essentially this model should take repetitions of spatial-temporal patterns of brain field into account at all functional levels, thus capturing both dynamic as well as hierarchical complexities of brain activity nested within a multi-scale operational architecture [9]. In a series of publications, Fingelkurts and Fingelkurts [4–7]

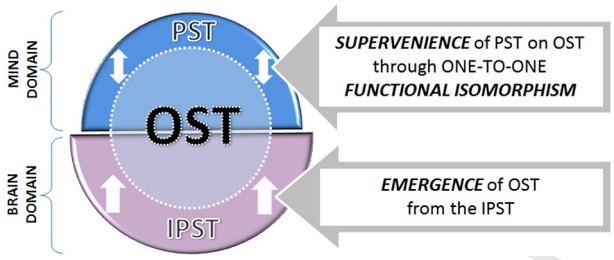

Fig. 2. Phenomenal, operational and physical levels of the brain–mind organization and their relation to emergentism and supervenience. Electromagnetic brain field constituting the OST level is the emergent property of brain itself (IPST level). The phenomenal level (PST) supervenes on the operational level (OST) and is functionally isomorphic to it. IPST indicates the *internal physical space–time* of the brain (violet color); OST indicates the *operational space–time* of the brain (indicated by white puncture line); PST indicates the *phenomenal space–time* of consciousness (blue color). In this model the OST level represents the constitutive mechanism of phenomenal consciousness; it ties the phenomenal (subjective) and neurophysiological (physical) levels together. (For interpretation of the references to color in this figure legend, the reader is referred to the web version of this article.)

have proposed the Operational Architectonics (OA) framework of brain–mind functioning centered around the notion of *operation* that satisfies these requirements. The notion of 'operation' has been chosen as the center of this OA theory of brain–mind functioning due to several reasons: it is a process lasting in time, present in both brain and mind functioning, and it has combinatorial nature (increasing complexity). All these features make 'operation' especially well suited for understanding and studying the mechanisms of how a conscious mind emerges from the physical brain (for a more detailed discussion see [8–10].

According to a general theory of brain–mind OA [4–10], the simplest mental/cognitive operations (responsible for elemental qualia or simple computations) are presented in the brain in the form of local 3D-fields produced by transient functional neuronal assemblies, while complex mental/cognitive operations (responsible for complex objects, images or thoughts) are brought into existence by joining a number of simple operations (temporal coupling of local 3D-fields by means of *operational synchrony*, OS) in the form of so-called *operational modules* (OM) of varied complexity and life-span. Therefore, brain OA is presented as a highly structured and dynamic extracellular electric field nested in spatial and temporal domains and spanning over a range of frequencies, thus forming a particular *operational space–time* (OST) in the brain [9] (Fig. 2). What is curious about the OST level of brain organization is that it intervenes between brain *internal physical space–time* (IPST) level where it literally resides, and the experiential/subjective phenomenal structure of a mind (*phenomenal space–time*, PST) to which it is isomorphic [9]. In this way, the OST level (i) has emergent properties relatively independent from the neurophysiological/neuroanatomical properties of the IPST level, and (ii) has a one-to-one correspondence with phenomenal (PST) level that supervenes on, and is ontologically inseparable from, the operational (OST) level (Fig. 2). The OST exists within brain internal physical space–time (IPST) and is best captured by the EEG measurement [4,6,7,9,10].

At the EEG level, simple mental operations (phenomenal qualities, primary cognitive operations and emotions) are equivalent to the EEG quasi-stationary segments (within which the local fields generated by transient functional neuronal assemblies are expressed) [4,8,9]. The quasi-stationary EEG segments within each local EEG signal are marked by boundaries in the form of *rapid transitional processes/periods* (RTPs) (Fig. 3, upper panel), which could be observed within a short-time window, within which EEG amplitude changes abruptly [6]. In comparison to the length of quasi-stationary segments, each RTP has a very short duration and can therefore be treated as a point or near-point [4,6]. The transition from one segment to another, then, reflects the moment of abrupt switching from one neuronal assembly's operation to another (Fig. 3, upper panel). Physically one could interpret such a transition as the offloading of entropy and the emergence of a new structure of the system (new neuronal assembly) [10]; see also [37,38]. In the physics literature, the events similar to RTPs are referred to as renewal (or critical) events [39,40]: namely, the events that reset the memory of the system [41]. This property is in fact a mathematical definition of a well-known physical phenomenon of "intermittency" and is compatible with self-organized criticality found both in physical systems [42,43] and in the brain [44–49]. Recently, it has been documented that RTPs in EEG are indeed "crucial events" [50,51].

Since the beginning and end of discrete operations performed by local neuronal assemblies are marked by sharp changes (RTPs) in the amplitude of local EEG signals, the simultaneous occurrence of such RTPs from different local

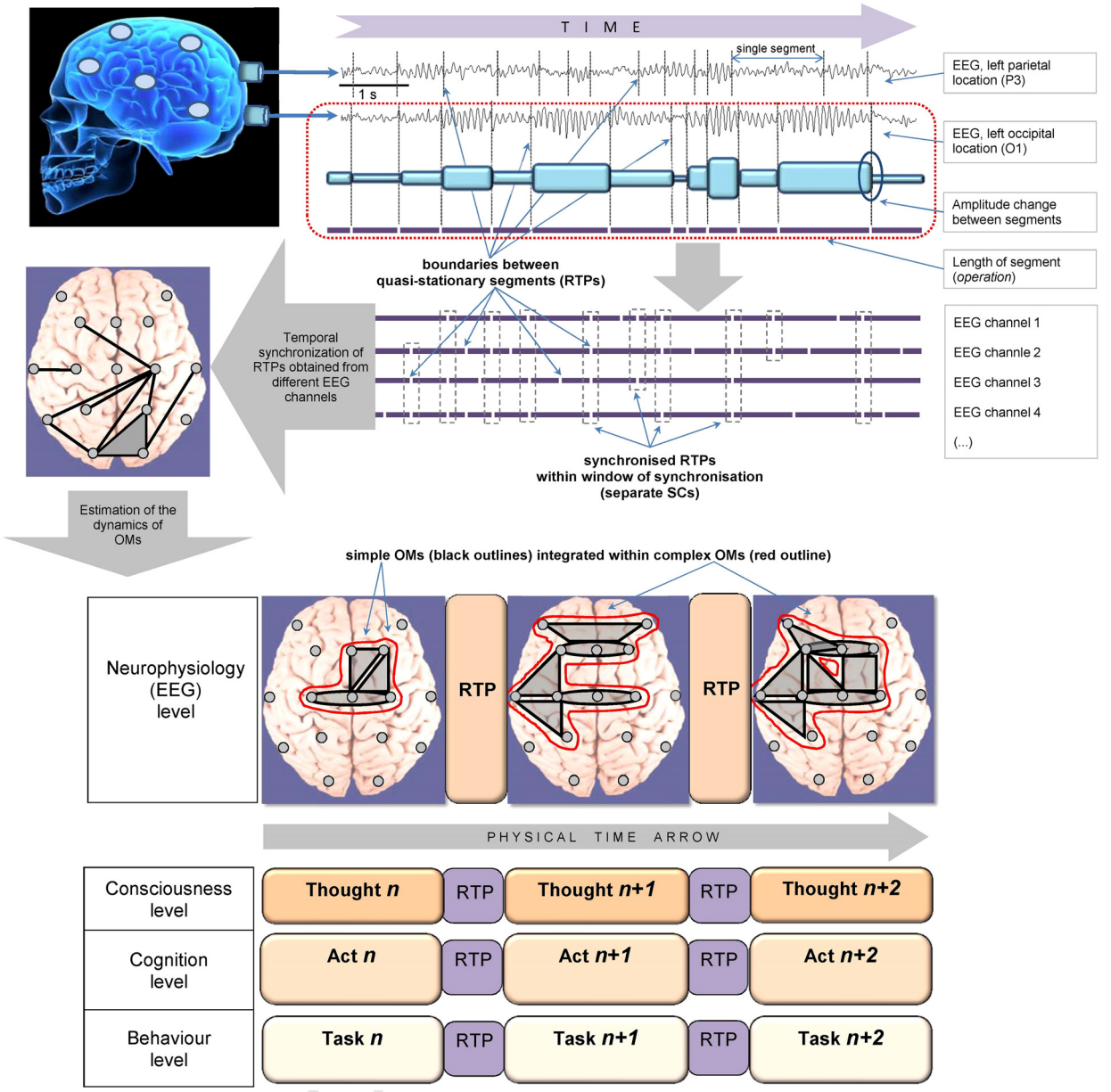

Fig. 3. Schematic illustration of EEG assessment of (a) neuronal assembly's dynamics and relation of this dynamics to simple operations and (b) large-scale conglomerates of synchronized neuronal assemblies in the form of operational modules (OMs) and their relation to a stream of complex operations or cognitive/conscious acts. Explanations are in the text. RTP – rapid transitional period (boundary between quasi-stationary EEG segments within the same local EEG signal); SC – synchrocomplex – momentary synchronization of RTPs among several local EEG signals within short temporal window of synchronization; Gray shapes illustrate individual OMs; Red line illustrates complex OMs. Low panel represents schematically the functional structures of phenomenological consciousness, cognition and behavior that functionally isomorphic with the structure of electrophysiological level. As an example, the simplest case is shown, when cognitive, phenomenal and behavioral operations/acts coincide in time (in most cases these relations are more complex). Cognitive, phenomenological, and behavioral levels illustrate the ever-changing stream of cognitive/phenomenal/behavioral acts, where each momentarily stable pattern is a particular cognitive/phenomenal/behavioral macro-operation (thought/image/act) separated by transitive fringes (or Rapid Transitional Periods; RTPs). (For interpretation of the references to color in this figure, the reader is referred to the web version of this article.)

EEG signals within the multichannel EEG recording could provide evidence of synchronization of simple operations performed by neuronal assemblies (located in different brain areas) that participate in the same functional act as a

group (Fig. 3, middle panel), e.g., executing a particular complex operation responsible for a subjective presentation of complex objects, scenes, concepts or thoughts [4,8–10]. Thus, the complex mental operations are reflected at the EEG level in the transitory spatiotemporal patterns formed by synchronized quasi-stationary segments separated by the RTPs, giving rise then to a completely new level of brain abstractness – *metastable brain states* [26] – which have been called *operational modules* (OM) [4,6,52] (Fig. 3, bottom panel). The OMs are metastable because of intrinsic differences in the activity between neuronal assemblies, which constitute every OM, each doing its own job while at the same time still retaining a tendency to be coordinated together within the same OM in order to execute the macro-operation [9].

Such a structure of the OM suggests that both *parallel* and *serial* processing may be just two sides of the same single underlying mechanism—synchrony of operations performed by neuronal assemblies. Parallel processing is executed by individual neuronal assemblies, while serial processing emerges as a result of the formation of OMs and their changes along with shifts in the process of actualization of objects in the physical or the mental world [5]. In this way, computationally, OMs have both classical, connectionist, and process architectures. For example, they resemble connectionist networks [53], since they may serve as associative, content-addressable memories, and they are distributed across many neural assemblies. Yet, the specific spatial-temporal patterns (OMs) per se are unitary, like symbols in classical logics [54]. And yet, each OM is a process, since it lasts as long as several operations that have particular continuity in time (and which are produced by different neuronal assemblies) are synchronized among each other during a given temporal interval [9].

In the OA model, the stream of phenomenological consciousness [55] expressed as the succession of complex cognitive operations, phenomenal images or thoughts is presented by the succession of discrete and relatively stable OMs, which are separated by rapid transitive periods (RTPs), i.e. abrupt changes of OMs (Fig. 3, bottom panel). Empirical evidence indicates [56–61] that at the critical point of transition in a mental state, e.g., during changes from one mental task/thought to another, the OM indeed undergoes a profound and rapid reconfiguration. In terms of the critical theory of physics [62–65] within the RTP between two consequent Oms, there is a biphasic process [10]: a brief episode when the drastic and abrupt increase in degrees of freedom among participating neuronal assemblies is accompanied by a sudden increase in entropy, information level and dimensionality, followed by a quick episode of reduction in the degrees of freedom of neuronal assemblies and rapid decrease in entropy, information level and dimensionality when the self-organization of a new presentational state emerges in the form of a new OM within the brain OST [9,10].

2. The topological approach: variants of the Borsuk–Ulam theorem

As stated in the Introduction, an advanced topological interpretation of the OA model might be based on new extensions of the Borsuk–Ulam Theorem (BUT). The concept of antipodal points (see Fig. 1) can be generalized to countless types of system signals, by introducing novel BUT variants that are region-based. A pair of opposite points can be used not just for the description of simple topological points, but also of lines, or perimeters, areas (Fig. 1B), regions, spatial patterns, images, temporal patterns, movements, paths, particle trajectories (Fig. 1C) [66–69], vectors (Fig. 1D), tensors, functions (Fig. 1E), algorithms, parameters, groups, range of data, symbols, signs, thermodynamic parameters (Fig. 1F), or, in general, *signals*. If we simply evaluate general nervous activity instead of 'signals' BUT leads naturally to the possibility of a region-based, not simply point-based, brain geometry. For instance, a brain region assessed through fMRI can have features such as area, diameter, average signal value, entropy and so on. One is thus allowed to describe brain functional and/or anatomical features in terms of antipodal points on a sphere [18,70]. It is noteworthy that BUT allows also the evaluation of the energetic nervous requirements. Indeed, there exists a physical link between the two spheres of different dimensions and their energetic features [69]. When two antipodal functions on a higher-dimensional structure project to a lower-dimensional structure, a single function is achieved [71,27]. This means that the single mapping function on the lower-dimensional structure displays values of energy parameters lower than the sum of two corresponding antipodal functions on the higher-dimensional structure (Fig. 1F). Therefore, in a metastable brain formed by structures with different dimensions, a decrease in dimensions gives rise to a decrease in energy. In such a way, a metastable brain/mind is achieved, in which the energetic changes do not depend anymore on thermodynamic parameters, but rather on affine connections, homotopies and continuous functions. An example is provided by a recent paper, where BUT allows the detection of Bayesian Kullback–Leibler divergence during unsure perception [71].

UNCORRECTED PROOF

Please cite this article in press as: Tozzi A, et al. Topodynamics of metastable brains. Phys Life Rev (2017), http://dx.doi.org/10.1016/j.plrev.2017.03.001

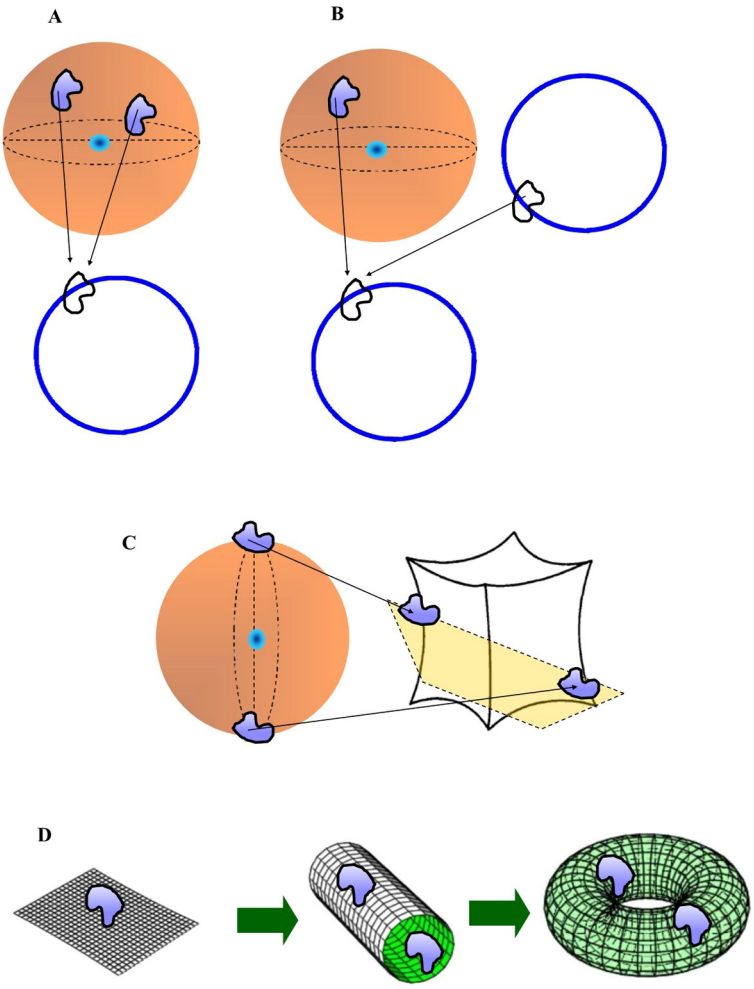

Fig. 4. Two features with signal matching do not need necessarily to be antipodal. Indeed, the applications of BUT can be generalized also on non-antipodal points on the same sphere (Fig. 4A), of non-antipodal points lying on two different structures (Fig. 4B). Figs. 4C and 4D show how BUT applies for structures with different types of curvatures.

Descriptively similar points and regions do not need necessarily to be opposite (antipodal), or embedded on the same structure (Figs. 4A and 4B) [18,19]. Thereafter, the applications of BUT can be generalized also for non-antipodal neighboring points (and/or regions) on a sphere. In effect, it is possible to evaluate matching signals, even if they are not exactly "opposite" each other. As a result, the antipodal point's restriction from the "standard" BUT is no longer needed, and one can also consider regions that are either adjacent or far apart. This BUT variant applies, provided there is a pair of regions on the sphere with the same feature value. We are thus allowed to say that the two points (or regions, or whatsoever) do not need necessarily to be antipodal, in order to be labeled together [18]. In brain terms, this means, for example, that two regions on the cortical surface with the same entropy values can be assessed together.

The original formulation of BUT describes the presence of antipodal points on spatial manifolds in every dimension, provided the manifold is a convex, positive-curvature structure (i.e., a ball). However, many brain functions are believed to occur on functional hyperbolic manifolds in the guise of a saddle, i.e., equipped with negative-curvature and concave shape. Therefore, it makes sense to look for antipodal points also on structures equipped with curvatures other than the convex one (Fig. 4C) [73]. Whether a system structure displays a concave, convex or flat appearance, does not matter: we may always find the points with matching descriptions predicted by BUT [71]. A single, planar

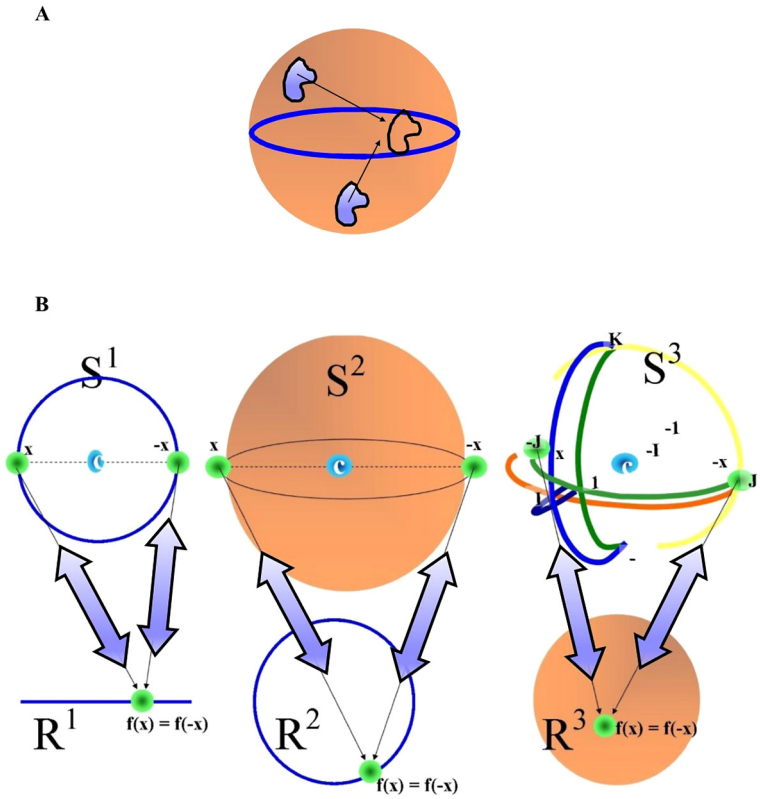

Fig. 5. A. The figure shows how a sphere may map on itself. Fig. 5B. The way BUT acts on structures of different dimensions is displayed: a 2-D circle, a 3-D sphere and a 4-D hypersphere. A symmetry, e.g., two antipodal points in higher dimensions, is said to be "broken" when it maps to a single point in one dimension lower. Note that the mapping is reversible from higher to lower dimensions, and vice versa (double-sided arrows).

description can be projected to higher dimensional donut-like structures (Fig. 4D), so that a torus stands for the most general structure which permits the description of matching points. For further details, see [71,74].

Although BUT has been originally described just in case of n being a natural number which expresses a structure embedded in a spatial dimension, nevertheless n can also stand for other types of numbers, when assessing the brain sphere. BUT can be used not just for the description of "spatial" dimensions equipped with natural numbers, but also for antipodal regions on brain spheres equipped with other kinds of dimensions, such as a temporal or a fractal one. This means, e.g., that a spherical structure can be made not just of space, but also of time. The dimension n might stand not just for a natural number, but also for an integer, a rational, an irrational or an imaginary one [71]. For example, n may stand for a fractal dimension, which is generally expressed by a rational number. This makes it possible for us to use the n parameter as a versatile tool for the description of systems' features.

Furthermore, matching points (or regions) might project to lower dimensions on the same structure (Fig. 5A). A sphere may map on itself: the projection of two antipodal points to a single point into a dimension lower can be internal to the same sphere. In this case, matching descriptions are assessed at one dimension of observation, while single descriptions come into play at a lower one, and vice versa. Such correlations are based on mappings, e.g., projections from one dimension to another. In many applications (for example, in fractal systems), we do not need the Euclidean space (the ball) at all: a system may display an intrinsic, *internal* point of view, and does not need to lie in any dimensional space [70]. Therefore, we may think that such a system just does exist by – and on – itself.

The BUT approach emphasizes the foremost role of symmetries in the evaluation of a metastable brain. Symmetries are real invariances that underline the world and occur at every level of systems' organization [74,75]. Bilinear forms of geometrical structures manifest symmetrical properties [76]. In other words, affine structures preserve parallel relationships. Symmetries are general structures of mathematical, physical and biological entities and provide a very broad approach, explaining also how network communities integrate or segregate information. It must be emphasized that symmetries are widespread and may be regarded as the most general feature of systems, perhaps more general

UNCORRECTED

than free-energy and entropy constraints too. Indeed, recent data suggest that thermodynamic requirements have close relationships with symmetries. The interesting observation that entropy production is strictly correlated with symmetry breaking in quasi-static processes paves the way to use system invariances for the estimation of both the free energy of metastable states, and the energy requirements of computations and information processing [77]. Thus, giving insights into symmetries provides a very general approach to every kind of systems function. A symmetry break occurs when the symmetry is present at one level of observation, but "hidden" at another level. A symmetry break is detectable at a lower dimension of observation (Fig. 5B).

Thereafter, we can state that single descriptions are broken (or hidden) symmetries, while matching descriptions are restored symmetries. In other words, a symmetry can be hidden at the lower dimension and restored when going one dimension higher. If we assess just single descriptions, we cannot see their matching descriptions: when we evaluate instead systems one dimension higher, we are able to see their hidden symmetries. This also means, that, going from a lower to a higher level of assessment, we find more information [74]: indeed, to make an example, a three-dimensional image encompasses more information than a two-dimensional one. In sum, symmetries, single and matching descriptions stand for the common language able to describe the metastable brain: BUT and its ingredients can be modified in different guises, in order to assess a wide range of brain functions. Although this field is nearly novel and still in progress, such a methodological approach has been already proved useful in the evaluation of brain symmetries, which allow us to assess the relationships, affinities and shape-deformations among BOLD activated areas [71]. Additionally, BUT has been used in the evaluation of cortical histological images previously treated with Voronoï tessellation [78,79]. The utilization of BUT presented here (see Section 3) upon the most comprehensive and neurobiologically plausible model of brain–mind functioning, e.g., the OA, shows yet another useful application of topological approaches in neuroscience.

3. Topodynamics of the brain–mind operational architectonics

In this section, we will integrate the OA model with the mathematical framework of BUT and its variants. In particular, we will focus on the two levels of OA described in Section 1:

i. the low level of brain–mind operational architectonics, which deals with the formation of transient neuronal assemblies and their dynamics delimited by RTPs in relation to simple mind operations (subsections 3.1, 3.2); and
ii. the high level of brain–mind operational architectonics, which deals with the formation of OMs through the synchronized operations of multiple transient neuronal assemblies in relation to complex mind operations, and their dynamics delimited by RTPs in relation to stream of consciousness (subsections 3.3, 3.4).

Along the discussion, we will also show how the real formalism for the description of BUT reinterpretations of the OA model can even reveal new insights not apparent from the neurophysiological standpoint by itself.

3.1. Nonlinear dynamics in brain–mind phenomenology

The transient neuronal assemblies and metastable OMs defined in Section 1 can be described in terms of abstract objects, and therefore assessed through the novel BUT variants described in Section 2. Indeed, BUT makes it possible to evaluate metastable brain dynamics in terms of projections from real to abstract phase spaces. Therefore, the nonlinear brain dynamics occurring during cognition and mentation can be assessed through more manageable linear techniques, in particular through projections and mappings. Indeed, BUT makes it possible for us to evaluate formally nonlinear brain dynamics, which occur during metastable cognition and consciousness, though in much simpler linear manner [71,80]. In brief, nonlinear dynamics are frequently studied through logistic maps equipped with Hopf bifurcations, where intervals are dictated by Feigenbaum constants. Tozzi and Peters [71] introduced an approach that offers a linear explanation of nervous nonlinearity and Hopf bifurcations, in terms of algebraic topology. Hopf bifurcation transformations (the antipodal points) can be described as paths or trajectories on abstract spheres embedded in dimensions that stand for the Feigenbaum constant's irrational number [81,82].

Isolated functions of local neuronal assemblies can be described in terms of abstract trajectories taking place on lower-dimensional structures, while globally coordinated activity among local neuronal assemblies stand for two

UNCORRECTED PROOF

Please cite this article in press as: Tozzi A, et al. Topodynamics of metastable brains. Phys Life Rev (2017), http://dx.doi.org/10.1016/j.plrev.2017.03.001

(or more) trajectories with matching description taking place on higher-dimensional structures. Note that the term "dimension" does not stand here for a spatial one. In this case, we are assessing a "functional" dimension which describes the degree of complexity: the more dimensions, the more complexity and information. Therefore, going from lower to higher complexity dimensions, we achieve an increase in matching, superimposed cortical patterns. Such a dimensional topological approach makes it possible to quantify the attractive but elusive phenomenological account of the mind, in terms of cognitive neuroscientific operational and experimental terms. According to phenomenalists, every human individual originally accepts over her/him a) an ever-changing spatial environment composed of manifold parts dependent on one another; b) other human individuals making manifold describable statements and c) these statements are dependent upon the environment [83,84]. When an individual becomes aware of some of the manifold parts of the environment outside or inside her/him, she/he states 'she/he is having an experience'. In a topological framework, the environment, the cortical layers and the describable statements can be embedded in different structures of various complexity dimensions, encompassing a different qualitative content and linked by projections. The object and its verbal counterpart stand for two antipodal points, while their matching description is achieved in the brain of the concrete human individual. It is noteworthy that the topological relationships among such three entities do not exist outside the triad: we cannot perceive the thoughts and the sensations of other people, but just project to them thoughts, statements and sensations analogous to ours. Subjective experiences relate to the environment just in the sense that the environment is able to modify the brain activity; thus, more accurately, they do not directly relate to the environment, but rather to complex brain activity variations.

In topological terms, the potential multi-variability of neuronal assemblies and their larger conglomerates is generated by the reciprocal mappings between lower-dimensional, short-term, local, metastable brain states and higher-dimensional, global ones. The topological concepts of mappings and projections helps us to assess metastability, if we take into account that lower-dimensional individual components of the brain/mind exhibit tendencies both to work autonomously, and to produce higher-dimensional, coordinated activity (equipped with matching descriptions). The concept of "projections" helps in elucidating a long-standing issue in science, namely, the cause-and-effect issue in the framework of OA. Current scientific experience is grounded on the tenets of causality, e.g., the relation between two processes where the first, the cause, is assumed to be responsible for the second, the effect. It is believed that the brain infers the causes underlying sensory events [85], or, in other words, is able to understand the causes when just the effects are known. This inferencing is not limited to conscious and high-level cognition, but it is also performed continually and effortlessly in unconscious perception [86].

We argue that, if we evaluate different spatial and temporal neural phenomena in the light of the "sameness" and projections instead of causality, we achieve a novel view of brain events, in touch with OA model. Inference is replaced by affine connections and mappings: to make an example, perceived shapes map into others, such as a coffee cup maps to a torus. This is in touch with philosophers [87] and scientists [88,89] who believe that inference is just a trick of the mind, i.e., the cause–effect relationships do not exist, being merely apparent correlations among events dictated by our natural, evolutionary instinct of mental association among conjoined events. In Hume's words, we tend to believe that things behave in a regular manner to the extent that behavior patterns of objects seem to persist into the future, and throughout the unobserved present. Chicharro and Ledberg [90] noticed that, because subsystems in the brain are often bidirectionally connected [91,92], this means that interactions rarely should be quantified in terms of cause-and-effect.

3.2. Metastability and emergence of topodynamic properties

The interaction among elementary, lower-dimensional neuronal systems, e.g., the neuronal assemblies, permits a synchronization of the stable microstates that takes place just in a higher dimension of complexity. This means that neuronal assemblies give rise to interactive information exchange of the essential variables, when projected to the higher-dimensional 'consensual decision' that is appropriate for each successive stage of behavioral/cognitive/mental performance (as specified in [26]). As we have already discussed in the Section 1, in the metastable regime of brain functioning, the interdimensional mapping between the two tendencies of autonomous fragmentation and cooperative integration among many distributed neuronal assemblies represents the coexistence of complementary, and not antagonistic, pairs [29,30]. Therefore, a topological concept of metastability may refer to transient, non-stationary processes where complexity increases in higher dimensions, leading to an "enlargement" of shared information. Note that, contrary to the synergetic approach mentioned above, which "compresses" and "squeezes" the effective num-

UNCORRECTED PROOF

Please cite this article in press as: Tozzi A, et al. Topodynamics of metastable brains. Phys Life Rev (2017), http://dx.doi.org/10.1016/j.plrev.2017.03.001

ber of degrees of freedom to a few order parameters, our topological metastable approach "dilutes" and "scatters" the message, when going from lower to higher dimensions. Because increasing complexity accrues from antipodal points with matching description, trajectories embedded in lower dimensions display a decrease in the number of dimensions, and therefore of information, compared with the same trajectories embedded in higher dimensions [72]. In sum, in a topological fashion, repetitions of spatial-temporal brain patterns stand for trajectories that, although starting from very simple lower-dimensional nested components, nevertheless are able to capture higher-dimensional cortical dynamics as well as hierarchical complexities of brain activity.

OA and topological projection share important features: they are processes persisting over time, they are present in both brain and mind functioning, and they have a combinatorial nature. In Section 1, we stated that revealing the nonstationary structure of EEG field stands for the proper technique able to assess the dynamic changes of brain spatial-temporal patterns in a way that is isomorphic with cognitive and phenomenal levels [8–10]. The term *isomorphic*, in topological terms, does not refer to a one-to-one correspondence, but rather to a correspondence that is doubled in the higher level. The OA framework is centered around the notion of "operation" [4–6]. This apparently vague concept can be better assessed and quantified in topological terms, because operations become here simple projections and mappings among abstract manifolds. According to OA, the simplest mental/cognitive operations are presented in the brain in the form of lower-dimensional local fields produced by transient functional neuronal assemblies, while complex mental/cognitive operations are brought into existence by joining the simple operations in the form of the higher-dimensional OMs considering BUT principles [71].

Topology gives an unexpected substantiation to the concept of the OST level of brain organization [8–10] that is intervening between the IPST level where it literally resides, and the PST to which it is isomorphic. Indeed, the OA theory states that the OST level a) displays emergent properties independent from the IPST level's neuro-physiological and neuro-anatomical properties, and b) has a one-to-one correspondence with PST level that supervenes on, and ontologically inseparable from the OST level. This relationship is well elucidated in terms of BUT and its variants (Fig. 6). As stated above, the only notable difference between OST and a topological framework is that the last does not display a one-to-one correspondence, but a one-to-two correspondence.

According to the OA theory, simple mental operations are equivalent to EEG quasi-stationary segments, the latter standing for the local fields generated by transient functional neuronal assemblies (Fig. 6). Such quasi-stationary segments are marked by boundaries within each local EEG, in the form of sharp RTPs [4,6]. Further, each RTP has a very short duration and can therefore be treated as a point or near-point, in guise of the points described by the classical BUT [20]. Note that BUT requires a function to be continuous, while the transition from one EEG segment to another reflects the moment of abrupt switching from one neuronal assembly's operation to another, and therefore is characterized by a transient loss of continuity [4,6]. Such apparent discrepancy is easily explained (Fig. 6, lower part). When, due to a change in environmental inputs, the continuity of a single perceived event is lost, a RTP occurs, and the phenomenal counterpart of this event vanishes in the brain/mind. In this brief instant, BUT does not hold anymore, and the inter-dimensional projections are temporarily lost. The continuity can be restored by a following incoming event, in order that novel, different matching projections are produced in the operational modules. Such a loss of continuity elucidates also the issue of the renewal process [41], which states that the temporary loss of projections resets the memory of the system.

3.3. Symmetry breaking, entropy, and information

In terms of physical critical theory and symmetries, according to OA theory a biphasic process within the RTP between two consequent OMs takes place [10]. A brief episode, characterized by a drastic and abrupt increase in symmetries and degrees of freedom among the participating neuronal assemblies, is accompanied by a sudden increase in entropy, information and dimensionality. This process is followed by quick episodes of symmetry breaks and reduction in the degrees of freedom of neuronal assemblies and rapid decrease in entropy, information and dimensionality [10]. The energetic variant of BUT comes into help in bringing more understand of these processes, because it states that, given a value of entropy in a lower dimension, it is twofold when projected in a higher dimension [25,69,74]. Godel's suggestion of abstract terms more and more converging to the infinity in the sphere of our understanding take us straight to a comparison with systems equipped with BUT antipodal points and regions. In terms of BUT, we achieve a progressive symmetry increase: starting from the symmetries endowed in the environment, we accomplish their substantial increase into the brain/mind [71].

UNCORRECTED PROOF

Please cite this article in press as: Tozzi A, et al. Topodynamics of metastable brains. Phys Life Rev (2017), http://dx.doi.org/10.1016/j.plrev.2017.03.001

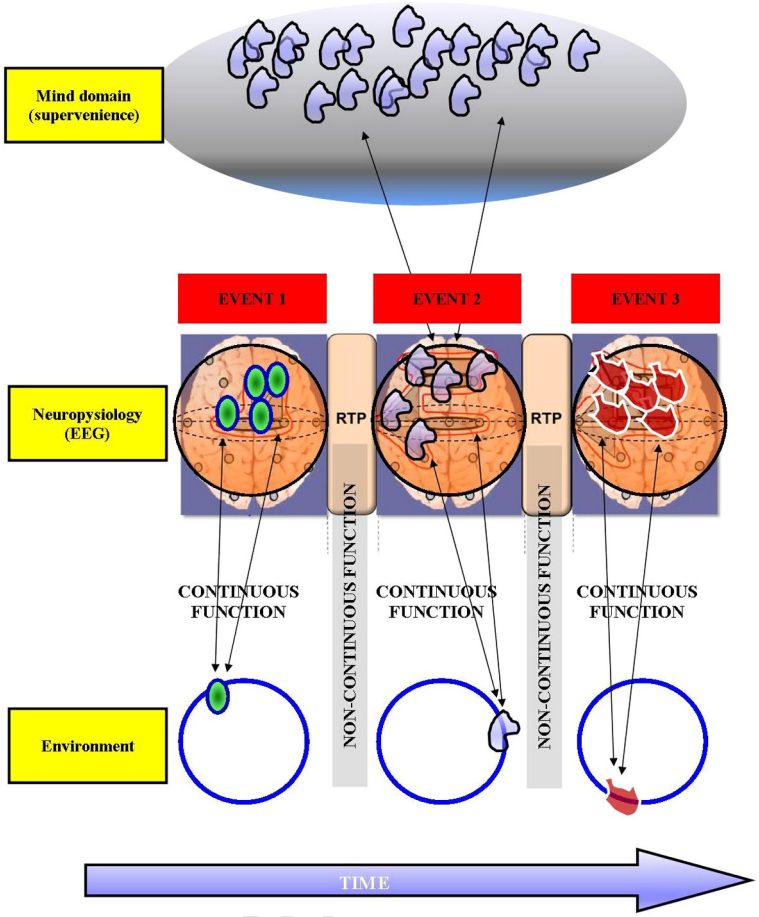

Fig. 6. Topological description of operational modules. We accomplish a composite multi-dimensional system in which each local constituent exhibits close projective relationships with the others. **In the lower part of Figure**, different events (1, 2 and 3) occurring in the surrounding environment (in which the individual's brain/mind is embedded/embodied) stand for different functions (depicted by different shapes). Such shapes, when projected in the brain operational modules described by EEG traces, give rise to matching descriptions. Note that, despite BUT requires a continuous function, the continuity is lost, due to a change in the environmental input from event 1 to event 2, and then to event 3. In this case, a RTP occurs and the preceding event in a sequence vanishes. The continuity is then restored by the following event, and novel matching projections occur in the operational modules. **Middle part of the Figure**: if we just consider OA synchronization of neural assemblies in terms of matching descriptions that correlate (through pairwise entropy) spatially remote neurophysiological events, we achieve a novel description of operational modules. **The upper part of the Figure** displays a topological description of the higher levels of the brain–mind organization. Note that the displayed circles and spheres do not stand for different spatial dimensions, but for different abstract dimensions of increasing complexity.

The OA model is not anatomical, rather it is about the structure and dynamics of the electromagnetic field. Electromagnetic fields can be evaluated, through a topological approach, in the general terms of particle trajectories taking place on donut-like manifolds. Indeed, the OA model can be described in the guise of multi-dimensional tori, projecting and mapping among levels which display different spatio-temporal features. As stated above, in the evaluation of OA activities at every spatio-temporal scale, we are allowed to assess antipodal *regions* instead of antipodal *points* [17,93]. BUT provides a way to evaluate changes of information among different anatomical and functional brain levels in a topological space, which is distinguished from purely functional or thermodynamical perspectives.

In the context of BUT we could name any brain location (with a particular neuronal assembly) a *worldsheet*, if all surrounding neuronal assemblies of its sub-regions contain at least one brain activity modeled as a string that describes a path followed by a moving particle. The term *cortical worldsheet* designates a region of the brain space completely covered by nervous activities [68] (Fig. 7). A 2D plane worldsheet can be rolled up to form the lateral surface of a 3D cylinder, termed a *worldsheet cylinder* [93]. Further, a *cortical* worldsheet cylinder maps to a *cortical worldsheet torus*, formed by bending the former until the ends meet. In sum, such a flattened worldsheet maps to a worldsheet

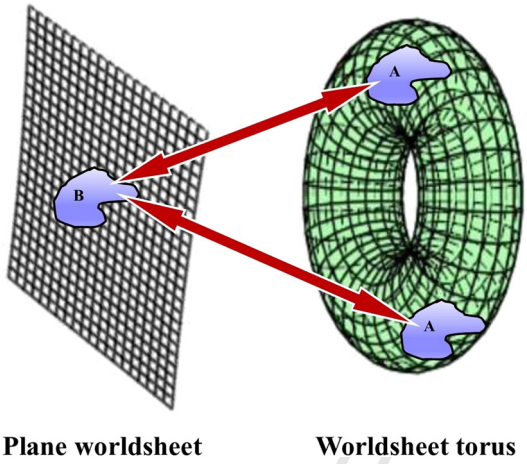

Fig. 7. Samples of OA patterns, illustrated in guise of geometrical shapes, are represented by the regions A and B on different structures with diverse dimensions. Regions A and B are examples of antipodal activities which lie on structures with various dimensions.

torus. This means that every brain activity can be assessed in terms of particle movements along the surface of multi-dimensional, donut-like toruses (Fig. 7). In sum, BUT and its variants entail that every kind of high-dimensional brain activity predicted by OA can be described in terms of donut-like structures [71]. This methodological advance, already used in limited trials, could be useful in order to achieve a unvarying operationalization of the OA across inter- and intra-cellular levels [94].

3.4. Topological "duality" and OA levels

As stated above, OA brain activity can be assessed either at functional micro-, meso- and macro-spatiotemporal scales of observation, or at intertwined levels with mutual interactions. We will show, based on topological findings, that nervous activities occurring in micro-levels project to single activities at macro-levels. This means that brain functions assessed at the higher scale of the whole brain necessarily display a counterpart in the lower ones, and vice versa. Consider Brouwer's fixed point theorem (FPT) [95]. Su [96] gives a nice illustration of the FPT: no matter how you continuously slosh the coffee around in a coffee cup, some point is always in the same position that it was before the sloshing began. And if you move this point out of its original position, you will eventually move some other point in the sloshing coffee back into its original position. In BUT terms, this means that not only we can always find a brain region containing an activity, but also that every activity comes together with another one, termed a *wired friend*. These observations lead to a *wired friend theorem*: every occurrence of a wired friend activity on the $n + 1$-dimensional structure maps to a fixed description, e.g., to another activity that belongs to an n-dimensional structure (Fig. 7) [68,93]. The significance of this is that we can always find an OA activity, embedded in a higher-dimensional brain macro-level, which is the topological description of another activity, embedded in a lower dimensional brain micro-level; and vice versa. This leads to a novel scenario, where all the levels described by OA are *dual* under topological transformation. The term *dual* refers to a situation where two seemingly different physical systems turn out to be equivalent. If two techniques or phenomena are related by a duality, one can be transformed into the other, so that one phenomenon ends up looking just like the other one [97].

One of the most successful entropy-based theories of brain function, i.e., the free-energy principle, requires the brain activity taking place in an ergodic phase space [98]. In physics and thermodynamics, the ergodic hypothesis states that, over long periods, the time spent by a system in a region of the microstates' phase space with the same energy is proportional to the region's volume, so that all accessible microstates are equiprobable over a long period of time [99]. In other words, ergodicity is a random process characterized by the time average of one sequence of events being the same as the ensemble average [100,101]. This also means that, in case of a Markov chain, as one increases the steps, there exists a positive probability measure at step n that is independent of the probability distribution at initial step 0 [102] However, widespread claims suggest that the brain is not fully ergodic. Indeed, many authors propose that the properties of brain fluctuations are inconsistent with the Markovian approximation [103], that the

UNCORRECTED PROOF

mean-square distance traveled by brain particles displays anomalous diffusion [104] and that the brain is weakly non-ergodic, as some phase space region may take extremely long times to be visited. An OA/topological approach provides a potential solution of the problem of using ergodic information measures in the supposed non-ergodic "physical setting" of brain activity. Indeed, both ergodic and non-ergodic brain conditions can be "unified", e.g., treated in terms of algebraic topology, just changing the dimension of the structure under investigation. We provide an example: taking a 2D disk, and a particle that may "ergodically" travel along its whole surface, when one projects such 2D structure one dimension higher, a 3D sphere is achieved. The latter is equipped with two antipodal regions where the particle can travel. Therefore, in higher dimensions, the particles are constrained to move just in some zones of the structure, and ergodicity is partially lost. This means that, in the context of the OA/topological brain, the discrepancy between ergodic and non-ergodic spaces stands just for a "dual" theory.

4. Predictions and new directions for future research

The new topodynamic approach derived from interrelating OA and the BUT topological framework throws a new light on the evidences provided by functional studies of the brain, which indeed are a subject of intense and increasing research. In this section, we will mention the most relevant predictions and new research directions directly related to the theme of this review paper: the empirically observable dimensional/symmetry/entropy increases, the new topological operationalization of chaotic dynamics and synchronization in the brain, the unification of coarse-grained scales of observation, and – perhaps most importantly – a new topodynamic description of the cerebral production mechanisms of syntactics and semantics. Subsequently, a new path for novel computers with nodes built into higher dimensions is finally considered.

4.1. The observable dimensional/symmetry/entropy increase

The main prediction of the BUT formulation in relation to Operational Architectonics is that the brain displays, apart from the "classical" four spatio-temporal dimensions, also other functional dimensions, where the OA mechanisms might take place: an increase of functional dimensions occurs as a result of the environmental stimuli impinging upon the brain processes. That is, the brain, rather than simply integrating sensory inputs and concentrating them into concepts as currently believed, appears to increase the complexity from the perceived physical object to the phenomenal object ("idea" of it) as suggested by the OA model [9,72]. Indeed, phenomenal objects can be described as complex patterns of qualities which are spatially extended and bounded to each other to form a unified item (Gestalt) with a particular meaningful categorization (semantics) immediately present for the subject [10]. More specifically, the BUT model predicts that an increase in dimensions and symmetries occurs from the environment, through the separate neuronal assemblies in primary sensory areas, to the higher coalitions of such neuronal assembles in the form of Operational Modules (OMs), and that informational entropy in the primary sensory areas must be lower than in the higher associative ones.

This prediction was confirmed recently in a fMRI study where the entropy/information in zones of fMRI images was assessed, in order to evaluate whether, as predicted by our model, the entropy is higher in associative cortices than in the primary ones [72]. The results of that study suggest that the brain operational functioning lies in dimensions higher than the environment and that a message coming from external inputs does not concentrate in a local brain spot, but rather is presented by a nonlocal complex OMs, as dictated by the OA framework. In such an operational architecture, each of the complex OMs is not just a sum of simpler OMs or of many neuronal assemblies, but rather a natural union of abstractions about simpler OMs [9,10]. Therefore, OMs have a rich combinatorial complexity and the ability to rapidly reconfigure themselves in accordance with the changing environmental input or mental activity.

Even though the OA is built on the electro-physiological field produced by the brain (EEG), some additional and complementary information could be extracted from the fMRI studies. And the BUT approach could be helpful here. A topological approach, which states that mappings among every brain signal and energetic information have the potential to be operationalized, makes it possible to extend the OA framework also in fMRI studies. As an example, let us consider the case of two brain states, one standing for a symmetry (the brain at rest), and another for a broken symmetry (the brain during a visual task). Our model sharply predicts the particular energetic values for both states (either in EEG or fMRI data), when they are functionally correlated [25,74]. Indeed, according to BUT, a single micro-area with symmetry breaking (e.g., lower-dimensional neuronal assemblies), necessarily projects to TWO areas

UNCORRECTED PROOF

Please cite this article in press as: Tozzi A, et al. Topodynamics of metastable brains. Phys Life Rev (2017), http://dx.doi.org/10.1016/j.plrev.2017.03.001

with preserved symmetry (e.g., a high-dimensional OA module). The single area in lower dimensions and the two areas with matching description need to display the same values of entropy. This allows us to recognize which zones of the brain are correlated during symmetry breaks, e.g., during the projective steps from higher to lower level of complexity, and vice versa.

Therefore, our framework is able to predict the following hypothetical results: if we find, during the visual task, say, three micro-areas with an entropy 1.08, we expect to find, during rest, six or more micro-areas with entropy = 1.08. In sum, by knowing just the entropy values for each local EEG (or BOLD-activated area), we are allowed to correlate two different brain states, e.g., a lower-dimensional state with symmetry breaking and a higher-dimensional state with preserved symmetries. The phenomenon of spontaneous breakdown of symmetry and restoration of symmetry in the EEG signals has been widely documented and analyzed by Freeman and colleagues [105,106]

4.2. The new topological operationalization of chaotic dynamics and synchronization in the brain

Another prediction is that the nonlinear dynamics required by OA can be tested through a topological approach. As stated above, nonlinear features of brain dynamics can be studied through logistic maps equipped with bifurcations, where intervals are dictated by Feigenbaum constants. In such framework of brain functioning at the edge of chaos, BUT topodynamics comes into play. As demonstrated by Tozzi and Peters [71], embracing brain nonlinearity in the framework of the BUT means that brain activity bifurcation transformations (the antipodal points) can be described as paths or trajectories on abstract spheres equipped with Feigenbaum dimensions. Such an approach facilitates the evaluation of nonlinear brain activity dynamics through simpler linear techniques. Our framework provides a topological mechanism which explains the elusive brain phenomena at the edge of chaos predicted by OA, cast in a physical/formal fashion with the potential of being operationalized.

The OA theory proposes that the simultaneous occurrence of RTPs from different local EEG signals provides evidence of synchronization of simple operations performed by different neuronal assemblies in order to execute a particular complex operation [4,10,61,107]. In topological terms, the synchronized quasi-stationary EEG segments separated by the RTPs are correlated with antipodal points in one dimension higher. The concepts of proximity (spatial as well as descriptive closeness, Peters [18]) and affine connections are also helpful in solving one of the problems raised by oscillations, e.g., how cooperation among so many "distant" sub-networks occurs seamlessly in real time. Thanks to the "continuous" mapping provided by BUT, a quantifiable explanation to the speed and balance of a system characterized by hierarchical and cross-hierarchical cooperating modules is achieved [45].

This explains the tendency of local EEG signals to be coordinated together within the same OM, in order to execute the macro-operation required to give rise to (a higher-dimensional level of) abstractness [9,10]. In this sense, the concepts of parallel and serial processing may be just two sides of the same underlying mechanism, e.g., a synchrony of operations performed by mappings and projections. Therefore, we may conclude that each OM is a projective process, since it lasts as long as several operations are synchronized among each other.

4.3. Unification of coarse-grained scales of observation

The new framework permits a topological duality among the different levels of OA, because it holds for all the types of spatiotemporal brain activities, independent of their inter- and intra-level relationships, strength, magnitude and boundaries. The generalization achieved allows the assessment of every possible OA's brain level, independent on its scale, specific features and local boundaries. Our topological investigation reveals that there must be at least one element in common among brain spatiotemporal activities that lie in different functional dimensions. In other words, there exists an assessable and quantifiable correspondence between micro-, meso- and macro-levels of OA brain levels. OA brain levels will always have some element in common: they do not exist in isolation, rather they are part of a large interconnected whole, with which they interact.

Therefore, the distinction among different coarse-grained levels of nervous activity does not count anymore, because nervous function at small, medium and large scales of neural observation turn out to be topologically equivalent. It allows a useful simplification in the assessment of brain activity. Because projections between dimensions describe neural phenomena spanning from the smallest to the highest scales, the distinction among different coarse-grained scales does not count anymore: indeed, nervous activity is topologically the same at small, medium and large scales of observation. In sum, two activities with matching description, embedded in two brain locations of different levels,

UNCORRECTED PROOF

Please cite this article in press as: Tozzi A, et al. Topodynamics of metastable brains. Phys Life Rev (2017), http://dx.doi.org/10.1016/j.plrev.2017.03.001

display the same features. Activities with matching ends (regions) in different cortical areas might also help to throw a bridge, for example, between sensation and perception. In the same guise, the relationships between the spontaneous and the evoked activity of the brain [108] take now a new significance: they become just two sides of the same coin, made of topologically-bounded dynamics.

4.4. Cerebral production mechanisms of syntactics and semantics

Another important prediction and new direction for future research involves the mechanisms of syntactics and semantics in the brain. According to the OA-topological model, it might be argued that the human brain processes syntactic and semantic elements through a change in functional/spatial dimensions. When presented with a proposition, the brain straightforwardly understands its grammar and discriminates whether it is correct or wrong, true or false. Unlike computers, the brain is able to identify signs of sequences in terms of both syntactic symbols and semantic meaning. It could be demonstrated, based on the current literature, that a testable algebraic topological approach gives helpful insights into the brain's computational activity during semantic recognition. Indeed, recent suggestions allow us to hypothesize that the semantic properties of a proposition, corresponding to the higher levels described by OA, are processed in brain dimensions higher than the syntactic ones. Further, we might show how, in a fully reversible process, the syntactic elements embedded in Broca's area can project into scattered semantic cortical zones. Thereafter, the presence of higher functional dimensions gives rise to an increase in the informational content of propositions. In order to explain that dimensional increase, we account for the dictates of the novel versions of the BUT and FPT.

In a very simplified view, the syntactic processing that occurs at one level of brain activity is projected to a higher level. This gives rise to semantic recognition, which encompasses more information. In our novel framework, syntax displays fewer dimensions than semantics in the central nervous system, so that semantic inputs have increased complexity. Therefore, the first task is to determine if the brain contains different dimensions, while the second is to describe nervous dynamics as vectors or tensors in pluri-dimensional phase spaces. The term 'brain *dimension*' may reflect either: a) levels of functional activity, b) or the number of components that pinpoint anatomical connections between cortical areas. The functional approach, based on complex network analysis of brain signals, assesses the multi-dimensionality of neural space in a brain model viewed as a complex dynamical system [109–111]. Apart from the *canonical* three dimensions, such technique is also capable of assessing other neural features such as frequency and magnitude, with each representing other possible dimensions [109].

The anatomical approach to brain dimensionality evaluates cortical locations [71,80]; and as recent advances indicate, brain trajectories may display four spatial dimensions – instead of the canonical three – during cortical spontaneous activity [79,80]. Such trajectories are described in terms of torus-shaped objects. Animals are shown to navigate by reading out a simple population vector of grid cell activity across multiple spatial scales [94]: this means that the behavior of population vectors, each lying in different anatomical dimensions embedded on instances of the functional torus, predicts neural and behavioral correlation to grid cell readout. An algorithm and model was developed to study how complex networks are organized by higher-order connectivity patterns, so as to reveal hubs and geographical elements not readily achieved by other methods. For further details, see [112]. It was demonstrated that information propagation units exhibit rich higher-order organizational structures.

In the same vein, real neural networks are not just random combinations of single network layers, but are instead organized in specific ways; these are dictated by hidden geometric correlations between layers, which permit the detection of multidimensional communities [113]. This is crucial for the BUT new models, because such multidimensionality enables trans-layer link prediction so that connections in one layer can be predicted by observing the hidden geometric structures of another layer. Defining "strings" as paths followed by a particle moving through space, our BUT model [74] provides a new formal framework for the distinctive characterization of semantics and syntactics. The brain localizations of syntactic and semantic processing as described in literature seem to agree with our topological model. The left anterior language area, e.g. Broca's area (left Brodmann area 44), is crucial for syntactic processing in speech production and perception [114,115]. This is despite the wide variability between individuals and the presence of diverse circuits not dedicated to just a single type of linguistic information processing [116]. While syntax seems to be localized in relatively fewer and smaller brain areas, semantics is instead scattered throughout vast areas of the cortical surface [117]. This would agree with a model encompassing BUT variants and FPT that regards semantic concepts as multiple antipodal strings on a torus surface, and syntactic concepts as single strings located

UNCORRECTED PROOF

Please cite this article in press as: Tozzi A, et al. Topodynamics of metastable brains. Phys Life Rev (2017), http://dx.doi.org/10.1016/j.plrev.2017.03.001

in specific brain zones. This also means that syntactic elements lie on higher brain dimensions than syntactic ones. According to the dictates of our BUT model, single strings capture less information than their matching descriptions embedded in higher projections. This is a seminal concept, and it is not necessarily intuitive. Note also that semantic information is not aggregated, but instead it is scattered in the brain. Syntactic symbols represent single sets of objects, while semantic meanings represent numerous sets of objects with matching description.

To sum up, an OA/topological or topodynamical approach makes it possible to build a feasible explanation for semantics processing in the brain. But it also suggests a new path for novel computers with nodes built into higher dimensions. Indeed, the fact that brain nodes can be embedded in higher dimensional spaces suggests the possibility of manufacturing computers equipped with pluri-dimensional nodes endowed in 3D geometric spaces. Yet a computer can be hypothesized having connections that are topologically 4D, although embedded in a simple 3D space. Such computers, implemented in ordinary 3D space, but equipped with nodes with the same number of neighbors as points in a 4D cube, could have the capability to perform semantic operations, due to more degrees of freedom.

5. Conclusions

In conclusion, we have achieved a topodynamic description of the main elements of the operational architectonics of brain–mind functioning. BUT and its extensions provide a methodological approach which makes it possible for researchers to study metastable brain/mind in terms of projections from real to abstract phase spaces, which is crucially important for building accurate computational and mathematical models of the brain–mind functioning (see also [118,119]). The real, measurable activity of the brain can now be described in terms of paths occurring on abstract structures. This leads to a consideration of affinities among multiple signals of brain activity, characterized as antipodal points on multi-dimensional structures endowed in abstract spaces. A shift in conceptualizations is evident in the BUT approach: the onset of the neuronal assemblies and their interactions within the operational modules is described in terms of sameness, closeness instantiated by their feature value vectors (e.g., amplitude, duration, and so on). The invaluable opportunity to treat elusive mental activities in terms of topological structures makes it possible for us to describe experience in the language of powerful analytical structures. Embracing OA model systems in the framework of algebraic topology [119,120] means that transformations (the antipodal points or regions) can be described as paths or trajectories on "abstract" structures: the BUT perspective makes possible a system's property located in the real space (the physical milieu's geometric space) to be translated to an abstract space (called the topological configuration space) and vice-versa, enabling us to achieve maps from one level to another. This puts in a new light the system interactions described by OA theory [4–10], in terms of affine connections and proximity (either spatial or descriptive closeness) among signals, in order to explain, for example, how network communities integrate or segregate information during complex mental activity. In sum, topodynamics of the metastable brain supplies us with richly sufficient statistics that helps us to elucidate the mechanisms of human brain/mind functioning. The paths described by BUT and its variants elucidate how the tight coupling among the different neural activities described by the OA model gives rise to self-organization where spatiotemporal patterns in one part of the brain, which are in charge of receiving and interpreting signals from other cortical parts, are closely intertwined at every spatio-temporal level. The AO model assessed in the light of a topological framework, therefore achieving the new topodynamic perspective, becomes one of the central information processing strategies of the advanced nervous system, including its semantic and syntactic 'computational' processes. The phenomenon seems traceable from an evolutionary point of view as well: whether the evolution of complexity in central nervous systems recapitulates essential topodynamic developments becomes an exciting possibility that could also open new research directions.

References

[1] Lehar S. Gestalt isomorphism and the primacy of subjective conscious experience: a Gestalt bubble model. Behav Brain Sci 2003;26:357–408.
[2] Khrennikov AYu. Information dynamics in cognitive, psychological and anomalous phenomena. Ser fundamental theories of physics. Dordrecht: Kluwer; 2004.
[3] Perlovsky LI. Modeling field theory for higher cognitive functions. Hershey, PA: Idea Group; 2006.
[4] Fingelkurts AA, Fingelkurts AA. Operational architectonics of the human brain biopotential field: towards solving the mind-brain problem. Brain Mind 2001;2:261–96.
[5] Fingelkurts AA, Fingelkurts AA. Mapping of the brain operational architectonics. In: Chen FJ, editor. Focus on brain mapping research. New York: Nova Science Publishers Inc; 2005. p. 59–98.

UNCORRECTED PROOF

Please cite this article in press as: Tozzi A, et al. Topodynamics of metastable brains. Phys Life Rev (2017), http://dx.doi.org/10.1016/j.plrev.2017.03.001

[6] Fingelkurts AA, Fingelkurts AA. Brain–mind operational architectonics imaging: technical and methodological aspects. Open Neuroimag J 2008;2:73–93.
[7] Fingelkurts AA, Fingelkurts AA. Operational architectonics methodology for EEG analysis: theory and results. Neuromethods 2015;91:1–59.
[8] Fingelkurts AA, Fingelkurts AA, Neves CFH. Phenomenological architecture of a mind and operational architectonics of the brain: the unified metastable continuum. New Math Nat Comput 2009;5:221–44.
[9] Fingelkurts AA, Fingelkurts AA, Neves CFH. Natural world physical, brain operational, and mind phenomenal space-time. Phys Life Rev 2010;7(2):195–249.
[10] Fingelkurts AA, Fingelkurts AA, Neves CFH. Consciousness as a phenomenon in the operational architectonics of brain organization: criticality and self-organization considerations. Chaos Solitons Fractals 2013;55:13–31.
[11] Bressler SL, Kelso JAS. Cortical coordination dynamics and cognition. Trends Cogn Sci 2001;5(1):26–36.
[12] Uhlhaas PJ, Singer W. Neuronal dynamics and neuropsychiatric disorders: toward a translational paradigm for dysfunctional large-scale networks. Neuron 2012;75:963–80.
[13] Tognoli E, Kelso JA. Enlarging the scope: grasping brain complexity. Front Syst Neurosci 2014;8:122.
[14] Willard S. General topology. Mineola, NY: Dover Pub., Inc.. ISBN 0-486-43479-6, 1970. xii+369 pp., MR0264581.
[15] Krantz SG. A guide to topology. Washington, DC: The Mathematical Association of America; 2009.
[16] Manetti M. Topology. Heidelberg: Springer; 2015.
[17] Naimpally SA, Peters JF. Topology with applications. Topological spaces near and far. Foreword by I.A. Taimanov. Hackensack, NJ: World Scientific Publishing Co. Pte. Ltd.. ISBN 978-981-4407-65-6, 2013. xvi+277 pp., MR 3075111.
[18] Peters JF. Computational proximity. Excursions in the topology of digital images. Intelligent systems reference library, vol. 102. Switzerland: Springer Int. Pub.; 2016.
[19] Peters JF, Tozzi A. Quantum entanglement on a hypersphere. Int J Theor Phys 2016:1–8. http://dx.doi.org/10.1007/s10773-016-2998-7.
[20] Borsuk M. Drei Sätze über die n-dimensional euklidische Sphäre. Fundam Math 1933;XX:177–90.
[21] Marsaglia G. Choosing a point from the surface of a sphere. Ann Math Stat 1972;43(2):645–6.
[22] Matoušek J. Using the Borsuk–Ulam theorem. Lectures on topological methods in combinatorics and geometry. Berlin, Heidelberg: Springer-Verlag; 2003.
[23] Beyer WA, Zardecki A. The early history of the ham sandwich theorem. Am Math Mon 2004;1:58–61.
[24] Moura E, Henderson DG. Experiencing geometry: on plane and sphere. Prentice Hall. ISBN 978-0-13-373770-7, 1996.
[25] Tozzi A, Peters JF. A symmetric approach elucidates multisensory information integration. Information 2017;8(1):4. http://dx.doi.org/10.3390/info8010004.
[26] Fingelkurts AA, Fingelkurts AA. Making complexity simpler: multivariability and metastability in the brain. Int J Neurosci 2004;114:843–62.
[27] Kelso JAS. Behavioral and neural pattern generation: the concept of neurobehavioral dynamical system (NBDS). In: Koepchen HP, editor. Cardiorespiratory and motor coordination. Berlin: Springer-Verlag; 1991.
[28] Kelso JAS. Dynamics patterns: the self-organization of brain and behaviour. Cambridge, MA: MIT Press; 1995.
[29] Kelso JAS. Coordination dynamics. In: Meyers RA, editor. Encyclopedia of complexity and systems sciences. Berlin: Springer; 2009. p. 1537–64.
[30] Kelso JAS, Engstrøm D. The complementary nature. Cambridge: MIT Press; 2006.
[31] Kelso JAS, Tognoli E. Toward a complementary neuroscience: metastable coordination dynamics of the brain; 2007.
[32] Haken H. Synergetics: an introduction. 3rd edition. Berlin: Springer-Verlag; 1983.
[33] Haken H. What can synergetics contribute to the understanding of brain functioning? In: Uhl C, editor. Analysis of neurophysiological brain functioning. Berlin: Springer-Verlag; 1999. p. 7–40.
[34] Freeman WJ. Origin, structure, and role of background EEG activity. Part 1. Analytic amplitude. Clin Neurophysiol 2004;115:2077–88.
[35] Miwakeichi F, Martinez-Montes E, Valdes-Sosa PA, Nishiyama N, Mizuhara H, Yamaguchi Y. Decomposing EEG data into space–time–frequency components using Parallel Factor Analysis. NeuroImage 2004;22:1035–45.
[36] Buzsaki G, Anastassiou CA, Koch C. The origin of extracellular fields and currents—EEG, ECoG, LFP and spikes. Nat Rev Neurosci 2012;13:407–20.
[37] Bak P. How nature works: the science of self-organized criticality. New York: Springer; 1996.
[38] Jensen HJ. Self-organized criticality: emergent complex behavior in physical and biological systems. Cambridge: Cambridge University Press; 1998.
[39] Bianco G, Grigolini P, Paradisi P. Fluorescence intermittency in blinking quantum dots: renewal of modulation? J Chem Phys 2005;123:174704.
[40] Silvestri L, Fronzoni L, Grigolini P, Allegrini P. Event- driven power-law relaxation in weak turbulence. Phys Rev Lett 2009;102:014502.
[41] Allegrini P, Menicucci D, Bedini R, Fronzoni L, Gemignani A, Grigolini P, et al. Spontaneous brain activity as a source of ideal 1/f noise. Phys Rev E 2009;80:061914.
[42] Bak P, Tang C, Wiesenfeld K. Self-organized criticality: an explanation of the 1/f noise. Phys Rev Lett 1987;59:381–4.
[43] Bak P. How nature works. Oxford, UK: Oxford University Press; 1997.
[44] Novikov E, Novikov A, Shannahoff-Khalsa D, Schwartz B, Wright J. Scale-similar activity in the brain. Phys Rev E 1997;56:R2387.
[45] Linkenkaer-Hansen K, Nikouline VV, Palva JM, Ilmoniemi RJ. Long-range temporal correlations and scaling behavior in human brain oscillations. J Neurosci 2001;21(4):1370–7.
[46] Freeman WJ. Evidence from human scalp electroencephalograms of global chaotic itinerancy. Chaos 2003;13(3):1067–77.
[47] Plenz D, Thiagarajan TC. The organizing principles of neuronal avalanches: cell assemblies in the cortex? Trends Neurosci 2007;30:101–10.
[48] Gong P, van Leeuwen C. Distributed dynamical computation in neural circuits with propagating coherent activity patterns. PLoS Comput Biol 2009;5(12):e1000611.

UNCORRECTED PROOF

Please cite this article in press as: Tozzi A, et al. Topodynamics of metastable brains. Phys Life Rev (2017), http://dx.doi.org/10.1016/j.plrev.2017.03.001

[49] Werner G. Viewing brain processes as critical state transitions across levels of organization: neural events in cognition and consciousness, and general principles. Biosystems 2009;96:114–9.
[50] Allegrini P, Paradisi P, Menicucci D, Gemignani A. Fractal complexity in spontaneous EEG metastable-state transitions: new vistas on integrated neural dynamics. Front Physiol 2010;1:128.
[51] Paradisi P, Allegrini P, Gemignani A, Laurino M, Menicucci D, Piarulli A. Scaling and intermittency of brain events as a manifestation of consciousness. AIP Conf Proc 2012;1510:151–61.
[52] Fingelkurts AA, Fingelkurts AA. Timing in cognition and EEG brain dynamics: discreteness versus continuity. Cogn Process 2006;7:135–62.
[53] Churchland PS, Sejnowski T. The computational brain. Cambridge: MIT; 1992.
[54] Fodor JA, Pylyshyn ZW. Connectionism and cognitive architecture: a critical analysis. Cognition 1988;28:3–71.
[55] James W. The principles of psychology, vol. I. New York: Dover; 1890.
[56] Fingelkurts AA, Fingelkurts AA, Ivashko RM, Kaplan AYa. EEG analysis of operational synchrony between human brain cortical areas during memory task performance. Vestn Moskovsk Univ Ser 16 Biol 1998;1:3–11 [in Russian].
[57] Fingelkurts AA, Fingelkurts AA, Krause CM, Kaplan AY, Borisov SV, Sams M. Structural (operational) synchrony of EEG alpha activity during an auditory memory task. NeuroImage 2003;20(1):529–42.
[58] Fingelkurts AA, Fingelkurts AA, Krause CM, Möttönen R, Sams M. Cortical operational synchrony during audio–visual speech integration. Brain Lang 2003;85:297–312.
[59] Fingelkurts AA, Fingelkurts AA, Kivisaari R, Pekkonen E, Ilmoniemi RJ, Kähkönen SA. Local and remote functional connectivity of neocortex under the inhibition influence. NeuroImage 2004;22(3):1390–406.
[60] Fingelkurts AA, Fingelkurts AA, Kivisaari R, Autti T, Borisov S, Puuskari V, et al. Opioid withdrawal results in an increased local and remote functional connectivity at EEG alpha and beta frequency bands. Neurosci Res 2007;58(1):40–9.
[61] Fingelkurts AA, Fingelkurts AA, Kivisaari R, Autti T, Borisov S, Puuskari V, et al. Methadone may restore local and remote EEG functional connectivity in opioid-dependent patients. Int J Neurosci 2009;119(9):1469–93.
[62] Prigogine I, Stengers I. Order out of chaos: man's new dialogue with nature. New York: Basic Books; 1984.
[63] Stanley HE. Introduction to phase transitions and critical phenomena. Oxford, UK: Oxford University Press; 1987.
[64] Marro J, Dickman R. Nonequilibrium phase transitions in lattice models. Cambridge, UK: Cambridge University Press; 1999.
[65] Haken H. Information and self-organization: a macroscopic approach to complex systems. New York: Springer; 2000.
[66] Borsuk M. Concerning the classification of topological spaces from the standpoint of the theory of retracts. Fundam Math 1958–1959;XLVI:177–90.
[67] Borsuk M. Fundamental retracts and extensions of fundamental sequences. Fundam Math 1969;1:55–85.
[68] Peters JF, Tozzi A. String-based Borsuk–Ulam theorem and wired friend theorem. 2016. arXiv preprint 1605, no. 02987v3.
[69] Peters JF, Tozzi A. From abstract topology to real thermodynamic brain activity. Cogn Neurodyn 2017. http://dx.doi.org/10.1007/s11571-0-17-943[illegible] [in press].
[70] Weeks JR. The shape of space. IInd edition. New York-Basel: Marcel Dekker, inc.; 2002.
[71] Tozzi A, Peters JF. A topological approach unveils system invariances and broken symmetries in the brain. J Neurosci Res 2016;94(5):351–65. http://dx.doi.org/10.1002/jnr.23720.
[72] Peters JF, Tozzi A, Ramanna S, Inan E. The human brain from [illegible]e: an increase in complexity from environmental stimuli to abstractions. Cogn Neurodyn 2017. http://dx.doi.org/10.1007/s11571-0-17-[illegible]2 [in press].
[73] Mitroi-Symeonidis FC. Convexity and Sandwich theorems. Eur J Res Appl Sci March 2015;1:9–11.
[74] Tozzi A, Peters JF. Symmetries, information and monster groups before and after the big bang. Information 2016;7(4):73. http://dx.doi.org/10.3390/info7040073.
[75] Weyl H. Symmetry. Princeton: Princeton University Press. ISBN 0-691-02374-3, 1982.
[76] Weyl H. Raum–Zeit–Materie. Vorlesungen über allgemeine Relativitätstheorie (space–time–matter). Dover Pubs, Inc.; 1918 [reprinted in H. Weyl (1952). Space–Time–Matter, trans. by H.L. Brose].
[77] Roldán É, Martínez I, Parrondo JMR, Petrov D. Universal features in the energetics of symmetry breaking. Nat Phys 2014;10(6):457–61. http://doi.org/10.1038/nphys2940.
[78] Peters JF, Tozzi A, Ramanna S. Brain tissue tessellation shows absence of canonical microcircuits. Neurosci Lett 2016;626:99–105. http://dx.doi.org/10.1016/j.neulet.2016.03.052.
[79] Peters JF, Ramanna S, Tozzi A, Inan E. Bold-independent computational entropy assesses functional donut-like structures in brain fMRI images. Front Human Neurosci 2017. http://dx.doi.org/10.3389/fnhum.2017.00038.
[80] Tozzi A, Peters JF. Towards a fourth spatial dimension of brain activity. Cogn Neurodyn 2016;10(3):189–99. http://dx.doi.org/10.1007/s11571-016-9379-z. PMID: 27275375.
[81] Kim I-S. Extensions of the Borsuk–Ulam theorem. J Korean Math Soc 1997;34(3):599–608.
[82] Schleicher D. Hausdorff dimension, its properties, and its surprises. Am Math Mon 2007;114(6):509–28. MR2321254.
[83] Avenarius R. Kritik Der Reinen Erfahrung von Richard Avenarius. Lepzig: CR Reisland; 1908.
[84] Russo Krauss C. L'empirio criticismo di Richard Avenarius tra psicofisiologia e teoria della consocenza. In: R. Avenarius, Il concetto umano di mondo; 2015.
[85] Parise CV, Spence C, Ernst MO. When correlation implies causation in multisensory integration. CurrBiol 2011;22(1):46–9.
[86] Körding KP, Beierholm U, Ma WJ, Quartz S, Tenenbaum JB, Shams L. Causal inference in multisensory perception. PLoS ONE 26 2007;2(9):e943.
[87] Hume D. A treatise of human nature: being an attempt to introduce the experimental method of reasoning into moral subjects. Penguin Classics; 1739–40 [new ed edition (31 Oct. 1985)].
[88] Libet B, Gleason CA, Wright EW, Pearl DK. Time of conscious intention to act in relation to onset of cerebral activity (readiness-potential). The unconscious initiation of a freely voluntary act. Brain 1983;106(Pt 3):623–42.

UNCORRECTED PROOF

[89] Bengson JJ, Kelley TA, Zhang X, Wang J-L, Mangun GR. Spontaneous neural fluctuations predict decisions to attend. J Cogn Neurosci 2014;26(11):2578–84.
[90] Chicharro D, Ledberg A. When two become one: the limits of causality analysis of brain dynamics. PLoS ONE 2012;7(3):e32466. http://dx.doi.org/10.1371/journal.pone.0032466.
[91] Friston K. Hierarchical models in the brain. PLoS Comput Biol 2008;4:e1000211.
[92] Barrett LF, Simmons WK. Interoceptive predictions in the brain. Nat Rev Neurosci 2015;16(7):419–29.
[93] Peters JF. Two forms of proximal physical geometry. Axioms, sewing regions together, classes of regions, duality, and parallel fibre bundles. Adv Math: Sci J 2016;5(2):241–68. arXiv:1608.06208v4.
[94] Marijuán PC, del Moral R, Navarro J. On eukaryotic intelligence: signaling system's guidance in the evolution of multicellular organization. Biosystems 2013;114(1):8–24. http://dx.doi.org/10.1016/j.biosystems.2013.06.005. Epub 2013 Jul 12.
[95] Volovikov Yu A. Borsuk–Ulam implies brouwer: a direct construction revisited. Am Math Mon 2008;115(6):553–6. http://dx.doi.org/10.2307/2975293.
[96] Su FE. Borsuk–Ulam implies brouwer: a direct construction. Am Math Mon 1997;104(9):855–9. MR1479992.
[97] Zwiebach Barton. A first course in string theory. Cambridge University Press. ISBN 978-0-521-88032-9, 2009.
[98] Friston K. The free-energy principle: a unified brain theory? Nat Rev Neurosci 2010;11(2):127–38.
[99] Barth A. Vorlesungen über Gastheorie, Leipzig, 1898 OCLC 01712811 ['Ergoden' on p. 89 in the 1923 reprint].
[100] Walters P. An introduction to ergodic theory. Springer. ISBN 0-387-95152-0, 1982.
[101] Alaoglu L, Birkhoff G. General ergodic theorems. Ann Math 1940;41(2):293–309.
[102] Feller W. An introduction to probability theory and its applications, vol. 2. Wiley; 1971.
[103] Fraiman D, Chialvo DR. What kind of noise is brain noise: anomalous scaling behavior of the resting brain activity fluctuations. Front Physiol 2012;3:307.
[104] Bianco S, Ignaccolo M, Rider MS, Ross MJ, Winsor P, Grigolini P. Brain, music, and non-Poisson renewal processes. Phys Rev E 2007;75:061911.
[105] Freeman WJ, Vitiello G. Nonlinear brain dynamics as macroscopic manifestation of underlying many-body field dynamics. Phys Life Rev 2006;3:93–118.
[106] Freeman WJ, Vitiello G. Vortices in brain waves. Int J Mod Phys B 2010;24:3269–95.
[107] Fingelkurts AA, Fingelkurts AA. Alpha rhythm operational architectonics in the continuum of normal and pathological brain states: current state of research. Int J Psychophysiol 2010;76:93–106.
[108] Tozzi A, Zare M, Benasich AA. New perspectives on spontaneous brain activity: dynamic networks and energy matter. Front Human Neurosci 2016. http://dx.doi.org/10.3389/fnhum.2016.00247.
Q7 [109] Kida T, Tanaka E, Kakigi R. Multi-dimensional dynamics of human electromagnetic brain activity. Front Human Neurosci 2016;19(9):713. http://dx.doi.org/10.3389/fnhum.2015.00713. eCollection 2015.
[110] Giusti C, Ghrist R, Bassett DS. Two's company, three (or more) is a simplex. Algebraic-topological tools for understanding higher-order structure in neural data. J Comput Neurosci 2016;41(1):1–14.
[111] Simas T, Chavez M, Rodriguez PR, Diaz-Guilera A. An algebraic topological method for multimodal brain networks comparisons. Front Psychol 2015;6(6):904. http://dx.doi.org/10.3389/fpsyg.2015.00904 [eCollection 2015].
[112] Tozzi A, Peters JF. Towards topological mechanisms underlying experience acquisition and transmission in the human brain. JF Integr Psych
Q8 Behav 2017. http://dx.doi.org/10.1007/s12124-017-9380-z.
[113] Kleineberg K-K, Boguñá M, Serrano MA, Papadopoulos F. Hidden geometric correlations in real multiplex networks. Nat Phys 2016. http://dx.doi.org/10.1038/nphys3812 [in press].
Q9 [114] Skeide MA, Friederici AD. The ontogeny of the cortical language network. Nat Rev Neurosci 2016;17:323–32. http://dx.doi.org/10.1038/nrn.2016.23.
[115] Stromswold K, Caplan D, Alpert N, Rauch S. Localization of syntactic comprehension by positron emission tomography. Brain Lang 1996;52:452–73.
[116] Sahin NT, Pinker S, Cash SS, Schomer D, Halgren E. Sequential processing of lexical, grammatical, and phonological information within Broca's area. Science 2009;326(5951):445–9.
[117] Huth AG, de Heer WA, Griffiths TL, Theunissen FE, Gallant JL. Natural speech reveals the semantic maps that tile human cerebral cortex. Nature 28 2016;532(7600):453–8. http://dx.doi.org/10.1038/nature17637.
[118] Sengupta B, Tozzi A, Cooray GK, Douglas PK, Friston KJ. Towards a neuronal gauge theory. PLoS Biol 2016;14(3):e1002400.
[119] Kozma R, Perlovsky L, editors. Neurodynamics of higher-level cognition and consciousness. Heidelberg: Springer; 2007.
[120] Krantz SG. Essentials of topology with applications. Boca Raton, FL: CRC Press; 2010. MR2554895.

UNCORRECTED PROOF

Highlights

- Novel topological findings allow the assessment of brain nonlinear dynamics.
- Relationships between brain functional dimensions and symmetries are elucidated.
- The mind/brain problem is tackled in terms of projections.

UNCORRECTED PROOF

Please cite this article in press as: Tozzi A, et al. Topodynamics of metastable brains. Phys Life Rev (2017), http://dx.doi.org/10.1016/j.plrev.2017.03.001

Available online at www.sciencedirect.com

ScienceDirect

Physics of Life Reviews 21 (2017) 46–55

PHYSICS of LIFE reviews

www.elsevier.com/locate/plrev

Reply to comment

Brain projective reality: Novel clothes for the emperor Reply to comments on "Topodynamics of metastable brains" by Arturo Tozzi et al.

Arturo Tozzi [a,*], James F. Peters [b,c], Andrew A. Fingelkurts [d], Alexander A. Fingelkurts [d], Pedro C. Marijuán [e]

[a] Center for Nonlinear Science, University of North Texas, 1155 Union Circle, #311427 Denton, TX 76203-5017, USA
[b] Department of Electrical and Computer Engineering, University of Manitoba, 75A Chancellor's Circle, Winnipeg, MB R3T 5V6, Canada
[c] Department of Mathematics, Adiyaman University, 02040 Adiyaman, Turkey
[d] BM-Science – Brain and Mind Technologies Research Centre, Espoo, Finland
[e] Bioinformation Group, Aragon Institute of Health Science (IACS), Aragon Health Research Institute (IIS Aragon), Zaragoza, 50009, Spain

Received 15 June 2017; accepted 16 June 2017
Available online 28 June 2017
Communicated by L. Perlovsky

First of all, we would like to gratefully thank all commentators for the attention and effort they have put into reading and responding to our review paper [this issue, Tozzi et al. [44]] and for useful observations that suggest novel applications for our framework. We understand and accept that some of our claims might appear controversial and raise skepticism, because the overall neural framework we have proposed is difficult to frame in established categories, given its strong multidisciplinary character. To make an example, Elsevier is publishing the British Neuroscience Association (BNA) 2017 Special Issue Collection. However, our paper could not fully fit in any of their Special Issues—attention, motivation, behavior; sensory and motor systems; novel treatments and translational neuroscience; genetics and epigenetics; learning and memory; neurodegenerative disorders and ageing; developmental neuroscience; neuronal, glial and cellular mechanisms; neuroendocrine and autonomic nervous systems; psychiatry and mental health; methods and techniques. Perhaps because our paper was mathematically, physically, biologically (neuroscientifically), and phenomenologically motivated from the start? Nevertheless, venturing in novel, fresh, testable proposals is badly needed in contemporary neuroscience, so to break into "the utter darkness of the inner mechanism of psychic acts… during the production of the concomitant phenomena of perception and thought, namely, feelings, consciousness and volition"—as Cajal had already observed in his opus magnus 'Textura'. But as he soberly confessed: "This ideal is still very distant" [38, p. 1,141]. In the pursuit of that very ideal, neuroscience and psychology have had, and continue to have, a plethora of movements and schools of thought: behaviorism, cognitivism, neural Darwinism, social

DOI of original article: http://dx.doi.org/10.1016/j.plrev.2017.03.001.
DOIs of comments: http://dx.doi.org/10.1016/j.plrev.2017.05.001, http://dx.doi.org/10.1016/j.plrev.2017.05.002, http://dx.doi.org/10.1016/j.plrev.2017.04.001, http://dx.doi.org/10.1016/j.plrev.2017.05.005, http://dx.doi.org/10.1016/j.plrev.2017.04.005, http://dx.doi.org/10.1016/j.plrev.2017.03.004, http://dx.doi.org/10.1016/j.plrev.2017.04.003, http://dx.doi.org/10.1016/j.plrev.2017.04.007, http://dx.doi.org/10.1016/j.plrev.2017.04.004.

* Corresponding author.
E-mail addresses: tozziarturo@libero.it (A. Tozzi), James.Peters3@umanitoba.ca (J.F. Peters), andrew.fingelkurts@bm-science.com (An.A. Fingelkurts), alexander.fingelkurts@bm-science.com (Al.A. Fingelkurts), pcmarijuan.iacs@aragon.es (P.C. Marijuán).

http://dx.doi.org/10.1016/j.plrev.2017.06.020
1571-0645/© 2017 Elsevier B.V. All rights reserved.

constructivism, Bayesian optimization...In our paper, we propose to go a step further, via the notion of topodynamics, towards "projectionism." In what follows, trying to elucidate the main features of this Emperor's new clothing, we proceed with the responses to the comments received.

1. Where are the proofs?

Among all the commentators, one (Lerner, [this issue]) has argued that the target paper is lacking the evidence of topological dynamics in the brain. It is somehow unexpected that Lerner fails to see the provided justifications and evidences that are discussed in much detail in the target paper itself. Even though this is a single case, we prefer to address it form the start, since it concerns the validity of our approach. At the same time, constricted by the space limitations of this reply, we can only provide very brief additional comments about that. As suggested by Erdi [this issue], looking at very recently published papers as well as at older ones through a topological lens, we find several methodological clues in favour of our framework.

A torus-like functional structure

An important theoretical prediction of our review paper has been already experimentally confirmed. A torus-like functional structure has been recently reported in functional landscapes' trajectories traced through dynamic EEG brain connectivity data (Xing et al., 2017). Additionally, in their comments Papo [this issue] and Friston [this issue] have pointed out that Finkelstein et al. (2015) demonstrated a 3D head-direction mechanism represented in azimuth × pitch toroidal coordinates in bats, which could support navigation in 3D space. Indeed, consistent with their toroidal model, head-direction pitch-cell tuning was unimodal, circular, and continuous within the available 360° of pitch. Furthermore, our model had predicted diffuse, long-range cortical interactions, in order to allow the brain to "build" the required multidimensional torus-like functional structure. In a recent work, Moore et al. (2017) measured neocortical sub- and supra-threshold dendritic membrane potential from distal-most dendrites in freely behaving rats, and demonstrated that dendritic action potentials firing rates were several-fold larger than somatic ones. Their data also point towards the occurrence of a hybrid, analog-digital coding in the dendrites, equipped with egocentric spatial maps comparable to pyramidal neurons (Moore et al., 2017). This confirms our own prediction that neural activity must not be limited to the "classical" extracellular somatic spikes, but must be extended to other neural structures, such as the dendrites.

Default mode network's symmetries

Tozzi and Peters (2016) described a functional torus occurring during the brain default mode network's activity. This torus must be equipped with antipodal points, i.e., a symmetry in which two brain areas are activated together with the same EEG frequency (or with the same fMRI entropy values). In turn, when the functional torus is "broken", e.g., during the deactivation of the default mode network, this kind of symmetry must be broken. A few years ago Fingelkurts and Fingelkurts (2010) published data that support the idea that in resting state two homologous (symmetrical) EEG channels exhibit the same frequency pattern. Indeed, they showed that analysis of EEG short-term spectral pattern (SP) types in different EEG channels within the same observation revealed that the same type of SP can be observed simultaneously in two EEG channels in 70% of observations during one minute EEG (notice that in the majority of cases these were homologous EEG channels – for example O1-O2 – and therefore have homologous functions).

Complex perceptual stimuli

In full agreement with our proposal that cortical neurons are significantly driven by interactions occurring across stimulus dimensions at all temporal levels and spatial scales, Sloas et al. (2016) were able to quantitatively describe the dependence between neural response and stimulus dimensions. More specifically, they demonstrated that auditory cortical neurons in mice are sensitive to interactions across dimensions, indicating significant integration across stimulus dimensions (such as center frequency, intensity, and bandwidth). This suggests that cortical representations of complex perceptual stimuli are not captured by low-dimensional characterizations.

Emotion and cognition

According to our framework, brain-mind operations (for instance, emotion and cognition) are dual in nature, i.e., they stand for the same activity with different descriptions, despite the fact that emotional states (the so-called emotional feelings) are often treated as different from cognitive states, such as those related to the perception of external stimuli. A recently published paper (LeDoux and Brown, 2017) supports this understanding. It challenges the conventional view which argues that emotions are programmed in subcortical circuits, and proposes instead that emotions are higher-order states instantiated in cortical circuits. They argue that conscious experiences, regardless of their content, arise from one and the same brain neurodynamic architectonics and propose a higher-order theory that accounts for

self-awareness of both conscious and emotional experiences (for a similar conceptualization, see also Fingelkurts et al., 2010a, 2013).

Topological findings

Two novel, recent findings throw a bridge between the Borsuk-Ulam theorem's antipodal points and the symmetric bidirectional connections in local cortical networks. In the first paper, a probabilistic mathematical analysis shows that the occurrences of bidirectional paths and non-random structures are closely linked in a network equipped with pairs of symmetric connections (Hoffmann and Triesch, 2017). This means that an overabundance of reciprocally connected pairs occurs, at least when pairs of neurons or neuronal assemblies are more likely to be connected than others. The second paper (Waskom and Wagner, 2017) is in touch with our prediction that the brain displays matching points (regions) encompassing higher mental functions. Indeed, these authors, examining fine-scaled subnetworks in targeted prefrontal regions, found that pairs of voxels with similar context preferences exhibit spontaneous correlations, approximately twice as large as those between pairs with opposite context preferences. As we have predicted, the regions' features must double, compared with regions encompassing lower mental functions. This means that the abstract representations that support goal-directed cognition are constrained by an intrinsic functional architecture, prompting new models of information representation in the association cortex.

Another recent study points towards a topological organization as an universal mechanism for local density control in cultured neural progenitor cells (NPCs). Kawaguchi et al. (2017) discovered that the NPCs' morphology and macroscopic patterns resulting from cell-to-cell interactions depend on interspersed topological defects with winding numbers of +1/2 and −1/2. Single-cell-level imaging around the defects clarified that cells not only concentrate at +1/2 defects, but also escape from −1/2 defects. A very similar mechanism of instability around (this time reversible) microcolumnar topological defects has been also recently proposed by Tozzi et al. (2017b), in order to explain the possible mechanisms underlying the neural code. Therefore, topological defects might be seen as a general mechanism in biology and neuroscience.

Intraneuronal mechanisms

In touch with Garreffa's comment [this issue], our framework supports the hypothesis that a preparatory, predictive coding is "a priori" located in the brain. Apart from the "classical" meso- and macro-level "predictive coding" accounts by Allen and Friston (2016), it has been recently demonstrated that the micro-level of neuronal intracellular activity is also involved (Mauger et al., 2016): neurons are equipped with a nuclear pool of polyadenylated transcripts that retain selected introns. Regulated intron retention in fully transcribed RNAs represents a mechanism to rapidly mobilize a pool of mRNAs in response to neuronal activity. This means that neurons encompass a stable reservoir of precursors that are then modified, according to the cellular requirements dictated by the different stimuli. In touch with this claim, recent observations underscore the instructive role of intrinsic mechanisms in synapse formation. Indeed, Sando et al. (2017) demonstrated that hippocampal circuits can develop independently of excitatory neurotransmission. This means that synapses assembled in the absence of activity are structurally mature. Loss of release did not disrupt the morphogenesis of presynaptic terminals and dendritic spines, suggesting that synaptic vesicular release of glutamate is unnecessary for synapse, assembly, morphogenesis and maintenance (Sando et al., 2017). See also Navarro et al. (2017) for a general description of the intraneuronal information processing mechanisms, which include tagging molecules for guidance of protein synthesis in postsynaptic spines, in concordance of presynaptic and postsynaptic neuronal activities. Summarizing, we could state that the above described intracellular mechanisms stand for a Kant's a priori, for a Friston's prior, and (in our terms) for a pool of symmetries, available into the neuron *before* its "interaction" with the environment. This means that the influential Locke's account of the mind as a "tabula rasa" filled with environmental sensations needs to be fully rejected.

Last news

A very recent paper, although not quoting us, provides additional support to our multidimensional account of the brain operational architectonics. Reimann et al. (2017) found, in the artificial micro-columnar network developed by the Blue Brain Project, several geometrical structures, termed cliques. The latter are multidimensional, and, in touch with our BUT, display pairwise correlations that increase with dimensions. The results of the study by Riemann et al. (2017) also confirm our theoretical conclusion that brain functions/operations are dual: the same features with matching description can be found both at the micro-levels (shown by Reimann et al. using a computational model of the neuronal network), and at the macro-levels of our multi-dimensional torus surrounding the whole, real, human brain.

2. Is our approach an oversimplification?

Starting from rather simple "abstract" claims, we have built a plausible general framework, able to elucidate disparate "real" phenomena of brain activity. Summarizing our novel topological approach, we observe that, just by taking into account projections among functional or real dimensions in a metastable brain (Fingelkurts and Fingelkurts, 2004, 2017), we achieve a system of mappings that fits very well with experimental results, as argued in the previous paragraphs. However, some commentators (Lerner directly, and, in a more nuanced way, Jausovec [this issue]) have expressed the concern that a mathematical/topological approach to systems features "talks" in rather general and abstract terms,leaving apart the overwhelming complexity of the human brain and the peculiar features of individuals and of single neural processes.

"The unreasonable power of topology in neuroscience"

We, however, in touch with recent claims, ask whether physics of the mind is possible, and whether it is possible to describe the mind based on the few first principles as physics does (Perlovsky, 2016). In our paper, we have tried to go a bit further—paraphrasing a seminal paper of Wigner (1960), we would like to highlight the "unreasonable power of topology in neuroscience". Indeed, elementary topological structures reveal entirely unforeseen connections in the study of brain function: they allow an unexpectedly close and accurate description of neural phenomena in these connections. Using Wigner's words, we may state that topology's enormous usefulness is something bordering on the mysterious, because, although we do not know why topology works so well, however its accuracy seems to override the concerns about its truth and consistency. Indeed, in spite the baffling complexity of the brain (Fingelkurts et al., 2010a), topology leads to the discovery, description, and assessment of certain neurophysiological regularities and invariant properties that can be formulated in terms of accurate mathematical concepts. In our paper, we tried to show how topology plays a sovereign role in the metastable brain affairs, so that the laws of the nervous activity can be formulated in the language of mathematicsand the language of mathematics offers a precise language of nature. Starting from a top-down approach (the neural topology), we tried to assess the apparently irreconcilable physical and psychological "coins" of the brain. In touch with a neutral monistic account of the brain, that emphasizes a common neutral element able to connect the brain and the mind (Fingelkurts et al., 2010b), we believe that the true bridge among them is the mathematics. Of course, this sort of "rationalism" is condemned to metaphysics, unless we do not provide (as we did) testable, empirical previsions, in touch with Quine's naturalized epistemology.

Dynamics of the metastable brain

In his comment, Jausovec [this issue] asked about the proofs of a metastable activity of the brain. We do not think that this is an objection, as he asked this rhetorical question and then answered by himself bringing several examples that show how the brain is indeed functioning in the metastable regime. In fact, a clean definition of metastability is provided in our paper, and it is sufficiently well explained why the neuronal assemblies as well as their larger spatio-temporal conglomerates are metastable. But we are aware that the concept of a metastable, multidimensional brain is not widely recognized and accepted yet, despite active work within this domain in neuroscience (for review see Fingelkurts and Fingelkurts, 2017). A lot of research is still left to be doneand topological concepts that take into account metastable principle might come into play. In this context, the Erdi's comment [this issue] is important. He suggested that a mathematical tool – neuropercolation – could be used to model the metastable regime of brain functioning. Indeed, neuropercolation allows modelling of the collective properties of interacting neural populations in brain networks that are near critical states, when the behavior of the system changes abruptly (Kozma et al., 2005). It provides a useful framework to describe abrupt transitions and critical phenomena in spatially distributed large-scale networks, in particular, in brain metastable networks with transient dynamics, as operational architectonics suggests(Fingelkurts et al., 2010a,b, 2013). Indeed, neuropercolation and topodynamics could be plausibly integrated due to the fact that they both use a topological approach to explore the relation between dynamical sub-systems (neuronal assemblies and their larger spatio-temporal conglomerates), where more abstract representations correspond to higherdimensional spaces (complex OMs).

In this respect, Lerner's critique [this issue] is difficult to tackle, because it relates to mathematical and formal details that have been largely referred to the cited literature. Unexpectedly,he did not go through our references at all. The answers to his questions, in particular concerning all the mathematical proofs, are clearly stated in our previous published and quoted papers, that plainly explain why a decrease in dimensions gives rise to a decrease in energy; why the energetic requirements depend on affine connections and continuous functions; why descriptively similar points and regions do not need necessarily to be antipodal; why two cortical regions with the same entropy values can be assessed together; why many brain functions are believed to occur on functional negative-curvature manifolds; why the term "dimension" does not stand for a spatial one, but for "functional" ones; why more dimensions mean more complexity and information; why the functional cortical paths can be compared to moving particles in a phase space; and finally why neuronal assemblies allow synchronization.

One of the standpoints of our building is the correlation among topological landmarks, information and thermodynamic entropies. This follows the route pursued by Ingarden and Górniewicz (1990), who gave a hierarchical classification of different concepts of shape of compact connected sets, the most general among them being the homological shape. Giving a probability distribution of shapes, we can define a shape entropy, a mean shape

and shape fluctuations. This enables a formulation of information thermodynamics of shape and its applications to different fields, including the physics of the brain.

A topological gauge theory for brain activity

In his comment, Friston[this issue] emphasizes the possible importance of a gauge theory for the assessment of brain function. Here we would like to stress that gauge theories can also be evaluated through the Borsuk-Ulam theorem. Indeed, the three main ingredients required to sketch a gauge theory are: 1) a system equipped with a symmetry and a correlated, measurable Lagrangian; 2) a continuous Lie group of local forces which break the symmetry locally; 3) one or more gauge fields, (possibly) external to the system, able to restore the broken symmetry and to keep the Lagrangian invariant, despite the local forces. The importance of such an approach rests upon the implicit ability to measure unknown quantities: if we know two of the ingredients (for example, the values of the Lagrangian and the total forces applied to the system), we can extrapolate and calculate the value of the third (for example, the gauge field), via procedures from differential geometry such as vectors' and tensors' projections. In a Borsuk-Ulam theorem context, the gauge field stands for the continuous function required to go from one level to another (see**Figure 1** for a simplified sketch).

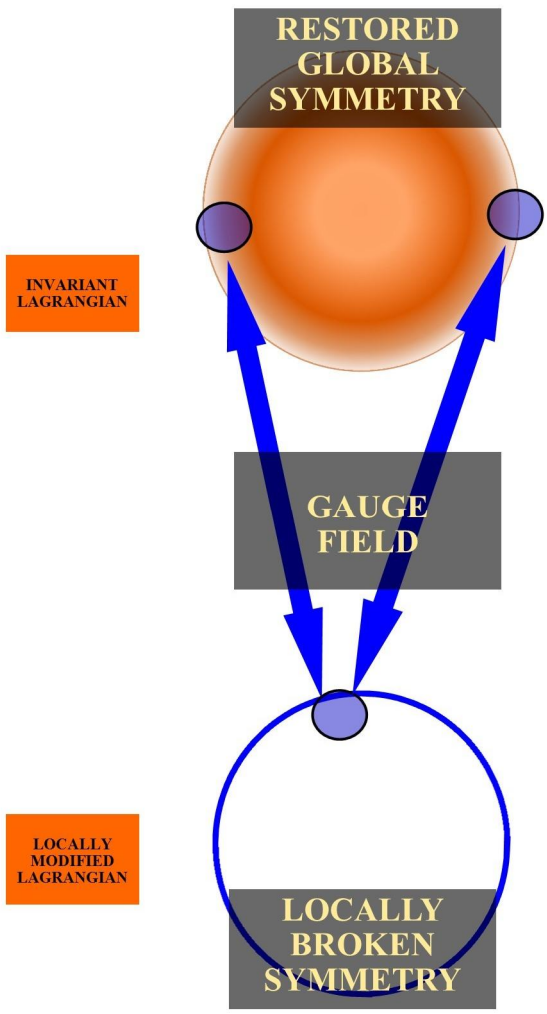

Figure 1. The Borsuk-Ulam theorem in the context of a gauge theory. As Borsuk-Ulam theorem and its variants require a function which needs to be continuous, a gauge theory requires a continuous gauge field. Modified from Tozzi et al., 2017c (forthcoming).

Possible biochemical correlates of brain fourth dimension
Concerning the possible neurophysiological mechanisms involved in our framework of brain multidimensional symmetries, we could achieve further insights by assessing the action mechanism of some active chemical substances. For instance, it is well known that high doses of lysergic acid diethylamide (LSD) may give to a subject the experience of additional spatial or temporal dimensions. Subjects under LSD report that static objects in three dimensions seem to move relative to one or more additional spatial dimensions (Katz et al, 1968). Under LSD, as compared to placebo, a huge increase in correlation among disparate regions in the brain occurs (Carhart-Harris et al., 2017). In particular, the visual cortex increases its connectivity with other brain areas: this helps to explain, in our framework, the increase of spatial and temporal dimensions reported by users. From a pharmacological point of view, LSD leads to cross-activation of 5-HT2A receptor heteromers for a very long time, and increases glutamate release in the cortical layers IV and V, leading to their excitation (Moreno et al., 2011). Therefore, because brain modules' increased synchronization/connectivity is both predicted by our model and artificially achieved via LSD intake, it is tempting to speculate that the features of a physiological four dimension of the brain activity could be correlated with the same biomolecular mechanisms as those that underlie the LSD abnormal subjective effects.

3. Possible further topodynamic developments of the metastable brain

Many commentators, seemingly aware (even more than us) of the hidden potentialities of topological approaches to brain function, propose to use topodynamic accounts also in neural contexts different from the ones we tackled, and in designing mathematical and computational models of fundamental brain-mind processes.

Novel approaches for brain topological dynamics
Garreffa [this issue] suggested to extend the "picture" described by the BUT also to the assessment of non-electric oscillatory activity. In this context, he introduced a mechanical hypothesis (hyper-oscillating system) as an additional operating entity that takes into account, aside of the well-known BOLD-related nervous functions, also the active role of cerebral vascular dynamics in brain function. He wonders whether it is possible to introduce a new "wired" signaling scenario, including cardiac activity and breathing, in Borsuk-Ulam theorem terms. This is in touch with very recent findings, suggesting that cerebrospinal fluid and intracranial venous volume react inversely to changes in intracranial arterial volume (Laganà et al., 2017). Garreffa also wondered whether electromagnetic brain field (EMBF) in IPST level of the brain operational architectonics is the only emergent level that can constitute the OST level, and whether other non-electrical phenomena could be eligible. Yes, indeed, the EMBF is related with other non-electrical fields in the brain and they are interrelated. In this respect, other oscillatory non-electrical phenomena could participate (to some extent, these interrelations are discussed in Fingelkurts et al., 2010a). Furthermore, Cankaya and Deli [this issue] suggested to complement the BUT calculations with the use of the matrix formulations borrowed from quantum mechanics, in order to assess brain activity states. Jausovek [this issue], in his turn, emphasized the possibility of applying our framework to study the individual differences in psychometric intelligence. Specifically, he believes that rate rapid transitional processes (RTPs) in brain activity and their synchronization among different brain locations could be strongly related to intelligence and its type. The preliminary data with RTP's synchrony (a.k.a. "operational synchrony") pointed that this might be a case (Fingelkurts and Fingelkurts, 2002), but further studies with a large sample of subjects are needed. Erdi [this issue] proposed to integrate topodynamics approach discussed in our target paper [Tozzi et al., 2017a, this issue] with neuropercolation model of neural populations with mixed local and non-local interactions.Henry [this issue] suggested the possibility to extend BUT in order to implement the current heterogeneous computing environments and hardware. He proposes very intriguing future scenarios that allow our model to be realized in practical computing applications. For example, he suggests extending topology and proximity in the current state-of-the-art of artificial deep learning neural networks, which are already able to generate a large number of feature vectors (i.e. signals) during training and classification. In order to pursue these useful suggestions, more advanced topological tools, as well as novel, more sophisticated forms of Borsuk-Ulam theorem are required. To make an example, instead of antipodal points or regions on the surface of a hypersphere (in our case, the brain), we could assess antipodal "Cech complexes", i.e., collections of intersecting neighborhoods (called balls) on the cortical surface. Such complexes could give us further reach in projections to higher-dimensional spaces. The trick is to consider the description of a Cech complex on the surface of a sphere: while in 3D the intersecting balls would be glued to the surface of a 3D hypersphere, in 2D the balls are intersection circles (all having elements in common).

Assessing complex phase spaces
As proposed by Friston [this issue] and Papo [this issue], the brain activity, instead of occurring in the "classical" Euclidean space of the central nervous system anatomy, might take place in metric and statistical functional spaces with particular geometries. To make an example, the sophisticated functional spaces of brain nonlinear dynamics suggested by Papo require manifolds much more complex than the "classical" 3D timespace. Topodynamics, with its

emphasis on symmetries on abstract manifolds, allows to embed brain trajectories, detected both by EEG and functional neurotechniques, on countless abstract manifolds, in order to improve the knowledge of their dynamics. Apart from the toroidal surfaces described in the main article (Tozzi et al., 2017a, this issue) other possible examples of abstract metric spaces where to cast nervous representation and inference problems are provided in **Figure 2**.
Furthermore, other mathematical/topological approaches are worth to be pursued: in such a vein, the brain antipodal points might stand for Riemannian toroidal surfaces. They can be (relatively) easily studied, because the mathematics able to explain trajectories on torus-like structures is already available. Further, in our target paper we did not talk about yet another peculiar feature of the Borsuk-Ulam theorem: the projections. We stated that matching descriptions in R^n map to a single description in R^{n-1}. But we did not take into account that both R^n and R^{n-1} could be embedded in a manifold of higher dimensions, say R^{n+1}. Considering this possibility means that the projections (imagine them as double-arrowed lines) from R^n *to* R^{n-1} might belong to a widerdimensional spectrum that includes also R^{n+1}. The above-mentioned double-arrowed lines could be of different length, depending on the distance between R^n and R^{n-1}. A different arrow length might stand for the intensity of the force required to make the mappings. The closer R^n is to R^{n-1}, the shorter the line, and the lesser the required energy to perform the projection. In sum, we achieve a single system, that we might call the "multi-BUT", equipped with three levels of dimensions, instead of the canonical two of the classical BUT. Considering projections takes us into a completely novel mathematical territory to explore: the fibre bundle territory.

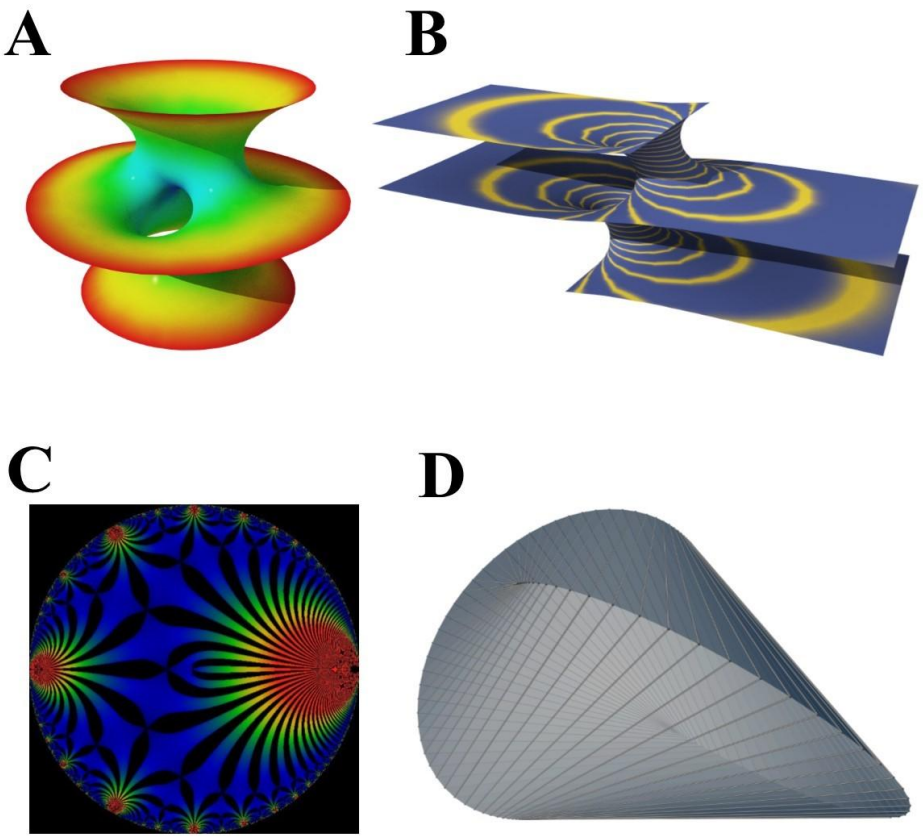

Figure 2. Possible abstract manifolds where to embed real brain activities. Changes in curvatures on such manifolds, in touch with information geometry, might stand for differences in mental or brain activities. **2A**: Costa's three ended, complete embedded, minimal surface. **2B**: Riemann's minimal surface; three levels are rendered, with a texture showing that the intersection with horizontal planes is circular. **2C**: Real part of the complex j-invariant as a function of the nome q on the unit disk. This type of repetitive modular oscillation has been recently found in the electric rhythms of the human EEG (Tozzi et al., 2017d). **2D**: Oloid surface, where patches can be flattened into a

plane; while rolling on a flat surface, its center of mass performs a motion different from a linear one. (Credits. **A** and **B**: Anders Sandberg, CC BY-SA 3.0; **C**: Linas Vepstas, CC BY-SA 3.0; **D**: KoenB, Share Alike 3.0 Unported).

Pairwise tool and the brain

As noted by Kakiashvili et al.'s [this issue], pairwise comparisons (PCs) could be "paired" with our topodynamical approach. This is in touch with their recent geometric interpretation of PCs in terms of the differential-geometric notion of holonomy, that might allow brain research to be directly related to intuitive, invariant geometric explanations in terms of abstract manifolds. For example, Oizumi et al. (2017) proposed a holistic framework, based on the same information geometry suggested by Friston [this issue]. Their measure of integration quantifies the strength of multiple causal influences among elements, by projecting the probability distribution of a system onto constrained manifolds. The amount of *integrated information* is geometrically interpreted as the divergence between the actual probability distribution of a system and an approximated probability distribution, where causal influences among elements are statistically disconnected. Further, Mailly et al. (2017) recently described a computerized method to build a multi-modal and multi-dimensional model of brain structures based on series of Acetylcholinesterase and Nissl stained sections, providing powerful tools for integration of observations derived from various technical approaches. In this context, another tool might come into play: the de Rham cohomology (Hazewinkel, 2001). It is a tool belonging both to algebraic and differential topology, capable of expressing basic topological information about smooth manifolds in a form particularly adapted to the concrete representation of computations and differential equations. Summarizing, such novel developments open the road to recognition of classical topological-geometric invariants, where the latter provide characteristic classes of simple geometric structures, such as closed compact manifolds, which are part of the Borsuk-Ulam theory.

Computational scenarios of neural Darwinism

If finally the king is naked, as suggested by Friston [this issue], and our projectionism holds true, what happens to a 3D (plus time) input (say the visual scene of a cat), when it is projected onto the higher-dimensional functional manifolds endowed in our brain? Does our central nervous system encompass two (or more) antipodal representations of the cat? Could the two (or more) mental images with matching description encompass, for example, both the emotional and rational aspects of the cat (such as tenderness and genus)? What if one of the antipodal images is located, say, in the insula (where emotions are produced), and the other in the frontal lobe (where rationality lies); or one image is located in the "what" ventral pathway (that describes the stored memory of the cat), and the other in the "where" dorsal pathway (that describes the bodily motor response of our organism to the cat's view)? Such theoretical 4D cat locations might explain why the brain code is believed to be sparse, and why a brain site for the consciousness has never been found. The several mental features of the cat (rational, emotional, motor responses to its view) might be scattered in different nervous areas with matching description, lying on different trajectories of the functional multidimensional torus. A computational model describing this scenario has been recently tackled by Tozzi and Peters (2017). They introduced a variant of Selfridge's Pandemonium (i.e., a winner-takes-all, hierarchic, Darwinian, parallel, neural architecture) that takes into account two novel architectural features, namely: a) "demons" able to recognize topological features of visual scene shapes, and b) low-level representations of objects in our environment mapped to higher-dimensional neural networks.

To conclude our reply, we would like to develop the "evolutionary" comment by Jausovec [this issue], with which we agree, when he mentions Jerison's views (1991) about the brain as a "mapping machine", in which maps are different representations of the external world, so that the number of these maps is related to the complexity of viewing and representing the environment. This is in complete agreement with our tenet that the brain function lies in dimensions higher that the external world. Recent descriptions of the projective architecture in the nervous systems of invertebrates (Hartenstein, 2017) and in the central nervous system of vertebrates (Wullimann, 2017) corroborate the amazing extension and complexity of their mapping systems. Indeed, "the topological inventions of life" (Marijuán, 1997) have represented the most fundamental evolutionary processing tool for the organism (and its central nervous system) *being in the world*. Our framework explains why hominids have larger brain, compared with other animals: the surplus of neurons, connections and nodes allow to assemble a larger (multidimensional) functional phase space, different from the environmental 3D plus time, where the more advanced human mental computations might take place. Therefore, the true reductionist level that explains the human mind is located in this large phase space, whatever its still unknown shape could be. It is also the gist of Friston's [this issue] elegant closing comment: the elusive phenomenon of consciousness has escaped "topodynamically" to higher dimensions.

REFERENCES

1) Allen M, Friston KJ. 2016. From cognitivism to autopoiesis: towards a computational framework for the embodied mind. Synthese, DOI 10.1007/s11229-016-1288-5
2) Carhart-Harris RL, Muthukumaraswamy S, Roseman L, Kaelen M, Droog W, et al. 2017. Neural correlates of the LSD experience revealed by multimodal neuroimaging. PNAS, 113 no. 17, 4853–4858, doi: 10.1073/pnas.1518377113
3) Chankaya MN, Deli E. 2017. Changes in brain entropy are related to abstract temporal topology. Comment on “Topodynamics of metastable brains” by Tozzi et al. Physics of Life Reviews, “this issue”.
4) Erdi P. From phase transitions to the topological renaissance. Comment on "Topdynamics of Metastable Brains" by Arturo Tozzi et al. Physics of Life Reviews, “this issue”.
5) Fingelkurts A.A., Fingelkurts A.A. Short-term EEG spectral pattern as a single event in EEG phenomenology. The Open Neuroimaging Journal, 2010, 4, 130-156.)
6) Fingelkurts AA, Fingelkurts AA, Neves CFH. Consciousness as a phenomenon in the operational architectonics of brain organization: Criticality and self-organization considerations. Chaos, Solitons & Fractals 2013; 55:13–31.
7) Fingelkurts AA, Fingelkurts AA, Neves CFH. Emergentist monism, biological realism, operations and brain–mind problem: Reply to comments on “Natural world physical, brain operational, and mind phenomenal space–time” by An.A. Fingelkurts, Al.A. Fingelkurts, C.F.H. Neves. Physics of Life Reviews 2010b;7(2): 264–268.
8) Fingelkurts AA, Fingelkurts AA, Neves CFH. Natural world physical, brain operational, and mind phenomenal space–time. Physics of Life Reviews 2010a; 7(2):195–249.
9) Fingelkurts AA, Fingelkurts AA. Exploring giftedness. In: Advances in Psychology Research, Vol. 9, Nova Science Publishers, 2002, pp. 137-155.
10) Fingelkurts AA, Fingelkurts AA. Information flow in the brain: Ordered sequences of metastable states. Information 2017, 8, 22; doi:10.3390/info8010022.
11) Fingelkurts AA, Fingelkurts AA. Making complexity simpler: multivariability and metastability in the brain. Intern. J. Neuroscience, 2004; 114:843–862.
12) Finkelstein A, Derdikman D, Rubin A, Foerster JN, Las L, Ulanovsky N. 2015. Three-dimensional head-direction coding in the bat brain. Nature 517, 159–164 (08 January 2015) doi:10.1038/nature14031
13) Friston. 2017. The Emperor’s new topology. Comment on "Topodynamics of Metastable Brains" by Arturo Tozzi et al. Physics of Life Reviews, “this issue”.
14) Garreffa G. 2017. The Physics Inside our Brain. Comment on "Topodynamics of Metastable Brains" by Arturo Tozzi et al. Physics of Life Reviews, “this issue”.
15) Hartenstein V. The Central Nervous System of Invertebrates. In: The Wiley Handbook of Evolutionary Neuroscience. Stephen V. Shepherd (ed.). John Wiley & Sons, Ltd. Chichester, UK, pp: 173-235.
16) Hazewinkel M. 2001. De Rham cohomology. Encyclopedia of Mathematics, Springer, ISBN 978-1-55608-010-4
17) Henry CJ. 2017. A Computational Discussion on Brain Topodynamics Comment on "Topodynamics of Metastable Brains" by Arturo Tozzi et al. Physics of Life Reviews, “this issue”.
18) Hoffmann FZ, Triesch J. 2017. Nonrandom network connectivity comes in pairs. Network Neurosci. Winter 2017, Vol. 1, No. 1, Pages: 31-41
19) Ingarden RS, Górniewicz L. 1990. Shape as an Information-Thermodynamical Concept and the Pattern Recognition Problem. Mathematische Nachrichten. 145, 1, 97–109. DOI: 10.1002/mana.19901450108
20) Jaušovec N. 2017. The neural code of thoughts and feelings: Comment on “Topodynamics of metastable brains” by Tozzi et al. Physics of Life Reviews, “this issue”.
21) Jerison, H., 1991. Brain Size and the Evolution of Mind. American Museum of Natural History, New York.
22) Kakiashvili T, Koczkodaj WW, Magnot J-P. 2017. Approximate reasoning by pairwise comparisons as a possible: Supplement to “Topodynamics of metastable brains” by Arturo Tozzi, et al. Physics of Life Reviews, “this issue”.
23) Katz MM, Waskow IE, Olsson J. 1968. Characterizing the psychological state produced by LSD". J Abnorm Psychol. 73 (1): 1-14. doi:10.1037/h0020114. PMID 5639999.
24) Kawaguchi K, Kageyama R, Sano M. 2017. Topological defects control collective dynamics in neural progenitor cell cultures. Nature (2017) doi:10.1038/nature22321
25) Kozma R, Puljic M, Balister P, Bollobas B, Freeman WJ. (2005) Phase transitions in the neuropercolation model of neural populations with mixed local and non-local interactions. Biol Cybern 92(6):367–379.
26) Laganà MM , Shepherd SJ, Cecconi P, Beggs CB. 2017. Intracranial volumetric changes govern cerebrospinal fluid flow in the Aqueduct of Sylvius in healthy adults. Biomedical Signal Processing and Control, 36, 84–92
27) LeDoux JE, Brown R. 2017. A higher-order theory of emotional consciousness. PNAS, Vol. 114 no. 10, E2016–E2025, doi: 10.1073/pnas.1619316114

28) Lerner VS. Letter to Editor: Comment on “Topodynamics of metastable brains” by Tozzi et al. Physics of Life Reviews, “this issue”
29) Mailly P, Haber SN, Groenewegen HJ, Deniaud J-M. 2017. A 3D multi-modal and multi-dimensional digital brain model as a framework for data sharing. Journal of Neuroscience Methods. Volume 194, Issue 1, 15 December 2010, Pages 56–63. http://doi.org/10.1016/j.jneumeth.2009.12.014
30) Marijuan PC. 1997. The topological inventions of life: From the specialization of multicellular colonies to the functioning of the vertebrate brain. World Futures 50 (1): 617-631.
31) Mauger O, Lemoine F, Scheiffele P. 2016. Targeted Intron Retention and Excision for Rapid Gene Regulation in Response to Neuronal Activity. Neuron. 2016 Dec 21;92(6):1266-1278. doi: 10.1016/j.neuron.2016.11.032.
32) Moore JJ, Ravassard PM, Ho D, Acharya L, Kees AL, Vuong C, Mehta MR. 2017. Dynamics of cortical dendritic membrane potential and spikes in freely behaving rats. Science. 2017 Mar 24;355(6331). pii: eaaj1497. doi: 10.1126/science.aaj1497. Epub 2017 Mar 9.
33) Moreno JL, Holloway T, Albizu L, Sealfon SC, González-Maeso J. 2011. Metabotropic glutamate mGlu2 receptor is necessary for the pharmacological and behavioral effects induced by hallucinogenic 5-HT2A receptor agonists. Neurosci Lett. 2011 Apr 15;493(3):76-9. doi: 10.1016/j.neulet.2011.01.046. Epub 2011 Jan 27.
34) Navarro J, del Moral R, Marijuán PC. Intraneuronal Computation. Charting the Signaling Pathways of the Neuron. In: The Wiley Handbook of Evolutionary Neuroscience. Stephen V. Shepherd (ed.). John Wiley & Sons, Ltd. Chichester, UK, pp: 49-87.
35) Oizumi M, Tsuchiya N, and Amari S-i. 2017. Unified framework for information integration based on information geometry. PNAS, vol. 113 no. 51, 14817–14822, doi: 10.1073/pnas.1603583113
36) Papo D. 2017. Beyond the anatomy-based representation of brain function: Comment on “Topodynamics of metastable brains” by Arturo Tozzi et al. Physics of Life Reviews, “this issue”.
37) Perlovsky LI. Physics of the Mind. Front SystNeurosci. 2016 Nov 15;10:84. eCollection 2016.
38) Ramon y Cajal S. 1899-1904. Textura del sistema nervioso del hombre y de los vertebrados. N. Moya. Madrid. pp:1141. English edition 1995, Oxford University Press, New York.
39) Reimann MW, Nolte M, Scolamiero M, Turner K, Perin R, et al. 2017. Cliques of Neurons Bound into Cavities Provide a Missing Link between Structure and Function. Front. Comput. Neurosci., 12 June 2017 | https://doi.org/10.3389/fncom.2017.00048
40) Sando R, Bushong E, Zhu Y, Huang M, Considine C, et al. 2017. Assembly of Excitatory Synapses in the Absence of Glutamatergic Neurotransmission. Neuron, 94, 2, 312–321.e3.
41) Sloas DC, Zhuo R, Xue H, Chambers AR, Kolaczyk E, Polley DB Sen K. 2016. Interactions across Multiple Stimulus Dimensions in Primary Auditory Cortex. eNeuro 11 August 2016, ENEURO.0124-16.2016; DOI: https://doi.org/10.1523/ENEURO.0124-16.2016
42) Tozzi A, Peters JF. 2016. Towards a Fourth Spatial Dimension of Brain Activity. Cognitive Neurodynamics 10 (3): 189–199. doi:10.1007/s11571-016-9379-z.
43) Tozzi A, Peters JF. 2017. A Novel Pandemonium Architecture Based on Visual Topological Invariants and Mental Matching Descriptions. viXra:1705.0223.
44) Tozzi A, Peters J, Fingelkurts AA, Fingelkurts AA, Marijuan P. 2017a. Topodynamics of metastable brains. Physics of Life Reviews, “this issue”.
45) Tozzi A, Peters JF, Ori O. 2017b. Cracking the barcode of fullerene-like cortical microcolumns. Neurosci Letters. 644, 100–106. http://dx.doi.org/10.1016/j.neulet.2017.02.064.
46) Tozzi A, Sengupta B, Peters JF, Friston KJ. 2017c. Gauge Fields in the Central Nervous System. In: The Physics of the Mind and Brain Disorders: Integrated Neural Circuits Supporting the Emergence of Mind, edited by Opris J and Casanova MF. New York, Springer; Series in Cognitive and Neural Systems. ISBN: 978-3-319-29674-6. Forthcoming.
47) Tozzi A, Peters JF, Jausovec N. 2017d. A repetitive modular oscillation underlies human brain electric activity. Neurosci Lett. 10.1016/j.neulet.2017.05.051 (in press).
48) Waskom ML, Wagner AD. 2017. Distributed representation of context by intrinsic subnetworks in prefrontal cortex. PNAS, vol. 114 no. 8 > Michael L. Waskom, 2030–2035
49) Wigner E. 1960. The Unreasonable Effectiveness of Mathematics in the Natural Sciences. In: Communications in Pure and Applied Mathematics, vol. 13, No. I. New York: John Wiley & Sons, Inc.
50) Wullimann MF. Nervous System Architecture in Vertebrates.In: The Wiley Handbook of Evolutionary Neuroscience. Stephen V. Shepherd (ed.). John Wiley & Sons, Ltd. Chichester, UK, pp: 236-278.
51) Xing M, Ajilore O, Wolfson OE, Abbott C, MacNamara A, et al. Thought Chart: Tracking Dynamic EEG Brain Connectivity with Unsupervised Manifold Learning. Brain Informatics and Health. Series: Lecture Notes in Computer Science, Year: 2016, Volume 9919, Page 149 DOI: 10.1007/978-3-319-47103-7_15

Progress in Biophysics and Molecular Biology 131 (2017) 494–496

Contents lists available at ScienceDirect

Progress in Biophysics and Molecular Biology

journal homepage: www.elsevier.com/locate/pbiomolbio

Postface: Heidegger's being and quantum vacuum☆

A dialogue between Martin Heidegger and a theoretical physicist, namely Richie, unveils the striking relationships between the Eastern and Western philosophical concepts of Being and the experimentally detectable quantum vacuum. We provide an account of long-standing theoretical issues, such Being, Entity, Existence and the unique role of human Thought in the world, and expound their possible physical counterparts.

RICHIE: Hi!

MARTIN: Hi! It has been a long time … How are you? What are you doing?

RICHIE: I'm studying the vacuum.

MARTIN: The vacuum?

RICHIE: Yes. In quantum field theory, the vacuum stands for the state with the lowest possible energy.

MARTIN: Do you mean that the vacuum state stands for an empty Nothing?

RICHIE: Not exactly … It is a mistake to think the vacuum as some absolutely empty void. The quantum vacuum is not truly empty, but contains instead fleeting electromagnetic waves and particles.

MARTIN: You talk about energy, electromagnetic waves, particles …

RICHIE: Yes. The quantum vacuum is the chunk of our Universe where energy and matter are the lowest possible.

MARTIN: What do you mean for energy and matter?

RICHIE: Energy and matter are the "real" part of our Universe. They are just two sides of the same coin. Indeed, in a state of very low energy, particles of matter cannot be produced. However, when the energy increases beyond a certain threshold, a particle is produced.

MARTIN: Are particles and energy characterized by essence? Are they entities? Or what else?

RICHIE: It depends on what you mean … According to you, what is Being? And Entity? Does the Being exist, or what?

MARTIN: There is a deep difference among Entity, Being and Existence. Science is able to study just the Entity, not the Being. Indeed, the Entity can be represented and reckoned, while the Being is not describable. In my writings, I attempted to turn away from questions concerning Entities to questions about Being, and to recover the most fundamental philosophical question: what does it mean for something to Be?

RICHIE: Mmm … difficult, but intriguing … do your Entities exist? What is Existence according to you? Does Existence mean that a stone, or an animal, or a human being, are located in time? Is Existence correlated with time passing?

MARTIN: Not exactly. I retain the term Existence just for humans. Stones and animals simply Are, while humans do Exist. Existence means to be-into, being-in-the-world. Existence lies into the glade of Being. Existence is a feature just of a human individual able to think, because it means consciousness. Stones and animals do not display consciousness. Indeed, human Thought is the truth of the Being.

RICHIE: You talk about a glade of Being. What about humans and consciousness? Do they stand into such glade? Or do they look at it from afar? Where are humans, and consciousness, located? What is the place of Existence?

MARTIN: The Being is a glade, where the home of Language is located. The human individual lives into the home of Language. We humans are gardeners of the Being, we take care of the Being, because we are the sole Entity able to think, although indistinctly, the Being. Through Language, humans are able to assess just the Entity, while there are no words in order to describe the Being. The Being lacks a representation, contrary to the Entity. The Being does not let himself to be represented as an object does.

RICHIE: In such a vein, I could try to answer your question about particles and energy. Particles and energy are Entities, describable and quantifiable by human language and by scientific accounts …

MARTIN: It is reasonable. Indeed, science, and also metaphysics, are able to describe and illustrate the Entity, rather that the Being. The scientific object of investigation is the Entity alone.

RICHIE: However, it's curious … my vacuum is similar to your Being … The quantum vacuum might very well stand for your glade of the Being.

MARTIN: I don't think so. If you, who are a scientist, study the vacuum, this means that the vacuum is not the Being, rather an Entity. Indeed, scientists are able to assess just Entities.

RICHIE: In this case, what you say does not hold true. Indeed, the vacuum displays features that are closer to the Being than to the Entity.

MARTIN: Which ones?

RICHIE: The vacuum that we scientists compare to a sort of undefined foam cannot be properly described by ordinary language. This is because quantum phenomena are weird, beyond the common sense, and escape every possible description. The vacuum obeys quantistic laws … That means that the vacuum cannot be uttered by the human Language. Our verbal skills are simply not fitted to pronounce the mechanisms of quantum dynamics, in the same way that it is unfeasible for humans to describe the Being. The language of Being cannot talk about the unspoken; the unspoken, in this case, is the Language of quanta. Quantum dynamics, as well as the Being, cannot be described through images or words.

☆ This postface is paying a homage to Albert Einstein and Rabindranath Tagore who carried out a famous discussion about the nature of reality, which took place at Einstein's house in Caputh, near Berlin, on July 30th, 1930. https://www.scienceandnonduality.com/wp-content/uploads/2014/09/einstein_tagore.pdf, visited on 01.08.2017.

http://dx.doi.org/10.1016/j.pbiomolbio.2017.07.009
0079-6107

MARTIN: Certainly, Existence is a structurally open possibility-for-Being. But … what about time? Existence is the Being into history. The human individual is fundamentally structured by its Temporality, or its concern with time.

RICHIE: Good question. To be sure, there is also another relationship between the foam of the vacuum and the glade of the Being. The quantum foam moves relentlessly, but time and causality do not apply inside it. Quantum phenomena are time-reversible and cause/effect associations entirely disappear. We are in front of a timeless foam, where the future and the past are lost into infinite bubbles.

MARTIN: There is still a problem to solve. A foremost one. Existence is the Being in time. Existence is finite and is into time. How can you explain the crucial step, from the Being's timelessness to the Existence thrown into the historical Universe? Can such a path be described when you start from a physical, indescribable Being?

RICHIE: Let me think about … Yes, I think it is possible, through a physical inquiry … Let's see … the microscopic quantum world located in the vacuum stands for the glade of Being, while the matter and energy of the macroscopic world stand for your Entities. The Entities are grounded, encompassed into the Being … and there is, I believe, a physical way to try to describe their strange relationship.

MARTIN: What is it? I'm very curious … And I do not know if I'm happy or I'm not … Indeed, we are trying to give physicality to my philosophy, and I'm not sure I like it …

RICHIE: The vacuum is a very dynamic system. It continuously produces fleeting particles from its energy, but such particles are called "virtual" because they are annihilated almost instantaneously. We are in front of the most counterintuitive, yet one of the most important, principles in quantum mechanics: vacuum is by no means empty nothingness, because it is full of various particles that are continuously fluctuating in and out of Entity. They appear, are Entities for a brief moment, and then disappear again. Every one blinks into Existence with its antimatter counterpart, then both quickly annihilate and fall back into the vacuum. Therefore, the energetic balance inside the vacuum is always zero. It is believed that such vacuum fluctuations, i.e., the constant appearance and disappearance of virtual particles, may have a connection with the "dark energy" that drives the accelerated expansion of the Universe.

MARTIN: If such virtual particles are so feeble that they not reach the status of Entity, how could the Entities in our observable Universe arise from the vacuum?

RICHIE: In very rough terms, it has been demonstrated that large energetic fluctuations in the vacuum are able to produce real particles that abruptly appear in our Universe. Some theories state that our Universe might have been generated from the vacuum. This process, called inflation, has been claimed in order to explain the Big Bang, i.e., the origin of our Universe. An abrupt change in the energy vacuum produced a huge number of particles, the ones we currently see in our Universe. In technical terms, and forgive me for this physical afterthought, it is feasible that a high energetic state of false vacuum abruptly felt towards a lower energetic basin of the real vacuum. This process led to an inflationary mechanism, e.g., the production of a huge amount of anti-gravitational energy which caused cosmic dilation and generation of real particles in our Universe.

MARTIN: Oh! I understand. Therefore, the Being is the Vacuum and the particles are the Entities. This means …

RICHIE: This means that it is possible to generate Entities from the Being. The glade of Being, due to a modification intrinsic to the same Being, is populated with Entities. And also with Existence, e.g., the human individual able to think. There is also another relationship between the Being and the quantum vacuum that must be kept into account. On the one hand the Being displays an infinite set of possibilities; on the other hand, the vacuum produces an infinite set of virtual particles. Just a few of them enter the real world in guise of real particles. It resembles the mechanism that gives rise to Entities and Existence from the Being.

MARTIN: Yes. It fits my framework. The Being is the truth and is also the Possible, i.e., the possibility of Entities and Existence. When the finite, time-embedded Existence arises from the vacuum of the Being, it "becomes" something that is still to be exploited, something that can be thought as posed.

RICHIE: But, on the other side, the rise of the Universe is something irreversible. That means a closure of our countless possibilities for being through time …

MARTIN: And that also means the finitude of time and our Being-towards-death, as I stated more than once …

RICHIE: Yes. As well as quantum dynamics needs an observer to be thought and assessed, the Being sets the human individual in order to take care of itself. Both quantum mechanics and the Being require consciousness able to cope with them, in order to be fully elucidated.

MARTIN: Indeed, Existence is defined by Care, a practically engaged mode of Being-in-the-world. Thinking is thinking about things originally discovered in our practical engagements.

RICHIE: Practical engagement is also the exploration of the vacuum, which involves a truthful relationship to our "thrownness" into a world that we are "always already" concerned with.

MARTIN: The Existence, that finds itself thrown into the world amidst things and with others, is thrown into its possibilities. Human individuals need to assume these possibilities, in order to assess the inmost individuality of the world. If I compare the vacuum with the Being, I lose the primeval openness of the Existence towards the Being. I just achieve the despicable openness to the "will to power" of the scientist and the contemporary human subject …

RICHIE: If you focus less on the way in which the structures of Being are revealed in everyday behavior and in subjects, and more on the way in which behavior itself depends on a prior "openness to being", you achieve what you require, i.e., that the Essence of being human is the maintenance of this openness.

MARTIN: Therefore, Thinking stands for a reflecting upon this more original way of discovering the world ….

[LOUDSPEAKER]: … passengers of the flight 1976 to the Black Forest …

MARTIN: It's my flight. I have to go.

RICHIE: OK. It has been a pleasure to meet you.

MARTIN: I am going to think about your quantum vacuum in my beloved Todtnauberg.

RICHIE: And I am going to my beloved CERN to think about your Being …

References

The above dialog is based on the following fundamental literature:

DeWitt, B.S., 1967. Quantum theory of gravity II. The manifestly covariant theory. Phys. Rev. 160, 1195–1239.
Ellwanger, U., 2012. From the Universe to the Elementary Particles. A First Introduction to Cosmology and the Fundamental Interactions. Springer-Verlag, Berlin Heidelberg, ISBN 978-3-642-24374-5.
Heidegger M. 1962 (1927). Being and Time. SCM Press, London.
Heidegger M. 2006 (1929). Che cos'è metafisica? Adelphi, Milano.
Heidegger M. 2013 (1946). Lettera sull'"Umanismo". Adelphi, Milano.
Moreva, E.V., Brida, G., Gramegna, M., Giovannetti, V., Maccone, L., Genovese, M., 2013. Time from quantum entanglement: an experimental illustration. Phys. Rev. A 89, 052122.
Wilson, C.M.G., Pourkabirian, J.A., Simoen, M., Johansson, J.R., Duty, T., et al., 2011. Observation of the dynamical Casimir effect in a superconducting circuit. Nature 479, 376–379.
Zeidler, E., 2011. Quantum Field Theory III: Gauge Theory. Springer-Verlag, Berlin, Heideberg.

Arturo Tozzi*
Center for Nonlinear Science, University of North Texas, 1155 Union Circle, #311427, Denton, TX 76203-5017, USA

Computational Intelligence Laboratory, University of Manitoba, Winnipeg, R3T 5V6 Manitoba, Canada

James F. Peters
Department of Electrical and Computer Engineering, University of Manitoba, 75A Chancellor's Circle, Winnipeg, MB R3T 5V6, Canada

Department of Mathematics, Faculty of Arts and Sciences, Adıyaman University, 02040 Adıyaman, Turkey

Computational Intelligence Laboratory, University of Manitoba, WPG, MB, R3T 5V6, Canada
E-mail address: james.peters3@umanitoba.ca.

Raquel del Moral, Pedro C. Marijuán
Grupo de Bioinformación/Bioinformation Group, Instituto Aragonés de Ciencias de la Salud (IACS), Instituto de Investigación Sanitaria Aragón (IIS), Edificio CIBA. Avda. San Juan Bosco, 13, 50009 Zaragoza, Spain
E-mail addresses: rdelmoral.iacs@aragon.es (R. del Moral), pcmarijuan.iacs@aragon.es (P.C. Marijuán).

* Corresponding author. Center for Nonlinear Science, University of North Texas, 1155 Union Circle, #311427, Denton, TX 76203-5017, USA.
E-mail address: tozziarturo@libero.it (A. Tozzi).

Available online 25 July 2017

Chapter 2

GAUGE FIELDS IN THE CENTRAL NERVOUS SYSTEM

Arturo Tozzi
Center for Nonlinear Science, University of North Texas
1155 Union Circle, #311427
Denton, TX 76203-5017 USA
Computational Intelligence Laboratory, University of Manitoba
Winnipeg R3T 5V6 Manitoba

Biswa Sengupta
Department of Engineering (Information Engineering)
University of Cambridge
Cambridge, United Kingdom

James F. Peters
Department of Electrical and Computer Engineering, University of Manitoba
75A Chancellor's Circle, Winnipeg, MB R3T 5V6 Canada and
Mathematics Department, Adıyaman University 02040 Adıyaman, Turkey

Karl J. Friston
Wellcome Trust Centre for Neuroimaging, University College London, London, United Kingdom

ABSTRACT

Recent advances in neuroscience highlight the complexity of the central nervous system (CNS) and call for general, multidisciplinary theoretical approaches. The aim of this chapter is to assess highly organized biological systems, in particular the CNS, via the physical and mathematical procedures of gauge theory – and to provide quantitative methods for experimental assessment. We first describe the nature of a gauge theory in physics, in a language addressed to an interdisciplinary audience. Then we examine the possibility that brain activity is driven by one or more continuous forces, called *gauge fields*, originating inside or outside the CNS. In particular, we go through the idea of *symmetries*, which is the cornerstone of gauge theories, and illustrate examples of possible gauge fields in the CNS. A deeper knowledge of gauge theories may lead to novel approaches to (self) organized biological systems, improve our understanding of brain activity and disease, and pave the way to innovative therapeutic interventions.

INTRODUCTION

Current technical advances in systems neuroscience (Dayan et al., 2013; Mattei, 2014; Huth et al., 2016; Taylor et al., 2016) try to establish causal relations between specific aspects of neuronal activity and system-level consequences. Multidisciplinary theoretical approaches, which offer a bridge connecting the scientific languages of biology, mathematics and physics, are clearly required. One might wonder if the unpredictable complexity of biology – neuroscience included – could hope for that kind of theories. An affirmative answer results from a treatment of living systems – and in particular the central nervous system (CNS) – via the physical and mathematical procedures of a gauge theory approach.

A possible role for gauge fields (Sengupta et al., 2016a) and symmetries (Tozzi and Peters 2016a) has been recently proposed in order to elucidate physiological and pathological features of brain activity. In the search for a dynamic interplay, a cross-over of the physics of elementary particles and cortical brain dynamics, gauge theory takes into account the possibility that brain activity is driven by one or more continuous forces represented by gauge fields, originating inside or outside the CNS. Three main ingredients are required to sketch gauge theory of the CNS:

- A system equipped with a symmetry and a correlated, measurable Lagrangian
- A continuous Lie group of local forces (transformations) which break the symmetry locally.
- One or more gauge fields, (possibly) external to the system, able to restore the broken symmetry and to keep the Lagrangian invariant, despite the local transformations.

The importance of such an approach rests upon the implicit ability to measure unknown quantities: if we knew two of the ingredients (for example, the values of the Lagrangian and the total forces applied to the system), we can extrapolate and calculate the value of the third (for example, the gauge field), via procedures from differential geometry. Indeed, vector projections can be used in order to assess CNS diseases in the powerful probabilistic framework of gradient descent trajectories along manifolds equipped with negative curvatures (Sengupta et al., 2016b).

The three above mentioned ingredients are interchangeable. System, local forces and gauge field may indeed play different

roles in the CNS, depending on our initial assignment. Sengupta et al. (2016a, 2016b) framed the required ingredients in the context of the free-energy principle and focused on the methodological implications of gauge theory for parameterisation and new inference schemes in data analysis. There are, however, other neurobiological possibilities, that speak to a neuronal gauge theory. It is conceivable that brain dynamics constitute more than one symmetry breaking and more than the expression of a single gauge field. A complex interaction among many actors might take place in the CNS, each with its specific role in preserving more than one Lagrangian – and our cognitive functions and associated pathologies could be the result of a mixture of many functional elements.

This paper comprises six sections, and extends neuronal gauge theories for brain function to consider several scenarios. The first section informally describes a gauge theory in physics. We address this introduction to a broad interdisciplinary audience and try to make it accessible to experts from different fields. The second section focuses on the features required for a gauge theory for the CNS; e.g., vector spaces and symmetries, while the third is an effort to describe what gauge theories bring on the table – in the evaluation of brain function. Section four provides the mathematical formalism for technical readers. In section five, we provide gauge theories within the framework of the free-energy principle. Finally, section six considers about other possible biological or functional candidates for brain symmetries/gauge fields.

1) WHAT IS A GAUGE THEORY?

A gauge theory is a field theory, in which the Lagrangian (a function that summarizes the dynamics of the system) is invariant under a continuous group of local transformations (Zeidler, 2011). The most important physical theories of the last centuries; i.e., electromagnetism, general relativity and quantum field theory, can be framed in gauge theories. The underlying concept is quite simple: *gauge* means *choice*. A *gauge* is nothing more than a *coordinate system* that varies depending on one's *location* with respect to some *base space*.

The cornerstones of gauge theories are the concept of *symmetries* and the Noether theorem, which states that for every continuous symmetry there is a conserved physical quantity. The global symmetry of the system is preserved, in spite of local changes, by a continuous force, called the *gauge field*. A gauge theory can be studied via normalized

mathematical procedures (t'Hooft, 1971), so that the local forces acting on each point of the system can be quantified and investigated through differential geometry. We will try to explain what a gauge theory is, conveying the geometric intuition rather than the rigorous formalism.

To illustrate the formalism, we might start with a ball, representing a system. Local forces, depicted as vectors, act just on a few zones of the ball surface (**figure 1A**). Indeed, vector spaces have noteworthy properties that make them attractive for representation models and for encoding complex structures as single multidimensional vectors (Snaider and Franklin, 2014). The ball is unfolded and flattened into a two-dimensional reconstruction, allowing the entire surface to be transferred to a bidimensional *circle* (**figure 1B**). The local forces are arbitrarily described as vectors of different lengths and orientations, originating from the circle surface (**figure 1B**). The local forces on the circle surface can be described in terms of a broken line (the dotted line in **figure 1C**). In this case, the symmetry is considered as locally *broken* or, better, *hidden*. In order to keep the global symmetry invariant, we need to introduce a balancing force (**figure 1D**). This force is the *gauge field*. When the gauge field comes into play, we obtain a system equipped with continuous and unbroken line (the dotted line parallel to the circle surface in **figure 1E**). This line stands for the Lagrangian, roughly corresponding to the global symmetry. In summary, if we want to keep the Lagrangian invariant, despite local changes, we have to transform the broken line of **figure 1C** into the continuous line of **figure 1E**, with the aid of a counteracting force. When a system preserves its own symmetry despite the action of local forces, it is said to be equipped with a gauge symmetry and we have a gauge theory.

When one sketches a gauge theory, one can arbitrarily choose a symmetry *a priori*: by *fixing a gauge*, the model then becomes easier to analyze mathematically. However, this does not automatically mean that every hypothesized gauge theory should be accepted as valid. Deciding exactly how to fix a gauge is a key issue: the tractability of the resulting problem is heavily dependent on the choice. Although gauge theories approach their task speculatively, they build entirely upon the results of the physical sciences. They must be not only logically, but also physically tenable. In sum, a gauge theory is an abstract conjecture that needs to be tested by empirical investigations. As an example, the Higgs boson was first hypothesized via a gauge symmetry (Higgs, 1964), then confirmed with the Large Hadron Collider.

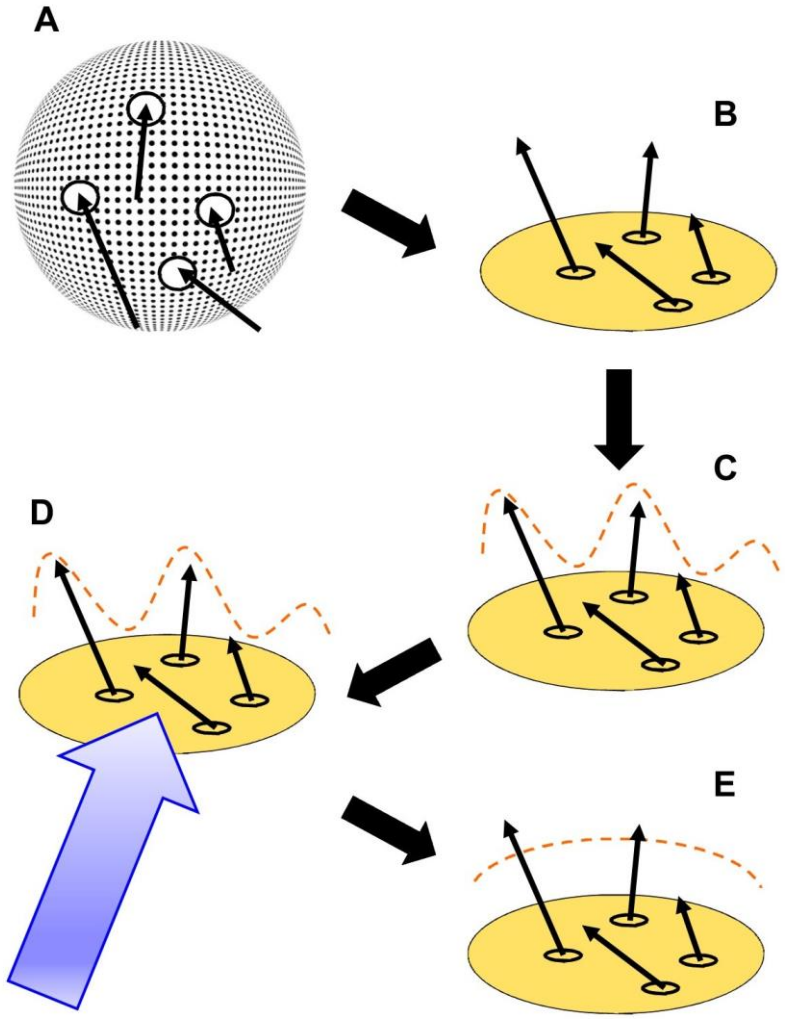

Figure 1. A geometrical illustration of a gauge theory. The gauge field, a sort of mathematical *deus ex machina*, balances local transformations. See text for further details.

2) IN SEARCH FOR SYMMETRIES IN THE CNS

In this section, we focus on the key problem in sketching a gauge theory for the CNS. To do this, we need a continuous symmetry to break and restore. The search for nervous symmetries is not easy. Due to our incomplete knowledge of brain function, we do not know exactly which, and how many, symmetries are hidden in the CNS. Furthermore, symmetries need to be constrained and it is unrealistic to seek – in biology – the mathematical simplicity of physics. Even if we knew the requisite symmetries, it is doubtful if our current technology would be able to calculate all the necessary variables at each point in the CNS. For example, recent studies suggest that

cognitive functions do not depend solely on electrical pulses, but on multifactorial intra- and extra-neuronal causes, involving supramolecular interactions among biologically active macromolecules (Tozzi, 2015). It is also important to remember that any hypothetical descriptions cannot unambiguously characterize the etiology of fluctuation properties, as similar symmetric properties may stem from qualitatively different generators, which may be difficult to distinguish with finite data (Papo 2014).

Despite these limitations, gauge theories could pave the way to a novel approach to organized living systems. The prevalence of complex fluctuations would allow not only treating the brain as a physical system, but also help classify cognitive processes as operators acting on symmetries. Moreover, the computational neuroscience community is currently undertaking an effort to provide a systematic way to characterize symmetry and asymmetry in the network structures of the connectome – by inspecting the eigenvalues of different types of connectivity matrices (Esposito et al., 2014). Gauge theories for the brain are reminiscent of a mechanism of homeostasis, in which: a) the conserved variable is a symmetry, often hidden from our observation, and b) the *balancing* force must be continuous. In what follows, we present a brief list of known symmetries in CNS that could be tested in the frame of a gauge theory. The following treatment recalls recent results by Tozzi and Peters (2016ab).

The brain generates scale-free fluctuation, even in the absence of exogenous perturbations (Papo 2014). It has been suggested that scaling properties allow cognitive processes to be framed in terms of complex but generic properties of brain activity at rest and, ultimately, during functional operations, limiting distributions, symmetries, and possibly their universality classes (Papo, 2014). The stability of spectrum exponents (of many neuronal processes) suggests that a universal scaling characterizes a large class of brain systems and physiological activities (de Arcangelis 2012). Complex scaling and intermittency are generic spatiotemporal properties of the brain and, more importantly, could contain information on how observable large-scale behaviours arise from the interactions of many small-scale processes (Papo 2014).

The $1/f^n$ structure – of time evolving neuronal activity – offers a parameterisation that summarizes the values of the frequency and amplitude of cerebral activity over a given time. This means that a high number of possible source configurations of brain currents, in different cortical areas (i.e., *local transformations*, such as gamma oscillations in somatomotor

cortex during states of enhanced vigilance, or alpha waves in posterior zones with the eyes open) give rise to a set of measured potentials characterized by a general scaling property. In a gauge theory, the global invariant power law might stand for the complete Lagrangian density of the total brain currents – and can therefore regarded as a global symmetry; while the local changes in frequency and amplitude are the local gauge symmetries. In summary, if we knew the frequencies and amplitudes of activity at each point of the brain, we could be able to estimate frequency and amplitude of the required, hypothetical gauge field.

Another neuronal symmetry has been recently discovered. A constant excitatory/inhibitory (E/I) ratio between the total amount of excitatory and inhibitory stimulation has been described, both in vitro and in vivo (Haider, 2006). The balance between the two opposing forces affects many cortical functions, such as feature selectivity and gain (Xue) and memory of past activity (Lombardi). The E/I ratio could also be interpreted as evidence of a homeostatic mechanism between strengthening and weakening processes in the adaptation of synaptic neuronal connections (de Arcangelis 2012). Homeostatic systems induce a distinction between inhibitory and excitatory connections that could contribute to symmetry breaking, leading to directed coupling and information transfer (Tognoli and Kelso, 2014). From our point of view, E/I ratio might be regarded as the Lagrangian of the intact and spontaneously active cerebral cortex. The experimental evaluation of local symmetry breakings in cerebral cortex could provide a map of the continuous forces acting on brain, in order that the gauge field could be calculated via differential geometry.

Thus far, gauge theories of CNS have been already proposed in the framework of quantum mind theories (Freeman and Vitiello, 2008; Matsui, 2001). Some of these models are equipped with a local gauge symmetry and resemble lattice gauge theory of high-energy physics. They are grounded on the notion of spontaneous symmetry breaking (Freeman and Vitiello, 2008). The symmetry that is broken is the rotational symmetry of the electric dipole of the vibrational field of water molecules. Environmental stimuli may therefore act as a trigger for the breakdown of such symmetry.

It has been suggested that the cerebral cortex exhibits a fairly uniform microarchitecture, e.g., the minicolumns, characterized by a modular connectivity with invariant properties (Casanova et al., 2011). Specifically, minicolumns exhibit a translational symmetry across their central axis and rotational symmetry;

i.e., displacement in different planes of section. Furthermore, they are equipped with transitive symmetry, with respect to geometric scaling of morphometric relations in different cortical areas, and with temporal symmetry of morphometric relations during cortical maturation. Evaluation of how architectonic relations among minicolumnar elements (e.g., pyramidal cells) are conserved under spatial and temporal variation might lead to a better understanding of diseases characterized by columnar anomalies, such as autism, schizophrenia, Alzheimer's and drug addiction (Opris and Casanova, 2014).

Last, but not the least, the free energy principle (FEP) for adaptive biotic systems (Friston, 2010) might be regarded as another symmetry hidden in the CNS (Sengupta et al., 2016). This is the most important candidate, because it encompasses all the above symmetries into a very general framework. Given its broad explanatory scope, we will return to the FEP later, in a dedicated section.

3) GAUGE THEORIES: WHAT ARE THEY GOOD FOR?

Gauge theories originate from physics. However, they could, in principle, be applied to countless fields of biology, such as cell structure, bodily physiology, and so on. In this chapter, we focus on the CNS. The first and most important question is the following: is it possible to transfer powerful gauge symmetries from their natural environment of physical particles to the *soft* (and much more complex) living structures of biology? In other words, are we allowed to sketch a gauge theory of brain function?

The importance of a gauge theory calls on the possibility of applying differential geometry to CNS activity, in order to quantify unknown, hidden or latent variables. The possibility of using vector spaces and geometrical structures instead of neurons and wires for a representation model of the CNS has been already explored. To give an example, a modular small-world topology in functional and anatomical cortical networks has been shown considered as an information processing architecture (Jarman). Furthermore, researchers have demonstrated that visual experience is two-scaled, with a smaller dimension at shorter length scales and another at longer scales (Sreekumar). Moreover, it has been proposed that entorhinal grid cells reflect a stable 2-dimensional manifold that contains the activity of individual neuronal representations, driven by continuous attractors (Yoon et al., 2013).

A central hypothesis, in this context, is that the information encoded in place-cell replay should reflect the topological structure of the experienced surroundings, thus capturing the spatial complexity of our environment (Wu and Foster, 2014). In order to use vectorial models in the assessment of the brain, the spatial characteristics of neuronal connectivity need to be considered. For this purpose, some scientists endow networks with a metric by embedding them into a physical space. This provides an adaptive rewiring model with a spatial distance function and a corresponding spatially adaptive (local) rewiring bias, which predicts observed connectivity architectures (Jarman). Further, by linking notions from Lagrangian and Hamiltonian mechanics of rigid bodies, some investigators have defined human shape as a Riemannian metric space, generalizing D'Arcy Thompson's classical formulation of mathematical morphology of shape and form, with the metric structure defined by the geodesic flow of coordinates connecting one shape to another (Djamanakova).

Software schemes offer tools for integrating structural and functional information across anatomical scales, thus connecting information across multiple physiological scales (Djamanakova et al., 2014). Also various neuro-epistemological approaches are based on vectors. This idea was first put forward by Alfred North Whitehead (Whitehead, 1919) and Kurt Lewin (Lewin, 1935) and then pursued, among others, by eliminative materialism (Churchland) and integration information theory (Tononi, 2007).

In common with the above, gauge theories also allow the projection from a *real*, external space onto an *abstract*, more manageable space equipped with sufficient statistics. However, a gauge framework is much more powerful and accurate (**figure 2**). Gauge fields have a practical advantage: their forces may be exactly calculated through a difficult, but feasible experimental energy-based variational approach. Gauge theories can be evaluated through topological tools such as the Borsuk-Ulam theorem (BUT). BUT states that (Borsuk 1933; Dodson, 1997):

Every continuous map $f : S^n \to R^n$ *must identify a pair of antipodal points (on* S^n*).*

This means that the sphere S^n maps to an n-dimensional, Euclidean space R^n (Tozzi and Peters, 2016b). Points on S^n are *antipodal*, provided they are diametrically opposite. For the use of BUT and its variants, see Peters and Tozzi (2016). It has

been recently proposed that symmetries lie on the S^n sphere in guise of antipodal points, while the broken symmetries lie on the corresponding R^n manifold (Tozzi and Peters, 2016a). Here, the gauge field stands for the continuous function required to go from a level to another (**figure 3**). This approach allows us to assess vector and tensor projections also by using the powerful tools of algebraic topology (Peters 2016).

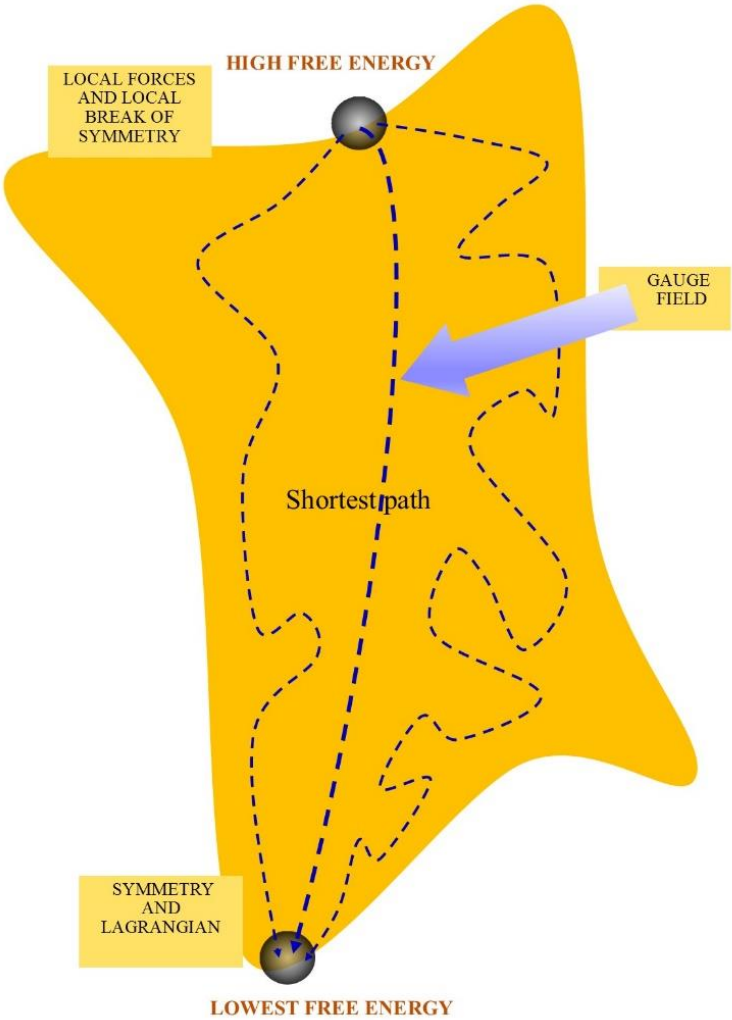

Figure 2. Neuronal phase spaces equipped with sufficient statistics allow a rigorous way of measuring distances on concave manifolds. This means that dynamics transporting one distribution of neuronal activity to another is given by the shortest path from point to higher energetic levels to lower ones. In mathematical terms, the gauge field is a Levi-Civita connection, which allows exponential mapping and parallel transport, following the steps of a Langevin equation. For further details, see Sengupta et al. (2016).

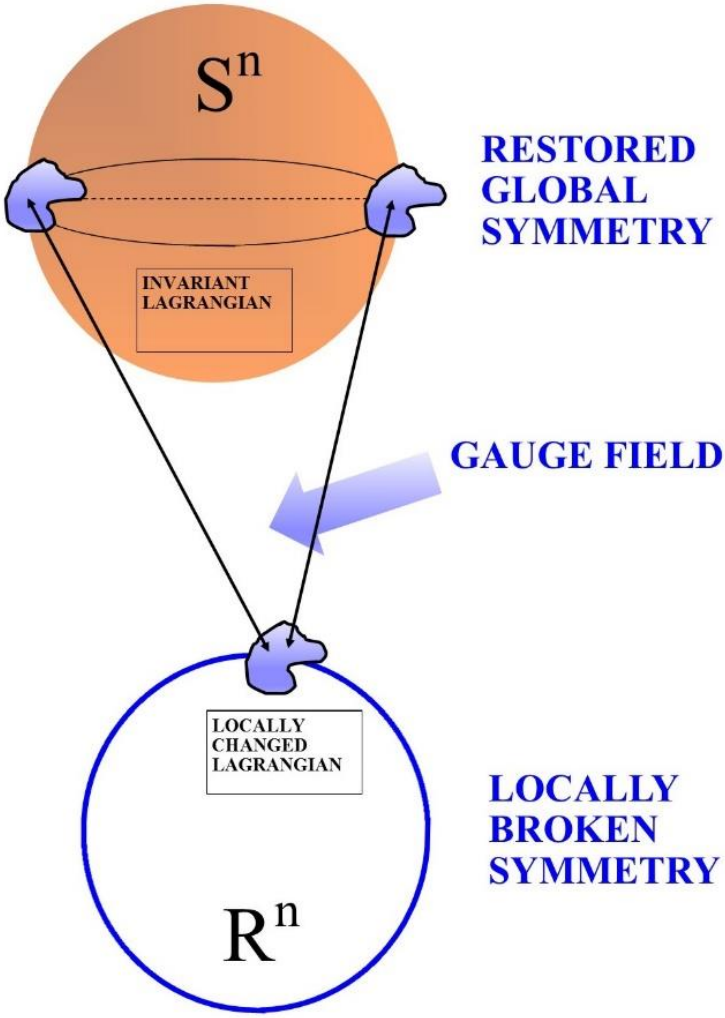

Figure 3. Borsuk-Ulam theorem and gauge fields. BUT and its variants require a function which needs to be continuous. In the same way, a gauge theory requires a gauge field which needs to be continuous.

4) MATHEMATICAL FORMALISM OF A CNS GAUGE THEORY

There are many possible ways to handle a gauge theory of the CNS in a differential geometric sense. Analytically, this is simple but the numerics can be tortuous. Sengupta et al. (2016) used Levi-Civita connections to project from an abstract space to another, more manageable space. Here we will focus instead on another type of transport, e.g., the Ehresmann connection.

As an example, we will consider the hypothetical case of a system of cerebral electric potentials equipped with a global invariant $1/f^n$ scaling symmetry. A procedure to quantitatively assess the required gauge fields is as follows. Neurophysiologic measures of brain activity in humans usually use a simple, non-invasive electroencephalogram (EEG). These measures exhibit significant 1/f-like power spectrum scaling (Pritchard, 1992). Subjects would undergo 10-20 EEG measurements during active concentration and rest, eyes open and closed. In **figure 4A**, as an example, we choose four random cerebral areas with hypothetical frequency and amplitude measures of EEG activity. The **n** value of recorded EEG segments could be estimated by fractal analysis techniques (Ihlen 2012). The most interesting cognitive phenomena occur in time windows shorter than seconds (Buzsáki and Watson, 2012). Consequently, EEG frequencies and amplitudes might be evaluated in sub-seconds frames.

Once acquired, data from each point of the cortex can be investigated using the formalism of differential geometry. Technically speaking, a continuous group of transformations is applied on the tangent bundle, then a local section of the principal bundle is chosen and the covariant derivative is calculated via an Ehresmann connection. Practically, this would involve the following. The cerebral hemispheres (**figure 4A**) are unfolded and flattened into a two-dimensional reconstruction (Van Essen, 2005), allowing the entire cortical surface to be transferred to an atlas **M** of $\mathbf{C}^{\mathbf{K}}$ (differentiable), $\mathbf{C}^{\infty}$ (smooth), finite dimensional manifolds, each one mapping a brain area (**figure 4B**). The set of power spectra describing each cortical area's frequencies and amplitudes now stand for a continuous group of local transformations acting on sections of **M**. **M** is arbitrarily equipped with a constant matrix **G** belonging to the SO(3) Lie group, isomorphic to the rotation group of the sphere (**figure 4B**).

M is a principal G-bundle ***P*** characterized by a trivial, smooth and differentiable fiber bundle, by vector bundles **E** and by a tangent bundle **TE** (**figure 4C**). The electrical forces are described by numbers, arranged in vectors and angles, representing the action **G** on a chosen local section **E** of ***P***. Four forces **G** are depicted in **Figure 4C** in the guise of four vector bundles **E** arising from four points **p** in the tangent space $\mathbf{T_p}$. They are equipped with four n-dimensional rotation angles $\boldsymbol{\varphi}(\varphi_1, \varphi_2, \ldots, \varphi_n)^T$ standing for the local $1/f^n$ scaling of each of the four brain areas. Rotations through tiny angles link nearby transformations of angles $\boldsymbol{\varphi}$ arising from points **p**. As a result, the linear approximation of the function **G** at **p** (and its angle $\boldsymbol{\varphi}$) in each dimension can be described by introducing a partial

derivative. In brief, changes in degrees of **φ** in selected brain areas match with different power spectra and hence with different electric configurations.

In a gauge theory, the geometric *link* between ***L*** and **φ** can be defined in terms of a connection form, the Ehresmann connection (Ehresmann, 1950). If we identify the horizontal space **H**, perpendicular to the vertical space **VE**, we can extrapolate the Ehresmann connection **ω**, which is a vector on **TE** (**figure 4C**). The Lagrangian density ***L*** is indeed a function of **TE** and **H**. It would be correct to formulate all rates of change of **ω** and **φ** in terms of covariant derivative, a linear differential operator in each associated **TE**, which allows different points (and their angles) to be compared. Mapping every vector **ω** of ***P*** into the bijective, diffeomorphic $\boldsymbol{P^I}$ space, enables one to derive a curvature form (**Figure 4D**). When the vectors $\boldsymbol{\omega^I}$ intersect the unique horizontal lift – corresponding to the invariant ***L*** – the angles **σ** are obtained.

The behavior of the vectors $\boldsymbol{\omega^I}$ and angles **σ** can be compactly written by point-wise vector addition of the partial derivatives of the function **G** at each point. As a result, we get a single vector: $\vec{\Omega} = \overrightarrow{\omega_1} + \overrightarrow{\omega_2} + \ldots + \overrightarrow{\omega_n}$. The angle **Σ** is introduced (**figure 4E**), standing for the interaction Lagrangian $\boldsymbol{L_{int}}$ and expressing the $1/f^n$ scaling values of vector addition obtained from our experimental procedure. If the lines ***L*** and **Ω** are parallel, **Σ** equals the zero, $\boldsymbol{L_{int}}$ equals ***L*** and the symmetry of the system is preserved. Otherwise, if ***L*** and **Ω** are not parallel (as is usual in physiological systems), **Σ** departs from zero, $\boldsymbol{L_{int}}$ is different from ***L*** and the system displays a broken or absent symmetry. In this case, in order to ensure the invariance of ***L*** and to restore the symmetry, we need to define a covariant derivative such that the derivative of **Σ** will again transform identically with **Σ**. According to the covariant version of gauge theories, the correction terms are reinterpreted as couplings to an additional divergent counter-term, the gauge field, by allowing the symmetry parameter to vary from place to place in the local coordinate system.

Figure 4F shows the above procedure in a very abridged form. If we ignore ***L*** and examine the vector **Ω** and its angle **Σ,** we observe nothing else than a single force. If we instead regard ***L*** as a vector, whose basis results from the scalar components of its vector space **v**, then **Ω** (and its angle **Σ**) turns out to be just one of the covariant components of ***L***. In order to keep ***L*** invariant, we need to add another component into **v**: we introduce the vector Ψ, equipped with the angle Θ (**figure 4F**). The angle **Θ** stands for the gauge field Lagrangian $\boldsymbol{L_{gf}}$ and expresses the global value of $1/f^n$ scaling of the required gauge

field. We are thus allowed to make accurate predictions of forces: we can extrapolate from **Θ** the values of time, frequency and amplitude of the gauge field required to keep invariant the $1/f^n$ scaling during cortical activity. This provides a practical example of how one can apply gauge theories operationally to electromagnetic recordings of the sort that are currently available in systems neuroscience.

A mathematical formulation for technical readers and a tutorial are provided in Sengupta et al. (2016), Supporting Information.

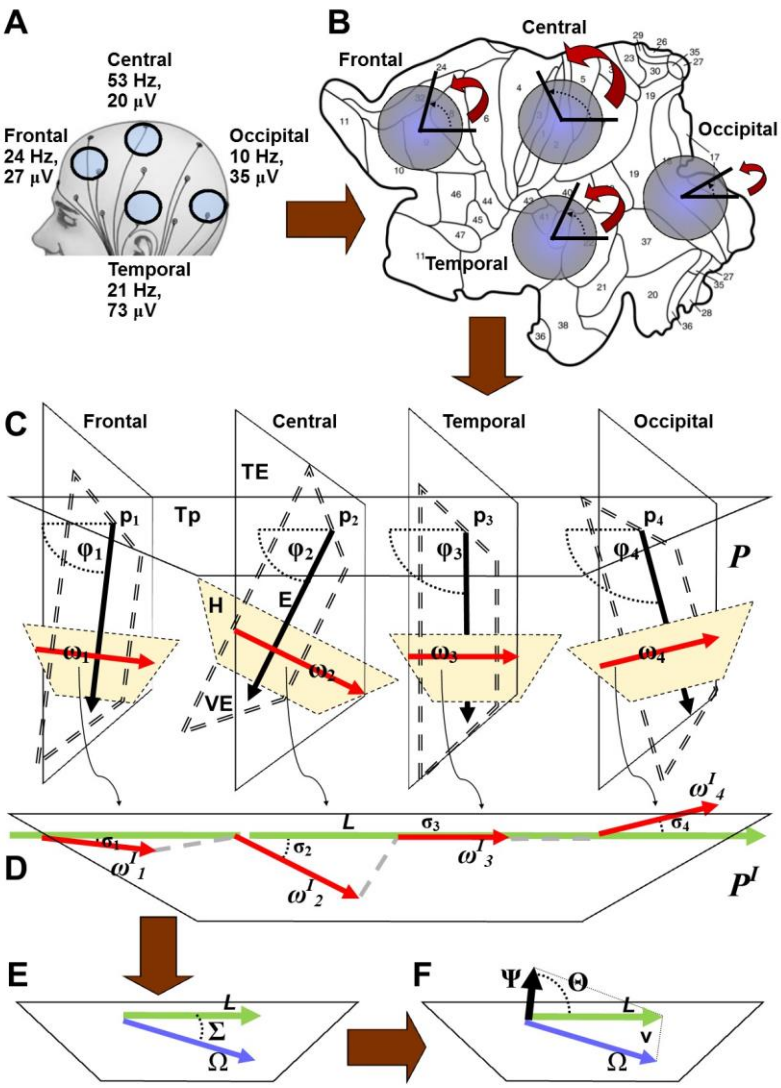

Figure 4. Dynamics of cortical electric fields, described in terms of sections of fiber bundles, jet manifolds, Lie groups and Ehresmann connections. See the main text for further details.

5) GAUGE THEORIES AND THE FREE-ENERGY PRINCIPLE

The free energy framework is the most natural candidate for a gauge theory of the CNS (Sengupta et al, 2016). The free energy principle says that self-organizing system that is at nonequilibrium steady-state with its environment must minimize its free energy, thus resisting a natural tendency to increase its disorder or entropy (Friston 2010). The principle of minimising variational free energy (an information theoretic construct for systems that attain non-equilibrium steady-state), is about trying to understand how homeostasis is maintained (Sengupta 2013). The free energy principle separates the agent (the internal states) from the environment (the external states), which encompasses the external and internal milieu. Because entropy is also the long-term average of *surprise*, the brain will appear to minimise surprise (aka *surprisal* or self information), in order to ensure that the probability of interoceptive and exteroceptive sensory states; i.e., the entropy of sensory exchanges with the environment remains low.

Agents can suppress surprise by changing the two things that surprise depends on: either they modify sensory input by acting on the world, thus minimizing prediction errors, or they adjust their perceptions, by changing their internal states, thus optimizing accuracy of predictions (Friston 2010). The feasibility of calculations based on entropy has been proved useful for a basic understanding of neuronal complexity. Research looking at fluctuations in brain signals provided evidence that the complexity of those signals, as measured by entropy, conveys important information about network dynamics, e.g., local and distributed processing (McDonough). Efficient algorithms to calculate transfer entropy values between two systems have been introduced, allowing the estimation of functional connectivity between different brain regions (Ma). Furthermore, resting-state fMRI data from the Human Connectome Project (Van Essen et al., 2013) were used to measure, through multiscale entropy, the extent of neural complexity in the BOLD signal (McDonough). These studies affirm a prediction of the principle of minimum (variational) free energy that necessarily entails a high degree of mutual information (relative entropy) among distributed representations in neural networks – and a necessary critical slowing of the sort seen in scale free dynamics (Friston et al., 2012).

The time average of variational free energy is essentially a proxy for entropy, therefore minimising entropy production corresponds to minimising variational free energy at each point

in time. Accordingly, we can treat variational free energy as a Lagrangian and, implicitly, a way of minimising entropy. One might imagine that the dynamics associated with this sort of Lagrangian are a necessary consequence of the resulting coupled dynamical system (with a random dynamical contracting set), and a resulting eigen-spectrum with a countably large number of eigenvalues and associated multi-Lorentzian spectral density. As above, tensor values of the required gauge field could be calculated via differential geometry. For example, if the tensors are measured in energy units, we can estimate how much energy (originating from an external or internal gauge field) is required by mental states, in order to minimize entropy and variational free energy at each point in time. **Table 1** recapitulates an account of a gauge theory based on the free-energy principle.

	PHYSICAL AND BIOLOGICAL CONTEXT	***VARIATIONAL FREE-ENERGY FORMALISM***	***POSSIBLE CORRESPONDING NERVOUS STRUCTURES***
SYSTEM	CNS	Brain as an inferential machine in non-equilibrium steady-state; an agent with its neuronal or internal states	CNS
LAGRANGIAN	Energetic homeostasis	Variational free-energy (sensory entropy)	CNS homeostasis
LOCAL FORCES	Continuous external stimuli coming from the environment, or internal stimuli coming from the body	External states producing local sensory perturbations in the agent and increase of prediction errors, which gives rise to a Kullback-Leibler divergence between sensation and prediction	Sensory pathways, from the periphery to the CNS, and their corresponding, coupled cortical layers 1-3, which convey bottom-up messages
GAUGE FIELD(S)	External continuous force	Precision weighting of prediction errors (implicit in the encoding of uncertainty), leading to minimization of prediction errors through action and/or perception; Levi-Civita connection, joining together physical spaces and phase spaces	Cortical layers 5-6; they convey top-down messages Visual attention Other unknown structures

Table 1. The ingredients of a gauge theory within the framework of the free-energy principle: See Sengupta et al (2016) for details

6) OTHER CANDIDATES FOR BRAIN GAUGE THEORIES

In summary, to sketch a CNS gauge theory, we require the neuronal homologues of the three ingredients: i.e., a system equipped with a symmetry, local forces and one or more gauge fields. Depending on our initial gauge choice, the three ingredients can be assessed in different combinations. Many possibilities arise, whose feasibility can be experimentally verified. In closing, we provide some discussion of further candidates for gauge fields.

Consciousness. In the search of the neural correlates of consciousness (Koch et al., 2016), gauge theories may provide a novel method to investigate this challenging phenomenon. In particular, when embedded in a gauge framework, consciousness no longer stands for unspecified brain activity, but for a quantifiable parameter that can be expressed in terms of vectors or tensors. Indeed, consciousness might correspond to a Levi-Civita connection; e.g., the gauge field. In absence of consciousness, the external states do not produce sensory perturbations; from the perspective of the free energy principle, this means, the symmetry of the variational free energy, e.g., the sensory entropy, cannot be restored. As an example, during sleep, in which consciousness is altered, a response to local sensory perturbations does not occur. In such a vein, if we assume that the system stands for the cortex, ascending arousal systems are potential candidates for gauge fields. The midbrain contains tonic neurons that ensure a continuous cortical neuromodulation. Tonic neurons are located in the locus coeruleus, in the dorsal raphe and central superior nuclei; e.g., along the pathway of the ventral branch of ascending arousal system, and in the reticular thalamic nucleus, which is the final step of the dorsal branch of the ascending arousal system (Nieuwenhuys et al., 2008). Recent data suggest that the neural correlates of consciousness might be associated with posterior cortical hot zones (Koch et al, 2016). If this was the case, we could be allowed to assimilate qualitative notions of conscious level into the quantitative gauge theoretic framework of cortical function.

Blood flow. If we hypothesize that the system is the entire CNS and the gauge field is located in other bodily systems, it is possible that local forces stand for the cortical oscillations evoked by the stimuli from the external environment, while the continuous gauge field stands for haemodynamic fluctuations. The idea that blood circulation influences brain activity dates

back to the pioneering work of Angelo Mosso (1896) and is still evident in brain mapping studies that predominate in modern neuroscience (Nieuwenhuys et al., 2008; Friston et al, 2014). A recent paper is particularly intriguing in this regard (Park et al., 2014). In humans, cardiovascular fluctuations underlie behaviourally relevant activation in multifunctional cortical areas. Neuronal events locked to heartbeats before stimulus onset predict the detection of a faint visual grating in the posterior right inferior parietal lobule and the ventral anterior cingulate cortex. Heartbeats therefore shape visual conscious experience, by contributing to neuronal representations. Similar coupling in the interoceptive domain would mean that the introception of autonomic signals might underlie subjectivity and sense of self (Park et al., 2014). Furthermore, emotions can be influenced by cardio-circulatory mechanisms. It has been demonstrated that short-term interoceptive fluctuations enhance perceptual and evaluative processes related to the processing of fear and threat. The processing of brief fear stimuli is selectively gated by their timing in relation to individual heartbeats and these interoceptive signals influence the detection of emotional stimuli at the threshold of conscious awareness, altering emotional judgments of fearful and neutral faces (Garfinkel et al., 2014). Resembling a novel version of Fechner law, gauge theories might quantitatively correlate stimuli and perceptual processing.

Environmental stimuli. In an *autopoietic* account of the gauge framework, the system might stand for the brain, equipped with self-sustained continuous forces producing local, self-generated perturbations. In this case, the best candidate for a gauge field is the continuous afference from the external world. In such a framework, the spontaneous activity of the brain cannot be simply reduced to background noise, uncorrelated to the system's response (Lombardi et al., 2012). We are presented with an auto-referential system, in which the role of spontaneous fluctuations is to preserve brain's internal symmetry. Homeostatic plasticity ensures that neuronal networks assume a sub-critical state, independently of the initial configuration. Surprisingly, increasing the external stimuli modifies the network set-point towards criticality (Priesemann 2015).

Time. It has been recently suggested that some brain functions could be dictated by the principle of minimum frustration, a concept borrowed from energetic landscapes of protein folding (Tozzi et al, 2016). The brain is equipped with many timescales, ranging from nanoseconds to several days. According to this novel formulation, structural changes in the

brain lead to energy decrease at very long CNS timescales. With the passage of time, the trajectories of neuronal processes, such as memory and perceptual recognition, tend towards the low-energy basins of narrow funnel-like attractors. As with the free energy principle, the minimum frustration principle states that the gradient descent (energy decrease) dictated by Langevin equations takes place over long brain timescales (see **Figure 2**). In such a vein, time becomes a gauge field. Indeed, at least at the non-relativistic scales typical of biological systems, time is a continuous function. This function can restore the global symmetry; e.g., the lowest possible variational free energy, which has been broken by local forces, e.g., environmental inputs. Time stands in this case for a known parameter, which affords the possibility to evaluate unknown parameters.

CONCLUSIONS

When emphasizing the circular causality between the nervous system and the world in which it is embodied, a proper consideration of this holistic aspect of information processing in the brain is required. Starting from this conceptual background, our aim was to introduce the general, abstract model of a physical gauge theory in biology and evaluate its possible implications for the CNS. Brain functions and neuropsychiatric diseases can be approached from the physicist's point of view – appealing to the basic observation that the CNS is an open system; continuously interacting with its environment. The ensuing dissipative character of the brain turns out – from a gauge theoretic perspective – to be the root of its dynamics, behaviour and persistence.

Such an approach holds promise because it directs us into new ways of thinking, offers new perspectives, and shows how it is possible to reformulate old problems. Gauge symmetries could lead to novel approaches to organized biological systems, improve our understanding of brain function and pave the way to innovative therapeutic strategies. To take some examples, visual attention, consciousness, spontaneous neuronal activity and functional regimes at the edge of criticality are impaired in many pathological conditions, such as autism, schizophrenia, drug addiction, Alzheimer Disease, depression *etc*. A potential medical application for gauge fields is epilepsy, in which, according to a gauge theory, the Lagrangian might be disrupted by pathological spikes. Seizures could be counteracted, or even removed, by carefully constructed 'artificial gauge fields' (e.g., via selective application of electric waves of specific frequency on target micro-areas, or via drugs) able to *recover* the

Lagrangian and restore the electric symmetry. We hope that this brief survey of the potential of a gauge theoretic approach hints at the possibility of such developments in the future.

BIBLIOGRAPHY

1. Borsuk, M. Drei s¨atze ¨uber die n-dimensionale euklidische sph¨are, Fundamenta Mathematicae XX (1933), 177–190.
2. Buzsáki, G., Watson, B.O. (2012). Brain rhythms and neural syntax: implications for efficient coding of cognitive content and neuropsychiatric disease. *Dialogues Clin. Neurosci*. 4, 345-367.
3. Casanova MF, El-Baz A, Switala A. Laws of conservation as related to brain growth, aging, and evolution: symmetry of the minicolumn. Front Neuroanat. 2011 Dec 26;5:66. doi: 10.3389/fnana.2011.00066. eCollection 2011.
4. Churchland PM. Neurophilosophy At Work. 2007. Cambridge Univ Pr ISBN-10: 0521864720. ISBN-13: 978-0521864725
5. Dayan, E., Censor N., Buch, E.R., Sandrini, M., and Cohen, L.G. (2013). Noninvasive brain stimulation: from physiology to network dynamics and back. *Nat. Neurosci.* 16, 838–844. doi: 10.1038/nn.3422
6. de Arcangelis L, Herrmann HJ. 2010. Learning as a phenomenon occurring in a critical state. PNAS 107: 3977-3981.
7. Djamanakova A, Tang X, Li X, Faria AV, Ceritoglu C, et al. Tools for Multiple Granularity Analysis of Brain MRI Data for Individualized Image Analysis. Neuroimage. 2014 Jun 26. pii: S1053-8119(14)00523-0. doi: 10.1016/j.neuroimage.2014.06.046. [Epub ahead of print]
8. Dodson, C.T.J. and P.E. Parker, A user's guide to algebraic topology, Kluwer, Dordrecht, Netherlands, 1997, xii+405 pp. ISBN: 0-7923-4292-5,MR1430097.
9. Ehresmann, C. (1950). Les connexions infinit´esimales dans un espace fibrée differentiable. *Colloque de Topologie*, Bruxelles, pp. 29–55.
10. Esposito U, Giugliano M, van Rossum M, Vasilaki E. Measuring Symmetry, Asymmetry and Randomness in Neural Network Connectivity. PLoS One. 2014 Jul 9;9(7):e100805. doi: 10.1371/journal.pone.0100805.

11. Ihlen, E.A. (2012). Introduction to multifractal detrended fluctuation analysis in matlab. *Front. Physiol.* 141, 1-18. doi: 10.3389/fphys.2012.00141
12. Freeman WJ, Vitiello G. Dissipation and spontaneous symmetry breaking in brain dynamics. J. Phys. A: Math. Theor. 41 (2008) 304042, (pp. 1-17). doi:10.1088/1751-8113/41/30/304042
13. Friston K (2010). The free-energy principle: a unified brain theory? Nature Reviews Neuroscience. 11:127-138. doi:10.1038/nrn2787.
14. Friston, K. (2013) Life as we know it. Journal of The Royal Society Interface 10
15. Friston, K., M. Breakspear and G. Deco (2012). "Perception and self-organized instability." Frontiers in Computational Neuroscience 6: 44.
16. Friston KJ, Kahan J, Razi A, Stephan KE, Sporns O. On nodes and modes in resting state fMRI. Neuroimage. 2014 May 24. pii: S1053-8119(14)00421-2. doi: 10.1016/j.neuroimage.2014.05.056.
17. Garfinkel SN, Minati L, Gray MA, Seth AK, Dolan RJ, Critchley HD. Fear from the heart: sensitivity to fear stimuli depends on individual heartbeats. J Neurosci. 2014 May 7;34(19):6573-82. doi: 10.1523/JNEUROSCI.3507-13.2014.
18. Gollisch T (2009). Throwing a glance at the neural code: rapid information transmission in the visual system. HFSP J 3(1): 36–46. doi: 10.2976/1.3027089
19. Haider B, Duque A, Hasenstaub AR, McCormick DA. Neocortical network activity in vivo is generated through a dynamic balance of excitation and inhibition. J Neurosci. 2006 Apr 26;26(17):4535-45.
20. Higgs PW. Broken Symmetries and the Masses of Gauge Bosons. Phys. Rev. Lett. 13, 508 – Published 19 October 1964. DOI: http://dx.doi.org/10.1103/PhysRevLett.13.508
21. Huth AG, de Heer WA, Griffiths TL, Theunissen FE, Gallant JL. Natural speech reveals the semantic maps that tile human cerebral cortex. Nature. 2016 Apr 28;532(7600):453-8. doi: 10.1038/nature17637.
22. Jarman N, Trengove C, Steur E, Tyukin I, van Leeuwen C. Spatially constrained adaptive rewiring in cortical networks creates spatially modular small world architectures. Cognitive Neurodynamics. April 2014. DOI: 10.1007/s11571-014-9288-y
23. Koch C, Massimini M, Boly M, Tononi G. Neural correlates of consciousness: progress and problems. Nat Rev Neurosci. 2016 Apr 20;17(5):307-21. doi: 10.1038/nrn.2016.22.
24. Jiang 2015

25. Lewin K. A dynamic theory of personality. McGraw_Hill Book Company, Inc. New York and London, 1935.
26. Lombardi F, Herrmann HJ, Perrone-Capano C, Plenz D, de Arcangelis L. Balance between excitation and inhibition controls the temporal organization of neuronal avalanches. Phys Rev Lett. 2012 Jun 1;108(22):228703. Epub 2012 May 31.
27. Ma C, Pan X, Wang R, Sakagami M. Estimating causal interaction between prefrontal cortex and striatum by transfer entropy. Cogn Neurodyn. 2013 Jun;7(3):253-61. doi: 10.1007/s11571-012-9239-4. Epub 2013 Jan 4.
28. Matsui T. Gauge Symmetry and Neural Networks. in "Fluctuating Paths and Fields"ed. by W.Janke et al., World Scientific (2001) pp. 271-280
29. Mattei, T.A. (2014). Unveiling complexity: non-linear and fractal analysis in neuroscience and cognitive psychology. *Front. Comput. Neurosci.* 21; 8:17. doi: 10.3389/fncom.2014.00017
30. McDonough IM, Nashiro K. Network complexity as a measure of information processing across resting-state networks: evidence from the Human Connectome Project. Front Hum Neurosci. 2014 Jun 10;8:409. doi: 10.3389/fnhum.2014.00409. eCollection 2014.
31. Milstein, J., Mormann, F., Fried, I., and Koch, C. (2009). Neuronal shot noise and Brownian 1/f2 behavior in the local field potential. *PLoS One*. 4, e4338. doi: 10.1371/journal.pone.0004338
32. Mosso A. Fear. Longmans, Green and Co. London New york, and Bombay. 1896
33. Nieuwenhuys R, Voogd J, van Huijzen C (2008) The Human Central Nervous System. Springer, Heidelberg
34. Xue M, Atallah BV, Scanziani M. Equalizing excitation–inhibition ratios across visual cortical neurons. Nature (2014) doi:10.1038/nature13321
35. Opris I, Casanova MF. Prefrontal cortical minicolumn: from executive control to disrupted cognitive processing. Brain. 2014 Jul;137(Pt 7):1863-75. doi: 10.1093/brain/awt359. Epub 2014 Feb 14.
36. Papo D. Functional significance of complex fluctuations in brain activity: from resting state to cognitive neuroscience. Front. Syst. Neurosci., 11 June 2014 | doi: 10.3389/fnsys.2014.00112
37. Park, H.D., Correia, S., Ducorps, A., Tallon-Baudry, C. (2014). Spontaneous fluctuations in neural responses to heartbeats predict visual detection. *Nat. Neurosci.*2014 Mar 9. [Epub ahead of print]. doi: 10.1038/nn.3671

38. Peters JF. 2016. Computational Proximity. Excursions in the Topology of Digital Images. Edited by Intelligent Systems Reference Library. Berlin: Springer-Verlag. doi:10.1007/978-3-319-30262-1.
39. Peters JF, Tozzi A. 2016. "Region-Based Borsuk-Ulam Theorem." *arXiv*.1605.02987
40. Priesemann V. Self-organization to sub-criticality. BMC Neuroscience 2015, 16(Suppl1):O19 http://www.biomedcentral.com/1471-2202/16/S1/O19
41. Pritchard, W.S. (1992). The brain in fractal time: 1/f-like power spectrum scaling of the human electroencephalogram. *Int. J. Neurosci*. 66, 119-129.
42. Sengupta B, Stemmler MB, Friston KJ. Information and efficiency in the nervous system--a synthesis. PLoS Comput Biol. 2013;9(7):e1003157. doi: 10.1371/journal.pcbi.1003157. Epub 2013 Jul 25.
43. Sengupta, Biswa, Arturo Tozzi, Gerald K. Cooray, Pamela K. Douglas, and Karl J. Friston. 2016a. "Towards a Neuronal Gauge Theory." PLOS Biology 14 (3): e1002400. doi:10.1371/journal.pbio.1002400.
44. Sengupta B, Friston KJ, Penny WD. 2016b Gradient-based MCMC samplers for dynamic causal modelling. Neuroimage. 2016 Jan 15;125:1107-18. doi: 10.1016/j.neuroimage.2015.07.043. Epub 2015 Jul 23.
45. Smith MA, Scholey AB (2014) Nutritional influences on human neurocognitive functioning. Front Hum Neurosci 8:358. doi: 10.3389/fnhum.2014.00358
46. Snaider J, Franklin S. "Vector LIDA." Procedia Computer Science 41 (2014): 188-203.
47. Sporns O (2013). Network attributes for segregation and integration in the human brain. Curr Opin Neurobiol. 23(2):162-71. doi: 10.1016/j.conb.2012.11.015.
48. Sreekumar V, Dennis S, Doxas I, Zhuang Y, Belkin M. The geometry and dynamics of lifelogs: discovering the organizational principles of human experience. PLoS One. 2014 May 13;9(5):e97166. doi: 10.1371/journal.pone.0097166. eCollection 2014.
49. 't Hooft G. Renormalizable Lagrangians for massive Yang-Mills fields. Nuclear Physics B. Volume 35, Issue 1, 1 December 1971, Pages 167–188
50. Taylor P, Hobbs JN, Burroni J, Siegelmann HT. The global landscape of cognition: hierarchical aggregation as an organizational principle of human cortical networks and functions. Sci Rep. 2015 Dec 16;5:18112. doi: 10.1038/srep18112.
51. Tognoli E, Scott Kelso JA. Enlarging the scope: grasping brain complexity. Front. Syst. Neurosci., 25 June 2014. doi: 10.3389/fnsys.2014.00122

52. Tononi G. Consciousness as integrated information: a provisional manifesto. Biol Bull. 2008 Dec;215(3):216-42.
53. Tozzi A. 2015. Information Processing in the CNS: A Supramolecular Chemistry? Cognitive Neurodynamics 9 (5): 463–77.
54. Tozzi A, Peters JF. 2016a. "A Topological Approach Unveils System Invariances and Broken Symmetries in the Brain." Journal of Neuroscience Research 94 (5): 351–65. doi:10.1002/jnr.23720.
55. Tozzi, A, Peters JF. 2016b. Towards a Fourth Spatial Dimension of Brain Activity. Cognitive Neurodynamics 10 (3): 189–99. doi:10.1007/s11571-016-9379-z.
56. Tozzi A, Fla Tor, Peters JF. 2016. "Building a Minimum Frustration Framework for Brain Functions in Long Timescales." J Neurosci Res. doi:10.1002/jnr.23748.
57. Van Essen, D.C. (2005). A Population-Average, Landmark- and Surface-based (PALS) atlas of human cerebral cortex. *Neuroimage*. 28, 635–666.
58. Whitehead AN. An enquiry concerning the principles of natural knowledge. Cambridge at the University Press, 1919.
59. Wu X, Foster DJ. Hippocampal replay captures the unique topological structure of a novel environment. J Neurosci. 2014 May 7;34(19):6459-69. doi: 10.1523/JNEUROSCI.3414-13.2014.
60. Yoon K, Buice MA, Barry C, Hayman R, Burgess N, Fiete IR. Specific evidence of low-dimensional continuous attractor dynamics in grid cells. Nat Neurosci. 2013 Aug;16(8):1077-84. doi: 10.1038/nn.3450. Epub 2013 Jul 14.
61. Zeidler, E. (2011). Quantum Field Theory III: Gauge Theory. Springer. doi: 10.1007/978-3-642-22421

Author's personal copy

Cogn Neurodyn
DOI 10.1007/s11571-017-9450-4

RESEARCH ARTICLE

Relationships between short and fast brain timescales

Eva Déli[1] · Arturo Tozzi[2] · James F. Peters[3,4]

Received: 10 April 2017 / Revised: 22 June 2017 / Accepted: 16 August 2017
© Springer Science+Business Media B.V. 2017

Abstract Brain electric activity exhibits two important features: oscillations with different timescales, characterized by diverse functional and psychological outcomes, and a temporal power law distribution. In order to further investigate the relationships between low- and high- frequency spikes in the brain, we used a variant of the Borsuk–Ulam theorem which states that, when we assess the nervous activity as embedded in a sphere equipped with a fractal dimension, we achieve two antipodal points with similar features (the slow and fast, scale-free oscillations). We demonstrate that slow and fast nervous oscillations mirror each other over time via a sinusoid relationship and provide, through the Bloch theorem from solid-state physics, the possible equation which links the two timescale activities. We show that, based on topological findings, nervous activities occurring in micro-levels are projected to single activities at meso- and macro-levels. This means that brain functions assessed at the higher scale of the whole brain necessarily display a counterpart in the lower ones, and vice versa. Our topological approach makes it possible to assess brain functions both based on entropy, and in the general terms of particle trajectories taking place on donut-like manifolds. Condensed brain activities might give rise to ideas and concepts by combination of different functional and anatomical levels. Furthermore, cognitive phenomena, as well as social activity can be described by the laws of quantum mechanics; memories and decisions exhibit holographic organization. In physics, the term duality refers to a case where two seemingly different systems turn out to be equivalent. This topological duality holds for all the types of spatio-temporal brain activities, independent of their inter- and intra-level relationships, strength, magnitude and boundaries, allowing us to connect the physiological manifestations of consciousness to the electric activities of the brain.

Keywords Quantum mechanics · Quantum cognition · Consciousness · Brain frequencies · Emotion regulation · Behavioral neuroscience · Borsuc Ulam theorem

✉ Arturo Tozzi
tozziarturo@libero.it

Eva Déli
eva.kdeli@gmail.com

James F. Peters
James.Peters3@umanitoba.ca

1 Institute for Consciousness Studies (ICS), Benczurter 9, Nyíregyháza 4400, Hungary

2 Center for Nonlinear Science, University of North Texas, 1155 Union Circle, #311427, Denton, TX 76203-5017, USA

3 Department of Electrical and Computer Engineering, University of Manitoba, 75A Chancellor's Circle, Winnipeg, MB R3T 5V6, Canada

4 Department of Mathematics, Adıyaman University, 02040 Adıyaman, Turkey

Introduction

Animals enhance their access to information—thus chances of survival—via the sensory system. The sensory organs are information grabbing machines; seeing further, smelling keener enables animals to gather nutrients (i.e., expanding time) and avoid physical dangers (i.e., time compression), an effective time machine that can lead to the relativity of time perception (Fingelkurts and Fingelkurts 2014). Interaction through sensory stimulus corresponds to energy-information exchange. The path, rhythms, extent and other physical qualities of brain

Published online: 23 August 2017

Author's personal copy

frequencies are finely regulated and turn the brain into a complex, yet subtle system. But the central nervous system is much more than a finely-regulated circuit board. Electric flows generate associations, meaning and memory in ways reminiscent of quantum networks. Quantum theory became a mainstream, accepted scientific idea for modeling mental phenomena (Khrennikov 2016) and the mind's quantum-like behavior is exploited in fields as diverse as search-engine optimization, psychology, economy, and sociology—in some cases for nearly a century. More than 70 recent national surveys, which examined the order effect of successive attitude questions, found quantum probability theory an impeccable predictor of human judgement (Wang et al. 2014). In quantum systems, outcome is highly dependent on the context of measurement and likewise, almost all cognitive processes, such as memory, decisions and perception, have contextual nature (Busemeyer and Bruza 2012). Therefore, quantum probability theory, which was invented to explain noncommutativity of measurements in physics, provides simple and surprisingly accurate predictive power in studying order effects in social and behavioral science (Brembs 2011; Nikolov et al. 2015; Pothos and Busemeyer 2013; Wang et al. 2014). In the brain, the appropriate temporal order of the cortex neuronal activation pattern triggers corresponding memories or experience, and forms a "temporal horizon". Reminiscent of the observer effect in quantum mechanics, the quantum-like evolution of the brain maintains the unity and permanence of the mind. Measurement (interaction) actively modifies the particle being measured, and in the brain it corresponds to cognitive change. The mental world is sectioned into a stable, stepwise progression of perception or learning, such as the empowering moment of riding a bike for the first time. This is the same for recognition, getting a joke, or meeting a friend. There is a moment of inspiration (loss, shame or fear), when a new balance is formed and understanding clicks. In line with this observation, it has been suggested that conscious awareness necessarily demands mental content being held "fixed", "frozen" within a discrete but continuous progressive present moment that stands for a phenomenal unity (Fingelkurts and Fingelkurts 2014). This occurs because spatial relationships, encoded in sensory stimulus, are translated into temporal rhythms, an orthogonal organization, by the place cells of the hippocampus (Ventriglia 2014). The brain's gradually improving responses to stimuli molded brain organization into the structural, organizational mirror of physical systems. Therefore, social interaction engenders particle-like features, such as uncertainty, hysteresis and territorial needs by the Pauli exclusion principle, which states that two fermions (pieces of matter) cannot be located in the same place.

The principle of static time shows that, by the standpoint of a hypothetical observer external to our Universe, the global cosmic structure is static and lacks temporal evolution (Moreva et al. 2013), hence changes remain local. In the brain, activation by stimulus is transient, because the global charge neutrality (i.e., the default mode network, DMN; we will discuss later about it) is automatically recovered via self-regulation (Deli 2016). Thus, the brain's global structure ensures stable personality throughout life, in spite of constant interaction with the environment. The brain transfers sensory stimulus via complex electromagnetic flows to the cortex, where a meaningful response is formulated and carried back by the same electromagnetic means. A constant flux of local electromagnetic potential differences in the complex neural landscape of the brain vary according to the principle of least action, but the resting brain's recurring electromagnetic activities form a highly reproducible harmonic function (Atasoy et al. 2016) that takes the form of a four dimensional hypersphere, in which toroidal oscillations (where two antipodal particles cannot never meet or become closer, due to their recurrent rotations) give rise to repetitive patterns of movements, thoughts, or memories (Tozzi and Peters 2016a). The coherent fluctuations in the spontaneous activity of the DMN show high metabolic rates and blood flow at rest, but deactivate when specific goal-directed behaviour or cognition is needed (Damoiseaux et al. 2006). Even in the absence of synaptic or anatomical connectivity, the DMN displays great autonomy and complexity, indicating its essential role as the ground state of the brain (Tozzi et al. 2016). Spontaneous fluctuations have been observed not only in electric activity, but also in various haemodynamic and metabolic parameters, as well as spontaneous fluctuations in the membrane potential, spontaneous spikes and neurotransmitter release (Kavalali et al. 2011; O'Donnell and Van Rossum 2014). In contrast, highly organized oscillation patterns, which reduce the degrees of freedom, are closely tied to specific mental activities, such as sensory processing (synfire chains, Abeles 1991).

The entropic consequence of energy-information exchange has been recognized by Landauer's famous principle. Hence, information accumulation in the brain, which is typical of sensory activation, corresponds to high entropy (Tozzi and Peters 2017). Sensory processing requires energy, which is satisfied by enhancing the oscillation frequencies in the brain. This information-energy relationship permits the consideration of cognitive processes based on thermodynamics, and ties mental operation into the general energy cycle of the physical environment—independent volition. Sensory information flow toward the cortex is an inextinguishable, pressing barrage of enhanced frequencies which activates the sensory cortex, which turns sensory information processing instinctive and involuntary. For example, reading and comprehending signs or deciphering stimuli occurs automatically, without

Author's personal copy

conscious intent and the musicality of a familiar tongue cannot be perceived. However, the brain's access to information by sensory perception is imperfect and limited (Pakhomov and Sudin 2013). Sensory flow is also inversed from left to right and upside down in the brain stem, which projects a small, upside-down image onto the back wall of the cortex. Sensory operation therefore is analogue to a camera obscura. The camera obscura (from Latin *vaulted darkened chamber*) is a box with a small opening or pinhole, which reflects a small, reversed image projected onto its back wall (Deli 2016; Peters 2017). Thus the brainstem effectively isolates the brain from its environment, and formulates an independent, inner world of the mind with its highly personal and subjective nature of experience, memories and ideas. The momentary projection of the temporal manifold depends on both the viewer and the self. The constantly changing, complex and elaborate mental world can only be accessed from the inside; for outside observers it is a holographic projection, which however appears strangely constant from childhood to old age.

In sum, we investigate the relations among nervous activities occurring in micro-, meso- and macro-levels of observation, in order to build a new hypothesis of consciousness and mental operation based on topological and quantum-like formalism. The electrical activity in the brain generates brainwaves, in which the low- and high-frequency bands determine opposite energy-information flows (Atmanspacher and Rotter 2008) that stand for the antipodal energetic poles of the brain's operational regulation by the Borsuk–Ulam theorem. Then we demonstrate that slow and fast nervous oscillations mirror each other over time via a sinusoid relationship, providing the possibility to link the two timescale activities through the Bloch theorem. Hence, cognitive phenomena, as well as social activity can be described by the laws of quantum mechanics, while memories and decisions exhibit holographic organization. The goal of this paper is to build a comprehensive theory that describes the operation of the mind, allowing us to connect the physiological manifestations of consciousness to the electric activities of the brain.

Materials and methods

Physical foundations

The classical view of a particle is point-like; however, in string theory it is a 1-dimensional object, which is considered the basis for consistently describing all of nature. In string theory, particle vibrations are motions of loops within a Calabi–Yau manifold, where field curvature changes are recorded by a holographic organization of a multidimensional waveform. This is also true in the mind. In the brain electromagnetic activity is often appears multidimensional. For example, resting state activity circumscribes a four dimensional hypersphere (Peters et al. 2017), in contrast to the three spatial dimensions of the physical world. Since the constantly changing cortical projection can be replayed repeatedly, past experiences inform present behavior and lead to far superior response. The mind also shows essential unity, which was recognized in philosophy well before science has investigated this question. A feeling of oneness with the body emerges from detailed representation of the body, via multiple sensory organs, in the brain (Guterstam et al. 2015), which gives rise to a single, unified experience. Conscious perception is never fractured: ambiguity forces a non-deterministic, quantum-like fluctuation between two possibilities (images, ideas, or concepts); for example, only one view of the Necker cube can be perceived at any one time. Indeed, although we can contemplate many possibilities, once we decide on a problem all other options cease to exist.

The non-intuitive and multifarious nature of mental operation, first proposed by philosophers and sages over the millennia of human civilization, can be successfully modeled by quantum probability (Brembs 2011; Pothos and Busemeyer 2009). The label "quantum" comes from that, in contrast with classical mechanics, certain quantities take on only discrete values. In quantum mechanics, particles have wavelike properties, and the Schrodinger equation governs their behavior. But quantum mechanics cannot predict with certainty the outcome of a simple experiment; it can only offer statistical information about the possible results. In contrast to classical systems, where measurement merely observes a preexisting quality, quantum measurement entails decoherence, which actively changes some property of the system being measured. Probabilistic assessment is often strongly context and order dependent, and individual states can form entangled, composite systems. Remarkably the same principles, that measurement corresponds to cognitive change (i.e., decoherence), appear to apply to the mind as well. Since human behavior is notoriously unpredictable, only statistical information can be gained about political views, shopping, or any other decision making activity. In the brain stimulus sparks oscillations that cross successive regulatory layers in their way to the neocortex and generate a response that restores the resting state of the brain and leads to discrete energy processing, which endows the mind with quantum characteristics.

The brain's identification with the body forms the basis of a homeostatic self-regulation (Guterstam et al. 2015). The mind is a cacophonous sensory kaleidoscope, peppered with transient ideas and possibilities that distill into a single decision or understanding. Even divergent sensory

Author's personal copy

perception and confusing, chaotic information load coalescence into a unified experience, decision or memory. Festinger's cognitive dissonance theory (1957) shows that cognitive or emotional discrepancy can force mental change, potentially even sacrificing core beliefs, in order to restore mental congruency. The constancy of self becomes particularly apparent when changes, even dramatic ones, affect the body or the brain. Such constancy turns the mind surprisingly particle-like, where ideas and thoughts form a highly fluid, malleable mental background, which is founded in electric activities of the brain and over which sensory interaction with the outside world becomes possible. Hence, we investigated the relationship between the background, resting activities to sensory activation in the brain.

Brainwaves: stimulus builds on the DMN

The prescient experiments of Libet (1985) have shown that volition show close correlation to the brain's background electrical fluctuations. However, cortical areas are universal processors tuned not so much for particular sensory modality, but rather for particular algorithms of incoming information processing (Pigarev and Pigareva 2015). During stimuli-evoked activity or cognitive demands, the brain transitorily exhibits functional conformations—other than the spontaneous ones—,which are linked with specific psychological correlates (Cole et al. 2014). The high frequency activity has been correlated, i.e., with perceptual binding and feedback/feedforward waves which improve the perception of external inputs (Buzsaki et al. 2013). The (environmental and internal) inputs cause changes in spike frequency in diverse cortical areas: the brain thus exhibits a high number of possible source configurations, such as gamma oscillations in somatomotor cortex during states of enhanced vigilance, or alpha waves in posterior zones with eyes open, and so on (Bastos et al. 2015). The resting modules form spatiotemporal symmetry vis-à-vis the primary sensory regions of the brain, indicating an organizational relationship between resting and evoked activities. To verify this idea, we have examined the relationship between low and high oscillations in the brain. Brain activity observed at both low and high temporal scales exhibits a $1/f^{\alpha}$-like power spectrum (He et al. 2010), including not just macroscopic electric oscillations, electroencephalography, magnetoencephalography and functional magnetic resonance imaging signals (He 2014), but also microscopic membrane potentials and fluctuations in neurotransmitter release (Milstein et al. 2009; Linkenkaer-Hansen et al. 2001). In particular, the temporal frequency spectrum of cerebral electric activity displays a scale-invariant behaviour $S(f) = 1/f^{\alpha}$, where $S(f)$ is the power spectrum, f is the frequency and α is an exponent that equals the negative slope of the line in a log power versus log frequency plot (Bakouie et al. 2017; Van de Ville et al. 2010; Pritchard 1992). Pink noise can be regarded as an intrinsic property of the brain characterizing a large class of neuronal processes (Fraiman and Chialvo 2012; He et al. 2010), suggesting the possibility that power law distributions contain information about how large-scale physiological and pathological outcomes arise from the interactions of many small-scale processes (de Arcangelis and Herrnann 2010). The emergence of power law distributions in the brain has been also correlated with the spontaneous appearance of high frequency neuronal avalanches (Beggs and Timme 2012). Therefore, both slow and fast oscillations are equipped with a power law structure.

The Borsuk–Ulam Theorem (Borsuk 1933) points out that, if a sphere S^n is mapped continuously into an-dimensional Euclidean space R^n, there is at least one pair of antipodal points on S^n which map onto the same point of R^n. The notation S^n stands for an n-sphere, which is a generalization of the circle (Weeks). An n-sphere is a n-dimensional structure of constant curvature, embedded in a convex $n + 1$ space. For example, a 2-sphere (S^2) is the 2-dimensional surface of a 3-dimensional ball (a beach ball is a good illustration). Examples of antipodal points are the poles of a sphere (Matoušek 2003). Tozzi and Peters (2016b) provide a mathematical treatment for technical readers.

The concept of antipodal points (also regions) can be used not just for the description of simple topological points or regions, but also of more complicated features, such as shapes of space (spatial patterns, i.e., area and diameter), of shapes of time (temporal patterns), vectors or tensors, functions, signals (Borsuk 1958–1959; Borsuk 1969; Peters 2016). If we simply evaluate systems activity instead of "signals", BUT leads naturally to the possibility of a region-based, not simply point-based, geometry. We are thus allowed to describe systems features as antipodal points on a n-sphere. If we map the two points on a $n-1$ sphere, we obtain a single point. This means that signal shapes can be compared (Weeks 2002; Peters 2016): the two antipodal points standing for systems features are assessed at one level of observation, while the single point at a lower level (Tozzi and Peters 2017). The BUT can be used not just for the evaluation of antipodal, but also of non-antipodal points on an n-sphere. We can consider regions on an n-sphere that are either adjacent or far apart (Tozzi et al. 2017a, b). And this BUT variants applies, provided there is a pair of regions on n-sphere with the same feature value. Therefore, the two points (or regions) do not need necessarily to be antipodal, in order to be described together (Peters 2016). This makes it possible to evaluate matching signals, even if they are not "opposite",

Author's personal copy

but "near" each other: the antipodal points restriction from the "standard" BUT is no longer needed. Although BUT was originally described just in case of n being a natural number which expresses a structure embedded in a spatial dimension, nevertheless the value of n can stand for other types of numbers. The n value of S^n can be also cast as an integer, a rational or an irrational number (Tozzi and peters 2016b). For example, we might regard functions or shapes as embedded in a sphere in which n do not stand for a spatial dimension, but for a fractal one. This makes it possible to use the n parameter as a tool for the description of nervous power laws.

Psychological findings greatly support the notion that the mental state and its beliefs play a crucial role in perception, motivation and choosing ones goals. For example, cholinergic modulation alters vigilance, by changing the quenching threshold, which determines the neuronal storage of activity pattern (Palma et al. 2012). Below a certain threshold inputs are suppressed as noise, and neural coding of the features occurs above it. Also, gamma-band activity in the alert monkey is largely an emergent property of cortex from the resting state waves (Bastos et al. 2014). Changes in slow oscillations modify fast oscillations and, inversely, incoming stimulus modifies the energy level of the resting state. Because higher energy base-level activity of the resting state might give rise to focused or stressful response, the brain's resting state determines the response's frequencies to stimulus and mental interaction is founded on the DMN (Tozzi et al. 2016).

Brainwaves: the role of oscillations in consciousness

Meijer and Geesink (2016) noticed how the particular spectrum of frequency bands point towards nature employing discrete eigenfrequencies or standing waves that match precisely with an acoustic scale, with sharp frequency ratios. Their findings touch upon the science of acoustics also, since they showed that the discrete frequencies could be modeled by music torus geometry. Geesink and Meijer (2016) proposed, based on an extensive literature survey, a hypothesis of a mathematical algorithm for coherent quantum frequencies, that may create stability of biological order. Their data point towards typical, discrete, coherent frequencies of electromagnetic waves able to stabilize or de-stabilize cells. This also stands for the central nervous system: electrical activity in the brain formulates a "wave-like" pattern, the so called brainwave, with a mean action potential rate of 4 Hz (Sengupta and Stemmler 2014). It is also thought that the greater and lower oscillations are associated with unrelated functional activity. Namely, the slow cortical activities correlate with spontaneous brain activity, the DMNs and the unconstrained, conscious cognition (i.e., mind-wandering or day dreaming propensities) (Christoff et al. 2016) or the dreaming state (Fox and Raichle 2007). In turn, during stimuli-evoked activity or cognitive demands, the brain transitorily exhibits functional conformations, which are linked with specific psychological correlates, such as sensory processing, perceptual binding and feedback/feedforward waves which improve the perception of external inputs (Patel et al. 2013) or negative emotional states (Seo et al. 2008; Zeeman 1976). The DMN, i.e., functionally and structurally connected regions show high metabolic activity and blood flow at rest, but deactivate when specific goal-directed behaviour or cognition is needed (Damoiseaux et al. 2006). In the brain, the direction of information (energy) transfer in the limbic structures is highly dependent on frequency; neocortical-limbic transfer occurs during slow theta waves (4–10 Hz), and data transfer reverses during gamma frequencies (30–130 Hz), among others. Low brain frequencies increase the degrees of freedom, forming complexity of higher dimensionality; whereas high brain frequencies are more deterministic and therefore allow fewer degrees of freedom and lower dimensionality (Buzsaki et al. 2013; Mazzucato et al. 2016). Since high frequencies serve sensory processing and other information enriched states, they can be considered high entropy states. In contrast, the increased degrees of freedom of the resting state might correspond to low entropy and permits the consideration of the brain energy-information cycle based on entropic considerations.

The energy need and information carrying capacity of brain waves is proportional to their frequencies. Since low- and high-frequency bands determine opposing energy-information flow, they can be considered as opposite energetic poles of the brain's operational regulation. The relationship between the low and high frequencies in the brain and the energy-information flow or direction (Fig. 1) allow us to represent scale-free brain frequencies as a sinusoid curve (Fig. 2), where the high and low frequencies appear to be energetic mirrors of each other. The Planck–Einstein relation expresses the correlation between energy (information) and the frequency (ν): $E = h\nu$. The high energy need of enhanced brain frequencies curtails the volume of vibrating brain tissue (the biological limit of timely energy supply), limiting the capacity for information transmission (Fig. 2, indicated by #1), whereas the rate of energy transmission approaches zero during the lowest frequencies (Fig. 2, indicated by #3). The inverse relationship of energy-information transmission leads to a power-law distribution between frequency bands (Penttonen and Buzsaki 2003). However, our account uncovers a deeper reason for the regulation and power law of electromagnetic activity in the brain: the principle of least action. Since the energy need, and the ability to transmit

Author's personal copy

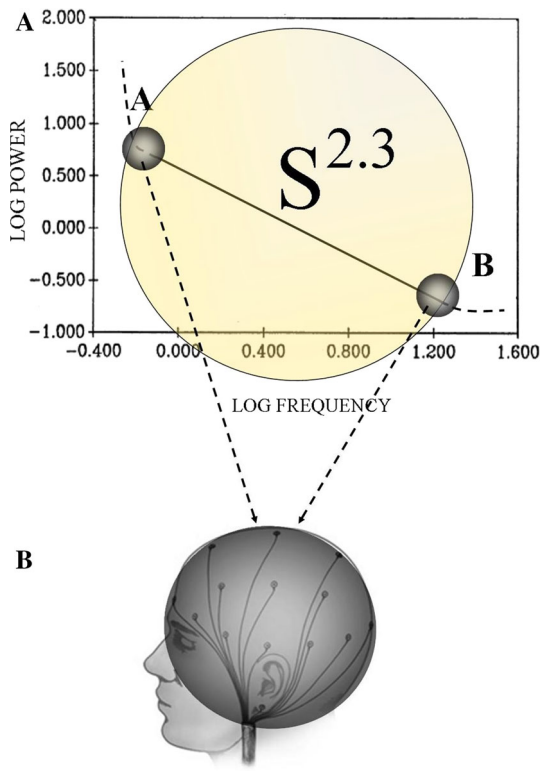

Fig. 1 **a** Log amplitude versus log frequency scatter plot of brain spikes detected by EEG techniques (modified from Pritchard). The Figure displays on the *x* axis the frequency (in Hz) and on the y axis the power (in μV^2) of the electric spikes. Note that the scale is logarithmic: it means that on the *x axis*, for example, $-0.400 = 0.39$ Hz, $0 = 1$ Hz, $0.4 = 2.52$ Hz, $1.2 = 16$ Hz and so on. In turn, on the y axis, $-1.000 = 0.1\ \mu V^2$, $-0.5 = 0{,}32\ \mu V^2$, $0.000 = 1\ \mu V^2$, $1.000 = 10\ \mu V^2$, and so on. The figure also depicts a fractal dimension, in this case equipped with the slope $\alpha = 2.3$. The BUT now comes into play: the *black circles* A and B, which respectively depict power laws at low- and high- brain frequency, stand for two antipodal points with matching description, embedded in a n-sphere with fractal exponent α (in this case, 2.3). Note that the Borsuk–Ulam theorem is not valid at the slope's tails, where the α exponent is lost (*dotted lines* on the *right* and *left* of the main slope). **b** The total fractal activity detected by different functional neurotechniques stands for the projection of the two antipodal points on a $n-1$ -manifold. A head mounted EEG is showed for sake of simplicity

information are proportional to the frequencies, the occurrence of higher frequencies in the brain dynamics decreases exponentially, but the occurrence of slow waves exponentially enhances. Their combined effect leads to power law of the brain's electromagnetic spectrum (Penttonen and Buzsaki 2003). The high energy need of enhanced brain frequencies curtails the volume of vibrating brain tissue, limiting its information transmission capacity, whereas the rate of energy transmission approaches zero during the lowest frequencies. As a consequence, the frequency-power relationship breaks down at both extremities and the curve develops a tail on both ends, shown by dotted lines on the right and left of the main slope (Fig. 1a).

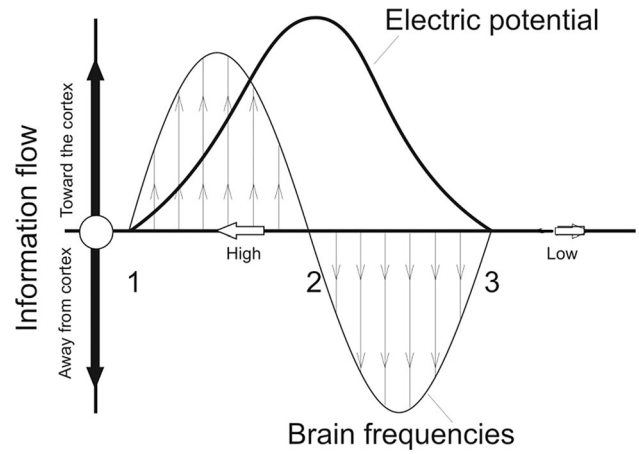

Fig. 2 The brain's changing energy balance due to stimulus over time (between the frequencies 1, 2 and 3). The brain frequencies change from high, on the *left* (#1), to low, toward the *right* (#3) and determine the direction of information flow in the brain (shown by *thin line*). The potential difference between the cortex and the limbic brain is indicated by *thick line*. The brain is energy neutral before stimulus (#1) and after a response (#3), but stimulus induces a potential difference between the cortex and the limbic brain (indicated by *2*). The high energy need of enhanced brain frequencies curtails the volume of vibrating brain tissue, limiting information transmission capacity (indicated by *#1*), whereas the energy transmission capacity disappears during the lowest frequencies (indicated by *#3*). Cortical activation extinguishes the energy of the stimulus (#2), but it generates apotential difference, which initiates a flow reversal that recovers the DMN (#3)

There is a rough positive correlation between brain size and animal size. However, thecerebrum's modular structure in birds is inefficient for growth, which effectively curtails the size of their brains. Neurons organize in microcolumnar layers in the mammalian cortex; a structure that can easily expand with growing brain size. During mammalian evolution, this organizational flexibility permitted a big expansion of brain, and consequently body size. Although four orders of magnitude separate the brain size of shrews from that of whales, the typical brain frequencies have remained astonishingly constant. Only the theta band, which is lower in humans (1–4 Hz) than in small animals such as rodents (6–10 Hz), shows notable difference (Buzsaki et al. 2013). Although axons with large conduction velocity facilitate information transmission, the remarkable evolutionary stability of brain frequencies across mammalian evolution with enormous differences in body size, brain size, and intellectual abilities is not understood. Even in the absence of stimulus, the connectome excitatory–inhibitory interactions produce harmonic functions. A parallel between brain oscillations and sound waves produced in a musical instrument, vibrations in a metallic plate, or electron wave function of a free particle given by the time-independent Schrödinger equation, have been proposed (Atasoy et al. 2016; Deli

Author's personal copy

2015, 2016). As harmonic oscillations emerge in physical systems in response to outside stimulus, in the brain seemingly reflecting the varied history of stimuli, wave form in the brain does not appear until 34th week in the fetus. For example, in instruments fitted vibrations, so called standing waves produce sound. The longest wave is called the fundamental, while multiple waves produce overtones. We propose that electromagnetic oscillations form in the brain in a similar vein. Just as a particular instrument can be recognized by its individual sound, brain oscillations (particularly in the lower-frequency range, which are produced by greater brain volume) are presumably fundamental and thus characteristic of the topographical shape and volume of the cortex. Thus, the frequencies can be considered the universal notes for the functioning brain. Just like in wind instruments, the higher notes are produced by reducing the vibrating volume; higher frequencies are produced by activating a smaller region of the brain's modular structures. In a musical instrument a standing wave is the result of the wave reflecting off the end of the tube and interfering with itself. In the brain the oscillations are reflected off the cortical surface. Neuronal activation on the cortical surface absorbs and extinguishes the energy of brain oscillations and forms standing waves between the limbic area (where the brain frequencies are spontaneously generated) and the cortical surface. Keeping the fundamental and overtones frequencies constant requires exact volume (or constant surface-volume ratio). However, brain volume increases as the radius cubed, whereas the cortical surface increases as the radius squared. As with wind instruments, in which the length is changed to modulate the sound, the evolutionary stability and universal regulatory code of brain frequencies is ensured by the increase of the cortical surface (area and/or square root of thickness) as the third power also. (Very small mammals, where the cortex does not fully surround the limbic brain, form exceptions.) The packaging of the disproportionally increasing cortical surface led to convolution, the formation of gyri and sulci, which inadvertently produced a more robust cortex. Indeed, the most convoluted cortices can be found in animals with the biggest brains, such as elephants and cetaceans. The linear relationship between the limbic and cortical region was overlooked in the recent study by Mota and Herculano-Houzel (2015), probably, by failing to account for the thick cortical mass of cetaceans (a substantial addition to limbic mass) in calculations. Because experience can accumulate in the immensely complex neuronal connections of the cortex, the folded cortical structure inadvertently enhances mental abilities, such as information processing, memory, and learning (Deaner et al. 2007). To face new challenges, old associations can be reconnected in a novel way. The complexity, convolution, and overall size of the neocortex of large mammals enable them to form close-knit, stable social groups based on compassion and kinship.

Interaction

The brain regulates itself by energy and charge conservation laws. Brain frequencies activate cortical assemblies of neurons, which generate a response and restore the brain's resting, equilibrium position (Mantini and Vanduffel 2013; Raichle and Snyder 2007). Thus oscillations can be viewed as a spring that moves energy (or information) in the form of electric current between the cortex and the limbic brain. The innate drive toward low entropy leads to a subtle regulation by the continuous and pervasive electromagnetic flows of the intact brain, giving rise to inexplicable, mysterious and highly involuntary mental processes. Bounding the space of holographic CFTs in string theory with complex systems has been shown recently (Perlmutter 2016). The importance of low entropy, corresponding to complexity, has been recognized in biology, evolution, aging (Lipsitz and Goldberger 1992), technological development (Levy 1994), innovation (Poutanen et al. 2016) and other fields. In the mind the spatial relationships of the physical world is replaced by an orthogonal "temporal horizon" of memories or experience. Temporal crystals have been created in the laboratory (Zhang et al. 2016), which allows us to conclude that such topological duality might holds for spatio-temporal brain activities also, independent of their inter- and intra-level relationships, strength, magnitude and boundaries. The brain frequencies determine the energy direction, neocortical-limbic transfer occurs during slow waves (positive emotions), and data transfer reverses during high frequencies; increasing frequencies are deterministic, generate excessive details and waste energy. High frequencies lead to painful and constricted feeling, which seems to last longer, as time *perception lengthens*, leading to impatience, called stress (Fredrickson and Joiner 2002; Yamada and Kawabe 2011). Amazingly, this is true even for unconscious stimuli (Oei et al. 2012). The detailed, deterministic oscillations narrow focus, reduce the degrees of freedom, illuminate differences, and lead to critical tendencies (Lupien et al. 2007). Such information accumulation therefore increases entropy and corresponds to a lack of confidence, which reduces trust, causing uncertainty, missed opportunities and failures. In contrast, energy accumulation in the brain is characterized by lack of details, allowing associative representations to emerge, producing confidence, trust, and belief. The willingness to work hard for rewards, even in cases of low probability of payout, is typical for a mind with high mental energy (Schultz 2007; Treadway et al. 2012). Trust and belief is the perception of temporal excess that encourages a patient, powerful, happy, and therefore satisfied mental state, which turns ambiguous situations into successful,

Author's personal copy

positive outcomes. The connection of slower oscillations with positive emotions, and enhanced brain frequencies with negative mental states has been corroborated in numerous studies (Bethell et al. 2012; Seo et al. 2008; Rudd et al. 2012). Emotions engender actions that modify the neuronal connections (modulating the mental energy), keeping them in constant flux that changes, modifies their meaning. In this way, the mind forms standing waves that are true to the local field. Such sophisticated homeostatic regulation based on entropy allows mammals and birds to be warm blooded, form the mysterious inner world of consciousness, display impressive learning ability and develop complex social life (McNally et al. 2012).

As the energy requirement of neuronal activation gradually extinguishes the information flow, it gives rise to an electric potential difference between the limbic and cortical areas, which reverses the flow via slow oscillations (Fig. 2, #2). The information flow reversal from the frontal toward occipital direction, and back toward the limbic region recovers the low entropy DMN. The sensory transmission toward the sensory cortex by fast oscillations and response by slow oscillations was confirmed in humans (Buzsaki et al. 2013), but should be typical in all mammals. Liu et al. (2015) examined the effects of high (40–100 Hz) and low frequency stimulation of rat central thalamus relay neurons in vivo. High frequency application caused widespread forebrain activation, whereas low brain frequency stimulation generated a jerking strain, possibly even convolution (Liu et al. 2015). The finding shows that electromagnetic flows in the brain correspond to energy-information exchange and polarity effects in normal brain's operation. Through long-term potentiation (Bliss and Lomo 1973) enhanced brain frequencies decrease the degrees of freedom by accumulating information (i.e., reducing trust) in the brain. Hence, normal social functioning depends on an abstract mental world of the resting state of the brain.

The unique and holographic nature of experience: the Bloch wave

A recent surge of publications examine the brain as a complex physical system, in which resting potential is characterized by a recurrent, highly reproducible harmonic function between the major modules of the brain (Atasoy et al. 2016; Peters et al. 2017; Tozzi et al. 2017b). Changes in extracellular parameters, regulated by information transmission, can be related to long-range nervous interactions and flows (Touboul 2012). Hence, quasi-neutral state can be described with slow to moderate electromagnetic fields and forces, which give rise to fast and slow brain oscillations. The local changes generate spatial currents which modulate ion flows (Pereira 2017), and in the brain electric potential differences between different modules give rise to oscillations that carry information, as globally coherent, large-scale waves in the delta, theta, alpha and beta bands that propagate with a variety of velocities. Their mean speed at each frequency band is proportional to temporal frequency, giving a range of 0.06–4.0 m/s, from delta to beta. Both ongoing activity and task-relevant intervals instigate large-scale coherent motion of the cortical signal that is measurable at the scalp (Alexander et al. 2016). Regions that are formed by resting state oscillations are located at opposite end of a spatial organization from primary sensory and motor regions; sitting at the top, most abstract representational hierarchy. Thus, the resting state is substantially insulated from direct environmental input, because energy-information exchange is meticulously regulated via the frequency conversion in the limbic system. It is intuitive and generally accepted that individual sensory experience, exemplified by Proust's Madelaine cookies, varies widely between people. Such subjective information-energy conversion turns the brain holographic. To clarify how the brain state might interpret stimulus, we calculated how the stimulus wave is shaped by the resting potential. Our topological approach showed that low- and high-frequency fractal spikes are correlated in the brain, because they display the same features (Fig. 1). This in touch with the claims of Pereira et al. (2017): in search for neural correlates of human brain activity, they suggested that a dynamical signature of conscious processing can be identified by means of a mathematical analysis of how the faster brain rhythms are nested in the slower ones.

Sensory activation zones are arranged evenly between the nodes of resting states, forming microscopic crystal-like symmetry (Margulies et al. 2016). This takes us into the realm of quantum dynamics. The issue of brain function correlated with quantum phenomena has been tackled by different Authors. To make an example, Pereira (2017) and Fernandes de Lima and Pereira (2017) investigated the mechanisms of neuroglial interactions involved in neural plasticity, highlighting the role of nonlinear interactions between glial membranes and synaptic terminals, based on the quantum dynamics of hydroionic waves within the neuropil. In this regard, hydroponic waves within the neuropil are considered to carry both physiological and cognitive functions. This crystal-like symmetry forms antipodal points, allowing calculation from a detected or measured point onto the opposite side of the diameter (corresponding to two points on the fractal slope). Once a matching description between slow and fast brain oscillations was established, we looked for a feasible equation able to link their reciprocal activities. We found a theory from an apparent far-flung branch, solid-state physics. In a periodically repeating environment (such as a lattice), the Bloch wave is a linear oscillation obtained by the product of (Floquet 1883; Traversa et al. 2013; Ahn and Hogan 2015): a periodic function with the same periodicity as the

Author's personal copy

lattice, a plane wave. In such a solid-state physics' system, the wave function Ψ for a particle has the form:

$$\Psi(x) = e^{ikr}u(x),$$

where Ψ is called a Bloch wave, x is its position, e^{ikr} is a plane wave (in which e is the Euler's number, i is the imaginary unit, k is a vector of real numbers called the *crystal wave vector*), and $u(x)$ is a periodic function with the same periodicity as the lattice. A mathematical treatment for technical readers is provided in the "Appendix".

Results

In a brain framework, we are allowed to look for the nervous correlates of the Bloch wave's equation (Fig. 3a): We may consider just the real part and put aside the imaginary part of the Bloch theorem.

The brain stands for a 2-D lattice. We are indeed allowed to unfold and flatten cerebral hemispheres into a two-dimensional reconstruction by computerized procedures (Van Essen 2005).

The periodic functions u stand for the spontaneous, slow brain oscillations which take place on the 2D brain lattice. We may conventionally state that u has the same periodicity of the brain lattice, because it corresponds to the nervous spontaneous oscillations.

The plane waves (the vectors of real numbers k) stand for the fast, task-evoked brain oscillations.

The Bloch waves stand for an unknown brain parameter able to link together the parameters u and k.

Figure 3b provides a simulation of the Bloch theorem applied to brain function. The picture shows that a change in slow oscillations leads to a change in fast oscillations, and vice versa.

Functional connectivity and the nodes of slow resting oscillations constrain the paths of emerging oscillation flows. Since the connectivity of functional hubs is frequency dependent, the information flow is dynamic and wave-like. Fast sensory oscillations can nest in the slow periodic function of these nodes. The brain's plasma-like operation encourages phase coherence in the collective flows of the extracellular space, in which long range connections modulate oscillation timing and frequencies. The nodes of resting potential in the brain might serve as stable deflection points that interfere with stimulus to create complex activation pattern.

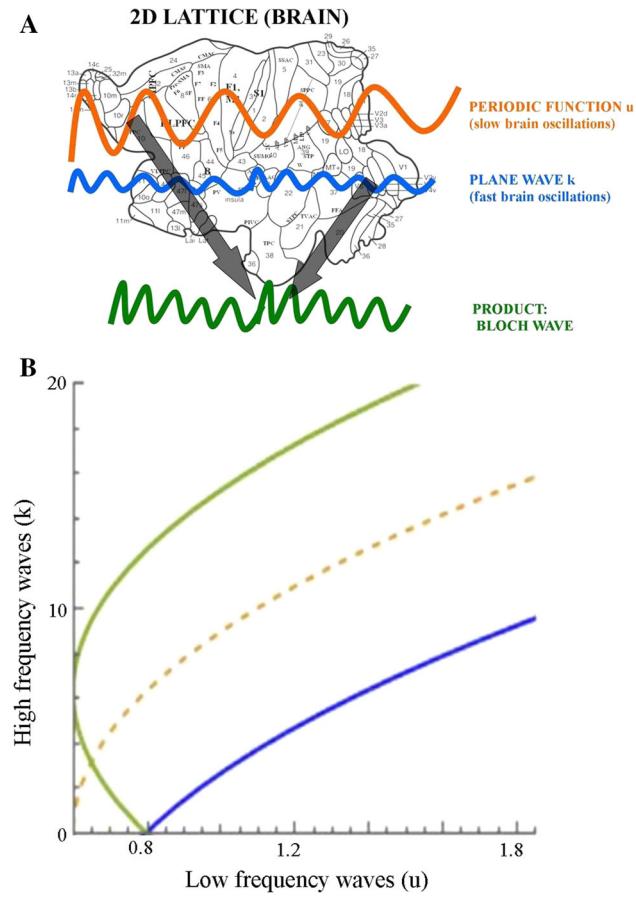

Fig. 3 **a** A rough sketch depicting the brain correlates of the Bloch theorem. **b**. Relationships between slow and fast brain oscillatory activity, according to the Bloch Theorem. A simulated plot of Bloch wave forms, for k (high frequency waves) on the y-axis, and u (low frequency waves) on the x-axis, is displayed. The brain spike frequencies are expressed in Hz (note that this time the scale is non-logarithmic). The *different lines* correspond to diverse values of the Bloch wave. Just the slow frequencies included in the fractal range are displayed, while the non-fractal slope tail on the left of Fig. 1a is excluded

Conclusions

A new hypothesis of consciousness and mental operation is proposed based on particle and quantum-like formalism. We show how the physiological manifestations of consciousness (such as emotions, memories and qualia) might arise out of the electromagnetic activities of the brain. The correlations between nervous fluctuations with different timescales and functional activity (the low- and the high- frequency spikes) can be represented by the Bloch theorem, because its periodic function can be replaced with the scale-free ultra-slow waves of the default mode networks, and its plane wave can be substituted with the fast brain spikes. In such a way, the increase in frequency of the slow electric oscillations leads to a predictable increase of the fast electric ones. Resting fluctuations of the brain exert a dominant role in regulating the brain's ability and potential to respond to sensory stimulus, leading to a functional inter-correlation between low and high oscillations, in which the momentary mental state reflects the brain's electromagnetic activity. Our

Author's personal copy

simulation showed that spontaneous fluctuations in cortical excitability might have a remarkable effect on the field potentials activity frequency spectrum as well as the spiking activity of neurons. Fluctuations in electromagnetic activity in the brain are intertwined with all other functions of the field potential, and the spiking activity of neurons. This "coupling" or nesting of many spikes subserves an important coordinating role and provides a logical structure for the integration of functional activity (Buzsáki and Watson 2012; Fox and Raichle 2007) via energy conservation and the principle of least action. In building the electromagnetic signal of stimulus on top of the resting brain's energy level, the brain operates according to the principle of least action, thereby forming a unique electric brain pattern, which is a holographic, highly subjective experience and mental world, characteristic of the individual, her past experiences and her current brain state. Such relativity of information content is linked to time perception and indeed reflection of relativity of time in general relativity. Moreover, the temporal expanse of mental concepts and feelings entails an orthogonal orientation against the field of gravity. In analogue to gravitational interaction of elementary fermions, mental interaction formulates a social field that plays crucial role in regulating thinking and behavior.

This hypothesis is supported by the observation that many types of behavioral variability follow a $1/f$ frequency distribution similar to that of spontaneous BOLD. Because higher frequencies have greater energy need and greater information carrying capacity, the regulation of the brain's electromagnetic activities show a power law relationship (Fox and Raichle 2007). The Bloch theorem might shed new light on the interpretation of the data from functional neuroimaging. If we were able to calculate the Bloch wave from the experimental records, we could obtain a simple factor which summarizes the behaviour of the brain's dynamical system—and which could also be compared with the real data from pairwise entropy studies (Watanabe et al. 2014). The "order parameter" might allow a better comprehension of cortical dynamics. This method could be used in the study of EEGs as well as fMRI neuroimaging. We also suggest other feasible applications of the Bloch theorem in different fields of neuroscience: for example, if we replace the brain with a lattice, we might evaluate the first Brillouin zone and quantify the Bloch waves in different functional states (for further details, see "Appendix"). The fact that the same Bloch wave may be obtained from different types of oscillations could explain the apparently chaotic behaviour of cortical fluctuations. If the Bloch waves change in different functional states (i.e., sensations, perceptions, emotions, mind wandering and so on), we might be able detect the underlying activity, starting just from the knowledge of the Bloch wave. Furthermore, the well-known relationships between Bloch waves, Floquet multipliers, Lyapunov exponents and limit-cycle attractors (see "Appendix") allow us to evaluate the brain oscillations' spatial fractals/temporal power laws in the context of dynamical system theories. To make an example, starting from the Lyapunov exponents endowed in the metastable brain at the edge of chaos (Beggs and Timme 2012), we might achieve a more manageable linear system, which depends just on the various brain timescales.

The brain communicates with the environment via the sensory system, which transform stimuli into the language of oscillations that propagate to the cortex. Therefore, stimulus triggers oscillations that are dependent both on the external input and the brain state. Hence, brain frequencies reflect the brain's integration into the environment via physical principles (which clearly governs the dynamics of the oscillations). Because the resting state of the brain is insulated from the environment by the sensory system, it can maintain low entropy. In the cortical brain sensory stimulus accumulates information and increases entropy. In the brain interaction (i.e., decoherence) changes mental energy (trust, confidence, etc.) by reorganizing the neuronal organization (the synaptic connections or their strength), while restoring the low entropy, i.e., resting state of the brain, which is insulated from the environment by the sensory system. This way the brain is a self-regulating system based on entropy. Since high entropy states correspond to information accumulation and high frequencies, the resting state of the brain forms low entropy that is automatically recovered via the energy state and stability of neuronal connections and their support cells. The highly debated role of sleep might very well play an important role in recovering the brain's low entropy state (Claussen and Hofmann 2012).

Electromagnetic activity in the brain is not arbitrary or accidental; it is directed by charge conservation laws. Shifting energy balances in the brain change the strength and orientation of synapses, which modifies the mental energy. This way the mind is a temporal gyrocompass, which, by restoring the resting state remains true to the local field. However, in the process, low brain frequencies accumulate energy (trust and confidence see, Neupert and Allaire 2012), whereas high brain frequencies accumulate information (leading to insecurity and fear). Therefore, over time, emotional interactions form a mental landscape (temporal field), which regulates the sensitivity of the brainstem, thus its reaction to the environment. In its constant interaction with the environment, the mind constantly changes and adapts! These way electromagnetic activities, which are wave-like, can manifest as point-like and irreversible moment-to-moment qualia of a quantum system. Hence, mental change and brain evolution is a stepwise progression, where interaction gradually

Author's personal copy

enhanced the brain's organizational symmetry vis-à-vis material systems. Thus energy-information equilibrium is low entropy, resting state, which ensures mental stability and it might be called low entropy principle. *The mind is an insulated, self-regulating system, which carefully controls energy-information exchange with the environment based on its entropy.* Low entropy principle might be present in other self-regulating systems in nature as well.

Studying particles of matter is very difficult due to their size and energy levels; examining the brain poses the opposite problem: the myriad possible ways to study it produce divergent, often confusing conclusions. However, the analog structure and operation of mind and matter holds great promise. With suitable corrections, understanding can be transferred between the fields of neurology and theoretical physics for the mutual benefit of both. This paper is intended as a first step toward building a comprehensive theory that describes the operation of the mind.

Appendix: Bloch waves and Floquet theorem

The Bloch theorem states that, if you multiply a plane wave by a periodic function, you obtain a Bloch wave, which expresses the energy eigenstates for a particle in a lattice, written as ψn_k, where n is a discrete index.

There are different Bloch waves with the same k, each one with a different periodic component u. Further, the same Bloch wave can be built in different ways, involving different vectors k and different periodic functions u. However, if we take into account just the first Brillouin zone of our lattice, we obtain that every Bloch state has a unique k.

The concept of Bloch theorem from solid-state physics—a second order differential equation-is about crystals in any number of spatial dimensions and deals in particular with the Schrödinger equation. However, it can be also applied in theory of ordinary differential equations, through the Floquet theorem (Floquet 1883). Indeed, the two theorems are almost equivalent (Floquet). The Floquet theorem, through a coordinate change in the lattice, transforms the original periodic system into a more manageable traditional linear system with constant, real coefficients. In other words, we map a fundamental matrix solution into a matrix function depending on the time, giving rise to a time-dependent change of coordinates. The Floquet theorem holds for any homogeneous, linear system of first order differential equations with a periodic coefficient matrix. Through a coordinate change in the lattice, the Floquet's theorem transforms the periodic system into a traditional linear system with constant, real coefficients.

We start from a linear first order differential equation:

$$\frac{d(x(t))}{dt} = A(t)x,$$

where $x(t)$ is a column vector of length n, and $A(t)$ is an $n \times n$ periodic matrix with period T.Then, for all $t \in R$:

$$\Phi(t+T) = \Phi(t)\Phi^{-1}(0)\Phi(T),$$

where $\Phi(t)$ is a fundamental matrix solution of the above differential equation $d(x(t)) \div dt = A(t)x$, and $\Phi^{-1}(0)$ $\Phi(T)$ is the monodromy matrix. Now consider the $n \times n$ matrices: B, P, Q, R: For each matrix B such that:

$$E^{TB} = \Phi^{-1}(0)\Phi(T),$$

there is a periodic (period T) matrix function $t \to P(t)$ such that:$\Phi(t) = P(t)E^{tB}$ for all $t \in R$. This representation is the Floquet normal form for the fundamental matrix $\Phi(t)$.

There is also a real matrix R and a real periodic function (period -2T) matrix function $t \to Q(t)$, which is continuous and periodic—such that:

$$\Phi(t) = Q(t)E^{tR} \quad \text{for all } t \in R.$$

The latter mapping gives rise to a time-dependent change of coordinates:

$$y = Q^{-1}(t)x,$$

under which the original system becomes a linear system with real constant coefficients $y = Ry$. The mapping of a fundamental matrix solution for such a differential equation into a (time-dependent) matrix function gives rise to a time-dependent change of coordinates, under which the original periodic system becomes a linear system with real constant coefficients $y = Ry$.

The eigenvalues of e^{TB} are called the characteristic multipliers of the system, while the characteristic exponent, called the Floquet exponent, is a complex μ such that $e^{\mu T}$ is a characteristic multiplier of the system. Floquet exponents are not unique and their real parts correspond to the Lyapunov exponents.

The linear differential equations with periodic coefficients have been widely used in many scientific fields. In particular, they provide a versatile tool for the stability analysis of physical systems equipped with a periodic steady-state and infinite memory, such as Brownian particles and circuit resonators (Traversa et al. 2013). The Floquet multipliers have been also used to assess the stability of periodic motion in natural rhythmic - movements in humans and machines-, not just in linear systems, but also in stochastic noise and in limit-cycle, nonlinear oscillators (Ahn and Hogan 2015).

Author's personal copy

References

Abeles M (1991) Corticonics: neural circuits of the cerebral cortex. Cambridge UniversityPress, New York

Ahn J, Hogan N (2015) Improved assessment of orbital stability of rhythmic motion with noise. PLoS ONE 10(3):e0119596. doi:10.1371/journal.pone.0119596

Alexander DM, Nikolaev AR, Jurica P, van Leeuwen C (2016) Global neuromagnetic cortical fields have non-zero velocity. PLoS ONE 11(3):E0148413. doi:10.1371/journal.pone.0148413

Atasoy S, Donnelly I, Pearson J (2016) Human brain networks function in connectome-specific harmonic waves. Nat Commun. doi:10.1038/ncomms10340

Atmanspacher H, Rotter S (2008) Interpreting neurodynamics: concepts and facts. Cogn Neurodyn 2(4):297–318

Bakouie F, Pishnamazi M, Zeraati R, Gharibzadeh S (2017) Scale-freeness of dominant and piecemeal perceptions during binocular rivalry. Cogn Neurodyn 11(4):319–326

Barbey AK, Colom R, Grafman J (2014) Distributed neural system for emotionalintelligence revealed by lesion mapping. Soc Cogn Affect Neurosci 9(3):265–272

Bastos AM, Briggs F, Alitto HJ, Mangun GR, Usrey WM (2014) Simultaneous recordings from the primary visual cortex and lateral geniculate nucleus reveal rhythmic interactions and a cortical source for gamma-band oscillations. J Neurosci 34(22):7639–7644. doi:10.1523/JNEUROSCI.4216-13.2014

Bastos AM, Litvak V, Moran R, Bosman CA, Fries P, Friston KJ (2015) A DCM study of spectral asymmetries in feedforward and feedback connections between visual areas V1 and V4 in the monkey. Neuroimage 108:460–475. doi:10.1016/j.neuroimage.2014.12.081 **(Epub 2015 Jan 10)**

Beggs JM, Timme N (2012) Being critical of criticality in the brain. Front Physiol 3:163

Bethell EJ, Holmes A, MacLarnon A, Semple S (2012) Evidence that emotion mediatessocial attention in rhesus macaques. PLoS ONE 7(8):e44387

Bliss T, Lomo T (1973) Long-lasting potentiation of synaptic transmission in the dentate areaof the anaesthetized rabbit following stimulation of the perforant path. J Physiol 232:331–356

Borsuk M (1933) Drei sätze über die n-dimensional euklidische sphäre. Fundam Math 1:177–190

Borsuk M (1958–1959) Concerning the classification of topological spaces from the standpoint of the theory of retracts. Fundam Math XLVI:177–190

Borsuk M (1969) Fundamental retracts and extensions of fundamental sequences. Fundam Math 1:55–85

Brembs B (2011) Towards a scientific concept of free will as a biological trait: spontaneous actionsand decision-making in invertebrates. Proc Biol sci R Soc 278(1707):930–939. doi:10.1098/rspb.2010.2325

Busemeyer JR, Bruza PD (2012) Quantum Models of cognition and decision. CambridgeUniversity Press, New York

Buzsáki G, Watson BO (2012) Brain rhythms and neural syntax: implications for efficient coding of cognitive content and neuropsychiatric disease. Dialog Clin Neurosci 4:345–367

Buzsaki G, Logothetis N, Singer W (2013) Scaling brain size, keeping timing: evolutionarypreservation of brain rhythms. Neuron 80(4):751–764

Christoff K, Irving Z, Fox KC, Spreng RN, Andrews-Hanna JR (2016) Mind-wandering as spontaneous thought: a dynamic framework. Nat Neurosci Rev. doi:10.1038/nrn.2016.113

Claussen JC, Hofmann UG (2012) Sleep, neuroengineering and dynamics. Cogn Neurodyn 6(3):211–214

Cole MW, Bassett DS, Power JD, Braver TS, Petersen SE (2014) Intrinsic and task-evoked network architectures of the human brain. Neuron 83(1):238–251. doi:10.1016/j.neuron.2014.05.014

Damoiseaux JS, Rombouts SA, Barkhof F, Scheltens P, Stam CJ et al (2006) Consistent resting-state networks across healthy subjects. Proc Natl Acad Sci USA 103(37):13848–13853 **(Epub 2006 Aug 31)**

de Arcangelis L, Herrmann HJ (2010) Learning as a phenomenon occurring in a critical state. Proc Natl Acad Sci 107:3977–3981

Deaner RO, Isler K, Burkart J, Van Schaik C (2007) Overall brain size, and notencephalization quotient, best predicts cognitive ability across non-human primates. Brain Behav Evol 70(2):115–124

Deli E (2015) The science of consciousness how a new understanding of space and time infers the evolution of the mind. Self-Published Hungary, Hungary

Deli E (2016) Consciousness, a cosmic phenomenon—a hypothesis. J Conscious Explor Res 7(11):910–930

Fernandes de Lima VM, Pereira Junior A (2016) The plastic glial-synaptic dynamics within the neuropil: a self-organizing system composed of polyelectrolytes in phase transition. Neural Plast. doi:10.1155/2016/7192427

Festinger L (1957) The theory of cognitive dissonance. Stanford University Press, Stanford

Fingelkurts AA, Fingelkurts AA (2014) Present moment, past, and future: mental kaleidoscope. Front Psychol 5:395. doi:10.3389/fpsyeg.2014.00395

Floquet G (1883) Sur les quations différentielles linéaires à coefficients périodiques. Ann Sci l'É.N.S. 2e série, tom 12:47–88

Fox MD, Raichle ME (2007) Spontaneous fluctuations in brain activity observed with functional magnetic resonance imaging. Nat Rev Neurosci 8:700–711

Fraiman D, Chialvo DR (2012) What kind of noise is brain noise: anomalous scaling behavior of the resting brain activity fluctuations. Front Physiol 3:307. doi:10.3389/fphys.2012.00307

Fredrickson BL, Joiner T (2002) Positive emotions trigger upward spirals toward emotional well-being. J Am Psychol Soc 13(2):172–175

Geesink HJH, Meijer DKF (2016) Quantum wave information of life revealed: an algorithm for electromagnetic frequencies that create stability of biological order, with implications for brain function and consciousness. NeuroQuantology. doi:10.14704/nq.2016.14.1.911

Guterstam A, Abdulkarim Z, Ehrsson HH (2015) Illusory ownership of an invisible bodyreduces autonomic and subjective social anxiety responses. Sci Rep 5:9831. doi:10.1038/srep09831

He BJ (2014) Scale-free brain activity: past, present, and future. Trends Cogn Sci 18(9):480–487

He BJ, Zempel JM, Snyder AZ, Raichle ME (2010) The temporal structures and functional significance of scale-free brain activity. Neuron 66(3):353–369. doi:10.1016/j.neuron.2010.04.020

Kavalali ET, Chung C, Khvotchev M, Leitz J, Nosyreva E, Raingo J, Ramirez DM (2011) Spontaneous neurotransmission: an independent pathway for neuronal signaling? Physiol (Bethesda) 26(1):45–53

Khrennikov A (2016) 'Social Laser': action amplification by stimulated emission of socialenergy. Philos Trans R Soc A 374(2058):20150094

Bliss CA, Kloumann, IM, Harris KD, Danforth CM, Dodds, PS (2012) Twitter reciprocalreply networks exhibit assortativity with respect to happiness pp 1–10 arXiv:1112.1010

Levy D (1994) Chaos theory and strategy: theory, applications, and managerial implications. Strateg Manag J 15:167–178

Libet B (1985) Unconscious cerebral initiative and the role of conscious will in voluntaryaction. Behav Brain Sci 8:529–566

Author's personal copy

Linkenkaer-Hansen K, Nikouline VV, Palva JM, Ilmoniemi RJ (2001) Long-range temporal correlations and scaling behavior in human brain oscillations. J Neurosci 21(4):1370–1377

Lipsitz LA, Goldberger AL (1992) Loss of "complexity" and aging: potential applications of fractals and chaos theory to senescence. JAMA 267:1806–1809

Liu J, Lee HJ, Weitz AJ, Fang Z, Lin P, Choy M, Lee JH (2015) Frequency selective control of cortical and subcortical networks by central thalamus. eLife 4:e09215

Lupien SJ, Maheu F, Tu M, Fiocco A, Schramek TE (2007) The effects of stress and stresshormones on human cognition. Implications for the field of brain and cognition. Brain Cogn 65(3):209–237

Mantini D, Vanduffel W (2013) Emerging roles of the brain's default mode network. The Neuroscientist. 19(1):76–87

Margulies DS, Ghosh SS, Goulas A, Falkiewicz M, Huntenburg JM, Langs G et al (2016) Situating the default-mode network along a principal gradient of macroscale cortical organization. Proc Natl Acad Sci. doi:10.1073/pnas.1608282113

Matoušek J (2003) Using the Borsuk–Ulam theorem. lectures on topological methods in combinatorics and geometry. Springer, Berlin

Mazzucato L, Fontanini A, La Camera G (2016) Stimuli reduce the dimensionality of cortical activity. Front Syst Neurosci. doi:10.3389/fnsys.2016.00011

McNally L, Brown SP, Jackson AL (2012) Cooperation and the evolution of intelligence. Proc R Soc B Biol Sci (April). doi:10.1098/rspb.2012.0206

Meijer DKF, Geesink HJH (2016) Phonon guided biology: architecture of life and conscious perception are mediated by toroidal coupling of phonon, photon and electron information fluxes at discrete eigenfrequencies. NeuroQuantology 14(4):718–755

Milstein J, Mormann F, Fried I, Koch C (2009) Neuronal shot noise and Brownian 1/f2 behavior in the local field potential. PLoS ONE 4(2):e4338. doi:10.1371/journal.pone.0004338

Moreva EV, Brida G, Gramegna M, Giovannetti V, Maccone L, Genovese M (2013) Time from quantum entanglement: an experimental illustration. Phys Rev A 89:052122

Mota B, Herculano-Houzel S (2015) Cortical folding scales universally with surface area andthickness, not number of neurons. Science 3(6243):74–77

Neupert SD, Allaire JC (2012) I think I can, I think I can: examining the within-personcoupling of control beliefs and cognition in older adults. Psychol Aging 2(2):145–152

Nikolov D, Oliveira DFM, Flammini A, Menczer F, Feb SI (2015) Measuring online social bubbles. Peer J Comput Sci. doi:10.7717/peerj-cs.38

O'Donnell C, Van Rossum MC (2014) Systematic analysis of the contributions of stochastic voltage gated channels to neuronal noise. Front Comput Neurosci 8:105. doi:10.3389/fncom.2014.00105

Oei NYL, Rombouts SARB, Soeter RP, van Gerven JM, Both S (2012) Dopamine modulates reward system activity during subconscious processing of sexual stimuli. Neuropsychopharmacology 37:1729–1737

Pakhomov A, Sudin N (2013) Thermodynamic view on decision-making process: emotions as a potential power vector of realization of the choice. Cogn Neurodyn 7(6):449–463

Palma J, Grossberg S, Versace M (2012) Persistence and storage of activity patterns in spiking recurrent cortical networks: modulation of sigmoid signals by after-hyperpolarization currents and acetylcholine. Front Comput Neurosci 6:42. doi:10.3389/fncom.2012.00042

Patel J, Schomburg EW, Berényi A, Fujisawa S, Buzsáki G (2013) Local generation and propagation of ripples along the septotemporal axis of the hippocampus. J Neurosci 33(43):17029–17041

Penttonen M, Buzsaki Gy (2003) Natural logarithmic relationship between brain oscillators. Thalamus Relat Syst 2(2):145–152

Pereira A (2017) Astroglial hydro-ionic waves guided by the extracellular matrix: an exploratory model. J Integr Neurosci 16(1):57–72

Pereira A Jr, Foz FB, Rocha AF (2017) The dynamical signature of conscious processing: from modality-specific percepts to complex episodes. Psychol Conscious Theory Res Pract. doi:10.1037/cns0000115

Perlmutter E (2016) Bounding the space of holographic CFTs with chaos. J High Energy Phys 2016:69

Peters JF (2016) Computational proximity. excursions in the topology of digital images, In: Peters JF (ed) pp 169–171. doi:10.1007/978-3-319-30262-1

Peters JF (2017) Foundations of computer vision. Computational geometry, visual image structures and object shape detection, intelligent systems reference library, vol 124. Springer, Berlin. doi:10.1007/978-3-319-52483-2

Peters JF, Ramanna S, Tozzi A, İnan E (2017) Bold-independent computational entropy assesses functional donut-like structures in brain fMRI images. Front Hum Neurosci 11:38

Pigarev IN, Pigareva ML (2015) The state of sleep and the current brain paradigm. Front Syst Neurosci 9:139. doi:10.3389/fnsys.2015.00139

Pothos EM, Busemeyer JR (2009) A quantum probability model explanation for violationsof 'l' derationacision theory. Proc R Soc B 276(1665):2171–2178

Pothos EM, Busemeyer JR (2013) Can quantum probability provide a new direction forcognitive modeling? Behav Brain Sci 36(03):255–274

Poutanen P, Soliman W, Ståhle P (2016) The complexity of innovation: an assessment and review of the complexity perspective. Eur J Innov Manag 19(2):189–213

Pritchard WS (1992) The brain in fractal time: 1/f-like power spectrum scaling of the human electroencephalogram. Int J Neurosci 66:119–129

Raichle ME, Snyder AZ (2007) A default mode of brain function: a brief history of anevolving idea. NeuroImage 37(4):1083–1090

Rudd M, Aaker J, Vohs K (2012) Awe expands people's perception of time, alters decisionmaking, and enhances well-being. Psychol Sci 23(10):1130–1136

Schultz W (2007) Reward signals. Scholarpedia 2(6):2184

Sengupta B, Stemmler MB (2014) Power consumption during neuronal computation. Proc IEEE 102:738–750

Seo D, Patrick CJ, Kennealy PJ (2008) Role of serotonin and dopamine systeminteractions in the neurobiology of impulsive aggression and its comorbidity with other clinical disorders. Aggress Violent Behav 13(5):383–395

Touboul J (2012) Mean-field equations for stochastic firing-rate neural fields with delays: derivation and noise-induced transitions. Phys D Nonlinear Phenom 241(15):1223–1244

Touroutoglou A, Lindquist KA, Dickerson BC, Barrett LF (2015) Intrinsicconnectivity in the human brain does not reveal networks for "basic" emotions. Soc Cogn Affect Neurosci 10(9):1257–1265

Tozzi A, Peters JF (2016a) Towards a fourth spatial dimension of brain activity. Cogn Neurodyn 10(3):189–199

Tozzi A, Peters JF (2016b) A topological approach unveils system invariances and broken symmetries in the brain. J Neurosci Res 94(5):351–365

Tozzi A, Peters JF (2017) The multidimensional world. Lambert Academic Publishing, Saarbrücken. ISBN-13: 978-3-330-03530-0

Tozzi A, Zare M, Benasich AA (2016) New perspectives on spontaneous brain activity: dynamic networks and energy matter. Front Hum Neurosci 10:247. doi:10.3389/fnhum.2016.00247

Author's personal copy

Tozzi A, Peters JF, Fingelkurts AA, Fingelkurts AA, Marijuán PC (2017a) Topodynamics of metastable brains. Phys Life Rev. doi:10.1016/j.plrev.2017.03.001

Tozzi A, Peters JF, Jausovec N (2017b) A repetitive modular oscillation underlies human brain electric activity. Neurosci Lett. doi:10.1016/j.neulet.2017.05.051

Traversa FL, Di Ventra M, Bonani F (2013) Generalized Floquet theory: application to dynamical systems with memory and Bloch's theorem for nonlocal potentials. Phys Rev Lett 110(17):170602

Treadway MT, Buckholtz JW, Cowan RL, Woodward ND, Li R, Ansari MS, Zald DH (2012) Dopaminergic mechanisms of individual differences in human effort -based decisionmaking. J Neurosci 32(18):6170–6176

Van de Ville D, Britz J, Michel CM (2010) EEG microstate sequences in healthy humans at rest reveal scale-free dynamics. PNAS 107(42):18179–18184. doi:10.1073/pnas.1007841107

Van Essen DC (2005) A population-average, landmark- and surface-based (PALS) atlas of human cerebral cortex. Neuroimage 28:635–666

Ventriglia F (2014) Random dispersion in excitatory synapse response. Cogn Neurodyn 8(4):327–334

Wang Z, Solloway T, Shiffrin RM, Busemeyer JR (2014) Context effects produced by question orders reveal quantum nature of human judgments. PNAS 111(26):9431–9436

Watanabe T, Hirose S, Wada H, Imai Y, Machida T, Shirouzu I, Konishi S, Miyashita Y, Masuda N (2014) Energy landscapes of resting-state brain networks. Front Neuroinform 25(8):12

Weeks JR (2002) The shape of space, 2nd edn. Marcel Dekker inc, New York-Basel

Yamada Y, Kawabe T (2011) Emotion colors time perception unconsciously. Conscious Cogn 20(4):1–7

Zeeman EC (1976) Catastrophe theory. Sci Am, 234(4):65–70, 75–83

Zhang J, Hess PW, Kyprianidis A, Becker P et al (2016) Observation of a discrete time crystal. arXiv:1609.08684

Critique of pure free energy principle.
Comment on "Answering Schrödinger's question: A free-energy formulation" by Maxwell James Désormeau Ramstead et al.

Arturo Tozzi (Corresponding Author)
Center for Nonlinear Science, University of North Texas
1155 Union Circle, #311427
Denton, TX 76203-5017, USA, and
Computational Intelligence Laboratory, University of Manitoba, Winnipeg, Canada
Winnipeg R3T 5V6 Manitoba
tozziarturo@libero.it

James F. Peters
Department of Electrical and Computer Engineering, University of Manitoba
75A Chancellor's Circle, Winnipeg, MB R3T 5V6, Canada and
Department of Mathematics, Adıyaman University, 02040 Adıyaman, Turkey,
Department of Mathematics, Faculty of Arts and Sciences, Adıyaman University
02040 Adıyaman, Turkey and Computational Intelligence Laboratory, University of
Manitoba, WPG, MB, R3T 5V6, Canada
james.peters3@umanitoba.ca

The paper by Ramstead et al. [1] [in this issue] reminds us the efforts of eminent scientists such as Whitehead and Godel. After having produced influential manuscripts, they turned to more philosophical issues, understanding the need for a larger formalization of their bounteous scientific results [2,3]. In a similar way, the successful free-energy principle has been generalized, in order to encompass not only the brain activity of the original formulation, but also the whole spectrum of life [1]. The final result is of prominent importance, because, in touch with Quine's naturalized epistemology [4] and Badiou's account of set theory [5], provides philosophical significance to otherwise purely scientific matters. The free energy principle becomes a novel paradigm that attempts to explain general physical/biological mechanisms in the light of a novel scientific ontology, the "variational neuroethology". The latter, seemingly grounded in a recursive multilevel reductionistic/emergentistic approach à la Bechtel [6], has also its roots in a rationalistic top-down approach that, starting from mathematical/physical general concepts (von Helmholtz's free energy), formulates experimentally testable (and falsifiable) theories.

Philosophical issues. One of the main concerns raised by generalizations of the free-energy principle is that it coped with individuals and evolution in rather vague and abstract terms. Is such a claim true? In order to tackle this problem, here we ask: what is meant by different organisms with peculiar systems features? The crux of Ramstead et al.'s argument is that organisms can be described in terms of (high dimensional) phase space induced by hierarchically nested Markov blankets. Then we ask: if different living beings display the common features of Markov blankets, might it be stated that they are "identical"? Has the free energy principle's notion of organisms anything to do with "identity"? Are biological systems (as described in a free energy principle context) identical? Do they stand for the same feature, or for two different features with something in common?
We recall Heidegger's account of the "principle of identity" [7]. It states that A=A. The formula expresses that one A is equal to another A. Hence, A is the same of A, because "identical" (from Greek) means: "the same".
However, in another possible version, the formula A=A speaks of "equality". A is A. It does not say that A is the same, but that every A is itself the same. Or, in other words, each thing itself is the same for itself with itself.
However, it could also be stated that A "belongs to" an identity with A. In this case, sameness is interpreted as a "belonging together". In "belonging together", the world "together" means: to be assigned and placed into the order of a together, to be established in the unity of a manifold, to be combined into the unity of a system. Such an assignment and placing occur thanks to connexions of the one with the other. Two interpretations are feasible: a) biological systems are determined by an identity as a feature of that identity; b) identity is represented as a feature of biological systems.
However, "belonging together" could also mean: the together is now determined by the belonging.
Therefore, the possibilities here are two: a) representing belonging in terms of the unit of together; b) experiencing this together in terms of belonging. The issue b) leads us to the psychological standpoint of the observer, i.e., to the original formulation of the free energy principle for brain activity. Indeed, the two features termed "brain" and "biological system" can also be thought as the same, so that both belong together in the same environmental milieu, and by virtue of the same milieu. If we attempt to represent together both the features as a coordination of perspectives, we can establish and explain this coordination either in terms of "brain" or "biological system". If the two features belong to each other, "biological system" belongs with "brain" in an identity, whose active assembly (amalgam) stems from that

"letting belong together" which we might call "mental representation". Identity becomes, in this version, a functional property of the event of mental representation.
In sum, identity can be presupposed either as a feature of biological systems, or a spring that flows from them. In this second account, the principle of identity becomes a watershed for the psychological origin of identity. We can therefore assess "brain" and "biological system" in terms of that which joins the two, by virtue of the event of mental representation. Thus, the term "biological system" displays the widest range of possible uses. In particular, it does not assess just "the same" thing, but also things that are "different". For example, the curvature shoreline of Vietri (southern Italy) and the edge of a bowl of water with similar curvature are components in feature vectors that supply the basis for common description. This implementation makes the free energy principle not just a launching platform for a novel interpretation of almost all the biological (and physical) phenomena, but also a suitable tool in order to evaluate the slight (objective and subjective) differences that make our world an astonishing realm of rich heterogeneity.

Physical and biological issues. The free energy principle is successful enough to justify its engagement in the assessment of a wide range of biological, physical, and also social, nonlinear systems. However, we want to draw the attention on less-explored issues, that might help to further investigate its powerful apparatus.

Pandemonium is a hierarchical, parallel processing, self-improving model, where "computational demons" perform non-trivial binary functions on two variables [8]. This architecture has been proposed also in order to elucidate brain functions, such as pattern recognition. The processing resembles a kind of natural evolution, by selecting outputs from the "best" processing demons. Indeed, Pandemonium introduces a "the winner-take-all" mechanism, in keeping with neural darwinism [9-12]: cognitive demons' selection generates new subdemons for trial and eliminates inefficient and weak ones, every time reweighting the assembly. The same concept might be extended to variational neuroethology, because competition among hierarchical nested Markov blankets might occur in every one of the four Tinbergen's levels of inquiry.

A role for non-stationary local fluctuations of temperature in Markov blankets merits exploring. For example, contrary to the common belief, the cortical temperature is not a stable parameter, rather the brain displays thermal gradients observed at many spatiotemporal scales [13]. Local changes in thermal properties may act as a dynamic variable, modulating presynaptic and postsynaptic events, sensory stimuli, behavioral changes, memory encoding and fine-tune activity-dependent processes [14-15]. Arguments concerning thermodynamics point towards a correlation between changes in temperature and message content. Indeed, modifications in temperature can be associated with variations in both thermodynamic and information entropies [16-17]. Temperatures encompass information about how large-scale biological outcomes arise from the interactions of many small-scale processes, so that thermal variations may lead to different probability outcomes. Ongoing fluctuations with complex thermal properties that vary across biological regions can be absorbed into a free energy framework [10]: to make an example, the critical slowing implicit in decrease of living systems' temperatures is mandated by any system that minimizes its energetic expenditure.

Time has a foremost role in variational neuroethology [1]. Indeed, in the free energy principle context, the entropy is simply that of the agent's own recognition density, and time is incorporated in the recognition density. The latter stands for the probabilistic representation $q(\delta \mid \mu)$ of the causes of sensory input, in which the internal states of the inferential machine are $\mu(t)$ and the causes $\delta \supset \{\tilde{x}, \theta, \gamma\}$, comprising hidden states $\tilde{x}(t)$, parameters θ and precisions γ (controlling the amplitude of the random fluctuations). Here we show how the arrow of time influences entropy production, in particular in systems displaying stochastic (random) properties governed by Brownian motion such as living beings and biomolecular processes [13,18,19]. Non-equilibrium steady-state systems are regulated not just by the (forward) standard, classic entropy per unit time, but also by another directional entropy: the (backward) time-reversed one [20]. In non-linear systems, the forward entropy exhibits lower randomness than the backward one, so that the total entropy production differs from the one produced by the sole standard entropy. Entropy production is represented in the following way:

$$\frac{1}{\kappa V \tau} \Delta_i^{\tau} S = h^R(P) - h(P) \geq 0,$$

in which $\frac{1}{\kappa V \tau} \Delta_i^{\tau} S$ stands for the entropy production of non-equilibrium steady state, $h^R(P)$ for the time-reversed entropy and $h(P)$ for the τ-entropy (i.e., the standard entropy per unit time τ). P denotes the coarse graining or partition.

During their time evolution, non-equilibrium steady-state biological systems (equipped with a hierarchy of Markov blankets) display an unexpected production of both thermodynamic and information entropy. In the context of variational neuroethology, this means that homogeneous environmental features enter the system's chains without special statistical correlation, and exit with a very fine statistical correlation due to their interaction inside living beings. This occurs because constraints, caused by the non-equilibrium steady-state and the generated randomness, impose stochastic boundary conditions at the borders of the Markov blankets. Time-reversal asymmetry provokes two opposite effects: on the one hand, time passing introduces probability biases and influences the evolution of a system capable of memory; on the other hand, the progressive, unforeseen changes in both Gibbs entropy [21] and information production leads to ageing and history-dependent organisms [22-23]. In sum, as times goes on, the recognition density\entropy described by the free energy principle displays an unpredicted variation, due to time-reversal asymmetry. This is another bias the living beings and their Markov blankets have to cope with.

REFERENCES

1) Ramstead MJD, Paul Benjamin Badcock PB, Friston KJ. 2017. Answering Schrödinger's question: A free-energy formulation. Physics of Life Reviews. https://doi.org/10.1016/j.plrev.2017.09.001.
2) Whitehead AN. 1929. Process and Reality (Gifford Lectures). Macmillan USA; 2Rev Edition, 1979.
3) Godel K. 1930-1964. Kurt Gödel: Unpublished Philosophical Essays. Rodriguez-Consuegra FA (Editor). Birkhäuser; 1995 edition.
4) Quine WVO. 1969. Epistemology Naturalized. In: Ontological Relativity and Other Essays. New York: Columbia University Press, 69–90.
5) Badiou A. 1988. Being and Event. Continuum. Edition 2011.
6) Bechtel, W. 2012. Understanding endogenously active mechanisms: A scientific and philosophical challenge. European Journal for the Philosophy of Science, 2, 233-248.
7) Heidegger M. 1957. Identity and difference. Harper & Row, Publishers (New York, Evanston, and London).
8) Selfridge OG. 1957. Pandemonium: a pradigm for learning. In: Mechanization of thought processes: proceedings of a Symposium held at the national Physical Laboratory, London: HMSO, 513-526.
9) McDowell JJ. 2010. Behavioral and neural Darwinism: Selectionist function and mechanism in adaptive behavior dynamics, Behavioural Processes 84, no. 1, May 2010, doi.org/10.1016/j.beproc.2009.k11.011.
10) Friston K. 2010. The free-energy principle: a unified brain theory? Nat Rev Neurosci 11(2):127-138. doi: 10.1038/nrn2787.
11) Rosenbaum DA. 2014. It's a Jungle in There: How Competition and Cooperation in the Brain Shape the Mind. Oxford University, ISBN 978-0-19-982977-4.
12) Edelman G. 2017. Neural Darwinisim, New Perspectives Quarterly, 31, (1):25-27.
13) Wang H, Wang B, Normoyle KP, Jackson K, Spitler K, et al. 2014. Brain temperature and its fundamental properties: a review for clinical neuroscientists. Front. Neurosci., 8;8:307 2014 | doi: 10.3389/fnins.2014.00307.
14) Long MA, Fee MS. 2008. Using temperature to analyse temporal dynamics in the songbird motor pathway. Nature456(7219):189-194.
15) Kalmbach AS, Waters J. 2012. Brain surface temperature under a craniotomy. J Neurophysiol. 108(11), 3138-3146.
16) Jizba P, Arimitsu T. 2001. The world according to Renyi: thermodynamics of fractal systems. AIP Conference Proceedings, 597, 341-348.
17) Jizba P., Korbel J. 2015. On q-non-extensive statistics with non-Tsallisian entropy. arXiv:1501.07386.
18) Kiviet DJ, Nghe P, Walker N, Boulineau S, Sunderlikova V, Tans SJ. 2014. Stochasticity of metabolism and growth at the single-cell level. Nature 514, 376–379. doi:10.1038/nature13582.
19) Ribrault C,Sekimoto K. TrillerA. 2011. From the stochasticity of molecular processes to the variability of synaptic transmission. Nat Rev Neurosci. 12, 375–387. doi:10.1038/nrn3025.
20) Gaspard P. 2005. Brownian motion, dynamical randomness and irreversibility. New J Phys. 7 77. doi:10.1088/1367-2630/7/1/077.
21) Cencini M, Falconi M, Olbrich E, Kantz H and Vulpiani A. 2000. Chaos or noise—difficulties of the distinction. Phys. Rev. E 62 427.
22) Carlson JM, Doyle J. 2002. Complexity and robustness. Proc Nat Acad Sci, 99, suppl. 1:2538-45.
23) Sherrington D. 2010. Physics and complexity. Phil Trans R Soc A 368, 1175–1189. doi:10.1098/rsta.2009.0208.

SCIENTIFIC FEDERATION
ABODE FOR RESEARCHERS

James F Peters, SF J Neuro Sci, 2017, 1:2

SciFed Journal of Neuroscience

Research Article Open Access

Towards Equations for Brain Dynamics and the Concept of Extended Connectome

*[1]James F Peters, [2]Arturo Tozzi, [3]Eva Déli

*[1]*Department of Electrical and Computer Engineering, University of Manitoba 75A Chancellor's Circle Winnipeg, MB R3T 5V6, Canada*

[2]*Center for Nonlinear Science, University of North Texas,1155 Union Circle, #311427, Denton, TX 76203-5017, USA*

[3]*Benczurter 9, Nyiregyhaza, 4400, Hungary*

Abstract

The brain is a system at the edge of chaos equipped with nonlinear dynamics and functional energetic landscapes. However, still doubts exist concerning the type of attractors or the trajectories followed by particles in the nervous phase space. Starting from a system governed by differential equations in which a dissipative strange attractor coexists with an invariant conservative torus, we developed a 3D model of brain phase space which has the potential to be operationalized and assessed empirically. We achieved a system displaying both a torus and a strange attractor, depending just on the initial conditions. Further, the system generates a funnel-like attractor equipped with a fractal structure. Changes in three brain phase parameters lead to modifications in funnel's breadth or in torus/attractor superimposition. We have found that the higher frequencies of evoked activities are more deterministic due to the greater funnel breadth with decreasing degrees of freedom. In contrast, the resting state is formed by lower frequencies represents greater degrees of freedom. Thus, our model explains a large repertoire of brain functions and activities, such as sensations/perceptions, memory and self-generated thoughts.

Keywords

Brain Dynamics; Strange Attractor; Invariant Torus; Nonlinear Systems

Introduction

The functional neocortex is the connectonome, a synoptically interconnected network of neurons. The energy need of synaptic activation depends of the frequency of use, which decreases the resistance over time. Thus, synaptic transmission is not a proportional with the energy of activation, but dependent on many factors, such as the synaptic conditions and state, neurotransmitter presence, chemical environment and the ATP/ADP ratio. These conditions may result in less, equal, or more energy being transferred than arrived at the bouton. Part of the energy transmitted from one neuron to the next creates a memory trace in the synapse, which enhances the efficiency of future transmissions. Therefore, the brain is a complex, non-linear system, formed by a large number of interacting and inter-dependent components which exhibit emergent properties, spontaneous self-organization, avalanches [1, 2, 3] and sensitivity to initial small changes. Synaptic transmission is susceptible to unpredictable behavior via the hierarchy of physical organization of the brain. Furthermore, it seems likely that the neural states might

***Corresponding author:** James F Peters, Department of Electrical and Computer Engineering, University of Manitoba 75A Chancellor's Circle Winnipeg, MB R3T 5V6, Canada. E-mail: James.Peters3@umanitoba.ca **Tel No**: 204 474 9755

Received August 15, 2017; **Accepted** September 16, 2017; **Published** September 29, 2017

Citation: James F Peters (2017) Towards Equations for Brain Dynamics and the Concept of Extended Connectome. SF J Neuro Sci 1:2.

Copyright: © 2017 James F Peters. This is an open-access article distributed under the terms of the Creative Commons Attribution License, which permits unrestricted use, distribution, and reproduction in any medium, provided the original author and source are credited.

be unique to specific mental states. The brain might be viewed as a single interconnected feedback system that can be described by mathematical phase space analysis, which can be flexibly and speedily reconfigured: many brain areas are capable of carrying out a variety of functions and are able to switch between those functions in a context-sensitive, dynamic fashion [4].

It has been proposed that the brain operates at the edge of chaos, near a critical regime, where the maximum information function lies between randomness and regularity [5, 6, 7]. The concept of nonlinear brain needs to be framed into the energy landscape theory, originally built for a statistical description of protein's potential surfaces [8, 9]. Such landscape is characterised not just by low-energy valleys - stationary points where the gradient vanishes -, but also by high-energy peaks and transition states. When nervous activity takes place, the energy tends to converge towards a stable state equipped with a minimum energy level, so that the interplay between neuronal structure and activity at many different spatiotemporal scales gives rise to functional "attractors" [10, 11] that emphasize the importance of random walks [12], metastability [13] and self-organized criticality [14]. Although the simplest candidate in which local minima might occur is a simple "fixed-point attractor", which is a funnel located in a functional phase space where trajectories converge as time progresses, other models have also been proposed: for example, resting state networks might emerge as structured noise fluctuations around a stable low firing activity equilibrium state in the presence of latent "ghost" multistable attractors. [15]. It has been also suggested that brain function does not exhibit erratic brain dynamics nor attractors, rather a stable sequence, called transient heteroclinic channel [13]. A foremost issue in such a context is the scale-free dynamics – also called $1/f^{\alpha}$ behavior, power law, self-similarity, fractal-like distribution [16, 17, 18, 19].

Conversely, it has been recently proposed that mental operations follow constrained, topological donut-like trajectories along preferential functional brain railways [20, 21, 22, 23, 24]. Experimental and theoretical clues allow us to conjecture that some brain activities are shaped in guise of a multidimensional torus. The theoretical claims of brain multidimensionality are widespread [3, 25, 26] as an example, models characterized by dimensionality reduction have been used in the study of human central nervous system [27]. It has been demonstrated that high dimensionality brain spontaneous activity structures occur, consisting of multiple, reproducible temporal sequences [28]. It has also been shown that the exceedingly diverse nonlinear selectivity in single-neuron activity in the prefrontal cortex is a signature of high-dimensional neural representations: crucially, this dimensionality is predictive of animal behaviour as it collapses in error trials [29]. In addition, recent findings suggest that nervous structures process information through topological as well as spatial mechanisms: for example, hippocampal place cells might produce topological templates in order to represent spatial information [30]. A torus displays a donut-like shape: it means that the trajectory followed by a particle inside it, is closed. To make an example, if one walks along one of the curves of a torus, she perceives in traversing in a straight trajectory, even though her environment is embedded in a higher dimension. The torus may be compared with a video game with biplanes in aerial combat: when a biplane flies off one edge of gaming display, it does not crash but rather it comes back from the opposite edge of the screen [31]. Mathematically speaking, the display edges have been "glued" together. Our brain exhibits similar behaviour, i.e., the unique ability to connect past, present and future events in a single, coherent picture [24, 32, 33], as if we were allowed to watch the three screens of past-present-future glued together in a mental kaleidoscope. The same occurs during other brain functions, e.g., memory retrieval, recursive imagination and mind wandering [34], in which concepts flow from one state to another. The torus is naturally visualized intrinsically, by ignoring any extrinsic properties a surface may have: in the same way, we humans perceive our thoughts intrinsically and naturally adopt "private", subjective or personal standpoints. The concept of personality corresponds very closely with the concept of the strange attractor [35]. If the brain is considered a chaotic system, accompanied by a quasi-attractor pattern in phase space, then a personality can be seen as a logical and necessary consequence. The brain, like other extremely complex systems, is unpredictable in the level of detail but roughly predictable on the level of structure. This means that the dynamics of its physical variables display a strange attractor with a complex structure. Thus, consciousness can be viewed as a phenomenon in Physics [36] and the complex neural dynamics of the brain can be studied in the framework of state space dynamics and criticality. In Physics, concepts of phase space transitions and the Renormalization Group are powerful tools for interpreting phenomena involving many scales of length and time in complex systems. The significance of these concepts lies

in their accounting for the emergence of different levels of new collective behaviors in complex systems, each level with its distinct ontology, organization and laws, as a new pattern of reality.

Earlier we have shown that the brain forms an energy structure, which is insulated from the environment. Thus, sensory interaction is carefully regulated based on energy/information exchange, which engenders self-organization and criticality [22]. Via via self-regulation the brain formulates low entropy, so called resting state.

In this multifaceted framework, a recently proposed three-dimensional, continuous, time-reversible system - governed by a set of first-order ordinary differential equations (ODEs) -comes into play. This system has an unusual property: it exhibits conservative behavior for some initial conditions, and dissipative for others [37]. The conservative regime has quasi-periodic orbits whose amplitude depends on the initial conditions, while the dissipative regime is chaotic. It means that, in the state space, a strange attractor coexists with an invariant torus. Our aim was to build a neural model, starting from the Sprott's ODEs, which might explain brain dynamics during different mental activities.

Materials and Methods

Sprott's Equations

We built a 3-dimensional phase space based on the unusual Sprott's system, equipped with no equilibrium points (stable or unstable) and only bounded orbits for all initial conditions. The system is described by the following ODEs:

$$\begin{aligned} \dot{x} &= y + 2xy + xz, \\ \dot{y} &= 1 - 2x^2 + yz, \\ \dot{z} &= x - x^2 - y^2. \end{aligned} \qquad (1)$$

The only possible solutions are (quasi)-periodic or chaotic, depending just on the starting point of the initial conditions. Notice that Sprott's images stand for the 4D case (x, y, z, t), with time as a (hidden) parameter on the derivatives.

We achieved the evaluable and measurable features described in Figure 1.

Figure 1: Depicts four measurable system's features. In this case, as an example, we displayed the system originating from the initial conditions 0.5002, -0.5, -0.0791. The solid circle A stands for the disk embedded into the strange attractor's maximum transversal diameter, while the solid line F for the diameter of the funnel lying into the strange attractor. The solid line L stands for the length of the funnel lying into the strange attractor, while the dotted circle T for the disk embedded into the torus's circumference

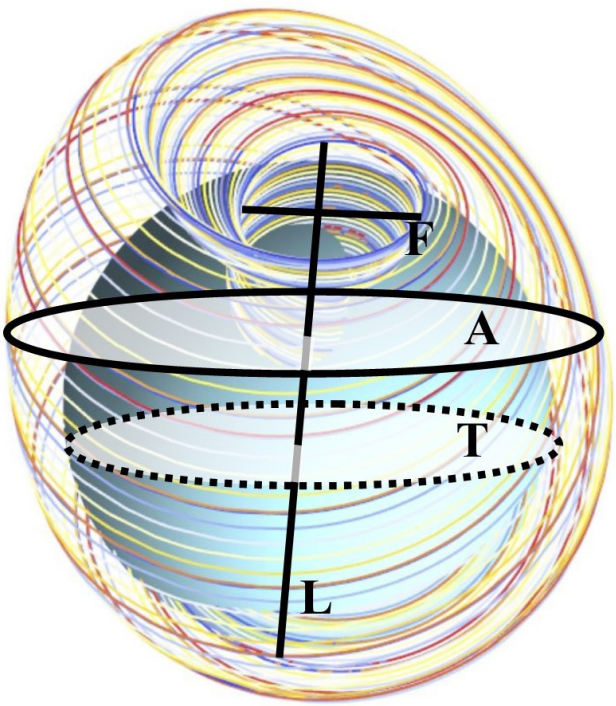

A Model of Brain Phase Space: The Extended Connectome

The next step was to evaluate whether it is possible to assess brain dynamics through our Sprott's system implementation. The natural candidate to the role of nervous phase space is the human connectome. According to the widely accepted description of the connectome's networks, the cortical and sub cortical structures form a hierarchical network, equipped with preferential pathways for fast communication and winner-takes-all mechanisms [38, 39]. However, recent papers unveil the role of a connectome that is more extended than previously believed, investigating network connections in different species: the Caenorhabditis elegans globally integrative rich club of neurons [40], the mouse micro scale cortico-thalamic pathway [41], the rodent peripheral nervous system connectivity and cortical midline structures [42], the human sub cortical connectome [43], thalamus [44] and basal ganglia - including striatum and put amen [45]. Taken together, such observations suggest that the nodes and the hubs of the connectome are not confined to the "higher" and phylogenetically recent structures, but are also diffused along the entire neural pathway; including the central and peripheral nervous system. It is possible that, in the years to come, the concept of connectome will be also extended to the peripheral receptors. Indeed, most peripheral structures play a crucial role in information processing: receptors perform complex neural computations that were thought to be carried out by sensory cortex and have a prominent role in sensory processing. As an example, the brain has outsourced some aspects of touch processing to the nerve endings in the fingertips [46]. In sum, we can state that the electric oscillatory activity of the extended connectome – shaped in guise of a phase space - gives rise to a free-energy landscape.

Our hypothesis is that external (or internal) inputs activate just a point on a 3D brain phase space (the connectome), and the activation of such a point leads to a trajectory displaying the shape of either a torus, or a strange attractor. The particle trajectories depend just on its initial location in the phase space.

We evaluated the system behavior during increases or decreases of every one of the three brain parameters, in order to detect which type of trajectory is achieved when a single change in x, y or z occurs. The values of some of the three coordinates were extracted from real-data plots of studies based on EEGs and fMRI neurotechniques (18, 29, 47, 48)

Results

We achieved a system displaying both a torus and a strange attractor, depending on the starting conditions, i.e., the initial points where the trajectories started their movements. Figure 2 shows the results of our implementation of Sprott's attractors with different initial conditions (x, y, z). A noteworthy result is that the strange attractors display funnel-shape morphology, with the appearance of a twisting funnel that dips in and out of the sphere: it means that the funnel is embedded in a fractal structure. The funnel is more or less narrow, depending on the initial conditions: to make an example, when x increases, the funnel is much narrower, while, when y increases, the funnel is larger. Depending from initial conditions, the strange attractor and the torus are more or less superimposed: i.e., when y changes, the strange attractor and the torus are closely intertwined, making difficult to evaluate whether a starting point leads to a fractal or non-fractal trajectory; vice versa, when z increases, the strange attractor surrounds the torus in guise of a cloud; furthermore, when x increases, the two structures are neatly separated.

In particular, we achieved the following results:

When the initial conditions are 0, 0, 0, the following system is displayed
L and T and are partially superimposed and intertwined.
T diameter = A diameter
F = high values (a large funnel)

When the initial conditions are 1, 0, 0
L and T are sharply separated
T < A
F = the minimum values (very narrow funnel's diameter)

When the initial conditions are 0, 1, 0
T (almost completely) includes and surrounds L.
T>A
A in partially embedded into T
F = the highest values (the widest funnel)

When the initial conditions are 0, 0, 1
A includes and surrounds T
A>T
T is embedded into A
F = low values (narrow funnel)

Figure 2: Implementation of Sprott's attractors for four different values of x,y and z. The black lines show the points zero on the respective axis. See the main text for further details

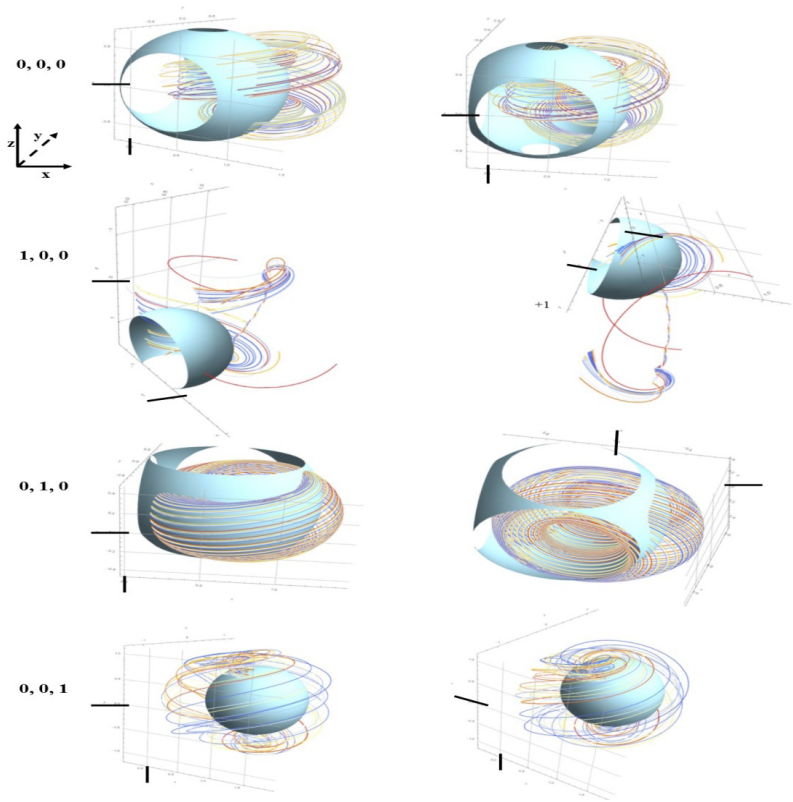

Conclusions

Self-organized criticality (SoC), a spontaneous dynamic state established and maintained in complex networks, is a universal characteristic of neural systems [49]. We investigated how the energy/information flow via synaptic transmission in the brain is related to psychological experiences, such as emotion and qualia. In the brain blood glucose levels are maintained by careful endocrine control, with the primary hormones insulin and glucagon acting in a complementary manner. The brain's high metabolism is ensured by the disproportionate consumption of oxygen and glucose. For example, the brain's local activity can be inferred by energetic changes registered by fMRI, PET, and EEG, because sensory stimulation is associated with a sharp increase in neuronal 2-deoxyglucose uptake [50]. In neurons, most ATP is dedicated to supporting synaptic transmission [51] and energy restrictions are often implicated in the brain's vulnerability to hypoxic-ischemic damage, and the reduction of consciousness. Thus, it is expected that the brain's available energy supply shows close relationship to the frequencies and amplitude of electric activation. Namely, the ATP/ADP ratio places an upper limit on the neurons energy use, which encourages the formation of frequencies away from their energetic mean value, leading to a power law of oscillation frequencies. In addition, the memories formed by the network of synaptic connections function as preferred paths that act as attractors in the phase space. Attractor networks naturally stabilize by seeking energy minima, and the relative positions of basins of attraction define the geometry of an energy landscape [4, 52]. As a result, the transition into an active attractor state occurs as a transition into an information/energy maximum.

Starting from the peculiar Sprott's system of ODEs, we built a neural testable model equipped with both a conservative torus and a dissipative strange attractor. When a moving particle starts its trajectory from a given position x, y, z in the 3D nervous phase space, we may predict whether it will fall in the torus or into the strange attractor. The funnel shape is fractal, and not just a simple fixed-point attractor. A narrower funnel means that the trajectory is constrained towards a small zone of the phase space. When the two structures are closely superimposed, we might hypothesize a state of phase transition at the

edge of the chaos, equipped with high symmetry, in which it is difficult to evaluate every single initial position: a slightly change in the starting point could indeed lead to completely different outcomes. When the torus and the strange attractor are clearly split, a single starting point gives rise to a sharply defined outcome. It means that in the latter case, the two conformations are neatly separated, as if the system went out of phase transition and a symmetry breaking occurred.

Looking for possible psychological correlates of our system, we hypothesize that the proposed scheme might stand for a large repertoire of brain functions and activities, such as sensations/perceptions, emotions, mood-state/affect, memory, abstraction, sequencing/planning, choice, judgment, creativity, self-generated thoughts [34]. For example, when the particle falls into the conservative torus conformation (where two antipodal particles cannot never meet or become closer, due to their recurring rotations) the correlated psychical activities could be either repetitive patterns of movements or thoughts, or preserved memories, or mind wandering, or unsure perceptions, in which different ideas are not properly melted together. In turn, when the particle falls into the dissipative strange attractor conformation (equipped with steep and narrow funnels), the correlated psychical activities could be driven by strong emotional impetus of survival, or motivation, focus, such as goals, pride, aggravation and others.

We might hypothesize that, due to external or internal inputs, changes take place in one or more of the three parameters. Such changes activate a single point of the 3D functional brain lattice, where a "particle 1" starts its trajectory into one of the two described dynamical conformations. When another input occurs, the corresponding variation in the parameters' value puts in motion a "particle 2" from a different starting point in the phase space. We might speculate that: a) either the particle 2' trajectory prevails and cancel the particle 1's; 2) or the two particles move at the same time, following each one its own orbit; 3) or the particle 1, following the activation of the starting point of the trajectory 2, switches from its trajectory to the trajectory 2, or to another one.

Our model also satisfies the brain free-energy constraints required by the most influential current brain theories [20, 53, 54, 55]. Indeed, spontaneous activity displays a lower energetic level than the evoked one. The energy need and information carrying capacity of brain waves is proportional to their frequencies [56] and all positive emotions and neutral mental states have smaller energy requirement than negative emotional states [57], showing the relationship between the energy need of brain oscillations to the physiological of mental, emotional experience. As stated above, we know that each spike has a certain consumption of ATP [58] and that each spike is formed by an oscillation, equipped with both amplitude and a frequency. During spontaneous activities, the frequency is very low, but the amplitude is substantial. In contrast, the high frequencies that emerge during evoked activities manifest only small amplitudes. For the Ohm's law, in the first case, the AMPLITUDE is determinant in energy consumption, whereas in the second case the energy consumption due to the amplitude of the oscillation is negligible, compared with the energy consumption due to its FREQUENCY. This means that the evoked brain activity, equipped with a mean spike frequency higher than the spontaneous activity, spends more energy. Due to their great energy need, great energy requiring activation, such as powerful stimulus or negative emotions represent a sharper funnel that can dramatically decrease the degrees of freedom, because the decrease in temporal dimensionality [20, 21]. However, the exponentially increasing energy gradient taxes the ATP production abilities of the brain and leads to mental, behavioral consequences manifested as lack of patience, aggravation and emotional breakdown. This occurs, because the ATP cannot keep up with the metabolic requirement of neural activation [55, 59]. Therefore, neurodegenerative pathways are thought to converge on energy failure, and synaptic terminals degenerate early in many neurodegenerative diseases associated with impaired energy metabolism [60].

This is in contrast to spontaneous activities, which are the physiological counterpart of the default mode network. This low-energy rewiring activity is characterized by low-frequency, high amplitude oscillations equipped with power laws, infinite correlation length and (probably) falling into strange attractors and phase transitions. Since the low frequencies extinguish information carrying capacity of the brain's electric activities, it leads to recurring, wayward thoughts with its psychological correlates (such as mind wandering or self-generated thoughts) [34]. During resting sensations, non-dissipative torus is restored. However, we have shown in our earlier work that the resting state is not immune from increasing frequencies [20, 21]. Accumulated emotional energies can interfere with the resting state, leading to more deterministic thought patters. Thus, ongoing brain activity is capable for the dynamic reconfiguration of

neural function [61] depending on the energy landscape.

Of course, ours is just an in-progress, provisional scheme. As suggested by Sprott himself (personal communication), we might also not to stop at three dimensions plus time, and we might take into account no integer dimensions too. For example, two interacting particles can be described as the motion of a single particle in a 6-dimensional space, where three of the dimensions characterize the particle position, and the other three characterize the components of velocity in each of the three spatial directions. A dynamical phase space's landscape (such as the brain) that consists of N interacting micro areas could be described by a single point moving in a 2N-dimensional phase space, although it will typically be the case that the dynamics is confined to a lower-dimensional subset of that very high-dimension space. It must also be kept into account that the torus, being structurally unstable in dynamical systems with dimensions greater than three, tends to evolve into a strange attractor. It means that, in long timescales, the trajectory inexorably falls into a funnel-like attractor equipped with the lowest possible energetic level, as proposed by protein-folding models based on the principle of minimum frustration [9].

References

1. Beggs JM, Plenz D (2004) Neuronal avalanches in neocortical circuits. J Neurosci 24**:** 5216-5229.

2. Tognoli E, Kelso JA (2014) Enlarging the scope: grasping brain complexity. Front Syst neurosci 8**:** 122.

3. Papo D (2014) Functional significance of complex fluctuations in brain activity: from resting state to cognitive neuroscience. Frontiers in Systems Neurosci 8**:** 112.

4. Amit DJ (1992) *Modeling Brain Function.* Cambridge: Cambridge University Press.

5. Arcangelis de L, Herrmann HJ (2010) Learning as a phenomenon occurring in a critical state. Proc Nat Acad Sci USA 107**:** 3977-3981.

6. Lombardi F, Herrmann HJ, Perrone Capano C (2012) Balance between Excitation and Inhibition Controls the Temporal. Organization of Neuronal Avalanches 108**:** 228703.

7. Zare M, Grigolini P (2013) Criticality and avalanches in neural network. Chaos Solitons and Fractals 55: 80-94.

8. Ferreiro DU, Cho SS, Komives EA (2005) The energy landscape of modular repeat proteins: topology determines folding mechanism in the ankyrin family. J Mol Biol 354**:** 679-692.

9. Sutto L, Latzer J, Hegler JA, et al. (2007) Consequences of localized frustration for the folding mechanism of the IM7 protein. Proc Natl Acad Sci 104**:** 19825-19830.

10. Vuksanovic V, Hövel P (2014) Functional connectivity of distant cortical regions: Role of remote synchronization and symmetry in interactions. NeuroImage 97**:** 1-8.

11. Watanabe T, Masuda N, Megumi F, et al. (2014) Energy landscape and dynamics of brain activity during human bistable perception. Nat Commun 28: 4765.

12. O'Donnell C, Van Rossum MC (2014) Systematic analysis of the contributions of stochastic voltage gated channels to neuronal noise. Front Comput Neurosci 8: 105.

13. Afraimovich V, Tristan I, Varona P, et al. (2013) Transient Dynamics in Complex Systems: Heteroclinic Sequences with Multidimensional Unstable Manifolds. Discontinuity, Nonlinearity and Complexity 21-41.

14. Bak P, Tang C, Wiesenfeld K (1987) Self-organized criticality: an explanation of the 1/f noise. Phys Rev Lett 59**:** 381-384.

15. Deco G, Jirsa VK (2012) Ongoing cortical activity at rest: criticality, multistability and ghost attractors. J Neurosci 32**:** 3366-3375.

16. Fraiman D, Chialvo DR (2012) What kind of noise is brain noise: anomalous scaling behaviour of the resting brain activity fluctuations. Frontiers in Physiology 3: 307.

17. Slomczynski W, Kwapien J, Zyczkowski K (2000) Entropy computing via integration over fractal measures. Chaos 10:180-188.

18. Milstein J, Mormann F, Fried I, et al. (2009) Neuronal shot noise and Brownian 1/f2 behavior in the local field potential. PLoS One 4: e4338.

19. Linkenkaer Hansen K, Nikouline VV, Palva JM, et al. (2001) Long-range temporal correlations and scaling behavior in human brain oscillations. Journal of Neuroscience 21: 1370-1377.

20. Sengupta B, Tozzi A, Coray GK, et al. (2016) Towards a Neuronal Gauge Theory. PLOS Biology 14: e1002400.

21. Tozzi A, Peters JF (2016) Towards a fourth spatial dimension of brain activity. Cognitive Neurodynamics 1-11.

22. Deli E, Peters J, Tozzi A (2017) Relationships between short and fast brain timescales. Cognitive Neurodynamics, in press.

23. Peters JF, Ramanna S, Tozzi A (2017) BOLD-independent computational entropy assesses functional donut-like structures in brain fMRI image. Frontiers Hum Neurosci.

24. Tozzi A, Peters JF, Fingelkurts AA, et al. (2017) Topodynamics of metastable brains. Physics of Life Reviews. http://dx.doi.org/10.1016/j.plrev.2017.03.001.

25. Tononi G (2008) Consciousness as Integrated Information: a Provisional Manifesto. The Biological Bulletin 215: 216-242.

26. Ponce Alvarez A (2015) Task-Driven Activity Reduces the Cortical Activity Space of the Brain: Experiment and Whole-Brain Modeling. PLoS Comput Biol 28: e1004445.

27. Garg R (2011) Full-brain auto-regressive modeling (FARM) using fMRI. Neuroimage 58: 416-441.

28. Mitra A (2015) Lag threads organize the brain's intrinsic activity. Proc Natl Acad Sci 112: 2235-2244.

29. Rigotti M, Barak O, Warden MR, et al. (2013) The importance of mixed selectivity in complex cognitive tasks. Nature 497: 585-590.

30. Dabaghian Y (2014) Reconceiving the hippocampal map as a topological template. eLife.

31. Weeks JR (2002) The shape of space. Second edition, Marcel Dekker inc New York-Basel.

32. Fingelkurts AA (2014) Present moment past and future: mental kaleidoscope. Front Psychol 5: 395.

33. Nyberg L (2010) Consciousness of subjective time in the brain. Proc Natl Acad Sci 107: 22356-22359.

34. Andrews Hanna JR, Ann NY (2014) The default network and self-generated thought: component processes, dynamic control and clinical relevance. Acad. Sci. 1316: 29-52.

35. Skrbina D (2017) Mind and Brain in Phase Space. http://www.bath.ac.uk/carpp/publications/doc_theses_links/d_skrbina.html

36. Werner G (2011) Consciousness Viewed in the Framework of Brain Phase Space Dynamics, Criticality, and the Renormalization Group. https://arxiv.org/ftp/arxiv/papers/1103/1103.2366.pdf

37. Sprott JC (2014) A dynamical system with a strange attractor and invariant tori. Physics Letters A 378: 1361-1363.

38. Van den Heuvel MP, Sporns O (2011) Rich-club organization of the human connectome. J Neurosci 31: 15775-15786.

39. Reese TM, Brzoska A, Yott DT, et al. (2012) Analyzing Self-Similar and Fractal Properties of the C elegans Neural Network. PLoS ONE 7: e40483.

40. Towlson EK, Vértes PE, Ahnert SE (2013) The rich club of the C. elegans neuronal connectome. J Neurosci 33: 6380-6387.

41. Oh SW, Harris JA, Ng L, et al. (2014) A mesoscale connectome of the mouse brain. Nature 508**:** 207-214.

42. Schmitt O, Eipert P, Hoffmann R, et al. (2014) Central and periph eral monosynaptic, polysynaptic and collaterals connectivity in the rat. Front Neuroinform Conference Abstract Neuroinformatics.

43. Looi JC, Walterfang M, Nilsson C, et al. (2014) The subcortical connectome: hubs, spokes and the space between - a vision for further research in neurodegenerative disease. Aust N Z J Psychiatry 48**:** 306-309.

44. Lenglet C, Abosch A, Yacoub E, et al. (2012) Comprehensive in vivo mapping of the human basal ganglia and thalamic connectome in individuals using 7T MRI. PLoS One 7**:** e29153.

45. Schmidt A, Denier N, Magon S, et al. (2015) Increased functional connectivity in the resting-state basal ganglia network after acute heroin substitution. Translat Psychiatry 5**:** e533.

46. Pruszynski JA, Johansson RS (2014) Edge-orientation processing in first-order tactile neurons. Nat Neurosci 17**:** 1404-1409.

47. Pritchard WS (1992) The brain in fractal time: 1/f-like power spectrum scaling of the human electroencephalogram. International Journal of Neuroscience 66: 119-129.

48. Miller KJ, Sorensen LB, Ojemann JG (2009) Power-Law Scaling in the Brain Surface Electric Potential. PLoS Comput Biol 5: e1000609.

49. Yada Y, Mita T, Sanada A, et al. (2017) Development of neural population activity toward self-organized criticality. Neuroscience 343: 55–65.

50. Lundgaard I, Li B, Xie L, et al. (2015) Direct neuronal glucose uptake heralds activity-dependent increases in cerebral metabolism. Nature Communications 6: 6807.

51. Pathak D, Shields LY, Mendelsohn BA, et al. (2015) The role of mitochondrially derived ATP in synaptic vesicle recycling. J Biol Chem 290: 22325-22336.

52. Street S (2016) Neurobiology as Information Physics. Front Syst Neurosci 10: 90.

53. Sengupta B, Stemmler MB, Friston KJ (2013) Information and efficiency in the nervous system-a synthesis. PLoS Comput Biol 9: e1003157.

54. Sengupta B, Laughlin SB, Niven JE (2013) Balanced excitatory and inhibitory synaptic currents promote efficient coding and metabolic efficiency. PLoS Comput Biol 9**:** e1003263.

55. Friston K (2010) The free-energy principle: a unified brain theory? Nat Rev Neurosci 11: 127-138.

56. Kao FC, Wang SR, Chang Yj (2015) Brainwaves Analysis of Positive and Negative Emotions. ISAA 1263-1266.

57. Saarimäki H, Ejtehadian LF, Glerean E, et al. (2017) Distributed affective space represents multiple emotion categories across the brain. bioRxiv.

58. Attwell D, Laughlin SB (2001) An energy budget for signaling in the grey matter of the brain. Journal of Cerebral Blood Flow Metabolism 21: 1133-1145.

59. Brown AM, Ransom BR (2015) Metab Brain Dis 30: 233.

60. Pathak D, Berthet A, Nakamura K (2013) Energy failure: does it contribute to neurodegeneration? Ann Neurol 74: 506-516.

61. Kirst C, Modes CD, Magnasco MO (2017) Shifting attention to dynamics: Self-reconfiguration of neural networks. *Curr Opin* Cell Biol 3: 132-140.

62. Haider B, Duque A, Hasenstaub AR, et al. (2006) Neocortical network activity in vivo is generated through a dynamic balance of excitation and inhibition. J Neurosci 26**:** 4535-4545.

63. He BJ, Zempel JM, Snyder AZ, et al. (2010) The temporal structures and functional significance of scale-free brain activity. Neuron 66: 353-369.

64. Newman MEJ (2005) Power laws, Pareto distributions and Zipf's law. Contemporary Physics 46: 323-351.

65. Xue M, Atallah BV, Scanziani M. Equalizing excitation-inhibition ratios across visual cortical neurons. Nature 511**:** 596-600.

66. Van de Ville D, Britz J, Michel CM (2010) EEG microstate sequences in healthy humans at rest reveal scale-free dynamics. Proc Natl Acad Sci USA 107: 18179-18184.

Citation: James F Peters (2017) Towards Equations for Brain Dynamics and the Concept of Extended Connectome. SF J Neuro Sci 1:2.

TOWARDS PLASMA-LIKE COLLISIONLESS TRAJECTORIES IN THE BRAIN

Arturo Tozzi (Corresponding Author)
Center for Nonlinear Science, University of North Texas
1155 Union Circle, #311427
Denton, TX 76203-5017, USA, and
Computational Intelligence Laboratory, University of Manitoba, Winnipeg, Canada
Winnipeg R3T 5V6 Manitoba
tozziarturo@libero.it

James F. Peters
Department of Electrical and Computer Engineering, University of Manitoba
75A Chancellor's Circle, Winnipeg, MB R3T 5V6, Canada and
Department of Mathematics, Adıyaman University, 02040 Adıyaman, Turkey,
Department of Mathematics, Faculty of Arts and Sciences, Adıyaman University
02040 Adıyaman, Turkey and Computational Intelligence Laboratory, University of
Manitoba, WPG, MB, R3T 5V6, Canada
james.peters3@umanitoba.ca

Eva Déli
Institute for Consciousness Studies (ICS) Benczurter 9 Nyiregyhaza, 4400
Hungary
eva.kdeli@gmail.com

Below is the unedited draft of the article that has been accepted for publication © *Neuroscience Letters, 2017, https://doi.org/10.1016/j.neulet.2017.10.016*

Plasma studies depict collisionless, collective movements of charged particles. In touch with these concepts, originally developed by the far-flung branch of high energy physics, here we evaluate the role of collective behaviors and long-range functional couplingsof charged particlesin brain dynamics. We build a novel, empirically testable, brain model which takes into account collisionless movements of charged particles in a system, the brain, equipped with oscillations. The model is cast in a mathematical fashion with the potential of being operationalized, because it can be assessed in terms of McKean-Vlasov equations, derived from the classical Vlasov equations for plasma. A plasma-like brain also elucidates cortical phase transitions in the context of a brain at the edge of chaos, describing the required order parameters. In sum, showing how the brain might exhibit plasma-like features,we go through the concept of holistic behavior of nervous functions.

In the true plasma, i.e., the fourth state of matter displayed at high energies, the particles' collective behavior is governed by: a) the reciprocal influences among the nearby charged particles embedded in a so called "Debye sphere", and b) by a plasma parameter, e.g., the average number of particles in the sphere (Sturrock, 1994; Goldston and Rutherford, 1995). In plasma, the spontaneous formation of spatial features takes place on a wide range of length scales on the boundary of a metastable state, giving rise to collisionless particles' collective movements (Cheng and Gamba 2012). A slight change in just one or two parameters is able to give rise to completely different particle trajectories and collisionless patterns.

We would not call brain function with the term *plasma*, but we will use instead the term *plasma-like*. The reason of our terminological choice is that, in true plasma, long-range correlations are preserved in order to avoid the large, disruptive electromagnetic fields which develop in presence of net charge. Furthermore, large systems of interacting particles should exhibit typical Debye lengths in order to be classified as "plasma" systems, and such parameter is still unknown in the brain. In its place, in brain we are in front of nearly neutral charges, e.g., a quasi-neutral state with slow to moderate electromagnetic fields and forces. Nevertheless, a similitude between brain and plasma collective dynamics is feasible, because, on temporal scales slower than plasma frequencies (about 10^{11} Hz) and at room temperature, plasma may be thought as a neutral fluid in which spontaneous electric fields are null. This description fits with the features of the human brain, that is equipped with a ratio between excitatory and inhibitory neurons collectively equaling the zero (Haider et al., 2006; Lombardi et al, 2012; Xue et al, 2014) and with long-range correlations. Experimental and theoretical clues allow us to conjecture that collisionless particles movements occur in the brain and that some nervous activities could be mediated by long-range extracellular flows (Linkenkaer-Hansen et al., 2001; Vuksanovic and Hövel, 2014; Gollo et al., 2017). It has been proposed that fluxes occurring in the complex intracellular web of molecular interactions could represent a universal feature of metabolic activity in living cells (Rossi et al., 2011; Prasad et al., 2014; Almaas et al, 2016). By implementing a flux balance analysis of an Escherichia coli strain, Almaas et al. (2016) showed that, whereas most metabolic reactions have low fluxes, the overall metabolic activity is dominated by reactions characterized by high ones. Cells respond to changes in growth conditions by reorganizing the rates of selected fluxes, predominantly within such a high-flux backbone. Li et al. (2015) suggestedthe presence of specific band-limited mechanismsof interregional oxygen correlation, driven by rhythmic or pseudo-oscillatory mechanisms. Traveling waves in humans may underlie processes involved in cortical activity's global coordination. For example, Alexander et al. (2016) evaluated whole head MEG, recorded during an observer-triggered apparent motion task. Episodes of globally coherent activity occurred in the delta, theta, alpha and beta bands of the signal in the form of large-scale waves, which propagated with a variety of velocities. Their mean speed at each frequency band was proportional to temporal frequency, giving a range of 0.06 to 4.0 m/s, from delta to beta. The wave peaks moved over the entire measurement array, during both ongoing activity and task-relevant intervals. Thist means that a large proportion of the cortical signal measurable at the scalp occurs as large-scale coherent motion. (Alexander et al., 2016).

Equations describing collisionless movements have been already used in the evaluation of large neuronal networks. Taking into account nets' specificity, topology, spatial extension and resulting space-dependent delays, Touboul (2012) developed a neural model based on stochastic analysis methods. He analyzed the collective behavior of mean-field limits of large-scale, spatially extended stochastic neuronal networks with delays. The asymptotic regime of such systems is characterized by integral-differential McKean–Vlasov equations. The latterare similar to usual neural field equations, but, because they incorporate noise levels as a parameter, they allow analysis of noise-induced transitions (Touboul, 2012). Deriving tractable reduced equations of biological neural networks, in order of capturing the macroscopic dynamics of neuronal sub-populations, has been a long-standing problem in computational neuroscience. Delarue et al. (2015) proposed a reduction of large-scale multi-population stochastic networks, based on the mean-field theory. They investigated the well-posedness of a networked integrate-and fire model describing an infinite population of neurons which interact with one another through their common statistical distribution. Inglis and Talay (2015) evaluated the convergence of a stochastic particle system that interacts through threshold hitting times towards a novel equation of McKean- Vlasov type. In this novel neurons' network model, a classical noisy integrate-and-fire model is coupled with a cable equation, in order to describe the dendritic structure of each neuron (Inglis and Talay, 2015). Furthermore, Galtier and Touboul (2013) derived, for a wide class of spiking neuron models, a system of differential equations of the type of the usual Wilson-Cowan systems. It describes the macroscopic activity of populations, under the assumption that synaptic integration is linear with random coefficients. Simulations of the reduced model showed a clear-cut agreement with real networks' macroscopic dynamics (Galtier and Touboul, 2013). In our paper, we will make a slightly different use of the McKean-Vlasov type equations, because they will be encompassed in a more general context: a brain function independent from subtending networks or large neural assemblies.

MATERIALS AND METHODS

The rationale. We hypothesize that the electromagnetic fields and currents generated by cortical neuronal spikes and other sources could be equipped with Vlasov-like, collisionless interactions. Such long-range interactions stand for an electrically quasi-neutral brain medium of unbound positive and negative particles. Classically, the relationship between an extracellular potential V_e (measured in Volts) and the current source density (measured in A m^{-2}) at a particular point of brain tissue is given by the Maxwell and Laplace equations (Buszaki et al., 2012). It is believed that multiple currents and sources combine linearly by the superimposition principle. However, if we take into account a plasma-like brain, the classical Ohmic equations are valid just in the narrow spatial limits of the Debye length, while, at a distance >>>Debye sphere (we might speculate that a value of >>>> Debye length needs to be at least in the range of centimeters in the brain), the time evolution of

the charged particles' distribution function is not anymore Maxwellian. Long-range interactionstake place, which can be mathematically evaluated in terms of collisionless equations. Indeed, a self-consistent collective electromagnetic field is produced by charged ions, so that the time evolution of long-range interactions among particles could be described by the Vlasov-Maxwell system of equations. In order to evaluate brain functions in a plasma-like context, we need to remove, from the classical Vlasov equation for highly charged plasma (Vlasov 1938), the useless (in our context) term which describes the distribution function for electrons, and to leave just the one for ions. In such a way, we are allowed to describe the dynamics of the brain as a system of charged particles in an electromagnetic field. With a suitable statistical treatment, the behavior of a large ensemble of random walks can be described by the equations of macroscopic diffusion (deBuyl et al., 2011). Therefore, a modified diffusion equation could describe the collective trajectories of the electromagnetic spikes in the brain (Syková and Nicholson, 2008).

Building a plasma-like model for brain activity. Here we introduce modified Vlasov equations lacking its *classical* term of free electrons: the so-called McKean-Vlasov equations. Indeed, applications of McKean-Vlasov model goes far beyond plasma physics and astrophysics, being now widely used also in biosciences (Bellomo et al., 2017). The latter equations, instead of mean charge moments, display number density, flow velocity and pressure moments (Dawson and Vaillancourt, 1995; Chayes and Panferov, 2010; Kotelenezand Kurtz, 2010). Note that these three variables can be described in terms of means of main observables and are functions just of position and time. In such a way, a self-consistent collective field comes into play, representing brain long-range behavior. Therefore, the brain currents display collective, plasma-like long range trajectories.

It has been recently proposed that mental operations, such as spontaneous activity and mind wandering, follow constrained, topological donut-like trajectories along preferential functional brain railways, shaped as a torus (Tozzi and Peters, 2016). In order to describe the movements of such trajectories, the plasma-like brain model is very helpful. If we depict brain fluxes as taking place on a torus, we notice that the collisionless trajectories can be described as movements in the toroidal space. If we now take into account equations on a n-torus, we can describe the time-evolution of probabilistic distribution of densities and their free energy functional (Chayes and Panferov, 2010). This treatment in terms of collisionless toroidal movements can be assessed through the McKean–Vlasov equation, that describes the time-evolution of a density $\rho = \rho(x, t)$, where $x \in T^d_L$, the d-dimensional torus of scale L. The equations states that:

$$\rho_t = \Delta_x \rho + \theta L^d \nabla_x \cdot \rho \Delta_x \left(V * \rho \right),$$

where V is a real-valued function of x, with the meaning of interaction potential. In addition, ρ is the density, θ the interaction (coupling) strength, e.g., the underlying density of the fluid, L is the torus scale, d the torus dimension, and * denotes the convolution in x. L^d stands for the volume factor. The term ∇denotes the divergence or the curl (rotation) of a vector field defined on a multi-dimensional domain. We now need to evaluate the brain counterparts. The value $\rho(x, t)$ has a probabilistic interpretation which we attribute to particle or the well-known value of fluid brain density. The value V stands for the interaction potential. It is assumed that ρ integrates to one. The dynamics is a gradient flow (with respect to a certain distance in the space of probability measures) for the *free energy* functional F. This means that, in touch with a long tradition of studies quantifying brain energy (Friston 2010; Sengupta et al., 2013), our model is also able to assess the required dynamics and free energy functional. Indeed, the dynamical equation can be recast into the form:

$$\frac{d}{dt} F_\theta \left(p \right) = -\int_{T_L^d} \rho \left| \nabla \log \frac{\rho}{e^{-\theta L^d V * \rho}} \right|^2 dx,$$

where the dynamics of the McKean-Vlasov equation is a gradient flow for $F_\theta \left(p \right)$, which is a free energy functional. For an in-depth discussion about this, see Chayes and Panferov (2010). For our proposed dynamical system, we expect the following behaviour:

a) Weak convergence to equilibrium, *e.g.*, the phase space density tends towards a time-independent measure.
b) Particles oscillate with smaller and smaller amplitude, but their speed, due to energy conservation, does not reach the zero. Therefore, the particles' behaviour will stand for a continuous function.
c) Some particles will get accelerated to larger speeds, so that the time-independent limiting phase space density will not have any more compact support.
d) The particles will display symmetric trajectories.

Summarizing, we require a sort of McKean-Vlasov equation for collective behavior of particles, which takes into account the following (brain) system features:

1) A torus, donut-like structure.
2) The presence of ions which are at charge equilibrium, e.g., positive charges=negative charges.
3) The presence of symmetric and continuous long-range trajectories.
4) The knowledge of the density value of the medium embedded into the sphere.

How to test our hypothesis? Previsions. Summarizing the previous paragraphs, both at rest and during spike potentials, the charged particles movements in the brain might be constrained by their electric interactions and

might display long-range plasma-like trajectories. Such collective movements can be described in terms of trajectories along a donut-like torus surface, excluding the central *hole* where intracellular currents take place. How to detect such collisionless spikes movements in real, experimental neurodata? Here the Borsuk-Ulam theorem (BUT) comes into play (Tozzi et al., 2017). Indeed, a less-known version of the BUT states that, given a continuous function, there must be two antipodal points with matching description on a two-dimensional torus (Vendruscolo et al., 2011). The theorem tells us that, if we project a fMRI brain image displaying some activity on a two-dimensional torus, we must find at least two activated regions that are antipodal. This theorem stands just in case the projected function is continuous: this is exactly the case of the hypothesized collisionless brain spikes. Therefore, the above-mentioned BUT variant allows us to evaluate, in fMRI neurodata, two of the required features of the hypothesized collisionless, long-range, plasma-like brain activity: such two features are the occurrence of symmetric activity and a continuous function. This means that, if we are able to find, in fMRI neuroimages projected on a 2-D torus, antipodal regions that are activated at the same time, the brain displays collisionless (plasma-like) activity.

RESULTS

In order to look for the antipodal points and the continuous function able to confirm our hypothesis of plasma-like nervous activity, we retrospectively assessed neurodata available from the literature. In particular, we evaluated fMRI images from Mitra etal. (2015). Their images display high-dimensional spontaneous activity structures, termed "lag threads", consisting of multiple reproducible temporal sequences. The lag threads were computed from real BOLD resting state rs-fMRI data in a group of 688 subjects, obtained from the Harvard-MGH Brain Genomics Superstruct Project (see Mitra 2015 for further technical details). Twenty-three original video frames (each one in three different projections) from Mitra et al. (2015) (**Figure, left pictures**) were arranged in order to provide the brain with a two-dimensional toroidal structure (**Figure, right pictures**), with the hole centered in the zone of the gray commissure. When the brain is assessed in terms of such donut-like structures, it is easy to see the frequent occurrence of antipodal points with matching activation (asterisks in the **right pictures**). This pattern was found in 18 of the 23 examined frames. In sum, in touch with the hypothesized occurence of collisionless, long-range trajectories in the brain, our data confirm the presence of both the required ingredients: symmetries and continuous function.

CONCLUSIONS

The occurrence of collisionless, plasma-like movements endowed in the brain currents allows us also to elucidate nervous phase transitions. The brain is sometimes described as a complex, non-linear system, formed by a large number of interacting and inter-dependent components which exhibit emergent properties, spontaneous self-organization and sensitivity to initial small changes (Bak et al, 1987; Tognoli and Kelso, 2014; Papo, 2014; Afraimovich et al., 2013). It has been proposed that the brain operates at the edge of chaos (Deco and Jirsa, 2012), near a critical regime, where the maximum information function lies between randomness and regularity (de Arcangelis and Herrmann, 2010; Zare and Grigolini, 2013). The treatment of nervous dynamics in terms of collisionless movements on a torus helps in elucidating both the claims that phase transitions occur in brain and their potential mechanisms. Furthermore, it allows us to predict which are the control phase parameters required in order to achieve the predicted nervous criticality. Touboul (2012) analyzed the collective behavior of mean-field limits of large-scale neuronal networks, characterized by a delayed integro-differential McKean–Vlasov equation. The authors identified, through bifurcation analysis, several qualitative transitions in the mean-field limit due to noise.

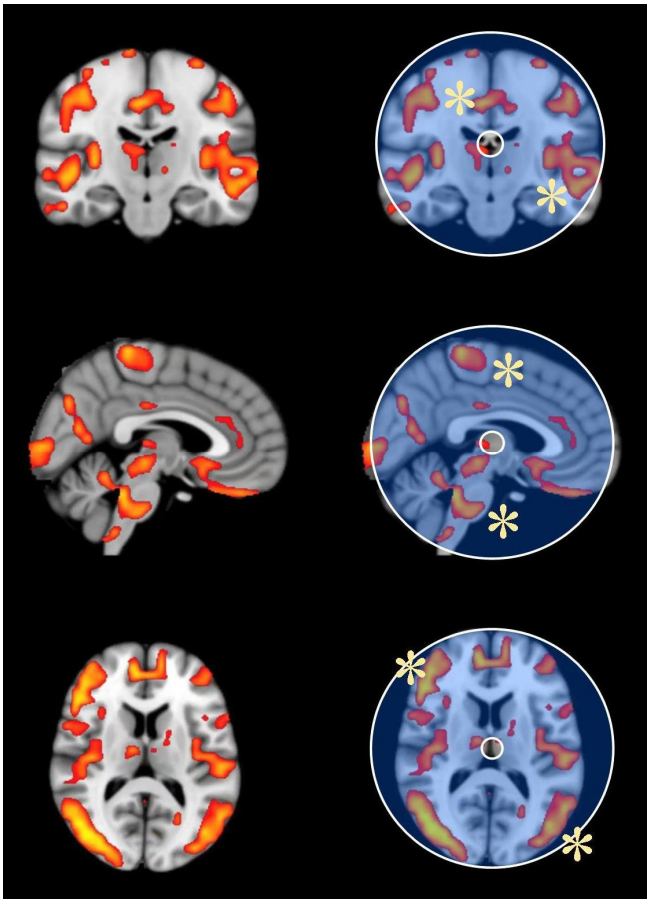

Figure. *The **left part** illustrates three of the 23 assessed video frames, showing brain activities computed from real BOLD resting state rs-fMRI data (Mitra 2015). Three different times and brain projections are displayed. The **right part** illustrates the images with the superimposition of a two-dimensional donut-like structure. Note the widely diffused presence of antipodal activated regions (asterisks).*

In particular, stabilization of spatially homogeneous solutions, synchronized oscillations, bumps, chaotic dynamics, wave or bump splitting were exhibited, arising from static or dynamic Turing–Hopf bifurcations (Touboul, 2012). It means that noise can be used in the evaluation of long-range collisionless nervous trajectories in nonlinear systems. In such a vein, Chayes and Panferov (2010), who studied the McKean–Vlasov equation on the finite tori of length scale L in d-dimensions, were able to derive the necessary and sufficient conditions for the existence of a phase transition (Gates and Penrose 1970). They found indications pointing to critical transitions at the value$\theta^1$of the interaction parameterθ described above. They showed that the uniform density is dynamically stable for $\theta<\theta^1$and that a *critical* transition occurs at $\theta= \theta^1$. They also showed that, under generic conditions such as L large, $d \geq 2$ and isotropic interactions, the phase transition is discontinuous and occurs at some $\theta_T<\theta^1$. In sum, McKean-Vlasov equations allow us to hypothesize the possible modalities of brain phase transitionsand to elucidate their control parameters.

In touch wih the old Golgi's claims concerning the presence of a fuctional nervous syncytium, recent developments start to unveil that the brain displays a *holistic* behavior (Friston, 2010), acting like a system with long-range interactions. Here we suggest that changes in a small number ofbrain parameters might lead to long-range nervous interactions. A large repertoire of brain functions and activities (Andrews-Hanna 2014) could be grounded on collective brain phenomena. Indeed, a plasma-like nervous behavior fits very well with the description of the consciousness and might also be responsible of maintaining perceptions, memories and thoughts. This approach, when implemented in a proper lattice or network, might provide a testable alternative to the well-consolidated neural models based on binary logic, such as McCullogh-Pitts neuron andHopfield networks, or on nonlinear interactions (Tozzi et al. 2016).By an operational point of view, in order to give testable previsions,we need to ask whether it is feasible to use McKean-Vlasov equations in the evaluation of EEG and fMRI patterns of spontaneous and evoked brain activity. It would not take a big effort to compare the nervous trajectories of the real temporal patterns described by previous studies with the theoretical results suggested by collisionless equations.

Furthermore, taking into account trajectories in nervous spaces, we could be able to predict whether they will fall in the donut-like torus suggested by Tozzi and Peters (2016). For example, we speculate that, when particles fall into the torus conformation (where two antipodal particles cannot never meet or become closer, due to their recurrent rotations) the correlated psychical activities could be either repetitive patterns of movements or thoughts, or preserved memories, or mind wandering.

REFERENCES

1) *Afraimovich V, Tristan I, Varona P, Rabinovich M. 2013.Transient Dynamics in Complex Systems: Heteroclinic Sequences with Multidimensional Unstable Manifolds. Discontinuity, Nonlinearity and Complexity**2,** 21-41.*
2) *Alexander DM, Nikolaev AR, Jurica P, van Leeuwen C. 2016. Global Neuromagnetic Cortical Fields Have Non-Zero Velocity. PLOS ONE 11(3):E0148413. DOI: 10.1371/journal.pone.0148413*
3) *Almaas E, Kovács B, Vicsek T, Oltvai ZN, Barabási AL. 2004.Global organization of metabolic fluxes in the bacterium Escherichia coli. Nature 427, 839-843, doi:10.1038/nature02289.*
4) *Andrews-Hanna JR,Smallwood J, Spreng RN. 2014. The default network and self-generated thought: component processes, dynamic control, and clinical relevance. Ann. N. Y. Acad. Sci. 1316, 29-52.*
5) *Bak P, Tang C, Wiesenfeld K. 1987. Self-organized criticality: an explanation of the 1/f noise. Phys. Rev. Lett.**59,**381–384.*
6) *Bellomo N, Degond P, Tadmor E (Eds.). 2017. Active Particles, Volume 1 Advances in Theory, Models, and Applications. Springer. Bernardinelli Y, Muller D, Nikonenko I. 2014. Astrocyte synapse structural plasticity. Neural Plast. 2014, 232105.*
7) *Buzsáki G, Anastassiou CA, Koch C. 2012. The origin of extracellular fields and currents — EEG, ECoG, LFP and spikes. Nature Reviews Neuroscience 13, 407-420.doi:10.1038/nrn3241.*
8) *Chayes L, Panferov V. 2010. The McKean–Vlasov Equation in Finite Volume. J Stat Phys 138: 351–380. DOI 10.1007/s10955-009-9913-z.*
9) *Cheng Y, Gamba IM. 2012. Numerical study of one-dimensional Vlasov–Poisson equations for infinite homogeneous stellar systems. Commun Nonlinear SciNumerSimulat 17 (2012) 2052–2061*
10) *Dawson D, Vaillancourt J. 1995. Stochastic McKean-Vlasov equations. Nonlinear Differential Equations and Applications NoDEA, Volume 2, Issue 2, pp 199-229.*
11) *deArcangelis L, Herrmann HJ. 2010. Learning as a phenomenon occurring in a critical state. Proc. Nat. Acad. Sci. USA **107,** 3977-3981.doi: 10.1073/pnas.0912289107.*
12) *deBuyl P, Mukamel D Ruffo S. 2011. Statistical mechanics of collisionless relaxation in a non-interacting system. Phil. Trans. R. Soc. A 2011 369, 439-452. doi: 10.1098/rsta.2010.0251*
13) *Deco G, Jirsa VK. 2012. Ongoing cortical activity at rest: criticality, multistability, and ghost attractors. J Neurosci**32,**3366-75. doi: 10.1523/JNEUROSCI.2523-11.2012.*
14) *Delarue F, Inglis J, Rubenthaler S, Tanré E. 2015. Global solvability of a networked integrate-and-fire model of McKean–Vlasov type. Ann. Appl. Probab. Volume 25, Number 4 (2015), 2096-2133.*
15) *Friston, K. 2010. The free-energy principle: a unified brain theory? Nat. Rev. Neurosci. 11, 127-138.*
16) *Galtier MN, Touboul J. 2013 Macroscopic equations governing noisy spiking neuronal populations with linear synapses. PLoS One. 13;8(11):e78917. doi: 10.1371/journal.pone.0078917. eCollection 2013.*

17) *Gates DJ, Penrose O. 1970. The van der Waals limit for classical systems. III. Deviation from the van der Waals-Maxwell theory. Comm. Math. Phys. Volume 17, Number 3 (1970), 194-209.*
18) *Goldston RJ, Rutherford PH. 1995. Introduction to Plasma Physics. CRC Press, Plasma Physics Series.*
19) *Gollo LL, Roberts JA, Cocchi L. 2017. Mapping how local perturbations influence systems-level brain dynamics. Neuroimage, pii: S1053-8119(17)30066-6. doi: 10.1016/j.neuroimage.2017.01.057.*
20) *Haider B, Duque A, Hasenstaub AR, McCormick DA. 2006. Neocortical network activity in vivo is generated through a dynamic balance of excitation and inhibition. J. Neurosci.* ***26,*** *4535-4545.*
21) *Inglis J, Talay D. 2015. Mean-Field Limit of a Stochastic Particle System Smoothly Interacting Through Threshold Hitting-Times and Applications to Neural Networks with Dendritic Component. SIAM J. Math. Anal., 47(5), 3884–3916. (33 pages)*
22) *Kotelenez PM, Kurtz TG. 2010 Macroscopic limits for stochastic partial differential equations of McKean–Vlasov type. Probab. Theory Relat. Fields (2010) 146:189–222. DOI 10.1007/s00440-008-0188-0*
23) *Lombardi F, Herrmann HJ, Perrone-Capano C, Plenz D, de Arcangelis L. 2012 Balance between Excitation and Inhibition Controls the Temporal Organization of Neuronal Avalanches.* ***108,*** *228703.*
24) *Li JM, Bentley WJ, Snyder LH. 2015. Functional connectivity arises from a slow rhythmic mechanism. ProcNatlAcadSci U S A. 12;112(19):E2527-35. doi: 10.1073/pnas.1419837112.*
25) *Linkenkaer-Hansen K, Nikouline VV, Palva JM, Ilmoniemi RJ. 2001. Long-range temporal correlations and scaling behavior in human brain oscillations. Journal of Neuroscience, 21(4), 1370-1377.*
26) *Mitra A, Snyder AZ, Blazey T, Raichle ME. 2015. Lag threads organize the brain's intrinsic activity. Proc Natl Acad Sci U S A. 112(17):E2235-44. doi: 10.1073/pnas.1503960112. Epub 2015 Mar 30.*
27) *Xue M, Atallah BV, Scanziani M. 2014. Equalizing excitation-inhibition ratios across visual cortical neurons. Nature* ***511,*** *596-600. doi: 10.1038/nature13321.*
28) *Papo D. 2014. Functional significance of complex fluctuations in brain activity: from resting state to cognitive neuroscience. Frontiers in Systems Neurosci.* ***8,*** *112.doi: 10.3389/fnsys.2014.00112.*
29) *Prasad A, Rossi C, Lamponi S, Pospíšil P, Foletti A. New perspective in cell communication: potential role of ultra-weak photon emission. J PhotochemPhotobiol B. 2014 Oct 5;139:47-53. doi: 10.1016/j.jphotobiol.2014.03.004. Epub 2014 Mar 15.*
30) *Rossi C, Foletti A, Magnani A, Lamponi S. 20111. New perspectives in cell communication: Bioelectromagnetic interactions. Semin Cancer Biol, 21(3):207-14. doi: 10.1016/j.semcancer.2011.04.003.*
31) *Sengupta B, Stemmler MB, Friston KJ. 2013. Information and efficiency in the nervous system--a synthesis. PLoSComput Biol.; 9(7):e1003157. doi: 10.1371/journal.pcbi.1003157.*
32) *Sturrock PA. 1994. Plasma Physics: An Introduction to the Theory of Astrophysical, Geophysical & Laboratory Plasmas. Cambridge University Press. ISBN 978-0-521-44810-9.*
33) *Syková E, Nicholson C. 2008. Diffusion in brain extracellular space. Physiol Rev. 88(4):1277-340. doi: 10.1152/physrev.00027.2007.*
34) *Tognoli E, Kelso JA. 2014. Enlarging the scope: grasping brain complexity. Front. Syst. neurosci****8,*** *122. doi: 10.3389/fnsys.2014.00122.*
35) *Touboul J. 2012. Mean-field equations for stochastic firing-rate neural fields with delays: Derivation and noise-induced transitions. Physica D: Nonlinear Phenomena. 241 (15):1223–1244. doi:10.1016/j.physd.2012.03.010*
36) *Tozzi A., Peters JF. 2016. Towards a fourth spatial dimension of brain activity.CognitiveNeurodynamics, 1-11, in press. DOI: 10.1007/s11571-016-9379-z*
37) *Tozzi A, Fla Tor, Peters JF. 2016. Building a minimum frustration framework for brain functions in long timescales. J Neurosci Res. In press.*
38) *Tozzi A, Peters JF, Fingelkurts AA, Fingelkurts AA, Marijuán PC. 2017. Topodynamics of metastable brains. Physics of Life Reviews, 21, 1-20. http://dx.doi.org/10.1016/j.plrev.2017.03.001.*
39) *Vendruscolo D, Desideri PE,Pergher PLQ. 2011. Some generalizations of the Borsuk-Ulam Theorem. Publicationesmathematicae 78(3)· April 2011*
40) *Vlasov AA. 1938. On Vibration Properties of Electron Gas. J. Exp. Theor. Phys. 8 (3): 291.*
41) *Vuksanovic V, Hövel P. 2014 Functional connectivity of distant cortical regions: Role of remote synchronization and symmetry in interactions. NeuroImage,* ***97,*** *1–8. DOI: 10.1016/j.neuroimage.2014.04.039.*
42) *Zare M, Grigolini P.2013 Criticality and avalanches in neural network. Chaos Solitons&Fractals****55,*** *80–94. DOI: 10.1016/j.chaos.2013.05.009.*

PROGRESS IN
Biophysics &
Molecular Biology
An International Review Journal

WHAT IS IT LIKE TO BE "THE SAME"?

Arturo Tozzi
Center for Nonlinear Science, University of North Texas, Denton, Texas 76203, USA
1155 Union Circle, #311427
Denton, TX 76203-5017 USA
tozziarturo@libero.it

James F Peters
Department of Electrical and Computer Engineering, University of Manitoba
75A Chancellor's Circle Winnipeg, MB R3T 5V6 CANADA and
Department of Mathematics, Adıyaman University, 02040 Adıyaman, Turkey
James.Peters3@umanitoba.ca

Below is the unedited draft of the article that has been accepted for publication © Progress in Biophysics & Molecular Biology, 2017.

A unifying principle underlies the organization of physical and biological systems. It relates to a well-known topological theorem which succinctly states that an activity on a planar circumference projects to two activities with "matching description" into a sphere. Here we ask: what does "matching description" mean? Has it something to do with "identity"? Going through different formulations of the principle of identity, we describe diverse possible meanings of the term "matching description". We demonstrate that the concepts of "sameness", "equality", "belonging together" stand for intertwined levels with mutual interactions. By showing that "matching" description is a very general and malleable concept, we provide a novel testable approach to "identity" that yields helpful insights into physical and biological matters. Indeed, we illustrate how a novel mathematical approach derived from the Borsuk-Ulam theorem, termed bio-BUT, might explain the astonishing biological "multiplicity from identity" of evolving living beings as well as their biochemical arrangements.

INTRODUCTION: SAMENESS AND MATCHING DESCRIPTIONS

The concept of "sameness" is the tenet of approximate reasoning, treatment of imprecision, assessment of physical systems and biological classification. Indeed, techniques such as pairwise comparison (Koczkodaj et al., 2017), rough sets and Fraenkel-Zermelo group theory are based on the concept of "equality" among different features. In particular, recently introduced versions of the Borsuk-Ulam theorem (BUT) state that a feature on a *n*-manifold projects to two points with "matching description" onto a *n*+1 manifold (Peters, 2016; Tozzi and Peters, 2016a). Starting from this rather simple and abstract claim, a fruitful general framework has been built which is able to elucidate disparate real physical and biological phenomena, from quantum entanglement (Peters and Tozzi, 2016) to brain activity (Tozzi et al. 2017a), from biological gauge theories (Tozzi et al., 2017b) to pre- big bang scenarios (Tozzi and Peters, 2016b).
Summarizing the novel topological approach, we may observe that, by taking into account projections on functional or real dimensions of physical and biological systems onto corresponding feature spaces, a system of mappings is achieved with "matching description" that fits very well with experimental results. This allows us to assess countless issues in far-flung scientific branches spaces (Angel and Leong, 1994; Benson et al., 2016; Giusti et al., 2016; Kida et al., 2016; Kleineberg et al, 2016; Simas et al., 2015). Nevertheless, what does "matching description" mean in a topological context? Matching descriptions are termed "descriptively near sets", i.e., two (or more) features that lie on the same manifold, but that have no points in common. In a semantic framework, a matching description encompasses all information about two nodes in two structures which semantically correspond to one another. In what follows, we will describe other possible meanings of matching description in different scientific contexts, providing testable examples. We will subsequently introduce a novel version of Borsuk-Ulam theorem (BUT), dubbed bio-BUT, that takes into account the overwhelming evolutionary complexification of living beings. Within the bio-BUT framework, we will use the concept of "matching description" in order to compare mathematical, physical and biological features of signals such as amplitude, duration and intensity.

THE PROBLEM OF CONNECTION AND UNITY

Some fundamental questions

Here we may ask, paraphrasing the seminal paper by Nagel (1974), what is it like to be a matching description? In order to tackle this issue, here we need to ask before: has matching description anything to do with "identity"? In the "classical" BUT, the matching features are just points, therefore a point is equal to another and we might easily state that they are "identical" (Borsuk, 1933). On the other hand, in the novel BUT variants, the matching features stand not just for simple topological points, but also for more intricate features, such as shapes of space (spatial patterns), shapes of time (temporal patterns), vectors, tensors, functions, signals, thermodynamic parameters, movements, trajectories, lexical structures (either syntactic or semantic), or most generally, symmetries and symmetry breaks (Peters et al., 2017; Matousek 2003). Thereafter, we may ask: apart from the two adimensional points of the classical BUT, are other types of matching features identical? When you compare a pair of "equal" features, how do you state that they are equal? Do they have the same feature, or two different features with something in common? In order to solve the issue, we analyze the "principle of identity" (Heidegger, 1957), which is one of the three tenets of classical logic.

First answer: sameness

The principle of identity states that A=A. The formula expresses, in its usual description, an equality of A and A. One A is equal to another A. Therefore, we can state that A is the same as A, because "identical" (from Greek and Latin) means: "**the same**". We will see how "matching description" standing for "sameness" can be found not just in the rather abstract disciplines of philosophy, logic and mathematics, but also in the "objective" accounts of physics and biology and in the "subjective" realm of single individual's mental activity.

Second answer: equality

In another version, the formula A=A speaks of "equality". A is A. It does not say that A is the same, but that **every A is itself the same**. Or, in other words, each thing itself is the same for itself and with itself.

Third answer: belonging together

It can also be stated that matching description "belongs to" an identity. In this case, sameness stands for a "**belonging together**". In "belonging together", the world "together" means to be assigned and placed into the order of a together, to be established in the unity of a manifold, **to be combined into the unity of a system**. Such assignment and placing occur

thanks to connections and mappings of the one with the other. Belonging together means that two features are put orderly into a common feature that is outlined against the background.
Therefore, two interpretations are feasible: a) matching description is determined by an identity as a feature of that identity; b) identity is represented as a feature of matching description.
To make an example, night and day belong together: if you say just "day", you do not yet acquire knowledge, if you not think the day as lasting until the night's onset. The night is night just because it stands for the day fading. Therefore, night and day are not just two interchangeable features; rather they have to be taken together. Two contrasting features such as night and day stand out in sharp relief just because they are two and meet one with each other.

Fourth answer: coincidentia oppositorum
Another possible interpretation for A=A might be extrapolated from Nicholas de Cusa (1440) and Giordano Bruno (1582): the so-called *coincidentia oppositorum*. As usual, the sign = can be understood either in terms of sameness, or equality, or belonging together. However, the two As stand for opposite, sometimes incompatible, apparently mutually excluding features or activities. In this case, we start from A different from B, where B= non A, or B= -A. At the end of the comparison, despite A is different from B, we achieve A=B, and therefore, just in terms of features A:

A = non A, or +A = -A

The As stand either for mathematical, or physical, or biological features. The principle of *coincidentia oppositorum* is in touch with the counter-intuitive failure of the principle of identity in quantum dynamics and in superimposition of wave/particles. This formulation is particularly useful in quantum dynamics, where experimental findings have "wrecked" the classical formulations of the principle of identity. To make an example, think about the Schrodinger cat. It is a paradox from quantum mechanics, represented by the possible states of a cat enclosed in a box together with a cyanide capsule. The wave function of the cat is described as a superposition of wave functions (one wave function corresponds to an intact capsule and live cat, while the other wave function corresponds to a broken capsule and a dead cat). Opening the box corresponds to cause the wave function to collapse into one of the two different states, denoted by $|\alpha \pm\rangle$, namely,

$$|\alpha\rangle = \sum_{n=0}^{\infty} \exp\left(\frac{-|\alpha|^2}{2}\right)\left(\frac{\alpha^{2n}}{n!}\right)^{1/2} \exp(\mathrm{i}n\phi)\,|n\rangle,$$

$$|-\alpha\rangle = \sum_{n=0}^{\infty} \exp\left(\frac{-|\alpha|^2}{2}\right)(-1)^n\left(\frac{\alpha^{2n}}{n!}\right)^{1/2} \exp(\mathrm{i}n\phi)\,|n\rangle,$$

where ϕ and $|\alpha\rangle$ represent the direction angle of excitation and the field strength, respectively (Gerile 2010). In effect, the cat be alive or dead in the same instant, so that the two coherent states (or, in our *coincidentia oppositorum* principle scenario, A = -A) are superimposed.

WHAT DOES MATCHING DESCRIPTIONMEAN IN BUT TERMS?

Here we describe some implications about the BUT counterparts of the above given definitions of the principle of identity. A BUT system, i.e., a system equipped with two manifolds in lower and higher dimensions and with reciprocal mappings, can be defined as follows (see **Figure 1**):

1) A single feature in lower dimensions specifies equality.
2) Two corresponding matching features in higher dimensions describe the same, the purely identical signal.
3) A BUT-oriented system describes signal values that belong together. In belonging together, the opposites do not disappear, rather they reach unity, although still existing separately, joined by a force that binds them together. In the BUT case, such force stands for the mappings between manifold of different dimensions. The whole BUT system may also describe the *coincidentia oppositorum*.

Lower dimensions. The equal is the single feature that stands alone in lower dimensions. In lower dimensions, we are assessing a single, undifferentiated, homogeneous feature; therefore, we cannot catch the differences between two

activities, the latter being distinguishable just in higher dimensions. The equal is correlated with the indistinguishable unity: indeed, it encompasses the whole feature description, leaving apart the possible differences endowed in the higher-dimensional systems' features. To make an example, by the standpoint of an observer located in the feature A and with an observational horizon limited to A, the BUT account in lower dimensions stands for the unity and for the complete available feature A description.

Higher dimensions. In turn, higher dimensions describe the standpoint of the separation. In higher dimensions, the differences between features become evident, as they can be separately assessed. Two features are the same just in case of the difference, the not-undifferentiated, the absence of singularity is thought. From the separation, the duality emerges. The same is never identified with the equal: the same expunges the risk to smooth the different in the always equal. The same may also stand for the reciprocal belonging together of different features, based on the assembly operated by the differences imposed by an observer. While the same joins the different in a primitive union, the equal scatters into the unity of what is one just for uniformity. In solving the different, the joining core of the same comes into light. In higher-dimensional levels, the same reaches the multiplicity of the almost incompatible. The BUT higher-dimensional account stands for the indeterminate and the unknown. Indeed, an observer located in one A cannot have knowledge of the antipodal A, placed at the opposite side of the high-dimensional manifold, and disjointed from the A where the observer stands. Therefore, our secluded observer in higher dimensions is able to catch neither the whole system, nor the possible existence of an identity, of a sameness, of a belonging together, of a matching description. The observer cannot encompass the whole system in a single sight. Incidentally, this might explain, for example, why we detect in our Universe the matter, but not the antimatter. BUT might also explain why we detect, by our standpoint inside the Universe, the arrow of time, e.g., the occurrence of time asymmetry.

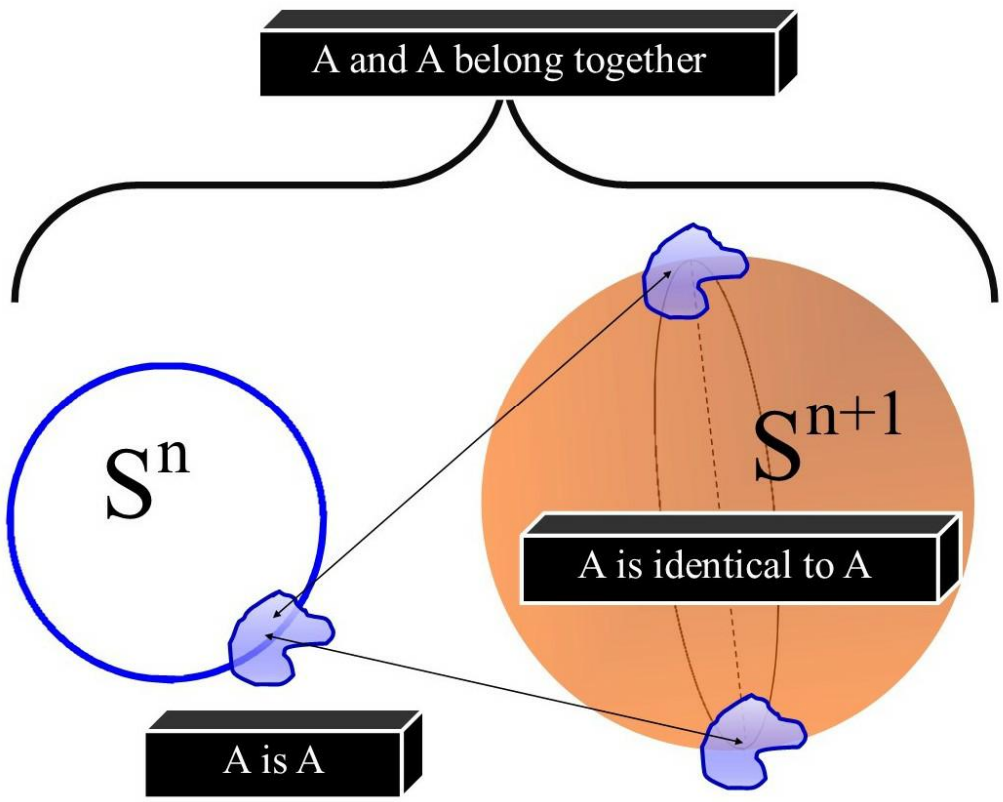

Figure 1. Topology and the principle of identity. The figure illustrates the Borsuk-Ulam theorem's counterparts of sameness, identity, belonging together (i.e., the first three answers to our main question). The shapes stand for the feature termed A.

A NOVEL BUT VARIANT IN MACROSCOPIC PHYSICS AND IN BIOLOGY

As stated above, our previous framework, developed through different papers in various scientific disciplines, suggests that BUT and its variants might explain relevant biological phenomena. To make an example, based on novel topological considerations, Tozzi et al. (2017b) have proposed a gauge symmetry for living cells. The reference system is the living cell, equipped with general symmetries standing for the intertwined biochemical, metabolic and signaling pathways that allow its global homeostasis. Environmental stimuli stand for "forces" able to locally break the symmetry of metabolic/signaling pathways, while the species-specific DNA is the gauge field that restores the global homeostasis after external perturbations. The authors applied BUT in order to operationalize a methodology in terms of topology/gauge fields and subsequently inquire about the evolution from inorganic to organic structures, proposing that, from prokaryotes to eukaryotes, an increase in complexity (standing in topological terms for an increase of dimensions on an abstract manifold) gave rise to a progressive increase of matching features (Chaisson 2010).

During evolution, life tends towards increase in complexity. The latter is an increase of dimensions in a manifold where the nth dimension stands for the level of complexity. To make a few examples, living beings have descriptively proximal appearance, their inorganic constituents have single description; seeds (as fibres) have single descriptions, fruits (projections from sets of fibres) have similar descriptions (for mathematical details, see the next paragraph). Such increase elucidates the countless biochemical functions of the more advanced living beings, such as mammals and primates. However, if an increase of matching description is correlated with an increase in dimensions (in the living cells' case, an increase in complexity), we would achieve a countless number of identical antipodal features, that are equal. Therefore, advanced cells might be equipped with a countless number of serial, monotonous, repeating features, which number increases with complexity, and the astonishing diversity of living beings would be lost (contrary to what happens in the real world).

Indeed, in terms of the principle of identity, our high complex macroscopic world is made of equal, but of different objects, achieved through the joining together of different microscopic particles endowed in lower levels of complexity. In particular, separation is a factor, achieved through oppositions against the undifferentiated, REQUIRED for life taking place. Two opposites prevail over the power of the singularity, because the order of life overtakes the primeval unity. The exit from the singularity gives rise to splits and to disjointed opposites, e.g., the huge variety evolving living beings. With increase in complexity (and therefore in dimensions) in living cells, the fixed points disappear, while differences and oppositions are produced in their full vitality.

Biology and topology: an intimate relationship. Every physical and biological structure has a history. Based on their features, every structure has a description. The physical and biological world is a collection of structures with shapes defined by fibre bundles of the form $X \xrightarrow{f} E \xrightarrow{\pi} B,$ where X is a set of particles, f maps X to a set of selected fibers (generators) E in an m-dimensional space, and π is a 1-1, continuous, bijective mapping that projects E onto a space B with a well-formed shape such that $\pi(e) \in \begin{cases} n-\text{dimensional space, n} \geq \text{m, or,} \\ n-\text{dimensional space, n} < \text{m,} \end{cases}$ for $e \in E,\ \pi(e) \in B.$

The collection of particles in X sweep out world canals as they move through space. Hence, the world canals defined by X resemble a multi-layer ham sandwich (layers of world sheets). For example, metabolic pathways are worldsheets, while homeostasis is intertwined worldsheets.

The fibres in E are selected segments (slices) of the sandwich in X. The projection π is a piecewise continuous mapping on E onto B. During evolution, life is a composition of fibre bundle projection mappings with concomitant dimensional changes (changes in complexity). Instead of a causality view of the physical structure, the origin of the species can be defined by projection mappings. Evolutionary systems are defined by sequences of projections of the form

$E \xrightarrow{\pi_1} B_1 \xrightarrow{\pi_2} B_2 \cdots B_i \xrightarrow{\pi_{i+1}} B_{i+1} \cdots \xrightarrow{\pi_k} B_{k+1}$ (evolved shape).

In other words, the fabric of the physical (and biological) world has an underlying fibre bundle structure, apart from thermodynamic and information relationships.

Projections among the structures of different dimensions are piecewise continuous. The projection $E \xrightarrow{\pi} B$ is piecewise continuous inasmuch as, for $A\ \delta\ B, A, B \subset E$ implies $\pi(A)\ \delta^{\wedge\wedge}\ \pi(B),$ i.e., whenever A is close to B in E, then $\pi(A) \in B$ is close to $\pi(B) \in B.$ The closeness of projects results from endowing the sets E and B with a

proximity relation with all projections defined in a proximity space $\left(E, B, \delta^{\wedge\wedge}\right)$, where $\delta^{\wedge\wedge}$ is a strong (overlap) Lodato proximity (Peters, 2016). In sum, world structures with changing shapes are defined by a collection of piecewise continuous projections.

A BIOLOGICAL VERSION OF THE BORSUK-ULAM THEOREM

Here we propose another development of BUT, termed bio-BUT, that can be useful in the experimental assessment of both macroscopic physical and biological (linear and nonlinear) systems. In plain terms, bio-BUT states that a single feature in n-dimensions, say A, projects to two matching points in n+1 -dimensions. The difference from the classical BUT is that, instead of achieving the two typical matching descriptions termed A and its opposite A, we achieve the two matching descriptions termed A and ΔA. In every subsequent mapping in higher dimensions, the diversity among the matching features increases, allowing a high rate of evolutionary variety. The identity (in the sense of equality or sameness) among matching features A gradually disappears, giving rise to more and more various living entities: in other words, the mapping from lower to higher dimensions gives rise to two features that are slightly different and belong together, instead of being the equal or the same. Therefore, life can be explained just by taking into account the total BUT system, and not just one of its manifolds.

In more technical terms, the Borsuk-Ulam theorem (BUT) from algebraic topology introduces a continuous mapping from an *n*-sphere into itself. A biological counterpart of BUT, dubbed bio-BUT, introduces a piecewise continuous mapping from signals in space time $\mathbb{R}^{3+1}$ into a k-dimensional space $\mathbb{R}^{k}$, $k \geq 1$, containing feature vectors that describe antipodal spacetime signals. In other words, antipodal signals in spacetime signal can have matching descriptions in a 1-dimensional space or matching descriptions in a k-dimensional space $\mathbb{R}^{3+1} \rightarrow \mathbb{R}^{k}$, $k \geq 1$. Let us briefly clarify the terms we are using in order to establish the bio-BUT.

***n*-sphere**. An *n*-sphere S^n is the set of points in Euclidean space $\mathbb{R}^{n+1}$ with unit distance to the origin (0,0,...,0), a point whose coordinates are $n+1$ zeros. An *n*-sphere is an *n*-dimensional manifold (Ghrist, 2014). That is, there is a continuous 1-1 map on the set of points on S^n onto $\mathbb{R}^{n}$. For example, $S = S^1$ denotes the Euclidean plane $\mathbb{R}^2$ and S^2 denotes the Euclidean 3-space $\mathbb{R}^3$. At the physical level, S^2 is the set of all points with unit distance from (0,0,0). The analogue of S^2 is the set of all points in the system (e.g., the brain), which physically is in the 3-space $\mathbb{R}^3$.

Antipodes. Let *x* be a point on S^n. The antipode of *x* is the point –*x* (Munkres,2000), i.e., the antipode of x is an opposite point on an *n*-sphere. For example, the antipode of a point x on the circumference of a circle is a point –x on that part of the circumference opposite *x*. Again, for instance, a physical analogue of Munkres antipode is the antipode of a cone at location x in one eye, i.e., a cone at the same location in the opposite eye. Another physical analogue of a Munkres antipode is an alternative description of a signal x, represented by a feature vector of the form $\Phi\left(\varphi_1\left(x\right), \cdots, \varphi_k\left(x\right)\right)$ with k components, where each $\varphi_i\left(x\right)$ is a feature value that represents an observation about the variable x.

Continuous Mapping. A continuous mapping $f : X \rightarrow Y$ is a correspondence between a point x in X and a point y = f(x) in Y, such that x and x' are close, then f(x) is close to f(x') (Naimpally and Peters, 2013). The physical analogue of a continuous mapping Φ: $\mathbb{R}^3 \rightarrow \mathbb{R}^k$ defines a correspondence between a set of signals in $\mathbb{R}^3$ and set of descriptions in $\mathbb{R}^k$. See **Table 1** for an example.

Piecewise Continuous Mapping. A piecewise continuous mapping $f : A \rightarrow B$ is a correspondence between a subset A in X and a subset B in Y, so that if a and a' are close in A, then f(a) and f(a') are close in B. In other words, we only assume that the closeness rule applies to a subset of the set X and a subset in the image space B that is a subset of the larger set Y, but does not necessarily apply to the larger sets X and Y. The physical analogue of a piecewise continuous mapping is a mapping Φ: $\mathbb{R}^{3+1} \rightarrow \mathbb{R}^k$ that is a correspondence between a set of signals A in $\mathbb{R}^{3+1}$ (spacetime) and a set of descriptions B in $\mathbb{R}^k$, so that if signals a and a' are close in A. Then description $\Phi\left(\varphi_1\left(a\right), \cdots, \varphi_k\left(a\right)\right)$ and description $\Phi\left(\varphi_1\left(a'\right), \cdots, \varphi_k\left(a'\right)\right), k \geq 1$ are close in B.

From the Borsuk-Ulam Theorem. If x is a point in S^n, then its antipode is the point –x. A continuous map $h: S^n \to S^n$ is antipode-preserving, provided h(x) = h(-x) for all $x \in S^n$.

A conjecture. There is a biological analogue of the Borsuk-Ulam Theorem. The following theorem proves this conjecture.

Towards the Bio-Borsuk-Ulam Theorem (bio-BUT). Given a signal a in $\mathbb{R}^{3+1}$, then its antipode is a signal –a in spacetime. A piecewise continuous map Φ: $\mathbb{R}^{3+1} \to \mathbb{R}^k$, $k \geq 1$ is antipode-preserving in spacetime, provided the antipodes have matching description, *i.e.*, $\Phi\left(\varphi_1(a),\cdots,\varphi_k(a)\right) = \Phi\left(\varphi_1(-a),\cdots,\varphi_k(-a)\right), k \geq 1$ for all signals α, -α $\in \mathbb{R}^{3+1}$.

Proof: Let x be a signal in a set of signals $X \subseteq \mathbb{R}^{3+1}$ and let –x be an antipodal signal in X. Every signal x has a description $\Phi\left(\varphi_1(x),\cdots,\varphi_k(x)\right) \in \mathbb{R}^k, k \geq 1,$ where $\varphi_i(x)$ is feature value for *x* and $\mathbb{R}^k$ is a feature space such that every point in $\mathbb{R}^k$ defined by the mapping Φ. Each antipodal signal –*x* occupies the same position as *x* after translation. Hence, $\Phi\left(\varphi_1(x),\cdots,\varphi_k(x)\right) = \Phi\left(\varphi_1(-x),\cdots,\varphi_k(-x)\right)$ after translation.

In other words, bio-BUT guarantees that the antipodal signals x, -x have matching descriptions in some k-dimensional spacetime, $k \geq 1$. In addition, bio-BUT relaxes the requirement that the domain and the range of the mapping Φ have the same dimension. For example, $\Phi\left(\varphi_1(x)\right)$ is 1-dimensional (i.e., only one perceived feature of signal *x* is described), whereas signal *x* itself is 3+1 dimensional in spacetime. **Table 1** provides analogues of mathematical structures underlying bio-BUT.

Structure(s)	**Mathematics**	**Physics**
2-sphere S^2	Euclidean space $\mathbb{R}^3$	Biosphere space
Antipodes (e.g., cones in left vs. right eye)	x, -x $\in \mathbb{R}^{3+1}$	Cone at x in left eye, cone at –x in right eye.
Antipodes (signal x vs. description of the signal)	x, -x $\in \mathbb{R}^3$	$\Phi\left(\varphi_1(x),\cdots,\varphi_i(x),\cdots,\varphi_k(x)\right)$ is a feature vector Φ with n observations that describes signal x. On the other side, $\Phi\left(\varphi_1(-x),\cdots,\varphi_i(-x),\cdots,\varphi_k(-x)\right)$ is a feature vector that describes signal –x, $k \geq 1$.

Table 1. Analogues of mathematical structures underlying bio-BUT.

Figure 2 provides an example on the evolution of two dynamical systems, according to bio-BUT. How does such decrease in feature homogeneity occur, in topological terms? It might occur through slightly changes in the strength of the projections. They could stand for slight changes in biological general symmetries, that give rise to an incomplete restoration of the locally broken Lagrangian.

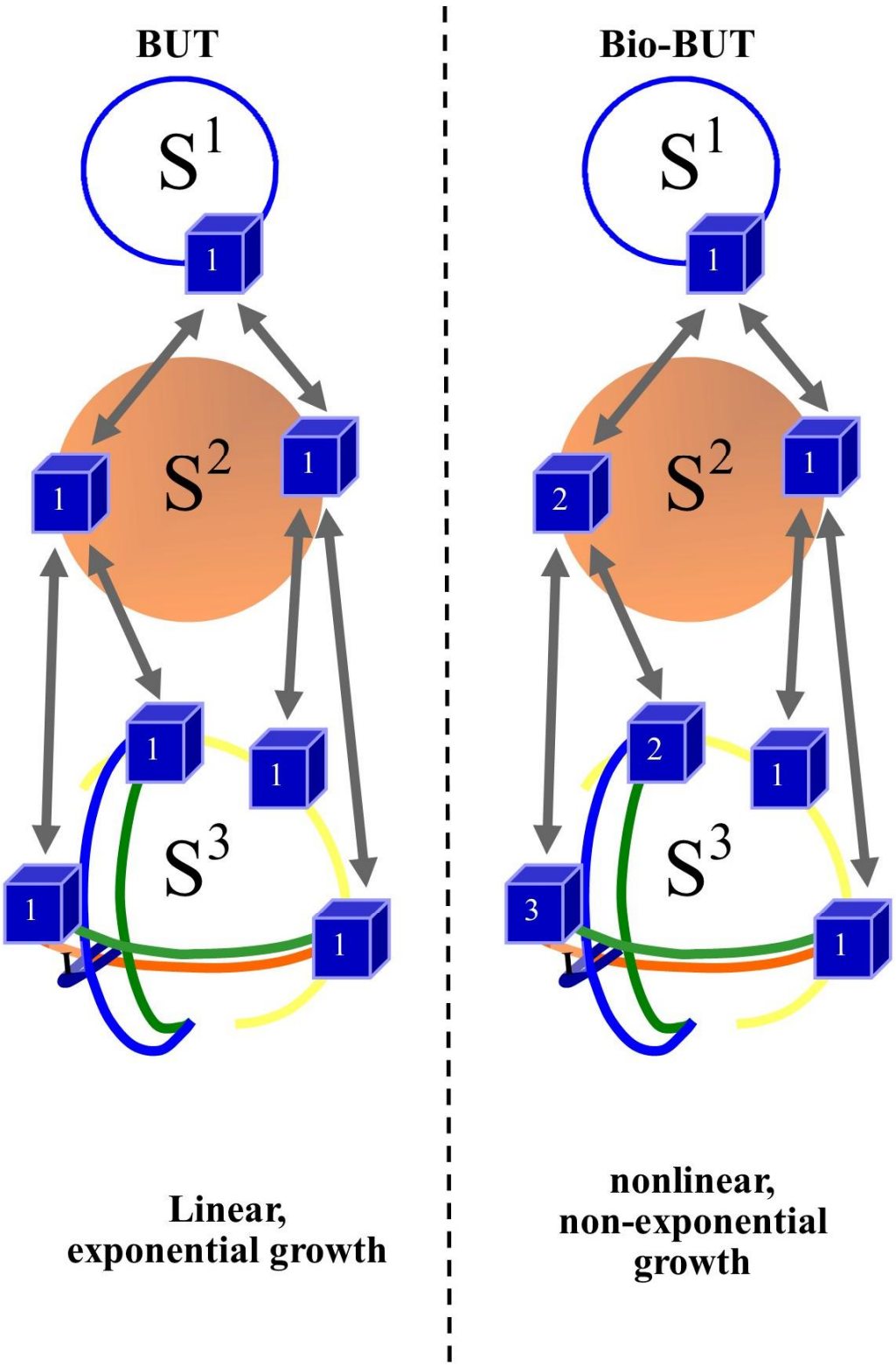

Figure 2. Evolution of two dynamical systems. In BUT terms (left side), every increase in manifold dimensions (in case of life, complexity) gives rise to redoubling of "the same" matching points. On the other side, in bio-BUT terms (right side), every increase in manifold dimensions gives rise to redoubling of matching points that "belong together", i.e., points that display slight different changes for every duplication. The two different dynamics may give rise to different systems' outputs, based on the dissimilar evolutions towards increases or decreases of manifolds' dimensions.

ASSESSMENT OF BRAIN FUNCTION IN TERMS OF THE IDENTITY PRINCIPLE

A further example from neuroscience shows how the identity principle and BUT may pave the way to novel approaches. We described the meaning of "belonging together". However, as we have seen before, "belonging together" can also mean: **the together is determined by the belonging**. Therefore, the possibilities here are two:

a) representing belonging in terms of the unit of together;

b) experiencing this together in terms of belonging.

This point b leads us into the psychological standpoint of the observer. Indeed, "thinking" and matching description can also be thought as the same, so that they belong together in the same, and by virtue of the same. If we attempt to represent together the thinking and matching description as a coordination, we can establish and explain the latter either in terms of thinking or in matching description. If thinking and matching description belong to each other, matching description belongs with thinking to an identity, whose active essence stems from that "letting belong together" which we call "mental representation". Identity becomes, in this version, a functional property of the event of mental representation.

Identity (including the ego, i.e., the subjective identity of the human individual) can be presupposed as a feature of the matching description, or as a spring that departs from it. In this account, the principle of identity becomes a spring into the psychological origin of identity. We can therefore assess matching description and thinking in terms of that which joins the two, by virtue of the event of mental representation. This allows us to assess brain function in terms of projections among manifolds with different dimensions.

CONCLUSION

We have shown how to generalize and operationalize the concept of BUT's matching description, correlating it with the principle of identity from logic and philosophy. We also provided applications in physics, biology and neuroscience. We defined BUT's "descriptively near sets" in terms of identity features: this concept might appear rather vague, because it refers not just to a physical content such as energy or vectors, but also to a semantic content, such as two "felines". Indeed, a possible concern is that a topological approach to systems features talks in rather general terms, leaving apart the peculiar features of single physical and biological processes. This paper highlights that the concept of matching description displays the widest range of possible uses, in particular when it is well developed. Although the BUT approaches to system features make higher level views of abstraction, nevertheless they do not leave apart a multifaced description of individuals. In particular, matching description does not assess just "the same" feature, but also features that are "different". Indeed, we have proposed a novel variant of BUT, termed bio-BUT, that elucidates the astonishing variety of living structures. Generation after generation, slight changes in DNA occur, and the same might happen during the life of the single individual, for example during ageing processes. This means that, if we were able to find the topological source of the above-mentioned slight changes in features A in single individuals, we might partially counteract ageing, or alleviate diseases due to an accelerated disarrangement of matching points.

Our framework also provides a lesson about our knowledge capabilities: the unity is never given directly, and knowledge is feasible just when coming back to unity. Therefore, we need to talk of unity BEFORE the separation. This implementation makes BUT and its variants not just the standpoint for a novel interpretation of a number of elusive biological and physical phenomena, but also a suitable tool in order to evaluate the slight (objective and subjective) differences that make our intellectual world an amazing realm of rich heterogeneity.

REFERENCES

1) Angel E, Leong P. 1994. Multidimensional dynamic programming on massively parallel computers. Computers & Mathematics with Applications. 27, 9–10: 67-75
2) Benson AR, Gleich DF, Leskovec J. 2016. Higher-order organization of complex networks. Science, 353, 6295: 163-166. DOI: 10.1126/science.aad9029
3) Borsuk M. 1933. Dreisatzeuber die n-dimensionale euklidischesphare.FundamentaMathematicae XX, 177–190.
4) Bruno G. 1582. De umbrisidearum. In: Jordani Bruni Nolani opera latine conscripta (Giordano Bruno the Nolan's Works Written in Latin), Dritter Band (1962) / curantibus F. Tocco et H. Vitell
5) Chaisson EJ. 2010. Energy Rate Density as a Complexity Metric and Evolutionary Driver. Complexity, v 16, p 27, 2011; DOI: 10.1002/cplx.20323.

6) Crabb MC, Jaworowski J. 2013. Aspects of the Borsuk-Ulam Theorem, J. of Fixed Point. Theory and Applications 13: 459–488, DOI 10.1007/s11784-013-0130-7, MR3122336.
7) de Cusa N. 1440. De doctaignorantia. English translation in Bond, H. Lawrence (ed.), Nicholas of Cusa: Selected Spiritual Writings, Classics of Western Spirituality. New York: Paulist Press, 1997.
8) Gerile, Sachuefu, Zhang, C.-H. Quantum entanglement in a system of Bose-Einstein condensate interacting with Schroddinger cat state, Optoelectronics Letters 6, no. 2, 1-4.
9) Ghrist R. 2014. Elementary Applied Topology, Amazon, ISBN: 978-1-5028-8085-1.
10) Giusti C, Ghrist R, Bassett DS. 2016. Two's company, three (or more) is a simplex. Algebraic-topological tools for understanding higher-order structure in neural data. Journal of Computational Neuroscience, 41; 1:1–14
11) Heidegger M. 1957. Identity and difference. Harper & Row, Publishers (New York, Evanston, and London).
12) Kida T, Tanaka E, Kakigi R. Multi-Dimensional Dynamics of Human Electromagnetic Brain Activity. Front Hum Neurosci. 2016 Jan 19;9:713. doi: 10.3389/fnhum.2015.00713. eCollection 2015.
13) Kleineberg K-K, Boguñá M, Serrano MA, Papadopoulos F. 2016. Hidden geometric correlations in real multiplex networks. Nature Physics, in press. doi:10.1038/nphys3812
14) Koczkodaj WW, Magnot J-P, Mazurek J, Peters JF, Rakhshani H, Soltys M, Strzałka D, Szybowski J, Tozzi A. 2017. On normalization of inconsistency indicators in pairwise comparisons. International Journal of Approximate Reasoning.86, 73–79. http://doi.org/10.1016/j.ijar.2017.04.005.
15) Matoušek J. 2003. Using the Borsuk–Ulam Theorem. Lectures on Topological Methods in Combinatorics and Geometry (Springer-Verlag Berlin Heidelberg).
16) Munkres JR. 2000. Topology, 2nd Ed. Prentice-Hall, Upper Saddle River, NJ, MR0464128
17) Nagel T. 1974. What Is It Like to Be a Bat? The Philosophical Review, 83, 4, 435-450.
18) Naimpally SA, Peters JF. 2013. Topological spaces via near and far. With a foreword by Iskander A. Taimanov. *World Scientific Publishing Co. Pte. Ltd., Hackensack, NJ*, 2013. xvi+277 pp. ISBN: 978-981-4407-65-6, MR3075111
19) Peters JF. 2016. Computational Proximity. Excursions in the Topology of Digital Images. Edited by Intelligent Systems Reference Library. Berlin: Springer-Verlag. doi:10.1007/978-3-319-30262-1.
20) Peters JF, Tozzi A. 2016. Quantum Entanglement on a Hypersphere. Int J Theoret Phys, 1–8. doi:10.1007/s10773-016-2998-7.
21) Peters JF, Ramanna S, Tozzi A, Inan E. 2017. Frontiers Hum Neurosci. BOLD-independent computational entropy assesses functional donut-like structures in brain fMRI image. doi: 10.3389/fnhum.2017.00038.
22) Simas T, Chavez M, Rodriguez PR, Diaz-Guilera A. 2015 An algebraic topological method for multimodal brain networks comparisons. Front Psychol. 6;6:904. doi: 10.3389/fpsyg.2015.00904. eCollection 2015.
23) Tozzi A, Peters JF. 2016a. A Topological Approach Unveils System Invariances and Broken Symmetries in the Brain. Journal of Neuroscience Research 94 (5): 351–65. doi:10.1002/jnr.23720.
24) Tozzi A, Peters JF. 2016b. Symmetries, Information and Monster Groups before and after the Big Bang. Information, 7(4), 73; doi:10.3390/info7040073.
25) Tozzi A, Peters JF, Fingelkurts AA, Fingelkurts AA, Marijuán PC. 2017a. Topodynamics of metastable brains. Physics of Life Reviews. http://dx.doi.org/10.1016/j.plrev.2017.03.001.
26) Tozzi A, Peters JF, Navarro J, Kun W, Lin B, Marijuán PC. 2017b. Cellular Gauge Symmetry and the Li Organization Principle. Progress in Biophysics and Molecular Biology. doi.org/10.1016/j.pbiomolbio.2017.06.004.

ARTICLE IN PRESS PLREV:973

Available online at www.sciencedirect.com

ScienceDirect

Physics of Life Reviews ••• (••••) •••–•••

PHYSICS of LIFE reviews

www.elsevier.com/locate/plrev

Comment

Einstein and the physics of the mind
Comment on "Physics of mind: Experimental confirmations of theoretical predictions" by Felix Schoeller et al.

Arturo Tozzi

Center for Nonlinear Science, University of North Texas 1155 Union Circle, #311427 Denton, TX 76203-5017 USA

Received 1 December 2017; accepted 19 January 2018

Communicated by J. Fontanari

Keywords: Special relativity; Brain; Central nervous system; Carnap; Einstein

Going through the intriguing paper by Schoeller et al. [7], we are gladly allowed to state that Carnap is back. He is back, due to the Authors' successful efforts to build a physics of the mind able to reduce biological issues to few fundamental physical principles and mathematical models. Also, Carnap's account turns to be stronger than ever, because the old-fashioned weapons of logical thinking, that he used as the groundwork of modern science, are here replaced by a more suitable type of process-logic, namely, dynamic logic. This novel approach, avoiding logical states until the very end of the processes and overturning the unsolvable computational complexity of the post-Gödelian logic, can be used as the foundation for psychology.

In touch with the Authors' strong (and appreciable) physicalist claims, we can take a step further: to encompass the dynamics described by the Queen of physics, i.e., special relativity, into the fruitful framework of dynamic logic. Indeed, the subjective perception of time could be assessed through the objective reference frame described by Einstein's four-dimensional spacetime in special relativity [2]. By the standpoint of an observer at rest, the moving object seems to modify with its speed. When the object approaches the light speed, time appears to slow down, compared with the time measured by the observer at rest. Nevertheless, another detectable change takes place too: a modification in object length. In Einstein's words, for an observer at rest, the length of a moving regulus is not invariant, because one of its dimensions shortens together with its speed increases. Therefore, in the inertial frame of special relativity, one of the three spatial dimensions varies, depending both on the observer's standpoint and the observed object's speed. This means that the inertial observer detects changes in the surface of the observed object, so that, for example, a cube appears more or less squeezed by the standpoint of two hypothetical observers, one at rest, and another traveling at the speed light [1]. According to different observer's standpoints, the information encompassed in the object appears modified at relativistic speeds. This means that the entropy endowed in an object surface is not an invariant and static

DOI of original article: https://doi.org/10.1016/j.plrev.2017.11.021.
E-mail address: tozziarturo@libero.it.

https://doi.org/10.1016/j.plrev.2018.01.009
1571-0645/© 2018 Elsevier B.V. All rights reserved.

Please cite this article in press as: Tozzi A. Einstein and the physics of the mind. Phys Life Rev (2018), https://doi.org/10.1016/j.plrev.2018.01.009

Einstein and the physics of the mind: Comment on "Physics of mind: experimental confirmations of theoretical predictions" by Felix Schoeller et al.

Arturo Tozzi
Center for Nonlinear Science, University of North Texas
1155 Union Circle, #311427 Denton, TX 76203-5017 USA
tozziarturo@libero.it

Below is the unedited draft of the article that has been accepted for publication © Physics of Life Reviews, 2018.

Going through the intriguing paper by Schoeller et al. (2018), we are gladly allowed to state that Carnap is back. He is back, due to the Authors' successful efforts to build a physics of the mind able to reduce biological issues to few fundamental physical principles and mathematical models. Also, Carnap's account turns to be stronger than ever, because the old-fashioned weapons of logical thinking, that he used as the groundwork of modern science, are here replaced by a more suitable type of process-logic, namely, dynamic logic. This novel approach, avoiding logical states until the very end of the processes and overturning the unsolvable computational complexity of the post-Gödelian logic, can be used as the foundation for psychology.

In touch with the Authors' strong (and appreciable) physicalist claims, we can take a step further: to encompass the dynamics described by the Queen of physics, i.e., special relativity, into the fruitful framework of dynamic logic. Indeed, the subjective perception of time could be assessed through the objective reference frame described by Einstein's four-dimensional spacetime in special relativity (Einstein, 1905). By the standpoint of an observer at rest, the moving object seems to modify with its speed. When the object approaches the light speed, time appears to slow down, compared with the time measured by the observer at rest. Nevertheless, another detectable change takes place too: a modification in object length. In Einstein's words, for an observer at rest, the length of a moving regulus is not invariant, because one of its dimensions shortens together with its speed increases. Therefore, in the inertial frame of special relativity, one of the three spatial dimensions varies, depending both on the observer's standpoint and the observed object's speed. This means that the inertial observer detects changes in the surface of the observed object, so that, for example, a cube appears more or less squeezed by the standpoint of two hypothetical observers, one at rest, and another traveling at the speed light (Chang, 1996). According to different observer's standpoints, the information encompassed in the object appears modified at relativistic speeds. This means that the entropy endowed in an object surface is not an invariant and static physical quantity, rather it depends on the observer: the faster the observer, the more information he gains about the object at rest being analyzed.

The above-mentioned Einstein's framework holds for objects or observers moving close to the light speed. Is it feasible to use the same framework in order to assess mental activities, that take place at very slow, non-relativistic speeds? Is it feasible to quantify the changes in information experienced by our mind, compared with the stationary physical information embedded in the objects we observe? During mental activity, although speed must be kept almost invariant because it is very far from the light speed, another of the parameters of Einstein's equations is modified: time. Indeed, our mind is able to subjectively dilate the time as a progressive present moment (Fingelkurts and Fingelkurts, 2014). Awareness requires mental content being held "fixed", "frozen" within a discrete but continuous "now" (James,1890; Revonsuo, 2003, Fingelkurts and Fingelkurts, 2014) of the mean duration of about 100 ms-few seconds (Pöppel,1988). In sum, in order to build a relativistic theory of the physics of the mind, we do not need to take into account what happens at light speed, rather what happens when time dilates in human inertial mental frames.

According to dynamic logic, a fundamental principle of the mind operation is a process "from vague to crisp". It describes how the brain/mind matches vague models to crisp projections from the retina, or, more generally, vague top-down models to sharp bottom-up signals. When projecting to the visual cortex, indistinct representations become crisper in 150 ms, therefore similar to the corresponding perception with opened eyes. It is noteworthy that only mental

representations that match retinal projections to the cortex are crisp and conscious. During learning, initial vague and uncertain models (standing for the Aristotelian potentialities) are associated with structures in the input signals (standing for the Aristotelian forms interacting with matter), in order that vague models become more and more definite during successive iterations. The dynamic logic processes also allow further steps, i.e., from vague to crisp perception to linguistic and cognitive components. The model provides a functional mental hierarchy which, occurring among layers of bottom-up and top-down signals, extends from sensory-motor representations at the bottom, to concepts of objects, contexts, situations, abstract cognition, up to a wide range of emotional processes and aesthetic emotions. It turns up that higher level models unify lower ones, in order to build more abstract and general concepts: driven by the knowledge instinct (or, in other words, motivated by aesthetic emotions) top-down and bottom-up projections are modified to match each other. In the language of the Authors' dynamic logic, vague-to-crisp perception processes (and the correlated imagination) can be assessed in terms of a massive mental time dilation. The latter stands for: a) in the relativistic case, to an inertial observer at rest who watches an object moving at light speed; b) in the non-relativistic case, to the conscious mind's dilated time, which allows modifications in object's perception. This means that the longer one imagines an object, the more the object changes, until it fades away in his mind. In the example provided by the Authors, even in the case of a simple everyday object, one fails to recollect all its details in absence of sensory information, due to the vagueness of imagination. Indeed, in the framework of a prolonged mental time dilation, abstract concepts are built on top of many levels of vague models, correspondingly they are even less accessible to consciousness.

Einstein's special relativity is based on invariant and non-invariant quantities. The latter, i.e., time and the axis parallel to the moving object, change according to the observer's subjective standpoint. Despite physics favors non-invariant quantities and focuses on the "hard" data coming from invariant frames, the opposite could be true for mental functions. Indeed, every brain is able to assess the non-invariant quantities of a relativistic-like inertial frame, giving rise to the astonishing differences in mental activity experienced by various individuals. Such differences might be quantified through the powerful physicalist approach suggested by dynamic logic. In the process of perception, due also to the dilation of the subjective time, "mind meets matter", top-down and bottom-up signals interact, and representations alternatively reach and loose crisp states corresponding to the Aristotelian actualities. Therefore, special relativity elucidates why, in dynamic logic, the top-down models and representations need to be vague and similar to Aristotelian potentialities.

REFERENCES

1) Chang M-C., Lai F, Chen W-C. 1996. Image shading taking into account relativistic effects. ACM Transactions on Graphics (TOG), 15(4), 265-300.
2) Einstein A. 1905. Zur Elektrodynamik bewegter Körper. Annalen der Physik (Berlin) (in German), Hoboken, NJ (published 10 March 2006), 322 (10), pp. 891–921, Bibcode:1905AnP...322..891E.
3) Fingelkurts AA, Fingelkurts AA. 2014. Present moment, past, and future: mental kaleidoscope. Frontiers in Psychology, 5:395. doi:10.3389/fpsyg.2014.00395.
4) James W. 1890. The Principles of Psychology, Vol. 1. New York, NY: Dover; 10.1037/10538-000.
5) Pöppel E. 1988. Mindworks: Time and Conscious Experience. Boston, MA: Harcourt Brace Jovanovich.
6) Revonsuo A. 2006. Inner Presence: Consciousness as a Biological Phenomenon. Cambridge: MIT Press.
7) Schoeller F, Perlovsky L, Arseniev D. Physics of mind: experimental confirmations of theoretical predictions. Phys Life Rev (2018), https://doi.org/10.1016/j.plrev.2017.11.021 [this issue].

Accepted Manuscript

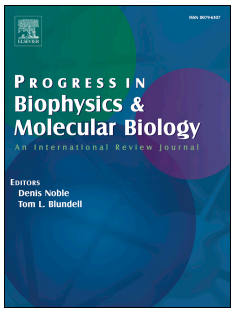

A timeless biology

Arturo Tozzi, James F. Peters, Clifford Chafin, Domenico De Falco, John S. Torday

PII: S0079-6107(17)30236-5

DOI: 10.1016/j.pbiomolbio.2017.12.002

Reference: JPBM 1302

To appear in: *Progress in Biophysics and Molecular Biology*

Received Date: 29 October 2017

Revised Date: 5 December 2017

Accepted Date: 6 December 2017

Please cite this article as: Tozzi, A., Peters, J.F., Chafin, C., De Falco, D., Torday, J.S., A timeless biology, *Progress in Biophysics and Molecular Biology* (2018), doi: 10.1016/j.pbiomolbio.2017.12.002.

This is a PDF file of an unedited manuscript that has been accepted for publication. As a service to our customers we are providing this early version of the manuscript. The manuscript will undergo copyediting, typesetting, and review of the resulting proof before it is published in its final form. Please note that during the production process errors may be discovered which could affect the content, and all legal disclaimers that apply to the journal pertain.

ACCEPTED MANUSCRIPT

A TIMELESS BIOLOGY

Arturo Tozzi (Corresponding Author)

Center for Nonlinear Science, University of North Texas, Denton, Texas 76203, USA
tozziarturo@libero.it

James F. Peters
Department of Electrical and Computer Engineering, University of Manitoba
75A Chancellor's Circle
Winnipeg, MB R3T 5V6 CANADA
James.Peters3@umanitoba.ca

Clifford Chafin
Roto9 Energy, Chapel Hill, NC, USA
cliff.chafin@gmail.com

Domenico De Falco
Second University of Naples, Dipartimento di Ingegneria Industriale e dell'Informazione, Aversa, Caserta, Italy
domenico.defalco@gmail.com

John S. Torday
Department of Pediatrics
Harbor-UCLA Medical Center, 1124 W.Carson Street
Torrance CA 90502
jtorday@labiomed.org

Contrary to claims that physics is timeless while biology is time-dependent, we take the opposite standpoint: physical systems' dynamics are constrained by the arrow of time, while living assemblies are time-independent. Indeed, the concepts of "constraints" and "displacements" shed new light on the role of continuous time flow in life evolution, allowing us to sketch a physical gauge theory for biological systems in long timescales. In the very short timescales of biological systems' individual lives, time looks like "frozen" and "fixed", so that the second law of thermodynamics is momentarily wrecked. The global symmetries (standing for biological constrained trajectories, i.e. the energetic gradient flows dictated by the second law of thermodynamics in long timescales) are broken by local "displacements" where time is held constant, i.e., modifications occurring in living systems. Such displacements stand for brief local forces, able to temporarily "break" the cosmic increase in entropy. The force able to restore the symmetries (called "gauge field") stands for the very long timescales of biological evolution. Therefore, at the very low speeds of life evolution, time is no longer one of the four phase space coordinates of a spacetime Universe: but it becomes just a gauge field superimposed to three-dimensional biological systems. We discuss the implications in biology: when assessing living beings, the underrated role of isolated "spatial" modifications needs to be emphasized, living apart the evolutionary role of time.

KEY WORDS: time; gauge theory; symmetries; constraints; informational entropy; evolution

INTRODUCTION

In order to emphasize the intrinsic failure of the physical laws in the assessment of the overwhelming biological complexity, it has been proposed that physics is essentially based on timeless dynamics, while irreversible time is a prominent feature of biota (Ulanowicz, 2017). Here we go through the opposite hypothesis, i.e., that macroscopic physics is time-constrained, while living beings tend towards an effort to "freeze" and "slow" the arrow of time. Perhaps, time does not exist at the micro-level of quantum vacuum and Planck scales (Rovelli, 1991). Yet, time modifies according to the Einstein special and general relativity (Einstein, 1905) at the relativistic macro-scales and at

ACCEPTED MANUSCRIPT

very high energies. However, at the meso-scales of the environmental niches that allow life, time is relatively stable. Here we show how such stability is very important for life evolution as we know it, and what it is like to be a living being closely depends on the stable, rather continuos time passing. Many current theories emphasize the foremost role of the "time" and "timescales" in different biological fields, from cellular function to neural activity (Linkenkaer-Hansen et al, 2001; Kravchick and Jordan, 2015; Papo, 2015). Is such a tenet true? Although stochastic variables and random fluctuations regulated by the Langevin and the Fokker-Planck equations frequently occur (Ribrault et al, 2011), biological activities are only partially Brownian, since they are "constrained". For example, the protein-folding final conformation is dictated by the minimum frustration principle on long evolutionaly timescales. Such principle states that proteins' energy decreases more than expected, as they assume conformations progressively more like the native state (Bryngelson and Wolynes, 1987; Ferreiro et al, 2011). A strong bias in the protein's surface energy landscape towards the lowest energetic basin occurs, overcoming the asperities of the rugged landscape (Onuchic et al., 1997; Sutto et al, 2007; Tozzi et al., 2016). In other words, proteins were enriched by evolution for sequences with the propensity to fold into the lowest energetic structures. Constraints also occur in countless other systems, from the nonlinear chaotic paths governed by strange attractors, to the structure of biological entities, ruled by their specific genetic pools. Despite the large number of different scenarios, the processes governing constraints on physical and biological systems may be generalized, taking into account the universal principle of the second law of thermodynamics, which states, in Planck's formulation, that "e*very process occurring in nature proceeds in the sense in which the sum of the entropies of all bodies taking part in the process is increased"*. In this framework, the concepts of "virtual displacement" - from the far-flung branch of analytical mechanics - come into play (Sommerfeld 1952; Landau and Lifshitz, 1976; Goldstein, 1980; Torby1984).

In this paper we will try to elucidate that, in the evolution of living beings, close relationships occur among displacements, information and time. Such findings make it possible to let us hypothesize a theory of time as a gauge field. The manuscript encompasses four sections. The first section describes the virtual and real constraints in the framework of a "frozen" time. The second section, taking into account probabilistic arguments, shows how is possible to insert virtual constraints on the Shannon entropy's plot, in order to correlate informational entropy with the arrow of time. The third section illustrates the procedure to sketch gauge theory based on the three above mentioned ingredients: constraints, probabilities and time. The fourth section describes an evolutionistic cosmic account based on the laws of symmetries.

1) VIRTUAL CONSTRAINTS

This section describes "virtual" and "real" constraints in the framework of a "frozen" time. Here we show how the natural paths of particle trajectories dictated by long timescales (standing in our case for the increase of thermodynamical entropy occurring in our Universe as time slowly passes) can be broken by the "virtual constraints", i.e., the very short timescales of the living beings, in which time is temporarily "frozen".

In technical terms, the key concept of virtual constraints is a dynamically imposed outer feedback control, so that the trajectory of a particle or an agent in the system's phase space can be "forced" towards the desired orbits and outputs (Canudas-de-Wit, 2004). Virtual constraints reduce the degrees of freedom, coordinating the evolution of the various links throughout a single variable. A closed-loop mechanism is achieved, wherein dynamic behaviour is fully determined by the evolution of simplest lower-dimension system (Stepp et al., 2010). The resulting system is called a "virtual limit system".

In mathematical terms, we define a set of $n-1$ outputs (or constraints):

$$y = \varphi(p,q) = \vec{q} - h(\theta, p) = \vec{q} - h(\theta, p(t)),$$

where y and $\varphi(p,q)$ are the outputs or constraints, $\vec{q} \in R^{n-1}$ is an $n-1$ dimensional real-valued vector that gives the actuated coordinates and velocities, p is the set of the design parameters, $\theta \in R$ is the unactuated variable, θ(q) is a function of the generalized coordinates of q. The latter equation describes the most general condition. In other words, constraints can be mathematically assessed through a well-established procedure that takes into account a wide range of systems' parameters.

An inner-feedback loop is used to perform output feedback linearization in a local domain, where the matrix is invertible:

$$\psi(q)u = k(q;\dot{q}) + v,$$

ACCEPTED MANUSCRIPT

where v is the outer feedback loop. Note that the equation includes a term $\dot{q}$ which depends on time, where the upper dot stands for the partial time derivative, i.e., $\dot{q} = \frac{\partial q}{\partial t}$ (Canudas-de-Wit, 2004).

If an outer feedback loop v is designed to zeroing the output y, we get a partially linearized system in the form:

$$\ddot{y} = v.$$

Then the full system dynamic is captured by the solutions of:

$$\alpha(\theta)\ddot{\theta} + \beta(\theta)\dot{\theta}^2 + \gamma(\theta) = 0,$$

together with the imposed constraint for mean q-value:

$$\bar{q} = h(\theta, p),$$

where $\theta(q)$, $\alpha(\theta)$, $\beta(\theta)$ and $\gamma(\theta)$ are scalar functions depending on the inner feedback loop.

In conclusion, the virtual constraints are forces external to the system's phase space (in our case, the increase of cosmic entropy achieved in very long timescales), able to modify an internal trajectory towards the required one (in our case, the temporary, short, local decreases of cosmic entropy occurring in living systems).

This process allows one to deal with high-dimensional systems with underactuated degree one, by only analyzing this second-order nonlinear equation.

In analytical mechanics the researchers cope with under-actuated Lagrangian systems of the form:

$$\frac{d}{dt}\left(\frac{\partial L}{\partial \dot{q}}\right) - \frac{\partial L}{\partial q} = B(q)u,$$

where q and $\dot{q}$ are vectors of generalized coordinates and velocities, $L(q;\dot{q})$ is a Lagrangian of the system, $B(q)$ is a matrix function of an appropriate dimension (with rank equal to the number of inputs) and u is a vector of independent control inputs. The under-actuation means that dim u< dim q, i.e., the number of actuators is less than the number of its degrees of freedom.

A virtual displacement is an assumed change of system coordinates occurring while time is held constant. It is called "virtual" rather than "real", since no actual displacement (in our case, the increase of entropy in a single place of the Universe where life occurs) takes place without the passage of time. Computerized simulations may be performed to see what happens to physical and biological paths when time is kept fixed, *e.g*, during the movements of animals in an environment, or during cytoplasmatic enzymatic reactions. For further details about the methodology, see **Figure 1**.

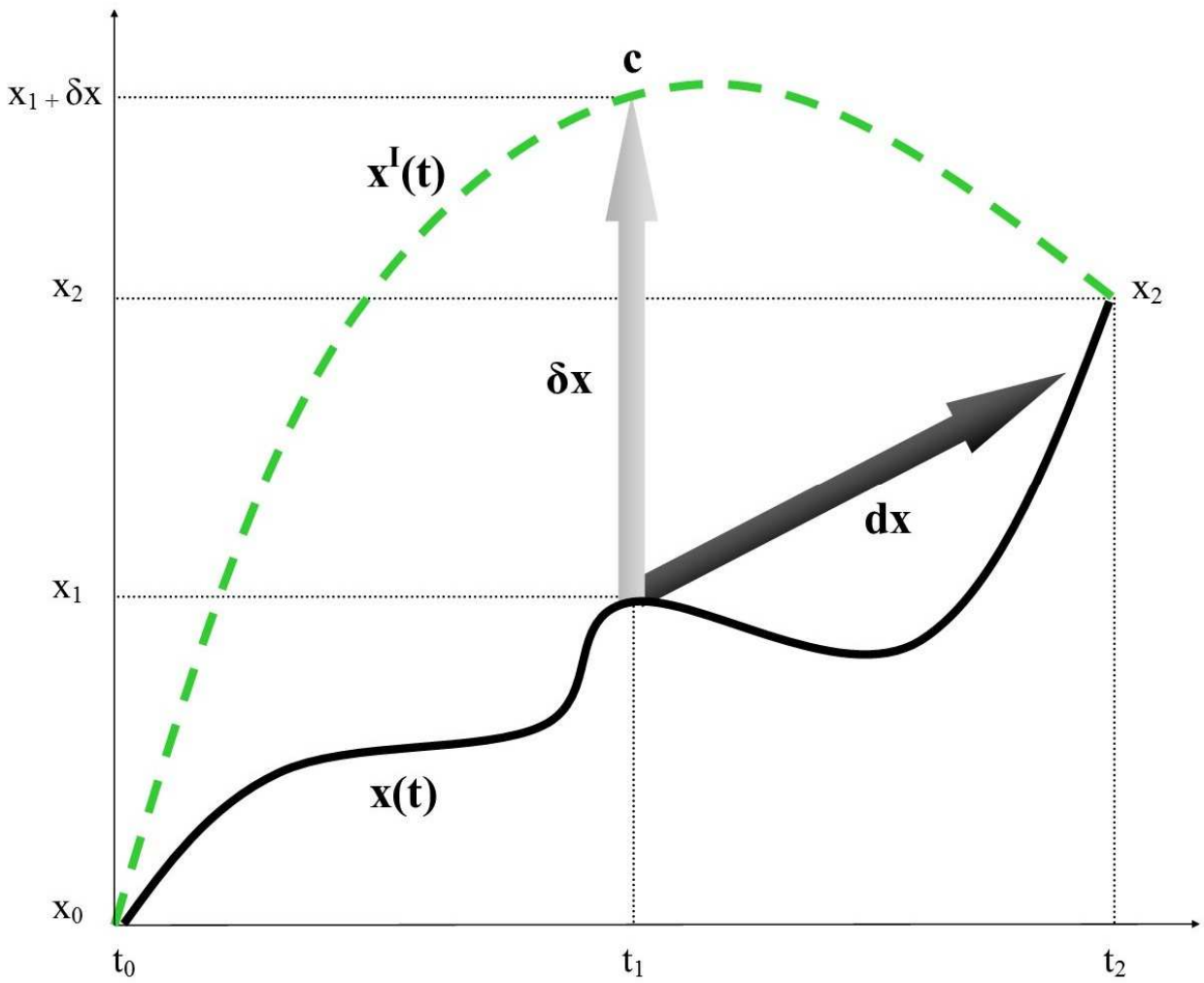

Figure 1. Real and virtual trajectories in a graph plotting time t on the X-axis and the space x on the Y-axis. The Figure evaluates two trajectories which both display a starting position at x_0 and an ending position at x_2. The black solid curve x(t) stands for the particle trajectory, while the dotted green curve $x^I(t)$ for a possible virtual trajectory. At position x_1 and time t_1, the virtual displacement δx (from x_1 to the point c) is illustrated (grey arrow). The regular displacement dx is a vector pointing in the direction of the motion (black arrow), which arises from differentiating with respect to time parameter along the path of the motion. In contrast, the virtual displacement δx is a tangent vector to the constraining manifold at a fixed time. It arises from the differentiation with respect to the enumerating paths of the motion, varied in a manner consistent with the constraints.

2) INFORMATION ENTROPY AND TIME

This section, taking into account probabilistic arguments, shows how is possible to locate virtual constraints on the Shannon entropy's plot, in order to correlate informational entropy with the arrow of time. Real displacements are governed by the second law of thermodynamics: in every system, either physical or biological, the thermodynamical entropy relentlessy increases from time T_0 to $T_2 = \infty$, until its maximum value. In our case, it is however preferable to use the informational entropy, instead of the thermodynamical one. Indeed, the two entropies are linked through the formula:

$S = k\,H$

ACCEPTED MANUSCRIPT
in which S is the thermodynamical entropy, k is the Bolztmann constant and H is the Shannon informational entropy. The informational entropy, apart from the invaluable advantage of quantifying the macroscopic states without a perfect knowledge of the microscopic ones, is not directly linked with time, allowing us to remove such parameter from our system. Indeed, the Shannon's plot of informational entropy does not encompass the parameter time. If we want to introduce the arrow of time on the Shannon's curve, we may superimpose another, third dimension to its classical 2-D plot (**Figure 2**). The vector of time $\boldsymbol{\zeta}$ lies in a plane forming an angle A with the 2-D plane of Shannon entropy. Note that the timescales expressed by the vector $\boldsymbol{\zeta}$ in the graphic may vary, depending on which system we are evaluating. As an example, if we take into account the system Universe, T_0 stands for the state of minimum entropy – the initial Big Bang -, while $T_2 = \infty$ stands for the state of maximum entropy, *i.e.*, the hypothetical final state of the Universe. Starting from the probability of a virtual constraint c, we may calculate the corresponding point T_1 on the arrow of time, in order to assess and quantify how much time is still required to reach $T_2 = \infty$ (which stands for the system's "real" final state at the energetic equilibrium). There is still an unknown, crucial parameter to measure: the value of the angle A, which is not implied to be constant, but could change in different examined systems.
If we know the value of of the angle A, we are allowed to recognize how long the biological system will take, in order to complete its biological path in cosmic times.
The next section answers the question: how can we find the value of the angle A? Here, the formalism of a gauge theory will come into play.

ACCEPTED MANUSCRIPT

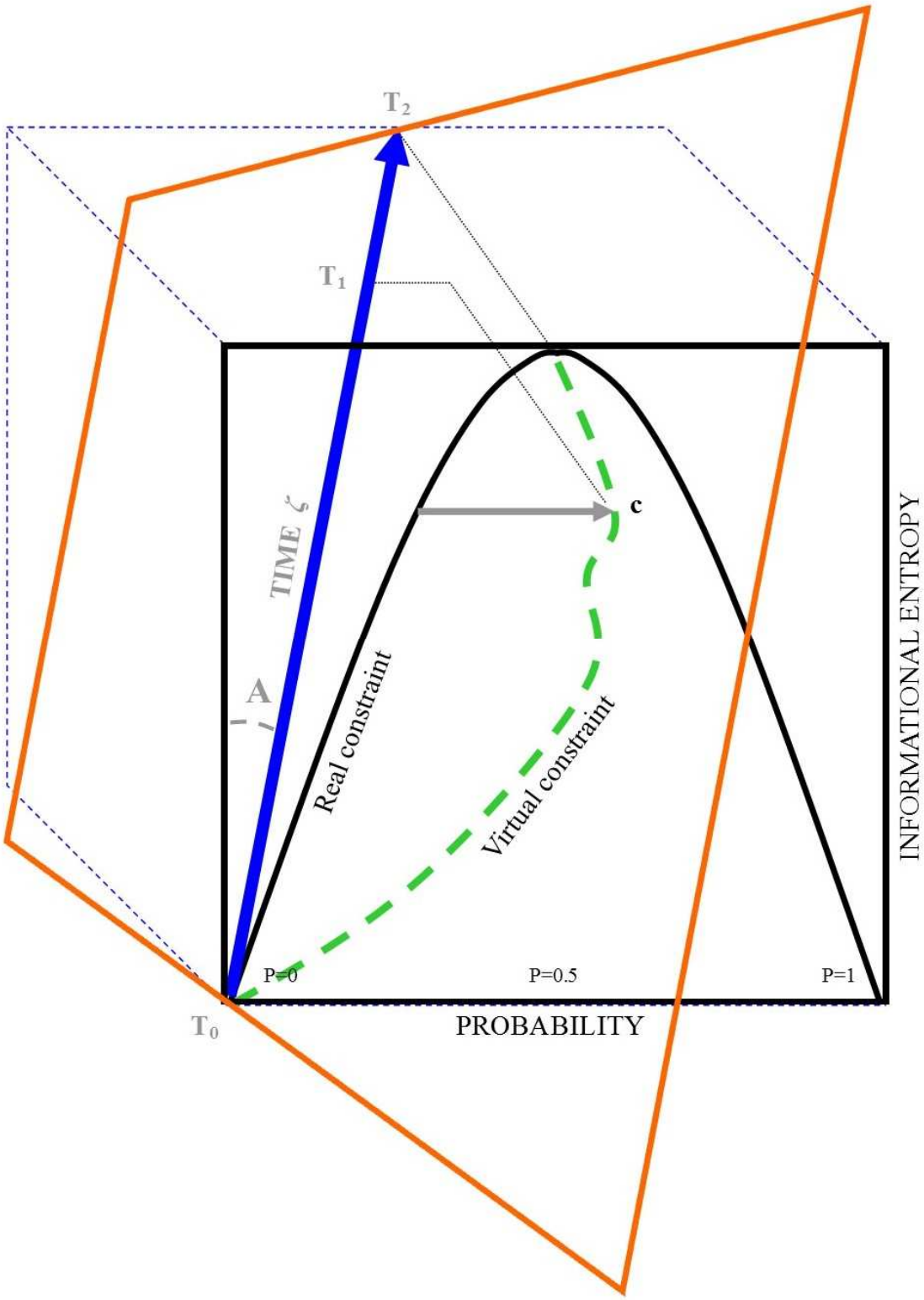

Figure 2. The informational entropy is plotted as a function of the random variable p, in the case of two possibilities with probabilities p and (1-p). The solid line black stands for the Shannon entropy (under ergodic conditions). The values p=0 and p=1 stand for the minimum entropy, p= 0.5 for the maximum entropy. The arrow of time ζ lies on a third coordinate of the phase space and is equipped with the angle A. Due to the energetic gradient flows dictated by the second law of thermodynamics, time, in its route from T_0 to $T_2 = \infty$, is correlated with an increase in informational

ACCEPTED MANUSCRIPT
entropy. Given a virtual displacement c on the virtual trajectory (dotted black line), the corresponding value of T_1 on the arrow of time can be calculated, provided the value of A is known.

3) GAUGE PROCEDURES

Here we illustrate the procedure in order to calculate the angle A, by sketching a gauge theory based on the three above mentioned ingredients: constraints, probabilities and time. In other words, we examine the possibility to build a differential geometry-based theory of the real (cosmic, long timescales) and virtual (biological, short timescales) trajectories' phase space. At first, we need a system equipped with real displacements - the real trajectories of particles or events in cosmic timescales - that stand for the continuous, global symmetries. Such symmetries are the energetic constraints that the second law of thermodynamics enforces on the system. While energetic gradient flows occur just in long timescales, in the very instant in which T is "frozen", fixed and equals to zero, virtual displacements occur. The latter stand for a continuous group of local transformations able to "break" the symmetry. The local loss of symmetry caused by living beings (a disturbance of the gradient flow) needs however to be ripristinated. In order to achieve this symmetry repair, we need to introduce a so-called gauge field, i.e., in our case, time, able to restore the gradient flow. Note that a gauge theory requires gauge fields to be continuous. Indeed, time, which is not continuous when approaching the light speed as dictated by Einstein's special relativity, nevertheless are almost continuous at the nonrelativistic timescales of the life.
There are many possible ways to deal with a theory of the virtual displacements in a differential geometric sense, for example by analyzing them in terms of sections of fibre bundles, jet manifolds and Ehresmann connections (Abraham and Marsden, 1978; Kolar and Michor, 1993; Lang, 1995). In order to quantify the required forces and in particular the angle A described in the previous paragraph, we proceeded as shown in **Figure 3**. The whole procedure is modified from Tozzi et al. (2017b). In the example described in **Figure 3A**, we depicted four areas (standing for the biological activity of four living beings in short timescales) as rotating circles, where rotations along the circumference stand for their probability densities. The geometric "link" between the real 3D manifold (depicted in **Figure 3A**) and an abstract manifold (depicted in **Figure 3B**) can be defined in terms of "connections" (Ehresmann 1950; Sengupta et al., 2016). According to the covariant version of a gauge theory, the correction terms are reinterpreted as couplings to an additional divergent counter term, the gauge field, by allowing the symmetry parameter to vary from place to place in the local coordinate system. **Figure 3E** illustrates the procedure. In other words, we need to introduce the vector ψ, equipped with the angle A, which stands fo the global value of the required gauge field. This procedure allows us to extrapolate from A the values of the gauge field required to keep the trajectories invariant under different virtual displacements.
Our framework resembles a gauge theory, but with some distinctions. The physical gauge theories are based on three tenets (Zeidler 2011):

a) The system is equipped with a continuous, preserved "global" symmetry (and a corresponding Lagrangian).
b) The system displays a continuous group of "local" transformations, equipped with a Lie group.
c) The Lagrangian is kept invariant under such local transformations by a "gauge field", i.e. a continuous force acting on the system.

The Lagrangian, through its connections with Noether's theorem, throws a bridge between symmetries and energetic requirements. However, the concept of the Lagrangian is slightly different in our model: instead of referring to the principle of least action and the "preservation" of a physical quantity as usual in gauge theories, it refers to the "dissipation" of a physical quantity through gradient flows.

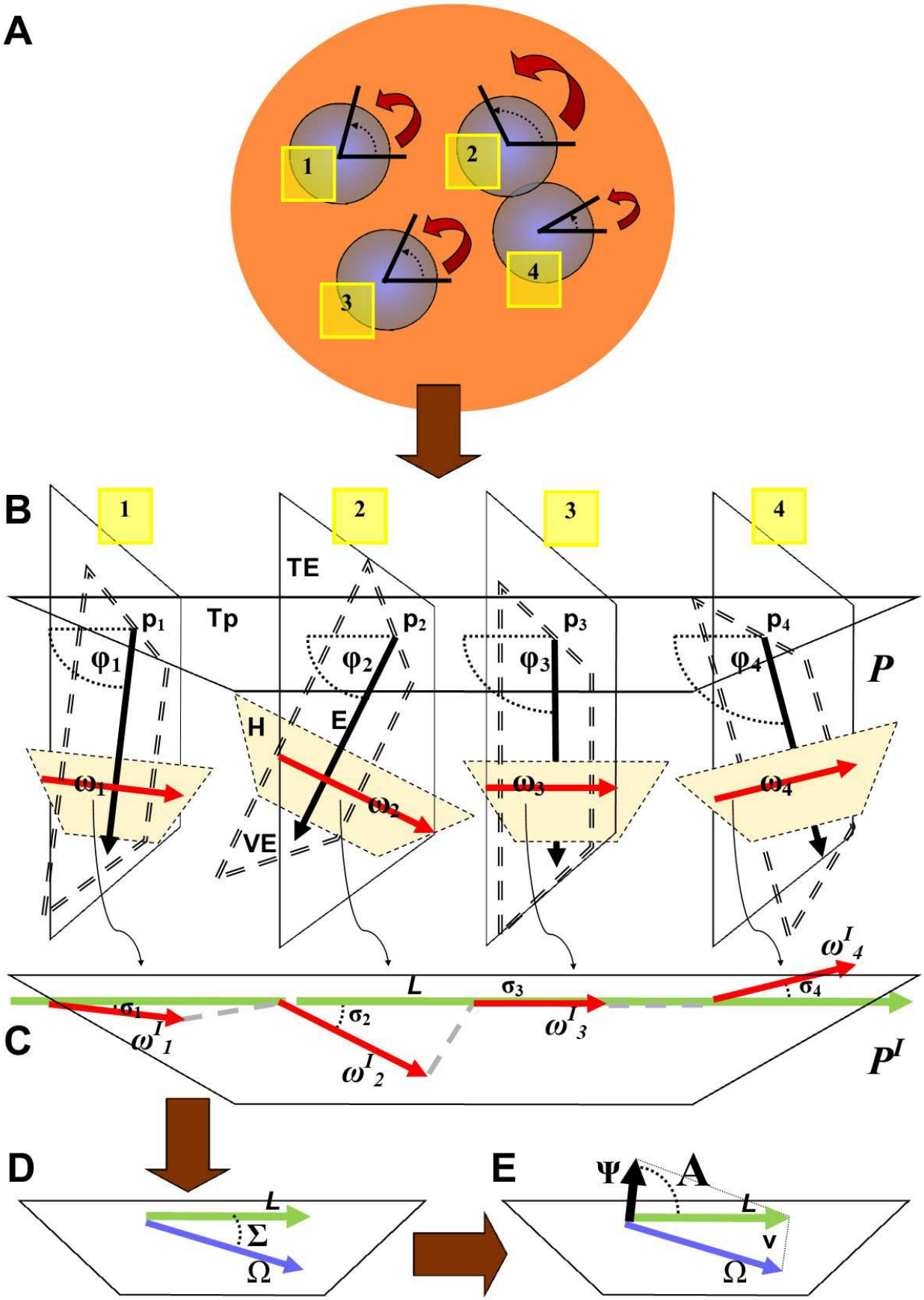
A
1
2
3
4
B
TE
Tp
p1
p2
p3
p4
φ1
φ2
φ3
φ4
P
H
E
VE
ω1
ω2
ω3
ω4
ωI 4
L
σ1
σ2
σ3
σ4
ωI 1
ωI 2
ωI 3
C
PI
D
L
Σ
Ω
E
Ψ
A
L
v
Ω

ACCEPTED MANUSCRIPT

Figure 3. Displacements in a system equipped with a global, invariant symmetry. The global symmetry stands for the constrained energetic paths towards a cosmic increase in entropy, dictated in long timescales by the second law of thermodynamics. Four virtual displacements, e.g., the anti-entropic activity of four living beings, are expressed as measures of probability states in four areas of a 3D system, at time kept fixed at zero. The four displacements' activity is expressed in terms of the circular movements taking place on a disk (**Figure 3A**) and mapped on a an abstract mathematical structure (**Figure 3B**). After a procedure of connection (**Figure 3C**) the gauge field (the vector ψ, equipped with our required angle A) can be calculated (**Figures 4D-E**). The gauge field stands here for time, continuous at the nonrelativistic timescales of the living beings. For further technical details about the mathematical apparatus, see Tozzi et al. (2017b).

4) CONCLUSION: SYMMETRIES AND EVOLUTION

We showed how the vector of time might stand for the energetic gradient of the system, locally "broken" by timeless perturbations. In analytical mechanics, the concept of virtual displacement - related to virtual work - is meaningful only when discussing a system subject to constraints on its motion. As stated above, this is the case of physical and biological activity. Because virtual displacements occur exclusively in space, the underrated role of the sole "spatial" modifications needs to be emphasized when assessing physical and biological activities. While virtual displacements take place, time is fixed and $\delta t = 0$, so that changes in physical/biological functions are independent of time passing. When time equals = 0, the real trajectory does not exist, because it is just the passing of time that gives rise to real displacements.

In this framework, the concepts of constraints and virtual displacement (Torby 1984) are going to be game changing. A virtual displacement is an assumed change of system coordinates occurring while time is held constant. It is called "virtual" rather than "real", since no actual displacement takes place with absence of time passing.

Therefore, we may draw a few conclusions:

1) In analytical mechanics, the concept of virtual displacement - related to virtual work - is meaningful only when discussing a system subject to constraints on its motion. As stated above, this is the case of biological activity.

2) Virtual displacements occur exclusively in space. The underrated role of the sole "spatial" modifications needs to be thus emphasized, when bearing in mind biological activities. Changes in spatial conformations may underline functional divisions in different zones of the biological melieu: for example, in touch with recent "neo-phrenonogical" claims (Tozzi, 2015), variations in psychological states could be correlated with different brain areas; further, various protein functions could depend just on spatial conformation's changes.

3) While virtual displacements take place, the time is fixed and $\delta t = 0$. The finding that changes in biological functions can be independent on the passage of time leads to several corollaries. To make an example, the role of pairwise entropy in neurofunctional studies needs to be re-evaluated: it takes into account the temporal overlapping of on\off states in brain subareas; however, if activity takes place in absence of time changes, such correlations become overestimated in the study of brain functions.

4) Virtual displacement mapping is an alternate name for parallax mapping, a system of three- dimensional displacement of surfaces, by which textures on flat surfaces give the illusion of depth. Virtual displacementmay therefore be the clue for a better comprehension of the three-dimensional perception (either visual, or acustic, tactile, chemical and so on) in living beings's nervous systems.

We would like to bring to the end with a remark concerning gauge theories. In touch with recent claims regarding the human brain activity (Sengupta et. al., 2016; Tozzi et al., 2017b) and cellular metabolism (Tozzi et al., 2017a), our work provides a further theoretical confirmation that gauge theories could be suitable not just for the canonical, well-estabilished assessment of physical particles and fields, but also for quantitative approaches to biological issues.

REFERENCES

1) Bryngelson, J.D. &Wolynes, P.G. Spin glasses and the statistical mechanics of protein folding. Proc. Natl. Acad. Sci. U S A. **84,** 7524-7528 (1987).

ACCEPTED MANUSCRIPT

2) Canudas-de-Wit, C. On the concept of virtual constraints as a tool for walking robot control and balancing. Annual Reviews in Control **28,** 157–166 (2004).
3) DeWitt, B.S. Quantum Theory of Gravity II. The Manifestly Covariant Theory. Phys. Rev. **160,** 1195-1239 (1967).
4) Ehresmann, C. Les connexions infinit´esimalesdans un espacefibrée differentiable. Colloque de Topologie, Bruxelles, pp. 29–55 (1950).
5) Einstein A. 1905. ZurElektrodynamikbewegterKörper. Annalen der Physik (Berlin) (in German), Hoboken, NJ (published 10 March 2006), 322 (10), pp. 891–921, Bibcode:1905AnP...322..891E
6) Ferreiro, D.U, Hegler, J.A., Komives E.A. &Wolynes, P.G. On the role of frustration in the energy landscapes of allosteric proteins. Proc Natl Acad Sci U S A. **108,** 3499-503 (2011).
7) Goldstein, H. Classical Mechanics (Addison-Wesley Publishing Co., Reading, Massachusetts, 1980).
8) Landau, L.L. &Lifshitz, M. Mechanics (Pergamon Press, Oxford, 1976).
9) Linkenkaer-Hansen, K., Nikouline, V.V., Palva, J.M., &Ilmoniemi R.J. Long-range temporal correlations and scaling behavior in human brain oscillations. J. Neurosci. **21**, 1370-1377 (2001).
10) Onuchic, J.N., Luthey-Schulten, Z. &Wolynes, P.G. Theory of protein folding: the energy landscape perspective. Annu. Rev. Phys Chem. **48,** 545-600 (1997).
11) Papo, D. How can we study reasoning in the brain? Front Hum Neurosci. **9,** 222 (2015).
12) Ribrault, C., Sekimoto, K. &Triller, A. From the stochasticity of molecular processes to the variability of synaptic transmission. Nat. Rev. Neurosci. **12,** 375–387 (2011).
13) Rovelli C. 1991. Time In Quantum Gravity: Physics Beyond The Schrodinger Regime. Physical Review D43, 442.
14) Sengupta B, Tozzi A, Coray GK, Douglas PK, Friston KJ. 2016. Towards a Neuronal Gauge Theory. PLOS Biology 14 (3): e1002400. doi:10.1371/journal.pbio.1002400.
15) Sommerfeld, A. Mechanics, Lectures on Theoretical Physics, vol. I (Academic Press, New York, 1952).
16) Stepp, C.E., Hillman, R.E. & Heaton, J.T. A virtual trajectory model predicts differences in vocal fold kinematics in individuals with vocal hyperfunction. J AcoustSoc Am. **127,** 3166-3176 (2010).
17) Sutto, L., Lätzer, J., Hegler, J.A., Ferreiro, D.U., &Wolynes, P.G. Consequences of localized frustration for the folding mechanism of the IM7 protein. Proc. Natl. Acad. Sci. U S A. 2007 **104,** 19825-19830 (2007).
18) Torby, B., 1984. Energy Methods. Advanced Dynamics for Engineers. HRW Series in Mechanical Engineering. United States of America: CBS College Publishing. ISBN 0-03-063366-4.
19) Tozzi A. 2015. Information Processing in the CNS: A Supramolecular Chemistry? Cognitive Neurodynamics 9 (5): 463–477.
20) Tozzi A, Fla Tor, Peters JF. 2016. Building a minimum frustration framework for brain functions in long timescales. J Neurosci Res.94(8): 702–716.
21) Tozzi A, Peters JF. 2017. Towards Topological Mechanisms Underlying Experience Acquisition and Transmission in the Human Brain. J.F. Integr. psych. behav. doi:10.1007/s12124-017-9380-z.
22) Tozzi A, Peters JF, Navarro J, Kun W, Lin B, Marijuán PC. 2017a. Cellular Gauge Symmetry and the Li Organization Principle. Progress in Biophysics and Molecular Biology. https://doi.org/10.1016/j.pbiomolbio.2017.06.004.
23) Tozzi A, Sengupta B, Peters JF, Friston KJ. 2017b. Gauge Fields in the Central Nervous System. 193-212. In: The Physics of the Mind and Brain Disorders: Integrated Neural Circuits Supporting the Emergence of Mind, edited by Opris J and Casanova MF. New York, Springer; Series in Cognitive and Neural Systems. ISBN: 978-3-319-29674-6. DOI10.1007/978-3-319-29674-6_9.
24) Ulanowicz RE. 2017. Preface: towards a global understanding of development and evolution. Progr Biophys Mol Biol, pii: S0079-6107(17)30178-5. In press.
25) Zeidler, E. Quantum Field Theory III: Gauge Theory. Springer-Verlag, Berlin, Heideberg (2011).

Journal of Neuroscience & Clinical Research

Research Article

A SCITECHNOL JOURNAL

The Thermodynamic Analysis of Neural Computation

Deli E[1]*, Peters JF[2] and Tozzi A[3]

Abstract

The brain displays a low-frequency ground energy confirmation, called the resting state, which is characterized by an energy/information balance via self-regulatory mechanisms. Despite the high-frequency evoked activity, e.g., the detail-oriented sensory processing of environmental data and the accumulation of information, nevertheless the brain's automatic regulation is always able to recover the resting state. Indeed, we show that the two energetic processes, activation that decreases temporal dimensionality via transient bifurcations and the ensuing brain's response, lead to complementary and symmetric procedures that satisfy the Landauer's principle. Landauer's principle, which states that information era- sure requires energy predicts heat accumulation in the system, this means that information accumulation is correlated with increases in temperature and lead to actions that recover the resting state. We explain how brain synaptic networks frame a closed system, similar to the Carnot cycle where the information/energy cycle accumulates energy in synaptic connections. In deep learning, representation of information might occur via the same mechanism.

Keywords

Energy/information exchange; Information erasure; Entropy; Landauer's principle; Carnot cycle; Deep learning

Introduction

The cortical brain is an evolutionary marvel which interacts with the outside world via self-regulation, based on its resting or ground state. The resting state, which is disturbed during stimulus and sensory processing, is recovered by automatic operations. In warm blooded animals, the brain's energy need multiplies although, the human brain represents only 2% of the body weight it receives 15% of the cardiac output, 20% of totals body oxygen consumption, and 25% of total body glucose utilization. It is thought that baseline energy consumption has been almost exclusively dedicated to neuronal signaling [1]. This almost constant and huge energy use maintains the brain's alertness, even during sleep by an active balance between inhibitory and excitatory neurons [2,3]. The slightest variation in excitation determines whether a spike is generated such a delicate balance of excitatory and inhibitory neurons turns the resting state into a highly energy requiring state [4-6]. Even in the absence of stimulus, the equal balance of excitatory and inhibitory neurons produces seemingly arbitrary bursts of resting state's activation [7]. This active balance between contrasting influences ensures the brain's ability for rapid, targeted response to environmental stimulus. For example, changes in inhibitory neurons increase frequencies and their energetic needs [4]. Via the sensory system, the brain partakes in the energy information exchange with the environment: the precarious energy balance turns interaction into a closed physical process: the thermodynamic entropy.

Entropy is a concept rooted in experience and experimental data different scientific fields (such as information theory or quantum mechanics) have their own, although related, definitions, with a significant amount of disagreement over diverse definitions of information and entropy [8,9]. To make just a few examples, it has been recently suggested that the negative work cost of erasure stands for negative entropy furthermore; entropy might drive order-increasing interactions, in closed systems and under special circumstances [10-12]. The brain's resting state allows the considerations of stimuli-related energy changes, based on the laws of thermodynamics. Sensory activation is coupled to information increase via enhanced frequencies so that the brain's energy/information cycle might form a closed thermodynamic system, similar to the Carnot cycle [13]. To gain better insight into the nature of entropy, here we investigate the role of stimulus during the entropic changes occurring during cognitive process. Landauer's principle (i.e., the erasure of information produces a minimal quantity of heat, proportional to the thermal energy) shows that a certain amount of work is necessary to erase a bit of information, dissipated as heat to the environment [14]. The needed amount of work couples with the function of uncertainty about the system, because information about the system reduces the cost of erasure. Likewise, the information value of stimuli, which determines the extent of response, is highly subjective. For example, the correlation of neuronal activation with visual stimulus is dynamic and mediated by intracortical mechanisms [15]. Furthermore, the oscillation dynamics of local neurons reflect the anatomical/functional occurrence of intra-cortical feedback, thalamocortical network, global signal propagation, synaptic clustering, network states and other residual activities well beyond the sensory value of inputs [16]. Thus, the connection between information and 'work' is the function of environmental entropy. Thus, applying Landauer's principle to the brain's cognitive process might uncover the thermodynamic nature of the energy information exchange during the sensory process.

One of the biggest puzzles in neuroscience is how comprehension and meaning emerge from the complex patterns of neural activity. Hemodynamic, metabolic parameters, membrane potential, electric spikes, neurotransmitter release have been studied [17-19]. EEG, lesion studies diffuse tensor imaging, MEG and fMRI analysis demonstrate that consciousness results from coherent, globally coordinated electric activities [20-25]. Since electric activities in the brain are correlated with conscious actions, the mind forms a unified experience by connecting sensory perception with mental states based on event related potentials [26,27]. An ensemble of cortical and subcortical regions, including the rostral anterior cingulate, precuneus, posterior cingulate cortex, posterior parietal cortex, dorsal prefrontal cortex, along with the caudate head, anterior claustrum and posterior thalamus, supports the occurrence and convergence of multiple resting state networks [28]. Resting state

***Corresponding author:** Eva Deli, Institute for Consciousness Research Nyiregyhaza Benczur ter 9, Hungary, Tel: 15073962613; E-mail: eva.kdeli@gmail.com

Received: January 25, 2018 **Accepted:** February 19, 2018 **Published:** February 27, 2018

SciTechnol International Publisher of Science, Technology and Medicine

All articles published in Journal of Neuroscience & Clinical Research are the property of SciTechnol, and is protected by copyright laws. Copyright © 2018, SciTechnol, All Rights Reserved.

network convergence might facilitate global communication and underpinning systems level integration in the human brain [29]. Local electromagnetic potential differences in the complex neural landscape vary according to the principle of least action, forming metastable changes of spatiotemporal patterns that are isomorphic with cognitive and phenomenal occurrences [30]. Via recurring, highly reproducible harmonic functions the brain's resting state has been shown to form the functional curvature of a four dimensional torus, which manifests itself as repetitive patterns of mental trajectories [31-35]. Even in the absence of synaptic anatomical connectivity, the resting state displays great autonomy and complexity, indicating its essential role as the ground state of the brain [36].

Biological organisms live with a temporal expiration date, determined by the access to air, water, food, mating, which modulates behavior between urgency and relaxation. The inner clock of activity is not connected to any local system, but results from a global temporal rhythm, which originates in midbrain dopamine neurons [37]. For example, sleep compresses the daytime firings of neurons in time. In fact, time turns into a relative experience, because intentional binding formulates the perception of time and gives rise to agency [38]. The importance of temporal considerations is further illustrated by the connection between deviations in time perceptions and diseases [39]. Major depression seems to slow time perception, whereas time passes at a jerky in schizophrenia [40]. Parkinson's disease is characterized by impairment in time control, as well as time delay. Therefore, time perception an elementary part of the formation of conscious experience, might be regulated by the energy/information cycle of the brain. Understanding the brain's energy/information exchange is critical, because disturbances in this cycle can cause health problems and disease without any obvious pathologic change in morphology.

The brain's gradually improving responses to stimuli have molded organization into a coherent, structural, organizational mirror of physical systems [41]. However, biological survival needs, such as water, food, reproduction, etc. are being dictated by relativity in time, formed by an oscillating motivation between urgency and relaxation. Mental operations, which form an increasingly improving mirror of the social environment, constantly respond to the environment and modify it, forming their common evolution. This way, environmental abstraction becomes integral part of a wholesome mental world, engendering an interconnected system which determines and governs thoughts, intentions and behavior according to the laws of physics.

Discussion Theoretical Foundations

Stimuli provide information input that leads to a thermodynamic relationship with the environment, in the form of the electric activities of the neuronal network. Because all evoked oscillations are greater than electric activities of the resting state and accompanied by entropic and dimensionality changes, the brain's information/energy cycle between stimulus and recovery of the resting state can be analyzed based on thermodynamics. Stimulus generates heat that can be assessed in terms of enhanced frequencies, synaptic modification. That way, the brain's responses to stimulus in the present state shapes its ability for future interactions. The energy devoted to neuronal connections satisfies Landauer's principle, which reflects sensory interaction based on energy/information exchange. Evoked states are information saturated, thus produce high entropy and involve high frequencies; these high frequencies are unstable and, due to their huge energy requirement, become energetically untenable over time.

Because the sensory system transforms spatial information into the temporal language of the oscillations, the brain is organized along temporal coordinates [42]. Here we analyze the brain's global energy/information cycle in terms of entropic and topological considerations, in view of the correlation between physiology and electric activities. We achieve generalizations that allow the assessment of the relationship of the brain's electric activities independent of their scale, magnitude, specific features and local boundaries-and cognitive experiences. We show that interconnected synaptic networks form a closed system, which leads to self-regulation based on energy/information transformations satisfying the Landauer's principle. Information accumulation corresponds to an increase in temperature indicated by enhanced frequencies, so that erasing information frees energy, which increases order through the energy accumulated in cortical synaptic connections. Therefore, self-regulation of activities is based on low entropy.

Brain activities do not exist in isolation; rather form a self-regulating, interconnected and coherent energy system. Moreover, brain models suggest that constantly changing nervous activities take place on different kinds of curvatures of the phase space [43]. Thus, activity can be assessed based on topological relationships. Topology suggests structures such as a toroidal view of activities and the projection of percepts to higher dimensional spaces as well as mappings of antipodal points on opposite perceived im- ages into hyperbolic manifolds [32]. Because disturbances in this self- regulating physical network might play a role in various pathologic conditions, we will take into account the relationship between temporal dimensionality and entropy, and the brain's evoked energy/information exchange (interaction). Energy availability limits information processing in the brain

The consideration of living organisms as open systems has a long tradition in the literature. ATP is used as the main energy source for metabolic functions and thus it supplies the energy need of neural spiking activities. Around 45% of the brain's baseline energy use in vivo is consumed on non-signaling processes [44,45]. In neurons, ATP consumption and ATP generation forms equilibrium between metabolic support and spiking activities. In an active brain, axonal ATP consumption is proportional to electric spiking activity. However, the expectation that the ATP production can satisfy liberally the energy need of signaling has been overturned. The surprising correlation between ATP levels and the generation of action potentials means that the increasing frequency of action potentials quickly deplete axonal energy levels [46]. This finding explains the existence of a complex energy supply network in neural tissue, in which multiple cell types and metabolic energy sources work in unison to maintain the ATP levels in axons. Nevertheless, nerve cells are unable to generate enough energy on their own to sustain their electrical activity. Axons depend on mitochondrial function to provide the necessary ATP levels. Both compound action potentials and axonal ATP content decrease in a stimulation frequency-dependent manner and ATP homeostasis actively relies on the presence of lactate. ATP decreases preceded or coincided with compound action potential decay confirm that energy depletion causes axonal failure. ATP supply in the white matter is limited and quickly depleted during cases of high frequency stimulation, such as, information processing in the brain (Figure 1). Because neurons cannot replenish their energy reserves fast enough during ATP depletion, e.g., such as in the case of high frequency activation, the brain's information processing forms a closed system. Because high frequencies can only use the available (and highly

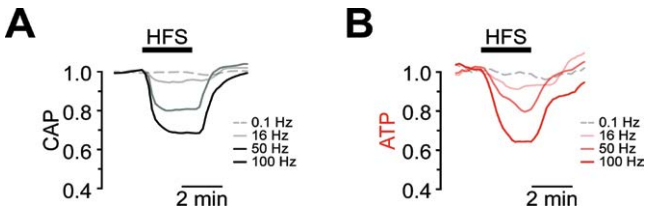

Figure 1: Compound action potentials (CAP) during high frequency stimulation (HFS).

limited) ATP supply, the path length of electric activity is proportional to the subjective information content of the stimulus and the ATP use is proportional to the path length. The limited axonal ATP supplies do not contribute to the processing of the stimulus any more than the ice melting to the sliding of the hockey puck. The low frequency response also has negligible energy use. Further- more, because sensory activation forms a closed loop around the resting state, the response must be complementary with the original stimulus in terms of entropy as well as temperature. For example, the temperature increase during stimulus must be complemented with a cooling down during sensory response. Therefore, path length represents the situation dependent energy need of information processing. The energy need of the maintenance of the readiness of the neural system is extremely high, because the noiseless spiking neural network can represent its input signals most accurately when excitatory and inhibitory currents are as strong and as tightly balanced as possible [47]. However, information transfer slides over the excitatory - inhibitory network with moderate energy input. Therefore the brain's tightly regulated energy/information exchange with the environment forms a closed system.

(A) The CAP area decreases over time during high-frequency stimulation (HFS). The decay amplitude deviates from the absence of HFS, indicated by the dashed line (0.1 Hz, used for normalization to 1.0), and increase progressively with the increase in stimulation frequency (16 Hz, 50 Hz, 100 Hz). (B) Axonal ATP levels also decrease with increasing stimulation frequency, reaching a new steady state level which depends on the stimulation frequency [46].

Relationship to the carnot cycle

The Carnot cycle offers an upper limit on the efficiency that any classical thermodynamic engine can achieve during the conversion of heat into work. No engine operating between two heat reservoirs can be more efficient than the corresponding Carnot engine.

The Carnot cycle is an idealization, since no classical engine is reversible and physical processes involve some increase in entropy. Surprisingly, the Carnot bound can be surpassed in microscopic systems, because thermal fluctuations induce transient decreases of entropy, allowing for possible violations of the Carnot limit. Such a miniaturized Carnot engine was realized using a single Brownian particle [47,48]. The Carnot cycle represents execution of work in a heat bath. The process consists of two isothermal processes, where the working substance is respectively in contact with thermal baths at different temperatures Th and Tc, connected by two adiabatic processes, where the substance is isolated and heat is neither delivered, nor absorbed. In the brain, neural activation is forwarded via synaptic connections, allowing the analysis of energy/ information exchange based on the principle of least action. We suggest that the nervous entropic changes in information and resting state display a thermodynamic relationship with the Carnot cycle. The cortical insulation of the limbic system, which lies on the top of the resting state, correlates with the occurrence of evoked potential. In turn, the evoked potential triggers electric activities that restore the resting state (Figure 2). This recurrent energy /information exchange forms a closed system and allows the examination of brain activity based on thermodynamic considerations. Landauer's principle shows how heat production is tied to information/energy transformations. The frequencies of the brain's evoked cycle reflect both its computational limit and the added heat of stimulus, which also determines the energy usage via synaptic changes.

The brain frequencies change from high, on the left (1), to low, toward the right (3), determining the direction of information flow in the brain (shown by thin line). The resting state of the brain is energy neutral before stimulus (1) and after a response (3). Evoked potential are illustrated by 2. The high energy need of enhanced brain frequencies induces an urgency (indicated by 1), whereas the high amplitude of the lowest frequencies permits an overarching, global connective and mental vision, indicated by 3.

The brain's energy/information cycle

In the brain, stimuli increase frequencies, which correlate with heat absorbed by the system, giving rise to an increase in temperature (Figure 3). This phase, marked DA in the picture, correspond to the Carnot cycle's adiabatic compression phase. In a classical gas, heat production is function of particles collisions, which is dependent on

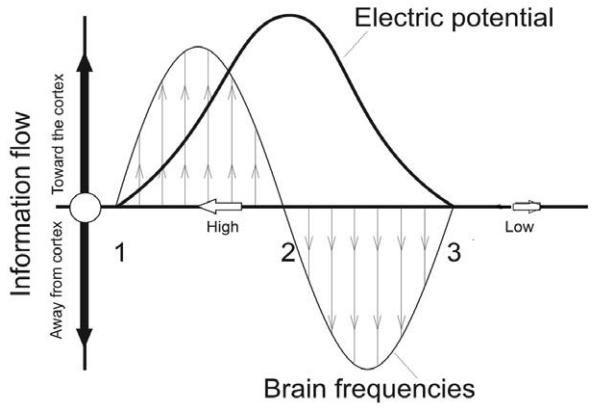

Figure 2: Changes in energy balance due to stimulus.

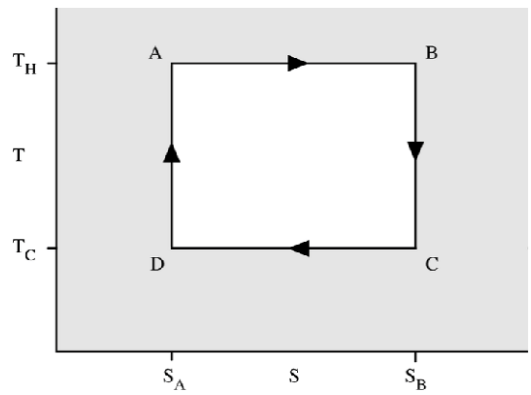

Figure 3: A Carnot cycle acting as a heat engine, illustrated on a temperature-entropy diagram.

the temperature and the number of particles (volume of the gas). In neural networks as well as in deep learning systems, network connections correlate with collisions. Therefore, the number of dimensions corresponds to the volume of the gas, whereas the depth of the network might represent the temperature of the system. The second phase, marked by AB, in which the frequencies spread throughout the whole cortex, stands for the isothermal expansion (the signal expands, exerting work). The third, relaxation phase, marked by BC, stands in the brain for evoked potentials reversing the direction of the electric flow on lower frequencies; the reduction of temperature exerts work, by accumulating energy in the complexity of synaptic connections. In this phase, meanings and concepts emerge, based on the subjective information value of the stimulus. The fourth phase, marked by CD, correlates with the contraction phase of the cycle: the brain's electric activities contract and recover the resting state.

The amount of thermal energy transferred in the process is the following:

$$Q = \int_B^A TDS$$

The area inside the cycle will then be the amount of work done by the system over the cycle.

$$W = \oint_V T = \oint_V (dQ - dU) = \oint_V (TdQ - dU) = \oint_V TdS = \oint_V dU = \oint_V TdS$$

Since dU is an exact differential, its integral over any closed loop is zero: it follows that the area inside the loop on a T-S diagram is equal to the total work performed the amount of energy transferred as work is

$W = \oint_V PdV = \oint_V TdS = (T_H - T_C)(S_B - S_C)$ The total amount of thermal energy transferred from the hot reservoir to the system will be

$$Q_H = T_H (S_B - S_C)$$

The efficiency η is defined to be:

$$\eta = \frac{W}{Q_H} = 1 = -\frac{T_C}{T_H}$$

Where

1. W is the work done by the system (energy exiting the system as work)
2. QC is the heat taken from the system (heat energy leaving the system)
3. QH is the heat put into the system (heat energy entering the system) TC is the absolute temperature of the cold reservoir
4. TH is the absolute temperature of the hot reservoir
5. SB is the maximum system entropy
6. SA is the minimum system entropy

The heat absorbed by the system toward order increasing transformation: Therefore, the amount of released heat corresponds to the entropy decrease (in- creasing synaptic complexity) of the system. The cycle takes place between a hot reservoir at temperature TH and a cold reservoir at temperature TC. The vertical axis displays the temperature, whereas the horizontal axis the entropy. In the brain, during the (DA) compression phase, the stimulus increases the frequencies, due to heat absorbed by the system. In neural networks as well as in deep learning systems the depth and number of connections of the network is related to the system's ability to produce work or to learning (AB): the frequencies spread throughout the whole cortex: the signal expands, exerting work. (BC): evoked potentials reverse the direction of the electric flow on lower frequencies (the temperature decreases, the energy leaves the system). CD: the electric activities contract and return to the resting state.

The brain's energy/information cycle

Determines the temporal dimensionality of electric activities in understanding, comprehension and learning Landauer's principle, originally developed for computation, was proven in increasingly sophisticated experiments and consequently, applicable for the tightly regulated environment of the brain [49-51]. According to the principle, information accumulation by electric activities of the brain during evoked states corresponds to enhanced temperature. Landauer's principle also shows that the recovery of the resting state frees energy for work, due to information/energy transformation. This process correlates with lower temperature. Decreasing frequencies form a sink of low information content and increasing degrees of freedom [52]. Thus, evoked activities modify the temporal field curvature and dimensionality via bifurcations in the brain's electric activities, whereas the resting, equilibrium state formulate Euclidean torus [32]. In contrast, decreasing frequencies increase the oscillations amplitude, thus activating greater brain regions, or modules [53]. Simultaneous activation of wider regions of the brain might engender mental coherence, ideas and learning. The potential assessment of neuronal activations and global cognitive processes in terms of brain energy cycle has immense potential in understanding various neural conditions, such as depression, PTSD and other neural disease.

Relationship between the resting state and learning

Sensory interaction increases between information content and entropy, but the living brain incessantly recovers its resting, low entropy state. Maintaining and restoring the resting state seems to be an inherent and essential part of healthy brain operation. Spontaneous brain activity, accounts for up to 70% of the great energy need of the brain [54]. Information input enhances frequencies and compresses time (by forming positive temporal curvature), which increases entropy, similar to a Brownian motion. In accordance with Landauer's principle, heat must be released when the resting state is restored [55]. Surprisingly, deep learning can also be divided into phases that constitute similar entropic effects and energetic transformations, consisting of compression of information and relaxation, which culminates in representation of information [56,57]. This entropy conservation in closed systems is expressed by the low entropy principle [58].

Entropic considerations of the brain's topology and activities: a mathematical treatment

Brain activities might follow particle paths traversing surfaces of geometric spaces formed by temporal rhythms of electric activities [52]. Thus, electric activities might manifest as dimensional structures, that change from n- dimensional (e.g., a two-dimensional disk) to n+1 -dimensional structure (e.g., negative curvature surface, which correspond to temporal expansion) and n-1 dimensional surface (positive temporal curvature surface, which correspond to temporal compression). Since the energy cost of sensory processing is proportional to frequencies, sensory information is translated into an energy signal in the brain. The sensory transmission toward

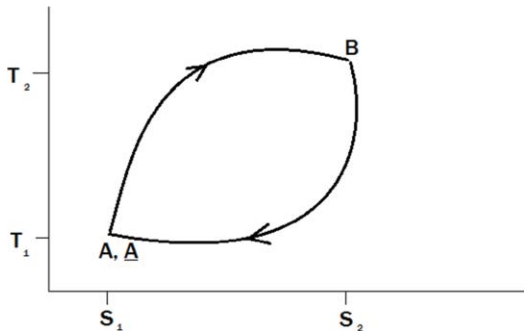

Figure 4: The entropic changes during a learning cycle.

the sensory cortex via fast oscillations, and response via slow oscillations, form the polarity effects of the brain's electromagnetic flows. Nevertheless, the strength and extent of synaptic connections (i.e. increasing synaptic complexity) differ before and after stimulus (Figure 4). The enhanced neural organization must be proportional with the release of thermal energy and consequent reduction of entropy. Therefore, stimulus, which increases temperature, might supply the energy to modulate synaptic strength or form new connections in the brain. The organizational constancy and charge neutrality of the resting state guarantees that the energy difference due to the released heat (as in a heat engine) leads to a higher order of the synaptic organization. Therefore, the brain is an active part of the environmental energy cycle.

A topological view of this synergy between the brain and the environmental energy cycles exhibits strong proximity both spatially and descriptively. The spatial strong proximity of the brain and environment is in the form of temporally overlapping cerebral energy and environmental energy readings (e.g., the occurrence energy highs and lows of the one set of readings overlaps with the occurrence similar readings of highs and lows in the other during the same timeframe) [59]. For example, let A and B represent nonempty sets of recordings of brain and environ- mental energy recordings that are temporally concomitant in situ. The spatial form of strong proximity is denoted by δ from the strong proximity axiom we have

$$A \overset{\omega}{\delta} B = A \cap B \neq \phi$$

i.e., the two sets of energy readings overlap [60]. There is also a descriptively strong proximity between the two sets of energy readings. The descriptive form of strong proximity is denoted by $\Re^n$. The subscript ϑ refers to a mapping $\vartheta : A \rightarrow \Re^n$ on the set of readings A into an n-dimensional feature space $\Re^n$, defined by $\vartheta(x)$ (a feature vector in $\Re^n$) that is a feature value of a reading x ∈ A. Similarly, there is a mapping $\vartheta : \mathrm{B} \rightarrow \Re^n$ on the readings in B into the feature space $\Re^n$. The two sets of energy readings with common descriptions give rise to a descriptive intersection (denoted by $\cap$) of the two sets:

$$\mathrm{A} \underset{\vartheta}{\cap} \mathrm{B} = \{\mathrm{x} \in \mathrm{A} \cup \mathrm{B} : \vartheta(x) \in \vartheta(x) \,\&\, \vartheta(x) \in \vartheta(\mathrm{B})\}$$

i.e., there is at least one cortical energy reading (e.g. cortical energy amplitude) in A that has the same description as an environmental energy reading (e.g. environmental energy amplitude) in B. From these structures, we can elicit a strong descriptive proximity between A and B in terms of

$$A \cap B \neq \phi \text{ Implies } A \underset{\vartheta}{\cap} B \neq 0$$

i.e., overlapping energy readings implies an overlap between the descriptions of the two sets of readings. This observation leads to the following descriptive proximity property:

$$A \overset{\omega}{\delta}_{\vartheta} B = A \underset{\vartheta}{\cap} B \neq \phi$$

The importance of this pair of proximities lies in the fact it is then possible to derive Leader uniform topologies on pairs of sets of energy readings. This is done in the following manner. Start with a collection of sets of cerebral energy readings

$\cup 2^{B_i}$) and a collection of environmental energy readings $\cup 2^{B_i}$ gathered during within the same timeframe. For each given subset A $\in \cup 2^{B_i}$, find all B $\in \cup 2^{B_i}$

Such that A B. Doing this for each given set of cerebral energy readings, leads to a collection of clusters of strongly near sets of readings. In effect, we have topologized the collections of energy readings by introducing a Leader uniform topology on the space of energy readings [61,62]. An important outcome of topologized energy readings is the introduction of a search space in which clusters of readings exhibit spatial and descriptive proximities. Moreover, our approach shows the role of observer in information processing: the history and current state of the brain is just as important in determining the degree of neuronal activation as the stimulus itself. Thus, the state of the observer i.e. the brain, determines the information value of the stimulus. This way, information processing in the brain is holographic. Thus, the degree of comprehension or understanding (manifested as increasing synaptic complexity) has a large subjective quality, the observer effect.

Conclusions

Physical principles often find application in other, seemingly unrelated fields, proving that the physical laws underline all of nature. The brain's immense energy use engenders a readiness on which interaction with the environment is possible. Recent data of compound action potentials during high frequency stimulation have shown that strong electrical activity reduces the ATP content of the axon. This way, the brain's electric activities depend on the temporary supply of energy sources, and thus the brain forms a closed system with respect to information processing. Here, in our investigation of brain processes, we analyzed the resting state in light of two important physical principles, the Carnot cycle and Landauer's principle. We traced back the brain electromagnetic activities onto these principles based on the principle of least action.

(A) Sensory information activates the neural system by enhancing the frequency of oscillations, which corresponds to changes in temperature. The increase in frequencies leads to positive temporal curvature, which compresses time perception. The entropy also increases between S1 to S2 (B) the second part of the cycle recovers the low entropy state and the Euclidean geometry. The slowing frequencies correspond to negative temporal curvature and to increases in time perception, which slows down the system. (A) The entropy decrease leads to order, manifested as synaptic complexity, underpinning concepts and meaning. Therefore, the energy increase between A and A, is supplied by sensory stimulus. Or in other words, perception of stimulus modifies mental organization.

The brain's fundamental regulation is founded on field effects of the resting state; in its constant interaction with the environment, the mind constantly changes and adapts. However, the maintenance of the resting state against the constant barrage of sensory activation by the

environment contributes to the brain's immense energy consumption. Sensory activation corresponds to information/entropy increase and the reduction of temporal dimensionality [32]. Landauer's principle in the brain means that evoked activities correspond to enhanced 'temperature,' whereas recovery of the resting state correlates with cooling down and the initial and final conditions differ in neural organization [55]. The incurred thermal energy might enhance neural organization, which engenders meaning, mental coherence and correlates with low entropy. Therefore, stimulus, which generates activation, might supply the energy to modulate synaptic strength or form new connections in the brain. Thus, Landauer's principle might explain the relationship between the electric activities of the brain and the physiological states of the mind. Two sides of the brain energy/information cycle are bound by the organizational constancy and charge neutrality of the resting state. The brain, as well as deep learning systems maintains a permanent readiness state, on which energy/information cycle with the environment can take shape. Therefore, both in the brain and in deep learning systems, Maxwell's demon can reverse the second law of thermodynamics. The existence of the stable resting state turns the brain into a globally static system. In this way, the brain's self-regulation utilizes the information input delivered by the environment, leading to an increase of its neural organization (mental capacity, corresponding to greater synaptic complexity). In a highly interconnected relationship, the brain is part of the thermodynamic cycle of the environment it modifies its environment, but it is evolved and changed by interaction. A connection between life processes and the entropic changes of the environment was suggested by Schrodinger 1945 and was further developed by Déli [58].We have shown that the constant barrage of information by the environment induces a thermodynamic cycle in the brain, similar to the Carnot cycle, which increases synaptic organization and complexity, i.e. order. The ability to transform information into energy seems to be the most essential quality of the brain. However, the brain is compelled by comprehension and interpretation of visual, auditory, tactile experience or taste by the stimulus. The brain neither engages nor controls the environment. Instead, the environment highjacks the brain to gather and process incoming information [41,58]. Furthermore, the environment extracts energy from the brain for sensory information: the environment provokes and extorts the brain's energy consumption needs. Feeding on complex organic compounds reduces the environment's entropy. Thus, evolution of life is part the environment's entropy management. The brain's immense energy use during its resting state ensures that very tiny changes in potential can trigger considerable activation and order increasing transformations. Thereby, thinking, memory and other conscious processes require minute computational costs. This permits us to uncover how energy/information transformations in the brain satisfy physical principles.

Reference

1. Shulman RG, Rothman DL, Hyder F (2009) Baseline brain energy supports the state of consciousness. Proc. Natl. Acad. Sci. USA 106: 11096-11101.
2. Dehghani N, Peyrache A, Telenczuk B, Le Van Quyen M, Halgren E (2016) Dynamic Balance of Excitation and Inhibition in Human and Monkey Neocortex Sci Rep 6: 23176.
3. Okun M, Lampl I (2009) Balance of excitation and inhibition.Scholarpedia 4:7467.
4. Gerd G, Dittrich P, Klaus-Peter Z (2011) Artificial wet neuronal networks from compartmentalised excitable chemical media. ERCIM NEWS 85: 30-32.
5. Kim JK, Fiorillo CD (2017) Theory of optimal balance predicts and explains the amplitude and decay time of synaptic inhibition Nature Communications 8: 14566.
6. Vladimir VK, Epstein IR (2011) Excitatory and inhibitory coupling in a one-dimensional array of Belousov-Zhabotinsky micro-oscillators: Theory. Physical Review E 84: 066209.
7. Luczak A, McNaughton BL, Harris KD (2015) Packet-based communication in the cortex. Nat. Rev. Neurosci 16: 745-755.
8. Duncan TL, Semura JS (2004) The Deep Physics Behind the Second Law: Infor- mation and Energy As Independent Forms of Bookkeeping. Entropy 6: 21-29.
9. Martin JS, Smith NA, Francis CD (2013) Removing the entropy from the definition of en- tropy: clarifying the relationship between evolution, entropy, and the second law of thermody- namic.cs. Evol. Educ. Outreach 6: 30.
10. Del Rio L, Berg EAJ, Renner R, Dahlsten O, Vedral V (2011) The thermodynamic meaning of negative entropy. Nature 474: 61-63.
11. Haji-Akbari A, Engel M, Keys AS, Zheng X, Rolfe G, et al. (2009) Disordered, quasicrystalline and crystalline phases of densely packed tetrahedra Nature 462: 773-777.
12. Haji-Akbari, A, M Engel, SC Glotzer (2011) Phase Diagram of Hard Tetrahedra Journal of Chemical Physics 135: 194-101.
13. Yamada Y, Kawabe T (2011) Emotion colors time perception unconsciously. Con- sciousness and Cognition. Elsevier Inc 20: 1-7.
14. Landauer R (1961) Irreversibility and heat generation in the computing process. IBM J Res Dev 5: 183-191.
15. Doiron B, Litwin-Kumar A, Rosenbaum R, Ocker GK, Josi AK (2016) The mechanics of state-dependent neural correlations. Nat. Neurosci 19: 383-393.
16. Wright NC, Hoseini MS, Wessel R (2016) Adaptation modulates correlated subthreshold re- sponse variability in visual cortex. J. Neurophysiol 118: 1257-1269.
17. Gazzaniga MS (2009) The Cognitive Neurosciences. (4th edtn). MIT Press. Cambridge, Massachusetts, United States.
18. Kavalali ET, Chung C, Khvotchev M, Leitzet J, Nosyreva E, et al. (2011) Spontaneous neurotransmission: an inde- pendent pathway for neuronal signaling? Physiology (Bethesda) 40: 45-53.
19. Donnell OC, Van Rossum MC (2014) Systematic analysis of the contributions of stochastic voltage gated channels to neuronal noise. Front. Comput. Neurosci 8: 105.
20. Jensen O, Gips B, Bergmann TO, Bonnefond M (2014) Temporal coding organized by cou- pled alpha and gamma oscillations prioritize visual processing. Trends Neuroscipii 37: 357-369.
21. Friston K (2010) The free-energy principle: a unified brain theory? Nat Rev Neurosci 11: 127-138.
22. Sporns O (2013) Network attributes for segregation and integration in the human brain. CurrOpinNeurobiol 23: 162-171.
23. Tozzi A (2015) Information Processing in the CNS: A Supramolecular Chemistry? Cognitive Neurodynamics 9: 463-477.
24. Koch C, Massimini M, Boly M, Tononi G (2016) Neural correlates of consciousness: progress and problems. Nat Rev Neurosci. Apr 9: 307-21.
25. Touboul J (2012) Mean-field equations for stochastic firing-rate neural fields with de- lays: Derivation and noise-induced transitions. Physica D: Nonlinear Phenomena 241: 1223-1244.
26. Guterstam A, Abdulkarim Z, Ehrsson HH (2015) Illusory ownership of an invisible body reduces autonomic and subjective social anxiety responses. Scientific Reports 5: 9831
27. Mancini F, Longo MR, Kammers MPM, Haggard P (2011) Visual distortion of body size modulates pain perception. Psychological Science APS 22: 325-330.
28. Bell PT1, Shine JM (2015) Estimating Large-Scale Network Convergence in the Human Functional Connectome. Brain Connect 5: 565-74.
29. Northoff G, Qin P, Nakao T (2010) Rest-stimulus interaction in the brain: a review. Trends Neurosci 33: 277-284.
30. Fingelkurts AA, Fingelkurts AA, Neves CFH (2009) Phenomenological architecture of a mind and operational architectonics of the brain: the unified metastable continuum. New Math Nat Comput 5: 221-244.

31. Atasoy S, Pearson J, Donnelly I (2016) Human brain networks function in connectome-specific harmonic waves. Nat. Commun: 7.
32. Tozzi A, Peters JF (2016a) Towards a Fourth Spatial Dimension of Brain Activity. Cognitive Neurodynamics 10: 189-199.
33. Tozzi A, Peters JF (2016b) A Topological Approach Unveils System Invariances and Broken Symmetries in the Brain. Journal of Neuroscience Research 94: 351-65.
34. Tozzi A (2016) Borsuk-Ulam Theorem Extended to Hyperbolic Spaces. In: Computational Proximity. Excursions in the Topology of Digital Images169-171.
35. Robinson PA, Zhao X, Aquino KM, Griffiths JD, Sarkar S et al. (2016) Eigenmodes of brain activity: Neural field theory predictions and comparison with experiment. Neuroimage 142: 79-98.
36. Teki S (2016) A Citation-Based Analysis and Review of Significant Papers on Timing and Time Perception. Frontiers in Neuroscience 10: 330.
37. Soares S, Atallah BV, Paton JJ (2016) Midbrain dopamine neurons control judgment of time. Science 354: 1273-1277.
38. Jo HG, Wittmann M, Hinterberger T, Schmidt S (2014) The readiness potential reflects intentional binding. Front. Hum. Neurosci 8: 421.
39. Kranick SM, Hallett M (2013) Neurology of volition. Exp. Brain Res 229: 313-327.
40. Stanghellini G, Ballerini M, Presenza S, Mancini M, Northoff G, et al. (2016) Abnormal Time Experiences in Major Depression: An Empirical Qualitative Study. Psychopathology 50: 125-140.
41. Déli E (2015) The Science of Consciousness. Self-published.
42. Fingelkurts AA, Fingelkurts AA (2014) Present moment, past, and future: mental kaleido- scope. Front. Psychol 5: 395.
43. Sengupta B, Tozzi A, Coray GK, Douglas PK, Friston KJ (2016) Towards a Neuronal Gauge Theory. PLOS Biology 14: e1002400.
44. Collell G, Fauquet J (2015) Brain activity and cognition: a connection from thermodynamics and information theory. Frontiers in Psychology 6: 818.
45. Engl E Attwell D (2015) Non-signalling energy use in the brain. J Physiol 593: 3417-3429.
46. Trevisiol (2017) eLife 2017. 6: e24241.
47. Koren V, Denave S (2017) Computational Account of Spontaneous Activity as a Signature of Predictive Coding. PLoS Computational Biology 13: e1005355.
48. Martinez IA, Roldan E, Dinis L, Petrov D, Parrondo JMR, et al. (2016) Brownian Carnot engine 12: 67–70.
49. Bérut A (2012) Experimental verification of Landauerâs principle linking information and thermodynamics. Nature (London) 483: 187-190.
50. Jeongmin H, Brian L, Scott D, Jeffrey B (2016) Experimental test of Landauer's principle in single-bit operations on nanomagnetic memory bits. Science Advances 2: e1501492.
51. Landauer R (1961) Irreversibility and heat generation in the computing process. IBM J Res Dev 5: 183 - 191.
52. Tozzi A, Peters JF (2017) Critique of pure free energy principle. Physics of Life Reviews.
53. Silva E, Crager K, Puce A (2016) On dissociating the neural time course of the processing of positive emotions. Neuropsychologia 83: 123-137.
54. Tomasi D, Wang GJ, Volkow ND (2013) Energetic cost of brain functional connectivity. PNAS 110: 13642-13647.
55. Pop-Jordanova N, Pop-Jordanov J (2005) Spectrum-weighted EEG frequency ("brain-rate") as a quantitative indicator of mental arousal. Prilozi 26: 35-42.
56. Shwartz-Ziv R, Tishby N (2017) Opening the black box of deep neural networks via information.
57. Gao X, Duan LM (2017) Efficient representation of quantum many-body states with deep neural networks. Nat Commun 8: 662.
58. Déli E (2017) Evaluation of Machâs Principle in a Universe with four spatial dimensions.
59. Peters JF (2016) Computational Proximity. Excursions in the Topology of Digital Images. Edited by Intelligent Systems Reference Library, Springer-Verlag, Berlin.
60. Peters JF (2016) Proximal physical geometry. Advances in Mathematics: Scientific Journal 5: 241-268.
61. Leader S (1959) On completion of proximity spaces by local clusters, Fundamenta Mathematicae 48: 201-216.
62. Peters JF (2015) Proximal Voronoi regions, convex polygons, Leader uniform topology, Advances in Mathematics 4: 1-5.

Author Affiliations

Top

[1]*Institute for Consciousness Research, Nyiregyhaza Benczur ter 9, Hungary*

[2]*Computational intelligence laboratory, university of Manitoba, Canada*

[3]*Center for nonlinear science, university of north Texas, 1155 union circle, 311427, Denton, TX 76203-5017, USA*

Submit your next manuscript and get advantages of SciTechnol submissions

- 80 Journals
- 21 Day rapid review process
- 3000 Editorial team
- 5 Million readers
- More than 5000 facebook fans
- Quality and quick review processing through Editorial Manager System

Submit your next manuscript at ● www.scitechnol.com/submission

Neuroscience Letters 678 (2018) 83–89

Contents lists available at ScienceDirect

Neuroscience Letters

journal homepage: www.elsevier.com/locate/neulet

Research article

Multidimensional brain activity dictated by winner-take-all mechanisms

Arturo Tozzi[a,b,*], James F. Peters[c,d]

[a] Center for Nonlinear Science, University of North Texas, 1155 Union Circle, #311427 Denton, TX 76203-5017, USA
[b] Computational Intelligence Laboratory, University of Manitoba, Winnipeg, R3T 5V6 Manitoba, Canada
[c] Department of Electrical and Computer Engineering, University of Manitoba, 75A Chancellor's Circle Drive, Winnipeg, MB R3T 5V6, Canada
[d] Department of Mathematics, Adıyaman University, 02040 Adıyaman, Turkey

ARTICLE INFO

Keywords:
Mind
Sensation
Perception
Evolution
Pattern recognition

ABSTRACT

A novel demon-based architecture is introduced to elucidate brain functions such as pattern recognition during human perception and mental interpretation of visual scenes. Starting from the topological concepts of invariance and persistence, we introduce a Selfridge pandemonium variant of brain activity that takes into account a novel feature, namely, demons that recognize short straight-line segments, curved lines and scene shapes, such as shape interior, density and texture. Low-level representations of objects can be mapped to higher-level views (our mental interpretations): a series of transformations can be gradually applied to a pattern in a visual scene, without affecting its invariant properties. This makes it possible to construct a symbolic multi-dimensional representation of the environment. These representations can be projected continuously to an object that we have seen and continue to see, thanks to the mapping from shapes in our memory to shapes in Euclidean space. Although perceived shapes are 3-dimensional (plus time), the evaluation of shape features (volume, color, contour, closeness, texture, and so on) leads to *n*-dimensional brain landscapes. Here we discuss the advantages of our parallel, hierarchical model in pattern recognition, computer vision and biological nervous system's evolution.

Pandemonium, initially introduced by [1] for Morse translation purposes, is a hierarchical, parallel processing, adaptive, self-improving model, where "computational demons" perform non-trivial binary functions on two variables. A Pandemonium architecture has been proposed also to elucidate some brain functions, such as pattern recognition during human perception. The process resembles natural evolution, by selecting the "best" processing demons and eliminating the relatively poor ones. A winner-take-all mechanism is introduced, because the cognition demon whose output far outshines the rest activates the "decision demon", responsible for the final output. The model is able to recognize, with no direct supervision, patterns which have not been specified, by using a feature weighting described as a form of hill-climbing. In keeping with the issue of "neural darwinism" [2], cognitive demons' selection generates new subdemons for trial and eliminates inefficient weak ones, every time reweighting the assembly. The brain is a selection system that put things together via pattern recognition [3] leading to perceptual categorization [4]. For the philosopher Hume, *ought* does not come from *is* [5]: instead, we build our thoughts on the basis of the brain's activity [6].

Here we introduce a novel version of Pandemonium, equipped two novel features (Fig. 1) that take into account recent claims from neuroscience. The first way to improve the Pandemonium is to allow its cognitive demons to compare retractions of shape contours in visual scenes through computational proximity, rather than trivial single-valued functions on two variables [7,8]. The feature demons in "classical" Pandemonium are built in order to perceive image features, such as, *e.g.*, short straight lines of the letter A. However, when we watch a segment in a visual scene, we perceive elements seemingly melted together in a single "complex of sensations" [9]. For example, we are able to detect, in the faintness of a rural scene at sunrise time, an increasingly distinct world of trees, hills and moving particles, *e.g.*, birds flying from one tree to another. We appear to be sewing pieces of a changing scene together. In touch with these observations, recent findings suggest that nervous structures process information through topological as well as spatial mechanisms. For example, hippocampal place cells create topological templates to represent spatial information [10–12]. Therefore, our novel cognitive demons will process topological, as well as spatial, image invariants.

The second feature of our Pandemonium is based on the recent claims that brain activities lie in functional dimensions higher than the 4D spacetime environment [13]. If such claims hold true, what happens to 3D (plus time) inputs (say a visual scene) when they are projected

* Corresponding author at: Center for Nonlinear Science, University of North Texas, 1155 Union Circle, #311427, Denton, TX, 76203-5017, USA.
E-mail addresses: tozziarturo@libero.it (A. Tozzi), James.Peters3@umanitoba.ca (J.F. Peters).

https://doi.org/10.1016/j.neulet.2018.05.014
Received 22 February 2018; Received in revised form 3 May 2018; Accepted 7 May 2018
Available online 08 May 2018
0304-3940/ © 2018 Elsevier B.V. All rights reserved.

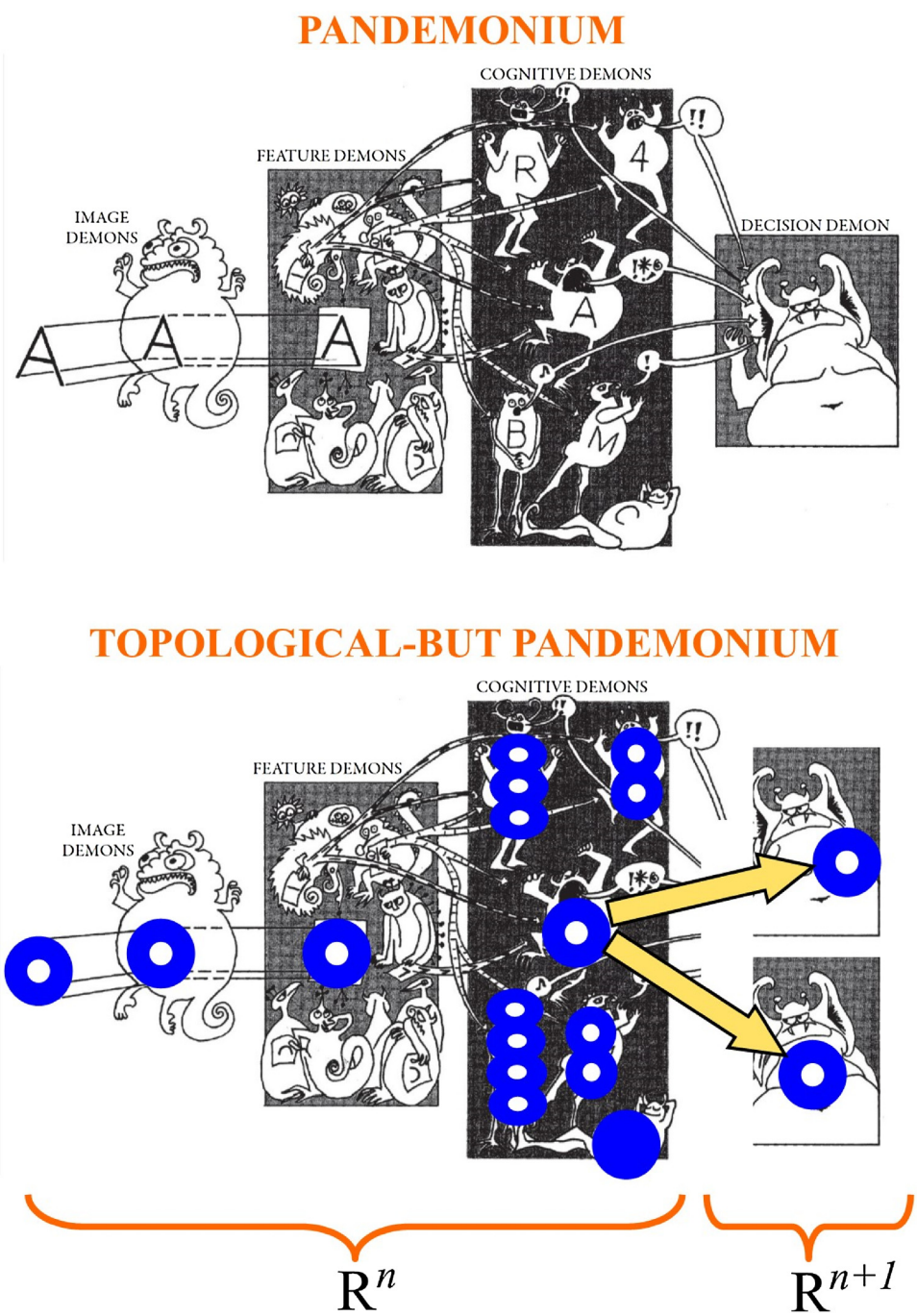

Fig. 1. Differences between the classical Pandemonium and the novel model.

onto higher brain dimensions? In our Pandemonium, the final brain output, *i.e.*, the motor response dictated by a single dominant cognitive demon, stands for TWO, instead of ONE, decision demons with matching description. We show how two matching descriptions in higher dimensions (in this case, the cognitive demons' level) give rise to a single description in lower dimensions (in this case, the decision demon's final output).

1. Image and feature demons recognize topological features from visual images

Here we show how to build Pandemonium's demons that recognize topological cues, instead of spatial ones, in visual images. There is a bridge between the polygonal partition of plane regions [14] and visual perception of shapes' proximities in polygonal-partitioned visual images [15–17]. See Fig. 2 for an example: the conjecture is that features demon, in touch with dynamical systems' accounts of random paths [18], would first hunt for features of the shapes in the scene nuclei, before moving outwards in the hunt for features of shapes in the larger picture.

An approximation of personal points-of-interest are shown as the vertices of a point cloud in Fig. 2B. This is an example of a Vietoris-Rips complex [16,19]. In lockstep with visual perception, triangular regions overlaying shapes in a visual scene are formed by joining neighboring pairs of points-of-interest with straight line segments. Imagine a video that records the continuous changes in lighting conditions in the daytime shop window display, illustrated in Fig. 2A. As the sun changes its position, the points-of-interest gradually modify, resulting in changing

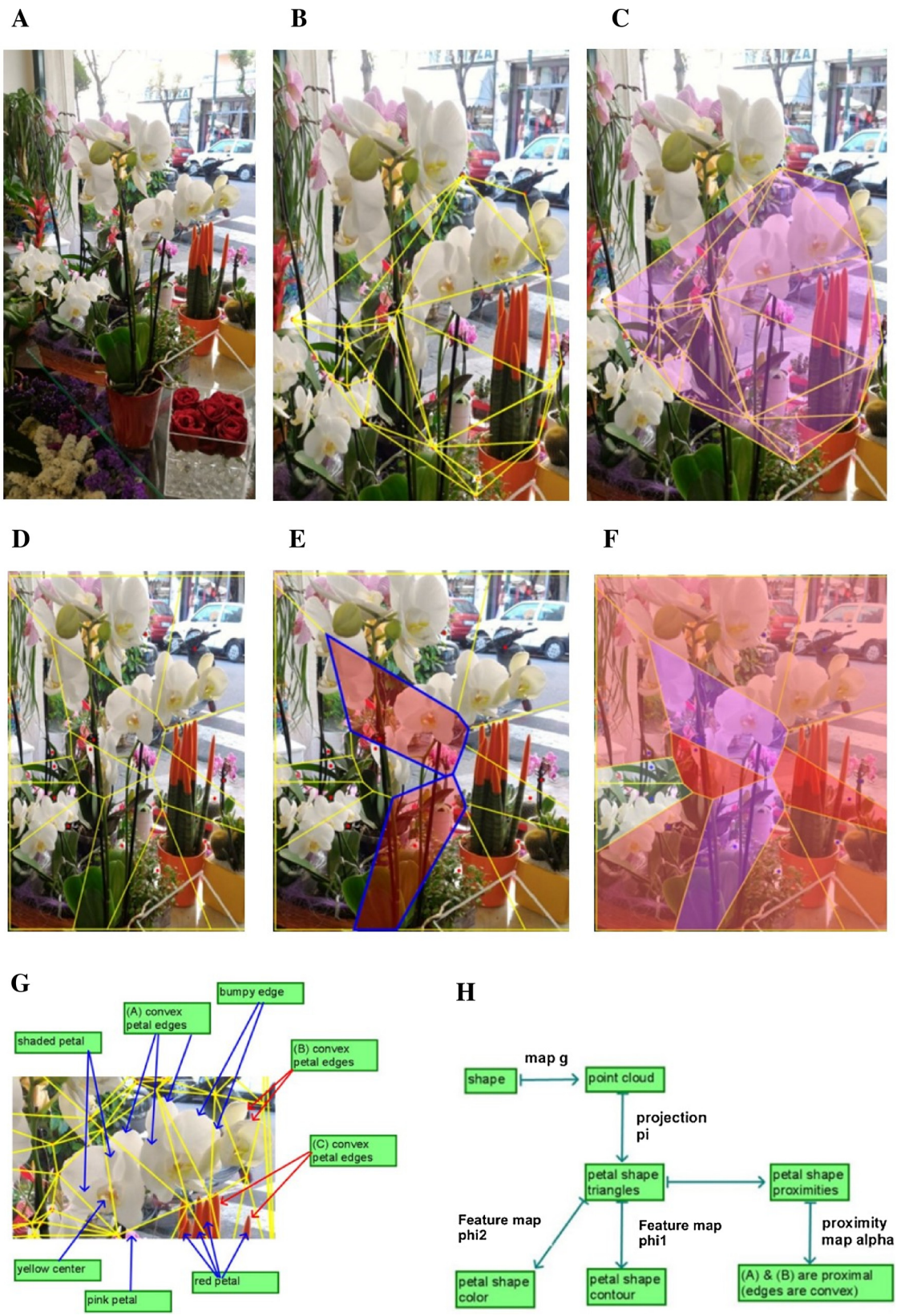

(caption on next page)

triangulations of the visual scene shapes. Mimicking the narrowing of a human viewer of visual scene shapes, clusters of triangles with common vertices are shown in Fig. 2C. Shapes become easier to measure and compare, whenever they are covered with known shapes such as triangles. Fig. 2**D–F** depict a polygonal view of the visual scene. The latter, called a Voronoï complex [15], provides larger, rounder regional views of the visual scene shapes. For example, a Vietoris-Rips complex covering a visual scene makes it easier for feature demons to detect

Fig. 2. A a visual scene containing a shop window flower display. 2 B suggests the focus of attention with a triangulation, facilitating a description of, *e.g.*, flower petal shapes. 2C: refinement of the focus of attention is provided by highlighted filled triangles in a collection of an Alexandroff nerve complex. 2D suggests a more enhanced view of the visual scene, in terms of decomposition into a collection of polygons with varying numbers of sides, reflecting greater or lesser importance in the scene perception. 2E gives further refinement of the focus of attention in terms of shapes of interest, encapsulated in highlighted polygons called scene nuclei. Notice that the dual nuclei polygons have a common edge. In effect, proximal nuclei are the center of attention in the inspection of the flower display. 2F shows polygons that are satellites of the scene nuclei. Only triangles adjacent to the nuclei qualify as nuclei satellites, that spread upwards and downwards, reflecting our attention's wandering from the initial scene focal points. 2G: feature demon mappings on triangular shapes in a Vietoris-Rips Complex. This triangulation is a refinement of the initial Vietoris-Rips complex in 2B. Smaller triangular regions make it easier to discern individual shape features such as color, contour, convexity. 2H: actions of a feature demon are represented as sequences of mappings in a fibre bundle. The fibres are points-of-interest in a point cloud, obtained as a slice of shape (map g). A projection mappingπon the point cloud onto a set of shape triangles in a Vietoris-Rips complex (covering the shapes in a visual scene) sets up the playground for a feature demon. Projections are a pair of feature mappings (also called projection mappings) from the Vietoris-Rips complex into color and contour features spaces, leading to characterizations of particular shapes, such as the flower petals in 2G. A proximity map α on the triangulated shapes in the Vietoris-Rips complex onto a set of proximities between shapes provides a cognition demon with bases for comparisons between shapes.

shape features in higher-dimensional spaces: smaller triangles make it easier to detect regional shapes. In Fig. 2G, quite a number of shapes features are displayed inside fairly small triangular regions, such as the triangles enclosing flower petals with convex regions. The actions of a feature demon are approximated with mappings in Fig. 2H, leading to shape feature spaces and shape proximities. The cognitive demons recognize not only shape features (such as, *e.g.*, the straight lines of the letter A), but also shape topological invariants (such as, the donut-like shape of a flower pot, or the proximities of the convex flower petals in Fig. 2G.

1.1. Decision demons allow higher-dimensional topological correlations between stimuli and brain energetic responses

Here we show how to build multi-dimensional decision demons, starting from lower-dimensional cognitive ones. We also show how decision demons embedded in higher functional brain dimensions are able to produce lower-dimensional bodily motor responses.

In our theoretical context of perception, the Borsuk-Ulam theorem (BUT) elucidates how we see an object and how we imagine it [13]. It is given in the following form [20]:

Let $f: S^n \to R^n$ be a continuous map. Then there exists $x \in S^n \subseteq R^{n+1}$ such that $f(x) = f(-x)$.

This means that antipodal (i.e., diametrically opposite) points on n-sphere S^n map to R^n, which is the n-dimensional Euclidean space [21]. The original formulation of BUT has been modified, resulting in different approaches [22]: continuous mappings are replaced by piecewise continuous mappings, antipodal points by antipodal regions with matching descriptions; furthermore, mappings are from S^n to R^k, $1 \leq k \leq n$ or $k \geq n$, which is the k-dimensional Euclidean space.

BUT explains how representations of objects in our environment are mapped to higher-dimensional views (our interpretations and coalescences), in order to achieve a form of pullback from descriptions to sources of descriptions, from a simplified view to multiple views of the same object. Indeed, a new form of shape theory (called homotopy) discovered by K. Borsuk [20] makes it possible to assess the properties that are preserved through deformation, stretching and twisting of objects [23,24]. Homotopy is a theory that explains how some shapes can be deformed into others [25]. In this context, the term "shape" means "exterior form" and "deformation" a mapping from one shape into another. A classic example is the deformation of a coffee cup into a torus. The combination of various forms of BUT and homotopy theory provides a methodological approach with countless possible applications, especially in helping us to understand how we acquire visual imagination. The theory of shape focuses on the global properties of geometric objects such as polyhedra and tori, neglecting the complications of the local structures of the objects [25]. What shape theory and BUT tell us is that cognitive processes relating to perception, storage, retrieval and reorganization interact with memory structures and construct a symbolic representation of the environment. For example, the mesh view in Fig. 3A can be viewed as visualization of one among many symbolic views of Leonardo DaVinci's Mona Lisa painting. In effect, an individual perceives [constructs] the features and events of the environment specified by this [pickup] information from the environment [26].

2. From cognitive to decision demons

In the sequel, the notion of antipodal point is extended to non-intersecting brain regions (standing for different decision demons). A region on the surface of an n-sphere S^n is a part (subset) of S^n. A surface region $\neg x$ is the antipode of x, provided $x \neq \neg x$ and x has the same feature values (characteristics) as $\neg x$. [27]. From a physics perspective, a cortical region (containing a decision demon) is a relativistic mass in a slice of space swept out by the region. The particles on a n-sphere are moving at a velocity v. For every cortical region with mass $x \in S^n$, we can always find $\neg x$ (the analog of the antipode $-x$ of a point on the surface of S^n) with the same characteristics of velocity and mass. In BUT-Pandemonium terms, we can always find two cortical decision demons with matching description. In effect, for the cortical energy $e_x = m_x v^2$, we can find its antipodal energy $e_{\neg x}$ for $\neg x \in S^n$. To achieve an antipodal energy $e_{\neg x}$, we weaken the original notion of antipodes, with $\neg x$ being a particle on S^nthat has characteristics that match those of $x \in S^n$. Let *reA*, reB be regions on S^n. A function $f: S^n \to R^k$ is piecewise continuous on S^n, provided *reA* close to reBimplies that $f(reA)$ is close to $f(reB)$.This leads to an energetic form of BUT (**energy-BUT**) for antipodal particles$x, \neg x \in S^n$:

Let $f: S^n \to R^k$ be a piecewise continuous map. Then there exists $x \in S^n \subseteq R^{n+1}$such that $f(x) = f(\neg x)$and $e_x = e_{\neg x}$.

Proof: $f(x)$, $f(\neg x)$ a feature vectors in R^{n+1}. Since, for each $x \in S^n$ there is $\neg x \in S^n$ with the same velocity and mass, the result follows: $f(x) = f(\neg x)$ and $e_x = e_{\neg x}$.

This means that two cortical decision demons with matching description display the same energetic level. As shown by [28], such energetic levels are experimentally assessable and quantifiable, in terms of entropy detected in fMRI images.

2.1. Cortical response fibres

This section introduces cortical response fibre bundles. They stand, in BUT-Pandemonium terms, for the decision demons' outputs that produce a bodily motor response to the original environmental stimuli. In general, a continuous mapping $\pi: E \to B$ is called a projection on a set of fibres E to B. Every element $e \in E$ is called a *fibre*, B is called a *fibre bundle base* and the collection of all mappings $\pi(e)$ is called a *fibre bundle*. The set E is a class of objects, so that each$e \in E$ has the same properties as every other member. The members of the class E are the result of a mapping $f: X \to E$.

In our BUT-Pandemonium framework, X is a set of visual objects (cognitive demons) that are mapped by f to a set $Cl_{re}E$ of brain's composite responses (a set of decision demons). Each object is a topological region of the visual field, making X a set of topological regions. Members of $Cl_{re}E$ are cortical cells (i.e., decision demons in cortical regions) found on the surface of an n-sphere S^n. The set $Cl_{re}E$ is a class of

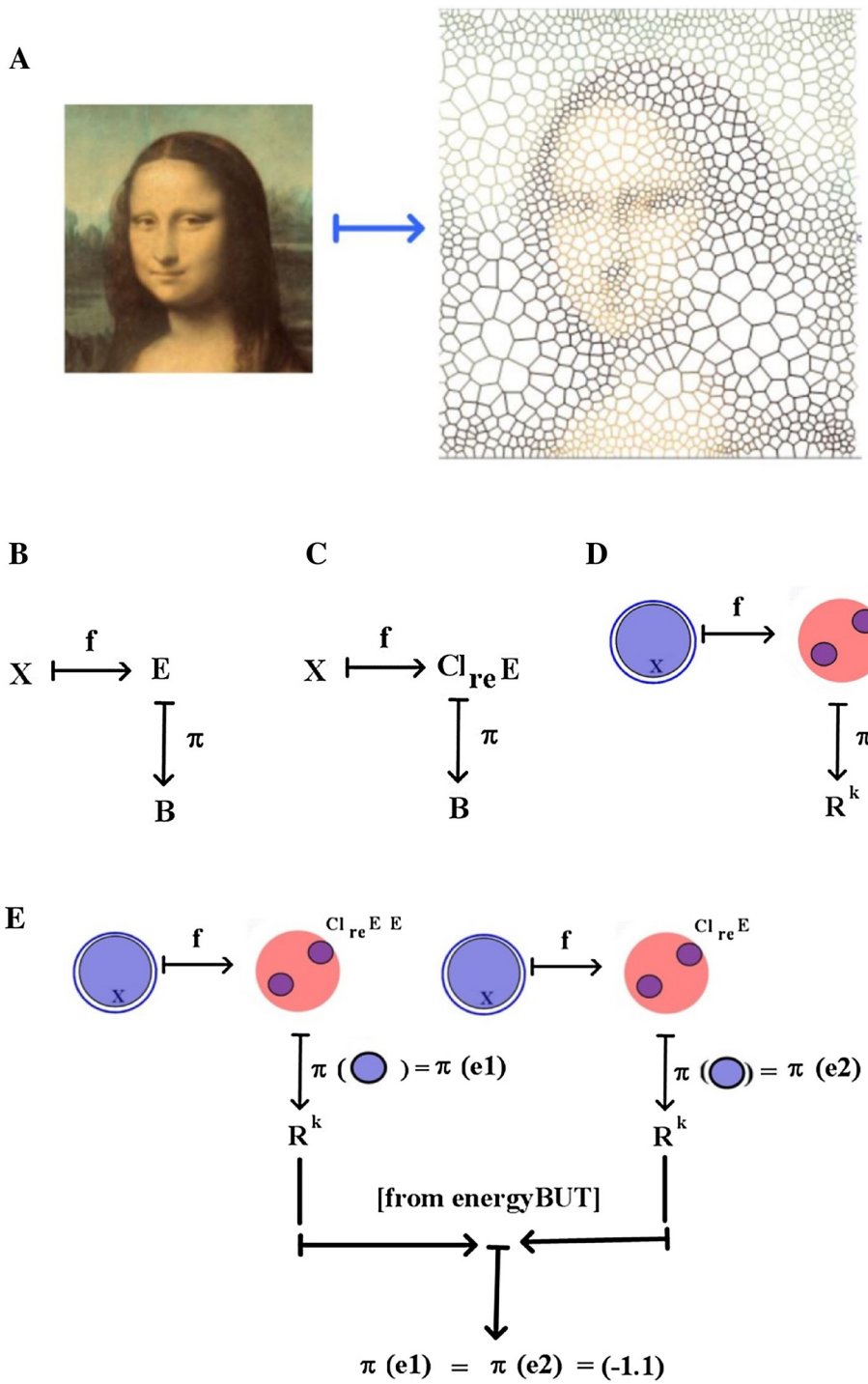

Fig. 3. A Mona Lisa shape deformably mapped to Mona Lisa Exterior Mesh Shapes. This mapping illustrates nascent persistence perception: we abstract away from very complex structures to arrive to a simpler, geometric view of the image as a collection of familiar convex polygons. 3B: framework for Cortical Fibre Bundles: general fibre mapπ. 3C: region-based fibre map π. 3D: VEP fibre map π. Here x represents a set of trajectories on a random network and $Cl_{re}E$ represents a class of small-world networks $Cl_{re}E \subset S^n$ that have been achieved with a change in lattices' dimensions. The mapping $\pi : Cl_{re}E \to R^k$is piecewise continuous from $Cl_{re}E$to cortical energy amplitudes. For $e \in Cl_{re}E$, $\pi(e) = (response) \in R^1$. **3E**: a pair of fibrations, denoted with π, are represented. It is also the case that $\pi(e1) = \pi(e2) = -1.1$, which is predicted by energyBUT.

elements, since their members have similar properties. Such properties can be easily assessed in terms of available experimental procedures, such as, *e.g.*, Visual Evoked Potential Response Amplitude.

Now we introduce the projection $\pi : Cl_{re}E \to B$, which is a piecewise continuous map on $Cl_{re}E$ to B, which is a set of response feature vectors in R^k. For simplicity, we assume that each feature vector$\pi(e) = (response) \in R^1$, where e is a fibre (cortical cell).

The cortical fibre bundle framework in Fig. 3C provides a platform for the application of energyBUT. From Fig. 3B, each visual region response $e1 \in Cl_{re}E$ (class of cortical regions) will have at least another matching cortical region response $e2 \in Cl_{re}E$. (Fig. 3D). Fig. 2D also illustrates the piecewise continuous mapping π on$Cl_{re}E$to $B = R^k$, $k = 1$. The assumption made here is that $Cl_{re}E$ and B are topological spaces and π is a homotopic mapping. In that case, the mapping π is an example of a *fibration*. That is, $\pi(e1)$is piecewise continuously transformed into$\pi(e2)$. In effect, there is always a path between the two shapes in B. The shapes in the situation in Fig. 3D are just points (1-dimensional vectors) in R^1 that represent visual responses. The set $\pi^{-1}(B) = Cl_{re}E$ (*cortical fibre bundle*) is an example of a region-based fibre bundle [27]. EnergyBUT viewed in the context of cortical fibre bundles is represented in Fig. 3E.

BUT variants and Borsuk's theory of shapes are closely allied to the concept of "persistence of perception". Our perception of an object continues, even when the object is out of sight. This is explained by viewing regions on the surface of a hypersphere as multiple representations of object shapes, mapped continuously to an object that

have seen and continue to see. It occurs thanks to the continuous mapping from shapes in our memory to shapes in Euclidean space. Persistence perception can be viewed as signals matching, real-scene visual signals that are collectively the umbra of physical shapes. For example, Fig. 3A displays the Mona Lisa painting impinging on the optic nerves: we map it to similar shape representations. Therefore, the use of "topological" feature demons might account for our knowledge of world objects, by borrowing a concept of invariance in topology. In touch with the concepts of perception of shapes and perception as shape mapping, a series of transformations can be endlessly and gradually applied to a pattern, without affecting its invariant properties. And, principal among the properties of world objects, is the shape, and the acquisition of persistent perception of object shapes, which we nicely explain with BUT variants.

3. Conclusions

We introduce a novel model of Pandemonium able to solve some of the doubts cast by Selfridge's original formulation. Indeed, contrary to template matching models [29] and gestalt accounts [30], Selfridge's model of pattern recognition postulates that an image is first perceived in terms of its basic individual elements/features, then is recognized as a whole object. Our model is equipped with feature demons able to identify topological invariants/global patterns at the very beginning, instead of straight or curved lines: this means that a global topological pattern can be recognized at the initial stages of sensation/perception. We introduce TWO decision demons, instead of one, that respond to the activation of the loudest cognitive demon. This explains a feature of human perception, e.g., error predictions based on overlapping features (for example, R and P, that are topologically equivalent, can be confused more frequently than R and B, or R and I). Our machine's final output stands for TWO (instead of ONE) decision demons with matching description: this means that, contrary to the classical Pandemonium which adopts a fully bottom-up approach that forgets the role of higher-hierarchical predictive codes, our Pandemonium points towards the presence of top-down brain constraints.

During sensation and perception, the individual's brain is forced to coalesce together environmental components, so that a complex interaction takes place between external affordances and the motivated humans who perceive them. The individual's ability to melt parts of the environment into a single perception is compelled and mandatory, rather than a free choice. The brain needs to perceive different elements together and cannot split them, because the perception may operate just in this way. The evolutionary advantage is self-evident: the perception of different elements is useless by itself, while the perception of complete objects, or concepts or ideas, is mandatory in order to survive in an explorable environment, full of possibilities, but also of dangers. The relationship between antipodal points with matching description is a topological one: the surface features of an object are "linked" together in a single complex of sensations through projections, affine connexions and proximity. The concept of *connexion* means that the joined parts of the environment are not necessarily in causal relationship, rather they are simply functionally correlated. Every individual, due to habituation, learns, from childhood forward, to join together the elements which are the most useful for his survival. Avenarius was the first to suggest that a Darwinian fight among different systems might take place in our own bodies and that the central nervous one exerts his prevalence among the others [31]. In our BUT-Pandemonium, the highest dimensional brain is able to control the anatomical/physiological levels equipped with lower dimensions and complexity. We hypothesize that the influence of inputs from different organs (such as intestinal bacteria) on the neocortex could be more limited than supposed, because the brain, located at higher levels of complexity, is able to dictate his own laws of preservation. The whole brain prevails and dictates behaviors, sometimes at the expenses of other organs: *e.g.*, in a cigarette smoker, the brain demands overcome the preservation of other systems, such as lungs or heart.

"Perception is based on information, not on sensations" [32]. The BUT-Pandemonium, rather than sensation-based, is information-based. This means that the human behavior is radically situated: individuals stand in an ecological relation to the environment, such that, to make predictions about their actions, one needs to assess their environmental niche and, especially, the information that "epistemically connects" the organism to its surroundings. An appropriate analysis of the environment, that can be provided in terms of BUT-Pandemonium, becomes crucial for an explanation of perceptually-guided behavior. Our work strengthens and brings to the front the primary question of "what" is perceived, before questions of mechanisms and material implementation are introduced [33]. Together with an emphasis on dynamical systems theory as a necessary methodology for investigating the structure of ecological information, our approach uses the modern tools of algebraic topology. Future work will assess whether other sensory cues, such as touch, display topological invariants that can be experimentally evaluated. Such invariants would encompass topological changes that occur not just in space, but also in time, as it occurs in our perceptions.

References

[1] O.G. Selfridge, Pandemonium: a pradigm for learning. In: mechanization of thought processes, Proceedings of a Symposium Held at the National Physical Laboratory, London: HMSO (2017) 513–526.

[2] D.A. Rosenbaum, It's a Jungle in There: How Competition and Cooperation in the Brain Shape the Mind, Oxford University, 2014 ISBN 978-0-19-982977-4.

[3] G. Edelman, Neural darwinisim, New Perspect. Q. 31 (1) (2017) 25–27 January 2017.

[4] J.J. McDowell, Behavioral and neural Darwinism: selectionist function and mechanism in adaptive behavior dynamics, Behav. Process. 84 (May (1)) (2010) 011, http://dx.doi.org/10.1016/j.beproc.2009.

[5] A.C. MacIntyre, Hume on is and ought, Philos. Rev. 68 (4) (1959) 451–468 URL: http://www.jstor.org/stable/2182491.

[6] G. Edelman, Wider than the Sky: The Phenomenal Gift of Consciousness, University Press, Yale, 2014, p. 2004.

[7] A. Di Concilio, C. Guadagni, J.F. Peters, S. Ramanna, Descriptive proximities: properties and interplay between classical proximities and overlap, Math. Comp. Sci. 12 (2018) 91–106 https://doi.org/10.1007/s11786-017-0328-y.

[8] M.Z. Ahmad, J.F. Peters, Proximal Cech complexes in approximating digital image object shapes. Theory and application, Theory Appl. Math. Comp. Sci. 7 (2) (2018) 81–123.

[9] E. Mach, Analysis of the Sensations, The Open Court Publishing Company, Chicago, 1885 1896.

[10] Y. Dabaghian, V.L. Brandt, L.M. Frank, Reconceiving the hippocampal map as a topological template, Elife 3 (2014) e03476.

[11] M. Arai, V. Brandt, Y. Dabaghian, The effects of theta precession on spatial learning and simplicial complex dynamics in a topological model of the hippocampal spatial map, PLoS Comp. Biol. 10 (6) (2014) e1003651.

[12] Z. Chen, S.N. Gomperts, J. Yamamoto, M.A. Wilson, Neural representation of spatial topology in the rodent hippocampus, Neural Comput. 26 (2014) 1–39.

[13] A. Tozzi, J.F. Peters, Towards a fourth spatial dimension of brain activity, Cogn. Neurodynamics 10 (2016) 189–199, http://dx.doi.org/10.1007/s11571-016-9379-z.

[14] P. Alexandroff, A.E. Farley (Ed.), EinfachsteGrundbegriffe der Topologie [Elementary Concepts of Topology trans, Dover Pubs., Inc., 19321961.

[15] J.F. Peters, Postscript. Where do shapes fit into the computer vision landscape, in: J. Kacprzyk, J.C. Jain (Eds.), Foundations of Computer Vision. Computational Geometry, Visual Image Structures and Object Shape Detection. Intelligent Systems Reference Library, Vol .124 Springer Int. Publishing AG, 2017, , http://dx.doi.org/10.1007/978-3-319-52483-2.

[16] J.F. Peters, Proximal nerve complexes. A computational topology, arXiv 1704 (2017) 1–16 no. 95909v1.

[17] J.F. Peters, E. İnan, Strongly proximal Edelsbrunner-Harer nerves, Proc. of the Jangjeon Math. Soc 19 (3) (2016) 563–582 Zbl 06665117.

[18] Karl Friston, The free-energy principle: a unified brain theory? Nat. Rev. Neurosci. 11 (2) (2010) 127–138, http://dx.doi.org/10.1038/nrn2787 Nature Publishing Group.

[19] R. Ghrist, Elementary applied topology, Createspace (2014) ISBN 978-1-5028-8085-7.

[20] K. Borsuk, Theory of Shape. Lecture Notes Series 28, MatematiskInstitut, Aarhus Universitet, 1971 MR0418088.

[21] J. Matoušek, Using the Borsuk–Ulam Theorem. Lectures on Topological Methods in Combinatorics and Geometry, Springer-Verlag, Berlin Heidelberg, 2003.

[22] A. Tozzi, J.F. Peters, A topological approach unveils system invariances and broken symmetries in the brain, J. Neurosci. Res. 94 (5) (2016) 351–365, http://dx.doi.org/10.1002/jnr.23720.

[23] W.A. Beyer, A. Zardecki, The early history of the ham sandwich theorem, Am. Math.

Mon. 111 (1) (2004) 58–61.
[24] M. Manetti, Topology, Springer, Heidelberg, 2015, http://dx.doi.org/10.1007/978-3-319-16958-3.
[25] K. Borsuk, J. Dydak, What is the theory of shape? Bull. Aust. Math. Soc. 22 (2) (1980) 161–198 MR0598690.
[26] H. Heft, The relevance of Gibson's ecological approach to perception for environment-behavior studies, in: G.T. Moore, R.W. Marans (Eds.), Adances in Environment, Behavior, and Design, Plenum Press, NY, 1997, pp. 71–107.
[27] J.F. Peters, Computational proximity, in: I.S.R. Library (Ed.), Excursions in the Topology of Digital Images, Springer-Verlag, Berlin, 2016, , http://dx.doi.org/10.1007/978-3-319-30262-1.
[28] A. Tozzi, J.F. Peters, From abstract topology to real thermodynamic brain activity, Cogn. Neurodynamics (2017), http://dx.doi.org/10.1007/s11571-017-9431-7.
[29] Y. Hirai, A template matching model for pattern recognition: self-organization of templates and template matching by a disinhibitory neural network, BiolCybern 38 (2) (1980) 91–101.
[30] A. Pastukhov, First, you need a Gestalt: an interaction of bottom-up and top-down streams during the perception of the ambiguously rotating human walker, Sci. Rep. 1 (April (1)) (2017) 1158, http://dx.doi.org/10.1038/s41598-017-01376-1.
[31] C. Russo Krauss, L'empiriocriticismo di Richard Avenarius tra psicofisiologia e teoria della consocenza, in: R. Avenarius (Ed.), Il Concetto Umano Di Mondo, Morcelliana, Brescia, 2015.
[32] J.J. Gibson, The Theory of Affordance in the Ecological Approach to Visual Perception, Erlbaum, Hillsdale, 1979.
[33] S.C. Rao, G. Rainer, E.K. Miller, Integration of what and where in the primate prefrontal cortex, Science 276 (May (5313)) (1997) 821–824.

Progress in Biophysics and Molecular Biology xxx (2018) 1–9

Contents lists available at ScienceDirect

Progress in Biophysics and Molecular Biology

journal homepage: www.elsevier.com/locate/pbiomolbio

Syntax meets semantics during brain logical computations

Arturo Tozzi [a, *], James F. Peters [b, c, d, e], Andrew A. Fingelkurts [f], Alexander A. Fingelkurts [f], Leonid Perlovsky [g, h]

[a] Center for Nonlinear Science, Department of Physics, University of North Texas, 1155 Union Circle, #311427, Denton, TX 76203-5017, USA
[b] Department of Electrical and Computer Engineering, University of Manitoba, 75A Chancellor's Circle, Winnipeg, MBR3T 5V6, Canada
[c] Department of Mathematics, AdıyamanUniversity, 02040 Adıyaman, Turkey
[d] Department of Mathematics, Faculty of Arts and Sciences, AdıyamanUniversity, 02040 Adıyaman, Turkey
[e] Computational Intelligence Laboratory, University of Manitoba, WPG, MB, R3T 5V6, Canada
[f] BM-Science – Brain and Mind Technologies Research Centre, Espoo, Finland
[g] Dept. Psychology and Dept. Engineering, Northeastern University, Boston, MA, USA
[h] Peter the Great Polytechnic University, St. Petersburg, Russia

ARTICLE INFO

Article history:
Received 16 December 2017
Received in revised form
26 April 2018
Accepted 23 May 2018
Available online xxx

Keywords:
Borsuk-ulam
Brouwer
Computation
Meaning
Truth
Syntactic

ABSTRACT

The discrepancy between syntax and semantics is a painstaking issue that hinders a better comprehension of the underlying neuronal processes in the human brain. In order to tackle the issue, we at first describe a striking correlation between Wittgenstein's Tractatus, that assesses the syntactic relationships between language and world, and Perlovsky's joint language-cognitive computational model, that assesses the semantic relationships between emotions and "knowledge instinct". Once established a correlation between a purely logical approach to the language and computable psychological activities, we aim to find the neural correlates of syntax and semantics in the human brain. Starting from topological arguments, we suggest that the semantic properties of a proposition are processed in higher brain's functional dimensions than the syntactic ones. In a fully reversible process, the syntactic elements embedded in Broca's area project into multiple scattered semantic cortical zones. The presence of higher functional dimensions gives rise to the increase in informational content that takes place in semantic expressions. Therefore, diverse features of human language and cognitive world can be assessed in terms of both the logic armor described by the Tractatus, and the neurocomputational techniques at hand. One of our motivations is to build a neuro-computational framework able to provide a feasible explanation for brain's semantic processing, in preparation for novel computers with nodes built into higher dimensions.
© 2018 Elsevier Ltd. All rights reserved.

Contents

1. Introduction: troubles with semantics 00
2. A logic link between syntactic and semantic issues 00
3. Looking for the neural correlates of syntax and semantics 00
4. A topological model of knowledge istinct 00
5. Concluding remarks 00
6. A philosophical CODA 00
Supplementary data 00
References 00

* Corresponding author.
E-mail addresses: tozziarturo@libero.it (A. Tozzi), james.peters3@umanitoba.ca (J.F. Peters), andrew.fingelkurts@bm-science.com (A.A. Fingelkurts), alexander.fingelkurts@bm-science.com (A.A. Fingelkurts), lperl@rcn.com (L. Perlovsky).

https://doi.org/10.1016/j.pbiomolbio.2018.05.010
0079-6107/© 2018 Elsevier Ltd. All rights reserved.

Please cite this article in press as: Tozzi, A., et al., Syntax meets semantics during brain logical computations, Progress in Biophysics and Molecular Biology (2018), https://doi.org/10.1016/j.pbiomolbio.2018.05.010

1. Introduction: troubles with semantics

Syntax assesses the relationships among the elements of linguistic expressions (Carnie, 2006): a property of the proposition is syntactic, provided it depends only on the symbols. Syntax is akin to grammar, which also includes phonology and orthography, such as the sounds and spellings of words (Martinich, 1996). Also, *syntax* refers to the presentation of symbols in a sequence that is valid as based on correctness of designated true/false values (Béziau, 2010). In turn, *semantics* assesses the relationships between expressions and extra-linguistic truths (Nerbonne, 1996). A property of the assertion is semantic, provided it depends only on the meaning. Semantics stands also for the logical "information flow" of linguistic expressions, such as in a sequence of arguments (Cruse, 2004). A central aspect in brain meaningful behavior is intentionality (Freeman, 2012): this means that semantic construction is not a passive process, rather a very active one performed by thinking agents (Capolupo et al., 2013). The problem is that syntactic properties are verifiable by computerized algorithms, while semantic properties are not, because the latter are based on the non-physicalist notion of truth. The issue of the unrelatability of syntax and semantics was first raised by Ludwig Wittgenstein. Indeed, the triumph of syntax depicted his seminal Tractatus Logico-Philosophicus (Wittgenstein, 1921) turned out to be incapable to solve the difficult logical and philosophical problems of syntactic versus semantics. That's why the so called "second" Wittgenstein (1953) rejected the philosophical scenario depicted in his own book and introduced the (almost) opposite semantic theory of "linguistic jokes". The issue was further complicated by the incompleteness theorems (Gödel, 1931) that demonstrated how, if one is limited to syntactic approaches, she is not capable to obtain truths. This means that, given a group of arithmetical axioms, there is always a true arithmetic proposition that cannot be demonstrated starting from the axioms, if we admit just syntactic methods (Segre, 1994; Mancosu, 1998). Hence, a paradox occurs: syntactic methods are inadequate to understand the complete properties of the same model that is easily understandable through semantics. This leads us to neuroscience and neurocomputation: despite the human thought is effortlessly able to grasp the semantic notion of truth, such non-physicalist truth cannot be verified by computers. Therefore, a) if unquestioned and consistent syntactic methods are used, then all truths cannot be proved; b) if the uncertain semantic models endowed in our brain are used, then all arithmetic truths possibly could be known, but the correctness of such models is ambiguous.

The challenge here is: could the pure logical and syntactic content described by the Tractatus be useful in the current neuroscientific debate? How do logical limitations look like, contemplated through the lenses of the neurocomputational models at hand? Is it feasible to achieve a computational implementation of the syntax, in order to make the Tractatus' tenets mathematically assessable and describable in semantic terms? Could computational syntax and brain semantics be treated through mathematical tools able to remove combinatorial complexity?

Herein we show how a semantic theory that links language and cognition, i.e., Perlovsky's joint language-cognitive model (Perlovsky and Sakai, 2014; Perlovsky, 2016), coupled with the topodynamic tenets of the recently proposed brain operational architectonics (Tozzi et al., 2017), is able to describe the very basic syntactic assumptions of the Tractatus. Further, we propose a new topological-computational approach so as to bridge between syntactic and semantic expressions in the human brain. An added motivation is to advance towards the construction of semantics-solving machines.

2. A logic link between syntactic and semantic issues

Here we show how two apparently unsuited approaches (the one equipped with syntactic and logical features, the other with semantic and computational structures) can be fruitfully joined, in order to logically describe the correlations between the language and the world.

"Deep" syntactics: Wittgenstein's logical correlations between the language and the world. Wittgenstein establishes in his *Tractatus* an isomorphism, a correlation and a quantitative articulation between the world (and its basic components) and language (and its basic components) (Fig. 1). These relationships are located in a fixed and immutable grid, the logical armor, embedded in a logical space where isomorphisms between the world and the language occur, through one-to-one-into projections. Starting from the simplest terms of this relationship, we have, on the world's side, the things, *i.e.*, the objects, simple and immutable. They stand for the unbridgeable border of the analysis and make up the irreducible substance of the world. From the language side, such simplest terms of the relationship stand for names, *i.e.*, words equipped with a meaning. From the world's side, the second level stands for the states of things, i.e., atomic facts, state of affairs, logical connections of things and links of objects. An objects' configuration is various, changing, irregular. Then, from the language side, the states of things stand for elementary propositions, *i.e.*, the atomic representations of the objects: they are independent one from each other, equipped with sense and characterized by truthful meaning. From the world side, the third higher step are the facts, i.e., configuration relationships, portrayals, logic of reality, subsistence of the states of things. From the language side, they stand for the composite propositions, *i.e.*, the propositions termed "molecular" that are the logic products of elementary propositions. They display the logic properties of language, but do not say anything else. Indeed, they have neither meaning, nor content; they just cope with the logical shape, unveiling the word armor. They are true and describe the real, despite the nettlesome fact that they do not define a primary, naïve, direct view. Their sense depends on the elementary propositions, because they are truth functions of the latter. The highest step stands, by one side, for the world itself: it is a limited whole, the logic space of the facts, a pure formal universality, a unique, essential structure that fixes up what happens. Note that the totality prevails on the simple level. The world's counterpart, at the highest level, is the language itself, which stands for the limit of the world. Life, the subject, the I, is located outside the world and language. Where the subject is located, nothing occurs. The subject, being out of the world, stands for the border, the non-content of the world. From the subject's location, the occurring experiences are available not through the ordinary syntax, rather through the immediacy of feeling. Accordingly, the role of philosophy is to proceed from the top to the bottom, from language to names. It is a top-down approach that starts from the higher level of the world and allows the analysis of the lower-levels, i.e., the states of things.

During the following years, Wittgenstein realized that his model was causing him troubles. The elementary, "atomic" structures of the Tractatus stand for both the names and the corresponding things in the world. Yet, how could one be sure that names and things are the very basic structures of the language and the world, respectively? How could one be sure that names and things cannot be split in further elementary components? How can I say that this is a "sword", and not just a collection of pieces, such as the blade, and so on? Therefore, the "second" Wittgenstein concluded that the human brain copes with indescribable "semantic" issues of words and things. Indeed, when presented with a proposition, the brain straightforwardly understands its grammar and discriminates

Please cite this article in press as: Tozzi, A., et al., Syntax meets semantics during brain logical computations, Progress in Biophysics and Molecular Biology (2018), https://doi.org/10.1016/j.pbiomolbio.2018.05.010

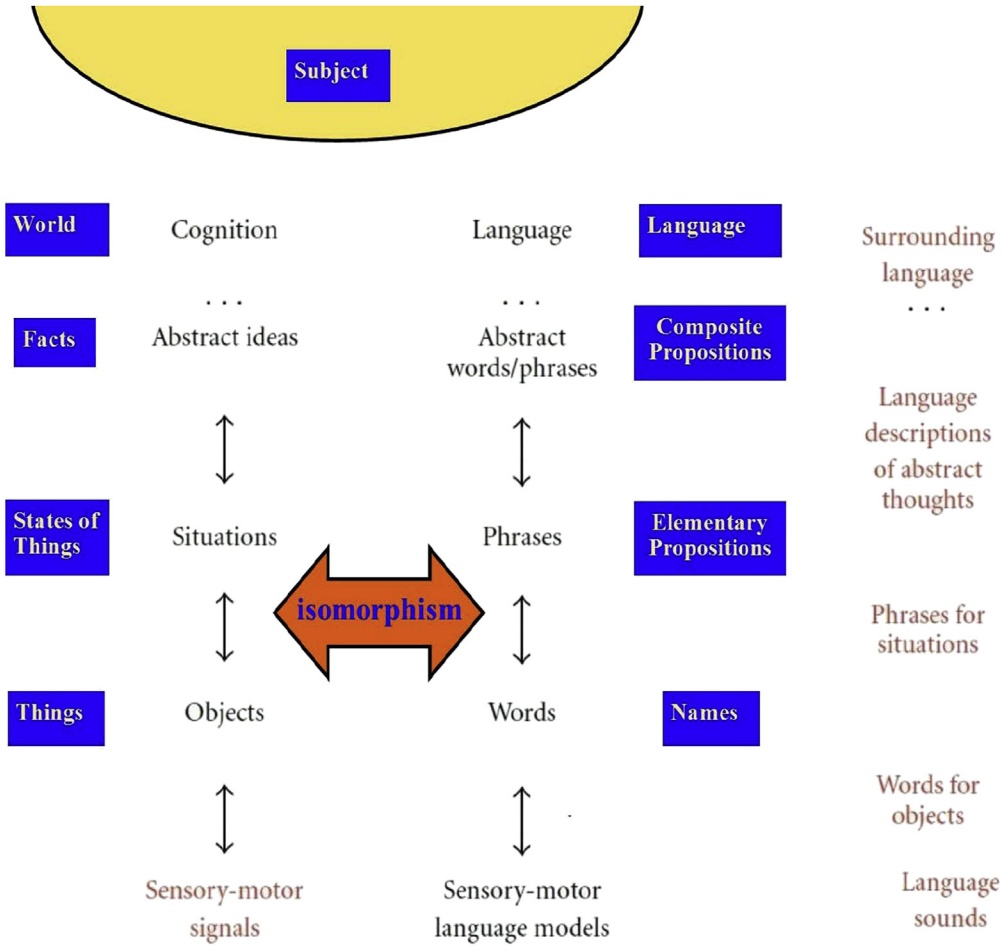

Fig. 1. Wittgenstein's isomorphic model (in dark squares) superimposed to Perlovsky's joint language-cognitive model. The latter depicts an entire hierarchy from sounds to words and phrases, until the highest concepts existing in culture. Both the models display parallel hierarchies of language and cognition (or world), where lower-level concepts and things project to higher levels equipped with meanings relevant to situations.

whether it is correct or wrong, true or false. Unlike computers, the brain is able to identify signs of sequences in terms of both syntactic symbols and semantic meaning. How do cope with the discrepancy between the logical syntax and the semantics endowed in our brains? Here, Perlovsky's account comes into play.

"Deep" semantics: Perlovsky's physical correlations between language, cognition and emotions. Perlovsky has developed a multi-level model of neural architecture that permits a computational description for the mental mechanisms of language, cognition and emotions (Perlovsky, 2011). A hetero-hierarchical structure occurs from sensory signals at the bottom, to highest concepts' representations at the top (Friston, 2010; Tozzi et al., 2017), while learning and recognition proceed in parallel with object perception. Concept representations stand for mental models of objects and situations. During visual perception, for instance, a mental model of the object stored in memory projects an image (top-down signals) onto the visual cortex, where it matches an image projected from retina (bottom-up signals). The brain, according to Perlovsky, makes use of "dynamic logic", i.e., a fuzzy process "from vague-to-crisp" (Ilin et al., 2014), where the degree of fuzziness is automatically set, corresponding to the accuracy of the learned models. In the process of learning, models become more and more accurate and association variables become crisper and crisper, so to increase and maximize the similarity between top-down and bottom-up messages. At each hierarchical level, concept-models encapsulate the mind's knowledge, generating top-down neural signals that interact with inputs (i.e., bottom-up signals). Knowledge is not static, rather a continuous process of adaptation and learning that takes place in order to understand the ever-changing surrounding world. Humans are equipped with what Perlovsky calls the "knowledge instinct", an inborn need, a drive to fit top-down and bottom-up signals that continuously improve our cognition. Given that cognition is inextricably linked with human language (Perlovsky, 2013), every mental semantic representation consists of two model aspects: cognitive and linguistic. Meanings are created by symbol-processes in the mind. Language plays a special role because, through its ability to accumulate cultural knowledge and communication among people, it provides grounding for abstract model-concepts at the higher levels of the mind hierarchy. Therefore, semantic issues, such as cognitive activities, language faculties, emotions, and also motivations, are mathematically assessable through a series of well-established equations, the "joint language-cognitive models" (Fig. 1). These equations maximize similarity without combinatorial complexity, due to the matching vagueness of similarity measures and the uncertainty of the model. In the process of learning and understanding input signals, models are adapted for their better representation, so that the similarity between models and signals increases. This increase in similarity satisfies the knowledge instinct and is mentally perceived as aesthetic emotions (Schoeller and Perlovsky, 2016).

Opposite to Wittgenstein's first model, Perlovsky's account

might be considered a fully semantic one. Indeed, he proposes Dynamic logic (DL), i.e., a variant to overcome limitations of "classical" logic (the one used by Wittgenstein, after Frege's and Russell's modifications). Classical logic is static (e.g., "this is a chair"), while DL is a process "from vague-to-crisp", or in other words, from a vague semantic representation, model, decision and plan, to crisp ones. DL could be viewed as a dynamic form of fuzzy logic that automatically sets a degree of fuzziness corresponding to the extent of the acuity each learned model with acuity measured on a continuous scale from 0 to 1. For technical readers, the mathematical account of Perlovsky's procedure is provided in Perlovsky (2011).

When Wittgenstein meets Perlovsky. As stated above, in the later period of his life, the so called "second" Wittgenstein dismissed the tenets of his own Tractatus. He realized that his syntactic "atomic facts" cannot be accurately described, because they just depend of the (semantic) communication context in which they are formulated (therefore, he started to talk about "linguistic jokes"). Here we will show that the late Wittgenstein was wrong, because the syntactic treasures of the Tractatus still hold true, when implemented through the Perlovsky's original account of semantics through fuzzy logic (Yoder, 2009). Perlovsky's tools are appropriate not just for the evaluation of every layer of mental hierarchies, cognitive as well as language models, but also for the Tractatus' content. Indeed, the first Wittgenstein's logical account of syntax and the Perlovsky's computational treatment of semantics display an unnoticed relationship. As illustrated in Fig. 1, a clear superimposition occurs between their accounts of language and cognition. In touch with the Tractatus, the joint language-cognitive model is organized in parallel hierarchies of language (words, texts) and cognitive models (world's mental representations). Near the bottom of these hierarchies, words refer to objects. Higher up, complex texts refer to complex situations. This means that words within texts refer to objects within situations (because situations are collections of objects), so that reference at higher levels corresponds to the words-objects relationships at lower levels. The highest levels (the most general models) can be predicted starting from the lower ones, because symbols are psychical processes that create meanings: they involve conscious as well as unconscious activities, concepts, emotions and models learned from culture, language and cognition. Therefore, Perlovsky's concept-model, built in order to maximize correspondence between the algorithm internal structure (semantic knowledge) and object recognition, establishes that the whole first Wittgenstein's' account is mathematically assessable and implementable through computational techniques at hand.

In sum, the tenets of the two influential frameworks may be superimposed, so that strict correspondences can be drawn between their single components and levels. This means that the two completely different approaches describe the same dynamics, and that syntax and semantics are not as far as we might believe. We may, therefore, draw the conclusion that syntax and semantics display combining features.

3. Looking for the neural correlates of syntax and semantics

In the previous section, we described a rather unexpected correlation between Wittgenstein's syntax and Perlovsky's semantics. In other words, we established a relationship between a purely logical approach to the language and testable psychological issues, such as emotions and subjectivity. The next step is to look for the neural correlates that would allow the unification of syntactic and semantic operations in the human brain. We need to transfer the above-mentioned syntactic and semantic matching account to the realm of the (natural and/or artificial) networks assessed by neuroscience. As we will illustrate in the next paragraphs, the possibility of such amalgamation lies in algebraic topology.

Entering topological issues. Our central hypothesis is that the human brain, due to its unique operational architectonics (Fingelkurts and Fingelkurts, 2001; Fingelkurts et al., 2010), processes syntactic and semantic elements through a change in functional and spatial dimensions. This hypothesis is rooted in the work of Walter Freeman related to intentionality. Throughout his studies, Freeman provided a comprehensive analysis of brain intentionality. He used the intentional action-perception cycle (Freeman, 1997; Freeman and Vitiello, 2006), in which individual neurons, neuron populations, and their supporting glia/vasculature architectures generate the cortical neurodynamics responsible for perception, cognition and behavior (Kozma and Freeman, 2009). According to this approach, brains are not passive receivers of information, but rather are the active agents that search for sensory input (Freeman, 2008; Capolupo et al., 2013). In topological terms, we may state that Wittgenstein's syntactic processing occurs at one operational level of brain activity, but projection is mapped to a higher functional/operational level where it is further processed (Tozzi et al., 2017). This extra processing gives rise to Perlovsky's semantic recognition, which encompasses far more information than the original Wittgenstein model. An explanation may be framed via new topological developments based on the Borsuk-Ulam and the Brouwer fixed-point theorems. Accordingly, we will hypothesize that the syntactic elements of a language lie on an *n-manifold*, while the semantic elements of a language lie on an *n+1 manifold*. The Borsuk-Ulam Theorem (BUT) states that there is a continuous function that maps antipodal points with matching descriptions into an n-dimensional space of real numbers. For technical readers, see: Borsuk (1933), Matousek (2003), Crabb and Jaworowski (2013), Tozzi and Peters (2016a), Peters (2016a,b). Continuous projections from an *n*-dimensional sphere to a *n*-dimensional Euclidean space lead to a string-based instance of BUT, termed strBUT. We consider a geometric structure with the characteristics of a *string* (Peters and Tozzi, 1016). By definition, a string on the surface of an n-sphere is a line that represents the path traced by a particle moving along its surface. In an abstract geometric space, a string, also termed *worldline* (Olive and Landsberg, 1989), is a region of space with either bounded or unbounded lengths. In evaluating a string-based BUT, we take into account antipodal sets instead of antipodal points (Petty, 1971). Indeed, in a point-free geometry (Di Concilio, 2013; Di Concilio et al., 2018), regions replace points as the primitives. If we assess a worldline in terms of a spatial region on the surface of an *n*-sphere, or in an *n*-dimensional normed linear space, strings can be defined as antipodal (Fig. 2A). Strings are *antipodal*, provided the regions encompassing the strings belong to disjoint parallel hyperplanes which have no points in common. A region is called a *worldsheet* if every one of its sub-regions contains at least one string. The term *worldsheet* designates a nonempty region of a space completely covered by strings, in which every member is a string. A 2D plane worldsheet can be rolled up to form the lateral surface of a 3D cylinder, named a worldsheet cylinder. Further, a worldsheet cylinder maps to a worldsheet torus, formed by bending the former until the ends meet (Fig. 2A). Hence, a flattened worldsheet maps to a worldsheet cylinder, and a flattened worldsheet cylinder maps to a worldsheet torus. This means that a bounded worldsheet cylinder is homotopically equivalent to a worldsheet torus.

The strings on different worldsheets are antipodal and descriptively near, i.e., they share a matching description. There is however a difference between the strings embedded in worldsheets of diverse dimensions. The higher the dimension of the worldsheet, the more information is encompassed in the strings on the same region, because of the higher number of coordinates.

Please cite this article in press as: Tozzi, A., et al., Syntax meets semantics during brain logical computations, Progress in Biophysics and Molecular Biology (2018), https://doi.org/10.1016/j.pbiomolbio.2018.05.010

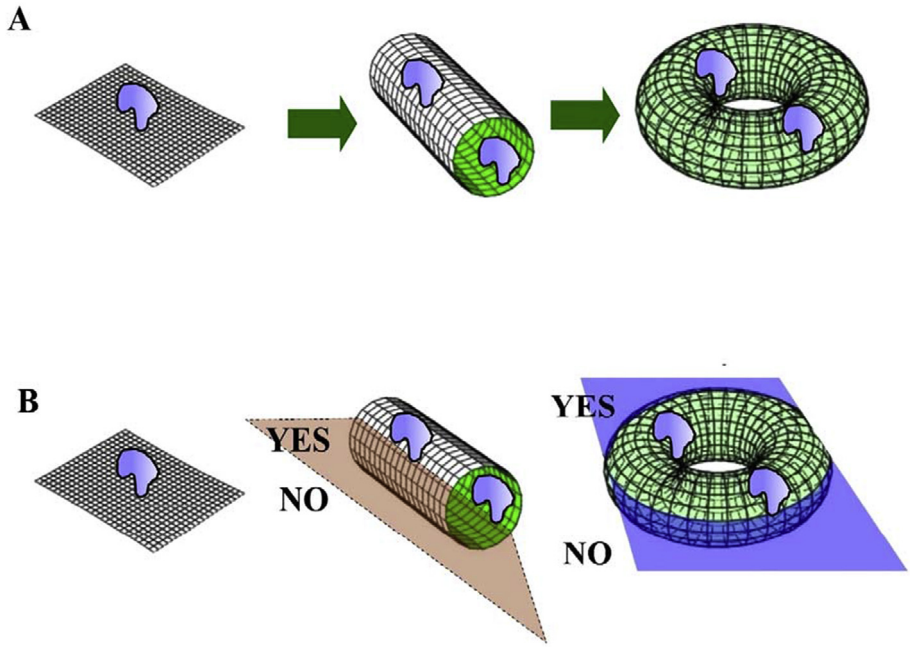

Fig. 2. AString mappings according to StrBUT. A string (blue spot) maps to a higher dimension, from the 2D worldsheet to the 3D worldsheets of the cylinder or torus. The strings on the three different structures are equipped with matching descriptions and are thus antipodal. Note that, for the classical BUT, a single string on the 2D worksheet maps to two opposite strings on the 3D worldsheets.
Figure 2B. Syntactic and semantic counterparts of strBUT. On the left, the blue spot stands for a bidimensional syntactic construct. Moving to one higher dimension achieves a third dimension. This further dimension stands for the semantic concept of a truth value as YES or NO to mean proof or contradiction. Thus, strings gain novel information when projected into structures of a higher dimension.

Strings contain more information than their projections in lower dimensions. This means that strBUT permits the evaluation of system features in higher dimensions—this in turn increases the amount of detectable information. For example, the 3D shape of a cat can be implied by the contour of its 2D shadow. For the process in reverse with complex points, a decrease in the number of dimensions implies that the lower dimensional space is occupied by simpler points. Therefore, strBUT provides a method to evaluate changes of information in a topological rather than in a thermodynamic framework: a projection mapping to a dimension at a lower level contains multiple mappings to a dimension at a higher level.

Next, we consider Brouwer's fixed point theorem (FPT). This theorem states that every continuous function from an n-sphere into an $n+1$ sphere has at least one fixed point (Brouwer, 1906). For example, FPT applies to a disk-shaped area to guarantee the existence of a fixed point behaving as a sort of whirlpool attracting moving particles. A coffee cup illustration of the FPT is given by Su (1997). Regardless of how the coffee is stirred without spilling, one point is always in the same position as occupied before the stirring commenced. Even more, if that point is moved out of its original position, then some other point is displaced back into its original position. In terms of the strBUT, the FPT means that an n-sphere always contains a string. Each string has a particular shape and also comes along together with another string, called a *wired friend* (Peters, 2016a,b). This leads to the *wired friend theorem*: the instance of a wired friend string with a particular shape on the structure S^n maps to a fixed description as another string that belongs to another structure S^{n+1} (Peters and Tozzi, 2016). The wired friend is recognizable by its shape, because the shape of a string is the silhouette of a wired friend string. We obtain maps of wired friend strings, projecting, from the 2D worksheet, to the cylinder worldsheet, to the torus worldsheet. Therefore, we can always find a structure of a higher dimension containing a string that is a description of another string mapped from a structure of lower dimension, and vice versa. In the next section, we show how this theorem has important consequences in the study of syntactic and semantic brain processing.

Why topology provides the logical chasm between syntactics and semantics. By means of strBUT and FTP, we can approach language in terms of both syntactics and semantics. We hypothesize that the syntactic elements of a language lie on an n-manifold, while the semantic elements of a language lie on an $n+1$ manifold. A syntactic proposition becomes a semantic argument when brain mechanisms project the proposition of one dimension onto a higher dimension for the argument, and the reverse process also applies. In logical terms, we define the syntactic proposition as $(p = q)^n$, where $n = 2$, and the semantic argument as $(p = q)^{n+1}$. At the higher dimension, we introduce the truth function such that the semantic argument returns True or False. For example, consider the syntactic preposition "the-skin-is-tender" and the semantic argument equipped with a truth function of True (or Yes): "*the skin is tender*". The truth value, of course, could be False (or Not) in the case of a disease affecting the skin. We write (the-skin-is-tender)^n and (*the skin is tender*)$^{n+1}$, where n stands for the abstract dimensions in which the proposition is embedded. The two propositions also stand for two groups, where the $n+1$ group encompasses the n-group as a subgroup. The $n+1$ group as equipped with a truth function (Yes or No) cannot be detected fully, if we look at just the n-group. This is because the n-group exhibits lesser dimensions than the $n+1$ group. When going from a semantic argument to a syntactic proposition, information may be lost at the proposition level due to the lower number of coordinates as mapped. This means that the semantic group is assessed first in the higher dimension than in the syntactic one. In topological terms, syntactic operations take place when strings as linguistic prepositions are placed in a 2D worldsheet, while semantic operations take place when strings as linguistic arguments are placed in

3D worldsheets for cylinders and toruses. Therefore, a group equipped with the further functionality of True or False is formed through a projective, continuous mechanism (Fig. 2B). In terms of the classical BUT, semantic elements encompass not just one, but two antipodal strings, equipped with a matching description. Such framework is useful when we assess the cortical counterparts of propositions. We contrast the two points lying on a higher dimension and the single point lying on a lower dimension. The main difference is that the two antipodal points as lying on a higher dimension form a group of themselves. That means that semantic processing can be assessed and operationalized solely if we take into account a context equipped with dimensions higher than that of syntactic symbols. Furthermore, when the dimension n increases, syntactic structures are compared with models existing one dimension higher to show similarities. The exponent $n+1$ simply means a higher spatial or functional dimension in the brain. As we will discuss later, computers equipped with nodes dedicated for higher spatial dimensions might be able to process semantic arguments too.

Why topology provides the neural chasm between syntactics and semantics. In the above Sections, we have hypothesized that the human brain processes syntactic and semantic elements through a change in functional or spatial dimensions. The syntactic processing that occurs at one level of brain activity is projected to a higher level; this gives rise to semantic recognition, which encompasses more information. Here we point at possible physical brain counterparts. In the central nervous system, syntax displays fewer dimensions than semantics, so that semantic inputs have increased complexity. The first task is to determine whether the brain contains different dimensions or not. The term brain *dimension* may reflect either a) functional/operational activity, or b) anatomical/functional connections between cortical areas in the form of spatio-temporal patterns. The functional approach a), based on complex network analysis of brain signals, assesses the multidimensionality of neural space in a brain model viewed as a complex dynamical system (Kida et al., 2016; Giusti et al., 2016; Simas et al., 2015). This approach describes nervous dynamics as vectors or tensors in pluri-dimensional phase spaces (Stemmler et al., 2015; Benson et al., 2016). Apart from the *canonical* three dimensions, is also capable of assessing other neural features, such as frequency and magnitude, each one representing other possible dimensions (Kida et al., 2016). The anatomical approach b) to brain dimensionality evaluates cortical locations (Tozzi and Peters, 2016a; 2016b); and as recent advances indicate, brain trajectories may display four spatial dimensions during cortical spontaneous activity, instead of the canonical three. Such trajectories are described in terms of torus-shaped objects. The brain representation of syntactic and semantic processing as described in literature seems to confirm our topological model. The left anterior language areas, e.g. Broca's area (left Brodmann area 44), are crucial for syntactic processing in speech production and perception (Skeide and Friederici, 2016; Stromswold et al., 1996). This is despite the wide variability between individuals and the presence of diverse circuits not dedicated just to a single type of linguistic information processing (Sahin et al., 2009). While syntax seems to be localized in relatively fewer and smaller brain areas, semantics is instead scattered throughout vast areas of the cortical surface (Huth et al., 2016). This is in agreement with our approach, that brings to existence a semantic hierarchy of linguistic thought, through the increasing complexity of joint operations that link many functional and transient neuronal assemblies in the brain (Benedetti et al., 2010), and a model encompassing StrBUT and the fixed-point theorem that regards semantic concepts as multiple antipodal strings on a torus surface—and syntactic concepts appearing as single strings located in specific brain zones (Fig. 3). This also means that semantics lies in a brain with higher dimensions than syntax.

According to the dictates of our strBUT model, single strings capture less information than their matching descriptions embedded in higher projections. Note that semantic information is not aggregated, rather is scattered and hierarchically organized in the brain, as brain operational architectonics predicts (Benedetti et al., 2010; Fingelkurts et al., 2003, 2010). Every part of this hierarchical, nested operational architecture is simultaneously present to every other part/component, forming a spatial co-presence of semantics (Fingelkurts et al., 2012). Syntactic symbols represent single sets of objects, while semantic meanings represent numerous sets of objects with matching description. By extension, we predict that, during the human brain development, the semantic processes precede the syntactic ones. Indeed, children exhibit a slow developmental segregation of syntax from semantics (Skeide and Friederici, 2016). The human embryo can already distinguish vowels *in utero*, but grammatical complexity is usually not fully mastered until at least 7 years (Piaget and Inhelder, 1958; Pinker, 2007). In the first three years, children rapidly acquire bottom-up processing skills, primarily implemented in the temporal areas. In a further stage until adolescence, top-down processes emerge gradually with the increasing structural connectivity of the left inferior frontal cortex (Skeide and Friederici, 2016). This

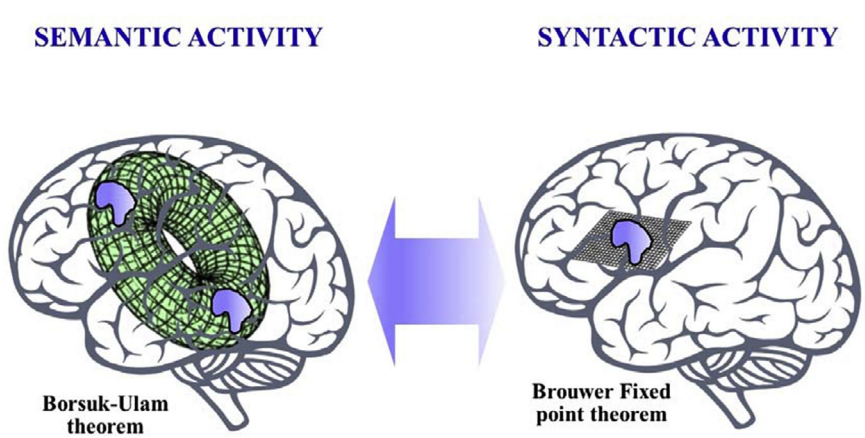

Fig. 3. The semantic and syntactic brain activity in a topological framework. Mappings take place between brain regions which are temporarily equipped with different functional dimensions. On the left, the strBUT dictates that higher dimensional activities lie on a torus, where scattered antipodal strings stand for the cortical areas activated during semantic activity. On the right, syntactic processes lie on a 2D structure. In this latter case, the movements of the more localized strings contained in the Broca's area are dictated by the FPT. Note that the process is fully reversible, depending on the direction of the continuous mapping from one dimension to another.

Please cite this article in press as: Tozzi, A., et al., Syntax meets semantics during brain logical computations, Progress in Biophysics and Molecular Biology (2018), https://doi.org/10.1016/j.pbiomolbio.2018.05.010

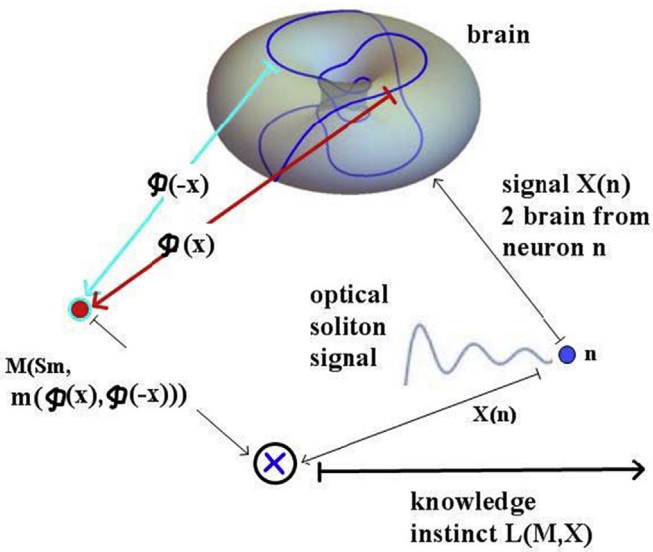

Fig. 4. Knowledge instinct L(M, X) is a cross product of mappings.

means that children are equipped with more semantics than adults. Nevertheless, these valuable insights provided by our topological tools need a further development, in order to incorporate the extra cognitive-emotional complexities of real or "deep" semantics; and it is here that Perlovsky's model comes into play.

4. A topological model of knowledge istinct

The striking correspondence between the first Wittgenstein's and Perlovsky's approaches tells us that we can use the powerful tool of the fuzzy logic for the syntactic/semantic assessment of the human language. Indeed, Wittgenstein emphasizes the correspondence between the world and the syntactic language, while Perlovsky analyzes the relationships between the world and human semantic perception. Putting together the two issues, we achieve a useful framework: Perlovsky's computations can be used in order to correlate the world and the two components of the human language. Here follows the procedure in order to operationalize the anticipated blend between the two approaches. We will show how, for example, in Tractatus' terms, primary prepositions might stand for higher-dimensional sets of the lower-dimensional words. In particular, as an example, we will focus on the computational treatment of one of the tenets of Perlovsky's approach, *i.e.*, what he calls "knowledge istinct".

Knowledge instinct and topological mappings. The derivation of knowledge is represented concisely as a fibre bundle. Briefly, a ***fibre bundle*** is a triple (E, π, B), where $\pi : E \rightarrow B$ is a projection mapping from a bundle space E to a base space B (Husemoller, 1994). Fibre bundles are on the threshold of an operational view of a complex collection of mappings that includes a projection mapping. This is the case, since it is a straightforward task to extract from a fibre bundle the steps of an algorithm (aka, precise prescription leading to implementations in different settings). The derivation of knowledge instinct L is quite complex. So, a concise view of this derivation provided by a fibre bundle is needed. A fibre bundle representation of the derivation of knowledge instinct L is given in Figs. 4 and 5. Each arrow $\mapsto$ in Fig. 5 represents a mapping. The **blue** arrows represent ordinary mappings that carry the derivation forward. The **blue** arrow represents a projection mapping from X(n) to the brain, which results in a gathering of antipodal evaluations of X(n), namely, $m(\varphi(X(n)), \varphi(-X(n)))$. A particular

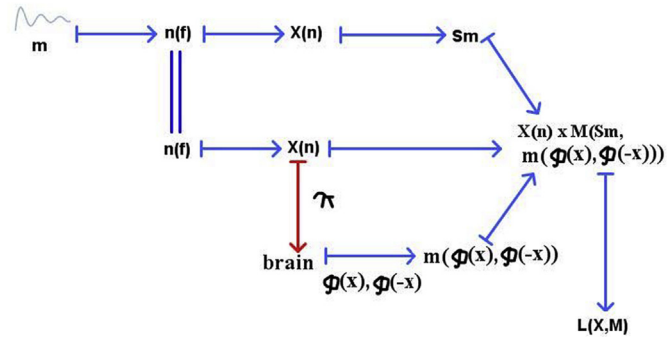

Fig. 5. Fibre bundle representation of knowledge instinct acquisition.

value of knowledge instinct $L(M, X)$results from a synthesis of two signals: $X(n)$and $M(Sm, m(\varphi(X(n)), \varphi(-X(n))))$.

Let us note that, by means of the above formal expressions, we are allowed to produce a preliminary synthesis on a realistic topological, multi-level fuzzy logic that accommodates the basics developments for a unified mathematical treatment of both syntax and semantics. Finally, it is a deep semantics where all instances of cognitive and emotional complexity may be included.

$$X(n) \otimes M(Sm, m(\varphi(X(n)), \varphi(-X(n)))) \rightarrow L(M, X),$$

where$X(n)$is the Gaussian of a signal impacting on neuron n and concept model $M(Sm, m(\varphi(X(n)), \varphi(-X(n))))$that includes input from cortical antipodal evaluations of X(n) from a toroidal view of the inner workings of the brain, *i.e.*, antipodal values $\varphi(X(n)), \varphi(-X(n))$originate a torus-shaped region of the brain. The cross product is mapped to knowledge instinct $L(M, X)$.

5. Concluding remarks

Starting from Wittgenstein's and Perlovsky's accounts, we have shown how semantic and syntactic abilities of the brain could be investigated in terms of algebraic topology. We also illustrated how the syntactic content of the Tractatus can be assessed in terms of the current neuroscientific language. Our review of the literature data reveals how the connectivity among the brain-active centers changes during the presentation of syntactic and semantic inputs (see Benedetti et al., 2010; Fingelkurts et al., 2003 among others), where semantic arguments are based on meaning for a truth function, while syntactic propositions on symbolic correctness and completeness. Further, we described how to use the powerful tools of fuzzy logic and topology for the systematic evaluation of human language and syntactic/semantics assessment. Building upon Perlovsky's computations blended with topological dynamic approaches, a new avenue appears in order to genuinely correlate the world and the two intrinsic components of human language - the syntactic/semantic multidimensionality of human words -.

It is noteworthy that these findings also prepare for a novel computational and logical approach beyond brain functions. Despite computers can process input on a 2D surface, they are not yet able to evaluate the truth function, based on meaning as True or False. Although massively parallel computers are available (Angel and Leong, 1994), their kind of multidimensionality does not tackle the outstanding problem of semantics. Indeed, the current multidimensional efforts in computer science focus on: either access methods (sets of multidimensional points giving computers support at the physical level (Gaede and Günther, 1998)), or digital signal processing (Pastizzo et al., 2002), or data sampling (Mersereau and Speake, 1983). Therefore, multiple dimensions are

Please cite this article in press as: Tozzi, A., et al., Syntax meets semantics during brain logical computations, Progress in Biophysics and Molecular Biology (2018), https://doi.org/10.1016/j.pbiomolbio.2018.05.010

currently used merely as representational devices for data analysis, causing a limitation in the potential of studies assessing artificial intelligence. The fact that brain nodes can be embedded in higher dimensional spaces suggests the possibility of manufacturing computers equipped with multidimensional nodes endowed in 3D geometric spaces. Yet a computer can be hypothesized having connections that are topologically 4D, though embedded in a simple 3D space. The latter computers, implemented in ordinary 3D space, but equipped with nodes with the same number of neighbors as points in a 4D cube, could have the capability to perform semantic operations. Complex semantics can be extracted from the statistics of input features using attractor neural networks (Ursino et al., 2009, 2010, 2011, 2014). These Authors focused on how similarity among objects, feature dominance and distinctiveness can be naturally encoded using a “simple” Hebbian training. Their model includes a lexical network, representing word-forms and a semantic network composed of several areas, each one coding for a different feature. They use a simple taxonomy of schematic objects, i.e., a vector of features, with shared categories and distinctive features (individual members). However, their model differs from ours, because what they address is the contra-hypothesis to ours, namely, that semantic meaning is represented in memory as a collection of features that *shrinks* and compacts the sum of previous sensory, motor, and emotional experiences.

6. A philosophical CODA

Our logical/topological approach embodies several previous suggestions by various authors. Hilbert's program states that every true proposition must be demonstrated starting from one of the available axioms. Except for those axioms, no other propositions are considered to have inherent truth value, rather they must necessarily be assessed through algorithms and computational processing. This means that a demonstrable proposition is syntactic, because it could be derived axiomatically by inspection of the symbols, independent on semantic meaning. However, the Gödel's first incompleteness theorem suggests that, given a group of arithmetical axioms, there will always be a true arithmetic to be discovered which cannot be demonstrated starting from the axioms suggested by Hilbert's approach. Indeed, the theorem states that, if we limit ourselves to syntactic methods of reasoning, then there will always be truths that are not accessible to us.

Syntactic models are inadequate to understand all the properties of an otherwise semantically understandable model. For example, our mental model of natural numbers cannot be completely characterized through syntactic methods. Further, how can we be sure that all the axioms are true? Their truth depends just on the universe of discourse, because the concept of truth has to do with semantics. According to formalists, axioms are indeed just starting points of linguistic jokes (Wittgenstein, 1953), so that the choice of an axiom looks like writing the rules of a table game. Therefore, every proposition, even if entirely false, is theoretically demonstrable, provided we start from an erratic group of faulty axioms.

Our model sheds new light on some of these issues. While Hilbert describes real objects in terms of mathematical axioms, we describe them in terms of projections and mappings. Maps from the lower syntactic dimension to the higher semantic dimension rule out the limitations invoked by Gödel's theorems. In a language, paraphrasing Charles Ball (Ferguslbon, Farwell, 1975), the groups of words and expressions are correlated both with their shapes and meanings, which pertain to the same conceptual sphere and to different dimensions. We could imagine that syntax works with individual symbols, while semantics works instead with groups of intrinsically correlated symbols. We mention in passing that we did not tackle the issue of the third linguistic subfield (together with syntax and semantics) of *pragmatics,* which investigates the ways in which context and use contribute to meaning (Mey, 2001). Our results form a platform model for a forthcoming interpretation of pragmatics, in terms of dimensions even higher than the semantic ones.

We conclude with excerpts from Wittgenstein's Philosophical Investigations (1953), where the author seems to foreshadow the topological computational model framework in which propositions are embedded:

> "Suppose someone said: every familiar word, in a book for example, actually carries an atmosphere with it in our minds, a 'corona' of lightly indicated uses. Just as if each figure in a painting were surrounded by delicate shadowy drawings of scenes, as it were in another dimension, and in them we saw the figures in different contexts (II_{VI})."

> "But how is it possible to see an object according to an interpretation?—The question represents it as a queer fact; as if something were being forced into a form it did not really fit. But no squeezing, no forcing took place here. When it looks as if there were no room for such a form between other ones you have to look for it in another dimension. If there is no room here, there is room in another dimension (II_{XI})."

Appendix A. Supplementary data

Supplementary data related to this article can be found at https://doi.org/10.1016/j.pbiomolbio.2018.05.010.

References

Angel, E., Leong, P., 1994. Multidimensional dynamic programming on massively parallel computers. Comput. Math. Appl. 27, 9–10, 67-75.
Benedetti, C., Marchetti, G., Fingelkurts, A.A., Fingelkurts, A.A., 2010. Mind operational semantics and brain operational architectonics: a putative correspondence. Open Neuroimaging J. 4, 53–69.
Benson, A.R., Gleich, D.F., Leskovec, J., 2016. Higher-order organization of complex networks. Science 353 (6295), 163–166. https://doi.org/10.1126/science.aad9029.
Béziau, J.-Y., 2010. Truth as a mathematical object. Principia 14 (1), 31–46.
Borsuk, M., 1933. Dreisatzeuber die n-dimensionaleeuklidischesphare. FundamentaMathematicae XX 177–190.
Brouwer, L.E.J., 1906. Uber abbildung von mannigfaltigkeiten. Math. Ann. 63 (1906), no. 2, 222–238, MR1511401.
Capolupo, A., Freeman, W.J., Vitiello, G., 2013. Dissipation of ‘dark energy’ by cortex in Knowledge retrieval. Phys. Life Rev. 10 (1), 85–94.
Carnie, A., 2006. Syntax: a Generative Introduction, second ed. Wiley-Blackwell, Oxford, ISBN 1-4051-3384-8.
Di Concilio, A., 2013. Point-free geometries: proximities and quasi-metrics. Math. Comput. Sci. 7 (1), 31–42. MR3043916.
Di Concilio, A., Guadagni, C., Peters, J.F., Ramanna, S., 2017. Descriptive proximities. Properties and interplay between classical proximities and overlap. Math. Comput. Sci. https://doi.org/10.1007/s11786-017-0328-y.
Crabb, M.C., Jaworowski, J., 2013. Aspects of the Borsuk-Ulam theorem. J. Fixed Point. Theory and Appl. 13, 459–488. https://doi.org/10.1007/s11784-013-0130-7. MR3122336.
Cruse, A., 2004. Meaning and Language: an Introduction to Semantics and Pragmatics. Oxford Textbooks in Linguistics.
Ferguson, C.A., Farwell, C.B., 1975. Words and sounds in early language acquisition. Language 51 (2), 419–439.
Fingelkurts, A.A., Fingelkurts, A.A., 2001. Operational architectonics of the human brain biopotential field: towards solving the mind-brain problem. Brain Mind 2 (3), 261–296.
Fingelkurts, A.A., Fingelkurts, A.A., Krause, C.M., Möttönen, R., Sams, M., 2003. Cortical operational synchrony during audio-visual speech integration. Brain Lang. 85 (2), 297–312.
Fingelkurts, A.A., Fingelkurts, A.A., Neves, C.F.H., 2010. Natural world physical, brain operational, and mind phenomenal space–time. Phys. Life Rev. 7, 195–249.
Fingelkurts, A.A., Fingelkurts, A.A., Neves, C.F.H., 2012. “Machine” consciousness and “artificial” thought: an operational architectonics model guided approach. Brain Res. 1428, 80–92.
Freeman, W.J., 1997. Nonlinear neurodynamics of intentionality. J. Mind Behav. 18

(2–3), 291–304.
Freeman, W., 2008. Nonlinear brain dynamics and intention according to Aquinas. Mind Matter 6 (2), 207–234.
Freeman, W.J., 2012. On the nature and neural mechanisms of mind force. Chaos Complex. Lett. 6 (1–2), 7–15.
Freeman, W.J., Vitiello, G., 2006. Nonlinear brain dynamics as macroscopic manifestation of underlying field dynamics. Phys. Life Rev. 3, 93–118.
Friston, K., 2010. The free-energy principle: a unified brain theory? Nat. Rev. Neurosci. 11, 127–138.
Gaede, V., Günther, O., 1998. Multidimensional access methods. ACM Comput. Surv. vol. 30 (2), 170–231 (CSUR) Surveys Homepage archive.
Giusti, C., Ghrist, R., Bassett, D.S., 2016. Two's company, three (or more) is a simplex. Algebraic-topological tools for understanding higher-order structure in neural data. J. Comput. Neurosci. 41 (1), 1–14.
Godel, K., 1931. Über formal unentscheidbareSätze der PrincipiaMathematica und verwandterSysteme. I. MonatsheftefürMathematik und Physik 38, 173–198.
Husemoller, D., 1994. Fibre Bundles, third ed. Springer-Verlag, New York, ISBN 0-387-94087-1, p. xx+353. MR1249482.
Huth, A.G., de Heer, W.A., Griffiths, T.L., Theunissen, F.E., Gallant, J.L., 2016. Natural speech reveals the semantic maps that tile human cerebral cortex. Nature 28 (532), 453–458. https://doi.org/10.1038/nature17637 (7600).
Ilin, R., Zhang, J., Perlovsky, L., Kozma, R., 2014 Feb. Vague-to-crisp dynamics of percept formation modeled as operant (selectionist) process, 2014 CognNeurodyn 8 (1), 71–80. https://doi.org/10.1007/s11571-013-9262-0.
Kida, T., Tanaka, E., Kakigi, R., 2016 Jan 19. Multi-dimensional dynamics of human electromagnetic brain activity. Front. Hum. Neurosci. 9, 713. https://doi.org/10.3389/fnhum.2015.00713 eCollection 2015.
Kozma, R., Freeman, W.J., 2009. The KIV model of intentional dynamics and decision making. Neural Network. 22 (3), 277–285.
Mancosu, P., 1998. From Brouwer to Hilbert, the Debate on the Foundations of Mathematics in 1920s. Oxford Univ. Press, ISBN 0-19-509631-2.
Martinich, A.P., 1996. The Philosophy of Language, III. Oxford University Press.
Matoušek, J., 2003. Using the Borsuk–ulam Theorem. Lectures on Topological Methods in Combinatorics and Geometry. Springer-Verlag Berlin Heidelberg.
Mersereau, R., Speake, T., Feb 1983. 1983. The processing of periodically sampled multidimensional signals. Acoustics, IEEE Trans. Speech Signal Process. 31 (1), 188–194.
Mey, J.L., 2001. 1993. Pragmatics: an Introduction, second ed. Blackwell, Oxford.
Nerbonne, J., 1996. The Handbook of Contemporary Semantic Theory. In: Lappin, S. (Ed.). Blackwell Publishing, Cambridge, MA.
Olive, D.I., Landsberg, P.T., Nov. 17, 1989. Introduction to string theory: its structure and its uses [and discussion]. Phil. Trans. Roy. Soc. Lond. Math. Phys. Sci. 329 (1605), 319–328. Physics and Mathematics of Strings.
Pastizzo, M.J., Erbacher, R.F., Feldman, L.B., 2002. Multidimensional data visualization. Behav. Res. Meth. Instrum. Comput. 34 (2), 158–162.
Perlovsky, L., 2011. Language and cognition interaction neural mechanisms. Comput. Intell. Neurosci. 2011 (2011), 454587. https://doi.org/10.1155/2011/454587.
Perlovsky, L., 2013. Language and cognition-joint acquisition, dual hierarchy, and emotional prosody. Front. Behav. Neurosci. 7, 123. https://doi.org/10.3389/fnbeh.2013.00123.
Perlovsky, L., 2016 Jan. Human consciousness is fundamental for perception and highest emotions, 2016 Behav. Brain Sci.. https://doi.org/10.1017/S0140525X15002216, 39:e191.
Perlovsky, L., Sakai, K.L., 2014 Dec. Language and cognition, 2014 Front. Behav. Neurosci. 16 (8), 436. https://doi.org/10.3389/fnbeh.2014.00436. eCollection 2014.
Peters, J.F., 2016a. Two forms of proximal physical geometry. Axioms, sewing regions together, classes of regions, duality, and parallel fibre bundles. Adv. Math., Sci. J. 5 (2), 241–268. Zbl 06810263.
Peters, J.F., 2016b. Computational Proximity. Excursions in the Topology of Digital Images. Intelligent Systems Reference Library, vol. 102. Springer. MR3727129.
Peters, J.F., Tozzi, A., 2016. String-based Borsuk-ulam Theorem and Wired Friend Theorem arXiv 1605, no. 02987v3, 1–17.
Petty, C.M., 1971. Equilateral sets in Minkowski spaces. Proc. Am. Math. Soc. 29, 369–374. MR0275294.
Piaget, J., Inhelder, B., 1958. The Growth of Logical Thinking from Childhood to Adolescence. New York: Basic Books [De la logique de l'enfant à la logique de l'adolescent (1955)].
Pinker, S., 2007. The Stuff of Thought: Language as a Window into Human Nature. Viking, New York, NY.
Sahin, N.T., Pinker, S., Cash, S.S., Schomer, D., Halgren, E., 2009. Sequential processing of lexical, grammatical, and phonological information within Broca's area. Science 326 (5951), 445–449.
Schoeller, F., Perlovsky, L., 2016 Aug. Aesthetic chills: knowledge-acquisition, meaning-making, and aesthetic emotions, 2016 Front Psychol 4 (7), 1093. https://doi.org/10.3389/fpsyg.2016.01093.
Segre, M., 1994. Peano's axioms in their historical context. Arch. Hist. Exact Sci. 48, 201–342.
Simas, T., Chavez, M., Rodriguez, P.R., Diaz-Guilera, A., 2015. An algebraic topological method for multimodal brain networks comparisons. Front. Psychol. 6 (6), 904. https://doi.org/10.3389/fpsyg.2015.00904 eCollection 2015.
Skeide, M.A., Friederici, A.D., 2016. The ontogeny of the cortical language network. Nat. Rev. Neurosci. 17, 323–332. https://doi.org/10.1038/nrn.2016.23.
Stemmler, M., Mathis, A., Herz, A.V.M., 2015. Connecting multiple spatial scales to decode the population activity of grid cells. Sci. Adv. 1 e1500816 18 December 2015.
Stromswold, K., Caplan, D., Alpert, N., Rauch, S., 1996. Localization of syntactic comprehension by positron emission tomography. Brain Lang. 52, 452–473.
Su, F.E., Nov., 1997. Borsuk-Ulam implies Brouwer: a direct construction. Am. Math. Mon. 104 (9), 855–859.
Tozzi, A., Peters, J.F., 2016a. Towards a fourth spatial dimension of brain activity. Cognit. Neurodynamics 10 (3), 189–199. https://doi.org/10.1007/s11571-016-9379-z.
Tozzi, A., Peters, J.F., 2016b. A topological approach unveils system invariances and Broken symmetries in the brain. J. Neurosci. Res. 94 (5), 351–365. https://doi.org/10.1002/jnr.23720.
Tozzi, A., Peters, J.F., Fingelkurts, A.A., Fingelkurts, A.A., Marijuán, P.C., 2017 Jul; 21. Topodynamics of metastable brains. Phys. Life Rev. 1–20. https://doi.org/10.1016/j.plrev.2017.03.001.
Ursino, M., Magosso, E., Cuppini, C., 2009. Recognition of abstract objects via neural oscillators: interaction among topological organization, associative memory and gamma band synchronization. IEEE Trans. Neural Network. 20, 316–335.
Ursino, M., Cuppini, C., Magosso, E., 2010. A computational model of the lexical-semantic system, based on a grounded cognition approach. Front. Psychol. 1, 1–221.
Ursino, M., Cuppini, C., Magosso, E., 2011. An integrated neural model of semantic memory, lexical retrieval and category formation, based on a distributed feature representation. Cognit. Neurodynamics 1–25.
Ursino, M., Cuppini, C., Magosso, E., 2014. A neural network for learning the meaning of objects and words from a featural representation. Neural Network. (63) https://doi.org/10.1016/j.neunet.2014.11.009. December 2014.
Wittgenstein, L., 1921. (1964). Tractatus logico-philosophicus e Quaderni 1914-1916. Collana Biblioteca di cultura filosofica. Einaudi, Torino.
Wittgenstein, L., 1953. Philosophical Investigations. Blackwell Publishing, ISBN 0-631-23127-7, 2001.
Yoder, L., 2009. Explicit logic circuits discriminate neural states. PLoS One 4 (1), e4154. https://doi.org/10.1371/journal.pone.0004154.

Please cite this article in press as: Tozzi, A., et al., Syntax meets semantics during brain logical computations, Progress in Biophysics and Molecular Biology (2018), https://doi.org/10.1016/j.pbiomolbio.2018.05.010

Cognitive Neurodynamics

THE INFORMATIONAL ENTROPY ENDOWED IN CORTICAL OSCILLATIONS

Arturo Tozzi[1], James F. Peters[2], Mehmet Niyazi Çankaya[3]

[1]*Center for Nonlinear Science, Department of Physics, University of North Texas, Denton, Texas 76203, USA*
1155 Union Circle, #311427 Denton, TX 76203-5017 USA
E-mail address: tozziarturo@libero.it **(corresponding Author)**
[2]*Department of Electrical and Computer Engineering, University of Manitoba*
75A Chancellor's Circle Winnipeg, MB R3T 5V6 Canada and
Department of Mathematics, Faculty of Arts and Sciences, Adıyaman University
02040 Adıyaman, Turkey
James.Peters3@umanitoba.ca
[3]*Deparment of Statistics, Faculty of Arts and Science, Usak University, Usak, Turkey*
mehmet.cankaya@usak.edu.tr

Below is the unedited draft of the article that has been accepted for publication © Cognitive Neurodynamics, 2018, https://doi.org/10.1007/s11571-018-9491-3.

ABSTRACT

A two-dimensional shadow may encompass more information than its corresponding three-dimensional object. Indeed, if we rotate the object, we achieve a pool of observed shadows from different angulations, gradients, shapes and variable length contours that make it possible for us to increase our available information. Starting from this simple observation, we show how informational entropies might turn out to be useful in the evaluation of scale-free dynamics in the brain. Indeed, brain activity exhibits a scale-free distribution that leads to the variations in the power law exponent typical of different functional neurophysiological states. Here we show that modifications in scaling slope are associated with variations in Rényi entropy, a generalization of Shannon informational entropy. From a three-dimensional object's perspective, by changing its orientation (standing for the cortical scale-free exponent), we detect different two-dimensional shadows from different perception angles (standing for Rènyi entropy in different brain areas). We show how, starting from known values of Rènyi entropy (easily detectable in brain fMRIs or EEG traces), it is feasible to calculate the scaling slope in a given moment and in a given brain area. Because changes in scale-free cortical dynamics modify brain activity, this issue points towards novel approaches to mind reading and description of the forces required for transcranial stimulation.

Keywords:
Rényi entropy, power laws, nervous system, scale-free, shadows, central nervous system

INTRODUCTION

Counter-intuitively, a 3D object might encompass less information than a 2D one(we do not see the hidden side of the moon). When observed from a given standpoint, an opaque 3D object could be less informative than a series of its 2D shadows (**Figure 1A**). Here we ask: is there a way to increase the information content of the shadow, to make it possible the detection of more details about the object, let us say a toy? The answer is positive, if we rotate the toy clockwise (or anticlockwise) along its central axis (**Figures 1B, 1C**). In this case, we achieve a pool of different shadows and shape contours with various angulations, able to increase our total available information. Therefore, 3D object's shadows (taken in its totality) are more informative, for a watching observer, whenever he moves. This "toy" analogy gives us the possibility to assess brain function in a novel way. For the purpose of this paper, the toy at rest stands for a given brain scale-free exponent, and its shadows for the corresponding Shannon entropy. In turn, the changes in location of the moving toy stand for changes in brain scale-free exponents, while the modifications in shadow's shape and its undulating contour stand for the corresponding Rènyi entropy (Rènyi 1961; Rènyi 1966; Peters 2017; Peters-Ramanna 2016).

Using our example of a toy as a 3D object and its moving shadows, the aim of this paper is to show how it is feasible to extract information about such toy, by looking at its moving shadows: in neurophysiological terms, we want to assess the relationships among scale-free exponents and generalized informational entropies in the brain. Furthermore, we would consider the recent advancement in the neurophenomenology research that established a link between a nested operational architectonics hierarchy of brain functioning (indexed by the EEG field) and the phenomenal (mental) level of brain organization (Fingelkurts and Fingelkurts, 2001; Fingelkurts et al., 2010). According to this line of research, the meanings, which subjectively (mentally) are experienced as thoughts or perceptions, can best be described objectively as created and carried by dynamic fields of neural activity of different sizes that are nested within the operational architectonics hierarchy that organize hundreds of millions of neurons and trillions of synapses (Fingelkurts et al., 2009, 2013a). We perform simulations in order to demonstrate how, starting from the Rènyi entropy easily detectable in neurodata series (e.g., from brain fMRI or EEG), it is feasible to calculate the cortical scale-free exponent in a given moment, and, consequently, the corresponding mental state.

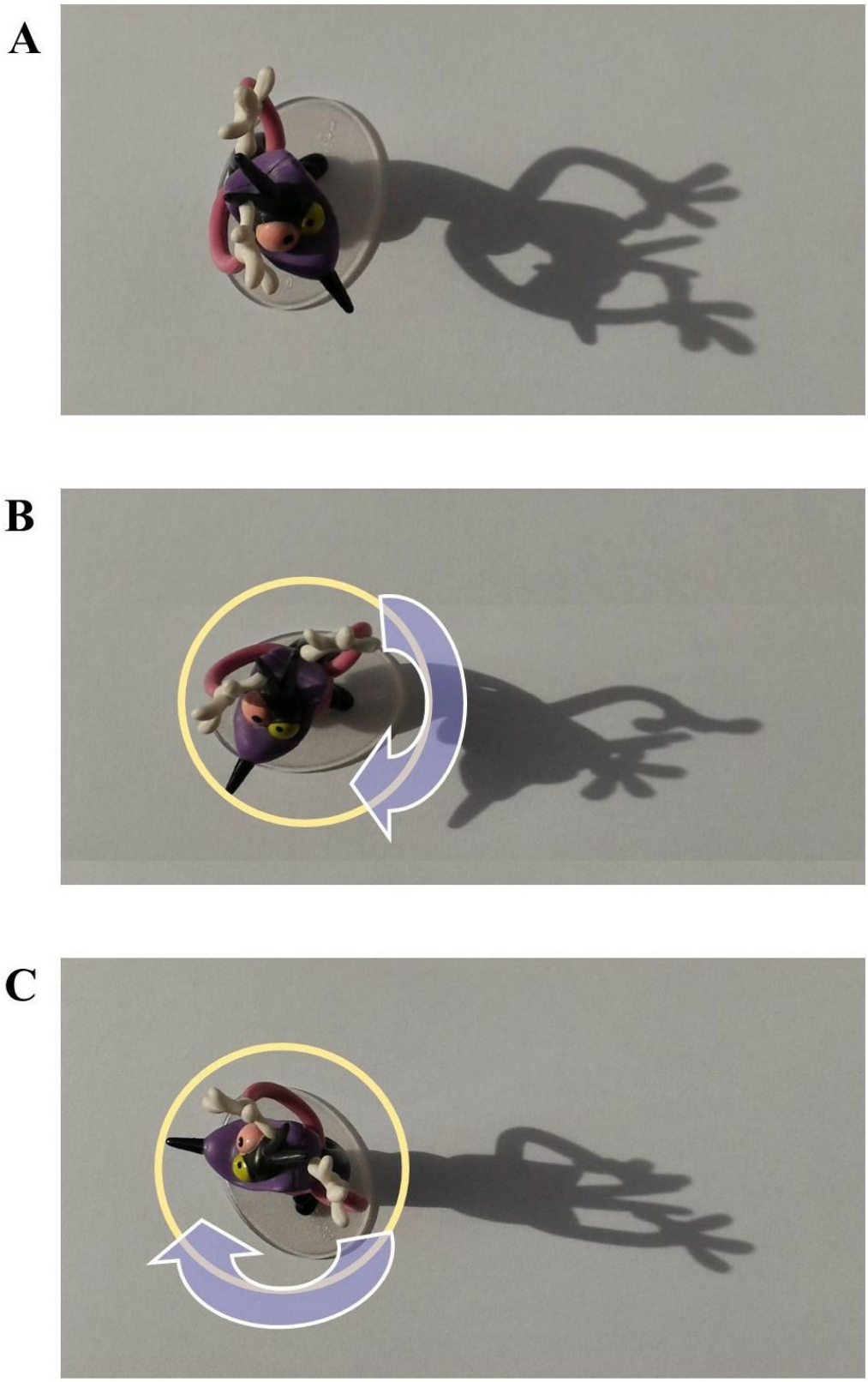

Figure 1. A toy under a light source. In **Figure 1A**, the 2D shadow offers more details of the 3D object than the view on the toy from above. **Figures 1B** and **1C** show how toy rotations lead to shadows with different shapes, and, consequently, with different information content. Therefore, a complete 360 degrees rotation of the object allows a complete evaluation of the shadows' shapes.

SHANNON ENTROPY ON A TOY

The brain activity, e.g., in our analogy the toy and its movements, can be described in terms of scale-free dynamics. Indeed, the brain activity observed at many spatiotemporal scales exhibits fluctuations with complex scaling behavior (Newman, 2005; Fingelkurts et al., 2010, 2013a), including not just cortical electric oscillations, but also membrane potentials and neurotransmitter release (Linkenkaer-Hansen et al., 2001; Fox and Raichle, 2007; Milstein et al., 2009). In particular, the frequency spectrum of the cerebral electric activity displays a scale-invariant behavior, characterized by a power spectrum, a frequency and an exponent that equals the negative slope (which we will term "scaling slope") of the line in a log power versus log frequency plot (Pritchard, 1992; Van de Ville et al., 2010). In simple terms, a scaling slope 1= stands for a horizontal line parallel to the x axis: the steeper the line, the higher the scale-free behaviour. The (spatial) fractals and (temporal) power laws can be regarded as intrinsic properties of the brain and characterize a large class of neuronal processes (de Arcangelis and Herrmann, 2010; He et al., 2010; Deli et al., 2017); moreover, pink noise distributions contain information about how large-scale physiological and pathological outcomes arise from the interactions of many small-scale processes (Jirsa et al., 2014).

Keeping this in mind, a given slope in a given moment of brain activity stands, in our example, for the toy at rest. Toy features can be described through their shadow, e.g., the Shannon entropy. The classical informational Shannon entropy is (Shannon 1948):

$$\mathrm{H(X)} = -\sum_{x \in X} \Pr(x) \log_2 \left[\Pr(x)\right].$$

The term X is a random variable with *n* possible outcomes, while $p_i = Pr(x)$, for i= 1, 2, 3, …*n*, is a probability distribution *Pr* on a finite set. Shannon entropy states that, under ergodic conditions, if we know the values of *Pr(x)*, we may obtain the values of $\mathrm{H(X)}$. In other words, $\mathrm{H(X)}$ is a probability density function that defines a generic probability distribution *Pr*such that, if we modify *Pr*, we obtain a different value of entropy on Shannon's curve. Hence, changing the probabilities usually occurs when we have prior information. In terms of the object depicted in **Figure 1A**, the steady toy stands for the systems' microstates, undetectable by macroscopic observers, while the shadow stands for the lower-dimensional Shannon entropy. Looking at the shadow (the Shannon entropy), we achieve otherwise undetectable information about opaque 3D objects, such as the toy features.

Now we need to find a brain functional counterpart for the moving toy, its changing shape and varying contours of shadows. Indeed, the cortical scale-free slopes are not constant, rather they display multiple possible exponents during various mental states. Despite a few skeptical studies (Tribukait and Eiken, 2016), it is widely accepted that different functional states - spontaneous fluctuations, task-evoked, perceptual and motor activity (Buszaki and Watson, 2012), cognitive demands (Buiatti et al., 2007; Fetterhoff et al., 2014), ageing (Suckling et al., 2008) - account for variations in scale-free exponents across cortical regions (Tinker and Velazquez, 2014; Wink et al., 2008). Accordingly, we may view brain activity as an ensemble of intertwined (mono)fractals, each with its own power slope and scaling range, each marking dynamical transitions between different response regimes (Papo, 2014; see also review Fingelkurts et al., 2013a). In terms of our toy, the whole brain activity stands for all the possible 360 degrees of rotation and their corresponding shadows.

INTRODUCING RENYI ENTROPY

The 360 degrees changes in toy angulation that gives rise to different shadows can be described in terms of Shannon entropy generalizations. Among the available ones (e.g., Tsallis, 1988), here we favour the one-parameter class of Rényi entropies (Rényi, 1966), a flexible and underestimated information-theory based index (Cambell, 1965). Rényi entropy (1961) is characterized by a changing parameter α andcan be defined as:

$$H_\alpha(X) = \frac{1}{1-\alpha} \sum_{\substack{i=1,\\ x \in X}}^{N} p_i^\alpha(x),$$

where $0 \le \alpha < \infty$ and $p_i^\alpha(x)$ is the probability of event x. The Rényi entropy approaches the Shannon entropy as α approaches 1. In other words, the Shannon entropy is a case of Rényi entropy in which α= 1. Rényi entropy has

applications in dynamical systems (Hentschel and Proccacia, 1983), coding (Cambell, 1965), information transfer (Jizba et al., 2012), theories in quantum mechanics, black holes' mutual information (Dong, 2016), assessment of human heartbeat fluctuations and coding/noncoding DNA sequences analysis (Costa et al., 2005). Rényi entropy has also been used to quantify ecosystems dynamics and diversity: from land cover types (Carranza et al., 2007; De Luca et al., 2011), to coastal dunes environments (Drius et al., 2013), from urban mosaics (Carranza et al., 2007) to species diversity in large areas (Rocchini et al., 2013).

WHY THE RENYI ENTROPY, INSTEAD OF THE SHANNON'S ONE?

This paragraph will be devoted to elucidate why Rényi entropy should be preferred, in order to assess brain activity. Shannon entropy depicts the discrete probabilities of an event in terms of a single curve. However, in many physical and biological cases, diversity cannot be reduced to a single index information, since all its aspects cannot be captured in a single statistic (Gorelick, 2006).Rényi entropy, in turn, depicts the discrete probabilities of an event in terms of many curves. Therefore, unlike Shannon entropy, Rényi entropy makes it possible to describe the system's status not just at a specific moment, but also when its trend *varies with time* (Müller et al., 2000; Patil and Taillie, 2001). Indeed, a complete characterization of landscape diversity can be achieved if, instead of a single index, a parametric family of indices is used, whose members have varying sensitivities to the presence of rare and abundant elements (Jost, 2007). Unlike Shannon entropy, which is single-valued, Rényi entropy is useful in measuring a range of information levels such as those in A-yeh and Peters (2016), the dynamics of non-stationary processes (Shaymov, Fradov, 2016) and the measuring of the distribution of entropy changes over time (see, *e.g*., Jauregui, Zunino, Lenzi, Mendes, Ribeiro, 2018). In other words, Rényi entropy offers a "continuum of possible diversity measures" (Ricotta and Avena, 2003) at diverse spatiotemporal scales, becoming increasingly regulated by the commonest when α gets higher. The change in α exponent can be regarded as a scaling operation that takes place not in the real, but in the data space (Podani, 1992): we are thus allowed to evaluate how changes of Rényi parameter influence the structure of information measures in the probability space of the scale-free dynamics. Diversity profiles are flat when the landscape is even, and steeply decrease as the landscape turns uneven (Jost, 2010). Therefore, Rényi's formulation allows a continuum of possible diversity measures which differ in their sensitivity to the rare and abundant elements in a landscape.

Because of its build-in pre-disposition to account for self-similar systems, Rényi entropy is an effective tool to describe multifractal systems (Jizba and Arimitsu, 2001). The generalized fractal dimensional and the Rényi exponent can be thought of as interchangeable. In technical terms, the Rényi parameter is connected via a Legendre transformation with the multifractal singularity spectrum. See Jizba and Arimitsu (2001) and Jizba and Korbel (2014) for technical details on mathematical proof. In particular, this means that Rényi entropy and scale-free exponent (and therefore the scaling slope) are strictly correlated. Therefore, changes in scaling slope lead to changes in the Rényi parameter, and vice versa (Słomczynski et al., 2000): scale-free systems lead to different probability outcomes, based solely on increases or decreases of the scaling slope. In sum, the "probabilistic" virtues of Rényi entropy represent a novel physics-based approach to probe brain scale-free dynamics, with the potential to lead to new insights into brain systems at all space-time scales and all levels of complexity.

Once elucidated why Rényi entropy is more suitable than Shannon's, in the next paragraph we will try to answer to the crucial question: what for? How might such a scheme help, in the experimental assessment of brain pink noise? Can the variations (fluctuations) in Rényi entropy can be correlated with the values of a circle perimeter (standing for 360 degrees angles of our toy example rotations)? Our moving toy might help to elucidate the issue. Indeed, toy rotations form an angle on a 360 degrees circumference, so that every angle corresponds to a different shadow, i.e., to a different value of Rényi entropy (**Figures1B** and **1C**). In neurophysiological terms, we are allowed to calculate the changes in brain scaling slopes, just by evaluating a full spectrum of the corresponding Rènyi entropies. The procedure will be described in the next paragraph.

WORKING ON RANDOMLY GENERATED ANGLES

Here we show the procedure in order to correlate our formulation of Rényi entropy with brain scale-free dynamics. We performed simulations of randomly generated angles (Çankaya et al., 2015) on a 2D circle. Every angle displays a random degree, so that their total sum stands for a 360 degrees full circle. The number of rays originating from the circle's center can be modelled through the cosine theorem, which states that:

$per_i^2 = b_i^2 + c_i^2 - 2b_i c_i Cos(\theta), i = 1,2, \dots n,$

where b and c (which could be randomly generated in simulations) are the length of rays originating from the circle's central point. The parameter per is one of the three sides of the triangle lying on the circle perimeter (**Figure 2, left side**). The randomly generated parameter θ stands for the angle between two rays, while n stands for the number of rays. The sum of per_i, namely $\sum_{i=1}^{n} per_i$, can be regarded as the circle's perimeter. Each set of perimeter values produces just one Rènyi entropy value: therefore, we replicated the simulation one hundred times.

Note that the fluctuations in Rényi entropy values depend just on the different perimeter values. In terms of brain assessment, we evaluate the cortical scale-free activity and the scaling slopes instead of evaluating random numbers. In such a vein, two cerebral hemispheres can be unfolded and flattened into a two-dimensional reconstruction by computerized procedures (Van Essen, 2005). In this model, the nervous electric activity occurs on a 2D brain surface with an approximated circular shape (**Figure 2, left side**). Perimeter values allow us to detect the nervous activity's travel lengths on the brain surface. After the brain signal's travel lengths have been achieved, the corresponding Rènyi Entropy values can be computed ("EntropyEstimation" package: https://cran.r-project.org/web/packages/EntropyEstimation/EntropyEstimation.pdf). **Figure 2, right side,** displays simulated Rényi values obtained from the perimeter values computed through the cosine theorem. In toy's terms, this means that a larger rotation gives rise to higher levels of information detectable from the shadows, while, in brain's terms, the higher the variations in scaling slopes, the higher the detected Rényi entropy and vice versa.

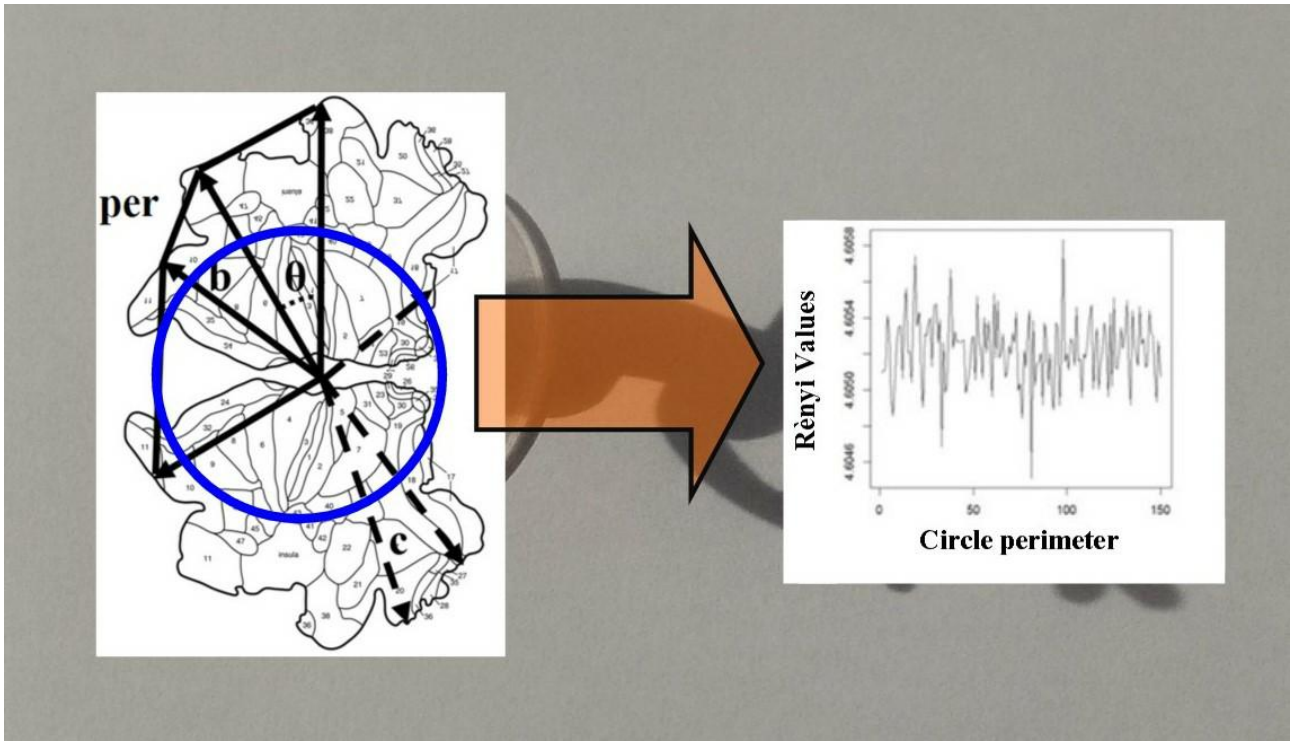

Figure 2. Renyi entropy' circle perimeter and its values (computed by the Renyi.z function in version 3.2.3 of R software) are superimposed, respectively, to the moving toy and its shadow. **Left part**: Cosine theorem for the evaluation of travel length Rényi entropies in a model of two-dimensional brain (modified from Van Essen, 2005). **Right part:** Simulated Rényi values for each circle's perimeter values for n=60 and a Rényi exponent=4; θ is generated from a uniform distribution in (0,1) and multiplied by 360. The Rènyi entropy values' bandwidth is around 4.6.

CONCLUSIONS

We showed that a clear correlation does exist in the brain between cortical scaling slope and brain activity evaluated in terms of probability states. Our approach enables us to achieve unknown scale-free exponents from known entropy changes, allowing us to evaluate the macro-states of the nervous system based on a sole order parameter, although we lack a perfect knowledge of its micro-states. In our simulations, random numbers generated from different distributions are able to modify the values of Rényi entropy: this means that the brain scale-free spectrum can be extrapolated, just starting from the values of entropy experimentally detected in EEG or fMRI traces. Considering the connection between brain activity dynamics and the mental states (Fingelkurts and Fingelkurts, 2001; Fingelkurts et al., 2009, 2010, 2013a), this observation paves the way to tackle the difficult issue of mind reading.

We hypothesize that, in order to optimize its functions, the brain could be equipped with intrinsic mechanisms of scaling features: in this framework, changes in scale-free exponents play a crucial role in information processing, leading to variations in entropy and probability of mental states. Empirical evidence suggests that cognitive tasks are modulated by the scale-free exponents of the brain fluctuation probability function, leading to a shrinking of multifractal spectrum and/or transitions from mono- to multi-fractal distributions (Popivanov et al., 2006; Fraiman and Chialvo, 2012).

This approach paves the way for novel approaches to already existing neural network models (Gravier et al., 2016; MegamNgouonkadi et al., 2016) and for innovative diagnostic and therapeutic strategies. For example, the widely-diffused method of pairwise entropy in neuroimaging techniques (Watanabe et al., 2014; Peters et al., 2017) might benefit of theRényi entropy-based approach. It is indeed feasible to start from known parameters of probability distribution, in order to achieve the unknown values of multifractal slopes. In particular, a change in Rényi exponent, caused by variations in scaling slopes, might lead to different probability outcomes, which can be calculated if just their pairwise entropies are known.
We also conjecture that the scale-free-like brain electric activity - setting aside their supposed relationships with self-organized criticality (Bak et al., 1987; Tozzi, 2015), nonequilibrium steady-state dynamics or second order phase transitions (Papo, 2014; Perkins et al., 2014; Tozzi, 2014; Tozzi and Peters, 2016) - could be modulated through the superimposition of an external electric currents characterized by carefully chosen scale-free exponents. This may have a practical application. For example, our results suggest that transcranial electrical stimulation's techniques need to take into account not only the amplitude and frequency of the applied waveforms (Reato et al., 2013), but also their scaling slope. A further tenable field of application are the diseases that have been linked to disturbance of brain networks - Alzheimer's disease, depression, attention deficit hyperactivity disorder, schizophrenia, autism (Fox and Raichle, 2007; Fingelkurts and Fingelkurts, 2010) -, meaning that they could be ameliorated, or even treated, by appropriate exogenous electromagnetic fields - e.g., via selective application of electric/magnetic waves of specific scale-free exponent on target micro-areas - able to "recover" and restore the physiological brain functions (Sunderam et al., 2009; Fingelkurts and Fingelkurts, 2010, 2015) and related subjective experiences (Fingelkurts et al., 2013b).

ACKNOWLEDGEMENTS

The Authors would like to thank Andrew and Alexander Fingelkurts for commenting upon an earlier version of this manuscript.

BIBLIOGRAPHY

1) A-yeh E, Peters JF (2016) Rényi entropy in measuring information levels in Voronoï tessellation cells with application in digital image analysis. Theory Appl Math Comput Sci 6(16):77–95
2) Bak P, Tang C, Wiesenfeld K (1987) Self-organized criticality: An explanation of the 1/f noise. Physical Review Letters, 59(4):381-384. PMID: 10035754
3) Buiatti M, Papo D, Baudonnière P-M, van Vreeswijk C(2007) Feedback modulates the temporal scale-free dynamics of brain electrical activity in a hypothesis testing task. Neuroscience 146:1400-1412. doi:10.1016/j.neuroscience.2007.02.048
4) Buzsáki G, Watson BO(2012) Brain rhythms and neural syntax: implications for efficient coding of cognitive content and neuropsychiatric disease. Dialogues in Clinical Neurosciences 4:345-367

5) CambellLL (1965) A coding theorem and Rényi entropy. Information and Control 8(4):423-429
6) Çankaya MN, Bulut YM, Doğru FZ, Arslan O (2015) A Bimodal Extension of the Generalized Gamma Distribution.RevistaColombiana de Estadística 38(2):371-378
7) Carranza ML, Acosta A, Ricotta C (2007)Analyzing landscape diversity in time: the use of Rényi's generalized entropy function. Ecological Indicators 7:505-510
8) Costa M, Goldberger AL, Peng CK (2005) Multiscale entropy analysis of biological signals. Phys Rev E Stat Nonlin Soft Matter Phys 71(2):021906
9) de Arcangelis L, Herrmann HJ(2010) Learning as a phenomenon occurring in a critical state. Proceedings of the National Academy of Sciences 107:3977-3981
10) De Luca E, Novelli C, Barbato F, Menegoni P, Iannetta M, Nascetti G (2011)Coastal dune systems and disturbance factors: monitoring and analysis in central Italy. Environmental Monitoring and Assessment 183: 437-450
11) Déli E, Tozzi A, Peters JF (2017) Relationships between short and fast brain timescales. Cognitive Neurodynamics11(6):539–552
12) Dong X(2016) The gravity dual of Rényi entropy. Nature Communications 7:12472. doi:10.1038/ncomms12472
13) Drius M, Malavasi M, Rosario Acosta AT, Ricotta C, Carranza ML (2013)Boundary-based analysis for the assessment of coastal dune landscape integrity over time. Applied Geography 45:41–48
14) Fetterhoff D, Opris I, Simpson SL, Deadwyler SA, Hampson RE, Kraft RA (2014) Multifractal analysis of information processing in hippocampal neural ensembles during working memory under Δ9-tetrahydrocannabinol administration. Journal of Neuroscience Methods pii: S0165-0270(14)00264-7. doi: 10.1016/j.jneumeth.2014.07.013
15) Fingelkurts AA,Fingelkurts AA (2001) Operational architectonics of the human brain biopotential field: Towards solving the mind-brain problem. Brain and Mind 2:261–296
16) Fingelkurts AA,Fingelkurts AA (2010) Alpha rhythm operational architectonics in the continuum of normal and pathological brain states: Current state of research. International Journal of Psychophysiology 76:93–106
17) Fingelkurts AA,Fingelkurts AA (2015) Operational architectonics methodology for EEG analysis: Theory and results. Neuromethods 91: 1–59, DOI 10.1007/7657_2013_60
18) Fingelkurts AA,Fingelkurts AA, Neves CFH (2009) Phenomenological architecture of mind and operational architectonics of the brain: The unified metastable continuum. New Math Nat Comput 5:221–244
19) Fingelkurts AA,Fingelkurts AA, Neves CFH (2010) Natural world physical, brain operational, and mind phenomenal space-time. Phys Life Rev 7:195–249
20) Fingelkurts AA,Fingelkurts AA, Neves CFH (2013a) Consciousness as a phenomenon in the operational architectonics of brain organization: Criticality and self-organization considerations. Chaos Solitons Fract 55: 13–31
21) Fingelkurts AA,Fingelkurts AA, Neves CFH (2013b) The structure of brain electromagnetic field relates to subjective experience: Exogenous magnetic field stimulation study. Presented at Neuroscience Finland 2013 Meeting: Optogenetics and brain stimulation, March 22, 2013, Helsinki, Finland.
22) Fox MD, Raichle ME (2007) Spontaneous fluctuations in brain activity observed with functional magnetic resonance imaging. Nature Review Neuroscience 8:700-711
23) Fraiman D, Chialvo DR (2012) What kind of noise is brain noise: anomalous scaling behavior of the resting brain activity fluctuations. Frontiers in Physiology 3:307 doi: 10.3389/fphys.2012.00307.
24) Gorelick R (2006) Combining richness and abundance into a single diversity index using matrix analogues of Shannon's and Simpson's indices. Ecography 29:525–530
25) Gravier A, Quek C, Duch W, Wahab A, Gravier-RymaszewskaJ(2016) Neural network modelling of the influence of channelopathies on reflex visual attention. CognNeurodyn. Feb;10(1):49-72. doi: 10.1007/s11571-015-9365-x. Epub 2015 Nov 9
26) He BJ, Zempel JM, Snyder AZ, Raichle ME(2010) The temporal structures and functional significance of scale-free brain activity. Neuron 66(3):353-369doi: 10.1016/j.neuron.2010.04.020.
27) Hentschel GHE, ProccaciaI (1983) The infinite number of generalized dimensions in fractals and strange attractors. Physica D 8(3):435-444
28) Jauregui M, Zunino L, Lenzi EK, Mendes RS, Ribeiro HV (2018)Characterization of time series via Rényi complexity-entropy curve. Proc R Soc Lond Ser A, Math Phys Eng Sci 498:74-85

29) Jirsa VK, Stacey WC, Quilichini PP, Ivanov AI, Bernard C (2014) On the nature of seizure dynamics. Brain 137(Pt 8), 2210-2230. doi: 10.1093/brain/awu133.
30) Jizba P, ArimitsuT (2001) The world according to Renyi: thermodynamics of fractal systems. AIP Conf Proc 597:341-348
31) Jizba P, Kleinert H, Shefaat M(2012)Rényi information transfer between financial time series. Physica A, 391(10): 2971
32) Jizba P, Korbel J(2014) Multifractal diffusion entropy analysis. Physica A 413:438-458
33) JostL (2007) Partitioning diversity into independent alpha and beta components. Ecology 88(10):2427-2439
34) JostL (2010) The relation between evenness and diversity. Diversity 2:207-232.
35) Linkenkaer-Hansen K, Nikouline VV, Palva JM., Ilmoniemi RJ. 2001. Long-range temporal correlations and scaling behavior in human brain oscillations. Journal of Neuroscience 21(4):1370-1377
36) MegamNgouonkadi EB, Fotsin HB, KabongNono M, LouodopFotsoPH (2016) Noise effects on robust synchronization of a small pacemaker neuronal ensemble via nonlinear controller: electronic circuit design. CognNeurodyn 2016 Oct;10(5):385-404. doi: 10.1007/s11571-016-9393-1. Epub 2016 Jun 11.
37) Milstein J, Mormann F, Fried I, Koch C (2009) Neuronal shot noise and Brownian 1/f2 behavior in the local field potential. PLoS One 4(2):4338 doi: 10.1371/journal.pone.0004338.
38) Müller F, Hoffmann-Kroll R, Wiggering H (2000) Indicating ecosystem integrity e theoretical concepts and environmental requirements. Ecological Modelling 130:13-23
39) Newman MEJ (2005) Power laws, Pareto distributions and Zipf's law. Contemporary Physics 46:323-351
40) Papo D (2014) Functional significance of complex fluctuations in brain activity: from resting state to cognitive neuroscience. Frontiers in Systems Neuroscience 8:112 doi: 10.3389/fnsys.2014.00112.
41) Patil GP, Taillie C (2001) A multiscale hierarchical Markov transition matrix model for generating and analyzing thematic raster maps. Environmental and Ecological Statistics 8:5-20
42) Perkins TJ, Foxall E, Glass L, Edwards R (2014) A scaling law for random walks on networks. Nature Communications 5:5121. doi: 10.1038/ncomms6121.
43) Peters JF (2017) Foundations of Computer Vision. Computational Geometry, Visual Image Structures and Object Shape Recognition. Springer Int. Pub. AG, DOI 10.1007/978-3-319-52483-2.
44) Peters JF, RamannaS (2016) Maximal nucleus clusters in Pawlak paintings. Nerves as approximating tools in visual arts. Proc Fed Conf on Comp Sci and Info Systems 8:199-202 DOI: 10.15439/2016F004.
45) Peters JF, Tozzi A, Ramanna S, İnanE (2017) The human brain from above: an increase in complexity from environmental stimuli to abstractions. Cognitive Neurodynamics 11(4):391–394
46) PodaniJ (1992) Space series analysis: processes reconsidered. Abstracta Botanica 16:25–29
47) Popivanov D, Stomonyakov V, Minchev Z, Jivkova S, DojnovP, et al. (2006)Multifractality of decomposed EEG during imaginary and real visual-motor tracking. Biological Cybernetics 94:149–156
48) Pritchard WS (1992) The brain in fractal time: 1/f-like power spectrum scaling of the human electroencephalogram. International Journal of Neuroscience 66:119-129
49) Reato D, Rahman A, Bikson M, Parra LC (2013)Effects of weak transcranial alternating current stimulation on brain activity-a review of known mechanisms from animal studies. Frontiers in Human Neuroscience 7:687
50) Rényi A (1961) On measures of entropy and information. Proc Fourth Berkeley Symp Math Stat and Probability vol I, Berkeley, CA, University of California Press 547-457,MR0132570
51) Rényi A (1966) On the amount of information in a random variable concerning an event. J Math Sci 1 30-33, MR0210263
52) Ricotta C, AvenaG (2003) On the relationship between Pielou's evenness and landscape dominance within the context of Hill's diversity profiles. Ecological Indicators 2:361–365
53) Rocchini D, Delucchi L, Bacaro G, Cavallini P, Feilhauer H, et al. (2013)Calculating landscape diversity with information-theory based indices: A GRASS GIS solution. Ecological Informatics 17:82–89
54) Shannon CE (1948) A Mathematical Theory of information. The Bell System Technical Journal 27:379-423.
55) Shalymov DS, Fradkov AL (2016)Dynamics of non-stationary processes that follow the maximum of the Rényi entropy principal. Proc R Soc Lond SerA Math Phys Eng Sci 472(2185):20150324
56) Słomczynski W, Kwapien J, Zyczkowski K (2000) Entropy computing via integration over fractal measures. Chaos 10(1):180-188
57) Suckling J, Wink AM, Bernard FA, Barnes A, BullmoreE (2008) Endogenous multifractal brain dynamics are modulated by age, cholinergic blockade and cognitive performance. Journal of Neuroscience Methods 174(2): 292-300. doi:10.1016/j.jneumeth.2008.06.037.

58) Sunderam S, Chernyy N, Peixoto N, Mason JP, Weinstein SL, et al. (2009) Seizure entrainment with polarizing low-frequency electric fields in a chronic animal epilepsy model. Journal of Neural Engineering 6(4):046009 doi: 10.1088/1741-2560/6/4/046009.
59) Tinker J, Velazquez JL (2014) Power law scaling in synchronization of brain signals depends on cognitive load. Frontiers in Systems Neuroscience 8:73 doi: 10.3389/fnsys.2014.00073.
60) Tozzi A (2014) Evolution: Networks and Energy Count. Nature 515:343 doi:10.1038/515343c.
61) Tozzi A (2015) How to Turn an Oscillation in a Pink One. Journal of Theoretical Biology 377:117–118 doi:10.1016/j.jtbi.2015.04.018.
62) Tozzi A, Peters JF (2016) Towards a fourth spatial dimension of brain activity. Cognitive Neurodynamics 10(3):189–199
63) Tribukait A, EikenO (2016) On the time course of short-term forgetting: a human experimental model for the sense of balance. Cognitive Neurodynamics 10(1):7–22
64) Tsallis C (1988) Possible generalization of Boltzman-Gibbs Statistics Journal of Statistical Physics 52(2):479-487
65) Van de Ville D, Britz J, Michel CM (2010)EEG microstate sequences in healthy humans at rest reveal scale-free dynamics PNAS 107(42):18179-18184 doi: 10.1073/pnas.1007841107.
66) Van Essen DC (2005) A Population-Average, Landmark- and Surface-based (PALS) atlas of human cerebral cortex. Neuroimage 28:635–666
67) Watanabe T, Masuda N, Megumi F, Kanai R, Rees G (2014) Energy landscape and dynamics of brain activity during human bistable perception. Nat Commun 28 5:4765 doi: 10.1038/ncomms5765.
68) Wink AM, Bullmore E, Barnes A, Bernard F, Suckling J (2008)Monofractal and multifractal dynamics of low frequency endogenous brain oscillations in functional MRI. Human Brain Mapping 29(7):791-801 doi: 10.1002/hbm.20593.

Neuroscience Letters 683 (2018) 138–143

Contents lists available at ScienceDirect

Neuroscience Letters

journal homepage: www.elsevier.com/locate/neulet

EEG dynamics on hyperbolic manifolds

Arturo Tozzi[a,b,*], James F. Peters[b,c], Norbert Jaušovec[d]

[a] Center for Nonlinear Science, Department of Physics, University of North Texas, Denton, TX, 76203, USA; 1155 Union Circle, #311427, Denton, TX, 76203-5017, USA
[b] Computational Intelligence Laboratory, University of Manitoba, Winnipeg, R3T 5V6, Manitoba, Canada; Department of Electrical and Computer Engineering, University of Manitoba, 75A Chancellor's Circle, Winnipeg, Manitoba, R3T 5V6, Canada
[c] Department of Macthematics, Adıyaman University, 02040, Adıyaman, Turkey; Department of Mathematics, Faculty of Arts and Sciences, Adıyaman University, 02040, Adıyaman, Turkey
[d] Department of Psychology, University of Maribor, Koroska Cesta 160, 2000, Maribor, Slovenia

ARTICLE INFO

Keywords:
Topology
Mirzakhani
Brain
Hyperbolic
Manifold
Polynomials

ABSTRACT

Biological activities, including cellular metabolic pathways, protein folding and brain function, can be described in terms of curved trajectories in hyperbolic spaces which are constrained by energetic requirements. Here, starting from theorems recently-developed by a deceased Field Medal young mathematician, we show how it is feasible to find and quantify the shortest, energy-sparing functional trajectories taking place in nervous systems' concave phase spaces extracted from real EEG traces. This allows neuroscientists to focus their studies on the few, most prominent functional EEG's paths and loops able to explain, elucidate and experimentally assess the rather elusive mental activity.

1. Introduction

The scientific knowledge of physical dynamics is currently more advanced than their biological counterparts, the latter still lacking the required explanatory depth. One of the main reasons for this disparity is that, while physics has been provided with powerful mathematical tools, biology has not. Physics works much better in the description of natural features, because we have recognized its subtending manifolds. To make an example, both general relativity and quantum mechanics describe Nature using mathematical structures, such as tensors and probability theory ([1–3]). Their subtending manifolds (*i.e.*, the phase spaces in which the corresponding activities take place) are well-known and have been experimentally confirmed: general relativity is described on a 3 + 1 dimensional pseudo-Riemannian manifold with tensor fields obeying certain partial differential equations (see, e.g., [4,5]), while quantum field theory is portrayed on an R^4 projective Hilbert space, with operator-valued fields obeying certain Lorentz-invariant partial differential equations and commutation relationships [6].

Concerning biology, to make an example, it is still difficult to understand the information content endowed in brain electroencephalogram (EEG) traces, or to find a definition for life [7,8]. There is no unequivocal definition of such biological dynamics, despite many proposals have been suggested. Apart from the intrinsic problems in describing such elusive phenomena, the very current limit is that the most of the proposed features - from the concept of homeostasis to organization, from adaptation to response to stimuli - are just descriptive. In sum, in neuroscience, as in biology in general, we lack the proper manifolds, and therefore we lack mathematically precise objectivity. This is a huge restraint, because the sole language able to describe in quantitative terms scientific issues is the mathematical one. If we leave apart math, we do not have the proper observables, and neural dynamics are made by observables.

The aim of this paper is to make an effort to provide a mathematical, operational, quantifiable definition of the dynamics of EEG real traces. In particular, to assess neurophysiological issues, we need at first to find the proper manifolds where their operations might take place. Therefore, our goal is to describe these phase spaces, by treating brain EEG activities and their corresponding gradient-descent Langevin equation, in terms of algebraic topology.

2. Towards the manifolds of brain activity

In terms of differential geometry treatments of probability measures, the manifold traced out by sufficient statistics displays negative curvature, *i.e.*, it is concave [9,10]. The term *manifold* refers to a topological space that is locally Euclidean, *i.e.*, a space described by the axioms and postulates of Euclidean geometry, including physical geometry [11]. Moving along this hyperbolic manifold's phase space (*i.e.*, a space with a geometry of constant negative scalar curvature, in which there are infinitely many lines parallel to a given line [12]) requires a

* Corresponding author at: Center for Nonlinear Science, Department of Physics, University of North Texas, Denton, TX, 76203, USA.
E-mail addresses: tozziarturo@libero.it (A. Tozzi), james.peters3@umanitoba.ca (J.F. Peters), norbert.jausovec@um.si (N. Jaušovec).

https://doi.org/10.1016/j.neulet.2018.07.035
Received 12 June 2018; Received in revised form 19 July 2018; Accepted 23 July 2018
Available online 24 July 2018
0304-3940/ © 2018 Elsevier B.V. All rights reserved.

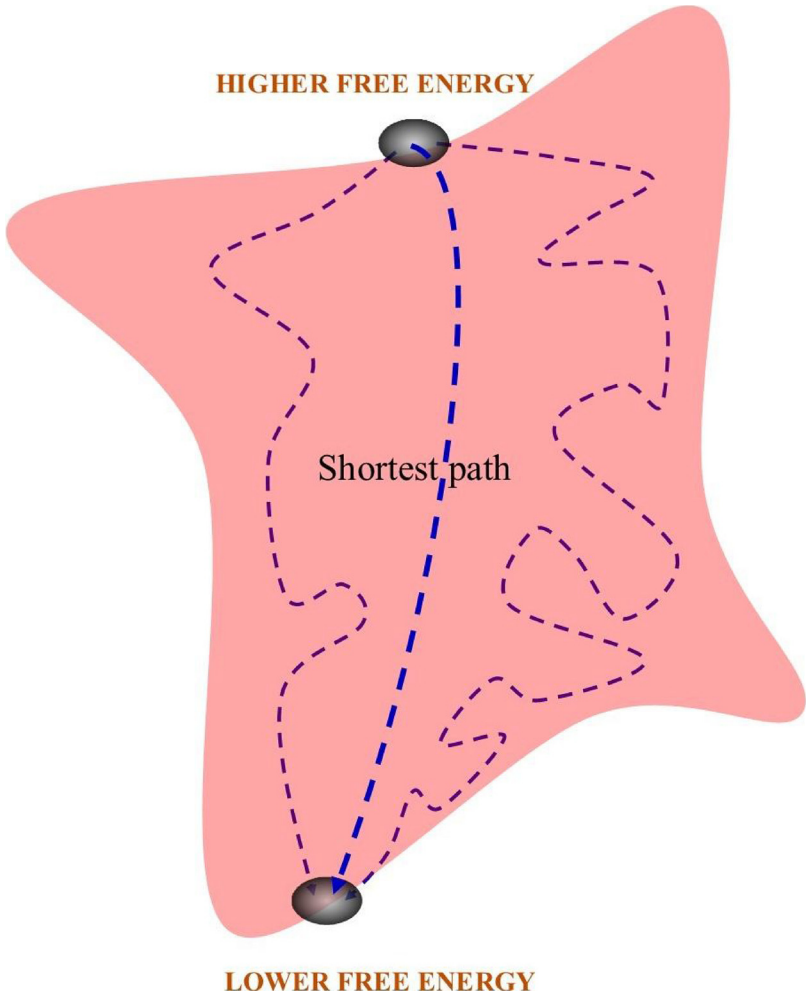

Fig. 1. Phase spaces equipped with sufficient statistics make it possible to rigorously measure distances on a hyperbolic manifold. Biological activities (including, *i.e.*, EEG neural function and protein folding) are here described in term of particles that, due to entropic dictates, tend to choose the shortest available path from points to higher energetic levels to lower ones, i.e., to follow the steepest descent direction in order to attain their nearest free energy minimum [33]. The Figure provides just an example, because in many other cases, such as metabolic and enzymatic cellular pathways, the trajectories can be far more complex. Such phenomena, that cannot be reduced just to jump over the free energy barriers, could be assessed through other approaches, such as, e.g., Monte-Carlo simulations. Modified from: Tozzi et al. [34].

distance measure that can be granted, for example, by Fisher information metric (Fig. 1). A pair of hypebolic planes are metrically equivalent, provided they have the same curvature. Is such a hyperbolic geodetic strategy able to describe living (and in particular nervous) dynamics, or is it just an axiomatically-adopted statistical method? In other words, are hyperbolic spaces viable, when we assess brain activity? The answer is affirmative, because the mathematical concept of concave manifold allows the generalization of the classical notion of Euclidean space. Because complex computational models are required in order to capture the cross-scale dynamics typical of neuroscientific issues [13], hyperbolic structures spread the methods of vector algebra and calculus from two- or three- dimensional Euclidean manifolds to functional spaces with every number of dimensions. Also, hyperbolic manifolds such as, *i.e.*, the Hilbert ones, are vector spaces equipped with an inner product that allows the quantification of lengths and angles. The concave spaces are essential tools in far-flung disciplines, from partial differential equations to quantum mechanics, from Fourier analysis (including heat transfer and EEG signal processing) to ergodic theory (including thermodynamics and information entropies). One might argue that the real dynamics of neural activities do not take place on hyperbolic phase spaces, rather on flat ones, such as the Euclidean world. This objection fades away, if we take into account that all the types of dynamics, both physical and biological, can be abstractly described on hyperbolic manifolds. Indeed, according to recent formulations of the Borsuk-Ulam theorem, matching descriptions between biological features can be provided, independent of the curvature of the subtending manifold [14]. In an operational language, this means that the steps of the nervous system's Langevin equation [15] experimentally detected in the flat, three-dimensional (plus time) Euclidean space, can be transported on a hyperbolic manifold, though, e.g., Levi-Civita or Ehresmann connections [16,17]. Therefore, neural dynamics can be successfully studied on abstract negative-curvature manifolds that mimic the real physical phase space where such processes occur. Here the work of Maryam Mirzakhani, the recently deceased 2014 Field Medal, comes into play, allowing us to calculate the number of trajectories in a hyperbolic phase space.

3. The Mirzakhani theorem

Mirzakhani [18] assessed the "geodesics" of hyperbolic surfaces. On a negative curved surface, geodetics simply stand for the shortest paths between two points. On hyperbolic manifolds, some geodesics are infinitely long (like the straight lines in the Euclidean plane), but others close up smoothly into a loop (like the circumference on a positive-curvature sphere). There are two types of closed geodetics (Fig. 2A and B): the very rare "simple" geodetics, that never intersect themselves, and the much more frequent ones that cut across themselves several times, before closing up. The number of the latter geodetics of a given length L grows exponentially, as their length grows. Mirzakhani demonstrated that also the number of the rare simple geodesics of length L grows, as L gets larger (Fig. 2C and D). However, she showed that, as the length of these simple geodetics grows, their number grows polynomially, instead of exponentially (Fig. 2E). The difference is subtle, but foremost. During an exponential growth, time (or space, or, in our case, the geodesics length) grows as a function K^n, where n is proportional to the size of the input and K is a constant [19]. In turn, during a

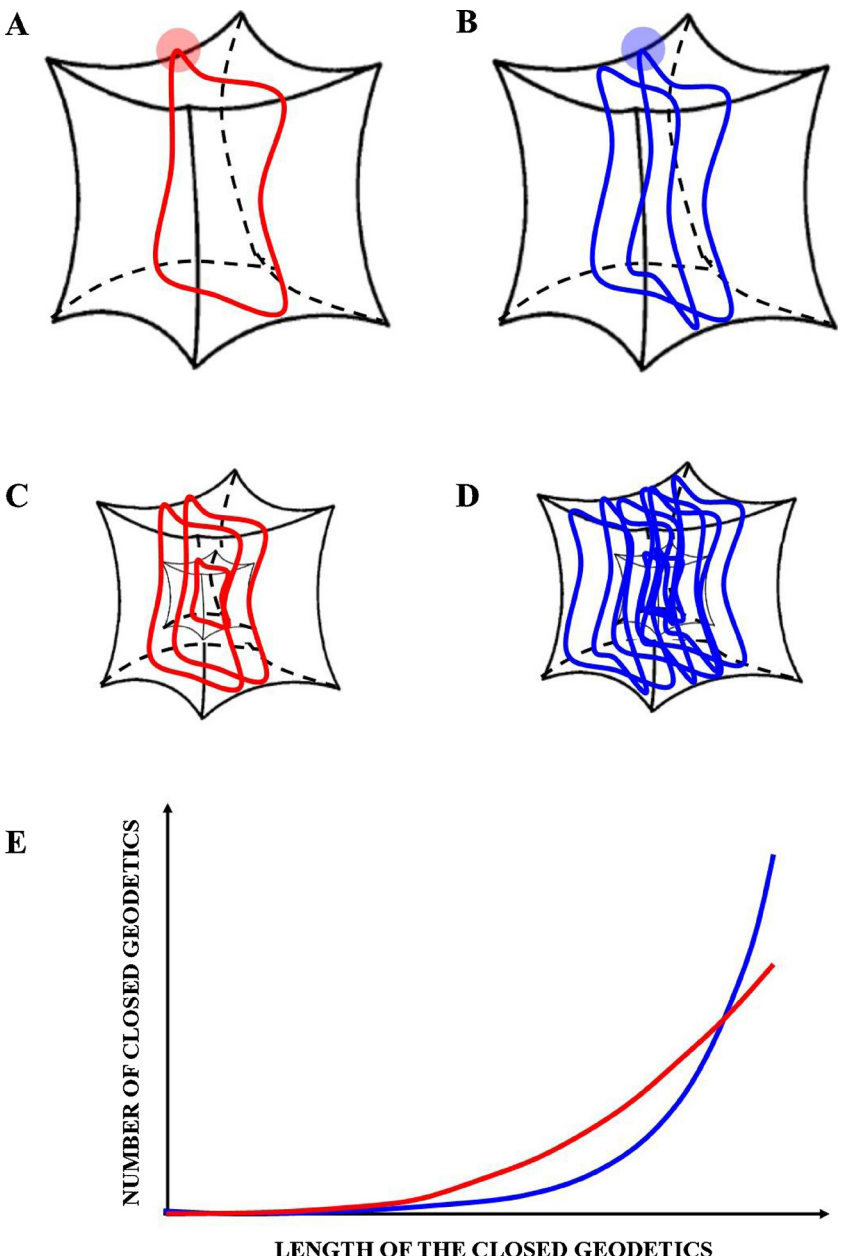

Fig. 2. In this oversimplified sketch, close geodetics on negative-curved manifolds are roughly illustrated. Fig. 2A displays a rare simple geodetics, while 2B depicts the more frequent type, the one that cuts across itself many times before closing up. The colored small circles stand for the point where the closure occurs. Fig. 2C and 2D illustrate the increase in number and length of geodetics, that occurs when a growth in manifold size takes place. The graph in Figure E shows how the two types of closed trajectories display a different behavior: the rare simple geodetics (red line) follow a polynomial growth, while the frequent ones (blue line) follow an exponential growth. (For interpretation of the references to colour in this figure legend, the reader is referred to the web version of this article).

polynomial growth, time (or space, or, in our case, the geodesics length) grows as a function n^k. In the sequel, we will provide the EEG counterparts of the Mirzakhani's findings, in order to operationalize her rather abstract theorem in terms of neural dynamics.

4. How to turn an EEG trace into a hyperbolic path

As an illustrative examlple, we assessed real data extracted from EEG responses to external stimuli. The data used in the present study were part of a larger experiment investigating the influence that gender has on brain responses to emotional stimuli [20]. Stimuli were color slides selected from the International Affective Pictures System [21] according to the valence dimension: emotionally positive (valence ratings from 7.2 to 8.2), neutral (valence ratings from 4.4 to 6.2), and negative (valence ratings from 1.3 to 2.0). The analyzed EEG data trace corresponds to a neutral stimulus (picture No. 5731; see Fig. 3A). EEG was recorded using a Quick-Cap with sintered (Silver/Silver Chloride; 8 mm diameter) electrodes. Using the Ten-twenty Electrode Placement System of the International Federation, the EEG activity was monitored over nineteen scalp locations (Fp1, Fp2, F3, F4, F7, F8, T3,T4, T5, T6, C3, C4, P3, P4, O1, O2, Fz, Cz and Pz). All leads were referenced to linked mastoids (A1 and A2), and a ground electrode was applied to the forehead. Additionally, vertical eye movements were recorded with electrodes placed above and below the left eye. Electrode impedance was maintained below 5 mk. The digital EEG data acquisition and analysis system (SynAmps) had a bandpass of 0.15–100.0 Hz. At cutoff frequencies, the voltage gain was approximately –6 dB. The 19 EEG traces were digitized online at 1000 Hz with a gain of 1000 (resolution of 084 mV/bit in a 16 bit A to D conversion), and stored on a hard disk. The EEG study was done according with Declaration of Helsinki and was approved by the Ethics Committee of the University of Maribor, Slovenia.

The question is whether the 2D traces detected by the above-mentioned EEg procedure can be detected on manifolds equipped with negative curvature. In other words, is it possible to transport EEG traces onto Riemannian hyperbolic manifolds? The answer is positive, if we perform a parallel transport of the two-dimensional trace on a three-dimensional hyperbolic manifold (Fig. 3B). Although parallel-transport

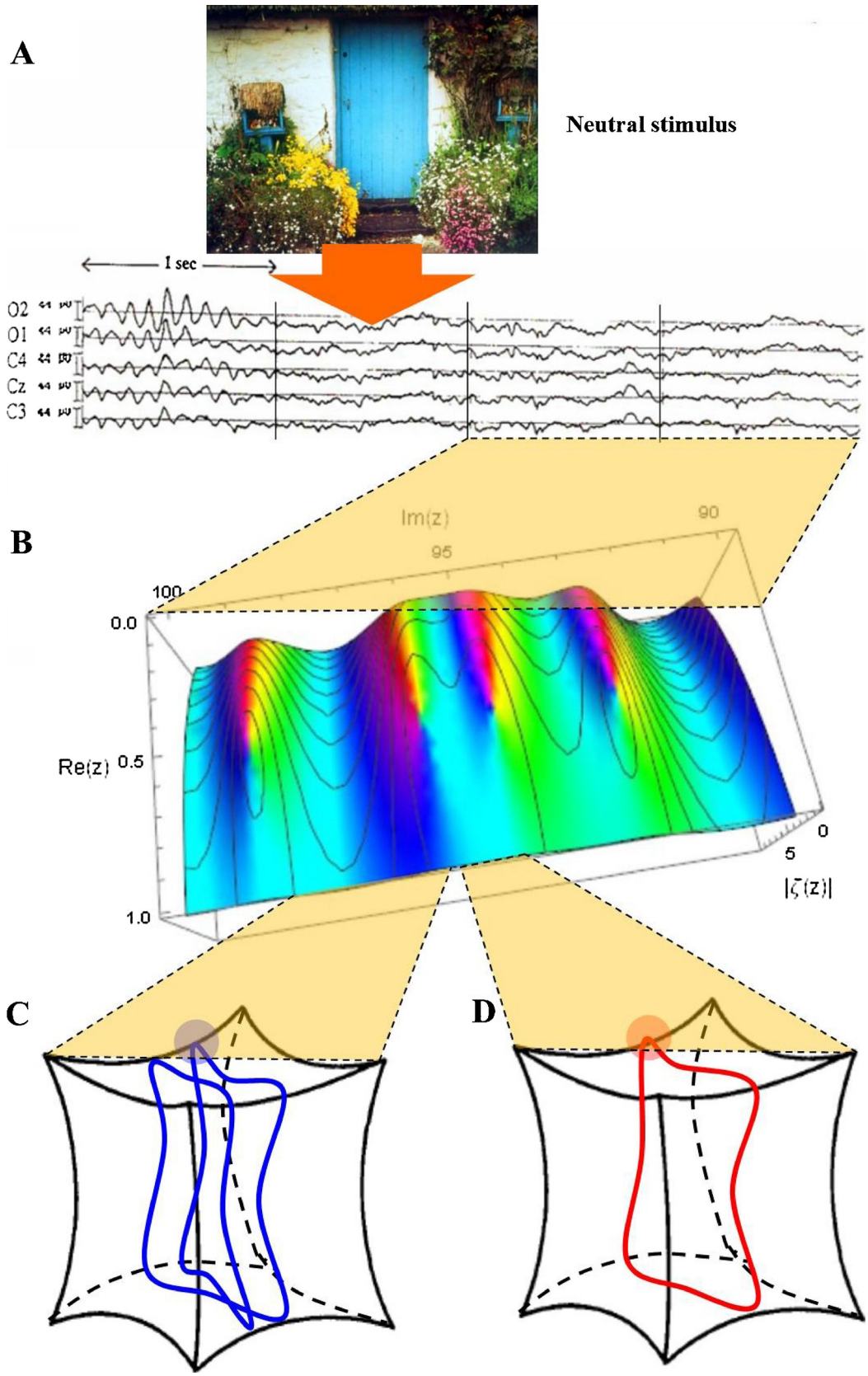

Fig. 3. How to transfer an EEG trace to a hyperbolic manifold. Fig. 3A depicts an EEG trace during and after a neutral visual stimulus. Fig. 3B: in this simulation, the two seconds of the EEG traces following the one-second stimulus are transported to a Riemannian, negative-curvature manifold. Therefore, Fig. 3B shows what the EEG trace looks like on a hyperbolic manifold. Fig. 3C-D: the paths described in Fig. 3B are converted in closed paths taking place on hyperbolic manifolds. Note that the path is closed when the EEG trace touches two times the subtending continuous line. Fig. 3C depicts a EEG pattern that leaves the central value and spends a long time in intersecting circles, before coming back to same value. Fig. 3D depicts a EEG pattern that leaves the central value and spends a short time in a single circle, before coming back to the same value.

requires the solution of a second-order differential equation, analysis shows us that we are allowed to use the first order approximation of the parallel transport, that we pursue in terms of solving geodesic equations for the sufficient statistics [22]. There are different routes one can take to achieve the goal: one needs to resort to one of the following generic transport procedures.

1) Ehresmann connection [17].
2) Levi-Civita connection [23].
3) We can formulate the Hessian operator on the Riemannian manifold in terms of the Laplace-Beltrami operator [24].
4) We can retain a first-order approximation and formulate descent directions that are orthogonal to the previous descent ones, through numerical analysis with the conjugate gradient-descent algorithm [25]. Routinely used in optimization, conjugate gradient descent methods have been used for gradient descent on manifolds traced out by energy functions such as the variational free-energy [26].

Starting from every one of the above-mentioned transport technique, we are able to achieve the mapping of the EEG trace illustrated in Fig. 3A to the hyperbolic Riemannian manifold depicted in Fig. 3B.

Our next goal is to describe such EEG hyperbolic paths in terms of the Mirzakhani theorem. In a previous paragraph, we stated that closed surfaces can be detected on a negative curved surface. Therefore, by using the same transport techniques described above, we achieve EEG paths that come back to the same EEG line's value (Fig. 3C and D). In case of our EEG traces' paths, such closed surfaces are circles on a hyperbolic manifold: every simple circle (corresponding to a Mirzakhani's "simple" geodetics) stands for a EEG path that comes back to the same value in less than 20 ms. More complex circles (corresponding to a Mirzakhani's more frequent geodetics) return to the same point (the central line of the EEG) in a variable, longer time: this means that some EEG traces, before coming back to their central values, describe one or more intersecting circles on the hyperbolic manifold. In other words, EEG traces spend a variable time up or down the central value, and then return to it, describing a variable number of circles which may or may not overlap.

4.1. The math subtending EEG'S neural dynamics

The theorem by Mirzakhani allows us to state that, if the size of a negative curved manifold is progressively increased, curved geodetics of increased length are achieved on its surface. This leads also to a quantifiable increase in their number. In neural terms, the increase in size of the manifold may stand for rather different systems' dynamical features: e.g., either a growth in energy, or in signal complexity, or in the neural units recruited in the brain during a mental task. Note that the Mirzakhani's very rare "simple" geodetics are of foremost importance, when translated in a neural context: indeed, they stand for the shortest paths, i.e., the steepest descent trajectory able to attain the system's nearest free energy minimum. To make a biological example, such kind of short and very efficient energetic paths are the ones that make the folding proteins less frustrated, therefore more efficient in performing their biochemical operations [27]. The Mirzakhani's framework tells us that, when the available free energy increases in the phase space, the most frustrated, and therefore least-performing, proteins display an exponential growth in their number of folding paths, while the less frustrated a polynomial one. The same holds for experimentally detected EEG traces.

Taking into account that the neural dynamics occur on hyperbolic phase spaces, two different EEG nervous activities can be assessed and carefully quantified: the first one is characterized by countless trajectories that slowly close up into loops, while the second one by less frequent trajectories that more quickly close up into loops. This faster activity, which stands for the best available trajectories from higher to lower free-energy states (according to the thermodynamic dictates), might be very important in order to explain the peculiar dynamics of the human brain's electric activity detected through EEG techniques. In turn, the slower activity might stand for the noisier, less efficient and more random dynamics taking place in the brain. The Mirzakhani's approach, when transferred to the neuroscientific realm, provides the recognition and quantification of both the slower and faster nervous activities, allowing researchers to focus efforts and experimental apparatus just on their favored ones. Indeed, these mathematical devices make it possible achieve graphs that illustrate the behavior of both the geodetics occurring in the biological system under evaluation (Fig. 2E).

4.2. Neuroscientific significance

Here we provide a few examples of the effectiveness of such kinds of purely mathematical approaches in the evaluation of biological issues. During a given brain activity (say during perception), several neural assemblies responsible for operations involved in this process are recruited and start to fire [28]. Furthermore, in this process, interactions occur among the members of the assembly (the neurons) as well as between several assemblies in order to mentally present the complex stimulus [29], giving rise to electric paths that take place in a functional hyperbolic phase space. For technical readers, such space can be built and quantitatively assessed through the authoritative tools of differential geometry, parallel transport and dynamics on manifolds described by Sengupta et al. [10]. Some of these trajectories are closed, others are not. In both real and artificial neural networks, these functional loops may follow linear, sigmoid, exponential or logarithmic responses [27,30]. While the most of the closed trajectories follow random walks, a few obey to the dictates of energy optimization, taking the shortest available paths [31]. Despite the random walks of neural ensembles have been proven to be able to encode input stimulus without any specific training [32], nevertheless, the faster, nonrandom, more efficient, polynomial paths of activation described by us are of foremost importance in the brain, because they allow better responses and energy sparing. It is not easy to detect such rare and peculiar polynomial activities among the others. When an increase of the given brain activity takes place (e.g., an increase in perceptive task load) and more neural assemblies are recruited, the closed trajectories on the negative curved manifold grow in number with exponential or polynomial behavior. The feasible operational procedure that we used is the following, provided just as one of the countless examples and possibilities. During a visual perceptual task, brain activity is detected through EEG techniques. At first, we will notice the activation of the visual primary sensory areas, then of the ventral/dorsal visual pathways and frontal areas. The next step is to project such three-dimensional EEG dynamics on a hyperbolic manifold, looking for the closed loops of this brain activity. Our experimental prevision is that, when more neuronal areas will be progressively recruited, we will observe a generalized exponential increase in EEG traces' loops. Furthermore, we will detect the simultaneous presence of a few loops displaying polynomial growth. The latter stand for the most efficient and powerful EEG activities related to the visual task under investigation. Therefore, due to the Mirzakhani's results, it becomes easier for neuroresearchers to detect and separate the two different types of EEG closed trajectories: the less useful grow exponentially, the more efficient ones grow polynomially. This allows scientists, when assessing the "mare magnum" of EEG brain oscillations, to "erase"from their analysis all the useless closed trajectories, and to focus just on the more interesting ones.

5. Conclusions

We made an effort to provide a feasible manifold model, where EEG nervous activities might take place, taking into account that physics is very successful in coping with the complexity of our world, while biology still lacks the required mathematical tools. For this reason, instead of inductively analyze the currently available empirical data,

we proposed to start from a very abstract mathematical framework, in order to formulate top-down previsions that can be experimentally tested.

Based on the recent literature, we introduced a negative curvature, concave, hyperbolic phase space where the functional trajectories of nervous EEG dynamics might take place. Such kind of manifold gave us the possibility to use the theorems developed by Maryam Mirzakhani, the first female mathematician honored with the prestigious Fields Medal Award (corresponding to the Nobel Prize for math), died in 2017 at just 40 years. Her approach allowed us to isolate and rigorously quantify the evolution of two different kinds of EEG neural responses: the exponential and the polynomial ones. It is noteworthy that, during a dynamical process taking place on a negative curvature manifold, at first the increase in polynomial growth is higher, when compared with the exponential one. In turn, when the dynamical process recruits more systems' units, the exponential growth prevails. Our approach suggests that, when assessing the dynamical activity of artificial or real neural networks, it would be preferable to focus the neuroresearch on the more efficient and significant polynomial responses, rather than the linear, sigmoid or exponential ones. Indeed, polynomial functions exhibit many desirable theoretical properties that make them best-suited for the study of nervous activity.

References

[1] H. Yilmaz, Relativity and quantum mechanics, Int. J. Theor. Phys. 21 (10/11) (1981) 871–902.

[2] C. Comte, Symmetry, relativity and quantum mechanics, Il Nuovo Cimento 111 B (8) (1996) 937–956.

[3] P.G. Fré, Gravity, a Geometrical Course. Vol. 1: Development of the Theory and Basic Physical Applications, Springer, 2013, https://doi.org/10.1007/978-94-007-5361-7.

[4] H. Weyl, 1955 [1913] The Concept of a Riemann Surface [Die Idee der Riemannschen Fläche (German)]. Dover, Mineola, NY, 2009, trans. by G.R. MacLane, xii + 191pp., ISBN-13: 978-0-486-47004-7, MR0166351.

[5] H. Weyl, 1988 [1st Ed. 1918, 2nd Ed. 1919, 3rd Ed. 1920]. Raum. Zeit. Materie (German) [Space. Time. Matter, Springer, Berlin, xvi + 349 pp., ISBN: 3-540-18290-X, MR0988402. Reprinted by Dover, NY, 1952, Trans. by H.L. Brose.

[6] M. Tegmark, The mathematical universe, Found. Phys. 38 (2) (2008) 101–150 February 2008.

[7] Chris P. McKay, What is life—and how do we search for it in other worlds? PLoS Biol. 2 (9) (2004) 302, https://doi.org/10.1371/journal.pbio.0020302 PMC 516796 Freely accessible. PMID 15367939.

[8] Edward N. Trifonov, Definition of life: navigation through uncertainties, J. Biomol. Struct. Dyn. 29 (4) (2012) 647–650, https://doi.org/10.1080/073911012010525017 Adenine Press, ISSN 0739-1102. Retrieved 12 January 2012.

[9] T. Tanaka, Information geometry of mean-field approximation, in: M. Opper, D. Saad (Eds.), Advanced Mean Field Methods: Theory and Practice, The MIT Press, 2001, pp. 259–273.

[10] B. Sengupta, A. Tozzi, G.K. Coray, P.K. Douglas, K.J. Friston, Towards a neuronal gauge theory, PLoS Biol. 14 (3) (2016) e1002400, https://doi.org/10.1371/journal.pbio.1002400.

[11] J.F. Peters, Two forms of proximal physical geometry. Axioms, sewing regions together, classes of regions, duality, and parallel fibre bundles, Adv. Math.: Sci. J. 5 (2) (2016) 214–268 ISSN 1857-8438 (electronic version), Zbl 1384.54015.

[12] J.G. Ratcliffe, Foundations of Hyperbolic Manifolds, 2nd ed., Springer, Berlin, 2006 ISBN-10: 0-387-33197-2.

[13] J. Bruineberg, C. Hesp, Beyond blanket terms: challenges for the explanatory value of variational (neuro-)ethology, Phys. Life Rev. 2017 (2017), https://doi.org/10.1016/j.plrev.2017.11.015.

[14] A. Tozzi, J.F. Peters, J. Navarro, W. Kun, B. Lin, P.C. Marijuán, Cellular gauge symmetry and the Li organization principle, Prog. Biophys. Mol. Biol. (2017), https://doi.org/10.1016/j.pbiomolbio.2017.06.004.

[15] P. Langevin, Sur la théorie du mouvement brownien, C. R. Acad. Sci. Paris 146 (1908) 530–533.

[16] T. Levi-Civita, Nozione di parallelismo in una varietà qualunque e conseguente specificazione geometrica della curvatura Riemanniana, Rend. Circ. Mat. Palermo 42 (1917) 73–205, https://doi.org/10.1007/bf03014898.

[17] C. Ehresmann, Les connexions infinitésimales dans un espace fibré différentiable, Colloque de Toplogie, Bruxelles, 1950, pp. 29–55.

[18] M. Mirzakhani, Growth of the number of simpleclosed geodesics on hyperbolic surfaces, Ann. Math. 168 (2008) (2008) 97–125.

[19] J.A. Wolf, Growth of finitely generated solvable groups and curvature of Riemanniann manifolds, J. Differ. Geom. 2 (4) (1968) 421–446.

[20] N. Jaušovec, K. Jaušovec, Emotional intelligence and gender: a neurophysiological perspective, in: A. Gruszka, G. Matthews, B. Szymura (Eds.), Handbook of Individual Differences in Cognition, Springer, New York, New York, NY, 2010, pp. 109–126 Retrieved from http://www.springerlink.com/index/10.1007/978-1-4419-1210-7_7.

[21] P.J. Lang, M.M. Bradley, B.N. Cuthbert, International Affective Picture System (IAPS): Affective Ratings of Pictures and Instructional Manual. Technical Report A-6, University of Florida, Bainesville, FL, 2005.

[22] E. Hairer, C. Lubich, G. Wanner, Geometric Numerical Integration: Structure Preserving Algorithms for Ordinary Differential Equations, Springer, 2004.

[23] W.M. Boothby, An Introduction to Differentiable Manifolds and Riemannian Geometry, Academic Press, 1986 ISBN 0-12-116052-1.

[24] J. Jost, Riemannian Geometry and Geometric Analysis, Springer-Verlag, Berlin, 2002 ISBN 3-540-42627-2.

[25] J.A. Snyman, Springer publishing. Practical Mathematical Optimization: An Introduction to Basic Optimization Theory and Classical and New Gradient-Based Algorithms, (2005) ISBN 0-387-24348-8.

[26] B. Sengupta, K.J. Friston, W.D. Penny, Efficient gradient computation for dynamical models, Neuroimage 98 (2014) 521–527, https://doi.org/10.1016/j.neuroimage.2014.04.040.

[27] A. Tozzi, Fla Tor, J.F. Peters, Building a minimum frustration framework for brain functions in long timescales, J. Neurosci. Res. 94 (8) (2016) 702–716.

[28] A.A. Fingelkurts, A.A. Fingelkurts, C.F.H. Neves, Natural world physical, brain operational, and mind phenomenal space-time, Phys. Life Rev. 7 (2010) 195–249.

[29] A.A. Fingelkurts, A.A. Fingelkurts, C.F.H. Neves, Consciousness as a phenomenon in the operational architectonics of brain organization: criticality and self-organization considerations, Chaos Solitons Fractals 55 (2013) 13–31.

[30] M.D. Zeiler, M. Ranzato, R. Monga, M. Mao, K. Yang, et al., On rectified linear units for speech processing, IEEE International Conference on Acoustics, Speech and Signal Processing (ICASSP), 2013, IEEE, 2013, pp. 3517–3521.

[31] O. Sporns, The non-random brain: efficiency, economy, and complex dynamics, Front. Comput. Neurosci. 5 (2011) 5, https://doi.org/10.3389/fncom.2011.00005 2011.

[32] J.B. George, G.M. Abraham, Z. Rashid, B. Amrutur, S.K. Sikdar, Random neuronal ensembles can inherently do context dependent coarse conjunctive encoding of input stimulus without any specific training, Sci. Rep. 8 (January (1)) (2018) 1403, https://doi.org/10.1038/s41598-018-19462-3.

[33] M.J.D. Ramstead, P.B. Badcock, K.J. Friston, Answering Schrödinger's question: a free-energy formulation, Phys. Life Rev. (2017), https://doi.org/10.1016/j.plrev.2017.09.001 2017 Sep 20. pii: S1571-0645(17)30140-9.

[34] A. Tozzi, B. Sengupta, J.F. Peters, K.J. Friston, Gauge fields in the Central nervous system.The physics of the mind and brain disorders: integrated neural circuits supporting the emergence of mind, in: J. Opris, M.F. Casanova (Eds.), Series in Cognitive and Neural Systems, Springer, New York, 2017, pp. 193–212, , https://doi.org/10.1007/978-3-319-29674-6_9 ISBN: 978-3-319-29674-6.

Available online www.jsaer.com

***Journal of Scientific and Engineering Research*, 2018, 5(7):413-419**

Research Article

ISSN: 2394-2630
CODEN(USA): JSERBR

A NOVEL BELT MODEL OF THE ATOM, COMPATIBLE WITH QUANTUM DYNAMICS

Alexander Yurkin[1], James F. Peters[2], Arturo Tozzi*[3]

[1] Russian Academy of Sciences, Moscow, Puschino, Russia
[2]CI Lab, University of Manitoba, Canada and Mathamatics, Adiyaman University, Adiyaman, Turkey
[3]University of North Texas, Department of physics, Denton, Texas, U.S.A

Abstract Here we provide a novel atomic, paraxial model in which a single belt of electrons surrounds the nucleus. The electronic belt is depicted in terms of broken lines and split wavy trajectories that intersect an axis, giving rise to small angles that can be accurately calculated. We demonstrate that the probabilistic electronic cloud of the atom described by quantum mechanics can be depicted in terms of an electronic belt, because its sizes closely match the descriptions given by de Broglie and Heisenberg. In touch with the claims of the two latter Authors, the wavy trajectories around the nucleus come back to a starting point, so that their orbits are stationary.

Keywords geometry; nucleus; electron; trajectories; geometrization of physics

Introduction

For descriptive purposes, the models of atoms [1 – 3] and molecules are generally represented as spheres. Thomson [12] was the first to provide, in 1904, an atomic model in terms of the motion of a ring of negatively-charged particles inside a uniformly electrified sphere. Another atomic nuclear model, in which an atom consists of a nucleus and electron shells, was then proposed by Rutherford in 1911 [13]. A geometric planetary model of the atomic structure was offered in the form of circle orbits of electrons around a nucleus by Bohr in 1922 [14], and in the form of elliptic orbits by Sommerfeld [1]. Here we propose a novel atomic model described on a two- dimensional manifold that can be generalized in terms of a three-dimensional spherical model.

Concerning the geometrical size [2] of the first atomic shell, the Bohr radius R_B is approximately:

$$R_B \approx 5{,}3 * 10^{-11}\ [\mathrm{m}]. \tag{1}$$

The speed v of the movement of an electron [3] on such first circular orbit is:

$$v \approx 0.0073c \approx 2{,}2 * 10^{6}\ \left[\frac{\mathrm{m}}{\mathrm{s}}\right], \tag{2}$$

where $c \approx 3 * 10^{8}\left[\frac{\mathrm{m}}{\mathrm{s}}\right]$.

The wavelength of this electron [3], in agreement with de Broglie's formula, is:

$$\lambda_e = \frac{2\pi\hbar}{m_e v} \approx 3{,}1 * 10^{-10}[\mathrm{m}], \tag{3}$$

where Plank constant is $\hbar \approx 1{,}05 * 10^{-34}$ [J $*$ s] and the mass of an electron is $m_e \approx 9{,}1 * 10^{-31}$[kg] .
The power of levels, that in Bohr's theory depends on the term n, are defined by the formula [2]:

$$E_n = -\frac{m_e e^4 Z^2}{2\hbar^2 n^2} \sim \frac{1}{n^2}, \tag{4}$$

where the main quantum number is $n = 1, 2, 3, \ldots$, e is a charge of an electron and Z is the atomic serial number.

De Broglie, due to his interpretation of the quantization rule in case of one-electron atom, took into account the phase wave running around an atomic nucleus on a circular orbit of an electron [3]. *If, in an orbit wavelength, λ_e keeps within an integer number of times, then the wave surrounding the nucleus will come back every time to a starting point equipped with the same phase and amplitude. In this case, the orbit turns out to be stationary.* De Broglie wrote down the formula of an orbit's stationarity, or the rule of quantization:

$$\frac{2\pi R}{\lambda_e} = n, \tag{5}$$

where R is the radius of a circular orbit and n is an integer which stands for the main quantum number.

For an orbit of Bohr's radius of $R = R_B$ and $n = 1$, the expression (5) will turn out to be:

$$\frac{2\pi R_B}{\lambda_e} = 1, \tag{6}$$

where

$$\lambda_e = 2\pi R_B. \tag{7}$$

The atomic nucleus' radius is accurately defined by the formula [2, 4]:

$$r = 1{,}3 * 10^{-15} A^{1/3} \text{ [m]}, \tag{8}$$

where A is the number of nucleons in a nucleus. Thus:

$$R >> r. \tag{9}$$

In our previous binomial atomic model [5], we provided a novel framework termed the *one belt model of the atom.* In [6], we described the required relationships among trajectories, angles and the four quantum numbers, demonstrating that our geometrical model does not contradict the Pauli principle. Further geometrical properties of this model were described in earlier works [7, 8]. In [5], a geometrical explanation of the splitting of atomic spectrum was provided. In [9], the possibility to transfer such geometric model to biology was suggested. The paper [5] also provides images of various trajectories, illustrating how they match the known models of electronic clouds in an atom [1]. The geometrical interpretation of particles' trajectories with integer and half-integer spin values has been separately given in [10], where attention was called to the ancient atomists Epicurus and Lucretius. This approach differs from Ishkhanov [4], who referred just to the ancient atomist Democritus.

In the present work, we build our model on the basis of both the de Broglie's hypothesis of the wave nature of particles [1 - 3] and the Heisenberg's uncertainty relation [1 - 3]. Our model displays a circular scale that is stretched six times, compared with the different treatment provided in [5, 9]. As well as in the previous works, we give a geometrical atomic description by using simple tools, such as compasses, a ruler and the same

paraxial approach widely used for the calculation of optical instruments. Also, our model does not contradict the probabilistic approaches of quantum theory [1-3]: indeed, the binomial distribution that stands for the main tenet of the probability theory [11], is also the cornerstone of our model [5].

The one belt model is nuclear, but not planetary. Nevertheless, it is possible to draw an analogy with our solar system, but without planets. Our model predicts one nucleus in the center of the atom (similar to the Sun), surrounded by an electronic belt (similar to a belt of asteroids between Mars and Jupiter).

The projection of our model to the drawing plane is provided in **Figure 1**. The general view of the belt model is represented in **Figure 1a**; a wavy trajectory for the first electronic orbit ($n = 1, K - shell$) is displayed in **Figure 1b**; the same trajectory extended in a horizontal tape is depicted in **Figure 1c**.

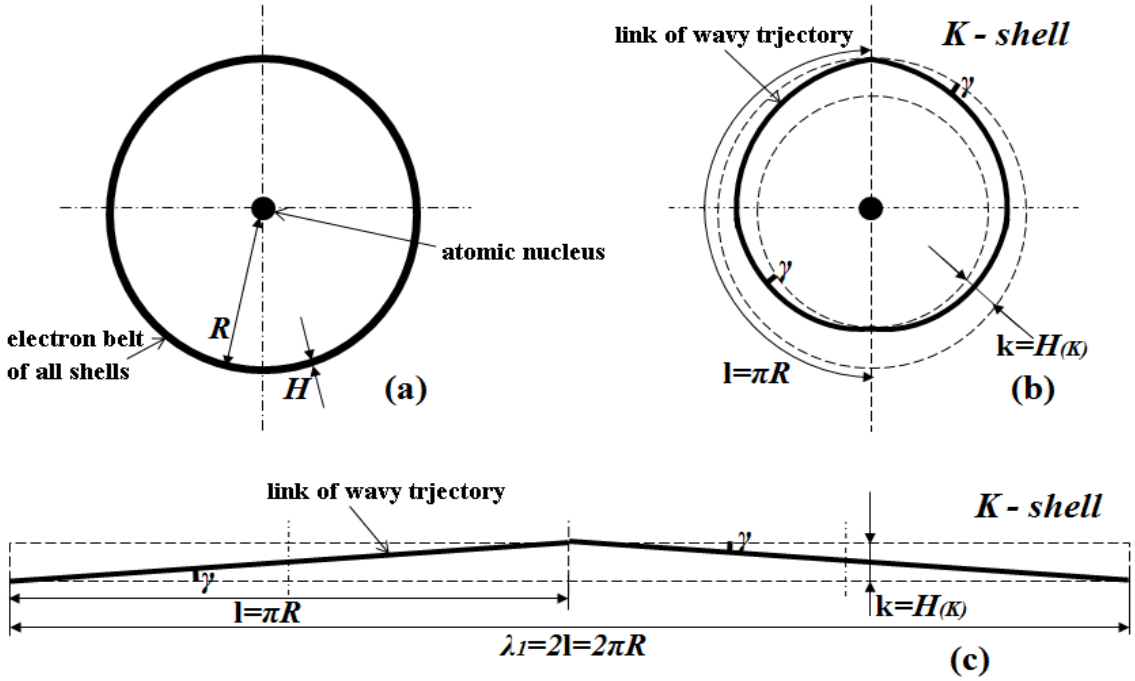

Figure 1: Belt model of the atom.

The plane of the drawing provides a general view of the projection displayed in (a). A wavy trajectory in illustrated in terms of curves (similar to the curves shown in [9]) of the first orbit (b). Note that the radial scale is here increased, compared with the picture (a); furthermore, the wavy trajectory is located in aconcentric coordinate grid with cells of $\mathrm{l} = \pi R$ length along a circle and a radial height of $\mathrm{k} = H_{(K)}$. The same trajectory described in (b) can be displayed on a horizontal tape (c); in this case, the wavy trajectory is located in a rectangular coordinate grid with cells length of $\mathrm{l} = \pi R$ and sells height of $\mathrm{k} = H_{(K)}$.

In our model, the electronic belt displays thickness H and is located at R distance from the nucleus. We assume that:

$$R >> H. \tag{10}$$

In our paraxial approach, we also assume that the speed of the movement of all the electrons on the orbits is identical according to the formula (2), and the length of the shortest wavy trajectory λ_1 equals the electron wavelength for the first electronic orbit ($n = 1, K - shell$):

$$\lambda_1 = \lambda_e \tag{11}$$

according to the formulae (3) and (7).

Generally, the electronic belt consists of several (up to eight [6]) electron shells termed K, L, M, etc., where

$H_{(K)}, H_{(L)}, H_{(M)}$ ... stand for the shells' thickness. The trajectories displayed by these shells settle down in every layer, as shown in [6]. Therefore, we will consider that all the shells are located within a thin electronic belt, where H is the belt thickness.

Our model consists of wavy trajectories. *In our paraxial model, we assume that wavy trajectories going around a nucleus come back to a given starting point, so that the orbits are stationary* in touch with the de Broglie's assumption given above. These trajectories have the appearance of cycles in homology theory, each with its own homology group [15 - 16].

In **Figure 2**, a pattern similar to **Figure 1a** is provided. In a reduced scale, projections to the drawing plane for $K - shell$ (a), $L - shell$ (b), $M - shell$ (c), and $N - shell$ (d) are provided.

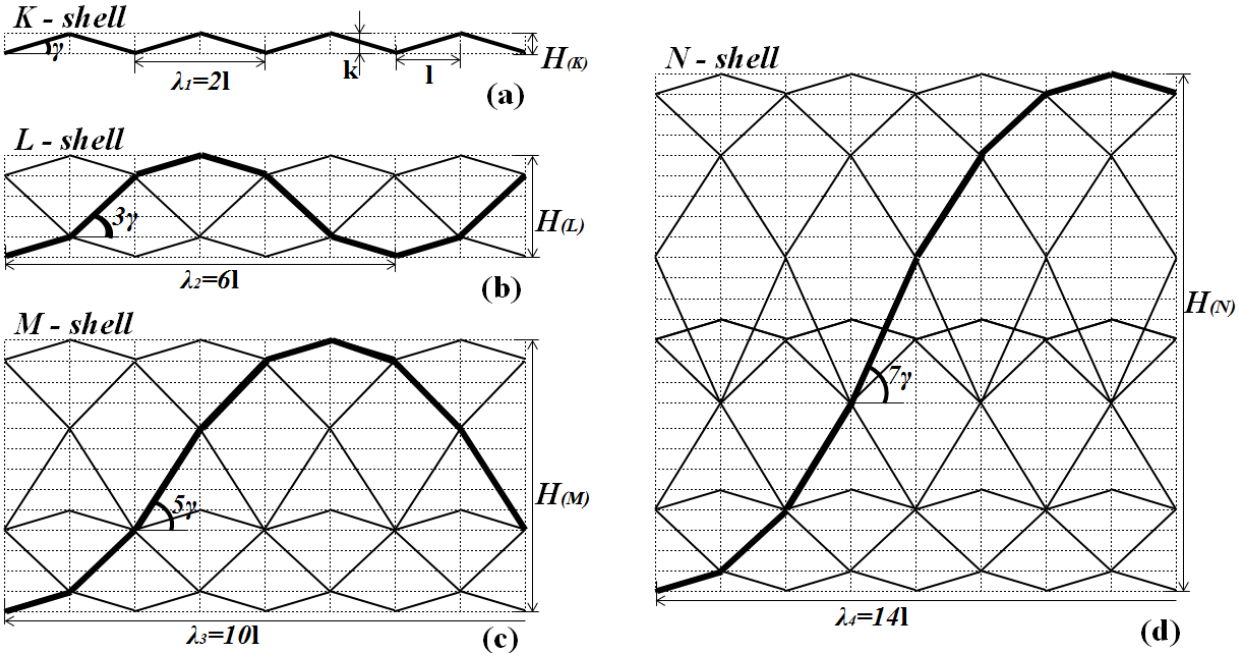

Figure 2: The first four shells of the atom. The thick lines depict wavy trajectories with a length of "waves" of $\lambda_1(a)$, $\lambda_2(b)$, $\lambda_3(c)$, $\lambda_4(d)$ *of* λ_{max}.

From **Figure 2**, some conclusions can be drawn:

•The $K - shell$ contains only one wavy trajectory with a length of "wave" $\lambda_1 = \lambda_{max} = 2\mathrm{l}$, height of $\nu_1 = \nu max = \mathrm{k} = H(K)$, and an angle p of inclination $p1 = pmax = \gamma$.

•The $L - shell$ contains two types of wavy trajectories with lengths of "waves" $\lambda_1 = 2\mathrm{l}$ and $\lambda_2 = \lambda_{max} = 6\mathrm{l}$, height

$\nu_1 = \mathrm{k}$ and $\nu_2 = \nu_{max} = 5\mathrm{k} = H_{(L)}$ and angles $p_1 = \gamma$, $p_2 = p_{max} = 3\gamma$.

•The $M - shell$ contains three types of wavy trajectories with lengths of "waves" $\lambda_1 = 2\mathrm{l}$, $\lambda_2 = 6\mathrm{l}$ and $\lambda_3 = 10\mathrm{l} = \lambda_{max}$, height $\nu_1 = \mathrm{k}$, $\nu_2 = 5\mathrm{k}$, $\nu_3 = 13\mathrm{k} = H_{(M)}$ and angles $p_1 = \gamma$, $p_2 = 3\gamma$, $p_3 = p_{max} = 5\gamma$, etc.

The length of wavy trajectories [6] depends on the number n and grows linearly:

$$\lambda_n = 2(2n - 1)\mathrm{l} \sim n. \tag{12}$$

The height of wavy trajectories and the thickness of a belt of electrons depend on the number n and grows quadratically:

$$\nu_n = (2n^2 - 2n + 1)\mathrm{k} \approx H(n) \sim n^2 \sim \lambda_n^2. \tag{13}$$

This corresponds, in Bohr's theory, to the square dependence of the distance from a nucleus to the orbits of an hydrogen atom [1].

The tilt angle of the links that gives rise to trajectories depends on the number n and grows linearly:

$$p_n = (2n-1)\gamma \sim n \sim \lambda_n. \tag{14}$$

If we take into account that the greatest number of shells in atom does not exceed the number of eight [6], then for the eighth shell (for $R - shell$) we will have:

$$\lambda_{max} = 30\text{l}, \tag{15}$$

$$\nu_{max} = 113\text{k}, \tag{16}$$

$$p_{max} = 15\gamma\,. \tag{17}$$

It is feasible to assume that, at further increases in the specified parameters characterizing an electronic belt, the system of trajectories goes beyond small angles, and the paraxial model won't take place. *In this case, our wavy trajectories around a nucleus won't come back to a starting point and the orbits won't be any more stationary.* Therefore, the atom becomes unstable.

As showed by our geometrical constructions and numerical calculations in [5, 6], the stationary distribution of energy among the trajectories' links gives rise to a dependence similar to the formula (4):

$$E_n \sim -\frac{1}{n^2}. \tag{18}$$

We are also allowed to write down the approximate dependence between the size of an atomic nucleus (8) and the elements of atomic shells:

$$p_n \sim \lambda_n \sim {\nu_n}^{1/2} \sim r. \tag{19}$$

The uncertainty of a coordinate Δx and an impulse Δp of micro-particle are defined by Heisenberg's relation:

$$\Delta x * \Delta p \gtrsim 2\pi\hbar. \tag{20}$$

The coordinates uncertainty of an interatomic electron [1] is commensurable with the atomic sizes and, more precisely, with the size of the first (Bohr's) orbit:

$$\Delta x \approx 10^{-10}\ [\text{m}]. \tag{21}$$

The probability to find an electron near a Bohr's orbit [2] is defined by expression (21). We assume that the thickness of an electronic belt in our model is:

$$H \approx \Delta x \approx 10^{-10}\ [\text{m}]. \tag{22}$$

According to the formulas (13), (16) and (22), the height of a cell (**Figures 1, 2**) of a coordinate grid in which the trajectories are placed will be:

$$\text{k} \approx H/100 \approx 10^{-12}\ [\text{m}]. \tag{23}$$

Because $\lambda_1 = 2\mathrm{l}$ (**Figures 1, 2**) therefore, due to (1) and (11), the length of a cell (**Figures 1, 2**) of a coordinate grid in which the trajectories are placed will be:

$$\mathrm{l} = \pi R_B \approx 10^{-10}\ [\mathrm{m}]. \tag{24}$$

In view of (23), the angle

$$\gamma \approx \mathrm{k}/\mathrm{l} \approx 10^{-2}\ [\mathrm{rad}]. \tag{25}$$

Then, a change of the values (23 – 25) in (12 – 14) allows the numerical estimation of the other elements of our model. In sum, through a simple geometrical construction achieved with compasses, a ruler and a paraxial approach, it is feasible to build a belt model of the atom with short height and long wavy trajectories (in comparison with the atomic radius) around the nucleus. In this paper, we limited ourselves to project our system of trajectories to the two-dimensional plane of the drawing. However, also three-dimensional pictures could be easily built: they would look like a thin (in paraxial approach) disk, or an almost flat toroidal shape with a nucleus in the center of this sphere.

Acknowledgments

We would like to thank Prof. S. Shnol, Prof. V. Mikhalevich, Dr. M. Mysakyan, Dr. A. Shemetov and Dr. O. Nersesyan for useful discussions.

References

[1]. K. A. Putilov and V. A. Fabrikant, Physics course. Vol. 3. Moscow: Fizmatgiz, 1960. (Russian)

[2]. I.V. Savelyev, Course of the general physics (Moscow: Nauka, Vol. 3, 1982). (Russian)

[3]. D. V. Sivykhin. Atomic and Nuclear Physics. Part 1. Atomic Physics. Moscow: Nauka, 1986. (Russian)

[4]. B. S. Ishkhanov, The Atomic Nucleus (Moscow University Physics Bulletin, 2012, Vol. 67, No. 1) pp. 1–24.

[5]. A.V. Yurkin, New, Binomial Model of Atom, Trajectories and Schemes of Energy of Splitting Levels of Atom (IOSR Journal of Engineering (IOSRJEN), www.iosrjen.org ISSN (e): 2250-3021, ISSN (p): 2278-8719 Vol. 07, Issue 02 (Feb. 2017), ||V1||) pp. 19-31).

[6]. A.V. Yurkin, On descriptive geometrical interpretation of the principle of Pauli, elements of the table of Mendeleyev and the Newtonian laminar current of liquid (Progress in physics, Vol. 12, issue 3, April-July) pp. 149.

[7]. A. V. Yurkin, Symmetric triangle of Pascal and arithmetic parallelepiped. On possibility of new evident geometrical interpretation of processes in long pipes. Lambert Academic Publishing, 2015, ISBN: 978-3-659- 38411-0 (ISBN: 978-3-8443-2275-0).

[8]. A.V. Yurkin, Silver ratios, Cardano's formula, and visual model of the second atomic shell (International Journal of Development Research, June, 2016 Vol. 06, Issue 06) pp. 8077-8084. www.journalijdr.com

[9]. A.V. Yurkin, A. Tozzi, J.F. Peters and P.C. Marijuán, Quantifying Energetic Dynamics in Physical and Biological Systems through a Simple Geometric Tool and Geodetic Curves (Progress in Biophysics and Molecular Biology, 131, 2017) pp. 153-161.

[10]. A.V. Yurkin, About new simple interpretation of trajectories of particles with various types of spin **(**IOSR Journal of Engineering (IOSRJEN) www.iosrjen.orgISSN (e): 2250-3021, ISSN (p): 2278-8719 Vol. 07, Issue 12 (December. 2017), ||V1||) pp. 47-50.

[11]. A. N. Kolmogorov, I .G. Zhurbenko and A.V. Prokhorov, Introduction to the theory of probability. Moscow: Nauka, 1995. (Russian)

[12]. J.J. Thomson, On the structure of the atom: An investigation of the stability and periods of oscillation of a number of corpuscles arranged at equal intervals around the circumference of a circle, with application of the results to the theory of atomic structure, Philosophical Magazine Series 6,7: 39 (1904): 237-265, DOI: 10.1080/14786440409463107.

[13]. E. Rutherford, The scattering of alpha and beta particles by matter, Philosophical Magazine 21 (1911): 669-688.

[14]. N. Bohr, Nobel Prize Lecture: The structure of the atom, In Niels Bohr: A Centenary Volume, Harvard University Press, 1985 [1922]: 91-97, ISBN 978-0-674-62415-3.

[15]. J.F. Peters, Proximal planar shape signatures. Homology nerves and descriptive proximity, Advances in Mathematics: Scientific Journal 6 (2017), no. 2, 71-85.

[16]. P. Giblin, Graphs, Surfaces and Homology, 3rd Ed., Cambridge University Press, 1977, 1981, 2010, ISBN 978-0-521-15405-5.

PREPRINT

Citation for this manuscript:
Tozzi, A. (2018, September 1). Sonny Liston and the torn tendon. https://doi.org/10.31236/osf.io/2p7w6

SONNY LISTON AND THE TORN TENDON

Arturo Tozzi, MD, PhD, AAP
Center for Nonlinear Science, University of North Texas, PO Box 311427, Denton, TX 76203-1427, USA
tozziarturo@libero.it

The first Liston-Clay fight in 1964 is still highly debated, because Liston quitted at the end of the sixth round claiming a left shoulder injury. Here we, based on the visual analysis of Sonny's movements during the sixth round, show how a left shoulder's rotator cuff tear cannot be the cause of the boxer failing to answer the bell for the seventh round.

KEYWORDS: boxing; Muhammad Ali; World Heavyweight Championship; Miami Beach; rotator cuff injury

The first fight between Sonny Liston and Cassius Clay took place on February 25, 1964 in Miami Beach. Liston failed to answer the bell for the seventh round and Clay was declared the winner by technical knockout (Remnick, 2000). The fight is one of the most controversial ever: it was the first time since 1919 that a World Heavyweight Champion had quit sitting on his stool. Liston said he had to quit because of a left shoulder injury (Tosches, 2000). However, there has been speculation since about whether the injury was severe enough to actually prevent him from continuing. It has been reported that Sonny Liston had been long suffering from shoulders' bursitis and had been receiving cortisone shots, despite his notorious phobia for needles (Assael 2016). In training for the Clay fight, it has been reported that he re-injured his left shoulder and was in pain when striking the heavy bag. He secretly resorted to heavy icing and ultrasound therapy after each training session. Immediately after the fight, Liston told broadcasters that he hurt the shoulder in the first round. Dr. Alexander Robbins, chief physician for the Miami Beach Boxing Commission, diagnosed Liston with a torn tendon in his left shoulder. During the night, a team of eight doctors inspected Liston's arm at St. Francis Hospital in Miami Beach and agreed that it was too badly damaged for Liston to continue fighting (Gallender 2012). The torn tendon had bled down into the mass of the biceps, swelling and numbing the arm. Those findings were confirmed in a formal investigation immediately after the fight by Florida State Attorney Richard Gerstein, who noticed that there was little doubt that Liston went into the fight with a sore or lame shoulder (Maule, 1964).
Here we provide an analysis of the fight movie, is order to evaluate whether Liston's left arm was damaged enough to prevent him to fight.

MATERIALS AND METHODS

Signs and symptoms rotator cuff injuries. Rotator cuff injuries range from acute reversible tendinitis to massive tears involving the supraspinatus, infraspinatus, and subscapularis. Despite traumatic rotator cuff tears may occur quickly or under heavy load (e.g., lifting a heavy weight) (Craig et al., 2017), the most common cause is repeated micro-trauma, which may occur over several weeks, months or years. In particular, repetitive overhead activities involving the rotator cuff are frequent in several overhead sports activities. To make an example, tennis players and baseball pitchers are especially vulnerable to overuse tears (Shaffer and Huttman, 2014; Menge et al., 2015). Indeed, imbalance between opposing muscle groups (the concentrically contracting muscles that generate force and the eccentrically contracting ones that control movement) may result in overuse injuries of the shoulder.
The main symptoms reported in rotator cuff injuries are: pain, weakness, instability, limited range of motion (ROM) (Moosikasuwan et al., 2005). Other associated symptoms may provide helpful information: swelling, numbness, loss of motion, catching or popping of the shoulder. Symptoms may be relatively acute, either following an injury, or associated with a known repetitive overuse activity. Inspection may reveal swelling, atrophy, asymmetry. Supraspinatus and infraspinatus atrophy can be observed in massive rotator cuff tears and in entrapments of the suprascapular nerve. Despite scapular winging is rare, scapulothoracic motion is often impaired. The biceps tendon can become inflamed and painful.

The active and passive ROM in all planes and scapulohumeral rhythm can be impaired. During active shoulder elevation, patients tend to have a decrease in glenohumeral and an increase in scapulothoracic joint motion (Steinbeck et al, 1998; Wuelker et al., 1998). Also, decreased active elevation with normal passive ROM is usually observed in rotator cuff tears, secondary to pain and weakness. When both active and passive ROM are equally decreased, this suggests onset of adhesive capsulitis. Overhand throwers often develop excess external rotation (up to 15-20°) on the throwing side, usually accompanied by loss of internal rotation on the same side. The impingement syndrome that can be associated with rotator cuff injuries tends to cause pain with elevation ranging from 60-120°. Significant weakness in external rotation is observed in large rotator cuff tears (infraspinatus and teres minor). The dropping of the arm with the elbow extended, in either thumbs down and up position, usually indicates a significant supraspinatus muscle tear. When the patient's shoulder is abducted to 90° and then the arm is lowered slowly to the side in the same arc of movement, severe pain or inability to slowly return the arm to the side indicates a rotator cuff tear. When the shoulder is forcibly forward flexed and internally rotated, the occurrence of pain indicates an overuse injury to the supraspinatus muscle and possibly to the biceps tendon. When the arm is maximally elevated through forward flexion, pain indicates a positive test result for impingement. When the shoulder and elbow are forward flexed to 90° and then the shoulder is internally rotated, pain indicates supraspinatus tendon and greater tuberosity impingement under the coracoacromial ligament and coracoid process. When the examiner forward flexes the arms to 90° and then forcibly internally rotates the shoulder, the occurrence of pain indicates supraspinatus tendonitis.

Assessing possible Liston's rotator cuff injuries. We carefully examined the frames of the original match movie. The assessed movie was taken from: Youtube. "Cassius Clay aka Muhammad Ali v Sonny Liston 1964". Published in 2012, Channel: MIchel Bresson. Length: 35 minutes and 36 seconds. In particular, we evaluated the sixth round, e.g., the round before Liston's quit. We examined the movements performed by both Sonny's arms, looking for the above described signs and symptoms of rotator cuff injuries. Also, we calculated how many times Liston used the right and the left arm the sixth round, in order to punch and counteract Clay's attacks.

RESULTS

No signs of arm swelling and numbing were detectable through a careful inspection of the single frames of the last, sixth round. Furthermore, no symptoms of shoulders' weakness, instability, limited range of motion were noticed. The active and passive range of shoulder joints motion was preserved. The internal and external rotations of the arms, together with flexion and extension of the elbows, did not seem to be impaired. During the sixth round, Sonny Liston raised the left arm 22 times and the right one just 3 times. He carried the right arm at belt level throughout the whole round. In sum, Liston moved the left arm in the ordinary way.

CONCLUSIONS

A rotator cuff tear is very common in sport activities characterized by repetitive lifting or overhead movements. As stated above, the diagnosis of rotator cuff tear in shoulder is characterized by peculiar signs and symptoms. It should be noticed that some rotator cuff tears are not painful, but may still result in arm weakness. At first, the pain may be mild and only occur when lifting the arm over the head. However, over time, the pain may become more noticeable. Shoulder pain and weakness increases with the severity of rotator cuff tear. In this case, the most important symptom is a reduction in shoulder function. In case of a small rotator cuff tear, the patient can often still raise the arm with or without pain, while moderate tears are usually very painful and impair motility. Indeed, partial rotator cuff tear may present just with mild shoulder pain, clicking during shoulder elevation, and mild shoulder weakness lifting the hand above shoulder height, or reaching behind the back. In turn, full thickness rotator cuff tear will generally cause severe shoulder pain and inability to lift the elbow away from the body. In some cases, the rotator cuff tear is so severe that a significant number of pain fibres are also torn, which can make them less painful, but very weak.

When inspecting the movie frames of the Liston-Clay match, the typical signs and symptoms of a rotator cuff tear (i.e., pain when lifting and lowering arm or following specific movements, and weakness when lifting or rotating the arm) were not noticed in Liston's boxing activity. Furthermore, in the sixth round, Liston used mostly the left arm, e.g., the one that was later said to be injured. If the boxer had the left-arm partially or totally injured, it would have used the right one, in order to avoid the pain and to address the left shoulder's impaired motility. This means that Liston's left arm was not damaged enough to prevent him to fight.

REFERENCES

1) Assael S. 2016. The Murder of Sonny Liston: Las Vegas, Heroin, and Heavyweights. Blue Rider Pr.
2) Craig R, Holt T, Rees JL. 2017. Acute rotator cuff tears. BMJ. 2017 Dec 11;359:j5366. doi: 10.1136/bmj.j5366.
3) Gallender PR. 2012. Sonny Liston - The Real Story Behind the Ali-Liston Fights. CreateSpace Independent Publishing Platform. ISBN-13: 978-1478185185

4) Maule T. 1964. "Yes, it was good and honest". Sports Illustrated: 20, March 9, 1964)..
5) Menge TJ, Byram IR, Boykin RE, Bushnell BD. 2015. Labrum and rotator cuff injuries in the throwing athlete. Phys Sportsmed. 2015 Feb;43(1):65-72. doi: 10.1080/00913847.2015.1005546. Epub 2015 Jan 20.
6) Moosikasuwan JB, Miller TT, Burke BJ. 2005. Rotator cuff tears: clinical, radiographic, and US findings. Radiographics. 2005 Nov-Dec;25(6):1591-607.
7) Remnick D. 2000. King of the World: Muhammed Ali and the Rise of an American Hero. Vintage Books Ed. ISBN: 978-0-375-70229-7 (0-375-70229-6)
8) Shaffer B, Huttman D. 2014. Rotator cuff tears in the throwing athlete. Sports Med Arthrosc Rev. 2014 Jun;22(2):101-9. doi: 10.1097/JSA.0000000000000022.
9) Steinbeck J, Liljenqvist U, Jerosch J. 1998. The anatomy of the glenohumeral ligamentous complex and its contribution to anterior shoulder stability. J Shoulder Elbow Surg. 1998 Mar-Apr. 7(2):122-6. [Medline].
10) Tosches N. 2000. The Devil and Sonny Liston. Little, Brown and Company (Boston, New York, London) .
11) Wuelker N, Korell M, Thren K. 1998. Dynamic glenohumeral joint stability. J Shoulder Elbow Surg. 1998 Jan-Feb. 7(1):43-52.

Neuroscience Letters 692 (2019) 41–46

Contents lists available at ScienceDirect

Neuroscience Letters

journal homepage: www.elsevier.com/locate/neulet

Research article

The common features of different brain activities

Arturo Tozzi[a,*], James F. Peters[b,c]

[a] Center for Nonlinear Science, University of North Texas 1155 Union Circle, #311427 Denton, TX 76203-5017, USA
[b] Department of Electrical and Computer Engineering, University of Manitoba, 75A Chancellor's Circle Winnipeg, MB R3T 5V6, Canada
[c] Department of Mathematics, Adıyaman University, 02040, Adıyaman, Turkey

ARTICLE INFO

Keywords:
Neurotechnique
Topology
Micro-level
Macro-level
Neural correlates

ABSTRACT

The term "brain activity" refers to a wide range of mental faculties that can be assessed either on anatomical/functional micro-, meso- and macro- spatiotemporal scales of observation, or on intertwined cortical levels with mutual interactions. Our aim is to show that every brain activity encompassed in a given anatomical or functional level necessarily displays a counterpart in others, i.e., they are "dual". "Duality" refers to the case where two seemingly different physical systems turn out to be equivalent. We describe a method, based on novel topological findings, that makes different manifolds (standing for different brain activities) able to scatter, collide and combine, in order that they merge, condense and stitch together in a quantifiable way. We develop a computational tool which explains how, despite their local cortical functional differences, all mental processes, from perception to emotions, from cognition to mind wandering, may be reduced to a single, general brain activity that takes place in dimensions higher than the classical three-dimensional plus time. This framework permits a topological duality among different brain activities and neuro-techniques, because it holds for all the types of spatio-temporal nervous functions, independent of their cortical location, inter- and intra-level relationships, strength, magnitude and boundaries.

1. Introduction

The brain activity has been classically divided into different functions. Philosophers (e.g., Kant and Locke) viewed the brain activity in terms of sensations, reasoning, intelligence. Similarly, in current neuroscience, the rather general term "brain activity" stands for a large repertoire of brain functions and mental faculties, such as attention and perception, emotions and cognition, memory and learning, higher cognitive processes (decision making, goal-directed choice, etc.) [1], mind wandering [2]. Many neuro-techniques have been developed throughout the years to assess brain activity at different levels of spatio-temporal observation and evaluate the mental correlates of nervous functions [3]. Every brain activity and experimental tool stands for an observational domain of the whole neuro-scientific discipline, able to evaluate a specific anatomical or functional scale. Some approaches assess brain activity at gross-grained levels of observation, such as EEG and lesion studies [4,5]. Others consider a meso-level of observation, e.g., localized brain areas and sub-areas, such as diffuse tensor imaging, MEG analysis and fMRI resting state functional connectivity [6]. Further approaches allow the assessment of more coarse-grained levels, e.g., microcolumns [7], or single-neuron function and structure Tozzi [8]. More reductionist approaches focus on the molecular levels of brain activity: see, for example, Jacobs et al. [9], Ekstrand et al. [10]. Other techniques favor an approach involving many functional and anatomical levels, tackling the issue of brain functions in terms of non-boundary wall domains spanning over every observational dimension and scale [11,12], so that far apart levels interact with each other (Touboul, 2012). Consciousness, for example, does not seem to be confined to a single level [13].

We explore the possibility to assess brain activities and their dimensional scales in terms of algebraic topology. We evaluate whether different mental faculties can be reduced to a more general one, and whether the division of mental faculties (e.g., the spit cognition/emotion) holds true. Topological concepts make it possible to achieve generalizations that allow the mathematical and empirical assessment of every possible brain activity, independent on its scale, magnitude, specific features and local boundaries. Each brain activity endowed in an anatomical or functional level necessarily displays a counterpart in other ones. This leads to novel scenarios, where different brain activities collide, combine and merge together in a testable way. Therefore, all the brain activities and neuro-techniques are *dual* under topological transformation. In physics, the term "dual" refers to a situation where two seemingly different phenomena turn out to be equivalent: the first can be transformed into the second, so that one ends up looking just like

* Corresponding author.
E-mail addresses: tozziarturo@libero.it, Arturo.Tozzi@unt.edu (A. Tozzi), James.Peters3@umanitoba.ca (J.F. Peters).

https://doi.org/10.1016/j.neulet.2018.10.054
Received 8 May 2018; Received in revised form 24 July 2018; Accepted 29 October 2018
Available online 29 October 2018
0304-3940/ © 2018 Elsevier B.V. All rights reserved.

the other [14].

2. Materials and methods

We provide the conceptual framework to assess brain activities in terms of topological shapes that move in multidimensional abstract environments.

2.1. Previous theories

Brain/mind relationships have been tackled by different standpoints, from philosophy – Averroes' unity of intellect, Autrecourt's many intellects (1340), Descartes' duality; Avenarius' empiriocriticism (1907); Dennett's Pandemonium (1991) - to psychology (Ibáñez et al., 2016) and neuroscience [15]. Current neuroscientists split the brain activity in different subsets of mental faculties [16]. Their experimental procedures aim to assess specific observational domains of mental faculties, looking for neural correlates of interacting mental functions [3]. Therefore, neuroscience relies on the tenet that the mind is a functional state of the brain and a clear cortical subdivision among different mental faculties does exist.

Nevertheless, there is no universally agreed definition of what brain/mind's distinguishing properties are. In cognitive neuroscience, "mind" refers to a set of "cognitive" faculties [1,17] i.e., the mental functions which give rise to information processing and embrace: consciousness, perception, attention, different types of memory, language, learning, thinking, judgement, action, attitudes and interaction in the physical, material, social, cultural world [18,19]. "Emotional" states (such as joy, fear, love, hate and so on) [20], alleged to be primitive and subjective, are not encompassed in the definition of the mind as such. Other scientists favor a more general definition of mind, which includes all mental faculties [21]. They argue that rational/emotional states cannot be separated, because, being of the same nature and origin, they should be considered all part of it as mind. We will describe how, despite the local cortical functional differences, mental processes can be reduced to a single, general brain activity.

2.2. Brain activities as moving strings

Brain activities taking place in nervous physical spaces can be assessed in terms of geometric structures, i.e., regions, areas or shapes embedded on the abstract geometric spaces' surface. Every nervous activity is modelled as a series of paths followed by particles traveling through brain's micro-, meso- or macro- areas. Brain activities taking place at lower-levels of observation (e.g., the neuronal level) can be depicted as structures equipped with n-dimensions, while brain activities taking place at higher-levels of observation (e.g., EEG spikes) can be depicted as $n+1$ -dimensional structures.

We term a geometric structure given by a single brain activity: "string" [22], which stands for a region on the surface of both the real cortical physical spaces and the abstract geometric ones. Because a string is the path followed by a particle moving through a single or many brain areas, its shape might display either zero or non-zero width, bounded or unbounded length. The brain is a collection of tiny regions of space, which are vibrant "strings" in ambient space time. A brain can be depicted as a collection of nervous activities in 3 + 1 space-time (an n-dimensional normed linear space) able to project to higher-dimensional functional spaces (an $n+1$-dimensional space). Continuous mappings from lower- to higher-dimensional structures lead to the Borsuk-Ulam theorem ([23,24]).

2.3. Borsuk-Ulam theorem (BUT)

BUT states that a single point on a circumference maps to two antipodal (diametrically opposite) points on a sphere. If we consider antipodal nervous activities confined to a single brain area (i.e., strings defined by the paths followed by cortical currents travelling through a 3 + 1 spacetime) instead of antipodal *points*, BUT leads to a region-based brain geometry ([25,26]), because, in a point-free geometry, regions replace points as the primitives [27,28]. Antipodal regions may also stand for the signals detected by different neuro-techniques, such as spatial/temporal patterns, trajectories, entropies, perceived shape boundary intensities ([28,29]). Hence, BUT provides a way to evaluate changes in information among different anatomical/functional brain levels in a topological space, distinguished from purely anatomical, functional or thermodynamic perspectives. A wide range of brain features (such as intraneuronal dynamics, EEG frequencies, BOLD activity) can be described in terms of antipodal geometric structures (strings) on $n+1$–dimensional structures. Brain signals of different scales and types can be compared, because the two antipodal points assessed at higher-dimensional scales of observation (e.g., EEG macro-levels) can be pulled back to single points at lower-dimensional scales (e.g., histological micro-levels) [26]. The two regions (or activities) do not need necessarily to be antipodal [29]. BUT can also assess non-antipodal features, provided there are a pair of regions, either adjacent or far apart, with the same feature vector ([30,31]). Even though BUT was originally described just for convex spheres, it is also possible to look for antipodal points on other structures [32]: whether a brain activity displays concave, convex or flat geometry, it does not matter, because we may always find the points with matching description predicted by BUT. A cortical projection $\pi(A, B) = E$ for A,B,E $\in$ {*collection* of cortical regions} is a mapping of a pair of cortical regions A,B to a single cortical region E [33,34].

The whole brain can be termed a "*worldsheet*" if every one of its subregions contains at least one string (a brain activity) [35]. In topological terms, "worldsheet" designates a nonempty region of a space completely covered by strings, in which every member is a string ([30,31]). A worldsheet is a special case of a world-volume traced by brain activities (strings) in the cortical 3 + 1 space-time. A brain activity occurs on a curved Riemannian surface of spatial dimension p in a cortical space-time of dimension $p + 1$.

2.4. Increase in brain functional dimensions

Brain theories are formulated in 4 space-time dimensions, where each point is defined by three space coordinates plus time [36]. The classical view of the 3D brain states that all anatomical and functional nervous constituents are bound to a worldsheet that can move within a 4-dimensional space (3 + 1 dimensional space-time). A distinctive feature of brain activities (strings) is their world-volume actions. For example, the complete action A_{M2} of a brain activity is defined with respect to the following:

A_{M2}: kinetic action,

$q = \pm 1$: electric charge of the brain activity,

$A^{[3]}$: 3-form gauge field,

W_3: world volume in 3-dimensional Euclidean space, so that $A_{M2} = A^{kin} \int_{W_3} A^{[3]}$.

This classical scheme has been recently "overthrown" by Peters et al. [37], who demonstrated that the total brain functional activity lies in dimension higher than the usual 3D (plus time) space. Functional increases in brain dimensions give rise to interesting consequences. Although strings embedded in the same wordsheet (i.e., brain activities embedded in the whole brain) are antipodal and share matching description, there is however a difference among the strings embedded in different brain areas. The higher the wordsheet's dimension, the more the information encompassed in strings on the same region, because the number of coordinates is higher. Because strings contain more information than their projections in lower dimensions, a region- and string-based BUT make it possible to evaluate systems features in higher-dimensions, leading to an increase in the amount of detectable information. For example, when you watch at a 3D cat embedded in a

3D plus time environment, your brain perceives a higher dimensional cat, encompassing not just the 3D image, but also its emotional content, the feline species, and so on. In turn, dropping down a dimension means that each region in the lower-dimensional space is simpler. Hence, BUT provides a way to evaluate changes of information among different brain activities in a topological fashion, in addition to the standard mathematical (Maartens, 2010 [35];) and thermodynamic [38] approaches.

2.5. Brouwer's fixed point theorem (FPT)

FPT states that every continuous function from a n-sphere of every dimension to itself has at least one fixed point [39]. FPT applies, e.g., to any disk-shaped area, where it guarantees the existence of a fixed point, which behaves like a whirlpool attracting moving particles. Su [40] gives a coffee cup illustration: no matter how you slosh the coffee around in a coffee cup, some point is always in the same position that it was before the sloshing began. If you move this point out of its original position, you will eventually move some other point in the sloshing coffee back into its original position. In nervous terms, the shape of brain activity, i.e., a string A (denoted str$A$), is the silhouette (the wiring of string str$A$.).

2.6. Wired friend theorem

Every occurrence of a wired friend of a string str$A$ with a particular shape with k features on an n-dimensional brane hypersphere S^n maps to a fixed description that belongs to a ball-shaped neighborhood in R^k.

In neuroscientific terms, we can always find a cortical region containing a single brain function (a string), and every function with a particular shape comes together with another one, termed a *wired friend*. Every occurrence of a wired friend string with a particular shape on the structure S^n maps to a fixed description, *e.g.* to another string that belongs to a manifold (or Euclidean space) with different dimensions. Every wired friend is recognizable by its shape, because the shape of a string is the silhouette of a wired friend string. Therefore, every brain activity (embedded in a higher-dimensional brain macro-level) is the topological description of another brain activity (embedded in a lower dimensional brain micro-level), and vice versa.

In sum, through the topological tools of BUT, FPT and multidimensional approaches, we may state that every brain activity (a string) is the description of another. In the sequel, we will show how the merging of different brain activities, occurring as result of the collision, combination and condensation between single strings [36,41], can be operationalized.

3. Results

We describe the computational tools that allow brain activities to be merged and reduced to just one. FPT tells us that different brain activities, when depicted as geometrical shapes, necessarily have at least a feature in common and are continually transforming into new homotopically equivalent ones. They influence each other by scattering and combining, to create bounded regions in the brain. Hence, brain activities can stick together to become *condensed*, e.g., worldsheets, portrayed as a collection of interacting elements of geometrical shapes. Fig. 1, **A, B** describe how to build a worldsheet encompassing brain activities.

3.1. The merging of brain activities: homotopy equivalence

Brain activity's shapes deform into another, as a result of the collision of a pair of separate shapes. Let a brain activity be represented in Fig. 1**C**. It evolves over time, as it twists and turns through the outer reaches of another one. Fig. 1**D** illustrates an inkling twisting brain activity appearing in the neighborhood of the first one. The two activities begin interacting, so that the first now has a region of space in common with the second (Fig. 1**E**). In effect, due to the interaction, they are partially stitched together. In Fig. 1**F**, a large area of the total brain space occupied by the first activity is partially absorbed by the second. Therefore, we have the birth of a condensed brain activity.

Recall that a brane (e.g., a brain) is a chunk of matter in the cosmos. Let br$A$, brB denote branes. The two branes br$A$, brB become at first connected via at least one open string (not shown) with ends on the branes (Fig. 1**G**), then a complete condensed brane is formed, with concentric branes having a tooth shape (Fig. 1**H**).

Here follows the mathematical treatment for technical readers. Let $f, g: X \to Y$ be a pair of continuous maps. E.g., let $f(X)$ and $g(X)$ be two brain activities with fixed endpoints (i.e., located in a given brain area). A *homotopy* [42] between f and g is a continuous map $H: X \times [0, 1] \to Y$ so that $H(x, 1) = g(x)$ and $H(x, 0) = f(x)$. The interest is in the possibility of deforming (transforming) one brain activity with a particular shape into another with a different shape. This means that the birth of different brain activities, evolving out of the interaction of initially disjoint branes, is allowed. Let $id_X: X \to X$ denote an identity map defined by $id_X(x) = x$. Similarly, $id_Y: Y \to Y$ is defined by $id_Y(t) = y$. The composition $f \circ g(X)$ is defined by $f \circ g(X) = f(g(X))$. Similarly, $g \circ f(X)$ is defined by $g \circ f(X) = g(f(X))$. The sets X and Y are homotopically equivalent, provided there are continuous maps so that $g \circ f(X) \cong \sim id_X(x)$ and $f \circ g \simeq id_y(y)$. [43]. Homotopically equivalent, evolving brain activity shapes which have the same homotopy type lead to a comparison of activities with seemingly varying shapes and sizes.

3.2. Example: homotopically equivalent shapes

A stitching action on a pair of equivalent brain activities is a homotopic mapping that splices them together. Brain activities occuring in branes br$A$, br$B$ are connected, provided there is at least one open string O (denoted by str$O$) with one extremity of str$O$ attached to br$A$ and with the other extremity of *strO* attached to br$B$. This is a further instance of the duality principle in physics. Open strings are strands ending on brain areas [36]. Strings str*O1,* str*O2* have nonempty intersection, provided both strings have extremities attached to the same point on a brain area. That is, one brain activity is the dual of another one, provided the first can be deformed into the second. Let K be a set of open strings and let 2^K be the collection of all subsets in K. The brane in Fig. 1**G** is an example of a Edelsbrunner-Harer nerve [43], which is a collection 2^K such that all nonempty subcollections of Nrv$K$ have a non-void common intersection, i.e., $\mathrm{Nrv}K = \{A \in 2^K: \cap A \neq \emptyset\}$. A sample nerve defined by the intersection of open strings str*O1,* str*O2* is shown in Fig. 1**I**.

In sum, when the two branes (two brain activities) are transformed into a new one, we have instance of their homotopy of equivalence, where the second brane that has completely absorbed the first. To make an example, the idea of "cat" arises from the perception of many single cats of different size, color, etc. This is an instance of the duality principle in brain theories: one brain activity is the dual of another, provided the perceived cat can be deformed into the imagined one. Therefore, there is no longer any difference between the cat I see and the cat I imagine. From what we have observed about BUT, FPT and topological shapes, non-colliding brain activities have at least a few features in common. Examples of such common brain features are: average gradient orientation of brane surface hills (upward slopes) and valleys (downward slopes), persistence (brane lifespan), local brane surface shape (*e.g.*, convex, concave), brane shape as a result of deformation from another shape (see, e.g., tooth shape in Fig. 1**H**), etc.

4. Conclusions

We showed how, despite their local cortical functional differences, mental processes can be reduced to a single, general brain activity. Brain activities, equipped either with antipodal or non-antipodal

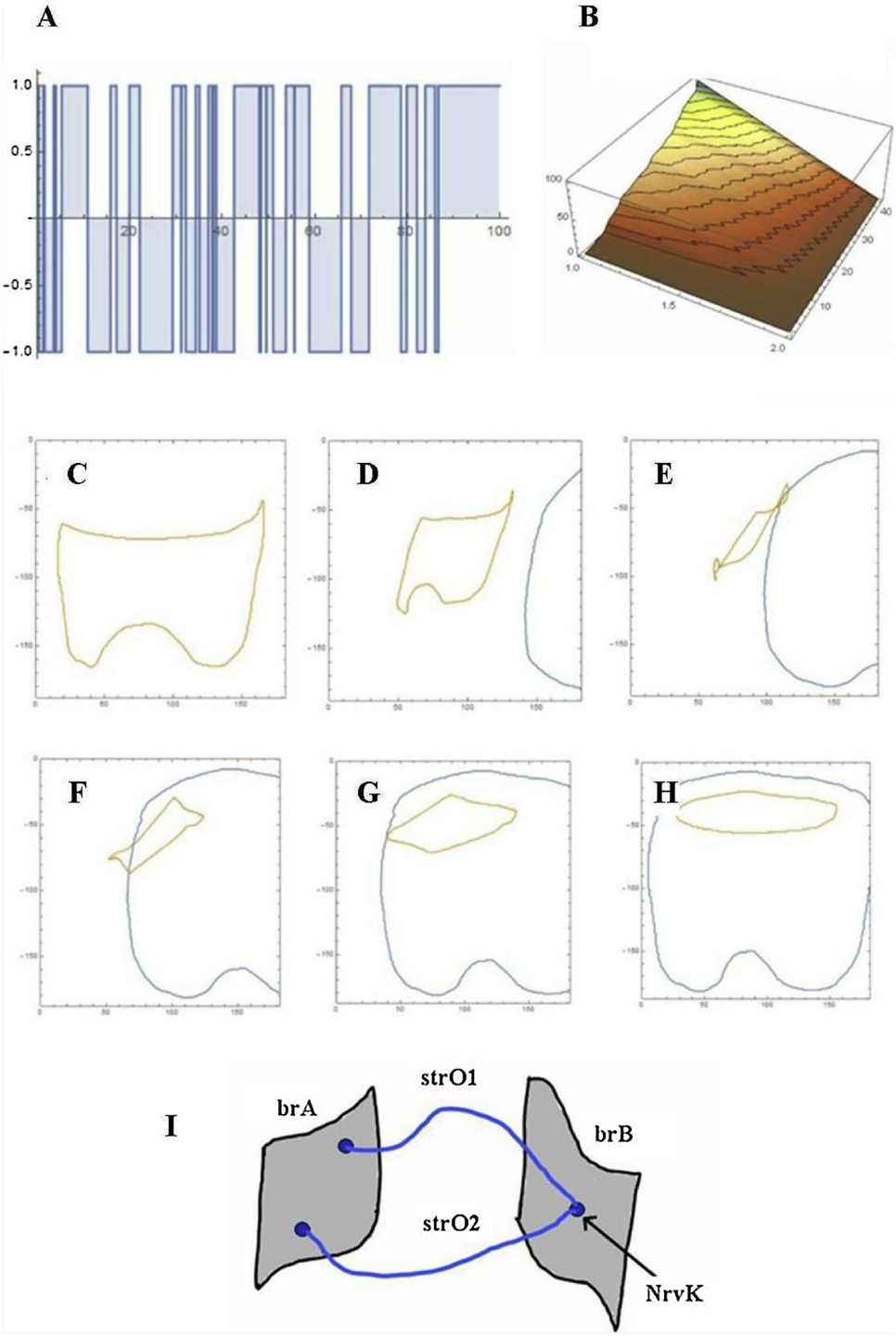

Fig. 1. A 2D representation of 40 brain activity collisions over 100 time steps. **B.** A 3D view of a brain activity collision process (0–100 seconds), in which a series of collisions results in their merging [41]. A worldsheet is represented by the 3D surface colliding with brain activities which stand for the vertical walls of the 3D box. **Figures C-H**. Homotopically equivalent shapes, standing for brain activities. A brain activity deform into another, as a result of the collision of a pair of separate activities. **C**: a brain activity (e.g., an emotion) at a given spatiotemporal level. Such level could be differently coarse-grained, e.g., might stand for every micro-, meso- or macro-level. **D**: two brain activities at two different levels. The second shape might stand, e.g., for a cognitive ability. **E**: interacting brain activities. **F**: dual brain activities. **G**: concentric brain activities. **H**: condensed brain activity: emotion and cognition have been merged. Fig. **I**. A set K of open strings strO1, strO2 have extremities on brain activities brA and br B. The extremities of strO1, strO2 meet in a common point on brain activity brB. Hence, nerve.

matching description and embedded in higher-dimensional nervous structures, map to a single activity in lower-dimensional ones, and vice versa. This means that there exists an assessable and quantifiable correspondence between the brain micro-, meso- and macro-levels assessed through a wide range of different neuro-techniques. Our framework holds for all the types of approaches to the brain, independent of their peculiar features, resolution, magnitude and boundaries.

The question is: what for? What are the real-world consequences of the duality among brain activities, by neuroscientists' viewpoint? The first consequence is that the distinction among different coarse-grained levels of nervous activity does not count anymore, because nervous function at small/medium/large scales of neural observation turn out to be topologically equivalent. This generalization points towards an assessable and quantifiable correspondence between different mental faculties. Our common-sense is used to conceive mind faculties as too far apart ever to communicate with one another, so that activities bounded on distant brain regions would never have direct contact: e.g., sensations and abstraction have seemingly very few in common. However, our topological investigation reveals that this belief is unfeasible, because there must be at least one element in common among brain activities that are apparently very distant from each other. Why does our mind separate brain activity in different mental faculties? The answer is straightforward, if we consider topological arguments. If we depict different mental faculties as abstract geometric shapes taking place in

the phase space our physical brain, they necessarily display at least a feature in common. Brain signals from two different mental faculties can be compared, because their shapes can be assessed together at higher-dimensional scales of observation. In the brain, every sub-region encompasses at least one mental faculty, which can be modeled as a shape in a topological space. In BUT terms, not only we find a brain region containing a mental faculty, but we also find a mental faculty, embedded in a cortical area, which is the topological description of another one, embedded in another area. In topological terms, mental faculties/shapes are continually transforming into new equivalent mental faculties/shapes. Cortical activities will always have some element in common: they do not exist in isolation, rather they are part of a large interconnected whole. Whether you experience pain or pleasure, or chomp on an apple, or compute a mathematical expression, or quote a proverb, or remember your childhood, or read Wittgenstein's *Tractatus*, it does not matter: the large repertoire of your brain functions can be described through the same topological apparatus.

The second consequence is that mental faculties, lying in multi-dimensional phase spaces, are dual. Tozzi et al. [44] described how lower-dimensional features can be assessed in the generic terms of particle trajectories traveling on higher-dimensional structures. In our brain scenario, particle movements are operationalized as functions occurring on structures equipped with different geometric curvatures. This methodological advance encompasses diverse brain models that claim for either concave, convex or flat nervous phase spaces ([45–47]). This means that the most of the brain theories are DUAL: e.g., their topological description is the same, despite the huge differences in the subtending manifolds and mechanisms. This useful simplification suggests that the level of observation is not significant when evaluating brain activities, because such levels are fully interchangeable. Because projections among dimensions describe neural phenomena spanning from the smallest to the highest scales, the distinction among different coarse-grained scales does not count anymore: nervous activity is topologically the same at small, medium and large scales of observation. This means, for example, that different types of cognitive studies assess the same topological activity, regardless of their dissimilar protocols and procedures.

Multichannel recordings reveal travelling waves of neural activity in multiple sensory, motor and cognitive systems at single-area (mesoscopic) and whole-brain (macroscopic) scales [48]. Such waves, both spontaneously generated by recurrent circuits and evoked by external stimuli, travel along brain networks at multiple scales, transiently modulating spiking and excitability as they pass. An appropriate projection mapping shows that, if two regions display matching features (e.g., the same intensity, or length, or pairwise entropy) [49], they stand for the same activity. Activities with matching ends (regions) in diverse cortical areas might also help to throw a bridge between spontaneous and evoked brain activities, which become just two sides of the same coin, made of topologically-bounded dynamics. Also, our topological account allows a characterization of the elusive phenomenon of "consciousness": the latter could topologically stand for the condensed brain activity that takes place in the highest-dimensional functional brain levels. In touch with of Cusa's [50] and Bruno's [51] claims, a sort of "coincidentia oppositorum" (our matching description?) occurs among the brain activities endowed in our skull, giving rise to consciousness. The tight coupling among different neural activities gives rise to brains that are in charge of receiving and interpreting signals from other cortical zones, in closely intertwined relationships at every spatio-temporal level. Topology becomes one of the central information processing strategies of the nervous system and allows us to achieve a general, testable, computational model of brain activity that keeps into account the functional subdivisions of mental functions.

References

[1] M.S. Gazzaniga, The Cognitive Neurosciences, fourth edition, MIT Press, 2009 ISBN: 9780262013413.

[2] J.R. Andrews-Hanna, J. Smallwood, R.N. Spreng, The default network and self-generated thought: component processes, dynamic control and clinical relevance, Ann. N. Y. Acad. Sci. 1316 (2014) 29–52.

[3] G. Abend, What are neural correlates neural correlates of? BioSocieties (2016) 1–24, https://doi.org/10.1057/s41292-016-0019-y.

[4] G. Buzsáki, B.O. Watson, Brain rhythms and neural syntax: implications for efficient coding of cognitive content and neuropsychiatric disease, Dialogues ClinNeurosci 4 (2012) 345–367.

[5] O. Jensen, B. Gips, T.O. Bergmann, M. Bonnefond, Temporal coding organized by coupled alpha and gamma oscillations prioritize visual processing, Trends Neurosci. (2014), https://doi.org/10.1016/j.tins.2014.04.001 pii: S0166-2236(14)00060-5.

[6] T. Watanabe, S. Kan, T. Koike, M. Misaki, S. Konishi, S. Miyauchi, N. Masuda, Network-dependent modulation of brain activity during sleep, NeuroImage 98 (2014) 1–10, https://doi.org/10.1016/j.neuroimage.2014.04.079.

[7] I. Opris, M.F. Casanova, Prefrontal cortical minicolumn: from executive control to disrupted cognitive processing, Brain 137 (July (Pt 7)) (2014) 1863–1875, https://doi.org/10.1093/brain/awt359 2014.

[8] A. Tozzi, Information Processing in the CNS: A Supramolecular Chemistry? Cogn. Neurodyn. 9 (5) (2015) 463–477.

[9] G.H. Jacobs, G.A. Williams, H. Cahill, J. Nathans, Emergence of novel color vision in mice engineered to express a human cone photopigment, Science 315 (5819) (2007) 1723–1725.

[10] M.I. Ekstrand, A.R. Nectow, Z.A. Knight, K.N. Latcha, L.E. Pomeranz, J.M. Friedman, Molecular profiling of neurons based on connectivity, Cell 157 (5) (2014) 1230–1242, https://doi.org/10.1016/j.cell.2014.03.059.

[11] K. Friston, The free-energy principle: a unified brain theory? Nat. Rev. Neurosci. 11 (2) (2010) 127–138, https://doi.org/10.1038/nrn2787.

[12] O. Sporns, Network attributes for segregation and integration in the human brain, CurrOpinNeurobiol 23 (2) (2013) 162–171, https://doi.org/10.1016/j.conb.2012.11.015.

[13] C. Koch, M. Massimini, M. Boly, G. Tononi, Neural correlates of consciousness: progress and problems, Nat. Rev. Neurosci. 17 (5) April) (2016) 307–321, https://doi.org/10.1038/nrn.2016.22.

[14] Zwiebach, Barton, A First Course in String Theory, Cambridge University Press, 2009 ISBN 978-0-521-88032-9.

[15] E. Başar, Brain Body Mind Oscillations in Scope of Uncertainty Principle, Springer, New York, 2010, p. 5 ISBN 1441961364.

[16] M.S. Gazzaniga, Shifting gears: seeking new approaches for mind/brain mechanisms, Annu. Rev. Psychol. 2013 (64) (2013) 1–20, https://doi.org/10.1146/annurev-psych-113011-143817 Epub 2012 Sep 17.

[17] M. Vandekerckhove, J. Panksepp, A neurocognitive theory of higher mental emergence: from anoetic affective experiences to noetic knowledge and autonoetic awareness, NeurosciBiobehav Rev. 35 (9) October) (2011) 2017–2025, https://doi.org/10.1016/j.neubiorev.2011.04.001 2011.

[18] A. George, The cognitive revolution: a historical perspective, Trends Cogn. Sci. (Regul. Ed.) 7 (2003).

[19] L.F. Almada, A. Pereira Jr, C. Carrara-Augustenborg, What affective neuroscience means for science of consciousness, Mens Sana Monogr. 11 (1) January) (2013) 253–273, https://doi.org/10.4103/0973-1229.100409 2013.

[20] A. Damasio, Feelings of emotion and the self, Ann. N. Y. Acad. Sci. 1001 (October) (2003) 253–261 2003.

[21] J.V. Oron Semper, J.I. Murillo, J. Bernacer, Adolescent emotional maturation through divergent models of brain organization, Front. Psychol. 7 (August (1263)) (2016), https://doi.org/10.3389/fpsyg.2016.01263 eCollection 2016.

[22] D.I. Olive, P.T. Landsberg, Introduction to string theory: its structure and its uses. Physics and mathematics of strings, Philos. Trans. Roy. Soc. Lond. (1989) 319–328 MR1043892.

[23] M. Borsuk, DreiSatze Uber Die N-Dimensionale EuklidischeSphare, FundamentaMathematicae XX (1933) 177–190.

[24] A. Tozzi, J.F. Peters, Towards a fourth spatial dimension of brain activity, Cogn. Neurodyn. 10 (3) (2016) 189–199, https://doi.org/10.1007/s11571-016-9379-z.

[25] J.F. Peters, S.A. Naimpally, Applications of near sets, Notices of the Amer, Math. Soc. 59 (4) (2012) 536–542, https://doi.org/10.1090/noti817.

[26] A. Tozzi, J.F. Peters, A topological approach unveils system invariances and broken symmetries in the brain, J. Neurosci. Res. 94 (5) (2016) 351–365, https://doi.org/10.1002/jnr.23720.

[27] A. Di Concilio, Point-free geometries: proximities and quasi-metrics, Math. Comp. Sci. 7 (1) (2013) 31–42 MR3043916.

[28] J.F. Peters, Computational Proximity. Excursions in the Topology of Digital Images. Edited by Intelligent Systems Reference Library, Springer-Verlag, Berlin, 2016, https://doi.org/10.1007/978-3-319-30262-1.

[29] J.F. Peters, Foundations of Computer Vision. Computational Geometry, Visual Image Structures and Object Shape Detection. Intelligent Systems Library 124, Springer Int. Pub. AB, 2016, https://doi.org/10.1007/978-3-319-52483-2.

[30] J.F. Peters, A. Tozzi, Region-Based Borsuk-Ulam Theorem, arXiv.1605.02987 (2016).

[31] J.F. Peters, A. Tozzi, String-Based Borsuk-Ulam Theorem, arXiv:1606.04031 (2016).

[32] F.C. Mitroi-Symeonidis, Convexity and sandwich theorems, Eur. J. Res. Appl. Sci. 1 (March) (2015) 9–11.

[33] J. Matoušek, Using the Borsuk–Ulam Theorem. Lectures on Topological Methods in Combinatorics and Geometry, Springer-Verlag, Berlin Heidelberg, 2003.

[34] M.C. Crabb, J. Jaworowski, Aspects of the borsuk-ulam theorem, J. Fixed Point Theory App. 13 (2013) 459–488, https://doi.org/10.1007/s11784-013-0130-7, MR3122336 2013.
[35] P.G. Fré, The branes: Three viewpoints, in Gravity, A Geometrical Course, Springer, 2013, https://doi.org/10.1007/978-94-007-5443-0_7 2013.
[36] A.-E. Davis, P. Brax, C. van de Bruck, Brane inflation and defect formation, Philos. Trans.: Math., Phys. Eng. Sci. 366 (1877) (2008) 2833–2842 Cosmology Meets Condensed Matter.
[37] J.F. Peters, A. Tozzi, S. Ramanna, E. Inan, The human brain from above: an increase in complexity from environmental stimuli to abstractions, Cogn. Neurodyn. (2017), https://doi.org/10.1007/s11571-017-9428-2.
[38] E.J. Marinec, Black holes and the phases of brane thermodynamics, Progress String Theory M-Theory 564 (2001) 117–145, https://doi.org/10.1007/978-94-010-0852-5_4.
[39] Volovikov, A. Yu, Borsuk-ulam implies Brouwer: a direct construction revisited, Am. Math. Mon. 115 (6) (2008) 553–556, https://doi.org/10.2307/2975293.
[40] F.E. Su, Borsuk-Ulam implies Brouwer: A direct construction, Am. Math. Mon. 104 (9) (1997) 855–859 MR1479992.
[41] E.J. Copeland, T.W.B. Kibble, Cosmic strings and superstrings, Proc. Math. Phys. Eng. Sci. 466 (2115) (2010) 623–657.
[42] M.M. Cohen, A Course in Simple Homotopy Theory, Springer-Verlag, New York-Berlin, 1973.
[43] J.F. Peters, E. Inan, Strongly proximal edelsbrunner-harer nerves, Proc. Jangjeon Math. Soc. 19 (3) (2016) 563–582.
[44] A. Tozzi, J.F. Peters, A.A. Fingelkurts, A.A. Fingelkurts, P.C. Marijuán, Topodynamics of metastable brains, Phys. Life Rev. (2017), https://doi.org/10.1016/j.plrev.2017.03.001.
[45] B. Sengupta, A. Tozzi, G.K. Coray, P.K. Douglas, K.J. Friston, Towards a neuronal gauge theory, PLoS Biol. 14 (3) (2016) e1002400, https://doi.org/10.1371/journal.pbio.1002400.
[46] B.P. Chamberlain, J. Clough, M.P. Deisenroth, Neural Embeddings of Graphs in Hyperbolic Space, arXiv:1705.10359 (2017).
[47] D. Papo, Beyond the anatomy-based representation of brain function: comment on "Topodynamics of metastable brains" by Arturo Tozzi et al, Phys. Life Rev. (2017), https://doi.org/10.1016/j.plrev.2017.04.005.
[48] L. Muller, F. Chavane, J. Reynolds, T.J. Sejnowski, Cortical travelling waves: mechanisms and computational principles, Nat. Rev. Neurosci. 19 (2018) 255–268, https://doi.org/10.1038/nrn.2018.20 2018.
[49] T. Kakiashvili, W.W. Koczkodaj, J.-P. Magnot, Approximate reasoning by pairwise comparisons, Phys. Life Rev. (2017), https://doi.org/10.1016/j.plrev.2017.04.001.
[50] Cusa, Nicholas of. 1440. On Learned Ignorance. tr. J Hopkins, Banning, Minneapolis, MN, 1985.
[51] G. Bruno, Jordani Bruni Nolani Opera Latineconscripta (Giordano Bruno the Nolan's Works Written in Latin), Dritter Band, Tocco F, Vitelli H, 1584 1962.

ARTICLE IN PRESS PLREV:1051

Available online at www.sciencedirect.com

ScienceDirect

Physics of Life Reviews ••• (••••) •••–•••

PHYSICS of LIFE reviews

www.elsevier.com/locate/plrev

Review

The multidimensional brain

Arturo Tozzi *

Center for Nonlinear Science, University of North Texas, 1155 Union Circle, #311427 Denton, TX 76203-5017, USA

Communicated by Prod Felix Schoeller

Abstract

Brain activity takes place in three spatial-plus time dimensions. This rather obvious claim has been recently questioned by papers that, taking into account the big data outburst and novel available computational tools, are starting to unveil a more intricate state of affairs. Indeed, various brain activities and their correlated mental functions can be assessed in terms of trajectories embedded in phase spaces of dimensions higher than the canonical ones. In this review, I show how further dimensions may not just represent a convenient methodological tool that allows a better mathematical treatment of otherwise elusive cortical activities, but may also reflect genuine functional or anatomical relationships among real nervous functions. I then describe how to extract hidden multidimensional information from real or artificial neurodata series, and make clear how our mind dilutes, rather than concentrates as currently believed, inputs coming from the environment. Finally, I argue that the principle "the higher the dimension, the greater the information" may explain the occurrence of mental activities and elucidate the mechanisms of human diseases associated with dimensionality reduction.
© 2019 Elsevier B.V. All rights reserved.

Keywords: Central nervous system; Big data; Neural networks; Topology; Phase space

0. Introduction

Physical or biological activities can be depicted in terms of moving particles embedded in three-dimensional space. In this simple, rather intuitive abstraction, the x, y and z axes stand for the canonical three spatial dimensions, while time passing is portrayed in terms of particles' trajectories [116] (Fig. 1A). For example, the trajectories displayed by the BOLD activation of cortical areas after a visual stimulus can be either drawn as interactive static plots or visualized as animations. However, the current increased availability of big data and innovative computational tools have led to to a growing interest for multidimensional approaches [17]. To understand what "multidimensionality" truly means, we need to think in more abstract terms than usual: while the visualization of low-dimensional data is relatively straightforward in a three-dimensional plot, it is not always obvious how to visualize high-dimensional datasets in a similarly intuitive way [33]. One possibility consists in adding further dimensions to the canonical ones, in order to attain other axes apart from x, y and z. If we introduce a further axis, the particles are allowed to

* Correspondence to: Center for Nonlinear Science, University of North Texas 1155 Union Circle, #311427 Denton, TX 76203-5017, USA.
E-mail addresses: tozziarturo@libero.it, Arturo.Tozzi@unt.edu.

https://doi.org/10.1016/j.plrev.2018.12.004
1571-0645/© 2019 Elsevier B.V. All rights reserved.

move in more than three dimensions (plus time) (Fig. 1B). This methodological step is highly profitable, because it allows the study of systems dynamics in higher dimensions, achieving more information about the particles' trajectories.

The trend towards multidimensional strategies is taking place in far-flung disciplines. Inspired by the periodic table, Reymond [82] grouped chemical compounds in a multidimensional space, in which neighbors have related properties; further, Cardesa et al. [9] uncovered energy cascades in five dimensions (three-dimensional space, time and scale) endowed in the turbulent flows of simple water-like fluids. This paves the way for similar analyses in geophysical and industrial flows, conducting and quantum fluids, plasmas. Not surprisingly, the assessment of the most complex object of all, e.g., the human brain, is also amenable to a multidimensional representation. As brain activities are portrayed as locations at different points in time, either linear/nonlinear nervous dynamics or neural functions/mental observables can be described in terms of scalars/vectors measured at different locations of multidimensional phase spaces. The key question here is: can further dimensions be added to the representation of brain activity? The choices at neuroscientist's disposal are manifold: they are allowed to insert all the axes they require (Fig. 1C), and to locate whatever parameter they want on the further axes, from spike frequencies to synchronized oscillations, from nonlinear fields to attractors, from color perceptual spaces to tactile qualities, from other spatial dimensions to the neural clusters' number (see Figs. 1B–F). Of course, to leave the realm of the pure abstraction and acquire scientific relevance, the arbitrarily chosen dimensions must provide testable hypotheses and experimental validation. In the following, I will describe recently-developed techniques that allow the use of extradimensions in neuroscience. I will then illustrate the multidimensional approach for a wide range of brain activities and mental functions. Furthermore, I will discuss how recent data point towards the real presence of hidden, further dimensions where nervous activity might take place. I will conclude that the brain operates in dimensions higher than its surrounding environment.

1. The unreasonable multidimensional power of the novel computational tools

Electroencephalography (EEG), functional MRI (fMRI) and magnetoencephalography (MEG) have been proven very useful in unveiling neural network dynamics taking place in the classical three spatial dimensions-plus time. However, the data extracted from these standard neurotechniques can be successfully assessed also in the language of innovative, sophisticated multidimensional tools [63]. In this Section, I describe new mathematical weapons that should allow to analyze in multidimensional contexts the huge data sets now commonly generated by standard experimental protocols [14]. Innovations make it feasible to scale efficiently to high dimensions: e.g., Shah and Koltun [91] introduced a clustering algorithm that untangles heavily mixed clusters and achieves high accuracy across multiple domains. It was successfully tested on large datasets of faces, hand-written digits, objects, newswire articles, protein expression levels and sensor readings from the Space Shuttle [91]. Another novel tool assesses the general multidimensional space that encompasses linear combinations of neuronal patterns: Rigotti and Fusi [83] proposed a method exploiting fMRI Repetition Suppression, in order to measure the hidden dimensionality in response to specific task conditions. This technique is able to detect microscopic overlaps even in brain areas that do not display discernible average differential BOLD signal, identifying the cortical circuits that integrate multiple independent information pathways. The importance of higher dimensionality lies in its relationships with the functionality of neural circuits: indeed, the dimensionality (measured, in this case, in terms of response vectors) is higher in areas involved in multistream integration and lower in regions where inputs from independent sources do not interact [83].

Another approach takes into account a feature that is generally hidden in standard series: the "fractal dimension" of data. The fact that the neural activity encompasses self-similarity at different temporal and spatial scales has been proven very useful for the assessment of biomedical analysis waveforms, in particular the complexity endowed in EEG time series [79,31,23]. In my framework, self-similarity might stand for a further (non-integer or fractional) dimension that allows the extraction of larger amounts of information from EEG and functional fMRI data sets [115]. Another important, recently developed issue is the "energy landscape analysis", a data-driven approach to neuroimaging [113], that has been used, in particular, for the assessment of fMRI series recorded from healthy individuals [22] and of energy landscapes shaping the dynamics of subcortical networks during resting state [39]. The latter authors evaluated alterations in energy landscapes after perturbation of subcortical networks' multidimensional parameters. Even slight network perturbations of different parameters (such as maximal number of attractors, unequal temporal occupations

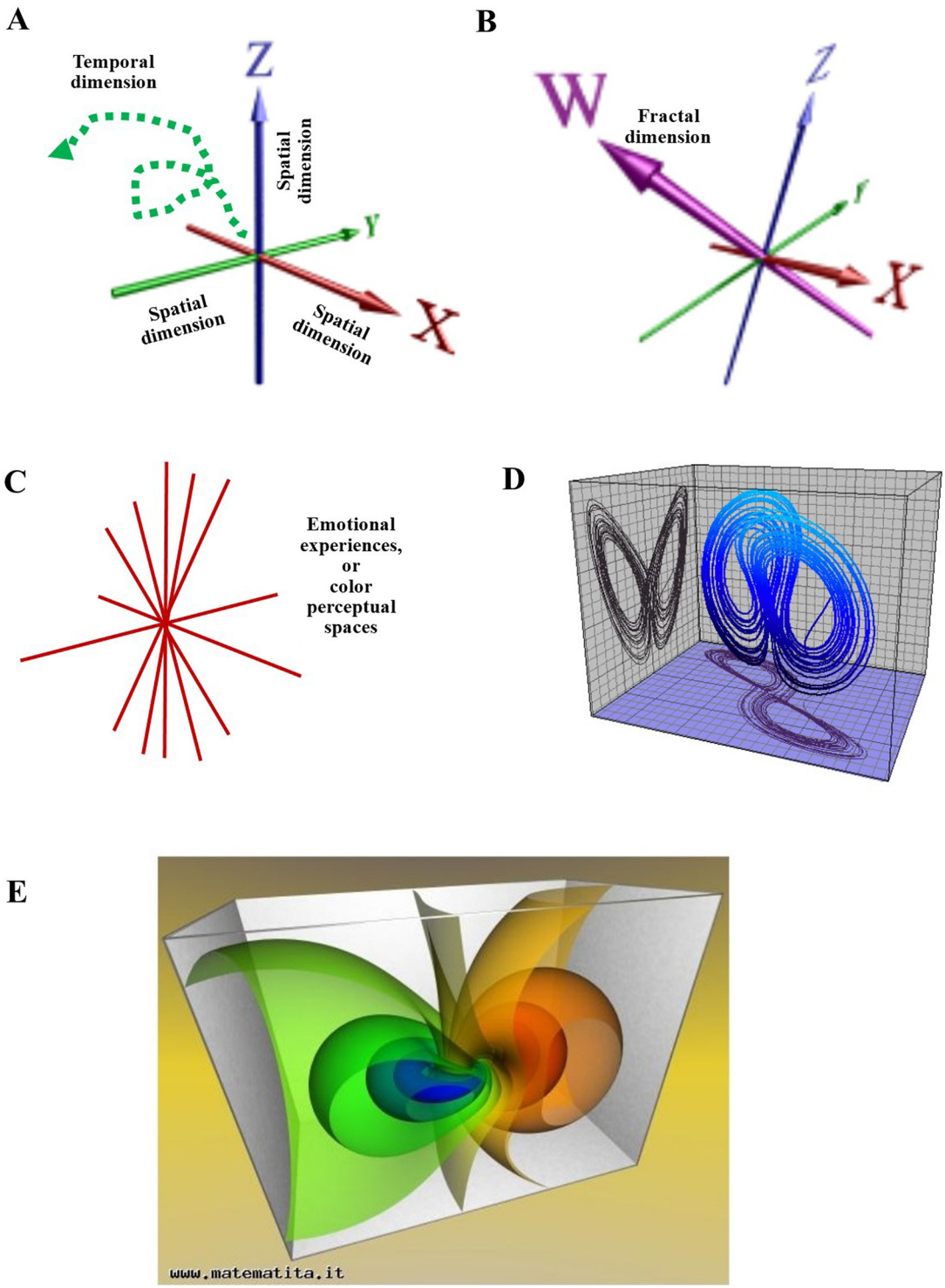

Fig. 1. Different ways to cope with further nervous dimensions. Fig. 1A depicts the canonical picture of three spatial dimension plus time. Time is described by a particle trajectory. Fig. 1B illustrates the arbitrary insertion of a further dimension, in this case a fractal one. Fig. 1C: a sheaf of functional multidimensions might stand for different mental or biological parameters (in this case, either emotions, or colors' perception). Fig. 1D: Multidimensional attractors produced by the complex, nonlinear dynamics of the brain at the edge of chaos. Fig. 1E. A Clifford torus, displaying four-dimensional, donut-like nervous spatial trajectories. Credits: Figs. 1A and 1B are modified from http://eusebeia.dyndns.org/4d/vis/01-intro; Fig. 1D is modified from https://www.mat.ucsb.edu/g.legrady/academic/courses/03w200a/multidimensional/index.html.

and readiness for system's reconfiguration) caused significant shifts in the energy landscape. Therefore, diverse nervous functions emerging due to the reconfiguration of the default brain network at rest can be easily assessed through the add of such multidimensional parameters.

The connectome turns multidimensional. Network science, an interdisciplinary spin-off of graph theory, envisages the brain in terms of the "connectome", i.e., a system of nodes and edges that describes the nervous system as a series of various interacting regions. Conventionally, connectome has been studied in terms of static or time-averaged links; however, recent improvements are starting to take into account also a dynamical component, i.e., the time-varying, non-permanent relationships among edges and nodes [52]. Complex network (graph-theory) analysis applied to MEG/EEG signals allows the assessment of both canonical and non-canonical dimensions, the latter standing for a series of non-spatial parameters, such as, e.g., spike frequencies, connectivity, activity magnitude and complex network properties [42,27]. Developments in source reconstruction algorithms are leading to novel neuronal metrics (standing, in my framework, for further dimensions) that can provide insights into the multidimensional dynamics of various neural representations [42]. The organization of complex networks can be assessed through higher-order connectivity patterns: such approaches allowed Benson et al. [5] to reveal unexpected hubs and geographical elements endowed in the very structure of the nervous connectome. On the other hand, Caiafa and Pestilli [8] described multidimensional arrays able to assess diffusion-weighted magnetic resonance data. They evaluated 1490 connectomes, thirteen tractography methods and three data sets and elucidated the relationships among nodes, edges, white matter fascicles and diffusion data. This method provides anatomical manipulation in multidimensions on white matter tracts, allowing either statistical inference, or the study of the white matter's geometrical organization. Novel statistical machine-learning methods, such as "multivariate pattern analysis", generate stimulus response models in a data-driven fashion that allows fMRI studies of dynamical functional network connectivity in human cognition [56]. Vergara et al. [108] developed an "information theoretical framework" that quantifies the information flowing among subsets of neural networks' functional domains. Clusters of cross domain mutual information point towards scarce information sharing between cognitive and sensory areas. These findings show that, when information theory is applied to states estimated from pairs of multi-network functional domains, additional, multidimensional features of connectivity can be easily unveiled.

The novel multidimensional tools might also help researchers to improve already existing neurotechniques. To make an example, the utility of the successful "independent vector analysis" is circumscribed, because of the extremely noisy nature and large variability of vector distributions. In order to overcome these limitations, Kuang et al. [46] proposed an adaptive fixed-point algorithm that analyzes multiple-subject complex-valued data, allowing an easier detection of the information in fMRI series. Their model, tested both on simulations and real fMRI data, achieves two goals: a) decomposing multi-subject complex-valued information, and b) addressing the troublesome problem of subjective variability of brain function [46]. The nervous connectome can be currently assessed not just in terms of anatomical or dynamical nodes derived from standard imaging neurotechniques, but also of molecular, cellular and neurochemical ones. Here we provide two recent examples. Sousa et al. [95] performed transcriptome sequencing of 16 regions of adult human, chimpanzee, and macaque brains. Integration with human single-cell transcriptomic data revealed global, regional and "cell-type-specific" species-expression differences in genes which denote distinct functional categories. Noori et al. [65] resorted to advanced data mining and supervised machine learning to develop a multiscale, multilayer "neurochemical connectome" of the rat brain. Their tool is freely available for systems analysis of motor, sensory, emotional and cognitive information processing. The last statement emphasizes the growing role of open sources in neuroscience. Advances in neuroimaging of healthy adults, including the ones driven by the Human Connectome Project, allow large free-available data sets to be investigated through recently developed computational tools [21], thus offering exciting prospects for accelerated progress in characterizing brain networks' anomalies [107].

The reverse is feasible too: back from higher to lower connectome dimensions. Despite their huge potentialities, high-dimensional reconstructions of the brain are currently plagued by a severe technical limitation: their computational cost. These restrictions can be tackled through a recently-introduced approach, termed "dimensionality reduction". Diverse dimension reduction techniques are available, from the popular "principal component analysis", to more advanced "factor analysis", including ICA, MAVE [64]. Ye et al. [117] assessed specific patterns encoded in the brain connectivity graphs of healthy subjects, in order to explain how high-dimensional, complex geometries can be mathematically embedded into lower dimensions. Their "tractography-derived" approach tested both linear

and nonlinear dimensionality reduction techniques and demonstrated that the most influential regions of the structural connectome, such as rich-club members, are more centrally mapped [117]. In turn, Heusser et al. [33] introduced "HypeTools", a Python toolbox for the visualization and manipulation of large, high-dimensional datasets. Dimensionality reduction was used in order to embed high-dimensional sets in a lower-dimensional space that allows simpler options for data manipulation. Just as the location of an object moving through a canonical space can be visualized in terms of a three-dimensional trajectory, HyperTools uses dimensionality reduction algorithms to create two- and three-dimensional paths for time series of high-dimensional observations [33]. Hence, multidimensional reconstructions extracted from real neurodata provide a huge amount of information; their main defect, i.e., computationally untreatable complexity, will be soon tackled by powerful, next-to-come advances that will achieve the proper dimensionality reduction.

In sum, this Section emphasizes how the recent free availability of big data sets which encompass thousands of features prompted the development of novel computational tools, able to cope with the underlying high-dimensional nature. This huge amount of information can be tackled in terms of paths tacking place in phase spaces of dimensions higher than the usual three plus time: indeed, every increase in dimensions leads to supplementary available information, in the same way as a sphere encompasses more information than a circle.

2. Topology and symmetries come into play

Once recognized the limitations of the classical techniques in accommodating brain activity, neuroscientists are trying to move beyond the classical approaches [77]. One of the most promising novel tools is topology, a branch of mathematics which allows the description of systems equipped with any number of dimensions. When topology meets the physics of the brain, we achieve a general model of neuronal activity that can be described in terms of multidimensional manifolds/computational geometry and has the potential to be operationalized. Indeed, topology works like a telescope and microscope at the same time: allowing to zoom into networks to find hidden neuronal structures and at the same time look at the larger cortical areas. In touch with old scholars [114,50] current scientists suggest that the world and its dynamics can be described in terms of mappings and projections taking place on topological structures [61]. Systems' properties of physical and biological spaces can be translated into abstract mathematical spaces, and *vice-versa*, leading to the development of higher dimensional constructs. Consistent with this trend, the last decade has seen an explosion of topological approaches in neuroscience, especially to understand neural codes [14] and to extract higher dimensional models of percept, concept, emotion, memory from experimental data [77]. For example, Baas [3] mapped sets of spike trains to a topological manifold, achieving a novel space with a structure richer enough to encompass non-trivial spatial stimuli. Recovering the manifold in which rats are moving, the author detected and separated the influence of the various stimuli that shape the neural (cognitive) space of spike trains. To sum up, topology allows to build phase spaces with more dimensions and therefore with more information to analyze: indeed, a particle moving in, say, five dimensions, describes more paths than a particle moving in the canonical three dimensions plus time.

The geometry inside: nested multilevel correlations. It has recently been argued that the real networks are not just random combinations of single features, rather are organized according to "hidden" geometric correlations between their layers [43]. These correlations allow the detection of multidimensional communities, e.g., sets of nodes that are simultaneously similar in multiple layers. Such kind of hidden multidimensionality enables accurate trans-layer link estimates, so that connections in one layer can be predicted by observing the hidden geometric space of another [43]. As suggested above, the recent availability of huge datasets leads to the necessity to develop methods able to extract as many hidden patterns as possible from experimentally detected traces. The challenge lies in transforming the detected patterns into scientific knowledge, using topological tools which are strictly intertwined with the complex network analysis and the language of graph theory. When connectivity exhibits integrated network topology, structural and functional features become more closely linked to each other, because direct structural connections mediate a larger proportion of neural communication within functional modules [26]. Complementing the conventionally-applied algebraic topology methods, Maletić and Zhao [55] proposed new "information entropy measures" for the characterization of multidimensional structures extracted from complex datasets. They assessed topological relationships, multilevel entropy measures and simplicial complexes endowed in taxi driver's cognitive maps, in order to track transitions to high-dimensional structures [55]. In turn, Merelli et al. [60] proposed a methodology, based on topological data analysis, that captures the changes of internal organization in complex systems: this means that the topological invariants

in multivariate time series can be used for the computation of a novel entropy measure, the so-called "weighted persistent entropy". This measure allows to track the nonlinear changes which are correlated with phase transitions and network reorganization.

[28] focused on "simplicial complexes", i.e., a construct from algebraic topology to assess higher-order networks, by capturing both emergent community structures and the dependence of the degree distribution on the number of the underlying dimensions [6]. It is noteworthy that higher-order networks have a natural geometric interpretation which describes the interactions between two or more nodes. Indeed, multidimensional networks might encompass simplicial complexes made not only by classic nodes and links, but also by triangles and tetrahedra glued along their faces. Simplicial complexes' network geometry attracts increasing attention, due to the wide range of possible applications, from data mining to Internet routing protocols [6]. The technique is promising for the assessment of neurodata extracted both from electrophysiological recordings in animal models and hemodynamic fluctuations in humans. The authors posit that simplicial complexes have the potential to eclipse graph theory in unraveling the fundamental mysteries of cognition [28].

Two is better than one. Last, but not least, another important concept from topology has recently come into play in neuroscience: the Borsuk–Ulam theorem (BUT), which states that two antipodal points on a sphere map to a single point on a circumference [7,57]. In neuroscientific terms, this means that a cortical region embedded in lower dimensions gives rise to two detectable regions with matching description in higher dimensions [105]. The dimensions described by BUT do not stand just for spatial ones (as in the case of a circle and a sphere), but also for abstract dimensions (such as biological complexity, fractional quantities, fractal dimensions) [72,103]. In BUT terms, every novel axis of the above-mentioned phase space stands for a different dimension. Indeed, the BUT perspective allows a feature (e.g., a shape, a trajectory, a vector or an energy) located in the three-dimensional environment to be translated to an abstract space of different dimensions, and vice versa. Achieving maps from one system to another, researchers are enabled to enrich and elucidate the information extracted from real neurodata [102].

Some of the BUT predictions have recently been confirmed, suggesting that this topological framework can be fruitfully used in neuroscience. The BUT predicts the presence of at least two brain regions equipped with the same features. Recent papers support this claim: for example, Karaman et al. [40] identified the existence of antipodal behavioral patterns of neural activities. Also, Hoffmann and Triesch [32] demonstrated that brain connectivity comes in pairs. They described, in a network in which connection probabilities are symmetric in pairs, the occurrence of abundant bidirectionally connected neuron pairs, which far exceeds what would be expected in a random network. The BUT framework envisages that a) matching cortical areas with different anatomical location might encompass the same mental faculty, and b) the activity of such a mental faculty halves when other ones occur in the brain. In touch with this prevision, Waskom and Wagner [112] stated that: "examining targeted prefrontal regions, we found that pairs of voxels with similar context preferences exhibited spontaneous correlations that were approximately twice as large as those between pairs with opposite context preferences."

The hidden relationships between symmetry breaking and multidimensionality. Many complex dynamical approaches to brain function have been proposed throughout the last years [16,4,120,100,18]. I would like to remark that one key point of these frameworks is that nonequilibrium phase transitions may lead to symmetry breaking [4,16,71]. In touch with my claim, Jirsa et al. [35], focusing on the left-right cortical symmetry, provided a bimodal description of the brain activity connected to behavioral dynamics. Moreover, it has been demonstrated that, when an acoustic stimulus frequency is systematically changed in an experimental setting, a spontaneous transition in coordination occurs at a critical frequency, in both motor behavior and brain activity [36]. The study of the temporal organization of large-scale brain networks in whole-brain resting fMRI data established that spontaneous transitions between networks of interacting brain areas are predictable [111]: more specifically, network activity is organized in a hierarchy of two distinct metastates (i.e., higher-order cognition and sensorimotor systems), such that transitions are more probable within, than between, metastates.

Dimensional reduction and symmetry break display close relationships. It has been even proposed that symmetry stands for features with matching description lying in higher dimensions, while the corresponding symmetry break for a single point lying one dimension lower [103]. Recent approaches highlighted the relationships between symmetry and energy requirements, because the former is strictly correlated with thermodynamic activity [86]. By introducing novel topological tools that analyze enthalpy, free-energy and entropy in fMRI neurodata, Tozzi and Peters [104] provided a testable approach to proceed from topology to thermodynamic of nervous activity/symmetry breaking. Hence,

during symmetry breaks and transitions from one functional state to another, changes in thermodynamic parameters and dimensions take place in the nervous system. This means that abstract topological approaches may represent real, energetic physical counterparts accessible to current neurotechniques.

A recent paper describes physical "gauge theories" in the context of the brain activity [90]. The authors assessed nervous activity through the physical and mathematical procedures of gauge theory, examining the possibility that brain function is driven by one or more continuous forces, called gauge fields, that originate inside or outside the CNS. In particular, their framework highlights the concept of symmetries, which represent the cornerstone of gauge theories. The approaches based on symmetry breaking allow a methodological assessment of brain dynamics, described and operationalized in terms of energetic gradient-descent trajectories taking place on curved paths of the nervous phase space. In touch with these symmetry issues, Robinson et al. [84] analyzed the activity eigenmodes of the bi-hemispheric brain and its spatial structure. They found that interhemispheric connections between homologous regions via the corpus callosum lead to splits which depend on symmetric or anti-symmetric activity between opposite areas. The symmetric properties of the lowest eigenmodes are able to constrain the interhemispheric connectivity strengths, so that, consistent with observations, spontaneous brain activity turns symmetric between hemispheres. In order to achieve and maintain the required brain function, neural activity needs to be tightly coordinated within the brain networks' manifolds. In this vein, Pillai and Jirsa [76] described structured flows on manifolds able to provide a formal description of behavior in terms of low-dimensional processes that emerge from the symmetric and invariant properties of network's dynamics. They found that symmetry breaking in network connectivity gives rise to timescales hierarchies, resulting in the emergence of attractive functional subspaces, so that behavior ultimately emerges when appropriate conditions imposed by energetic constraints upon the couplings are satisfied. In short, a topological, abstract framework, consisting of brain symmetric functions lying on multidimensional manifolds, describes the general thermodynamic and information principles [59,60] that predict how behavior and task rules are represented in the real brain.

In sum, this Section suggests that the best available strategy to tackle the elusive issue of nervous multidimensionality is to make use of the proper topological weapons. The current state of the art suggests that the very general and "deductive" topological approaches afford accurate previsions that can be tested in the proper scientific experimental setting. This is because abstract topology displays a real energetic counterpart that can be measured in the nervous system.

3. A journey into mental hidden dimensions

In the previous Section, I described how additional nervous dimensions, suggested by simulations or extrapolated from real neuro-data sets, stand for methodological devices that allow mathematical treatment of the brain activity. Here I will focus on multidimensional (anatomical or functional) structures that may implement it in the central nervous system. Indeed, recent papers point indirectly towards the human brain as truly encompassing hidden dimensions. This claim is doomed to be highly controversial, because the mind of a human observer, perhaps due to evolutionary constraints, is not capable to perceive, or even imagine, spaces and structures made up of four or more dimensions.

The hidden dimensions of perceptual spaces. A "perceptual space" of a sensory domain is a mental workspace of points (or vectors, or tensors) that capture similarities and differences in judgments and enables further processing such as classification and naming [118,109]. Perceptual spaces are not traceable to single-neuron properties, because they span across all the sensory cues: from colors to environmental sounds, from faces recognition to auditory textures, from tactile quality to odor. The best studied, i.e., the color's perceptual space, is correlated with the three cone absorption spectra and is believed to lie in more than three dimensions-plus time [109]. Combinatorial strategies are needed in order to represent each separate neuronal population in high-dimensional spaces. The authors focused on a ten-dimensional domain of visual textures, assessed through psychophysical measurements in human observers. The multidimensional approach to color vision suggests two combinatorial strategies of perceptual space's representation: 1) the first is based on projections onto coordinate-like axes equipped with Euclidean geometry, while 2) the second is based on activity patterns. Such patterns are scattered throughout the whole multidimensional space, which is equipped with peculiar global curvatures [109]. Multiple types of local image statistics capture different dimensions, such as luminance distributions, spatial contrast, oriented segments and corners, allowing the analysis of textures, surfaces and forms [110]. Such multifaceted visual processing is difficult to assess, because of the very high dimensionality and the interaction of different kinds of statistics. In order to tackle the problem, Victor et al. [110] focused on binary images

on a square lattice, using a reduced set of stimuli able to tap several kinds of local statistics. Assessing 16 subjects in a ten-parameter (ten-dimensional, in my terminology) space, the authors found that local image statistics shapes a perceptual space which is highly stereotyped across observers. The same approach and experimental treatment might hold for other cues. For example, during complex sounds processing, auditory cortex neurons integrate across multiple dimensions of sound (such as center frequency, intensity and bandwidth), and not just across the few ones detected by traditional studies [94]. The latter authors built an evolutionary algorithm and a statistical method for nonlinear regression that allow a quantitative exploration of cortical responses to five-dimensional auditory stimuli in mice. In summary, sensory cortical neurons seem to be driven by interactions across different inputs dimensions, in ways that are not detected by low-dimensional characterizations [19].

Stimuli modify the dimensionality of cortical activity. Recent works assessing connectome arrangements provide indirect proofs of human brain multidimensionality. Mazzucato et al. [58] evaluated the activity of ensembles of simultaneously recorded neurons and demonstrated that stimuli change the dimensionality of cortical activity: the more the network's ensemble size grows, the more neurons are recruited, the more the dimensions. In particular, the default mode network displays higher dimensionality, compared with other nervous functional networks. In touch with these claims, Zamora-López et al. [119] compared the connectomes of C. elegans, cats, macaques and humans with surrogate networks in which either modules or hubs were destroyed, showing that functional complexity always decreases in the perturbed networks. A comparison between simulated and empirically attained resting-state functional connectivity suggests that the human brain at rest has the largest complexity allowed by its anatomical connectome. Roland et al. [85] examined the space-time dynamics of excitation/inhibition in dendrites and axons, over four visual areas of ferrets exposed to scenes with stationary and moving objects. The visual stimuli broke the tight balance, such that networks exhibited longer episodes of net excitation, followed by a compensatory mechanism of net inhibition. Within 80 milliseconds, the excitation-inhibition's space-time dynamics produced a flow on a low three-dimensional manifold that reduced the complexity of neuron interactions over the whole network. In contrast to pure temporal dynamics, low dimensional flows evolved to distinguish the simple visual scenes [85].

The discovery of stimulus-induced synchronization in the visual cortex suggests that the correlations among low-level stimulus features are encoded by the temporal relationship between neuronal discharges. Therefore, temporal coherence might represent a signature of perceptual grouping, providing a link between temporal coordination and cognitive functions [93]. Performing chronic multisite recordings from the visual cortex of anesthetized cats and monkeys trained to solve cognitive tasks, these authors assigned different coding functions to low-dimensional dynamics features (such as synchronized oscillations and phase shifts) and high-dimensional non-linear ones. They proved that the low-dimensional dynamics, characterized by synchronized oscillations and large-scale correlations, are nothing more than the results of computations performed in the high-dimensional state-space of recurrently coupled networks. In brief, the multiplicity of the neural architecture in different sensory systems provides the opportunity to compare their dissimilar solutions to two common requirements: the need for dimensionality reduction and the effectiveness of the higher-order statistical structure inherent in natural sensory inputs [118]. In the reminder, I will discuss an alternative way to elucidate the relationships between the different dimensionalities of the brain and the environment.

Emotions and goals in extra dimensions. A few experimental examples illustrate how multidimensional approaches can be used to assess various mental activities. Emotional states (also termed emotional feelings) are traditionally viewed as innately programmed in subcortical areas [48]. Are such emotional experiences embedded in a complex, high-dimensional categorical mental space? Claims about the geometric organization of the semantic space of emotion have sparked intense debate, in particular among authors who support modified versions of the "higher-order theory of consciousness" [47]. This theory investigates the relationships between conscious states and higher-order representations, predicting that the latter portray oneself as being in particular mental states [47]. It is tempting to trace the described higher-order mental activities to dimensional considerations. In order to quantify the boundaries between emotion categories, Cowen et al. [11] analyzed a series of self-reported emotional states elicited by short videos. The array of reported emotional experiences was assessed in terms of discrete and dimensional geometries. The videos elicited 27 distinct varieties of reported emotional experience uncovering gradients of emotions (e.g., from anxiety to fear to horror to disgust) corresponding to smooth variation in affective dimensions, such as valence and dominance. As stated above, the temporal sequence of a brain activity can be represented as a trajectory (termed in this case a "thought chart") in a phase space. Assuming the topological space containing all the possible brain states to be a very high-dimensional manifold, Xing et al. [116] proposed an unsupervised manifold learning framework to

reconstruct and visualize such huge structure and to provide a novel data-driven framework for brain states' classifications. They examined the temporal EEG connectomes of 20 healthy volunteers, both at rest and during an emotion regulation task. A computerized procedure of nonlinear dimensionality reduction was then performed, in order to reconstruct and embed the learned manifold in a lower-dimensional Euclidean space. The thought charts of resting and emotion regulation task turned out to describe two distinct trajectories on the high-dimensional topological space. Such an approach has potential applications in neurofeedback, via real-time thought chart visualization, as it allows new trajectories to be inserted on-line through out-of-sample embedding Xing et al. [116].

Patterns in sensory cortex are organized across circuits equipped with an intrinsic functional architecture, arranged along relevant stimulus dimensions [112]. Waskom and Wagner examined whether similar organizational principles might also underlie distributed representations of more abstract information, such as rules or goals. Because the human prefrontal cortex supports goal-directed behavior by representing task context information through higher-order processes, they used multivariate decoding and spontaneous correlations' analysis to show that context representations are distributed across subnetworks within the prefrontal cortex. They found that pairs of voxels with similar context preferences exhibited spontaneous correlations, twice as large as those between pairs with opposite context preferences. Such subnetwork organization was stable across both task-engaged and resting states, suggesting that the abstract multidimensional representations supporting goal-directed cognition are constrained by an intrinsic functional architecture. In turn, Agus et al. [1] investigated psychology undergraduates' performances on problems presented in both verbal-numerical and graphical-pictorial formats. The best predictor of good performance turned out to be the confidence in solution correctness under the condition of time pressure administration. This finding suggests that the occurrence of a graphical facilitation could be the result of a multifactorial interaction among multiple contextual and individual dimensions (such as, e.g., visuo-spatial and numerical prerequisites, statistical anxiety, attitudes towards statistics and the confidence in response correctness), rather than being strictly related to the problem presentation format [1]. This lends support to the notion that brain function's multidimensionality may also refer to the subjective features of the studied population.

Consciousness: the multidimensional device of the brain? Recent claims suggest that brain modifications correlated with consciousness may reflect the action of projective transformations. In particular, Rudrauf et al. [87] introduced a mathematical model of embodied consciousness, in which the spatial field of consciousness is described in terms of projective geometry under the control of a process of active inference. Such spatial field, according to the authors, would be able to combine multisensory evidence with prior beliefs in memory. The single individual's standpoints and perspectives are selected according to his preferences, so that the choice of projective frames governs how expectations are transformed by consciousness [87]. An increasing interest has been raised by the integrated information theory of consciousness [98,44]. However, this framework is plagued by practical and theoretical problems. Indeed, measuring integrated information from neuronal signals requires the problematic assessment of all the elements at the same time; furthermore, the interpretation of the required spatial partition becomes rather vague in continuous time-series variables extracted from nonlinear dynamics. In order to tackle these issues, Tajima and Kanai [97] correlated the topological dimensionality of shared continuous attractor dynamics with integrated information. The effects of unobserved nodes on the attractor dynamics can be assessed using "delay-embedding techniques", able to quantify the dimensionality of an embedded attractor even in case of partial observations [97]. In touch with the above-mentioned gauge theories of the brain, topological dimensionality points towards a critical property of integrated information, i.e., its invariance to general coordinate transformations. This means that topological approaches allow the extension of the current notions of integrated information theory of consciousness to continuous dynamical systems too [97].

Whereas a pairwise causal influence between two neural elements can be assessed with existing methods, the quantification of multiple influences poses two major mathematical problems: overestimation and non-causal confounding influences. To solve these problems, Oizumi et al. [70] derived a measure of integrated information where causal influences among elements are statistically disconnected. Integrated information is here geometrically interpreted as the divergence between the actual probability distribution of a system and an approximated one. This framework allows a methodological unification of a wide range of information theoretic measures, such as mutual information, transfer entropy, stochastic interaction and integrated information. Such a novel concept of "geometrical integrated information" is very promising, as it quantifies the strength of multiple causal influences among elements, by simply projecting the probability distribution of complex systems onto constrained multidimensional manifolds.

In this section, I showed how experimentally detectable mental functions can be assessed in terms of changes in nervous dimensions. I concluded that mental processes such as sensations, perceptions, emotions and consciousness are associated with aspects of neural dynamics occurring in hidden nervous dimensions.

4. Multidimensional lessons from virtual and real neurodata

Multidimensional lessons from artificial neuronal networks. Within the brain networks, tens of millions of multidimensional geometrical structures have been recently uncovered. Reimann et al. [81] assessed a virtual network of artificial cortical neurons, using simplicial complexes' techniques that assess the routes of network information flows. In response to virtual stimuli, synaptically connected neurons are bounded into multidimensional geometrical structures, termed functional cliques. Functional cliques evolve in a stereotypical sequence towards the transitory appearance of more and more complex structures, up to eleven dimensions. The more neurons in a clique, the higher the dimension of the resulting geometric object. Higher-dimensional cliques temporarily assemble to enclose high-dimensional holes (referred to as cavities by the authors). The brain would therefore react to stimuli by building a tower of temporary multidimensional blocks, starting with mono-dimensional rods, then bi-dimensional planks, three-dimensional cubes and more complex multidimensional geometries. Experiments were then performed on real brain tissue, suggesting that, during development, the brain constantly rewires in order to build as many high-dimensional structures as possible [81].

Multidimensional lessons from human neurodata. Because the nervous symmetric states display dimensions higher than the asymmetric ones, the space of interest might not just refer to abstract dynamical neural manifolds, but also to detectable physical cortical locations. In this vein, Stemmler et al. [96] demonstrated that animals can navigate by reading out a simple population of grid cell activity across multiple spatial scales. The population vectors' combination at different microscopic dimensions allows to predict neural and behavioral correlates of multiscale grid cell readout, encompassing both entorhinal grid cells and hippocampal place cells. Despite the spatial activity of a single grid cell cannot constitute a metric, a hierarchically organized ensemble provides a distance measure [96]. The human brain exhibits the ability, peculiar among the living beings, to connect past, present and future events in a coherent picture, as if Homo sapiens was allowed to watch past-present-future glued together in a sort of mental kaleidoscope [102,24]. This observation led to the hypothesis that the brain activity might take place on a multidimensional torus. Indeed, recent findings suggest that the trajectories followed by human thoughts during mind-wandering and/or memory retrieval might take place in the functional space of a donut-like, four-dimensional (plus time) hypersphere, undetectable in the usual three dimensions (plus time) (Figure E). A retrospective evaluation of fMRI data, looking for the topological hallmarks of a fourth dimension, appears to be consistent with the existence of a functional hypersphere [102]. Such hypersphere is made observable through "hallmarks" on the brain surface, i.e., the simultaneous activation of areas opposite each other. The three-dimensional "shadows" of a four-dimensional torus are a direct consequence of the BUT, which predicts that "antipodal points" will be simultaneously activated in a multidimensional brain.

The last, but not the least, novel topological techniques of "computational proximity" provided evidence that a four-dimensional nervous activity does exist: in other words, a ceaseless, functional four-dimensional cap surrounds the brain [73]. The authors introduced a method for the measurement of hidden temporal patterns of entropy/information in fMRI data, based on image tessellation into small polygons encompassing dissimilar entropic content. During spontaneous brain activity, this method highlighted entropic patterns that closely resemble the trajectories foreseen by the presence of a brain hypersphere.

Does the brain activity lie in dimensions higher than the environment? Topological models predict that: 1) increases in anatomical/functional dimensions and symmetries might occur in the path from lower to higher activities of the brain; therefore, 2) information in the primary sensory areas is lower than in the higher associative ones. Contrary to common belief, this framework points towards a brain that progressively increases the complexity of the perceived object: an imagined (or perceived) dog encompasses more information than the real dog, because the former is filled with novel emotional and cognitive meanings (for example, when watching a dog, one might think: "how nice is it!" "it is a canid", and so on). In order to demonstrate the counter-intuitive hypothesis that the brain activity might occur in dimensions higher than the three-dimensional (plus time) environment, Peters et al. [74] retrospectively assessed fMRI series and found that, during visual stimulation, the Rényi entropy (i.e., information) is higher in associative cortices than in the visual primary ones. Therefore, rather than distillate the message from the external world, our

brain scatters the incoming input in higher functional dimensions. A recent paper by Dasgupta et al. [15] substantiates the idea that the insects' nervous system too displays such increases in dimensions, compared with the environment. The authors assessed fruit flies during performance of a similarity search-for example task. The fly's olfactory circuit assigns similar neural activity patterns to similar odors, so that behaviors learned from one odor are used when a similar one is experienced. Surprisingly, flies solve this problem with a variant of a computer science algorithm termed "locality-sensitive hashing", that spreads the incoming message across many group of neurons, instead of concentrating it on a few ones [15].

In touch with these claims, Axelrod et al. [2] argued that we generate internal experience through the simultaneous activation of different cognitive systems, interrelated in higher dimensions. In order to test the hypothesis that our mental experience is mediated by a combination of activities of multiple cognitive processes, the authors evaluated four fMRI experiments with the same participants. They found that, during a self-generated mental activity (in their case, recalling personal memories), three cognitive processes (retrieving memory of events, building a vivid scene in our mind, moving back in time) are pooled over in order to operate simultaneously. Therefore, the subjective impression that each of our internal experiences is a unitary, indivisible entity is accomplished by the brain through a combination of different components, that might lie in higher dimensions. This also means that the concept of the "grandmother neuron" is likely condemned to disappear.

In this Section, I provided the "strongest" available claims, i.e., the recently published papers that more explicitly point towards the possible existence of real brain extra-dimensions. Once again, I stress that even these extreme approaches are built upon topological weapons. This is not purely coincidental, because topology seems to stand for a higher-order approach able to catch the otherwise elusive presence of hidden neural dimensions of the anatomical/functional structure of the brain.

5. Brains in higher dimensions: what next?

Despite the limitations due to the still insufficient computational power of the currently available algorithms, the study of hidden nervous dimensions is a promising approach. It is therefore legitimate to ask about the possible future developments of such powerful tools. In this review, I limited my description to the hidden dimensions of the brain; however, recent studies start to highlight other underestimated actors displaying the computational powers previously believed to be exclusive of the brain. Here are a few examples. In previous Sections, we noticed that the best candidate for the role of multidimensional neural phase space is the nervous connectome. However, the standard description of the connectome confined to cortical/subcortical structures [106] might not suffice. Indeed, recent paper point towards the connectome's nodes and hubs not just confined to the "higher" structures of the brain, but also extended to the central and peripheral nervous systems [49,99,69,89,54]. This means that multidimensionality might not be restricted to the brain, rather it might encompass the whole nervous system. Despite the integration of somatosensory information is generally assumed to be a function of the central nervous system, Du et al. [20] described fully functional GABAergic communication within rodent peripheral sensory ganglia. Sensory neurons express major proteins necessary for GABA synthesis and release GABA in response to depolarization: this means that sensory ganglia can modulate transmission of pain-related signals from the peripheral sensory nerves to the CNS [20]. In addition, it has been demonstrated that peripheral receptors play a role not just in information processing and perceptual synthesis, but may also have cognitive effects (for a review, see [101]). For example, Pruszynski and Johansson [80] reported that first-order neurons in the tactile system provide signal edge orientation, via both intensity and temporal structure of their responses. These peripheral neurons perform feature extraction computations that were typically attributed just to cortical neurons. These findings point towards nervous peripheral structures, such as somatosensory ganglia and receptors, representing a hitherto underappreciated site of sensory integration. Therefore, it is possible that, in next years, the concept of connectome will be also extended to the peripheral receptors, which reflect the abstract understanding of the immediate environment [34]. This enlarged framework of nervous activity offers a potential target for multidimensional approaches to neural function that are not circumscribed to the brain [20].

The last frontier: looking for the biochemical nervous correlates of further dimensions. Once assumed that multidimensional brain dynamics may occur, could its neurophysiological mechanisms be hypothesized? The incorporation of cellular and transcriptional data on individual nodes with network models of the connectome enabled the assessment

the microscopic mechanisms underpinning the macroscopic organization of the whole-brain networks [13]. Further insights could be provided through the assessment of the pharmacodynamics of active chemical substances [88]. For instance, high doses of lysergic acid diethylamide (LSD) cause the subjective report of additional spatial or temporal dimensions' perception. Individuals under the effect of LSD describe static objects in three dimensions that seem to move relative to additional spatial dimensions [41]. Carhart-Harris et al. [10] described how LSD provokes increased correlation among different brain regions, compared with placebo. The reported increases in connectivity between visual cortex and other brain areas might help to explain the subjective account of spatial and temporal dimensions' increase. LSD leads to a prolonged cross-activation of 5-HT2A receptor heteromers and to increase in glutamate release in specific cortical layers [62,78]: hence, it might be speculated that the functional occurrence of brain additional dimensions could be correlated with the biomolecular mechanisms underlying the mental effects associated with the use of active mental substances.

Is it feasible to build a real (or artificial) neural network to detect (or simulate) multidimensional brain activities? A recent experimental technique could contribute to solve this crucial question, throwing an unexpected bridge between biophysical neural function and... the devices of theoretical physics. A magnetic field with the proper angulation is able to modify the trajectory and the voltage difference of a given electric current. This phenomenon is termed "Hall effect" [30]. A similar process, called "quantum Hall effect" [66], occurs when an electric charge is sandwiched between two surfaces cooled down to near absolute-zero temperature. When such two-dimensional apparatus is exposed to a strong magnetic field, the electric amount that it can conduct becomes "quantized". This phenomenon is straightforwardly elucidated, if we just consider it as occurring in four, instead of the canonical three, spatial dimensions [121,45,122]. In operational terms, Lohse et al. [53] built a two-dimensional waveguide for light flow and superimposed complex oscillatory patterns that act as a manifestation of higher-dimensional coordinates. They used a two-dimensional lattice consisting of superlattices along the x and y axes. Each superlattice is achieved by superimposing two standing waves of different wavelength (Fig. 2A). A third wave is introduced along the x direction: this corresponds to tilting the long lattice along the x-axis' one-dimensional path (Fig. 2B). Lohse et al. [53] and Zilberberg et al. [122] provided the wavelengths, the angles and the proper equations required in order to detect the four-dimensional quantum Hall effect. Two different responses are attained: 1) a linear one (two-dimensional) along the axis x, and 2) a nonlinear one (four-dimensional) along the axis y (Fig. 2C). In sum, the authors provided a relatively simple approach able to describe peculiar quantum dynamics is terms of pure oscillations. Here I ask: could such "four-dimensional-building apparatus" be transferred, with the due amendments, to the neuroscientific field, in order to assess and quantify the presence of further spatial dimensions in the brain? I speculate that the typical conformation of the waves located in the lattice might be achieved by using real nervous oscillations of different frequency. The required waves might stand for the nervous electric oscillations detected *in vivo* through well-known neurotechniques such as EEG and fMRI. Therefore, the superimposition of neural waves of different wavelengths might produce the superlattice illustrated in Fig. 2A. The superimposition of further brain waves (Fig. 2B) might give rise to both (two-dimensional) linear and (four-dimensional) nonlinear nervous dynamics. My theoretical claim would allow to transfer the framework of the four-dimensional quantum Hall effects provided by Lohse et al. [53] to the realm of neuroscience, in order to: a) describe the real multidimensional brain dynamics and b) demonstrate the feasibility of a synthetic nervous network equipped with four spatial dimensions (plus time), instead of the classical three (plus time).

Dimensional changes in human diseases. To better understand, diagnose, and treat psychiatric primary and secondary disorders, it is crucial to achieve deeper insights into brain circuits in health and disease, both in humans and animal models [107], in order to elucidate abnormal brain connectivity and network dysfunction [25,13]. For example, Odish et al. [68] demonstrated the presence of longitudinal modifications of the structural connectome in (pre) Huntington's disease, compared with healthy controls: these dynamics correlated with changes in clinical and cognitive measures. Other brain disorders, including schizophrenia and Alzheimer's disease are associated with specific lesions, more likely to be located in the connectomic hubs [12]. Furthermore, diffusion tensor imaging-based studies, together with multi-shell tractography and probabilistic fiber tracking, have identified also in Parkinson's disease global and local connectome disruptions (reduced global clustering and efficiency, as well as increased global path length) and extensive patterns of reduced connectivity [38,92]. Gleichgerrcht et al. [29] provided evidence that epilepsy too is likely to be correlated with abnormal function within specific brain networks. Last, but not least, the Human Connectome Project, gathering data from healthy young adults aged 21–35, is achieving a high-quality dataset for comparability with other populations. Their ongoing studies include: Amish Connectome Mental Illness,

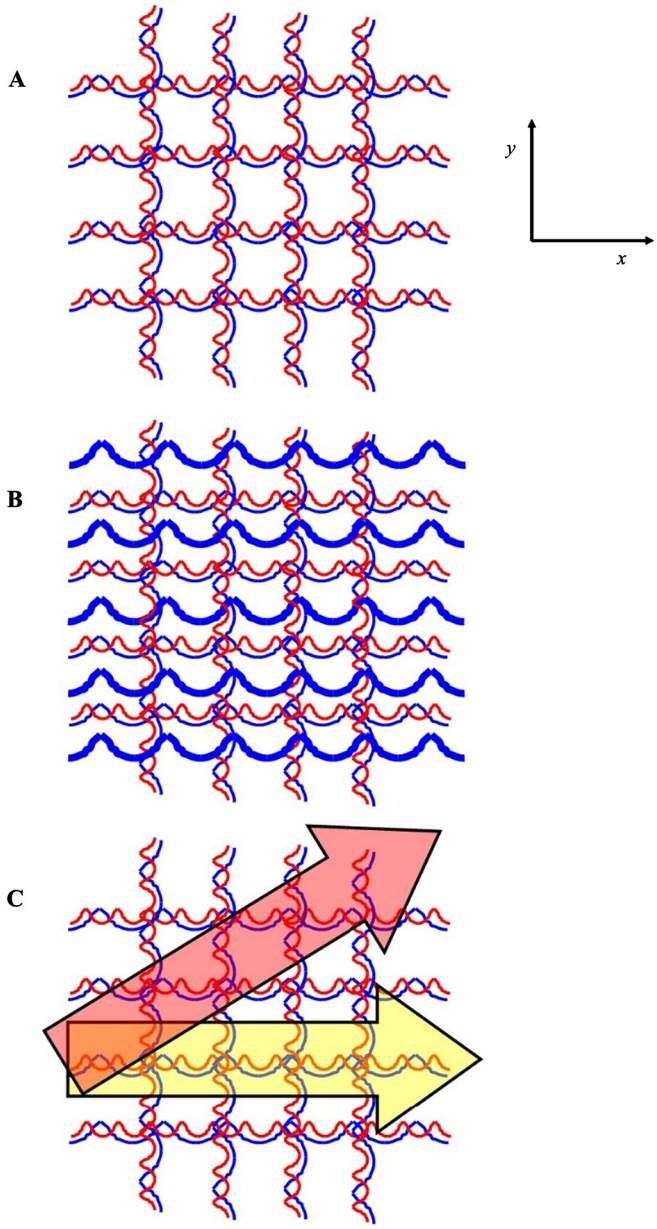

Fig. 2. Four-dimensional physical activities taking place on a two-dimensional superlattice. Fig. 2A depicts a topological lattice equipped with two waves of different wavelength (red and blue thin lines). Fig. 2B: another wave (blue thick line) with the proper wavelength and angulation is superimposed to the lattice along the direction x. In the experimental assessment of Lohse et al. [53], the proper angulation of the third wave is achieved by tilting the lattice. Fig. 2C: the superimposition of the three waves gives rise to two different motions: a two-dimensional, linear one along the axis x (yellow arrow), and a four-dimensional, nonlinear one, along the axis y (red arrow). Modified from Lohse et al. [53].

Anxiety and Depression in Teenagers, Human Connectomes for Low Vision, Blindness, Sight Restoration (https://www.humanconnectome.org/disease-studies).

One could readily anticipate that multidimensional approaches to network theory will allow a novel level of assessment of human diseases, currently undetectable by standard techniques. The problems to tackle are huge, because the large number of different network organizations and fiber tracts' connections make changes detectable enough to distinguish groups not sufficient to diagnose the disease of an individual patient [37]. Nevertheless, just to give an example of the huge potentialities of the novel approaches, these challenges could be addressed by a multidimensional

description of structural, functional, effective and dynamic connectomes. Simulated lesion studies of both targeted and random removal allowed the visual assessment of generated abnormalities in brain connectivity and the inspection of topological alterations in neural connections [117,12]. Kang et al.'s [39] suggest that energy landscape analysis could be an important tool to investigate the brain networks' alterations correlated with brain diseases. Neurodevelopmental brain disorders might arise from imbalances in excitatory and inhibitory (E/I) brain circuitry that cannot be captured by the classical low-dimensional model. O'Donnell et al. [67] combined computational simulations with analysis of in vivo two-photon Ca2+ imaging data, recorded from the somatosensory cortex of a mice model of Fragile-X Syndrome [67]. Their results suggest that the basic E/I imbalance model should incorporate higher dimensional approaches, which could better capture the multifaceted computational functions of neural circuits.

Recent approaches demonstrate the feasibility of precision medicine paradigms in the assessment of complex, multifactorial diseases [51]. For example, patients affected by the Type 2 diabetes (T2D) display a wide range of phenotypes and susceptibilities to diabetes-related complications, including neurologic impairment. Li et al. [51] developed a precision medicine approach that characterizes the complexity of these patient populations. The use of high-dimensional electronic medical records, genotype data from more than 11,000 individuals and topology-based patient-patient networks allowed the authors to identify three distinct subgroups of T2D, characterized by different complications and outcomes. A genetic association analysis of the emergent T2D subtypes was also performed, in order to identify subtype-specific genetic markers. This technique highlighted thousands of single-nucleotide polymorphisms which map to unique genes, specific to the three T2D subtypes [51]. The use of novel meta-analytic approaches in neuroscience has been described by Crossley et al. [13], who applied network analysis methods to previously published studies and/or publicly accessible databases. This strategy of combining connectivity with other brain features, termed "meta-connectomics", shows how network analysis of task-based neuroimaging studies can be used in order to infer functional co-activation from primary data of regional activations. This approach, relating cognition to functional network topology, shows that the brain is composed of cognitively specialized functional subnetworks or modules, linked by a rich club of less specialized regions. Furthermore, meta-connectomics makes it possible to correlate meta-analytic maps of disorder-related MRI abnormalities with the complex topology of the healthy connectome.

In conclusion, the examples provided in this Section suggest once again that brain multidimensionality is a novel exciting field of research, potentially able to provide integrative insights into nervous organization. It is easy to foresee that the hidden dimensions of the brain, either abstract or real, will play a prominent role in the future assessment of both neural function at different coarse-grained levels, and psychiatric disorders.

6. Conclusions: it's not true, but I still believe it

In this paper, I emphasized how numerous clues in the recent literature point towards the possibility to assess brain activities in terms of multidimensional phase spaces. Powerful computational methods allow the extraction of a large amount of otherwise inaccessible information from the massive neurodata sets already available in literature and in the web. I stressed that such hidden information can be more easily extracted, when embedded in multidimensional phase spaces. I showed how such novel approaches in multi-dimensions could be useful in the assessment of countless brain activities, from perceptions to consciousness, from emotions to probabilistic reasoning, and so on.

However, a last, crucial issue needs to be tackled: are nervous multidimensions a convenient technical device, or do they reflect genuine brain features? In the experimental assessment of nervous activity, two ways are viable in order to cope with multidimensions. In many of the papers quoted in this review, extra-dimensions stand for a technical device used just for methodological purposes, which makes it possible to deal with the overwhelming complexity of the nervous activity. There is, however, another conceivable use of additional dimensions. Some of the above-mentioned authors provided further axes in order to describe true brain extra-dimensions: this means that these added dimensions are not mere abstractions. Yet, the borders between the two approaches are not so neat at all, because the standard math that usually assesses networks and brain function is unable to detect the required high-dimensional structures and spaces. This may also explain why it is so hard to understand the brain. It is difficult to understand whether these papers consider neural activity somehow analogous to a multidimensional structure, or we are asked to believe that the brain actually is, or contains, one. In spite of the abundance of both proofs and available methods for the empirical assessment of imperceptible hidden dimensions, this type of multidimensional realism of the brain may not be readily accepted, because of our limited three-dimensional perception. But then, does it really matter? As

suggested by Petlevski [75], the topological models of multidimensional brain offer a very large conceptual module encompassing all the branches of neuroscience, including human diseases.

To sum up, are we in front of a multidimensional brain, or a three-dimensional brain that operates in multidimensions? The answer may just not matter, as long as the novel models are able to elucidate nervous processing and provide testable hypotheses. Apart from epistemological debates on the realism or anti-realism of entities and theories, what matters now is that the study of changes in brain dimensions is a promising novel tool. Approaching brain multidimensions, a large amount of deductive rationalism is required, because this framework is about mappings and projections among different activity levels. We must remind that, while neural networks are known to exhibit rich, lower-order connectivity patterns at the level of individual nodes and edges, higher-order organization is still largely unexplored. I believe that a complete description of nervous phenomena can only be achieved by looking at their higher levels, where differences are more easily detectable and assessable.

Acknowledgements

The Author would like to thank David Papo for the precious and skillful suggestions.

References

[1] Agus M, Peró-Cebollero M, Penna MP, Guàrdia J. Comparing psychology undergraduates' performance in probabilistic reasoning under verbal-numerical and graphical-pictorial problem presentation format: what is the role of individual and contextual dimensions? EURASIA J Math Sci Tech Ed 2015;11(4):735–50. https://doi.org/10.12973/eurasia.2015.1382a.

[2] Axelrod V, Rees G, Bar M. The default network and the combination of cognitive processes that mediate self-generated thought. Nat Hum Behav 2017;1:896–910. https://doi.org/10.1038/s41562-017-0244-9.

[3] Baas NA. On the concept of space in neuro science. Curr Opin Syst Biol 2017;1:32–7.

[4] Beggs JM, Timme N. Being critical of criticality in the brain. Front Physiol 2012;3:163. https://doi.org/10.3389/fphys.2012.00163.

[5] Benson AR, Gleich DF, Leskovec J. Higher-order organization of complex networks. Science 2016;353:163–6. https://doi.org/10.1126/science.aad9029.

[6] Bianconi G, Rahmede C. Network geometry with flavor: from complexity to quantum geometry. Phys Rev E 2016;93(3):032315. https://doi.org/10.1103/PhysRevE.93.032315.

[7] Borsuk K. Dreisatzeuber die n-dimensionale Euklidischesphare. Fundam Math 1933;XX:177–90.

[8] Caiafa CF, Pestilli F. Multidimensional encoding of brain connectomes. Sci Rep 2017;7(1):11491. https://doi.org/10.1038/s41598-017-09250-w.

[9] Cardesa JI, Vela-Martín A, Jiménez J. The turbulent cascade in five dimensions. Science 2017;357(6353):782–4. https://doi.org/10.1126/science.aan7933. Epub 2017 Aug 17.

[10] Carhart-Harris RL, Muthukumaraswamy S, Roseman L, Kaelen M, Droog W, et al. Neural correlates of the LSD experience revealed by multimodal neuroimaging. Proc Natl Acad Sci USA 2017;113(17):4853–8. https://doi.org/10.1073/pnas.1518377113.

[11] Cowen AS, Keltner D. Self-report captures 27 distinct categories of emotion bridged by continuous gradients. Proc Natl Acad Sci USA 2017;114(38):E7900–9. https://doi.org/10.1073/pnas.1702247114.

[12] Crossley NA, Mechelli A, Scott J, Carletti F, Fox PT, et al. The hubs of the human connectome are generally implicated in the anatomy of brain disorders. Brain 2014;137(8):2382–95. https://doi.org/10.1093/brain/awu132.

[13] Crossley NA, Fox PT, Bullmore ET. Meta-connectomics: human brain network and connectivity meta-analyses. Psychol Med 2016;46(5):897–907. https://doi.org/10.1017/S0033291715002895.

[14] Curto C. What can topology tell us about the neural code? Bull Am Math Soc 2016;54(1). https://doi.org/10.1090/bull/1554.

[15] Dasgupta S, Stevens CF, Navlakha S. A neural algorithm for a fundamental computing problem. Science 2017;358(6364):793–6. https://doi.org/10.1126/science.aam9868.

[16] de Arcangelis L, Herrmann HJ. Learning as a phenomenon occurring in a critical state. Proc Natl Acad Sci 2010;107:3977–81.

[17] Dekker J, Belmont AS, Guttman M, Leshyk VO, Lis JT, et al. The 4D nucleomeproject. Nature 2017;549(7671):219–26. https://doi.org/10.1038/nature23884.

[18] Dehghani-Habibabadi M, Zare M, Shahbazi F, Usefie-Mafahim J, Grigolini P. Neuronal avalanches: where temporal complexity and criticality meet. Eur Phys J E, Soft Matter 2017;40(11):101. https://doi.org/10.1140/epje/i2017-11590-8.

[19] Dmochowski JP, Ki JJ, DeGuzman P, Sajda P, Parra LC. Extracting multidimensional stimulus-response correlations using hybrid encoding-decoding of neural activity. NeuroImage 2017. https://doi.org/10.1016/j.neuroimage.2017.05.037. pii: S1053-8119(17)30429-9 [Epub ahead of print].

[20] Du X, Hao H, Yang Y, Huang S, Wang C, et al. Local GABAergic signaling within sensory ganglia controls peripheral nociceptive transmission. J Clin Invest 2017;127(5):1741–56. https://doi.org/10.1172/JCI86812.

[21] Eickhoff S, Nichols TE, Van Horn JD, Turner JA. Sharing the wealth: neuroimaging data repositories. NeuroImage 2016;124(Pt B):1065–8. https://doi.org/10.1016/j.neuroimage.2015.10.079.

[22] Ezaki T, Watanabe T, Ohzeki M, Masuda N. Energy landscape analysis of neuroimaging data. Philos Trans A Math Phys Eng Sci 2017;375(2096). pii: 20160287. https://doi.org/10.1098/rsta.2016.0287.

[23] Fetterhoff D, Opris I, Simpson SL, Deadwyler SA, Hampson RE, Kraft RA. Multifractal analysis of information processing in hippocampal neural ensembles during working memory under Δ9-tetrahydrocannabinol administration. J Neurosci Methods 2014. pii: S0165-0270(14)00264-7. https://doi.org/10.1016/j.jneumeth.2014.07.013.
[24] Fingelkurts AA, Fingelkurts AA. Present moment, past, and future: mental kaleidoscope. Front Psychol 2014;5:395.
[25] Fornito A, Zalesky A, Breakspear M. The connectomics of brain disorders. Nat Rev Neurosci 2015;16(3):159–72. https://doi.org/10.1038/nrn3901.
[26] Fukushima M, Betzel RF, He Y, van den Heuvel MP, Zuo XN, Sporns O. Structure-function relationships during segregated and integrated network states of human brain functional connectivity. Brain Struct Funct 2017. https://doi.org/10.1007/s00429-017-1539-3.
[27] Garcia JO, Ashourvan A, Muldoon SF, Vettel J, Bassett DS. Applications of community detection techniques to brain graphs: algorithmic considerations and implications for neural function. Proc IEEE 2018;106(5):846–67. https://doi.org/10.1109/JPROC.2017.2786710.
[28] Giusti C, Ghrist R, Bassett D. Two's company, three (or more) is a simplex: algebraic-topological tools for understanding higher-order structure in neural data. J Comput Neurosci 2016 Aug;41(1):1–14. https://doi.org/10.1007/s10827-016-0608-6.
[29] Gleichgerrcht E, Kocher M, Bonilha L. Connectomics and graph theory analyses: novel insights into network abnormalities in epilepsy. Epilepsia 2015 Nov.;56(11):1660–8. https://doi.org/10.1111/epi.13133.
[30] Hall E. On a new action of the magnet on electric currents. Am J Math 1879;2(3):287–92. https://doi.org/10.2307/2369245.
[31] He BJ, Zempel JM, Snyder AZ, Raichle ME. The temporal structures and functional significance of scale-free brain activity. Neuron 2010;66(3):353–69. https://doi.org/10.1016/j.neuron.2010.04.020.
[32] Hoffmann FZ, Triesch J. Nonrandom network connectivity comes in pairs. Netw Neurosci 2017;1(1):31–41. https://doi.org/10.1162/NETN_a_00004.
[33] Heusser AC, Ziman K, Owen LLW, Manning JR. HyperTools: a Python toolbox for visualizing and manipulating high-dimensional data. arXiv:1701.08290v1, 2017.
[34] Japyassú HF, Laland KN. Extended spider cognition. Anim Cogn 2017;20(3):375–95.
[35] Jirsa VK, Fuchs A, Kelso JAS. Connecting cortical and behavioural dynamics: bimanual coordination. Neural Comput 1998;10:2019–45.
[36] Jirsa VK, Friedrich R, Haken H, Kelso JAS. A theoretical model of phase transitions in the human brain. Biol Cybern 1994;71(1):27–35.
[37] Kaiser M. The potential of the human connectome as a biomarker of brain disease. Front Human Neurosci 2013;7:484. https://doi.org/10.3389/fnhum.2013.00484.
[38] Kamagata K, Zalesky A, Hatano T, Di Biase MA, El Samad O, et al. Connectome analysis with diffusion MRI in idiopathic Parkinson's disease: evaluation using multi-shell, multi-tissue, constrained spherical deconvolution. NeuroImage: Clin 2018;17:518–29. https://doi.org/10.1016/j.nicl.2017.11.007.
[39] Kang J, Pae C, Park HJ. Energy landscape analysis of the subcortical brain network unravels system properties beneath resting state dynamics. NeuroImage 2017 Apr.;149:153–64. https://doi.org/10.1016/j.neuroimage.2017.01.075.
[40] Karaman B, Murat Demirer R, Bayrak C. Modeling the antipodal connectivity structure of neural communities. AIMS Neurosci 2016;3(2):163–80. https://doi.org/10.3934/Neuroscience.2016.2.163.
[41] Katz MM, Waskow IE, Olsson J. Characterizing the psychological state produced by LSD. J Abnorm Psychol 1968;73(1):1–14. https://doi.org/10.1037/h0020114. PMID 5639999.
[42] Kida T, Tanaka E, Kakigi R. Multidimensional dynamics of human electromagnetic brain activity. Front Human Neurosci 2016;9:713. https://doi.org/10.3389/fnhum.2015.00713.
[43] Kleineberg K-K, Boguñá M, Ángeles Serrano M, Papadopoulos F. Hidden geometric correlations in real multiplex networks. Nat Phys 2016;12:1076–81. https://doi.org/10.1038/nphys3812.
[44] Koch C, Massimini M, Boly M, Tononi G. Neural correlates of consciousness: progress and problems. Nat Rev Neurosci 2016;17(5):307–21. https://doi.org/10.1038/nrn.2016.22.
[45] Kraus YE, Ringel Z, Zilberberg O. Four-dimensional quantum Hall effect in a two-dimensional quasicrystal. Phys Rev Lett 2013;111:226401.
[46] Kuang LD, Lin QH, Gong XF, Cong F, Calhoun VD. Adaptive independent vector analysis for multi-subject complex-valued fMRI data. J Neurosci Methods 2017;281:49–63. https://doi.org/10.1016/j.jneumeth.2017.01.017.
[47] Lau H, Rosenthal D. Empirical support for higher-order theories of conscious awareness. Trends Cogn Sci 2011;15(8):365–73. https://doi.org/10.1016/j.tics.2011.05.009.
[48] LeDoux JE, Brown R. A higher-order theory of emotional consciousness. Proc Natl Acad Sci USA 2017 Feb. https://doi.org/10.1073/pnas.1619316114. pii: 201619316.
[49] Lenglet C, Abosch A, Yacoub E, De Martino F, Sapiro G, Harel N. Comprehensive in vivo mapping of the human basal ganglia and thalamic connectome in individuals using 7T MRI. PLoS ONE 2012;7:e29153. https://doi.org/10.1371/journal.pone.0029153.
[50] Lewin K. A dynamic theory of personality. New York and London: McGraw-Hill Book Company, Inc.; 1935.
[51] Li L, Cheng WY, Glicksberg BS, Gottesman O, Tamler R, et al. Identification of type 2 diabetes subgroups through topological analysis of patient similarity. Sci Transl Med 2015;7(311):311ra174. https://doi.org/10.1126/scitranslmed.aaa9364.
[52] Li A, Cornelius SP, Liu Y-Y, Wang L, Barabási A-L. The fundamental advantages of temporal networks. Science 2017 Nov;358(6366):1042–6. https://doi.org/10.1126/science.aai7488.
[53] Lohse M, Schweizer C, Price HM, Zilberberg O, Bloch I. Exploring 4D quantum Hall physics with a 2D topological charge pump. Nature 2018;553:55–8. https://doi.org/10.1038/nature25000.
[54] Looi JC, Walterfang M, Nilsson C, Power BD, van Westen D, et al. The subcortical connectome: hubs, spokes and the space between – a vision for further research in neurodegenerative disease. Aust NZ J Psychiatry 2014;48:306–9. https://doi.org/10.1177/0004867413506753.
[55] Maletić S, Zhao Y. Multilevel integration entropies: the case of reconstruction of structural quasi-stability in building complex datasets. Entropy 2017;19(4):172. https://doi.org/10.3390/e19040172.
[56] Mandelkow H, de Zwart JA, Duyn JH. Linear discriminant analysis achieves high classification accuracy for the BOLD fMRI response to naturalistic movie stimuli. Front Human Neurosci 2016;10:128. https://doi.org/10.3389/fnhum.2016.00128.

[57] Matoušek J. Using the Borsuk–Ulam theorem. Lectures on topological methods in combinatorics and geometry. Berlin, Heidelberg: Springer-Verlag; 2003.
[58] Mazzucato L, Fontanini A, La Camera G. Stimuli reduce the dimensionality of cortical activity. Front Syst Neurosci 2016;10:11. https://doi.org/10.3389/fnsys.2016.00011.
[59] Meijer DKF. Information: what do you mean? Syntropy J 2013;3:1–49. http://www.lifeenergyscience.it/english/2013-eng-3-01.pdf.
[60] Merelli E, Piangerelli M, Rucco M, Toller D. A topological approach for multivariate time series characterization: the epileptic brain. In: Conference: 9th EAI conference on bio-inspired information and communications technologies, BICT 2015, New York; 2015.
[61] Milton R, Babichev A, Dabaghian Y. A topological approach to synaptic connectivity and spatial memory. BMC Neurosci 2015;16(Suppl 1):P44. https://doi.org/10.1186/1471-2202-16-S1-P44. License: CC BY 4.0.
[62] Moreno JL, Holloway T, Albizu L, Sealfon SC, González-Maeso J. Metabotropic glutamate mGlu2 receptor is necessary for the pharmacological and behavioral effects induced by hallucinogenic 5-HT2A receptor agonists. Neurosci Lett 2011;493(3):76–9. https://doi.org/10.1016/j.neulet.2011.01.046. Epub 2011 Jan 27.
[63] Morone F, Roth K, Min B, Stanley HE, Makse HA. Model of brain activation predicts the neural collective influence map of the brain. Proc Natl Acad Sci USA 2017;114(15):3849–54. https://doi.org/10.1073/pnas.1620808114.
[64] Nylen EL, Wallisch P. Dimensionality reduction. In: Neural data science; 2017. p. 223–48.
[65] Noori HR, Schöttler J, Ercsey-Ravasz M, Cosa-Linan A, Varga M, Toroczkai Z, et al. A multiscale cerebral neurochemical connectome of the rat brain. PLoS Biol 2017;15(7):e2002612. https://doi.org/10.1371/journal.pbio.2002612.
[66] Novoselov KS, Jiang Z, Zhang Y, Morozov SV, Stormer HL, et al. Room-temperature quantum Hall effect in graphene. Science 2007;315(5817):1379.
[67] O'Donnell C, Gonçalves JT, Portera-Cailliau C, Sejnowski TJ. Beyond excitation/inhibition imbalance in multidimensional models of neural circuit changes in brain disorders. eLife 2017;6:e26724. https://doi.org/10.7554/eLife.26724.
[68] Odish OF, Caeyenberghs K, Hosseini H, van den Bogaard SJ, Roos RA, Leemans A. Dynamics of the connectome in Huntington's disease: a longitudinal diffusion MRI study. Neuromage: Clin 2015;9:32–43. https://doi.org/10.1016/j.nicl.2015.07.003.
[69] Oh SW, Harris JA, Ng L, Winslow B, Cain N, et al. A mesoscale connectome of the mouse brain. Nature 2014;508:207–14. https://doi.org/10.1038/nature13186.
[70] Oizumi M, Tsuchiya N, Amari SI. Unified framework for information integration based on information geometry. Proc Natl Acad Sci USA 2016;113(51):14817–22. https://doi.org/10.1073/pnas.1603583113.
[71] Papo D. Functional significance of complex fluctuations in brain activity: from resting state to cognitive neuroscience. Front Syst Neurosci 2014;8:112.
[72] Peters JF. Computational proximity. In: Peters JF, editor. Excursions in the topology of digital images; 2016. p. 169–71. https://doi.org/10.1007/978-3-319-30262-1.
[73] Peters JF, Ramanna S, Tozzi A, İnan E. Bold-independent computational entropy assesses functional donut-like structures in brain fMRI images. Front Human Neurosci 2017;11:38. https://doi.org/10.3389/fnhum.2017.00038.
[74] Peters JF, Tozzi A, Ramanna S, Inan E. The human brain from above: an increase in complexity from environmental stimuli to abstractions. Cogn Neurodyn 2017. https://doi.org/10.1007/s11571-0-17-9428-2.
[75] Petlevski S. Modeling the model: the world beyond the immediate sensorium. In: Markič O, Strle T, Kolenik T, Kordeš U, Gams M, editors. Proceedings of the 20th international multiconference information society – is 2017. Volume B – Cognitive science. Ljubljana: Institut "JožefŠtefan"; 2017. p. 44–7.
[76] Pillai AS, Jirsa VK. Symmetry breaking in space-time hierarchies shapes brain dynamics and behavior. Neuron 2017;94(5):1010–26. https://doi.org/10.1016/j.neuron.2017.05.013.
[77] Posina VR. Higher dimensional algebraic study of brain functions. 2015-05-27 T 11:29:04 UTC, 2015.
[78] Preller KH, Schilbach L, Pokorny T, Flemming J, Seifritz E, Vollenweider FX. Role of the 5-HT2A receptor in self- and other-initiated social interaction in LSD-induced states – a pharmacological fMRI study. J Neurosci 2018. pii: 1939-17. https://doi.org/10.1523/JNEUROSCI.1939-17.2018.
[79] Pritchard WS. The brain in fractal time: 1/f-like power spectrum scaling of the human electroencephalogram. Int J Neurosci 1992;66:119–29.
[80] Pruszynski JA, Johansson RS. Edge-orientation processing in first-order tactile neurons. Nat Neurosci 2014;17:1404–9. https://doi.org/10.1038/nn.3804.
[81] Reimann MW, Nolte M, Scolamiero M, Turner K, Perin R, Chindemi G, et al. Cliques of neurons bound into cavities provide a missing link between structure and function. Front Comput Neurosci 2017;11:48. https://doi.org/10.3389/fncom.2017.00048.
[82] Reymond J-L. The chemical space project. Acc Chem Res 2015;48(3):722–30. https://doi.org/10.1021/ar500432k.
[83] Rigotti M, Fusi S. Estimating the dimensionality of neural responses with fMRI repetition suppression. appears in proceedings of the 5th NIPS workshop on machine learning and interpretation in neuroimaging. Montreal, 2015. arXiv:1605.03952v1, 2016.
[84] Robinson PA, Zhao X, Aquino KM, Griffiths JD, Sarkar S, Mehta-Pandejee G. Eigenmodes of brain activity: neural field theory predictions and comparison with experiment. NeuroImage 2016;142:79–98. https://doi.org/10.1016/j.neuroimage.2016.04.050. Epub 2016 May 6.
[85] Roland PE, Bonde LH, Forsberg LE, Harvey MA. Breaking the excitation-inhibition balance makes the cortical network's space-time dynamics distinguish simple visual scenes. Front Syst Neurosci 2017;11:14. https://doi.org/10.3389/fnsys.2017.00014.
[86] Roldán E, Martínez IA, Parrondo JMR, Petrov D. Universal features in the energetics of symmetry breaking. Nat Phys 2014;10:457–61. https://doi.org/10.1038/nphys2940.
[87] Rudrauf D, Bennequin D, Granic I, Landini G, Friston K, Williford K. A mathematical model of embodied consciousness. J Theor Biol 2017;428:106–31. https://doi.org/10.1016/j.jtbi.2017.05.032.
[88] Schartner MM, Carhart-Harris RL, Barrett AB, Seth AK, Muthukumaraswamy SD. Increased spontaneous MEG signal diversity for psychoactive doses of ketamine, LSD and psilocybin. Sci Rep 2017;7:46421. https://doi.org/10.1038/srep46421.

[89] Schmitt O, Eipert P, Hoffmann R, Morawska P, Klünker A, et al. Central and peripheral monosynaptic, polysynaptic and collaterals connectivity in the rat. Front Neuroinform Conference Abstract: Neuroinformatics 2014. https://doi.org/10.3389/conf.fninf.2014.18.00058.
[90] Sengupta B, Tozzi A, Coray GK, Douglas PK, Friston KJ. Towards a neuronal gauge theory. PLoS Biol 2016;14(3):e1002400. https://doi.org/10.1371/journal.pbio.1002400.
[91] Shah SA, Koltun V. Robust continuous clustering. Proc Natl Acad Sci USA 2017;114(37):9814–9. https://doi.org/10.1073/pnas.1700770114.
[92] Shah A, Lenka A, Saini J, Wagle S, Naduthota RM, et al. Altered brain wiring in Parkinson's disease: a structural connectome-based analysis. brain connect 2017;7(6):347–56. https://doi.org/10.1089/brain.2017.0506.
[93] Singer W, Lazar A. Does the cerebral cortex exploit high-dimensional, non-linear dynamics for information processing? Front Comput Neurosci 2016;10:99.
[94] Sloas DC, Zhuo R, Xue H, Chambers AR, Kolaczyk E, Polley DB, et al. Interactions across multiple stimulus dimensions in primary auditory cortex. eNeuro 2016;3(4). pii: ENEURO.0124-16.2016. https://doi.org/10.1523/ENEURO.0124-16.2016.
[95] Sousa AMM, Zhu Y, Raghanti MA, Kitchen RR, Onorati M, et al. Molecular and cellular reorganization of neural circuits in the human lineage. Science 2017;358(6366):1027–32. https://doi.org/10.1126/science.aan3456.
[96] Stemmler M, Mathis A, Herz AVM. Connecting multiple spatial scales to decode the population activity of grid cells. Sci Adv 2015;1:e1500816.
[97] Tajima S, Kanai R. Integrated information and dimensionality in continuous attractor dynamics. Neurosci Consciousness 2017;2017(1):1–9. https://doi.org/10.1093/nc/nix011.
[98] Tononi G. Consciousness as integrated information: a provisional manifesto. Biol Bull 2008;215(3):216–42.
[99] Towlson EK, Vértes PE, Ahnert SE, Schafer WR, Bullmore ET. The rich club of the C. elegans neuronal connectome. J Neurosci 2013;33:6380–7. https://doi.org/10.1523/JNEUROSCI.3784-12.2013.
[100] Tozzi A. Evolution: networks and energy count. Nature 2014;515:343. https://doi.org/10.1038/515343c.
[101] Tozzi A. Information processing in the CNS: a supramolecular chemistry? Cogn Neurodyn 2015;9(5):463–77.
[102] Tozzi A, Peters JF. Towards a fourth spatial dimension of brain activity. Cogn Neurodyn 2016;10(3):189–99. https://doi.org/10.1007/s11571-016-9379-z.
[103] Tozzi A, Peters JF. A topological approach unveils system invariances and broken symmetries in the brain. J Neurosci Res 2016;94(5):351–65. https://doi.org/10.1002/jnr.23720.
[104] Tozzi A, Peters JF. From abstract topology to real thermodynamic brain activity. Cogn Neurodyn 2017;11:283. https://doi.org/10.1007/s11571-017-9431-7.
[105] Tozzi A, Peters JF, Fingelkurts AA, Fingelkurts AA, Marijuán PC. Topodynamics of metastable brains. Phys Life Rev 2017. https://doi.org/10.1016/j.plrev.2017.03.001.
[106] Van den Heuvel MP, Sporns O. Rich-club organization of the human connectome. J Neurosci 2011;31:15775–86. https://doi.org/10.1523/JNEUROSCI.3539-11.2011.
[107] Van Essen DC, Barch DM. The human connectome in health and psychopathology. World Psychiatry 2015;14(2):154–7. https://doi.org/10.1002/wps.20228.
[108] Vergara VM, Miller R, Calhoun V. An information theory framework for dynamic functional domain connectivity. J Neurosci Methods 2017;284:103–11. https://doi.org/10.1016/j.jneumeth.2017.04.009.
[109] Victor JD, Rizvi SM, Conte MM. Two representations of a high-dimensional perceptual space. Vis Res 2017;137:1–23. https://doi.org/10.1016/j.visres.2017.05.003.
[110] Victor JD, Thengone DJ, Rizvi SM, Conte MM. A perceptual space of local image statistics. Vis Res 2017;117:117–35. https://doi.org/10.1016/j.visres.2015.05.018.
[111] Vidaurrea D, Smith SM, Woolricha MW. Brain network dynamics are hierarchically organized in time. Proc Natl Acad Sci USA 2017;114(48):12827–32. https://doi.org/10.1073/pnas.1705120114.
[112] Waskom ML, Wagner AD. Distributed representation of context by intrinsic subnetworks in prefrontal cortex. Proc Natl Acad Sci USA 2017;114(8):2030–5. https://doi.org/10.1073/pnas.1615269114.
[113] Watanabe T, Hirose S, Wada H, Imai Y, Machida T, et al. Energy landscapes of resting-state brain networks. Front Neuroinform 2014;8:12. https://doi.org/10.3389/fninf.2014.00012.
[114] Whitehead AN. An enquiry concerning the principles of natural knowledge. Cambridge University Press; 1919.
[115] Wiltshire TJ, Euler MJ, McKinney TL, Butner JE. Changes in dimensionality and fractal scaling suggest soft-assembled dynamics in human EEG. Front Physiol 2017;8:633. https://doi.org/10.3389/fphys.2017.00633. eCollection 2017.
[116] Xing M, Ajilore O, Wolfson O, Leow A. Thought chart: tracking dynamic EEG brain connectivity with unsupervised manifold learning. In: Brain informatics and health; 2016. p. 149–57.
[117] Ye AQ, Ajilore O, Conte G, GadElkarim J, Thomas-Ramos G, et al. The intrinsic geometry of the human brain connectome. Brain Inf 2015;2(4):197–210. Epub 2015 Nov 7.
[118] Zaidi Q, Victor J, McDermott J, Geffen M, Bensmaia S, Cleland TA. Perceptual spaces: mathematical structures to neural mechanisms. J Neurosci 2013;33(45):17597–602. https://doi.org/10.1523/JNEUROSCI.3343-13.2013.
[119] Zamora-López G, Chen Y, Deco G, Kringelbach ML, Zhou C. Functional complexity emerging from anatomical constraints in the brain: the significance of network modularity and rich-clubs. Sci Rep 2016;6:38424. https://doi.org/10.1038/srep38424.
[120] Zare M, Grigolini P. Chaos, solitons & fractals criticality and avalanches in neural networks. Chaos Solitons Fractals 2013;55:80–94. http://doi.org/10.1016/j.chaos.2013.05.009.
[121] Zhang S-C, Hu J. A four-dimensional generalization of the quantum Hall effect. Science 2001;294:823–8.
[122] Zilberberg O, Huang S, Guglielmon J, Wang M, Chen KP, et al. Photonic topological boundary pumping as a probe of 4D quantum hall physics. Nature 2018;553(7686):59–62. https://doi.org/10.1038/nature25011.

TOPOLOGY OF HUMAN PERCEPTION

James F. Peters (corresponding Author)
Department of Electrical and Computer Engineering, University of Manitoba
75A Chancellor's Circle
Winnipeg, MB R3T 5V6 Canada and
Department of Mathematics, Adıyaman University, 02040 Adıyaman, Turkey
james.peters3@umanitoba.ca

Arturo Tozzi
Center for Nonlinear Science, University of North Texas
1155 Union Circle, #311427
Denton, TX 76203-5017 USA
tozziarturo@libero.it
Arturo.Tozzi@unt.edu

ABSTRACT

During the exploration of the surrounding environment, the brain links together external inputs, giving rise to perception of a persisting object. During imaginative processes, the same object can be recalled in mind even if it is out of sight. Here, topological theory of shape provides a mathematical foundation for the notion of persistence perception. In particular, we focus on ecological theories of perception, that account for our knowledge of world objects by borrowing a concept of invariance in topology. We show how a series of transformations can be gradually applied to a pattern, in particular to the shape of an object, without affecting its invariant properties, such as boundedness of parts of a visual scene. High-level representations of objects in our environment are mapped to simplified views (our interpretations) of the objects, in order to construct a symbolic representation of the environment. The representations can be projected continuously to an environmental object that we have seen and continue to see, thanks to the mapping from shapes in our memory to shapes in Euclidean space.

Keywords:
Brain; Borsuk-Ulam theorem; sensation; environment; ecological theory; Gibson.

Theoretical physics teaches us that the intimate micro-structure of the world consists of elements in perpetual movement, interacting with each other in a framework of probabilities, energy fields and vacuum. However, when we see a segment in a visual scene in the environment, we perceive elements seemingly melted together in a single complex of sensations. To make an example, we are able to detect, in the indistinctness of a rural scene at sunrise time, an increasingly distinct world of trees, hills, valleys and moving particles, e.g., birds flying from one tree to another. In effect, we appear to be sewing pieces of a changing scene together. How does the brain join different significant elements, giving rise to a single, stable perception of a scene? How does the brain imagine or recall objects that are out of sight? These two problems need to be tackled not at the microscopic atomic or sub-atomic level, nor at the galactic level, but at an intermediate macroscopic level where living beings stand. A noteworthy approach to understanding the mechanisms of direct perception is to start at the ecological level. Indeed, this article introduces a shape-based explanation of James J. Gibson's theory of persistence perception (Gibson, 1950). Throughout the second half of the twentieth century, he (1966, 1971, 1979) developed a unique theory in perceptual science, namely the ecological theory of perception (ETP), which stresses the importance of the relationships of the individual and the environment (Heft, 1997). The foundation for perception is ambient, ecologically available, direct information, as opposed to peripheral or internal sensations. The human (and/or animal) individual is embedded in the surrounding environment and the perception is strictly linked to searching movements, because changing awareness of the connectedness of the components of a scene occurs *in situ*, and not in a static context. The environment contains real, perceivable opportunities (called "affordances") for an individual's actions. Affordances are properties of the perceived environment (Gibson, 1979; Gibson, 1986; Lu, 2013) that provide paths to merged structures, shapes and actions. For example, the more chances children are given to directly perceive and interact with their environment, the more affordances they discover, and the more accurate their perceptions become over the passage of time. Perceiving is essentially exploratory (Heft, 1997). It consists in the acquisition of objective knowledge, by assembling diverse views of an object to form its abstract representation. In effect, a perceptual system is formed by vision, movements of the

eyes, head and entire body. Ecological theories argue that perception of persisting surfaces depends on the perception of specific structures, invariant over time. Recognition (perceiving) objects entails continuous mappings between our representations of objects and in-the-world ones. In effect, perception can be explained by our discovery of equivalent configurations (form, shapes) of objects (Heft 1997; Rock, 1983).

Visual information is carried in two separate pathways in our brain (Mishkin et al., 1983). Visual identification of objects is enabled by the multisynaptic cortico-cortical ventral pathway, which interconnects the striate, prestriate, and inferior temporal areas. On the other side, visual location of objects is made possible by the dorsal pathway, which runs dorsally, interconnecting the striate, prestriate and inferior parietal areas. Therefore, the visual system separates processing of an object's form and color ("what") from its spatial location ("where") (Rao et al., 1997).Recent findings suggest that nervous structures process information through topological as well as spatial mechanisms. For example, it is has been hypothesized that hippocampal place cells create topological templates to represent spatial information (Dabaghian, 2014; Arai, 1014; Chen, 2014; Tozzi et al., 2018). Developments in studies which consider the role of embodied cognition and action in psychology can be seen to support this basic position about hippocampal place cells. In particular, in this article, we show that novel incarnations of the "classical"Borsuk-Ulam theorem lead to a better comprehension and assessment of several features of direct perception and imagination.

TOPOLOGY COMES INTO PLAY

Borsuk-Ulam theorem. Topology, which assesses the properties that are preserved through deformations, stretching and twisting of objects, is a underrated methodological approach with countless possible applications (Willard, 1970; Krantz, 2009; Manetti, 2015). The Borsuk-Ulam theorem or BUT, cast in a quantitative fashion which has the potential of being operationalized, is a universal principle underlying a number of natural phenomena. In particular, we will show that BUT and its variants allow the assessment of perceptual features in terms of affinities and projections from real spaces to representations in feature spaces. It is noteworthy that BUT and its variants talk about projections, connections, not about cause-and-effect relationships (Tozzi and Peters, 2016a). Briefly, BUT states that, if a single point on a circumference projects to a higher spatial dimension, it gives rise to two antipodal points with matching description on a sphere, and vice versa(Borsuk, 1933; Marsaglia, 1972; Matoušek, 2003; Beyer, 2004). This means that the two antipodal points are assessed at one level of observation in terms of description, while a single point is assessed at a lower level (Tozzi 2016b), i.e., point location vs. point description. Points on a sphere are "antipodal", provided they are diametrically opposite (Henderson, 1996). Examples of antipodal points are the poles of a sphere. This means, e.g., that there exist on the earth surface at least two antipodal points with the same temperature and pressure. BUT looks like a translucent glass sphere between a light source and our eyes: we watch two lights on the sphere surface instead of one. But the two lights are not just images, they are also real with observable properties, such as intensity and diameter.

Variants of the Borsuk-Ulam theorem. The concept of antipodal points can be generalized to countless types of system signals. The two opposite points can be used not just for the description of simple topological points, but also oflines, or perimeters, areas, regions, spatial patterns, images, temporal patterns, movements, paths, particle trajectories (Borsuk, 1969; Peters and Tozzi, 2016b), vectors, tensors, functions, algorithms, parameters, groups, range of data, symbols, signs, thermodynamic parameters, or, in general, signals. If we simply evaluate nervous activity instead of "signals", BUT leads naturally to the possibility of a region-based, not simply point-based, brain geometry, with many applications. A region can have indeed features such as area, diameter, illumination, average signal value, and so on. We are thus allowed to describe system features as antipodal points on a sphere (Weeks, 2004; Peters, 2016).

Descriptively similar points and regions do not need necessarily to be opposite, or on the same structure(Peters, 2016; Peters and Tozzi 2016a). Therefore, the applications of BUT can be generalized also on non-antipodal neighboring points and regions on an sphere. In effect, it is possible to evaluate matching signals, even if they are not "opposite", but "near" each other. As a result, the antipodal points restriction from the "standard" BUT is no longer needed, and we can also consider regions that are either adjacent or far apart. And this BUT variant applies, provided there are a pair of regions on the sphere with the same feature value. We are thus allowed to say that the two points (or regions, or whatsoever) do not need necessarily to be antipodal, in order to be labeled together (Peters 2016).

The original formulation of the BUT describes the presence of antipodal points on spatial manifolds in every dimension, provided the manifold is a convex, positive-curvature structure (*i.e*, a ball). However, many brain functions occur on manifolds endowed with other types of geometry: for example, the hyperbolic one encloses complete Riemannian *n*-manifolds of constant sectional curvature -1 and concave shape (*i.e*, a saddle) (Sengupta et al., 2016). We are thus allowed to look for antipodal points also on structures equipped with kinds of curvature other than the convex one (Mitroi-Symeonidis, 2015). Or, in other words, whether a system structure displays a concave, convex or flat

appearance, does not matter: we may always find the points with matching description predicted by BUT(Tozzi, 2016). A single description on a plane can be projected to higher dimensional donut-like structures, in order that a torus stands for the most general structure which permits the description of matching points. For further details, see Peters and Tozzi (2016b).
Although BUT has been originally described just in case of *n* being a natural number which expresses a structure embedded in a spatial dimension, nevertheless the value of *n* in the brain sphere can also stand for other types of numbers (Tozzi et al., 2017). The BUT can be used not just for the description of "spatial" dimensions equipped with natural numbers, but also of antipodal regions on brain spheres equipped with other kinds of dimensions, such as a temporal or a fractal one (Tozzi,2019). This means, e.g., that spherical structures can be made not just of space, but also of time. The dimension *n* might stand not just for a natural number, but also for an integer, a rational, an irrational or an imaginary one. For example, *n* may stand for a fractal dimension, which is generally expressed by a rational number. This makes it possible for us to use the *n* parameter as a versatile tool for the description of systems' features.
Furthermore, matching points(or regions) might project to lower dimensions on the same structure. A sphere may map on itself: the projection of two antipodal points to a single point into a dimension lower can be internal to the same sphere. In this case, matching descriptions are assessed at one dimension of observation, while single descriptions at a lower one, and vice versa. Such correlations are based on mappings, e.g., projections from one dimension to another.In many applications (for example, in fractal systems), we do not need the Euclidean space (the ball) at all: a system may display an intrinsic, *internal* point of view, and does not need to lie in any dimensional space (Weeks, 2002). Therefore, we may think that the system just does exist by - and on – itself.

The foremost role of symmetries. Symmetries are real invariances that underline the world and occur at every level of systems' organization (Weyl, 1982). Bilinear forms of geometrical structures manifest symmetrical properties (Weyl, 1918). In other words, affine structures preserve parallel relationships. Symmetries are the most general features of mathematical, physical and biological entities and provide a very broad approach, explaining also how network communities integrate or segregate information. It must be emphasized that symmetries are widespread and may be regarded as the most general feature of systems, perhaps more general than free-energy and entropy constraints too. Indeed, recent data suggest that thermodynamic requirements have close relationships with symmetries. The interesting observation that entropy production is strictly correlated with symmetry breaking in quasi-static processes paves the way to use system invariances for the estimation of both the free energy of metastable states, and the energy requirements of computations and information processing (Roldán, 2014). Thus, giving insights into symmetries provides a very general approach to every kind of systems function. A symmetry break occurs when the symmetry is present at one level of observation, but "hidden" at another level. A symmetry break is detectable at a lower dimension of observation. Thus, we can state that single descriptions are broken (or hidden) symmetries, while matching descriptions are restored symmetries. In other words, a symmetry can be hidden at the lower dimension and restored when going one dimension higher. If we assess just single descriptions, we cannot see their matching descriptions: when we evaluate instead systems one dimension higher, we are able to see their hidden symmetries. In sum, symmetries, single descriptions and matching descriptions are the common language among different real sciences.

In sum, BUT displaysversatile formulations thatcan be modified in different fashions, in order to achieve a wide range of uses in neuroscience, such as multisensory integration, neural histological images tessellation, brain symmetries, Kullback-Leibler divergence during perception, detection of a brain functional 3-sphere. For further details, see Tozzi and Peters (2016a and 2016b). In the next paragraphs, we will focus on the role of BUT and its variants in direct perception and object recalling, taking into account Gibson's incisive observations.

PERCEPTION OF SHAPES AND PERCEPTION AS SHAPE MAPPING

In such a theoretical context of perception,theBorsuk-Ulamtheoremhelps elucidate the tenets of the ETP and explains how we see an object and how we imagine it (Tozzi and Peters, 2016b). Briefly, BUT explains how high-level representations of objects in our environment are typically mapped to simplified views (our interpretations and coalescences) of the objects. And these mappings described by BUT can sometimes be reversed (*inversed*) to achieve a form of pullback from descriptions to sources of descriptions, from a simplified view to multiple views of the same object. Indeed, a new form of shape theory (called homotopy) discovered by K. Borsuk makes it possible to assess the properties that are preserved through deformation, stretching and twisting of objects (Beyer, 2004; Manetti, 2015). Homotopy is a theory of shape deformation (Borsuk, 1971; Borsuk and Dydak, 1980), e.g., how some shapes can be deformed into other shapes. In this context, the term "shape" means "exterior form" and a "deformation" is a mapping from shape into another one. A classical example is the deformation of a coffee cup into a torus. The combination of

various forms of BUT and homotopy theory provides a methodological approach with countless possible applications, especially in helping us understand perception and how we acquire visual imagination. The theory of shape, in simple terms, focuses on the global properties of geometric objects such as polyhedra and tori, neglecting the complications of the local structures of the objects (Borsuk and Dydak, 1980). What shape theory and BUT tell us about visual image acquisition echoes the Gibsonian view of perception: *cognitive processes relating to perception, storage, retrieval and reorganization interact with memory structures and construct a symbolic representation of the environment*. For example, mesh view in **Figure 1** can be viewed as visualization of one among many symbolic views of Leonardo DaVinci's Mona Lisa painting. In effect, an individual perceives [constructs] the features and events of the environment specified by this [pickup] information from the environment (Heft, 1997).

In particular, BUT variants and Borsuk's theory of shapes are closely allied to Gibson's view of *persistence of perception* (Gibson, 1979; Natoulas, 1992). That is, our perception of an object continues, even when the object is out of sight. This can concisely be explained by viewing regions on the surface of a hypersphere as multiple representations of object shapes, mapped continuously to an ecological object that have seen and continue to see. It occurs thanks to the continuous mapping from shapes in our memory to shapes in Euclidean space. In effect, persistence perception can be viewed as signals matching, real-scene visual signals that are collectively the umbra of physical shapes.

Every physical shape has a basic geometry characterized by a bounded region of space with a nonempty interior. Thanks to shape boundaries, each shape separates the perception of shapes into two regions, namely, that part of space that is exterior outside a shape and that part of space that is in the interior of a shape.

The perception of shape of an object **A** with **boundary** bdy_A and **interior** int_A is concomitant with the changing of a shape as it moves with velocity v_A through spacetime. By taking into account the mass of a shape and its velocity as it moves in spacetime with varying speeds, it is then possible to arrive at a mathematical model of perceived shape with energy E with mass m and momentary velocity v, namely,

$E \approx m$ (spacetime energy of a perceived shape), i.e.,

$E = mv^2$.

It has also been observed by L. Suskind (2008) that energy is a shape shifter. Putting these observations together, we arrive at the following useful lemma.

Lemma A. (Based on an Observation by L. Susskind). The mass of the brain is proportional to its shape-shifting energy.

From Lemma A, we derive a shape function

$$shA\left(bdy_A, \text{int}_A, v_A\right),$$

which depends on the momentary values of bdy_A (boundary of a shape sh_A), int_A (interior of a shape sh_A), and v_A (momentary velocity of shape sh_A). The function sh_A (based on recent results in Peters (2020)) represents the combined results of the movement and shape-changing of object A, *i.e.*, the momentary energy of object A.

Theorem. The mass of an object is derivable from its changing shape and momentary velocity.

Proof: By definition, the shape of an object A (our sh_A) travelling in spacetime with velocity v_A, has a boundary bdy_A and an interior int_A. Let

$sh_A : \square \times \square \times \square \to \square$ (mapping of a real valued trio to a real value),

be a scalar mapping represented by $sh_A\left(bdy_A, \text{int}_A, v_A\right)$ so that $sh_A\left(bdy_A, \text{int}_A, v_A\right) = sh_A\left(\vec{r}\right)$ is assigned to each brain cell p with position vector $\vec{r}$. In addition, $\text{div}\, sh_A$ denotes the divergence of the vector field and $grad\ sh_A$ denotes the gradient (change in direction) of the scalar field sh_A.

The differential operator $\Delta sh_A\left(bdy_A, \text{int}_A, v_A\right)$ is the Laplace delta of function sh_A at a point $\left(bdy_A, \text{int}_A, v_A\right)$. Also, recall that the Hamilton nabla operator ∇ provides a convenient shorthand for standard partial derivatives. The Laplace delta Δsh_A is defined by

$$\Delta sh_A = \text{div}\, grad\ sh_A = \nabla \cdot \left(\nabla sh_A\right) = \frac{\partial^2 sh_A}{\partial bdy_A^2} + \frac{\partial^2 sh_A}{\partial \text{int}_A^2} + \frac{\partial^2 sh_A}{\partial v_A^2}.$$

In that case, the energy E_A of object A at any given instant is the value of Δsh_A. In effect,

$$\Delta sh_A \mapsto E_A\left(\text{energy of brain } A\right),$$

i.e., Δsh_A maps to shape energy E_A. Then, from Lemma A, the mass m_A of object A is proportional to its shape-shifting energy, defined by

$$m_A = \frac{1}{v_A^2} \times \left[\Delta sh_A\right] = \frac{1}{v_A^2} \times \left[E_A\right] = \frac{E_A}{v_A^2}\left(\text{brain mass } m_A \approx \text{ shape-shifting energy } E_A\right). \square$$

Hence, object mass m_A varies relative to its shape-shifting energy. The important side-effect of object shape-changing energy is that it provides a platform as well as a foundation for the perception of shape. That is, shape perception will tend to vary as object mass m_A varies as its shape morphs with velocity v_A at each instant during its lifetime as it moves through space.

To make an example, **Figure 1**displays the Mona Lisa painting impinging on the optic nerves: we map it to similar shape representations, such as the Mona Lisa mesh. Gibson accounted for our knowledge of world objects by borrowing a concept of invariance in topology: a series of transformations can be endlessly and gradually applied to a pattern without affecting its invariant properties (Gibson,1950). And, principal among the properties of world objects, is shape and the acquisition of persistent perception of object shapes, which we nicely explain with BUT variants.

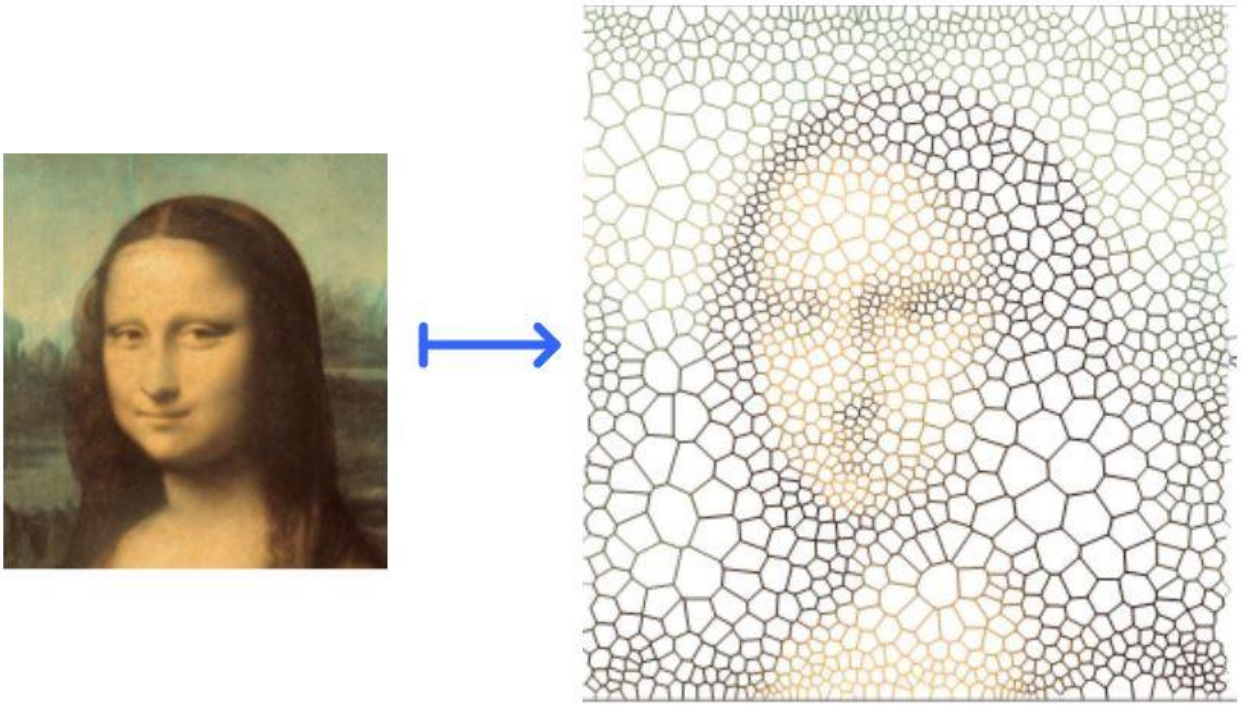

Figure 1. Mona Lisa shape deformably mapped to Mona Lisa Exterior Mesh Shapes. This mapping illustrates nascent Gibsonian persistence perception: we abstract away from the very complex structures in Da Vinci's painting to arrive a simpler, geometric view of the image as a collection of familiar convex polygons. Modified from: Tozzi and Peters (2018).

A TOPOLOGICAL APPROACH TO "ASKNOT WHAT'S INSIDE YOUR HEAD, BUT WHAT YOUR HEAD'S INSIDE OF"

We start from the simplest and most natural standpoint: an individual (either human or animal) embedded in his environment(Russo-Krauss, 2015). The environment stands for what surrounds the organisms that perceive and behave, in order that both are joined together in a inseparable couple. In topological terms, we may say that the individual is embedded in a spatial three-dimensional ball. Thus, the individual stands in front of the surrounding spatial environment, shaped in guise of a sphere. The environment is not theone of the "traditional" physics: indeed, it can be described through – and is made of - the triad of "medium", "substance" and "surfaces" perceived by the individual. The ecological surface stands for the "classical" geometric plane, while the ecological medium for the standard geometrical space. In such a guise, the object features that the individual perceives are just the interface between surfaces, in order that information is embedded into the light (natural or artificial) surrounding them. The most stable, long-lasting perception of the individual is the base upon which he stands, e.g., the ground, the horizontal surface under his feets. When the individual raises his eyes, he perceives the sky, or the ceiling. The middle zone between the ground and the sky is the medium. The objects, e.g., something which can be handled, stand vertically in the medium. The permanent objects are just surface features which can be perceived on long timescales. For our purposes, it is noteworthy that the human (and also animal) individual splits the environment, in which he moves and finds novel affordances, in three components: the ground and the sky, which join together at the horizon, and the intermediate zone, the medium. We are thus allowed to split the three-dimensional ball into three slices: the sky on the top, the ground on the bottom and the intermediate zone in the middle. In topological terms, the brain splits the environment in different closed subsets. In this framework, a theorem, closely linked to the Borsuk-Ulam theorem, comes into play: the Lusternik–Schnirelmann theorem (LST). It states that, if a sphere is covered by n+1 open sets, then one of them

contains a pair of antipodal points. In other words, every time you split a sphere in three parts, there is always one of them which contains an entire diameter, where the antipodal points lie (**Figure 2A**). With this theorem, we are guaranteed at least a pair of exactly opposite points on a sphere (Dodson and Parker, 1997). According to LST, one of the three slices must necessarily contain some antipodal points, e.g., surface features with matching description. When an individual move around and looks for something (i.e., an object), his brain focuses on one of the three slices of the n-sphere. If we state that the individual attention is driven by one of the slices, we may term such slice as the one containing antipodal points. In other words, the individual needs to find, in one of the three slices in which he separates his environment (the sky, the ground and the medium), a pair of antipodal points equipped with matching description. The latter, by an ecological point of view, share something perceivable in common. Note that, according to the forms of the BUT, the points do not need necessarily to be antipodal. It means that two points embedded in one of the three closed sets do not need to be opposite to be described together. The antipodal points, according to one of the BUT variants, do not need to be simple *points*, but they could have different features. They could be spatial objects or shapes, but also matching movements, or they may display a temporal scale. In the latter case, the shapes are not called objects, but events.

Once we have established a topological framework for objects in the environment, how does the process of perception occur in our brain (mind)?When two antipodal points (or functions) are joined together according to BUT and its variants, they are perceived together, in order that the individual sees (or hears, or touches) a complex of sensations representing the object. According to one of the BUT features (the mapping from a higher to a lower dimension),the dimensions of the surrounding environment need to be reduced when they "enter" our brain. To make an example, we will take into account the multisensory integration, a mental phenomenon occurring when two stimuli from different cues are perceived together (e.g., the view of a running ambulance and the sound of its siren, **Figure 2A**). In a topological view, BUT (and its variants) nicely applies to multisensory integration: two environmental stimuli from different sensory modalities display similar features, when mapped into cortical neurons. For example, an observer stands in front of the surrounding environment. An ambulance is embedded in the environment. The observer perceives, through his different sense organs such as ears and eyes, the sounds and the movements of the ambulance. The latter stands for an object embedded in the three-dimensional sphere. The two different sensory modalities (sounds and movements) stand for non-antipodal points on the sphere's circumference. Even if objects belonging to opposite regions can either be different or similar, depending on their features (Peters, 2016), however they must share the same features. In our case, both sounds and movements come from the same object embedded in the sphere, i.e., the ambulance. The two non-antipodal points project to a two-dimensional layer, the brain cortex - where multisensory neurons lie - and converge into a single multisensory signal (**Figure 2B**). According to the dictates of the BUT, such a single point contains a "melted" messages from the two modalities, which takes into account the features of both (Tozzi and Peters, 2016b).

Contrary to the standard theories of perception, which emphasize the input processing and an Helmotzian distinction between fixed, innate sensations and variable, learned perceptions, ETP proposes a novel approach. A mutual relationship occurs between the individual and the environment. The perceptive experience is direct and immediate. Information is directly taken from the environment, with no mediations. According to ETP, the real word is the phenomenic one. The ETP concept of a smart mechanism able to extract the invariants from the input stream means that the active subject puts in relationships and connexions the objects through his senses, with no need for mental processing in order to build them. The truth corresponds to the immediate perception, which is a *datum* in our brain. Topology nicely explains this interesting feature which is common not just to perceptions, but also to higher mental activities. Indeed, the antipodal point do not stand just for spatial features, such as an object, but also for temporal sequences. It means that the brain is constrained to link together not just spatial elements in an object, but also temporal events in a concept, an idea, a proposition, a hope, a desire and so on. Furthermore, the individual can be embedded not just in a spatial n-sphere, but also in a n-sphere in which n stands for the time, according to the dictates of the BUT variants. Also many spheres with different times are possible: it means that the individual is "constrained" to link past and future events, it is not a choice of his own.

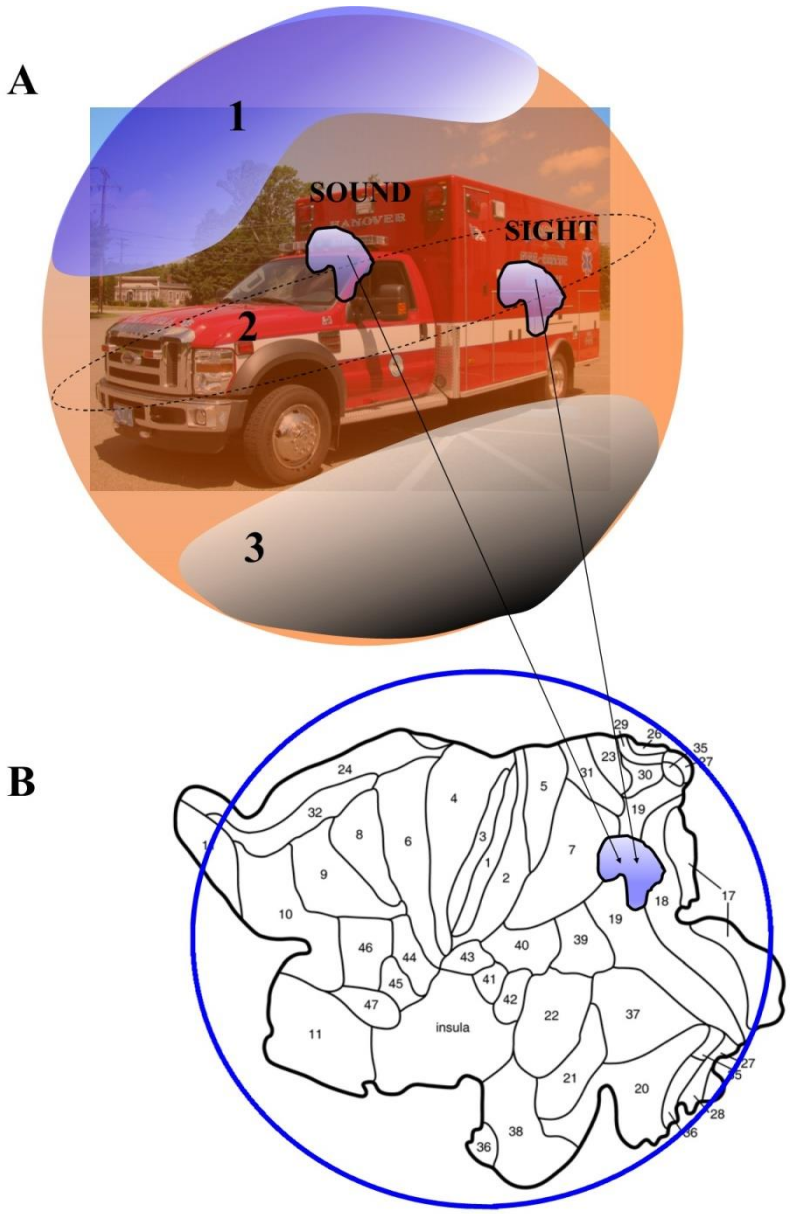

Figure 2A. The three closed regions predicted by the Lusternik–Schnirelmann theorem are named 1,2 and 3. Once achieved two points with matching description embedded into one of the three closed regions (in this case, the region 2), they can be projected (**Figure 2B**) to a single point onto a 2D brain model (modified from Van Essen, 2005).

CONCLUSIONS

This paper introduces a possible foundation of a general theory of perception based on some findings of algebraic topology. Such a foundation is inspired by – and partly agrees with – the Gibsonian approach to visual perception. Indeed, our paper provides a link between the Ecological Theory of Perception (Gibson ETP) and the topological framework of BUT and its variants, able to explain the mechanisms of perception. Although Gibson stated that space is a myth, a ghost, a fake produced by geometry, a topological approach sheds new light on his own theory. According to this novel conception, the individual's brain (or mind) is forced to coalesce together some components of the environment, in a complex interaction between external affordances and the motivated humans who perceive them. The melting of parts of the environment into a single perception is thus compelled, and is not a free choice made by the individual. The brain needs to perceive different elements together and cannot split them, because the perception may occur and operate just in this way.

The evolutionary advantage is self-evident: the perception of different elements is useless by itself, while the perception of a complete object, or of a concept or an idea, is mandatory in order to survive in an explorable environment, full of

possibilities, but also of dangers. In sum, the need to join things together in a single perception is mandatory for our brain (mind). It is important to emphasize that the antipodal points with matching description do not need to be causally correlated: their relationship is a topological one, meaning that the surface features of an object are "linked" together in a single complex of sensations by projections, affine connexions and proximity. In other words, the concept of *connexion* means that the joined parts if the environment are not necessarily in causal relationship, rather they are simply functionally correlated. The individual, with the habituation, learns, from childhood forward, to join together the elements which are more useful for his surviving.

"Perception is based on information, not on sensations" (Gibson, 1979). This means that ETP, rather than sensation-based, is information-based, because emphasizes an analysis of the environment (in terms of affordances), and the concomitant specificational information that the organism detects about such affordances. The human behaviour is radically situated. In other words, you cannot make predictions about human behaviour unless you know what situation or context or environment the human in question was in. Individuals stand in an ecological relation to the environment, such that to adequately explain some behaviour it is necessary to study the environment or niche in which it took place and, especially, the information that "epistemically connects" the organism to the environment. Thus, an appropriate analysis of the environment, made in terms of BUT and its variants, becomes crucial for an explanation of perceptually guided behaviour.

Gibson's work strengthens and brings to the front the primary question of "what" is perceived, before questions of mechanisms and material implementation are introduced (Rao et al., 1997). Together with a contemporary emphasis on dynamical systems theory as a necessary methodology for investigating the structure of ecological information, the Gibsonian approach, particularly in the light of the modern tools of algebraic topology, has maintained its relevance and applicability to neuroscience.

ACKNOWLEDGEMENTS.

The research by J.F. Peters has been supported by the Natural Sciences &Engineering Research Council of Canada (NSERC) discovery grant 185986, Instituto Nazionale di Alta Matematica (INdAM) Francesco Severi, Gruppo Nazionale per le Strutture Algebriche, Geometriche e Loro Applicazioni grant 9 920160 000362, n.prot U 2016/000036 and Scientific and Technological Research Council of Turkey (TŰBİTAK) Scientific Human
Resources Development (BIDEB) under grant no: 2221-1059B211301223.
The Authors would like to thank also Rosa Del Prete for her skillful suggestions.

REFERENCES

1) Arai M, Brandt V, Dabaghian, Y. 2014. The effects of theta precession on spatial learning and simplicial complex dynamics in a topological model of the hippocampal spatial map. PLoS Comp. Bio. 10 (6): e1003651.
2) Beyer WA, Zardecki A. 2004. The early history of the ham sandwich theorem. American Mathematical Monthly, 111, n. 1:58-61
3) Borsuk, K. 1933.Drei sätzeüber die n-dimensional euklidische sphäre, FundamentaMathematicae XX, 177–190.
4) Borsuk K. 1958-1959. Concerning the classification of topological spaces from the standpoint of the theory of retracts, Fund. Math., XLVI, 321-330, MR0104216.
5) Borsuk K. 1969. Fundamental retracts and extensions of fundamental sequences, Fund. Math. 64(1), 55–85, MR0243520.
6) Borsuk K. 1971. Theory of Shape. Lecture Notes Series 28, Matematisk Institut, Aarhus Universitet, MR0418088
7) Borsuk K, Dydak J. What is the theory of shape? Bull. Austral. Math. Soc. 22 (1980), no. 2, 161-198, MR0598690.
8) Chen Z, Gomperts SN, Yamamoto J, Wilson MA. 2014. Neural representation of spatial topology in the rodent hippocampus. Neural Comput. 26, 1–39.
9) Dabaghian Y, Brandt VL, Frank LM. 2014. Reconceiving the hippocampal map as a topological template. Elife 3, e03476.
10) Dodson CTJ, Parker PE. 1997. A user's guide to algebraic topology, Kluwer, Dordrecht, Netherlands, 1997, xii+405 pp. ISBN: 0-7923-4292-5, MR1430097.
11) Gibson JJ. 1950. The Perception of the Visual World. Greenwood Press, Westpost, Conn.
12) Gibson JJ. 1966. The senses considered as perceptual systems. Boston: Houghton-Mifflin.
13) Gibson JJ. 1971. The information available in pictures. Leonardo 4, 27-35.
14) Gibson JJ. 1979. The theory of affordance in the ecological approach to visual perception. Hillsdale, Erlbaum.

15) Gibson JJ. 1986. The ecological approach to visual perception. Boston: Houghton-Mifflin.
16) Heft H. 1997. The relevance of Gibson's ecological approach to perception for environment-behavior studies. In G.T. Moore, R.W. Marans, Adances in Environment, Behavior, and Design. Plenum Press, NY, 1997, 71-107.
17) Krantz SG. 2009. A guide to topology, The Mathematical Association of America, Washington, D.C.
18) Lu J, Cheng L. 2013. Perceiving and interacting affordances: A new model of human-affordance interactions. Integr. Psych. Behav. 47, 142-155.
19) Manetti M. 2015. Topology, Springer, Heidelberg. DOI 10.1007/978-3-319-16958-3.
20) Marsaglia G. 1972. Choosing a Point from the Surface of a Sphere. Annals of Mathematical Statistics 43 (2): 645–646. doi:10.1214/aoms/1177692644.
21) Matoušek J. 2003. Using the Borsuk–Ulam Theorem. Lectures on Topological Methods in Combinatorics and Geometry. Springer-Verlag Berlin Heidelberg.
22) Mishkin M, Ungerleider LG, Macko KA. 1983. Object vision and spatial vision: two cortical pathways. Trends in Neurosciences, 6:414–417.
23) Mitroi-Symeonidis F-C. 2015 Convexity and sandwich theorems. European Journal of Research in Applied Sciences, vol. 1, pp. 9-11
24) Natsoulas T. 1992. The tunnel effect, Gibson's perception theory, and reflective seeing, Psychol. Res. 54, 160-174.
25) Henderson DW. 1996. Experiencing geometry on plane and sphere. Prentice Hall. ISBN 978-0-13-373770-7.
26) Peters JF. 2016. Computational Proximity. Excursions in the Topology of Digital Images. (I. S. R. Library, Ed.). Berlin: Springer-Verlag. DOI: 10.1007/978-3-319-30262-1.
27) Peters JF. 2020. Computational Geometry, Topology and Physics of Digital Images with Applications. Shape Complexes, Optical Vortex Nerves and Proximities. Springer Int. Pub. AG, Cham Switzerand, in press.
28) Peters JF, Tozzi A. 2016a. Region-Based Borsuk-Ulam Theorem. arXiv:1605.02987v2.
29) Peters JF, Tozzi A. 2016b. String-Based Borsuk-Ulam Theorem. arXiv:1606.04031.
30) Rao SC, Rainer G, Miller EK. 1997. Integration of what and where in the primate prefrontal cortex.Science. 1997 May 2;276(5313):821-4.
31) Rock I. 1983. The logic of perception. MIT Press, Cambridge, MA.
32) Roldán E, Martínez IA, Parrondo JMR, Petrov D. 2014. Universal features in the energetics of symmetry breaking. Nature Physics 10, 457–461. doi:10.1038/nphys2940
33) Russo Krauss C. 2015. L'empiriocriticismo di Richard Avenarius tra psicofisiologia e teoria della consocenza, in R. Avenarius, Il concetto umano di mondo, Morcelliana, Brescia.
34) Sengupta B, Tozzi A, Coray GK, Douglas PK, Friston KJ. 2016. Towards a Neuronal Gauge Theory. PLOS Biology 14 (3): e1002400. doi:10.1371/journal.pbio.1002400.
35) Susskind, L. (2008) The Black Hole War. Hachette Book Group, Inc.
36) Tozzi A. 2016. Borsuk-Ulam Theorem Extended to Hyperbolic Spaces. In Computational Proximity. Excursions in the Topology of Digital Images, edited by J F Peters, 169–171. doi:10.1007/978-3-319-30262-1.
37) Tozzi A, Peters JF. 2016a. Towards a fourth spatial dimension of brain activity. Cognitive Neurodynamics, 1–11. DOI: 10.1007/s11571-016-9379-z
38) Tozzi A, Peters JF. 2016b. A topological approach unveils system invariances and broken symmetries in the brain. Journal of Neuroscience Research, 94(5), 351–365. http://doi.org/10.1002/jnr.23720.
39) Tozzi A, Peters JF, Fingelkurts AA, Fingelkurts AA, Marijuán PC. 2017. Topodynamics of metastable brains. Physics of Life Reviews, 21, 1-20. http://dx.doi.org/10.1016/j.plrev.2017.03.001.
40) Tozzi A, Peters JF. 2018. Multidimensional brain activity dictated by winner-take-all mechanisms. Neuroscience Letters, 678 (21):83-89. https://doi.org/10.1016/j.neulet.2018.05.014.
41) Tozzi A, Peters JF, Fingelkurts A, Fingelkurts A, Perlovsky L. 2018. Syntax meets semantics during brain logical computations. Progr Biophys Mol Biol, 140: 133-141. https://doi.org/10.1016/j.pbiomolbio.2018.05.010.
42) Tozzi A. 2019. The multidimensional brain. Physics of Life Reviews. doi: https://doi.org/10.1016/j.plrev.2018.12.004. In press.
43) Van Essen, D.C. (2005). A Population-Average, Landmark- and Surface-based (PALS) atlas of human cerebral cortex. Neuroimage. 28, 635–666.
44) Weeks JR. 2002. The shape of space, IInd edition. Marcel Dekker, inc. New York-Basel.
45) Weyl H. 1918. Raum−Zeit−Materie. Vorlesungen über allgemeine Relativitäts theorie (Space—Time—Matter). Reprinted in H. Weyl (1952). Space—Time—Matter, trans. By H.L. Brose, Dover Pubs, Inc.
46) Weyl H. 1982. Symmetry. Princeton: Princeton University Press. ISBN 0-691-02374-3.
47) Willard S. 1970. General topology, Dover Pub., Inc., Mineola, NY, xii +369pp, ISBN: 0-486-43479-6 54-02, MR0264581.

Available online at www.IJournalSE.org

Emerging Science Journal

Vol. 3, No. 2, April, 2019

Topology of Black Holes' Horizons

Arturo Tozzi [a*], James F Peters [b]

[a] *Center for Nonlinear Science, University of North Texas, 1155 Union Circle, #311427, Denton, TX 76203-5017, USA*

[b] *Department of Electrical and Computer Engineering, University of Manitoba, 75A Chancellor's Circle, Winnipeg, MB R3T 5V6, Canada*

Abstract

The Möbius strip spacetime topology and the entangled antipodal points on black hole surfaces, recently described by 't Hooft, display an unnoticed relationship with the Borsuk-Ulam theorem from algebraic topology. Considering this observation and other recent claims which suggest that quantum entanglement takes place on the antipodal points of a S^3 hypersphere, a novel topological framework can be developed: a feature encompassed in an S^2 unentangled state gives rise, when projected one dimension higher, to two entangled particles. This allows us to achieve a mathematical description of the holographic principle occurring in S^2. Furthermore, our observations let us to hypothesize that a) quantum entanglement might occur in a four-dimensional spacetime, while disentanglement might be achieved on a motionless, three-dimensional manifold; b) a negative mass might exist on the surface of a black hole.

Keywords:

Borsuk-Ulam Theorem;
Antipodal Points;
Quantum Entanglement;
Holographic Principle;
t'Hooft;
Möbius Strip.

Article History:

Received:	26	January	2019
Accepted:	03	April	2019

1- Introduction

The spacetime topology of a black hole has been recently described in four dimensions [1, 2]. The impenetrable, continuous curtain surrounding the black hole, termed firewall, displays antipodal quantum states with matching description. This also means that particles emerging at opposite sides of the 4-dimensional hypersphere are strongly entangled. In turn, recent claims suggest that quantum entanglement can be assessed in terms of opposite features on a 4D hypersphere. Indeed, Peters and Tozzi [3, 4] showed that a separable state can be achieved for each of the entangled particles lying in S^2, just by embedding them in a higher dimensional S^3 space. The Authors view quantum entanglement as the simultaneous activation of signals in a 3D space mapped into a S^3 hypersphere. Because the particles are entangled at the S^2 level and un-entangled at the S^3 hypersphere level, a composite system is achieved, in which each local constituent is equipped with a pure state.

It is noteworthy that both the issues, i.e., the black hole's antipodal points and the entanglement on a hypersphere, are assessable through the framework described by the Borsuk-Ulam theorem (BUT), which states that e*very continuous map* $f: S^n \to R^n$ *must identify a pair of antipodal points* – diametrically opposite points on an n-sphere [5, 6]. Points are *antipodal*, provided they are diametrically opposite [7-9]. Examples of antipodal points are the endpoints of a line segment, or opposite points along the circumference of a circle, or poles of a sphere, or the opposite quantum states with matching description embedded in the 't Hooft's four-dimensional black hole surface [10-12]. In other words, the BUT states that two features with matching description are mapped to a single feature one dimension lower, provided the function under assessment is continuous. In the case of 't Hooft's account of black holes, the continuity is preserved, because the firewalls of their surfaces are continuous. In the sequel, we will show how the BUT is correlated with the holographic principle and will draw unexpected consequences.

* **CONTACT**: Tozziarturo@libero.it

DOI: http://dx.doi.org/10.28991/esj-2019-01169

© This is an open access article under the CC-BY license (https://creativecommons.org/licenses/by/4.0/).

2- Holographic Principle and Topological Mappings

The possibility dictated by the BUT to proceed from higher to lower dimensions and vice versa leads us to the realm of the holographic principle (HP). It states that the description of a volume of space can be thought of as encoded on a lower-dimensional boundary to the region [13, 14]. The theory suggests that the entire universe can be seen as two-dimensional information on the cosmological horizon. In HP, information (albeit quantum states evolving in spacetime) can be represented as a hologram, explainable via the theory of topological deformation retracts [15]. A deformation retract is a mapping of the boundary of a shape (surface) to its skeleton [16]. In the context of black holes, we have a deformation of quantum states in their neighborhood. Here we show how, starting from the 't Hooft black hole equipped with quantum strates entangled on its horizon, an algebraic topological description of the HP can be provided.

The derivation of the holographic principle is represented concisely as a fibre bundle. Briefly, a ***fibre bundle*** is a triple $(E,\ \pi, B)$, where $\pi: E \to B$ is a projection mapping from a bundle space E to a base space B [17]. Fibre bundles are on the threshold of an operational view of a complex collection of mappings that includes a projection mapping. This is the case, since it is a straightforward task to extract from a fibre bundle the steps of an algorithm (aka, precise prescription leading to implementations in different settings, such as a black hole's horizon equipped with antipodal points). A fibre bundle representation of the holographic principle L is given in Figure 1, that illustrates how the holographic manifold $L(M,X)$ can be extracted from a cross product of mappings:

$$\begin{aligned} &X(n) \otimes M\left(m\left(\varphi(X(n)), \varphi(-X(n))\right)\right) \to L(M,X) \\ &X \otimes M \to L(M,X) \\ &L(M,X), \end{aligned} \tag{1}$$

Where $X(n)$ is the Hamiltonian of a quantum signal impacting on the particle n and an antipodal gathering $M(m(\varphi(X(n)), \varphi(-X(n))))$ that includes input from black hole's antipodal evaluations of $X(n)$ from a spherical view of the black hole's horizon, i.e., antipodal values $\varphi\big(X(n)\big), \varphi\big(-X(n)\big)$ originated from a circle-shaped region of the horizon. That is, the mapping.

$$X \otimes M \to L(M,X) \tag{2}$$

Models the mapping of the accumulation $\otimes$ accruing from the interaction of the results of the mappings X and M to the holographic manifold $L\ (M,X)$, which displays a dimension lower than the black hole's 4D surface.

Concerning Figure 1, each arrow $\longmapsto$ represents a mapping. The arrows depict both ordinary mappings that carry the derivation forward and a projection mapping from $X(n)$ to the black hole's horizon, which results in a gathering of antipodal evaluations of $X(n)$, namely, $m(\varphi\big(X(n)\big), \varphi\big(-X(n)\big))$. A particular value of a holographic manifold $L\ (M,X)$ results from a synthesis of two signals: $X(n)$ and $M(m(\varphi\big(X(n)\big), \varphi\big(-X(n)\big)))$.

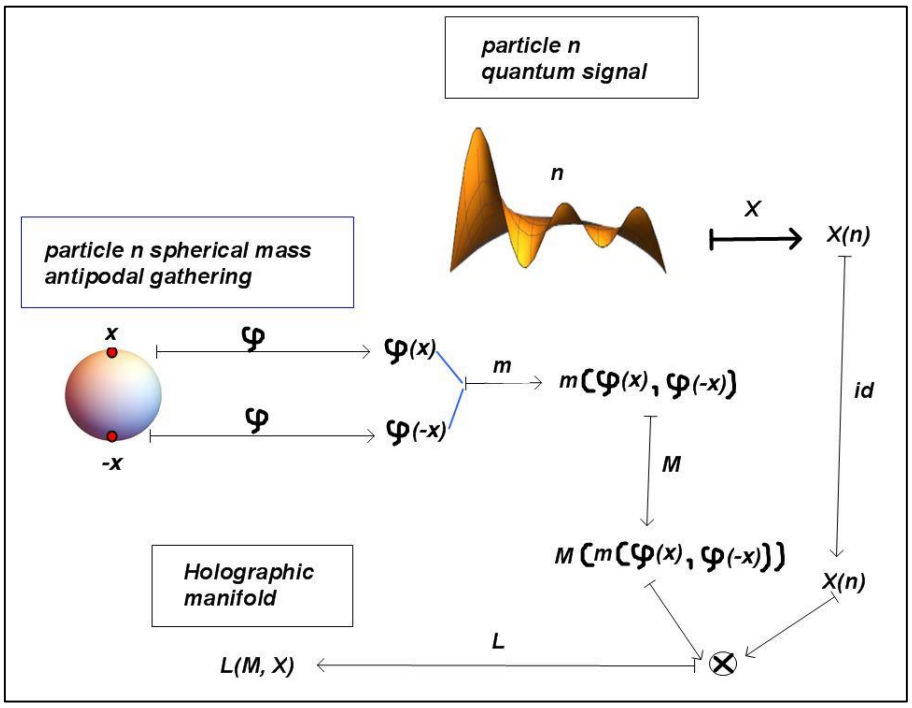

Figure 1. Fibre bundle representation the holographic principle and its relationships with black holes. The picture illustrates the procedure to achieve a topological correlation between black hole's surface and the holographic principle. See text for further details.

3- Black Hole Dynamics on a Möbius Strip

The entangled antipodal points on black hole surfaces described by ‘t Hoof trequire spacetime topology displaying a time-like Möbius strip [1]. The Möbius strip, also called the twisted cylinder, is a one-side surface equipped with just one boundary [18, 19], when embedded in three-dimensional Euclidean space. A Möbius strip can be built by taking a paper strip and giving it a half-twist, then joining the ends in order to form a loop. This means that a line that starts from the seam down the middle meets back at the seam, but at the other side. If continued, the line meets the starting point, in a point that is double the length of the original strip. This single continuous curve may be described either through a parameterized subset of a three-dimensional Euclidean space, or through cylindrical polar coordinates. Topologically, the Möbius strip can be defined as the square [0, 1] × [0, 1], with its top and bottom sides identified by the relation $(x, 0) \sim (1 - x, 1)$ for $0 \leq x \leq 1$.

In ‘t Hooft’s terms, the mapping obtained by making a trip around the black hole’s Möbius strip is a CPT inversion that allows time to change sign at the horizon.

In the previous paragraphs, we showed how the BUT, which copes with projections and mappings among different functional dimensions, has been proven suitable for the description of black hole’s antipodal features. Here we show how the BUT’s antipodal features with matching description can be assessed in terms of closed paths on a Möbius strip. This allows us to evaluate the system’s dynamics in terms of paths and trajectories taking place onto the well-established, easily manageable phase space of a twisted cylinder. Because the techniques of algebraic topology that assess the BUT features are quite complex, difficult to approach and quantify, a framework is required that allows the description of the BUT’s matching features in terms of dynamics taking place in phase spaces. This means that the scenario described by the BUT can be transported to a peculiar phase space, i.e., a Möbius strip, in order that antipodal points can be tackled in terms of trajectories taking place on a rather simple abstract manifold.

Our aim is to achieve the transport of the BUT’s antipodal points to the one-side surface of such twisted cylinder. If we embed the trajectories of two BUT matching functions x and –x (Figure 2A) on a Möbius strip, we achieve a closed, continuous loop where the two functions are allowed to travel along constrained trajectories. It is easy to see that a piece of strip of a given length, standing for a time interval, may display both x and –x at the same time (Figure 2B). The BUT dictates are preserved because, even if the two matching features are simultaneous, they do not have points in common: indeed, they lie on the opposite surface of the same strip. In black holes’ terms, this means that the oscillations’ trajectories of two areas which activate together can be followed in subsequent times, even when their matching activation has disappeared (Figure 2C).

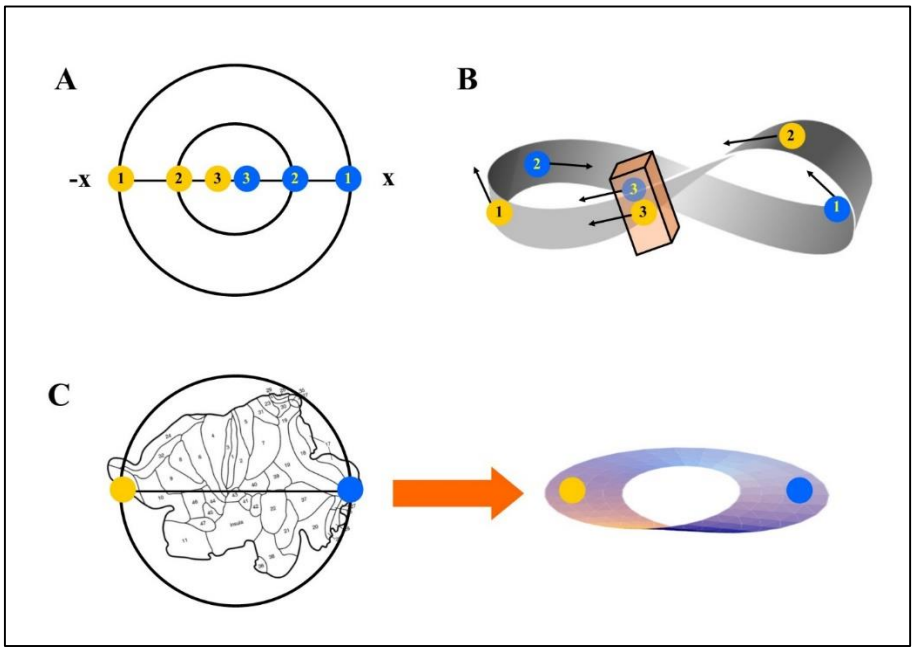

Figure 2. Transport of the BUT theorem on a Möbius strip. Figure 2A. Changing the radius of the hypersphere makes the antipodal points more or less close. Close to the center, the two points (marked with the number 3) are almost superimposed. Figure 2B. The movements of the antipodal points can be described in terms of trajectories on a Möbius strip. The parallelepiped stands for a slice of time, where both the antipodal features occur simultaneously. Figure 2C. A theoretical example from neuroscience is provided. A cerebral hemisphere is unfolded and flattened into a two-dimensional reconstruction [26] that can be embedded into a circular manifold. When two antipodal areas display simultaneously a feature in common, e.g., the same value of pairwise entropy [27], we achieve a topological description assessable in terms of BUT (left side). Such two areas and their subsequent dynamics can be easily visualized and assessed in terms of trajectories taking place on an abstract twisted cylinder (right side).

4- Introducing Time in the BUT Framework

The account of the cosmic holographic principle is generally provided by a framework which takes for granted that the event horizon is equipped with two spatial dimensions plus time. However, another possibility does exist, in order to describe a holographic manifold. A question arises: is it just a coincidence that the parameter time is not contemplated in two important formulas describing the Universe and the holographic principle? Indeed, both the Bekenstein-Hawking and Wheeler-De Witt equations take into account a static state of the related phenomena. Here the Moreva et al.'s results come into play [20]. These Authors experimentally described how an observer located inside the Universe perceives the time flow, while a hypothetical external observer perceives the Universe as motionless. According to their framework, entanglement discloses time as an emergent phenomenon. By running their experiment in two different modes ("observer" and "super-observer" mode) they showed how the same energy-entangled Hamiltonian eigenstate can be perceived as evolving by the internal observers that test the correlations between a clock subsystem and the rest, whereas it is static for the super-observer [21]. If we describe the Moreva et al.'s framework in terms of the BUT, we achieve the following topological result: an "observer" lies on a S^3 manifold, while a "superobserver" on a S^2 manifold. Indeed, the higher-dimensional manifold displays the coordinate of time, while the lower-dimensional does not. In physical terms, a manifold equipped with four dimensions (the three spatial dimensions plus time) encompasses two features with matching description. In turn, if we keep the dimension of time equal to zero (therefore removing it), we achieve a manifold, equipped with just three (spatial) dimensions, that encompasses just a single feature.

In sum, joining together the above-mentioned frameworks, it might be hypothesized that quantum entanglement occurs in spacetime, while disentanglement is achieved onto a motionless, three-dimensional manifold. Therefore, we may introduce the holographic principle in the following BUT terms: a motionless feature lying in a lower-dimensional stationary S^2 manifold gives rise to two moving features on a higher dimensional S^3 manifold, where time flow occurs. In other words, a feature encompassed in an unentangled state characterized by absence of time gives rise, when projected in one dimension higher (where time is not anymore zero), to two entangled particles. And vice versa.

5- Antipodal Masses: a Hypothesis

The above-mentioned frameworks allow to compare curved spacetime manifolds with structures equipped with antipodal symmetries. It is generally agreed that a black hole tends to deform the space around it, creating a vortex that captures nearby chunks of matter. The evolution of black holes can be represented by a Schwarzschild Spacetime Embedding Diagram [22]. In this approach, an embedding diagram for the vortex for a black hole can be visualized as a rubber sheet onto which a heavy mass is dropped. When an initial mass in increasing, the black hole's radius increases, burgeoning to a new mass with increasing gravitational pull. This observation allows us to tackle the issue in terms of antipodal points on black holes. Indeed, the different modes of the mass of a chunk of matter in the neighborhood of a black hole might reveal mass as an emergent phenomenon. The antipodal spacetime scenario for a chunk of matter being sucked into (of in the neighborhood of) a black hole is shown in Figure 3 in a Penrose diagram, that is a conformal compactification of 2D Minkowski space. Using such a diagram to represent the evolution of soft particles populating spacetime was first suggested by Gerard 't Hooft [1, 2].

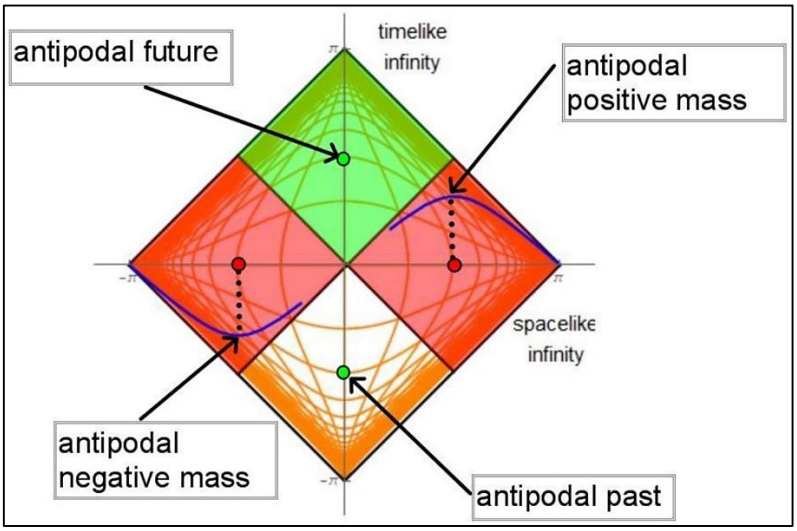

Figure 3. Evolution of chunks of soft matter in the neighborhood of a black hole. Antipodal spacetime is represented with a Penrose diagram, which also mimics the behavior of matter in the neighborhood of a black hole. Vertically, the green region represents future time and the orange region represents past time in the lifespan of a chuck of matter. Horizontally, the concave down blue geodesic line in the red region $+\pi$ represents the positive mass of a chuck matter on the S^4 surface of a black hole, whereas the concave up blue geodesic line in the red region $-\pi$ represents the negative mass of a chunk of matter on the opposite surface.

Indeed, Penrose diagrams are able to capture the causal relations between antipodal points in spacetime. It is used to represent the infinities (timelike infinities vertically in two regions representing spacetime past and future, and spacelike infinities representing the evolution of the mass of a chunk of matter on the surface of a black hole). Figure 3 extends 't Hooft's model, using the horizontal axis to represent the masses of soft matter [23-25]. The relationship between chunks of matter and a black hole in the neighborhood of surrounding ones, represented by the Penrose diagram in Figure 3, says to us that, as well as it is feasible to achieve antipodal points with matching features on a black hole horizon, we are allowed to hypothesize the simultaneous presence on the horizon of particles with positive and negative mass.

6- Conclusion

We showed how black holes' antipodal points can be described in terms of BUT. This led us to an algebraic topological description of the HP. The correlation between black hole's surface and HP allows a fibre bundle representation, standing for an algorithm that can be implemented in softwares. The BUT approaches [28, 29] are fruitful, because they allow the formulation of intriguing theoretical claims, suggesting a) the possible presence of antipodal positive and negative masses on black hole horizons and b) a feature encompassed in an unentangled state characterized by absence of time might give rise to entangled particles, when mapped to a four-dimensional spacetime. Because 't Hooft tackles antipodal entangled quantum states in terms of opposite points on a S^3 hypersphere, his account might hold also for the 4-dimensional Minkowskian manifold of the general relativity. Therefore, we are in front of a potential unification of quantum mechanics and general relativity on a S^3 manifold.

Results from different disciplines point towards the BUT as a universal principle to quantitatively assess otherwise elusive biological/physical activities [30-32]. In this topological context, systems operations become projections among different levels, giving rise to apparently emergent properties in higher dimensions. Here we showed how the features described by BUT, occurring on an orientable manifold with positive-curvature, can be assessed in terms of paths on a non-orientable manifold, i.e., a Möbius strip. The possibility to locate oscillations on a Möbius strip allows the assessment of simultaneous activities that are spatially separated. It must also be taken into account that the BUT requirements, such as two features with no points in common and the proper mappings, are fully preserved when projected to a Möbius strip. The transport of the BUT apparatus to a Möbius strip displays also another valuable advantage: because the mapping achieved by making a trip around a twisted cylinder is an inversion, this permits the preservation of the invariance under inversions, therefore obeying to the laws of conservation of energy and information [30, 33]. In sum, the study of patterns on a twisted cylinder (instead of a three-dimensional Euclidean phase space) is justified by the BUT framework and might pave the way to the detection of unexpected relationships among different synchronous physical activities.

7- Conflict of Interest

The authors declare no conflict of interest.

8- References

[1] 't Hooft, Gerard. "Virtual Black Holes and Space–Time Structure." Foundations of Physics 48, no. 10 (January 30, 2018): 1134–1149. doi:10.1007/s10701-017-0133-0.

[2] 't Hooft, Gerard. "Black Hole Unitarity and Antipodal Entanglement." Foundations of Physics 46, no. 9 (May 5, 2016): 1185–1198. doi:10.1007/s10701-016-0014-y.

[3] Peters, James F., and Arturo Tozzi. "Quantum Entanglement on a Hypersphere." International Journal of Theoretical Physics 55, no. 8 (April 11, 2016): 3689–3696. doi:10.1007/s10773-016-2998-7.

[4] Zhou, Jun, Hong-yi Fan, and Jun Song. "A New Two-Mode Thermo- and Squeezing-Mixed Optical Field." Chinese Physics B 26, no. 7 (June 2017): 070301. doi:10.1088/1674-1056/26/7/070301.

[5] Borsuk, Karol. "Drei Sätze über die n-dimensionale euklidische Sphäre." Fundamenta Mathematicae 20, no. 1 (1933): 177-190.

[6] Henderson, David Wilson, and Daina Taimina. Experiencing geometry: in Euclidean, spherical, and hyperbolic Spaces. Pearson College Division, 2001. ISBN-13: 978-0130309532.

[7] Matousek, Jiri, Anders Björner, and Günter M. Ziegler. Using the Borsuk-Ulam theorem: lectures on topological methods in combinatorics and geometry. Springer Science & Business Media, 2003. ISBN: 3-540-00362-2.

[8] Borsuk, Karol. "Errata to the paper" Fundamental retracts and extensions of fundamental sequences" Fundamenta Mathematicae 64 (1969), pp. 55-85." Fundamenta Mathematicae 3, no. 64 (1969): 375.

[9] Borsuk, M., and Anna Gmurczyk. "On homotopy types of 2-dimensional polyhedra." Fundamenta Mathematicae 109, no. 2 (1980): 123-142.

[10] Dodson, Christopher T., and Phillip E. Parker. A user's guide to algebraic topology. Vol. 387. Springer Science & Business Media, 1997. ISBN: 0-7923-4292-5, MR1430097.

[11] Krantz, Steven G. “A Guide to Topology” (2009). doi:10.5948/upo9780883859179.

[12] Manetti, Marco. “Topology.” UNITEXT (2015). doi:10.1007/978-3-319-16958-3.

[13] Hooft, Gerard'T. "Dimensional reduction in quantum gravity." arXiv preprint gr-qc/9310026 (1993).

[14] Susskind, Leonard. “The World as a Hologram.” Journal of Mathematical Physics 36, no. 11 (November 1995): 6377–6396. doi:10.1063/1.531249.

[15] Ahmed, Nasr, and H. Rafat. “Topological Origin of Holographic Principle: Application to Wormholes.” International Journal of Geometric Methods in Modern Physics 15, no. 08 (August 2018): 1850131. doi:10.1142/s0219887818501311.

[16] Hatcher, Allen. “Algebraic topology”, 2005. ISBN-13: 978-0521795401.

[17] Husemoller, D. "Fibre bundles Third edition." Graduate Texts in Mathematics 20 (1994). ISBN: 0-387-94087-1, MR1249482.

[18] Möbius, A.F. "The band appears in his." (1858): 519.

[19] Starostin, E. L., and G. H. M. van der Heijden. “The Shape of a Möbius Strip.” Nature Materials 6, no. 8 (July 15, 2007): 563–567. doi:10.1038/nmat1929.

[20] Moreva, Ekaterina, Giorgio Brida, Marco Gramegna, Vittorio Giovannetti, Lorenzo Maccone, and Marco Genovese. “Time from Quantum Entanglement: An Experimental Illustration.” Physical Review A 89, no. 5 (May 20, 2014). doi:10.1103/physreva.89.052122.

[21] Moreva, Ekaterina, Giorgio Brida, Marco Gramegna, Vittorio Giovannetti, Lorenzo Maccone, and Marco Genovese. “Entanglement Discloses Time as an Emergent Phenomenon.” CLEO: 2014 (2014). doi:10.1364/cleo_qels.2014.fw1a.8.

[22] Zaslavskii, O. B. “Acceleration of Particles Near the Inner Black Hole Horizon.” Physical Review D 85, no. 2 (January 18, 2012). doi:10.1103/physrevd.85.024029.

[23] Mitra, Abhas. "Kruskal coordinates and mass of Schwarzschild black holes." arXiv preprint astro-ph/9904162 (1999).

[24] Parzygnat, A.J. Krkuskel-Szekeres coordinates and Penrose diagrams, (2014). URL: http://www.physik.uniregensburg.de/forschung/wegscheider/gebhardt_files/skripten/Lect04KruskalCoord.pdf.

[25] Mitra, Abhas. "The Mass of the Oppenheimer-Snyder black hole." arXiv preprint astro-ph/9904163 (1999).

[26] Van Essen, David C. “A Population-Average, Landmark- and Surface-Based (PALS) Atlas of Human Cerebral Cortex.” NeuroImage 28, no. 3 (November 2005): 635–662. doi:10.1016/j.neuroimage.2005.06.058.

[27] Tozzi, Arturo, James F. Peters, Andrew A. Fingelkurts, Alexander A. Fingelkurts, and Pedro C. Marijuán. “Topodynamics of Metastable Brains.” Physics of Life Reviews 21 (July 2017): 1–20. doi:10.1016/j.plrev.2017.03.001.

[28] Moura, E., D.G. Henderson. “Experiencing geometry: on plane and sphere”. (1996) ISBN 978-0-13-373770-7.

[29] Peters, James F., Arturo Tozzi, and Sheela Ramanna. “Brain Tissue Tessellation Shows Absence of Canonical Microcircuits.” Neuroscience Letters 626 (July 2016): 99–105. doi:10.1016/j.neulet.2016.03.052.

[30] Tozzi, Arturo, and James F. Peters. “From Abstract Topology to Real Thermodynamic Brain Activity.” Cognitive Neurodynamics 11, no. 3 (March 14, 2017): 283–292. doi:10.1007/s11571-017-9431-7.

[31] Sengupta, Biswa, Arturo Tozzi, Gerald K. Cooray, Pamela K. Douglas, and Karl J. Friston. “Towards a Neuronal Gauge Theory.” PLOS Biology 14, no. 3 (March 8, 2016): e1002400. doi:10.1371/journal.pbio.1002400.

[32] Tozzi, Arturo, and James F. Peters. “A Topological Approach Unveils System Invariances and Broken Symmetries in the Brain.” Journal of Neuroscience Research 94, no. 5 (February 16, 2016): 351–365. doi:10.1002/jnr.23720.

[33] Tozzi, Arturo. “The Multidimensional Brain.” Physics of Life Reviews (January 2019). doi:10.1016/j.plrev.2018.12.004.

entropy

MDPI

Article

Entropy Balance in the Expanding Universe: A Novel Perspective

Arturo Tozzi [1,*] and James F. Peters [2]

1 Center for Nonlinear Science, Department of Physics, University of North Texas, Denton, TX 76203, USA
2 Department of Electrical and Computer Engineering, University of Manitoba, 75A Chancellor's Circle, Winnipeg, MB R3T 5V6, Canada; james.peters3@umanitoba.ca
* Correspondence: tozziarturo@libero.it

Received: 14 March 2019; Accepted: 14 April 2019; Published: 17 April 2019

Abstract: We describe cosmic expansion as correlated with the standpoints of local observers' co-moving horizons. In keeping with relational quantum mechanics, which claims that quantum systems are only meaningful in the context of measurements, we suggest that information gets ergodically "diluted" in our isotropic and homogeneous expanding Universe, so that an observer detects just a limited amount of the total cosmic bits. The reduced bit perception is due the decreased density of information inside the expanding cosmic volume in which the observer resides. Further, we show that the second law of thermodynamics can be correlated with cosmic expansion through a relational mechanism, because the decrease in information detected by a local observer in an expanding Universe is concomitant with an increase in perceived cosmic thermodynamic entropy, via the Bekenstein bound and the Laudauer principle. Reversing the classical scheme from thermodynamic entropy to information, we suggest that the cosmological constant of the quantum vacuum, which is believed to provoke the current cosmic expansion, could be one of the sources of the perceived increases in thermodynamic entropy. We conclude that entropies, including the entangled entropy of the recently developed framework of quantum computational spacetime, might not describe independent properties, but rather relations among systems and observers.

Keywords: quantum vacuum; Bekenstein bound; cosmological constant; ergodicity

1. Introduction

Relational properties among quantum systems are the most fundamental elements to construct quantum mechanics, instead of being independent properties [1,2]. This strong claim, suggested by relational formulations of quantum mechanics, has been supported by recent papers, which state that the experimentally detected correlations in Bell tests strongly contradict the tenet of local realism, i.e., the properties of the physical world are independent of our observation of them [3]. According to relational formulations of quantum mechanics, features of quantum systems such as superposition and entanglement are manifested through the rules of counting the alternatives, without explicitly calling out the reference system. For example, wave function and reduced density matrix can be derived from the relational probability amplitude matrix [4].

Therefore, quantum mechanics has been reformulated as a theory that describes physical systems in terms of observer-dependent relational properties. This framework is inspired by the key idea behind special relativity, i.e., that the details of an observation depend on the reference frame of the observer. In this paper, we aim to use relational properties to describe two well-known physical phenomena, such as thermodynamic and information entropy, in terms of dependence from an observer embedded in their comoving cosmic horizon. In touch with relational quantum mechanics, our aim is to show that entropies do not describe independent properties, rather relations among systems and

observers: this means that the complete description of information and thermodynamic entropies is only meaningful in the context of measurements performed by anobserver. Further, we show how this relational framework might be extended to also encompass the recently-developed theory of quantum computational spacetime and related entanglement entropy [5].

2. The Role of Entropies

2.1. Information

Information is a measurable physical quantity that, according to many scholars, might stand for the most general paradigm to investigate cosmological, physical and biological systems. It has been claimed that the physical world is made up of information itself [6], so that our Universe is assessable in pure terms of information. The idea that information is the fundamental physical quantity dates back to F.W. Kantor [7].By then, different information-related perspectives have been developed, from the hypothesis that the Universe is a giant digital computer [8,9], to the suggested link among information theory, statistical thermodynamics and the probabilistic nature of quantum mechanics [10–13], from computational loop quantum gravity [14] to connections between information and the Bekenstein–Hawking entropy [15,16].Therefore, information sits at the core of physics, leading to the proposal of the "it from bit" dogma [17]: every field or particle exists because of its observation. In our Universe, information, as well as energy, cannot be created or destroyed, i.e., the total number of cosmic bits must be kept constant. The conservation of information is derived from quantum field theory, via the quantum Liouville theorem [18].Indeed, quantum field theory (and information conservation) works both forward and backward in time. The probabilistic combination of pure states keeps the same set of probabilities. In other words, because time evolution is unitary, it is also reversible, i.e., no information can ever get lost: an observer is theoretically allowed, starting from any time-like slice, to run time backwards and compute what happened earlier. Therefore, the amount of information is invariant in our cosmos: the number of bits encompassed in the whole Universe cannot modify, even if the theory of "the world as a hologram" holds true [19,20].

One of the raised concerns against the paradigm of information preservations, i.e., the "black hole information paradox" related to the hypothetical loss of information inside black holes, has been solved: these puzzling cosmic bodies might release the "trapped" information through the Hawking radiation, until they evaporate [21–23]. It has been observed that the entropy of a black hole corresponds to the logarithm of a number of possible equally probable measurement choices u of the observer outside the event horizon. In effect, for entropy defined by

$$H(u) = \int_0^L \rho(n,x)\ln(\rho(n,x))dx, \tag{1}$$

we obtain a plot, representing symmetry of measurement choices of the observer inside the event horizon (amplitude going up one side the of a hill) and the observer outside the event horizon (amplitude going down the other side of a hill).

To avoid confusion or misconceptions, we need to make clear the difference between event and commoving horizons. The event horizon is the largest distance from which light emitted now can ever reach the observer in the future. The comoving horizon (also termed particle horizon) is the largest distance from which light could have reached the observer by a specific time: it stands for the space assessable by local observers [24]. The total amount of information encompassed in the event horizon is unvarying. Here we will show how the uncontroversial statement related to the conservation of cosmic information in the event horizon leads to unexpected consequences by the standpoint of a local observer embedded inside their own commoving cosmic horizon. Indeed, changes in entropy occur inside an asymptotically flat Friedmann–Robertson–Walker Universe when dust, radiation and black holes cross the cosmological commoving horizon and disappear [25].

2.2. Thermodynamic Entropy

In the previous paragraph, we stated that information is constant in our Universe. This may sound weird to anyone familiar with the second law of thermodynamics, which says that "every process occurring in nature proceeds in the sense in which the sum of the entropies of all bodies taking part in the process is increased" (Planck's formulation). How can such opposite claims be consistent? The microscopic laws of physics are reversible: despite irreversibility that comes out due to coarse graining to a larger effective scale, the microscopic information does not get lost. Indeed, the entropy described by the second law is the sum of the entropies of many macroscopic local objects. Macroscopic physical systems, like the observable Universe, are not just regulated by stochastic variables and random fluctuations, but also by constraints given by the arrow of time.Despite the large number of different suggested scenarios and paradigms, the processes governing time constraints of physical and biological systems may be generalized, if we consider the universal principle of the second law of thermodynamics [26–28]. Therefore, the positive arrow of time observed in the macroscopic Universe (due to the time-reversal symmetry violation) is strictly correlated with the second law of thermodynamics. In thermodynamics, information I can be defined as the negation of thermodynamic entropy S [29]:

$$\mathrm{I} = -\mathrm{S}. \tag{2}$$

In this account, a single bit of thermodynamic entropy stands for the distinction between two alternative states in a physical system. As a result, thermodynamic entropy of the Universe is proportional to the total number of distinguishable states encompassed in the cosmos: the higher the number of states, the higher the entropy. We will see in the sequel how thermodynamic entropy and information can be correlated, setting aside Shannon's account [30].

3. Cosmic Expansion Comes into Play

The Universe is expanding. It has been hypothesized that our Cosmos arose from a perturbation in the quantum vacuum, when an inflationary mechanism, correlated with a false vacuum state, led to the production of cosmic matter and to the huge expansion that took place 1^{-35} s after the Big Bang [31]. Vacuum quantum fluctuations (dictated by the Heisenberg energy-time uncertainty principle) could have been able to cause, through an inflaton-based mechanism, the occurrence of the Big Bang, characterized by very high density and temperature state [32–35]. At the very beginning, 1^{-43} s after the Big Bang, our Universe was equipped with an energy of 10^{19} GeV and a temperature of 10^{32} K; its horizon was 10^{-25} cm large and the density 10^{96} kg/m^3. By then, the temperature halved every double expansion. At 10^{-36} s, the energy lowered to 10^{16} GeV, and at 10^{-32} s the temperature decreased to 10^{28} K. The cosmic inflationary expansion at 10^{-35} s stands for the standard explanation for experimentally detected cosmic features such as isotropicity, homogeneity, symmetry and zero curvature. It is noteworthy that the Universe underwent a rapid expansion so that, from the above-mentioned horizon diameter of 10^{-25} at 10^{-43}, it reached the size of about onemeter diameter at 10^{-32} s. Another gentler inflationary period started approximately 4.5 billion years ago [36]. Currently, 13.79 billion years after its birth, our Universe is still accelerating, slowly proceeding towards thermal death [37]. In our cosmic era, from our standpoint of local observers, the visible cosmological horizon is 10^{29} cm, the cosmic density is 10^{-29} gr/cm^3, the matter corresponds to one atom/m^2 and the space is expanding at a speed of about 67–74 km/s per megaParsec, with slightly different values according to different techniques [38].

How did (and still does) cosmic expansion occur? It has been correlated with the quantum vacuum, a material medium capable of polarization and equipped with its own electric permittivity, permeability and dielectric constant. The quantum vacuum is believed to display a negative pressure (an anti-gravitational force) that equals its energy density and causes the accelerated expansion of the current Universe. One of the feasible explanations of the quantum vacuum'santi-gravitational strength is the repulsive dark energy, which is correlated with the cosmological constant. The current

consensus states that the cosmological constant gives rise to a negative pressure: indeed, the amount of energy in a container full of vacuum increases when the volume increases. The dark energy amount encompasses 73% of the whole Universe. This paradigm leads to a straightforward conclusion: due to the cosmic expansion, the density of "visible" matter and radiation is diluting inside observers' commoving horizons. What about information? In the next paragraphs, we will elucidate how it is feasible to correlate cosmic expansion with information and thermodynamic entropy.

4. Linking Cosmic Expansion, Information and Thermodynamic Entropy

Cosmic expansion leads to an unexpected consequence: for a local observer enclosed in a given cosmological comoving horizon constrained by the light speed, the information density (bits/cosmic volume unity) is decreasing with time passing. This also means that observers perceive thermodynamic entropy as increasing. How is it possible? Here we illustrate the route that allows the correlation in a common theoretical framework of the relationships between thermodynamic entropy and information. The total entropy embedded inside the observer's comoving horizon can be quantified through the Bekenstein bound, because the entropy must be finite in the sphere delimited by this horizon. The Bekenstein bound is an upper limit on the thermodynamic entropy S—or the information I, according to Shannon [30]—endowed in a space region equipped with a given amount of energy. In other words, the Bekenstein bound stands for the maximum quantity of information required to describe a physical system down to the quantum level. The universal form of the bound can be described as follows [39,40]:

$$\mathrm{Ssys} = \zeta \frac{AEK}{hc} \tag{3}$$

where S_{sys} is the cosmic thermodynamic entropy detectable by the observer, A is the area of the local observer's horizon, E is the energy including matter (the total mass–energy of the Universe consists of about 10^{69} Joule), $\hbar$ is the reduced Planck constant, c is the speed of light, k is the Boltzmann constant, ζ is a factor such that $0 < \zeta < 1$.

Setting ζ to one in the case of the total S_{sys}, we are allowed to quantify the thermodynamic information, by partitioning the factor into a relative information component ($\zeta_I = 1 - \zeta_S$) and a relative entropy component ($\zeta_S = 1 - \zeta_I$) [41]:

$$\mathrm{I_{sys}} = \zeta \mathrm{I} \frac{AEK}{hc} = (1 - \zeta \mathrm{S}) \frac{AEK}{hc}. \tag{4}$$

In the case of cosmic expansion, we achieve a decrease of information density in the space inside the observer's comoving horizon.In other words, the number of detectable bits declines.This means that information exits from the observer's comoving horizon, according to the formula:

$$\Delta \mathrm{I_{sys}} = \frac{\Delta Esurr}{kT} = \Delta \zeta \mathrm{S} \tag{5}$$

where T is the temperature. Note that temperature decreases with cosmic expansion, contributing to the cosmic budget of the thermodynamic entropy.

Here the Landauer principle comes into play: any logically irreversible manipulation of information, such as the erasure of a bit, must be accompanied by a corresponding entropyincrease in either the information-processing apparatus, or its environment [42]. The minimum possible amount of energy required to erase one bit of information is called the "Landauer limit":

$kT\ln 2$.

When one bit of logical information is lost, the amount of entropy generated is at least k ln 2, so that the energy which must eventually be emitted to the environment is $E \geq kT \ln 2$. To provide an example, at 20 °C, the Landauer limit represents an energy of approximately 0.0172 eV, or 2.75 zJ [43].

Due to our lack of knowledge of cosmic topology and shape, we cannot be sure that the system formed by the local observer's event and comoving horizons are physically closed systems; in spite of

this uncertainty, our general framework holds the same. Indeed, an increase in the number of physical states corresponding to each logical state means that, for an observer (a human "observer" embedded in its constrained comoving horizon) who is keeping track of the logical state of the system but not of its the physical state, the number of possible physical states has increased; in other words, entropy has increased from the standpoint of our observer.

In the whole Universe, the total expansion leaves the thermodynamic entropy of relativistic particles (such as photons, gravitons and neutrinos) unchanged. This occurs because the entropy of a gas of relativistic particles is proportional to the number of particles, which is invariant as the cosmos expands [44]. Therefore, if we assess the thermodynamic entropy inside the volume of the event horizon, the number of photons in that volume does not change. However, local observers embedded in their comoving horizon perceive a decrease in information (which gets more diluted), and therefore an increase in thermodynamic entropy. In sum, our theoretical account states that the cosmic expansion dictated by the cosmological constant of the quantum vacuum leads both to local decreases in information and increases in thermodynamic entropy in the spacetime accessible to local observers. A single observer detects the same macro-cosmic features everywhere and different observers detect the same macro-cosmic features (i.e., the Universe is homogeneous and isotropic), therefore it is feasible to extend our framework to every observer in the entire Universe.

5. Entangled Spacetime and Comoving Horizons: An Unexpected Link

We disregard quantum decoherence breaking due to afluctuating environment, working instead with the approximated hypothesis that quantum entanglement is maintained at infinite distance. In this context, our lack of knowledge of quantum issues in fluctuating environments in terms of objective and computable physical phenomena might be a great lack—also, for instance, in terms of pilot wave evolution in a noisy environment, in which the superposition of quantum states cannot be maintained and rebuilt on distances larger than the De Broglie length [45–47]. However, the recently-developed framework of quantum computational spacetime highlights the foremost role of entanglement entropy [5]. This leads us inside the spherical comoving horizon perceived by a local observer. Indeed, relationships do exist among the comoving horizon, quantum entanglement and information entropies. Recent claims suggest that quantum entanglement can be assessed in terms of opposite features on a four-dimensional hypersphere. It has been proposed that a separable state can be achieved for each of the entangled particles lying in S^2, just by embedding them in a higher dimensional S^3 space [48,49]. These authors view quantum entanglement as the simultaneous activation of signals in a 3D space mapped into a S^3 hypersphere. The particles are entangled at the S^2 level and un-entangled at the S^3 hypersphere level, therefore a composite system is achieved, in which each local constituent is equipped with a pure state. It is noteworthy that the two issues of a comoving horizon and entanglement on a hypersphere are assessable through the framework described by the Borsuk–Ulam theorem, which states that "every continuous map $f : S^n \to R^n$ must identify a pair of antipodal points"—diametrically opposite points on an n-sphere [50,51]. This means that at least some of the entropy values detected at opposite sides of the spherical comoving horizon display matching description, i.e., they are entangled.

In sum, in touch with the premises of quantum computational spacetime, a cosmic observer is merged inside a spherical comoving horizon that must necessarily display the entanglement entropy required by the theory.

6. Conclusions

Here we partially explain the occurrence of the second law of thermodynamics through the issue of the cosmic expansion, that leads to a diluted information for a local observer, and, consequently, to their detection of increases in thermodynamic entropy. The canonical approach is reverted: here we start from information, and reach the entropy, and not vice versa as generally assumed. It is noteworthy that information is also linked with the Shannon entropy, that holds for ergodic systems: The Universe is ergodic, because it is homogeneous and isotropic, at least at macroscales [52]. Our approach is based

upon the relational formulations of quantum mechanics, where information is considered the most general paradigm to investigate cosmological and physical systems.

Therefore, (at least a part of) the increase in thermodynamic entropy might be correlated with cosmic expansion. Our hypothesis leads to (theoretically) testable previsions. When (and if) cosmic expansion decreases or relapses, the entropy perceived by local observers embedded in their comoving horizon must decrease, or even relapse. Furthermore, we predict that, due to cosmic dilation, the thermodynamic entropy detectable by local observers is increased in the current cosmic era, compared with previous periods.

Our suggestions are in touch with the results of [53]. These authors described how an observer located inside the Universe perceives time flow, while a hypothetical external observer perceives the Universe as motionless. According to [54], entanglement discloses time as an emergent phenomenon. By running their experiment in two different modes ("observer" and "super-observer" mode) they showed how the same energy-entangled Hamiltonian eigenstate can be perceived as evolving by the internal observers that test the correlations between a clock subsystem and the rest, whereas it is static for the super-observer. This means that, in touch with both our account and relational quantum mechanics, the description of cosmic quantities, such as thermal history or time passing, is meaningful in the framework of measurements performed by anobserver. The above-mentioned approximated hypothesis, i.e., that quantum entanglement is maintained at infinite distance (as it happens in the absence of environment in zero-noise quantum mechanics), can be improved by introducing the concept of "super-observer", that replaces the non-existence of quantum decoupled observers. The observer is still considered as part of a quantum super-system, while the existence of a "super-observer" who watches the system, interacts with it, but does not form quantum super-super-systems is admitted. This framework comes out of the fact that the measure is basically a statistical (and hence classical and quantum-incoherent) output of interactions between systems embedded in a large-scale classical system. The observer is a classical system quantum-decoupled (by the noise) with the measured system: in the relational quantum mechanical approach, this property is attributed (implicitly) to the super-observer.

As stated above, the Cosmic Background Radiation points towards our Universe as strongly isotropic and homogeneous at cosmic macroscales. Inflationary expansion explains why the primeval 10^{90} causally-disconnected quantum "seeds" [31] led to the experimentally detected homogeneity and isotropy. Still, inflation would have amplified minute quantum fluctuations (pre-inflation) into slight density ripples of over- and under-density (post-inflation).Here the concept of hyperuniformity comes into play, i.e., the anomalous suppression of density fluctuations on large length scales occurring in amorphous cellular structures of ordered and disordered materials [55].The evolution of a given set of initial points takes place when, through Lloyd iterations, each point is replaced by the center mass of its Voronoi cell. This corresponds to a gradient descent algorithm which allows a progressive, general convergence to a random minimum in the potential energy surface. Klatt et al. [55] report that systems equipped with different initial configurations (such as, e.g., either hyper-fluctuating, or anisotropic, or relatively homogeneous point sets), converge towards the same high degree of uniformity after a relatively small number of Lloyd iterations (about 10^5).This means that, in the systems' final states, independent of the initial conditions, the cell volumes become uniform and the dimension less total energy converges towards values comparable to the deep local energy minima of the optimal lattice. Therefore, we are allowed to describe the cosmic evolution suddenly after the Big Bang in terms of Lloyd iterations, where the initial quantum seeds stand for initial point sets, progressively converted to point sets with a centroidal Voronoi diagram. In other words, the tiny perturbations in the primeval Universe which seed the later formation of cosmic macro-structures might stand for the starting points of the subsequent processes described in terms of Voronoi cells. This would permit observers to achieve, starting from countless different possible conformations of the primeval Universe, the detected isotropic and homogeneous Cosmic Background Radiation. Indeed, after just 10^5 iterations, every

possible initial system must converge towards an hyperuniform state, where observers perceive energy as very low and uniformity degree as very high.

Author Contributions: Contributions: conceptualization, A.T. and J.F.P.; methodology, A.T. and J.F.P.; software, A.T.; validation, A.T.; formal analysis, A.T. and J.F.P.; investigation, A.T.; resources, A.T.; data curation, A.T. and J.F.P.; writing—original draft preparation, A.T.; writing—review and editing, A.T. and J.F.P.; visualization, A.T.; supervision, A.T.; project administration, A.T.; funding acquisition, A.T.

Funding: This research received no external funding.

Conflicts of Interest: The authors declare no conflict of interest.

References

1. Rovelli, C. Relational Quantum Mechanics. *Int. J. Theor. Phys.* **1996**, *35*, 1637–1678. [CrossRef]
2. Smerlak, M.; Rovelli, C. Relational EPR. *Found. Phys.* **2007**, *37*, 427–445. [CrossRef]
3. The BIG Bell Test Collaboration. Challenging local realism with human choices. *Nature* **2018**, *557*, 212–216. [CrossRef]
4. Yang, J.M. A Relational Formulation of Quantum Mechanics. *Sci. Rep.* **2018**, *8*, 13305. [CrossRef]
5. Zizzi, P. Entangled spacetime. *Mod. Phys. Lett. A* **2018**, *33*, 1850168. [CrossRef]
6. Bekenstein, J.D. Black holes and information theory. *arXiv* **2003**, arXiv:quant-ph/0311049.
7. Kantor, F.W. *Information Mechanics*; Wiley-Interscience: Hoboken, NJ, USA, 1977; ISBN 10: 0471029688/13: 9780471029687.
8. Schmidhuber, J. Algorithmic Theories of Everything. *arXiv* **2000**, arXiv:quant-ph/0011122.
9. Zenil, H. *A Computable Universe: Understanding and Exploring Nature as Computation with a Foreword by Sir Roger Penrose*; World Scientific Publishing Company: Singapore, 2012.
10. Jaynes, E.T. Information Theory and Statistical Mechanics. *Phys. Rev.* **1957**, *106*, 620. [CrossRef]
11. Lloyd, S. Ultimate physical limits to computation. *Nature* **2000**, *406*, 1047–1054. [CrossRef]
12. Marzuoli, A.; Rasetti, M. Computing Spin Networks. *Ann. Phys.* **2005**, *318*, 345–407. [CrossRef]
13. Fuentes-Guridi, I.; Girelli, F.; Livine, E. Holonomic Quantum Computation in the Presence of Decoherence. *Phys. Rev. Lett.* **2005**, *94*, 020503. [CrossRef]
14. Zizzi, P.A. Quantum computationtoward quantum gravity. *Gen. Relat. Gravit.* **2001**, *33*, 1305–1318. [CrossRef]
15. Görnitz, T. Abstract Quantum Theory and Space-Time Structure, I. Ur Theory and Bekenstein-Hawking Entropy. *Int. J. Theoret. Phys.* **1988**, *27*, 527–542. [CrossRef]
16. Von Weizsäcker, C.F. *The Structure of Physics*; Görnitz, T., Lyre, H., Eds.; Springer: Dordrecht, The Netherlands, 2006; ISBN 978-1-4020-5235-4.
17. Wheeler, J.A. Information, physics, quantum: The search for links. In *Zurek, Wojciech Hubert. Complexity, Entropy, and the Physics of Information*; Addison-Wesley: Redwood City, CA, USA, 1990; ISBN 9780201515091.
18. Zeidler, E. *Quantum Field Theory III: Gauge Theory*; Springer: Berlin/Heideberg, Germany, 2011.
19. Hooft, G. Dimensional Reduction in Quantum Gravity. *arXiv* **1993**, arXiv:gr-qc/9310026.
20. Susskind, L. The World as a Hologram. *arXiv* **1994**, arXiv:hep-th/9409089.
21. Hawking, S. Particle Creation by Black Holes. *Commun. Math. Phys.* **1975**, *43*, 199–220. [CrossRef]
22. Hawking, S. Information loss in black holes. *Phys. Rev. D* **2005**, *72*, 084013. [CrossRef]
23. Gyongyosi, L. A statistical model of information evaporation of perfectly reflecting black holes. *Int. J. Quantum Inf.* **2014**, *12*, 1560025. [CrossRef]
24. Davis, T.M.; Lineweaver, C.H. Expanding Confusion: Common Misconceptions of Cosmological Horizons and the Superluminal Expansion of the Universe. *Publ. Astron. Soc. Aust.* **2013**, *21*, 97–109. [CrossRef]
25. Davis, T.M.; Davies, P.C.W.; Lineweaver, C.H. Black hole versus cosmological horizon entropy. *arXiv* **2003**, arXiv:astro-ph/0305121.
26. Bryngelson, J.D.; Wolynes, P.G. Spin glasses and the statistical mechanics of protein folding. *Proc. Natl. Acad. Sci. USA* **1987**, *84*, 7524–7528. [CrossRef]
27. Ferreiro, D.U.; Hegler, J.A.; Komives, E.A.; Wolynes, P.G. On the role of frustration in the energy landscapes of allosteric proteins. *Proc. Natl. Acad. Sci. USA* **2011**, *108*, 3499–3503. [CrossRef]
28. Tozzi, A.; Fla, T.; Peters, J.F. Building a minimum frustration framework for brain functions in long timescales. *J. Neurosci. Res.* **2016**, *94*, 702–716. [CrossRef]

29. Beck, C. Generalized information and entropy measures in physics. *Contemp. Phys.* **2009**, *50*, 495–510. [CrossRef]
30. Shannon, C.E. A Mathematical Theory of information. *Bell Syst. Tech. J.* **1948**, *27*, 379–423, 623–656. [CrossRef]
31. Veneziano, G. A Simple/Short Introduction to Pre-Big-Bang Physics/Cosmology. *arXiv* **1998**, arXiv:hep-th/9802057v2.
32. Penrose, R. Cycles of Time. In *An Extraordinary New View of the Universe*; Alfred, A., Ed.; Knopf: New York, NY, USA, 2011.
33. Mandelstam, L.; Tamm, I. The uncertainty relation between energy and time in nonrelativistic quantum mechanics. *J. Phys. (USSR)* **1945**, *9*, 249–254.
34. Vaidman, L. Minimum time for the evolution to an orthogonal quantum state. *Am. J. Phys.* **1992**, *60*, 182–183. [CrossRef]
35. Uffink, J. The rate of evolution of a quantum state. *Am. J. Phys.* **1993**, *61*, 935. [CrossRef]
36. Ellwanger, U. From the Universe to the Elementary Particles. In *A First Introduction to Cosmology and the Fundamental Interactions*; Springer: Berlin/Heidelberg, Germany, 2012; ISBN 978-3-642-24374-5.
37. Bars, I.; Terning, J. *Extra Dimensions in Space and Time*; Springer: Berlin, Germany, 2009; ISBN 978-0-387-77637-8.
38. Ade, P.A.R.; Aghanim, N.; Arnaud, M.; Ashdown, M.; Aumont, J.; Baccigalupi, C.; Banday, A.j.; Barreiro, R.B.; Bartlett, J.G.; Bartolo, N.; et al. Planck 2015 results. XIII. Cosmological parameters. *Astron. Astrophys.* **2016**, *594*, A13. [CrossRef]
39. Bekenstein, J.D. Black Holes and Entropy. *Phys. Rev. D* **1973**, *7*, 2333–2346. [CrossRef]
40. Bekenstein, J.D. Generalized second law of thermodynamics in black-hole physics. *Phys. Rev. D* **1974**, *9*, 3292–3300. [CrossRef]
41. Street, S. Neurobiology as Information Physics. *Front. Syst. Neurosci.* **2016**, *10*, 90. [CrossRef] [PubMed]
42. Landauer, R. Irreversibility and heat generation in the computing process. *IBM J. Res. Dev.* **1961**, *5*, 183–191. [CrossRef]
43. Bérut, A.; Arakelyan, A.; Petrosyan, A.; Ciliberto, S.; Dillenschneider, R.; Lutz, E. Experimental verification of Landauer's principle linking information and thermodynamics. *Nature* **2012**, *483*, 187–190. [CrossRef]
44. Lineweaver, C.H.; Egan, C. Life, gravity and the second law of thermodynamics. *Phys. Life Rev.* **2008**, *5*, 225–242. [CrossRef]
45. Ozawa, M. Universally valid reformulation of the Heisenberg uncertainty principle on noise and disturbance in measurement. *Phys. Rev. A* **2003**, *67*, 042105. [CrossRef]
46. Chiarelli, P. Can fluctuating quantum states acquire the classical behavior on large scale? *J. Adv. Phys.* **2013**, *2*, 139–163.
47. Chiarelli, P. The Gravity of the Classical Klein-Gordon field. *Symmetry* **2019**, *11*, 322. [CrossRef]
48. Peters, J.F.; Tozzi, A. Quantum Entanglement on a Hypersphere. *Int. J. Theor. Phys.* **2016**, *55*, 3689–3696. [CrossRef]
49. Zhou, J.; Fan, H.-Y.; Song, J. A new two-mode thermo- and squeezing-mixed optical field. *Chin. Phys. B* **2017**, *26*, 070301. [CrossRef]
50. Borsuk, K. Dreisatze uber die n-dimensionaleeuklidischesphare. *Fundam. Math.* **1933**, *XX*, 177–190. [CrossRef]
51. Tozzi, A.J.F.; Peters, A.A.; Fingelkurts, A.A.; Fingelkurts, P.C.; Marijuán, P.C. Topodynamics of metastable brains. *Phys. Life Rev.* **2017**, *21*, 1–20. [CrossRef]
52. Clifton, T.; Clarkson, C.; Bull, P. Isotropic blackbody cosmic microwave background radiation as evidence for a homogeneous universe. *Phys. Rev. Lett.* **2012**, *109*, 051303. [CrossRef]
53. Moreva, E.V.G.; Brida, M.; Gramegna, V.; Giovannetti, L.; Maccone, M. Genovese. Time from quantum entanglement: An experimental illustration. *Phys. Rev. A* **2013**, *89*, 052122. [CrossRef]
54. Moreva, E.V.; Brida, G.; Gramegna, M.; Giovannetti, V. Entanglement discloses Time as an emergent phenomenon. In Proceedings of the CLEO: QELS_Fundamental Science, San Jose, CA, USA, 8–13 June 2014. [CrossRef]
55. Klatt, M.A.; Lovrić, J.; Chen, D.; Kapfer, S.C.; Schaller, F.M.; Schönhöfer, P.W.A.; Gardiner, B.S.; Smith, A.-S.; Schröder-Turk, G.E.; Torquato, S. Universal hidden order in amorphous cellular geometries. *Nat. Commun.* **2019**, *10*, 811. [CrossRef]

© 2019 by the authors. Licensee MDPI, Basel, Switzerland. This article is an open access article distributed under the terms and conditions of the Creative Commons Attribution (CC BY) license (http://creativecommons.org/licenses/by/4.0/).

ARTICLE IN PRESS PLREV:1112

Available online at www.sciencedirect.com

ScienceDirect

Physics of Life Reviews ••• (••••) •••–•••

PHYSICS of LIFE reviews

www.elsevier.com/locate/plrev

Comment

The Borsuk-Ulam theorem solves the curse of dimensionality: Comment on "The unreasonable effectiveness of small neural ensembles in high-dimensional brain" by Alexander N. Gorban et al.

Arturo Tozzi [a,*], James F. Peters [b,c]

[a] *Center for Nonlinear Science, Department of Physics, University of North Texas, 1155 Union Circle, #311427, Denton, TX 76203-5017, USA*
[b] *Department of Electrical and Computer Engineering, University of Manitoba, 75A Chancellor's Circle, Winnipeg, MB R3T 5V6, Canada*
[c] *Department of Mathematics, Adıyaman University, 02040 Adıyaman, Turkey*

Received 18 April 2019; accepted 23 April 2019

Communicated by L. Perlovsky

Gorban et al. [7] correlate multidimensional data spaces with high-dimensional nervous activities. This task requires huge computational power: indeed, the extraction of maximum value from the massive amount of gathered datasets entails newly-developed approaches for combining data-driven methods, physical modeling and algorithms capable of learning with limited, weak, or biased labels (Mars et al. [9]; Bergen et al. [3]).

On the other hand, when novel features are added in data mining, multiple measurements are combined and increases in data set dimensionality are achieved, the performance of the available classifiers tends to degrade (Barbour [1]). This excruciating issue is termed "the curse of dimensionality". When dimensions increase, the classifier's performance augments until the optimal number of features is reached. However, further increases in dimensionality result in performance decrease (Fig. 1A). In plain terms, the more the dimensions, the less the information available. This is a painstaking problem, if we want to think of the brain in terms of a multidimensional machine, as suggested by a growing amount of recent studies (see, for example, Bellmund et al. [2]; for a review, see Tozzi [16]).

The problem of the curse of dimensionality can be formulated in terms of geometry and topology too (Kůrková [8]). A n-sphere is a n-dimensional structure with positive (convex) curvature embedded in a $n+1$ Euclidean space, called a $n+1$-ball (Matousek [10]). For example, a circumference (1-dimensional sphere) surrounds a cd-rom (2-dimensional ball), while a thin plastic surface (2-dimensional sphere) surrounds a beach ball (3-dimensional ball). A 3-sphere (also called glome, or hypersphere) is a 3-dimensional elliptic surface, embedded in a 4-dimensional ball. What counts here is that the more the n-dimensions of the sphere, the less its volume, so that the hyperspheres' volumes tend to zero as their dimensionality tends to infinity (Fig. 1B). Indeed, in higher dimensions, the ball volume has a tendency to be concentrated near the equator (Fig. 1C). The volume of an n-sphere in terms of the volume of an $(n-2)$-ball of the same radius is:

DOI of original article: https://doi.org/10.1016/j.plrev.2018.09.005.
* Corresponding author.
E-mail addresses: tozziarturo@libero.it, Arturo.Tozzi@unt.edu (A. Tozzi), James.Peters3@umanitoba.ca (J.F. Peters).

https://doi.org/10.1016/j.plrev.2019.04.008
1571-0645/© 2019 Elsevier B.V. All rights reserved.

Please cite this article in press as: Tozzi A, Peters JF. The Borsuk-Ulam theorem solves the curse of dimensionality: Comment on "The unreasonable effectiveness of small neural ensembles in high-dimensional brain" by Alexander N. Gorban et al.. Phys Life Rev (2019), https://doi.org/10.1016/j.plrev.2019.04.008

$$V_n(R) = \frac{2\pi R^2}{n} V_{n-2}(R)$$

Using two-dimension recursion formulas, it is easy to notice that the volume of an n-sphere of radius R approaches zero as n tends to infinity (Wang 2005). At each iteration, the new factor being multiplied into the volume is proportional to 1/n, while the constant of proportionality $2\pi R^2$ is independent of n.

This counter-intuitive observation explains why the available information encompassed in a spherical volume decreases with increases in sphere's dimensions: as n-dimensionality augments, a larger percentage of the data tend to reside outside the equatorial feature space, which is the sole volume available for our observation. While the data encompassed in a few dimensions are packed and therefore easily detectable, the addition of further dimensions leads to "stretch" such data across that dimension, leaving them further apart. This causes the occurrence of extremely sparse information in higher dimensions, so that distance measures start losing their effectiveness to detect dissimilarity and become meaningless.

How to avoid the curse of dimensionality, when assessing multidimensional neural phase spaces? Apart from the canonical techniques used to achieve the "blessing of dimensionality" (Pereda et al., 2018), another, novel approach is available: the Borsuk-Ulam theorem (BUT), which has been widely used in physics, biology and neuroscience (for a review, see: Tozzia et al., 2017). The theorem states that (Borsuk 1933):
Every continuous map must identify a pair of antipodal points (on S^n).
In other words, if a sphere S^n is mapped continuously into a *n*-dimensional Euclidean space R^n, there is at least one pair of antipodal points on S^nmapping onto the same point of R^n. A pair of points are antipodal on a sphere, provided they are diametrically opposite each other. The poles of a sphere is an example. In the hands of K. Borsuk, BUT provides a building block in shape theory (Borsuk and Dydak, 1980). In the recent years, the BUT's ingredients (antipodal points, *n* exponent and projections from lower to higher dimensions) have been modified to achieve a wide range of BUT variants. For an introduction, see Peters, 2016 and for a survey, see Tozzi et al., 2017. In these novel versions, the "points" are replaced by "regions", which stand for either mathematical, physical or biological features (Peters 2016). The term "matching description" means that the sets of regions display common feature values or symmetries. A symmetry break occurs when the symmetry is detectable at one level of observation, but is "hidden" at another level (Roldàn et al., 2014). Because BUT tells us that we can find, on an *n*-dimensional sphere, a pair of opposite points that have the same encoding on an *n*-1 sphere, this means that symmetries can be found when evaluating the system in higher dimensions, while they disappear (are hidden or broken) when we assess the same system in one dimension lower.

A BUT variant, termed **energy-BUT**, is particularly useful in our context (Tozzi and Peters, 2017). A physical link does exist between the abstract concept of BUT and the energetic features of a system of two spheres $S^n$and S^{n-1}. We start from a manifold S^n equipped with a pair of antipodal features, standing for a symmetry. When these opposite features map to a *n*-Euclidean manifold (where S^{n-1} lies), a symmetry break/dimensionality reduction occurs, and a single feature is achieved. This means that the single mapping function on S^{n-1} displays energy parameters lower than the two corresponding antipodal functions on S^n (**Figure D**). Therefore, decreases in dimensions give rise to energy decreases. In such a way, BUT yields physical quantities, because a system is achieved in which energetic changes occur among different dimensional levels. Energy-BUT concerns not just energy, but also information, providing a way to evaluate decreases in information in topological, other than thermodynamic, terms. Indeed, two antipodal features encompass more information than their single projection in a lower dimension.
Since the existence of one pair of mappings between different dimensions implies an overall change in thermodynamic and informational parameters, BUT is allowed to solve the curse of dimensionality. When a S^n sphere increases in dimensions, a single feature (say, a bit of information inS^2) becomes two features with matching description (say, two bits in S^3) (**Figure D**). It is easy to see that the BUT-framed information amplifications occurring in high dimensions are concentrated near the equator, i.e., where the hypersphere's volume available for data assessment is located. Despite the expansion of dimensionsshrinks the spherical volume leading to loss of information, the above-described BUT mechanism compensates and restores this failure, leading to an increase in information in higher-dimensional spheres.

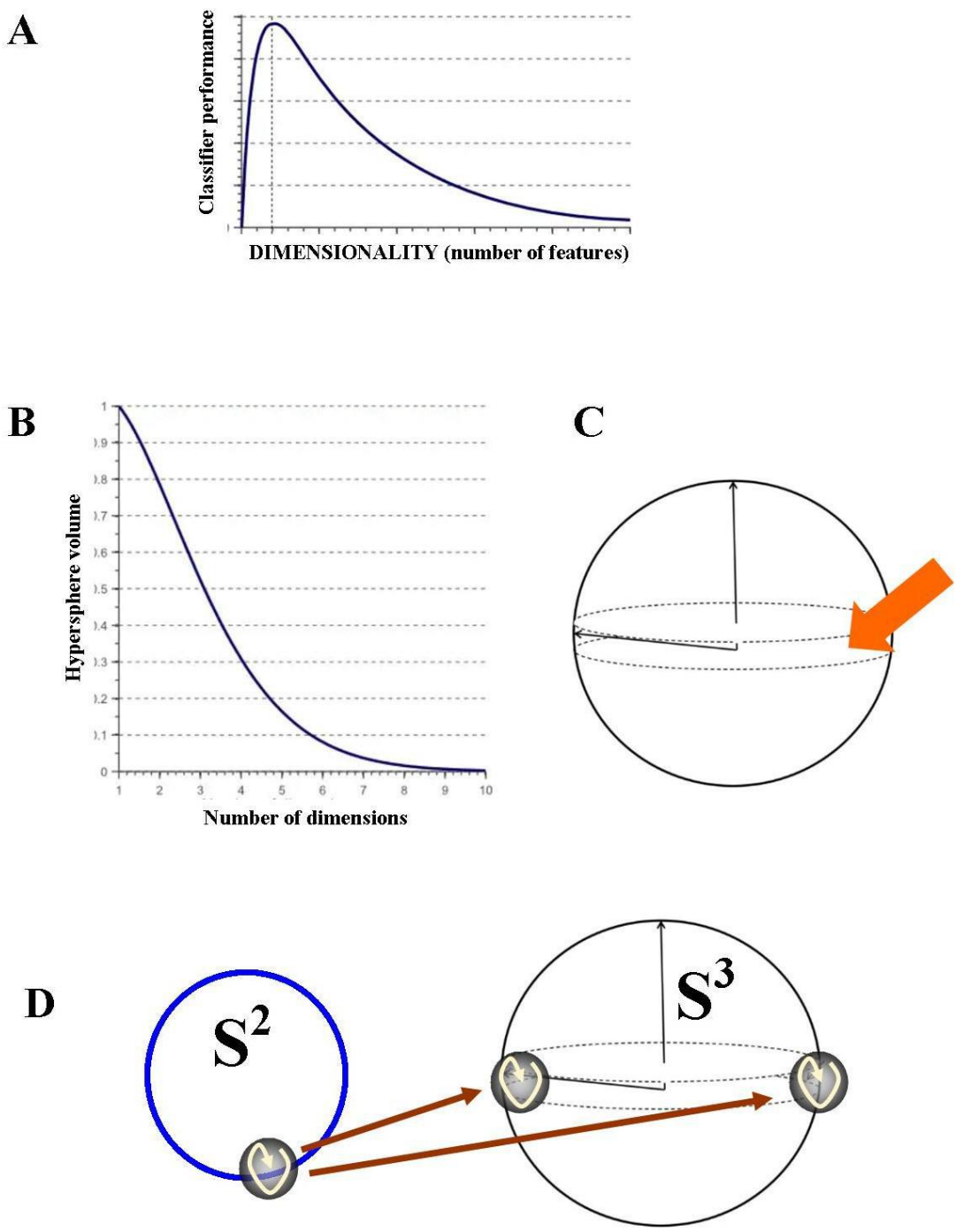

Figure. How to solve the curse of dimensionality through the algebraic topological weapon of BUT. **Figure A:** an increase in number of measurements impairs classifier performance. **Figure B:** when assessing positive-curvature manifolds (spheres), an increase in dimensions leads to a decrease in volume. **Figure C**: Counterintuitively, the volume of high-dimensional balls is concentrated near their borders, in particular near their equator (red arrow). **Figure D**: in BUT terms, the manifold S^2 displays a single feature conformation (black oval containing a curved arrow), which becomes two features with matching description when mapped to a manifold S^3 . It this case, the two antipodal features stand for two symmetric functions equipped with the same information content. In sum, a dimensional increase is correlated with an increase in available information, despite the spherical volume is decreased. **Figures A, B**: Modified from: http://www.visiondummy.com/2014/04/curse-dimensionality-affect-classification/; **Figure C**: modified from Gorban and Tyukin (2017); **Figure D**: modified from Tozzi et al., 2018.

REFERENCES

1. Barbour DL. 2019. Precision medicine and the cursed dimensions. npj Digital Medicine, 2(4).
2. Bellmund JLS, Gardenfors P, Moser EI, Doeller CF. 2018. Navigating cognition: spatial codes for human thinking. Science, 362 (6415), eeat6766.
3. Bergen KJ, Johnson PA, de Hoop MV, Beroza GC. 2019. Machine learning for data-driven discovery in solid Earth geosciences. Science, 363 (6433): eaau0323. DOI: 10.1126/science.aau0323.
4. Borsuk K. 1933. Dreisatzeuber die n-dimensionale euklidischesphare. Fundamenta Mathematicae, XX, 177–190.
5. Borsuk K, Dydak J. 1980. What is the theory of shape? Bull. Austral. Math. Soc. 22, 161-198.
6. Gorban AN, Tyukin IY. 2017. Stochastic separation theorems. Neural Networks, 94: 255-259. https://doi.org/10.1016/j.neunet.2017.07.014.
7. Gorban AN, Makarov VA, Tyukin IY. 2018. The unreasonable effectiveness of small neural ensembles in high-dimensional brain. Phys Life Rev. https://doi.org/10.1016/j.plrev.2018.09.005.
8. Kůrková V. 2019. Some insights from high-dimensional spheres: Comment on "The unreasonable effectiveness of small neural ensembles in high-dimensional brain" by Alexander N. Gorban et al. Phys Life Rev. https://doi.org/10.1016/j.plrev.2019.03.014.
9. Mars RB, Passingham RE, Jbabdi S. 2018. Connectivity Fingerprints: From Areal Descriptions to Abstract Spaces. Trends Cogn Sci. 2018 Sep 18. pii: S1364-6613(18)30209-2. doi: 10.1016/j.tics.2018.08.009.
10. Matoušek J. 2003. Using the Borsuk–Ulam Theorem. Lectures on Topological Methods in Combinatorics and Geometry. Berlin Heidelberg: Springer-Verlag.
11. Pereda E, García-Torres M, Melián-Batista B, Mañas S, et al. 2018. The blessing of Dimensionality: Feature Selection outperforms functional connectivity-based feature transformation to classify ADHD subjects from EEG patterns of phase synchronisation. PLoS One. 13(8):e0201660. doi: 10.1371/journal.pone.0201660.
12. Peters JF. 2016. Computational Proximity. Excursions in the Topology of Digital Images. Edited by Intelligent Systems Reference Library. Berlin: Springer-Verlag. doi:10.1007/978-3-319-30262-1.
13. Roldán É, Martínez I, Parrondo JMR, Petrov D. 2014. Universal features in the energetics of symmetry breaking. Nature Physics, 10(6), 457–461. http://doi.org/10.1038/nphys2940.
14. Tozzi A, Peters JF. 2017. From abstract topology to real thermodynamic brain activity. Cognitive Neurodynamics, 11(3) 283–292. Doi:10.1007/s11571-017-9431-7.
15. Tozzi A, Peters JF, Fingelkurts AA, Fingelkurts AA, Marijuán PC. 2017. Topodynamics of metastable brains. Physics of Life Reviews, 21, 1-20. http://dx.doi.org/10.1016/j.plrev.2017.03.001.
16. Tozzi A. 2019. The multidimensional brain. Physics of Life Reviews. doi: https://doi.org/10.1016/j.plrev.2018.12.004.
17. Wang X. 2005. Volumes of Generalized Unit Balls. Mathematics Magazine, 8(5):390–395.

Author's personal copy

Cognitive Neurodynamics (2019) 13:417–428
https://doi.org/10.1007/s11571-019-09539-8

REVIEW PAPER

Points and lines inside human brains

Arturo Tozzi[1] · James F. Peters[2,3]

Received: 13 January 2019 / Revised: 17 April 2019 / Accepted: 30 April 2019 / Published online: 7 May 2019
© Springer Nature B.V. 2019

Abstract

Starting from the tenets of human imagination, *i.e.*, the concepts of lines, points and infinity, we provide a biological demonstration that the skeptical claim "human beings cannot attain knowledge of the world" holds true. We show that the Euclidean account of the point as "that of which there is no part" is just a conceptual device produced by our brain, untenable in our physical/biological realm: currently used terms like "lines, surfaces and volumes" label non-existent, arbitrary properties. We elucidate the psychological and neuroscientific features hardwired in our brain that lead us humans to think to points and lines as truly occurring in our environment. Therefore, our current scientific descriptions of objects' shapes, graphs and biological trajectories in phase spaces need to be revisited, leading to a proper portrayal of the real world's events: miniscule bounded physical surface regions stand for the basic objects in a traversal of spacetime, instead of the usual Euclidean points. Our account makes it possible to erase of a painstaking problem that causes many theories to break down and/or being incapable of describing extreme events: the unwanted occurrence of infinite values in equations. We propose a novel approach, based on point-free geometrical standpoints, that banishes infinitesimals, leads to a tenable physical/biological geometry compatible with human reasoning and provides a region-based topological account of the power laws endowed in nervous activities. We conclude that points, lines, volumes and infinity do not describe the world, rather they are fictions introduced by ancient surveyors of land surfaces.

Keywords Continuum · Physical equations · Topology · Curvature · Infinity

Throughout the centuries, different skeptical claims have been proposed, from doubts about the possibility of knowledge/certainty, to the doctrine that true knowledge is uncertain, to concerns about the limitations of human mind. Here we will focus on the skeptical tenet that "human beings cannot attain knowledge of the external world". Throughout the centuries, such skeptical claim has been just tackled through logical weapons (for a survey, from Pyrrho to Erasmus, from Montaigne to Feyerabend and Fogelin, see: Popkin and Maia Neto 2007). However, logic does not describe the world, rather the human interpretation of the world. Indeed, our brain works with models. Demarcation among objects and things is somewhat arbitrary, because our mind tends to exclude the continuity among the world's structures. We tend to draw a line of separation among things that we judge different, arbitrarily excluding or including issues in our description, to achieve positive demarcations that allow a pragmatic treatment of the world based on regularity and uniformity (Bonzon 2017; Kim and Lim 2017). In touch with set theory, our mind, equipped with logic weapons, tends to split the set of the entire world in different, arbitrary subsets that do not really stand, in terms of quantum dynamics, for different things (Mizraji and Lin 2017; Peters et al. 2017). The same scientific concept of "observable" is based on the choice of variables in an experimental setting: scientists, putting aside most of the variables, focus their efforts on a few features. For example, elementary particles are fully defined just in terms of three experimental observables, *i.e.*, charge, spin and mass (Seiden 2005), putting aside, for practical purposes, less "useful" features.

✉ Arturo Tozzi
tozziarturo@libero.it; Arturo.Tozzi@unt.edu

James F. Peters
James.Peters3@umanitoba.ca

[1] Center for Nonlinear Science, University of North Texas, 1155 Union Circle #311427, Denton, TX 76203-5017, USA

[2] Department of Electrical and Computer Engineering, University of Manitoba, 75A Chancellor's Circle, Winnipeg, MB R3T 5V6, Canada

[3] Department of Mathematics, Adıyaman University, 02040 Adıyaman, Turkey

Author's personal copy

We will proceed as follows. In the first section, we will describe how the most successful description of the world, i.e., mathematics, is based on Euclidean geometry. Then, we will show how Euclidean geometry is intrinsically unable to describe the physical and biological world surrounding us. In the sequel, we will analyze feasible alternatives to Euclidean points and lines, in order to quantitatively describe the world. Then, in Sect. 2, we will provide an example of the feasible use of such novel techniques, tackling the issue of removing the troublesome concept of infinity from mathematical formulas.

Mining the authority of mathematics

Our physical and biological world can be described in terms of mathematical definitions, postulates, relations, theorems, formulas, equations and algorithms. Despite the claims that math is a collection of abstractions invented by our minds, it is astonishingly successful in order to explain and quantify a lot of issues of our world (Wigner 1960). Indeed, math elucidates many physical phenomena, such as the interaction of photons and physical surfaces, the diffraction of light with prisms, the apparent influence of speed on moving masses, and so on. Novel branches of math—such as algebraic topology, group theory and functional analysis—leading to far-flung approaches that include nonlinear dynamics in physics and chemistry—start to unveil also the mysteries of otherwise previously unclassifiable issues, such as weather, thrust, interactions and structure of neuro-systems (albeit minds) and the collective behaviors of societies.

A huge portion of our mathematics of the physical world is based on the amazingly simple Euclidean geometry. Indeed, starting from very straightforward assumptions and theorems such as those found in Euclid's geometry, it is feasible to build also non-Euclidean geometries with the convergence of parallel lines (Aleksandrov 1969) and complex manifolds able to explain issues such as those in quantum mechanics. One of the main components of Euclidean geometry is the point, that stands for the most fundamental object. The first definition of a point (prior to Euclid) is given by the Pythagoreans: a point is a monad having position. Euclid begins his geometry with the definition of a point [that of which there is no part] (Def. 1, Euclid 300 BCE) and the extremities of a line are points (Def. 2). Euclid's Def. 1 is interpreted by T.L. Heath to mean that a point is that which is indivisible in parts. Therefore, we are confronted with a primitive notion defined only by axioms that it must satisfy, i.e., the point upon which the whole apparatus is built, meaning that geometry cannot be described in terms of previously defined real objects or structures. Here we ask whether the zero-substance point holds true in our physical world and extend our analysis also to other Euclidean objects, such as lines, surfaces, volumes and so on.

The physical unfeasibility of Euclidean points and surfaces

Despite the huge influence of the Euclidean geometry in current scientific approaches, its internal framework is fatally flawed from the very beginning, if we want to use it to describe physical (and also biological) phenomena. The geometric points described by Euclid, originally defined as "that which have no part", are not equipped with any diameter, area, volume, or other physical features such as height, density, weight. Many constructs of Euclidean geometry are represented by a set of points, that stand for infinite collections of objects that conform to certain axioms. In particular, the Euclidean point is posited as something which has location but zero diameter. However, it is widely recognized that our world is quantized, and that a minimum length does exist, *i.e.*, the Planck size. Instead of a Euclidean point, we arrive at a region-based view of points in which every point is a spatial region (Peters 2016b) with measurable diameter as well as location of its centroid. The quantization of matter leads to one of the hallmarks of spacetime, namely, Planck's constant. This allowed scientists to formulate frameworks, such as string theories (Duff 1996; de Haro et al. 2013) and quantum gravity (Rovelli and Smolin 1988; Muxin 2011), in which our reality is quantized, and therefore discontinuous. Thus, a real manifold must be made of separable units, and is not a continuum with no holes. However, such an approach *does not hold true* for the Euclidean manifolds. In the sequel, we will show how and why an Euclidean geometric structure (such as points, lines, surfaces, volumes) cannot display a real counterpart, and are therefore useless in the description of our physical world.

Paraphrasing Aristotle's account of continuity and indivisibility (ARISTOTLE PHYSICS Book VI, Part 1), things are said to be "continuous" if their extremities are one, "in contact" if their extremities are joined together, and "in succession" if there is nothing of their own kind intermediate between them (Bradwardine 1330). Nothing that is termed "continuous" can be composed of "indivisibles": to make an example, an Euclidean line cannot be composed of points, the line being continuous and the point indivisible. Indeed, the extremities of two Euclidean points can neither be one (since of an indivisible there can be no extremity as distinct from some other part), nor together (since that which has no parts can have no extremity, the extremity and the thing of which the extremity is distinct). Moreover, if that which is continuous is composed of Euclidean points, these points must be either continuous, or

Author's personal copy

in contact with one another. Therefore, indivisibles cannot be continuous: one thing can be in contact with another only if whole is in contact with whole or part with part or part with whole. But since indivisibles have no parts, they must be in contact with one another as whole with whole. And if they are in contact with one another as whole with whole, they will not be continuous. For Euclid, that which is continuous has distinct parts, and these parts into which it is indivisible need to be spatially separate. In particular, concerning the line, an Euclidean point cannot be in succession to another in such a way that length can be composed of points. Indeed, things are in succession, provided there is nothing of their own kind intermediate between them, whereas that which is intermediate between points is always a line, or a region of a surface. Again, if the Euclidean length (i.e., the line) could be composed of indivisibles, it could be divided into indivisibles, since each is divisible into the parts of which it is composed. But, as stated above, no continuous thing is divisible into things without parts. Nor can there be anything of any other kind intermediate between the parts: if there could be any such thing, it must be either indivisible or divisible, and if it is divisible, it must be divisible either into indivisibles or into divisibles that are infinitely divisible, in which case it is continuous.

In sum, because the Euclidean line is either continuous or depicted as an infinite set of zero-mass points, it does not describe real lines, that are made of a set of contiguous multi-mass regions.

The problem of a physical continuum becomes more murky, if we consider what means mathematically for a mapping between spatial regions to be continuous. Let $f : X \rightarrow Y$ be a mapping on X into Y, so that $f(x) \in Y$ for $x \in X$. In the context of proximity spaces, a point x is near a region or set of points A, provided $f(x)$ is near $f(A)$(Naimpally and Warrack 1970). In other words, a function proximally continuous, provided the function preserves pairs of sets so that whenever $\{x\}, A$ are near (in the same proximity), so too $f(x), f(A)$ are near (Peters 2014). Put another way, a function f is continuous, provided the image $f(x)$ of every point of adherence $x \in X$ is a point of adherence in the set $f(A)$(Smirnov 1952).

Again from a mathematics perspective, it is an axiom in proximity space theory that the closeness of a point to a cell complex that is a collection of 0-cells (vertexes) implies that the point is either on the boundary or within the cell complex. By contrast, a physically continuous mapping from a computational proximity perspective (Peters 2016a) imply that the closeness of a physical region such as an atom χ to another physical region such as a collection of atoms A means that χ is the in the neighbourhood of A, not that χ is in A.In other words, as anticipated by old philosophers too (Autrecourt and About 1340), closeness of points and sets in mathematics is quite different from the closeness of points and sets in the physical world. Instead of the conventional closeness of points and sets, the axiomatic foundations of the descriptive closeness of points and sets has been recently introduced (Di Concilio et al 2018). In the context of descriptive proximity, the closeness of points and cell complexes is viewed in terms of overlapping descriptions of the points and the sets. In other words, a feature vector that describes a point and the feature vector that describes a cell complex overlap without requiring that the descriptive closeness of a point x and cell complex A implies the inclusion of the point x in the cell complex.

As for the line, the same applies also for other Euclidean structures, such as two-dimensional surfaces and three-dimensional volumes. Indeed, every continuous Euclidean manifold (whatsoever its dimensions may be) is divisible into divisibles that are infinitely divisible: if it were divisible into indivisibles, we should have an indivisible in contact with an indivisible, since the extremities of closed manifolds that are continuous with one another are one and are in contact. This means that a collection of n-dimensional Euclidean structures cannot give rise, when joined together, to a $n + 1$ dimensional manifold. Therefore, the Euclidean points, lines, surfaces, volumes cannot exist in the real world. In particular, considering that physical space is quantized and that the minimum possible length is the Planck one, a real "point" cannot exhibit zero mass. Furthermore, at Planck length, another problem arises for an hypothetical basic "point": many theories predict that the minimum separable structure, *i.e.*, the string, lies in 10–11 dimensions, rather than being *a* dimensional. Therefore, in the real world, also the simplest structure, *i.e.*, the real point, must be a spatial region that displays nonzero mass in spacetime, otherwise it cannot exist. Furthermore, as stated above, it is also difficult to talk about real lines, surfaces, volumes, given the indefiniteness and vagueness of their Euclidean definition and structure.

Further possibilities to cope with the physical reality

In the previous paragraph, we showed that the concept of Euclidean points and n-dimensional manifolds do not hold true for the description of our real world, because every physical structure cannot be built starting from nonzero mass ones. An Euclidean line does not exist in the real world, because a real line must be composed of spatial subregions, and this is not compatible with the Euclidean tenets. It might be objected that a line could be made of points made of bosons, that, satisfying the Bose–Einstein condensate theory, can be described as superimposed. However, a real line in our world must be composed of

Author's personal copy

matter, i.e., fermions that are subject to the principle of locality: therefore, a point made of fermions cannot be superimposed to another one, because they must occupy different locations in space. It might also be objected that a line could be made of different points that are not superimposed, rather they are separated by a small void, but it is not the case of the Euclidean line's description.

Our results suggest that it's time to change our approach. It is clear, from our account, that the Euclidean axiomatic system cannot hold in the real world. The Euclidean point is just a conceptual device, and the same holds for its consequences: lines, surfaces, volumes. The physical impossibility of points holds also for "surfaces". For example, in weighting, since many years, there is the problem to take into account where the mass surface ends, because there are always, without solution of continuity, "layers" of air molecules more or less interacting with the "solid", part of which does influence the "weighted mass" also in the most accurate measurements. That is already a fact long since in precision metrology: "the non-uniqueness in these cases comes from thickness of the adherent interface layer(s), having an effect different from zero on the actual dimensions of the object, i.e., adding additional mass to the object with possibly time-dependent variability" (Pavese and Charki 2016).

Is it feasible to provide definitions of points and manifolds other than the Euclidean ones, in order to overtake its fatal limitations in the description of physical matters?

Despite there exist several regions-based accounts of space/time, due to Roeper, Menger, Tarski and others (Shapiro and Hellman 2017), the most of them, contrary to our approach, follow the Aristotelian theme that continua are not composed of points. A more recent view of a point by M. Simon (1901) moves closer to physical points. According to such an approach, a point is the limit of localization. More in keeping with the contemporary view of a point as a property of duration, a theory of extensive connection and atomicity of actual entities has been built (Whitehead 1929). The notion of extensive connection brings us full circle to an expansion of cellular topology and physical proximity space theory, in which a point stands for the minimal part of overlapping regions of physical space, such as overlapping perimeters of vortex atoms that live together in motion continua with limited duration. In other words, a point is a finite region of space with non-zero area, while a line is drawn from one region to another (Peters 2016a).

One region A includes another region B, whenever every region connected to B is also connected to A (Whitehead 1929). In other words, region A is connected to region B, provided there is a path from any subregion of B to a subregion of A. The extremity of a connecting path between subregions is itself a subregion with measurable area, albeit a tiny subregion that has the appearance of a point in Euclides' surveyer-like geometry.

We may state that a region of space is the maximum distance between subregions (intervals) of its bounding edge. This definition allows the description of a point as a single abstract spatial vertex: in other words, our physical reality can be described in terms of multiple surface spacetime vortices, in which each vortex is a funnel reaching down to a physical limit, called a vertex. Examples are provided in Fig. 1. This approach permits us to remove the unwanted Euclidean geometry from the quantitative assessment of our world.

A humanly reasonable Euclidean geometry

Despite the usefulness of Euclidean geometry, our results suggest that it's time to change our approach to the geometry of physical surfaces, because Euclid describes totally abstract surface regions. It is also feasible to deliver a psychological explanation for the Euclid's successful mathematical description of the world. Indeed, taking into account recent neuroscientific findings, we are allowed to hypothesize why our mind seems to recognize in the surrounding environment Euclidean points, lines, surfaces, volumes, despite the fact that they cannot, according to our account, exist in reality. Over the last few years, studies of receptive field properties in several mammalian visual brain structures, such as the lateral geniculate nucleus and the primary sensitive cortex, have suggested the existence of cell classes with unique functional response properties (Van Hooser et al. 2005; Viswanathan and Nieder 2017). To make an example, the cells of the cortical visual area V1 display basic receptive field properties, such as orientation selectivity, direction selectivity, bar length and end-stopping (Duffy and Hubel 2007). Further, similar to the primary visual cortex, orientation sensitivity was closely reflected by the receptive fields properties also in extra-cortical structures, such as the lateral geniculate nucleus (Li et al. 2018). Therefore, many experimental suggestions dating back just a few years suggest that our brain is equipped with neurons, located in cortical and extra-cortical areas, that selectively fire when our sight perceives angles, surfaces, lines, contours. And such angles, surfaces, lines, contours do not exist in the real world, provided that the borders of the objects cannot be as well sharply delimited as suggested by Euclidean geometry.

Our perception is perhaps an evolutionary mechanism that permits us to cope with our external, rather visual, world, in order to avoid dangers and harms. The detection by sight of geometrical issues in the environment (such as points, lines, contours and so on) does not necessarily describe the real world, but rather stands for a sort of internal map based on species-specific, innate

Author's personal copy

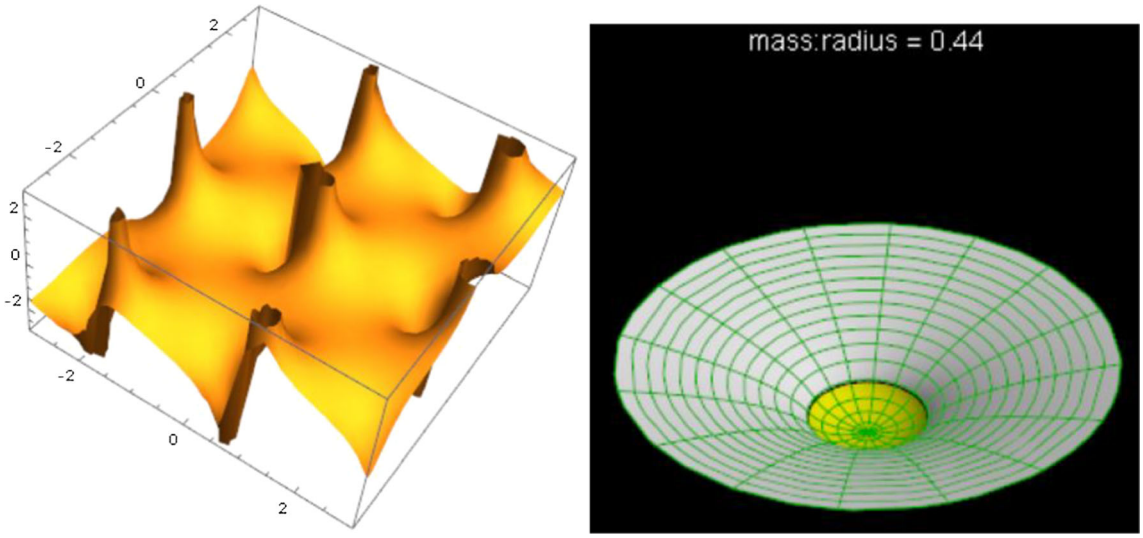

Fig. 1 Examples of sample vortices. **Left**: a Weierstrass-Zeta mathematical model for multiple surface spacetime vortices, in which each vortex is a funnel reaching down to a physical limit called a vertex. **Right**: black hole vortex (initial mass radius 0.44 km) formation. It results from steadily increasing strong gravitational force that pulls neighboring chunks of matter into its funnel winding down to the squish level. Therefore, massive chunks of matter are squeezed to the diameter of a vortex

interpretations of the physical reality. We are rather firmly wired, if not actually hardwired, to think of the abstractions represented by such programs as realities. The whole idea in biology is after all to respond to survival situations quickly and effectively, rather than to question or contemplate their deeper nature. In Karl Friston's terms (2010), the brain is an inferential machine that compares the real world with an internal map, pre-existent in our mind. Therefore, it might be suggested that what we see is just partially real: indeed, we might ask whether other animals, such as, e.g., an ant equipped with olfactive-tactile perceptions rather than our visual ones, or a bat (Nagel 1974), are able to recognize points and lines. Indeed, some response properties, such as linearity of spatial summation, contrast gain, dependence of receptive field size on eccentricity and interlaced arrangement of cortical neurons, vary from species to species (Van Hooser et al. 2005; Mazade and Alonso 2017). To make an example, despite the fact that a squirrel has greater visual acuity and a physically larger V1 than some mammals that have orientation maps in V1, it is not provided of such maps (Van Hooser et al. 2005). In turn, electrophysiological recordings in awake and anesthetized turtles reveal that their dorsal cortex is sensitive to the spatial structure of natural images, and their receptive fields are not entirely uniform across space (Fournier et al. 2018). Therefore, the mapping and representation of visual space in turtle's three-layered cortex differ from those found in mammalian primary visual cortex. This means that, contrary to the mammalian primary visual cortex, the turtle dorsal cortex performs a global, rather than local, analysis of the visual scene (Fournier et al. 2018). This means that, in animals different from us, spatial information can be found both at the single-neuron and population scales and a clear retinotopic mapping of thalamocortical projections is not detectable.

Our sensations and perceptions (and therefore our world) depend on the activity of our cortex. A recent study points towards this hypothesis. Indeed, Armenta Salas et al. (2018) showed that intracortical microstimulation in primary somatosensory cortex (S1) is a method of inducing discriminable artificial sensation. In a tetraplegic human with microelectrode arrays implanted in S1, the Authors reported replicable elicitations of sensations in both the cutaneous and proprioceptive modalities. Therefore, the direct activation of the cortex is able to achieve naturalistic percepts that closely mimic the body's natural physiological capabilities.

Tackling the problem of infinity in physics and biology

We showed, in the previous paragraphs, that infinity does not exist in our physical and biological world, rather it is a technical device correlated with our mathematical formulations of the world issues. In their theories and models dealing with formulas that describe finite, measurable quantities, physicists do not appreciate the occurrence of unwished infinite values. Indeed, with the exception of various forms of conformal infinity (Frauendiener 2000; Sommers 1978), mathematical infinity—indeterminate infinite results in which, for example, solutions of the

Author's personal copy

gravitational field equations cannot be continued (Bergmann 1989)—prevents scientific issues to provide practical formulas that correspond to, or at least approximate, the real observables. For example, in case of bodies with infinite gravitational mass and/or energy, equations become intractable and useless, since their results would be always the same, regardless of objects' position, mass and movement. In some cases, infinite results mean that the used theory is approaching the point where it fails. A classic example is the black holes' mathematical singularity: the commonest solutions of the general relativity's equations allow for zero-size finite mass distributions, leading to infinite density, e.g., a point where general relativity breaks down and is incapable of appropriately describing events. Other examples are the Newtonian gravity and Coulomb's law of electrostatics at r = 0. Although infinity can be used in physics, scientists require for practical purposes the final result being physically meaningful: e.g., in quantum field theory, infinities are treated through procedures such as renormalization ('t Hooft 1971).

The concept of infinity is a painful concern also, e.g., in fullerenic issues. To make an example, Chan et al. (2016) carried out large-scale computational quantum chemistry calculations to obtain heats of formation for C60 and some higher fullerenes, using the DSD-PBE-PBE/cc-pVQZ double-hybrid density functional theory method. However, they noticed a slow convergence to the graphene limit, which they attributed to the relatively small proportion of fullerene carbons that are in "low-strain" regions. Indeed, it would take tens, if not hundreds, of thousands of carbons for a fullerene to roughly approach the limit. Other problems linked with infinity arise when researchers try to assess asymptotic shapes of symmetrical fullerene ball, that is a flat-sided polyhedron whose edges have an average curvature radius of order $R^{2/3}$ (Witten and Li 1993).

Here we propose a different way to cope with the enigmatic results of the infinity in the description of physical equations, holding out the possibility of a physical geometry (Peters 2016a) that is region-based instead of point-based. This approach leads to a form of Desarguesian affine space in which locally parallel lines converge (Zaka and Peters 2019). We infer scaling of the shape and energy of a space-enclosing elastic sheet such as a large fullerene ball of linear dimension R. Stretching deformation is crucial in determining the optimal shape, in conjunction with bending. The asymptotic shape of a symmetrical fullerene ball is a flat-sided polyhedron whose edges have an average curvature radius of order R2/3. The predicted asymptotic energy is concentrated in these edges and is of orderR1/3. Analogous edges with this scaling property should occur generally in elastic sheets with discrete disclinations.

Infinity as the continuation of a straight line in affine geometry

As stated above, unqualified infinity cannot be any of the physical observables which we either can assess or measure: when we set out to investigate the infinity, we must leap beyond simple physical concepts and use mathematics. Inspired by Nicholas de Cusa' treatment of infinity (de Cusa 1440; Tozzi and Peters 2017a), here we illustrate how to use mathematical and geometrical features to undertake physical infinity. If one wants to assess finite physical measurements leading to infinity, one needs at first to consider finite mathematical figures and topological manifolds, together with their features and relations. Next, one must apply these relations in a projective way. Thirdly, one must thereafter, in a still more highly transformed way, apply the relations of these infinite figures to the general concept of mathematical infinity, which is altogether independent even of all figures and manifolds.

Let us start, in touch with de Cusa's accounts, with the picture of mathematical infinite, which will be represented by a straight line. One can maintain that, if there were an infinite line, it would be a straight one, or, for example, an infinite triangle, circle or sphere. Since the latter three figures display infinite sides, as will be shown, they can also be described in terms of infinite lines. First of all, an infinite line would be a straight one. The circle's diameter is a straight line, and its circumference is a curved line greater than the diameter. If the curved line becomes less curved in proportion to the increased circle's circumference, then the maximum circle's circumference, which cannot be greater, is minimally curved and therefore maximally straight (Fig. 2a). Indeed, in the Figure, the arcs of the larger circle are less curved than the smaller ones. Therefore, the straight line will be the arc of the maximum circle, which cannot be greater. An infinite line is necessarily the straightest; and to it no curvature is opposed. In the same way, every manifold with positive curvature, such as, for example, a triangle, or a circumference, or a sphere, can be described in terms of an infinite line standing for a maximum triangle, or a maximum circle, or a maximum sphere. Indeed, an infinite line is whatever is present in the curvature of a finite line: a line finite in length can be longer and straighter, therefore the maximum line is the longest and straightest. If figures are describable by a finite line, and if an infinite line is all-the-things-with-respect-to-which a finite line is in infinity, then it follows that an infinite line stands also for a triangle, a circle, and a sphere.

How is it possible that an infinite line is a side of a triangle? Since any two sides of any triangle cannot, if conjoined, be shorter than the third, this means that, in the case of a triangle whose one side is infinite, the other two

Author's personal copy

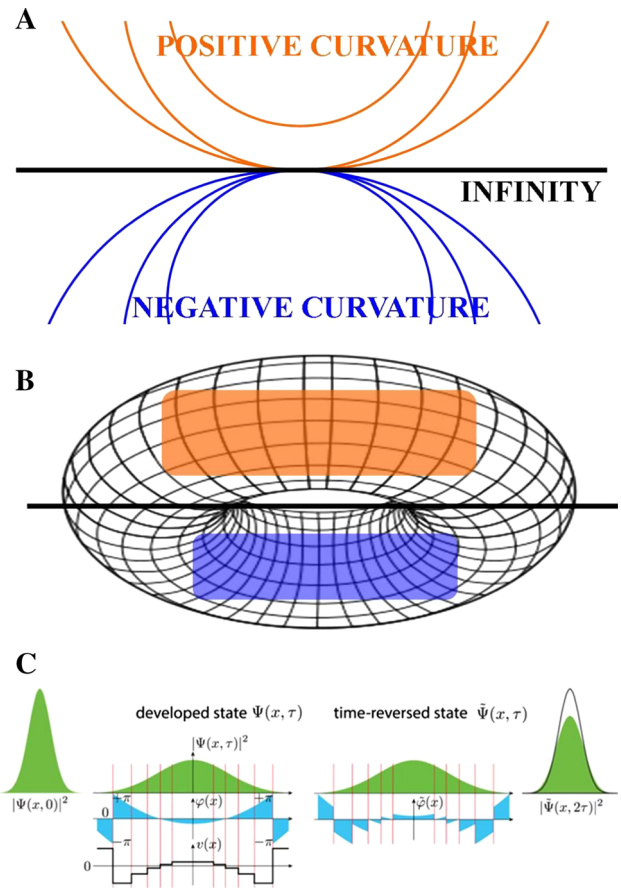

Fig. 2 Curvature changes in biological and physical systems. **a** given a physical system described by progressively increasing curves on a positive-curvature manifold, the occurrence of infinity (straight line) can be removed by taking into account progressively decreasing curves on a negative-curvature manifold. **b** by placing physical observables on a toroidal manifold, one achieves a correspondence between positive and negative curvatures, thus erasing the unwanted occurrence of infinity. **c** Time-reversal according to Lesovik et al. (2019). From the second ("developed state") to the third ("time-reversed state") panel, the Authors modified the phase of the wave-function in every tiny area, so that the lines with positive curvatures in the second panel become lines with negative curvatures in the third one

sides are not shorter, i.e., they are both infinite. Since there cannot be more than one infinite thing, an infinite triangle cannot be composed of a plurality of lines, even though it is the greatest and simplest triangle. And because it is a triangle—something which it cannot be without three lines—it will be necessary that the one infinite line be three lines, and that the three lines be one most simple line. And similarly, regarding the angles: for there will be only one infinite angle; and this angle is three angles, and the three angles are one angle. Nor will this maximum triangle be composed of sides and angles; rather, the infinite line and angle are one and the same thing, so that the line is the angle, because the triangle is the line. The larger the one angle, the smaller are the other two. Now, any one angle can be increased almost but not completely up to the size of two right angles. Nevertheless, let us hypothesize that it is increased completely up to the size of two right angles, while the triangle remains nonetheless a triangle. In that case, it will be obvious that the triangle has one angle that comprises the three angles and that the three angles are one. In the same manner, one can state that a triangle is a line, and an infinite line is a maximum triangle. For any two sides of a quantitative triangle are, if conjoined, as much longer than the third side as the angle which they form is smaller than two right angles. Hence, the larger the angle, the less the lines and the smaller its surface. Therefore, if, by hypothesis an angle could be two right angles, the whole triangle would be resolved into a simple line. Hereby it is evident that an infinite line is a maximum triangle. Next, by applying the same reasoning and the proper rotations, it is feasible to show that an infinite triangle is also an infinite circle and an infinite sphere.

In sum, an infinite line has been shown to be all that which is in the possibility of every finite line and manifold: a triangle is extracted from a line, and an infinite line from an infinite triangle. Hence, an important speculative consideration can be inferred: infinity is correlated with finite manifolds. Because infinite curvature is infinite straightness, this means that an infinite manifold can be described in opposite terms: it is not a thing and is not any other thing; it is not here and is not there; it is unqualifiedly free from all things and is beyond all things; is above the negation of all things. By a physicist's standpoint, this explains why physical theories leading to infinite values are awfully problematic and difficult to cope with. In the next paragraph, starting from the above-mentioned de Cusa's account, we propose a geometrically-framed method to solve the problem of infinity in physical systems.

Geometric removal of infinity in physical and biological formulas: an example

In the previous section, the result was reached that infinity can be expressed by a straight line with zero-curvature. How to use this observation, in the mathematical treatment of physical finite systems whose equations lead to the unwanted infinity? When one has a physical system of equations, he may project it into a positive-curvature manifold through well-described geometrical procedures (Frankel 2011). If the equations tend towards infinity, and therefore give meaningless results, one is allowed to remove the infinity by projecting the same physical equations on a negative-curvature manifold. Given equations' trajectories moving in a convex phase space, when they tend to converge towards a zero-curvature manifold, the undesirable infinity is approximated. To remove the obstacle, we could describe the same equations on an

Author's personal copy

opposite, concave phase space. Indeed, recent work has shown that the appropriate isometric space for embedding complex networks—and in particular the neural multidimensional ones, such as the human connectome (Tozzi 2019)—is not the flat Euclidean space, but rather a negatively curved hyperbolic space (Sengupta et al. 2016; Tozzi et al. 2018). Hyperbolic space has the property that power-law degree distributions, strong clustering and hierarchical community structure emerge naturally when random graphs are embedded in positive-curvature manifolds. It is therefore logical to exploit the structure of the hyperbolic space for useful embeddings of complex networks: in touch with this claim, it has been demonstrated that, when applied to the task of classifying vertices of complex networks, hyperbolic space embeddings outperform the Euclidean space ones (Chamberlain et al. 2017). To provide an operational example, the steps of the Langevin equation (Langevin 1908) experimentally detected in the three-dimensional (plus time) Euclidean space can be transported to a hyperbolic manifold, though, e.g., Levi–Civita or Ehresmann connections (Levi–Civita 1917; Ehresmann 1950). This allows us to assess dynamics inside abstract negative-curvature manifolds that mimic the real physical phase space where such processes occur. This procedure has been tackled by Tozzi et al. (2018), who showed that biophysical activities, including cellular metabolic pathways, protein folding and brain function, can be described in terms of curved trajectories in hyperbolic spaces which are constrained by energetic requirements. The transition and the relationships between the positive- and negative-curvature manifolds are described in Fig. 2b, for sake of simplicity, as taking place on the opposite sides (one convex, one concave) of a single multidimensional torus. A recent, very interesting approach shows that changes in curvatures, apart from removing infinity from physical equations, are able to reverse time too. Indeed, Lesovik et al. (2019) used variations in curvatures to reverse the arrow of time (Fig. 2c). This means that, once again in touch with the 1440 de Cusa's account, a trajectory taking place on a positive-curvature manifold can be counteracted by one taking place on a negative-curvature manifold.

Other solutions to the problem of infinity were introduced in Geroch et al. Kronheimer Geroch, Penrose (1972), leading to computable solutions (Frauendiener 2000; Zenginoglu 2007). The basic approach is to rewrite metrics defined in terms of points at infinity with tractable, computable metrics that sidestep infinite planes and points at infinity such as those shown in Fig. 3.

Here is an example. The Minkowski spacetime metric in polar coordinates is $g = dt^2 - dr^2 - r^2 d\sigma^2$, where $d\sigma^2$ is the metric of the unit sphere. To achieve confomal rescaling of g, the null coordinates $u = t - r$ and $v = t + r$ are introduced, to obtain

$$g = dudv - \frac{1}{4}(v-u)^2 d\sigma^2.$$

The coordinates u and v range over the complete real line, provided $v - u \geq 0$. This infinite range is compactified, using $u = \tan U, v = \tan V$, and new null coordinates ranging over $\left(-\frac{\pi}{2}, \frac{\pi}{2}\right)$, resulting in

$$g = \frac{1}{4\cos^2 U \cos^2 V}\left[4dUdV - \sin^2(V-U)d\sigma^2\right],$$

which is not defined at $U = \pm\frac{\pi}{2}, V = \pm\frac{\pi}{2}$. To resolve this problem, a new metric is extracted from g, namely,

$$g_{new} = 4dUdV - \sin^2(V-U)d\sigma^2.$$

g_{new} is the tractable metric of the Einstein cylinder, which means that Minkowski space is now conformable embedded into the Einstein cylinder (Frauendiener 2000).

A foremost topic: nervous fractals and power laws

In this paragraph, we will tackle the issue of a point-free description of (spatial) fractals and (temporal) power laws. Scale-invariant behaviors have been shown to be ubiquitous in nature, as well as in the brain, and explain well the underlying dynamics of many natural phenomenon, and how we perceive the surrounding environment (Papo 2014; Fox et al. 2015; de Arcangelis et al. 2006; Lübeck 2004). It is noteworthy that fractals display an astonishing analogy with de Cusa's logical concept of "coincidentia oppositorum", both displaying self-similarity at all scales and magnitudes of observation. The frequency spectrum of cerebral activity exhibits a scale-invariant behavior $S(f) = 1/f^n$, where **S(f)** is the power spectrum, **f** is the frequency and n is the power spectral density. The latter is termed fractal "dimension" and equals the negative slope of the line in a log power versus frequency scatter plot (Milstein et al. 2009; Pritchard 1992). Power law distributions contain information on how large-scale physiological and pathological outcomes arise from the interactions of many small-scale processes. leading also to self-organized criticality (de Arcangelis and Herrmann 2010; Jirsa et al. 2014). A recently introduced version of the Borsuk-Ulam theorem (BUT), termed re-BUT, states that there is a continuous mapping between regions in topological spaces (Peters 2016a). In simpler words, a single region in lower dimensions maps to two matching regions in higher dimensions, provided the function is continuous (Tozzi and Peters 2016). Note that, instead of the canonical points described in the standard BUT, in re-

Author's personal copy

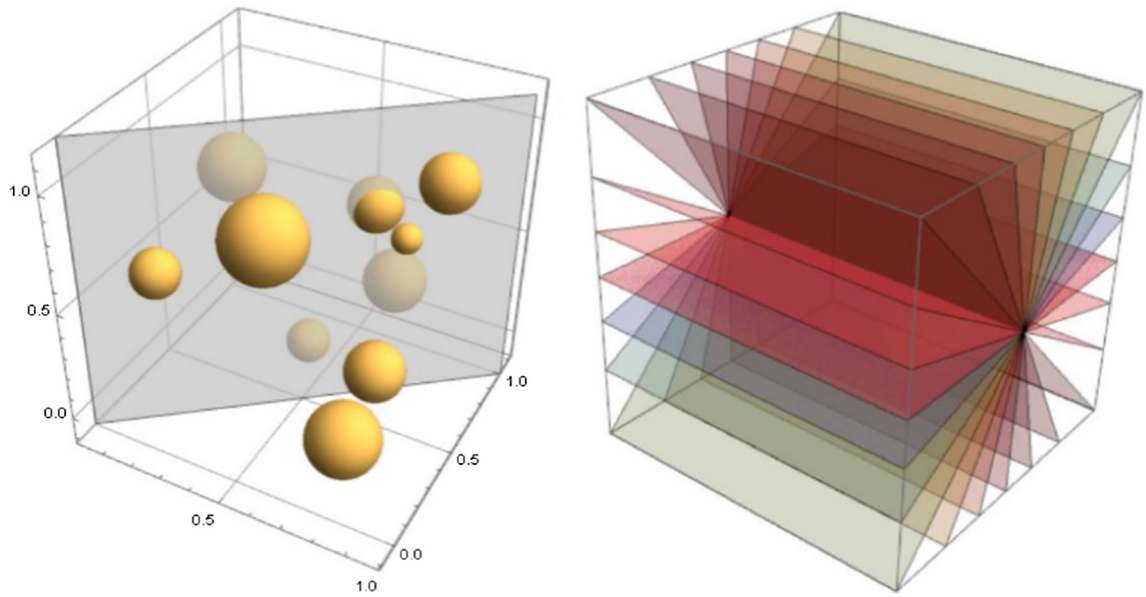

Fig. 3 Conformable infinity at computable points near, but not at ideal points. **Left side**: Tractable point on spheres in spacetime that are sliced by an infinite plane. Ideal points on the infinite plane are replaced with non-ideal points that are computable. **Right side**: Those parts of a sheaf of infinite places that intersect with computable lines are computable up to but not including the ideal points

BUT a point-free description (i.e., based on regions) is provided (Fig. 4a). Is it suitable to make use of re-BUT (and therefore of point-free geometry) in the description of fractals and power laws? Tozzi and Peters (2016) showed that the dimensions involved in BUT and re-BUT could be Hausdorff (fractal) as well as spatial (Fig. 4b). Indeed, the fractal account gives rise to a dimension greater than the "classical" one-dimension which is generally attributed to the "normal" curves embedded in a standard Euclidean space. In Fig. 4b, we used, as an example, a dimension corresponding to the value of 1.3.

In sum, point-free descriptions, through the use of topological weapons such as the re-BUT, can be extended to encompass the description of brain's fractal dynamics too.

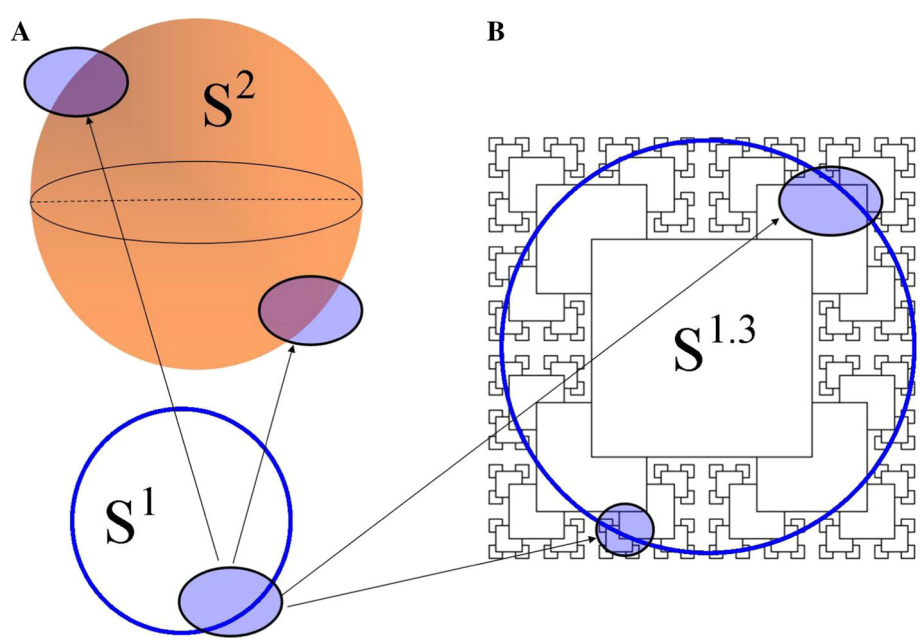

Fig. 4 A point-free topology allows description of fractals. **a** the novel BUT variant, termed re-BUT, describes a pointless feature (blue shape) on a two-dimensional circle S^1. When projected onto a sphere S^2, two pointless features with matching description are achieved (blue shapes). **b** the pointless feature on S^1 can be projected not just to S^2, but also to the fractal structure $S^{1.3}$. Therefore, we achieve two pointless features in $S^{1.3}$ (blue shapes): they stand for two matching descriptions, because they depict the same fractal structure, self-similar at different magnifications and coarse-grained scales. (Color figure online)

Author's personal copy

Conclusions: removing points, lines and infinity

Here we ask whether one of the basic building blocks of Euclidean geometry, *i.e.*, the point, holds true in our physical world. Given our negative answer, we concluded that the Euclidean manifolds cannot properly describe the real world. Our observation suggests the need for a viable alternative to Euclidean geometry, despite its current utmost importance in the description of the reality surrounding us. Indeed, the Euclidean geometry, after many centuries from its first formulation, still stands for the main tenet of the ensuing mathematical and physical developments. Starting from its postulates and theorems, it has been feasible to consider exception conditions, such as curved space, that are more in keeping with the relativistic spacetime. Furthermore, Euclidean geometry allowed to work our way toward non-Euclidean geometries (Johnstone 1983), R. Descartes's vortex geometry, sweeping comprehensive cellular complexes in Whiteheadean closure finite weak topology, V.G. Boltyanskii and V.A. Efremovich intuitive combinatorial topology, Edelsbrunner-Harer computational topology, Cech-Efremovich-Lodato-Naimpally-DiConcilio proximity spaces (Di Concilio 2013), K. Borsuk shape theory (Borsuk 1958, 1969), P.G. Tait's knots (1877). Such improvements led to J.S. Birman's braids, links, knots and mapping class groups that allow amazingly simple solutions to problems in quantum mechanics and to W.T. Kelvin's knotted and knitted vortex atoms (Kelvin 1867). This also led to a deep understanding of Helmholz's discovery (Helmholz 1858) of simple vortex rings and the vexing problem of vortex motion in perfect liquids, as well as the elucidation of thermodynamic properties of gases.

Further, we showed that points and lines are programs running in mammalian brains, able to capture predictable consistencies in the external world, in forms that are both compact and supportive of fast, first-level approximations even in slow, neuron-based brains. So, while a ball is not much like a point, it is enough like a point for a human or canine brain to use a point-like approximation of it to move a hand (or snout) to the right location to catch it when thrown (Bollinger 2018). Even though quantum uncertainty adamantly informs us that higher levels of detail always requires higher energy costs, our mammalian-brain mathematics treat this paradox as "minor detail" that can be overlooked in our formal treatments of the physical world (Barranca et al. 2018).

It is assumed by physicists, due to pragmatic issues, that no measurable quantity or event might have infinite values. Indeed, any physical theory needs to provide operational formulas that correspond, to or at least approximate, reality (e.g., Iyer and Petters 2007). As an example, if any object of infinite gravitational mass were to exist, any use of the formula in order to quantify the gravitational force would lead to a useless infinite result. The formula would be useful neither to compute the force between two objects of finite mass, nor to compute their motions. Sometimes, an infinite result of a physical quantity may mean that the theory being used is approaching the point where it fails. We provided a novel conceptual framework to theoretically solve the problem of the occurrence of infinity in physical equations. We compared (a) finite quantities to curved lines endowed in positive-curvature manifolds, and (b) intractable infinity to a straight line. In order to restore the equations and erase the straight line of infinity, we project the quantities onto curved lines endowed in negative-curvature manifolds.

We achieved at first a physical system's description on, say, the convex surface of a manifold. In order to avoid the occurrence of infinite when the curvature approaches the zero, we projected such description to the concave surface of a manifold, through a long list of available and well-studied procedures of vectorial and tensorial transport: e.g., Ehresmann connections (Tozzi et al. 2017), parallel transport on Riemannian manifolds (Sengupta et al. 2016), and so on. In other words, we need at first to project a physical phenomenon which tends to intractable infinity onto a positive-curvature manifold, such as a triangle, or a sphere, or a donut-like manifold, arriving at a physical geometry useful in the physical sciences (see, e.g., Peters 2016a; Tozzi and Peters 2017b). Indeed, when the phenomenon's calculations tend towards infinity, we achieve an unwanted flat line. To go back to a tractable description, we need now to introduce a negative-curvature manifold, corresponding to a modified physical phenomenon, where finite operations might take place.

We would like to bring to an end with a prediction: an intellectually satisfying and experimentally meaningful resolution of the apparent conflicts between quantum mechanics and classical physics, including general relativity, will not be possible until the Euclidean conceptual barrier we have described in our paper is fully overcome (Bollinger, personal communication). In particular, recognizing that "time" must also be "unEuclidified" should rather dramatically alter how we perceive and use to represent both quantum and classical time, making them more of a continuum in which the level of temporal detail once again depends on the resources applied. By then, using mathematical abstractions that no longer relegate spatial and temporal uncertainty "only" to the quantum domain, many of the seemingly insurmountable barriers between quantum and classical quite likely will disappear.

Author's personal copy

References

Aleksandrov AD (1969) Non-Euclidean geometry. In: Alexsandrov AD, Kolmogorov AN, Lavrent'ev MA (eds) Mathematics: its content methods and meaning. The MIT Press, Cambridge. ISBN 0-486-40916-3

Armenta Salas M, Bashford L, Kellis S, Jafari M, Jo H et al (2018) Proprioceptive and cutaneous sensations in humans elicited by intracortical microstimulation. Elife 7:e32904. https://doi.org/10.7554/elife.32904

Autrecourt, Nicholas of. About 1340. The universal treatise. Marquette University Press, Milwaukee, Wisconsin, 1971

Barranca VJ, Huang H, Li S (2018) The impact of spike-frequency adaptation on balanced network dynamics. Cogn Neurodyn 13(1):105–120

Bergmann PG (1989) Quantum gravity at spatial infinity. Gen Relativ Gravit 21(3):271–278

Bollinger T (2018) Fundamental as fewer bits. FQXi essay contest 2017, Jan 2018. https://fqxi.org/data/essay-contest-files/Bollinger_FQXi_Essay_2017_.pdf

Bonzon P (2017) Towards neuro-inspired symbolic models of cognition: linking neural dynamics to behaviors through asynchronous communications. Cogn Neurodyn 11(4):327–353

Borsuk K (1958) Concerning the classification of topological spaces from the standpoint of the theory of retracts. FundamentaMathematicae XLVI:177–190

Borsuk K (1969) Fundamental retracts and extensions of fundamental sequences. FundamentaMathematicae 1:55–85

Bradwardine T (1330) about 1330, De continuo (On the Continuum). In: Murdoch JE (ed) geometry and the continuum in the fourteenth century: a philosophical analysis of Thomas Bradwardine's Tractatus de continuo. Ph.D. thesis, University of Wisconsin, 1957

Chamberlain BP, Clough J, Deisenroth MP (2017) Neural embeddings of graphs in hyperbolic space. arXiv:1705.10359

Chan B, Kawashima Y, Katouda M, Nakajima T, Hirao K (2016) From C60 to infinity: large-scale quantum chemistry calculations of the heats of formation of higher fullerenes. J Am Chem Soc 138(4):1420–1429

de Arcangelis L, Herrmann HJ (2010) Learning as a phenomenon occurring in a critical state. Proc Natl Acad Sci 107:3977–3981

de Arcangelis L et al (2006) Self-organized criticality model for brain plasticity. Phys Rev Lett 96:028107

de Cusa N (1997) 1440. De doctaignorantia. English translation. In: Bond HL (ed) Nicholas of Cusa: selected spiritual writings, classics of western spirituality. Paulist Press, New York

de Haro S, Dieks D, 't Hooft G, Verlinde E (2013) Forty years of string theory reflecting on the foundations. Found Phys 43(1):1–7

Di Concilio A (2013) Point-free geometries: proximities and quasi-metrics. Math Comput Sci 7(1):31–42. https://doi.org/10.1007/s11786-013-0140-2

Di Concilio A, Guadagni C, Peters JF, Ramanna S (2018) Descriptive proximities. Properties and interplay between classical proximities and overlap. Math Comput Sci 12:91–106. https://doi.org/10.1007/s11786-017-0328-y

Duff M (1996) M-theory (the theory formerly known as strings). Int J Mod Phys A 11(32):5623–5641

Duffy KR, Hubel DH (2007) Receptive field properties of neurons in the primary visual cortex under photopic and scotopic lighting conditions. Vis Res 47(19):2569–2574

Ehresmann C (1950) Les connexions infinitésimales dans un espace fibrée differentiable. Colloque de Topologie. Bruxelles, pp 29–55

Fournier J, Müller CM, Schneider I, Laurent G (2018) Spatial information in a non-retinotopic visual cortex. Neuron 97(1):164–180. https://doi.org/10.1016/j.neuron.2017.11.017

Fox KC, Spreng RN, Ellamil M, Andrews-Hanna JR, Christoff K (2015) The wandering brain: meta-analysis of functional neuroimaging studies of mind-wandering and related spontaneous thought processes. Neuroimage 1(111):611–621. https://doi.org/10.1016/j.neuroimage.2015.02.039

Frankel T (2011) The geometry of physics: an introduction, IIIrd edn. Cambridge University Press, Cambridge. ISBN 978-1-107-60260-1

Frauendiener, 2000. Conformal infinity. Living Reviews in Relativity, http://www.springer.com/us/livingreviews/articles/volume3/2000-4frauendiener

Friston K (2010) The free-energy principle: a unified brain theory? Nat Rev Neurosci 11(2):127–138

Geroch R, Kronheimer EH, Penrose R (1972) Ideal points in space-time. Proc R Soc London A 327:545–567

Helmholz H (1858) Uber integrale derhydrodynamicsGleichungenwelchederWirbelbewegungentsprechen. J fur die reine und angewandteMathematik, 55, 25–55, [On the integrals of the hydronamical equations, which express vortex motion], trans. by Tait PG. Phil Mag 33: 485–512

Iyer SV, Petters AO (2007) Light's bending angle due to black holes: from the photon sphere to infinity. Gen. Relativ. Grav. 39:1563–1582

Jirsa VK et al (2014) On the nature of seizure dynamics. Brain J Neurol 137:2210–2230

Johnstone PT (1983) The point of pointless topology. Bull Am Math Soc 8(1):41–53

Kelvin L (Thomson W) (1867) On vortex atoms. Proc R Soc Edinb 6:94–105

Kim S-Y, Lim W (2017) Dynamical responses to external stimuli for both cases of excitatory and inhibitory synchronization in a complex neuronal network. Cogn Neurodyn 11(5):395–413

Langevin P (1908) Sur la théorie du mouvementbrownien. C R Acad Sci Paris 146:530–533

Lesovik GB, Sadovskyy IA, Suslov MV, Lebedev AV, Vinokur VM (2019) Arrow of time and its reversal on the IBM quantum computer. Sci Rep 9:4396

Levi-Civita T (1917) Nozione di parallelismo in una varietà qualunque e conseguente specificazione geometrica della curvatura Riemanniana. Rend Circ Mat Palermo 42:73–205. https://doi.org/10.1007/bf03014898

Li H, Fang Q, Ge Y, Li Z, Meng J, Zhu J, Yu H (2018) Relationship between the dynamics of orientation tuning and spatiotemporal receptive field structures of Cat LGN Neurons. Neuroscience 377:26–39. https://doi.org/10.1016/j.neuroscience.2018.02.024

Lübeck S (2004) Universal scaling behavior of non-equilibrium phase transitions. Int J Mod Phys B 18:3977–4118

Mazade R, Alonso JM (2017) Thalamocortical processing in vision. Vis Neurosci 34:007. https://doi.org/10.1017/s0952523817000049

Milstein J et al (2009) Neuronal shot noise and Brownian 1/f2 behavior in the local field potential. PLoS ONE 4:e4338

Mizraji E, Lin J (2017) The feeling of understanding: an exploration with neural models. Cogn Neurodyn 11(2):135–146

Muxin H (2011) Cosmological constant in loop quantum gravity vertex amplitude. Phys Rev D 84(6):064010

Nagel T (1974) What is it like to be a bat? Philos Rev 83(4):435–450. https://doi.org/10.2307/2183914

Naimpally SA, Warrack BD (1970) Proximity spaces. Cambridge University Press, Cambridge

Papo D (2014) Functional significance of complex fluctuations in brain activity: from resting state to cognitive neuroscience. Front Syst Neurosci 8:112

Author's personal copy

Pavese F, Charki A (2016) Some important features of the proposed new definition of the International System of Units (SI): realization and hierarchical problems that the users should know about. Int J Metrol Qual Eng 7:403. https://doi.org/10.1051/ijmqe/2016023

Peters JF (2014) Topology of digital images: visual pattern discovery in proximity spaces. Springer, Berlin. https://doi.org/10.1007/978-3-642-57845-2

Peters JF (2016a) Computational proximity. Excursions in the topology of digital images. Springer International Publishing, New York City. https://doi.org/10.1007/978-3-319-30262-1

Peters JF (2016b) Two forms of proximal, physical geometry.Axioms, sewing regions together, classes of regions, duality and parallel fibre bundles. Adv Math Sci J 5(2):241–268

Peters JF, Tozzi A, Ramanna S, İnan E (2017) The human brain from above: an increase in complexity from environmental stimuli to abstractions. Cogn Neurodyn 11(4):391–394

Popkin RH, Maia Neto JR (eds) (2007) Skepticism: an anthology. Prometheus Books, Amherst. ISBN 1591024749, ISBN 13: 9781591024743

Pritchard WS (1992) The brain in fractal time: 1/f-like power spectrum scaling of the human electroencephalogram. Int J Neurosci 66:119–129

Rovelli C, Smolin L (1988) Knot theory and quantum gravity. Phys Rev Lett 61(10):1155–1958

Seiden A (2005) Particle physics. A comprehensive introduction. Addison-Wesley, Boston. ISBN 0-8053-8736-6

Sengupta B, Tozzi A, Cooray GK, Douglas PK, Friston KJ (2016) Towards a neuronal gauge theory. PLoS Biol 14(3):e1002400. https://doi.org/10.1371/journal.pbio.1002400

Shapiro S, Hellman G (2017) Frege meets aristotle: points as abstracts. Philos Math 25(1):73–90. https://doi.org/10.1093/philmat/nkv021

Simon M (1901) Euclid und die sechsplanimetrischen Bucher, vol 8. Teubner, Leipzig

Smirnov JM (1952) On proximity spaces. Math. Sb. (N.S.) 31(73):543–574 (Engish translation, Am Math Soc Trans Ser 2(38): 5–35 (1964)) (**in Russian**)

Sommers P (1978) The geometry of the gravitational field at space-like infinity. J Math Phys 19:549–554

't Hooft G (1971) Renormalizable Lagrangians for massive Yang-Mills fields. Nucl Phys B 35:167–188

Tait PG (1877) On knots. Trans R Soc Edinb 28:273–317

Tozzi A (2019) The multidimensional brain. Phys Life Rev. https://doi.org/10.1016/j.plrev.2018.12.004

Tozzi A, Peters JF (2016) A topological approach unveils system invariances and broken symmetries in the brain. J Neurosci Res 94(5):351–365. https://doi.org/10.1002/jnr.23720

Tozzi A, Peters JF (2017a) What does it mean "the same"? Prog Biophys Mol Biol. https://doi.org/10.1016/j.pbiomolbio.2017.10.005

Tozzi A, Peters JF (2017b) From abstract topology to real thermodynamic brain activity. Cogn Neurodyn 11(3):283–292

Tozzi A, Sengupta B, Peters JF, Friston KJ (2017) Gauge fields in the central nervous system. In: Opris J, Casanova MF (eds) The physics of the mind and brain disorders: integrated neural circuits supporting the emergence of mind. Series in cognitive and neural systems. Springer, New York. ISBN 978-3-319-29674-6

Tozzi A, Peters JF, Jaušovec N (2018) EEG dynamics on hyperbolic manifolds. Neurosci Lett 683:138–143. https://doi.org/10.1016/j.neulet.2018.07.035

Van Hooser SD, Heimel JA, Nelson SB (2005) Functional cell classes and functional architecture in the early visual system of a highly visual rodent. Prog Brain Res 149:127–145

Viswanathan P, Nieder A (2017) Visual receptive field heterogeneity and functional connectivity of adjacent neurons in primate frontoparietal association cortices. J Neurosci 37(37):8919–8928. https://doi.org/10.1523/jneurosci.0829-17.2017

Whitehead AN (1929) Process and reality. An essay in cosmology. The Free Press, New York

Wigner EP (1960) The unreasonable effectiveness of mathematics in the natural sciences. Richard Courant lecture in mathematical sciences delivered at New York University, May 11, 1959. Commun Pure Appl Math 13:1–14

Witten TA, Li H (1993) Asymptotic shape of a fullerene ball. Europhys Lett 23:51–55

Zaka O, Peters JF (2019) Isomorphic-dilations of the skew-fields constructed over parallel lines in the Desargues affine plane. arXiv, 1904, no. 01496, 1–15 DOI: arXiv:1904.01469v1

Zenginoglu (2007) A conformal approach to numerical calculations of asymptotically flat spacetimes. Dissertation, Mathematisch-NaturwissenschaftlichenFacultat der Universitat Potsdam and Max Planck Institut fur Gravitationphysic Albert Einstein Institute and arXiv 0711.0873v2, 2007

Publisher's Note Springer Nature remains neutral with regard to jurisdictional claims in published maps and institutional affiliations.

Article | Published: 18 September 2019

Electrical and synaptic integration of glioma into neural circuits

Humsa S. Venkatesh, Wade Morishita, Anna C. Geraghty, Dana Silverbush, Shawn M. Gillespie, Marlene Arzt, Lydia T. Tam, Cedric Espenel, Anitha Ponnuswami, Lijun Ni, Pamelyn J. Woo, Kathryn R. Taylor, Amit Agarwal, Aviv Regev, David Brang, Hannes Vogel, Shawn Hervey-Jumper, Dwight E. Bergles, Mario L. Suvà, Robert C. Malenka & Michelle Monje

Nature **573**, 539–545 (2019) | Download Citation

21k Accesses | **6** Citations | **884** Altmetric | Metrics

Abstract

High-grade gliomas are lethal brain cancers whose progression is robustly regulated by neuronal activity. Activity-regulated release of growth factors promotes glioma growth, but this alone is insufficient to explain the effect that neuronal activity exerts on glioma progression. Here we show that neuron and glioma interactions include electrochemical communication through bona fide AMPA receptor-dependent neuron–glioma synapses. Neuronal activity also evokes non-synaptic activity-dependent potassium currents that are amplified by gap junction-mediated tumour interconnections, forming an electrically coupled network. Depolarization of glioma membranes assessed by in vivo optogenetics promotes proliferation, whereas pharmacologically or genetically blocking electrochemical signalling inhibits the growth of glioma xenografts and extends mouse survival. Emphasizing the positive feedback mechanisms by which gliomas increase neuronal excitability and thus activity-regulated glioma growth, human intraoperative electrocorticography demonstrates increased cortical excitability in the glioma-infiltrated brain. Together, these findings indicate that synaptic and electrical integration into neural circuits promotes glioma progression.

Associated Content

Nature | News & Views

Dangerous liaisons as tumour cells form synapses with neurons

Andres Barria

Sections | Figures | References

Abstract
Data availability
Code availability
References
Acknowledgements
Author information
Ethics declarations
Additional information
Extended data figures and tables

Ethics declarations
Additional information
Extended data figures and tables
Supplementary information
Source data
Rights and permissions
About this article
Further reading
Comments

1 Comment | Nature | Arturo Tozzi cns

Recommend | Tweet | Share | Sort by Newest

Start the discussion…

Arturo Tozzi cns • 7 minutes ago

CANCER AND EVOLUTION?

Given the ability of different tumours to produce electric synapses (see the papers in this special Issue, apart from this one: https://www.nature.com/arti..., https://www.nature.com/arti..., https://www.nature.com/arti..., https://www.nature.com/arti..., one might wonder whether such ability might have had evolutionary importance in the development of the central nervous systems (CNS) of Primates, and, in particular, humans.
Indeed, it could be at least theoretically hypothesized that (low-grade?) tumours might successfully be inserted in the hosts' CNS and, instead of causing death or functional impairment, to provide an evolutionary advantage, e.g., in terms of increased neuronal connections and/or improved neural functions.

Arturo Tozzi
Center for Nonlinear Science, Department of Physics, University of North Texas, Denton, Texas, USA
tozziarturo@libero.it
Arturo.Tozzi@unt.edu

Abstract
Data availability
Code availability
References
Acknowledgements
Author information
Ethics declarations
Additional information
Extended data figures and tables
Supplementary information
Source data
Rights and permissions
About this article
Further reading
Comments

Progress in Biophysics and Molecular Biology 150 (2020) 153–159

Contents lists available at ScienceDirect

Progress in Biophysics and Molecular Biology

journal homepage: www.elsevier.com/locate/pbiomolbio

Towards dewetting monoclonal antibodies for therapeutical purposes

Tozzi Arturo

Center for Nonlinear Science, Department of Physics, University of North Texas, 1155 Union Circle, #311427, Denton, TX, 76203-5017, USA

ARTICLE INFO

Article history:
Received 28 May 2019
Received in revised form
22 August 2019
Accepted 7 September 2019
Available online 13 September 2019

Keywords:
Influenza a virus
Immunology
Immunotherapy
Receptor
Tumors

ABSTRACT

Dewetting transition - a concept borrowed from fluid mechanics - is a physiological process that takes place inside the hydrophobic pores of ion channels. This transient phenomenon causes a metastable state that forbids water molecules to cross microscopic receptor cavities. This leads to a decreased conductance, a closure of the pore and, subsequently, severe impairment of cellular performance. We suggest that artificially-provoked dewetting transition in ion channel hydrophobic pores might stand for a molecular candidate to erase detrimental organisms, such as viruses, bacteria, and cancer cells. We describe a novel type of high-affinity monoclonal antibody, that: a) targets specific trans-membrane receptor structures of harmful or redundant cells; b) is equipped with lipophilic and/or hydrophobic fragments that prevent physiological water flow inside ion channels. Therefore, we achieve an artificial dewetting transition inside receptor cavities, that causes discontinuity within transmembrane ionic flows, channel blockage, and subsequent damage of morbid cells. As an example, we describe dewetting monoclonal antibodies that target the M2 channel of the Influenza A virus: they might prevent water from entering pores thus leading to virion impairment.

© 2019 Elsevier Ltd. All rights reserved.

Contents

1. Factors influencing dewetting in physical systems . . . 154
2. Dewetting phenomena in biological structures . . . 155
3. Dewetting monoclonal antibodies come into play . . . 156
4. Conclusions . . . 158
Aknowledgements . . . 158
References . . . 158

In fluid mechanics, dewetting is a process occurring at solid–liquid or liquid–liquid interfaces. Dewetting stands for the rupture of the thin, liquid continuous film on the substrate surface, leading to formation of irregular patterns of droplets. The opposite process is called spreading. Four stages can be recognized as dewetting proceeds (Sharmaa and Reiterb (1996)): (a) film rupture; (b) hole expansion and coalescence to form a polygonal "cellular" pattern. The dry patches augment when the material is gathered in the rim surrounding the growing hole; (c) disintegration of polymer ridges into spherical drops, due to Rayleigh instability. The droplets size and spacing may vary over several orders of magnitude, since dewetting process starts from randomly formed holes inside the film. A two-tier surface exhibits a two-stage wetting transition: first impalement at microscale texture, then at nanoscale; (d) fingering instability of hole rims during their expansion (Sharmaa and Reiterb (1996)).

This process, borrowed by physics, has been recently extended to describe also microscopic biological phenomena. In particular, dewetting transitions may occur inside the hydrophobic pores of cellular ion channels. In the narrowest, more hydrophobic parts of receptor holes, a metastable state of dewetting transition forbids water molecules to get inside the cavities, leading to a decrease in conductance channel closure, and impairment of cellular activity. We show how this peculiar process can be artificially produced to alter the physiological activity of noxious pathogens, such as

E-mail addresses: tozziarturo@libero.it, Arturo.Tozzi@unt.edu.

https://doi.org/10.1016/j.pbiomolbio.2019.09.001
0079-6107/© 2019 Elsevier Ltd. All rights reserved.

viruses, bacteria and tumoral cells. In particular, we suggest the manufacture of monoclonal antibodies (against cellular receptors) equipped with lipophilic/hydrophobic caps. In the sequel, we will term these antibodies DEMA (DEwetting Monoclonal Antibodies). Once they link monoclonal targets, their artificial hydrophobic device blocks water flow inside receptors, contributing to malfunction of pathological organisms.

1. Factors influencing dewetting in physical systems

Various physical processes cause, modify and interphere with dewetting phenomena. One of the most important factors is the **spreading coefficient**. It settles on the spontaneous spreading and dewetting for an oil drop placed on a liquid substrate (i.e., water) with ambient gas. The formula of such coefficient S is (Rosen, 2004; Leroux et al., 2008):

$$S = \gamma_{gw} - \gamma_{go} - \gamma_{ow}$$

where γ_{gw} is the gas-water surface tension, γ_{go} is the gas-oil surface tension and γ_{ow} is the oil water surface tension (measured inside the fluids before they are brought in contact). When $S > 0$, spontaneous spreading occurs; in turn, dewetting occurs for $S < 0$. In most dewetting experiments, a thin polymer film is spun onto a substrate. Even in case of $S < 0$, the film does not dewet immediately when located in a metastable state, e.g., when the temperature is below the polymer glass transition temperature. Annealing this metastable film above its glass transition temperature increases the mobility of the polymer-chain molecules, leading to dewetting (Karapanagiotis and Gerberich, 2005).

Temperature. Solid films are usually metastable or unstable in their deposited state. When heated to higher temperatures, they dewet or agglomerate to form islands (Thompson, 2012). This process, driven by surface energy minimization, occurs via surface diffusion well below a film melting temperature, especially when the film is very thin. Films pre-patterning may contribute to the building of ordered arrays of particles and complex patterns of partially dewetted structures, providing insights into the effects of surface energy anisotropy and facets on shape evolution (Thompson, 2012).

Type of substrate (at room temperature). Rahe et al. (2012) reported the formation of extended molecular layers of C(60) molecules on a dielectric surface at room temperature. In sharp contrast to previous C(60) adsorption studies on prototypical ionic crystal surfaces, a wetting layer was obtained, when calcite (CaCO(3))(10 14) surface is chosen as the substrate. Non-contact atomic force microscopy data confirms an excellent match between hexagonal lattice of the molecular layer and peculiar unit cell dimensions. The difference observed microscopically upon C(60) adsorption on CaCO(3)(10 14) compared to other dielectric surfaces was explained by a macroscopic picture that takes into account surface energies. This example demonstrates that a simple surface-energy based approach provides a valuable estimate for choosing molecule-insulator systems suitable for molecular self-assembly at room temperature (Rahe et al., 2012).

Hole growth, fingering instability, drop diameters and film thickness. Sharmaa and Reiterb (1996) found an excellent match between theoretical predictions and experimental results concerning instabilities and various stages of dewetting of thin (<60 nm) films on coated substrates. Thin polystyrene films (>10 nm), prepared on silicon wafers with three different nano-sized (~1 nm) coatings, dewet spontaneously above the glass transition temperature, leading to the growth of cylindrical holes with wavy rims. In the case of films that are much thicker than the coating, the wettability of the substrate by polystyrene has no influence on the number density of holes. This is explained by the dominating influence of long-range Lifshitz–van der Waals interactions originating from the bulk substrate. In later stages, polygon diameter is rather independent of the coating: this is explained by the insensitivity of the first stages to the coating properties and by the competition between Rayleigh instability (leading to droplets) and drainage from ridges (leading to coalescence). On the contrary, hole growth, fingering instability and drop diameters are highly affected by the surface properties (wettability) of coatings. An increase in film thickness (h) decreases the number density of initial holes ($\alpha h-4$), increases the polygon diameter ($\alpha h2$), augments the drop diameter, and makes the fingering instability stronger.

Wettability of the fluid, vibration, superhydrophobic structures. Several natural superhydrophobic structures display hierarchical two-tier roughness (Boreyko et al., 2011). The wetting and dewetting properties of two-tier roughness is a function of working fluid wettability, where the surface tension of water/ethanol drops is tuned by the mixing ratio. When the ethanol concentration of deposited drops was gradually increased on one-tier control samples, the impalement of the microtier-only surface occurred at a lower ethanol concentration, compared with the nanotier-only surface. The corresponding two-tier surface exhibited two-stage wetting transition, first due to impalement of the microscale texture, then to the nanoscale one. Subsequently, the impaled drops were subjected to vibration-induced dewetting. Both drops impaling one-tier surfaces and two-tier roughness could not be dewetted. However, on the two-tier surface, drops impaling just the microscale roughness exhibited a full dewetting transition upon vibration. Therefore, it has been suggested that two-tier roughness is essential for preventing catastrophic, irreversible wetting of superhydrophobic surfaces (Boreyko et al., 2011).

Electrowetting and detachment of droplets from solid surfaces. Electrowetting on superhydrophobic surfaces (EWOSS) can be generated by an alternating current signal, often leading to droplet impalement (Lapierre et al., 2013). To avoid this unwanted occurrence, either superhydrophobic surfaces must show robustness to high pressure, or an external energy must be used to dewet the droplets. Lapierre et al. (2013) described a novel approach to actuate liquid droplets via a modulated EWOSS signal (MEWOSS). This technique, that allows dewetting caused by periodic vibrations induced through electrowetting actuation, permits the investigation of a huge range of superhydrophobic surfaces. Detachment of droplets from solid surfaces is a a crucial process in practical applications, such as heat transfer and digital microfluidics. Electrowetting actuations with square pulse signals were used to detach droplets from hydrophobic surfaces (Lee et al., 2014). The threshold voltage for droplet detachment turned out to be almost constant for various droplet volumes ranging from 0.4 to 10 μL. Also, droplets can be detached more easily when the width of applied pulse is well-matched to the spreading time. When the droplet was actuated by a double square pulse, the threshold voltage was reduced by ~20% from that for a single square pulse actuation. Finally, droplets can be detached from the solid bottom surface without using a top needle electrode (Lee et al., 2014).

Active matter wetting transition. Sándor et al. (2017) showed that, in the presence of random pinning substrates, sterically interacting self-propelled disks exhibit transitions among different states. In particular, we are in front of an example of active matter wetting transition: starting from a phase of separated cluster state, the disks can spread out and homogeneously cover the substrate. This transition is regulated by disk density, substrate strength, cluster size (that dips at the wetting-dewetting transition) and fraction of sixfold coordinated particles (that drops when dewetting occurs) (Sándor et al., 2017).

In sum, a huge range of physical factors, that can be fine-tuned in experimental settings, may contribute to the attainment and preservation of dewetting regimes in countless systems equipped with solid–liquid or liquid–liquid interfaces. In the sequel, the above-mentioned phenomena will permit us to build strategies to influence the dynamics of droplet formation inside biological channels of pathogenic agents.

2. Dewetting phenomena in biological structures

Dewetting processes have been identified in many biological contexts. In case of living agents, dewetting occurs at solid-liquid interface (i.e., cellular structures and the water surrounding them). Dewetting contributes to cellular layer stability and mechanical responses, therefore representing a physiological process that contributes to metabolic patterns and homeostasis. Cellular layer stability was investigated by Douezan and Brochard-Wyart (2012), who showed that cohesive cellular layers deposited on non-adhesive substrates are metastable and dewet with a mechanism of nucleation and growth of dry patches. Two mechanisms contribute to compromise the integrity of cellular layers: indeed, dewetting can be induced either chemically by a non-adhesive surface treatment, or physically by a decrease in the substrate rigidity. The interpretation of cellular opening dynamics in terms of dewetting of viscous films can be used to estimate parameters characterizing the mechanical response of cellular layers.

Cell–cell and cell–tissue contacts between extracellular matrix and cell surface glycocalix. Cell adhesion is controlled by an interplay among membrane elasticity, short-range (lock-and-key) forces mediated by cell surface receptors and short-/long-range nonspecific interactions (Sackmann and Bruinsma, 2002). Cell adhesion, once explored through simplified models that mimic cell and tissue surfaces, enable local measurements of cellular shape changes and adhesion forces. Cell adhesion can be described in terms of first-order dewetting transitions that allow formation of adhesion plaques and permit very low receptor densities. The glycocalix repeller molecules, with their dewetting force, play a key role for the control of adhesion transition and mechanical stability of the adhering cells, by relaxing the strength of the binding forces. Because the stress fibers that stabilize adhesion domains are counteracted by leverage enforced by hydrodynamic shear forces (Sackmann and Bruinsma, 2002), this means that dewetting processes stand for a crucial issue in cell adhesion.

Tanaka et al. (2005) assessed wetting and dewetting of hydrated biopolymer layers mediating cell–cell and cell–tissue contacts, i.e., the extracellular matrix and the cell surface glycocalix. The sum of the net effects of the various interfacial forces, that is referred to as the disjoining pressure, was used as a semi-quantitative measure to describe the thermodynamics of hydrated interlayers. Disjoining pressures were measured through external forces to maintain the equilibrium distance between two parallel surfaces (in case of living cells, the two parallel surfaces stand for two neighboring plasma membranes). Using artificial models of extracellular matrix and glycocalix, Tanaka et al. (2005) described stable cell–cell contacts in terms of the wetting (or spreading) of complex fluids on polymer surfaces. The adjustment of wetting interactions via thin hydrating layers enabled them to transform three-dimensional cell membranes into quasi-two-dimensional films on macroscopically large surfaces. Fine-tuning of local conditions at the interface allowed selective wetting of native cell membranes on microstructured polysaccharide films. In sum, this approach suggests a large potential for individual detection of biological functions in confined geometries.

Substrate stiffness. On a surface, living tissues can either form a droplet-like cell aggregate or spread as a monolayer of migrating cells (Alert and Casademunt, 2018). These processes of tissue wetting and/or spreading depend on the mechanical properties of the substrate, such as stiffness. Taking into account that cells exert larger active traction forces, Alert and Casademunt (2018) showed the occurrence of tissue wetting transition at a critical substrate stiffness that decreases with tissue size. On substrates with stiffness gradient, the tissue spreads faster on the stiffer side. Furthermore, the tissue can wet the substrate on the stiffer side, while dewetting from the softer one. The stiffer-side interface can transiently drag the softer-side interface toward increasing stiffness, against its spreading tendency. These two effects related to stiffness gradients result in directed tissue migration, i.e., a phenomenon that can be produced by both dewetting on the soft side and hydrodynamic interactions between tissue interfaces.

Lipid bilayers and droplets. The behavior of lipid bilayer is crucial to understand biological processes such as ions trafficking between cells (Vargas et al., 2014). The standard procedures to explore the properties of lipid bilayer and hemifused states, that typically use either supported membranes or vesicles, have several shortcoming in terms of bio-relevance or accessibility for measurements. Vargas et al. (2014) studied the formation of individual free-standing hemifused states between cell membranes, using an optimized microfluidic scheme that allows for simultaneous optical and electrophysiological measurements. At first, two model membranes were formed at a desired location within a microfluidic device, using a variation of the droplet interface bilayer technique. Then, the two model membranes were brought into contact, forming a single hemifused state. For all tested lipids, the hemifused state between free-standing membranes was created within hundreds of milliseconds, i.e. several orders of magnitude faster than previously reported. Formation of hemifused state was a two stage process, whereas the second stage can be explained as a dewetting process in no-slip boundary condition. The formed hemifusion states are long-living and can be triggered by the proper electric fields (Vargas et al., 2014).

Lipid droplets, i.e., the dispersed phase of an oil-in-water emulsion in aqueous cytosol, are almost ubiquitous intracellular organelles with fundamental roles in cellular metabolism. They store oil-based reserves of metabolic energy and components of membrane lipids. Lipid droplets are. Their unique architecture is characterized by an interface between the dispersed oil phase and the aqueous cytosol, that permits dewetting. This mechanism enables cells to use emulsified oil according to their requirements for metabolic energy or membrane synthesis. The regulation of phospholipid surfactants composition at the surface of lipid droplets is crucial both for their own homeostasis and for protein targeting to their surfaces (Thiam et al., 2013). This emphasizes the importance of basic biophysical principles of emulsions for lipid droplet biology.

Opening of transendothelial cell macroapertures (TEMs) in pathogenic bacteria. Pathogenic bacteria can cross from blood vessels to host tissues by opening of TEMs. To induce TEM opening, bacteria intoxicate endothelial cells with proteins that disrupt their contractile cytoskeletal network. Cell membrane tension is no longer resisted by contractile fibers, leading to the opening. Gonzalez-Rodriguez et al. (2012) modeled the opening of TEMs as a new form of dewetting. Their model predicted the minimum radius for hole nucleation, the maximum TEM size, and the dynamics of their opening, in agreement with experimental data. The physical model was then coupled with biological experimental data to reveal that proteins missing in metastasis control the line tension at the rim of the TEM and opposes its opening. More, their studies clearly show that, while liquid dewetting is irreversible, cellular dewetting is transient.

Hydrophobic binding cavity of protein active sites, channels

and receptors. The interactions of proteins and their phase behavior are influenced by their own relationships with the surrounding hydration waters. Rego et al. (2019) found that, akin to extended hydrophobic surfaces, proteins situate their hydration waters at the edge of a dewetting transition, making them susceptible to unfavorable perturbations. The strength of the unfavorable potential needed to trigger dewetting is roughly the same for all the assessed proteins, depending just on the width of the hydration shell being perturbed (Rego et al., 2019). Analyzing the solvation of protein active sites, Young et al. (2010) observed a drying transition in the narrow hydrophobic binding cavity of Cox-2. They identified five proteins that, in molecular dynamics simulations, underwent drying transitions in their active sites. Because these cavities need not to desolvate before binding hydrophobic ligands, they often exhibit very large binding affinities. Furthermore, the Authors demonstrated that drying in protein cavities is not unique to Cox-2. The dynamics of confined water in capillaries and nanotubes suggests that ion cell gating may involve not just modifications in the pore geometry, but also transitions between water-filled and empty states. Webb et al. (2015) studied the molecular mechanisms of GoSlo-SR-5-6, a novel large-conductance Ca2+-activated K+ channel agonist. According to their results, the bulky D ring of GoSlo inserts into a hydrophobic pocket between the S4S5L and S6C and perturbs the interaction between these two regions, resulting in channel opening and voltage sensor activation. A straightforward explanation supporting their suggestion could be a state of dewetting transition.

To provide another example from human pathogens, the heptameric structure of the small mechanosensitive channel of Escherichia coli (MscS) displays a relatively wide (7–15 Å), yet highly hydrophobic, transmembrane pore, that exhibits dewetting and low conductance (Anishkin and Sukharev, 2004). Indeed, irrespective of the initial conditions, simulations converged towards the same state of intermittent vapor-liquid transitions. The pore is water-filled in the wider part and empty in the narrow hydrophobic hole. The polar gain-of-function substitution L109S resulted in a stable hydration of the entire pore. Steered passages of Cl(−) ions through the narrow part of the pore consistently produced partial ion dehydration, when the proper force of 200–400 pN was used. This means that the crystal MscS structure does not represent an open state, and that the MscS gate (that is similar to the nicotinic ACh receptor) involves a vapor-lock mechanism. This means that limited changes of geometry or surface polarity can locally switch the regime between water-filled (conducting) and empty channels.

Summarizing this Section, a straightforward conclusion can be drawn. When water and ions are enclosed within the subnanometer, narrow cellular confines of a ion channel hydrophobic pore, they exhibit an odd behavior (Aryal et al., 2015): near a critical point, a stochastic liquid-vapor water phase transitions takes place (Anishkin and Sukharev, 2004). These transient vapor states are "dewetted", i.e. devoid of water molecules within all, or part of, the pore. The crucial question is: what are the physiological implications of the dewetting transitions taking place inside the ion channels of living cells? The decreased amount of water molecules inside receptors leads to impaired conductance, energetic barriers to ion transit and closure of the channel, in a process termed "hydrophobic gating". It is noteworthy that the principles underlying the metastable dynamical state of hydrophobic gating require a very small tube radius and interactions with a strongly hydrophobic lining (Lapierre et al., 2013).

3. Dewetting monoclonal antibodies come into play

The recently-developed concept of "supramolecular chemistry" suggests that complex chemical entities, including the ones correlated with dewetting transition, can be reversibly built, starting from molecular components bound together by labile non-covalent interactions (Lehn, 2007; Tozzi, 2015). Through self-organized, self-assembled and dynamic transitory processes, the storage of information occurs at the molecular level, while its retrieval, transfer and processing at the supramolecular one. Crowding-induced changes in self-assembling macromolecules point towards systems capable of generating well-defined functional supramolecular architectures (Foffi et al., 2013). Sequential self-organization on increasing scale in non-equilibrium systems leads to the emergence of novel features/properties at each level. Incorporating dewetting transitions in this perspective appears particularly relevant for the development of novel drugs. In this Section, we consider the possibility to build high-affinity monoclonal antibodies able to dewet the ion channels of target cells, thus leading to their impairment and, possibly, death. Antibodies with high affinity for receptors of pathological cells could be equipped with lipophilic structures, covalently attached, e.g., to their Fc region. These hydrophobic/lipophilic components must serve two purposes: a) to prevent water to penetrate inside the receptor ionic channels; b) to avoid immune Fc-mediated responses. In plain terms, we could state that, thanks to DEMA, a sort of cork provides a tight seal that prevents water to fill the receptor channels of pathogenic cells, causing collapse of unwanted organisms. DEMA could be used to counteract different types of pathogenic cells, such as viral, bacterial and tumoral ones. In the sequel, we will provide the example of Influenza A M2 proton channel, in an effort to develop a novel drug able to neutralize the virion.

An example: building DEMA against influenza A virus M2 receptor. The transmural, pH-regulated Matrix-2 (M2) proton channel is a crucial element of influenza A virus envelope (Pielak and Chou, 2011; Rossman et al., 2010). The M2 channel is a homotetramer consisting of helices stabilized by two disulfide bonds. The extracellular N-terminal domain encompasses the residues 1–23, while the transmembrane segment (TMS) (residues 24–46) forms the pore of the ion channel and is one of the targets of amantadine (Fig. 1, **bottom**). In turn, the intracellular C-terminal domain (residues 47–97) plays roles in virus budding and assembly. The crucial residues are the imidazole of His37 (pH sensor) and the indole of Trp41 (gate). Activated by low pH, M2 leads to proton conductance essential for viral replication. Furthermore, M2 regulates the virion core acidity, contributes to receptor-mediated endocytosis, promotes viral replication inside the nucleus of the infected cell, supplies the formation of filamentous strains, membrane scission, stabilization and release of the budding virion (Thomaston et al., 2015; Ichinohe et al., 2010). M2 is the target of several broadly neutralizing antibodies against influenza A, even if clinical results are still lacking and/or under clinical development (Cho and Wrammert, 2016; Fiers et al., 2009). M2 is the target of anti-influenza A drugs too. In particular, aminoadamantanes are specific M2 channel blockers that lead to incomplete viral uncoating an failure in promoting infection (Cady et al., 2010). However, the M2 gene is susceptible to relatively frequent mutations, so that the emergence of resistant strains has led to partial discontinuation of aminoadamantanes (Homeyer et al., 2016).

We suggest to use DEMA as a novel drug against all the strains of Influenza A (Fig. 1, **top**). The very structure of M2 let us hypothesize that a monoclonal antibody that prevents water to enter the M2 channel might disrupt Influenza A pathogenetic activity. Indeed, water plays a foremost role in M2 functioning (Fig. 2A). The channel, highly selective for protons, is activated by low pH and has a low conductance. Conduction mechanism involves: a) the exchange of protons between the His37 imidazole moiety, responsible for proton selectivity and pH modulation, and b) the water confined to the M2 bundle interior. Water molecules within the pore form

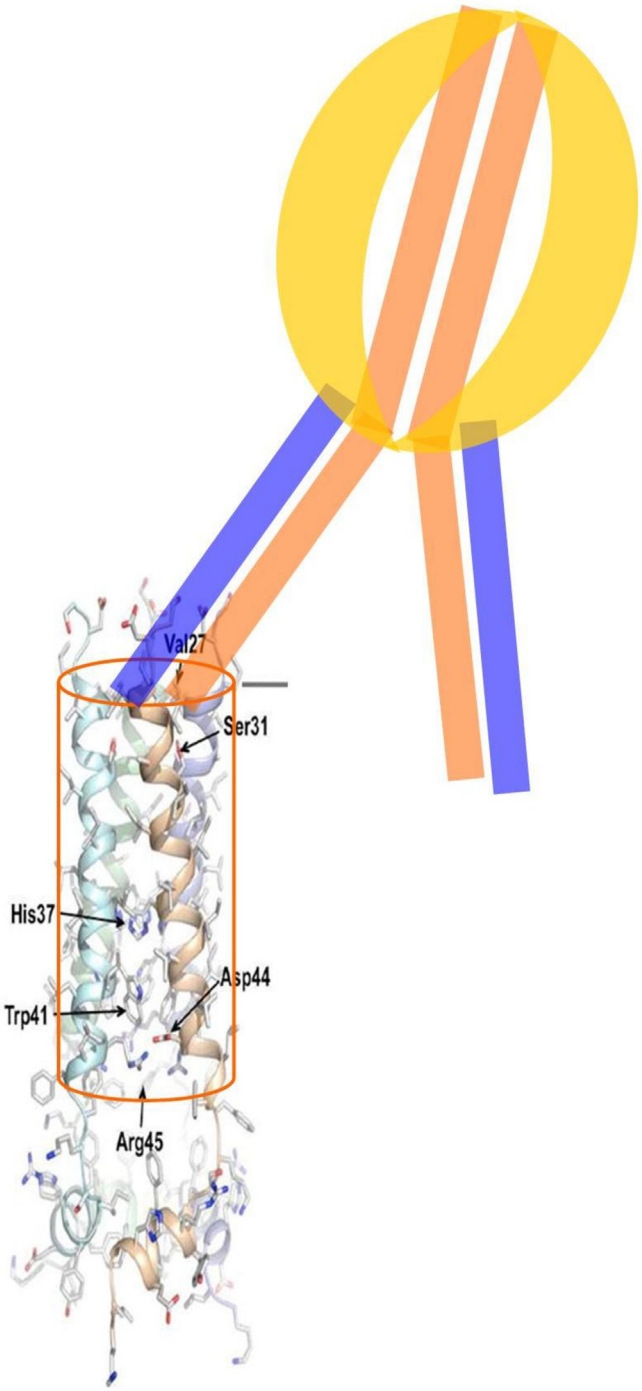

Fig. 1. Bottom: high resolution structures of the AM2 channel domain. Solution structure of residues 18–60 in 1,2-Dihexanoyl-sn-Glycero-3-Phosphocholine micelles at pH 7.5 (Modified from Pielak and Chou, 2011). **Top**: Dewetting antibody (DEMA) against the Val27 area. The Fc region of this artificial antibody is surrounded by an hydrophobic structure (yellow shape). Channel and antibody are drawn to scale: the transmembrane section (red cylinder) is about 30 Å long.

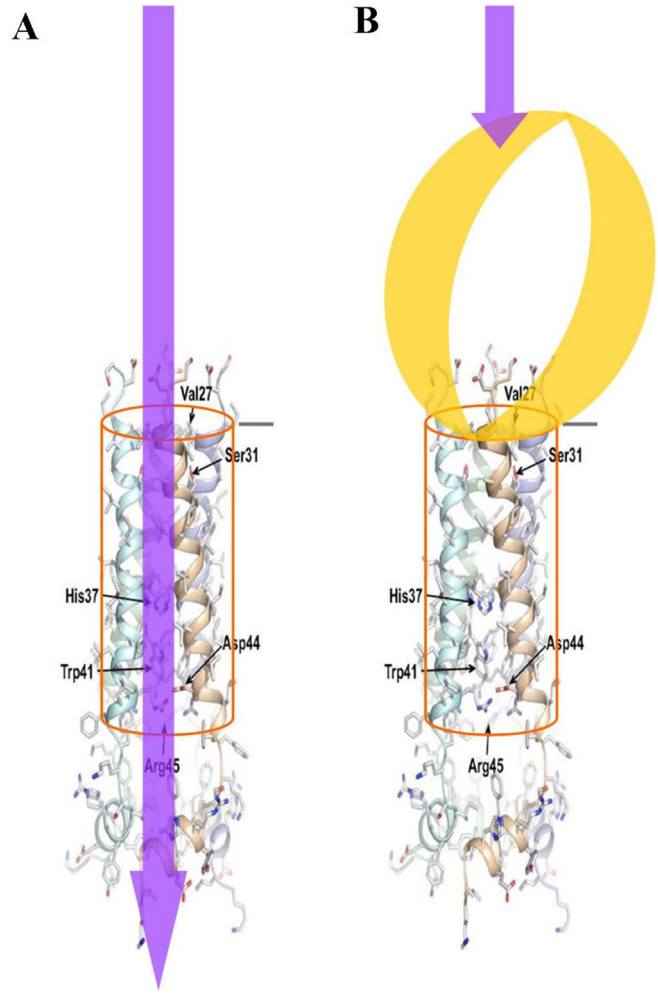

Fig. 2. Water flow inside M2 channel. **2A**: In physiological conditions, water is allowed to flow inside the M2 channel, giving rise to proton gradients crucial for pathogenic activity of Influenza A virus. **2B**: When a DEMA targets the upper part of the M2 receptor, its hydrophobic component prevents water to go through the M2 receptor channel (**right side**), leading to impairment of virionic metabolic pathways.

hydrogen-bonded networks or "water wires", from the channel entrance to His37. When a proton gradient occurs, conformational changes facilitate asymmetric diffusion through the channel. Indeed, protons diffusing through the channel need not be localized to a single His37 imidazole, but rather they may be delocalized over the entire His-box and associated water clusters. Furthermore, pore-lining carbonyl groups stabilize hydronium ions through second-shell interactions that involve the bridging of water molecules. A ring of methyl groups from Val27 tightens the N-terminal side of the pore to ~3.1 Å, narrowing the entrance and preventing water molecules from penetrating the channel (Pielak and Chou, 2011). Small motion or "channel breathing" may thus be required for water to enter the pore. It is widely accepted that water molecules are needed inside the channel cavity for supporting proton conduction. Water molecules, provided with a diameter of ~3 Å, start to exhibit liquid–vapor transitions and stochastic switches between wet and dry states within a hydrophobic pore of diameter less than ~14 Å. The most dynamic range for these transitions is between 9 and 12 Å: below this range, the pore will be largely dewetted (Aryal et al., 2015). The pore widens after Ser31 and becomes the widest at Gly34 position, that is equipped with an inner diameter of ~6 Å. The channel then narrows towards the C terminus, as the sidechains of His37 and Trp41 constrict the inner diameter to 1.7 and 1.4 Å, respectively.

The presence of a hydrophobic (or lipophilic) part located on the constant chain of DEMA, could, according to our theoretical previsions, stop water flow inside the M2 channels (Fig. 2B), leading to viral malfunction and, possibly, removal from the infected human body.

4. Conclusions

We showed how dewetting transition, characterized by an unusual behavior of water supramolecular assembly, stands for an increasingly important principle that has been already used to assess countless morphological and/or functional biological structures, such as protein cavities, extracellular matrix and glycocalix, lipid droplets, lipid bilayers, cell adhesion, macroapertures opening in endothelial cells. In the narrowest, more hydrophobic part of cellular channels, a metastable state of dewetting transition of water molecules takes place, leading to decrease of conductance and closure of the pore.

Several clues point towards the occurrence of dewetting transitions also in nervous cells. Indeed, it is believed that dewetting transition might occur in a wide range of ion channel receptors of the central nervous system (Aryal et al., 2015; Tozzi et al., 2016). Here we provide a few examples:

a) Pentameric ligand-gated ion channels (PLGC), that mediate fast neurotransmission in the nervous system. Nerve signaling in humans and chemical sensing in bacteria both rely on the controlled opening and closing of the ion-conducting pore in PLGC (Zhu and Hummer, 2010).
b) Tetrameric "P-loop" cation channels. This superfamily encompasses various potassium, sodium, and calcium selective channels, the non-selective TRP and cyclic-nucleotide-gated channels. The ability of these channels to select between different cations and to be gated by a diverse range of biochemical and biophysical stimuli enables them to play fundamental roles in the control of nearly all forms of cellular electrical activity.
c) Voltage-gated potassium channels.
d) Small conductance and large conductance Ca2+-activated channels.
e) MthK channels.
f) Two-pore domain channels: this is another subfamily of potassium channels thought to lack a classical bundle-crossing gate.
g) TWIK-1.

Neuronal activity is mediated through changes in the probability of stochastic transitions between open and closed states of ion channels (Cannon et al., 2010). Dewetting transition could lead to increase of inhibition in neurons, therefore influencing the inhibitory/excitatory (E/I) ratio (Xue et al., 2014). Excitation and inhibition are always matched: an optimal E/I ratio across neurons is maintained, despite fluctuating cortical activity levels, through the appropriate strengthening or weakening of inhibitory synapses. E/I ratio is stable, both in vitro and in the intact and spontaneously active cerebral cortex, not only in individual pyramidal neurons (Haider et al., 2006), but also across multiple cortical neurons (Xue et al., 2014) and during neural avalanches (Lombardi et al., 2012). The relationships between the two opposing forces in the mammalian cerebral cortex affect several cortical functions, such as feature selectivity and gain (Xue), memory of past activity. E/I ratio could thus be interpreted as the evidence of a homeostatic mechanism between strengthening and weakening processes in the adaptation of real synapses, both at the single neuron state and at the network excitability level (Lombardi et al., 2012; Tognoli and Kelso, 2014). Therefore, dewetting transition may stand for an important regulatory mechanism, that, influencing neuronal E/I ratio, allows the physiological activities of the brain. The possibility to modulate dewetting transitions through DEMA could be used to counteract neurological diseases through fresh developed drugs.

Our account of dewetting transition paves the way for innovative strategies. To make an example, dewetting enables researchers to build synthetic asymmetric model membranes with lipid composition/architecture that mimics the outer membrane of human pathogens, such as Pseudomonas aeruginosa. Maktabi et al. (2019) described a microfluidic technique for fabricating monodisperse asymmetric giant unilamellar vesicles, equipped with Gram-negative bacterial outer membrane lipid composition. They generated 50–150 μm diameter water-in-oil-in-water double emulsions that simulate the inner and outer leaflets of the lipid bilayer (Maktabi et al., 2019). Extraction processes by ethanol and micropipette aspiration triggered adhesive interaction between the two lipid monolayers assembled on the water-oil and oil-water interfaces (i.e., dewetting transition), forcing them to contact and to form lipid bilayer membranes that resemble Gram negative bacterial walls.

The last, but not the least, dewetting mechanisms can be used to achieve novel therapeutic weapons against a wide range of diseases. Apart from the above-described DEMA, other totally different approaches might take advantage of dewetting transitions. The possibility to artificially modulate dewetting processes could lead to the development of new drugs (with mechanisms different from DEMA) that might be relevant in development, regeneration, self-immunity, infection and cancer. For example, dewetting can be inhibited or prevented by factors other than DEMA: e.g., by photocrosslinking the thin film prior to annealing, or by incorporating nanoparticle additives into the film, or by modifying temperature, vibration, alternating currents, and so on. Also, surfactants may have a significant effect on the spreading coefficient: as more surfactant molecules are absorbed into the interface, the system free-energy decreases together with surface tension, eventually causing the system to become completely wet. And vice versa.

Aknowledgements

I would like to thank Jose Joaquim Souza Melo, who made me aware of dewetting transition.

References

Alert, R., Casademunt, J., 2018. Role of substrate stiffness in tissue spreading: wetting transition and tissue durotaxis, 2018 Oct 25 Langmuir. https://doi.org/10.1021/acs.langmuir.8b02037 [Epub ahead of print].
Anishkin, A., Sukharev, S., 2004. Water dynamics and dewetting transitions in the small mechanosensitive channel MscS. Biophys. J. 86 (5), 2883–2895, 2004 May.
Aryal, P., Sansom, M.S., Tucker, S.J., 2015. Hydrophobic gating in ion channels. J. Mol. Biol. 427 (1), 121–130. https://doi.org/10.1016/j.jmb.2014.07.030.
Boreyko, J.B., Baker, C.H., Poley, C.R., Chen, C.H., 2011. Wetting and dewetting transitions on hierarchical superhydrophobic surface. Langmuir 27 (12), 7502–7509. https://doi.org/10.1021/la201587u.
Cady, S.D., Schmidt-Rohr, K., Wang, J., Soto, C.S., Degrado, W.F., Hong, M., 2010. Structure of the amantadine binding site of influenza M2 proton channels in lipid bilayers. Nature 463 (7281), 689–692. https://doi.org/10.1038/nature08722.
Cannon, R.C., O'Donnell, C., Nolan, M.F., 2010 Aug 12. Stochastic ion channel gating in dendritic neurons: morphology dependence and probabilistic synaptic activation of dendritic spikes. PLoS Comput. Biol. 6 (8) https://doi.org/10.1371/journal.pcbi.1000886 pii: e1000886.
Cho, A., Wrammert, J., 2016. Implications of broadly neutralizing antibodies in the development of a universal influenza vaccine, 2016 Apr Curr. Opin. Virol. 17, 110–115. https://doi.org/10.1016/j.coviro.2016.03.002. Epub 2016 Mar 28.
Douezan, S., Brochard-Wyart, F., 2012. Dewetting of cellular monolayers. Eur. Phys. J. E (EPJ E), - Soft Matter 35 (5), 34. https://doi.org/10.1140/epje/i2012-12034-9, 2012 May.
Fiers, W., De Filette, M., El Bakkouri, K., Schepens, B., Roose, K., et al., 2009. M2e-based universal influenza A vaccine. Vaccine 27 (45), 6280–6283. https://doi.org/10.1016/j.vaccine.2009.07.007, 2009 Oct 23.
Foffi, G., Pastore, A., Piazza, F., Temussi, P.A., 2013. Macromolecular crowding: chemistry and physics meet biology (Ascona, Switzerland, 10-14 June 2012). Phys. Biol. 10 (4), 040301.
Gonzalez-Rodriguez, D., Maddugoda, M.P., Stefani, C., Janel, S., Lafont, F., et al., 2012

May 25. Cellular dewetting: opening of macroapertures in endothelial cells. Phys. Rev. Lett. 108 (21), 218105.
Haider, B., Duque, A., Hasenstaub, A.R., McCormick, D.A., 2006 Apr 26. Neocortical network activity in vivo is generated through a dynamic balance of excitation and inhibition. J. Neurosci. 26 (17), 4535–4545.
Homeyer, N., Ioannidis, H., Kolarov, F., Gauglitz, G., Zikos, C., et al., 2016. Interpreting thermodynamic profiles of aminoadamantane compounds inhibiting the M2 proton channel of influenza a by free energy calculations. J. Chem. Inf. Model. 56 (1), 110–126. https://doi.org/10.1021/acs.jcim.5b00467.
Ichinohe, T., Pang, I.K., Iwasaki, A., 2010. Influenza virus activates inflammasomes via its intracellular M2 ion channel. Nat. Immunol. 11 (5), 404–410. https://doi.org/10.1038/ni.1861.
Karapanagiotis, Ioannis, Gerberich, William W., 2005. Polymer film rupturing in comparison with leveling and dewetting. Surf. Sci. 594 (1–3), 192–202. https://doi.org/10.1016/j.susc.2005.07.023.
Lapierre, F., Coffinier, J., Boukherroub, R., Thomy, V., 2013. Electro-(de)wetting on Superhydrophobic surfaces. Langmuir 29 (44), 13346–13351. https://doi.org/10.1021/la4026848.
Lee, S.J., Hong, J., Kang, K.H., Kang, I.S., Lee, S.J., 2014. Electrowetting-induced droplet detachment from hydrophobic surfaces. Langmuir 30 (7), 1805–1811. https://doi.org/10.1021/la404344y.
Lehn, J.M., 2007. From supramolecular chemistry towards constitutional dynamic chemistry and adaptive chemistry. Chem. Soc. Rev. 36 (2), 151–160.
Leroux, Frédéric, Campagne, Christine, Perwuelz, Anne, Gengembre, Léon, 2008. Polypropylene film chemical and physical modifications by dielectric barrier discharge plasma treatment at atmospheric pressure. J. Colloid Interface Sci. 328 (2), 412–420. https://doi.org/10.1016/j.jcis.2008.09.062. PMID 18930244.
Lombardi, F., Herrmann, H.J., Perrone-Capano, C., Plenz, D., de Arcangelis, L., 2012 Jun 1. Balance between excitation and inhibition controls the temporal organization of neuronal avalanches. Phys. Rev. Lett. 108 (22), 228703. Epub 2012 May 31.
Maktabi, S., Schertzer, J.W., Chiarot, P.R., 2019. Dewetting-induced formation and mechanical properties of synthetic bacterial outer membrane models (GUVs) with controlled inner-leaflet lipid composition. Biochim. Soft Matter 15 (19), 3938–3948. https://doi.org/10.1039/c9sm00223e, 2019 May 15.
Pielak, R.M., Chou, J.J., 2011. Influenza M2 proton channels. Biochim. Biophys. Acta 1808 (2), 522–529. https://doi.org/10.1016/j.bbamem.2010.04.015, 2011 Feb.
Rahe, P., Lindner, R., Kittelmann, M., Nimmrich, M., Kühnle, A., 2012 May 14. From dewetting to wetting molecular layers: C60 on CaCO3(10 14) as a case study. Phys. Chem. Chem. Phys. 14 (18), 6544–6548. https://doi.org/10.1039/c2cp40172j.
Rego, N.B., Xi, E., Patel, A.J., 2019. Protein hydration waters are susceptible to unfavorable perturbations, 2019 Feb 6 J. Am. Chem. Soc. 141 (5), 2080–2086. https://doi.org/10.1021/jacs.8b11448. Epub 2019 Jan 22.
Rosen, M.J., 2004. Surfactants and Interfacial Phenomena, third ed. Wiley-Interscience, Hoboken, New Jersey. p. 244. ISBN 978-0-471-47818-8. OCLC 475305499.
Rossman, J.S., Jing, X., Leser, G.P., Lamb, R.A., 2010. Influenza virus M2 protein mediates ESCRT-independent membrane scission. Cell 142 (6), 902–913. https://doi.org/10.1016/j.cell.2010.08.029.
Sackmann, E., Bruinsma, R.F., 2002. Cell adhesion as wetting transition? ChemPhysChem 3 (3), 262–269, 2002 Mar 12.
Sándor, C., Libál, A., Reichhardt, C., Olson Reichhardt, C.J., 2017. Dewetting and spreading transitions for active matter on random pinning substrates. J. Chem. Phys. 146 (20), 204903. https://doi.org/10.1063/1.4983344, 2017 May 28.
Sharmaa, A., Reiterb, G., 1996. Instability of thin polymer films on coated substrates: rupture, dewetting, and drop formation. J. Colloid Interface Sci. 178 (Issue 2), 383–399. https://doi.org/10.1006/jcis.1996.0133, 25 March 1996.
Tanaka, M., Rehfeldt, F., Schneider, M.F., Mathe, G., Albersdörfer, A., et al., 2005. Wetting and dewetting of extracellular matrix and glycocalix models. J. Phys. Condens. Matter 17 (9). https://doi.org/10.1088/0953-8984/17/9/022.
Thiam, A.R., Farese Jr., R.V., Walther, T.C., 2013. The biophysics and cell biology of lipid droplets. Nat. Rev. Mol. Cell Biol. 14, 775–786. https://doi.org/10.1038/nrm3699.
Thomaston, J.L., Alfonso-Prieto, M., Woldeyes, R.A., Fraser, J.S., Klein, M.L., Fiorin, G., DeGrado, W.F., 2015. High-resolution structures of the M2 channel from influenza A virus reveal dynamic pathways for proton stabilization and transduction. Proc. Natl. Acad. Sci. U. S. A 112 (46), 14260–14265.
Thompson, C.V., 2012. Solid-state dewetting of thin films. Annu. Rev. Mater. Res. 42, 399–434. https://doi.org/10.1146/annurev-matsci-070511-155048.
Tognoli, E., Scott Kelso, J.A., 25 June 2014. Enlarging the scope: grasping brain complexity. Front. Syst. Neurosci. https://doi.org/10.3389/fnsys.2014.00122.
Tozzi, A., 2015. Information Processing in the CNS: A Supramolecular Chemistry? Cognitive Neurodynamics, vol. 9, pp. 463–477, 5.
Tozzi, A., Tor, Fla, Peters, J.F., 2016. Building a minimum frustration framework for brain functions in long timescales. J. Neurosci. Res. 94 (8), 702–716.
Vargas, J.N., Seemannab, R., Fleury, J.B., 2014. Fast membrane hemifusion via dewetting between lipid bilayers. Soft Matter 10, 9293–9299.
Webb, T.I., Kshatri, A.S., Large, R.J., Akande, A.M., Roy, S., et al., 2015 Feb 17. Molecular mechanisms underlying the effect of the novel BK channel opener GoSlo: involvement of the S4/S5 linker and the S6 segment. Proc. Natl. Acad. Sci. U. S. A. 112 (7), 2064–2069. https://doi.org/10.1073/pnas.1400555112.
Xue, M., Atallah, B.V., Scanziani, M., 2014. Equalizing excitation–inhibition ratios across visual cortical neurons. Nature. https://doi.org/10.1038/nature13321.
Young, T., Hua, L., Huang, X., Abel, R., Friesner, R., Berne, B.J., 2010. Dewetting transitions in protein cavities. Proteins 78 (8), 1856–1869. https://doi.org/10.1002/prot.22699.
Zhu, F., Hummer, G., 2010. Pore opening and closing of a pentameric ligand-gated ion channel, 2010 Nov 16 Proc. Natl. Acad. Sci. U. S. A. 107 (46), 19814–19819. https://doi.org/10.1073/pnas.1009313107. Epub 2010 Nov 1.

Volume 151 | March 2020 | ISSN 0079-6107

ELSEVIER

An International Review Journal

PROGRESS IN BIOPHYSICS & MOLECULAR BIOLOGY

EDITORS
DENIS NOBLE
TOM L. BLUNDELL
PETER KOHL

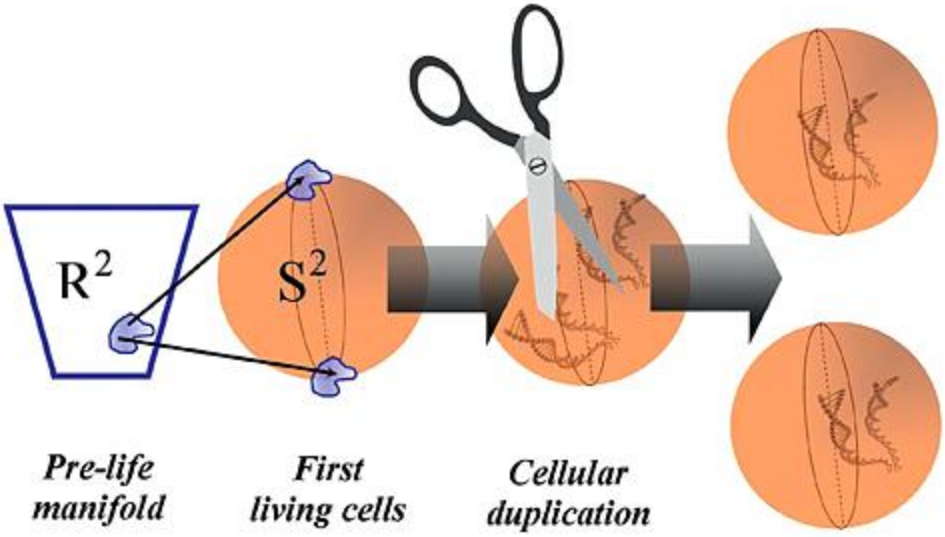

Progress in Biophysics and Molecular Biology 151 (2020) 1–13

Contents lists available at ScienceDirect

Progress in Biophysics and Molecular Biology

journal homepage: www.elsevier.com/locate/pbiomolbio

Projective mechanisms subtending real world phenomena wipe away cause effect relationships

Arturo Tozzi [a, *], David Papo [b]

[a] Center for Nonlinear Science, Department of Physics, University of North Texas, 1155 Union Circle, #311427, Denton, TX, 76203-5017, USA
[b] Fondazione Istituto Italiano di Tecnologia, Ferrara, Italy

ARTICLE INFO

Article history:
Received 13 May 2019
Received in revised form
16 October 2019
Accepted 10 December 2019
Available online 12 December 2019

Keywords:
Causality
Topology
Borsuk-Ulam theorem
Fixed point theorem
Non-Hermitian systems
Uhlenbeck theorem
Dewetting transition
Kneser graphs

ABSTRACT

Causal relationships lie at the very core of scientific description of biophysical phenomena. Nevertheless, observable facts involving changes in system shape, dimension and symmetry may elude simple cause and effect inductive explanations. Here we argue that numerous physical and biological phenomena such as chaotic dynamics, symmetry breaking, long-range collisionless neural interactions, zero-valued energy singularities, and particle/wave duality can be accounted for in terms of purely topological mechanisms devoid of causality. We illustrate how simple topological claims, seemingly far away from scientific inquiry (e.g., "given at least some wind on Earth, there must at all times be a cyclone or anticyclone somewhere"; "if one stirs to dissolve a lump of sugar in a cup of coffee, it appears there is always a point without motion"; "at any moment, there is always a pair of antipodal points on the Earth's surface with equal temperatures and barometric pressures") reflect the action of non-causal topological rules. To do so, we introduce some fundamental topological tools and illustrate how phenomena such as double slit experiments, cellular mechanisms and some aspects of brain function can be explained in terms of geometric projections and mappings, rather than local physical effects. We conclude that unavoidable, passive, spontaneous topological modifications may lead to novel functional biophysical features, independent of exerted physical forces, thermodynamic constraints, temporal correlations and probabilistic a priori knowledge of previous cases.

© 2019 Elsevier Ltd. All rights reserved.

Contents

1. Introduction . . . 2
2. Topological approach . . . 2
3. The hairy ball theorem in physics and biology . . . 3
   3.1. Exceptional points in non-Hermitian biological networks . . . 4
4. Topological accounts of living cells and brains . . . 4
   4.1. Ergodic systems and the Brouwer fixed point theorem . . . 5
   4.2. Sensations and Lusternik–Schnirelmann theorem . . . 5
5. The biophysical meaning of the borsuk-ulam theorem . . . 6
   5.1. A BU theorem-based explanation of the universal self-similarity of particles? . . . 6
   5.2. Physical properties of the BU theorem explain particle/wave duality in the double slit experiment . . . 7
   5.3. Collisionless interactions in plasma-like fluids . . . 8
   5.4. BU theorem, symmetry and symmetry breaking . . . 8
   5.5. Graph theory comes into play: Kneser graphs and the BU theorem . . . 8
6. Concluding remarks: when causality fades away . . . 10
   References . . . 11

* Corresponding author.
E-mail addresses: Arturo.Tozzi@unt.edu (A. Tozzi), papodav@gmail.com (D. Papo).

https://doi.org/10.1016/j.pbiomolbio.2019.12.002
0079-6107/© 2019 Elsevier Ltd. All rights reserved.

1. Introduction

« La Geométrie qui ne doit qu'obéir à la Physique quand elle se réunit avec elle, lui commande quelquefois ».

D'Alembert, *Essai d'une nouvelle théorie de la résistance des fluides*, 1752.

The scientific method prescribes that theoretical claims must be empirically tested in the proper experimental setup. Causality represents one of the pillars of the scientific method and can be defined as follows: "The substance S is responsible for (or contributes to) the state of affairs p that is obtained at a subsequent time t", where S may stand for active or passive, inanimate or living, non-sentient or intelligent, wholly active or inactive, free or constrained contributors (modified from Freddoso, 1988). For example, the evaluation of adverse drug reactions in pharmacodynamics is based on a small number of tenets (Naranjo et al., 1981; Mouton et al., 2017):

(a) Temporal correlation between the alleged cause and the reported effect.
(b) A priori knowledge of previous cases describing the same hypothetical correlation.
(c) The feasibility to repeat the chain of events, through proper experimental settings.
(d) When the cause is discontinued, the system under assessment frequently returns to its original conditions. This means that the reported symptoms disappear and bodily integrity is restored.

Cause effect relationships are often interpreted as establishing dependencies between events. The core of causality lies in the occurrence of path-connected sets or subsets, i.e., the presence of features that can be joined together. Events are bound into causal chains by two relations: spatio-temporal continuity (at least in macroscopic phenomena) and statistical relevance (Van Fraassen, 1977).

However, the assessment of cause effect relationships is frequently a difficult venture. Critiques to causality have been raised throughout the centuries by philosophers, theologicians and theoreticians such as Pyrrho, Al-Ghazali, Nicholas of Autrecourt, 1971 (1340), John of Mirecourt (Franzinelli, 1958), William of Ockham (1974), Berkeley, Hume, Montaigne, Wittgenstein, Feyerabend, Fogelin (Popkin and Maia Neto, 2007), and Van Fraassen (1977). Unpredictable correlations might prevent scientific queries on causality (Nebeker et al., 2004; Davies et al., 2011; Loke, 2012; Saedder et al., 2015). Features are often unknown or hard to observe, and system boundaries and dynamics may be irregular and indistinct, blurring cause effect relationships. Limitations to causality may not stem from observational limitations, and may be intrinsic to the nature of the system. For instance, the classical causal formulation does not faithfully account for systems where causality may be *conditional*, i.e. when the occurrence of some events *a* and *b* is mutually conditional upon each other (Bartoletti et al., 2015), or *circular*, whereby global parameters created by the intrinsic interactions among the individual parts of a system in turn govern the behavior of the individual parts. In general, causal relations are hard to define in complex systems, where a great number of degrees of freedom interact non-linearly and non-locally, giving rise to non-trivial phenomenologies, e.g. in plasma flows and brain dynamics, or in contexts where quantum effects cannot be neglected, e.g. double slit experiments or quantum entanglement. Causal explanations are by no means the only ones consistent with the scientific method. Alternative ones, e.g. mechanistic, dynamical, and probabilistic explanations, have long been used to account for observed phenomena in various fields.

For instance, it has been recently argued that physical and biological phenomena can be explained in terms of topological properties of the system under consideration (Huneman, 2010). While causal and mechanistic explanations respectively account for observed process or performed function in terms of chains of causal factors or interactions, and of entities or processes organized to produce them, in topological explanations phenomenology is characterized in terms of topological features of the system (Kostić, 2018). In the sequel, we will show how topological projections work in real contexts and what are the physical or biological mechanisms leading to mappings among different dimensions in real-world paths and trajectories. Once established that there is an opportunity to treat systems in terms of topological structures, we will describe how to make the leap from the simple, almost intuitive topological theorems to hugely generic events.

2. Topological approach

Topology is a branch of mathematics that studies the properties of objects that are invariant under smooth deformation e.g. stretching and twisting, of shape and size (Bourbaki, 1966; Bredon, 1997; Dodson and Parker, 1997; Peters, 2016). Topological properties may play a role analogous to that of symmetry (Golubitsky and Stewart, 2015), supplying structure and coherence to the laws of nature (Gross, 1996), to a large extent irrespective of the particular domain, provided the system under consideration is endowed with the appropriate structure (Papo, 2019).

Some fundamental processes in physics may have an intrinsically topological nature. A notable example is that of phase transitions, that recent research has shown to be understandable in purely topological terms, at least under certain conditions (Franzosi et al., 2000; Donato et al., 2016; Pettini et al., 2019). In alternative, topological descriptions may represent an efficient and robust way to highlight the properties of a given system at appropriate scales (Robinson, 2013). A further example is represented by the intrinsic unconventional superconductivity in a two-dimensional superlattice recently reported by Cao et al. (2018), that cannot be explained by weak electron–phonon interactions. The superlattice is achieved by stacking two sheets of graphene twisted relative to each other by a small angle. For twist angles of about 1.1°—the first 'magic' angle (Jiang et al., 2019)—the electronic band structure of this 'twisted bilayer graphene' exhibits flat bands near zero Fermi energy, resulting in insulating states at half-filling.

Topological approaches can be applied not only to physical phenomena, but also to biological ones. In a biological context, one studies the topological properties of "fields" of large numbers (or expanses) of biological molecules that share some form of neighborhood smoothness with regard to a specific metric, e.g. density, orientation, charge, or any of a number of field-like, "smoothness dominated" metrics. For instance, Gaiha et al. (2019) used network theory to study mutationally constrained epitopes of HIV protein structure data. Epitopes containing amino acids with multiple interactions within the three-dimensional structure of an HIV protein are prevented from escaping and tend to bind to protective HLA types. This demonstrates the topological importance of individual amino acid residues: a slight change in these small elements allows distinguishing individuals who naturally control HIV, even in the absence of protective HLA alleles. In the sequel, we will provide other examples of changes in topological features leading to modifications in living beings.

Data from far-flung scientific disciplines point towards topological issues as universal rules for elusive physical and biological

activities. The role of topology as an explanatory factor has been recognized in a great number of fields, ranging from condensed matter physics, to biology and neuroscience, from quantum computing (Collins, 2006), to data mining and data analysis. In networked systems, topology has been shown to be key to processes, e.g. synchronization, in systems of coupled oscillators (Pecora and Carroll, 1998; Boccaletti et al., 2006; Arenas et al., 2008). For a survey of the countless applications of topology, from pre-big bang scenarios, to quantum entanglement, emergence of life and neuroscience, see Peters et al. (2017a and 2017b); Peters and Tozzi (2016). In this topological context, system operations become projections among different levels, that give rise to apparently emergent properties in higher dimensions. Topological approaches suggest that system properties in physical/biological spaces can be translated to abstract mathematical properties, and vice versa: this means that complete descriptions of a wide range of phenomena can be reached just by looking at their higher levels, where the differences are easily detectable. In sum, topological modifications suggest that we are dealing with mathematical mappings and projections among different activity levels, instead of cause/effect relationships. Topological alterations provide by themselves physically and biologically quantifiable effects.

In the remainder of this article, we illustrate ways in which physical and biological phenomena can be explained in terms of the underlying topology, in contexts that both classical deductive and inductive logics no longer hold, without relying upon the thermodynamic constraints, fields and forces that are usually employed in the explanation of causal relationships. Specifically, we review phenomena originating from geometrical effects rather than local physics, and show how some fundamental topological theorems (see Table 1) afford a straightforward explanation of otherwise puzzling physical and biological phenomena.

3. The hairy ball theorem in physics and biology

Suppose that some aspect of a living system, e.g. a cell membrane, is described in terms of a continuous function, e.g. surface tension. Hairy Ball Theorem (HBT) ensures the presence of at least one point (or tiny area) where this function disappears; this means that the cellular membrane must display at least a small area where surface tension vanishes. However, inside this area, called singularity, energy gets lost: therefore, this approach seems to run counter to thermodynamic constraints. This difficulty can be solved in terms of mathematical/topological approaches. Indeed, the effect resulting from HBT must be compensated for through the mathematical device called "bubble phenomenon". This concept is borrowed from Uhlenbeck's singularity removal theorem for four-dimensional Yang-Mills connections to higher dimensions. The point with vanishing continuous tangent stands for a removable singularity inside a punctured ball. Inside the singularity, uniform convergence of conformally invariant equations occurs. This means that many positive-energy solutions (instantons) on the spherical manifold are concentrated near this tiny area, where they converge towards a trivial pointwise solution. Close to the singularity dictated by HBT, a bubble-tree domain can be drawn (Uhlenbeck, 1982a,b). Provided the norm of the curvature is sufficiently small, bubble trees allow removing the singularity and transforming gauge fields into a smooth field (Tao and Tian, 2004; Meyer and Rivière, 2003). In our case, this means that the surface tension, apparently vanished in a tiny area of the spherical cellular membranes of living cells, can be recovered by constructing bubbles on bubbles that restore the energy lost inside the singularity.

Theoretical singularities with vanishing surface tension display a biophysical counterpart in cellular membranes: the channel cavities. Within the channels of cellular membranes, the surface tension gets almost lost and difficult to detect and measure. The procedure suggested by Uhlenbeck allows for the quantification of the real surface tension of every channel that apparently displays a zero value of such tension.

One may wonder why we should care about the values of surface tension inside the channels of a living cell. The relevance of this seemingly rather unimportant issue becomes clearer if we consider the process of dewetting transition (Sharmaa and Reiterb, 1996; Thompson, 2012; Li et al., 2019). Dewetting, i.e. the retraction of a fluid from a surface it was forced to cover, is a general mechanism of cellular functioning, which has been described in lipid droplets and

Table 1
Some fundamental topological theorems.

Theorems

Hairy ball theorem (HBT). There is no non-vanishing continuous tangent vector field on an even-dimensional n-sphere (Eisenberg ad Guy R. 1979). This ensures the presence of at least one point where vectors (and/or tensors) disappear. Two naïve descriptions assert that "whenever one attempts to comb a hairy ball flat, there will always be at least one tuft of hair at one point on the ball", and "given at least some wind on Earth, there must at all times be a cyclone or anticyclone somewhere".

Ham sandwich theorem (HST). For every positive integer n, given n measurable "objects" in n-dimensional Euclidean space, it is possible to divide all of them in half with a single $(n-1)$-dimensional hyperplane (Matoušek, 2003; Beyer and Zardecki, 2004). To provide an example, "given globs of ham, bread, and cheese (in any shape), placed any way you like, there exists one flat slice of a knife (a plane) that will bisect each of the ham, bread, and cheese".

Brouwer fixed point theorem (FPT). Every continuous function from an n-sphere of any dimension to itself has at least one fixed point (Volovikov and Yu, 2008; Crabb and Jawaworski, 2013). In particular, FPT applies to any disk-shaped area, where it guarantees the existence of a fixed point, i.e., a sort of whirlpool that attracts moving particles. A coffee cup illustration has been provided: "no matter how you slosh the coffee, some point is always in the same position that it was before the sloshing began".

Lusternik–Schnirelmann theorem (LST). If a sphere is covered by n+1 open sets, then one of them contains a pair of antipodal points. In other words, every time you split a sphere in three parts, one of the three must encompass an entire diameter (Dodson and Parker, 1997). One of the three slices must necessarily contain some antipodal surface features with matching description.

Borsuk-Ulam theorem (BU theorem). A general topological principle underlies the organization of physical and biological systems. It relates to a well-known and rather simple theorem, the BU theorem, which states that, provided the function under assessment is continuous, two points with matching description in a higher dimension map to a single point in lower dimensions (Borsuk, 1933; Matoušek, 2003). In plain terms, this means that at any moment, there is always a pair of antipodal points on the Earth's surface with equal temperatures and barometric pressures. In the last years, the original formulation of BU theorem has been modified, providing useful extensions (Borsuk, 1969; Tozzi et al., 2017):

a Antipodal points can be replaced by regions or shapes with matching descriptions (Tozzi and Peters, 2016a), allowing comparisons of shapes, trajectories, functions, vectors, particle trajectories, entropies, bits (Tozzi and Peters, 2017a).
b The features need not be antipodal, and may simply share no common points (Tozzi et al., 2016a).
c BU theorem variants hold not just for convex structures such as circumferences and spheres described by the classical theorem, but also for flat and concave ones, which better describe the intricate trajectories of real system dynamics (Sengupta et al., 2016).
d The dimensions described by BU theorem are not necessarily spatial ones (as in the case of circles and spheres), but may also be of an abstract nature (Tozzi et al., 2017): the crucial issue is that matching descriptions allow commensurability between (real or abstract) entities equipped with different (real or abstract) dimensions.

bilayers (Thiam et al., 2013; Vargas et al., 2014), extracellular matrix and glycocalix (Tanaka et al., 2005), protein cavities (Young et al., 2010), openings of endothelial cells (Gonzalez-Rodriguez et al., 2012), mechanosensory channels (Anishkin and Sukharev, 2004), cell adhesion (Sackmann and Bruinsma, 2002). This mechanism is characterized by a very unusual behaviour of supramolecular water assemblies: when water and ions are enclosed within the narrowest sub-nanometer confines of ion channel hydrophobic pore, a peculiar stochastic liquid-vapour water phase transition takes place near a given critical point (Aryal et al., 2015). These transient vapour states are "dewetted", i.e. effectively devoid of water molecules within all or part of the pore. The decreased amount of liquid state water molecules inside the channels leads to hydrophobic gating and is associated with impaired conductance, energy barriers to ion transit and, ultimately, channel closure. A narrow hydrophobic gate region may disfavor liquid-phase water, leading to local dewetting, which will form an energetic barrier to water and ion permeation without steric occlusion of the pore (Rao et al., 2019). Because metastable dynamical states of hydrophobic gating require both very small radius and interactions with strongly hydrophobic linings (Boreyko et al., 2011; Lapierre et al., 2013), knowledge of the surface of channels is imperative. Indeed, such knowledge might lead to the development of drugs able to modify channel surface tension and, therefore, to selectively interfere with the biological activities of cellular receptors.

Many prominent phenomena originate from geometrical effects rather than from local physics. Laver and Forgan (2010) examined the consequences of HBT for the lattice of flux lines that form when a magnetic field is applied to a type-II superconducting crystal. Discontinuities must exist in lattice shape as a function of field direction relative to the crystal. Extraordinary, "unconventional" flux line lattice shapes that spontaneously break the underlying crystal symmetry are remarkably likely across both conventional and unconventional type-II superconductors. The study of flux line lattice (FLL) shapes and orientations forms a cornerstone in the understanding of both conventional and unconventional superconductivity. Unusual FLL structures are rather likely for purely geometrical reasons, because the FLL must comply with the HBT. HBT makes it clear that "unconventional" FLL structures are not exclusive to unconventional superconductors and therefore do not necessarily imply unconventional superconductivity. Although geometry decrees that the FLL must cleave to HBT, it is local physics that determines exactly how this is achieved (Laver and Forgan, 2010). To provide another example, application of the HT to the analysis of the surface instabilities inherent for liquid/vapour interfaces were reported by Bormashenko (2015). When a continuous tangential velocity field exists on the surface of the liquid sample which is homeomorphic to a ball, zero velocity points will be necessarily present at the surface. The author applied HBT to the analysis of the surface instabilities occurring under the rapid evaporation of polymer solutions. The ensuing zero velocity points, necessarily present at the surface under Marangoni instability, enable direct visualization of instabilities. HBT is also key to the characterization of the magnetic field in plasma physics. In fusion plasma physics, a surface spanned by magnetic field lines is referred to as a flux surface. Flux surfaces are particularly important in describing static magnetic hydrodynamic equilibria. The knowledge of equilibrium flux surfaces is critical and defines much of the geometry of the fusion experiment. If the shape of flux surfaces that contains both magnetic field lines and current lines is closed and orientable, it must be homeomorphic to either a sphere S^2, a torus, or a connect sum of tori. Since the magnetic field is nowhere vanishing and tangent to the surface, HBT rules out the possibility of a sphere.

3.1. Exceptional points in non-Hermitian biological networks

The singular points prescribed by HBT are ubiquitous in non-Hermitian systems, i.e., in systems that do not obey conservation laws, as they exchange energy with the surrounding environment. In such systems, spectral singularities in the parameter space called *exceptional points*, where two resonant modes of the Hamiltonian become degenerate, emerge for some values of the control parameters. Non-Hermitian degeneracies are associated with rich and complex phenomenology, a property that is taken advantage of in quantum resonance, optics and photonics, in particular in the fields of coupled-cavity laser sources, sensors, absorbers, nonlinear resonators, spatial mode converters and isolators (Miri and Alù, 2019).

Recently, neural networks have been characterized as non-Hermitian systems (Amir et al., 2016; Tanaka and Nelson, 2018). Indeed, the brain exhibits features often associated with these singularities:

1 Non-conservative elements with gain and loss are correlated with the dynamic inhibitory/excitatory balance discovered in neocortical neurons (Haider et al., 2006).
2 Phase transitions dramatically altering macroscopic system behaviour (Tognoli and Kelso, 2014).
3 Imaginary values required by non-Hamiltonian systems (that can support entirely real eigenvalue spectra) (Tozzi et al., 2016).
4 Non-Hermitian components of the covariance matrix, whose eigenvectors can be interpreted as the fields corresponding to temporally uncorrelated and spatially orthogonal sources in the brain (Marzetti et al., 2008).
5 The sharp frequency oscillations produced by brain activity might correspond to the peculiar topology of eigenvalue surfaces near exceptional points described by Gong et al. (2018).

Ultimately then, some important aspects of system-level brain phenomenology can be understood in terms of properties of non-Hermitian random matrices, and in particular of localized eigenfunctions, that arise naturally in sparse neural networks (Amir et al., 2016; Tanaka and Nelson, 2018).

4. Topological accounts of living cells and brains

In biological systems, tiny changes in topological features might lead to alterations in macroscopic behavior. Here we provide a few examples that demonstrate how small modifications in topology may lead to novel functional biological features.

6 Mohan et al. (2019) explored the tuning effect of receptor dimerization, i.e., a fundamental mechanism by which most cytokines and growth factors activate Type-I transmembrane receptors. They designed a series of dimer ligands for the erythropoietin receptor, in which the distance and angle between monomers were varied. They demonstrated that topology differentially affects the strength of activation and pathways: different EpoR complex topologies elicit either full, or partial, or null agonism. This means that ligand-induced topological changes in the extracellular domains (ECDs) of dimeric receptors can affect signaling output.
7 The control of cell fate through oriented cell division is imperative for organ development. Basal epidermal progenitor cells divide parallel or perpendicular to the basement membrane to self-renew or produce differentiated stratified layers. Box et al. (2019) found that mouse embryos defective for the planar cell polarity (PCP) gene, Vangl2, exhibit increased perpendicular divisions and hyperthickened epidermis. Surprisingly, this is not due to defective Vangl2 function in the epidermis, but to

changes in cell geometry and packing that arise from the open neural tube characteristic of PCP mutants. This means that local tissue architecture, rather than cortical PCP cues, regulates the decision between symmetric and stratifying divisions, allowing flexibility for basal cells to adapt to the needs of the developing tissue.

8 The rate of AIDS progression in untreated HIV-1 infection has a variable outcome, that is affected by variation in the genes encoding a patient's human leukocyte antigen (HLA) proteins (McMichael and Carrington, 2019). This genetic association between HLA and AIDS progression has been attributed to differences in T cell recognition of HLA-bound HIV-derived peptide epitopes. Indeed, epitopes containing amino acids with multiple topological interactions within the three-dimensional structure of an HIV protein are constrained from escape and tend to bind to protective HLA types.

9 Brookes and Riccio (2019) elucidated how genome architecture is essential for transcriptional activation in nervous system development. During neuronal differentiation, genome topology, as well as RNA topology (Frank-Kamenetskii, 2013), are now regarded as key factors that contribute to transcriptional regulation. This means that the dynamic organization of chromatin within the nucleus impacts gene activation in response to extrinsic signaling and during neuronal differentiation. Further, they highlighted how alteration of genome topology is associated with neurological disorders.

Also HST, BFT and LST provide feasible biological realizations. If we consider the concept of life, we notice that its definition is rather qualitative, because it takes into account complex concepts such as homeostasis, organization, growth, adaptation, and response to stimuli (McKay, 2004; Trifonov, 2012). One of the most frequent definitions of life involves cellular duplication, i.e., the ability of living beings to produce new individual organisms (offspring), either asexually from a single parent organism, or sexually from two. The concept of reproduction can be topologically treated, providing us with a mathematical definition of one of the foremost traits of life. Every cell gives rise to two identical "progeny": this means that, thanks to continuous mapping among manifolds, monocellular life and its primeval birth can be defined and operationalized in terms of the BU theorem and HST. Starting from unique assemblies of macromolecules, a living cell can be topologically built and two progenitors can be achieved from an ancestral cell. In this context, life becomes the mathematical, quantifiable phenomenon reflecting the continuous function required by the BU theorem (Fig. 1**, left).** HST comes into play at the stage of cellular division, when a single cell gives rise to two indistinguishable ones. We achieve antipodal points not due to the changes in dimensions that the BU theorem suggests, but rather by a SPLIT of S^2 into two identical parts (see Fig. 1**, right** for further details). Thanks to the ham sandwich approach, antipodal regions on a sphere are viewed as tiny balls sliced by a hyperplane. This leads to a fresh view of cell division; it becomes the result of splitting a sphere into two identical hyperspheric offspring cells.

4.1. Ergodic systems and the Brouwer fixed point theorem

Successful biophysical theories such as the free-energy principle (Friston, 2010) require that living activities take place within ergodic phase spaces. This means that, over long periods, the time spent by a system in a region with the same energy is proportional to the volume of the region, so that all accessible microstates are equiprobable over a long period of time (Barth, 1923; Walters, 1982; Alaoglu and Birkhoff, 1940; Feller, 1971). On the other hand, many biological systems, such as the brain, may violate this condition

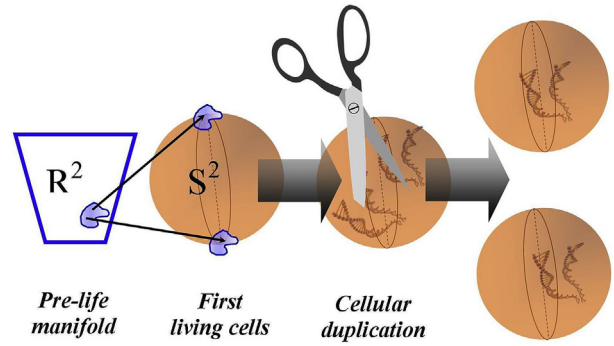

Fig. 1. Topological framework for cellular duplication. The **left side** of the figure displays a two-dimensional manifold R^2 (standing for pre-biological assemblies of macromolecules) and a three-dimensional sphere S^2 (standing for the first organization of membrane-delimited living cells). The process can be described in terms of the BU theorem for different values of dimensions: indeed, from a single feature on R2 that maps to two matching features on S^2, and vice versa. Features stand here for those foremost biological parts, where more than one copy is required, in order to generate life: biochemical paths, nucleic acid conformation, and so on. The **right side** of the figure illustrates how, due to the ham-sandwich theorem, the three-dimensional cell with two antipodal regions can be split into two three-dimensional spheres, each one equipped with one of the antipodal features. This occurs during cellular division: a manifold separates into two manifolds with the same dimension.

(Bianco et al., 2007). A topological approach elucidates this controversial issue. Both ergodic and non-ergodic conditions can be treated in terms of algebraic topology, just by changing the dimensions of the structure under investigation. At first, we consider particles traveling "ergodically" along the whole surface of a two-dimensional disk; we then consider the corresponding three-dimensional sphere, achieved through higher-dimensional mappings. In the higher-dimensional case, our particles are constrained to move inside the surface areas corresponding to antipodal points. This means that particles cannot meet, and, because they cannot walk across the whole surface of the three-dimensional sphere, the system ergodicity is lost. As a result, the system is ergodic in lower dimensions, but non-ergodic in higher ones.

Here is where FPT comes into play. In biological contexts, FPT dictates that we can always find a region containing a single feature, and every feature (for the BU theorem) comes together with another one, termed a "wired friend" (Tozzi et al., 2018a). Every occurrence of a wired friend on a lower-dimensional structure maps to a fixed description, e.g. to another feature belonging to a manifold with higher dimensions. Therefore, FPT and the BU theorem allow one to understand biological features that are embedded in a higher-dimensional macro-level to be a topological description that is embedded within a lower-dimensional micro-level, and vice versa.

4.2. Sensations and Lusternik–Schnirelmann theorem

Recent interpretations of human perception focus on the simplest and most natural standpoint: an individual (either human or animal) embedded in her environment (Gibson, 1979; Russo-Krauss, 2015). In topological terms, the individual is embedded in a spatial three-dimensional ball, because her surrounding spatial environment is shaped as a sphere. In the framework of ecological approaches to visual perception (Gibson, 1986), the environment perceived by the individual is not a physical one, but rather is described by the triad: "medium", "substance" and "surfaces" (Gibson, 1950). The most stable, long-lasting perception is the ground upon which the observer stands, i.e., the horizontal surface under her feet. When the individual raises her eyes, she perceives the sky or the ceiling. The middle zone between the ground and the

sky stands for the medium, where objects, e.g., something which can be handled, stand vertically. For our topological purposes, it is noteworthy that the human individual splits her surrounding environment in three components: the ground and the sky, which join together at the horizon, and the intermediate zone, the medium. Therefore, the three-dimensional ball is split in three slices: the sky on the top, the ground on the bottom and the intermediate zone in the middle. Indeed, the brain spontaneously tends to part the environment in different closed subsets. In this context, LST might be very helpful. It states, in plain terms, that one of the three slices must necessarily contain some surface features with matching description. When an individual focuses her glance on one of the three slices of her surrounding three-dimensional sphere, her attention is driven by the slice containing antipodal points. Therefore, "attention" becomes a mental attitude that permits individuals to find, inside one of the three slices (the sky, the ground and the medium), a pair of features that share something perceivable in common. The matching features could stand for spatial objects or shapes, but also for matching movements: in the latter case, the shapes are not called objects, but events. In sum, LST provides a topological explanation of the psychological spontaneous mechanisms underlying human attention and perception.

5. The biophysical meaning of the borsuk-ulam theorem

The BU theorem has been invoked in the characterization of a wide range of physical/biological systems, from quantum entanglement to cellular homeostasis, from gauge theories to multidimensional neural activity (see Peters and Tozzi, 2016; Peters et al., 2017; Tozzi and Peters, 2016b, 2017b; c; Tozzi, 2019), to network phenomena such as incoherence-mediated remote synchronization in which two noncontiguous parts of the network are identically synchronized, while the dynamics of the intermediate part is statistically incoherent (Zhang et al., 2017). The mirror network structure symmetry proposed to underly mediated remote synchronization bears an obvious relation with the disjointed antipodal points with matching description described by the BU theorem. We refer the reader to Tozzi et al. (2017) for a survey of the countless applications of the BU theorem. To provide a trivial example of the huge potentialities of the BU theorem, we can state as follows: when a soap bubble spontaneously achieves the proper spherical shape, it is mandatory for its circumference to display at least two antipodal points with matching features (such as, e.g., the same superficial tension), independent of spatio-temporal constraints and probabilistic considerations.

Here, we illustrate the role of the BU theorem in two phenomena involving light rays, i.e., optical reflection (gravitational lensing), and oscillatory interference (double slit experiments). If one shines a light through a clear sphere onto a plane, there will be a point in the overlapping images of the near and far side of the sphere that includes two maximally distant points. This rather qualitative suggestion leads in a straightforward way to the concept of gravitational lensing. A gravitational lens is a distribution of matter (e.g., a galactic cluster) between a distant source and an observer on the Earth. Light is bent from the source, as it travels towards the observer. The amount of bending is one of the predictions of the general theory of relativity (Einstein, 1936). The light from a distant galaxy diverges due to the gravitational effects of a foreground celestial body, which acts like a lens and makes the distant source appear either distorted or magnified. This mechanism can be explained in terms of BU theory: projections give rise to deflection of light rays through a passive mechanism (Fig. 2). In the BU theorem framework, a three-dimensional hidden cosmic body emits a three-dimensional oscillatory light beam that intersects a four-dimensional gravitational lens, giving rise to the two

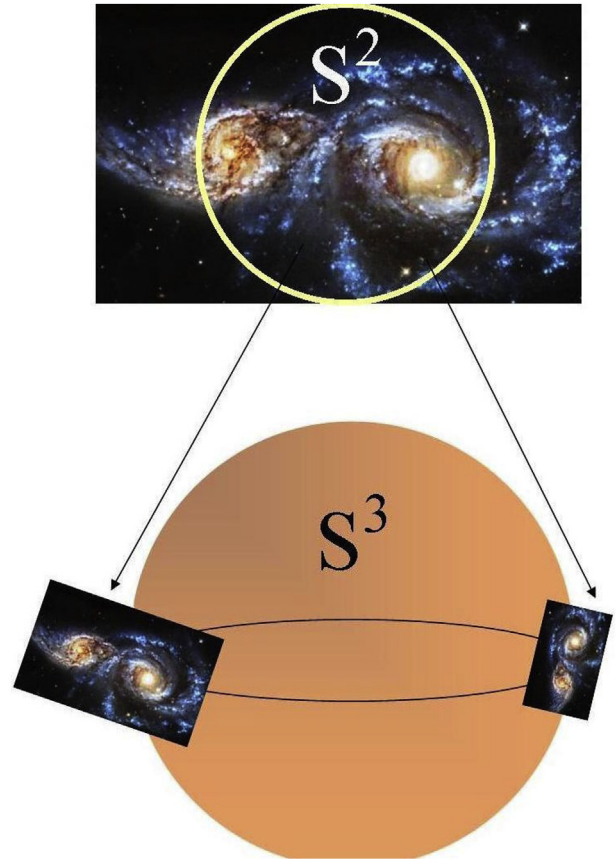

Fig. 2. Relationships between gravitational lenses and the BU theorem. Light rays from the three-dimensional galactic structure S^2 are reflected when approaching the four-dimensional gravitational lens S^3. This leads to two matching descriptions of the galactic structure.

images with matching description detectable by we observers on the Earth. Note that the gravitational lens can be thought of as a 4-D (rather than 3-D) manifold, time adding the additional dimension to the spatial manifold.

5.1. A BU theorem-based explanation of the universal self-similarity of particles?

One may wonder whether one of the most fundamental problems in particle physics, i.e., the universal self-similarity of particles that allows photons from the other side of the universe to be understood in terms of electrons (or other particles) "just like" the ones in our lab here, might be interpretable as applications of a collection of very-high-dimension BU theorem hyperspheres combined to create a latticework of antipodal identities, in which every electron (or other particle) is ultimately linked to every other one. Why? When supervising Richard Feynman's thesis, Wheeler once proposed the wild idea that there is "only one electron in the universe", traveling forward in time as an electron, then backwards from the end of the universe to the beginning as an anti-electron, then bounding forward again as a different electron: is sum, a lattice of antipodal duals whose "podes" are literally the start and end of time itself. Feynman pointed out that there simply is not enough antimatter in the universe to make the symmetry implied by Wheeler's idea possible. But Feynman appreciated the fundamental idea of forwards-and-backwards antipodal time symmetry in electrons to such an extent that it formed the basis of his diagram-based approach to quantum electrodynamics (QED); it can be

interpreted as a smaller-scale application of the idea of a lattice of the BU theorem antipodal "bounce point" identities of electrons and positrons, those two particle types being the forward and backward paths between the antipodes of each interlinked hypersphere.

5.2. Physical properties of the BU theorem explain particle/wave duality in the double slit experiment

Double-slit experiments illustrate the probabilistic nature of quantum mechanical phenomena, as they suggest that light and matter display features of both waves and particles (Ma and Blume, 1995). A wave is split into two separate waves which later recombine into a single wave. The wave nature of light causes the oscillations passing through the slits to interfere (Fig. 3A). Indeed, the Huygens–Fresnel principle allows one to understand each point on a wavefront as generating a secondary wavelet. The disturbance at any subsequent point can be found by summing the contributions of the individual wavelets at that point. When the two waves are in phase, the summed amplitude is maximum; when in anti-phase, they cancel, so that the summed intensity is zero (Ament et al., 2011). These features, known as constructive and destructive interferences, produce bright and dark bands on the detection screen, a result that would not be expected if light consisted of classical particles (Fig. 3C). Light is found to be absorbed as individual particles (not waves) at discrete points of the screen so that th e interference pattern appears through the varying density of particle hits on the detection screen. Therefore, double slit experiments prove the complementarity principle: photons behave as either particles or waves, but cannot be observed as both simultaneously.

Understanding a phenomenon in terms of the BU theorem requires the presence of a few ingredients:

(1) Two manifolds with different dimensions, independent of their curvature (either convex, or flat, or concave).
(2) A continuous function.
(3) A projective force that allows mappings from one dimension to another.
(4) Two (or more) matching features, possibly (but not necessarily) antipodal.

The double-slit experiment's setting provides all the required ingredients (Fig. 3B):

(1) The higher-dimensional manifold stands for the three-dimensional space between the double-slit barrier and the detection screen, and can be described in terms of an S^2 sphere. The lower-dimensional manifold stands for the two-dimensional detection screen $\mathbb{R}^2$.
(2) The required continuous function stands for the relative intensity of the intersecting waves.
(3) The projective force stands for the light trajectories traveling throughout the medium.
(4) The matching features are the areas of the S^2 manifold where the relative intensities are equal. The two features with matching descriptions stand for symmetrical structures endowed in the interfering waves. Indeed, the occurrence of symmetric refraction patterns is in touch with the claims by Revelli et al. (2019), who demonstrated that interference patterns in resonant inelastic x-ray scattering disclose the symmetry of electronic excited states, in the same way as elastic scattering does for the ground state. The single feature, located on the surface of the 2D screen, stands for a single value of relative intensity.

The stripes produced on the screen, caused by repeated shots of single particles, stand for the zones of high (dark stripes) and absent relative intensity (white stripes). Continuous waves, which give rise to the dark stripes on the screen, are produced when the interference is constructive. In turn, when the two waves cancel and their summed intensity is zero (destructive interference), the function becomes discontinuous: therefore, the BU theorem does not hold anymore and the points cannot be detected (white stripes).

The double-slit experiment can be understood in terms of the BU theorem (Fig. 3). When a plane wave crosses two slits of the proper size, it is split in two different waves that interfere with each other and reach the detection screen (Fig. 3A). In a BU theorem account, the two interfering waves are located inside a sphere S^2, in the three-dimensional space between the two slits and the screen (Fig. 3B). The interference patterns detected by Revelli et al. (2019) suggesting that there exist interfering oscillations that display

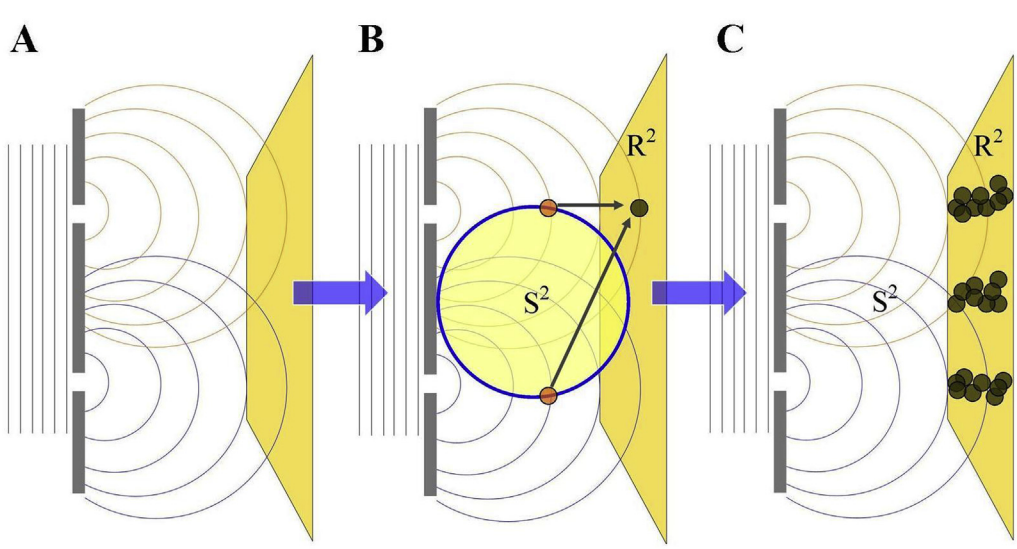

Fig. 3. Topology meets double slit experiments. 3A: A plane wave (or a laser beam) crosses two slits, giving rise to two superimposing oscillations. Fig. 3B describes the BU theorem incarnation of the double slit experiment, while **3C** illustrates the interference pattern caused by bright and dark bands on the detection screen. See text for further details.

matching descriptions in S^2. Quantum mechanics prescribes that when the two waves reach the two-dimensional screen S^2, they generate a single detection point. In BU theorem terms, this means that two features with matching description in S^2 project to a single feature in S^2 (Fig. 3B). Therefore, BU theorem-framed projections describe the counterintuitive quantum notion of light as equipped with both oscillatory and particle-like behavior in the double-slit experiment: the continuous, oscillatory components of the quantum wave are located inside the three-dimensional manifold S^2, while the discrete particle components are located inside the two-dimensional manifold S^2 (Fig. 3C).

This is in touch with relational formulations of quantum mechanics, that suggest relational properties among quantum systems as the most fundamental issue of the microscopic realm (Rovelli, 1996; Smerlak and Rovelli, 2007). This approach, which discards real, observer-independent quantum properties (Yang, 2018), has recently been substantiated by The BIG Bell Test Collaboration's findings (2018). Experimentally detected correlations in Bell tests contradicted local realism, and the claim that the properties of the physical world are independent of our observation does not hold true.

5.3. Collisionless interactions in plasma-like fluids

Plasma, i.e., the fourth state of matter at high energies, is characterized by collective movements of charged particles. Long-range correlations are required to avoid the large disruptive electromagnetic fields in presence of net charge. The collective behavior is governed by the reciprocal influences among nearby charged particles embedded in a "Debye sphere" (Sturrock, 1994; Goldston and Rutherford, 1995). A self-consistent collective electromagnetic field is produced by charged ions inside this system of interacting particles, so that time evolution of long-range interactions can be described by the Vlasov-Maxwell system of equations (Vlasov, 1938). The spontaneous formation of spatial features takes place on a wide range of length scales on the boundary of a metastable state (Cheng and Gamba, 2012): this means that very slight changes in just a few parameters give rise to completely different patterns. Consistent with the concepts developed by high energy physics, the role of collective behaviors of charged particles and long-range functional couplings has been evaluated also in brain dynamics, in terms of McKean-Vlasov equations of macroscopic diffusion, that are derived from the classical Vlasov ones for plasma (Tozzi et al., 2018b; Syková and Nicholson, 2008; deBuyl et al., 2011). In BU theorem terms, when collisionless dynamical structures modify their collective shape and reach the proper conformation, the ensuing topological changes lead to the achievement of antipodal points with matching description (Fig. 4): this explains the spontaneous, cause-free occurrence of the long-range interactions that characterize this type of dynamical systems.

5.4. BU theorem, symmetry and symmetry breaking

Topological explanations allow the removal of energetic requirements in scientific descriptions. Indeed, topological changes have the advantage of describing energetic features not subject to the second law of thermodynamics. This is due to the link between thermodynamics and symmetries. Symmetry, a type of invariance occurring when an object does not change under a set of transformations, is the most general feature of countless types of systems. Symmetries, widespread at every level of organization, can be regarded as the most general feature of systems, more general than free-energy and entropy constraint. The recent observation that, in quasi-static processes, entropy production is strictly correlated with symmetry breaking paves the way to use system invariance for the estimation of enthalpy and energy requirements in computational processing (Roldán et al., 2014).

Symmetry breaking consists of sudden change in the set of available states (Roldán et al., 2014). In a spontaneous symmetry break (SSB), the underlying laws are invariant under a transformation, but the system as a whole is modified. This allows a biophysical structure cast in a symmetric state to end up in an asymmetric one. In the case of finite systems with metastable states, the confinement is not strict: the system can "jump" from one region to another (Friston, 2010; Fraiman and Chialvo, 2012). In the SSB framework, the BU theorem is a welcome benefit, because symmetries can be assessed in terms of antipodal points on a hypersphere. Symmetries (standing for antipodal self-similarities) enclosed in the abstract spaces of n-dimensional spheres can be evaluated in terms of projections on lower-dimensional manifolds (standing for broken symmetries). "Hidden" would be a better term than "broken", because the symmetry is always there. Symmetries, hidden at a lower level, are restored at a higher level of analysis: a symmetry break occurs when symmetry is detectable at one level of observation and "hidden" at another. These steps do not obey to the second law of thermodynamics, nor causal relationships, because the law gets unnoticed during projective topological operations. Once established that energetic issues are correlated with topology, what happens to information when proceeding from higher to lower dimensions? Information decreases, because less dimensions have less coordinates, and therefore less information (for a thorough treatment, see Tozzi and Peters, 2019).

A recent paper studying self-organization and symmetry breaking during intestinal organoid development (Serra et al., 2019) seems to corroborate the usefulness of topological explanations of biophysical dynamics. Intestinal organoids are three-dimensional artificial structures that mimic intestinal cell-type composition and tissue organization. The development of cell populations of organoids derived from a single intestinal stem cell is driven by transient activation of the transcriptional regulator YAP1. When a first symmetry-breaking event occurs (in topological terms, a decrease in dimension), a fraction of identical cells in a symmetrical sphere (in topological terms, features with matching description) differentiate into Paneth cells. The latter generate the stem-cell niche and asymmetric structures, such as crypts and villi. Cell-to-cell variability in YAP1, emerging in symmetrical spheres, leads to symmetry-breaking events and formation of the first Paneth cells. This means that single cells exposed to a uniform growth-promoting environment (in topological terms, a continuous function) display the intrinsic ability to generate emergent, self-organized behavior that results in the formation of complex multicellular asymmetric structures.

5.5. Graph theory comes into play: Kneser graphs and the BU theorem

In combination with graph theory, the BU theorem acquires combinatorial significance that gives rise to fruitful applications in the assessment of topological relationships devoid of causality. This point can be understood by describing dynamical systems obeying the BU theorem in terms of Kneser graphs. The Kneser graph $KG_{n,k}$ is a simple graph whose vertices correspond to the subsets with k elements of a set with n elements, in which two vertices are connected if they correspond to disjoint subsets (Albertson and Boutin, 2007). For example, $KG_{5,2}$ displays five n elements, e.g. $\{1,2,3,4,5\}$, that can be matched in pairs of k-elements subsets, e.g. $\{1,2\}$, $\{3,5\}$, and so on (Fig. 5A). These subset pairs correspond to matching descriptions in the BUT framework. Although vertex- and edge-transitive, a Kneser graph is not as regular as it might appear at first sight. If we start from a vertex and follow the allowed

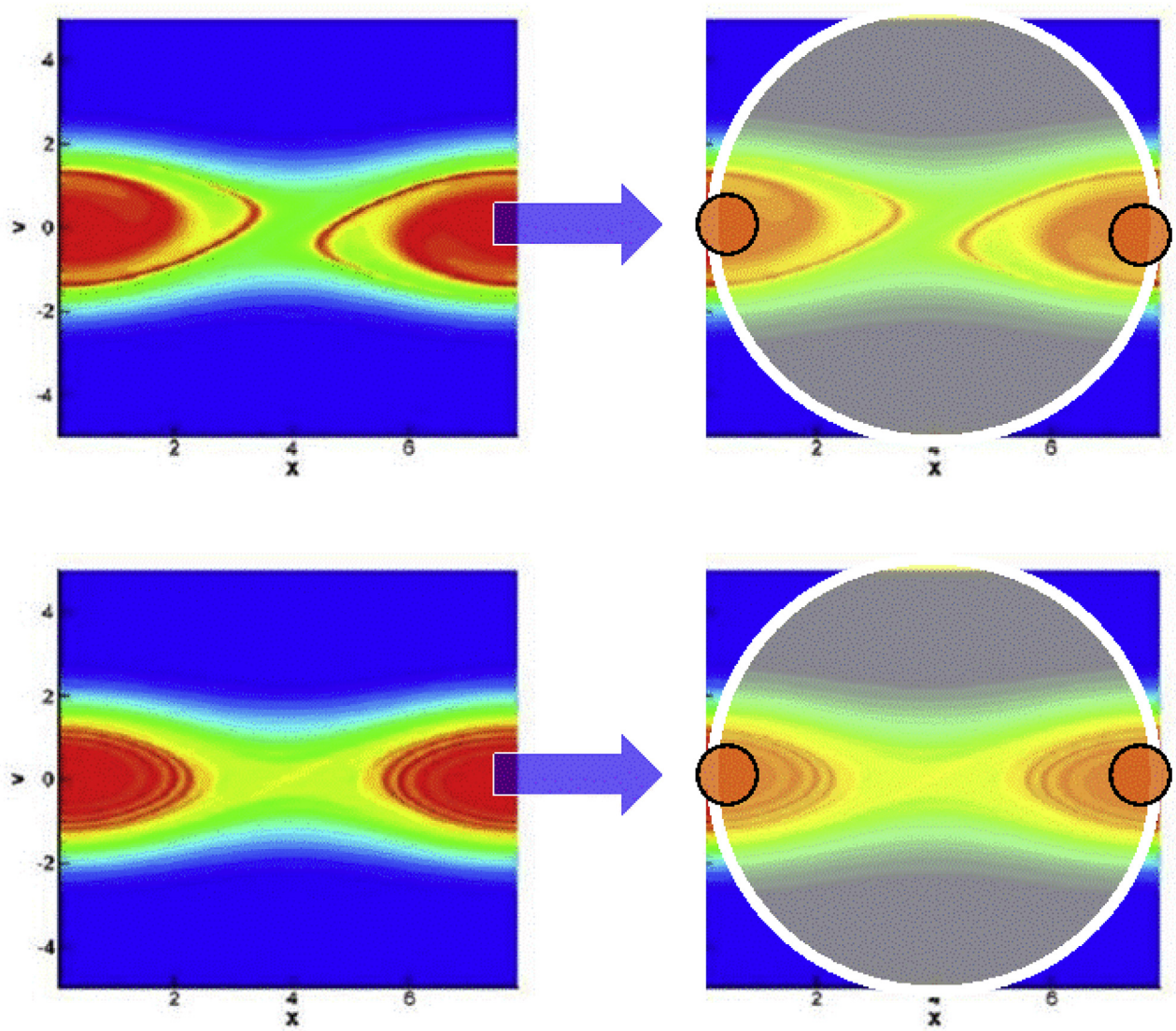

Fig. 4. Left side: two examples of long-range interactions of collective movements of collisionless particles in plasma (modified from Cheng and Gamba, 2012). A slight change in just one or two parameters gives rise to rather different patterns. **Right side**: the BU theorem interpretation of the two examples of collisionless movements. Plasma currents are embedded in spheres equipped with antipodal features displaying matching description (red circles).

trajectories, we notice that the paths are constrained, so that just some dynamical configurations and steps are permitted in a short number of moves. For example, in $KG_{5,2}$, a path starting from one vertex, say $\{1,2\}$, cannot proceed towards $\{1,4\}$ in a single step. The sequence of mandatory "moves" is described by the so-called "chromatic number", that stands for the smallest number of colors needed to paint the vertices, so that no two adjacent vertices share the same color (Skiena, 1990; Pemmaraju and Skiena, 2003). The chromatic number of a generic Kneser graph $KG_{n,k}$ is $n - 2k + 2$for instance, the $KG_{5,2}$ graph requires three colors in any proper coloring (Fig. 5B).

One important property of the Kneser graph is the occurrence of a large gap between the chromatic number $\chi(KG_{n,k})$ and the fractional chromatic number $\chi_f(KG_{n,k})$. The latter stand for the minimum value a/b such that the graph G can be covered by a independent sets, where each vertex occurs in at least b of them. Coloring hypergraphs display strong computational hardness, therefore allowing the quantitative assessment a large number of operations (Fig. 5D). When $n \geq 3k$, and for $n \leq 27$, all the connected Kneser graphs encompass a Hamiltonian cycle, except for $KG_{5,2}$. A Hamiltonian cycle is a traceable, circular path in an undirected or directed graph that visits each vertex exactly once (Fig. 5C). In turn, $KG_{5,2}$. displays a Hamiltonian path, but no Hamiltonian cycle. It is called "hypohamiltonian", meaning that, although it has no Hamiltonian cycle, the deletion of any vertex makes it Hamiltonian (Albertson and Boutin, 2007).

To demonstrate the close relationship between Kneser graphs and the BU theorem, we need to introduce the LST and the Kneser conjecture. The LST guarantees the existence of at least a pair of exactly opposite points on a sphere, as required by the BU theorem. The LST holds for both open and closed sets. The Kneser conjecture states that, whenever the n -subsets of a $(2n + k)$-set are divided into $k + 1$ classes, then two disjoint subsets end up in the same class (Kneser, 1955). In other words, for every $k > 0$ and $n > 2k$, $\chi(KG_{n,k}) = n - 2k + 2$, where χ denotes the chromatic number. The Kneser conjecture for chromatic numbers was solved by Lovász (1978) using the BU theorem. Therefore, there must exist two disjoint k-sets colored i, in touch with the BU theorem's

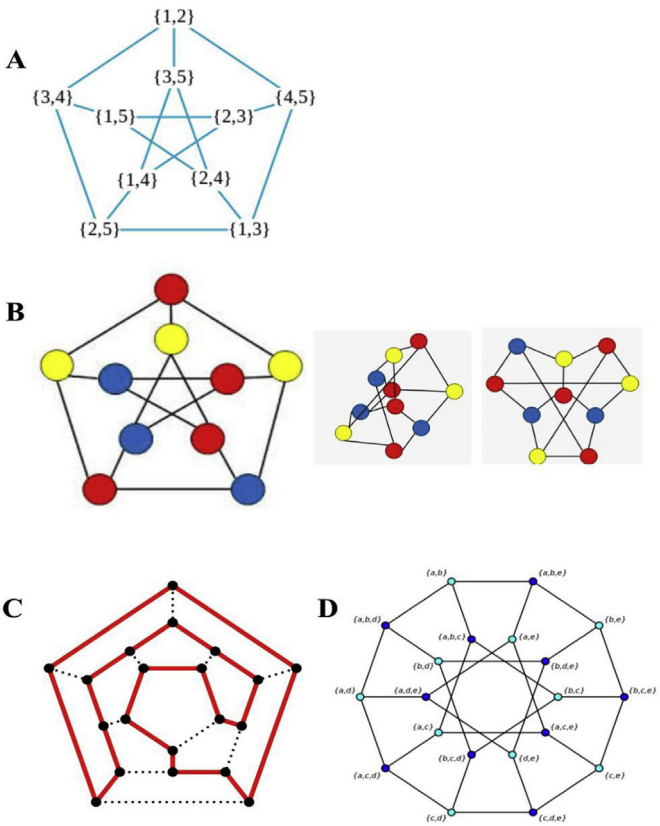

Fig. 5. A: The graph $KG_{5,2}$ is provided as an example for Kneser graphs. Fig. 5B illustrates the required coloring of the vertices. Note that, as shown in the central and right frames, the graph's shape is not constrained: different configurations of vertexes are feasible, provided the relationships among the sub-set *k* elements are kept invariant. Fig. 5C: a Hamiltonian cycle on a dodecahedron. Fig. 5D depicts a more complicated structure, termed the Bipartite Kneser Graph. This means that different possible graphs can be used, depending on the requirement of the experimental setting.
Sources: A: https://fr.wikipedia.org/wiki/Graphe_de_Kneser#/media/File:Kneser-5-2.svg; B: spring-of-mathematics.tumblr.com; C: https://en.wikipedia.org/wiki/Hamiltonian_path#/media/File:Hamiltonian_path.svg; D: https://commons.wikimedia.org/wiki/File:BipartiteKneserGraph.svg

requirement of two points with matching description. Altogether, the dynamics of the BU theorem matching descriptions take place on higher-dimensional systems that display the combinatorial configuration of a Kneser graph. This means that, in a physical/biological dynamical system, only the few trajectories and paths that require the shortest number of steps are allowed. Thus, the dynamical evolution of the system becomes predictable once endowed with a proper representation described by antipodal points generated in higher dimensions.

6. Concluding remarks: when causality fades away

Contemporary approaches to explanations in scientific theories are generally predicated upon causal mechanisms. Here we argued that some important physical and biological phenomena can be explained in terms of their topological properties without resorting to cause and effect relationships. We illustrated how topological theorems and their recently-developed variants can be used to make sense of observed phenomena in physics, biology and neuroscience. In particular, we discussed some implications of the presence of antipodal, fixed and zero-points in dynamical systems, showing how topological-related events, such as shape and dimensions modifications, generate changes in features that obey strict topological requirements. These changes do not require causality, as no forces are needed to mediate the interactions underlying these spontaneous mechanisms. It is noteworthy that in many cases (e.g., soap bubbles, closed random walks and spontaneous brain activity) spatiotemporal shape modifications take place passively, not requiring (internal or external) forces. Variations in shapes are associated with phenomena such as the emergence of symmetries or the occurrence of features with matching description, that can be generated irrespective of energetic constraint. The main points were illustrated with key physical and biological phenomena. The biophysical gist of simple topological concepts allows description of real word phenomena devoid of energetic constraints and cause effect explanations, because proper mappings and projections replace forces and fields in physical and biological dynamics, leading to causality-free scientific explanations.

We described topological theorems and their recently-developed variants, highlighting the possible use in physics, biology, neuroscience. The tremendous power of the BU theorem has been successfully used in many applications, from math to logic, from physics to biology and statistics. This allowed us to throw an operational bridge between the BU theorem and double-slit experiments: a topology-framed explanation suggests that the continuous, oscillatory component of the quantum light wave is located inside a three-dimensional manifold, while the discrete particle component is inside a two-dimensional one. This is in keeping with relational formulations of quantum mechanics, that suggest relational properties among quantum systems as the most fundamental issue of the microscopic realm (Rovelli, 1996; Smerlak and Rovelli, 2007). This approach, that discards real, observer-independent quantum properties (Yang, 2018), has been recently substantiated by The BIG Bell Test Collaboration's findings (2018). Experimentally detected correlations in Bell tests contradict local realism: therefore, the claim that the physical world's properties are independent of our observation does not hold true.

A recent paper published in Nature, that examines self-organization and symmetry breaking during intestinal organoid development, seems to corroborate the expediency of our topological framework when approaching biophysical dynamics. Intestinal organoids are three-dimensional artificial structures that mimic intestinal cell-type composition and tissue organization. Serra et al. (2019) analyzed self-organizing development of cell populations of organoids derived from a single intestinal stem cell, driven by transient activation of the transcriptional regulator YAP1. When a first symmetry-breaking event occurs (in topological terms, a decrease in dimensions), a fraction of identical cells in a symmetrical sphere (in topological terms, features with matching description) differentiate into Paneth cells. The latter generate the stem-cell niche and asymmetric structures, such crypts and villi. Cell-to-cell variability in YAP1, emerging in symmetrical spheres, leads to symmetry-breaking events and formation of the first Paneth cells. Therefore, single cells exposed to a uniform growth-promoting environment (in topological terms, a continuous function) display the intrinsic ability to generate emergent, self-organized behavior that results in the formation of complex multicellular asymmetric structures.

Further theoretically feasible applications of topological explanations can be proposed in domains including sociology and earth geology. For instance, sociological phenomena might be not just cause and effect relationships, but also topological changes in temporal paths. This could lead to projection-based description of events, rather than causality-related mappings and projections, instead of forces. Consistent with this claim, the role of virus–virus interactions has been recently addressed in antiviral immunity (Domingo-Calap et al., 2019). The authors demonstrated that viral

escape from interferon (IFN)-based innate immunity is a social process, in which IFN-stimulating viruses determine the fitness and altruistic traits of neighboring ones. The link with the BU theorem is patent, if we take into account that, in well-mixed populations, spatial structure determines whether IFN shutdown can evolve. Therefore, fundamental social evolution rules dictated by shape constraints govern viral innate immunity evasion. Concerning earth geology, Aubert and Finlay (2019) studied geomagnetic jerks, i.e., abrupt changes in the second time derivative - the secular acceleration - of Earth's magnetic field. Recent jerks have been linked to short-lived, temporally alternating and equatorially localized pulses of secular acceleration observed in satellite data, associated with rapidly alternating flows at Earth's core surface. The authors showed that jerks could be caused by the arrival of localized Alfvén wave packets radiated from sudden buoyancy releases inside the core. This means that an interaction occurs between slow core convection and rapid hydromagnetic waves. The possibility to reproduce jerks in terms of the BU theorem offers a new way to probe the physical properties of Earth's deep interior.

In conclusion, we described how topological abstract theorems work in the real world, arguing that biophysical connotations of topological modifications do not require cause effect relationships: this permits us to cope with the deep uncertainty frequently detected during the scientific assessment of countless systems. Important issues still to be addressed are those of temporal emergence and scale-dependence of topological explanations, the main point being that each explanation, causal, mechanistic, topological etc. of a given phenomenon may be optimal in a given context or at a given scale, but may not rule out the validity of other explanations at other levels. For instance, while topological explanations may under certain circumstances be valid when considering "time snapshots" to assert that these relationships cannot be assessed using ordinary cause and effect, the development of the smoothness-dominated metrical fields over which such assertions can be made require powerful application of temporal causality over a broad scale. Embedding cell division and double-slit quantum interference examples within historical time leads to models in which relationships become long-term examples of globally constrained traditional cause effect, with such causality exhibiting itself the emergence of smooth metrics that are locally micro-scale cause and effect-based and entropic. This would not invalidate the importance of a more "snapshot-based" assessment of the resulting topologies, but it would add important details that would relate such assessments more specifically and more carefully to traditional cause effect relationships.

References

Alaoglu, L., Birkhoff, G., 1940. General ergodic theorems. Ann. Math. 41 (2), 293–309.

Albertson, M.O., Boutin, D.L., 2007. Using determining sets to distinguish Kneser graphs. Electron. J. Combinator 14 (1), R20. MR 2285824.

Ament, L.J.P., van Veenendaal, M., Devereaux, T.P., Hill, J.P., van den Brink, J., 2011. Resonant inelastic x-ray scattering studies of elementary excitations. Rev. Mod. Phys. 83, 705.

Amir, A., Hatano, N., Nelson, D.R., 2016. Non-Hermitian localization in biological networks. Phys. Rev. E 93. https://doi.org/10.1103/PhysRevE.93.042310, 042310.

Anishkin, A., Sukharev, S., 2004. Water dynamics and dewetting transitions in the small mechanosensitive channel MscS. Biophys. J. 86, 2883–2895.

Arenas, A., Díaz-Guilera, A., Kurths, J., Moreno, Y., Zhou, C., 2008. Synchronization in complex networks. Phys. Rep. 469, 93–153.

Aryal, P., Sansom, M.S., Tucker, S.J., 2015. Hydrophobic gating in ion channels. J. Mol. Biol. 427, 121–130.

Aubert, J., Finlay, C.C., 2019. Geomagnetic jerks and rapid hydromagnetic waves focusing at Earth's core surface. Nat. Geosci. 12, 393–398.

Autrecourt, Nicholas of About 1340, 1971. The Universal Treatise. Marquette University Press, Milwaukee, Wisconsin.

Barth, A., 1923. Vorlesungen über Gastheorie. Leipzig: 1898. OCLC 01712811. ('Ergoden' on p.89 in the 1923 reprint).

Bartoletti, M., Cimoli, T., Pinna, G.M., Zunino, R., 2015. Models of circular causality. In: International Conference on Distributed Computing and Internet Technology. Springer, Cham, pp. 1–20.

Beyer, W.A., Zardecki, A., 2004. The early history of the ham sandwich theorem. Am. Math. Mon. 111 (1), 58–61.

Bianco, S., Ignaccolo, M., Rider, M.S., Ross, M.J., Winsor, P., Grigolini, P., 2007. Brain, music, and non-Poisson renewal processes. Phys. Rev. E 75, 061911.

Boccaletti, S., Latora, V., Moreno, Y., Chavez, M., Hwang, D.U., 2006. Complex networks: structure and dynamics. Phys. Rep. 424 (4–5), 175–308.

Boreyko, J.B., Baker, C.H., Poley, C.R., Chen, C.H., 2011. Wetting and dewetting transitions on hierarchical superhydrophobic surface. Langmuir 27, 7502–7509.

Bormashenko, E., 2015. Surface instabilities and patterning at liquid/vapor interfaces: exemplifications of the "hairy ball theorem". Colloids. Interface Sci. Commun. 5, 5–7. https://doi.org/10.1016/j.colcom.2015.04.003. March 2015.

Borsuk, K., 1933. Drei sätze über die n-dimensionale euklidische sphare. Fundam. Math. XX, 177–190.

Borsuk, K., 1969. Fundamental retracts and extensions of fundamental sequences. Fundum. Math. 64 (1), 55–85.

Bourbaki, N., 1966. Elements of Mathematics. General Topology 1, Chapters 1–4. Translated from the French. Reprint of the 1966 Edition. Springer-Verlag, Berlin, ISBN 3-540-19374-X, 1989. viii+437, MR0979294.

Box, K., Joyce, B.W., Devenport, D., 2019. Epithelial geometry regulates spindle orientation and progenitor fate during formation of the mammalian epidermis. eLife 8, e47102. https://doi.org/10.7554/eLife.47102.

Bredon, G.E., 1997. Topology and Geometry, Corrected 3rd Printing of the 1993 Original. Graduate Texts in Mathematics. Springer-Verlag, NY xiv + 557 pp., MR 1700700.

Brookes E, Riccio A. Location, location, location: nuclear structure regulates gene expression in neurons. Curr. Opin. Neurobiol.. Https://doi.org/10.1016/j.conb.2019.03.009.

Cao, Y., Fatemi, V., Fang, S., Watanabe, K., Taniguchi, T., et al., 2018. Unconventional superconductivity in magic-angle graphene superlattices. Nature volume 556, 43–50.

Cheng, Y., Gamba, I.M., 2012. Numerical study of one-dimensional Vlasov–Poisson equations for infinite homogeneous stellar systems. Commun. Nonlinear Sci. Numer. Simul. 17 (2012), 2052–2061.

Collins, G.P., 2006. Computing with quantum knots. Sci. Am. 294 (4), 56–63.

Crabb, M.C., Jawaworski, J., 2013. Aspects of the Borsuk-Ulam theorem. J. of Fixed Point Theory and Applications 13, 459–488. https://doi.org/10.1007/s11784-013-0130-7. MR3122336.

Davies, E.C., Rowe, P.H., James, S., et al., 2011. An investigation of disagreement in causality assessment of adverse drug reactions. Pharm. Med. 25 (1), 17–24. https://doi.org/10.2165/11539800-000000000-00000.

de Buyl, P., Mukamel, D., Ruffo, S., 2011. Statistical mechanics of collisionless relaxation in a non-interacting system. Phil. Trans. R. Soc. A 2011 369, 439–452. https://doi.org/10.1098/rsta.2010.0251.

Dodson, C.T.J., Parker, P.E., 1997. A User's Guide to Algebraic Topology. Kluwer, Dordrecht, Netherlands, ISBN 0-7923-4292-5, 1997, xii+405 pp, MR1430097.

Domingo-Calap, P., Segredo-Otero, E., Durán-Moreno, M., Sanjuán, R., 2019. Social evolution of innate immunity evasion in a virus. Nature Microbiology.

Donato, I., Gori, M., Pettini, M., Petri, G., De Nigris, S., Franzosi, R., Vaccarino, F., 2016. Persistent homology analysis of phase transitions. Phys. Rev. E 93 (5), 052138.

Einstein, A., 1936. Lens-like action of a star by the deviation of light in the gravitational field. Science 84 (2188), 506–507.

Eisenberg, M., Guy, R., 1979. A proof of the hairy ball theorem. Am. Math. Mon. 86 (7), 571–574. https://doi.org/10.2307/2320587.

Feller, W., 1971. An Introduction to Probability Theory and its Applications, vol. 2. Wiley.

Fraiman, D., Chialvo, D.R., 2012. What kind of noise is brain noise: anomalous scaling behavior of the resting brain activity fluctuations. Front. Physiol. 3, 307.

Frank-Kamenetskii, M.D., 2013. RNA topology. Artif. DNA PNA XNA 4 (2), 35–36. https://doi.org/10.4161/adna.24680, 2013 Apr 1.

Franzinelli, A., 1958. Questioni inedite di Giovanni de Mirecourt sulla conoscenza (Sent. I, q. 2–6). In: Franzinelli, A. (Ed.), I Sent., Qq. 2–6, Rivista Critica di Storia della Filosofia, 13/3, pp. 319–340.

Franzosi, R., Pettini, M., Spinelli, L., 2000. Topology and phase transitions: paradigmatic evidence. Phys. Rev. Lett. 84 (13), 2774.

Freddoso, A.J., 1988. Medieval aristotelianism and the case against secondary causation in nature. In: Morris, T.V. (Ed.), Divine and Human Action: Essays in the Metaphysics of Theism. Cornell University Press, Ithaca, NY, pp. 74–118.

Friston, K., 2010. The free-energy principle: a unified brain theory? Nat. Rev. Neurosci. 11 (2), 127–138.

Gaiha, G.D., Rossin, E.J., Urbach, J., Landeros, C., Collins, D.R., et al., 2019. Structural topology defines protective CD8+ T cell epitopes in the HIV proteome. Science 3 (6439), 480–484. https://doi.org/10.1126/science.aav5095, 364.

Gibson, J.J., 1950. The Perception of the Visual World. Greenwood Press, Westpost, Conn.

Gibson, J.J., 1979. The Theory of Affordance in the Ecological Approach to Visual Perception. Erlbaum, Hillsdale.

Gibson, J.J., 1986. The Ecological Approach to Visual Perception. Houghton-Mifflin, Boston.

Goldston, R.J., Rutherford, P.H., 1995. Introduction to Plasma Physics. CRC Press, Plasma Physics Series.

Golubitsky, M., Stewart, I., 2015. Recent advances in symmetric and network dynamics. Chaos 25 (9), 097612.

Gong, Z., Ashida, Y., Kawabata, K., Takasan, K., Higashikawa, S., Ueda, M., 2018.

Topological phases of non-Hermitian systems. Phys. Rev. X 8, 031079.
Gonzalez-Rodriguez, D., Maddugoda, M.P., Stefani, C., Janel, S., Lafont, F., Cuvelier, D., Lemichez, E., Brochard-Wyart, F., 2012. Cellular dewetting: opening of macro-apertures in endothelial cells. Phys. Rev. Lett. 25 (21), 218105, 108.
Gross, D.J., 1996. The role of symmetry in fundamental physics. Proc. Natl. Acad. Sci. U.S.A. 93 (25), 14256–14259.
Haider, B., Duque, A., Hasenstaub, A.R., McCormick, D.A., 2006. Neocortical network activity in vivo is generated through a dynamic balance of excitation and inhibition. J. Neurosci. 26, 4535–4545. https://doi.org/10.1523/JNEUROSCI.5297-05.2006.
Huneman, P., 2010. Topological explanations and robustness in biological sciences. Synthese 177 (2), 213–245.
Jiang, Y., Lai, X., Watanabe, K., Taniguchi, T., Haule, K., et al., 2019. Charge order and broken rotational symmetry in magic-angle twisted bilayer graphene. Nature 573, 91–95, 2019.
Kneser, M., 1955. Aufgabe 300. Jahresber. Dtsch. Math. Ver. 58.
Kostić, D., 2018. Mechanistic and topological explanations: an introduction. Synthese 195 (1), 1–10.
Lapierre, F., Coffinier, J., Boukherroub, R., Thomy, V., 2013. Electro- (de)wetting on Superhydrophobic surfaces. Langmuir 29, 13346–13351.
Laver, M., Forgan, E.M., 2010. Magnetic flux lines in type-II superconductors and the 'hairy ball' theorem. Nat. Commun. 1. Article number: 45.
Li, J., Ha, N.S., Liu, T.L., van Dam, R.M., Kim, C.-J., 2019. Ionic-surfactant-mediated electro-dewetting for digital microfluidics. Nature 572, 507–510.
Loke, Y.K., 2012. Adverse drug reactions. Br. J. Clin. Pharmacol. 73 (6), 908–911. https://doi.org/10.1111/j.1365-2125.2012.04235.x, 2012 Jun.
Lovász, L., 1978. Kneser's conjecture, chromatic numbers and homotopy. J. Comb. Th. A 25, 319–324.
Ma, Y., Blume, M., 1995. Interference of fluorescence x rays and coherent excitation of core levels. Rev. Sci. Instrum. 66, 1543.
Marzetti, L., Del Gratta, C., Nolte, G., 2008. Understanding brain connectivity from EEG data by identifying systems composed of interacting sources. Neuroimage 42, 87–98. https://doi.org/10.1016/j.neuroimage.2008.04.250, 2008.
Matoušek, J., 2003. Using the Borsuk-Ulam Theorem. Lectures on Topological Methods in Combinatorics and Geometry. Written in Cooperation with Anders Björner and Günter M. Ziegler. Springer-Verlag, Berlin, ISBN 3-540-00362-2, 2003. xii+196, MR1988723.
McKay, Chris P., 2004. What is life—and how do we search for it in other worlds? PLoS Biol. 2 (2), 302. https://doi.org/10.1371/journal.pbio.0020302 (9).
McMichael, A.J., Carrington, M., 2019. Topological perspective on HIV escape. Science 364 (6439), 438–439. https://doi.org/10.1126/science.aax4989.
Meyer, Y., Rivière, T., 2003. Partial regularity results for a class of stationary Yang-Mills fields in high dimension. Rev. Matemática Iberoam. 19, 195–219.
Miri, M.-A., Alù, A., 2019. Exceptional points in optics and photonics. Science 363 (6422), eaar7709. https://doi.org/10.1126/science.aar7709.
Mohan, K., Ueda, G., Kim, A.R., Jude, K.M., Fallas, A.J., et al., 2019. Topological control of cytokine receptor signaling induces differential effects in hematopoiesis. Science 364 (6442). https://doi.org/10.1126/science.aav7532 eaav7532.
Mouton, J.P., Mehta, U., Rossiter, D.P., Maartens, G., Cohen, K., 2017. Interrater agreement of two adverse drug reaction causality assessment methods: a randomised comparison of the liverpool adverse drug reaction causality assessment tool and the world health organization-uppsala monitoring centre system. PLoS One 12 (2), e0172830. https://doi.org/10.1371/journal.pone.0172830.eCollection.2017, 2017 Feb 24.
Naranjo, C.A., Busto, U., Sellers, E.M., Sandor, P., Ruiz, I., et al., 1981. A method for estimating the probability of adverse drug reactions. Clin. Pharmacol. Ther. 30 (2), 239–245, 1981 Aug.
Nebeker, J.R., Barach, P., Samore, M.H., 2004. Clarifying adverse drug events: a clinician's guide to terminology, documentation, and reporting. Ann. Intern. Med. 140 (10), 795–801. https://doi.org/10.7326/0003-4819-140-10-200405180-00017. PMID 15148066.
Ockham of W, 1974. In: Boehner, Philotheus, Gedeon, Gál, et al. (Eds.), Opera Philosophica, vol. I. Franciscan Institute, St. Bonaventure, NY.
Papo, D., 2019. Gauging functional brain activity: from distinguishability to accessibility. Front. Physiol. 10, 509.
Pecora, L.M., Carroll, T.L., 1998. Master stability functions for synchronized coupled systems. Phys. Rev. Lett. 80 (10), 2109.
Pemmaraju, S., Skiena, S., 2003. Computational Discrete Mathematics: Combinatorics and Graph Theory in Mathematica. Cambridge University Press, Cambridge, England.
Peters, J.F., 2016. Computational proximity. Excursions in the topology of digital images. In: Intelligent Systems Reference Library. Springer-Verlag, Berlin. https://doi.org/10.1007/978-3-319-30262-1.
Peters, J.F., Tozzi, A., 2016. Quantum entanglement on a hypersphere. Int. J. Theor. Phys. 1–8. https://doi.org/10.1007/s10773-016-2998-7.
Peters, J.F., Tozzi, A., Ramanna, S., Inan, E., 2017. The human brain from above: an increase in complexity from environmental stimuli to abstractions. Cogn. Neurodynamics 11 (4), 391–394. https://doi.org/10.1007/s11571-0-17-9428-2.
Pettini, G., Gori, M., Franzosi, R., Clementi, C., Pettini, M., 2019. On the origin of phase transitions in the absence of symmetry-breaking. Phys. A Stat. Mech. Appl. 516, 376–392.
Popkin, R.H., Maia Neto, J.R. (Eds.), 2007. Skepticism: an Anthology. Prometheus Books, ISBN 1591024749 (ISBN13: 9781591024743).
Rao, S., Klesse, G., Stansfeld, P.J., Tucker, S.J., Sansom, M.S.P., 2019. A heuristic derived from analysis of the ion channel structural proteome permits the rapid identification of hydrophobic gates. PNAS July 9 (28), 13989–13995. https://doi.org/10.1073/pnas.1902702116, 2019 116.
Revelli, A., Moretti Sala, M., Monaco, G., Becker, P., Bohatý, L., et al., 2019. Resonant inelastic x-ray incarnation of Young's double-slit experiment. Sci. Adv. 5 (1), eaav4020 https://doi.org/10.1126/sciadv.aav4020.
Robinson, M., 2013. Topological Signal Processing. Springer, Berlin.
Roldán, E., Martínez, I.A., Parrondo, J.M.R., Petrov, D., 2014. Universal features in the energetics of symmetry breaking. Nat. Phys. 10, 457–461. https://doi.org/10.1038/nphys2940.
Rovelli, C., 1996. Relational quantum mechanics. Int. J. Theor. Phys. 35, 1637–1678.
Russo Krauss, C., 2015. L'empiriocriticismo di Richard Avenarius tra psicofisiologia e teoria della consocenza. In: Avenarius, R. (Ed.), Il concetto umano di mondo. Morcelliana, Brescia.
Sackmann, E., Bruinsma, R.F., 2002. Cell adhesion as wetting transition? ChemPhysChem 12, 262–269.
Saedder, E.A., Lisby, M., Nielsen, L.P., Bonnerup, D.K., Brock, B., 2015. Number of drugs most frequently found to be independent risk factors for serious adverse reactions: a systematic literature review. Br. J. Clin. Pharmacol. 80 (4), 808–817. https://doi.org/10.1111/bcp.12600.PMCID:PMC4594723, 2015 Oct.
Sengupta, Biswa, Tozzi, Arturo, Cooray, Gerald K., Douglas, Pamela K., Friston, Karl J., 2016. Towards a neuronal gauge theory. PLoS Biol. 14 (3), e1002400 https://doi.org/10.1371/journal.pbio.1002400.
Serra, D., Mayr, U., Boni, A., Lukonin, I., Rempfler, M., et al., 2019. Self-organization and symmetry breaking in intestinal organoid development. Nature 569, 66–72. https://doi.org/10.1038/s41586-019-1146-y.
Sharmaa, A., Reiterb, G., 1996. Instability of thin polymer films on coated substrates: rupture, dewetting, and drop formation. JColloid Interface Sci178, 383–399.
Skiena, S., 1990. Implementing Discrete Mathematics: Combinatorics and Graph Theory with Mathematica. Addison-Wesley, Reading, MA.
Smerlak, M., Rovelli, C., 2007. Relational EPR. Found. Phys. 37, 427–445.
Sturrock, P.A., 1994. Plasma Physics: an Introduction to the Theory of Astrophysical. Geophysical & Laboratory Plasmas. Cambridge University Press, ISBN 978-0-521-44810-9.
Syková, E., Nicholson, C., 2008. Diffusion in brain extracellular space. Physiol. Rev. 88 (4), 1277–1340. https://doi.org/10.1152/physrev.00027.2007.
Tanaka, H., Nelson, D.R., 2018. Non-Hermitian Quasi-Localization and Ring Attractor Neural Networks arXiv:1811.07433.
Tanaka, M., Rehfeldt, F., Schneider, M.F., Mathe, G., Albersdorfer, A., Neumaier, K.R., Purrucker, O., Sackmann, E., 2005. Wetting and dewetting of extracellular matrix and glycocalix models. J. Phys. Condens. Matter 17, 9.
Tao, T., Tian, G., 2004. A singularity removal theorem for Yang-Mills fields in higher dimensions. J. Am. Math. Soc. 17 (3), 557–593.
The BIG Bell Test Collaboration, 2018. Challenging local realism with human choices. Nature 557, 212–216.
Thiam, A.R., Farese Jr., R.V., Walther, T.C., 2013. The biophysics and cell biology of lipid droplets. Nat RevMolecular Cell Biol 14, 775–786.
Thompson, C.V., 2012. Solid-state dewetting of thin films. Ann. Rev.Mater. Res. 42, 399–434.
Tognoli, E., Kelso, J.A.S., 2014. Enlarging the scope: grasping brain complexity. Front. Syst. Neurosci. https://doi.org/10.3389/fnsys.2014.00122.
Tozzi, A., 2019. The multidimensional brain. Phys. Life Rev. https://doi.org/10.1016/j.plrev.2018.12.004.
Tozzi, A., Peters, J.F., 2016a. A topological approach unveils system invariances and broken symmetries in the brain. J. Neurosci. Res. 94 (5), 351–365. https://doi.org/10.1002/jnr.23720.
Tozzi, A., Peters, J.F., 2016b. Towards a fourth spatial dimension of brain activity. Cogn. Neurodynamics 10 (3), 189–199. https://doi.org/10.1007/s11571-016-9379-z.
Tozzi, A., Peters, J.F., 2017a. From abstract topology to real thermodynamic brain activity. Cogn. Neurodynamics 11 (3), 283–292. https://doi.org/10.1007/s11571-017-9431-7.
Tozzi, A., Peters, J.F., 2017b. Towards topological mechanisms underlying experience acquisition and transmission in the human brain. Integr. Psychol. Behav. Sci. 51 (2), 303–323. https://doi.org/10.1007/s12124-017-9380-z.
Tozzi, A., Peters, J.F., 2019. The Borsuk-Ulam theorem solves the curse of dimensionality: comment on "the unreasonable effectiveness of small neural ensembles in high-dimensional brain" by Alexander N. Gorban et al. Phys. Life Rev. https://doi.org/10.1016/j.plrev.2019.04.008.
Tozzi, A., Peters, J.F., Jausovec, N., 2016. A repetitive modular oscillation underlies human brain electric activity. Neurosci. Lett. 653, 234–238. https://doi.org/10.1016/j.neulet.2017.05.051.
Tozzi, A., Peters, J.F., Fingelkurts, A.A., Fingelkurts, A.A., Marijuán, P.C., 2017. Topodynamics of metastable brains. Phys. Life Rev. 21, 1–20. https://doi.org/10.1016/j.plrev.2017.03.001.
Tozzi, A., Peters, J.F., Fingelkurts, A., Fingelkurts, A., Perlovsky, L., 2018a. Syntax meets semantics during brain logical computations. Progr. Biophys. Mol. Biol. 140, 133–141. https://doi.org/10.1016/j.pbiomolbio.2018.05.010.
Tozzi, A., Peters, J.F., Deli, E., 2018b. Towards plasma-like collisionless trajectories in the brain. Neurosci. Lett. 662, 105–109. https://doi.org/10.1016/j.neulet.2017.10.016.
Trifonov, E.N., 2012. Definition of life: navigation through uncertainties. J. Biomol. Struct. Dyn. 29 (4), 647–650. https://doi.org/10.1080/073911012010525017. Adenine Press.
Uhlenbeck, K., 1982a. Connections with L^p bounds on curvature. Commun. Math. Phys. 83 (1), 31–42.

Uhlenbeck, K., 1982b. Removing singularities in Yang-Mills fields. Commun. Math. Phys. 83, 11–29.
Van Fraassen, B.C., 1977. The pragmatics of explanation. Am. Phil. Q. 14 (2), 143–150.
Vargas, J.N., Seemannab, R., Fleury, J.B., 2014. Fast membrane hemifusion via dewetting between lipid bilayers. Soft Matter 10, 9293–9299.
Vlasov, A.A., 1938. On vibration properties of electron gas. J. Exp. Theor. Phys. 8 (3), 291.
Voloviko, Yu, A., 2008. Borsuk-ulam implies brouwer: a direct construction revisited. Am. Math. Mon. 115 (6), 553–556. https://doi.org/10.2307/2975293.
Walters, P., 1982. An Introduction to Ergodic Theory. Springer, ISBN 0-387-95152-0.
Yang, J.M., 2018. A relational formulation of quantum mechanics. Sci. Rep. 8, 13305.
Young, T., Hua, L., Huang, X., Abel, R., Friesner, R., Berne, B.J., 2010. Dewetting transitions in protein cavities. Proteins 78, 1856–1869.
Zhang, L., Motter, A.E., Nishikawa, T., 2017. Incoherence-mediated remote synchronization. Phys. Rev. Lett. 118, 174102.

Author's personal copy

Cognitive Neurodynamics (2020) 14:339–345
https://doi.org/10.1007/s11571-020-09574-w

RESEARCH ARTICLE

Removing uncertainty in neural networks

Arturo Tozzi[1] · James F. Peters[2,3]

Received: 23 August 2019 / Revised: 24 January 2020 / Accepted: 19 February 2020 / Published online: 27 February 2020
© Springer Nature B.V. 2020

Abstract

Neuroscientists draw lines of separation among structures and functions that they judge different, arbitrarily excluding or including issues in our description, to achieve positive demarcations that permits a pragmatic treatment of the nervous activity based on regularity and uniformity. However, uncertainty due to disconnectedness, lack of information and absence of objects' sharp boundaries is a troubling issue that prevents these scientists to select the required proper sets/subsets during their experimental assessment of natural and artificial neural networks. Starting from the detection of metamorphoses of shapes inside a Euclidean manifold, we propose a technique to detect the topological changes that occur during their reciprocal interactions and shape morphing. This method, that allows the detection of topological holes development and disappearance, makes it possible to solve the problem of uncertainty in the assessment of countless dynamical phenomena, such as cognitive processes, protein homeostasis deterioration, fire propagation, wireless sensor networks, migration flows, and cosmic bodies analysis.

Keywords Holes · Grid · Homology · Shapes · Uncertainty

Introduction

Demarcation among objects and things is somewhat arbitrary, because our mind tends to exclude the continuity among hidden or unknown structures of the world (Fort 1919; Popkin and Maia Neto 2007; Autrecourt 1340; Tozzi and Peters 2019). In touch with set theory, observers tend to spatially and temporally split the set of the entire world in different, sometimes arbitrary, subsets. This concept seems straightforward in math, and in particular in topology, where, the Jordan theorem states that exist an "inside" and an "outside" region (Ghrist 2014; Arkhangelskii 2001; Terasawa 2004). The tremendous power of topological set and cell complex theory (Peters 2018a, b; Cooke and Finney 1967; Alexandroff 1961) has been successfully used in many applications, from math to logic, from physics to biology, from neuroscience to statistics. In a covering of a finite, bounded plane region, for example, there are three elementary cells to consider, namely, 0-cells (vertexes), 1-cells (edges) and 2-cells (filled triangles). The core of set and cell complex theory lies in the occurrence of path-connected sets or subsets on surfaces containing punctures (holes), i.e., the presence of elements which are (more or less arbitrarily) joined together and separated from the external environment. There is an analogy between usual presence of tiny pores (punctures) in physical surfaces and aberrant surface punctures (large holes) and, for example, protein homeostasis in the human body, namely, healthy neuronal homeostasis versus aberrant neuronal perturbations (Harnack et al. 2015) and cellular mechanics (translation, folding and clearance) of the proteome (Morimoto and Cuervo 2009).

A serious problem arises when we grasp that, in many applications, a system's object shapes are unknown and apparently disconnected, making it very difficult to find and recognize the proper subtending sets' very presence and/or dynamics (Déli et al. 2017; Wang and Hu 2019).

✉ Arturo Tozzi
tozziarturo@libero.it; Arturo.Tozzi@unt.edu

James F. Peters
James.peters3@umanitoba.ca

1 Center for Nonlinear Science, Department of Physics, University of North Texas, 1155 Union Circle, #311427, Denton, TX 76203-5017, USA

2 Department of Electrical and Computer Engineering, University of Manitoba, Winnpeg, MB R3T 5V6, Canada

3 Department of Mathematics, Adıyaman University, 02040 Adıyaman, Turkey

Author's personal copy

The boundaries of object shapes may be very irregular and indistinct, leading to a knowledge of the split between shape interiors and boundaries which hampers shape approximation and measurement (Tozzi and Peters 2017; Rao 2018; Sen et al. 2019). In this paper, we will start from moving objects, i.e., features which can be described by a function from time to its corresponding spatial object (Gäuting et al. 2000). Similarly, a moving region related to a moving object displays mappings from time to a region object, i.e., a feature consisting of one or several connected components called faces, each of which may or may not have holes inside it (Schneider and Behr 2006). In this paper, in order to tackle the painstaking issues related to unavailable topological spatial relationships and intrinsic uncertainty, we tackle the goal to assess the trajectories of undefined/disjointed/disconnected sets or subsets: in particular, we consider changes in topological features of two unknown spatial shapes moving inside a two-dimensional grid.

Materials and methods

Several approaches to the study of moving and region objects use procedures of data analysis arising from persistent homology, whose early roots (for connected components) trace back to SizeTheory (Verri et al. 1993; Verri and Uras 1997), later generalized to higher dimensions (Edelsbrunner et al. 2002; Edelsbrunner and Morozov 2012). Among the models which assess topological relationships, i.e., the topological properties of a given spatial relationship (Corcoran and Jones 2018), the most successful are the Intersection Model (Egenhofer 1991) and the Region Connection Calculus (Randell et al. 1992). Still, both these approaches and their generalizations (Schneider and Behr 2006) assume that the locations of connected objects, modeled as subsets of R^2, are accurately known. This is not always the case, because confounding factors may cause uncertainty in spatial data detection: among them, the most significant are incompleteness, due to lack of information, and vagueness, resulting from objects not having crisp or sharp boundaries (Worboys 1998). We aim to evaluate spatial objects whose geometries and shapes change over time: we will term these objects with the above-mentioned definition of moving regions (Liu and Schneider 2011) and will propose a model able to detect their conceivable topological modifications.

In technical terms, our goal was to achieve topological features to describe intersection or union of spatial moving disconnected regions in a two-dimensional Abelian lattice. At first, we built a two-dimensional grid made by 10×10 squares, each standing for a single pixel. The grid is composed of 100 white squares, representing empty locations. We randomly generated a pair of two-dimensional objects with different shapes, free to move inside the grid with unpredictable trajectories. The presence and movements of object shapes inside a video frame are pinpointed in terms their centers of mass (centroids). Over time, the shadows of shapes can overlap and sometimes merge, depending on the reflections (projections of the light blocked by the shapes). We benefited from the fact that a moving region whose location and extend change over time can imply topological changes such as hole formation and disappearance.

Hole detection was based on snapshots captured at instants termed observations. We formally defined a basic topological change, i.e., hole formation, between two consecutive observations (Amad and Peters 2018; Peters 2020). A hole is a bounded surface region that absorbs light. Shapes themselves are defined by their surface holes (e.g., spaces between an automobile grid, tire well, open windows). The detection method, modified from Gäuting et al. (2000), uniquely maps a unit, by partitioning the observations before and after the changes. A moving region can have different holes at different time intervals, and different changes between two same states may occur. For example, from a simple region to asingle region with holes, either a hole is formed inside the region (termed *hole form*), or the region touches itself at two ends (termed *region self-touch*).

The grid was equipped with sensors able to detect just a single feature: an empty square (a white pixel) fully surrounded by eight filled squares (red pixels). In other words, optical sensors, unable to detect object's shapes, occurrence and movements, are able to spot just the dynamical presence and disappearance of holes in the grid. Here follows the sensors' detection algorithm. At the Earth's near-ground level, holes can be found in surface object punctures and atmospheric water vapor puncture. From a video camera perspective, holes are regions that absorb light (Peters 2020). Both types of holes vary minutely in size and extent over time. To provide an example, atmospheric holes are continuously varying in location due to changing atmospheric pressure plasmas (Overzet et al. 2010). Variations in atmospheric holes also vary due to

Author's personal copy

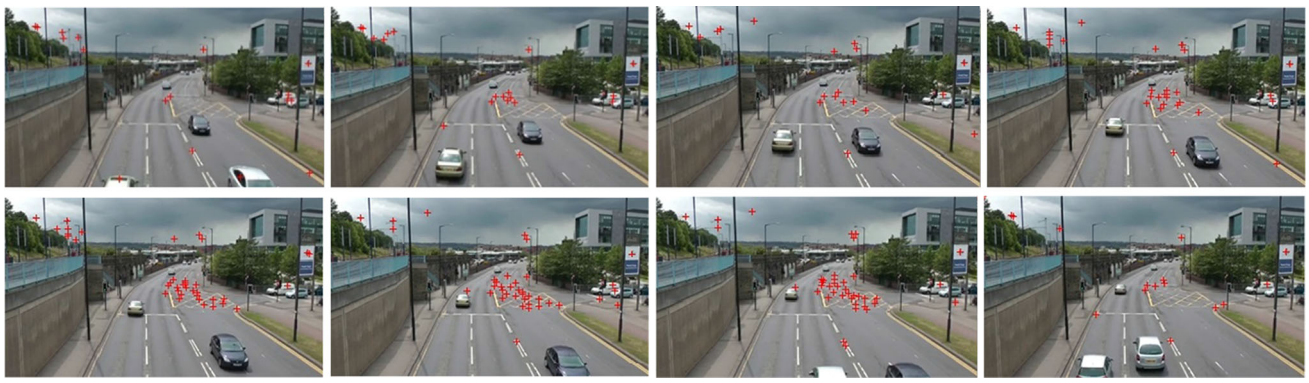

Fig. 1 Centroids on holes in a sequence of video frames. Each + (red plus sign) identifies the centroid of a hole. The locations of the holes in these video frames vary from moment due varying atmospheric conditions. (Color figure online)

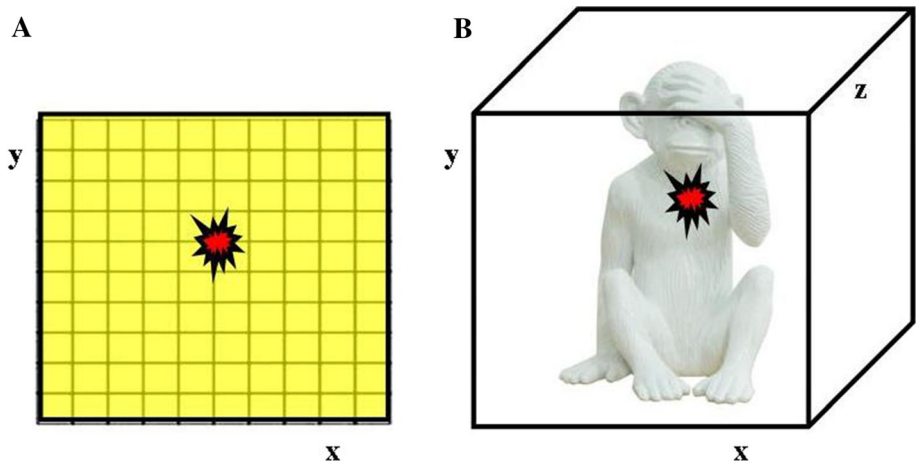

Fig. 2 Sample centroid holes, illustrated as red stars. **a** Centroid in a two-dimensional region at: (x, y) = (0.396, 0.554). **b** Centroid in a three-dimensional region at (x, y, z) = (0.0005, 0.0504,-0.7149)

movements of water molecules in the air and shifting sunlight conditions. Evidence of this can be seen in the sequence of video frames in the Fig. 1 below. Sample centroids (holes) of 2D and 3D regions are shown in Fig. 2.

The *centroid of a region* is the center of mass of the region. Let (x_i, y_j), $i = 1, \ldots, n$, $j = 1, \ldots, n$ be the coordinates of the points in an $n \times m$ region. And let (x_c, y_c) be the coordinates of the region centroid. Then the centroid of this 2D region is located at

$$(x_c, y_c) = \left(\frac{1}{n} \sum_{i=1}^{n} x_i, \frac{1}{n} \sum_{j=1}^{n} y_j \right)$$

Similarly, a centroid in a 3D region such as the regions in the video frames in the Fig. 1 is located at

$$(x_c, y_c, z_c) = \left(\frac{1}{m} \sum_{i=1}^{m} x_i, \frac{1}{m} \sum_{j=1}^{m} y_j, \frac{1}{m} \sum_{k=1}^{m} z_k \right)$$

The algorithm used to find the centroids of holes (dark regions) found in the video frames in the Fig. 1 is given next.

Author's personal copy

Input: Colour image **img** in a video frame.
Output: Centroids on holes recorded in a video frame.

Img → imgGrey % Convert img to greyscale.

imgGrey → imgBW % Convert imgGrey to binary.

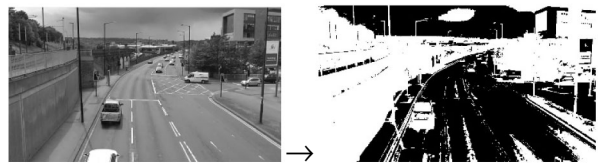

find centroids of holes % Mark holes with +
End **Algorithm** Centroids of Video Frame Holes.

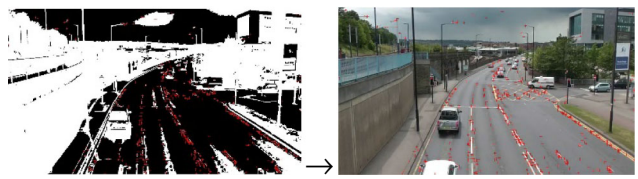

Results

Our technique allows the detection of holes in consecutive video frames that contain moving object shapes traveling in the 10 × 10 grid.

The Figure illustrates three on the countless possible distributions of the centroids of holes. At first, we assess the case of two intersecting moving shape shadows (Fig. 3a). Also, we consider the case which can be explained as shape reflection (projection the light blocked by a shape) resulting the formation of surface holes (Fig. 3b). Our account can be generalized to reflections of multiple moving object shapes whose dynamics include pinpointing the centroids of interior shape holes as well as reflected light leading to shadow holes (Fig. 3c). It is noteworthy that the knowledge of a single video frame parameter, i.e., the presence of pixels in the interior of the holes arising from the dynamical interaction of the moving shapes, allows us to achieve knowledge about topological features of otherwise undetectable objects. Indeed, even if an observer was unaware of the two moving objects' shapes and trajectories, that observer would be still able to extract useful information, simply looking at the detection screening that signals the presence (and disappearance) of holes. Although no information is available concerning the two objects' shape, nevertheless the observer is still able to detect and quantify their dynamics and interactions.

Conclusions

Concerning the biophysical realm, many accounts of our real world, both philosophical and biological, are used to consider a living being as an individual, self-preserving, unique subject equipped with borders, such as cellular membranes, envelopments, Markov blankets, and so on. The canonical illustration of biological organisms depicts "something" equipped with some peculiar activity, confined into itself, which struggles against (and cooperates with) the external world, in order to keep its entropy as low as possible and devoted to self-preservation (Ramstead et al. 2019). However, despite such stereotypical descriptions, the things get much more complicated when we approach the real word and its physical/biological content, in particular the brain function. The demarcation among objects, things and living beings could be somewhat arbitrary, and the same holds for set theory too. The same limitation holds for the very concept of evolution, which is based on species. Our concept of species is very arbitrary, because it throws not experimentally demonstrated borders among living beings. If we think to different populations of Homo. despite we are used to consider Sapiens, Neandertals, Denisovians, Floresians as different species, genetic studies undoubtedly point towards their ancient ibridation, which occurred more than once in different prehistoric contexts (Slon et al. 2018). Concerning our DNA, the delimitation of a species from another is sometimes difficult, due, e.g., to the presence in animal genome of viral

Author's personal copy

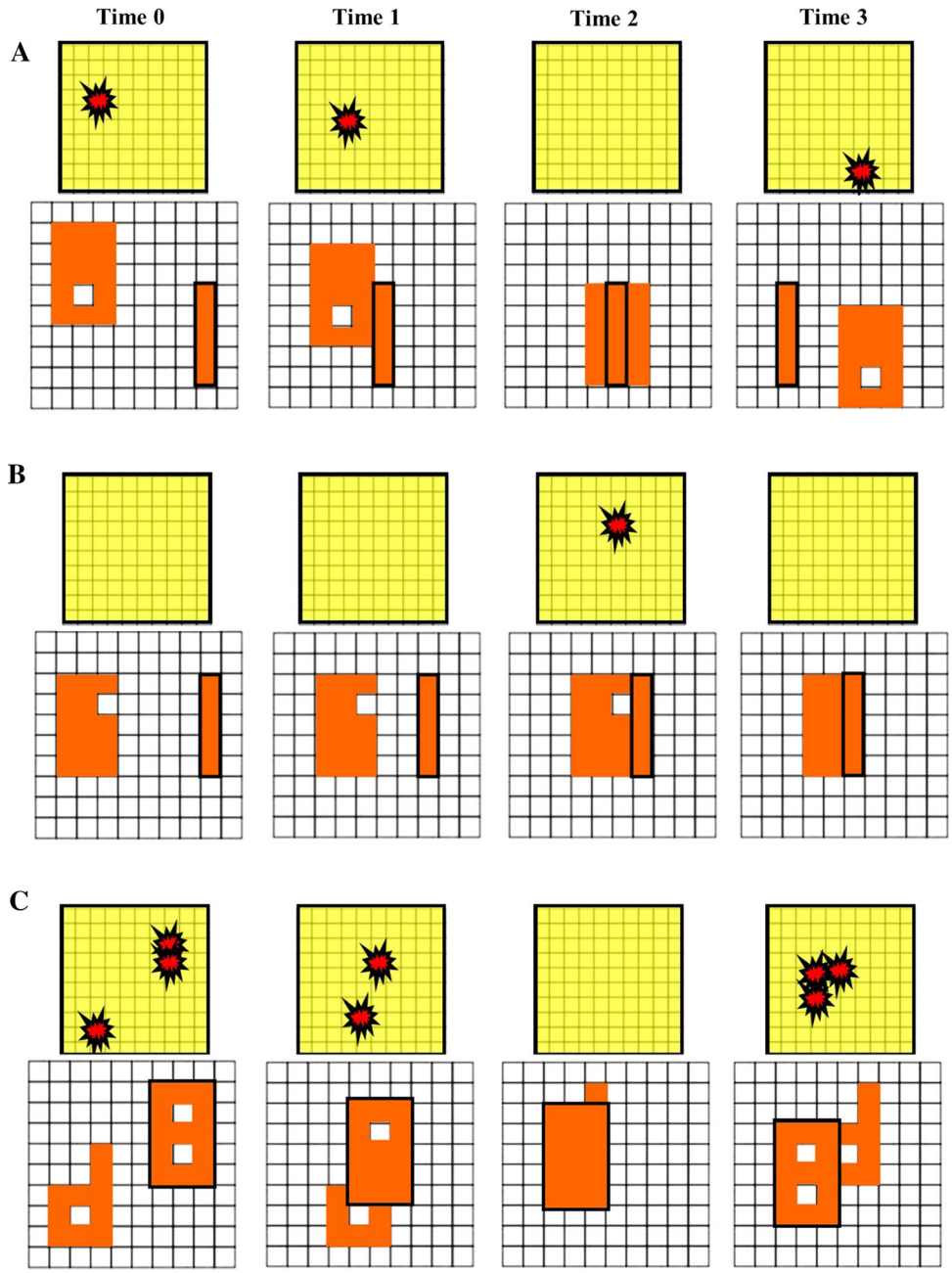

Fig. 3 Moving regions in a two-dimensional grid. The upper parts of each of the three figures (yellow grids) display the detection screening for hole recognition: when sensors detect holes, they fire inside the corresponding pixels (red stars). The lower part of the three figures (white grids encompassing red shapes) illustrates moving regions traveling inside a 10 × 10 grid. **a** Depicts the union of two objects, one with a hole and one without. **b** Displays a case of hole formation, when two shapes with ho holes interact and merge. **c** Depicts the dynamics of two moving shapes equipped with a different number of holes. (Color figure online)

and bacterial sequences. To make an example, the horizontal transmission of genetic material is able to overtake the so-called "species-specific" barriers (Chen et al. 2018), making sometimes difficult to clearly encompass individual living beings in a given species.

Given these premises, our aim here was to describe a technique to detect topological information from unknown and (possibly) disconnected spatial dynamic physical shape homeostasis features. We showed how unidentified interactions between two shapes on a two-dimensional grid give rise to modifications in topological features which can be detected and quantified. This means that topological changes pave the way to several possible applications in far-flung scientific disciplines. To provide a few examples, the detection of moving regions' holes might allow to assess the extent of a spreading forest fire, or the coverage of two mobile networking devices (Liu and Schneider 2011). The study of these topological changes might also help researchers to improve the performance of wireless sensor networks (Worboys and Duckham 2006) and the knowledge of neuronal homeostasis that counteracts long-term perturbations of neural activity and protein homeostasis in terms of is folding dynamics (Tozzi et al. 2016). Also, topological detection in network models might provide insights in both global structure and local node interactions, either in natural or artificial neural networks

Author's personal copy

and in lattice percolation procedures. Further, unknown patterns assessed through topological weapons could be useful in understanding economic and sociologic trends of migratory fluxes (Ignacio and Darcy 2019). Our technique of hole detection makes it possible to assess the discrete dynamic changes and multi-dynamic clustering occurring in the brain as well as at the macroscales of galaxies, cosmic bodies and Megaparsec web-like cosmic matter distribution, describing the topological invariants of their subtending networks (Pranav et al. 2016) and, possibly, providing better insights in dark matter and vacuum energy. Our account might also provide unexpected insights in the physiological neural mechanisms of figure-ground perception, in scenes where near surfaces occlude multiple contours and borders at different depths, producing alignments that are improbable except under conditions of occlusion. Indeed, in touch with our account, Gillam and Grove (2011) hypothesized that figure-ground and hole perception can be determined solely by properties of ground, in the absence of any figural shape, or surround, factors. The last, but not the least, the foremost role of holes seems to corroborate the recently-introduced axiomatic foundations of the descriptive closeness of points and sets, which aims to overtake the conventional closeness of points and sets (Di Concilio et al. 2018). In the context of descriptive proximity, the closeness of points and sets can be viewed in terms of their overlapping descriptions of punctured surface homeostasis that delineate detectable holes with high acuity.

References

Alexandroff P (1961) Elementary concepts of topology. Dover Publications Inc., Ne w York

Amad MZ, Peters JF (2018) Maximal centroidal vortices in triangulations. A descriptive proximity framework in analyzing object shapes. Theory Appl Math Comput Sci 8(1):39–59

Arkhangelskii AV (2001) [1994]. Extremally-disconnected space. In: Hazewinkel M (eds) Encyclopedia of mathematics. Springer, Berlin. ISBN 978-1-55608-010-4

Autrecourt, Nicholas of. About 1340. The Universal Treatise. Marquette University Press, Milwaukee, Wisconsin (1971)

Chen J, Quiles-Puchalt N, Chiang YN, Bacigalupe R, Fillol-Salom A et al (2018) Genome hypermobility by lateral transduction. Science 362(6411):207–212. https://doi.org/10.1126/science.aat5867

Cooke GE, Finney RL (1967) Homology of cell complexes. Princeton University Press, Princeton

Corcoran P, Jones CB (2018) Stability and statistical inferences in the space of topological spatial relationships. IEEE Access 6:18907–18919. https://doi.org/10.1109/ACCESS.2018.2817493

Déli E, Tozzi A, Peters JF (2017) Relationships between short and fast brain timescales. Cognit Neurodyn 11(6):539–552

Di Concilio A, Guadagni C, Peters JF, Ramanna S (2018) Descriptive proximities. Properties and interplay between classical proximities and overlap. Math Comput Sci 12:91–106. https://doi.org/10.1007/s11786-017-0328-y

Edelsbrunner H, Morozov D (2012) Persistent homology: theory and practice. In: European Congress of Mathematics, Krakow, 2–7 July 2012, European Mathematical Society, pp 31–50

Edelsbrunner H, Letscher D, Zomorodian A (2002) Topological persistence and simplification. Discrete Comput Geom. https://doi.org/10.1007/s00454-002-2885-2

Egenhofer MJ (1991) Reasoning about binary topological relations. In: Symposium on spatial databases. Springer, pp 141–160

Fort C (1919). The book of damned. Prometheus Books, 1991

Gäuting RH, Bäohlen MH, Erwig M, Lorentzos CSJNA, Schneider M, Vazirgiannis M (2000) A foundation for representing and querying moving objects. ACM Trans Database Syst 25(1):142

Ghrist R (2014) Elementary applied topology. Amazon. ISBN 978-1-5028-8085-1

Gillam BJ, Grove PM (2011) Contour entropy: a new determinant of perceiving ground or a hole. J Exp Psychol Human Percept Perform 37(3):750–757

Harnack D, Pelko M, Chaillet A, Chitour Y, van Rossum MCW (2015) Stability of neuronal networks with homeostatic regulation. PLoS Comput Biol. https://doi.org/10.1371/journal.pcbi.1004357

Ignacio PSP, Darcy IK (2019) Tracing patterns and shapes in remittance and migration networks via persistent homology. EPJ Data Sci 8:1. https://doi.org/10.1140/epjds/s13688-018-0179-z

Liu H, Schneider M (2011) Tracking continuous topological changes of complex moving regions. In: Proceeding SAC '11. Proceedings of the 2011 ACM symposium on applied computing. TaiChung, Taiwan. ACM, New York, NY, USA, pp 833–838. ISBN 978-1-4503-0113-8. https://doi.org/10.1145/1982185.1982366

Morimoto RI, Cuervo AM (2009) Protein homeostasis and aging: taking care of proteins from the cradle to the grave. J Gerontol A Biol Sci Med Sci 64A(2):167–170

Overzet LJ, Jung D, Mandra MA, Goeckner M, Dufour T, Dussart R, Lefaucheux P (2010) RF impedance measurements of DC atmospheric micro-discharges. Eur Phys J D 60:449–454. https://doi.org/10.1140/epjd/e2010-00274-5

Peters JF (2018a) Proximal planar shapes. Correspondence between triangulated shapes and nerve complexes. Bull Allahabad Math Soc 33:113–137

Peters JF (2018b) Proximal vortex cycles and vortex nerve structures. Non-concentric, nesting, possibly overlapping homology cell complexes. J Math Sci Model 1(2):56–72

Peters JF (2020) Computational geometry, topology and physics of digital images. Shape complexes, optical vortex nerves and proximities. Springer, Cham. https://doi.org/10.1007/978-3-030-22192-8

Popkin RH, Maia Neto JR (eds) (2007) Skepticism: an anthology. Prometheus Books. ISBN 1591024749; ISBN13 9781591024743

Pranav P, Edelsbrunner H, van de WeygaertR Vegter G, Kerber M et al (2016) The topology of the cosmic web in terms of persistent Betti numbers. Mon Not R Astron Soc 465(4):4281–4310. https://doi.org/10.1093/mnras/stw2862

Ramstead MJD, Constant A, Badcock PB, Friston KJ (2019) Variational ecology and the physics of sentient systems. Phys Life Rev 31:188–205. https://doi.org/10.1016/j.plrev.2018.12.002

Randell DA, Cui Z, Cohn AG (1992) A spatial logic based on regions and connection. In: Proceedings 3rd international conference on knowledge representation and reasoning

Rao AR (2018) An oscillatory neural network model that demonstrates the benefits of multisensory learning. Cognit Neurodyn 12(5):481–499

Author's personal copy

Schneider M, Behr T (2006) Topological relationships between complex spatial objects. ACM Trans Database Sys 31(1):39–81

Sen S, Daimi SN, Watanabe K, Takahashi K, Bhattacharya J, Saha G (2019) Switch or stay? Automatic classification of internal mental states in bistable perception. Cognit Neurodyn 14:95–113. https://doi.org/10.1007/s11571-019-09548-7

Slon V, Mafessoni F, Vernot B, de Filippo C, Grote S et al (2018) The genome of the offspring of a Neanderthal mother and a Denisovan father. Nature 561:113–116

Terasawa J (2004) Extremally disconnected spaces. In: Hart KP, Nagata J, Vaughan JE (eds) Encyclopedia of general topology. Elsevier, Amsterdam. https://doi.org/10.1016/b978-044450355-8/50092-1

Tozzi A, Peters JF (2017) From abstract topology to real thermodynamic brain activity. Cognit Neurodyn 11(3):283–292

Tozzi A, Peters JF (2019) Points and lines inside human brains. Cognit Neurodyn 13(5):417–428

Tozzi A, Tor Fla, Peters JF (2016) Building a minimum frustration framework for brain functions in long timescales. J Neurosci Res 94(8):702–716

Verri A, Uras C (1997) Metric-topological approach to shape representation and recognition. Image Vis Comput 14:189–207

Verri A, Uras C, Frosini P, Ferri M (1993) On the use of size functions for shape analysis. Biol Cybern 70:99–107

Wang P, Hu J (2019) A hybrid model for EEG-based gender recognition. Cognit Neurodyn 13(6):541–554

Worboys M (1998) Imprecision in finite resolution spatial data. GeoInformatica 2(3):257–279

Worboys M, Duckham M (2006) Monitoring qualitative spatiotemporal change for geosensor networks. Int J Geogr Inf Sci 20:1087–1108

Publisher's Note Springer Nature remains neutral with regard to jurisdictional claims in published maps and institutional affiliations.

frontiers in Computational Neuroscience

METHODS
published: 22 April 2020
doi: 10.3389/fncom.2020.00034

Topological View of Flows Inside the BOLD Spontaneous Activity of the Human Brain

Arjuna P. H. Don[1], *James F. Peters*[1]*, *Sheela Ramanna*[2] *and Arturo Tozzi*[1,3]

[1] Computational Intelligence Laboratory, University of Manitoba, Winnipeg, MB, Canada, [2] Applied Computer Science, University of Winnipeg, Winnipeg, MB, Canada, [3] Department of Physics, University of North Texas, Denton, TX, United States

Spatio-temporal brain activities with variable delay detectable in resting-state functional magnetic resonance imaging (rs-fMRI) give rise to highly reproducible structures, termed cortical lag threads, that propagate from one brain region to another. Using a computational topology of data approach, we found that persistent, recurring blood oxygen level dependent (BOLD) signals in triangulated rs-fMRI videoframes display previously undetected topological findings, i.e., vortex structures that cover brain activated regions. Measure of persistence of vortex shapes in BOLD signal propagation is carried out in terms of Betti numbers that rise and fall over time during spontaneous activity of the brain. Importantly, a topology of data given in terms of geometric shapes of BOLD signal propagation offers a practical approach in coping with and sidestepping massive noise in neurodata, such as unwanted dark (low intensity) regions in the neighborhood of non-zero BOLD signals. Our findings have been codified and visualized in plots able to track the non-trivial BOLD signals that appear intermittently in a sequence of rs-fMRI videoframes. The end result of this tracking of changing lag structures is a so-called persistent barcode, which is a pictograph that offers a convenient visual means of exhibiting, comparing, and classifying brain activation patterns.

Keywords: Betti Numbers, brain activity, fMRI video, persistence bar code, topological data analysis

OPEN ACCESS

Edited by:
Tatyana Sharpee,
Salk Institute for Biological Studies,
United States

Reviewed by:
Tuo Zhang,
Northwestern Polytechnical University,
China
Valeri Makarov,
Complutense University of Madrid,
Spain

***Correspondence:**
James F. Peters
james.peters3@umanitoba.ca

Received: *30 October 2019*
Accepted: *30 March 2020*
Published: *22 April 2020*

Citation:
Don APH, Peters JF, Ramanna S and Tozzi A (2020) Topological View of Flows Inside the BOLD Spontaneous Activity of the Human Brain. Front. Comput. Neurosci. 14:34. doi: 10.3389/fncom.2020.00034

1. INTRODUCTION

Point clouds are a natural outcome of a topology of data approach in tracking intermittent as well as persistent BOLD signals in different sections of the brain. A point cloud is a collection of sampled pinpointed places in a subregion (Ghrist, 2014). A topology of data circumvents noise in data and focuses on those data that persist over time (Edelsbrunner and Harer, 2010). Computational topology of data provides a practical method in isolating, measuring, and classifying persistent lag structures BOLD signals in each rs-fMRI video frame that are mapped to point clouds in a finite, bounded region in an n-dimensional Euclidean metric space. It has been observed that brain activity in one region of the brain propagates to others with variable temporal delay (Mitra et al., 2015; Matsui et al., 2016; Park et al., 2019), giving rise to brain activity lag (delay) structures. Lag threads are temporal sequences of propagated brain activities (Mitra et al., 2015). Lag structures in fMRI video frames are rich source of point clouds. Triangulated brain point clouds are a source of brain activation area shapes that appear intermittently in different cortical regions during a rs-fMRI video such as the four videos provided by Mitra et al. (2015). Selected barycenters of triangles in a triangulated cortical point cloud are connected to form vortexes covering each brain

activation region with its own distinctive shape. Each vortex in a triangulated rs-fMRI video frame is a collection of connected cycles (see, e.g., the lower half of **Figure 1**) that make it possible to approximate, measure, track and compare brain activation region shapes. A vortical view of brain activity first appeared in Freeman (2009).

Each vertex in a triangulated brain activation region point cloud is represented by a feature vector containing useful information such as activation region area and representative Betti number (Giusti et al., 2015). Traditionally, the more intuitive geometric forms of Betti numbers are counts of cells (vertexes, edges, filled triangles), cycle counts or surface hole counts (Zomorodian, 2001). A particularly useful intuitive form of geometric Betti number is a count of the number of connected vortex cycles covering an activation subregion (Peters, 2020). Less frequently used algebraic Betti numbers (counts of the number of generators in a free Abelian group; Munkres, 2000) also provide insight concerning the inner workings of cycles in triangulated brain activation regions. We first consider the persistence of geometric numbers (vortex cycle counts) over sequences of sequences of triangulated rs-FMRI video frames. Later, in **Appendix B**, the persistence of algebraic Betti numbers is also considered to obtain an alternative view of the changing character of connected cycles in triangulated rs-FMRI lag threads in three regions of the brain.

Tracking the appearances of the Betti number of a brain activation vortex containing a particular number of connected cycles leads to the construction of a persistence barcode (see the top half of **Figure 1**) in which a Betti number appears in a video frame, disappears afterward and possibly reappears one or more times in later video frames. 2D (planar) as well as 3D (volumetric) persistent barcodes provide an easy-to-read means of tracking intermittent BOLD signals in a sequence of rs-fMRI video frames.

The origin of topological data analysis and persistent homology can be traced back to Edelsbrunner et al. (2000, 2001). A common approach is to build a continuous shape (graphs) on top of data to detect complex topological and underlying geometric structures (Carlsson, 2009; Chazal and Michel, 2017). This shape is called a simplicial complex or a nested family of simplicial complexes and the process of shape construction is commonly referred to a filtration (Zomorodian, 2001). One of the fundamental tools in computational topology is persistent homology (Zomorodian and Carlsson, 2005), which is a powerful tool to compute, study, and efficiently encode multiscale topological features of nested families of simplicial

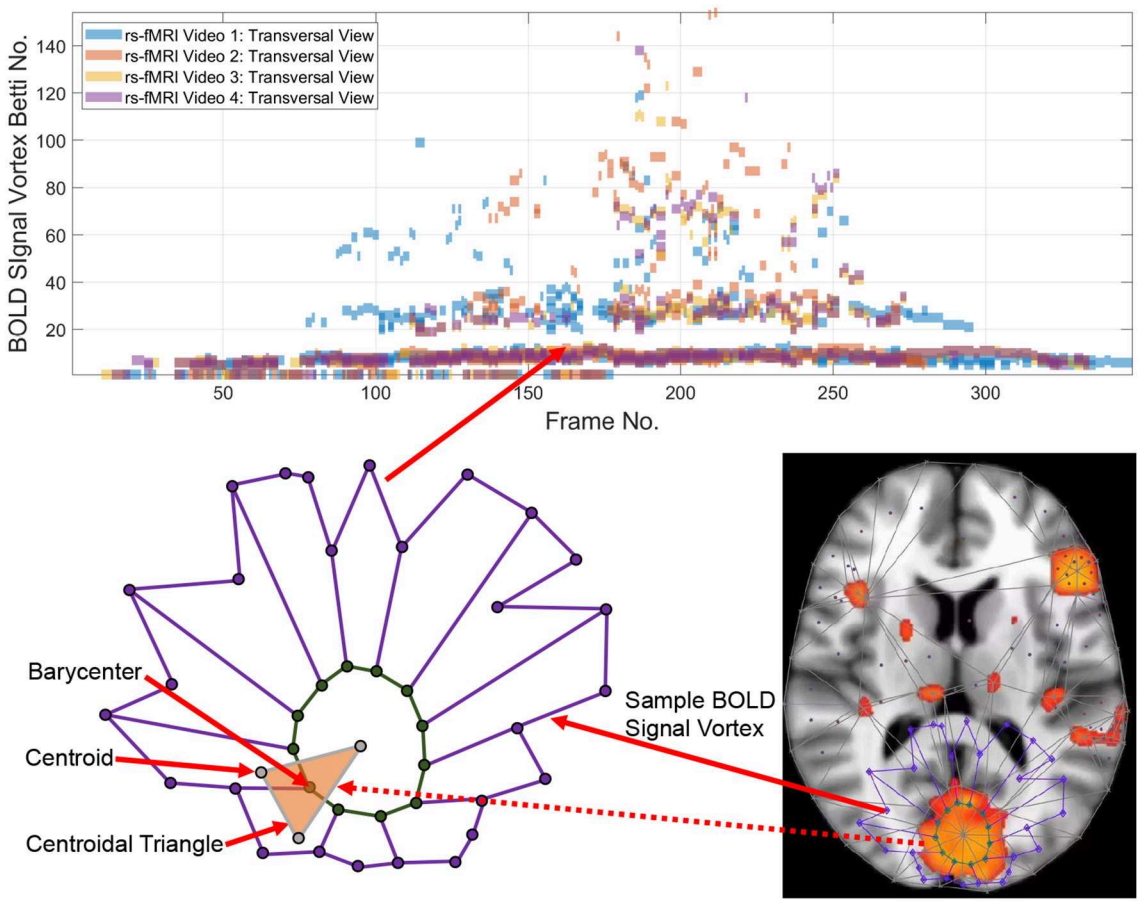

FIGURE 1 | Betti numbers for a rs-fMRI BOLD signal vortex on a Transversal view for four videos.

complexes and topological spaces (Edelsbrunner and Harer, 2008).

Earlier studies of brain networks primarily focused on a graph-theoretic approach where the brain regions and their connections are encoded as a graph (i.e., a network of nodes and edges) and cycles (representing complex behaviors). Such networks were modeled and analyzed with methods such as Q-modularity (Meunier et al., 2009) or with network measures such as betweeness centrality (Bullmore and Sports, 2009). Brain networks with weighted edges where problems of selecting thresholds for edge weights and dealing with sparse edges can be found in Achard and Bullmore (2007) and van Wijk et al. (2010). This has led to application of persistent homology to the problem of determining multiple thresholds derived from more than one network. A brain network can be considered as the 1-skeleton of a simplicial complex, where the 0-dimensional hole is the connected component, and the 1-dimensional hole is a cycle (Chung et al., 2019). The number of k-dimensional holes of a simplicial complex is its k-th Betti number. Persistent homology-based multiscale hierarchical modeling was proposed in Lee et al. (2011b), Petri et al. (2014), Giusti et al. (2015), Sizemore et al. (2018), and Chung et al. (2019) to name a few. Here, graph filtration is used to build these networks in a hierarchically manner. Filtration is the process of connecting edges to form a graph.

Betti numbers computed during this filtration process have been used for further statistical analysis such as Pearson correlation to MRI image data (Chung et al., 2015) and various metrics for similarity and distances assessments (Lee et al., 2011a; Chung et al., 2019). 0-dimensional holes (β_0 or zeroth Betti numbers) have been computed during the graph filtration process and a persistent barcode has been constructed for subsequent statistical analysis (Cassidy et al., 2015; Chung et al., 2017). However, the *cycle* concept is extremely important to the study of behavior diffusion and integration of the brain network. In persistent homology, cycles are measured using the first or one-dimensional Betti Number (β_1). In Chung et al. (2019), the one dimensional Betti numbers are used to measure cycle and the significance of the number of cycles is evaluated using the Kolmogorov–Smirnov (KS) distance.

For geometric representations of rs-fMRI lag threads, an incisive form of statistical analysis of the geometry is given in terms of edge density and Eigen values (Giusti et al., 2015). The results of this form of geometry-based statistical analysis are given in **Appendix A**.

In contrast to earlier approaches, we use computational geometry to detect lag thread shapes in fMRI video frames using a *geometric* Betti number that counts the total number of connected cycles forming a vortex (nested, usually non-concentric, connected cycles) derived from the triangulation of brain activation regions. We build on our previous work in Peters et al. (2017), Don and Peters (2019), and Peters (2020), to evaluate real BOLD resting state rs-fMRI videos from Mitra et al. (2015).

Here, the video frames are processed directly to obtain Betti numbers by triangulating the transversal, sagittal, and coronal sections of the fRMI video frames and constructing vortexes through a process of filtration. Rather than constructing graphs of brain networks and analysing cycles in the network, we analyze cycles by processing the video frames. The vortexes correspond to the changing activation areas in the video frames. The number of vortexes in a frame represents the most relevant areas of change. Higher Betti number values imply that the change is closer to the center of the section of the brain. To the best of our knowledge, this method of detecting cycles in persistent homology is novel and a preliminary version of this paper appeared in Don A. P. et al. (2019).

2. MATERIALS AND METHODS

2.1. Theory

The basic approach is to introduce a geometric representation of brain activation regions in terms of intersecting cycles that are sequences of path-connected vertexes on the barycenters of triangles forming vortices (Don and Peters, 2019; Peters, 2020). Each vortex is a collection of connected cycles called a vortex nerve. Of particular interest are those nerves that have a maximal collection of triangles of a common vertex in the triangulation of a finite, bounded planar region. In our case, the planar region is a rs-fMRI video frame. A vortex nerve results from the triangulation of the sections of each rs-fMRI brain video frame. A centroid (also called a seed point), is used as a vertex in the triangulation of a video frame. A barycenter on a such a triangle is in a high light intensity video frame region between the dark regions, which we refer to as *holes*.

Definition 1 (Hole). A ***hole*** is a collection of contiguous low intensity voxels. The ***centroid of a hole*** is the center of mass of the hole. In an rs-fMRI video frame, the holes are in background regions containing dark (low intensity) voxels and the foreground regions are filled with mainly orange voxels. Sample centroids of brain activation region holes are given in **Figure 1**.

Using Delaunay triangulation (Delaunay, 1934; Yung et al., 2016), each pair of closest neighboring centroids of holes become the vertexes of edges of triangles covering brain activation regions in rs-fMRI videos. Each line segment drawn between closest pairs of centroids becomes the edge of a triangle in the Delaunay triangulation of an rs-fMRI video frame. The concept of a hole is crucial to this work, since edges drawn between barycenters in the interior of adjacent centroidal triangles reveal paths of high intensity voxels between brain activation region holes.

Definition 2 (Barycenter of centroidal triangle). Recall that the median line of a triangle is a line drawn from a vertex to the midpoint of the opposite side of the triangle. The ***barycenter of a centroidal triangle*** is the point of intersection of the median lines of the triangle. A sample barycenter is given in **Figure 1**.

The barycenters of centroidal triangles covering brain activation regions are always between holes. Barycenters are stepping stones in the construction vortex cycles.

Definition 3 (Barycentric cycle). A ***barycentric cycle*** is a sequence of edges drawn between neighboring barycenters of adjacent centroidal triangles.

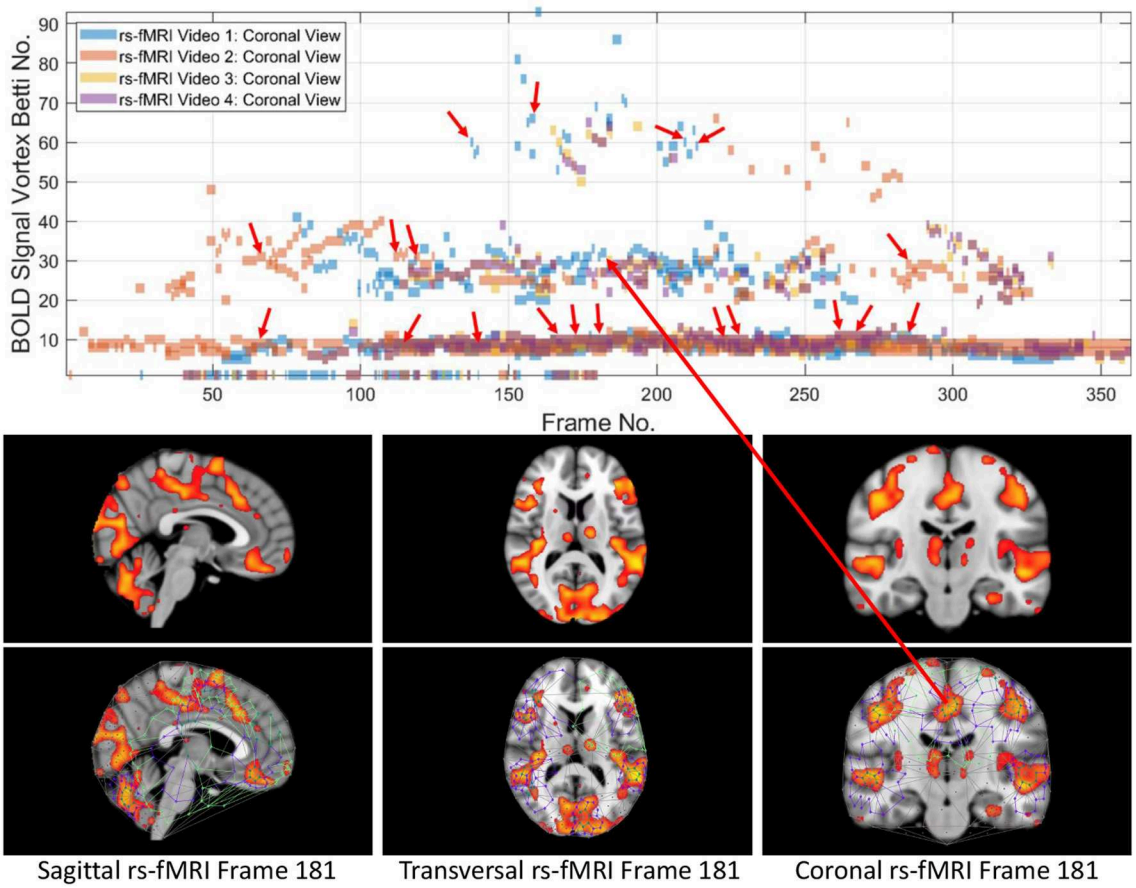

FIGURE 2 | Coronal persistence barcode with Betti numbers as vortex cycle counts in a rs-fMRI video frame (see text for further details).

As a result, connected barycenters model paths for high intensity voxels recorded in a brain activity video frame. Barycentric cycles are the basic building blocks in the construction of local vortexes covering triangulated brain activation regions.

Definition 4 (Local Vortex (briefly, Vortex)). A ***local vortex*** is a collection of nesting, usually non-concentric barycentric cycles. The simplest vortex contains a single barycentric cycle (see, for example, the vortex in **Figure 3**).

2.2. Betti Numbers on a Triangulated Brain Activation Region

Betti numbers provide a computational topology perspective on the structure of brain activation subregions. In our case, the ***Betti number*** β_1 tells us either the number of connected vortex cycles in a vortex on a triangulated brain activation region (***geometric view***). Later, in **Appendix B**, we also introduce and apply the Betti number β_α, which is a count of the number of generators in a free Abelian group representation of an rs-fMRI video frame vortex (***algebraic view***). The focus here is on the persistent geometric Betti numbers across sequences of triangulated video frames. Each such Betti number is mapped to an entry in a persistent barcode (see top half of **Figure 1**). This topology of data pictographs is useful in representing the persistence of the brain activation region shapes found in rs-fMRI brain video sections. From an intuitive perspective, there are three types of geometric Betti numbers, namely, $\beta_0, \beta_1, \beta_2$, introduced in Zomorodian (2001).

Definition 5 (β_0). The ***Betti number*** $\boldsymbol{\beta_0}$ is a count of the total number of elementary cell complexes, which are vertexes, edges and filled triangles attached to each other in a triangulated region.

Definition 6 (β_1). The ***Betti number*** $\boldsymbol{\beta_1}$ is a count of the number cycles.

Each β_1 in a persistent barcode (Ghrist, 2008) represents the number of connected barycentric cycles covering an activation area of the brain.

Definition 7 (β_2). The ***Betti number*** $\boldsymbol{\beta_2}$ is a count of the number of holes. In our case, $\boldsymbol{\beta_2}$ is a count of the number of contiguous low intensity voxels in brain activation regions in an rs-fMRI video.

Definition 8 (C_0 vortex cycle). ***cycle*** $\boldsymbol{C_0}$ is the ***innermost cycle in a vortex***. In our case, the sequence of

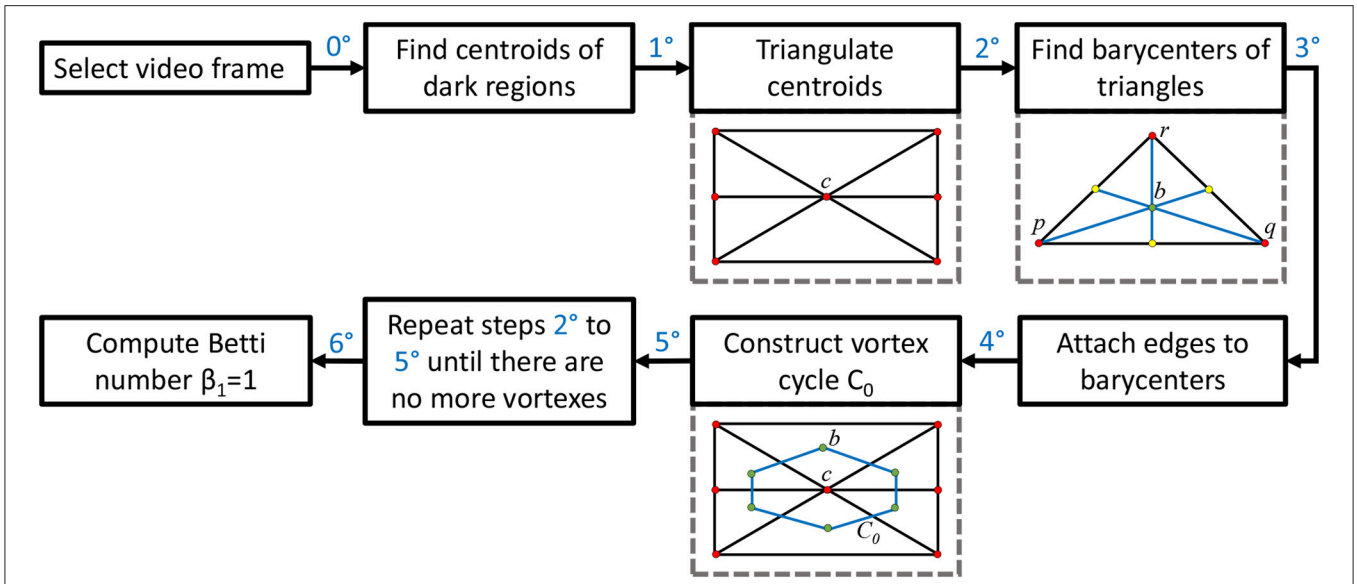

FIGURE 3 | Method flow graph.

edges connected between barycenters of adjacent triangles with a common vertex, collectively called an Alexandroff nerve (Alexandroff, 1965) forms the *cycle* C_0. Notice that cycle C_0 will always be in the interior of a brain activation region containing high intensity voxels.

Definition 9 (C_1). In a vortex with 2 nested cycles, ***cycle*** $\boldsymbol{C_1}$ is the vortex cycle that has only C_0 in its interior. In effect, cycle C_1 is a collection of path-connected vertices on a sequence of edges surrounding C_0. Cycle C_1 usually overlaps the boundary of a high intensity brain activation region in an rs-fMRI video frame.

Definition 10 (Bridge Segment). A ***bridge segment*** is an edge attached between vertices on a pair of neighboring cycles. Let *cycA*, *cycB* be a pair of neighboring cycles (i.e., there are no cycles in between *cycA* and *cycB*) and let p be a vertex on *cycA* and q, a vertex on *cycB*. The edge $\overline{pq}$ is a bridge segment. Edge $\overline{cj}$ between vertices c and j is a bridge segment and there is no bridge segment between vertices c and i in **Figure 5**.

In the main body of this paper, we give barcoded video results for the more intuitive geometric Betti number counts of vortex cycles on triangulated brain activation regions. Later, in **Appendix B**, we give examples of both geometric and algebraic forms of Betti numbers. A repetition of the same β_1 across a sequence of consecutive frames tells us that a similar vortex shape recurs in these frames. The geometric Betti number of a vortex containing two cycles with k bridge segments attached between the pair of vortex cycles equals k + 2 (Don and Peters, 2019).

For example, the Betti number β_0 of the vortex in the lower half of **Figure 1** equals 12 and $\beta_1 = 1$, since there are 12 cycle edges and there is only one cycle in the vortex shown.

2.3. rs-fMRI Lag Threads Having Descriptive Proximity

A pair of objects are descriptively proximal (near each other), provided the objects have the same description (Di Concilio et al., 2018). A ***feature vector*** provides a description of an object. In this work, feature vector (Betti number, area) describes a subregion of a rs-fMRI brain region. Rather than a purely theoretical, abstract approach to descriptive proximity spaces, the focus here is on computational descriptively proximities. Briefly, computational descriptive proximity includes algorithms as well as structures such as set intersection, union and closure and proximity space axioms introduced in Peters (2020). Descriptive proximites provide mathematical framework useful in measuring, comparing, and classifying (1) lag structures and threads across frames in the same video or (2) lag structures and threads across frames in different rs-fMRI videos. For example, in terms of (1), ($\mathcal{B}_t$, inner vortex cycle area) = (100, 100 mm^2) describes a brain activation subregion in the transversal brain section in frames 10 and 75 in **Figure 7**. In terms of (2), Let $\mathcal{B}_s, \mathcal{B}_t, \mathcal{B}_c$ be Betti numbers for the sagittal, transversal and coronal brain regions. The feature vector $(\mathcal{B}_s, \mathcal{B}_t, \mathcal{B}_c)$ is used to describe and compare lag threads in frames across different videos. This is an important advantage that accrues from the application of computational descriptive proximities.

2.4. Methods

This section briefly introduces the method used to derive vortex cycles on triangulated video frames (steps 0 through 5) and their geometric Betti numbers (step 6), which are used to construct persistent barcode for rs-fMRI videos. The fMRI videos (of 688 subjects) used in this work were obtained from the Harvard-MGH Brain Genomics Superstruct Project (Buckner et al., 2014). Each video contains 360 frames that exhibit the propagation of

BOLD signals in the sagittal, transversal and coronal sections of the human brain (see, e.g., the middle row of **Figure 2**). Let K be a rs-fMRI video frame. The steps to obtain triangulation vortexes covering the brain activation regions shown in **Figure 2** are exhibited in the flow graph in **Figure 3**.

$\mathbf{0^0}$ After selecting a video frame, find the centroids (centers of mass) of the dark background regions. Holes are identified by binarizing each video frame.

$\mathbf{1^0}$: Triangulate the centroids of the tiny dark regions inside the brain activation regions in K. A sample centroidal triangle is shown in **Figure 1**.

$\mathbf{2^0}$: Find the barycenter of every centroidal triangle $\triangle$ in K. Each barycenter is a voxel representing a high BOLD signal situated between centroids.

$\mathbf{3^0}$: Connect the barycenters where there is the greatest concentration of centroidal triangles $\triangle$s with a common vertex. Recall that the vertex common to a collection of triangles is an example of an Alexandroff nerve (Alexandroff, 1965) (see, e.g., the collection of centroidal triangles with a common vertex covered by the inner vortex cycle in **Figure 1**). In this work, the focus is on finding maximal Alexandroff nerves.

$\mathbf{4^0}$: Construct vortex cycles on the barycenters of centroidal triangles $\{\triangle\}$ along the boundary of C_0.

$\mathbf{5^0}$: Repeat steps $\mathbf{2^0}$ through $\mathbf{4^0}$ until there are no more vortexes covering subregions containing nonzero BOLD signals. The end result is a collection of connected nesting non-concentric cycles that form a *vortex*. Once these vortexes are generated, the next step is to compute the β_1 for each vortex that has been found in each of the triangulated video frames. Notice that there is usually more than one vortex in video frame.

$\mathbf{6^0}$: Compute Betti number. Count the number of non-single edge (main) cycles in a vortex plus the number of signal edge cycles connected between the main vortex cycles. This process is repeated for each brain section in every frame containing sagittal, trasversal and coronal brain sections in each of the sample rs-fMRI videos.

To construct a Betti number-based persistent barcode, insert a bar in a pictograph (an easy-to-read visualization of brain activity instants accumulated in what is known as a homology barcode Ghrist, 2014), using rs-fMRI video frame number (x-axis) and its corresponding Betti Number (y-axis) (shown in the top half of **Figure 1**).

3. RESULTS

3.1. Part 1. Edge Density and Eigen Value Statistics

Since the focus of this study of brain activation in rs-fMRI videos is on the formation of nesting cycles (vortexes) covering the interior brain activation regions, we consider the edge densities and eigenvalues that reflect the levels of connectedness of these activation region cycles.

3.1.1. Edge Density

In this work, edge density quantifies the connectedness in the vortex representation of a brain activation region in a rs-fMRI video frame. Specifically, ***edge density*** is proportional to the product of the number of vortex bridge segments between cycles $\times$ the number of cycle vertices. Mathematically, we have

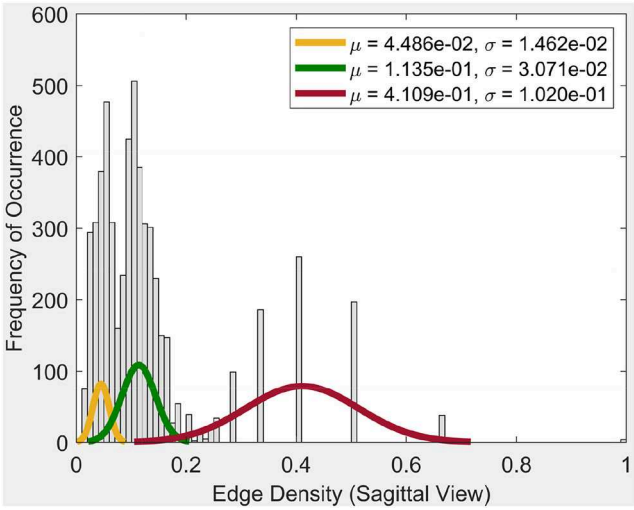

FIGURE 4 | Edge density of sagittal view.

$$E = \text{number of bridge segments between vortex cycles.}$$
$$V = \text{number of vortex cycle vertices.}$$
$$EdgeDensity = 2\left[\frac{E}{V(V-1)}\right].$$

An increase in the number of bridge segments E between vortex cycles results in higher edge density. This can happen in the case where there is more than one bridge segment connected to a vortex cycle. An increase in the number of vortex cycle vertices V with no change in the number of bridge segments, leads to a lower edge density. This occurs whenever the number of dark regions increase in a brain activation region, which leads to an increase in the number of centroidal triangles. This also leads to an increase in the number of barycenters. Physically, each barycenter pinpoints the location of high intensity in a brain activation region. Each vortex cycle vertex represents a barycenter on brain activation region triangle.

Frequency of occurrence in the plot in **Figure 4**, for example, is the number of times a certain edge density appears in the cycles. Whenever a certain edge density appears, the plot will show the frequency of occurrence as 1. If it reappears, the frequency of occurrence will be 2. So it will increase the said value for the occurrence by 1, each time it appears.

From the plot for the Sagittal view in **Figure 4**, it can be seen that each distribution can be represented using three normal distributions. Observe that the left-most normal distribution has a mean $\mu = 0.04$ and a standard deviation $\sigma = 0.014$ but it has a lower edge density compared to the other two (middle, right) distributions. The middle normal distribution has $\mu = 0.11$ and a $\sigma = 0.03$. This distribution has the highest frequency of occurrence of edges. The right normal distribution has a $\mu = 0.41$ and a $\sigma = 0.1$ and has the second highest edge frequency.

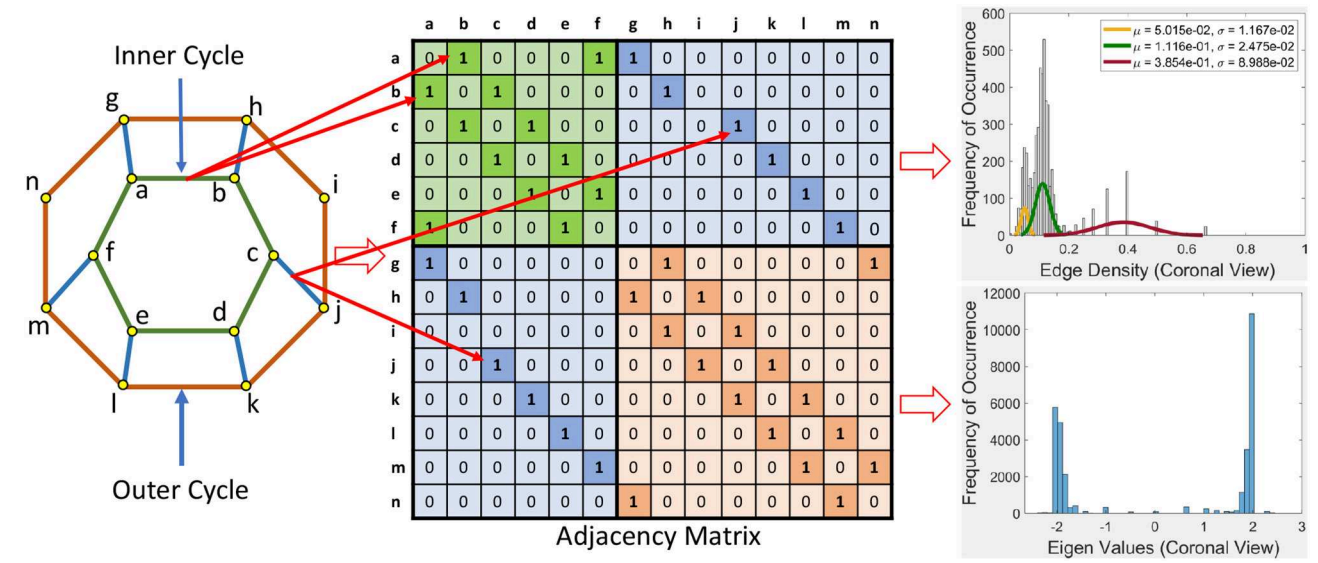

FIGURE 5 | Adjacency matrix representation of cortical vortex Connectedness.

When we consider the cycles that are generated by these edge density values, we can observe the following. In order to get a edge density value close to 0.4, there needs to be single cycle with a lower number of vertices. For example, in the case where there is a single cycle with three vertices (i.e., a triangle), we have the edge density of 0.66. This represents the highest value attainable in vortex cycles. Any single or multiple cycles will have a lower edge density than 0.66. In other words, higher the number of cycles and vertices in a cycle; the lower the edge density. Hence, in **Figure 4**, it can be observed that the highest frequencies of occurrence of edges is for edge densities between 0.1 and 0.2. For further evidence of this, see the plots for transversal and coronal views given in 9 and 10 reported in **Appendix A**.

3.1.2. Eigenvalue Spectrum

This section briefly introduces an eigenvalue spectrum representation of the eigen values derived from the connectivity relations between cortical vortex cycles. A number λ is an ***eigenvalue*** of a linear transformation A (our adjacency matrix), provided there is a vector $x \neq 0$ so that $A(x) = \lambda x$. The vector x called an ***eigenvector***. Eigen values are computed using an ***adjacency matrix*** A, which is a $n \times n$ square matrix where n is the number of vertices in a vortex cycle. Here, an ***eigenvalue spectrum*** is defined by an activation matrix view of the connectedness between vertices in a vortex representation of brain activation regions in rs-fMRI videos. Each adjacency matrix represents the connectivity in vortex cycles. To help visualize the connectivity between vertexes in a vortex, a color-coding scheme is given. That is, the vertices on each vortex cycle edge are color-coded as shown in **Figure 5**. In this color-coding scheme, sub-matrix (a–f) represents inner cycle vertexes (color-coded Green ■). The Sub-matrix (g–n) represents cycle vertexes (color-coded Orange ■). The other two sub matrices represent the bridge segment vertexes (color-coded Blue ■).

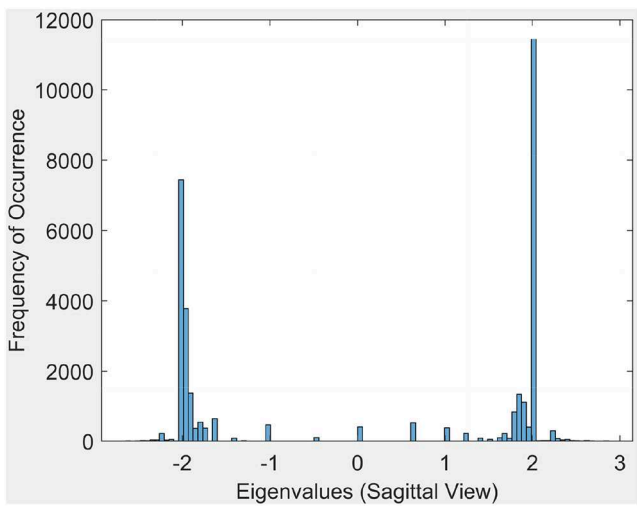

FIGURE 6 | Eigen values for the sagittal view.

A bridge segment between vortex cycles with its ending vertices on neighboring cycles has its connectivity represented by a cell containing 1 in the two sub-matrices (color-coded Blue ■) that are not on the main diagonal as illustrated in **Figure 5**. The bridge segment $\overline{cj}$ is represented by 1s in cells (c,j) and (j,c). If a vortex cycle has an edge between two vertices in locations i and j the cycle, it is represented symmetrically by 1 in a matrix cell (i,j) and a corresponding cell (j,i). For example if there is a edge between vertices 4 and 6 then cells (4, 6) and (6, 4) is 1 in the corresponding adjacency matrix.

Each eigenvalue plot encapsulates results of the sagittal, transversal and coronal views of brain activations recorded in rs-fMRI videos. Each plot represents 12 separate brain section videos = 3 brain sections × 4 original composite videos (i.e., we

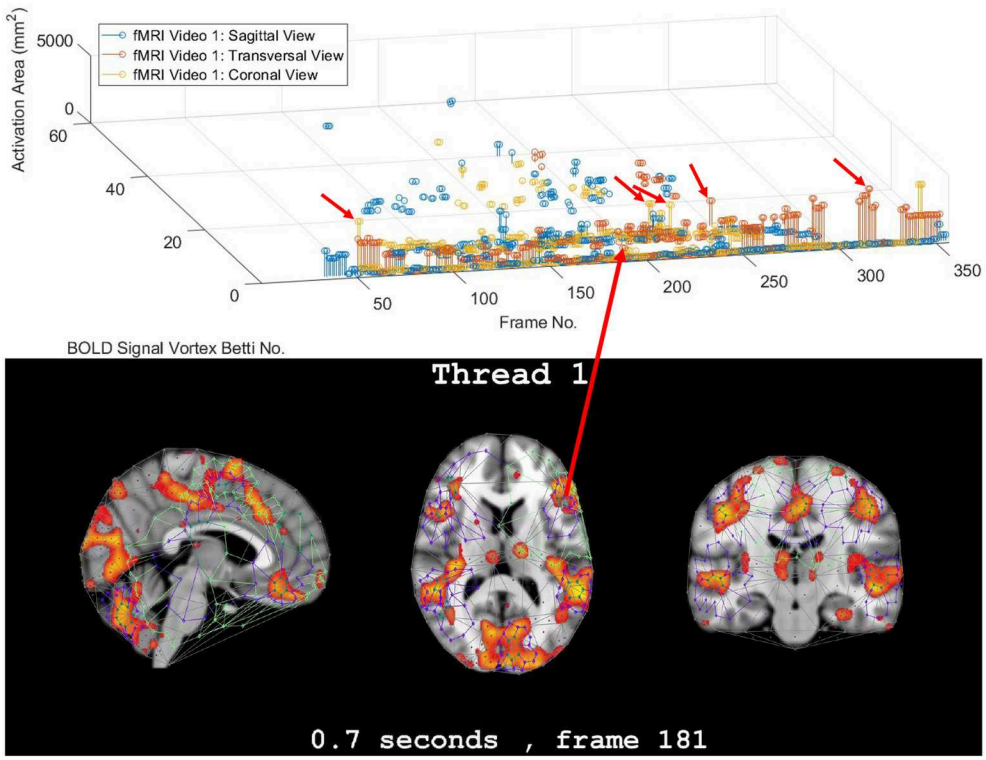

FIGURE 7 | Frame-Betti number-Area for rs-fMRI BOLD signal vortexes on three brain regions.

have extracted three separate brain section videos from each of the four original composite videos). The separated brain section videos made it possible for us to carry out statistical analysis based on the triangulation of the centroids on holes found in the brain activation regions of each brain section in the reported experimental results recorded in the original four videos.

Example 1. In **Figure 5**, connectivity between vertices on vortex cycles are color-coded. For instance, the connectivity between vertexes a and b on the inner cycle in **Figure 5** is represented by a green cell ■ containing a 1 in (b, a) (row b and column a) and by a green cell containing a 1 in (a, b) (row a and column b). ■

Sample results for the eigenvalue spectrum for the sagittal view of brain activation regions is recorded in the plot in **Figure 6**. Plots of the eigenvalue spectrum for the transversal and coronal views are given in **Appendix A**.

3.2. Part 2. Derivation of Persistent Brain Activation Subregion Signature

Each triangulated BOLD signal propagation subregion has a signature defined by the vector (frame number, cycle count Betti number, inner vortex cycle area). This leads to the production of four triangulated rs-fMRI videos available at Don A. et al. (2019), that are part of the University of Manitoba Vortex Signature Project. Vortexes have been derived from each of the triangulation of the BOLD signal activation regions in each of the brain sections in the video frames in the four rs-fMRI videos from Buckner et al. (2014).

A straightforward outcome of the derived vortexes is a rich source of new means of describing individual BOLD signal activation regions as well as a bridge to various forms of descriptions of lag threads. For example, each vortex has a Betti number (count of the number of connected cycles) and various cycle areas. Each of the three brain regions in each frame in the Harvard Brain Genomics rs-fMRI videos has its own vortex and, consequently, its own Betti number. Typically, each video frame will have more than one Betti number derived from vortexes on the multiple brain activation subregions.

In this study, the focus is on the area of the inner cycle of a BOLD signal subregion vortex. This is the case, since each inner cycle lies entirely within the interior of an activation subregion. Hence, an inner cycle area is a reliable approximation of a brain activation area. In sum, geometric Betti numbers and inner vortex cycle area help gauge the extent of an activation subregion. Considered either separately or taken together, a vortex on brain activation subregion provides the basis for a subregion signature, i.e., a distinctive characteristic of a brain activation subregion in a rs-fMRI video frame. For example, (frame number, Betti number) = (140, 60), (200, 60), (210, 60) provides a signature for the coronal brain region in frames 140, 200, and 210 in **Figure 2**. Betti number 60 is an example of a brain activation subregion characteristic that persists over a sequence of video frames. The vector (frame number, Betti number, inner vortex cycle area) =

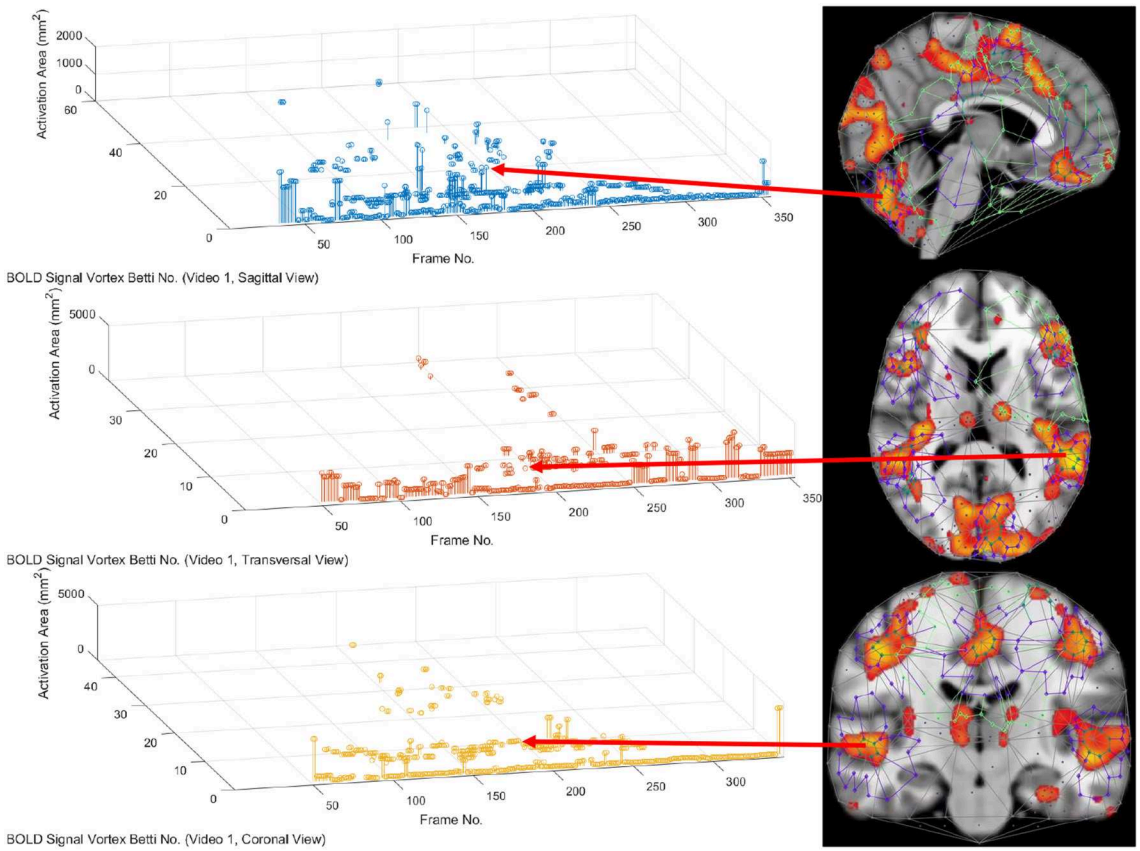

FIGURE 8 | 3D persistence barcode for 3 rs-fMRI BOLD signal propagated in brain regions.

(180, 40, 10 mm^2) depicts a brain activation subregion in the sagittal brain region in **Figure 7**. A repetition of the same Betti number for the same brain region across multiple video frames defines a lag thread pattern. For example, $\mathcal{B}_s = \mathcal{B}_t = \mathcal{B}_c = 100$ for the sagittal, transversal and coronal brain regions defines a lag thread pattern for multiple frames in **Figure 7**.

The gaps between the sequences of contiguous bars are important, since gaps in a particular row of pictograph bars indicates rs-fMRI video frames that do not have the same level of brain activity represented by bars in the row. The proximity of the bars (not necessarily contiguous) in a pictograph row call attention to BOLD signals that are close to each other, temporally. Repeated bars in a pictograph row indicate a repeated (persistent) level of brain activity recorded in rs-fMRI video frames. An example of a pictograph row containing multiple, contiguous bars can be seen in row 30 (Betti numbers = 30) in **Figure 2**. Contiguous bars in a pictograph row indicate the closeness in time of the corresponding brain activity.

Examples of pictograph rows containing multiple, non-contiguous bars can be seen in rows 10 and 60 (Betti numbers = 10 and 60) in **Figure 2**. A byproduct of the inspection of a sequence of contiguous bars (geometric β_1 Betti numbers) in a persistent barcode row can lead to the production of a reduced rs-fMRI video containing only video frames with either activation sub-regions with the same Betti number or a new video containing frames with activation sub-regions, each with a different β_1 (vortex cycle count) Betti number.

3.3. Part 3. Confirmation of Highly Reproducible Lag Thread Topography

From 3D barcodes in **Figure 7** as well as in **Figure 8**, Betti number-area patterns can be detected within frames in the same video. That is, one can find many examples of brain activation subregion Betti number (and corresponding subregion area in a lag thread in one video frame) that are reproduced in a lag thread in a different video frame. In other words, the Betti number-area combination persists across different frames. Many examples of this Betti number-area persistence phenomenon can be detected in the two sample 3D homology barcodes when compared with similar 3D homology barcodes derived from the frames in the videos available at the University of Manitoba Vortex Project at Don A. et al. (2019). These persistent repetitions in the topography detected in different lag threads confirm the observation that there are commonalities in signal propagation within each lag thread (Mitra et al., 2015).

3.4. Summary of Findings

This study of the Betti numbers and inner vortex areas of rs-fMRI BOLD signal propagation subregions of the brain confirms and supplements earlier findings given in Mitra et al. (2015). A main

result of this study of the persistence of brain activation subregion features confirms the contention that the topography of lag threads is highly reproducible. Starting with the Betti number of connected cycles derived from triangulated brain activation regions found in rs-fMRI videos, it is apparent that the vortexes on brain activation subregions appear over and over in the lag threads across different rs-fMRI video frames. In other words, we find that there are commonalities in BOLD signal propagation within each lag thread.

The question whether intrinsic brain activity contains reproducible temporal sequences is revisited. It is confirmed that a human resting state fMRI (rs-fMRI) contains persistent (repeatable) highly reproducible lag structure. The answer to this question is given twofold. This is done first in terms of Betti numbers that are counts of the number of connected cycles in vortexes on triangulated brain activation subregions. We introduce a 2D persistence pictograph (barcode) that exhibits the appearance, disappearance, and repeated reappearance of Betti numbers across lag threads in sequences of rs-fMRI video frames. In addition, the reproducibility question is also answered in terms of the introduction of a video frame-Betti number-vortex cycle area combination in 3D persistence barcodes that facilitates a check on how often these features of lag threads appear during a rs-fMRI session.

Concluding Remarks

This study considers Betti numbers that are counts of the number of connected barycentric cycles in vortexes on triangulated brain activation regions. In terms of the area occupied by a vortex on a brain activation subregion, we have only considered the area of the interior of the innermost barycentric cycle of each vortex. Also of interest and of considerable importance is the area in the interior of other cycles that includes the inner vortex cycle. Future work would expand the derivation of persistent barcodes to include the zeroth as well as the oneth Betti numbers. In working toward the approximation of the area of brain activation subregion shapes, the areas in the interior of the other cycles (summing on the innermost vortex cycle area) would be considered.

DATA AVAILABILITY STATEMENT

The dataset for this study can be found at the following URL: https://drive.google.com/drive/folders/1NxZ1Ydcuhzrdmgav-DxIGrbg-pq5GCI8?usp=sharing.

AUTHOR CONTRIBUTIONS

JP designed the materials and methods. AD developed the code and tools. AT and JP analyzed the data and performed the research. SR contributed to the research and writing of the paper.

FUNDING

This research has been supported by the Natural Sciences & Engineering Research Council of Canada (NSERC) discovery grants 185986 and 194376, Instituto Nazionale di Alta Matematica (INdAM) Francesco Severi, Gruppo Nazionale per le Strutture Algebriche, Geometriche e Loro Applicazioni grant 9 920160 000362, n.prot U 2016 / 000036.

ACKNOWLEDGMENTS

Authors acknowledge the NSERC Discovery Grants program for this research. This manuscript has been released as a Pre-print at https://www.biorxiv.org/content/10.1101/809293v2.

SUPPLEMENTARY MATERIAL

The Supplementary Material for this article can be found online at: https://www.frontiersin.org/articles/10.3389/fncom.2020.00034/full#supplementary-material

REFERENCES

Achard, S., and Bullmore, E. (2007). Efficiency and cost of economical brain functional networks. *PLoS Comput. Biol.* 3:e30017. doi: 10.1371/journal.pcbi.0030017

Alexandroff, P. (1965). *Elementary Concepts of Topology*. New York, NY: Dover Publications, Inc.

Buckner, R. L., Roffman, J. L., and Smoller, J. W. (2014). Brain Genomics Superstruct Project (GSP). *Harvard Dataverse*. doi: 10.7910/DVN/25833

Bullmore, E., and Sports, O. (2009). Complex brain networks: graph theoretical analysis of structural and functional systems. *Nat. Rev. Neurosci.* 10, 186–198. doi: 10.1038/nrn2575

Carlsson, G. (2009). Topology and data. *Bull. Am. Math. Soc.* 46, 255–308. doi: 10.1090/S0273-0979-09-01249-X

Cassidy, B., Rae, C., and Solo, V. (2015). "Brain activity: conditional dissimilarity and persistent homology," in *ISBI, 12th International Symposium on Biomedical Imaging* (New York, NY: IEEE), 1356–1359.

Chazal, F., and Michel, B. (2017). An introduction to topological data analysis: fundamental and practical aspects for data scientists. *arXiv* 1710, 1–38. doi: 10.1142/9789813144446_0001

Chung, M., Hanson, J., Ye, J., Davidson, R., and Pollak, S. (2015). Persistent homology in sparse regression and its application to brain morphometry. *IEEE Trans. Med. Imaging* 34, 1928–1939. doi: 10.1109/TMI.2015.2416271

Chung, M., Lee, H., DiChristofano, A., Ombao, H., and Solo, V. (2019). Exact topological inference of the resting-state brain networks in twins. *Netw. Neurosci.* 3, 674–694. doi: 10.1162/netn_a_00091

Chung, M., Vilalta-Gil, V., Lee, H., Rathouz, P., Lahey, B., and Zald, D. (2017). "Exact topological inference for paired brain networks via persistent homology. Information processing in medical imaging," in *IPMI, Lecture Notes in Computer Science, 10265* (Springer), 299–310.

Delaunay, B. (1934). Sur la sphère vide. *Izvestia Akad. Nauk SSSR, Otdelenie Matematicheskii i Estestvennyka Nauk* 7, 793–800.

Di Concilio, A., Guadagni, C., Peters, J., and Ramanna, S. (2018). Descriptive proximities. Properties and interplay between classical proximities and overlap. *Springer Math. Comput. Sci.* 12, 91–106. doi: 10.1007/s11786-017-0328-y

Don, A., Peters, J., Ramanna, S., and Tozzi, A. (2019). *Vortex Signature Project*. Available online at: https://drive.google.com/drive/folders/1NxZ1Ydcuhzrdmgav-DxIGrbg-pq5GCI8?usp=sharing

Don, A. P., and Peters, J. F. (2019). Ghrist barcoded video frames. Application in detecting persistent visual scene surface shapes captured in videos. *Theory Appl. Math. Comput. Sci.* 9, 14–27. doi: 10.1007/978-3-030-22192-8

Don, A. P., Peters, J. F., Ramanna, S., and Tozzi, A. (2019). Topological inference from spontaneous activity structures in FMRI videos with persistence barcodes. *Cold Spring Harb. Lab.* 2019:809293. doi: 10.1101/809293

Edelsbrunner, H., and Harer, J. (2008). Persistent homology. A survey. *Contemp. Math.* 453, 257–282. doi: 10.1090/conm/453/08802

Edelsbrunner, H., and Harer, J. (2010). *Computational Topology. An Introduction*. Providence, RI: American Mathematical Society.

Edelsbrunner, H., Letscher, D., and Zomorodian, A. (2000). "Topological persistence and simplification," in *41st Annual Symposium on Foundations of Computer Science*, (Los Alamitos, CA: IEEE Comput. Soc. Press), 454–463.

Edelsbrunner, H., Letscher, D., and Zomorodian, A. (2001). Topological persistence and simplification. *Springer Discr. Comput. Geometry* 28, 511–533. doi: 10.1007/s00454-002-2885-2

Freeman, W. (2009). Vortices in brain activity: their mechanism and significance for perception. *Neural Netw.* 22, 491–501. doi: 10.1016/j.neunet.2009.06.050

Ghrist, R. (2008). Barcodes: the persistent topology of data. *Bull. Am. Math. Soc.* 45, 61–75. doi: 10.1090/S0273-0979-07-01191-3

Ghrist, R. (2014). *Elementary Applied Topology*. Philadelphia, PA: University of Pennsylvania.

Giusti, C., Pastalkova, E., Curto, C., and Itskov, V. (2015). Clique topology reveals intrinsic geometric structure in neural correlations. *Proc. Nat. Acad. Sci. U.S.A.* 112, 1355–1360. doi: 10.1073/pnas.1506407112

Lee, H., Chung, M., Kang, H., Kim, B.-N., and Lee, D. (2011a). "Computing the shape of brain networks using graph filtration and Gromov-Hausdor metric," in *MICCAI, Lecture Notes in Computer Science, 6892* (Toronto, ON: Springer), 302–309.

Lee, H., Chung, M., Kang, H., Kim, B.-N., and Lee, D. (2011b). "Discriminative persistent homology of brain networks," in *ISBI, IEEE International Symposium on Biomedical Imaging* (Chicago, IL), 841–844.

Matsui, T., Murakami, T., and Ohki, K. (2016). Transient neuronal coactivations embedded in globally propagating waves underlie resting-state functional connectivity. *Proc. Nat. Acad. Sci. U.S.A.* 113, 6556–6561. doi: 10.1073/pnas.1521299113

Meunier, D., Lambiotte, R., Fornito, A., Ersche, K., and Bullmore, E. (2009). Hierarchical modularity in human brain functional networks. *Front. Neuroinform.* 3:2009. doi: 10.3389/neuro.11.037.2009

Mitra, A., Snyder, A. Z., Blazey, T., and Raichle, M. (2015). Lag threads organize the brain's intrinsic activity. *Proc. Nat. Acad. Sci. U.S.A.* 112, E2235–E2244. doi: 10.1073/pnas.1503960112

Munkres, J. (2000). *Topology, 2nd Edn.* Englewood Cliffs, NJ: Prentice-Hall.

Park, Y. B., Shim, M. M., James, O., and Park, H. (2019). Possible links between the lag structure in visual cortex and visual streams using fMRI. *Sci. Rep.* 9, 4283–4293. doi: 10.1038/s41598-019-40728-x

Peters, J. (2020). *Computational Geometry, Topology and Physics of Digital Images with Applications. Shape Complexes, Optical Vortex Nerves and Proximities*. Cham: Springer Int. Pub.

Peters, J., Ramanna, S., Tozzi, A., and Inan, E. (2017). Bold-independent computational entropy assesses functional donut-like structures in brain fMRI images. *Front. Hum. Neurosci.* 11:38. doi: 10.3389/fnhum.2017.00038

Petri, G., Expert, P., Turkheimer, F., Carhart-Harris, R., Nutt, D., Hellyer, P. J., et al. (2014). Homological scaffolds of brain functional networks. *J. R. Soc. Interface* 11:20140873. doi: 10.1098/rsif.2014.0873

Sizemore, A. E., Giusti, C., Kahn, A., Vettel, J., Betzel, R., and Bassett, D. (2018). Cliques and cavities in the human connectome. *J. Comput. Neurosci.* 44, 115–145. doi: 10.1007/s10827-017-0672-6

van Wijk, B., Stam, C., and Daffertshofer, A. (2010). Comparing brain networks of different size and connectivity density using graph theory. *PLoS ONE* 5:e13701. doi: 10.1371/journal.pone.0013701

Yung, C., Choi, G.-T., Chen, K., and Lui, L. (2016). Trim: triangulating images for efficient registration. *arXiv cs.GR* 1605, 1–13. doi: 10.1016/j.jvcir.2018.07.005

Zomorodian, A., and Carlsson, G. (2005). Computing persistent homology. *Discrete Comput. Geomet.* 33, 249–274. doi: 10.1007/s00454-004-1146-y

Zomorodian, A. F. (2001). *Computing and comprehending topology: persistence and hierarchical morse complexes* (Ph.D. thesis). Department of Computer Science; University of Illinois at Urbana-Champaign, Chicago, IL., United States.

Conflict of Interest: The authors declare that the research was conducted in the absence of any commercial or financial relationships that could be construed as a potential conflict of interest.

Copyright © 2020 Don, Peters, Ramanna and Tozzi. This is an open-access article distributed under the terms of the Creative Commons Attribution License (CC BY). The use, distribution or reproduction in other forums is permitted, provided the original author(s) and the copyright owner(s) are credited and that the original publication in this journal is cited, in accordance with accepted academic practice. No use, distribution or reproduction is permitted which does not comply with these terms.

ResearchGate

See discussions, stats, and author profiles for this publication at: https://www.researchgate.net/publication/341111780

Gastroesophageal and gastric ultrasound in children: the state of the art

Article *in* Journal of Ultrasound · May 2020

DOI: 10.1007/s40477-020-00471-w

CITATIONS
0

READS
29

5 authors, including:

Raffaele Minella
Azienda Sanitaria Locale Napoli 3 Sud
48 PUBLICATIONS **1,093** CITATIONS

SEE PROFILE

Rocco Minelli
Department Life and Health "V. Tiberio", University of Molise, Via Francesco De Sa…
16 PUBLICATIONS **6** CITATIONS

SEE PROFILE

Eugenio Rossi
Azienda Ospedaliera di Rilievo Nazionale Santobono Pausilipon
163 PUBLICATIONS **254** CITATIONS

SEE PROFILE

Cremone Gaetana
Azienda Ospedaliera Universitaria OO.RR. S.Giovanni di Dio e Ruggi d'Aragona
8 PUBLICATIONS **8** CITATIONS

SEE PROFILE

Some of the authors of this publication are also working on these related projects:

Project My philosophical papers View project

Project Fixed point theory View project

All content following this page was uploaded by Raffaele Minella on 18 October 2020.

The user has requested enhancement of the downloaded file.

Journal of Ultrasound
https://doi.org/10.1007/s40477-020-00471-w

REVIEW PAPER

Gastroesophageal and gastric ultrasound in children: the state of the art

Raffaele Minella[1] · Rocco Minelli[2] · Eugenio Rossi[3] · Gaetana Cremone[4] · Arturo Tozzi[5]

Received: 2 April 2020 / Accepted: 23 April 2020
© Società Italiana di Ultrasonologia in Medicina e Biologia (SIUMB) 2020

Abstract
In previous years, the role of gastroesophageal (GE) ultrasound as a diagnostic tool in gastroesophageal reflux disease (GERD) has been disputed. Most authors believe that it is difficult to diagnose GERD without correlation studies between esophageal pathology and ultrasonographic signs. Indeed, there are many anatomic descriptions of the normal GE junction. The fact that GERD diagnosis was made by morphological studies was believed to be an incorrect deduction. We revisit the pathophysiologic data concerning the gastroesophageal junction and gastric function and review the data in the literature of the past 30 years.

Keywords Gastroesophageal reflux disease · Lower esophageal sphincter · Gastric emptying time · Ultrasound

Introduction

Gastroesophageal reflux disease (GERD) is complex and involves changes that lead to the failure of normal anti-reflux mechanisms. Esophageal damage is a consequence of delayed gastric emptying time (GET) and hiatal hernia, but it is considered a motor defect. The anti-reflux barrier is a well-defined anatomic region that is the result of a delicate balance between the lower esophageal sphincter and the crural diaphragm. The phrenoesophageal ligament and the gastric sling fibers of the gastric cardia also contribute to the functioning of the barrier. In case of anatomic laxity or increased intragastric pressure, the barrier does not guarantee its function, and reflux occurs [1].

Ultrasonographic aspects

The gastroesophageal region and gastric motor function can be studied by means of ultrasonography. The main ultrasound parameters that are considered in the literature are the following:

1) The length of the abdominal tract of the esophagus was measured only on the longitudinal scans from the point at which the esophagus traversed the diaphragm to the gastroesophageal region identified on the sonogram by a small triangular pad of gastric folds radiating from the cardia [2] (Fig. 1).
2) The esophageal wall thickness was measured on the anterior wall at the midpoint of the abdominal esophagus [2] (Fig. 2).
3) The gastroesophageal angle (angle's His) was delimited within the tangent line passing from the left fornix of the stomach and the line of the esophageal wall [3] (Fig. 3).
4) The esophageal diameter was measured from serosa to serosa in longitudinal scans [4] (Fig. 4).

The reference values of these parameters are not well established, despite many articles and reviews [5–7]. In

✉ Rocco Minelli
rocco.minelli@libero.it

1 Primary Care Pediatrician, ASLNA3Sud Torre del Greco, Italy

2 Department Life and Health "V. Tiberio", University of Molise, Francesco De Sanctis st 1, 86100 Campobasso, Italy

3 Unit of Radiology and Ultrasound, A.O.R.N. Santobono-Pausilipon, Pausilipon Hospital, Naples, Italy

4 Department of Radiology Hospital G. Fucito, Mercato San Severino, Salerno, Italy

5 Center for Nonlinear Science, Department of Physics, University of North Texas, Denton, TX 76203, USA

Published online: 02 May 2020

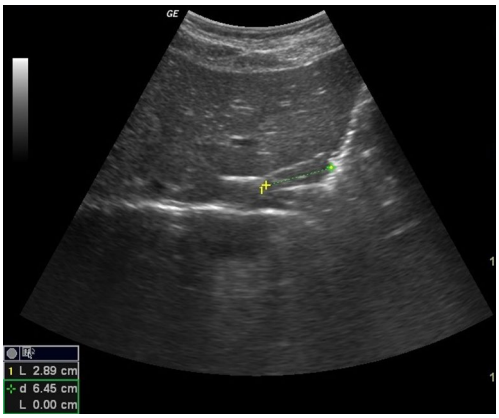

Fig. 1 Longitudinal scan showing the length of the abdominal tract of the esophagus

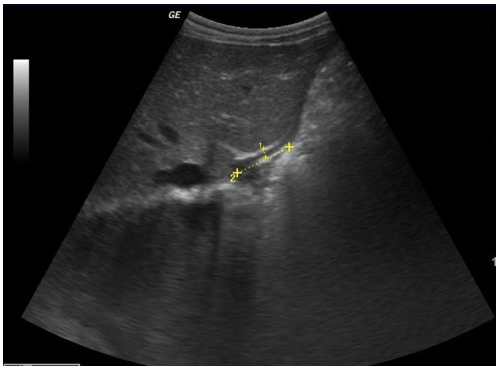

Fig. 2 Longitudinal scan showing that the esophageal wall thickness was measured on the anterior wall at the midpoint of the abdominal esophagus

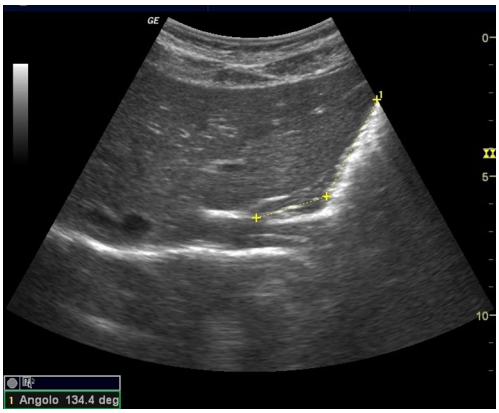

Fig. 3 Longitudinal scan showing the gastroesophageal angle

effect, the design of each study lacks randomization or pathological controls, and is conducted in only a few patients, or is statistically incorrect. The results are expert opinions because of the low level and quality of the evidence. The

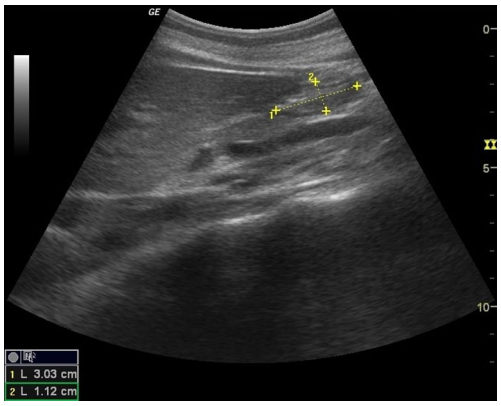

Fig. 4 Longitudinal scan from serosa to serosa

stomach, too, can be studied by ultrasonography, but at present only functional studies are performed regarding motor activity. The GET was calculated by measuring the cross-section of the gastric antrum corresponding to the sagittal plane passing through the superior mesenteric vein (as a point of reference) to obtain scanning consistency. The cross-section of the gastric antrum shows an elliptic shape at this level, and its area in cubic centimeters was measured by the following formula: $\pi\, a \times b\, /4$ (a: longitudinal diameter, b: anteroposterior diameter). The stomach was considered empty when the section area of the antrum returned to the baseline value and persisted unchanged for at least 30 min. The final GET was calculated in relation to the start of the meal. In controls, the final GET of a standard meal is 180 min [8]. Another intriguing feature of functional ultrasound of the stomach is the study of fundus accommodation. Gastric accommodation, in fact, is an important mechanism in comprehending the pathophysiology of functional disorders of the stomach. In 2000, Olafsdottir et al. demonstrated that gastric accommodation ultrasonography is a noninvasive imaging test [9] during the ingestion of a meal, with the proximal stomach acting as a reservoir by increasing its volume without a significant change in intragastric pressure. For proximal stomach measurements, two standardized sonographic sections were chosen by placing the transducer at the left subcostal margin and tilting it cranially. First, a sagittal section of the stomach was obtained, with the left renal pelvis in a longitudinal projection and the left lobe of the liver and the tail of the pancreas serving as internal landmarks. The stomach area was outlined by tracing the inner echogenic layer, corresponding to the interface between the soup and the mucosa of the gastric wall, from the top margin of the fundus and 7 cm downward along the axis of the stomach (sagittal section, sa). Then, the transducer was rotated 90° clockwise to obtain an oblique frontal gastric section. In this case, the left hemidiaphragm, the top margin of the fundus, and the liver parenchyma served as

landmarks. In this way, it is feasible to measure the maximal oblique frontal diameter (ofd), which is located within 7 cm along the long axis of the proximal stomach. An approximate volume of the proximal stomach (av) was calculated by combining these two measures (av = sa × ofd). The av values were used to compute the individual emptying fraction of the proximal stomach, defined as (av1 min-av actual)/av1 min. Time zero was defined as the end of the ingestion period of 5 min. The field of application of gastric proximal ultrasound examination is currently confined to the study of functional disorders of the gastrointestinal (GI) tract in accordance with Rome IV Pediatric, but it is an important prospective tool for the complex evaluation of patients with gastroesophageal reflux.

Historical review

The 2009 ESPGHAN guidelines [10] suggest that these tests are not recommended for the routine evaluation of GERD in children. The guidelines of 2018 [11] modify in part these recommendations, suggesting that at present, ultrasound has no role as a routine diagnostic tool for GERD in children, but this test may be useful for evaluating other conditions that might mimic GERD, including, most importantly, pyloric stenosis in the infant population. Abdominal ultrasound may also pick up other diagnoses that may trigger symptoms of discomfort and vomiting, including diagnoses such as hydronephrosis, ureteropelvic obstruction, gallstones, and ovarian torsion. Like barium swallow X-ray, ultrasound can detect hiatal hernia and the length and position of the lower esophageal sphincter (les) relative to the diaphragm and magnitude of the gastroesophageal angle of His. It has also been proposed as a diagnostic test for gastric dysmotility, which may have implications from a reflux perspective. In 1993, Gomes et al. demonstrated that the length of the abdominal esophagus is fundamental in reflux studies [13]. In 2003, the same authors validated the sonographic method. In 1994, Westra affirmed the ability of the ultrasonographic measurement to diagnose symptomatic gastroesophageal reflux [14]. In 2001, Esposito et al. [2] concluded that the visualization of the GE junction and the measurement of the abdominal esophagus are achievable with real-time sonography. Many studies were performed in the subsequent years to demonstrate the feasibility of ultrasonography in diagnosing GERD, but none was performed with the correct design; therefore, each contribution must be considered an expert opinion. Cucchiara et al. demonstrated that the GET in patients with functional dyspepsia [8–12] and cystic fibrosis [15] was delayed. The field of application of gastric proximal ultrasound examination is at present confined to the study of functional disorders of the GI tract in accordance with Rome IV Pediatric, or in evaluating rehabilitation in anorexia, but it is an important prospective tool for the complex evaluation of patients with gastroesophageal reflux [6, 16–18].

Conclusion

The evaluation of children with gastroesophageal reflux disease requires an accurate ultrasonographic approach, but ultrasound requires more and accurate studies for complete validation.

Compliance with ethical standards

Conflict of interest The authors declare that they have no conflict of interest.

Informed consent All procedures followed were in accordance with the ethical standards of the responsible committee on human experimentation (institutional and national) and with the Helsinki declaration of 1975, and its late amendments. Additional informed consent was obtained from all patients for which identifying information is not included in this article.

Human and animal rights This article does not contain any studies with human or animal subjects performed by any of the authors.

References

1. Tack J et al (2018) Pathophysiology of gastroesophageal reflux disease. Gastroenterology 154:277–288
2. Esposito F et al (2001) Transabdominal sonography of the normal gastroesophageal junction in children. J Clin Ultrasound 29:326–331
3. Halkiewicz F et al (2000) Ultrasound picture of gastroesophageal junction in children with reflux disease. Med Sci Monit 6:96–99
4. Hashemi H et al (2009) Diagnostic efficacy of distal esophagus ultrasonography in diagnosis of gastroesophageal reflux disease in children. Res J Biol Sci 4:71–76
5. Savino A et al (2012) Us in the diagnosis of gastroesophageal reflux in children. Pediatr Radiol 42:515–524
6. Di Serafino M, Severino R, Lisanti L, Rocca R, Scarano E (2016) Dysphagia lusoria: an uncommon cause of dysphagia. J Hepatol Gastroint Dis 2(134):2. https://doi.org/10.4172/2475-3181.1000134
7. Di Serafino M, Mercogliano C, Vallone G (2015) Ultrasound evaluation of the enteric duplication cyst: the gut signature. J Ultrasound 19(2):131–133. https://doi.org/10.1007/s40477-015-0188-8
8. Cucchiara S et al (1995) Real time ultrasound reveals gastric motor abnormalitiesin children investigated for dyspeptic symptoms. Pediatr Gastroenterol Nutr. 21:446–453
9. Olafsdottir E et al (2000) Impaired accommodation of the proximal stomach in children with recurrent abdominal pain. J Pediatr Gastroenterol Nutr 30:157–163
10. Vandenplas Y et al (2009) Pediatric gastroesophageal reflux clinical practice guidelines: joint recommandations of the north american society for pediatric gastroenterology, hepatology and nutrition (naspghan) and the european society for pediatric gastroenterology, hepatology and nutrition (espghan). J Pediatr Gastronetrol Nutr 49:498–547

11. Rosen N et al (2018) Pediatric gastroesophageal reflux clinical practice guidelines: joint recommandations of the north american society for pediatric gastroenterology, hepatology and nutrition (naspghan) and the european society for pediatric gastroenterology, hepatology and nutrition (espghan). J Pediatr Gastronetrol Nutr 66:516–554
12. Tufano A, Minelli R, Rossi E et al (2020) Inferior epigastric artery pseudoaneurysm secondary to port placement during a robot-assisted laparoscopic radical cystectomy. J Ultrasound. https://doi.org/10.1007/s40477-020-00442-1
13. Gomes H et al (2003) Ultrasonography and gastric emptiyng in children: valuidation of a sonographic method and determination of physiological and pathological patterns. Pediatr Radiol 33:522–529
14. Westra SJ et al (1994) Symptomatic gastroesophageal reflux: diagnosis with ultrasound. J Pediatr Gastroenterol Nutr 19:58–64
15. Cucchiara S et al (1996) Us measurement of gastric emptying time in aptients with cystic fibrosis and effect of ranitidine on delayed gastric emptying. J Pediatr Gastroenterol Nutr 128:485–488
16. Corvino A, Sandomenico F, Setola SV et al (2019) Added value of contrast-enhanced ultrasound (CEUS) with Sonovue® in the diagnosis of inferior epigastric artery pseudoaneurysm: report of a case and review of literature. J Ultrasound 22:485–489. https://doi.org/10.1007/s40477-019-00398-x
17. Di Serafino M et al (2017) A case of esophageal perforation: clinical and diagnostic management in emergency medicine. Emerg Care J 13:6848. https://doi.org/10.4081/ecj.2017.6848
18. Esposito F, Di Serafino M, Mercogliano C et al (2019) The pediatric gastrointestinal tract: ultrasound findings in acute diseases. J Ultrasound 22:409–422. https://doi.org/10.1007/s40477-018-00355-0

Publisher's Note Springer Nature remains neutral with regard to jurisdictional claims in published maps and institutional affiliations.

View publication stats

Author's personal copy

Foundations of Science
https://doi.org/10.1007/s10699-020-09708-7

Are Borders Inside or Outside?

Arturo Tozzi[1]

Accepted: 27 September 2020
© Springer Nature B.V. 2020

Abstract
When a boat disappears over the horizon, does a distant observer detect the last moment in which the boat is visible, or the first moment in which the boat is not visible? This apparently ludicrous way of reasoning, heritage of long-lasting medieval debates on decision limit problems, paves the way to sophisticated contemporary debates concerning the methodological core of mathematics, physics and biology. These ancient, logically-framed conundrums throw us into the realm of bounded objects with fuzzy edges, where our mind fails to provide responses to plain questions such as: given a closed curve with a boundary (say, a cellular membrane) how do you recognize what is internal and what is external? We show how the choice of an alternative instead of another is not arbitrary, rather points towards entirely different ontological, philosophical and physical commitments. This paves the way to novel interpretations and operational approaches to challenging issues such as black hole singularities, continuous time in quantum dynamics, chaotic nonlinear paths, logarithmic plots, demarcation of living beings. In the sceptical reign where judgements seem to be suspended forever, the contemporary scientist stands for a sort of God equipped with infinite power who is utterly free to dictate the rules of the experimental settings.

Keywords Infinity · Boundary · Jordan curve theorem · Bradwardine · Nicholas of autrecourt

Take an object with a border separating the internal from the external. We might ask: is the boundary inside or outside the object? At the very edge of the closed curve, does the last point of the internal occur, or the first point of the external? Medieval scholars confronted diverse types of these challenges that are currently termed "limit decision problems". The ancient theologians/philosophers/scientists used the weapons available to them, i.e., Aristotelian analytic arguments and thought experiments, to appraise the limits and degrees of "powers" such as time, length, weight, distance, and so on (Offredus 1478; Nielsen 1982). Here I examine the subtleties of limit decision problems going through apparently silly questions such as: "the present time stands for: the current instant, or the last instant

✉ Arturo Tozzi
tozziarturo@libero.it; Arturo.Tozzi@unt.edu

[1] Department of Physics, Center for Nonlinear Science, University of North Texas, 1155 Union Circle #311427, Denton, TX 76203-5017, USA

Published online: 06 October 2020

Author's personal copy

of the past, or the first instant of the future?" It is straightforward to claim that this intricate way of reasoning is perplexing for the baffled modern-day readers. Who cares about weird medieval enterprises such as the search for "*incipit*" and "*desinit*" (i.e., the "beginning" and the "end")? What is the practical gist of absurd questions such as: "when we look at a boat disappearing over the horizon, does exist the last instant in which we see the boat, or the first instant in which we do not see the boat?" (O'Donnell 1939). What these apparently idle remarks bring on the operational table of the pragmatic scientific method?

I will show in the sequel that these issues are not as bizarre as one might believe. The quite different solutions to this kind of difficulties were not delivered by medieval scholars just to satisfy a whim, rather to explain, assess and quantify different issues, including physical and biological ones. I will proceed as follows. At first, I will describe the practice of medieval limit decision problems from a general point of view. The ensuing specific chapters will treat physical and biological issues, portraying the medieval (and current) treatments of specific themes such as time, space, lengths and so on. Recounting how the ancient authors considered all options relative to these troublesome issues, my goal is tripartite. My first goal is to show to the baffled reader how the choice of an alternative instead of another is not arbitrary, rather it is points towards fully different ontological, philosophical, physical, and biological commitments. My second goal is to breathe new life into forgotten concepts tackled by Medieval scholars, turning them into precious gifts from the past. My third goal, the most important, is to demonstrate how these treasures from ancient times can be helpful (I would say: game changing) to tackle current mathematical, physical and biological issues under a novel methodological light.

1 Decision Limit Problems: an Historical Leitmotiv

Ancient scholars, particularly Oxonians and Parisian middle-age authors, were fond of the subtilities and endeavours of the troublesome problem of limits. Figure 1, upper part, provides a general sketch of the challenges they faced. Take a line encompassing a segment bounded by two endpoints. When you evaluate the tiny spots remarkably close to the two endpoints, how do you define them? To make an example, what do you call the endpoint termed "beginning" in Fig. 2a? Do you call it the last point before the beginning, of do you call it the first point after the beginning? The first move of medieval philosophers/scientists was to consider the problem of time passing, i.e., the *primo et ultimo istanti* (the first and the last instant), and *incipit* and *desinit* (the beginning and the end) (Shapiro and Shapiro 1965; Heytesbury 1979). Is this very moment the last instant after the past ones, or is it an instant of the present, or is it the first instant before the future ones? The issue is related to the Aristotelian dilemma: does the present instant cease to be when it is, or when it is not? (Trifogli 2017). Either this instant now is, and immediately afterwards will not be, or this instant now is not, and immediately beforehand it was. Successively, the temporal challenge of the *primo et ultimo istanti* was used to cope with other types of *maximum and minimum* magnitudes such as weights, or spatial distances (Walker 2018). Here you are a typical set off: "an object cannot be seen from every distance, because there can be a distance so great that the object cannot be seen from it, and because there can be a minimum distance brought closed to the vision from which a visible thing cannot be seen".

Medieval scholars' next step was to relate the limit problem of spatial bodies to gnoseology and epistemology. What about the medium instant between the whole time in which the thing can be seen, and the whole time in which it cannot be seen? In this medium

Author's personal copy

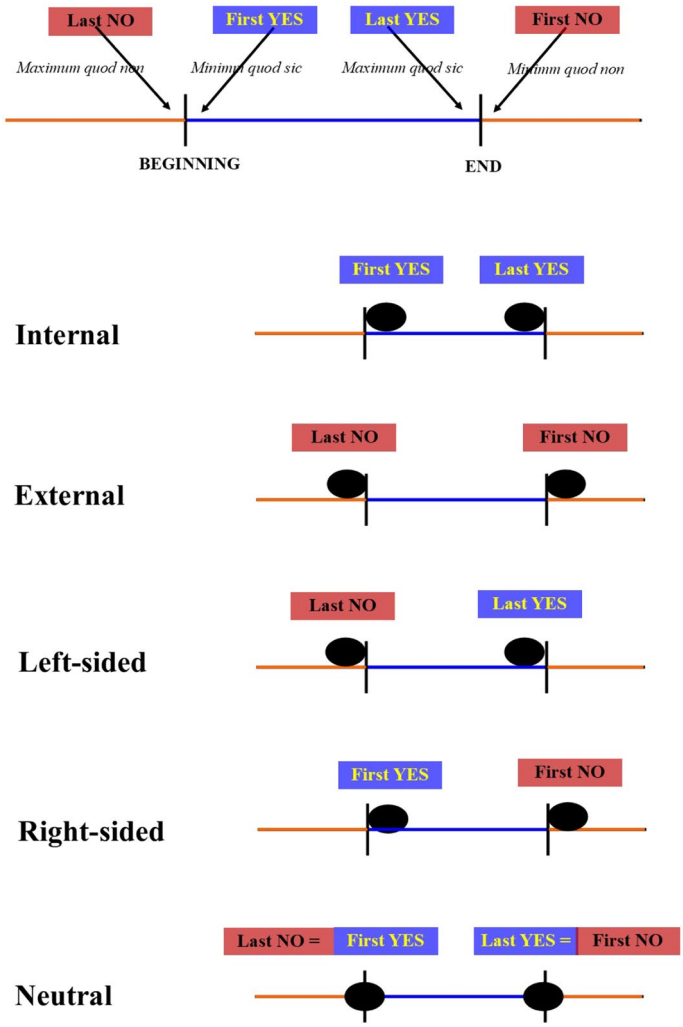

Fig. 1 Different kinds of decision limit problems. The Figure on the top outlines the overall pattern described in this paper. When you mark with black dots the endpoints (beginning and end) of a given segment (blue line), you are allowed to perform different choices inside the tiny area close to the endpoints: you may choose to consider the last point before the line (termed "the last NO" in logical terms, and "*maximum quod non*" in medieval terminology), and so on. Note that, according the analytic geometry's conventions, the points at the extreme left stand for the first ones, because numbers grow from left to right along the X-axis. Following such convention, the nomenclature would be inverted: our "Last NO" would stand for the "First NO". However, we favoured a different choice, because we wanted to emphasize that, in our context, the first yes and the last yes refer just to the segment under examination, and not to the full length of the line. (Color figure online)

instant, can the thing be seen, or cannot (O'Donnell 1939)? When a boat disappears over the horizon, what is the instant (o the minimum spatial range) of change between the whole state of visibility and that of non-visibility? The limit problem of spatial bodies became strictly correlated with human perceptions, because it involves what was called "intension and remission" of sensations: What is the smallest amount of matter that permits us to

Author's personal copy

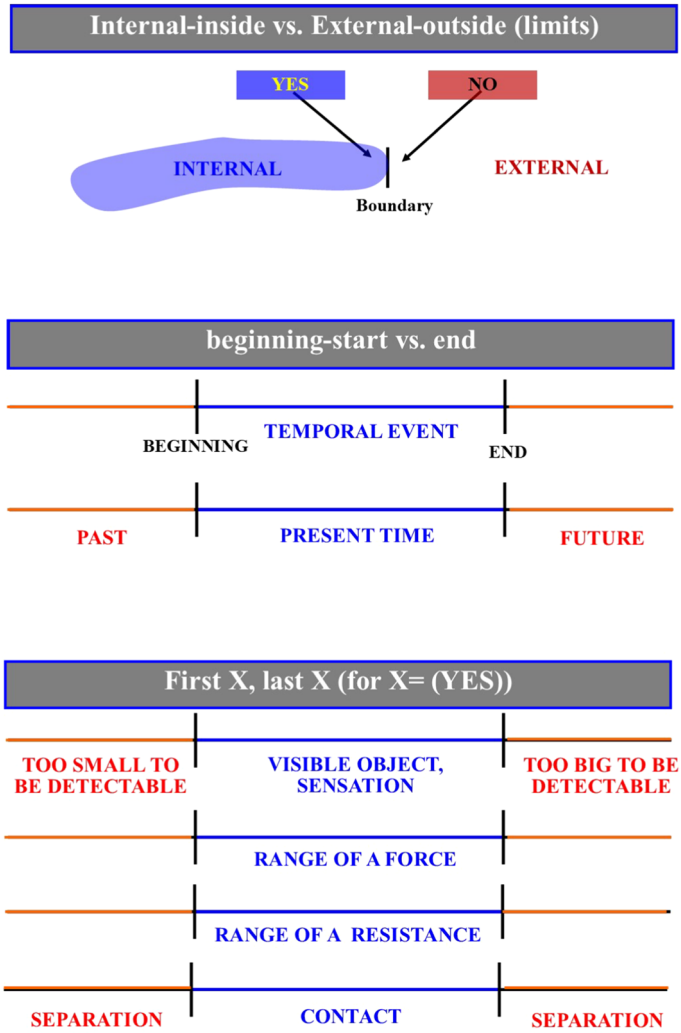

Fig. 2 The basic dichotomies of our logical approach are here correlated with the basic scientific issues tackled by our paper. Note that the phase spaces where these logical operations may take place can be various: such phase spaces may refer either to borders in time, or real spaces, mathematical or qualitative spaces

define an object? How much is an object divisible into particles so small that, once these particles are dispersed, the object no longer exercises influence on the senses (Autrecourt 1940)? What does it mean that an object is too small, or too big, to be detected? The next move of the volitional scholars was to turn to the ranges of forces, such as pressure, or heat, and so on. Can an active capacity (force) be measured against a passive capacity (resistance)? Take a force: there must be a range in which the capacity can act or be acted upon, and another range in which it cannot act or be acted upon, and not both. If you can lift one hundred pounds, you can lift fifty pounds too. Conversely, if you can see a grain of millet from the distance of a mile, you can also see a skyscraper at the same distance.

Author's personal copy

The force under evaluation, they reasoned, should only be able to take a value in the range on which it is measured from zero and the value which serves as its boundary. The last, but not the least, the case of the separation of two surfaces on the assumption of direct contact was frequently appraised as a hypothetical experimental setting invoked to deny the existence of natural and artificial vacuum (Grant 1973).

To visualize the viable choices and relationships, we will use the informative sketches envisioned by Murdoch (1964). A black dot marks the left or right side of the segment's endpoint, according to the location where the scholar decided to pinpoint the event under examination. For example, Fig. 1, Internal points says that the author is favouring the choice of internal points: in case of the human lifespan, he means that life goes from the first moment of existence (birth; FIRST YES) to the last moment of existence (death; LAST YES). In turn, Fig. 1, External points says that the author is favouring the choice of external points: he means that life goes from the last moment of non-existence before birth (LAST NO), to the first moment of non-existence after death (FIRST NO). The choice depicted in Fig. 1, Left-side was made by scholars who did not believe in the first instant of motion, rather did believe in the last instant of motion. In turn, Fig. 1, Right-side was kept by scholars who believed in the first instant of motion but did not believe in the last instant of motion.

All the examples provided so far describe the dividing-point as mandatory located either before or after the segment's endpoint. The dividing-point was assigned by the most of Medieval scholars to one of the sides of the segment, and not to both, due to the principle of non-contradiction: "contradictory propositions cannot both be true at the same time and in the same sense". "If it is yes, it cannot be no": a point cannot be common to both the sides an endpoint. Nevertheless, a few strong-willed Medieval scholars realized that another intriguing possibility was left to their investigations: continuum and infinity (Bradwardine 1955). Examining the treatment of space, time, and local motion provided by Aristotle's Physics, they grasped that terms such as "begins" and "ceases" have connections with the nature and properties of continua. They understood that the dividing endpoint point can be common to both the sides, so that "the last no" and "the first yes" are superimposed and inextricable (Fig. 1, Neutral). The same holds for "the last yes" and "the first no". In the sequel, I will examine the medieval account of specific limit problems, such as the first temporal instant, the first moment is which a force is applied, and so on. I will use their lessons to assess contemporary challenges in scientific fields such as mathematics, physics and biology. A general sketch summarizing the scientific problems I will encounter in the sequel can be found in Fig. 2.

The Figure on the top outlines the overall pattern described in this paper. When you mark with black dots the endpoints (beginning and end) of a given segment (blue line), you are allowed to perform different choices inside the tiny area close to the endpoints: you may choose to consider the last point before the line (termed "the last NO" in logical terms, and "*maximum quod non*" in medieval terminology), and so on. Note that, according the analytic geometry's conventions, the points at the extreme left stand for the first ones, because numbers grow from left to right along the X-axis. Following such convention, the nomenclature would be inverted: our "Last NO" would stand for the "First NO". However, we favoured a different choice, because we wanted to emphasize that, in our context, the first yes and the last yes refer just to the segment under examination, and not to the full length of the line.

The Figures below illustrate the different choices to assess decision limit problems. For sake of clarity, we termed the different assortments of choices with the arbitrary names of Internal, External, Left-sided, Right-sided, Neutral, based on the location of the points

Author's personal copy

close to the segment's endpoints. Every scheme can be used with different meaning in dissimilar scientific contexts. See text for further details.

2 Lessons from the Past 1: Current Insights in Physical Issues

Paradoxical properties of the temporal flow uncovered by Medieval scholars might be scientifically valuable. "Beginning" may be expounded by meaning that in the present instant a thing or a process is, and immediately prior to the present instant it was not (Fig. 1, Internal) (Heytesbury 1979). "Beginning" may be also expounded in the opposite way (Fig. 1, External) (Trifogli 2017). In turn, people like Heytesbury (1984) favoured Fig. 1, Left-sided when evaluating the "beginning" of time, and Fig. 1, Right-sided when evaluating the "ceasing" of time. There was the logical necessity to ascribe the dividing point to one of the two sides as an attribute of time itself. Likewise, theological concerns pointed towards the endpoint as a discrete entity: points and lines must be immediate to one another and not superimposed, because God's knowledge of them must be clear and distinct (Sylla 1998). Other scholars like Bradwardine took an opposite way, that is more interesting for our purposes: they declared that time flows continuously (Hannan and Villanova 2016). If time is continuous, the present instant does not exist, and movements in the past denote movements in the present and the future too (Fig. 1, Neutral).

This way of reasoning brings us to contemporary issues, suggesting the astounding possibility to treat time in quantum dynamics as a continuous parameter, rather than discrete. It is generally accepted that time is quantized, the smallest quantity of time being the Planck time (Wesson 1980). Nevertheless, the role of time in quantum dynamics is ambiguous: it is noteworthy that time plays a role neither in Wheeler-DeWitt equations, nor in the formulation of entangled states. Moreva et al. (2013) went so far as to state that the Universe is motionless for a hypothetical external observer: time exists just for observers inside the universe, because it is an emergent phenomenon arising from quantum entanglement. Any God-like observer outside the cosmos sees a static, unchanging Universe, just as the Wheeler-DeWitt equations predict. We propose, in touch with relativity that considers time as one of the four coordinates making the fabric of spacetime, to establish time in quantum dynamics in a peculiar way. Each physical system is associated with a (topologically) separable complex Hilbert space H with inner product $\langle\varphi|\psi\rangle$. We suggest to correlate the parameter time with the infinite-dimensional Hilbert space. If we use one of the countless coordinates of the quantum Hilbert space to locate time, we achieve a time that is continuous. But there is even more to it. In touch with Bradwardine, continuous time does not require to a single instant to be separated by the others, because the instant that separates two timeframes is common to both the segments. When Bradwardine (1955) states that "there is not a first instant of being and a first instant of nonbeing because they overlap" (Fig. 1, Neutral), he makes a leap that will pave the way to infinity in philosophy, mathematics, biophysics… and theology. Once it becomes senseless to talk about past, present, and future, the argument of contingent futures is inadequate to tackle the theological issue of predestination and free will. God's atemporality is opposed to the temporal flow of the universe and humankind, so that statements concerning future states or objects can be verified just retrospectively (Hannan and Villanova 2016). It is exactly what occurs during quantum measurements: the observer (the scientist, the researcher) cannot predict a priori the outcome of the experiment, because the quantum states are noncommutative and superimposed. Unless he finalizes the experiment and

Author's personal copy

achieves decoherence, the researcher cannot be aware of the result: he is allowed, in touch with Bradwardine's analysis, to look at the results just retrospectively.

Defending Aristotle's contention that nature is a material plenum, medieval authors denied the existence of separate, continuously extended vacuum, either small or large (Grant 1973). They proceeded as follows: if two plane surfaces, initially in uniform mutual contact with no air intervening, are separated in such manner that they remain continuously parallel, a vacuum is temporarily produced, until the newly-formed cavity is progressively filled by the expanding air surrounding the two surfaces. In opposition to this tradition, Blasius of Parma proposed an imaginative solution based on extrinsic boundaries (Fig. 1, External) which denied the first moment of surfaces' separation (Grant 1973; Pelacani 2005). This unusual procedure prevents the occurrence of a vacuum: if the surfaces do not split, vacuum cannot occur. In touch with this line of argument, we turn to a present-day question. How can the event horizon of a black hole be demarcated? By the standpoint of an observer falling inside the black hole, the event horizon is not perceivable at all. In turn, the event horizon is clearly detectable by an observer at rest far from the black hole (Bekenstein 1973; Gogberashvili (2019); . This subjective fuzziness in coping with boundaries in extreme physics leads us to an even more intricate problem: the singularity inside the black hole (Hawking 2005). What and where are the boundaries of black holes' singularities? If I choose to consider the border as located in the area external to the singularity (Fig. 1, External), I achieve the conventional view of the black hole as information-sucker. In touch with Blasius de Parma's account of the vacuum, the choice of external limits allows us to exclude the possibility to detect any information located inside the black hole. However, medieval authors also suggest another possibility: what if I consider the black hole's boundaries according to the scheme depicted in Fig. 1, Internal? In this case, we ponder the singularity in terms of the last internal point, with no relationships with the external. The black hole singularity becomes an entity independent of the surrounding space, possibly leading to wormholes. Studying the interior of rotating black holes coupled to a massless scalar field in asymptotically flat spacetime, Chesler (2019) noticed that the existence of a null singularity at the Cauchy horizon and a central spacelike singularity at radius $r = 0$ is required. In touch with the choice described in Fig. 1, Internal.

According to Albert of Saxony and Buridan, a moving body is continuously and successively in another place (Thijssen 2009). Local motion stands for a separate entity different from the moving body and the crossed space, in the same way as the concept of whiteness may be thought despite the absence of a detectable white body. A question (not obvious for us at all) arose: do the celestial spheres move just locally with respect to its parts? If God decides to reverse the circular movement of the sky from West to East, then the local motion will lack an external point of reference. The Universe is not located in a surrounding container that might act as a reference frame, and yet it can move locally. In other words, is it feasible to detect the local motion of an object, when a reference frame in not available to my observation? The answer of medieval scholars such as Oresme was straightforward: yes, it is feasible, because the detection of movement is grounded in human perception. Oresme rejects the movement in relation to an external point of reference: the circular motion of the heaven depends just on the fact that it is another way than it was before (Thijssen 2009). This "anti-reference" approach, conflicting with the tenets of Einstein's relativity, is amazingly close to recent claims in quantum mechanics. This theory has been reformulated as an approach that describes physical systems in terms of observer-dependent relational properties (Tozzi and Peters, 2019a). This means that the properties of the physical world are reliant on our observation (Rovelli 1996; Smerlak

Author's personal copy

Fig. 3 Different possibilities to cope with internal and external boundaries. Figure 3a illustrates a logistic plot: progressive bifurcations occur when increasing the phase parameter on the axis x. The starting point of every bifurcation stands for the "last no". Figure 3b depicts an exponential (dotted line) and a linear (solid line) curve: note that the points at the extreme right stand, respectively, for the first no and the last yes. Figure 2c depicts the rotations of a four-dimensional Clifford torus: during the movements, the same point (red and blue dots) is alternatively internal and external to the donut-like structure. The video is available here: "A stereographic projection of a Clifford torus performing a simple rotation" https://en.wikipedia.org/wiki/Clifford_torus#/media/File:Clifford-torus.gif

and Rovelli 2007; Zizzi 2018). Recent papers support this disconcerting statement, demonstrating that experimentally detected correlations in Bell tests strongly contradict the tenets of local realism (The BIG Bell Test Collaboration 2018). In touch with Oresme's claim, the relational formulations of quantum mechanics strikingly state that features of quantum systems, such as superposition and entanglement, are demonstrated through the rules of counting the alternatives, without explicitly calling out the reference system (Yang 2018). This suggests that the dichotomy relativity-quantum mechanics can be related not just to the wave-particle duality described by quantum mechanics, but also to the existence of reference frames described by relativity. Indeed, the reference frames give rise to the relativity of the temporal order which describes whether physical events are successive or simultaneous.

The choice of Fig. 1, left-sided permits to physicists and biologists to shed fully novel light on ubiquitous behaviours that subtends countless natural and artificial phenomena: nonlinear and chaotic dynamics. Collective systems equipped with a large number of interacting and inter-dependent components are characterized by non-equilibrium dynamics, self-organized criticality that operates at the edge of chaos, metastable state of second-phase transitions, spontaneous avalanches, universal power laws, and so on (Bak et al. 1987; Perkins et al. 2014). Chaotic systems display dependence from initial conditions, positive Lyapunov exponents, attractors. These systems are apt to live close to a metastable state of second-order phase transitions, characterized by infinite correlation length, countless functional dimensions, spontaneous avalanches and universal power laws (de Arcangelis and Herrmann 2010; Sherrill et al. 2020). To understand how the choice of Fig. 1, left-sided fits in the discourse, take the bifurcation plot of logistic maps (Fig. 3a), a behaviour that is typical of systems at the edge of criticality. The logistic map is a one-dimensional nonlinear difference equation used in dynamic systems theory (Jordan and Smith 2007; Richardson et al. 2014). It is visualized on a bifurcation diagram as a function of a fixed phase parameter located on the axis x. When the phase parameter increases, a growing number of doubling bifurcations progressively takes place, until a chaotic state is reached (Smith 2013). What are the boundaries of a single bifurcation? These boundaries cannot occur after the beginning of a bifurcation, because the split gives rise to two, instead of one, lines. Also, the boundaries cannot occur after the end of a bifurcation for the same reason. Therefore, to assess the length of a bifurcation we need to calculate the first point before the beginning of the bifurcation (the last NO in Fig. 3a) and the last point before the end of the bifurcation (the last YES in Fig. 3a): this matches the scheme illustrated in Fig. 1, left-sided.

Similar discrepancies might occur when scientists assess two different graphs: the exponential and the linear plot (Fig. 3b). While the beginning of both the plots can be described with "the first YES", the end of the two lines displays a different behaviour. The end of the linear line must be described in terms of "the last YES", while the end of the exponential curve must be described in terms of "the first NO" after the plateau. Indeed,

Author's personal copy

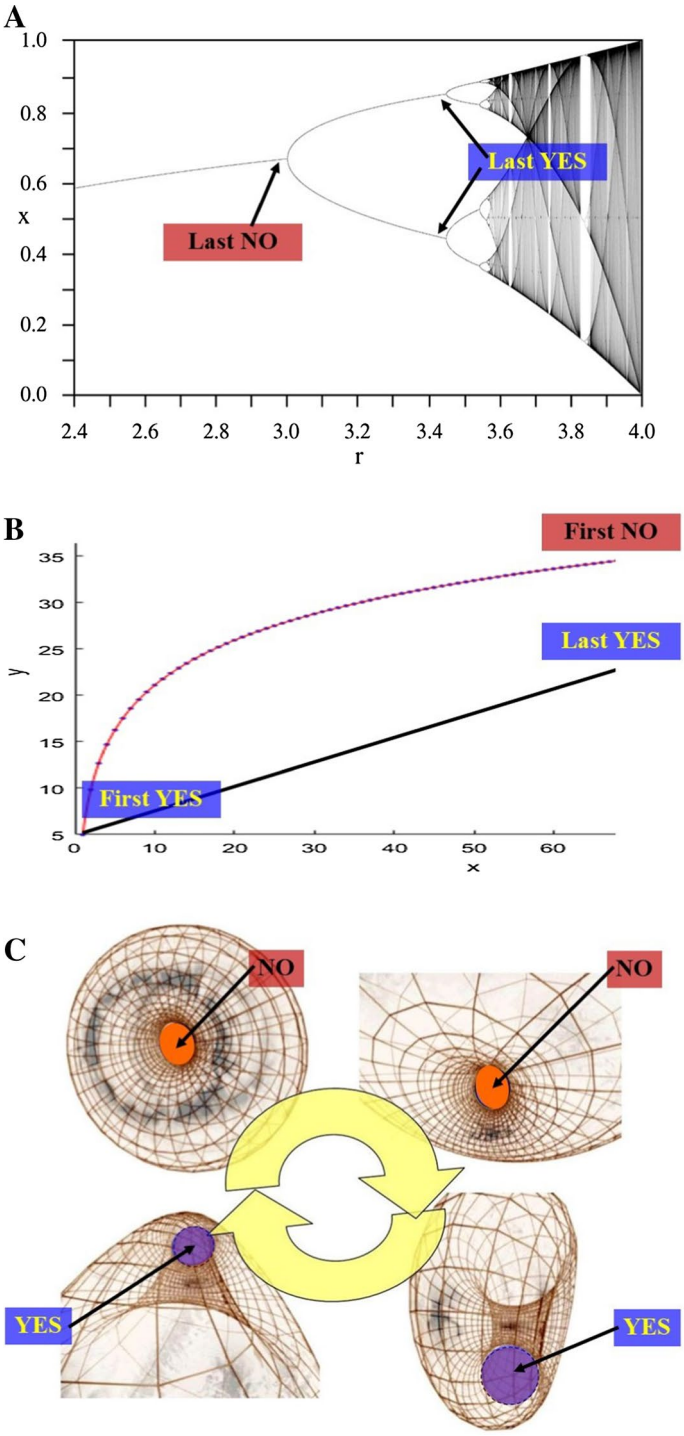

Author's personal copy

the exponential curve converges towards a point external to the highest value in the axis y, but never touches it. Therefore, we can state that the linear dynamics adhere to the scheme in Fig. 1, Internal, while the exponential dynamics adhere to the scheme in Fig. 1, Right side.

The *Liber sex principiorum* (the book of the six principles), dated about 1150, describes the Aristotelian cosmic spheres in terms of a structure that closely resembles a four-dimensional torus, i.e., a donut-like structure that has been used to describe the nervous dynamics of the brain activity (Tozzi 2019). The anonymous author (Porretano 2009) states that "controversy arises concerning the border of the sphere (i.e., the *Primum Mobile*, the outermost moving sphere in the geocentric model of the universe). Nothing is outside the sphere; however, a locus cannot be given in such a sphere, because the sphere itself is the locus that surrounds; then, once admitted that the sphere is local, it must also be admitted that something does exist outside the sphere, in which the site of the border is located; however, nothing exists outside the sphere border, therefore the sphere is nowhere. Indeed, nothing does exist outside itself; in turn, no place is the place of itself; once admitted that the sphere is local, it must be also admitted that the extreme border of the sky must be else than itself; however, nothing is beyond itself and, therefore, the border is nowhere. It must be admitted that talking about these arguments is somewhat weird, obscure and against the experience of our senses." If you look at the movements of a hypersphere, you appreciate a strikingly analogy: the same point becomes alternatively external or internal in a rotating hypersphere (Fig. 2c). This means that, in a few cases of formally developed mathematical concepts, it is almost impossible to decide whether a point is internal or external. In other words, it is not feasible to provide a distinction between the cases depicted in Fig. 1, Internal and Fig. 1, External. This brings us to the troublesome dilemma of the boundaries, that will be tackled in the next Section.

3 Lessons from the Past 2: Current Insights in Biological Issues

Augustine identified the Being with the Good and the Evil with the Not-Being. Hints of this conception are still visible in the current notions of set theory and topology, where the attention is drawn towards the closed, compact, continuous, bounded manifolds, rather than towards fuzzier and untreatable concepts such as open lines and manifolds without boundaries. Despite this reassuring commitment towards simpler concepts, the troubles are not over: if the closed curves are intersections pertinent of both internal and external, how can I make a distinction between inside and outside? If the boundaries can be located both inside and outside, what does make me sure that the interior does not extend throughout the exterior? Or, in turn, why couldn't the external fill the internal? When considering physical and biological features, the issue is related to the indeterminacy of object delimitation and the difficulty to quantify its boundaries. For example, in the case of a porous membrane of a living cell, where does the cytoplasm finish and where the surrounding environment start? Are membrane pores and channels part of the interior of the cell, or of the surrounding environment? These seemingly negligible concerns may be crucial in several fields. Take, e.g., metrology: when you are evaluating a microscopic object, weight measurement might be affected by the surrounding electronic cloud (Tozzi and Papo 2020). In vertebrates, the central and peripheral nervous system are segregated at the cellular level (Suter and Jaworski 2019), because physical barriers and combinations of attractive and repulsive cues control cell behaviors at the dividing line. However, especially

Author's personal copy

during nervous system development, neurons and signals negotiate the boundary zone: a small number of select cells traverse the boundary and connect the two components (Suter and Jaworski 2019). Boundaries can be regulated through cellular micro-components too: to provide an example, the capability of proteins and nucleic acids to undergo liquid–liquid phase separation is a vital molecular principle that permits cells to quickly and reversibly compartmentalize their components into non–membrane-bound sub-compartments (Frottin et al. 2019).

The distinction between internal and external limits provides a subtle, intriguing difference that can be fully appreciated if we consider biological entities. If a scientist favours the approach in Fig. 1, Internal he is providing internal limits to living beings. Once equipped with internal boundaries, living beings become homeostatic, self-sustaining entities provided with an ontological status that sharply separates them from external environment. Living cell become confined structures split from the surrounding environment. In turn, if a scientist favours the approach in Fig. 1, External he is suggesting that external limits to living beings occur. The choice of external limits lean towards the scientific/philosophical view of dynamic systems theory (Friston 2010): moving objects, events, cellular automata and living beings are structures embodied/embedded in the environment, with which they establish relational interactions (Ceruti and Damiano 2018).

In chemistry, stochastic activation rate is conventionally defined by the mean first passage time (MFPT) of a Brownian particle to a small target. Likewise, in biological gradient/descent apparatuses of Bayesian machines, the stochastic activation rate is set on the mean of the first passage time around the goal, i.e., the local minimum (Constant et al. 2019). Schuss et al. (2017) proposed a different approach in cellular biology, which sets the time scale of activation not anymore to MFPT, rather to the "mean time of the first among many arrivals" of particles at the target. According to this approach, termed Statistics of the extreme, fast activation processes occurring in living cells require a biological activation time that is not anymore necessarily exponential. For example, the fertilization rate does not depend anymore on the number and redundancy of the spermatozoa, rather it depends on the time required by the first spermatozoon to reach the egg (Fig. 1, Internal). This means that, in the field of optimal random search, just one arrive counts, while the other arrivals are not useful. This also means that an incomplete knowledge of the event does not preclude the possibility to predict the outcome. Here the Lévy's zero–one law comes into play: if we are learning gradually all the information that determines the outcome of an event, then we will become gradually certain what the outcome will be. Certain types of events will either almost surely happen or almost surely not happen, because their probability is either zero or one: e.g., in an infinite sequence of coin-tosses, a sequence of 100 consecutive heads must necessarily occur. Therefore, even if you do not have knowledge of all the collected data of system dynamics (e.g., you cannot know the trajectories of all the spermatozoa), you expect that the results always tend towards either zero, or one. In other words, your statistical knowledge of all the intermediate steps does not matter: a spermatozoon will always either fertilize, or not fertilize, the egg. In touch with this account, it has been recently proposed that loners, i.e., individuals out of sync with a coordinated majority, could be critical to understanding collective and social behavior and multicellular development, enabling diversification of life-history strategies (Rossine et al. 2020).

The present-day solution of the boundary problem lies in topology. This branch of mathematics provides a very general and abstract concept of space: intuitively, a topological space is characterized by its shape and holes, and not by the distance between the points (Dodson and Parker 1997). Thanks to its ability to assess systems properties in

Author's personal copy

terms of abstract mathematical spaces, topology displays three useful operational features. At first, topology allows the assessment of the elusive networks subtending systems dynamics, such as, e.g., transitions from ring-shaped to tree-shaped network arrangement. Topological spaces have been used in the context of complex network analysis and graph theory (Kleinberg et al. 2016), looking for, e.g., integrated network topology connectivity (Fukushima et al. 2017), multilevel entropy measures (Maletic and Zhao 2017), and simplicial complexes (Giusti et al. 2016; Bianconi and Rahmede 2016) which capture emergent community structures. Other network applications involve gene topology (Flavahan et al. 2019; Achar et al. 2020), hidden symmetries (Golubitsky and Stewart 2015), phase transitions (Pettini et al. 2019), unconventional superconductivity (Cao et al. 2018), quantum computing (Collins 2006), HIV proteins arrangement (Gaiha et al. 2019), receptor dimerization (Mohan et al. 2019).

Concerning the second useful operational feature, systems changes can be tackled in terms of theorems from algebraic topology. Algebraic theorems suggest that tiny changes in topological features may lead to alterations in macroscopic behavior of physical/biological systems (Tozzi and Papo 2020). We refer the reader to Tozzi et al. (2017) for a survey of the numerous physical and biological counterparts of the Borsuk-Ulam theorem ("at any moment, there is always a pair of antipodal points on the Earth's surface with equal temperatures and barometric pressures"). To provide an example that demonstrates how small modifications in topology may lead to novel functional biological features, take a perfectly spherical soap bubble: due to the Borsuk-Ulam theorem, there must exist at least two antipodal points on its spherical surface with identical values of surface tension. When the soap bubble is deformed, the spherical shape gets lost: this leads to the disappearance of antipodal points with the same surface tension.

Concerning the last, but not the least, useful operational feature, topology defines the closeness of sets of points with their neighbourhoods. In plain words, topology talks about the relationships between a single point and the points surrounding it. This approach is exactly what we are looking for the mathematical treatment of the boundary problem: given a spherical object, are the boundary points located inside or outside the sphere? In topological terms, when I calculate the area of the interior, must I also include the tiny surface covered by the boundary? The Jordan Curve Theorem (JCT) says that any planar continuous simple closed curve separates the plane in two disjoint regions, i.e., an "interior" region bounded by the curve and an "exterior" region containing all the nearby and far away unbounded points (Jordan 1893). The boundary is the common element of the bounded and the unbounded components. It must be stressed that the solution provided by topology and mathematics is straightforward: leaving apart technicalities, we can plainly state that in topology every point can be considered either internal, or external. Indeed, the borders can be indifferently approached from the inside and the outside of an object. Despite this mathematical designation of the boundary problem, practical difficulties in decision limit problems concerning physical/biological systems are not solved at all (Koczkodaj et al. 2017; Tozzi and Peters 2019): what is a set, and more importantly, how to provide a boundary to a set? Paraphrasing ancient scholars, we may ask: in topology, does the principle of non-contradiction hold? If the boundary points described by the Jordan theorem are both internal/not internal, the principle of non-contradiction (and also of identity!) breaks down. The problem is also more distressing, if we consider fractal structures such as the topological Cantor set, which is totally disconnected and is equipped with points that at the same time spread apart and are packed together.

How to get out of this wood? There is a chance and is a good one: to get rid of… points. Here the theory of descriptive nearness comes into play, allowing us to deal with

Author's personal copy

subsets that share some common properties even if they are not spatially close (Di Concilio et al. 2018). Set descriptions arise from the connection between relations on an object space and relations on the corresponding feature space, so that they do not require the use of points as marks to perform operations. Other types of point-free geometries have been used for different purposes, such as: to compute relative stabilities among different experimental structures of organic molecules (Noé et al. 2019), to address the problem of detecting the curvature of a free probing particle inside a magnetic field (Bonalda et al. 2019), to identify the topological holes that continuously appear and disappear in a series of movie frames (Tozzi and Peters 2020). In case of uncertainty due to lack of information and absence of sharp boundaries, we can delimit the interior through a ciclic chain-wise set of pixels, instead of a conventional boundary line (Don et al. 2020). In these sophisticated approaches, the points are removed and replaced by complex structures that consider topological vortices and Betti numbers. Therefore, the requirement of points and boundaries for the description of systems and phenomena fades away, as indirectly suggested many centuries ago.

4 Conclusion: Different Choices, Different Meanings

We showed how medieval approaches to decision limit problems can be actualized, providing fresh insights in ongoing scientific issues. We conclude that in mathematics, physics and biology, the border between the external and the internal is conventionally stipulated for practical and operational purposes. The feasibility to detect, identify and characterize a boundary depends on the technology and equipment available to the researchers. Since the choice of the point's location is arbitrary, the verbs "to start" and "to end" become just relative terms. The attribution of the division to one or another segment is just a logical, not real necessity: in modern terms, we may call it a metalinguistic necessity.

In the 14th Century, Buridan wondered why constant forces have not been detected in nature if they are required for motion (Grant and Nelson 1962). He noticed that, although these rules (we could say in modern terms: scientific laws) are conditional and true, they are almost never found to produce their effects in the real world. Nevertheless, if the ideal conditions stated in the rules are observed, everything would occur just as the rules assert: this means that the rules are not useless or fictitious. The inference for Buridan is straightforward: although these conditions are not fulfilled by natural powers, it is nevertheless possible to them to be fulfilled by divine power, i.e., by *Potentia Dei infinita*. God sometimes forgets about His *Potentia Dei Ordinata* that rules our physical world and guarantees the regularity of the natural laws. Rather, He sometimes opts for actions out of the ordinary paths of events, such as miracles. Paraphrasing these ancient and forgotten scholars, we could nowadays state that our scientists make the same methodological approach when performing their experiments: mimicking the *Potentia Dei infinita*, they carefully shape a strict experimental setting, thoroughly determining the quantitative parameters according to their own will. Therefore, the experimental results stand for the data achieved by a Divinity (the scientist) who artificially sculpts the environment where the predicted event under examination must take place. Buridan provided an effort to upholding the tenet of the Christian faith of God's omnipotence, while clinging to defensible epistemological position that guarantees the application of human reason. The case of the modern scientist is far from different. According to the concept of *Potentia Dei infinita*, only by means of secondary cause is God (the scientist) able to provoke

Author's personal copy

effects. Scientists are under some obligation, and this serves to eliminating their arbitrary interference in the normal course of events.

The distinction between God's ordained (laws of nature) and absolute powers (strict experimental setting) safeguards the contention that scientists must exercise restraint to guarantee natural certitude, in the meantime preserving the normal course of events. Even if God annihilates an object that the observer is watching, the observer continues to perceive the object. It is exactly what happens when scientists examine quantum systems, perturbing and annihilating them through instrumental measures. Still, there is a difference between the infinite powerful God and the current scientists. One of the limits of medieval God's infinite power was that He must be constrained by the same logical principles that He created by Himself. God Himself cannot escape logic. In turn, scientific investigation is an empirical enterprise that is not automatically framed on logical premises. Scientist are not necessarily exceedingly reasonable and coherent. The same Isaac Newton, who haughtily stated: "*hypotheses non fingo"* ("I do not contrive hypotheses"), spent half of his life looking for historical forecasts in Johannes' Apocalypse, that he thought was a prophetical holy book. Scientists may have exotic intuitions that could, against all odds, be subsequently confirmed by ensuing experiments. Illogicity is sometimes the key for serendipitous discoveries. This means that illogical premises could be scientifically fruitful, if, and only if, scientists are capable to test and confirm them in a painstaking experimental setting.

References

Achar, Y. J., Adhil, M., Choudhary, R., Gilbert, N., & Foiani, M. (2020). Negative supercoil at gene boundaries modulates gene topology. *Nature, 577*, 701–705.

Autrecourt N. 1940. The Universal Treatise. Marquette University Press, Milwaukee, Wisconsin, 1971.

Badiou, A. (2015). *Being and Event*. London: Bloomsbury.

Bak, P., Tang, C., & Wiesenfeld, K. (1987). Self-organized criticality: an explanation of the 1/f noise. *Physical Review Letters*, *59*, 381–384.

Bekenstein, J. D. (1973). Black holes and entropy. *Physical Review D, 7*(8), 2333–2346.

Bianconi, G., & Rahmede, C. (2016). Network geometry with flavor: From complexity to quantum geometry. *Physical Review E*, *93*(3), 032315. https://doi.org/10.1103/PhysRevE.93.032315.

Bonalda D, Seveso L, Paris MGA. 2019. Quantum sensing of curvature. arXiv:1903.06905.

Borsuk, K. (1933). Dreisatzeuber die n-dimensionale euklidischesphare. *Fundamenta Mathematicae, 20*(1), 177–190.

Bradwardine, Thomas (1349?), 1955 [B-TP], *Tractatus proportionum seu de proportionibus velocitatum in motibus*, (H. Lamar Crosby, Jr. ed. and trans.) in Thomas of Bradwardine His Tractatus de Proportionibus. Its Significance for the Developement of Mathematical Physics, Madison, WI: University of Wisconsin Press.

Cao, Y., Fatemi, V., Fang, S., Watanabe, K., Taniguchi, T., et al. (2018). Unconventional superconductivity in magic-angle graphene superlattices. *Nature, 556*, 43–50.

Ceruti, M., & Damiano, L. (2018). Plural embodiment(s) of mind. Genealogy and guidelines for a radically embodied approach to mind and consciousness. *Frontiers in Psychology*. https://doi.org/10.3389/fpsyg.2018.02204.

Chesler PM. 2019. Singularities in rotating black holes coupled to a massless scalar field. arXiv:1905.04613

Collins, G. P. (2006). Computing with quantum knots. *Scientific American, 294*(4), 56–63.

Constant, A., Ramstead, M. J. D., Veissière, S. P. L., & Friston, K. (2019). Regimes of expectations: An active inference model of social conformity and human decision making. *Frontires in Psychology*. https://doi.org/10.3389/fpsyg.2019.00679.

de Arcangelis, L., & Herrmann, H. J. (2010). Learning as a phenomenon occurring in a critical state. *Proceedings of the National Academy of Sciences, 107*, 3977–3981.

Di Concilio, A., Guadagni, C., Peters, J. F., & Ramanna, S. (2018). Descriptive proximities. Properties and interplay between classical proximities and overlap. *Mathematics in Computer Science, 12*, 91–106.

Author's personal copy

Dodson, C. T. J., & Parker, P. E. (1997). *A user's guide to algebraic topology*. Dordrecht: Kluwer.

Don, A. P., Peters, J. F., Ramanna, S., & Tozzi, A. (2020). Topological view of flows inside the bold spontaneous activity of the human brain. *Frontiers in Computational Neuroscience*. https://doi.org/10.3389/fncom.2020.00034.

Flavahan, W. A., Drier, Y., Johnstone, S. E., Hemming, M. L., Tarjan, D. R., et al. (2019). Altered chromosomal topology drives oncogenic programs in SDH-deficient GISTs. *Nature, 575*, 229–233.

Friston, K. (2010). The free-energy principle: A unified brain theory? *Nature Reviews Neuroscience, 11*(2), 127–138. https://doi.org/10.1038/nrn2787.

Frottin, F., Schueder, F., Tiwary, S., Gupta, R., Körner, R., et al. (2019). The nucleolus functions as a phase-separated protein quality control compartment. *Science, 365*(6451), 342–347. https://doi.org/10.1126/science.aaw9157.

Fukushima, M., Betzel, R. F., He, Y., van den Heuvel, M. P., Zuo, X. N., & Sporns, O. (2017). Structure-function relationships during segregated and integrated network states of human brain functional connectivity. *Brain Structure and Function*. https://doi.org/10.1007/s00429-017-1539-3.

Gaiha, G. D., Rossin, E. J., Urbach, J., Landeros, C., Collins, D. R., et al. (2019). Structural topology defines protective CD8+ T cell epitopes in the HIV proteome. *Science, 364*(6439), 480–484. https://doi.org/10.1126/science.aav5095.

Giusti, C., Ghrist, R., & Bassett, D. (2016). Two's company, three (or more) is a simplex: Algebraic-topological tools for understanding higher-order structure in neural data. *Journal of Computational Neuroscience*, *41*(1), 1–14. https://doi.org/10.1007/s10827-016-0608-6.

Gogberashvili, M. (2019). Can quantum particles cross a horizon? *International Journal of Theoretical Physics, 58*, 3711–3725.

Golubitsky, M., & Stewart, I. (2015). Recent advances in symmetric and network dynamics. *Chaos, 25*(9), 097612.

Grant, E. (1973). Medieval explanations and interpretations of the dictum that 'nature abhors a vacuum'. *Traditio, 291973*, 327–355.

Grant, E., & Nelson, B. (1962). Hypotheses in late medieval and early modern science. *Daedalus, 91*(3), 599–616.

Hannan S, Villanova PMR. 2016. The Envious Instant: Material Conditions of Truth in Thomas Bradwardine https://hcommons.org/app/uploads/sites/1000608/2017/06/The_Envious_Instant_Material_Conditions.pdf

Hawking, S. (2005). Information loss in black holes. *Physical Review D, 72*(8), 084013. https://doi.org/10.1103/PhysRevD.72.084013.

Heytesbury W. 1979. *William of Heytesbury on "Insoluble" Sentences*, (Paul V. Spade ed. and transl.), Toronto: Pontifical Institute of Medieval Studies.

Heytesbury, W. (1984). *On maxima and minima. Synthese historical library (text and study in the history of logic and philosophy)*. Dordrecht: Springer.

Jordan C. 1893. Cours d'analyse, 1, Gauthier-Villars.

Jordan, D. W., & Smith, P. (2007). *Non-linear ordinary differential equations: Introduction for scientists and engineers* (4th ed.). Oxford: Oxford University Press.

Kleineberg, K.-K., Boguñá, M., Ángeles Serrano, M., & Papadopoulos, F. (2016). Hidden geometric correlations in real multiplex networks. *Nature Physics, 12*, 1076–1081. https://doi.org/10.1038/nphys3812.

Koczkodaj, W. W., Magnot, J.-P., Mazurek, J., Peters, J. F., Rakhshani, H., Soltys, M., et al. (2017). On normalization of inconsistency indicators in pairwise comparisons. *International Journal of Approximate Reasoning, 86*, 73–79. https://doi.org/10.1016/j.ijar.2017.04.005.

Maletic, S., & Zhao, Y. (2017). Multilevel integration entropies: The case of reconstruction of structural quasi-stability in building complex datasets. *Entropy*, *19*(4), 172. https://doi.org/10.3390/e19040172.

Mohan, K., Ueda, G., Kim, A. R., Jude, K. M., Fallas, A. J., et al. (2019). Topological control of cytokine receptor signaling induces differential effects in hematopoiesis. *Science*. https://doi.org/10.1126/science.aav7532.

Moreva, E. V., Brida, G., Gramegna, M., Giovannetti, V., Maccone, L., & Genovese, M. (2013). Time from quantum entanglement: An experimental illustration. *Physical Review A, 89*, 052122.

Murdoch, J. E. (1964). *Superposition, congruence and continuity in the Middle Ages. L'aventure de la science. Histoire de la pensée*. XII Paris: Hermann.

Nielsen, L. O. (1982). Thomas Bradwardine's treatise on 'incipit' and 'desinit': Edition and introduction. *Cahiers de l'Institute du Moyen Age Grec et Latin, 42*, 1–83.

Noé, F., Olsson, S., Köhler, J., & Wu, H. (2019). Boltzmann generators: Sampling equilibrium states of many-body systems with deep learning. *Science*. https://doi.org/10.1126/science.aaw1147.

Author's personal copy

O' Donnell JR. 1939. Appendix: Questio de qua respondit Magister Nicholas de Utricuria. In. Nicholas of Autrecourt. *Mediaeval Studies, I. Pontifical Institute of Mediaeval Studies*, Toronto, Canada.

Offredus A. 1478. De primo et ultimo instanti ad defensionem communis opinionis adversus Petrum Mantuanum. Publisher Salomon, Bernard, ca. 1506-ca. 1561. Facsimile Publisher, 2016, ISBN-13: 978–9333632997.

Pelacani B. 2005. Questiones circa tractatum proportionum Magistri Thome Braduardini. Editor, Biard J. S. Rommevaux, Paris.

Perkins, T. J., Foxall, E., Glass, L., et al. (2014). A scaling law for random walks on networks. *Nature Communications, 5*, 5121.

Pettini, G., Gori, M., Franzosi, R., Clementi, C., & Pettini, M. (2019). On the origin of phase transitions in the absence of symmetry-breaking. *Physica A: Statistical Mechanics and its Applications, 516*, 376–392.

Porretano G. 2009. Libro dei sei principi. Eds., Paparella F. Bompiani, Testi a Fronte.

Richardson, M. J., Dale, R., & Marsh, K. L. (2014). Complex dynamical systems in social and personality psichology. In H. T. Reis & C. M. Judd (Eds.), *Handbook of research methods in social and personality psychology* (2nd ed.). Cambridge: Cambridge University Press.

Rossine, F. W., Martinez-Garcia, R., Sgro, A. E., Gregor, T., & Tarnita, C. E. (2020). Eco-evolutionary significance of "loners". *PLOS biology*. https://doi.org/10.1371/journal.pbio.3000642.

Rovelli, C. (1996). Relational quantum mechanics. *International Journal of Theoretical Physics, 35*, 1637–1678.

Schuss, Z., Basnayakey, K., & Holcmany, D. (2017). Redundancy principle for optimal random search in biology. *BioRxiv*. https://doi.org/10.1101/210443.

Shapiro, H., & Shapiro, C. (1965). De primo et ultimo instanti Des Walter Burley. *Archiv für Geschichte der Philosophie, 47*(1–3), 157–173.

Sherrill SP, Timme NM, Beggs JM, Newman EL. 2020. Correlated activity favors synergistic processing in local cortical networks in vitro at synaptically relevant timescales. Network Neuroscience. 1–20.

Smerlak, M., & Rovelli, C. (2007). Relational EPR. *Foundations of Physics, 37*, 427–445.

Smith, R. (2013). Period doubling, information entropy, and estimates for Feigenbaum's constants. *International Journal of Bifurcation and Chaos, 23*(11), 1350190.

Suter, T. A. C. S., & Jaworski, A. (2019). Cell migration and axon guidance at the border between central and peripheral nervous system. *Science*. https://doi.org/10.1126/science.aaw8231.

Sylla, D. E. (1998). God, indivisibles, and logic in the later middle ages: Adam Wodeham's response to Henry of Harclay. *Medieval Philosophy and Theology, 7*(1), 69–87.

The BIG Bell Test Collaboration. (2018). Challenging local realism with human choices. *Nature, 557*, 212–216.

Thijssen JMMH. 2009. The Debate over the nature of motion: John Buridan, Nicole Oresme and Albert of Saxony. With an edition of John Buridan's "Quaestiones super libros Physicorum, secundum ultimam lecturam", Book III, Q. 7. Early science and medicine, 14, /3, *Evidence and Interpretation: Studies on Early Science and Medicine in Honor of John E. Murdoch*, 186–210.

Tozzi, A., Peters, J. F., Fingelkurts, A. A., Fingelkurts, A. A., & Marijuán, P. C. (2017). Topodynamics of metastable brains. *Physics of Life Reviews, 21*, 1–20. https://doi.org/10.1016/j.plrev.2017.03.001.

Tozzi, A. (2019). The multidimensional brain. *Physics of Life Reviews, 31*, 86–103. https://doi.org/10.1016/j.plrev.2018.12.004.

Tozzi, A., & Peters, J. F. (2019). Points and lines inside our brains. *Cognitive Neurodynamics, 13*(5), 417–428. https://doi.org/10.1007/s11571-019-09539-8.

Tozzi, A., & Papo, D. (2020). Projective mechanisms subtending real world phenomena wipe away cause effect relationships. *Progress in Biophysics and Molecular Biology, 151*, 1–13. https://doi.org/10.1016/j.pbiomolbio.2019.12.002.

Tozzi, A., & Peters, J. F. (2020). Removing uncertainty in neural networks. *Cognitive Neurodynamics, 14*, 339–345. https://doi.org/10.1007/s11571-020-09574-w.

Trifogli, C. (2017). Walter burley on the incipit and desinit of an instant of time. *Vivarium, 55*(1–3), 85–102.

Yang, J. M. (2018). A relational formulation of quantum mechanics. *Scientific Reports, 8*, 13305.

Walker GF. (2018). Nicholas of Autrecourt' Quaestio de intensione visionis revisited: the schola Oxoniensis and Parisian masters on limit decision problems. In: Goubier F, Roques M, Duba W, Schabel C. Brill (ed.), *The Instant of Change in Medieval Philosophy and Beyond*. Academic Pub, ISBN-13: 978-9004367913

Wesson, P. S. (1980). The application of dimensional analysis to cosmology. *Space Science Reviews, 27*(2), 117. https://doi.org/10.1007/bf00212237.

Zizzi, P. (2018). Entangled spacetime. *Modern Physics Letters A, 33*, 1850168.

Author's personal copy

Publisher's Note Springer Nature remains neutral with regard to jurisdictional claims in published maps and institutional affiliations.

Arturo Tozzi does not like to be on focus. Looking for unexpected, hidden multidisciplinary relationships, he publishes in rather heterogeneous scientific journals. He terms his methodology "testable rationalism": experimental previsions arising from top-down, deductive mathematical approaches. He is a M.D., Ph.D., Pediatrician and Adjunct Assistant Professor in Physics.

THREE OPTIONS AGAINST SARS-CoV-2: PEDIATRIC SERA, MITHRIDATIZATION, DEWETTING ANTIBODIES

Arturo Tozzi
Center for Nonlinear Science, Department of Physics, University of North Texas, Denton, Texas, USA
tozziarturo@libero.it
Arturo.Tozzi@unt.edu

Here we suggest three feasible options that could be useful in COVID-19 medical management.

1) COVID-19: CHILDREN SERA FOR PASSIVE ANTIBODY THERAPY?

Among the potential treatment options for COVID-19 [1], passive antibody therapy has been suggested. Because infusions of antibody-laden blood have been fruitful in prior outbreaks such as the SARS epidemic and the 1918 flu pandemic, it has been proposed to use human convalescent sera from individuals recovered from COVID-19 [2]. Supporting the idea of using plasma from previously affected patients, a preliminary study suggests that macaques do not develop a coronavirus infection the second time they are exposed [3]. Nevertheless, it is well known that children display less severe symptoms when infected by SARS-CoV-2 [4]: this means that it might be hypothesized that sera from pediatric population could be experimented as a promising option for containing COVID-19, both in prevention and treatment.

REFERENCES

1) *Baden LR, Rubin EJ. 2020. Covid-19 — The Search for Effective Therapy. N Engl J Med 2020. DOI: 10.1056/NEJMe2005477.*
2) *Casadevall A, Pirofski LA. 2020. The convalescent sera option for containing COVID-19. J Clin Invest. 2020 Mar 13. pii: 138003. doi: 10.1172/JCI138003.*
3) *Bao L, Deng W, Gao H, Xiao C, Liu J, et al. 2020. Reinfection could not occur in SARS-CoV-2 infected rhesus macaques. BiorXiv, doi: https://doi.org/10.1101/2020.03.13.990226.*
4) *Lu X, Zhang L, Du H, Zhang J,Li YY, et al. SARS-CoV-2 Infection in Children. N Engl J Med 2020. DOI: 10.1056/NEJMc2005073.*

2) MILD COVID-19 SYMPTOMS AND LOW VIRAL LOAD: A FORM OF MITHRIDATIZATION?

SARS-CoV-2 positive patients with few/no symptoms and modest levels of detectable viral RNA in the oropharynx have been described [1]. This claim, together with the observation that SARS-CoV-2 displays a well-known decay rate both in aerosols and various surfaces [2], suggests an intriguing possibility: when an otherwise healthy subject is exposed to a very low viral load, a partial immunization might occur that prevents severe COVID-19 forms. This mechanism, that we might term "mithridatization", has been already described in animal models of the 2009 pandemic influenza virus, where decreasing the challenge dose resulted in reduction in clinical signs and delay in virus production in the upper respiratory tract [3]. This would mean that a low-dose challenge with SARS-CoV-2 might be administered to decrease the COVID-19 symptomatology, in particular in fragile patients.

REFERENCES

1) *Zou L, Ruan F, Huang M, Liang L, Huang H, et al. 2020. SARS-CoV-2 Viral Load in Upper Respiratory Specimens of Infected Patients. N Engl J Med 2020; 382:1177-1179. DOI: 10.1056/NEJMc2001737.*
2) *van Doremalen N, Bushmaker T, Morris DH, Holbrook MG, Gamble A, et al. 2020. Aerosol and Surface Stability of SARS-CoV-2 as Compared with SARS-CoV-1. N Engl J Med, DOI: 10.1056/NEJMc2004973.*
3) *Marriott AC, Dove BK, Whittaker CJ, Bruce C, Ryan KA, et al. 2014. Low dose influenza virus challenge in the ferret leads to increased virus shedding and greater sensitivity to oseltamivir. PLoS One, 9(4):e94090. doi: 10.1371/journal.pone.0094090.*
4) *Peiris JS, Chu CM, Cheng VC, Chan KS, Hung IF, et al. 2003. Clinical progression and viral load in a community outbreak of coronavirus-associated SARS pneumonia: a prospective study. Lancet. 2003 May 24;361(9371):1767-72.*

3) DEWETTING ANTIBODIES AGAINST VIROPORINS MIGHT CONTRIBUTE TO DECREASE 2019-nCoV INFECTION SPREAD

Dewetting transition is transient phenomenon taking place inside the hydrophobic pores of ion channels that forbids water molecules to cross microscopic receptor cavities and leads to impairment of cellular performance. It has been recently suggested that artificially-provoked dewetting transition in ion channel hydrophobic pores might stand for a molecular candidate to erase viruses, bacteria and cancer cells, and to block autoimmune activities. A novel type of high-affinity monoclonal antibody has been suggested, that is equipped with lipophilic and/or hydrophobic fragments that prevent physiological water flow inside ion channels and targets specific trans-membrane receptor structures of influenza viruses. Here we suggest that these dewetting monoclonal antibodies targeting the 2019-nCoV viroporin channels, sprayed in the nasal cavities, might lead to virion impairment, thus preventing inter-human viral transmission.

In fluid mechanics, dewetting stands for the rupture of the thin, liquid continuous film on the solid–liquid or liquid–liquid interfaces, leading to formation of irregular patterns of droplets (Sharmaa, 1996; Sharmaa and Reiterb, 1996; Sackmann and Bruinsma, 2002; Anishkin and Sukharev, 2004; Rosen 2004; Tanaka et al., 2005; Karapanagiotis and Gerberich, 2005; Leroux et al., 2008; Young et al., 2010; Boreyko et al., 2011; Thompson 2012; Gonzalez-Rodriguez et al. 2012; Douezan and Brochard-Wyart, 2012; Rahe et al., 2012; Lapierre et al., 2013; Thiam et al., 2013; Lee et al., 2014; Vargas et al., 2014; Sándor et al., 2017; Alert and Casademunt 2018; Rego et al., 2019). This process, borrowed by physics, has been recently extended to describe also microscopic biological phenomena. In particular, dewetting transitions may occur inside the hydrophobic pores of cellular ion channels. In the narrowest, more hydrophobic parts of receptor holes, a metastable state of dewetting transition forbids water molecules to get inside the cavities, leading to a decrease in conductance channel closure, and impairment of cellular activity. Tozzi (2020) proposed that this peculiar process can be artificially produced to alter the physiological activity of noxious pathogens, such as viruses, bacteria and tumoral cells. In particular, the manufacture of monoclonal antibodies (against cellular receptors) has been suggested, equipped with lipophilic/hydrophobic caps. In the sequel, we will term these antibodies DEMA (DEwetting Monoclonal Antibodies). Once they link monoclonal targets, their artificial hydrophobic device blocks water flow inside receptors, contributing to malfunction of pathological organisms. The factors influencing dewetting in physical systems, in biological structures and also in nervous cells are described by Tozzi (2020).
In brief, a huge range of physical factors, that can be fine-tuned in experimental settings, may contribute to the attainment and preservation of dewetting regimes in countless systems equipped with solid–liquid or liquid–liquid interfaces. Summarizing, when water and ions are enclosed within the sub-nanometer, narrow cellular confines of a ion channel hydrophobic pore, they exhibit an odd behavior (Aryal et al., 2015): near a critical point, a stochastic liquid-vapor water phase transitions takes place (Anishkin and Sukharev, 2004). These transient vapor states are "dewetted", i.e., devoid of water molecules within all, or part of, the pore. The decreased amount of water molecules inside receptors leads to impaired conductance, energetic barriers to ion transit and closure of the channel, in a process termed "hydrophobic gating". It is noteworthy that the principles underlying the metastable dynamical state of hydrophobic gating require a very small tube radius and interactions with a strongly hydrophobic lining (Lapierre et al., 2013).
In the sequel, the above-mentioned physiological phenomenon of dewetting transition will permit us to build strategies to influence the dynamics of droplet formation inside biological channels of 2019-nCoV viroporin channels.

TOWARDS DEWETTING MONOCLONAL ANTIBODIES

In this Section, we consider the possibility to build high-affinity monoclonal antibodies able to dewet the ion channels of target cells, thus leading to their impairment and, possibly, death. Antibodies with high affinity for receptors of pathological cells could be equipped with lipophilic structures, covalently attached, e.g., to their Fc region. These hydrophobic/lipophilic components must serve two purposes: a) to prevent water to penetrate inside the receptor ionic channels; b) to avoid immune Fc-mediated responses. In plain terms, we could state that, thanks to DEMA, a sort of cork provides a tight seal that prevents water to fill the receptor channels of pathogenic cells, causing collapse of unwanted organisms. DEMA could be used to counteract different types of pathogenic cells, such as viral, bacterial and tumoral ones. In the sequel, we will provide the example of Influenza A M2 proton channel, in an effort to develop a novel drug able to neutralize the virion. In Tozzi (2020), we provided an example, describing how to build D**EMA against influenza A virus M2 receptor** (Pielak and Chou, 2011; Rossman et al., 2010; Cho and Wrammert, 2016; Fiers et al., 2009; Cady et al., 2010; Homeyer et al., 2016).
The following paragraph is from Tozzi (2020), including the Figures. We suggest to use DEMA as a novel drug against all the strains of Influenza A (**Figure 1, top**). The very structure of M2 let us hypothesize that a monoclonal antibody that prevents water to enter the M2 channel might disrupt Influenza A pathogenetic activity. Indeed, water plays a foremost role in M2 functioning (**Figure 2A**). The channel, highly selective for protons, is activated by low pH and has a low conductance. Conduction mechanism involves: a) the exchange of protons between the His37 imidazole moiety, responsible for proton selectivity and pH modulation, and b) the water confined to the M2 bundle interior. Water molecules within the pore form hydrogen-bonded networks or "water wires", from the channel entrance to His37.

When a proton gradient occurs, conformational changes facilitate asymmetric diffusion through the channel. Indeed, protons diffusing through the channel need not be localized to a single His37 imidazole, but rather they may be delocalized over the entire His-box and associated water clusters. Furthermore, pore-lining carbonyl groups stabilize hydronium ions through second-shell interactions that involve the bridging of water molecules. A ring of methyl groups from Val27 tightens the N-terminal side of the pore to ~3.1 Å, narrowing the entrance and preventing water molecules from penetrating the channel (Pielak and Chou, 2011). Small motion or "channel breathing" may thus be required for water to enter the pore. It is widely accepted that water molecules are needed inside the channel cavity for supporting proton conduction. Water molecules, provided with a diameter of ~3 Å, start to exhibit liquid–vapor transitions and stochastic switches between wet and dry states within a hydrophobic pore of diameter less than ~14 Å. The most dynamic range for these transitions is between 9 and 12 Å: below this range, the pore will be largely dewetted (Aryal et al., 2015). The pore widens after Ser31 and becomes the widest at Gly34 position, that is equipped with an inner diameter of ~ 6 Å. The channel then narrows towards the C terminus, as the sidechains of His37 and Trp41 constrict the inner diameter to 1.7 and 1.4 Å, respectively.
The presence of a hydrophobic (or lipophilic) part located on the constant chain of DEMA, could, according to our theoretical previsions, stop water flow inside the M2 channels (**Figure 2B**), leading to viral malfunction and, possibly, removal from the infected human body.

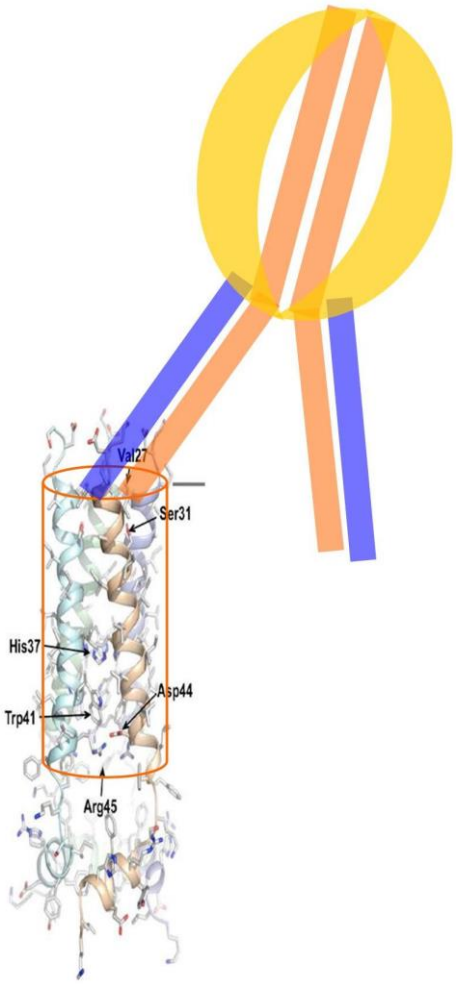

Figure 1. **Bottom**: high resolution structures of the AM2 channel domain. Solution structure of residues 18–60 in 1,2-Dihexanoyl-sn-Glycero-3-Phosphocholine micelles at pH 7.5 (Modified from Pielak and Chou, 2011). **Top**: Dewetting antibody (DEMA) against the Val27 area. The Fc region of this artificial antibody is surrounded by an hydrophobic structure (yellow shape). Channel and antibody are drawn to scale: the transmembrane section (red cylinder) is about 30 Å long. From: Tozzi (2020).

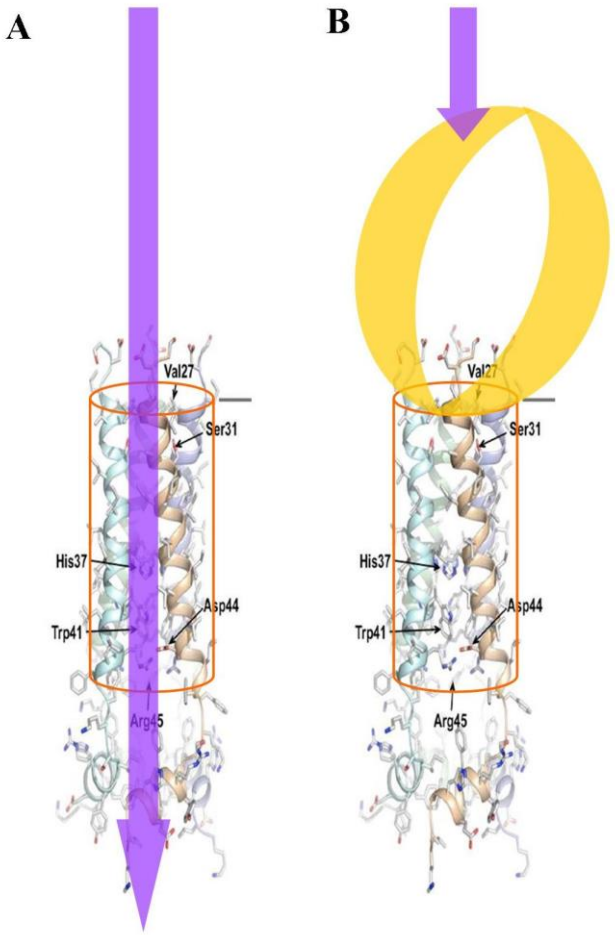

Figure 2. Water flow inside M2 channel. **2A**: In physiological conditions, water is allowed to flow inside the M2 channel, giving rise to proton gradients crucial for pathogenic activity of Influenza A virus. **2B**: When a DEMA targets the upper part of the M2 receptor, its hydrophobic component prevents water to go through the M2 receptor channel (**right side**), leading to impairment of virionic metabolic pathways. From: Tozzi (2020).

CORONAVIRUS CHANNELS

Our account of dewetting transition paves the way for innovative strategies. To make an example, dewetting enables researchers to build synthetic asymmetric model membranes with lipid composition/architecture that mimics the outer membrane of human pathogens, such as Pseudomonas aeruginosa (Maktabi et al., 2019).

Here we take into account the 2019 novel coronavirus 2019-nCoV, recently announced by the World Health Organization. Bioinformatics analysis on a virus genome is available and has been compared with other related coronavirus genomes: overall, the genome of 2019-nCoV has 89% nucleotide identity with bat SARS-like-CoVZXC21 and 82% with that of human SARS-CoV (Chan et al., 2020). Recent studies on coronaviruses have described the presence of a viroporin, i.e., a ion-channel protein (**Figure 3**). The latter is generated by the CoV E protein when it forms homotypic interactions which allows it to oligomerise (Schoeman and Fielding, 2019). Viroporins are viral-encoded membrane pore-forming proteins that can modulate cellular ion channels; they have been suggested to regulate and function in multiple stages of the viral life cycle, from viral entry to assembly and release, and even pathogenesis (Schoeman and Fielding, 2019).

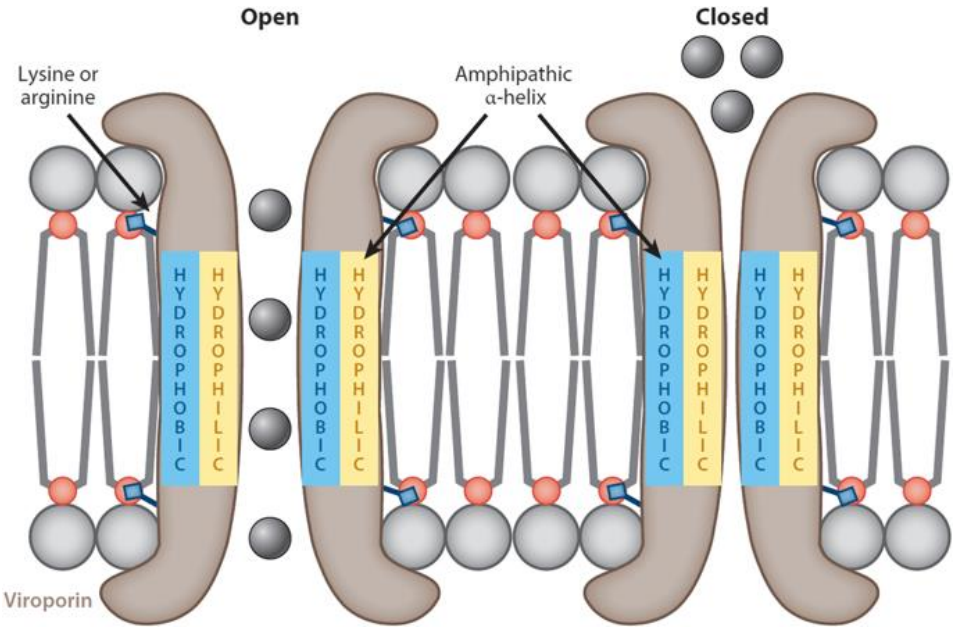

Figure 3. Coronaviruses' viroporin structure and motifs. For further details about this Figure, see Schoeman and Fielding (2019).

SUGGESTIONS

Dewetting transition, characterized by an unusual behavior of water supramolecular assembly, stands for an increasingly important feature that has been already used to assess countless morphological and/or functional biological structures, such as protein cavities, extracellular matrix and glycocalix, lipid droplets, lipid bilayers, cell adhesion, macroapertures opening in endothelial cells. In the narrowest, more hydrophobic part of cellular channels, a metastable state of dewetting transition of water molecules takes place, leading to decrease of conductance and closure of the pore.

Dewetting mechanisms can be used to achieve novel therapeutic weapons against a wide range of diseases. Further, the possibility to artificially modulate dewetting processes could lead to the development of new drugs (with mechanisms different from DEMA) that might be relevant in development, regeneration, self-immunity, infection and cancer.
Here we suggest to build a dewetting monoclonal antibody against the viroporins of 2019-nCoV (or against other viral channels characterized by dewetting transition). Once achieved a drug, it could be sprayed into the nose. Indeed, administred through the nose, such monoclonal dewetting antibody might contribute to inactivate the virions in the human airways, before 2019-nCoVs are able to link to the host's cellular membranes.

REFERENCES

1) Alert R, Casademunt J. 2018. Role of Substrate Stiffness in Tissue Spreading: Wetting Transition and Tissue Durotaxis. Langmuir. 2018 Oct 25. doi: 10.1021/acs.langmuir.8b02037. [Epub ahead of print]
2) Anishkin A, Sukharev S. 2004. Water dynamics and dewetting transitions in the small mechanosensitive channel MscS. Biophys J. 2004 May;86(5):2883-95.
3) Aryal P, Sansom MS, Tucker SJ. Hydrophobic gating in ion channels. J Mol Biol. 2015, 427(1):121-30. doi: 10.1016/j.jmb.2014.07.030.
4) Boreyko JB, Baker CH, Poley CR , and Chen CH . Wetting and Dewetting Transitions on Hierarchical Superhydrophobic Surface. Langmuir, 2011, 27 (12), pp 7502–7509 DOI: 10.1021/la201587u
5) Cannon RC, O'Donnell C, Nolan MF. Stochastic ion channel gating in dendritic neurons: morphology dependence and probabilistic synaptic activation of dendritic spikes. PLoS Comput Biol. 2010 Aug 12;6(8). pii: e1000886. doi: 10.1371/journal.pcbi.1000886.
6) Cady SD, Schmidt-Rohr K, Wang J, Soto CS, Degrado WF, Hong M. 2010. Structure of the amantadine binding site of influenza M2 proton channels in lipid bilayers. Nature. 463 (7281): 689–92. doi:10.1038/nature08722

7) Chan JF, Kok KH, Zhu Z, Chu H, To et al. 2020. Genomic characterization of the 2019 novel human-pathogenic coronavirus isolated from a patient with atypical pneumonia after visiting Wuhan. Emerg Microbes Infect. 2020 Dec;9(1):221-236. doi: 10.1080/22221751.2020.1719902.
8) Cho A, Wrammert J. 2016. Implications of broadly neutralizing antibodies in the development of a universal influenza vaccine. Curr Opin Virol. 2016 Apr;17:110-115. doi: 10.1016/j.coviro.2016.03.002. Epub 2016 Mar 28.
9) Douezan S, Brochard-Wyart F. 2012. Dewetting of cellular monolayers. Eur Phys J E Soft Matter. 2012 May;35(5):34. doi: 10.1140/epje/i2012-12034-9.
10) Fiers W, De Filette M, El Bakkouri K, Schepens B, Roose K, et al. 2009. M2e-based universal influenza A vaccine. Vaccine. 2009 Oct 23;27(45):6280-3. doi: 10.1016/j.vaccine.2009.07.007.
11) Gonzalez-Rodriguez D, Maddugoda MP, Stefani C, Janel S, Lafont F, et al. Cellular dewetting: opening of macroapertures in endothelial cells. Phys Rev Lett. 2012 May 25;108(21):218105
12) Homeyer N, Ioannidis H, Kolarov F, Gauglitz G, Zikos C, et al. 2016. Interpreting Thermodynamic Profiles of Aminoadamantane Compounds Inhibiting the M2 Proton Channel of Influenza A by Free Energy Calculations. Journal of Chemical Information and Modeling. 56 (1): 110–26. doi:10.1021/acs.jcim.5b00467
13) Ichinohe T, Pang IK, Iwasaki A. 2010. Influenza virus activates inflammasomes via its intracellular M2 ion channel. Nature Immunology. 11 (5): 404–10. doi:10.1038/ni.1861
14) Foffi G, Pastore A, Piazza F, Temussi PA (2013) Macromolecular crowding: chemistry and physics meet biology (Ascona, Switzerland, 10-14 June 2012). Phys Biol 10(4):040301
15) Haider B, Duque A, Hasenstaub AR, McCormick DA. Neocortical network activity in vivo is generated through a dynamic balance of excitation and inhibition. J Neurosci. 2006 Apr 26;26(17):4535-45.
16) Karapanagiotis, Ioannis; Gerberich, William W. (2005). "Polymer film rupturing in comparison with leveling and dewetting". Surface Science 594 (1–3): 192–202. doi:10.1016/j.susc.2005.07.023.
17) Lapierre F, Coffinier J, Boukherroub R, Thomy V. Electro-(de)wetting on Superhydrophobic surfaces. Langmuir, 2013, 29 (44), pp 13346–13351. DOI: 10.1021/la4026848
18) Lee SJ, Hong J, Kang KH, Kang IS, Lee SJ. Electrowetting-Induced Droplet Detachment from Hydrophobic Surfaces. Langmuir, 2014, 30 (7), pp 1805–1811. DOI: 10.1021/la404344y
19) Lehn JM (2007) From supramolecular chemistry towards constitutional dynamic chemistry and adaptive chemistry. Chem Soc Rev 36(2):151-160.
20) Leroux, Frédéric; Campagne, Christine; Perwuelz, Anne; Gengembre, Léon (2008). "Polypropylene film chemical and physical modifications by dielectric barrier discharge plasma treatment at atmospheric pressure". Journal of Colloid and Interface Science 328 (2): 412–20.doi:10.1016/j.jcis.2008.09.062. PMID 18930244.
21) Lombardi F, Herrmann HJ, Perrone-Capano C, Plenz D, de Arcangelis L. Balance between excitation and inhibition controls the temporal organization of neuronal avalanches. Phys Rev Lett. 2012 Jun 1;108(22):228703. Epub 2012 May 31.
22) Maktabi S, Schertzer JW , Chiarot PR. 2019. Dewetting-induced formation and mechanical properties of synthetic bacterial outer membrane models (GUVs) with controlled inner-leaflet lipid composition. Biochim Soft Matter. 2019 May 15;15(19):3938-3948. doi: 10.1039/c9sm00223e.
23) Pielak RM, Chou JJ. 2011. Influenza M2 proton channels. Biochim Biophys Acta. 2011 Feb; 1808(2): 522–529. doi: 10.1016/j.bbamem.2010.04.015.
24) Rahe P, Lindner R, Kittelmann M, Nimmrich M, Kühnle A. From dewetting to wetting molecular layers: C60 on CaCO3(10¯14) as a case study. Phys Chem Chem Phys. 2012 May 14;14(18):6544-8. doi: 10.1039/c2cp40172j.
25) Rego NB, Xi E, Patel AJ. 2019. Protein Hydration Waters Are Susceptible to Unfavorable Perturbations. J Am Chem Soc. 2019 Feb 6;141(5):2080-2086. doi: 10.1021/jacs.8b11448. Epub 2019 Jan 22.
26) Rosen MJ. (2004). Surfactants and Interfacial Phenomena (3rd ed.). Hoboken, New Jersey: Wiley-Interscience. p. 244. ISBN 978-0-471-47818-8. OCLC 475305499.
27) Rossman JS, Jing X, Leser GP, Lamb RA. 2010. Influenza virus M2 protein mediates ESCRT-independent membrane scission. Cell. 142 (6): 902–13. doi:10.1016/j.cell.2010.08.029
28) Sackmann E, Bruinsma RF. 2002. Cell adhesion as wetting transition? Chemphyschem. 2002 Mar 12;3(3):262-9.
29) Sándor C, Libál A, Reichhardt C, Olson Reichhardt CJ. 2017. Dewetting and spreading transitions for active matter on random pinning substrates. J Chem Phys. 2017 May 28;146(20):204903. doi: 10.1063/1.4983344.
30) Schnell JR, Chou JJ. 2008. Structure and mechanism of the M2 proton channel of influenza A virus. Nature, 451:591–595.
31) Schoeman D, Fielding BC. 2019. Coronavirus envelope protein: current knowledge. Virology Journal volume 16, Article number: 69.
32) Sharmaa A, Reiterb G. 1996. Instability of Thin Polymer Films on Coated Substrates: Rupture, Dewetting, and Drop Formation. Journal of Colloid and Interface Science. Volume 178, Issue 2, 25 March 1996, Pages 383–399. doi:10.1006/jcis.1996.0133

33) Tanaka M, Rehfeldt F, Schneider MF, Mathe G, Albersdörfer A, et al. Wetting and dewetting of extracellular matrix and glycocalix models. 2005 Journal of Physics: Condensed Matter Volume 17 Number 9. doi:10.1088/0953-8984/17/9/022
34) Thiam AR, Farese Jr RV, Walther TC. The biophysics and cell biology of lipid droplets. Nature Reviews Molecular Cell Biology 14, 775–786 (2013) doi:10.1038/nrm3699
35) Thomaston JL, Alfonso-Prieto M, Woldeyes RA, Fraser JS, Klein ML, Fiorin G, DeGrado WF. 2015. High-resolution structures of the M2 channel from influenza A virus reveal dynamic pathways for proton stabilization and transduction. Proceedings of the National Academy of Sciences of the United States of America. 112 (46): 14260–5.
36) Thompson CV. Solid-State Dewetting of Thin Films (2012). Annual Review of Materials Research. Vol. 42: 399-434. DOI: 10.1146/annurev-matsci-070511-155048
37) Tozzi A. 2015. Information Processing in the CNS: A Supramolecular Chemistry? Cognitive Neurodynamics 9 (5): 463–477.
38) Tozzi A, Fla Tor, Peters JF. 2016. Building a minimum frustration framework for brain functions in long timescales. J Neurosci Res, 94(8): 702–716.
39) Tozzi A. 2020. Towards Dewetting Monoclonal Antibodies For Therapeutical Purposes. Progress in Biophysics and Molecular Biology, 150:153-159. https://doi.org/10.1016/j.pbiomolbio.2019.09.001.
40) Vargas JN, Seemannab R, Fleury JB. Fast membrane hemifusion via dewetting between lipid bilayers. Soft Matter, 2014,10, 9293-9299
41) Young T, Hua L, Huang X, Abel R, Friesner R, Berne BJ. Dewetting transitions in protein cavities. Proteins [2010, 78(8):1856-1869]. DOI: 10.1002/prot.22699
42) Webb TI, Kshatri AS, Large RJ, Akande AM, Roy S, et al. Molecular mechanisms underlying the effect of the novel BK channel opener GoSlo: Involvement of the S4/S5 linker and the S6 segment. Proc Natl Acad Sci U S A. 2015 Feb 17;112(7):2064-9. doi: 10.1073/pnas.1400555112.
43) Zhu F, Hummer G. 2010. Pore opening and closing of a pentameric ligand-gated ion channel. Proc Natl Acad Sci U S A. 2010 Nov 16;107(46):19814-9. doi: 10.1073/pnas.1009313107. Epub 2010 Nov 1.

Author's personal copy

Foundations of Science (2021) 26:245–255
https://doi.org/10.1007/s10699-020-09674-0

A Topological Approach to Infinity in Physics and Biophysics

Arturo Tozzi[1] · **James F. Peters**[2,3]

Published online: 26 May 2020
© Springer Nature B.V. 2020

Abstract
Physical and biological measurements might display range values extending towards infinite. The occurrence of infinity in equations, such as the black hole singularities, is a troublesome issue that causes many theories to break down when assessing extreme events. Different methods, such as re-normalization, have been proposed to avoid detrimental infinity. Here a novel technique is proposed, based on geometrical considerations and the Alexander Horned sphere, that permits to undermine infinity in physical and biophysical equations. In this unconventional approach, a continuous monodimensional line becomes an assembly of countless bidimensional lines that superimpose in quantifiable knots and bifurcations. In other words, we may state that Achilles leaves the straight line and overtakes the turtle.

Keywords Donut-like · Infinity · Paths · Physical geometry · Networks · Alexander horned sphere

1 Introduction

Excluding conformal infinity (Frauendiener 2000), the occurrence of infinite results in physical and biophysical formulas prevents experimental descriptions of real observables (Bergmann 1989). For example, when assessing bodies with infinite gravitational mass and/or energy, equations become untreatable and lead to failures in theories. A standard example is the mathematical singularity of black holes, where the commonest solutions of the equations of general relativity allow for zero-size, finite mass distributions. This leads to infinite density, e.g., singularities where relativity breaks down. The same occurs when

✉ Arturo Tozzi
tozziarturo@libero.it; Arturo.Tozzi@unt.edu

James F. Peters
James.Peters3@umanitoba.ca

1 Center for Nonlinear Science, Department of Physics, University of North Texas, 1155 Union Circle, #311427, Denton, TX 76203-5017, USA

2 Department of Electrical and Computer Engineering, University of Manitoba, 75A Chancellor's Circle, Winnipeg, MB R3T 5V6, Canada

3 Department of Mathematics, Faculty of Arts and Sciences, Adıyaman University, 02040 Adıyaman, Turkey

Author's personal copy

biological dynamics give rise to nonlinear chaotic paths, where the trajectories become gradually more and more unpredictable. The problem becomes troublesome, if we think that infinity is hidden also in the most unlikely discipline, i.e., quantum mechanics. Despite quantum description is framed on the concept of indivisible elements, it must be stressed that its postulates dictate dynamics taking place inside a Hilbert space of infinite dimensions. In quantum mechanics, infinity runs out the door and comes back in the window. To make the problem more intricate, recent claims suggest that infinite sets cannot be reduced to finite sets (in technical terms, the Connes conjecture is refutable). Indeed, it seems that infinity cannot be reduced to finite, at least in peculiar contexts such as von Neumann algebras (Ji et al. 2020). The problem is worsened by the Mandelstamm-Tamm inequality for quantum systems (Mandelstam and Tamm 1945), that dictates a general lower bound for the lifetime of all quantum states in terms of reasonable measures of uncertainty of the energy in a system, even if the standard deviation is infinite. Indeed, according to the Heisenberg principle, the time-energy uncertainty relation (Busch 2008) has the following formulation:

$$\Delta T \Delta E \geq \frac{\hbar}{2}, \tag{1}$$

where ΔT is the duration of a system perturbation and ΔE is the change in energy in a quantum jump of the system. In such a quantum jump, it is possible a quantum of unbounded energy. Heisenberg argued that there is imprecision within which the instant of transition between system states is specifiable via the time-energy relation (Heisenberg 1927). This means that significant fluctuations in the duration of system particle energy may occur in a very short time interval, which results in the uncertainty of the temporal coordinates, starting and ending instants. In turn, very short time intervals lead to huge fluctuations in energy of quanta which tend towards infinite values. As a consequence of the time-energy uncertainty relation, there is uncertainty for both ΔT (indeterminate variations in system change intervals) and ΔE (indeterminate energy fluctuations that can either infinitesimally small or tending towards infinity).

In sum, although infinity can be used in physics and biophysics, scientists require for practical purposes the final results to be physically meaningful: e.g., in quantum field theory, infinities are treated through procedures such as renormalization (Hooft 1971). Here we propose a fully novel, topologically-framed, approach to the issue of infinity in scientific equations.

2 Geometrical Concepts of Infinity

The concept of infinity is strictly correlated with the long-standing geometrical problem concerning the line: is a line composed of indivisibles, or is it an infinitely divisible continuum? Throughout the centuries, many different answers have been provided to this painstaking question (Bell 2005). For example, Aristotle, Al Ghazali and Averroes stated that a line is not composed of atoms, but rather of parts divisible without an end (Aristotle 1980). Democritus, Leucippus and Epicurus maintained that a continuous line is composed of indivisible bodies. Pythagoras, Plato and Walter de Chatton (about 1323) claimed that a line is composed by a finite number of indivisibles, while others by an infinite number of indivisibles. In this latter group, Henry of Harclay (1275–1317) stated that a line is composed by an infinite number of immediately joined indivisibles, while the Bishop of

Author's personal copy

Lincoln that it is composed by an infinite number of indivisibles which are mediate to one another. According to the more sophisticated mathematical approach of Richard Kilvington (about 1302–1360), a continuum stands for infinite sets of integers containing infinite subsets with intrinsic and extrinsic quantifiable boundaries. Adam of Whodeham (death: 1358) suggested that one infinite can be greater than another. In turn, Bradwardine, outstripping the contemporary mathematical views, believed that a continuum is not composed of indivisible points, but of mutually joined parts, i.e., an infinite number of mediate indivisibles that are not points (Bradwardine 1328–1335). William of Ockham said that a continuum whose parts form a unity is distinct from a contiguum of juxtaposed things. In the following centuries, the issue was tackled by foremost authors, including Isaac Barrow, Leibnitz, Guillame de L'Hópital, Euler, Berkeley, until the continuum was described in terms of infinitesimals by Bernard Bolzano, Augustin-Louis Cauchy, Karl Weierstrass, Richard Dedekind (Dedekind 1963). Different solutions were proposed, until Georg Cantor introduced the theory of transfinite numbers that led to the modern concept of abstract set (Cantor 1961). In Cantor's view, it was numbers, rather than geometric points, that are equipped with objective significance.

Critical reactions were put forward by Brentano, Peirce, Poincaré (Poincaré 1946), Brouwer, Hermann Weyl. Enthrallingly, Wittgenstein stated that infinite objects cannot occur in our world, because infinity is just a logical concept of the possibilities of the language: he said that, if two calculations give rise to different results, it is not a fault, neither a contradiction, because the observer is always allowed to change the rules of the joke he is playing (Waismann 1979). By the way, this is what happens when the four-dimensional account of relativity breaks down inside the black hole singularity, so that we are required to introduce in our tale the infinite-dimensional account of quantum Hilbert spaces. Apart from the most advanced contemporary theories—see Abram Robinson (1996), Bridges (1999), Lawvere (1980), it is assumed in calculus and theory of function that between any two rational points there are rational points. For every convergent series of such fractions there is just one limiting points: this collection of limiting points it termed continuous. In particular, in modern topology, a continuum is defined as a compact connected subset of a topological space.

2.1 Infinity as a Straight Line in an Unusual Historical Geometrical Approach

One of the most striking treatments of infinity is the one by Nicolas de Cusa (de Cusa 1440), that allows to use mathematical and geometrical features to undertake physical infinity. de Cusa pictures the infinite as a straight line. Infinite circles or spheres can be described in terms of infinite lines: when the diameter becomes less curved in proportion to the increased circumference, then the maximum circumference, which cannot be greater, is minimally curved and therefore maximally straight. An infinite line is necessarily the straightest, so that no curvature is opposed. In the same way, every infinite manifold with positive curvature (an infinite triangle, an infinite square) can be described in terms of an infinite maximum line that is the longest and straightest. Nor will this maximum manifold be composed of sides and angles; rather, the infinite line and angle are one and the same thing, so that the line is the angle, because the manifold is the line. In sum, an infinite line stands, according to de Cusa, for all that which is in the possibility of every finite line and manifold. Hence, a speculative inference can be made, namely, infinity is correlated with finite manifolds. In current scientific terms, de Cusa's account sounds as follows: given a physical system described by progressively increasing curves on a positive-curvature

Author's personal copy

manifold, the unwanted occurrence of a straight line (standing for infinite value in equations) can be erased by adding progressively decreasing curves on an opposite negative-curvature manifold. In sum, infinity can be expressed by a straight line with zero-curvature. This observation has been used in the mathematical treatment of physical finite systems whose equations lead to the unwanted infinity by Tozzi and Peters (2019a), who employed geometrical procedures (Frankel 2011), Langevin equations (Langevin 1908), Levi–Civita and Ehresmann connections (Levi-Civita 1917; Ehresmann 1950).

3 Topology Comes into Play

In this paragraph, we suggest a geometrically-framed method to solve the problem of infinity in physical systems. If one wants to assess finite physical measurements leading to infinity, one needs at first to consider *bounded as well as unbounded geometrical shapes* and topological manifolds, together with their features and relations (Naimpally and Peters 2013; Guadagni 2014; Di Concilio et al. 2018, Peters 2020a, b). Next, one must apply these relations in a projective way. Thirdly, one must thereafter, in a still more highly transformed way, apply the relations of these infinite figures to the general concept of mathematical infinity, which is altogether independent even of all figures and manifolds.

3.1 Alexander Horned Sphere: A Toroidal Phase Space for Both Infinite and Discrete Lines

To make the description of a line that assesses quantitative values of both indivisible and divisible features, we propose to use a peculiar torus-like phase space, modified from the pathological object termed horned sphere (Alexander 1924). An Alexander horned sphere (AHS) is a topological structure made up of a countable union of compact sets. The mapping of AHS is homeomorphic with the ball B^3, its boundary being a sphere (Fig. 1a). AHS, together with its inside, stands for a topological 3-ball which is simply connected (i.e., every finite, simple closed curve can be shrunk to a point by a sequence of retraction mappings while staying inside). However, the outer complement of the solid is not simply connected and its fundamental group is not finitely generated. This provides an example of a wild embedding in E^3: the exterior is not simply connected (unlike the exterior of the usual round sphere). This means that a closed curve linking a torus in the above construction cannot be shrunk to a point without touching the horned sphere (Fig. 1b, c). Because AHS displays an uncountable infinity of wild points which are the limits of the sequences, it has also been used to describe wild embeddings in quantum states (Asselmeyer-Maluga 2018). Furthermore, the set of nonlocally flat points is a Cantor set. AHS displays branch points on the sphere (roughly, the "ends" of the horns), since any neighborhood of a limit contains a horned complex.

What matters in our framework is that the bifurcation paths approaching an infinite number are disjoined, i.e., no bifurcation is in touch with another on the opposite side (Fig. 1c). To treat together both finite and infinite quantities, we require an AHS torus-like structure equipped with two different functional areas (Fig. 2):

(a) a circular section, on which indivisible features can be evaluated.

Author's personal copy

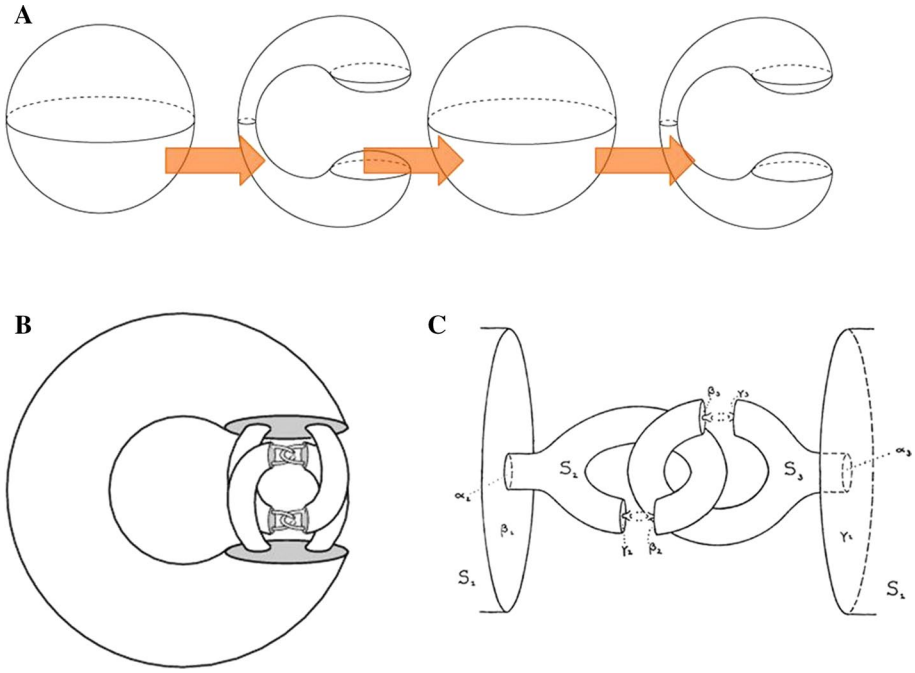

Fig. 1 Alexander Horned sphere (AHS). **a** AHS can be built from a positive-curvature manifold with genus zero. **b**, **c** AHS at different magnifications. **c** displays the original draw and nomenclature provided by Alexander (1924)

(b) a branched section, equipped with ad libitum infinite bifurcations, on which continuum can be evaluated. This means that the continuum inside a one-dimensional line is treated in terms of superimposition of countless lines in two dimensions.

4 Mathematical Treatment of Infinity Via the Alexander Horn

Concerning AHS and the more general problem of the number of links in knots, linking numbers λ (sum of the number of crossing points in a knot) as well as enhanced linking numbers have been introduced (Livingston 2003). A link is a collection of closed curves in three-dimensional space without self-intersections. A link with one component is called a knot. Examples of links with two components are shown in Fig. 3. In the study of knots (especially AHS), linking numbers can become unbounded (approaching infinite numbers of crossing points) rather quickly. For example, a two-component linking number is denoted by $\lambda(K, L)$, which ranges over the set of integers $2, 3, ..., \infty$.

Also, AHS allows the introduction of geometric computable solutions to the problem of infinity. The basic approach is to rewrite metrics defined in terms of points at infinity with tractable, computable metrics that sidestep infinite planes and points at infinity. This permits to assess conformable infinity at computable points near, but not at, ideal points. In other words, ideal points on the infinite plane are replaced with non-ideal points that are computable, because they intersect sheets of infinite places. Here we provide an example

Author's personal copy

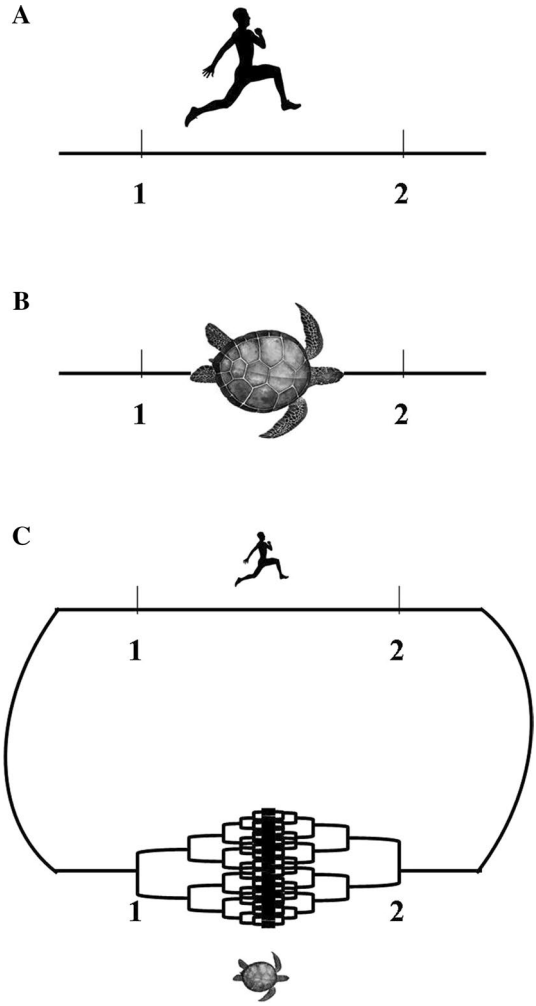

Fig. 2 The geometric line in terms of divisible (**a**) and indivisible (b) components. **c** depicts the two sides of an Alexander horn torus, encompassing both divisible (upper part) and indivisible (lower part) components

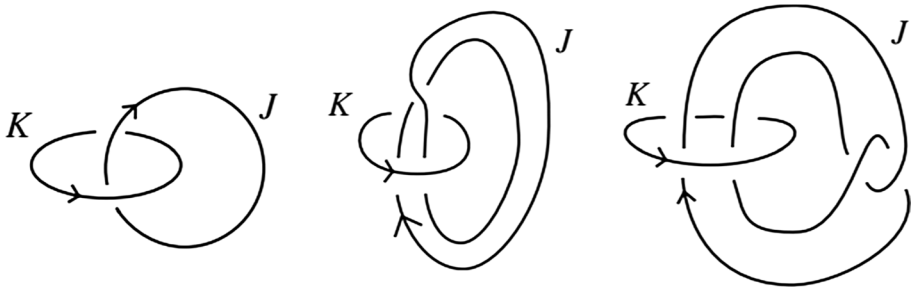

Fig. 3 Examples of 2-component links. From: Livingston (2003)

Author's personal copy

from physics (Frauendiener 2000). The Minkowski spacetime metric in polar coordinates is

$$\tilde{g} = dt^2 - dr^2 - r^2 d\sigma^2, \tag{2}$$

where $d\sigma^2$ is the metric of the unit sphere. Let $\tilde{g}$ be a function defined on physical space–time manifold, i.e., a space that is locally Euclidean. To achieve conformal rescaling of a spinor wave function $\tilde{g}$ (Penrose 1976), the null coordinates $u = t - r, v = t + r$ are introduced to put the Minkowski line-element into the following form:

$$\tilde{g} = dudv - \frac{1}{4}(v-u)^2 d\sigma^2. \tag{3}$$

The coordinates u and v range over the complete real line, provided $u - v \geq 0$. This infinite range is compactified (every cover of the space has a finite subcover (Naimpally and Peters 2013)) by transforming the range space with appropriate functions with null coordinates U, V ranging over the open interval $\left(-\frac{\pi}{2}, +\frac{\pi}{2}\right)$, e.g., $u = \tan U, v = \tan V$, resulting in

$$\tilde{g} = \frac{1}{4\cos^2 U \cos^2 V}\left[4dudv - \sin^2(V-U)\right] d\sigma^2. \tag{4}$$

This Minkowski metric is not defined for U, V at the boundary points of the open interval. Next, consider a second space–time metric $g = \Omega^2 \tilde{g}$, which is the metric of the Einstein cylinder ε. To adapt the metric g to a space–time physical system, where the cylinder ε lives, space–time coordinates are introduced, namely, $T = U + V, R = V - U$. Then define g to be

$$g = dT^2 - dR^2 - \sin^2 R d\sigma^2. \tag{5}$$

In effect, the Minkowski space is conformably embedded into the Einstein cylinder ε.

5 Alexander Torus in the Study of Physical and Biophysical Continuum: An Operational Example

Linear dynamics of physical and biological systems can be described in terms of trajectories taking place inside manageable donut-like manifolds equipped with genus one. However, widespread nonlinear dynamics might take place, such as paths at the edge of chaos, power law and free scale phenomena, systems' bifurcations, iterative maps, ordinary differential equations, Bayesian issues, temperature chaos detected in four-dimensional Edwards-Anderson models with Gaussian disorder to low temperatures (Wang et al. 2018). Here we ask: if we consider linear dynamics as indivisible, and non-linear chaotic dynamics as continuous, is it feasible to build a single donut-like phase space where both these dynamics might be mapped? The answer is positive, if we consider AHS. Both the linear and nonlinear paths can be arranged inside a phase space consisting of an AHS. This relatively simple general description of both the trajectories as taking place inside horned torus-shaped manifolds allows to standardize the assessment of a wide range of natural and artificial paths, from time series analysis to iterative maps, from population dynamics to temperature.

Countless linear biological trajectories, including nervous dynamics, can be tackled in terms of paths of different curvatures embedded in a three-dimensional phase space

Author's personal copy

(Tozzi and Peters 2019b). As an example, here we provide a simulation of a linear flow that turns out chaotic when crossing a physical obstacle (Fig. 4a). To map these dynamical paths to AHS, a projection mapping can be performed that allows the mirror image of a flow trajectory to be copied to the AHS surface (Fig. 4b), i.e., map each point in a flow trajectory onto to AHS surface. Such projections can be achieved through available methodologies of vectorial and tensorial transport, such as Ehresmann connections (Tozzi et al. 2017) or parallel transport on Riemannian manifolds (Sengupta et al. 2016). It is noteworthy that different kinds of nonlinear paths can be assessed through this procedure: to make an example, Fig. 4c illustrates the case of two mirror logistic plots embedded in an AHS. In sum, when we place physical or biological observables on the surface of AHS, we achieve the description of their different trajectories inside a single, peculiar donut-like phase space.

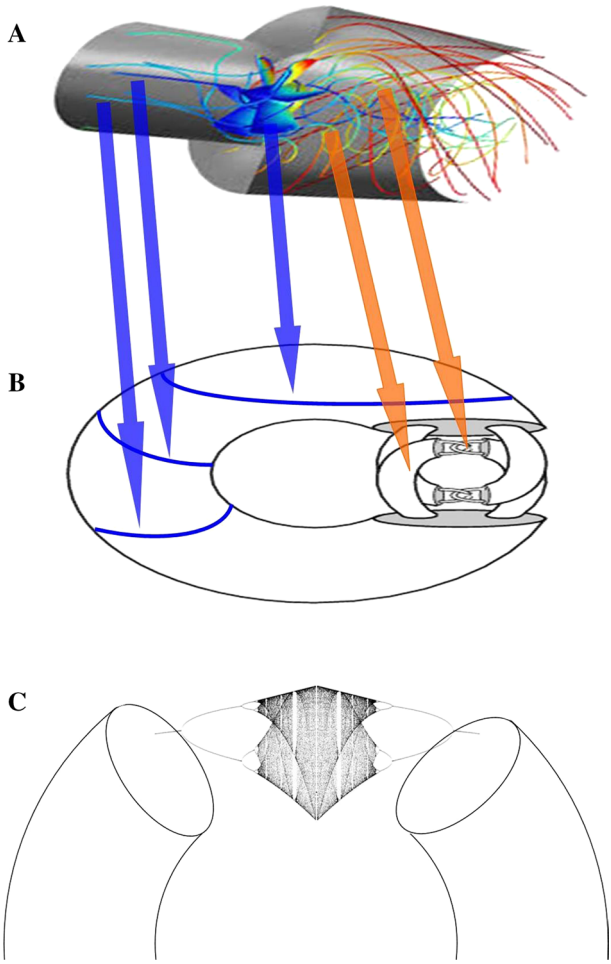

Fig. 4 Mapping of real systems flows to AHS. Widespread physical and biological linear paths (**a**) can be described in terms of trajectories taking place the toroidal side of AHS (blue arrows and curved lines in **b**). In turn, non-linear trajectories can be projected to the branched section of the HAS (red arrows). Modified from: CFD Moduule. https://www.technic.com.au/products/cfd/ (Retrieved 2018). **c** One of the feasible modifications of the Alexander horned sphere. Here two opposite logistic plots are inserted into the branched section of the horned torus

Author's personal copy

6 Conclusion: Solving Infinity

It is assumed by scientists, due to pragmatic issues, that no measurable quantity or event has infinite values. Indeed, any physical and/or biophysical theory needs to provide operational tools that correspond to, or at least approximate, reality (e.g., Iyer and Petters 2007). Consider, for example, if any object of infinite gravitational mass were to exist, any use of the formula in order to quantify the gravitational force would lead to a useless infinite result. The formula would be useful neither to compute the force between two objects of finite mass, nor to compute their motions. Sometimes an infinite result of a physical quantity may mean that the theory being used is approaching the point where it fails.

To solve the problem of the meaningless occurrence of infinity in scientific equations, a novel geometrically-framed conceptual framework has been proposed here, based on a geometric perspective. The mapping of real systems' paths to AHS permits us to achieve manageable representations of countless physical and biological trajectories inside peculiar donut-like phase spaces. This allows to simplify the measurement procedures, because toroidal paths have been widely studied in several fields, such as in modular wavelets, admissibility and frame conditions, lifting admissible functions, transformations and dilations, reconstruction formulas, natural tensor products, required Lie groups and extra modular groups (Tozzi et al. 2018; Calixto et al. 2015; Wang et al. 2015).

Thinking to the everlasting quarrel dating back to the ancient Greeks, a question arises. This paper is devoted to the notion of infinity as it appears in exact sciences: what kind of infinity is meant in the text? Is it an actual or potential infinity? In philosophy of mathematics and physics, the abstraction of actual infinity involves the acceptance (if the axiom of infinity is included) of infinite entities as given, actual and completed objects. These might include the set of natural numbers, extended real numbers, transfinite numbers, or even an infinite sequence of rational numbers. Actual infinity is to be contrasted with potential infinity, in which a non-terminating process (such as "add 1 to the previous number") produces a sequence without the last element, and where each individual result is finite and is achieved in a finite number of steps. As a result, potential infinity is often formalized using the concept of limit. Therefore, no problems arise in physical and biological frameworks when coping with the concept of potential infinity. Furthemore, a conceptual leap is provided here: in this novel framework based on the Alexander horn, a continuous monodimensional line stands for a set of innumerable bidimensional lines that overlay in quantifiable knots and bifurcations.

Compliance with Ethical Standards

Conflict of interest On behalf of all authors, the corresponding author states that there is no conflict of interest.

References

Alexander, J. W. (1924). An example of a simply connected surface bounding a region which is not simply connected. *Proceedings of the National Academy of Sciences, 10*, 8–10.

Aristotle (1980). Physics, 2 volumes, trans. Cornford and Wickstead. Loeb Classical Library, Cambridge, MA: Harvard University Press and Heinemann.

Author's personal copy

Asselmeyer-Maluga, T. (2018). Hyperbolic groups, 4-manifolds and Quantum Gravity. arXiv:1811.04464.

Bell, J. L. (2005). *The continuous and the infinitesimal in mathematics and philosophy*. Milan: Polimetrica S.A.

Bergmann, P. G. (1989). Quantum gravity at spatial infinity. *General Relativity and Gravitation, 21*(3), 271–278.

Bradwardine, T. (1328–1335). Tractatus de continu. Trans by Murdoch JE. Quoted in Edward Grant ed., a source book in Medieval science. Cambridge, Massachusetts: Harvard University Press, 1974.

Bridges, D. (1999). Constructive mathematics: A foundation for computable analysis. *Theoretical Computer Science, 219*, 95–109.

Busch, P. (2008). The time-energy uncertainty relation. *Lecture Notes in Physics, 734*, 73–105. https://doi.org/10.1007/978-3-540-73473-4_3.

Calixto, M., Guerrero, J., & Roşca, D. (2015). Wavelet transform on the torus: A group theoretical approach. *Applied and Computational Harmonic Analysis, 38*(1), 32–49. https://doi.org/10.1016/j.acha.2014.03.001.

Cantor, G. (1961). *Contributions to the founding of the theory of transfinite numbers*. New York: Dover.

de Cusa, N. (1440). De docta ignorantia. English translation in Bond, H. Lawrence (ed.), Nicholas of Cusa: Selected Spiritual Writings, Classics of Western Spirituality. New York: Paulist Press, 1997.

Dedekind, R. (1963). *Essays on the theory of numbers*. New York: Dover.

Di Concilio, A., Guadagni, C., Peters, J. F., & Ramanna, S. (2018). Descriptive proximities. Properties and interplay between classical proximities and overlap. *Mathematics in Computer Science, 12*(1), 91–106. https://doi.org/10.1007/s11786-017.0328-y.

Ehresmann, C. (1950). *Les connexion s infinitésimales dans un espace fibré différentiable* (pp. 29–55). Bruxelles: Colloque de Toplogie.

Frauendiener, J. (2000). Conformal infinity. *Living Reviews in Relativity, 3*, 4.

Frankel, T. (2011). The geometry of physics: An introduction. Cambridge University Press; IIIrd Ed. ISBN-13: 978-1107602601.

Guadagni, C. (2014). Bornological Convergences on Local Proximity Spaces and Metric Spaces. Ph.D. Thesis, Universitá degli Studi di Salerno.

Heisenberg, W. (1927). Über den anschaulichen Inhalt der quantentheoretischen Kinematik und Mechanik. Zeitschrift f`ur Physik, 43: 172–198.

Iyer and Petters. (2007). Light's bending angle due to black holes: from the photon sphere to infinity. *General Relativity and Gravitation, 39*, 1563–1582.

Ji, Z., Natarajan, A., Vidick, T., Wright, J., & Yuen, H. (2020). MIP*=RE. arXiv:2001.04383.

Langevin, P. (1908). Sur la théorie du movement brownien. *Comptes rendus de l'Académie des Sciences Paris, 146*, 530–533.

Lawvere, F. W. (1980). Toward the description in a smooth topos of the dynamically possible motions and deformations of a continuous body. *Cahiers de Topologie et Géométrie Différentielle Catégoriques, 21*, 377–392.

Levi-Civita, T. (1917). Nozione di parallelismo in una varietà qualunque e conseguente specificazione geometrica della curvatura Riemanniana. *Rendiconti del Circolo Matematico di Palermo, 42*, 73–205. https://doi.org/10.1007/bf03014898.

Livingston, C. (2003). Enhanced linking numbers. *The American Mathematical Monthly, 110*(5), 361–385. https://doi.org/10.1080/00029890.2003.11919975.

Mandelstam, L., & Tamm, I. (1945). The uncertainty relation between energy and time in nonrelativistic quantum mechanics. *Journal of Physics (USSR), 9*, 249–254.

Naimpally, S. A., & Peters, J. F. (2013). Topology with applications. topological spaces via near and far. World Scientific Pub. Co., Ltd., Singapore, xvi+277 pp. ISBN: 978-981-4407-65-6, MR3075111.

Peters, J. F. (2020a). *Computational geometry, topology and physics of digital images with applications Shape complexes, optical vortex nerves and proximities* (p. xxv+440). Switzerland: Springer. https://doi.org/10.1007/978-3-030-22192-8.

Peters, J. F. (2020b). Ribbon complexes and their approximate descriptive proximities. Ribbon & vortex nerves, Betti numbers and planar division, Bull. Allahabad Math. Soc., in press; also, arXiv 1911.09014v6.

Penrose, R. (1976). Nonlinear gravitons and curved tensor theory. *General Relativity and Gravitation, 7*, 31–52.

Poincaré, H. (1946). Foundations of science, trans. G. Halsted, New York: Science Press.

Robinson, A. (1996). *Non-standard analysis*. Princeton: Princeton University Press.

Sengupta, B., Tozzi, A., Coray, G. K., Douglas, P. K., & Friston, K. J. (2016). Towards a neuronal gauge theory. *PLOS Biology, 14*(3), e1002400. https://doi.org/10.1371/journal.pbio.1002400.

Author's personal copy

Hooft, G. T. (1971). Renormalizable Lagrangians for massive Yang-Mills fields. *Nuclear Physics B, 35*, 167–188.

Tozzi, A., Peters, J. F., Fingelkurts, A. A., Fingelkurts, A. A., & Marijuán, P. C. (2017). Topodynamics of metastable brains. *Physics of Life Reviews, 21*, 1–20. https://doi.org/10.1016/j.plrev.2017.03.001.

Tozzi, A., Peters, J. F., Fingelkurts, A., Fingelkurts, A., & Perlovsky, L. (2018). Syntax meets semantics during brain logical computations. *ProgrBiophys Mol Biol, 140*, 133–141. https://doi.org/10.1016/j.pbiomolbio.2018.05.010.

Tozzi, A., & Peters, J. F. (2019a). Points and lines inside our brains. *Cognitive Neurodynamics*. https://doi.org/10.1007/s11571-019-09539-8.

Tozzi, A., & Peters, J. F. (2019b). Points and lines inside our brains. *Cognitive Neurodynamics, 13*(5), 417–428. https://doi.org/10.1007/s11571-019-09539-8.

Wang, B. Q., Zhou, W. G., & X-H., (2015). A local wavelet transform on the torus T2. *International Journal of Wavelets, Multiresolution and Information Processing, 13*(04), 1550027. https://doi.org/10.1142/S0219691315500277.

Waismann, F. (1979). Wittgenstein and the Vienna Circle: Conversations. Rowman & Littlefield. ISBN-13: 978-0064973106.

Wang, W., Wallin, M., & Lidmar, J. (2018). Chaotic temperature and bond dependence of four-dimensional Gaussian spin glasses with partial thermal boundary conditions. *Physical Review E, 98*, 062122.

Publisher's Note Springer Nature remains neutral with regard to jurisdictional claims in published maps and institutional affiliations.

Arturo Tozzi is an adjunct assistant professor at the Center for Nonlinear Science, University of North Texas, U.S.A. He is also a M.D. and a pediatrician at the ASL Na2 Nord, Italy. He favours multidisciplinary research, looking for unexpected relationships between mathematical and biophysical issues. His main interest involves neuroscience from a topological perspective, in particular the brain as a multidimensional device.

James F. Peters is a professor in the Department of Electrical & Computer Engineering, University of Manitoba, Canada and adjunct professor in the Department of Mathematics, Adiyaman University, Turkey. His research interests are geometric topolology, computational geometry, topology and physics, focusing on CW topological spaces and local descriptive proximity clustering theory.

Author's personal copy

Synthese
https://doi.org/10.1007/s11229-020-02895-7

Information-devoid routes for scale-free neurodynamics

Arturo Tozzi[1] · **James F. Peters**[2,3,4,5]

Received: 18 April 2020 / Accepted: 26 September 2020
© Springer Nature B.V. 2020

Abstract

Neuroscientists are able to detect physical changes in information entropy in the available neurodata. However, the information paradigm is inadequate to describe fully nervous dynamics and mental activities such as perception. This paper suggests explanations to neural dynamics that provide an alternative to thermodynamic and information accounts. We recall the Banach–Tarski paradox (BTP), which informally states that when pieces of a ball are moved and rotated without changing their shape, a synergy between two balls of the same volume is achieved instead of the original one. We show how and why BTP might display this physical and biological synergy meaningfully, making it possible to model nervous activities. The anatomical and functional structure of the central nervous system's nodes and edges makes it possible to perform a sequence of moves inside the connectome that doubles the amount of available cortical oscillations. In particular, a BTP-based mechanism permits scale-invariant nervous oscillations to amplify and propagate towards widely separated brain areas. Paraphrasing the BTP's definition, we could state that: when a few components of a self-similar nervous oscillation are moved and rotated throughout the cortical connectome, two self-similar oscillations are achieved instead of the original one. Furthermore, based on topological structures, we illustrate how, counterintuitively, the amplification of scale-free oscillations does not require information transfer.

✉ Arturo Tozzi
tozziarturo@libero.it; Arturo.Tozzi@unt.edu

James F. Peters
james.peters3@umanitoba.ca

1 Center for Nonlinear Science, University of North Texas, 1155 Union Circle, #311427, Denton, TX 76203-5017, USA

2 Department of Electrical and Computer Engineering, University of Manitoba, 75A Chancellor's Circle, Winnipeg, MB R3T 5V6, Canada

3 Department of Mathematics, Adıyaman University, 02040 Adıyaman, Turkey

4 Department of Mathematics, Faculty of Arts and Sciences, Adıyaman University, 02040 Adıyaman, Turkey

5 Computational Intelligence Laboratory, University of Manitoba, Winnipeg, MB R3T 5V6, Canada

Published online: 01 November 2020

Author's personal copy

Keywords Banach–tarski paradox · Brain · Power law · Fractal · Oscillations · Information

Broadly successful information theory permits the appraisal of general features of physical/biological systems, suggesting that our world (including ourselves) is made up of a fundamental physical assembly termed information (Shannon 1948; Bekenstein 2003). Over time, numerous information-related perspectives have been portrayed: e.g., information theory has been correlated with statistical thermodynamics, Renyi entropy, Bekenstein–Hawking entropy, quantum mechanics, and so on (Jaynes 1957; Lloyd 2000; Marzuoli and Rasetti 2005; Bromiley et al. 2010; Cafaro et al. 2016; Tozzi et al. 2018). After the launch of the slogan "it from bit" (Wheeler 1990), neuroscientists asked themselves whether physical information could be used to describe and quantify brain activity, mental functions and their neural correlates (Tozzi and Peters 2016). Noteworthy attempts are free-energy Bayesian approaches (Friston 2010) based on energy budgets (Attwell and Laughlin 2001), and pairwise entropy extracted from fMRI neurodata (Watanabe et al. 2013, 2014). Neuroscientists are providing an effort to correlate modifications in sensations and perceptions with changes in brain informational content, investigating the neural correlates of mental tasks in terms of information entropy. Nonetheless, it is quite clear that something is amiss with the duet information/nervous activity. Just observing simple pictures and sequences of video frames, it easy to grasp that information entropy is inadequate to assess and classify the activities and the high-dimensional topological structures that we term mental functions. The entropic content of different photographs can be accurately quantified through several available techniques (see, e.g., Allen and Triantaphillidou 2009). Looking at simple pictures, it can be noticed that a grey picture displays zero entropy, while a coarse-grained picture with black, grey and white tiny dots displays the highest levels of entropy (Fig. 1A, B). From the standpoint of the naïve observer, both the pictures are a collection of meaningless spots devoid of content. In turn, photographs depicting, say, a tender infant or a pleasant landscape display values of entropy relatively close to each other, even though the photographs are imbued with fully different meaning and sense (Fig. 1C, D). These latter pictures produce vivid perceptions that trigger emotions, reasoning, thoughts, i.e., in short, all sorts of psychological activities. This means that correlation information/sensation does not suffice for, or is irrelevant, when it comes to understanding cognitive functions. Perhaps, making an even stronger claim, perception and psychological functions of the observer are not correlated at all with the physical informational content of sensed objects. Therefore, the efforts of neuroscientists to quantify the changes in brain information entropy during different mental tasks are doomed to failure, because the entropic modifications detected through the available neuro-techniques (such as, e.g., EEG, fMRI, tractography) could not be correlated with mental activities.

Even if it is assumed that brain states do carry information, there is a lack of evidence to justify the claim that cognitive activity involves, or depends on, extracting information. Here we propose a process, devoid of information transfer, that makes it possible to duplicate (we could say: clone) brain activities in different areas of the central nervous system. In particular, we show how and why the Banach–Tarski paradox (BTP) from set-theoretic geometry permits the replication of one of the foremost features of brain oscillations: the occurrence of power laws.

Author's personal copy

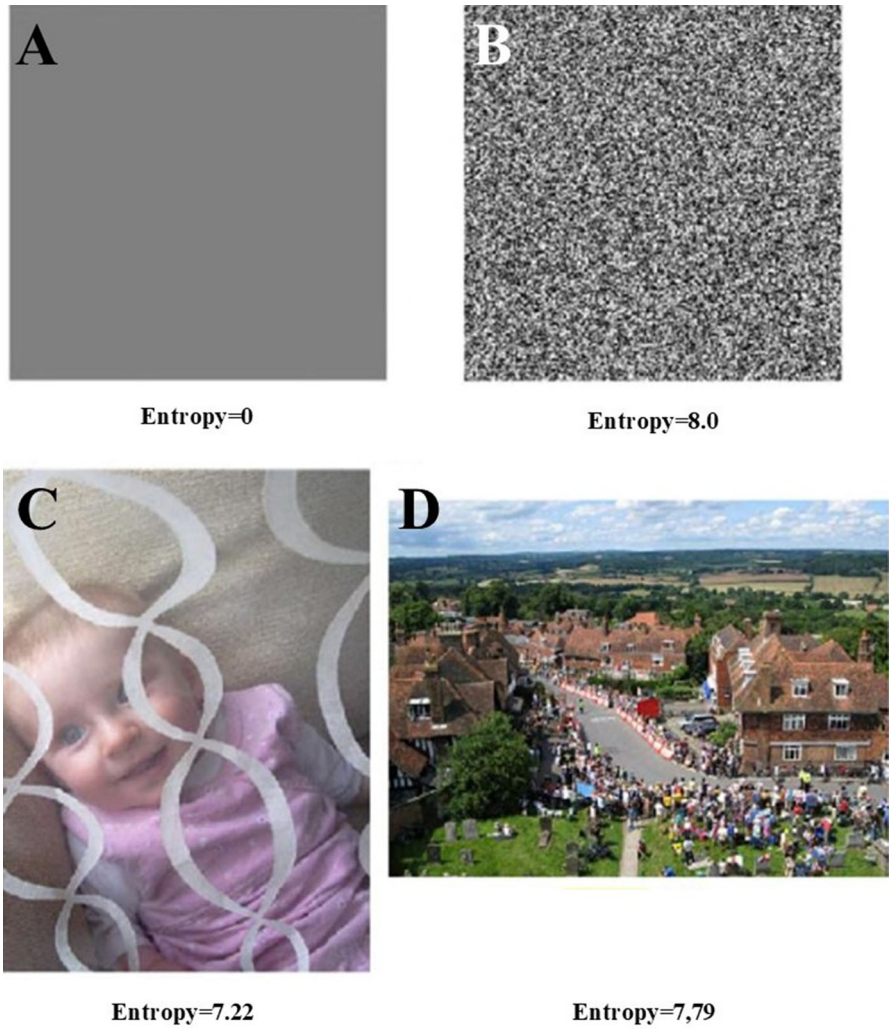

Fig. 1 Entropy level in different pictures. Modified from: Allen and Triantaphillidou (2009)

1 A physical meaning for the banach tarski paradox

The Banach–Tarski paradox (BTP) from set-theoretic geometry suggests that a solid 3-dimensional ball decomposed into at least five disjoint subsets can be reassembled in a different way to yield two identical copies of the original ball (Banach and Tarski 1924; Churkin 2010). In plain words, given any two volumes A, B in the Euclidean space R^3 such that each volume is bounded and has nonvoid interior, volume A can be partitioned (cut into separate pieces) into a sufficient number of sub-volumes and moved by rigid motions (translations and rotations) to construct a copy of B. This can be proved using the Axiom of Choice (Aliprantis and Border 2006). That is, if

Author's personal copy

2^A is a collection of nonempty sets X of a nonvoid set A, there is always a mapping $f : 2^A \rightarrow 2^A$ defined by $f(A_i \in 2^A) = \bigcup_{\substack{i \in I \\ A_i \in 2^A}} A_i = A$. In effect, the Axiom of Choice tells us that we can always find an index i and choose subsets A_i so that the union of the subsets gives us back the original set A. The Banach–Tarski paradox is a glorious extension of the Axiom of Choice. When pieces of a ball are moved and rotated without changing their shape, we achieve two balls, instead of the original one. Figure 2 illustrates how a few cuts, followed by simple geometric rotations and translations, allow the duplication of a mathematical structure without volumetric modification. The paradox goes against the everyday experience because common sense presupposes changes in volume when objects are split. Any physical analogy would involve division into two objects with the same volume, but half the density of the original. The case of BTP is different: contrary to a physical sphere which is equipped with a finite number of atoms, the pieces described by BTP are infinitely divisible, i.e., they encompass an infinite number of points. Each piece here is so infinitely complex that it is immeasurable, or, in physical words, it does not have a well-defined measurable volume. These pieces are highly pathological in nature, so that their construction requires the use of the axiom of choice.

The BTP is about a ball that, counterintuitively (not necessarily paradoxically), can be decomposed into disjoint pieces whose subsequent composition leads to two balls, both the same size as the original ball. It is a kind of cloning procedure, and the minimum number of pieces required is astonishingly small, namely five. In quest for alternatives to information accounts of the brain activity, the next step is to ask: could BTP be useful in describing nervous dynamics? When coping with the central nervous system, what is the object or the event separable in at least five pieces that can be cloned by dissection and reconstruction? Our effort is constrained by a few dictates: we need to split a ball (or, in our case, some features of nervous activity) into amorphous, non-measurable sets where the volume measure does not count. Does there exist in the brain and the nervous system a feature, a neural assembly, a system, a dynamical process that obeys the conditions and geometric properties dictated by BF?

The answer is affirmative if we consider scale-free dynamics. When Fourier analysis of brain waves is performed, it can be observed that the frequency spectrum of the cerebral activity exhibits a scale-invariant behavior (Mandelbrot 1967; Pritchard 1992):

$$\mathrm{S(f)} = 1/\mathrm{f}^{\mathrm{n}},$$

where S(f) is the power spectrum, f the frequency and n the power spectral density. The power spectral density, also termed the "fractal dimension", equals the negative slope of a log power versus frequency scatter plot (Milstein et al. 2009). It is noteworthy that fluctuations with complex scaling properties are spontaneously generated by the brain even in the absence of exogenous perturbations or changes in controlling parameters (Papo 2014). Such scale-invariant behavior is not restricted to cortical electric activity but has been also detected in spontaneous neurotransmitter release (Fox and Raichle

Author's personal copy

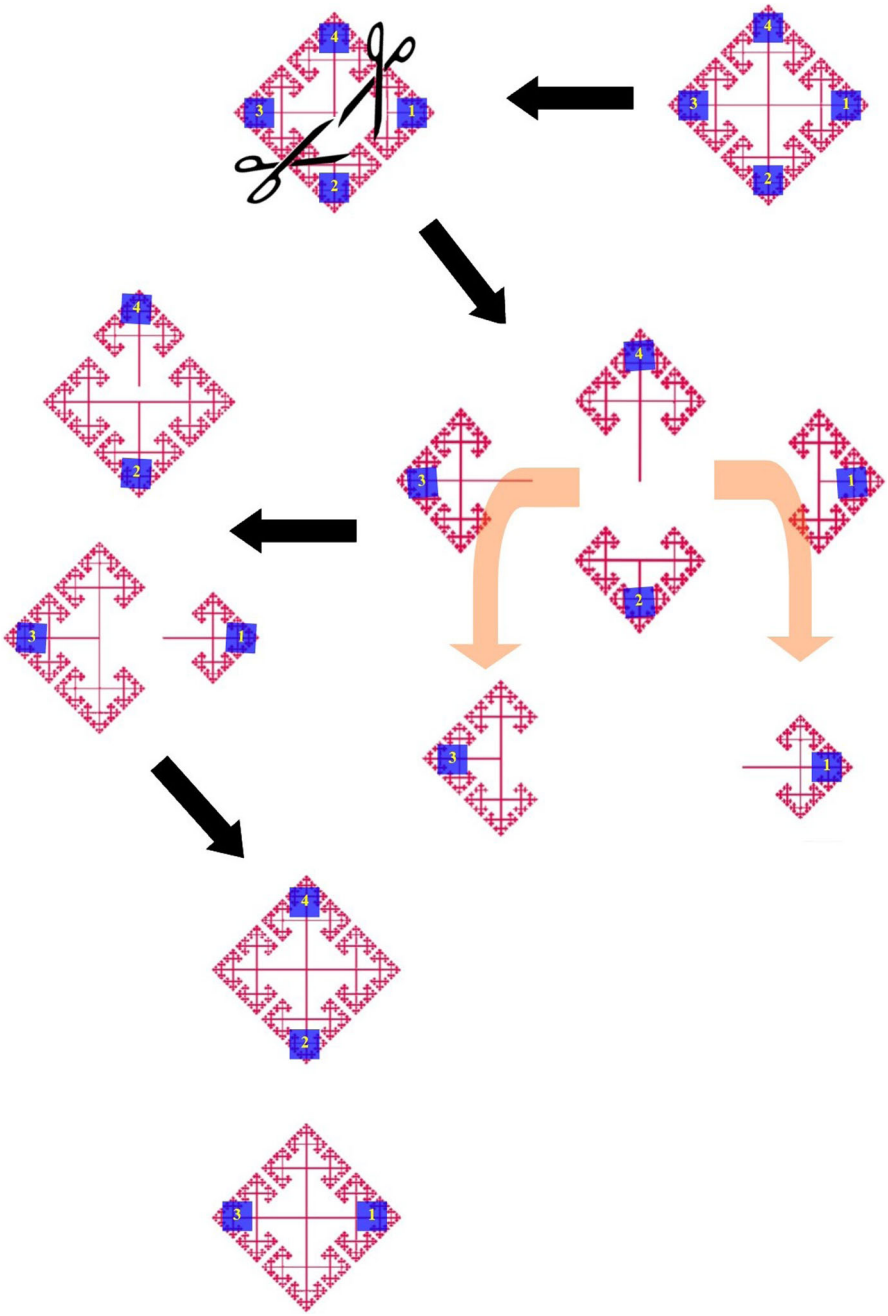

Fig. 2 This classical example illustrates the operations required by BTP through decomposition into sets. Starting from a single manifold, once performed a series of cuts and translations, two manifolds are achieved equal to the original one. Note that, if we include the parent (original manifold) as one of the pieces, we get a total of five, that is the minimum number of pieces required to let BTP work

Author's personal copy

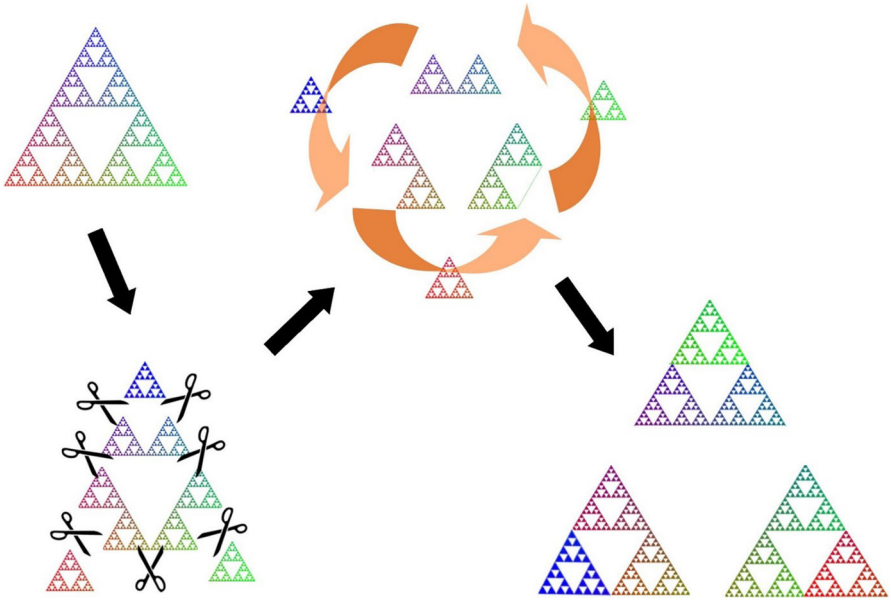

Fig. 3 Decomposition in three pieces of a Sierpinski triangle, a fractal manifold made of triangles. A few cuts and a rotational movement allow to achieve three Sierpinski triangles, starting from just one

2007). Universal scaling stands for a general spatio-temporal property of physiological and pathological brain signals. The emergence of power law distributions has been interpreted in terms of self-organized criticality (Lübeck 2004), a mechanism of slow energy accumulation and fast energy redistribution that drives the system towards a critical state (De Arcangelis and Herrmannn 2010). It has been proposed that the same cognitive processes can be framed in terms of complex activities equipped with scaling properties (Sengupta and Stemmler 2014). Power law distributions contain information on how large-scale physiological and pathological outcomes arise from the interactions of many small-scale processes: this means that the volume where a single process takes place does not count anymore (Tinker and Velazquez 2014; Kawe et al. 2019).

Therefore, it is suitable to make use of scale-free oscillations (both "spatial" fractals and/or "temporal" power laws) to build a BTP framework of the nervous activity. Indeed, scale-free nervous oscillations display the same features required by the BTP set-theoretic decomposition: these nervous oscillations are non-measurable sets with no well-defined volume and absence of mass conservation. The occurrence of power laws makes it possible to detect the same oscillatory pattern at different levels of observation, independent of the neuronal volume being considered. Fractals and power laws repeat themselves from the micro- to the macro-levels of observation, unchanged when split and reunited. Paraphrasing the BTP's formulation, we could say that: when at least five components of a scale-invariant nervous oscillation are moved, translated and rotated without changing their shape, we achieve two scale-invariant nervous oscillations instead of the original one. In other words, we suggest that the proper

Author's personal copy

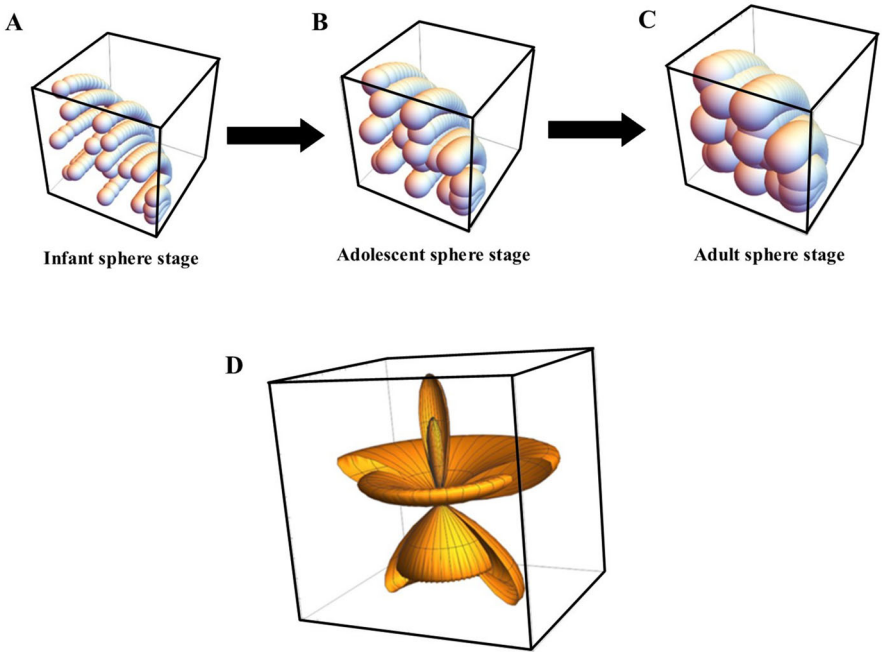

Fig. 4 Burgeoning growth BTP stages. **a** The beginning BTP stage starts with multiple tiny infant spheres (i.e., spherical composite vertexes in a nexus) that continuously form multiple sequences of contiguous spacetime spheres. **b** The growth of BTP spherical divisions leads to contiguous adolescent spheres. **c** Next, in a spacetime, seemingly a Hegelian synthesis stage, BTP spherical divisions that form path-connected vortexes lead to a nexus of contiguous adult spheres. **d** BTP process viewed as a piecewise division of one sphere into the interior of another sphere. In this case, a single sphere serves as a generator of another sphere

sequence of moves duplicates the scale free oscillations generated (spontaneously or not) by the central nervous system.

2 Power laws meet the banach Tarski paradox

In the previous paragraph, we described the theoretical background to link two apparently irreconcilable frameworks, i.e., the abstract mathematical apparatus of BTP and the impalpable scale-free dynamics occurring in the nervous system. In this paragraph we seek to operationalize their partnering in the real-world system of the human brain. We show how it is feasible to physically/biologically illustrate the counterintuitive claim that both objects and nervous processes can be duplicated without changes in volume, energy, information. The canonical example of one sphere which becomes two spheres after a series of cuts and rotations/translations has been previously illustrated in Fig. 2. Here we describe how, with the choice of just a few cuts, a fractal manifold can be decomposed into three structures with matching description (Fig. 3). Technically, BTP makes it possible to achieve k copies of a ball in the Euclidean n-space from one, for any integers $n \geq 3$ and $k \geq 1$, by using the Lie rotation group SO(n).

Author's personal copy

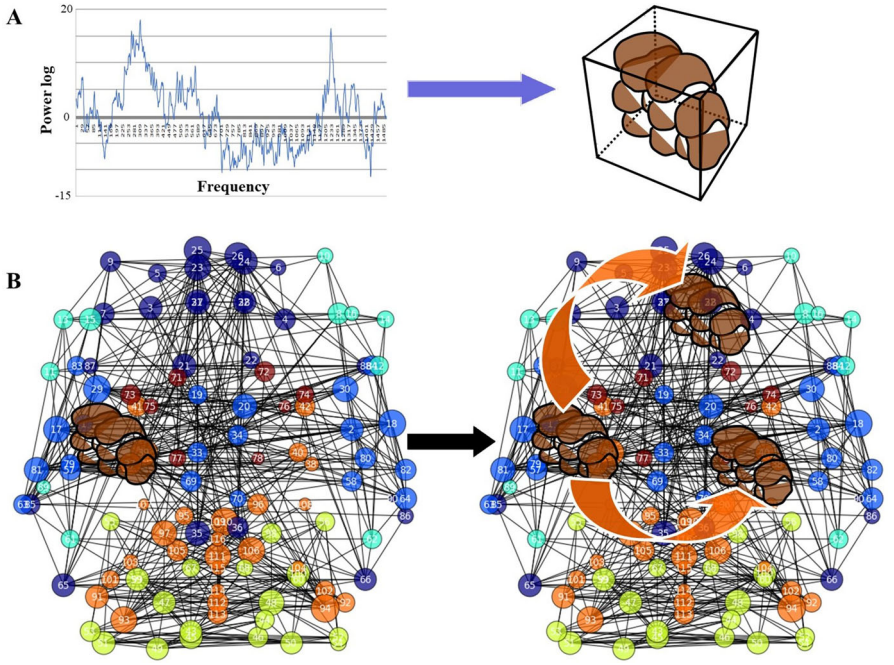

Fig. 5 Theoretical example of how BTP could be able to duplicate brain oscillations throughout different cortical areas. **a** Scale-free oscillations experimentally detected in the brain through Fourier analysis (left) and their illustration in terms of multiple tiny spheres (right). **b** Scale-free oscillations are located inside a single area of the connectome, described here in terms of Python/FSL Resting State Pipeline. The pipeline is a collection of steps that can be used to process a single subject's resting state raw data into a node-based correlation matrix representing connectivity among different cortical regions. **c** BTT comes into play: with the proper translations and rotations (not shown here) along the edges and the nodes of the connectome, the scale-free oscillations are split in different chunks with matching description. Due to the scale-invariant behavior of power law oscillations, every chunk displays the same features of the original scale-free oscillation. This allows us to achieve a "duplication", a "cloning" of the original seed oscillation in two (or more) oscillations with the same pink noise located in different areas of the connectome. Modified from: https://wiki.biac.duke.edu/biac:analysis:resting_pipeline

Here we consider the Sierpinski triangle, a fractal fixed set with the overall shape of an equilateral triangle, subdivided recursively into smaller equilateral triangles (Ali et al. 2019). Figure 3 shows how three Sierpinski triangles can be achieved, starting from just one. Therefore, with the proper choice of cuts and translations, scale-free structures obey the BTP dictates.

The paradox can be also used in another slightly different way, allowing the assessment of physical and biological dynamics (Fig. 4). In this case, the main issue is not the split of pieces, rather the growth of BTP stages. We start with multiple spherical composite vertexes in a nexus. In the sequel, multiple sequences of contiguous spacetime spheres are produced (Fig. 4A–C). BTP can be also viewed as a piecewise division of one sphere into the interior of another sphere (Fig. 4D). The BTP process starts with a single sphere serving as a generator of another sphere. The required pieces are not "solids" in the usual sense, rather infinite scatterings of vertexes standing for physi-

Author's personal copy

cal counterparts of points in an algebraic topology (Alexandroff 1935; Peters 2020). These vertexes represent the minuscule spacetime chunks in shape assemblies that are the basic building blocks of vortex nerve structures in a CW topology (Peters 2018, 2019). Therefore, the multiple spacetime spherical divisions illustrated in Fig. 4D lead to incarnation of multiple generators of offspring spheres that are pivots in path-connected vortical structures, which have high affinity to complex-valued activation functions (Özgür et al. 2020). A path can then be traced from the surface of a parent sphere (call it e1) along the surface of a child sphere (call it e2), stretching in an unbounded fashion to a nexus of contiguous new offspring spheres, forming the collection of BTP generators $\{e_1, e_2, \ldots, e_k\}, k \to \infty$. In effect, the algebraic Betti number for a burgeoning BTP sphere is $\beta_\alpha = k$ in a free Abelian group representation of a sequence of BTP sphere divisions (Don et al. 2020).

In group theory, a group is defined by a nonempty set G together with a binary operation denoted by + . In G, there is a zero element 0 and every member g in G has an inverse − g so that g − g = 0. G is Abelian, provided g + g′ = g′ + g for all members g, g′ in G. Recall that a finite group G is cyclic, provided every element g in G can be written as an integer multiple of a generating element h in G so that

$$g = h + h + \cdots + h = nh, \quad n > 0.$$

In effect, every member of a cyclic group can be written as linear combination of a generating element (called a generator). A finite free Abelian group G has a collection of generators of cyclic subgroups so that every member of G can be written as a linear combination of its generating elements. These observations lead to a concise way of pigeonholing free Abelian groups so that each pigeonhole is identified by a single number named after Enrico Betti by Poincare (Peters 2020). A Betti number is a count of the number of generators in a free Abelian group.

Vortex cycles containing vertices that are path-connected provide a rich source of free Abelian groups with concise characterizations with Betti numbers. In such vortexes, there are distinguished vertices h (path generator) so that every path between vertexes can be written as a linear combination of h. In effect, every vortex introduced here has a free Abelian group representation, concisely identified by its Betti number.

In sum, independent of volumetric parameters, we achieve the growth of one (Fig. 4D) or many (Fig. 4A–C) spheres through a well-defined series of stages.

The next step is to use this approach to evaluate the flows of the scale-free nervous oscillations taking place in the brain. Once shown that fractal structures can grow and modify according to the BTP dictates, we need to find their nervous counterparts. We require two ingredients: (a) scale-free oscillations; (b) a manifold where rotations and translation can take place. The nervous scale-free oscillations are fully available in the brain and have been described in the previous paragraphs. Concerning the manifold, we will utilize the node-based correlation matrix of the human brain termed connectome (Van den Heuvel and Sporns 2011). The anatomical and functional connections described by the connectome display the proper edges, nodes, angles, bifurcations and standard reciprocal relationships that allow us to perform the rotations and translations required by BTP. Despite the claim that cortical connections are arranged in self-similar patterns is controversial (see: Sporns 2006 vs. Reese et al. 2012), in this

Author's personal copy

paper we do not require the connectome to be fractal by itself, because we use it just as a static manifold, a locally Euclidean setting for our operations.

Figure 5 provides a tentative description of how a nervous BTP could work in the case of brain oscillations being equipped with scale-free temporal dynamics (i.e., the temporal power law counterparts of the above-described spatial fractals). Cortical oscillations are characterized by pink noise, i.e., by power law spectrum: therefore, they are self-invariant at different temporal and spatial scales and can be assessed in terms of growing spheres (Fig. 5A). Starting from an oscillation equipped with power law spectrum in a given area of the connectome (Fig. 5B, left), we are allowed to perform translation and rotation operations (not shown in Figure), achieving in other areas of the connectome two (or more) oscillations with the same feature, i.e., with the same power law spectrum (Fig. 5B, right).

In sum, we could state that, due to a BTP mechanism, a neuronal oscillation in a brain area is cloned in other areas with minimum energetic consumption.

3 Conclusions

This paper has three starting-points: (a) measures based on syntactic information alone are not sufficient to describe brain activity exhaustively; (b) there is large-scale spatial coherent neural activity across the brain; (c) the brain is a multi-scale system with dynamics at different time scales. The paper makes an additional point though: the BanachTarski-Paradox (BTP) can be employed to specify (b) or (c), and thus complement information measures as in (a) to characterize brain activity more completely. We described nervous propagation through BPT, showing how a sequence of moves related to scale-free brain oscillations allows cloning, duplication and increases in the number of cortical waves. We assessed brain activity in terms of BPT neurodynamics across different time scales, looking at interlevel relations connecting adjacent levels of activity. The fact that BTP might work in physical and biological systems would mean, as already suggested by Tozzi and Papo (2020), that topological changes may give rise to modifications devoid of thermodynamic constraints and topological superimposition, so that events occur that do not require an identifiable cause. Against all informational odds, it is noteworthy that BTP can be used to describe duplications of nervous oscillations that do not entail information transfer. Although the moves dictated by BTP in the physical/biological setting of the connectome require at least a small amount of energy to be performed, they do not require information transfer. To elucidate this intricate issue, we need to start from symbolic dynamics, a topological tool that has been already used to address interlevel relations between micro- and macro-states in complex systems equipped with deep structure (Atmanspacher 2016). In symbolic dynamics, we consider "flows", that stand for compact metric spaces with homeomorphism groups (Furstenberg 1967). An infinite discrete group G is equipped with an action termed G-flow, made of closed, G-invariant subflows (Glasner et al. 2019). Two dynamical systems or sets are termed disjoint if at least one of them is minimal, i.e., it is not equipped with further subflows (Glasner and Weiss 2018). When the subset is minimal, it is devoid of Bernoulli flows, or, in an alternative formulation, the processes with entropy zero are disjoint from Bernoulli flows. This means there

Author's personal copy

is no input from the preceding spatial proximal subflow to the next iteration, i.e., the distal subflow and, even more important, no information transfer occurs when the two subsets are disjoint. It is noteworthy that the "pieces" described by HBT display the same ingredients and features required by disjointed dynamical systems in topological dynamics: indeed, BTP subflows are related to the geometric study of fixed points of a self-mapping on a metric space. In a geometry of fixed points of a self-mapping on a metric space, new generalized contractive conditions have been established that ensure a self-mapping having a fixed disc or a fixed circle (Özgür and Taş 2019). In other words, we may state that HBT is characterized by an infinite discrete group split by an arbitrary free Abelian group of rotation through the axiom of choice, giving rise to at least five subflows. Every different subflow (every "piece") is minimal and disjoint from the others. In sum, in both symbolic dynamics and BPT approaches, fine-grained state dynamics are mapped onto coarser-grained (symbolic) state dynamics in such a way that the dynamics are topologically conjugate. It might be objected that in this case BTP-cloning is not "information-devoid", because moving across levels typically changes the granularity of phase space partitions. Also, a kind of syntactic information can be associated with any such partition: since the partitions are different, this could stand for an information flow across levels. However, even if these objections hold true, this would not be an information flow due to causal interaction. To further corroborate our suggestion that no information transfer occurs among the subflows, it must be emphasized that four of the five sets described in the BTP construction are not Lebesgue-measurable: this means that no information is lost, since the information never existed.

An important limitation must be considered: even though neurodynamics shows scale-free behavior over time (or frequency) scales, the frequency range over which power-law behavior persists is extremely limited in the brain. Indeed, the power spectral density can be detected just in the frequency range of about 0.1–40 Hz, while the tails do not display power laws. This means that the ideal picture of the Sierpinski triangle, which is self-affine over all length scales, cannot be achieved in the brain. In other words, power-law behavior in the brain does not cover infinite frequencies/amplitudes, but rather it covers just a discrete interval. Since the BTP significantly works with infinities, the question arises how such infinities may or may not be consequential for phenomena in our finite world. Here a novel technique comes in to play which makes it possible to undermine infinity in biophysical issues correlated with pink noise (Tozzi and Peters 2020). This approach suggests the possibility of mapping real systems' paths to a manifold, which corresponds to an Alexander Horned sphere (AHS). AHS is equipped with one arm where white noise takes place, and another arm where pink noise takes place. This approach allows us to achieve manageable representations, because a continuous mono-dimensional line becomes an assembly of countless superimposed bi-dimensional lines, giving rise to quantifiable knots and bifurcations. Therefore, techniques do exist that are able to overtake the limitation of extending a real-world discrete phenomenon to abstract infinite phenomena.

In this paper, we focused on the BTP as a tool to explain scale-free neurodynamics. In addition, BTP can be also used in other ways, such as, e.g., to motivate some coupling between different kinds of dynamics. The object to be cloned could be an abstract structure, such as an attractor in the phase space in which the dynamics is

Author's personal copy

represented. Another possibility is to argue that a BTP-type cloning might give rise to large-scale coherence in neurodynamics. A next step would be to compare it to alternative approaches explaining large-scale coherence in brain dynamics, such as functional connectivity in recurrent/recursive networks, and to look for the proper network to use. To provide an example, it has been recently demonstrated that recurrent activity in the mouse vibrissal somatosensory neurons can drive input-specific amplification during behavior (Peron et al. 2020). In touch with this computational modelling which implements amplification and allows pattern completion, the operations required by BTP could be guaranteed by local recurrent circuits and spatially intermingled neurons with similar receptive fields/increased connectivity.

The last, but not the least, the brain vortexes and Betti numbers recently described in cortical lag threads (Don et al. 2020) can be duplicated with simple spatial transformations (the passage of oscillations through brain wires), without energy transfer. This is a fruitful operation, because it leads to a new form of Borsuk-Ulam theorem (BUT) in terms of Betti numbers. In fact, the underlying mechanism in instantiations of BUT (Tozzi and Peters 2017) provides a terse description of the inner workings of BTP in the context of neuro-dynamics. Here are two examples: (a) Antipodal, symmetric vortexes serving as generators of offspring spheres dictated by BTP on the surface of a sphere have the same algebraic Betti number (count of the number of generators), with an underlying geometric Betti number (e.g., count of the number of cycles in each vortex). This form of BUT carries over into the study of symmetric activation regions in rs-FMRI videos; (b) BTP -produced antipodal, symmetric vortexes on the surface of a sphere have the same algebraic Betti number (count of the number bridge segments $\times$ 2 attached between vortex cycles).

In conclusion, a BTP-based approach facilitates tackling brain issues from an unusual standpoint. Against all informational odds, it is noteworthy that BPT can be used to describe duplications of nervous oscillations that do not entail information transfer.

References

Alexandroff, P. (1932, 1961). *Elementary concepts of topology*. New York: Dover Pubs Inc. ISBN 0-486-60747-X.

Ali, A., Rafique, H., Arshad, T., Alqarni, M. A., Chauhdary, S. H., & Bashir, A. K. (2019). A fractal-based authentication technique using Sierpinski triangles in smart devices. *Sensors (Basel)*. https://doi.org/10.3390/s19030678

Allen, E., & Triantaphillidou, S. (2009). *The Manual of Photography* (10th ed.). Abdingdon, Oxon: Taylor and Francis Group.

Atmanspacher, H. (2016). On macrostates in complex multi-scale systems. *Entropy, 18*(12), 426. https://doi.org/10.3390/e18120426

Attwell, D., & Laughlin, S. B. (2001). An energy budget for signaling in the grey matter of the brain. *Journal of Cerebral Blood Flow and Metabolism, 21*(10), 1133–1145. https://doi.org/10.1097/00004647-200110000-00001

Banach, S., & Tarski, A. (1924). Sur la décomposition des ensembles de points en parties respectivement congruentes. *Fundamenta Mathematicae, 6,* 244–277.

Bekenstein, J. D. (2003). Black holes and information theory. arXiv:quant-ph/0311049.

Author's personal copy

Bromiley, P. A., Thacker, N. A., & Bouhova-Thacker, E. (2010). Shannon entropy, Renyi entropy, and information. Tina 2004-004, Statistic and Inf Series, Imaging Sci. and Biomed. Eng., Univ. of Manchester, UK

Aliprantis, C. D., & Border, K. C. (2006). *Odds and Ends*. Berlin: Springer. ((**ISBN-10 3-540-29586-0**)).

Cafaro, C., Ali, S. A., & Giffin, A. (2016). Thermodynamic aspects of information transfer in complex dynamical systems. *Physical Review E, 2016*(93), 022114.

Churkin, V. A. (2010). A continuous version of the Hausdorff–Banach–Tarski paradox. *Algebra and Logic, 49*(1), 81–89. https://doi.org/10.1007/s10469-010-9080-y

de Arcangelis, L., & Herrmann, H. J. (2010). Learning as a phenomenon occurring in a critical state. *Proceedings of the National Academy of Sciences, 107,* 3977–3981.

Don, A. P., Peters, J. F., Ramanna, S., & Tozzi, A. (2020). Topological view of flows inside the BOLD spontaneous activity of the human brain. *Frontiers in Computational Neuroscience*. https://doi.org/10.3389/fncom.2020.00034

Fox, M. D., & Raichle, M. E. (2007). Spontaneous fluctuations in brain activity observed with functional magnetic resonance imaging. Nature reviews. *Neuroscience, 8,* 700–711.

Friston, K. (2010). The free-energy principle: A unified brain theory? *Nature Reviews Neuroscience, 11*(2), 127–138. https://doi.org/10.1038/nrn2787

Furstenberg, H. (1967). Disjointness in ergodic theory, minimal sets, and a problem in diophantine approximation. *Mathematical Systems Theory, 1,* 1–49.

Glasner, E., & Weiss, B. (2018). On the disjointness property of groups and a conjecture of Furstenberg. arXiv:quant-ph/0311049.

Glasner, E., Tsankov, T., Weiss, B., & Zucker, A. (2019) Bernoulli disjointness. arXiv:quant-ph/0311049.

Jaynes, E. T. (1957). Information theory and statistical mechanics. *Physical Review, 106,* 620.

Kantor, F. W. (1977). *Information Mechanics*. Hoboken: Wiley.

Kawe, T. N. J., Shadli, S. M., & McNaughton, N. (2019). Higuchi's fractal dimension, but not frontal or posterior alpha asymmetry, predicts PID-5 anxiousness more than depressivity. *Scientific Reports, 9*(1), 19666. https://doi.org/10.1038/s41598-019-56229-w

Lloyd, S. (2000). Ultimate physical limits to computation. *Nature, 406,* 1047–1054. https://doi.org/10.1038/35023282

Lübeck, S. (2004). Universal scaling behavior of non-equilibrium phase transitions. *International Journal of Modern Physics B, 18,* 3977–4118.

Mandelbrot, B. (1967). How long is the coast of Britain? Statistical self-similarity and fractional dimension. *Science, 56*(3775), 636–638.

Marzuoli, A., & Rasetti, M. (2005). Computing spin networks. *Annals of Physics, 318,* 345–407.

Milstein, J., Mormann, F., Fried, I., & Koch, C. (2009). Neuronal shot noise and Brownian 1/f2 behavior in the local field potential. *PLoS ONE, 4*(2), e4338. https://doi.org/10.1371/journal.pone.0004338

Ȯzgȕr, N., Taş, N., & Peters, J. F. (2020). New complex-valued activation functions. *An International Journal of Optimization and Control Theories & Applications, 10*(1), 66–72. https://doi.org/10.11121/ijocta.01.2020.00756

Özgür, N., & Taş, N. (2019). Pata Zamfirescu type fixed-disc results with a proximal application. arXiv:quant-ph/0311049.

Papo, D. (2014). Functional significance of complex fluctuations in brain activity: From resting state to cognitive neuroscience. *Frontiers in Systems Neuroscience, 8,* 112.

Peron, S., Pancholi, R., Voelcker, B., Wittenbach, J. D., Ólafsdóttir, H. F., et al. (2020). Recurrent interactions in local cortical circuits. *Nature, 579*(7798), 256–259. https://doi.org/10.1038/s41586-020-2062-x ((**Epub 2020 Mar 4**)).

Peters, J. F. (2018). Proximal vortex cycles and vortex nerves. Non-concentric, nesting, possibly overlapping homology cell complexes. *Journal of Mathematical Sciences and Modelling, 1*(2), 80–85.

Peters, J. F. (2019). Vortex nerves and their proximities. Nerve Betti numbers and descriptive proximity. *Bulletin of The Allahabad Mathematical Society, 34*(2), 263–276.

Peters, J. F. (2020). *Computational geometry, topology and physics of digital images with applications. Shape complexes, optical vortex nerves and proximities*. Cham: Springer.

Pritchard, W. S. (1992). The brain in fractal time: 1/f-like power spectrum scaling of the human electroencephalogram. *The International Journal of Neuroscience, 66,* 119–129.

Reese, T. M., Brzoska, A., Yott, D. T., & Kelleher, D. J. (2012). Analyzing self-similar and fractal properties of the C. elegans neural network. *PLoS ONE, 7*(10), e40483. https://doi.org/10.1371/journal.pone.0040483

Author's personal copy

Sengupta, B., & Stemmler, M. B. (2014). Power consumption during neuronal computation. *Proceedings of the IEEE, 102,* 738–750.

Shannon, C. E. (1948). A mathematical theory of information. *The Bell System Technical Journal, 27,* 379–423.

Sporns, O. (2006). Small-world connectivity, motif composition, and complexity of fractal neuronal connections. *Biosystems, 85*(1), 55–64. https://doi.org/10.1016/j.biosystems.2006.02.008

Tinker, J., & Velazquez, J. L. (2014). Power law scaling in synchronization of brain signals depends on cognitive load. *Frontiers in Systems Neuroscience, 8,* 73. https://doi.org/10.3389/fnsys.2014.00073

Tozzi, A., & Peters, J. F. (2016). A topological approach unveils system invariances and broken symmetries in the brain. *Journal of Neuroscience Research, 94*(5), 351–365. https://doi.org/10.1002/jnr.23720

Tozzi, A., & Peters, J. F. (2017). From abstract topology to real thermodynamic brain activity. *Cognitive Neurodynamics, 11*(3), 283–292. https://doi.org/10.1007/s11571-017-9431-7

Tozzi, A., Peters, J. F., & Cankaya, M. N. (2018). The informational entropy endowed in cortical oscillations. *Cognitive Neurodynamics, 12*(5), 501–507. https://doi.org/10.1007/s11571-018-9491-3

Tozzi, A., & Papo, D. (2020). Projective mechanisms subtending real world phenomena wipe away cause effect relationships. *Progress in Biophysics and Molecular Biology, 151,* 1–13. https://doi.org/10.1016/j.pbiomolbio.2019.12.002

Tozzi, A., & Peters, J. F. (2020). A topological approach to infinity in physics and biophysics. *Foundations of Science*. https://doi.org/10.1007/s10699-020-09674-0

Van den Heuvel, M. P., & Sporns, O. (2011). Rich-club organization of the human connectome. *Journal of Neuroscience, 31,* 15775–15786. https://doi.org/10.1523/JNEUROSCI.3539-11.2011

Wheeler, J. A. (1990). Information, physics, quantum: The search for links. In W. H. Zurek (Ed.), *Complexity, Entropy, and the Physics of Information*. Redwood City: Addison-Wesley.

Watanabe, T., Hirose, S., Wada, H., Imai, Y., Machida, T., et al. (2013). A pairwise maximum entropy model accurately describes resting-state human brain networks. *Nature Communications, 4,* 1370. https://doi.org/10.1038/ncomms2388

Watanabe, T., Kan, S., Koike, T., Misaki, M., Konishi, S., et al. (2014). Network-dependent modulation of brain activity during sleep. *NeuroImage, 98,* 1–10. https://doi.org/10.1016/j.neuroimage.2014.04.079

Publisher's Note Springer Nature remains neutral with regard to jurisdictional claims in published maps and institutional affiliations.

Author's personal copy

Cognitive Neurodynamics (2021) 15:349–357
https://doi.org/10.1007/s11571-020-09598-2

RESEARCH ARTICLE

Neural computing in four spatial dimensions

Arturo Tozzi[1] · Muhammad Zubair Ahmad[2] · James F. Peters[2]

Received: 20 July 2019 / Revised: 26 April 2020 / Accepted: 11 May 2020 / Published online: 18 May 2020
© Springer Nature B.V. 2020

Abstract

Relationships among near set theory, shape maps and recent accounts of the Quantum Hall effect pave the way to neural networks computations performed in higher dimensions. We illustrate the operational procedure to build a real or artificial neural network able to detect, assess and quantify a fourth spatial dimension. We show how, starting from two-dimensional shapes embedded in a 2D topological charge pump, it is feasible to achieve the corresponding four-dimensional shapes, which encompass a larger amount of information. Synthesis of surface shape components, viewed topologically as shape descriptions in the form of feature vectors that vary over time, leads to a 4D view of cerebral activity. This novel, relatively straightforward architecture permits to increase the amount of available qbits in a fixed volume.

Keywords Hall effect · Oscillations · Fourth dimension · Brain · Neuronal network

Multidimensional approaches are a novel field of research, with a potential to provide insights into neural organization (Tozzi 2019). However, these approaches are technically demanding to cope with elusive multidimensional activities. The recent onset of datasets encompassing thousands of features has led to the development of novel tools, such as feature selection, to model the underlying high-dimensional settings of neurodata generation (Garcia et al. 2018). Despite feature selection techniques allow the reduction of the data dimensionality and improve algorithms' performance (Dmochowski et al. 2017), huge data volume makes learning tasks computationally demanding. Increasing features' quantity/complexity results in reduced computational efficiency of algorithms. Most of the algorithms in use, developed for neural datasets of small size, cannot cope with the emerging Big Data problems. Therefore, novel tools are required to quantify multidimensional issues related to neuronal systems.

In quantum computing, quantum properties can be used to represent and structure data (stored in terms of qbits), providing an amount of information higher than the classical computers. Here we describe a novel neural computing tool that is able, starting from simple shapes traces encompassed in a two-dimensional lattice, to detect information from a fourth spatial dimension. We aim to transfer the framework of the quantum Hall effects provided by Lohse et al. (2018) to the realm of brain computing, to demonstrate the feasibility of a synthetic quantum network equipped with four spatial dimensions (plus time), instead of the classical three (plus time).

We will describe 4D neural computing in terms of a computational device able to cope with *shape maps*, i.e., shapes' assessment at various hierarchical levels of synthesis. At first, we will define the fundamental structure for neural maps construction; then we will provide the operational steps for achieving 4D neural computing. We will also show that shape maps provide an expanded view of the Borsuk–Ulam Theorem (Tozzi et al. 2017), which allows to increase the amount of available qbits.

✉ Arturo Tozzi
tozziarturo@libero.it; Arturo.Tozzi@unt.edu

Muhammad Zubair Ahmad
ahmadmz@myumanitoba.ca

James F. Peters
James.Peters3@umanitoba.ca

[1] Center for Nonlinear Science, University of North Texas, 1155 Union Circle, #311427, Denton, TX 76203-5017, USA

[2] Department of Electrical and Computer Engineering, University of Manitoba, 75A Chancellor's Circle, Winnipeg, MB R3T 5V6, Canada

Author's personal copy

Introducing shape maps

In near set theory, we consider a space K and a probe function $\phi : 2^K \to \mathbb{R}^n$(Peters 2007, 2014). Given a small neighborhood $U \subset K$, we construct the fiber bundle $(K_\Phi, K, \pi, \phi(U))$. Here, K_Φ is termed the *glossa* (a set paired with description (Ahmad and Peters 2018)), i.e., a space where each $k \in K$ is paired with $\phi(k)$, due to the local trivialization property. This structure can be described as follows:

$$\phi(U) \to K_\Phi \xrightarrow{\pi} K.$$

To define classical set theoretic operations incorporating description, we introduce the notion of *descriptive intersection* (Di Concilio et al. 2018). Let $A, B \subset K$ and $\phi : 2^K \to \mathbb{R}^n$. A descriptive intersection is defined as:

$$A \bigcap_\Phi B = \{x \in A \cup B : \phi(x) \in \phi(A) \text{ and } \phi(x) \in \phi(B)\}.$$

Note that a descriptive intersection of sets A, B consists of all the elements. in either A or B, having the same description. In other words, sets A and B are close, provided there is at least one pair of elements a in A and b in B that are close descriptively. Implicit here are two forms of near sets, i.e., overlapping spatially near sets with (figure 8 shape) and disjoint (non-overlapping) descriptively near sets containing shapes with the same description, e.g., A = {}. B = {} with shape in common to A and B. In effect, members of the descriptive intersection of a pair of sets (e.g., neurons, brain signals) are a source of fibers and concomitant information in the form of closeness for what we call a topological charge pump. It follows that all the elements in $A \cap B$ are included in the descriptive intersection. We can represent this definition in terms of fiber bundle structure and classical set theoretic operations as follows:

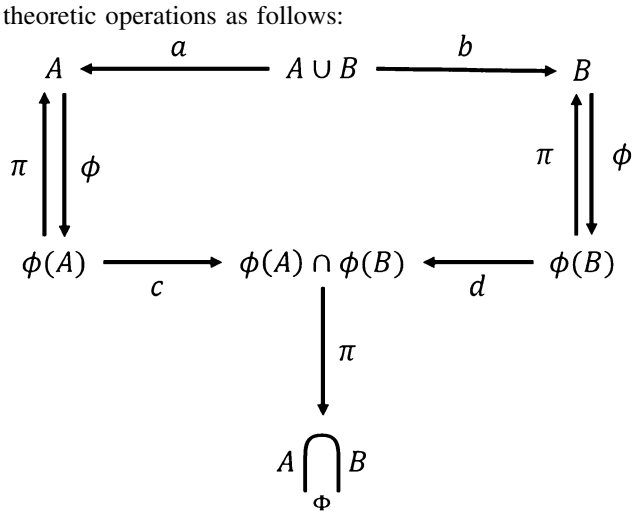

Note that the arrows are used here as connections in a topological sense, i.e., to establish descriptive intersection and union in fiber bundles.

Once established the notion of descriptive intersection, the next step is to define a descriptive union. Four different possible definitions have been discussed by Ahmad and Peters (2018): they consider either elements in $A \cup B$(non-restrictive), or $A \cap B$(restrictive), or few values of description (descriptive discriminatory), or all possible values (descriptive nondiscriminatory). Here we will evaluate just the *non-restrictive and descriptive discriminatory union*. Given $A, B \subset K$ and $\phi : 2^K \to \mathbb{R}^n$, non-restrictive and descriptive discriminatory union is described as follows:

$$A \bigcup_{\phi=\{i,j\}} B = \{x \in A \cup B : \phi(x) = i or \phi(x) = j\}.$$

A non-restrictive and descriptive discriminatory union of sets A, B consists of all the elements of A and B that have matching description feature values {i, j}, with features such as shape energy and mass, decided a priori. A more detailed account of the properties of this union is given in Ahmad and Peters (2018). In terms of classical set theoretic operations and fiber bundles, the latter definition can be described in the following terms:

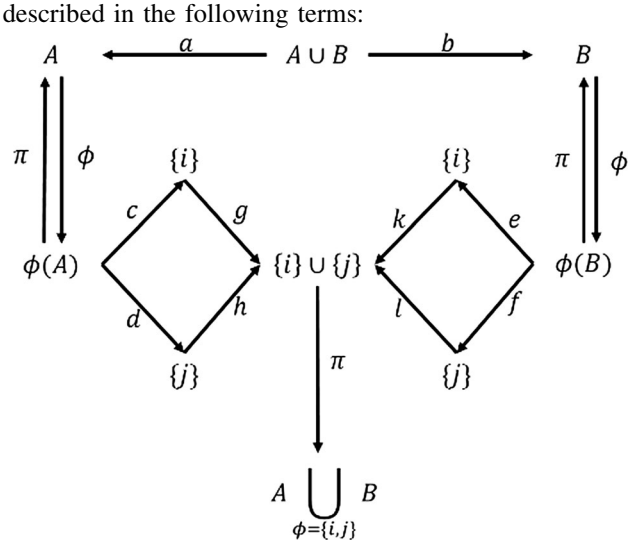

Shapes in terms of synthesis

The next step is to define representation of a shape as a synthesis. We begin with a set of shapes $\{Sh_i\}_{i\in\mathbb{Z}}$ with no description attached to them. For simplicity, we assume them as embedded in a 2-dimensional space. This set of shapes is said to be at synthesis level 0, which is represented as S_0. To attach description to these shapes, we use a probe function $\phi_1 : 2^{S_0} \to \mathbb{R}^n$ at level 0 and achieve a gloss presented as $\{Sh_i \to \phi_1(Sh_i)\}_{i\in\mathbb{Z}}$, standing for the synthesis

Author's personal copy

level 1 or S_1. In other words, each shape synthesis spirals upward to more informative views of each shape and geometrically is a vortex with a shape at its center (level 0). We move onto the next level of synthesis, attaching another description to the one already attached in S_1. Thus, S_2 is constructed using a probe function $\phi_2 : 2^{S_1} \rightarrow \mathbb{R}^n$. The corresponding glossa can be represented as $\{Sh_i \rightarrow \phi_1(Sh_i) \rightarrow \phi_2(\phi_1(Sh_i))\}_{i\in\mathbb{Z}}$. We generalize for the mth synthesis level S_m, using the probe function $\phi_m : 2^{S_m} \rightarrow \mathbb{R}^n$. This means that the glossa at S_m can be written as $\{Sh_i \rightarrow \phi_1(Sh_i) \rightarrow \cdots \rightarrow \phi_{m-1} \ (\cdots \phi_1(Sh_i)) \rightarrow \phi_m(\phi_{m-1} \cdots \phi_1(Sh_i))\}_{i\in\mathbb{Z}}$. In sum, we define a family of functions that can be collectively termed as shape maps. Let $s_i^{i+1} : S_i \rightarrow S_{i+1}$, be a map between the synthesis levels, then for a shape representation with m synthesis levels the shape maps are $\mathbb{S}_m = \{s_i^{i+1}\}_{i=1,2,\cdots,m-1}$.

Figure 1a shows a shape map encompassing different levels of synthesis. The shapes Sh_i, exist at S_0 the zeroth level of synthesis. At S_1, descriptions are attached to each shape with the help of a probe function ϕ_1. At the next level of synthesis, a description is attached to the description of each of the objects by ϕ_2. Similarly, increasing the levels of synthesis, we increase the number of descriptions until, at S_n, a description is attached to the previous level using ϕ_n. At the highest level, the

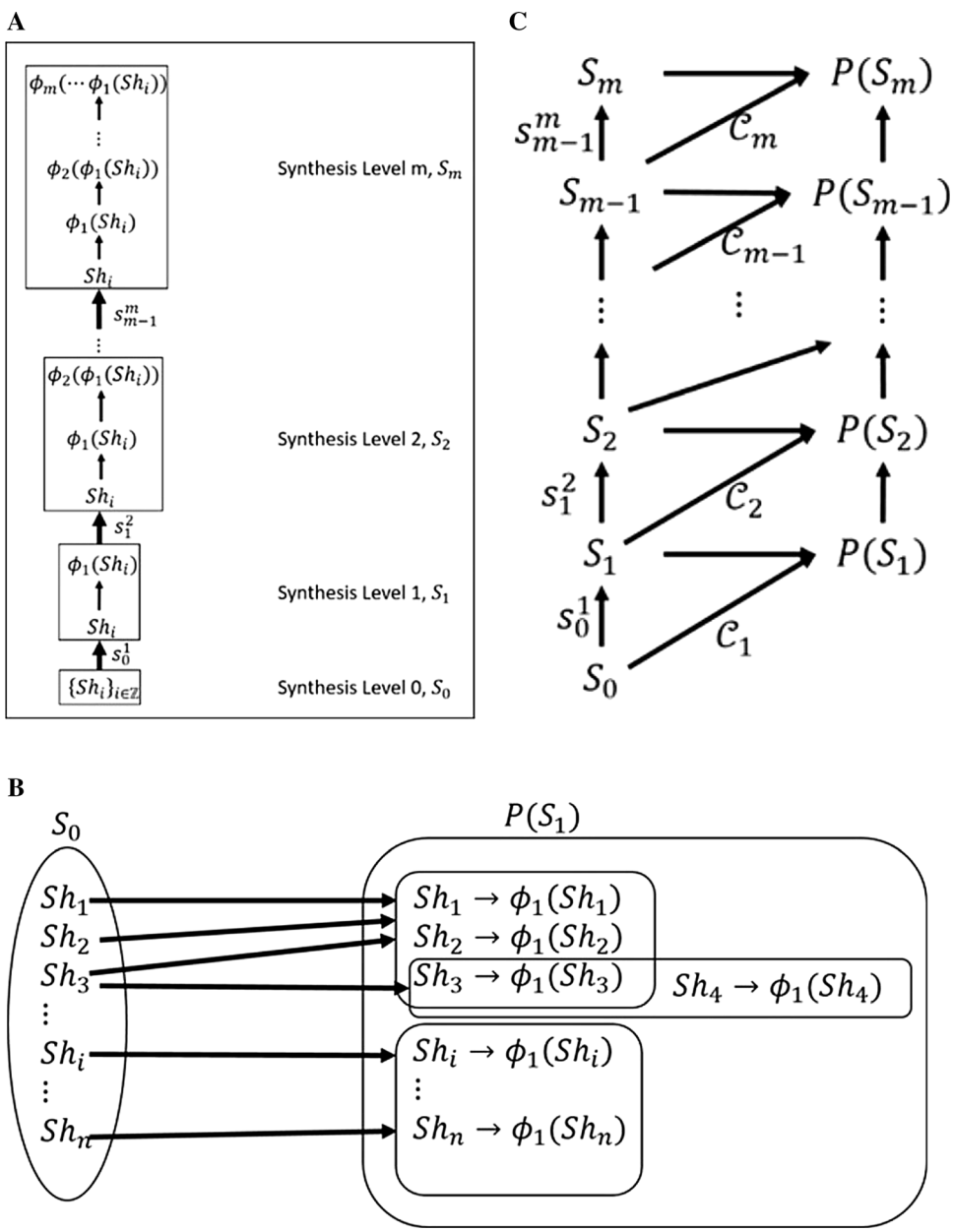

Fig. 1 Topological steps of shape maps construction. **a** Shape maps with n-levels of synthesis. **b** Shape maps lead to shapes clustered and glued together using descriptive intersection. **c** Shape description diagram for m-synthesis levels. See text for further details. The arrows are used here as topological steps of shape maps constructions

Author's personal copy

description can be written as a composition of maps $\phi_n(\phi_{n-1}\cdots\phi_1(Sh_i))$.

Once achieved shapes representation with the desired level of synthesis, we need to "organize" them according to a general description throughout all the levels. By "organizing" we mean clustering the shapes into sets based on some similarity criterion. Here the previously described near set paradigm comes into play. For this purpose, the descriptive intersection (Di Concilio et al. 2018) and the non-restrictive and descriptive discriminatory union (Ahmad and Peters 2018) are used. It is noteworthy there just one descriptive intersection is feasible, while the number of non-restrictive and descriptive discriminatory union depends on the number of pairs of descriptions $\{i,j\}$ selected a priori. We have set of descriptive set theoretic operators for each S_m. Let us represent this set at synthesis level j as:

$$\mathcal{O}^j = \left\{ \bigcap_{\Phi}, \left\{ \bigcup_{\phi=A_i\in A} \right\}_{i\in\mathbb{Z}} \right\},$$
$$\textit{where } A = \left\{ x \in 2^{\textit{Codomain}(\phi_j)} : |x| = 2 \right\}.$$

In this set, we achieve both descriptive intersection and a selection of the possible non-restrictive and descriptive discriminatory unions. Further, if we take into account any of these operators for S_i, the synthesis assesses the descriptions attached at S_i and provides again the elements of the S_{i-1} level. This is clear from the arrow diagrams illustrated in Fig. 1a, which show how the descriptive set theoretic operations return the elements in the base space K, rather than the ones in the glossa K_Φ. We assume that each of the operators in $\mathcal{O}^j$ can be used for a single set, instead of canonical binary operator. The same applies for the descriptive union in which all the elements with a priori decided descriptions are returned. We define a family of maps, which clusters the elements in S_i based on the application of operators in $\mathcal{O}^i$:

$$\mathcal{C}_i = \left\{ c^i_j = s^i_{i-1}\left(\mathcal{O}^i_j(S_{i-1})\right) \right\}_{j=1,2,\ldots,|\mathcal{O}^i|},$$
where $\mathcal{O}^i_j$ is the jth element of the set $\mathcal{O}^i$.

This map clusters the elements in S_i based on some similarity measure. If we consider the non-restrictive and descriptive discriminatory union with $\phi = \{i,j\}$ as the similarity measure, then it results in clustering all the shapes with description value of either i or j. Every operator in $\mathcal{O}^i$ results in a different cluster (set) of S_i elements. Because each $c^i_j : S_{i-1} \to S_i$, their union to form $\mathcal{C}_i$ results in a new space $P(S_i)$, built by clustering the S_i elements. Hence, we can represent this as $\mathcal{C}_i : S_{i-1} \to P(S_i)$. An example of this map is illustrated in Fig. 1b. This Figure also illustrates the beginning of a hyper Borsuk–Ulam Theorem (Borsuk 1957–1958; Matoušek 2003; Tozzi and Peters 2016a). The introduction of a hyper-BUT paves the way to techniques for shape detection, "bunching" (clustering), classification, building (disparate shapes are synthesized to form new shapes for future reference), and shape analysis in a high-dimensional space (Tozzi and Peters 2016a, b). Shape building, also called bulk building, allows new shapes to be achieved. The hierarchical view of shape maps leads to two forms of synthesis, namely, shape-gluing (descriptive intersection) and shape agglomeration (descriptive union). We define another family of maps for synthesis level m represented as $\mathfrak{C}_m = \{C_i\}_{i=1,2,\ldots m}$, termed *clustering maps*. This allows to build a diagram termed *shape description diagram,* illustrated in Fig. 1c.

A tool from theoretical physics

Here we ask: is it feasible to assess and quantify how oscillations may generate multidimensional computations? More specifically, is it feasible to build a real or an artificial oscillatory network able to simulate an otherwise undetectable fourth spatial dimension? The answer is affirmative. Recent experimental findings describe a technique that throws an operational bridge between theoretical physics and quantum computing. At first, we explore the "Hall effect" (Hall 1879) observed in 2D systems with low temperatures and strong magnetic fields in which conductance σ map to quantized values defined by

$$\sigma = \nu\frac{e^2}{h},\ e = \text{charge, h} = 6.6\times10^{-34}\,\text{kg m}^2/\text{s},\ \nu = \text{filling factor},$$

i.e., the production of potential difference transverse to electric current, upon application of a magnetic field perpendicular to current.

Magnetic fields with the proper angulation are able to bend electric rays. A comparable phenomenon, called "quantum Hall effect", occurs in quantum dynamics (Novoselov et al. 2007). An electric charge sandwiched between two surfaces behaves like a two-dimensional material: when this material is cooled down to near absolute-zero temperature and subjected to a strong magnetic field, the amount that it can conduct becomes "quantized", leading to the so-called quantum Hall effect (Tozzi 2019). This puzzling phenomenon is easily explained, if we take into account that it occurs in four, instead of the canonical three, spatial dimensions (Zhang and Hu 2001; Kraus et al. 2013; Zilberberg et al. 2018). Lohse et al. (2018) found a (relatively) simple way to probe four-dimensional quantum physical phenomena, starting from an artificial, two-dimensional dynamic system, a superlattice termed "2D topological charge pump". The light flowing through the

Author's personal copy

two-dimensional superlattice behaves according to the predictions of the four-dimensional quantum Hall effect. The Authors provided a two-dimensional waveguide equipped with patterns acting as manifestations of higher-dimensional coordinates: in operational terms, they built a 2D lattice consisting of superlattices along the *x* and *y* axes.

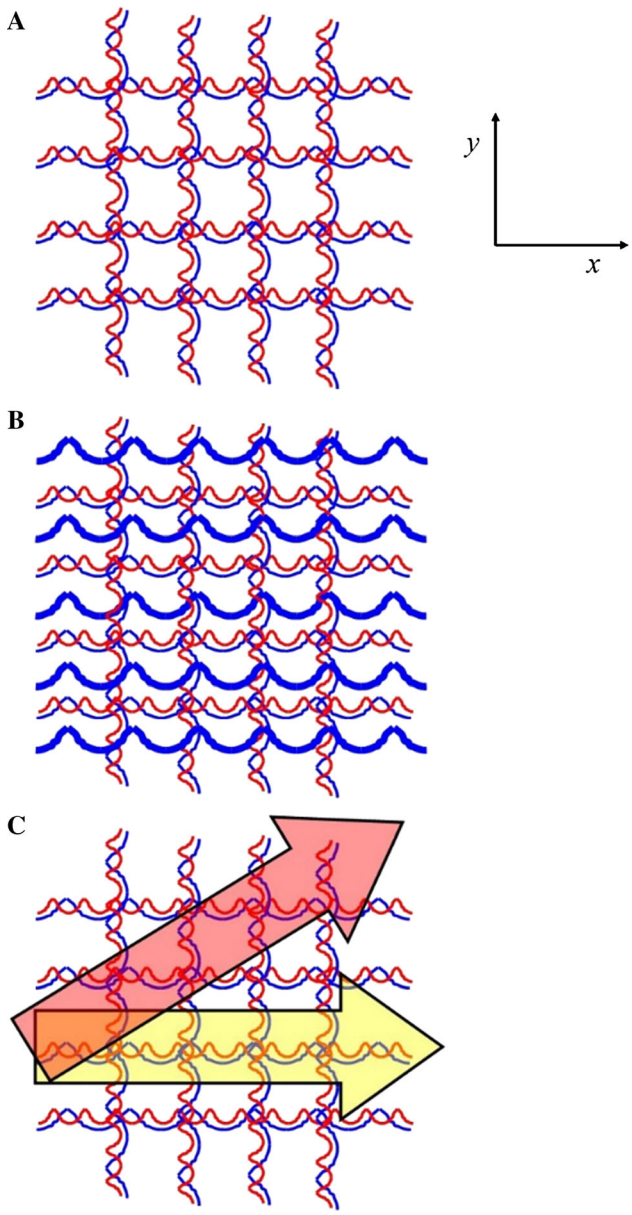

Fig. 2 4D physical activities on a 2D superlattice, according to Lohse et al. (2018). **a** Illustrates a topological lattice with two waves of different wavelength (red and blue thin lines). **b** Depicts a third wave (blue thick line) with the proper wavelength and angulation (not shown here) superimposed to the lattice along the x direction. The required angulation of the third wave might also be achieved by tilting the lattice. **c** The superimposition of the three waves gives rise to two different paths: a 2D linear one along the x axis (yellow arrow), and a nonlinear 4D one along the y axis (red arrow). (Color figure online) Modified from Tozzi (2019)

Each superlattice is achieved by superimposing two standing waves of different wavelength (Fig. 2a). When a third wave is introduced along the *x* direction, this corresponds to tilting the long lattice along a one-dimensional path shadowing the axis x, carefully choosing the proper inclination (Fig. 2b). Lohse et al. (2018) and Zilberberg et al. (2018) provided the proper measures (e.g., angles, equations) to detect the 4D spacetime quantum Hall effect. Their procedure on 2D topological charge pumps allows the achievement of dynamics along the y axis that are equivalent to movements in four spatial dimensions. In effect, shape vectors (σ, e, v, t) have components that describe time-varying shapes relative to the changing temporal (spacetime) component t. They lead to two different responses: a linear one (two-dimensional response with fixed v) along the axis x and a nonlinear one (four-dimensional response with time-varying σ relative to e, v) (Fig. 2c). In sum, the Authors provide a technique which describes quantum dynamics in terms of pure oscillations. Here we ask: could such procedure be transferred, with the due corrections, to quantum computing, in order to build a spatial four-dimensional device where quantum computational operations might take place?

Neural computations in the form of shape maps

In the previous paragraph, we showed that Lohse et al.'s (2018) approach, i.e., a 2D topological charge pump, holds true for the assessment of the unusual multidimensional phenomenon occurring in quantum dynamics' Hall effect. Here we aim to show how, with the proper amendments, their four-dimensional- apparatus could be also used to build, assess and quantify a further spatial dimension of neural networks endowed in two-dimensional lattices. In other terms, our aim is to explore 4D shapes using 2D functional lattices, where the constructing basis in the x and the y dimensions are superlattices, i.e., periodic layered structures derived from the superposition of two stationary waves of different wavelengths. Our goal is to correlate shape maps to Lohse' et al.'s 2D lattice oscillations, the latter standing for the S_0 at the Oth level of synthesis (Fig. 3, lowest part). The entire topological pump stands for the space K, while its horizontal and vertical oscillations stand, respectively, for $A, B \subset K$. The topological pump's phase φ_x (which is the pump parameter, achieved when pumping is performed by moving the long lattice along x) stands for the probe function φ_1 displayed in Fig. 1a. The topological pump's phase φ_y (which stands for a transverse superlattice phase that depends linearly on x, and which varies with φ_x changes) stands for the probe function φ_2. Note that φ_x lies at the S_1 level of synthesis, while φ_y at the S_2 level. In sum, when φ_x is modified, we achieve changes in φ_y, which lead to a quantized non-

Author's personal copy

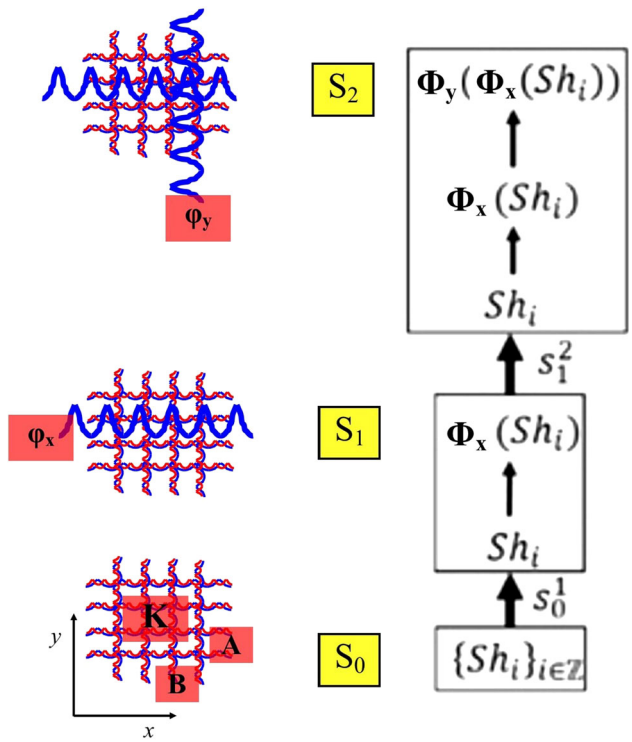

Fig. 3 Near set theory's and shape maps' lexicon can be used to describe the operations taking place on the 2D topological charge pump too. The yellow squares describe the levels of synthesis, while the red ones the near set theory's counterparts of the Lohse et al.'s lattice

linear response along y: such nonlinear response stands for the four-dimensional features in the topological space K. Note that, when an adiabatic pump cycle of the 2D topological charge pump is performed (Fig. 4), we achieve periodic modulation along closed trajectories, both on the horizontal and vertical plane (curves φ_x and φ_x in the upper part of the Fig. 4). In a full pump cycle, these closed trajectories cover a closed surface which lies in the 4D parameter space (middle part of Fig. 4). Our model allows the assessment of antipodal points in higher dimensions, due to the hyper-BUT dictates (Fig. 4, lower part). When evaluating 2D signals in 4D phase spaces, we achieve a multidimensional structure equipped with antipodal features with matching description.

Conclusions

The benefits in using near sets in biomedical signal analysis, camouflage detection, human pattern recognition, c cellular division trails, zero-shot recognition and visual pattern classification are clearly recognized in the literature. Linking these developments with our unconventional combination of disciplines in network science and mathematics, we proposed a new form of neural computation using four spatial dimensions and sketch the preliminary theoretical steps to detect, asses and quantify a fourth spatial dimension using a neural network. In particular, we aimed to transfer the framework of the quantum Hall effect provided by Lohse et al. (2018) to the realm of neural computation, in order to: a) describe real multi-dimensional brain dynamics and b) demonstrate the feasibility of a synthetic network equipped with four spatial dimensions (plus time), instead of the classical three (plus time). We provided the theoretical apparatus to link two-dimensional topological charge pump to topological shape maps, achieving neural computing in four spatial dimensions. Indeed, working on a properly manipulated two-dimensional quantum lattice such as the topological charge pump, it is feasible to build a transverse oscillation standing for the whole system's four-dimensional component. We showed how the superimposition of waves of different frequency and orientation produces the required superlattice's functional reticulum. When the latter is crossed by other waves of different frequency along its x axis, both (two-dimensional) linear and (four-dimensional) nonlinear dynamics are accomplished. The superimposition of the proper waves gives rise to two quantifiable and assessable different motions: a linear one along the x axis, and a nonlinear one along the y axis. The oscillatory response along the y axis stands for the artificial network's component displaying the fourth spatial dimension.

The question is: why might scientist perform computations in four spatial dimensions, instead of the canonical three? How can real information be detected though a multidimensional apparatus? How much could neural computing profit from operations taking place in higher dimensions? The use of abstract mathematical language in multi-dimensions is justified if it helps to simplify our available techniques in neuroscience or design new applications (e.g., neurotechnology or neurodata tools). This might contribute to improve, for example, automatic classification of internal mental states during bistable perception (Sen et al. 2020), connectivity-based features of EEG signals for object recognition (Tafreshi et al. 2019), uncertainty removal in neural networks (Tozzi and Peters 2020). In Fig. 5, we provided an additional effort to simplify the very abstract concepts of high dimensional topology and to highlight their efficacy. We started from a three-dimensional network embedded in a convex manifold, where the quantum Hall effect is re-used for computational purposes (Fig. 5a). In operational terms, the network in Fig. 5a of specific oscillatory interactions in superlattices might be used also to assess more conventional neural network architectures, such as, e.g., manifolds representing electrophysiological thresholds of groups oscillating neurons already formulated in four dimensions

Author's personal copy

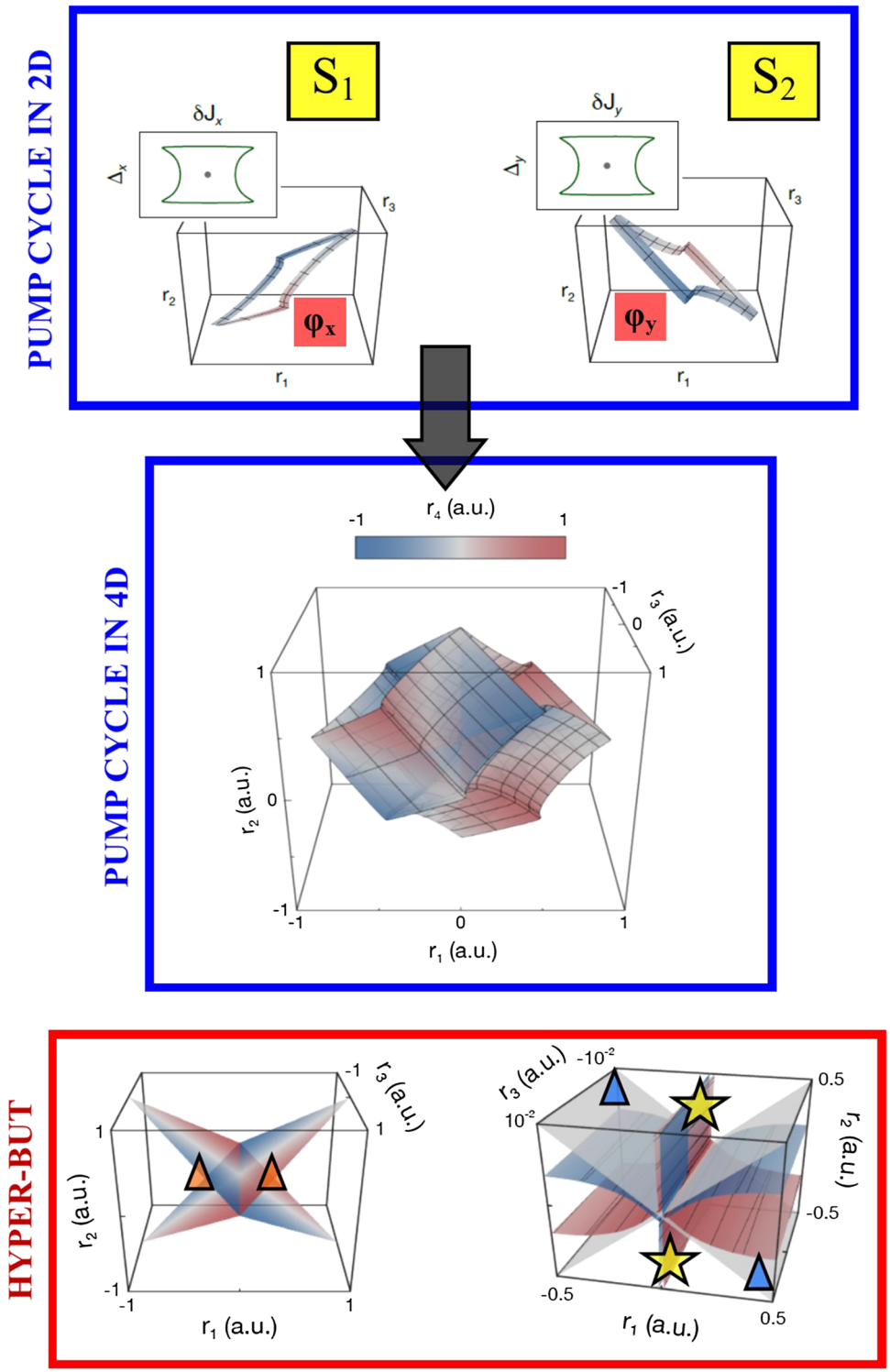

Fig. 4 Adiabatic pump cycle in different dimensions. Note that the paths in 2D give rise to a multifaceted manifold in 4D. The lower part of the Figure (embedded in a red square) illustrates how the Borsuk–Ulam theorem holds true for the 2D topological charge pump. Indeed, inside the transformed parameter space where singularities correspond to planes that touch at the origin, it is easy to detect several antipodal points with matching description (green and blue triangles, yellow stars). See Lohse et al. (2018) for further details and the legenda of the plots depicted here. (Color figure online)

(Izhikevich 2010), or spiking neural network models of mental imagery (Riley and Davies 2020), or neurocomputational models of semantic memory (Ursino et al. 2018). In our framework, fast and slow oscillations computing concepts of sets (e.g., union, intersection) may stand for both classes or operations in near set theory. The same equivalence rules hold between classical set-theory and neural networks (e.g., like the classical McCulloch-Pits models) and between near sets and fiber bundles in 4 spatial dimensions. Once achieved an output signal (a shape) in three dimensions (Fig. 5b), we projected it to a four-dimensional hypersphere (Fig. 5d). This approach

Author's personal copy

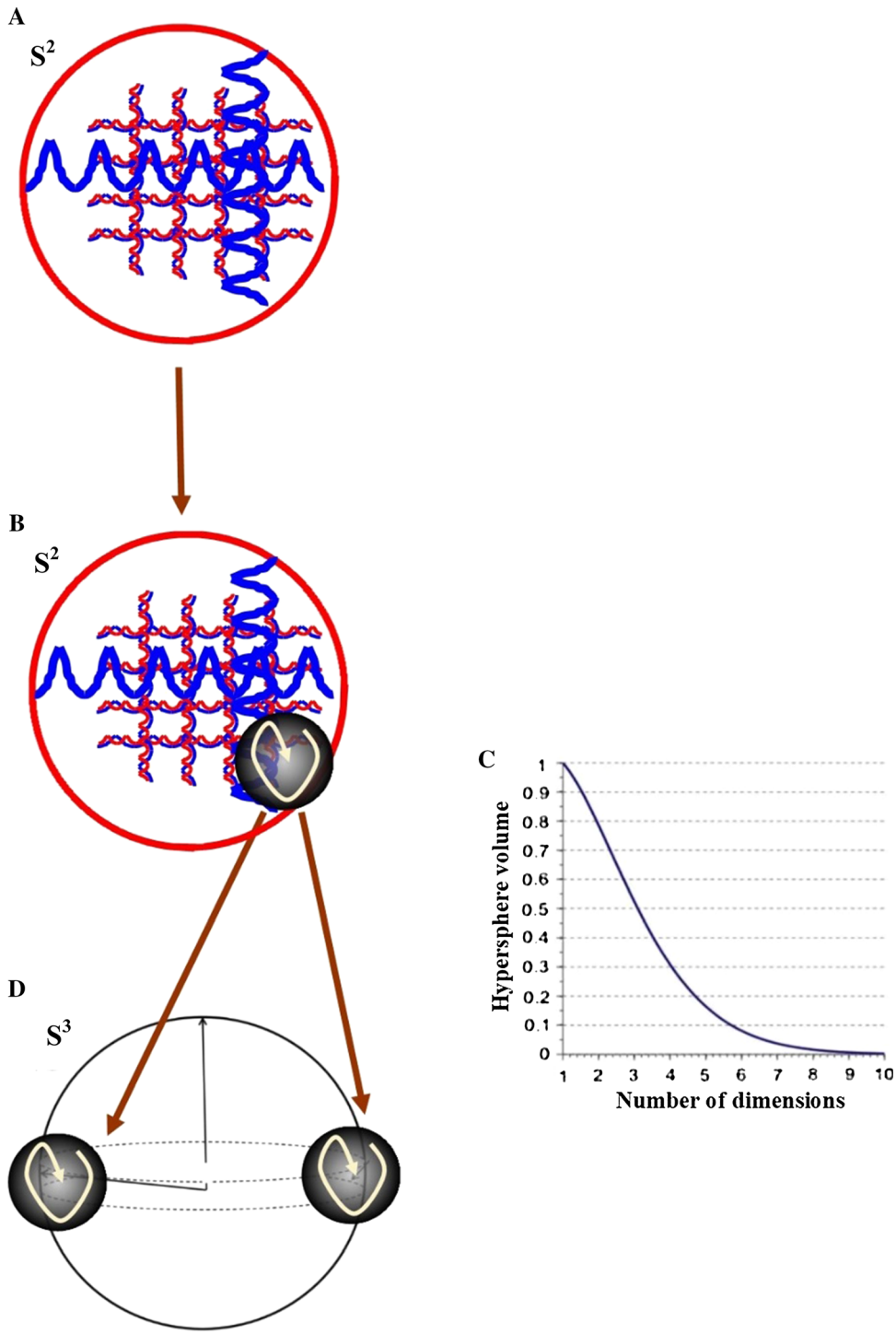

Fig. 5 A simplified sketch of the suggested four-dimensional network. The Quantum Hall effect explains how a high-level description of a neural network could detect very general forms of information from a SPATIAL fourth dimension. **a** Three dimensional appearance of neuro-oscillatory activity in a Quantum Hall effect context. Different waves in the neural network superimpose according the dictates of near sets symbols. An output (the shape in **b**) is produced in the three-dimensional manifold and is projected to a four-dimensional manifold in **d**, where, counterintuitively (**b**), a bigger amount of information can be stored in smaller amount of space

allows us to use projections and fiber bundles to make geometrical sense of extra "spatial" dimensions, so that we can move along an internal direction without carrying us away from the particular space–time point at which we are situated. This might explain fiber-independent coactivation of opposite fMRI activity, as suggested by Tozzi and Peters (2016a). In particular, when projecting qbits (a shape can be described in terms of qbits) from lower to higher dimensions, their number increases (Fig. 5d), due to the dictates of the recently-developed variants of the Borsuk–Ulam theorem (Tozzi and Peters 2019). The shape projection from three to four spatial dimensions allows us to achieve TWO shapes with matching description, because the mappings takes place one dimensions higher. This means that a four-dimensional quantum computer amplifies the message, but does not require increases in phase

Author's personal copy

space's volume: indeed, going in higher dimensions, the manifold volume does not increase, while the information does (Fig. 5c) (Tozzi and Peters 2019). In other words, the interaction among different waves produces a novel functional dimension, i.e., a higher dimensional phase space where computational operations take place more efficiently at the same energetic cost.

To provide a theoretical operational example, in a visual two-dimensional scene the presence of the shape causes a deformation in two-dimensional topological charge pumps. The resulting four-dimensional wave represents neurons firing in different sections of the brain (Don et al. 2020) and a corresponding computer's response to the introduction of object shape parameters (geometry, feature vectors) in its oscillatory lattice. Therefore, four-dimensional oscillation is the main feature that leads to multiple shape vectors, i.e., each four-dimensional oscillation results in a corresponding shape description. Further, shape feature vector components have the x and y axes that can be arranged in varying orientations according to different required shape reconstructions, making it possible to achieve an increase in discriminatory power and detectable features. The last, but not the least, different neuronal activities might exhibit different four-dimensional hidden components, that, once detected, could be experimentally assessed and quantified.

References

Ahmad MZ, Peters JF (2018) Descriptive unions. A fibre bundle characterization of the union of descriptively near sets, arXiv:1811.11129

Borsuk K (1957–1958) Concerning the classification of topological spaces from the standpoint of the theory of retracts. XLVI:177–190

Di Concilio A, Guadagni C, Peters JF, Ramanna S (2018) Descriptive proximities. Properties and interplay between classical proximities and overlap. Math Comput Sci 12(1):91–106. https://doi.org/10.1007/s11786-017.0328-y

Dmochowski JP, Ki JJ, DeGuzman P, Sajda P, Parra LC (2017) Extracting multidimensional stimulus-response correlations using hybrid encoding-decoding of neural activity. Neuroimage. https://doi.org/10.1016/j.neuroimage.2017.05.037

Don A, Peters JF, Ramanna S, Tozzi A (2020) Topological view of flows inside the BOLD spontaneous activity of the human brain. Front Comput Neurosci. https://doi.org/10.3389/fncom.2020.00034

Garcia JO, Ashourvan A, Muldoon SF, Vettel J, Bassett DS (2018) Applications of community detection techniques to brain graphs: algorithmic considerations and implications for neural function. Proc IEEE. https://doi.org/10.1109/jproc.2017.2786710

Hall E (1879) On a new action of the magnet on electric currents. Am J Math 2(3):287–292. https://doi.org/10.2307/2369245

Izhikevich EM (2010) Dynamical systems in neuroscience—the geometry of excitability and bursting. ISBN: 9780262514200

Kraus YE, Ringel Z, Zilberberg O (2013) Four-dimensional quantum Hall effect in a two-dimensional quasicrystal. Phys Rev Lett 111:226401

Lohse M, Schweizer C, Price HM, Zilberberg O, Bloch I (2018) Exploring 4D quantum Hall physics with a 2D topological charge pump. Nature 553:55–58. https://doi.org/10.1038/nature25000

Matoušek J (2003) Using the Borsuk–Ulam theorem. Lectures on topological methods in combinatorics and geometry. Springer, Berlin

Novoselov KS, Jiang Z, Zhang Y, Morozov SV, Stormer HL et al (2007) Room-temperature quantum Hall effect in graphene. Science 315(5817):1379

Peters JF (2007) Near sets. Special theory about nearness of objects. Fundam Inf 75(1–4):407–433

Peters JF (2014) Topology of digital images. Visual pattern discovery in proximity spaces. In: Intelligent systems reference library. Springer, Berlin, pp 1–342, vol 63. ISBN 978-3-642-53844-5. https://doi.org/10.1007/978-3-642-53845-2

Riley SN, Davies J (2020) A spiking neural network model of spatial and visual mental imagery. Cogn Neurodyn 14:239–251. https://doi.org/10.1007/s11571-019-09566-5

Sen S, Daimi SN, Watanabe K et al (2020) Switch or stay? Automatic classification of internal mental states in bistable perception. Cogn Neurodyn 14:95–113. https://doi.org/10.1007/s11571-019-09548-7

Tafreshi TF, Daliri MR, Ghodousi M (2019) Functional and effective connectivity based features of EEG signals for object recognition. Cogn Neurodyn 13:555–566. https://doi.org/10.1007/s11571-019-09556-7

Tozzi A (2019) The multidimensional brain. Phys Life Rev. https://doi.org/10.1016/j.plrev.2018.12.004 **(in press)**

Tozzi A, Peters JF (2016a) Towards a fourth spatial dimension of brain activity. Cogn Neurodyn 10(3):189–199. https://doi.org/10.1007/s11571-016-9379-z

Tozzi A, Peters JF (2016b) A topological approach unveils system invariances and broken symmetries in the brain. J Neurosci Res 94(5):351–365. https://doi.org/10.1002/jnr.23720

Tozzi A, Peters JF (2019) The Borsuk–Ulam theorem solves the curse of dimensionality: comment on "the unreasonable effectiveness of small neural ensembles in high-dimensional brain" by Alexander N. Gorban et al. Phys Life Rev. https://doi.org/10.1016/j.plrev.2019.04.008

Tozzi A, Peters JF (2020) Removing uncertainty in neural networks. Cogn Neurodyn. https://doi.org/10.1007/s11571-020-09574-w

Tozzi A, Peters JF, Fingelkurts AA, Fingelkurts AA, Marijuán PC (2017) Topodynamics of metastable brains. Phys Life Rev 21:1–20. https://doi.org/10.1016/j.plrev.2017.03.001

Ursino M, Cuppini C, Cappa SF et al (2018) A feature-based neurocomputational model of semantic memory. Cogn Neurodyn 12:525–547. https://doi.org/10.1007/s11571-018-9494-0

Zhang S-C, Hu J (2001) A four-dimensional generalization of the quantum Hall effect. Science 294:823–828

Zilberberg O, Huang S, Guglielmon J, Wang M, Chen KP et al (2018) Photonic topological boundary pumping as a probe of 4D quantum Hall physics. Nature 553(7686):59–62. https://doi.org/10.1038/nature25011

Publisher's Note Springer Nature remains neutral with regard to jurisdictional claims in published maps and institutional affiliations.

Cognitive Neurodynamics
https://doi.org/10.1007/s11571-021-09668-z

RESEARCH ARTICLE

Topology of eeg wave fronts

Arturo Tozzi[1] · Edward Bormashenko[2] · Norbert Jausovec[3]

Received: 24 June 2020 / Revised: 7 January 2021 / Accepted: 29 January 2021
© The Author(s), under exclusive licence to Springer Nature B.V. part of Springer Nature 2021

Abstract
Whenever one attempts to comb a hairy ball flat, there will always be at least one tuft of hair at one point on the ball. This seemingly worthless sentence is an informal description of the hairy ball theorem, an invaluable mathematical weapon that has been proven useful to describe a variety of physical/biological processes/phenomena in terms of topology, rather than classical cause/effect relationships. In this paper we will focus on the electrical brain field—electroencephalogram (EEG). As a starting point we consider the recently-raised observation that, when electromagnetic oscillations propagate with a spherical wave front, there must be at least one point of the tangential components of the vector fields where the electromagnetic field vanishes. We show how this description holds also for the electric waves produced by the brain and detectable by EEG. Once located these zero-points in EEG traces, we confirm that they are able to modify the electric wave fronts detectable in the brain. This sheds new light on the functional features of a nonlinear, metastable nervous system at the edge of chaos, based on the neuroscientific model of Operational Architectonics of brain-mind functioning. As an example of practical application of this theorem, we provide testable previsions, suggesting the proper location of transcranial magnetic stimulation's coils to improve the clinical outcomes of drug-resistant epilepsy.

Keywords Topology · Nervous activity · Poincaré–brouwer theorem · Electromagnetic · Epilepsy

Introduction

Spontaneous topological modifications in physical/biological systems may lead to novel functional features, indirectly dependent of exerted physical forces (Tozzi and Papo 2020). Here we consider one of the most intriguing theorems of algebraic topology, the "hairy ball" theorem (HBT, or Poincaré–Brouwer theorem), due to Poincaré (1885), later proved for even-dimensional spheres in 1912 by L.E.J. Bower, which states that there is no non-vanishing continuous tangent vector field on even-dimensional *n*-spheres (Brouwer 1912; Milnor 1978; Eisenberg and Guy 1979). A naïve description asserts that "given at least some wind on Earth, there must at all times be a cyclone or anticyclone somewhere". HBT ensures the presence of at least one point on the sphere where any continuous tangent vector field on the sphere must disappear. HBT relates several physical phenomena to non-local topological effects, rather than to local physics (Tozzi and Papo 2020; Bormashenko 2016). Indeed, HBT has been used to analyze nematic solid shells deformations (Modes and Warner 2012), nanoparticle chains growth (DeVries et al. 2007), flux line patterns occurring when a magnetic field is applied to a type-II superconducting crystal (Layer and Forgan 2010), patterns arising from dynamic surface—Marangoni-like-instabilities (Bormashenko 2015) and the spin-base invariant formalism of Dirac fermions (Gies and St 2015). Novel feasible applications of HBT have been recently suggested (Tozzi and Papo 2020) for the assessment of cell membrane surface tension, Uhlenbeck's singularity removal theorem (Uhlenbeck 1982; Tao and Tian 2004), dewetting transitions (Sharma and Reiter 1996; Li et al. 2019), unconventional superconductors (Laver and Forgan 2010), surface instabilities inherent for liquid/vapor

✉ Arturo Tozzi
arturo.tozzi@napoli2nord.it; tozziarturo@libero.it

Edward Bormashenko
edward@ariel.ac.il

1 Center for Nonlinear Science, Department of Physics, University of North Texas, 1155 Union Circle, #311427, Denton, TX 76203-5017, USA

2 Chemical Engineering Department, Engineering Faculty, Ariel University, P.O.B. 3, 407000 Ariel, Israel

3 Ruperce 46, 2229 Malecnik, Slovenia

Published online: 17 February 2021

Content courtesy of Springer Nature, terms of use apply. Rights reserved.

interfaces (Bormashenko 2015), non-Hermitian degeneracies (Miri and Alù 2019) which naturally arise in sparse neural networks (Amir et al. 2016). HBT describes the collective dynamics of particles in spherical crystals (Yao 2019): in particular, it predicts defect-driven synchronized breathing modes, emerging around disclinations related to disruption of crystalline order (Yao 2019). Furthermore, HBT zero-velocity points appear in numerous physical problems, including rolling of solid bodies (Bormashenko and Kazachkov 2017) and Leidenfrost droplets (Bormashenko 2019). Concerning singularities in rotating black holes, Chesler (2019) stated that "decayng fluxes… necessitate the existence of a null singularity at the Cauchy horizon". This claim suggests another unnoticed application of HBT.

Here we start from the recent observation that HBT is also able to describe electromagnetic waves propagation (Bormashenko 2016). When oscillations in a given medium display wave fronts topologically equivalent to a sphere, there must be at least one point of the wave front where electromagnetic fields' vectors, speed and Poynting vector equal zero. There exist certain so-called "dark directions", well-known to engineers designing antennas (Liang et al. 2013), devoid of energy transport (Chen et al. 2019) and unavoidable for electromagnetic fields generated by multipoles characterized by vector spherical harmonics (Chen et al. 2019). Here we make an effort to describe the restrictions imposed by HBT on the spatial distribution of vectors $\vec{E}$ in the propagating electric waves extracted from electroencephalogram (EEG) traces. Provided that the electric waves propagate spherically on the cerebral cortex, HBT dictates the occurrence of at least one point on the cortical surface at which vectors of the electric fields equal zero. In other words, when a continuous tangential velocity field exists on a surface homeomorphic to a ball, zero velocity points will be necessarily present at the surface. We show how this observation has major implications for the assessment of brain metastability, as well as for clinical applications: for example, the search for target zones for the use of transcranial magnetic stimulation (TMS).

Materials and methods

Hairy ball theorem and wave fronts propagation in physical systems

The "hairy ball" theorem suggests that, given a ball with hairs all over it, it is impossible to comb the hairs so that all the hairs lay flat. Some hair must be sticking straight up (Su 2021). Instead of hairs, consider propagation of electromagnetic fields, when the wave front (i.e. the surface of the constant phase) displays a shape that is topologically equivalent to a sphere (i.e., the surface is characterized by the Euler number $\chi = 2$). In this case, the vectors of the electric $\vec{E}$ and magnetic $\vec{H}$ fields form continuous tangential fields (Fig. 1a). HBT demands that the tangential component of the continuous vector field, defined on the surface topologically equivalent to a sphere, will be zero in at least one point located on the surface. For further details, see Liang et al. 2013, Bormashenko 2016, Chen et al. 2019. Therefore, according to HBT, both $\vec{E}$ and $\vec{H}$ have at least one point where fields are zero. When both the fields simultaneously equal zero in the same point, we achieve $\vec{E} = 0$, $\vec{H} = 0$, due to the equivalence $\vec{H} = \hat{n} \times \vec{E}$, where $\hat{n}$ is the unit vector normal to the wave front. In the same point, the Poynting vector $\vec{S} = \frac{c}{4\pi}\vec{E} \times \vec{H}$ equals zero too. Because the group velocity of electromagnetic wave in this direction is zero, no transport of energy in the direction normal to the wave front in this point is possible and the "dark direction" is formed, whatever the physical source field could be (Liang et al. 2013, Chen et al. 2019). To provide an example, consider the hypothetical field (either electromagnetic or hydrodynamic, and so on) in Fig. 1b, where the wave progression of the vectors displays a positive-curvature front. According to the HBT dictates, a point with zero value must exist on the wave front (Fig. 1c), which causes a local perturbation of the field and leads to wave front deformation (Fig. 1d).

The vector field in principle may be normal to the surface in this point. Apparently it is impossible for the vectors of the electric and magnetic field to be normal to the surface of the constant phase (in other words parallel to the wave vector), due to the transverse nature of the electromagnetic field. It is noteworthy that the vectors of electric and magnetic fields will possess a zero point placed on the wave front at any given time, if the surface of the constant phase keeps the shape topologically equivalent to a sphere. It is also worth to be underlined that HBT holds not just for spherical manifolds, but also for every manifold with positive-curvature, provided its genus is zero. For example, Cummins et al. (2018) analyzed the motion of wind dispersed plants, reporting a vortex of recirculating air, which is detaching owing the flow passing through the pappus (Fig. 1e). The occurrence of stagnation points (in this case two instead of one) can be noticed where the air velocity at the vortex surface is zero. The dandelion example suggests that the manifold does not need necessarily to be a sphere: HBT just requires that such manifold should be topologically equivalent to a sphere. This observation will have important implications in the following.

Content courtesy of Springer Nature, terms of use apply. Rights reserved.

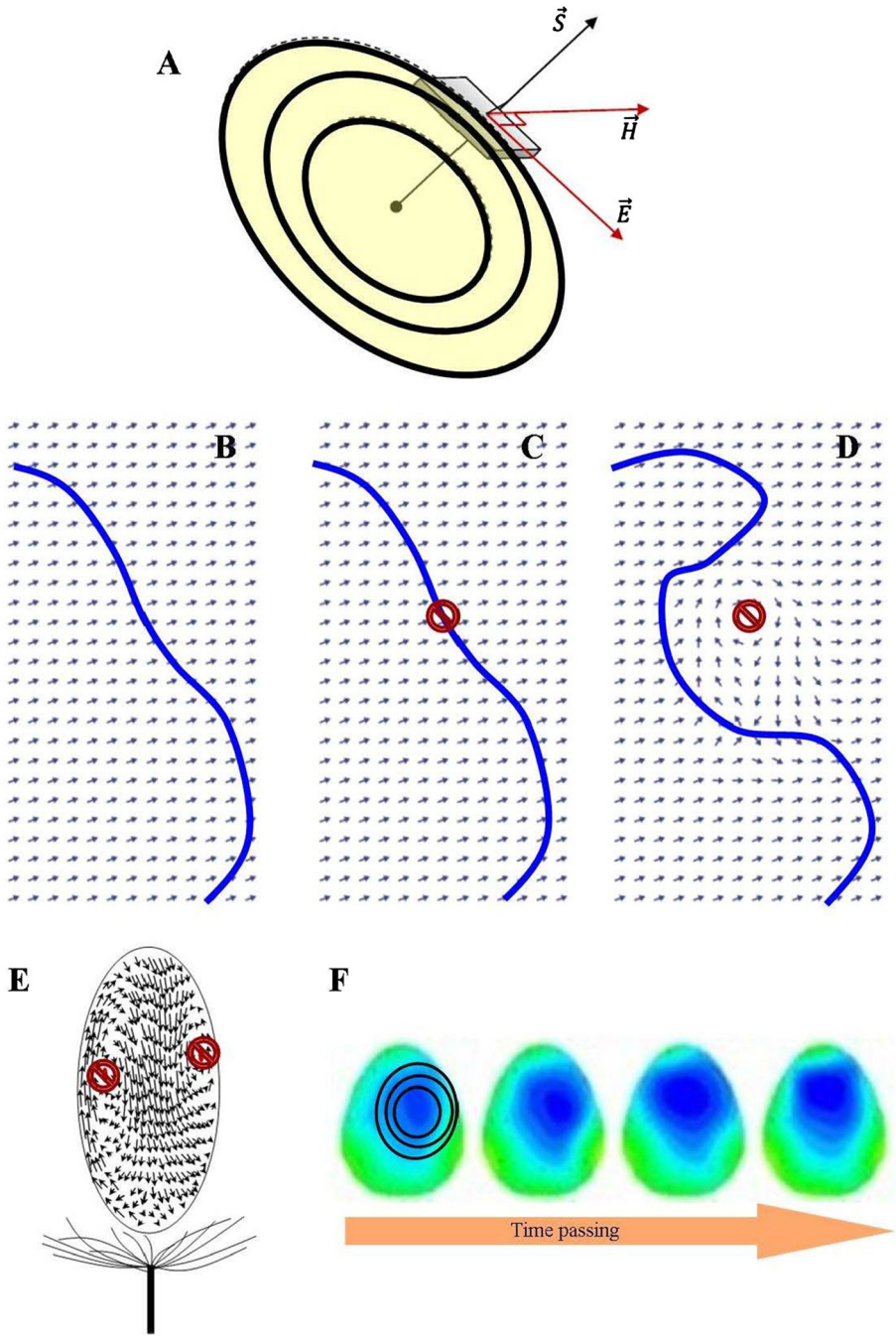

Fig. 1 Schematic illustration of pattern propagation of oscillations in physical systems, including the brain. **a** Propagating electromagnetic wave. $\vec{S}$ stands for the Poynting vector. Note that the concentric patterns of electric propagation give rise to a wave front with a surface topologically equivalent to a sphere. Modified from Bormashenko (2016). **b–d**. Simulation of a hypothetical world sheet in spacetime depicting a generic flow equipped with a positive-curvature wave front (modified from Beekman 2011). When the wave front proceeds (1b), the occurrence of the tangential components of vectors (1c) leads to modifications in vectors trajectories and, consequently, to distortions in the wave front (1d). In this simulation, the vanishing point of the wave front predicted by HBT is illustrated by a prohibition sign. **e**. Sketch of dandelion and the vortexes it generates. The arrows illustrate the field of velocities at the vortex surface. The two prohibition signs depict the stagnation points dictated by HBT. Modified from Cummins et al. (2018). **f**. The concentric, positive-curvature patterns typical of electromagnetic fields can be also found when examining the electric waves' temporal propagation in two-dimensional EEG traces

Looking for HBT in nervous electric waves

In the sequel, we provide an effort to use HBT to analyze the EEG electric activity of the brain. We choose to focus on the ELECTRIC $\vec{E}_{\text{field}}$ of the brain, rather than the MAGNETIC field $\vec{H}$, because the former is more powerful and easier to detect through simple EEG techniques. Indeed, the circular patterns and wave fronts of electric waves propagation can be easily identified in real EEG traces. This is in touch with the recently-described novel mechanism for large-scale coordination in the human brain: traveling waves of theta and alpha oscillations (Zhang et al. 2018). The authors found contiguous clusters of cortex with oscillations at specific frequencies within 2–15 Hz, displaying spatial phase gradients. Further, Zhang et al. (2018) also suggested that the direction of this wave propagation correlated with the spatial orientation of local frequency gradients. EEG traces do encompass electric waves with sphere-like wave fronts (Fig. 1f). The requirement of spherical currents is satisfied when we analyze brain electric activity: indeed, the shape of flux

Content courtesy of Springer Nature, terms of use apply. Rights reserved.

surfaces that contains current lines is closed and orientable in the brain, so that it is homeomorphic to a sphere S^2. Since the electric field in the brain is nowhere vanishing and tangent to the surface, HBT rules out the possibility to describe nervous oscillations as taking place on a sphere. Also, the "dark directions" can be predicted for the electric field generated by brain, when the field appears on the cortical surface topologically equivalent to a sphere.

According to HBT, the circular propagation of concentric electric waves must display zero-points on their wave fronts. It is worth to be emphasized that only "tangential" components of vector fields become zero on the surfaces topologically equivalent to a sphere. Further, when electric waves propagate from a given brain area, the wave front must necessarily be locally perturbed by these zero-points. For the purpose of this study to assess whether and how HBT permits a novel description of electric fields' propagation in the brain, we analyzed EEG traces of three subjects that were presented emotional visual stimuli, according to the procedure described by Jaušovec and Jaušovec (2010). The emotional stimuli were color slides selected from the International Affective Pictures System (Lang et al. 2005) according to the valence dimension: emotionally positive (valence ratings from 7.2 to 8.2), neutral (valence ratings from 4.4 to 6.2), and negative (valence ratings from 1.3 to 2.0). The discrimination of picture categories occurred during passive viewing and was internally driven—the respondents were not asked to make any judgments or motor responses. EEG was recorded using a Quick-Cap with sintered (Silver/Silver Chloride; 8 mm diameter) electrodes. Using the Ten-twenty Electrode Placement System of the International Federation, the EEG activity was monitored over nineteen scalp locations (Fp1, Fp2, F3, F4, F7, F8, T3,T4, T5, T6, C3, C4, P3, P4, O1, O2, Fz, Cz and Pz) during the visual task. ll leads were referenced to linked mastoids (A1 and A2), and a ground electrode was applied to the forehead. Additionally, vertical eye movements were recorded with electrodes placed above and below the left eye. The digital EEG data acquisition and analysis system (SynAmps) had a bandpass of 0.15–100.0 Hz. At cutoff frequencies, the voltage gain was approximately—6 dB. The 19 EEG traces of the three subjects were digitized online at 1000 Hz with a gain of 1000 (resolution of 084 μV/bit in a 16 bit A to D conversion), and stored on a hard disk. Epochs were automatically screened for artifacts. All epochs showing amplitudes above ± 50 microV (less than 3%) were excluded, to avoid that the traces could be artifacts of the visualizing algorithm while plotting the EEG power maps. The EEG study was done according with Declaration of Helsinki and was approved by the Ethics Committee of the University of Maribor, Slovenia.

To practically identify the occurrence of zero-points of electric activity in the real EEG traces, we evaluated two different plots: a) the raw data, i.e., a table displaying the electric values in μV in every cortical area for every time in ms; 2) a 2-D temporal reconstruction of EEG waves. We evaluated the changes in electric activity occurring in the first 500 ms after the presentation of emotional stimuli.

Results

According to our topological approach, the concentric wave fronts of EEG electric activity can be assessed in terms of HBT. When EEG traces display zero values in some areas at a given time, predictable changes in electric wave fronts must occur elsewhere. Looking at the table of EEGs raw data from the three subjects presented with visual stimuli, we detected the occurrence of about 15–20 zero-points/500 ms, with different electrode scalp locations and different timing (Fig. 2). We did not find a predictable path in both timing and location of the newly-formed zero-points.

To compare the occurrence of zero-points in raw data with the modifications of electric wave fronts, we examined the corresponding EEG 2D temporal plots from the three subjects (Fig. 3a). A spatio-temporal correlation can be found between the sudden occurrence of zero-points and the subsequent onset of warped wave fronts. Indeed, almost ubiquitously, the occurrence of a zero-point is followed with a delay of 20–30 ms by the formation of a wave front in areas far apart the zero-points. See Fig. 3b for further details.

In particular, in Fig. 3a, the 14 detected zero-points were followed by the above-described, predictable electric wave front pattern in 13/14 (92.85%) cases.

Therefore, the occurrence of zero-points is able to modify the circular propagation of electric waves and to give rise to deformations of the wave fronts. In the case of the electric activity of the brain during visual stimulation, the occurrence of wave front modifications can be visually predicted when examining the location and the timing of the zero-points in the EEG two-dimensional plots.

Discussion

Starting from the observation that HBT constraints the vectors' spatial distribution of electric and magnetic fields in the far Fraunhofer region (Bormashenko 2016), we used this simple theorem from algebraic topology to describe the electric activity (EEG) of the brain. Indeed, the vectors of electric fields are equipped at least with one zero point placed on the wave front at any given time, when the wave

Content courtesy of Springer Nature, terms of use apply. Rights reserved.

	[FP1]	[FP2]	[F3]	[F4]	[C3]	[C4]	[P3]	[P4]	[O1]	[O2]	[F7]	[F8]	[T3]	[T4]	[T5]	[T6]	[CZ]	[FZ]	[PZ]
0 ms	-5,8992	0,0882	-11,8091	-6,9042	-12,1666	-20,875	-20,7427	-8,5803	-8,6899	-2,656	-5,7335	-2,5231	-7,9839	0,0896	-12,0214	4,8835	-16,5696	-11,6985	-15,2734
10	6,5155	11,7284	6,3929	9,2941	2,6449	5,4186	-6,6799	-2,8306	-10,02	-7,9681	5,3751	13,6067	3,8574	16,129	-0,2671	7,4584	1,7913	5,6693	-4,6995
20	14,3517	12,7866	13,141	14,3395	13,6654	19,3649	10,7229	5,9266	-4,7883	-6,6401	7,8835	13,9671	11,303	16,4875	11,398	5,8602	14,9575	12,9584	12,4718
30	13,9996	13,0511	12,697	13,5428	18,9553	19,276	23,5553	7,0765	-0,798	-7,4369	13,1691	14,2374	16,3265	11,2903	19,3232	3,9068	18,8983	11,6085	22,3226
40	-1,6729	0,3527	-0,444	2,3899	10,1389	6,8399	15,557	8,2264	2,1281	1,328	-0,4479	-1,8022	8,7015	4,8387	13,4461	8,6127	6,9861	-1,2598	11,8391
50	-4,0502	-5,5556	-6,3041	-5,3994	-2,5568	-5,6851	2,2852	4,5113	8,0692	10,9783	0,4479	-6,7583	-2,9603	-15,5018	3,4728	5,061	-6,807	-8,189	-0,5423
60	1,2327	0,0882	-3,2852	-3,9832	-5,2017	-8,6165	-4,922	3,4498	7,8031	9,0305	-2,4188	-0,7209	-0,5382	0,1792	-1,3357	5,061	-8,867	-5,4893	-5,1514
70	3,5219	-1,1464	-6,8368	-4,1602	-19,3079	-21,1415	-23,9068	-15,126	-7,7145	-1,9478	-1,3438	-1,2615	-9,3294	-3,853	-12,8228	-0,3552	-24,8097	-9,8988	-27,2933
80	-3,3458	-9,2593	-7,8135	-14,0739	-13,3128	-35,3542	-17,3149	-21,2295	-2,9262	-4,1611	-2,2396	-6,2176	-2,3324	-9,5878	-1,5138	-9,8557	-26,5114	-17,0979	-28,3778
90	-6,6916	-17,284	-10,9212	-22,6599	-10,3152	-28,9585	-6,5041	-10,3494	0,532	-5,5777	-4,0314	-17,5715	1,2559	-12,5448	5,699	-9,0566	-22,7497	-21,5973	-13,2851
100	-1,6729	-7,1429	-1,3319	-6,8157	7,3176	-1,8654	15,9086	6,015	9,0446	0,0885	5,2856	-3,6044	11,9309	-4,7491	16,4737	0	-3,4035	-9,9888	9,3086
110	4,6665	2,1164	0,0888	1,3277	12,8719	7,0175	22,3248	9,5533	12,5914	1,328	8,1523	3,8747	12,4692	7,5269	21,4604	-0,6215	7,8818	-2,1597	17,5328
120	0,5283	-0,97	-4,3507	-3,2751	2,1159	4,175	7,7346	9,0226	0,532	4,4267	2,1501	-4,055	6,9971	1,7025	7,8362	4,5283	-1,1644	-5,8493	6,1455
130	-9,5091	-5,291	-8,0799	-3,3636	-2,8212	6,5734	2,7247	11,1455	1,2414	6,9057	-2,7772	0,0885	1,4353	4,9283	6,7676	8,7014	-4,6574	-8,279	3,1631
140	-0,4402	4,2328	-5,3274	6,1075	1,7633	12,9691	8,5256	13,7992	11,616	11,0668	-1,6125	7,5693	2,5118	-0,8065	9,35	12,8746	-0,5374	-1,2598	6,507
150	1,761	4,7619	-2,9301	2,4784	3,7029	6,9287	6,0646	7,6957	10,9953	4,7809	-2,3292	1,9824	2,0632	3,3154	7,3909	1,687	2,1496	0,6299	5,3321
160	-4,1382	0,4409	-3,9068	-4,3372	-5,8188	-13,8574	-1,3184	-7,9611	4,9656	-1,6822	-5,2856	-2,8835	-1,3456	-6,362	4,0962	-9,8557	-10,8374	-7,1091	-8,1338
170	-2,1131	3,6155	-4,9723	3,2751	1,058	-4,3527	9,4045	-1,2384	15,5176	6,1974	-12,3628	6,3077	-1,7941	5,6452	11,309	0,444	0,1791	0,18	3,615
180	-1,1446	-4,5855	-7,5472	-9,1171	-1,1461	-10,5707	3,5157	-11,4993	2,7488	-6,8172	-4,4793	-7,3891	4,575	-11,0215	6,5895	-11,2764	-8,6879	-10,0787	-3,8861
190	-0,9685	-3,2628	-0,7991	-5,842	3,7029	-2,7537	5,5372	-2,0345	4,1676	-1,8592	6,7189	-3,0638	8,1633	5,3763	6,0552	-3,6404	-2,8661	-4,6794	1,8979
200	4,4904	0,5291	-8,1687	-8,6745	-2,2923	-3,2867	2,5489	0	2,8375	-0,4427	-2,7772	-3,4242	4,0368	-3,3154	2,5824	-9,5893	-9,0461	-8,6389	1,7171
210	0,7924	-3,8801	-5,505	-8,2319	-3,2621	-4,4415	4,0431	1,5922	5,143	-0,4427	5,196	-7,1187	3,1397	-5,1971	5,4319	-0,2664	-13,8827	-9,1789	-0,0904
220	-2,7295	-5,5556	-5,4162	-8,8515	-5,1135	-8,0835	1,7579	-3,8036	7,1824	-0,8853	-2,9563	-13,3363	2,2427	-15,681	7,2128	-8,6127	-11,9122	-7,4691	-5,3321
230	-6,0753	-8,7302	-13,3185	-12,7462	-13,8417	-14,5681	-4,6583	-1,5922	5,143	5,2236	-3,8522	-10,633	-5,3824	-3,853	0,089	-2,3085	-14,8679	-15,1181	-5,4225
240	-11,8864	-15,5203	-22,1976	-22,8369	-25,6557	-16,8776	-8,7014	-4,069	3,7242	7,1713	-17,8275	-19,0133	-16,5956	-6,0932	-7,2128	-0,9767	-22,2123	-23,847	-10,4835
250	-19,6346	-20,194	-25,394	-28,2363	-26,7137	-22,1186	-5,1857	-9,9956	5,675	1,6822	-18,813	-22,2573	-14,6221	-12,8136	-3,5619	-3,5516	-29,1984	-30,8661	-13,1948
260	-11,2701	-10,6702	-14,2064	-15,0476	-8,5519	-13,8574	3,252	-2,4768	12,9461	8,3223	-14,8712	-11,0836	-4,0368	-8,3333	4,8976	1,687	-16,5696	-16,4679	-5,784
270	-2,2012	-7,7601	-8,2575	-11,0644	2,2923	-6,6622	6,3283	-0,3538	12,5028	4,9579	-6,9877	-13,7869	3,8574	-12,9032	8,6376	1,7758	-9,6731	-10,5287	-1,2653
280	-1,761	-4,9383	-4,7947	-5,7535	11,7258	3,4644	15,6449	11,9416	19,3305	15,9363	-4,5689	-5,7671	8,0736	3,0466	16,2956	3,5516	1,7017	-6,2992	9,6701
290	-1,5849	-2,1164	-2,131	-3,0095	9,698	6,3069	11,2503	14,7722	15,5176	10,5356	-7,8835	-3,244	4,8441	1,4337	11,5761	3,5516	0,8957	-3,7795	6,6878
300	16,2888	12,8748	9,1454	15,1361	17,8973	19,0095	18,6333	22,5564	18,7985	12,6605	3,4938	12,0748	6,9971	11,4695	12,9118	10,9212	15,1366	12,6884	19,521
310	20,8673	16,7548	13,2297	15,4016	14,2826	11,5479	16,1723	13,18	14,8969	6,6401	3,9418	12,4352	10,4956	4,3011	12,4666	5,7714	10,2105	14,0382	13,5563
320	16,4649	14,8148	6,6593	12,9232	-2,2041	-1,5989	4,131	3,7152	4,0789	2,0363	6,6271	10,9935	-1,9735	-4,4803	2,6714	3,818	-3,8513	9,1789	0,8134
330	20,1629	17,0194	5,7714	11,507	-16,0458	0	-2,9005	2,9191	2,2168	-1,9478	0,9854	11,8946	-5,203	6,1828	-2,7605	4,3507	-6,0009	8,279	-1,5364
340	16,4649	14,6384	2,4861	9,7367	-7,9348	5,0633	0,791	1,2384	4,0789	-6,286	2,0605	11,7143	-1,1662	7,6165	4,5414	0,2664	-8,1505	3,8695	-3,3439
350	6,6916	8,1129	-1,7758	3,6291	0,3527	2,1319	3,252	-0,1769	3,0149	-6,9057	-3,8522	2,7934	2,7809	3,4946	5,699	-0,8879	-9,2253	-0,27	-3,7054
360	9,245	6,7019	1,2431	3,5406	7,7584	5,0633	12,6566	3,2729	11,084	-0,6197	5,5543	5,677	8,9706	4,2115	14,9599	6,3041	-5,1948	-2,0697	3,8861
370	9,5091	3,2628	0,1776	-2,8325	6,3478	-6,3957	9,844	-6,5458	8,3352	-6,8172	1,3438	-0,5407	6,1	5,0179	13,268	-1,687	-7,7026	-4,9494	-0,5423
380	11,4462	6,7019	4,2619	-1,1507	9,1691	-2,9314	8,5256	-5,7497	5,941	-3,6299	16,4838	3,7846	9,8677	2,5986	11,4871	-1,5094	-1,3435	-3,7795	0,2711
390	7,9243	2,7337	-1,5094	-5,3994	4,7609	-9,5936	6,3283	-6,2804	8,8672	-2,3904	2,0605	-2,0725	5,3824	-4,3907	9,1719	-5,505	-6,18	-9,5388	-2,169
400	3,8741	-2,4691	-2,3973	-7,7893	-0,1763	-16,5223	3,8673	-7,2534	8,2465	-2,1248	0	-2,6132	3,8574	-3,5842	8,9047	1,4206	-10,2105	-10,8886	-4,6995
410	5,9872	-1,2346	0,6215	-6,7272	-6,8768	-15,9005	2,461	-8,4034	7,0051	-3,8955	5,3751	-4,7759	1,9735	-6,8996	7,6581	-5,4162	-12,8974	-7,919	-6,5974
420	2,3773	-2,5573	-4,6171	-5,9305	-4,4964	-8,883	5,8888	-5,5728	7,0938	0,4427	1,523	-7,1187	0,1794	-6,7204	9,7952	-3,2852	-11,9122	-6,8391	-3,8861
430	5,3709	0,6173	-3,2852	-9,3826	4,32	-6,0404	11,9534	-3,9805	12,5914	-1,7707	-0,4479	-10,5429	4,7544	-7,1685	13,6242	0	-9,4044	-7,649	1,0845
440	6,3394	-0,7055	1,2431	-5,1339	4,7609	-5,4186	7,9982	-5,3958	5,7637	-4,2497	-7,0773	-2,9736	4,575	-5,4659	11,4871	-2,131	-5,6426	-2,6997	-2,0786
450	17,3454	2,7337	6,2153	2,921	3,8792	-1,066	2,461	-7,0765	2,3941	-7,5255	11,1982	-0,811	2,8706	-0,7168	5,0757	-1,1543	-1,2539	5,2193	-5,5129
460	16,2888	10,0529	6,0377	7,7893	5,8188	8,4388	0,0879	-1,3268	1,0641	-5,0465	4,748	4,3253	1,8838	2,3297	2,4043	7,5472	4,747	9,5388	-4,338
470	9,4211	7,3192	4,2619	3,7176	-2,0278	0,6218	-5,0978	-2,6537	-3,2809	-2,8331	0	4,4154	-2,8706	14,6057	-0,6233	10,9212	-4,8365	3,4196	-8,4953
480	4,0502	-0,6173	-8,3463	-8,586	-11,285	-15,4564	-3,4278	-10,1725	-1,5074	-6,5516	1,2542	-4,2352	-5,0235	-0,1792	2,0481	-3,6404	-16,7488	-9,5388	-12,291
490	-8,4526	-15,4321	-16,515	-25,3153	-21,6002	-25,8494	-8,5256	-14,7722	-5,143	-7,8796	-9,4961	-19,8243	-13,9045	-11,2903	-2,2262	-6,1265	-29,5567	-24,027	-17,8039
	[FP1]	[FP2]	[F3]	[F4]	[C3]	[C4]	[P3]	[P4]	[O1]	[O2]	[F7]	[F8]	[T3]	[T4]	[T5]	[T6]	[CZ]	[FZ]	[PZ]

Fig. 2 Raw data from EEG activity in a subject who underwent emotional stimuli. The results are plotted as electric activity (in μV) across different brain areas vs time locations (in ms). The red squares illustrate the electrode location and the timing of the electric activity almost equaling zero μV

front's shape is topologically equivalent to a sphere. In this study, we showed that zero-points can be reliably identified in EEG signals and that they give rise to predictable wave fronts of electric diffusion. In what follows we will place our findings in the context of brain-mind research, as well as provide an illustrative example for a clinical application.

Brain-mind research and HBT

Here we argue that a physical and biological phenomenon such as chaotic dynamics in the brain can be accounted for in terms of a purely topological mechanism (Tozzi and Peters 2017; Zhao et al. 2020). One of the most promising theoretical neural frameworks is the general theory of brain-mind operational architectonics (OA) (Fingelkurts and Fingelkurts 2004). According to OA, the simplest mental/cognitive operations are correlated with local 3D-fields produced by transient functional neuronal assemblies, while complex mental/cognitive operations are produced by joining a number of simple operations (temporal coupling of local 3D-fields by means of *operational synchrony*, OS) in form of metastable *operational modules* (OM) of varied life-span. Nested OA displays a peculiar brain *operational space–time* (OST) (Fig. 4b) that is best

Content courtesy of Springer Nature, terms of use apply. Rights reserved.

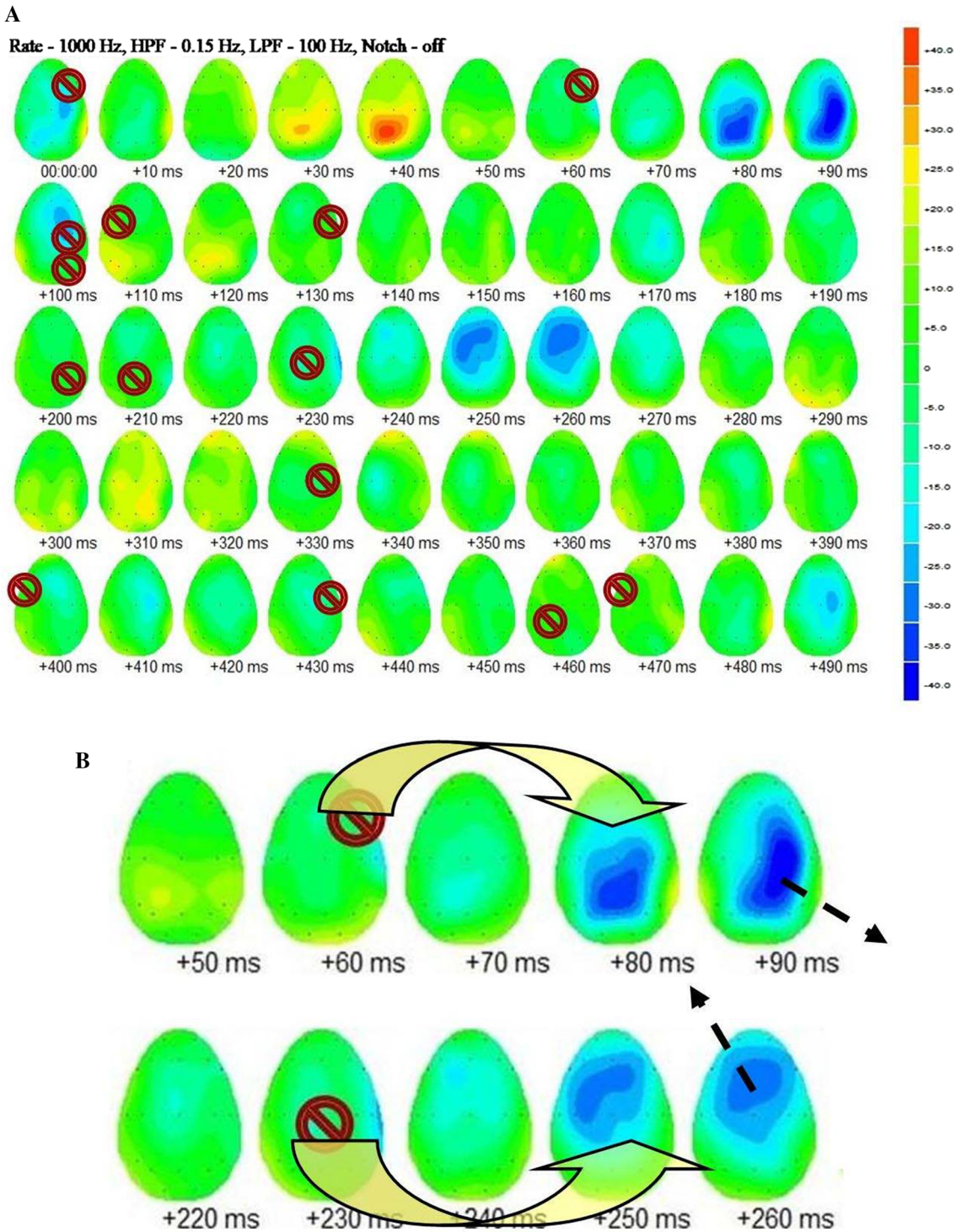

Fig. 3 The role of HBT in modifying the electric activity of the brain in a subject presented with visual stimuli. The prohibition signs illustrate the points where electric zero-values occur in the first 500 ms after the stimuli. Note the occurrence of wave fronts, depicted as concentric increases or decreases of cool and warm colors. Figure 3b. Magnification of two short frames from the Fig. 3a. When the vanishing zero-points (prohibition signs) appear in a given area, concentric wave fronts (blue concentric areas) arise in different areas after about 20–30 ms (curved arrows) and tend to propagate in a direction opposite to the zero-points (straight dotted arrows). Therefore, the occurrence of vanishing zero-points allows to predict the rise and the progression of the ensuing electric wave front

Content courtesy of Springer Nature, terms of use apply. Rights reserved.

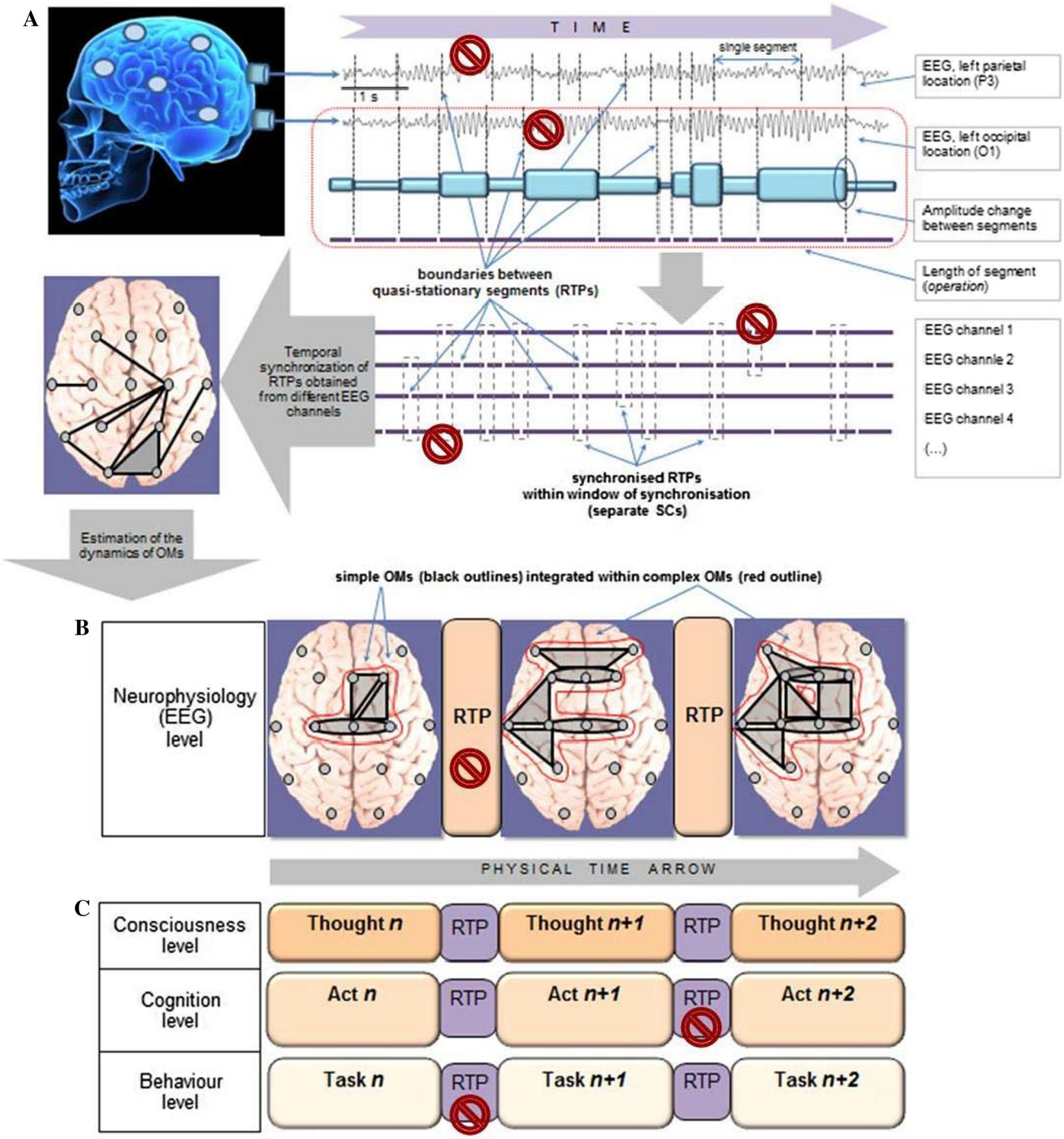

Fig. 4 Schematic illustration of the Operational Architectonics methodology and possible relation to HBT. All RTPs should be HBT zero-points: here, for sake of simplicity, just a few HBT zero-points are illustrated (prohibition signs). It must be reminded, however, that all RTPs should be HBT zero-points. **a–c**. Schematic illustration of EEG assessment of (a) neuronal assembly's dynamics and relation of this dynamics to simple operations and (b) nested large-scale conglomerates of synchronized neuronal assemblies in the form of nested operational modules (OMs) and (c) their relation to a stream of complex operations or cognitive/conscious acts. RTP–rapid transitional period (boundary between quasi-stationary EEG segments within the same local EEG signal); SC–synchrocomplex—momentary synchronization of RTPs among several local EEG signals within short temporal window of synchronization; Gray shapes illustrate individual (simple)OMs; Red line illustrates complex OMs. Figure 4c schematically depicts the functional structures of phenomenological consciousness, cognition and behavior functionally isomorphic with the structure of electrophysiological level. Cognitive, phenomenological, and behavioral levels illustrate the ever-changing stream of cognitive/phenomenal/behavioral acts, where each momentarily stable pattern is a particular cognitive/phenomenal/behavioral macro-operation (thought/image/act) separated by transitive fringes (RTPs). This figure is modified from Tozzi et al. (2017)

Content courtesy of Springer Nature, terms of use apply. Rights reserved.

captured by EEG measurement (Fingelkurts and Fingelkurts 2017). At the EEG level, simple mental operations (phenomenal qualities, emotions, and so on) are equivalent to the EEG quasi-stationary segments, within which the local fields generated by transient functional neuronal assemblies are expressed. The quasi-stationary EEG segments within each local EEG signal are marked by boundaries in the form of *rapid transitional processes/periods* (RTPs) (Fig. 4a), i.e., abrupt EEG amplitude changes observed within a short-time window. We suggest that RTPs could be correlated with the occurrence of HBT zero-points. Indeed, in comparison to the length of quasi-stationary segments, each RTP has a very short duration and can therefore be treated as a point, i.e., the HBT zero-point of our topological approach. Furthermore, the number of RTPs fits well with the number of HBT zero points: the number of RPTs per each minute local-EEG (at least during restful wakefulness with closed eyes) is about 61–351, depending on the frequency range, with a progressive increase from delta to gamma frequency range (Fingelkurts and Fingelkurts 2015; Fingelkurts and Fingelkurts 2019). In turn, the RTP range of temporal durations is produced on timescales corresponding to 100–900 ms range, while the occurrence of zero-points is followed by changes in electric wave fronts after 20–30 ms.

The transition from one segment to another reflects the moment of abrupt switching from one neuronal assembly's operation to another (Fig. 2a). The events similar to RTPs are referred to as renewal (or critical) events: namely, the crucial events that reset the memory of the system. This property is correlated with the physical phenomenon of "intermittency" and is compatible with self-organized criticality found both in physical systems and in the brain. Since the beginning and the end of discrete operations performed by local neuronal assemblies are marked by sharp changes (RTPs) in the amplitude of local EEG signals, the simultaneous occurrence of such RTPs from different local EEG signals within the multichannel EEG recording could provide evidence of synchronization of simple operations performed by neuronal assemblies (located in different brain areas) that participate in the same functional act as a group (Fig. 4b), e.g., executing a particular complex operation responsible for a subjective presentation of complex objects, scenes or thoughts. HBT can be correlated with the general theory of brain-mind OA, that considers the brain as a metastable system (Fingelkurts and Fingelkurts 2004, 2017): in HBT terms, the complex mental operations (reflected in the transitory spatiotemporal EEG patterns formed by synchronized quasi-stationary segments separated by the RTPs) could be correlated with the HBT-related electric zero-points that give rise to RTPs (Fig. 3c).

In sum, the general theory of brain-mind operational architectonics implies that the EEG encompasses HBT zero-points. These zero-points provide a topological explanation for the crucial events that reset the memory of the metastable brain activity and that explain both simpler and more sophisticated mental operations.

A clinical application of HTB

Once established the occurrence of events dictated by HBT, the next question is: has this observation testable applications? Can we use topology to improve our therapeutic options against human neurological diseases? Below we illustrate one of the potential clinical applications of HBT. Let us consider the case of epilepsy. The occurrence of points where brain oscillations vanish provides us with a novel way to use transcranial magnetic stimulation (TMS), a focal electrical brain stimulation induced by powerful magnetic fields (Yu et al. 2013; Chung et al. 2019; Kohli and Casson 2019). Low frequency repetitive rTMS (0.3–1 Hz) decreases cortical excitability, suggesting a potential therapeutic advantage for patients with drug-resistant epilepsy (Jan et al. 2017; Gersner et al. 2016). Chen et al. (2016) retrospectively analyzed the evidence for the efficacy of TMS in drug-resistant epilepsy, evaluating studies that used rTMS of any frequency, duration, intensity and setup (focal or vertex treatment). Excruciatingly, the evidence for efficacy of rTMS for reduction in seizure rate/frequency is still lacking, due to the extreme variability in outcome reporting (Jan et al. 2017). There is still no agreement on optimized stimulation parameters and patterns of rTMS for epilepsy, because TMS effects vary across individuals and depend on a large number of factors: frequency, number of stimuli within a train, stimulation intensity, type of coil, coil position, duration of stimulation, and inter-train interval.

In this uncertain context, an HBT approach to epileptic seizures suggests that the area of onset of pathological spikes might be characterized by an impaired amount of topologically vanishing points: in particular, it might be hypothesized an increase in number of zero points (Fig. 5a). The occurrence of vanishing points gives us the possibility to draw a testable prevision: to achieve the best therapeutic effect in epilepsy, rTMS treatments must use not solid, coherent beams, rather hollow magnetic beams, i.e., cylindrical beams with internal cavities devoid of magnetic stream. Indeed, the use of cylindrical hollow beams is suggested by HBT-related topology: when a sphere with genus zero becomes a torus (i.e., a manifold with genus equal or higher than one), HBT no longer holds. To provide an example, the Fig. 5b, left side, illustrates the rotation of a rigid ball around a fixed axis OO_1: it is easy to see that O and O_1 are zero velocity points, in touch with

Content courtesy of Springer Nature, terms of use apply. Rights reserved.

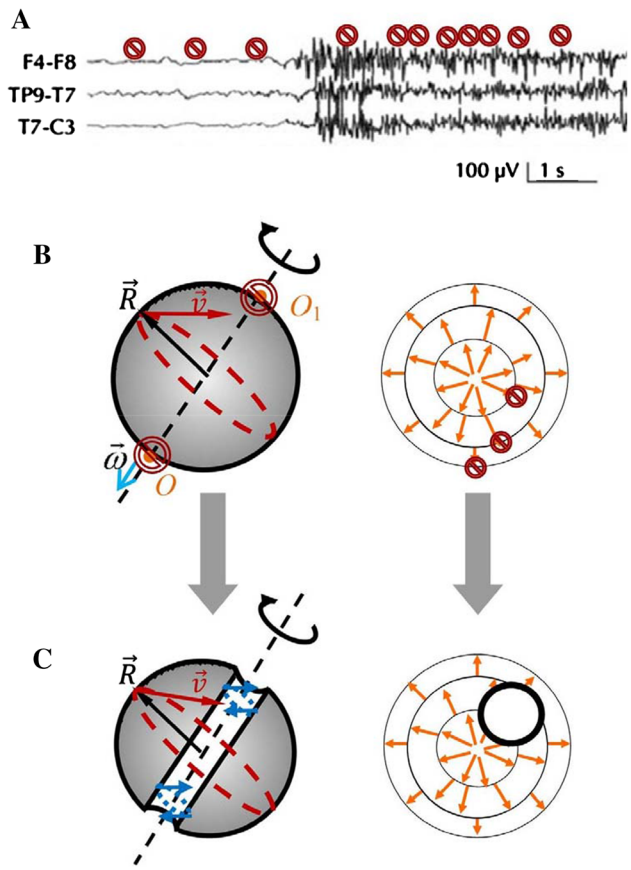

Fig. 5 **a** Recorded surface EEG (displayed in a bipolar transverse montage) showing a left parietal EEG seizure onset. Modified from: Beleza et al. (2010). The number of vanishing points (prohibition signs) is depicted as increasing after the seizure onset. **b**. Rotation of a rigid ball (left) compared with an electric concentric wave front (right). In both cases, the occurrence of zero-points (prohibition signs) is required by HBT. Modified from: Bormashenko and Kazachkov (2017). **c**. The occurrence of a torus removes the zero-points in both the rigid ball and the electric wave front. See text for further details

HBT's dictates. In turn, the zero velocity points disappear when the ball is drilled completely through, because HBT does not hold anymore in case of a manifold being a torus with genus one (Fig. 5c, left side). The same holds for the circular wave fronts of the brain electric activity (Fig. 5b–c, right side): in rTMS, terms, the hollow beam corresponds to the production of a torus inside the circular wave front (Fig. 5c, right side). In case of a manifold with genus one artificially provoked by rTMS's external waves, HBT does not hold anymore: this means that the normal electric activity of the brain with impaired zero-points can be restored. In a HBT account, epilepsy can be compared to Marangoni-like instabilities: the pathological zero-points are modified by rTMS-mediated forces, reversing the unwanted seizure oscillations and restoring the normal cortical function.

In sum, a topological approach based on HBT suggests that the pathological effects of epileptic wave fronts might be restored by using an unconventional type of transcranial magnetic stimulation.

To sum up, clear-cut topological theorems, such as, e.g., the Borsuk-Ulam theorem described by Tozzi et al. (2017), can be used to make sense of experimentally observed neuroscientific phenomena. Here we discussed the implications of HBT-correlated zero-valued points in nervous dynamical systems, describing how mathematical-related events, such as vector modifications, generate changes in brain features that comply with strict topological requirements.

References

Amir A, Hatano N, Nelson DR (2016) Non-Hermitian localization in biological networks. Phys Rev E 93:042310. https://doi.org/10.1103/PhysRevE.93.042310

Beekman AJ (2011) Vortex duality in higher dimensions. Casimir PhD series. urn:isbn:9789085931133

Beleza P, Rémi J, Feddersen B, Peraud A, Noachtar S (2010) Epidural and foramen-ovale electrodes in the diagnostic evaluation of patients considered for epilepsy surgery. Epileptic Disord 12(1):48–53. https://doi.org/10.1684/epd.2010.0297

Bormashenko E (2015) Surface instabilities and patterning at liquid/vapor interfaces: Exemplifications of the "hairy ball theorem. Coll Interf Sci Commun 5:5–7. https://doi.org/10.1016/j.colcom.2015.04.003

Bormashenko E (2016) Obstructions imposed by the poincaré-brouwer (hairy ball) theorem on the propagation of electromagnetic waves. J Electromagnet Waves Appl. https://doi.org/10.1080/09205071.2016.1169226

Bormashenko E (2019) Motion of the liquid on the surface of Leidenfrost droplets and the hairy ball theorem. Surf Innov 7(2):101–103

Bormashenko E, Kazachkov A (2017) Rotating and rolling rigid bodies and the "hairy ball" theorem. Am J Phys 85:447

Brouwer LEJ (1912) Über abbildung von mannigfaltigkeiten. Math Ann 71:97–115

Chen R, Spencer DC, Weston J, Nolan SJ (2016) Transcranial magnetic stimulation for the treatment of epilepsy. Cochrane Database Syst Rev. https://doi.org/10.1002/14651858.CD011025.pub2

Chen W, Chen Y, Liu W (2019) Singularities and poincaré indices of electromagnetic multipoles. Phys Rev Lett 122:153907

Chesler PM (2019) Singularities in rotating black holes coupled to a massless scalar field. arXiv:1905.04613

Chung SW, Sullivan C, Rogasch NC, Hoy KE, Bailey NW et al (2019) The effects of individualised intermittent theta burst stimulation in the prefrontal cortex: a TMS-EEG study. Hum Brain Mapp 40(2):608–627. https://doi.org/10.1002/hbm.24398

Court JH, Raven J (1995) Manual for Raven's progressive matrices and vocabulary scales. Section 7: research and references: summaries of normative, reliability, and validity studies and references to all sections. Oxford, England: Oxford Psychologists Press/San Antonio, TX: The Psychological Corporation

Cummins C, Seale M, Macente A, Certini D, Mastropaolo E et al (2018) A separated vortex ring underlies the flight of the dandelion. Nature 562(7727):414–418. https://doi.org/10.1038/s41586-018-0604-2

Content courtesy of Springer Nature, terms of use apply. Rights reserved.

DeVries GA, Brunnbauer HY, Jackson AM, Long B, Neltner BT et al (2007) Divalent metal nanoparticles. Science 315(5810):358–361

Eisenberg M, Guy R (1979) A proof of the hairy ball theorem. Am Math Mon 86(7):571–574. https://doi.org/10.2307/2320587

Fingelkurts AA, Fingelkurts AA (2004) Making complexity simpler: multivariability and metastability in the brain. Int J Neurosci 114:843–862. https://doi.org/10.1080/00207450490450046

Fingelkurts AA, Fingelkurts AA (2015) Operational architectonics methodology for EEG analysis: theory and results. Neuromethods 91:1–59. https://doi.org/10.1007/7657_2013_60

Fingelkurts AA, Fingelkurts AA (2017) Information flow in the brain: ordered sequences of metastable states. Information. https://doi.org/10.3390/info8010022

Fingelkurts AA, Fingelkurts AA (2019) Placing pure experience of eastern tradition into the neurophysiology of Western tradition. Cogn Neurodyn 13:121–123

Gersner R, Oberman L, Sanchez MJ, Chiriboga N, Kaye HL et al (2016) H-coil repetitive transcranial magnetic stimulation for treatment of temporal lobe epilepsy: a case report. Epilepsy Behav Case Rep 2016(5):52–56. https://doi.org/10.1016/j.ebcr.2016.03.001

Gies H, St L (2015) Global surpluses of spin-base invariant fermions. Phys Lett B 743:415–419

Jan MM, Alsallum MS, Sadler MR (2017) Transcranial magnetic stimulation and epilepsy. Int J Med Sci Clin Invent 4(10):3256–3260. https://doi.org/10.18535/ijmsci/v4i10.07ICV2015:52.82

Jaušovec N, Jaušovec K (2010) Emotional intelligence and gender: a neurophysiological perspective. In: Gruszka A, Matthews G, Szymura B (eds) Handbook of individual differences in cognition. Springer, New York, pp 109–126

Kohli S, Casson A (2019) Machine learning validation of EEG+tACS artefact removal. J Neural Eng. https://doi.org/10.1088/1741-2552/ab58a3

Lang PJ, Bradley MM, Cuthbert BN (2005) International affective picture system (IAPS): Affective ratings of pictures and instructional manual. Technical report A-6. Bainesville, FL. University of Florida

Layer M, Forgan EM (2010) Magnetic flux lines in type-II superconductors and the "hairy ball theorem." Nature Comm 1:45

Li J, Ha NS, Liu TL, van Dam RM, Kim C-J (2019) Ionic-surfactant-mediated electro-dewetting for digital microfluidics. Nature 572:507–510

Liang L, Hum SV (2013) A low-profile antenna with quasi-isotropic pattern for UHF RFID applications. IEEE Antennas Wirel Propag Lett 12:210–213

Milnor J (1978) Analytic proofs of the "hairy ball"theorem, and the Brouwerfixed point theorem. Am Math Mon 85(7):521–524

Miri M-A, Alù A (2019) Exceptional points in optics and photonics. Science. https://doi.org/10.1126/science.aar7709

Modes CD, Warner M (2012) Responsive nematic solid shells: topology, compatibility and shape. EPL 2012(97):36007

Poincaré H (1885) Sur les courbes définies par le èquations différentielle. J Math Pures et Appl 4(1):167–244

Sharmaa A, Reiterb G (1996) Instability of thin polymer films on coated substrates: rupture, dewetting, and drop formation. J Coll Interf Sci 178:383–399

Su FE. 2021. Hairy ball theorem. https://math.hmc.edu/funfacts/hairy-ball-theorem/

Tao T, Tian G (2004) A singularity removal theorem for Yang-Mills fields in higher dimensions. J Amer Math Soc 17(3):557–593

Tozzi A, Papo D (2020) Projective mechanisms subtending real world phenomena wipe away cause effect relationships. Prog Biophys Mol Biol 151:1–13. https://doi.org/10.1016/j.pbiomolbio.2019.12.002

Tozzi A, Peters JF (2017) From abstract topology to real thermodynamic brain activity. Cogn Neurodyn 11(3):283–292. https://doi.org/10.1007/s11571-017-9431-7

Tozzi A, Peters JF, Fingelkurts AA, Fingelkurts AA, Marijuán PC (2017) Topodynamics of metastable brains. Phys Life Rev 21:1–20. https://doi.org/10.1016/j.plrev.2017.03.001

Uhlenbeck K (1982) Connections with L^p bounds on curvature. Comm Math Phys 83(1):31–42

Yao Z (2019) Command of collective dynamics by topological defects in spherical crystals. Phys Rev Lett 122:228002

Yu K, Wang J, Deng B, Wei X (2013) Synchronization of neuron population subject to steady DC electric field induced by magnetic stimulation. Cogn Neurodyn 7:237–252

Zhang H, Watrous A1, Patel A, Jacobs J (2018) Theta and Alpha Oscillations Are Traveling Waves in the Human Neocortex. Neuron 98(6):1269-1281.e4. https://doi.org/10.1016/j.neuron.2018.05.019

Zhao J, Qin Y, Che Y, Ran H, Li J (2020) Effects of network topologies on stochastic resonance in feedforward neural network. Cogn Neurodyn 14:399–409

Publisher's Note Springer Nature remains neutral with regard to jurisdictional claims in published maps and institutional affiliations.

Content courtesy of Springer Nature, terms of use apply. Rights reserved.

Terms and Conditions

Springer Nature journal content, brought to you courtesy of Springer Nature Customer Service Center GmbH ("Springer Nature").

Springer Nature supports a reasonable amount of sharing of research papers by authors, subscribers and authorised users ("Users"), for small-scale personal, non-commercial use provided that all copyright, trade and service marks and other proprietary notices are maintained. By accessing, sharing, receiving or otherwise using the Springer Nature journal content you agree to these terms of use ("Terms"). For these purposes, Springer Nature considers academic use (by researchers and students) to be non-commercial.

These Terms are supplementary and will apply in addition to any applicable website terms and conditions, a relevant site licence or a personal subscription. These Terms will prevail over any conflict or ambiguity with regards to the relevant terms, a site licence or a personal subscription (to the extent of the conflict or ambiguity only). For Creative Commons-licensed articles, the terms of the Creative Commons license used will apply.

We collect and use personal data to provide access to the Springer Nature journal content. We may also use these personal data internally within ResearchGate and Springer Nature and as agreed share it, in an anonymised way, for purposes of tracking, analysis and reporting. We will not otherwise disclose your personal data outside the ResearchGate or the Springer Nature group of companies unless we have your permission as detailed in the Privacy Policy.

While Users may use the Springer Nature journal content for small scale, personal non-commercial use, it is important to note that Users may not:

1. use such content for the purpose of providing other users with access on a regular or large scale basis or as a means to circumvent access control;
2. use such content where to do so would be considered a criminal or statutory offence in any jurisdiction, or gives rise to civil liability, or is otherwise unlawful;
3. falsely or misleadingly imply or suggest endorsement, approval , sponsorship, or association unless explicitly agreed to by Springer Nature in writing;
4. use bots or other automated methods to access the content or redirect messages
5. override any security feature or exclusionary protocol; or
6. share the content in order to create substitute for Springer Nature products or services or a systematic database of Springer Nature journal content.

In line with the restriction against commercial use, Springer Nature does not permit the creation of a product or service that creates revenue, royalties, rent or income from our content or its inclusion as part of a paid for service or for other commercial gain. Springer Nature journal content cannot be used for inter-library loans and librarians may not upload Springer Nature journal content on a large scale into their, or any other, institutional repository.

These terms of use are reviewed regularly and may be amended at any time. Springer Nature is not obligated to publish any information or content on this website and may remove it or features or functionality at our sole discretion, at any time with or without notice. Springer Nature may revoke this licence to you at any time and remove access to any copies of the Springer Nature journal content which have been saved.

To the fullest extent permitted by law, Springer Nature makes no warranties, representations or guarantees to Users, either express or implied with respect to the Springer nature journal content and all parties disclaim and waive any implied warranties or warranties imposed by law, including merchantability or fitness for any particular purpose.

Please note that these rights do not automatically extend to content, data or other material published by Springer Nature that may be licensed from third parties.

If you would like to use or distribute our Springer Nature journal content to a wider audience or on a regular basis or in any other manner not expressly permitted by these Terms, please contact Springer Nature at

onlineservice@springernature.com

biophysica

MDPI

Article

Nervous Activity of the Brain in Five Dimensions

Arturo Tozzi [1,*], James F. Peters [2,3], Norbert Jausovec [4], Arjuna P. H. Don [5], Sheela Ramanna [6], Irina Legchenkova [7] and Edward Bormashenko [7]

1 Center for Nonlinear Science, Department of Physics, University of North Texas, Denton, TX 76203, USA
2 Department of Electrical and Computer Engineering, University of Manitoba, 75A Chancellor's Circle, Winnipeg, MB R3T 5V6, Canada; James.Peters3@umanitoba.ca
3 Department of Mathematics, Faculty of Arts and Sciences, Adıyaman University, 02040 Adıyaman, Turkey
4 Ruperce 46, 2229 Malecnik, Slovenia; norbertjausovec@gmail.com
5 Computational Intelligence Laboratory, University of Manitoba, Winnipeg, MB R3T 2N2, Canada; pilippua@myumanitoba.ca
6 Applied Computer Science, University of Winnipeg, Winnipeg, MB R3B 2E9, Canada; s.ramanna@uwinnipeg.ca
7 Chemical Engineering Department, Engineering Faculty, Ariel University, P.O. Box 3, Ariel 407000, Israel; ilegchenkova@gmail.com (I.L.); edward@ariel.ac.il (E.B.)
* Correspondence: tozziarturo@libero.it

Abstract: The nervous activity of the brain takes place in higher-dimensional functional spaces. It has been proposed that the brain might be equipped with phase spaces characterized by four spatial dimensions plus time, instead of the classical three plus time. This suggests that global visualization methods for exploiting four-dimensional maps of three-dimensional experimental data sets might be used in neuroscience. We asked whether it is feasible to describe the four-dimensional trajectories (plus time) of two-dimensional (plus time) electroencephalographic traces (EEG). We made use of quaternion orthographic projections to map to the surface of four-dimensional hyperspheres EEG signal patches treated with Fourier analysis. Once achieved the proper quaternion maps, we show that this multi-dimensional procedure brings undoubted benefits. The treatment of EEG traces with Fourier analysis allows the investigation the scale-free activity of the brain in terms of trajectories on hyperspheres and quaternionic networks. Repetitive spatial and temporal patterns undetectable in three dimensions (plus time) are easily enlightened in four dimensions (plus time). Further, a quaternionic approach makes it feasible to identify spatially far apart and temporally distant periodic trajectories with the same features, such as, e.g., the same oscillatory frequency or amplitude. This leads to an incisive operational assessment of global or broken symmetries, domains of attraction inside three-dimensional projections and matching descriptions between the apparently random paths hidden in the very structure of nervous fractal signals.

Keywords: higher dimensions; brain; neurodata; Fourier analysis; fractal

check for updates

Citation: Tozzi, A.; Peters, J.F.; Jausovec, N.; Don, A.P.H.; Ramanna, S.; Legchenkova, I.; Bormashenko, E. Nervous Activity of the Brain in Five Dimensions. *Biophysica* **2021**, *1*, 38–47. https://doi.org/10.3390/biophysica1010004

Received: 11 January 2021
Accepted: 18 February 2021
Published: 22 February 2021

Publisher's Note: MDPI stays neutral with regard to jurisdictional claims in published maps and institutional affiliations.

Copyright: © 2021 by the authors. Licensee MDPI, Basel, Switzerland. This article is an open access article distributed under the terms and conditions of the Creative Commons Attribution (CC BY) license (https://creativecommons.org/licenses/by/4.0/).

1. Introduction

The activity of the nervous system takes place in dimensions higher than the conventional spatial three plus time. This counterintuitive claim has been put forward in terms of multidimensional approaches such as simplicial complexes encompassing synaptic connections [1], neural codes for navigating cognition [2], and rhythm and synchrony in cortical network models [3]. For a review, see Tozzi [4]. Karl Friston [5] highlighted how "invariances or symmetries afforded by projections onto high dimensional spaces... may not reveal themselves through local scrutiny of the surface data acquired from the brain in action, but may require . . . " the use of high-dimensional manifolds. Higher-dimensional nervous trajectories have been located in phase spaces consisting of genus-zero hypersphere S^3 or genus-one Clifford torus [6]. It has been suggested that brain functions such as mind-wandering and memory retrieval could be explained by the functional occurrence

of imperceptible further spatial dimensions [7]. Here we ask, starting from the standard neurodata available in three dimensions plus time, does there exist an operational procedure to assess the corresponding four-dimensional trajectories? Is it feasible to assess in higher dimensions the three-dimensional paths detected during customary data collection? We describe here a viable option, i.e., the projection of three-dimensional data achieved from real experimental series to a four-dimensional hypersphere. In particular, we aim to map electroencephalographic (EEG) oscillations to an S^3 hypersphere or, in other words, to achieve orthographic projections of brain signal patches via quaternions.

The development of quaternions, first proposed by Hamilton [8], has been quite slow, due to the painstaking issue of the non-commutativity of quaternion multiplicity [9]. In recent years, technical improvements to avoid non-commutativity have made quaternions feasible to explore quantum mechanics, attitude control, computer graphics, and robust image hashing [10,11]. Quaternions have been also useful in neural network research and modeling patterns of EEG signals. Quaternion-based signal analysis techniques have been used to extract features related to motor imagery in various mental states, granting signals classification in decision trees, in support vector machine and in k-nearest neighbor techniques [12]. Li and Wang [13] assessed drive-response synchronization for quaternion-valued shunting inhibitory cellular neural networks with mixed delays: the occurrence of almost periodic solutions, achieved through the Banach fixed point theorem, led to novel state-feedback controllers that ensured global exponential synchronization. The last, but not the least, a novel quaternion-valued singular spectrum analysis for EEG multichannel analysis has been introduced to solve the excruciating problem of noise in extracted sources [14]. In this paper, we explore the possibility to use global visualization methods for exploiting quaternion maps of EEG traces. We describe how a quaternionic description of brain activity provides many operational benefits apart from the assessment of the multidimensional brain activity. We describe how these operational benefits greatly improve the extraction of useful information from neurodata.

2. Materials and Methods

We provided a methodological effort to map two- and three-dimensional EEG oscillations extracted from real neurodata to four-dimensional S^3 hyperspheres. We used four-dimensional quaternions to represent orthographic projections of brain signals' images onto the manageable surface of a three-dimensional sphere.

2.1. EEG Traces

We analyzed EEG traces of subjects at rest. EEG was recorded using a Quick-Cap with sintered (silver/silver chloride; 8 mm diameter) electrodes. Using the Ten-twenty Electrode Placement System of the International Federation, the EEG activity was monitored over 19 scalp locations (Fp1, Fp2, F3, F4, F7, F8, T3, T4, T5, T6, C3, C4, P3, P4, O1, O2, Fz, Cz, and Pz). ll leads were referenced to linked mastoids (A1 and A2), and a ground electrode was applied to the forehead. Additionally, vertical eye movements were recorded with electrodes placed above and below the left eye. The digital EEG data acquisition and analysis system (SynAmps) had a bandpass of 0.15–100.0 Hz. At cutoff frequencies, the voltage gain was approximately -6 dB. The 19 EEG traces were digitized online at 1000 Hz with a gain of 1000 (resolution of 084 μV/bit in a 16 bit A to D conversion) and stored on a hard disk. Epochs were automatically screened for artifacts. All epochs showing amplitudes above ± 50 microV (less than 3%) were excluded, to avoid that the traces could be artifacts of the visualizing algorithm while plotting the EEG power maps. The EEG study was done according with Declaration of Helsinki and was approved by the Ethics Committee of the University of Maribor, Slovenia.

The traces assessed in this study were extracted from three scalp areas, corresponding to the central electrodes Cz, Fz, and Pz. We choose these vertex locations because they are known to display the lowest occurrence of extra-cerebral artifacts.

2.2. Quaternion Maps

A vast assortment of feasible quaternion-driven variants and higher-dimensional visual representation strategies is available, resulting in the technical achievement of very intricate quaternion maps. The two most widely used classes of quaternion visualization are based on: (a) visual geometric context and (b) parallel coordinates [15]. In this paper, we favor the more manageable geometric view. Since the mathematical procedures have been thoroughly described, in this paper, we choose a plain approach for non-technical readers. The website https://quaternions.online/provides an introduction to three-dimensional quaternion graphics. See also, for an affordable treatment of quaternions, Hart (2014) [16].

In the EEG trace illustrated in Figure 1A, every single point of the plot (amplitude versus time) can be described by three vectors, each lying on a different spatial coordinate x, y, or z (depicted in Figure 1A as green, red, and blue arrows, respectively). We will term these three vectors "triad." In the case of the two-dimensional EEG plots, we assume that one of the three coordinates equals zero. Figure 1B illustrates a triad of vectors (standing for a single point of the EEG plot) embedded in a cubic manifold. Further, the quaternion trajectories of a triad of vectors can be depicted as arcs moving inside a three-dimensional spheric frame encompassing the axes x, y, and z (Figure 1C). The movements of the arc are dictated by the constraints of the axis rotation and the Euler angle (Hart, 2014) [16]. All the single triads from EEG traces can be projected to a hyperspheric manifold, either using punctiform (Figure 1D) or uniform orthographic projections.

The multidimensional concept of "n-sphere" is crucial to grasp the concept of quaternions. A n-sphere is a n-dimensional structure embedded in n + 1 spaces termed n + 1 balls [17]. To make an example, a circumference (1-dimensional sphere) surrounds a cd-rom (2-dimensional ball), while a plastic surface (2-dimensional sphere) surrounds a beach ball (3-dimensional ball). A 3-sphere (also called glome or hypersphere) is a 3-dimensional elliptic surface embedded in a 4-dimensional ball. In other words, a glome is an object with positive curvature in a Euclidean 4-dimensional space, formed by all the points at constant distance from a fixed central point [18]. It is noteworthy that three-dimensional data, such as, e.g., different activated cortical areas in fMRI pictures, can be approached in terms of circular trajectories on 3-spheres. The use of hyperspheres in data analysis and data mining displays several advantages, since information extrapolated from three-dimensional manifolds can be visualized by a single mathematical structure, the glome. See Figure 2 for further details.

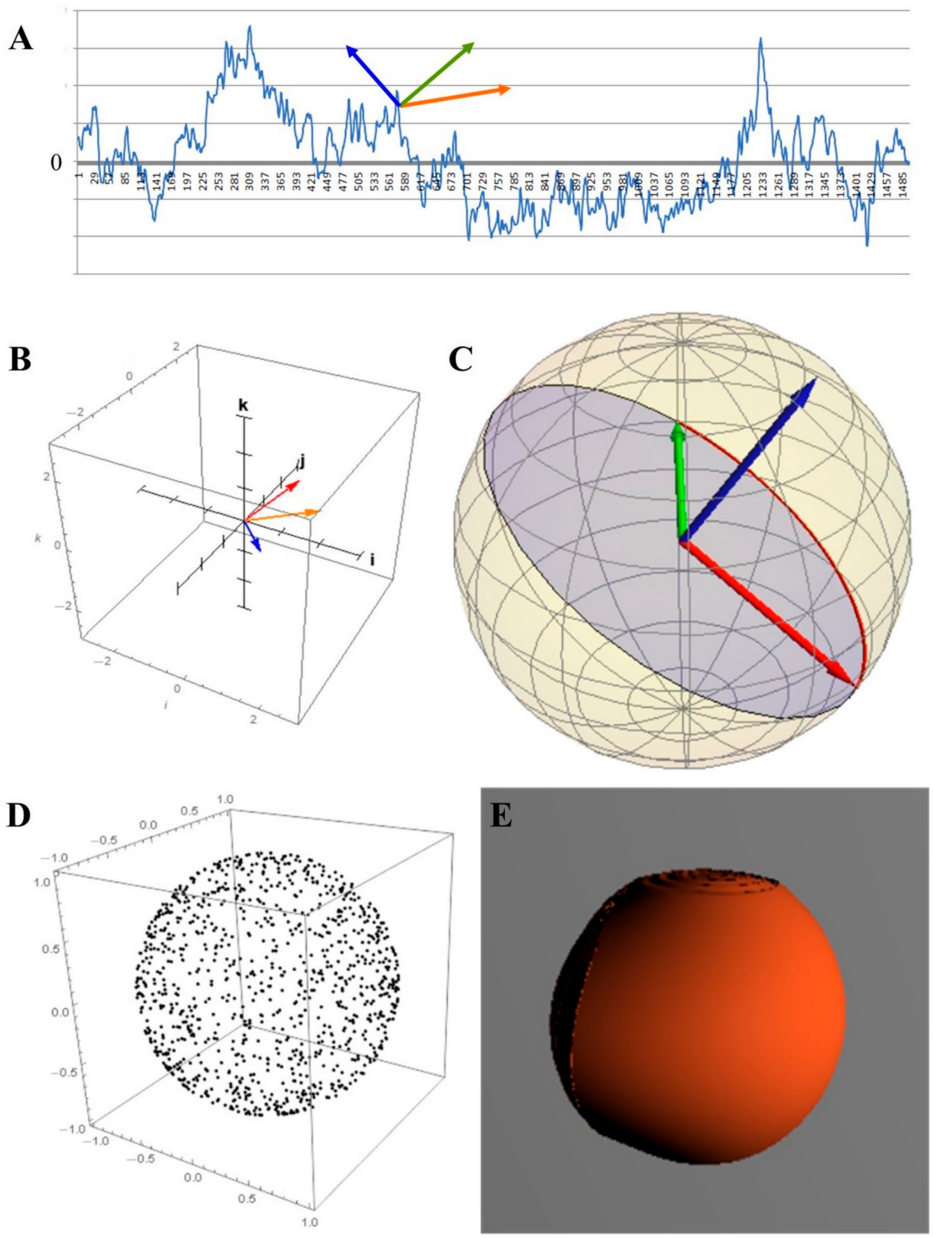

Figure 1. Quaternion mappings of a three-dimensional electroencephalographic traces (EEG) wave to a four-dimensional hypersphere. (**A**). EEG oscillations mean detected from the three central electrodes Cz, Fz, and Pz. The plot displays time in milliseconds (axis x) versus amplitude in mV (axis y). The three vectors standing for a single point of the plot are depicted by green, red, and blue arrows, respectively. (**B**). A barebones quaternionic projection relative to the three vectors making a triad. (**C**). Three-dimensional quaternion projection inside a sphere. (**D**). Punctiform orthographic projection of a brain signal spike (amplitude) onto the surface of a sphere via quaternion sphere. (**E**). Uniform orthographic projection of brain signals onto the surface of a sphere, achieved after projecting signal vectors via quaternionic maps.

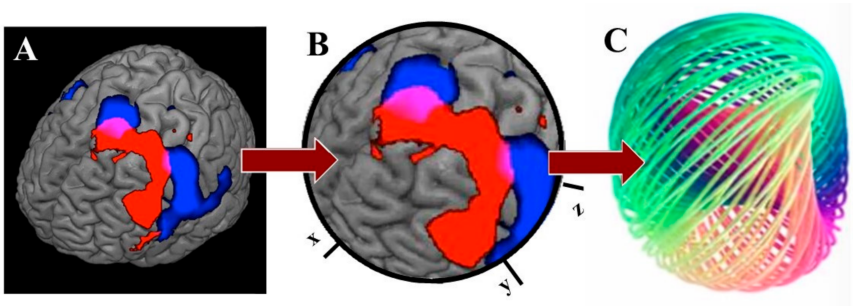

Figure 2. Feature extraction from a three-dimensional dataset to a four-dimensional hypersphere. (**A**). A three-dimensional fMRI (Functional Magnetic Resonance Imaging) neuroimage displays different activated areas, painted as blue and red spots on the surface of the cortical hemispheres. (**B**). The blue and red spots are mapped to the surface of a three-dimensional ball equipped with the canonical axes x, y, and z. (**C**). A technique termed Hopf fibration [19] allows the projection of the spots from the 2-sphere onto a glome, so that every point on the 2-sphere matches a single circular trajectory on the 3-sphere. Modified from [20].

In more technical terms, a map of a glome equipped with Sp(1) or SU(2) Lie groups can be projected onto a three-dimensional surface [6]. The circular trajectories on the 3-sphere match the compact, simply connected symplectic Lie group Sp(1) equipped with quaternionic 1×1 unitary matrices. The 3-sphere is parallelizable as a differentiable manifold, with a principal U(1) bundle over the 2-sphere. The 3-sphere's Lie group structure is Sp(1), which is equipped with quaternionic 1×1 unitary matrices [21]. The symmetries of the quaternionic manifold display a number system like the complex numbers, but with three imaginary quantities, instead of just one Orthographic projections derived from a sphere with center (0,0,0) with unit vectors α, β, γ, express the excess in any shape as an orthographic projection on the surface of a sphere (Tait 1867). We express an arc as DF and an angle on the surface of the sphere the quaternion as $\beta\alpha^{-1}\gamma$, i.e., $DF = \beta\alpha^{-1}\gamma$.

Summarizing, the use of quaternions makes it possible to utilize the spatial coordinates of every point placed inside a three-dimensional plot. The three spatial coordinates become single points, i.e., triads, inside four-dimensional hyperspheres. In the sequel, we will describe how brain signal patches derived from Fourier analysis can be represented geometrically as inputs to quaternions.

2.3. Fourier Analysis

Through Fourier analysis, quaternions provide a cumulative fractal view of multiple brain signals, described in terms of orthogonal projections on the surface of the brain viewed as a sphere. Indeed, it has been demonstrated that a Fourier analysis extracted by raw EEG data is able to describe the scale-free dynamics endowed in nervous oscillations [22–24], since cortical electric waves observed at different spatiotemporal scales exhibit a frequency spectrum characterized by scale-invariant behavior and power spectrum [25–27].

Fourier analysis was achieved through a designed MATLAB-based software. The frequencies were obtained with resolution of 0.25 Hz (Figure 3A).

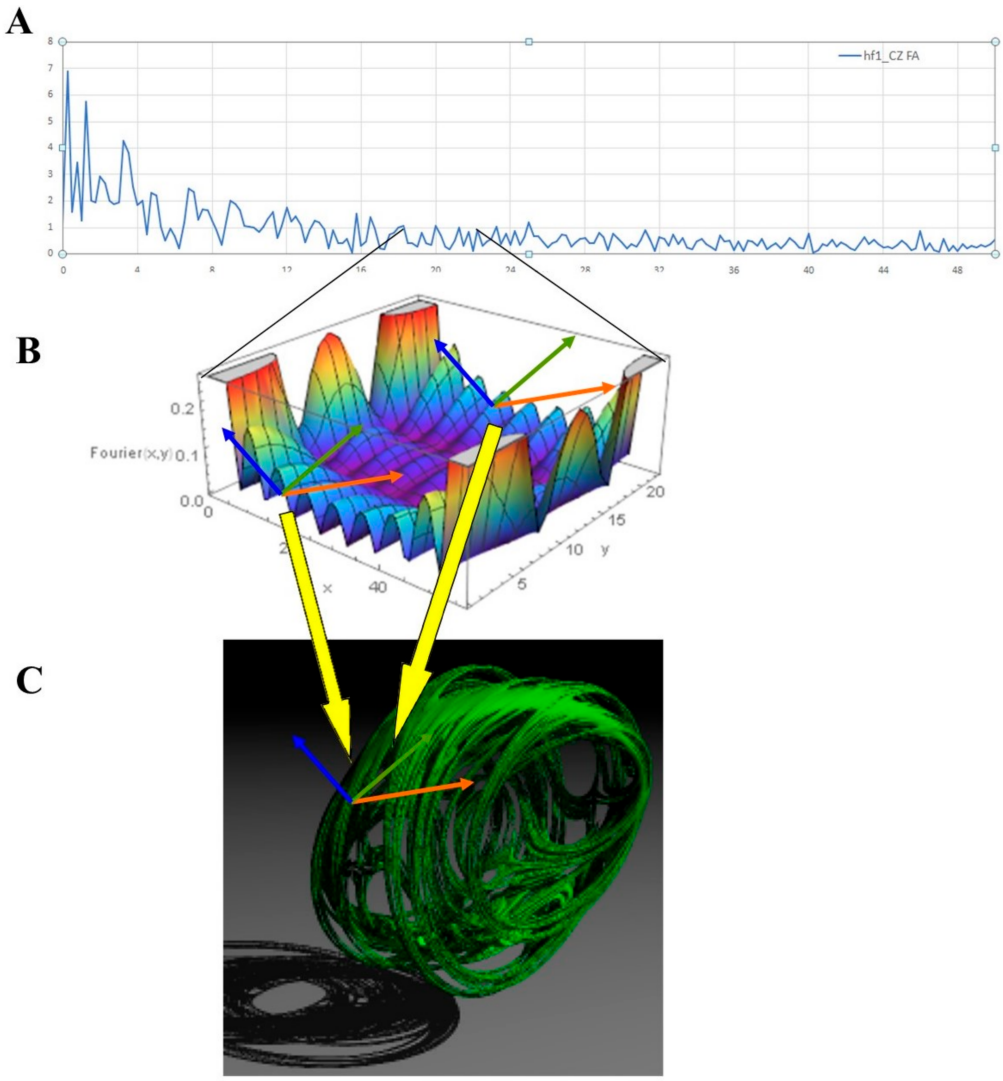

Figure 3. Quaternion simulation of non-uniform orthographic projection of brain fractal signals onto a fragmented sphere. (**A**) Two-dimensional Fourier analysis of an EEG trace. The x axis displays the frequencies in Hertz and the y axis, the amplitude in mV. (**B**). Three-dimensional magnification of a short trace from the plot in (**A**). (**C**) View of the orthographic projection of scale-free brain signal patches on continuous curves (represented by green threads and their shadows) via a quaternion. Note that two triads with matching description in three dimensions (i.e., equipped with the same orientation of the three axes) illustrated in (**B**) project (yellow arrows) to a single triad in four dimensions.

Once achieved a three-dimensional counterpart of the two-dimensional brain signal patches treated with Fourier analysis (Figure 3B), we took a step further, i.e., we used three-dimensional fractal quaternionic orthographic projections and mapped the triads in four dimensions.

3. Results

We performed simulations to show how it is feasible to achieve four-dimensional quaternionic projections from the two-dimensional data of the Fourier analysis that depicts the scale-free activity of the brain.

The three-dimensional triads achieved through Fourier analysis (Figure 3B) were projected to a four-dimensional quaternionic manifold, illustrated in terms of orthographic projections in three-dimensional spaces (Figure 3C). These ortographic projections are described by points (triads) on three-dimensional arcs located inside a sphere. Note that the

triads with matching description in the three-dimensional plot (e.g., the two identical triads depicted in Figure 3B) converge towards a single triad in the four-dimensional hypersphere. This means that temporally distant three-dimensional trajectories equipped with the same features (say, the same amplitude or the same frequency) come to be superimposed inside the quaternionic map. Therefore, repetitive spatiotemporal patterns undetectable in three dimensions plus time are easily enlightened in four dimensions plus time.

Next, we simulated the temporal progression of Fourier analysis' EEG scale-free dynamics in four dimensions plus time. Figure 4 portrays models of four-dimensional quaternionic orthographic projections of nervous fractal paths extracted from EEGs' Fourier analysis. The bumps illustrated in the four-dimensional fractal quaternionic plot (see, e.g., Figure 4D,E) stand for varying brain signal amplitudes crossing the surfaces of the nervous phase spaces.

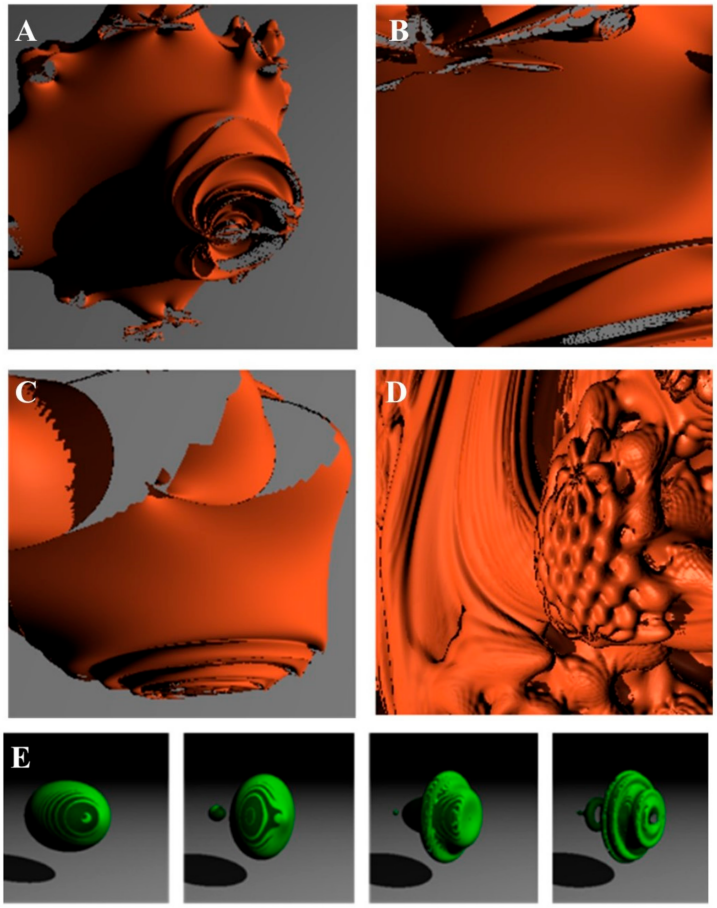

Figure 4. (**A**–**D**) Simulations of orthographic projections of scale-free brain signal patches onto the surface of a sphere via quaternions. Every picture stands for a quaternion surface closeup, where magnifications of the fractal structure of the hypersphere, depicted as three-dimensional views of the quaternion, can be seen. To make an example, (**A**) illustrates a planetary view of a non-uniform orthographic projection of brain signals onto a fragmented sphere. (**E**) Fractal-view (from the top to the bottom) of the orthographic projection of temporal sequences of brain signals patches on continuous curves represented by pulsating (vibrating) green threads and their shadows via a quaternion. This sequence stands for a spacetime view of the quaternionic mappings and encompasses a hidden time scale for the sequence of orange orthographic projections. No scale bar is needed, since the orthographic projections are scale-free.

4. Conclusions

We simulated quaternion orthographic projections of brain signals, using fractal traces from Fourier analysis of EEG plots. The recent, exciting innovations in quaternion-valued

neural networks, such as, e.g., the ones suggested by [13,28], pave the way to test an intriguing hypothesis, i.e., the recently proposed claim that the brain activity takes place in multidimensional spaces. It is noteworthy that, apart from the quaternionic maps described in this paper, other methods are available to assess higher dimensional activities of nervous networks. It has been recently suggested that hidden spatial dimensions of nervous activity could be methodologically assessed and quantified in terms of oscillations inside two-dimensional superlattices equipped with quantum Hall effects [29]. The superimposition of waves of different wavelengths gives rise to both (two-dimensional) linear and (four-dimensional) nonlinear dynamics [30,31]. Both the approaches, i.e., quantum Hall effects and quaternion-valued neural networks, would allow the transfer of mathematical/physical issues to the realm of neuroscience in order to: (a) describe the real multidimensional brain dynamics and (b) implement synthetic nervous networks equipped with four spatial dimensions (plus time), instead of the classical three (plus time). A crucial question is still unanswered: apart from the assessment of the multidimensional brain model, may quaternionic maps provide other insights that could be useful to describe the conventional three-dimensional neural dynamics? The answer is positive. Quaternionic mapping stands for a versatile technique that has been widely used in different experimental contexts. To make a few examples, Hanson and Thakur [15] used quaternion to expose global spatial relationships among amino acid residue structures within proteins, allowing them to assess global residue alignment in crystallographic data and statistical orientation properties in nuclear magnetic resonance. The visualizations resulting from quaternion spaces enables comparisons of absolute as well as relative orientations, because it permits, e.g., either to ascertain the stereochemical nature of proteins or to visualize global and local residue orientation properties of nucleic acids.

Importantly, quaternionic views of brain activity lead to a descriptive proximity topological characterization [32] of the activities of different neural functions that are descriptively close. This is made possible by the recent introduction of approximate descriptive proximity [33], which facilitates the computation of the distance between feature vectors used to represent and describe the shapes of brain signal patches. Thanks to the description of a fourth spatial dimension, quaternion-based feature vectors provide a formal basis for the approximate descriptively proximal assessment of the closeness of spatially separated brain activities, either by the same brain or by different brains at different times. A quaternion mapping embodies the full three degree-of-freedom transformation from the three-dimensional identity frame triad to a four-dimensional frame triad. This means that a quaternionic representation is much simpler than the usual representation using a triple of orthogonal three-dimensional vectors [15]. The three spatial coordinates of every point inside a three-dimensional plot become a single point inside a four-dimensional hypersphere. In particular, the points located close to each other on the hypersphere's surface (although temporally distant) display similar coordinates in three dimensions: in other words, these points are equipped with matching description. This allows quaternions to naturally expose global similarities among spatially far apart residues in a protein complex, no matter how near or how distant, extending the analysis to far between components of multi-part structures [15]. Quaternion mappings onto a hypersphere disclose properties of the dynamic systems' spatial orientation, making easier to detects hidden features such as global or broken symmetries, zones of speed convergence, domains of attraction inside three-dimensional projections, convergence among apparently random paths [28]. Therefore, quaternions provide an alternative methodology to the widely diffused methods of time-lagged mutual information and autocorrelation functions that have been used to evaluate the periodic features of the continuous EEG signal [34,35]. The last, but not the least, an intriguing hypothesis can be raised: as well as Fruchart et al. [36] investigated hidden non-commutative dualities (i.e., mathematical mappings that reveal links between apparently unrelated systems) in twisted kagome lattices, quaternionic movements could be used to detect neural responses not predicted by standard symmetry

analysis. This would allow the assessment of self-dualities in brain dynamics, which are dictated by non-commuting responses.

In sum, mapping EEG oscillations to an S^3 hypersphere is accomplished with orthographic projections of vectors inherent in brain signal patches via quaternions; this relatively straightforward approach leads to the possibility to enlighten hidden symmetries, in particular, in nervous neurodata.

Author Contributions: All the Authors had full access to all the data in the study and take responsibility for the integrity of the data and the accuracy of the data analysis. All the Authors equally contributed to: study concept and design, acquisition of data, analysis and interpretation of data, drafting of the manuscript, critical revision of the manuscript for important intellectual content, statistical analysis, obtained funding, administrative, technical, and material support, study supervision. All authors have read and agreed to the published version of the manuscript.

Funding: This research received no external funding.

Conflicts of Interest: The authors declare no conflict of interest.

References

1. Reimann, M.W.; Nolte, M.; Scolamiero, M.; Turner, K.; Perin, R.; Chindemi, G.; Dłotko, P.; Levi, R.; Hess, K.; Markram, H. Cliques of Neurons Bound into Cavities Provide a Missing Link between Structure and Function. *Front. Comput. Neurosci.* **2017**, *11*, 48. [CrossRef]
2. Bellmund, J.L.S.; Gardenfors, P.; Moser, E.I.; Doeller, C.F. Navigating cognition: Spatial codes for human thinking. *Science* **2018**, *362*, eeat6766. [CrossRef]
3. Chariker, L.; Shapley, R.; Young, L.-S. Rhythm and Synchrony in a Cortical Network Model. *J. Neurosci.* **2018**, *38*, 8621–8634. [CrossRef]
4. Tozzi, A. The multidimensional brain. *Phys. Life Rev.* **2019**, *31*, 86–103. [CrossRef] [PubMed]
5. Friston, K. The Emperor's new topology: Comment on "Topodynamics of metastable brains" by Arturo Tozzi et al. *Phys. Life Rev.* **2017**, *21*, 26–28. [CrossRef]
6. Tozzi, A.; Peters, J.F. Towards a Fourth Spatial Dimension of Brain Activity. *Cogn. Neurodyn.* **2016**, *10*, 189–199. [CrossRef] [PubMed]
7. Peters, J.F.; Ramanna, S.; Tozzi, A.; İnan, E. Bold-Independent Computational Entropy Assesses Functional Donut-Like Structures in Brain fMRI Images. *Front. Hum. Neurosci.* **2017**, *11*, 38. [CrossRef]
8. Hamilton, W.R. On Quaternions; or on a new System of Imaginaries in Algebra (letter to John T. Graves). *Philos. Mag.* **1844**, *25*, 489–495.
9. Tate, P.G. *An Elementary Treatise on Quaternions*; Clarendon Press: Oxford, UK, 1867.
10. Hosny, K.M.; Khedr, Y.M.; Khedr, W.I.; Mohamed, E.R. Robust Color Image Hashing Using Quaternion Polar Complex Exponential Transform for Image Authentication. *Circuits Syst. Signal Process.* **2018**, *37*, 5441–5462. [CrossRef]
11. Ayzenberg, A. Torus action on quaternionic projective plane and related spaces. *arXiv* **2019**, arXiv:1903.03460.
12. Batres-Mendoza, P.; Montoro-Sanjose, C.R.; Guerra-Hernandez, E.I.; Almanza-Ojeda, D.L.; Rostro-Gonzalez, H.; Romero-Troncoso, R.J.; Ibarra-Manzano, M.A. Quaternion-Based Signal Analysis for Motor Imagery Classification from Electroencephalographic Signals. *Sensors* **2016**, *16*, 336. [CrossRef]
13. Li, Y.; Wang, H. Almost periodic synchronization of quaternion-valued shunting inhibitory cellular neural networks with mixed delays via state-feedback control. *PLoS ONE* **2018**, *13*, e0198297. [CrossRef]
14. Enshaeifar, S.; Kouchaki, S.; Took, C.C.; Sanei, S. Quaternion Singular Spectrum Analysis of Electroencephalogram with Application in Sleep Analysis. *IEEE Trans. Neural Syst. Rehabil. Eng.* **2016**, *24*, 57–67. [CrossRef] [PubMed]
15. Hanson, A.J.; Thakur, S. Quaternion maps of global protein structure. *J. Mol. Graph. Model.* **2012**, *38*, 256–278. [CrossRef] [PubMed]
16. Hart, V.; Segerman, H. The Quaternion Group as a Symmetry Group. *arXiv* **2014**, arXiv:1404.6596v1.
17. Giblin, P. *Graphs, Surfaces and Homology*; Cambridge University Press: Cambridge, UK, 2010.
18. Weeks, J.R. The shape of space: How to visualize surfaces and three-dimensional manifolds. *Pure Appl. Math.* **1985**, *96*, 197–210.
19. Hopf, H. *Collected Papers/Gesammelte Abhandlungen*; Springer: Berlin, Germany; New York, NY, USA, 2001.
20. Johnson, N. A Visualization of the Hopf Fibration. 2015. Available online: https://nilesjohnson.net/hopf.html (accessed on 22 September 2020).
21. Ozdemir, F.; Özekes, H. On the Homomorphisms of the Lie Groups SU(2) and S3. *Abstr. Appl. Anal.* **2013**, *2*, 1–5. [CrossRef]
22. Pritchard, W.S. The brain in fractal time: 1/f-like power spectrum scaling of the human electroencephalogram. *Int. J. Neurosci.* **1992**, *66*, 119–129. [CrossRef]
23. Fingelkurts, A.A.; Fingelkurts, A.A.; Neves, C.F.H. Natural world physical, brain operational, and mind phenomenal space-time. *Phys. Life Rev.* **2010**, *7*, 195–249. [CrossRef]

24. Buzsáki, G.; Watson, B.O. Brain rhythms and neural syntax: Implications for efficient coding of cognitive content and neuropsychiatric disease. *Dialogues Clin. Neurosci.* **2012**, *4*, 345–367.
25. Van de Ville, D.; Britz, J.; Michel, C.M. EEG microstate sequences in healthy humans at rest reveal scale-free dynamics. *Proc. Natl. Acad. Sci. USA* **2010**, *107*, 18179–18184. [CrossRef] [PubMed]
26. Jirsa, V.K.; Stacey, W.C.; Quilichini, P.P.; Ivanov, A.I.; Bernard, C. On the nature of seizure dynamics. *Brain* **2014**, *137 Pt 8*, 2210–2230. [CrossRef]
27. de Arcangelis, L.; Herrmann, H.J. Learning as a phenomenon occurring in a critical state. *Proc. Natl. Acad. Sci. USA* **2010**, *107*, 3977–3981. [CrossRef] [PubMed]
28. Oliveros-Muñoz, J.M.; Jiménez-Islas, H. Hyperspherical path tracking methodology as correction step in homotopic continuation methods. *Chem. Eng. Sci.* **2013**, *97*, 413–429. [CrossRef]
29. Tozzi, A.; Ahmad, M.Z.; Peters, J.F. Neural computing in four spatial dimensions. *Cogn. Neurodyn.* **2020**. [CrossRef]
30. Lohse, M.; Schweizer, C.; Price, H.M.; Zilberberg, O.; Bloch, I. Exploring 4D quantum Hall physics with a 2D topological charge pump. *Nature* **2018**, *553*, 55–58. [CrossRef]
31. Zilberberg, O.; Huang, S.; Guglielmon, J.; Wang, M.; Chen, K.P.; Kraus, Y.E.; Rechtsman, M.C. Photonic topological boundary pumping as a probe of 4D quantum Hall physics. *Nature* **2018**, *553*, 59–62. [CrossRef]
32. Di Concilio, A.; Guadagni, C.; Peters, J.F.; Ramanna, S. Descriptive proximities, properties and interplay between classical proximities and overlap. *Math. Comp. Sci.* **2018**, *12*, 91–106. [CrossRef]
33. Peters, J.F. *Computational Geometry, Topology and Physics of Digital Images with Applications. Shape Complexes, Optical Vortex Nerves and Proximities*; Springer Nature: Cham, Switzerland, 2020; p. xxv+440. [CrossRef]
34. von Wegner, F. Partial Autoinformation to Characterize Symbolic Sequences. *Front. Physiol.* **2018**, *9*, 1382. [CrossRef]
35. von Wegner, F.; Laufs, H.; Tagliazucchi, E. Mutual information identifies spurious Hurst phenomena in resting state EEG and fMRI data. *Phys. Rev. E* **2018**, *97*, 022415. [CrossRef]
36. Fruchart, M.; Zhou, Y.; Vitelli, V. Dualities and non-Abelian mechanics. *Nature* **2020**, *577*, 636–640. [CrossRef]

MRM_02 short.qxp_Hrev_master 15/02/21 15:58 Pagina 5

Multidisciplinary Respiratory Medicine 2021; volume 16:741

pagepress

OPEN ACCESS

SHORT REPORT

Do gene-environment interactions play a role in COVID-19 distribution? The case of Alpha-antitrypsin, air pollution and COVID-19

Nicola Murgia,[1] Angelo Guido Corsico,[2] Gennaro D'Amato,[3] Cara Nichole Maesano,[4] Arturo Tozzi,[5] Isabella Annesi-Maesano[4]

[1]*Section of Occupational Medicine, Respiratory Diseases and Toxicology, University of Perugia, Italy*
[2]*Center for Diagnosis of Inherited α1-Antitrypsin Deficiency, Department of Internal Medicine and Therapeutics, Pneumology Unit, Fondazione IRCCS Policlinico San Matteo, University of Pavia, Italy*
[3]*Division of Respiratory and Allergic Diseases, Department of Chest Diseases, High Specialty A. Cardarelli Hospital, and Medical School of Specialization in Respiratory Diseases, Federico II University of Naples, Italy*
[4]*INSERM and Sorbonne University, Epidemiology of Allergic and Respiratory Diseases Department, IPLESP, Paris, France*
[5]*Center for Nonlinear Science, Department of Physics, University of North Texas, Denton TX, USA*

ABSTRACT

Background: Gene-environment interactions are relevant for several respiratory diseases. This communication raises the hypothesis that the severity of COVID-19, a complex disease where the individual response to the infection may play a significant role, could partly result from a gene-environment interaction between air-pollution and Alpha-1 Antitrypsin (AAT) genes.
Methods: To evaluate the impact of the AAT and air pollution interaction on COVID 19, we introduced an AAT*air pollution global risk score summing together, in each country, an air pollution score (ozone, nitrogen dioxide and fine particulate matter) and an AAT score (which sums the ranked frequency of MZ, SZ, MS). We compared this global score with the ranking of European countries in terms of death number per million persons.
Results: The ranking of the AAT*air pollution global risk score matched the ranking of the countries in terms of the observed COVID-19 deaths per 1M inhabitants namely in the case of the first European countries: Belgium, UK, Spain, Italy, Sweden, France. We observed parallelism between the number of COVID deaths and the AAT*air pollution global risk in Europe. AAT anti-protease, immune-modulating and coagulation-modulating activities may explain this finding, although very speculatively.
Conclusions: Even if further studies taking into account genetic background, population density, temporal dynamics of individual epidemics, access to healthcare, social disparities and immunological response to SARS-CoV2 are needed, our preliminary observation, urges to open a discussion on gene-environment interactions in COVID-19.

Key words: AAT; COVID-19; environment; air pollution.

Correspondence: Nicola Murgia, Section of Occupational Medicine, Respiratory Diseases and Toxicology, University of Perugia, Piazzale Gambuli, 06128 Perugia, Italy. Tel. +39.075.5784488. E-mail: nicola.murgia@unipg.it

Contributions: NM, conceptualization, investigation, original draft writing; AGC, AT, validation, manuscript review and editing; GDA, conceptualization, manuscript review and editing; CNM, methodology, manuscript review and editing; IAM, conceptualization, formal analysis, supervision, original draft writing.

Conflict of interest: The authors declare that they have no competing interests, and all authors confirm accuracy.

Availability of data and materials: Available from the corresponding author on reasonable request.

Ethics approval and consent to participate: Not applicable.

Consent for publication: Not applicable.

MRM_02 short.qxp_Hrev_master 15/02/21 15:58 Pagina 6

Introduction

Gene-environment interactions are thought to be critical for several respiratory diseases such as cancer, emphysema and asthma. They could contribute also to the respiratory infection caused by SARS-CoV-2 that deeply affects the lung by increasing the risk of suffering from a severe form of the disease (COVID-19) in susceptible individuals. Genetic susceptibility to SARS-CoV2 has been studied: some critical immunogenetic pathways (*e.g.,* interferon related) have been identified and interconnection with other important system (*e.g.,* renine-angiotensin-aldosterone) in infection progression has been proposed [1]. Another relevant factor in the pathogenesis of COVID-19 seems to be Alpha-1 Antitrypsin (AAT) which shown an inhibitory effect on transmembrane serine protease 2 (TMPRSS2), key protease for SARS-CoV2 infection [2]. AAT deficiency (AATD) is a genetic condition resulting from the inheritance of two abnormal alpha-1 (Z) antitrypsin genes (ZZ) impacting AAT production, a protein which protects the lungs from inflammation caused by infection and inhaled irritants Individuals with the AAT genetic defect do not release alpha-1-antiprotease from the liver, and present low levels of the protein in serum and alveoli. Consequently, alveoli lack antiprotease protection from external aggressions. Although this deficiency is rare, other more frequent AAT gene combinations exist (SZ, SS, MS, MZ among the commonest) that also modulate AAT production [3]. Gene involvement in COVID 19 is supported by the fact that ethnic differences in AATD alleles might explain national differences in COVD-19 fatality, although only partly [4].

For some authors, air pollution may play a role in SARS-CoV2 infection and COVID-19 severity [5]. However, it is not clear yet if airborne pollutants are directly involved in causing a more severe form of the disease or are the chronic diseases correlated to air pollution (cardiovascular and respiratory) to make the subject more prone to the detriment effect of the infection [6].

In this short report we raise the hypothesis according to which the severity of COVID-19 could partly result from a gene-environment interaction between air pollution and AAT genes that impair lung and immunological response to SARS-COV-2 action and boost an exaggerated inflammatory response, responsible of COVID-19 lung damage.

To explore the impact of the AAT and air pollution interaction on COVID 19, we consider the situation in Europe, where AAT Deficiency has been both mapped and quantified and air pollution exposure data are available. Similar data are not available in the rest of the world.

Methods

To explore the impact of the AAT and air pollution interaction on COVID-19, we consider the situation in Europe, where both AAT Deficiency has been mapped and quantified and air pollution exposure data are available. Similar data are not available in the rest of the world.

AAT Deficiency frequencies according to major genotypes was drawn by the results of an international study [3] and air pollution level by the European Environmental Agency (https://www.eea.europa.eu/themes/air). COVID-19 death numbers were provided by https://coronavirus.jhu.edu/map.html.

To evaluate the impact of the AAT and air pollution interaction on COVID 19, we introduced a AAT*air pollution global risk score summing together, in each country, an air pollution score (which sums exposure levels (low=1, medium=2, high=3) for each of three major pollutants (ozone, nitrogen dioxide and fine particulate matter) and an AAT score (which sums the ranked frequency of MZ, SZ, MS deficits according to five classes from absent =1 to elevated=5). We compared this global score with the ranking of countries in terms of death number per million persons.

Results

The ranking of the AAT*air pollution global risk score matched the ranking of the countries in terms of the observed COVID-19 deaths per 1M inhabitants namely in the case of the first European countries: Belgium (1385), Spain (949), Italy (875), UK (838), France (780) (Figure 1).

Discussion

We observed an ecological parallelism between the number of COVID-19 deaths and the AAT*air pollution global risk in Europe.

This observation is supported by biological plausibility. As a matter of fact there is an increasing evidence of the role of inflammation/AAT imbalance in making COVID-19 more severe [7] which is influenced by air pollution: AAT has an inhibitory effect on important infection and disease mediators, such as ADAM-17 [2] , and down-regulate the production of IL-6, IL-8, IL-1b, and TNF-a, key mediators in the "cytokine storm" observed in severe COVID-19 pneumonia patients and possibly related to a macrophage activation syndrome and a secondary haemophagocytic lymphohistiocytosis [8]. Pneumothorax and pneumomediastinum are well-known complications of ventilated COVID-19 patients, explained by the use of higher pressures and larger tracheal tubes, but also by diffuse alveolar damage which may contribute to air leakage. It is unclear if antiproteases play a protective role in SARS-CoV-2 alveolar damage, but AAT deficiency has previously been identified as a predisposing factor for pneumothorax [9]. Systemic thrombosis could be another important mechanism of lung and systemic damage in COVID-19 patients. In a recent survey, patients with severe AAT deficiency had a higher mortality from pulmonary embolism than the reference population [10]. This finding has not been explained, but may be related to an increased complement activation, as evidenced by patients with AAT deficiency who show an increased cleavage of complement C3 component in C3d [11]. Moreover, the crosstalk between complement, coagulation and the vascular system is actually considered one of the most important factors in determining coagulation abnormalities and thrombosis seen in the more severe COVID-19 patients [12]. Complement system can be activated by virus-IgG or virus-IgM immunocomplexes or by virus IgA immunocomplexes, through mannose-binding lectin linked to both viral N glycan and IgA [13].

One concern about our findings may raise up from the observation of a very low prevalence of COPD, which is one typical clinical outcome in AAT-deficiency, in patients hospitalized for COVID-19. However, COPD was strongly associated with the more severe forms of COVID-19, requiring mechanical ventilation and ICU admission [14].

The main limitation of our observation is that many other factors could explain the overlap between environment and Covid-19. One of the most important is population density which could contribute substantially to environmental pollution. However there is increasing evidence of a role of air pollution in Covid-19 mortality taking into account also population density, as well other important factors such as family size, house crowding, percentage of private mobility use and socio-economical deprivation[15].

MRM_02 short.qxp_Hrev_master 15/02/21 15:58 Pagina 7

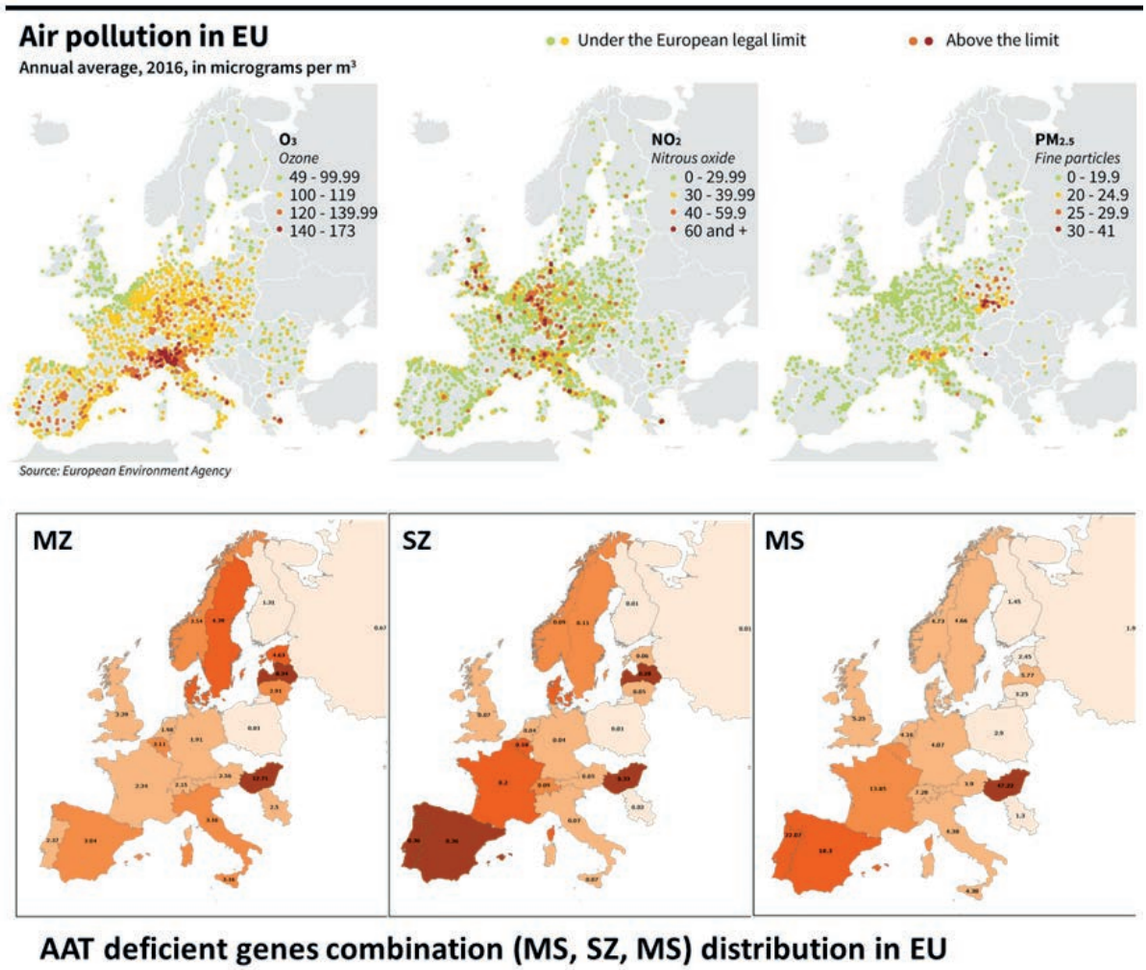

Figure 1. **Air pollution and alpha-1 antitrypsin (ATT) genes combinations distribution in EU.**

Large genetic studies on the interaction between the human genome and SARS-CoV-2 infection are already ongoing (for example https://www.covid19hg.org/), but they do not explain COVID-19 severity entirely and they do not consider environmental interactions. Further studies considering population density, temporal dynamics of individual epidemics, access to healthcare, social disparities and immunological response to SARS-CoV-2 are needed. Adhering to the precautionary principle, however, suggests air pollution emissions must be diminished now to protect individuals.

Conclusions

Our observation, though very preliminary, should help to open a discussion on gene-environment interactions in COVID-19. Moreover, even if most of the research is still ongoing, respiratory doctors and other specialists should be aware of emerging clinical predisposing factors and their interactions with host immunity ad coagulation, which would make more susceptible the patients to the consequences of SARS-CoV-2 infection.

References

1. McCoy K, Peterson A, Tian Y, Sang Y. Immunogenetic association underlying severe COVID-19. Vaccines (Basel) 2020;8:E700.
2. de Loyola MB, Dos Reis TTA, de Oliveira GXLM, da Fonseca Palmeira J, Argañaraz GA, Argañaraz ER. Alpha-1-antitrypsin: A possible host protective factor against Covid-19. Rev Med Virol 2020:e2157.
3. Blanco I, de Serres FJ, Fernandez-Bustillo E, Lara B, Miravitlles M. Estimated numbers and prevalence of PI*S and PI*Z alleles of alpha1-antitrypsin deficiency in European countries. Eur Respir J 2006;27:77-84.
4. Shapira G, Shomron N, Gurwitz D. Ethnic differences in alpha-1 antitrypsin deficiency allele frequencies may partially explain national differences in COVID-19 fatality rates. FASEB J 2020;34:14160-5.
5. Pozzer A, Dominici F, Haines A, Witt C, Münzel T, Lelieveld J. Regional and global contributions of air pollution to risk of death from COVID-19. Cardiovasc Res 2020;116:2247-53.
6. Barouki R, Kogevinas M, Audouze K, Belesova K, Bergman A, Birnbaum L, et al. The COVID-19 pandemic and global

MRM_02 short.qxp_Hrev_master 15/02/21 15:58 Pagina 8

environmental change: Emerging research needs. Environ Int 2020;146:106272.
7. McElvaney OJ, McEvoy NL, McElvaney OF, Carroll TP, Murphy MP, Dunlea DMP, et al. Characterization of the inflammatory response to severe COVID-19 illness. Am J Respir Crit Care Med 2020;202:812-21.
8. Gonagle D, Sharif K, O'Regan A, Bridgewood C. The role of cytokines including interleukin-6 in COVID-19 induced pneumonia and macrophage activation syndrome-like disease. Autoimmun Rev 2020;19:102537.
9. Boone PM, Scott RM, Marciniak SJ, Henske EP, Raby BA. The genetics of pneumothorax. Am J Respir Crit Care Med 2019;199:1344-57.
10. Tanash HA, Ekström M, Wagner P, Piitulainen E. Cause-specific mortality in individuals with severe alpha 1-antitrypsin deficiency in comparison with the general population in Sweden. Int J Chron Obstruct Pulmon Dis 2016;11:1663-9.
11. O'Brien ME, Fee L, Browne N, Browne N, Carroll TP, Meleady P, et al. Activation of complement component 3 is associated with airways disease and pulmonary emphysema in alpha-1 antitrypsin deficiency. Thorax 2020;75:321-30.
12. Cugno M, Meroni PL, Gualtierotti R, Griffini S, Grovetti E, Torri A, et al. Complement activation in patients with COVID-19: A novel therapeutic target. J Allergy Clin Immunol 2020;146:215-7.
13. Matricardi PM, Dal Negro RW, Nisini R. The first, holistic immunological model of COVID-19: Implications for prevention, diagnosis, and public health measures. Pediatr Allergy Immunol 2020;31:454-70.
14. Lippi G, Henry BM. Chronic obstructive pulmonary disease is associated with severe coronavirus disease 2019 (COVID-19). Respir Med 2020;167:105941.
15. e Angelis E, Renzetti S, Volta M, Donato F, Calza S, Placidi D, et al. COVID-19 incidence and mortality in Lombardy, Italy: an ecological study on the role of air pollution, meteorological factors, demographic and socioeconomic variables. Environ Res 2021;195:110777.

Received for publication: 7 January 2021. Accepted for publication: 11 January 2021
This work is licensed under a Creative Commons Attribution-NonCommercial 4.0 International License (CC BY-NC 4.0).
©Copyright: the Author(s), 2021
Licensee PAGEPress, Italy
Multidisciplinary Respiratory Medicine 2021; 16:741
doi:10.4081/mrm.2021.741

Philosophia
https://doi.org/10.1007/s11406-021-00359-x

Why Should Natural Principles Be Simple?

Arturo Tozzi[1]

Received: 6 January 2021 / Accepted: 10 March 2021
© The Author(s), under exclusive licence to Springer Nature B.V. 2021

Abstract
One of the criteria to a strong principle in natural sciences is simplicity. The conventional view holds that the world is provided with natural laws that must be simple. This common-sense approach is a modern rewording of the medieval philosophical/theological concept of the Multiple arising from (and generated by) the One. Humans need to pursue unifying frameworks, classificatory criteria and theories of everything. Still, the fact that our cognitive abilities tend towards simplification and groupings does not necessarily entail that this is the way the world works. Here we ask: what if singularity does not pave the way to multiplicity? How will we be sure if the Ockham's razor holds in real life? We will show in the sequel that the propensity to reduce to simplicity the relationships among the events leads to misleading interpretations of scientific issues. We are not going to take a full sceptic turn: we will engage in active outreach, suggesting examples from biology and physics to demonstrate how a novel methodological antiunitary approach might help to improve our scientific attitude towards world affairs. We will provide examples from aggregation of SARS-Cov-2 particles, unclassified extinct creatures, pathological brain stiffness. Further, we will describe how antiunitary strategies, plagiarising medieval concepts from William od Ockham and Gregory of Rimini, help to explain novel relational approaches to quantum mechanics and the epistemological role of our mind in building the real world.

Keywords Neuroscience · COVID-19 · Dickinsonia · Sphere packing · Relational quantum mechanics

"Natural principles must be simple". Motivated by Hilbert's 24th problem, Hipolito (2019) suggests that the Free Energy Principle (Friston, 2010) takes a seemingly mathematical complex domain and must be reduced to something simple. The author follows the common belief that the world must be fitted with

✉ Arturo Tozzi
tozziarturo@libero.it; arturo.tozzi@aslnapoli2nord.it

[1] Center for Nonlinear Science, Department of Physics, University of North Texas, 1155 Union Circle, #311427, Denton, TX 76203-5017, USA

Published online: 16 April 2021

unifying natural laws and that the simplicity of a model is relevant to estimating inductive inference, predictive accuracy and explanatory power (Goodman, 1959; Foster & Martin, 1966. Akaike, 1973; Forster & Sober, 1994; Harman, 1999; Baker, 2003). This approach is a reminder of ever-present medieval hints from ancient scholastics (Oreskes et al., 1994), such as the Ockham's razor and the Neoplotinian tenet that the Multiple must be generated from (and by) the One. Here we ask: why there must be unifying laws? Why do we need theoretical simplicity, either syntactic (i.e., simplicity) or ontological (i.e., parsimony)? In touch with set theory, observers tend to build various arbitrary sets which do not necessarily stand for different objects or events (Friedman, 1974; Tozzi & Peters, 2020a). Our biggest problem is perhaps the mental way we cope with everyday life using analogy, i.e., the common-sense identity of relation between apparently unrelated objects or features (Hesse, 1974; Chater, 1999; Sowa & Majumdar, 2003). Through analogy, our brain tries to make sense of the unpredictable features of the ceaseless environmental inputs (Hofstadter and Sander, 2011; Koczkodaj et al., 2017). Yet, Mc Ginn's cognitive closure (McGinn, 1994) suggests that our intrinsically limited minds are prevented to know the reality subtending our perceptions. Think to the Wittgenstein's lion, or the Nagel's bat, or to medieval theologians who gave for granted that God must exist just because the most of humankind believes in God. Since the times of Hermes Trismegistus, countless scholars (both philosophers and scientists) have been used to proceed from the One to the Multiple and to justify the Ockham's razor (Barnes, 2000; Kelly, 2004).

Still, some authors disagree. For example, Ackerman (1961) and Bunge (1961) challenge the role of simplicity in inductive inference and the justifiability of simplicity criteria in theory evaluation. In Alain Badiou's opinion, the One is just an operation on a subtending manifold, since the Multiple gives rise to the One, and not vice versa (Badiou, 1888). This approach rejects the classical approach: God → Multiplicity, then One/Simple → Multiple/Complex. Likewise, Deleuze and Guattari (1980) introduced a theory of a unity that is multiple in itself. They point towards non-hierarchical connections opposed to the tree-like conceptions of knowledge based on dualist categories and binary choices. Apart from the above-mentioned philosophical issues, things are not as simple as believed also in mathematics. It is remarkable that the same Hilbert was puzzled by Godel's and Tarki's theorems which prevented his efforts towards simplicity and unification of mathematical foundations. Since the One is generally believed as infinite, and since a mathematical infinite can be a multiple of another (Tozzi & Peters, 2020b), we may state, together with the medieval thinker Henry of Harclay, what follows: the fact that we humans are able to think to infinity and to the One does not scientifically imply that infinity and the One really exist in the Universe (Sylla, 1998a, 1998b). We will show in the sequel that the attitude towards simplicity leads to misleading interpretations of scientific issues. Despite our destructive criticism, we are not going to take a sceptic turn. Indeed, our aim is to show how antiunitary methodological approaches shed light on fully underrated features.

1 Against Ochkam's Razor: Physical and Biological Account

In quantum dynamics, the demarcation problem and the failure of the principle of locality cause severe troubles to the otherwise untouchable Aristotelian principle of identity (Tozzi & Peters, 2018): if A does not anymore equal A, how could the Unity and the Simple be defined? To make things even worse, the quantum field theory describes the Universe as permeated by at least 24 fields (possibly more), each one corresponding to a single elementary particle: too many to be reduced to Simplicity. If the Universe is suffering a progressive quantum decoherence and decrease in number of symmetries, this means that there must have been at the beginning something very symmetric, therefore overly intricate and complex. Obviously, this not compatible with the concept of One preceding the Multiple.

At times, straightforward phenomena can be more puzzling than believed. To provide a baffling example, hot water freezes faster than cold water, as suggested by the temperature dependent Mpemba effect. Counterintuitively, a hot system can be cooled faster that an identical system initiated at a lower temperature. How do we explain this anomalous behaviour? In this case, a unifying principle cannot save us. In nonequilibrium thermodynamic systems, the energetic state closer to the ground state may take a longer time to reach the lowest energetic basin (Lu & Raz, 2017). See Fig. 1 for further details. This means that, under the proper conditions, a cold system can heat up faster than the same system initiated at a higher temperature. This also means that the mechanisms underlying the Mpemba effect requires a complex explanation which casts doubt on the existence of a sole subtending principle.

Then comes biology. Life is not reducible to simplicity: just looking at the intricate patterns of the plots and tables illustrating cellular metabolic pathways, it is self-evident that things are not simple at all. The same limitation holds for the very concept of evolution: the demarcation among living beings is somewhat arbitrary. Our concept of species is very unacquainted since the borders among living beings are often not experimentally proven. One of the most typical examples is the enigmatic Dickinsonia, an extinct lineage that does not fit within known animal phyla. Dated about 571-541 million years ago, it is a marine genus of fossils belonging to the early communities of Ediacara Biota, i.e., the oldest fossil evidence for the appearance of animals (Ivantsov, 2007). Tentatively assigned to the animal kingdom (Bobrovskiy et al., 2018), the mobile Dickinsonia lacks convincing evidence of mouth, gut and anus and possibly fed via external absorption and digestion of organic matter through its ventral surface. We classify Sapiens, Neandertals, Denisovans, Floresiensis as distinct species of the genus Homo, despite genetic studies point towards multiple ancient hybridizations (Gibbons, 2017; Slon et al., 2018; Massilani et al., 2020). Concerning our DNA, species demarcation is at times difficult, due, e.g., to the occurrence of viral and bacterial sequences in animal genomes. The horizontal transmission and lateral transduction of genetic material described by Chen et al. (2018) and D'Angiolo et al. (2020) may overtake the canonical "species-specific" barriers, making it difficult to sharply incorporate individual beings in the framework of a single species. We may state that horizontal transmission of genetic material makes evolutionary trajectories of living beings unpredictable and

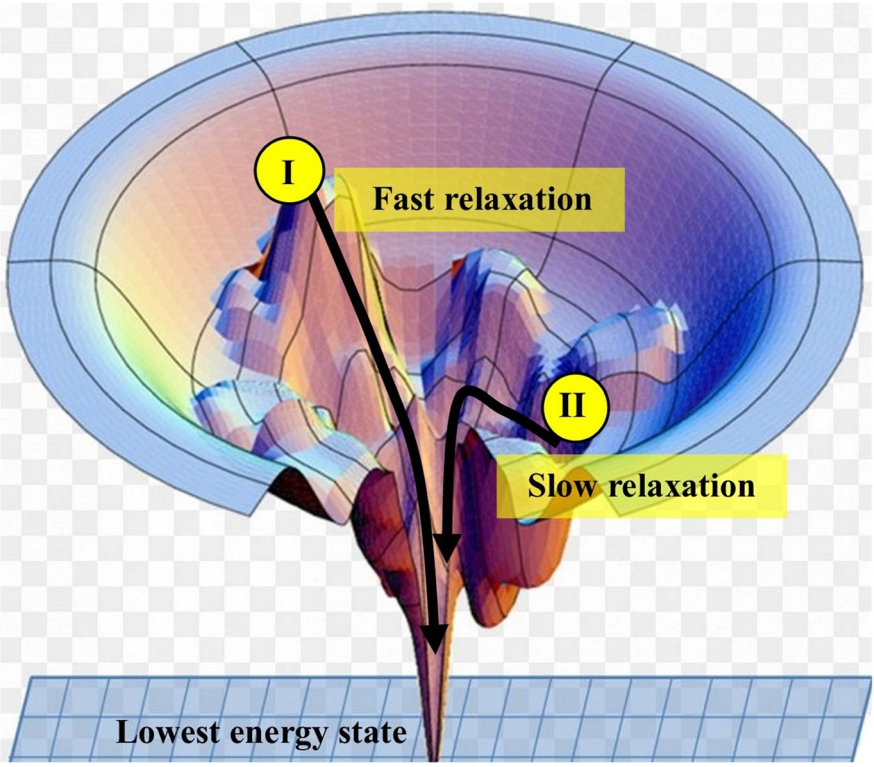

Fig. 1 Potential energy basin of water cooling explain the Mpemba effect. The hotter point of departure (yellow circle I) takes less time to reach the freezing temperature (termed: lowest energy state) compared with the colder point of departure (yellow circle II)

irreducible to the One, in touch with Deleuze and Guattari's model (1980). The very concept of the evolutionary life proceeding from monocellular to multicellular beings could be misleading. Indeed, recent studies star to unveil a more complicated state of affairs... see Bhowmik and Krishnamurthy (2019).

2 The Scientific Virtues of Methodological Antiunitary Approaches

Here we show how the switch from one-to-multiple approaches to antiunitary methodology might contribute to unravel intriguing scientific conundrums. For example, a question has been raised during these frantic months of pandemics: why do elder people suffer from more severe COVID-19 symptoms compared with children (see, e.g., Parri et al., 2020; Qiu et al., 2020)? Despite attempts at explanations generally focus on the foremost role of the spike protein, our approach suggests to look for underrated issues. SARS-Cov-2 particles are not just made of RNA and viral proteins (Chen et al., 2020), but also of a lipid wall "stolen" from the endoplasmic reticulum-Golgi intermediate compartment (ERGIC) of the human host (Brian

& Baric, 2005; Appenzeller-Herzog & Hauri, 2006). After intracellular assembly, virions are transported to the cell surface and released by exocytosis (Risco et al., 2002; Risco et al., 2002) (Fig. 2a). It is well documented that biochemical, morphological and functional modifications of ERGIC membranes occur at different ages and during senescence (Cho et al., 2011; Torres-González et al., 2012; Brown & Naidoo, 2012; Udono et al., 2015; Calvo-Rodríguez et al., 2016; Liu et al., 2018; Su et al., 2018; Janikiewicz et al., 2018; Despres et al., 2019; Chadwick & Lajoie, 2019). This means that SARS-Cov-2 changes its "skin" when jumps from old to young hosts and vice versa. Since human ERGIC membranes display different arrangements with time passing, the SARS-Cov-2 particles produced in the tissues of children are phenotypically different from the particles produced in the tissues of elder people (Fig. 2b). The different features of SARS-Cov-2 emerging from old and young cells might contribute to variations in viral load, infectivity and clinical severity.

The intrinsic impossibility to reduce functional affairs to unifying, antiunitary principles is self-evident also in neuroscience. Recent claims suggest that the brain activity takes place in multidimensional phase spaces. For a review, see Tozzi (2019). When I see a cat in front of me, I perceive not just the three-dimensional image of the cat, but also countless mental features of the cat (emotional features: "how tender!", cognitive features: "this is a Feline", linguistic features, and so on). In other words, we (quite improperly) use the same word "cat" to describe both the real perceived animal and the imagined animal. Incidentally, another existential quantifier would be required in logic to discern between the object and its mental image. The common belief is that biophysical phenomena take place in Euclidean phase spaces (Bellmund et al., 2018). Still, recent work has shown that the appropriate isometric space for embedding complex networks (in particular the neural multidimensional phase space) is not the flat Euclidean space, but rather negatively curved hyperbolic spaces (Sengupta et al., 2016; Chamberlain et al., 2017). Embeddings in hyperbolic spaces outperform Euclidean spaces since they allow a more manageable treatment of the required thermodynamic equations, such as, e.g., the Fokker-Plank equations (Sengupta et al., 2016).

The current paradigm in neuroscience is framed on a basic unitary principle: the brain activity can be explained in terms of the action potentials and the nervous circuits which generate the electric spikes crossing the central nervous system. However, recent insight point towards the brain activity (including cognitive functions) as mediated not just by spikes, but also by a countless number of other heterogeneous factors such as macromolecules, transitory changes in protein conformation, glial cells, extracellular matrix, peripheral receptors, substrate patterning, intestinal bacteria, immune system, prion-based mechanisms, metabolic status, nutritional factors, hormones breathing, heartbeats, light, and so on. For a review, see Tozzi (2015). Here we suggest that another still unexplored issue might contribute to modify the brain activity, i.e., a correlation between rheology and neurological disease. It is well-known that electromagnetic waves propagate more slowly and with lower frequencies when traveling through more liquid mediums (Ogilvie & Proctor, 2003). Concerning the viscoelastic properties of the brain tissue, differences in stiffness among dissimilar neural structures and areas have been described (Budday et al.,

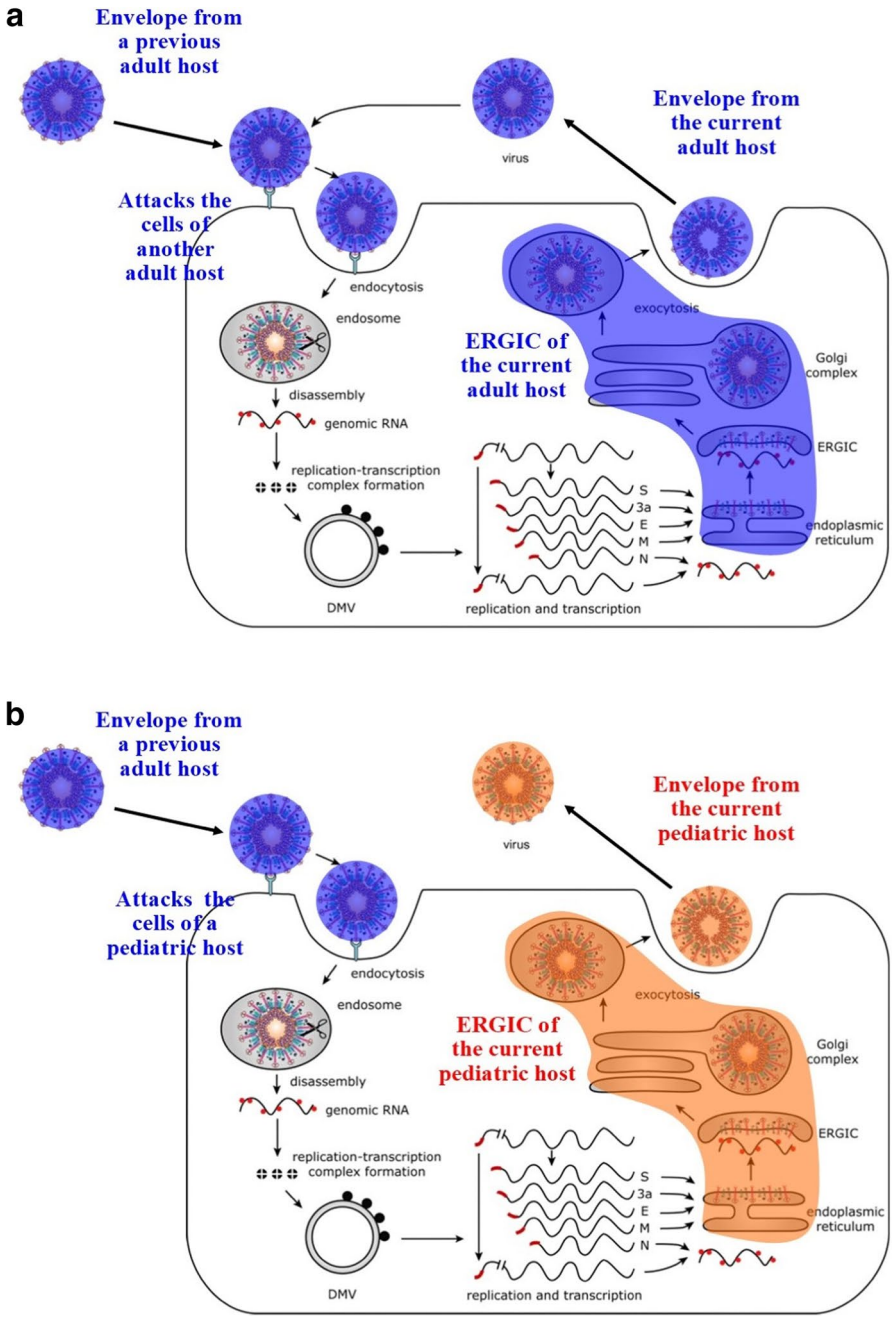

Fig. 2 Replication pathway of SARS-Cov-2. The ERGIC of the adult host's cell, painted in blue (**a**), is different from the ERGIC of the child host's cell, painted in red (**b**). This means that the virions released by elder host cells (blue spheres) are phenotypically different from the virions released by young host cells (red spheres). Modified from: de Haan and Rottier (2006)

2017; Ranta et al., 2017; Miceli et al., 2017): in particular, decreased stiffness and viscosity can be detected in patients with clinical diagnosis of Alzheimer's disease (AD) and several dementia subtypes (Murphy et al., 2011; ElSheikh et al., 2017; Gerischer et al., 2017; Del Giudice et al., 2017; Shamaev & Shumilova, 2018). Furthermore, AD is characterized by significant increases in slow wave EEG activity in different brain areas (Waninger et al., 2016). This might mean that the decreases in brain stiffness occurring in AD can be correlated with the experimentally detected pathological decline of EEG frequencies. We speculate that two different regimes of brain electric oscillations take place: the healthy brain tissue displays higher values of viscoelastic indexes and encompasses higher EEG frequencies, while the AD brain tissue displays a more liquid behavior and encompasses lower EEG frequencies. This would pave the way to the use of drugs such as mannitol (Shaltiel-Karyo et al., 2013), hyaluronic acid and osmolytes to restore the impaired brain viscoelastic features in AD.

In physics and biology, a foremost issue testifies that the relationships between the one and the multiple are more intricate than suggested by the plain and reassuring account of the Ockham's razor. Nonlinear dynamics, single-parameter bifurcations, random graphs, complex and/or chaotic systems prove that things and facts are not as simple and predictable as believed until half a century ago. In touch with this observation, Turalska and West (2018) made an astonishing achievement, demonstrating that the Mittag-Leffler equations are able to describe the movements of a single component belonging to a collective system. In touch with Bechtel's multilevel emergentism (2008), this confirms how higher systemic levels modify the dynamics of the lower ones and vice versa, causing an intermingling of the One and the Multiple that cannot be resolved by a trivial reduction to the One and to the Simple.

Here you are a biological example of emergence from aggregation, against too strict holistic approaches based on the First Principles. Viruses may spread not just as single particles, but also as collective aggregates reminiscent of bacterial biofilms (Segredo-Otero & Sanjuán, 2019; Millen et al., 2019; Thoulouze & Alcover, 2011; Andreu-Moreno & Sanjuán, 2020; Leeks et al., 2019). For example, close evaluation of available microscopic photographs and videos of SARS-CoV-2 virions shows that their round particles squeeze and stick into each other (Fig. 3a), progressively aggregating in small clusters that fill the available liquid space (Fig. 3b). It could be boosted by the fact that the spike proteins can be tilted by up to ~90° relative to the membrane, giving their head an unexpected orientational freedom (Watanabe et al., 2020; Ke et al., 2020; Turoňová et al., 2020). In the extracellular milieu, viral particles tend to aggregate in interconnected globular networks of progressively growing assemblies (Fig. 3c-d). The possibility to achieve collective dynamical behavior may provide invaluable advantages to SARS-CoV-2, such as, e.g., best sphere packaging and inner core sanctuary spared by immunologic and environmental noxae (Fu et al., 2016; Teich et al., 2016). In sum, virionic clusters might stand for an unnoticed collective mechanism that on one hand contributes to viral spread, on another hand stands for a potential target leading to novel antiviral strategies.

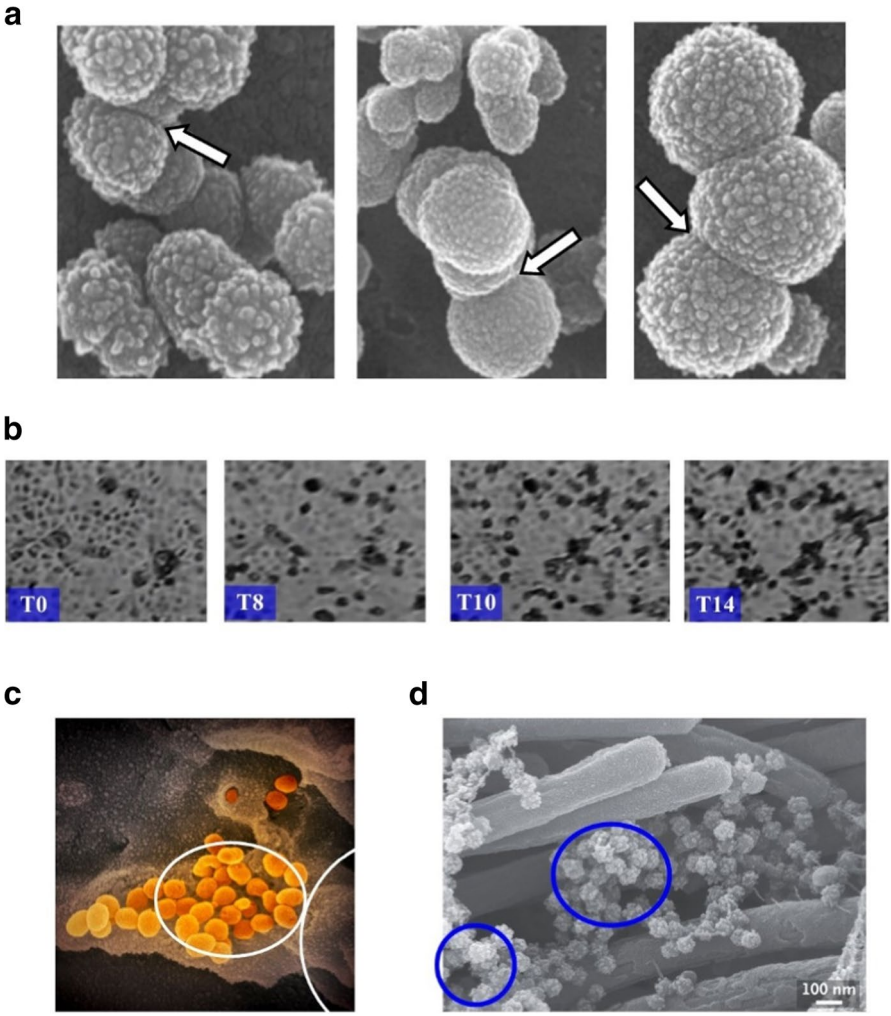

Fig. 3 Interaction of coronavirus particles detected by transmission electron microscope at different magnifications. **a**. SARS-CoV particles have been found either isolated or in aggregates. The arrows highlight the adhesion areas between different squeezed virions. Modified from Lin et al. (2004). **b**. Movie frames illustrating the temporal outcome of SARS-CoV-2 virion production and growth in the supernatant of infected cultured cells. Modified from: https://www.youtube.com/watch?v=qTt3P5V8M1A&feature=youtu.be. Note the progressive crowding of virion particles: this leads small clusters to converge in bigger clusters. **c**. SARS-CoV-2 virions emerging from the surface of infected cultured cells. Small clusters tend to converge, giving rise to larger aggregates (round shapes). Modified from: https://www.flickr.com/photos/niaid/albums/72157712914621487. **d**: spreading of SARS-CoV-2 inoculated into human bronchial epithelial cells (modified from Ehre, 2020)

3 Conclusions

Every science is based on the available knowledge related to its own specific content. Progress is pursued through a progressive accumulation of conclusions, making

us closer to the subtended unifying principles. This standard way to think and proceed was endorsed also in pre-scientific eras: think, e.g., to Thomas Aquinas, who maintains that every science is a single and simple habit of the intellect, consisting of the unity of its formal object. To provide another example, Peter Auriol, answering to the question: "whether the habit acquired from theological study be one of many?" states that science is ONE habit of the intellect, generated by sequentially acquired demonstrations (Spade, 1972). We make progress from one conclusion to another, since every conclusion sheds light on the middle terms of the syllogism and improves the knowledge of other conclusions. Science is the science of the conclusions, and conclusions allow us to mentally grasp the underlying principles, i.e., the first truths. A single act of the intellect simultaneously grasps the truth of the principle and the truth of the conclusion.

Despite our severe critique of his razor, Ockham's philosophy could still make a huge contribution to this debate. Ockham is notorious just for his Razor, as Ravel is notorious just for his Bolero, despite their (scientific and musical) output is overwhelmingly rich of almost forgotten treasures. To unravel the freshness of Ockham's thought, we will start from an epistemological account of quantum mechanics. Quantum mechanics has been interpreted by influential scientists as a reference-frame theory pertaining to observer-dependent relational properties (Smerlak & Rovelli, 2007; Yang, 2018). Relational formulations of quantum mechanics have been experimentally supported by recent papers that contradict the tenets of local realism (The BIG Bell Test Collaboration, 2018; Proietti et al., 2019), the same local realism which states that: "the properties of the physical world are independent from the observer". In the fascinating Wigner's friend paradox, John is sealed in a lab and measures a particle, while Nicholas stands outside. Suppose that John is entangled with Nicholas in such a way that they perceive that the particles they measure are correlated. According to quantum mechanics, particles are allowed to occupy both John's and the Nicholas' locations at once, i.e., they are superimposed. However, when John observes his particle, the same act of observing "collapses" the particle to just one spot, so that John detects the two particles as not anymore superimposed. Yet for Nicholas the superposition remains: he will detect the collapse occurring when he will make a measurement of his own particle sometime later. This means that John's and Nicholas' experiences are frankly conflicting. The Wigner's friend paradox, once believed to be just an exotic *gedankenexperiment*, has been recently experimentally challenged. Bong et al. (2020) found, again, an irreconcilable mismatch between John's and Nicholas' observations. Their conclusions were that the unitary, deterministic evolution of isolated systems and the non-unitary, probabilistic state update after a quantum measurement are hard to reconcile at all coarse-grained scales, including the macro-scales of the observers. Therefore, the slogan "every observed event exists absolutely, not relatively" could be physically erroneous.

Here a philosophical concept from our medieval past comes into play and might help to solve the conundrum. In the question 19 of the second quodlibet, William of Ockham asks whether the proposition "*hoc est corpus meum*" ("this is my body") is literally true as uttered by the priest at mass (Ockham, 1991). According to Ockham, to every spoken proposition corresponds some mental proposition. When the priest utters the first words "*hoc est*", the body of Christ

does not exist yet in the Eucharist, because the words "*hoc est*" are not themselves determinate enough to fix the meaning intended by the speaker. Indeed, the priest's utterance in the middle of the phrase is true as mental proposition, but it is not yet true as spoken proposition, because the subsequent words "*corpus meum*" have not yet been pronounced. According to Ockham, a mental proposition is true at the beginning and at the end, because it exists as a whole all at once. This means that a mental proposition can be termed "*ens permanens*" (a permanent entity). In turn, a spoken proposition exists just successively and not all at once, so that it is true at the end but not at the beginning of the utterance. This means that a spoken proposition can be termed "*ens successivum*" (a successive entity). The spoken proposition is not true at the beginning, rather it is true at the end of the utterance. Coming back to relational quantum mechanics, we may state that reality itself is different at the beginning and at the end of the utterance, or, in non-linguistic setups, we may state that reality itself is different at the beginning and at the end of the experimental procedures to detect quantum phenomena. To provide an example, at the beginning of quantum entanglement measurements nobody knows which quantum state will be detected after the experiment has been performed. Quantum reality stands for an *ens successivum* such that only a part of it exists at any given time.

A further leap is required to proceed towards a novel epistemological approach to quantum mechanics: from relationism to interactionism. This means that the role of time, underrated and almost despised in quantum mechanics (Moreva et al., 2014), must be kept into account, since a deep difference does exist inside a quantum state before and after the observer's measurement. To move onwards, we are required to go back to Gregory of Rimini and his theory of *complexe significabile* (Zupko, 1994). Gregory of Rimini suggests that the intuition of a preposition and the comprehension of its meaning are two different mental acts (Dal, 1956). The subject who agrees to a scientific issue does not keep into account the proposition or its conclusion, rather he keeps into account what does the proposition mean, or its truth (sic *esse vel* sic *non esse*). The simple apprehension and intuition of a proposition are not yet scientific knowledge, the latter requiring intensionality and agreement: you do not need water as it is, rather you need water because you are thirsty. Therefore, the object of the scientific knowledge does not consist of the simple demonstration, rather it consists of the total (unitary) meaning of the conclusion independent of the same proposition. The object of the scientific knowledge is termed "*complexe significabile*", i.e., the "that clause" introduced by the Oxonensis Adam of Wodeham and exported by Gregory to the University of Paris (Nannini, 2015). "*Homo est albus*" stands neither for "*homo*", nor for "*albedo*", rather it stands for a total meaning which is different from both real objects and mental entities. "*Homo est albus"* becomes a distinct entity, separate from the subject "*homo*" and the predicate "*est albus*", since it does match neither the "*homo*", nor "*est albus*". Therefore, the object of scientific knowledge becomes the mental process of agreement to the possible true meanings.

Gregory's *complexe significabile* was condemned in 1277 by the scholars of the University of Paris, because they reputed his approach unnecessarily expanding the eternal truths: to provide an example, the phrase "the Father is correlated with the

Son" might point towards something different from the Father and the Son. Leaving apart Gregory's ultimate output concerning divine realities, we may state, in fully agreement with him, that the activity of the human mind produces fictious entities. For in the end our mental activity increases the number of entities, so that our subjectivity multiplies concepts by default. If such entities and concepts are real of fictitious, it does not matter anymore: what counts is that the possible meaning of a proposition becomes the real meaning in relational quantum mechanics.

Acknowledgments The Author would like to thank Vittorio Tozzi, M.D., Ospedale Cardarelli (Naples, Italy), for the useful suggestions.

Authors' Contribution The Author had full access to all the data in the study and take responsibility for the integrity of the data and the accuracy of the data analysis. The Author performed: study concept and design, acquisition of data, analysis and interpretation of data, drafting of the manuscript, critical revision of the manuscript for important intellectual content, statistical analysis, obtained funding, administrative, technical, and material support, study supervision.

Declarations

The author warrants that the article is original, does not infringe on any copyright or other proprietary right of any third part, is not under consideration by another journal, and has not been previously published.

Conflict of Interest The Author does not have any known or potential conflict of interest including any financial, personal or other relationships with other people or organizations within three years of beginning the submitted work that could inappropriately influence, or be perceived to influence, their work.

Human and Animal Rights and Informed Consent This research does not contain any studies with human participants or animals performed by the Author.

References

Ackerman, R. (1961). Inductive simplicity. *Philosophy of Science, 28*, 162–171.

Akaike, H. (1973). Information theory and the extension of the maximum likelihood principle. In B. Petrov & F. Csaki (Eds.), *Second International Symposium on Information Theory*. Akademiai Kiado.

Andreu-Moreno, I., & Sanjuán R. (2020). Collective viral spread mediated by virion aggregates promotes the evolution of defective interfering particles. *mBio, 11*(1). https://doi.org/10.1128/mBio.02156-19.

Appenzeller-Herzog, C., & Hauri, H.-P. (2006). The ER-Golgi intermediate compartment (ERGIC): In search of its identity and function. *Journal of Cell Science, 2006*(119), 2173–2183. https://doi.org/10.1242/jcs.03019.

Badiou, A. (1888). Being and event. Bloomsbury, London (2015).

Baker, A. (2003). Quantitative parsimony and explanatory power. *British Journal for the Philosophy of Science, 54*, 245–259.

Barnes, E. C. (2000). Ockham's razor and the anti-superfluity principle. *Erkenntnis, 53*, 353–374.

Bechtel, W. (2008). Mental Mechanisms: Philosophical Perspectives on Cognitive Neuroscience. Lawrence Erlbaum Associates. ISBN: 978-0-8058-6333-8.

Bellmund, L. S., Gärdenfors, P., Moser, E. I., & Doeller, C. F. (2018). Navigating cognition: Spatial codes for human thinking. *Science, 362*(6415), eaat6766. https://doi.org/10.1126/science.aat6766.

Bhowmik, S., & Krishnamurthy, R. (2019). The role of sugar-backbone heterogeneity and chimeras in the simultaneous emergence of RNA and DNA. *Nature Chemistry, 11*, 1009–1018.

Bobrovskiy, I., Hope, J. M., Ivantsov, A., Nettersheim, B. J., Hallmann, C., & Brocks, J. J. (2018). Ancient steroids establish the Ediacaran fossil Dickinsonia as one of the earliest animals. *Science., 361*(6408), 1246–1249. https://doi.org/10.1126/science.aat7228.

Bong, K.-W., Utreras-Alarcón, A., Ghafari, F., Liang, Y.-C., Tischler, N. et al. (2020). A strong no-go theorem on the Wigner's friend paradox. *Nature Physics, 16*, 1199–1205.

Brian D.A., Baric R.S. 2005. Coronavirus Genome Structure and Replication. In: Enjuanes L. (eds) Coronavirus Replication and Reverse Genetics. Current Topics in Microbiology and Immunology, vol 287. Springer.

Brown, M. K., & Naidoo, N. (2012). The endoplasmic reticulum stress response in aging and age-related diseases. *Frontiers in Physiology, 3*, 263. https://doi.org/10.3389/fphys.2012.00263.

Budday S, Sommer G, .Haybaeck J, Steinmann P, Holzapfel GA, Kuhl E. 2017. Rheological characterization of human brain tissue. Acta Biomaterialia, 60, 315-329. https://doi.org/10.1016/j.actbio.2017.06.024.

Bunge, M. (1961). The weight of simplicity in the construction and assaying of scientific theories. *Philosophy of Science, 28*, 162–171.

Calvo-Rodríguez, M., García-Durillo, M., Villalobos, C., & Núñez, L. (2016). In vitro aging promotes endoplasmic reticulum (ER)-mitochondria Ca 2+ cross talk and loss of store-operated Ca 2+ entry (SOCE) in rat hippocampal neurons. *Biochimica et Biophysica Acta, 1863*(11), 2637–2649. https://doi.org/10.1016/j.bbamcr.2016.08.001.

Chadwick, S. R., & Lajoie, P. (2019). Endoplasmic reticulum stress coping mechanisms and lifespan regulation in health and diseases. *Frontiers in Cell and Development Biology, 7*, 84. https://doi.org/10.3389/fcell.2019.00084.

Chamberlain, B.P., Clough, J., Deisenroth, M.P. (2017). Neural Embeddings of Graphs in Hyperbolic Space. arXiv:1705.10359.

Chater, N. (1999). The search for simplicity: A fundamental cognitive principle. *The Quarterly Journal of Experimental Psychology, 52A*, 273–302.

Chen, J., Quiles-Puchalt, N., Chiang, Y. N., Bacigalupe, R., Fillol-Salom, A., et al. (2018). Genome hypermobility by lateral transduction. *Science, 362*(6411), 207–212. https://doi.org/10.1126/science.aat5867.

Chen, Y., Liu, Q., & Guo, D. (2020). Emerging coronaviruses: Genome structure, replication, and pathogenesis. *Journal of Medical Virology, 92*(4), 418–423. https://doi.org/10.1002/jmv.25681.

Cho, J.-H., Saini, D. K., Karunarathne, W. K. A., Kalyanaraman, V., & Gautam, N. (2011). Alteration of Golgi structure in senescent cells and its regulation by a G protein γ subunit. *Cellular Signalling, 23*(5), 785–793. https://doi.org/10.1016/j.cellsig.2011.01.001.

D'Angiolo, M., De Chiara, M., Yue, J. X., Irizar, A., Stenberg, S., et al. (2020). A yeast living ancestor reveals the origin of genomic introgressions. *Nature, 587*, 420–425. https://doi.org/10.1038/s41586-020-2889-1.

Dal, P. M. (1956). la teoria del "significato totale" della proposizione nel pensiero di Gregorio da Rimini. *Rivista Critica di Storia della Filosofia, 11*(3/4), 287–311.

de Haan, C. A., & Rottier, P. J. M. (2006, 2006). Hosting the severe acute respiratory syndrome coronavirus: Specific cell factors required for infection. *Cellular Microbiology*. https://doi.org/10.1111/j.1462-5822.2006.00744.x.

Del Giudice, F., Tassieri, M., Oelschlaeger, C., & Shen, A. Q. (2017). When microrheology, bulk rheology, and microfluidics meet: Broadband rheology of hydroxyethyl cellulose water solutions. *Macromolecules, 50*(7), 2951–2963. https://doi.org/10.1021/acs.macromol.6b02727.

Deleuze, G., Guattari, F. (1980). A Thousand Plateaus: Capitalism and Schizophrenia. Ed. Bloomsbury Publishing PLC, 1988, EAN: 9780485113358.

Despres, J., Ramdani, Y., di Giovanni, M., Bénard, M., Zahid, A., et al. (2019). Replicative senescence of human dermal fibroblasts affects structural and functional aspects of the Golgi apparatus. *Experimental Dermatology, 28*(8), 922–932. https://doi.org/10.1111/exd.13886.

Ehre, C. (2020). SARS-CoV-2 infection of airway cells. *The New England Journal of Medicine, 383*, 969. https://doi.org/10.1056/NEJMicm2023328.

ElSheikh M, Arani A, Perry A, Boeve BF, Meyer FB, 2017 et al. MR Elastography demonstrates unique regional brain stiffness patterns in dementias. AJR. American Journal of Roentgenology 209(2):403-408. https://doi.org/10.2214/AJR.16.17455.

Forster, M., & Sober, E. (1994). How to tell when simpler, more unified, or less ad hoc theories will provide more accurate predictions. *British Journal for the Philosophy of Science, 45*, 1–35.

Foster, M., & Martin, M. (1966). *Probability, confirmation, and simplicity: Readings in the philosophy of inductive logic*. The Odyssey Press.

Friedman, M. (1974). Explanation and scientific understanding. *Journal of Philosophy, LXXI*, 1–19.

Friston, K. (2010). The free-energy principle: A unified brain theory? *Nature Reviews. Neuroscience, 11*(2), 127–138.

Fu, L., Steinhardt, W., Zhao, H., Socolar, J. E. S., & Charbonneau, P. (2016). Hard sphere packings within cylinders. *Soft matter. Royal Society of Chemistry, 12*(9), 2505–2514.

Gerischer LM, Fehlner A, Köbe T, Prehn K, Antonenko D, 2017 et al. Combining viscoelasticity, diffusivity and volume of the hippocampus for the diagnosis of Alzheimer's disease based on magnetic resonance imaging. Neuroimage Clin. 18:485-493. https://doi.org/10.1016/j.nicl.2017.12.023.

Gibbons, A. (2017). Neandertals mated early with modern humans. *Science, 357*(6346), 14. https://doi.org/10.1126/science.357.6346.14.

Goodman, N. (1959). Recent developments in the theory of simplicity. *Philosophy and Phenomenological Research, 19*, 429–446.

Harman, G. (1999). Simplicity as a pragmatic criterion for deciding what hypotheses to take seriously. In G. Harman (Ed.), *Reasoning, meaning and mind*. Oxford University Press.

Hesse, M. (1974). *The structure of scientific inference*. Macmillan.

Hipolito, I. (2019). A simple theory of every 'thing'. *Physics of Life Reviews.* https://doi.org/10.1016/j.plrev.2019.10.006.

Hofstadter, D., Sander, E. (2011). Surfaces and Essences: Analogy as the Fuel and Fire of Thinking. Basic Books.

Ivantsov, A. Y. (2007). Small Vendian transversely articulated fossils. *Paleontological Journal., 41*(2), 113–122. https://doi.org/10.1134/S0031030107020013.

Janikiewicz, J., Szymański, J., Malinska, D., Patalas-Krawczyk, P., Michalska, B., et al. (2018). Mitochondria-associated membranes in aging and senescence: Structure, function, and dynamics. *Cell Death & Disease, 9*(3), 332. https://doi.org/10.1038/s41419-017-0105-5.

Ke, Z., Oton, J., Qu, K., Cortese, M., Zila, V., et al. (2020). Structures and distributions of SARS-CoV-2 spike proteins on intact virions. *Nature.* https://doi.org/10.1038/s41586-020-2665-2.

Kelly, K. (2004). Justification as truth-finding efficiency: How Ockham's razor works. *Minds and Machines, 14*, 485–505.

Koczkodaj, W. W., Magnot, J.-P., Mazurek, J., Peters, J. F., Rakhshani, H., Soltys, M., Strzałka, D., Szybowski, J., & Tozzi, A. (2017). On normalization of inconsistency indicators in pairwise comparisons. *International Journal of Approximate Reasoning., 86*, 73–79. https://doi.org/10.1016/j.ijar.2017.04.005.

Leeks, A., Sanjuán, R., & West, S. A. (2019). The evolution of collective infectious units in viruses. *Virus Research, 265*, 94–101. https://doi.org/10.1016/j.virusres.2019.03.013.

Lin, Y., Yan, X., Cao, W., Wang, C., Feng, J., et al. (2004). Probing the structure of the SARS coronavirus using scanning electron microscopy. *Antiviral Therapy, 9*(2), 287–289.

Liu, L., Wang, J., Feng, J., Yao, M., Hao, C., et al. (2018). Serum Golgi protein 73 is a marker comparable to APRI for diagnosing significant fibrosis in children with liver disease. *Scientific Reports, 8*(1), 16730. https://doi.org/10.1038/s41598-018-34714-y.

Lu, Z., & Raz, O. (2017). Nonequilibrium thermodynamics of the Markovian Mpemba effect and its inverse. *PNAS, 114*(20), 5083–5088.

Massilani, D., Skov, L., Hajdinjak, M., Gunchinsuren, B., Tseveendorj, D., et al. (2020). Denisovan ancestry and population history of early east Asians. *Science, 370*(6516), 579–583. https://doi.org/10.1126/science.abc1166.

McGinn, C. (1994). The problem of philosophy. *Philosophical Studies, 76*(2–3), 133–156. https://doi.org/10.1007/bf00989821.

Miceli, S., Ness, T. V., Einevoll, G. T., & Schubert, D. (2017). Impedance Spectrum in cortical tissue: Implications for propagation of LFP signals on the microscopic level. *eNeuro, 4*(1). https://doi.org/10.1523/ENEURO.0291-16.2016.

Millen, S., Gross, C., Donhauser, N., Mann, M. C., Péloponèse Jr., J. M., & Thoma-Kress, A. K. (2019). Collagen IV (COL4A1, COL4A2), a component of the viral biofilm, is induced by the HTLV-1 Oncoprotein tax and impacts virus transmission. *Frontiers in Microbiology, 10*, 2439. https://doi.org/10.3389/fmicb.2019.02439.

Moreva, E.V., Brida, G. Gramegna, M., Giovannetti, V. (2014). Entanglement discloses Time as an emergent phenomenon. 2014 Conference: CLEO: QELS_Fundamental Science. https://doi.org/10.1364/CLEO_QELS.2014.FW1A.8.

Murphy, M. C., Huston III, J., Jack Jr., C. R., Glaser, K. J., Manduca, A., et al. (2011). Decreased brain stiffness in Alzheimer's disease determined by magnetic resonance elastography. *J MagnReson Imaging., 34*(3), 494–498. https://doi.org/10.1002/jmri.22707.

Nannini, A. (2015). Pierre Ceffons di Clairvaux. La questione dei significabilia complexe intorno al 1350. I. Edizione della quaestio 25 della Lectura super I Sententiarum. Rivista Di Filosofia Neo-Scolastica - 2015 - 4.

Ockham, W. (1991). Quodlibetal questions. Eds. Freddoso AJ, Kelley FE. Yale University Press.

Ogilvie, G. I., & Proctor, M. R. E. (2003). On the relation between viscoelastic and magnetohydrodynamic flows and their instabilities. *Journal of Fluid Mechanics, 476*, 389–409. https://doi.org/10.1017/S0022112002003051.

Oreskes, N., Shrader-Frechette, K., & Belitz, K. (1994). Verification, validation, and confirmation of numerical models in the earth sciences. *Science, 263*, 641–646.

Parri, N., Lenge, M., & Buonsenso, D. (2020). Children with Covid-19 in pediatric emergency departments in Italy. *NEJM*. https://doi.org/10.1056/NEJMc2007617.

Proietti, M., Pickston, A., Graffitti, F., Barrow, P., Kundys, D., et al. (2019). Experimental test of local observer independence. *Science Advances, 5*(9), eaaw9832. https://doi.org/10.1126/sciadv.aaw9832.

Qiu, H., Wu, J., Hong, L., Luo, Y., Song, Q., & Chen, D. (2020). Clinical and epidemiological features of 36 children with coronavirus disease 2019 (COVID-19) in Zhejiang, China: An observational cohort study. *The Lancet Infectious Disease*. https://doi.org/10.1016/S1473-3099(20)30198-5.

Ranta, R., Le Cam, S., Tyvaert, L., & Louis-Dorr, V. (2017). Assessing human brain impedance using simultaneous surface and intracerebral recordings. *Neuroscience, 343*.

Risco, C., Rodríguez, J. R., López-Iglesias, C., Carrascosa, J. L., Esteban, M., & Rodríguez, D. (2002). Endoplasmic reticulum-Golgi intermediate compartment membranes and vimentin filaments participate in vaccinia virus assembly. *Journal of Virology, 76*(4), 1839–1855.

Segredo-Otero, E., & Sanjuán, R. (2019). The effect of genetic complementation on the fitness and diversity of viruses spreading as collective infectious units. *Virus Research, 267*, 41–48. https://doi.org/10.1016/j.virusres.2019.05.005.

Sengupta, B., Tozzi, A., Coray, G. K., Douglas, P. K., & Friston, K. J. (2016). Towards a neuronal gauge theory. *PLOS Biology, 14*(3), e1002400. https://doi.org/10.1371/journal.pbio.1002400.

Shaltiel-Karyo, R., Frenkel-Pinter, M., Rockenstein, E., Patrick, C., Levy-Sakin, M., et al. (2013). A blood-brain barrier (BBB) disrupter is also a potent α-synuclein (α-syn) aggregation inhibitor: A novel dual mechanism of mannitol for the treatment of Parkinson disease (PD). *The Journal of Biological Chemistry, 288*(24), 17579–17588. https://doi.org/10.1074/jbc.M112.434787.

Shamaev, A. S., & Shumilova, V. V. (2018). Calculation of natural frequencies and damping coefficients of a multi-layered composite using homogenization theory. *IFAC-PapersOnLine, 51*(2), 126–131. https://doi.org/10.1016/j.ifacol.2018.03.022.

Slon, V., Mafessoni, F., Vernot, B., de Filippo, C., Grote, S., et al. (2018). The genome of the offspring of a Neanderthal mother and a Denisovan father. *Nature, 561*, 113–116.

Smerlak, M., & Rovelli, C. (2007). Relational EPR. *Foundations of Physics, 37*, 427–445.

Sowa, J. F., & Majumdar, A. K. (2003). *Analogicalal reasoning. Conceptual structures for knowledge creation and communication, proceedings of ICCS 2003*. Springer-Verlag.

Spade, P. V. (1972). The unity of a science according to Peter Auriol. *Franciscan Studies, 32*, 203–217.

Su, Y., Wang, P., Shen, H., Sun, Z., Xu, C., et al. (2018). The protein kinase D1-mediated classical protein secretory pathway regulates the Ras oncogene-induced senescence response. *Journal of Cell Science, 131*(6), jcs207217. https://doi.org/10.1242/jcs.207217.

Sylla, E. D. (1998a). God, indivisibles, and logic in the later middle ages: Adam Wodeham's response to Henry of Harclay. *Medieval Philosophy and Theology, 7*(1998), 69–87.

Sylla, D. E. (1998b). God, indivisibles, and logic in the later middle ages: Adam Wodeham's response to Henry of Harclay. *Medieval Philosophy and Theology, 7*(1), 69–87.

Teich, E. G., et al. (2016). 'Clusters of polyhedra in spherical confinement', proceedings of the National Academy of Sciences. *National Acad Sciences, 113*(6), E669–E678.

The BIG Bell Test Collaboration. (2018). Challenging local realism with human choices. *Nature, 557*, 212–216.

Thoulouze, M. I., & Alcover, A. (2011). Can viruses form biofilms? *Trends in Microbiology, 19*(6), 257–262. https://doi.org/10.1016/j.tim.2011.03.002.

Torres-González, E., Bueno, M., Tanaka, A., Krug, L. T., & Cheng, D.-S. (2012). Role of endoplasmic reticulum stress in age-related susceptibility to lung fibrosis. *American Journal of Respiratory Cell and Molecular Biology, 46*(6), 748–756. https://doi.org/10.1165/rcmb.2011-0224OC.

Tozzi, A. (2015). Information processing in the CNS: A Supramolecular chemistry? *Cognitive Neurodynamics, 9*(5), 463–477.

Tozzi, A. (2019). The multidimensional brain. *Physics of Life Reviews, 31*, 86–103. https://doi.org/10.1016/j.plrev.2018.12.004.

Tozzi, A., & Peters, J. F. (2018). What it is like to be "the same"? *Progress in Biophysics and Molecular Biology., 133*, 30–35. https://doi.org/10.1016/j.pbiomolbio.2017.10.005.

Tozzi, A., & Peters, J. F. (2020a). Removing uncertainty in neural networks. *Cognitive Neurodynamics, 14*, 339–345. https://doi.org/10.1007/s11571-020-09574-w.

Tozzi, A., & Peters, J. F. (2020b). A topological approach to infinity in physics and biophysics. *Foundations of Science*. https://doi.org/10.1007/s10699-020-09674-0.

Turalska, M., & West, B. J. (2018). Fractional dynamics of individuals in complex networks. *Frontiers of Physics, 6*, 110. https://doi.org/10.3389/fphy.2018.00110.

Turoňová, B., Sikora, M., Schürmann, C., Hagen, W. J. H., Welsch, S., et al. (2020). In situ structural analysis of SARS-CoV-2 spike reveals flexibility mediated by three hinges. *Science.* https://doi.org/10.1126/science.abd5223.

Udono, M., Fujii, K., Harada, G., Tsuzuki, Y., Kadooka, K., et al. (2015). Impaired ATP6V0A2 expression contributes to Golgi dispersion and glycosylation changes in senescent cells. *Scientific Reports, 5*, 17342.

Waninger, S., Ahlfors, S., Stikic, M., Korszen, S., Berka, C., et al. (2016). Identification of neurophysiological biomarkers of mci using resting state EEG. *Alzheimer & Dementia, 12*(7, Supplement), P882. https://doi.org/10.1016/j.jalz.2016.06.1823.

Watanabe, Y., Allen, J. D., Wrapp, D., McLellan, J. S., & Crispin, M. (2020). Site-specific glycan analysis of the SARS-CoV-2 spike. *Science, 369*(6501), 330–333. https://doi.org/10.1126/science.abb9983.

Yang, J. M. (2018). A relational formulation of quantum mechanics. *Scientific Reports, 8,* 13305.

Zupko, J. (1994). How it played in the rue de Fouar re: The reception of Adam wodeham's theory of the _Complexe Significable_ in the arts faculty at Paris in the mid-fourteenth century. *Franciscan Studies, 54*(1), 211–225.

Publisher's Note Springer Nature remains neutral with regard to jurisdictional claims in published maps and institutional affiliations.

Foundations of Science
https://doi.org/10.1007/s10699-021-09798-x

A Geometric Milieu Inside the Brain

Arturo Tozzi[1] · **Alexander Yurkin**[2] · **James F. Peters**[3,4]

Accepted: 6 May 2021
© The Author(s), under exclusive licence to Springer Nature B.V. 2021

Abstract
The brain, rather than being homogeneous, displays an almost infinite topological genus, since it is punctured with a high number of "cavities". We might think to the brain as a sponge equipped with countless, uniformly placed, holes. Here we show how these holes, termed topological vortexes, stand for nesting, non-concentric brain signal cycles resulting from the activity of inhibitory neurons. Such inhibitory spike activity is inversely correlated with its counterpart, i.e., the excitatory spike activity propagating throughout the whole brain tissue. We illustrate how Pascal's triangles and linear and nonlinear arithmetic octahedrons are capable of describing the three-dimensional random walks generated by the inhbitory/excitatory activity of the nervous tissue. In case of nonlinear 3D paths, the trajectories of excitatory spiking oscillations can be depicted as the operation of filling the numbers of octahedrons in the form of "islands of numbers": this leads to excitatory neuronal assemblies, spaced out by empty areas of inhibitory neuronal assemblies. These mathematical procedures allow us to describe the topology of a brain of infinite genus, to represent inhibitory neurons in terms of Betti numbers and to highlight how spike diffusion in neural tissues is generated by the random activation of tiny groups of excitatory neurons. Our approach suggests the existence of a strong mathematical background subtending the intricate oscillatory activity of the central nervous system.

Keywords Arithmetic figures · Central nervous system · Nonlinear · Excitatory/inhibitory ratio · Neurons

✉ Arturo Tozzi
tozziarturo@libero.it; Arturo.Tozzi@unt.edu

Alexander Yurkin
alvl1yurkin@rambler.ru

James F. Peters
james.peters3@umanitoba.ca

1 Center for Nonlinear Science, University of North Texas, 1155 Union Circle, #311427, Denton, TX 76203-5017, USA

2 Russian Academy of Sciences, Moscow, Puschino, Russia

3 Department of Electrical and Computer Engineering, University of Manitoba, 75A Chancellor's Circle, Winnipeg, MB R3T 5V6, Canada

4 Mathematics Department, Adiyaman University, Adiyaman, Turkey

Published online: 13 May 2021

Content courtesy of Springer Nature, terms of use apply. Rights reserved.

1 Introduction

The brain is a Riemannian manifold with genus zero. In other words, the brain does not contain holes: this tenet is implicitly assumed by the most influential accounts of the nervous activity (Friston & Ao, 2012; Telley et al., 2019). Genus is a particular topological invariant linked to the Euler characteristic that is generally used to classify 2D manifolds, but it can be generalized in higher dimensions too. In this paper, we will tackle the issue of a scarcely observed topological property of the brain that goes against the mainstream "genus zero opinion". Come to thing of it, it could be stated that the brain exhibits countless holes, because the neural tissue encompasses neurons devoid of excitatory spikes, i.e., the neural tissue displays transient neuronal "punctures" with inhibitory activity (Hodge et al., 2019). This means that the brain is equipped with a countless, or at least very high, number of holes surrounding the excitatory spiking neurons. We will term these holes "brain vortexes" (Don et al., 2020). Assuming that the brain is isotropic/homogeneous at very large scales and that the excitatory/inhibitory ratio is constant, the tissue concentration of these holes must be homogeneous too. To make a trivial example, we might think to the brain as a sponge equipped with countless and uniformly placed holes. Here we will try to answer to crucial questions: how are brain vortexes produced during nervous activity? Can they be described in mathematical terms, i.e., within the geometric dynamics on a 3D manifold of infinite genus? Is the brain depending on mathematical rules? What are the topological features, peculiarities and predictable physical consequences of a brain described in terms of a Riemannian manifold with high, almost infinite, genus? To answer these questions, we introduce a deterministic geometric model that permits visual constructions of linear (without any acceleration) and nonlinear (with the simplest uniformly acceleration) random walks in three-dimensional spaces. Our model is derived from the Pascal's triangle, an array of the binomial coefficients widely used in numerous contexts. Its applications in mathematics extend to algebra, calculus, trigonometry, plane and solid geometry. Pascal's Triangle is widely used in algebra and probability/combinatorics (Edwards, 2013), since it allows us to find without tedious computations the number of subsets of r elements that can be formed from a set with n distinct elements (Brothers, 2012). In the real world, this leads into the topic of graph theory, such as, e.g., turning mapping information into structures such as shortest paths, airplane routes and airport control, Dijkstra's algorithm, computer graphics, engineering, search algorithms and data management. Other examples of the scientific utility of Pascal's triangle can be provided. In a triangular portion of a grid, the number of shortest grid paths from a given node to the top node is the corresponding entry in Pascal's triangle. Proton Nuclear Magnetic Resonance displays an inherent geometry in which Pascal's triangles has a prominent role (Hore, 1983).

In the following, we will show how Pascal's triangle-derived model may describe the paths of random walks that produce brain vortexes and short- and long-range nervous oscillations.

Content courtesy of Springer Nature, terms of use apply. Rights reserved.

2 Geometric Models of Random Walks

Simple visual geometric models are required to make it easy to understand the description of complex phenomena (Klein, 1956; Sommerfeld, 1973). Recursive formulas to calculate the step-shaped Pascal's triangle at various initial conditions and during random walks processes have been suggested.

Pascal's arithmetic triangle, its analogues, generalizations and possible applications of visual geometric models have been thoroughly carried out (Yurkin, 2013, 2016, 2018; Yurkin et al., 2018). Novel, stepwise form for Pascal's triangle (1D), two-sided (2D) and multidimensional generalizations can be achieved in linear models of random walks (Kolmogorov et al., 1995). Yurkin (1995) proposed an optical laser scheme standing for a nonlinear 1D walk in a system of rays; further, a real laser nonlinear 2D random walk in a system of rays was carried out. Nonlinear and non-Markovian random walks were described by Fedotov and Korabel (2015). Sarkar and Maiti (2017) portrayed a symmetric random walk on a regular tetrahedron, an octahedron and a cube. In the 1D case (along a straight line), a random walk (linear and nonlinear) can occur along two mutually perpendicular directions (right, left) inside an arithmetic triangle (the triangle has two corners on his base and one on his top) (Kolmogorov et al., 1995). In the 2D case, a random walk (linear and nonlinear) can be carried out in four different directions (forward, back, right, left) inside an arithmetic square (the square has four corners) (Yurkin, 2019a).

Linear and nonlinear 3D random walks has been described as visual linear and nonlinear 3D models in form of arithmetic octahedrons (Yurkin,). In the 3D case of a Pascal's triangle, random walks (both linear and nonlinear) can be carried out in six different directions (forward, backward, right, left, up, down) inside an arithmetic regular octahedron equipped with six vertices. For further details, see Yurkin (). Sequential iterations of octahedrons composed of small cubes describe the number of walks from the initial cell (initial cube) to the final cell (final cube). In the linear case, neighboring empty cells will densely fill the linear arithmetic octahedrons at the next iterations, without leaving any gaps or

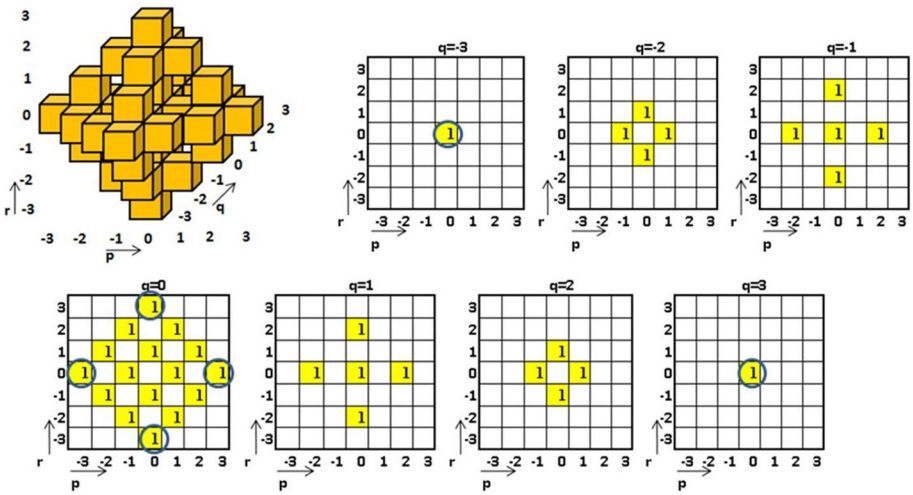

Fig. 1 The second iteration ($n = 2$) of the nonlinear arithmetic octahedron consists of 36 cubes. The Figures $q = \pm 1$ show the formation of separate structures of numbers ("islands of numbers"). Modified from: Yurkin (2019b, 2019c)

Content courtesy of Springer Nature, terms of use apply. Rights reserved.

empty spaces. In turn, a 3D nonlinear random walk in a volume can be described as octahedrons not tightly filled with cubes (branching cells). See Fig. 1 for further details. Some empty cells inside the octahedrons (white cubes or gaps) will be filled with yellow cubes at the next iteration, some empty cells will be filled after every iteration, and so on. For big *n* numbers, the relative quantity of the empty cells or gaps (related to the general quantity of cells in nonlinear octahedron) decreases with increases in number n.

3 Brain Random Walks Come Into Play

The iterations illustrated in in the previous paragraph permit the classification of different types of random walks in the form of the following table:

	Linear random walk (one unit steps, perpendicular each others)	**Nonlinear random walk** (first one unit steps, second two units steps, third three unit steps, ets., perpendicular each others)
3D case	• Steps of constant length along six perpendicular directions in octahedron • Gaps and "islands of numbers" are absent in a linear arithmetic octahedron	• Steps of increasing length along six perpendicular directions in octahedron • Gaps and "islands of numbers" appear and disappear in different areas in a nonlinear arithmetic octahedron after several iterations. The relative quantity of the empty cells or gaps decreases with increases in *n*

The self-organized brain oscillations in the central nervous system encompass spontaneous excitability that produce bifurcations. Indeed, the brain is a non-linear electromagnetic-activation oscillatory system at the edge of chaos with inter-dependent modules (Fraiman & Chialvo, 2012; Tognoli & Kelso, 2013; Tozzi et al., 2016; Wang et al., 2017; Xu & Wang, 2014). The occurrence of genetic-driven spontaneous oscillations during the brain development has been widely studied in both real and syntetic models. It is well-known that spontaneous cortical electric fluctuations occur before the 35th week of gestation (Krueger & Garvan, 2014) and are more frequently detectable in immature synapses (Kavalali et al., 2011). The neocortical circuits not just display rich spontaneous dynamics engaged by sensory inputs but are also able to generate outputs independent of external stimuli (Yuste et al., 2005). Trujillo et al. (2019) highlighted how structural and transcriptional changes in network activity spontaneously follow fixed genetic programming in human neocortical organoid models, producing random phase-amplitude coupling that resembles human neonatal EEG features. The transcriptional or epigenetic heterogeneity related to early biases in cell fate choices can be stochastic in nature (Soldatov et al., 2019; Velasco et al., 2019; Wang et al., 2019). These data highlight the critical role of spontaneous electromagnetic induction in the formation of an economical self-organized neuronal network. Given the predominant role of nonlinear stochastic paths in brain dynamics, the above-described Pascal's triangle-framed recursive formulas of geometric linear/nonlinear assemblies may find application to understand the nonlinear activity of neuronal oscillations' 3D random walks. In touch with the framework theorized by Pascal's triangle iterations, it is well-known that neural crest cells differentiate through a series of stereotypical lineage-restriction binary decisions that involve coexpression/competition of genes driving alternative fate programs (Soldatov et al., 2019). During migration, multipotent neural crest cells follow a

Content courtesy of Springer Nature, terms of use apply. Rights reserved.

progression of fate bifurcations that can be formalized as a series of sequential binary decisions assessable in terms of Pascal's triangle.

The spatiotemporal balance of the brain activity is kept equalized by varying the strengths of neuronal excitation (E) and inhibition (I) (Haider et al., 2006; Xue et al., 2014). A constant, steady E/I ratio does exist between the total amount of excitatory and inhibitory stimulation, both in vitro and in the intact cortex, both at the single neuron level and at the network excitability level (Sengupta & Stemmler, 2014; Sengupta et al., 2013). Excitation and inhibition are deeply matched: an optimal E/I ratio across neurons is always retained, despite the fluctuations in cortical levels' activity. E/I ratio stands for a homeostatic mechanism between strengthening and weakening processes in the adaptation of real synapses. Homeostasis triggers a discrepancy between inhibitory and excitatory connections that could contribute to symmetry breaking and leads to directed coupling and information transfer (Tognoli). E/I ratio could be regarded as the whole symmetry of the intact cerebral cortex. In terms of the Pascal's triangle model, the filled cells stand for single excitatory neurons, while the empty cells produced inside the octahedrons stand for inhibitory neurons (Fig. 2). After a few iterations, the empty cells will be progressively filled with yellow cubes: this means that areas of inhibition and excitation continuosly appear and disappear when further iterations take place during the expansion of the spike oscillation.

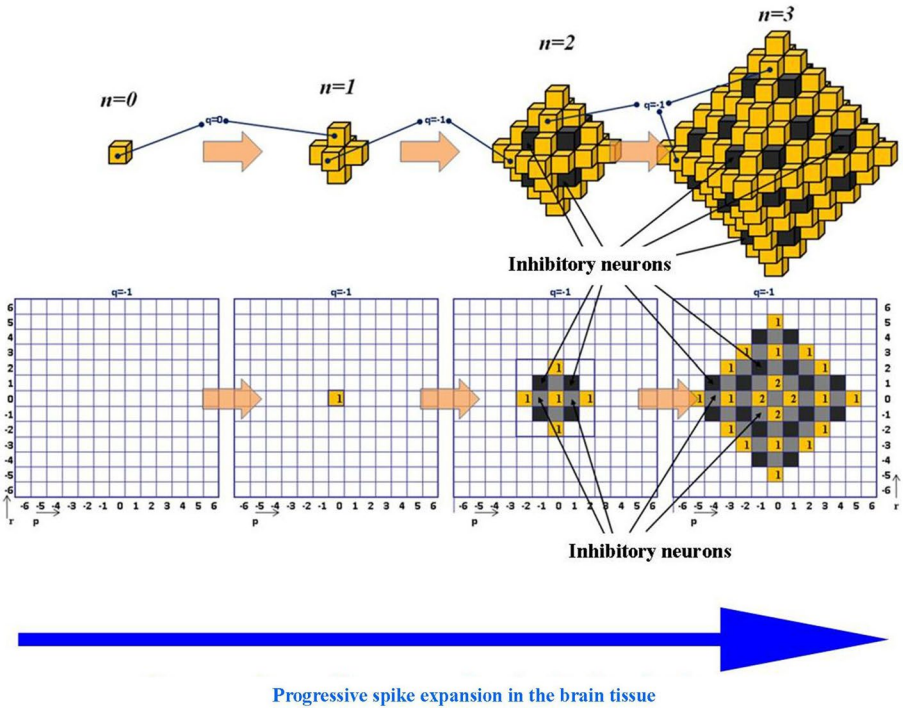

Fig. 2 Neural oscillation expansion and neuronal excitatory/inhibitory occurrence in terms of random walks taking place inside a 3D lattice. In our nonlinear octahedron model, inhibitory neurons look like dark gaps, while excitatory neurons like yellow filled cubes. Modified from: Yurkin (2019b, 2019c)

Content courtesy of Springer Nature, terms of use apply. Rights reserved.

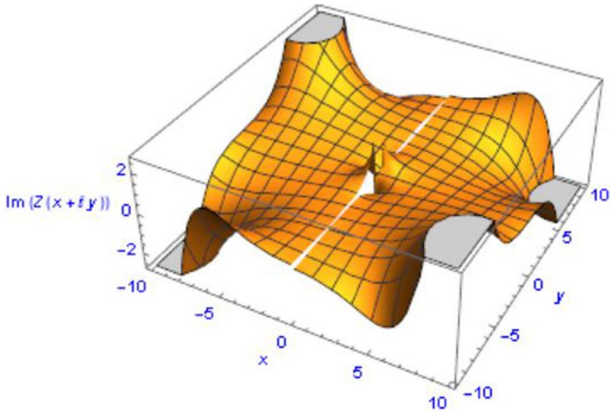

Fig. 3 A Riemannian surface with the center of the surface punctured with a hole

3.1 Vortex Cycles in Brain Spikes

A punctured manifold is analogous to a physical/biological space with holes. This means that we need to work on a manifold that is Riemannian. Briefly, a manifold is a topological space that is locally Euclidean (i.e., around every point, there is a neighborhood that is topologically the same as the open unit ball in R^n). A Riemann surface is a surface-like configuration that covers the complex plane with several, and in general infinitely many, "sheets". A sample Riemannian surface is shown in Fig. 3. It is easy to notice that the center of the surface is punctured with a hole, which stands, in our framework, for a rupture of neuronal excitability due to inhibitory components. Inhibitory neurons can be modelled as vortex cycles (Don et al., 2020; Peters, 2018, 2020) with induced order proximity of spiraling hole vortexes (Ahmad & Peters, 2019). The rim of this brain vortex cycle represents the edge of an inhibitory neuronal assembly. The inner cycles for a vortex reaching inward represent excitatory brain pull. Therefore, the brain can be depited as nesting, non-concentric vortex cycles embedded in a punctured Riemann surface (Weyl, 1955).

In this context, a novel formulation of the Borsuk Ulam theorem (BUT) might be of great help: the Vortex-BUT, which works on a manifold with holes. There are three forms of vortexBUT:

- Physical geometry vortex BUT (pevBUT): each pair of antipodal vortex hypersphere surface points $S^{n-1}(R^n)$ maps to the Euclidean space R^n.
- Region-based vortex BUT (revBUT): each pair of antipodal vortex hypersphere surface regions in $2^{S^{n-1}}$ (2^{R^n}) region points map to the Euclidean space 2^{R^n}(Peters, 2016).
- Descriptive vortex BUT (phivBUT): each pair of anitipodal vortex surface points OR regions maps to R^k, $k \geq 1$.

Each glial structure is an example of a massive vortex cycle. A punctured physical surface is a surface populated by vortices: this allows us to start viewing punctured brain surfaces using vortexBUT. The one very different thing about the new form of BUT is that we replace the Borsuk-Ulam use of S^n with V^n, a vortex in n-dimensional space. Then the simplest form of vortexBUT is defined by a continuous function

$$f : V^n \rightarrow R^n$$

Content courtesy of Springer Nature, terms of use apply. Rights reserved.

so that f(x) = f(− x) for antipodal points x, − x on V^n.

Several variants of BUT have been provided in the very last years to assess brain functions (Tozzi et al., 2017). Why do we need another BUT variant? The answer is straightforward, if we consider that single neurons may have an impact on surround firing statistics and even on simple behaviors. Exploiting the advantages of a simple cortex, Hemberger et al. (2019) examined the influence of single pyramidal neurons on their surrounding cortical circuits. Brief activations of single neurons triggered reliable sequences of firing in tens of other excitatory/inhibitory cortical neurons, reflecting cascading activity through local networks. The evoked pyramidal patterns extended over hundreds of micrometers from their source over up to 200 ms. In touch with a vortexBUT account of the brain, simultaneous activation of pyramidal cell "pairs" (i.e., neuronal activities with matching description as dicatated by BUT) stand for balanced control of population activity, preventing paroxysmal amplification. Single cortical pyramidal neurons can generate rapidly evolving and non-random firing sequences, in touch once again with our Pascal triangle's model (Hemberger et al., 2019).

4 Conclusions

Our account of deterministic models equipped with visual constructions of linear and non-linear 3D random walks through arithmetic figures displays interesting geometric and algebraic topological properties. The minuscule regions between brain cells have the appearance of cavities or holes in donut-shaped activation regions. From (Don et al., 2020), we know that brain activation regions have vortical structures defined by nested, possibly intersecting brain signal cycles resulting from the activity of inhibitory neurons. Here we observe that these brain activation region vortexes reside in a Riemannian space, since each brain vortex cycle does not have a sub-cycle that resides in the vortex. The brain, rather than being homogeneous, embodies a real, smooth Riemanning manifold in the sense that at each cell $p(x, y, z, t)$ (point in a 4D spacetime setting) we can describe a piecewise smooth mapping $f : \mathrm{R}^n \to \mathrm{R}$ defined by $\nabla f = \frac{\partial f}{\partial x} + \frac{\partial f}{\partial y} + \frac{\partial f}{\partial z} + \frac{\partial f}{\partial t}$ that maps the rate of change of p to a real number. In effect, a collection of brain cells has its own differential geometry. In 4D spaces, the rate of change of brain activity oscillates piecewise continuously in spiraling vortices represented by ∇f, encompassing linear random walks, in which the achieved arithmetic octahedron is densely filled with numbers. Each of these vortexes has its own ∇f represented by a free group providing its seeds in fMRI videos quantified with Betti numbers. In this context, a Betti number equals the number of generators of a free group representation (Munkres, 1984) of basin activation vortexes. These cortical Betti numbers arise naturally at a varying pace over spatio-temporal episodes in brain activity. In a Riemannian model of brain activity, f(p) and f(p′) loom as fixed points inasmuch as f(p) = p and f(p′) = p′ for the varying brain cell rates of change of $\nabla f(p), \nabla f(p')$. This view of brain cell activations residing on a Riemanning manifold represents a straightforward extension of the 2D view of a Riemannian surface (Weyl, 1955). Due to our lack of knowledge, we cannot specify whether our nervous Riemannian manifold with genus zero displays compactness or non-compactess. In case of compactness, we are in front of algebraic geometry rather than just geometry and our title should be "An Algebraic, topological and Geometric Milieu Inside the Brain" instead of just "A Geometric Milieu Inside the Brain".

Content courtesy of Springer Nature, terms of use apply. Rights reserved.

In cortical 4D spaces encompassing nonlinear random walks, the achieved arithmetic octahedron is not fully filled with numbers, since it contains gaps. Gaps, "islands of numbers" and separate structures of numbers appear and disappear inside the octahedron in the nonlinear 3D case after many iterations (Figs. 1 and 2). For high n numbers, the relative quantity of the empty cells or gaps (relative to the total number of cells in the nonlinear octahedron) decreases with increases in n. In sum, for nonlinear 3D cases, we can speak of filling the numbers of the arithmetic octahedron in the form of "islands of numbers" or separate structures of numbers, until a given threshold is reached. This leads us into the realm of a nonlinear brain punctured with inhibitory components that break the topological order of the neuronal tissue and propagating oscillations. The fact that physical constraints, such as the ones described by Pascal's triangle permutations, limit the range of brain activity has been largely recognized in brain growth. Tripathy et al. (2018) reported that Mast1, espressed just in postmitotic neuronal dendritic and axonal compartments, is associated with the microtubule cytoskeleton. Mice with Mast1 microdeletions display peculiar macroscopic features, such as enlarged corpus callosum and smaller cerebellum, in absence of megalencephaly. These opposite findings (abnormal increase vs abnormal reduction) let us to hypothesize that the macroscopic growth of the brain tissue is regulated by physical constraints: keeping invariant the brain size (i.e., in absence of megaloencephaly), the central nervous tissue of animals harboring Mast1 microdeletions undergoes a general rearrangement. In physical/mathematical terms, a three-dimensional lattice (standing for the whole brain mass) harbors vectors and tensors which product (including excitatory and inhibitory neurons) must be held constant. When lattice perturbations occur (e.g., the case of cytoskeleton's genetic Mast1 alterations), one of the tensors modifies. To keep invariant the tensor product, another tensor need to vary: in simpler words, the fact that more axons cross the midline in Mast1 Leu278 del mice means that the size of other structures (in this case, the cerebellum) must decrease. In touch with this observation, Tripathy et al. (2018) report that, in animals harboring Mast1 microdeletions, the PI3K/AKT3/mTOR pathway is unperturbed, whereas Mast2 and Mast3 levels are diminished, indicative of a dominant-negative mode of action.

In our framework, the combinatorial properties of the Pascal's triangle are correlated with the mathermatical operations leading to brain spikes, through iterated random walk patterns. The occurrence of inhibitory cells in terms of "hollows" in the very structure of the brain tissue permits us to consider the topological features of a high-genus manifold, compared with genus-zero manifolds. What does the occurrence of a neural manifold of very high genus physically mean? There are many ways to generalize the notion of genus to higher dimensions, e.g., Heegaard genus in algebraic topology, arithmetic and geometric genus in algebraic geometry (Almgren & Thurston, 1977). Feldman et al. (1996) tackled the issue of the topological properties of infinite genus Riemann surfaces. They introduced a class of infinite genus Riemann surfaces, specified by means of a few geometric axioms, to which the classical theory of compact Riemann surfaces up to and, including the Torelli Theorem, extends. The axioms are flexible enough to encompass many interesting examples, such as the heat curve and a connection to the periodic Kadomcev–Petviashvilli equation. Apart from the mentioned accounts, our results suggest the feasibility of another intriguing operational approach, which allows us to generalize the notion of genus to higher dimensions through another powerful weapon: the Betti number. The brain might stand for a manifold equipped with a Betti number corresponding to the number of inhibitory neurons. Betti numbers are topological objects proved to be invariants by Poincaré that are used to extend the polyhedral formula to higher dimensional spaces. Informally, the kth Betti number refers

Content courtesy of Springer Nature, terms of use apply. Rights reserved.

to the number of path-connected edges (Kaczynski et al., 2004) embedded in surface holes. In case of a brain tissue with n vortex cycles and k edges attached between each of the cycles, the Betti number $= n + k$ (Don et al., 2020; Manschot et al., 2012). The brain is a dynamical system where the genus continuously changes because inhibitory cells' activity may vary. If the brain displays a high genus, the population of excitatory neurons cannot incresase beyond a given threshold because, in topological terms, the potential squeezing leaves always holes that cannot be reduced to a single point. Our model provides another way to generate inhibitory activity: the progressive iterations of random walks in an expanding excitatory neural activity lead to the production of hollows. These hollows stand for places that can be filled by inhibitory neurons. Therefore, inhibitory structures might spontaneously appear when nonlinear excitatory random walks start to occur in the nervous structures.

Experimental data achieved from the available neurotechniques suggest that our brain oscillations are balanced through a persistent excitatory/inhibitory (E/I) ratio. Here the concept of hyperuniformity comes into play. In amorphous cellular structures of ordered and disordered materials, anomalous suppression of density fluctuations takes place on large length scales (Klatt et al., 2019). A set of initial points evolves through Lloyd iterations since each point can be replaced by the centre mass of its Voronoi cell. A gradient descent algorithm is produced that permits a progressive convergence towards a minimum in the potential energy surface. Klatt et al. (2019) discovered that systems equipped with different initial configurations converge towards the same degree of uniformity after 10^5 Lloyd iterations. This means that, independent of the initial conditions, adult brain's cell volumes become uniform and the dimensionless total energy converges towards values comparable to the local energy minima. Therefore, we propose to describe brain oscillation expansion in terms of Lloyd iterations. In the nervous case, the seeds stand for the initial point sets (i.e., one or few excited neurons) which are converted into centroidal Voronoi diagrams. The tiny perturbations in the brain oscillations that seed the ensuing development of excitatory macro-structures might stand for the starting spots of the process described by Klatt et al. (2019) in terms of Voronoi cells and described by us in terms of Pascal's triangle models. Since every system must converge towards an hyperuniform state after a finite number of iterations (Tozzi & Peters, 2019), the brain starts from countless different possible spike conformations and then achieves the extremely high degree of uniformity typical of its neuronal E/I ratio.

In sum, we showed how relatively simple geometric and mathematical concepts might subtend the very mechanisms of intricate and nonlinear brain activities.

Author Contributions All the Authors had full access to all the data in the study and take responsibility for the integrity of the data and the accuracy of the data analysis. All the Authors equally contributed to: study concept and design, acquisition of data, analysis and interpretation of data, drafting of the manuscript, critical revision of the manuscript for important intellectual content, statistical analysis, obtained funding, administrative, technical, and material support, study supervision.

Funding This research did not receive any specific grant from funding agencies in the public, commercial, or not-for-profit sectors.

Declarations

Conflict of interest The authors declare that they have no conflict of interest.

Content courtesy of Springer Nature, terms of use apply. Rights reserved.

Ethical approval The authors warrant that the article is original, does not infringe on any copyright or other proprietary right of any third part, is not under consideration by another journal, and has not been previously published.

Human rights This research does not contain any studies with human participants or animals performed by any of the Authors.

References

Ahmad, M. Z., & Peters, J. F. (2019). Proximity induced by order relations (pp. 1–22). arXiv:1903.05532v2

Almgren, F. J., Jr., & Thurston, W. P. (1977). Examples of unknotted curves which bound only surfaces of high genus within their convex hulls. *Annals of Mathematics. Second Series, 105*(3), 527–538. https://doi.org/10.2307/1970922

Brothers, H. J. (2012). Finding e in Pascal's triangle. *Mathematics Magazine, 85*, 51. https://doi.org/10.4169/math.mag.85.1.51

Don, A. P., Peters, J. F., Ramanna, S., & Tozzi, A. (2020). Topological view of flows inside the BOLD spontaneous activity of the human brain. *Frontiers in Computational Neuroscience*. https://doi.org/10.3389/fncom.2020.00034

Edwards, A. W. F. (2013). The arithmetical triangle. In Wilson, R., & Watkins, J.-J. (Eds.), *Combinatorics: Ancient and modern* (pp. 166–180). Oxford University Press.

Fedotov, S., & Korabel, N. (2015). Nonlinear and non-Markovian random walk: self-organized anomaly. arXiv:1505.02625v1.

Feldman, J., Knörrer, H., & Trubowitz, E. (1996). Infinite genus Riemann surfaces. Toronto 1995. In J. B. Carrell, & R. Murty (Eds.), Canadian Mathematical Society/Société mathématique du Canada 1945–1995. Volume/Tome 3 (pp. 91–112). Canadian Mathematical Society.

Fraiman, D., & Chialvo, D. R. (2012). What kind of noise is brain noise: Anomalous scaling behavior of the resting brain activity fluctuations. *Frontiers in Physiology*. https://doi.org/10.3389/fphys.2012.00307

Friston, K., & Ao, P. (2012). Free energy, value, and attractors. *Computational and Mathematical Methods in Medicine, 2012*, 937860. https://doi.org/10.1155/2012/937860

Haider, B., Duque, A., Hasenstaub, A. R., & McCormick, D. A. (2006). Neocortical network activity in vivo is generated through a dynamic balance of excitation and inhibition. *Journal of Neuroscience, 26*(17), 4535–4545

Hemberger, M., Shein-Idelson, M., Pammer, L., & Laurent, G. (2019). Reliable sequential activation of neural assemblies by single pyramidal cells in a three-layered cortex. *Neuron*. https://doi.org/10.1016/j.neuron.2019.07.017

Hodge, R. D., Bakken, T. E., Miller, J. A., Smith, K. A., Barkan, E. R., et al. (2019). Conserved cell types with divergent features in human versus mouse cortex. *Nature, 573*(7772), 61–68. https://doi.org/10.1038/s41586-019-1506-7

Hore, P. J. (1983). Solvent suppression in Fourier transform nuclear magnetic resonance. *Journal of Magnetic Resonance, 55*(2), 283–300. https://doi.org/10.1016/0022-2364(83)90240-8

Kaczynski, T., Mischaikov, K., & Mrozek, M. (2004). *Computational homology*. Springer. ISBN 0-387-40853-3

Kavalali, E. T., Chung, C., Khvotchev, M., Leitz, J., Nosyreva, E., Raingo, J., & Ramirez, D. M. (2011). Spontaneous neurotransmission: an independent pathway for neuronal signaling? *Physiology (bethesda, Md.), 26*(1), 45–53. https://doi.org/10.1152/physiol.00040.2010

Klatt, M. A., Lovrić, J., Chen, D., Kapfer, S. C., Schaller, F. M., et al. (2019). Universal hidden order in amorphous cellular geometries. *Nature Communications, 10*, 811

Klein, F. (1956). *About so-called non-Euclidean geometry. About the geometry bases. Collection of classical works on Lobachevsky's geometry and development of its ideas*. Gosizdat.

Kolmogorov, A., Zhurbenko, I., & Prokhorov, A. (1995). *Introduction to the theory of probability*. Nauka.

Krueger, C., & Garvan, C. (2014). Emergence and retention of learning in early fetal development. *Infant Behavior & Development, 37*(2), 162–173. https://doi.org/10.1016/j.infbeh.2013.12.007

Manschot, J., Pioline, B., & Sen, A. (2012). From black holes to quivers. *High Energy Physics*. https://doi.org/10.1007/JHEP11(2012)023

Munkres, J. R. (1984). *Elements of algebaic topology*. Perseus Publishing.

Peters, J. F. (2016). *Computational proximity. Excursions in the topology of digital images*. Springer. ISBN 978-3-379-30260-7, Zbl1382-68008.

Content courtesy of Springer Nature, terms of use apply. Rights reserved.

Peters, J. F. (2018). Proximal vortex cycles and vortex nerve structures. Non-concentric, nesting, possibly overlapping homology cell complexes. *Journal of Mathematical Sciences and Modelling, 1*(2), 80–85. ISSN 2636-8692.

Peters, J. F. (2020). *Computational geometry, topology and physics. Shape complexes, optical vortex nerves and proximities in digital images*. Springer. ISBN 979-3-030-23191-1, Zbl 07098311.

Sarkar, J., & Maiti, S. I. (2017). Symmetric random walks on regular tetrahedra, octahedra, and hexahedra. *Calcutta Statistical Association Bulletin, 69*(1), 110–128

Sengupta, B., Laughlin, S. B., & Niven, J. E. (2013). Balanced excitatory and inhibitory synaptic currents promote efficient coding and metabolic efficiency. *PLoS Computational Biology, 9*, e1003263

Sengupta, B., & Stemmler, M. B. (2014). Power consumption during neuronal computation. *Proceedings of the IEEE, 102*, 738–750

Soldatov, R., Kaucka, M., Kastriti, M. E., Petersen, J., Chontorotzea, T., et al. (2019). Spatiotemporal structure of cell fate decisions in murine neural crest. *Science, 364*(6444), eaas9536. https://doi.org/10.1126/science.aas9536

Sommerfeld, A. (1973). Cognition ways in physics. Collection of papers, p. 157. Editor: Smorodinsky, J. Moscow: Nauka. (Klein, Riemann und die mathematische Physik. Naturwiss (1919), 7.

Telley, L., Agirman, G., Prados, J., Amberg, N., Fièvre, S., et al. (2019). Temporal patterning of apical progenitors and their daughter neurons in the developing neocortex. *Science, 364*(6440), eaav2522. https://doi.org/10.1126/science.aav2522

Tognoli, E., & Kelso, J. S. (2013). On the brain's dynamical complexity: Coupling and causal influences across spatiotemporal scales. *Advances in Cognitive Neurodynamics (III), (Iii)*, 259–265. https://doi.org/10.1007/978-94-007-4792-0

Tozzi, A., & Peters, J. F. (2019). Entropy balance in the expanding universe: A novel perspective. *Entropy, 21*(4), 406. https://doi.org/10.3390/e21040406

Tozzi, A., Peters, J. F., Fingelkurts, A. A., Fingelkurts, A. A., & Marijuán, P. C. (2017). Topodynamics of metastable brains. *Physics of Life Reviews, 21*, 1–20. https://doi.org/10.1016/j.plrev.2017.03.001

Tozzi, A., Zare, M., & Benasich, A. A. (2016). New perspectives on spontaneous brain activity: Dynamic networks and energy matter. *Frontiers in Human Neuroscience, 10*, 247. https://doi.org/10.3389/fnhum.2016.00247

Tripathy, R., Leca, I., van Dijk, T., Weiss, J., van Bon, B. W., et al. (2018). Mutations in MAST1 cause mega-corpus-callosum syndrome with cerebellar hypoplasia and cortical malformations. *Neuron, 100*(6), 1354–1368. https://doi.org/10.1016/j.neuron.2018.10.044

Trujillo, C. A., Gao, R., Negraes, P. D., Yeo, G. W., Voytek, B., & Muotri, A. R. (2019). Complex oscillatory waves emerging from cortical organoids model early human brain network development. *Cell Stem Cell, 25*(4), 558-569.E7. https://doi.org/10.1016/j.stem.2019.08.002

Velasco, S., Kedaigle, A. J., Simmons, S. K., Nash, A., Rocha, M., et al. (2019). Individual brain organoids reproducibly form cell diversity of the human cerebral cortex. *Nature, 570*, 523–527

Wang, R., Fan, Y., & Wu, Y. (2019). Spontaneous electromagnetic induction promotes the formation of economical neuronal network structure via self-organization process. *Science and Reports, 9*(1), 9698. https://doi.org/10.1038/s41598-019-46104-z

Wang, Y., Wang, R., & Zhu, Y. (2017). Optimal path-finding through mental exploration based on neural energy field gradients. *Cognitive Neurodynamics, 11*(1), 99–111. https://doi.org/10.1007/s11571-016-9412-2

Weyl, H. (1955). *The concept of a Riemann surface*. By MacLane, G.R., Dover Pub. Inc., NY.

Xu, X., & Wang, R. (2014). Neurodynamics of up and down transitions in a single neuron. *Cognitive Neurodynamics, 8*(6), 509–515. https://doi.org/10.1007/s11571-014-9298-9

Xue, M., Atallah, B. V., & Scannziani, M. (2014). Equalizing excitation-inhibition ratios across visual cortical neurons. *Nature, 511*, 596–600

Yurkin, A. (1995). System of rays in lasers and a new feasibility of light coherence control. *Optics Communications, 114*, 393

Yurkin, A. (2013). *New binomial and new view on light theory. About one new universal descriptive geometric model*. Lambert Academic Publishing. ISBN 978-3-659-38404-2.

Yurkin, A. (2016). On descriptive geometrical interpretation of the principle of Pauli, elements of the table of Mendeleyev and the Newtonian laminar current of liquid. *Progress in Physics, 12*, 149–169

Yurkin, A. (2018). And where are fluctuations in quantum-mechanical wave function? *Advances in Theoretical & Computational Physics, 1*(1.1-7).

Yurkin, A. (2019a). Computing stiks against random walk. *Advances in Theoretical & Computational Physics, 2*(1.1-6).

Yurkin, A. (2019b). Fractions of arithmetic octahedron and random walk. *International Journal of Engineering Technology Research Management (iJETRM), 3*(5).

Content courtesy of Springer Nature, terms of use apply. Rights reserved.

Yurkin, A. (2019c). Visual models and classification of 1D, 2D, and 3D random walk. *European Journal of Advances in Engineering and Technology (EJAET), 6*(2), 42–53

Yurkin, A., Peters, J. F., Tozzi, A. (2018). A novel belt model of the atom, compatible with quantum dynamics. *Journal of Scientific and Engineering Research, 5*(7):413–419. www.jsaer.com.

Yuste, R., McLean, J. N., Smith, J., & Lansner, A. (2005). The cortex as a central pattern generator. *Nature Reviews Neuroscience, 6*, 477–483. https://doi.org/10.1038/nrn1686

Publisher's Note Springer Nature remains neutral with regard to jurisdictional claims in published maps and institutional affiliations.

Arturo Tozzi is a M.D., Pediatrician in Naples Italy. He also works with The Center for Nonlinear Science, Denton Texas, USA. He does not like to be on focus. Looking for unexpected, hidden multidisciplinary relationships, he publishes in rather different Journals (e.g., nuts in Nature, New England Journal of Medicine, Physics of Life Reviews, PLOS Biology, Cognitive Neurodynamics, etc) and fields (biology, physics, math, philosophy, history, medicine, and, above all, neuroscience).

Alexander Yurkin is a member of Russian Academy of Sciences. Pupil of the mathematicians Vladislav Mikhalevich and Vasily Dikusar, he is a leading expert in geometric accounts of physical and biological processes. In particular, he studies linear and nonlinear systems' dynamics in terms of iterations of geometric figures, such as octahedrons and Pascal's triangles.

James F. Peters is Professor at Department of Electrical and Computer Engineering, University of Manitoba, Winnipeg, Canada. His research focuses on establishing frameworks for the study of the closeness of structures on triangulated finite bounded surface regions filled with holes in a space K endowed with a spatial or descriptive proximity relation. In Alexandroff-Hopf-Whitehead CW (Closure finite Weak) complexes on K, e.g., this leads to the discovery of proximal sub-complexes and proximal nerve structures that are close to each other either spatially or descriptively. Of particular interest is the detection, characterization, analysis, measurement, rate of change, energy, and classification of shapes of nesting, non-overlapping skeletal vortexes, forming what are known as optical vortex nerves.

Content courtesy of Springer Nature, terms of use apply. Rights reserved.

Terms and Conditions

Springer Nature journal content, brought to you courtesy of Springer Nature Customer Service Center GmbH ("Springer Nature").

Springer Nature supports a reasonable amount of sharing of research papers by authors, subscribers and authorised users ("Users"), for small-scale personal, non-commercial use provided that all copyright, trade and service marks and other proprietary notices are maintained. By accessing, sharing, receiving or otherwise using the Springer Nature journal content you agree to these terms of use ("Terms"). For these purposes, Springer Nature considers academic use (by researchers and students) to be non-commercial.

These Terms are supplementary and will apply in addition to any applicable website terms and conditions, a relevant site licence or a personal subscription. These Terms will prevail over any conflict or ambiguity with regards to the relevant terms, a site licence or a personal subscription (to the extent of the conflict or ambiguity only). For Creative Commons-licensed articles, the terms of the Creative Commons license used will apply.

We collect and use personal data to provide access to the Springer Nature journal content. We may also use these personal data internally within ResearchGate and Springer Nature and as agreed share it, in an anonymised way, for purposes of tracking, analysis and reporting. We will not otherwise disclose your personal data outside the ResearchGate or the Springer Nature group of companies unless we have your permission as detailed in the Privacy Policy.

While Users may use the Springer Nature journal content for small scale, personal non-commercial use, it is important to note that Users may not:

1. use such content for the purpose of providing other users with access on a regular or large scale basis or as a means to circumvent access control;
2. use such content where to do so would be considered a criminal or statutory offence in any jurisdiction, or gives rise to civil liability, or is otherwise unlawful;
3. falsely or misleadingly imply or suggest endorsement, approval , sponsorship, or association unless explicitly agreed to by Springer Nature in writing;
4. use bots or other automated methods to access the content or redirect messages
5. override any security feature or exclusionary protocol; or
6. share the content in order to create substitute for Springer Nature products or services or a systematic database of Springer Nature journal content.

In line with the restriction against commercial use, Springer Nature does not permit the creation of a product or service that creates revenue, royalties, rent or income from our content or its inclusion as part of a paid for service or for other commercial gain. Springer Nature journal content cannot be used for inter-library loans and librarians may not upload Springer Nature journal content on a large scale into their, or any other, institutional repository.

These terms of use are reviewed regularly and may be amended at any time. Springer Nature is not obligated to publish any information or content on this website and may remove it or features or functionality at our sole discretion, at any time with or without notice. Springer Nature may revoke this licence to you at any time and remove access to any copies of the Springer Nature journal content which have been saved.

To the fullest extent permitted by law, Springer Nature makes no warranties, representations or guarantees to Users, either express or implied with respect to the Springer nature journal content and all parties disclaim and waive any implied warranties or warranties imposed by law, including merchantability or fitness for any particular purpose.

Please note that these rights do not automatically extend to content, data or other material published by Springer Nature that may be licensed from third parties.

If you would like to use or distribute our Springer Nature journal content to a wider audience or on a regular basis or in any other manner not expressly permitted by these Terms, please contact Springer Nature at

onlineservice@springernature.com

Chaos, Solitons and Fractals 152 (2021) 111351

Contents lists available at ScienceDirect

Chaos, Solitons and Fractals

Nonlinear Science, and Nonequilibrium and Complex Phenomena

journal homepage: www.elsevier.com/locate/chaos

Quaternionic views of rs-fMRI hierarchical brain activation regions. Discovery of multilevel brain activation region intensities in rs-fMRI video frames☆

Arjuna P.H. Don[a], James F. Peters[a,d,*], Sheela Ramanna[c], Arturo Tozzi[a,b]

[a] Computational Intelligence Laboratory, University of Manitoba,WPG, MB, R3T 5V6, Canada
[b] Department of Physics, University of North Texas, Denton, TX, United States
[c] Applied Computer Science Department, University of Winnipeg,WPG, MB, R3B 2E9, Canada
[d] Department of Mathematics, Faculty of Arts and Sciences, Adiyaman University, 02040 Adiyaman, Turkey

ARTICLE INFO

Article history:
Received 21 February 2021
Revised 11 July 2021
Accepted 5 August 2021

2010 MSC:
30G35 (hypercomplex variables quaternions)
57M05 (free group presentations)
57M60 (group action on cell complexes)
76M23 (vortex methods)

Keywords:
Betti number
Brain activation region
CW space
Cell complex
Cycle
Free group presentation
Multi-level intensities
Quaternion
rs-fMRI
Shape
Vortex

ABSTRACT

This paper introduces quaternionic views of multi-level brain activation region intensities in resting-state functional magnetic resonance imaging (rs-fMRI) videos. Quaternions make it possible to explore rs-fMRI brain activation regions in a 4D space in which there are varying brain activation intensities in spiralling activation cycles (each with its own intensity). As a result, there is a natural formation of multi-level cycles that form pyramidal vortex shapes with varying diameters. These pyramidal vortexes reflect the fractality (self-similarity) of clusters of similar multilevel brain activation region cycles. Using a computational topology of data approach, we have found that persistent, recurring **clusters of spiraling cycles** resulting from blood oxygen level dependent (BOLD) signals in triangulated rs-fMRI video frames. Each brain activation region cycle is a **cell complex**, which is a collection path-connected vertexes that has no end vertex. Measurement of persistence of spiraling vortex shapes in BOLD signal propagation regions is carried out in terms of Betti numbers (counts of distinguished cycle vertexes called generators) that rise and fall over time during spontaneous activity of the brain. A main result given here is that every quaternionic brain activation region vortex has a free group presentation. In addition, we introduce 3D barcodes of brain activation videos that help visualize and quantify the fractality of clusters of multilevel vortexes arising naturally from triangulated brain activation regions in rs-fMRI video frames. We have made freely available downloadable archives of videos that exhibit the resulting clusters of spiraling brain activation cycles.

© 2021 Elsevier Ltd. All rights reserved.

1. Introduction

The development of quaternionic algebra, was first proposed by Hamilton [1] and introduced by Tait [2]. In the past decade, multi-channel quaternionic models have found wide spread use in color image processing. Quaternion Wavelet Transform-based image processing has been used extensively in [3–7]. In [8], a quaternionic framework was applied to color image smoothing and segmentation. The authors in [9] generalized the conventional complex-type moments (CTMs) for gray-scale images to color images as quaternion-type moments (QTMs) using quaternion algebra with application to typical image processing tasks. In [10], quaternion polar harmonic transforms (QPHTs) were developed based on quaternion algebra for a more compact and discriminative representation of color images. In [11], a quaternion invariance based hashing algorithm to fuse complementary visual features was proposed.

More recently, a low rank quaternion approximation model to better estimate the singular values of the underlying low-rank quaternion matrix for color images was proposed [12]. In [13], a theoretical analysis of the performance of multi-channel quaternion image processing vs. independent channel processing was discussed. A quaternion anti synchronization model of fractional uni-

☆ Multilevel brain activation intensities in rs-fMRI images.

* Corresponding author at: Computational Intelligence Laboratory, University of Manitoba,WPG, MB, R3T 5V6, Canada.
E-mail address: james.peters3@umanitoba.ca (J.F. Peters).

https://doi.org/10.1016/j.chaos.2021.111351
0960-0779/© 2021 Elsevier Ltd. All rights reserved.

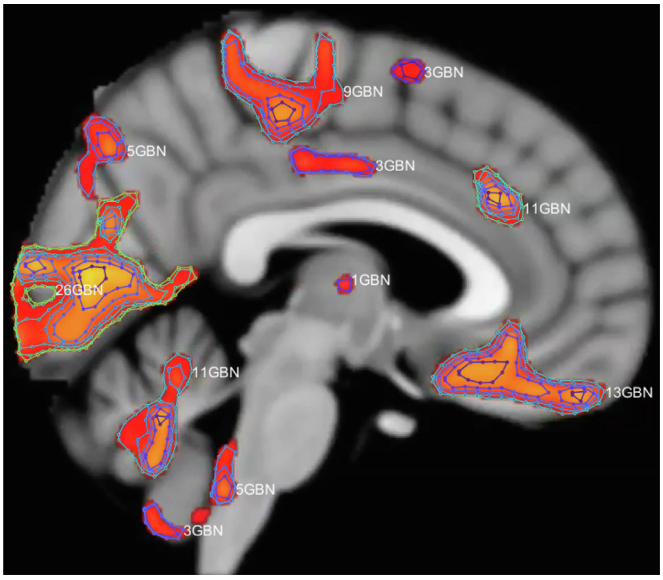

Fig. 1. Vortexes on a sample Sagittal view of a fMRI video frame. (Frame 159 Thread 1).

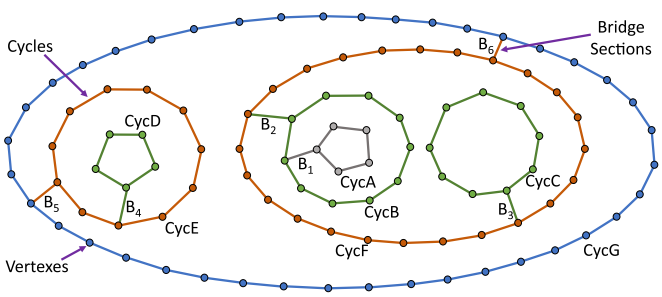

Fig. 2. Nested Brain Activation Region with Spiraling Cycles Forming Vortexes.

fied model with quaternion variables was studied in [14]. In [15], the possibility of using global visualization methods for exploiting four-dimensional quaternion maps of three-dimensional EEG traces was discussed.

In contrast, this paper introduces quaternions in a topology of data approach in the study of persistent, recurring blood oxygen level dependent (BOLD) signals in triangulated rs-fMRI video frames. Detected activation regions within each video frame display multi-level, spiraling vortex structures that cover brain activated regions with high fractality (see, e.g., Fig. 1). The findings reported here represent a significant advance over our earlier findings [16]. Measurement of persistence of varying vortex shapes during BOLD signal propagation is carried out in terms of Betti numbers (counts of vortex cycle generating elements) that rise and fall over time during spontaneous activity of the brain. The utility of quaternionic views of hierarchical brain activation regions in rs-fMRI video frames stems of from the discovery of nested brain activation region vortex cycles[1]. For example, varying multi-level vortical structures within a video frame snapshot of the Sagittal view of the brain are shown in Fig. 1. Vortex signatures such as 13GBN in Fig. 1 indicate the operation of 13 voxels that function as cycle generating elements. Geometrically, each brain activation region vortex is a collection of multiple nested cycles (sub-vortices) with varying intensities as shown in Fig. 2. For example, sub-vortex vor$E$ contains nested cycles Cyc$D$, Cyc$E$ attached to each other via bridge edge B_4. The varying intensity levels of the cycles in Sub-vortex vor$E$ are represented by edges with different colors (e.g., green $\boldsymbol{p}$ ●——● $\boldsymbol{q}$ for Cyc$D$ and red $\boldsymbol{p}$ ●——● $\boldsymbol{q}$ for Cyc$E$ in Fig. 2). Taken together, the collection of voxels (colored dots) are path-connected via varying numbers of moves either right or left from a distinguished voxel (called a generator) to reach any other point in the 13GBN vortex.

[1] For examples, see https://drive.google.com/drive/folders/13e7YhjxUEmZOTN9BMa9QuDk7rKrGPiOZ?usp=sharing

2. Preliminaries

This section briefly introduces the structures that are the building blocks in a brain activation region vortex found in triangulated rsfMRI video frames. For details, see [17, chapters 1 & 3].

2.1. Voxels, edges and filled triangles

There are two types of picture elements in video frames, namely,

4D voxel is a 4-dimensional video frame picture element v with coordinates (x, y, γ, t), where x and y are horizontal and vertical coordinates of v, γ is the intensity of v (either 1 or 0 in a binary frame and 0 (black),..., 255 (white) in a greyscale frame), elapsed time t ranging from clock tick t_0 at the start of a video and clock tick t_{end} at the end of a video.

6D voxel is a 6-dimensional video frame picture element v with coordinates $(x, y, \gamma_r, \gamma_g, \gamma_b, t)$, where x and y are horizontal and vertical coordinates of v, $\gamma_r, \gamma_g, \gamma_b$ are the red (r) ●, green (g) ●, blue (b) ● intensities of v-color channels (ranging in the interval 0 (lowest color intensity),..., 255 (highest color intensity) in an RBG frame), elapsed time t ranging from clock tick t_0 at the time of appearance of the initial frame in a video to clock tick t_{end} for the final frame at the end of a video.

2.2. Cycles and vortexes

In triangulated rs-fMRI video frames, cycles and vortexes are examples of cell complexes that are constructed from combinations of simpler building blocks, namely, 0-cells (single voxels), 1-cells (edges) and 2-cells (filled triangles). A **1-cycle** is a collection of voxels that are path-connected and with no end-voxel. A **vortex** is a collection of nested 1-cycles that are attached to each other via bridge edges. Every vortex vor$E$ on a triangulated video frame has a geometric presentation denoted by |vor$E$| [[18], p. 239]. A **bridge edge** is an edge attached between voxels on neighboring (adjacent) 1-cycles in a vortex. The endpoints (voxels) on a bridge are called **generators**, since bridge voxel g is the entrance to a cycle through which any other voxel v in the cycle can be reached via k moves. Hence, each vortex v in a cycle can be written as $v = kg$.

2.3. Cyclic groups and free group presentations of cycles and vortexes

Definition 1. A **cyclic group** G on a video frame has a binary operation + (move) on a finite collection of voxels that includes a generator voxel g, identity element 0 (representing zero moves). Every voxel in G equals kg (k moves to the right of g) and has an inverse $-v$ (k moves to the left of g).

Lemma 1. *Every cycle in a video frame has a cycle group representation.*

Proof. Immediate from Def. 1. □

Definition 2. A **free group** G on a video frame has a binary operation + (move) on a finite collection of generatore voxels $g_1, \ldots, g_n$,

identity element 0 (representing zero moves). Every voxel v in G can be written as linear combination of the generators, e.g.,

$$v = k_1 g_1 + \cdots + k_n g_m = \sum_{\substack{i=1\\ j=1}}^{n,m} k_i g_j.$$

Vortexes in triangulated video frames can be represented concisely as free groups.

Definition 3. Let 2^K be the collection of cell complexes in a video frame K, vortex $|\text{vor}E| \in 2^K$, basis $\mathcal{B} \in |\text{vor}E|$, k_i the ith integer coefficient in a linear combination $\sum_{i,j} k_i g_j$ of generating elements $g_j \in \mathcal{B}$. A free group G **representation** of $|\text{vor}E|$ is a continuous self-map $f : 2^K \to 2^K$ defined by

$$f(|\text{vor}E|) = \left\{ v := \sum_{i,j} k_i g_j : v \in |\text{vor}E|, g_j \in \mathcal{B} \right\}$$
$$= \overbrace{\boldsymbol{G}(\{\boldsymbol{g_1}, \ldots, \boldsymbol{g}_{|\mathcal{B}|}\}, +)}^{|\text{vor}\boldsymbol{E}| \mapsto \text{free group}\boldsymbol{G}}.$$

Theorem 1. *Every cycle in a video frame has a free group presentation.*

Proof. From Lemma 1, every cycle has cyclic group presentation (call it G). From Def. 2, G is a free group. □

Theorem 2. *Every vortex on a video frame has a free group presentation.*

Proof. Let K be a video frame and let $f : K \to K$ be a continuous self-map defined as in Def. 3. The desired result follows. □

2.4. Bridge edges and betti numbers

The end voxels on each bridge edge are a source of generators on vortexes in video frames. A **Betti number** is a count of the number of generators in a free group. We know from Theorem 2, that every video frame vortex has a free group presentation. Hence, Betti numbers provided a concise means of indexing, measuring and comparing vortexes in video frames.

Remark 1. The end voxels on each bridge in a vortex vor$E$ are generators in the free group representation G of vor$E$. Hence, if G represents a vortex containing k bridges, then the Betti number $\beta(G) = 2k$, since each bridge in G contributes a pair of generators for the vortex free group.

Example 1. In Fig. 2, we have one super vortex vor$E$ whose boundary is cycle Cyc$G$. Vortex vor$E$ contains a pair of sub-vortexes vorE_1 containing cycles Cyc$E$, Cyc$D$ attached via bridge brB_4 and vorE_2 containing cycles Cyc$A$, Cyc$B$, Cyc$C$ attached to each other via bridges brB_1, brB_2, brB_3. Sub-vortexes vorE_1, vorE_2 are attached to the boundary cycle Cyc$G$ via a pair bridges brB_5, brB_6. Hence, the Betti number for vortex vor$E$ is

$$\beta(\text{vor}E) = 2(\text{br}Count) = 2 \times 6 = 12.$$

Example 2. In Fig. 1, video frame indexing is achieved in the following way in terms of 11 vortexes shown in the Sagittal view of varying brain activation spirals, namely,

$$\beta(\text{vor1}GBN) = 1(occurence).$$
$$\beta(\text{vor3}GBN) = 3(occurences).$$
$$\beta(\text{vor5}GBN) = 2(occurences).$$
$$\beta(\text{vor9}GBN) = 1(occurence).$$
$$\beta(\text{vor11}GBN) = 2(occurences).$$
$$\beta(\text{vor13}GBN) = 1(occurence).$$
$$\beta(\text{vor26}GBN) = 1(occurence).$$

Hence, the index for this video frame is

$$\begin{aligned}\beta(\text{fr}E) &= 1 + 3 \times 3 + 5 \times 2 + 9 \times 1 + 11 \times 2 + 13 + 26\\ &= 1 + 9 + 10 + 9 + 22 + 13 + 26\\ &= 70.\end{aligned}$$

3. Quaternionic views of voxels in video frames

Several instances of different representations of varying levels of voxel intensities in changing brain activation regions for color rs-fMRI video frames are introduced, based on earlier work. One of the most famous representations is the cubed representation of color using RGB values as XYZ coordinates and every pixel can be written as a vector drawn from the origin to the corresponding color values [19]. For example, vectors r = (255,0,0), g = (0,255,0) and b = (0,0,255) and any color can be represented by the linear combination of the three vectors as $V_c = k_r r + k_g g + k_b b$ where k_r, k_g and k_b are scalars that determines the value of each color.

The usual representation of a quaternion is $a + b\vec{i} + c\vec{j} + d\vec{k}$. Where i,j and k are vectors. When a = 0, it is called a pure quaternion. In order to represent color pixels, pure quaternions are used where each pixel can be denoted as $k_r\vec{i} + k_g\vec{j} + k_b\vec{k}$.

3.1. Representing voxels in color video

Color video frames that are captured with various video cameras and other imaging equipment most of the time produce images. Picture elements in video frame are called voxels or superpixels. A voxel in color video frame has Red, Green and Blue channels that vary depending on the reflected light recorded by a video camera. Apart from RGB representation there are other color representations of images that include HSV where each voxel has Hue, Saturation and Variance which is closer to how humans perceive color. Most of the image processing algorithms use grayscale representation of images, where RGB or HSV values are converted to a single variable that represents the value as a difference in gray value (usually between 0 to 255). But this grayscale representation is a limiting factor in image segmentation since different color channels may have similar or very close grayscale values, and cannot be separated efficiently using a threshold value. The conventional color image processing approach involves grayscale methods on each color stream separately and then combining the results to obtain the final result. The biggest drawback with this approach is the disregard for the correlation of the three color channels, which loses the entirety of three channels [8,20].

3.2. Quaternion rotation distance

Given the usual quaternion in the form, $q = a + bi + cj + dk$, consider two quaternions q_1 and q_2. The angular distance between two quaternions q_1 and q_2 can be expressed as $\theta = 2cos^{-1}(real(z))$ where product $z = q_1 * conjugate(q_2)$. As q_1 approaches q_2, the angle of z goes to 0, and z approaches the unit quaternion.

Using the quaternion data type syntax, the angular distance is calculated as shown in Algorithm 1:

4. Methodology

This section describes the methodology that includes the steps which were taken to obtain the vortexes on the fMRI video frames.

Step (1) Convert the fMRI frame to a quaternion matrix. Then calculate the color distance to each pixel from the origin $(0 + 0i + 0j + 0k)$. The obtained values are shown by the 3D plot after Step 1.

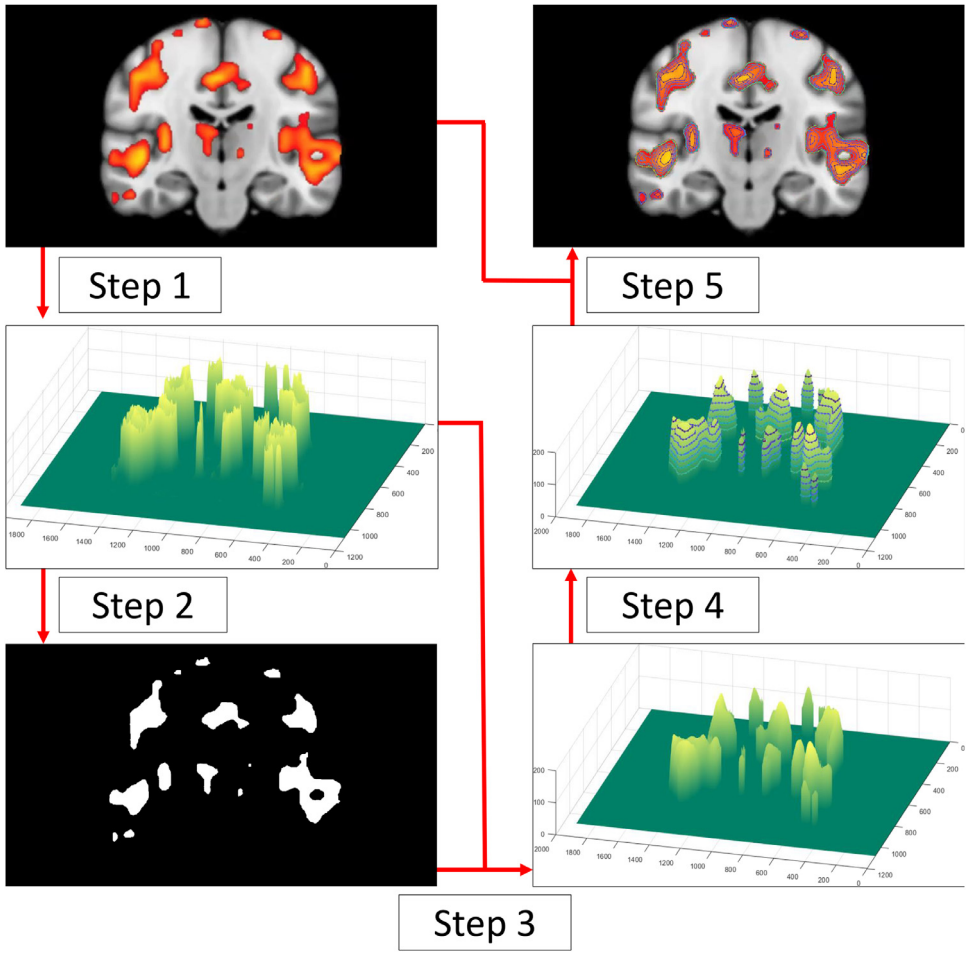

Fig. 3. Step by step method to obtain vortexes.

Algorithm 1: Angular Distance

input : Quaternions q_1 and q_2
output: Angular distance (angDist) between q_1 and q_2

```
deltaQuat = q1* conj(q2);
realPart = real(deltaQuat);
if rpart<0 then
    realPart = -realPart;
angDist = 2.*acos(realPart);
```

Step (2) Separate the active region of the brain from the other areas. This is obtained by using a threshold value of 0.8. Any pixel higher than the threshold will be marked as 1 or 0 otherwise. Hence a binary image is obtained as a result of Step 2.

Step (3) Perform morphological operations on the activated areas to separate the boundary region from the interior. Here, the activated area is shrunk to obtain the interior of the activated area using the color distance matrix (result of Step 1). The resulting color distance matrix is shown as a 3D plot as a result of Step 3.

Step (4) Draw vortexes using activation levels of the interior regions of the brain. In this step, the boundary of each activated area in each level is used to generate vertices for the cycles.

Step (5) Superimpose the obtained cycles onto the fMRI frame.

Fig. 3 shows the steps taken to obtain the cycle complex for each frame.

5. Results

This section presents experimental results which highlights varying brain activation intensities in spiralling activation cycles each with its own intensity. The inner cycles represent activation regions with the highest intensity (brightness). The geometric Betti number is a representation of brightness of the activation area. Three sample fMRI frames are given by Figs. 1, 5 and 6. Fig. 5 shows the coronal view of the brain in frame 197 in video thread 1. There are several inherent qualities of the Spiraling Cycles Forming Vortexes (SCFV) and Geometric Betti Numbers (GBN) that stand out in the sample video frame. The SCFV vortexes in the sample frame are labeled as Vortexes A to G (VtxA to VtxG). One distinguishing feature is that these vortexes are highly reproducible when the activation regions they cover have similar underlying features. For example, consider features area and brightness. Regions labelled VtxA, VtxB,VtxD and VtxE and their GBNs are similar (Fig. 4).

It is noteworthy that SCFVs depend not only on the area of the activation region, but also on the distribution of the brightness levels in each activation region. For example, in Fig. 5, the area covered by the VtxC vortex is comparatively larger than area covered by the VTXF. However, the GBN value for VtxF is higher because it has more levels of brightness (intensities) in its activation regions and has two internal generator cycles. One of the advantages of the

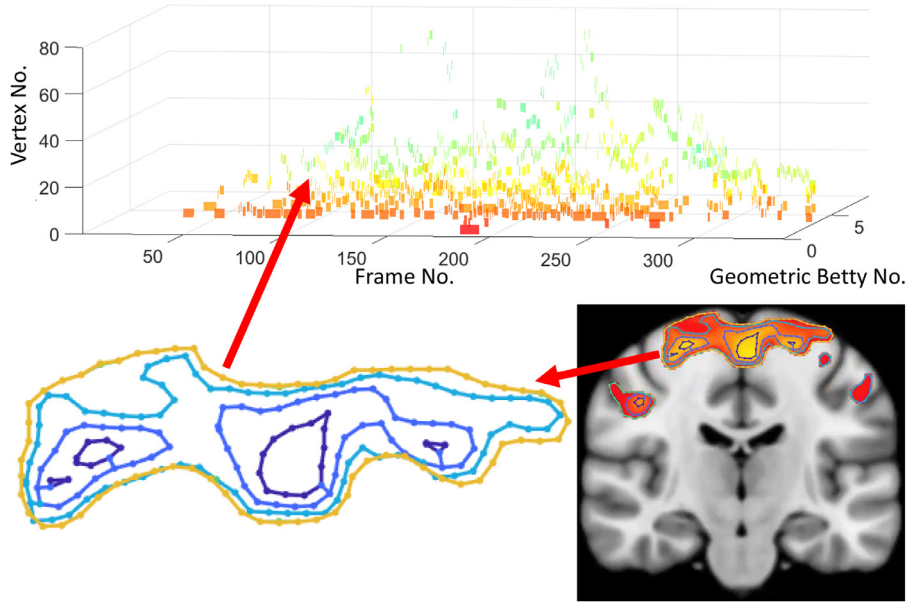

Fig. 4. Generation of 3D barcodes using vortex cycle Betti numbers.

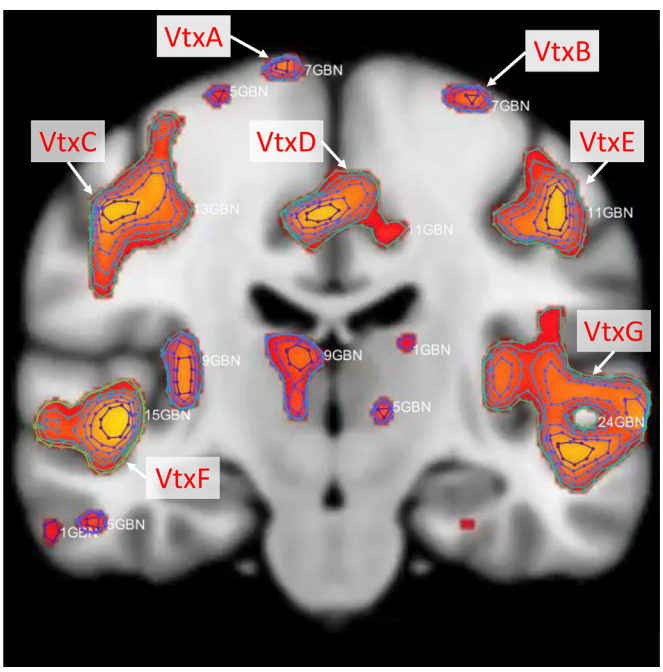

Fig. 5. Vortexes on a sample Coronal view of a fMRI video frame. (Frame 197 Thread 1).

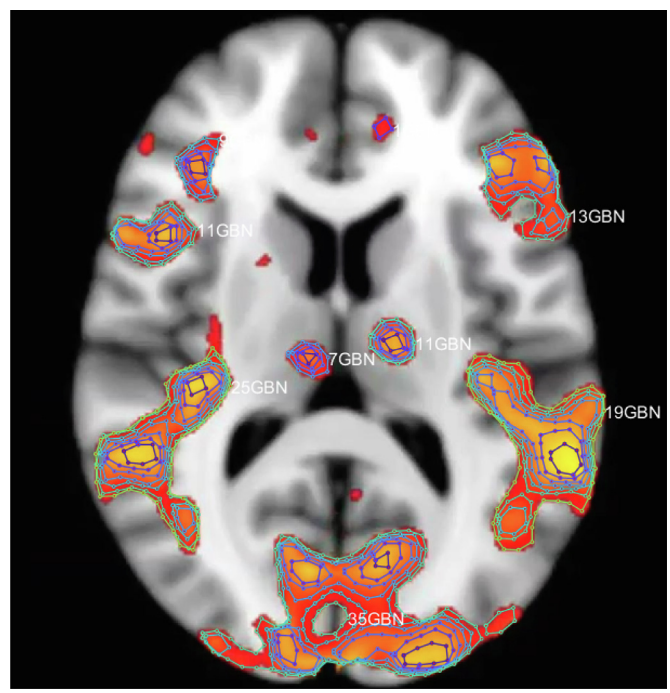

Fig. 6. Vortexes on a sample Traversal view of a fMRI video frame. (Frame 184 Thread 1).

discovering Spiraling Cycles Forming Vortexes method is that this method can accommodate inner holes in the activation regionsfor any SCFV in Fig. 5. The same correlation between SCFV and their corresponding GBN values can be seen in Figs. 1 and 6.

5.1. Edge density and eigen value statistics

5.1.1. Edge density

Edge density in a vortex nerve determines connectedness in the vortex representation of a brain activation region in a rs-fMRI video frame. The edge density is calculated as a ratio between edges (line segments between two vertices) and vertices in a vortex nerve. The value of edge density for a graph varies between 0 and 1. A graph without any edges between its vertices will have 0 edge density, while a complete graph, where each vertex is connected to every other vertex, will have an edge density of 1. Since the vortex nerves in this paper are simple undirected graphs, the edge density is defined as:

$$EdgeDensity = \frac{2E}{V(V-1)} \tag{1}$$

where E is the number of edges and V is the number of vertices in the vortex nerve. If the vortex nerve has an edge density close to the maximum number of possible edges, it is considered to be a dense vortex nerve. Similarly, if the vortex nerve has only a few edges, it is considered as sparse. Hence, the determination of

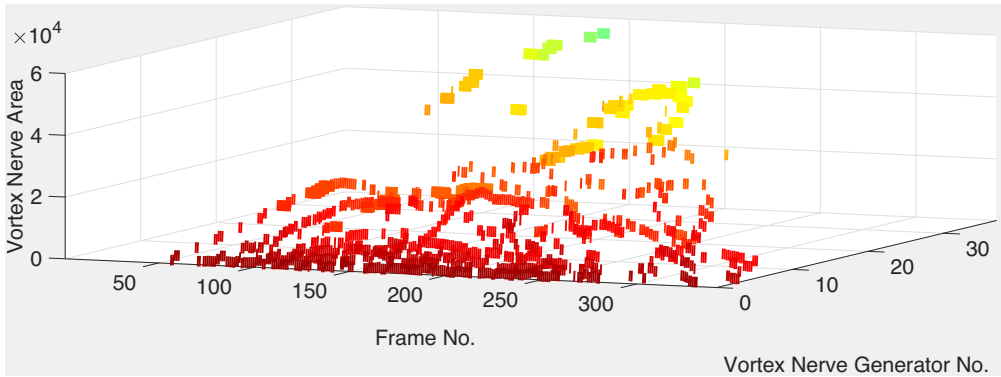

Fig. 7. Vortex Nerve Area Vs Vortex Nerve Generator No. Vs Frame No., 3D Barcode.

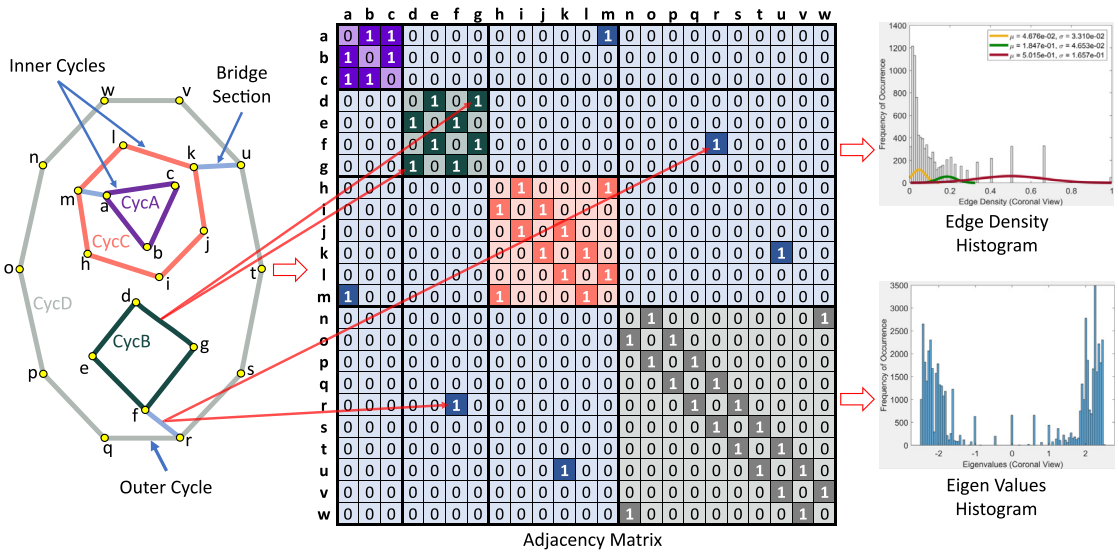

Fig. 8. The adjacency matrix that represents the vortex cycles and bridge segments. Which helps to generate the edge density histogram and eigen value histograms.

whether a vortex nerve is a dense or sparse is relative and depends on the type of nerve [21] (Fig. 7).

Higher edge density implies that there are more edges between vertices in the vortex cycle. But since we only draw a single bridge segment between cycles, the edge density decreases when the number of cycles increases. As a consequence, when the number of cycles increases, the edge density decreases. As an example, for the vortex nerves used in this paper, the maximum value obtained for edge density is 1, in the case of a single cycle with three vertices. (ex: This is the case of triangle, where each vertex is connected to every other vertex). The next highest edge density value that can be obtained is, $2/3 = 0.666$ where a single cycle with four vertices is considered. Single or multiple cycles will have an edge density lower than 0.66. In other words, higher the number of cycles and vertices in a cycle, the lower the edge density.

Another characteristic to note is that larger number of cycles leads to brighter activation regions. Which means that the edge density is inversely proportional to the brightness of the activation region. Also when the area of the activation region increases, the number of vertices in the cycles increase. This is because the cycles gets larger with the activation region area. Hence, edge density is inversely proportional to both brightness and area of activation regions.

Frequency of occurrence in the plot in Fig. 9(a) shows the number of times a certain edge density appears in the cycles. Whenever a certain edge density appears, the plot will show the frequency of occurrence as 1. If it reappears, the frequency of occurrence for that value will be increased by 1. From the plot for the Coronal view in Fig. 9(a), it can be seen that each distribution can be represented using three normal distributions. Observe that the left-most normal distribution has a mean $\mu = 0.04676$ and a standard deviation $\sigma = 0.0331$ and has the highest frequency of occurrence when compared to the other two (middle, right) distributions. The middle normal distribution has $\mu = 0.1847$ and $\sigma = 0.04653$. This distribution has the lowest frequency of occurrence of edge densities. The right normal distribution has a $\mu = 0.05015$ and $\sigma = 0.01657$ and has the second highest frequency of occurrence. Hence, in Fig. 9(a), it can be observed that the highest frequencies of occurrence of edges is for edge densities between 0 and 0.1.

5.1.2. Eigenvalue spectrum

Eigenvalues are a special set of scalars associated with a linear system of equations. This section briefly introduces an eigenvalue spectrum which is the representation of the eigen values derived from the connectivity relations between cycles in a vortex nerve. A scalar λ is a eigenvalue of a linear transformation provided there is a vector $x(x \neq 0)$ so that $A(x) = \lambda x$, where vector x called an eigenvector. Eigen values are computed using an adjacency matrix A, which is a n $\times$ n square matrix where n is the number of vertices in a vortex nerve. Here, an eigenvalue spectrum is defined by an

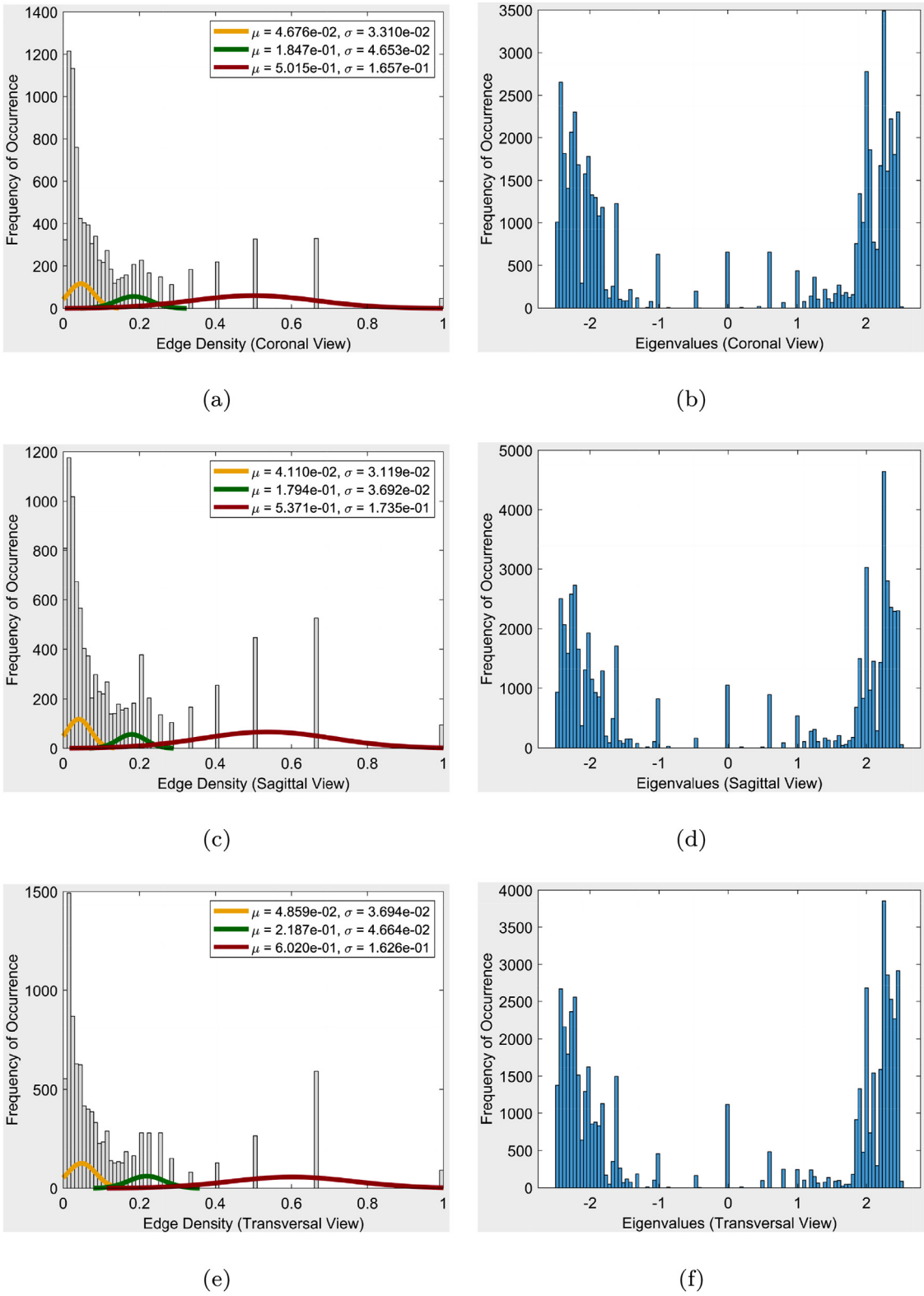

Fig. 9. Edge density and eigen value histograms for each brain view.

activation matrix view of the connectedness between vertices in a vortex representation of brain activation regions in rs-fMRI videos.

Each adjacency matrix represents the connectivity in vortex cycles (see Fig. 8). A color coding is used to mark each cycle and bridge segments between cycles separately. The example shown in Fig. 8 has 4 cycles that are interconnected using three bridge sections. The innermost cycle (coded in purple) is a triangle and is represented first using symmetric sub matrix (a-c). Recall, that vortex nerves are simple undirected graphs with no duplicate edges, no loops (an edge from some vertices back to itself)and each connection between vertices is undirected. The diagonal of the sub matrix has 0 for all positions because none of the vertices are con-

nected to themselves. Each edge (a line segment that connects two vertices) in the cycle is represented by 1 in the sub-matrix. If there is no edge between corresponding vertices, then the edge is represented as 0. A connection between vertices a and b is represented by two, (a,b) and (b,a), matrix positions.

Similarly, cycle CycB is represented in the adjacency matrix is coded with color green. The order of the cycles that are represented in the sub-diagonal matrices in the adjacency matrix is not important. For example, cycle CycC can be represented before CycA. CycC and outermost cycle CycD is shown in colors orange and gray in the adjacency matrix.

A bridge segment between vortex cycles with its ending vertices on neighboring cycles has its connectivity represented by the sub matrices that are away from the main diagonal. These sub matrices are color coded as blue and represent connectivity between cycles. Since they are also bi-directional, each edge is represented by two symmetrical positions in the adjacency matrix. For example the bridge segment fr between CycB and CycD is represented by matrix positions (f,r) and (r,f).

Fig. 9(b) shows the frequency of occurrence of each eigen value for the coronal view of the brain activation regions recorded in 4 rs-fMRI videos. Since adjacency matrix is symmetrical for undirected vortex nerves, all the eigen values are real [22].

6. Conclusion

The paper calls attention to the discovery of spiraling intensities (brightness levels) forming cycles in each brain activation region in rs-fMRI video frames. Geometrically, this means that typically there are multiple cycles forming a staircase rising to a plateau in an activation region vortex. What we are calling a vortex is a collection of cycles. Each cycle is a collection of path-connected frame picture elements (voxels) with edges attached between voxels that form a path. In other words, each brain activation region forms a collection of nested cycles attached to other, each with its own level of intensity represented visually with a particular color. The edges of a single activation region cycle represent a uniform brightness level identified in a quaterionic view of video frame voxel intensities. The brightness level of the voxels of a brain activation region cycle is visualized with a single color. A simplified approach to indexing of brain activation region vortexes is made possible by considering the Betti number of the vortex. Lower Betti numbers indicate lower numbers of vortex cycle brightness levels (less intense brain activation region). Higher Betti numbers point to brain activation regions indicate higher numbers of vortex cycle brightness levels (more intense brain activation region).

Declaration of Competing Interest

This statement is to certify that no conflict of interest exists in the submission of this manuscript. Also, the manuscript is approved for publication by all authors. The work described is original research that has not been published previously, and not under consideration for publication elsewhere.

CRediT authorship contribution statement

Arjuna P.H. Don: Conceptualization, Investigation, Formal analysis, Supervision, Writing – original draft. **James F. Peters:** Methodology, Validation, Software, Writing – original draft. **Sheela Ramanna:** Methodology, Resources, Writing – original draft, Writing – review & editing. **Arturo Tozzi:** Investigation, Writing – review & editing.

Acknowledgment

Authors acknowledge the NSERC Discovery Grants program (#194376) for this research.

References

[1] Hamilton. On quaternions; or on a new system of imaginaries. Algebra 1843. Letter to John T. Graves
[2] Tait P. An elementary treatise on quaternions. An elementary treatise on quaternions. Oxford: Clarendon Press; 1867.
[3] Zhou J, Xu Y, Xiaokang, Yang. Quaternion wavelet phase based stereo matching for uncalibrated images. Pattern Recognit Lett 2007;28(12):1509–22.
[4] Chan WL, Choi H, Baraniuk RG. Coherent multiscale image processing using dual-tree quaternion wavelets. IEEE Trans Image Process 2008;17(7):1069–82.
[5] Xu Y, Yang X, Song L, Traversoni L, Lu W. QWT: retrospective and new applications. Geometric algebra computing. Bayro-Corrochano E, Scheuermann G, editors. London: Springer; 2010. doi:10.1007/978-1-84996-108-0_1.
[6] Ginzberg P, Walden AT. Matrix-valued and quaternion wavelets. IEEE Trans Signal Process 2013;61(6):1357–67.
[7] Chai P, Luo X, Zhang Z. Image fusion using quaternion wavelet transform and multiple features. IEEE Access 2017;5:6724–34.
[8] Subakan ÖN, Vemuri BC. A quaternion framework for color image smoothing and segmentation. Int J Comput Vis 2011;91(3):233–50.
[9] Chen B, Shu H, Coatrieux G, Chen G, Sun X, Coatrieux JL. Color image analysis by quaternion-type moments. J Math Imaging Vis 2015;51(1):124–44.
[10] Li YN. Quaternion polar harmonic transforms for color images. IEEE Signal Process Lett 2013;20(8):803–6.
[11] Li YN, Wang P, Su YT. Robust image hashing based on selective quaternion invariance. IEEE Signal Process Lett 2015;22(12):2396–400.
[12] Chen Y, Xiao X, Zhou Y. Low-rank quaternion approximation for color image processing. IEEE Trans Image Process 2020;29:1426–39.
[13] Marco SD. Theoretical analysis of quaternion image matching performance. In: Proceedings SPIE 11399, mobile multimedia/image processing, security, and applications; 2020.
[14] Mahmoud EE, Higazy M, Alotaibi H, Abo-Dahab S, Abdel-Khalek S, Khalil E. Quaternion anti-synchronization of a novel realizable fractional chaotic model. Chaos Solitons Fractals 2021;144:1–20.
[15] Tozzi A, Peters JF, Jausovec N, Legchenkova I, Bormashenko E. Nervous activity of the brain in five dimensions. BioPhysica 2021;1(1):38–47. doi:10.3390/biophysica1010004.
[16] Don AP, Peters JF, Ramanna S, Tozzi A. Topological view of flows inside the bold spontaneous activity of the human brain. Front Comput Neurosci 2020;14:34.
[17] Peters J. Computational geometry, topology and physics of digital images with applications. Shape complexes, optical vortex nerves and proximities. Cham, Switzerlan: Springer Nature; 2020. xxv+440 pp.,ISBN 978-3-030-22191-1/hbk; 978-3-030-22192-8/ebook, Zbl07098311
[18] Rotman J. The theory of groups. An introduction.. Boston, Mass: Allyn and Bacon, Inc; 1965. xiii+305 pp., MR0204499, reviewed by R.C. Lyndon
[19] Ramella G, Sanniti Di Baja G. A new technique for color quantization based on histogram analysis and clustering. Int J Pattern Recognit Artif Intell 2013;27(03):1360006.
[20] Koschan A, Abidi M. Digital color image processing. John Wiley & Sons; 2008.
[21] Coleman TF, Moré JJ. Estimation of sparse jacobian matrices and graph coloring blems. SIAM J Numer Anal 1983;20(1):187–209.
[22] Brouwer AE, Haemers WH. Spectra of graphs. Springer Science & Business Media; 2011.

TROUBLES WITH SHANNON'S ACCOUNT OF THE ENTROPY IN THE CONTINUOUS CASE

Arturo Tozzi
Center for Nonlinear Science, Department of Physics, University of North Texas, Denton, Texas, USA
tozziarturo@libero.it

According to Shannon, the entropy for continuous stochastic processes has many properties analogous to the entropy for discrete processes. Nevertheless, there are some mathematical and physical problems with Shannon's account. The obstacle arises in chapter 21 (Shannon 1948), when Shannon describes the continuous case of the entropy of ergodic ensemble of functions (i.e., the entropy of a set of functions together with a probability measure).
Two possibilities may occur:

1) The entropy in the discrete case is related to the logarithm of the PROBABILITY of long sequences of samples and to the NUMBER of the probable sequences of long length,
2) the entropy in the continuous case is related to the logarithm of the PROBABILITY DENSITY of long sequences of samples and to the VOLUME of the probable sequences of long length in the function space.

This divergence follows from Shannon's requirement of systems under assessment to be ergodic, thus allowing the continuous space to be divided into many small cells. Indeed, the key property and main tenet of the Shannon's account of entropy, both discrete and continuous, is the occurrence of ergodicity, such that every generated sequence displays the same statistical properties. If an ensemble is ergodic, each function is the set typical of the ensemble: each function can be expected to go through all the convolutions of any of the functions of the set. The presence of ergodicity leads to the statistical homogeneity required by Shannon to treat the entropy of discrete noiseless channels, of discrete channels with noise and of continuous channels.

In the case of white noise and large n, there is a well-defined volume (at least in the logarithmic sense) of high probability, and within this volume the probability density is relatively uniform (in the logarithmic sense). Shannon demonstrates that the region of high probability is a sphere of radius $\sqrt{nN}$ in the discrete case, while in the continuous case the volume of high probability is the squared radius of a sphere having the same volume.

However, it is well-known that the more the dimensions of the sphere, the less its volume (Kůrková V. 2019). In higher-dimensional spheres, the ball volume tends to be concentrated near the equator, approaching the zero as their dimensionality tends to infinity. If the volume of the higher-dimensional ball is progressively "shrunken" inside the sphere, this means that the system's ergodicity gets lost. This also means that the volume of the probable sequences of long length in the function space, which is a typical parameter of the entropy in the continuous case, does not hold anymore in multidimensions.

When the ergodicity is not guaranteed, the operation performed by Shannon of dividing the continuum of messages and signals into a large but finite number of homogeneous small regions is doomed to failure. Therefore, the concept of Shannon entropy is undermined by its very foundations since its ergodic tenet is not viable in the real multidimensional world.

Furthermore, Shannon portrays his stochastic ergodic systems in terms of random walks, white noise, Markov paths. It has been shown that this approach is not profitable when random walks occur in phase spaces of dimensions higher than two. The more the dimensions, the more the (seemingly) stochastic paths are constrained, because their trajectories cannot resume to the starting point. This means that high-dimensional tracks, ubiquitous in real world physical/biological phenomena, cannot be operationally treated in terms of closed paths. This also means that memoryless events disconnected from the past such as Markov chains cannot exist in high dimensions. For further details, see: Tozzi (2020).

REFERENCES

1) Kůrková V. 2019. Some insights from high-dimensional spheres: Comment on "The unreasonable effectiveness of small neural ensembles in high-dimensional brain" by Alexander N. Gorban et al. Phys Life Rev. https://doi.org/10.1016/j.plrev.2019.03.014.
2) Shannon CE. 1948. A Mathematical Theory of information. The Bell System Technical Journal 27:379-423.
3) Tozzi A. 2021. Random Walks Are Not So Random, After All. viXra:2010.0002.

BioSystems 211 (2022) 104584

Contents lists available at ScienceDirect

BioSystems

journal homepage: www.elsevier.com/locate/biosystems

An economic approach to energy budgets: HOW many resources should living organisms spare?

Arturo Tozzi

Center for Nonlinear Science, Department of Physics, University of North Texas, 1155 Union Circle, #311427, Denton, TX, 76203-5017, USA

ARTICLE INFO

Keywords:
Economics
ATP
Energy budget
Cellular activity
Ageing
Prebiotic

ABSTRACT

Ramsey's economic theory of saving (RTS) estimates how much of its commodities a nation should save to safeguard the well-being of future generations. Since RTS retains many attractive qualities such as simplicity, strength, breadth and generality, here we ask if it would be useful to investigate biophysical issues. Specifically, we focus on a biological topic that lends itself as a backdrop for the study of the imbalance between intake and expenditure, i.e., the evaluation of the multicellular living organisms' energetic requirements and constraints. Our problem is to find at each time the optimum distribution and the right balance of the cellular energy budget between consumption and storage: how much must a living organism spare to increase its chances of survival over long periods? To give an operational example, we discuss the ATP requirements in the central nervous system during the spontaneous and the evoked activity of the brain, showing that the experimentally detected values of energetic expenditure during neural computations match well with the estimations provided by RTS. Suggesting how to find the optimum allocation of the available energy between expenditure and saving at each time, RTS approaches to biological energy budgets may have a wide range of experimental applications, such as: a) optimization of the long-term survival chances of either immortalized cell cultures, or beneficial bacterial colonies and exogenous probiotic mixtures; b) eradication of detrimental biofilms, such as, e.g., heart valves' Streptococcus colonies; c) novel anti-stress and anti-ageing strategies.

1. Introduction

Every living organism requires energy for maintenance, growth and reproduction, since the whole dynamics of cell fate decisions and regulatory networks rely on ATP levels and cellular energy budgets (Kerr et al., 2019). The energy budget provides useful information concerning cellular metabolic state, embryogenesis (Song et al., 2019), dysfunction of signalling pathways (Papkovsky and Zhdanov, 2021), aberrant activity of ATP-producing proteins (Zhdanov et al., 2011). To provide an example, organisms exposed to suboptimal conditions (e.g., starvation, pharmacological treatment, diabetes, cancer) face an a priori cost of fighting stress in terms of metabolic resources (see, e.g., Smolders et al., 2003; Schmidt et al., 2021). The experiments concerning influence of energy availability on regulatory network dynamics usually evaluate how energy budgets affect both the microscopic cell behaviour (Kerr et al., 2019) and the mechanistic connections of sub-organismal processes. However, energy budgets can be calculated not just at the micro-levels of cellular activity, but also at different macro-levels of living systems' activities. Furthermore, the metabolic cost of animal growth, which quantifies the amount of energy required to synthesize a unit of biomass, is a key factor for the making of ontogenetic energy budgets (Ferral et al., 2020). Also, energy budgets provide the proper operational framework to examine the acquisition of energy resources at higher degrees of organization, such as those at the population and ecosystem levels (Murphy et al., 2018).

We ask whether the storing capacity of the living organisms' energy pathways can be quantitatively assessed through mathematical models. Here the Ramsey's economic theory of saving (RTS) comes into play (Ramsey 1928), providing a simple and profitable mathematical apparatus generalizable enough to be used for the assessment of energy budgets. "How much of its income should a nation save for the next generations?" The question was put forward and successfully tackled by the versatile 25 years old "economist" Frank Plumpton Ramsey in 1928, two years before his unexpected death (Misak 2020). Inspired by Ramsey's rather general mathematical/economical approach to saving, we will provide an effort to mathematically cope with biological issues related with energy budget. In particular, we will ask to ourselves the following tantamount question: "how much of its energy budget should

E-mail address: tozziarturo@libero.it.

https://doi.org/10.1016/j.biosystems.2021.104584
Received 13 October 2021; Received in revised form 11 November 2021; Accepted 18 November 2021
Available online 26 November 2021

a living organism save over time for the most efficient long-term survival?". Also, we will tackle the next obvious question: "Why should we use RTS to assess the energy budget of living organisms?"

2. RAMSEY'S model: the original account

"How much of its output should a nation save over time and across generations?". In touch with the Classical-Utilitarianism calculus, Ramey believed that an accurate balancing is required between use and storage. He identified the best match between attainable and desirable utility streams over time and across generations (Misak 2020). Indeed, immediate energetic consumption produces utility now but reduces the opportunities in the future, while energetic saving reduces utility now and increases it in the future. Ramsey requires to invest an amount which may have no immediate payoff but may nevertheless produce a big payoff for future generations.

The key elements of RTS are individuals' lifetime well-beings who are subject to resource constraints (Ramsey 1928). The demographic profile over time is taken to be given, such that the future numbers of people are seen as exogenous and predictable (Dasgupta 1969). Since these individuals are considered identical, a single individual at each date may be assumed, removing any distinction between time and generations. Economic uncertainty is not an option, since the economy, assumed to be closed to international trade, is endowed with a single, non-depreciating commodity that can be worked by labour to produce output at each date. Ramsey's approach neglects the differences between distinct kinds of goods and labour, so that we are allowed to simply speak of general quantities such as capital, consumption and labour without considering their particular forms.

Ramsey's model makes other simplifying assumptions (Parfit 1984):

1) The future is assumed to be deterministic and infinitely long.
2) The community goes on forever.
3) The community will be always maintaining the same size. Therefore, the population is assumed to be constant.
4) The community will be always maintaining the same capacity for aversion to labour and enjoyment.
5) The community will be always governed by the same motives in accumulation.
6) Inventions, technical innovations and improvements in organization are not allowed.
7) No misfortunes, such as earthquakes, wars, catastrophes, will occur to sweep away the nation's accumulations.

Since some of the output can be either invested to increase the commodity's stock or consumed immediately, the practical problem is to find the optimum allocation of output at each date between consumption and investment. Ramsey argues that savings plus consumption must equal the income (Ramsey 1928):

$$\frac{dc}{dt} + x = f(a, c) \tag{1}$$

where x(t) is the total rate of consumption or expenditure in a community and a(t) is the total rate of labour in a community. Further, c(t) is the capital (i.e., the stock of the commodity that serves to produce output) at time t, while c_0 is the given capital with which the nation starts at t=0, dc/dt are the savings and f(a,c) is the income. All the terms x, a and c are functions of one independent variable, the time, with $t \to \infty$.

A series of mathematical steps leads Ramsey to his main results, i.e., a general rule stating that the rate of saving multiplied by the marginal utility of money should always be equal to the maximum possible rate minus the actual rate of utility enjoyed. The corresponding equation is:

$$\frac{dc}{dt} = f(a, c) - x = \frac{B - (U(x) - V(\alpha))}{u(x)} \tag{2}$$

U(x) is the total rate of utility of a rate of consumption x, while u(x), which never increases, is the marginal rate of utility of a rate of consumption x. We'd like to remind that the economic utility is the satisfaction or benefit derived by consuming a product (Kahneman and Tversky, 1979). Therefore, the marginal utility of a good/service describes how much pleasure or satisfaction is gained from an increase in consumption (Castro and Araujo 2019). Furthermore, V(a) is the total rate of disutility of a rate of labour a, while v(a), which never decreases, is the marginal rate of disutility of a rate of consumption x. Indeed, labour supply is an exogenously given constant which is unpleasant and characterized by disutility. The difference U(x) - V(a) is the net enjoyment per unit of time: this value is a maximum subject to the condition that x equals what can be produced with a and c. The term B (Bliss) is the maximum obtainable rate of enjoinment which, with time passing, approaches asymptomatically to a certain finite limit.

After a few steps (see Ramsey 1928), the main equation can be rewritten as follows:

$$B - W(y) = \frac{dW}{dy}(rc - y) \tag{3}$$

Where rc is the unearned income, W(y) = U(x) - V(a) is the total marginal utility of an unearned income available for consumption, while w (y) is the corresponding marginal utility. The term y stands for x – pa, i.e., the consumption minus the earned income. The plot of eq. (3) displays the concave function illustrated in Fig. 1.

Despite its qualities, RTS has some weaknesses with regard to its simplifying assumptions and rigid requirements. For example, the Ramsey's model points to very high saving rates. According to Ramsey, over half of resources must be saved: i.e., an income of £ 500 per annum requires an amount that should be saved of about £ 300 per annum. Another thorny issue is that the passage of time for an individual is not the same as for generations, so that an individual's lifetime well-being is different from intergenerational well-being. Despite RTS adopts the shortcut to provide the short-term and the long-term well-beings with the same functional form, there is little evidence to suggest that such simplification holds in the real-world's intergenerational life. Also, Ramsey assumes that time is a continuous and not a discrete variable, perhaps because the mathematics is simpler.

In the last decades, many scholars provided efforts to overtake the limitations of the otherwise powerful Ramsey's theory. Less stringent accounts have been offered that consider less constrained situations, e.g., introducing novel factors such as moderate changes with the external, opening the economy to trade, and so on. For a survey of the new developments, see Koopmans (1965); Solow (1974); Mirrlees (1967); Arrow et al. (2012). For example, Dasgupta and Heal (1974)

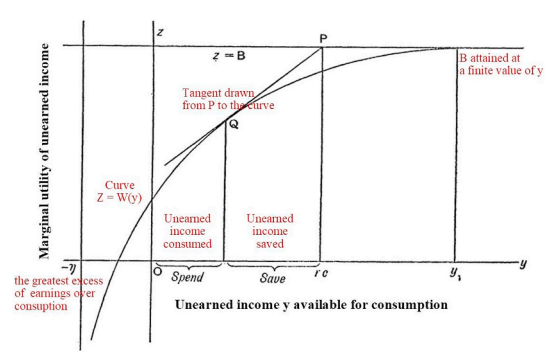

Fig. 1. The behaviour of long-term communities according to the Ramsey's account. The utility is assumed to be an increasing and strictly concave function which is bounded above. Bliss turnpike is beyond our reach, but we can measure how close we are to it to determine the trade-off between consumption and saving at each point of time. Once identified the amount of unearned income available for consumption (rc in the Figure), the consumed and the saved unearned incomes can be easily calculated. Modified from Ramsey (1928).

delivered a RTS extension including natural capital in production which, referred to biological models, would allow the introduction of phenotypical, epigenetic, genotypical and evolutionary improvements in the cellular capabilities of labour/energetic production.

To sum up, the results achieved by Ramsey display surprising generality. The original formulation of RTS evaluates how much natural capital a nation should save. Yet, put in terms of maximal utility over the long run, RTS provides a general scheme which could be profitably used to assess recent hot topics such as exhaustible resources, climate change, nuclear waste disposal (Misak 2020). We will see in the next chapter that RTS leads to a valuable operational result: in biology, given a known amount of energy available for cellular consumption, the consumed and the saved energies can be estimated.

3. RAMSEY'S model: the biological counterpart

RTS provides a basic and broad mathematical apparatus for the evaluation of many scientific issues, such as, in our case, living organisms' energy budgets. Our biological problem is to find at each time the optimum distribution between the consumed and the saved energy, or in other words, to determine the right balance between consumption and investment. Our goal is to answer to the question: how much can be spared at a given value of energy?

Starting from the energy available for consumption, the quantity of energy to spare in order to achieve the highest benefit for the future and for the next generations is easily calculated. Erasing any distinction between time passing and generations, living beings are taken to be identical, so that the occurrence of a single individual at each date may be assumed. The intentions are assumed always realized, while the amount of available sources is assumed always fully deployed and the labour e fully employed. Since Ramsey does not incorporate uncertainty about future possibilities, we consider individual's life as characterized:

a) By one and only energetic source.
b) By an exogenous constant, termed cellular labour, which produces at each date an output consisting of energy.

In touch with RTS, the future survival of living organisms is seen as exogenous and predictable, having the external factors a negligible effect on their survival. The cellular economy is assumed to be closed to energetic changes with other living beings. This means that some of the produced energy can be used to increase the energy stock, while the remainder can be consumed immediately. No mention is made of possible phenotypic, epigenetic, genotypic, evolutionary improvements in cellular capability of labour or ability to achieve a larger quantity of available sources. In touch with Ramsey's account, the anticipated energy production at each moment equals the sum of intended storage and intended consumption. Since the living being is in equilibrium at each moment, the intended saving equals the intended investment at each moment.

The biological counterpart to RTS runs as follows: in a living system the energetic savings plus the consumption must equal the income. The foremost consequence of the application of RTS to the energy budget of living organisms is that the consumed and the spared values of energy can be easily calculated looking at the plot of the concave function. Fig. 2 illustrates the biological counterpart of the concave economic function described in Fig. 1.

Generally speaking, Ramsey's biological problem can be cast equally as, "how much of a living organism's energetic production should it consume?" The biological consequences of a RTS approach to living organism's energetic dynamics are straightforward. Since the amount of available sources is assumed not to waste or decrease in benefit, the gross energetic investment equals the net energetic investment. If the consumption is lower than the energetic production at a given time, the investment is positive and the amount of the available sources increases; in turn, if the consumption exceeds the energetic production at a given

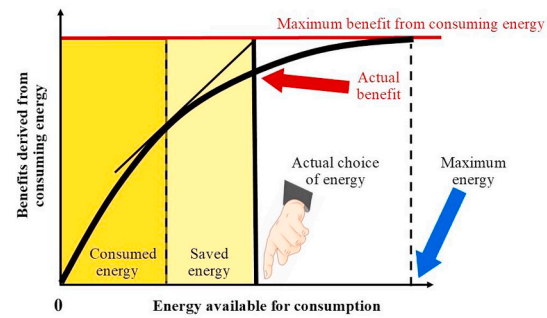

Fig. 2. Living organisms' energy budget according to the Ramsey's plot. In our biological context, the utility stands for the cellular benefits derived by energetic consumption. The concave curve describes how much benefit (actual benefit) is gained by the living organism from an increase in energy consumption (the actual choice of energy). The plot also says that the more is spared, the sooner the highest benefits will be reached.

time, the investment is negative and the amount of available sources is doomed to decline. When sources are available, the produced energy is always >0. When the use of available energy increases, the resulting benefits are always positive. It is noteworthy that the resulting benefits depend solely on the quantity of available energy. After the consumption of a certain quantity of energy, the resulting benefits reach a plateau, and further increases in energy are not able to improve anymore the benefits. When the benefits are the highest possible, the spared energy is zero, since the tangent parallels the maximum.

To provide an operational example of the implications of RTS in biological issues, here we will examine the energy budget of the central nervous system (CNS) performing neural computations during its spontaneous and evoked (e.g., perceptive) activities. Following the nomenclature of the previous chapter, in the case of the CNS the capital c stands for the available stock of ATP (expressed in μmol/gr/min) that serves to produce the required outputs, while x(t) is the total rate of consumption or expenditure inside the CNS. Also, a(t) is the total rate of labour produced by nervous substructures and dc/dt are the savings, while f(a,c) is the income. The most important factor, i.e., W(y) = U(x) - V(a) stands for the CNS benefits derived from consuming energy. The term B (Bliss) is the maximum obtainable benefit from consuming energy, corresponding to the best available perception, i.e., the maximum information attainable by the perceptual activity of the CNS.

The brain activity needs a continuous energy supply (Sengupta and Stemmler, 2014), estimated at about 40 μmol of ATP/gr of brain grey matter/min (Attwell and Laughlin, 2001). The brain displays two different typical activities:

1) The spontaneous activity. Generated in the absence of explicit tasks, it has been correlated with "resting-state" or "default-network activity" (Raichle 2010). This low-frequency activity utilizes electric spikes below the alpha waves (<8 Hz) (Tozzi et al., 2016). The spontaneous activity of the brain requires a certain amount of energy, considering that ATP consumption at the mean rate of 4 Hz is 3.29×10^9 molecules of ATP/neuron/sec.
2) The evoked activity. It is elicited during tasks such as intentional movements, memory, perception. Characterized by local boosts in spike frequency, this high-frequency activity utilizes electric spikes in the range of the beta and gamma waves (>13 Hz) (Raichle and Gusnard 2002). Since every additional spike requires 6.5 μmol/ATP/gr/min (Attwell and Laughlin, 2001), the evoked activity of the brain demands a much bigger amount of energy, enthalpy consumption and free-energy production, compared with the spontaneous activity (Tozzi et al., 2016).

The energy supply of the CNS is correlated with information processing in the brain (Sengupta et al., 2013). During the evoked activity

of the brain, increases in spike frequency (and therefore increases in ATP consumption) confer benefits to the human cognitive abilities. In particular, during the evoked activity of perception, high-frequency feedforward currents project from the primary sensitive areas to the frontal cortex. The use of gamma frequencies around 40 Hz guarantees to the brain the highest information capacity, therefore improving the mental ability to sharply perceive things from the surrounding environment (Meador et al., 2002; Beldzik et al., 2019). This means that, at least in theory, the best available perception would be achieved with an energetic consumption of about 260 μmol/ATP/gr/min, corresponding to an electric brain frequency around 40 Hz. In the Ramsey's plot, this ATP value of 260 would stand for the maximum energy able to guarantee the maximum benefit, i.e., to guarantee the best available perception (Fig. 3). Though, it is well-known that the maximum increase in energy consumption which can be sustained by the muscular vessels of the brain is about 120 μmol of ATP/gr/min, corresponding to a frequency of just 18 Hz (Hochachka 2020). This means that the CNS is not capable of handling the hypothetical consumption of 260 μmol/ATP/gr/min during the optimal perceptual frequency of 40 Hz. Therefore, the overall power consumption of the CNS must be minimized through buffer strategies (Sengupta et al., 2013; Howarth et al., 2012). Nervous mechanisms are required to promote energetic efficiency and balance the equilibrium between consumed/saved ATP without exceeding the "threshold" of 120 μmol/ATP/gr/min.

To provide an example, Fig. 3 portrays the Ramsey's concave function in two different energetic cases of perceptive activity of the CNS. In Fig. 3A, the chosen amount of ATP available for perceptual neural computations is about 130 μmol/gr/min. This value, standing for about half of the maximum available ATP at 40 Hz, guarantees just a partial perceptive benefit. When the tangent is drawn from the line of the best available perception to the concave curve, we achieve a large amount of spared ATP and a small amount of used ATP, the latter corresponding to low brain frequencies of about 4 Hz. In turn, in Fig. 3B, the chosen amount of ATP is much higher, i.e., about 210. This value guarantees a very high perceptive benefit, almost reaching the best available perception. Drawing the tangent as before, we achieve an amount of used ATP that is close to the "threshold" of 130.

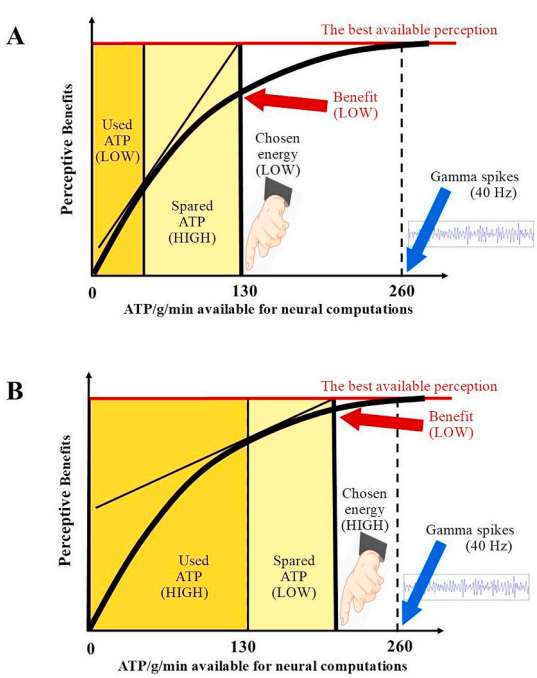

Fig. 3. Ramsey's model in case of perceptive activity of the central nervous system. In Fig. 3A and B, two distinct values of ATP available for perceptual neural computations are chosen, i.e., 130 and 210, respectively. The maximum value of ATP is 260, corresponding to the best perceptive frequency of 40 Hz. Note how different initial levels of energy (lower in **3A** and higher in **3B**) lead to completely different outcomes of perceptual benefit and consumed/saved energy. In both the cases, the energy of the CNS during perceptive activity matches the values of the Ramsey's concave curve. See text for further details.

Therefore, the energetic expenditure of neural computations detected by experimental procedures agrees with the estimations provided by the concave curve of Ramsey's plot. In accordance with the empirical results, RTS allows the evaluation of the brain's storage capacity during energetically expensive activities. Contrary to the RTS economic account which emphasizes the saved income, our RTS account of perception takes a slightly different view: while a portion of the produced energy is consumed immediately by the CNS, the remainder is NOT stored in order to increase the energetic stock, rather it is employed to spare the used energy. Therefore, the Ramsey's model might stand for one of the feasible strategies of nervous cells to minimize the constraints of energy consumption and maximize the benefits of energy storing, contributing to the balance of the quantitative tradeoff between energy use and information processing in the CNS.

4. Conclusions

Our paper deals with the explanation of Ramsey's economic theory of saving (RTS) applied to biological issues, specifically to the study of the imbalance between intake and expenditure, consumption and storage. For our part, our aim was to cast Ramsey's economic problem in terms of: "how much of a living organism's energetic production should it consume?" We found that Ramsey's model might provide a well-grounded mathematical framework to describe the energy budget of living organisms. The evaluation of energy budgets requires quantities that can be (relatively easily) operationally assessed. For example, the cellular energy budget can be measured through different available techniques that facilitate the comparison of different cells, such as direct measurement, extracellular flux analysis, high-resolution respirometry, fluorescent dye kits (Schmidt et al., 2021), specific bioenergetic signatures such as respiration, glycolytic flux, Krebs cycle activity, ATP levels, total biomass, NAD(P)H, Ca2+, mitochondrial pH, membrane potential, redox state (Papkovsky and Zhdanov, 2021), the measure of changes in glycogen, lipid, and protein budgets (Smolders et al., 2003). It is noteworthy that the energy budget concerns not just cells, but also complex organisms: e.g., the number of calories in case of sporting activities can be quantitatively assessed. We also showed how, thanks to RTS, it is feasible to estimate how much energy can be used and stored by the CNS to retain the maximum information capacity during the perceptive activity.

At this point it comes to wonder: what for? Why should we provide an effort to correlate seemingly disparate fields such as the economic theory of saving and the cellular energy budget? The answer is straightforward: such comparison is very promising. Suggesting an interest in the distant future that is worth to be considered, RTS allows to calculate the amount of energy that a living individual must spare in order to optimize its chances to survive longer and in good health. RTS's plot says how much energy must be spared from the available stock of the cellular budget to maximize the energy available for consumption. Indeed, high energetic consumption impairs the future well-being of the cell, while larger amount of reservoir might preserve the organism for longer times. RTS could be useful to compare the long-term effects of different energetic options. To provide a practical example, do the benefits of energetic expensive activities such as bodybuilding overcome the long-term damages? Does sport at competitive levels in children contribute to extend their well-being and lifetime? Furthermore, the knowledge of the proper quantity of cellular energy to store and spare might pave the way to novel anti-stress, beauty treatments and anti-ageing approaches.

The system-nation described by RTS reminds cell cultures, in which the parameters are strictly standardised and the energetic sources/flows

carefully regulated. Ramsey's assumption that the community goes on forever in a world with an indefinite future lends itself well with the "infinite life" assumption adopted for cell colonies such as, e.g., Caco-2, the immortalized cell line of human colorectal adenocarcinoma cells (Marziano et al., 2019). In this peculiar case, the Ramsey's plot provides us with a useful information: how much energy must be provided to achieve the best preservation and longest survival of a cell culture to ensure the welfare of its future generations? In accordance with this line of reasoning, RTS might also contribute to improve the survival of beneficial bacterial colonies and biofilms, such as, e.g., endogenous saprophytic intestinal bacteria or exogenous probiotic mixtures (Giannetti et al., 2017), or to obliterate detrimental biofilms, such as, e.g., cardiac valvular colonies of harmful Streptococcal strains (Hosokawa et al., 2018).

We want to end with a more speculative insight. While individuals often save for their children, Ramsey asks how much society should save. In touch with this account, RTS implementation in the study of living organisms suggests that increases in intracellular energetic levels might lead to increases in stable phenotypes and decision-making capabilities. If the cells with sub-threshold intracellular energy are forced to adopt a singular phenotype and a specific cell fate, this could mean that energetic differences among different cells may help to explain the experimentally detected variability in cellular decision-making across biological systems.

Declaration of competing interest

The author warrants that the article is original, does not infringe on any copyright or other proprietary right of any third part, is not under consideration by another journal, and has not been previously published.

The Author does not have any known or potential conflict of interest including any financial, personal or other relationships with other people or organizations within three years of beginning the submitted work that could inappropriately influence, or be perceived to influence, their work.

This research did not receive any specific grant from funding agencies in the public, commercial, or not-for-profit sectors.

This research does not contain any studies with human participants or animals performed by the Author.

The Author had full access to all the data in the study and take responsibility for the integrity of the data and the accuracy of the data analysis. The Author performed: study concept and design, acquisition of data, analysis and interpretation of data, drafting of the manuscript, critical revision of the manuscript for important intellectual content, statistical analysis, obtained funding, administrative, technical, and material support, study supervision.

Data availability

No data was used for the research described in the article.

References

Arrow, K.J., Dasgupta, P., Goulder, L.H., Mumford, K.J., Oleson, K., 2012. Sustainability and the measurement of wealth. Environ. Dev. Econ. 17 (3), 317–355.
Attwell, D., Laughlin, S.B., 2001. An energy budget for signaling in the grey matter of the brain. J. Cerebr. Blood Flow Metabol. 21 (10), 1133–1145.
Beldzik, E., Domagalik, A., Beres, A., Marek, T., 2019. Linking visual gamma to task-related brain networks-a simultaneous EEG-fMRI study. Psychophysiology 56 (12), e13462. https://doi.org/10.1111/psyp.13462.
Castro, L.C., Araujo, A.S., 2019. Marginal utility & its diminishing methods. Int. J. Tax. Econ. Manag. 36–47.
Dasgupta, P., 1969. On the concept of optimum population. Rev. Econ. Stud. 36 (3), 295–318.
Ferral, N., Gomez, N., Holloway, K., Neeter, H., Fairfield, M., et al., 2020. The extremely low energy cost of biosynthesis in holometabolous insect larvae. J. Insect Physiol. 120, 103988 https://doi.org/10.1016/j.jinsphys.2019.103988.
Giannetti, E., Maglione, M., Alessandrella, A., Strisciuglio, C., De Giovanni, D., et al., 2017. A mixture of 3 bifidobacteria decreases abdominal pain and improves the quality of life in children with irritable bowel syndrome: a multicenter, randomized, double-blind, placebo-controlled, crossover trial. J. Clin. Gastroenterol. 51 (1), e5–e10. https://doi.org/10.1097/MCG.0000000000000528.
Hochachka, P.W., 2020. Muscles as Molecular and Metabolic Machines. Taylor & Francis Ltd. EAN: 9780367227807.
Hosokawa, S., Okayama, H., Hiasa, G., Kawamura, G., Shigematsu, T., et al., 2018. Isolated left atrial infective mural endocarditis. Intern. Med. 57 (7), 957–960. https://doi.org/10.2169/internalmedicine.9559-17.
Howarth, C., Gleeson, P., Attwell, D., 2012. Updated energy budgets for neural computation in the neocortex and cerebellum. J. Cerebr. Blood Flow Metabol. 32 (7), 1222–1232. https://doi.org/10.1038/jcbfm.2012.35.
Kahneman, D., Tversky, A., 1979. Prospect theory: an analysis of decision under risk. Econometrica 47 (2), 263–292. https://doi.org/10.2307/1914185.
Kerr, R., Jabbari, S., Johnston, I.G., 2019. Intracellular energy variability modulates cellular decision-making capacity. Sci. Rep. 9 (1), 20196 https://doi.org/10.1038/s41598-019-56587-5.
Koopmans, T.C., 1965. On the Concept of Optimal Economic Growth. Pontificiae Academiae Scientiarum Scripta Varia, 28. Reprinted in T.C. Koopmans, vol. 1966. The Econometric Approach to Development Planning, Amsterdam: North Holland.
Marziano, M., Tonello, S., Cantù, E., Abate, G., Vezzoli, M., et al., 2019. Monitoring Caco-2 to enterocyte-like cells differentiation by means of electric impedance analysis on printed sensors. Biochim. Biophys. Acta Gen. Subj. 1863 (5), 893–902. https://doi.org/10.1016/j.bbagen.2019.02.008.
Meador, K.J., Ray, P.G., Echauz, J.R., Loring, D.W., Vachtsevanos, G.J., 2002. Gamma coherence and conscious perception. Neurology 59 (6). https://doi.org/10.1212/WNL.59.6.847.
Misak, C., 2020. Frank Ramsey: A Sheer Excess of Powers Copertina Rigida – 13 Febbraio 2020. OUP, Oxford. -13: 978-0198755357.
Mirrlees, J.A., 1967. Optimum growth when technology is changing. Rev. Econ. Stud. 34 (1), 95–124.
Murphy, C.A., Nisbet, R.M., Antczak, P., Garcia-Reyero, N., Gergs, A., et al., 2018. Incorporating suborganismal processes into dynamic energy budget models for ecological risk assessment. Integrated Environ. Assess. Manag. 14 (5), 615–624. https://doi.org/10.1002/ieam.4063.
Papkovsky, D.B., Zhdanov, A.V., 2021. Cell energy budget platform for multiparametric assessment of cell and tissue metabolism. Methods Mol. Biol. 2276, 305–324. https://doi.org/10.1007/978-1-0716-1266-8_23.
Parfit, D., 1984. Reasons and Persons. Oxford University Press, Oxford.
Raichle, M.E., Gusnard, D.A., 2002. Appraising the brain's energy budget. Proc. Natl. Acad. Sci. U. S. A. 99 (16), 10237–10239. https://doi.org/10.1073/pnas.172399499.
Raichle, M.E., 2010 Apr. 2010. Two views of brain function. Trends Cognit. Sci. 14 (4), 180–190. https://doi.org/10.1016/j.tics.2010.01.008.
Ramsey, F.P., 1928. A mathematical theory of saving. Econ. J. 38 (152), 543–559.
Schmidt, C.A., Fisher-Wellman, K.H., Neufer, P.D., 2021. From OCR and ECAR to energy: perspectives on the design and interpretation of bioenergetics studies. J. Biol. Chem. 297 (4), 101140 https://doi.org/10.1016/j.jbc.2021.101140.
Sengupta, B., Laughlin, S.B., Nieven, J.E., 2013. Balanced excitatory and inhibitory synaptic currents promote efficient coding and metabolic efficiency. PLoS Comput. Biol. 9, e1003263.
Sengupta, B., Stemmler, M.B., 2014. Power consumption during neuronal computation. Proc. IEEE 102 (Issue 5), 738–750. https://doi.org/10.1109/JPROC.2014.2307755.
Smolders, R., De Boeck, G., Blust, R., 2003. Changes in cellular energy budget as a measure of whole effluent toxicity in zebrafish (Danio rerio). Environ. Toxicol. Chem. 22 (4), 890–899.
Solow, R.M., 1974. Intergenerational equity and exhaustible resources. Rev. Econ. Stud. 41 (Symposium Issue), 29–45.
Song, Y., Park, J.O., Tanner, L., Nagano, Y., Rabinowitz, J.D., Shvartsman, S.Y., 2019. Energy budget of Drosophila embryogenesis. Curr. Biol. 29 (12), R566–R567. https://doi.org/10.1016/j.cub.2019.05.025.
Tozzi, A., Zare, M., Benasich, A.A., 2016. New perspectives on spontaneous brain activity: dynamic networks and energy matter. Front. Hum. Neurosci. 10, 247. https://doi.org/10.3389/fnhum.2016.00247.
Zhdanov, A.V., Favre, C., O'Flaherty, L., Adam, J., O'Connor, R., et al., 2011. Comparative bioenergetic assessment of transformed cells using a cell energy budget platform. Integr Biol (Camb. 3 (11), 1135–1142. https://doi.org/10.1039/c1ib00050k.

BioSystems 215–216 (2022) 104652

Contents lists available at ScienceDirect

BioSystems

journal homepage: www.elsevier.com/locate/biosystems

Bipolar reasoning in feedback pathways

Arturo Tozzi

Center for Nonlinear Science, Department of Physics, University of North Texas, Denton, TX, USA, 1155 Union Circle, #311427, Denton, TX, 76203-5017, USA

ARTICLE INFO

Keywords:
Bipolar fuzzy set
Decision making problem
Non-classical logic
Scholasticism
Transcranial magnetic stimulation

ABSTRACT

Instead of the conventional 0 and 1 values, bipolar reasoning uses −1, 0, +1 to describe double-sided judgements in which neutral elements are halfway between positive and negative evaluations (e.g., "uncertain" lies between "impossible" and "totally sure"). We discuss the state-of-the-art in bipolar logics and recall two medieval forerunners, i.e., William of Ockham and Nicholas of Autrecourt, who embodied a bipolar mode of thought that is eminently modern. Starting from the trivial observation that "once a wheat sheaf is sealed and tied up, the packed down straws display the same orientation", we work up a new theory of the bipolar nature of networks, suggesting that orthodromic (i.e., feedforward, bottom-up) projections might be functionally coupled with antidromic (i.e., feedback, top-down) projections via the mathematical apparatus of presheaves/globular sets. When an entrained oscillation such as a neuronal spike propagates from A to B, changes in B might lead to changes in A, providing unexpected antidromic effects. Our account points towards the methodological feasibility of novel neural networks in which message feedback is guaranteed by backpropagation mechanisms endowed in the same feedforward circuits. Bottom-up/top-down transmission at various coarse-grained network levels provides fresh insights in far-flung scientific fields such as object persistence, memory reinforcement, visual recognition, Bayesian inferential circuits and multidimensional activity of the brain. Implying that axonal stimulation by external sources might backpropagate and modify neuronal electric oscillations, our theory also suggests testable previsions concerning the optimal location of transcranial magnetic stimulation's coils in patients affected by drug-resistant epilepsy.

1. Introduction

The notion of bipolarity relies on the presence of two kinds of entities of diametrically opposed nature, i.e., a positive and a negative entity (Amgoud et al., 2008). Bipolar reasoning considers a positive side, a negative side and their close relationships (Zhang 1998). Whereas the logical space of classical logics is based on the dyadic relationships 0,1 which does not support computational assessment of unknown propositions, the logical space of bipolar logics (BL) is based on the triadic relationships −1, 0, +1 which supports computational coexistence of the two bipolar variables. Double-sided judgements, widely utilized in biophysical and social phenomena such as top-down/bottom-up, cooperation/competition and interests/conflict of interests, have been especially used in argumentation frameworks (Amgoud et al., 2008; Cayrol and Lagasquie-Schiex 2013). Countless subfields of engineering, economic, social disciplines, decision making, etc. display uncertainty problems that cannot be portrayed through the unipolar 0,1 information of the standard two-valued logic. In turn, multipolar information allows the description of systems in which information is either incomplete, or not fully reliable, or vague and fuzzy, or contradictory, or deficient (Dalkili and Demirtas, 2021; Tozzi and Peters, 2020).

Here we focus on a peculiar kind of bipolarity, i.e., the bipolarity between feedforward and feedback projections in biological and artificial neural networks (Sherrill et al., 2021). In particular, hierarchical counterstream via feedforward and feedback connections is a major and simple organizing principle of the cerebral cortex (Payeur et al., 2021; Varga et al., 2021). The orthodromic (i.e., feedforward, bottom-up) and antidromic (i.e., feedback, top-down) brain activity has been tackled via mathematical/topological weapons such as algebraic topology, near set theory and category theory (Tozzi et al., 2017a; Peters et al., 2017). Nevertheless, these theoretical approaches to nervous functions are constrained by soaring abstraction and vagueness in defining regular structures and nearness relations, thus preventing the formulation of sharp experimental previsions (Wolski 2013). The main goal of this paper is to overcome these difficulties, showing how the mathematical apparatus of presheaves/globular sets provides theoretical examples of applications in feedforward/feedback bipolar networks.

We will proceed as follows. At first, we will discuss the different

E-mail address: tozziarturo@libero.it.

https://doi.org/10.1016/j.biosystems.2022.104652
Received 13 January 2022; Received in revised form 26 February 2022; Accepted 26 February 2022
Available online 2 March 2022
0303-2647/© 2022 Elsevier B.V. All rights reserved.

types of bipolar judgement and their subtending logics. Then, we will tackle the past and the future developments of bipolar logics. At first, we will provide an historical overview of two medieval precursors of bipolar logics, i.e., as William of Ockham and Nicholas of Autrecourt. Next, we will show how double-sided judgements can be very useful to tackle current and next-to-come methodological issues such as orthodromic/antidromic feedback networks. Then, we will provide a mathematical description of presheaves/sheaves/globular sets, using their intricate mathematical apparatus to analyze orthodromic and antidromic activities of the nervous system. After that, we will provide operational and theoretical examples of feasible applications in different disciplines, suggesting experimental previsions that are testable with the current available technologies.

2. The present: state–OF–the-art in bipolar logics

To tackle uncertainty problems, various types of logical approaches involving bipolar judgements have been introduced. Here we describe two of the most successful logical accounts of bipolar reasoning, i.e., the bipolar fuzzy set and the paraconsistent logics.

Various Bipolar Logics (BL) have been introduced in the very last decades, such as, e.g., the bipolar fuzzy set theory for bipolar reasoning (Zhang 1998) and its variants/extensions (Akram 2013; Chen et al., 2014; Zhang 2017; Lee and Hur, 2019; Riaz and Tehrim, 2020; Dalkili and Demirtas, 2021). Fuzzy concrete domains bring together qualitative and quantitative reasoning and are therefore appropriate for representing bipolarity and imprecision (Hudelot et al., 2008). A bipolar scale is a totally ordered set with an interior element 0 termed "neutral" which divides positive from negative evaluations (Dubois and Prade H. 2008). Different types of bipolar judgements have been described in the literature of bipolar fuzzy sets. Here we, following Dubois and Prade (2008), will provide an effort to unify these types in a broader, simpler and more manageable framework. We will consider two cases of bivariate polarity: symmetric and asymmetric.

1) The first and simplest case involves **symmetric bipolarity**, in which the negative is the inverse mirror of the positive and the positive is the inverse mirror of the negative. The values can be ordered into a unidimensional linear list, i.e., a straight line equipped with two extremities −1 and +1 and a middle point 0 (Table 1, upper part). Unlike two-valued logics where 0 and 1 stands for true and false, here −1 stands for false, +1 stands for true and 0 stands for half-true. The two mirror images are comparable and mutually exclusive. Their relation is bipolar, reflexive, symmetric, transitive crisp or fuzzy, commutative, associative, distributive and monotonic (Palladino and Palladino, 2007).
2) The second case involves **asymmetric bipolarity**, in which the totally ordered negative scale is distinct from the totally ordered positive scale, since they separately evaluate positive and negative information. In this case two dimensions (i.e., the positive and the negative) are involved, such that the values can be distributed within a two-dimensional space (Table 1, lower part). Note that the neutral level is located at one extremity of the scale in both the positive and the negative scale. To make an example, the negative pole of a bipolar relation is the unipolar relation formed with all the negative and zero values in the negative side of the bipolar relation. The asymmetric bipolarity is the union of the positive and the negative scales and no associativity may occur for finite scales. Unlike the symmetric case, each bipolar comparison operator leads to a different resolution.

Two general cases of asymmetric bipolarity can be described:

Table 1
Examples of symmetric and asymmetric bipolarity in different scientific fields. Text modified from: Dubois and Prade (2008).

	SYMMETRIC BIPOLARITY			
	-1	0	+1	
General framework of bipolar relationships	negative	Neutral		positive
Three-valued logic with neutral truth value	false	half-true		true
Probability theory	impossible	Uncertain		totally sure
	ASYMMETRIC BIPOLARITY			
	-1	0	+1	
Argumentation in favour and against ill-known events	in disfavour	Doubtful		in favour
Plausibility	impossible	non-impossible		guaranteed possible
Belief	believe ¬p	Believe neither p nor ¬p, due to our ignorance		believe p
Confidence in an event	background knowledge: constraints to how the world behaves (e.g., physical laws and common sense decreasing the possible worlds)	Uncertain		data: empirical observation of the world leads to positive token of support
When observations accumulate	negative information: conjunctive aggregation	missing information		positive information: disjunctive aggregation
Bipolar reasoning in information theory	negative information: what is considered impossible	Uncertain		positive information: what is granted as possible
Incomplete information	possible	Doubtful		necessary
Rough set theory	elements not belonging to the subset A	elements with unknown membership		elements belonging to the subset A

a) A case characterized by the coexistence of positive and negative poles with duality relation. An item is judged according to two independent evaluations performed on the same data, one in favour and one against. This is the case of formal argumentation and paraconsistent logics. In turn, in uncertainty theory characterized by incomplete information, the weak evaluation of an item may be the complement of the positive evaluation of the contrary item.
b) A "strongest" case, characterized by the fact that the negative and the positive parts of the information are of different nature and just partially related through minimum consistency requirements. In this case, the positive image is not a mirror image of the negative image, since the negative and the positive pieces of information cannot be aggregated using the standard principles of information merging. For example, two separate possibility distributions can be disjoint in knowledge representation. A situation that is not impossible is not necessarily guaranteed as possible if not explicitly permitted; in turn, what is guaranteed possible should not be impossible. When observations accumulate, background knowledge increases, positive information aggregates disjunctively and negative information aggregates conjunctively.

Table 2 shows that the three values −1, 0, +1 have a different meaning according to the scientific field under evaluation, such as, e.g., probability theory, 3-valued logic with neutral truth value, uncertainty and boundary problems, information theory, and so on.

Paraconsistent logics (henceforward PCLs) suggest that not every contradiction entails arbitrary absurdities (Jaśkowski 1948; da Costa and Newton, 1974). PCLs reject two tenets of the classical Aristotelian logic: the principle of explosion (henceforward PEX) and the law of noncontradiction (henceforward LNC).

PEX asserts that *ex falso quodlibet,* i.e., from falsehood -or from contradiction-anything follows:

$$p \wedge \neg p \rightarrow q$$

i.e., for any statements p and q, if p and not-p are both true, then it logically follows that q is true. Once a contradiction has been asserted, both a positive statement and its own negation can be proven true. The inference from p and ¬p to an arbitrary conclusion leads to inconsistencies in formal axiomatic systems, making it impossible to distinguish truth from falsehood. To avoid the danger of meaningless statements implicit in PEX, the law of noncontradiction (LNC) comes to the rescue:

$$\neg(p \wedge \neg p)$$

Since contradictories cannot be simultaneously true, LNC removes the inconsistency from the beginning and neutralizes PEX.

PCLs, together with other non-classical logics such as relevance and minimal logic (Johansson, 1937), suggest that the classical *ex falso quodlibet* is incorrect (Priest and Routley, 1989) since the inference from p and ¬p to an arbitrary conclusion does not hold (Varzi 2000). A logic is paraconsistent iff it is not the case for all sentences p, q that $p, \neg p \vdash q$. This means that we cannot be certain of the truth of any proposition which is irreducible to PEX (Copleston 1974).

As an example, during argumentation one states "I said this", while another "no. I said that", even though something is clear to both. Everything which appears to be true is true according to the two contenders, even at the risk to predicate the truth and the falsity of the same thing in the logical discourse. People taking part in the discussion may disagree while being (self-) consistent, using some vague terms either purposefully or unintentionally (Ciuciura 2013). Conclusions are not really demonstrated, since the opposite conclusions can be drawn from the evidence of each one of the contenders. This approach is very similar to what suggested by the PCLs' non-adjunctive discursive logic: "from the fact that a thesis P and a thesis Q have been advanced in a discourse it does not follow that the thesis $P \vee Q$ has been advanced, because it may happen that P and Q have been advanced by different persons" (Jaśkowski 1999).

Nowadays BL and PCLs are largely used in disparate fields such as bipolar reasoning, bipolar clustering, conflict resolution coordination, equilibrium relations, protocol design for cooperation and coordination in multiagent decision analysis (Zhang 1998), multivalued social graphs, multivalued social network models (Chen et al., 2014), representation of preferences in artificial intelligence or in cognitive psychology (Amgoud et al., 2008), inclusion degrees of a rough set (Chen et al., 2014), evaluation of brain imaging (Hudelot et al., 2008). Da Silva Neves and Livet (2008) proposed that bivariate bipolarity of emotions (negative, neutral, positive) might provide the tools for emotional reasoning that helps to discriminate between deduction, induction and abduction. Also, BT has been used in decision making. e.g., when a group of friends chooses the movie to watch, when the products of a magazine are ordered, when three professors vote against a candidate applying for an academic job (Chen et al., 2014). BL has also been utilized to create algorithms for multiple attribute decision making problems in planning a children hospital (Hashim et al., 2018). The last, but not the least, bipolarity is involved in choices concerning spatial relations such as above and below, left and right, etc (Hudelot et al., 2008).

Table 2
Different types of directional paths.

ASYMMETRIC BIPOLARITY

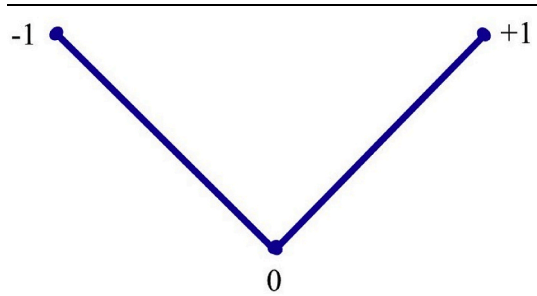

feedback circuit	neither feedforward, nor feedback	feedforward circuit
retrograde direction	neither anterograde, nor retrograde	anterograde direction
antidromic path	stationary path	orthodromic path
backpropagation	absence of propagation	propagation
bottom-up route	unknown route	top-down route

3. The past: medieval forerunners of bipolar logics

Middle-ages thinkers provided accounts of oppositions, antitheses and contrasts that, rather astonishingly, match up well with the most advanced logical bipolar theories. One of the foremost descriptions of the concept of contraries can be found in the Medieval Quodlibetal Questions by William of Ockham (1991). He states that the name "contraries" can be taken in different ways, since every distinction can be either real, formal or of reason (Ockham, Quodlibetal 1.3). The

opposition can be either (5.17, 5.24):

I. Between real things outside the mind,
II. Or between noncomplex (i.e., simple) and complex (i.e., combined) signs of things.

Noncomplex and complex signs of contraries are real mental qualities which correspond to opposition of reason. Thoughts are expressed by mental words which are signs of true things (1.6). The names (either mental, spoken or written predicable) are conceptually distinct from one another, although they are not really diverse (3.2).

The mental opposition between noncomplex signs has four modes (5.17):

1) Contraries. They are signs of those things that signify positively and affirmatively, since no negation should be posited in their definition.
   a) Some contraries cannot be predicated on the same thing simultaneously, but only successively. To make an example, "a human being is white" and "a human being is black" may occur one after the other but cannot exist at the same moment in the same subject. The same God does not have the power to produce infinitely many things simultaneously, rather He virtually and simultaneously contains infinitely many effects that can be produced successively (3.1).
   b) Other contraries cannot be truly predicated either at the same time or successively (e.g., "whiteness" and "blackness").
2) Privative. One of the signs signifies positively (e.g., the disposition), while the other signs signifies both what is positively/affirmatively and what is opposite privatively (e.g., the privation). In the nominal definition of privation, a negation precedes the disposition that is opposed to it, so that the privation signifies the disposition negatively. For example, blindness is not a real thing in the eye, since "blind" is a human being (or an eye) that does not have the vision it ought to have by nature. Therefore, some signs signify by positing and affirming, while others signify by taking away and denying. While which is not an entity is altogether nothing, privations are truly something, since the latter are either concepts of the mind, or spoken things, or things outside the soul.
3) Relative. There are relative names that cannot be predicated of the same thing in the same respect relative to the same thing (e.g., equal and unequal, similar and dissimilar).
4) Contradictories. These signs cannot be predicated of the same thing at the same thing and are such that one of them signifies something affirmatively (e.g., human being) and the other precisely the same thing negatively while indeterminately signifying anything affirmatively (e.g., nonhuman being).

The mental opposition between complex signs has three modes:

1) The signs have the same subject and predicate, but one is affirmative and the other is negative (e.g., "Socrates is an animal" and "Socrates is not an animal"). One must be universal and the other particular, or both must be particular.
2) Contrary complex signs have the same subject and predicate, but one is a universal affirmative and the other a universal negative. The terms must be taken significatively, otherwise they are not opposed. For example, "the expression *every human being* is a common term with a universal sign" and "the expression *no human being* is a common term with a universal sign" are both true, hence are not contraries.
3) Virtual (not formal) contradictories. These complex signs must have the same subject and cannot be both true at the same time. "No animal is running" and "some human being is running" are not opposed as contraries or contradictories, since they have not the same subject. However, they are opposed since "some human being is running" implies the contradictory "no animal is running". Therefore, subalternates (e.g., "every A is B" and "some A is B″) and subcontraries (e.g., "some A is B″ and "some A is not B″) are not opposed.

Furthermore, Ockham makes subtle distinctions between slightly different cases involving the linguistic concepts of "false" and "true", suggesting how a proposition can be first true and afterward false, or vice versa (Ockham, Quodlibetal 4.4, 5.17):

a) "Socrates talks". This proposition is true in the instant in which Socrates talks. If Socrates does not talk, this proposition is false.
b) "Socrates will talk tomorrow". This proposition is invariably true from always until tomorrow, but it will not be true anymore by tomorrow. Before tomorrow nothing can modify the truth value of this proposition, since it is true now and will never become false before tomorrow. The truth of this proposition does not have a beginning, but has an end, i.e., tomorrow. A proposition cannot change from being true to being false before the time at which the revealed thing is to occur. If a proposition is true at a given time, then it has been true at every past time. Indeed, every true present-tense proposition has a necessary past-tense counterpart.
c) "Socrates will not talk tomorrow". This proposition is invariably false from always until tomorrow, but is invariably true after tomorrow. The truth of this proposition does have a beginning (i.e., tomorrow), but lacks an end.
d) "Caesar once existed and does not exist now" is true and false in this instant. Caesar both exists and does not exist in this place, since before or after cannot exist into a single instant (4.11).
e) "The priest on the altar starts to utter: *hoc est* …". Until the priest does not fully utter *hoc est Corpus Christi*, the body of Christ does not exist yet in the Eucharist. The priest's utterance in the middle of the phrase is true as mental proposition, but it is not yet true as spoken proposition, because the words *Corpus Christi* have not yet been pronounced (2.19). Reality itself can be different at the beginning and at the end of an utterance. A mental proposition is true at the beginning and at the end since it exists all at once as a whole (ens permanens). In turn, a spoken proposition exists just successively and not all at once (ens successivum), so that it is true at the end and not at the beginning (2.19). For further details, see Tozzi (2021).

True and false predicated of a whole proposition are distinct it the way that a term is distinct from a proposition of which is not part: e.g., true is not a part of the proposition "Socrates is wise", even though the term true is truly predicated of this proposition. In turn, the (abstract names) "truth" and "falsity" are not things distinct from true and the false propositions. The names "truth" and "falsity" are connotative names, not absolute names (a connotative name signifies one thing primarily and another secondarily, e.g., "white" signifies the white subject primarily and the whiteness itself secondarily). If a proposition has truth, then it holds for absolute terms, but not for connotative terms. This means that truth can be falsity in the same way as a proposition can be false. But the proposition "truth is falsity" should be denied, in just the way that "a true proposition is a false proposition" should be denied. If no proposition exists, a human being is still truly an animal, while "a human being is an animal" is not true.

Note that the notion of bipolarity in Ockham's accounts of contraries frequently displays asymmetric bipolarity. To provide a few examples, Ockham describes privation (blind) and disposition (sight), dissimilar and similar, beliefs and evident knowledge (1.1), nonhuman being and human being, "which is not an entity is altogether nothing" and "privations are truly something". Ockham's account of contraries is related with bipolar logics also in another subtle way. In touch with the three values −1, 0, +1 of bipolar reasoning, Ockham suggests that there is a priority between the opposition of the two contrary extremes and the opposition of the middle and of the contrary extremes, since an extreme is opposed to an extreme prior to the middle's being opposed to an extreme (3.7).

In conclusion, Ockham's foresight concerning the modern bipolar logics can be summarized by his own proposition "if two thinks are not sufficient to truth, a third is needed" (1.8).

Nicholas Of Autrecourt: A forerunner of paraconsistent logics. Paraconsistent logics (henceforward PCLs), first put forward in 1910–1929 by the Russians Vasil'év and Oreov, were formalized around the 50s by the Polish Jaśkowski (1948) and the Brazilian da Costa and Newton (1974). Leaving apart the logical treatment tackled by the French Parvipontians Adam Balsham and William of Soissons in the 12th-century (Priest 2011), PEX has been accepted as self-evident throughout the centuries. However, the critique to PEX (and to the law of noncontradiction LNC) put forward by PCLs has been anticipated in writings dating back to the first half of the 14th century. The 50-year--old Nicholas of Autrecourt, a Master of Arts in the Parisian arts faculty and *baccalaureus and licentiatus* in theology, was condemned in 1347 by the papal court in Avignon after allegations of false teaching. About 60 articles of either "false, or erroneous, suspect, presumptuous, dangerous, or heretic" propositions were collected and publicly recanted in Avignone and Paris (Kaluza 1995).

Here we focus on Autrecourt's condemned articles concerning LNC, which he calls the *primum principium*. The Latin articles reproduced here are numbered according to the Chartolarium Universitatis Parisiensis (Deniflis and Chatelain, 1891):

It roughly translates to:
Starting from LNC, it follows that:

- *From the fact that one thing is, it cannot be inferred the fact that another thing is (5)*
- *From the fact that one thing is, it cannot be inferred that another thing is not (6)*
- *From the fact that one thing is not, it cannot be inferred that another thing is (7)*
- *From the fact that one thing is not, it cannot be inferred that another thing is not (8)"*

Therefore, Autrecourt suggests that the following logical propositions cannot be inferred from LNC:

$p \rightarrow q$

$p \rightarrow \neg q$

$\neg p \rightarrow \neg q$

$\neg p \rightarrow q$

This means that:

$\neg(p \vee \neg p) \rightarrow \neg(q \vee \neg q)$

Consequently,

$\neg(p \wedge \neg p) \rightarrow \neg(q \vee \neg q)$

Since $p \wedge \neg p \rightarrow q$ is false, Autrecourt rejects PEX, in touch with paraconsistent logics (Fitch 2013).

The logical and epistemological strength of LNC in Autrecourt's writings is matter of controversy. It has been suggested that he bears a dual interpretation of the certitude provided by LNC (Groarke 1984). On the one hand, Autrecourt holds the conventional scholastic view that LNC stands for the foremost principle ensuring firm ground upon which

Item, dixi, proh dolor, in primo principio[3] quando legi Sententias et in epistola secunda et sexta, quas scripsi contra Bernardum[4], quod ex eo quod una res est, non potest evidenter evidentia deducta ex primo principio inferri, quod alia res sit (5). — *Falsam et revocandam.*

Item, dixi in locis predictis quod ex eo, quod una res est, non potest evidenter inferri quod alia res non sit (6). — *Falsam et revocandam.*

Item, dixi in locis predictis quod ex eo, quod una res non est, non potest evidenter evidentia deducta ex primo principio inferri, quod alia res non sit (8). — *Falsam et revocandam.*

Item, dixi locis predictis quod ex eo, quod una res non est, non potest evidenter inferri, quod alia res sit (7). — *Falsam et revocandam, quanquam aliqui dicant eam veram esse.*

to build the truth. For example, in the second letter to Bernard, he writes that there is no other certitude but the certitude of LNC, except for the certitudes of faith (De Rijk 1994). He asserts that every syllogism can be reduced to the truth of LNC through immediate or mediate operations. On the other hand, Autrecourt raises elsewhere questions about the steadiness of his own belief in LNC. The last chapters of the Tractatus (conceivably written later) appear to somewhat deny the absolute certitude previously guaranteed by LNC. The most contentious paragraphs (O'Donnell, 1942; pg. 237, chapter: *an omne illud quod apparet sit*) are reproduced here:

Octava conclusio est quod non omnes propositiones possunt ostendi esse evidentes per primum principium; nam cum primo principio oportet assumere aliquid quod contineat conclusionem in actu; minor non, quemadmodum major et principium primum, videlicet in potentia.

Nona conclusio est, quod aliquis posset per consuetudinem aut alias resilire, ut non assentiret indubitanter ei, quod est primum principium esse verum utpote, si sic nutriretur, ut sibi diceretur, quod est aliquod agens omnipotens, quod potest facere contrarium et quod non debet ipsum movere evidentia, quia oppositum potest stare cum ea ut declararetur in multis.

Decima conclusio est quod non posset non assentire quin esset sibi clarum et evidens.

Here an objection is raised, put forward in Giles' Letter to Nicholas too: the fact that God can make miracles seems to deny the existence of LNC (De Rijk 1994). God can annihilate every proposition by miracle, and, if He should do so, LNC would not be valid, since it would not even exist. This means that the possibility to distinguish, e.g., between the propositions "God exists" and "God does not exist" fades away. If contradictories signify the same, the firmness of LNC is undermined beyond repair. Autrecourt suggests elsewhere in the Treatise that the only thing which guarantees the certitude of the first principles is our firm belief that we know them clearly and evidently. In Autrecourt's opinion, the knowledge of appearances cannot rely on LNC, since what is known through LNC is analytic and devoid of factual information (Beuchot, 2005).

In touch with the critique to PNC, it is noteworthy that a variant of PCLs, i.e., the relevance logic, asserts that antecedent and consequent of implications must be relevantly related. It is remarkable that this correlation is explicitly required by the same Autrecourt, who plainly states that the antecedent and the subsequent must share their contents. The consequent cannot be inferred from a doubtful antecedent, since antecedent and consequent obey the principle of identity and must be identical. According to Autrecourt, a priori demonstrations hold just when the identity A = A occurs between the consequent and the antecedent (dal Pra, 1952; Maccagnolo 1953). In Autrecourt the cognitive borders between logical and psychological approaches are rather fuzzy. The dichotomy lies in the fact that he sometimes stresses empiricism, another times Revelation. For example, he writes in a letter to Giles that it is unclear whether the consequent is equal to the antecedent, since it is not discernible whether a perceived thing is simple and indivisible (De Rijk 1994). Only God comprehends all the things in a single, simple apprehension. The strongest way to provide a bridge between mental contents and their supposed noumenal correlates is to build a probability, though *probable* in the mere sense of being of worthier assent than its contradictory opposite (McDermott 1973).

In conclusion, Autrecourt's account is in touch with paraconsistent logics: they both aim to remove not just PEX, but also LNC. Also, it is noteworthy that the unfeasibility of $p \wedge \neg p \rightarrow q$ is frequently observed also in the argumentation of natural language, e.g., when two men hold opposite conclusions.

4. The future: backpropagation of antidromic paths

In the sequel, we will examine directional paths equipped with different degrees of feedforward and feedback trajectories. Feedforward/feedback trajectories are well fit to describe a widespread array of neural networks, either artificial or natural. To make an example, the study of biofeedback circuits in the nervous system never ceases to surprise. It has been recently discovered that fine-tune limb movements in mice are modulated not only by signals from the motor system, but also by tactile feedbacks targeting the brainstem cuneate nucleus (Conner et al., 2021). Various examples of directional pathways exhibiting bipolarity are illustrated in Table 2.

Note that all the triads in Table 2 display the two-dimensional asymmetric type of bivariate polarity. In terms of bipolar fuzzy sets, the membership degree [0,+1] implies that the element satisfies the property (in our case, the occurrence of feedforward trajectories), while [−1,0] implies that the element satisfies the implicit counter-property (in our case, the occurrence of feedback trajectories) (Chen et al., 2014). See Fig. 1A. In turn, the membership degree [0,0] implies that the path does exhibit neither orthodromic nor antidromic features (in our case, the path stands still). Further, the membership degree [−1,+1] implies a bidirectional path that exhibits both orthodromic and antidromic features (in our case, the path simultaneously takes two opposite trajectories) (Fig. 1A).

Researchers are still trying to figure out how the brain might perform backpropagation to solve credit assignment problems. Here the presheaf category from category theory and algebraic topology comes into play (Bredon, 1997), providing a structure rich enough to convey a feasible explanation of orthodromic and antidromic paths in neural networks. As an example of presheaf, think to a sheaf of wheat, sealed and tied up with twine supply: in this case, the countless straws with various orientation are compacted in well-ordered tiny sections, where they display coherent behavior and matching description (Fig. 1B). The same happens in tractography, the recently introduced neuroanatomic technique which allows the identification of well-defined anatomical white matter structures resembling presheaves (Fig. 1C).

We will describe here the mathematical apparatus that will be used in the sequel to describe the feedforward and backpropagation in neural circuits. We will talk at first about composition of functions. When working with a specific input value (named either $x \in X$, or another letter), the composition of functions (denoted by the symbol $\circ$):

$$g\ of(x) \tag{1}$$

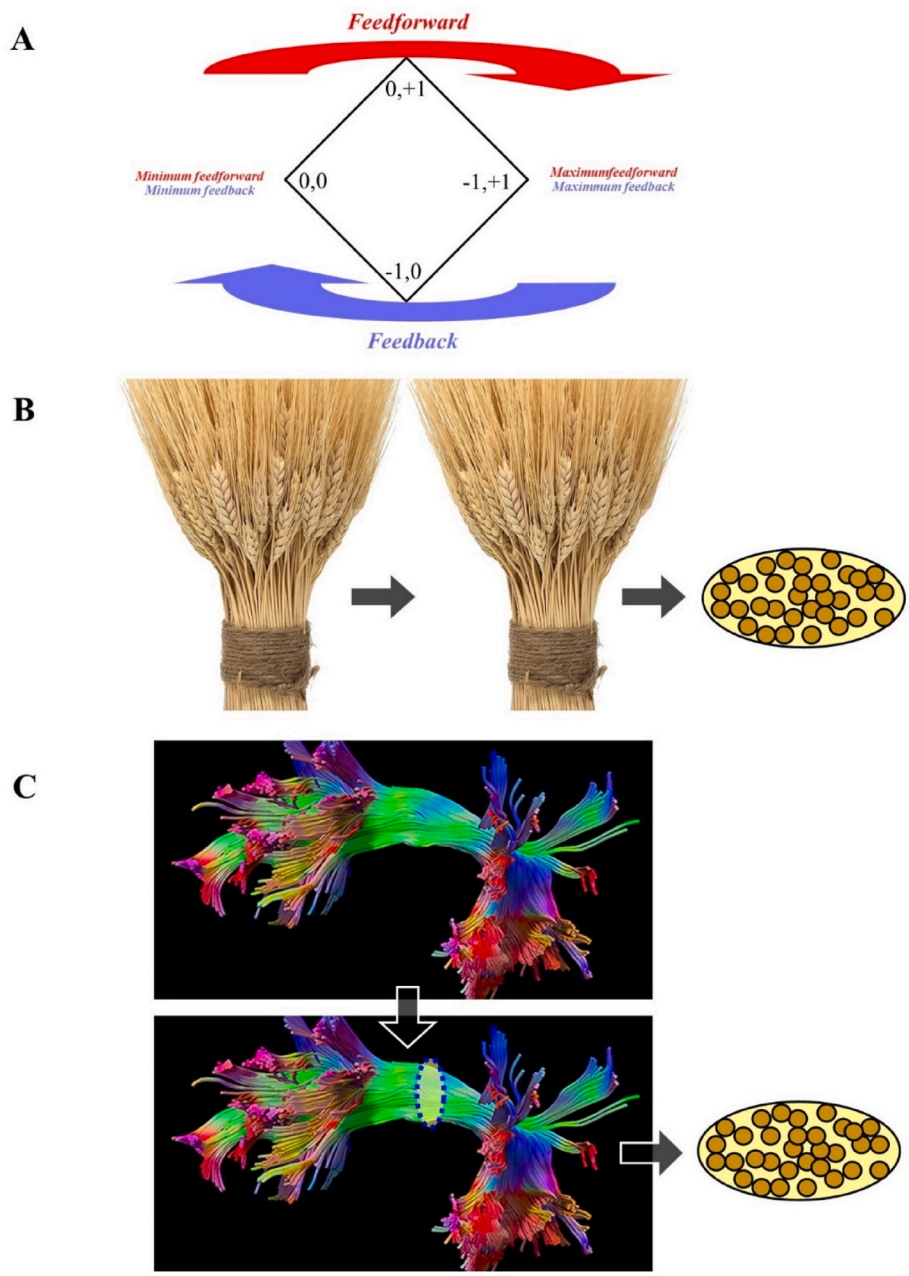

Fig. 1. A. Bipolar relationships between propagation and backpropagation. See text for further details. Fig. 1B-C. Examples of presheaves-like structures in the real world. Fig. 1B: a wheat sheaf displays a cross-section in which the straws, rather being scattered, are remarkably close one each other. Fig. 1C: diffusion MRI maps white matter bundles and assesses their structural integrity. Note that the white matter bundles display close analogy with the wheat straws depicted in Fig. 1B. Modified from: http://brain.labsolver.org/.

is defined by:

$$(g\ of)\ (x) = g(f(x)) \tag{2}$$

In other words, take the function f(x) and put it in place of x in the function g, so that the output of f is used as the input of g (Bergman, 2011). In case of two functions:

$$f : X \rightarrow Y\ and\ g :\ Y \rightarrow Z, \tag{3}$$

then g∘f is a function from X to Z, so that:

$$g\ of : X \rightarrow Z \tag{4}$$

This is where globular sets and presheaves come into play. The category of globes is a category whose objects are natural numbers, while a globular set is a geometric shape for higher structures, standing to simplicial sets as globes to simplices.

A globular set is a presheaf on the category of globes (Kashiwara and Schapira, 1994; Bredon, 1997), i.e., a particular kind of contravariant functor which helps to capture sections:

$$gSet :\ = PSh(G) \tag{5}$$

To achieve a presheaf F in the topological space W (standing for our universe of discourse), two requirements are needed: gluability and uniqueness (Street, 2000; Simpson, 2011).

Once these requirements are satisfied, for each open X ⊂ W, the restriction map is a homeomorphism

$$\rho w, X :\ F(W) \rightarrow F(X) \tag{6}$$

such that $\rho_{w,w}$ is an identity.

Therefore, in terms of the category of globes, the globular set X ∈ gSet is a sequence of sets $X_0, X_1, X_2,.., X_n$, i.e., a collection of the set of n-globes $\{X_n\}_{n \in N} \subset W$, that is equipped with pairs of functions:

$$\{S_{n,}\ t_n : X_{n+1} \rightarrow X_n\}_{n \in N} \tag{7}$$

such that the following globular identities hold:

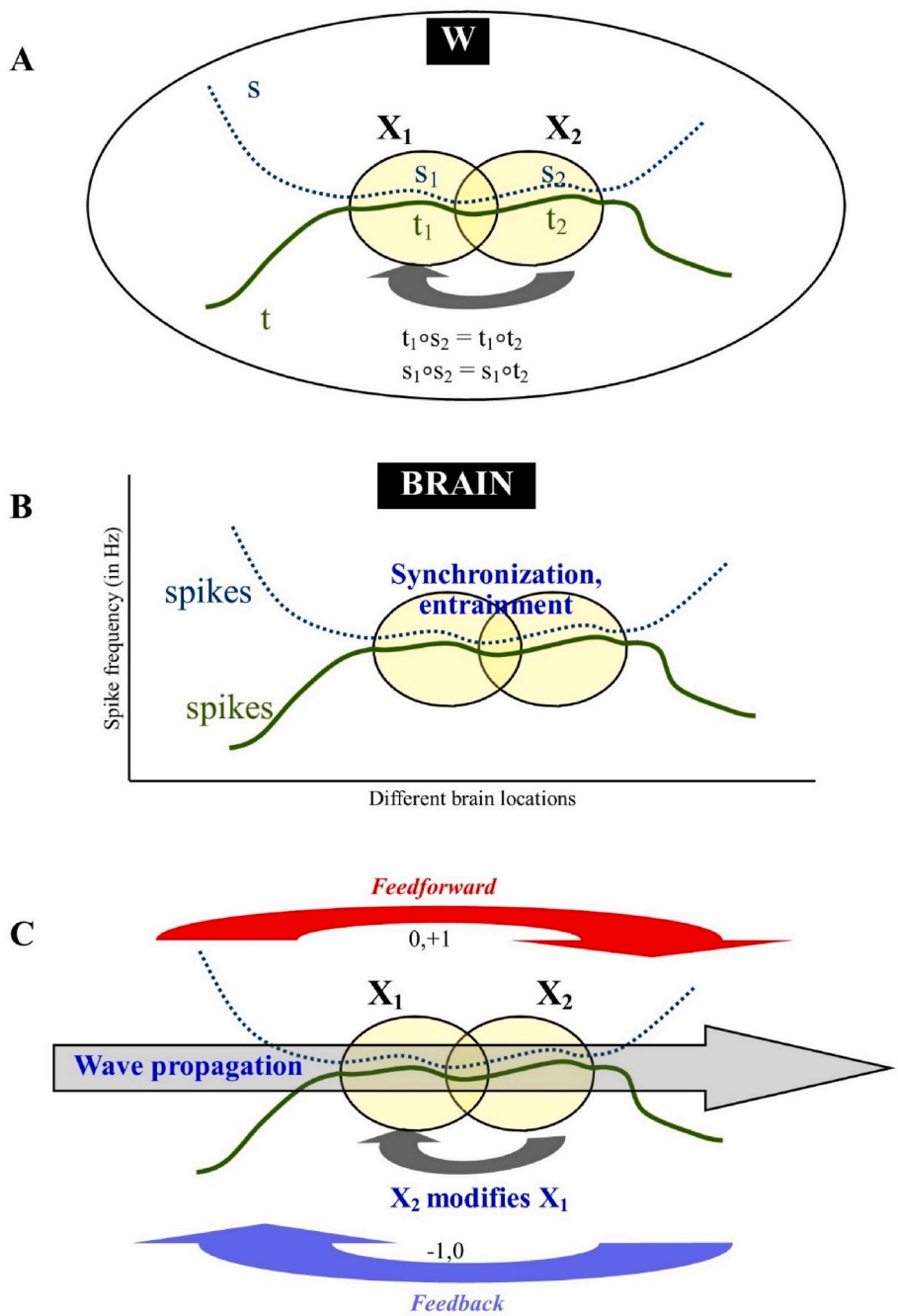

Fig. 2. A. Geometric counterparts of the abstract concept of globular sets/presheaves in the universe of discourse W. The nomenclature is described in the main text. For further details, see: https://ncatlab.org/nlab/show/globular+set#references. Fig. 2B: concerning the universe of discourse termed "brain", the globular sets allow to explain how and why spikes of different incoherent frequencies are synchronized in certain brain areas. Fig. 2C. A nervous theory of globular sets suggests that antidromic spikes do exist, so that X_2 exerts effects on X_1. Note that the orthodromic and the antidromic flows correspond to asymmetric bivariate polarity between feedforward/feedback trajectories.

$$S_n o S_{n+1} = S_n o t_{n+1} \tag{8}$$

and

$$t_n o S_{n+1} = t_n o t_{n+1} \tag{9}$$

where s and t stand for the two sections termed, respectively, source and target (Fig. 2A).

Note that X_n may also stand for directed edges at level n.

A further constraint is required: no reflexive globular sets do exist, or, in other words, do not exist degeneracy maps going back in the opposite direction $X_1 \rightarrow X_2$ (Simpson, 2011).

Our next step will be to use globular sets and presheaves to sketch a neural model able to describe the nervous orthodromic and antidromic activities taking place in cortical tissues. Sheaf theory is subtle enough that seemingly similar constructions yield vastly different invariants. Slight changes in the definition of stalks, restriction maps and the underlying topological base spaces lead to fully different results. Since our aim is just to provide network theorists with a novel methodological tool for the evaluation of bipolar networks, the explicit construction of the proper presheaf is beyond the scope of this paper.

Consider a brain area W, equipped with two functions termed s and t (Fig. 2A). They diverge everywhere, apart from a cortical subarea (i.e., a subset of W) which encompasses X_1 and X_2, with $X_1 \cap X_2$. If in subarea $X_1 \cap X_2$ the above-mentioned constraints are satisfied and the topological concept of presheaf holds, the two functions s and t have an unusual behavior, i.e., they do not diverge inside the subsets X_1 and X_2, rather display coherence, equality and matching description. Globular sets and presheaf theory require that the composition of functions occurring

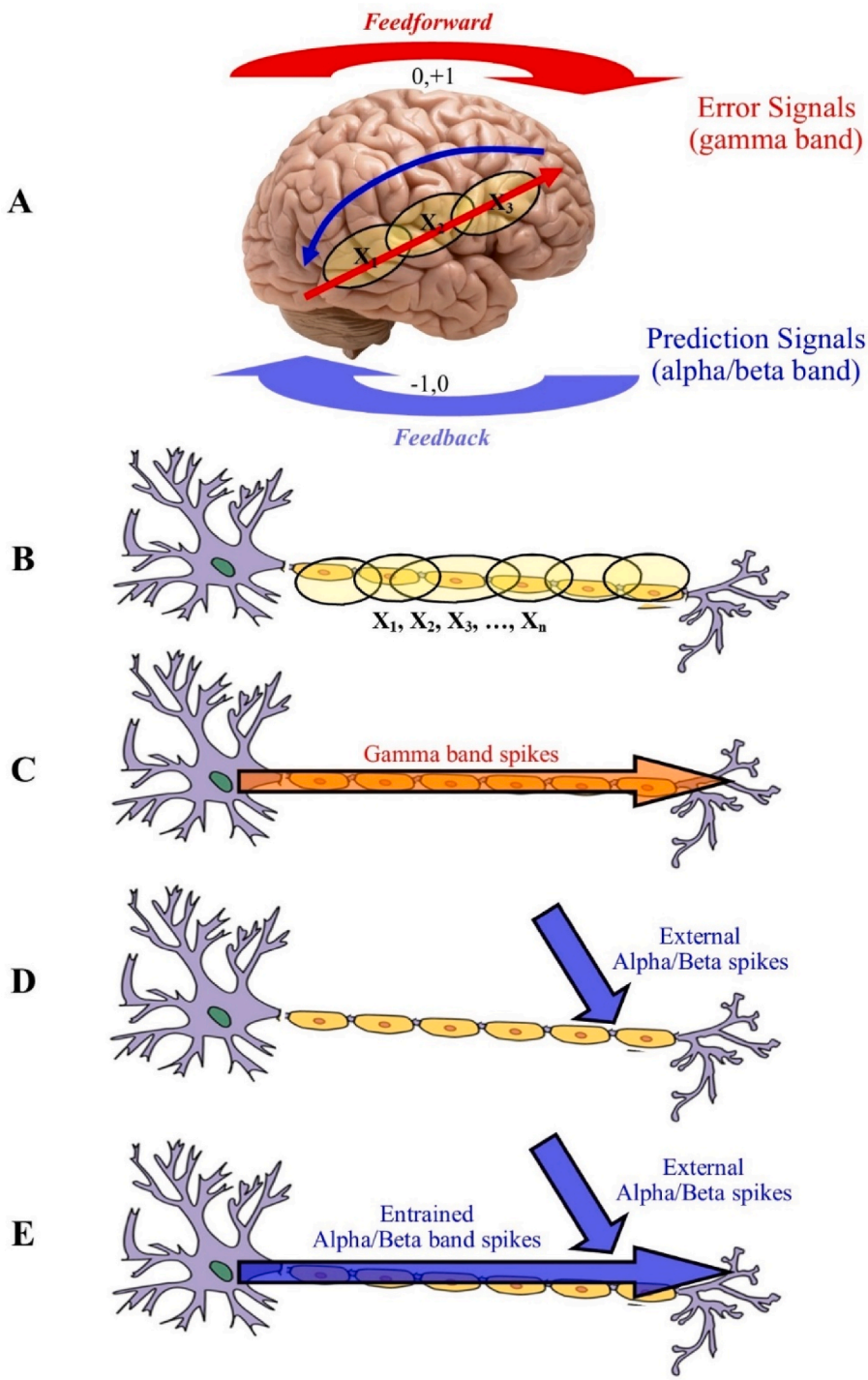

Fig. 3. Orthodromic and antidromic currents in the human brain. Fig. 3A. An example of feedforward and feedback projections in the brain. The globular sets are superimposed to the corresponding gamma feedforward spikes. Fig. 3B–E. Procedure to experimentally test whether presheaves do exist in the brain. Fig. 3B: according to presheaf models, the neuronal axon must be equipped with globular set's intersecting subsets. The soma is on the left of the depicted neuron. The yellow circles superimposed to the axon illustrate the intersecting subsets of a globular set. Fig. 3C–E provide an example of the proposed procedure. Take a neuron that produces gamma bursts (Fig. 3C). The red arrow superimposed to the axon illustrates the standard, orthodromic axonal propagation of gamma-spikes. According to presheaf theories, if an external and continuous beta spike is applied to the distal axon (blue arrow in Fig. 3D), the neuron will generate entrained beta bursts, instead of the previous gamma bursts (Fig. 3E). (For interpretation of the references to colour in this figure legend, the reader is referred to the Web version of this article.)

inside the subset $X_1 \cap X_2$ does not diverge as it does in other subsets. Furthermore, the functions s_2 and t_2 in X_2 precede the functions s_1 and t_1 in X_1, so that the output of the cortical subarea X_2 is used as the input of the cortical subarea X_1. This means that changes in functions occurring in X_2 lead to corresponding antidromic changes in the orthodromic functions occurring in X_1. In general terms, we can state that source and targets in X_1 follow sources and targets in X_2. Also, there is an equivalence between:

1) X_1 sources that follow X_2 sources and X_1 sources that follow X_2 targets.
2) X_1 targets that follow X_2 sources and X_1 targets that follow X_2 targets.
3) X_1 targets that follow X_2 sources and X_1 targets that follow X_2 targets.

In brief, X_2 functions (source and target) point towards and modify X_1 functions (source and target). Therefore, X_2 controls X_1, and not vice versa.

Summarizing, the brain activity assessed in terms of presheaves/globular sets might explain different features of neural functions (Fig. 2B-C):

1) It elucidates why brain oscillations equipped with different spike frequency and amplitude tend to converge and coalesce towards single functional areas, where overlapping and matching

synchronized frequencies/amplitudes contribute to keep the signal steady (Fig. 2B).

2) It suggests that a hierarchical oscillatory activation occurs inside single functional areas, where the oscillations are constrained to follow strict temporal sequences.
3) It explains the occurrence of feedforward flows and back-propagation: when an entrained oscillation propagates from A to B, changes in B frequency leads to changes in A frequency (Fig. 2C). This means that orthodromic (i.e., feedforward, bottom-up) projections are functionally coupled with antidromic (i.e., feedback, top-down) projections.

This last, counterintuitive observation has foremost implications in the study of the brain activity and f artificial neural networks, as we will see in the sequel.

5. PRESHEAVES/GLOBULAR sets for the evaluation of feedforward/feedback trajectories: testable previsions

In the previous sections, we showed how the mathematical apparatus of globular sets/presheaves might provide a well-grounded mathematical framework to assess network phenomena characterized by propagation and backpropagation. In this Section we are going to provide testable experimental and theoretical examples of feasible applications in neuroscience and network theory.

Orthodromic and antidromic currents in the human brain. Neuronal feedforward pathways are associated with enhanced gamma (30–70 Hz) oscillations, whereas feedback projections, which account for a large portion of all connections between neurons in the thalamo-cortical system, selectively modulate alpha/low-beta (8–15 Hz) oscillations (Mejias et al., 2016; Michalareas et al., 2016; Sikkens et al., 2019). The interplay between hierarchically organized feedforward (bottom-up) and feedback (top-down) signaling involves intricate dynamics across multiple (intralaminar, interlaminar, interareal, and whole cortex) scales involved in attentional processes, predictive coding, executive control (Mejias et al., 2016). Information propagates in opposite directions through visual areas during bottom-up intake of current stimuli and top-down processes of memory or attention (Bastos et al., 2015; Zheng and Colgin, 2015; Michalareas et al., 2016). In working memory and its volitional control, an interplay occurs between network gamma oscillations in superficial cortical layers and alpha/beta in deep cortical layers (Miller et al., 2018). To provide an example, Fig. 3A describes the case of prediction and errors signals in the Bayesian brain. In terms of presheaf theory, a change in frequency occurring in the cortical location X_2 leads also to a change in frequency in the cortical location X_1. This means that the brain electric frequency might be controlled antidromically, so that distal frequencies might be able to modify proximal frequencies. Therefore, presheaf models would help to describe the neurophysiology of brain stimulation via external sources such as transcranial magnetic stimulation (henceforward TMS), i.e., a focal electric brain stimulation induced by powerful magnetic fields (Chung et al., 2016; Jan et al., 2017; Kohli and Casson, 2019).

TMS protocols are divided into single-pulse, paired-pulse and repetitive TMS (henceforward rTMS). Extracellular electromagnetic stimulations produce electrical fields in both myelinated and unmyelinated axons (Rattay, 1986; Basser and Roth, 1991), generating hyperpolarized regions in cell membranes (Rattay et al., 2012). Intracranial cortical stimulation induces selective activation across cell types and layers (Komarov et al., 2019), while external brain gamma stimulation modulates motor performance/GABA-A-ergic interneuron activity (Guerra et al., 2018; McDermott et al., 2018). The origins, cellular mechanisms and functional effects of rTMS are unidentified (Benali

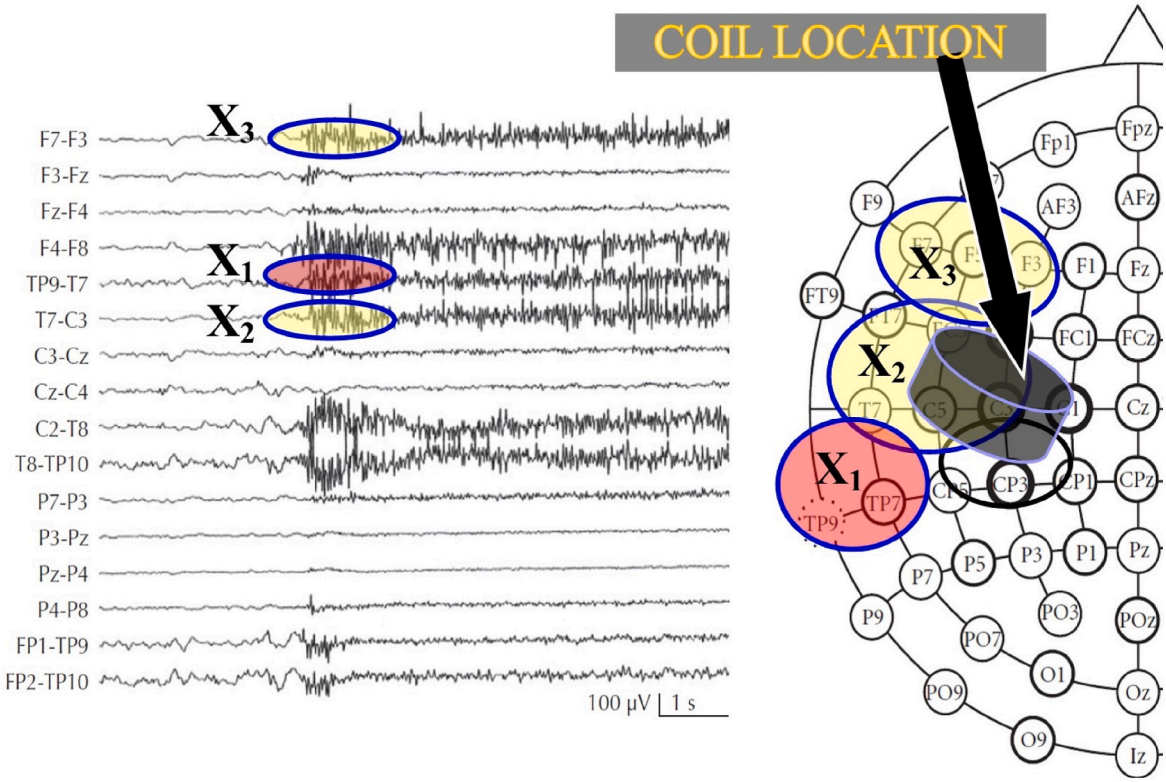

Fig. 4. Application of presheaves in different contexts of feedforward and feedback paths. **Left**. Recorded surface EEG (displayed in a bipolar transverse montage) showing a left parietal EEG seizure onset. The red circle stands for the area of onset of the seizure X_1, while the yellow circles for the areas of seizure propagation X_2 and X_3. Modified from: Beleza et al. (2010). **Right**. EEG mount illustrating the globular sets involved in the seizure depicted in Fig. 4A, left. Starting from the area X_1 of onset, the seizure propagates through the areas X_2 and X_3. Our model predicts that a transcranial stimulation with coils located in X_2 (dark cylinder) might counteract the seizure. (For interpretation of the references to colour in this figure legend, the reader is referred to the Web version of this article.)

et al., 2011). At present, there is no systematic method to predict which neural elements will be activated by a given stimulation regime (Komarov et al., 2019), since spike initiation site may change for short and long pulses (Rattay et al., 2012) and every individual has different rhythmic firing pattern in response to burst stimulation (Chung et al., 2019).

Our model sheds new light on the mechanisms of rTMS, suggesting that axonal stimulations from external sources might modify the frequency charges of the involved neurons. Fig. 3B–E illustrate a theoretical example of a neuron firing at, say, 30 Hz. If we apply on the axon an external 10-Hz current, our model predicts that the neuron will synchronize its output frequency towards 10-Hz. Due to the mathematical constraints of presheaves, we suggest that the 10-Hz external axonal stimulation might be able to antidromically backpropagate from the neuronal axon to the body. Despite our scarce knowledge of antidromic oscillations' effects on neural information processing, experimental data point towards the possibility that external axon modulation affects frequency encoding in neurons, before and after it is convoyed. Axons are not only information carriers, rather their trunks are endowed with ionotropic and metabotropic receptors for transmitters/neuromodulators (DeMaegd and Stein, 2018). Neuromodulator effects on axons generate ectopic spiking, characterized by ion potentials backpropagating towards different sites independent of incoming synaptic events. Increasing ectopic spike frequency leads to delayed peripheral bursts, reductions in spike number/burst duration, and modifications in sensory firing frequency. Computational models demonstrate that antidromic action potentials can alter sensory encoding in neurons with slow ionic conductances (DeMaegd and Stein, 2018). During γ-tACS over the right temporal lobe, Santarnecchi et al. (2019) observed functional connectivity of bilateral temporal lobes after stimulation, caused by EEG increase in γ spectral power over bilateral temporal lobes.

In sum, in the context of a globular set theory-framed approach, axonal neuromodulation might have the role to produce rapid frequency changes also in sites far from the stimulated axon. This paves the way to the application of presheaves in different contexts regarding feedforward/feedback paths, such as the use of rTMS in human disease. Specific high frequency rTMS has been already approved for the treatment of major depression. Low frequency rTMS (0.3–1 Hz) are less studied, but its ability to decrease cortical excitability suggests a potential therapeutic effect in patients affected by drug-resistant epilepsy (Jan et al., 2017). Even though conventional rTMS stimulators activate only superficial cortical areas, it is feasible to reach deep epileptic foci (such as, for example, in temporal lobe epilepsy) using specially designed H-coils which provide low frequency rTMS (Gersner et al., 2016). Chen et al. (2016) retrospectively analyzed the evidence for the efficacy of TMS in drug-resistant epilepsy compared with available treatments. They evaluated studies that used rTMS of any frequency, duration, intensity, and setup (focal or vertex treatment) on patients of different ages. Given the extreme variability in techniques and outcome reporting, the evidence for efficacy of rTMS for reduction in seizure rate, seizure frequency and mean number of epileptic discharges is still lacking (Jan et al., 2017). The main problem is that there is still no agreement on optimized stimulation parameters and patterns of rTMS for epilepsy. TMS effects are erratic across individuals and depend on frequency, number of stimuli within a train, stimulation intensity, type of coil, coil position, duration of stimulation and inter-train interval.

Our approach suggests the proper coil location for transcranial magnetic stimulation in epilepsy. In case of epileptic seizures, our model hypothesizes that the onset area of pathological spikes might extend to other regions through a mechanism of synchronization linked with the transient formation of globular sets. Once hypothesized that synchronous pathological spikes might occur inside functional globular sets, a novel mathematical framework for epilepsy is achieved that is worth to be investigated. If the presheaf framework holds true, the starting epileptic focus (standing for X_1) propagates to the surrounding brain areas (standing for X_2), giving rise to synchronized pathological waves with matching description/zero divergence (Fig. 4). The activation of areas X_2 (e.g., through transcranial stimulation with coils located in X_2) are therefore able to modify the oscillatory activity of the initial locus of epilepsy onset X_1. This means that the areas surrounding the locus of seizure onset keep the seizure active, and not vice versa. This suggests an easily testable prevision: to achieve the best therapeutic effect and confirm that the mathematical apparatus of globular sets holds true in epilepsy, rTMS treatments must not focus on the first focus of onset of epilepsy, rather on the surrounding areas where the pathological spikes propagate (Fig. 4).

The occurrence of back-propagation is a widespread phenomenon identified in different systems and at different levels of observation. For example, a chemical counterpart of the above-described mathematical retrograde path defined by globular sets has been implicitly described in literature. Wang et al. (2020) studied catalyzed chemical reactions (such as the ubiquitous click reactions in living cells) which provoke increases in free-energy/enthalpy in the medium. They discovered that these energetic increases generate long-range mechanical perturbations that permit to speed the mobility of the Brownian diffusion of reactants and nearby solvent. In other words, contrary to the chemistry dogma that molecular diffusion and chemical reaction are unrelated, some reactions can boost the surrounding reactants and solvents, increasing their speed and mobility. The Authors also elucidated a noteworthy issue: if you want to keep a stable concentration gradient and a constant fluid density, you need to counterbalance the above-described effects of boosted diffusion molecules/anterograde diffusion by using backflow of solvent molecules. This new boosting mechanism in chemistry corresponds to the same backpropagation processes described by preseheaves and globular sets. The boosting mechanism is remarkable also for another reason: we speculate that, when the chemical boost is prolonged and self-sustained enough, the backpropagation might contribute to provide the energy required to start life from chemical reactions and preserve the living organism's efforts to survive via homeostatic balance. Back-propagation can be found also in the brain (Smith et al., 2013). During the sensitive cue period, "feed-forward" signals flow from granular to supragranular/infragranular layers in the primate temporal cortex. In turn, during the sensitive delay period, reverse "feed-back" signals flow from infragranular to supragranular layers (Takeuchi et al., 2011). This reversal of signal flow suggests that the temporal cortex differentially recruits its laminar circuits for sensory and mnemonic processing.

6. Conclusions

We showed that the mathematical apparatus of presheaves/globular sets gives us the possibility to treat feedforward paths and backpropagation in terms of category theory. The key question is: what is the rationale for choosing the intricate mathematical apparatus of presheaves to approach bipolarity in network theory? The local-to-global machinery of algebraic topology seems poised to provide the perfect tools for gathering disparate neural activities into a coherent whole. To provide an example concerning the human central nervous system, presheaves offer invaluable benefits for the analysis of nervous activities: a) they generalize the local systems that are so ubiquitous in the brain areas and subareas; b) they have powerful applications to the topology of algebraic and the analytic complex varieties of singular spaces such as the nervous phase spaces (Dimca, 2004); c) they make available a suitable notion of "general coefficient systems" that could be useful for the assessment of nonlinear nervous dynamics; d) they stand for common methods of comparison between different cohomology theories of general topological spaces (Bredon, 1997); e) they provide foundations of near sets that can be used to describe brain areas and subareas (Wolski, 2013). Also, globular sets allow to analyze the stability of synchronous states in dynamical systems such as the brain (Papo and Buldú, 2019), shedding new light of the still unknown mechanisms of spike synchronization. Presheaves permit us to draw previsions that can

be experimentally tested with the current neuro-technologies, such as, e.g., a counterintuitive claim: when an entrained oscillation propagates from the brain area A to a brain area B, changes in spike frequency in B lead to changes in spike frequency in A.

Since the size of the globular sets may vary, presheaves can be used for the assessment of different coarse-grained nervous structures at the micro-, meso- and macro-levels of observation. The human ability to re-identify objects at different times and across observation gaps leads to the phenomenon termed "object persistence" (Fields, 2013). The computational tasks required by object persistence can be tackled in terms of presheaf theory both at the microscopic level of histological microcolumns (Tozzi et al., 2017b) and at the macroscopic level of brain functional/anatomical areas. Concerning the micro-levels of observation, we suggest that the globular sets could be located inside the multilayer arrangement of the cortex, in particular in the layer IV of the primary sensory occipital areas of the Primates, where large amounts of granular cells process the visual information coming from the thalamus. In this sub-cortical milieu, the role of the globular sets' enduring coalescence of functions would be threefold:

1. Synchronize oscillatory patterns.
2. Stabilize information content.
3. Produce unambiguous, long-lasting percepts.

Concerning the macro-levels of brain analysis, the face-selective response to static images of famous and unfamiliar faces is mediated by neural activity in the occipital/posterior temporal cortex, across the fusiform face area (henceforward FFA) (Axelrod et al., 2019). FFA recognizes faces despite the underlying noise and the huge number of conflicting inputs, so that the brain will be always able to recognize Jennifer Aniston, independent of her dresses, make-up or haircut. If we consider FFA in terms of a sheaf F equipped with, say, two globular sets $X_1 \cap X_2$, a change occurring in X_2 will also involve X_1. Since the FFA subareas X_1 and X_2 are synchronized, they must always display matching description: this ensures stability to the percept and explains why face recognition is always constant, despite the changes in environmental inputs. Also, a presheaf approach might help to elucidate the issue of memory. We speculate that memory could be stored in globular sets that allow preservation and flexibility of the information. If memories are scattered throughout the brain as suggested by the sparse code theory, they could be encompassed in dispersed globular sets that display the same content in different locations (in X_1, X_2, …,X_n). Therefore, the labile stability of information content might be granted by the globular set apparatus endowed in brain structures, in which the ubiquitous divergence among functions equals zero.

Our approach paves the way to novel attitudes towards issues at the border between biophysics and philosophy. The treatment and transmission of information is a physical process that must be regulated by the Landauer Principle, regardless of the underlying computational logic (Bormashenko, 2019). Physical Bayesian theories consider the brain as an inferential machine which requires priors. These priors can be mathematically assessed in terms of presheaves that keep information stable. Two subsets $X_1 \cap X_2$ could stand not just for two "spatially" separated structures, but also for two "temporally" separated events, i.e., two ensuing temporal windows. The dictates of globular sets theory require that the event X_1 at time t_1 must follow the event X_2 at time t_2. This means that events in t_2 can influence events in t_1. This counterintuitive claim does not break any physical law, if we think to priors in terms of abstract mental activities such as predictions, volitions, goals. X_1 becomes real only when the event predicted by mental activities occurs in the external world. Therefore, we speculate that real events X_1 occurring in the world are generated by the predictions X_2 created by our mental Bayesian priors. This mathematical approach provides a response to one of the most controversial philosophical issues concerning the relationships between the "mental" and the "real world": presheaves might explain how the elusive, immaterial mental activity provokes physical effects in the real world.

We described how and why Nicholas of Autrecourt can be considered to have pioneered the current paraconsistent logics. Here we suggest novel lines of research involving Autrecourt and PCLs. He states that the ultimate reason why the evident truths (including LNC) are to be accepted is that they please our minds, since a being is nobler that another if naturally pleases men more (Kennedy et al., 1971). In touch with Aristotle, the optimistic concept of *cosmic goodness* is the pivotal point of Autrecourt's thought. Since the universe has complete goodness, falsehood is the evil of intellect. The intellect is not made for being pleased with the false, so that it can be stated that "what appears is, what is evident is true" (McDermott 1973). The concept of cosmic goodness recalls the modern notion of the anthropic principle, asserting that the scientific scrutiny of the Universe would not even be possible if the laws of the universe had been incompatible with the development of life (Dicke 1961). Since humans have survived and are still here, this means that the evolution did not let our senses to believe to false cues. This takes us in the logical world of PCLs, where our intellect provides an effort to grab not just the being, but also the non-being (Maccagnolo 1953). In touch with Autrecourt's cosmic goodness, PCLs hold that no true theory would ever contain inconsistencies. PCLs and the gnoseological belief in truth provided by the human evolution allow the intrinsic mechanisms of damage control to restore the contradictions generated by the unavoidable errors intrinsic in every information system.

A further connection can be found among Autrecourt, PCLs and quantum mechanics (Brown 1993). For quite a long time, logic has tried to cope with the problems raised by Heisenberg's uncertainty and the microscopic features of quantum dynamics (henceforward QD) (Heathcote 2021). Compared with the common sense of the macroscopic life and with special relativity, QD displays very different behaviors and features, starting from the very subtending mathematical structure (Yilmaz, 1981; Comte, 1996; Fré, 2013). QD is described on an infinite-dimensional projective Hilbert space, where vectors with different bases are sets of equivalence classes (Tegmark 2008). In other words, the microscopic world of quantum dynamics displays different bases that are the source of the rather counterintuitive physical effects faced during experimental observations. In the macroscopic world, the binary operation of multiplication is commutative, i.e., changing the order of the operands does not change the result (Goodman, 2003). This means that: $ab = ba$. In turn, the QD's linear operators representing a pair of physical variables do not commute, rather are mutually complementary. This means that $cd \neq dc$. Examples of complementary quantum properties that cannot all be observed or measured simultaneously are position and momentum, energy and duration, spin on different axes, wave and particle, entanglement and coherence, and so on (Kalckar et al., 1996). Here Autrecort comes into play, when he writes in the Tractatus that two points can touch with each retaining its own different position. This seemingly weird statement is in touch with the quantum concept of bosons' superposition (i.e., identical bosons can occupy the same quantum state), since bosons are not subject to the Pauli exclusion principle. Autrecourt declares in the Condemnations that a transition occurs from one state to the contradictory one in the absence of a real intrinsic change of any of the terms. Connectives such as "¬" do not mean anything, since they are syncategorematic terms lacking denotation and ontological status (Thijssen 1990). In touch with Ockham, Autrecourt seems to support the thesis that we have no knowledge of things outside the word, but only of terms: God and creatures become nothing. In accordance with this medieval insight, recent approaches interpret quantum mechanics as a reference-frame theory pertaining to observer-dependent relational properties (Yang 2018). Remarkably, these radical formulations of quantum mechanics have been experimentally supported by a recent reliable paper (The BIG Bell Test Collaboration 2018). In agreement with PCLs and Autrecourt's Ockhamism, The BIG Bell Test Collaboration seems to contradict the tenets of the local realism and suggests that the properties of the physical

world are dependent from the observer.

In conclusion, we provided feasible examples of applications of presheaves/globular sets in network theory. Many natural and artificial neural networks (e.g., Hopfield 1982) are equipped with bipolar paths: a feedforward path which guarantees the anterograde propagation of the message and a feedback path which regulates the anterograde message and ensures its retrograde backpropagation. Our theoretical approach provides the first step towards a fully novel mathematical type of neural network in which message backpropagation is provided by the same feedforward fibers. This would allow computational neural networks to spare the bulky occurrence of dedicated feedback circuits.

Statement

The undersigned Author transfer all copyright ownership of the manuscript, in the event the work is published.

The undersigned author warrants that the article is original, does not infringe on any copyright or other proprietary right of any third part, is not under consideration by another journal, and has not been previously published.

The Author does not have any known or potential conflict of interest including any financial, personal or other relationships with other people or organizations within three years of beginning the submitted work that could inappropriately influence, or be perceived to influence, their work.

This research did not receive any specific grant from funding agencies in the public, commercial, or not-for-profit sectors.

This research does not contain any studies with human participants or animals performed by the Author.

The Author had full access to all the data in the study and take responsibility for the integrity of the data and the accuracy of the data analysis. The Author performed: study concept and design, acquisition of data, analysis and interpretation of data, drafting of the manuscript, critical revision of the manuscript for important intellectual content, statistical analysis, obtained funding, administrative, technical, and material support, study supervision.

Conflicts of interest

The Author does not have any known or potential conflict of interest including any financial, personal or other relationships with other people or organizations within three years of beginning the submitted work that could inappropriately influence, or be perceived to influence, their work.

References

Akram, M., 2013. Bipolar fuzzy graphs with applications. Knowl. Base Syst. 39, 1–8, 2013.

Amgoud, L., Cayrol, C., Lagasquie-Schiex, M.C., Livet, P., 2008. On bipolarity in argumentation frameworks. Int. J. Intell. Syst. 23 (10), 1062–1093. https://doi.org/10.1002/int.20307. Special Issue: Bipolar Representations of Information and Preference Part 2: Reasoning and Learning.

Axelrod, V., Rozier, C., Malkinson, T.S., Lehongre, K., Adam, C., et al., 2019. Face-selective neurons in the vicinity of the human fusiform face area. Neurology 22; 92 (4), 197–198. https://doi.org/10.1212/WNL.0000000000006806.

Basser, P.J., Roth, B.J., 1991. Stimulation of a myelinated nerve axon by electromagnetic induction. Med. Biol. Eng. Comput. 29 (3), 261–268.

Bastos, A.M., Vezoli, J., Bosman, C.A., Schoffelen, J.M., Oostenveld, R., et al., 2015. Visual areas exert feedforward and feedback influences through distinct frequency channels. Neuron 21 (2), 390–401. https://doi.org/10.1016/j.neuron.2014.12.018, 85.

Beleza, P., Rémi, J., Feddersen, B., Peraud, A., Noachtar, S., 2010. Epidural and foramen-ovale electrodes in the diagnostic evaluation of patients considered for epilepsy surgery. Epileptic Disord. 12 (1), 48–53. https://doi.org/10.1684/epd.2010.0297, 2010 Mar.

Benali, A., Trippe, J., Weiler, E., Mix, A., Petrasch-Parwez, E., et al., 2011. Theta-burst transcranial magnetic stimulation alters cortical inhibition. J. Neurosci. 31 (4), 1193–1203. https://doi.org/10.1523/JNEUROSCI.1379-10.2011.

Bergman, C., 2011. Universal Algebra: Fundamentals and Selected Topics. CRC Press, ISBN 978-1-4398-5129-6.

Beuchot, M., 2005. Nicholas of Autrecourt. In: Gracia, J.J.E. (Ed.), A Companion to Philosophy in the Middle Ages. Noone TB, ISBN 9780631216728. https://doi.org/10.1002/9780470996669.

Bormashenko, E., 2019. Generalization of the Landauer principle for computing devices based on many-valued logic. Entropy 21 (12), 1150. https://doi.org/10.3390/e21121150.

Bredon, G.E., 1997. Sheaf Theory. Springer-Verlag, New York, ISBN 978-0-387-94905-5.

Brown, B., 1993. Old quantum theory: a paraconsistent approach. Proceedings of the Philosophy of Science Association 2, 397–441.

Cayrol, C., Lagasquie-Schiex, M.-C., 2013. Bipolarity in argumentation graphs: towards a better understanding. Int. J. Approx. Reason. 54 (7), 876–899. https://doi.org/10.1016/j.ijar.2013.03.001. September 2013.

Chen, J., Li, S., Ma, S., Wang, X., 2014. Polar Fuzzy Sets: an Extension of Bipolar Fuzzy Sets. Fuzzy Logical Algebras and its Applications. https://doi.org/10.1155/2014/416530. |Article ID 416530 |, 2014.

Chen, R., Spencer, D.C., Weston, J., Nolan, S.J., 2016. Transcranial magnetic stimulation for the treatment of epilepsy. Cochrane Database Syst. Rev. (8), CD011025 https://doi.org/10.1002/14651858.CD011025.pub2.

Comte, C., 1996. Symmetry, relativity and quantum mechanics. Il Nuovo Cimento 111 B (8), 937–956.

Conner, J.M., Bohannon, A., Igarashi, M., Taniguchi, J., Baltar, N., Azim, E., 2021. Modulation of tactile feedback for the execution of dexterous movement. Science 374 (6565), 316–323. https://doi.org/10.1126/science.abh1123.

Copleston, F.C., 1974. The logical empiricism of Nicholas of Autrecourt. Proceedings of the Aristotelian Society. New Series 74, 249–262, 1973 - 1974.

Chung, S.W., Hill, A.T., Rogasch, N.C., Hoy, K.E., Fitzgerald, P.B., 2016. Use of theta-burst stimulation in changing excitability of motor cortex: a systematic review and meta-analysis. Neurosci. Biobehav. Rev. 43–64. https://doi.org/10.1016/j.neubiorev.2016.01.008.

Chung, S.W., Sullivan, C., Rogasch, N.C., Hoy, K.E., Bailey, N.W., et al., 2019. The effects of individualised intermittent theta burst stimulation in the prefrontal cortex: a TMS-EEG study. Hum. Brain Mapp. 40 (2), 608–627. https://doi.org/10.1002/hbm.24398.

Ciuciura, J., 2013. Non-adjunctive discursive logic. Bulletin of the Section of Logic 42 (3).

da Costa, Newton, C.A., 1974. On the theory of inconsistent formal systems. Notre Dame J. Formal Logic 15, 497–510.

dal Pra, M., 1952. La fondazione dell' empirismo e le sue aporie nel pensiero di nicola di Nicola di Autrecourt. Riv. Critic Stor. Filosof. 7 (5), 384–402.

Da Silva Neves, R., Livet, P., 2008. Bipolarity in human reasoning and affective decision making. Int J Intelligent systems 23 (8), 898–922. https://doi.org/10.1002/int.20299.

Dalkili, O., Demirtas, N., 2021. Bipolar fuzzy soft (D-)metric spaces. Commun. Fac. Sci. Univ. Ank. Ser. A1 Math. Stat. 70 (1), 64–73. https://doi.org/10.31801/cfsuasmas.774658.

DeMaegd, M.L., Stein, W., 2018. Long-distance modulation of sensory encoding via axonal neuromodulation. In: Sensory Nervous System. Thomas Heinbockel, IntechOpen. https://doi.org/10.5772/intechopen.74647.

De Rijk, L.M., 1994. Nicholas of Autrecourt: His Correspondence with Master Giles and Bernard of Arezzo. Brill Academic Pub, Leiden, New York, Koln. -10: 9004099883.

Deniflis, H., Chatelain, A., 1891. Chartolarium Universitatis Parisiensis. Tomus II, Sectio Prior. Parisiis, Ex Typis Fratrum Delalain.

Dicke, R.H., 1961. Dirac's cosmology and mach's principle. Nature 192 (4801), 440–441. https://doi.org/10.1038/192440a0.

Dimca, A., 2004. Sheaves in Topology. Springer-Verlag Berlin Heidelberg, ISBN 978-3-642-18868-8.

Dubois, D., Prade, H., 2008. An introduction to bipolar representations of information and preference. Int. J. Intell. Syst. 23 (8), 866–877. Wiley, ⟨10.1002/int.20297⟩. ⟨hal-03356864⟩.

Fields, C.A., 2013. The principle of persistence, Leibniz's law, and the computational task of object Re-identification. Hum. Dev. 56, 147–166. https://doi.org/10.1159/000350206.

Fitch, R., 2013. Nicholas of Autrecourt and the mastery of reason. D (Dallas, 1978) 116 (3), 168–189.

Fré, P.G., 2013. Gravity, a Geometrical Course, vol. 1. Springer. https://doi.org/10.1007/978-94-007-5361-7. Development of the Theory and Basic Physical Applications.

Gersner, R., Oberman, L., Sanchez, M.J., Chiriboga, N., Kaye, H.L., et al., 2016. H-coil repetitive transcranial magnetic stimulation for treatment of temporal lobe epilepsy: a case report. Epilepsy Behav Case Rep 5, 52–56. https://doi.org/10.1016/j.ebcr.2016.03.001, 2016.

Goodman, F., 2003. Algebra: Abstract and Concrete, Stressing Symmetry, vol. 2e. Prentice Hall, ISBN 0-13-067342-0.

Groarke, L., 1984. On Nicholas of Autrecourt and the law of non-contradiction. Dialog. Can. Phil. Rev. 23 (Issue 1), 129–134. https://doi.org/10.1017/S0012217300019181.

Guerra, A., Suppa, A., Bologna, M., D'Onofrio, V., Bianchini, E., et al., 2018. Boosting the LTP-like plasticity effect of intermittent theta-burst stimulation using gamma transcranial alternating current stimulation. Brain Stimul 11 (4), 734–742. https://doi.org/10.1016/j.brs.2018.03.015.

Hashim, R.M., Gulistan, M., Smarandache, F., 2018. Applications of neutrosophic bipolar fuzzy sets in HOPE foundation for planning to build a children hospital with different types of similarity measures. Symmetry 2018 10 (8), 331. https://doi.org/10.3390/sym10080331.

Heathcote, A., 2021. Countability and self-identity. Euro Jnl Phil Sci 11, 109. https://doi.org/10.1007/s13194-021-00423-z.

Hopfield, J.J., 1982. Neural networks and physical systems with emergent collective computational abilities. Proc. Natl. Acad. Sci. Unit. States Am. 79, 2554–2558.
Jan, M.M., Alsallum, M.S., Sadler, M.R., 2017. Transcranial magnetic stimulation and epilepsy. International Journal of Medical Science and Clinical Inventions 4 (10), 3256–3260. https://doi.org/10.18535/ijmsci/v4i10.07.ICV.2015:52.82.
Jaśkowski, S., 1948. Rachunek zdań dla systemów dedukcyjnych sprzecznych. Studia Societatis Scientiarum Torunensi (Sectio A) 1 (5), 55–77.
Jaśkowski, S., 1999. Log. Log. Philos. 7, 49. Zbl 1013.03004).
Johansson, I., 1937. Der Minimalkalkül, ein reduzierter intuitionistischer Formalismus. Compos. Math. 4, 119–136.
Kalckar, J., Bohr, N., Rosenfeld, L., Rüdinger, E., Aaserud, F., 1996. Foundations of Quantum Physics II (1933-1958). Elsevier, ISBN 978-0-444-89892-0, p. 210. Retrieved 2011-10-24.
Kashiwara, M., Schapira, P., 1994. Sheaves on manifolds, Grundlehren der Mathematischen Wissenschaften, vol. 292. Springer-Verlag, Berlin, New York, ISBN 978-3-540-51861-7.
Kaluza, Z., 1995. Nicolas d'Autrecourt. Ami de la vérité. In: Histoire littéraire de la France, vol. 42 (Paris).
Kennedy, L.A., Arnold, R.E., Millward, A.E., 1971. The Universal Treatise of Nicholas of Autrecourt. Marquette University press, Milwaukee, Wisconsin.
Kohli, S., Casson, A., 2019. Machine learning validation of EEG+tACS artefact removal. J. Neural. Eng. https://doi.org/10.1088/1741-2552/ab58a3 (in press).
Komarov, M., Malerba, P., Golden, R., Nunez, P., Halgren, E., Bazhenov, M., 2019. Selective recruitment of cortical neurons by electrical stimulation. PLoS Comput. Biol. 15 (8), e1007277 https://doi.org/10.1371/journal.pcbi.1007277.
Lee, J.-G., Hur, K., 2019. Bipolar fuzzy relations. Mathematics 7 (11), 1044. https://doi.org/10.3390/math7111044, 2019.
Maccagnolo, E., 1953. Metafisica E gnoseologia in nicolò D'Autrecourt. Riv. Filos. Neo-Scolastica 45 (1), 36–53.
McDermott, C., 1973. Direct sensory awareness: a Tibetan view and a medieval counterpart. Philos. East W. 23 (3), 343–360, 1973.
McDermott, B., Porter, E., Hughes, D., McGinley, B., Lang, M., et al., 2018. Gamma band neural stimulation in humans and the promise of a new modality to prevent and treat Alzheimer's disease. J Alzheimers Dis 65 (2), 363–392. https://doi.org/10.3233/JAD-180391.
Mejias, J.G., Murray, J.D., Kenned, H., Wang, X.-J., 2016. Feedforward and feedback frequency-dependent interactions in a large-scale laminar network of the primate cortex. Sci. Adv. 2 (11), e1601335 https://doi.org/10.1126/sciadv.1601335.
Michalareas, G., Vezoli, J., van Pelt, S., Schoffelen, J.-M., Kennedy, H., Fries, P., 2016. Alpha-beta and gamma rhythms subserve feedback and feedforward influences among human visual cortical areas. Neuron 89 (2), 384–397. https://doi.org/10.1016/j.neuron.2015.12.018, 2016 Jan 20.
Miller, E.K., Lundqvist, M., Bastos, A.M., 2018. Working memory 2.0. Neuron 100 (2), 463–475. https://doi.org/10.1016/j.neuron.2018.09.023, 2018 Oct 24.
O'Donnell, J.R., 1942. The Philosophy of Nicholas of Autrecourt and His Appraisal of Aristotle. Mediaeval Studies, pp. 97–125. https://doi.org/10.1484/J.MS.2.306538.
Ockham, W., 1991. In: Freddoso, A.J., Kelley, F.E. (Eds.), Quodlibetal Questions. Yale University Press, New Haven & London.
Palladino, D., Palladino, C., 2007. Logiche Non Classiche. Un'introduzione, Carocci Ed. -13: 978-8843040025.
Papo, D., Buldú, J.M., 2019. Brain synchronizability, a false friend. Neuroimage 196, 195–199. https://doi.org/10.1016/j.neuroimage.2019.04.029.
Payeur, A., Guerguiev, J., Zenke, F., Richards, B.A., Naud, R., 2021. Burst-dependent synaptic plasticity can coordinate learning in hierarchical circuits. Nat. Neurosci. 24, 1010–1019.
Peters, J.F., Ramanna, S., Tozzi, A., İnan, E., 2017. Bold-independent computational entropy assesses functional donut-like structures in brain fMRI images. Front. Hum. Neurosci. 11, 38. https://doi.org/10.3389/fnhum.2017.00038.
Priest, G., Routley, R., 1989. Applications of paraconsistent logic. In: Priest, Routley and Norman. Philosophia Verlag, Munich.
Priest, G., 2011. What's so bad about contradictions?. In: Priest, Beall and Armour-Garb, the Law of Non-contradiction. Clarendon Press, Oxford.
Rattay, F., 1986. IEEE Trans. Biomed. Eng. 33 (10), 974–977.
Rattay, F., Paredes, L.P., Leao, R.N., 2012. Strength-duration relationship for intra-versus extracellular stimulation with microelectrodes. Neuroscience 214, 1–13. https://doi.org/10.1016/j.neuroscience.2012.04.004, 2012 Jul 12.
Riaz, M., Tehrim, S.T., 2020. On bipolar fuzzy soft topology with decision-making. Soft Comput. 24, 18259–18272. https://doi.org/10.1007/s00500-020-05342-4.
Santarnecchi, E., Sprugnoli, G., Bricolo, E., Costantini, G., Liew, S., et al., 2019. Gamma tACS over the temporal lobe increases the occurrence of Eureka! moments. Sci. Rep. 9 (1), 5778. https://doi.org/10.1038/s41598-019-42192-z.
Sherrill, S.P., Timme, N.M., Beggs, J.M., Newman, N.L., 2021. Partial information decomposition reveals that synergistic neural integration is greater downstream of recurrent information flow in organotypic cortical cultures. PLoS Comput. Biol. https://doi.org/10.1371/journal.pcbi.1009196.
Sikkens, T., Bosman, C.A., Olcese, U., 2019. The role of top-down modulation in shaping sensory processing across brain states: implications for consciousness. Front. Syst. Neurosci. https://doi.org/10.3389/fnsys.2019.00031.
Simpson, C., 2011. Homotopy Theory of Higher Categories - from Segal Categories to N-Categories and beyond. Cambridge University Press, ISBN 9780511978111.
Smith, S.L., Smith, I.T., Branco, T., Häusser, M., 2013. Dendritic spikes enhance stimulus selectivity in cortical neurons in vivo. Nature 503 (7474), 115–120. https://doi.org/10.1038/nature12600.
Street, R., 2000. The petit topos of globular sets. J. Pure Appl. Algebra 154 (1–3), 299–315. https://doi.org/10.1016/S0022-4049(99)00183-8.
Takeuchi, D., Hirabayashi, T., Tamura, K., Miyashita, Y., 2011. Reversal of interlaminar signal between sensory and memory processing in monkey temporal cortex. Science 331 (6023), 1443–1447. https://doi.org/10.1126/science.1199967.
Tegmark, M., 2008. The mathematical universe. Found. Phys. 38 (2), 101–150. February 2008.
The BIG Bell Test Collaboration, 2018. Challenging local realism with human choices. Nature 557, 212–216.
Thijssen, J.M.M.H., 1990. The "semantic" articles of Autrecourtss condemnation. New proposals for an interpretation of the articles 57, 155–175, 1, 30, 31, 35, 57 and 58. Archives d'histoire doctrinale et littéraire du Moyen Age, 1990a. https://www.jstor.org/stable/44403829. Librairie Philosophique J. Vrin.
Tozzi, A., Peters, J.F., Fingelkurts, A.A., Fingelkurts, A.A., Marijuán, P.C., 2017a. Topodynamics of metastable brains. Phys. Life Rev. 21, 1–20. https://doi.org/10.1016/j.plrev.2017.03.001.
Tozzi, A., Peters, J.F., Ori, O., 2017b. Cracking the barcode of fullerene-like cortical microcolumns. Neurosci. Lett. 644, 100–106. https://doi.org/10.1016/j.neulet.2017.02.064.
Tozzi, A., Peters, J.F., 2020. Removing uncertainty in neural networks. Cognitive Neurodynamics 14, 339–345. https://doi.org/10.1007/s11571-020-09574-w.
Tozzi, A., 2021. Why should natural principles Be simple? Philosophia 1–15. https://doi.org/10.1007/s11406-021-00359-x, 2021 Apr 16.
Varga, B., Soós, B., Jákli, B., Bálint, E., Somogyvári, Z., Négyessy, L., 2021. Network path convergence shapes low-level processing in the visual cortex. Front. Syst. Neurosci. https://doi.org/10.3389/fnsys.2021.645709, 24 May 2021.
Varzi, A., 2000. Supervaluationism and paraconsistency. In: Batens, D., Mortensen, C., Priest, G., Van Bendegem, J.-P. (Eds.), Frontiers of Paraconsistent Logic. Baldock: Research Studies Press), pp. 279–297.
Wang, H., Park, M., Dong, R., Kim, J., Cho, Y.-K., et al., 2020. Boosted molecular mobility during common chemical reactions. Science 369, 537–541. https://doi.org/10.1126/science.aba8425, 6503.
Wolski, M., 2013. Toward foundations of near sets: (pre-)sheaf theoretic approach. Math. Comput. Sci. 7 (1), 125–136. MR3043923.
Yang, J.M., 2018. A relational formulation of quantum mechanics. Sci. Rep. 8, 13305.
Yilmaz, H., 1981. Relativity and quantum mechanics. Int. J. Theor. Phys. 21 (10/11), 871–902.
Zhang, X.W., 2017. Bipolar-value fuzzy soft lie subalgebras. IOP Conf. Ser. Mater. Sci. Eng. 231, 1–9.
Zhang, W.-R., 1998. YinYang bipolar fuzzy sets. Fuzzy Syst. Conf. 1, 835–840.
Zheng, C., Colgin, L.L., 2015. Beta and gamma rhythms go with the flow. Neuron 85 (2), 236–237. https://doi.org/10.1016/j.neuron.2014.12.067, 2015 Jan 21.

proceedings

MDPI

Proceeding Paper

Informational Approaches Lead to Formulations of Quantum Mechanics on Poincaré Disks †

Arturo Tozzi

Center for Nonlinear Science, Department of Physics, University of North Texas, Denton, TX 76203-5017, USA; tozziarturo@libero.it

† Presented at the Conference on Theoretical and Foundational Problems in Information Studies, IS4SI Summit 2021, Online, 12–19 September 2021.

Abstract: A novel methodological approach requires the observer to investigate the information accessible outside the object under scrutiny. The object becomes an "hole" devoid of information, surrounded by a container that is no longer a passive structure. We use this container-framed attitude for a mathematical attempt to take a step towards the unexploited unification of general relativity and quantum mechanics. We show that the tenets of quantum mechanics, i.e., the observable A, the autostates ψa, and the Schrodinger equation for the temporal evolution of states, can be described in terms of oscillatory paths taking place on negative-curvature Poincaré disks.

Keywords: manifold; Hilbert space; observer; measurement; Avicenna

check for updates

Citation: Tozzi, A. Informational Approaches Lead to Formulations of Quantum Mechanics on Poincaré Disks. *Proceedings* **2022**, *81*, 20. https://doi.org/10.3390/proceedings2022081020

Academic Editor: Mark Burgin

Published: 10 March 2022

Publisher's Note: MDPI stays neutral with regard to jurisdictional claims in published maps and institutional affiliations.

Copyright: © 2022 by the author. Licensee MDPI, Basel, Switzerland. This article is an open access article distributed under the terms and conditions of the Creative Commons Attribution (CC BY) license (https://creativecommons.org/licenses/by/4.0/).

1. Introduction

The ancient Aristotelian concepts of active and potential intellects (henceforward AI and PI) display a viable counterpart to the modern-day theory of information. Alexander of Aphrodisias, Al-Farabi, and Avicenna suggested that past, present, and future knowledge is fully endowed in omniscient and everlasting AI, which is fixed, supralunar, external to the body, and shared by all individuals [1]. Each individual displays their own PI, i.e., the personal ability to grab chunks of AI. The current concept of Shannon's/Wheeler's total cosmic information (henceforward TCI) is analogous: TCI is eternal and can be neither created nor annihilated. AI and TCI both have a problem with the principle of individuation: how is the thing A identified as distinguished from the thing B? If two files contain the same fixed quantity of bits, what is the difference between their qualitative (we could use the term "semantic") content? This raises doubts as whether the tenet of TCI as an unlimited, eternal whole holds true. The comparison between AI/PI and TCI has two opposite paradoxical consequences: on one hand, it wipes out the concept of Holy, Divine knowledge and leaves just the quantitative concept of physical information; on the other hand, it reintroduces a metaphysical component, i.e., the presence of a vague, eternal, indefinable substance permeating the universe. It looks like TCI allows the metaphysical concept of God to sneak in the back of scientific issues. Do scientists extract the information endowed in the object, or do they build information not existing inside the object? Is our qualitative mental information discovered, or is it invented? Recent papers suggest that quantum mechanics is a reference-frame theory pertaining to observer-dependent relational properties. Amazingly, these radical relational formulations of quantum mechanics have been experimentally supported: it has been demonstrated that the properties of the physical world are dependent on the observer as opposed to the tenets of local realism [2]. Once our pars destruens against the concept of TCI is completed, a pars construens is strongly required. We suggest a new methodology according to which the observer does not investigate the information endowed in the thing, but rather investigates the information outside the thing [3]. The thing becomes a "hole" devoid of information inside a surrounding environment that is no longer a passive container, but rather an active

structure enabling the examination of its content. In the sequel, we will use this approach to amend our critique of information: in particular, we will suggest a new approach to the curvatures, i.e., the "containers", subtending quantum dynamics.

2. *Pars construens:* Hyperbolic Dynamics and Quantum Mechanics

We will tackle the issue of the unexploited unification of general relativity (GR) and quantum mechanics (QM), which prevent a proper understanding of the micro- and macroscopic world [4,5]. GR assumes a 3+1-dimensional pseudo-Riemannian manifold with tensor fields, whereas QM assumes a R^4 projective Hilbert space with operator-valued fields [6]. The projective infinite-dimensional Hilbert space of the QM's microscopic world displays countless bases that are the source of the counterintuitive physical effects experienced during experimental observation. Our approach, based on the evaluation of the "container" instead of the "content", suggests a curvature-based mathematical approach to QM. We examine the possibility that the oscillatory dynamics described by QM might take place on microscopic negative-curvature, hyperbolic continuous manifolds. This novel manifold stands for the container encompassing the QM's Hilbert spaces. In particular, we describe how the tenets of quantum mechanics, such as the observable A, the autostates ψa, and the Schrodinger equation for the temporal evolution of states, might work very well on a Poincaré disk equipped with rotational groups.

2.1. *Before Measuring*

Every quantum physical system is described by a (topologically) separable complex Hilbert space of states H with inner product, in which each vector can be decomposed in the linear combination of other vectors [7]. Every observable A in the space H is associated with an hermitian linear self-adjoint operator and with an orthonormal basis of vectors, i.e., the base of its autostates ψa [8,9]. The autovalue a of the operator A displays one or more autostates ψa. Since each autovalue a depicts a possible value of A, ψa forms a compete set, i.e., a wave function, standing for the superposition of all the ψa. Before the measurement of the observable A, all the autostates ψa are superimposed, giving rise to a wave function that completely describes the state of the system:

$$A\ \psi a = a\ \psi a \tag{1}$$

In search of relationships between the dynamics of quantum oscillations and the movements on a hyperbolic manifold, we suggest that the features of the Hilbert space, the observable A, and the autostates ψa before and after measuring could be described in terms of their negative-curvature counterparts on the Poincaré disk. Since the spectrum of an operator corresponds to the set of its autovalues that can be discrete or continuous, the continuous manifold of the Poincaré disk is split in tessellated areas, giving rise to countless discrete tiles. The physical pattern occurring before the experimental measurement can be illustrated in terms of the virtually uncountable number of ψa, each one filling a single tile of the Poincaré disk (Figure 1A). From the standpoint of the observer, most autostates ψa are difficult to access, since the most of them are in the periphery of the Poincaré sphere. In turn, from the standpoint of the observer, it is much easier to assess the largest tiles in the center of the Poincaré disk. We shall see in the sequel that this observation has considerable implications after the experimental measurement. The QM wavefunction evolves in time according to the time-dependent Schrödinger equation [10]. Considering this postulate, one of the most important features of our QM hyperbolic model is that the continuous QM Poincaré disk is not at all a static manifold; rather, it is equipped with rotations that provide the tiles with effortless physical movements. This permit shifts of the tessellated areas from the center to the periphery of the disk surface, and vice versa (Figure 1B). Once we have described the dynamic tiles detectable by the observer before measuring, we will describe what happens to the tiles after the measurement.

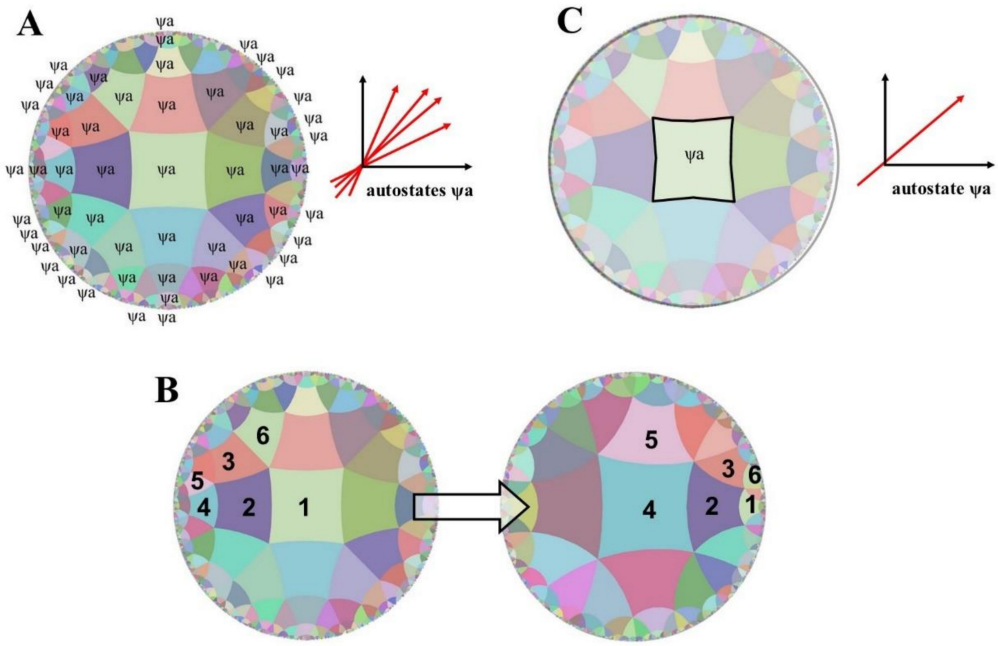

Figure 1. An observable of a QM system is portrayed in terms of a collection of tiles on a hyperbolic Poincaré disk. The tiles are painted in different colors to emphasize that each tessellation corresponds to a single autostate ψa. (**A**) Before the experimental measurement of the observable A, all the autostates ψa are detectable, and no preferential autostate can be chosen. The wave function of the autostates ψa is described by a sheaf of vectors lying on orthonormal basis (right Figure). (**B**) The operations occurring on the Poincaré disk permit the movement of every tile. For the sake of clarity, some of the tiles are numbered to show their movements from the initial state (left) to the final state (right). In long periods of time, every QM wave necessarily crosses the central tile of the Poincaré disk: to provide an example, the peripheral tile 4 in the left figure moves towards the center of the disk in the right figure. (**C**) After the experimental measurement of the observable A, the system collapses, and a single "frozen" autostate ψa becomes detectable in our observation frame, i.e., in the central tile. The wave function of the autostates ψa is now described by a single vector lying on orthonormal basis (right Figure). Modified from: Rendering Hyperbolic Spaces—Hyperbolica Devlog #3 (https://www.youtube.com/watch?v=pXWRYpdYc7Q, accessed on 30 December 2021).

2.2. After Measuring

After the experimental measurement of the observable A, the system collapses towards one of its ψa autostates, chosen based on probability. Every ψa corresponds to a physical state in which, after the measurement of A, one finds one of the values a_n or $a_{(f)}$, so that just a single autostate ψa becomes detectable (Figure 1C). We suggest that the very operation of measurement selects a single tile located inside the rotating Poicaré disk. Incidentally, the movements must be random, because QM, according to another of its postulates, is described by statistical results of continuous probability, where the square module of the vector coefficients stand for probabilities. Before the measurement, the tiles are free to move on the surface of the Poincaré disk, following hyperbolic paths. In turn, the experimental measurement "freezes" the movements of the tessellated areas so that, after the experiment, a single motionless tile can be detected by the standpoint of the observer. The experimental procedure of measurement generates a stationary window of observation located at the center of the Poincaré disk, where the largest tile stands for the tessellation that is the most accessible to the observer. To provide an analogy, think to the inspection of a single "frozen" frame extracted from a long video sequence. Paraphrasing [11], pathologies associated with the possible existence of many unitarity inequivalent representations on the hyperbolic disk disappear, since the whole operation of QM measurement is realized by choosing only one representation, i.e., the ψa located in the central tile.

3. Conclusions

Several attempts have been provided to describe QM in terms of hyperbolic manifolds. See, e.g., [12–16]. Though these authors claim that hyperbolic manifolds are just methodological tools to approach QM, our container-framed attitude suggests that hyperbolic manifolds are part of the description of QM. We suggest that QM might really take place on non-Euclidean hyperbolic manifolds, in the same way that GR really takes place on Euclidean manifolds. In this new physical framework, the macroscopic Euclidean world is like a container encompassing sub-microscopic regions where a negative-curvature fabric includes the waves and paths described by QM.

Funding: This research received no external funding.

Institutional Review Board Statement: Not applicable.

Informed Consent Statement: Not applicable.

Data Availability Statement: Not applicable.

Conflicts of Interest: The author declares no conflict of interest.

References

1. Dales, R.C. *The Problem of the Rational Soul in the Thirteenth Century*; Brill: Leiden, The Netherlands; New York, NY, USA; Köln, Germany, 1995.
2. The BIG Bell Test Collaboration. Challenging local realism with human choices. *Nature* **2018**, *557*, 212–216. [CrossRef] [PubMed]
3. Tozzi, A.; Peters, J.F. Information-devoid routes for scale-free neurodynamics. *Synthese* **2021**, *199*, 2491–2504. [CrossRef]
4. Curtright, T.L.; Fairlie, D.B.; Zachos, C.K. *A Concise Treatise on Quantum Mechanics in Phase Space*; World Scientific: Singapore, 2014; ISBN 9789814520430.
5. Piazza, L.; Lummen, T.T.; Quiñonez, E.; Murooka, Y.; Reed, B.W.; Barwickm, B.; Carbonem, F. Simultaneous observation of the quantization and the interference pattern of a plasmonic near-field. *Nat. Commun.* **2015**, *6*, 6407. [CrossRef] [PubMed]
6. Tegmark, M. The Mathematical Universe. *Found. Phys.* **2008**, *38*, 101–150. [CrossRef]
7. Cassinelli, G.; Lahti, P. Quantum mechanics: Why complex Hilbert space? *Philos. Trans. A Math. Phys. Eng. Sci.* **2016**, *375*, 20160393. [CrossRef] [PubMed]
8. Dirac, P.A.M. The Fundamental Equations of Quantum Mechanics. *Proc. R. Soc. A Math. Phys. Eng. Sci.* **1925**, *109*, 642–653. [CrossRef]
9. Gisin, N.; Fröwis, F. From quantum foundations to applications and back. *Philos. Trans. A Math Phys. Eng. Sci.* **2018**, *376*, 20170326. [CrossRef]
10. Batygin, K. Schrödinger evolution of self-gravitating discs. *Mon. Not. R. Astron. Soc.* **2018**, *475*, 5070–5084. [CrossRef]
11. Cartas-Fuentevilla, R.; Berra-Montiel, J.; Meza-Aldama, O. Hyperbolic ring-based formulation for thermo field dynamics, quantum dissipation, entanglement, and holography. *Eur. Phys. J. C* **2020**, *80*, 603. [CrossRef]
12. Ruppeiner, G. Riemannian geometry in thermodynamic fluctuation theory. *Rev. Mod. Phys.* **1995**, *67*, 605. [CrossRef]
13. Khrennikov, A. Hyperbolic quantum mechanics. *Adv. Appl. Clifford Algebras* **2003**, *13*, 1–9. [CrossRef]
14. Cariñena, J.F.; Rañada, M.F.; Santander, M. The quantum free particle on spherical and hyperbolic spaces: A curvature dependent approach. *J. Math. Phys.* **2011**, *52*, 072104. [CrossRef]
15. Iomin, A. Exponential spreading and singular behavior of quantum dynamics near hyperbolic points. *Phys. Rev. E* **2013**, *87*, 054901. [CrossRef] [PubMed]
16. Kollár, A.J.; Fitzpatrick, M.; Houck, A.A. Hyperbolic lattices in circuit quantum electrodynamics. *Nature* **2019**, *571*, 45–50. [CrossRef] [PubMed]

Philosophia
https://doi.org/10.1007/s11406-022-00576-y

To Know them, Remove their Information: An Outer Methodological Approach to Biophysics and Humanities

Arturo Tozzi[1,2]

Received: 9 September 2021 / Revised: 20 March 2022 / Accepted: 11 August 2022
© The Author(s), under exclusive licence to Springer Nature B.V. 2022

Abstract
Set theory faces two difficulties: formal definitions of sets/subsets are incapable of assessing biophysical issues; formal axiomatic systems are complete/inconsistent or incomplete/consistent. To overtake these problems reminiscent of the old-fashioned principle of individuation, we provide formal treatment/validation/operationalization of a methodological weapon termed "outer approach" (OA). The observer's attention shifts from the system under evaluation to its surroundings, so that objects are investigated from outside. Subsets become just "holes" devoid of information inside larger sets. Sets are no longer passive containers, rather active structures enabling their content's examination. Consequences/applications of OA include: a) operationalization of paraconsistent logics, anticipated by unexpected forerunners, in terms of advanced truth theories of natural language; b) assessment of embryonic craniocaudal migration in terms of Turing's spots; c) evaluation of hominids' social behaviors in terms of evolutionary modifications of facial expression's musculature; d) treatment of cortical action potentials in terms of collective movements of extracellular currents, leaving apart what happens inside the neurons; e) a critique of Shannon's information in terms of the Arabic thinkers' active/potential intellects. Also, OA provides an outer view of a) humanistic issues such as the enigmatic Celestino of Verona's letter, Dante Alighieri's "Hell" and the puzzling Voynich manuscript; b) historical issues such as Aldo Moro's death. Summarizing, we suggest that the safest methodology to quantify phenomena is to remove them from our observation and tackle an outer view, since mathematical/logical issues such as selective information deletion and set complement rescue incompleteness/inconsistency of biophysical systems.

Keywords Non-classical logic · Richard Avenarius · Aganglionosis · Paolo and Francesca · Scholastics · Zermelo-Fraenkel theory

✉ Arturo Tozzi
tozziarturo@libero.it; arturo.tozzi@alsnapoli2nord.it

Extended author information available on the last page of the article

Published online: 02 September 2022

Set theory has always made significant contributions to logic, mathematics, topology, etc. But we can ask the question: what is a set? Most mathematicians adopt the naive point of view that what is meant by a set is intuitively clear (Munkres, 1999). In turn, logicians provided set theory axiomatizations where each axiom expresses a foundational property of the sets. Though, even the best available set axiomatization, viz. the Zermelo-Fraenkel set theory (Zermelo, 1930; Fraenkel et al., 1973), does not help in gauging the appropriate experimental setting for physical and biological scientific questions (Day, 2012). The axiom of infinity ZF7 requires the existence of a set having infinitely many members: it is not the case with the limited number of elements included in physical and biological sets. Further, the fuzziness of concepts such as life and internal/external in biology makes the quantitative use of sets very challenging. Think, for example, to the current dilemmas in defining the boundaries of disease (Doust et al., 2017). There are problems also for the sets and subsets of the formal systems, i.e., the sets of axioms along with rules of symbolic manipulation that permits the derivation of new theorems. Computer programs can in principle use algorithms to enumerate all the theorems of the system, removing every statement not resulting from the same theorems. A set of axioms is complete if a statement (or its negation) is provable from the axioms, while a set of axioms is consistent if there is no statement such that both the statement and its negation are provable from the axioms (Siavashi, 2016).

Gödel's incompleteness theorems showed that a) for any consistent formal system of basic arithmetic capable of modelling natural numbers, there will always be statements that are true but unprovable within the system (Gödel, 1931); b) the system cannot demonstrate its own consistency. In sum, a complete and consistent finite list of axioms can never be created in formal systems of basic arithmetic: if novel axioms are added to make the system complete, the price to pay is that the system becomes inconsistent. The earliest formulations of Gödel's incompleteness theorems concerned the arithmetic system of Principia Mathematica and the Hilbert's program for the set of mathematical axioms. By then, incompleteness theorems' demonstration has been extended to any effective formal system.

Summarizing, we got two problems:

a) We do not have a strict methodological definition of set to validate the description of biophysical and humanistic issues.
b) A formal axiomatic system cannot be simultaneously complete and consistent: either it is complete and inconsistent, of incomplete and consistent.

In the sequel we will provide an effort to show how these two problems can be overtaken via topological and logical arguments. We suggest a shift in investigators' interest from the object under assessment to its surrounding environment. The evaluated system turns out to be just a subset devoid of information inside a larger set. This procedure leads, as we shall see, to physical as well as biological consequences able to provide novel theoretical and methodological approaches to old problems from far-flung branches.

1 Towards "Punctured" Subsets

How a set (or a subset) can be distinguished from another? This question takes us back to ancient disputes concerning the principle of individuation, regarded as fundamental around 1275–1350 for solving philosophical as well as physical and theological problems (Gracia, 1991). How is a thing identified as distinguished from other things? Does an (ontological, or logical, or both) criterion exist that individuates the indivisible members of the kind for which it is given? The problem is far from removed from contemporary science and philosophy. Since Aristotle, different notions of individuation have been proposed (Regis, 1976). The principle of individuation is the form for Augustine, the matter for Avicenna, the *materia signata* for Thomas of Aquinas. Duns Scoto introduced the *haecceitas*, a peculiar feature of both the indistinct matter and the form which allows an object to be exactly *hic et nunc*, achieving its unmistakable singularity (Clatterbaugh, 1972). William of Ochkam claimed that there is no time for pointless discussions, since the universals are not ontological entities, rather conceptual issues. A young Leibniz suggested that the individual is a positive metaphysical entity which is both distinguishable from other individuals and an indivisible unity (Koszkalo, 2017).

We will focus on a rather neglected interpretation of the principle of individuation, i.e., the double negation theory, first put forward (possibly) by Henry of Ghent. Henry ponders that the cause of individuation that makes a substance individual must be something twice negative (Koszkalo, 2017). The first negation concerns the divisibility of an individual: in the hierarchical Porphyry's tree of species and genera, the lowest species contains no subdividing species and is therefore called individual, which means indivisible. The second negation concerns the identity: a given individual is different from another individual. The double negation operates both from the internal, removing any multiplication and diversity from a given subset, and from the external, excluding any identity with other subsets. In the next paragraphs, we will use this negative approach to the principle of individuality to cope with sets and subsets.

Individuality as Negation: The Operational Approach Take a subset x of a set U, where x stands for a formal axiomatic system (Fig. 1A). If the universe of the discourse x (encompassing a subset of U and a certain number of axioms) is assessed just from the "internal" standpoint, there are troubles with Godel's theorems. If an observer evaluates just the observed system x without regard to U, the subsequent theory of the "internal" view of x must be either incomplete, or inconsistent. To reach the completeness and consistency of x, that's only one shot: to look at the whole set U encompassing x. In other words, the "content" (i.e., the subset x) could be axiomatically assessed by studying its "container" (i.e., the set U). In touch with ancient claims dating back to the twelfth century (Porretano, 2009), the container is no longer a passive structure including its content, rather becomes an active structure enabling the formal treatment of its content. Summarizing, to attain a formal axiomatic system that is complete and consistent, we need to remove the formal

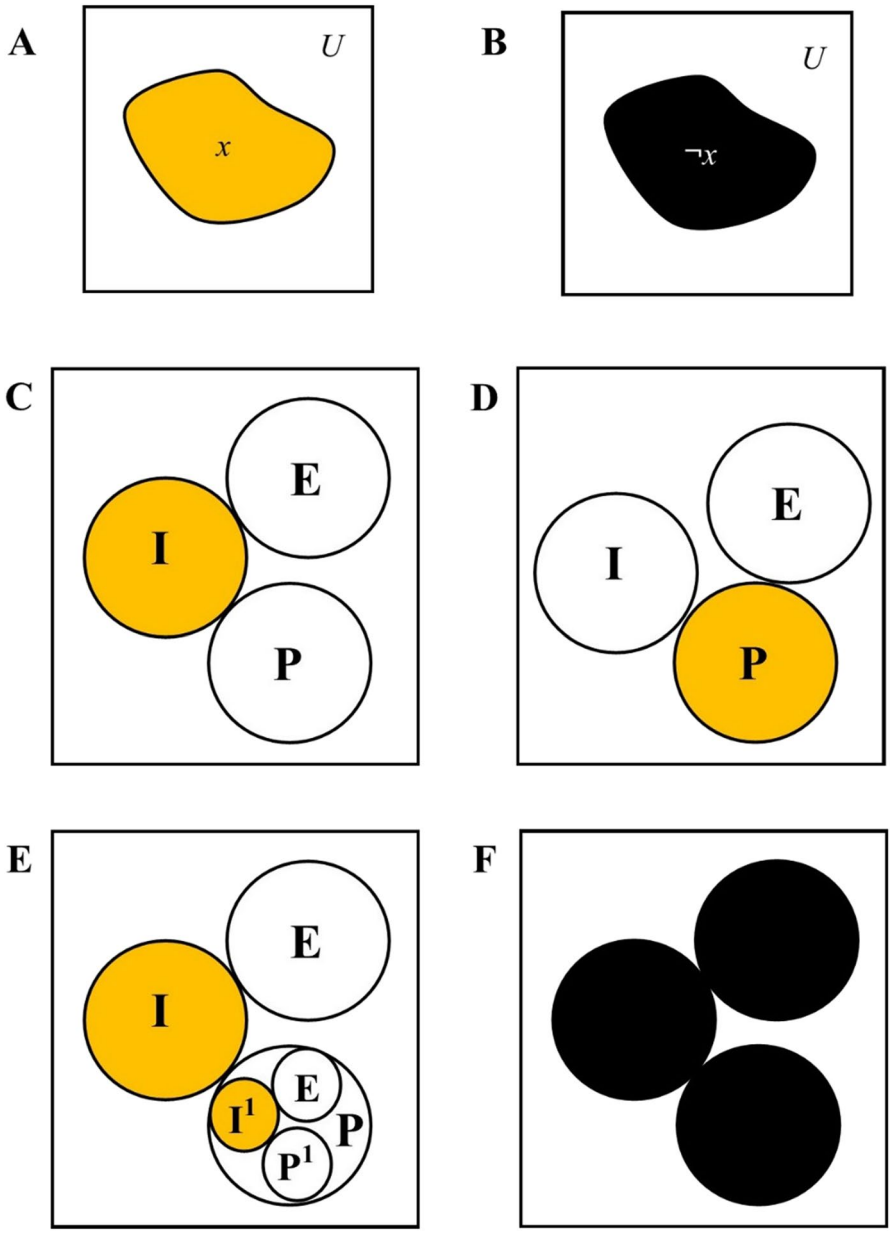

Fig. 1 **A**. Venn diagram for a subset *x* inside a square set *U*. **B**. By shading the region inside the subset *x*, the complement ¬x is acheived. Figure 2C-F. A square set *U* encompassing different subsets with diverse topological relationships. The orange subsets stand for the universe of discourse that the observer is analyzing at that moment. Figure 1C. The subset I intersects both the subsets E and P. Figure 1D. In this case, it is the subset P that intersects both I and E. **E**. The subset I intersects the subset E and the subset P, the latter encompassing a subset where I^I intersects both the subsets E^I and P^I. **F**. The three subsets, their reciprocal relationships and their further subdivisions are not recognizable anymore, since they have been "erased" (black areas) from the square set *U*

system itself from our analysis and to focus on its surroundings. This strategy consists of the logical operation of the complement of x, i.e., the removal of x from U. The complement of x is the set of elements excluding x within the larger set U. Since the larger set U contains all the elements under study, the subset x is not analyzed by an internal standpoint, rather by an external one. In logical language, the complement of x is achieved by turning x into $\neg x$ (Fig. 1B).

In sum, the best way to guarantee the completeness and consistence to our universe of discourse (i.e., the subset x) is to remove x itself and to introduce the external set U. We will term this novel methodological weapon "outer approach" (OA). In our outer framework, contrary to the belief of philosophers like Giulio Cesare Vanini, the negation precedes the affirmation (Palumbo, 1878). The elements under examination and their topological relationships are no longer the object of our interest, rather they become empty holes inside manifolds with genus > 1 (Figs. 1C-F). We could define them "punctured subsets", since the subsets under examination can be assessed in terms of holes, Betti numbers, vortices (Don et al., 2020). When a set inside a genus-zero manifold turns out to be a hole inside a genus-one manifold, we achieve the completeness of the content inside our "hole". It is noteworthy that a "punctured" approach to manifolds can be partially tackled by no point geometries, that emphasize the role of holes and voids in the quantitative assessment of scientific issues (Di Concilio et al., 2018). To provide a working example, the occurrence of holes in video frames has been used for objects movements' recognition.

Validation of Punctured Sets To ensure the foundation of our novel methodological OA, we are required to provide a stricter logical account. Once attained that the complement of x can be achieved by turning x into $\neg x$, the Aristotelian logical principles become problematic. By one hand, the identity principle is compromised since x has been artificially turned into $\neg x$. This problem is easily fixed, if we consider, in touch with Ockham, that a proposition entailing a contradiction encompasses two extremes that are not distinct entities, rather just distinct terms. Since contradictions concern just the concepts in the observer's mind, there is no contradiction in the real physical/biological entity under investigation (Ockham, 1991, quodlibet 1.2). On another hand, the law on noncontradiction (henceforward LNC) does not hold anymore. This problem is difficult to tackle, since we might ask to ourselves: if we turn x into $\neg x$, does the system preserve its consistency? The answer is negative. Nevertheless, two ways are available to restore the impaired consistency:

a) The duality principle (De Morgan duality) comes into play (Kleene, 1952). The members of each pair are said dual to each other when all the values and operations are switched simultaneously. To provide an example, the duality principle permits to the Boolean algebra to remain unchanged when all dual pairs (such as, e.g., 0 and 1, $\wedge$ and $\vee$) are unchanged (Boole, 2003). For every proposition involving logical addition and multiplication ("or" and "and"), there is a corresponding proposition in which the words "addition" and "multiplication" are interchanged.

b) Another way to restore the consistency in our system (i.e., our universe of discourse) is to use a paraconsistent logical approach, in which x and $\neg x$ are not mutually exclusive, rather they are complementary.

Paraconsistent logics (henceforward PCLs), reject LNC, suggesting that not every contradiction entails arbitrary absurdities. (Jaśkowski, 1948; da Costa, 1974;). PCLs states that the classical logical rule *ex falso quodlibet* is incorrect since it cannot be inferred that p and ¬p lead to arbitrary conclusions (Priest & Routley, 1989; Varzi, 2000). A logic is paraconsistent iff it is not the case for all sentences p, q that p, $\neg p \rightarrow q$ (Priest, 2011). In plain terms, PCLs hold when two contenders draw from their own evidence opposite conclusions which are not really demonstrated (Ciuciura, 2013). As stated by Jaśkowski (1999), "from the fact that two theses P and Q have been advanced in a discourse it does not follow that the thesis $P \vee Q$ has been advanced, since P and Q could have been advanced by different persons".

The underrated empiriocriticst Richard Avenarius (1843–1896), who investigated the laws of experience and knowledge (Russo Krauss, 2015), can be considered to have pionereed PCLs. In his Kritik (Avenarius, 1908) he postulated an axiom of knowledge stating that every human individual initially assumes: a) a spatial environment composed of manifold parts standing in relation of dependence to one another, and b) other human individuals making manifold describable statements. Every individual's experience always finds together, inextricably joined, both the I and the environment. The two components form an unbreakable enduring coordination (Avenarius and Russo Krauss, 2017), since a not-I is assigned to every I. No complete description of what is found by the experience can be drawn regardless of the two components taken together. Therefore, the original experience of the human individual goes against a split between p and ¬p. What is found by the experience is twofold, consisting of an inextricably intermingled persistence of both I and not-I. Therefore, it can be stated that Avenarius, in touch with PCLs, implicitly undermines not just the ontological component of PNC, but also its very logical component.

2 Living Beings from Outside

Our OA stands for a methodological tool to investigate living systems. The focus shifts from the analysis of the living structure to the analysis of his own external environment. This methodological operation brings to extremes the main tenet of dynamic systems theory: "the living beings are embedded/embodied in their environmental niche" (Friston, 2010). The object of scientific study, viz. the living cell, becomes a sort of behaviorist black box, totally devoid of information. The best information available for the biologists comes from the environment where life is embedded. Considering that the cells can modify their surroundings, the study of the environmental changes allows to investigate what happens inside the cell too. We are no longer looking for the information inside living agents, rather

for the changes in baseline information inside the environment. The OA approach suggests that, if a biologist wants to study a bacterial colony, he must not look at the colony, rather at the changes in the surrounding environment such as variations in temperature, humidity, chemical gradients, and so on.

Muscles of Facial Expression in Extinct Species of the Genus Homo Physical anthropologists have usually avoided the study of human facial expressions and nonverbal communication, leaving their interpretation mostly to psychologists (LaBarre, 1947; Birdwhistell, 1970). Primate muscles of facial expression (mimetic muscles) are unique in that they function either to open and close the apertures of the face or tug the skin into intricate movements (Goodmurphy and Ovalle, 1999). The importance of the face as a critical variable in social intelligence is related to positive fitness consequences (Fridlund, 1994; Schmidt & Cohn, 2001). The mimetic musculature, a discernible signal of others' social intentions, transmits close-proximity social information such as emotional states, individual recognition, mate, infant/caregiver interaction, promotion of social acceptance, moderation of the effects of social negative actions, territorial intentions and conflict of interests with strangers or competitors (Preuschoft, 2000; Burrows et al., 2006). Facial expressions are coordinated with social interaction and language at several levels (Stringer & Andrews, 2005), such as the use of mimetic muscles to articulate speech sounds (Massaro, 1998), the contribution of facial movements to the syntactic structure (Bavelas et al., 1997) and the conversational signals (Ekman et al., 1979). Although many studies have described facial muscular features in Primate species (Pellatt, 1979; Swindler and Wood, 1982; Gibbs et al., 2002), scarce data are available in ancient species of the genus Homo. We suggest, motivated by our OA methodological approach, that he current state of research in facial expression, combined with the topical interest in social intelligence as a driving force in human evolution, calls for the study of mimetic muscles in paleoanthropology.

The arrangement of mimetic muscles in modern *Homo sapiens* and in extinct human species such as, e.g., *Homo neanderthalensis*, *erectus*, *heidelbergensis* and *ergaster* (Fig. 2), could be compared to provide phylogenetic perspective to the evolution of facial expression and its role in human social intelligence. The attachments of facial muscles could be evaluated relative to known bony landmarks, such as the Frankfurt Horizontal, nasion, infra-orbital foramen, zygomaticomaxillary and zygomaticotemporal sutures, maxillary incisive and mandibular incisive fossae, mental foramen. Once projected the surface attachments of every mimetic muscle to a computerized model of the skull, the bony origin of the following muscles of facial expression could be evaluated: corrugator supercilii (Benedetto and Lahti, 2005), levator labii superioris, zygomaticus minor (Ferreira et al., 1997), zygomaticus major (Spiegel and DeRosa, 2005; Mowlavi and Wilhelmi, 2004), caninus, nasalis alar part, mentalis, quadratus labii inferioris, triangularis. In turn, due to the lack of well-defined bony markings (Stranding, 2004), the following muscles of facial expression cannot be evaluated, neither in modern nor in extinct human species: orbicularis

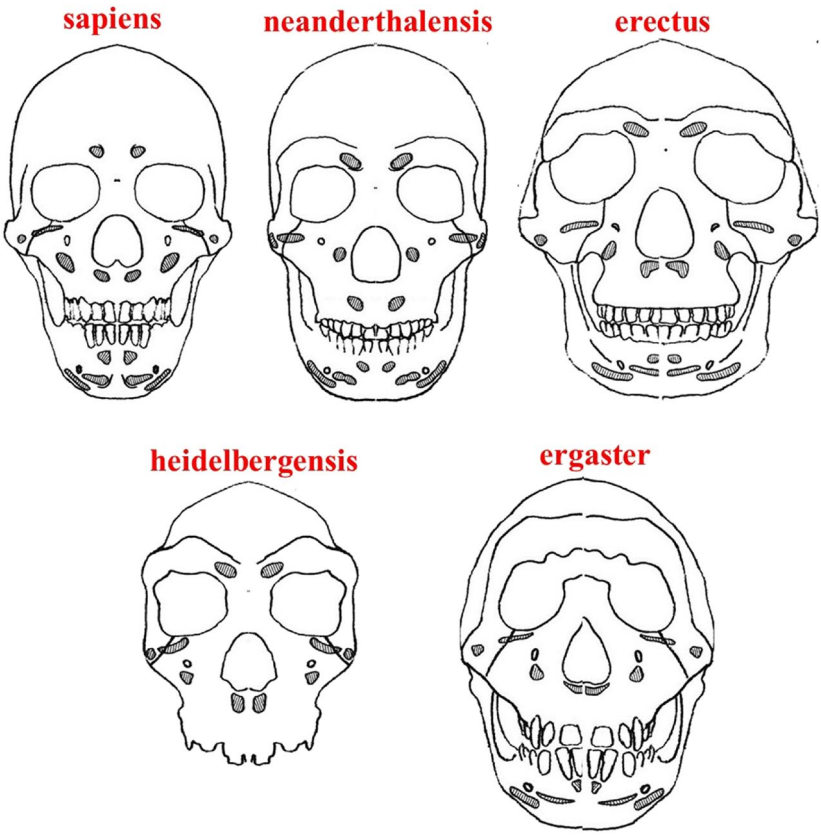

Fig. 2 Schematic illustration of the bony attachments of several mimetic muscles in five different hominin species. The skulls and the cranium are shown in frontal view. The skulls are drawn so that their total vertical lengths are the same

oculi pars orbitalis, Horner's muscle, levator labii superioris alaeque nasi, depressor septi nasi, nasalis (traverse part), incisivi labii superioris, buccinator, incisivi labii inferioris, platysma. It has been suggested that the complexity of mimetic muscles increases from the most primitive Primates to the *Hominidae*, with the highest level of complexity to be found in *Homo sapiens* (Gregory, 1929; Schultz, 1969). As species get more closely related to *Homo sapiens* and social networks become more intricate, it is held that their communicative facial repertoire and underlying facial musculature might become more elaborate (Huber, 1930; Preuschoft, 2000). However, the legitimacy of this hypothetical, hierarchical phylogenetic model has been called into question. For example, Burrows and Smith (2003) found greater complexity in the facial muscles of *Otolemur* than previously reported, while Burrows et al. (2006) advised that we are not allowed to claim greater complexity in *Homo* facial expression musculature compared with *Pan troglodytes*.

Turing Spots and Hirschsprung Disease: An Unusual Theoretical Relationship During prenatal embryonic development, cells from the neural crest migrate rostro-caudally inside the gut to form the myenteric and submucosal plexuses. In Hirschsprung disease (HD) neurons are missing from the distal parts of the intestine, leading to pathological aganglionic and hypoganglionic zones (Hirschsprung, 1888; Han et al., 2018). The unpredictable length of the impaired intestine is a troublesome issue that sometimes prevents surgeons to fully remove the pathological segment and restore intestinal motility (Miele et al., 2000; Genser et al., 2013). We ask: does the intestinal colonization in HD follow a predictable pattern? Here Turing's reaction–diffusion model (RD) comes into play (Turing, 1952). RD describes a system of chemical substances where random disturbances are caused by the competition between two active components termed activators and inhibitors (Deca, 2017). The balance between excitatory and inhibitory inputs produces different diffusion patterns of the traveling chemical substances (Kondo & Miura, 2010). RD has been proven useful to describe the formation of travelling waves and wave-like phenomena, as well as self-organized patterns like stripes, hexagons or dissipative solitons. These patterns dubbed "Turing patterns" have been used to explain a wide range of biological features, including leopard spots, zebra stripes, shark denticles, zebrafish markings, avian feathers, lung branching morphogenesis (Xu et al., 2017), hippocampal grid cell's firing patterns (Kondo et al., 2009; Cooper et al., 2018). We hypothesize that an RD-like mechanism might explain the lack of neuronal colonization of the distal gut in HD. OA suggests a model of gut colonization where reagents (i.e., the neuroblasts from the neural crest) enter a cylinder (i.e., the enteric wall) from an extremity (i.e., the proximal gut) and homogeneously diffuse towards the other extremity (i.e., the distal gut). The neural density in HD could progressively decrease in the distal areas due to local inhibition factors counteracting the rostro-caudal diffusion of the neural progenitors. RD modeling of gut colonization requires a slightly modified Turing's activator-inhibitor model. For technical readers, see: Xu et al. (2017); Cooper et al. (2018). The initial conditions may vary across different simulations (Fig. 3A). A fine-tuning of several parameters may be performed either by defining the center of a spot in an initiator row of a given number and radius, or by choosing a spatial discretization and a sufficient small-time step to ensure numerical stability, or by changing the concentrations of the two active reagents. This means that unchanged concentrations of activator lead to a constant number of neurons throughout the whole physiological gut (Fig. 3B, left side). In turn, decreases in activator and/or increases in inhibitor lead in HD to anomalous neuronal diffusion and impaired nervous density (Fig. 3B, right side).

The next question is: what is the biological rationale of a RD model for HD? HD is an embryonic disorder caused by the lack of neuroblasts' craniocaudal migration, differentiation and maturation from the neural crests by the fifth to the twelfth week of human gestation. The earlier the migration ceases, the longer the aganglionic segment will be, leading to more severe constipation. AO suggests that defects in neuroblasts differentiation and accelerated ganglion cell destruction may contribute to the disorder. Despite it is well known that mutations of several genes are involved in HD (Auricchio et al., 1999; Tang 2012; Jiang et al., 2015; Alves et al., 2013), causes

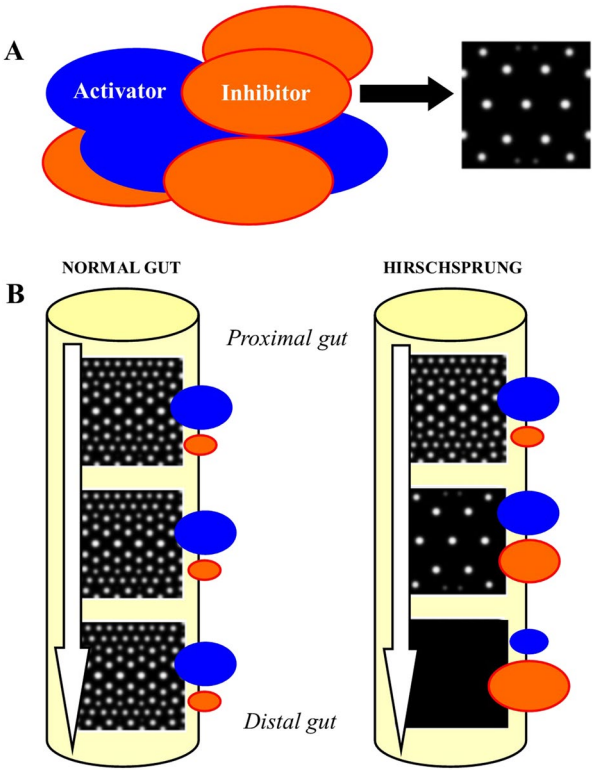

Fig. 3 **A**: Simulation of Turing's spots production. The circles **in the left picture** illustrate the concentration on activators (blue circles) and inhibitors (red circles). Their interaction generates spotted patterns in a two-dimensional lattice (**right picture**). The white spots **in the right picture** stand for the neural density in the intestinal layer. **B, left side**. In the healthy embryonal gut, the neuronal progenitors from neural crest progressively colonize the intestinal wall following a proximal–distal progression (white arrow). The final number of neurons will be approximately the same in all the segments of the adult gut. **B, right side**. In HD, the number of neurons tends distally to decrease during embryonal colonization, leading to the occurrence of hypo/aganglionic distal segments. In terms of RD, the progression (white arrow) is counteracted by the higher concentration of inhibitory factors in the distal gut (red circles)

other than the genetic ones might contribute to the incomplete migration of neural progenitors. RD models suggest the possible occurrence in the distal gut's environment of local factors inhibiting the canonical cranio-caudal progression of neuroblasts. Embryonic cell migration takes place on an underlying tissue domain which is itself growing over the time scale of days in which this phenomenon occurs, suggesting that cell migration/colonization is strongly affected by the tissue domain growth (Landman et al., 2003) through chemotactic migration models which closely resemble RD models. If a strict interaction between activating and inhibitory factors occurs in the distal gut, the cross-relationships among different genes products may alter the balance of rostro-caudal neuroblast colonization. Models of mouse megacolon, Waardenburg-Shah syndrome and early Xenopus embryos revealed that interactions among PAX3 EGR2, CX32 promoter, MITF SOX9 and SOX10 lead to impaired formation of neural crest precursors (Bondurand et al., 2000, 2001; Lee et al., 2000; Taylor and LaBonne, 2005).

In sum, RD models for intestinal migration of neuroblasts predict that the subtle balance between the concentrations of activators and inhibitors produces aganglionic, hypoganglionic or normoganglionic gut segments. A further unnoticed option must be considered: the occurrence of an hyperganglionic intestine, characterized by hyperplasia of submucosal and myenteric plexuses (Tozzi et al., 1999). In RD terms, hyperganglionosis might stand for the absence of the distal inhibitors (see Fig. 3B,

left side) required for the normal development of the healthy gut. Further, HD may be associated with the Waardenburg syndrome, which displays pigmentation changes resembling Turing-like patterns. An animal counterpart of human aganglionic megacolon, viz. the congenital abnormality of overo spotted horses termed "white foal syndrome" (McCabe et al., 1990), is characterized by lethal intestinal obstruction together with a nearly all-white RD-like coat. The correlation between RD models and the real pattern of neural intestinal colonization is experimentally testable. The medical advantage would be the possibility to estimate of intestine length to remove during surgical procedures for HD.

3 Human Brains from Outside

OA may have consequences when psychologists and neuroscientists approach mental functions. According to a bodily view of pain, pains are objects located in body parts (Nie, 2021). To quote Ockham, pain is in the foot, not in the head (Ockham, 1991, 1–12). This would mean that mental representations can be studied from outside the brain. The cognitive functions of the central nervous system such as sensations, memory etc. (Gazzaniga, 2013) become "holes" devoid of information that pave the way to a negative definition not just of mental activities, but also of the same consciousness. An OA formulation of consciousness suggests the following definition: "the consciousness is all that we cannot refer to the environment surrounding us". A shift is required from our mental activity termed attention (i.e., the selective focus on a discrete aspect of information manifested by an attentional bottleneck) to negative formulations. Therefore, we agree with Clark and Chalmers (1998), who advocate the active role of the environment in driving cognitive processes. Since human reasoners tend to lean heavily of environmental supports, the world plays an active causal role, becoming part of the cognitive process.

Extracellular Flows in the Brain Leaving temporarily apart what happens inside the neurons, OA suggests to assess the action potentials in terms of extracellular currents of charged particles. Starting from the claim that the brain currents exhibit long-range connections and collisionless collective behavior taking place inside the underrated extracellular neuronal space, we will discuss here how the extracellular electromagnetic currents generated by cortical neural sources could obey to Vlasov-like equations.

Extracellular matrix is a key player in nervous intercellular communication (Tozzi, 2015). Nervous networks depend not only on wired communication channels such as chemical/electrical synapses and ephaptic transmission, but also on signals diffusion in the extracellular spaces (Marcoli et al., 2015). Extracellular fluid, cerebro-spinal fluid and blood might have a role in handling information through signals diffusion along energy gradients in poorly delimited extracellular matrix, permitting widespread intercellular communication (Agnati and Fuxe, 2000; Agnati et al., 2010). Contrary to the common belief, the contribute of diffusive currents must not be neglected, being of magnitude comparable with the Ohmic currents. Sustained periods of neuronal output up to 84 s modify local extracellular ion concentration by

several mM (Halnes et al., 2015). Slow diffusive currents induce local changes of the extracellular potential in the order of a few tens mV. Modifications in extracellular space volume and/or geometry may affect the clearance of metabolites, neuroactive substances and toxic products, and modify the diffusion of neuroactive substances, impacting upon synaptic and extra-synaptic transmission, neuron–glia communication and ionic homeostasis (Syková et al., 1999). The non-uniform osmotic-induced cellular shrinkage produces residual extracellular space that temporarily traps diffusing molecules and slows macroscopic diffusion (Chen & Nicholson, 2000). Pan et al. (2014) confirmed, through microelectrode arrays recordings in cultured neurons, that extracellular action potentials' signal amplitude depends on the impedance of micro-tunnels. The local differences in astrocytes tiling, extracellular space fluid and extracellular matrix composition suggest that plastic brain compartments do exist in the central nervous system (Marcoli et al., 2015; Halnes et al., 2015), since the transient occurrence of local voids, e.g., the synaptic gaps that increase the tortuosity of the extracellular space, can be produced within minutes by perisynaptic astrocyte processes (Bernardinelli et al., 2014).

It is widely recognized that the Maxwell and Laplace equations provide a connection between the extracellular potential V_e (measured in Volts) and the current source density (measured in A m^{-2}) at every location of the brain tissue (Buzsáki et al., 2012), since multiple currents combine linearly due to the superimposition principle. However, the classical Ohmic equations hold just inside the narrow limits of the Debye layer (i.e., the region close to the membrane with the strongest concentration gradients), since the time evolution of the charged particles' distribution function is not anymore Maxwellian at distance $>>>$ Debye sphere. Pods et al. (2013) introduced a three-dimensional model of cylindric axons embedded in the extracellular fluid, based on the Poisson-Nernst-Planck equations of electrodiffusion. Special attention was paid to the Debye layer. They found both a signal component stemming directly from the intracellular electric field, and a peculiar extracellular local field potentials waveform (Pods et al., 2013). The occurrence and evolution of long-range interactions can be mathematically described in terms of a self-consistent collective electromagnetic field produced by charged ions. Since the main mechanism of molecular transport within extracellular spaces is the diffusion, and since the brain acts like a porous medium for substances that do not cross cellular boundaries, the well-established diffusion equations could be used to describe the collective trajectories of large molecular ensembles (Syková & Nicholson, 2008). Modified Vlasov-Maxwell equations (Vlasov 1938; Kotelenez & Kurtz, 2010) might be able to describe brain dynamics in terms of a system of charged particles interacting with the electromagnetic field produced by the cortical currents. In sum, long-range behavior can be portrayed in terms of extracellular space/interstitial fluids containing collisionless chemical ions that give rise to self-consistent collective fields (Fig. 4A).

The collective movements of extracellular molecular diffusion are constrained, among other factors (Wu & Shuai, 2015), by two crucial macroscopic parameters that modify the nervous architecture and the geometric alignment (Chen & Nicholson, 2000; Buszaki et al., 2012): the cortical interstitial volume fraction α

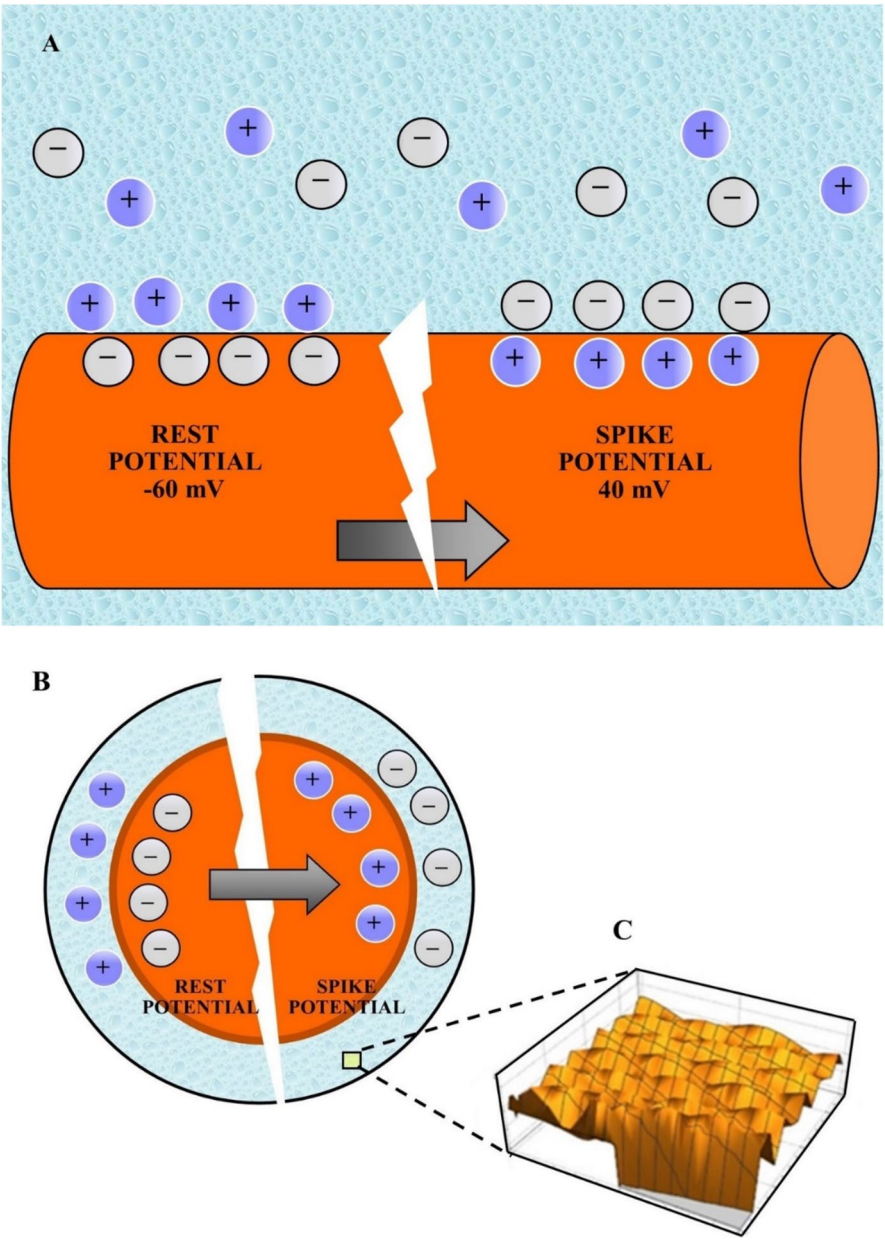

Fig. 4 Schematic illustration of neuronal intracellular/extracellular ionic movements. The intracellular axonal compartment is painted in red. **A**. Rest and spikes potentials (left and right, respectively) exhibit reverted ion concentrations in the intra- and extra- neuronal spaces. **B**. An oversimplified spherical model of McKean-Vlasov collective movements portrays the brain as a rigid ball containing charged particles, e.g., extracellular and intracellular ions. The intracellular neuronal compartment (inner red circle), consisting of about 85% of the brain volume, is surrounded by the thinner extracellular space (outer circle). The extracellular charged particles display reciprocal long-range interactions collectively described by the collisionless equations. **C** illustrates a simulation of particle movements in a tiny zone of the extracellular compartment. These theoretical plots might be compared with real EEG or fMRI neurodata

(i.e., the extracellular volume/total tissue volume) (Xie et al., 2013; Syková et al., 1999) and the tortuosity of the interstitial space, which reflects the hindrance imposed to the matrix by geometric constraints (Syková & Nicholson, 2008; Nicholson et al., 2011). Depicting the brain currents in terms of fluxes taking place inside a sphere (Figs. 4B-C), the long-range collisionless trajectories can be described as collective movements in the extracellular space. It is noteworthy that the time-evolution of such collisionless spherical movements can be assessed via the above-mentioned modified McKean–Vlasov equations. For further details, see: Chayes and Panferov (2010); Tozzi et al. (2018).

4 Humanities from Outside

In humanities, due to the intrinsic lack of the" trial and error" inductive methods typical of the experimental procedures of hard sciences, metaphorical expressions about our world and its various segments rarely develop into well-defined, quantifiable, measurable, testable and operationalizable structures. OA suggests different interpretations of social and poetic matters, providing extensive rework and fresh philosophical and textual implications.

Celestino's controversial letter The Capuchin friar Celestino of Verona was one of the main whistle-blowers of Giordano Bruno. Tortured and sentenced by the Inquisition in 1587, the heretic Celestino met Bruno in the Venetian prison where both were locked up between 1592 and 1593. Confined at San Severino Marche, Celestino wrote in May 1599 to the Holy Office of the Roman Inquisition to seek an audience. Summoned by the Inquisitors, he moved to Rome between June and July 1599. His request is reported in the official archives of the Holy Office. The minutes of the sitting of the Congregation run as follows (Firpo, 1949):

> "Feria V, 3 iunii 1599. Fratis Celestini de Verona, ordinis Cappucinorum, lectis litterris datis in civitate Sancti Secerini adhoc S. Officium scriptis, die sexta maii, decretum quod ad S. Officium et deponat quae sibi occurrunt."

Still, on 8 July 1599, a surprising minute is reported in the same archive. Here you are the extant report of the proceedings we are interested in (Firpo, 1949):

> [4]"Feria V, 8 iulii 1599. Fratris Celectini, filii quondam Lactantii Arigoni de Verona, subdiaconi ordinis fratrum monorum congregationis Cappucinorum, letta copia litterarum ab ipso, ut creditur, sciptarum 20 iunii proxime praeteriti Inquisitori Venetiarum, Sanctissimus mandavit fieri diligentiam pro reperiendo autore dictarum litterarum per comparationem scripturae, et apud superiores Cappuccinorum, nec non ex scripturis eiusdem fratris Celectini in processu".

In brief, the report says that the Pope (and the Brotherhood) read the copy of a letter sent to the Venetian Inquisitor on June the 20th. This letter was believed to be written by Celestino. To uncover the author of this manuscript, the Pope asked

for a comparison with previous Celestino's writings. The result of the comparison is unknown: what we know so far is that Celestino was taken to the same roman prison where Giordano Bruno was confined and was burnt alive in *Campo dei Fiori* in September, five months before Bruno himself suffered the same fate in the same place. What is certain is that a very speedy trial was concluded against Celestino, following procedures that were unusual for the otherwise careful and meticulous Roman Inquisition. How to explain the letter received by the Venetian Inquisitor? Influent scholars such as Firpo (1949), Marchetti (1979) and Maifreda (2018) unanimously held that the letter was anonymous. Once he came to know of the anonymous letter, the Pope Clemens VIII, suspecting that Celestino himself was behind the unsigned manuscript, asked for his Capuchin brothers who held his previous writings. Summarizing, the standard version argues in favour of self-denunciation: Celestino wrote to the Roman Inquisition and (anonymously) to the Venetian Inquisitor to inform himself.

However, looking carefully at the extant report, an alternative version is worth to be put forward. The minute does not explicitly contend that the letter was anonymous. Furthermore, it is not stated that the Pope read the original manuscript, rather he went through a copy. The phrase: "*ab ipso, ut creditor, scriptarum*" ("the letter believed to be written by Celestino") might mean exactly the opposite of what has been traditionally convened. An unorthodox account of the minute can be hypothesized: the Pope (and the Brotherhood) read a copy of the letter signed by Celestino previously sent to the Venetian Inquisitor. Though, the Pope and the Brotherhood noticed something suspicious concerning the manuscript, something against the ascription to Celestino. That's why the letter "was believed to be written by Celestino": it was signed by him, but it seemed like the manuscript was not in Celestin's wheelhouse. This interpretation implies that the Pope had reason to believe that the letter sent to the Venetian Inquisitor was not by Celestino, despite his signature. The Pope guessed that somebody was trying to pass himself off as Celestino. This unconventional interpretation paves the way to a fully novel understanding of Celestino's trial. Our role ends here: once we have raised the issues, it is not our task to speculate on alternative explanations for such an intricate affair.

Dante Aligheri's "amor, ch'a nullo amato…": an "ex nihilo" account of "a nullo" The renewed verse V, 104 of Dante Alighieri's "Hell" (Giacalone, 1982) is one of the most celebrated not just of the Divine Comedy, but also of the worldwide literature. Nevertheless, its meaning is still controversial and highly debated.

"Amor, ch'a nullo amato amar perdona": the mainstream account points towards the following meanings:

1) "Love, that spares none of the loved from loving in return".
2) Or "Love, that does not allow not to love back".
3) Or "Love, that, when one is loved, does not allow that it be refused".
4) Or "if you love someone, that love will give back to you".

In the *Amor Cortese*'s framework, summarized by Andrea Cappellano's "De Amore", love is a power unescapably pushing men towards women and vice versa, forcing everyone who is loved to love in turn (Malato, 2018). However, this conventional reading does not sound logical: why do I have necessarily to love anyone who loves me? The neo-Plotinian, medieval account of a God who loves its Creatures suggests that reverberation and mirroring of Love occurs among entities equipped with different levels of Being (Katz, 1950). Nevertheless, the claim "Love, which does not allow NOT to love back" is against the ordinary experience when referred to the everyday love affairs among human beings. We suggest a OA-framed interpretation: the words "a nullo" can be taken in the sense of the Latin "ex nihilo", i.e., "from nothing". In Dante's context, "ex nihilo" may stand for different meanings at diverse informative levels. In a philosophical and theological sense, Dante's "ex nihilo" might refer to the long-standing controversy about God's Creation "ex nihilo", i.e., a God who creates without manipulation of pre-existing matter (Gilson, 1955). The idea that "nothing comes from nothing", first appeared in Parmenides' Physics. In the following centuries, creation ex nihilo became a typical christian issue (see, e.g., Basilio de Cesarea, 1990) against the Platonic concept of uncreated matter. During the Medieval ages, the proposition "ex nihilo, nil fit ("out of nothing, comes nothing") was used by Scholastic theologians to claim that the Universe needs God as its cause, since something cannot be created from Nothing (Duncan, 2011). This account is strictly correlated with the controversial Averroes' and Aquinas' account of causality. The cause/effect issue was tackled by the 1277 Condemnations, that provided a sharp critique of the "heretical" account of God as the First Cause able to produce just the First Effects (Klima et al., 2007; Marmura 2000). It is noteworthy that the Condemnations, that also dismissed Andrea Cappellano's "De Amore". Therefore, in Dante's Chant V, "ab nihilo" could stand for "sine causa", in touch with the 1277 Condemnations.

Love is described here as a power issuing from nothing at all, "ab nihilo". Just like God is the First Cause who creates the world from nothing, Love lets people fall in love without recognizable causal relationships and preexisting background. Love, at least in the case of the illegitimate passion that links Paolo and Francesca, arises from absolute ignorance. In the social context of an adulterous love, "from nothing" might stand for: "ignoring the rules, the canonical laws". A love affair out of the sacrament of wedding must be condemned. Therefore, Love might correspond to the "for del dritto amore" mentioned in Hell XXX, 39, i.e., "love as a passion outside every rule of the legitimate Love".

Summarizing, if we consider our account as holding true, or at least possible, the proper semantic meaning of the verse "Amor, ch'a nullo amato amar perdona" would be:

1) "Love, that forgives the loved to love from nothingness".
2) Or "Love, that forgives who is loved to love back, against the laws".
3) Or "Love, that allows who is loved to love, also against natural and human laws".
4) "The power of love holds also against the natural laws and order, and against God's will.

Other feasible interpretations, also raising from the same "ex nihilo"'s account suggested by OA, could be:

1) "Love, that allows, starting from nothing, an individual to love the loved one".
2) Or "Love, that forgives to love from nothingness the loved".
3) Or "Love, that absolves who loves the loved with no reason".

In summary, a free translation of Dante's verse could be: "Love is a strong, unreasonable power outside natural and human laws, which allows one to love another against all odds". This also testifies how Dante was fully aware of the theological and philosophical debates occurring before and after the 1277 Condemnations.

The mysteries of the Voynich manuscript The Voynich manuscript (Beinecke MS 408) is a baffling fifteenth-century codex including weird and elaborated illustrations such as otherworldly plants, unfamiliar constellations, herbal medicine drawings and enigmatic images of naked women swimming though fantastical tubes and green baths (Skinner et al., 2017). The manuscript is written by an unknown author in an unknown language and alphabet. From the rediscovery in 1912 by rare books dealer Wilfrid Voynich, its language has eluded decipherment (Clemens & Harkness, 2016). The 240-page manuscript is believed running left to right, with most of the characters composed of one or two simple pen strokes. The format is one column in the page body, with slightly indented right margin and with paragraph divisions, often with stars in the left margin (Shailor). OA suggested us to visually inspect the ink in digital reproductions (available at Beinecke Rare Book and Manuscript Library, Yale University: http://beinecke.library.yale.edu/dl_crosscollex/SearchExecXC.asp?srchtype=CNO and here: http://ixoloxi.com/voynich/pdf/en/vms-quire1-en.pdf). It can be demonstrated that the codex is partially written from right to left (Fig. 5). Therefore, contrary to the common belief, at least some rows of the Voynich manuscript run from right to left.

5 Recent History from Outside

History, by its own nature, copes with intricate combination of theoretically and empirically wavering occurrences. This prevents a deepening of human events' dynamics through testable experimental procedures. Concept development and modelling, as well as others that might contribute to quantification of historical events, are strongly required. Take, for example, the kidnapping of the former Italian Prime Minister and then President of the relative majority party Christian Democracy Aldo Moro (Drake, 1995). At 9 o'clock of March 16th, 1978, he was kidnapped in Rome by left terrorists of the Red Brigades (Gotor, 2018). His body was found 55 days after in the trunk of a Renault 4 car. According to the official version, confirmed by the same brigatists ten years after the event, killers brought him to a parking garage and shot him with two weapons, the body lying on the back inside the car trunk. This reconstruction of Moro's death is still highly debated (Moro, 1998; Cucchiarelli, 2016). The photographs

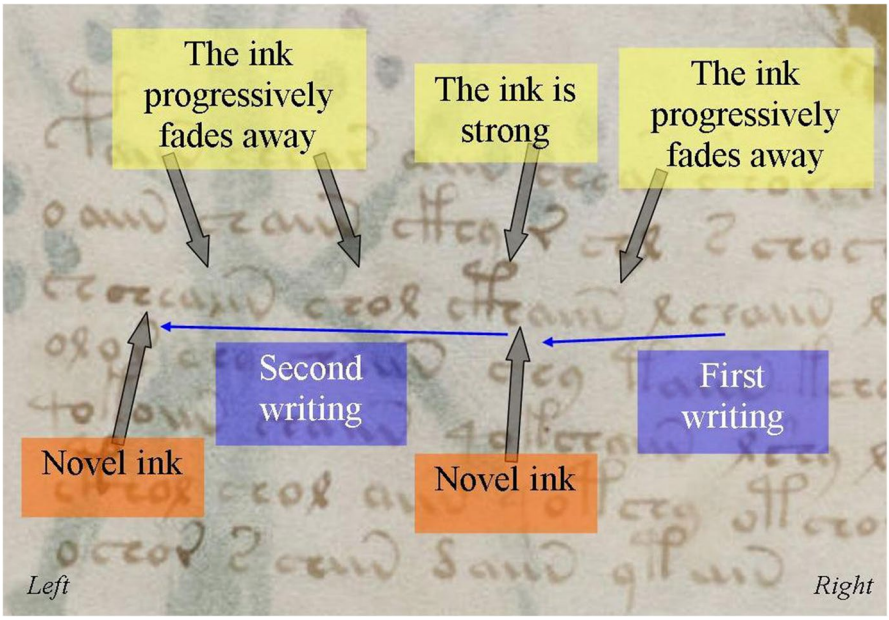

Fig. 5 Magnified view of the Voynich manuscript. In the row under examination, the pen stroke ran from right to left. When the ink started to fade, the Author dipped once again the pen in the ink and kept writing. This means that some rows are written from right to left, contrary to the common belief

taken during the body inspection (Questura di Roma, 1978) and the official report of the autopsy (Commissione, 1989) are freely available on Gero Grassi's website: http://www.gerograssi.it/cms2/index.php. Instead of looking at the body and the wounds, an OA approach suggest the investigation of outer elements, such as the jacket, gilet, cravat, shirt and underwear. The question here is: is it feasible to infer from the clothes the temporal sequence of the bullets and the position of Moro's body during the shots? Going through the autopsy report, it can be inferred that just two of the bullets pierced the jacket. The two holes in the jacket can be superimposed solely to two of the breaks: the entry wounds termed 1 and 2 in Fig. 6, left side. During body inspection, after the removal of the gilet, the cravat looked ruffled and disarrayed (Fig. 7A). The explanation is straightforward, if we consider that the doctors reported the presence of napkins under the gilet, assembled to stop previous bleeding. The cravat's displacement could have been caused by the insertion of the napkins under the gilet after the first shots (Fig. 7B). Looking at the breaks detectable on the cravat, it can be noticed that they were produced by bullets shot after the insertion of napkins. These holes correspond to the ones termed 5, 6 and 8 (and, possibly, 4) (Fig. 7C). In sum, contrary to the official version of one-step execution inside the car trunk with the body lying supine, OA points towards a multi-step execution, the first phases taking place outside the car. According to our analysis, the temporal series of events was the following: at first the President, standing upright or seated, was shot by a few bullets. Then the killers put napkins under the gilet to stop the haemorrhage. It followed the sequence of shots 5, 6 and 8 (and, possibly, 4) that pierced the cravat already dislocated by the napkins.

Fig. 6 **A**. Entry breaks on Moro's gilet (blue spots). The two holes passing through the jacket are marked in yellow. Note that the two yellow holes piercing the jacket do not match any of the blue holes piercing the gilet. **B**. Once relocated the jacket via computer simulation, it is easy to notice that only two blue dots match the yellow dots, i.e., the blue dots termed 1 and 2. The location of the jacket during the shots that reached the holes 1 and 2 corresponds to an individual standing vertical. Therefore, Moro was upright, rather than lying on the back inside the car, when he was reached by these bullets

Another last sequence was thrown when the body was already lying on the back inside the car: indeed, a bullet was found stucking the trunk's metal below Moro's corpse.

In sum, OA is helpful in detecting hidden features in photographs of deceased subjects, contributing to elucidate cold forensic cases. We suggest that a closer computer-aided investigation of clothing can be used to shed new light on controversial historical events in which pictures are available: to provide a theoretical example, it would be feasible to describe the series of shots that reached Benito Mussolini's body during his contentious execution.

6 Information from Outside

The old-fashioned concept of active and potential intellects has a feasible counterpart in the modern-day notion of information. Here we show how this claim leads to unexpected, troubling consequences. Aristotle distinguishes between the active and

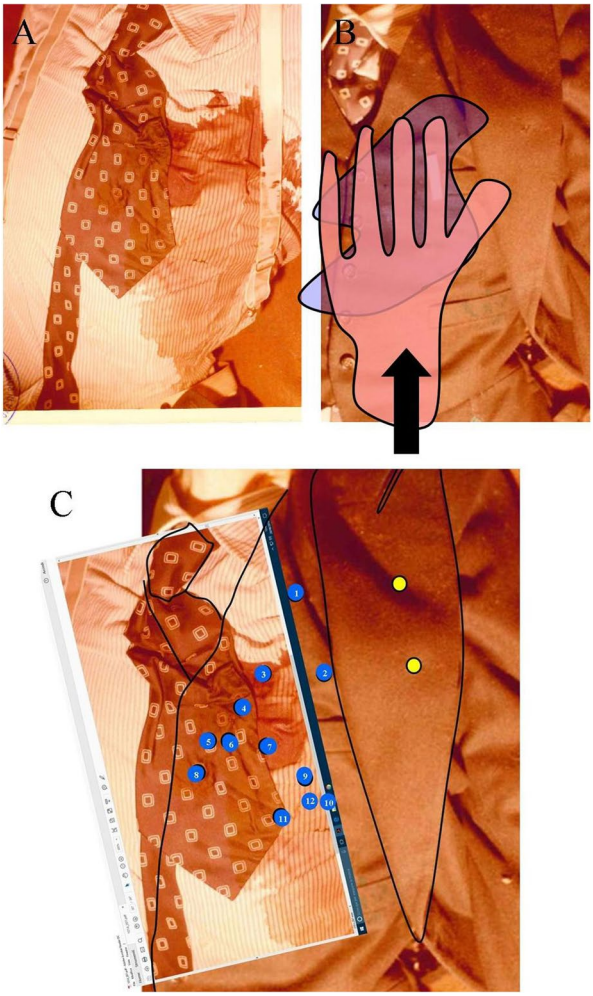

Fig. 7 **A**. The cravat under the gilet was warped and the necktie misplaced. This suggests that napkins were inserted under the gilet after the first shots to stop the bleeding (Fig. 7B). **C**. Superimposition of the entry breaks and the ruffled cravat. The borders of the gilet and the jacket are highlighted (black lines). It is easy to notice that the holes in the ruffled cravat match the shoots 5, 6 and 8 (and, possibly, 4). This means that the bullets reaching the cravat were not shot during the first phases of the execution

the potential intellect (see *De Anima*: III,5 and Metaphysics: XII, 7–10). To know something, every man must be equipped with the ability to know it. This individual skill is the potential intellect, to be boosted by training and exercise. The active intellect is required to transform the potential knowledge of the potential intellect into actual knowledge. Some scholars such as Alexander of Aphrodisias merged the mortal, passive, potential intellect with the body and equated the omniscient, separable, impassible, unmixed, divine, immortal active intellect with the "unmoved mover" (Bazán, 1989). In touch with OA, the Arabic thinkers Al-Farabi, Avicenna and Averroes located the active intellect outside the human soul, fully separated from the human being (Dales, 1995). Two hierarchical emanations take place:a) from the First Cause to the supernal realm and b) from the transcendent active intellect to the lower world. The illumination of the human (potential) intellect is achieved through its conjunction with the transcendent (active) intellect (Davidson, 1992). In sum, the

whole human knowledge, past, present and future, is included in the active intellect, external to the body and shared by all the individuals. According to his skills, possibilities and available technology, the potential intellect of every individual catches a part of the fixed and stable cosmic knowledge provided by the active intellect.

Translating the account of the active intellect into the current concept of information and information entropies (Shannon, 1948; Dick, 1981; Wheeler, 1990), we achieve the notion of total cosmic information. Cosmic information, which is eternal since it can be neither created nor annihilated, could be either finite is the Universe is closed, or infinite if the Universe is open. It stands for the general active intellect, partially available for the potential intellect of every huma individual. To provide an example, take a scientist studying an object. Fitted with natural skills and powered by technological devices, he extracts chunks of the total information endowed in the object. The more the available technology, the more the scientist's potential intellect gets information from the agent intellect (in this case, the information encompassed inside the object under investigation). For example, when a scientist wants to scrutinize the infrared light emitted by an object, he requires a proper detector since his natural skills are not powerful enough to detect this feature. The more the scientist explores each possible feature of the object, the more he gets close to the complete knowledge. Things come to a full circle when we examine once again Richard Avenarius' links with PCLs. The Avenarius' I and the not-I are strictly correlated, although none of them prevails. This is a standpoint of the philosophical attitude termed "neutral monism": despite the I (i.e., the human mind) and the not-I (i.e., the body and the environment) have equal dignity, they must be subordinated to something neutral, hierarchically placed above them. Among the disparate efforts throughout the centuries to find this neutral principle, the attempt provided by Sayre (1976) is noteworthy. He presented an original approach to the subject of the mind–body problem, linking the physical sciences with the sciences of human behavior and suggesting that the neutral principle above the mind and the body is the cybernetic concept of information. This means that the conceptual step from PCLs to active intellect/information is not a difficult road.

One might ask: what for? What does a rather analogical comparison between Aristotle's, Avicenna's and Averroe's intellects and Shannon's and Wheeler's information bring on the table? An outer approach to this question provides a striking response. The ancient accounts suggest a divine source for the active intellect, either angelic/supralunar, or a direct emanation of God. Nevertheless, the corresponding account of cosmic information as an unlimited, immortal whole has problems with the principle of individuation. As previously stated, the problem of individuation is far from removed from contemporary science and philosophy. How are things identified as distinguished from other things? How can the homogeneous matter give rise to different forms and qualities? These ancient questions are still relevant in far flung fields, in particular in the hotly debated field of information, since we might ask: if two files contain the same number of bits, which is the difference between their available information? The information enclosed in two expanded memories with the same number of bits is different by the inquirer's standpoint. For example, two 1 GB Drive flash USBs might encompass either a Depeche Mode album or the second Symphony of Shostakovich, it does not matter. This leads to biological

questions. Even though the human cells have the same DNA, a hepatocyte and a cardiac cell are clearly different: does it mean that their principle of individuation depends on their phenotype, or by the different bodily environment in which they are embedded? Do they encompass the same amount of information?

In sum, the same fixed quantity of bits does not lead to the detection of the same available qualitative (we could use the term "semantic") content. This raises doubts as whether the tenet of the cosmic information extracted by the human mind holds true. Also, critiques have been raised to the role of information in mental activity, casting doubts on the adequacy of the information paradigm to describe the brain functions and on the assumed relationships between changes in entropies detected by the available neuro-techniques and mental tasks (Tozzi & Peters, 2020).

The comparison between active intellect and information has paradoxically two opposite consequences: by one side it eradicates the divine concept of the knowledge and leaves just the quantitative concept of information; by another side, however, it introduces once again a metaphysical component, i.e., the presence of a vague, eternal substance permeating the universe and devoid of scientifically recognizable meaning. In other words, when we, in touch with the concept of the agent intellect, consider the cosmic information as the largest number of bits, we are only allowing the metaphysical concept of God to sneak in the back of scientific matters. Therefore, a crucial question arises: when the scientist takes information from the object, is he extracting the information endowed in the object, or is it building information that does not exist inside the object? Is our qualitative mental information discovered, or is it invented? Do we really think that there is something there, outside us and inside the object? Isn't "an object encompassing the highest number of bits" a metaphysical concept?

The OA approach provides an alternative account: what is believed to be extracted from an object is not really extracted, rather is produced by our minds by removing the object from our mental analysis. Could we state, paraphrasing Aristotle, that semantic information is not actually any real thing before being thought by human individuals? Could we say that the mind is potentially whatever is thinkable, though actually is nothing until it has thought? Is active knowledge identical with its object? Is potential knowledge prior in time to actual knowledge? Is the knowledge alone the cause that produces the action? Does time exist without a clock? In terms of information and active/potential intellects, we can just come to an end with a slogan: *without a thermometer, an object does not have a temperature*.

7 Conclusions

We advocate a methodological innovation, i.e., an outer view of biophysical and humanistic issues. OA outcomes include the possibility that the setting choices of living systems are influenced by hidden variables correlated with still unknown environmental factors. In is well-known that the living organisms must be equipped with homeostatic mechanisms to cope with external changes in pH, temperature, osmolarity, bacteria, viruses, etc. Here we ask: how do the living organisms cope with changes in environmental factors that have been less scientifically explored?

Are living beings equipped with still unknown homeostatic devices to tackle least studied external changes such as, e.g., magnetic fields, infrasounds, cosmic rays, visual or tactile noise, etc.? Are there hidden, still unexplored peripheral or internal receptors sensitive to different types of environmental changes? Active research of new receptors in ongoing. For a survey, see Tozzi (2015). Here we provide just a few of the recently described examples. The hypothesis that the brain might be equipped with a natural external noise-cancelling circuit like the technology of Active Noise Control (Rauschecker et al., 2010) has been recently confirmed by Schneider et al. (2018), who described a dynamic sensory filter involving motor cortical inputs to the auditory cortex that selectively suppress the predictable acoustic consequences of movement. Shivaraju et al. (2021) discovered that mouse and human airway basal stem cells sense hypoxia and respond by differentiating into protective neuroendocrine cells to mitigate tissue damage. The last, but not the least, ultrasonic inaudible components of the human infant cry influence hemodynamic responses in the breast region of unaware mothers (Doi et al., 2019). This amazing latter finding suggests that the ultrasonic components of the acoustic signal play a role in human mother–infant interaction.

To show the huge potentialities of OA in scientific inquiry, we propose the last example, which demonstrates how an outer view might provide fresh insights in the interpretation of already achieved scientific results. According to OA, it might be hypothesized that a factor outside our body, say, e.g., the bacteria on our skin, could contribute to keep constant our bodily temperature. This claim is easily testable: do germfree rats have a temperature lower that the rats normally exposed to microbes? Looking at the literature, we found a paper by Kluger et al. (1990) which tested whether the gut flora is able to influence the body temperature of rodents. Both germfree mice and rats given nonabsorbable antibiotics showed a marked decrease in both their daytime and nighttime temperatures. While the Authors concluded that their results support the hypothesis that gut flora has a tonic stimulatory effect on the body temperature of rodents, OA suggests a different explanation for this long ago acquired experimental finding: a factor outside the body (the skin bacteria), could contribute to keep constant the bodily temperature.

Declarations The undersigned Author transfer all copyright ownership of the manuscript, in the event the work is published.

The undersigned author warrants that the article is original, does not infringe on any copyright or other proprietary right of any third part, is not under consideration by another journal, and has not been previously published.
The Author does not have any known or potential conflict of interest including any financial, personal or other relationships with other people or organizations within three years of beginning the submitted work that could inappropriately influence, or be perceived to influence, their work.
This research did not receive any specific grant from funding agencies in the public, commercial, or not-for-profit sectors.
This research does not contain any studies with human participants or animals performed by the Author.
The Author had full access to all the data in the study and take responsibility for the integrity of the data and the accuracy of the data analysis. The Author performed: study concept and design, acquisition of data, analysis and interpretation of data, drafting of the manuscript, critical revision of the manuscript for important intellectual content, statistical analysis, obtained funding, administrative, technical, and material support, study supervision.

References

Agnati, L. F., & Fuxe, K. (2000). Volume transmission as a key feature of information handling in the central nervous system possible new interpretative value of the Turing's B-type machine. *Progress in Brain Research, 125*, 3–19.

Agnati, L. F., Guidolin, D., Guescini, M., Genedani, S., & Fuxe, K. (2010). Understanding wiring and volume transmission. *Brain Research Reviews, 64*, 137–159.

Alexander, D. M., Nikolaev, A. R., Jurica, P., & van Leeuwen, C. (2016). Global Neuromagnetic Cortical Fields Have Non-Zero Velocity. *PLoS ONE, 11*(3), E0148413. https://doi.org/10.1371/journal.pone.0148413

Alves, M. M., Sribudiani, Y., Brouwer, R. W., Amiel, J., Antiñolo, G., et al. (2013). Contribution of rare and common variants determine complex diseases-Hirschsprung disease as a model. *Developmental Biology*, 382(1), 320–9. https://doi.org/10.1016/j.ydbio.2013.05.019.

Auricchio, A., Griseri, P., Carpentieri, M. L., Betsos, N., Staiano, A., Tozzi, A., et al. (1999) Double Heterozygosity for a RET Substitution Interfering with Splicing and an EDNRB Missense Mutation in Hirschsprung Disease. *The American Journal of Human Genetics*, 64(4), 1216–21. https://doi.org/10.1086/302329.

Avenarius, R., (1908). *Kritik Der Reinen Erfahrung von Richard Avenarius*. C.R. Reisland.

Avenarius, R., Russo Krauss, C. (2017). Osservazioni sul concetto di oggetto della psicologia. FedOA - Federico II University Press. ISBN: 978-88-6887-016-4.

Basilio di Cesarea. (1990). *Sulla Genesi*. Mario Naldini (eds.), Fondazione Lorenzo Valla - Arnoldo Mondadori Editore.

Bavelas, J. B., & Chovil, N. (1997). Faces in dialogue. In J. A. Russell & J. M. Fernandez-Dols (Eds.), *The psychology of facial expression* (pp. 334–346). Cambridge University Press.

Bazán, B. C. (1989). On "First Averroism" and its Doctrinal Background, in Of Scholars, Savants, and their Texts. Studies in Philosophy and Religious Thought. Essays in Honor of Arthur Hyman, Peter Lang, New York-Bern-Frankfurt am Main-Paris, pp. 9–22.

Benedetto, A. V., & Lahti, J. G. (2005). Measurement of the anatomic position of the corrugator supercilii. *Dermatologic Surgery, 8*(Pt 1), 923–927.

Bernardinelli, Y., Muller, D., & Nikonenko, I. (2014). Astrocyte synapse structural plasticity. *Neural Plasticity, 2014*, 232105.

Beuchot, M. (2005). Nicholas of Autrecourt. In: A Companion to Philosophy in the Middle Ages. Eds: Gracia JJE, Noone TB. ISBN:9780631216728. https://doi.org/10.1002/9780470996669.

Birdwhistell, R. L. (1970). *Kinesics and context*. University of Pennsylvania Press.

Bondurand, N., Pingault, V., Goerich, D. E., Lemort, N., Sock, E., et al. (2000). Interaction among SOX10, PAX3 and MITF, three genes altered in Waardenburg syndrome. *Human Molecular Genetics*, 2000, 9(13), 1907–17.

Bondurand, N., Girard, M., Pingault, V., Lemort, N., Dubourg, O., Goossens, M. (2001). Human Connexin 32, a gap junction protein altered in the X-linked form of Charcot-Marie-Tooth disease, is directly regulated by the transcription factor SOX10. Human Molecular Genetics. 10(24), 2783–95.

Boole, G. (1854).An Investigation of the Laws of Thought. Prometheus Books, 2003. ISBN 978-1-59102-089-9.

Burrows, A. M., & Smith, T. D. (2003). Muscles of facial expression in Otolemur, with a comparison to Lemuroidea. *Anatomical Record, 274A*, 827–836.

Burrows, A. M., Waller, B. M., Parr, L. A., & Bonar, C. J. (2006). Muscles of facial expression in the chimpanzee (Pan troglodytes): Descriptive, comparative and phylogenetic contexts. *Journal of Anatomy, 208*, 153–167.

Buzsáki, G., Anastassiou, C. A., & Koch, C. (2012). The origin of extracellular fields and currents — EEG, ECoG, LFP and spikes. *Nature Reviews Neuroscience, 13*, 407–420. https://doi.org/10.1038/nrn3241

Chayes, L., & Panferov, V. (2010). The McKean–Vlasov Equation in Finite Volume. *Journal of Statistical Physics, 138*, 351–380. https://doi.org/10.1007/s10955-009-9913-z

Chen, K. C., Nicholson, C. (2000). Changes in brain cell shape create residual extracellular space volume and explain tortuosity behavior during osmotic challenge. Proceedings of the National Academy of Sciences of the United States of America. 97(15), 8306–11.

Ciuciura, J. (2013). Non-adjunctive discursive logic. *Bulletin of the Section of Logic*. 42(3).

Commissione Parlamentare d'inchiesta sulla strage di via Fani sul sequestro e l'assassinio di Aldo Moro e sul terrorismo in Italia. 1989. *Verbale di descrizione ed identificazione del cadavere e di autopsia (Aldo Moro)*. Vol. 45, Doc. XXIII, n.5: 649–662.

Cooper, R. L., Thiery, A. P., Fletcher, A. G., Delbarre, D. J., Rasch, L. J., Fraser, G. J. 2018. An ancient Turing-like patterning mechanism regulates skin denticle development in sharks. *Science Advances*. 2018, 4(11):eaau5484. https://doi.org/10.1126/sciadv.aau5484. eCollection 2018 Nov.

Clark, A., Chalmers, D. J. (1998). Analysis, 58:10.23.

Clatterbaugh, K. C. (1972). Individuation in the ontology of Duns Scotus. *Franciscan Studies., 32*, 65–73.

Clemens, R., Harkness, D. (2016). The Voynich Manuscript. Yale Univ Pr. ISBN-13: 978–0300217230.

Cucchiarelli, P. (2016). Morte di un presidente. Quello che né lo Stato né le BR hanno mai raccontato sulla prigionia e l'assassinio di Aldo Moro. Ponte alle Grazie, Firenze.

da Costa, N. C. A. (1974). On the Theory of Inconsistent Formal Systems. *Notre Dame Journal of Formal Logic, 15*, 497–510.

Dales, R. C. (1995). The Problem of the Rational Soul in the Thirteenth Century, Leiden- New- York Köln, Brill.

Davidson, H. A. (1992). *Alfarabi, Avicenna, and Averroes, on Intellect: Their Cosmologies*. Oxford University Press.

Day, T. (2012). Computability, Godel's incompleteness theorem, and an inherent limit on the predictability of evolution. *Journal of the Royal Society, Interface, 9*(69), 624–639. https://doi.org/10.1098/rsif.2011.0479

Deca, D. (2017) Grid Cells-From Data Acquisition to Hardware Implementation: A Model for Connectome-Oriented Neuroscience. In J. Opris and M. F. Casanova (Eds.), *The Physics of the Mind and Brain Disorders: Integrated Neural Circuits Supporting the Emergence of Mind*, Pages 493–511. ISBN: 978–3–319–29674–6. Springer.

Deniflis, H., Chatelain, A. (1891). Chartolarium Universitatis Parisiensis. Tomus II, Sectio Prior. Parisiis, ex typis fratrum Delalain.

Di Concilio, A., Guadagni, C., Peters, J. F., & Ramanna, S. (2018). Descriptive proximities. Properties and interplay between classical proximities and overlap. *Mathematics in Computer Science, 12*, 91–106. https://doi.org/10.1007/s11786-017-0328-y

Dick, P. K. (1981). Valis. Mariner Books ed.

Doi, H., Sulpizio, S., Esposito, G., Katou, M., Nishina, E., et al. (2019). Inaudible components of the human infant cry influence haemodynamic responses in the breast region of mothers. *The Journal of Physiological Sciences, 69*, 1085–1096.

Don, A. P., Peters, J. F., Ramanna, S., & Tozzi, A. (2020). Topological View of Flows inside the BOLD Spontaneous Activity of the Human Brain. *Frontiers in Computational Neuroscience*. https://doi.org/10.3389/fncom.2020.00034

Doust, J., Walker, M. J., & Rogers, W. A. (2017). Current Dilemmas in Defining the Boundaries of Disease. *Journal of Medicine and Philosophy, 42*(4), 350–366. https://doi.org/10.1093/jmp/jhx009

Drake, R. (1995).The Aldo Moro Murder Case. Harvard University Press, 1995.

Duncan, D. (2011). Faith Science: Where Faith and the Scientific Method Collide. Tate Pub & Enterprises Llc. ISBN-13: 978–1617390067.

Ekman, P. (1979). About brows: Emotional and conversational signals. In M. von Cranach, K. Foppa, W. Lepenies, & D. Ploog (Eds.), *Human ethology: Claims and limits of a new discipline* (pp. 169–222). Cambridge University Press.

Ferreira, L.M., Minami, E., Pereira, M.D., Chohfi, L.M., Andrews, J.de M., 1997. [Anatomical study of the levator labii superioris muscle] [Article in Portuguese] *Revista da Associação Médica Brasileira*, 43, 185-188.

Firpo, L. (1949). Il processo di Giordano Bruno. Estratto congiunto: Quaderni della Rivista storica italiana, n. 1.

Fitch R. 2013. Nicholas of Autrecourt and the mastery of reason. DT 116,3: 168–189.

Fraenkel, A., Bar-Hillel, Y., Lévy, A. (1973). Foundations of Set Theory. North-Holland.N 0016–2736. First published in 1958.

Fridlund, A. (1994). *Human facial expression: An evolutionary view*. Academic Press.

Friston, K. (2010). The free-energy principle: A unified brain theory? *Nature Reviews Neuroscience, 11*(2), 127–138. https://doi.org/10.1038/nrn2787

Gazzaniga, M. S. (2013). Shifting gears: Seeking new approaches for mind/brain mechanisms. *Annual Review of Psychology, 2013*(64), 1–20. https://doi.org/10.1146/annurev-psych-113011-143817

Genser, L., Manceau, G., Karoui, M., Breton, S., Brevart, C., et al. (2013). Postoperative and long-term outcomes after redo surgery for failed colorectal or coloanal anastomosis: retrospective analysis of 50 patients and review of the literature. *Diseases of the Colon and Rectum*. 56(6), 747–55. https://doi.org/10.1097/DCR.0b013e3182853c44.

Giacalone, G. (1982). Alighieri D. La Divina Commedia. Commento e postille critiche di Giuseppe Giacalone; Angelo Signorelli (Ed.), Roma.

Gibbs, S., Collard, M., & Wood, B. (2002). Soft-tissue anatomy of the extant hominoids: A review and phylogenetic analysis. *Journal of Anatomy, 200*, 3–49.

Gilson, E. (1955). *History of Christian Philosophy in the Middle Ages*. Sheed and Ward.

Gödel, K. (1931). Über formal unentscheidbare Sätze der Principia Mathematica und verwandter Systeme, I. *Monatshefte Für Mathematik Und Physik, 38*(1), 173–198. https://doi.org/10.1007/BF01700692

Goodmurphy, C. W., & Ovalle, W. K. (1999). Morphological study of two human facial muscles: Orbicularis oculi and corrugator supercilii. *Clinical Anatomy, 12*, 1–11.

Gotor, M. (2018). Aldo Moro- Lettere dalla Prigionia. ed. "Gli Struzzi", Giulio Einaudi Editore, Torino.

Gracia, J. J. E. (1991). The Centrality of the Individual in the Philosophy of the Fourteenth Century. *History of Philosophy Quarterly., 8*(3), 235–251.

Gregory, W. K. (1929). *Our Face from Fish to Man*. G.P. Putnam's Sons.

Halnes, G., Mäki-Marttunen, T., Keller, D., Pettersen, K. H., Einevoll, G. T. (2015). The effect of ionic diffusion on extracellular potentials in neural tissue. arXiv:1505.06033v2.

Han, J. W., Youn, J. K., Oh, C., Kim, H. Y., Jung, S. E., Park, K. W. (2018). Why Do the Patients with Hirschsprung Disease Get Redo Pull-Through Operation? *European Journal of Pediatric Surgery*. https://doi.org/10.1055/s-0038-1667038.

Hirschsprung, H. (1888). StuhlträgheitNeugeborener in Folge von Dilatation und Hypertrophie des Colons. *JahrbuchfürKinderheilkunde Und physischeErziehung. Berlin., 27*, 1–7.

Huber, E. (1930). Evolution of facial musculature and cutaneous field of trigeminus. Part I. *The Quarterly Review of Biology, 5*, 133–188.

Jaśkowski, S. (1948). Rachunek zdań dla systemów dedukcyjnych sprzecznych. *Studia Societatis Scientiarum Torunensi (Section A), 1*(5), 55–77.

Jaśkowski, S. (1999). Log. Log. Philos. 7, 35–56 (Zbl 1013.03004), p. 49.

Jiang, Q., Arnold, S., Heanue, T., Kilambi, K. P., Doan, B., et al. (2015). Functional loss of semaphorin 3C and/or semaphorin 3D and their epistatic interaction with ret are critical to Hirschsprung disease liability. *American Journal of Human Genetics*. 96(4), 581–96. https://doi.org/10.1016/j.ajhg.2015.02.014.

Katz, J. (1950). The philosophy of Plotinus. Presentative book from the Enneads. Appleton-Century-Crofts, Inc..

Kleene, S. C. (1952) Introduction to metamathematics. D. Van Nostrand Co., Inc., New York, N. Y. Imprint: North Holland, 1980, ISBN: 9780720421033.

Klima, G., Allhoff, F., Vaidya, A. J. (2007). Selection from the Condemnation of 1277. In: Medieval Philosophy. Essential readings with commentary. Blackwell Publishing Ltd.

Kluger, M. J., Conn, C. A., Franklin, B., Freter, R., & Abrams, G. D. (1990). Effect of gastrointestinal flora on body temperature of rats and mice. *American Journal of Physiology, 258*(2 Pt 2), R552–R557. https://doi.org/10.1152/ajpregu.1990.258.2.R552

Kondo, S., Iwashita, M., Yamaguchi, M. (2009). How animals get their skin patterns: fish pigment pattern as a live Turing wave. *The International Journal of Developmental Biology*. 53(5–6), 851–6. https://doi.org/10.1387/ijdb.072502sk.

Kondo, S., Miura, T. (2010). Reaction-diffusion model as a framework for understanding biological pattern formation. *Science*. 329(5999), 1616–20. https://doi.org/10.1126/science.1179047.

Koszkalo, M. (2017). Scholastic sources of Wilhelm Leibnitz's treatise Disputatio metaphysica de principio individui. *Roczniki Filozoficzne, LXV, 2*, 23–55.

Kotelenez, P. M., & Kurtz, T. G. (2010). 2010 Macroscopic limits for stochastic partial differential equations of McKean–Vlasov type. *Probability Theory and Related Fields, 146*, 189–222. https://doi.org/10.1007/s00440-008-0188-0

LaBarre, W. (1947). The cultural basis of emotions and gestures. *Journal of Personality, 16*, 49–68.

Landman, K. A., Pettet, G. J., Newgreen, D. F. (2003). Mathematical models of cell colonization of uniformly growing domains. *Bulletin of Mathematical Biology*. 65(2), 235–62.

Lee, M., Goodall, J., Verastegui, C., Ballotti, R., Goding, C. R. (2000). Direct regulation of the Microphthalmia promoter by Sox10 links Waardenburg-Shah syndrome (WS4)-associated hypopigmentation and deafness to WS2. *The Journal of Biological Chemistry*. 275(48), 37978–83.

Maifreda, G. (2018). Io dirò la verità. Editori Laterza, Bari.
Malato, E. (2018). Dizionario della Divina Commedia. Salerno Editrice, Roma.
Marchetti, V. (1979). Celestino da Verona. Dizionario Biografico degli Italiani, Vol. 23.
Marcoli, M., Agnati, L. F., Benedetti, F., Genedani, S., Guidolin, D., Ferraro, L., Maura, G., Fuxe, K. (2015). On the role of the extracellular space on the holistic behavior of the brain. *Reviews in the Neurosciences*. 26(5), 489–506. https://doi.org/10.1515/revneuro-2015-0007.
Marmura, M. E. (2000). *Al Ghazali*. Brigham Young University Press.
Massaro, D. W. (1998). *Perceiving talking faces*. MIT Press.
McCabe, L., Griffin, L. D., Kinzer, A., Chandler, M., Beckwith, J. B., McCabe, E. R. (1990). Overo lethal white foal syndrome: equine model of aganglionic megacolon (Hirschsprung disease). *American Journal of Human Genetics*. 36(3), 336–40.
Miele, E., Tozzi, A., Staiano, A., Toraldo, C., Esposito, C., Clouse, R. E. (2000). Persistence of abnormal gastrointestinal motility after operation for Hirschsprung's disease. *The American Journal of Gastroenterology*, 95(5), 1226–30. https://doi.org/10.1111/j.1572-0241.2000.02014.x.
Moro, A. C. (1998). Storia di un delitto annunciato. Le ombre del caso Moro. Editori Riuniti.
Mowlavi, A., & Wilhelmi, B. J. (2004). The extended SMAS facelift: Identifying the lateral zygomaticus major muscle border using bony anatomic landmarks. *Annals of Plastic Surgery, 52*, 353–357.
Munkres, J. (1999). Topology. Pearson College Div; 2nd edition. ISBN-10: 0131816292.
Nicholson, C., Kamali-Zare, P., & Tao, L. (2011). Brain extracellular space as a diffusion barrier. *Computing and Visualization in Science, 14*, 309–325.
Nie, C. (2021). Can a Bodily Theorist of Pain Speak Mandarin? *Philosophia*. https://doi.org/10.1007/s11406-021-00353-3
Ockham, W. (1991). Quodlibetal Questions. Volumes 1 and 2, Quodlibets 1–7. Freddoso AJ and Kelley FE (Eds.). Yale Library of Medieval Philosophy, Yale University Press.
Palumbo, F. (1878). Giulio Cesare Vanini e i suoi tempi. Stabilimento Tipografico N. Jovene.
Pan, L., Alagapan, S., Franca, E., DeMarse, T., Brewer, G. J., & Wheeler, B. C. (2014). Large Extracellular Spikes Recordable From Axons in Microtunnels. *IEEE Transactions on Neural Systems and Rehabilitation Engineering, 22*(3), 453.
Pellatt, A. (1979). The facial muscles of three African primates contrasted with those of Papio ursinus. *South African Journal of Science, 75*, 436–440.
Pods, J., Schönke, J., & Bastian, P. (2013). Electrodiffusion Models of Neurons and Extracellular Space Using the Poisson-Nernst-Planck Equations—Numerical Simulation of the Intra- and Extracellular Potential for an Axon Model. *Biophysical Journal, 105*(1), 242–254. https://doi.org/10.1016/j.bpj.2013.05.041
Porretano, G. (2009). Libro dei sei principi. Ed. Paparella F. Bompiani testi a fronte
Priest, G., Routley, R. (1989). Applications of Paraconsistent Logic. in Priest, Routley and Norman. Philosophia Verlag.
Priest, G. (2011). What's so bad about contradictions? In: Priest, Beall and Armour-Garb, The Law of Non-Contradiction. Clarendon Press.
Preuschoft, S. (2000). Primate faces and facial expressions. *Social Research, 67*, 245–271.
Questura di Roma. (1978). Fascicolo dei rilievi tecnici eseguiti in giorno 9 Maggio 1978, in via Michelangelo Caetani, ove è stata rinvenuta l'autovettura Renault con a bordo il cadavere dell'On. Aldo Moro. Gabinetto Regionale di Polizia Scientifica.
Rauschecker, J. P., Leaver, A. M., Mühlau, M. (2010). Tuning out the noise: Limbic-auditory interactions in tinnitus. *Neuron*, 2010 66(6), 819–826. https://doi.org/10.1016/j.neuron.2010.04.032.
Regis, E., Jr. (1976). Aristotle's "Principle of Individuation." *Phronesis, 21*(2), 157–166.
Russo Krauss, C. (2015). L'empiriocriticismo di Richard Avenarius tra psicofisiologia e teoria della consocenza, in R. Avenarius, Il concetto umano di mondo, Morcelliana, Brescia.
Sayre, K. (1976). Cybernetics and the Philosophy of Mind. Routledge Library Editions: philosophy of mind.
Schmidt, K. L., & Cohn, J. F. (2001). Human Facial Expressions as Adaptations: Evolutionary Questions in Facial Expression Research. *Yearbook of Physical Anthropology, 44*, 3–24.
Schneider, D. M., Sundararajan, J., Mooney, R. (2018). A cortical filter that learns to suppress the acoustic consequences of movement. *Nature*, 561, 391–395.
Schultz, A. H. (1969). *The Life of Primates*. Universe Books.
Shailor, B. A. Beinecke, M. S. (nd) 408; Beinecke Rare Book And Manuscript Library, General Collection Of Rare Books And Manuscripts, Medieval And Renaissance Manuscripts. Yale University. https://beinecke.library.yale.edu/collections/highlights/voynich-manuscript.
Shannon, C. E. (1948). A Mathematical Theory of information. *The Bell System Technical Journal, 27*, 379–423.

Shivaraju, M., Chitta, U. K., Grange, R. M. H., Jain, I. H., Capen, D., et al. (2021). Airway stem cells sense hypoxia and differentiate into protective solitary neuroendocrine cells. *Science, 371*(6524), 52–57. https://doi.org/10.1126/science.aba0629

Siavashi, E. (2016). On the Reliability of the Meta-Mathematical Notions Defined by Gödel's Coding Method. *Teorema: Revista Internacional de Filosofía*, 35(1), 5–12.

Skinner, S., Prinke, R. T., Zandbergen, Rene. (2017). The Voynich Manuscript: The World's Most Mysterious and Esoteric. Watkins Pub Ltd. SBN-13: 978–1786780775.

Syková, E., Roitbak, T., Mazel, T., Simonová, Z., & Harvey, A. R. (1999). Astrocytes, oligodendroglia, extracellular space volume and geometry in rat fetal brain grafts. *Neuroscience, 91*(2), 783–798.

Syková, E., & Nicholson, C. (2008). Diffusion in brain extracellular space. *Physiological Reviews, 88*(4), 1277–1340. https://doi.org/10.1152/physrev.00027.2007

Spiegel, J. H., & DeRosa, J. (2005). The anatomical relationship between the orbicularis oculi muscle and the levator labii superioris and zygomaticus muscle complexes. *The Journal of Plastic and Reconstructive Surgical, 116*, 1937–1942.

Stranding, S. (2004). *Gray's Anatomy* (39th ed.). Churchill Livingstone.

Stringer, C., & Andrews, P. (2005). *The complete world of Human evolution*. Thames & Hudson.

Swindler, D. R., & Wood, C. D. (1982). *An Atlas of Primate Gross Anatomy*. Robert E. Krieger Publishing.

Tang, C. (2012). Genome-wide copy number analysis uncovers a new HSCR gene: NRG3. *PLoS Genetics, 8*(5), e1002687. https://doi.org/10.1371/journal.pgen.1002687

Taylor, K. M., Labonne, C. (2005). SoxE factors function equivalently during neural crest and inner ear development and their activity is regulated by SUMOylation. *Developmental Cell*, 9(5), 593–603.

Tozzi, A., Staiano, A., Tramontano, A., Miele, E., Toraldo, C. (1999). Hyperganglionosis and Hirschsprung's disease. *Journal of Pediatric Gastroenterology and Nutrition* 05/1999; 28(5). https://doi.org/10.1097/00005176-199905000-00132.

Tozzi, A. (2015). Information Processing in the CNS: A Supramolecular Chemistry? *Cognitive Neurodynamics, 9*(5), 463–477.

Tozzi, A., Peters, J. F., & Deli, E. (2018). Towards plasma-like collisionless trajectories in the brain. *Neuroscience Letters, 662*, 105–109. https://doi.org/10.1016/j.neulet.2017.10.016

Tozzi, A., & Peters, J. F. (2020). Information-devoid routes for scale-free neurodynamics. *Synthese*. https://doi.org/10.1007/s11229-020-02895-7

Turing, A. M. (1952). The chemical basis of morphogenesis. *Philosophical Transactions of the Royal Society, B: Biological Sciences*, 237(641), 37–73.

Varzi, A. (2000). Supervaluationism and Paraconsistency. In D. Batens, C. Mortensen, G. Priest and J-P. Van Bendegem (Eds.), Frontiers of Paraconsistent Logic, pp. 279–97. Research Studies Press.

Vlasov, A. A. (1938). On Vibration Properties of Electron Gas. *Journal of Experimental and Theoretical Physics, 8*(3), 291.

Wheeler JA. 1990. Information, physics, quantum: The search for links. In Zurek, Wojciech Hubert (Eds.). Complexity, Entropy, and the Physics of Information. Addison-Wesley. ISBN 9780201515091. OCLC 21482771.

Wu, X. X., & Shuai, J. (2015). Effects of extracellular potassium diffusion on electrically coupled neuron networks. *Physical Review e: Statistical, Nonlinear, and Soft Matter Physics, 91*(2), 022712.

Xie, L., Kang, H., Xu, Q., Chen, M. J., Liao, Y., Thiyagarajan, M., O'Donnell, J., Christensen, D. J., Nicholson, C., Iliff, J. J., et al. (2013). Sleep drives metabolite clearance from the adult brain. *Science, 342*, 373–377.

Xu, H., Sun, M., Zhao, X. (2017). Turing mechanism underlying a branching model for lung morphogenesis. *PLoS One*, 12(4), e0174946. https://doi.org/10.1371/journal.pone.0174946.

Zermelo, E. (1930). Über Grenzzahlen und Mengenbereiche. *Fundamenta Mathematicae., 16*, 29–47. https://doi.org/10.4064/fm-16-1-29-47

Publisher's Note Springer Nature remains neutral with regard to jurisdictional claims in published maps and institutional affiliations.

Springer Nature or its licensor holds exclusive rights to this article under a publishing agreement with the author(s) or other rightsholder(s); author self-archiving of the accepted manuscript version of this article is solely governed by the terms of such publishing agreement and applicable law.

Authors and Affiliations

Arturo Tozzi[1,2]

[1] Center for Nonlinear Science, Department of Physics, University of North Texas, Denton, TX, USA

[2] ASL Napoli 2 Nord, Distretto 45, Caivano, Naples, Italy

biomedicines

MDPI

Review

Unusual Mathematical Approaches Untangle Nervous Dynamics

Arturo Tozzi [1,*] and Lucio Mariniello [2]

[1] Center for Nonlinear Science, University of North Texas, Denton, TX 76203-5017, USA
[2] Department of Pediatrics, University Federico II, 80131 Naples, Italy
* Correspondence: tozziarturo@libero.it

Abstract: The massive amount of available neurodata suggests the existence of a mathematical backbone underlying neuronal oscillatory activities. For example, geometric constraints are powerful enough to define cellular distribution and drive the embryonal development of the central nervous system. We aim to elucidate whether underrated notions from geometry, topology, group theory and category theory can assess neuronal issues and provide experimentally testable hypotheses. The Monge's theorem might contribute to our visual ability of depth perception and that the brain connectome can be tackled in terms of tunnelling nanotubes. The multisynaptic ascending fibers connecting the peripheral receptors to the neocortical areas can be assessed in terms of knot theory/braid groups. Presheaves from category theory permit the tackling of nervous phase spaces in terms of the theory of infinity categories, highlighting an approach based on equivalence rather than equality. Further, the physical concepts of soft-matter polymers and nematic colloids might shed new light on neurulation in mammalian embryos. Hidden, unexpected multidisciplinary relationships can be found when mathematics copes with neural phenomena, leading to novel answers for everlasting neuroscientific questions. For instance, our framework leads to the conjecture that the development of the nervous system might be correlated with the occurrence of local thermal changes in embryo–fetal tissues.

Keywords: monocular cue; microcolumn; infinity topoi; globular set; embryonal neurulation; neurodata; geometry; topology; group theory; category theory

Citation: Tozzi, A., Mariniello, L. Unusual Mathematical Approaches Untangle Nervous Dynamics. *Biomedicines* **2022**, *10*, 2581. https://doi.org/10.3390/biomedicines10102581

Academic Editor: Masaru Tanaka

Received: 12 August 2022
Accepted: 10 October 2022
Published: 14 October 2022

Publisher's Note: MDPI stays neutral with regard to jurisdictional claims in published maps and institutional affiliations.

Copyright: © 2022 by the authors. Licensee MDPI, Basel, Switzerland. This article is an open access article distributed under the terms and conditions of the Creative Commons Attribution (CC BY) license (https://creativecommons.org/licenses/by/4.0/).

1. Introduction

Mathematics displays the curious operational feature to be able to describe and predict biophysical issues, despite our scarce knowledge of the relationships between abstract models and descriptive experimental results [1–3]. Mathematics works in the real world, even if we do not know why [4–6]. It has also been used as a unifying language/framework for the description of neuroscientific issues. Different mathematical fields have been used to cope with neural matters and to tackle the cognitive functions of the brain. In particular, computational neuroscience has provided an effort to go through the intricate matters of the neural activity at different coarse-grained levels [7–10]. Our approach in this paper will be slightly different. Our objective is not to discuss mathematics applied to neurodata. We will not consider the areas of calculus and analysis, i.e., the mathematical branches encompassing multivariable calculus, functional analysis and numerical analysis that allow the computation of the ordinary/partial differential equations arising in many neuroscientific applications. We will not focus on the mathematics subtending the implementation of various neurotechniques such as EEG, fMRI, network reconstruction, etc. [11–18]. Rather, our main objective is to highlight unnoticed relationships linking mathematical abstract concepts to the neuronal activity which subtends the very function of the central nervous system.

We will proceed as follows. Every chapter will be devoted to a different area of neuroscience. Macro-, meso- and microneuroanatomy, nervous development and visual

perception will be tackled in purely mathematical terms. In particular, approaches from manifold mathematical branches, such as geometry, topology, group theory and category theory will be used to tackle these issues. We will describe the neurobiological counterparts of braid groups, elliptic curves, micronetworks, liquid crystals, Monge's theorem, cohomology groups and shaves. We will provide a survey of mathematical methodologies and their neuroscientific counterparts that might contribute to improve our knowledge of the central nervous system. Furthermore, we will suggest next-to-come, feasible mathematical developments which may prove potentially helpful in the experimental assessment of brain dynamics.

2. Mathematics and the Anatomy on the Central Nervous System

In this chapter, we will describe how mathematical concepts might be useful to quantitatively assess anatomical structures of the central and peripheral nervous systems. We will provide three examples and different coarse-grained anatomic scales. First, we will show how knots and braid groups provide a scarcely explored approach to elucidate the arrangement of nervous fibers at the mesoscopic scales of the ascending pathways. Second, we will show that the mathematical concept of elliptic curves might be used to evaluate interhemispheric connections at mesoscopic scales. Third, we will show how the successful mathematical approaches based on neural networks might be unexpectedly extended to the microscopic scale of neuronal membranes.

2.1. Macroscopic Scale: Braid Groups, Nerve Fibers and Somatotopic Maps

Here the focus is focused on the anatomical intertwining of fibers in both the central and peripheral nervous systems. The description of intermingling peripheral nerves and mingling grey/white matter can be appraised in terms of knot theory and braid groups [19]. Knots can be turned one into another via three-dimensional space deformations, giving rise to assemblies with associative and commutative properties [20]. A braid is a collection of strands between two parallel planes [21]. Braids are termed isotopic when, keeping their endpoints fixed, they can be twisted into each other without cutting the strands. The operations of composition allow braids to be joined to achieve new ones. Given a set of braids with a fixed number of strands, its group structure is provided by generators and fusion rules such as, e.g., associativity, crossing, braiding/unbraiding, intertwining, the composition and sequence of elementary braids, and so on. In algebraic topology, a well-established link does exist between braids and knots. Is it always possible to transform a knot into a closed braid? For example, the Alexander theorem states that every knot or link in three-dimensional Euclidean space is the closure of a braid [22]. Nevertheless, the correspondence between knots and braids is not one-to-one because a single knot may have many braid representations. The Markov theorem provides the moves to relate closed braids representing the same knot type [23].

Biology suggests several examples of living structures that stand for feasible counterparts of mathematical knots and braids. For example, tissue morphogenesis is produced by coordinated regional changes in cell shape driven by localized contractions of actomyosin "braids" [24]. The existence of a wire-like flow of electrons and ions along cytoskeletal elements conveying messages from the cell membrane to the nucleus has been demonstrated [25]. The three-dimensional space of neural connections is severely constrained by physical factors, such as the anatomical overlap of neuronal arbors and the available axonal space to make synapses. Indeed, specific neuron-type patterns of distance-dependent connectivity are correlated with peculiar overlaps between the dendritic and axonal ramifications, so that the diverse branching patterns of individual arbors of the same neuronal type is able to influence higher-order connections [26,27].

Incorporating the mathematical/topological perspective of knot theory in neuroscience appears particularly relevant for understanding peculiar brain functions such as, e.g., how the brain represents and processes environmental stimuli. The arrangement of nervous fibers might stand for an example of isotopic braids describing the evolution of multi-

particle systems with two spatiotemporal extremities: a beginning and an end. Just as the knots are embeddings of closed lines in the three-dimensional space and cannot be reduced to simple circles by a continuous deformation [28], the nerves are structures that do not completely disentangle after being pulled from both ends. The nervous fibers connecting distinct structures of the peripheral and the central nervous systems are shaped as braids. For example, consider the sensory inputs from the external world detected by the peripheral nervous fibers: these inputs follow a multisynaptic, ascending path towards the more proximal areas of the central nervous system. See Figure 1A,B for further details. This means that, if we term "braid group" as the whole nervous tract between the peripheral receptors and cortical areas, we are allowed to term "knots" as the intermediate multisynaptic steps. Figure 1C tells us that the anatomical nervous structures studied by tractography can also be described in terms of braids.

The overwhelming complexity of the mammalian nervous system makes It extremely difficult to map nervous anatomical structures to mathematical manifolds equipped with knots and braids. Given the objective obstacle to find the proper group generators, why should we care to describe the nervous paths in the tricky terms of braid groups? What are the (methodological, philosophical, explanatory, medical) benefits? Our suggestion is twofold:

(a) Simple changes in the location and arrangement of nerves could explain the activity of the central nervous system.
(b) The external inputs follow specific nervous paths which are assessable in the mathematical terms of braid groups.

The theoretical occurrence of a link between the anatomical conformation of the nerves expressed in terms of knots/braids and brain activity would mean that different braiding rules might give rise to different nervous functions. Fully different perceptions such as olfactive, auditory, tactile and visive perceptions could be explained by diverse configurations of the braids connecting every external receptor to the corresponding sensitive cortex. In touch with the suggestion that sensitive pathway conformations might affect cue perception, Guillamón-Vivancos et al. [29] suggest that, despite the tactile information simultaneously activating the tactile and visual neural pathways during the embryonic stage, the pathways reorganize after birth to permit the separate processing of visual and tactile information.

It is well-established that neural pathways are topographically organized in maps that are highly preserved from the periphery to the cortex [30]. This could be explained by the occurrence of isotopic braids in nervous fibers: as the strands between the starting and the ending points (i.e., the nervous fibers between the peripheral receptor and the corresponding cortical projection) display the same intermingled conformation, they might carry the same message. This hypothesis does not require that the external message stands strictly in a 1:1 relationship with the corresponding cortical area. Due to the braid rules, the relationship between the two extremities of the braids could be either injective or surjective, bijective and so on. Therefore, in a mathematical braid framework, the arrangement of the cortical somatotopic maps could be correlated with the arrangement of the peripheral nervous fibers. The connections between the two extremities might give rise to reversible or irreversible topological knots, respectively, standing for labile functional activities and stable anatomical tracts. This means that at least a part of human brain diseases might depend on the anatomical configuration of peripheral nerve fibers. Instead of looking for alterations in the central nervous systems, it would be reasonable to look for neuropathological features in the braids and knots of the peripheral nervous fibers.

In sum, braid groups could be the key to explaining the perceptual variations between different sensitive cues such as sight and hearing. Indeed, different braids conformations might generate distinct computational processes in the corresponding primary sensory cortex.

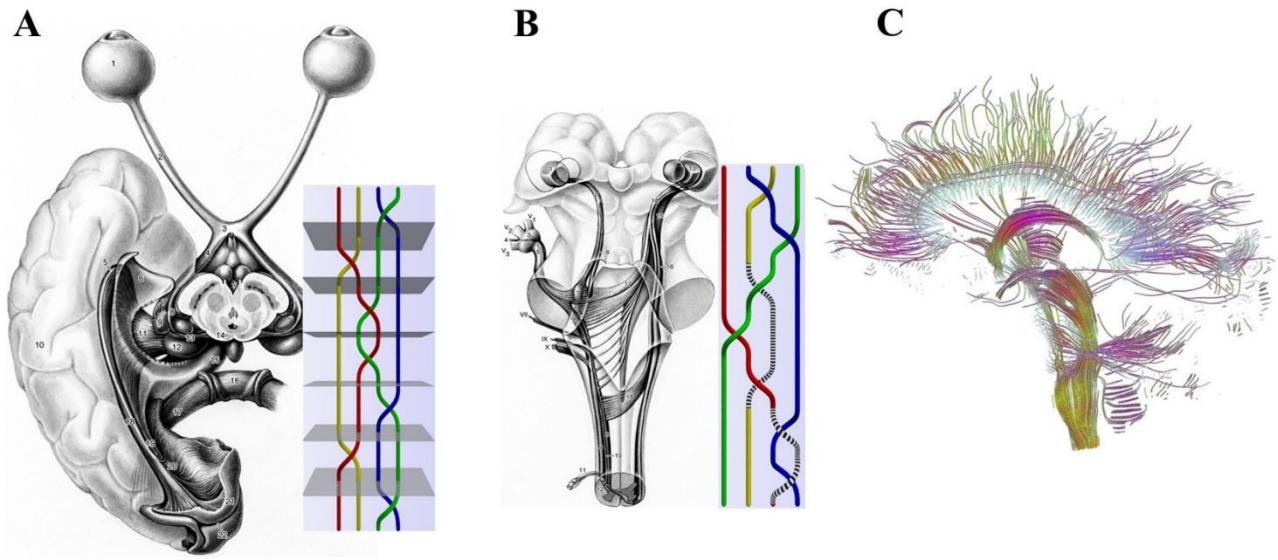

Figure 1. (**A**,**B**). Comparison of nervous connections in the central/peripheral nervous systems and mathematical examples of braid groups. The figures illustrate the retino–geniculo–cortical projection in a ventral view (**A**), the central connections of the trigeminal nerve in a sagittal view (**B**) and their hypothetical braid counterparts. Modified from: [31] For further details, see [32]. (**C**). The anatomical nervous structures detectable by tractography can be described in terms of braids. Modified from: [33]—"Brain dataset courtesy of Gordon Kindlmann at the Scientific Computing and Imaging Institute, University of Utah, and Andrew Alexander, W. M. Keck Laboratory for Functional Brain Imaging and Behavior, University of Wisconsin-Madison".

2.2. Mesoscopic Scale: Are There Elliptic Curves in the Brain?

Elliptic curves, generated through cubic equations, are characterized by two-dimensional paths devoid of either cusps or intersections. Elliptic curves are enclosed in two-dimensional finite algebraic fields. They can be defined in terms of points, integer numbers and rational numbers [34,35]. Many neurotechniques, e.g., EEG, fMRI, diffusion tensor imaging and diffusion tensor tractography, describe nervous structures (such as tracts, commissures, fasciculi, radiations) arranged as arcs that roughly resemble elliptic curves [36]. Starting from this remark, a mathematical account can be drawn which hypothesizes the occurrence of abstract structures underlying the anatomy and function of mesoscopic nervous pathways. The question is: what for? What do elliptic curves bring to the table when investigating nervous paths? Elliptic curves might stand for the abstract counterpart of the anatomical neural projections endowed in the finite field of the central nervous system. A brain including elliptic curves could be operationally partitioned in numbered areas containing either integer or rational numbers. This approach would allow us to treat these brain areas via the powerful weapons of algebraic geometry, complex analysis, number theory and representation theory. Being elliptic curve abelian [37], they must be equipped with intrinsic symmetries that are hidden at first sight. The occurrence of hidden symmetries would allow long-range, simultaneous activation of neurons located in distant brain areas. It is of note that half of the elliptic curves display a finite number of rational numbers, while the other half display an infinite number of rational numbers [38]. In operational terms, this means that half of the nervous patterns are continuous and half are discontinuous, i.e., arranged in discrete spatiotemporal steps. Last but not least, the solutions of the elliptic cubic curve are confined to a spatial region that is topologically equivalent to a torus. Therefore, as suggested by Tozzi et al. [39], the anatomical and functional nervous trajectories could be assessed in terms of trajectories occurring inside a torus.

2.3. Microscopic Scale: Towards a Transient Microconnectome Made of Tunneling Nanotubes?

Standard neuroscience textbooks tell us that neurons communicate via axons, dendrites and synapses, generating a sort of holistic structure that can be assessed via the mathematical weapons of network theory and dynamical systems theory. In dynamical systems, simple elements spontaneously aggregate into larger and more ordered structures, giving rise to different self-sustaining waves such as traveling waves, rotating waves and standing and reflected waves/spirals [40]. In nonequilibrium systems characterized by the self-organization of collective particles, input-driven local fluctuations lead to the emergence of larger-scale ordering [41,42]. This is the case not just of artificial devices such as shape-changing robotic active matter but also of biological assemblies [43]. For example, cellular self-organization promotes the follicle pattern in avian skin [44]. Self-organization generates processes such as crystallization which contributes to unusual self-assemblies of small and rigid organic molecules (such as proteins, viruses, nucleic acids, nervous structures), to colloids gathering in liquid crystals, to gold nanocrystal superlattices, etc. [45]. It has been suggested that the brain is a dynamical system at the edge of chaos characterized by random fluctuations [46–50]. Here the human connectome comes into play, i.e., the hierarchical anatomical and functional network of the cortical/subcortical structures that can be mathematically described by net theory. The connectome is characterized by random walks, preferential pathways for fast communication and winner-takes-all mechanisms [51–54].

Recently discovered microscopic entities could deeply modify the current paradigm of the neural connectome. Tunneling nanotubes (TNTs) are F-actin-based, transient tubular connections [55] that allow the active transfer of vesicles, organelles and small molecules between adjacent cells [56,57]. The occurrence of TNTs in primary neurons and astrocytes has been theoretically correlated with the short-range transmission of electrical signals [58–60]. Developing neurons form transient TNTs that both enhance electrical coupling with distant astrocytes and allow the transfer of polyglutamine aggregates between neuronal cells [61]. TNTs are not stable structures as their lengths vary with the distance between the connected cells [60], and their lifetime may range from a few minutes up to several hours [62,63]. The occurrence of TNTs with their peculiar transient features changes our notion of the human connectome made of stable nodes/edges and long-standing connections between brain areas [64]. Indeed, TNTs might provide a microscopic intercellular neural network with peculiar features, namely, the nodes are not stable and the edges appear, modify and vanish with passing time. As the extremities of TNTs link two cellular structures, the dogma of the cell as an individual unit might be questioned [57]. A microscopic narrative of connectome also provides an alternative explanation to the observation that some network branches are visited more than others, generating nervous dynamics which are slightly nonergodic.

3. Mathematics and the Embryonic Development of the Nervous System

Soft-matter polymers and embryonal neurulation. The development of multicellular living beings involves morphogenetic processes that shape embryo–fetal structures through the self-organized activity of pluripotent stem cells [65]. The orchestrated movement of cellular groups requires genetic as well as mechanical and molecular interactions between cells and their surrounding environment [65,66]. Migrating cells respond to various stimuli such as cortical tension, luminal pressure and size [67], local changes in tissue architecture [68] as well as topographical, adhesive and chemoattractant cues [69–72] and duplication of existing regions [73]. Changes in substrate stiffness trigger collective cell migration, suggesting that tissue mechanics combines with molecular effectors to coordinate morphogenesis [66]. We, focusing on the morphogenetic dynamical processes characterized by cooperative interaction and the collective migration of numerous cellular units [41], describe here an unnoticed biophysical process that might underlie the very structure of the systems of vertebrates. The embryo–fetal development of the central and

peripheral nervous systems is of foremost importance as the growth of the neuronal tissue is correlated with the growth of a wide range of non-nervous structures [74].

Brain-derived signals are involved in embryogenetic regulation, providing long-range interactions among separate structures. During embryogenesis, unexpected interactions have been described between the nervous system and numerous craniofacial and trunk skeletal elements [75,76]. For instance, multipotent Schwann cell precursors detach from their nerve fiber commitment to become mesenchymal, chondroprogenitor and osteoprogenitor cells [77]. In addition, a link has been found between two apparently unrelated processes, gastrulation and neural crest migration, via changes in tissue mechanics [66]. In the sequel, we aim to portray embryonal neurulation in terms of condensed colloidal self-matter and its liquid/crystalline phase.

Cellular structures could be viewed as building blocks characterized by liquid/crystalline phases of condensed soft matter, in which order and fluidity coexist [78]. Liquid–liquid phase separation allows intracellular organization within distinct compartments of bacteria and eukaryotes [79,80]. The phase transitions drive proteins to aggregate into cytoplasmatic and nuclear-condensed fluid bodies, generating nonuniform localization patterns and subcellular compartmentalization. Biomolecular condensates include membrane protein clusters, cytoplasmic P granules [81], histone locus body, heterochromatin domains [82], protoplasmic gelation [83], amyloid-like assemblies [84] and intrinsically disordered mixed-charge domains. Liquid-phase condensates can be viewed as reaction centers where some components become enriched for processing or storage within cells. For example, Garcia Quiroz et al. [85] found that the keratinocytes of the stratified squamous epithelium undergo a vinegar-in-oil type of liquid–liquid phase separation, crowding the cytoplasm with increasingly viscous protein droplets able to drive squamous formation.

Compounds made of "liquid crystals" display properties between conventional liquids and solid crystals that can be experimentally studied in vitro [86–90]. Mundoor et al. [91] produced building blocks of a molecular–colloidal liquid crystal made of micrometer-long inorganic silica-coated disks, dispersed in a crystalline fluid composed of molecular rods. Field-induced motion caused by the magnetic fields elicited colloidal interactions between the disks in the nematic hosts and generated various symmetric conformations with different tangential surface orientations (Figure 2A). Within a range of temperature and concentration, the freely diffusing rods arranged themselves orthogonally to the solvent molecules, producing a biaxial liquid crystal. Mundoor et al. [92] demonstrated that the dispersion of the isotropic-charged colloidal disks in the nematic host composed of molecular rods produces isotropic, nematic and smectic columnar organizations (Figure 2A). While regular polymeric materials respond in a linear fashion to external stimuli such as high temperature, liquid crystal polymers display nonlinear and much faster macroscopic changes [93]. It is feasible to realize low symmetry condensed matter phases in systems with building blocks of dissimilar shapes and sizes. During the embryo–fetal differentiation of the central nervous system, the bodily architecture recalls isotropic, nematic and smectic columnar arrangements [94]. See Figure 2B for further details. It is noteworthy that biaxial nematics can be produced either through long inorganic nanorods and short organic molecules, or board-like molecules or component mixtures, paving the way to future approaches focused on organic structures. The experimental clues point towards a relationship between the biological elements (in our case, the nervous elements) and the phase changes, e.g., the assembly of the developing synaptic active zone requires the liquid phase of the scaffold molecules [95].

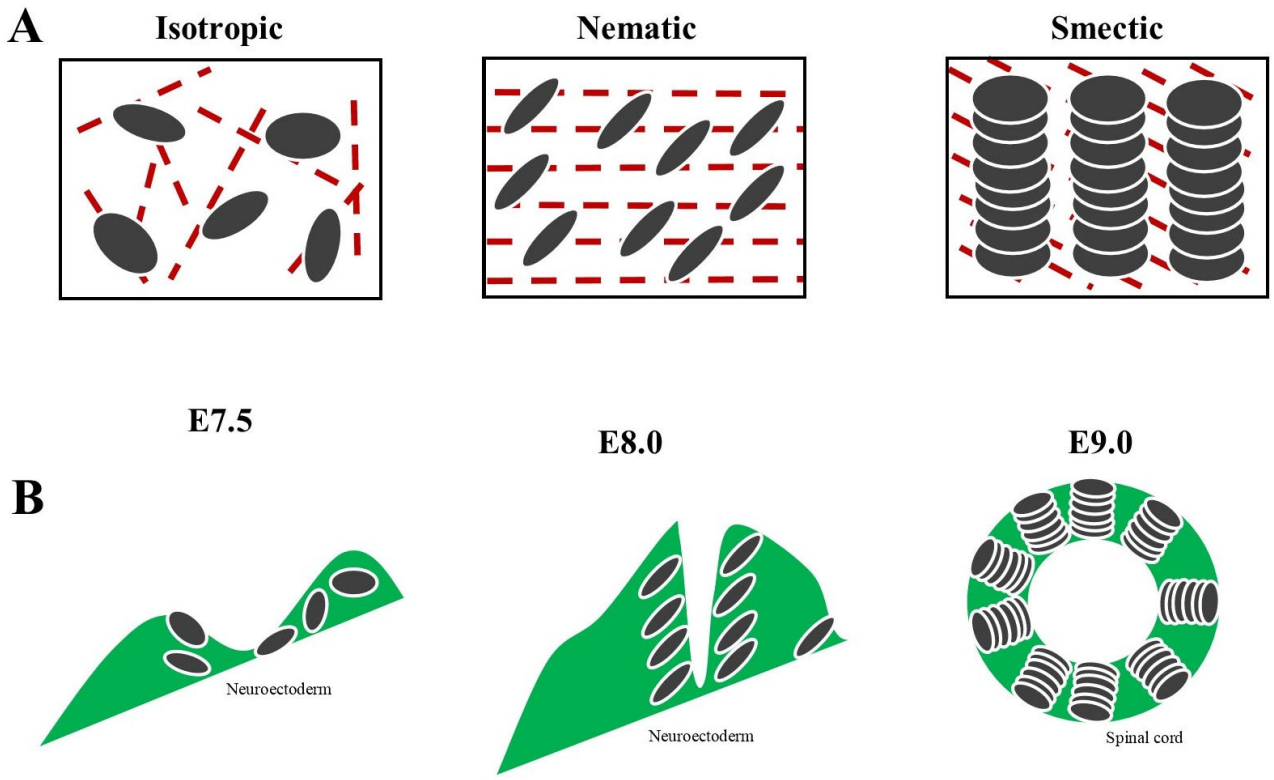

Figure 2. Comparison of two seemingly uncorrelated phenomena, i.e., liquid crystal phases and embryonic development of the nervous system. (**A**) Mixtures of molecular/colloidal rods and disks of fluid-condensed matter give rise to temperature-dependent columnar chains displaying different uniaxial symmetries. Depending on the structural arrangement, we achieve isotropic, nematic and smectic liquid crystals. For further details, see [91]. (**B**) Schematic transverse sections of neurulation in the mouse embryo at different stages of development. While the primitive confined neuroectoderm at E.75 recalls isotropic liquid crystals (**left picture**), the converging neural folds at E8.0 remind the arrangement of nematic liquid crystals (**middle picture**). In turn, the spinal cord at E.9.0 evokes the typical arrangement of smectic liquid crystals (**right picture**). For further details, see [94].

Summarizing, we suggest investigating the relationship between the processes of liquid crystals arrangements and the formation of embryonic nervous structures. To further scrutinize this hypothetical correlation, we provide a testable hypothesis. The collective phenomena of colloidal interactions between disks in the nematic hosts described by Mundoor et al. [91,92] are thermotropic, i.e., they are temperature-driven and temperature-dependent. Increases in temperature in the nematic colloidal fluids lead to unusual transitions towards more ordered states. When the temperature is lowered, symmetry-breaking phase transitions lead at first to the transition from isotropic liquid to nematic phases and then to a liquid–crystal smectic phase [78]. In touch with classical polymer physics, Kießling et al. [96] observed a systematic deformation of the viscous cellular matter upon temperature changes. This framework enables us to draw an intriguing suggestion that correlates the differences in cellular temperature with the developmental outcomes of the nervous system. Within biological cells, transient temperature spikes and short-distance heat fluxes have been detected [97]. Such nonstationary local fluctuations in cellular temperature are also worth exploring in the nervous system. Indeed, differences exist between the temperatures of the cell body and neurites [98]. Further, the neocortex displays thermal gradients at various spatiotemporal coarse graining [49]. The membrane temperature can modify the neuronal activity via adjustments in the opening and closing rates of ion channels [99]. Local changes in temperature can modulate

presynaptic and postsynaptic events, sensitive stimuli and memory encoding [100,101]. As fluctuations in thermic flows are correlated with variations in thermodynamic/information entropies, a correlation might also be hypothesized between temperature changes and the message content [102,103].

Summarizing, the development of the central and peripheral nervous systems could be correlated with the local thermal changes occurring in embryo–fetal tissues. The fact that the embryonal neurulation occurs at different temperatures in different animals does not invalidate our theoretical account as every species-specific embryogenic temperature might lead to anatomical modifications in the adult nervous system.

4. Mathematics and Visual Perception

In this chapter, we will describe how mathematical approaches might be helpful to assess the features of visual perception. The research area of visual perception is huge, including, e.g., the modelling and control of visual perception, visual perception learning, static and motion-based visual illusions and visual–perception models related to the mathematical aspects of dynamic visual cryptography [104–110]. Here we will show how the Monge's theorem might provide a novel operational approach to the dazzling phenomenon of depth perception (DP). DP, crucial for everyday action, is the visual ability of humans and other sighted animals to perceive both the distance of an object and its three-dimensional solid structure [111]. Many anatomical structures and sources of information contribute to produce DP in different animals. Among the most important mechanisms subtending DP, binocular and monocular perception are worth a mention [112].

Binocular depth perception relies on two main mechanisms, i.e., stereopsis and retinal binocular disparity [113,114]. Stereopsis depends on the fact that many animals adjust their two eyes to place the image of an object on the fovea, where acuity is the highest. In turn, retinal binocular disparity suggests that, as our eyes are separated, the images of the object fall at different locations on the left and right retinas [115]. The visual system melts these two images to quantify the depth of the location of the object. In turn, monocular depth perception provides depth information when viewing a scene with one eye [116]. Many sources of information from the image and its surrounding environment produce monocular DP, including, e.g., relative size (distant objects subtend smaller visual angles than near objects), texture gradient, occlusion, contrast differences (e.g., texture gradient, illumination and shading), motion parallax, etc. [117]. To make an example, the first studies on DP involved aircraft pilots during take-off and landing, showing that texture analysis and motion detection are the most relevant features for the perception of solid structures [118]. For depth perception at close range, stereopsis is the most precise mechanism but is available only to a few vertebrates. In turn, motion parallax is used by many species, including vertebrates as well as invertebrates. Compared to other animals, humans display the best performance regarding depth resolution [119].

In the last decades, it has been demonstrated that shape detection also depends on higher cognitive activities such as previous experience/memory, context-dependent size interpretation and whether the observer is "expecting" to see the shape. Accumulating evidence suggests that the main three computational goals (determining surface depth order, gauging depth intervals and representing three-dimensional surface geometry and object shape) are provided by different hierarchical stages of cortical processing [120]. The integration of right and left eye information generates cortical three-dimensional representations of the visual environment [121]. For instance, in mammals such as mice that use stereoscopic cues to guide their behavior, neurons in the primary visual cortex V1 are sensitive to binocular disparity. In sum, the complex response of DP is built up from multiple environmental inputs and different intermingling distal and proximal nervous processes.

Here we suggest another novel monocular mechanism that might contribute to DP. Our approach is based on a theorem from geometry, the Monge's theorem (MT). MT states the following: given three nonoverlapping circles of distinct radii in a two-dimensional

Euclidean plane, the intersection points of each of the three pairs of external tangent lines lie on a single line [122]. See Figure 3A for a pictorial rendering.

MT implies that the projections arising from three separated objects (i.e., two- or three-dimensional circles) give rise to a line that is external to the three objects. MT has been operationally used to calculate the correct camera position for the wearing examination of the cutting edge of the hob, by calculating the inner points of the Monge cuboid and their parallel shifting (defined by the bijective Monge projections) bordered by a surface [123]. Further, MT is still valid even if the plane is equipped with non-Euclidean metrics [124].

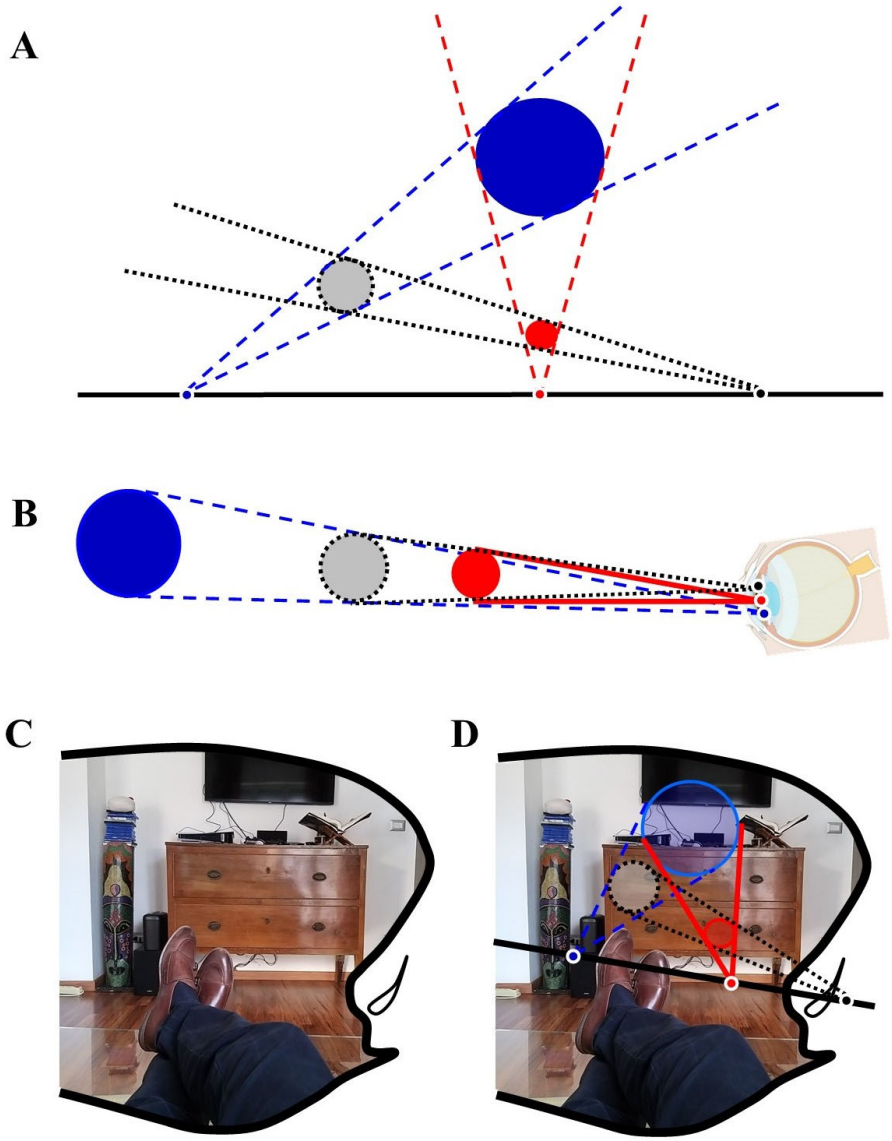

Figure 3. Monge's theorem (MT) for the evaluation of depth perception. (**A**) Pictorial rendering of MT. (**B**) MT can be used to investigate the physiological mechanism of depth perception. The line on the eye lens corresponds to the line joining the projections from three objects embedded in the environment. (**C**) A subject lying upon his sofa with his right eye closed. "In a frame formed by the ridge of my eyebrow, by my nose and my moustache, appears a part of my body, so far as visible, with its environment" [125]. (**D**) An example of the monocular depth perception of MT drawn from Figure 3C. Three objects with different distances from the eye are projected to a black line on the eye lens, according to the MT rules.

We suggest locating the line external to the three objects in the eye lens (Figure 3B). This line is produced by three sensed objects located in the environment. Due to the MT, the projections of the three objects on the eye lens are slightly far apart from one another. The line is subsequently projected from the eye lens to the retina, giving rise to retinal objects that are slightly far apart from each other. This simple, monocular mechanism might stand for a mathematical device that promotes our three-dimensional perception of the world (Figure 3C,D).

5. Discussion

Our theoretical account emphasizes how mathematical rules might shape the structure and activity of biological entities. The theoretical implications of our account suggest that simple changes in the arrangement of the anatomical and functional nervous structures might elucidate (at least partially) the activity of the central nervous system. In touch with D'Arcy Thompson [65], it could be stated that the arrangement and the pattern contribute to the biological function. Geometric constraints are powerful factors which are able to define shape, size and cell distributions, drive crucial biological phenomena and give rise to deterministic patterns that are predictable and reproducible. For example, methods to develop the spatial and temporal control of stem cell-derived epithelial organoids have been described, thereby rendering a stochastic process more deterministic [126]. A mathematical-framed approach to scientific matters provides a metatheoretic starting point that might be termed "testable rationalism": sharp experimental previsions arising from top–down, deductive mathematical approaches. Mathematical weapons such as group structure and generator operations point towards a new approach to long-standing questions concerning human sensation and perception. This leads to the hint that the very intermingling of nervous structures might contribute to brain functions. As the dynamical processes of living systems display cooperative interaction of many units, we are allowed to portray the development of the central/peripheral nervous systems in terms of assemblies of building blocks dictated by mathematical constraints.

We want to give a further theoretical suggestion, this time drawn from category theory and group theory [127–130]. Once a wheat sheaf is sealed and tied up, the packed-down straws display the same orientation. This trivial observation brings us into the realm of presheaves/globular sets that allows a simple assessment of diverging and superimposing functions. A mathematically well-founded assessment of elusive nervous activities in terms of presheaves as well as the hierarchical information transmission inside globular sets provide fresh insights on different neural issues. Presheaves also permit the tackling of the nervous phase spaces in terms of the theory of infinity categories, i.e., an approach founded on equivalence, rather than equality [131]. The key to unlocking the activity of the brain does not lie in single neurons, or single neuronal assemblies or single neural modules, rather in its abstract functional phase spaces where equivalence and not identity holds. Here we will explain this time in technical terms, a novel theoretical approach to nervous paths based on infinity topoi. This permits us to introduce Lurie's theory of infinity topoi [132] to describe and quantify the paths taking place inside the brain phase spaces. As sheaf-theoretic methods are powerful and flexible enough to allow generalizations of neural paths, Lurie's theory enjoys formal properties that suggest novel functional phase spaces where brain activities might take place.

Every category of sheaves of abelian groups contains derived functors called cohomology groups [133] that can be defined as follows:

$$H^n (X,G)$$

where X is a topological space, and G an abelian group [131].

This means that the cohomology group H^n (X,G) can be defined in terms of sheaf cohomology:

$$H^n_{sheaf} (X,\underline{G})$$

where $\underline{G}$ stands for the constant sheaf on X. Remember that a sheaf is a presheaf that satisfies the gluing axiom.

Lurie [131] generalized this approach to non-abelian cohomology H^1 (X,G), also taking into account the fact that the coefficient system G is not constant and may display different values. This is the case for the brain phase spaces. Specifying G is equivalent to specifying the Eilenberg–MacLane space K(G,1), together with a base point. This observation suggests that the proper coefficients G for non-abelian cohomology H^1 (X,G) are not groups but rather homotopy types, i.e., purely combinatorial entities such as simplicial sets. Sheaves of homotopy types on X can be used as coefficients, achieving a theory of infinite stacks (in groupoids) on X. Stacks, that are required to satisfy a descent condition only for covering, satisfy the Whitehead theorem: a pointed stack (E,η) can be achieved, for which π_i(E, η) is a trivial sheaf for all i > 0, such that E is not contractible. If K is a simplicial set, then the cohomology of X with coefficients K can be defined as:

$$H_{jj}(X,K) = \pi_0 (F(X))$$

where H_{jj} is the Joyal–Jardine homotopy theory of simplicial presheaves on X, and F is a fibrant replacement for the constant simplicial presheaf with value K on X [131].

In brain terms, if X stands for the manifold where nervous oscillations take place, and G stands for an operation performed by the brain (say, the oscillatory activity), the following conclusions can be drawn together with Lurie [131]:

(1) If X is paracompact, H (X, K) is the set of homotopy classes from X into K.
(2) If X is paracompact space of finite covering dimension, then Lurie's theory of stacks is equivalent to the Joyal–Jardine homotopy theory.

The definition of a sheaf depends just on the open sets of a topological space, rather than the individual points; this means that open sets could be replaced by other objects. The stalk F_x of a sheaf F captures the properties of a sheaf "around" a point x ∈ X, generalizing the germs of functions.

In neuroscientific words, we can state the following: even if one looks at smaller and smaller neighborhoods when single neuronal assemblies or tiny brain areas are investigated, no single neighborhood is small enough such that some limit can be taken into account [134]. In terms of nervous issues, this means that a nervous object of investigation, e.g., either the single neurons, or the single brain modules or an assembly of neural waves with the same frequency, stand in relation to each other in many ways. Single neural structures do not count anymore, rather the whole brain activity counts. Summarizing, an infinity topoi approach to neural dynamics suggests that nervous activities can be described in terms of sheaves and presheaves leading us into the realm of the ∞-topos, i.e., a ∞-category of ∞-stakes on a topological space that is correlated to ordinary topos. We are faced with two entirely different approaches to brain dynamics:

(1) The customary concept of equality suggests the occurrence of a strict relationship between two entities (say, two neurons or two neural waves on the brain surface).
(2) Lurie's concept of equivalence of ∞-topos suggests that two entities (say, two neurons or two neural waves on the brain surface) stand in relation to each other in many ways.

In this latter account, the relationships between the entities can be studied in terms of the different forms correlated with homotopy paths, explaining why apparently matching cortical oscillations give rise to highly different interindividual responses.

6. Conclusions

We went through unusual mathematical approaches to assess several aspects of the nervous activity. The translational implications of our account are manifold. For instance, the Monge's theorem suggests a new methodological approach to cope with our visual ability of depth perception. Further studies are required to confirm whether the human brain might use this theorem to achieve visual depth through monocular vision. This

would lead to a better comprehension of the peripheral visual mechanisms and would suggest that the peripheral receptors perform advanced computations previously believed to be of exclusive pertinence to the central nervous structures. Our suggestion that the brain connectome can be tackled in terms of tunnelling nanotubes sheds new light on the studies concerning the human connectome. We propose that the human connectome can be tackled not just at the macrolevel of the connection of brain areas or at the mesolevel of neurons linked by axons/dendrites but also at the microlevel of intermembrane connexions among neuronal calls. This suggests a highly reductionistic approach where factors of the size of angstrom may dictate macroscopic behavior and pathological outcomes. The fact that the multisynaptic ascending fibers connecting the peripheral receptors to the neocortical areas can be assessed in terms of knot theory/braid groups suggests a novel approach to predict fiber regeneration during abnormal human nervous development and after trauma. Further, the physical concepts of soft-matter polymers and nematic colloids applied to neurulation in mammalian embryos lead to the conjecture that the development of the nervous system might be correlated with local thermal changes in embryo–fetal tissues. It suggests that the artificial embryos created for experimental and translational purposes can be manipulated through the relatively simple local modification of temperature.

Showing that natural three-dimensional natural rock fragments reproduce the Plato's cube, Domokos et al. [135] found that distinct fragment patterns tend towards ubiquitous, standard icosahedral and octahedral shapes which can be formulated in terms of Archimedean lattices [136]. The spontaneous occurrence of distinctive self-assembled artificial structures could be compared with the design of natural organic crystalline materials, such as the nervous structures. In particular, both artificial and natural quasicrystal structures can generate fullerenic-like self-assemblies grounded on simple, overarching geometric rules [45,137–145]. The same fullerenic structures have been recently proposed to explain the features of cortical microcolumns that can be flattened to form fullerene-like, two-dimensional lattices [146,147]. As a final remark, we would like to emphasize that our experimental predictions can be demonstrated via current technologies. Concerning, for example, the theoretical correlation between the embryonal mechanisms of nervous growth and liquid crystals, the recent availability of artificial embryonic structures from the aggregates of mammalian stem cells [148–152] provides an exciting possibility to study in vitro the developmental processes.

In sum, we suggest that under-rated geometrical and topological concepts may not just shed new light of the dynamics of the central and peripheral nervous systems but may also provide hints towards feasible translational applications.

Author Contributions: A.T. and L.M. equally contributed to: study concept and design, acquisition of data, analysis and interpretation of data, drafting of the manuscript, critical revision of the manuscript for important intellectual content, statistical analysis, obtained funding, administrative, technical, material support and study supervision. All authors have read and agreed to the published version of the manuscript.

Funding: This research did not receive any specific grant from funding agencies in the public, commercial or not-for-profit sectors.

Institutional Review Board Statement: Not applicable.

Informed Consent Statement: This research does not contain any studies with human participants or animals undertaken by the authors.

Data Availability Statement: All data and materials generated or analyzed during this study are included in the manuscript. The authors had full access to all the data in the study and take responsibility for the integrity of the data and the accuracy of the data analysis.

Conflicts of Interest: The authors do not have any known or potential conflict of interest including any financial, personal or other relationships with other people or organizations within three years

of beginning the submitted work that could inappropriately influence, or be perceived to influence, their work.

References

1. Benacerraf, P. What Numbers Could not Be. *Philos. Rev.* **1965**, *74*, 47–73. https://doi.org/10.2307/2183530.
2. Maddy, P. Believing the Axioms, II. *J. Symb. Log.* **1988**, *53*, 736–764. https://doi.org/10.2307/2274569.
3. Beckers, S.; Eberhardt, F.; Halpern, J.Y. Approximate Causal Abstraction. *arXiv:1906.11583v2* , **2019**, 210.
4. Wigner, E. The Unreasonable Effectiveness of Mathematics in the Natural Sciences. *Communications on Pure and Applied Mathematics* **1960**, *13*, 1–14.
5. Lakoff, G.; Nunez, R. *Where Mathematics Come From: How The Embodied Mind Brings Mathematics Into Being*, Reprint ed.; Basic Books: New York, NY, USA, 2001; ISBN-13: 978-0465037711.
6. Sejnowski, T.J. The unreasonable effectiveness of deep learning in artificial intelligence. *Proc. Natl. Acad. Sci. USA* **2020**, *117*, 30033–30038. https://doi.org/10.1073/pnas.1907373117.
7. Giusti, C.; Ghrist, R.; Bassett, D. Two's company, three (or more) is a simplex: Algebraic-topological tools for understanding higher-order structure in neural data. *J. Comput. Neurosci*. **2016**, *41*, 596. https://doi.org/10.1007/s10827-016-0608-6.
8. Morone, F.; Roth, K.; Min, B.; Stanley, H.E.; Makse, H.A. Model of brain activation predicts the neural collective influence map of the brain. *Proc. Natl. Acad. Sci. USA* **2017**, *114*, 3849–3854. https://doi.org/10.1073/pnas.1620808114.
9. Kang, J.; Pae, C.; Park, H.J. Energy landscape analysis of the subcortical brain network unravels system properties beneath resting state dynamics. *Neuroimage* **2017**, *149*, 153–164. https://doi.org/10.1016/j.neuroimage.2017.01.075.
10. Yamazaki, T.; Igarashi, J.; Yamaura, H. Human-scale Brain Simulation via Supercomputer: A Case Study on the Cerebellum. *Neuroscience* **2021**, *462*, 235–246. https://doi.org/10.1016/j.neuroscience.2021.01.014.
11. Friston, K.J.; Williams, S.; Howard, S.; Frackowiak, R.S.; Turner, R. Movement-related effects in fMRI time-series. *Magn Reson Med*. **1996**, *35*, 346–355. https://doi.org/10.1002/mrm.1910350312.
12. Bhagalia, R.; Kim, B. Spin saturation artifact correction using slice-to-volume registration motion estimates for fMRI time series. *Med. Phys*. **2008**, *35*, 424–434. https://doi.org/10.1118/1.2826555.
13. Whittingstall, K.; Bartels, A.; Singh, V.; Kwon, S.; Logothetis, N.K.. Integration of EEG source imaging and fMRI during continuous viewing of natural movies. *Magn. Reson. Imaging* **2010**, *28*, 1135–1142. https://doi.org/10.1016/j.mri.2010.03.042.
14. Ostwald, D.; Porcaro, C.; Bagshaw, A.P. Voxel-wise information theoretic EEG-fMRI feature integration. *NeuroImage* **2011**, *55*, 1270–1286. https://doi.org/10.1016/j.neuroimage.2010.12.029.
15. Mirsattari, S.M.; Ives, J.R.; Leung, L.S.; Menon, R.S. EEG monitoring during functional MRI in animal models. *Epilepsia* **2007**, *48* (Suppl. S4), 37–46. https://doi.org/10.1111/j.1528-1167.2007.01240.x.
16. Stoll, S.; Infanti, E.; de Haas, B.; Schwarzkopf, D.S. Pitfalls in post hoc analyses of population receptive field data. *Neuroimage* **2022**, *263*, 119557. https://doi.org/10.1016/j.neuroimage.2022.119557.
17. Perez, D.L.; Nicholson, T.R.; Asadi-Pooya, A.A.; Bègue, I.; Butler, M.; Carson, A.J.; David, A.S.; Deeley, Q.; Diez, I.; Edwards, M.J.; et al. Neuroimaging in Functional Neurological Disorder: State of the Field and Research Agenda. *NeuroImage: Clin.* **2021**, *30*, 102623. https://doi.org/10.1016/j.nicl.2021.102623.
18. Raimondo, L.; Oliveira, .A.; Heij, J.; Priovoulos, N.; Kundu, P.; Leoni, R.F.; van der Zwaag, W. Advances in resting state fMRI acquisitions for functional connectomics. *NeuroImage* **2021**, *243*, 118503. https://doi.org/10.1016/j.neuroimage.2021.118503.
19. Lukyanova, O.; Nikitin, O. Modeling of extrasynaptic information transfer in neural networks using braid theory. *Procedia Comput. Sci.* **2018**, *145*, 306–311.
20. Cromwell, P.R. *Knots and Links*; Cambridge University Press: Cambridge, UK, 2004.
21. Artin, E. Theory of braids. *Ann. of Math*. **1947**, *48*, 101–126.
22. Alexander, J. A lemma on a system of knotted curves. *Proc. Natl. Acad. Sci. USA* **1923**, *9*, 93–95. https://doi.org/10.1073/pnas.9.3.93.
23. Birman. J.S. Knots, links, and mapping class groups. In *Annals of Math Study*; Princeton University Press: Princeton, NJ, USA, 1974; Volume 82.
24. Bailles, A.; Collinet, C.; Philippe, J.-M.; Lenne, P.-F.; Munro, E.; Lecuit, T. Genetic induction and mechanochemical propagation of a morphogenetic wave. *Nature* **2019**, *572*, 467–473.
25. Frieden, B.R.; Gatenby, R.A. Signal transmission through elements of the cytoskeleton form an optimized information network in eukaryotic cells. *Sci. Rep.* **2019**, *9*, 6110.
26. Reimann, M.W.; Horlemann, A.-L.; Ramaswamy, S.; Muller, E.B.; Markram, H. Morphological Diversity Strongly Constrains Synaptic Connectivity and Plasticity. *Cereb Cortex*. **2017**, *27*, 4570–4585. https://doi.org/10.1093/cercor/bhx150. https://doi.org/10.1093/cercor/bhx150.
27. Lukyanova, O.; Nikitin, O. Neuronal topology as set of braids: Information processing, transformation and dynamics. *Opt. Mem. Neural Netw.* **2017**, *26*, 172–181. https://doi.org/10.3103/S1060992X17030043.
28. Wu, F.Y. Knot theory and statistical mechanics. *Rev. Mod. Phys.* **1992**, *64*, 1099–1131.
29. Guillamón-Vivancos, T.; Aníbal-Martínez, M.; Puche, L.; Moreno-Bravo, J.A.; Valdeolmillos, M.; Martini, F.J.; López-Bendito, G. Input-dependent segregation of visual and somatosensory circuits in the mouse superior colliculus. *Science* **2022**, *377*, 845–850. https://doi.org/10.1126/science.abq2960.

30. Imam, N.; Finlay, B.L. Self-organization of cortical areas in the development and evolution of neocortex. *Proc. Natl. Acad. Sci. USA* **2020**, *117*, 29212–29220. https://doi.org/10.1073/pnas.2011724117.
31. A journey through the mathematical theory of braids, available online at: http://matematita.science.unitn.it/braids/summary.html (accessed on 31 Oct 2021).
32. Nieuwenhuys, R.; Voogd, J.; van Huijzen, C. *The Human Central Nervous System*, 4th ed.; Springer: Berlin/Heidelberg, Germany, 2008.
33. Diffusion tensor MRI datasets, available online at:http://www.sci.utah.edu/~gk/DTI-data/ (accessed on 31 Oct 2021)
34. Gebel, J.; Pethő, A.; Zimmer, H.G. Computing Integral Points on Elliptic Curves. *Acta Arith* **1994**, *68*, 171–192.
35. Heath-Brown, D.R. The average analytic rank of elliptic curves. *Duke Math. J.* **2004**, *122*, 591–623. https://doi.org/10.1215/S0012-7094-04-12235-3.
36. Alizadeh, M.; Kozlowski, L.; Muller, J.; Ashraf, N.; Shahrampour, S.; Mohamed, F.B.; Wu, C.; Sharan, A. Hemispheric Regional Based Analysis of Diffusion Tensor Imaging and Diffusion Tensor Tractography in Patients with Temporal Lobe Epilepsy and Correlation with Patient outcomes. *Sci. Rep.* **2019**, *9*, 215. https://doi.org/10.1038/s41598-018-36818-x.
37. Kühne, L. Equidistribution in Families of Abelian Varieties and Uniformity. *arXiv* **2021**, arXiv:2101.10272.
38. Smith, A. 2∞-Selmer groups, 2∞-class groups, and Goldfeld's conjecture. *arXiv* **2017**, arXiv:1702.02325.
39. Tozzi. A.; Peters, J.F.; Fingelkurts, A.A.; Fingelkurts, A.A.; Marijuán, P.C. Brain projective reality: Novel clothes for the emperor. Reply to comments on "Topodynamics of metastable brains" by Tozzi et al. *Phys. Life Rev.* **2017**, *21*, 46–55. https://doi.org/10.1016/j.plrev.2017.06.020.
40. Bhattacharya, S.; Iglesias. P.A. Controlling excitable wave behaviors through the tuning of three parameters. *Biol. Cybern.* **2019**, *113*, 61–70.
41. Lovecchio, E.; Allegrini, P.; Geneston, E.; West, B.J.; Grigolini, P. From self-organized to extended criticality. *Front. Physiol.* **2012**, *3*, 98. https://doi.org/10.3389/fphys.2012.00098.
42. Chvykov, P.; Berrueta, T.A.; Vardhan, A.; Savoie, W.; Samland, A.; Murphey, T.D.; Wiesenfeld, K.; Goldman, D.I.; England, J.L. Low rattling: A predictive principle for self-organization in active collectives. *Science* **2021**, *371*, 90–95. https://doi.org/10.1126/science.abc6182.
43. Linneweber, G.A.; Andriatsilavo, M.; Dutta, S.B.; Bengochea, M.; Hellbruegge, L.; Liu, G.; Ejsmont, R.K.; Straw, A.D.; Wernet, M.; Hiesinger, P.R.; et al. A neurodevelopmental origin of behavioral individuality in the *Drosophila* visual system. *Science* **2020**, *367*, 1112–1119. https://doi.org/10.1126/science.aaw7182.
44. Shyer, A.E.; Rodrigues, A.R.; Schroeder, G.G.; Kassianidou, E.; Kumar, S.; Harland, R.M. Emergent cellular self-organization and mechanosensation initiate follicle pattern in the avian skin. *Science* **2017**, *357*, 811–815. https://doi.org/10.1126/science.aai7868.
45. Montis, R.; Fusaro, L.; Falqui, A.; Hursthouse, M.B.; Tumanov, N.; Coles, S.J.; Threlfall, T.L.; Horton, P.N.; Sougrat, R.; Lafontaine, A.; et al. Complex structures arising from the self-assembly of a simple organic salt. *Nature* **2021**, *590*, 275–278. https://doi.org/10.1038/s41586-021-03194-y.
46. Bengson, J.J.; Kelley, T.A.; Zhang, X.; Wang, J.-L.; Mangun, G.R. Spontaneous Neural Fluctuations Predict Decisions to Attend. *J. Cogn. Neurosci.* **2014**, *26*, 2578–2584. https://doi.org/10.1162/jocn_a_00650.
47. Ribrault, C.; Sekimoto, K.; Triller, A. From the stochasticity of molecular processes to the variability of synaptic transmission. *Nat. Rev. Neurosci.* **2011**, *12*, 375–387. https://doi.org/10.1038/nrn3025.
48. Zare, M.; Grigolini, P. Criticality and avalanches in neural networks. *Chaos, Solitons Fractals* **2013**, *55*, 80–94. https://doi.org/10.1016/j.chaos.2013.05.009.
49. Wang, B.; Ewang, H.(.; Normoyle, K.P.; Ejackson, K.; Espitler, K.; Sharrock, M.F.; Miller, C.M.; Ebest, C.; Ellano, D.; Du, R. Brain temperature and its fundamental properties: A review for clinical neuroscientists. *Front. Neurosci.* **2014**, *8*, 307. https://doi.org/10.3389/fnins.2014.00307.
50. Papo, D. Functional significance of complex fluctuations in brain activity: From resting state to cognitive neuroscience. *Front. Syst. Neurosci.* **2014**, *8*, 112. https://doi.org/10.3389/fnsys.2014.00112.
51. Sporns, O.; Tononi, G.; Kötter, R. The Human Connectome: A Structural Description of the Human Brain. *PLOS Comput. Biol.* **2005**, *1*, e42. https://doi.org/10.1371/journal.pcbi.0010042.
52. Reese, T.M.; Brzoska, A.; Yott, D.T.; Kelleher, D.J. Analyzing Self-Similar and Fractal Properties of the C. elegans Neural Network. *PLoS ONE* **2012**, *7*, e40483. https://doi.org/10.1371/journal.pone.0040483.
53. Betzel, R.F.; Griffa, A.; Avena-Koenigsberger, A.; Goñi, J.; Thiran, J.-P.; Hagmann, P.; Sporns, O. Multi-scale community organization of the human structural connectome and its relationship with resting-state functional connectivity. *Netw. Sci.* **2013**, *1*, 353–373. https://doi.org/10.1017/nws.2013.19.
54. Pang, J.C.; Gollo, L.L.; Roberts, J.A. Stochastic synchronization of dynamics on the human connectome. *NeuroImage* **2021**, *229*, 117738. https://doi.org/10.1016/j.neuroimage.2021.117738.
55. Goodman, S.; Naphade, S.; Khan, M.; Sharma, J.; Cherqui, S. Macrophage polarization impacts tunneling nanotube formation and intercellular organelle trafficking. *Sci. Rep.* **2019**, *9*, 14529. https://doi.org/10.1038/s41598-019-50971-x.
56. Ariazi, J.; Benowitz, A.; De Biasi, V.; Boer, M.D.; Cherqui, S.; Cui, H.; Douillet, N.; Eugenin, E.A.; Favre, D.; Goodman, S.; et al. Tunneling Nanotubes and Gap Junctions–Their Role in Long-Range Intercellular Communication during Development, Health, and Disease Conditions. *Front. Mol. Neurosci.* **2017**, *10*, 333. https://doi.org/10.3389/fnmol.2017.00333.

57. Sartori-Rupp, A.; Cervantes, D.C.; Pepe, A.; Gousset, K.; Delage, E.; Corroyer-Dulmont, S.; Schmitt, C.; Krijnse-Locker, J.; Zurzolo, C. Correlative cryo-electron microscopy reveals the structure of TNTs in neuronal cells. *Nat. Commun.* **2019**, *10*, 342. https://doi.org/10.1038/s41467-018-08178-7.
58. Abounit, S.; Zurzolo, C. Wiring through tunneling nanotubes—From electrical signals to organelle transfer. *J. Cell Sci.* **2012**, *125*, 1089–1098. https://doi.org/10.1242/jcs.083279.
59. Wang, X.; Gerdes, H.-H. Long-distance electrical coupling via tunneling nanotubes. *Biochim. Et Biophys. Acta (BBA) Biomembr.* **2012**, *1818*, 2082–2086. https://doi.org/10.1016/j.bbamem.2011.09.002.
60. Austefjord, M.W.; Gerdes, H.-H.; Wang, X. Tunneling nanotubes. *Commun. Integr. Biol.* **2014**, *7*, e27934. https://doi.org/10.4161/cib.27934.
61. Costanzo, M.; Abounit, S.; Marzo, L.; Danckaert, A.; Chamoun, Z.; Roux, P.; Zurzolo, C. Transfer of polyglutamine aggregates in neuronal cells occurs in tunneling nanotubes. *J. Cell Sci.* **2013**, *126*, 3678–3685. https://doi.org/10.1242/jcs.126086.
62. Gurke, S.; Barroso, J.F.V.; Gerdes, H.-H. The art of cellular communication: Tunneling nanotubes bridge the divide. *Histochem. Cell Biol.* **2008**, *129*, 539–550. https://doi.org/10.1007/s00418-008-0412-0.
63. Seyed-Razavi, Y.; Hickey, M.J.; Kuffová, L.; McMenamin, P.G.; Chinnery, H.R. Membrane nanotubes in myeloid cells in the adult mouse cornea represent a novel mode of immune cell interaction. *Immunol. Cell Biol.* **2012**, *91*, 89–95. https://doi.org/10.1038/icb.2012.52.
64. Van Essen, D.C.; Smith, S.M.; Barch, D.M.; Behrens, T.E.J.; Yacoub, E.; Ugurbil, K. The WU-Minn Human Connectome Project: An overview. *NeuroImage* **2013**, *80*, 62–79. https://doi.org/10.1016/j.neuroimage.2013.05.041.
65. Thompson, D.W. *On Growth and Form*; Dover Pubns: Mineola, NY, USA, 1992; ISBN-10:0486671356.
66. Barriga, E.H.; Franze, K.; Charras, G.; Mayor, R. Tissue stiffening coordinates morphogenesis by triggering collective cell migration in vivo. *Nature* **2018**, *554*, 523–527.
67. Chan, C.J.; Costanzo, M.; Ruiz-Herrero, T.; Mönke, G.; Petrie, R.J.; Bergert, M.; Diz-Munoz, A.; Mahadevan, L.; Hiiragi, T. Hydraulic control of mammalian embryo size and cell fate. *Nature* **2019**, *571*, 112–116. https://doi.org/10.1038/s41586-019-1309-x.
68. Box, K.; Joyce, B.W.; Devenport, D. Epithelial geometry regulates spindle orientation and progenitor fate during formation of the mammalian epidermis. *eLife* **2019**, *8*, e47102. https://doi.org/10.7554/elife.47102.
69. Dabaghian, Y.; Brandt, V.L.; Frank, L.M. Reconceiving the hippocampal map as a topological template. *eLife* **2014**, *3*, e03476. https://doi.org/10.7554/elife.03476.
70. Babichev, A.; Dabaghian, Y.A. Topological Schemas of Memory Spaces. *Front. Comput. Neurosci.* **2018**, *12*, 27. https://doi.org/10.3389/fncom.2018.00027.
71. Dabaghian, Y. Through synapses to spatial memory maps via a topological model. *Sci. Rep.* **2019**, *9*, 572. https://doi.org/10.1038/s41598-018-36807-0.
72. Dai, W.; Guo, X.; Cao, Y.; Mondo, J.A.; Campanale, J.P.; Montell, B.J.; Burrous, H.; Streichan, S.; Gov, N.; Rappel, W.-J.; et al. Tissue topography steers migrating *Drosophila* border cells. *Science* **2020**, *370*, 987–990. https://doi.org/10.1126/science.aaz4741.
73. Kebschull, J.M.; Richman, E.B.; Ringach, N.; Friedmann, D.; Albarran, E.; Kolluru, S.S.; Jones, R.C.; Allen, W.E.; Wang, Y.; Cho, S.W.; et al. Cerebellar nuclei evolved by repeatedly duplicating a conserved cell-type set. *Science* **2020**, *370*, abd5059. https://doi.org/10.1126/science.abd5059.
74. Karzbrun, E.; Khankhel, A.H.; Megale, H.C.; Glasauer, S.M.K.; Wyle, Y.; Britton, G.; Warmflash, A.; Kosik, K.S.; Siggia, E.D.; Shraiman, B.I.; et al. Human neural tube morphogenesis in vitro by geometric constraints. *Nature* **2021**, *599*, 268–272. https://doi.org/10.1038/s41586-021-04026-9.
75. Herrera-Rincon, C.; Pai, V.P.; Moran, K.M.; Lemire, J.M.; Levin, M. The brain is required for normal muscle and nerve patterning during early Xenopus development. *Nat. Commun.* **2017**, *8*, 587.
76. Soldatov, R.; Kaucka, M.; Kastriti, M.E.; Petersen, J.; Chontorotzea, T.; et at. Spatiotemporal structure of cell fate decisions in murine neural crest. *Science* **2019**, *364*, eaas9536. https://doi.org/10.1126/science.aas9536.
77. Xie, M.; Kamenev, D.; Kaucka, M.; Kastriti, M.E.; Zhou, B.; Artemov, A.V.; Storer, M.; Fried, K.; Adameyko, I.; Dyachuk, V.; et al. Schwann cell precursors contribute to skeletal formation during embryonic development in mice and zebrafish. *Proc. Natl. Acad. Sci. USA* **2019**, *116*, 15068–15073. https://doi.org/10.1073/pnas.1900038116.
78. Qian, Q.; Nakamura, J.; Fallahi, S.; Gardner, G.C.; Manfra, M.J. Possible nematic to smectic phase transition in a two-dimensional electron gas at half-filling.. *Nat. Commun.* **2017**, *8*, 1536. https://doi.org/10.1038/s41467-017-01810-y.
79. Hartmann, R.; Singh, P.K.; Pearce, P.; Mok, R.; Song, B.; Díaz-Pascual, F.; Dunkel, J.; Drescher, K. Emergence of three-dimensional order and structure in growing biofilms. *Nat. Phys.* **2018**, *15*, 251–256. https://doi.org/10.1038/s41567-018-0356-9.
80. Ladouceur, A.-M.; Parmar, B.S.; Biedzinski, S.; Wall, J.; Tope, S.G.; Cohn, D.; Kim, A.; Soubry, N.; Reyes-Lamothe, R.; Weber, S.C. Clusters of bacterial RNA polymerase are biomolecular condensates that assemble through liquid–liquid phase separation. *Proc. Natl. Acad. Sci. USA* **2020**, *117*, 18540–18549. https://doi.org/10.1073/pnas.2005019117.
81. Brangwynne, C.P.; Eckmann, C.R.; Courson, D.S.; Rybarska, A.; Hoege, C.; Gharakhani, J.; Julicher, F.; Hyman, A.A. Germline P Granules Are Liquid Droplets That Localize by Controlled Dissolution/Condensation. *Science* **2009**, *324*, 1729–1732. https://doi.org/10.1126/science.1172046.
82. Strom, A.R.; Emelyanov, A.V.; Mir, M.; Fyodorov, D.V.; Darzacq, X.; Karpen, G.H. Phase separation drives heterochromatin domain formation. *Nat.* **2017**, *547*, 241–245. https://doi.org/10.1038/nature22989.
83. Nguyen, T.A.; Le, S.; Lee, M.; Fan, J.-S.; Yang, D.; Yan, J.; Jedd, G. Fungal Wound Healing through Instantaneous Protoplasmic Gelation. *Curr. Biol.* **2020**, *31*, 271–282.e5. https://doi.org/10.1016/j.cub.2020.10.016.

84. Boke, E.; Ruer, M.; Wühr, M.; Coughlin, M.; Lemaitre, R.; Gygi, S.P.; Alberti, S.; Drechsel, D.; Hyman, A.A.; Mitchison, T.J. Amyloid-like Self-Assembly of a Cellular Compartment. *Cell* **2016**, *166*, 637–650. https://doi.org/10.1016/j.cell.2016.06.051.
85. Quiroz, F.G.; Fiore, V.F.; Levorse, J.; Polak, L.; Wong, E.; Pasolli, H.A.; Fuchs, E. Liquid-liquid phase separation drives skin barrier formation. *Science* **2020**, *367*, aax9554. https://doi.org/10.1126/science.aax9554.
86. Iwabata, K.; Sugai, U.; Seki, Y.; Furue, H.; Sakaguchi, K. Applications of Biomaterials to Liquid Crystals. *Molecules* **2013**, *18*, 4703–4717. https://doi.org/10.3390/molecules18044703.
87. Mitov, M. Cholesteric liquid crystals in living matter. *Soft Matter* **2017**, *13*, 4176–4209. https://doi.org/10.1039/c7sm00384f.
88. Sargazi, M.; Linford, M.R.; Kaykhaii, M. Liquid Crystals in Analytical Chemistry: A Review. *Crit. Rev. Anal. Chem.* **2018**, *49*, 243–255. https://doi.org/10.1080/10408347.2018.1512399.
89. Termine, R.; Golemme, A. Charge Mobility in Discotic Liquid Crystals. *Int. J. Mol. Sci.* **2021**, *22*, 877. https://doi.org/10.3390/ijms22020877.
90. Bisoyi, H.K.; Li, Q. Liquid Crystals: Versatile Self-Organized Smart Soft Materials. *Chem. Rev.* **2021**, *122*, 4887–4926. https://doi.org/10.1021/acs.chemrev.1c00761.
91. Mundoor, H.; Wu, J.-S.; Wensink, H.H.; Smalyukh, I.I. Thermally reconfigurable monoclinic nematic colloidal fluids. *Nature* **2021**, *590*, 268–274. https://doi.org/10.1038/s41586-021-03249-0.
92. Mundoor, H.; Park, S.; Senyuk, B.; Wensink, H.H.; Smalyukh, I.I. Hybrid molecular-colloidal liquid crystals. *Science* **2018**, *360*, 768–771. https://doi.org/10.1126/science.aap9359.
93. Iqbal, D.; Samiullah, M.H. Photo-Responsive Shape-Memory and Shape-Changing Liquid-Crystal Polymer Networks. *Materials* **2013**, *6*, 116–142. https://doi.org/10.3390/ma6010116.
94. Chen, V.S.; Morrison, J.P.; Southwell, M.F.; Foley, J.F.; Bolon, B.; Elmore, S.A. Histology Atlas of the Developing Prenatal and Postnatal Mouse Central Nervous System, with Emphasis on Prenatal Days E7.5 to E18.5. *Toxicol. Pathol.* **2017**, *45*, 705–744. https://doi.org/10.1177/0192623317728134.
95. McDonald, N.A.; Fetter, R.D.; Shen, K. Assembly of synaptic active zones requires phase separation of scaffold molecules. *Nat.* **2020**, *588*, 454–458. https://doi.org/10.1038/s41586-020-2942-0.
96. Kießling, T.R.; Stange, R.; Käs, A.J.; Fritsch, A.W. Thermorheology of living cells—Impact of temperature variations on cell mechanics. *New J. Phys.* **2013**, *15*, 045026. https://doi.org/10.1088/1367-2630/15/4/045026.
97. Sotoma, S.; Zhong, C.; Kah, J.C.Y.; Yamashita, H.; Plakhotnik, T.; Harada, Y.; Suzuki, M. In situ measurements of intracellular thermal conductivity using heater-thermometer hybrid diamond nanosensors. *Sci. Adv.* **2021**, *7*, eabd7888. https://doi.org/10.1126/sciadv.abd7888.
98. Tanimoto, R.; Hiraiwa, T.; Nakai, Y.; Shindo, Y.; Oka, K.; Hiroi, N.; Funahashi, A. Detection of Temperature Difference in Neuronal Cells. *Sci. Rep.* **2016**, *6*, 22071. https://doi.org/10.1038/srep22071.
99. Xu, Y.; Ma, J.; Zhan, X.; Yang, L.; Jia, Y. Temperature effect on memristive ion channels. *Cogn. Neurodynamics* **2019**, *13*, 601–611. https://doi.org/10.1007/s11571-019-09547-8.
100. Long, M.A.; Fee, M.S. Using temperature to analyse temporal dynamics in the songbird motor pathway. *Nature* **2008**, *456*, 189–194. https://doi.org/10.1038/nature07448.
101. Kalmbach, A.S.; Waters, J. Brain surface temperature under a craniotomy. *J. Neurophysiol.* **2012**, *108*, 3138–3146. https://doi.org/10.1152/jn.00557.2012.
102. Jizba, P.; Arimitsu, T. The world according to Renyi: Thermodynamics of fractal systems. *AIP Conf. Proc.* **2001**, *597*, 341–348.
103. Jizba, P.; Korbel, J. On q-non-extensive statistics with non-Tsallisian entropy. *arXiv* **2015**, arXiv:1501.07386.
104. Lu, G.; Saunoriene, L.; Gelžinis, A.; Petrauskiene, V.; Ragulskis, M. Visual integration of vibrating images in time. *Opt. Eng.* **2018**, *57*, 093107. https://doi.org/10.1117/1.OE.57.9.093107.
105. Bach, M. *Optische Täuschungen und Andere Außergewöhnliche Sehphänomene*; Amazon.com, Inc.: Bellevue, WA, USA, 2022; ISBN 978-3-942825-97-9.
106. Slotnick, S.D. Visual Memory and Visual Perception Recruit Common Neural Substrates. *Behav. Cogn. Neurosci. Rev.* **2004**, *3*, 207–221. https://doi.org/10.1177/1534582304274070.
107. Read, J.C. Visual Perception: Monovision Can Bias the Apparent Depth of Moving Objects. *Curr. Biol.* **2019**, *29*, R738–R740. https://doi.org/10.1016/j.cub.2019.06.035.
108. Read, J.C.; Cumming, B.G. Visual Perception: Neural Networks for Stereopsis. *Curr. Biol.* **2017**, *27*, R594–R596. https://doi.org/10.1016/j.cub.2017.05.013.
109. Fleming, R.W. Visual perception: Colour brings shape into stark relief. *Curr. Biol.* **2022**, *32*, R272–R273. https://doi.org/10.1016/j.cub.2022.01.077.
110. Wexler, M.; van Boxtel, J.J. Depth perception by the active observer. *Trends Cogn. Sci.* **2005**, *9*, 431–438. https://doi.org/10.1016/j.tics.2005.06.018.
111. Chen, M.K.; Liu, X.; Wu, Y.; Zhang, J.; Yuan, J.; Zhang, Z.; Tsai, D.P. A Meta-device for Intelligent Depth Perception. *Adv. Mater.* **2022**, 2107465. https://doi.org/10.1002/adma.202107465.
112. Read, J.C. Binocular Vision and Stereopsis Across the Animal Kingdom. *Annu. Rev. Vis. Sci.* **2021**, *7*, 389–415. https://doi.org/10.1146/annurev-vision-093019-113212.
113. Chopin, A.; Chan, S.W.; Guellai, B.; Bavelier, D.; Levi, D.M. Binocular non-stereoscopic cues can deceive clinical tests of stereopsis. *Sci. Rep.* **2019**, *9*, 5789. https://doi.org/10.1038/s41598-019-42149-2.

114. Mitsudo, H. Neural Mechanism Underlying Stereoscopic Depth Perception: Why are the Two Eyes Aligned? *Brain Nerve* **2021**, *3*, 1225–1229. https://doi.org/10.11477/mf.1416201921.
115. Ding, J.; Levi, D.M. A unified model for binocular fusion and depth perception. *Vis. Res.* **2020**, *180*, 11–36. https://doi.org/10.1016/j.visres.2020.11.009.
116. Thompson, L.; Ji, M.; Rokers, B.; Rosenberg, A. Contributions of binocular and monocular cues to motion-in-depth perception. *J. Vis.* **2019**, *19*, 2–2. https://doi.org/10.1167/19.3.2.
117. Harris, J.M.; Wilcox, L.M. The role of monocularly visible regions in depth and surface perception. *Vis. Res.* **2009**, *49*, 2666–2685. https://doi.org/10.1016/j.visres.2009.06.021.
118. Forrester, J.V.; Dick, A.D.; McMenamin, P.G.; Roberts, F.; Pearlman, E. Physiology of vision and the visual system. In *The Eye*, 4th ed.; Saunders Ltd., Philadelphia, United States; **2016**; pp. 269–337.e2. https://doi.org/10.1016/b978-0-7020-5554-6.00005-8.
119. Schaeffel, F. Vergleichende Betrachtung von Lichtempfindlichkeit, Tiefenwahrnehmung und Bewegungswahrnehmung bei Tier und Mensch Comparative analysis of light sensitivity, depth and motion perception in animals and humans. *Der Ophthalmol.* **2017**, *114*, 997–1007. https://doi.org/10.1007/s00347-017-0568-x.
120. Anzai, A.; DeAngelis, G.C. Neural computations underlying depth perception. *Curr. Opin. Neurobiol.* **2010**, *20*, 367–375. https://doi.org/10.1016/j.conb.2010.04.006.
121. Boone, H.C.; Samonds, J.M.; Crouse, E.C.; Barr, C.; Priebe, N.J.; McGee, A.W. Natural binocular depth discrimination behavior in mice explained by visual cortical activity. *Curr. Biol.* **2021**, *31*, 2191–2198.e3. https://doi.org/10.1016/j.cub.2021.02.031.
122. Walker, W. Monge's Theorem in Many Dimensions. *Math. Gaz.* **1976**, *60*, 185–188.
123. Balajti, Z.; Dudás, I. The Monge theorem and its application in engineering practice. *Int. J. Adv. Manuf. Technol.* **2017**, *91*, 739–749. https://doi.org/10.1007/s00170-016-9763-1.
124. Ermis, T.; Gelisgen, O. Does the monge theorem apply to some non-euclidean geometries? *Glob. J. Adv. Res. Class. Mod. Geom.* **2021**, *10*, 122–127.
125. Mach, E. *Contributions to the Analysis of Sensations*; The Open Court Publishing Co: Chicago, IL, USA, 1897.
126. Gjorevski, N.; Nikolaev, M.; Brown, T.E.; Mitrofanova, O.; Brandenberg, N.; DelRio, F.W.; Yavitt, F.M.; Liberali, P.; Anseth, K.S.; Lutolf, M.P. Tissue geometry drives deterministic organoid patterning. *Science* **2022**, *375*, eaaw9021. https://doi.org/10.1126/science.aaw9021.
127. Kra, I. Cohomology of kleinian groups. *Proc. Natl. Acad. Sci. USA* **1969**, *63*, 655–660. https://doi.org/10.1073/pnas.63.3.655.
128. Dummit, D.S.; Foote, R.M. *Abstract Algebra*, 3rd ed.; WolframAlpha: Hoboken, NJ, USA, 2003; ISBN 0-471-43334-9.
129. Stasheff, J.D. Continuous cohomology of groups and classifying spaces. *Bull. Am. Math. Soc.* **1978**, *84*, 513–531. https://doi.org/10.1090/s0002-9904-1978-14488-7. ISSN 0002-9904.
130. Minchenko, A.; Ovchinnikov, A. Triviality of differential Galois cohomology of linear differential algebraic groups. *Commun. Algebra* **2019**, *47*, 5094–5100. https://doi.org/10.1080/00927872.2019.1612416.
131. Lurie, J. On Infinity Topoi. arXiv **2003**, *arXiv:math/0306109*.
132. Lurie, J. Higher Topos Theory. arXiv **2008**, *arXiv:math/0608040*.
133. Grothendieck, A. Sur quelques points d'algèbre homologique, I. *Tohoku Math. J.* **1957**, *9*, 119–221. https://doi.org/10.2748/tmj/1178244839. .
134. Serre, J.-P. Faisceaux Algebriques Coherents. *Ann. Math.* **1955**, *61*, 197. https://doi.org/10.2307/1969915.
135. Domokos, G.; Jerolmack, D.J.; Kun, F.; Török, J. Plato's cube and the natural geometry of fragmentation. *Proc. Natl. Acad. Sci. USA* **2020**, *117*, 18178–18185. https://doi.org/10.1073/pnas.2001037117.
136. Twarock, R.; Luque, A. Structural puzzles in virology solved with an overarching icosahedral design principle. *Nat. Commun.* **2019**, *10*, 4414. https://doi.org/10.1038/s41467-019-12367-3. .
137. Palotás, J.; Martens, J.; Berden, G.; Oomens, J. The infrared spectrum of protonated buckminsterfullerene C60H+. *Nat. Astron.* **2019**, *4*, 240–245. https://doi.org/10.1038/s41550-019-0941-6.
138. McGrath, R.; Sharma, H.R.; Smerdon, J.A.; Ledieu, J. The memory of surfaces: Epitaxial growth on quasi-crystals. *Philos. Trans. R. Soc. London. Ser. A: Math. Phys. Eng. Sci.* **2012**, *370*, 2930–2948. https://doi.org/10.1098/rsta.2011.0220.
139. Koju, V.; Robertson, W.M. Excitation of Bloch-like surface waves in quasi-crystals and aperiodic dielectric multilayers. *Opt. Lett.* **2016**, *41*, 2915–2918. https://doi.org/10.1364/ol.41.002915.
140. Mustafa, M.-E.; Amin, M.; Siddiqui, O.; Tahir, F.A. Quasi-Crystal Metasurface for Simultaneous Half- and Quarter-Wave Plate Operation. *Sci. Rep.* **2018**, *8*, 15743. https://doi.org/10.1038/s41598-018-34142-y.
141. Wang, P.-Y.; Mason, T.G. A Brownian quasi-crystal of pre-assembled colloidal Penrose tiles. *Nature* **2018**, *561*, 94–99. https://doi.org/10.1038/s41586-018-0464-9.
142. Bosi, S.; Da Ros, T.; Spalluto, G.; Prato, M. Fullerene derivatives: An attractive tool for biological applications. *Eur. J. Med. Chem.* **2003**, *38*, 913–923. https://doi.org/10.1016/j.ejmech.2003.09.005.
143. Nierengarten, I.; Nierengarten, J.-F. Fullerene Sugar Balls: A New Class of Biologically Active Fullerene Derivatives. *Chem. Asian J.* **2014**, *9*, 1436–1444. https://doi.org/10.1002/asia.201400133.
144. Kazemzadeh, H.; Mozafari, M. Fullerene-based delivery systems. *Drug Discov. Today* **2019**, *24*, 898–905. https://doi.org/10.1016/j.drudis.2019.01.013.
145. Gülseren, G.; Saylam, A.; Marion, A.; Özçubukçu, S. Fullerene-Based Mimics of Biocatalysts Show Remarkable Activity and Modularity. *ACS Appl. Mater. Interfaces* **2021**, *13*, 45854–45863. https://doi.org/10.1021/acsami.1c11516.

146. Tozzi, A.; Peters, J.F.; Ori, O. Fullerenic-topological tools for honeycomb nanomechanics. Toward a fullerenic approach to brain functions. *Full- Nanotub. Carbon Nanostructures* **2017**, *25*, 282–288. https://doi.org/10.1080/1536383x.2017.1283618.
147. Tozzi, A.; Peters, J.F.; Ori, O. Cracking the barcode of fullerene-like cortical microcolumns. *Neurosci. Lett.* **2017**, *644*, 100–106. https://doi.org/10.1016/j.neulet.2017.02.064.
148. Telley, L.; Agirman, G.; Prados, J.; Amberg, N.; Fièvre, S.; Oberst, P.; Bartolini, G.; Vitali, I.; Cadilhac, C.; Hippenmeyer, S.; et al. Temporal patterning of apical progenitors and their daughter neurons in the developing neocortex. *Science* **2019**, *364*, eaav2522. https://doi.org/10.1126/science.aav2522.
149. Daoud, A.M.P.; Popovic, M.; Dondorp, W.J.; Bustos, M.T.; Bredenoord, A.L.; Lopes, S.M.C.D.S.; Brink, S.C.V.D.; Roelen, B.; De Wert, G.M.W.R.; Heindryckx, B. Modelling human embryogenesis: Embryo-like structures spark ethical and policy debate. *Hum. Reprod. Updat.* **2020**, *26*, 779–798. https://doi.org/10.1093/humupd/dmaa027.
150. Yang, J.; Fu, H.; Tam, C.; Liu, P. Expanded potential: The key to synthetic embryo?. *Curr. Opin. Genet. Dev.* **2020**, *64*, 72–77. https://doi.org/10.1016/j.gde.2020.06.008.
151. Tomoda, K.; Kime, C. Synthetic embryology: Early mammalian embryo modeling systems from cell cultures. *Dev. Growth Differ.* **2021**, *63*, 116–126. https://doi.org/10.1111/dgd.12713.
152. Tarazi, S.; Aguilera-Castrejon, A.; Joubran, C.; Ghanem, N.; Ashouokhi, S.; Roncato, F.; Wildschutz, E.; Haddad, M.; Oldak, B.; Gomez-Cesar, E.; et al. Post-gastrulation synthetic embryos generated ex utero from mouse naive ESCs. *Cell* **2022**, *185*, 3290–3306.https://doi.org/10.1016/j.cell.2022.07.028.

Journal of NeuroPhilosophy 2022;1(2):222-239

Front Waves of Chemical Reactions and Travelling Waves of Neural Activity

Yidi Zhang*, Shan Guo†, Mingzhu Sun‡, Lucio Mariniello§, Arturo Tozzi‖, Xin Zhao**

Abstract

Travelling waves crossing the nervous networks at mesoscopic/macroscopic scales have been correlated with different brain functions, from long-term memory to visual stimuli. Here we investigate a feasible relationship between wave generation/propagation in recurrent nervous networks and a physical/chemical model, namely the Belousov–Zhabotinsky reaction (BZ). Since BZ's nonlinear, chaotic chemical process generates concentric/intersecting waves that closely resemble the diffusive nonlinear/chaotic oscillatory patterns crossing the nervous tissue, we aimed to investigate whether wave propagation of brain oscillations could be described in terms of BZ features. We compared experimentally detected oscillations during the spontaneous activity of the brain with BZ-like concentric waves simulated by a recently introduced artificial network. The observed overlap and agreement between simulated and measured oscillatory patterns suggests that changes in cortical areas' neural activity might be described in terms of a recognizable diffusion pattern. We describe biological plausibility, benefits and limits of our approach and discuss the relationship among BZ-like networks, Pandemonium-like architectures and the spontaneous activity of the brain.

Key Words: central nervous system, chaos, chemical reaction, spontaneous activity, BOLD activity, nonlinear dynamics

DOI: 10.5281/zenodo.7254050

Introduction

Travelling waves of neural activity, spontaneously generated by intrinsic circuits or evoked by external stimuli, cross the brain at single-area and whole-brain scales (Muller *et al.*, 2018; Zhang *et al.*,

Corresponding author: Arturo Tozzi
Address: *Institute of Robotics and Automatic Information System, Nankai University, Tianjin, China. †Institute of Robotics and Automatic Information System, Nankai University, Tianjin, China. ‡Institute of Robotics and Automatic Information System, Nankai University, Tianjin, China. §Department of Pediatrics, University Federico II, Naples. ‖Center for Nonlinear Science, Department of Physics, University of North Texas, Denton, USA, **Institute of Robotics and Automatic Information System, Nankai University, Tianjin, China.
e-mail ✉ tozziarturo@libero.it
Received: 1 September 2022; **Accepted:** 23 October 2022

2018). These spatiotemporal cortical patterns have been correlated with a variety of mental functions, from long-term memory consolidation to processing of visual stimuli (**Figure 1**). It has been hypothesized that synchronous occurrence of neural oscillations in different neural populations might assist information transfer among these populations (Akam and Kullmann, 2010). A broad computational and mathematical literature on travelling waves in neural networks has been produced, focusing on theoretical mechanisms for wave spreading. Here we ask whether wave generation and propagation in recurrent nervous networks might be correlated with extant physical/chemical models. A chemical system termed Belousov–Zhabotinsky reaction (BZ), though an incomplete analogy to the cortical activity, provides a suggestive template for waves radiating from brain sub-areas. BZ describes an unusual, nonlinear chemical oscillator: in presence of bromine and an acid, concentric circles are effortlessly and incessantly produced in a Petri dish, giving rise to simultaneous, intersecting wave fronts which intermingle and/or reciprocally annihilate (**Figure 2A**). BZ models of noise-induced order have been used for chemical computations describing far from equilibrium nonlinear dynamics and chaotic evolution. BZ-like computational models rely on geometrically constrained excitable chemical mediums which make use of changes in reagents concentrations to transmit information. This approach has been proven useful in different contexts such as, e.g., image processing, Voronoi diagram, logical computations. Zhang et al. (2012) designed circuits that reproduce the typical oscillatory patterns of BZ. Their circuits consist of planar, geometrically constrained, binary adder chemical devices that perform not just two-bit, but also multi-bit logical computations. Sun and Zhao (2013) and Guo et al. (2014) further described how one-bit decoders can be extended through cascade methods to design two-bit, three-bit, or higher bit binary decoders.

BZ-like travelling waves can be used to investigate physical and/or biological phenomena: for example, they mimic the cardiac electrical waves and resemble the oscillations of certain bacterial colonies (Cincotti *et al.,* 2019). Here we tackle the BZ issue from the standpoint of the brain cortical activity: does a correlation exist between the configurations of BZ oscillations and brain waves? The answer could be positive, if we consider that the vibrations inside a BZ medium create a pattern of simultaneous and/or successive concentric waves across the surface that closely resemble the travelling waves produced in the cortex by the impact of afferent action potentials. Instead of precise zero-lag synchrony, a range of flexible phase relationships might produce waves of various shapes including plane, radial and spiral waves, and complex spatiotemporal patterns.

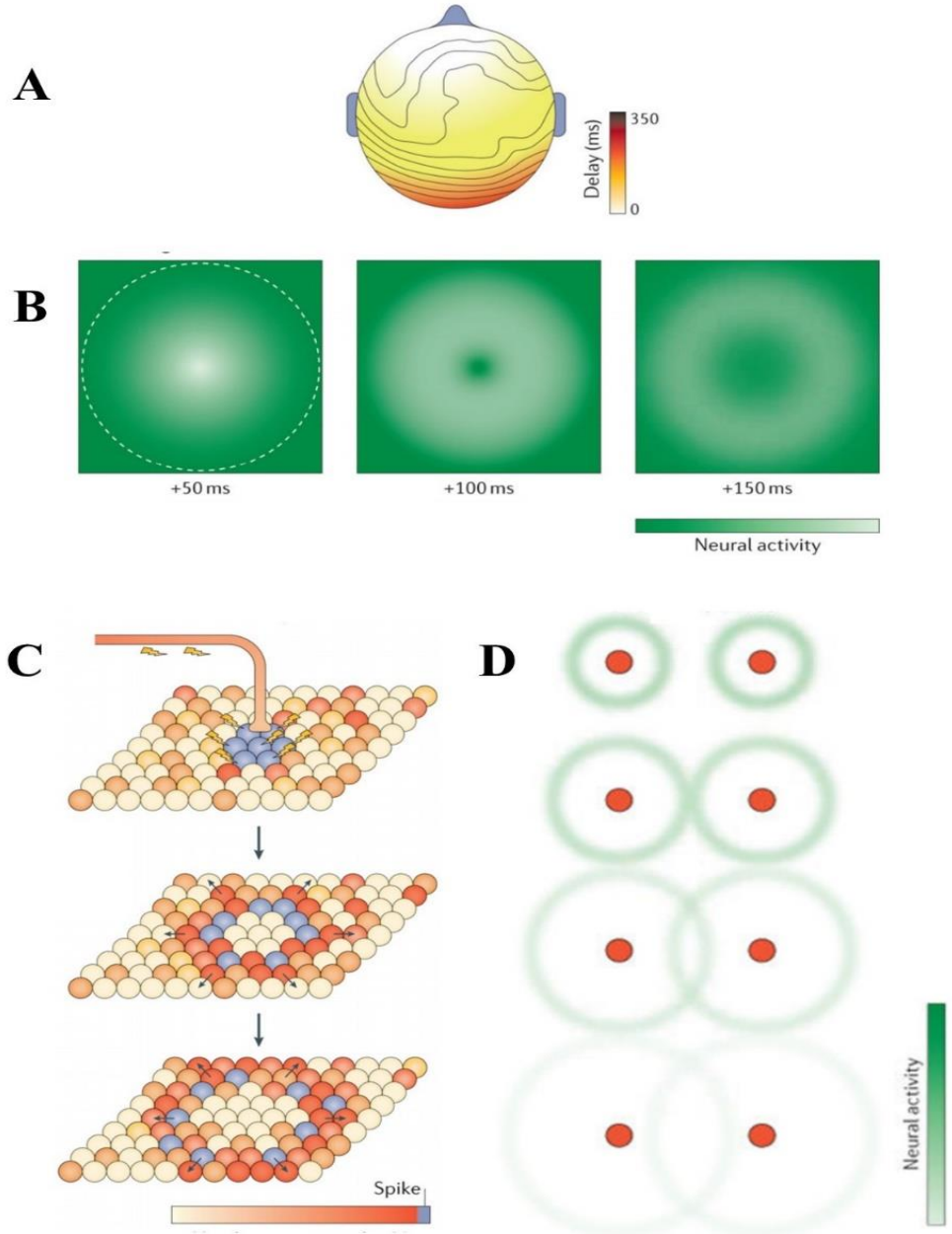

Figure 1. Examples of cortical travelling waves. **Figure 1A**. The slow oscillations of deep non-rapid-eye-movement sleep are reported in terms of a travelling wave moving globally from anterior to posterior regions (modified from Massimini et al. 2004). **Figure 1B**. A model for stimulus-evoked responses in the visual cortex. Within the response zone, the activity pattern might take two main forms: either stationary bumps of activity (not shown here) or travelling waves (illustrated in the picture). Modified from Muller et al. (2018). **Figure 1C**. Schematic model for wave generation in topographic networks of neurons with local random connections. Spheres represent neurons whose membrane potential is indicated by colour. In waking states, cortical networks with strong background display local stimulation that elicits waves weakly entraining neuronal spiking (Muller *et al.,* 2018). **Figure 1D**. Interaction between sparse, weakly interacting cortical waves. It has been hypothesized that such oscillations might generate a symmetric global wave field when passing through each other. Modified from Muller et al. (2018) and Perrard et al. (2016).

Brain activity has another common ground with BZ: both display oscillations characterized by chaotic features and self-organizing activity under the influence of specific stimuli (Fraiman and Chialvo, 2012; Zare and Grigolini, 2013; Qu *et al.,* 2014; Tozzi *et al.,* 2017); both exhibit "excitability", i.e., the sudden occurrence of patterns, such as the neural avalanches, emerging in an apparently quiescent medium (Tyukin *et al.,* 2019). Starting from these premises, we tested whether BZ-like mechanisms might underlie the oscillatory behavior of fMRI BOLD activation during spontaneous activity of the brain. To pursue our goal, we introduced a novel computational model of nervous activity, i.e., a BZ-like circuit that mimics the oscillations arising from single cortical subareas and propagating (non-homogeneously and non-ergodically) towards different cortical locations. We compared the simulated waves produced by our BZ network with available real neurodata and found that the propagation of nervous oscillations in the brain matches the propagation of the simulated waves generated by of our BZ-like circuit.

Materials and Methods

Our aim was to compare innovative artificial circuits simulating the typical BZ waves with the real patterns of oscillations extracted from fMRI movies of the spontaneous activity of the brain.

Previous circuits based on Belousov-Zhabotinsky reaction. In previous studies, BZ has been described in terms of circuits that reproduce the typical front waves and superimposing oscillatory patterns of this unusual chemical reaction (**Figure 2A**). For further details and the master equations, see Zhang et al. (2012); Sun and Zhao (2013); Guo et al. (2014). The basic unit of the circuit, termed binary adder unit (BAU), consists of simple straight-line boundaries. BAU was implemented with a number of tools, such as unidirectional transmission, T-shaped and cross-propagation structures (**Figures 2B-D**). Due to its geometrically constrained structure, BAU performs the addition of binary information without the need of ruling clocks or adjustments in parameters. Methodologies borrowed by adders building in digital circuits permits to couple single-bit BAUs and produce two-bit binary adders and, as the number of bits increases, more complex multi-bit binary decoders. The latter can be designed via nesting and cascade methods that link n-bit decoders ($n \geq 2$) with ($n - 1$)-bit decoders, so that every n-bit decoder includes the simpler structure of a ($n - 1$)-bit decoder. This iterative process produces both simple (One-way propagation, Osmotic propagation, Delayed propagation) and complex circuits (Adders, Memory, Decoders, Comparators). Simulations have demonstrated the feasibility of such a combinatory logical circuit able to convert binary information from n input lines to a maximum of $2n$ unique output lines (Guo *et al.,*

2014). Multi-bit digital comparators allow not just the assessment of two multi-bit binary numbers one bit after another, but also the use of the Boolean terms 0 and 1 to describe the results. In sum, quite simple basic units can be combined via special connection methods in network models that mimic the behavior of BZ concentric oscillations, making it possible to produce more elaborate computational functions.

Entering the brain activity: lag threads. High-dimensional structures with variable delay termed "lag threads" have been found in the brain during spontaneous activity, consisting of multiple, highly reproducible temporal sequences that propagate from one brain region to another. Mitra et al. (2015) suggested that the brain activity encompasses both single and multiple lag threads. We retrospectively evaluated video frames showing lag threads computed from real BOLD resting state rs-fMRI data. Data were extracted from 688 subjects (Harvard-MGH Brain Genomics Superstruct Project). We examined 54 images from four sets of movies (Threads 1, 2, 3 and 4) including transverse sections of the brain. The videos are freely-available: http://www.pnas.org/content/suppl/2015/03/24/1503960112.DCSupplemental.

Building the proper circuits. The next step was to build a BZ-like artificial circuit appropriate to describe real lag threads. Instead of the usual neural models such as McCulloch-Pitts Neurons, Hopfield networks and so on (Hopfield 1982; Tozzi *et al.,* 2016), we used a node-like structure especially designed for simulation of both single lag threads and the superposition of multiple lag threads. This novel network, rather different from the adder units, decoders and comparators portrayed in previous papers (Zhang *et al.,* 2012; Sun and Zhao, 2013), describes neuronal unities at different levels of observation, from the micro-to the macro-level. Indeed, a BZ-like neural unit (provided with input and output channels) may stand both for a large cortical area and for a small group of neurons.

To keep the model as simple as possible, the basic node-like structures (neuronal units) inspired by lag threads are rectangular ring channels equipped with input and output channels. The circuit permits different paths according to the temporal sequence of signals propagation in real threads. The number of inputs and outputs mimics the number of threads: e.g., **Figures 2B-C** show two inputs and two outputs channels.

To achieve the proper propagation sequence between nodes, we introduced one-way transmission structures:

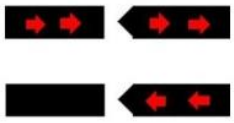

where signals are unidirectional, e.g., they are allowed to travel just from left to right and not vice versa. The addition of unidirectional transmission structures to input channels prevents signal output through the input channel.

The very features of a basic BZ-like circuit suggest that two different paths may occur (Sun and Zhao, 2013):

a) signal transmission from inputs to outputs (**Figures 2B-C**).

b) signal annihilation when two front waves meet (**Figure 2D**).

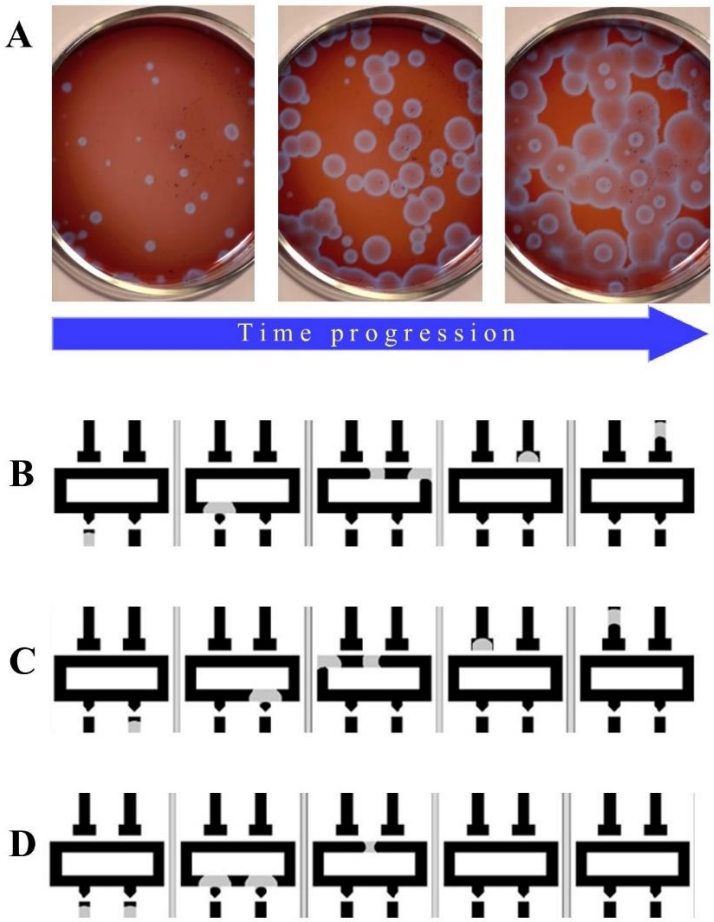

Figure 2. Comparison between travelling waves produced by chemical BZ and by one-bit digital comparators. **Figure 1A**: Two-dimensional BZ in a Petri dish. The typical configuration of wave sources produces circular and spiral oscillations, as shown in these frames modified from: https://www.youtube.com/watch?v=jRQAndvF4sM. Note how the temporal evolution of the numerous chemical wave fronts leads to their merging, superimposition or annihilation. **Figure 1B-D**: Three different possible patterns of wave propagation in basic one-bit digital comparators. **Figures 2B-C** show how a single wave propagating from a single input channel (bottom) is able to reach a single output channel (top) after a wave bifurcation. **Figure 1D** shows how two waves propagating from two different input channels are not able to reach the output channels, because their gathering leads to mutual annihilation.

Simulations of BZ-like concentric patterns on brain-like templates. Once achieved a BZ-like network simulating lag threads, our aim was to assess whether the concentric oscillatory paths produced by our circuit could be superimposed with the real concentric oscillatory paths detectable in the video frames of BOLD resting state rs-fMRI activity. According to Mitra et al. (2015), each brain activity encompasses not just single, but also multiple lag threads. Our aim was to simulate the two threads shown in Figure 6 from Mitra et al. (2015). Both these two threads display four nodes, but the temporal order of their wave propagation is different.

The basic unit, i.e., the rectangular-shaped channel with two inputs and two outputs channels, can be expanded via nesting and cascading processes to build multi-bit digital comparators. We connected and combined several basic units to build the complex lag threads described in **Figures 3A and 3B**. **Figure 3A** illustrates the circuit designed for the description of thread 1, consisting of four (neuronal) units and ad hoc connections among them. The yellow arrows depict the direction of signal transmission. The signal input starts from the left side of the node 1 and enters the node 1 through the unidirectional transmission structure designed to prevent the signal from the opposite direction to output through the input channel. When the signal propagates to the rectangular-shaped channel, it splits in two wave fronts. After passing through half a rectangle in different directions, their wave fronts meet at the opposite side, enter the gap into the T-shaped structure and continue to node 2. Summarizing, the input enters node 1, crosses nodes 2 and 3 and the output exits node 4.

Figure 3B illustrates the circuit designed for thread 2, consisting of four neuronal units and the corresponding connections too. The red arrows depict the direction of signal transmission. This time, the input enters node 4, crosses nodes 3 and 1 and the output exits node 2. It is noteworthy that the connection between nodes 1 and 2 is the same in the two threads, so that signals always propagate from node 1 to 2. The sequence that crosses the nodes 1 and 2 is termed “lag thread motif”.

Mitra stated that the spontaneous activity of the brain is achieved through the superposition of multiple threads. Therefore, we produced a more intricate circuit encompassing multiple lag threads. **Figure 3C** illustrates two-threaded superposition (thread 1 and 2). The yellow and red arrows depict the direction of signal transmission in thread 1 and 2, respectively. Note that the two signals stand for simultaneous inputs for two different channels. Signal 1 from thread 1 and signal 2 from thread 2 simultaneously reach the output channels in node 2 and node 3, respectively. Therefore, signal 1 outputs node 4 after crossing node 3, while signal 2 outputs node 2 after crossing node 1. This is in touch with the observation that signal transmission is constrained in threads: for example, in the two threads

1 and 2 of **Figure 3C**, the node 1 is able to transmit signals just from left to right, while the node 4 is able to transmit signals both from left to right and right to left.

In case of a single thread, the node-like structure is a unit with a single input and a single output; in a two-threaded superposition, the node-like structure is a unit with two inputs and two outputs; in a three-threaded superposition, the node like structure is a unit with three inputs and three outputs, and so on. Increasing the number of threads, more complex structures are achieved that permit higher number of computations.

BZ-like circuits generate synthetic oscillations that tend to propagate, converge, merge/annihilate and so on, giving rise to travelling waves that closely resemble the real oscillations detectable in the chemical BZ. The next step was to incorporate our synthetic oscillations in a template resembling the brain shape and anatomical structure in transverse projection. Using our BZ-like circuits, we generated random concentric wave fronts and projected them to the brain template (**Figure 3D**). We randomly generated simultaneous waves arising from different starting points inside the brain template to investigate their intersections and interactions.

Results

We found that the patterns of signal transmission in simulated BZ-like travelling waves match the oscillatory patterns detectable in the spontaneous activity of the brain. The experimental data from real BOLD resting state rs-fMRI data agree well with our simulated wave fronts, showing a good superimposition. The neural wave fronts closely resemble the BZ-like concentric circles embedded in the brain template. Indeed, matching features between the simulated and real oscillations were found in 85% of the 54 examined frames and in 65% of all detectable oscillations, independent of brain location and time window.

Concerning interactions and superpositions between distinct oscillations, two different cases can be described both in real and simulated travelling waves:

1) a single wave gives rise to a wave front that proceeds through the cortical areas. 2) Two waves cancel one each other when they start to merge and overlap.

To provide an example of the case 1, the upper part of **Figure 4A** illustrates the signals of thread 3 from 0.4s to 1.1s, while the lower part of **Figure 4A** illustrates the corresponding artificial signals produced by BZ-like circuits. The two travelling waves, the real and the simulated one, display the same progression throughout the brain template. To provide an example of the case 2, see **Figure 4B**, which illustrates two waves that annihilate when intersecting.

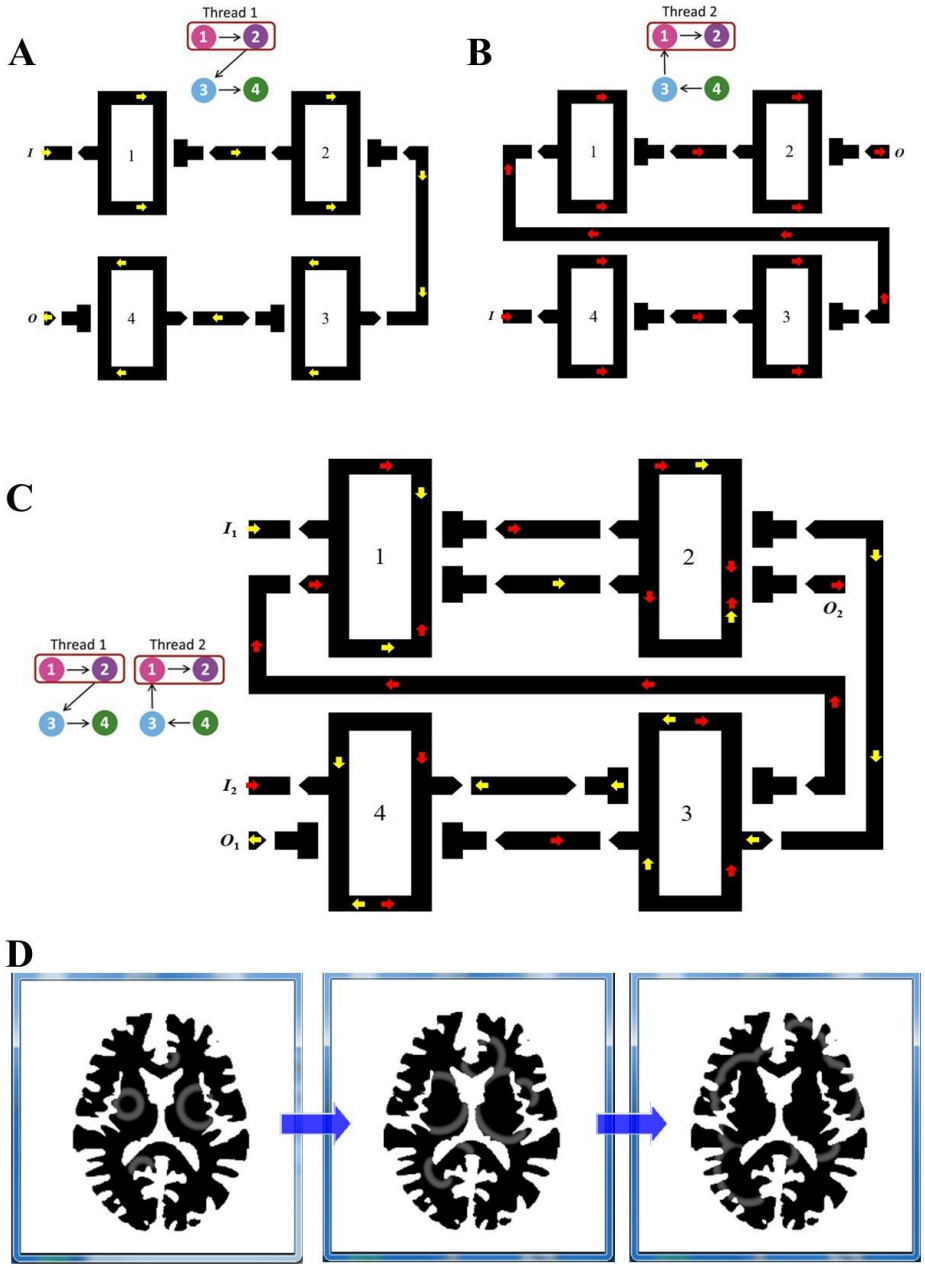

Figure 3. The lag threads detectable in the spontaneous activity of the brain can be described in terms of BZ-like circuits. **Figures 3A-B** illustrate simulations with four neuronal unities inspired by the lag threads described in the video frames of BOLD resting state rs-fMRI activity. The arrows depict the direction of signal transmission from the input to the output. The numbers 1,2,3,4 designate four rectangular structures, each one standing for a neuronal unit. **Figure 3A**. Simulation of signal crossing in thread 1. **Figure 3B**. Simulation of signal crossing in thread 2. **Figure 3C**. Simulation of two simultaneous signals crossing in threads 1 and 2. The yellow arrows show the signals of thread 1, the red arrows the signals of thread 2. **Figure 3D**. Simulation of the temporal evolution of three simulated BZ-like concentric patterns inside a brain-like template. Modified from Mitra et al.'s movies.

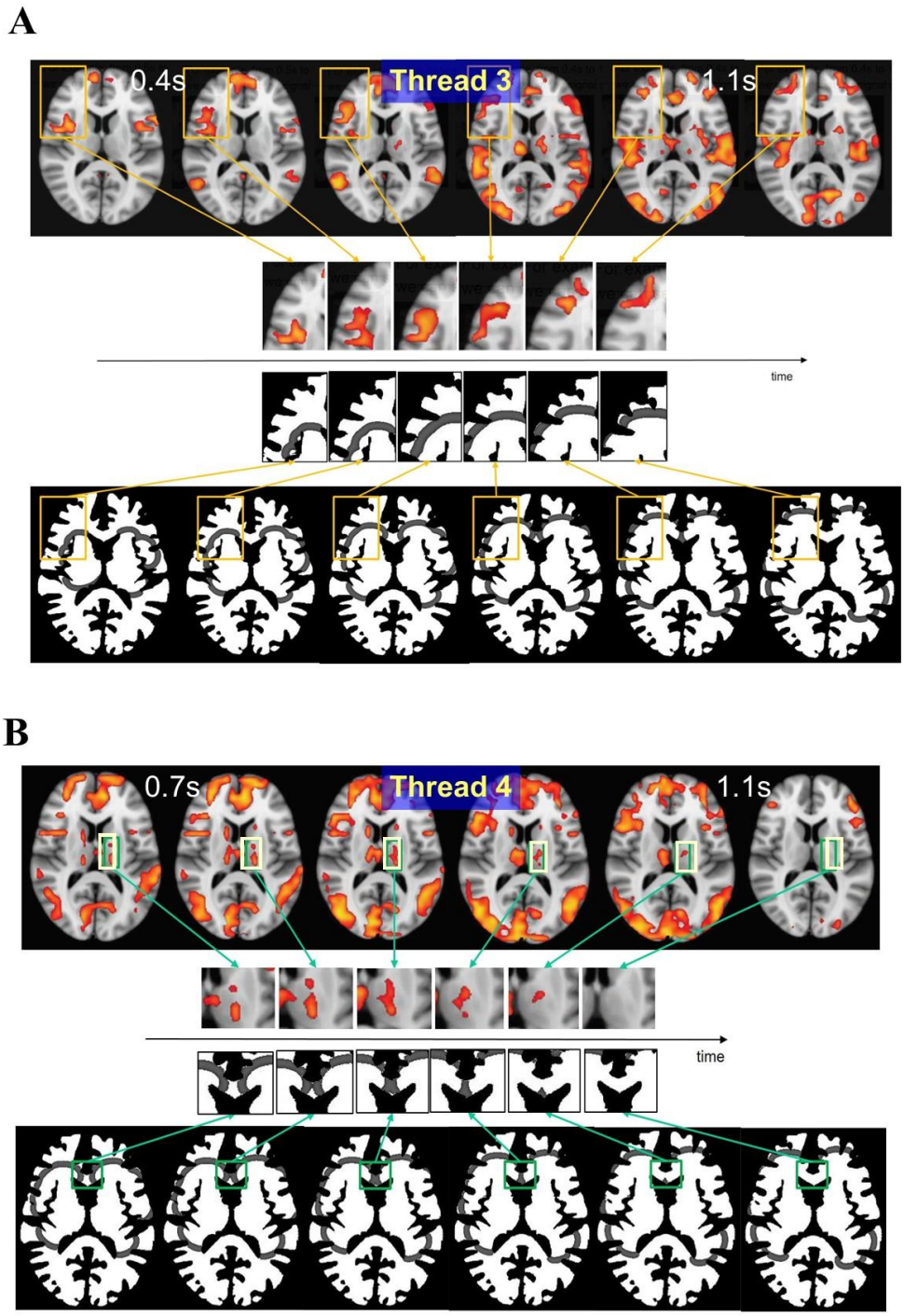

Figure 4. Comparison between wave fronts from real lag thread frames (**upper part**) and from simulations with the novel BZ-like circuit (**lower part**). The paths of the travelling waves can be easily detected and compared in both BZ simulations and real fMRI data. **Figure 4A** illustrates the progression of a real and a simulated single wave, while **Figure 4B** illustrates the annihilation of two simultaneous waves.

We found agreement between the waves produced by the spontaneous activity of the brain and the waves simulated by the novel network. This means that the diffusive paths detected in BOLD neuronal activity can be described in terms of BZ-like models and their master equations.

Conclusions

We found BZ-correlated dynamics in video frames of BOLD resting state rs-fMRI activity. The matching of theoretical BZ models and real patterns of neural activity allows us to achieve two goals. The first goal is the possibility to reproduce and standardize neural waves propagation in order to investigate different cognitive activities. To make use of video frames of BOLD resting state rs-fMRI activity as the domain of BZ, we began with two recently developed concepts:

a) each brain activity encompasses single or multiple lag threads (Mitra *et al.,* 2015);

b) chemical signal processors based on the BZ platform are available (Zhang *et al.,* 2012).

To mimic both single lag threads and the superposition of multiple lag threads, we designed relatively simple BZ-like structures where random oscillations propagate through a small number of nodes. We found that the oscillatory patterns of neuronal activity produced by simulations based on BZ fully overlap the oscillatory patterns detected in the brain during spontaneous activity. Therefore, the behavior of BZ travelling waves is very similar to the behavior of brain travelling waves: this suggests that logical devices based on the space-time interaction of travelling excitation oscillations is well-suited for experimental implementation in neuroscience (see also: Gomez-Molina *et al.,* 2017).

In this paper we assessed just coarse-grained macro-levels of observation and analysis: this led us to describe nodes at the level of cortical subareas equipped with inputs and outputs. Nevertheless, if we consider micro-levels of observation and analysis, nodes might also stand, e.g., for single neurons or micro-columnar circuits. A crucial question arises: is it feasible to generalize the description of nodes in BZ-like circuits, independent of the chosen coarse-graining? The answer is positive, because generalizations do not impair the broad description provided by threads. Indeed, BZ-like reactions provide a good sketch of both single threads and their subsequent superposition. In this paper we implemented just two-threads superpositions, while a more intricate superposition of multiple threads would require further exploration.

The matching of theoretical BZ models and real patterns of neural activity allows us also to achieve a second goal: to posit that the brain encompasses a recognizable diffusion pattern spreading throughout nervous structures. Cincotti et al. (2019) brought a new level of complexity to BZ by combining multiple wave sources in a so-called "threaded ring" configuration. The order in the fluids is never perfect, because contaminations and impurities may affect the values of order parameters. For example, a dust particle in the proper chemical medium may trigger spontaneous BZ waves consisting of concentric rings moving outward from the particle. In other cases, circular BZ wave fronts perturbed by obstacles (see the movie: https://www.youtube.com/watch?v=jRQAndvF4sM) transform into spirals and/or scroll rings, i.e., ring-shaped sources emitting circular waves which propagate both inwardly and outwardly from the source. It is noteworthy that impurities are always *local*, which means that they are small and affect just limited spaces of the medium. Peculiar local configurations termed *vortices* can be temporarily achieved when oscillations wind around a central point. Because vortices might also stand for topological defects in the crystalline order of a medium (Beekman *et al.,* 2017), this leads us into the field of superfluids and superconductors, where Kosterlitz-Thouless transitions (which describe ordered state at low temperature and completely disordered state at high temperature) are caused by topological defects in two-dimensional manifolds (Kosterlitz and Thouless, 1973). In neural terms, this means that each type of order (also the order of the brain activity) has its own type of topological defects, which presumably can undergo similar unbinding transitions caused by vortices. In touch with these claims, Don et al. (2020) used computational topology on triangulated rs-fMRI videoframes to detect vortex structures covering activated regions of the brain. During spontaneous activity of the brain, measure of persistence of vortex shapes was carried out in terms of Betti numbers that rise and fall over time (Don *et al.,* 2020).

To link up travelling neural oscillations to brain mechanisms of computations, virtues, defects and biological plausibility of our novel BZ-like network are here explained. We proposed a BZ-like network producing concentric waves from random multifocal sources located in a two-dimensional manifold. Although centered on binary operations like most neural networks, our network simulates the progression of concentric waves and their superposition through an operation of binary addition. In terms of biological counterparts, our model requires numerous nervous spots located in the central nervous system that spontaneously generate random oscillations propagating in concentric waves throughout the brain. When the oscillations produced by multifocal sources interact, they collide and merge, allowing us to achieve dynamics that are reproducible by BZ-like networks. Therefore, the main requirement for the biological plausibility of our model is the occurrence of spontaneous travelling waves in the brain. Indeed, the brain cortex is crossed by scattered

spontaneous waves whose frequencies and speeds are consistent with slow conduction (Davis *et al.,* 2020). It is well established that spontaneous travelling waves in the brain are endogenously generated and are not triggered by explicit tasks (Northoff 2018). This "intrinsic" brain activity has been associated not just with resting-state or default-mode network (Tozzi et at. 2016), but also with disused circuits (Newbold *et al.,* 2020) and increased target-evoked neuronal responses/perceptual sensitivity (Davis *et al.,* 2020). Comparison between the oscillations produced by our model and the oscillations detected in fMRI traces suggests that the front waves of scattered spontaneous oscillations are circular and tend to propagate in concentric, expanding circles.

Our model permits the assessment of front waves' interactions: instead of investigating input features such as probability-weighted connections, activation functions, learning rates, thresholds and hidden layers, our BZ-like network focuses on the relationships between the various outputs, i.e., the concentric waves generated by point sources.

The process looks like natural evolution, by selecting the "best" concentric wave and eliminating the relatively poor ones, so that a single output from a very few spots far outshines the rest. Therefore, we suggest a winner-take-all approach, in touch with Pandemonium-like architectures (Selfridge 1957). Spontaneously generated concentric waves subtend a hierarchical, self-improving model able to perform non-trivial binary functions (Tozzi and Peters, 2018). A Pandemonium-based architecture have been already proposed to elucidate not just cellular homeostasis (Liu *et al.,* 2019), but also brain functions such as pattern recognition and mental interpretation of visual scenes (McDowell, 2010; Edelman, 2017). Here we propose to extend Pandemonium-based architectures also to the spontaneous activity of the brain, so that, in touch with "neural darwinism" (Rosenbaum, 2014), the concentric scattered waves become a selection system. The waves interaction described by our model might help explain a puzzling finding. It has been uncovered that neurons coordinate the strength of their excitatory and inhibitory inputs to establish and maintain a constant excitation/inhibition (E/I) ratio. E/I ratio is thought to be essential for circuit function and stability (Xue *et al.,* 2014; Sengupta 2013; Sengupta 2014; He and Cline, 2019) and is rather stable at different magnifications (He *et al.,* 2018). E/I ratio stability can be exposed as various coarse-grained levels of analysis, such as individual pyramidal neurons in vitro and in vivo (Haider *et al.,* 2006), ensemble of multiple cortical neurons (Xue *et al.,* 2014) neural avalanches (Lombardi et a., 2012), circuit assembly, intact and spontaneously active cerebral cortex. How a balance of excitatory to inhibitory inputs is established and subsequently maintained remains a matter of debate (He and Cline, 2019). To provide an example, Xue et al. (2014) suggested that optimal E/I ratio across neurons is maintained, despite fluctuating cortical activity

levels, due to strengthening or weakening of synapses (Xue *et al.,* 2014). Our model suggests that the E/I ratio could be controlled (among other factors) by oscillations' collisions: when wave fronts interact, their merging gives rise to annihilation and intensification that provide a natural balance between excitatory and inhibitory inputs.

BZ-like circuits stand for an approach to neural networks different from the standard ones. The combination of the elementary modules, i.e., binary adder unit, allow the achievement of both series and parallel processing. Because of the intricate nature of excitable mediums and the high dependency on synchronized inputs both in chemical and in nervous settings, BZ-like networks require careful control of signals timing to achieve binary addition. Indeed, one of the main troubles with our model is time representation, since the human brain encompasses waves with different speeds, taking longer or shorter times to reach a target area. The same occurs inside the neural fibers of different diameter and diverse myelination. In our model, due to the scarce homogeneity of the connections between nodes, it takes different time for signals to pass through one node to another. To overcome the difficulty and achieve the required synchronous binary addition, a slight change in the channel length could be required. Since the signals are transmitted throughout the channels at the same speed, the lag time can be monitored and modified in two ways:

a) either by changing the channel length between nodes:

b) or, since the speed of the signal slows down as it passes through the gap, by modifying the lag time with the addition of several channel gaps:

When examining the very concept of lag thread, the term "lag" is a key innovation point, suggesting that it is worth to be incorporated in artificial nervous circuits. However, is it feasible to weight threads? The suggestion of Mitra et al. (2015) that different threads occupy different weights in brain activities is difficult to describe in the context of BZ-like approaches. For example, suppose that the weight of thread 1 is higher than the weight of thread 2. When simultaneous signals in thread 1 and 2 cross the structure, the signal 1 will obliterate the signal 2. This means that a functionally significant weight difference between distinct threads occurs. In turn, if the sole signal 2 crosses the circuit, it is left undisturbed. Further studies are required to design the proper structure able to treat differently signals coming from diverse threads.

Our network allows to appraise nonlinear dynamics in the plain terms of superimposing waves. In touch with our model, it is noteworthy that fluctuations of cortical activity are neither purely synchronous, nor spatially disorganized noise processes (Davis *et al.,* 2020). The matching of theoretical BZ models and real patterns of neural activity suggests that the occurrence of chaotic, non-linear activity during brain activity is correlated with peculiar topological and geometrical arrangements of the subtending neural circuits. BZ models for neural activity predict that the subtle balance between concentric oscillations produces nonlinear chaotic patterns of wave propagation. In touch with the BZ framework, the brain has been described as a complex, non-linear system operating at the edge of chaos, characterized by inter-dependent components, spontaneous self-organization and emergent properties (Tognoli and Kelso, 2013; Yan *et al.,* 2013; Xu and Wang, 2014; Kim and Lim 2015). Funnel-like locations in nervous phase spaces converge towards the shortest path as time progresses (Watanabe *et al.,* 2013; Tozzi *et al.,* 2016; Sengupta *et al.,* 2016; Wang *et al.,* 2017). Distinct nonlinear functional regimes have been described both in the central nervous system and in artificial neural networks (Deco and Jirsa, 2012; Touboul 2012; Afraimovich *et al.,* 2013). In agreement with brain dynamics, the solutions of BZ equations describe a wide range of nonlinear behaviors, including the formation of travelling waves and attractor-like phenomena, as well as self-organized patterns. BZ-like network models are relatively straightforward since they are equipped with simple logical devices such as Boolean gates, adders, counters, memory cells. Apart from the lengths of the channels and the proper arrangement of nodes and edges, no other adjustments, such as phase parameters or fine-tuning, is required by our network. This suggests that the emergence of nonlinear dynamics could be strictly correlated with the geometric and topological arrangement of the channels where wave propagation takes place. In the description of nonlinear neural issues, wave bifurcations might stand for phase transitions, while BZ dynamics might replace Hopfield networks and/or Hodgkin-Huxley/reaction diffusion models (Hopfield 1982; Yang and Wu, 2018). Therefore, the key to understand chaotic dynamics might lie in the constrained shapes of circuits, nodes and edges that provide the very arrangement of physical/biological networks. Paraphrasing the adage that the function creates the organ, our BZ-like model suggests that in a neural network the arrangement creates the function.

Acknowledgements

This research was jointly supported by the National Key R&D Program of China (grant 2018YFB1304900), the National Natural Science Foundation of China (grants U1813210 and U1613220), and the Natural Science Foundation of Tianjin (grants 14JCZDJC31800 and 14ZCDZGX00801).

References

Afraimovich V, Tristan I, Varona P, Rabinovich JM. Transient Dynamics in Complex Systems: Heteroclinic Sequences with Multidimensional Unstable Manifolds. Discontinuity, Nonlinearity and Complexity 2013; 2(1): 21-41.

Akam T, Kullmann DM. Oscillations and filtering networks support flexible routing of information. Neuron 2010; 67:308–320.

Beekman AJ, Nissinen J, Wu K, Liu K,Slager R-J, et al. Dual gauge field theory of quantum liquid crystals in two dimensions. Physics Reports 2017; 683:1-110.

Cincotti A, Maucher F, Evans D, Chapin BM, Horner K, et al. Threaded Rings that Swim in Excitable Media. Phys Rev Lett 2019; 123, 258102

Davis ZW, Muller L, Martinez-Trujillo J, Sejnowski T, Reynolds JH. Spontaneous travelling cortical waves gate perception in behaving primates. Nature 2020; 587:432–436.

Deca D. Grid Cells-From Data Acquisition to Hardware Implementation: A Model for Connectome-Oriented Neuroscience. In: The Physics of the Mind and Brain Disorders: Integrated Neural Circuits Supporting the Emergence of Mind, edited by Opris J and Casanova MF. New York, Springer; Series in Cognitive and Neural Systems 2017;493-511.

Deco G, Jirsa VK. Ongoing cortical activity at rest: criticality, multistability, and ghost attractors. J Neurosci. 2012; 7;32(10):3366-75. doi: 10.1523/JNEUROSCI.2523

Don AP, Peters JF, Ramanna S, Tozzi A. Topological View of Flows inside the BOLD Spontaneous Activity of the Human Brain. Front Comput Neurosci 2020; DOI: 10.3389/fncom.2020.00034.

Edelman G. Neural Darwinisim, New Perspectives Quarterly. January 2017; 31(1):25-27.

Fraiman D, Chialvo DR. What kind of noise is brain noise: Anomalous scaling behavior of the resting brain activity fluctuations. Frontiers in Physiology 2012; 1–11. http://doi.org/10.3389/fphys.2012.00307.

Gomez-Molina JF, Corredor M, Restrepo-Velasquez AA, Ricoy UM. Computer models for ions under electric and magnetic fields: random walks and relocation of calcium in dendrites depends on timing and population type. IFMBE proceedings. In: VII Latin American Congress on Biomedical Engineering CLAIB 2016, Bucaramanga, Santander, Colombia, October 26th -28th, 2016.

Guo S, Sun M-Z,Han J-D, Zhao X. Digital Comparator in Excitable Chemical media. Int. Journ. of Unconventional Computing 2014; 0:1–15.

Haider B, Duque A, Hasenstaub AR, McCormick DA. Neocortical network activity in vivo is generated through a dynamic balance of excitation and inhibition. The Journal of Neuroscience 2006; 26:4535-4545.

He H-Y, Shen W, Zheng L, Guo X, Cline HT. Excitatory synaptic dysfunction cell-autonomously decreases inhibitory inputs and disrupts structural and functional plasticity. Nat Commun 2018;9(1):2893.

He H-y, Cline HT. What Is Excitation/Inhibition and How Is It Regulated? A Case of the Elephant and the Wisemen. J Exp Neurosci 2019; 13: 1179069519859371.

Hopfield JJ. Neural networks and physical systems with emergent collective computational abilities. PNAS 1982; 79: 2554–2558.

Kim SY, Lim W. Frequency-domain order parameters for the burst and spike synchronization transitions of bursting neurons. Cogn Neurodyn 2015; 9(4):411-21.

Liu N, Matsumura H, Kato T, Ichinose S, Takada A, et al. Stem cell competition orchestrates skin homeostasis and ageing. Nature 2019; 568(7752):344-350.

Lombardi F, Herrmann J, Perrone-Capano C, Plenz D, de Arcangelis L. Balance between Excitation and Inhibition Controls the Temporal Organization of Neuronal Avalanches. Physical Review Letters 2012; 108:228703

Kosterlitz JM, Thouless DJ. Ordering, metastability and phase transitions in two-dimensional systems. Journal of Physics C: Solid State Physics 1973; 6 (7):1181–1203.

Massimini M, Huber R, Ferrarelli F, Hill S, Tononi G. The sleep slow oscillation as a travelling wave. J Neurosci 2004; 24:6862–6870.

McDowell JJ.Behavioral and neural Darwinism: Selectionist function and mechanism in adaptive behavior dynamics, Behavioural Processes 2010; 84. doi.org/10.1016/j.beproc.2009.k11.011

Mitra A, Synder AZ, Blazey T, Raichle ME Lag threads organize the brain's intrinsic activity. Proc Natl Acad Sci USA 2015; 112(17):2235-2244.

Muller L, Reynaud A, Chavane F, Destexhe A. The stimulus-evoked population response in visual cortex of awake monkey is a propagating wave. Nat Commun 2014; 5:3675.

Muller L, Chavane F, Reynolds J, Sejnowski TJ. Cortical travelling waves: mechanisms and computational principles. Nature Reviews Neuroscience 2018; 19: 255–268.

Newbold DJ, Laumann TO, Hoyt CR, Petersen SE, Snyder AZ, Dosenbach NUF. Plasticity and Spontaneous Activity Pulses in Disused Human Brain Circuits. Neuron 2020; https://doi.org/10.1016/j.neuron.2020.05.007.

Northoff G. The brain's spontaneous activity and its psychopathological symptoms – "Spatiotemporal binding and integration". Prog Neuropsychopharmacol Biol Psychiatry 2018; 80(Pt B):81-90.

Xu X, Wang R. Neurodynamics of up and down transitions in a single neuron. Cogn Neurodyn 2014; 8(6):509-15.

Xue M, Atallah BV, Scanziani M. Equalizing excitation-inhibition ratios across visual cortical neurons. Nature 2014; 511:596-600.

Qu J, Wang R, Du CYY. Oscillations and synchrony in a cortical neural network. Cognitive Neurodynamics 2014; 8(2):157–166.

Perrard S, Fort E, Couder Y. Wave-based Turing machine: time reversal and information erasing. Phys Rev Lett 2016; 117:094502.

Rosenbaum DA. It's a Jungle in There: How Competition and Cooperation in the Brain Shape the Mind. Oxford University, 2014.

Selfridge OG. Pandemonium: a pradigm for learning. In: Mechanization of thought processes: proceedings of a Symposium held at the national Physical Laboratory, London: HMSO, 2017, 513-526.

Sengupta B, Laughlin SB, Niven JE. Balanced Excitatory and Inhibitory Synaptic Currents Promote Efficient Coding and Metabolic Efficiency. PLoS Comput Biol 2013; 9(10): e1003263.

Sengupta B, Tozzi A, Cooray GK, Douglas PK, Friston KJ. Towards a Neuronal Gauge Theory. PLOS Biology 2016; 14(3), e1002400.

Sun M-Z and Zhao X. Multi-bit binary decoder based on Belousov-Zhabotinsky reaction. The Journal of Chemical Physics 2013; 138, 114106.

Tognoli E, Kelso JS. On the Brain's Dynamical Complexity: Coupling and Causal Influences Across Spatiotemporal Scales. Advances in Cognitive Neurodynamics (III) 2013; 259–265.

Touboul J. Mean-field equations for stochastic firing-rate neural fields with delays: Derivation and noise-induced transitions. Physica D: Nonlinear Phenomena. 2012; 241(15):1223–1244.

Tozzi A, Fla T, Peters PJ. Building a minimum frustration framework for brain functions in long timescales. J Neurosci Res 2016; 94(8):702–716.

Tozzi A, Zare M, Benasich AA. New Perspectives on Spontaneous Brain Activity: Dynamic Networks and Energy Matter. Front Hum Neurosci 2016; 10:247.

Tozzi A, Peters JF, Fingelkurts AA, Fingelkurts AA, Marijuán PC. Topodynamics of metastable brains. Phys Life Rev 2017; 21:1-20.

Tozzi A, Peters JF. Multidimensional brain activity dictated by winner-take-all mechanisms. Neuroscience Letters, 2018; 678 (21):83-89.

Tyukin IY, Iudin D, Iudin F, Tyukina T, Kazantsev V, et al. Simple model of complex dynamics of activity patterns in developing networks of neuronal cultures. PLoS One 2019; 14(6):e0218304.

Wang Y Wang R, Zhu Y. Optimal path-finding through mental exploration based on neural energy field gradients. Cogn Neurodyn 2017; 11(1):99-111.

Watanabe T., Hirose S, Wada H, Imai Y, Machida T, Shirouzu I, Masuda N. A pairwise maximum entropy model accurately describes resting-state human brain networks. Nature Communications, 2013; 4:1370.

Yang Y, Wu M. Rhythmicity and waves in the cortex of single cells. Philos Trans R Soc Lond B Biol Sci 2018; 373(1747):20170116. doi: 10.1098/rstb.2017.0116.

Zare M, Grigolini P. Chaos, Solitons & Fractals Criticality and avalanches in neural networks. Chaos, Solitons and Fractals 2013: 55:80–94.

Zhang G-M, Wong I, Chou M-T, Zhao X. Towards constructing multi-bit binary adder based on Belousov- Zhabotinsky reaction. J Chem Phys 2012; 136:164108.

Zhang H, Watrous AJ, Patel A, Jacobs J. Theta and alpha oscillations are traveling waves in the human neocortex. Neuron 2018; 98:1269–1281.

Authors hold copyright with no restrictions. Based on its copyright *Journal of NeuroPhilosophy* (JNphi) produces the final paper in JNphi's layout. This version is given to the public under the Creative Commons license (CC BY). For this reason authors may also publish the final paper in any repository or on any website with a complete citation of the paper.

Neural Processing Letters
https://doi.org/10.1007/s11063-022-11099-8

Ramsey's Theory Meets the Human Brain Connectome

Arturo Tozzi[1]

Accepted: 6 December 2022
© The Author(s), under exclusive licence to Springer Science+Business Media, LLC, part of Springer Nature 2022

Abstract
Ramsey's theory (RAM) from combinatorics and network theory goes looking for regularities and repeated patterns inside structures equipped with nodes and edges. RAM represents the outcome of a dual methodological commitment: by one side a top-down approach evaluates the possible arrangement of specific subgraphs when the number of graph's vertices is already known, by another side a bottom-up approach calculates the possible number of graph's vertices when the arrangement of specific subgraphs is already known. Since natural neural networks are often represented in terms of graphs, we propose to use RAM for the analytical and computational assessment of the human brain connectome, i.e., the distinctive anatomical/functional structure provided with vertices and edges at different coarse-grained scales. We retrospectively examined the literature regarding graph theory in neuroscience, looking for hints that might be related to the RAM framework. At first, we establish that the peculiar network required by RAM, i.e., a graph characterized by every vertex connected with all the others, does exist inside the human brain connectome. Then, we argue that the RAM approach to nervous networks might be able to trace unexpected functional interactions and unexplored motifs shared between different cortical and subcortical subareas. Furthermore, we describe how remarkable RAM outcomes, such as the Ramsey's theorem and the Ramsey's number, might contribute to quantify novel properties of neuronal networks and uncover still unknown anatomical connexions.

Keywords Computer science · Machine learning · Extremal set theory · Turán's theorem · Ramsey's theorem

1 Introduction

Graphs are discrete mathematical structures equipped with vertices joined by edges [13, 39]. They represent the common, general manifolds subtending the phase spaces of our logical, mathematical, physical, chemical, biophysical and biological worlds. The Ramsey's theory (RAM) from combinatorics and network theory examines the intrinsic mathematical features endowed in graphs [18]. Suggesting the general conditions for the existence of

✉ Arturo Tozzi
tozziarturo@libero.it

1 Center for Nonlinear Science, Department of Physics, University of North Texas, 1155 Union Circle, #311427, Denton, TX 76203-5017, USA

orderly substructures with regular properties, RAM advocates that large sets of elements (say numbers, points, planes, objects, image tessellations and so on) unavoidably contain repetitive geometric patterns [9]. Problems in RAM are usually tackled in terms of edge-coloured graphs such as, e.g., no matter how you n-color the edges, when the graph is large enough you will always find certain subgraphs with monochromatic edge labelling. A typical example of RAM is the problem of friends and strangers, which proves that at a gathering of any six people some three of them are either mutual acquaintances or complete strangers to each other.

RAM probes the emergence of the order that arises when different kinds of structures grow large enough. Hence, it has been profitably used in far-flung scientific fields. Interesting applications include game theory, decision making, metamathematics, communications, approximation algorithms, harmonic analysis, ergodic theory, convex and computational geometry, probabilistic method versus constructions, information retrieval in computer science, dual source codes, MaxSAT NP-hard computation problems, lower bound arguments for Parallel Random-Access Machine and for Boolean function computation [25, 29, 30].

Here we suggest using RAM for the assessment of the anatomical and functional neural network known as the human brain connectome. The cortical and subcortical areas of the central nervous system form a hierarchy characterized by community structures of densely interconnected brain subareas, each one standing for a graph vertex [27, 28, 36]. These networks can be described at different coarse-grained scales, from single neurons to neuronal populations and nervous tissue's macroscale, corresponding to the various levels of spatial resolution of the currently available imaging techniques. Even though the nervous networks' graphs are often too large to be manually analysed, advanced methods such as graph database and analysis libraries have been combined to search for/identify remarkable subgraph patterns and motifs inside the ever-increasing amount of connectomics data sets [24]. We will proceed as follows. At first, we will provide a gentle introduction to RAM and its theorems. Then, we will retrospectively go through the literature to ascertain whether RAM could be used to look for unknown, regular substructures hidden in the human connectome.

2 Materials and Methods

By an operational standpoint, the aim of Ramsey's theory is to answer to one of the two following reversed questions:

(1) Given a certain graph with n vertices, do subgraphs with specific features exist? In this case, researchers look for the unknown number of potential subgraphs encompassed in graphs with already known numbers n of vertices.
(2) Given a subgraph with specific features, which is the number n of vertices that a certain graph must have to encompass such subgraph? In this reverse case, researchers look for the required graphs with sufficiently many edges to contain already known structures as subgraphs. RAM calculates how many elements of a certain structure must be counted to guarantee the existence of a certain property.

Here we focus on the Ramsey's theorem (RT) and the Ramsey's number, two of the most distinguished RAM outcomes. RT refers just to complete graphs K_n, i.e., graphs in which every pair of distinct vertices n is connected by a unique undirected edge. To provide an example, Fig. 1a illustrates a K_6 complete graph. RT states that a complete monochromatic sub graph will always be found in any edge color labelling of a large enough complete graph [17]. To provide an example, let the edges of K_6 be coloured with two colours, e.g., black

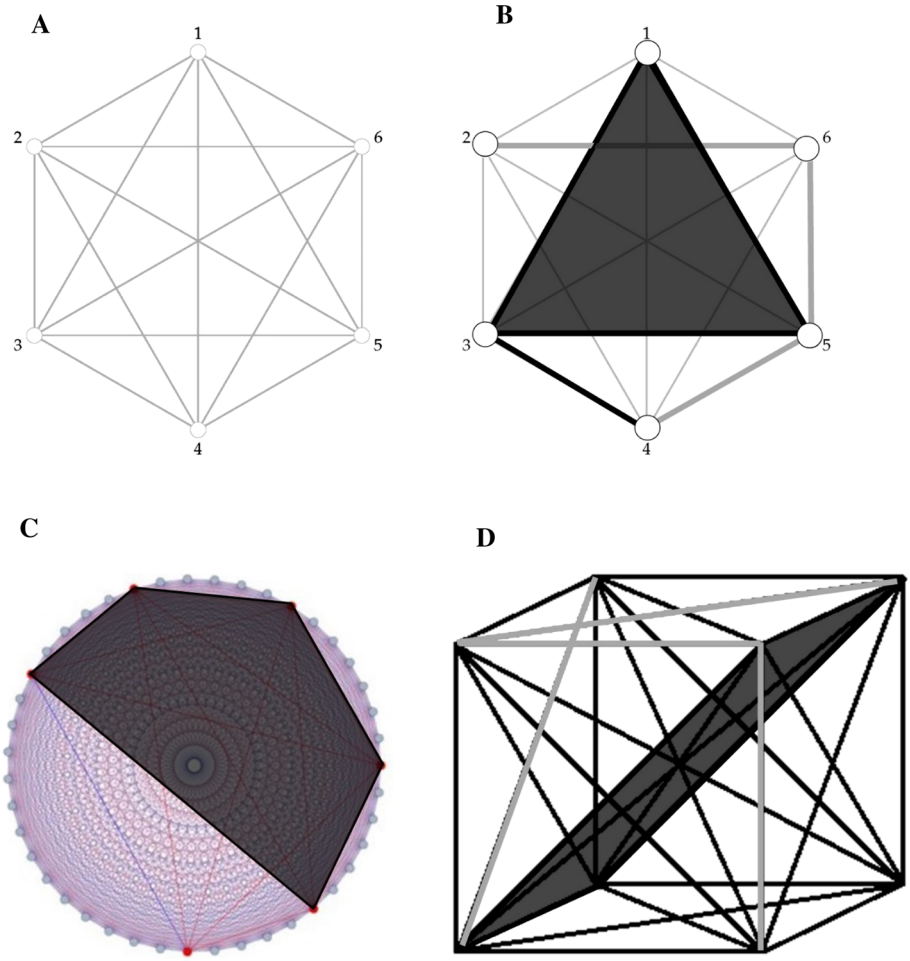

Fig. 1 a–b. Ramsey's theorem in case of Ramsey's number R(3,3) = 6. **a** A complete K_6 graph, geometrically forming the edge set of an exahedron with 15 edges. **b** Every pair of vertices is connected with a black or grey edge. No matter how the black or grey lines are arranged, there will always be a triangle that is either black, or grey. One of the many available black triangles is portrayed. **c** Ramsey's theorem in case of Ramsey's number R(5, 5) = 43. The best coloring of the complete graph K43 contains monochromatic figures (the black pentagon in Figure) sitting on 5 nodes. Modified from: Molnár et al. [25]. **d** Ramsey's theorem in the case of a complete three-dimensional graph with 8 edges, i.e., a hypercube. The Figure shows that the hypercube can contain, among countless others, a black rectangle, i.e., a monochromatic K4 with four coplanar vertices. Modified from: https://sites.google.com/site/pointlesslargenumberstuff/home/2/grahamsnumber

and grey, representing two different features (Fig. 1b). If two vertexes are connected by, say, a black edge, this means that they both display the black feature. According to RT, no matter how you colour with black or grey the edges of K_6, you cannot avoid the existence of:

(a) either a triangle whose three sides are all black,
(b) or a triangle whose three sides are all grey (Fig. 1b).

The conclusion is straightforward: whatever colours are used, there will always be at least one monochromatic figure (that is, a figure with all the edges of the same color). Since n vertices correspond to about n^2 edges, there are many ways to color the edges.

Therefore, for each pair of positive integers k and l there exists an integer R(k,l) (known as the Ramsey number) such that any graph with R(k,l) nodes contains a clique with at least k nodes or an independent set with at least l nodes. The general formula of the Ramsey's number reads:

$$R(k, l) = V$$

where k stands for the number of sides of the figure coloured with one color, l stands for the number of sides of the figure coloured with another color, R(k,l) is an integer depending on both k and l, and V stands for the number of vertexes [2]. The two terms (k,l) suggest that we are using a 2-coloring of the edges. In other words, the Ramsey's number is the minimum number of vertices V = R(k,l) such that all undirected simple graphs of order v contain a clique of order k or an independent set of order l. RT states that such a number exists for all k and l. Another statement of RT sounds as follows: for integers k,$l > = 2$, there exists at least a positive integer R(k,l) such that no matter how the complete graph $K_{R(k,l)}$ is two-colored, it will contain a subgraph K_k or a subgraph K_l. The above-mentioned K_6 example is conventionally described by the formula:

$$R(3, 3) = 6$$

The formula reads as follows: if you have a complete graph with the edges forming either a tree-sided black figure or a tree-sided grey figure, the complete graph must display at least 6 vertexes. In case of a subset of at least three completely uniform edges, RT guarantees that such subset is provided by a hexagonal graph. We will see in the sequel that the coloured graphs' black colors may stand for biophysical features such as, e.g., the spiking cerebral areas, while the grey colors for the non-spiking cerebral areas.

RT copes with the existence of monochromatic subsets characterized by connected edges of just one colour. Nevertheless, when the number n of the complete graphs' vertices increases, the number of possible colorings becomes very intricate. The Ramsey's numbers for the smallest values of K_n are known: for example, R(3,3) = 6 and R(4,4) = 18. Yet, when considering the huge available number of subgraphs with different colors, the Ramsey's number becomes almost impossible to calculate [1]. For higher K_n, only approximate bounds of the Ramsey's number are known [3]: for example R(5,5) is only known to lie in the range 43–49 (Fig. 1c), while R(6,6) = 102–165. It is worth mentioning that RT works also for multidimensional graphs [19]. The example of the hypercube is provided in Fig. 1d. In this case, RT allows us to answer to the following questions:

(a) What is the smallest number of dimensions of a n-dimensional hypercube, in which all vertex pairs form lines that all are colored with one of two colors (say black or grey), such that there must exist a monochromatic complete graph of four coplanar vertices? The answer is four.
(b) What is the smallest number of edges of a hypercube such that all the available colorings will contain a monochromatic K^4 with four coplanar vertices? The answer is eight.

Apart from RT, RAM includes other useful theorems that could be helpful to improve the graph theoretical analysis of the human brain connectome. A subfield of RAM, i.e., the extremal graph theory (EGT), describes graphs with sufficiently many edges to encompass the required structures as intermediate-sized subgraphs [7, 8, 35]. Interesting possibilities could be given by manifold, intriguing EGT theorems [5, 11, 26]. We will focus here just

on one of them, i.e., the Dirac's theorem, which states that very *n*-vertex simple graph all of whose vertices have degree at least *n/2* has a Hamilton cycle, i.e., is a path that visits each vertex exactly once.

2.1 Ramsey's Theorem and the Mathematics of the Human Brain Connectome

In the last decades, graph theoretical analysis was used to generate different kinds of graphs, such as the widely-diffused neural, convolutional and recurrent networks [40]. Concerning the neuroscientific field, the human brain connectome's networks have been mapped through a vast array of different techniques. Brain connectivity patterns (both anatomical and functional) are classified is terms of statistical dependencies (functional connectivity) or of causal interactions (effective connectivity) among various neural units, allowing neuroscientists and medical doctors to make inferences regarding human cognition, behaviour and nervous disorders [14]. Anatomical human brain connectome's graphs equipped with up to 1015 vertices and several thousand edges have been attained [16]. Starting from the Human Connectome Project's freely available data relative to 413 healthy human young adults (http://www.humanconnectome.org/documentation/S500), Fellner et al. [16] evaluated the frequent graph edges and subgraphs extracted from hundreds of high-quality MR images. The frequent edges were computed through the Budapest Reference Connectome Server [34], in which the edge frequency threshold k% can be selected. The resulting connectome contains only the edges present in at least k% of the subjects. In literature, every node roughly corresponds to an anatomically labelled area or subarea of the gray matter, while every edge corresponds to the axonal fibers connecting different areas or subareas. Still, the complete graphs' vertices do not refer to the neuronal microscopic level, rather represent larger Region of Interests that are densely connected to each other.

We propose to use the RT framework for the assessment of neuronal networks, in order to improve our knowledge of the connectivity among different brain subareas. To tackle our goal, we went retrospectively through the literature, looking for tacit remarks pointing towards the occurrence of RAM structures in the human brain connectome. We aimed to look for the occurrence in the human brain connectome's datasets provided by Fellner et al. [16] of the complete subgraphs (all-to-all connected brain regions) required by RT.

3 Results

3.1 Do Complete Graphs Exist in the Human Connectome?

Our RAM approach to real nervous networks requires the existence in the human brain connectome of rather peculiar graphs, i.e., graphs that are technically referred as complete. Therefore, the question is: does the human brain connectome contain graphs in which every pair of distinct brain subareas is connected by a unique edge? Examining the published data, we found that the answer is affirmative, thanks to the works of You et al. [37] and Fellner et al. [15, 16]. You et al. [37], exploring the design space of various relational graphs based on average path length and clustering coefficient, describe the features of complete graphs of fully connected layers. Fellner et al. [16] provided an effort to map the complete graphs of the human brain networks. Assessing the human braingraphs of 413 subjects from the dataset of the Human Connectome Project, each one consisting of 463 nodes, they listed the complete subgraphs present in at least the 80% of the available samples. Figure 2a provides an example

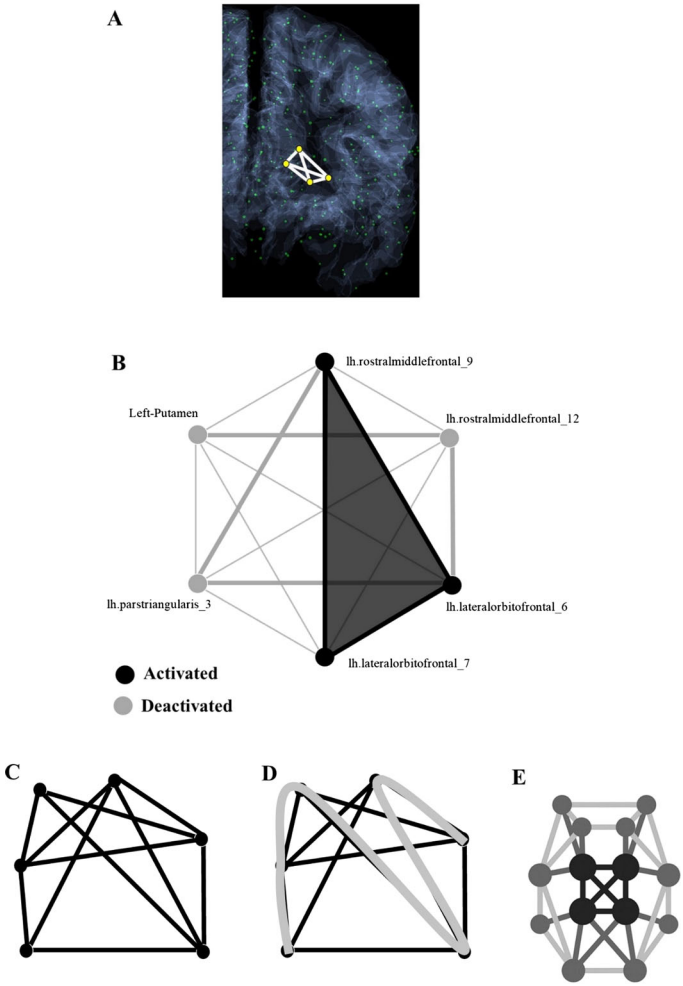

Fig. 2 **a** A complete subgraph with four vertices endowed in the human connectome. This K4 graph connects four anatomical zones, termed: Left-Caudate, Left-Pallidum, Left-Putamen and Left-Thalamus-Proper. Modified from Fellner et al. [16]. **b** In this K6 graph, every vertex stands for one of the anatomical subareas of the connectome described by Fellner et al. [16]. Each vertex is illustrated as a black dot (an activated brain subarea) or a grey dot (a deactivated brain subarea). When an edge links two vertexes with the same colour, the edge will be of the same colour. The figure depicts the occurrence of a black triangle with black edges in which three brain subareas are simultaneously activated. **c**–**e** Dirac's theorem and the human brain connectome. Given a simple graph with 6 vertices (**c**), a path visiting each vertex exactly once (grey line) is allowed if all the vertices have a degree at least n/2 (**d**). In the case of **c**, the degree is at least three. **e** in turn, the Dirac's theorem does not hold when the whole connectome is assessed as a single graph. In this simplified sketch of the bilateral human connectome [38], every vertex of this 14-vertices graph does not display more than 6 edges: this means that a path visiting every vertex exactly once is forbidden by the Dirac's theorem

of a K_4 subgraph detected by graph theoretical analysis. It is noteworthy that many of the complete subgraphs are located in the striatum and that just a few of them display nodes in both the hemispheres. Further, the right hippocampus and the right amygdala occur in much more complete subgraphs than the left ones, while the left thalamus-proper, the left putamen and the left pallidum occur in much more complete subgraphs than the right ones [16].

For our RAM purposes, the required nervous subgraphs must be equipped with a number of vertices ≥ 6. Fellner et al. [16] found fourty-eight K_6 and two K_7 complete subgraphs endowed in about 80% of the assessed connectomes, mostly (forty-two) located in the left hemisphere. Below are a few examples of the K_6 subgraphs detected in the human central nervous system:

(a) Left-Putamen, lh.lateralorbitofrontal_6, lh.lateralorbitofrontal_7, lh.parstriangularis_3, lh.rostralmiddlefrontal_12, lh.rostralmiddlefrontal_9. This subgraph is illustrated in Fig. 2b.
(b) Left-Putamen, lh.lateralorbitofrontal_4, lh.lateralorbitofrontal_6, lh.parstriangularis_3, lh.rostralmiddlefrontal_12, lh.rostralmiddlefrontal_9
(c) Right-Accumbens-area, Right-Caudate, Right-Hippocampus, Right-Pallidum, Right-Putamen, Right-Thalamus-Proper
(d) Right-Amygdala, Right-Caudate, Right-Hippocampus, Right-Pallidum, Right-Putamen, Right-Thalamus-Proper
(e) Left-Caudate, Left-Putamen, Left-Thalamus-Proper, lh.precentral_11, lh.precentral_4, lh.precentral_7
(f) Left-Caudate, Left-Putamen, lh.caudalanteriorcingulate_1, lh.caudalanteriorcingulate_2, lh.rostralanteriorcingulate_1, lh.rostralanteriorcingulate_2

Just two K_7 complete subgraphs have been found in the human central nervous system, both located in the left hemisphere:

(a) The first one connects the left putamen with six vertices in the left frontal lobe. The seven vertices correspond to the following anatomical zones: Left-Putamen, lh.lateralorbitofrontal_4, lh.lateralorbitofrontal_6, lh.lateralorbitofrontal_7, lh.parstriangularis_3, lh.rostralmiddlefrontal_12, lh.rostralmiddlefrontal_9
(b) the second one connects the left caudate and the left putamen to five left frontal areas. The seven vertices correspond to the following anatomical zones: Left-Caudate, Left-Putamen, lh.lateralorbitofrontal_7, lh.medialorbitofrontal_2, (lh.rostralanteriorcingulate_1, lh.rostralmiddlefrontal_12, lh.rostralmiddlefrontal_9

3.2 RAM in Neuroscience: Operational Issues

In the previous paragraph, going through the published literature, we confirmed the existence in the human brain connectome of the complete subgraphs equipped with at least six vertices required by RT. The next step is to illustrate some of the RAM procedures that could be used to assess neuronal networks. To provide an example, Fig. 2b illustrates one of the K_6 complete subgraphs endowed in the human connectome, in which every vertex stands for a different anatomical brain subarea [16]. We propose to use complete subgraphs to investigate the dynamics of activated and deactivated brain areas. In a neuroscientific context, the coloured graphs' black color can be replaced by cerebral areas that are currently active, while the coloured graphs' grey color can be replaced by cerebral areas that are currently inactive. Therefore, each vertex can be represented either as a black dot standing for an activated subarea, or a grey dot standing for a deactivated subarea. When an edge links two vertexes that

simultaneously display the same color, the edge is depicted with the same colour. In Fig. 2b, for example, three subareas are simultaneously activated and can be therefore portrayed as a black triangle with black edges. RT suggests that, in each of the forty-eight K_6 complete subgraphs endowed in the human brain connectome, there must always be at least three brain subareas that are simultaneously either activated or deactivated.

Apart from the opportunity to predict the simultaneous activation of brain subareas (i.e., the vertices of complete graphs) connected by neural paths (i.e., the edges of complete graphs), RT also suggests other useful applications. The Ramsey's number predicts the features and the arrangement of the complete networks potentially underlying the experimentally detected activated subareas. To make an example, if the simultaneous activation of four subareas is identified in which every pair of vertices is connected by a unique edge, RT dictates that the ensuing quadrangle must be encompassed inside a complete graph equipped with at least 18 vertices. This means that at least 18 brain subareas must be involved. This bottom-up approach paves the way to the possibility to discover unexplored connexions among hidden brain subareas that are simultaneously activated (or deactivated).

To provide an example of the countless possibilities of the extremal graph theory in the study of nervous connectomics, we will examine a viable application of the Dirac's theorem. Contrary to complete graphs, simple graphs (Fig. 2c) do not contain graph loops and multiple edges [10, 12]. Since the simple graph displays vertices with degree at least $n/2$, the Dirac's theorem dictates that a path crossing each vertex exactly once must unavoidably occur (Fig. 2d). This means that the existence of Hamiltonian paths is mandatory inside the substructures endowed in the human brain connectome. In turn, a path that crosses each vertex exactly once is not allowed when the macro-structure of the whole connectome is assessed in terms of a huge, single and simple graph. In this case, the simple graph's requirements of the Dirac's theorem are not guaranteed (Fig. 2e). This means that quick paths visiting just once a series of brain subareas are allowed, while quick paths visiting just once all the brain areas are not allowed. This suggests that a nervous path must be redundant to cross the whole brain, being required to cross a single node at least ≥ 2 times.

In conclusion, RAM suggests a twofold novel approach to the study of the brain connections:

(1) to start from a known complete network and look for the brain subareas that must necessarily be simultaneously activated.
(2) to start from the simultaneously activated brain subareas and look for the subtending, unknown complete network.

4 Conclusions

We suggest that a Ramsey's theory-framed narrative of human brain's connectome dynamics could be able to provide alternative approaches in respect to graph theoretical analysis of neuronal networks. One of the widely used theorem from RAM is the Ramsey's theorem (RT). RT descriptions are usually tackled in terms of edge-coloured complete graphs, such that the theorem guarantees a monochromatic coloring in any two-edge-coloured vertex complete graph. Concerning neuroscience, we suggested that, given six brain areas arranged in a complete graph, three of them must be simultaneously activated or deactivated.

Graph theory is becoming a widely diffused tool to cope with the current availability of large amounts of neuroscientific data. Yet, brain network reconstruction with complex

network representation involves biased theoretical assumptions that affect networks reconstruction and properties [22]. Some authors consider neurodata as the vectors of amplitudes of a multivariate signal, while others compare the similarity matrix computed between signals from different brain regions or look for features that are invariant under continuous deformations [6]. To assess nervous dynamics and describe the intrinsic taxonomy of neural architectures, several studies used different types of networks [21]. For example, topological data analysis delivers tools that describe the shape of data in terms of holes or cavities [33]. This successful method, based on the notion of simplicial complexes, provides results robust under continuous data deformation [31]. Of course, every one of the available methods comes with pros and cons, but we are not going to discuss them. What interest us is that RT requires the existence of distinctive complete graphs endowed in the human brain connectome, such that every pair of distinct brain subareas must be connected by a unique undirected edge. These peculiar graphs, although not frequent, do exist in the human brain connectome [16]. Complete graphs are well represented in real biological neural networks, in particular in the structures displaying densely connected "rich club property" [4, 38]. As stated above, complete graphs provide us with the operational opportunity to treat neuronal networks in terms of RT. Another invaluable advantage of complete graphs is that no anatomical contiguity is required among the brain subareas located in every vertex. To provide an example, take the two vertices that have been termed lh.rostralmiddlefrontal_9 and Left-Putamen in Fig. 2b. The very configuration of the complete graph permits to move and locate the two above mentioned anatomical areas in whatsoever vertex, since every subarea must be adjacent to every other. This means that the brain subareas belonging to complete graphs must always display functional connectivity, even though they are anatomically far apart. Relatively straightforward networks are achieved that are more manageable and easier to build, compared with the usual networks that make up the human brain connectome.

As stated above, RT can be operationally used to solve two inverse questions. On one hand, in any graph in which all points are connected by either black lines or grey lines, a large subset of the graph that is either all black or all grey is guaranteed. On the other hand, every uniform subset (no matter how it is great) is unavoidably encompassed in a graph with a well-known minimum number of vertices.

RAM could be used also in neuroscientific disciplines different from connectomics [23]. Take, for example, the Holland's hexagon model, widely used for the experimental evaluation of vocational interests [20]. This model consists of a complete graph that incorporates six interrelated interest areas, each one standing for a vertex: Realistic, Investigative, Artistic, Social, Enterprising, and Conventional. A RAM approach suggests that at least three of these six features must be either present or absent in subjects undergoing MRI and voxel-based morphometry to investigate the psychometric relationships between vocational interests and abilities (see, e.g., Schroeder et al. [32]). Another feasible possibility is to correlate RT with the Boolean logic. In our example of Fig. 2b, the activation/deactivation of brain subareas might correspond to the Boolean functions YES/NO. This means that, with the proper adjustments, RAM could be also used to assess complete graph-like Boolean networks.

By an epistemological standpoint, a RAM approach to neuronal issues suggests that, leaving apart specifically committed physical/biological explanations, the simultaneous activation of connectome subareas (usually detected through pairwise comparison techniques) might stand for a nervous mechanism exclusively depending on the inherent graph arrangement.

Author contribution The Author had full access to all the data in the study and take responsibility for the integrity of the data and the accuracy of the data analysis. The Author performed: study concept and design, acquisition of data, analysis and interpretation of data, drafting of the manuscript, critical revision of the

manuscript for important intellectual content, statistical analysis, obtained funding, administrative, technical, and material support, study supervision.

Funding This research did not receive any specific grant from funding agencies in the public, commercial, or not-for-profit sectors.

Declaration

Conflict of interest The Author does not have any known or potential conflict of interest including any financial, personal or other relationships with other people or organizations within three years of beginning the submitted work that could inappropriately influence, or be perceived to influence, their work.

Human participants This research does not contain any studies with human participants or animals performed by the Author.

References

1. Ajtai M, Komlós J, Szemerédi E (1980) A note on Ramsey numbers. J Combin Theory Ser A 29(3):354–360. https://doi.org/10.1016/0097-3165(80)90030-8
2. Allen P (2008) Covering two-edge-coloured complete graphs with two disjoint monochromatic cycles. Comb Probab Comput 17(4):471–486
3. Angeltveit V, McKay BD (2017) R(5,5)≤48. http://arxiv.org/abs/1703.08768
4. Ball G, Aljabar P, Zebari S, Tusor N, Arichi T, Merchant N et al (2014) Rich-club organization of the newborn human brain. Proc Natl Acad Sci U S A 111(20):7456–7461. https://doi.org/10.1073/pnas.1324118111
5. Bárány I, Valtr P (1998) A positive fraction Erdos-Szekeres theorem. Discrete Comput Geom 19:335–342. https://doi.org/10.1007/PL00009350
6. Billings J, Saggar M, Hlinka J, Keilholz S, Petri G (2021) Simplicial and topological descriptions of human brain dynamics. Netw Neurosci 5(2):549–568. https://doi.org/10.1162/netn_a_00190
7. Bollobás B (2004) Extremal graph theory. Dover Publications, New York
8. Bondy JA (1971) Pancyclic graphs I. J Comb Theory Ser B 11(1):80–84
9. Bondy JA, Murty USR (2008) Graph theory. Springer; 3rd printing 2008 ed. ISBN-13: 978-1846289699
10. Bronshtein IN, Semendyayev KA (2004) Handbook of mathematics, 4th edn. Springer, New York
11. Büyükçolak J, Gözüpek D, Özkan S, Shalom M (2019) On one extension of Dirac's theorem on Hamiltonicity. Discret Appl Math 252:10–16. https://doi.org/10.1016/j.dam.2017.01.011
12. Christofides D, Kühn D, Osthus D (2012) Edge-disjoint Hamilton cycles in graphs. J Comb Theory Ser B 102(5):1035–1060
13. Diestel R (2018) Graph theory. Springer, 5th edn. ISBN-13: 978-3662575604
14. Farahani FV, Karwowski W, Lighthall NR (2019) Application of graph theory for identifying connectivity patterns in human brain networks: a systematic review. Front Neurosci. https://doi.org/10.3389/fnins.2019.00585
15. Fellner M, Varga B, Grolmusz V (2020) The frequent network neighborhood mapping of the human hippocampus shows much more frequent neighbor sets in males than in females. PLoS ONE 15(1):e0227910. https://doi.org/10.1371/journal.pone.0227910
16. Fellner M, Varga B, Grolmusz V (2020) The frequent complete subgraphs in the human connectome. PLoS ONE 15(8):e0236883. https://doi.org/10.1371/journal.pone.0236883
17. Graham RL, Rothschild BL (1971) Ramsey's theorem for n-parameter sets. Trans Am Math Soc 159:257–292. https://doi.org/10.2307/1996010
18. Graham RL, Rothschild BL, Spencer JH (1990) Ramsey theory, 2nd edn. Wiley, New York
19. Hindman N, Strauss D (1998) 18 Multidimensional ramsey theory. In: Hindman N, Strauss D (eds) Algebra in the Stone-Cech compactification theory and applications volume 27 in the series De Gruyter expositions in mathematics. https://doi.org/10.1515/9783110809220.369
20. Holland JL (1997) Making vocational choices: a theory of vocational personalities and work environments. Psychological Assessment Resources, Inc, Lutz, FL, 3.è
21. Khan A, Sohail A, Zahoora U, Qureshi AS (2020) A survey of the recent architectures of deep convolutional neural networks. Artif Intell Rev 53:5455–5516

22. Korhonen O, Zanin M, Papo D (2021) Principles and open questions in functional brain network reconstruction. Hum Brain Mapp. https://doi.org/10.1002/hbm.25462
23. Laughlin DC (2013) The intrinsic dimensionality of plant traits and its relevance to community assembly. J Ecol. https://doi.org/10.1111/1365-2745.12187
24. Matelsky JK, Reilly EP, Johnson EC et al (2021) DotMotif: an open-source tool for connectome subgraph isomorphism search and graph queries. Sci Rep 11:13045. https://doi.org/10.1038/s41598-021-91025-5
25. Molnár B, Varga M, Toroczkai Z, Ercsey-Ravasz M (2018) A high-performance Analog Max-SAT solver and its application to Ramsey numbers. http://arxiv.org/abs/801.06620
26. Motzkin TS, Straus EG (1965) Maxima for graphs and a new proof of a theorem of Turán. Can J Math 17:533–540. https://doi.org/10.4153/CJM-1965-053-6
27. Peters JF, Tozzi A, Deli E (2017) Towards equations for brain dynamics and the concept of extended connectome. SF J Neuro Sci 1:1
28. Reese TM, Brzoska A, Yott DT, Kelleher DJ (2012) Analyzing self-similar and fractal properties of the C. elegans neural network. PLoS ONE 7(10):e40483. https://doi.org/10.1371/journal.pone.0040483
29. Roberts FS (1984) Applications of Ramsey theory. Discret Appl Math 9(3):251–261
30. Rosta V (2004) Ramsey theory applications. Electron J Combin 11:DS13
31. Salnikov V, Cassese D, Lambiotte R (2018) Simplicial complexes and complex systems. Eur J Phys 40(1):014001
32. Schroeder DH, Haier RJ, Tang CY (2012) Regional gray matter correlates of vocational interests. BMC Res Notes 5:242. https://doi.org/10.1186/1756-0500-5-242
33. Sizemore AE, Karuza EA, Giusti C, Bassett DS (2018) Knowledge gaps in the early growth of semantic feature networks. Nat Hum Behav 2:682–692
34. Szalkai B, Kerepesi C, Varga B, Grolmusz V (2017) Parameterizable consensus connectomes from the human connectome project: the budapest reference connectome server v3.0. Cognit Neurodyn 11(1):113–116
35. Szemerédi E (1975) On sets of integers containing no k elements in arithmetic progression. Acta Arith 27(585):199–245
36. Sporns O, Tononi G, Kötter R (2005) The human connectome: a structural description of the human brain. PLoS Comput Biol 1(4):e42. https://doi.org/10.1371/journal.pcbi.0010042
37. You J, Leskovec J, He K, Xie S (2020) Graph structure of neural networks. http://arxiv.org/abs/2007.06559
38. van den Heuvel MP, Sporns O (2011) Rich-club organization of the human connectome. J Neurosci 31(44):15775–15786. https://doi.org/10.1523/JNEUROSCI.3539-11.2011
39. Wilson RJ (2010) Introduction to graph theory. Prentice Hall; 5th edn. ISBN-13 978-0273728894
40. Zhou J, Cui G, Hu S, Zhang Z, Yang C et al (2020) Graph neural networks: a review of methods and applications. AI Open 1(2020):57–81

Publisher's Note Springer Nature remains neutral with regard to jurisdictional claims in published maps and institutional affiliations.

Springer Nature or its licensor (e.g. a society or other partner) holds exclusive rights to this article under a publishing agreement with the author(s) or other rightsholder(s); author self-archiving of the accepted manuscript version of this article is solely governed by the terms of such publishing agreement and applicable law.

The NEW ENGLAND JOURNAL of MEDICINE

August 4, 2022
N Engl J Med 2022; 387:397-407
DOI: 10.1056/NEJMoa2203067

ORIGINAL ARTICLE

Low-Dose Subcutaneous or Intravenous Monoclonal Antibody to Prevent Malaria

Richard L. Wu, M.D., Azza H. Idris, M.D., Ph.D., Nina M. Berkowitz, M.P.H., Myra Happe, Ph.D., Martin R. Gaudinski, M.D., Christian Buettner, Ph.D., Larisa Strom, M.P.H., Seemal F. Awan, M.D., LaSonji A. Holman, F.N.P., Floreliz Mendoza, R.N., Ingelise J. Gordon, R.N., Zonghui Hu, Ph.D., et al., for the VRC 614 Study Team*

CONCLUSIONS

In this small trial, L9LS administered intravenously or subcutaneously protected recipients against malaria after controlled infection, without evident safety concerns. (Funded by the National Institute of Allergy and Infectious Diseases; VRC 614 ClinicalTrials.gov number, NCT05019729.)

Comments

Arturo TOZZI, MD
Aug 09, 2022

ANOPHELES' PERI-EQUATORIAL MIGRATION VIA CORIOLIS FORCES

Most of the Plasmodium-carrying Anopheles spp. (henceforward mosquitoes) increase in individuals' number during the wet season and decrease during the dry season. It has been demonstrated that female pregnant mosquitoes can be transported by wind currents for hundreds of kilometers every night, at altitudes of at least 140-500 meters. It could be hypothesized that mosquitoes leave the African Northern peri-equatorial zones during the beginning of the dry season, crossing the near-equatorial trough to migrate towards the wetter African Southern peri-equatorial zones. Looking for wet seasons to lay their eggs, mosquitoes might employ the peri-equatorial Coriolis force to cross the equator from the North to the South, and viceversa. In order to migrate towards the wet zones, mosquitoes might make use of their halteres, i.e., small club-shaped organs able to detect the Coriolis forces. This would suggest that the best period to administer the short-lived monoclonal antibodies could be before the beginning of the wet season (i.e., February-March in the Northern hemisphere and Sectember-October in the Southern hemisphere).

Cognitive Neurodynamics
https://doi.org/10.1007/s11571-023-09978-4

RESEARCH ARTICLE

Towards a single parameter for the assessment of EEG oscillations

Arturo Tozzi[1] · James F. Peters[2]

Received: 6 February 2022 / Revised: 9 January 2023 / Accepted: 31 January 2023
© The Author(s), under exclusive licence to Springer Nature B.V. 2023

Abstract
The single macroscopic flow on the boundary of a closed curve equals the sum of the countless microscopic flows in the enclosed area. According to the dictates of the Green's theorem, the counterclockwise movements on the border of a two-dimensional shape must equal all the counterclockwise movements taking place inside the shape. This mathematical approach might be useful to analyse neuroscientific data sets for its potential capability to describe the whole cortical activity in terms of electric flows occurring in peripheral brain areas. Given a map of raw EEG data to coloured ovals in which different colours stand for different amplitudes, the theorem suggests that the sum of the electric amplitudes measured inside every oval equals the amplitudes measured just on the oval's edge. This means that the collection of the vector fields detected from the scalp can be described by a novel, single parameter summarizing the counterclockwise electric flow detected in the outer electrodes. To evaluate the predictive power of this parameter, in a pilot study we investigated EEG traces from ten young females performing Raven's intelligence tests of various complexity, from easy tasks (n = 5) to increasingly complex tasks (n = 5). Despite the seemingly unpredictable behavior of EEG electric amplitudes, the novel parameter proved to be a valuable tool to to discriminate between the two groups and detect hidden, statistically significant differences. We conclude that the application of this promising parameter could be expanded to assess also data sets extracted from neurotechniques other than EEG.

Keywords Brain · Electroencephalogram · Differential equation · Amplitude · EEG mounting

Introduction

The circulation of flows around a two-dimensional closed curve can be described by the integral of a two-dimensional vector field, which exemplifies the "macroscopic" circulation around the boundary of the closed curve. In turn, the "microscopic" circulation inside the enclosed surface can be depicted in terms of numerous small, closed curves which represent the vector field's propensity to circulate at that location. It is noteworthy that the microscopic flows match the curl i.e., a vector operator able to define the infinitesimal circulation of vector fields in three-dimensional spaces (Schey 1997; Vines et al., 2021). Here the Green's theorem from vector calculus comes into play, suggesting that the sum of all the microscopic circulations occurring in the area delimited by the closed curve equals the macroscopic circulation occurring on the curve's edge (Green, 1828; Cauchy 1846; Arfken 1985). The Green's theorem holds only for curves oriented counterclockwise, such that the border is defined as a positively oriented boundary surrounding the two-dimensional region.

In this paper we provided an effort to assess neuroscientific issues in terms of the powerful theoretical apparatus dictated by the Green's theorem. In particular, we focus on two-dimensional data sets extracted from EEG traces during Raven's intelligence tests of various complexity, from easy tasks to difficult tasks. Once the electric oscillations have been extracted from the EEG traces, we used the Green's theorem which gives us the opportunity to use a single parameter to describe the nervous dynamics. We suggest that this novel parameter could be useful to

✉ Arturo Tozzi
tozziarturo@libero.it

James F. Peters
james.peters3@umanitoba.ca

[1] Center for Nonlinear Science, University of North Texas, 1155 Union Circle, #311427, Denton, TX 76203-5017, USA

[2] Department of Electrical and Computer Engineering, University of Manitoba, 75A Chancellor's Circle, Winnipeg, MB R3T 5V6, Canada

Published online: 15 May 2023

describe at least part of the brain electric activity when the latter is assessed not just through EEG, but also through other neurotechniques such as e.g., fMRI and magnetoencephalography.

Patients and methods

EEG data

We analysed EEG traces of young female students (n = 10, mean age: 21 years) that were presented a non-verbal test of Raven's Advanced Progressive Matrices Plus used to quantify general human intelligence and abstract reasoning (Mazhirina et al., 2016; Zhuo et al., 2021). Half of the subjects (n = 5) were assessed with less difficult items (henceforward Raven Easy), while the other half (n = 5) were assessed with increasingly complex items (henceforward Raven Difficult). The procedures are described by Jaušovec and Jaušovec (2005 and 2010), accomplished according to the Declaration of Helsinki and approved by the Ethics Committee of the University of Maribor, Slovenia. The EEG was recorded while students were performing the two different tasks, using a Quick-Cap with sintered (Silver/Silver Chloride; 8 mm diameter) electrodes. The EEG activity was recorded over nineteen scalp locations (i.e., Fp1, Fp2, F3, F4, F7, F8, T3, T4, T5, T6, C3, C4, P3, P4, O1, O2, Fz, Cz and Pz) according to the International Federation's Ten-twenty Electrode Placement System. A ground electrode was applied to the forehead and ll leads were referenced to linked mastoids (A1 and A2). The bandpass of the digital EEG data acquisition and analysis system (SynAmps) was 0.15–100.0 Hz. The voltage gain was approximately –6 dB at cutoff frequencies. Every EEG trace was digitized online at 1000 Hz with a gain of 1000 (resolution of 084 μV/bit in a 16 bit A to D conversion) and stored on a hard disk. All epochs showing amplitudes above ± 50 microV (< 3%) were automatically removed from computations to avoid the occurrence of artifacts of the visualizing algorithm while plotting the EEG power maps. The raw data extracted from the experimental EEG activity, i.e., the matrices displaying the electric values in μV/milliseconds for every cortical area, were plotted in terms of a series of two-dimensional coloured ovals, different colours standing for different amplitudes (Fig. 1A). Every oval illustrates a one-millisecond time frame.

The Green's theorem for the appraisal of EEG data

As stated above, the electric flows extracted from EEG data can be illustrated as front waves of different colours taking place on two-dimensional ovals, the latter summarizing the scalp locations of the EEG electrodes. In touch with the Green's theorem's counterclockwise requirement, we conventionally regarded the EEG positive amplitudes as taking place anticlockwise and the EEG negative amplitudes as taking place clockwise (Fig. 1A). The next step was to describe the electric amplitudes in every EEG oval frame in terms of a vector field, i.e., a quantity displaying magnitude and direction (angle) at every particular location (Fig. 1B). Using the Green's theorem's dictates to assess EEG data sets, we may state what follows: the sum of the amplitudes detectable inside an oval (i.e., the vector field described in Fig. 1B) must equal the values of amplitude detected on the surface of the same oval (i.e., the counterclockwise flow taking place on the oval's surface is illustrated by the red path in Fig. 1B). This means that a single flow detectable on the border of an oval timeframe is capable of operationally summarize the whole electric oscillations detectable in the enclosed surface.

Once established that the flows on the surface of two-dimensional manifolds can be assessed in terms of the flows taking place of their edge, our next step was to operationally find the appropriate neuroscientific counterpart. The flows taking place on the oval's edge correspond to the electrodes lying on the peripheral, outer borders of the EEG mounting (Fig. 1C). Therefore, we evaluated the values of all the electric amplitudes detectable in the following peripheral scalp locations: Fp1, Fp2, O1, O2, F7, F8, T3, T4, T5 and T6, while the central electrodes F3, F4, T3, T4, T5, T6, C3, C4, P3, P4, Fz, Cz and Pz were excluded from our analysis (Fig. 1D).

This means that for every timeframe (corresponding to 1 ms) we summed the values of the electric amplitudes experimentally detected in the outer locations Fp1, Fp2, O1, O2, F7, F8, T3, T4, T5, T6 and achieved μV/milliseconds plots. The sum can be expressed by a single value, i.e., a novel parameter able to summarize the EEG electric activity of the brain. We compared the values of this single parameter achieved from the subjects undergoing the Raven Easy and Raven Difficult tests. An independent two-sample, unpaired Student's t test was used to determine if the means of two sets of data were significantly different from each other.

Results

The patients were clustered in two groups: Easy and Difficult Raven test. The amplitudes measured in the outer EEG electrodes (henceforward outer amplitudes) were summed and plotted in μV/milliseconds for a time length of 500 ms. To provide an example, Fig. 2A illustrates the plot extracted from one of the subjects attending a Raven

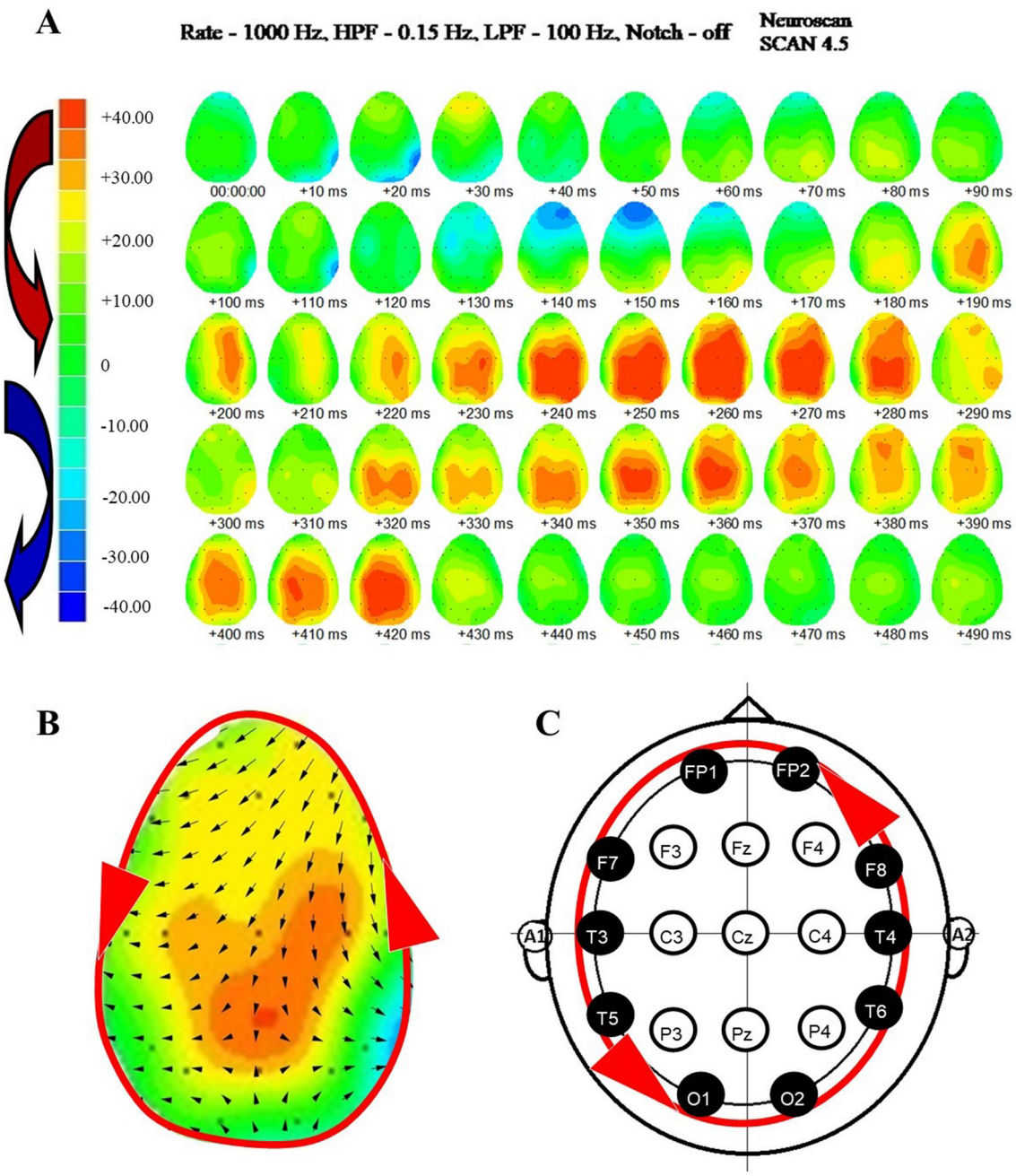

Fig. 1 EEG traces and the corresponding electric flows. **A** Fifty ovals illustrate a 500 ms, two-dimensional reconstruction of EEG waves from a subject performing a Raven Easy task. The different colours measure different detectable electric amplitudes (in μV) across different brain areas. The positive flows are conventionally deemed to occur anticlockwise (red curved arrow), while the negative flows clockwise (blue curved arrow). Although the EEG has been recorded using time windows of one millisecond, the Figure shows just the images taken every 10 ms. **B** Magnification of a single frame displaying a hypothetical vector field's grid (black arrows inside the oval). According to the Green's theorem, the counterclockwise flow (red circle with arrows) surrounding the EEG trace's boundary equals all the flows taking place on the enclosed vector field. **C** Once the counterclockwise circle is projected to a standard EEG mounting, the Green's theorem dictates that the flow taking place on the boundary can be measured by looking just at the external electrodes (highlighted in black)

Easy test. Each point of the line represents the sum of the amplitudes detected every millisecond in the peripheral scalp locations Fp1, Fp2, O1, O2, F7, F8, T3, T4, T5, T6.

The mean ± SD of outer amplitude was 267,7,414, 244 ± 521,106 μV for the patients who underwent the Easy Raven test, while 213,7,800,816 ± 266,8129 μV for

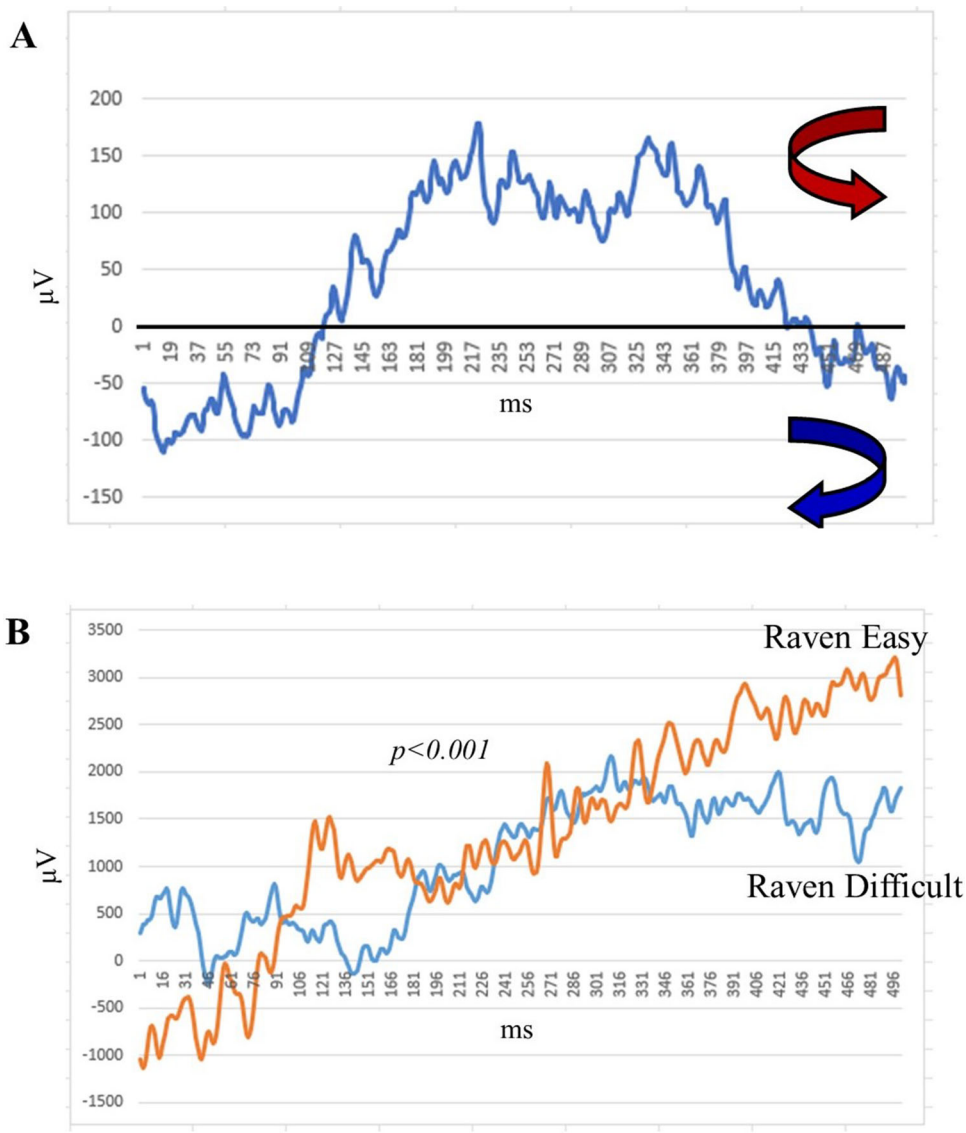

Fig. 2 **A** The plot (µV/milliseconds) depicts the sum of the outer amplitudes, i.e., the amplitudes detected in the locations corresponding to the electrodes Fp1, Fp2, O1, O2, F7, F8, T3, T4, T5, T6 during a Raven Easy task. The figure is drawn from the data of the coloured EEG plot illustrated in Fig. 1A. **B** Comparison of two plots summarizing the outer amplitudes mean in the five Raven Easy and in the five Raven Difficult tests

the patients who underwent the Difficult Raven test. The Student's t test showed that the means of two sets of outer amplitudes (Raven Easy vs. Raven Difficult) were significantly different from each other ($p < 0.001$). Therefore, significant differences in outer amplitude oscillations related to different test difficulty were observed. It is noteworthy that the soaring values of SD suggest a huge variability in the EEG amplitude values. Despite such seemingly unpredictable behavior of the electric amplitudes, the novel, single parameter which summarizes the outer amplitudes of the peripheral electrodes proved to be a very valuable tool. Indeed, the novel parameter enabled hidden statistically significant differences to be detected, leading to a powerful operational distinction between the two groups under examination.

Discussion

The Green's theorem says that every counterclockwise path on the border of a closed line conveys the vector fields' behaviour taking place inside the area surrounded by the border. The two-dimensional Green's theorem and its three-dimensional counterpart, i.e., the Stoke's theorem, have been widely used in different scientific fields. To provide an example, they were used to assess the relationships between the charges and the scalar potentials' horizon-values in black holes (Gibbons and Perry, 1978; Heusler 1998), suggesting the intriguing possibility to evaluate the internal flows of black holes by means of the holographic principle applied to their surfaces. In this paper, we used the Green's theorem to describe the electric

activity of the human brain in terms of the flows taking place on particular locations of the EEG mounting, i.e., the peripheral, outer electrodes. We found that a single parameter is able to summarize the general activity of the brain and to find statistically different outcomes in populations performing different cognitive operations. Even though we chose to focus on the specific task of the human intelligence, every experimentally detectable cognitive task can be assessed through the Green's theorem, from visual perception to memory, from intention to decision making, and so on (Cisek 2019). We evaluated the relatively short time windows of 500 ms in an effort to detect the very initial changes in brain activity during intelligence tasks and predict next-to-come, longer latency behaviours. Nevertheless, every technically achievable time window (either longer or even shorter) can be explored through the Green's theorem. We chose to focus on EEG traces since we had at our disposal the rough data sets available from the published papers of the lamented Norbert Jausovec. However, the Green's theorem can be used to investigate the nervous flows and oscillatory wave fronts achieved from different neurotechniques, such as, e.g., fMRI, magnetoencephalography and so on.

Our description of counterclockwise flows taking place in two-dimensional nervous traces can be extended also to the description of their three-dimensional counterparts. While the Green's theorem depicts the two-dimensional case, the above mentioned Stoke's theorem illustrates the three-dimensional case (Pontryagin 1959). In Fig. 3A, a three-dimensional EEG headmodel is illustrated. For the right-hand rule of vector calculus, the length of every vector (the red arrows in Figure) summarizes the microscopic curl activity taking place in the corresponding scalp location. Note that some arrow turns clockwise, while others counterclockwise (not illustrated in Figure). For the Stoke's theorem, the counterclockwise activity taking place on the EEG border equals the sum of all the counterclockwise activities depicted by the red vectors.

The study of Green's Theorem in terms of a piecewise smooth boundary formed by a pair differentiable functions P and Q is a source of a variety of applications (Zenisek 1999; Tewari, R., Vinodchandran, N.V. (2012)). It has been proved that, whenever the following conditions for a pair of simple, closed curves (named after Jordan) are satisfied, then Green's theorem holds (Craven, 1964).

When the simple (no loops), closed curves P and Q are close enough (Fig. 3B), then the line integral $\oint_C (Pdx + Qdy)$ is approximately the same as the area of the region R within a piecewise smooth boundary traced by P and Q, i.e., whenever we have:

C = simple (no self-intersections) Jordan Curve.

R = bounded region enclosed by the curve C (see Fig. 3C for an example).

P(x,y), Q(x,y) = functions differentiable at all points of R and continuous on C ∪ R.

Therefore,

$\frac{\partial Q}{\partial x} - \frac{\partial P}{\partial Y} = Riemann$ integrable difference on R. Then

$$\oint_c (Pdx + Qdy) = \iint_R \left[\frac{\partial Q}{\partial x} - \frac{\partial P}{\partial Y}\right] dxdy$$

The conditions set forth by Craven (1964) for the Green's theorem hold true with the pair of curves P, Q shown in Fig. 3B, C. Indeed, the cycles (simple, closed curves) traced by the differentiable functions P and Q are represented in the displays of brain waves. Obviously, P and Q together provide a boundary region R of the space occupied by the brain, viewed here in a planar fashion. In the case where $\frac{\partial Q}{\partial x} - \frac{\partial P}{\partial y}$ is a divergence, we know that Green's theorem holds. From a practical standpoint, this means that Green's theorem gives an approach to

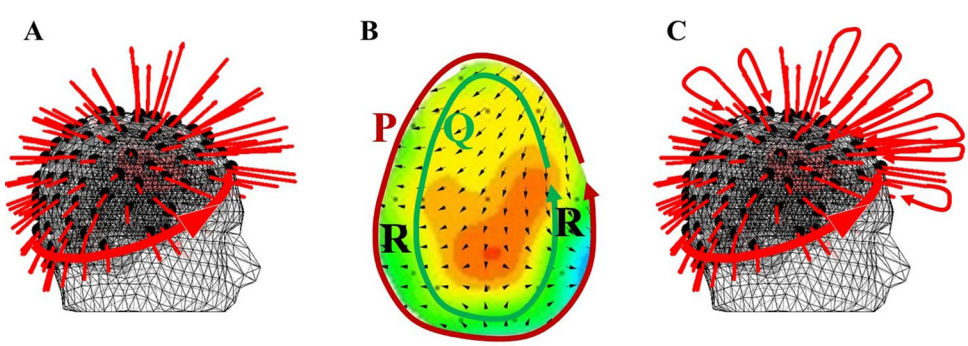

Fig. 3 **A** Orientations of the lead fields in the XYZ directions for headmodel dipoli for a superficial source. The single macroscopic value equalling the sum of all the microscopic vectorial activities (arrows) is outlined by the thick counterclockwise circle. Modified from: https://www.fieldtriptoolbox.org/workshop/oslo2019/forward_modeling/ **B** A pair of differentiable functions P and Q on an EEG oval. In the basic scenario described by the Green's Theorem, P and Q are simple, closed curves that form the boundary R and the line integral C on Pdx + Qdy is a measurement of the area occupied by the region R. **C** The red arrows of Fig. 3A can be described in terms of cycles and overlapping cycles standing for the vortexes formed by nested cycles

measuring the brainwave region bounded by P and Q in terms of the line integral $\oint_C (Pdx + Qdy)$, knowing that what we have found is the area of the region bounded by P and Q. In Fig. 3C, this observation is applied to multiple bounded regions in pairs of overlapping cycles of brain activity vortexes. We now have a means of comparing the areas of bounded regions within different vortexes formed by nested cycles resulting from brain activity. These nested brain activity cycles are consistent with what we know about vortexes found in the nested, non-concentric cycles in electromagnetic wave forms (Baldomir, and Hammond, 1996).

To sum up, what do we achieve when using the Green's theorem to evaluate nervous flows? A short answer to this question is: we arrive at a straightforward means of measuring the area of the region R bounded by a pair of nested curves commonly found in cortical activity vortexes. The collection of the vector fields detected from the scalp can be described by a single parameter, i.e., the counterclockwise electric flow occurring on the border of the EEG oval images. That is, we glean information inside the shape traced by nested curves arising from brain activity.

Acknowledgements To the memory of Norbert Jausovec. He and his precious EEG data go on living in our hearts and manuscripts.

References

Arfken G (1985) Gauss's theorem. Mathematical methods for physicists, 3rd edn. Academic Press, Orlando, FL

Baldomir D, Hammond P, (1996) Geometry of electromagnetic systems. Oxford Science Publications.

Cauchy A (1846) Sur les intégrales qui s'étendent à tous les points d'une courbe fermée. Comptes Rendus 23:251–255

Cisek P (2019) Resynthesizing behavior through phylogenetic refinement. Atten Percept Psychophys 81:2265–2287. https://doi.org/10.3758/s13414-019-01760-1

Craven BD (1964) A note on Green's theorem. J Austr Math Soc 4(3):289–292

Gibbons GW, Perry MJ (1978) Black holes and thermal green functions. Proc Royal Soc Lond Math Phys Sci 358(1695):467–494

Green G (1828) An essay on the application of mathematical analysis to the theories of electricity and magnetism. Journal f ur die reine und angewandte Mathematik Vol 39, 1 (1850) pp 73–89, Vol 44, 4 (1852) pp 356–74, and Vol 47, 3 (1854) pp 161–221

Heusler M (1998) Stationary Black Holes: uniqueness and beyond. Living Rev Relativ 1998, 1(1): 6 https://doi.org/10.12942/lrr-1998-6

Jaušovec N, Jaušovec K (2010) Emotional Intelligence and Gender: A Neurophysiological Perspective. In: Gruszka A, Matthews G, Szymura B (ed), Handbook of Individual Differences in Cognition (pp 109–126). New York, NY: Springer New York. Retrieved from http://www.springerlink.com/index/https://doi.org/10.1007/978-1-4419-1210-7_7.

Jausovec N, Jausovec K (2005) Differences in induced gamma and upper alpha oscillations in the human brain related to verbal/performance and emotional intelligence. Int J Psychophys 56(3):223–235. https://doi.org/10.1016/j.ijpsycho.2004.12.005

Mazhirina KG, Mel'nikov ME, Pokrovskii MA, Petrovskii ED, Savelov AA, Shtark MB (2016) Raven's progressive matrices in the lexicon of dynamic mapping of the brain (MRI). Bull Exp Biol Med 160(6):850–856. https://doi.org/10.1007/s10517-016-3325-2

Pontryagin LS (1959) Smooth manifolds and their applications in homotopy theory. American Mathematical Society Translations, Ser. 2, Vol. 11, American Mathematical Society, Providence, R.I., pp 1–114

Schey HM (1997) Div, Grad, Curl, and all that: an informal text on vector calculus, 3rd edn. W. W. Norton, New York

Tewari R, Vinodchandran NV (2012) Green's theorem and isolation in planar graphs. Inf Comput 215:1–7

Vines SK, Anderson BJ, Allen RC, Denton RE, Engebretson MJ, Johnson JR, Burch JL (2021) Determining emic wave vector properties through multi-point measurements: The wave curl analysis. J Geophys Res Space Phys 126(4):e2020JA028922 https://doi.org/10.1029/2020JA028922.

Zenisek A (1999) Green's theorem from the viewpoint of applications. Appl Math 44(1):55–80

Zhuo T, Huang Q, Kankanhalli M (2021) Unsupervised abstract reasoning for raven's problem matrices. IEEE Trans Image Process 2021(30):8332–8341. https://doi.org/10.1109/TIP.2021.3114987

Publisher's Note Springer Nature remains neutral with regard to jurisdictional claims in published maps and institutional affiliations.

Springer Nature or its licensor (e.g. a society or other partner) holds exclusive rights to this article under a publishing agreement with the author(s) or other rightsholder(s); author self-archiving of the accepted manuscript version of this article is solely governed by the terms of such publishing agreement and applicable law.

Organisms Diversity & Evolution
https://doi.org/10.1007/s13127-023-00613-y

ORIGINAL ARTICLE

Non-ultrametric phylogenetic trees shed new light on Neanderthal introgression

Arturo Tozzi[1]

Received: 6 May 2022 / Accepted: 28 April 2023
© Gesellschaft für Biologische Systematik 2023

Abstract

Ultrametric spaces are widely used to depict evolutionary times in phylogenetic trees since they assume that every population/species is located at the tips of bifurcating branches of the same length. The discrete branching of ultrametric trees permits the measurement of distances between pairs of individuals that are proportional to their divergence time. Here the traditional ultrametric concept of bifurcating and divergent phylogenetic tree is overturned and a new type of non-ultrametric diagram is introduced. The objective of this study is the description of gene flows in branching species/populations in terms of converging trees instead of bifurcating trees. To provide an operational example, the paleoanthropological issue of the date of Neanderthal genome's introgression in non-African humans is examined. Neanderthals and ancient humans are not anymore two species that exchange chunks of DNA, rather become a single, novel cluster of extant hominins that must be considered by itself. The novel converging, non-ultrametric phylogenetic trees permit the calibration of molecular clocks with a twofold benefit. When the date of the branching of two population/species from a common ancestor is known, the novel approach allows to calculate the time of subsequent introgressions. On the contrary, when the date of the introgression between two population/species is known, the novel approach allows to detect the time of their previous branching from a common ancestor.

Keywords Triangle inequality · Sets · Molecular clock · Hominins

Introduction

Phylogenetic analysis protocols entail various steps, from the identification of sets of homologous sequences to the download of the achieved sequences, ending up with the production of a phylogenetic tree (PT) inferred from the aligned sequences (Soares et al., 2017; Tamura et al., 2011). PTs depict morphological/genetic evolutionary relationships among populations or species (Woese, 2000). Unlike other evolutionary diagrams such as additive trees and cladograms, the PT abscissa describes the amount of change of a given character that occurred over time, while the ordinate describes the evolutionary time. PT makes use of bifurcating branches in which the tips stand for groups of descendants' populations/species and the nodes for their common ancestors. The branch lengths are proportional to the inferred evolutionary distance among the specimens under investigation (Hall, 2013). Rooted PT of clustering sequences is generally set in ultrametric spaces, i.e. non-Euclidean spaces in which all the tips are equidistant from the root. To provide an example, the widely used UPGMA and WPGMA methods (i.e. unweighted and weighted pair group methods with arithmetic mean) generate ultrametric trees characterized by the constant rate assumption that the distances from the root to every branch tip are equal (Sokal & Michener, 1958). Therefore, ultrametric trees are very useful to describe a peculiar aspect of the evolutionary history, i.e. the divergence time among populations/species (Page & Holmes, 1998).

Here an alternative approach to ultrametric trees, i.e. a novel non-ultrametric phylogenetic tree (NUPT) is proposed which allows the description of gene flows in terms of convergent instead of divergent branches. The model is illustrated and its theoretical advantages and operational implications are discussed, providing an example drawn from the paleoanthropological issue of ancient hominins'

✉ Arturo Tozzi
tozziarturo@libero.it

[1] Center for Nonlinear Science, Department of Physics, University of North Texas, 1155 Union Circle, Denton, TX #31142776203-5017, USA

Published online: 10 June 2023

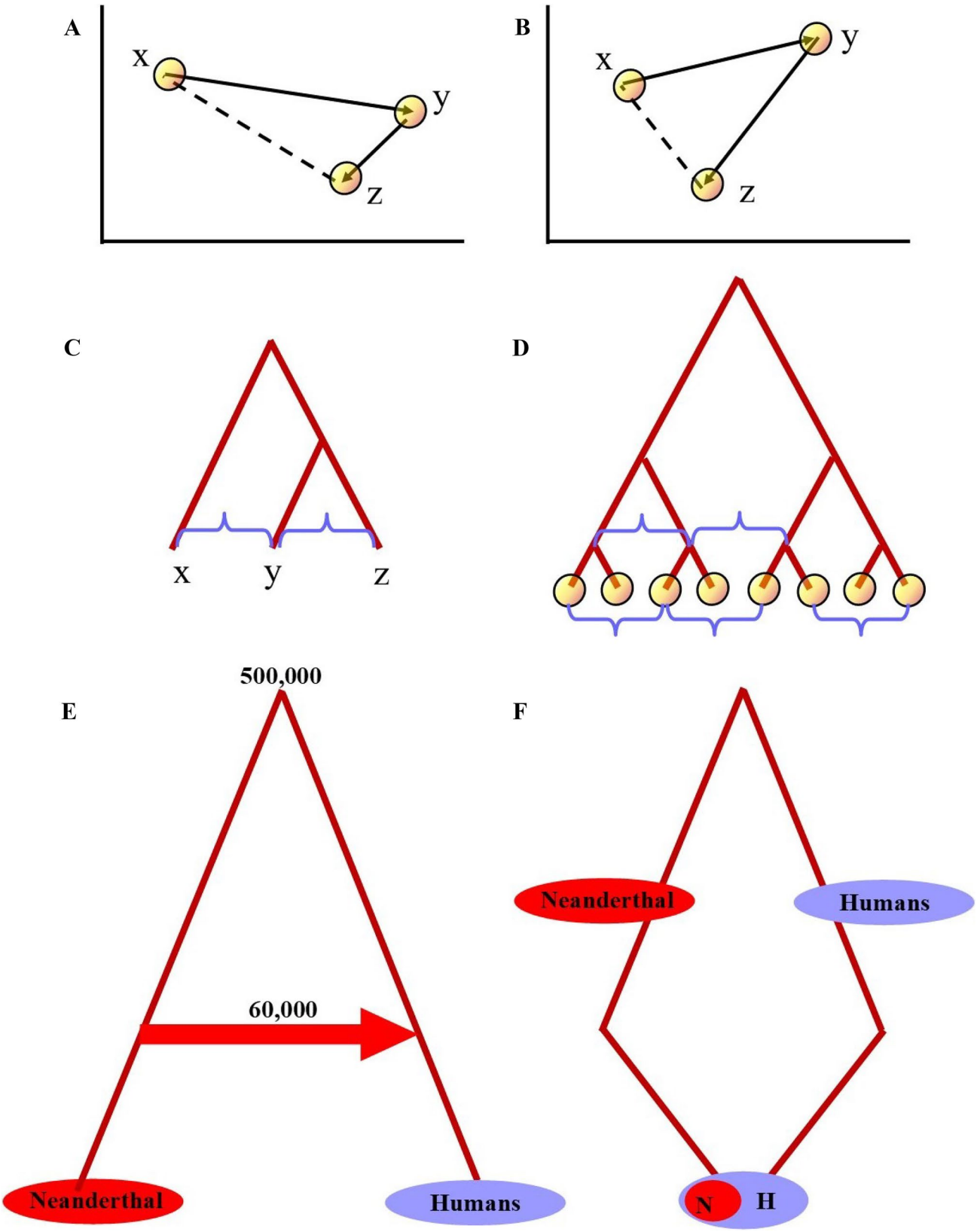
A
x
y
z
B
x
y
z
C
x
y
z
D
E
500,000
60,000
Neanderthal
Humans
F
Neanderthal
Humans
N
H

◂**Fig. 1-D** Composition and arrangement of ultrametric spaces. **A** According to the standard Euclidean geometry, triangle inequality means that every side of a triangle cannot be longer than the sum of the other two. **B** In the non-Euclidean case, strong triangle inequality comes into play so that just triangles with two or three sides of the same length are allowed. **C** An ultrametric tree is shaped as a triangle grid generated by the steps among x, y and z. Note that the distances between the branches are accurately preserved. The points x, y and z may stand not just for the vertices of equilateral or isosceles triangles, but also for features such as biological taxa, populations and species. **D** Regular branching tree of a translational invariant ultrametric space. The population/species are represented by the yellow balls at the tips of the distal branches, while the distances among the population/species are provided by the tree itself, according to the hierarchy of the balls' sets and subsets. **E** Phylogenetic ultrametric tree of genetic flows between Neanderthals and ancient non-African humans (termed "humans" for sake of clarity). The split and introgression dates (500,000 and 60,000 years ago, respectively) are tentative and based on the current literature. If the two available sets are deemed to be separated, they can be located inside a diverging branching tree. **F** New NUPT of genetic flows between Neanderthals and non-African humans. In this case, the two sets partially superimpose, giving rise to phylogenetic trees that are convergent instead of bifurcating. Therefore, a large set of modern extant hominins is achieved which encompasses as subsets both introgressed Neanderthals and ancient humans

DNA introgression in Late Pleistocene Homo sapiens. Putative gene flows from archaic hominins to Homo sapiens suggest a very intricate evolutionary history characterized by a single of multiple episodes of gene flow between populations/species (Prüfer et al., 2017). For example, genome sequencing of various hominins' specimens points towards gene flows among Neanderthals, Denisovans, unknown archaic groups and early modern humans (Hajdinjak et al., 2021; Meyer et al., 2012; Prüfer et al., 2014; Reich et al., 2010).

The focus here is on the genetic relationships between Neanderthals and modern humans. The inferred timing of their last common ancestor is a hotly debated matter since small variations in the weighed parameters lead to very different estimates of their divergence time (Meyer et al., 2016). Mixed results from studies of cranial variation, ancient DNA, human mutation rate, mitochondrial sequence comparisons and average value of linkage disequilibrium suggest that the lineages leading to modern humans and Neanderthals diverged between 300,000 and 600,000 years ago, with little subsequent admixture (Krings et al., 1997; Noonan et al., 2006; Serre et al., 2004). More radical suggestions date back the last common ancestor to pre-800,000 years ago (Gómez-Robles A, 2019). It has been suggested that an introgression from Neanderthals to non-African human ancestors occurred 37,000–86,000 years ago, most likely between 47,000 and 65,000 years ago (Posth et al., 2017; Sankararaman et al., 2012). In the sequel, it is made clear how and why the novel NUPT approach sheds new light on the times of divergence and introgression of Neanderthals and ancient non-African human populations.

Materials and methods

Ultrametric diverging trees: what, when and why

Ultrametric trees rely on the mathematical concept of ultrametricity, which is closely related to the concept of triangle inequality. In plane geometry, triangle inequality states that the length of every side of the triangle is lower than or equal to the sum of the other two, such that:$d(x,z) \leq d(x,y) + d(y,z)$where x, y and z are the three vertices of a triangle and d is the distance between every pair of vertices (Fig. 1A). In this case, the triangle lies in the classical Euclidean space.

Yet, there exist a strongest version of triangle inequality, such that:$d(x,z) \leq \max[d(x,y), (y,z)]$

In plain words, the rule of strong triangle inequality suggests the sole occurrence of peculiar triangles, i.e. equilateral or isosceles with the basis smaller than the other two sides (Fig. 1B). Those triangles do not lie in Euclidean space, rather in a space termed ultrametric. This non-Euclidean space can be depicted either as a triangular grid where the distances are always preserved (Fig. 1C), or as a tree-like hierarchy of triangles/balls (Fig. 1D).

The ultrametric assumption requires that a tree must display the following unusual properties:

1) The ultrametric distances are described by steps that are unavoidably discrete: continuum is not allowed.
2) The ultrametric-based clocks rely on the assumption that the temporal distance always corresponds to the total time multiplied by a constant.
3) Different ultrametric balls do not have points in common. This leads to counterintuitive outcomes:
4) In an ultrametric space, two balls cannot overlap.
5) In an ultrametric space, two balls always keep the same spacing and fixed distance.

Scientists use DNA sequence data gathered from hominin samples to test models of archaic admixture such as, in our case, the Neanderthal gene flow in modern non-African humans. To evaluate recombination events and build PT, scientists infer the date of the last genetic exchange between the ancestral populations/species by measuring the extent of admixture linkage disequilibrium (Sankararaman et al., 2016). A widely used procedure for dating gene flow in target populations/species evaluates a set of single nucleotide polymorphisms at which a single randomly chosen allele is derived relative to an ancestor (Sankararaman et al., 2016; Wall, 2000). Traditionally, scientists have preferred ultrametric trees for ancestral state reconstruction and phylogenetic inference because of their unvaluable practical advantages. Discrete branchings of ultrametric trees are

characterized by a distance between any pair of (modern) sequences that is plainly proportional to their divergence time (Gavryushkin et al., 2016). In ultrametric trees, the amount of change in living populations/species is related to the amount of time (Cusimano & Renner, 2014). This allows the building of molecular clocks able to correlate phenotypic evolution and genomic/molecular/protein sequence data with branch lengths. Indeed, the molecular clock assumption suggests that the mutation rates are always constant on all the branches. This means that the mutation distances are proportional to the divergence time and equal between any pair of modern sequences and their most recent common ancestor (Page & Holmes, 1998).

Ultrametric trees have been used to build up PTs of gene flows among disparate hominins. Several tasks have been accomplished such as the genome sequence of Neanderthals from the Altai Mountains and Vindija Cave (Prüfer et al., 2017), the putative date of interbreeding between Neanderthals and modern humans (Sankararaman et al., 2012), the Neanderthal ancestry in Initial Upper Palaeolithic European humans (Hajdinjak et al., 2021), the Denisovan and Neanderthal gene flow in Icelandic genomes (Skov et al., 2020), the ancient gene flow from early modern humans into Eastern Neanderthals (Kuhlwilm et al., 2016) and the genetic evidence for archaic admixture in Africa (Hammer et al., 2011). It is noteworthy that the statistic across pairs of introgressed alleles is expected to have an exponential decay with genetic distance since linkage disequilibrium decays at a constant rate per generation. This means that recombination events are expected to break down the genetic segments shared by different populations/species such as modern humans and Neanderthals (Sankararaman et al., 2012).

Even though ultrametric trees are favoured by scientists to ascertain gene flows between populations/species, they have some limitations. Distances between populations/species have been successfully used to shed light into their evolutionary past (Zhivotovsky, 2001). The resulting scenarios are generally understood to be a snapshot of the data, in the sense that they can be used as a starting point to guide exploration of a dataset. However, only in rare cases are the distances assumed to have arisen under a molecular clock (i.e. to satisfy the ultrametric property). The molecular clock assumption is generally expected to hold below the species level, which is the reason why tools like UPGMA have been applied successfully in these types of studies. In general, trees that do not have the same amount of time between the tips and the roots and cannot be regarded as being properly ultrametric, unless the cases in which evolution is strictly proportional to time. Indeed, the rates of neutral evolution on large time scales are neither constant nor are they a function of mutation alone. Since human evolution, including that of the fossil populations from which genomes may be recovered, is far from mutation drift equilibrium, variation in population size through time and across populations can be expected. Moreover, modifications in the population size change the degree to which mildly deleterious and mildly fitness-enhancing mutations may behave as though they are neutral.

Towards a novel converging tree

Given these premises, we suggest a non-ultrametric alternative to the widespread ultrametric trees, i.e. a novel PT able to assess recombination events in evolutionary times. Ultrametric trees entail the philosophical and methodological implication that PTs are bifurcating. Every branch leads to a single population/species that is kept conceptually distinct from the others, even in the event of introgressive episodes (Fig. 1E). Therefore, in ultrametric trees, the tips (i.e. the population or the species under assessment) shall be regarded as separated sets. A variant of PT is proposed here in which the ultrametric assumption is partially lessened. In the novel framework, the two population/species undergoing introgression give rise to a SINGLE population, so that the branching tree tends to converge in a single cluster, rather than bifurcating in two smaller clusters (Fig. 1F). In mathematical terms, the non-overlapping sets located at the numerous tips of bifurcating ultrametric trees become overlapping subsets located at the unique tip of convergent NUPT.

To describe NUPT characterized by converging instead of bifurcating trees, a novel type of diagram is operationally required for gene flows calculation. The diagram for the assessment the novel NUPT approach consists of a square. A square has been chosen since all the sides and the angles must be identical both to preserve translational symmetries and to avoid non-replicable distortions due to confounding factors such as geometric transformations, projections, displacement, shift operators, affine connexions and parallel transport. The diagram, illustrated in Fig. 2, describes the relationships between two branching population/species, termed Ancient Sample I and Ancient Sample II. The grid on the left portrays a temporal clock with time running from the past (top) to the present-day (bottom). The left and the right sides of the square represent, respectively, the branching of the Ancient Sample I and of the Ancient Sample II after the split from a common ancestor. The upper side of the square is calibrated on the supposed dating of the Ancient Samples I and II's bifurcation from a common ancestor. The lower side of the square describes the merging of the Ancient Samples I and II's DNAs in the extant population/species. The lower side of the square encompasses a percent scale from 0 to 100% which measures both the amount of Ancient Sample I's DNA still preserved in the current population/species and the amount of Ancient Sample II's DNA still preserved in the current population/species.

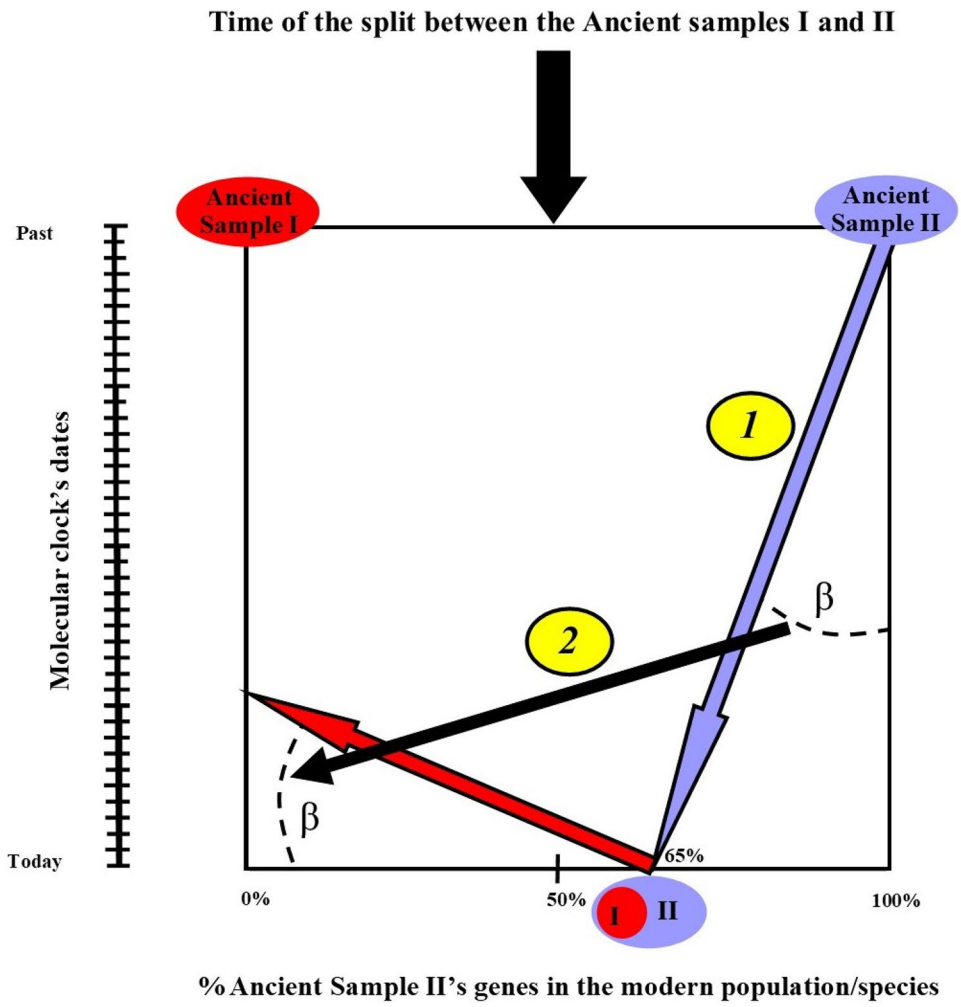

Fig. 2 Novel non-ultrametric approach for detection of genetic flows timing. After the split (upper side of the square) at a given time in the past, two branches are generated: the branch of the Ancient Sample I (left side) and the branch of the Ancient Sample II (right side). When the Ancient Sample II's DNA is introgressed by the Ancient Sample I's DNA (or vice versa), the final result is a single modern population/species containing percentages of both the genetic materials. To provide an example, the figure suggests that in the lower side of the square the 65% of the single modern population's DNA comes from the Ancient Sample II, while the remaining 35% from the Ancient Sample I. The arrow from the upper right vertex to the lower side of the square gives rise to the angle β. The two numbered yellow circles illustrate the two steps of the procedure described in the main text

The procedure requires two further steps, illustrated by the two numbered yellow circles in Fig. 2.

1) The first step consists of drawing a line from the right upper vertex of the Ancient Sample II's right side of the square to a percent value of the lower side. This percent value stands for the estimated percentage of the Ancient Sample's II DNA still preserved in the modern population/species. The operation of drawing the line leads to the formation of the angle β.
2) The second step consists of translating the angle β to the lower part of the diagram, with one of the vertices located at the chosen percent value. A triangle is formed such that one of its sides meets the Ancient Sample I's left side of the square at one point. This point corresponds to the date of the Ancient Sample I's DNA introgression in the Ancient Sample II's DNA.

In the next section, we will examine the specific procedure related with Neanderthals and ancient non-African humans relationships.

Results

Two divergent population/species of Neanderthals and non-African archaic humans branching from a common ancestor are located on the left and the right sides of the square, respectively. The calibration of the temporal clock portrayed on the left grid may vary according to the available estimates. Two possible dates for the split between Neanderthals and ancient non-African humans, namely 400,000 and 600,000 years ago, are provided by Fig. 3A and B, respectively. After the split (upper side of the square) at a given time in the past, two branches were generated: the branch of the Neanderthals (left side) and the branch of the ancient non-African humans (right side).

The percent scale in the lower side of the square quantifies the percentage amount of ancient human's DNA and Neanderthal's DNA preserved in the current non-African human populations. Therefore, the first step consists of drawing a line from the right upper vertex of the ancient humans to the 96% value on the lower side. Indeed, estimates suggest that the modern population of non-Africans

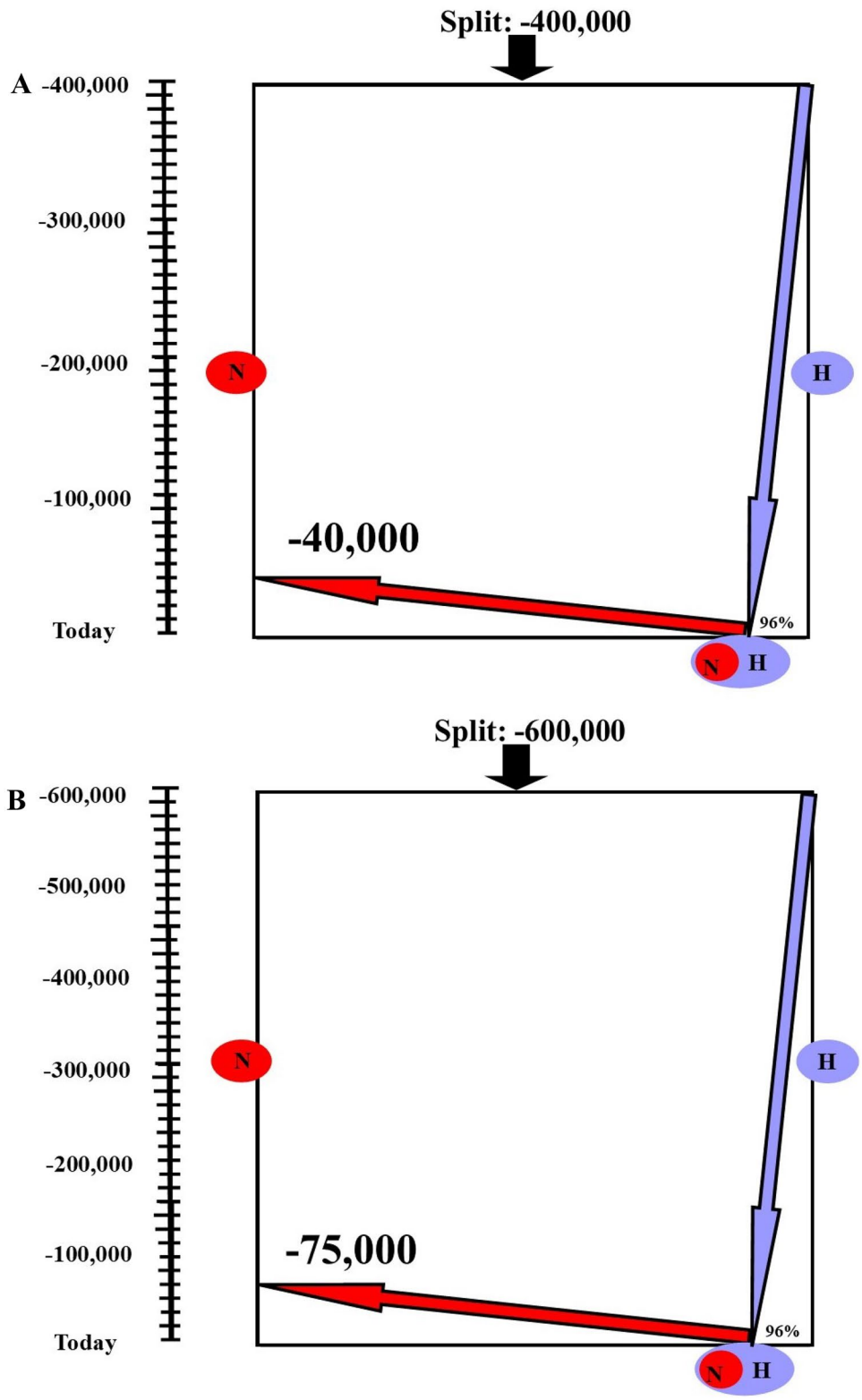

Fig. 3 Neanderthals (red square termed N) and ancient non-African humans (blue square termed H) branching from a common ancestor. Two scenarios are illustrated, each of them relying on a square with distinct molecular clock calibration. Our method suggests what follows: if the split took place 400,000 years ago, the introgression occurred about 40,000 years ago (**A**); if the split took place 600,000 years ago, the introgression occurred about 75,000 years ago (**B**)

preserves about 96% of archaic human ancestors' DNA, while the 4% is provided by the Neanderthal's DNA introgression. The arrow from the upper right vertex to the lower side of the square gives rise to the angle β, which stands for the current non-African humans' genomic divergence after the Neanderthals/ancient non-African humans split. The second step consists of translating the angle β to the lower side of the square, with one of the vertices located at the

value of 96%. One of the sides of the triangle formed by the angle β meets the Neanderthal's left side of the square in a point corresponding to the date of the Neanderthal's DNA introgression in the archaic humans.

If the split between Neanderthals and archaic humans is estimated at 400,000 years ago, the Neanderthal introgression took place about 40,000 years ago (Fig. 3A). As an alternative, if the split between Neanderthals and archaic humans is estimated at 600,000 years ago, the Neanderthal introgression took place about 75,000 years ago (Fig. 3A).

These findings lend themselves to manifold conclusions that will be tackled in the next section.

Conclusions

We propose a new operational approach to phylogenetic trees, termed NUPT, able to estimate the date of introgression between two branching populations or species, e.g. Neanderthals and ancient non-African humans. NUPT is an extension of traditional clustering methods in phylogenetics and provides a useful resource in a scientific stage where there is increasing amounts of evidence for introgression or reticulate evolution (Garrick et al., 2019). In particular, our primary purpose was to calculate the time of Neanderthal's DNA introgression in modern non-African humans. Our assumption is straightforward: when the ancient human DNA was introgressed by Neanderthal DNA, the end result is a converging, single modern population containing both the genetic materials.

Our square allows the graphic depiction of many parameters related to the genetic dynamics occurring between two populations or species. For example, the estimates suggesting that about 96% of the single modern population's DNA comes from ancient humans, while about 4% from Neanderthals, can be graphically depicted in the lower side of our square by drawing just a few lines. A low amount of genetic divergence between two species that subsequently tend to converge suggests that their merging occurred very later after their original split. Such amount of genetic divergence can be graphically depicted by the angle β, which is correlated with the current population/species' genomic divergence occurred after the split between the two populations/species. The lower the angle β, the closer to the current-day the introgression took place.

The temporal grid can be calibrated in different ways according to the various estimated dates of the original split between Neanderthals and ancient non-African humans. Our method accomplishes a valuable result, i.e. the different calibration of the molecular clock leads to different temporal estimates of the introgressive event. The date of introgression modifies according to the choice of the temporal grid: if the split between Neanderthals and ancient non-African humans took place 400,000 years ago, the introgression occurred about 40,000 years ago; if the split took place 600,000 years ago, the introgression occurred about 75,000 years ago.

Our novel NUPT approach has another twofold virtue. If the alleged date of the bifurcation between two population/species from a common ancestor is known, the method allows to calculate the date of their subsequent introgression. In turn, if the date of the introgression between two population/species is known, the method allows to detect the date of their previous split from a common ancestor. Researchers need simply to change the order of the operations one and two on the square: the angle β is drawn at first of the lower side of the square, then it is translated to the left side of the square. In this case, the upper side of the square is not calibrated on the supposed dating of the Ancient Samples I and II's bifurcation from a common ancestor. The vertex of the achieved angle will meet the left side of the square in a point corresponding to the dating of the split between the two populations/species.

Discussion

In this study, a new approach for estimating rooted ultrametric, non-fully bifurcating phylogenetic trees is anticipated. The premise here is that the widely used ultrametric trees do not describe exactly the state of matter (Balaban et al., 2019) since they favour the description of the differences between population/species, instead of their similarities. In turn, our novel NUPT approach considers the clustering of populations/species instead of their distinctions. Starting from two overlapping sets with a few features in common, a coalescent model of phylogenetic tree can be built that is characterized by converging branches. The paper is concerned with the problem of introgression between two species. As such, we aim to provide a novel method to overcome the issue that distances used for reconstructing the evolutionary past between species need not be ultrametric. In particular, a simple procedure to build non-ultrametric phylogenetic trees is proposed to calculate the hypothetical date of interbreeding among different populations/species.

In this paper, we focus on the instance of Neanderthal's DNA introgression in modern non-African humans. Nevertheless, the novel procedure can be generalized to all the cases of genetic recombination between populations/species, ranging from introgression to hybridization, from reticulation to repeated lineage splitting and lineage fusion, i.e. the complete merging of two or more populations resulting in a single panmictic group (Pickrell and Pritchard, 2012; Garrick et al., 2014; Hunley et al., 2016; Garrick et al., 2020). NUPT allows the prediction of the branching date between two populations/species when the

amount of genetic material's introgression is known. This could be useful for the assessment of far-flung issues, such as interbreeding of wild and domestic animal populations, creation and fitness of new artificial varieties of hybrid plants and the study of the evolution of SARS-Cov-2 after the conjectured split of common coronavirus ancestors from bat and pangolin strains (Touati et al., 2020).

NUPT has limitations. The use of sequence divergence to date the nodes in non-ultrametric trees of different hominins groups (see Prüfer et al., 2017) is complicated by mixture among lineages. When the novel population is the product of merging between groups that have been evolving independently for a while, phylogenetic trees will sample sequences from both lineages and will make the population resemble, without corrections for admixture, the root state more than it would if it had continued evolving at a rate proportional to time.

Furthermore, the NUPT assumption cannot be fully consistent in two cases:

1) When the conversion of ancestral variation among-group is achieved via random genetic drift occurring at different rates.
2) When sequences that were polymorphic in the ancestral population subsequently segregate in the two branched lineages and in the admixed population.

Nevertheless, leaving apart the abovementioned limitations, NUPT leads to intriguing theoretical consequences. The hot disputes between the Out-Of-Africa and multiregional evolution models of human evolution in the Pleistocene (Wolpoff et al., 2000; Bräuer et al., 2004; Groucutt et al., 2015; Montinaro et al., 2021) can be tackled in terms of ancient populations, instead of species. These populations are able to diverge, converge and clustering in a worldwide network of genic exchanges that leads to "modern humans", i.e. individuals characterized by local genetic differences.

Acknowledgements The author would like to thank his intellectual brother Norbert Jausovec, who gave precious suggestions and instructive insights. Norbert, sadly, left us a few months ago.

Author contribution The author performed: study concept and design, acquisition of data, analysis and interpretation of data, drafting of the manuscript, critical revision of the manuscript for important intellectual content, statistical analysis, obtained funding, administrative, technical, material support and study supervision.

Data availability All data generated or analyzed during this study are included in the manuscript.

Declarations

Ethics statement This research does not contain any studies with human participants or animals performed by the Author.

Conflict of interest The authors declare no competing interests.

Disclaimer The author had full access to all the data in the study and take responsibility for the integrity of the data and the accuracy of the data analysis. The author warrants that the article is original, does not infringe on any copyright or other proprietary right of any third part, is not under consideration by another journal and has not been previously published.

References

Balaban, M., Moshiri, N., Mai, U., Jia, X., & Mirarab, S. (2019). TreeCluster: Clustering biological sequences using phylogenetic trees. *PLoS ONE, 14*(8), e0221068. https://doi.org/10.1371/journal.pone.0221068

Bräuer, G., Collard, M., & Stringer, C. (2004). On the reliability of recent tests of the Out of Africa hypothesis for modern human origins. *The Anatomical Record. Part A, Discoveries in Molecular, Cellular, and Evolutionary Biology, 279*(2), 701–7. https://doi.org/10.1002/ar.a.20064

Cusimano, N., & Renner, S. S. (2014). Ultrametric trees or phylograms for ancestral state reconstruction: Does it matter? *Taxon*. 63(4), 721–726. https://www.jstor.org/stable/taxon.63.4.721

Garrick, R. C., Benavides, E., Russello, M. A., Hyseni, C., & Edwards, D. L. (2014). Lineage fusion in Galápagos giant tortoises. *Molecular Ecology, 23*(21), 5276–90. https://doi.org/10.1111/mec.12919

Garrick, R. C., Banusiewicz, J. D., Burgess, S., Hyseni, C., & Symula, R. E. (2019). Extending phylogeography to account for lineage fusion. *Journal of Biogeography, 46*(2), 268–278. https://doi.org/10.1111/jbi.13503

Garrick, R. C., Hyseni, C., & Arantes, I. C. (2020). Efficient summary statistics for detecting lineage fusion from phylogeographic datasets. *Journal of Biogeography, 47*(10), 2129–2140. https://doi.org/10.1111/jbi.13932

Gavryushkin, A., & Drummond, A. J. (2016). The space of ultrametric phylogenetic trees. *Journal of Theoretical Biology, 403*, 197–208. https://doi.org/10.1016/j.jtbi.2016.05.001

Gómez-Robles A. (2019). Dental evolutionary rates and its implications for the Neanderthal–modern human divergence. *Science Advances, 5*(5). https://doi.org/10.1126/sciadv.aaw1268

Groucutt, H. S., Petraglia, M. D., Bailey, G., Scerri, E. M. L., & Parton, A. (2015). Rethinking the dispersal of Homo sapiens out of Africa. *Evolutionary Anthropology, 24*(4), 149–164. https://doi.org/10.1002/evan.21455

Hajdinjak, M., Mafessoni, F., Skov, L., Vernot, B., & Hübner, A. (2021). Initial Upper Palaeolithic humans in Europe had recent Neanderthal ancestry. *Nature, 592*, 253–257.

Hall, B. G. (2013). Building phylogenetic trees from molecular data with MEGA. 2013. *Molecular Biology and Evolution, 30*(5), 1229–1235. https://doi.org/10.1093/molbev/mst012

Hammer, M. F., Woerner, A. E., Mendez, F. L., Watkins, J. C., & Wall, J. D. (2011). Genetic evidence for archaic admixture in Africa. *PNAS, 108*(37), 15123–15128. https://doi.org/10.1073/pnas.1109300108

Hunley, K. L., Cabana, G. S., & Long, J. C. (2016). The apportionment of human diversity revisited. *American Journal of Physical Anthropology, 160*(4), 561–569.

Krings, M., Stone, A., Schmitz, R. W., Krainitzki, H., & Stoneking, M. (1997). Neanderthal DNA sequences and the origin of modern humans. *Cell, 90*(1), 19–30. https://doi.org/10.1016/S0092-8674(00)80310-4

Kuhlwilm, M., Gronau, I., Hubisz, M. J., de Filippo, C., & Prado-Martinez, J. (2016). Ancient gene flow from early modern humans

into Eastern Neanderthals. *Nature, 530*(7591), 429–433. https://doi.org/10.1038/nature16544

Meyer, M., Arsuaga, J.-L., Nagel, S., Aximu-Petri, A., & Martínez, I. (2016). Nuclear DNA sequences from the Middle Pleistocene Sima de los Huesos hominins. *Nature, 531*, 504–507.

Meyer, M., Kircher, M., Gansauge, M.-T., Li, H., & Racimo, F. (2012). A high-coverage genome sequence from an archaic Denisovan individual. *Science, 338*(6104), 222–226.

Montinaro, F., Pankratov, V., Yelmen, B., Pagani, L., & Mondal, M. (2021). Revisiting the out of Africa event with a deep-learning approach. *American Journal of Human Genetics, 108*(11), 2037–2051. https://doi.org/10.1016/j.ajhg.2021.09.006

Noonan, J. P., Coop, G., Kudaravalli, S., Smith, D., Krause, J., Alessi, J., Chen, F., Platt, D., Pääbo, S., & Pritchard, J. K. (2006). Sequencing and analysis of Neanderthal genomic DNA. *Science, 314*, 1113–1118.

Page, R., & Holmes, E. (1998). Molecular evolution: A phylogenetic approach. Blackwell Science ISBN 0–86542–889–1.

Pickrell, J., & Pritchard. (2012). Inference of population splits and mixtures from genome-wide allele frequency data. *Nature Precedings*, 1–1

Posth, C., Wißing, C., Kitagawa, K., Pagani, L., & van Holstein, L. (2017). Deeply divergent archaic mitochondrial genome provides lower time boundary for African gene flow into Neanderthals. *Nature Communications, 8*, Article number: 16046.

Prüfer, K., de Filippo, C., Grote, S., Mafessoni, F., & Korlević, P. (2017). A high-coverage Neanderthal genome from Vindija Cave in Croatia. *Science, 358*(6363), 655–658. https://doi.org/10.1126/science.aao1887

Prüfer, K., Racimo, F., & Patterson, N. (2014). The complete genome sequence of a Neanderthal from the Altai Mountains. *Nature, 505*, 43–49. https://doi.org/10.1038/nature12886

Reich, D., Green, R., Kircher, M., Krause, J., & Patterson, N. (2010). Genetic history of an archaic hominin group from Denisova Cave in Siberia. *Nature, 468*, 1053–1060. https://doi.org/10.1038/nature09710

Sankararaman S, Mallick, S., Patterson, N., & Reich, D. (2016). The combined landscape of Denisovan and Neanderthal ancestry in present-day humans. *Current Biology, 26*(9), 1241–1247. Published online 2016 Mar 28. https://doi.org/10.1016/j.cub.2016.03.037

Sankararaman, S., Patterson, N., Li, H., Pääbo, S., & Reich, D. (2012). The date of interbreeding between Neanderthals and modern humans. *PLOS Genetics*. https://doi.org/10.1371/journal.pgen.1002947

Serre, D., Langaney, A., Chech, M., Teschler-Nicola, M., Paunovic, M., Mennecier, P., Hofreiter, M., Possnert, G., & Pääbo, S. (2004). No evidence of Neanderthal mtDNA contribution to early modern humans. *PLoS Biology, 2*, e57. https://doi.org/10.1371/journal.pbio.0020057

Skov, L., Coll Macià, M., Sveinbjörnsson, G., et al. (2020). The nature of Neanderthal introgression revealed by 27,566 Icelandic genomes. *Nature, 582*, 78–83.

Soares, A., Râbelo, R., & Delbem, A. (2017). Optimization based on phylogram analysis. *Expert Systems with Applications, 78*, 32–50. https://doi.org/10.1016/j.eswa.2017.02.012

Sokal, R., & Michener, C. (1958). A statistical method for evaluating systematic relationships. *University of Kansas Science Bulletin, 38*, 1409–1438.

Tamura, K., Peterson, D., Peterson, N., Stecher, G., Nei, M., & Kumar, S. (2011). MEGA5: Molecular evolutionary genetics analysis using maximum likelihood, evolutionary distance, and maximum parsimony methods. *Molecular Biology and Evolution, 28*, 2731–2739.

Touati, R., Haddad-Boubaker, S., Ferchichi, I., Messaoudi, I., Elloumi, O., A., et al. (2020). Comparative genomic signature representations of the emerging COVID-19 coronavirus and other coronaviruses: High identity and possible recombination between Bat and Pangolin coronaviruses. *Genomics, 112*(6), 4189–4202. https://doi.org/10.1016/j.ygeno.2020.07.003

Wall, J. D. (2000). Detecting ancient admixture in humans using sequence polymorphism data. *Genetics, 154*(3), 1271–1279.

Woese, C. R. (2000). Interpreting the universal phylogenetic tree. *PNAS, 97*(15), 8392–8396. https://doi.org/10.1073/pnas.97.15.8392

Wolpoff, M. H., Hawks, J., & Caspari, R. (2000). Multiregional, not multiple origins. *American Journal of Physical Anthropology, 112*(1), 129–136. https://doi.org/10.1002/(SICI)1096-8644(200005)112:1%3c129::AID-AJPA11%3e3.0.CO;2-K

Zhivotovsky, L. A. (2001). Estimating divergence time with the use of microsatellite genetic distances: Impacts of population growth and gene flow. *Molecular Biology and Evolution, 18*(5), 700–709.

Publisher's Note Springer Nature remains neutral with regard to jurisdictional claims in published maps and institutional affiliations.

Springer Nature or its licensor (e.g. a society or other partner) holds exclusive rights to this article under a publishing agreement with the author(s) or other rightsholder(s); author self-archiving of the accepted manuscript version of this article is solely governed by the terms of such publishing agreement and applicable law.

BioSystems 232 (2023) 105018

Contents lists available at ScienceDirect

BioSystems

journal homepage: www.elsevier.com/locate/biosystems

Short Communication

Laws of taxation for multicellular organisms: The economics of sleep

Arturo Tozzi

Center for Nonlinear Science, Department of Physics, University of North Texas, 1155 Union Circle, #311427, Denton, TX, 76203-5017, USA

ARTICLE INFO

Keywords:
Syncope
Electroencephalography
Spike frequency
Volterra equations
Inelastic commodity

ABSTRACT

In macro-public finance, the Ramsey rule (RR) concerns variable taxation to maximize social welfare and economic efficiency in a purely competitive monopolistic system. To extract tax revenue with the least loss of utility to the representative individual, RR dictates that optimal, proportionate taxes should be such as to diminish in the same proportion the production of each commodity taxed. The sources of supply that are inelastic, i.e., necessities/utilities, must be taxed more. We hypothesize that the Ramsey's economical approach might provide a general mechanism to investigate far-flung biological issues, such as preys/predators dynamics, food restriction in ecological niches, local changes in blood flow in rival or complementary organs of multicellular organisms. In particular, RR suggests a quantifiable relationship between the physiological decrease in cortical spike frequency occurring during sleep and energy consumption. Since small decreases in spike frequency during sleep are correlated with large decreases in the amount of consumed ATP, the brain could be considered an inelastic commodity which can be "taxed" more than other organs, allowing the whole organism to spare energy. Shedding light on the energy budget of the central nervous system, RR improves our knowledge of cerebral perfusion during sensory-evoked responses and tissue hypoxia caused by decreased blood flow, suggesting that energy from outside can be provided to counteract brain ischemia. In sum, the economical approach provided by Ramsey stands for a useful methodological tool that could be used in biological contexts to investigate the dynamical correlations among different organs in multicellular organisms.

1. Introduction

The Ramsey rule concerns the introduction of taxes in a public monopoly with no foreign trade, in which commodities' price regulation is adjusted to maximize both social welfare and statal earning (Ramsey, 1927; Boiteux 1956). Contrary to the stable equilibrium provided by absence of taxes, the Ramsey's approach paves the way for progressive income taxes and indirect taxation (Mulligan and Sala-i-Martin, 1998). Ramsey's premises sound as follows: if individuals were the same, the best policy option for a public monopoly is to lump sum taxes. Yet individuals are not the same in the real world, therefore a second-best policy solution is needed, consisting of an array of different taxes inside a system of taxation that is not uniform (Misak 2020).

In this paper, we aim to "borrow" the Ramsey rule from the economic field of macro-public finance to assess biological issues. In particular, we focus on the energy budget of the mammalian central nervous system, assessing.

1) Physiological conditions, such as sleep and task-evoked brain activity.
2) Pathological conditions, such as acute decrease of blood supply leading to brain tissue ischemia.

We discuss how the relationships between the Ramsey's economic framework and the energy requirements/constraints of the central nervous system make it possible to predict the frequency of the electric spikes and the amount of ATP spent in different settings, including sleep and task-related cerebral activation. We show that the Ramsey's framework can be also used to shed light on other biological issues, such as the blood supply of different organs in multicellular living organisms, the response of prey's population to changes in hunter's population and the case of food restriction in ecological niches. We conclude that the potential application of the Ramsey rule to biological affairs might stand for a useful methodological tool to shed light on unnoticed biological correlations. Further, the Ramsey rule suggests novel therapeutical approaches to counteract injuries in multicellular organisms and restore the proper functioning of impaired organs.

E-mail address: tozziarturo@libero.it.

https://doi.org/10.1016/j.biosystems.2023.105018
Received 5 July 2023; Received in revised form 30 August 2023; Accepted 30 August 2023
Available online 4 September 2023
0303-2647/© 2023 Elsevier B.V. All rights reserved.

2. The Ramsey rule in macro-public finance

The dictates of the Ramsey rule are illustrated in Fig. 1A. The plot displays the quantity demand on the axis x and the price on the axis y. Ramsey assumes that the utility is a non-homogeneous quadratic function, so that the supply curves can be illustrated in terms of straight lines (red lines I and II). When the tax is kept constant (red lines I and II), changes in quantity demanded are linearly correlated with increases in price: the more the quantity, the more the price, and vice versa. The demand (the blue line) is expressed in terms of a Hicksian demand function, indicating how an economic agent would react to changes in the price of a good, if the agent is guaranteed the same previous utility. Ramsey suggests that the net utility is maximum when tax income is infinitesimal (Ramsey, 1927). Sufficiently small taxes can be described as a Taylor approximation, making the blue demand curves linear in the relevant range. The current price is given by the intersection between the red and the blue lines (green dot I). When tax is raised (red line II), the intersection between the red line II and the blue line (green dot II) reveals decreases in quantity demanded and increases in price.

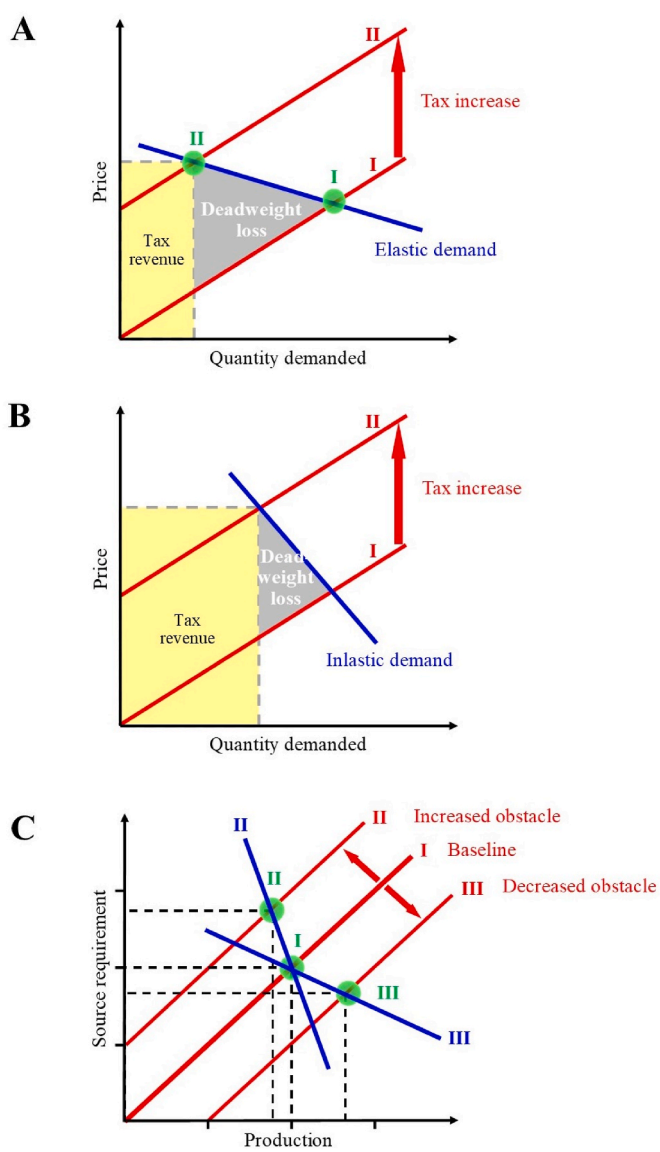

Fig. 1. Ramsey rule in economics and biophysics. Fig. 1A–B. Geometric analysis of the Ramsey rule after and before tax increase, in the two cases of elastic (Fig. 1A) and inelastic (Fig. 1B) demands. Fig. 1C. Putative use of the Ramsey rule to assess physical and biological issues. The Figure provides a rather general sketch that will be used in the next paragraphs to tackle manifold biological issues. See the main text for details.

Ramsey asks: when a tax revenue needs to be raised, how can the public monopoly minimize the unavoidable losses? In other terms, how much taxes on specific commodities must be increased or decreased by the public monopoly in order to optimize individual utility? He concludes that, in case of rivals (e.g., wine and beer) or complementary (e.g., tea and sugar) goods, optimal taxes should reduce in the same proportion the production of each taxed commodity to leave unchanged the proportions in which they are consumed (Gruber 2015). After raising the tax on a commodity, the state gets some revenue, corresponding to the shaded yellow area under the demand curve. Since raising taxes decreases production, some quantity demanded disappears (the grey area) and cannot be taxed anymore. Therefore, the state suffers losses too, corresponding to the shaded grey area under the demand curve, namely, the excess burden of deadweight losses, which stands for the difference in production and consumption of a given product or service. By the consumer's standpoint., the entire shaded grey and yellow area is what the consumer is willing to pay to avoid the tax.

Fig. 1A depicts the blue line of elastic demand, but there is also the case of inelastic demand (Fig. 1B). Price elasticity of demand is the change in quantity demand of a commodity in response to price change. It is the ratio between percentage changes in quantity and price, so that the demand is elastic when the quotient is greater than one and inelastic when smaller than one. Concerning elastic commodities, the change in quantity demanded is greater than the change in its price. In elasticity of demand, little change in the price of goods results in substantial change in quantity demanded, and vice versa. Decreases in price lead to significant increases in demand, resulting in increases in total spending and revenues of the seller. Elastic goods include luxury items that are subjected to infrequent change purchases. Elastic good also include brand-name food and beverages, such as spirits, Coca-Cola, cereals or candy bars. In this case, increases in price due to taxes will affect the demand, leading consumers to stop purchasing the commodity and shift to available substitute.

Demand is considered inelastic if the quantity demand for a good or service remains almost constant despite changes in price within a specific period. The percentage change in quantity demanded is less than in price. Large change in the price of goods results in little change in quantity demanded, and vice versa. The demand is insensitive such that consumers buy nearly the same amount as the price increases, leading to decreases in the seller's total revenue. When demand is more inelastic than supply, consumers bear a greater proportion of the tax burden than producers do. Inelastic commodities are usually necessities without acceptable substitutes, such as utilities, telecommunications, bus travel, oil, petrol, car fuel in short run, medical insurance, salt, rice, eggs, livestock. Inelastic goods include also the commodities for which consumers are addicted such as cigarettes, beer, etc.

The blue line is shallow in elastic demand (Fig. 1A) and steep in inelastic demand (Fig. 1A). In a perfectly elastic demand, the blue line must be parallel to the x axis. In the case of elastic demand, the total revenue and price move in opposite direction, whereas in the case of inelastic demand move both in the same direction. When taxes are increased, the excess burden of deadweight losses, i.e., the grey area, is higher in case of elastic than inelastic goods (Fig. 1B). In turn, the tax revenue, i.e., the yellow area, is higher for inelastic than elastic goods. In technical terms, in case of independent commodities, the optimal tax on each good should be inversely proportional to price elasticities. In colloquial terms, the taxation of inelastic goods provides economic advantages to the state, compared with the taxation of elastic goods. By taxing elastic goods, the government earns less and loses more. Therefore, the Ramsey rule suggests that, to lower deadweight loss and maximize social welfare, commodities which are inelastic must be taxed more in order to provide higher earnings to the state.

Summarizing, the Ramsey rule concerns goods pricing in a public monopoly with the purpose of maximizing social welfare and covering

the fixed costs. The following conclusions can be drawn.

1) When taxes are fixed, increases in price lead to decreases in quantity demanded, while decreases in quantity demanded lead to increases in price.
2) Production must be depressed to raise a revenue.
3) Every increase in taxes corresponds to both an increase in price and a decrease in quantity demand, while every decrease in taxes corresponds to both a decrease in price and an increase in quantity demand.
4) Differences in price and demand occur between the lines of elastic or inelastic demand, leading to areas of deadweight loss of value and of tax revenue that are bigger for inelastic demand than for elastic demand.
5) The more the commodity is inelastic, the more it must be taxed.

In the sequel, we will see that the economical sketch provided by the Ramsey's approach can be used to tackle biological issues such as, e.g., various brain activities including sleep and task-related increase in electric spikes frequency.

Towards the Ramsey rule in biophysical affairs: the general framework. Could the dictates of the Ramsey rule be used to investigate the general features of physical and biological affairs? A viable solution is suggested in Fig. 1C. The plot illustrates a general scheme where the produced quantity is displayed on the axis x and the amount of the resources that can be spent on the axis y. Together with Ramsey, we assume that, at least for small adjustments, the produced quantity is always linearly correlated with the resource requirement such that the red lines I, II and III are straight. This means that the more the produced quantity, the more the resource requirement, and vice versa. Every value on the red line I (e.g., the green dot I) defines a parallelepipedal surface (dotted figure).

Every organism is characterized by a physiological baseline, corresponding to a default state (red line I). Departures from the default state can be caused by increased (red line II) and decreased (line III) obstacles to the baseline activity. To achieve the best advantage, the organism would react to deviations from the baseline. Novel equilibria would be achieved, exemplified by different parallelepipedal surfaces (demarcated by the green dots II and III) that can be quantitatively compared.

Summarizing, three parameters can be estimated when assessing biophysical issues through the Ramsey rule.

1) the parameter on the axis x, standing for the produced quantity.
2) the parameter on the axis y, standing for the required energy.
3) The parameters on the red lines. They correspond to the default state of the organism (**red line I**), to the state of the organism after an obstacle has been posed (**red line II**), to the state of the organism after an obstacle has been removed (**red line III**).

According to the Ramsey rule, the knowledge of two parameters leads automatically to the knowledge of the unknown third. For instance, when a quantifiable obstacle occurs (red line II) and the produced quantity can be experimentally computed on the axis x, the unknown amount of the required energetic resource on the axis y can be easily calculated (green dot II). In turn, if the values on the axes x and y are known (e.g., the green dot III), the unknown red line III can be drawn. Once identified the percent deviation of the obstacle from the baseline, we can quantify how far from the red line I we should draw the parallel red line III. Note that the blue lines could have different slopes, configurating the economical situations of elastic or inelastic demand. The steeper the blue line, the more the biological phenomenon will be inelastic, such that small decreases in quantity production will lead to great changes in energetic requirement.

In the sequel, we will give practical examples illustrating the dynamical responses provided by physical and/or biological organisms to optimize systemic utility.

3. The Ramsey rule and the central nervous system

We hypothesize that the Ramsey's rule concerning monopoly in macro-public finance could be used to investigate the energy budget of the central nervous system, improving our knowledge of neuroscientific issues such as sleep energetics, brain tissue hypoxia, and so on.

The brain requires a large amount of energy, mostly derived from glucose metabolism (Cuenoud et al., 2020). The brain corresponds to 2% of the human body mass yet it accounts for ~20% of the energy consumed (Fox and Raichle, 2007; Raichle, 2010). Almost 20–60% of the energy allocated for the brain supports the cortical grey matter's metabolic rate, including brain "housekeeping" under the isoelectric state, action potentials and transmembrane potentials restoration (Sengupta et al., 2013). The required energy is mainly generated from ATP hydrolysis, tightly correlated to changes in energy demand under various brain activities (Du et al., 2008). For example, the energy required for memory formation in fruit flies corresponds to ~10mJ/bit (Girard et al., 2023). During resting, a single human cortical neuron consumes 4.7 billion ATPs per second and the brain 5.7 kg ATP per day (Zhu et al., 2012).

The production of electric spikes requires energetic costs that can be quantified. ATP consumption at the "baseline" mean rate of 4 Hz is 3.29 $\times$ 10^9 molecules of ATP/neuron/sec, while each additional spike requires 6.5 μmol/ATP/gr/min (Attwell and Laughlin, 2001). A spike's oscillation combines amplitude and frequency. For the Ohm's law, the electric spikes' energy consumption due to the *amplitude* is negligible as compared with energy consumption due to the *frequency* (Tozzi et al., 2016). Therefore, the higher the spike frequency, the higher the energetic cost, quantifiable through the amount of ATP consumption. This means that evoked activities of the brain such as perceptual and motor tasks require local increases in spike frequency, compared with the spontaneous activity. Beta and gamma waves generated during task performance require additional energy consumption of ~5% (Attwell and Laughlin, 2001; Sengupta et al., 2013). It is noteworthy that recent technologies such as cerebral tissue perfusion's real-time monitoring have made biochemical energetic analysis widely available and accessible (Smolders et al., 2003; Schmidt et al., 2021; Si et al., 2023).

The cerebral blood flow is another factor that must be considered when assessing the brain energy budget via the Ramsey rule. Being not capable of glucose storage, the brain can be considered a monopoly that requires a continuous supply of energy sources provided by the cerebral blood flow (Takahashi 2022). The latter can be regulated in response to neuronal activity so as to ensure adequate supply of glucose to meet the neuronal metabolic demands of the grey matter (Takahashi 2022).

The alleged dictates of the Ramsey rule in the biological context of the central nervous system can be illustrated by a plot displaying the spike frequency on the axis x and the amount of ATP consumption on the axis y (Fig. 2A). It can be assumed that spike frequency and ATP consumption are linearly correlated (**red line I**), such that the energetic steps from low-frequency spontaneous activity to high-frequency task activity can be quantified. When the blood flow is kept constant throughout the brain (**red line I**), changes in spike frequencies are linearly correlated with increases in ATP consumption: the more the spike frequency, the more the ATP consumed, and vice versa. Small decreases in blood flow can be described by the **red line II**, while small increases by the **red line III**. When the blood flow locally decreases (**red line II**), increases in ATP consumption and decreases in spike frequency simultaneously occur (**green dot II**).

If we want to investigate the putative nervous counterparts of the Ramsey's rule, we are required to establish a few equivalences.

a) Ramsey's equilibrium without taxation stands for the default mode network at the system's baseline.
b) The cost stands for the ATP quantity required to go from lower to higher Hz in a given brain area.

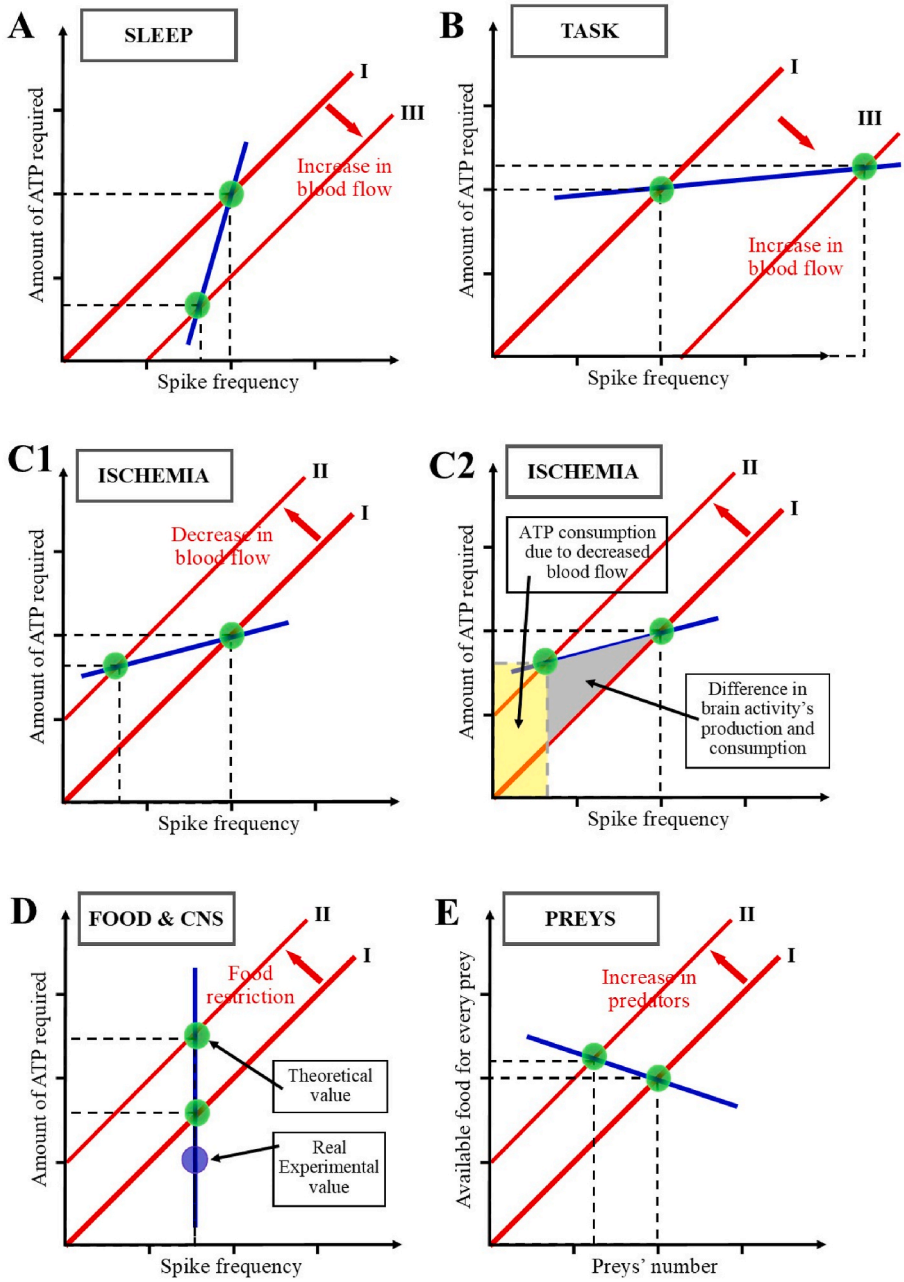

Fig. 2. Putative geometric analysis of the Ramsey rule in different biological settings. Fig. 2A–C cope with the brain's energy budget before and after changes in cerebral lood flow caused by different factors, i.e., sleep (Fig. 2A), task-related activities (Fig. 2B), cerebral ischemia (Fig. 2C1–2C2) and the relationship between food availability and spike frequency (Fig. 2D). Fig. 2E illustrates a biological example concerning the relationships between changes in number of preys/predators and food availability. See the main text for further details.

c) The profit stands for the physiological activity gained by increase in Hz to perform the job.
d) The produced quantity stands for the spike frequency.
e) The quantity demanded stands for the ATP required to produce every type of spikes,
f) The tax baseline stands for the blood intake required to produce the brain activity at rest.
g) During task, an increase in quantity demand is achieved.

In the sequel, we will provide a few examples that illustrate how the Ramsey rule could (and could not) be used to investigate nervous issues.

Sleep. The above-described methodological approach leads to our first neuroscientific application of the Ramsey rule, i.e., the case of sleep. Thanks to the connections among CBF, BOLD, CMRO2 and CMRGlu, changes in blood flow have been detected both during awake states and sleep (Davis et al., 1998; Elvsåshagen et al., 2019; Park et al., 2021). The metabolic relationship between CBF and CMRO2 is still being investigated, with recent models adopting the action of glymphatic system as an additional player (DiNuzzo et al., 2023; Holstein-Rønsbo et al., 2023). It has been established that the brain blood flow increases of ~4–26% during slow-wave sleep and of about 80% during REM sleep (Douglas 2011). In mammal models, the arteriole diameter and the cerebral blood volume increase 2–5 times more during sleep than the increases evoked by sensory stimulation (Turner et al., 2020). Marked increases in amplitude and decreases in frequency of bilateral low-frequency oscillations have been found during sleep, with neural activity being substantially larger than the neural activity elicited by sensory-evoked responses (Stevner et al., 2019; Schreiner et al., 2021). Therefore, matching the Ramsey rule's previsions, experimental findings suggest that increases in blood flow during sleep are correlated with decreases in both spike frequency and energy consumption (Fig. 2A).

In touch with the Ramsey's previsions, increase in blood flow, decrease in spike frequency and decrease in energy consumption take place during sleep. If the Ramsey rule holds true, the experimental

knowledge of two factors leads automatically to the calculation of the unknown third. For example, the known values of blood flow and spike frequency leads to extrapolate the unknown value of energy consumption. Note that the Ramsey rule does not hold for very low frequencies, where the amount of ATP consumption reaches the zero on the axis x. Therefore, it can be predicted that sparing energy during sleep holds only for a certain range of spike frequency.

The Figure suggests that the demand is rather inelastic (steep blue line), leading to the prediction that small decreases in spike frequency during sleep are correlated with large decreases in energy consumption. This means that the brain can be "taxed" more than other organs during sleep, since the deadweight loss is lower than in other organs. Therefore, the Ramsey framework suggests that sleep is a very convenient and affordable activity for the whole living organism, allowing to spare large amounts of energy at the expenses of higher cognitive activities.

Task-related brain hyperperfusion. During sensory-evoked responses, increase in cerebral blood flow leads to simultaneous increases in number of spikes and ATP consumption (Lin et al., 2010). It would be tempting to believe that task-induced neuronal activation, characterized by higher spike frequencies with higher energy demands, would require very large increases of both ATP production and cerebral blood flow. However, contrary to this claim, the energy demand of task-induced brain activation is small relative to the hyperemic response. Indeed, increases in cerebral blood flow are large (about 58%), compared with relatively small increases in ATP (about 15%) (Lin et al., 2010). This scenario is outlined in Fig. 2B. The Ramsey rule holds true also in this case, where a paradoxical increase of spike frequency occurs despite a small increase of required energy. It is noteworthy that the blue line is shallow as in case of elastic demands. This issue will be deepened further in the conclusions.

Syncope, EEG & brain perfusion. Cerebral perfusion represents a single parameter encompassing various phenomena such as arterial pressure, vascular anatomy, viscosity, regional variations of vascular tone, etc (Pranevicius and Pranevicius, 2009). Cerebral ischemia can be caused by several factors, such as hypoperfusion during normothermia or incomplete hypothermia, vaso-vagal depression, syncope (Levy and Parcella, 1987). Cerebral ischemia in animal models brings down cortical blood flow to <2 ml/100 g/min, depleting levels of ATP throughout the whole brain (Marcy and Welsh, 1984) and generating long-term metabolic changes (Tukacs et al., 2023). During spontaneous and induced vasovagal reaction, the total blood volume and the tissue oxygenation strongly decrease in the central nervous system, compensated by a slight blood volume pooling in the lower body part (van Dijk et al., 2014). Following vasodepressor syncope, a slowdown in EEG activity occurs, characterized by generalized high-amplitude waves followed by frequency reduction at 1.5–3 Hz (Ammirati et al., 1998; Aebi et al., 2019). Slow-flat-slow patterns are correlated with more severe cerebral hypoperfusion (Solbiati and Sheldon. 2014). Also, brain electrical activity during acute ischemic stroke and subsequent hyper-acute cerebral tissue hypoperfusion leads to increases in delta and theta EEG power (Ajčević et al., 2021). Increases in slower EEG frequency bands also occur as early as ~10–15 s during cerebral hypoperfusion following cardiac arrest (Razavi and Meador, 2016).

In touch with the Ramsey's framework, the effective outflow pressure could be taken as uniform throughout the brain. As dictated by the Ramsey rule, decreases in cerebral blood flow during ischemia lead to decreases in spike frequency corresponding to specific values of ATP consumption (Fig. 2C1). If the Ramey rule holds true, the knowledge of the flow perfusion and of the EEG spike frequency permits to quantify the unknown amount of ATP required by the brain to compensate the injury. This would mean that the amount of external energy to administer during ischemia to avoid long-term brain damage could be quantified. Yet, if the values of EEG spike frequency and energy consumption are known during a brain ischemic attack, the percentage of cerebral flow reduction might be calculated. Fig. 2C2 suggests that, after the occurrence of an obstacle interfering with the baseline state, there is a leftover amount of energy (corresponding to the grey area) that gets lost and cannot be used anymore, while there is a beneficial part (corresponding to the yellow area) that can be fruitfully used by the organism.

Food restriction and the central nervous system. The effects of food restriction on the central nervous system suggest that metabolic states are able to dynamically regulate the neocortical energy budget. Nevertheless, the Ramsey rule does not hold in case of food restriction. The Ramsey rule would predict that spike frequency preservation during food restriction might give rise to increase in ATP consumption (see the theoretical value illustrated in Fig. 1D). However, it has been experimentally demonstrated that food restriction does not increase, rather reduces by 29% the utilization of synaptic ATP in the visual cortex (Padamsey et al., 2022). Neuronal excitability is nonetheless preserved by compensatory increases in input resistance and depolarized resting potentials. This means that neurons under food restriction spike at similar rates as controls but spend less ATP (see the experimental value illustrated in Fig. 1D).

Therefore, the Ramsey rule doesn't always apply to biological issues and researchers needed to be careful with its use.

Summarizing, the Ramsey rule is a useful methodological tool to elucidate some issues concerning the central nervous system's dynamics. In the next chapter, we will tackle other biological potential applications of the Ramsey rule.

4. The Ramsey rule and multiorgan living systems

Modifications in energy budgets are an ecologically relevant parameter for livings systems embedded in their biological niches (Smolders et al., 2003). Biophysical constraints related to animal body mass, energy expenditure for maintenance, growth, reproduction and heat-dissipation, represent an a priori cost deeply impacting metabolic resources (Dyer et al., 2023). The Ramsey's framework suggests that living beings' energetic requirements can be used to test physiological responses under the same exposure regime and link cellular effects to other endpoints within the same population (Smolders et al., 2003). Note that the requirements of a living organism can be compared with Ramsey's demand of a monopoly. The use the Ramsey's rule in biology underlies a general framework: *when an obstacle occurs to the physiological dynamics of multiorgan living systems, organ production is lowered and more resources are spent*. An available amount of energy is left for the organism, while another part is irreparably lost for the organism. In the next paragraphs we will describe feasible and unfeasible applications of the Ramsey rule to biological issues.

Nutrients and organ efficiency. The Ramsey rule might be used to analyze the introduction of variable intake of nutrients in an energetically self-sufficient multicellular system, in order to maximize both the well-being of each organ and the total energetic efficiency of the whole organism (Aytaç 2018). In Ramsey's jargon: the extraction from the organism of revenue (with the least loss of utility to the single organ) requires that the optimal amount of nutrients (expressed in terms of increases or decreases in flow to single organs) should be such as to diminish in the same proportion the production of each involved organ. Increases or decreases in blood flow may occur in different organs due to either physiological conditions like the activation of the adrenergic system during running to avoid predators, or to pathological conditions such as stroke. The Ramsey rule might answer to the questions.

a) When the energetic requirements need to be raised, how can the whole organism minimize the unavoidable losses?
b) How much the whole organ might increase or decrease the local blood flow to optimize the well-functioning of every one of its single organs?

In case of rival organs (e.g., skin and hearth while running) or complementary organs (e.g., gut and kidney after eating), local changes in blood flow should reduce in the same proportion the specific activity

of each involved organ in order to leave unchanged the proportions in which they are used. Here is how Ramsey's framework could work. After decreases in blood flow inside a given organ, the whole organism gets some revenue, corresponding to the shaded yellow area under the demand curve in Fig. 1A. In turn, the whole organism suffers losses too, corresponding to the shaded grey area under the demand curve in Fig. 1A, standing for the difference in production and consumption of a given organ. Since local decreases in blood flow lead to reductions in organ's production, some quantity demanded disappears (the grey area in Fig. 1A) and cannot be used anymore. By the single organ's standpoint., the entire shaded grey and yellow area in Fig. 1A is what the organ is willing to pay to compensate the locally decreased blood flow.

Food restriction in ecological niches. Ramsey's rule could also be used to tackle population dynamics in relatively closed ecological niches, the latter corresponding to a monopolistic competition. Take, for example, the dynamics between prey and predator illustrated in Fig. 2E. The number of preys is displayed on the x axis and the available food for every prey on the axis y. The perturbing factor acting as an obstacle for preys is the increase in number of predators (red line II). When predators increase in number, a decrease in number of preys occur. Still, a decrease in preys' number means an increase in available food for the surviving preys. From a real-world perspective, if the number of predators is known, the Ramsey's rule permits to calculate the amount of required food when the remnant preys decrease in number, and, vice versa, the number of preys when the amount of consumed food is known. If the number of preys and the amount of consumed food are both known, the Ramsey rule allows to quantify the number of predators.

The Ramsey rule could be used to complement the Lotka–Volterra equations, i.e., the nonlinear differential equations that illustrate the oscillating dynamics of two interacting species (Lotka, 1910; Zhu et al., 2023). The Lotka–Volterra equations and the Ramsey rule have some features in common and differ on some things. In both, the fluctuating numbers of predators and prey observed in natural populations can be described by a single variable. However, the Lotka–Volterra model assumes that the preys, unless subject to predation, have unlimited food supply and exponential growth, while the Ramsey's framework assumes that the growth is always linear. Yet, the Ramsey rule, being more sensitive to small changes than the Lotka–Volterra equations, might better describe the micro-dynamics occurring between preys and predators. Further, the Ramsey rule might be better equipped in detecting the interactions between species and populations that are not fixed but change over time (Park et al., 2023).

Hormone homeostasis. It would be tempting to use the Ramsey rule to investigate the role of the hormones, i.e., the biological molecules sent to distant organs in multicellular organisms. To provide an example, the thyroid hormones in the human body could be evaluated. In Ramsey's terms.

a) The cost could stand for the ATP required to produce fT3.
b) The earning would be the achievement of the baseline stability guaranteed by the fT3 homeostasis.
c) The tax baseline would be the ATP required to produce fT3.
d) The tax increase would be the decrease in ATP reservoirs required to produce fT3.

However, the Ramsey rule cannot be used in this case. Indeed, the whole organism tends towards a state of homeostasis, so that the earning cannot be quantifiable in biological terms, but just in terms of rather qualitative concepts such as well-being, baseline stability and body preservation.

5. Conclusions

We showed that the economical sketch drawn by the Ramsey rule could be used to assess the brain function, shedding new light on nervous energetic mechanisms that underlie phenomena like sleep and tissue hypoxia. Also, we described how the Ramsey rule's economic dictates can be used to tackle other biological issues such as preys/predators relationships and food shortage in ecological niches. Summarizing, the Ramsey rule applied to biology concerns the occurrence of obstacles in a living systems or group of living systems that try to maximize their welfare and cover their fixed energetic costs. The following inferences can be drawn.

1) Increases in obstacles lead organisms to produce less and spend more.
2) Increase or decreases in obstacles to the system's stable functioning represent departures from the baseline that are able modify the energetic requirement and the production of the quantity demanded.
3) When the obstacles are removed, increases in energetic requirement linearly lead to decreases in production of the quantity demanded, while decreases in production of quantity demanded linearly lead to augmented energetic requirement.
4) Changes in the values of three different biological parameters can be quantified through a powerful mathematical apparatus borrowed from economic disciplines.

Differences in produced quantity and energetic requirement generate different biological settings that resemble the economic concept of elastic or inelastic demand. The Ramsey's framework suggests that some biological situations can be described in terms of elastic demand, while others in term of inelastic demand. For instance, being the blue curve very steep, sleep falls within the case of inelastic demand (Fig. 2A). This means that small decreases in spike frequency during sleep ends up saving large quantities of ATP. In turn, the demand is insensitive such that the brain generates nearly the same spike frequency as the ATP consumption increases. Living organisms must optimize systemic utility at the expenses of their singular components: when demand is more inelastic than supply, the single components will bear a greater proportion of the tax burden than the whole living system will. Therefore, the Ramsey rule suggests that, to both maximize the well-being of the whole organism and spare energy, organs with inelastic behavior such as the brain during sleep must be "taxed" heavily. These findings confirm that sleep is a vital function of the brain which stands for a necessary "good" without acceptable substitutes.

When the blue line is shallow, biological phenomena fall within the case of elastic demand. This is the case for task-evoked brain activity (Fig. 2B), central nervous system ischemia ((Fig. 2C), prey/predator relationships (Fig. 2E). Little changes in energetic expense result in substantial change in quantity produced, and vice versa. By "taxing" elastic commodities, the whole organism earns less and loses more. Indeed, decreases in energetic requirement lead to significant increases in demand, resulting in organism's increases in total spending and revenues. Increases in price due to taxes for elastic commodities will lead consumers to stop using the commodity, shifting to available substitute. This suggests that cerebral perfusion during sensory-evoked responses might be blocked after a certain amount of energy is consumed, not being the highly expensive cerebral activity any more advantageous for the organism.

Apart from being a resourceful tool ensuring public goods/entitlements to be financed by efficient taxation, the Ramsey rule displays another invaluable advantage, i.e., it is quantitatively expressed as a quantitative differential equation that, working like a Euler–Lagrange equation, can be applied to other disciplines (Barro and Sala-i-Martin, 2004). However, there are limitations to the use of the Ramsey rule. For exempting savings from income-tax, we must suppose the taxes imposed only for a very short time. Further, Ramsey suggests that savings as future consumption should be taxed too. Besides, we might be justified to raise revenue by placing bounties or subsides on some commodities and taxes on others. The greatest criticism to the Ramsey rule of optimal taxation is that the indispensable commodities have low price elasticity of demand, while luxury goods have not (Aytaç 2018).

This calls for high tax rates on necessities and low tax rates on luxury commodities, introducing conflict between efficiency and social justice (Nahata et al., 2007). As illustrated above, there are also cases, such as food restriction in the brain and hormone homeostasis, in which the Ramsey rule fails to describe biological issues. Ramsey assumes that the quantities on the axis x and y are linearly correlated: for example, spike frequency and ATP consumption in Fig. 2A are on a straight line. This assumption of linearity cannot be taken for granted in biological systems and needs experimental confirmation or rejection. Still, the potential occurrence of nonlinear correlation between the quantities on the axis x and y does not invalidate the Ramsey's approach. Indeed, with the proper calculations, the baseline straight curve could be rather easily replaced by a curved one.

It could be speculated that the legitimacy of the Ramsey rule in contexts different from economics could be endorsed by testing it on other physical and biological phenomena. For instance, it could be conjectured that the relationship between ageing and bodily energy consumption might obey the Ramsey dictates, as well as earthquakes' seismic waves amplitude and ground energy. To stay in the field of human biology, a theoretical relationship obeying the Ramsey rule could be explored between the volume of intestinal gases and the contraction/dilation of the gut walls. Other issues worth investigating are the relationships between muscle contraction and ATP expenditure, or between changes in colonic pH and intestinal motility. Do these phenomena obey elastic or inelastic dictates? For instance, being the muscles more essential for mammals than large brains, could the muscular apparatus be compared with inelastic commodities?

In conclusion, we argue that the Ramsey rule borrowed from macroeconomics seems a promising candidate to investigate the dynamics of (at least) some physical and biological phenomena.

Ethics approval and consent to participate

This research does not contain any studies with human participants or animals performed by the Author.

Consent for publication

The Author transfers all copyright ownership, in the event the work is published. The undersigned author warrants that the article is original, does not infringe on any copyright or other proprietary right of any third part, is not under consideration by another journal, and has not been previously published.

Availability of data and materials

All data and materials generated or analyzed during this study are included in the manuscript. The Author had full access to all the data in the study and takes responsibility for the integrity of the data and the accuracy of the data analysis.

Funding

This research did not receive any specific grant from funding agencies in the public, commercial, or not-for-profit sectors.

Authors' contributions

The Author performed: study concept and design, acquisition of data, analysis and interpretation of data, drafting of the manuscript, critical revision of the manuscript for important intellectual content, statistical analysis, obtained funding, administrative, technical, and material support, study supervision.

Declaration of competing interest

The authors declare that they have no known competing financial interests or personal relationships that could have appeared to influence the work reported in this paper.

Data availability

No data was used for the research described in the article.

References

Aebi, Mathias R., Bourdillon, Nicolas, Meziane, Hadj B., Nicol, Edward, Jérôme Barral, et al., 2019. Cardiovascular and cerebral responses during a vasovagal reaction without syncope. Front. Neurosci. 13, 2019. https://doi.org/10.3389/fnins.2019.01315, 10 December 2019.

Ajčević, M., Furlanis, G., Miladinović, A., et al., 2021. Early EEG alterations correlate with ctp hypoperfused volumes and neurological deficit: a wireless EEG study in hyper-acute ischemic stroke. Ann. Biomed. Eng. 49, 2150–2158. https://doi.org/10.1007/s10439-021-02735-w, 2021.

Ammirati, Fabrizio, Colivicchi, Furio, Di Battista, Giancarlo, Garelli, Fausto Fiume, Santini, Massimo, 1998. Electroencephalographic correlates of vasovagal syncope induced by head-up tilt testing. Stroke 29 (11), 2347–2351. https://doi.org/10.1161/01.STR.29.11.2347Stroke, 1998;29.

Attwell, D., Laughlin, S.B., 2001. An energy budget for signaling in the grey matter of the brain. J. Cerebr. Blood Flow Metabol. 21 (10), 1133–1145.

Aytaç, Deniz, 2018. Optimal taxation of consumption in the scope of changing. Taxes and taxation trends. In: Jolanta Iwin-Garzy?ska. https://doi.org/10.5772/intechopen.74378.

Barro, Robert J., Sala-i-Martin, Xavier, 2004. Growth Models with Consumer Optimization. Economic Growth, second ed. McGraw-Hill, New York, ISBN 978-0-262-02553-9, p. 91.

Boiteux, M., 1956. Sur la gestion des Monopoles Publics astreints a l'equilibre budgetaire. Econometrica 24 (No. 1), 22–40. https://doi.org/10.2307/1905256. Jan., 1956.

Cuenoud, Bernard, Özlem Ipek, Shevlyakova, Maya, Beaumont, Maurice, Cunnane, Stephen C., et al., 2020. Brain NAD is associated with ATP energy production and membrane phospholipid turnover in humans. Front. Aging Neurosci. 12, 2020. https://doi.org/10.3389/fnagi.2020.609517.

Davis, Timothy L., Kwong, Kenneth K., Weisskoff, Robert M., Rosen, Bruce R., 1998. Calibrated functional MRI: mapping the dynamics of oxidative metabolism. Proc. Natl. Acad. Sci. USA 95 (4), 1834–1839. https://doi.org/10.1073/pnas.95.4.1834.

DiNuzzo, Mauro, Dienel, Gerald A., Behar, Kevin L., Petroff, Ognen A., Helene Benveniste, et al., 2023. Neurovascular coupling is optimized to compensate for the increase in proton production from nonoxidative glycolysis and glycogenolysis during brain activation and maintain homeostasis of pH, pCO2 , and pO2, 2023 May 7 J. Neurochem.. https://doi.org/10.1111/jnc.15839. Online ahead of print.

Douglas, Neil J., 2011. Respiratory physiology. In: Kryger, Meir, Roth, Thomas, William, C. (Eds.), Principles and Practice of Sleep Medicine, 2017.

Du, Fei, Zhu, Xiao-Hong, Zhang +3, Yi, Chen, Wei, 2008. Tightly coupled brain activity and cerebral ATP metabolic rate. Proc. Natl. Acad. Sci. USA 105 (17), 6409–6414. https://doi.org/10.1073/pnas.0710766105.

Dyer, Alexander, Brose, Ulrich, Berti, Emilio, Rosenbaum, Benjamin, Myriam, R., Hirt, 2023. The travel speeds of large animals are limited by their heat-dissipation capacities. PLoS Biol. https://doi.org/10.1371/journal.pbio.3001820.

Elvsåshagen, Torbjørn, Mutsaerts, Henri JMM., Zak, Nathalia, Norbom, Linn B., Quraishi, Sophia H., et al., 2019. Cerebral blood flow changes after a day of wake, sleep, and sleep deprivation. NeuroImage Volume 186 (1), 497–509. https://doi.org/10.1016/j.neuroimage.2018.11.032. February 2019.

Fox, M.D., Raichle, M.E., 2007. Spontaneous fluctuations in brain activity observed with functional magnetic resonance imaging. Nat. Rev. Neurosci. 8, 700–711.

Girard, Maxime, Jiang, Jiamu, van Rossum, Mark CW., 2023. Estimating the Energy Requirements for Long Term Memory Formation arXiv:2301.09565.

Gruber, Jonathan, 2015. Public Finance and Public Policy, fifth ed. Worth Publishers. -13 978-1464143335 : .

Holstein-Rønsbo, Stephanie, Gan, Yiming, Giannetto, Michael J., Rasmussen, Martin Kaag, Sigurdsson, Björn, et al., 2023. Glymphatic influx and clearance are accelerated by neurovascular coupling. Nat. Neurosci. 26 (6), 1042–1053. https://doi.org/10.1038/s41593-023-01327-2. Epub 2023 Jun 1.

Levy, W.J., Parcella, P.A., 1987. Electroencephalographic evidence of cerebral ischemia during acute extracorporeal hypoperfusion. J. Cardiothorac. Anesth. 1 (4), 300–304. https://doi.org/10.1016/s0888-6296(87)80041-8, 1987 Aug.

Lin, Ai-Ling, Fox, Peter T., Jean Hardies, +1, Gao, Jia-Hong, 2010. Nonlinear coupling between cerebral blood flow, oxygen consumption, and ATP production in human visual cortex. Proc. Natl. Acad. Sci. USA 107 (18), 8446–8451. https://doi.org/10.1073/pnas.0909711107.

Lotka, A.J., 1910. Contribution to the theory of periodic reaction. J. Phys. Chem. 14 (3), 271–274. https://doi.org/10.1021/j150111a004.

Marcy, V.R., Welsh, F.A., 1984. Correlation between cerebral blood flow and ATP content following tourniquet-induced ischemia in cat brain. J. Cerebr. Blood Flow Metabol. 4 (3), 362–367. https://doi.org/10.1038/jcbfm.1984.53, 1984 Sep.

Misak, C., 2020. Frank Ramsey: A Sheer Excess of Powers. OUP, Oxford. -13 978 : -0198755357.
Mulligan, Casey B., Sala-i-Martin, Francesc Xavier, 1998. The Optimum Quantity of Money: Theory and Evidence (March 1997). NBER Working Paper No. w5954. https://ssrn.com/abstract=225734. Available at SSRN:
Nahata, Babu, Izyumov, Alexei, Busygin, Vladimir, Anna, Mishura, 2007. Application of Ramsey model in transition economy: a Russian case study. Energy Econ. 29 (1), 105–125. https://doi.org/10.1016/j.eneco.2005.09.011. January 2007.
Padamsey, Zahid, Katsanevaki, Danai, Dupuy, Nathalie, Nathalie, L., Rochefort, 2022. Neocortex saves energy by reducing coding precision during food scarcity. Neuron 110 (Issue 2), P280–P296. E10, January 19, 2022.
Park, S., Hong, H., Kim, R.Y., Ma, J., Lee, S., Ha, E., Yoon, S., Kim, J., 2021. Firefighters have cerebral blood flow reductions in the orbitofrontal and insular cortices that are associated with poor sleep quality. Nat. Sci. Sleep 13, 1507–1517. https://doi.org/10.2147/NSS.S312671.
Park, Youngjai, Shimada, Takashi, Son, Seung-Woo, Park, Hye Jin, 2023. Invasion and interaction determine population composition in an open evolving ecological system. Chaos 33 (6), 063151. https://doi.org/10.1063/5.0142978, 2023 Jun 1.
Pranevicius, Mindaugas, Pranevicius, Osvaldas, 2009. Can processed EEG monitoring detect postural cerebral ischemia or cerebral hypoperfusion? Circulation 84 (24), 122. No. 1.
Raichle, M.E., 2010. Two views of brain function. Trends Cognit. Sci. 14 (4), 180–190. https://doi.org/10.1016/j.tics.2010.01.008. Epub 2010 Mar 4.
Ramsey, F.P., 1927. A contribution to the theory of taxation. Econ. J. 37 (145). Mar., 1927.
Razavi, Babak, Meador, Kimford, 2016. Dynamics of quantitative EEG changes during cerebral hypoperfusion (I11.002). Neurology (16 Suppl. ment), 86. April 05, 2016.
Schmidt, Cameron A., Fisher-Wellman 2, Kelsey H., Neufer, P Darrell, 2021. From OCR and ECAR to energy: perspectives on the design and interpretation of bioenergetics studies. J. Biol. Chem. 297 (4), 101140 https://doi.org/10.1016/j.jbc.2021.101140, 2021 Oct.
Schreiner, T., Petzka, M., Staudigl, T., et al., 2021. Endogenous memory reactivation during sleep in humans is clocked by slow oscillation-spindle complexes. Nat. Commun. 12, 3112. https://doi.org/10.1038/s41467-021-23520-2.
Sengupta, B., Stemmler, M.B., Friston, K.J., 2013. Information and efficiency in the nervous system–a synthesis. PLoS Comput. Biol. 9 (7), e1003157 https://doi.org/10.1371/journal.pcbi.1003157.
Si, J., Li, M., Zhang, X., et al., 2023. Cerebral tissue oximeter suitable for real-time regional oxygen saturation monitoring in multiple clinical settings. Cogn Neurodyn 17, 563–574. https://doi.org/10.1007/s11571-022-09847-6.
Smolders, Roel, De Boeck, Gudrun, Blust, Ronny, 2003. Changes in cellular energy budget as a measure of whole effluent toxicity in zebrafish (Danio rerio). Environ. Toxicol. Chem. 22 (4), 890–899, 2003 Apr.
Solbiati, Monica, Sheldon, Robert, 2014. Syncope: how the EEG helps in understanding clinical findings. Brain 137 (Issue 2), 309–311. https://doi.org/10.1093/brain/awt363. February 2014.
Stevner, A.B.A., Vidaurre, D., Cabral, J., et al., 2019. Discovery of key whole-brain transitions and dynamics during human wakefulness and non-REM sleep. Nat. Commun. 10, 1035. https://doi.org/10.1038/s41467-019-08934-3, 2019.
Takahashi, Shinichi, 2022. Metabolic contribution and cerebral blood flow regulation by astrocytes in the neurovascular unit. Cells 11 (5), 813. https://doi.org/10.3390/cells11050813, 2022.
Tozzi, A., Zare, M., Benasich, A.A., 2016. New perspectives on spontaneous brain activity: dynamic networks and energy matter. Front. Hum. Neurosci. 10, 247. https://doi.org/10.3389/fnhum.2016.00247.
Tukacs, V., Mittli, D., Hunyadi-Gulyás, É., et al., 2023. Chronic cerebral hypoperfusion-induced disturbed proteostasis of mitochondria and MAM is reflected in the CSF of rats by proteomic analysis. Mol. Neurobiol. 60, 3158–3174. https://doi.org/10.1007/s12035-023-03215-z, 2023.
Turner, Kevin L., Gheres, Kyle W., Proctor, Elizabeth A., J Drew, Patrick, 2020. Neurovascular coupling and bilateral connectivity during NREM and REM sleep. Elife. https://doi.org/10.7554/eLife.62071.
van Dijk, J.G., Thijs, R.D., van Zwet, E., Tannemaat, M.R., van Niekerk, J., Benditt, D.G., et al., 2014. The semiology of tilt-induced reflex syncope in relation to electroencephalography changes. Brain 137, 576–585.
Zhu, Xiao-Hong, Qiao, Hongyan, Du, Fei, Xiong, Qiang, Liu, Xiao, et al., 2012. Quantitative imaging of energy expenditure in human brain. Neuroimage 60 (4), 2107–2117. https://doi.org/10.1016/j.neuroimage.2012.02.013, 2012 May 1.
Zhu, Zhenliang, Chen, Yuming, Chen, Fengde, Zhong, Li, 2023. Complex dynamics of a predator-prey model with opportunistic predator and weak Allee effect in prey. J. Biol. Dynam. 17 (1), 2225545 https://doi.org/10.1080/17513758.2023.2225545, 2023 Dec.

Acta Biotheoretica (2023) 71:23
https://doi.org/10.1007/s10441-023-09474-6

REGULAR ARTICLE

The First Nucleic Acid Strands May Have Grown on Peptides via Primeval Reverse Translation

Arturo Tozzi[1] · **Marco Mazzeo**[2]

Received: 5 April 2023 / Accepted: 25 October 2023
© Prof. Dr. Jan van der Hoeven stichting voor theoretische biologie 2023

Abstract

The central dogma of molecular biology dictates that, with only a few exceptions, information proceeds from DNA to protein through an RNA intermediate. Examining the enigmatic steps from prebiotic to biological chemistry, we take another road suggesting that primordial peptides acted as template for the self-assembly of the first nucleic acids polymers. Arguing in favour of a sort of archaic "reverse translation" from proteins to RNA, our basic premise is a Hadean Earth where key biomolecules such as amino acids, polypeptides, purines, pyrimidines, nucleosides and nucleotides were available under different prebiotically plausible conditions, including meteorites delivery, shallow ponds and hydrothermal vents scenarios. Supporting a protein-first scenario alternative to the RNA world hypothesis, we propose the primeval occurrence of short two-dimensional peptides termed "selective amino acid- and nucleotide-matching oligopeptides" (henceforward SANMAOs) that non-covalently bind at the same time the polymerized amino acids and the single nucleotides dispersed in the prebiotic milieu. In this theoretical paper, we describe the chemical features of this hypothetical oligopeptide, its biological plausibility and its virtues from an evolutionary perspective. We provide a theoretical example of SANMAO's selective pairing between amino acids and nucleosides, simulating a poly-Glycine peptide that acts as a template to build a purinic chain corresponding to the glycine's extant triplet codon GGG. Further, we discuss how SANMAO might have endorsed the formation of low-fidelity RNA's polymerized strains, well before the appearance of the accurate genetic material's transmission ensured by the current translation apparatus.

Keywords Nucleoside triphosphates · Prebiotic chemistry · RNA world · Origin of life · Polypeptide

Extended author information available on the last page of the article

Published online: 10 November 2023

1 Introduction

In a stable and unrestricted milieu, the minimum genetic requirement for a vital cell capable of autonomous growth counts no less than 300 genes to ensure at least cytosolic metabolism and genomic expression and preservation (Hutchison III et al. 2016; Thornburg et al. 2022). The huge structural and functional demands of extant living cells are difficult to reconcile with the enigmatic steps from inorganic to biological chemistry. In particular, the origin of the translation system is a chicken-and-egg conundrum: which came first, genes or proteins? (Wolf and Koonin 2007). An influential hypothesis put forward by Gilbert (1986) suggests that RNA was the first macromolecule in the prebiotic world, long before functional proteins and hence DNA (Kirschning 2021). The RNA-world hypothesis assumes that life on Earth started with self-recognizing and self-replicating RNA molecules, supposedly RNA ribozymes or prototypical ribonucleotide reductases (Fusz et al. 2005; Lundin et al. 2015; Schneider et al. 2018; Becker et al. 2019). Only later proteins became the catalysts of life, contributing to the genetic takeover of DNA as the information-storage molecule (Müller et al. 2022). Variant theories suggest the occurrence of pristine pre-RNA systems such as, e.g., a heterogeneous chimeric nucleic acid structure where purine deoxyribonucleosides, pyrimidine ribonucleosides and non-canonical bases may have coexisted in the same geochemical scenario (Schneider et al. 2018; Bhowmik and Krishnamurthy 2019; Xu et al. 2020). However, objections have been raised to the RNA world hypothesis, being RNA polymers' catalytic repertoire too small, chemically too homogeneous and constrained by low yield/slow turnover (Kirschning 2021).

Otherwise, the extant cooperation among peptides, small molecules, coenzymes and metal-based cofactors points towards primeval coevolution of different proto-metabolic biomolecules at a system level (Kroiss et al. 2019; Kirschning 2021). Also, it has been suggested a primordial peptide synthesis without ribosomes, evoking a primeval RNA-peptide world. Alternatively, there existed a stage prior to the RNA world termed the "polypeptide" or the "protein world" (Milner-White and James 2019), in which amino acids pairing was mandatory to allow peptide-to-peptide information transfer and ensuing synthesis of one protein sequence from another (Root-Bernstein 1982). The hypothesis is attractive, since amino acids and even peptides are easier to chemically synthesize from simple chemicals than nucleotides (Milner-White and James 2019). Further, as we will see in the sequel, simple amino acidic polymers display better binding and catalytic properties compared with RNA chains (Milner-White and James 2019).

Here we will tackle the chicken–egg problem regarding the duality between nucleic acids and proteins from a new peptidic perspective. Given the almost infinite possibilities of combinations among amino acids and nucleic acids in long timescales, it is likely that complex molecules equipped with biological activity spontaneously arose in ancient abiotic environments (Kitadai and Maruyama 2018). The real problem is not so much the spontaneous formation of complex biomolecules, but their preservation through duplication mechanisms and subsequent transmission to the next generation. The central dogma of molecular

biology states that information is transferred from DNA to protein through an RNA intermediate, apart from a few reverse transcriptases (Wolf and Koonin 2007; Chandramouly et al. 2021). Going against this dogma, we will describe the possibility that the first peptides were "retro-translated" to nucleic acid polymers. We will suggest the primeval occurrence of a short, amino acidic polymer termed "selective amino acid- and nucleotide-matching oligopeptide" (henceforward SANMAO). SANMAO was able to non-covalently bind the amino acids endowed in a peptidic chain and to selectively pair them with the single nucleosides scattered in the abiotic medium. We will describe the chemical features of this hypothetical oligopeptide, its biological plausibility and evolutionary virtues.

2 From Amino Acids to Nucleotides

The RNA world hypothesis suggests that the peptidic synthesis under prebiotic conditions was initiated by RNA molecules (Wolf and Koonin 2007). It has been proposed that non-canonical RNA bases established a rudimental and inaccurate peptide synthesis directly on RNA (Bhowmik and Krishnamurthy 2019), starting from covalently connected chimeric molecules made of peptide and RNA (Müller et al. 2022). Since the formation of peptide bonds via direct binding of amino acids to RNA templates (Yarus 1998) is stereochemically implausible, it is more likely that the primeval RNA acted as a template to synthetize aminoacylating ribozymes (Wochner et al. 2011; Torres de Farias and José 2020; Müller et al. 2022). Initially, RNA must have gained the ability to catalyze the synthesis of just small peptides (Müller et al. 2022). Translation might have started with ribozyme-catalyzed reactions involving abiogenic amino acids, followed by aspecific, non-templated synthesis of increasingly versatile peptides (Wolf and Koonin 2007). The specific amino acids recognition by proto-tRNAs might have depended just on the physical affinity between amino acids and their cognate codons/anticodons (Wolf and Koonin 2007). In the sequel, we will suggest another theory for the onset of peptide translation.

2.1 A Scenario for the Evolution of Translation: Towards a Proteic Beginning

We propose a peptide-first model in which oligopeptides capable of molecular recognition spontaneously appeared. Terminologically, we will consider oligopeptides as chains of aminoacids ≤ 20 residues, while polypeptides > 20 (Apostolopoulos et al. 2021). Here follows a list of the virtues of a peptide-first model:

1. Peptides' and proteins' polymers are easier to abiotically synthetize than nucleic acids' (Fusz et al. 2005).
2. Peptide bonds are more chemically stable than RNA bonds, the latter being more prone to hydrolysis (Schiller 2016).
3. The extant peptides and proteins have a wider breadth of chemical moieties for molecular recognition, displaying strong affinities for various types of small molecules.

4. Peptides and proteins have a much broader repertoire and efficiency as catalysts than RNAs and ribozymes. For example, the Ser-His and Gly-Gly oligopeptide can catalyze peptide bond formation (Schiller 2016), while the Pro-Pro dipeptide and the Pro-x-x-Phe tetrapeptide (x = any amino acid) display aldol condensation activity, i.e., the most significant carbon–carbon bond-forming reaction (Schiller 2016).
5. Proteins have a greater potential for the evolution of a variety of binding and catalytic capacities than RNA (Wolf and Koonin 2007).
6. Action of peptides as templates has been already demonstrated for self-replicating α-helix peptides (Schiller 2016).
7. It has been suggested that amino acids and peptides drove the evolution of translation through the intermediate stage of peptidic proto-ligases forming covalent bonds (Frenkel-Pinter et al. 2019).
8. Cationic side chains incorporated into proto-peptides possibly interacted with negatively charged RNA, catalyzing RNA oligomerization (Frenkel-Pinter et al. 2019).

In sum, several reasons plead for a versatile polypeptide world at the very origin of life. We will see in the sequel that the main problem is to understand how primeval peptides were able to produce their own copies. We suggest that, in a proteic world at the dawn of life, the issue of information transmission could be tackled through the production of nucleic acids' polymers from spontaneously generated peptidic templates. We require a sort of "reverse translation", a primitive "protein-dependent RNA polymerase" which might provide some kind of chemical correspondence between amino acids and their extant cognate triplets (Wolf and Koonin 2007; Biro 2007).

2.2 Information Transmission from Amino Acids to Nucleotides?

We explore the possibility that some peptides were "retro-translated" into nucleic acid polymers by an oligopeptide, namely SANMAO, able to selectively pair the polymeric amino acids and the single nucleotides scattered in the abiotic medium. Once a specific series of nucleotides was brought near, covalent links were established, speeding up non-stochastic formation of biologically relevant RNA chains.

Our aim is to look for the likely chemical and biological attributes of SANMAO. In has been suggested that the first peptides were short, glycine-rich peptidic chains supplied with randomly alternating L/D racemic amino acids. Since short polypeptides flicker between structureless conformations rather than staying fixed in one, enantiomeric ring/chain structures devoid of tertiary structure were favored at the expense of helical conformations (Milner-White and Russell 2008). Like a few extant peptides that are metamorphic, i.e., quickly switch between different folds with different functions (Lella and Mahalakshmi 2017; Dishman et al. 2021), it is feasible that the early oligopeptides explored many different conformations and moved so quickly between different states that no fixed conformation was detectable (Milner-White and James 2019). The commonest primeval polypeptide conformation might

have been the nest, i.e., a biologically active 3–6 residue peptide (Milner-White and Russell 2008). For example, the synthetic hexapeptide Ser–Gly–Ala–Gly–Lys–Thr has been shown to bind phosphate, while other nests can either bind iron–sulfur centers for electrons storage/transfer, or form polymeric channels characterized by potassium-driven transmembrane potentials (Milner-White and James 2019).

SANMAO must be formed by the amino acids available on the Hadean Earth. If we hypothesize that the primordial soup might have contained ~ 10 natural amino acids and peptides < 5 amino acids each, the possible SANMAO's sequence combinations amount to ~ 110,000 (Schiller 2016). To bring this number down, it should be noted that not all the possible amino acid pairs are available for bonding and higher affinities generate more persisting biomolecules (Root-Bernstein 1982; Biro 2007; Lella and Mahalakshmi 2017; Frenkel-Pinter et al. 2020). The most abundant amino acids are (and possibly were) the structurally versatile Gly and Ala (Trifonov 2004).

Peptide flexibility is guaranteed by the small, rotating Gly, rigidity is guaranteed by Ala, Tyr, Trp, Phe and conformation changes are guaranteed by His. The hydrosulphiric bonds of Cys and Met confer resistance to denaturation, while Pro causes α- and β-chains disruption. The outer peptidic surfaces are rich of negative-charged Lys, Arg, His, while the inner surfaces are rich of hydrophobic amino acids. Occasionally, peptidic chains may exert opposite biological effects. To make an example, cationic poly(Leu-Lys) peptides favor mononucleotide diphosphates' oligomerization and increase the abundance of long RNA oligomers (Frenkel-Pinter et al. 2020), while (Leu-Lys)n or (Leu-Lys-Lys-Leu)n peptides exhibit RNA hydrolysis activities (Frenkel-Pinter et al. 2020).

Amino acids with complex side chains such as the aromatic and the cationic ones are thought to be late recruitments to the genetic code (Wolf and Koonin 2007). Despite long-range electrostatics generated by cationic amino acids (i.e., Arg, His, and Lys) plays at present a more dominant role than peptide conformation (Frenkel-Pinter et al. 2019), it must be stressed that the cationic amino acids were not abundant on the prebiotic Earth (Frenkel-Pinter et al. 2020). When coping with the primordial mediums, it must be also kept into account that different environments display different temperatures, pH and redox gradients (Holm et al. 2006; Baaske et al. 2007; Russell et al. 0; Fryer 2012; Postec et al. 2015; Lamadrid et al. 2017; Preiner et al. 2018; Cartwright and Russell 2019; Boyd et al. 2020; Russell and Ponce 2020). These variations deeply influence peptides formation, kinetics, folding and biological activity.

Our SANMAO's scenario requires a mechanism for the elongation of the nucleosides' growing chain similar to the extant mechanism for biological nucleic acids synthesis, where the 3′ end of the incoming nucleotide forms a covalent phosphodiester with the 5′ end of the previous nucleotide. In touch with our requirement, a plausible mechanism of ribose 3′ OH orientation has been suggested which favors the formation of 5′–3′, rather than the more probable 5′–2′ linkage (Carter Jr and Kraut 1973).

The prebiotic peptide catalysis of phosphodiesters, an issue that seems vital for the SANMAO hypothesis and may represent a link between prebiotic chemistry and the RNA world, has been investigated by Wieczorek et al. (2013). The authors used

the catalytic L-dipeptides Ser-His and Ala-His to achieve condensation of activated RNA monomers into short RNA chains, proceeding through an intermediate reaction in which dipeptides covalently bind to nucleotide monophosphates.

It is worth mentioning that SANMAO does not require polymerase, hydrolase and ligase activity. Indeed, nucleotides' polymers can spontaneously self-assemble even in abiotic environments, where the energy to form the phosphodiester bonds between the sugar base of one nucleotide and the phosphate group of the adjacent nucleotide is easily available. The biological task of SANMAO is not to create phosphodiester bonds, but rather to guarantee and expedite the possibility that two given nucleotides get closer to each other, increasing the chances of their spontaneous polymerization.

Now, we are finally ready, in the next section of the Results, to build a SANMAO and describe its interactions.

3 Results

Here we provide a simulation of an hypothetical oligopeptide supplied with the SANMAOs' required biochemical features. SANMAO must display two active zones: the first active zone selectively links a specific amino acid located in a template polypeptide, while the second active zone selectively links isolated purines or pyrimidines.

To give a proof-of-concept example, we substantiate the chemical steps from Gly to its extant corresponding codon, i.e., the triplet codon GGG. Our scenario meets specific requirements:

1. We need a peptide acting as a template for the synthesis of nucleic acids chains. For sake of simplicity, we will use a gly-gly dipeptide, the simplest to generate in every plausible primeval scenario.
2. Also, we need the spontaneous occurrence of a pool of different nucleotides dispersed in the primordial milieu, including at least a few guanosine monofosfate molecules.
3. Then, we need an oligopepeptide (namely, SANMAO) able to link selectively via non-covalent interactions both the Gly and the Guanosyn monofosfate.

Among the countless feasible SANMAO conformations, we suggest a six-amino acids long oligopeptide capable of binding both Gly and Guanosyn monofosfate. Starting from the N-terminus, our SANMAO displays the following PQGQPG sequence:

Pro1-Gln2-Gly3-Gln4-Pro5-Gly6.

The hydrophilic Glu2/Gln4 and the hydrophobic Gly3/Gln6 are small, devoid of steric hindrance and provide SANMAO's conformation flexibility. Our SANMAO allows the following non-covalent interactions (Fig. 1):

a. The acidic Glu2 and Glu4 bind the two carbonyl groups of the gly-gly dipeptide.

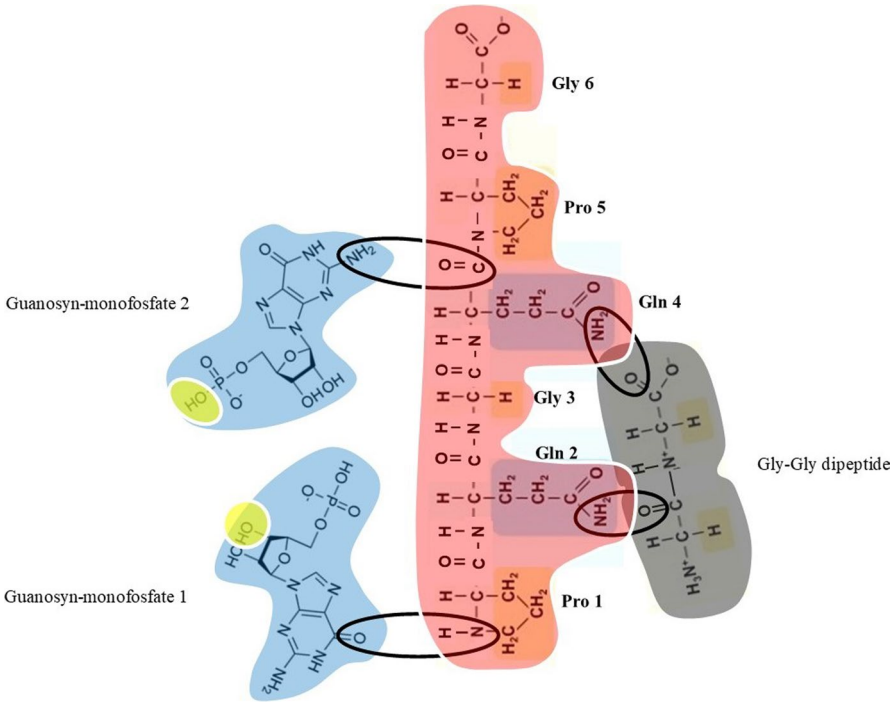

Fig. 1 Theoretical steps leading to the formation of Guanosyn polymers starting from a Gly-Gly dipeptide and an oligomer with PQGQPG sequence. The Gly-Gly dipeptide (right) acts as a template for the polymerization of the purine corresponding to Gly, i.e., the guanosyn-monofosfate (left). The hollow circles depict the molecular surfaces linked by non-covalent bonds. The yellow circles depict the molecular surfaces of the guanosyn-monofosfate where the covalent phosphodiester bonds will take place. For the sake of simplicity, the figure illustrates the formation of just two of the three guanosyns forming the triplet codon GGG. (Color figure online)

b. The hydrophobic Pro1 and Gln2 bind the first molecule of guanosine monofosfate.
c. The hydrophobic Pro5 and Gly6 bind the second molecule of guanosine monofosfate.

SANMAO attains proximity between the two molecules of guanosine monofosfate, thus expediting the formation of a covalent phosphodiester bond between the 5′ end of the first guanosine monofosfate and the 3′ end of the second guanosine monofosfate.

Checking for the biological plausibility of the PQGQPG sequence, we ran UniProtKB for peptide search. The PQGQPG sequence can be found in bacteria, fungi and eukaryotes such as *Acinetobacter baumannii* 99,063, *Streptomyces* sp. PRh5, *Oceanicoccus sagamiensis*, the fungal plant pathogen *Colletotrichum fioriniae* PJ7, the roundworm *Ancylostoma ceylanicum*, the African malaria mosquito *Anopheles gambiae*, the common eastern firefly *Photinus pyralis*, the Atlantic salmon *Salmo salar*, the European red deer *Cervus elaphus hippelaphus* and also Homo sapiens. In

humans and other mammals, the PQGQPG sequence can be detected in various collagen proteins. Also, the RCSB Protein Data Bank observed the PQGQPG sequence in the *Pseudomonas aeruginosa*'s minor pseudopilin XcpW, a type II secretion machinery carrying virulence factors into the extracellular space (Franz et al. 2011). The PQGQPG sequence, which deletion does not impair protein function, is located in a pseudolipin's unstructured proteic extremity that is relatively hydrophobic and intrinsically disordered.

Therefore, our theoretical SANMAO sequence is not just biologically plausible, but can also be currently found in different taxonomical domains and kingdoms.

Thanks to SANMAO, the extremities of the two nucleotides can be arranged in close proximity, thus facilitating spontaneous covalent bond formation. The transient interactions provided by SANMAO allow peptidic chains to act as templates to build increasingly longer chains of nucleic acids that roughly correspond to the amino acids of the template polypeptide. At this stage, it does not matter whether the nucleic acids chains are made either of RNA, DNA, uncanonical nucleosides or unconventional mixtures.

When nucleic acids are achieved from a prototype peptidic template, SANMAO allows the reverse operation too. The novel nucleic acid polymer may serve as template for building a copy of the prototype polypeptide. Figure 2 summarizes the complete theoretical sequence. In the primordial milieu containing biomolecules and polymers (Fig. 2A), different SANMAOs link specific amino acids placed inside a template peptide (Fig. 2B). Then, every SANMAO links the corresponding nucleotidic triplet, giving rise to a progressively longer nucleic acid polymer (Fig. 2C). Next, the nucleic acid polymer (Fig. 2D), through the same SANMAOs (Fig. 2E), uses the scattered amino acids available in the primordial milieu to produce a copy of the template peptide (Fig. 2F). Note that every SANMAO (say SANMAO 1) may also act as template peptide for another SANMAO (say SANMAO 2), the whole procedure leading to the duplication of the same SANMAO 1.

4 Conclusions

This paper provides a theoretical attempt to elucidate the primeval transmission of symbolic information between proteins and nucleic acids, outlining a theoretical model of "reverse translation" from short peptides to nucleic acid oligomers at the origin of life. For one polymer to faithfully transmit symbolic information to another polymer, even one built from the same composite parts, there has to be some kind of integral stoichiometric relationship between their strands. The Watson–Crick double helix solves this problem in a unique way, because the backbone structures of RNA and DNA have largely overlapping stable helix parameters. This problem has been quantitatively discussed by Carter Jr and Kraut (1973), who showed that extended polypeptide strands curve in such a way that their stable conformations include helix parameters matching those of double-stranded RNA if and only if the number of amino acids is exactly twice the number of nucleotide bases in the RNA. Such stoichiometric equivalence appears to be essential for the reproducible templating of one polymer by another. These data are in touch with our account. It might be

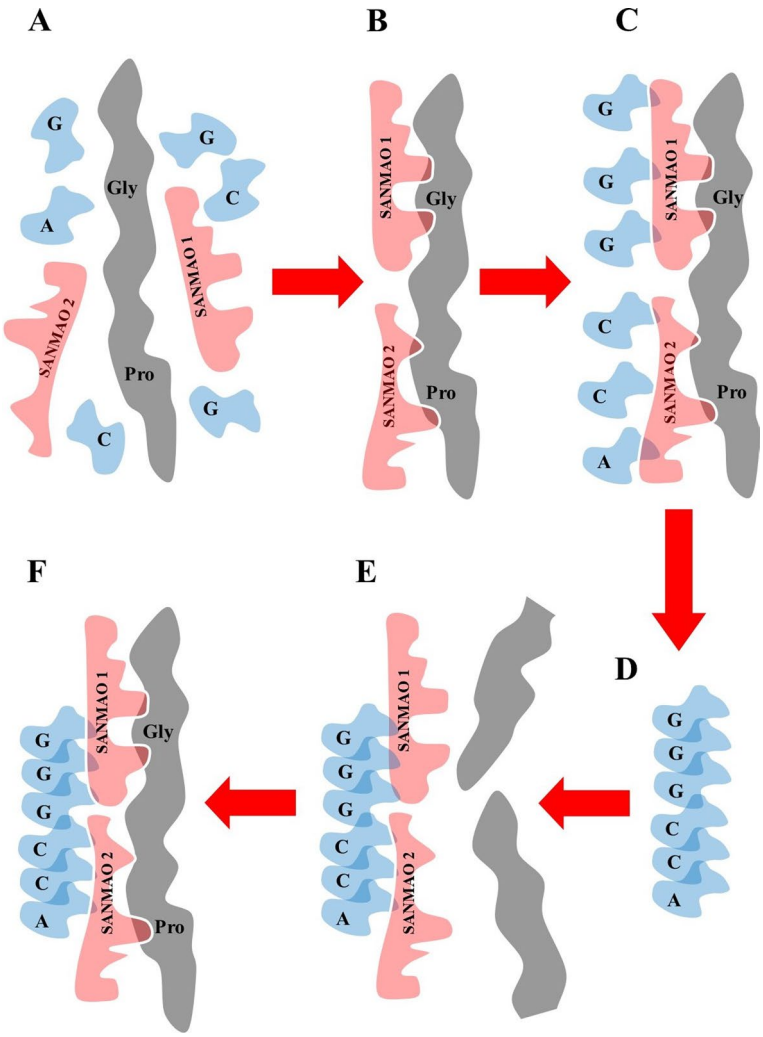

Fig. 2 Theoretical switching from template peptides to nucleic acid polymers and vice versa. The blue shapes stand for single nucleosides where *A* adenine, *C* cytosine and *G* guanine. A template polymer is depicted in grey and two of its amino acids (Gly and Pro) are highlighted. Two structurally different SANMAO molecules (red shapes) correlate distinct amino acids with specific nucleosides. For more details, see the main text. (Color figure online)

objected that the model presented in Figs. 1 and 2 is fanciful in two dimensions and that the authors would have to construct the corresponding models carefully in three dimensions in order to convey even a modicum of reality. However, the available data concerning the primeval medium point towards peptides lacking a three-dimensional structure (Milner-White and James 2019).

We suggest the random appearance on the Hadean Earth (about 4 billion years ago) of oligopeptides (SANMAOs) able to link both the amino acids and the

purines/pyrimidines scattered in the primeval abiotic medium. SANMAOs acted as a buffer between amino acids and nucleic acids, promoting a sort of "reverse translation" from peptidic templates to nucleotidic polymers.

Three fundamental premises underlie our scientific effort to address the issue of the first cellular replication and to tackle the proteins/nucleic acids' chicken–egg problem via the SANMAO hypothesis:

1. The occurrence of a primeval environment with a continuous source of freely available energy is required for the spontaneous synthesis of biomolecules' polymers. Many energetically plausible paths from inorganic settings to the first living cells have been outlined (Sousa et al. 2013). For example, the energetic sources for early organic synthesis and systems reactions could have been derived from the proton gradients at the hydrothermal vents-ocean alkaline interface (Sousa et al. 2013; Damer and Deamer 2020). The nanopores formed by the Fe-rich saponite sheets might have acted as confined microenvironments capable of preserving biopolymers precursors from the detrimental effects of the aqueous medium (Ménez et al. 2018). Then, manifold isolated chemical compartments generated mingled agglomerates able to last for long until the SANMAO's replication processes began.
2. Physical constraints must be kept into account. Physical rules allow biomolecular mixtures, in particular peptides, to self-assemble and cooperate, generating self-organizing hierarchies of polymeric materials (Jacobs 2021; Trivedi et al. 2022; McMullen et al. 2022).
3. The previous prebiotic formation of complex biomolecules is mandatory. The availability of amino acids, polypeptides, proteins, purines, pyrimidines, nucleosides and nucleotides is required under prebiotically plausible conditions on the Hadean Earth. The challenge is to trace plausible physical–chemical processes that permit biomolecules' abiotic formation and self-regenerating catalytic cycles from a handful of simple compounds such as cyanide, water ammonia, and so on (Becker et al. 2019; Wołos et al. 2020).

Hence, the availability of the amino acids and peptides in prebiotic settings must be investigated. Primordial amino acids and Gly-Gly and cyclo(Gly-Gly) oligopeptides were exogenously delivered to the Hadean Earth (and possibly to the Noachian Mars) by comets and asteroids through hypervelocity impact shocks (Shimoyama and Ogasawara 2002; Holm et al. 2015; Ménez et al. 2018; Eigenbrode et al. 2018). In the interstellar medium, carbon atoms' condensation on the surface of cold cosmic dust leads to the spontaneous formation of isomeric polyglycine peptides (Krasnokutski et al. 2022; Broadley et al. 2022). Simulations of impacts of Fe-bearing meteorites/asteroids on CO_2- and N_2-rich oceans suggest that glycine and alanine can be spontaneously synthetized from mixtures of Fe, Ni, Mg_2SiO_4, H_2O, CO_2 and N_2 (Takeuchi 2020). Also, amino acids and peptides may have appeared on the Hadean earth under different geochemical scenario, including Fischer–Tropsch-type synthesis (Russell et al. 2010; Rouméjon and Cannat 2014), Miller and Urey's spark discharge, Sutherland's cyanosulfidic

protometabolism (Holm et al. 2015; Takeuchi 2020; Kirschning 2021), Strecker synthesis (Ménez et al. 2018), alkylation of indole with pyruvate followed by amination under hydrothermal conditions (Ménez et al. 2018), etc. The starting blocks for building amino acids are usually pyruvate, carbohydrate-containing molecules, carboxylic acids, ammonium, glutamate, glutamine, aspartate, H_2S and thiosulfate (Kirschning 2021). Complex amino acid such as tryptophan can be abiotically formed beneath the Atlantis Massif during a serpentinites' late alteration stage, via Friedel–Crafts reactions catalyzed by iron-rich saponite clays (Ménez et al. 2018). It is noteworthy that amino acids synthesis may occur under various conditions of water supply, pH and temperature, leading, e.g., to the production of phenols that are a moiety of tyrosine (Russell et al. 2010), of phenylalanyl-phenylalanine and tyrosyl-tyrosine oligomers (Milner-White and Russell 2008), of high yields of alanine, glutamate, phenylalanine and tyrosine (Milner-White and Russell 2008). Polypeptides can be produced abiotically also in extreme conditions. For example, dry glycine polymers are formed at pressures up to ~ 250 atm during thermal cycling between 0 and 250 °C (Milner-White and Russell 2008). Further, possible amino acids ancestors like depsipeptides produce polypeptides during dry-down cycles under mild conditions (Frenkel-Pinter et al. 2019).

In a SANMAO scenario, the first peptides, utilizing the nucleotides spontaneously generated in the primeval medium, acted as a template for nucleic acid polymerization. Therefore, the next step is to investigate the availability of nucleic acids in prebiotic settings.

The building blocks of RNA and DNA, i.e., the purine/pyrimidine nucleobases and their structural isomers, have been detected in carbonaceous meteorites, possibly generated by photochemical reactions in the interstellar medium and subsequently incorporated into asteroids (Oba et al. 2022). When incubated with impact and volcanic rock glasses at room temperature, ribonucleoside triphosphates are converted to a steady polyribonucleic acid of 90–150 nucleotides in length (Jerome et al. 2022). Still, purines and pyrimidines, in particular adenine, may be abiotically formed both in seafloor hydrothermal environments and shallow ponds. Purines synthesis is feasible along a pathway based on the reaction of formamidopyrimidine precursors with ribose, whereas pyrimidines require a further step involving aminooxazoles (Becker et al. 2019). Fischer–Tropsch type reactions on carbonaceous chondrites in the presence of NH_3 and short heating up to 600 °C generate the familiar nucleobases, although at very low conversions (Preiner et al. 2018). An abiotic one-pot scenario has been suggested to generate purines, pyrimidines and also 5′-mono- and diphosphates in the same environment, driven solely by wet–dry cycles occurring at low temperatures in a few separated shallow ponds (Becker et al. 2019). Wet–dry cycles allow mononucleotide mixtures' polymerization up to > 100 nucleotides in length (Kirschning 2021). While isocyanates in combination with sodium nitrite generate methylated nucleosides (Schneider et al. 2018), the uranosyl-selective prebiotic synthesis of purine deoxyribonucleosides uses intermediates from the prebiotic synthesis of pyrimidines, leading to a mixture of deoxyadenosine, deoxyinosine, cytidine and uridine (Xu et al. 2020). Dry heating combinations of glycine, alanine, valine, lysine, asparagine and glutamine produce pterin riboside at

160–200 °C for 4–6 h (Preiner et al. 2018). When ultramafic rocks are exposed to fluids, the alkalinity may promote abiotic formation of pentoses, particularly ribose (Holm et al. 2006). Also, water-soluble polyphosphates like cyclotriphosphate can be generated in the vicinity of volcanoes (Kirschning 2021).

In sum, experimental and theoretical approaches suggest that key biomolecules such as amino acids, polypeptides, purines, pyrimidines, nucleotides and nucleotides were available under various prebiotically plausible conditions, including meteorites delivery, shallow ponds and hydrothermal vents scenarios. Nevertheless, biomolecules' prebiotic formation is not an easy process, being bonds formation kinetically frustrated by high energy barriers (Frenkel-Pinter et al. 2019). This would mean that spontaneously generated biomolecular polymers of reasonable length were present on the Hadean Earth, but not abundant (Preiner et al. 2018; Takeuchi 2020).

Another problem is the scarce fidelity of the first SANMAO mechanism of protein translation. Indeed, structural organization and cell order distribution of granular systems (Wanjura et al. 2019) suggest that every hierarchical level adds complexity during assembly at the expense of increases in random errors (Michel and Yunker 2019). This would mean that the first efforts to transmit the genetic material to the offspring, i.e., the first random couplings between amino acids and nucleosides, were unavoidably prone to errors. Being the primeval translational mechanisms not as accurate and efficient as the modern triplet-based version (Wolf and Koonin 2007; Schiller 2016), the ancient peptides gave rise to polymerized strains of low-fidelity RNA. Nevertheless, the many mistakes of the primeval "reverse-transational" mechanism were possibly effective to enlarge the number of codon combinations. Then, the natural selection of strong affinity intermolecular interactions and the decreased entropy of the best couplings led to increased stabilization over long timescales (Schiller 2016). Due to decoding systems' evolutionary pressures (Otten et al. 2020; Torres de Farias and José 2020), the subsequent emergence and selection of RNA drove the separation of catalytic and genetic functions (Schiller 2016). Then, repetition and duplication of simple peptidic and nucleic acids polymers took progressively place (Milner-White and James 2019). Synergy and co-evolution among diverse classes of molecules including polyesters and depsipeptides contributed to attenuate hydrolysis rates, promote folding/solubility and accelerate ligand binding/catalysis (Frenkel-Pinter et al. 2020). Actually, cationic proto-peptides significantly increase the thermal stability of folded RNA structures, while RNA increases by > 30-fold the depsipeptides' lifetime (Frenkel-Pinter et al. 2020).

Our model holds true even in the case in which the stereochemical hypothesis of the origin of the genetic code was false. Indeed, SANMAO does not necessarily require stereochemical relationships between amino acids and codons and/or anticodons. Further, covalent interactions between the peptide moiety and the nascent nucleic acid should also be taken into account (Müller et al. 2022). The SANMAO model hypothesizes that non-covalent interactions such as hydrogen bonds allow information flow from the template peptide to the nucleic acids. Yet, the model can be reasonably modified assuming the presence of covalent bonds between the SANMAO oligopeptide and the growing nucleic acid fragments. Each template amino acid (such as, e.g., Gly) could match a single SANMAO oligopeptide covalently linked with a nucleotide fragment that corresponds to the

amino acid codon (such as, e.g., GGG in the case of Gly), leading to the formation of covalent phosphodiester bonds and nucleoside fragments. To support this claim, it has been hypothesized that a natural tendency to interactions between pre-mRNA molecules and peptidated-RNAs sustained the catalytic role in the phase that triggered the genetic code origin (Di Giulio 2015). Di Giulio's model suggests that the pairing between peptidated-RNAs and pre-mRNAs involving a base number greater than three would represent the first form of the genetic code, followed by a natural evolutionistic tendency towards the more efficient triplet conformation. Therefore, the origin of enzymatic catalysis could be traced to the early relationship between nucleotides and amino acid components, via an intermediate formed by tRNA-like molecules covalently linked to polypeptides (Di Giulio 1997). The genetic code would result from a very long era of interactions among peptidated-RNAs, the extant tmRNAs representing the molecular fossils of the evolutionary stages that led to the appearance of the first mRNAs.

Catalytic and reproducing systems prone to Darwinian selection eventually developed, generating versatile and resilient metabolic "hypercycles" that circumvented the potential "error catastrophe" due to the formation of long strings of random sequences (Mossela and Steel 2005). Further, thousands of metabolic innovations on earlier phylogenetic branches were facilitated by horizontal gene transfers, breeding stepwise adaptation to successive environments and ensuing regulatory adaptations (Pang and Lercher 2018).

It has been argued that life emerged many times via multiple different historical pathways (Kempes and Krakauer 2021). If life spontaneously arose on the Hadean Earth from rather trivial non-organic assemblies, why it has not been produced de novo after the appearance of the last universal common ancestor (LUCA)? We suggest a straightforward answer: any viable effort after LUCA to produce unprecedented life was doomed to fail because of natural selection. After LUCA, the likely newcomers generated from organic precursors of low complexity would have been too fragile to compete with well-adapted LUCA's heirs equipped with consolidated selective advantage and plastic immune memory (Ferro et al. 2019; Bernheim et al. 2021; Wein and Sorek 2022).

Our work has a limitation, i.e., the molecules presented here have not been synthesized and no molecular modelling has been performed. Our fully theoretical model would require experimental support, by achieving the proposed hexapeptide commercially from a custom peptide-synthesis company to investigate the proposed interactions, possibly using a technique such as surface plasma resonance. In addition to testing for the existence of interactions, there would also be the need to test for their specificity and catalytic properties, as our model would appear to require that different peptide sequences form interactions with different amino acids.

In sum, in touch with the literature, we assume that life is a spontaneous process consisting of self-assembly of complex molecules. Focusing on the crucial step of protein translation, we propose, this time against the literature and the central dogma of molecular biology, an unusual but plausible scenario in which peptides lead to nucleic acid polymers.

Author Contributions The authors equally contributed to: study concept and design, acquisition of data, analysis and interpretation of data, drafting of the manuscript, critical revision of the manuscript for important intellectual content, statistical analysis, obtained funding, administrative, technical, and material support, study supervision.

Funding This research did not receive any specific grant from funding agencies in the public, commercial, or not-for-profit sectors.

Data Availability All data and materials generated or analyzed during this study are included in the manuscript. The authors had full access to all the data in the study and take responsibility for the integrity of the data and the accuracy of the data analysis.

Declarations

Conflict of interest The authors do not have any known or potential conflict of interest including any financial, personal or other relationships with other people or organizations within three years of beginning the submitted work that could inappropriately influence, or be perceived to influence, their work.

Ethical Approval This research does not contain any studies with human participants or animals performed by the authors.

Consent for Publication The authors transfer all copyright ownership, in the event the work is published. The undersigned authors warrant that the article is original, does not infringe on any copyright or other proprietary right of any third part, is not under consideration by another journal, and has not been previously published.

References

Apostolopoulos V, Bojarska J, Chai T-T, Elnagdy S, Kaczmarek K et al (2021) A global review on short peptides: frontiers and perspectives. Molecules 26(2):430. https://doi.org/10.3390/molecules26020430

Baaske P, Weinert F, Duhr S, Lemke K, Russell MJ, Braun D (2007) Extreme accumulation of nucleotides in simulated hydrothermal pore systems. Proc Natl Acad Sci USA 104:9346–9351

Becker S, Feldmann J, Wiedemann S, Okamura H, Schneider C et al (2019) Unified prebiotically plausible synthesis of pyrimidine and purine RNA ribonucleotides. Science 366(6461):76–82. https://doi.org/10.1126/science.aax2747

Bernheim A, Millman A, Ofir G et al (2021) Prokaryotic viperins produce diverse antiviral molecules. Nature 589:120–124. https://doi.org/10.1038/s41586-020-2762-2

Bhowmik S, Krishnamurthy R (2019) The role of sugar-backbone heterogeneity and chimeras in the simultaneous emergence of RNA and DNA. Nat Chem 11:1009–1018

Biro JC (2007) The Proteomic Code: a molecular recognition code for proteins. Theor Biol Med Model 4:45. https://doi.org/10.1186/1742-4682-4-45

Boyd ES, Amenabar MJ, Poudel S, Templeton AS (2020) Bioenergetic constraints on the origin of autotrophic metabolism. Philos Trans A 378(2165):20190151. https://doi.org/10.1098/rsta.2019.0151. (**published online 6 Jan 2020**)

Broadley MW, Bekaert DV, Piani L et al (2022) Origin of life-forming volatile elements in the inner Solar System. Nature 611:245–255. https://doi.org/10.1038/s41586-022-05276-x

Carter CW Jr, Kraut J (1973) A proposed model for interaction of polypeptides with RNA. Proc Natl Acad Sci USA 71(2):283–287. https://doi.org/10.1073/pnas.71.2.283

Cartwright JH, Russell MJ (2019) The origin of life: the submarine alkaline vent theory at 30. Interface Focus. https://doi.org/10.1098/rsfs.2019.0104

Chandramouly G, Zhao J, McDevitt S, Rusanov T, Hoang T et al (2021) Polθ reverse transcribes RNA and promotes RNA-templated DNA repair. Sci Adv 7(24):eabf1771. https://doi.org/10.1126/sciadv.abf1771. (**published online 11 June 2021**)

Damer B, Deamer D (2020) The hot spring hypothesis for an origin of life. Astrobiology. https://doi.org/10.1089/ast.2019.2045

Di Giulio M (1997) On the RNA world: evidence in favor of an early ribonucleopeptide world. J Mol Evol 45:571–578

Di Giulio M (2015) A model for the origin of the first mRNAs. J Mol Evol 81:10–17

Dishman AF, Tyler RC, Fox JC, Kleist AB, Prehoda KE et al (2021) Evolution of fold switching in a metamorphic protein. Science 371(6524):86–90. https://doi.org/10.1126/science.abd8700

Eigenbrode JL, Summons RE, Steele A, Freissinet C, Millan M et al (2018) Organic matter preserved in 3-billion-year-old mudstones at Gale crater, Mars. Science 360(6393):1096–1101. https://doi.org/10.1126/science.aas9185

Ferro K, Peuß R, Yang W, Rosenstiel P, Schulenburg H, Kurtz J (2019) Experimental evolution of immunological specificity. Proc Natl Acad Sci USA 116(41):20598–20604. https://doi.org/10.1073/pnas.1904828116

Franz LP, Douzi B, Durand E, Dyer DH, Voulhoux R, Forest KT (2011) Structure of the minor pseudopilin XcpW from the *Pseudomonas aeruginosa* type II secretion system. Acta Crystallogr D 67:124–130

Frenkel-Pinter M, Haynes JW, Martin C, Petrov AS, Burcar BT et al (2019) Selective incorporation of proteinaceous over nonproteinaceous cationic amino acids in model prebiotic oligomerization reactions. Proc Natl Acad Sci USA 116(33):16338–16346. https://doi.org/10.1073/pnas.1904849116

Frenkel-Pinter M, Haynes JW, Mohyeldin AM et al (2020) Mutually stabilizing interactions between proto-peptides and RNA. Nat Commun 11:3137

Fryer P (2012) Serpentinite mud volcanism: observations, processes, and implications. Annu Rev Mar Sci 4:345–373. https://doi.org/10.1146/annurev-marine-120710-100922

Fusz S, Eisenführ A, Srivatsan SG, Heckel A, Famulok M (2005) A ribozyme for the aldol reaction. Chem Biol 12(8):941–950. https://doi.org/10.1016/j.chembiol.2005.06.008

Gilbert W (1986) Origin of life: the RNA world. Nature 319:618. https://doi.org/10.1038/319618a0

Holm NG, Dumont M, Ivarsson M, Konn C (2006) Alkaline fluid circulation in ultramafic rocks and formation of nucleotide constituents: a hypothesis. Geochem Trans 7:7

Holm NG, Oze C, Mousis O, Waite JH, Guilbert-Lepoutre A (2015) Serpentinization and the formation of H_2 and CH_4 on celestial bodies (planets, moons, comets). Astrobiology 15(7):587–600. https://doi.org/10.1089/ast.2014.1188

Hutchison CA III, Chuang R-Y, Noskov VN, Assad-Garcia N, Deerinc TJ et al (2016) Design and synthesis of a minimal bacterial genome. Science. https://doi.org/10.1126/science.aad6253

Jacobs WM (2021) Self-assembly of biomolecular condensates with shared components. Phys Rev Lett 126:258101 (**Published 24 June 2021**)

Jerome CA, Kim H-J, Mojzsis SJ, Benner SA, Biondi E (2022) Catalytic synthesis of polyribonucleic acid on prebiotic rock glasses. Astrobiology 22(6):629–636. https://doi.org/10.1089/ast.2022.0027

Kempes CP, Krakauer DC (2021) The multiple paths to multiple life. J Mol Evol 89:415–426

Kirschning A (2021) The coenzyme/protein pair and the molecular evolution of life. Nat Prod Rep 38(5):993–1010. https://doi.org/10.1039/d0np00037j

Kitadai N, Maruyama S (2018) Origins of building blocks of life: a review. Geosci Front 9(4):1117–1153

Krasnokutski SA, Chuang K-J, Jäger C, Ueberschaar N, Henning TH (2022) A pathway to peptides in space through the condensation of atomic carbon. Nat Astron 6:381–386

Kroiss D, Ashkenasy G, Braunschweig AB, Tuttle T, Ulijn RV (2019) Catalyst: can systems chemistry unravel the mysteries of the chemical origins of life? Chem 5:1917–1920

Lamadrid HM, Donald Rimstidt J, Schwarzenbach EM, Klein F, Ulrich S et al (2017) Effect of water activity on rates of serpentinization of olivine. Nat Commun 8:16107

Lella M, Mahalakshmi R (2017) Metamorphic proteins: emergence of dual protein folds from one primary sequence. Biochemistry 56(24):2971–2984. https://doi.org/10.1021/acs.biochem.7b00375. (**Publication Date 1 June 2017**)

Lundin D, Berggren G, Logan DT, Sjöberg B-M (2015) The origin and evolution of ribonucleotide reduction. Life 5(1):604–636. https://doi.org/10.3390/life5010604

McMullen A, Muñoz Basagoiti M, Zeravcic Z et al (2022) Self-assembly of emulsion droplets through programmable folding. Nature 610:502–506

Ménez B, Pisapia C, Andreani M, Jamme F, Vanbellingen QP et al (2018) Abiotic synthesis of amino acids in the recesses of the oceanic lithosphere. Nature 564(7734):59–63. https://doi.org/10.1038/s41586-018-0684-z. (**Epub 7 Nov 2018**)

Michel JA, Yunker PJ (2019) Structural hierarchy confers error tolerance in biological materials. Proc Natl Acad Sci USA 116(8):2875–2880. https://doi.org/10.1073/pnas.1813801116

Milner-White EJ (2019) Protein three-dimensional structures at the origin of life. Interface Focus 9(6):20190057. https://doi.org/10.1098/rsfs.2019.0057(Publishedonline18Oct2019)

Milner-White EJ, Russell MJ (2008) Predicting the conformations of peptides and proteins in early evolution. Biol Direct 3:3. https://doi.org/10.1186/1745-6150-3-3

Mossela E, Steel M (2005) Random biochemical networks: the probability of self-sustaining autocatalysis. J Theor Biol 233(3):327–336. https://doi.org/10.1016/j.jtbi.2004.10.011

Müller F, Escobar L, Xu F, Węgrzyn E, Nainytė M et al (2022) A prebiotically plausible scenario of an RNA–peptide world. Nature 605:279–284

Oba Y, Takano Y, Furukawa Y, Koga T, Glavin DP et al (2022) Identifying the wide diversity of extraterrestrial purine and pyrimidine nucleobases in carbonaceous meteorites. Nat Commun 13:2008

Otten R, Pádua RAP, Adrian Bunzel H, Nguyen V, Pitsawong W et al (2020) How directed evolution reshapes the energy landscape in an enzyme to boost catalysis. Science 370(6523):1442–1446. https://doi.org/10.1126/science.abd3623

Pang TY, Lercher MJ (2018) Each of 3,323 metabolic innovations in the evolution of *E. coli* arose through the horizontal transfer of a single DNA segment. Proc Natl Acad Sci USA 116(1):187–192. https://doi.org/10.1073/pnas.1718997115

Postec A, Quéméneur M, Bes M, Mei N, Benaïssa F et al (2015) Microbial diversity in a submarine carbonate edifice from the serpentinizing hydrothermal system of the Prony Bay (New Caledonia) over a 6-year period. Front Microbiol. https://doi.org/10.3389/fmicb.2015.00857

Preiner M, Xavier JC, Sousa FL, Zimorski V, Neubeck A et al (2018) Serpentinization: connecting geochemistry, ancient metabolism and industrial hydrogenation. Life 8(4):41. https://doi.org/10.3390/life8040041

Root-Bernstein RS (1982) Amino acid pairing. J Theor Biol 94(4):885–894. https://doi.org/10.1016/0022-5193(82)90083-2

Rouméjon S, Cannat M (2014) Serpentinization of mantle-derived peridotites at mid-ocean ridges: mesh texture development in the context of tectonic exhumation. Geochem Geophys Geosyst 15(6):2354–2379. https://doi.org/10.1002/2013GC005148Citations:55. (**First published 23 May 2014**)

Russell MJ, Ponce A (2020) Six 'Must-Have' minerals for life's emergence: olivine, pyrrhotite, bridgmanite, serpentine, fougerite and mackinawite. Life 10(11):291. https://doi.org/10.3390/life10110291

Russell MJ, Hall AJ, Martin W (2010) Serpentinization as a source of energy at the origin of life. Geobiology 8(5):355–371. https://doi.org/10.1111/j.1472-4669.2010.00249.x

Schiller MR (2016) The minimotif synthesis hypothesis for the origin of life. J Transl Sci 2(5):289–296. https://doi.org/10.15761/JTS.1000154(Publishedonline19July2016)

Schneider C, Becker S, Okamura H, Crisp A, Amatov T et al (2018) Noncanonical RNA nucleosides as molecular fossils of an early earth-generation by prebiotic methylations and carbamoylations. Angew Chem Int Ed Engl 57(20):5943–5946. https://doi.org/10.1002/anie.201801919. (**Epub 17 April 2018**)

Shimoyama A, Ogasawara R (2002) Dipeptides and diketopiperazines in the Yamato-791198 and Murchison carbonaceous chondrites. Orig Life Evol Biosph 32(2):165–179. https://doi.org/10.1023/a:1016015319112

Sousa FL, Thiergart T, Landan G, Nelson-Sathi S, Pereira IAC et al (2013) Early bioenergetic evolution. Philos Trans R 368(1622):20130088. https://doi.org/10.1098/rstb.2013.0088. (**Print 19 July 2013**)

Takeuchi Y (2020) Y Furukawa, T Kobayashi, T Sekine, N Terada & T Kakegawa Impact-induced amino acid formation on Hadean Earth and Noachian Mars. Sci Rep 10:9220

Thornburg ZR, Bianchi DM, Brier TA, Smith HO, Glass JI et al (2022) Fundamental behaviors emerge from simulations of a living minimal cell. Cell 185(2):345–360. https://doi.org/10.1016/j.cell.2021.12.025

Torres de Farias S, José MV (2020) Transfer RNA: The molecular demiurge in the origin of biological systems. Prog Biophys Mol Biol 153:28–34. https://doi.org/10.1016/j.pbiomolbio.2020.02.006

Trifonov EN (2004) The triplet code from first principles. J Biomol Struct Dyn 22:1–11

Trivedi M, Saxena D, Ng WK et al (2022) Self-organized lasers from reconfigurable colloidal assemblies. Nat Phys 18:939–944. https://doi.org/10.1038/s41567-022-01656-2

Wanjura CC, Gago P, Matsushima T, Blumenfeld R (2019) Structural evolution of granular systems: theory. arXiv:1904.06549 (Submitted on 13 April 2019)

Wein T, Sorek R (2022) Bacterial origins of human cell-autonomous innate immune mechanisms. Nat Rev Immunol 22:629–638. https://doi.org/10.1038/s41577-022-00705-4

Wieczorek R, Dörr M, Chotera A, Luisi PL, Monnard P-A (2013) Formation of RNA phosphodiester bond by histidine-containing dipeptides. ChemBioChem 14(2):217–223. https://doi.org/10.1002/cbic.201200643

Wochner A, Attwater J, Coulson A, Holliger P (2011) Ribozyme-catalyzed transcription of an active ribozyme. Science 332(6026):209–212. https://doi.org/10.1126/science.1200752

Wolf YI, Koonin EV (2007) On the origin of the translation system and the genetic code in the RNA world by means of natural selection, exaptation, and subfunctionalization. Biol Direct 2:14. https://doi.org/10.1186/1745-6150-2-14

Wołos A, Roszak R, Żądło-Dobrowolska A, Beker W, Mikulak-Klucznik B (2020) Synthetic connectivity, emergence, and self-regeneration in the network of prebiotic chemistry. Science 369(6511):eaaw1955. https://doi.org/10.1126/science.aaw1955

Xu J, Chmela V, Green N et al (2020) Selective prebiotic formation of RNA pyrimidine and DNA purine nucleosides. Nature 582:60–66. https://doi.org/10.1038/s41586-020-2330-9

Yarus M (1998) Amino acids as RNA ligands: a direct-RNA-template theory for the code's origin. J Mol Evol 47(1):109–117

Publisher's Note Springer Nature remains neutral with regard to jurisdictional claims in published maps and institutional affiliations.

Springer Nature or its licensor (e.g. a society or other partner) holds exclusive rights to this article under a publishing agreement with the author(s) or other rightsholder(s); author self-archiving of the accepted manuscript version of this article is solely governed by the terms of such publishing agreement and applicable law.

Authors and Affiliations

Arturo Tozzi[1] · Marco Mazzeo[2]

✉ Arturo Tozzi
tozziarturo@libero.it

Marco Mazzeo
maz.marco@hotmail.it

[1] Center for Nonlinear Science, Department of Physics, University of North Texas, 1155 Union Circle, #311427, Denton, TX 76203-5017, USA

[2] Erredibi Srl, Via Pazzigno 117, 80146 Naples, Italy

Filomat 38:3 (2024), 793–802
https://doi.org/10.2298/FIL2403793P

Published by Faculty of Sciences and Mathematics,
University of Niš, Serbia
Available at: http://www.pmf.ni.ac.rs/filomat

Geometric realizations of homotopic paths over curved surfaces

James F. Peters[a], Roberto Alfano[b], Peter Smith[c], Arturo Tozzi[d], Tane Vergili[e,*]

[a]*Department of Electrical & Computer Engineering, University of Manitoba, Winnipeg, MB, R3T 5V6, Canada and Department of Mathematics, Adıyaman University, 02040 Adıyaman, Türkiye*
[b]*RMG, Design Department, Unit 2A, Wheatstone Road, Swindon SN3 5XX, England, United Kingdom*
[c]*Faculty of Technology, University of Sunderland, Edinburgh Building, City Campus, Chester Road, Sunderland, SR1 3SD, United Kingdom*
[d]*Center for Nonlinear Science, University of North Texas, 1155 Union Circle, 311427, Denton, TX 76203-5017, United States of America*
[e]*Department of Mathematics, Karadeniz Technical University, 61080 Trabzon, Türkiye*

Abstract. This paper introduces geometric realizations of homotopic paths over simply-connected surfaces with non-zero curvature as a means of comparing and measuring paths between antipodes with either a Feynman path integral or Woodhouse contour integral, resulting in a number of extensions of the Borsuk Ulam Theorem. All realizations of homotopic paths reside on a Riemannian surface S, which is simply-connected and has non-zero curvature at every point in S. A fundamental result in this paper is that for any pair of antipodal surface points, a path can be found that begins and ends at the antipodal points. The realization of homotopic paths as arcs on a Riemannian surface leads to applications in Mathematical Physics in terms of Feynman path integrals on trajectory-of-particle curves and Woodhouse countour integrals for antipodal vectors on twistor curves. Another fundamental result in this paper is that the Feynman trajectory of a particle is a homotopic path geometrically realizable as a Lefschetz arc.

1. Introduction

This paper introduces a path-Borsuk-Ulam Theorem, stemming from three main forms of paths over curved surfaces that have been identified, namely,

1° **Poincaré Contour paths** were introduced by Poincaré in 1892 in his analysis situs paper [17]. In a contour path, each subpath is an infinitely small contour on a manifold [17, p. 240]. Recently, N.M.J. Woodhouse [23] introduced contour integrals defined on twistor curves on a complex manifold.

2° **Whitehead Homotopic paths** were introduced during the late 1940s by J.H.C. Whitehead [21, 22] and S. Lefschetz [6], elaborated in [14–16]. For Whitehead, a *path* is a continuous map $h : [0, 1] \to S$, *i.e.*, a map from the unit interval to a space S. For Lefschetz, a *homotopic path* h in an arcwise connected space S is

2020 *Mathematics Subject Classification*. Primary 55P62; Secondary 54E05.
Keywords. antipode, Borsuk-Ulam Theorem, geometric realization, path, Whitehead Homotopy Theory.
Received: 14 April 2023; Accepted: 06 August 2023
Communicated by Hari M. Srivastava
The research has been supported by the Natural Sciences & Engineering Research Council of Canada (NSERC) discovery grant 185986 and Instituto Nazionale di Alta Matematica (INdAM) Francesco Severi, Gruppo Nazionale per le Strutture Algebriche, Geometriche e Loro Applicazioni grant 9 920160 000362, n.prot U 2016/000036 and Scientific and Technological Research Council of Turkey (TÜBİTAK) Scientific Human Resources Development (BIDEB) under grant no: 2221-1059B211301223.
* Corresponding author: Tane Vergili
Email addresses: james.peters3@umanitoba.ca (James F. Peters), roberto.alfano@physics.org (Roberto Alfano), peter.smith@sunderland.ac.uk (Peter Smith), tozziarturo@libero.it (Arturo Tozzi), tane.vergili@ktu.edu.tr (Tane Vergili)

simply a map of a directed (= oriented) closed arc $\widehat{v_0, v_1}$ into S [6, p. 158]. A space is arcwise connected provided every vector in the space S is on a path containing an initial vector and a terminal vector such as the arcs in Figure 1.

3° **Feynman paths** were introduced by R.P. Feynman in his thesis completed in 1942 [3, p. xiv]. A *Feynman path* is a trace of the trajectory of a particle between fixed endpoints [3, p. xiv], providing a framework for a path integral, also introduced by Feynman[3] and elaborated by R.P. Feynman and A.R. Hibbs in [4]. A *Penrose path* over a twistor curve (from R. Penrose's 1968 paper [13]) and its refinement by R.S. Ward in his 1977 thesis [20] supervised by Penrose, is a form of Feynman path in which the trajectory of a particle is over a twistor curve.

The original Borsuk-Ulam Theorem (BUT) [2] from K. Borsuk in 1933 is given in terms of antipodal vectors $\vec{p}, -\vec{p}$ on the surface of an n-dimensional Euclidean sphere S^n, defined by

$$S^n = \left\{(x_1, \ldots, x_{n+1}) \in \mathbb{R}^{n+1}\ ,\ x_1^2 + \cdots + x_{n+1}^2 = 1,\ n \geq 2\right\}.$$

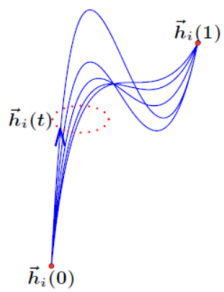

Figure 1: Discrete paths $h : I_d \to S$ with all $t \in I_d$.

Points on the surface of a sphere are *antipodal* provided the points are diametrically opposite each other. Examples of antipodal vectors are the poles on the surface of a planet.

In 1933, K. Borsuk introduced the following theorem.

Theorem 1.1. (**Borsuk-Ulam Theorem**) [2, p. 178] *For every continuous map $f : S^n \to \mathbb{R}^n$, there exists $\vec{p} \in S^n$ such that $f(\vec{p}) = f(-\vec{p})$.*

Remark 1.2. *Theorem 1.1 is a translation from German, which is given by J. Matoušek [9, p. 21].*

Remark 1.3. *The basis for Theorem 1.1 came from K. Borsuk's thesis completed in 1930 [1]. Ulam is credited by Borsuk (in a footnote [2, p. 178]) with the idea codified in Theorem 1.1, which Ulam stated as a conjecture. In effect, Borsuk proved Ulam's conjecture in 1933. In 1930, L. Lusternik and S. Shnirel'man introduced the nonvoid intersection of sets of closed surface curves that have antipodal vectors in common.*

Theorem 1.4. (**Lusternik-Shnirel'man Theorem**) [7] *For any cover $F_1, \ldots, F_{n+1}$ of the sphere S^n by $n+1$ closed sets, there is at least one set containing a pair of antipodal points common to $F_i, -F_i$ (i.e., $F_i \cap -F_i \neq \emptyset$).*

Remark 1.5. *Theorem 1.4 is a translation from Russian, which is given by J. Matoušek [9, p. 21].*

Theorem 1.4 contrasts with Theorem 1.1. In the Lusternik-Shnirel'man Theorem 1.4, there is a closed set F_i that is a cover of a sphere S^n and that has an opposite set $-F_i$, in which the sets $F_i, -F_i$ contain antipodal points such that $F_i \cap -F_i \neq \emptyset$. This sharply contrasts with the Borsuk-Ulam Theorem, which asserts there is a continuous map f from S^n into $\mathbb{R}^n$ over a surface containing antipodal surface vectors $\vec{p}, -\vec{p}$ such that $f(\vec{p}) = f(-\vec{p})$. Also, Theorem 1.4 concludes with the observation that the intersection of $F_i, -F_i$ is nonvoid

but the values of the shared antipodal points are not given. In the LS theorem formulation, it is possible that the antipodal points in $F_i \cap -F_i$ have different values. By contrast, in the Theorem 1.1 formulation, it is asserted that the antipodal points map to the same value.

Given a path $h : I \to S^n$, let $T = \{t_i\}$ be an ordered and countable subset of I, where $0 < t_i < t_{i+1} < 1$ such that $h(t_i) \neq h(t_{i+1})$. We then have $I_d = \{0, 1\} \cup T$, which is called a *discrete unit interval*.

Example 1.6. *Given a path $h : I \to S^n$, let $T_{0.0001} = \{t_i\}$ be a countable and ordered subset of I such that $0 < t_i < t_j < 1$ for all $i < j$, and $|h(t_i) - h(t_{i+1})| = 0.00001$ for all i. Then $I_d = \{0, 1\} \cup T_{0.00001}$ is a discrete unit interval.*

2. Preliminaries

More recent versions of the Borsuk-Ulam Theorem (see, *e.g.*, [11, §68,p.405], [19, p.266],[9, §2.1,p. 23]) require the map $f : S^n \to \mathbb{R}^n$ to be continuous. The map f is continuous provided for each subset $E \subset S^n$, if a point $\vec{p}$ is arbitrarily close to E (*i.e.*, $\inf_{\vec{e}\in E} |\vec{p} - \vec{e}| = 0$), then $f(\vec{p})$ is arbitrarily close to $f(E)$. However, in keeping with an interest in the geometric realization of discrete paths as surface arcs containing points with gaps between them, we consider discrete maps.

Definition 2.1. *Let S be a Riemannian surface. Given a path $h : I \to S$, a discrete path is a map $h : I_d \to S$ where I_d is a discrete unit interval of I. (We will also denote the discrete path by h.) Here $\vec{h}(0)$ and $\vec{h}(1)$ are the initial and terminal points in S, respectively, and $\vec{h}(t) \in S$ for all $t \in I_d$.*

Example 2.2. *Discretely close surface points $\vec{p}, \vec{q}$ such as close water molecules always have a minute gap between them.*

Example 2.3. *The discrete unit interval I_d is a collection of discretely close points $t, t' \in I_d$ such that $t' = t_{i\pm1}$.*

Definition 2.4. *A map $f : S^n \to \mathbb{R}^n$ is said to be discrete provided for each subset $E \subset S^n$, if a point $\vec{p}$ is discretely close to E, then $f(\vec{p})$ is close to $f(E)$.*

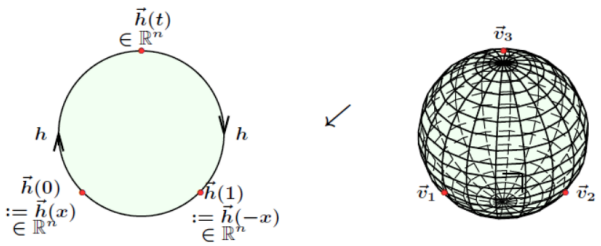

Figure 2: The left-slanting arrow ↙ reads *collapses to*, *e.g.*, ◂ ↙ ▹, *i.e.*, collapse a left-pointing solid triangle to its boundary. For example, collapse a sphere S to a circle containing a discrete path $h : I_d \to S$ with $\vec{h}(0) = \vec{h}(x) \in \mathbb{R}^2$, antipodal to $\vec{h}(1) = \vec{h}(-x) \in \mathbb{R}^2$, with $\vec{h}(t) \in \mathbb{R}^2$ for $t \in I_d \setminus \{0, 1\}$.

Example 2.5. *A sample discrete path $h : I_d \to S$ on the surface of a Riemannian sphere is shown in Figure 2. This path begins at vector $\vec{h}(0) \in \mathbb{R}^n$ at $\vec{v}_1$ on the surface of S and ends at vector $\vec{h}(1) \in \mathbb{R}^n$, which is the value of antipode of $\vec{v}_1$. The assumption made here is that $\vec{h}(0)$ and $\vec{h}(1)$ have the same value such as identical temperature.*

That is, a *discrete path* $h : I_d \to S$ is a map from the discrete unit interval $I_d \subset I$ (for $I = [0, 1]$) to a bounded, simply connected surface S with non-zero curvature. Path h is discrete, since there are gaps between all points $\vec{h}(t) \in S$ between 0 and 1 in $I_d \subset [0, 1]$. The surface S is *simply connected* provided every path h has

end points $h(0), h(1) \in S$ and h has no self-loops.

Paths either lie entirely on a surface in the planar case or lie on a surface and, possibly, puncture a surface in the non-planar case. Paths that puncture a surface are called cross-cuts. A *cross cut path* P (also called an *ideal arc* [10, §3, p.11]) has both ends in P and path interior in the interior of S.

Remark 2.6. *Homotopic paths were introduced by J.H.C. Whitehead [21]. For Whitehead, a path $h : [0, 1] \to X$ is a continuous map from the unit interval to a cell complex X. In the pursuit of discrete paths in a curved space, the focus is on 0-cells (single points) and 1-cells (arcs) in an n-dimensional Riemannian space S. A single surface vector is a 0-cell.*

Definition 2.7. *[5] An arc is a curvilinear line segment attached to a pair of 0-cells.*

Definition 2.8. *A pair of vectors v_0, v_1 is path-connected provided there is a sequence of 0-cells starting with v_0 and ending with v_1 in such a way that v_0, v_1 are attached to a Lefschetz arc. If such an arc exists between a pair of 0-cells v_0 and v_1 in this sequence (i.e., each pair v_0 and v_1 in the sequence of 0-cells are path connected), a collection of Leftschetz arcs corresponding to this sequence is called a discrete Lefschetz arc. We will denote the discrete Lefschetz arc between v_0 and v_1 by $\widehat{v_0, v_1}$.*

Proposition 2.9. *There is a discrete Lefschetz arc between each pair of 0-cells.*

Proof. Immediate from Definition 2.8. □

Example 2.10. *All vectors on the circle in Figure 2 are path-connected, since, from Proposition 2.9, there is a Lefschetz arc between each pair of vectors.*

3. Antipodal and Non-Antipodal Path Borsuk-Ulam Theorem

This section introduces results for the geometric realization of homotopic paths in surface arcs.

Lemma 3.1. *Every discrete path constructs a discrete Lefschetz arc.*

Proof. Given a path $h : I \to X$, let $h : I_d \to X$ be a discrete path. Then the collection

$$\{h(0), h(1)\} \cup \{h(t_i) \ : \ t_i \in I_d\}$$

forms a sequence of path connected 0-cells in X, hence it forms a discrete Lefschetz arc between $h(0)$ and $h(1)$. □

Theorem 3.2. *The endpoints of a discrete Lefschetz arc can be the same.*

Proof. Given two path connected 0-cells $\vec{v}_0$ and $\vec{v}_1$, we know that there is a discrete Lefschetz arc from $\vec{v}_0$ to $\vec{v}_1$. One can reverse the direction of arcs (since it can be considered to be a discrete path) so that the union of the discrete Lefschetz arcs $\widehat{v_0, v_1}$ and $\widehat{v_1, v_0}$ will form a discrete Lefschetz arc $\widehat{v_0, v_0}$. □

Next, consider the geometric realization of discrete homotopic path as a discrete arc and which constructs a vector field.

Theorem 3.3. *Every discrete path constructs a vector field.*

Proof. Let $h : I_d \to S$ be a discrete path. From Lemma 3.1, h constructs a discrete arc $\widehat{h(0), h(1)}$ on a surface S. Consequently, each $\vec{h}(t) \in \widehat{h(0), h(1)}$ has a location $(x_1, \dots) \in S$ with its own magnitude and direction S, *i.e.*, every $\vec{h}(t)$ is a vector in S. Hence, h constructs a vector field. □

Lemma 3.4. *Let $\vec{v}_1, \vec{v}_2$ be antipodal vectors on the surface of an n-sphere S^n. There exists a discrete path h with vectors that are antipodal on a surface S^n.*

Proof. Let $\vec{v}_1, \vec{v}_2$ be antipodal vectors on the surface of an n-sphere S^n. Since S^n is path connected, there is a discrete Lefschetz arc $\widehat{\vec{v}_1, \vec{v}_2}$. The collection of Lefschetz arcs (hence the discrete Lefschetz arc itself) forms a discrete path $h : I_d \to S^n$ with $\vec{h}(0) = \vec{v}_1$ and $\vec{h}(1) = \vec{v}_2$. Hence, a discrete path can be defined for every pair of antipodal points on S^n. □

From what we have observed about discrete paths on the surface of a sphere, we obtain the following theorem.

Theorem 3.5. (**Path-Borsuk-Ulam Theorem**) *Given a continuous map $f : S^n \to \mathbb{R}^n$ (hence a discrete map), there exist a discrete path $h : I_d \to \mathbb{R}^n$ and a point $\vec{p} \in S^n$ such that $h(0) = f(\vec{p}) = f(-\vec{p})$. In fact, h forms a discrete loop based at $f(\vec{p})$.*

Proof. It is obvious that a continuous map $f : S^n \to \mathbb{R}^n$ is also a discrete map. From Theorem 1.1 (Borsuk-Ulam Theorem), we know that there is a point $\vec{p} \in S^n$ such that $f(\vec{p}) = f(-\vec{p})$. Consider a sequence of points $\{\vec{v}_t\} \subset S^n$ indexed over a discrete interval I_d such that $\vec{v}_0 = \vec{p}$, $\vec{v}_1 = -\vec{p}$, and two consequtive terms $\vec{v}_t, \vec{v}_{t+1}$ are discretely close for all $t \in I_d$. Then consider the image of this sequence $\{f(\vec{v}_t)\}_{t \in I_d}$. This set can be considered as the image of the discrete path $h : I_d \to \mathbb{R}^n$ defined by $h(t) = f(\vec{v}_t)$. In fact, h is a discrete loop. □

Remark 3.6. *An immediate consequence of Theorem 3.5 is that, for any pair of antipodal surface points, we can always introduce a discrete path h that begins and ends at the antipodal points such as places that have same latitude and longitude. For example, the antipode of Winnipeg, Manitoba, Canada with coordinates 49°.53′N, 97°.8′W is Port-aux-Français, Kerguelen, French Southern Territories.*

Example 3.7. *An example of a discrete path that begins and ends at antipodal surface points is shown in Figure 2.*

Observe that a path can be constructed between any pair of surface vectors. This observation leads to more general form of Theorem 3.5.

Theorem 3.8. (**Non-antipodal path-BUT**) *Let the discrete unit interval I_d be an index set for vectors $v_0, \ldots, v_t, \ldots, v_1$, $t \in I_d$ in S^n in a continuous map $f : S^n \to \mathbb{R}^n$ such that $f(v_0) = f(v_1)$ for some $v_0, v_1 \in S^n$. There is a discrete path $k : I_d \to \mathbb{R}^n$ with endpoints $f(v_0), f(v_1)$ that are values in $\mathbb{R}^n$ such that $k(0) = k(1)$.*

Proof. Let $h : I \to S^n$ be a path from v_0 to v_1 and $h : I_d \to S^n$ be its associated discrete path. Then the composition $k = f \circ h$ is a discrete path in $\mathbb{R}^n$ with endpoints $f(v_0)$ and $f(v_1)$ so that $k(0) = k(1)$. □

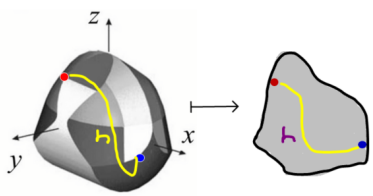

Figure 3: 2D and 3D views of discrete paths on a Gomboc Riemannian surface.

Example 3.9. *An example of a discrete path that begins and ends at antipodal surface vectors on a bumpy Riemannian sphere (aka Gomboc sphere) is shown in Figure 3.*

Example 3.10. *An example of a discrete path $h : S^2 \to \mathbb{R}^3$ on a 3D Gomboc Riemannian surface is shown in Figure 3. The same path is also depicted on a 2D slice of the 3D surface. In keeping with Theorem 3.8, each vector $\vec{h}(v_t)$ is a signal value from the path h. For example, if we let the discrete path be an optical field flow containing a stream of photons reflected from a Riemannian surface, then there are number of possible signal values for $\vec{h}(v_t)$,* e.g.,

1° *wavelength of* $\vec{h}(v_t)$.
2° *frequency of* $\vec{h}(v_t)$.
3° *electron voltage of* $\vec{h}(v_t)$.
4° *lumens (luminosity) of* $\vec{h}(v_t)$.
5° *gradient of* $\vec{h}(v_t), t \in I_d$, *which would be perpendicular to the surface at* (x, y, z), *defined by*

$$grad(\vec{h}(v_t)) = \frac{\partial \vec{h}}{x} i + \frac{\partial \vec{h}}{y} j + \frac{\partial \vec{h}}{z} k.$$

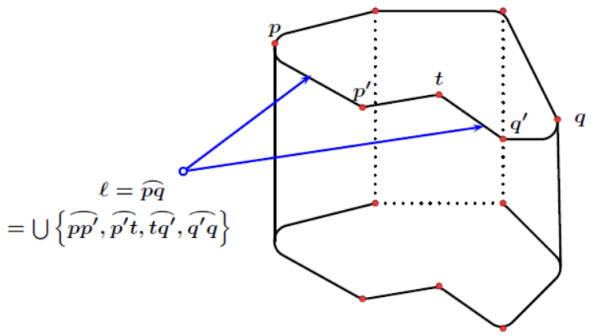

Figure 4: Trajectory of a particle over twistor curve realizable as the union of a sequence of sub-arcs on Lefschetz arc $\ell = \widehat{pq}$ on a R.S. Ward hypersurface $\mathbb{C}S$ [20, p.62].

4. Feynman Trajectories of a Particle

This section introduces particle trajectories as continuous paths over the curvature of space-time, which leads to the counterpart of the discrete path results already given. The transition from discrete paths results from the geometry of space-time generated by quantum processes [8], which is in keeping with the observation by R. Penrose [13] that the link between space-time curvature and quantum processes such as those found in Feynman trajectory of a particle is supplied by the use of twistors. A *twistor space* is a complex manifold $\mathbb{C}M$. For example, a Lefschetz arc in curved space-time is a R.S. Ward hypersurface $\mathcal{S}$ twistor [20, p.56], which is a complex curve ℓ in $\mathbb{C}\mathcal{S}$.

Example 4.1. *A sample twistor curve* $\ell \in \mathbb{C}S$ *is shown in Fig. 4, which is a geometric realization of a Feynman trajectory of a particle (see Def. 4.2), which leads to a space-time view of a Lefschetz arc (see Def. 4.2 and Lemma 4.5).*

Definition 4.2. *The trajectory of a particle in a 2-plane in curved space-time is a map*

$$h : \mathbb{R}^2 \times S^2 \to \mathbb{R}^2 \times S^2$$

defined by

$$h(t_{t_x}) = \widehat{t_{t_x}, t_{t_{x_i}}} \cup \bigcup \widehat{t_{t_{x_i}}, t'_{t'_{x'_i}}} \quad t, t' \in \mathbb{R}, x_i \in S^2, i \in I,$$

in which each $\widehat{t_{t_{x_i}}, t'_{t'_{x'_i}}}$ *is a space-time line segment in a curve* ℓ *starting with subarc* $\widehat{t_{t_{x_0}}, t_{t_{x_i}}}$ *in a Lefschetz arc at times* t_t *(instant* t *in region time* t*) with index* i *in the unit interval* $I = [0, 1]$ *is mapped to an arcwise-connected set,* i.e, *the line segments in the trajectory are attached to each other and starting with* $\widehat{t_{t_{x_0}}, t_{t'_{x_i}}}$, *there is a path from any subarc a sequence of subarcs can be traversed to reach an ending subarc* $\widehat{t_{t_{x_n}}, t'_{t'_{x_{n'}}}}$ *in a N.M.J. Woodhouse [23] twistor space* $\mathbb{R}^2 \times S^2$ *with metric signature* $++--$.

Remark 4.3. *From Definition 4.2, the vectors in $h(t_{x_i})$ are J.H.C. Whitehead zero cells [21] in an arcwise-connected space $\mathbb{R}^2 \times S^2$.*

Definition 4.4. *A Lefschetz arc E is a curve ℓ attached between a pair of 0-cells p, p'. We assume the curve ℓ is dense and the points in ℓ are path-connected, i.e., between every pair of points q, q' in ℓ, there is a sequence of sub-arcs traversable between q and q'.*

Lemma 4.5. *A trajectory of a particle is realizable as a Lefschetz arc.*

Proof. From Definition 4.2, a trajectory h is a curve ℓ that starts and ends with a 0-cell and is the union of subarcs in an arcwise-connected space. Hence, from Definition 4.4, the trajectory h is realizable as a Lefschetz arc. □

Example 4.6. *A sample trajectory of a particle as a Lefschetz arc over a twistor curve realized as a Lefschetz arc $\ell = \widehat{pq}$ with endpoints (0-cells) $\vec{p}, \vec{q}$ and which is the union of sub-arcs is shown in Figure 4.*

Definition 4.7. *The unit $I = [0, 1] \in \mathbb{R}$ is the set of all real values in the closed interval with initial value 0 and ending 1 and an unbounded number of consecutive everywhere dense subintervals of real values between 0 and 1. That is, every real number x in a subinterval of $A \subset I$ has another real number $x' \in A$ that is arbitrarily close to x.*

Lemma 4.8. *The trajectory of a particle is continuous.*

Proof. From Definition 4.7, I is dense and is the index set for the points in the trajectory of a particle. A particle moving along the Lefschetz curve can be observed at any real value in the unit interval $I = [0, 1]$ (see J.J. Sakurai and J. Napolitano [18, p. 37]). Let h be the trajectory of a particle t_{t_x}. One can consider this trajectory as a curve $\ell : I \to Im\ h$ defined by $\ell(t) = t_{t_{x_i}}$ with $\ell(0) = t_{t_x}$. Since ℓ is continuous, for any close pair i, j in I will be mapped to close pair $t_{t_{x_i}}$ and $t_{t_{x_j}}$ and hence close points in $\mathbb{R}^2 \times S^2$ will be mapped to two close trajectories. Hence, h is continuous. Then if $i, i' \in I$ are close, then $t_{x_i}, t_{x_{i'}}$ are close. Hence, the trajectory h is continuous. □

Remark 4.9. *In the proof of Lemma 4.8, we considered a trajectory of a particle as a curve, parametrized on the closed interval $[0, 1]$. However, in 1-D Quantum Mechanics, this is not the case, i.e.. The points of the trajectory may have an infinite number of possible values so that they may not be limited in $[0, 1]$ but rather are lying in $(-\infty, \infty)$. For more details, see J.J. Sakurai and J. Napolitano [18, pp. 37-42].*

Example 4.10. *Given a trajectory h, consider the set $J = \{t_i\}_{i \in I}$ of the instants of time of occurrence of the points in the trajectory of a particle over a vector field. The map $g : I \to \mathbb{R}$ defined by $g(i) = t_i$ is continuous, since for every arbitrarily close pair i and j, t_i and t_j are also arbitrarily close.*

5. Feynman Path Integral

In this section, it is observed that a Feynman path is continuous (Lemma 5.2), which leads to the results in Theorem 5.4 and Theorem 5.5 for Feynman paths, which are consequences of the Borsuk-Ulam Theorem.

Definition 5.1. *[4, p. 31] A Feynman path is a function $H : \mathbb{R}^2 \times S^2 \to S^2$ defined by $H(t_{t_x}) = x$ for a particle at point x at time t_t.*

Lemma 5.2. *Every Feynman path is continuous.*

Proof. Let $H : \mathbb{R}^2 \times S^2 \to S^2$ be a Feynman path, defined by $H(t_{t_{x_a}}) = x_a$ which is the trajectory h of a particle at point x_a at time t_t. Let ℓ represent that a particle travels over during its trajectory and let $H(t_{t_{x_a}}) = x_a$ be a point in ℓ. For simplicity, the curve ℓ is referred to as the trajectory of a particle. During the passage of a particle over ℓ, ℓ has no gaps in it. Since a trajectory map h is continuous, two close points $t_{t_{x_a}}$ and $t_{t_{x_b}}$ will lead us two close points x_a and x_b in ℓ at time t_t. Hence, a Feynman path h is continuous. □

Remark 5.3. *In Lemma 5.2, the continuity of a Feynman path H is explained in terms of the closeness (nearness) paradigm from [12, §1.5, p. 8], instead of the abstract (less intuitive) $\epsilon - \delta$ view of continuity. This approach befits the character of the trajectory of a particle over a curve ℓ, where the trajectory of a particle and the curve ℓ (without gaps) are traced by the particle in its trajectory. Just as pairs of points in the curve ℓ can be arbitraily close, so too, from Lemma 4.8, the vectors $H(t_{t_{x_a}}), H(t_{t_{x_b}})$ in the trajectory of a particle can be arbitrarily close.*

The value of a path between points a and b on a curve ℓ (the positions of a particle trajectory at times t_a, t_b, respectively), is $K(b, a)$, defined in a complex space $\mathbb{C}S$ with respect to Planck's constant $\hbar$ by Feynman and Hibbs [4, p. 45] by

$$\begin{aligned}
V(x,t) &= \textit{Potential energy of particle with mass } m.\\
L &= \frac{m}{2}\dot{x}^2 - V(x,y) \text{ (\textit{Lagragian} for the system).}\\
S[b,a] &= \int_{t_a}^{t_b} L(\dot{x},x,t)dt\\
a,b &= \textit{ points on a twistor curve.}\\
K(b,a) &= \int_a^b e^{\left(\frac{i}{\hbar}\right)S[b,a]}\mathcal{D}x(t).
\end{aligned}$$

A Feynman path $H : \mathbb{R}^2 \times S^2 \to S^2$ over a curved space S^2 can be considered as $H = pr_2 \circ h$, the composition of its corresponding trajectory map $h : \mathbb{R}^2 \times S^2 \to \mathbb{R} \times S^2$ and the second projection map $pr_2 : \mathbb{R}^2 \times S^2 \to S^2$. Given a fixed point b_h on ℓ, define $\alpha : S^2 \to \mathbb{R}^2$ by $\alpha(\vec{a}) = K(b_h, a)$ where $K(b_h, a)$ is the value of the trajectory h containing points b_h, a in a segment $\widehat{b_h, a}$ in a curve ℓ starting at a and terminating at b_h.

Theorem 5.4. (**Feynman Path Theorem**) *Given a map $\alpha : S^2 \to \mathbb{R}^2$, there exists $\vec{a}$ in S^2 such that $\alpha(\vec{a}) = \alpha(-\vec{a})$.*

Proof. From Lemma 5.2, a Feynman path H is continuous and so that α is also continuous. Hence, from Theorem 1.1, we obtain the desired result, $\alpha(\vec{a}) = \alpha(-\vec{a})$ for antipodal points $a, -a$ in a Feynman path H. □

Theorem 5.5. (**Feynman Trajectory-of-Particle Theorem**) *The Feynman trajectory of a particle satisfies Borsuk-Ulam Theorem 1.1. Let $H : S^2 \to \mathbb{R}^2$ be the trajectory of a particle on the surface of sphere. There is at least one pair vectors $\vec{p}, \vec{p'} \in S^2$ such that $H(\vec{p}) = H(\vec{p'})$.*

Proof. From Lemma 5.2, a Feynman trajectory is continuous. Hence, from Theorem 1.1, we obtain the desired result for antipodal points $\vec{p}, -\vec{p} \in S^n$ in the Feynman trajectory h. □

Theorem 5.6. (**Feynman Path Integral Theorem**) *There exists a Feynman path with an initial path integral $K(b_h, a)$ for an initial vector $\vec{a}$ that equals the path integral $K(b_h, -a)$ for a later vector $-\vec{a}$, which may or may not be the antipode of vector $\vec{a}$.*

Proof. $K(b_h, a)$ are Feynman path integrals that resonate (have values) for a particle that has gradients on either two different surface curvatures along a surface curve ℓ or on the same surface curvature on a path ℓ' for a boomerang trajectory that follows a path that is a cycle. In either case, choose an intermediate point b_h in the path between $\vec{a}$ and b_h so that the two segments on ℓ have the same length. In that case, $K(b_h, a) = K(b_h, -a)$. □

Remark 5.7. *The significance of Theorem 5.6 is that the endpoints on a particle trajectory curve ℓ need not be antipodal points. That is, Theorem 5.6 is more general than Theorem 5.4.*

6. Woodhouse Borsuk-Ulam Theorem

This section gives three results for N.M.J. Woodhouse contour integrals [23, p. 198], defined with respect to the set of all real α-planes that has topology $\mathbb{R}^2 \times S^1$, which is compactified by adding S^1 representing α-planes that lie in the null cone at ∞. First, consider

$$\xi = x_1 + ix_2 \text{ and } \tau = t_1 + it_2, \text{ representing } \alpha\text{-planes as surfaces, with}$$
$$w = \xi + \bar{z}\tau,\ \bar{w} = \bar{\xi} + z\bar{\tau}, \text{ constant for } z = e^{i\theta}, \text{ where}$$
$$z = e^{i\theta} \text{ determines orientation of } \alpha\text{-plane.}$$
$$\phi(w, \bar{w}, z) = \frac{1}{2\pi} \oint_{|z|=1} f(w, \bar{w}, z) \frac{dz}{z}, \text{ expanded to obtain}$$
$$\phi(w, \bar{w}, z) = \frac{1}{2\pi} \oint_{|z|=1} f(\xi + \bar{z}\tau, \bar{\xi} + z\bar{\tau}, z) \frac{dz}{z}.$$

Let $\Phi : S^2 \to \mathbb{C}$ be a map defined by $\Phi(\vec{p}) = \phi(w_{\vec{p}}, \bar{w}_{\vec{p}}, z)$, where $w_{\vec{p}}$ is the point representing $\vec{p}$ on the equilateral circle $S_{\vec{p}}$ on S^2 which is passing through $\vec{p}$. The function Φ can be realized as a function $\Phi : S^2 \to \mathbb{R}^2$ as $\mathbb{C}$ and $\mathbb{R}^2$ are homeomorphic.

Definition 6.1. *The contour integral $\Phi : S^2 \to \mathbb{R}^2$ is a smooth function, since ϕ is a smooth function on a twistor space [23]. That is, Φ is continuous.*

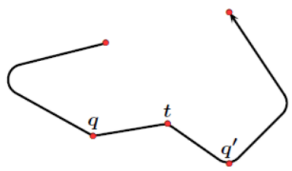

Figure 5: Woodhouse contour integrals on sub-twistor curve antipodes $\boldsymbol{q}, \boldsymbol{q}'$ with $\oint_{\widehat{qt0}} = \oint_{\widehat{tq'0}}$.

Theorem 6.2. *The contour integral Φ satisfies the Borsuk-Ulam Theorem.*

Proof. From Definition 6.1, the contour integral $\Phi : S^2 \to \mathbb{R}^2$ is a continuous function. The result follows from Theorem 1.1, *i.e.*, there exist antipodes $\vec{p}, -\vec{p}$ on a twistor curve in $\mathbb{R}^2 \times S^2$ such that $\Phi(p) = \Phi(-p)$. □

Corollary 6.3. *The map Φ also satisfies the path-Borsuk-Ulam Theorem given in Theorem 3.5.*

Proof. Take $n = 2$ and replace the continuous map $f : S^n \to \mathbb{R}^n$ with $\Phi : S^2 \to \mathbb{R}^2$ in the proof of Theorem 3.5. □

Example 6.4. *Sample contour integrals on sub-twistor vectors that are antipodal are shown in Figure 5.*

Theorem 6.5. *Let ϕ, ϕ' be the Woodhouse contour integrals over a twistor curve ℓ and let p, p' be any two distinct points on ℓ. Then there are Φ, Φ' such that $\Phi(p) = \Phi'(p')$.*

Proof. Replace the Feynman path integral with the Woodhouse contour integral in the proof of Theorem 5.6, and the desired result follows. That is, we can always find a point q between p, p' on the twistor ℓ such that $\Phi(p) = \Phi'(p')$. □

Remark 6.6. *Theorem 6.5 covers a broader spectrum of twistor length measurements than Theorem 6.2. That is, for any pair of distinct vectors on a twistor curve, we can always find an intermediate vector so that the contour integrals over the resulting twistor sub-arcs have equal value.*

Example 6.7. *Sample contour integrals on sub-twistor curves $\widehat{\boldsymbol{v_1}, \boldsymbol{v_2}}, \widehat{\boldsymbol{v_2}, \boldsymbol{v_3}}$ with end points that may or may not be non-antipodal are shown in Figure 6.*

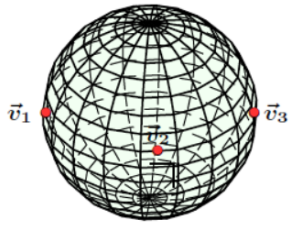

Figure 6: Woodhouse contour integrals on sub-twistor curves $\widehat{v_1, v_2}, \widehat{v_2, v_3}$ with $\oint_{\widehat{v_1,v_2}} 0 = \oint_{\widehat{v_2,v_3}} 0$.

7. Concluding Remarks

The focus in path Borsuk-Ulam Theorem 3.5 is on a homotopic path between antipodes on the surface of a sphere S^n mapped to real values in $\mathbb{R}^n$. The geometry underlying the Borsuk-Ulam Theorem looms up, for example, in the realization of a homotopic path as an arc stretching over a planetary curved surface between one location and another location at varying space-times with the same latitude and longitude. In this paper, the Borsuk-Ulam Theorem is an emperor with new clothes, namely,

1° *How to look:* consider either a discrete or continuous homotopic paths between antipodes.
2° *Geometric realization:* endpoints of twistor curves that are either antipodal or non-antipodal.
3° *Length-of-arc measure: e.g.*, measure with either a Feynman path integral or Woodhouse contour integral over arcs having antipodal endpoints.

References

[1] K. Borsuk, *On retractions and related sets*, Ph.D. thesis, University of Warsaw, Warsaw, Poland, 1930.
[2] K. Borsuk, *Drei sätze über die n-dimensionale euklidische sphäre*, Fundamenta Mathematicae **XX** (1933), 177–190.
[3] R.P. Feynman, *The principle of least action in quantum mechanics*, Ph.D. thesis, Princeton University, Princeton, N.J., 1942.
[4] R.P. Feynman and A.R. Hibbs, *Quantum mechanics and path integrals, extended edition, preface by D.F. Styer*, Dover Publications, Inc., Mineola, NY, 2010.
[5] S. Lefschetz, *Applications of algebraic topology. Graphs and networks, the Picard-Lefschetz Theory and Feynman Integrals, (applied mathematical sciences)*, vol. 16, Springer-Verlag, New York-Heidelberg, 1976.
[6] S. Lefschetz, *Introduction to topology*, Princeton University Press, Princeton, N.U., 1976.
[7] L. Lusternik and S. Shnirel'man, *Topological problems in variational problems (Russian)*, Issledowatelskii Institut Matematiki i Mechaniki pri O.M.G.U., Moscow **17** (1930), no. 1, 166–217.
[8] L.J. Mason, *Twistors in curved space-time*, Ph.D. thesis, Wadham College, Oxford University, Oxford, U.K., 1985.
[9] J. Matoušek, *Using the borsuk-ulam theorem. lectures on topological methods in combinatorics and geometry* written in cooperation with Anders Björner and Günter M. Ziegler, Springer-Verlag, Berlin, 2003.
[10] L. Mosher, *Tiling the projective foliation space of a punctured surface*, Trans. Amer. Math. Soc. **306** (1988), no. 1, 1–70.
[11] J.R. Munkres, *Elements of algebraic topology, 2nd ed.*, Perseus Publishing, Cambridge, MA, 1984.
[12] S.A. Naimpally and J.F. Peters, *Topology with applications. Topological spaces via near and far*, World Scientific, Singapore, 2013.
[13] R. Penrose, *Twistor quantization and curved space-time*, Int. J. of Theor. Phys. **1** (1968), no. 1, 61–99.
[14] J.F. Peters, *Ribbon complexes & their approximate descriptive proximities. Ribbon & vortex nerves, Betti numbers and planar divisions*, Bull. Allahabad Math. Soc. **35** (2020), no. 1, 31–53.
[15] J.F. Peters, *Homotopic nerve complexes with free group presentations*, Int. Online Conf. Algebraic and Geometric Methods of Analysis, 25-28 May 2021, Odesa, Ukraine, Institute of Mathematics of the National Academy of Sciences of Ukraine, Taras Shevchenko National University of Kyiv and Kyiv Mathematical Society, 2021, dedicated to the memory of Yuriy Trokhymchuk (17.03.1928-18.12.2019), arXiv:2106.13586, pp. 110–111.
[16] J.F. Peters and T. Vergili, *Fixed point property of amenable planar vortexes*, Appl. Gen. Topol. **22** (2021), no. 2, 385–397.
[17] J.H. Poincaré, *Sur l'analysis situs*, Comptes Rendus Acad. Sci. Paris **115** (1892), 633–636.
[18] J.J. Sakurai and J. Napolitano, *Modern quantum mechanics*, Cambridge University Press, U.K., 2021.
[19] E.H. Spanier, *Algebraic topology*, McGraw-Hill Book Co., New York-Toronto, Ontario, Canada, 1966.
[20] R.S. Ward, *Curved twistors spaces*, Ph.D. thesis, St. John's College, Oxford University, Oxford, U.K., 1977.
[21] J.H.C. Whitehead, *Combinatorial homotopy. I*, Bulletin of the American Mathematical Society **55** (1949), no. 3, 213–245, Part 1.
[22] J.H.C. Whitehead, *Combinatorial homotopy. II*, Bulletin of the American Mathematical Society **55** (1949), no. 5, 453–496, Part 2.
[23] N.M.J. Woodhouse, *Contour integrals for the ultrahyperbolic wave equation*, Proc. Roy. Soc. London Ser. A **438** (1992), no. 1902, 197–2006.

STUDY PROPOSAL: TOWARDS STREPTOCOCCAL INFECTIONS WITH NONSPECIFIC SYMPTOMS

Arturo Tozzi
Center for Nonlinear Science, Department of Physics, University of North Texas, Denton, Texas, USA
1155 Union Circle, #311427 Denton, TX 76203-5017 USA
tozziarturo@libero.it

PREMISE

In 2023, increases in scarlet fever's incidence have been detected throughout Europe. Based on general pediatricians' experience, we hypothesize that a shift has occurred in both group A streptococcus (GAS) clinical findings and age of onset. Therefore, we propose to evaluate whether the well-standardized signs and symptoms leading to GAS diagnosis still hold.

STUDY DESIGN

Children of every age (also <3 years) with fever, but without the specific diagnostic signs and symptoms of GAS infection, will undergo Strep test throat swab (swab 1). All the positive children will be treated with the standard therapy of 10-days amoxicillin. After the therapy, another swab will be performed on the treated children (swab 2).

POSSIBLE OUTCOMES

1) If swab 2 will be still positive, this means that children are either carriers, or, very rarely, therapy-resistant.
2) If swab 2 will be negative, this means that children underwent a GAS infection characterized by nonspecific signs and symptoms.
We also expect that the age of GAS infection could be lower than suggested in literature, i.e., that GAS currently also infects children <3 years.

Open Peer Review on Qeios

Mental Recognition of Objects via Ramsey Sentences

Arturo Tozzi[1]

1 University of North Texas

Funding: No specific funding was received for this work.

Potential competing interests: No potential competing interests to declare.

Abstract

Dogs display vast phenotypic diversity, including differences in height, skull shape, tail, etc. Yet, humans are almost always able to quickly recognize a dog, despite no single feature or group of features are critical to distinguish dogs from other objects/animals. In search of the mental activities leading human individuals to state *"I see a dog*", we hypothesize that the brain might extract meaningful information from the environment using Ramsey sentences-like procedures. To turn the proposition *"I see a dog"* in a Ramsey sentence, the term dog must be replaced by a long and complex assertion consisting only of observational terms, existential quantifiers and operational rules. The Ramsey sentence for *"I see a dog"* sounds: "*There is at least an entity called dog which satisfies the following conditions: it is an animal, it has four legs, …, etc, …, and is something that I have in my sight*". We discuss the biological plausibility and the viable neural correlates of a Ramsey-like mechanism in the central nervous system. We accomplish a brain-inspired, theoretical neural architecture consisting of a parallel network that requires virtually no memory, is devoid of probabilistic choices and can analyze huge but finite amounts of unique visual details, combining them in a single concept. In sum, Ramsey sentence stands for a versatile tool that can be used not just as a methodological device to cope with biophysical affairs, but also for a model to describe the real functioning of cognitive operations such as sensation and perception.

Arturo Tozzi

Center for Nonlinear Science, Department of Physics, University of North Texas, Denton, Texas, USA; 1155 Union Circle, #311427 Denton, TX 76203-5017 USA.

tozziarturo@libero.it

Keywords: theoretical terms; non-observable entity; sparce code; neural network, symbolic reasoning.

Introduction

As John was passing by, he saw a dog under a tree. He said to himself: *I' see a dog*'. John says the same words when he sees a dog collar, when he hears barking, when he catches the typical smell of dog in an empty room. In all these cases, John is almost always capable of recognizing a dog. What happens in John's brain when he watches a dog? How does John recognize that he is watching a dog? We will leave apart auditory, olfactive, tactile cues and will confine ourselves to the assessment of a specific case related with visual cues, i.e., a human individual who watches an object, a painting, a sketch, a photo illustrating something that he terms "a dog". Scientists tackled the issue and formulated manifold responses. Some scholars provide a holistic account of perceptive contents, suggesting that the observed object displays as a whole emergent properties that cannot be found zooming in any part of its constituents (Pastukhov 2017). In turn, others contend that an image is first perceived in terms of its basic individual elements/features, then is recognized (Grainger et al., 2008). Others suggest that the visual system might split the processing of an object's form and color ("what") from its spatial location ("where") (Rao et al., 1997). Others believe that quick recognition of things like dogs involve both category-specific computational hubs in the ventral visual stream and distributed cortical memory networks (Woolnough et al., 2020). Further, template matching models of pattern recognition suggests that mental comparison takes place between external inputs and internal schemes (Hirai 1980).

We will take a different turn. At first, we will break the concept of dog into its component parts, looking for the minimal features or traits that allow human observers to recognize that this is a dog. The problem is twofold:

1. By one side, the visual and non-visual features allowing John to say "*I see a dog*" must be defined.
2. By another side, despite dogs are among the most variable mammals, John is almost always able to quickly recognize that this is a dog. Therefore, the second problem sounds as follows: looking at different images depicting manifold canine breeds, how does it happen that John is almost always able to state "*I see a dog*"?

We will conclude that no single feature or group of features allow John to distinguish the dog from other objects or animals, nevertheless John is always able to recognize that this is a dog. To solve this seeming contradiction, a theory of sensation and perception can be built using an approach borrowed from the last writings of Frank Plumpton Ramsey, just before his premature death in 1930. We will suggest that the brain might use Ramsey language-like procedures to extract

meaningful information from the environment. Further, we will examine the biological plausibility and the possible neural correlates of a Ramsey-like mechanism in the brain.

Defining Dogs with Ramsey Sentences

How does John recognize a dog? We will analyze both the visual and non-visual features that allow John to state "*I see a dog*". The Oxford Learners' Dictionary defines the dog as an animal with four legs and a tail, often kept as a pet or trained for work such as hunting or guarding buildings. The dog can also be defined as a highly variable domestic mammal (Canis familiaris) closely related to the gray wolf. Yet, these definitions are rather general. How many features of a dog are required to say "this is a dog"? How many features of different dogs are required to identify the dog's breed?

We could say that John recognizes a dog because it is an animal, but it is a too vague concept. We could say that John recognizes a dog because it has four legs, but John is able to recognize a dog even if, unfortunately, has three legs. We could say that John recognizes a dog because is a domesticated descendant of the wolf, but he is able to easily recognize a dog even if he is unaware of phylogenesis and evolution. We could say that John recognizes a dog through its genome sequencing (Hayward et al., 2016; Plassais et al., 2019; Letko et al., 2023), but he can recognize a dog even if he never heard about DNA. We could say that John recognizes a dog because it has an upturning tail, but he can recognize a dog even if, unfortunately, has a cut tail. Despite there are many different shapes for dog tails, from straight up to curled or corkscrew, John says that he recognizes that it is a dog. The same holds for the weight, the height, the eye gaze, the facial expression, the body posture, the manifold coats of different breeds, the different-shaped snout, the Carnivorans-like teeth arrangement for cutting meat, the non-retractable claws, etc. We could say that John recognizes a dog because it is uniquely adapted to human behavior, having acquired the ability to understand and communicate with humans. But John effortlessly recognizes also a wild dog.

In sum, our examples suggest that no single observable and non-observable feature or group of features are critical to define the dog and distinguish it from other objects or animals. Nevertheless, the lack of explicit identifying features and the huge morphological and behavioral diversity between breeds do not prevent John to be almost always able to recognize that he is seeing a dog. To resolve this apparent contradiction, we are going to introduce the Ramsey sentence and show how it could be used to describe the mental activities that lead John to state "*I see a dog*".

The proposition "*I see a dog*" can be turned in a Ramsey sentence. Ramsey introduced a technique of examining a scientific theory by means of long and complex formal propositions (Ramsey 1931), later termed "Ramsey Sentences" by Hempel (1958). Ramsey's account is built on the observation that scientific theories often describe abstract, theoretical terms such as "*spin*" and "*electron*" that cannot be observed and are difficult to distinguish from the metaphysical terms so often encountered in philosophy (Carnap 1966). A finitely axiomatized scientific theory T can be formulated in a formal language of first order predicate logic (Hintikka 1998), where the predicates are usually divided into two groups, namely the observational terms (O1, O2,…, On) and the non-observational terms (N1, N2,…, N2). Therefore, the theory can be expressed as:

$$T = O1, O2, \ldots On; N1, N2, \ldots Nn.$$

Aiming to build scientific theories by means of both existential propositions and explicit definitions representing experiences, Ramsey removed the theoretical entities Nn from T. Non-observable entities can be tackled through second order variables X, i.e., primitive observation terms not referring to individuals, but to properties of individuals or relations between individuals. A Ramsey's sentence is achieved, i.e., a second-order, extended observational statement where the theoretical terms and/or postulates are replaced by a high but finite number of variables and observables bound to initial existential quantifiers ∃. In formal terms:

$$TR = \exists X1\ \exists X2 \ldots \exists Xn, O1, O2, \ldots On.$$

Where the proposition TR stands for the Ramsey sentence of T.

Theoretical terms are replaced by the assertion that "*there is at least one entity that displays the same formal connection with the observational properties that the theory T and that satisfies certain conditions*". For example, instead of explicitly using theoretical terms such as "*electron*", a long and complex proposition can be drawn that goes through all the cases satisfying the laws and consequences, so that the term "*electron*" turns out to designate the conjunction of all the properties needed to specify the meaning of the term, such as, e.g., the properties 1, 2, 3, plus 4,5,6, plus the additional properties 7,8, etc.

The same Ramsey humbly asked to himself: is it necessary to use such intricate definition for the legitimate use of theory? The answer is positive. According to functionalistic scholars, Ramsey sentences provide empirically adequate descriptions of the things that can be described just by observational terms (Berardi and Steila, 2015; Lowther 2022). The Ramsey–Carnap approach, or Ramseyfication, has been widely used to assess scientific issues such as, e.g., infrared spectroscopy in analytical chemistry (Toppel 2021). Further, David Lewis (1972) suggested to use Ramsey sentences to tackle mental issues. He introduced a general method for constructing Ramsey sentences to define mental operations such as pain. All the mental state terms related with pain are removed from the statement and replaced by variables X plus existential quantifiers:

$$\exists X1\ \exists X2\ \exists X3\ \exists X4, \ldots \exists Xn.$$

In this case, the variable X includes:

a. Quantifiers that range over mental states.
b. Terms that denote stimulations/behavior.
c. Terms that specify various causal relations among them.

In the sequel, we suggest to look at the Ramsey sentence in realist terms, advising that it is not just a useful methodological tool, but might also be a reliable model to explain cognitive mental processes such as sensation and perception.

Could Ramsey Sentences be performed by Human Brains?

We argue that the term "*dog*" can be treated as a theoretical term in a Ramsey's sentence. For children who never saw a dog, the dog stands for a theoretical entity. Only with time, habituation and social consensus children learn to climb the steps from theoretical to observable entities, becoming able to say: "*I see a dog*". Therefore, the mental schemes that allow human individuals to say: "*I see a dog*" require time and training to give a meaning to the observed object. In touch with this observation, it has been reported that face looking in monkeys is not innate, rather experience is required for the formation/maintenance of face domains (Arcaro et al., 2017).

Our aim is to provide a Ramsey sentence for the (apparently) trivial assertion:

> *"I see a dog".*

To achieve Ramseyfication, the assertion can be modified in:

> *"I have a dog in my sight".*

Then, it can be described in Ramsey's terms through second order variables do not referring to individual dogs, but to properties/relations among dogs:

> *"There is at least an entity called dog which satisfies the following conditions: it is an animal, it has four legs, it is a domesticated descendant of the wolf,…, etc, …, and is something that I have in my sight".*

All the observable features encompassed in the concept of "*dog*" must be explicitly expressed using a long but finite list of dog-related features that can be empirically confirmed.

In sum, a Ramsey sentence can be used to assess how the human brain perceives and recognizes a dog. The next step will be to evaluate the biological feasibility and the viable neural correlates for Ramsey sentences.

Subcortical and cortical areas related to visual sensation and perception have been widely investigated (Hayama et al., 2016). When a dog is in front of John's eyes, the sequence of neuronal activation can be followed throughout John's visual system (**Figure 1**). We hypothesize that in the short 280–400 ms time window that occurs from the view of the dog to the assertion "*I see a dog*", the brain performs manifold parallel computations. Every parallel neural channel examines one of the numerous observational terms X of a Ramsey sentence (namely, every single feature of the dog), combining to produce a single final output that turns out to be the assertion "*I see a dog*" (**Figure 1**). We accomplish a logical-mathematical framework in the form of a Ramsey sentence, which is useful in reasoning about the unification of analytic observables and concept.

The next step is to look for feasible neural correlates of this Ramsey-like mechanism. Clues point towards the biological plausibility of Ramsey-like processes that occur in the brain during cognitive processes such as sensation and perception. To start with, the Ramsey's account requires manifold parallel channels able to simultaneously perform computations

related with different dog features. To watch and recognize a dog requires simultaneous parallel information processing in sensorimotor, associative and limbic circuits modulated by both sensory cues and previous learning (Macpherson et al., 2021). It is noteworthy that the nervous system is a distributed large-scale network characterized by parallel processing loops. In touch with a Ramsey framework, widespread inter-area fluctuation modes transmit sensory data and task responses through parallel non-interfering channels, so that the neocortical sensory processing overcomes the substantial variability of neuronal sensory responses and generates reliable sensory discrimination (Ebrahimi et al., 2022). Parallel computing and parallelization strategies are widely used in theoretical neuroscience and artificial neural networks' optimization to perform human-like tasks, to capture neuron and synapse dynamics and to deal with data processing, pattern recognition and classification (Liu et al., 2016; Pastur-Romay et al., 2017; Ben-Nun and Hoefler, 2018; Peres and Rhodes, 2022; Kanwisher et al., 2023). Compared with sequential architectures, parallel neural network architectures display optimized performance, higher efficiency, better flexible behavioral control (Hikosaka et al., 1999; Åström and Koker, 2011, Peres and Rhodes, 2022). Furthermore, parallel training is robust and capable of yielding accurate long-term predictions in realistic scenarios (Ribeiro and Aguirre, 2018), facilitating performance of complex and simultaneous behaviors (Macpherson et al., 2021). In the central nervous system, the sparce, parallel pathways underlying Ramsey sentences require in the final stages inputs convergence towards the assertion "*I see a dog*". In touch with this claim, it has been demonstrated that, despite the extreme sparseness of the magnocellular LGN inputs to the macaque primary visual cortex, the V1 produces robust orientation selectivity/continuity in the orientation map, together with simple/complex classification (Chariker et al., 2016). While the neocortex at rest displays single pattern of functional connections, different areas share co-fluctuations and task-related information within 300 s after the onset of the sensory stimulus (Ebrahimi et al., 2022).

The Ramsey's account of sensation and perception suggest that the brain analyses huge amounts of single visual details in a sparce code manner. In agreement with this hypothesis, the representation of semantic processing, that is crucially engaged when judgements are formulated based on association or conceptual similarity (Jackson et al., 2015), is scattered throughout vast areas of the cortical surface (Huth et al, 2016). Another crucial item of the Ramsey sentences, namely, the existential quantifiers, display well-known neural correlates. BOLD fMRI studies point towards the existence of a large-scale fronto-parietal network contributing to specific aspects of logical quantifiers' comprehension (Olm et al., 2014; Zhan et al., 2017; Heim et al., 2020). All the quantifiers (e.g., "at least three") recruit both the right inferior parietal cortex, suggesting that a numerosity component contributes to quantifier comprehension, and the thalamus/anterior cingulate, suggesting an involvement of selective attention (McMillan et al., 2005). A Ramsey-like account of perception and sensation requires the involvement of numerous mental processes including attention, motivation, memory formation and extinction. In touch with this account, separate neuronal mice subpopulations in the central amygdala selectively encode a wide range of different salient stimuli from various sensory modalities with distinct valences and physical properties (Yang et al., 2023). Furthermore, evidence has been found for a specific role of subregions in the medial parietal cortex for the rapid recognition of distinctive entities such as faces and scenes (Woolnough et al., 2020). The Ramsey's framework commands a reductionistic interpretation of widely used complexity measures, providing a feasible account for the spatial and temporal autocorrelation phenomena that explain various measures of network topology and capture individual and regional variations (Shinn et al., 2023). Describing different visual properties as related and

intertwined, Ramsey-like models suggest that a comprehensive picture based on cortical population dynamics is required to explain function, hinting to a system that is less feedforward and more dominated by intracortical signals than previously thought.

In sum, clues from the literature point toward the possibility to build a realistic Ramsey-like model for the cognitive operation of the brain.

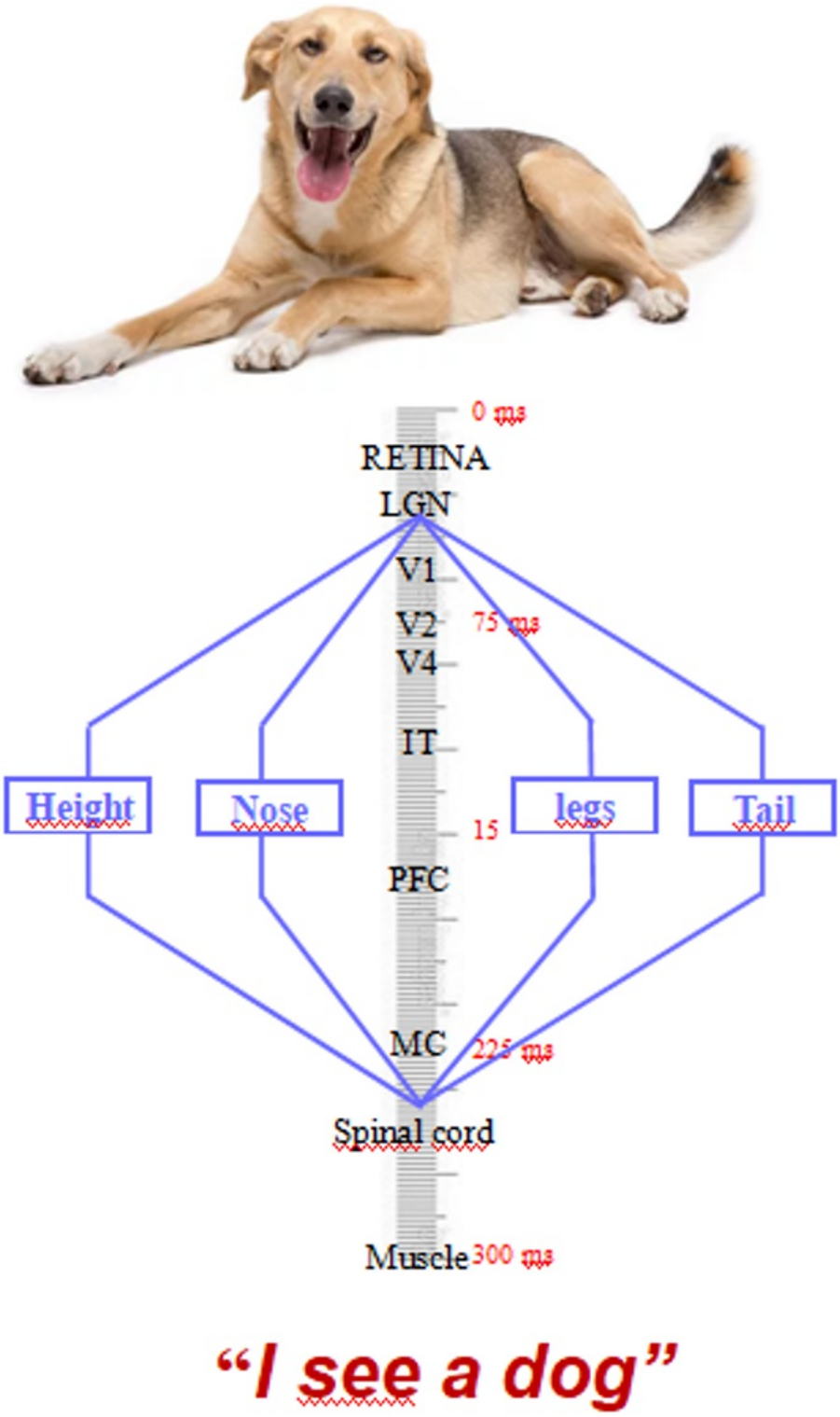

Figure 1. A Ramey-like account of human sensation and perception. The graduated scale at the centre illustrates the latency time (in milliseconds) along the human visual pathway. When an human individual sees a dog, the retina is first activated after 20–40 ms, then they follow the lateral geniculate nucleus (LGN), the primary, secondary and tertiary visual cortices (V1, V2, V3, V4), the infero-temporal area (IT), the prefrontal cortex (PFC), the motor cortex (MC) and the peripheral effectors that generate, after >280 ms, the motor output leading to the assertion *"I see a dog"* (modified from Grimaldi et al., 2023). The Figure depicts four parallel paths, every one processing a single observable variable related with the concept of dog. Just four of the numerous available parallel pathways are illustrated. The

Ramsey-like nervous circuitry is characterized by proximal divergence, central parallel processing and distal convergence.

Conclusions

The human mind is almost always able to recognize a dog, despite dog breeds vary widely in shape, size, color, etc. We suggest that this cognitive phenomenon can be tackled via a methodological and functional approach based on Ramsey sentences. A Ramsey-like approach to the cognitive activities such as sensation and perception suggests that mental states can be intended in terms of parallel and simultaneous activation of specific cortical subareas. A Ramsey-like approach suggests that the brain does not split the environment perceived as a whole in manifold components, rather manifold components act as inputs to analytically build the mental representation of the surrounding environment. In terms of computer science, fitting, optimization and objective function of the target output are not anymore achieved via learning algorithms (Kanwisher et al., 2023), rather via a huge but finite number of parallel computations, each one regarding a single feature of the input's training data. This means that Ramsey sentences might contribute to the human ability to represent relations between concepts, to code relationships between items sharing basic conceptual properties (e.g., dog and wolf) and to simultaneously represent associative links between dissimilar items co-occurring in peculiar contexts (e.g., dog and bone) within a single, unified concept (Jackson et al., 2015).

The possibility to use Ramsey sentences in neuroscientific contexts leads to intriguing outcomes. First of all, criticism can be levelled at the concepts of pair correlation and predictive code in the brain. The paradigm of pair correlations suggests that different brain regions work together in a coordinated and strongly correlated manner, where sensory responses result from comparisons between bottom-up inputs and contextual predictions (Uran et al., 2022), achieving a collection of morphisms, i.e., maps between objects and their mental representation. In other words, the brain would recognize a dog by performing pair correlation between the immaterial dogs stored in the brain and the one that is currently watched. On the contrary, the Ramsey's account points towards the counterintuitive hypothesis that the brain does not perform matching between external visual inputs and an internal database, or between a model output and a target output matching the error. All the content of a dog that can be observed is explicitly expressed in a long and complex formal sentence generated in the parallel circuitry of the brain. No mental interpretation of vague, non-observable entities is required, rather observational terms capable of empirical confirmation are achieved. This means that the concept of the dog arises naturally from the parallel flow occurring in different subcortical and cortical areas, without the need of pre-stored mental concepts of the dog and of comparison among observable variables expressed in terms of atomic propositions. Paraphrasing Ramsey, the concept of a dog must be built out of simple observational facts, leaving apart the use of a set of axioms and a dictionary of correspondence rules that translates the primary language into the secondary language. Theoretical terms contribute to the observational component of a theory not through bridge laws connecting theoretical and observational concepts, rather the only bridge principle is the given theory itself (Hintikka 1997). Further, a Ramsey-like circuitry permits the addition of parallel lines to perform always new atomic propositions o improve and enlarge the very definition of terms such as "*dog*".

A Ramsey-like approach to cognitive activities cast doubts on the utility of the energetically expensive long-term memory storage in the brain. Engrams of specific memories are thought to be distributed and stored in ensembles of neurons across multiple brain regions that are functionally connected, via cross-regional recruitment of presynaptic neurons initiated by downstream memory neurons (Lavi et al., 2022; Roy et al., 2022). The Ramsey account suggests that the brain is a collection of numerous but finite functional units, everyone performing a single operation. The concept of dog arises from the simultaneous, sparce activation of many single parallel processes. What is termed memory ends up depending on the countless sparce sources that have been activated together, keeping in mind that the same anatomical unity can be recruited during different cognitive tasks. In long times, the single, variable features of a dog (such as breed, cheek features, neck length, and so on) have been gathered in scattered and parallel brain circuits. In touch with this theoretical account, it has been demonstrated in monkeys that environmental inputs drive neuronal activity by sculpting cortical domain formation (Arcaro et al., 2017). Selective viewing behavior at birth bias category-specific visual responses toward retinotopic representation, with no need of category-specific templates.

Another outcome of using Ramsey sentences for the assessment of human cognitive activities is the demise of probabilistic and Bayesian accounts of choices and beliefs (Cazettes et al., 2023). Probabilistic and classical inference patterns have been suggested to subtend both artificial and natural neural networks. Looking for the statistics of features in images, artificial and natural systems might use gradient descent learning that builds representations that are more sensitive to common features (Benjamin et al., 2022). Bayesian accounts point towards the brain as an inferential machine equipped with a priori beliefs (Ramstead et al., 2020). For instance, a Bayesian inference semantics for probabilistic reasoning in natural language successfully deals with various probabilistic semantic phenomena, including generalised quantifiers (Bernardy et al., 2019). On the contrary, Ramsey sentences guarantee neural multiplexing that does not require outputs based on pondering of probabilities. The Ramsey sentence displays a crucial component that runs counter probabilistic interpretations of human choices and beliefs, namely the existential quantifier. Thanks to the existential quantifier, the assertion "*I see a dog*" must be treated as an evolving existential statement such as "*there is at least one thing termed dog that…*". The assertion becomes a shorthand expression of all the judgements and beliefs about dogs whose consequences will meet the future successfully or not. The possibility that "*I see a dog*" might be determined in a way that John is unable to statistically anticipate must not be foreclosed, since "*I see a dog*" is open to John's future revision due to further additions made within the scope of the quantifier (Misak 2020). Leaving apart probabilistic accounts, we suggest that a Selfridge's Pandemonium-like "the-winner-takes-all" mechanism (Tozzi and Peters, 2018) might provide a plausible account subtending the coalescence of the single observational features in the final output.

The use of a Ramsey-like approach to human cognitive activities has limitations. It has been objected that Ramsey sentences do not carry out a genuine elimination of theoretical concepts (Majer 1989; Koslow 2008). It has been pointed out that Ramsey sentences cannot provide a satisfactory formalism to functionalism, being just a type of behaviourism plus a cardinality constraint on the number of relations between mental-relevant events (Lowther 2022). Another objection can be raised: Ramsey sentences could be unfeasible in the human brain, since they would require a huge amount of time and computational power. The objection concerning time is easily removed if we consider that parallel networks are able to simultaneously perform a finite but huge number of operations. Yet, the requisite of high amount of computational

power for the functioning of Ramsey-like's brain mechanisms is not necessarily bad. It is well-known that huge, overparametrized neural networks do help for robustness, i.e., for the ability of computer systems to cope with both erroneous inputs and errors during execution. Bubeck et al. (2021) investigated the balance between the size of a neural network (i.e., the number of neurons k) and its robustness as measured by the Lipschitz constant of the data fitting model $f \in Fk(\psi)$). To accomplish a robust two-layers neural network and perfectly fit the data, a huge amount of information is required, corresponding to one neuron per datapoint (Bubeck and Sellke, 2022). In sum, the large size of a network required by Ramsey sentences permits the achievement of optimal smoothness robustness.

Apart from neuroscience, Ramsey approaches could be used for the evaluation of other biological systems too. For example, Ramsey sentences could provide a systematic perspective on the intercellular wiring of the human immune system. The human immune system's distributed network of cells circulating throughout the body is dynamically connected via interactions between cell-surface proteomes (Shilts et al., 2022). Ramsey sentences might be used to systematically map direct protein interactions and receptor wiring across the surface proteins detectable on human leukocytes.

To sum up, the Ramsey sentence might stand for a versatile device that can be used not just as a methodological tool to cope with biophysical affairs, but also as a reliable model to describe the real functioning of biological systems.

References

- Ajabi, Z., Keinath, A.T., Wei, XX. et al. Population dynamics of head-direction neurons during drift and reorientation. Nature 615, 892–899 (2023). https://doi.org/10.1038/s41586-023-05813-2
- Andrews-Hanna JR, Smallwood J, Spreng RN (2014) The default network and self-generated thought: component processes, dynamic control and clinical relevance. Ann N Y Acad Sci 1316:29-52.
- Arcaro, M., Schade, P., Vincent, J. et al. Seeing faces is necessary for face-domain formation. Nat Neurosci 20, 1404–1412 (2017). https://doi.org/10.1038/nn.4635
- Åström, Freddie; Rasit Koker. 2011. A parallel neural network approach to prediction of Parkinson's Disease. Expert Systems with Applications, Volume 38, Issue 10, 15 September 2011, Pages 12470-12474. https://doi.org/10.1016/j.eswa.2011.04.028
- Ben-Nun, Tal; Torsten Hoefler. 2018. Demystifying Parallel and Distributed Deep Learning: An In-Depth Concurrency Analysis. arXiv:1802.09941v2 [cs.LG] 15 Sep 2018
- Benjamin AS, Ling-Qi Zhang, Cheng Qiu, Alan A Stocker, Konrad P Kording. 2022. Efficient neural codes naturally emerge through gradient descent learning. Nat Commun. 2022 Dec 29;13(1):7972. doi: 10.1038/s41467-022-35659-7.
- Berardi S, Silvia Steila. 2015. An intuitionistic version of Ramsey's Theorem and its use in Program Termination. Annals of Pure and Applied Logic, Volume 166, Issue 12, December 2015, Pages 1382-1406. https://doi.org/10.1016/j.apal.2015.08.002.
- Bernardy, Jean-Philippe; Rasmus Blanck, Stergios Chatzikyriakidis, Shalom Lappin, Aleksandre Maskharashvili. 2019. Bayesian Inference Semantics: A Modelling System and A Test Suite. Proceedings of the Eighth Joint Conference on

Lexical and Computational Semantics (*SEM), pages 263–272

- Minneapolis, June 6–7, 2019.
- Bubeck Sébastien; Mark Sellke. 2022. A Universal Law of Robustness via Isoperimetry. arXiv:2105.12806
- Bubeck S, Li Y, Nagaraj D. 2021. A Law of Robustness for Two-Layers Neural Networks. Proceedings of Machine Learning Research vol 134:1–17, 2021 34th Annual Conference on Learning Theory.
- Carnap R. 1966. An Introduction to the Philosophy of Science. Dover Publications, 1995, ISBN-13 : 978-0486283180
- Cazettes, F., Mazzucato, L., Murakami, M. et al. 2023. A reservoir of foraging decision variables in the mouse brain. Nat Neurosci (2023). https://doi.org/10.1038/s41593-023-01305-8
- Chariker, Logan; Robert Shapley and Lai-Sang Young. 2016. Orientation Selectivity from Very Sparse LGN Inputs in a Comprehensive Model of Macaque V1 Cortex. Journal of Neuroscience 7 December 2016, 36 (49) 12368-12384; DOI: https://doi.org/10.1523/JNEUROSCI.2603-16.2016
- Ebrahimi, S., Lecoq, J., Rumyantsev, O. et al. 2022. Emergent reliability in sensory cortical coding and inter-area communication. Nature 605, 713–721 (2022). https://doi.org/10.1038/s41586-022-04724-y
- Edelman G. 2017. Neural Darwinisim, New Perspectives Quarterly. January 2017, 31, no. 1, 25-27.
- Fenk, L.A., Riquelme, J.L. & Laurent, G. Interhemispheric competition during sleep. Nature 616, 312–318 (2023). https://doi.org/10.1038/s41586-023-05827-w
- Gazzaniga MS. 2009. The Cognitive Neurosciences, Fourth Edition. MIT Press. ISBN: 9780262013413
- Gazzaniga MS. 2013. Shifting gears: seeking new approaches for mind/brain mechanisms. Annu Rev Psychol. 2013;64:1-20. doi: 10.1146/annurev-psych-113011-143817. Epub 2012 Sep 17.
- Grainger Jonathan; Arnaud Rey, Stéphane Dufau. 2008. Letter perception: from pixels to pandemonium. Trends Cogn Sci. 2008 Oct;12(10):381-7. doi: 10.1016/j.tics.2008.06.006.
- Grimaldi Antoine; Amélie Gruel, Camille Besnainou, Jean-Nicolas Jérémie, Jean Martinet, and Laurent U. Perrinet. 2023. Precise Spiking Motifs in Neurobiological and Neuromorphic Data. Brain Sci. 2023, 13(1), 68; https://doi.org/10.3390/brainsci13010068
- Hayama, Sara; Linda Chang, Kazim Gumus, George R. King, Thomas Ernst. 2016. Neural correlates for perception of companion animal photographs. Neuropsychologia. 2016 May; 85: 278–286. doi: 10.1016/j.neuropsychologia.2016.03.018
- Hayward, J. J. et al. Complex disease and phenotype mapping in the domestic dog. Nat. Commun. 7, 10460 (2016).
- Heim Stefan, Corey T McMillan 4, Christopher Olm 4, Murray Grossman. 2020. So Many Are "Few," but so Few Are Also "Few" - Reduced Semantic Flexibility in bvFTD Patients. Front Psychol. 2020 Apr 3;11:582. doi: 10.3389/fpsyg.2020.00582.
- Hempel CG. 1958. The theoretician's dilemma: A study in the logic of theory construction. Minnesota Studies in the Philosophy of Science 2:173-226.
- Hikosaka, Okihide; Hiroyuki Nakahara, Miya K. Rand, Katsuyuki Sakai, Xiaofeng Lu, et al. 1999. Parallel neural networks for learning sequential procedures. Trends in Neurosciences, Volume 22, Issue 10, October 1999, Pages 464-471. https://doi.org/10.1016/S0166-2236(99)01439-3
- Hintikka J. 1998. Ramsey Sentences and the Meaning of Quantifiers. Philosophy of Science, Vol. 65, No. 2, pp. 289-

305 (17 pages); https://www.jstor.org/stable/188262

- Hirai Y. 1980. A template matching model for pattern recognition: self-organization of templates and template matching by a disinhibitory neural network. BiolCybern. 1980;38(2):91-101.
- Huth AG, de Heer WA, Griffiths TL, Theunissen FE, Gallant JL. 2016. Natural speech reveals the semantic maps that tile human cerebral cortex. Nature. 28;532(7600):453-8. doi: 10.1038/nature17637.
- Jackson, R, Hoffman, P, Pobric, G & Lambon Ralph, MA 2015. The nature and neural correlates of semantic association vs. conceptual similarity. Cerebral Cortex, vol. 25, no. 11, pp. 4319-4333. https://doi.org/10.1093/cercor/bhv003
- Kanwisher, Nancy; Meenakshi Khosla, Katharina Dobs. 2023. Using artificial neural networks to ask 'why' questions of minds and brains. Trends in Neurosciences, Volume 46, Issue 3, P240-254, March 2023. DOI: https://doi.org/10.1016/j.tins.2022.12.008
- Koslow, Arnold. 2008. The Representational Inadequacy of Ramsey Sentences. Theoria, https://doi.org/10.1111/j.1755-2567.2006.tb00948.x
- Lavi, Ayal; Megha Sehgal, Andre F. de Sousa, Anna Okabe, Cameron Bear, Alcino J. Silva. 2022. Local memory allocation recruits memory ensembles across brain regions. Neuron Volume 111, Issue 4, P470-480.E5, DOI: https://doi.org/10.1016/j.neuron.2022.11.018
- Letko, Anna; Benoît Hédan, Anna Snell, Alexander C Harris, Vidhya Jagannathan, et al. 2023. Genomic Diversity and Runs of Homozygosity in Bernese Mountain Dogs. Genes (Basel). 2023 Mar 4;14(3):650. doi: 10.3390/genes14030650.
- Lewis, David. 1970. How to define theoretical terms. Journal of Philosophy, 67 (13): 426–446, doi:10.2307/2023861, JSTOR 2023861
- Liu, X., Zeng, Y., Zhang, T. et al. Parallel Brain Simulator: A Multi-scale and Parallel Brain-Inspired Neural Network Modeling and Simulation Platform. Cogn Comput 8, 967–981 (2016). https://doi.org/10.1007/s12559-016-9411-y
- Lowther, T.S. 2022. Behaviourism in Disguise: The Triviality of Ramsey Sentence Functionalism. Axiomathes 32, 101–121 (2022). https://doi.org/10.1007/s10516-020-09511-w
- Macpherson, Tom; Masayuki Matsumoto, Hiroaki Gomi, Jun Morimoto, Eiji Uchibe, Takatoshi Hikida. 2021. Parallel and hierarchical neural mechanisms for adaptive and predictive behavioral control. Neural Networks Volume 144, December 2021, Pages 507-521. https://doi.org/10.1016/j.neunet.2021.09.009
- Majer U. 1989. Ramsey's Conception of Theories: An Intuitionistic Approach. History of Philosophy Quarterly. Vol. 6, No. 2, 233-258.
- McDowell JJ. 2010. Behavioral and neural Darwinism: Selectionist function and mechanism in adaptive behavior dynamics, Behavioural Processes 84, no. 1, May 2010, doi.org/10.1016/j.beproc.2009.k11.011
- Misak C. 2020. Frank Ramsey: A Sheer Excess of Powers. OUP Oxford. ISBN-13 : 978-0198755357
- Olm Christopher A; Corey T McMillan 1, Nicola Spotorno 1, Robin Clark 2, Murray Grossman 1. 2014. The relative contributions of frontal and parietal cortex for generalized quantifier comprehension. Front Hum Neurosci. 2014 Aug 7;8:610. doi: 10.3389/fnhum.2014.00610.
- McMillan Corey T, Robin Clark, Peachie Moore, Christian Devita, Murray Grossman. 2005. Neural basis for generalized

quantifier comprehension. Neuropsychologia. 2005;43(12):1729-37. doi: 10.1016/j.neuropsychologia.2005.02.012.

- Pastukhov A. 2017. First, you need a Gestalt: An interaction of bottom-up and top-down streams during the perception of the ambiguously rotating human walker. Sci Rep. 2017 Apr 25;7(1):1158. doi: 10.1038/s41598-017-01376-1.
- Pastur-Romay L A, A B Porto-Pazos, F Cedron, A Pazos. 2017. Parallel Computing for Brain Simulation. Curr Top Med Chem. 2017;17(14):1646-1668. doi: 10.2174/1568026617666161104105725.
- Peres, Luca; Oliver Rhodes. 2022. Parallelization of Neural Processing on Neuromorphic Hardware. Front. Neurosci., 10 May 2022 Volume 16 - 2022 | https://doi.org/10.3389/fnins.2022.867027
- Plassais, J., Kim, J., Davis, B.W. et al. Whole genome sequencing of canids reveals genomic regions under selection and variants influencing morphology. Nat Commun 10, 1489 (2019). https://doi.org/10.1038/s41467-019-09373-w
- Ramsey FP. 1931. Theories, in The Foundations of Mathematics and Other Logical Essays, R. B. Braithwaite (ed.), London: Routledge, pp. 212–236.
- Ramstead, Maxwell, Karl J Friston, Inês Hipólito. 2020. Is the Free-Energy Principle a Formal Theory of Semantics? From Variational Density Dynamics to Neural and Phenotypic Representations. Entropy (Basel). 2020 Aug 13;22(8):889. doi: 10.3390/e22080889.
- Rao SC, Rainer G, Miller EK. 1997. Integration of what and where in the primate prefrontal cortex. Science. 1997 May 2;276(5313):821-4.
- Ribeiro, Antônio H., Luis A. Aguirre. 2018. “Parallel Training Considered Harmful?”: Comparing series-parallel and parallel feedforward network training. Neurocomputing, Volume 316, 17 November 2018, Pages 222-231. https://doi.org/10.1016/j.neucom.2018.07.071
- Rosenbaum DA. 2014. It’s a Jungle in There: How Competition and Cooperation in the Brain Shape the Mind. Oxford University, ISBN 978-0-19-982977-4.
- Roy, D.S., Park, YG., Kim, M.E. et al. 2022. Brain-wide mapping reveals that engrams for a single memory are distributed across multiple brain regions. Nat Commun 13, 1799 (2022). https://doi.org/10.1038/s41467-022-29384-4
- Selfridge OG. 2017. Pandemonium: a pradigm for learning. In: Mechanization of thought processes: proceedings of a Symposium held at the national Physical Laboratory, London: HMSO, 513-526.
- Shinn, M., Hu, A. Turner, L. et al. 2023. Functional brain networks reflect spatial and temporal autocorrelation. Nat Neurosci 26, 867–878 (2023). https://doi.org/10.1038/s41593-023-01299-3
- Shilts, J., Severin, Y., Galaway, F. et al. A physical wiring diagram for the human immune system. Nature 608, 397–404 (2022). https://doi.org/10.1038/s41586-022-05028-x
- Toppel, M. 2021. Applying Ramseyfication to Infrared Spectroscopy. Erkenn (2021). https://doi.org/10.1007/s10670-021-00506-6
- Tozzi A, Peters JF. 2018. Multidimensional brain activity dictated by winner-take-all mechanisms. Neuroscience Letters, 678 (21):83-89. https://doi.org/10.1016/j.neulet.2018.05.014.
- Uran, Cem; Alina Peter, Andreea Lazar, Pascal Fries, Wolf Singer, Martin Vinck. 2022. Predictive coding of natural images by V1 firing rates and rhythmic synchronization. Neuron, Volume 110, Issue 7, P1240-1257.E8. DOI: https://doi.org/10.1016/j.neuron.2022.01.002
- Yang, T., Yu, K., Zhang, X. et al. 2023. Plastic and stimulus-specific coding of salient events in the central amygdala.

Nature 616, 510–519 (2023). https://doi.org/10.1038/s41586-023-05910-2

- Woolnough, Oscar; Patrick S. Rollo, Kiefer J. Forseth, Cihan M. Kadipasaoglu, Arne D. Ekstrom, Nitin Tandon. 2020. Category Selectivity for Face and Scene Recognition in Human Medial Parietal Cortex. Current Biology Volume 30, Issue 14, P2707-2715.E3, Doi: https://doi.org/10.1016/j.cub.2020.05.018
- Zhan Jiayu; Xiaoming Jiang 1 2, Stephen Politzer-Ahles 3, Xiaolin Zhou. 2017. Neural correlates of fine-grained meaning distinctions: An fMRI investigation of scalar quantifiers. Hum Brain Mapp. 2017 Aug;38(8):3848-3864. doi: 10.1002/hbm.23633.

STUDY PROPOSAL: TOWARDS STREPTOCOCCAL INFECTIONS WITH NONSPECIFIC SYMPTOMS

Arturo Tozzi
Center for Nonlinear Science, Department of Physics, University of North Texas, Denton, Texas, USA
1155 Union Circle, #311427 Denton, TX 76203-5017 USA
tozziarturo@libero.it

PREMISE

In 2023, increases in scarlet fever's incidence have been detected throughout Europe. Based on general pediatricians' experience, we hypothesize that a shift has occurred in both group A streptococcus (GAS) clinical findings and age of onset. Therefore, we propose to evaluate whether the well-standardized signs and symptoms leading to GAS diagnosis still hold.

STUDY DESIGN

Children of every age (also <3 years) with fever, but without the specific diagnostic signs and symptoms of GAS infection, will undergo Strep test throat swab (swab 1). All the positive children will be treated with the standard therapy of 10-days amoxicillin. After the therapy, another swab will be performed on the treated children (swab 2).

POSSIBLE OUTCOMES

1) If swab 2 will be still positive, this means that children are either carriers, or, very rarely, therapy-resistant.
2) If swab 2 will be negative, this means that children underwent a GAS infection characterized by nonspecific signs and symptoms.
We also expect that the age of GAS infection could be lower than suggested in literature, i.e., that GAS currently also infects children <3 years.

Preprints (www.preprints.org) | NOT PEER-REVIEWED | Posted: 19 October 2022 doi:10.20944/preprints202210.0263.v1

Review

Biological Relevance of Intestinal Gases in Healthy Humans

Arturo Tozzi[1,2] and Raffaele Minella[3]

1. Center for Nonlinear Science, Department of Physics, University of North Texas, Denton, Texas 76203, USA
2. 1155 Union Circle, #311427, Denton, TX 76203-5017 USA; tozziarturo@libero.it
3. Primary Care Pediatrician, ASL NA3 Sud, Torre del Greco, Italy; raffaele-minella@libero.it

ABSTRACT

Intestinal gases are usually discarded as physiologically inert, useless sub-products of colonic fermentation that must be expelled to prevent discomfort and meteorism. Starting from the observation that many living beings use exogenous and/or endogenous gases to attain evolutionary benefits, we question whether intestinal gases in healthy humans could have underestimated physiological effects, either intestinal or extra-intestinal. We examine gaseous volume, composition, source and local distribution in proximal as well as distal gut, providing extensive data that may serve as reference for future studies. We analyze each one of the most abundant intestinal gases and describe their diffusive patterns, active trans-barrier transport dynamics, chemical properties, intra-/extra-intestinal metabolic effects mediated by intracellular, extracellular, paracrine and distant actions. Discussing the physical properties of the whole intestinal gaseous mixture, we illustrate how changes in volume/pressure can be generated by two different mechanisms, namely, physical muscular gut contraction and biological colonic fermentation, with quite different metabolic outcomes. The experimental gas laws suggest that the gaseous exchanges between lumen and bloodstream are impaired by muscular contraction and improved by muscular relaxation. In turn, the surface-area-to-volume ratio suggests that the gaseous exchanges are impaired by microorganismal overproduction and improved by microorganismal reduction. Further, theoretical stochastic approaches from probability theory indicate that the non-turbulent, random paths of gas molecules inside colonic haustra do not homogenously spread over the whole mucosal surface. This means that the intestinal area available for lumen/blood metabolic exchanges is much less than expected not just in disease states, but also in healthy individuals.

Keywords: nitrogen; oxygen; carbon dioxide; methane; hydrogen sulfide; sulfur dioxide; cyanide; gasotransmitter; Boyle's law

INTRODUCTION

Many living beings make use of the mechanical and/or chemical properties of gases to increase their likelihood of survival. For example, planktonic heterotrophic prokaryotes (Staley 1980) and certain Haloarchaea (Völkner et al., 2020) modify their overall cellular density by inflating and deflating gas-filled cytoplasmatic micro-structures. These structures, termed gas vesicles, allow microorganisms to float vertically and reach different depths in water columns (Pfeifer 2014), preventing halophilic microorganisms' osmotic shock in high-salted environments and malfunctioning of light-driven proton pumps (Oren 2012; Talapatra et al., 2013). While gas vesicles are highly permeable to gases (i.e., oxygen, nitrogen, hydrogen, carbon dioxide, carbon monoxide, methane and even perfluorocyclobutane) that diffuse from the environment to the cytoplasm in a passive way (Pfeifer 2012), gases can be also produced in an active way by other living organisms. For instance, carbon monoxide is actively produced by the aeriform cells (Larimer et al., 1962) of the deadly Siphonophore Physalia physalis (namely, the Portuguese man of war), which lives at the sea water/air interface and uses an enlarged float filled with gas as a sail to travel by wind (Munro et al, 2019). Exchanges of exogenous gases are crucial for respiration in plants (Ishizaki 2015) and animals supplied with circulatory systems. To provide an example familiar to us, the human body introduces O_2 and expells CO_2 through the lungs, making chemical use of the inhaled atmospheric gases to attain aerobic cellular respiration.

© 2022 by the author(s). Distributed under a Creative Commons CC BY license.

Preprints (www.preprints.org) | NOT PEER-REVIEWED | Posted: 19 October 2022 doi:10.20944/preprints202210.0263.v1

In this paper, we will focus on one of the major gaseous reservoirs in the human body, i.e., the intestine. Although emphasis has been traditionally given to the gastrointestinal complaints caused by "excess gas" such as belching, flatulence, abdominal bloating and distension, emerging evidence suggests that intestinal gases bring intestinal and extra-intestinal benefits. We will describe the underrated physiological roles of the gases that can be found in the healthy human intestine, trying to answer the following questions:

1) Which types of exogenous and exogenous gases can be found in the human intestine?
2) How are the endoluminal gases generated and/or dispersed?
3) Do intestinal endoluminal gases have physiological roles?

We will proceed as follows. At first, we will analyse the volume, composition, local distribution and source of intestinal gas in healthy human individuals. Then, we will describe the intra-/extra-intestinal physiological roles of every one of the most abundant intestinal gases. Lastly, we will tackle the unexplored issue of the general physical properties of the intestinal gases and their intraluminal/extraluminal effects, stressing that gaseous mixing, transport and trans-barrier exchanges are strictly correlated with the intestinal motor patterns.

INTESTINAL GASES: GENERALITIES

Quite variable gaseous concentrations can be measured in intestinal lumen, faeces and breath, depending on the quantity and quality of the ingested food, the host/bacterial metabolic processes and the technique used for the assay (Blachier et al., 2021). The total weight of human intestinal gas amounts to just a few grams, while the total gaseous intestinal volume can be quantified, with a certain approximation, in ≈100-500 cm^3 (Badley et al., 1993; Schiller et al, 2005; Wang et al., 2021). The source of intestinal gas is twofold (Roccarina et al., 2010):

1) Exogenous swallowed air.
2) Endogenous gases produced by:
   a) Intraluminal fabrication by the host organism.
   b) Intraluminal fabrication by commensal microorganisms.
   c) Trans-membrane diffusion from bloodstream into the intestinal lumen.

The human intestinal gas' composition varies along the different gastrointestinal tracts. See the **Table** for quantitative details. Swallowed air is the major source of nitrogen (N_2) and oxygen (O_2), while carbon dioxide (CO_2) comes both from swallowed air and intestinal production. A large amount of intestinal gases is generated by microorganismal fermentation in the human colon from the dynamic crosstalk between microbiota and host metabolism (Singhal and Shah, 2020). These gases include carbon dioxide (CO_2), hydrogen (H_2), methane (CH_4) (Levitt 1971; Wang et al., 2021). The sum of N_2, O_2, CO_2, H_2 and CH_4 accounts for more than 99% of the expelled intestinal gas (Roccarina et al., 2010). The remaining 1% is composed of various odoriferous substances including hydrogen sulfide (H_2S), sulfur dioxide (SO_2), sulphur-containing mercaptans, ammonia (NH_3), indole, skatole, volatile amines, short chain fatty acids, plus acetic acid, propanoic acid, butyric acid, isobutyric acid, pentanoic acid, valeric acid, etc (Heresbach et al., 1995; Montalto et al., 2009; Wang et al., 2021). The gaseous production varies according to the age. To provide an example, the intestinal gases and faecal short-chain fatty acids produced by preterms' gut microbiota increase during the first 4 weeks of life (Wang et al., 2021). The dietary uptake deeply affects the amount of some intestinal gases depends on. In particular, some fermenting foods are known to increase intestinal gas production (Scaldaferri et al., 2013):

a) Non-absorbable carbohydrates such as lactulose and mannitol.

Preprints (www.preprints.org) | NOT PEER-REVIEWED | Posted: 19 October 2022 doi:10.20944/preprints202210.0263.v1

b) Incompletely absorbed carbohydrates such as lactose, fructose, sorbitol.
c) Sulfur-rich foods such as beans, pork, onions, cabbage and cauliflower.

A we shall see later, some gaseous substances can be detected after carbohydrate load using breath tests as markers of colonic carbohydrate fermentation (Wang et al., 2021).

	Atmosphere	Stomach	Colon	Flatus	Breath
Nitrogen (N_2)	78	≈78	≈65	≈59	78
Oxygen (O_2)	21	≈15	≈2	≈4	16
Carbon dioxide (CO_2)	0.04	≈7	≈10	≈9	4
Hydrogen (H_2)	Traces	Traces	≈3	≈21	Traces
Methane (CH_4)	Traces	0	≈15	≈7	Traces
Hydrogen sulfide (H_2S)	Traces	0	Traces	Traces	Traces
Sulfur dioxide (SO_2)	Traces	Traces	Traces	Traces	0

Table. Approximate percentage of different gases in various human anatomical districts. Intestinal gases may occur in widely different proportions in each bowel region, depending on manifold factors. Concerning blood gases, they are defined as the mixture of gases dissolved in the fluid fraction of blood or transported by carriers such as., e.g., haemoglobin and urea nitrogen (Walker et al., 1990). Data extracted from: Levitt (1971); Roccarina et al. (2010); Sahakian et al. (2010); Modesto et al. (2022).

Gaseous exchanges between intestinal lumen and blood. Most of the intestinal gases cross barrier between the intestinal lumen and the blood by means of passive mechanisms governed by the Fick's law of diffusion (Michenkova et al, 2021). In the human gut, the gradient between the gaseous mixture's partial pressures in the intestinal lumen and in the bloodstream dictates the direction of gases exchanges. The formula provided by Forster (1968) summarizes the physiological basis of passive gas exchange in the intestine:

$$\frac{d(VP_L)}{dt} \quad \frac{1}{P_B - 47} = -k\,(P_L - Pc)$$

Where V is the total intraluminal gaseous volume, P_L and Pc are, respectively, the partial intraluminal and extraluminal gaseous pressures, P_B is the barometric pressure and 47 is the pure pressure of water at 37°. K is a transfer coefficient depending on the type of gas, e.g., N_2 diffuses through the epithelial intestinal barrier slowly than O_2 and CO_2.
The values of mesenteric perfusion and intestinal microcirculation contribute to gaseous exchanges. The total colonic blood flow is ≈18 mL/min per 100 g of colonic tissue, much lower in the muscularis layer (≈11mL /min per 100 g of muscularis tissue) than in the mucosa-submucosa (≈28 mL /min per 100 g of mucosal-submucosal tissue) (Hulten et al., 1976).
Since gases have been traditionally deemed to diffuse freely and passively, previous studies mainly focused on gaseous production/reactivity rather than diffusion/transport (Rodriguez-Grande and Konsman 2018). Still, the discovery of gas pores has raised the intriguing possibility of active cellular modulation of gas diffusion. Indeed, some gases can cross different compartments by means of transmembrane channels. Recent observations suggest that that the highly conserved and widely diffused

Preprints (www.preprints.org) | NOT PEER-REVIEWED | Posted: 19 October 2022 doi:10.20944/preprints202210.0263.v1

intramembrane channels termed aquaporins transport not just water molecules, but also gases (Herrera and Garvin, 2011; Zhang et al., 2019). Aquaporin channels represent a major transcellular route for water and gas transport also in the gastrointestinal tract (Zhu et al., 2016). Different aquaporin isoforms have been found in the stomach, small and large intestine, everyone preferentially distributed in distinct gut segments and cell types (Liao et al., 2021). For instance, a water, glycerol and H_2O_2 transporting channel expressed in colonic epithelial cells, namely Aquaporin 3, affects epithelial tight junction integrity and permeability (Yde et al., 2021).

Flatus' patterns. As the healthy human individual generates 0.6-1.8 L of gas per day, it follows that discard must be continuous. The mechanisms of removal are manifold: microorganismal consumption, host consumption, absorption into the systemic circulation and ensuing expulsion mainly through the breath, belching, eructation and, above all, flatus (Hasler 2006; Montalto et al., 2009; Sahakian et al., 2010). The data concerning flatus' frequency and volume vary widely, with some subjects passing gas more often than others. The mean total volume ranges in different studies from ≈260 (Manichanh et al., 2013) to ≈705 ml/die, with an upper limit of 1800 (Tomlin et al., 1991). On their usual diet, subjects pass gas from ≈7 (Manichanh et al., 2013) to ≈10 daytime evacuations, with an upper limit of 20 (Furne and Levitt, 1996). The record of abdominal symptoms is rare in healthy subjects (≈0.4 discomfort/pain per day) (Manichanh et al., 2013). Gender, age, and methane production had no significant influence on flatus frequency and volume (Furne and Levitt, 1996). Flatus is produced also during the sleeping period, but the rate is significantly lower than the daytime (median: 16 and 34 ml/h, respectively) (Tomlin et al., 1991). Larger volumes of flatus are produced after meals. Fiber-free diet reduces the total daily volume, suggesting that fermentation gases make the highest contribution to normal flatus volume (Tomlin et al., 1991). The addition to the diet of 10 g/day of the nonabsorbable disaccharide lactulose increases flatus frequency to ≈19 times/die (Furne and Levitt, 1996). On flatulogenic diet, increased gas production leads to increase in number not just of gas evacuations (≈22/day), but also of abdominal symptoms (≈3 mean discomfort/pain per day) (Manichanh et al., 2013).

Intestinal motility. Gaseous mixing, transport and trans-barrier exchanges are strictly correlated with bowel movements. Gas is actively propelled by the inner circular and longitudinal musculature, moving along the gut independent of solids and liquids (Azpiroz 2005). Two main motor patterns have been detected, especially in the healthy human colon:

a) Peristalsis followed by propagation. Wave-like muscular contractions along the intestinal length drive strong fluid flows both forward and backward, with the average movement pushing from the proximal to the distal gut (Cheng et al., 2020). The following quantitative data are taken from Chen et al. (2017). **Simultaneous pressure waves** are the most prominent propulsive motor pattern, since their fast-propagating contractions lead to gas expulsion and anal sphincter relaxation. These transient increases in intraluminal pressure covering the entire colon length are characterized by ~30 episodes/h frequency, ~15 sec pressure duration, ~32 cm propagation distance, ~15 mmHg average amplitude, fast rate of rise up to ~20 mmHg in ~8 s, slower rate of return to baseline in ~12 s. Passing of intraluminal material takes a few seconds from one end of the colon to another, with speeds up to 10 cm/s. Rhythmic low frequency of ~0.5–1 cycle/min occurs, suggesting the presence of a stimulus-dependent pacemaker, likely the interstitial cells of Cajal endowed in the deep muscular plexus (Sanders et al., 2006; Huizinga et al., 2021).

b) Segmentation followed by mixing and absorption. Non-propagating muscular contractions drive weak flows that lead to increased mixing (Codutti et al., 2022). The following quantitative data are taken from Chen et al. (2017). **Isolated haustral boundary pressure transients** are common, short-lasting pressure increases ranging in amplitude 5–230 mmHg,

Preprints (www.preprints.org) | NOT PEER-REVIEWED | Posted: 19 October 2022 doi:10.20944/preprints202210.0263.v1

lasting 30–180 min and occurring simultaneously in many haustral segments spaced 4-5 cm apart, but not in adjacent segments. These pressure transients display a typical 3 cycles/min rhythmicity in the human colon, likely associated with electrical slow wave activity generated by the interstitial cells of Cajal endowed in the submucosal plexus (Huizinga et al., 2014). **Intra-haustral segmentation** activity is characterized by isolated pressure transients covering the size of an haustra, i.e., 3–5 cm. A distinctive, synchronized intra-haustral cyclic motor pattern at 3–6 cycles/min is exhibited. These waves occur for 2 to 10 min, 0–6 times /hour and abruptly alternate with erratic patterns resembling the small intestine' segmentation motor pattern. Their propagation at 2 ± 1 cm/s in antegrade or retrograde direction suggests once again the presence of a dominant pacemaker. The **antegrade** and **retrograde pressure waves** roughly display the same features: ~2/h frequency, ~20 seconds pressure duration, ~29 cm propagation distance, ~16 mmHg average amplitude and ~5 cm/s propagation velocity.

Intestinal transit and the correlated intraluminal pressure can be also modified by a series of viscero-somatic reflexes triggered by intraluminal lipidic nutrients and by mechanical stimulations like rectal distension, intra-abdominal volume load, etc (Azpiroz 2005). Besides gut musculature contractions, also boosts in abdominal pressure caused by coughing, body movements, talking and drinking lead to increases in luminal pressure (Chen et al., 2017). Symptoms perception depends on intraluminal gas distribution and gut motor response to gas loads (Harder et al., 2003). Similar magnitude of gas retention produces more abdominal symptoms during jejunal than rectal infusion, whereas abdominal distension is similar. The colon is more compliant during quasi-static distensions than during rapid barostatic balloon distensions at 10 ml/s (Barucha et al., 2001).

In sum, the healthy intestine is characterized by two major motor patterns, i.e., high-amplitude, lumen-obliterating neurogenic waves and rhythmic trains of shallow, low-amplitude myogenic waves (Amedzrovi Agbesi and Chevalier, 2022). We will see in the sequel that these different patterns lead to different outcomes regarding not just gaseous fluid dynamics, but also gaseous metabolic outcomes.

Gaseous volumetry in gut segments. The intestine has an oro-anal length of ≈5 m, two-third of which refers to the small intestine. The gut surface area is ~32 m^2, of which about two refers to the colon (Helander and Fändriks, 2014). In the undisturbed gut of healthy subjects, extreme volumetric variability can be appreciated in every compartment depending on extra-intestinal pressure, intestinal walls contraction and quantity/quality of ingested foods. In presence of food and fluid, the small bowel, which is empty and closed most of the time, moves more frequently than the colon (Fang et al., 2009). With a large degree of approximation (Pritchard et al., 2014; Nilsson et al, 2015; van Meegdenburg et al., 2015), the ascending colon has a mean volume of ≈200 mL, the transverse colon of ≈185 mL, the descending colon of ≈175 mL and the rectosigmoid colon of ≈200 mL (including the feces). In the ascending colon, 10% increases occur 90-240 minutes after feeding as the meal residue enters the cecum (Schiller et al., 2005). The human mean fluid volume is lower in fasting colon that in fasting small bowel (≈13 versus ≈54 mL, respectively) (Schiller et al., 2005). Fluid is not homogeneously distributed, rather it is provisionally confined in separated fluid pockets that increase in number after meals (mean number ≈5) (Schiller et al., 2005). The total colonic fluid volume in almost entirely stored (~95%) in the few fluid pockets (~10%) larger than 1 mL (Goelen et al., 2021).

In conclusion, since fluids and faeces occupy just a relatively small volume (a few dozen mL and ≈200 mL, respectively), it can safely be said that the partially relaxed colon's intraluminal volume is filled by gases for the most part.

Preprints (www.preprints.org) | NOT PEER-REVIEWED | Posted: 19 October 2022 doi:10.20944/preprints202210.0263.v1

Preprints (www.preprints.org) | NOT PEER-REVIEWED | Posted: 19 October 2022 doi:10.20944/preprints202210.0263.v1

PHYSIOLOGY OF INDIVIDUAL INTESTINAL GASES

Here we will describe the physical/biological features and metabolic effects of each one of the main intestinal gases. We will show how intestinal gases, conventionally believed as biologically inert, provide instead countless physiological effects. Our main goal will be to point out that gas production, consumption, excretion and disposal in different gut compartments take part in the hemostasis of manifold physiological processes involving not only the gut, but also extra-intestinal organs (Montalto et al., 2009). For example, we will show how four small gaseous molecules previously considered as toxic gases, namely hydrogen sulfide (H_2S), nitric oxide (NO), carbon monoxide (CO) and sulfur dioxide (SO_2), have been recently assigned to the mammalian family og gasotransmitters (Huang et al., 2021). Gasotransmittes are signalling molecules that freely diffuse through the intestinal cellular membranes, playing crucial physiological and pathophysiological roles in many processes such as stomach acid release, smooth muscles relaxation, local blood flow adjusting, inflammation activation, angiogenesis, heart contractility control, etc (Verbeure et al., 2021).

Nitrogen (N_2). Nitrogen supplies the main fraction of intestinal gases. Its concentration varies greatly with the diet, especially in the distal gut (Modesto et al., 2022). It has long been believed that the intestinal N_2 entirely came from swallowed air. However, the gut commensals Klebsiella and Clostridiales strains might produce ~0.01% of the standard nitrogen requirement for humans (Igai et al., 2016). Also, Helicobacter pylori produces NH_3 using uric acid as a substrate to achieve local gastric acid neutralization (Naito et al., 2018). Compared with other gases like O_2 and CO_2, N_2 gradient diffusion between lumen and blood is much slower (Levitt 1971). This means that most of the intestinal N is not absorbed, rather is propelled towards the distal intestinal tracts. While a N_2 partial pressure gradient from the intestinal lumen to the blood does exist in the duodenum and upper small bowel, downhill gradients occur from blood to intestinal lumen in the colon, in particular after beans meals. The gradient established by CO_2, CH_4 and H_2 produced by commensal bacteria drives N_2 diffusion from the bloodstream into the colon (Levitt 1971). Therefore, the gastric N_2 comes entirely from swallowed air, while a certain amount of N_2 in flatus comes from blood diffusion.
Contrary to the inert nitrogen from the inhaled/exhalated atmospheric air, the intestinal N_2 plays a role in nitrogenous compound metabolism. In the lumen of the small intestine, amino acids from alimentary sources and endogenous proteins from enterocytes are deaminated, hydrolysed, incorporated or degraded by the microbiota, in particular by Bacteroidetes (Davila et al., 2013; Bergen and Wu, 2009; Reese et al., 2018). N_2 supply and recycling from the small intestine is crucial also for colonic digestion, building and absorption of endoluminal proteins/aminoacids (Reese et al., 2018). Nitrogen-derived molecules like nitrated short-chain fatty acids are energy substrates for both colonocytes and peripheral tissues (Davila et al., 2013). When the dietary supply of N_2 for the synthesis of dispensable amino acids is deficient, urea nitrogen absorption from the large intestine is used for increasing body protein synthesis and deposition (Mansilla et al., 2015). Residual undigested luminal proteins and recovered amino acids, rather than being absorbed, can play the role of precursors for the synthesis of numerous metabolic end products (Davila et al., 2013). These bioactive products affect physiological processes, locally in the gut as well as systemically after absorption (Lundberg and Weitzberg 2013; Carlström et al., 2020). For example, reactive nitrogen oxides such as nitric oxide (NO), nitrite, nitrate, nitrated fatty acids, N-nitrosamines peroxynitrite, S-nitrosothiols are continuously manufactured in the colon (Lundberg and Weitzberg 2013; Carlström et al., 2020). The N_2-derived ammonia (NH_3), produced by colonic intestinal bacterial urease from uric acid, is used not just by the surrounding bacteria as a nitrogen source for amino acid synthesis (Naito et al., 2018), but also by enterocytes via glutamate, glutamine, citrulline, and urea synthesis (Bergen and Wu, 2009). Able to diffuse through the pores of the human Aquaporin 1 (Michenkova et al, 2021), NH_3 can be systemically absorbed and cause hepatic encephalopathy in patients with liver cirrhosis.
In sum, intestinal N_2 is crucially involved in the nitrogenous compound metabolism that is mandatory for the survival of both intestinal host cells and microorganismal commensals.

Preprints (www.preprints.org) | NOT PEER-REVIEWED | Posted: 19 October 2022 doi:10.20944/preprints202210.0263.v1

Oxygen (O_2). Oxygen concentration progressively declines throughout the gut. The atmosphere contains about 21% O_2, while the stomach approximately 15-16%. This means that some of the swallowed O_2 is adsorbed through the intestinal vessels. Most of the O_2 has been removed in the colon, falling to ≈2% of the total gaseous amount (Modesto et al., 2022). Growing evidence points toward a facilitating role for the human Aquaporin 1, abundantly distributed in the endothelial cells of the gastrointestinal tract, in O_2 transport (Zhu et al., 2016; Zwiazek et al., 2017). In the colon, O_2 tends to diffuse from the bloodstream into the lumen, due to its low pressure. However, at very high O_2 intraluminal pressures, mammals can absorb O_2 through their intestines. Experiments in rodent and porcine models, inspired by loaches that use intestinal air breathing to survive under extensive hypoxia, demonstrated that intra-rectal O_2 delivery attains significant systemic oxygenation (Okabe et al., 2021; Mountford et al., 2021).

The role of the atmospheric oxygen is mainly correlated with the aerobic respiration, which requires O_2 transport from the lungs to the peripheral tissues via haemoglobins. In turn, the role of O_2 in the intestinal lumen is manifold. First, the scarce amount of intraluminal colonic O_2 favours the proliferation of essential anaerobic commensals (Levitt 1971). In turn, the microbiome contributes to maintain the hypoxic environment of the intestine that is critical for mucosal cells' nutrient absorption, intestinal barrier function and innate/adaptive immune responses (Singhal and Shah, 2020). Genes dependent on hypoxia-inducible factors contribute to epithelium maintenance, nutrient absorption and immune regulation (Singhal and Shah, 2020). Further, the hypoxic condition of the large intestine makes various fermenting bacteria able to produce acetic acid, CH_4 and HS2 as energy sources (Naito et al., 2018).

Oxygen is also a crucial component to build active molecules with profound intestinal and extra-intestinal effects. For example, the O_2-derived hydrogen peroxide (H_2O_2) is a major redox signaling molecule with effects on growth and differentiation. Produced by cell-surface NADPH Oxidase enzymes, H_2O_2 shapes both the colonic epithelial surface environment and the colonic bacterial growth, in particular Citrobacter's growth (Miller et al., 2020). The process is favoured by the water channel Aquaporin-3 that accelerates H_2O_2 uptake and intracellular accumulation, leading to downstream intracellular signalling (Miller et al., 2010). Moreover, the epithelial release of reactive oxygen species such as H_2O_2 toward the intestinal lumen provides an innate mucosal defensive mechanism after chronic inflammation, as well as after exposure to dysbiotic microbiota (Singh et al., 2018; Burgueño et al., 2019).

Oxygen enters the composition of the a gaseous signalling molecule's endothelial biosynthesis, namely the nitric oxide (NO), the first of the four known gasotransmitters to be discovered. NO is generated from O_2, L-arginine and NADPH by the enzyme nitric oxide synthase (NOS) that reduces organic nitrates (Carlström et al., 2020). Three different NOS isoforms exist: the neuronal, the endothelial and the inducible NOS, the latter mainly produced by macrophages to cope with inflammatory stress factors (Verbeure 2021). Displaying a half-life time of a few seconds, the extremely active NO freely diffuses across membranes. Supposed to be mostly active at the site of production and the surrounding cells, NO engenders transient paracrine and autocrine effects (Verbeure et al., 2021). NO is a key regulator in processes like blood vessel dilatation, anti-inflammatory activity, feeding behaviour, glucose metabolism. Acting as a neurotransmitter for non-adrenergic, non-cholinergic inhibitory neurons, NO promotes relaxation of the fundic area after a meal. Via intracellular signalling in enteroendocrine cells, NO (together with other gasotransmitters) plays a role in the release of gut peptides such as gastrin, cholecystokinin, secretin, motilin, ghrelin, glucagon-like peptide 1 and 2 (Verbeure et al., 2021). Indeed, gut peptides regulate a number of physiological processes in different gut segments through NO-mediated pathways. For instance, NO promotes CCK-mediated prevention of oesophageal acid reflux during digestion, gastrin release, motilin-mediated contractility of gastric smooth muscles, CCK-mediated neurogenic vasodilatation in mesenteric and cerebral arteries, GLP-1-mediated endothelium-dependent vasodilatation, CCK2Rs-mediated inhibition on motor activity in distal colon, etc. For a survey, see Verbeure et al. (2021). Further, bacteria-dependent NO formation from dietary nitrate has been associated with blood vessels' endothelium vasodilation and increasing blood flow in the cardiovascular system (Carlström et al., 2020).

Preprints (www.preprints.org) | NOT PEER-REVIEWED | Posted: 19 October 2022 doi:10.20944/preprints202210.0263.v1

In sum, intestinal O_2 contributes to gut homeostasis in a roundabout way. By one side, its shortage in the distal gut promotes the homeostasis of anaerobic commensals essential to host's survival. By another side, O_2 is one of the main constituents of powerful active molecules that affect physiological phenomena well beyond the gut.

Carbon dioxide (CO_2). Carbon dioxide is generated in various intestinal segments. The CO_2 content in the stomach is much higher than the swallowed air (5-9 vs 0.04%), since carbon dioxide is locally produced during the periods of high gastric acid secretion via HCl neutralization by dietary bicarbonates (McIver et al., 1926; Levitt 1971). Carbon dioxide partially diffuses from the proximal intestinal lumen into the blood, but its absorption rate is not enough to prevent accumulation in the duodenum and proximal jejuneum. More jejunal CO_2 is generated by the degradation of dietary triglycerides to fatty acids (Ritz et al., 1993). CO_2 movements across cellular membranes are not just passive, but also depend to a small extent on active transport performed by aquaporin channels (Michenkova et al, 2021). The amount of CO_2 has increased to ≈10.0% in the colon, with large variations depending on the diet (Modesto et al., 2022). Although CO_2 diffuses much more rapidly than H_2, CH_4, N_2, and O_2 (Scaldaferri et al., 2013), the volume of the intestinal-produced CO_2 is greater than the volume passed in flatus, since a part of the intraluminal gas diffuses into the bloodstream (Levitt 1971). Colonic CO_2 is a fermentative subproduct of the bicarbonate/acid reaction performed by commensals such as Bifidobacteria and butyrate-producing Clostridial clusters (Heresbach et al., 1995; Rivière et al., 2016). Short-chain fatty acids (acetate, propionate and butyrate) are the dominant fermentation acids that accumulate to high concentrations in the colon (Louis et al., 2022). The extreme acid load associated with high colonic p CO_2 is partially counteracted by the proximal colon epithelium's apical membrane, that provides a significant resistance towards CO_2 diffusion and confers cellular protection (Endeward and Gros, 2005).

The intestinal CO_2 enters red blood cells and is converted to carbonic acid, which dissociates to hydrogen ion and bicarbonate. Two-thirds of the bicarbonate diffuses out into the plasma, is converted back to CO_2, in the lungs and expelled by exhalation. Apart from the well-known roles in cellular respiration and peripheral chemoreceptors' activation during hypoxia (Oikawa et al., 2003; Akaishi et al., 2019), CO_2 is involved in manifold metabolic reactions. For instance, CO_2 enters the composition of Carbon monoxide (CO), one of the four known gasostransmitters. Contrary to the very short-lived and labile NO, H_2S and SO_2, the hemoglobin-binded CO is a relatively stable molecule with half-life time up to 4 h (Verbeure et al., 2021). Its biological functions are mainly related to the activation of soluble guanylyl cyclase and, to a less extent, cytochrome P450 inhibition (Verbeure et al., 2021). CO is synthesized by two enzymes. The inducible heme oxygenase 1, located in gastric epithelial cells/lamina propria's inflammatory cells, is activated during inflammation/oxidative stress. For example, HO-1 macrophages' production is stimulated by the bacterial lipopolysaccharide. The CO produced by HO-1 acts on intestinal bacteria to cause release of adenosine triphosphate, which in turn activates inflammasome response and interlukin-1β production (Naito et al., 2018). In turn, the heme oxygenase 2 is constitutively active and more broadly expressed: it can be found within the jejuneal myenteric and submucosal plexuses, vascular endothelial cells, liver, brain (Verbeure et al., 2021). CO is an important regulator of acute and chronic inflammation in the gastrointestinal tract.

A crucial intermediate of carbon dioxide and carbon metabolism is the lactate, a readily combusted fuel which can be shuttled throughout the body as energy source (Mahan 2021). A relatively small number of lactate-utilizing colonic species can metabolize lactate to short-chain fatty acids, butyrate, acetate and propionate (Wang et al. 2020; Louis et al., 2022). Some bacteria like Bacteroides and Firmicutes are susceptible to growth inhibition by relevant concentrations of lactate and acetate, whereas other bacteria like the lactate-producer Bifidobacterium adolescentis are resistant (Wang et al., 2020). By increasing expansion of intestinal stem-cells, Paneth and goblet cells, the lactic acid produced in anaerobic conditions by Bifidobacterium and Lactobacillus spp. contributes to intestinal epithelial development (Lee at al., 2018). Further lactate may work as a whole-body metabolite acting

Preprints (www.preprints.org) | NOT PEER-REVIEWED | Posted: 19 October 2022 doi:10.20944/preprints202210.0263.v1

as a potent signaling molecule in the central nervous system, impacting neuron/astrocyte activity in brain areas well beyond the neuronal diffusion zone (Mahan 2021)

In sum, intestinal CO_2 is produced in in various intestinal segments in different ways. Carbon dioxide's metabolites play direct roles in pH homeostasis, energy production and intestinal anti-inflammatory responses.

Methane (CH_4). Methane is produced by the human enteric microflora through anaerobic fermentation of both endogenous and exogenous carbohydrates (Sahakian et al., 2010). The human colonic concentration of methane is ≈14% (Modesto et al., 2022), with differences observed according to the amount of ingested fermentable dietary residues, time of the day and individual variations (Naito et al., 2018). To make a comparison, cattle produce ≈250-500 Lt of methane every day (Johnson and Johnson, 1995), with an estimated emission rate of 95-150 g/animal/day (Sejian et al., 2011). Just one/two third of healthy human adults produce methane (Roccarina et al., 2010; Ishaq and Peter. 2016). Children start producing CH_4 at about two years (Levitt 1971). Contrary to H_2, the colonic CH_4 production is relatively constant throughout the day (Levitt 1971). Human CH_4 is produced in extremely anaerobic conditions not by bacteria, but by methanogenic microorganisms of the Archea domain (Gandhi et al., 2021). The Archea Methanobrevibacter smithii is able to reduce CO_2, methanol, or acetate to CH_4, using H_2 as an electron donor (Miller et al., 1982 Hylemon et al., 2018). Tiny amounts of CH_4 can be produced under hypoxic conditions to counteract intracellular oxygen radical production not just by Archea microorganisms, but also by host components such as, e.g., rat mitochondrial subfractions and bovine endothelial cell cultures (Boros et al., 2015). In this case, CH_4 is generated from phosphatidylcholine metabolites containing both electron donor and acceptor groups (Ghyczy et al., 2008). Like H_2, the intraluminal colonic CH_4 diffuses to the blood for gradient concentration, enters the splanchnic circulation and is excreted through the breath (Bond et al., 1971; Zaorska et al., 2021). Analysis of respiratory methane provides approximative measure of CH_4 production (Sahakian et al., 2010; Schneider et al., 2020; McKay et al., 1985), revealing that methane concentration varies from 1 to 20 ppm as measured by exhaled CH_4 (Naito et al., 2018)

Evidence suggests that CH_4 may not be inert as previously thought (Sahakian et al., 2010). Methane significantly influences the enteric nervous system's cholinergic pathway, increasing contraction amplitudes (Park et al., 2014). In guinea pig ileum, CH_4 delayed ileal peristaltic conduction velocity by increasing contractility (Jahng et al., 2012). In radiolabelling experiments of small intestinal infusion, CH_4 slowed dogs' and guinea pigs' small intestinal transit, by increasing bowel contractions oral and aboral to the stimulus (Pimentel et al., 2006; Lee at al. 2013). The increases in contractile activity correlated with CH_4 production have been associated with constipation-predominant irritable bowel syndrome (Pimentel et al., 2006; Sahakian et al., 2010). Further, abundance in methanogenic bacteria has been positively correlated with slowed intestinal transit time (Attaluri et al., 2010; Triantafyllou et al., 2014) and chronic intestinal pseudo-obstruction (Khan et al., 2022). In turn, Rifaximin has been shown to improve chronic constipation by altering methane production (Ghoshal et al., 2018). It is noteworthy that patients with irritable bowel syndrome are characterized not just by reduction of methane producing microorganisms, but also by reduction of butyrate producing bacteria, known to improve intestinal barrier function (Pozuelo et al., 2015).

In mammals, during hypoxic events such as haemorrhagic shock, CH_4 production and subsequent mitochondrial redox regulation/oxidative phosphorylation improves basal respiration (Boros et al., 2015; Mészáros et al., 2017; Bársony et al., 2020). Mitochondria themselves can be sources of endogenous CH_4 under oxido-reductive stress conditions. During hypoxic condition, various colonic bacteria produce chemical compounds that can be used as energy source, such as acetic acid, CH_4 and HS_2 (Naito et al., 2018). Also, lines of evidence suggest that exogenous CH_4 exerts anti-inflammatory, anti-apoptotic and antioxidative effects (Mészáros et al., 2017; Zaorska et al., 2021). Methane modulates leukocyte activation (Boros et al., 2012) and plays shielding roles in hepatitis (He et al., 2016), acute lung injury (Sun et al., 2017), diabetic retinopathy, spinal cord ischemia/reperfusion injury and sepsis (Li et al., 2019).

Preprints (www.preprints.org) | NOT PEER-REVIEWED | Posted: 19 October 2022 doi:10.20944/preprints202210.0263.v1

In sum, intestinal CH_4 is produced by intestinal commensal anaerobia in approximately one-two third of healthy humans. Methane delays intestinal transit and compensates oxido-reductive stress conditions. Its extra-intestinal effects are so extended, that a few researchers are starting to suggest that CH_4 could stand for a fifth gasotransmitter apart from NO, CO, H_2S and SO_2.

Hydrogen (H_2). In healthy individuals, H_2, which accounts for ≈3% of the colonic gases, is almost entirely produced by the dietary fiber's intraluminal fermentation performed by anaerobic commensals in the large intestine (Modesto et al., 2022). Hydrogen is a by-product of ingested fermentable substrates including non-absorbable oligosaccharides such as beans/lactulose (90%) and poorly absorbed proteins, short chain fatty acids and alcohols (10%). The amount of lactose in a glass of milk generates 500–1,000 ml of H_2 after bacterial fermentation. Hydrogen-producer species are abundant in the gut microbiota and include not just the two major colonic phyla, i.e., Firmicutes and Bacteroidetes, but also members of the genera Roseburia, Ruminococcus, Eubacterium (Hylemon et al., 2018; Naito et al., 2018). It is remarkable that many hydrogen cross-feeding microbes have evolved. The three main hydrogenotrophic colonic groups are the sulfate-reducing bacteria (such as Desulfovibrio), the methanogenic archaea and the reductive acetogens (Carbonero et al., 2012; Scaldaferri et al., 2013; Smith et al., 2021). Luminal colonic H_2 freely diffuses between the lumen and the blood, the net movement depending on the pressure gradient. Colonic H_2 absorption is highly effective at low colonic hydrogen accumulation rates, but not at higher accumulation rates (Hammer 1993). Therefore, about 15% of H_2 diffuses back into the bloodstream, with the rest passing as flatus. The colonic H_2 absorbed by the blood is cleared by the lungs. The time taken for H_2 to appear in the breath after ingestion of a standard load of glucose or lactose is used to determine whether the upper gastrointestinal tract has been colonized by H_2 producing bacteria (Hammer 1993; Carbonero et al., 2012; Wilder-Smith et al., 2018).

Colonic hydrogen leads to the production of short-chain fatty acids like butyrate. When H_2 is not fully metabolized, fermentation may be incomplete and intermediates such as lactate, succinate, and ethanol may accumulate (Scaldaferri et al., 2013). Physiological H_2 concentrations have been shown to have antioxidant properties, protecting the healthy colonic mucosa from oxidative insults and preventing inflammation/carcinogenesis (Carbonero et al., 2012). Also, roles on local intestinal motility have been suggested for H_2. It shortened guinea pigs' colonic transit by 47% in the proximal colon, but just by 10% in the distal colon (Jahng et al., 2012).

In sum, intestinal H_2 is major byproduct of colonic fermentative metabolism. Hydrogen preserves the healthy colonic mucosa from oxidative insults and might have a role in shortening colonic transit.

Hydrogen sulfide (H_2S). In healthy humans, the most of H_2S is a by-product of colonic bacterial metabolism (Linden 2014). Cysteine catabolic bacteria and, to a lower extent, sulfate-reducing bacteria produce H_2 using as substrates both dietary and endogenous compounds of organic and inorganic nature (Guo et al., 2016; Blachier et al., 2021). Two enzymatic trans-sulfuration pathways are involved in H_2S production, i.e., the cystathionine gamma-lyase in the vascular system's smooth muscles, and the cystathionine beta-synthase in both central and intestinal nervous systems (Guo et al., 2016; Verbeure et al., 2021). To generate H_2S in an anaerobic watery environment like the human colon, some requirements must be satisfied, e.g., high-concentration of sulfate ions and organic substances as carbon source and sulfate-reducing bacteria like Desulfovibrio bacteria (Naito et al., 2018). Sulfate reduction and methanogenesis seems to be mutually exclusive in the colon and this is possibly linked to sulfate availability, which favours H_2S instead of CH_4 production (Scaldaferri et al., 2013). Hydrogen sulfide is produced also by endogenous cellular enzymes expressed in intestine, liver, kidney and brain (Sahakian et al., 2010). In particular, H_2S is synthetized by specific enzymatic pathways in different intestinal cell types, including neurons and smooth muscle (Jimenez et al., 2017). Vegetables like garlic and onions contain the natural H_2S donor allicin and therefore generate a large amount of colonic H_2S (Benavides et al., 2007).

Preprints (www.preprints.org) | NOT PEER-REVIEWED | Posted: 19 October 2022 doi:10.20944/preprints202210.0263.v1

Intraluminal and faecal colonic H_2S concentrations are rather variable and may reach 3.4 mmol/L in human stools (Guo 2016; Blachier et al., 2021).

H_2S is an important energy substrate in colonocytes because its mitochondrial oxidization results in ATP synthesis (Blachier et al., 2021). However, when the intracellular H_2S concentration is pushed locally above the healthy limit and exceeds the colonocyte capacity for its oxidation, the mitochondrial respiratory chain is inhibited and the energy metabolism is impaired (Blachier et al., 2021). Too high luminal H_2S concentration affects the integrity of the mucosal layer, leading to increase in inflammatation.

Together with CO, NO and SO_2, H_2S is regarded as an endogenous gasotransmitter (Wu et al. 2017). Its biology is a still developing area of research. Although less studied that the other three, H_2S has been found to act as a signalling molecule immediately after release. It has been demonstrated that H_2S affects intestinal motility, promoting colonic transit (Nalli et al., 2017). It has been recently suggested that exogenous H_2S might exert an excitatory effect on colonic motility, through Substance P release from afferent nerves together with activation/deactivation of different Ca2+ channels in smooth muscle cells (Quan et al., 2022). Inhibition of H_2S biosynthesis increases motility, while H_2S donors cause smooth muscle relaxation and inhibition of propulsive motor patterns (Jimenez et al., 2017). Recent reports provide evidence for crosstalk between NO and H_2S in colonic smooth muscle. NO generates H_2S via cGMP/PKG pathway, while H_2S increases NO-induced cGMP levels. Further, H_2S and its oxidation product polysulfide can activate nociceptors expressed in sensory nerves, displaying effects on visceral nerve hypersensitivity (Chassard et al., 2012). After high protein meals, the H_2S donor amino acid l-cysteine suppresses ghrelin release from the rat stomach, reducing appetite for a long time (Verbeure et al., 2021). Colonic H_2S stimulates GLP-1 release, improving glycemia in male mice. Considering its short half-life time, H_2S possibly achieves this effect by stimulating nearby colonic cells instead of ileal cells after plasmatic transport (Pichette et al., 2017). High concentrations of hydrogen sulfide produced by bysulfate-reducing bacteria are involved in gut inflammation through detrimental mechanisms of toxicity, pH lowering and inhibition of the beneficial lactic acid bacteria (Dordević et al., 2021).

Recent, still controversial findings suggest that endogenous H_2S might play roles in angiogenesis and smooth muscle vascular relaxation (Linden 2014; Wu et al. 2017). Abnormal H_2S metabolism is associated with diseases including heart failure, hypertension, atherosclerosis, asthma, diabetes and neurodegenerative diseases (Wu et al. 2017). Increased expression of various H_2S-producing enzymes could be correlated with ulcerative colitis and human colonic cancer development (Cai et al., 2014; Guo et al., 2016). H_2S displays a bell-shaped pharmacology, whereby lower (endogenous) H_2S production promotes, while higher (generated from exogenous H_2S donors) inhibits colorectal cell tumoral proliferation.

In sum, H_2S is an endogenous gasotransmitter produced almost exclusively in the colon as a by-product of colonic bacterial metabolism. Hydrogen sulfide produces ambivalent physiological effects, depending on its intracellular concentration.

Sulfur dioxide (SO_2). Previously regarded as a highly toxic gas smelling of burnt matches detectable in atmospheric pollutants, sulfur dioxide is not harmful if ingested in low concentration with food. One of the main sources of SO_2 in the human body comes from the addition of sulfites to food products due to their bacteriostatic, bactericidal and antioxidant properties. Sulfites are regarded as safe for consumption at concentrations up to 5000 parts per million (Irwin et al., 2017). Sulfur dioxide is used as a preservative termed E220 for dried fruits, food starches, wine/beer fermentation and medications to prevent oxidation and changes in pigment (Zamboni et al., 2011). Also, SO_2 or its conjugate base bisulfite is endogenously produced during intestinal fermentation. Generated through cysteine metabolism and ingested sulphur's conversion, SO_2 is an intermediate product of sulfur-oxidizing bacteria and sulfate-reducing organisms, in particular Desulfovibrio genus. Variation in the distribution of sulfate-reducing microbial communities have been detected in healthy mice (Kushkevych et al., 2019). Usually, the healthy individuals' colonocytes are able to absorb and detoxify the gas. Sulfur dioxide is generated also in mammalian cardiovascular tissues from

Preprints (www.preprints.org) | NOT PEER-REVIEWED | Posted: 19 October 2022 doi:10.20944/preprints202210.0263.v1

sulfur-containing amino acids (Huang et al., 2016). Interactions occur between SO_2 and the other gasotransmitter H_2S, the latter regulating some SO_2 pathways (Huang et al., 2021).

Although its biological role in mammalian biology is not well understood, SO_2 is regarded as the fourth gasotransmitter. Very small amounts of SO_2 display cytoprotective, antioxidant and anti-inflammatory properties that ameliorate colitis in rats, reversing inflammatory features like oxidative stress, NF-κ B and inflammasome activation, endoplasmic reticulum autophagy, p53 activation and apoptosis (Banerjee et al., 2019). Endogenous sulfur dioxide in low concentrations regulates cardiac and blood vessel function, triggering endothelium-dependent vasodilation and myocardial antioxidant defense reserve (Want et al., 2011). Relatively recent studies showed that SO_2 ameliorates systemic and pulmonary hypertension, prevents atherosclerosis development and protects against myocardial ischemia-reperfusion injury (Huang et al., 2016).

At high concentrations, SO_2 displays manifold adverse effects, especially on the colonocytes. High SO_2 levels cause colonocyte's cell death, goblet cell loss, crypt architectural distortion and superficial mucosal ulceration, leading to permeability and barrier function shortfall. Still controversial data suggest that high SO_2 levels may be linked with ulcerative colitis (Teigen et al.,2019). One of the key deleterious effects of SO_2 consists of impairment of short chain fatty acids metabolism. Competition for the available intestinal hydrogen occurs between sulphur-reducing bacteria and short chain fatty acids-producing bacteria, causing reversible inhibition of butyrate oxidation. This leads to decreases in butyrate acid, that is vital in providing up to 70% of the energy metabolism required by the colonocytes. High SO_2 concentrations cause endothelium-independent vasodilation mediated via calcium channels, leading to harmful inotropic effects on cardiac output function. An association has been found between sulfur dioxide and increase in ischemic heart disease, heart failure and arrhythmia, mainly due to mitochondrial dysfunction in cardiac muscles (Qin et al., 2016).

In sum, intestinal SO_2 is both ingested with the food and produced by intestinal bacteria via sulfur conversion. Like a two-faces Janus, sulfur dioxide is a beneficial antioxidant and anti-inflammatory molecule at low doses and an extremely dangerous poison at high doses.

In conclusion, the gaseous mixture is composed by a large number of gases, each one characterized by its own sources, dynamics, metabolism, biological effects.

Preprints (www.preprints.org) | NOT PEER-REVIEWED | Posted: 19 October 2022 doi:10.20944/preprints202210.0263.v1

PHYSICAL PROPERTIES OF THE INTESTINAL GASEOUS MIXTURE

Here we will analyze the effects of physical laws on intestinal gases physiology, describing how the physical interplay between gaseous volume and luminal surface impacts absorption and mixing. We will consider just the whole mixture of different gases, leaving apart the differences among each gas. According to the Dalton's law of partial pressures in ideal gases, the pressure of a mixture of non-reactive gases equals the sum of the pressures of all the constituent gases. Further, the Amagat's law states that the volume of a gas mixture equals the sum of the volumes of the component gases, when the temperature and the pressure are held constant. Taken together, the two theorems suggest that gas particle identity plays no role in determining both final pressure and volume of the intestinal gaseous mixture.

Modifications in intestinal gaseous volumes may have a twofold cause:

1) Physical factors, e.g., changes in luminal pressure and temperature.
2) Biological factors, e.g., changes in diet and intestinal microorganisms' metabolism.

We will argue that the two distinct causes of gaseous volumetric modification lead to fully different absorptive outcomes.

Gaseous volumetric changes due to intestinal physical factors: Boyle's law. Trans-barrier gaseous exchanges do not depend on the intraluminal pressure, rather on the difference between the partial gaseous pressures in lumen and in blood. Though, the intraluminal pressure retains an indirect, deep effect on gas exchanges. It is well-known that variations in the three main physical gaseous parameters, i.e., pressure, volume and temperature, cause modifications in gut diameter, flow volume, fluids velocity (Uno 2018). For instance, analytical Poiseuille-flow simulations suggest that oppositely directed contractile waves are useful for mixing and favouring nutrient absorption. Indeed, two colliding contractile waves moving toward one another cause blobs of silicone injected into the embryonic chicken's intestine to be squeezed together (Amedzrovi Agbesi and Chevalier, 2022).

Pressure, volume and temperature are linked to each other through the experimental gas laws (Webster 1965; Randsoe and Hyldegaard, 1985). Even though these laws hold for a given mass of an ideal gas within a closed system, they can be also used to describe the behavior of real gases such as the intestinal gaseous mixture in the confined environment of colonic haustra.

Charles's law states that the temperature and the volume are in direct proportion when the gas pressure is held constant. One of its formulations reads:

$V/T = k$

Where V is the gaseous volume, T is the gaseous temperature and k is a constant such that every 1°C increase in temperature leads to 1/273 increase in volume.

Gay-Lussac's law states that the temperature and the gas pressure are in direct proportion when the gas volume is held constant. One of its formulations reads:

$P/T = k$

Where P is the gaseous pressure, T is the gaseous temperature, and k is a constant such that every 1°C increase in temperature leads to 1/273 increase in pressure.

About the intestinal gases, the two laws can be formulated as follows:

a) Charles' law: keeping the gaseous pressure constant, slightly decreases (1/273) in the gaseous volume occur when the gut temperature decreases of 1°C.
b) Gay-Lussac' law: keeping the gaseous volume constant, slightly decreases (1/273) in the gaseous pressure occur when the gut temperature decreases of 1°C.

Preprints (www.preprints.org) | NOT PEER-REVIEWED | Posted: 19 October 2022 doi:10.20944/preprints202210.0263.v1

Being the range of gut temperatures very narrow (about 37-40°C) (Dokladny et al., 2005; Ruddock et al., 2014), increases or decreases in temperature will produce very small changes in volume and pressure. This means that the effects of the Charles' and Gay-Lussac' laws are negligible in the colon.

For a third experimental gas law, i.e., the Boyle's law, the story is different. The law states that the absolute pressure exerted by an ideal gas is inversely proportional to the volume it occupies, when the temperature and the amount of gas remain unchanged. One of its formulations reads:

$P \cdot V = k$

Where P s the gas pressure, V is the gaseous volume and k is a constant such that the volume doubles when the volume halves.

About the intestinal gases, the Boyle's law can be formulated as follows: Keeping the colon temperature constant, the gut gaseous volume halves when the gut pressure due to gut contraction doubles (**Figure 1A**). Among the three examined experimental laws of gases, the Boyle's law has the deepest physiological implications. It suggests that every change in gut pressure leads to significant changes in intraluminal gaseous volume, and vice versa. When the muscular relaxation causes increases in gut diameter and decreases in intraluminal pressure, the gaseous mass tends to fill a larger intraluminal volume. This means that the amount of fixed gaseous mass per unit volume, namely the gaseous density, has been modified. See **Figure 1B** for further details.

Intestinal movements have a deep effect on nutrients' intraluminal persistence and absorption. Small intestine's fluid dynamics simulations suggest that the average flow velocity is the key feature to control absorption efficiency and bacterial growth (Codutti et al., 2022). Alternating the two contraction patterns of peristalsis and segmentation, the gut switches between different flow regimes, optimizing nutrient absorption and minimizing bacterial overgrowth (Codutti et al., 2022). The slower the flow speed, the longer the gaseous mixture persists in the gut, the more the intraluminal gases are exchanged with the blood. When the gaseous volume is augmented due to muscular relaxation, a larger amount of mucosal surface is available, leading to increases in trans-barrier metabolic exchanges between the lumen and the bloodstream.

Summarizing, the Boyle's experimental gas law suggests a twofold effect on the gut function: gaseous exchanges between intestinal lumen and blood are impaired by muscular contraction and improved by muscular dilation.

Gaseous volumetric changes due to intestinal biological factors: surface-area-to-volume ratio. A puzzling phenomenon has been reported, i.e., the colonic absorption of H_2 is highly effective at low colonic accumulation rates, but ineffective at the higher accumulation rates occurring after ingestion of non-absorbable carbohydrates (Hammer 1993). An unnoticed physical/biological factor might shed new light on this experimental observation. When the volume of colonic gas increases due to microorganismal fermentative reactions, the surface area per unit volume cannot be overlooked. This factor, termed surface-area-to-volume ratio (henceforward SA:V), suggests that body size and shape are mathematically interconnected. Changes in volume are not linearly correlated with changes in surface, since volumes tend to increase much more than areas. For instance, when the sphere's radius increases, the volume expansion is proportional to the radius' cube (r^3) while the surface expansion is proportional just to the radius' square (r^2). Therefore, the smaller sphere displays relatively more surface (and a higher SA:V) compared with the bigger sphere. To provide a rough example, an eukaryotic cell with radius 2 displays a surface of 4 and a volume of 9, while an eukaryotic cell with radius 3 displays a surface of 9 and a volume of 29. The phenomenon is ubiquitous: a wide range of living systems exhibits robust SA:V homeostasis at different coarse-grained scales, from neurons to elephants (Harris and Theriot 2018; Beaulieu-Laroche al., 2021). SA:V has been widely utilized to evaluate cellular packing, animal water loss, heat transfer during thermoregulation, etc (Glazier 2010; Hales at al., 2017; Nguyen et al., 2019).

The large surfaces (relative to their volumes) displayed by tiny organisms permit plentiful exchanges of nutritive substances between the internal and the external, compared with the small surfaces (relative to their volumes) displayed by larger organisms. About

Preprints (www.preprints.org) | NOT PEER-REVIEWED | Posted: 19 October 2022 doi:10.20944/preprints202210.0263.v1

the colonic gas produced by fermentation, every intraluminal gaseous bubble displays a surface available for lumen/blood trans-barrier gaseous exchanges. SA:V dictates that enhanced microorganismal production of intraluminal gases leads to large increases in gaseous bubble's volumes and small increases in their surface (**Figure 1C**). The bigger gaseous bubbles have less capability of performing lumen/blood metabolic exchanges, compared with the smaller ones. This means that a high volume of colonic gas (corresponding to a small SA:V) stands for a detrimental outcome that impairs gaseous exchanges, adsorption, catalysis and reactions across the intestinal barrier. Despite the SA:V mechanism and the Boyle's law mechanism may both lead to increases in gaseous volumes, they exert opposite metabolic effects. While the increases in gaseous volume due to Boyle's law mechanism cause decreases in gaseous density (**Figure 1B**), the increases in gaseous volume due to SA:V cause increases in gaseous density (**Figure 1C**).

Summarizing, SA:V ratio suggests that the gaseous exchanges between the intestinal lumen and the bloodstream are impaired by microorganismal overproduction and improved by microorganismal decreased production.

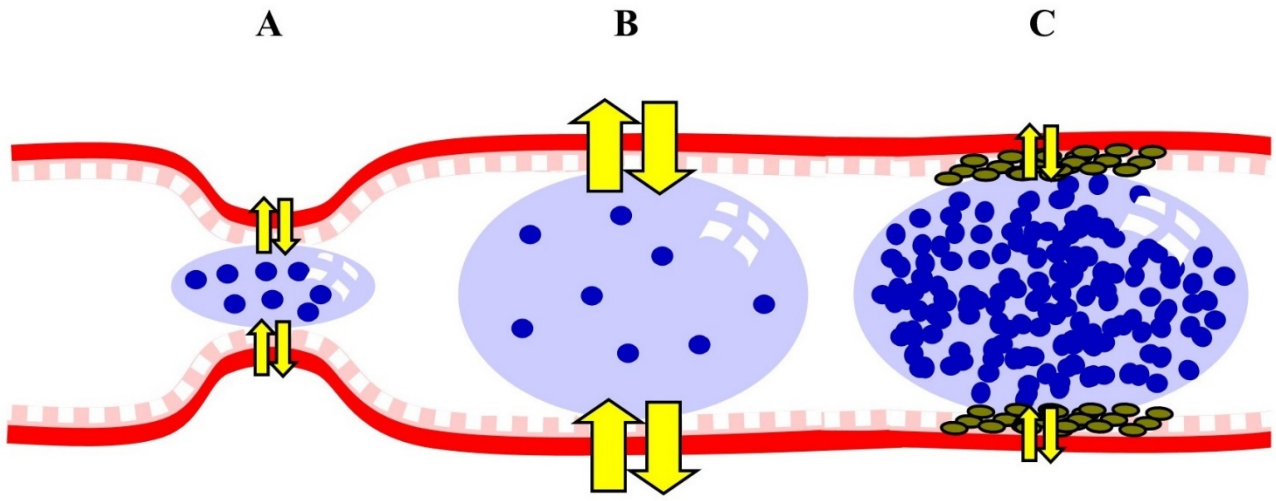

Figure 1. Effects of intraluminal volumetric modifications on intestinal gaseous absorption. Intraluminal gas bubbles with varying surfaces and volumes are illustrated inside a contractile intestinal segment. **Figure 1A**. Due to the Boyle's law, muscular contraction leads to decrease in gaseous volumes. The subsequent decrease in gaseous surface leads to impaired lumen/blood metabolic exchanges (small yellow arrows). **Figure 1B**. Due to the Boyle's law, muscular dilation leads to increased gaseous volumes. The subsequent increase in gaseous surface leads to improved lumen/blood metabolic exchanges (big yellow arrows). Note that the gaseous density, illustrated by the blue dots standing for single gas molecules, is lower, compared with Figure A. **Figure 1C**. Large amounts of fermenting microorganisms (green ovals) in a relaxed gut lead to increase in gaseous volumes. Despite the increases in gaseous surface and gaseous density, SA:V dictates that the lumen/blood metabolic exchanges are less effective (small yellow arrows) than in Figure B.

Preprints (www.preprints.org) | NOT PEER-REVIEWED | Posted: 19 October 2022 doi:10.20944/preprints202210.0263.v1

Gaseous random walks in colonic haustra. An overlooked factor in gut dynamics research is the hydrodynamic flow. Are intestinal gaseous movements laminar or turbulent? The best available quantitative approach to tackle the complexity of turbulent flows consists of the dimensionless Reynolds number (henceforward Re), which describes the ratio of inertial/viscous forces:

$$Re = \frac{\rho \cdot L \cdot u}{\mu}$$

where ρ is the fluid density (kg/m^3), L is the characteristic linear dimension (the cylinder's diameter in m), u is the fluid velocity (m/s) and μ is the dynamic viscosity (kg/m · s). Re differentiates between laminar (Re < 2,100) and turbulent flows (Re > 3,000) (Wygnanski and Champagne, 2006). Simulations can be performed through freely available calculators, such as, e.g., https://www.omnicalculator.com/physics/reynolds-number. Reynolds number simulation of intestinal gas produces the following result: gaseous density ρ = ≈1.18 kg/m^3, dynamic viscosity μ = ≈0.000018 Kg/m · s, colonic fluid velocity u = ≈ 0.01 m/s, while the characteristic linear dimension L equals the intestinal diameter, which ranges from ≈ 0.08 m in the caecum to ≈ 0.055 m in the rectum (Uno, 2018). Since the Reynolds number turns out to be ≈ 30.0 in all the intestinal segments, gaseous flows in the gut are always laminar. Therefore, gaseous flows do not display the vorticity that is the hallmark of turbulent flows (Sturm et al., 2012; Kalmár-Nagy and Bak, 2019).

Unconstrained, random movements of gaseous molecules occur in the undisturbed environment of the segmented haustra. In probability theory, a "random process" (the term "random" is roughly interchangeable with "stochastic") is a sequence of variables whose outcomes do not follow a deterministic pattern, rather their evolution is described by probability distributions (Paul and Baschnagel, 2013). Since no preferential flow direction does exist, the state of a stochastic process cannot be accurately predicted by the knowledge of its previous and current states. A "random walk" is a path consisting of a succession of random steps in a mathematical space (Codling et al., 2008). A "Brownian motion" depicts the random fluctuations of particles inside a fluid at thermal equilibrium (Blomberg et al., 2020). "Ergodicity" is a random process in which all the accessible microstates in a phase space are equiprobable over a long period of time (Walters, 1982). The concepts of random processes, random walks, Brownian motion and ergodicity are used to approach classic, relativistic and quantum systems (Gong et al., 2021) such as, e.g., light, liquids/gases motion, genome organization's heterogeneity, protein concentrations' fluctuations, signal processing, gambling, evolution, ecological processes, etc (Elowitz et al., 2002; Finn and Misteli, 2019; Pontes-Filho et al., 2020; Klosin et al. 2020; Casacio et al., 2021; Wooller et al., 2021).

It might be tempting to believe that the gaseous random walks tend to uniformly spread inside the segmented colonic haustra, disrupting the initially clumpy distribution of gas bubbles. Though, we will show here that gaseous random walks in colonic haustra cannot spread homogeneously. An unappreciated factor must be regarded when coping with random walks, i.e., the number of dimensions of the phase space where the movements take place. Stochastic approaches are not profitable when random walks occur in phase spaces of dimensions higher than two: the higher the phase space's dimensions, the less the possibility that random walks return to the starting point. Indeed, random walks in two-dimensional lattices (**Figure 2A**) have unity probability of reaching any point (say, the starting point) as the number of steps approaches infinity (**Figure 2B**). Consider a random walk on a lattice of dimension D^d. The probability $p^{(d)}$ that a random walk returns to the origin is: $p(1) = p(2) = 1$ (McCrea and Whipple, 1940). This means that a particle almost surely will get back to the starting point in case of two-dimensional random walks. To provide an example, it has been stated that "a drunk man will find his way home, but a drunk bird may get lost forever". A drunk man randomly walking around the streets arranged in a square grid will always go back home. Yet, in case of random walks in phase spaces equipped with dimensions higher than two (**Figure 2D**), the probability to reach the starting point decreases with increases in number of dimensions (Domb, 1954; Finch 2003) (**Figure 2E**). Indeed, $p(d)<1$ for $d>2$, so that, for example, $p(3)=0.3405$, $p(5)=0.1351$, $p(8)=0.079$, and so on (Montroll, 1956). A drunk bird, that, unlike the drunk man, can fly in three dimensions instead

Preprints (www.preprints.org) | NOT PEER-REVIEWED | Posted: 19 October 2022 doi:10.20944/preprints202210.0263.v1

of just two, will not get back to its nest. Since three-dimensional random walks exhibit an extremely low probability to return by chance to the starting point, we are allowed to state that the (apparently stochastic) trajectories occurring in three-dimensional phase spaces are hampered and constrained. In case of two-dimensional random walks, ergodicity is guaranteed by the fact that all the accessible microstates are equiprobable over a long period of time (**Figure 2C**). In turn, random walks taking place in high dimensions cannot be fully ergodic, because every point (say, the starting point) cannot be easily crossed more than once (**Figure 2F**). This means that the trajectories in three-dimensional systems are unable to homogenously fill the whole phase space, leading to a loss of the same ergodicity that is fully guaranteed in two dimensions. In touch with this observation, significant deviations from Brownian motion have been uncovered in a variety of animate and inanimate systems such as, e.g., the movements of avian predators or bird flocks (Metzler 2014; Vilk et al., 2022). Ergodicity breaking has been observed uniquely at the micro-scale of observation, while it is hidden at large-scale interpatch observation (Vilk et al., 2022).

About the gut, this means that the undisturbed random diffusion of gas (i.e., the gaseous random walks) inside a colonic pocket (i.e., inside a three-dimensional phase space) impacts gaseous permeability rates and trans-membrane exchanges. The gaseous mixture's three-dimensional random paths do not diffuse ergodically, therefore they cannot reach all the regions of the haustral mucosa (i.e., all the partitions of the phase space). Since the particle probability to reach the starting point is 0.3405 for three-dimensional random walks, this means that the amount of colonic area available for lumen/blood metabolic exchanges has fallen by ≈two thirds. Therefore, changes in gut permeability could be caused not just by well-studied noxae like, e.g., intestinal epithelium's increased apoptosis, altered permeability, impaired tight junctions' porosity, zonulin-mediated diseases, leaky gut syndrome and so on (Camilleri, 2019; Obermüller et al., 2020; Tajik et al., 2020), but also by the physiological stochastic dynamics of the gases confined in the colonic haustra of healthy individuals.

Preprints (www.preprints.org) | NOT PEER-REVIEWED | Posted: 19 October 2022 doi:10.20944/preprints202210.0263.v1

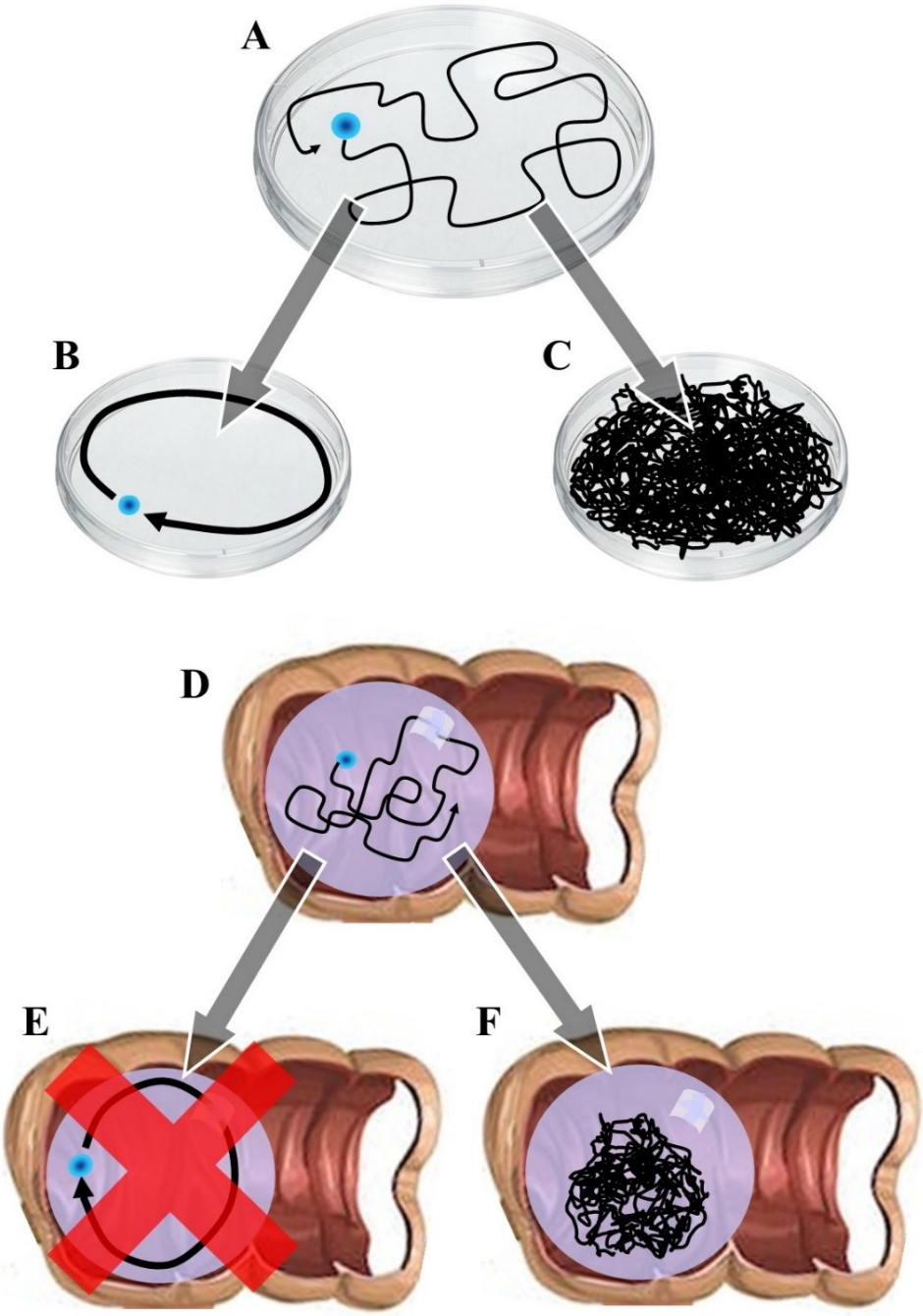

Figure 2. Random walks in phase spaces with different dimensions. **Figure 2A** illustrates a two-dimensional random walk with its starting point (blue dot). Two dimensional random paths tend to form recurrent closed paths (**Figure 2B**) and to fill the whole available surface (**Figure 2C**). **Figure 2D** illustrates a three-dimensional random walk of a gaseous particle confined in a gaseous bubble inside a colonic haustrum. Three-dimensional random paths cannot form recurrent, closed paths (**Figure 2E**) and cannot fill the whole available volume (**Figure 2F**).

Preprints (www.preprints.org) | NOT PEER-REVIEWED | Posted: 19 October 2022 doi:10.20944/preprints202210.0263.v1

Preprints (www.preprints.org) | NOT PEER-REVIEWED | Posted: 19 October 2022 doi:10.20944/preprints202210.0263.v1

CONCLUSIONS

We discussed the production and storage mechanisms of intestinal gases, emphasizing their biological roles and growing importance in human physiology and pathology. Rather than waste material discarded by host's and microbiome's biological reactions, the intestinal gaseous mixture affects energy metabolism, gut transit regulation, immunity, paracrine and eccrine regulation, bacterial proliferation, blood musculature control, gut metabolic exchanges with blood and breath, etc. Being intestinal gas' volume and composition important factors for the experimental assessment of gut microbiome, functional disorders, bowel perforation diagnostics, etc (Modesto et al., 2022), the quantitative data provided in this review may be helpful in basic research and translational medicine. An important operational feature of intestinal gases is that some of them are detectable in exhaled breath. Measurement of breath hydrogen and methane excretion after ingestion of test-carbohydrates is a valuable, non-invasive and inexpensive diagnostic test that provides crucial information concerning gastrointestinal disorders (Hammer, 2022). Breath test is useful in the diagnosis of carbohydrate maldigestion syndromes, small intestinal bacterial overgrowth, methane-associated constipation, evaluation of bloating/gas, etc (Rezaie et al., 2017). ^{13}C-breath tests is used to detect Helicobacter pylori infection, quantify gastric emptying time and screen pancreatic exocrine and liver function (Keller et al, 2021). Orally administered urea containing isotopically labelled CO_2 is hydrolysed by the urease produced in large quantities by Helicobacter pylori. Urea is then hydrolysed to ammonia and carbon dioxide, which diffuses into the blood and is excreted by the lungs (Savarino et al., 1999). Yet, more standardization is required regarding indications for breath tests' methodology, performance and results interpretation (Keller et al., 2021).

A few intestinal gases, namely hydrogen sulfide (H_2S), nitric oxide (NO), carbon monoxide (CO) and sulfur dioxide (SO_2), are classified among the gasotrasmitters. To fall within the definition of gasotransmitter, the gasous molecule must be generated endogenously and must exert regulatory (rather than toxic) effects (Pacher 2021). Interestingly, all these molecules are either produced by mitochondrial enzymes, and/or display significant effects on mitochondria, suggesting ancient regulatory roles in bacterial species (Wareham et al., 2018). It has been recently suggested that another molecule could be counted among the mammalian gasotransmitters, namely, cyanide. We agreed not to talk about cyanide in the previous chapters because its effects on the gastrointestinal tract are still unknown. Exposure to cyanide occurs via cigarette smoking, smoke inhalation during plastics combustion, drinking cyanide-contaminated water or ingestion of large amounts of edible plants like apricot kernel, flaxseed, cassava, almonds, Chinese cabbage, radish (Lee and Kwon, 2009). Further, endogenous cyanide production has been demonstrated by various mammalian enzymes from endogenous and exogenous substrates (Cipollone and Visca, 2007). For instance, apricot cyanogenic glycosides can be converted into thiocyanate by human hepatic and colonic cells (Lee and Kwon, 2009). Some bacteria like Pseudomonas aeruginosa are cyanide-producing too. Hydrogen cyanide is readily soluble in water and in biological fluids, where it usually exists in the volatile undissociated form. While cyanide at high concentrations is a cytotoxic agent exerting harmful effects via inhibition of the mitochondrial Complex IV, cyanide at low concentrations stimulates mitochondrial electron transport and promotes ATP production, resulting in cell proliferation stimulation (Randi et al., 2021). A few, tenuous clues point towards a possible involvement of cyanide in the physiology of the intestinal tract. Studies evaluating dietetic regular intake of ^{14}C-labelled cyanide in rats suggest that the stomach accounts for 18% of the total injected radioactivity. Most of the cyanide is excreted in the urine and only small amounts are found in the faeces, indicating intestinal absorption into the body fluid (Okoh et al., 1982).

Intestinal motility is emerging as a deal-breaker in a variety of unexpected topics. Traditionally, the wide inter-individual heterogeneity in microbiota composition has been associated with physiological variables and population-wide differences in human lifestyle (Vujkovic-Cvijin et al., 2020). For example, industrialized infants have a paucity of microbiotic gene cassettes involved

Preprints (www.preprints.org) | NOT PEER-REVIEWED | Posted: 19 October 2022 doi:10.20944/preprints202210.0263.v1

in human milk utilization, compared with Tanzanian hunter-gatherers' infants (Olm et al., 2022). Still, bowel movement quality is recently emerging as a strong source of heterogeneity in human gut microbiota profiles (Vujkovic-Cvijin et al., 2020). It is becoming increasingly clear that different intestinal contraction patterns may cause changes in fluid dynamics. Propulsion, reflux and mixing lead to modifications in the intestinal microbiota, since obliterating waves induce considerable bolus mixing due to an upstream vortex, while colliding waves create a high-pressure region characterized by rapid fluid flow, high shear stress and radial mixing upon annihilation (Amedzrovi Agbesi and Chevalier, 2022). We provided an effort to correlate intestinal gaseous changes in volume or density with modifications in gaseous mixing and trans-barrier diffusion. We showed that increases in gas volume due to two different mechanisms (namely, physical muscular gut contraction and biological colonic fermentation) lead to different metabolic outcomes. The Boyle's experimental gas law suggests that the gaseous exchanges between lumen and bloodstream are decreased by muscular contraction and augmented by muscular relaxation. The surface/volume ratio suggests that these exchanges are reduced by microorganismal overproliferation and increases improved by microorganismal decline.

It is noteworthy that the two mechanisms may also exert synergic effects. For instance, volumetric gaseous increases during intestinal obstruction are caused by both muscular relaxation and increased colonic fermentation, allowing the two simultaneous mechanisms to provide counterbalanced effects on the inter-barrier gaseous exchanges. Therefore, at least to some extent, the physiological gaseous turnover tends to be neither increased nor decreased in case of intestinal dilation. The distinction between physical and biological causes of intestinal volumetric changes might shed new light also on the puzzling phenomenon of pneumatosis intestinalis, i.e., the radiographing finding of gas in the mucosa, submucosa, muscular layers or mesentery (Ho et al., 2007; Albright 2019). A variety of contributing factors have been suggested to explain the pathogenesis of intramural gas accumulation (St Peter et al., 2003; Blair et al., 2015; Sugihara and Okada, 2017):

a) Mechanical pressure from pulmonary diseases like chronic obstructive pulmonary disease.
b) Progressive diffusion of high-pressure intraluminal gas inside the bowel wall.
c) Infiltration of gas-producing microorganisms inside the impaired bowel wall. The mucosal derangement and the subsequent increase in mucosal permeability would allow gas-forming bacteria to enter the bowel wall and locally produce gas.
d) Intraluminal bacterial overgrowth.
e) Excessive H_2 excretion due to lack of H_2-consuming intestinal bacteria (Levitt and Olsson, 1995). It has been suggested that rapid H_2 diffusion from the lumen into intramural gas bubbles would cause N_2, O_2, and CO_2 to diffuse from the bloodstream into the bubbles. As a result, the bubble would expand and persist indefinitely as long as intraluminal H_2 continues to diffuse (Levitt and Olsson, 1995). The phenomenon, termed gas cysts' counterperfusion supersaturation, occurs mainly near the blood vessels of the colonic mesenteric border (Florin and Hills, 1995).

Our account suggests that intraluminal increases in gaseous volume due to microbial fermentation could be the main factor that increases the gaseous pressure exerted in the haustral pockets. In the confined haustral volumes, local increases in gaseous pressure may reach high intraluminal values, overtaking the counter-pressure exerted by the blood flow and impacting the allometric relationships governing the biophysics of the mucosal cells. Therefore, we speculate that the best mechanism to explain intestinal pneumatosis is to consider that high-pressure transitory waves might allow intraluminal gases to passively diffuse inside the gut wall.

Along the "gut-brain-axis", the intestinal microbiota influences functions, development and disease of both the enteric and the central nervous systems. Intestinal bacteria deliver a wide range of mammalian neurotransmitters, including dopamine, norepinephrine, serotonin, gamma-aminobutyric acid (Strandwitz 2018). Some gases that can be found in the gut exert well-known effects on both the peripheral intestinal neurons and the central neurons. For example, NO, apart from the above-described effects on the intestinal neurons, is synthesized "on demand" in the brain from postsynaptic terminals and is involved in neuronal signaling, volume transmission, retrograde modulation of presynaptic electrical activity, transmitter release (Rodriguez-Grande and Konsman

Preprints (www.preprints.org) | NOT PEER-REVIEWED | Posted: 19 October 2022 doi:10.20944/preprints202210.0263.v1

2018; Del-Bel and De-Miguel, 2018). Hydrogen sulfide, apart from promoting colonic transit and affecting intestinal motility/visceral nerve hypersensitivity, is also a neuromodulator that enhances NMDA-induced currents in hippocampal neurons (Abe and Kimura, 1996; Nagai et al., 2004) and mediates the reciprocal brain interactions between glial calcium waves and neuronal activity (Guo et al., 2016).

Other gases that can be found in the gut are known to exert effects on the central neurons, but their roles on the intestinal neurons is still controversial. For example, ammonia, due to the NH_3 -permeable channels, can be systemically absorbed causing hepatic encephalopathy in patients with liver cirrhosis (Rodriguez-Grande and Konsman 2018). Further, N_2 hyperbaric exposure induces narcosis targeting the striatum and the substantia nigra compacta (Rostain and Lavoute, 2016). A role of H_2O_2 as intercellular signaling molecule/neuromodulator in the brain is becoming increasingly apparent (Ledo et al., 2022).

Here we suggest a testable hypothesis, i.e., that the intestinal submucosal and myenteric neurons might be sensitive to NH_3 and H_2O_2 as the central neurons are. Having these gases well-studied metabolic effects on the central neurons, it is theoretically possible that they could have metabolic effects also on the intestinal neurons, considering that cell-produced volatile substances often regulate neighbouring cells in a paracrine fashion (Herrera and Garvin, 2011). This notion is supported by the ability of H_2O_2 to diffuse in the extracellular space of the living rodent brain over 100 μm within its 2.2 seconds average half-life (Ledo et al., 2022). The in vivo H_2O_2 brain diffusion coefficient of about 2.5×10^{-5} cm^2/s makes it theoretically possible for intraluminal-generated H_2O_2 to reach the intestinal nervous system. Since H_2O_2 can be transported through Aquaporin 3 in colonic epithelial cells (Yde et al., 2021), it might be able to reach at least the neurons of the submucosal plexus.

In sum, we suggest that still unknown effects of intestinal gases on the myenteric and submucosal neurons are (possibly) waiting to be discovered.

The last, but not the least, our physical account indicates that gaseous mixing and absorption are far from optimum even in the healthy gut. Two mechanisms contribute to weaken the gaseous exchanges between the lumen and the bloodstream:

a) The absence of turbulence in the intestinal content's flows. Turbulence is a dissipative phenomenon characterized by mathematically untreatable fluctuating instabilities. The breakdown of the continuum flow assumption that is characteristic of the Navier-Stokes equations (Barber and Emerson, 2002) leads to unsteady flow conditions and to the onset of the hallmark of turbulence, i.e., the occurrence of vortices, eddies and swings at different length scales (Sturm et al., 2012). Overflowed surfaces are subject to counter-rotating foci, separation and saddle points, extinction and even inversion of the velocity (Ma et al., 2020). While the intrinsic unpredictability of turbulence contributes to enhance fluid mixing and improve diffusive exchanges, the laminar flows displayed by intestinal fluids must generate just a small amount of intraluminal mixing and metabolic exchanges.
b) The random walks' failure to cover the entire phase space. In the (relatively) quiet colonic pockets' environment, the gaseous particles can stochastically reach just one third of the entire mucosal surface, leaving apart large "patches" of colonocytes where metabolic trans-barrier exchanges cannot be fully realized.

Therefore, next-to-come experimental studies concerning intestinal absorption might take into account that a large, quantifiable fraction of the intestinal surface is not available for fluid exchanges between the lumen and the bloodstream.

In conclusion, intestinal gases have always had a bad reputation from the standpoints of aesthetics, etiquette, and ethics. Things have come to such pass that a proposal in Malawi has been brought up in 2011 to criminalize public flatulence (Pfeifer, 2020). Nevertheless, in stark contrast to this negative reputation, intestinal gases have a wide range of physiological as well as pathological

Preprints (www.preprints.org) | NOT PEER-REVIEWED | Posted: 19 October 2022 doi:10.20944/preprints202210.0263.v1

effects not just on various intestinal segments, but also on extra-intestinal organs. Viewed as toxic gases and/or environmental toxins until a few years ago, many gaseous molecules have been recently "promoted" to the role of biologic mediators (Pacher 2021). The capability to metabolically interact with the intestinal wall and to cross the barrier between the lumen and the bloodstream makes intestinal gases a versatile tool to achieve intracellular, extracellular, paracellular, paracrine as well as distant actions, both in a state of well-being and in response to manifold noxae.

REFERENCES

1) Akaishi T, Onishi E, Abe M, Toyama H, Ishizawa K. et al. 2019. The human central nervous system discharges carbon dioxide and lactic acid into the cerebrospinal fluid. Fluids Barriers CNS. 2019 Mar 29;16(1):8. doi: 10.1186/s12987-019-0128-7.
2) Albright, J.W. 2019. Signs of Air in Bowel Wall. In: Eltorai, A., Hyman, C., Healey, T. (eds) Essential Radiology Review. Springer, Cham. https://doi.org/10.1007/978-3-030-26044-6_95
3) Amedzrovi Agbesi, Richard J.; Nicolas R. Chevalier. 2022. Flow and mixing induced by single, colinear, and colliding contractile waves in the intestine. Phys. Rev. Fluids 7, 043101 – Published 15 April 2022
4) Attaluri A, Jackson M, Valestin J, Rao SS. Methanogenic flora is associated with altered colonic transit but not stool characteristics in constipation without IBS. Am J Gastroenterol 2010; 105: 1407–1411.
5) Azpiroz F. 2005. Intestinal gas dynamics: mechanisms and clinical relevance. Gut; 54(7): 893–895. doi: 10.1136/gut.2004.048868
6) Badley AD, Camilleri M, O'Connor MK. 1993. Noninvasive measurement of human ascending colon volume. Nucl Med Commun;14(6):485-9.
7) Banerjee, Sharmistha; Sumit Ghosh, Krishnendu Sinha, Sayantani Chowdhury, Parames C Sil. Sulphur dioxide ameliorates colitis related pathophysiology and inflammation. Toxicology. 2019 Jan 15;412:63-78. doi: 10.1016/j.tox.2018.11.010.
8) Barber RW, Emerson DR. 2002. The Influence Of Knudsen Number On The Hydrodynamic Development Length Within Parallel Plate Micro-channels. WIT Transactions on Engineering Sciences. Volume 36, DOI10.2495/AFM020191
9) Bársony A, Vida N, Gajda A, Rutai A, Mohácsi A, et al. 2020. Methane Exhalation Can Monitor the Microcirculatory Changes of the Intestinal Mucosa in a Large Animal Model of Hemorrhage and Fluid Resuscitation. Front. Med., Sec. Intensive Care Medicine and Anesthesiology; https://doi.org/10.3389/fmed.2020.567260
10) Beaulieu-Laroche L, Brown NJ, Hansen M, Toloza EHS, Sharma J,, et al. 2021. Allometric rules for mammalian cortical layer 5 neuron biophysics. Nature 600, 274–278 (2021). https://doi.org/10.1038/s41586-021-04072-3
11) Bergen WG, Wu G. 2009. Intestinal Nitrogen Recycling and Utilization in Health and Disease . The Journal of Nutrition, Volume 139, Issue 5, May 2009, Pages 821–825, https://doi.org/10.3945/jn.109.104497
12) Bharucha AE, Hubmayr RD, Ferber IJ, Zinsmeister AR. 2001. Viscoelastic properties of the human colon. 2001. Am J Physiology, Volume 281Issue 2, Pages G459-G466. https://doi.org/10.1152/ajpgi.2001.281.2.G459
13) Bergen WG, Wu G. 2009. Intestinal nitrogen recycling and utilization in health and disease. J Nutr;139(5):821-5. doi: 10.3945/jn.109.104497.

Preprints (www.preprints.org) | NOT PEER-REVIEWED | Posted: 19 October 2022 doi:10.20944/preprints202210.0263.v1

14) Blachier F, Andriamihaja M, Larraufie P, Ahn E, Lan A, Kim E. 2021. Production of hydrogen sulfide by the intestinal microbiota and epithelial cells and consequences for the colonic and rectal mucosa. Am J Physiol Gastrointest Liver Physiol; 320(2):G125-G135. doi: 10.1152/ajpgi.00261.2020.
15) Blair HA, Baker R, Albazaz R. 2015. Pneumatosis intestinalis an increasingly common radiological finding, benign or life-threatening? A case series. BMJ Case Rep
16) Blomberg SP, Rathnayake SI, Moreau CM. 2020. Beyond Brownian Motion and the Ornstein-Uhlenbeck Process: Stochastic Diffusion Models for the Evolution of Quantitative Characters. Am Nat. 195(2):145-165. doi: 10.1086/706339.
17) Bond Jr. J.H., Engel, R.R., Levitt, M.D. (1971) Factors influencing pulmonary methane excretion in man. An indirect method of studying the in situ metabolism of the methane-producing colonic bacteria. The Journal of Experimental Medicine. 133, 572–588.
18) Boros, M., Ghyczy, M., Érces, D. et al. (2012) The anti-inflammatory effects of methane. Crit Care Med. 40, 1269–1278.
19) Boros M, Tuboly E, Mészáros A, Amann A. 2015. The role of methane in mammalian physiology-is it a gasotransmitter? J Breath Res;9(1):014001. doi: 10.1088/1752-7155/9/1/014001.
20) Burgueño JF; Fritsch J, Santander AM, Brito N, Fernández I, et al. 2019. Intestinal Epithelial Cells Respond to Chronic Inflammation and Dysbiosis by Synthesizing H2O2. Front Physiol;10:1484. doi: 10.3389/fphys.2019.01484.
21) Cai W-J, Wang MJ, Ju Li-H, Wang C, Zhu Y-C. 2014. Hydrogen sulfide induces human colon cancer cell proliferation: Role of Akt, ERK and p21. Cell Biology International; Volume34, Issue6, Pages 565-572. https://doi.org/10.1042/CBI20090368
22) Camilleri M. Leaky gut: mechanisms, measurement and clinical implications in humans. Gut. 2019 Aug;68(8):1516-1526. doi: 10.1136/gutjnl-2019-318427. Epub 2019 May 10.
23) Carbonero F, Benefiel A, Gaskins H. 2012. Contributions of the microbial hydrogen economy to colonic homeostasis. Nat Rev Gastroenterol Hepatol 9, 504–518. https://doi.org/10.1038/nrgastro.2012.85
24) Carlström M, Moretti CH, Weitzberg E, Lundberg JO. 2020. Microbiota, diet and the generation of reactive nitrogen compounds. Free Radical Biology and Medicine, Volume 161, Pages 321-325. https://doi.org/10.1016/j.freeradbiomed.2020.10.025
25) Casacio CA, Madsen LS, Terrasson A, Waleed M, Barnscheidt K, et al. 2021. Quantum-enhanced nonlinear microscopy. Nature 594, 201–206. https://doi.org/10.1038/s41586-021-03528-w
26) Chassard C, Dapoigny M, Scott KP, et al. 2012. Functional dysbiosis within the gut microbiota of patients with constipated-irritable bowel syndrome. Aliment. Pharmacol Ther 2012; 35: 828–838.
27) Chen J-H, Yu Y, Yang Z, Yu W-Z, Chen WL, et al. 2017. Intraluminal pressure patterns in the human colon assessed by high-resolution manometry. Scientific Reports volume 7, Article number: 41436
28) Cheng, H.M., Mah, K.K., Seluakumaran, K. (2020). Motility: Peristalsis, Segmentation, Haustration and Mass Movement. In: Defining Physiology: Principles, Themes, Concepts. Volume 2. Springer, Cham. https://doi.org/10.1007/978-3-030-62285-5_10
29) Cipollone, R; P. Visca, Is there evidence that cyanide can act as a neuromodulator? IUBMB Life 59, 187–189 (2007).
30) Codling EA, Plank MJ, Benhamou S. 2008. Random walk models in biology. J R Soc Interface. 2008 Aug 6;5(25):813-34. doi: 10.1098/rsif.2008.0014.
31) Codutti A, Cremer J, Alim K. 2022. Changing Flows Balance Nutrient Absorption and Bacterial Growth along the Gut. Phys. Rev. Lett. 129, 138101
32) Davila A-M, Blachier F, Gotteland M, Andriamihaja M, Benetti P-H, et al. 2013. Intestinal luminal nitrogen metabolism: role of the gut microbiota and consequences for the host. Pharmacol Res;68(1):95-107. doi: 10.1016/j.phrs.2012.11.005

Preprints (www.preprints.org) | NOT PEER-REVIEWED | Posted: 19 October 2022 doi:10.20944/preprints202210.0263.v1

33) Del-Bel E, De-Miguel FF. 2018. Extrasynaptic Neurotransmission Mediated by Exocytosis and Diffusive Release of Transmitter Substances. Front Synaptic Neurosci. 2018; 10: 13. doi: 10.3389/fnsyn.2018.00013

34) Dokladny, Karol; Pope L Moseley, Thomas Y Ma. Physiologically relevant increase in temperature causes an increase in intestinal epithelial tight junction permeability. Am J Physiol Gastrointest Liver Physiol. 2006 Feb;290(2):G204-12. doi: 10.1152/ajpgi.00401.2005.

35) Domb C. 1954. On Multiple Returns in the Random-Walk Problem. Proc. Cambridge Philos. Soc. 50, 586-591.

36) Dordević, Dani; Simona Jančíková MonikaVítězová, Ivan Kushkevych. Hydrogen sulfide toxicity in the gut environment: Meta-analysis of sulfate-reducing and lactic acid bacteria in inflammatory processes. Journal of Advanced Research. Volume 27, January 2021, Pages 55-69. https://doi.org/10.1016/j.jare.2020.03.003

37) Elowitz MB, Levine AJ, Siggia ED, Swain PS. 2002. Stochastic Gene Expression in a Single Cell. Science, Vol. 297, Issue 5584, pp. 1183-1186. DOI: 10.1126/science.1070919.

38) Endeward V, Gros G. 2005. Low carbon dioxide permeability of the apical epithelial membrane of guinea-pig colon. J Physiol;567(Pt 1):253-65. doi: 10.1113/jphysiol.2005.085761.

39) Fang Y-H, Chen C-X, Zhang B-L. 2009. Effect of small bowel preparation with simethicone on capsule endoscopy. J Zhejiang Univ Sci B; 10(1): 46–51. doi: 10.1631/jzus.B0820148

40) Finch SR. 2003. Pólya's Random Walk Constant. §5.9 in Mathematical Constants. Cambridge, England: Cambridge University Press, pp. 322-331.

41) Finn EH, Misteli T. 2019. Molecular basis and biological function of variability in spatial genome organization. Science. Vol. 365, Issue 6457. DOI: 10.1126/science.aaw9498.

42) Florin TH, Hills BA. 1995. Does counterperfusion supersaturation cause gas cysts in pneumatosis cystoides coli, and can breathing heliox reduce them? Lancet, Volume 345, Issue 8959, Pages 1220-1222. https://doi.org/10.1016/S0140-6736(95)91996-1

43) Forster RE. 1968. Physiological basis of gas exchange in the gut. Annals New York Acad Sci. Volume150, Issue 1. Gastrointestinal Gas, pages 4-12. https://doi.org/10.1111/j.1749-6632.1968.tb19024.x

44) Furne, J K; M D Levitt. Factors influencing frequency of flatus emission by healthy subjects. Dig Dis Sci. 1996 Aug;41(8):1631-5. doi: 10.1007/BF02087912.

45) Gandhi A, Ayesha Shah, Michael P. Jones, Natasha Koloski, Nicholas J. Talley, et al. Methane positive small intestinal bacterial overgrowth in inflammatory bowel disease and irritable bowel syndrome: A systematic review and meta-analysis. Gut Microbes. 2021; 13(1): 1933313. Published online 2021 Jun 30. doi: 10.1080/19490976.2021.1933313

46) Ghoshal, Uday C, Deepakshi Srivastava, Asha Misra. A randomized double-blind placebo-controlled trial showing rifaximin to improve constipation by reducing methane production and accelerating colon transit: A pilot study. Indian J Gastroenterol. 2018 Sep;37(5):416-423. doi: 10.1007/s12664-018-0901-6.

47) Ghyczy M, Torday C, Kaszaki J, Szabó A, Czóbel M, Boros M. 2008. Hypoxia-induced generation of methane in mitochondria and eukaryotic cells: an alternative approach to methanogenesis. Cell Physiol Biochem;21(1-3):251-8. doi: 10.1159/000113766.

48) Glazier DS. 2010. A unifying explanation for diverse metabolic scaling in animals and plants. Biological Reviews. 85 (1): 111–138. doi:10.1111/j.1469-

49) Goelen J, Alexander B, Wijesinghe HE, Evans E, Pawar G, et al. 2021. Quantification of Fluid Volume and Distribution in the Paediatric Colon via Magnetic Resonance Imaging. Pharmaceutics;13(10):1729. doi: 10.3390/pharmaceutics13101729.

50) Gong M, Wang S, Zha C, Chen M-C, Huang H-L, et al. 2021. Quantum walks on a programmable two-dimensional 62-qubit superconducting processor. Science, Vol. 372, Issue 6545, pp. 948-952. DOI: 10.1126/science.abg7812.

Preprints (www.preprints.org) | NOT PEER-REVIEWED | Posted: 19 October 2022 doi:10.20944/preprints202210.0263.v1

51) Guo F-F, Yu T-C, Hong J, Fang J-Y. 2016. Emerging Roles of Hydrogen Sulfide in Inflammatory and Neoplastic Colonic Diseases. Front. Physiol., Sec. Gastrointestinal Sciences. https://doi.org/10.3389/fphys.2016.00156
52) Hales T, Adams M, Bauer G, Dang TS, Harrison J, et al. 2017. A Formal Proof of the Kepler Conjecture. Forum of Mathematics, Pi. 5: e2. doi:10.1017/fmp.2017.1.
53) Hammer HF. 1993. Colonic hydrogen absorption: quantification of its effect on hydrogen accumulation caused by bacterial fermentation of carbohydrates. Gut. 1993 Jun; 34(6): 818–822. doi: 10.1136/gut.34.6.818
54) Harder H, Serra J, Azpiroz F, Passos MC, Aguadé S, Malagelada J-R. 2003. Intestinal gas distribution determines abdominal symptoms. Gut;52(12):1708-13. doi: 10.1136/gut.52.12.1708.
55) Harris LK, Theriot JA. 2018. Surface Area to Volume Ratio: A Natural Variable for Bacterial Morphogenesis. Trends Microbiol. 2018 Oct; 26(10): 815–832.
56) Hasler, William L. 2006. Gas and Bloating. Gastroenterol Hepatol (N Y). 2006 Sep; 2(9): 654–662. PMID: 28316536
57) He, R., Wang, L.P., Zhu, J.L. et al. (2016) Methane-rich saline protects against concanavalin A-induced autoimmune hepatitis in mice through anti-inflammatory and anti-oxidative pathways. Biochem Biophys Res Commun. 470, 22–28.
58) Helander HF, Fändriks L. 2014. Surface area of the digestive tract – revisited. Scand J Gastroenterol;49(6):681-9. doi: 10.3109/00365521.2014.898326.
59) Heresbach D, Flouríe B, Briet F, Achour L, Rambaud JC, Messing B. 1995. Effect of colonic fermentation on respiratory gas exchanges measured in the postabsorptive state. Am J Clin Nutr;62(5):973-8. doi: 10.1093/ajcn/62.5.973.
60) Herrera M, Garvin JL. 2011. Aquaporins as gas channels. Pflugers Arch;462(4):623-30. doi: 10.1007/s00424-011-1002-x.
61) Ho, Lisa M, Erik K Paulson, William M Thompson. Pneumatosis intestinalis in the adult: benign to life-threatening causes. AJR Am J Roentgenol. 2007 Jun;188(6):1604-13. doi: 10.2214/AJR.06.1309.
62) Huang YQ, Jin HF, Zhang H, Thang CS, Du JB. Interaction among Hydrogen sulfide and other gasotransmitters in mammalian Physiology and Pathophysiology. Adv Exp Med Biol 2021; 1315: 978-981
63) Huizinga J, Chen JH, Fang Zhu Y. et al. 2014. The origin of segmentation motor activity in the intestine. Nat Commun 5, 3326. https://doi.org/10.1038/ncomms4326
64) Huizinga JD, Hussain A, Chen J-H. 2021. Interstitial cells of Cajal and human colon motility in health and disease. Am J Physiol Gastrointest Liver Physiol321(5):G552-G575. doi: 10.1152/ajpgi.00264.2021
65) Hulten L, Jodal M, Lindhagen J, Lundgren O. 1976. Colonic blood flow in cat and man as analyzed by an inert gas washout technique. Gastroenterology. 70(1):36-44.
66) Hylemon PB; Harris SC, Ridlon JM. 2018. Metabolism of hydrogen gases and bile acids in the gut microbiome. FEBS Lett;592(12):2070-2082. doi: 10.1002/1873-3468.13064.
67) Igai K, Itakura M, Nishijima S, Tsurumaru H, Suda W, et al. 2016. Nitrogen fixation and nifH diversity in human gut microbiota. Scientific Reports volume 6, Article number: 31942
68) Ishaq Suzanne L., Peter L. 2016. Moses and André-Denis G. Wright. The Pathology of Methanogenic Archaea in Human Gastrointestinal Tract Disease. The Gut Microbiome. Implications for Human Disease, Edited by Gyula Mozsik . DOI: 10.5772/64637
69) Ishizaki K. 2015. Development of schizogenous intercellular spaces in plants. Front. Plant Sci, Sec. Plant Physiology. https://doi.org/10.3389/fpls.2015.00497
70) Hammer, Heinz F.; Mark R. Fox, Jutta Keller, Silvia Salvatore, Guido Basilisco, et al. European guideline on indications, performance, and clinical impact of hydrogen and methane breath tests in adult and pediatric patients: European Association for Gastroenterology, Endoscopy and Nutrition, European Society of Neurogastroenterology and Motility, and

Preprints (www.preprints.org) | NOT PEER-REVIEWED | Posted: 19 October 2022 doi:10.20944/preprints202210.0263.v1

European Society for Paediatric Gastroenterology Hepatology and Nutrition consensus. United European Gastroenterol J. 2022 Feb; 10(1): 15–40. Published online 2021 Aug 25. doi: 10.1002/ueg2.12133

71) Irwin, Sally V.; Peter Fisher, Emily Graham, Ashley Malek, Adriel Robidoux. Sulfites inhibit the growth of four species of beneficial gut bacteria at concentrations regarded as safe for food. PLoS One. 2017; 12(10): e0186629. Published online 2017 Oct 18. doi: 10.1371/journal.pone.0186629

72) Jahng J, Jung IS, Choi EJ, Conklin JL, Park H. 2012. The effects of methane and hydrogen gases produced by enteric bacteria on ileal motility and colonic transit time. Neurogastroenterol Motil ;24(2):185-90, e92. doi: 10.1111/j.1365-2982.2011.01819.x.

73) Jimenez, M; V Gil, M Martinez-Cutillas, N Mañé, and D Gallego. Hydrogen sulphide as a signalling molecule regulating physiopathological processes in gastrointestinal motility Br J Pharmacol. 2017 Sep; 174(17): 2805–2817. Published online 2017 Jul 27. doi: 10.1111/bph.13918

74) Johnson K. A., D. E. Johnson. Methane emissions from cattle. Journal of Animal Science, Volume 73, Issue 8, August 1995, Pages 2483–2492, https://doi.org/10.2527/1995.7382483x

75) Kalmár-Nagy, T., Bak, B.D. 2019. An intriguing analogy of Kolmogorov's scaling law in a hierarchical mass–spring–damper model. Nonlinear Dyn 95, 3193–3203 (2019). https://doi.org/10.1007/s11071-018-04749-x.

76) Keller, J; Heinz F. Hammer, Paul R. Afolabi, Marc Benninga, Osvaldo Borrelli. European guideline on indications, performance and clinical impact of 13C-breath tests in adult and pediatric patients: An EAGEN, ESNM, and ESPGHAN consensus, supported by EPC. United European Gastroenterol J. 2021 Jun; 9(5): 598–625. doi: 10.1002/ueg2.12099

77) Khan MZ, Lyu R, McMichael J, Gabbard S. 2022. Chronic Intestinal Pseudo-Obstruction Is Associated with Intestinal Methanogen Overgrowth. Dig Dis Sci;67(10):4834-4840. doi: 10.1007/s10620-021-07343-1.

78) Klosin A, Oltsch F, Harmon T, Honigmann A, Jülicher F. 2020. Phase separation provides a mechanism to reduce noise in cells. Science. Vol. 367, Issue 6476, pp. 464-468. DOI: 10.1126/science.aav6691.

79) Kushkevych, Ivan; Oľga Leščanová, Dani Dordević, Simona Jančíková, Jan Hošek,et al. The Sulfate-Reducing Microbial Communities and Meta-Analysis of Their Occurrence during Diseases of Small–Large Intestine Axis. J Clin Med. 2019 Oct; 8(10): 1656. Published online 2019 Oct 11. doi: 10.3390/jcm8101656

80) Larimer JL, Ashby EA. Float gases, gas secretion and tissue respiration in the Portuguese man-of-war, Physalia. J. Cell. Comp. Physiol. 1962;60:41–47. doi: 10.1002/jcp.1030600106.

81) Ledo A, Fernandes E, Salvador A, Laranjinha J, Barbosa RM. 2022. In vivo hydrogen peroxide diffusivity in brain tissue supports volume signaling activity. Redox Biology; Volume 50, April 2022, 102250

82) Lee, Jiyeon ; Hoonjeong Kwon. Conversion of Apricot Cyanogenic Glycosides to Thiocyanate by Liver and Colon Enzymes. Toxicol Res. 2009 Mar;25(1):23-28. doi: 10.5487/TR.2009.25.1.023.

83) Lee, K.N., Lee, O.Y., Koh, D.H., Sohn, W., Lee, S.P., Jun, D.W.,Lee, H.L., Yoon, B.C., Choi, H.S., Hahm, J.S. (2013) Association between Symptoms of Irritable Bowel Syndrome and Methane and Hydrogen on Lactulose Breath Test. Journal of Korean medical science. 28, 901-907.

84) Lee Y-S, Kim T-Y, Kim Y, Lee S-H, Kim S, et al. 2018. Microbiota-Derived Lactate Accelerates Intestinal Stem-Cell-Mediated Epithelial Development. Cell Host Microbe;24(6):833-846.e6. doi: 10.1016/j.chom.2018.11.002.

85) Levitt MD. 1971. Volume and Composition of Human Intestinal Gas Determined by Means of an Intestinal Washout Technic. N Engl J Med 1971; 284:1394-1398. DOI: 10.1056/NEJM197106242842502

86) Levitt MD, Olsson S. 1995. Pneumatosis cystoides intestinalis and high breath H2 excretion: insights into the role of H2 in this condition. Gastroenterology;108(5):1560-5. doi: 10.1016/0016-5085(95)90707-6.

87) Li, Z.Y., Jia, Y.F., Feng, Y. et al. (2019) Methane alleviates sepsis-induced injury by inhibiting pyroptosis and apoptosis: in vivo and in vitro experiments. Aging. 11, 1226–1239.

Preprints (www.preprints.org) | NOT PEER-REVIEWED | Posted: 19 October 2022 doi:10.20944/preprints202210.0263.v1

88) Liao S, Li G, Lv L, Mei Z. 2021. The regulatory roles of aquaporins in the digestive system. Genes & Diseases; Volume 8, Issue 3, Pages 250-258. https://doi.org/10.1016/j.gendis.2019.12.011

89) Linden DR. 2014. Hydrogen Sulfide Signaling in the Gastrointestinal Tract. Antioxid Redox Signal. 2014 Feb 10; 20(5): 818–830. doi: 10.1089/ars.2013.5312

90) Louis P, Duncan SH, Sheridan PO, Walker AW, Flint H. 2022. Microbial lactate utilisation and the stability of the gut microbiome. Gut Microbiome, 3, E3. doi:10.1017/gmb.2022.3.

91) Lundberg JO, Weitzberg E. 2013. Biology of nitrogen oxides in the gastrointestinal tract. Gut;62(4):616-29. doi: 10.1136/gutjnl-2011-301649.

92) Ma A, Gibeau B, Ghaemi S. 2020. Time-resolved topology of turbulent boundary layer separation over the trailing edge of an airfoil. Journal of Fluid Mechanics, Volume 891, A1. DOI: https://doi.org/10.1017/jfm.2020.106.

93) Mahan VL. 2021. Effects of lactate and carbon monoxide interactions on neuroprotection and neuropreservation. Med Gas Res;11(4):158-173. doi: 10.4103/2045-9912.318862.

94) Manichanh, Chaysavanh ; Anat Eck, Encarna Varela, Joaquim Roca, José C Clemente, et al. Anal gas evacuation and colonic microbiota in patients with flatulence: effect of diet. Gut. 2014 Mar;63(3):401-8. doi: 10.1136/gutjnl-2012-303013. Epub 2013 Jun 13.

95) Mansilla, Wilfredo D; Daniel A Columbus, John K Htoo, Cornelis FM de Lange. Nitrogen Absorbed from the Large Intestine Increases Whole-Body Nitrogen Retention in Pigs Fed a Diet Deficient in Dispensable Amino Acid Nitrogen. The Journal of Nutrition, Volume 145, Issue 6, June 2015, Pages 1163–1169, https://doi.org/10.3945/jn.115.212316

96) McIver MA, Redfield AC, Benedict EB. 1926. Gaseous exchange between the blood and the lumen of the stomach and intestines. https://doi.org/10.1152/ajplegacy.1926.76.1.92

97) McCrea WH, Whipple FJW. 1940. Random Paths in Two and Three Dimensions. Proc. Roy. Soc. Edinburgh 60, 281-298.

98) Meli R, Pirozzi C, Pelagalli A. 2018. New Perspectives on the Potential Role of Aquaporins (AQPs) in the Physiology of Inflammation. Front. Physiol., Sec. Integrative Physiology. https://doi.org/10.3389/fphys.2018.00101

99) Mészáros AT, Szilágyi AL,Juhász L, Tuboly E, Érces D, et al. 2017. Mitochondria As Sources and Targets of Methane. Front. Med.,Sec. Intensive Care Medicine and Anesthesiology. https://doi.org/10.3389/fmed.2017.00195

100) Metzler R, Jeon J-H, Cherstvya AG, Barkaid E. 2014. Anomalous diffusion models and their properties: non-stationarity, non-ergodicity, and ageing at the centenary of single particle tracking. Phys Chem Chem Phys,16, 24128-24164. https://doi.org/10.1039/C4CP03465A

101) Michenkova M, Taki S, Blosser MC, Hwang HJ, Kowatz T. 2021. Carbon dioxide transport across membranes. Interface Focus;11(2):20200090. doi: 10.1098/rsfs.2020.0090. DOI: 10.1098/rsfs.2020.0090.

102) Miller EW, Dickinson BC, Chang CJ. 2010. Aquaporin-3 mediates hydrogen peroxide uptake to regulate downstream intracellular signaling. PNAS, 107 (36) 15681-15686. https://doi.org/10.1073/pnas.1005776107

103) Miller TL, Wolin MJ, de Macario EC, Macario AJ. 1982. Isolation of Methanobrevibacter smithii from human feces. Appl Environ Microbiol. 1982 Jan; 43(1): 227–232. doi: 10.1128/aem.43.1.227-232.1982

104) Miller BM, Liou MJ, Zhang LF, Nguyen H, Litvak Y, et al. 2020. Anaerobic respiration of NOX1-derived hydrogen peroxide licenses bacterial growth at the colonic surface. Cell Host Microbe; 28(6): 789–797.e5. doi: 10.1016/j.chom.2020.10.009

105) Modesto, A., Cameron, NR., Varghese, C, Peters N, Stokes B, et al. et al. 2022. Meta-Analysis of the Composition of Human Intestinal Gases. Dig Dis Sci 67, 3842–3859. https://doi.org/10.1007/s10620-021-07254-1

106) Montalto M, Di Stefano M, Gasbarrini A, Corazza GR. 2009. Intestinal gas metabolism. Digestive and Liver Disease Supplements; Volume 3, Issue 2, Pages 27-29. https://doi.org/10.1016/S1594-5804(09)60015-2

Preprints (www.preprints.org) | NOT PEER-REVIEWED | Posted: 19 October 2022 doi:10.20944/preprints202210.0263.v1

107) Montroll EW. 1956. Random Walks in Multidimensional Spaces, Especially on Periodic Lattices. J. SIAM 4, 241-260.

108) Mountford PA, Leiphrakpam PD, Weber HR, McCain A, Scribner RM, et al. 2021. Colonic Oxygen Microbubbles Augment Systemic Oxygenation and CO2 Removal in a Porcine Smoke Inhalation Model of Severe Hypoxia. Biorxiv; doi: https://doi.org/10.1101/2021.12.08.466665.

109) Munro C, Vue Z, Behringer RB, Dunn CW. 2019. Morphology and development of the Portuguese man of war, Physalia physalis. Sci Rep;9(1):15522. doi: 10.1038/s41598-019-51842-1

110) Naito Y, Uchiyama K, Takagi T. 2018. Redox-related gaseous mediators in the gastrointestinal tract. J Clin Biochem Nutr;63(1):1-4. doi: 10.3164/jcbn.18-56.

111) Nalli AD, Bhattacharya S, Wang H, Kendig DM, Grider JR, Murthy KS. 2017. Augmentation of cGMP/PKG pathway and colonic motility by hydrogen sulfide. Am J Physiol Gastrointest Liver Physiol;313(4):G330-G341. doi: 10.1152/ajpgi.00161.2017.

112) Nguyen TD, Kadri OE; Sikavitsas VI, Voronov RS. 2019. Scaffolds with a High Surface Area-to-Volume Ratio and Cultured Under Fast Flow Perfusion Result in Optimal O2 Delivery to the Cells in Artificial Bone Tissues. Applied Sciences. 9 (11): 2381. doi:10.3390/app9112381.

113) Nilsson M, Sandberg TH, Poulsen JL, Gram M, Frøkjaer JB, et al. 2015. Quantification and variability in colonic volume with a novel magnetic resonance imaging method.. Neurogastroenterol Motil;27(12):1755-63. doi: 10.1111/nmo.12673.

114) Obermüller B, Frisina N, Meischel M, Singer G, Stanzl-Tschegg S, et al. 2020. Examination of intestinal ultrastructure, bowel wall apoptosis and tight junctions in the early phase of sepsis. Sci Rep;10(1):11507. doi: 10.1038/s41598-020-68109-9.

115) Oikawa S, Hirakawa H, Kusakabe T, Hayashida Y. 2003. Effect of CO2 on Cardiovascular Regulation in Conscious Rats. In: Pequignotì JM, Gonzalez C, Nurse CA, Prabhakar NR, Dalmaz Y. (eds) Chemoreception. Advances in Experimental Medicine and Biology, vol 536. Springer, Boston, MA. https://doi.org/10.1007/978-1-4419-9280-2_60

116) Okabe R, Chen-Yoshikawa TF, Yoneyama Y, Kobayashi E, Date H, Takebe T. 2021. Mammalian enteral ventilation ameliorates respiratory failure. Clinical And Translational Resource And Technology Insights| Volume 2, Issue 6, P773-783.E5. DOI:https://doi.org/10.1016/j.medj.2021.04.004

117) Okoh, P N; G A Pitt. The metabolism of cyanide and the gastrointestinal circulation of the resulting thiocyanate under conditions of chronic cyanide intake in the rat. Can J Physiol Pharmacol . 1982 Mar;60(3):381-6. doi: 10.1139/y82-055.

118) Olm, Matthew R; , Dylan Dahan, Matthew M Carter, Bryan D Merrill, Feiqiao B Yu, et al. Robust variation in infant gut microbiome assembly across a spectrum of lifestyles. Science. 2022 Jun 10;376(6598):1220-1223. doi: 10.1126/science.abj2972. Epub 2022 Jun 9.

119) Oren A. 2012. The Function of Gas Vesicles in Halophilic Archaea and Bacteria: Theories and Experimental Evidence. Life 2013, 3(1), 1-20; https://doi.org/10.3390/life3010001.

120) Pacher P. 2021. Cyanide emerges as an endogenous mammalian gasotransmitter. Proceedings of the National Academy of Sciences of the United States of America. 118 (25): e2108040118. doi:10.1073/pnas.2108040118.

121) Paul W, Baschnagel J. 2013. Stochastic Processes: From Physics to Finance. Springer Science & Business Media. ISBN 978-3-319-00327-6.

122) Park YM, Lee YJ, Hussain Z, Lee YH, Park H. 2017. The effects and mechanism of action of methane on ileal motor function. Neurogastroenterol Motil;29(9). doi: 10.1111/nmo.13077.

123) Pichette J, Fynn-Sackey N, Gagnon J. 2017. Hydrogen Sulfide and Sulfate Prebiotic Stimulates the Secretion of GLP-1 and Improves Glycemia in Male Mice. Endocrinology;158(10):3416-3425. doi: 10.1210/en.2017-00391.

Preprints (www.preprints.org) | NOT PEER-REVIEWED | Posted: 19 October 2022 doi:10.20944/preprints202210.0263.v1

124) Pfeifer, F. 2012. Distribution, formation and regulation of gas vesicles. Nat Rev Microbiol 10, 705–715. https://doi.org/10.1038/nrmicro2834.

125) Pfeifer F. 2014. Haloarchaea and the Formation of Gas Vesicles. Life 2015, 5(1), 385-402; https://doi.org/10.3390/life5010385.

126) Pfeifer, K. (2020). The Normative Significance of Flatulence: Aesthetics, Etiquette, and Ethics. IAFOR Journal of Arts & Humanities, 7(1). https://doi.org/10.22492/ijah.7.1.02

127) Pimentel M, Lin HC, Enayati P, van den Burg B, Lee H-R, et al. 2006. Methane, a gas produced by enteric bacteria, slows intestinal transit and augments small intestinal contractile activity. Gastrointstinal and Liver Physiology, Volume 290,Issue 6, Pages G1089-G1095. https://doi.org/10.1152/ajpgi.00574.2004

128) Pontes-Filho S, Lind P, Yazidi A, Zhang J, Hammer H, et al. 2020. A neuro-inspired general framework for the evolution of stochastic dynamical systems: Cellular automata, random Boolean networks and echo state networks towards criticality. Cognitive Neurodynamics volume 14, pages 657–674.

129) Pozuelo, M; Suchita Panda, Alba Santiago, Sara Mendez, Anna Accarino, et al. Reduction of butyrate- and methane-producing microorganisms in patients with Irritable Bowel Syndrome. Sci Rep. 2015 Aug 4;5:12693. doi: 10.1038/srep12693.

130) Pritchard SE, Marciani L, Garsed KC, Hoad CL, Thongborisute W, et al. 2014. Fasting and postprandial volumes of the undisturbed colon: normal values and changes in diarrhea-predominant irritable bowel syndrome measured using serial MRI. Neurogastroenterol Motil; 26(1): 124–130. doi: 10.1111/nmo.12243

131) Qin, Guohua; Meiqiong Wu, Jiaoxia Wang, Zhifang Xu, Jin Xia, Nan Sang. Sulfur Dioxide Contributes to the Cardiac and Mitochondrial Dysfunction in Rats. Toxicological Sciences, Volume 151, Issue 2, June 2016, Pages 334–346, https://doi.org/10.1093/toxsci/kfw048

132) Quan, Xiaojing; Wei Chen, Bin Qin, Jinhai Wang, Hesheng Luo, Fei Dai. The excitatory effect of hydrogen sulfide on rat colonic muscle contraction and the underlying mechanism. J Pharmacol Sci. 2022 Jul;149(3):100-107. doi: 10.1016/j.jphs.2022.04.004. Epub 2022 Apr 21.

133) Randi, Elisa B ; Karim Zuhra, Laszlo Pecze, Theodora Panagaki, Csaba Szabo. Physiological concentrations of cyanide stimulate mitochondrial Complex IV and enhance cellular bioenergetics. Proc Natl Acad Sci U S A. 2021 May 18;118(20):e2026245118. doi: 10.1073/pnas.2026245118.

134) Randsoe T, Hyldegaard O. 1985. Effect of oxygen breathing on micro oxygen bubbles in nitrogen-depleted rat adipose tissue at sea level and 25 kPa altitude exposures. J Appl Physiol (1985). 2012 Aug;113(3):426-33. doi: 10.1152/japplphysiol.00193.2012.

135) Reese AT, Pereira FC, Schintlmeister A, Berry D, Wagner M, et al. 2018. Microbial nitrogen limitation in the mammalian large intestine. Nat Microbial; 3(12): 1441–1450. doi: 10.1038/s41564-018-0267-7

136) Rezaie, Ali; Michelle Buresi, Anthony Lembo, Henry Lin, Richard McCallum, et al. Hydrogen and Methane-Based Breath Testing in Gastrointestinal Disorders: The North American Consensus. Am J Gastroenterol. 2017 May; 112(5): 775–784. Published online 2017 Mar 21. doi: 10.1038/ajg.2017.46

137) Ritz P, Cloarec D, Beylot M, Champ M, Charbonnel B, et al. 1993. Effects of colonic fermentation on respiratory gas exchanges following a glucose load in man. Metabolism;42(3):347-52. doi: 10.1016/0026-0495(93)90085-3.

138) Rivière A, Selak M, Lantin D, Leroy F, De Vuyst L. 2016. Bifidobacteria and Butyrate-Producing Colon Bacteria: Importance and Strategies for Their Stimulation in the Human Gut. Front. Microbiol., Sec. Microbial Symbioses. https://doi.org/10.3389/fmicb.2016.00979

139) Roccarina D, Lauritano EC, Gabrielli M, Franceschi F, Ojetti V, Gasbarrini A. 2010. The role of methane in intestinal diseases. Am J Gastroenterol;105(6):1250-6. doi: 10.1038/ajg.2009.744

Preprints (www.preprints.org) | NOT PEER-REVIEWED | Posted: 19 October 2022 doi:10.20944/preprints202210.0263.v1

140) Rodriguez-Grande B, Konsman J-P. 2018. Gas Diffusion in the CNS. J Neurosci Res;96(2):207-218. doi: 10.1002/jnr.24077.

141) Rostain J-C, Lavoute C. 2016. Neurochemistry of Pressure-Induced Nitrogen and Metabolically Inert Gas Narcosis in the Central Nervous System. Compr Physiol;6(3):1579-90. doi: 10.1002/cphy.c150024.

142) Ruddock, Alan D; Garry A Tew, Alison J Purvis. Reliability of intestinal temperature using an ingestible telemetry pill system during exercise in a hot environment. J Strength Cond Res. 2014 Mar;28(3):861-9. doi: 10.1519/JSC.0b013e3182aa5dd0.

143) Sahakian AB, Jee S-R, Pimentel M. 2010. Methane and the gastrointestinal tract. Dig Dis Sci;55(8):2135-43. doi: 10.1007/s10620-009-1012-0.

144) Sanders KM, Koh SD, Ward SM. 2006. Interstitial cells of Cajal as pacemakers in the gastrointestinal tract. Annu Rev Physiol;68:307-43. doi: 10.1146/annurev.physiol.68.040504.094718.

145) V Savarino 1, S Vigneri, G Celle. The 13C urea breath test in the diagnosis of Helicobacter pylori infection. Gut. 1999 Jul;45 Suppl 1(Suppl 1):I18-22. doi: 10.1136/gut.45.2008.i18.

146) Scaldaferri F, Nardone O, Lopetuso LR, Petito V, Bibbò S, et al. 2013. Intestinal gas production and gastrointestinal symptoms: from pathogenesis to clinical implication. Eur Rev Med Pharmacol Sci;17 Suppl 2:2-10.

147) Schiller C, Fröhlich C-P, Giessmann T, Siegmund W, Mönnikes H, et al. 2005. Intestinal fluid volumes and transit of dosage forms as assessed by magnetic resonance imaging. Aliment Pharmacol Ther;22(10):971-9. doi: 10.1111/j.1365-2036.2005.02683.x.

148) Schneider, C., Wutzke, K.D. & Däbritz, J. Methane breath tests and blood sugar tests in children with suspected carbohydrate malabsorption. Sci Rep 10, 18972 (2020). https://doi.org/10.1038/s41598-020-75987-6

149) Sejian V, Lal R, Jeffrey Lakritz, Thaddeus Ezeji. Measurement and prediction of enteric methane emission. Int J Biometeorol. 2011 Jan;55(1):1-16. doi: 10.1007/s00484-010-0356-7.

150) Singh AK, Hertzberger RY, Knausa UG. 2018. Hydrogen peroxide production by lactobacilli promotes epithelial restitution during colitis. Redox Biol; 16: 11–20. doi: 10.1016/j.redox.2018.02.003

151) Singhal R, Shah YM. 2020. Oxygen battle in the gut: Hypoxia and hypoxia-inducible factors in metabolic and inflammatory responses in the intestine. J Biol Chem;295(30):10493-10505. doi: 10.1074/jbc.REV120.011188.

152) Smith, N.W., Shorten, P.R., Altermann, E. et al. 2021. Examination of hydrogen cross-feeders using a colonic microbiota model. BMC Bioinformatics 22, 3. https://doi.org/10.1186/s12859-020-03923-6

153) Sturm H, Dumstorff G, Busche P, Westermann D, Lang W. 2012. Boundary Layer Separation and Reattachment Detection on Airfoils by Thermal Flow Sensors. Sensors (Basel, Switzerland). DOI:10.3390/s121114292.

154) Sun, A.J., Wang, W.H., Ye, X.J. et al. (2017) Protective effects of methane-rich saline on rats with lipopolysaccharide-induced acute lung injury. Oxid Med Cell Longev, 7430193.

155) Staley, J.T. The gas vacuole: An early organelle of prokaryote motility? Origins Life Evol Biosphere 10, 111–116 (1980). https://doi.org/10.1007/BF00928662.

156) St Peter SD, Abbas MA, Kelly KA. 2003. The spectrum of pneumatosis intestinalis. Arch Surg;138(1):68-75. doi: 10.1001/archsurg.138.1.68.

157) Strandwitz P. 2018. Neurotransmitter modulation by the gut microbiota. Brain Res;1693(Pt B):128-133. doi: 10.1016/j.brainres.2018.03.015.

158) Sturm H, Dumstorff G, Busche P, Westermann D, Lang W. 2012. Boundary Layer Separation and Reattachment Detection on Airfoils by Thermal Flow Sensors. Sensors (Basel, Switzerland). DOI:10.3390/s121114292.

159) Sugihara Y, Okada H. Pneumatosis Cystoides Intestinalis. N Engl J Med. 2017 Dec 7. 377 (23):2266.

Preprints (www.preprints.org) | NOT PEER-REVIEWED | Posted: 19 October 2022 doi:10.20944/preprints202210.0263.v1

160) Tajik, N., Frech, M., Schulz, O. et al. Targeting zonulin and intestinal epithelial barrier function to prevent onset of arthritis. Nat Commun 11, 1995 (2020). https://doi.org/10.1038/s41467-020-15831-7

161) Talapatra S, Hong J, McFarland M, Nayak AR, Zhang C. 2013. Characterization of biophysical interactions in the water column using in situ digital holography. Journal Marine Ecology Progress Series. Volume 473, Pages 29-51.

162) Teigen, Levi M.; Zhuo Geng, Michael J. Sadowsky, Byron P. Vaughn, Matthew J. Hamilton, Alexander Khoruts. 2019. Dietary Factors in Sulfur Metabolism and Pathogenesis of Ulcerative Colitis. Nutrients. 2019 Apr; 11(4): 931.Published online 2019 Apr 25. doi: 10.3390/nu11040931

163) Tomlin, J; C Lowis, and N W Read. Investigation of normal flatus production in healthy volunteers. Gut. 1991 Jun; 32(6): 665–669. doi: 10.1136/gut.32.6.665.

164) Triantafyllou, Konstantinos, Christopher Chang, Mark Pimentel. 2014. Methanogens, methane and gastrointestinal motility. J Neurogastroenterol Motil. 2014 Jan;20(1):31-40. doi: 10.5056/jnm.2014.20.1.31.

165) Uno Y. 2018. Colonic transit time and pressure based on Bernoulli's principle. Clin Exp Gastroenterol;11:153-163. doi: 10.2147/CEG.S153676.

166) van Meegdenburg MM, Heineman E, Broens PMA. 2015. Dyssynergic defecation may aggravate constipation: results of mostly pediatric cases with congenital anorectal malformation. Am J Surgery; Volume 210, Issue 2, P357-364. DOI:https://doi.org/10.1016/j.amjsurg.2014.09.038

167) Verbeure W, van Goor H, Mori H, van Beek AP, Tack J; van Dijk PR. 2021. The Role of Gasotransmitters in Gut Peptide Actions. Front Pharmacol; 12: 720703. doi: 10.3389/fphar.2021.720703

168) Vilk O, Orchan Y, Charter M, Ganot N, Toledo S, et al. 2022. Ergodicity Breaking in Area-Restricted Search of Avian Predators. Phys. Rev. X 12, 031005.

169) Völkner K, Jost A, Pfeifer F. 2020. Accessory Gvp Proteins Form a Complex During Gas Vesicle Formation of Haloarchaea. Front. Microbiol., 12 November 2020 | https://doi.org/10.3389/fmicb.2020.610179.

170) Vujkovic-Cvijin, I., Sklar, J., Jiang, L. et al. Host variables confound gut microbiota studies of human disease. Nature 587, 448–454 (2020). https://doi.org/10.1038/s41586-020-2881-9

171) Walker HK, Hall WD, Hurst JW, editors. 1990. Clinical Methods: The History, Physical, and Laboratory Examinations. 3rd edition. Boston: Butterworths.

172) Walters P. 1982. An Introduction to Ergodic Theory, Springer, ISBN 0-387-95152-0.

173) Wang XB, Jin HF, Tang CS, Du JB. 2011. The biological effect of endogenous sulfur dioxide in the cardiovascular system. Eur J Pharmacol. 670 (1): 1–6. doi:10.1016/j.ejphar.2011.08.031. PMID 21925165.

174) Wang SP, Rubio LA, Duncan SH, Donachie GE, Holtrop G, et al. 2020. Pivotal Roles for pH, Lactate, and Lactate-Utilizing Bacteria in the Stability of a Human Colonic Microbial Ecosystem. mSystems. 2020 Sep-Oct; 5(5): e00645-20. doi: 10.1128/mSystems.00645-20

175) Wang X, Li J, Li N, Guan K, Yin D, et al. 2021. Evolution of Intestinal Gases and Fecal Short-Chain Fatty Acids Produced in vitro by Preterm Infant Gut Microbiota During the First 4 Weeks of Life. Front. Pediatr, Sec. Pediatric Gastroenterology, Hepatology and Nutrition, https://doi.org/10.3389/fped.2021.726193

176) Wareham, L. K. ; H. M. Southam, R. K. Poole, Do nitric oxide, carbon monoxide and hydrogen sulfide really qualify as ‘gasotransmitters’ in bacteria? Biochem. Soc. Trans. 46, 1107–1118 (2018).

177) Webster C. 1965. The discovery of Boyle's law, and the concept of the elasticity of air in seventeenth century. Archive for the History of Exact Sciences, 2 (6): 441–502.

178) Wilder-Smith CH, Olesen SS, Materna A, Drewes AM. 2018. Fermentable Sugar Ingestion, Gas Production, and Gastrointestinal and Central Nervous System Symptoms in Patients With Functional Disorders. Gastroenterology;155(4):1034-1044.e6. doi: 10.1053/j.gastro.2018.07.013.

Preprints (www.preprints.org) | NOT PEER-REVIEWED | Posted: 19 October 2022 doi:10.20944/preprints202210.0263.v1

179) Wooller MJ, Bataille C, Druckenmiller P, Erickson GM, Groves P., et al. 2021. Lifetime mobility of an Arctic woolly mammoth. Science, Vol. 373, Issue 6556, pp. 806-808. DOI: 10.1126/science.abg1134.

180) Wu, D., Li, M., Tian, W. et al. Hydrogen sulfide acts as a double-edged sword in human hepatocellular carcinoma cells through EGFR/ERK/MMP-2 and PTEN/AKT signaling pathways. Sci Rep 7, 5134 (2017). https://doi.org/10.1038/s41598-017-05457-z

181) Wygnanski IJ, Champagne FH. 2006. On transition in a pipe. Part 1. The origin of puffs and slugs and the flow in a turbulent slug. Journal of Fluid Mechanics. Volume 59, Issue 2. On transition in a pipe. Part 1. The origin of puffs.

182) Yde, Jonathan; Stephen J Keely, Hanne B Moeller. Expression, regulation and function of Aquaporin-3 in colonic epithelial cells. Biochim Biophys Acta Biomembr. 2021 Jul 1;1863(7):183619. doi: 10.1016/j.bbamem.2021.183619.

183) Zamboni, Cibele B.; Medeiros, Ilca M. M. A.; de Medeiros, José A. G. (October 2011). Analysis of Sulfur in Dried Fruits Using NAA (PDF). 2011 International Nuclear Atlantic Conference - INAC 2011. ISBN 978-85-99141-03-8.

184) Zaorska E, Gawryś-Kopczyńska M, Ostaszewski R, Koszelewski D. 2021. Methane, a gut bacteria-produced gas, does not affect arterial blood pressure in normotensive anaesthetized rats. Biorxiv, doi: https://doi.org/10.1101/2021.03.31.437828

185) Zhang Y, Xu K, Liu Y, Erokwu BO, Zhao P, et al. 2019. Increased cerebral vascularization and decreased water exchange across the blood-brain barrier in aquaporin-4 knockout mice. PLoS One;14(6):e0218415. doi: 10.1371/journal.pone.0218415.

186) Zhu C, Chen Z, Jiang Z. 2016. Expression, Distribution and Role of Aquaporin Water Channels in Human and Animal Stomach and Intestines. Int. J. Mol. Sci. 2016, 17(9), 1399; https://doi.org/10.3390/ijms17091399

187) Zwiazek JJ, Xu H, Tan X, Navarro-Ródenas A, Morte A. 2017. Significance of oxygen transport through aquaporins. Sci Rep;7:40411. doi: 10.1038/srep40411.

BioSystems 238 (2024) 105192

Contents lists available at ScienceDirect

BioSystems

journal homepage: www.elsevier.com/locate/biosystems

Flock members experience gas pressures higher than lone individuals

Arturo Tozzi

Center for Nonlinear Science, Department of Physics, University of North Texas, 1155 Union Circle, #311427, Denton, TX, 76203-5017, USA

ARTICLE INFO

Keywords:
Collective behavior
Topological distance
Flow
Cohesion

ABSTRACT

Local interactions between flock members in absence of centralized control generate collective dynamics characterized by coherent large-scale patterns. We investigate whether aggregates of individuals like birds, swarms and fishes behaving in concert with their neighbors may modify the physical properties of the fluid medium in which they are embedded. Using the K-Nearest Neighbors algorithm to simulate collective animal behavior, we showed that the occurrence of collective dynamics can modify the physical parameters of the phase space in which the interacting individuals' trajectories take place. This means that lone individuals experience the nearby fluid medium (i.e., the air in case of birds/insects and the water in case of fishes) differently from flock members. In particular, our framework suggests that a bird belonging to a group and acting collectively with its neighbors perceives the nearby atmosphere as denser, compared with an isolated bird.

1. Introduction

Collective animal behavior emerges from simple local rules of interaction among neighbor individuals in absence of centralized control (Ballerini et al., 2008; Cavagna et al., 2010). Self-organized global order consists of coherent and collective large-scale patterns generated in large interacting systems (Bialek et al., 2012; Mora et al., 2016). Scale-free changes in the behavioral state of one animal affect and are affected by those of all other animals, no matter how large the group is (Cavagna et al., 2010). Numerical models as well as experimental findings suggest that the mechanism of group formation is universal, transcending the detailed nature of its components (Attanasi et al., 2015). Computational models assessing collective animal behavior like bird flocks are based on a few empirical rules (Reynolds 1987):

1) Attraction among individuals grants cohesion of the aggregation, ensuring that no bird remains isolated.
2) Short-range repulsion zone of the order of the wingspan prevents dangerous proximity and avoids collisions, thereby preserving individual integrity (Ballerini et al., 2008).
3) Alignment of the velocities allows birds to fly in the same direction, keeping similar speed and direction.
4) Noise must be kept into account when drawing the proper equations (Giardina 2008).

The experimentally assessable interacting flock members' physical features include shape, movement, density and structure, as well as subtler features such as directional polarity, average group speed, marginal speed, changes in flock shape, local density-density correlations, information transfer, topological distance, bearing angle, distance to nearest neighbors, two-points correlation function, coexistence of multiple timescales, etc. (Cavagna et al., 2022; Bialek et al., 2012; Chen et al., 2023).

Here, using two-points correlation function, we asked whether lone individuals might experience physical forces differently from groups of interacting individuals. We exploited the K-Nearest Neighbors (k-NN) algorithm to evaluate whether increases in the number of interactions among neighbor individuals lead to physical changes in the surrounding environment. In particular, we investigated whether lone birds experience the air masses surrounding them differently from birds belonging to flocks.

2. K-NN algorithms and collective behaviour

To evaluate the interactions among individuals during collective behavior, we focused on the K-Nearest Neighbors algorithm, also known as KNN or k-NN (Cover and Hart, 1967; Holmes and Adams, 2003). It is a nonparametric, supervised learning algorithm that uses proximity to catalogue the grouping of individual data points in a phase space (Rajagopalan and Lall, 1999). It is usually used as a classification algorithm based on the assumption that similar points can be found near one another (Bang-Jensen et al., 2004). It does not require prior assumptions as to the form of the variables' joint probability density function (Rajagopalan and Upmanu, 1999).

E-mail address: tozziarturo@libero.it.

https://doi.org/10.1016/j.biosystems.2024.105192
Received 8 January 2024; Received in revised form 14 March 2024; Accepted 15 March 2024
Available online 16 March 2024
0303-2647/© 2024 Elsevier B.V. All rights reserved.

We coloured each point of the two-dimensional plane with the class that would be assigned to it using the k-NN algorithm, so that the 0/1 values were conventionally color-coded red and blue. In terms of collective animal behaviour, the 0/1 values had the following meaning:

1) The 1-valued blue shapes stood for the space occupied by interacting flock members.
2) The 0-valued red shapes stood for the space occupied by the fluid medium (either gaseous in case of birds or insects, or liquid in case of fishes) surrounding the interacting flock members.

To provide a few examples, the blue shapes might stand either for bird flocks, or mating swarms of mosquitoes and midges, or for a school of fish, while the red shapes might stand for the surrounding air or water provided with physical parameters like pressure, density, temperature, local turbulence, etc.

We performed a k-NN algorithm simulation on an original picture depicting red and blue shapes (**Figure**). We run the Stanford Vision and Learing Lab's interactive K-Nearest Neighbors Demo (http://vision.stanford.edu/teaching/cs231n-demos/knn/) using the following parameters:

a) Number of points: 60 (corresponding to the number of individuals is a flock).
b) Metric: L1 norm (Lasso regression).
c) Number of neighbors (K) = 1–7.

As far as we are concerned with collective animal behaviour, the k-NN algorithm's most relevant parameter is the K value, i.e., an arbitrary number defining how many neighbors will be checked to determine the classification of a specific query point, i.e., a single individual (Lipsky and Porat, 2008). The number of neighbors K entails the similarity between a single point and the surrounding ones such that the higher the K, the higher the number of assessed correlations between adjacent points. The higher the number K, the higher the likelihood for neighbor individuals to perform the same physical movements (Patwardhan et al., 2023). In biological terms, this means that the higher the number K, the more the single individuals like birds, insects and fishes will behave in concert with their neighbors, displaying the same physical features like speed, or polarization, or direction, or bearing angle, etc. When the minimum default value of 1 is assigned to K, only one neighbor is used for the prediction and the instance will be assigned to the same class as its single nearest neighbor. In turn, when K corresponds to the maximum number of available data points, all the individuals in the flock are used for prediction.

We ended up selecting a number K corresponding to odd numbers between 1 and 7 for two reasons. First, it is recommended to have an odd number for K to avoid ties in classification. Second, it has been established that every bird in a flock interacts on average with a fixed number of six to seven nearest neighbors, independent of density fluctuations (Ballerini et al., 2008; Bialek et al., 2012). This interaction with the 6–7 closest neighbors does not depend on the metric distance or a fixed-size neighborhood, but rather on the topological distance (Niizato et al., 2014; Kumar and De, 2021). In brief, the best way to assess any change in physical parameters during collective animal behavior is to evaluate what happens to the surrounding environment when 6–7 neighbor individuals act collectively.

The Figure suggests that the higher the K, the more the blue shapes are extended. In turn, the higher the K, the more the red shapes shrink. The red surface covers 40.625% of the total surface of the original two-dimensional picture, while it covers 28.125% of the total surface of the picture corresponding to K = 7. This suggests that the stronger the physical correlation among neighbors, the smaller the surface occupied by the nearby physical environment.

3. Energy & pressure during neighbours interactions

Once established that increases in K lead to shrinking of red shapes and dilation of blue shapes, the next step is to look for k-NN algorithm's feasible physical counterparts. By a physical standpoint, the blue shapes might represent individuals performing collective movements, while the red shapes might represent fluid objects mixed with these individuals. The red shapes might stand for fluid physical systems (henceforward FPS) surrounding the flock members. FPS are provided with experimentally quantifiable amounts of energy, volume and surface. To give an example in terms of collective animal behavior, the blue shapes could stand for bird flocks flying in the air. The air (corresponding to the red shapes) could be supplied with physical features such as friction, variation in pressures, density, etc.

Our k-NN simulations suggested that increases in K lead to decreases in red shapes' surfaces. This means that the larger the aggregates of individuals with the same behavior (blue shapes), the lower the surface of the nearby FPS (red shapes). The FPS' surface tension can be experimentally calculated and expressed in energy per unit area (J/m^2). If the energy endowed in FPS is preserved, decreases in surface lead to increases in surface tension. The layout holds not just for the two-dimensional phase space described in the original two-dimensional picture, but also for three-dimensional phase spaces. In three-dimensional phase spaces, the higher the number K, the smaller the FPS' volume. The pressure exerted by FPS can be experimentally calculated and expressed in $P = J/m^3$, corresponding to the fixed amount of energy J stored inside FPS per unit volume. If the amount of energy stored in FPS is kept constant, increases in K lead to decreases in FPS volume. Therefore, the pressure inside three-dimensional FPS increases when K increases.

Boyle's law suggests that the pressure is directly proportional to the

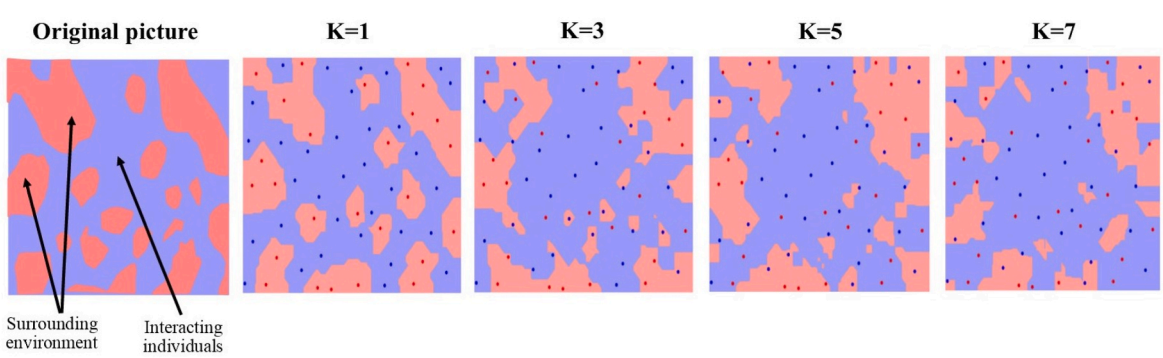

Fig. 1. K-Nearest Neighbors algorithm's processing of a two-dimensional phase space consisting of shapes of different colors, standing for interacting flock members performing collective movements (blue) and the surrounding fluid medium (red). As the number of neighbors K increases, the surface of the red shapes decreases and the surface of the blue shapes increases.

density of any fluid object (Webster 1965). If the temperature is kept constant, increases in pressure lead to increases in fluid object's density. Therefore, increases in number K lead also to changes in FPS' density. This means that flying flock members behaving collectively experience an atmosphere that is denser, compared with the atmosphere experienced by lone birds.

Summarizing, by the standpoint of a flock with collective movements, our framework suggests what follows: when interactions among neighbors strengthen, the density, the pressure and the surface tension exerted by the nearby air are perceived as increased by every individual belonging to the group.

4. Conclusions

We argued that collective dynamics modify the physical parameters perceived by neighbor flock members, depending on the amount of their aggregation. A bird acting collectively with other 5–6 birds will perceive a given pressure from the surrounding air, while a lone bird will perceive a pressure that is lower. We contend that the k-NN algorithm is not just a methodological device for objects classification, but rather displays a physical counterpart too. The higher the similarity between a single point and the surrounding ones (expressed by higher values of K), the more the fluid objects embedded in the phase space are shrunken. Being the red shapes physical fluids that encompass an amount of energy and exert a certain pressure, increases in K lead to increase in the pressure exerted by the red shapes on the blue shapes.

Self-organized systems often exhibit emergent properties that cannot be detected when examining their single components (Chvykov et al., 2021; Hu et al., 2022). The modifications in physical parameters described in this paper are not apparent, rather are real phase space's rearrangements that emerge from collective behavior (Gal and Kronauer, 2022). We found that, compared with a lone individual, the perception of physical parameters varies by the standpoint of an individual belonging to a flock. Hence, changes in air density can be detected and analyzed only by examining self-assembled clusters of birds that are weakly coupled (Bormashenko et al., 2020). These emergent modifications in the medium's physical parameters might contribute to explain some remarkable features of the bird flocks' behavior. We argue that the changes in phase space's properties might provide a trade-off between grouping and motor efficiency optimization (Noda et al., 2016). To provide an example, the energy required to compress a gas to a certain volume can be calculated by multiplying the difference between the gas pressure and the external pressure by the change in volume, such that:

$$(Pi - Pe) \times \Delta V$$

This means that the pressure exerted by flock members contributes to increase the pressure inside FPS, with effects on the flocks' dynamics. Yet, the fact that the density within the flock is nonhomogeneous, as birds are packed more tightly at the border than the center (Ballerini et al., 2008), might be explained by the fact that the pressure exerted by the surrounding air is higher on the boundary of the aggregation. In close similarity with the complex patterns displayed by birds' collective escape under predation (Papadopoulou et al., 2022), it could be hypothesized that the closer the high-pressure FPS is perceived by the flock members, the higher the frequency of their collective turning maneuvers. Further, it could be conjectured that nearest neighbors are more likely to be found on the sides rather than in the direction of motion (Giardina 2008) in order to avoid the increased pressure caused by the surrounding FPS. We propose the introduction of a relative physical quantity, namely the k-nearest neighbors pressure, which stands for a change in pressure depending on the relationships among the flock members inside the phase space. We define this quantity "relative" (Mazzuco et al., 2021) because it rests on the capability of flock members to interact and produce emergent phenomena.

In conclusion, we suggest that the very collective dynamics among neighbor birds could alter the physical features of the nearby environment. This claim could be generalized to other types of collective movements in which physical parameters such as volumes, surfaces, magnetic field's density, etc., can modify. For instance, different degrees of biological aggregation, such as cell–cell adhesion processes or clusters of migrating cells, may lead to changes in volume energy densities (Cox and Smith, 2014). Another feasible example of highly varying biological aggregation might consist of oral biofilms harbouring microbial clusters interspersed with salivary fluid (Perez-Tanoira et al., 2019; Simon-Soro et al., 2022; Martínez-Hernández et al., 2023). Interacting individuals displaying collective behavior might be regarded not just as passive objects inside energy fields' gradients, but rather in terms of active agents able to modify the energy gradients surrounding them.

CRediT authorship contribution statement

Arturo Tozzi: Writing – review & editing, Writing – original draft, Visualization, Validation, Supervision, Software, Resources, Project administration, Methodology, Investigation, Funding acquisition, Formal analysis, Data curation, Conceptualization.

Declaration of competing interest

The author warrants that the article is original, does not infringe on any copyright or other proprietary right of any third part, is not under consideration by another journal, and has not been previously published.

The Author does not have any known or potential conflict of interest including any financial, personal or other relationships with other people or organizations within three years of beginning the submitted work that could inappropriately influence, or be perceived to influence, their work.

This research did not receive any specific grant from funding agencies in the public, commercial, or not-for-profit sectors.

This research does not contain any studies with human participants or animals performed by the Author.

The Author had full access to all the data in the study and take responsibility for the integrity of the data and the accuracy of the data analysis. The Author performed: study concept and design, acquisition of data, analysis and interpretation of data, drafting of the manuscript, critical revision of the manuscript for important intellectual content, statistical analysis, obtained funding, administrative, technical, and material support, study supervision.

Data availability

No data was used for the research described in the article.

References

Attanasi, Alessandro, Cavagna, Andrea, Del Castello, Lorenzo, Giardina, Irene, Jelic, Asja, et al., 2015. Emergence of collective changes in travel direction of starling flocks from individual birds' fluctuations. J. R. Soc. Interface 12 (108), 20150319. https://doi.org/10.1098/rsif.2015.0319.

Ballerini, M., Cabibbo, N., Candelier, R., Cavagna, A., E Cisbani, I., et al., 2008. Interaction ruling animal collective behavior depends on topological rather than metric distance: evidence from a field study. Proc. Natl. Acad. Sci. U.S.A. 105 (4), 1232–1237. https://doi.org/10.1073/pnas.0711437105.

Bang-Jensen, J., Gutin, G., Yeo, A., 2004. When the greedy algorithm fails. Discrete Optim. 1, 121–127, 2004.

Bialek, William, Cavagna, Andrea, Giardina, Irene, Mora, Thierry, Silvestri, Edmondo, et al., 2012. Statistical mechanics for natural flocks of birds. Proc. Natl. Acad. Sci. U.S.A. 109 (13), 4786–4791. https://doi.org/10.1073/pnas.1118633109, 2012 Mar 27.

Bormashenko, Edward, Fedorets, Alexander A., Frenkel, Mark, Dombrovsky, Leonid A., Nosonovsky, Michael, 2020. Clustering and self-organization in small-scale natural and artificial systems. Philos Trans A Math Phys Eng Sci 378 (2167), 20190443. https://doi.org/10.1098/rsta.2019.0443, 2020 Mar 20.

Cavagna, A., Cimarelli, Alessio, Giardina, Irene, Viale, Massimiliano, 2010. Scale-free correlations in starling flocks. PNAS June 107 (26), 11865–11870. https://doi.org/10.1073/pnas.1005766107, 14, 2010.

Chen, Xiaowen, Winiarski, Maciej, Puścian, Alicja, Knapska, Ewelina, Walczak, Aleksandra M., Mora, Thierry, 2023. Generalized glauber dynamics for inference in biology. Phys. Rev. X 13, 041053.

Chvykov, Pavel, Berrueta, Thomas A., Vardhan, Akash, Savoie, William, Samland, Alexander, et al., 2021. Low rattling: a predictive principle for self-organization in active collectives. Science 371 (6524), 90–95. https://doi.org/10.1126/science.abc6182.

Cover, T., Hart, P., 1967. Nearest neighbor pattern classification. IEEE Trans. Inf. Theor. 13 (1, January 1967).

Cox, Brian N., Smith, David W., 2014. On strain and stress in living cells. J. Mech. Phys. Solid. 71 (November 2014), 239–252. https://doi.org/10.1016/j.jmps.2014.07.001.

Gal, Asaf, Kronauer, Daniel J.C., 2022. The emergence of a collective sensory response threshold in ant colonies. Proc. Natl. Acad. Sci. USA 119 (23), e2123076119. https://doi.org/10.1073/pnas.2123076119.

Giardina, Irene, 2008. Collective behavior in animal groups: theoretical models and empirical studies. HFSP J. 2 (4), 205–219. https://doi.org/10.2976/1.2961038, 2008 Aug.

Holmes, C.C., Adams, N.M., 2003. Likelihood inference in nearest-neighbour classification models. Biometrika 90 (2003), 99–112.

Hu, Jiliang, Amor, Daniel R., Barbier, Matthieu, Bunin, Guy, Gore, Jeff, 2022. Emergent phases of ecological diversity and dynamics mapped in microcosms, 2022 Oct 7 Science 378 (6615), 85–89. https://doi.org/10.1126/science.abm7841. Epub 2022 Oct 6.

Kumar, V., De, R., 2021. Efficient flocking: metric versus topological interactions. R. Soc. Open Sci. https://doi.org/10.1098/rsos.202158, 8202158202158.

Lipsky, O., Porat, E., 2008. Approximated pattern matching with the L 1, L 2 and L∞ metrics. In: Amir, A., Turpin, A., Moffat, A. (Eds.), String Processing and Information Retrieval. SPIRE 2008. Lecture Notes in Computer Science, 5280. Springer, Berlin, Heidelberg. https://doi.org/10.1007/978-3-540-89097-3_21.

Martínez-Hernández, M., Reyes-Grajeda, J.P., Hannig, M., et al., 2023. Salivary pellicle modulates biofilm formation on titanium surfaces. Clin. Oral Invest. 27, 6135–6145. https://doi.org/10.1007/s00784-023-05230-9, 2023.

Mazzuco, S., Suhrcke, M., Zanotto, L., 2021. How to measure premature mortality? A proposal combining "relative" and "absolute" approaches. Popul. Health Metrics 19 (1), 41. https://doi.org/10.1186/s12963-021-00267-y, 2021 Oct 26.

Mora, Thierry, Walczak, Aleksandra M., Del Castello, Lorenzo, Ginelli, Francesco, Melillo, Stefania, et al., 2016. Local equilibrium in bird flocks. Nat. Phys. 12 (12), 1153–1157. https://doi.org/10.1038/nphys3846.

Niizato, Takayuki, Murakami, Hisashi, Gunji, Yukio-Pegio, 2014. Emergence of the scale-invariant proportion in a flock from the metric-topological interaction. Biosystems 119, 62–68. https://doi.org/10.1016/j.biosystems.2014.03.001, 2014 May.

Noda, T., Fujioka, K., Fukuda, H., Mitamura, H., Ichikawa, K., Arai, N., 2016. The influence of body size on the intermittent locomotion of a pelagic schooling fish. Proc. R. Soc. A B 283, 290–291. https://doi.org/10.1098/rspb.2015.3019.

Patwardhan, Siddharth, Rao, Varun K., Fortunato, Santo, Radicchi, Filippo, 2023. Epidemic spreading in group-structured populations. Phys. Rev. X 13, 041054.

Perez-Tanoira, Ramón, Aarnisalo, Antti, Haapaniemi, Aaro, Saarinen, Riitta, Kuusela, Pentti, Kinnari, Teemu J., 2019. Bacterial biofilm in salivary stones, 2019 Jun Eur. Arch. Oto-Rhino-Laryngol. 276 (6), 1815–1822. https://doi.org/10.1007/s00405-019-05445-1. Epub 2019 Apr 26.

Rajagopalan, Balaji, Upmanu, Lall, 1999. A k-nearest-neighbor simulator for daily precipitation and other weather variables. Surface Water and Climate. https://doi.org/10.1029/1999WR900028.

Reynolds, C.W., 1987. Flocks, Herds, and Schools:A Distributed Behavioral Model. ACM SIGGRAPH, 87. Anaheim, California.

Simon-Soro, Aurea, Ren, Zhi, Krom, Bastiaan P., Hoogenkamp, Michel A., Cabello-Yeves, Pedro J., et al., 2022. Polymicrobial aggregates in human saliva build the oral biofilm, 2022 Feb 22 mBio 13 (1), e0013122. https://doi.org/10.1128/mbio.00131-22. Epub 2022 Feb 22.

Webster, C., 1965. The discovery of Boyle's law, and the concept of the elasticity of air in seventeenth century. Arch. Hist. Exact Sci. 2 (6), 441–502.

signals

MDPI

Review

Approaching Electroencephalographic Pathological Spikes in Terms of Solitons

Arturo Tozzi

Center for Nonlinear Science, Department of Physics, University of North Texas, 1155 Union Circle, #311427, Denton, TX 76203, USA; tozziarturo@libero.it

Abstract: A delicate balance between dissipative and nonlinear forces allows traveling waves termed solitons to preserve their shape and energy for long distances without steepening and flattening out. Solitons are so widespread that they can generate both destructive waves on oceans' surfaces and noise-free message propagation in silica optic fibers. They are naturally observed or artificially produced in countless physical systems at very different coarse-grained scales, from solar winds to Bose–Einstein condensates. We hypothesize that some of the electric oscillations detectable by scalp electroencephalography (EEG) could be assessed in terms of solitons. A nervous spike must fulfill strict mathematical and physical requirements to be termed a soliton. They include the proper physical parameters like wave height, horizontal distance and unchanging shape; the appropriate nonlinear wave equations' solutions and the correct superposition between sinusoidal and non-sinusoidal waves. After a thorough analytical comparison with the EEG traces available in the literature, we argue that solitons bear striking similarities with the electric activity recorded from medical conditions like epilepsies and encephalopathies. Emerging from the noisy background of the normal electric activity, high-amplitude, low-frequency EEG soliton-like pathological waves with relatively uniform morphology and duration can be observed, characterized by repeated, stereotyped patterns propagating on the hemispheric surface of the brain over relatively large distances. Apart from the implications for the study of cognitive activities in the healthy brain, the theoretical possibility to treat pathological brain oscillations in terms of solitons has powerful operational implications, suggesting new therapeutical options to counteract their detrimental effects.

Keywords: electrodes; critically ill patients; juvenile absence epilepsy; nonlinear Schrödinger equation; Korteweg-de Vries equation; Peregrine soliton

check for updates

Citation: Tozzi, A. Approaching Electroencephalographic Pathological Spikes in Terms of Solitons. *Signals* **2024**, *5*, 281–295. https://doi.org/10.3390/signals5020015

Academic Editors: Ran Xiao and Quanying Liu

Received: 27 February 2024
Revised: 22 April 2024
Accepted: 26 April 2024
Published: 1 May 2024

Copyright: © 2024 by the author. Licensee MDPI, Basel, Switzerland. This article is an open access article distributed under the terms and conditions of the Creative Commons Attribution (CC BY) license (https://creativecommons.org/licenses/by/4.0/).

1. Introduction

Solitons are single, spatially localized waves that travel without changing their shape and size [1]. Due to a delicate balance between dissipative effects and nonlinear dynamics, solitons are coherent structures propagating in space and time at a constant velocity without attenuation, distortion, or energy loss [2,3]. At least in an idealized framework, the stability and stationarity of soliton's analytical solutions are confirmed against non-integrable perturbations [4] (Ye et al., 2020) so that frictional effects like viscosity do not cause solitons to decay over time [5]. The energy of solitons is carried adiabatically through the medium, i.e., without transferring heat or mass [6]. Since the energy transfer to shorter wavelength regions is difficult, solitons reach a state of thermodynamic equilibrium that allows them to evolve for a long time without damping [7,8]. Solitons are naturally observed or artificially produced in different macro-, meso- and microscopic settings, playing key roles in the context of out-of-equilibrium nonlinear systems. They can be found in space plasmas, solar winds, planetary magnetospheres, marine and fluvial surface gravity waves, telegraph lines [9], high-speed silica fiber-optic telecommunication, optical coherence tomography, photorefractive crystals [10], micromechanical systems [11], magnetic matter, superconductors [12], Bose–Einstein condensates [13], etc. Their occurrence in ionic crystals, crystalline

solids and nematic liquid crystals [14] suggests a role for solitons in the physical properties of solids at high temperatures [11]. It has been conjectured that soliton-like mechanisms could also underlie biological phenomena like electron/proton transport along proteins' helices [15,16] as well as cardiac action potentials [17].

Still, attempts have been made to describe the MICROSCOPIC nervous activity of the central nervous system in terms of solitons [18]. It has been conjectured that the standard Hodgkin–Huxley model of the neurons' action potential could be piezoelectrically coupled with synchronized soliton pressure pulses generated inside the lipids of biological membranes [19] and influenced by thermodynamic variables like voltage, temperature, pressure, chemical potentials [17]. According to this controversial model, the traveling solitons are localized in the membrane, do not spread out in the surrounding medium, do not release heat, and can modify the local membrane density and thickness [20,21].

Here, we take a different turn, suggesting another potential approach to assess the nervous electric spikes in the context of solitary waves. Looking at the central nervous system's nervous activity at the MACROSCOPIC scale, we argue that some of the brain electric oscillations detected by electroencephalography (EEG) could be mathematically and biophysically approached in terms of solitons' motion. We contend that the electric oscillation spikes attained by scalp EEG monitoring techniques resemble, in many respects, solitary waves. Since an electric wave must fulfill strict mathematical and physical requirements in order to be termed a soliton, we will analytically examine the manifold physical features of solitary waves and will look for their feasible counterparts in the cortical electric activity measurable on the scalp. In sum, by delving into the potential existence of solitons within EEG signals, we explore various nonlinear medium features and physical properties, such as energy expression, wavelength, phase velocity, and wave height. We conclude that soliton-related analytical methods could be effectively employed in the study of EEG signals.

2. Nonlinear Media and Solitons

Solitons are naturally robust to perturbations as they travel with little dissipation over long timeframes [22] (Rowley et al., 2022). The peculiar coherence of these highly localized wave packets can be attributed to the fact that the tendency for a wave pulse to disperse is exactly balanced by nonlinear effects occurring in the propagation medium [5]. While the linear and nonlinear effects acting alone would cause the wave to decay, in the right combination, they lead to waves that persist stably and compactly as they propagate, periodically returning to the initial state.

Numerous natural and artificial phenomena are characterized by the slight nonlinear dynamics required to generate solitons. Looking for a model of soliton-like EEG oscillations, we must first look for the possible presence of nonlinear dynamics in the central nervous system.

Nervous Nonlinear Medium

Solitons require a dissipative physical medium characterized by a certain degree of nonlinearity. In keeping with this claim, nervous nonlinear dynamics have been ubiquitously detected in both experimental settings and ecologically valid conditions [23,24]. Using brain network analysis, data-driven approaches and machine learning [25], various types of nonlinear dynamic behavior have been found in the wave series extracted from EEG data sets [23]. Nonlinear dynamics in the central nervous system consist of phase transitions, branching processes, metastability, limit cycles, self-oscillations, non-stationarity, neuronal avalanches, chaotic behavior and collective phenomena with the emergence of order [26,27]. Increasing evidence suggests that cortical neuronal networks operate near a critical state where balanced activity patterns support optimal information processing, scale-free correlations and the emergence of adaptive collective behavior [26].

Therefore, it can be stated that the nonlinear dynamics required by a nervous soliton-like model are widely diffused in the brain.

3. Equations for Solitons

In mathematical terms, solitons stand for one of the countless possible solutions for different types of nonlinear wave equations [6]. In particular, the Korteweg-de Vries equation (KdVE), originally developed to describe weakly nonlinear wave propagation in shallow water, admits analytic solutions representing solitons. KdVE equation can be written as

$$\partial_t \Phi + \partial^3{}_x \Phi - 6\Phi\partial_x \Phi = 0$$

where ∂_x and ∂_t are partial derivatives of x and t, Φ stands for the height displacement of the water surface from its equilibrium height. KdVE implies an equilibrium between dispersion $\partial^3{}_x\Phi$ and advection $\Phi\partial_x\Phi$, the latter standing for the particle transport provided by bulk motion and velocity of the fluid. KdVE can describe soliton systems in which the particles are driven by fluid pressure [28] as well as soliton turbulence in ocean waves [29]. The Benjamin–Bona–Mahony equation (BBME) is a KdVE variant for modeling long surface gravity waves of small amplitude, propagating uni-directionally in 1+1 dimensions. Yet, a particle-based fluid trajectory description of multi-soliton interactions can be achieved by the Kadomtsev–Petviashvili equation (KPE), i.e., a two-dimensional version of KdVE.

Apart from KdVE, BBME, and KPE, other wave equations display soliton solutions. The most prominent is the one-dimensional nonlinear Schrödinger equation (NLSE), an example of integrable systems of nonlinear partial differential equations owning an infinite set of conservation laws. NLSE stands for a universal tool to model the dynamical evolution in dispersive media of weakly nonlinear, varying packets of quasi-monochromatic waves [30]. Among the manifold versions, the linearly damped and driven NLSE can be expressed in the dimensionless form:

$$iu_t + \frac{1}{2}\, u_{xx} + |\, u\,|^2\, u = f - i\gamma u$$

where f = f(x,t) is the driving (or forcing) of the system, $i\gamma u$ is the linear damping of strength $\gamma > 0$ [31]. Depending on the chosen physical setting, different NLSE formulations provide different results according to the values of the dispersive nonlinear coefficients [30]. NLSE has a wide range of applications, including, e.g., the slow evolution of wave amplitude in shallow waters of uniform depth, the irregular wave trains propagating in deep water, superconductivity devices, nonlinear optics, etc. [32]. Concerning Bose–Einstein condensates, the soliton's behavior can be described by a variant of the NLSE referred to as the Gross–Pitaevskii equation (GPE) [30,33]. In this case, the velocities of single particles are determined by the phase of the wave function. Figure 1 illustrates a few examples of soliton solutions to various nonlinear wave equations.

Therefore, every attempt to look for hints of nervous solitons requires electric solitary waves to obey explicit nonlinear wave equations.

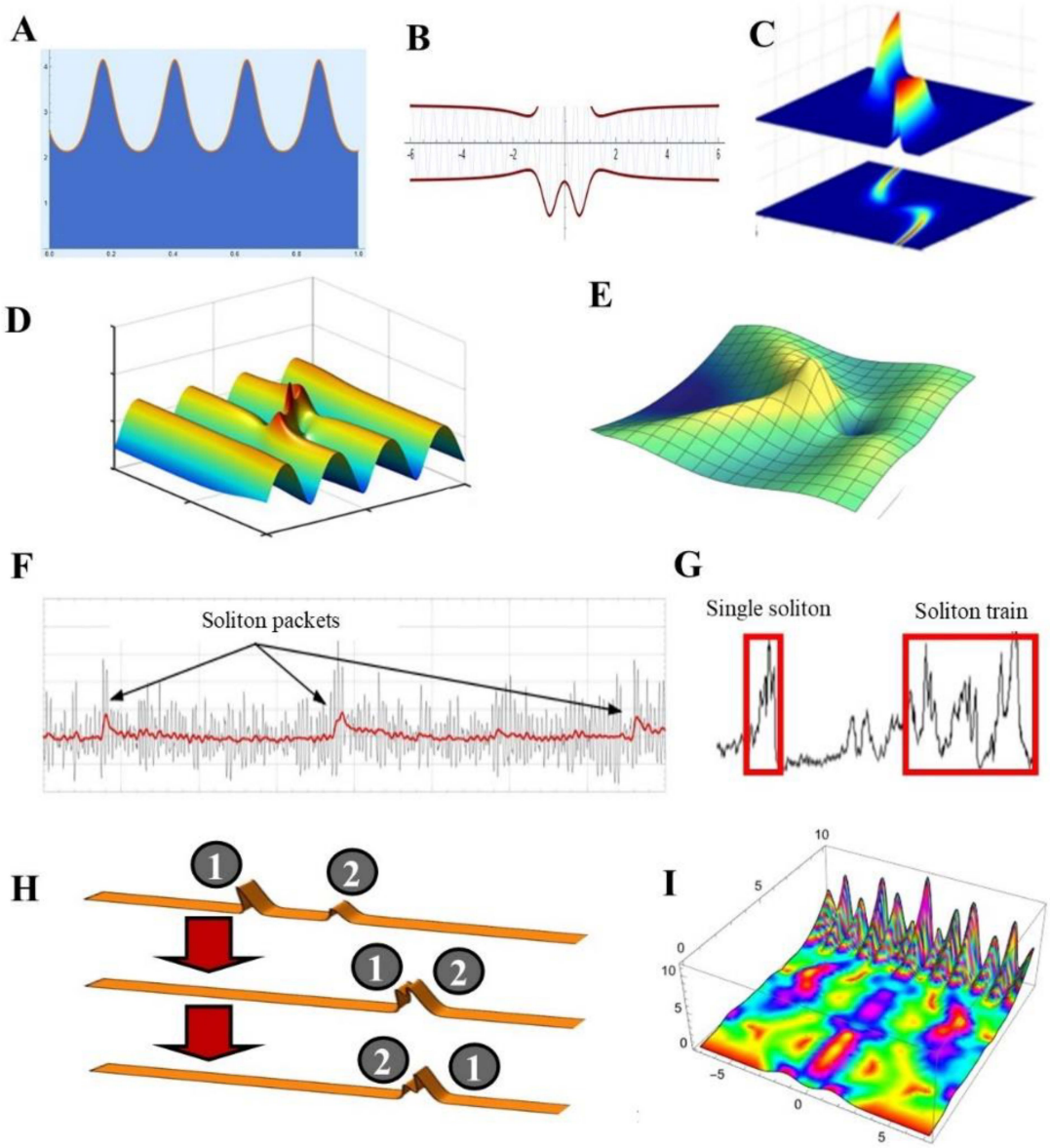

Figure 1. Features of different types of solitons. (**A**) A cnoidal wave is a periodic traveling-wave solution of KdVE. It refers to surface waves whose wavelength is large compared to the water depth; modified from https://demonstrations.wolfram.com/CnoidalWavesFromKortewegDeVriesEquation/ (accessed on 4 March 2024) (**B**) Formation of a rogue wave in the deep ocean, modeled using LNSE; modified from https://demonstrations.wolfram.com/RogueOceanWaves/ (accessed on 4 March 2024) (**C**) Top figure: example of dynamic behavior of an optical soliton with spatio-temporal dispersion, based on variable–coefficient NLSE. Bottom Figure: Time evolution of the soliton position x(t) interpreted in terms of wave streamlines obeying NLSE; modified from [34]. (**D**) Peregrine soliton solution based on a periodic-wave background generated by an NLSE variant; modified from [4]. (**E**) Soliton solution of the integrable focusing NLSE with spectral data consisting of a pair of conjugate poles of order 2n; modified from [35]. (**F**) Soliton trains (packets) in shallow water wind waves. The wave train (black) is achieved by low-pass filtering of the data (red); modified from [29]. (**G**) Single soliton and soliton trains detected for a month in the solar wind's pressure; modified from [36]. (**H**) Weakly nonlinear two-soliton propagation in shallow water described by KdVE; modified from https://demonstrations.wolfram.com/SolitonsFromTheKortewegDeVriesEquation/ (accessed on 4 March 2024) (**I**) NLSE-derived soliton profile perturbed by a periodic potential; modified from https://demonstrations.wolfram.com/SolutionOfANonlinearSchroedingerEquation/ (accessed on 4 March 2024).

Solitons in the Electrical Domain and in EEG Spikes

Solitons may be produced in the context of the electrical domain, both at the macro-, meso- and micro-levels of observation. The occurrence of electrostatic solitons is ubiquitous in macroscopic contexts such as two-fluid astrophysical plasmas, planetary magnetospheres and lunar wakes [3]. In solar wind, the interplanetary magnetic fields provide favorable conditions for solitons formation [36]. In space plasmas, nonlinear electrostatic solitary waves can be interpreted in terms of ion- and electron-acoustic solitons propagating parallel to the ambient magnetic field. Concerning the micro-levels of observation, electromagnetic fields and saturable nonlinear dielectrics may influence solitary waves' shape and behavior [37]. Self-reinforcing magnetic solitons have been generated in Bose–Einstein condensates from atoms with different spins [38]. In nematic and cholesteric liquid crystals, external electric fields drive the collective reorientation of nematic molecules. This process generates solitons representing self-trapped "bullets" that move with high speed, perpendicularly to the electric field and to the initial alignment direction [14,39]. The above-mentioned nonlinear wave equations have been widely used to cope with electric as well as external uniform magnetic fields inside the discrete nonlinear electrical lattices used for electrical transmission [40].

Once the solitons can be generated in an electromagnetic milieu, the question is whether they could occur in the hemispheric electric field detected by scalp EEG. The fact that NLSE may govern soliton propagation on spherical surfaces of electromagnetic fields traveling in coiled optical fibers [41] provides an indirect hint that solitons can be uncovered inside spherical electric fields [42]. Further, it has been shown that electric or magnetic monopole pairs can interact with Coulombic fields equipped with the SO(3) rotations typical of spherical surfaces [43].

Therefore, the nervous electric activity detected on the scalp could be assessed by using nonlinear wave equations with solitons solutions.

4. The Remarkable Physical Features of Solitons

Solitons' solutions can be given analytically by using mathematical devices such as first-order Fourier analysis and statistical analysis [6,44]. Different solutions of KdVE, BBME, NLSE, KPE and GPE generate different types of propagating solitons characterized by distinct physical features and various wave shapes. The physical parameters to assess the presence and the dynamics of solitons are manifold. They include surface elevation, wave height, phase velocity (i.e., the rate at which the wave phase propagates), wavelength, spatiotemporal evolution of the normalized force as a function of a fixed or infinite horizontal distance, breathing period and maximum intensity, trajectories, velocities, acceleration, medium depth, material parameters [2,45]. In fluid media like seas or channels, also surface tension, density, gravity, channel height, water depth, carrier frequency and amplitude of the background wave [44] conspire to generate the solitons' features.

Therefore, when looking for the theoretical occurrence of solitons in EEG traces, the above-mentioned physical parameters must be taken into account.

4.1. Different Shapes for Different Solitary Waves

One of the most distinguished features of solitons is the shape, so different from the usual sine waves (Figure 1). Solitary waves include W-shaped, bright, dark, kink-dark, singular, kink antikink solitons [34,40], cnoidal waves (Figure 1A), abnormally large waves (also termed "freak" or "rogue" waves), "thick" or "top-table" solitons, algebraic solitons, solitons of different polarities [46], multi-solitons with doubly-localized peaks [1], etc. Unlike "bright" solitons, which locally amplify the surrounding medium, "dark" solitons stand for a local decrease in the wave amplitude able to cause a depression [44]. Dark solitons on the surface of water might influence extreme events like tsunamis, such that an almost flat ocean surface may evolve into a singular, destructive rogue wave with high amplitude, as energy is conveyed in the central zone from the surrounding areas [44] (Figure 1B). Contrary to the usual solitons that keep their profile unchanged during propa-

gation, the Peregrine soliton displays a double spatio-temporal localization characterized by progressive, standardized and cyclic changes in shape [47] (Figure 1D). Apart from the ones described above, other parameters may influence the large variety of solitons' shapes. These parameters include hyperbolic function solutions, elliptic parameters for cnoidal waves, variable–coefficient functions, modulation instability gain [34], the Sine–Gordon expansion method [40], etc. Furthermore, periodic traveling-wave solutions may give rise to "trains" of many solitons (Figure 1F). This occurs in the solar wind; whereas weak shock waves produce only single soliton pulses, strong shocks produce trains of solitons [36] (Figure 1G).

Therefore, when looking for the possible occurrence of solitary waves in EEG traces, it is mandatory to carefully evaluate whether the shape of the electric spikes matches the features of solitons.

4.2. Solitons in Healthy EEG Traces

The occurrence of solitons in EEG traces from healthy individuals has been conjectured. Sen [48] generated action potential-like solitons resembling EEG-like surface waves on a synthetic brain connectome in response to surface deformations produced by local pinch. Yet, part of the electric activity of the healthy human brain is characterized by nervous electric spikes that are reminiscent of solitons. For instance, the neuronal activity in the medial entorhinal cortex displays peculiar ultraslow periodic oscillations from tens of seconds to minutes. Further, electrocorticographic studies suggest that alpha and theta oscillations generate traveling waves propagating in a posterior-to-anterior direction at $\sim$0.25–0.75 m/s [49,50]. The last, but not the least significant, electrical recordings and spectral analysis from many brain regions exhibit neural oscillations at multiple spatial scales that, like solitons, are non-sinusoidal [50].

Therefore, theoretical mathematical findings, as well as implicit cues from neurophysiological studies, suggest the possibility that at least part of the normal electric EEG activity might involve solitons.

4.3. Solitons in Pathological EEG Traces

Reviewing the neuroscientific literature, it is easy to notice that quite a few EEG electric spikes detectable in disease states look like solitons [51]. Emerging from the noisy background of normal electric activity, high-amplitude, low-frequency EEG solitary waves of different shapes can be observed in various human diseases. A few EEG snapshots are illustrated in Figure 2.

1. Figure 2A illustrates a case of Herpesvirus-6 limbic encephalitis with lateralized periodic discharges over the left temporal region, with no apparent inter-discharge interval between the spike-and-wave complexes (modified from [52] Gélisse et al. (2023).
2. Figure 2B illustrates a bilateral synchronous symmetrical delta burst pattern with almost flat amplitude during burst intervals, recorded during wakefulness in the advanced stages of subacute sclerosing panencephalitis in an adult patient; modified from [53].
3. Figure 2C illustrates an example of a 3 to 4 Hz generalized spike-wave in a child affected by juvenile absence epilepsy; modified from https://www.epilepsy.com/what-is-epilepsy/syndromes/juvenile-absence-epilepsy (accessed on 23 March 2024).
4. Figure 2D illustrates a typical EEF in a case of sporadic Creutzfeldt–Jacob disease. Note the disease-typical periodic sharp wave complexes that occur in the middle and late stages; modified from https://www.eurocjd.ed.ac.uk/images/typical-eeg-sporadic-cjd (accessed on 23 March 2024).
5. Figure 2E illustrates an EEG snapshot showing a right temporal focal seizure in an adult. A focal slowing occurs in the temporal region; modified from [54].
6. Figure 2F illustrates the coexistence of focal and generalized epileptiform discharges in a 7-year-old boy with benign childhood epilepsy with occipital paroxysms [55].

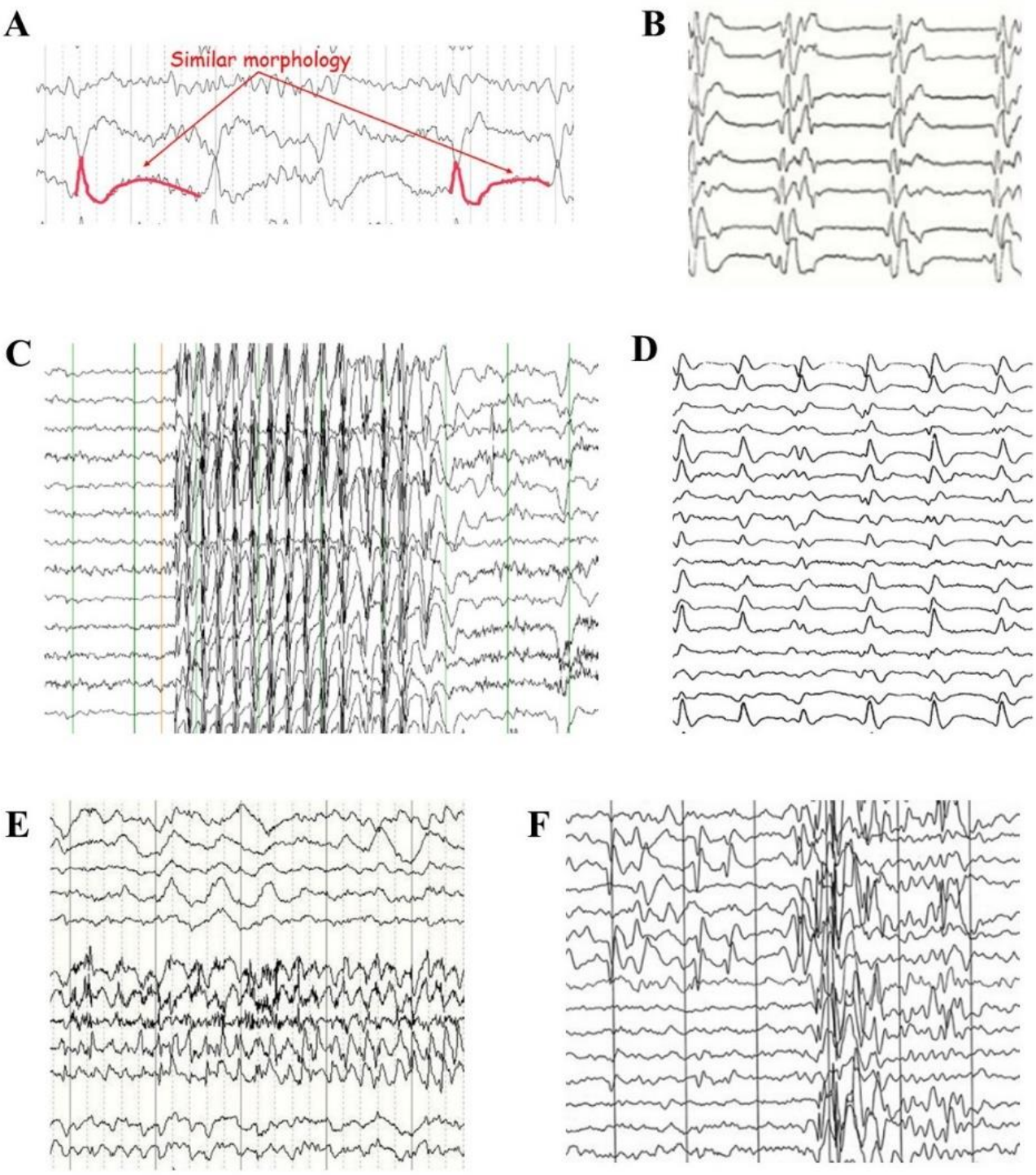

Figure 2. Pathological EEG patterns resembling trains of solitons. (**A**) Herpesvirus-6 limbic encephalitis; modified from [52]. (**B**) Typical "metronomic" delta burst pattern with almost flat amplitude during burst intervals, recorded during advanced stages of subacute sclerosing panencephalitis; modified from [53]. (**C**) Juvenile absence epilepsy; modified from https://www.epilepsy.com/what-is-epilepsy/syndromes/juvenile-absence-epilepsy (accessed on 23 March 2024) (**D**) Creutzfeldt–Jacob disease; modified from https://www.eurocjd.ed.ac.uk/images/typical-eeg-sporadic-cjd (accessed on 23 March 2024) (**E**) EEG snapshot showing a right temporal focal seizure; modified from [54]. (**F**) Coexistence of focal and generalized epileptiform discharges in a 7-year-old boy with benign childhood epilepsy with occipital paroxysms [55]. Similarities between solitons and pathological EEG patterns can be identified by comparing the waves illustrated in Figures 1 and 2.

Distinct medical conditions, including critically ill patients, encephalitis and epilepsy, are characterized by EEG traces with features that remind solitons trains, i.e., repeated patterns or stereotyped activity with or without interchange intervals, at an approximately regular rate or intervals [55]. Just as solitons, pathological EEG waveforms may display relatively uniform morphology and duration. Like solitons, pathological EEG oscillations can travel on the hemispheric surface of the brain over relatively large distances, and, like solitons, neither tend to flatten out nor steepen and topple over. Further, some pathological EEG waves display double spatio-temporal localization with cyclic changes in shape, just as Peregrine solitons.

Summarizing, the occurrence in EEG traces of features and shapes corresponding to various types of solitary waves suggests that some pathological brain electric activities might represent the biological counterpart of physical solitons.

5. Dynamics of Solitary Waves

Solitons travel long distances with no need for leading or trailing waves. The soliton's wave crest can be much higher than the surrounding waves [29]. Since the velocity depends on the wave's amplitude and height, a soliton is slower than its carrier waves. In addition, the velocity of solitons can be increased by an acceleration induced by an external water flow. When the distance along the surface approaches zero, a sharp rise of the wave crest can be detected above the rest of the deep fluid medium. The deeper the water, the more negative the nonlinearity parameter and the higher the possibility of generating rogue solitons, characterized by large-amplitude oscillations with height two times larger than the wave train [32]. When the soliton disappears, a defocusing process takes place in which the instantaneous frequencies in front become lower than those behind it [32].

5.1. Interactions between Solitons

Time-reversible interactions among multiple solitons, carriers, and media occur in both natural and artificial settings. When a carrier wave enters the soliton, its amplitude drops to zero; when it exits, its amplitude returns to the previous value [44]. Two colliding solitons penetrate through each other, exchange their amplitude and velocity and emerge fully intact as the exact pulses that entered the collision [2,45] (Figure 1H). At first, the two waves would align to temporarily reproduce the initial sine wave before separating again and repeating the same cycle. The higher amplitude wave is narrower and faster than the wave with the minor amplitude. Heart- and bell-shaped-cusp optical solitons can be produced by two-wave superposition (see the Figures in [28]). Though 90% of the soliton collisions occur between pairs of solitons, the remnant collisions involve multiple solitons [46]. Multi-spot soliton packets bound together with the appropriate relative phase can be achieved in saturable Kerr nonlinear media by simply shifting the refractive index with harmonic transverse modulations [56].

Therefore, theoretical multiple soliton-like waves detectable in EEG traces are required to preserve their shape after collision.

5.2. Dynamics of Solitary Waves

Viable examples of interactions between solitons can be found in pathological EEG traces. For instance

(a) Figure 2E illustrates the coexistence of generalized normal and focal pathological discharges that are spatially separated.
(b) Figure 2F illustrates the coexistence of generalized and focal epileptiform discharges that are spatially mixed.

Hence, it is theoretically possible that EEG waves could be produced by the transient superposition of diverse solitary waves from different brain areas. In touch with this claim, models of soliton conduction in microscopic branchlets with polarized microstructure suggest that linear superposition of two oppositely directed traveling waves might occur [2,45]. The resulting wave made of superimposed solitons can be resolved at late times into separate

single solitons, making it possible to uncover the cortical source of every one of the solitary oscillations [32].

Therefore, clues from the physical literature and pathological EEG traces let us argue that the superposition of solitons might occur in the electrical fields produced by cortical activity.

6. Solitons' Generation

Due to their inability to form spontaneously from noisy and/or dissipative systems, solitons' generation relies on the occurrence of external perturbations (Figure 1I) [23]. Artificial solitons can be engineered via different techniques in a wide range of media. A steady train of water waves with a well-defined shape can be produced in a shallow water regime by driving a piston at one end of the tank. The solitary waves may either ricochet back and forth or be absorbed at the other end with a porous material acting as an artificial beach [6,44]. In contrast to homogeneous media in which stable multi-peaked solitons do not exist, localized "lumps" of light can be produced in slightly nonlinear diffractive media such as glass, photonic lattices and optical fibers [33,56] by manipulating the light in miniaturized semiconductor chips [57]. In nonlinear silica optical fiber systems, the spreading due to dispersion and the intensity-dependent refraction due to nonlinearity are extremely balanced to generate solitons traveling in the waveguide for long distances [34]. In this case, the production of compact soliton beams is driven by femtosecond pulses oriented towards the transverse dimension [5], allowing ultrafast switching rates of several terahertz. Yet, solitons made of repulsively interacting atoms have been produced in microcavities and Bose–Einstein condensates [58]. Every soliton generated at each boundary of the box propagates in a uniform background density, colliding with one another in a way that can be controlled [59].

Therefore, a model that predicts soliton propagation in the mammalian central nervous system must carefully describe how solitary waves could be produced in the electromagnetic milieu produced by the neural tissue.

Generation of Neuronal Solitons

We stated that surface solitons might emerge from (and may interact with) electromagnetic fields like the ones detected on the scalp, a question arises: how could solitary waves be physically produced in the nervous tissue? Different theoretical possibilities might be considered:

(a) The nervous solitons detectable on the scalp are electric waves produced by the underlying neuronal tissue. In this case, solitons are produced INSIDE the electric fields.
(b) The nervous solitons detectable on the scalp are pressure waves that only later become electric currents. In this case, solitons are produced OUTSIDE the electric fields. This can be accomplished in several ways, including the piezoelectric effect, e.g., a simple electromechanical interaction between the mechanical stress and the electrical fields.

Another distinction could be made concerning the anatomical source of these theoretical nervous solitons:

(c) The nervous solitons can be naturally produced in the healthy brain.
(d) The nervous solitons can be produced in the pathological brain, e.g., by the spared tissue adjacent to injured areas.

In summation, further studies are needed to elucidate the possible mechanisms underlying solitons generation in the central nervous system.

7. Conclusions

We suggested that the central nervous system's nervous macroscopic activity could be assessed in terms of solitons. Particularly, we argued that the brain electric oscillations detected by scalp EEG monitoring could be described as solitary waves. Going through

many examples, we claimed that solitons resemble, in many respects, the cortical electric spikes. Solitons are very versatile, being able to generate both destructive waves in the ocean and noise-free messages in optic fibers. They have the potential to achieve powerful and reliable information processing in different fields, including telecommunications networks in electronics, optical computing and signal control [60], as well as practical applications in ultra-sharp pulse/edge generation and high-speed metrology [37]. The main questions are as follows: what does the potential relationship between solitons and cortical electric field bring to the table? What are the beneficial outcomes, operational qualities and methodological advantages?

Considering that solitons may carry just a modest amount of information when viewed as a code, what extent of information can be extracted from them in the context of brain activity? Solitons would allow the electric, noise-free transport of messages without dissipation. The low signal-to-noise ratio (S/N ratio) of scalp EEG often acts as a bottleneck, limiting the widespread application of EEG technology. If solitons do occur in EEG traces, they might be utilized to enhance the S/N ratio of scalp EEG recordings. Indeed, solitons stand for bits of information that are robust to perturbations and noise, highly stable over long timeframes and able to recover spontaneously even after complete disruption [23]. Solitons in Bose–Einstein condensates could function as qubits with long lifetimes of the order of a few seconds [61]. While isolated solitons can only encode single bits, two or more coupled solitons could boost transmission capacity by encoding more than one bit of information at a time. Also, charged soliton pulses could be used as a substrate for memory storage since they carry details of the input deformation parameters [48]. Further, multidimensional solitons in nematic and cholesteric liquid crystals can be used as vehicles for the two-dimensional delivery of micro-cargos [38]. Therefore, the theoretical occurrence of EEG soliton-like waves in the brain might provide benefits from a physiological and evolutionary standpoint.

The functional contributions of solitary waves to brain activity in healthy individuals could be manifold. It has been suggested that soliton pulses and surface waveforms might cooperate to identify incoming signals, help focus attention and retrieve memory [48]. Traveling waves could be behaviorally relevant in supporting brain connectivity and correlation between task events [49]. Ultraslow sequences of solitary traveling oscillations might couple circuits across extended time scales, serving as a template for new sequence formation during navigation. Since the mutual attraction of multiple solitons traveling in optical fibers can generate bound states, we speculate that solitary waves could help the phase synchronization of cortical networks [50]. Solitons' production could compensate for maladjustments of one variable by fine-tuning another one, providing a theoretical explanation for the effects of anesthetics [17,19,20]. Further, cortical traveling waves might contribute to the hierarchical organization of each brain region by unidirectional communication between arbitrarily paired areas [50].

We argued that if a correlation does exist between solitons and pathological EEG patterns, this similarity could be harnessed to identify certain diseases through the detection and analysis of solitons. Therefore, if the soliton-like EEG modalities could be somehow disrupted. The elimination of the soliton that the proper procedures might lead to a recovery of the brain's healthy state. Potential detrimental solitons correlated with medical conditions might be countered and neutralized in various ways. Since solitons are produced by a delicate balance between nonlinear and dissipative forces like viscosity, a pharmacologically induced modification of the brain viscosity might lead to the derangement of pathological solitons. Further, solitons display peculiar physical features like non-sinusoidal waves that could be theoretically manipulated by focal electrical brain stimulation induced by external magnetic fields, namely, by transcranial magnetic stimulation (TMS) [62,63]. In pathological states, the ordinary EEG oscillations deviate from the norm. In this case, our model of nervous solitons based on Schrodinger-like equations predicts that pathological spikes could be correlated with changes in the anatomical/functional location of the electric sources. Figure 3 provides a proof-of-concept example of brain

EEG waves treated in terms of the Schrodinger equation. In the healthy brain, the energy sources are arranged in a regular order along the straight line connecting two scalp electrodes (Figure 3A). This generates a regular wave with well-defined periodicity and rhythm. When a disease occurs, e.g., an epileptic focus, one of the energy sources turns off its location on the straight line (Figure 3B). This divergence perturbs the wave profile: even slight changes in the location of energy sources can vary the potential, leading to waves with fully different shapes. To restore the healthy wave, an appropriately located external current could be given via TMS to counteract the effects of the displaced energy source (Figure 3C). Note that the profile wave in Figure 3 is drawn from the classical Schrodinger equation that holds just for microscopic systems subject to the laws of quantum mechanics. Nevertheless, the example can be generalized to macroscopic systems like EEG traces when considering NLSE instead of the classical Schrodinger equation.

Therefore, artificial manipulation of harmful solitons in the nervous tissue can be achieved by superimposing TMS external currents to counteract the pathological electric waves. This might have consequences for medical treatment. For instance, the proper external current might contribute to modify the harmful solitons produced during epileptic discharge, bringing healing to the convulsive symptoms.

The possible relationships between solitary waves and brain activities pave the way to novel lines of research. We focused on the spikes extracted from EEG traces, but the universe of the discourse could also be extended to the oscillations detected by other experimental procedures like fMRI and local field potential electrophysiology. When nonlinear effects occur in silica optical fibers, the momentum and the medium dispersion might coincide. This generates a "phase matching" that allows solitons to emit a special kind of low-intensity radiation called resonant radiation [33]. It could be speculated that this radiation could be found also in EEG traces. The property of solitons to interact with each other in a nonlinear medium suggests that they could also be analyzed in terms of elastically colliding particles that do not interact with each other and do not perturb the wave [46,64]. When the soliton propagates through the medium, the particles are accelerated until the wave has left the region. After the interaction, the particles become motionless again, but their positions have shifted. The particles' single trajectories are influenced only by wave velocity, while their movement is governed by the current flow. This suggests that solitons at the interface of two biological fluid mediums might be useful to move or mix particles, contributing to the intra- and extra-cellular transport mechanisms.

In summation, research concerning relationships and interactions between solitons and the electric waves produced by the central nervous system still requires attention, but the premises are so promising that the field would be worth exploring.

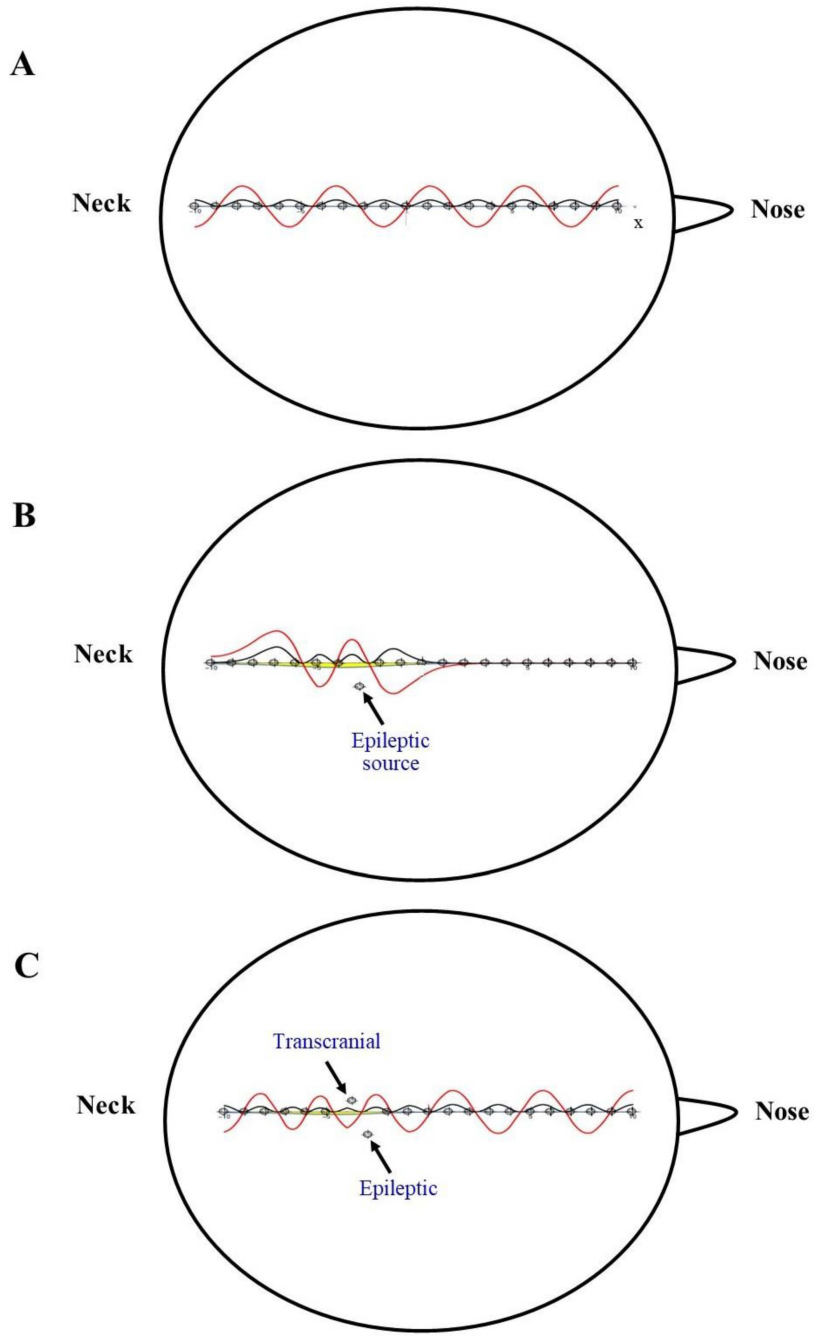

Figure 3. Schrödinger wavefunctions in a continuously varying potential field. The red oscillations stand for the wavefunctions, and the black ones stand for the probability density. The plot of the Schrödinger equation is embedded in a head contour. The plot represents an EEG wave spreading across the scalp electrodes between the neck and the nose. Solutions of the one-dimensional Schrödinger equation with quantum number 10 are provided in a potential-energy field V(x), which can be varied by moving a series of locators (the little circles). Even small changes in position of one or more locators modify the potential energy field, generating waves with fully different heights, frequencies, shapes and periodicities. In the example, when the elementary periodic wave (**A**) is disrupted by a change in position of one locator (**B**), it can be restored by changing the position of another locator (**C**). In the context of a human disease like epilepsy, this means that the healthy oscillation (**A**) disrupted by epileptic foci (**B**) could be restored by the proper transcranial current (**C**); modified from https://demonstrations.wolfram.com/SchroedingerWavefunctionsInAContinuouslyVaryingPotential/ (accessed on 3 March 2024).

Funding: This research did not receive any specific grant from funding agencies in the public, commercial or not-for-profit sectors.

Data Availability Statement: All data and materials generated or analyzed during this study are included in the manuscript. The author had full access to all the data in the study and takes responsibility for the integrity of the data and the accuracy of the data analysis.

Conflicts of Interest: The author declares no conflict of interest.

References

1. Chabchoub, A.; Slunyaev, A.; Hoffmann, N.; Dias, F.; Kibler, B.; Genty, G.; Dudley, J.; Akhmediev, N. The Peregrine Breather on the Zero-Background Limit as the Two-Soliton Degenerate Solution: An Experimental Study. *Front. Phys.* **2021**, *9*, 633549. [CrossRef]
2. Poznanski, R.R.; Cacha, L.A.; Al-Wesabi, Y.M.; Ali, J.; Bahadoran, M.; Yupapin, P.P.; Yunus, J. Solitonic conduction of electrotonic signals in neuronal branchlets with polarized microstructure. *Sci. Rep.* **2017**, *7*, 2746. [CrossRef]
3. Sharma, A.; Malik, H.K.; Kumar, H.; Goyal, S. Effect of magnetic field on electromagnetic soliton evolution by different pulses. *J. Theor. Appl. Phys.* **2019**, *13*, 31–37. [CrossRef]
4. Ye, Y.; Bu, L.; Wang, W.; Chen, S.; Baronio, F.; Mihalache, D. Peregrine Solitons on a Periodic Background in the Vector Cubic-Quintic Nonlinear Schrödinger Equation. *Front. Phys.* **2020**, *8*, 596950. [CrossRef]
5. Minardi, S.; Eilenberger, F.; Kartashov, Y.V.; Szameit, A.; Röpke, U.; Kobelke, J.; Schuster, K.; Bartelt, H.; Nolte, S.; Torner, L.; et al. Three-dimensional light bullets in arrays of waveguides. *Phys. Rev. Lett.* **2010**, *105*, 263901. [CrossRef]
6. Redor, I.; Barthélemy, E.; Michallet, H.; Onorato, M.; Mordant, N. Experimental Evidence of a Hydrodynamic Soliton Gas. *Phys. Rev. Lett.* **2019**, *122*, 214502. [CrossRef]
7. Krylov, S.F.; Yankov, V.V. The role of solitons in strong turbulence. *Zhurnal Eksperimental Teor. Fiz.* **1980**, *79*, 8246.
8. Diebel, F.; Timotijević, D.V.; Jović Savić, D.M.; Denz, C. Soliton formation by interacting Airy beams. In *Complex Light and Optical Forces X*; Proceedings Volume 9764; SPIE: Basel, Switzerland, 2016; p. 97640S. [CrossRef]
9. Kayum, A.; Ara, A.; Barman, H.K.; Ali Akbar, M. Soliton solutions to voltage analysis in nonlinear electrical transmission lines and electric signals in telegraph lines. *Results Phys.* **2020**, *18*, 103269. [CrossRef]
10. Bouchet, T.; Marsal, N.; Sciamanna, M.; Wolfersberger, D. Two dimensional Airy beam soliton. *Sci. Rep.* **2022**, *12*, 9064. [CrossRef] [PubMed]
11. Manley, M.E.; Sievers, A.J.; Lynn, J.W.; Kiselev, S.A.; Agladze, N.I.; Chen, Y.; Alatas, A. Intrinsic localized modes observed in the high-temperature vibrational spectrum of NaI. *Phys. Rev. B* **2009**, *79*, 134304. [CrossRef]
12. Kachulin, D.; Dyachenko, A.; Zakharov, V. Soliton Turbulence in Approximate and Exact Models for Deep Water Waves. *Fluids* **2020**, *5*, 67. [CrossRef]
13. Strecker, K.E.; Partridge, G.B.; Truscott, A.G.; Hulet, R.G. Formation and propagation of matter-wave soliton trains. *Nature* **2002**, *417*, 150–153. [CrossRef] [PubMed]
14. Li, B.-X.; Borshch, V.; Xiao, R.-L.; Paladugu, S.; Turiv, T.; Lavrentovich, O.D. Electrically driven three-dimensional solitary waves as director bullets in nematic liquid crystals. *Nat. Commun.* **2018**, *9*, 2912. [CrossRef] [PubMed]
15. Ciblis, P.; Cosic, I. The Possibility of Soliton/Exciton Transfer in Proteins. *J. Theor. Biol.* **1997**, *184*, 331–338. [CrossRef]
16. Sinkala, Z. Soliton/exciton transport in proteins. *J. Theor. Biol.* **2006**, *241*, 919–927. [CrossRef]
17. Heimburg, T. The thermodynamic soliton theory of the nervous impulse and possible medical implications. *Prog. Biophys. Mol. Biol.* **2022**, *173*, 24–35. [CrossRef]
18. Heimburg, T.; Jackson, A.D. On soliton propagation in biomembranes and nerves. *Proc. Natl. Acad. Sci. USA* **2005**, *102*, 9790–9795. [CrossRef]
19. Andersen Søren, S.L.; Jackson, A.D.; Heimburg, T. Towards a thermodynamic theory of nerve pulse propagation. *Prog. Neurobiol.* **2009**, *88*, 104–113. [CrossRef]
20. Heimburg, T.; Jackson, A.D. On the action potential as a propagating density pulse and the role of anesthetics. *arXiv* **2006**, arXiv:physics/0610117. [CrossRef]
21. Johnson, A.S.; Winlow, W. The Soliton and the Action Potential—Primary Elements Underlying Sentience. *Front. Physiol.* **2018**, *9*, 357787. [CrossRef]
22. Rowley, M.; Hanzard, P.H.; Cutrona, A.; Bao, H.; Chu, S.T.; Little, B.E.; Morandotti, R.; Moss, D.J.; Oppo, G.L.; Totero Gongora, J.S.; et al. Self-emergence of robust solitons in a microcavity. *Nature* **2022**, *608*, 303–309. [CrossRef]
23. Hernandez, C.I.; Kargarnovin, S.; Hejazi, S.; Karwowski, W. Examining electroencephalogram signatures of people with multiple sclerosis using a nonlinear dynamics approach: A systematic review and bibliographic analysis. *Front. Comput. Neurosci.* **2023**, *17*, 1207067. [CrossRef]
24. Poikonen, H.; Zaluska, T.; Wang, X.; Magno, M.; Kapur, M. Nonlinear and machine learning analyses on high-density EEG data of math experts and novices. *Sci. Rep.* **2023**, *13*, 8012. [CrossRef]
25. Luo, C.; Li, F.; Li, P.; Yi, C.; Li, C.; Tao, Q.; Zhang, Y.; Yao, D.; Yin, G.; Song, P.; et al. A survey of brain network analysis by electroencephalographic signals. *Cogn. Neurodyn.* **2022**, *16*, 17–41. [CrossRef]

26. Meisel, C.; Olbrich, E.; Shriki, O.; Achermann, P. Fading Signatures of Critical Brain Dynamics during Sustained Wakefulness in Humans. *J. Neurosci.* **2013**, *33*, 17363–17372.
27. Mahgoub, A.; Qaraqe, M. Automatic detection of ictal activity in EEG using synchronization and chaos-based attributes. *Med. Biol. Eng. Comput.* **2023**, *61*, 3387–3396. [CrossRef]
28. Alquran, M.; Jaradat, I.; Yusuf, A.; Sulaiman, T.A. Heart-cusp and bell-shaped-cusp optical solitons for an extended two-mode version of the complex Hirota model: Application in optics. *Opt. Quant. Electron.* **2021**, *53*, 26. [CrossRef]
29. Costa, A.; Osborne, A.R.; Resio, D.T.; Alessio, S.; Chrivì, E.; Saggese, E.; Bellomo, K.; Long, C.E. Soliton Turbulence in Shallow Water Ocean Surface Waves. *Phys. Rev. Lett.* **2014**, *113*, 108501. [CrossRef]
30. Karjanto, N. The nonlinear Schrödinger equation: A mathematical model with its wide-ranging applications. *arXiv* **2019**, arXiv:1912.10683.
31. Fotopoulos, G.; Frantzeskakis, D.J.; Karachalios, N.I.; Kevrekidis, P.G.; Koukouloyannis, V.; Vetas, K. Extreme wave events for a nonlinear Schrödinger equation with linear damping and Gaussian driving. *Commun. Nonlinear Sci. Numer. Simul.* **2020**, *82*, 105058. [CrossRef]
32. Xia, W.; Ma, Y.; Dong, G.; Zhang, J.; Ma, X. Emergence of Solitons from Irregular Waves in Deep Water. *J. Mar. Sci. Eng.* **2021**, *9*, 1369. [CrossRef]
33. Rubino, E.; McLenaghan, J.; Kehr, S.C.; Belgiorno, F.; Townsend, D.; Rohr, S.; Kuklewicz, C.E.; Leonhardt, U.; König, F.; Faccio, D. Negative-Frequency Resonant Radiation. *Phys. Rev. Lett.* **2012**, *108*, 253901. [CrossRef] [PubMed]
34. Liu, F.-F.; Lü, X.; Wang, J.-P. Dynamical behavior and modulation instability of optical solitons with spatio-temporal dispersion. *Phys. Lett. A* **2024**, *496*, 129317. [CrossRef]
35. Bilman, D.; Buckingham, R. Large-Order Asymptotics for Multiple-Pole Solitons of the Focusing Nonlinear Schrödinger Equation. *J. Nonlinear Sci.* **2019**, *29*, 2185–2229. [CrossRef]
36. Shah, A.; Rehman, S.-U.; Haque, Q.-U.L.; Mahmood, S. Solitons and Turbulence in Solar Wind at 1 au: Multi-satellite Data and FDTD Simulations. *Astrophys. J.* **2020**, *890*, 1. [CrossRef]
37. Bradley, P.J.; De Angelis, C. Soliton dynamics and surface waves at the interface between saturable nonlinear dielectrics. *Opt. Commun.* **1996**, *130*, 205–218. [CrossRef]
38. Chai, X.; Lao, D.; Fujimoto, K.; Ramas, C. Magnetic soliton: From two to three components with SO(3) symmetry. *Phys. Rev. Res.* **2020**, *3*, L012003. [CrossRef]
39. Shen, Y.; Dierking, I. Dynamics of electrically driven solitons in nematic and cholesteric liquid crystals. *Commun. Phys.* **2020**, *3*, 14. [CrossRef]
40. Yamgoué, S.B.; Deffo, G.R.; Tala-Tebue, E.; Pelap, F.B. Exact solitary wave solutions of a nonlinear Schrödinger equation model with saturable-like nonlinearities governing modulated waves in a discrete electrical lattice. *Chin. Phys. B* **2018**, *27*, 126303. [CrossRef]
41. Körpınara, T.; Demirkola, R.C.; Körpınara, Z. Soliton propagation of electromagnetic field vectors of polarized light ray traveling along with coiled optical fiber on the unit 2-sphereS^2. *Rev. Mex. Fis.* **2020**, *65*, 626. [CrossRef]
42. Lima, F.M.S. What Exactly is the Electric Field at the Surface of a Charged Conducting Sphere? *Reason* **2018**, *23*, 1215–1223. [CrossRef]
43. Wabnig, J.; Resch, J.; Theuerkauf, D.; Anmasser, F.; Faber, M. Numerical Evaluation of a Soliton Pair with Long Range Interaction. *arXiv* **2022**, arXiv:2210.13374.
44. Chabchoub, A.; Kimmoun, O.; Branger, H.; Hoffmann, N.; Proment, D.; Onorato, M.; Akhmediev, N. Experimental Observation of Dark Solitons on the Surface of Water. *Phys. Rev. Lett.* **2013**, *110*, 124101. [CrossRef] [PubMed]
45. Xiao, Y.; Wang, P.; Zhang, J.; Guo, T.; Gao, R.; Ren, S. Controllable soliton propagation of Airy-Gaussian beams under the fractional effect. *Optik* **2021**, *243*, 167431. [CrossRef]
46. Didenkulova, E. Soliton turbulence in weakly nonlinear and weakly dispersive media. In Proceedings of the EGU General Assembly 2021, Online, 19–30 April 2021; p. EGU21-552. [CrossRef]
47. Peregrine, D.H. Water waves, nonlinear Schrödinger equations and their solutions. *J. Austral. Math. Soc. B* **1983**, *25*, 16–43. [CrossRef]
48. Sen, S. A global method of generating action potentials and EEG oscillations in a topological surface network. *BiorXiv* **2022**. biorXiv:2022-06. [CrossRef]
49. Zhang, H.; Watrous, A.J.; Patel, A.; Jacobs, J. Theta and Alpha Oscillations Are Traveling Waves in the Human Neocortex. *Neuron* **2018**, *98*, P1269–P1281.e4. [CrossRef]
50. Cole, S.R.; Voytek, B. Brain Oscillations and the Importance of Waveform Shape. *Trends Cogn. Sci.* **2017**, *21*, 137–149. [CrossRef]
51. Handa, P.; Mathur, M.; Goel, N. Open and free EEG datasets for epilepsy diagnosis. *arXiv* **2021**, arXiv:2108.01030.
52. Gélisse, P.; Tatum, W.O.; Crespel, A.; Jallon, P.; Kaplan, P.W. Determining ICU EEG periodic patterns and why it matters. *J. Neurol.* **2023**, *270*, 4744–4752. [CrossRef]
53. Gadoth, N. Subacute Sclerosing Pan-Encephalitis (SSPE)—Past and Present. In *Pathogenesis of Encephalitis*; Hayasaka, D., Ed.; IntechOpen: London, UK, 2011. [CrossRef]
54. Chari, G.; Yadav, K.; Nishijima, D.; Omurtag, A.; Zehtabchi, S. Improving the ability of ED physicians to identify subclinical/electrographic seizures on EEG after a brief training module. *Int. J. Emerg. Med.* **2019**, *12*, 11. [CrossRef] [PubMed]

55. Fernández-Torre, J.L. First Chapter: Interictal EEG. In *Atlas of Epilepsies*; Panayioutopoulos, C., Ed.; Springer: Berlin/Heidelberg, Germany, 2010.
56. Kartashov, Y.V.; Vysloukh, V.A.; Torner, L. Soliton trains in photonic lattices. *Opt. Express* **2004**, *12*, 2831–2837. [CrossRef] [PubMed]
57. Genevet, P.; Barland, S.; Giudici, M.; Tredicce, J.R. Cavity Soliton Laser Based on Mutually Coupled Semiconductor Microresonators. *Phys. Rev. Lett.* **2008**, *101*, 123905. [CrossRef]
58. Fritsch, A.R.; Guo, S.; Koh, S.M. Dark solitons in Bose–Einstein condensates: A dataset for many-body physics research. *Mach. Learn.: Sci. Technol.* **2022**, *3*, 047001. [CrossRef]
59. Halperin, E.J.; Bohn, J.L. Quench-produced solitons in a box-trapped Bose-Einstein condensate. *Phys. Rev. Res.* **2020**, *2*, 043256. [CrossRef]
60. Gaur, D.S.; Purohit, A.; Mishra, A.K. Trapping and guiding soliton through Airy pulse. *Opt. Commun.* **2024**, *556*, 130300. [CrossRef]
61. Shaukat, M.I.; Castro, E.V.; Terças, H. Quantum dark solitons as qubits in Bose-Einstein condensates. *Phys. Rev. A* **2017**, *95*, 053618. [CrossRef]
62. Chung, S.W.; Sullivan, C.; Rogasch, N.C.; Hoy, K.E.; Bailey, N.W. The effects of individualized intermittent theta burst stimulation in the prefrontal cortex: A TMS-EEG study. *Hum Brain Mapp* **2019**, *40*, 608–627. [CrossRef]
63. Kohli, S.; Casson, A. Machine learning validation of EEG tACS artefact removal. *J. Neural. Eng.* **2019**, *17*, 016034. [CrossRef]
64. Hirota, R. Exact Solution of the Korteweg–de Vries Equation for Multiple Collisions of Solitons. *Phys. Rev. Lett.* **1971**, *27*, 1192–1194. [CrossRef]

Disclaimer/Publisher's Note: The statements, opinions and data contained in all publications are solely those of the individual author(s) and contributor(s) and not of MDPI and/or the editor(s). MDPI and/or the editor(s) disclaim responsibility for any injury to people or property resulting from any ideas, methods, instructions or products referred to in the content.

Neohelicon
https://doi.org/10.1007/s11059-024-00752-x

Norse burial practices and medieval fear of revenants in the myth of Ragnarök

Arturo Tozzi[1]

© Akadémiai Kiadó, Budapest, Hungary 2024

Abstract
After the introduction of the Christian religion, a traumatic shift took place in the Norse approach to death rituals. Transition went with strains between the ancient era of cremation and the new inhumation period. We argue that the myth of Ragnarök, written after Icelandic Christianization, might refer to the Norse mythical past of funeral pyres as opposed to the Christian funeral practices. We provide novel insights about the role of Odin, who is swallowed by Fenrir as if he has been buried in the ground, and of Surtr, who burns the world to restore the purifying role of the flames. Yet, the fear among Norse people for dead revenants can be traced in the Ragnarök myth, in which malevolent and benevolent characters return from death. Ragnarök sets out how to cope with revenants either to keep them quiet, or counteract their evil powers, or fully remove their menace. Concerns about revenants were more compelling for Medieval Norsemen after Christianization, when the corpses could not be any longer destroyed/purified by the fire, but rather had to lie in the earth with easy access to return from death. Summarizing, we argue that: (a) Ragnarök outlines the transition from Norse to Christian burial practices and the ways Norsemen coped with this trauma; (b) Ragnarök is also a history of revenants, in which Norsemen strive to deal with the uncanny powers of dead.

Keywords Edda · Snorri Sturlson · Völuspá · Cosmogony · Ahmad Ibn Fadlan · Baldr funeral

✉ Arturo Tozzi
tozziarturo@libero.it

[1] Center for Nonlinear Science, Department of Physics, University of North Texas, 1155 Union Circle, #311427, Denton, TX 76203-5017, USA

Published online: 24 September 2024

Introduction

The Norse myth of the end of the world, namely the myth of Ragnarök, portrays the twilight and the fate of the gods (Schjødt, 2019). The main sources are the Poetic Edda, sections Völuspá and Vafþrúðnismál, and the Prose Edda of Snorri Sturlson (1179–1241), section Gylfaginning (Gisli Sigurðsson, 2013). The dating of the Eddas is a vexed question (Gunnell & Lassen, 2013, pp. 25–44). It has been hypothesized that Voluspa was composed before the 11th century, partly based on older material from oral tradition (Vésteinn Ólason, 2013). The final rendering of the myth, e.g., the extant Eddas, were compiled in a Christian milieu by Icelandic authors around the first half of the 13th century, a few centuries after the Norse golden age. Iceland was legally converted to Christianity around the year 1000, but Scandinavian pagan beliefs survived for long periods (Eiríkur Eiríksson, 1971). It is not known whether Ragnarök had been slightly or heavily influenced by Christian thinkers. Also, it is unclear whether the saga portrays the 13th -14th century Icelandic viewpoint on the preceding pagan history (Kanerva, 2018). It has not been decided whether there ever was a coherent Ragnarök tradition (Schjødt, 2020), although the archeological record uncovers various 10th -11th century carved crosses and stones depicting events from Ragnarök (Bailey, 2002; Kermode, 2005; Schulte, 2007).

The analogies between Ragnarök and Christian sources – i.e., the Old Testament, the Book of Revelation (Schjødt et al., 2020), the 8th century Wessobrunn Prayer, the 9th century poem Muspilli (Pakis, 2009), the 9th century poem Heliand and the medieval liturgical homilies – suggest that the saga could be an example of cultural transferring or syncretic superposition between the ancient Norse and the late Medieval European Christians (Schjødt, 2019). Similarities have been reported between the Ragnarök and various eschatological traditions, including early Judaism, Graeco-Roman myths, Sybilline Oracles (Bugge, 1867), ancient Iranian traditions. Some authors hypothesize for Ragnarök an Indo-European pre-Christian background handed down in a Christian medieval context (Hultgård, 2022). The purpose of the Eddas' writers has been harshly contended. Did they want to preserve for posterity the original Pagan poetry, or defend the Norse beliefs paganism by countering the advance of the new religion (Stern, 2016)? Alternatively, do they want to match the old beliefs with the new ones, assimilating the pagan past with the Christian message (Samplonius, 2013)? Scholars decode Ragnarök as a mythical account of cyclic natural events like the daily rotation of the sun or the succession of the seasons, while others suggest a poetic rendering of the geothermal events occurring in the inhospitable Icelandic inland (Patel, 2017) or during the catastrophic volcanic winter of 536 AD (Gräslund & Price, 2012).

In this manuscript, we take a different stand on the myth of Ragnarök. We start from the traumatic passage occurred in Norse death rituals after Christianization around the 10-13th century, when burials were imposed and replaced the ancient funeral pyres taking place on the decks of the ships. We argue that Ragnarök might describe the anguish caused by the new inhumation rites that dethroned centuries-long pagan burial practices. Further, we argue that Ragnarök might describe the fear of revenants coming back to life and the ways to counteract, mitigate or neutralize their malevolent influence.

Preparation for death: Norsemen vs. Christians

In the European Medieval times, preparation after death was both a spiritual and a material affair deemed to be crucial both for the physical afterlife of the deceased and the well-being of who outlived him (Caciola, 1996; Simpson, 2003). The funerary practices in Norse Age are testified by the archaeological evidence of many burials (Roderick, 1968; Steinsland & Meulengracht, 1998) and by literary sources, e.g., the Ahmad ibn Fadlan's impressive account dated 922 AD (Brøndsted, 1965) and the description of the Baldr funeral in the prose Edda. It is noteworthy that preparation for death and afterlife has been extensively studied in the 13th Iceland, i.e., in the historical, cultural and religious milieu in which the Eddas were compiled.

Ancient Norse funerals. Norse funerals were intense events involving narrative performance of rites and rituals to honor the deceased and facilitate his journey to the realm of the gods. Practices varied widely across the Norse world, based on the social status, local customs and religious beliefs. Cremation and inhumation were both common. According to Snorri, cremation was favored by early Norsemen, who believed that the fire's smoke would carry the deceased's spirit to the afterlife. Odin wanted the dead warriors being burned together with all their goods on the decks of the ships to take them in the Valhalla, the boat symbolizing the journey to the afterlife and the flame representing transformation and renewal from life to death (Brøndsted, 1965). Although it is misleading to give a general overview out of one report specific for one occasion, some details from Ibn Fadlan's account are worth to be mentioned. He writes that the wealthiest and eminent Norsemen were clothed in fine garments and placed on top of their boats hauled ashore, surrounded by rich foods, strong drink, everyday items, gaming sets, sailing equipment, weapons, jewelry and even livestock and slaves "volunteered" to be slain and burned together with their masters. The act of lighting the pyre was an important ritual, performed by the dead man's nearest kinsman. Then people came, each bringing a burning brand and throwing it on the pyre. It might be speculated that massive and grim women like the Fadlan's "Angel of Death" could be involved in some Norse ritualistic practices. The funeral could be drawn out for days, consisting of commemorative rituals, feasts and games. Places like lakes, clearings and around large trees could serve as the central location (Anders, 2005). Then, the burned ashes were thrown in sea or taken to a burial, where large mounds of stones were raised (Kanerva, 2013). Most Norse funerals involved cremation or inhumation on land, an exception being the Baldr's funeral, in which the flaming ship was pushed out to sea. When many warriors died together, several bodies were laid out in the hull of the largest ship, with their leader and his weapons in the centre (Ratican, 2020).

Norse Funerals in Ragnarök. In the Ragnarök myth, there is a plenty of references to the ancient Norse funerals and burials. For instance, the boats symbolizing the journey to the afterlife are well represented in Ragnarök, carrying the Gods' enemies to the final battlefield: "Naglfar will be loosened from its moorings, the ship of that name… And in this flood Naglfar will be carried along (Gylfaginning; Snorri Sturluson, 1987, p. 53). "Then there will also arrive there Fenriswolf and the Midgard serpent. By then Loki will also have arrived there and Hrym and with him all the frost giants, but with Loki will be Hel's people (Völuspá; Snorri Sturluson, 1987, p. 54)."

In the same way that the Norse funerals usually took place on the ground, also the gods' death occurs on the land. As the funeral boats were hauled ashore during Norse cremations, during Ragnarök the evil passengers were disembarked to reach the fated battlefield. Just like large clearings served as the central location for the Norse burial rituals, the final battle in Ragnarök takes place in a huge esplanade: "The field Vígrídr is a hundred leagues in each direction (Gylfaginning; Snorri Sturluson, 1987, p. 54)".

According to the Norse *weltanschauung*, no one can escape the fate, including gods themselves. Throughout the Norse poetry, there are constant reminders of the threat of Ragnarök (Lassen, 2021). Gods are fully aware that they are doomed to die, so much that Odin himself obsessively tries to pursue knowledge of the cause of his own death (Swain, 2016, pp. 14–22). Despite fate is sealed, gods' bravery enables them to face the death with dignity (Wijianto, 2020). They are fully aware of the continuous cycles of birth, death and rebirth occurring in the cosmic history. Therefore, it can be hypothesized that Odin marches willingly towards death. He behaves as if he was preparing his own funeral. Like the wealthiest dead Norsemen were clothed in fine garments, the most eminent among the gods is dressed to die before the final battle: "Odin will ride in front with golden helmet and fine coat of mail and his spear called Gungnir (Gylfaginning; Snorri Sturluson, 1987, p. 54)". The other gods and the human warriors from Valhalla have fine clothes too: "The Æsir will put on their war gear, and so will all the Einheriar (Gylfaginning; Snorri Sturluson, 1987, p. 54)". The fact that they, like Odin, are preparing for their own death recalls the historical fact that the bodies of many warriors who died together were laid out in the hull of the largest ship, with their leader in the centre (Ratican, 2020). Odin offers his body as a sacrifice for the rebirth of the world, his death being glorified as the result (Wijianto, 2020). We suggest that, like the servants who wish to die with their chieftain, Odin goes voluntarily towards the death, playing the role of the slave "rewarded" for his faithful service.

The pyre of Norse funerals symbolizes the transformative power of fire seen as the vehicle to carry the deceased to their destination in the afterlife (Conti, 2021). It is mandatory that the world burns to be born again, the fire having a purifying and regenerative double valency. He who burns everything in the end is Surtr, who "will fling fire over the earth and burn the whole world (Gylfaginning; Snorri Sturluson, 1987, p. 54)". Despite Surtr is one of the main opponents of the gods during Ragnarök, he is not a fully negative character: "his sword is exceeding good: from it radiance shines brighter than from the sun". We believe it is not a case that the final fire is caused by him: since the central ritual of lighting the Norse funeral pyre was performed by the dead man's nearest kinsman, we speculate that Surtr could be much closer to Odin than currently believed. In Scandinavian folklore, possibly due to the weathering action of the tides, fire must be symbolically associated with water to have a termination effect (De Ceglia, 2023, pp. 253–256). That's why the burned ashes were sometimes thrown in sea. In the same way, during the Ragnarök, everything sinks into the water: "The sun will go dark, earth sinks in the sea (Völuspá; Snorri Sturluson, 1987, p. 55)". The Massive and grim women having key roles in Norse funerals are also present in Voluspa, where an old giantess brings the brood of Fenrir. The offspring of this terrific woman is correlated with the deaths of the gods (Völuspá; Larrington, 1996)". The funeral ritual could be drawn out for days, consist-

ing of commemorative rituals, feasts and games. Likewise, the gods survived to the final destruction of the old world gather to remember old times: "After that Baldr and Hod will arrive from Hel. Then they will all sit down together and talk and discuss the mysteries and speak of the things that had happened in former times (Gylfaginning; Snorri Sturluson, 1987, p. 56)."

In sum, our textual reading suggests that the myth of Ragnarök describes, among other topics, the ancient Norse funerals in which the eminent chieftain was ultimately burned.

Towards Christian burials. Pagan funeral practices shifted over time throughout Northern Europe, especially once Christianity began to impact the Norse beliefs. As the centuries wore on and the new religion took hold, funerals begun to combine both Norse and Christian practices. The elaborate Norse procedures became simpler and more practical as Christianity crept across Scandinavia, cremation being gradually replaced with burial as the primary funerary method (De Ceglia, 2023, pp. 256–261). When someone converted to Christianity, their offspring could remain pagan and bury them in a pagan fashion. Alternatively, Christian offspring could bury their pagan parents in a Christian fashion. For instance, when his son converted to Christianity, the powerful king Gorm was exhumed from his enormous burial mound and reburied beneath a Christian church (Kanerva, 2018). Around 900, an Icelandic female character wished to be buried at the floodmark because she did not want to be interred in unholy ground, as the land was still pagan (Kanerva, 2018). Hybrid burials between pagan and Christian traditions have been uncovered in the United Kingdom, indicating shifts in ritual practice as the Scandinavians incomers slowly assimilated to these new regions (Paterson, 2017). While Norse graves were usually full of fine jewelry and weaponry, the Christian burials, much smaller and modest, were restricted to clothing accessories.

A slow transition did occur between the earliest Norse period called by Snorri Sturlson the "cremation age" and the more recent times of the burial mounds (Snorri Sturluson, 2010). The ensuing evolution of funeral practices towards Christian burial innovations could have been traumatic, possibly leading to resistance to novelty by large selections of Norse population. It has been suggested that a tense longing for flames crosses the Norse sagas, were the characters look back with regret on a mythical past in which the evil is destroyed by the walls of the funeral pyres' fire (De Ceglia, 2023, pp. 253–256). For instance, it has been contended that Norsemen are used to burn their beloved quickly such that they go to afterlife that very moment, while Arabs (and Christians) throw them to the ground where they are devoured by maggots (Brøndsted, 1965).

Therefore, the myth of Ragnarök might reflect the radical transition from Norse to Christian burial practices, depicting how the Norse people dealt with the trauma. In touch with this hypothesis, some verses in the Eddas point towards the description of Christian burials. An event occurring during the Ragnarök's final battle could be correlated with the historical introduction of Christian burials in the Norse society. In the same way that a Christian burial requires inhumation, Odin is swallowed by Fenrir and vanishes from the word: "The wolf will swallow Odin. That will be the cause of his death (Gylfaginning; Snorri Sturluson, 1987, p. 54)" Odin, who was preparing his own funeral as the final sacrifice to purify the world, is unexpectedly

eaten, disappearing as if he was buried in the ground. Instead of being cremated on the ground of a ship, Odin finds himself interred in the Christian way. The fact that Odin's son Vithar avenges his father by slaying the Wolf does not imply that the Norse tradition of the ancient funeral pyres has been restored. Everything falls into place only when Sutr burns the whole world, allowing the ancient funeral pyres to regenerate the world.

In sum, a few clues in the myth of Ragnarök suggest that the authors intended to make a connection between the ancient, magnificent pyres and the recent, controversial inhumations practices. In the next chapters, at first we will describe the Scandinavian Middle Ages' fear for dead and burials, then we will argue that it could be connected with the dreadful events described in the myth of Ragnarök.

Medieval, Icelandic revenants

Looking for relationships between the Norse burial practices and the myth of Ragnarök, the first step is to switch our account and tackle the crucial issue of the reanimated corpses revived from death, i.e., the entities termed revenants. Revenants were regarded as part of the natural world in the Scandinavian Medio eve (Tomaini, 2018). It was believed that a kind of vitality remained in the human corpse, being the dead embedded in a liminal space from where they could still enter the world of the living (Kanerva, 2011; De Ceglia, 2023, pp. 8–10). Communities dealt with their dead as continual, albeit non-living members, imbued of mythic and symbolic functions.

Despite their fondness to go to battle, and despite their religion provided a noticeable psychological support for the fearless warriors eager to reach Valhalla (Lindow, 1997; Schjødt, 2011), Norsemen were nevertheless fearful of the mysteries of death. We have knowledge of Norse dead people who did not rest in their graves as far as it is written in the medieval Icelandic Family Sagas (Clover, 1985). Undead subjects appeared to Northmen in dreams and visions not as ethereal ghosts as in other Medieval contexts, rather in physical recognisable bodies, often looking ominous and frightful (Merkelbach, 2012, pp. 10–11). Revenants could have both benevolent and malevolent behaviour and effects. The restless evil individuals haunted their own families and neighbors especially at night, causing fear, illness, insanity and death, until the nearby places become deserted (Kanerva, 2018). "Whenever birds landed on Þórólfr's grave, they fell down dead (Martin, 2005)". Night and darkness are especially scary. In the sagas, it is very dangerous to go out after sunset. Many events concerning malevolent undead took place in the autumn: as winter approaches, people believe that dead have begun to walk again, causing the livings all sorts of trouble (Kanerva, 2013): shepherds who did not come home could be found dead, completely coal-black, every bone broken (Martin, 2005). The revenants in medieval sagas could even act as agents of order, whose restlessness is connected to past deeds of those still living that have caused psychosocial conflicts and social disequilibrium within their community (Kanerva, 2011). Alive people had to be very careful in performing funeral rites to put a brake to evil revenants.

How to prevent posthumous evildoers. Many of the funeral rites described in the Icelandic tales were intended to provide to the deceased a quiet afterlife. When the

character died well-prepared, he continued to peacefully take part in the lives of the living with protective and benevolent functions (Kanerva, 2013). In turn, some individuals were anticipated to return posthumously with evil intentions. The potential candidates included strong-minded charismatic persons, subjects died in angry emotional states or with unresolved conflicts, strange-looking and awkward evildoers, individuals skilled in witchcraft or equipped with supernatural skills such as being capable of becoming berserkers in battle, people provided with extraordinary appearance such as wolf-grey hair, or females of remarkable size (Kanerva, 2015).

The anticipated posthumous restlessness could be prevented by preparing the corpses with the appropriate rituals (Vésteinn Ólason, 2003). Only persons with high social status were able to inactivate posthumous restlessness and control the authority of the dead (Kanerva, 2013). The preparation of the corpse was carefully disposed. Dead might be approached from behind, sometimes by the shoulders. The head might be covered with a cloth so that nobody could accidentally look into the dead's eyes, being the glance of the dead harmful. The eyes, mouth and nostrils might be closed and fingernails cut. The corpse might be carried out through an opening created in the wall of the house, so that the deceased would not know its way back (Kanerva, 2013).

Once the corpse reached the final destination, other control practices might help prevent further restlessness. The body could be physically hindered through obstacles like stones, intended to prevent dead evildoers from exiting their mound. Other times, the wall of the mound of stones was built so tall that only a bird could fly over it (Kanerva, 2013). Distance was reputed a foremost factor in determining the power of the dead, who was sometimes buried in a place so remote that the men must stay overnight on their trip. In the Artic Circle, the rituals to neutralize revenants were much more physical than the Continental ones. In Icelandic sagas, the hero had to engage in hand-to-hand combat with the restless dead, who frequently has superhuman strength (Örnólfur Thorsson, 2005). When somebody did not accomplish alone the removal of a perilous revenant, he might request help also from his reluctant rivals, since the law required that they agree to help with the burial (Kanerva, 2013). If all the above-mentioned control procedures fail, the best effective methods of disposing of a revenant was to decapitate the body with a sword, or to burn his body (Kanerva, 2013).

In the next paragraph, we will discuss the occurrence of potential revenants in the myth of Ragnarök.

Revenants in the Ragnarök saga. In Eddic poetry, the dead could be waked up against their own will by heathen gods and goddesses. In the same Völuspá, Óðinn wakes up a völva (Kanerva, 2013). Characters returned from death are widely mentioned in the myth of Ragnarök, where both benevolent and malevolent revenants come back to life. The evildoers, i.e., the people from Hel, and the gods' Champions, i.e., the warriors of Valhalla, return from death to fight each other: "Across the sea will come Muspell's troops with Loki at the helm (Völuspá; Snorri Sturluson, 1987, p. 55)" "The Æsir will put on their war gear, and so will all the Einheriar (Gylfaginning; Snorri Sturluson, 1987, p. 54)". After the end of the world, a few gods will be back from death. Baldr, who sat in the Hel-hall after his death, turns back to life. While Odin was associated by the Medieval Christian audience with God and Loki with Satan or the Antichrist, Baldr was associated with prosperity and fertility of the

spring season, in the same way as the second coming of Jesus Christ will wash away of the old, flawed gods (Swain, 2016, pp. 29–34).

Norsemen believed that dead individuals were embedded in a liminal space from where they could still escape. Death did not come suddenly, rather was a continuous path where the boundaries with life are blurred and slippery. This seems to recall the fact that the gods were sleeping at the beginning of Ragnarök: "Heimdallr will stand up and blow mightily on Giallhorn and awaken all the gods and they will hold a parliament together (Gylfaginning; Snorri Sturluson, 1987, p. 54)". It is tempting to speculate that the gods, at first suspended between life and death, were reanimated by the Heimdallr's horn (Kozák, 2021). Legends spread all over the world, including Greenland, recommend people to try to be quiet and well-behaved during the start of the hauntings, since loud noises make the spirits of the land angry (Merkelbach, 2012, p. 21). In touch with this suggestion, the same seems to hold for the dwarfs, who make a loud roar while the gods are at council. Just like the revenants try to leave their tombstones, the dwarfs groan at the stone doors.

It was not uncommon that bodies changed their features because of the intense frost. The corpses are described in sagas as turning black, swollen and very heavy ("His body became too heavy for the two oxen and men transporting the corpse to carry"), suggesting an emotional condition of anger that is still present in the corpse, ready to go out in revenants (Kanerva, 2018). Likewise, the Midgard Serpent was described as exceptionally heavy, such that no god possessed the strength to lift him (Gylfaginning; Snorri Sturluson, 1987, p. 53). Also, the fact that the more frightening beasts are freed might suggest that they were imprisoned in a sort of limb between life and death. "all the fetters and bonds will snap and break. Then Fenriswolf will get free. Then the ocean will surge up on to the lands because of the Midgard Serpent will fly into a giant rage and make its way ashore (Gylfaginning; Snorri Sturluson, 1987, p. 53)". Fenris' regained freedom and the Midgard Serpent's lethal raid might remind the return from the exile of death of malignant corpses, carrying pestilence and death. Nobody was safe from revenants, especially in the dark of the Northern frozen nights. In Ragnarök, "…the wolf will swallow the sun, and people will think this is a great disaster. Then the other wolf will catch the moon, and he also will cause much mischief. The stars will disappear from the sky (Gylfaginning; Snorri Sturluson, 1987, p. 53)". The frightening situation in which both sun and moon are devoured, followed by a frozen dark, is the best background for dead people to come back from death (Schjødt, 2019).

When a Norse died well-prepared, he continued to provide peace and security to his community. This is also the case of Baldr, who benefitted from an elaborate funeral. Accordingly, some events in Ragnarök remind the Viking procedures to prevent dead individuals to come back to life. The corpses were carried out through an opening created in the wall of the house, so that the deceased would not know their way back to the house. This brings to mind that "Amid this turmoil the sky will open and from it wil ride the sons of Muspell. Surt will ride in front… And when they ride over Bifrost it will break (Gylfaginning; Snorri Sturluson, 1987, p. 53)". The destruction of Bifröst, the bridge used by gods to travel between the Realms, forces them to stay still in one place, no way to get back.

In Icelandic sagas and in Ragnarök, the fingernails of the dead individual must be cut to help the gods before their final battle. A ritual precept by the Pythagorean school (VI sec. B.C) states: "Spit on your hair clippings and nail parings". The precept might concern the magic powers of hair and nails that permit people to exert power on other individuals (Pitagora, 2018). After the Odin's death, Vidarr blocks the Fenrir's lower jaw with his foot: "…Vídarr will come forward and step with one foot on the lower jaw of the wolf… With one hand he will grasp the wolf's upper jaw and tear apart its mouth and this will cause the wolf's death (Gylfaginning; Snorri Sturluson, 1987, p.54)". This reminds us that the bodies of individuals with anticipated posthumous restlessness were physically hindered through stones to prevent them from exiting their mound. The final battle with the mutual slaughter of humans, gods and monsters recalls the heroes of the Northmen sagas who had to engage in hand-to-hand combat with the restless and strong dead. In case of obstinate restlessness, one of the best methods of disposing of a revenant was to decapitate the body with a sword. In touch with this observation, Vithar breaks Fenrir's jaws and then pierces with a sword: "with his hand he lets his blade pierce Hvedrung's son heart. So is his father avenged (Völuspá; Snorri Sturluson, 1987, p. 55)". In the Norse sagas, when a character did not accomplish alone the removal of a perilous revenant, he might request help also from his rivals. In touch with this observation, the gods require the final assistance of none other than their most perilous enemy, i.e., Surtr, who burns the world and puts an end to all the restless dead.

The fear of death is not fully removed even after the destruction of the restless' undecayed corpse. When the revenant's ashes were thrown to the see, it might occur that they fled to the mainland. It happened once in an Icelandic saga that a cow licked some of it from a stone and subsequently gave birth to a bull that killed one of the characters (Kanerva, 2013). Accordingly, the threat of terrific attacks is not over in Ragnarök, even after the magnificent rebirth of the world and the gods. Indeed, the last verses of Voluspa portend the comeback of evil even in the new peaceful world, with the appearance of the nasty dragon Nithhogg (Völuspá; Larrington, 1996)". This means that the battle against the revenants is won, but not the war.

In sum, revenants are everywhere in Ragnarök, representing one of the greatest fears of the valiant Northmen warriors. We are entitled to hypothesize that the events described in the Ragnarök saga set out how to cope with revenants either to keep them quiet, or to counteract their evil powers, or to fully remove their menace.

Conclusions

The myth of Ragnarök is still an enigma, starting from the dispute over its date. It is not known whether the myth is based on older material from oral tradition and how much it has been influenced by Christian thinkers through cultural transferring or syncretic superposition (Wijianto, 2020). There is disagreement regarding the alleged relationships between Ragnarök, Christian sources and ancient eschatological traditions from all over the world (Samplonius, 2001). It is not even clear the purpose of the writers, whether they want to maintain the original Pagan poetry, or countering the advance of the new faith, or integrate the pagan folklore with the Christian

lesson, or describe Icelandic geothermal events (Mallory & Adams, 1997). In this manuscript, we provide an effort to build a new perspective that might shed new light on the meaning of the myth of Ragnarök. We present excerpts dedicated to Ragnarök from both the Edda books. The excerpts from the Prose Edda (section Gylfaginning) are provided in the translation of Anthony Faulkes (Snorri Sturluson, 1987), while the excerpts from the Poetic Edda (poems Völuspá and Vafþrúðnismál) are provided in the translation of Carolyne Larrington (Larrington, 1996).

Going through both the Eddas, we argued that many verses and phrases might be interpreted as the description and illustration of ancient Norse funeral practices. We provide many examples in the two books suggesting that the authors remain torn between the ancient funeral practices and the new burial rituals which become widespread during Northmen Christianization. Furthermore, we proposed a fresh interpretation about the main characters - in particular Odin, Fenrir, Surtr and Baldr - inserted in the context of the ancient and new death rituals. In our approach to the myth of Ragnarök, the fire of the funeral pyres takes a constructive role that permits the regeneration of the gods and the world, as opposed to the inhumation practices imposed by the early Christianization of Scandinavia and Iceland.

Yet, we focused on the unnoticed occurrence of benevolent and malevolent dead revenants in the Ragnarök myth. References to burial practices and ways to cope with corpses are scattered throughout the whole manuscripts. We suggest that this was kind a way to exorcize the fear of death that was always present in Norse folklore, despite their fearless warriors' look. We argue that the Ragnarök tale hints at the ritual practices used by Northmen to ward off the negative influence of restless dead. This might represent an attempt by Norse people to make peace with their own nightmares and the frightening darkness of the cold Scandinavian nights. This issue was even more compelling for Medieval Northmen after Christianization, when the corpses could not be any longer destroyed (and/or purified) by the fire. Having to lie on the ground instead of being burned to ashes, the dead could easily come back from death. It has been pointed out that undead characters appeared mostly in Northern sagas narrating the Christian conversion of prominent Icelanders, in a context in which the tensions between the old and the new religion were relentlessly mounting (Merkelbach, 2012, pp. 7–10). It's no coincidence that, after the advent of Christianity, the first Iceland revenants were described as hell-bound pagan souls raising from their burial grounds (De Ceglia, 2023, pp. 265–270).

We conclude that the Ragnarök myth can be read and interpreted at various levels, but the social, cultural, political and religious milieu of the Christian Medieval Iceland in which it has been written must be always taken into account.

References

Anders, A. (2005). Behind heathendom: Archaeological studies of Old Norse religion. *Scottish Archaeological Journal*, *27*(2), 105–138. https://doi.org/10.3366/saj.2005.27.2.105

Bailey, R. N. (2002). Scandinavian myth on Viking-period stone sculpture in England. In G. Barnes & M.C. Ross (Eds.), *Old Norse myths, literature, and society* (pp. 15–23). Centre for Medieval Studies, University of Sydney.

Brøndsted, J. (1965). *The vikings*. (Trans., K. Skov) (pp. 301–305). Penguin Books.

Bugge, S. (1867). *Norroen Folkvæði, Islansk Samling af Folkelige Oldtidsdigte om Nordens Guder og Heroer almindelig Kaldet Sæmundr Edda inns fróða* [Icelandic collection of ancient folk poems about the gods and heroes of the North commonly called very erudite Sæmundr' Edda]. Christiania 1867.

Caciola, N. (1996). Wraiths, revenants and ritual in medieval culture. *Past & Present*, *152*(1), 3–45. https://doi.org/10.1093/past/152.1.3.

Clover, C. J. (1985). Icelandic family sagas. Old Norse-Icelandic literature. A critical guide. In C. J. Clover, & J. Lindow (Eds.), *Islandica* (Vol. 45, pp. 239–315). Cornell University Press.

Conti, M. (2021). *Apocalisse e Ragnarǫk: elementi cristiani nella Vǫluspá*. MA thesis, Facoltà di Lettere e Filosofia, Corso di laurea magistrale in Linguistica, La Sapienza, Roma.

De Ceglia, F. P. (2023). *Vampyr*. Giulio Einaudi Editore.

Eiríkur Eiríksson, J. (1971). Jón Hnefill Aðalsteinsson. Kristnitakan á Íslandi [Christianity in Iceland]. *Kirkjuritið*, *37*(4), 71–74.

Gisli Sigurðsson. (2013). Vǫluspá as the product of an oral tradition: What does that entail? In T. Gunnell, & A. Lassen (Eds.), *The Nordic apocalypse. Approaches to Vǫluspá and Nordic days of judgment* (pp. 45–62). Brepols.

Gräslund, B., & Price, N. (2012). Twilight of the gods? The 'dust veil event' of A.D. 536 in critical perspective. *Antiquity*, *86*, 428–443.

Gunnell, T., & Lassen, A. (Eds.). (2013). *The Nordic apocalypse. Approaches to Vǫluspá and Nordic days of judgment*. Brepols.

Hultgård, A. (2022). *The end of the world in Scandinavian mythology. A comparative perspective on Ragnarök*. Oxford University Press.

Kanerva, K. (2011). The role of the dead in medieval Iceland: A case study of Eyrbyggja Saga. *Collegium Medievale*, *24*, 23–49.

Kanerva, K. (2013). Messages from the Otherworld: The roles of the dead in medieval Iceland. In M. H. Jacobsen (Ed.), *Deconstructing death: Changing cultures of death, dying, bereavement and care in the Nordic countries* (pp. 111–130). University Press of Southern Denmark.

Kanerva, K. (2015). Having no power to return? Suicide and posthumous restlessness in medieval Iceland. *Thanatos*, *4*(1), 57–79.

Kanerva, K. (2018). Restless dead or peaceful cadavers? Preparations for death and afterlife in medieval Iceland. I. In A. Lahtinen, & M. Korpiola (Eds.), *Dying prepared in medieval and early Modern Northern Europe* (pp. 18–43). Brill.

Kermode, P. M. C. (2005). *Manx crosses or The inscribed and sculptured monuments of the Isle of Man from about the end of the fifth to the beginning of the thirteenth century* (reprint of 1907 Bemrose ed., pp. 96–218). Elibron Classics.

Kozák, J. A. (2021). The echo of creation. Parallels between Old Norse cosmogony and eschatology. *Temenos. Nordic Journal of Comparative Religion*, *57*(1), 103–126.

Larrington, C. (Ed.). (1996). *The Poetic Edda* (Revised Edition 2014). Oxford University Press.

Lassen, A. (Ed.). (2021). *Odin's ways: A guide to the pagan god in medieval literature* (1st ed., pp. 95–111). Routledge.

Lindow, J. (1997). Murder and vengeance among the gods: Baldr in Scandinavian mythology. *Folklore Fellows' Communications Helsinki: Suomalainen Tiedeakatemia*, *262*, 79–80.

Mallory, J. P., & Adams, D. Q. (Eds.). (1997). *Encyclopedia of Indo-European culture*. Taylor & Francis.

Martin, J. D. (2005). Law and the (Un)Dead: Medieval models for understanding the hauntings in Eyrbyggja saga. *Saga-Book: Viking Society for Northern Research*, *29*, 67–82.

Merkelbach, R. (2012). *'Hann lá eigi kyrr': Revenants and a haunted past in the sagas of Icelanders*. Master's Thesis, University of Cambridge.

Pakis, V. A. (2009). The literary status of Muspilli in the history of scholarship: Two peculiar trends. *Amsterdamer Beiträge zur älteren Germanistik*, *65*, 41–60. https://doi.org/10.1163/9789042032118_006

Patel, S. S. (2017). The Blackener's Cave. *Archaeology*, *70*(3), 36–41.

Paterson, C. (2017). A tale of two cemeteries: Viking burials at Cumwhitton and Carlisle, Cumbria. In E. Cambridge, & J. Hawkes (Eds.), *Crossing boundaries: Interdisciplinary approaches to the art, material culture, language and literature of the early medieval world* (pp. 149–159). Oxbow Books.

Pitagora (2018). Simboli (Ttrans., G. Ruiu) (pp. 58–59). La Vita Felice.

Ratican, C. (2020). *The other body: Persons in Viking age multiple burials in Scandinavia and the Western diaspora*. Retrieved January 14, 2023, (pp. 27–41), https://doi.org/10.17863/CAM.54718

Samplonius, K. (2001). Sibylla borealis: Notes on the structure of Vǫluspá. In K.E. Olsen, A. Harbus, & T. Hofstra (Eds.), *Germanic texts and Latin models: Medieval reconstructions* (pp. 185–229). Peeters.

Samplonius, K. (2013). The background and scope of Vǫluspá. In T. Gunnell, & A. Lassen A (Eds.), *The Nordic apocalypse: Approaches to 'Völuspá' and Nordic days of judgement* (pp. 113–146). Brepols.
Schjødt, J. P. (2011). The warrior in Old Norse religion. Ideology and power in the Viking and middle ages: Scandinavia, Iceland, Ireland, Orkney and the Faeroes. In G. Steinsland, G. J. Vidar, J. E. Sigurðsson, I. Rekdal, & Beuermann (Eds.), *The Northern world* (pp. 269–295). Brill.
Schjødt, J. P. (2019). The Ragnarǫk myth in Scandinavia. In J. Althoff, J. D. Berrens, & T. Pommerening (Eds.), *Finding, inheriting or borrowing? The construction and transfer of knowledge in antiquity and the Middle Ages* (pp. 365–371). Transcript.
Schjødt, J. P., Lindow, J., & Andrén, A. (Eds.). (2020). *The pre-Christian religions of the North; history and structures*. Brepols.
Schulte, M. (2007). Memory culture in the Viking ages: The runic evidence of formulaic patterns. *Scripta Islandica. University of Uppsala*, *58*, 57–73.
Simpson, J. (2003). Repentant soul or walking corpse? Debatable apparitions in medieval England. *Folklore*, *114*, 389–402.
Snorri Sturluson (1987). *Edda* (Trans. and ed., A. Faulkes). Denrt J.M. Everyman.
Snorri Sturluson. (2010). *Heimskringla: History of the kings of Norway* (Ed., L.M. Hollander). University of Texas Press.
Steinsland, G., & Meulengracht, S. P. (1998). *Människor och makter i vikingarnas värld* [People and powers in the world of the Vikings] (Trans., H.O. Sjöström) (pp. 83–93). Ordfront.
Stern, F. L. (2016). Ragnarǫk: alternativas de interpretação da escatologia escandinava [Ragnarōk: Alternative interpretations of Scandinavian eschatology]. *Sacrilegens, Revista dos Alunos do Programa de Pós-graduação em Ciência da Religião* da *UFJF, 13,*39–58.
Swain, N. (2016). *A comparison of the Norse gods, Odin aand Loki, with emphasis placed on their roles during Ragnarök {the twilight of the gods} and Christian imagery within the poetic Edda and the prose Edda*. BA Dissertation Module HY30340, Department of History and Welsh History, Aberystwyth University.
Tomaini, T. (2018). *Dealing with the dead. Mortality and community in medieval and early modern Europe* (pp. 97–128). Brill.
Vésteinn Ólason, V. (2003). The un/grateful dead: From Baldr to Bægifótr. In M.C. Ross (Ed.) *Old Norse myths, literature and society* (pp. 153–171). University Press of Southern Denmark.
Vésteinn Ólason, V. (2013). Voluspá and time. In T. Gunnell, & A. Lassen (Eds.), *The Nordic apocalypse: Approaches to 'Völuspá' and Nordic days of judgement* (pp. 25–44). Brepols.
Wijianto, A. (2020). Comparative literature study of motif differences in Ragnarok and the book of Revelation. *Lire Journal (Journal of Linguistics and Literature)*, *4*(1), 50–63.

Publisher's Note Springer Nature remains neutral with regard to jurisdictional claims in published maps and institutional affiliations.

Springer Nature or its licensor (e.g. a society or other partner) holds exclusive rights to this article under a publishing agreement with the author(s) or other rightsholder(s); author self-archiving of the accepted manuscript version of this article is solely governed by the terms of such publishing agreement and applicable law.

WAS THE HITTITE KING MUWATALLI II KILLED?

Arturo Tozzi
Center for Nonlinear Science, Department of Physics, University of North Texas, Denton, Texas, USA
tozziarturo@libero.it

In this brief note, we cast doubts on the death of the great Hittite king Muwatalli II. Going through the prayer CTH 383 in which the king's impiety against the priestess of the Sun-goddness of Arinna is emphasized and condemned, we argue that Muwatalli II was dismissed and killed: "*he paid for it with his head*".

Muwatalli II, first-rank son, legitimate heir and successor of the Hittite king Mursili II, ascended the throne around 1295 B.C. Moving the capital of the Hittite kingdom from the vulnerable Hattusa to the more manageable southern town of Tahrunthassa (Catalogue of Hittite Texts CTH 81, CTH 85), Muwatalli II made a political and religious breakthrough that (possibly) met strong inner opposition (Bryce 2005). The highly divisive shift was (possibly) also caused by the royal wish to favour the cult of the Storm God of Lighting as an alternative to the widely venerated Sun-goddness of Arinna. After the transfer, Muwatalli II appointed his youngest and ambitious brother Hattusili as Governor of the Upper Land and King of the land of Hapkis (CTH 81). Muwatalli II made war against the aggressive Ramesses II's Egyptian kingdom, taking part in the first ever recorded battle, the battle of Kadesh in 1274 B.C.

Muwatalli II (possibly) favoured his second-rank son Urhi-Teshub who (possibly) flanked him in his last years. Nevertheless, a few texts seem to suggest that Urhi-Teshup (possibly) ran counter to his father's wishes (CTH 89, CTH 387). When Muwatalli II died around the year 1272 B.C., he (apparently) left no "first rank" male heirs. Therefore, Urhi-Teshup took the crown, flanked by his powerful uncle Hattusili. A few years later (about 1265 B.C.) the 50-years-old uncle deposed the nephew and assumed the kingship with the name of Hattusili II, beginning a ca. 28-years long reign together with his beloved wife, the chief priestess Puduhepa. It is noteworthy that both Urhi-Teshub and Hattusili II were largely unpopular among their own people (CTH 86, CTH 105, CTH 590). Their ascensions to the throne were classified as unlawful not just by parts of the Hittite aristocracy, but also by their Assyrian, Babylonian and Egyptian royal counterparts (CTH 155, CTH 172, CTH 173).

We focus here on an overlooked detail that sheds new light on the fate of Muwatalli II. The Hattusili's prayer of exculpation to the Sun-goddness of Arinna (CTH 383) encompasses a plea of king Hattusili and his wife Puduhepa concerning the sins of the former Hittite kings (Lebrun 1980). The Figure shows the tablet CTH 383 and a magnification of the lines that we are going to assess.

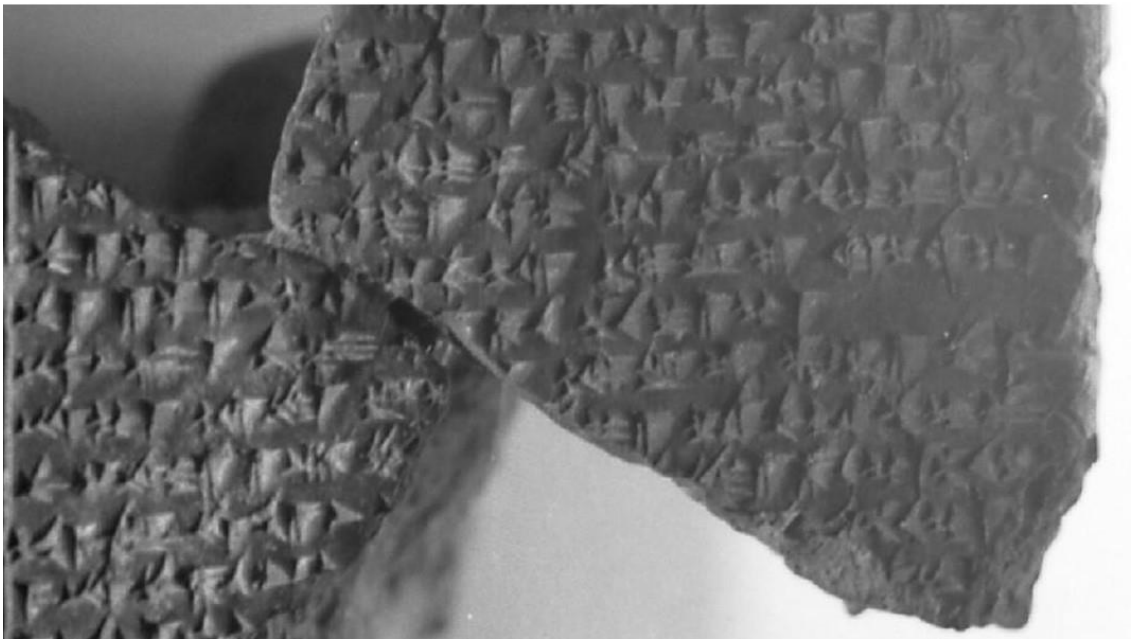

The tablet CTH 383 and its magnification. Modified from: https://www.hethport.adwmainz.de/fotarch/bildausw.php?n=Bo%202057&b=+N03606+N03607+N03608+N03707+N03913+N03914+N04089+N04090+N04092+BoFN00381+BoFN00382+Phb01272+Phb01273

Among other issues, the prayer describes an episode occurred during the reign of Muwatalli II. The king brought a formal trial against his own stepmother Danuhepa, who was the chief priestess of the Sun-goddness of Arinna and the powerful last wife and widow of his father Mursili II. The case led to the (possibly transient) downfall of Danuhepa and to the ruin of her sons and followers. Both Urhi-Teshup (CTH 297) and Hattusili III (CTH 383) seemed eager to lessen their own responsibility in Muwattalli II's haunting of Danuḫepa, being (apparently) concerned about the possible revenge by the Sun goddess of Arinna to them. It is worth mentioning that Danuḫepa was (possibly) restored to royal favour after Muwatalli II's death.

In the prayer CTH 383, Hattusili aims to dissociate himself from his brother Muwatalli II, explicitly stating that he is not involved into the matter of the ruination of Danuhepa's son. In particular, he states what follows:

"The one who did that evil thing (i.e., Muwatalli II) has become a God (i.e., has already died). He stepped down from the road and paid for it with his head. ...The one who has carried out the matter of Danuhepa, that one has already paid for it himself." (Singer, 2002).

The crucial passage states that (Del Monte 2003):

^{15}*na-at IŠ-TU* SAG.D[U-*Š*]*Ú ka-ru-ú pa-ra- a šar-ni-*⌜*ik*⌝*-ta*

Which means: *"(Muwatalli II) paid for it with his head"*.

The words "SAG.DU" and "šarnink" stand, respectively, for "head" and "to compensate". It is noteworthy that the same words are used in Telipinu's edict (CTH 19):

^{52}*nu* SAG.DU-*na-az šar-ni-ik-du*

with the same meaning: *"(the king who did evil things against his brothers or sisters) will pay with his head"*.

In sum, the text CTH 383 clearly states that Muwatalli II was dismissed and killed.
Who did it to Muwatalli II? Hit men sent either by Hattusili, or Urhi-Teshub, or Danuhepa? Unknown sons of Mursili II? A Palace plot? A popular uprising against the king's decision to turn deities or to change the capital?

REFERENCES

1) Bryce T. 2005. The Kingdom of the Hittites. Oxford University Press, Oxford. ISBN-13: 978-0199281329.
2) Del Monte G. 2003. Antologia della letteratura ittita. Servizio Editoriale Universitario di Pisa.
3) Lebrun R. 1980. Hymnes et prières hittites, Louvain-la-Neuve, pp. 309-328.
4) Singer I. 2002. Hittite prayers. Ed. Hoffner JR HA. Society of Biblical Literature, Atlanta, Georgia.

SANSEVERO CHAPEL'S DECORO SCULPTURE IN LIGHT OF RIPA'S ICONOGRAPHY

Arturo Tozzi
Center for Nonlinear Science, Department of Physics, University of North Texas, Denton, Texas, USA
1155 Union Circle, #311427 Denton, TX 76203-5017 USA
tozziarturo@libero.it

The Sansevero Chapel displays a well-conceived design, in which Ripa's iconographic references play an important role. We argue that di Sangro at times distorts Ripa's iconography to illustrate the difficult path awaiting the Mason apprentice. *Decorum,* one of the first sculptures the visitor encounters on their left upon entering the Chapel, lacks two iconographic Ripa's features that would have been very dear to di Sangro: the amaranth, which recalls his studies in natural Palingenesis, and the symbol of Mercury, a highly significant element in both alchemical and Masonic contexts. In the first steps of the initiatory path, the unwelcome absence of the symbol of Mercury prevents the still confused apprentice from perfecting his knowledge. This also explains the absence of amaranth: without the knowledge of initiatory alchemical wisdom, it is not possible to resurrect life, both real and spiritual. As the initiate progresses through the Chapel in a counterclockwise direction, more and more alchemical and Masonic elements begin to appear before his eyes, indicating that he is on the right track in his long journey.

Raimondo di Sangro (1710–1771), Prince of Sansevero, is renowned for his astonishing Neapolitan Chapel (de Ceglia et al. 2024). We examine some Sansevero Chapel's sculptures in light of Cesare Ripa's iconography. Many of the works in the Sansevero Chapel representing abstract concepts follow the conventional code of allegorical representation derived from Ripa's *Iconology*, dating back to 1593. This work written "for poets, painters and sculptors" was highly influential in the 17th century, especially in the field of pictorial and sculptural artistic representation. The treatise, which had fallen out of use by the 18th century, came back into vogue thanks to Sansevero's interest. Indeed, a new edition of *Iconology* compiled by Abbot Cesare Orlandi and published between 1764 and 1767 is dedicated to Raimondo di Sangro, who was its patron (Mandowsky 1939). The 80-year-old Corradini, who came to Naples in the service of the Prince, created 36 models in baked clay, likely representing the original ideas for all the sculptures requested by the patron (Cioffi 1994). It should be noted that both di Sangro and Corradini were freemasons and this may have influenced the iconography of the sculptures they conceived. Some argue that the iconography of the statues in the Chapel is not a precise application of Ripa's work, but this is refuted both by the faithful reproduction of many symbols and by the documented passion di Sangro had for *Iconologia,* to the point of funding a new edition.
Di Sangro made the chapel for various purposes. He wanted a funeral chapel of the highest Neapolitan aristocracy to glorify the patron's family, with the males embodying nobility of the sword and the females nobility of spirit. He wanted to reaffirm the antiquity of the family's aristocracy and illustrate the sanctity of the family. The Chapel displays other interpretative levels too, depending on knowledge of hermetic and Masonic traditions. It might be interpreted either as an allegorical representation of the Masonic initiatory path, where disciplines and virtues are needed to achieve the Great Work, or as the Visible temple of di Sangro's Brothers of the Rose of the Grand Order, or as a Hermetic temple. It is noteworthy that di Sangro wished to preserve the iconography of all the works. He expressed the wish that his heirs always strive to maintain the family church in perfect condition and, above all, to ensure that the decoration remains unchanged down to the smallest detail (di Sangro 1771). He made an exception to the aforementioned prohibition for the painting of the ceiling and four sculptures, including *Decorum*. This exception was authorized by him only on the condition that his eldest son maintained the same virtue symbolized by each sculpture.
In short, the structure of the Chapel reveals a well-conceived initial design, in which Ripa's iconographic references play a very important role.

Several sculptures in the Sansevero Chapel (such as *Decorum*, *The Sweetness of the Marital Yoke*, *Modesty*, *Sincerity*, *Self-Control*, *Education*, and *Divine Love*) slightly differ in certain details from Ripa's traditional representation. See **Figure** for further details. While some of these variations seem to be guided by di Sangro and Corradini's aesthetic and stylistic criteria, other changes are puzzling and worthy of further investigation.

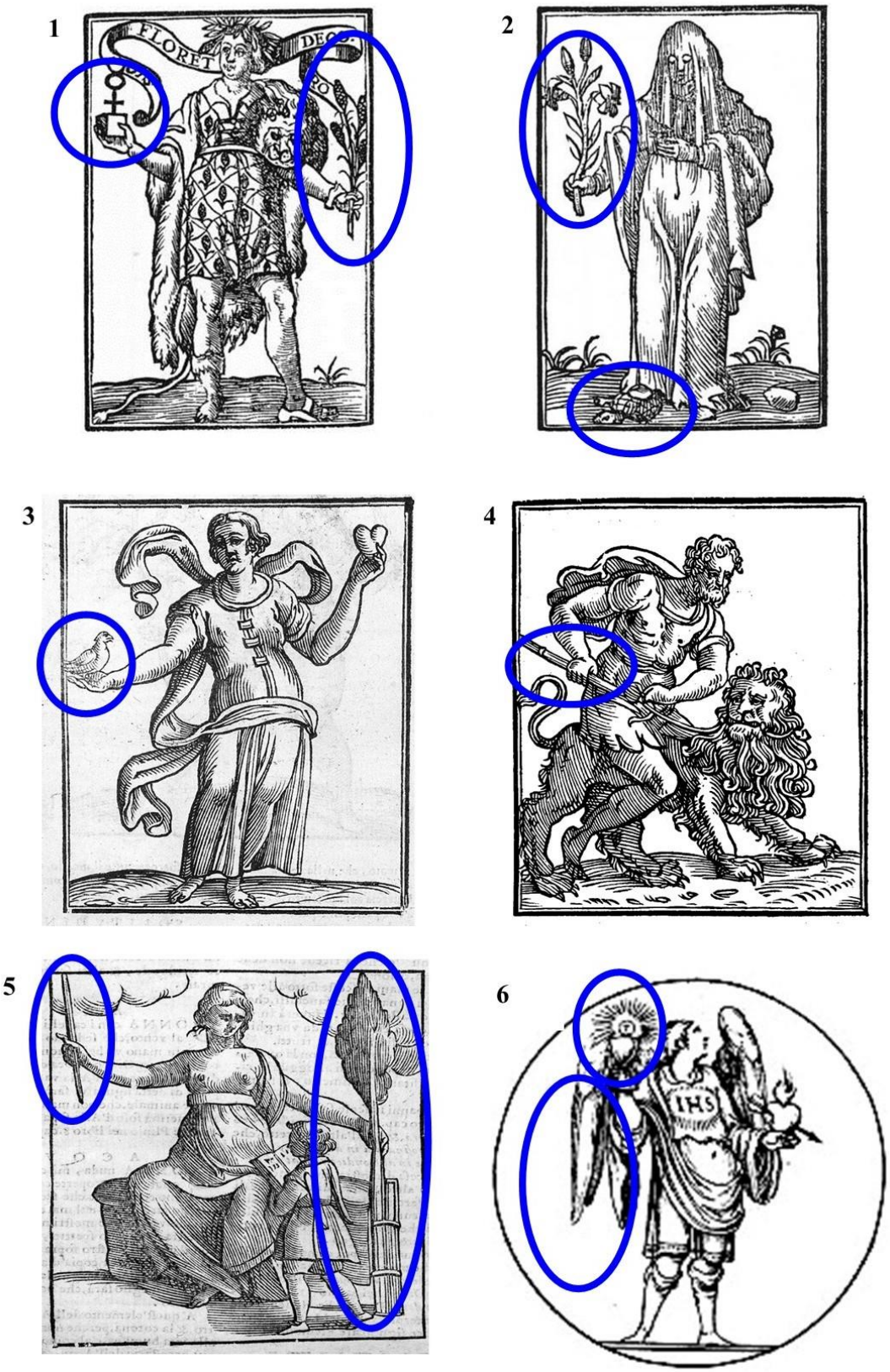

Figure. Ripa's iconography for the abstract concepts of *Decorum* (**Figure 1**), *Modesty* (**Figure 2**), *Sincerity* (**Figure 3**), *Self-Control* (**Figure 4**), *Education* (**Figure 5**), and *Divine Love* (**Figure 6**). The blue circles illustrate the differences between the Sansevero Chapel's sculptures and the corresponding Ripa's iconographic attributes.

Attributed to Corradini, *Decorum* celebrates the virtues of Raimondo's great-grandfather's wife. Corradini's *Decorum* does not perfectly follow Ripa's Iconography, as the amaranth is not present in the young boy's left hand. The amaranth ("which does not wither") is an everlasting plant that has the characteristic of never decaying. Ripa uses the image of the amaranth as a symbol of immortality and of the righteousness of public behavior (Pizzorusso 2018). The amaranth flower, once picked, does not dry out and decay like others but comes back to life when moistened with water. This behaviour strikingly recalls the studies on natural Palingenesis by di Sangro, during which he claimed to revive small animals, such as river crabs, after rehydrating them (Di Sangro 2016).
Yet, the square topped with the symbol of Mercury is missing from the young boy's right hand. This omission is striking, especially considering the alchemical meanings of the symbol of Mercury. The ideogram of Mercury has a tripartite structure representing the Moon, the Sun and the Earth and synthesizes the three astrological archetypes, namely the feminine, the masculine and the material substrate. Yet, in alchemical terms, mercury, along with sulfur, is the primordial element present in all metals.
Summarizing, *Decorum* lacks two important Ripa's iconographic elements that would have been very dear to di Sangro: the amaranth, which recalls his studies in natural Palingenesis, and the symbol of Mercury, a highly significant element in both alchemical and Masonic contexts.

We suggest an interpretation of the absence in the *Decoro* sculpture of the two crucial Ripa's symbols. The right hand of *Decorum* is hidden from view as it is bent behind the back, as if hiding something between their fingers, namely, the symbol of Mercury. Since the alchemical symbol of Mercury had to be hidden, the youth in *Decoro* is forced to keep his right hand behind his back to conceal it. One might think that di Sangro hid the symbol of Mercury because, during the design phase of the Chapel shortly before the 1750, he was compelled to conceal his Masonic initiatory path due to pressures from the more conservative religious authorities of the Kingdom of Naples (Spruit 2006). But this hypothesis does not hold up when considering that the chapel is scattered with more or less explicit Masonic symbols that certainly would not have escaped the watchful ecclesiastical censors.
We suggest that *Decoro*, one of the first sculptures the visitor encounters on their left upon entering the Sansevero Chapel, could represent the first steps of the initiatory path, in which the apprentice is still confused and far from the truth. The unwelcome absence of the alchemical symbol of Mercury prevents the operator from perfecting the Great Work, making the attainment of renewed life impossible. This explains the absence of amaranth in the left hand of the youth in *Decoro*: without the knowledge of initiatory alchemical wisdom provided by Mercury, it is not possible to resurrect life, both real and spiritual.

As the initiate progresses through the Chapel in a counterclockwise direction, alchemical and Masonic elements begin to appear before their eyes. The truth is still hidden in *Modesty* and the underlying bas-relief *Noli me Tangere*, while the physical and metaphysical bonds start to be broken in Queirolo's *Disinganno*. With Christ giving sight to a blind man in the Sammartino's bas-relief of *Disinganno*, the initiatory alchemical and Masonic journey proceeds with the attainment of true sight through the use of reason connected to a profound Christian experience. Then the initiate comes across Queirolo's *Sincerity* holding in her right hand a caduceus, a well-known alchemical symbol. It is noteworthy that all the versions of Ripa's Iconography from 1603 to 1779 do not display this caduceus. This time, Sansevero subverts Ripa's iconographic description by intentionally adding an alchemical symbol, indicating that the initiate is on the right track in his long journey.

In conclusion, while almost always faithful to Ripa's iconography, in some cases di Sangro distorts it in order to illustrate the difficult path that awaits the Mason apprentice.

REFERENCES

1) Cioffi Martinelli R. 1994. La cappella Sansevero. Arte barocca e ideologia massonica. 2 Ed., 1 aprile 1994. ISBN-13: 978-8885651418.
2) de Ceglia FP; Maraschi A, Monno A, Tempesta G. 2024. In Search of the Phoenix in Eighteenth-Century Naples. Raimondo di Sangro, Nature Mimesis, and the Production of Counterfeit Stones between Palingenesis, Alchemy, Art, and Economy. Nuncius, 06 Mar 2024.
3) di Sangro R. 1771. Testamento. Archivio Notarile, Naples, Francesco de Maggio, fol. 62.
4) di Sangro R. 2016. Breve nota di quel che si vede in casa di Raimondo di Sangro Principe di Sansevero. IVth Ed., Colonnese Editore, Napoli.
5) Mandowsky E. 1939. Richerche intorno all'iconologia di Cesare Ripa. La Bibliofilia, disp 7 and 8, app. II.
6) Pizzorusso C. 2018. I fiori di Innsbruck: Lorenzo Lippi e Pietro Andrea Mattioli. Rivista di Letterature moderne e comparate. Vol. LXXI, nuova serie, Fasc. 4, ottobre-dicembre 2018
7) Ripa C. 1613. Iconologia, Eredi di Matteo Florimi, Siena.
8) Spruit L. 2006. Supplica - di Raimondo Di Sangro. Alos ISBN-13: 978-8888247281

TOWARDS A HIGH GENUS COSMIC MANIFOLD

Arturo Tozzi
Center for Nonlinear Science, Department of Physics, University of North Texas, Denton, Texas, USA
1155 Union Circle, #311427, Denton, TX 76203-5017, USA
tozziarturo@libero.it

ABSTRACT

The universe is punctured with a high number of black holes that might stand for topological "holes" or "cavities". Starting from this observation, we discuss the possibility to think over the universe in terms of a manifold of very high genus (henceforward VHGM), rather than an isotropic and homogeneous manifold of genus zero. We argue about the feasibility and the likely physical consequences of a cosmic VHGM approach. In ΛCDM, a topological surface of very high genus might guarantee highly stable, topologically ordered structures protected against small perturbations, leading to fine-tuning and consistency of cosmic parameters. In non-standard cosmological models, a VHGM framework might help to elucidate spatial features like extra-dimensions, compactified universes, spacetime foam, multi-loops string interactions. Groups of almost infinite surface diffeomorphisms might also generate topological defects, impurities, passages and handles that connect different regions at either micro-, meso- or macroscopic physical scales, shedding light on the accelerated expansion of the Universe, on wormholes, on multiverse and bubble universes. VHGM might also contribute to the nonlocal interactions that are typical of quantum entanglement and to information and energy storage, with special attention to the quantum vacuum discrepancy and the holographic approaches. In conclusion, the theoretical possibility of a cosmic VHGM suggests a strong and methodologically manageable mathematical background subtending the mechanical, dynamical, energetic and informational features of the spacetime fabric in both ΛCDM and non-standard cosmological models.

Keywords: cosmology; astrophysics; ΛCDM; geometric topology; Planck results.

INTRODUCTION

The universe, isotropic and homogeneous at very large scales, can be regarded as a spatially flat, genus-zero four-dimensional manifold (de Bernardis et al., 2000). The assumption that the universe does not contain holes is implicitly taken for granted by the most influential accounts (Planck Collaboration 2016). Here we release a version that goes against the mainstream "genus-zero tenet". We argue that the cosmic manifold exhibits countless "handles" or "cavities" due to the occurrence of black holes that break its continuity. Very high genus manifolds (henceforward VHGMs) are mathematical objects pulled out when conventional, finite-genus systems' descriptions are inadequate. The higher the genus, the more complex the surface and/or the manifold. In mathematical jargon, the VHGM's groups of homeomorphisms, diffeomorphism and big mapping class groups, including the Riemannian ones, exhibit quantifiable algebraic and topological properties that affect one each other (Aramayona et al., 2020; Aougab et al., 2021; Mann and Rafi, 2023). The "holes" can be understood in a variety of topological ways, including regions, handles, punctures, loops, vortices, groups of symmetries, etc.
The question is: assuming our hypothesis is true and the universe can be described in terms of a high genus manifold, what are the physical outcomes? We will argue that the rich VHGM's topological features can be used to assess complex physical structures at different coarse-grained levels of observation, from the micro- to the meso- and the macro-scale. VHGMs can be used not just for the description of topological features, but also of spatial features (e.g., lines, perimeters, areas, volumes), images, spatial and temporal patterns, particle trajectories, vectors, tensors, functions, range of data, thermodynamic parameters, defects, impurities, signals (Tozzi et al., 2017). A list of feasible VHGM applications in physical and cosmic contexts is portrayed in **Table**. In each of the following chapters, our goal will be twofold:

1) To illustrate the feasible physical properties of a hypothetical manifold of very high, almost infinite genus.
2) To use VHGM to describe and/or assess both non-standard cosmological models and the standard, 6-parameter lambda cold dark matter model (henceforward ΛCDM), which continues to supply an excellent fit to the cosmic microwave background data at high and low redshift (Aghanim et al., 2020).

To sum up, we claim that the abstract topological manifolds of very high or infinite genus may have fascinating applications across various fields in physics, theoretical physics and astrophysics.

Spatial & geometric features	
	extra-dimensions
	compactified universes
	spacetime foam
	exotic cosmic topologies
	imaginary numbers in quantum mechanics
Highly stable structures	
	fine-tuning
	constant cosmic parameters
Impurities and defects, passages or handles	
	multiverse and bubble universes
	wormholes
	accelerated expansion of the Universe
Systems Dynamics interactions	
	strings interactions like splitting and joining
	multi-loops string interactions
Scale-free dynamics, chaotic dynamics	
	fractal-like distribution
Nonlocal interactions	
	quantum entanglement
Thermodynamic features	
	quantum vacuum discrepancy
	black hole thermodynamics
	holographic universe
Temporal dimensions	
	cosmic evolution

Table. Potential physical properties of topological objects with very high genus. The cosmic features that might be potentially described by high genus topological objects are displayed.

SPATIAL & GEOMETRIC FEATURES

The holes may represent systems with a highly flexible or "deformable" geometry characterized by a high number of possible shapes or sizes. In differential topology and in geometric group theory, but also in physics, VHGM may play crucial roles in building exotic, differentiable structures with unusual spatial properties, in which the high dimensional, smooth manifold structure differs from the canonical ones. Topological holes can be used to assess infinite-dimensional moduli spaces in which the parameters describing the system's geometry can vary in an almost infinitely complex way. High genus surfaces can be also equipped with more rigid structures consisting of translation constructions (Hooper 2013). Since the holes may represent not just natural numbers, but also integers, rationals, irrationals and imaginary numbers (Tozzi et al., 2017), they can be used to assess the the complex plane's mathematics subtending quantum dynamics.

In higher-dimensional physical theories, the geometry of the extra dimensions can be highly nontrivial, with bulky effects on the large-scale structure on the universe (Bars and Terning, 2009; Watts et al., 2017). In string theory, the universe is often modeled with extra dimensions that can be compactified in complicated ways through Calabi-Yau manifolds (Douglas 2015). These compactified universes may include "multi-connected" spaces with repeating regions that can be assimilated to the concept of VHGM.

Surfaces of almost infinite genus could arise in scenarios where fluctuations become extreme. Particularly in case of higher-dimensional spaces or complex boundary conditions, the number of holes, handles and path integrals increase without bounds. In the context of quantum gravity and in more exotic scenarios like certain models of loop quantum gravity and string theory, the concept of the universe as a smooth manifold is challenged at the Planck scale's high energy

regimes, where the spacetime is thought to dynamically behave like a "foam" with large fluctuations in geometry and topology (Davis 1994; Carlip 2023).
The homogeneous and isotropic large-scale structure described by the cosmological principle in ΛCDM is usually modeled as a 3-dimensional spatial manifold with relatively simple topologies involving either flat, convex or concave spaces (Boylan-Kolchin 2023). Yet, there is room for other hypothetical spacetime structures where space is not simply connected but rather is characterized by a high number of topological features and a large variety of shapes. Infinite-genus manifolds embrace different structures that could theoretically match the shape of the universe, including:

1) The infinite Loch Ness monster surface, equipped with an orientable surface of infinite genus that displays only one end (Valdez 2009; Arredondo and Ramírez Maluendas, 2017). Its metrizable topological surface provides an example of chaotic groups of countable products' homeomorphisms (Zhukova and Korotkov, 2022).
2) The two ends surface termed Jacob's ladder surface (Ghys 1995).
3) The groups with no planar ends and with self-similar end spaces (Aougab et al., 2021).
4) The Weierstrass' one-ended, periodic minimal surfaces (Thayer 2012).
5) The Veech groups of tame translation surfaces, where every end has genus (Ramírez Maluendas and Valdez 2017).
6) The blooming Cantor trees with infinite number of handles and wild translation surfaces (Randecker 2018).
7) Parabolic or infinite translation surfaces with wild singularities. In this case, there is a failure of the classical Gauss-Bonnet formula for translation surfaces, which relates the cone angle of the singularities (geometry) to the genus of the surface (topology) (Randecker 2018).

It should be noted that non-trivial spatial topologies of the universe may give rise to potentially measurable signatures in the cosmic microwave background. To date, machine learning approaches have been used to classify viable topologies of the microwave background, at least in the test case of small toroidal universes (Tamosiunas et al., 2024).

HIGHLY STABLE, TOPOLOGICALLY ORDERED STRUCTURES

The holes may represent a highly stable, topologically ordered phase of matter where the large number of topological features protects against small perturbations, as in the case of topological quantum computing. Surfaces of almost infinite genus can be also associated with low-dimensional topology, infinite cyclic knot group and knot complements, i.e., the space left after removing a knot from a three-dimensional space (Conway and Powell, 2023).
In this metatheoretic cosmic context, the holes may represent a highly stable, topologically ordered structure of the universe where the large number of topological features protect against small perturbations. This suggests that a VHGM approach to the universe might contribute to solve the fine-tuning problem, constraining the cosmic parameters to remain constant within tight limits (Landsman 2016).

IMPURITIES AND DEFECTS, "PASSAGES" AND "HANDLES"

The holes may represent the systems' impurities that affect the conductive or magnetic properties, especially in certain models of spin liquids or quantum Hall states. To provide an example, colloidal platinum nanocrystals produced from the same synthesis batch may display intertwined topological defects that include size variations, lattice distortions, structural degeneracies, strain (Kim et al., 2020). These tiny differences in structure may generate non-trivial topologies that lead to systems dynamics' modifications and energetic frustration, unexpectedly influencing the system's physical properties (Kim et al., 2020).
In chaotic inflationary models characterized by a process of eternal inflation, the universe is thought to spawn an almost infinite number of "bubble universes" or "pocket universes" that become isolated from one another but are potentially connected through an almost infinite number of complex topological structures (Fialko et al, 2015). These connections could manifest through the presence of bridges between different regions. In the VHGM context, the hypothetical wormholes can be thought of as handles that connect different regions of either spacetime or multiverse. It has been conjectured that billions of microscopic wormholes could be responsible for the current accelerated expansion of the universe, where the visible horizon is 10^{29}, expanding at a speed of 74,3±2,1 km/sec per megaparsec. In a VHGM framework, the effective cosmological constant depends on the Gauss-Bonnet coupling and the wormhole density, attaining an effective dark energy sector of topological origin (Tsilioukas et al, 2024)

SYSTEMS DYNAMIC INTERACTIONS

The holes may represent the number of possible configurations involving different physical quantities. High topological complexity with an unbounded number of degrees of freedom describes physical systems with an enormous number of interaction pathways, including particles, fields, vortices, connections, charge configurations, excitations, phase transitions, chaotic bifurcations, etc.

The holes may represent loops, cycles, fluxes and vortices hinting at conserved quantities in dynamical systems. This approach has remarkable methodological and operational implications. For instance, when assessing the variance in observables' measurement during scattering events, the classical regime characterized by negligible uncertainty may emerge because of an infinite set of relationships among multiloop amplitudes in a momentum-transfer expansion (Cristofoli et al., 2021). VHGM could represent a high number of quantum loops or topological excitations, corresponding to physical systems that have complex boundary conditions or nontrivial vacuum states, leading to topological fluctuations of the spacetime at the quantum level.

In string theory, high genus surfaces can be used to describe different classes of interactions. For instance, the worldsheet of a propagating string can be modeled as a two-dimensional surface where strings interactions such as splitting and joining correspond to different topologies (Demulder et al., 2023). In perturbative string theory, the worldsheet surface's almost infinite genus is related to the number of loops in the string interactions, characterized by the vanishing capacity of the ideal boundary (Davis 2005). When the higher-order corrections to string interactions involve more loops, the surface's genus tends to increase. It is noteworthy that, in a cosmic VHGM context, the countable series of the above-mentioned infinite genus Loch Ness monster's loops may stand for string interactions.

SCALE-FREE DYNAMICS, CHAOTIC BEHAVIOUR

The holes may represent scale-free dynamics, namely (spatial) fractal-like distribution, (temporal) power laws, $1/f\alpha$ behavior, self-similarity, scale-invariant structure. A surface with fractal structure displays the same topological features repeating at each scale and generating almost infinite complexity at all scales (Hernández et al., 2017). Also, the holes may represent chaotic behavior, where sensitivity to initial conditions, density of closed orbits of homeomorphism groups and their countable products are correlated with high genus topological features (Zhukova and Korotkov, 2022).

If the universe has a fractal structure either at small or large scales as suggested by a few authors (see, e.g., Dickau 2009), the cosmic distribution of matter may not be homogeneous, but instead follow a fractal-like distribution, generating an almost infinitely complex, self-similar pattern that might involve surfaces of very high genus. This is also the case of the Everett III's formulation of quantum mechanics (Everett III 1957), where the number of the branching trees of all the possible outcomes is almost infinite and can therefore be described by a VHGM mathematical approach.

NONLOCAL INTERACTIONS

The holes may represent nonlocal interactions. In this case, information is spread out across the entire area of a high genus surface, with no single "local" description being sufficient. Non-local covers of infinite-type surfaces have different possible homeomorphism types (Biringer et al., 2024) so that complex space connectivity can be used to assess physical nonlocal interactions, especially in the cases of quantum entanglement and topological phases of matter.

If spacetime itself was modeled as a surface of very high genus, this could imply that distant regions of the universe are connected in a highly intricate and nonlocal manner. Nonlocality could manifest through the presence of particles connected by topologically nontrivial paths. This is the case with quantum entanglement.

A Riemann surface with very high genus can be thought of as having an indefinite number of handles or punctures corresponding to the moduli spaces of highly intricate geometric structures. This means that the holes may represent "passages" that can be visualized as "handles" connecting different elements at either the micro-, meso- or macroscopic physical scales.

THERMODYNAMIC FEATURES

The holes may represent thermodynamic parameters like energy. In physical contexts, energetic changes do not depend anymore on thermodynamic parameters, but rather on topological features like affine connections, projections, homotopies and continuous functions (Tozzi and Papo, 2017). Yet, random surfaces of infinite genus may describe the large-N thermodynamic limits that can be reached in statistical mechanics as well as in string theory.

The holes may represent information storage. A surface of almost infinite genus could store an almost infinite amount of topological information, particularly in the thermodynamic limit where the number of the components (e.g., particles, strings or signals) goes to infinity, their behavior becoming indefinitely complex (La 1991). This explains why certain theoretical models of quantum memory or holographic systems are described as supplied with vast or even infinite information capacity.
In conformal field theory and topological quantum field theory, surfaces of almost infinite genus can be used to model systems where the number of topological interactions or degrees of freedom becomes unbounded. The fact that an almost infinite entropy might correspond to an almost infinite number of possible cosmic configurations could be relevant in situations where the number of accessible microstates is extremely large, as is the case of black hole thermodynamics or cosmical systems undergoing phase transitions. Also, a VHGM-like approach with the energy endowed inside the topological holes might help to solve the scale discrepancy between the observed vacuum energy of just 10^{-9} J/m^3 and the theoretical quantum vacuum energy of 10^{133} j/m^3 (Henke 2017).
Black hole's exponential complexity is a matter of fact in the holographic dictionary. When coping with isolated, single-sided, non-evaporating black holes, reconstruction of interior outgoing modes is always exponentially complex (Engelhardt et al., 2021). The "quantum extremal surface" appears to encode the amount of holographic entanglement entropy that has radiated away from the black hole, evolving over the black hole's lifetime exactly as expected if information escapes (Engelhardt and Wall, 2014). New results show that an infinite number of black holes configurations are conceivable in dimensions higher than three, leading to a full range of possible topologies for the horizon as well as the domain of outer communication (Khuri and Rainone, 2022).

TEMPORAL DIMENSIONS

The holes may represent not just "spatial" dimensions, but also other kinds of dimensions such as the temporal ones. This means that a high genus topological structure can be made not just of space, but also of time, portraying the temporal evolution of the universe. Certain approaches to quantum gravity suggest that the topology of the universe could evolve over time, acquiring more and more topological complexity, possibly approaching an almost infinite genus in some future state. Therefore, the evolutionary processes of the universe might be studied via VHGM methodologies.

Summarizing, the abstract mathematical framework described by VHGM can be fruitfully used to investigate physical systems that are characterized by a very high amount of geometric, mechanical, dynamical, energetic, informational interactions and/or configurations. Some applications of VHGM are highly theoretical but are crucial for studying the limits in applications like quantum Hall effects and topological insulators. In our paper, we narrowed our list of feasible applications, focusing on the issue of a VHGM-like physical universe in both non-standard cosmological models and ΛCDM.

CONCLUSIONS

The universe regarded as a topological manifold of high genus is a speculative idea. Direct experimental evidence is lacking and none of the widely accepted cosmological models posit the universe as having a very high genus. Nevertheless, several theoretical backgrounds in modern physics implicitly allow for such a possibility, especially when considering the relationship between complex topological features and the spacetime structure.
While mathematically possible, a very high genus universe must face serious challenges. Observational evidence and the current understanding of cosmology suggest that, if such complexity exists, it may be hidden beyond the reach of current experiments. An objection may be raised concerning the cosmic microwave background (henceforward CMB), which describes a large-scale cosmic manifold that is isotropic and homogeneous, providing strong constraints on the possible topologies of the universe (Linker et al, 2024). The answer to this objection is that CMB was emitted from the surface of last scattering about 379,000 years after the Big Bang, while the most recent candidates for the oldest-known black holes date back to 400 million years after the Big Bang (Maiolino et al., 2024). This means that the primeval, continuous, uniform, isotropic and homogeneous manifold carved by CMB preceded the onset of singularities like the first black holes. Starting from an isotropic and homogeneous universe after the Big Bang, the production of many generations of black holes might have pierced the spatiotemporal continuum, progressively leading to a universe equipped with higher and higher genus. Moreover, the introduction of very high topological complexity into a physical model might raise issues of stability and energy. Almost infinite genus might imply an almost infinite amount of energy or complexity in spacetime, which could be physically problematic. This issue could be solved by considering that this huge amount of energy could be hidden inside the cosmic holes.

It could be speculated that a cosmic VHGM approach could help to elucidate the mystery of the physical nature of the dark sector of the universe. However, when comparing the topological properties of the large-scale dark matter distribution in various cosmological models, the ΛCDM and warm dark matter models produce nearly identical genus curves, indicating no topological differences in structure formation (Watts et al., 2017). In turn, the quintessence model produces significant differences in the strength and redshift evolution of non-Gaussian modes associated with higher cluster and lower void abundances (Watts et al., 2017).
To oppose to these drawbacks, there is one advantage to using a VHGM approach, namely the possibility of using the tools at our disposal such as the Teichmüller's infinite-dimensional spaces, that allow not just the mathematical classification of the elements of big mapping class groups, but also the assessment of countless physical systems including geodesic currents, foliations, laminations (Saric 2018).

It would be obvious to think that black holes are too small to affect the macrocosm, but it is not the case. Supermassive black holes can deeply influence the macroscopic structure of the spacetime, regulating cool gas accretion in massive galaxies (Wang et al., 2024). Still, micrometer-scale waves simulating black hole ringdown signatures are able to modify the background velocity field via intricate wave–vortex interactions (Švančara et al., 2024). Further, simulated postmerger gravitational-wave signals generated by binary black hole coalescence produce deep changes in nonlinear spacetime dynamics (Mitman et al., 2024). Galactic overdensities around ancient supermassive black holes support the idea that the most distant black holes grow within huge dark matter halos (Mignoli et al., 2020), generating gigantic high-power jets that represent the largest galaxy-made structures (Oei et al., 2024). Information change between black holes and spacetime is another clue testifying the effects of the black holes on cosmic structures (Chesler et al., 2019).

We showed that very high genus manifolds could be theoretically acknowledged also in ΛCDM (Aghanim et al., 2020). A VHGM-like approach could explain why the ΛCDM universe is highly connected and displays a very high number of quantum loops and topological excitations. Another theoretical source of cosmic "holes" could be represented by the occurrence of cosmic voids, i.e., vast pockets that are on average less dense than the universe. Making up together at least 80% of the universe's volume, such "bubbles" can span hundreds of millions of light-years (Contarini et al., 2022). Here, contrary to the usual efforts to evaluate how the expansion of the universe would affect the number and density of voids, we emphasize the possible effects of the voids on the cosmic manifold.
The holes may represent also biological features. Apart from the VHGM applications in physics, aspects of biological complexity like large interaction networks (e.g., indefinitely scaling neural networks, protein folding, metabolic pathways, cell signaling networks, ecosystems), and spatial or temporal self-similar structures (e.g., vascular systems, evolutionary processes), can be approximated to intricate, high genus topological structures in which the complexity could dramatically increase.

In sum, while there is no direct evidence to suggest that the universe has a topological manifold of infinite genus, certain theoretical frameworks, especially quantum gravity and string theory, open the door to such a possibility. Surfaces of infinite genus could model exotic, fractal, chaotic structures of spacetime, especially at very small or very large scales. But there is also room for a VHGM-like interpretation of the standard ΛCDM model.

DECLARATIONS

Ethics approval and consent to participate: This research does not contain any studies with human participants or animals performed by the Author.
Consent for publication: The Author transfers all copyright ownership, in the event the work is published. The undersigned author warrants that the article is original, does not infringe on any copyright or other proprietary right of any third part, is not under consideration by another journal, and has not been previously published.
Availability of data and materials: all data and materials generated or analyzed during this study are included in the manuscript. The Author had full access to all the data in the study and take responsibility for the integrity of the data and the accuracy of the data analysis.
Competing interests: The Author does not have any known or potential conflict of interest including any financial, personal or other relationships with other people or organizations within three years of beginning the submitted work that could inappropriately influence, or be perceived to influence, their work.
Funding: This research did not receive any specific grant from funding agencies in the public, commercial, or not-for-profit sectors.
Authors' contributions: The Author performed: study concept and design, acquisition of data, analysis and interpretation of data, drafting of the manuscript, critical revision of the manuscript for important intellectual content, statistical analysis, obtained funding, administrative, technical, and material support, study supervision.
Acknowledgements: none.

REFERENCES

1) Aghanim N, Y. Akrami, F. Arroja, M. Ashdown, J. Aumont, et al. 2020. Planck 2018 results - I. Overview and the cosmological legacy of Planck. A&A Volume 641, A1. DOI: https://doi.org/10.1051/0004-6361/201833880
2) Aougab, T., Patel, P. & Vlamis, N.G. 2021. Isometry groups of infinite-genus hyperbolic surfaces. Math. Ann. 381, 459–498 (2021). https://doi.org/10.1007/s00208-021-02164-z
3) Aramayona, Javier; Priyam Patel, Nicholas G Vlamis. 2020. The First Integral Cohomology of Pure Mapping Class Groups. International Mathematics Research Notices, Volume 2020, Issue 22, November 2020, Pages 8973–8996, https://doi.org/10.1093/imrn/rnaa229
4) Arredondo JA, Ramírez Maluendas C. 2017. On the Infinite Loch Ness monster. Commentationes Mathematicae Universitatis Carolinae, 58 (4): 465–479. doi:10.14712/1213-7243.2015.227.
5) Bars, I.; Terning, J. 2009. *Extra Dimensions in Space and Time*; Springer: Berlin, Germany. ISBN 978-0-387-77637-8.
6) Boylan-Kolchin, Michael. 2023. Stress testing Λ CDM with high-redshift galaxy candidates. Nat Astron . 2023;7(6):731-735. doi: 10.1038/s41550-023-01937-7. Epub 2023 Apr 13.
7) Biringer, Ian; Yassin Chandran, Tommaso Cremaschi, Jing Tao, Nicholas G. Vlamis, et al. 2024. Covers of surfaces. arXiv:2409.03967v2
8) Carlip S. 2023. Spacetime foam: a review. Rep. Prog. Phys. 86 066001. DOI 10.1088/1361-6633/acceb4
9) Chesler, Paul M.; Ramesh Narayan, Erik Curiel. 2019. Singularities in Reissner-Nordström black holes. arXiv:1902.08323
10) Contarini, Sofia; Alice Pisani, Nico Hamaus, Federico Marulli, Lauro Moscardini, Marco Baldi. 2022. The perspective of voids on rising cosmology tensions. arXiv:2212.07438, last revised 5 Feb 2024
11) Conway, Anthony; Mark Powell. 2023. Embedded surfaces with infinite cyclic knot group. Geometry & Topology 27:2 (2023) 739–821. DOI: 10.2140/gt.2023.27.739
12) Cristofoli, Andrea; Riccardo Gonzo, Nathan Moynihan, Donal O'Connell, Alasdair Ross, et al. 2021 . The Uncertainty Principle and Classical Amplitudes. arXiv:2112.07556v1. latest version 29 May 2024
13) Davis, Simon. 1994. The Four-Point Function On A Surface Of Infinite Genus. Modern Physics Letters AVol. 09, No. 14, pp. 1299-1307. https://doi.org/10.1142/S021773239400112XCited by:3 (Source: Crossref)
14) Davis, Simon. 2005. Effectively Closed Infinite-Genus Surfaces And The String Coupling. International Journal of Modern Physics AVol. 20, No. 04, pp. 821-850. https://doi.org/10.1142/S0217751X05021245
15) de Bernardis, P., Ade, P., Bock, J. et al. A flat Universe from high-resolution maps of the cosmic microwave background radiation. Nature 404, 955–959 (2000). https://doi.org/10.1038/35010035
16) Demulder, Saskia; Sibylle Driezen, Bob Knighton, Gerben Oling, Ana L. Retore, et al., 2025. Exact approaches on the string worldsheet. arXiv:2312.12930. last revised 28 Jan 2024
17) Dickau, Jonathan J. 2009. Fractal cosmology. Chaos, Solitons & Fractals. 41 (4): 2103–2105. Bibcode:2009CSF....41.2103D. doi:10.1016/j.chaos.2008.07.056. ISSN 0960-0779.
18) Douglas, Michael R. 2015. Calabi–Yau metrics and string compactification. Nuclear Physics B, Volume 898, September 2015, Pages 667-674
19) Engelhardt, Netta; Aron C. Wall. 2014. Quantum Extremal Surfaces: Holographic Entanglement Entropy beyond the Classical Regime. arXiv:1408.3203, last revised 14 Jan 2015.
20) Engelhardt, Netta; Geoff Penington, Arvin Shahbazi-Moghaddam. 2021. Finding Pythons in Unexpected Places. arXiv:2105.09316
21) Everett III, Hugh. 1957. “Relative State” Formulation of Quantum Mechanics. Rev. Mod. Phys. 29.
22) Fialko O.; B. Opanchuk, A. I. Sidorov, P. D. Drummond, J. Brand. 2015. Fate of the false vacuum: Towards realization with ultra-cold atoms. Europhysics Letters, Volume 110, Number 5, EPL 110 56001. DOI 10.1209/0295-5075/110/56001
23) Ghys É. 1995. Topologie des feuilles génériques. Annals of Mathematics, Second Series, 141 (2): 387–422, doi:10.2307/2118526.
24) Henke, Christian. 2017. Quantum vacuum energy in General Relativity. arXiv:1712.08518. Last revised 7 Feb 2019.
25) Hernández, J., Israel Morales, Ferrán Valdez. 2017. The Alexander Method for Infinite-Type Surfaces. The Michigan mathematical Journal. DOI:10.1307/MMJ/1561773633Corpus
26) Hooper, W. Patrick. 2013. Grid Graphs and Lattice Surfaces Get access Arrow. International Mathematics Research Notices, Volume 2013, Issue 12, 2013, Pages 2657–2698, https://doi.org/10.1093/imrn/rns124
27) Kim, Byung Hyo; Junyoung Heo, Sungin Kim, Cyril F Reboul, Hoje Chun, et al. 2020. Critical differences in 3D atomic structure of individual ligand-protected nanocrystals in solution. Science. 2020 Apr 3;368(6486):60-67. doi: 10.1126/science.aax3233.
28) Khuri, Marcus A.; Jordan F. Rainone. 2022. Black Lenses in Kaluza-Klein Matter. arXiv:2212.06762. last revised 11 Jul 2023

29) La, HoSeong. 1991. Thermodynamics of handles. Annals of Physics, Volume 205, Issue 2, 1 February 1991, Pages 458-472
30) Landsman, K. 2016. The Fine-Tuning Argument: Exploring the Improbability of Our Existence. In: Landsman, K., van Wolde, E. (eds) The Challenge of Chance. The Frontiers Collection. Springer, Cham. https://doi.org/10.1007/978-3-319-26300-7_6
31) Linker, P., Ozel, C., Pigazzini, A. et al. 2024. A K-Theory Approach to Characterize Admissible Physical Manifolds. Int J Theor Phys 63, 68 (2024). https://doi.org/10.1007/s10773-024-05608-9
32) Maiolino, R., Scholtz, J., Witstok, J. et al. A small and vigorous black hole in the early Universe. Nature 627, 59–63 (2024). https://doi.org/10.1038/s41586-024-07052-5
33) Mann, Kathryn; Kasra Rafi. 2023. Large-scale geometry of big mapping class groups. Geometry & Topology 27:6 (2023) 2237–2296 DOI: 10.2140/gt.2023.27.2237
34) Mignoli Marco; Roberto Gilli, Roberto Decarli, Eros Vanzella, Barbara Balmaverde, et al. 2020. Web of the giant: Spectroscopic confirmation of a large-scale structure around the z = 6.31 quasar SDSS J1030+0524. Astronomy & Astrophysics. Volume 642, October 2020, DOI: https://doi.org/10.1051/0004-6361/202039045
35) Mitman, Keefe; Macarena Lagos, Leo C. Stein, Sizheng Ma, Lam Hui, et al. 2023. Nonlinearities in Black Hole Ringdowns. Phys. Rev. Lett. 130, 081402 – Published 22 February 2023
36) Oei, M.S.S.L., Hardcastle, M.J., Timmerman, R. et al. Black hole jets on the scale of the cosmic web. Nature 633, 537–541 (2024). https://doi.org/10.1038/s41586-024-07879-y
37) Planck Collaboration. 2016. Planck 2015 results. XIII. Cosmological parameters. Astronomy & Astrophysics, Volume 594, id.A13, 63 pp.
38) Ramírez Maluendas C, Valdez F. 2017. Veech groups of infinite-genus surfaces. Algebraic & Geometric Topology 17 529–560. DOI: 10.2140/agt.2017.17.529
39) Randecker A. 2018. Wild translation surfaces and infinite genus. Algebraic & Geometric Topology 18, 2661–2699. DOI: 10.2140/agt.2018.18.2661.
40) Saric, Dragomir. 2018. Thurston's boundary for Teichmüller spaces of infinite surfaces: the length spectrum. Proc. Amer. Math. Soc. 146 (2018), no. 6, 2457–2471.
41) Švančara, P., Smaniotto, P., Solidoro, L. et al. Rotating curved spacetime signatures from a giant quantum vortex. Nature 628, 66–70 (2024). https://doi.org/10.1038/s41586-024-07176-8
42) Tamosiunas, Andrius; Fernando Cornet-Gomez, Yashar Akrami, Stefano Anselmi, Javier Carrón Duque, et al. 2024. Cosmic topology. Part IVa. Classification of manifolds using machine learning: a case study with small toroidal universes. Journal of Cosmology and Astroparticle Physics, Volume 2024, September 2024. DOI 10.1088/1475-7516/2024/09/057
43) Thayer, Edward C. 2012. Higher-Genus Chen–Gackstatter Surfaces and The Weierstrass Representation for Surfaces of Infinite Genus. Experimental Mathematics, Volume 4, 1995 - Issue 1, Pages 19-39. https://doi.org/10.1080/10586458.1995.10504305
44) Tozzi A, Papo D. 2020. Projective mechanisms subtending real world phenomena wipe away cause effect relationships. Progress in Biophysics and Molecular Biology. 151:1-13. DOI: 10.1016/j.pbiomolbio.2019.12.002.
45) Tozzi A, Peters JF, Fingelkurts AA, Fingelkurts AA, Marijuán PC. 2017. Topodynamics of metastable brains. Physics of Life Reviews, 21, 1-20. http://dx.doi.org/10.1016/j.plrev.2017.03.001.
46) Tsilioukas, Stylianos A.; Emmanuel N. Saridakis, Charalampos Tzerefos. 2024. Dark energy from topology change induced by microscopic Gauss-Bonnet wormholes. Phys. Rev. D 109, 084010 – Published 5 April 2024
47) Valdez F. 2009 Infinite genus surfaces and irrational polygonal billiards. Geom Dedicata 143, 143 (2009). https://doi.org/10.1007/s10711-009-9378-x
48) Wang, T., Xu, K., Wu, Y. et al. Black holes regulate cool gas accretion in massive galaxies. Nature 632, 1009–1013 (2024). https://doi.org/10.1038/s41586-024-07821-2
49) Watts, Andrew L.; Pascal J. Elahi, Geraint F. Lewis, Chris Power. 2017. Large-scale structure topology in non-standard cosmologies: impact of dark sector physics. Monthly Notices of the Royal Astronomical Society, Volume 468, Issue 1, June 2017, Pages 59–68, https://doi.org/10.1093/mnras/stx375
50) Zhukova N. I.; G. Korotkov. 2022. Chaotic behaviour of countable products of homeomorphism groups. Pages 1287-1312. https://doi.org/10.1080/10236198.2022.2090838 CrossMark LogoCrossMark